Scientific and Technical Aerospace Reports

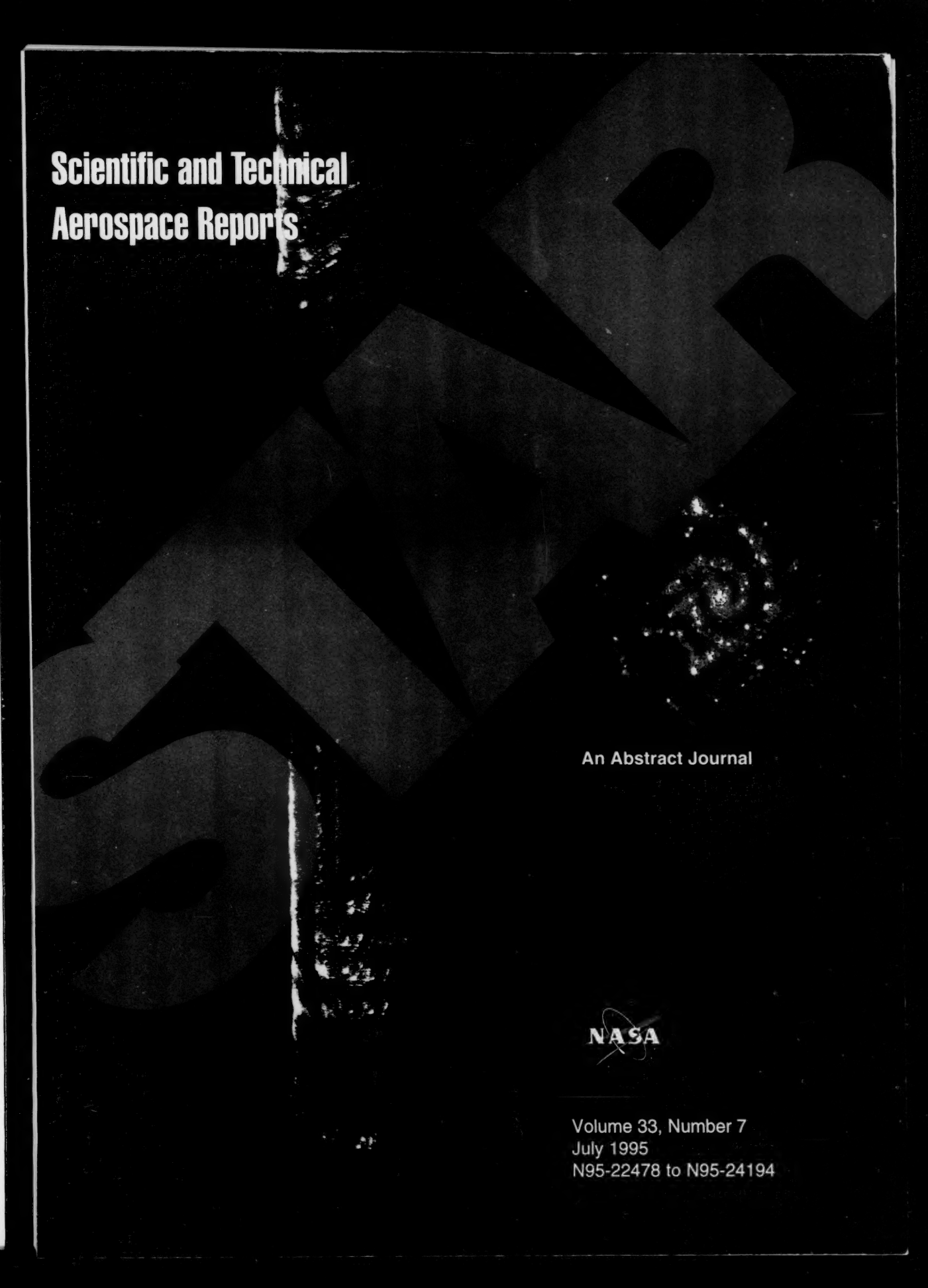

An Abstract Journal

NASA

Volume 33, Number 7
July 1995
N95-22478 to N95-24194

The NASA STI Office ... in Profile

Since its founding, NASA has been dedicated to the advancement of aeronautics and space science. The NASA Scientific and Technical Information (STI) Office plays a key part in helping NASA maintain this important role.

The NASA STI Office provides access to the NASA STI Database, the largest collection of aeronautical and space science STI in the world. The Office is also NASA's institutional mechanism for disseminating the results of its research and development activities.

Specialized services that help round out the Office's diverse offerings include creating custom thesauri, translating material to or from 34 foreign languages, building customized databases, organizing and publishing research results ... even providing videos.

For more information about the NASA STI Office, you can:

- **Phone** the NASA Access Help Desk at (301) 621-0390
- **Fax** your question to the NASA Access Help Desk at (301) 621-0134
- **E-mail** your question via the **Internet** to help@sti.nasa.gov
- **Write** to:

NASA Access Help Desk
NASA Center for AeroSpace Information
800 Elkridge Landing Road
Linthicum Heights, MD 21090-2934

Scientific and Technical Aerospace Reports

Scientific and Technical Aerospace Reports (STAR), is published each month as a major product of the NASA Scientific and Technical Information (STI) Office.

Inside this issue you will find:

- **Front Matter** containing a typical citation and abstract sample explaining the standard format, including codes for ordering reports
- **An Abstract Section** containing citations and abstracts of reports and publications that provide comprehensive coverage of worldwide aerospace-related topics including aeronautics and space science technology. *STAR* lists published and publicly available reports entered into the NASA STI Database during the four weeks preceding publication of this issue. These citations and abstracts are listed by subject categories.
- **An Index Section**
  - Subject
  - Personal author
  - Corporate source
  - Contract number
  - Report number
- **An Appendix** containing a guide for ordering cited reports, registering with the NASA STI Office, and using the available products and services. Additionally, price schedules, phone numbers, and addresses are included in this information packed section.

NASA also sponsors the companion journal, *NASA Open Volumes on Aerospace (NOVA)*, which lists abstracts of the open literature on aerospace subjects available worldwide. *NOVA* is for internal NASA use only, available from the NASA Center for AeroSpace Information (CASI).

Entries found in *STAR* are available through the NASA online retrieval service, RECON.

The NASA STI Office gathers information through national and international agreements and exchanges and makes this information available to the NASA community and to the public in many forms through various outlets.

For additional information on the NASA STI Office, call the NASA Access Help Desk at (301) 621-0390, or write to:

NASA Center for AeroSpace Information
800 Elkridge Landing Road
Linthicum Heights, Maryland 21090-2934

US ISSN 0036-8741

This publication was prepared by the NASA Center for AeroSpace Information,
800 Elkridge Landing Road, Linthicum Heights, MD 21090-2934, (301) 621-0390.

Volume 33 Number 7 / July 1995

TABLE OF CONTENTS

AERONAUTICS For related information see also *Astronautics.*

01 AERONAUTICS (GENERAL) **1607**

02 AERODYNAMICS **1607**
Includes aerodynamics of bodies, combinations, wings, rotors, and control surfaces; and internal flow in ducts and turbomachinery. For related information see also *34 Fluid Mechanics and Heat Transfer.*

03 AIR TRANSPORTATION AND SAFETY **1609**
Includes passenger and cargo air transport operations; and aircraft accidents. For related information see also *16 Space Transportation* and *85 Urban Technology and Transportation.*

04 AIRCRAFT COMMUNICATIONS AND NAVIGATION **1611**
Includes digital and voice communication with aircraft; air navigation systems (satellite and ground based); and air traffic control. For related information see also *17 Space Communications, Spacecraft Communications, Command and Tracking* and *32 Communications and Radar.*

05 AIRCRAFT DESIGN, TESTING AND PERFORMANCE **1611**
Includes aircraft simulation technology. For related information see also *18 Spacecraft Design, Testing and Performance* and *39 Structural Mechanics.* For land transportation vehicles see *85 Urban Technology and Transportation.*

06 AIRCRAFT INSTRUMENTATION **1613**
Includes cockpit and cabin display devices; and flight instruments. For related information see also *19 Spacecraft Instrumentation* and *35 Instrumentation and Photography.*

07 AIRCRAFT PROPULSION AND POWER **1614**
Includes prime propulsion systems and systems components, e.g., gas turbine engines and compressors; and onboard auxiliary power plants for aircraft. For related information see also *20 Spacecraft Propulsion and Power, 28 Propellants and Fuels,* and *44 Energy Production and Conversion.*

08 AIRCRAFT STABILITY AND CONTROL **1614**
Includes aircraft handling qualities; piloting; flight controls; and autopilots. For related information see also *05 Aircraft Design, Testing and Performance.*

09 RESEARCH AND SUPPORT FACILITIES (AIR) **1616**
Includes airports, hangars and runways; aircraft repair and overhaul facilities; wind tunnels; shock tubes; and aircraft engine test stands. For related information see also *14 Ground Support Systems and Facilities (Space).*

ASTRONAUTICS For related information see also *Aeronautics.*

12 ASTRONAUTICS (GENERAL) **1617**
For extraterrestrial exploration see *91 Lunar and Planetary Exploration.*

13 ASTRODYNAMICS ..... **N.A.**
Includes powered and free-flight trajectories; and orbital and launching dynamics.

14 GROUND SUPPORT SYSTEMS AND FACILITIES (SPACE) ..... **N.A.**
Includes launch complexes, research and production facilities; ground support equipment, e.g., mobile transporters; and simulators. For related information see also *09 Research and Support Facilities (Air).*

15 LAUNCH VEHICLES AND SPACE VEHICLES **1619**
Includes boosters; operating problems of launch/space vehicle systems; and reusable vehicles. For related information see also *20 Spacecraft Propulsion and Power.*

16 SPACE TRANSPORTATION **1619**
Includes passenger and cargo space transportation, e.g., shuttle operations; and space rescue techniques. For related information see also *03 Air Transportation and Safety* and *18 Spacecraft Design, Testing and Performance.* For space suits see *54 Man/System Technology and Life Support.*

17 SPACE COMMUNICATIONS, SPACECRAFT COMMUNICATIONS, COMMAND AND TRACKING ..... **N.A.**
Includes telemetry; space communications networks; astronavigation and guidance; and radio blackout. For related information see also *04 Aircraft Communications and Navigation* and *32 Communications and Radar.*

N.A.—No abstracts were assigned to this category for this issue.

18 SPACECRAFT DESIGN, TESTING AND PERFORMANCE 1620
Includes satellites; space platforms; space stations; spacecraft systems and components such as thermal and environmental controls; and attitude controls. For life support systems see *54 Man/System Technology and Life Support.* For related information see also *05 Aircraft Design, Testing and Performance, 39 Structural Mechanics,* and *16 Space Transportation.*

19 SPACECRAFT INSTRUMENTATION ..... N.A.
For related information see also *06 Aircraft Instrumentation* and *35 Instrumentation and Photography.*

20 SPACECRAFT PROPULSION AND POWER 1624
Includes main propulsion systems and components, e.g., rocket engines; and spacecraft auxiliary power sources. For related information see also *07 Aircraft Propulsion and Power, 28 Propellants and Fuels, 44 Energy Production and Conversion,* and *15 Launch Vehicles and Space Vehicles.*

CHEMISTRY AND MATERIALS

23 CHEMISTRY AND MATERIALS (GENERAL) 1626

24 COMPOSITE MATERIALS 1627
Includes physical, chemical, and mechanical properties of laminates and other composite materials. For ceramic materials see *27 Nonmetallic Materials.*

25 INORGANIC AND PHYSICAL CHEMISTRY 1631
Includes chemical analysis, e.g., chromatography; combustion theory; electrochemistry; and photochemistry. For related information see also *77 Thermodynamics and Statistical Physics.*

26 METALLIC MATERIALS 1638
Includes physical, chemical, and mechanical properties of metals, e.g., corrosion; and metallurgy.

27 NONMETALLIC MATERIALS 1646
Includes physical, chemical, and mechanical properties of plastics, elastomers, lubricants, polymers, textiles, adhesives, and ceramic materials. For composite materials see *24 Composite Materials.*

28 PROPELLANTS AND FUELS 1652
Includes rocket propellants, igniters and oxidizers; their storage and handling procedures; and aircraft fuels. For related information see also *07 Aircraft Propulsion and Power, 20 Spacecraft Propulsion and Power,* and *44 Energy Production and Conversion.*

29 MATERIALS PROCESSING 1653
Includes space-based development of products and processes for commercial application. For biological materials see *55 Space Biology:*

ENGINEERING For related information see also *Physics.*

31 ENGINEERING (GENERAL) 1654
Includes vacuum technology; control engineering; display engineering; cryogenics; and fire prevention.

32 COMMUNICATIONS AND RADAR 1655
Includes radar; land and global communications; communications theory; and optical communications. For related information see also *04 Aircraft Communications and Navigation* and *17 Space Communications, Spacecraft Communications, Command and Tracking.* For search and rescue see *03 Air Transportation and Safety,* and *16 Space Transportation.*

33 ELECTRONICS AND ELECTRICAL ENGINEERING 1659
Includes test equipment and maintainability; components, e.g., tunnel diodes and transistors; microminiaturization; and integrated circuitry. For related information see also *60 Computer Operations and Hardware* and *76 Solid-State Physics.*

34 FLUID MECHANICS AND HEAT TRANSFER 1664
Includes boundary layers; hydrodynamics; fluidics; mass transfer and ablation cooling. For related information see also *02 Aerodynamics* and *77 Thermodynamics and Statistical Physics.*

35 INSTRUMENTATION AND PHOTOGRAPHY 1687
Includes remote sensors; measuring instruments and gauges; detectors; cameras and photographic supplies; and holography. For aerial photography see *43 Earth Resources and Remote Sensing.* For related information see also *06 Aircraft Instrumentation* and *19 Spacecraft Instrumentation.*

36 LASERS AND MASERS 1690
Includes parametric amplifiers. For related information see also *76 Solid-State Physics.*

37 MECHANICAL ENGINEERING **1692**
Includes auxiliary systems (nonpower); machine elements and processes; and mechanical equipment.

38 QUALITY ASSURANCE AND RELIABILITY **1697**
Includes product sampling procedures and techniques; and quality control.

39 STRUCTURAL MECHANICS **1698**
Includes structural element design and weight analysis; fatigue; and thermal stress. For applications see *05 Aircraft Design, Testing and Performance* and *18 Spacecraft Design, Testing and Performance.*

GEOSCIENCES For related information see also *Space Sciences.*

42 GEOSCIENCES (GENERAL) **1701**

43 EARTH RESOURCES AND REMOTE SENSING **1717**
Includes remote sensing of earth resources by aircraft and spacecraft; photogrammetry; and aerial photography. For instrumentation see *35 Instrumentation and Photography.*

44 ENERGY PRODUCTION AND CONVERSION **1725**
Includes specific energy conversion systems, e.g., fuel cells; global sources of energy; geophysical conversion; and windpower. For related information see also *07 Aircraft Propulsion and Power, 20 Spacecraft Propulsion and Power,* and *28 Propellants and Fuels.*

45 ENVIRONMENT POLLUTION **1731**
Includes atmospheric, noise, thermal, and water pollution.

46 GEOPHYSICS **1735**
Includes aeronomy; upper and lower atmosphere studies; ionospheric and magnetospheric physics; and geomagnetism. For space radiation see *93 Space Radiation.*

47 METEOROLOGY AND CLIMATOLOGY **1741**
Includes weather forecasting and modification.

48 OCEANOGRAPHY **1743**
Includes biological, dynamic, and physical oceanography; and marine resources. For related information see also *43 Earth Resources and Remote Sensing.*

LIFE SCIENCES

51 LIFE SCIENCES (GENERAL) **1744**

52 AEROSPACE MEDICINE **1748**
Includes physiological factors; biological effects of radiation; and effects of weightlessness on man and animals.

53 BEHAVIORAL SCIENCES **1749**
Includes psychological factors; individual and group behavior; crew training and evaluation; and psychiatric research.

54 MAN/SYSTEM TECHNOLOGY AND LIFE SUPPORT **1750**
Includes human engineering; biotechnology; and space suits and protective clothing. For related information see also *16 Space Transportation.*

55 SPACE BIOLOGY ..... **N.A.**
Includes exobiology; planetary biology; and extraterrestrial life.

MATHEMATICAL AND COMPUTER SCIENCES

59 MATHEMATICAL AND COMPUTER SCIENCES (GENERAL) ..... **N.A.**

60 COMPUTER OPERATIONS AND HARDWARE **1752**
Includes hardware for computer graphics, firmware, and data processing. For components see *33 Electronics and Electrical Engineering.*

61 COMPUTER PROGRAMMING AND SOFTWARE **1753**
Includes computer programs, routines, algorithms, and specific applications, e.g., CAD/CAM.

62 COMPUTER SYSTEMS **1761**
Includes computer networks and special application computer systems.

63 CYBERNETICS **1766**
Includes feedback and control theory, artificial intelligence, robotics and expert systems. For related information see also *54 Man/System Technology and Life Support.*

64 NUMERICAL ANALYSIS **1785**
Includes iteration, difference equations, and numerical approximation.

65 STATISTICS AND PROBABILITY **1793**
Includes data sampling and smoothing; Monte Carlo method; and stochastic processes.

66 SYSTEMS ANALYSIS **1794**
Includes mathematical modeling; network analysis; and operations research.

67 THEORETICAL MATHEMATICS **1795**
Includes topology and number theory.

PHYSICS For related information see also *Engineering.*

70 PHYSICS (GENERAL) **1798**
For precision time and time interval (PTTI) see *35 Instrumentation and Photography*; for geophysics, astrophysics or solar physics see *46 Geophysics, 90 Astrophysics*, or *92 Solar Physics.*

71 ACOUSTICS **1799**
Includes sound generation, transmission, and attenuation. For noise pollution see *45 Environment Pollution.*

72 ATOMIC AND MOLECULAR PHYSICS **1800**
Includes atomic structure, electron properties, and molecular spectra.

73 NUCLEAR AND HIGH-ENERGY PHYSICS **1816**
Includes elementary and nuclear particles; and reactor theory. For space radiation see *93 Space Radiation.*

74 OPTICS **1819**
Includes light phenomena and optical devices. For lasers see *36 Lasers and Masers.*

75 PLASMA PHYSICS **1829**
Includes magnetohydrodynamics and plasma fusion. For ionospheric plasmas see *46 Geophysics.* For space plasmas see *90 Astrophysics.*

76 SOLID-STATE PHYSICS **1838**
Includes superconductivity. For related information see also *33 Electronics and Electrical Engineering* and *36 Lasers and Masers.*

77 THERMODYNAMICS AND STATISTICAL PHYSICS **1847**
Includes quantum mechanics; theoretical physics; and Bose and Fermi statistics. For related information see also *25 Inorganic and Physical Chemistry* and *34 Fluid Mechanics and Heat Transfer.*

SOCIAL SCIENCES

80 SOCIAL SCIENCES (GENERAL) **1853**
Includes educational matters.

81 ADMINISTRATION AND MANAGEMENT **1853**
Includes management planning and research.

82 DOCUMENTATION AND INFORMATION SCIENCE **1854**
Includes information management; information storage and retrieval technology; technical writing; graphic arts; and micrography. For computer documentation see *61 Computer Programming and Software.*

83 ECONOMICS AND COST ANALYSIS **1864**
Includes cost effectiveness studies.

84 LAW, POLITICAL SCIENCE AND SPACE POLICY ..... **N.A.**
Includes NASA appropriation hearings; aviation law; space law and policy; international law; international cooperation; and patent policy.

85 URBAN TECHNOLOGY AND TRANSPORTATION **1864**
Includes applications of space technology to urban problems; technology transfer; technology assessment; and surface and mass transportation. For related information see *03 Air Transportation and Safety, 16 Space Transportation,* and *44 Energy Production and Conversion.*

SPACE SCIENCES For related information see also *Geosciences.*

88 SPACE SCIENCES (GENERAL) ..... **N.A.**

89 ASTRONOMY **1865**
Includes radio, gamma-ray, and infrared astronomy; and astrometry.

90 ASTROPHYSICS **1867**
Includes cosmology; celestial mechanics; space plasmas; and interstellar and interplanetary gases and dust. For related information see also *75 Plasma Physics.*

91 LUNAR AND PLANETARY EXPLORATION **1869**
Includes planetology; and manned and unmanned flights. For spacecraft design or space stations see *18 Spacecraft Design, Testing and Performance.*

92 SOLAR PHYSICS **1870**
Includes solar activity, solar flares, solar radiation and sunspots. For related information see also *93 Space Radiation.*

93 SPACE RADIATION **1871**
Includes cosmic radiation; and inner and outer earth's radiation belts. For biological effects of radiation see *52 Aerospace Medicine.* For theory see *73 Nuclear and High-Energy Physics.*

GENERAL

Includes aeronautical, astronautical, and space science related histories, biographies, and pertinent reports too broad for categorization; histories or broad overviews of NASA programs.

99 GENERAL **1872**

SUBJECT INDEX **I-1**

PERSONAL AUTHOR INDEX **I-119**

CORPORATE SOURCE INDEX **I-135**

CONTRACT NUMBER INDEX **I-155**

REPORT NUMBER INDEX **I-159**

APPENDIX **A-1**

TYPICAL CITATION AND ABSTRACT

NASA SPONSORED — ON MICROFICHE

ACCESSION NUMBER → **N95-10148*#** National Aeronautics and Space Administration. Lewis Research Center, Cleveland, OH. ← CORPORATE SOURCE

TITLE → **EFFECTS OF A FORWARD-SWEPT FRONT ROTOR ON THE FLOWFIELD OF A COUNTERROTATION PROPELLER**

AUTHORS → M. Nallasamy (NYMA, Inc., Brook Park, OH.) and Gary G. Podboy Aug. 1994 19 p Presented at the 30th Joint Propulsion Conference, Indianapolis, IN, 27-29 Jun. 1994; sponsored by AIAA, ASME, SAE, and ASEE ← PUBLICATION DATE

CONTRACT OR GRANT → (Contract NAS3-27186; RTOP 538-03-11)

REPORT NUMBERS → (NASA-TM-106671; E-8994; NAS 1.15:106671; AIAA Paper 94-2694) Avail: CASI HC A03/MF A01; 6 functional color pages ← AVAILABILITY SOURCE AND PRICE CODE

The effects of a forward-swept front rotor on the flowfield of a counterrotation model propeller at takeoff conditions at zero degree angle of attack are studied by solving the unsteady three-dimensional Euler equations. The configuration considered is an uneven blade count counterrotation model with twelve forward-swept blades on the fore rotor and ten aft-swept blades on the aft rotor. The flowfield is compared with that of a reference aft-swept counterrotation geometry and Laser Doppler Velocimeter (LDV) measurements. At the operating conditions considered, the forward-swept blade experiences a higher tip loading and produces a stronger tip vortex compared to the aft-swept blade, consistent with the LDV and acoustic measurements. Neither the solution nor the LDV data indicated the formation of a leading edge vortex. The predicted radial distribution of the circumferentially averaged axial velocity at the measurement station agreed very closely with LDV data, while crossflow velocities showed poor agreement. The discrepancy between prediction and LDV data of tangential and radial velocities is due in part to the insufficient mesh resolution in the region between the rotors and in the tip region to track the tip vortex. The vortex is diffused by the time it arrives at the measurement station. The uneven blade count configuration requires the solution to be carried out for six blade passages of the fore rotor and five passages of the aft rotor, thus making grid refinement prohibitive.

Author

VOLUME 33 NUMBER 7 / July 1995

Scientific and Technical Aerospace Reports

A Monthly Publication of the National Aeronautics and Space Administration

01 AERONAUTICS (GENERAL)

N95-24025*# National Aeronautics and Space Administration. Lewis Research Center, Cleveland, OH.

RESEARCH AND TECHNOLOGY, 1994

Jan. 1995 171 p

(NASA-TM-106764; E-9207; NAS 1.15:106764) Avail: CASI HC A08/MF A02

This report selectively summarizes the NASA Lewis Research Center's research and technology accomplishments for the fiscal year 1994. It comprises approximately 200 short articles submitted by the staff members of the technical directorates. The report is organized into six major sections: Aeronautics, Aerospace Technology, Space Flight Systems, Engineering and Computational Support, Lewis Research Academy, and Technology Transfer. A table of contents and author index have been developed to assist the reader in finding articles of special interest. This report is not intended to be a comprehensive summary of all research and technology work done over the past fiscal year. Most of the work is reported in Lewis-published technical reports, journal articles, and presentations prepared by Lewis staff members and contractors. In addition, university grants have enabled faculty members and graduate students to engage in sponsored research that is reported at technical meetings or in journal articles. For each article in this report a Lewis contact person has been identified, and where possible, reference documents are listed so that additional information can be easily obtained. The diversity of topics attests to the breadth of research and technology being pursued and to the skill mix of the staff that makes it possible. Author

N95-23506# AVRO International Aerospace, Woodford (England). Engineering Test Facilities.

HEALTH AND USAGE MONITORING SYSTEMS: CORROSION SURVEILLANCE

J. D. Smart and D. C. Weetman (Real Time Corrosion Management Ltd., Grandby Row, England.) *In* AGARD, Corrosion Detection and Management of Advanced Airframe Materials Jan. 1995 11 p (For primary document see N95-23496 07-26)

Copyright Avail: CASI HC A03/MF A03

N95-23519# Department of the Air Force, Tinker AFB, OK.

OKLAHOMA CITY AIR LOGISTICS CENTER (USAF) AGING AIRCRAFT CORROSION PROGRAM

Donald E. Nieser *In* AGARD, Corrosion Detection and Management of Advanced Airframe Materials Jan. 1995 12 p (For primary document see N95-23496 07-26)

Copyright Avail: CASI HC A03/MF A03

02 AERODYNAMICS

Includes aerodynamics of bodies, combinations, wings, rotors, and control surfaces; and internal flow in ducts and turbomachinery.

For related information see also *34 Fluid Mechanics and Heat Transfer.*

N95-22666*# National Aeronautics and Space Administration. Ames Research Center, Moffett Field, CA.

FLOW VISUALIZATION STUDIES OF VTOL AIRCRAFT MODELS DURING HOVER IN GROUND EFFECT

Nikos J. Mourtos (San Jose State Univ., CA.), Stephane Couillaud (San Jose State Univ., CA.), Dale Carter (San Jose State Univ., CA.), Craig Hange, Doug Wardwell, and Richard J. Margason Jan. 1995 48 p Original contains color illustrations

(RTOP 505-68-32)

(NASA-TM-108860; A-95025; NAS 1.15:108860) Avail: CASI HC A03/MF A01; 28 functional color pages

A flow visualization study of several configurations of a jet-powered vertical takeoff and landing (VTOL) aircraft model during hover in ground effect was conducted. A surface oil flow technique was used to observe the flow patterns on the lower surfaces of the model. There were significant configuration effects. Wing height with respect to fuselage, the presence of an engine inlet duct beside the fuselage, and nozzle pressure ratio are seen to have strong effects on the surface flow angles on the lower surface of the wing. This test was part of a program to improve the methods for predicting the hot gas ingestion (HGI) for jet-powered vertical/short takeoff and landing (V/STOL) aircraft. The tests were performed at the Jet Calibration and Hover Test (JCAHT) Facility at Ames Research Center. Author

N95-22802*# National Aeronautics and Space Administration. Langley Research Center, Hampton, VA.

WING PRESSURE DISTRIBUTIONS FROM SUBSONIC TESTS OF A HIGH-WING TRANSPORT MODEL

Zachary T. Applin, Garl L. Gentry, Jr., and M. A. Takallu (Lockheed Engineering and Sciences Co., Hampton, VA.) Jan. 1995 442 p

(RTOP 505-59-10-13)

(NASA-TM-4583; L-17380; NAS 1.15:4583) Avail: CASI HC A19/MF A04

A wind tunnel investigation was conducted on a generic, high-wing transport model in the Langley 14- by 22-Foot Subsonic Tunnel. This report contains pressure data that document effects of various model configurations and free-stream conditions on wing pressure distributions. The untwisted wing incorporated a full-span, leading-edge Krueger flap and a part-span, double-slotted trailing-edge flap system. The trailing-edge flap was tested at four different deflection angles (20 deg, 30 deg, 40 deg, and 60 deg). Four wing configurations were tested: cruise, flaps only, Krueger flap only, and high lift (Krueger flap and flaps deployed). Tests were conducted at free-stream dynamic pressures of 20 psf to 60 psf with corresponding chord Reynolds numbers of 1.22 x 10(exp 6) to 2.11 x 10(exp 6) and Mach numbers of 0.12 to 0.20. The angles of attack presented range from 0 deg to 20 deg and were determined by wing configuration. The angle of sideslip ranged from minus 20 deg to 20 deg. In general, pressure distributions were relatively insensitive to free-stream speed with exceptions primarily at high angles of attack or high flap deflections. Increasing trailing-edge Krueger flap significantly reduced peak suction pressures and steep gradients on the wing at high angles of attack.

Installation of the empennage had no effect on wing pressure distributions. Unpowered engine nacelles reduced suction pressures on the wing and the flaps. Author

N95-22917*# Lockheed-Fort Worth Co., Fort Worth, TX.
EULER TECHNOLOGY ASSESSMENT PROGRAM FOR PRELIMINARY AIRCRAFT DESIGN EMPLOYING SPLITFLOW CODE WITH CARTESIAN UNSTRUCTURED GRID METHOD Report, 1 Feb. - 1 Aug. 1994
Dennis B. Finley Mar. 1995 100 p
(Contract NAS1-19000; RTOP 505-68-30-03)
(NASA-CR-4649; NAS 1.26:4649) Avail: CASI HC A05/MF A02

This report documents results from the Euler Technology Assessment program. The objective was to evaluate the efficacy of Euler computational fluid dynamics (CFD) codes for use in preliminary aircraft design. Both the accuracy of the predictions and the rapidity of calculations were to be assessed. This portion of the study was conducted by Lockheed Fort Worth Company, using a recently developed in-house Cartesian-grid code called SPLITFLOW. The Cartesian grid technique offers several advantages for this study, including ease of volume grid generation and reduced number of cells compared to other grid schemes. SPLITFLOW also includes grid adaptation of the volume grid during the solution convergence to resolve high-gradient flow regions. This proved beneficial in resolving the large vortical structures in the flow for several configurations examined in the present study. The SPLITFLOW code predictions of the configuration forces and moments are shown to be adequate for preliminary design analysis, including predictions of sideslip effects and the effects of geometry variations at low and high angles of attack. The time required to generate the results from initial surface definition is on the order of several hours, including grid generation, which is compatible with the needs of the design environment. Author

N95-23095*# Boeing Defense and Space Group, Seattle, WA.
EULER TECHNOLOGY ASSESSMENT FOR PRELIMINARY AIRCRAFT DESIGN EMPLOYING OVERFLOW CODE WITH MULTIBLOCK STRUCTURED-GRID METHOD Technical Report, 1 Feb. - 1 Aug. 1994
David A. Treiber and Dennis A. Muilenburg Hampton, VA NASA Mar. 1995 66 p
(Contract NAS1-18762; RTOP 505-68-30-03)
(NASA-CR-4651; NAS 1.26:4651) Avail: CASI HC A04/MF A01

The viability of applying a state-of-the-art Euler code to calculate the aerodynamic forces and moments through maximum lift coefficient for a generic sharp-edge configuration is assessed. The OVERFLOW code, a method employing overset (Chimera) grids, was used to conduct mesh refinement studies, a wind-tunnel wall sensitivity study, and a 22-run computational matrix of flow conditions, including sideslip runs and geometry variations. The subject configuration was a generic wing-body-tail geometry with chined forebody, swept wing leading-edge, and deflected part-span leading-edge flap. The analysis showed that the Euler method is adequate for capturing some of the non-linear aerodynamic effects resulting from leading-edge and forebody vortices produced at high angle-of-attack through C(sub Lmax). Computed forces and moments, as well as surface pressures, match well enough useful preliminary design information to be extracted. Vortex burst effects and vortex interactions with the configuration are also investigated. Author

N95-23182*# Wayne State Univ., Detroit, MI. Dept. of Mathematics.
ACTIVE CONTROL OF PANEL VIBRATIONS INDUCED BY A BOUNDARY LAYER FLOW Technical Report, 31 Aug. 1990 - 31 Oct. 1994
Pao-Liu Chow 24 Jan. 1995 30 p
(Grant NAG1-1175)
(NASA-CR-197867; NAS 1.26:197867) Avail: CASI HC A03/MF A01

The problems of active and passive control of sound and vibration has been investigated by many researchers for a number of years. However, few of the articles are concerned with the sound and vibration with flow-structure interaction. Experimental and numerical studies on the coupling between panel vibration and acoustic radiation due to flow excitation have been done by Maestrello and his associates at NASA/Langley Research Center. Since the coupled system of nonlinear partial differential equations is formidable, an analytical solution to the full problem seems impossible. For this reason, we have to simplify the problem to that of the nonlinear panel vibration induced by a uniform flow or a boundary-layer flow with a given wall pressure distribution. Based on this simplified model, we have been able to consider the control and stabilization of the nonlinear panel vibration, which have not been treated satisfactorily by other authors. Although the sound radiation has not been included, the vibration suppression will clearly reduce the sound radiation power from the panel. The major research findings are presented in three sections. In section two we describe results on the boundary control of nonlinear panel vibration, with or without flow excitation. Sections three and four are concerned with some analytical and numerical results in the optimal control of the linear and nonlinear panel vibrations, respectively, excited by the flow pressure fluctuations. Finally, in section five, we draw some conclusions from research findings. Derived from text

N95-23185*# Lockheed Aeronautical Systems Co., Marietta, GA.
AN ASSESSMENT OF VISCOUS EFFECTS IN COMPUTATIONAL SIMULATION OF BENIGN AND BURST VORTEX FLOWS ON GENERIC FIGHTER WIND-TUNNEL MODELS USING TEAM CODE Contractor Report, 1 Feb. - 1 Aug. 1994
Tim A. Kinard, Brenda W. Harris, and Pradeep Raj Hampton, VA NASA Mar. 1995 82 p
(Contract NAS1-19000; RTOP 505-68-30-03)
(NASA-CR-4650; NAS 1.26:4650) Avail: CASI HC A05/MF A01

Vortex flows on a twin-tail and a single-tail modular transonic vortex interaction (MTVI) model, representative of a generic fighter configuration, are computationally simulated in this study using the Three-dimensional Euler/Navier-Stokes Aerodynamic Method (TEAM). The primary objective is to provide an assessment of viscous effects on benign (10 deg angle of attack) and burst (35 deg angle of attack) vortex flow solutions. This study was conducted in support of a NASA project aimed at assessing the viability of using Euler technology to predict aerodynamic characteristics of aircraft configurations at moderate-to-high angles of attack in a preliminary design environment. The TEAM code solves the Euler and Reynolds-average Navier-Stokes equations on patched multiblock structured grids. Its algorithm is based on a cell-centered finite-volume formulation with multistage time-stepping scheme. Viscous effects are assessed by comparing the computed inviscid and viscous solutions with each other and experimental data. Also, results of Euler solution sensitivity to grid density and numerical dissipation are presented for the twin-tail model. The results show that proper accounting of viscous effects is necessary for detailed design and optimization but Euler solutions can provide meaningful guidelines for preliminary design of flight vehicles which exhibit vortex flows in parts of their flight envelope. Author

N95-23193*# Joint Inst. for Advancement of Flight Sciences, Hampton, VA.
AN APPROXIMATE THEORETICAL METHOD FOR MODELING THE STATIC THRUST PERFORMANCE OF NON-AXISYMMETRIC TWO-DIMENSIONAL CONVERGENT-DIVERGENT NOZZLES M.S. Thesis - George Washington Univ.
Craig A. Hunter Mar. 1995 51 p
(Contracts NCC1-14; NCC1-24; RTOP 537-07-20)
(NASA-CR-195050; NAS 1.26:195050) Avail: CASI HC A04/MF A01

An analytical/numerical method has been developed to predict the static thrust performance of non-axisymmetric, two-dimensional convergent-divergent exhaust nozzles. Thermodynamic nozzle performance effects due to over- and underexpansion are modeled using one-dimensional compressible flow theory. Boundary layer development and skin friction losses are calculated using an approximate integral momentum method based on the classic karman-Polhausen solution. Angularity effects are included with these two models in a computational Nozzle Performance Analysis Code, NPAC. In four different case studies, results from NPAC are compared to experimental data obtained from subscale nozzle testing to demonstrate the capabilities and limitations of the NPAC method. In several cases, the NPAC prediction matched experimental gross thrust efficiency data to within 0.1 percent at a design NPR, and to within 0.5 percent at off-design conditions. Author

N95-23218*# Old Dominion Univ., Norfolk, VA. Dept. of Aerospace Engineering.
AERODYNAMIC DESIGN OPTIMIZATION WITH SENSITIVITY ANALYSIS AND COMPUTATIONAL FLUID DYNAMICS Final Report, period ending 31 May 1995

Oktay Baysal Mar. 1995 8 p
(Grant NAG1-1188)
(NASA-CR-197419; NAS 1.26:197419) Avail: CASI HC A02/MF A01

An investigation was conducted from October 1, 1990 to May 31, 1994 on the development of methodologies to improve the designs (more specifically, the shape) of aerodynamic surfaces of coupling optimization algorithms (OA) with Computational Fluid Dynamics (CFD) algorithms via sensitivity analyses (SA). The study produced several promising methodologies and their proof-of-concept cases, which have been reported in the open literature. Author

N95-23250*# National Aeronautics and Space Administration. Ames Research Center, Moffett Field, CA.
EXPERIMENTAL RESULTS FOR A HYPERSONIC NOZZLE/AFTERBODY FLOW FIELD
Frank W. Spaid (McDonnell-Douglas Aerospace, Saint Louis, MO.), Earl R. Keener (Eloret Corp., Palo Alto, CA.), and Frank C. L. Hui Mar. 1995 106 p
(RTOP 505-70-62)
(NASA-TM-4638; A-94119; NAS 1.15:4638) Avail: CASI HC A06/MF A02

This study was conducted to experimentally characterize the flow field created by the interaction of a single-expansion ramp-nozzle (SERN) flow with a hypersonic external stream. Data were obtained from a generic nozzle/afterbody model in the 3.5 Foot Hypersonic Wind Tunnel at the NASA Ames Research Center, in a cooperative experimental program involving Ames and McDonnell Douglas Aerospace. The model design and test planning were performed in close cooperation with members of the Ames computational fluid dynamics (CFD) team for the National Aerospace Plane (NASP) program. This paper presents experimental results consisting of oil-flow and shadow graph flow-visualization photographs, afterbody surface-pressure distributions, rake boundary-layer measurements, Preston-tube skin-friction measurements, and flow field surveys with five-hole and thermocouple probes. The probe data consist of impact pressure, flow direction, and total temperature profiles in the interaction flow field. Author

N95-23462*# Toledo Univ., OH.
ENHANCED ANALYSIS AND USERS MANUAL FOR RADIAL-INFLOW TURBINE CONCEPTUAL DESIGN CODE RTD Final Contractor Report
Arthur J. Glassman Cleveland NASA Mar. 1995 24 p
(Grant NAG3-1165; RTOP 505-69-50)
(NASA-CR-195454; E-9538; NAS 1.26:195454) Avail: CASI HC A03/MF A01

Modeling enhancements made to a radial-inflow turbine conceptual design code are documented in this report. A stator-endwall clearance-flow model was added for use with pivoting vanes. The rotor calculations were modified to account for swept blades and splitter blades. Stator and rotor trailing-edge losses and a vaneless-space loss were added to the loss model. Changes were made to the disk-friction and rotor-clearance loss calculations. The loss model was then calibrated based on experimental turbine performance. A complete description of code input and output along with sample cases are included in the report. Author

N95-23669*# Tennessee Univ., Tullahoma, TN. Space Inst.
SUPERSONIC LAMINAR FLOW CONTROL RESEARCH Semiannual Report No. 2, Jul. - Dec. 1994
C. F. Lo Dec. 1994 64 p
(Grant NAG2-881)
(NASA-CR-197938; NAS 1.26:197938) Avail: CASI HC A04/MF A01

The objective of the research is to understand supersonic laminar flow stability, transition and active control. Some prediction techniques will be developed or modified to analyze laminar flow stability. The effects of super laminar flow with distributed heating and cooling on active control will be studied. The primary tasks of the research applying to the NASA/Ames Proof of Concept (POC) and Laminar Flow Supersonic Wind Tunnel (LFSWT) nozzle design with laminar flow control are as follows: (1) predictions of supersonic laminar boundary layer stability and transition; (2) effects of wall heating and cooling for supersonic laminar flow control; and (3) performance evaluation of POC and LFSWT nozzles design with wall heating and cooling effects applying at different locations and various length. A paper addressing the effect of heating and cooling strips on boundary layer stability of nozzles and test sections of supersonic wind tunnels is included as an appendix. Derived from text

N95-23787# National Inst. for Fusion Science, Nagoya (Japan).
EFFECT OF SATELLITE HELICAL HARMONICS ON THE STELLARATOR CONFIGURATION
V. D. Pustovitov (Kurchatov, I. V. Inst. of Atomic Energy, Moscow, USSR.) Dec. 1994 46 p Submitted for publication Sponsored by Internnational Science Foundation
(ISSN 0915-633X)
(NIFS-328) Avail: CASI HC A03/MF A01

We discuss the problem of self-consistent analytical description of stellarators with a helical field which has, besides the main harmonic, two nearest satellites with the same period in the toroidal angle. The expression for the flux function explicitly incorporating the effect of such satellites on the shape of magnetic surfaces is obtained. It is shown that they produce the shift of magnetic surfaces. The expression for this shift is derived. Two problems are considered where the behavior of B(exp 2) on a magnetic surface is important: Pfirsch-Schluter current at the presence of satellites and possibility of fulfillment of quasisymmetry condition (B(exp 2) on a magnetic surface does not depend on one of the angular Boozer coordinates) at least at a single magnetic surface. It is shown that the effect of satellite harmonics on the magnitude of Pfirsch-Schluter current turns out to be much smaller than it was predicted earlier on the basis of simplified model where the shift related with satellites was not taken into account. It is shown that quasisymmetry condition in a configuration with two satellites can be fulfilled only in linear approximation in helical field. The analysis is performed for conventional stellarators with planar circular axis making use of stellarator expansion. Author

N95-23283*# Mississippi State Univ., Mississippi State, MS. Dept. of Aerospace Engineering.
CROSSFLOW INSTABILITY CONTROL ON A SWEPT-WING: PRELIMINARY STUDIES Abstract Only
David H. Bridges *In* Hampton Univ., 1994 NASA-HU American Society for Engineering Education (ASEE) Summer Faculty Fellowship Program Dec. 1994 p 63 (For primary document see N95-23276 07-99)
Avail: CASI HC A01/MF A02

N95-23294*# Texas A&M Univ., College Station, TX. Dept. of Aerospace Engineering.
CONTROL OF FLOW SEPARATION IN AIRFOIL/WING DESIGN APPLICATIONS Abstract Only
Thomas A. Gally *In* Hampton Univ., 1994 NASA-HU American Society for Engineering Education (ASEE) Summer Faculty Fellowship Program Dec. 1994 p 75 (For primary document see N95-23276 07-99)
Avail: CASI HC A01/MF A02

N95-23333*# California Univ., Davis, CA. Dept. of Mechanical and Aeronautical Engineering.
HIGH-LIFT FLOW-PHYSICS FLIGHT EXPERIMENTS ON A SUBSONIC CIVIL TRANSPORT AIRCRAFT (B737-100) Abstract Only
Cornelis P. vanDam *In* Hampton Univ., 1994 NASA-HU American Society for Engineering Education (ASEE) Summer Faculty Fellowship Program Dec. 1994 p 115 (For primary document see N95-23276 07-99)
Avail: CASI HC A01/MF A02

03 AIR TRANSPORTATION AND SAFETY

Includes passenger and cargo air transport operations; and aircraft accidents.

For related information see also *16 Space Transportation* and *85 Urban Technology and Transportation.*

N95-23201# Manchester Univ. (England). Dept. of Pure and Applied Physics.
COLLABORATIVE RESEARCH ON AIRCRAFT ICING AND CHARGING PROCESSES IN ICE Final Annual Technical Report, 1 Sep. 1992 - 31 Aug. 1994

C. P. Saunders 1 Sep. 1994 44 p
(Grant AF-AFOSR-0376-91)
(AD-A285102; EOARD-TR-94-07) Avail: CASI HC A03/MF A01

This study is into the electrification processes that occur when ice crystals collide with other bodies. The work is of relevance to the charging of ice pellets falling in thunderstorms when they collide with ice crystals, and to the charging of aircraft when they fly through ice phase precipitation. The study relates the thunderstorm field measurements made over recent years to the laboratory simulations of thunderstorm conditions. Charging is shown to be dependent on the water content in the cloud, on the ice crystal sizes, on the speed of impact, and on the temperature. Several theories to account for this charge transfer behavior are discussed, including measurements of a charge layer at an ice interface that may be indicative of charge being available for transfer during ice particle collisions. The major conclusion is that all the proposed mechanisms have problems in accounting for the observed charging behavior. Further field studies are needed in which the growth or sublimation state of ice pellets in thunderstorms may be identified so that laboratory simulations can be made more relevant. DTIC

N95-23598# National Transportation Safety Board, Washington, DC.
REPORT OF PROCEEDINGS: AVIATION ACCIDENT INVESTIGATION SYMPOSIUM. VOLUME 2: PARTICIPANT PRESENTATIONS
1994 331 p Symposium held in Tysons Corner, VA, 29-31 Mar. 1994
(PB94-917007; NTSB/RP-94/02-Vol-2) Avail: CASI HC A15/MF A03

Volume 2 contains presentations made by participants in the Safety Board's Aviation Accident Investigation Symposium held at Tysons Corner, Virginia, from March 29 through 31, 1994. Volume 1 contains the Safety Board's responses to a number of recommendations made by the aviation industry during the symposium. The symposium provided a forum for the aviation industry to discuss and critique Safety Board programs and practices, as well as procedures used during aviation accident investigations. Participants included representatives from U.S. air carriers, airframe and engine manufacturers, aviation associations and unions, government officials and interested parties, as well as foreign investigative authorities and manufacturers. Author

N95-23609# National Transportation Safety Board, Washington, DC.
AIRCRAFT ACCIDENT REPORT. RUNWAY OVERRUN FOLLOWING REJECTED TAKEOFF. CONTINENTAL AIRLINES FLIGHT 795, MCDONNELL DOUGLAS MD-82, N18835, LAGUARDIA AIRPORT, FLUSHING, NY, 2 MARCH 1994
1995 89 p
(PB95-910401; NTSB/AAR-95/01) Avail: CASI HC A05/MF A01

This report explains the accident involving Continental Airlines flight 795, an MD-82 airplane, which experienced a runway overrun following a rejected takeoff from runway 13 at LaGuardia Airport, Flushing, New York, on March 2, 1994. Safety issues discussed in the report include the availability of takeoff performance data for flightcrews, the proper functioning of pitot/static heat systems, the duration of cockpit voice recordings, and problems associated with passenger evacuations from airplanes. Safety recommendations concerning these issues were addressed to the Federal Aviation Administration and to Continental Airlines, Inc. Author

N95-24012# Wichita State Univ., Wichita, KS.
THE AIRLINE QUALITY REPORT, 1994
Brent D. Bowen (Nebraska Univ., Omaha, NE.) and Dean E. Headley Apr. 1994 48 p
(NIAR-94-11) Avail: CASI HC A03/MF A01

The Airline Quality Rating was developed and first announced in early 1991 as an objective method of comparing airline performance on combined multiple factors important to consumers. Development history and calculation details for the AQR rating system are detailed in The Airline Quality Rating (NIAR Report 91-11) issued in April, 1991, by the National Institute for Aviation Research at Wichita State University. A full reporting of the monthly Airline Quality Rating scores for 1991 and 1992 is available in Airline Quality Report 1992 (NIAR Report 92-11) and Airline Quality Rating Report 1993 (NIAR Report 93-11) by contacting Wichita State University. The Airline Quality Rating 1994 (NIAR Report 94-11) is a summary of month-by-month quality ratings for the nine major domestic U.S. airlines operating during 1993. Using the Airline Quality Rating (AQR) system and monthly performance data for each airline for the calendar year of 1993, individual and comparative ratings are reported. This research monograph, NIAR Report 94-11, contains a brief summary of the AQR methodology, detailed data and charts that track comparative quality for major domestic airlines across the 12 month period of 1993, and industry average results. Also, comparative Airline quality Rating data for 1992 is included to provide a longer term view of quality in the industry. Author

N95-24024# Civil Aeromedical Inst., Oklahoma City, OK.
AIRCRAFT FIRES, SMOKE TOXICITY, AND SURVIVAL: AN OVERVIEW Final Report
Arvind K. Chaturvedi and Donald C. Sanders Feb. 1995 7 p
(DOT/FAA/AM-95/8) Avail: CASI HC A02/MF A01

In-flight fires in modern aircraft are rare, but post-crash fires do occur. Cabin occupants frequently survive initial forces of such crashes but are incapacitated from smoke inhalation. According to an international study, there were 95 fire-related civil passenger aircraft accidents world-wide over a 26-year period, claiming approximately 2400 lives. Between 1985-1991, about 16% (32) of all US transport aircraft accidents involved fire and 22% (140) of the deaths in these accidents resulted from fire/smoke toxicity. Our laboratory database (1967-1993) indicates that 360 individuals in 134 fatal fire-related civil aircraft (air carrier and general aviation) accidents had carboxyhemoglobin saturation levels, with or without cyanide in blood, high enough to impair performance. Combustion toxicology is now moving from a descriptive to a mechanistic phase. Methods for gas analyses have been developed and combustion/animal-exposure assemblies have been constructed. Material/fire-retardant toxicity and interactions between smoke gases are being studied. Relationships between gas exposure concentrations, blood levels, and incapacitation onset are being established in animal models. Continuing basic research in smoke toxicity will be necessary to understand its complexities, and thus enhance aviation safety and fire survival chances. Author

N95-24050# Wichita State Univ., Wichita, KS. National Inst. for Aviation Research.
A MULTIBODY/FINITE ELEMENT ANALYSIS APPROACH FOR MODELING OF CRASH DYNAMIC RESPONSES
Deren Ma Apr. 1994 210 p
(NIAR-94-3) Avail: CASI HC A10/MF A03

Occupant models are robust tools for gaining insight into the gross motion of ground vehicle or aircraft occupants and evaluating loads and deformations of their critical parts in the studies of crashworthiness. One of the most important issues in occupant modeling is how the large motion of rigid segments of occupants such as the limbs and the small deformations of flexible bodies such as the spine column are handled. In this dissertation, mathematical models of the occupants with a finite element model of the spine are developed based on the principles of the rigid/flexible multibody dynamics and finite element methods along with numerical techniques. An exhaustive study of the occupant modeling and post-crash dynamic behavior of the vehicle occupants under various crash environments is performed by both experimental and analytical means. With the validated occupant model containing the lumbar spine, the gross motion of occupant segments, including displacements, velocities and accelerations are evaluated. The spinal axial loads, bending moments, shear forces, internal forces, nodal forces, and deformation time histories are also determined. In addition, variables such as Head Injury Criteria (HIC), Severity Index (SI) and Dynamic Response Index (DRI) are evaluated to determine possibilities of the injuries in particular crash scenario. This detailed information helps assess the level of spinal injury, determine mechanisms of spinal injury, and design and develop better occupant safety devices. Derived from text

N95-24065# Federal Aviation Administration, Washington, DC. Flight Standards Service.
OCEANIC OPERATIONS: AN AUTHORITATIVE GUIDE TO OCEANIC OPERATIONS
Sep. 1994 243 p
(FAA-AFS-550; FAA-AC-91-70) Avail: CASI HC A11/MF A03

This advisory circular (AC) contains information and guidance to be used by operators and pilots planning oceanic flights. Information is presented on the following topics: United States aviation and the International Civil Aviation Organization; oceanic operations for all aircraft in all geographic areas; North Atlantic operations; Northern Pacific operations; Southern Pacific operations; Caribbean operations; Gulf of Mexico operations; long-range

navigation; helicopter oceanic operations; crew training for oceanic operations; general aviation short-range aircraft oceanic operations; polar flights; and oceanic operations to the former Soviet Union and other Soviet Block nations. CASI

N95-24071# Civil Aeromedical Inst., Oklahoma City, OK.
A REVIEW OF CIVIL AVIATION FATAL ACCIDENTS IN WHICH LOST/DISORIENTED WAS A CAUSE/FACTOR: 1981-1990 Final Report
William E. Collins Jan. 1995 11 p
(DOT/FAA/AM-95/1) Avail: CASI HC A03/MF A01

The National Transportation Safety Board (NTSB) analyzes circumstances and data from civil aviation accidents and describes one or more causes and/or related factors to help explain each accident. Among the formally accepted NTSB categories of accident causation is one termed 'lost/disoriented;' that term generally differs from 'spatial disorientation' and refers more to a loss of geographic awareness and, perhaps, resulting confusion on the part of the pilot. The present study was undertaken to provide information regarding the circumstances surrounding these fatal general aviation accidents in recent years, and to define demographic and behavioral characteristics of the 'lost/disoriented' pilots. Those reports were examined and analyzed in terms of type of accident, age and experience of pilots, actions of pilots, night or day, and other conditions. The computer search yielded a total of 120 accidents in which 'lost/disoriented' was among the findings noted by investigators of general aviation accidents for the 10-year period. Those accidents resulted in 169 fatalities. Related causes and circumstances associated with the accidents were analyzed and categorized. 'Lost/disoriented' accident frequency for the 1981-90 period peaked at 22 fatal accidents in 1985 and declined steadily thereafter. 75% of the pilots had no instrument rating, 64% of the accidents were associated with adverse weather, and just over half occurred at night. Other analyses suggest that educational efforts should continue to emphasize proper flight planning and the flight hazards of adverse weather conditions so that the recently lowered rates of 'lost/disoriented' accidents can be maintained or improved. Author

N95-24105# National Transportation Safety Board, Washington, DC.
AVIATION ACCIDENT INVESTIGATION SYMPOSIUM. VOLUME 1: INDUSTRY RECOMMENDATIONS AND SAFETY BOARD RESPONSES
17 Mar. 1994 73 p Symposium held in Tysons Corner, VA, 29-31 Mar. 1994
(PB94-917005; NTSB/RP-94/01-Vol-1) Avail: CASI HC A04/MF A01

Volume 1 contains the Safety Board's responses to a number of recommendations made by the aviation industry during the Safety Board's Aviation Accident Investigation Symposium. The symposium provided a forum for the aviation industry to discuss and critique Safety Board programs and practices, as well as procedures used during aviation accident investigations. Participants included representatives from U.S. air carriers, airframe and engine manufacturers, aviation associations and unions, government officials and interested parties, as well as foreign investigative authorities and manufacturers. Author (revised)

04 AIRCRAFT COMMUNICATIONS AND NAVIGATION

Includes digital and voice communication with aircraft; air navigation systems (satellite and ground based); and air traffic control.

For related information see also *17 Space Communications, Spacecraft Communications, Command and Tracking* and *Communications and Radar.*

N95-23393* National Aeronautics and Space Administration. Ames Research Center, Moffett Field, CA.
CUEING LIGHT CONFIGURATION FOR AIRCRAFT NAVIGATION Patent
Mary K. Kaiser, inventor (to NASA) and Walter J. Johnson, inventor (to NASA) 24 May 1994 9 p Filed 27 Aug. 1992
(NASA-Case-ARC-11982-1; US-Patent-5,315,296;
US-Patent-Appl-SN-935939; US-Patent-Class-340-946;
US-Patent-Class-73-178H; US-Patent-Class-340-953;
US-Patent-Class-340-961; US-Patent-Class-340-981;
US-Patent-Class-362-62; Int-Patent-Class-G08B-21/00) Avail: US Patent and Trademark Office

A pattern of light is projected from multiple sources located on an aircraft to form two clusters. The pattern of each cluster changes as the aircraft flies above and below a predetermined nominal altitude. The initial patterns are two horizontal, spaced apart lines. Each is capable of changing to a delta formation as either the altitude or the terrain varies. The direction of the delta cues the pilot as to the direction of corrective action.
Official Gazette of the U.S. Patent and Trademark Office

N95-23565# Civil Aeromedical Inst., Oklahoma City, OK.
THE ROLE OF FLIGHT PROGRESS STRIPS IN EN ROUTE AIR TRAFFIC CONTROL: A TIME-SERIES ANALYSIS Final Report
Mark B. Edwards (Oklahoma Univ., Oklahoma City, OK.), Dana Fuller (Oklahoma Univ., Oklahoma City, OK.), O. U. Vortac (Oklahoma Univ., Oklahoma City, OK.), and Carol A. Manning Jan. 1995 13 p
(DOT/FAA/AM-95/4) Avail: CASI HC A03/MF A01

Paper flight progress strips (FPS's) are currently used in the United States en route air traffic control system to document flight information. Impending automation will replace these paper strips with electronic flight data entries. In this observational study, control actions, communication events, and computer interactions were recorded and analyzed using time-series regression models. Regression models were developed to predict FPS activities (Writing, Manipulating, Looking) at different levels of traffic complexity, for individuals and teams of air traffic controllers. The ability to predict FPS manipulations was modest, but prediction of looking at FPS's was poor. Overall, these data indicate that: (1) flight strip activities were similar for individuals and for the data-side controllers in the team (whose primary responsibility is the strips); and (2) flight strip activity for teams was predictable from the radar-side controller's actions, but not the data-side controller's actions. Author

N95-23318*# Saint Cloud State Coll., MN. Dept. of Electrical Engineering.
DIFFERENTIAL GPS AND SYSTEM INTEGRATION OF THE LOW VISIBILITY LANDING AND SURFACE OPERATIONS (LVLASO) DEMONSTRATION Abstract Only
James M. Rankin *In* Hampton Univ., 1994 NASA-HU American Society for Engineering Education (ASEE) Summer Faculty Fellowship Program Dec. 1994 p 100 (For primary document see N95-23276 07-99)
Avail: CASI HC A01/MF A02

05 AIRCRAFT DESIGN, TESTING AND PERFORMANCE

Includes aircraft simulation technology.

For related information see also *18 Spacecraft Design, Testing and Performance* and *39 Structural Mechanics.* For land transportation vehicles see *85 Urban Technology and Transportation.*

N95-22510# Army Research Lab., Watertown, MA. Materials Directorate.
RATIONALE FOR THE MODULAR AIR-SYSTEM VULNERABILITY ESTIMATION NETWORK (MAVEN) METHODOLOGY Final Report, Jan. - Jun. 1994
Lisa K. Roach Sep. 1994 26 p
(DA Proj. 1L1-62618-AH-80)
(AD-A285797; ARL-TR-581) Avail: CASI HC A03/MF A01

The air community has long had a need for a new vulnerability/lethality (V/L) methodology, one usable by the triservice community. Current models range from manual calculations of total vulnerable area (Av) to complex models of incendiary functioning, fragment penetration, and fire initiation with component fault tree damage modes. Most, if not all, of these models make use of expected value, or deterministic, methods which do not accurately reflect the actual, observed phenomenology. In addition, technological advances in system design and weapon lethality have outpaced the growth of these models. While the community has tried to come to grips with these more complex systems and phenomenology, clearly, the existing models have not. The purpose of this report is to describe the rationale behind the development of a new stochastic, point-burst vulnerability

model for air systems which supports the myriad of analyses the air community must perform, as well as to discuss, in general, the technical requirements which generated this need. DTIC

N95-22806*# National Aeronautics and Space Administration. Flight Research Center, Edwards, CA.

FLIGHT TEST OF THE X-29A AT HIGH ANGLE OF ATTACK: FLIGHT DYNAMICS AND CONTROLS

Jeffrey E. Bauer, Robert Clarke, and John J. Burken Washington Feb. 1995 70 p

(RTOP 505-64-30)

(NASA-TP-3537; H-1984; NAS 1.60:3537) Avail: CASI HC A04/MF A01

The NASA Dryden Flight Research Center has flight tested two X-29A aircraft at low and high angles of attack. The high-angle-of-attack tests evaluate the feasibility of integrated X-29A technologies. More specific objectives focus on evaluating the high-angle-of-attack flying qualities, defining multiaxis controllability limits, and determining the maximum pitch-pointing capability. A pilot-selectable gain system allows examination of tradeoffs in airplane stability and maneuverability. Basic fighter maneuvers provide qualitative evaluation. Bank angle captures permit qualitative data analysis. This paper discusses the design goals and approach for high-angle-of-attack control laws and provides results from the envelope expansion and handling qualities testing at intermediate angles of attack. Comparisons of the flight test results to the predictions are made where appropriate. The pitch rate command structure of the longitudinal control system is shown to be a valid design for high-angle-of-attack control laws. Flight test results show that wing rock amplitude was overpredicted and aileron and rudder effectiveness were underpredicted. Flight tests show the X-29A airplane to be a good aircraft up to 40 deg angle of attack. Author

N95-22829*# National Aeronautics and Space Administration. Flight Research Center, Edwards, CA.

DIRECT ADAPTIVE PERFORMANCE OPTIMIZATION OF SUBSONIC TRANSPORTS: A PERIODIC PERTURBATION TECHNIQUE

Martin D. Espana and Glenn Gilyard Washington Mar. 1995 45 p

(RTOP 505-69-10)

(NASA-TM-4676; H-2040; NAS 1.15:4676) Avail: CASI HC A03/MF A01

Aircraft performance can be optimized at the flight condition by using available redundancy among actuators. Effective use of this potential allows improved performance beyond limits imposed by design compromises. Optimization based on nominal models does not result in the best performance of the actual aircraft at the actual flight condition. An adaptive algorithm for optimizing performance parameters, such as speed or fuel flow, in flight based exclusively on flight data is proposed. The algorithm is inherently insensitive to model inaccuracies and measurement noise and biases and can optimize several decision variables at the same time. An adaptive constraint controller integrated into the algorithm regulates the optimization constraints, such as altitude or speed, without requiring and prior knowledge of the autopilot design. The algorithm has a modular structure which allows easy incorporation (or removal) of optimization constraints or decision variables to the optimization problem. An important part of the contribution is the development of analytical tools enabling convergence analysis of the algorithm and the establishment of simple design rules. The fuel-flow minimization and velocity maximization modes of the algorithm are demonstrated on the NASA Dryden B-720 nonlinear flight simulator for the single- and multi-effector optimization cases. Author

N95-22949*# Old Dominion Univ., Norfolk, VA. Dept. of Aerospace Engineering.

A CFD STUDY OF COMPLEX MISSILE AND STORE CONFIGURATIONS IN RELATIVE MOTION Final Report, period ending 30 Sep. 1994

Oktay Baysal Mar. 1995 6 p

(Grant NAG1-1150)

(NASA-CR-197912; NAS 1.26:197912) Avail: CASI HC A02/MF A01

An investigation was conducted from May 16, 1990 to August 31, 1994 on the development of computational fluid dynamics (CFD) methodologies for complex missiles and the store separation problem. These flowfields involved multiple-component configurations, where at least one of the objects was engaged in relative motion. The two most important issues that had to be addressed were: (1) the unsteadiness of the flowfields (time-accurate and efficient CFD algorithms for the unsteady equations), and (2) the generation of grid systems which would permit multiple and moving bodies in the computational domain (dynamic domain decomposition). The study produced two competing and promising methodologies, and their proof-of-concept cases, which have been reported in the open literature: (1) Unsteady solutions on dynamic, overlapped grids, which may also be perceived as moving, locally-structured grids, and (2) Unsteady solutions on dynamic, unstructured grids. Author

N95-22953*# National Aeronautics and Space Administration. Langley Research Center, Hampton, VA.

INTEGRATED AERODYNAMIC/DYNAMIC/STRUCTURAL OPTIMIZATION OF HELICOPTER ROTOR BLADES USING MULTILEVEL DECOMPOSITION

Joanne L. Walsh, Katherine C. Young, Jocelyn I. Pritchard (Army Vehicle Structures Lab., Hampton, VA.), Howard M. Adelman, and Wayne R. Mantay (Army Aviation Systems Command, Hampton, VA.) Jan. 1995 52 p

(RTOP 505-63-36-06; DA Proj. 1L1-6241-A-47-AB)

(NASA-TP-3465; L-17233; NAS 1.60:3465; ARL-TR-518) Avail: CASI HC A04/MF A01

This paper describes an integrated aerodynamic/dynamic/structural (IADS) optimization procedure for helicopter rotor blades. The procedure combines performance, dynamics, and structural analyses with a general-purpose optimizer using multilevel decomposition techniques. At the upper level, the structure is defined in terms of global quantities (stiffness, mass, and average strains). At the lower level, the structure is defined in terms of local quantities (detailed dimensions of the blade structure and stresses). The IADS procedure provides an optimization technique that is compatible with industrial design practices in which the aerodynamic and dynamic designs are performed at a global level and the structural design is carried out at a detailed level with considerable dialog and compromise among the aerodynamic, dynamic, and structural groups. The IADS procedure is demonstrated for several examples. Author

N95-23161# National Aerospace Lab., Amsterdam (Netherlands).

REVIEW OF AERONAUTICAL FATIGUE INVESTIGATION IN THE NETHERLANDS DURING THE PERIOD MARCH 1991-MARCH 1993 Technical Paper

J. B. deJonge 16 Mar. 1993 33 p See also PB92-223437

(PB95-139184; NLR-TP-93109-U) Avail: CASI HC A03/MF A01

A brief review is given of work performed in the Netherlands in the field of aeronautical fatigue. Where possible, applicable references have been presented. NTIS

N95-23217*# Princeton Univ., NJ. Dept. of Mechanical and Aerospace Engineering.

AN INVESTIGATION OF HELICOPTER DYNAMIC COUPLING USING AN ANALYTICAL MODEL Final Report

Jeffrey D. Keller 7 Mar. 1995 23 p

(Grant NAG2-561)

(NASA-CR-197420; NAS 1.26:197420) Avail: CASI HC A03/MF A01

Many attempts have been made in recent years to predict the off-axis response of a helicopter to control inputs, and most have had little success. Since physical insight is limited by the complexity of numerical simulation models, this paper examines the off-axis response problem using an analytical model, with the goal of understanding the mechanics of the coupling. A new induced velocity model is extended to include the effects of wake distortion from pitch rate. It is shown that the inclusion of these results in a significant change in the lateral flap response to a steady pitch rate. The proposed inflow model is coupled with the full rotor/body dynamics, and comparisons are made between the model and flight test data for a UH-60 in hover. Results show that inclusion of induced velocity variations due to shaft rate improves correlation in the pitch response to lateral cycle inputs. Author

N95-23390* National Aeronautics and Space Administration. Ames Research Center, Moffett Field, CA.

AERODYNAMIC SURFACE DISTENSION SYSTEM FOR HIGH ANGLE OF ATTACK FOREBODY VORTEX CONTROL Patent

Peter T. Zell, inventor (to NASA) 5 Jul. 1994 10 p Filed 8 Feb. 1993

(NASA-Case-ARC-11979-1; US-Patent-5,326,050;

US-Patent-Appl-SN-014584; US-Patent-Class-244-75R;
US-Patent-Class-244-199; Int-Patent-Class-B64C-5/00) Avail: US Patent and Trademark Office

A deployable system is introduced for assisting flight control under certain flight conditions, such as at high angles of attack, whereby two inflatable membranes are located on the forebody portion of an aircraft on opposite sides thereof. The members form control surfaces for effecting lateral control forces if one is inflated and longitudinal control forces if both are inflated.

Official Gazette of the U.S. Patent and Trademark Office

N95-23395* National Aeronautics and Space Administration. Ames Research Center, Moffett Field, CA.

LIFT ENHANCING TABS FOR AIRFOILS Patent

James C. Ross, inventor (to NASA) 15 Mar. 1994 9 p Filed 8 Feb. 1993
(NASA-Case-ARC-11990-1; US-Patent-5,294,080;
US-Patent-Appl-SN-014581; US-Patent-Class-244-215;
US-Patent-Class-244-216; Int-Patent-Class-B64C-9/16) Avail: US Patent and Trademark Office

A tab deployable from the trailing edge of a main airfoil element forces flow onto a following airfoil element, such as a flap, to keep the flow attached and thus enhance lift. For aircraft wings with high lift systems that include leading edge slats, the slats may also be provided with tabs to turn the flow onto the following main element.

Official Gazette of the U.S. Patent and Trademark Office

N95-23666 Defence Science and Technology Organization, Melbourne (Australia). Air Operations Div.

ENHANCEMENT OF F/A-18 OPERATIONAL FLIGHT MEASUREMENTS: DATA REPORT FOR PHASE 1

B. A. Woodyatt, J. Bennett, and S. D. Hill Aug. 1994 73 p
(DSTO-TR-0049; AR-008-910) Copyright Avail: Issuing Activity (DSTO Aeronautical and Maritime Research Lab., GPO Box 4331, Melbourne, Victoria 3001, Australia)

This report describes the procedures used in the processing of approximately 300 hours of flight maintenance data from the F/A-18's Maintenance Status Display and Recording System (MSDRS). A Flight Path Reconstruction (FPR) program and a modified F/A-18 mathematical model from the US Naval Air Warfare Center Aircraft Division (NAWC-AD) were used to enhance these flight data in resolution and frequency. DSTO's Airframes and Engines Division (AED) will use these enhanced flight data to obtain a representative flight load spectrum. The load spectrum will be used in a full scale fatigue test of the empennage and aft fuselage of an F/A-18, the Australian contribution to the International Follow-On Structural Test Program (IFOSTP). IFOSTP is a joint collaboration between the Canadian Forces (CF) and the Royal Australian Air Force (RAAF) to appraise structural modifications to the F/A-18 designed to achieve a service life of 6000 hours. Author

N95-24091# General Accounting Office, Washington, DC. National Security and International Affairs Div.

REPORT TO THE SECRETARY OF DEFENSE. UNMANNED AERIAL VEHICLES: NO MORE HUNTER SYSTEMS SHOULD BE BOUGHT UNTIL PROBLEMS ARE FIXED

Mar. 1995 19 p
(GAO/NSIAD-95-52; B-259256) Avail: CASI HC A03/MF A01; GAO, PO Box 6015, Gaithersburg, MD 20877 HC

The Department of Defense is acquiring the Hunter Short-Range Unmanned Aerial Vehicle (UAV) for use by the Army, Navy and Marine Corps. The Hunter is a pilotless aircraft resembling a small airplane that is controlled from a ground station. It is intended to perform reconnaissance, target acquisition, and other military missions by flying over enemy territory and transmitting video imagery back to ground stations for use by military commanders. This report reviews the Hunter program to determine: (1) whether it has been demonstrated to be logistically supportable; (2) whether performance deficiencies found in prior testing have been resolved; and (3) whether it represents a valid joint-service effort as mandated by Congress. Derived from text

N95-23317*# Mississippi State Univ., Mississippi State, MS. Dept. of Aerospace Engineering.

THIN TAILORED COMPOSITE WING FOR CIVIL TILTROTOR Abstract Only

Masoud Rais-Rohani *In* Hampton Univ., 1994 NASA-HU American Society for Engineering Education (ASEE) Summer Faculty Fellowship Program Dec. 1994 p 99 (For primary document see N95-23276 07-99)
Avail: CASI HC A01/MF A02

06 AIRCRAFT INSTRUMENTATION

Includes cockpit and cabin display devices; and flight instruments.

For related information see also *19 Spacecraft Instrumentation* and *35 Instrumentation and Photography.*

N95-22578* National Aeronautics and Space Administration. Pasadena Office, CA.

VIRTUAL REALITY FLIGHT CONTROL DISPLAY WITH SIX-DEGREE-OF-FREEDOM CONTROLLER AND SPHERICAL ORIENTATION OVERLAY Patent

Brian C. Beckman, inventor (to NASA) (Jet Propulsion Lab., California Inst. of Tech., Pasadena, CA.) 14 Feb. 1995 14 p Filed 23 Apr. 1993
Supersedes N93-30416 (31 - 11, p 3251)
(Contract NAS7-918)
(NASA-Case-NPO-18733-1-CU; US-Patent-5,388,990;
US-Patent-Appl-SN-056503; US-Patent-Class-434-38;
US-Patent-Class-434-43; US-Patent-Class-434-307R;
US-Patent-Class-434-372; US-Patent-Class-364-578;
US-Patent-Class-395-152; US-Patent-Class-345-8) Avail: US Patent and Trademark Office

A virtual reality flight control system displays to the pilot the image of a scene surrounding a vehicle or pod having six degrees of freedom of acceleration or velocity control by the pilot and traveling through inertial space, the image itself including a superimposed figure providing the pilot an instant reference of orientation consisting of superimposed sets of geometric figures whose relative orientations provide the pilot an instantaneous feel or sense of orientation changes with respect to some fixed coordinate system. They include a first set of geometric figures whose orientations are fixed to the pilot's vehicle and a second set of geometric figures whose orientations are fixed with respect to a fixed or interstellar coordinate system. The first set of figures is a first set of orthogonal great circles about the three orthogonal axes of the flight vehicle or pod and centered at and surrounding the pilot's head, while the second set of figures is a second set of orthogonal great circles about the three orthogonal axes of a fixed or interstellar coordinate system, also centered at and surrounding the pilot's head.

Official Gazette of the U.S. Patent and Trademark Office

N95-24030*# National Aeronautics and Space Administration. Ames Research Center, Moffett Field, CA.

TRISTAR 1: EVALUATION METHODS FOR TESTING HEAD-UP DISPLAY (HUD) FLIGHT SYMBOLOGY

R. L. Newman (Crew Systems Consultants, San Marcos, TX.), L. A. Haworth, G. K. Kessler (Naval Air Test Center, Patuxent River, MD.), D. J. Eksuzian (Naval Air Development Center, Warminster, PA.), W. R. Ercoline (Krug Life Sciences, Inc., Houston, TX.), R. H. Evans (Air Force Instrument Flight Center, Randolph AFB, TX.), T. C. Hughes (Aeronautical Systems Div., Wright-Patterson AFB, OH.), and L. F. Weinstein (Krug Life Sciences, Inc., Houston, TX.) Feb. 1995 88 p
(RTOP 505-64-36)
(NASA-TM-4665; A-94141; NAS 1.15:4665; TR-94-A-019;
NAWCADPAX-95-10-RTR; AL-CF-TR-1994-0159) Avail: CASI HC A05/MF A01

The first in a series of piloted head-up display (HUD) flight symbology studies (TRISTAR) measuring pilot task performance was conducted at the NASA Ames Research Center by the Tri-Service Flight Symbology Working Group (FSWG). Sponsored by the U.S. Army Aeroflightdynamics Directorate, this study served as a focal point for the FSWG to examine HUD test methodology and flight symbology presentations. HUD climb-dive marker dynamics and climb-dive ladder presentations were examined as pilots

performed air-to-air (A/A), air-to-ground (A/G), instrument landing system (ILS), and unusual attitude (UA) recover tasks. Symbolic presentations resembled pitch ladder variations used by the U.S. Air Force (USAF), U.S. Navy (USN), and Royal Air Force (RAF). The study was initiated by the FSWG to address HUD flight symbology deficiencies, standardization, issue identification, and test methodologies. It provided the mechanism by which the USAF, USN, RAF, and USA could integrate organizational ideas and reduce differences for comparisons. Specifically it examined flight symbology issues collectively identified by each organization and the use of objective and subjective text methodology and flight tasking proposed by the FSWG. Author

07 AIRCRAFT PROPULSION AND POWER

Includes prime propulsion systems and systems components, e.g., gas turbine engines and compressors; and onboard auxilliary power plants for aircraft.

For related information see also *20 Spacecraft Propulsion and Power, 28 Propellants and Fuels,* and *44 Energy Production and Conversion.*

N95-23088*# Colorado Univ., Boulder, CO. Dept. of Aerospace Engineering Sciences.

HIGH-PERFORMANCE PARALLEL ANALYSIS OF COUPLED PROBLEMS FOR AIRCRAFT PROPULSION Progress Report, Jun. 1994 - Jan. 1995

C. A. Felippa, C. Farhat, P.-S. Chen, U. Gumaste, M. Leoinne, and P. Stern Feb. 1995 51 p Original contains color illustrations

(Grant NAG3-1273)

(NASA-CR-197440; CU-CAS-95-03; NAS 1.26:197440) Avail: CASI HC A04/MF A01 4 functional color pages

This research program deals with the application of high-performance computing methods to the numerical simulation of complete jet engines. The program was initiated in 1993 by applying two-dimensional parallel aeroelastic codes to the interior gas flow problem of a by-pass jet engine. The fluid mesh generation, domain decomposition and solution capabilities were successfully tested. Attention was then focused on methodology for the partitioned analysis of the interaction of the gas flow with a flexible structure and with the fluid mesh motion driven by these structural displacements. The latter is treated by an ALE technique that models the fluid mesh motion as that of a fictitious mechanical network laid along the edges of near-field fluid elements. New partitioned analysis procedures to treat this coupled 3-component problem were developed in 1994. These procedures involved delayed corrections and subcycling, and have been successfully tested on several massively parallel computers. For the global steady-state axisymmetric analysis of a complete engine we have decided to use the NASA-sponsored ENG10 program, which uses a regular FV-multiblock-grid discretization in conjunction with circumferential averaging to include effects of blade forces, loss, combustor heat addition, blockage, bleeds and convective mixing. A load-balancing preprocessor for parallel versions of ENG10 has been developed. It is planned to use the steady-state global solution provided by ENG10 as input to a localized three-dimensional FSI analysis for engine regions where aeroelastic effects may be important. Author

N95-23222*# Moller International, Inc., Davis, CA.

EVALUATION OF THERMAL BARRIER AND PS-200 SELF-LUBRICATING COATINGS IN AN AIR-COOLED ROTARY ENGINE Final Contractor Report

Paul S. Moller Cleveland, OH NASA Mar. 1995 39 p

(Contract NAS3-26309; RTOP 324-02-00)

(NASA-CR-195445; E-9493; NAS 1.26:195445) Avail: CASI HC A03/MF A01

This project provides an evaluation of the feasibility and desirability of applying a thermal barrier coating overlaid with a wear coating on the internal surfaces of the combustion area of rotary engines. Many experiments were conducted with different combinations of coatings applied to engine components of aluminum, iron and titanium, and the engines were run on a well-instrumented test stand. Significant improvements in specific fuel consumption were achieved and the wear coating, PS-200, which was invented at NASA's Lewis Research Center, held up well under severe test conditions. Author

N95-23550*# National Aeronautics and Space Administration. Lewis Research Center, Cleveland, OH.

SENSITIVITY OF COMBUSTION-ACOUSTIC INSTABILITIES TO BOUNDARY CONDITIONS FOR PREMIXED GAS TURBINE COMBUSTORS

Douglas Darling, Krishnan Radhakrishnan (NYMA, Inc., Brook Park, OH.), and Ayo Oyediran (AYT Corp., Brook Park, OH.) Mar. 1995 8 p Presented at the Central/Western States Sections Joint Technical Meeting, San Antonio, TX, 23-26 Apr. 1995; sponsored by the Combustion Institute

(Contract NAS3-27186; RTOP 537-02-21)

(NASA-TM-106890; E-9530; NAS 1.15:106890) Avail: CASI HC A02/MF A01

Premixed combustors, which are being considered for low NOx engines, are susceptible to instabilities due to feedback between pressure perturbations and combustion. This feedback can cause damaging mechanical vibrations of the system as well as degrade the emissions characteristics and combustion efficiency. In a lean combustor instabilities can also lead to blowout. A model was developed to perform linear combustion-acoustic stability analysis using detailed chemical kinetic mechanisms. The Lewis Kinetics and Sensitivity Analysis Code, LSENS, was used to calculate the sensitivities of the heat release rate to perturbations in density and temperature. In the present work, an assumption was made that the mean flow velocity was small relative to the speed of sound. Results of this model showed the regions of growth of perturbations to be most sensitive to the reflectivity of the boundary when reflectivities were close to unity. Author

N95-24053*# Union Carbide Industrial Gases, Inc., Tonawanda, NY. Linde Div.

AIRBORNE ROTARY AIR SEPARATOR STUDY Interim Report

A. Acharya, C. F. Gottzmann, and J. J. Nowobilski Cleveland, OH NASA Dec. 1990 64 p

(Contract NAS3-25560)

(NASA-CR-189099; E-9583; NAS 1.26:189099) Avail: CASI HC A04/MF A01

Several air breathing propulsion concepts for future earth-to-orbit transport vehicles utilize air collection and enrichment, and subsequent storage of liquid oxygen for later use in the vehicle emission. Work performed during the 1960's established the feasibility of substantially reducing weight and volume of a distillation type air separator system by operating the distillation elements in high 'g' fields obtained by rotating the separator assembly. This contract studied the capability test and hydraulic behavior of a novel structured or ordered distillation packing in a rotating device using air and water. Pressure drop and flood points were measured for different air and water flow rates in gravitational fields of up to 700 g. Behavior of the packing follows the correlations previously derived from tests at normal gravity. The novel ordered packing can take the place of trays in a rotating air separation column with the promise of substantial reduction in pressure drop, volume, and system weight. The results obtained in the program are used to predict design and performance of rotary separators for air collection and enrichment systems of interest for past and present concepts of air breathing propulsion (single or two-stage to orbit) systems. Author

08 AIRCRAFT STABILITY AND CONTROL

Includes aircraft handling qualities; piloting; flight controls; and autopilots.

For related information see also *05 Aircraft Design, Testing and Performance.*

N95-22674*# McDonnell-Douglas Aerospace, Long Beach, CA. Transport Aircraft.

GUIDANCE AND CONTROL REQUIREMENTS FOR HIGH-SPEED ROLLOUT AND TURNOFF (ROTO) Final Report

Steve H. Goldthorpe, Alan C. Kernik, Larry S. McBee, and Orv W. Preston Jan. 1995 127 p

(Contract NAS1-19703; RTOP 538-04-13-01)
(NASA-CR-195026; NAS 1.26:195026) Avail: CASI HC A07/MF A02

This report defines the initial requirements for designing a research high-speed rollout and turnoff (ROTO) guidance and control system applicable to transport class aircraft whose purpose is to reduce the average runway occupancy time (ROT) for aircraft operations. The requirements will be used to develop a ROTO system for both automatic and manual piloted operation under normal and reduced visibility conditions. Requirements were determined for nose wheel/rudder steering, braking/reverse thrust, and the navigation system with the aid of a non-real time, three degree-of-freedom MD-11 simulation program incorporating airframe and gear dynamics. The requirements were developed for speeds up to 70 knots using 30 ft exit geometries under dry and wet surface conditions. The requirements were generated under the assumptions that the aircraft landing system meets the current Category III touchdown dispersion requirements and that aircraft interarrival spacing is 2 nautical miles. This effort determined that auto-asymmetric braking is needed to assist steering for aft center-of-gravity aircraft. This report shows various time-history plots of the aircraft performance for the ROTO operation. This effort also investigated the state-of-the-art in the measurement of the runway coefficient of friction for various runway conditions. Author

N95-22908*# Massachusetts Inst. of Tech., Cambridge, MA. Dept. of Aeronautics and Astronautics.

DESIGN OF HIGH PERFORMANCE MULTIVARIABLE CONTROL SYSTEMS FOR SUPERMANEUVERABLE AIRCRAFT AT HIGH ANGLE OF ATTACK Final Report

Lena Valavani [1995] 3 p
(Grant NAG1-1088)
(NASA-CR-197661; NAS 1.26:197661) Avail: CASI HC A01/MF A01

The main motivation for the work under the present grant was to use nonlinear feedback linearization methods to further enhance performance capabilities of the aircraft, and robustify its response throughout its operating envelope. The idea was to use these methods in lieu of standard Taylor series linearization, in order to obtain a well behaved linearized plant, in its entire operational regime. Thus, feedback linearization was going to constitute an 'inner loop', which would then define a 'design plant model' to be compensated for robustness and guaranteed performance in an 'outer loop' application of modern linear control methods. The motivation for this was twofold; first, earlier work had shown that by appropriately conditioning the plant through conventional, simple feedback in an 'inner loop', the resulting overall compensated plant design enjoyed considerable enhancement of performance robustness in the presence of parametric uncertainty. Second, the nonlinear techniques did not have any proven robustness properties in the presence of unstructured uncertainty; a definition of robustness (and performance) is very difficult to achieve outside the frequency domain; to date, none is available for the purposes of control system design. Thus, by proper design of the outer loop, such properties could still be 'injected' in the overall system. Author

N95-22954*# National Aeronautics and Space Administration. Lewis Research Center, Cleveland, OH.

STABLE H(INFINITY) CONTROLLER DESIGN FOR THE LONGITUDINAL DYNAMICS OF AN AIRCRAFT

Hitay Oezbay (Ohio State Univ., Columbus, OH.) and Sanjay Garg Feb. 1995 53 p
(RTOP 505-62-50)
(NASA-TM-106847; E-9421; NAS 1.15:106847) Avail: CASI HC A04/MF A01

This report discusses different approaches to stable H infinity controller design applied to the problem of augmenting the longitudinal dynamics of an aircraft. Stability of the H infinity controller is investigated by analyzing the effects of changes in the performance index weights, and modifications in the measured outputs. The existence of a stable suboptimal controller is also investigated. It is shown that this is equivalent to finding a stable controller, whose infinity norm is less than a specified bound, for an unstable plant which is determined from parametrization of all H infinity controllers. Examples are given for a gust alleviation and a command tracking problem. Author

N95-23389* National Aeronautics and Space Administration. Ames Research Center, Moffett Field, CA.

ENGINES-ONLY FLIGHT CONTROL SYSTEM Patent

Frank W. Burcham, inventor (to NASA), Glenn B Gilyard, inventor (to NASA), Joseph L. Conley, inventor (to NASA), James F. Stewart, inventor (to nASA), and Charles G. Fullerton, inventor (to NASA) 19 Jul. 1994 18 p Filed 28 May 1992
(NASA-Case-ARC-11944-1; US-Patent-5,330,131;
US-Patent-Appl-SN-889347; US-Patent-Class-244-75R;
US-Patent-Class-244-7R; US-Patent-Class-244-182;
US-Patent-Class-244-51; Int-Patent-Class-B64C-19/00) Avail: US Patent and Trademark Office

A backup flight control system for controlling the flightpath of a multi-engine airplane using the main drive engines is introduced. The backup flight control system comprises an input device for generating a control command indicative of a desired flightpath, a feedback sensor for generating a feedback signal indicative of at least one of pitch rate, pitch attitude, roll rate and roll attitude, and a control device for changing the output power of at least one of the main drive engines on each side of the airplane in response to the control command and the feedback signal.
Official Gazette of the U.S. Patent and Trademark Office

N95-23392*# Georgia Tech Research Inst., Atlanta, GA. Contracting Support Div.

FLUTTER ANALYSIS OF COMPOSITE BOX BEAMS Final Administrative Report, 21 Sep. 1993 - 20 Sep. 1994

Dewey H. Hodges and Matthew Greenman 21 Feb. 1995 14 p
(Grant NGT-50981)
(NASA-CR-197931; NAS 1.26:197931) Avail: CASI HC A03/MF A01

The dynamic aeroelastic instability of flutter is an important factor in the design of modern high-speed, flexible aircraft. The current trend is toward the creative use of composites to delay flutter. To obtain an optimum design, we need an accurate as well as efficient model. As a first step towards this goal, flutter analysis is carried out for an unswept composite box beam using a linear structural model and Theodorsen's unsteady aerodynamic theory. Structurally, the wing was modeled as a thin-walled box-beam of rectangular cross section. Theodorsen's theory was used to get 2-D unsteady aerodynamic forces, which were integrated over the span. A free-vibration analysis is carried out. These fundamental modes are used to get the flutter solution using the V-g method. Future work is intended to build on this foundation. Author

N95-23410*# Minnesota Univ., Minneapolis, MN. Dept. of Aerospace Engineering and Mechanics.

FEEDBACK CONTROL LAWS FOR HIGHLY MANEUVERABLE AIRCRAFT Annual Report, 1 Feb. 1995 - 31 Jan. 1996

William L. Garrard and Gary J. Balas 31 Jan. 1995 11 p
(Grant NAG1-1380)
(NASA-CR-197944; NAS 1.26:197944) Avail: CASI HC A03/MF A01

During this year, we concentrated our efforts on the design of controllers for lateral/directional control using mu synthesis. This proved to be a more difficult task than we anticipated and we are still working on the designs. In the lateral-directional control problem, the inputs are pilot lateral stick and pedal commands and the outputs are roll rate about the velocity vector and side slip angle. The control effectors are ailerons, rudder deflection, and directional thrust vectoring vane deflection which produces a yawing moment about the body axis. Our math model does not contain any provision for thrust vectoring of rolling moment. This has resulted in limitations of performance at high angles of attack. During 1994-95, the following tasks for the lateral-directional controllers were accomplished: (1) Designed both inner and outer loop dynamic inversion controllers. These controllers are implemented using accelerometer outputs rather than an a priori model of the vehicle aerodynamics; (2) Used classical techniques to design controllers for the system linearized by dynamics inversion. These controllers acted to control roll rate and Dutch roll response; (3) Implemented the inner loop dynamic inversion and classical controllers on the six DOF simulation; (4) Developed a lateral-directional control allocation scheme based on minimizing required control effort among the ailerons, rudder, and directional thrust vectoring; and (5) Developed mu outer loop controllers combined with classical inner loop controllers. Derived from text

N95-23671*# National Aeronautics and Space Administration. Lewis Research Center, Cleveland, OH.

MOTOR DRIVE TECHNOLOGIES FOR THE POWER-BY-WIRE (PBW) PROGRAM: OPTIONS, TRENDS AND TRADEOFFS

Malik E. Elbuluk (Akron Univ., Akron, OH.) and M. David Kankam Mar. 1995 14 p Presented at the National Aerospace and Electronics Conference, Wright-Patterson AFB, OH, 23-27 May 1995; cosponsored by the IEEE and the Aerospace and Electronics Systems Society

(RTOP 233-02-03)

(NASA-TM-106885; E-9521; NAS 1.15:106885) Avail: CASI HC A03/MF A01

Power-By-Wire (PBW) is a program involving the replacement of hydraulic and pneumatic systems currently used in aircraft with an all-electric secondary power system. One of the largest loads of the all-electric secondary power system will be the motor loads which include pumps, compressors and Electrical Actuators (EA's). Issues of improved reliability, reduced maintenance and efficiency, among other advantages, are the motivation for replacing the existing aircraft actuators with electrical actuators. An EA system contains four major components. These are the motor, the power electronic converters, the actuator and the control system, including the sensors. This paper is a comparative literature review in motor drive technologies, with a focus on the trends and tradeoffs involved in the selection of a particular motor drive technology. The reported research comprises three motor drive technologies. These are the induction motor (IM), the brushless dc motor (BLDCM) and the switched reluctance motor (SRM). Each of the three drives has the potential for application in the PBW program. Many issues remain to be investigated and compared between the three motor drives, using actual mechanical loads expected in the PBW program. Author

N95-23297*# California Univ., Davis, CA. Dept. of Mechanical and Aeronautical Engineering.

ANALYSIS OF THE LONGITUDINAL HANDLING QUALITIES AND PILOT-INDUCED-OSCILLATION TENDENCIES OF THE HIGH-ANGLE-OF-ATTACK RESEARCH VEHICLE (HARV) Abstract Only

Ronald A. Hess *In* Hampton Univ., 1994 NASA-HU American Society for Engineering Education (ASEE) Summer Faculty Fellowship Program Dec. 1994 p 79 (For primary document see N95-23276 07-99)

Avail: CASI HC A01/MF A02

N95-23314*# Old Dominion Coll., Norfolk, VA. Dept. of Aerospace Engineering.

INNER LOOP FLIGHT CONTROL FOR THE HIGH-SPEED CIVIL TRANSPORT Abstract Only

Brett A. Newman *In* Hampton Univ., 1994 NASA-HU American Society for Engineering Education (ASEE) Summer Faculty Fellowship Program Dec. 1994 p 96 (For primary document see N95-23276 07-99)

Avail: CASI HC A01/MF A02

N95-23319*# Saint Louis Univ., Cahokia, IL. Dept. of Aerospace Engineering.

PRELIMINARY IDENTIFICATION OF BUFFET PROBLEMS IN HIGH SPEED CIVIL TRANSPORT Abstract Only

Krishnaswamy Ravindra *In* Hampton Univ., 1994 NASA-HU American Society for Engineering Education (ASEE) Summer Faculty Fellowship Program Dec. 1994 p 101 (For primary document see N95-23276 07-99)

Avail: CASI HC A01/MF A02

N95-23325*# Tennessee Univ. Space Inst., Tullahoma, TN.

HANDLING QUALITIES OF THE HIGH SPEED CIVIL TRANSPORT Abstract Only

U. Peter Solies *In* Hampton Univ., 1994 NASA-HU American Society for Engineering Education (ASEE) Summer Faculty Fellowship Program Dec. 1994 p 107 (For primary document see N95-23276 07-99)

Avail: CASI HC A01/MF A02

09 RESEARCH AND SUPPORT FACILITIES (AIR)

Includes airports, hangars and runways; aircraft repair and overhaul facilities; wind tunnels; shock tubes; and aircraft engine test stands.

For related information see also *14 Ground Support Systems and Facilities (Space).*

N95-23011*# National Aeronautics and Space Administration. Langley Research Center, Hampton, VA.

DYNAMIC RESPONSE TESTS OF INERTIAL AND OPTICAL WIND-TUNNEL MODEL ATTITUDE MEASUREMENT DEVICES

R. D. Buehrle, C. P. Young, Jr. (North Carolina State Univ., Raleigh, NC.), A. W. Burner, J. S. Tripp, P. Tcheng, T. D. Finley, and T. G. Popernack, Jr. Feb. 1995 44 p

(RTOP 505-59-54-01)

(NASA-TM-109182; NAS 1.15:109182) Avail: CASI HC A03/MF A01

Results are presented for an experimental study of the response of inertial and optical wind-tunnel model attitude measurement systems in a wind-off simulated dynamic environment. This study is part of an ongoing activity at the NASA Langley Research Center to develop high accuracy, advanced model attitude measurement systems that can be used in a dynamic wind-tunnel environment. This activity was prompted by the inertial model attitude sensor response observed during high levels of model vibration which results in a model attitude measurement bias error. Significant bias errors in model attitude measurement were found for the measurement using the inertial device during wind-off dynamic testing of a model system. The amount of bias present during wind-tunnel tests will depend on the amplitudes of the model dynamic response and the modal characteristics of the model system. Correction models are presented that predict the vibration-induced bias errors to a high degree of accuracy for the vibration modes characterized in the simulated dynamic environment. The optical system results were uncorrupted by model vibration in the laboratory setup. Author

N95-23192*# National Aeronautics and Space Administration. Lewis Research Center, Cleveland, OH.

NASA LOW-SPEED AXIAL COMPRESSOR FOR FUNDAMENTAL RESEARCH

Charles A. Wasserbauer (Sverdrup Technology, Inc., Brook Park, OH.), Harold F. Weaver, and Richard G. Senyitko (Sverdrup Technology, Inc., Brook Park, OH.) Feb. 1995 13 p

(Contract NAS3-25266; RTOP 505-62-52)

(NASA-TM-4635; E-9016; NAS 1.15:4635) Avail: CASI HC A03/MF A01

A low-speed multistage axial compressor built by the NASA Lewis Research Center is described. The purpose of this compressor is to increase the understanding of the complex flow phenomena within multistage axial compressors and to obtain detailed data from a multistage compressor environment for use in developing and verifying models for computational fluid dynamic code assessment. The compressor has extensive pressure instrumentation in both stationary and rotating frames of reference, and has provisions for flow visualization and laser velocimetry. The compressor will accommodate rotational speeds to 1050 rpm and is rated at a pressure ratio of 1.042. Author

N95-24019# Los Alamos National Lab., NM.

NTS-SPILL TEST FACILITY WIND TUNNEL EXHAUST PLUME CHARACTERIZATION

R. Kerr, H. Goldwire, D. Smith, J. Rawlings, T. Schaffer, and J. Robson Jul. 1994 8 p Presented at the 1994 Chemical Analysis By Laser Interrogation of Proliferation Effluents (CALIOPE ITR) Interim Technical Review, Livermore, CA, 26-28 Apr. 1994

(Contract W-7405-eng-48)

(DE95-003630; UCRL-JC-118476; CONF-9404162-14) Avail: CASI HC A02/MF A01

The exhaust plume of the NTS-STF wind tunnel has been characterized to demonstrate its suitability as a target for CALIOPE experiments. Smoke from grenades has been released in multiple quantities and at different positions inside the tunnel. The smoke plumes have been recorded on video tape. The wind velocity profile has also been determined with a moveable array of miniature vane anemometers. These measurements will

be used to determine the vapor concentration pathlength as part of the ground truth. DOE

N95-23299*# Old Dominion Coll., Norfolk, VA. Dept. of Mechanical Engineering.
SYSTEM IDENTIFICATION OF THE LARGE-ANGLE MAGNETIC SUSPENSION TEST FIXTURE (LAMSTF) Abstract Only
Jen-Kuang Huang *In* Hampton Univ., 1994 NASA-HU American Society for Engineering Education (ASEE) Summer Faculty Fellowship Program Dec. 1994 p 81 (For primary document see N95-23276 07-99)
Avail: CASI HC A01/MF A02

N95-23304*# Old Dominion Coll., Norfolk, VA. Dept. of Mechanical Engineering.
OPTIMIZED DESIGN OF A HYPERSONIC NOZZLE Abstract Only
Ramesh Krishnamurthy *In* Hampton Univ., 1994 NASA-HU American Society for Engineering Education (ASEE) Summer Faculty Fellowship Program Dec. 1994 p 86 (For primary document see N95-23276 07-99)
Avail: CASI HC A01/MF A02

N95-23309*# New Jersey Inst. of Tech., Newark, NJ. Dept. of Chemical Engineering, Chemistry and Environmental Science.
DESIGN OF A VARIABLE AREA DIFFUSER FOR A 15-INCH MACH 6 OPEN-JET TUNNEL Abstract Only
Norman W. Loney *In* Hampton Univ., 1994 NASA-HU American Society for Engineering Education (ASEE) Summer Faculty Fellowship Program Dec. 1994 p 91 (For primary document see N95-23276 07-99)
Avail: CASI HC A01/MF A02

12 ASTRONAUTICS (GENERAL)

For extraterrestrial exploration see *91 Lunar and Planetary Exploration.*

N95-22947*# National Aeronautics and Space Administration, Washington, DC.
SPACE SCIENCE FOR THE 21ST CENTURY. STRATEGIC PLAN FOR 1995-2000
Sep. 1994 26 p
(NASA-TM-110546; NAS 1.15:110546) Avail: CASI HC A03/MF A01

This publication is one of three volumes in 'Space Science for the 21st Century', the Office of Space Science Strategic plan for 1995-2000. The other two volumes are the recently released Integrated Technology Strategy and the Education Plan, which is in preparation at this publication date. The Science Plan was developed by the Office of Space Science (OSS) in partnership with the Space Science Advisory Committee. The mission of the OSS is to seek answers to fundamental questions about: the galaxy and the universe; the connection between the Sun, Earth, and Heliosphere; the origin and evolution of planetary systems; and the origin and distribution of life in the universe. The strategy to answer these questions includes completing the means to survey the universe across the entire electromagnetic spectrum; completing the survey of cosmic rays through their highest energies, and of interstellar gas; carrying out a basic new test of the Theory of General Relativity; completing development of the means to understand the mechanisms of solar variability and its effects on Earth; completing the first exploration of the inner and outer frontiers of the heliosphere; determining the plasma environments of the solar system planets and how those environments are affected by solar activity; completing development of the means to finish the reconnaissance of the entire solar system from the Sun to Pluto; beginning the comprehensive search for other planets around other stars; resuming surface exploration of solar system bodies to understand the origin and evolution of the Sun's planetary system; continuing the study of biogenic compounds and their evolution in the universe; and searching for indicators of past and present conditions conducive to life. Derived from text

N95-23262*# National Aeronautics and Space Administration. Lyndon B. Johnson Space Center, Houston, TX. Space Station Program Office
STS-61 MISSION DIRECTOR'S POST-MISSION REPORT
Ronald L. Newman Jan. 1995 146 p
(NASA-TM-104803; S-780; NAS 1.15:104803) Avail: CASI HC A07/MF A02

To ensure the success of the complex Hubble Space Telescope servicing mission, STS-61, NASA established a number of independent review groups to assess management, design, planning, and preparation for the mission. One of the resulting recommendations for mission success was that an overall Mission Director be appointed to coordinate management activities of the Space Shuttle and Hubble programs and to consolidate results of the team reviews and expedite responses to recommendations. This report presents pre-mission events important to the experience base of mission management, with related Mission Director's recommendations following the event(s) to which they apply. All Mission Director's recommendations are presented collectively in an appendix. Other appendixes contain recommendations from the various review groups, including Payload Officers, the JSC Extravehicular Activity (EVA) Section, JSC EVA Management Office, JSC Crew and Thermal Systems Division, and the STS-61 crew itself. This report also lists mission events in chronological order and includes as an appendix a post-mission summary by the lead Payload Deployment and Retrieval System Officer. Recommendations range from those pertaining to specific component use or operating techniques to those for improved management, review, planning, and safety procedures. Author

N95-23549*# National Aeronautics and Space Administration. Marshall Space Flight Center, Huntsville, AL.
LDEF MATERIALS RESULTS FOR SPACECRAFT APPLICATIONS: EXECUTIVE SUMMARY
A. F. Whitaker, comp. and D. Dooling, comp. (D2 Associates, Huntsville, AL.) Washington Mar. 1995 27 p Conference held in Huntsville, AL, 27-28 Oct. 1992; sponsored by the University of Alabama, the Alabama Space Grant Consortium, and the Society of Advanced Materials and Process Engineers
(NASA-CP-3261; M-745; NAS 1.55:3261) Avail: CASI HC A03/MF A01

To address the challenges of space environmental effects, NASA designed the Long Duration Exposure Facility (LDEF) for an 18-month mission to expose thousands of samples of candidate materials that might be used on a space station or other orbital spacecraft. LDEF was launched in April 1984 and was to have been returned to Earth in 1985. Changes in mission schedules postponed retrieval until January 1990, after 69 months in orbit. Analyses of the samples recovered from LDEF have provided spacecraft designers and managers with the most extensive data base on space materials phenomena. Many LDEF samples were greatly changed by extended space exposure. Among even the most radially altered samples, NASA and its science teams are finding a wealth of surprising conclusions and tantalizing clues about the effects of space on materials. Many were discussed at the first two LDEF results conferences and subsequent professional papers. The LDEF Materials Results for Spacecraft Applications Conference was convened in Huntsville to discuss implications for spacecraft design. Already, paint and thermal blanket selections for space station and other spacecraft have been affected by LDEF data. This volume synopsizes those results. Author

N95-23750*# National Aeronautics and Space Administration. Lyndon B. Johnson Space Center, Houston, TX.
MODELING ACTIONS AND OPERATIONS TO SUPPORT MISSION PREPARATION
Jane T. Malin, D. P. Ryan (Metrica, Inc., Houston, TX.), and D. L. Schreckenghost (Metrica, Inc., Houston, TX.) *In* JPL, Third International Symposium on Artificial Intelligence, Robotics, and Automation for Space 1994 Oct. 1994 p 385-388 (For primary document see N95-23672 07-63)
Avail: CASI HC A01/MF A03

N95-23751*# CRI Space, (Denmark).
CRI PLANNING AND SCHEDULING FOR SPACE
Mads Aarup *In* JPL, Third International Symposium on Artificial Intelligence, Robotics, and Automation for Space 1994 Oct. 1994 p 289-392 (For primary document see N95-23672 07-63)
Avail: CASI HC A01/MF A03

N95-23752*# MATRA Marconi Space, Toulouse (France).
BENEFITS OF ADVANCED SOFTWARE TECHNIQUES FOR MISSION PLANNING SYSTEMS
A. Gasquet, Y. Parrod, and A. DeSaintVincent *In* JPL, Third International Symposium on Artificial Intelligence, Robotics, and Automation for Space 1994 Oct. 1994 p 393-396 (For primary document see N95-23672 07-63)
Avail: CASI HC A01/MF A03

N95-23758*# Carnegie-Mellon Univ., Pittsburgh, PA. The Robotics Inst.
HIGH PERFORMANCE TECHNIQUES FOR SPACE MISSION SCHEDULING
Stephen F. Smith *In* JPL, Third International Symposium on Artificial Intelligence, Robotics, and Automation for Space 1994 Oct. 1994 p 419-422 (For primary document see N95-23672 07-63)
(Contracts NCC2-531; F30602-90-C-0119)
Avail: CASI HC A01/MF A03

N95-23759*# Tokyo Univ. (Japan). Dept. of Aeronautics an Astronautics.
APPLICATIONS OF DYNAMIC SCHEDULING TECHNIQUE TO SPACE RELATED PROBLEMS: SOME CASE STUDIES
Shinichi Nakasuka and Tetsujiro Ninomiya *In* JPL, Third International Symposium on Artificial Intelligence, Robotics, and Automation for Space 1994 Oct. 1994 p 423-426 (For primary document see N95-23672 07-63)
Avail: CASI HC A01/MF A03

N95-23760*# Office National d'Etudes et de Recherches Aerospatiales, Toulouse (France).
SOLUTION AND REASONING REUSE IN SPACE PLANNING AND SCHEDULING APPLICATIONS
Gerard Verfaillie and Thomas Schiex *In* JPL, Third International Symposium on Artificial Intelligence, Robotics, and Automation for Space 1994 Oct. 1994 p 427-430 (For primary document see N95-23672 07-63)
Avail: CASI HC A01/MF A03

N95-23761*# Honeywell Technology Center, Minneapolis, MN.
EMPIRICAL RESULTS ON SCHEDULING AND DYNAMIC BACKTRACKING
Mark S. Boddy and Robert P. Goldman *In* JPL, Third International Symposium on Artificial Intelligence, Robotics, and Automation for Space 1994 Oct. 1994 p 431-434 (For primary document see N95-23672 07-63)
Avail: CASI HC A01/MF A03

N95-23763*# SRI International Corp., Menlo Park, CA. Artificial Intelligence Center.
INTEGRATING PLANNING AND REACTIVE CONTROL
David E. Wilkins and Karen L. Myers *In* JPL, Third International Symposium on Artificial Intelligence, Robotics, and Automation for Space 1994 Oct. 1994 p 435-442 (For primary document see N95-23672 07-63)
(Contract F30602-90-C-0086)
Avail: CASI HC A01/MF A03

N95-23764*# Florida Inst. of Tech., Melbourne, FL. Computer Science Program.
AUTOMATIC GENERATION OF EFFICIENT ORDERINGS OF EVENTS FOR SCHEDULING APPLICATIONS
Robert A. Morris *In* JPL, Third International Symposium on Artificial Intelligence, Robotics, and Automation for Space 1994 Oct. 1994 p 443-447 (For primary document see N95-23672 07-63)
Avail: CASI HC A01/MF A03

13 ASTRODYNAMICS

Includes powered and free-flight trajectories; and orbital and launching dynamics.

No abstracts in this category.

14 GROUND SUPPORT SYSTEMS AND FACILITIES (SPACE)

Includes launch complexes, research and production facilities; ground support equipment, e.g., mobile transporters; and simulators.

For related information see also *09 Research and Support Facilities (Air).*

N95-23679*# Siemens A.G., Vienna (Austria). Knowledge Systems Lab.
OPERATOR PROCEDURE VERIFICATION WITH A RAPIDLY RECONFIGURABLE SIMULATOR
Yumi Iwasaki, Robert Engelmore, Gary Fehr, and Richard Fikes *In* JPL, Third International Symposium on Artificial Intelligence, Robotics, and Automation for Space 1994 Oct. 1994 p 37-40 (For primary document see N95-23672 07-63)
(Contract NCC2-537; NAG2-581; ARPA Order 8607)
Avail: CASI HC A01/MF A03

N95-23702*# National Aerospace Lab., Tokyo (Japan).
CONCEPT VERIFICATION OF THREE DIMENSIONAL FREE MOTION SIMULATOR FOR SPACE ROBOT
Osamu Okamoto, Teruomi Nakaya, and Brett Pokines (Virginia Polytechnic Inst. and State Univ., Blacksburg, VA.) *In* JPL, Third International Symposium on Artificial Intelligence, Robotics, and Automation for Space 1994 Oct. 1994 p 153-156 (For primary document see N95-23672 07-63)
Avail: CASI HC A01/MF A03

N95-23711*# Tokyo Inst. of Tech. (Japan). Dept. of Mechano-Aerospace Engineering.
DEVELOPMENT OF THE DYNAMIC MOTION SIMULATOR OF 3D MICRO-GRAVITY WITH A COMBINED PASSIVE/ACTIVE SUSPENSION SYSTEM
Kazuya Yoshida, Shigeo Hirose, and Tadashi Ogawa *In* JPL, Third International Symposium on Artificial Intelligence, Robotics, and Automation for Space 1994 Oct. 1994 p 197-200 (For primary document see N95-23672 07-63)
Avail: CASI HC A01/MF A03

N95-23734*# Kawasaki Heavy Industries Ltd., Kakamigahara (Japan). Space Systems Engineering Div.
TELEROBOTICS TEST BED FOR SPACE STRUCTURE ASSEMBLY
M. Kitami, K. Ogimoto, F. Yasumoto (Kawasaki Heavy Industries Ltd., Akashi, Japan.), T. Katsuragawa (Kawasaki Heavy Industries Ltd., Akashi, Japan.), T. Itoko (Kawasaki Heavy Industries Ltd., Akashi, Japan.), Y. Kurosaki (Kawasaki Heavy Industries Ltd., Akashi, Japan.), S. Hirai (Ministry of International Trade and Industry, Tsukuba, Japan.), and K. Machida (Ministry of International Trade and Industry, Tsukuba, Japan.) *In* JPL, Third International Symposium on Artificial Intelligence, Robotics, and Automation for Space 1994 Oct. 1994 p 309-312 (For primary document see N95-23672 07-63)
Avail: CASI HC A01/MF A03

15 LAUNCH VEHICLES AND SPACE VEHICLES

Includes boosters; operating problems of launch/space vehicle systems; and reusable vehicles.

For related information see also *20 Spacecraft Propulsion and Power.*

N95-24032*# Auburn Univ., AL. Dept. of Aerospace Engineering.
AERODYNAMIC FLIGHT CONTROL TO INCREASE PAYLOAD CAPABILITY OF FUTURE LAUNCH VEHICLES Final Report, 20 Jan. 1994 - 19 Jan. 1995
John E. Cochran, Jr. 28 Feb. 1995 9 p
(Contract NAS8-39131)
(NASA-CR-197704; NAS 1.26:197704) Avail: CASI HC A02/MF A01

The development of new launch vehicles will require that designers use innovative approaches to achieve greater performance in terms of pay load capability. The objective of the work performed under this delivery order was to provide technical assistance to the Contract Officer's Technical Representative (COTR) in the development of ideas and concepts for increasing the payload capability of launch vehicles by incorporating aerodynamic controls. Although aerodynamic controls, such as moveable fins, are currently used on relatively small missiles, the evolution of large launch vehicles has been moving away from aerodynamic control. The COTR reasoned that a closer investigation of the use of aerodynamic controls on large vehicles was warranted. Derived from text

N95-23332*# Old Dominion Coll., Norfolk, VA.
MULTIDISCIPLINARY DESIGN OPTIMIZATION USING GENETIC ALGORITHMS Abstract Only
Resit Unal *In* Hampton Univ., 1994 NASA-HU American Society for Engineering Education (ASEE) Summer Faculty Fellowship Program Dec. 1994 p 114 (For primary document see N95-23276 07-99)
Avail: CASI HC A01/MF A02

16 SPACE TRANSPORTATION

Includes passenger and cargo space transportation, e.g., shuttle operations; and space rescue techniques.

For related information see also *03 Air Transportation and Safety* and *18 Spacecraft Design, Testing and Performance.* For space suits see *54 Man/System Technology and Life Support.*

N95-23093*# Lockheed Engineering and Sciences Co., Houston, TX.
STS-59 SPACE SHUTTLE MISSION REPORT
Robert W. Fricke, Jr. Jun. 1994 52 p Sponsored by NASA. Johnson Space Center
(NASA-TM-110527; NSTS-08291; NAS 1.15:110527) Avail: CASI HC A04/MF A01

The STS-59 Space Shuttle Program Mission Report summarizes the Payload activities as well as the Orbiter, External Tank (ET), Solid Rocket Booster (SRB), Redesigned Solid Rocket Motor (RSRM), and the Space Shuttle main engine (SSME) systems performance during the sixty-second flight of the Space Shuttle Program and sixth flight of the Orbiter vehicle Endeavor (OV-105). In addition to the Orbiter, the flight vehicle consisted of an ET designated as ET-63; three SSME's which were designated as serial numbers 2028, 2033, and 2018 in positions 1, 2, and 3, respectively; and two SRB's which were designated BI-065. The RSRM's that were installed in each SRB were designated as 360W037A (welterweight) for the left SRB, and 360H037B (heavyweight) for the right SRB. This STS-59 Space Shuttle Program Mission Report fulfills the Space Shuttle Program requirement as documented in NSTS 07700, Volume 8, Appendix E. That document requires that each major organizational element supporting the Program report the results of its hardware evaluation and mission performance plus identify all related in-flight anomalies. The primary objective of the STS-59 mission was to successfully perform the operations of the Space Radar Laboratory-1 (SRL-1). The secondary objectives of this flight were to perform the operations of the Space Tissue Loss-A (STL-A) and STL-B payloads, the Visual Function Tester-4 (VFT-4) payload, the Shuttle Amateur Radio Experiment-2 (SAREX-2) experiment, the Consortium for Materials Development in Space Complex Autonomous Payload-4 (CONCAP-4), and the three Get-Away Special (GAS) payloads. Derived from text

N95-23094*# Lockheed Engineering and Sciences Co., Houston, TX.
STS-62 SPACE SHUTTLE MISSION REPORT
Robert W. Fricke, Jr. May 1994 59 p Sponsored by NASA. Johnson Space Center
(NASA-TM-110450; NSTS-08290; NAS 1.15:110450) Avail: CASI HC A04/MF A01

The STS-62 Space Shuttle Program Mission Report summarizes the Payload activities as well as the Orbiter, External Tank (ET), Solid Rocket Booster (SRB), Redesigned Solid Rocket Motor (RSRM), and the Space Shuttle main engine (SSHE) systems performance during the sixty-first flight of the Space Shuttle Program and sixteenth flight of the Orbiter vehicle Columbia (OV-102). In addition to the Orbiter, the flight vehicle consisted of an ET designated as ET-62; three SSME's which were designated as serial numbers 2031, 2109, and 2029 in positions 1, 2, and 3, respectively; and two SRB's which were designated BI-064. The RSRM's that were installed in each SRB were designated as 360L036A (lightweight) for the left SRB, and 36OWO36B (welterweight) for the right SRB. This STS-62 Space Shuttle Program Mission Report fulfills the Space Shuttle Program requirement as documented in NSTS 07700, Volume 8, Appendix E. That document requires that each major organizational element supporting the Program report the results of its hardware evaluation and mission performance plus identify all related in-flight anomalies. The primary objectives of the STS-62 mission were to perform the operations of the United States Microgravity Payload-2 (USMP-2) and the Office of Aeronautics and Space Technology-2 (OAST-2) payload. The secondary objectives of this flight were to perform the operations of the Dexterous End Effector (DEE), the Shuttle Solar Backscatter Ultraviolet/A (SSBUV/A), the Limited Duration Space Environment Candidate Material Exposure (LDCE), the Advanced Protein Crystal Growth (APCG), the Physiological Systems Experiments (PSE), the Commercial Protein Crystal Growth (CPCG), the Commercial Generic Bioprocessing Apparatus (CGBA), the Middeck Zero-Gravity Dynamics Experiment (MODE), the Bioreactor Demonstration System (BDS), the Air Force Maui Optical Site Calibration Test (AMOS), and the Auroral Photography Experiment (APE-B). Derived from text

N95-23187*# Lockheed Engineering and Sciences Co., Houston, TX.
STS-61 SPACE SHUTTLE MISSION REPORT
Robert W. Fricke, Jr. Feb. 1994 53 p Sponsored by NASA Johnson Space Center
(NASA-TM-110545; NSTS-08288; NAS 1.15:110545) Avail: CASI HC A04/MF A01

The STS-61 Space Shuttle Program Mission Report summarizes the Hubble Space Telescope (HST) servicing mission as well as the Orbiter, External Tank (ET), Solid Rocket Booster (SRB), Redesigned Solid Rocket Motor (RSRM), and the Space Shuttle main engine (SSME) systems performance during the fifty-ninth flight of the Space Shuttle Program and fifth flight of the Orbiter vehicle Endeavour (OV-105). In addition to the Orbiter, the flight vehicle consisted of an ET designated as ET-60; three SSME's which were designated as serial numbers 2019, 2033, and 2017 in positions 1, 2, and 3, respectively; and two SRB's which were designated BI-063. The RSRM's that were installed in each SRB were designated as 360L023A (lightweight) for the left SRB, and 360L023B (lightweight) for the right SRB. This STS-61 Space Shuttle Program Mission Report fulfills the Space Shuttle Program requirement as documented in NSTS 07700, Volume 8, Appendix E. That document requires that each major organizational element supporting the Program report the results of its hardware evaluation and mission performance plus identify all related in-flight anomalies. The primary objective of the STS-61 mission was to perform the first on-orbit servicing of the Hubble Space Telescope. The servicing tasks included the installation of new solar arrays, replacement of the Wide Field/Planetary Camera I (WF/PC I) with WF/PC II, replacement of the High Speed Photometer (HSP) with the Corrective Optics Space Telescope Axial Replacement (COSTAR), replacement of rate sensing units (RSU's) and electronic control units (ECU's), installation of new magnetic sensing systems and fuse plugs, and the repair of the Goddard High Resolution Spectrometer (GHRS). Secondary objectives were to perform the requirements of the IMAX Cargo Bay Camera (ICBC), the IMAX Camera, and the Air Force Maui Optical Site (AMOS) Calibration Test.

Derived from text

N95-23275* National Aeronautics and Space Administration. Lyndon B. Johnson Space Center, Houston, TX.
TOYS IN SPACE, 2 (Videotape)
Dexter Herbert, ed. 24 Jun. 1993 *Its* Liftoff to Learning Series Videotape: 37 min. 53 sec. playing time, in color, with sound
(NASA-TM-110541; NONP-NASA-VT-95-43944) Avail: CASI VHS A02/BETA A22

In this educational video from the 'Liftoff to Learning' series, astronauts from the STS-54 Mission (Mario Runco, John Casper, Don McMonagle, Susan Helms, and Greg Harbaugh) explain how microgravity and weightlessness in space affects motion by using both mechanical and nonmechanical toys (gravitrons, slinkys, dart boards, magnetic marbles, and others). The gravitational effects on rotation, force, acceleration, magnetism, magnetic fields, center of axis, and velocity are actively demonstrated using these toys through experiments onboard the STS-54 Mission flight as a part of their spaceborne experiment payload. CASI

N95-23664* National Aeronautics and Space Administration. Lyndon B. Johnson Space Center, Houston, TX.
ENDEAVOR: NOW AND THEN (Videotape)
22 Sep. 1992 *Its* Liftoff to Learning Series Videotape: 19 min. 5 sec. playing time, in color, with sound
(NASA-TM-110539; NONP-NASA-VT-95-43942) Avail: CASI VHS A02/BETA A22

In this educational 'Liftoff to Learning' video series, astronauts from STS-49 Space Shuttle Mission (Thomas Akers, Bruce Melnick, Pierre Thuot, Kathy Thorton, Kevin Chilton, and Richard Hieb) compare their mission aboard the Space Shuttle Endeavor and their shuttle with its namesake, the ship 'Endeavor', commanded by Captain James Cook of England in the late 1700's. Using historical paintings, drawings, and computer graphics, Cook's Endeavor is brought to life. Its voyage path, problems, biological experiments, and discoveries are shown and compared to the modern-day Endeavor, its mission and experiments. The Space Shuttle Endeavor was named in 1988, through a nation-wide school contest. It is the fifth Space Shuttle to be built and employs new technology in its design, for example, its drag shoot for shuttle landings. One part of the STS-49 Mission was the retrieval of the Intel satellite. CASI

N95-23665* National Aeronautics and Space Administration. Lyndon B. Johnson Space Center, Houston, TX.
ALL SYSTEMS GO! (Videotape)
2 Sep. 1992 *Its* Liftoff to Learning Series Videotape: 33 min. 34 sec. playing time, in color, with sound
(NASA-TM-110542; NONP-NASA-VT-95-43945) Avail: CASI VHS A02/BETA A22

In this educational 'Liftoff to Learning' video series, astronauts from STS-40 Space Shuttle Mission (F. Drew Gaffney, Millie Hughes-Fulford, Rhea Seddon, James Bagia, Bryan O'Connor, Tamara Jernigan, and Sidney Gutierrez) show, using footage and highlights from their mission, how microgravity causes changes in the human body. The STS-40 was a mission of spaceborne experiments concerned with the physiological, biological, and chemical changes that occur in the human body as a result of microgravity. Different experiments are shown and their significance are explained. CASI

N95-24027* National Aeronautics and Space Administration, Washington, DC.
SPACE SHUTTLE MISSION: STS-67
Mar. 1995 56 p
(NASA-TM-110509; NAS 1.15:110509; NASA-News-Release-95-18) Avail: CASI HC A04/MF A01

The Space Shuttle Endeavor, scheduled to launch March 2, 1995 from NASA's Kennedy Space Center, will conduct NASA's longest Shuttle flight prior to date. The mission, designated STS-67, has a number of experiments and payloads, which the crew, commanded by Stephen S. Oswald, will have to oversee. This NASA press kit for the mission contains a general background (general press release, media services information, quick-look facts page, shuttle abort modes, summary timeline, payload and vehicle weights, orbital summary, and crew responsibilities); cargo bay payloads and activities (Astro 2, Get Away Special Experiments); in-cabin payloads (Commercial Minimum Descent Altitude Instrumentation Technology Associates Experiments, protein crystal growth experiments, Middeck Active Control Experiment, and Shuttle Amateur Radio Experiment); and the STS-67 crew biographies. The payloads and experiments are described and summarized to give an overview of the goals, objectives, apparatuses, procedures, sponsoring parties, and the assigned crew members to carry out the tasks. CASI

17 SPACE COMM., SPACECRAFT COMM., COMMAND & TRACKING

Includes telemetry; space communications networks; astronavigation and guidance; and radio blackout.

For related information see also *04 Aircraft Communications and Navigation* and *32 Communications and Radar.*

N95-23754*# Malin Space Science Systems, San Diego, CA.
AUTOMATIC COMMANDING OF THE MARS OBSERVER CAMERA
Michael Caplinger *In* JPL, Third International Symposium on Artificial Intelligence, Robotics, and Automation for Space 1994 Oct. 1994 p 401-404 (For primary document see N95-23672 07-63)
(Contract JPL-959060)
Avail: CASI HC A01/MF A03

N95-23756*# NYMA, Inc., Cleveland, OH.
DESIGN AND IMPLEMENTATION OF AN EXPERIMENT SCHEDULING SYSTEM FOR THE ACTS SATELLITE
Mark J. Ringer *In* JPL, Third International Symposium on Artificial Intelligence, Robotics, and Automation for Space 1994 Oct. 1994 p 409-412 (For primary document see N95-23672 07-63)
Avail: CASI HC A01/MF A03

18 SPACECRAFT DESIGN, TESTING AND PERFORMANCE

Includes satellites; space platforms; space stations; spacecraft systems and components such as thermal and environmental controls; and attitude controls.

For life support systems see *54 Man/System Technology and Life Support.* For related information see also *05 Aircraft Design, Testing and Performance, 39 Structural Mechanics,* and *16 Space Transportation.*

N95-22542* National Aeronautics and Space Administration, Washington, DC.
HEY! WHAT'S SPACE STATION FREEDOM? (Videotape)
Dutch vonEhrenfried 1992 Videotape: 28 min. 49 sec. playing time, in color, with sound
(NASA-TM-110531; NONP-NASA-VT-95-42907) Avail: CASI VHS A02/BETA A22

This video, 'Hey! What's Space Station Freedom?', has been produced as a classroom tool geared toward middle school children. There are three segments to this video. Segment One is a message to teachers presented by Dr. Jeannine Duane, New Jersey, 'Teacher in Space'. Segment Two is a brief Social Studies section and features a series of Presidential Announcements by President John F. Kennedy (May 1961), President Ronald Reagan (July 1982), and President George Bush (July 1989). These historical announcements are speeches concerning the present and future objectives of the United States' space programs. In the last segment, Charlie Walker, former Space Shuttle astronaut, teaches a group of middle school children, through models, computer animation, and actual footage, what Space Station Freedom is, who is involved in its construction, how it is to be built, what each of the modules on the station is for, and how long and in what sequence this construction will occur. There is a brief animation segment where, through the use of cartoons, the children fly up to Space Station Freedom as astronauts, perform several experiments and are given a tour of the station, and fly back to Earth. Space Station Freedom will take four years to build and will have three lab modules, one from ESA and another from Japan, and one habitation module for the astronauts to live in. CASI

N95-22667*# National Aeronautics and Space Administration. Lewis Research Center, Cleveland, OH.

QUICK LOOK REPORT OF ACCELERATION MEASUREMENTS ON MIR SPACE STATION DURING MIR-16

Richard DeLombard and Melissa J. B. Rogers (Tal-Cut Co., Beachwood, OH.) Jan. 1995 89 p Original contains color illustrations

(RTOP 963-60-0D)

(NASA-TM-106835; E-9396; NAS 1.15:106835) Avail: CASI HC A05/MF A01; 14 functional color pages

The NASA Microgravity Science and Applications Division (MSAD) sponsors the Space Acceleration Measurement System (SAMS) to support microgravity science experiments with microgravity acceleration measurements. In the past, SAMS was flown exclusively on the NASA Orbiters. MSAD is currently sponsoring science experiments participating in the Shuttle-Mir Science Program in cooperation with the Russians on the Mir space station. Included in the complement of MSAD experiments and equipment is a SAMS unit installed on the Mir space station. On 25 August 1994, the SAMS unit was launched on a Russia Progress vehicle to the Mir space station. The SAMS unit will support science experiments from the U.S. and Russia in a manner similar to the Orbiter missions by measuring the microgravity environments during the experiment operations. In October 1994, the SAMS unit recorded data on Mir for over fifty-three hours in seven different time periods to survey possible locations for future experiments. This report presents a quick look at the data and the microgravity environment during the time periods in which SAMS data were acquired. The Mir acceleration data were examined to ascertain gross attributes of the data. This report does not present an exhaustive examination of all possible activities due to the short time available to prepare this quick look report and due to the absence of complete timeline information during the SAMS recording time periods. Appendices A, B and C provide plots of the SAMS data for an overview of the microgravity environment at the times that data were recorded. Appendix D describes the procedures to access SAMS data by file transfer protocol (ftp) utilizing the internet. Appendix E contains a user comment sheet. Author

N95-22868# Los Alamos National Lab., NM.

ON-ORBIT SCIENCE IN A SMALL PACKAGE: MANAGING THE ALEXIS SATELLITE AND EXPERIMENTS

Diane Roussel-Dupre, Jeffrey J. Bloch, Doug Ciskowski, Robert Dingler, Cindy Little, Meg Kennison, William C. Priedhorsky, Sean Ryan, and Richard Warner (AeroAstro, Inc., Herndon, VA.) 1994 14 p Presented at the Annual Meeting of the Society of Photo-Optical Instrumentation Engineers, San Diego, CA, 24-29 Jul. 1994

(Contract W-7405-eng-36)

(DE94-014426; LA-UR-94-2180; CONF-940723-2) Avail: CASI HC A03/MF A01

The Array of Low Energy X-ray Imaging Sensors (ALEXIS) satellite is Los Alamos' first attempt at building and flying a small, low cost, rapid development, technology demonstration and scientific space mission. The ALEXIS satellite contains the two experiments: The ALEXIS telescope array, (which consists of six EUV/ultrasoft x-ray telescopes utilizing multilayer mirrors, each with a 33 degree field-of-view), and a VHF ionospheric experiment called BLACKBEARD. The spacecraft is controlled exclusively from a grand station located at Los Alamos. The 113-kg ALEXIS satellite was launched by a Pegasus booster into a 750 x 850 km, 70 degree inclination orbit on April 25, 1993. Due to damage sustained at the time of launch, ground controllers did not make contact with the satellite until late June. By late July, full satellite operations had been restored through the implementation of new procedures for attitude control. Science operations with the two onboard experiments began at that time. This paper discusses our experience gained in launching and managing this small scientific and technology demonstration satellite. DOE

N95-23188*# Rockwell International Corp., Downey, CA. Space Systems Div.

STRUCTURAL ARRANGEMENT TRADE STUDY. VOLUME 1: REUSABLE HYDROGEN COMPOSITE TANK SYSTEM (RHCTS) AND GRAPHITE COMPOSITE PRIMARY STRUCTURES (GCPS). EXECUTIVE SUMMARY

14 Mar. 1995 30 p Prepared in cooperation with Northrop Grumman Corp., Los Angeles, CA; North American Aviation, Inc., Tulsa, OK; and Hercules, Inc., Wilmington, DE

(Contracts NCC8-39; NCC1-193)

(NASA-CR-197685; NAS 1.26:197685; SSD95D0069-Vol-1) Avail: CASI HC A03/MF A01

This volume is the first of a three volume set that discusses the structural arrangement trade study plan that will identify the most suitable configuration for an SSTO winged vehicle capable of delivering 25,000 lbs to a 220 nm circular orbit at 51.6 deg inclination. The Reusable Hydrogen Composite Tank System (RHCTS), and Graphite Composite Primary Structures most suitable for intertank, wing and thrust structures are identified. This executive summary presents the trade study process, the selection process, requirements used, analysis performed and data generated. Conclusions and recommendations are also presented. Derived from text

N95-23189*# Rockwell International Corp., Downey, CA. Space Systems Div.

STRUCTURAL ARRANGEMENT TRADE STUDY. VOLUME 3: REUSABLE HYDROGEN COMPOSITE TANK SYSTEM (RHCTS) AND GRAPHITE COMPOSITE PRIMARY STRUCTURES (GCPS). ADDENDUM

14 Mar. 1995 257 p Prepared in cooperation with Northrop Grumman Corp., Los Angeles, CA; North American Aviation, Inc., Tulsa, OK; and Hercules, Inc., Wilmington, DE

(Contracts NCC8-39; NCC1-193)

(NASA-CR-197687; NAS 1.26:197687; SSD95D0069-Vol-3) Avail: CASI HC A12/MF A03

This volume is the third of a 3 volume set that addresses the structural trade study plan that will identify the most suitable structural configuration for an SSTO winged vehicle capable of delivering 25,000 lbs to a 220 nm circular orbit at 51.6 deg inclination. The most suitable Reusable Hydrogen Composite Tank System (RHCTS), and Graphite Composite Tank System (GCPS) composite materials for intertank, wing and thrust structures are identified. Vehicle resizing charts, selection criteria and back-up charts, parametric costing approach and the finite element method analysis are discussed. Derived from text

N95-23249*# National Aeronautics and Space Administration. Lyndon B. Johnson Space Center, Houston, TX.

MIR HARDWARE HERITAGE Reference Publication, 1977-1994

David S. F. Portree Mar. 1995 220 p Revised

(NASA-RP-1357; S-789; NAS 1.61:1357) Avail: CASI HC A10/MF A03

The heritage of the major Mir complex hardware elements is described. These elements include Soyuz-TM and Progress-M; the Kvant, Kvant 2, and Kristall modules; and the Mir base block. Configuration changes and major mission events of the Salyut 6, Salyut 7, and Mir multiport space stations are described in detail for the period 1977-1994. A comparative chronology of U.S. and Soviet/Russian manned spaceflight is also given for that period. The 68 illustrations include comparative scale drawings of U.S. and Russian spacecraft as well as sequential drawings depicting missions and mission events. Author

N95-23260*# North Carolina Univ., Greensboro, NC.

COMPUTATIONAL CONTROL OF FLEXIBLE AEROSPACE SYSTEMS Annual Report

Lonnie Sharpe, Jr. and Ji Yao Shen Dec. 1994 74 p

(Grant NAG1-1436)

(NASA-CR-197902; NAS 1.26:197902) Avail: CASI HC A04/MF A01

The main objective of this project is to establish a distributed parameter modeling technique for structural analysis, parameter estimation, vibration suppression and control synthesis of large flexible aerospace structures. This report concentrates on the research outputs produced in the last two years. The main accomplishments can be summarized as follows. A new version of the PDEMOD Code had been completed based on several incomplete versions. The verification of the code had been conducted by comparing the results with those examples for which the exact theoretical solutions can be obtained. The theoretical background of the package and the verification examples has been reported in a technical paper submitted to the Joint Applied Mechanics & Material Conference, ASME. A brief USER'S MANUAL had been compiled, which includes three parts: (1) Input data preparation; (2) Explanation of the Subroutines; and (3) Specification of control variables. Meanwhile, a theoretical investigation of the NASA MSFC two-dimensional ground-based manipulator facility by using distributed parameter modeling technique has been conducted. A new

mathematical treatment for dynamic analysis and control of large flexible manipulator systems has been conceived, which may provide an embryonic form of a more sophisticated mathematical model for future modified versions of the PDEMOD Codes. Derived from text

N95-23398*# Dayton Univ., OH. Dept. of Engineering Management and Systems.
INTEGRATING O/S MODELS DURING CONCEPTUAL DESIGN, PART 1
Annual Report, 1 Jul. - 31 Dec. 1994
Charles E. Ebeling 31 Dec. 1994 78 p
(Grant NAG1-1327)
(NASA-CR-197903; NAS 1.26:197903) Avail: CASI HC A05/MF A01

The University of Dayton is pleased to submit this report to the National Aeronautics and Space Administration (NASA), Langley Research Center, which integrates a set of models for determining operational capabilities and support requirements during the conceptual design of proposed space systems. This research provides for the integration of the reliability and maintainability (R&M) model, both new and existing simulation models, and existing operations and support (O&S) costing equations in arriving at a complete analysis methodology. Details concerning the R&M model and the O&S costing model may be found in previous reports accomplished under this grant (NASA Research Grant NAG1-1327). In the process of developing this comprehensive analysis approach, significant enhancements were made to the R&M model, updates to the O&S costing model were accomplished, and a new simulation model developed. This is the 1st part of a 3 part technical report. Author

N95-23399*# Dayton Univ., OH. Dept. of Engineering Management and Systems.
INTEGRATING O/S MODELS DURING CONCEPTUAL DESIGN, PART 2
Annual Report, 1 Jul. - 31 Dec. 1994
Charles E. Ebeling 31 Dec. 1994 158 p
(Grant NAG1-1327)
(NASA-CR-197904; NAS 1.26:197904) Avail: CASI HC A08/MF A02

This report documents the procedures for utilizing and maintaining the Reliability & Maintainability Model (RAM) developed by the University of Dayton for the National Aeronautics and Space Administration (NASA) Langley Research Center (LaRC) under NASA research grant NAG-1-1327. The purpose of the grant is to provide support to NASA in establishing operational and support parameters and costs of proposed space systems. As part of this research objective, the model described here was developed. Additional documentation concerning the development of this model may be found in Part 1 of this report. This is the 2nd part of a 3 part technical report. Author

N95-23400*# Dayton Univ., OH. Dept. of Engineering Management and Systems.
INTEGRATING O/S MODELS DURING CONCEPTUAL DESIGN, PART 3
Annual Report, 1 Jul. - 31 Dec. 1994
Charles E. Ebeling 31 Dec. 1994 71 p
(Grant NAG1-1327)
(NASA-CR-197905; NAS 1.26:197905) Avail: CASI HC A04/MF A01

Space vehicles, such as the Space Shuttle, require intensive ground support prior to, during, and after each mission. Maintenance is a significant part of that ground support. All space vehicles require scheduled maintenance to ensure operability and performance. In addition, components of any vehicle are not one-hundred percent reliable so they exhibit random failures. Once detected, a failure initiates unscheduled maintenance on the vehicle. Maintenance decreases the number of missions which can be completed by keeping vehicles out of service so that the time between the completion of one mission and the start of the next is increased. Maintenance also requires resources such as people, facilities, tooling, and spare parts. Assessing the mission capability and resource requirements of any new space vehicle, in addition to performance specification, is necessary to predict the life cycle cost and success of the vehicle. Maintenance and logistics support has been modeled by computer simulation to estimate mission capability and resource requirements for evaluation of proposed space vehicles. The simulation was written with Simulation Language for Alternative Modeling II (SLAM II) for execution on a personal computer. For either one or a fleet of space vehicles, the model simulates the preflight maintenance checks, the mission and return to earth, and the post flight maintenance in preparation to be sent back into space. THe model enables prediction of the number of missions possible and vehicle turn-time (the time between completion of one mission and the start of the next) given estimated values for component reliability and maintainability. The model also facilitates study of the manpower and vehicle requirements for the proposed vehicle to meet its desired mission rate. This is the 3rd part of a 3 part technical report. Author

N95-23532# Sandia National Labs., Albuquerque, NM.
MOVING MASS TRIM CONTROL FOR AEROSPACE VEHICLES
R. D. Robinett, B. A. Rainwater, and S. A. Kerr 1994 17 p Presented at the American Institute of Aeronautics and Astronautics Missile Sciences Conference, Monterey, CA, 7-9 Nov. 1994
(Contract DE-AC04-94AL-85000)
(DE95-002602; SAND-94-2746C; CONF-9411142-4) Avail: CASI HC A03/MF A01

A moving mass trim controller increases the accuracy of axisymmetric, ballistic vehicles. The MMTC is different than other moving mass schemes because it generates an angle-of-attack (AOA) directly from the mass motion. The nonlinear equations of motion for a ballistic vehicle with one moving point mass are derived and provide the basis for a detailed simulation model. The full nonlinear equations are linearized to produce a set of linear, time-varying autopilot equations. These autopilot equations are analyzed and used to develop theoretical design tools for the creation of MMTC's for both fast and slow spinning vehicles. A fast spinning MMTC is designed for a generic artillery rocket that uses principal axis misalignment to generate trim AOA. A slow spinning is designed for a generic reentry vehicle that generates a trim AOA with a center of mass offset and aerodynamic drag. The performance of both MMTC's are evaluated with the detailed simulation. DOE

N95-23781# Massachusetts Inst. of Tech., Lexington, MA. Lincoln Lab.
CALCULATION OF SATELLITE DRAG COEFFICIENTS
Edward M. Gaposchkin 18 Jul. 1994 57 p
(Contract F19628-90-C-0002)
(AD-A285118; MIT-TR-998; ESC-TR-93-293) Avail: CASI HC A04/MF A01

Calculation of Cd for satellites using accommodation coefficients is reviewed. A phenomenological model for accommodation coefficients due to Hurlbut, Sherman, and Nocilla is used to obtain values for the accommodation coefficients for average satellite materials, thermosphere constituents and temperatures, and satellite velocities using a number of laboratory measurements. There is a significant difference between these results and the traditional method of calculating Cd. These differences contribute as much as 20% error in use of thermosphere models for calculation of satellite drag. DTIC

N95-24049# National Aerospace Lab., Tokyo (Japan).
DYNAMICAL MODEL AND NUMERICAL SIMULATIONS FOR ENGINEERING TEST SATELLITE-6
Isao Yamaguchi and Takashi Kida Jun. 1994 19 p In JAPANESE
(ISSN 0389-4010)
(NAL-TR-1239) Avail: CASI HC A03/MF A01

This report derives the dynamical model of Engineering Test Satellite-VI (ETS-VI), which is a large-scale high-performance test satellite launched by H-II rocket in the summer launch window of 1994. The mission of ETS-VI is to establish the bus technology necessary for realizing a 2-ton-class geosynchronous three-axis stabilized application satellite. The National Aerospace Laboratory is participating in the on-orbit flight experiments of ETS-VI for the system identification and attitude control. Numerical simulation software have been developed and used to check the on-board control algorithm before launch. This paper describes their details. Author

N95-22814*# National Aeronautics and Space Administration. Lewis Research Center, Cleveland, OH.
UTILIZING A TDRS SATELLITE FOR DIRECT BROADCAST SATELLITE-RADIO PROPAGATION EXPERIMENTS AND DEMONSTRATIONS
James E. Hollansworth *In* JPL, Addendum to the Proceedings of the Third International Mobile Satellite Conference (IMSC 1993) 1993 p 13-18 (For primary document see N95-22813 07-32)
Avail: CASI HC A02/MF A01

N95-23279*# Old Dominion Coll., Norfolk, VA. Dept. of Engineering Management.
A MANUFACTURING DATABASE OF ADVANCED MATERIALS USED IN SPACECRAFT STRUCTURES Abstract Only
Han P. Bao *In* Hampton Univ., 1994 NASA-HU American Society for Engineering Education (ASEE) Summer Faculty Fellowship Program Dec. 1994 p 59 (For primary document see N95-23276 07-99)
Avail: CASI HC A01/MF A02

N95-23700*# National Space Development Agency, Tokyo (Japan).
DESIGN AND DEVELOPMENT STATUS OF ETS-7, AN RVD AND SPACE ROBOT EXPERIMENT SATELLITE
M. Oda, T. Inagaki, M. Nishida, K. Kibe, and F. Yamagata *In* JPL, Third International Symposium on Artificial Intelligence, Robotics, and Automation for Space 1994 Oct. 1994 p 143-147 (For primary document see N95-23672 07-63)
Avail: CASI HC A01/MF A03

N95-23713*# National Space Development Agency, Tsukuba (Japan). Systems Engineering Dept.
AUTOMATIC SATELLITE CAPTURE AND BERTHING WITH ROBOT ARM (ASCABRA)
Noriyasu Inaba, Yasufumi Wakabayashi, and Takahiko Iijima *In* JPL, Third International Symposium on Artificial Intelligence, Robotics, and Automation for Space 1994 Oct. 1994 p 205-208 (For primary document see N95-23672 07-63)
Avail: CASI HC A01/MF A03

N95-23719*# Hitachi Ltd., Kawasaki (Japan). Systems Development Lab.
AUTONOMOUS SPACECRAFT EXECUTIVE AND ITS APPLICATION TO RENDEZVOUS AND DOCKING
Fuminobu Komura, Masatoshi Furuya, Toshiro Sasaki, Robert L. Anderson (TRW Systems Group, Redondo Beach, CA.), and Roy K. Tsugawa (TRW Systems Group, Redondo Beach, CA.) *In* JPL, Third International Symposium on Artificial Intelligence, Robotics, and Automation for Space 1994 Oct. 1994 p 235-238 (For primary document see N95-23672 07-63)
Avail: CASI HC A01/MF A03

N95-23721*# Hughes Information Technology Corp., Aurora, IL.
THE STARPICKER EXPERT SYSTEM: A PROBLEM IN EXPERTISE CAPTURE
David Smith and G. Martin Hudson *In* JPL, Third International Symposium on Artificial Intelligence, Robotics, and Automation for Space 1994 Oct. 1994 p 245-248 (For primary document see N95-23672 07-63)
Avail: CASI HC A01/MF A03

N95-23726*# National Aerospace Lab., Tokyo (Japan).
TRUSS STRUCTURE TELE-MANIPULATION EXPERIMENT USING ETS-7
Kohtaro Matsumoto, Seishiroh Kibe, Isao Yamaguchi, Takashi Kida, Sachiko Wakabayashi, Hiroshi Ueno (Shimizu Corp., Japan.), Hitoshi Sato (Shimizu Corp., Japan.), Shigeru Aoki (Shimizu Corp., Japan.), and Tetsuji Yoshida (Shimizu Corp., Japan.) *In* JPL, Third International Symposium on Artificial Intelligence, Robotics, and Automation for Space 1994 Oct. 1994 p 275-278 (For primary document see N95-23672 07-63)
Avail: CASI HC A01/MF A03

N95-23727*# Communications Research Lab., Koganei (Japan).
ANTENNA-ASSEMBLING MECHANISM TEST ON ETS-7
Yoshiaki Suzuki, Shinichi Kimura, Tetsuo Takahashi, Kazuo Nakamura (NEC Corp., Ikebe, Japan.), and Hajime Morikawa (NEC Corp., Ikebe, Japan.) *In* JPL, Third International Symposium on Artificial Intelligence, Robotics, and Automation for Space 1994 Oct. 1994 p 279-284 (For primary document see N95-23672 07-63)
Avail: CASI HC A02/MF A03

N95-23799*# European Space Agency. European Space Research and Technology Center, ESTEC, Noordwijk (Netherlands).
EURECA 11 MONTHS IN ORBIT: INITIAL POST FLIGHT INVESTIGATION RESULTS
Alan Dover, Roberto Aceti, and Gerhard Drolshagen *In* NASA. Langley Research Center, LDEF: 69 Months in Space. Third Post-Retrieval Symposium, Part 1 Feb. 1995 p 23-35 (For primary document see N95-23796 07-99)
Avail: CASI HC A03/MF A04

N95-23803*# T and M Engineering, Glendora, CA.
EFFECT OF THE SPACE ENVIRONMENT ON MATERIALS FLOWN ON THE EURECA/TICCE-HVI EXPERIMENT
Carl R. Maag, Tim J. Stevenson (Mare Crisium, Old Carisbrooke, England.), William G. Tanner (Baylor Univ., Waco, TX.), and Janet Borg (Centre National de la Recherche Scientifique, Orsay, France.) *In* NASA. Langley Research Center, LDEF: 69 Months in Space. Third Post-Retrieval Symposium, Part 1 Feb. 1995 p 65-70 (For primary document see N95-23796 07-99)
Avail: CASI HC A02/MF A04

N95-23822*# National Aeronautics and Space Administration. Langley Research Center, Hampton, VA.
STATUS OF LDEF CONTRIBUTIONS TO CURRENT KNOWLEDGE OF METEOROID AND MANMADE DEBRIS ENVIRONMENTS AND THEIR EFFECTS ON SPACECRAFT IN LEO Abstract Only
William H. Kinard *In its* LDEF: 69 Months in Space. Third Post-Retrieval Symposium, Part 1 Feb. 1995 p 255 (For primary document see N95-23796 07-99)
Avail: CASI HC A01/MF A04

N95-23823*# National Aeronautics and Space Administration. Lyndon B. Johnson Space Center, Houston, TX.
LDEF METEOROID AND DEBRIS SPECIAL INVESTIGATION GROUP INVESTIGATIONS AND ACTIVITIES AT THE JOHNSON SPACE CENTER
Thomas H. See (Lockheed Engineering and Sciences Co., Houston, TX.), Jack L. Warren (Lockheed Engineering and Sciences Co., Houston, TX.), Michael E. Zolensky, Clyde A. Sapp (Lockheed Engineering and Sciences Co., Houston, TX.), Ronald P. Bernhard (Lockheed Engineering and Sciences Co., Houston, TX.), and Claire B. Dardano (Lockheed Engineering and Sciences Co., Houston, TX.) *In* NASA. Langley Research Center, LDEF: 69 Months in Space. Third Post-Retrieval Symposium, Part 1 Feb. 1995 p 257-273 (For primary document see N95-23796 07-99)
Avail: CASI HC A03/MF A04

N95-23824*# Departement d'Etudes et de Recherches en Technologie Spatiale, Toulouse (France).
MICROMETEOROIDS AND DEBRIS ON LDEF COMPARISON WITH MIR DATA
Jean-Claude Mandeville and Lucinda Berthoud *In* NASA. Langley Research Center, LDEF: 69 Months in Space. Third Post-Retrieval Symposium, Part 1 Feb. 1995 p 275-285 Sponsored by European Commission (For primary document see N95-23796 07-99)
Avail: CASI HC A03/MF A04

N95-23825*# National Aeronautics and Space Administration. Langley Research Center, Hampton, VA.
SMALL CRATERS ON THE METEOROID AND SPACE DEBRIS IMPACT EXPERIMENT
Donald H. Humes *In its* LDEF: 69 Months in Space. Third Post-Retrieval Symposium, Part 1 Feb. 1995 p 287-322 (For primary document see N95-23796 07-99)
Avail: CASI HC A03/MF A04

N95-23826*# National Aeronautics and Space Administration. Langley Research Center, Hampton, VA.
LONG TERM MICROPARTICLE IMPACT FLUXES ON LDEF DETERMINED FROM OPTICAL SURVEY OF INTERPLANETARY DUST EXPERIMENT (IDE) SENSORS
C. G. Simon (Institute for Space Science and Technology, Inc., Gainesville, FL.), J. P. Oliver (Institute for Space Science and Technology, Inc., Gainesville, FL.), W. J. Cooke (Institute for Space Science and Technology, Inc., Gainesville, FL.), K. I. Downey (Institute for Space Science and Technology, Inc., Gainesville, FL.), and P. C. Kassel *In its* LDEF: 69 Months in Space. Third Post-Retrieval Symposium, Part 1 Feb. 1995 p 323-336 (For primary document see N95-23796 07-99)

(Grant NAG1-1218)
Avail: CASI HC A03/MF A04

N95-23827*# Kent Univ., Canterbury (England). Unit for Space Sciences.
PENETRATION RATES OVER 30 YEARS IN THE SPACE AGE
J. A. M. McDonnell and J. M. Baron *In* NASA. Langley Research Center, LDEF: 69 Months in Space. Third Post-Retrieval Symposium, Part 1 Feb. 1995 p 337-351 Sponsored by Science and Engineering Research Council (For primary document see N95-23796 07-99)
Avail: CASI HC A03/MF A04

N95-23835*# Kent Univ., Canterbury (England). Unit for Space Sciences.
MICRO-ABRASION PACKAGE CAPTURE CELL EXPERIMENT ON THE TRAILING EDGE OF LDEF: IMPACTOR CHEMISTRY AND WHIPPLE BUMPER SHIELD EFFICIENCIES
Howard J. Fitzgerald and Hajime Yano *In* NASA. Langley Research Center, LDEF: 69 Months in Space. Third Post-Retrieval Symposium, Part 1 Feb. 1995 p 445-457 Sponsored by European Social Fund, Overseas Research Studentship, Daiwa Anglo-Japanese Foundation, and the Anglo-American Educational Exchange Scholarship Fund (For primary document see N95-23796 07-99)
Avail: CASI HC A03/MF A04

N95-23843*# POD Associates, Inc., Albuquerque, NM.
DIMENSIONAL SCALING FOR IMPACT CRATERING AND PERFORATION
Alan J. Watts and Dale Atkinson *In* NASA. Langley Research Center, LDEF: 69 Months in Space. Third Post-Retrieval Symposium, Part 1 Feb. 1995 p 523-535 (For primary document see N95-23796 07-99)
Avail: CASI HC A03/MF A04

19 SPACECRAFT INSTRUMENTATION

For related information see also *06 Aircraft Instrumentation* and *35 Instrumentation and Photography.*

N95-23864*# Jet Propulsion Lab., California Inst. of Tech., Pasadena, CA.
USE OF THE AIRBORNE VISIBLE/INFRARED IMAGING SPECTROMETER TO CALIBRATE THE OPTICAL SENSOR ON BOARD THE JAPANESE EARTH RESOURCES SATELLITE-1
Robert O. Green, James E. Conel, Jeannette vandenBosch, and Masanobu Shimada (National Space Development Agency, Ohashi, Japan.) *In its* Summaries of the 4th Annual JPL Airborne Geoscience Workshop. Volume 1: AVIRIS Workshop 25 Oct. 1993 p 77-80 Sponsored by NASDA (For primary document see N95-23844 07-42)
Avail: CASI HC A01/MF A03

20 SPACECRAFT PROPULSION AND POWER

Includes main propulsion systems and components, e.g., rocket engines; and spacecraft auxilliary power sources.

For related information see also *07 Aircraft Propulsion and Power, 28 Propellants and Fuels, 44 Energy Production and Conversion,* and *15 Launch Vehicles and Space Vehicles.*

N95-22885# Sandia National Labs., Albuquerque, NM.
SENSOR-BASED CONTROL OF ROCKET THRUST CHAMBER FEATURE LOCATION FOR AUTOMATED BRAZE PASTE DISPENSING
Dan J. Schmitt, Jim L. Novak, John E. Maslakowski (Rockwell International Corp., Canoga Park, CA.), and Gregory P. Starr (New Mexico Univ., Albuquerque, NM.) 1994 12 p Presented at the 5th World Conference on Robotics Research, Cambridge, MA, 27-29 Sep. 1994
(Contract DE-AC04-94AL-85000)
(DE94-016559; SAND-94-1646C; CONF-9409163-2) Avail: CASI HC A03/MF A01

A sensor-based control system has been developed for locating key features on rocket thrust chamber assemblies for automated braze paste dispensing. The system uses a non-contact Multi-Axis Seam Tracking (MAST) sensor to locate these features. The MAST sensor measures capacitance variations between the sensor and thrust chamber surface to produce four varying voltages for control purposes. The sensor information is used to locate the thrust chamber surface and to guide the robotic paste dispensing equipment along the seams in real-time. Experiments demonstrate that seams can be tracked at 50 mm/sec within the accuracy required for braze paste dispensing. DOE

N95-22905# Los Alamos National Lab., NM.
ALERT-DERIVATIVE BIMODAL SPACE POWER AND PROPULSION SYSTEMS
M. G. Houts, W. A. Ranken, and J. J. Buksa 1994 10 p Presented at the 12th Symposium on Space Nuclear Power and Propulsion, Albuquerque, NM, 8-12 Jan. 1995
(Contract W-7405-eng-36)
(DE95-002754; LA-UR-94-3660; CONF-950110-9) Avail: CASI HC A02/MF A01

Safe, reliable, low-mass bimodal space power and propulsion systems could have numerous civilian and military applications. This paper discusses potential bimodal systems that could be derived from the ALERT space fission power supply concept. These bimodal concepts have the potential for providing 5 to 10 kW of electrical power and a total impulse of 100 MN-s at an average specific impulse of 770 s. System mass is on the order of 1000 kg. DOE

N95-23221*# National Aeronautics and Space Administration. Lewis Research Center, Cleveland, OH.
NASA 30 cm ION THRUSTER DEVELOPMENT STATUS
Michael J. Patterson, Thomas W. Haag, Vincent K. Rawlin, and Michael T. Kussmaul (NYMA, Inc., Brook Park, OH.) Mar. 1995 17 p Presented at the 30th Joint Propulsion Conference, Indianapolis, IN, 27-29 Jun. 1994; cosponsored by AIAA, ASME, SAE, and ASEE
(Contract NAS3-27186; RTOP 232-02-03)
(NASA TM-106842; NAS 1.15:106842; AIAA Paper 94-2849) Avail: CASI HC A03/MF A01

A 30 cm diameter xenon ion thruster is under development at NASA to provide an ion propulsion option for missions of national interest and it is an element of the NASA Solar Electric Propulsion Technology Applications Readiness (NSTAR) program established to validate ion propulsion for space flight applications. The thruster has been developed to an engineering model level and it incorporates innovations in design, materials, and fabrication techniques compared to those employed to conventional ion thrusters. The performance of both functional and engineering model thrusters has been assessed including thrust stand measurements, over an input power range of 0.5-2.3 kW. Attributes of the engineering model thruster include an overall mass of 6.4 kg, and an efficiency of 65 percent and thrust of 93 mN at 2.3 kW input power. This paper discusses the design, performance, and lifetime expectations of the functional and engineering model thrusters under development at NASA. Author

N95-23240*# National Aeronautics and Space Administration. Lewis Research Center, Cleveland, OH.
FUNCTIONAL TESTING OF THE SPACE STATION PLASMA CONTACTOR
Michael J. Patterson, John A. Hamley, Timothy R. Sarver-Verhey (NYMA, Inc., Brook Park, OH.), and George C. Soulas (NYMA, Inc., Brook Park, OH.) Mar. 1995 16 p Presented at the 30th Joint Propulsion Conference, Indianapolis, IN, 27-29 Jun. 1994; cosponsored by AIAA, ASME, SAE and ASEE
(RTOP 478-43-10)
(NASA-TM-106841; E-9405; NAS 1.15:106841; AIAA Paper 94-3308)
Avail: CASI HC A03/MF A01

A plasma contactor system has been baselined for the International Space Station Alpha (ISSA) to control the electrical potentials of surfaces to eliminate/mitigate damaging interactions with the space environment. The system represents a dual-use technology which is a direct outgrowth of the NASA electric propulsion program and, in particular, the technology development effort on ion thruster systems. The plasma contactor subsystems include a hollow cathode assembly, a power electronics unit, and an expellant management unit. Under a pre-flight development program these subsystems are being developed to the level of maturity appropriate

for transfer to U.S. industry for final development. Development efforts for the hollow cathode assembly include design selection and refinement, validating its required lifetime, and quantifying the cathode performance and interface specifications. To date, cathode components have demonstrated over 10,000 hours lifetime, and a hollow cathode assembly has demonstrated over 3,000 ignitions. Additionally, preliminary integration testing of a hollow cathode assembly with a breadboard power electronics unit has been completed. This paper discusses test results and the development status of the plasma contactor subsystems for ISSA, and in particular, the hollow cathode assembly. Author

N95-23261*# Pennsylvania State Univ., University Park, PA. Dept. of Mechanical Engineering.

FUNDAMENTAL PHENOMENA ON FUEL DECOMPOSITION AND BOUNDARY LAYER COMBUSTION PROCESSES WITH APPLICATIONS TO HYBRID ROCKET MOTORS Semiannual Progress Report

Kenneth K. Kuo, Y. C. Lu, Martin J. Chiaverini, and George C. Harting 8 Nov. 1994 26 p

(Contract NAS8-39945)

(NASA-CR-197919; NAS 1.26:197919) Avail: CASI HC A03/MF A01

An experimental study on the fundamental processes involved in fuel decomposition and boundary layer combustion in hybrid rocket motors is being conducted at the High Pressure Combustion Laboratory of the Pennsylvania State University. This research should provide a useful engineering technology base in the development of hybrid rocket motors as well as a fundamental understanding of the complex processes involved in hybrid propulsion. A high pressure slab motor has been designed and manufactured for conducting experimental investigations. Oxidizer (LOX or GOX) supply and control systems have been designed and partly constructed for the head-end injection into the test chamber. Experiments using HTPB fuel, as well as fuels supplied by NASA designated industrial companies will be conducted. Design and construction of fuel casting molds and sample holders have been completed. The portion of these items for industrial company fuel casting will be sent to the McDonnell Douglas Aerospace Corporation in the near future. The study focuses on the following areas: observation of solid fuel burning processes with LOX or GOX, measurement and correlation of solid fuel regression rate with operating conditions, measurement of flame temperature and radical species concentrations, determination of the solid fuel subsurface temperature profile, and utilization of experimental data for validation of a companion theoretical study (Part 2) also being conducted at PSU. Author

N95-23450*# National Aeronautics and Space Administration. Lewis Research Center, Cleveland, OH.

OVERVIEW OF THE SOLAR DYNAMIC GROUND TEST DEMONSTRATION PROGRAM AT THE NASA LEWIS RESEARCH CENTER

Richard K. Shaltens Mar. 1995 9 p

(RTOP 233-03-0B)

(NASA-TM-106876; E-9501; NAS 1.15:106876) Avail: CASI HC A02/MF A01

The Solar Dynamic (SD) Ground Test Demonstration (GTD) program demonstrates the availability of SD technologies in a simulated space environment at the NASA Lewis Research Center (LERC) vacuum facility. Data from the SD GTD program will be provided to the joint U.S. and Russian team which is currently designing a 2 kW SD flight demonstration power system. This SD technology has the potential as a future power source for the International Space Station. This paper reviews the goals and status of the SD GTD program. A description of the SD GTD system includes key design features of the system, subsystems and components. Author

N95-23790*# Sverdrup Technology, Inc., Brook Park, OH.

AN RL10A-3-3A ROCKET ENGINE MODEL USING THE ROCKET ENGINE TRANSIENT SIMULATOR (ROCETS) SOFTWARE Final Report

Michael Binder Cleveland, OH Jul. 1993 13 p

(Contract NAS3-25266; RTOP 593-12-00)

(NASA-CR-190786; E-9585; NAS 1.26:190786) Avail: CASI HC A03/MF A01

Steady-state and transient computer models of the RL10A-3-3A rocket engine have been created using the Rocket Engine Transient Simulation (ROCETS) code. These models were created for several purposes. The RL10 engine is a critical component of past, present, and future space missions; the model will give NASA an in-house capability to simulate the performance of the engine under various operating conditions and mission profiles. The RL10 simulation activity is also an opportunity to further validate the ROCETS program. The ROCETS code is an important tool for modeling rocket engine systems at NASA Lewis. ROCETS provides a modular and general framework for simulating the steady-state and transient behavior of any desired propulsion system. Although the ROCETS code is being used in a number of different analysis and design projects within NASA, it has not been extensively validated for any system using actual test data. The RL10A-3-3A has a ten year history of test and flight applications; it should provide sufficient data to validate the ROCETS program capability. The ROCETS models of the RL10 system were created using design information provided by Pratt & Whitney, the engine manufacturer. These models are in the process of being validated using test-stand and flight data. This paper includes a brief description of the models and comparison of preliminary simulation output against flight and test-stand data. Author

N95-23791*# Sverdrup Technology, Inc., Brook Park, OH.

PREDICTED PERFORMANCE OF AN INTEGRATED MODULAR ENGINE SYSTEM Final Report

Michael Binder and James L. Felder Jul. 1993 18 p

(Contract NAS3-25266; RTOP 584-04-11)

(NASA-CR-190787; E-9586; NAS 1.26:190787) Avail: CASI HC A03/MF A01

Space vehicle propulsion systems are traditionally comprised of a cluster of discrete engines, each with its own set of turbopumps, valves, and a thrust chamber. The Integrated Modular Engine (IME) concept proposes a vehicle propulsion system comprised of multiple turbopumps, valves, and thrust chambers which are all interconnected. The IME concept has potential advantages in fault-tolerance, weight, and operational efficiency compared with the traditional clustered engine configuration. The purpose of this study is to examine the steady-state performance of an IME system with various components removed to simulate fault conditions. An IME configuration for a hydrogen/oxygen expander cycle propulsion system with four sets of turbopumps and eight thrust chambers has been modeled using the Rocket Engine Transient Simulator (ROCETS) program. The nominal steady-state performance is simulated, as well as turbopump thrust chamber and duct failures. The impact of component failures on system performance is discussed in the context of the system's fault tolerant capabilities. Author

N95-23439*# Rockwell International Corp., Canoga Park, CA. Rocketdyne Div.

NON-INTRUSIVE MEASUREMENTS IN A ROCKET ENGINE COMBUSTOR

S. Farhangi, V. T. Gylys, and R. J. Jensen *In* NASA. Marshall Space Flight Center, Eleventh Workshop for Computational Fluid Dynamic Applications in Rocket Propulsion Jul. 1993 p 1619-1634 (For primary document see N95-23412 07-34)

Avail: CASI HC A03/MF A10

N95-23640*# Auburn Univ., AL. Dept. of Aerospace Engineering.

IGNITION TRANSIENT CALCULATIONS IN THE SPACE SHUTTLE SOLID ROCKET MOTOR

Rhonald M. Jenkins and Winfred A. Foster, Jr. *In* NASA. Marshall Space Flight Center, Eleventh Workshop for Computational Fluid Dynamic Applications in Rocket Propulsion, Part 1 Jul. 1993 p 571-595 (For primary document see N95-23615 07-34)

Avail: CASI HC A03/MF A10

N95-23655*# National Aeronautics and Space Administration. Marshall Space Flight Center, Huntsville, AL.

NUMERICAL STUDY OF BASE PRESSURE CHARACTERISTIC CURVE FOR A FOUR-ENGINE CLUSTERED NOZZLE CONFIGURATION

Ten-See Wang *In its* Eleventh Workshop for Computational Fluid Dynamic Applications in Rocket Propulsion, Part 1 Jul. 1993 p 941-961 (For primary document see N95-23615 07-34)

Avail: CASI HC A03/MF A10

23 CHEMISTRY AND MATERIALS (GENERAL)

N95-22918*# Boeing Defense and Space Group, Seattle, WA.
EVALUATION OF ADHESIVE MATERIALS USED ON THE LONG DURATION EXPOSURE FACILITY Report, Oct. 1989 - Jan. 1995
H. W. Dursch, B. K. Keough, and H. G. Pippin Hampton, VA NASA Mar. 1995 58 p
(Contracts NAS1-18224; NAS1-19247; RTOP 506-43-61-02; RTOP 233-03-02-04)
(NASA-CR-4646; NAS 1.26:4646) Avail: CASI HC A04/MF A01

The adhesive and adhesive-like materials flown on LDEF included epoxies and silicones (including lap shear specimens), conformal coatings, potting compounds, and several tapes and transfer films. With the exception of the lap shear specimens, these materials were used in the fabrication and assembly of the experiments such as bonding thermal control surfaces to other hardware and holding individual specimens in place, similar to applications on other spacecraft. Typically, the adhesives were not exposed to solar radiation or atomic oxygen. Only one adhesive system was used in a structural application. This report documents all results of the Materials and Systems SIG investigation into the effect of long term low Earth orbit (LEO) exposure of these materials. Results of this investigation show that if the material was shielded from exposure to LDEF's external environment, the 69 month exposure to LEO had, in most cases, minimal effect on the material. Author

N95-22919*# Rockwell International Corp., Downey, CA. Space Systems Div.
LOW EARTH ORBIT THERMAL CONTROL COATINGS EXPOSURE FLIGHT TESTS: A COMPARISON OF U.S. AND RUSSIAN RESULTS Report, 8 Nov. - 12 Aug. 1993
A. C. Tribble, R. Lukins, E. Watts, S. F. Naumov, and V. K. Sergeev Hampton, VA NASA Mar. 1995 64 p
(Contract NAS1-19243; RTOP 233-03-02-02)
(NASA-CR-4647; NAS 1.26:4647) Avail: CASI HC A04/MF A01

Both the United States (US) and Russia have conducted a variety of space environment effects on materials (SEEM) flight experiments in recent years. A prime US example was the Long Duration Exposure Facility (LDEF), which spent 5 years and 9 months in low Earth orbit (LEO) from April 1984 to January 1990. A key Russian experiment was the Removable Cassette Container experiment, (RCC-1), flown on the Mir Orbital Station from 11 January 1990 to 26 April 1991. This paper evaluates the thermal control coating materials data generated by these two missions by comparing: environmental exposure conditions, functionality and chemistry of thermal control coating materials, and pre- and post-flight analysis of absorptance, emittance, and mass loss due to atomic oxygen erosion. It will be seen that there are noticeable differences in the US and Russian space environment measurements and models, which complicates comparisons of environments. The results of both flight experiments confirm that zinc oxide and zinc oxide orthotitanate white thermal control paints in metasilicate binders (Z93, YB71, TP-co-2, TP-co-11, and TP-co-12), are the most stable upon exposure to the space environment. It is also seen that Russian flight materials experience broadens to the use of silicone and acrylic resin binders while the US relies more heavily on polyurethane. Author

N95-23270*# National Aeronautics and Space Administration. Lewis Research Center, Cleveland, OH.
ATOMIC OXYGEN DURABILITY EVALUATION OF PROTECTED POLYMERS USING THERMAL ENERGY PLASMA SYSTEMS
Bruce A. Banks, Sharon K. Rutledge, Kim K. deGroh, Curtis R. Stidham (Sverdrup Technology, Inc., Brook Park, OH.), Linda Gebauer (Cleveland State Univ., OH.), and Cynthia M. LaMoreaux (Cleveland State Univ., OH.) Feb. 1995 17 p Presented at the International Conference on Plasma Synthesis and Processing of Materials, Denver, CO, 21-25 Feb. 1993; sponsored by The Metallurgical Society
(Contract NAS3-25266; RTOP 506-41-4A)
(NASA-TM-106855; L-9452; NAS 1.15:106855) Avail: CASI HC A03/MF A01

The durability evaluation of protected polymers intended for use in low Earth orbit (LEO) has necessitated the use of large-area, high-fluence, atomic oxygen exposure systems. Two thermal energy atomic oxygen exposure systems which are frequently used for such evaluations are radio frequency (RF) plasma ashers and electron cyclotron resonance plasma sources. Plasma source testing practices such as ample preparation, effective fluence prediction, atomic oxygen flux determination, erosion measurement, operational considerations, and erosion yield measurements are presented. Issues which influence the prediction of in-space durability based on ground laboratory thermal energy plasma system testing are also addressed. Author

N95-23477# Japan Atomic Energy Research Inst., Tokyo (Japan).
ANNUAL REPORT OF THE OSAKA LABORATORY FOR RADIATION CHEMISTRY JAPAN ATOMIC ENERGY RESEARCH INSTITUTE, (NO. 26)
Mar. 1994 64 p
(DE94-785277; JAERI-M-94-017) Avail: CASI HC A04/MF A01

The annual research activities of Osaka Laboratory for Radiation Chemistry, JAERI during the fiscal year of 1992 (April 1, 1992 - March 31, 1993) are described. The research activities were conducted under the two research programs: the study on laser-induced organic chemical reactions and the study on basic radiation technology for functional materials. Detailed descriptions of the activities are presented in the following subjects: laser-induced organic synthesis, modification of polymer surface by laser irradiation, radiation-induced polymerization, preparation of fine particles by gamma ray irradiation, and electron beam dosimetry. The operation report of the irradiation facilities is also included. DOE

N95-24004*# National Aeronautics and Space Administration. Lewis Research Center, Cleveland, OH.
MICROGRAVITY COMBUSTION SCIENCE: 1995 PROGRAM UPDATE
Howard D. Ross, ed., Suleyman A. Gokoglu, ed., and Robert Friedman, ed. Apr. 1995 55 p Presented at the 3rd International Microgravity Combustion Workshop, Cleveland, OH, 11-13 Apr. 1995 Original contains color illustrations
(RTOP 962-22-00)
(NASA-TM-106858; E-9456; NAS 1.15:106858) Avail: CASI HC A04/MF A01; 4 functional color pages

Microgravity greatly benefits the study of fundamental combustion processes. In this environment, buoyancy-induced flow is nearly eliminated, weak or normally obscured forces and flows can be isolated, gravitational settling or sedimentation is nearly eliminated, and temporal and spatial scales can be expanded. This document reviews the state of knowledge in microgravity combustion science with the emphasis on NASA-sponsored developments in the current period of 1992 to early 1995. The subjects cover basic research in gaseous premixed and diffusion-flame systems, flame structure and sooting, liquid droplets and pools, and solid-surface ignition and flame spread. They also cover applied research in combustion synthesis of ceramic-metal composites, advanced diagnostic instrumentation, and on-orbit fire safety. The review promotes continuing research by describing the opportunities for Principal Investigator participation through the NASA Research Announcement program and the available NASA Lewis Research Center ground-based facilities and spaceflight accommodations. This review is compiled by the members and associates of the NASA Lewis Microgravity Combustion Branch, and it serves as an update of two previous overview reports. Author

N95-24142# California Univ., Berkeley. Lawrence Berkeley Lab, CA.
CHEMICAL SCIENCES DIVISION Annual Report, 1993
Oct. 1994 100 p
(Contract DE-AC03-76SF-00098)
(DE95-002655; LBL-35769) Avail: CASI HC A05/MF A02

The Chemical Sciences Division (CSD) is one of eleven research Divisions of the Lawrence Berkeley Laboratory, a DOE National Laboratory. In FY 1993, the Division made considerable progress on developing two end-stations and a beamline to advance combustion dynamics at the Advanced Light Source (ALS). In support of DOE's national role in combustion research and chemical science, the beamline effort will enable researchers from around the world to make fundamental advances in understanding the structure and reactivity of critical reaction intermediates and transients, and in understanding the dynamics of elementary chemical reactions. The Division has continued to place a strong emphasis on full compliance with environmental health and safety guidelines and regulations and has made progress in technology transfer to industry. Finally, the

Division has begun a new program in advanced battery research and development that should help strengthen industrial competitiveness both at home and abroad. DOE

N95-23909*# National Aeronautics and Space Administration. Lewis Research Center, Cleveland, OH.
ATOMIC OXYGEN INTERACTIONS WITH PROTECTED ORGANIC MATERIALS ON THE LONG DURATION EXPOSURE FACILITY (LDEF)
Bruce A. Banks, Kim K. deGroh, Justine L. Bucholz (Ohio Aerospace Inst., Brook Park, OH.), and Michael R. Cales (Cleveland State Univ., OH.) *In* NASA. Langley Research Center, LDEF: 69 Months in Space. Third Post-Retrieval Symposium, Part 2 Feb. 1995 p 737-753 (For primary document see N95-23896 07-99)
Avail: CASI HC A03/MF A03

N95-23914*# Boeing Defense and Space Group, Seattle, WA.
ORGANIC MATRIX COMPOSITE PROTECTIVE COATINGS FOR SPACE APPLICATIONS
Harry W. Dursch and Pete George *In* NASA. Langley Research Center, LDEF: 69 Months in Space. Third Post-Retrieval Symposium, Part 2 Feb. 1995 p 825-842 (For primary document see N95-23896 07-99)
(Contract NAS1-19427)
Avail: CASI HC A03/MF A03

24 COMPOSITE MATERIALS

Includes physical, chemical, and mechanical properties of laminates and other composite materials.

For ceramic materials see *27 Nonmetallic Materials.*

N95-22563* National Aeronautics and Space Administration. Lewis Research Center, Cleveland, OH.
METHOD OF PRODUCING A SILICON CARBIDE FIBER REINFORCED STRONTIUM ALUMINOSILICATE GLASS-CERAMIC MATRIX COMPOSITE Patent
Narottam P. Bansal, inventor (to NASA) 14 Feb. 1995 4 p Filed 16 Sep. 1993 Supersedes N94-15929 (32 - 3, p 934) Division of abandonded US-Patent-Appl-SN-892054, filed 4 Jun. 1992
(NASA-Case-LEW-15263-2; US-Patent-5,389,321;
US-Patent-Appl-SN-128007; US-Patent-Appl-SN-892054;
US-Patent-Class-264-60; US-Patent-Class-264-63; US-Patent-Class-264-166; US-Patent-Class-264-332; US-Patent-Class-501-8; US-Patent-Class-501-95)
Avail: US Patent and Trademark Office

A SrO-Al2O3-2SrO2 (SAS) glass ceramic matrix is reinforced with CVD SiC continuous fibers. This material is prepared by casting a slurry of SAS glass powder into tapes. Mats of continuous CVD-SiC fibers are alternately stacked with the matrix tapes. This tape-mat stack is warm-pressed to produce a 'green' composite. Organic constituents are burned out of the 'green' composite, and the remaining interim material is hot pressed.
Official Gazette of the U.S. Patent and Trademark Office

N95-22683# Northwestern Univ., Evanston, IL.
INVESTIGATION OF MECHANICAL PROPERTIES AND THEIR RELATION TO THE INTERNAL STRUCTURE OF NANOCRYSTALLINE METALS AND COMPOSITES
J. R. Weertman and W. P. Murphy Jul. 1994 17 p
(Contract DE-FG02-86ER-45229)
(DE95-001151; DOE/ER-45229/34) Avail: CASI HC A03/MF A01

A new compaction unit was installed for consolidation at high temps. SANS of nanocrystalline (n-) Pd and Cu confirms presence of pores close to the grain size; high scattering angles indicated large amounts of hydrogen (H). Confirmation was obtained from prompt gamma activation analysis. Compaction at high temps, preheating the powders before compacting, or a post-consolidation anneal, greatly lowers the H content. SANS showed that annealing expands voids in samples with high H content, but voids shrink if the H has been removed. Elastic modulus in n-Fe was measured using a nanoindenter; results indicate that the diminution of modulus in n-metals can be explained entirely on the basis of porosity. Detailed x ray measurements were made on n-Pd to examine the frequency of twins and stacking faults; results will be compared to TEM. A new chamber is being constructed for the inert gas condensation equipment, for improved vacuum. DOE

N95-22833 Army Armament Research, Development and Engineering Center, Watervliet, NY.
NOTCH-TIP DAMAGE AND TRANSLAMINAR FRACTURE TOUGHNESS MEASUREMENTS FROM CARBON/EPOXY LAMINATES Final Report
J. H. Underwood and M. T. Kortschot Mar. 1994 19 p Limited Reproducibility: More than 20% of this document may be affected by microfiche quality
(AD-A280101; ARCCB-TR-94010) Avail: CASI HC A03

Notched (0/+45/90/-45) carbon/epoxy laminates were used to study translaminar fracture, where through-thickness cracking propagates across fibers and laminae. Radiographs of damage were compared with crack growth determined from load-versus-deflection plots using elastic fracture mechanics. Comparison of damage at the notch tip with fracture mechanics evaluation identified some material/test conditions for which a critical value of fracture toughness is a useful concept. For other condition the extent of damage in the specimen showed that the concept of fracture toughness is not directly applicable. DTIC

N95-22928*# National Aeronautics and Space Administration. Langley Research Center, Hampton, VA.
THREE-DIMENSIONAL CTOA AND CONSTRAINT EFFECTS DURING STABLE TEARING IN A THIN-SHEET MATERIAL
D. S. Dawicke (Analytical Services and Materials, Inc., Hampton, VA.), J. C. Newman, Jr., and C. A. Bigelow (Federal Aviation Administration, Atlantic City, NJ.) Feb. 1995 26 p
(RTOP 538-02-10-01)
(NASA-TM-109183; NAS 1.15:109183) Avail: CASI HC A03/MF A01

A small strain theory, three-dimensional elastic-plastic finite element analysis was used to simulate fracture in thin sheet 2024-T3 aluminum alloy in the T-L orientation. Both straight and tunneled cracks were modeled. The tunneled crack front shapes as a function of applied stress were obtained from the fracture surface of tested specimens. The stable crack growth behavior was measured at the specimen surface as a function of applied stress. The fracture simulation modeled the crack tunneling and extension as a function of applied stress. The results indicated that the global constraint factor, alpha(sub g), initially dropped during stable crack growth. After peak applied stress was achieved, alpha(sub g) began to increase slightly. The effect of crack front shape on alpha(sub g) was small, but the crack front shape did greatly influence the local constraint and through-thickness crack-tip opening angle (CTOA) behavior. The surface values of CTOA for the tunneled crack front model agreed well with experimental measurements, showing the same initial decrease from high values during the initial 3mm of crack growth at the specimen's surface. At the same time, the interior CTOA values increased from low angles. After the initial stable tearing region, the CTOA was constant through the thickness. The three-dimensional analysis appears to confirm the potential of CTOA as a two-dimensional fracture criterion. Author

N95-22940# Delaware Univ., Newark, DE. Dept. of Physics and Astronomy.
NANOPHASE MATERIALS: SYNTHESIS, PROPERTIES, APPLICATIONS Final Report
George C. Hadjipanayis, ed. and Richard W. Siegl, ed. Sep. 1994 824 p *Its* NATO ASI Series E: Applied Sciences, Volume 260
(Contract N00014-93-1-0667)
(AD-A286013) Avail: CASI HC A99/MF A10

This document focuses on the following topics: Chemical Synthesis of Nanophase Materials; Preparation of Gamma Fe2Oe Particles; Synthesis of III-V Semiconductor Particles from Organometallic Precursors; Synthesis of Nanostructured Catalysts and Catalytic Supports; Formation of Magnetic Spinel Iron Oxide in Solution; Synthesis of Nanoscale Iron Oxide Structures Using Protein Cages and Polysaccharide Networks; Gas Evaporation and Electron Microscopical Observation of Small Particles; Nanoparticles from a Supersaturated Vapor; Formation and Phase ANalysis of Surface Oxides on Ultrafine Particles of Fe; Y(x)Zr(1-x)O(2-x/2) Nanophase Powders Prepared by a Vaporization/Condensation Process in a Solar Furnace; and Synthesis and Characterization of Iron-Magnesium Bimetallic Particles
DTIC

N95-23025*# National Aeronautics and Space Administration. Goddard Space Flight Center, Greenbelt, MD.

ENVIRONMENTAL, SAFETY, AND HEALTH CONSIDERATIONS: COMPOSITE MATERIALS IN THE AEROSPACE INDUSTRY

Huai-Pu Chu, comp. Oct. 1994 234 p Conference held in Mesa, AZ, 20-21 Oct. 1994 Sponsored by Aerospace Industries Association and Suppliers of Advanced Composite Materials Association

(RTOP 313-00-00)

(NASA-CP-3289; Rept-95B00035; NAS 1.55:3289) Avail: CASI HC A11/MF A03

The Aerospace Industries Association, Suppliers of Advanced Composite Materials Association, and the National Aeronautics and Space Administration co-sponsored a conference on 'Environmental, Safety, and Health Considerations--Composite Materials in the Aerospace Industry.' The conference was held in Mesa, Arizona, on October 20-21, 1994. Seventeen papers were presented in four sessions including general information, safety, waste, and emissions from composites. Topics range from product stewardship, best work practice, biotransformation of uncured composite materials, to hazardous waste determination and offgassing of composite materials. For individual titles, see N95-23026 through N95-23039.

N95-23026*# Dow Chemical Co., Midland, MI.

A ROADMAP FOR REGULATORY SURVIVAL IN THE 1990s

R. S. Sayad, S. B. McCollister, and R. D. Olson *In* NASA. Goddard Space Flight Center, Environmental, Safety, and Health Considerations: Composite Materials in the Aerospace Industry Oct. 1994 p 1-13 (For primary document see N95-23025 07-24)

Avail: CASI HC A03/MF A03

There have been many changes over the last several years in the ways that we're required to label, handle, and dispose of the products of our manufacturing processes...and we all know there will be more, not fewer, environmental regulations to deal with in the years to come. It is important to be aware of how a chemical is listed by federal or state regulations or recommending bodies. For example, if a chemical has been listed by OSHA, IARC (International Agency for Research on Cancer), or NTP (the National Toxicology Program) as a carcinogen, this listing will trigger hazard communication requirements. It may cause restrictions on the levels of a chemical that you may release into the air or water as well as how you manage your plant wastes. Understanding how a chemical is listed is the first critical step in overall compliance. Once a chemical makes one of these lists as a hazardous material or a carcinogen, your emissions, labelling, or MSD sheets may need to be changed in order to comply with federal or state regulations. Being fully aware of how the chemicals you use are listed by all pertinent bodies is the essential compass that you must have to follow the regulatory road map. Author

N95-23027*# Du Pont de Nemours (E. I.) and Co., Wilmington, DE.

PRODUCT STEWARDSHIP IN THE COMPOSITES INDUSTRY

Donald C. Aldrich and Edmund A. Merriman *In* NASA. Goddard Space Flight Center, Environmental, Safety, and Health Considerations: Composite Materials in the Aerospace Industry Oct. 1994 p 15-29 (For primary document see N95-23025 07-24)

Avail: CASI HC A03/MF A03

The definition and purpose of Product Stewardship is discussed. Its' impact in the composites industry is stated. The report also outlines 12 ways that Product Stewardship can be utilized by consumers.

Derived from text

N95-23028*# Northrop Grumman Corp., Los Angeles, CA.

HEALTH, SAFETY AND ENVIRONMENTAL REQUIREMENTS FOR COMPOSITE MATERIALS

Kathleen A. Hazer *In* NASA. Goddard Space Flight Center, Environmental, Safety, and Health Considerations: Composite Materials in the Aerospace Industry Oct. 1994 p 31-45 (For primary document see N95-23025 07-24)

Avail: CASI HC A03/MF A03

The health, safety and environmental requirements for the production of composite materials are discussed. The areas covered include: (1) chemical identification for each chemical; (2) toxicology; (3) industrial hygiene; (4) fire and safety; (5) environmental aspects; and (6) medical concerns.

Derived from text

N95-23029*# Northrop Grumman Corp., Los Angeles, CA.

AEROSPACE INDUSTRIES ASSOCIATION (AIA) WORK PRACTICES REPORT FOR COMPOSITES

Jackie Luca *In* NASA. Goddard Space Flight Center, Environmental, Safety, and Health Considerations: Composite Materials in the Aerospace Industry Oct. 1994 p 47-83 (For primary document see N95-23025 07-24)

Avail: CASI HC A03/MF A03

In an effort to gain a better understanding of effective safety and health work practice controls for composite manufacturing operations, the Aerospace Industries Association (AIA) Occupational Safety and Health Committee established a Composites Task Group. The group's task was to provide AIA members with recommendations for minimizing occupational exposure risk and to determine research needs and information gaps. The strategy included a review of toxicological information on composites, a review of member company experience and control methods, and interaction with other professional organizations who share an interest in composite work practices. Derived from text

N95-23030*# Occupational Safety and Health Administration, Salt Lake City, UT. Health Response Team.

SKIN EXPOSURE: ASSESSING THE HAZARD IN THE WORKPLACE

Kevin Cummins *In* NASA. Goddard Space Flight Center, Environmental, Safety, and Health Considerations: Composite Materials in the Aerospace Industry Oct. 1994 p 85-106 (For primary document see N95-23025 07-24)

Avail: CASI HC A03/MF A03

An outline of the Occupational Safety and Health Agency's concerns of skin exposure to hazardous chemicals is presented, followed by the corresponding slide narrations. Specifically, dermatitis and skin absorption as compared to lung absorption are addressed. Lung versus skin exposure is examined for glycol ethers and acrylamide. Examples of skin exposure include PBC's in transformers, toluene and xylene from autobody work, polynuclear aromatics (PNA's) among Coke oven workers, toluene diisocyanate (TDI), and occupational chemical exposures in an academic medical center. Permeation through gloves in the semiconductor industry is addressed as evidence for the need to assess the effectiveness of PPE (Personal Protective Equipment). This leads to the revisions of the PPE standard and the Safety and Health Program standard. CASI

N95-23031*# Air Force Systems Command, McClellan AFB, CA. Advanced Composites Program Office.

MISHAP RISK CONTROL FOR ADVANCED AEROSPACE/COMPOSITE MATERIALS

John M. Olson *In* NASA. Goddard Space Flight Center, Environmental, Safety, and Health Considerations: Composite Materials in the Aerospace Industry Oct. 1994 p 107-120 (For primary document see N95-23025 07-24)

Avail: CASI HC A03/MF A03

Although advanced aerospace materials and advanced composites provide outstanding performance, they also present several unique post-mishap environmental, safety, and health concerns. The purpose of this paper is to provide information on some of the unique hazards and concerns associated with these materials when damaged by fire, explosion, or high-energy impact. Additionally, recommended procedures and precautions are addressed as they pertain to all phases of a composite aircraft mishap response, including fire-fighting, investigation, recovery, clean-up, and guidelines are general in nature and not application-specific. The goal of this project is to provide factual and realistic information which can be used to develop consistent and effective procedures and policies to minimize the potential environmental, safety, and health impacts of a composite aircraft mishap response effort. Author

N95-23032*# Gordon (Rex B.).

FIRE HAZARD CONSIDERATIONS FOR COMPOSITES IN VEHICLE DESIGN

Rex B. Gordon *In* NASA. Goddard Space Flight Center, Environmental, Safety, and Health Considerations: Composite Materials in the Aerospace Industry Oct. 1994 p 127-135 (For primary document see N95-23025 07-24)

Avail: CASI HC A02/MF A03

Military ground vehicles fires are a significant cause of system loss,

equipment damage, and crew injury in both combat and non-combat situations. During combat, the ability to successfully fight an internal fire, without losing fighting and mobility capabilities, is often the key to crew survival and mission success. In addition to enemy hits in combat, vehicle fires are initiated by electrical system failures, fuel line leaks, munitions mishaps and improper personnel actions. If not controlled, such fires can spread to other areas of the vehicle, causing extensive damage and the potential for personnel injury and death. The inherent fire safety characteristics (i.e. ignitability, compartments of these vehicles play a major roll in determining rather a newly started fire becomes a fizzle or a catastrophe. This paper addresses a systems approach to assuring optimum vehicle fire safety during the design phase of complex vehicle systems utilizing extensive uses of composites, plastic and related materials. It provides practical means for defining the potential fire hazard risks during a conceptual design phase, and criteria for the selection of composite materials based on its fire safety characteristics. Author

N95-23033*# EXTRA Research, Inc., Salt Lake City, UT.
BIOTRANSFORMATION OF AN UNCURED COMPOSITE MATERIAL
Clement J. Welsh (Utah Univ., Salt Lake City, UT.), Michael J. Glass (Utah Univ., Salt Lake City, UT.), Brian Cheslack, Robert Pryor, Duan K. Tran, and Gail Bowers-Irons *In* NASA. Goddard Space Flight Center, Environmental, Safety, and Health Considerations: Composite Materials in the Aerospace Industry Oct. 1994 p 143-167 (For primary document see N95-23025 07-24)
Avail: CASI HC A03/MF A03

The feasibility of biologically degrading prepreg wastes was studied. The work was conducted with the intention of obtaining baseline data that would facilitate the achievement of two long-range goals. These goals are: (1) the biological remediation of the hazardous components in the prepreg wastes, and (2) providing the potential for recycling the prepreg waste fibers. The experiments examined a prepreg that employs an bismaleimide resin system. Initial results demonstrated an obvious deterioration of the prepreg material when incubated with several bacterial strains. The most active cultures were identified as a mixture of 'Bacillus cereus' and 'Pseudomonas sp'. Gas chromatography analyses revealed seven primary compounds in the resin mixture. Biotransformation studies, using the complete prepreg material, demonstrated on obvious loss of all seven organic compounds. Gas chromatography-mass spectrometry analyses resulted in structure assignments for the two primary components of the resin. Both were analogs of Bisphenol A; one being bismaleimide, and the other being Bisphenol A containing a diglycidyl moiety. The 'diglycidyl analog' was purified using thin-layer chromatography and the biotransformation of this compound (at 27 ug/ml bacterial culture) was monitored. After a seven-day incubation, approximately 40% of the organic compound was biotransformed. These results demonstrate the biotransformation of the prepreg resin and indicate that biological remediation of the prepreg wastes is feasible. Author

N95-23034*# Adherent Technologies, Inc., Albuquerque, NM.
CHEMICAL RECYCLING OF SCRAP COMPOSITES
Ronald E. Allred and Richard M. Salas *In* NASA. Goddard Space Flight Center, Environmental, Safety, and Health Considerations: Composite Materials in the Aerospace Industry Oct. 1994 p 177-188 (For primary document see N95-23025 07-24)
(Contract F08635-93-C-0109)
Avail: CASI HC A03/MF A03

There are no well-developed technologies for recycling composite materials other than grinding to produce fillers. New approaches are needed to reclaim these valuable resources. Chemical or tertiary recycling, conversion of polymers into low molecular weight hydrocarbons for reuse as chemicals or fuels, is emerging as the most practical means for obtaining value from waste plastics and composites. Adherent Technologies is exploring a low-temperature catalytic process for recycling plastics and composites. Laboratory results show that all types of plastics, thermosets as well as thermoplastics, can be converted in high yields to valuable hydrocarbon products. This novel catalytic process runs at 200 C, conversion times are rapid, the process is closed and, thus, nonpolluting, and no highly toxic gas or liquid products have been observed so no negative environmental impact will result from its implementation. Tests on reclamation of composite materials show that epoxy, imide, and engineering thermoplastic matrices can be converted to low molecular weight hydrocarbons leaving behind the reinforcing fibers for reuse as composite reinforcements in secondary, lower-performance applications. Chemical recycling is also a means to dispose of sensitive or classified organic materials without incineration and provides a means to eliminate or reduce mixed hazardous wastes containing organic materials. Author

N95-23035*# McDonnell-Douglas Aerospace, Saint Louis, MO. Analytical Chemical Lab.
OFFGASSING TEST METHODOLOGY FOR COMPOSITE MATERIALS
Abstract Only
Dale A. Scheer *In* NASA. Goddard Space Flight Center, Environmental, Safety, and Health Considerations: Composite Materials in the Aerospace Industry Oct. 1994 p 189 (For primary document see N95-23025 07-24)
Avail: CASI HC A01/MF A03

A significant increase in the use of composite materials has occurred during the past 20 years. Associated with this increased use is the potential for employees to be exposed to offgassing components from composite systems. Various components in composite systems, particularly residual solvents, offgas under various conditions. The potential for offgassing to occur increases as a composite material is heated either during cure or during lay-up operations. Various techniques can be employed to evaluate the offgassing characteristics of a composite system. A joint effort between AIA and SACMA resulted in the drafting of a proposed test method for evaluating the offgassing potential of composite materials. The purpose of testing composite materials for offgassing is to provide the industrial hygienist with information which can be used to assess the safety of the workplace. This paper outlines the proposed test method and presents round robin testing data associated with the test method. Also in this presentation is a discussion of classes of compounds which require specialized sampling techniques. Author (revised)

N95-23036*# Composites Services Corp.
SOCIETY OF THE PLASTIC INDUSTRY PROCESS EMISSION INITIATIVES
Joseph McDermott *In* NASA. Goddard Space Flight Center, Environmental, Safety, and Health Considerations: Composite Materials in the Aerospace Industry Oct. 1994 p 191-207 (For primary document see N95-23025 07-24)
Avail: CASI HC A03/MF A03

At first view, plastics process emissions research may not seem to have much bearing on outgassing considerations relative to advanced composite materials; however, several parallel issues and cross currents are of mutual interest. The following topics are discussed: relevance of plastics industry research to aerospace composites; impact of clean air act amendment requirements; scope of the Society of the Plastics Industry, Inc. activities in thermoplastic process emissions and reinforced plastics/composites process emissions; and utility of SPI research for advanced polymer composites audiences. CASI

N95-23037*# National Aeronautics and Space Administration. Goddard Space Flight Center, Greenbelt, MD.
OUTGASSING CONSIDERATIONS FOR COMPOSITES IN SPACE APPLICATIONS
Petar Arsenovic and Huai-Pu Chu *In its* Environmental, Safety, and Health Considerations: Composite Materials in the Aerospace Industry Oct. 1994 p 209-218 (For primary document see N95-23025 07-24)
Avail: CASI HC A02/MF A03

Composites have been increasingly used in the construction of spacecraft. However, unlike metals, composites must be used with particular discretion in space applications because of their outgassing properties. For example, the outgas materials may cause serious contamination problems and affect the performance of delicate instruments. This paper presents an overview of the testing procedure and acceptance criteria for outgassing selection of spacecraft materials. Since composites can contain and absorb moisture which will outgas in space as water vapor, the test results of moisture absorption and desorption of a composite material are discussed also. Author

N95-23038*# Air Force Inst. of Tech., Wright-Patterson AFB, OH.
MODELING AEROSOL EMISSIONS FROM THE COMBUSTION OF COMPOSITE MATERIALS

J. A. Roop, D. J. Caldwell, and K. J. Kuhlmann *In* NASA. Goddard Space Flight Center, Environmental, Safety, and Health Considerations: Composite Materials in the Aerospace Industry Oct. 1994 p 219-230 (For primary document see N95-23025 07-24)
Avail: CASI HC A03/MF A03

The use of advanced composite materials (ACM) in the B-2 bomber, composite armored vehicle, and F-22 advanced tactical fighter has rekindled interest concerning the health risk of burned or burning ACM. The objective of this work was to determine smoke production from burning ACM and its toxicity. A commercial version of the UPITT II combustion toxicity method developed at the University of Pittsburgh, and subsequently refined through a US Army-funded basic research project, was used to established controlled combustion conditions which were selected to evaluate real-world exposure scenarios. Production and yield of toxic species varied with the combustion conditions. Previous work with this method showed that the combustion conditions directly influenced the toxicity of the decomposition products from a variety of materials. Author

N95-23039*# Grace (W. R.) and Co., Lexington, MA.
AQUEOUS ALTERNATIVES FOR METAL AND COMPOSITE CLEANING
JoAnn Quitmeyer *In* NASA. Goddard Space Flight Center, Environmental, Safety, and Health Considerations: Composite Materials in the Aerospace Industry Oct. 1994 p 231-238 (For primary document see N95-23025 07-24)
Avail: CASI HC A02/MF A03

For many years the metalworking industry has cleaned metal and composite substrates with chlorinated solvents. Recently, however, health and disposal related environmental concerns have increased regarding chlorinated solvents, including 1,1,1-trichloroethane, trichloroethylene, methylene chloride, or Freon'. World leaders have instituted a production ban of certain ozone depleting chlorofluorocarbons (CFC's) by 1996. The Occupational Safety and Health Administration (OSHA) has instituted worker vapor exposure limitations for virtually all of the solvents used in solvent-based cleaners. In addition, the United States Environmental Protection Agency (EPA) has defined nearly all solvent-based cleaners as 'hazardous'. Cradle to grave waste responsibility is another reason manufacturers are trying to replace chlorinated solvents in their cleaning processes. Because of these factors, there now is a world wide effort to reduce and/or eliminate the use of chlorinated solvents for industrial cleaning. Waterbased cleaners are among the alternatives being offered to the industry. New technology alkaline cleaners are now available that can be used instead of chlorinated solvents in many cleaning processes. These waterbased cleaners reduce the release of volatile organic compounds (VOC's) by as much as 99 percent. (The definition and method of calculation of VOC's now varies from region to region.) Hazardous waste generation can also be significantly reduced or eliminated with new aqueous technology. This in turn can ease worker exposure restrictions and positively impact the environment. This paper compares the chemical and physical properties of this aqueous cleaners versus chlorinated solvents. Derived from text

N95-23258*# National Aeronautics and Space Administration. Lewis Research Center, Cleveland, OH.
EFFECTS OF DELAMINATIONS ON THE DAMPED DYNAMIC CHARACTERISTICS OF COMPOSITE LAMINATES: MECHANICS AND EXPERIMENTS
D. A. Saravanos and D. A. Hopkins Feb. 1995 34 p
(RTOP 505-63-5B)
(NASA-TM-106862; E-9467; NAS 1.15:106862) Avail: CASI HC A03/MF A01

Analytical and experimental work is presented on the damped free-vibration of delaminated laminates and beams. A laminate theory is developed where the unknown kinematic perturbations induced by a delamination crack are treated as additional degrees of freedom. The generalized stiffness, inertia and damping matrices of the laminate are formulated. An analytical solution is developed for the prediction of natural frequencies, modes and modal damping in composite beams with delamination cracks. Evaluations of the mechanics on various cantilever beams with a central delamination are performed. Experimental results for the modal frequencies and damping of composite beams with a single delamination are also presented and correlations between analytical predictions and measured data are shown. The effects of delamination vary based on crack size, laminate configuration, and mode order. The implications of the mechanics in developing delamination detection techniques are also discussed. Author

N95-23463*# National Aeronautics and Space Administration. Lewis Research Center, Cleveland, OH.
A COUPLED LAYERWISE ANALYSIS OF THE THERMOPIEZOELECTRIC RESPONSE OF SMART COMPOSITE BEAMS BEAMS
H.-J. Lee and D. A. Saravanos (Ohio Aerospace Inst., Cleveland, OH.) Mar. 1995 39 p Presented at the 36th Structures, Structural Dynamics, and Materials Conference, New Orleans, LA, 10-13 Apr. 1995; cosponsored by AIAA, ASME, AHS, and ASC
(RTOP 505-63-5B)
(NASA-TM-106889; E-9528; NAS 1.15:106889; AIAA Paper 95-1101)
Avail: CASI HC A03/MF A01

Thermal effects are incorporated into previously developed discrete layer mechanics for piezoelectric composite beam structures. The updated mechanics explicitly account for the complete coupled thermoelectromechanical response of smart composite beams. This unified representation leads to an inherent capability to model both the sensory and actuator responses of piezoelectric composite beams in a thermal environment. Finite element equations are developed and numerical results are presented to demonstrate the capability of the current formulation to represent the behavior of both sensory and active smart structures under thermal loadings. Author

N95-23537 Rutherford Appleton Lab., Chilton (England).
NONLINEAR THERMOVISCOELASTIC BEHAVIOUR IN COMPLEX MATERIALS
A. D. Irving, B. R. Clayton, and T. Dewson Jul. 1994 23 p Prepared in cooperation with Nottingham Univ.
(PB95-140653; RAL-94-073) Avail: Issuing Activity (National Technical Information Service (NTIS))

This paper is concerned with the development of a quantitative analysis method that can extract the mixed linear and nonlinear dynamical response of a thermoviscoelastic process in complex materials. A tractable set of simultaneous equations with well behaved coefficients can be generated by taking time series moments of a suitably truncated Volterra series expansion. This moment hierarchy is a set of inhomogeneous nonlinear integral equations, based on a vector multidimensional convolution form of the Volterra functional series expansion. The hierarchy developed is used to analyze the time dependent thermoviscoelastic properties of resin matrix composite materials. Estimates of the temporal response of the measured deformation gradient to the measured mechanical and thermal forces were then used to predict the out of sample stress field values. These predictions demonstrated that the response functions provided a good, locally time invariant, representation of the thermoviscoelastic process. The range of applied loads span a significant region of the phase space for the specimen and the estimated response function values and steady state transport coefficients remained constant over this range. NTIS

N95-23551*# National Aeronautics and Space Administration. Marshall Space Flight Center, Huntsville, AL.
PERMEABILITY TESTING OF COMPOSITE MATERIAL AND ADHESIVE BONDS FOR THE DC-XA COMPOSITE FEEDLINE PROGRAM
A. T. Nettles Washington Mar. 1995 13 p
(NASA-TM-108483; NAS 1.15:108483) Avail: CASI HC A03/MF A01

Hercules IM7/8552 carbon/epoxy and Hysol EA 9394 epoxy adhesive bonded between composite/titanium were tested for permeability after various numbers of thermal cycles between 100 C and liquid nitrogen (-196 C). The specimens were quenched from the 100 C temperature into liquid nitrogen to induce thermal shock into the material. Results showed that the carbon/epoxy system was practically impermeable even after 12 thermal cycles. The EA 9394 adhesive bondline was more permeable than the carbon/epoxy, but vacuum mixing minimized the permeability and kept it within allowable limits. Thermal cycling had little effect on the permeability values of the bondline specimens. Author

N95-23924# Rochester Univ., NY.
MICROSTRUCTURAL BEHAVIOR OF NONEQUILIBRIUM SYSTEMS Final Report, 1 Mar. 1986 - 31 May 1993

J. C. M. Li Nov. 1994 16 p
(Contract DE-FG02-85ER-45201)
(DE95-004450; DOE/ER-45201/T2) Avail: CASI HC A03/MF A01

The major achievements made during this period are as follows: (1) negative creep in metallic glasses and mechanochemical spinodal decomposition; (2) magnetic domain structure at shear bands and annealing embrittlement of metallic glasses; (3) etch pits along shear bands in metallic glasses; (4) increase of Curie temperature by rapid heating; (5) molecular dynamics simulation of melting; (6) nanoporous materials; (7) dislocation-crack interactions; (8) recovery processes of deformed structure; and (9) differences in deformation mechanisms between metals and polymers. A brief discussion is given for each achievement. DOE

N95-23277*# Iowa State Univ. of Science and Technology, Ames, IA. Dept. of Aerospace Engineering and Engineering Mechanics.
IDEALIZED TEXTILE COMPOSITES FOR EXPERIMENTAL/ANALYTICAL CORRELATION Abstract Only
Daniel O. Adams *In* Hampton Univ., 1994 NASA-HU American Society for Engineering Education (ASEE) Summer Faculty Fellowship Program Dec. 1994 p 57 (For primary document see N95-23276 07-99)
Avail: CASI HC A01/MF A02

N95-23288*# Boston Univ., MA. Dept. of Aerospace and Mechanical Engineering.
FABRIC GEOMETRY DISTORTION DURING COMPOSITES PROCESSING Abstract Only
Julie Chen *In* Hampton Univ., 1994 NASA-HU American Society for Engineering Education (ASEE) Summer Faculty Fellowship Program Dec. 1994 p 69 (For primary document see N95-23276 07-99)
Avail: CASI HC A01/MF A02

N95-23300*# Florida Univ., Gainesville, FL. Dept. of Aerospace Engineering, Mechanical and Engineering Science.
INTERLAMINAR SHEAR TEST METHOD DEVELOPMENT FOR LONG TERM DURABILITY TESTING OF COMPOSITES Abstract Only
Peter G. Ifju *In* Hampton Univ., 1994 NASA-HU American Society for Engineering Education (ASEE) Summer Faculty Fellowship Program Dec. 1994 p 82 (For primary document see N95-23276 07-99)
Avail: CASI HC A01/MF A02

N95-23502# Virginia Univ., Charlottesville, VA. Center for Electrochemical Science and Engineering.
THE DETECTION AND ANALYSIS OF GALVANIC DAMAGE IN BMI/GRAPHITE FIBER COMPOSITES
S. R. Taylor and G. L. Cahen, Jr. *In* AGARD, Corrosion Detection and Management of Advanced Airframe Materials Jan. 1995 12 p Sponsored by Virginia Center for Innovative Technology and Naval Air Warfare Center (For primary document see N95-23496 07-26)
Copyright Avail: CASI HC A03/MF A03

N95-23900*# National Aeronautics and Space Administration. Langley Research Center, Hampton, VA.
SURFACE CHARACTERIZATION OF LDEF CARBON FIBER/POLYMER MATRIX COMPOSITES
Holly L. Grammer (Virginia Polytechnic Inst. and State Univ., Blacksburg, VA.), James P. Wightman (Virginia Polytechnic Inst. and State Univ., Blacksburg, VA.), Philip R. Young, and Wayne S. Slemp *In its* LDEF: 69 Months in Space. Third Post-Retrieval Symposium, Part 2 Feb. 1995 p 601-612 (For primary document see N95-23896 07-99)
(Grant NAG1-1186)
Avail: CASI HC A03/MF A03

N95-23910*# National Aeronautics and Space Administration. Marshall Space Flight Center, Huntsville, AL.
TREND ANALYSIS OF IN-SITU SPECTRAL REFLECTANCE DATA FROM THE THERMAL CONTROL SURFACES EXPERIMENT (TCSE)
Donald R. Wilkes (AZ Technology, Huntsville, AL.), P. S. LeMaster (AZ Technology, Huntsville, AL.), Richard J. Mell (AZ Technology, Huntsville, AL.), Edgar R. Miller (AZ Technology, Huntsville, AL.), and James M. Zwiener *In* NASA. Langley Research Center, LDEF: 69 Months in Space. Third Post-Retrieval Symposium, Part 2 Feb. 1995 p 755-769
(For primary document see N95-23896 07-99)
Avail: CASI HC A03/MF A03

25 INORGANIC AND PHYSICAL CHEMISTRY

Includes chemical analysis, e.g., chromatography; combustion theory; electrochemistry; and photochemistry.

For related information see also *77 Thermodynamics and Statistical Physics.*.

N95-22517# Lehigh Univ., Bethlehem, PA. Center for Surface Studies.
INFRARED STUDY OF CARBON DEPOSITS ON BIMETALLIC CATALYSTS
R. P. Eischens 1994 6 p
(Contract DE-FG02-86ER-13612)
(DE95-000902; DOE/ER-13612/T1) Avail: CASI HC A02/MF A01

The study investigated coke deposited on alumina, on platinum/alumina, and on bimetallic/alumina catalysts. The interest in coke is based on coke deposition being the limited factor in the processes used to produce gasoline. The success of the bimetallic catalysts can be related to their effect on coke deposition. The consensus view has been that coke deposits on catalysts are a complex species composed of carbon and hydrogen in which the hydrogen/carbon ratio is inversely related to the temperature to which the coke has been heated. A new factor was introduced when infrared studies detected bands at 1580 and 1470/cm. Isotropic substitution studies showed that these bands are due to an oxygenated species similar to a carboxylate. During the fifth year of the project, it was shown that the oxygen needed to convert hydrocarbons to carboxylate are provided by the more basic hydroxyls on the alumina surface. Carboxylates were not observed in coke deposited on zeolites under conditions which produced carboxylates on alumina. This difference is attributed to the absence of strongly basic hydroxyl groups in zeolites. During the final sixth year this work was extended to show that treatment of alumina with hydrogen sulfide eliminates carboxylate formation. Results from this study are discussed. DOE

N95-22575# Alabama Univ., University, AL. Dept. of Chemistry.
MAGNETIC RESONANCE AND OPTICAL SPECTROSCOPIC STUDIES OF CAROTENOIDS Progress Report, 1 Dec. 1991 - - 30 Nov. 1994
L. D. Kispert May 1994 14 p
(Contract DE-FG05-86ER-13465)
(DE95-003729; DOE/ER-13465/9) Avail: CASI HC A03/MF A01

It is the authors goal to study the role of the host lattice in the formation of carotenoid cation radicals, dications, and excited singlet states. Particular emphasis is being placed on determining what is special about carotenoids that natural photosynthetic systems require them for photoprotection and also as components for electron transport processes. The authors are thus manipulating the host matrix so as to characterize the function and the structure of carotenoids and their cation radicals and dications in different dielectric media. To understand their properties, we have carried out Simultaneous Electrochemistry and Electron Paramagnetic Resonance (SEEPR), Simultaneous Electrochemistry and Optical Spectroscopy; Simultaneous Electrochemistry and Resonance Raman, Electron-Nuclear Double Resonance (ENDOR), Chemically Induced Dynamic Electron Polarization (CIDEP), two dimensional NMR, and optical measurements of carotenoids and carotenoid cation radicals. Carotenoid excited states were formed optically and studied by picosecond spectroscopy in different dielectric media. The carotenoid cation radicals were formed electrochemically, photolytically, catalytically, and radiolytically in different hosts matrices. The structures of carotenoids available to us from commercial or philanthropically inclined sources differ so widely that the effects of a particular feature cannot be systematically assessed. In order to reduce the structural variables, several novel carotenoids were synthesized. Most are unsymmetrical 7(prime)-apo-7(prime)-phenyl(beta)-carotenes in which the phenyl ring is substituted with different electron-withdrawing or electron-donating groups. DOE

N95-22677# Los Alamos National Lab., NM.
MOCVD OF GALLIUM AND CALCIUM SULFIDES FOR IMPROVED PHOSPHOR PROCESSING
N. M. Peachey, J. A. Samuels, B. F. Espanoza, C. D. Adams, D. C. Smith,

R. C. Dye, R. T. Tuenge (Planar Systems, Inc., Beaverton, OR.), C. F. Schaus (Planar Systems, Inc., Beaverton, OR.), and C. N. King (Planar Systems, Inc., Beaverton, OR.) 1994 11 p Presented at the Materials Week 1994, Rosemont, IL, 3-7 Oct. 1994
(Contract W-7405-eng-36)
(DE95-000918; LA-UR-94-3179; CONF-941016-1) Avail: CASI HC A03/MF A01

Recently, doped calcium thiogallate CaGa2S4 phosphors have been investigated for use in electroluminescent flat panel displays. The current technique used for the deposition of thin film calcium thiogallate is sputtering. Unfortunately, this requires a high temperature annealing process to provide the desired crystallinity of the phosphor. Recent efforts have focused on the possible use of metal-organic chemical vapor deposition (MOCVD) to produce the CaGa2S4 layer. The use of MOCVD provides an attractive alternative to sputtering since it does not require heating above the melting temperatures of the glass substrates used for the display panels. To accomplish this, the deposition of both Ga2S3 and CaS is investigated as these compounds are intermediate steps in the development of the phosphor deposition. Uniform, crystalline films of both Ga2S3 and CaS were deposited and the process shows promise for successful deposition of the CaGa2S4 phosphor. DOE

N95-22681# Argonne National Lab., IL.
HYDROGEN VIBRATIONAL DENSITY OF STATES OF ADSORBED WATER ON RARE-EARTH MODIFIED ZIRCONIA
C. K. Loong, L. E. Iton, and Masakuni Ozawa (Nagoya Inst. of Tech., Japan.) 20 Jul. 1994 9 p Presented at the Neutron Scattering, Sendai, Japan, 11-14 Oct. 1994
(Contract W-31-109-eng-38)
(DE95-001127; ANL/IPNS/CP-83105; CONF-9410165-5) Avail: CASI HC A02/MF A01

Rare-earth (RE) doped ZrO2 prepared by a method of coprecipitation from aqueous solution shows many properties such as good thermal stability and large surface area (approximately) 80 sq m/g that are suitable for use as catalyst supports and sorbents for a variety of molecules. The authors have measured the vibrational densities of states of surface hydroxyl groups as well as physisorbed water molecules in La(0.1)Zr(0.9)O(1.95) and Nd(0.1)Zr(0.9)O(1.95) by inelastic neutron scattering. The spectrum of dry RE-ZrO2 exhibits a peak at about 455 meV characteristic of the O-H stretch vibrations of surface hydroxyl groups. At a submonolayer coverage of H2O this peak broadens and shifts to a slightly lower energy. At higher coverage three bands, corresponding to the O-H stretch (approximately) 430 meV, H-O-H bend (approximately) 200 meV) and vibrational motion (approximately) 80 meV, were observed. The decreasing energy and larger width of the OH stretch band with increasing H2O coverage indicate the influence of hydrogen bonding on the motion of water molecules. DOE

N95-22710 Department of the Navy, Washington, DC.
LIGHT EMISSION-OR-ABSORBANCE-BASED BINDING ASSAYS FOR POLYNUCLEIC ACIDS Patent
David A. Kidwell, inventor (to Navy) 26 Jul. 1994 25 p Filed 15 Jan. 1993
(AD-D016557; US-Patent-5,332,659; US-Patent-Appl-SN-004009; US-Patent-Class-435-6) Avail: US Patent and Trademark Office

A target polynucleic acid strand may be detected within a sample. A sensing strand of complementary polynucleic acid is labelled, at at least two internucleotide phosphate groups, with labels which vary their electronically interaction with each other, and thus their emission or absorption spectra, depending upon whether the sensing strand is bound to target polynucleic acid in the sample. DTIC

N95-22722# Sandia National Labs., Livermore, CA.
CHEMICAL VAPOR DEPOSITION IN LOW PRESSURE BATCH FURNACES
W. G. Houf and J. F. Grcar 1993 7 p Presented at the 10th International Heat Transfer Conference, Brighton, England, 14-18 Aug. 1994
(Contract DE-AC04-94AL-85000)
(DE95-003035; SAND-93-8685C; CONF-940809-7) Avail: CASI HC A02/MF A01

A two-dimensional axisymmetric model for low pressure chemical vapor deposition in a multiwafer batch reactor has been developed. The model includes a rigorous description of multicomponent species transport, gas phase chemistry, surface chemistry, convective heat transfer, wafer heat conduction, and surface-to-surface radiative exchange with specular reflection and partially transmitting quartz surfaces. The model is designed to execute rapidly on a small computer workstation so that it may be used by semiconductor manufacturing companies in the selection of optimum processing conditions. The model has been used to simulate the deposition of polysilicon films from silane gas. Predictions from the model are found to be in good agreement with the reactor deposition data from a commercial reactor. Simulations have been performed to explore the aspects of scaling such reactors to larger wafer diameters. DOE

N95-22764# Argonne National Lab., IL.
EVALUATION OF NEUTRON TECHNIQUES FOR ILLICIT SUBSTANCE DETECTION
C. L. Fink, B. J. Micklich, T. J. Yule, P. Humm, L. Sagalovsky, and M. M. Martin 1994 5 p Presented at the 13th International Conference on the Application of Accelerators in Research and Industry, Denton, TX, 7-10 Nov. 1994
(Contract W-31-109-eng-38)
(DE95-002988; ANL/TD/CP-83462; CONF-941129-9) Avail: CASI HC A01/MF A01

The authors are studying inspection systems based on the use of fast neutrons for detecting illicit substances such as explosives and drugs in luggage and cargo containers. Fast neutron techniques can determine the quantities of light elements such as carbon, nitrogen, and oxygen in a volume element. Illicit substances containing these elements are characterized by distinctive elemental densities or density ratios. They discuss modeling and tomographic reconstruction studies for fast-neutron transmission spectroscopy. DOE

N95-22795# Michigan Univ., Ann Arbor, MI. Dept. of Geological Sciences.
PRECISE DETERMINATIONS OF THE ISOTOPIC COMPOSITIONS AND ATOMIC WEIGHTS OF MOLYBDENUM, TELLURIUM, TIN AND TUNGSTEN USING ICP SOURCE MAGNETIC SECTOR MULTIPLE COLLECTOR MASS SPECTROMETRY
Der-Chuen Lee and A. N. Halliday 1994 22 p Presented at the Alfred O. Nier Symposium on Inorganic Mass Spectrometry, Durango, CO, 10-12 May 1994
(Contract DE-FG02-94ER-14412)
(DE95-003003; CONF-940556-4) Avail: CASI HC A03/MF A01

Precise determinations of the isotopic compositions of molybdenum, tellurium, tin and tungsten were obtained utilizing an inductively coupled plasma source (ICP) magnetic sector mass spectrometer equipped with multiple collectors. The results of this study are comparable to those measured by conventional and negative thermal ionization mass spectrometry (TIMS and NTIMS) and the values recommended by the International Union of Pure and Applied Chemistry (IUPAC), but with improvement in precision by up to two orders of magnitude. The isotopic abundances and atomic weight for each element calculated from the data obtained in this study are also in excellent agreement with previously published values. The only disagreement between this study and IUPAC recommended values is for tellurium. However, with the exception of Te-130, the Te data are in good agreement with those reported in a recent study by De Laeter. The results of this study demonstrate the capability of this new instrument to produce precise and reproducible isotopic data for elements that are difficult to ionize and measure with TIMS. Furthermore, the greater precision of isotopic measurements possible with the ICP source multiple collector magnet sector mass spectrometer greatly enhances the prospects for research on the distribution and isotopic compositions of these elements in terrestrial and meteoritic materials. DOE

N95-22857# Argonne National Lab., IL.
ON THE FORMATION OF IRON(3) OXIDES VIA OXIDATION OF IRON(2)
Roberta Bongiovanni (Turin Univ., Italy.), Exio Pelizzetti (Turin Univ., Italy.), Enrico Borgarello (Enericerche S.p.A., Milan, Italy.), and Dan Meisel 1994 25 p
(Contract W-31-109-eng-38)
(DE94-018392; ANL/CHM/PP-79404) Avail: CASI HC A03/MF A01

Formation of iron oxides in aqueous salt solutions is reviewed. The

discussion is focused on the oxidation of iron(II) and the following hydrolysis process that leads to the formation of a solid phase from homogeneous solutions. Results from our own studies on the kinetics of the oxidation reactions and the ensuing growth processes are presented. DOE

N95-22869# California Univ., Berkeley. Lawrence Berkeley Lab, CA.
TURBIDITY OF A NEAR CRITICAL IONIC FLUID
T. Narayanan and K. S. Pitzer Apr. 1994 12 p Presented at the 12th Symposium on Thermophysical Properties, Boulder, CO, 19-24 Jun. 1994
(Contract DE-AC03-76SF-00098)
(DE94-014916; LBL-35519; CONF-940633-6) Avail: CASI HC A03/MF A01

We report the critical behavior of osmotic compressibility (chi tau), that was deduced from turbidity, in an ionic fluid mixture comprised of tetra-n-butylammonium picrate in a low dielectric solvent, 1-dodecanol. The liquid-liquid phase separation in this system is driven, predominantly, by Coulombic interactions. Measurements covered the reduced temperature, t, range 7 x 10(exp -5) less than or equal t less than or equal 7 x 10(exp -2). The critical behavior of chi tau indicates a crossover from the mean field to the Ising critical exponent, as the critical temperature (Tc) is approached. DOE

N95-22876# Brookhaven National Lab., Upton, NY.
PARTICLE SIZE DEPENDENCE IN FISCHER-TROPSCH SYNTHESIS
D. Mahajan, E. Zuckerman, and A. Kobayashi 1994 17 p Presented at the Coal Liquefaction and Gas Conversion Contractors' Review Conference, Pittsburgh, PA, 7-8 Sep. 1994
(Contract DE-AC02-76CH-00016)
(DE95-003124; BNL-60794; CONF-9409168-9) Avail: CASI HC A03/MF A01

The use of ultrafine particle (UFP) iron catalysts in slurry-phase Fischer-Tropsch (F-T) synthesis was investigated. Two systems were selected: (1) NANOCAT(trademark) or MACH-1, a commercially available unsupported Fe2O3 material with mean particle diameter (MPD) of 3 nm (surface area (SA) = 255 sq m.g(exp -1), and density (d) = 0.05 g.mL(exp -1)) ; and (2) an unsupported Fe2O3 material from BASF with MPD of 20-80 nm (SA = 16-20 sq m.g(exp -1), and d = 5.25 g.mL(exp -1)). For reference, the UCI catalyst with MPD of 32.5 (mu)m SA = 232 sq m.g(exp -1), and d = 0.80 g.mL(exp -1); composition (wt%): Fe2O3 = 69.6, K2O = 5.1 SiO2 = 8.3, CuO = 2.6; loss on ignition (LOI) = 14.8 was also included. After slurried catalyst reduction with CO at 280 C, F-T activity data were collected at 240 C and 0.78 MPa with balanced gas (H2/CO is approximately 2/1). A run was also completed with MACH-1 at 260 C and 2.77 MPa. At 240 C, 0.78 MPa, and gas-hourly-space-velocity (GHSV) of 4.5-4.7 NL.gFe(sup -1).h(exp -1), space-time-yields (STY) of hydrocarbon products were 0.36, 0.26, and 0.54 kg.kgFe(sup-1).h(exp -1) for BASF, MACH-1, and UCI respectively. The corresponding alpha values obtained from Anderson-Schulz-Flory (ASF) plots (in the C(sub 3)-C(sub 7) range) were 0.60, 0.57, and 0.50. A Moessbauer study on a MACH-1 sample, quenched after 199 hours at 260 C, indicated that MACH-1 was in the magnetic phase. EXAFS and Moessbauer measurements on several unreduced, freshly reduced, and quenched UFP samples are in progress. The H2/CO stoichiometry used is relevant to natural gas-derived syngas. Future runs will utilize these data for development of UFP catalysts for oxygenates synthesis with CO2-rich syngas. DOE

N95-22886# Sandia National Labs., Albuquerque, NM.
MODELING NO(X) EMISSIONS IN TURBULENT JET FLAMES: EFFECTS OF BUOYANCY AND RADIATION
Andrew E. Lutz and James E. Broadwell (California Inst. of Tech., Pasadena, CA.) 1994 24 p Presented at the Western States Section of the Combustion Institute Spring Meeting, Davis, CA, 21-22 Mar. 1994
(Contract DE-AC04-94AL-85000)
(DE94-016621; SAND-94-8586C; CONF-940397-3) Avail: CASI HC A03/MF A01

This paper presents the Two-Stage Lagrangian model for predicting chemical kinetics in turbulent jet flames. The model uses two perfectly stirred reactors to represent chemical reactions in regions of homogeneously mixed fluid and diffusion layers within the structure of a turbulent jet. Entrainment of surrounding fluid into the reactors is derived from experimental correlations, including the effects of buoyancy on the entrainment rate. Complete chemical kinetic mechanisms for hydrocarbon oxidation and nitrogen chemistry are retained in the model at modest computational expense. The model includes a simple but useful sub-model for energy loss from the flame via thermal radiation transfer. Examples in this paper include NO(x) emission predictions from hydrogen and methane flames, in comparison to experimental data. The model predictions demonstrate the importance of simultaneously considering buoyancy and radiation in almost all flames. Recent experiments and numerical studies suggest a somewhat different view of turbulent combustion from that on which the Two-Stage Lagrangian model was originally based. This view and the corresponding model modifications are described. This paper introduces a diffusion flame model that provides a more realistic representation of burning within diffusive regions of turbulent jet flames. To describe this model, the authors present analytical solutions for a flame-sheet with infinitely fast chemistry and numerical diffusion flame solutions for finite rate chemistry. DOE

N95-22887# Brookhaven National Lab., Upton, NY. Safeguards, Safety and Nonproliferation Div.
REMOTE DETECTION OF TRACE EFFLUENTS USING RESONANCE RAMAN SPECTROSCOPY
Arthur J. Sedlacek and Carl L. Chen 1994 8 p Presented at the Tactical Technologies and Wide Area Surveliance International Symposium, Chicago, IL, 2 Nov. 1993
(Contract DE-AC02-76CH-00016)
(DE94-016858; BNL-49542; CONF-9311173-2) Avail: CASI HC A02/MF A01

The authors discussed the potential of the resonance Raman chemical sensor as a remote sensor that can be used for gases, liquids or solids. This spectroscopy has the fundamental advantage that it is based on optical fingerprints that are insensitive to environmental perturbations or excitation frequency. By taking advantage of resonance enhancement, the inelastic scattering cross-section can increase anywhere from 4 to 6 orders of magnitude which translate into increased sensing range or lower detection limits. It was also shown that differential cross-sections as small as 10(exp - 27) sq cm/sr do not preclude the use of this technique as being an important component in one's remote-sensing arsenal. The results obtained in the early 1970's on various pollutants and the more recent work on atmospheric water cast a favorable light on the prospects for the successful development of a resonance Raman remote sensor. Since many of the chemicals important in the manufacture of narcotics are aromatics with strong UV/VIS absorption, it is expected that many will have pronounced resonance enhancements. DOE

N95-23064# Surface/Interface, Inc., Mountain View, CA.
CHARGE DISTRIBUTION ANALYSIS OF CATALYSTS UNDER SIMULATED REACTION CONDITIONS Technical Progress Report No. 6, 1 Jan. 1994 - 31 Mar. 1994
F. Freund 1994 58 p
(Contract DE-AC22-92PC-92106)
(DE95-003526; DOE/PC-92106/T6) Avail: CASI HC A04/MF A01

The surface charge characteristics of iron oxides at various temperatures were studied. The sulfidation reaction of iron oxide powder samples was performed under an atmosphere of H2S, and the surface charge properties of the resulting iron sulfides was studied. DOE

N95-23092*# MVA, Inc., Norcross, GA.
TRANSMISSION ELECTRON MICROSCOPE STUDIES OF EXTRATERRESTRIAL MATERIALS Final Report
Lindsay P. Keller 31 Jan. 1995 121 p
(Contract NAS9-18992)
(NASA-CR-188363; NAS 1.26:188363) Avail: CASI HC A06/MF A02

Transmission Electron Microscopy, X-Ray spectrometry and electron-energy-loss spectroscopy are used to analyse carbon in interplanetary dust particles. Optical micrographs are shown depicting cross sections of the dust particles embedded in sulphur. Selected-area electron diffraction patterns are shown. Transmission Electron Microscope specimens of lunar soil were prepared using two methods: ion-milling and ultramicrotomy. A combination of high resolution TEM imaging and electron diffraction is used to characterize the opaque assemblages. The opaque assemblages analyzed in this study are dominated by ilmenite with lesser rutile and spinel exsolutions, and traces of Fe metal. Derived from text

N95-23122# Sandia National Labs., Albuquerque, NM.
INFLUENCE OF POROSITY AND TWO-PHASE FLOW ON DIFFUSIONAL/THERMAL INSTABILITY OF A DEFLAGRATING ENERGETIC MATERIAL
S. B. Margolis (Sandia National Labs., Livermore, CA.) and F. A. Williams (California Univ., San Diego, La Jolla, CA.) Nov. 1994 39 p
(Contract DE-AC04-94AL-85000)
(DE95-002592; SAND-94-8409) Avail: CASI HC A03/MF A01

The combustion of condensed materials is known to admit diffusional/thermal instabilities that can lead to various oscillatory modes of burning. In the present work, asymptotic analyses are developed for nonsteady multi-phase deflagration of porous energetic solids, such as degraded nitramine propellants, that experience significant gas flow in the solid preheat region and are characterized by the presence of exothermic reactions in a bubbling melt layer at their surfaces. Relative motion between the gas and condensed phases is taken into account in both regions, and the derived asymptotic model is analyzed to obtain an explicit solution for steady, planar deflagration and a dispersion relation describing its linear stability. The latter determines a pulsating neutral stability boundary in the nondimensional activation energy - disturbance wavenumber plane beyond which nonsteady, nonplanar solutions are anticipated. Focusing on the realistic limit of small ratios of gas-phase to condensed-phase density and thermal conductivity, it is shown that the effect of a nonzero porosity alpha(sub s) of the unburned solid material is generally destabilizing, by an amount proportional to alpha(sub s)(1-alpha(sub s))(sup -1), relative to the nonporous case. This effect arises both from the lower combustion temperature of the porous energetic material and from the gas-phase diffusion of heat from the reaction zone towards the porous preheat region. These results therefore suggest that degraded propellants, which exhibit greater porosity than their undamaged counterparts, may be especially prone to nonsteady deflagration. DOE

N95-23164# Massachusetts Inst. of Tech., Cambridge, MA. Energy Lab.
CONVERSION OF LIGHT HYDROCARBON GASES TO METAL CARBIDES FOR PRODUCTION OF LIQUID FUELS AND CHEMICALS
A. F. Diaz, A. J. Modestino, J. Pride, J. B. Howard, J. W. Tester, and W. A. Peters Aug. 1994 7 p
(Contract DE-AC22-92PC-92111)
(DE95-000362; FE-MIT-92111-7; DOE/PC-92111/T6) Avail: CASI HC A02/MF A01

A milestone in the project was reached during the reporting period with the completion of the thermal plasma reactor. A mechanical wheel-type powder feeder was procured in May from Miller Thermal, Inc., of Appleton, WI, following a successful shakedown testing of the feeder in April. Magnesium oxide powder fed at 6 g/min for about 20 seconds into the interelectrode arc region of an argon plasma at nominal overall power levels of 4.05 kW, 7.5 kW and 14.5 kW exhibited a noticeable change in color from white (pre-plasma) MgO to gray (post-plasma) powder, with the post-14.5 kW plasma powder exhibiting the greatest change in color. An alarm system that would alert the operator to cooling water failure and inadequate draft in the exhaust chimney was also installed in May. In June, the power line from the oscillator to the gun was replaced with thick-wall (i.e. extra strong) copper pipe to reduce ohmic power losses. Also during June, a solids sampler with a sintered filter cup was fabricated to replace a cascade impactor which was inhibiting gas flow through the probe system. Furthermore, the final stage of equipment construction, the installation of a pressure relief system, was completed in June. The entire experimental setup is due for inspection by the MIT Safety Office in the near future. After this office approves the apparatus for routine operation, a scoping run with methane and CaO/MgO can be performed. DOE

N95-23202# Lehigh Univ., Bethlehem, PA.
ETHANOL SYNTHESIS AND WATER GAS SHIFT OVER BIFUNCTIONAL SULFIDE CATALYSTS
K Klier, R. G. Herman, and M. Deemer Jun. 1994 5 p
(Contract DE-FG22-91PC-91301)
(DE94-017376; DOE/PC-91301/11) Avail: CASI HC A01/MF A01

During this quarter, the cesium formate-doped and the undoped molybdenum disulfide previously prepared were sent out to Galbraith Laboratories for elemental analysis for cesium, molybdenum, and sulfur. A new Na/MoS2 catalyst was prepared under an inert atmosphere by an intercalation technique using sodium metal dissolved in liquid ammonia. This sample will be fully characterized. An all-glass apparatus was constructed for carrying out systematic intercalation procedures with alkali metals dissolved in liquid ammonia. This apparatus will insure that the dispersed catalysts are prepared in an oxygen/moisture-free environment. The stainless steel continuous flow high pressure/high temperature catalyst testing system was rebuilt and the analytical end of the unit was upgraded. DOE

N95-23252*# Iowa Univ., Iowa City, IA. Dept. of Chemistry.
SUPPORTED TRANSITION METAL CATALYSTS FOR PARA- TO ORTHO-HYDROGEN CONVERSION Final Report
Christopher J. Brooks, Wei Wang, and Darrell P. Eyman May 1994 106 p
(Grant NAG3-893)
(NASA-CR-197907; NAS 1.26:197907) Avail: CASI HC A06/MF A02

The main goal of this study was to develop and improve on existing catalysts for the conversion of ortho- to para-hydrogen. Starting with a commercially available Air Products nickel silicate, which had a beta value of 20, we were trying to synthesize catalysts that would be an improvement to AP. This was accomplished by preparing silicates with various metals as well as different preparation methods. We also prepared supported ruthenium catalysts by various techniques using several metal precursors to improve present technology. What was also found was that the activation conditions prior to catalytic testing was highly important for both the silicates and the supported ruthenium catalysts. While not the initial focus of the research, we made some interesting observations into the adsorption of H2 on ruthenium. This helped us to get a better understanding of how ortho- to para-H2 conversion takes place, and what features in a catalyst are important to optimize activity. Reactor design was the final area in which some interesting conclusions were drawn. As discussed earlier, the reactor catalyst bed must be constructed using straight 1/8 feet OD stainless steel tubing. It was determined that the use of 1/4 feet OD tubing caused two problems. First, the radius from the center of the bed to the wall was too great for thermal equilibrium. Since the reaction of ortho- to para-H2 is exothermic, the catalyst bed center was warmer than the edges. Second, the catalyst bed was too shallow using a 1/4 feet tube. This caused reactant blow-by which was thought to decrease the measured activity when the flow rate was increased. The 1/8 feet tube corrected both of these concerns. Derived from text

N95-23339# Lehigh Univ., Bethlehem, PA.
NO DECOMPOSITION IN NON-REDUCING ATMOSPHERES Technical Progress Report, Jun. 1994 - Aug. 1994
K. Klier, R. G. Herman, and I. Jirka Sep. 1994 14 p
(Contract DE-FG22-93PC-93222)
(DE95-004324; DOE/PC-93222/4) Avail: CASI HC A03/MF A01

This report summarizes the results obtained during optimization of conditions of ion exchange of Co(2+) cations into zeolite A. The results are summarized as follows: The Co(2+) species were introduced into Na A zeolite by contacting the zeolite with aqueous solution of cobalt (II) nitrate at pH approximately 6 and pH approximately 11. In both cases the expected ion exchange stoichiometry 1 Co(2+): 2 Na(1+) was exceeded, indicating intracavital precipitation and precipitation extraneous to the zeolite grains of excess cobalt species which likely consist of hydroxyoxides. All cobalt appeared to be divalent. Distribution of the Co(2+) species was initially uniform in the preparation carried out at pH 6 but prolonged heat treatment resulted in the enrichment of cobalt in the external surface region of the zeolite. At pH 11, the initial distribution was nonuniform, with the Co(2+) species enriched at the surface. The preparation did not achieve the intended exchange stoichiometry and indicated rather that more or less undefined cobalt (II) hydroxyoxide supported by the zeolite material, which could also be partially exchanged with cobalt, has been produced. Because in the catalytic applications reproducibility is essential, further preparations aiming at the desired exchange stoichiometry have been initiated in which lower pH will prevent precipitation of the hydroxyoxides. However, all the samples will be tested for NO decomposition to obtain a qualitative comparison between ion-exchanged and impregnated CoNaA zeolites. DOE

N95-23345# Wisconsin Univ., Madison, WI.
ORGANOMETALLIC CHEMISTRY OF BIMETALLIC COMPOUNDS Progress Report, Jan. 1992 - Jul. 1995

C. P. Casey Jul. 1994 21 p
(Contract DE-FG02-85ER-13406)
(DE95-004436; DOE/ER-13406/9) Avail: CASI HC A03/MF A01

Four main projects at the interface between organometallic chemistry and homogeneous catalysis were pursued. All were designed to give increased understanding of the mechanisms of organometallic reactions related to homogeneous and heterogeneous catalysis. In addition, a minor study involving eta(exp 5)-to eta(exp 1)-cyclopentadienyl ring slippage in catalysis was completed. DOE

N95-23348# Pacific Northwest Lab., Richland, WA.
KRYPTON ISOTOPE ANALYSIS USING NEAR-RESONANT STIMULATED RAMAN SPECTROSCOPY
C. A. Whitehead, B. D. Cannon, and J. F. Wacker Dec. 1994 22 p
(Contract DE-AC06-76RL-01830)
(DE95-005061; PNL-10203) Avail: CASI HC A03/MF A01

A method for measuring low relative abundances of Kr-85 in one liter or less samples of air has been under development here at Pacific Northwest Laboratory. The goal of the Krypton Isotope Laser Analysis (KILA) method is to measure ratios of 10(exp -10) or less of Kr-85 to more abundant stable krypton. Mass spectrometry and beta counting are the main competing technologies used in rare-gas trace analysis and are limited in application by such factors as sample size, counting times, and selectivity. The use of high-resolution lasers to probe hyperfine levels to determine isotopic abundance has received much attention recently. In this study, we report our progress on identifying and implementing techniques for trace Kr-85 analysis on small gas samples in a static cell as well as limitations on sensitivity and selectivity for the technique. High-resolution pulsed and cw lasers are employed in a laser-induced fluorescence technique that preserves the original sample. This technique, is based on resonant isotopic depletion spectroscopy (RIDS) in which one isotope is optically depleted while preserving the population of a less abundant isotope. The KILA method consists of three steps. In the first step, the 1s(sub 5) metastable level of krypton is populated via radiative cascade following two-photon excitation of the 2p(sub 6) energy level. Next, using RBDS, the stable krypton isotopes are optically depleted to the ground state through the 1s(sub 4) level with the bulk of the Kr-85 population being preserved. Finally, the remaining metastable population is probed to determine Kr-85 concentration. The experimental requirements for each of these steps are outlined below. DOE

N95-23360# Los Alamos National Lab., NM.
SIMULATION OF ABSORPTION EDGE DENSITOMETRY
Sin-Tao Hsue and M. Collins Nov. 1994 12 p
(Contract W-7405-eng-36)
(DE95-004393; LA-12874-MS) Avail: CASI HC A03/MF A01

A method for simulating absorption edge densitometry has been developed. This program enables one to simulate spectra containing any combination of special nuclear materials (SNM) in solution. The method has been validated with an analysis method using a single special nuclear material in solution or a combination of two types of SNM separated by a Z of 2. This computer simulation has been used to explore the bias caused by the presence of, for example, plutonium in a determination of uranium concentration. The authors have also used this program to explore better methods of analyzing densitometry data. DOE

N95-23380# California Univ., Berkeley. Lawrence Berkeley Lab, CA.
DIFFUSION BEHAVIOR OF LYSOZYME IN AQUEOUS AMMONIUM SULFATE SOLUTIONS UNDER VARYING SOLUTION CONDITIONS AS DETERMINED BY DYNAMIC LIGHT SCATTERING
U. M. Fornefeld, D. E. Kuehner, H. W. Blanch, and J. M. Prausnitz Dec. 1994 24 p
(Contract DE-AC03-76SF-00098)
(DE95-004821; LBL-36510) Avail: CASI HC A03/MF A01

As proteins gain significance in commercial applications such as pharmaceuticals, detergents, organic waste management and cosmetics, efficient and economical recovery of these valuable biomolecules is of increasing importance. The salting-out process has found widespread application in the area of protein separations. To date, salt-induced precipitation of proteins from complex aqueous solutions remains largely an empirical process; no comprehensive model exists to predict salting-out phase equilibria in protein solutions. Rational predictive models for salt-induced precipitation will, therefore, be of great value in protein purification, both on the preparative and the analytical scale. Any attempt to model theoretically salt-induced protein precipitation must include the known physics of protein interactions in aqueous solution. With this in mind, it is crucial to acknowledge that protein precipitation is fundamentally an aggregation process. In order to incorporate aggregation effects into ongoing efforts to model salting out of proteins, it is necessary to quantify the degree of aggregation as a function of solution conditions. Therefore, dynamic light scattering measurements were performed with a well-studied protein, hen-egg-white lysozyme, under several solution conditions. DOE

N95-23381# Lawrence Livermore National Lab., Livermore, CA.
ETHYLENE OXIDATION CHEMISTRY IN A WELL-STIRRED REACTOR
N. Marinov and P. Malte (Washington Univ., Seattle, WA.) Sep. 1994 45 p
(Contract W-7405-eng-48)
(DE95-004823; UCRL-ID-118564) Avail: CASI HC A03/MF A01

Ethylene is an important intermediate in the combustion of methane, larger aliphatic hydrocarbons, and aromatics. Detailed fuel-lean C2H4H2O/air well-stirred reactor data by Thornton were used to analyze reported combustion chemistry mechanisms and the development of this study's ethylene oxidation mechanism. The data set had been obtained for the temperature range 1,003 to 1,253 K and ethylene-oxygen equivalence ratio range 0.086 to 0.103, at atmospheric pressure. Mechanisms were derived from reaction sets of Westbrook and Pitz, and Dagaut, Cathonnet and Boettner. Examination of each reported mechanism indicated unusually large kinetic rates for the vinyl decomposition reaction were used in order to obtain agreement with the Thornton data set. An ethylene oxidation model was developed in order to address the mechanistic problems of the previous models. This study's mechanism well simulated the overall rate of ethylene oxidation and concentration profiles of CO, CO2, H2, CH2O, C2H2, CH3OH, CH4, and C2H6. Successful predictions by the model were dependent on a new high temperature vinyl oxidation reaction route, C2H3 + O2 = CH2CHO + O with a branching ratio of 1.19--1.21 at 1,053 K to 1.63--2.47 at 1,253 K. The branching ratio values were dependent upon the extent of fall-off for the C2H3 + O2 = CH2O + HCO reaction. DOE

N95-23476# Japan Atomic Energy Research Inst., Tokyo (Japan).
EXTRA.M: A COMPUTING CODE SYSTEM FOR ANALYSIS OF THE PUREX PROCESS WITH MIXER SETTLERS FOR REPROCESSING
Shoichi Tachimori Mar. 1994 188 p
(DE94-785273; JAERI-1331) Avail: CASI HC A09/MF A02

A computer code system EXTRA.M, for simulation of transient behavior of the solutes in a multistage countercurrent extraction process, was developed aiming to predict the distribution and chemical behaviors of actinide elements, i.e., U, Pu, Np, and of technetium in the Purex process of fuel reprocessing. The mathematical model is applicable to a complete mixing stagewise contactor such as mixer settler and to the Purex, with tri-n-butylphosphate (TBP) and nitric acid system. The main characteristics of the EXTRA.M are as follows: (1) Calculation of distribution ratios of the solutes is based on numerical equations of which parameter values are to be determined by a best fit method with a number of experimental data; (2) Total of 18 solutes (U(IV), U(VI), Pu(III), Pu(IV), Pu(V), Pu(VI), Np(IV), Np(V), Np(VI), Tc(IV), Tc(V), Tc(VI), Tc(VII), Zr(IV), HNO3, hydrazine, hydroxylamine nitrate and nitrous acid) are treated and rate equations of total 40 chemical reactions involving these solutes are incorporated; (3) Instantaneous change of flow conditions, i.e., concentration of the solutes and flow rate of the feeding solutions, is contrived by computation; and (4) Reflux or bypass mode calculation, in which an aqueous raffinate stream is transferred to the preceding bank or stage, is possible. The present report explains the concept, assumptions and characteristics of the model, the material balance equations including distribution and reaction rate equations and their solution method, and the usefulness of the model by showing some examples of the verification results. A description and source program of EXTRA.M1, as an example, are listed in the annex. DOE

N95-23481# Praxair, Inc., Tonawanda, NY.
OXYGEN ENRICHED COMBUSTION SYSTEM PERFORMANCE STUDY. PHASE 2: 100 PERCENT OXYGEN ENRICHED COMBUSTION IN REGENERATIVE GLASS MELTERS Final Report

G. B. Tuson, H. Kobayashi, and M. J. Campbell Aug. 1994 124 p
(Contract DE-FC07-88ID-12833)
(DE95-004212; DOE/ID-12833/1) Avail: CASI HC A06/MF A02

The field test project described in this report was conducted to evaluate the energy and environmental performance of 100% oxygen enriched combustion (100% OEC) in regenerative glass melters. Additional objectives were to determine other impacts of 100% OEC on melter operation and glass quality, and to verify on a commercial scale that an on-site Pressure Swing Adsorption oxygen plant can reliably supply oxygen for glass melting with low electrical power consumption. The tests constituted Phase 2 of a cooperative project between the United States Department of Energy, and Praxair, Inc. Phase 1 of the project involved market and technical feasibility assessments of oxygen enriched combustion for a range of high temperature industrial heating applications. An assessment of oxygen supply options for these applications was also performed during Phase 1, which included performance evaluation of a pilot scale 1 ton per day PSA oxygen plant. Two regenerative container glass melters were converted to 100% OEC operation and served as host sites for Phase 2. A 75 ton per day end-fired melter at Carr-Lowrey Glass Company in Baltimore, Maryland, was temporarily converted to 100% OEC in mid- 1990. A 350 tpd cross-fired melter at Gallo Glass Company in Modesto, California was rebuilt for permanent commercial operation with 100% OEC in mid-1991. Initially, both of these melters were supplied with oxygen from liquid storage. Subsequently, in late 1992, a Pressure Swing Adsorption oxygen plant was installed at Gallo to supply oxygen for 100% OEC glass melting. The particular PSA plant design used at Gallo achieves maximum efficiency by cycling the adsorbent beds between pressurized and evacuated states, and is therefore referred to as a Vacuum/Pressure Swing Adsorption (VPSA) plant. DOE

N95-23495# California Univ., Berkeley. Lawrence Berkeley Lab, CA.
CARBON MONOXIDE OXIDATION OVER THREE DIFFERENT STATES OF COPPER: DEVELOPMENT OF A MODEL METAL OXIDE CATALYST Ph.D. Thesis
G. G. Jernigan Oct. 1994 200 p
(Contract DE-AC03-76SF-00098)
(DE95-004682; LBL-36383) Avail: CASI HC A09/MF A03

Carbon monoxide oxidation was performed over the three different oxidation states of copper -- metallic (Cu), copper (I) oxide (Cu2O), and copper (II) oxide (CuO) as a test case for developing a model metal oxide catalyst amenable to study by the methods of modern surface science and catalysis. Copper was deposited and oxidized on oxidized supports of aluminum, silicon, molybdenum, tantalum, stainless steel, and iron as well as on graphite. The catalytic activity was found to decrease with increasing oxidation state (Cu is greater than Cu2O which is greater than CuO) and the activation energy increased with increasing oxidation state (Cu, 9 kcal/mol less than CuO, 14 kcal/mol less than CuO, 17 kcal/mol). Reaction mechanisms were determined for the different oxidation states. Lastly, NO reduction by CO was studied. A Cu and CuO catalyst were exposed to an equal mixture of CO and NO at 300 - 350 C to observe the production of N2 and CO2. At the end of each reaction, the catalyst was found to be Cu2O. There is a need to study the kinetics of this reaction over the different oxidation states of copper. DOE

N95-23545*# Massachusetts Univ., Lowell, MA. Center for Atmospheric Research.
THEORETICAL CALCULATIONS OF PRESSURE BROADENING COEFFICIENTS FOR H2O PERTURBED BY HYDROGEN OR HELIUM GAS Final Report
Robert R. Gamache and James B. Pollack Jan. 1995 44 p
(Contract NCC2-5029)
(NASA-CR-197345; NAS 1.26:197345) Avail: CASI HC A03/MF A01

Halfwidths were calculated for H2O with H2 as a broadening gas and were estimated for He as the broadening species. The calculations used the model of Robert and Bonamy with parabolic trajectories and all relevant terms in the interaction potential. The calculations investigated the dependence of the halfwidth on the order of the atom-atom expansion, the rotational states, and the temperature in the range 200 to 400K. Finally, calculations were performed for many transitions of interest in the 5 micrometer window region of the spectrum. The resulting data will be supplied to Dr. R. Freedman for extracting accurate water mixing ratios from the analysis of the thermal channels for the Net Flux experiment on the Galileo probe. Author

N95-23554 Helsinki Univ. of Technology, Espoo (Finland). Lab. of Forest Products Chemistry.
SCANDINAVIAN SYMPOSIUM ON SURFACE CHEMISTRY
P. Stenius and L. Sarvaranta 1994 148 p Conference held in Espoo, Einland, 15-17 Jun. 1994 Limited Reproducibility: More than 20% of this document may be affected by microfiche quality
(PB95-140687; ISBN-951-22-2166-7) Avail: Issuing Activity (National Technical Information Service (NTIS))

The following topics are discussed: (1) molecular forces between surfaces; (2) flocculation and floc structure; (3) dispersions and surfaces of minerals; (4) foams and thin liquid films; (5) emulsions; (6) new instrumentation; (7) polymer/surfactant interactions; (8) biosurfaces; and (9) poster sessions. NTIS

N95-23573# Los Alamos National Lab., NM.
ELECTROCHEMICAL STUDIES OF PEROVSKITE MIXED CONDUCTORS
E. L. Brosha, B. W. Chung, and F. H. Garzon 1994 6 p Presented at the 1994 Fall Meeting of the Materials Research Society (MRS), Boston, MA, 28 Nov. - 2 Dec. 1994
(Contract W-7405-eng-36)
(DE95-003704; LA-UR-94-3930; CONF-941144-15) Avail: CASI HC A02/MF A01

Research into the growth of high-quality single crystal thin films of high transition temperature (Tc) superconductors have stimulated interest in other perovskite metal oxides with a variety of physical properties. Thin films of perovskite materials are among the major focal research areas for optical, sensor, electronic, and superconducting applications. Two lanthanum-based oxygen/electronic conducting perovskite oxides of particular interest for high temperature fuel cell electrodes and interconnects and for other electrochemical applications such as oxygen separation devices are La(1-x)Sr(x)MnO(3-y) and La(1-x)Sr(x)CoO(3-y). The La-based perovskites are valuable for these technologies because they reduce interfacial resistances by eliminating the need for a three phase contact area (gas, metal electrode, electrolyte). In addition, these oxides may also serve a valuable role as novel catalysts or catalytic supports; however, little is known about what catalytic properties they may possess. Fundamental study of the electrochemical, diffusional oxygen transport, and surface catalytic properties of these materials can be greatly simplified if the complications associated with the presence of grain boundaries and multiple crystallite orientations can be avoided. Therefore, single crystals of these La-based perovskites become highly desirable. In this work, the authors report the structural and electrical properties of highly oriented thin films of La(0.84)Sr(0.16)MnO3 and La(0.8)Sr(0.2)CoO3 grown on single crystal Y-ZrO2 substrates. In addition, the authors have demonstrated growing, in situ, epitaxial multilayer perovskite/fluorite/perovskite configurations for fundamental fuel cell modeling. DOE

N95-24007# Sandia National Labs., Albuquerque, NM.
CHEMICAL RECOGNITION SOFTWARE
J. S. Wagner, M. W. Trahan, W. E. Nelson, P. J. Hargis, Jr., and G. C. Tisone 1994 11 p Presented at the Optical Sensing for Environmental and Process Monitoring, McLean, VA, 7-10 Nov. 1994
(Contract DE-AC04-94AL-85000)
(DE95-003346; SAND-94-2817C; CONF-9411144-3) Avail: CASI HC A03/MF A01

We have developed a capability to make real time concentration measurements of individual chemicals in a complex mixture using a multispectral laser remote sensing system. Our chemical recognition and analysis software consists of three parts: (1) a rigorous multivariate analysis package for quantitative concentration and uncertainty estimates; (2) a genetic optimizer which customizes and tailors the multivariate algorithm for a particular application; and (3) an intelligent neural net chemical filter which pre-selects from the chemical database to find the appropriate candidate chemicals for quantitative analyses by the multivariate algorithms, as well as providing a quick-look concentration estimate and consistency check. Detailed simulations using both laboratory fluorescence data and computer synthesized spectra indicate that our software can make accurate concentration estimates from complex multicomponent mixtures, even when the mixture is noisy and contaminated with unknowns. DOE

N95-24181# National Aerospace Lab., Tokyo (Japan).
EFFECTS OF JET STRENGTH ON NOx FORMATION IN PREMIXED IMPINGING JET COMBUSTION WITH MINIMUM HEAT LOSSES
Lin Xie and Shigeru Hayashi Jun. 1994 9 p Original contains color illustrations
(ISSN 0389-4010)
(NAL-TR-1237T) Avail: CASI HC A02/MF A01

NOx formation in the turbulent combustion of premixed methane/air mixtures in an impinging jet combustor with minimum heat losses was investigated. Experiments were carried out at atmospheric pressure and an inlet temperature of 323K. Equivalence ratios ranged from 0.5 to 1.0 while mass loadings of the combustor ranged from 1.23 to 4.94 kg/cu ms, where the mass loading is defined as the mass flow rate of mixture per combustor volume. Impingement of jets of the mixtures produced a turbulent flow field in a spherical ceramic shell placed in a cubic ceramic chamber for minimizing heat losses from the combustion field to the ambient. The NOx formation rates were predicted using the Zeldovich mechanism and were compared with the measurements. It was found that the level of NOx produced in the turbulent flame is proportional to the residence time except for very fuel-lean conditions, which suggest that NOx was formed via the 'thermal NOx mechanism' rather than the 'prompt NOx mechanisms'. Changes in turbulence levels did not affect the NOx formation rate. Significant reduction of NOx emissions observed in previous studies of impinging jet combustion in a closed chamber may have been caused by increased heat losses and elimination of spatial temperature gradient in the burnt gas, rather than the intense mixing caused by impingement jets. The NOx formation rates predicted by the Zeldovich mechanisms were lower than those measured in the turbulent flame by approximately an order of magnitude, particularly under fuel-lean conditions. Author

N95-23504# Defence Research Establishment Pacific, Victoria (British Columbia).
THE USE OF ELECTROCHEMICAL IMPEDANCE SPECTROSCOPY TO PREDICT THE CORROSION OF ALUMINUM-LITHIUM ALLOYS IN MARINE ENVIRONMENTS
D. R. Lenard, J. G. Moores, P. R. Roberge (Royal Military Coll. of Canada, Kingston, Ontario.), and E. Halliop (Royal Military Coll. of Canada, Kingston, Ontario.) *In* AGARD, Corrosion Detection and Management of Advanced Airframe Materials Jan. 1995 12 p (For primary document see N95-23496 07-26)
Copyright Avail: CASI HC A03/MF A03

N95-23643*# National Aeronautics and Space Administration. Lewis Research Center, Cleveland, OH.
SPRAY COMBUSTION EXPERIMENTS AND NUMERICAL PREDICTIONS
Edward J. Mularz (Army Research Lab., Cleveland, OH.), Daniel L. Bulzan, and Kuo-Huey Chen (Toledo Univ., OH.) *In* NASA. Marshall Space Flight Center, Eleventh Workshop for Computational Fluid Dynamic Applications in Rocket Propulsion, Part 1 Jul. 1993 p 645-665 (For primary document see N95-23615 07-34)
Avail: CASI HC A03/MF A10

N95-23644*# Rockwell International Corp., Canoga Park, CA. Rocketdyne Div.
PROGRESS IN ADVANCED SPRAY COMBUSTION CODE INTEGRATION
Pak-Yan Liang *In* NASA. Marshall Space Flight Center, Eleventh Workshop for Computational Fluid Dynamic Applications in Rocket Propulsion, Part 1 Jul. 1993 p 667-687 (For primary document see N95-23615 07-34)
Avail: CASI HC A03/MF A10

N95-23645*# National Aeronautics and Space Administration. Marshall Space Flight Center, Huntsville, AL.
CFD ANALYSIS OF SPRAY COMBUSTION AND RADIATION IN OMV THRUST CHAMBER
M. G. Giridharan (CFD Research Corp., Huntsville, AL.), A. Krishnan (CFD Research Corp., Huntsville, AL.), A. J. Przekwas (CFD Research Corp., Huntsville, AL.), and K. Gross *In its* Eleventh Workshop for Computational Fluid Dynamic Applications in Rocket Propulsion, Part 1 Jul. 1993 p 689-715 (For primary document see N95-23615 07-34)
Avail: CASI HC A03/MF A10

N95-23646*# Alabama Univ., Huntsville, AL. Dept. of Chemical Engineering.
DEVELOPMENT OF AN ATOMIZATION METHODOLOGY FOR SPRAY COMBUSTION
S. P. Seung, C. P. Chen, and Y. S. Chen (Engineering Sciences, Inc., Huntsville, AL.) *In* NASA. Marshall Space Flight Center, Eleventh Workshop for Computational Fluid Dynamic Applications in Rocket Propulsion, Part 1 Jul. 1993 p 717-747 (For primary document see N95-23615 07-34)
Avail: CASI HC A03/MF A10

N95-23797*# National Aeronautics and Space Administration. Marshall Space Flight Center, Huntsville, AL.
LDEF ENVIRONMENT MODELING UPDATES
Tim Gordon (Applied Science Technology, Inc., Littleton, CO.), Ray Rantanen (ROR Enterprises, Athol, ID.), and Ann F. Whitaker *In* NASA. Langley Research Center, LDEF: 69 Months in Space. Third Post-Retrieval Symposium, Part 1 Feb. 1995 p 3-11 (For primary document see N95-23796 07-99)
Avail: CASI HC A02/MF A04

N95-23798*# National Aeronautics and Space Administration. Langley Research Center, Hampton, VA.
OUTGASSING PRODUCTS FROM ORBITER TPS MATERIALS
Gale A. Harvey, Tom J. Lash, and J. Richard Rawls *In its* LDEF: 69 Months in Space. Third Post-Retrieval Symposium, Part 1 Feb. 1995 p 13-20 (For primary document see N95-23796 07-99)
Avail: CASI HC A02/MF A04

N95-23804*# European Space Agency. European Space Research and Technology Center, ESTEC, Noordwijk (Netherlands).
MATERIAL INSPECTION OF EURECA FIRST FINDINGS AND RECOMMENDATIONS
Marc VanEesbeek, Michael Froggatt, and Georges Gourmelon *In* NASA. Langley Research Center, LDEF: 69 Months in Space. Third Post-Retrieval Symposium, Part 1 Feb. 1995 p 71-86 (For primary document see N95-23796 07-99)
Avail: CASI HC A03/MF A04

N95-23836*# Institute for Space Science and Technology, Inc., Gainesville, FL.
SECONDARY ION MASS SPECTROMETRY (SIMS) ANALYSIS OF HYPERVELOCITY MICROPARTICLE IMPACT SITES ON LDEF SURFACES Abstract Only
C. G. Simon, A. J. Buonaquisti (North Carolina State Univ., Raleigh, NC.), D. A. Batchelor (North Carolina State Univ., Raleigh, NC.), J. L. Hunter (North Carolina State Univ., Raleigh, NC.), D. P. Griffis (North Carolina State Univ., Raleigh, NC.), V. Misra (North Carolina State Univ., Raleigh, NC.), D. R. Ricks (North Carolina State Univ., Raleigh, NC.), J. J. Wortman (North Carolina State Univ., Raleigh, NC.), D. E. Brownlee (Washington Univ., Seattle, WA.), and S. R. Best (Auburn Univ., AL.) et al *In* NASA. Langley Research Center, LDEF: 69 Months in Space. Third Post-Retrieval Symposium, Part 1 Feb. 1995 p 459-460 (For primary document see N95-23796 07-99)
(Grant NAG1-1218)
Avail: CASI HC A01/MF A04

N95-23837*# Technische Hochschule, Darmstadt (Germany). Dept. of Material Science.
SIMS CHEMICAL AND ISOTOPIC ANALYSIS OF IMPACT FEATURES FROM LDEF EXPERIMENTS AO187-1 AND AO187-2
Frank J. Stadermann, Sachiko Amari (Washington Univ., Saint Louis, MO.), John Foote (Washington Univ., Saint Louis, MO.), Pat Swan (Washington Univ., Saint Louis, MO.), Robert M. Walker (Washington Univ., Saint Louis, MO.), and Ernst Zinner (Washington Univ., Saint Louis, MO.) *In* NASA. Langley Research Center, LDEF: 69 Months in Space. Third Post-Retrieval Symposium, Part 1 Feb. 1995 p 461-473 (For primary document see N95-23796 07-99)
Avail: CASI HC A03/MF A04

N95-23897*# National Aeronautics and Space Administration. Langley Research Center, Hampton, VA.
SUMMARY AND REVIEW OF MATERIALS SPECIAL INVESTIGATION GROUP EVALUATIONS OF HARDWARE FROM THE LONG DURATION EXPOSURE FACILITY
Ann F. Whitaker (National Aeronautics and Space Administration. Marshall Space Flight Center, Huntsville, AL.), Joan Funk, H. Gary Pippin (Boeing Defense and Space Group, Seattle, WA.), and Harry Dursch (Boeing Defense and Space Group, Seattle, WA.) *In its* LDEF: 69 Months in Space. Third Post-Retrieval Symposium, Part 2 Feb. 1995 p 539-553 (For primary document see N95-23896 07-99)
(Contract NAS1-19247)
Avail: CASI HC A03/MF A03

N95-23898*# Boeing Defense and Space Group, Seattle, WA.
RECENT RESULTS FROM LONG DURATION EXPOSURE FACILITY MATERIALS TESTING
H. Gary Pippin and Harry W. Dursch *In* NASA. Langley Research Center, LDEF: 69 Months in Space. Third Post-Retrieval Symposium, Part 2 Feb. 1995 p 555-565 (For primary document see N95-23896 07-99)
(Contract NAS1-19247)
Avail: CASI HC A03/MF A03

26 METALLIC MATERIALS

Includes physical, chemical, and mechanical properties of metals, e.g., corrosion; and metallurgy.

N95-22531# Argonne National Lab., IL. Chemistry Div.
STRUCTURE, MELTING, AND REACTIVITY OF NICKEL CLUSTERS FROM NUMERICAL SIMULATIONS
J. Jellinek and Z. B. Guevenc 1994 24 p Presented at the North Atlantic Treaty Organization (NATO) Advanced Research Workshop on the Sxnergy Between Dynamics and Reactivity, Dryme, Scotland, 3-8 Jul. 1994
(Contract W-31-109-eng-38)
(DE95-002911; ANL/CHM/CP-84263; CONF-9407108-2) Avail: CASI HC A03/MF A01

The subject of the discussion is structural and dynamical properties of nickel clusters as derived from numerical simulations. A brief description of the potential energy functions used to represent the intracluster interactions and the interaction of a Ni13 cluster with a D2 molecule is given in Section 2, which also contains a sketch of the theoretical and computational methodologies utilized. A sample of results on structures of nickel clusters of different sizes is presented in Section 3. The evolution of the patterns and peculiarities of the intracluster dynamics with the cluster energy, which leads to structural isomerization and solid-to-liquid-like transitions, is discussed in Section 4. In Section 5 the authors present and discuss results on the Ni13 + D2 collision system. In particular, they analyze the dynamics of the reactive channel of the interaction (i.e., dissociative adsorption of the molecule on the cluster) as defined by the initial rovibrational state of D2, the system collision energy, and the structure and temperature of Ni13. The calculated data are compared with the available experimental results and a 'tuning' of the cluster-molecule interaction potential based on the interplay between theory and experiment is performed. A brief summary is given in Section 6. DOE

N95-22532# Michigan Univ., Ann Arbor, MI. Dept. of Nuclear Engineering.
THE ROLE OF GRAIN BOUNDARY CHEMISTRY AND STRUCTURE IN THE ENVIRONMENTALLY-ASSISTED INTERGRANULAR CRACKING OF NICKEL-BASE ALLOYS Progress Report, 1 Aug. 1993 - 31 Jul. 1994
G. S. Was Jul. 1994 37 p
(Contract DE-FG02-85ER-45184)
(DE95-002941; DOE/ER-45184/10) Avail: CASI HC A03/MF A01

Creep tests conducted in both primary water at controlled potentials and in inert argon show that the water environment provides an enhancement in creep rate by a factor of 5-10 over that in argon, regardless of the applied potential. Cracking is most severe in the water tests, but correlates best with the amount of creep strain, supporting a creep damage accumulation model. Creep experiments on carbon doped heats of Ni-16Cr-9Fe support earlier findings that the creep rate and the amount of intergranular (IG) cracking are strong functions of the amount of carbon in solution. Experiments on two heats containing the same amount of carbon in solution, but one of which contains grain boundary carbides, show that carbides are ineffective in preventing IG cracking if the amount of carbon in solution is low. Grain boundary misorientation studies confirm that thermal treatments which produce a larger proportion of CSL boundaries exhibit significantly lower creep rates (by 10x) and have a higher yield strength (by 25 MPa). In support of these studies, an electron backscattering pattern (EBSP) imaging system for use in an environmental scanning electron microscope (ESEM) has just recently been completed to provide determination of grain boundary misorientation on small grain (30 microns) samples. In addition, a multiple constant load test (MCLT) system has just been completed to provide for the simultaneous and independent creep testing of up to three samples in high temperature water. DOE

N95-22571# Argonne National Lab., IL. Chemistry Div.
SOLVATION OF ISOLATED TRANSITION METAL IONS
Stephen R. Wasserman and Kathleen A. Carrado 1994 6 p
(Contract W-31-109-eng-38)
(DE95-002978; ANL/CHM/PP-79757) Avail: CASI HC A02/MF A01

X-ray absorption spectroscopy is used to study the structure of transition metal ions as they encounter excess solvent and dissolve, more particularly, Cu in bentonite, with methanol solvent. The distance between the Cu ion and the oxygen atom increases by 0.03 +/- 0.01 angstrom as the Cu atom enters solution; the bond distance between the Cu ions and oxygen ligands in the slurries of the clays is the same as in aqueous solutions. DOE

N95-22576# Sandia National Labs., Albuquerque, NM.
ANALYSIS OF PHYSIOCHEMICAL PROCESSES DURING SOLDER AGING
K. L. Erickson, P. L. Hopkins, and P. T. Vianco Nov. 1994 59 p
(Contract DE-AC04-94AL-85000)
(DE95-003811; SAND-94-0691) Avail: CASI HC A04/MF A01

A model describing the diffusion-controlled growth of multiple intermetallic layers and the displacement of the interfaces between layers was developed and implemented in a one-dimensional computer code based on the method-of-lines. The model can accommodate cases involving: (1) finite initial layer thicknesses, (2) rate-limiting interfacial reactions, (3) multiple and variable diffusion coefficients, and (4) finite material boundaries. Additionally, the effects of nucleation can be modeled empirically. A transformation of the spatial coordinate circumvented the need to remesh the growing and (or) shrinking layers. Results from the one-dimensional code were verified by comparing the numerical results with analytical solutions for simple systems involving two, three, and five layers. The computer code was applied to analysis of the intermetallic layer growth that occurred in solder aging experiments that were done with 100Sn and 63Sn-37Pb solders. The analyses indicated that intermetallic layer growth was consistent with a bulk diffusion mechanism involving Cu and (or) Sn and variable diffusion coefficients that should reflect some enhanced diffusion during early layer growth. The enhanced diffusion can be accounted for empirically using a variable diffusion coefficient that is a function of layer thickness. DOE

N95-22592# Argonne National Lab., IL. Experimental Facilities Div.
THERMAL OUTGASSING STUDIES ON MACHINABLE TUNGSTEN AND TZM MOLYBDENUM ALLOY
C. Liu, R. W. Nielsen, Y. Li, D. Ryding, and T. M. Kuzay 1994 14 p Presented at the 41st Annual American Vacuum Society Symposium, Denver, CO, 24-28 Oct. 1994
(Contract W-31-109-eng-38)
(DE95-002984; ANL/XFD/CP-82916; CONF-941001-7) Avail: CASI HC A03/MF A01

Machinable tungsten and molybdenum alloys are extensively used as safety shutters and optical slits at the Advanced Photon Source (APS) front ends. These materials may present a vacuum problem because of their porosity. Also, an environmentally hazard-free cleaning procedure has to be developed for these materials. We have chosen specially heat-treated machinable tungsten with a density of 18 g/cm(exp 3) for safety shutters and TZM (a molybdenum alloy containing 0.5% titanium and approximately 0.1% zirconium) for optical slits. Thermal outgassing tests have been

performed for a machinable tungsten set with a total surface area of 4500 cm(exp 2) and a 2.8 x 4.6 x 32.6 cm(exp 3) piece of TZM. A cleaning procedure using alkaline detergent ultrasonic washes and vacuum furnace baking was used before outgassing measurements. Outgassing rates 10 hours after initial pump down at room temperature are 1.6 x 10(exp -10) Torr l s(exp -1) cm(exp -2) for machinable tungsten and 6.0 x 10(exp -10) Torr l s(exp -1) cm(exp -2) for TZM. The outgassing rates 24 hours after an in situ bake at 160 C for two days decreased to 2.2 x 10(exp -12) Torr l s(exp -1) cm(exp -2) for machinable tungsten and 2.2 x 10(exp -11) Torr l s(exp -1) cm(exp -2) for TZM. Optical studies confirmed that the TZM sample is more porous than the machinable tungsten sample. Further studies of a denser TZM sample show that the outgassing rate decreases as the porosity decreases. The outgassing rate 24 hours after a 48-h bake at 160 C reached 7.4 x 10(exp -12) Torr l s(exp -1) cm(exp -2) for the denser TZM sample. DOE

N95-22594# Argonne National Lab., IL. Materials Science Div.
X-RAY DIFFRACTION CHARACTERIZATION OF DEFECT BEHAVIOR IN NANOCRYSTALLINE NICKEL DURING ANNEALING
J. A. Eastman, M. A. Beno, G. S. Knapp, and L. J. Thompson Sep. 1994 5 p Presented at the 2nd International Conference on Nanostructured Materials, Stuttgart, Germany, 3-7 Oct. 1994
(Contract W-31-109-eng-38)
(DE95-002992; ANL/MSD/CP-82603; CONF-941039-1) Avail: CASI HC A01/MF A01

Nanocrystalline nickel samples were annealed while collecting high angle x-ray diffraction data in order to correlate changes in strain and defect content with changes in grain size. The microstrain broadening magnitude decreased rapidly prior to any grain growth, while the Debye-Waller parameter was not reduced significantly prior to the onset of grain growth. DOE

N95-22608# International Centre for Theoretical Physics, Trieste (Italy).
ELECTRICAL RESISTIVITY OF LIQUID ALKALI METALS AND NON-LOCAL PSEUDOPOTENTIAL
Iijaz Shah and M. Anis Alam Sep. 1993 6 p
(DE94-627417; IC-93/294) Avail: CASI HC A02/MF A01 (US Sales Only)

Norm conserving, nonlocal, fully screened and transferable pseudopotentials developed by Bachelet, Hamann, and Schulter have been used to calculated the electrical resistivities of alkali metals. The results agree well with those obtained through experiments. DOE

N95-22609# Instituto de Engenharia Nuclear, Rio de Janeiro (Brazil).
STUDY OF RADIATION DAMAGES IN AISI 316 AND 347 STEELS Ph.D. Thesis [ESTUDO DE DANOS POR IRRADICAO EM ACOS AISI 316 E 347]
Goncalo Rodrigues dosSantos Mar. 1993 223 p In PORTUGESE
(DE94-627480; INIS-BR-3343) Avail: CASI HC A10/MF A03 (US Sales Only)

The CV-28 cyclotron at IEN (Nuclear Engineering Institute) has been used to simulate, in a short time scale, uniform He concentrations produced during neutron irradiation of metals by (n, alpha) reactions. Helium was implanted at concentrations of 1 to 300 ppm in 100 micron thick sheet samples of AISI 316 and 347 SS by degrading a 28 MeV alpha particle beam with a rotating energy degrader. The effects of He on the mechanical properties of the steels were studied by both nondestructive (positron annihilation) and destructive tests (tensile, creep, TEM, and SEM). The positron lifetime measurements of irradiated and annealed samples were used as the base to discuss the He diffusion mechanism. Activation energies of 0.34 +/- 0.04 eV for 316 SS and 0.57 +/- 0.06 eV for 347 SS characterized a dissociative process above 650 C. TEM analyses have suggested the Ostwald ripening process for bubble growth over the full range of He concentrations studied. It was shown, in agreement with theoretical calculations, that by themselves the displacements produced during the helium implantation, at rate of 1.8 x 10(exp -3) d pa/ppm, were not sufficient to cause significant changes in ductility. However, a strong ductility loss with increasing He concentration was observed for both types of steel for tensile tests at 25 C, as well as in creep at 750 C over the range of strain (100 to 200 MPa). Finally, it was shown that charged particle simulation associated with positron annihilation techniques provides a fast, relatively low cost, and useful method to study different kinds of neutron damage in materials. DOE

N95-22686# Oak Ridge National Lab., TN.
INVESTIGATION OF DEPTH-AREA RELATIONSHIPS ASSOCIATED WITH NANOINDENTATIONS
L. Riester and M. K. Ferber 1994 12 p Presented at the Conference on Plastic Deformation of Ceramics, Snowbird, UT, 7-12 Aug. 1994
(Contract DE-AC05-84OR-21400)
(DE95-001353; CONF-940865-3) Avail: CASI HC A03/MF A01

Determination of hardness from indentation testing requires the measurement of the contact area. For indents generated at very low loads (less than 20 mN) or shallow depths (less than 250 nm), optical methods do not have sufficient resolution. One approach utilized in current state-of-the-art mechanical properties microprobes (MPM) involves the measurement of indenter depth. Calculation of the plastic area then requires a relation between depth and contact area. This relation is generally derived either by assuming the indenter is perfectly sharp ('Ideal Indenter' assumption) or by calibrating the shape using materials having known hardness and elastic modulus values. The validity of both approaches was examined by using a Scanning Force Microprobe (SFM) to measure the actual dimensions of the residual impressions made by the MPM. The SFM data revealed that the 'Ideal Indenter' assumption underestimates the actual plastic area. This result accounts for the fact that hardness values measured with the MPM are typically higher than those obtained with conventional hardness testers. DOE

N95-22724# Sandia National Labs., Livermore, CA.
TEMPERATURE EFFECTS ON HYDROGEN-INDUCED CRACKING IN AN IRON-BASED SUPERALLOY
N. R. Moody, S. L. Robinson, J. E. Angelo, and M. W. Perra 1994 10 p Presented at the 5th International Conference on Hydrogen Effects on Material Behavior, Moran, WY, 11-15 Sep. 1994
(Contract DE-AC04-94AL-85000)
(DE95-003037; SAND-95-8435C; CONF-940945-3) Avail: CASI HC A02/MF A01

Effects of temperature on hydrogen-induced crack growth susceptibility were studied in the iron-based superalloy using hydrogen charged samples. The measured crack growth rates increased by more than two orders of magnitude as temperature increased from 253 to 298 K. Crack grow rates then decreased at higher temperature. Fracture in all samples was initiated by fracture of matrix carbides followed by microvoid formation at slip band intersections and failure of interconnecting slip band segments. Most interestingly, the fracture surfaces appeared identical for any given applied stress intensity suggesting that fracture occurs at a critical hydrogen concentration. A transient model for impurity atom interaction with a blocked edge dislocation array was then applied to the data and showed reasonably good agreement between predicted and measured crack growth rates. This agreement supports the concept that fracture occurs when hydrogen reaches a critical concentration at the slip band intersections and the observation that rates are controlled by the diffusivity of hydrogen through the lattice. Moreover, the results show that microvoid formation at slip band intersections is the dominant event in the fracture process. DOE

N95-22732# Westinghouse Hanford Co., Richland, WA.
AN INVESTIGATION INTO THE EFFECTS OF HYDROGEN ON THE FRACTURE AND DEFORMATION OF ALLOY X-750 Ph.D. Thesis
D. M. Symons 1994 158 p
(Contract DE-AC11-93PN-38195)
(DE95-003206; WAPD-T-3003) Avail: CASI HC A08/MF A02

This study investigated the effect of hydrogen on the fracture of a nickel-base superalloy, Alloy X-750 in the solution treated and aged (HTH) condition. The effect of hydrogen was examined through tensile testing and fracture toughness testing incorporating observations from scanning electron microscopy and light microscopy. The elongation for tensile specimens tested at 3.33 x 10(exp -4) s(exp -1) was reduced from 21% for noncharged specimens to 7.3% for 5.7 ppm hydrogen and was further reduced to 3.5% for 65 ppm hydrogen. The fracture surface for all specimens was intergranular ductile dimples with minimal transgranular dimple fracture. The elongation further decreased as the strain rate was decreased for the hydrogen-charged specimens while for the noncharged specimens no strain rate effect was observed. Prestraining prior to charging dramatically decreased elongation after hydrogen charging, though in all cases the flow stress was achieved prior to failure. The intergranular failure mechanism in Alloy X-750 was a microvoid initiation process at grain boundary carbides

followed by void growth and coalescence. The effect of hydrogen was also investigated through fracture toughness testing. A model based on a strain modified critical stress criterion was shown to correlate the fracture behavior as a function of hydrogen well. The embrittlement phenomenon may be explained by a reduction of the interfacial strength of the carbide-matrix interface due to hydrogen with possible secondary effects of HELP (hydrogen enhanced local plasticity) and a local hydrogen pressure at the carbide-matrix interface reducing the void initiation strain. DOE

N95-22835# Sandia National Labs., Albuquerque, NM.
PULSED ION BEAM SURFACE TREATMENT FOR PREPARING RAPIDLY SOLIDIFIED CORROSION RESISTANT ALLOY SURFACES
R. G. Buchheit, L. M. Maestas, D. C. McIntyre, R. W. Stinnett, and J. B. Greenly (Cornell Univ., Ithaca, NY.) 1994 5 p Presented at the 186th Meeting of the Electrochemical Society, Miami, FL, 9-14 Oct. 1994
(Contract DE-AC04-94AL-85000)
(DE94-012072; SAND-94-1328C; CONF-941063-1) Avail: CASI HC A01/MF A01

IBEST (Ion BEam Surface Treatment) uses a series of 60 to 100 ns ion beam pulses to deposit energy in the topmost 2 to 20 micrometers of a metal surface to melt it. Areas as large as 1000 sq cm can be treated by a single pulse. Treated regions that experienced melt were smoother after ion beam treatment. DOE

N95-22840 International Centre for Theoretical Physics, Trieste (Italy).
NON LOCAL PSEUDOPOTENTIALS, TRANSPORT PROPERTIES OF LIQUID NOBLE METALS
Ijaz Shah and M. Anis AnisAlam Sep. 1993 6 p Sponsored by NSRDB Limited Reproducibility: More than 20% of this document may be affected by microfiche quality
(DE94-627416; IC-93/293) Avail: CASI HC A02 (US Sales Only)

Norm conserving, non local, fully screened and transferable pseudopotentials developed by Bachelet, Hamann and Schulter have been used to calculate the electrical resistivities of liquid noble metals. The results agree well with those obtained through experiments. DOE

N95-22893# Bettis Atomic Power Lab., West Mifflin, PA.
THE HYDROGEN EMBRITTLEMENT OF ALLOY X-750
Douglas M. Symons and Anthony W. Thompson (California Univ., Berkeley. Lawrence Berkeley Lab, CA.) 1994 11 p
(Contract DE-AC11-93PN-38195)
(DE95-003207; WAPD-T-3053) Avail: CASI HC A03/MF A01

This study investigated the mechanism of hydrogen embrittlement in Alloy X-750 through tensile testing and fracture toughness testing. The failure mode in this material was ductile intergranular fracture through microvoid coalescence. This microvoid initiation sites appear to be the grain boundary chromium carbides based upon the size and the spacing of the microvoids as well as upon plateau etching. The elongation decreased from 21% with no hydrogen to 3.5% with 65 ppm hydrogen at 25 C while no degradation was observed at -196 C. This suggests that the HELP mechanism plays a role in the fracture process. It was shown that prestraining, cold work, prior to charging decreased elongation. Specimens plastically strained to 5% and 10% plastic strain prior to hydrogen charging and strained to failure after the charging at a rate of 3.33 x 10(exp 4)s(exp -1), failed near the flow stress. This is consistent with the need for local plasticity at the grain boundaries not observable in the bulk. The results of this study are consistent with the mechanism of hydrogen embrittlement as a combination of the reduction in particle interfacial energy and the HELP mechanism, though, a hydrogen pressurization mechanism or a local increase in the void growth rate can not be discounted. DOE

N95-22934# International Centre for Theoretical Physics, Trieste (Italy).
KKR-CPA CALCULATIONS OF DENSITY OF STATES AND SOFT X RAY EMISSION FROM DISORDERED LI-MG ALLOYS
S. S. Rajput, R. M. Singru, and R. Prasad Jan. 1994 11 p
(DE94-628882; IC-94/25) Avail: CASI HC A03/MF A01 (US Sales Only)

The density of states (DOS) and soft X ray spectra from disordered Li(1-x)Mg(x) alloys have been calculated by using the charge self-consistent KKR-CPA method. We find that the DOS at the Fermi energy (E(sub F)) shows an interesting behaviour as a function of x; it first increases in the range x=0.0 to 0.14, then shows a flat behaviour in the range x approx. 0.14 to 0.20 and finally decreases smoothly from x = 0.20 to 0.60. We show that this behaviour of the DOS is related to the development of a neck in the Fermi surface and its smearing due to disorder scattering. Theoretical results for the soft X ray emission spectra are compared with experimental results and are found to be in good accord. DOE

N95-23057# International Centre for Theoretical Physics, Trieste (Italy).
A MODEL FOR THE METAL-NONMETAL TRANSITION IN METAL-MOLTEN SALT SOLUTIONS
D. Yurdabak, Z. Akdeniz, and M. P. Tosi (Scuola Normale Superiore, Pisa, Italy.) Mar. 1994 6 p
(DE94-628490; IC-94/50) Avail: CASI HC A02/MF A01 (US Sales Only)

We outline a theory for the metal - nonmetal transition occurring in solutions of alkali metals in molten alkali halides as governed by a balance between the binding of ionic clusters by localized electrons and the excess free energy of an ionic assembly screened by metallic electrons. In the model the transition is driven by the composition dependence of the screening length. The theory is amenable to an analytic solution within the mean spherical approximation when Thomas-Fermi screening is used and the ions are described by charged hard spheres. DOE

N95-23121# Oak Ridge National Lab., TN.
CALCULATIONS OF ALLOY PHASES WITH A DIRECT MONTE-CARLO METHOD
J. S. Faulkner (Florida Atlantic Univ., Boca Raton, FL.), Yang Wang (Florida Atlantic Univ., Boca Raton, FL.), E. A. Horvath (Florida Atlantic Univ., Boca Raton, FL.), and G. M. Stocks 1994 9 p Presented at the 16th Materials Research Society (MRS) Fall Meeting, Boston, MA, 30 Nov. - 5 Dec. 1992
(Contracts DE-AC05-84OR-21400; DE-FG05-89ER-45392)
(DE94-018963; CONF-921101-144) Avail: CASI HC A02/MF A01

A method for calculating the boundaries that describe solid-solid phase transformations in the phase diagrams of alloys is described. The method is first-principles in the sense that the only input is the atomic numbers of the constituents. It proceeds from the observation that the crux of the Monte-Carlo method for obtaining the equilibrium distribution of atoms in an alloy is a calculation of the energy required to replace an A atom on site i with a B atom when the configuration of the atoms on the neighboring sites, kappa, is specified, delta H(sub kappa)(A yields B) = E(sub B)(kappa) - E(sub A)(kappa). Normally, this energy difference is obtained by introducing interatomic potentials, v(sub ij), into an Ising Hamiltonian, but the authors calculate it using the embedded cluster method (ECM). In the ECM an A or B atom is placed at the center of a cluster of atoms with the specified configuration K, and the atoms on all the other sites in the alloy are simulated by the effective scattering matrix obtained from the coherent potential approximation. The interchange energy is calculated directly from the electronic structure of the cluster. The table of delta H(sub kappa)(A yields B)'s for all configurations K and several alloy concentrations is used in a Monte Carlo calculation that predicts the phase of the alloy at any temperature and concentration. The detailed shape of the miscibility gaps in the palladium-rhodium and copper-nickel alloy systems are shown. DOE

N95-23132# Oak Ridge National Lab., TN.
LONG-TERM AGING OF TYPE 308 STAINLESS STEEL WELDS: EFFECTS ON PROPERTIES AND MICROSTRUCTURE
D. J. Alexander, J. M. Vitek, and S. A. David 1994 6 p Presented at the 3rd International Conference on Trends in Welding Research, Gatlinburg, TN, 1-5 Jun. 1992
(Contract DE-AC05-84OR-21400)
(DE94-018961; CONF-9206173-12) Avail: CASI HC A02/MF A01

Multipass gas tungsten arc welds with type 308 stainless steel filler metal in type 304L base plate have been aged at 400, 475, or 550 C for times up to 5,000 h. The changes in mechanical properties as a result of these agings have been followed with tensile, impact, and fracture toughness testing, using subsize tensile, half-size Charpy, and 0.45T compact specimens, respectively. The changes in the microstructure were evaluated with optical and transmission electron microscopy. Relatively little change was observed in the tensile properties for any of the aging treatments, but significant embrittlement was observed in the impact and fracture toughness testing. The transition temperatures increased rapidly for aging at 475 or

550 C, and more slowly for aging at 400 C. The upper-shelf energies and the fracture toughness showed similar responses, with only a small decrease for 400 C aging, but much greater and rapid decreases with aging at 475 or 550 C. Aging at 400 or 475 C resulted in the spinodal decomposition of the ferrite phase in the weld metal into iron-rich alpha and chromium-enriched alpha prime. In addition, at 475 C G-phase precipitates formed homogeneously in the ferrite and also at dislocations. At 550 C carbides formed and grew at the ferrite-austenite interfaces, and some ferrite transformed to sigma phase. These changes must all be considered in determining the effect of aging on the fracture properties. DOE

N95-23186*# National Aeronautics and Space Administration. Marshall Space Flight Center, Huntsville, AL.

THE CORROSION PROTECTION OF 2219-T87 ALUMINUM BY ORGANIC AND INORGANIC ZINC-RICH PRIMERS

M. D. Danford, M. J. Mendrek, and D. W. Walsh (California Polytechnic State Univ., San Luis Obispo, CA.) Washington Feb. 1995 18 p

(NASA-TP-3543; M-771; NAS 1.60:3543) Avail: CASI HC A03/MF A01

The behavior of zinc-rich primer-coated 2219-T87 aluminum in a 3.5-percent Na-Cl was investigated using electrochemical techniques. The alternating current (ac) method of electro-chemical impedance spectroscopy (EIS), in the frequency range of 0.001 to 40,000 Hz, and the direct current (dc) method of polarization resistance (PR) were used to evaluate the characteristics of an organic, epoxy zinc-rich primer and an inorganic, ethyl silicate zinc-rich primer. A dc electrochemical galvanic corrosion test was also used to determine the corrosion current of each zinc-rich primer anode coupled to a 2219-T87 aluminum cathode. Duration of the EIS/PR and galvanic testing was 21 days and 24 h, respectively. the galvanic test results demonstrated a very high galvanic current between the aluminum cathode and both zinc-rich primer anodes (37.9 micro A/cm(exp 2) and 23.7 micro A/cm(exp 2) for the organic and inorganic primers, respectively). The PR results demonstrated a much higher corrosion rate of the zinc in the inorganic primer than in the organic primer, due primarily to the higher porosity in the former. Based on this investigation, the inorganic zinc-rich primer appears to provide superior galvanic protection and is recommended for additional study for application in the solid rocket booster aft skirt. Author

N95-23215*# Eloret Corp., Palo Alto, CA.

COMPUTATIONAL STUDIES OF METAL-METAL AND METAL-LIGAND INTERACTIONS Report, 1 Oct. 1991 - 30 Jun. 1994

Leslie A. Barnes 22 Jul. 1994 10 p

(Contract NCC2-741)

(NASA-CR-197862; NAS 1.26:197862) Avail: CASI HC A02/MF A01

Accurate calculations on the bond length, dipole moment, and harmonic frequency of CO are presented, using large basis sets and high levels of electron correlation. The geometric structure, force constants and binding energies of Cr(CO)6 and Cr(CO)5 are computed using large basis sets and high levels of electron correlation. The molecule O4(+) is studied, using large basis sets and high levels of electron correlation, including the CASSCF, CASSI,and CASPT2 methods. Binding energies, geometries and frequencies are computed. Symmetry breaking is a particular problem for the antisymmetric stretch, which is addressed using the CASSI method. The symmetry breaking problem in O4(+) has also been studied using the Brueckner coupled-cluster method. This gives results in good agreement with CASSI. A multi-region numerical integration scheme is investigated for use in Density Functional Calculations. This scheme is found to give comparable results to a widely used scheme based on the Euler-Maclaurin technique. Author

N95-23496# Advisory Group for Aerospace Research and Development, Neuilly-Sur-Seine (France). Structures and Materials Panel.

CORROSION DETECTION AND MANAGEMENT OF ADVANCED AIRFRAME MATERIALS [LA DETECTION DE LA CORROSION ET LA GESTON DES MATERIAUX AVANCES ENTRANT DANS LA CONSTRUCTION DES CELLULES]

Jan. 1995 240 p In ENGLISH and FRENCH Presented at the 79th Meeting of the AGARD Structures and Materials Panel, Seville, Spain, 5-6 Oct. 1994 Original contains color illustrations

(AGARD-CP-565; ISBN-92-836-1011-3) Copyright Avail: CASI HC A11/MF A03

A Specialists' Meeting on Corrosion Detection and Management of Advanced Airframe Materials was held to present the current knowledge base of corrosion, degradation, detection and prevention and to identify the research and development issues which must be addressed in order to ensure long service life and low maintenance costs of NATO aircraft. The Meeting concentrated on corrosion detection, test methodology for environmental assessment, mechanistic evaluation, corrosion prevention methods, and materials selection and design to prevent environmental degradation. For individual titles, see N95-23497 through N95-23519.

N95-23497# Defence Research Agency, Farnborough, Hampshire (England). Structural Materials Centre.

THE CORROSION AND PROTECTION OF ADVANCED ALUMINIUM - LITHIUM AIRFRAME ALLOYS

C. J. E. Smith, D. L. Bartlett, and J. A. Gray *In* AGARD, Corrosion Detection and Management of Advanced Airframe Materials Jan. 1995 9 p (For primary document see N95-23496 07-26)

Copyright Avail: CASI HC A02/MF A03

The corrosion and stress corrosion cracking behavior of 8090-T81 and 2091-T84 sheet and 8090-T8171 plate aluminum-lithium alloys tested under laboratory and marine exposure conditions are compared with aerospace aluminium alloys currently in service. Initial results are also presented on the corrosion performance of a metal matrix composite aluminium alloy. The corrosion protection of aluminium-lithium alloys is discussed and progress on the development of chromate-free systems and their application to advanced aluminium alloys is described. Author

N95-23498# Deutsche Forschungs- und Versuchsanstalt fuer Luft- und Raumfahrt, Cologne (Germany).

EXFOLIATION CORROSION AND STRESS CORROSION CRACKING BEHAVIOUR OF Al-Li ALLOYS

Reinhold Braun *In* AGARD, Corrosion Detection and Management of Advanced Airframe Materials Jan. 1995 12 p (For primary document see N95-23496 07-26)

Copyright Avail: CASI HC A03/MF A03

The exfoliation corrosion and stress corrosion cracking (SCC) behavior of damage tolerant sheet and plate materials of aluminum-lithium based alloys in underaged tempers was studied performing different accelerated tests. The EXCO test (ASTM G34) produced blistering and mild exfoliation corrosion. The modified EXCO test suggested by Lee and Lifka proved to be more severe than the standard EXCO test. When exposed to the cyclic acidified salt fog (MASTMAASIS test according to ASTM G85, Annex A2), the Al-Li alloys studied suffered severe exfoliation. The MASTMAASIS test reproduced marine exposure results for conventional 2024-T351 and 7075-T7351 plates and the limited data for aluminium-lithium based 8090-T81 and 2091-T84 sheets published in the literature. Therefore, it seems to be a promising testing technique to predict the service performance of high strength aluminum alloys. Static loading tests indicated very high SCC resistance for 8090-T8171 and 2091-T8X51 plates in longitudinal and long transverse directions. Environmentally assisted cracking occurred in the latter alloys when stress was applied in the short transverse direction. Threshold stresses below 100 MPa were obtained from alternate immersion tests (ASTM G44) and from permanent immersion tests in an aqueous solution of 0.5 M NaCl plus 0.1 M LiCl plus 0.05 M NaHCO3 plus 0.05 M Na2CO3. Using the latter synthetic environment, the slow strain rate testing technique indicated sensitivity to stress corrosion cracking for recrystallized 8090-T81 and 2091-T84 sheet materials. Author

N95-23499# Middle East Technical Univ., Ankara (Turkey).

EFFECT OF LOADING DIRECTION AND LONG-TERM AGING ON FATIGUE-CRACK GROWTH IN Al-Li ALLOY 2090

M. Anik and M. Doruk *In* AGARD, Corrosion Detection and Management of Advanced Airframe Materials Jan. 1995 9 p (For primary document see N95-23496 07-26)

Copyright Avail: CASI HC A02/MF A03

The effect of prolonged exposures up to 1000 Hr at 150, 165 and 180 C on the fatigue-crack were studied in the Al-Li alloy 2090 using the direct current potential drop technique, and results compared with crack growth rates determined in salt water. The CCT specimens, 40 x 200 mm in size, were taken from the sheet material with a thickness of 1.6 mm. Since one of the purposes of this work was to investigate the directionality of fatigue-crack growth behavior, the specimens were machined in the grainflow direction (L-T), long-transverse direction (T-L) and 45 deg to

rolling direction (L + 45 deg). The pretreatment applied before the aging consisted of solutionizing at 550 C for one hour followed by 6 percent stretching. According to the air results, the fatigue-crack behavior did not vary significantly with specimen orientations tested in this study. On the other hand, the long-term aging was found to have a pronounced effect on the crack growth kinetics, demonstrated by growth rates which increased up to about 8 fold following aging for 1000 Hr. The rate of the salt-water induced fatigue-crack growth was higher at low values, but lower at high values of Delta K, relative to those obtained in air. Whereas the reduction in roughness induced crack closure effect is believed to be responsible for enhancement at low stress intensity ranges the retardation at high Delta K-values may be attributed to crack-tip electrochemistry, whereby intermetallics with high cathodic efficiency are thought to play a role.

Author

N95-23500# Naval Air Warfare Center, Warminster, PA. Aircraft Div.

CORROSION OF LANDING GEAR STEELS

E. U. Lee, J. Kozol, J. B. Boodey, and J. Waldman *In* AGARD, Corrosion Detection and Management of Advanced Airframe Materials Jan. 1995 12 p (For primary document see N95-23496 07-26)

Copyright Avail: CASI HC A03/MF A03

A study was conducted on the corrosion behavior of landing gear steels, AerMet 100, 300M, AF1410, HYTUF and 4340. This study included investigations of stress corrosion cracking and immersion corrosion in an aqueous 3.5 percent NaCl solution, salt spray corrosion in a fog chamber of atomized aqueous 5 percent NaCl solution, humidity corrosion in an atmosphere of vapor from distilled water and hydrogen embrittlement. AF1410 steel is most resistant to stress corrosion cracking, and it is followed by AerMet 100, 0.20C AF1410, HYTUF, 300M and 4340 steels. The immersion corrosion and salt spray corrosion rates of an AerMet 100 steel are 33-40 percent and 13-20 percent those of a 300M steel. In a humidity chamber, AerMet 100 steel is not corrodible in 110 days, whereas 300M steel is quite susceptible to humidity corrosion. Compared to 300M steel, AerMet 100 steel is less susceptible to hydrogen embrittlement.

Author

N95-23501# KOMPOZIT Corp., Kaliningrad (Russia).

SPECIFIC FEATURES OF CORROSION BEHAVIOR OF STAINLESS MARAGING STEELS FOR AEROSPACE APPLICATION

V. B. Spiridonov and V. V. Sharapov *In* AGARD, Corrosion Detection and Management of Advanced Airframe Materials Jan. 1995 4 p (For primary document see N95-23496 07-26)

Copyright Avail: CASI HC A01/MF A03

Specific features of the embrittlement of stainless Cr-Ni maraging steels by environmental or N2O4 media are considered by the example of steel 03Kh11N10M2Tu-VD. Results of corrosion tests and fractographic and microanalytical investigations are presented. The method of accelerated testing of these steels for stress corrosion cracking is described. Author

N95-23502# Virginia Univ., Charlottesville, VA. Center for Electrochemical Science and Engineering.

THE DETECTION AND ANALYSIS OF GALVANIC DAMAGE IN BMI/GRAPHITE FIBER COMPOSITES **c24**

S. R. Taylor and G. L. Cahen, Jr. *In* AGARD, Corrosion Detection and Management of Advanced Airframe Materials Jan. 1995 12 p Sponsored by Virginia Center for Innovative Technology and Naval Air Warfare Center (For primary document see N95-23496 07-26)

Copyright Avail: CASI HC A03/MF A03

The use of graphite fiber polymer matrix composites (GFPMC) in multi-material assemblies which must maintain mechanical integrity in aqueous environments has focused attention on the galvanic degradation of these materials. Of recent concern to the aerospace industry is the galvanic degradation of bismaleimide (BMI)-graphite fiber (GF) composites when galvanically coupled to an active metal (e.g. aluminum). A detailed understanding of the damage process, both in terms of mechanism and extent, has not been possible because of the lack of sensitive method to detect, quantify, and characterize damage in this material system. This study has used electro-chemical impedance spectroscopy (EIS) to monitor material interfacial changes in an 8-ply, 0 deg, unidirectional BMI-GF composite subjected to cathodic and anodic polarization in NaCl solutions, exposure to caustic solutions, and galvanic coupling to a series of metals (Al, Fe, Cu, Ti) in NaCl solutions. Cathodic polarization was found to produce porous electrode behavior which was attributed to breakdown of the fiber/matrix interface and subsequent moisture ingress. This is in contrast to caustic exposure which did not show a porous electrode response, presumably due to general BMI solvation. These electrochemical results in combination with mechanical shear tests performed in an array of chemical and electrochemical conditions indicate that long-lived reaction intermediates, e.g. peroxide and superoxide radicals, generated during the oxygen reduction reaction on graphite, not hydroxyl ions, are the key damaging species. This will have important implications to the development of more damage resistant polymer chemistries. The sensitivity of EIS has also indicated that couples to titanium, proposed to be a benign couple, caused changes in the impedance spectra similar to those for low cathodic overpotentials. The long term implications of these latter changes on composite durability are not known at this time, but warrant further evaluation. Author

N95-23503# Institute for Aerospace Research, Ottawa (Ontario). Structures, Materials and Propulsion Lab.

DOUBLE PASS RETROREFLECTION FOR CORROSION DETECTION IN AIRCRAFT STRUCTURES **c74**

J. P. Komorowski, S. Krishnakumar, R. W. Gould, N. C. Bellinger, F. Karpala (Diffracto Ltd., Windsor, Ontario.), and O. L. Hageniers (Diffracto Ltd., Windsor, Ontario.) *In* AGARD, Corrosion Detection and Management of Advanced Airframe Materials Jan. 1995 12 p (For primary document see N95-23496 07-26)

Copyright Avail: CASI HC A03/MF A03

An optical double pass retroreflection surface inspection technique (D Sight) used for visualizing surface distortions, depressions or pertrusions has been adapted as a rapid, enhanced visual inspection method inspection of large external aircraft surfaces. A project to fully characterize the D Sight indications of corrosion damage in lap splices is currently active. Over 150 large transport aircraft fuselage lap splice specimens have been collected. D Sight Aircraft Inspection System - (DAIS) 250C has been developed and tested both in the laboratory and in the field. In laboratory tests lap splices retrieved from retired aircraft and subjected to accelerated corrosion and lap splices naturally corroded in-service were inspected with DAIS, eddy current, X-ray, shadow moire and subjected to tear down. It has been shown that the DAIS 250C is capable of locating corrosion pillowing indicative of a thickness loss as low as 2 percent. The first field trial of the DAIS 250C was based on two service bulletins requiring inspection of longitudinal and circumferential lap splices on the 737-200 aircraft from BS 259.5 to BS 1016. The DAIS 250C inspection, including analysis and report, took 36 man-hours. The recommended technique in the SB was close visual inspection and the time required according to the service bulletins, was 278 man-hours. Author

N95-23504# Defence Research Establishment Pacific, Victoria (British Columbia).

THE USE OF ELECTROCHEMICAL IMPEDANCE SPECTROSCOPY TO PREDICT THE CORROSION OF ALUMINUM-LITHIUM ALLOYS IN MARINE ENVIRONMENTS **c25**

D. R. Lenard, J. G. Moores, P. R. Roberge (Royal Military Coll. of Canada, Kingston, Ontario.), and E. Halliop (Royal Military Coll. of Canada, Kingston, Ontario.) *In* AGARD, Corrosion Detection and Management of Advanced Airframe Materials Jan. 1995 12 p (For primary document see N95-23496 07-26)

Copyright Avail: CASI HC A03/MF A03

In order to acquire some experience with the behavior of aluminum-lithium alloys in the marine environment, the Defense Research Establishment Pacific compared panels made from Aluminum Alloy (AA) 2090 and 8090 sheet with the conventional alloys AA 7075 and 2024, respectively, in several tests involving long term exposure to sea water fog and full or partial immersion in sea water. The results of these were then compared with the results of a new technique, developed by the Royal Military College of Canada for the analysis of electrochemical impedance measurements, that was performed on these alloys in simulated sea water. The long term exposure tests indicated that corrosion problems could occur with aluminum-lithium alloys in the marine environment. The 8090 alloy was found to suffer from severe localized attack, including intergranular cracking, along edges that were immersed in sea water. The 2090 alloy, however, appeared to offer some advantages over its 7075-T6 counterpart, as it was more resistant to corrosion at its edges, even though it suffered as much or more corrosion on the rolled surfaces. On some 2090 panels,

the corrosion resistance of the edges was found to be enhanced by cold work associated with shearing. Polarization resistance measurements were generally consistent with the results of the long term exposure tests, although they predicted corrosion rates for the rolled surfaces of the 8090 and 7075 alloys that were apparently too high. The angle of depression of the Nyquist plots appeared to correlate with the number of corrosion sites within a given area and was in good agreement with visual observations of the long term exposure panels. Author

N95-23505# Defence Research Agency, Farnborough, Hampshire (England). Structural Materials Centre.

NON-DESTRUCTIVE DETECTION OF CORROSION FOR LIFE MANAGEMENT **c38**

David A. Bruce *In* AGARD, Corrosion Detection and Management of Advanced Airframe Materials Jan. 1995 8 p (For primary document see N95-23496 07-26)

Copyright Avail: CASI HC A02/MF A03

In recent years, aircraft operators have been driven to increased use of Non-Destructive Evaluation (NDE) to ensure airworthiness during life extensions for ageing aircraft or as an integral part of a damage tolerant lifting philosophy. Major airframe static and fatigue tests are routinely used to highlight problem areas on airframes where design limitations or changes of usage may lead to early failures. The results of such tests become progressively less reliable as the age of the airframe increases and the operating conditions diverge from those under which the tests were conducted. Increased inspection, whether by visual or other means is usually the only alternative to wholesale refurbishment or replacement of aircraft or components. Almost all of the development to date of NDE techniques for corrosion detection and characterization has been concentrated on existing airframe materials, principally Aluminum alloys and steels. The current capabilities of corrosion detection techniques will be reviewed and current research aimed at areas where there is a requirement for improved detection capability will be described. New materials, such as Polymer Matrix Composites, will experience different types of 'corrosive' deterioration. The capability of NDE methods to detect material degradation in new composite materials will be discussed. Finally, reliance on NDE, choice of NDE technique and optimal scheduling of inspections all require an assessment of the reliability of NDE methods. It will be shown that a range of NDE techniques with differing capabilities and characteristics will be required to ensure compatibility with maintenance schedules if full use is to be made of NDE for life management of structures which may be subject to corrosion. Author

N95-23506# AVRO International Aerospace, Woodford (England). Engineering Test Facilities.

HEALTH AND USAGE MONITORING SYSTEMS: CORROSION SURVEILLANCE **c01**

J. D. Smart and D. C. Weetman (Real Time Corrosion Management Ltd., Grandby Row, England.) *In* AGARD, Corrosion Detection and Management of Advanced Airframe Materials Jan. 1995 11 p (For primary document see N95-23496 07-26)

Copyright Avail: CASI HC A03/MF A03

A predictive method of determining the inspection requirements for specific areas of individual aircraft could offer major advantages in terms of safety and maintenance and repair costs. An approach such as Health and Usage Monitoring in Service, in which the condition of components is monitored whilst in operation, would allow inspection requirements to be minimized and maintenance to be carried out as it becomes necessary. To use such an approach on aircraft would require very sensitive monitoring techniques. Modern electrochemical corrosion instrumentation could offer the required levels of sensitivity for detecting and characterizing the corrosion processes which precede the development of observable damage. This paper details a program carried out to assess the suitability of such electrochemical monitoring instrumentation for aerospace applications and to assess the feasibility of producing an aircraft system on which a predictive corrosion monitoring system could be based. Author

N95-23507# National Aerospace Lab., Amsterdam (Netherlands).

EDDY CURRENT DETECTION OF PITTING CORROSION AROUND FASTENER HOLES **c38**

J. H. Heida and W. G. J. tHart *In* AGARD, Corrosion Detection and Management of Advanced Airframe Materials Jan. 1995 10 p Sponsored by Royal Netherlands Air Force (For primary document see N95-23496 07-26)

Copyright Avail: CASI HC A02/MF A03

An evaluation of the eddy current technique for the detection and depth assessment of corrosion around fastener holes in F-16 lower wing skins is described. The corrosion type in this structure is pitting corrosion at the countersink edge of the fastener holes. Due to a corrosion clean-up limit of only 1.5 - 2.5 percent, a maximum thickness reduction in the range of 0.08 - 0.32 mm is allowed (depending on local skin thickness). This specifies the needed sensitivity for in-service corrosion inspection. In the evaluation use was made of specimens cut out of the F-16 lower wing skin structure. In total twelve specimens were exposed to an accelerated corrosion test (EXCO-test). Eddy current inspection of the specimens with installed fasteners was performed with a standard eddy scope and four different eddy current probes. After the eddy current inspection cross-sections of the twelve-specimens were made to determine the extent of pitting corrosion at the countersink edges. After evaluation of the inspection results the following conclusions can be drawn: for in-service detection of countersink edge corrosion standard visual inspection is the preferred technique regarding the simplicity, sensitivity and reliability of inspection; and for the purpose of depth assessment the eddy current technique is capable of detecting countersink edge corrosion with a depth from about 0.1 mm. Due to the corrosion clean-up limit of only 1.5 - 2.5 percent (0.08 - 0.32 mm), however, the eddy current technique is considered not applicable for in-service depth assessment of countersink edge corrosion in F-16 lower wing skins. Author

N95-23508# Belgian Center for Corrosion Study, Brussels (Belgium). Center for Corrosion Study.

IN-SITU DETECTION OF SURFACE PASSIVATION OR ACTIVATION AND OF LOCALIZED CORROSION: EXPERIENCES AND PROSPECTIVES IN AIRCRAFT

A. Pourbaix *In* AGARD, Corrosion Detection and Management of Advanced Airframe Materials Jan. 1995 5 p (For primary document see N95-23496 07-26)

Copyright Avail: CASI HC A01/MF A03

The surveillance of the actual conditions of materials in aircrafts and the analysis of the influence of flight or standby conditions require detection methods that give quantitative and instantaneous results and that are related to the real degradation process. Electrochemical methods derived from methods used in laboratory have proven to be of interest. The scientific concepts and the instrumentation are generally easily applicable to field conditions; some effort is necessary to develop relevant sensors. The first example applies to the phosphating of carbon steels before painting. The characterization of surface passivation or reactivity can be of interest before and during the surface conversion processes. The second example applies to the detection of crevice corrosion, as may occur in riveted joints. Author

N95-23509# Belgian Center for Corrosion Study, Brussels (Belgium). Center for Corrosion Study.

TEST METHOD AND TEST RESULTS FOR ENVIRONMENTAL ASSESSMENT OF AIRCRAFT MATERIALS

A. Pourbaix *In* AGARD, Corrosion Detection and Management of Advanced Airframe Materials Jan. 1995 4 p (For primary document see N95-23496 07-26)

(Contracts DAJA45-83-C-0011; DAJA45-83-C-0041)

Copyright Avail: CASI HC A01/MF A03

A study was conducted to identify whether life prediction of high strength aluminum alloys for aircrafts can be determined from short term accelerated atmospheric corrosion tests. The method used is a wet and dry method with electrochemical measurements to characterize the formation or destruction of passive layers. The materials tested include high strength steel 4130, precipitation hardening 15-7 Mo-PH steel and aluminum alloys 6061, 7075 and 2024 with different heat treatments and surface conditions. It appears that the ranking of different Al alloys depends on the type of atmosphere (chloride or acid). The method also clearly showed the detrimental effect of chromated cadmium plating on the hydrogen embrittlement of high strength steel. Corrosion processes of aluminum and high strength steels were clearly identified and useful recommendations could be derived from such tests. Author

N95-23510# Deutsche Aerospace A.G., Munich (Germany).
CORROSION PROTECTION MEASURES FOR CFC/METAL JOINTS OF FUEL INTEGRAL TANK STRUCTURES OF ADVANCED MILITARY AIRCRAFT
Claus D. Hamm *In* AGARD, Corrosion Detection and Management of Advanced Airframe Materials Jan. 1995 11 p (For primary document see N95-23496 07-26)
Copyright Avail: CASI HC A03/MF A03

Assembly of carbon fiber composites (CFC) and aluminum structures shall be avoided in unprotected conditions. The more noble CFC could cause fatal galvanic corrosion on the aluminum part. Adequate protection methods for electrical isolation of these dissimilar materials shall be adopted. Adhesion of the coatings on both the CFC and aluminum substrate during exposure to the simulated fuel tank environment is an essential requirement for corrosion protection and fuel tightness of the joint. In a sequence of material and functional tests for selection of adequate coatings and associated materials as well as galvanic corrosion and integral tank aspects have been taken into account. Additional to the static panel test for paint adhesion corrosion tests under dynamic loading and corrosive environment were performed. Based on the experience of these investigations the selected combinations of the coatings, sealants and associated materials were applied on structural tank box for final evaluation. This test article represented the section of a fuselage integral fuel tank structure. For simulation of the complete in-service spectrum, during the life of an aircraft structure, static and dynamic loads were induced. The internal tank environment was simulated by water as fuel replacement and by pressurization of the compartment. Resistance of the CFC/aluminum joint to galvanic corrosion and liquid tightness of the selected integral tank concept proved excellent under simulated conditions. Author

N95-23511# Deutsche Airbus G.m.b.H., Bremen (Germany).
CORROSION PREVENTION WITH ENVIRONMENTALLY COMPLIANT MATERIALS: A DESIGN CHALLENGE
C. W. Matz *In* AGARD, Corrosion Detection and Management of Advanced Airframe Materials Jan. 1995 6 p (For primary document see N95-23496 07-26)
Copyright Avail: CASI HC A02/MF A03

In order to eliminate hazardous properties many well proven materials and processes for corrosion prevention have to be replaced. Examples are chromates in primers, sealants and pretreatment processes; and cadmium as plating material and solvents, which usage shall be significantly reduced. The replacement materials often do meet the usual requirements completely. Examples are given how the deficit in performance can be overcome by design changes and supplemental measures. Author

N95-23512# National Aeronautics and Space Administration. Langley Research Center, Hampton, VA.
NEW NONDESTRUCTIVE TECHNIQUES FOR THE DETECTION AND QUANTIFICATION OF CORROSION IN AIRCRAFT STRUCTURES **c38**
W. P. Winfree, K. E. Cramer, P. H. Johnston, and M. Namkung *In* AGARD, Corrosion Detection and Management of Advanced Airframe Materials Jan. 1995 6 p (For primary document see N95-23496 07-26)
Copyright Avail: CASI HC A02/MF A03

An overview is presented of several techniques under development at NASA Langley Research Center for detection and quantification of corrosion in aircraft structures. The techniques have been developed as part of the NASA Airframe Structural Integrity Program. The techniques focus on the detection of subsurface corrosion in thin laminated structures. Results are presented on specimens with both manufactured defects, for calibration of the techniques, and on specimens removed from aircraft. Author

N95-23513# Air Products and Chemicals, Inc., Allentown, PA.
ORGANIC COATING TECHNOLOGY FOR THE PROTECTION OF AIRCRAFT AGAINST CORROSION **c27**
Charles R. Hegedus, Stephen J. Spadafora, and Anthony T. Eng (Naval Air Warfare Center, Warminster, PA.) *In* AGARD, Corrosion Detection and Management of Advanced Airframe Materials Jan. 1995 12 p Original contains color illustrations (For primary document see N95-23496 07-26)
Copyright Avail: CASI HC A03/MF A03

Coating systems on military and commercial aircraft perform a variety of functions. Clearly, the most critical of these is the protection of aircraft structures from environmental degradation. Protective coatings serve as the primary defense against corrosion of aircraft metallic alloys, as well as degradation of other materials such as polymeric composites. Traditional coatings for aircraft include epoxy primers and polyurethane topcoats. Primers normally contain high concentrations of corrosion inhibitors, such as chromates, and they are designed to provide superior adhesion and corrosion protection. Polyurethane topcoats are formulated to enhance protection and durability; they also provide desired optical effects (i.e., anesthetics or camouflage). More recently, alternative coatings have been developed, such as self-priming topcoats, flexible primers, temporary and multi-functional coatings. These new developments reflect trends in protective coatings technology, changes in aircraft operational requirements/capabilities, and, most dramatically, concerns over environmental protection and worker safety. This issue has created a drive toward coatings with low (possibly zero) concentrations of volatile organic compounds (VOC's) and non-toxic corrosion inhibitors. In turn, these changes have led to concerns over long-term performance, especially protection against corrosion. This paper reviews current organic coatings technology for the protection of aircraft structures and discusses future needs and trends based on advancing technology, environmental concerns, and operational requirements. Author

N95-23514# KOMPOZIT Corp., Kaliningrad (Russia).
PROBLEMS OF PREDICTING MATERIAL PROPERTY RETENTION DURING LONG TERM SERVICE **c38**
Yu. P. Gordeev and A. M. Khomutov *In* AGARD, Corrosion Detection and Management of Advanced Airframe Materials Jan. 1995 6 p (For primary document see N95-23496 07-26)
Copyright Avail: CASI HC A02/MF A03

A procedure of materials-science studies accompanying the process of product development, manufacture and service is offered. It provides correct selection of materials, trustworthy prediction of their behavior, high reliability of their operation in products of space-rocket application. Reliable prediction of material behavior during long-term service is achieved by breaking up the complex effect of the environment into individual factors and by analyzing the effect of each factor on the properties of the material. Author

N95-23515# Naval Air Warfare Center, Warminster, PA. Aircraft Div.
CORROSION DETECTION AND MONITORING OF AIRCRAFT STRUCTURES: AN OVERVIEW
V. S. Agarwala, P. K. Bhagat (Federal Aviation Administration, Atlantic City, NJ.), and G. L. Hardy (Wright Lab., Wright-Patterson AFB, OH.) *In* AGARD, Corrosion Detection and Management of Advanced Airframe Materials Jan. 1995 6 p (For primary document see N95-23496 07-26)
Copyright Avail: CASI HC A02/MF A03

Corrosion occurs on both military and civilian aircraft as a result of operation in corrosive environments and utilization of less than optimum corrosion preventive measures during fabrication. For low usage rate systems such as military aircraft, corrosion treatment constitutes a high cost maintenance action because corrosion effects can be life limiting mainly due to the fact that current techniques require extensive material loss for reliable detection of corrosion. For high usage systems such as commercial aircraft, corrosion may constitute a safety problem. A recent study by the U.S. Air Force at Tinker Air Force Base has demonstrated that while off-the-shelf nondestructive inspection equipment has some capability for detecting and quantifying aircraft corrosion, significant improvements in both detection and quantification are still required. Results of this study will be briefly reviewed along with discussions relating to some new and innovative inspection technology for detecting corrosion. New concepts and techniques for corrosion monitoring, i.e., detection of onset of corrosion or breakdown of corrosion protection system, will also be discussed. Advances in electrochemical measurements, thermal imaging, and optical scanning for chemical changes are providing some new research and development opportunities. Finally, concepts relating to damage-revealing chemicals and coatings which may revolutionize the detection and management of corrosion in our systems will be discussed. Author

N95-23516# Deutsche Aerospace A.G., Munich (Germany).
EXPERIENCE OF IN-SERVICE CORROSION ON MILITARY AIRCRAFT
H. J. Voss *In* AGARD, Corrosion Detection and Management of Advanced

Airframe Materials Jan. 1995 18 p (For primary document see N95-23496 07-26)
Copyright Avail: CASI HC A03/MF A03

To prevent corrosion of military aircraft the design has to be performed with respect to a careful material selection and an effective surface protection treatment of the materials. Protective treatment on aircraft against moisture, humidity, salty atmosphere, industrial environment, hydraulic fluids, fuel, de-icing fluids, combat chemicals etc. is necessary to meet the operation requirements of the aircraft throughout its operational life. Occurring corrosion detected during maintenance shows that not in every case the requirements above can avoid corrosion problems. This report will show some selected examples of in-service corrosion under investigation of the causes. Inspection and repair methods are shown; further recommendations for corrosion prevention and control to reduce corrosion problems based on practical experiences will be given. Author

N95-23517# Naval Air Station, Norfolk, VA.
US NAVY OPERATING EXPERIENCE WITH NEW AIRCRAFT CONSTRUCTION MATERIALS
G. T. Browne *In* AGARD, Corrosion Detection and Management of Advanced Airframe Materials Jan. 1995 19 p (For primary document see N95-23496 07-26)
Copyright Avail: CASI HC A03/MF A03

This paper addresses the U.S. Navy's experience and problems encountered with new aircraft construction material in the highly corrosive naval operating environment, including: experience with carbon bismaleimide (BMI) and epoxy matrices composite, new aluminum alloys and metal to composite joint repair of honeycomb and monolithic composite structure in fleet activities ashore and afloat; problems experienced with electromagnetic interference (EMI) protection, systems currently in use, and the development of corrosion inhibiting conductive (EMI) sealant; and fastener compatibility for joining carbon composite to metals, H-60 and H-53 helicopter problems, and corrective actions. Author

N95-23518# Aerospatiale, Toulouse (France). Avions Div.
CORROSION IN SERVICE EXPERIENCE WITH AIRCRAFT IN FRANCE
M. J. Frustie and P. Gauthier (CTMS, Toulouse, France.) *In* AGARD, Corrosion Detection and Management of Advanced Airframe Materials Jan. 1995 7 p In FRENCH (For primary document see N95-23496 07-26)
Copyright Avail: CASI HC A02/MF A03

The objective of this communication is to present from a comparison of observed corrosions on modern airplanes (Airtbus, ATR) and corrosions on older airplanes (Transall, Caravelli) the progress realized in the control of corrosion, based on the adaption of materials and better performing protection. It's necessary today to adapt the techniques and constraints of the new legislative dispositions concerning the environment which bring to research the new materials and protection system. Transl. by CASI

N95-23519# Department of the Air Force, Tinker AFB, OK.
OKLAHOMA CITY AIR LOGISTICS CENTER (USAF) AGING AIRCRAFT CORROSION PROGRAM **c01**
Donald E. Nieser *In* AGARD, Corrosion Detection and Management of Advanced Airframe Materials Jan. 1995 12 p (For primary document see N95-23496 07-26)
Copyright Avail: CASI HC A03/MF A03

Because of projected reductions in future defense budgets, less money will be available for new aircraft acquisitions. Consequently, many of the current aircraft will have to be maintained well into the twenty-first century. As they continue to age, the time-dependent effects of material degradation, due to corrosion, will become more significant. Having to maintain aircraft three to four times their original design life presents a unique new set of complex technical problems and challenges. The primary concern is the reduction of airframe fatigue life and static strength due to widespread corrosion damage, fatigue, embrittlement, material loss due to corrosion, intergranular corrosion attack, fretting and stress concentrations. In an effort to ensure continued airworthiness and flight safety, an aggressive program plan has been developed and implemented at Tinker AFB to try to solve the corrosion problems and fatigue related problems to present the occurrence of catastrophic structural failures. The program consists of (1) invasive disassembly of a complete C/KC-135 and sections of B-52 and Boeing 707 aircraft, (2) corrosion documentation/information system development, (3) analysis and testing the effects of corrosion on structural integrity, as well as corrosion growth rates, (4) corrosion modeling and development of C/KC-135 service life extension strategies, (5) and comprehensive evaluation of nondestructive inspection/testing (NDI/NDT) equipment for hidden corrosion detection and quantification. This program has been extensively coordinated with USAF Wright Labs, AFOSR, Naval Air Warfare Center, FAA Aging Aircraft Center, NASA Langley, industry and academia. Author

N95-23571# Los Alamos National Lab., NM.
PREPARATION OF HIGH QUALITY YBa2Cu3O(7-DELTA) THICK FILMS ON FLEXIBLE Ni-BASED ALLOY SUBSTRATES WITH TEXTURED BUFFER LAYERS
X. D. Wu, S. R. Foltyn, P. Arendt, J. Townsend, I. H. Campbell, P. Tiwari, W. X. Jia, J. O. Willis, M. P. Maley, and J. Y. Coulter et al 1995 7 p Presented at the Applied Superconductivity Conference, Boston, MA, 16-21 Oct. 1994
(Contract W-7405-eng-36)
(DE95-003686; LA-UR-94-3789; CONF-941013-1) Avail: CASI HC A02/MF A01

High current YBa2Cu3O(7-delta) YBCO thick films on flexible nickel substrates with textured buffer layers were deposited by using ion beam assisted deposition (IBAD). Pulsed laser deposited YBCO films were not only c-axis oriented with respect to the film surface but also strongly in-plane textured. The in-plane mosaic spread of YBCO films was approximately 10 deg. A critical current density of 8 x 10(exp 5) A/sq cm was obtained at 75 K and zero field for thin YBCO films. It was also demonstrated that thick YBCO films with a high critical current and excellent magnetic field dependence at liquid nitrogen temperature can be obtained on flexible nickel substrates by using the textured buffer layers. Issues encountered in producing the films were discussed. DOE

N95-23980 Westinghouse Savannah River Co., Aiken, SC.
CHARACTERIZATION OF TYPE 304L STAINLESS STEEL SOLID-STATE CLOSURE WELDS FOR RADIOACTIVE WASTE CONTAINMENT
S. L. West 1994 52 p Presented at the 27th Annual International Metallographic Society Meeting, Montreal, Canada, 24-27 Jul. 1994 Limited Reproducibility: More than 20% of this document may be affected by microfiche quality
(Contract DE-AC09-89SR-18035)
(DE94-016539; WSRC-MS-94-0149; CONF-940793-2) Avail: CASI HC A04

Radioactive wastes, generated during years of nuclear materials production, will be vitrified in glass and sealed in canisters. These cylindrical canisters are fabricated from 0.375 in. (9.5 mm) thick Type 304L stainless steel plates and are 24 in. (61 cm) in diameter and 118 in. (3 m) tall with a forged nozzle. The canisters will be sealed by resistance upset welding with a 5 in. (12.7 cm) diameter, 0.5 in. (1.27 cm) thick, slightly oversized plug welded into the nozzle. A parametric study recommended a range of production welding variables based on mechanical tests and metallography. Intentionally 'cold' welds produced with low currents and short times exhibited insufficient interface length and lack-of-bonding. At very high currents, long weld times and low force, maximum heating occurred with significant melting at the top, which makes process stability a concern. All welds made between these extremes exhibited predominantly solid-state bonding. Little variation in microstructure between welds was found along much of the interface with changes in current, force and time. Hardness traverses across the welds showed higher values at the interface, indicative of the worked microstructure. Crevices formed at the top and bottom during plastic flow of the material, and grain sizes varied along the interface from differences in dynamic recrystallization and grain growth. The degree of melting at the top was the most significant difference among welds made within the recommended parameter range. DOE

N95-23983# Comision Nacional de Energia Atomica, Buenos Aires (Argentina).
EFFECT OF DIFFERENT IONS ON THE ANODIC BEHAVIOUR OF ALLOY 800 CHLORIDE SOLUTIONS AT HIGH TEMPERATURE
C. J. Lafont and M. G. Alvarez 1993 5 p Presented at the 2nd Argentine Sessions on Materials Science, La Plata, Argentina, 25-28 Oct. 1993
(DE94-634944; INIS-AR-066; CONF-9310181) Avail: CASI HC A01/MF A01 (US Sales Only)

The anodic behaviour and passivity breakdown of alloy 800 in sodium bicarbonate and sodium phosphate aqueous solutions were studied in the temperature range from 100 C to 280 C by means of electrochemical techniques. The effect of phosphate or bicarbonate additions on the pitting susceptibility and pitting morphology of the alloy in chloride solutions was also examined. Experiments were performed in the following solutions: 0.1M NaHCO3, at 100 C, 200 C, 280 C; 0.06M NaH2PO4 + 0.04M Na2HPO4, at 100 C, 200 C and 280 C, and 0.1M NaCl with different additions of bicarbonate ion (0.02M, 0.05M and 0.1M) and phosphate ion (0.01M, 0.05M and 0.1M) at 100 C and 280 C. The anodic polarization curves of alloy 800 in deaerated 0.1M NaHCO3 and 0.06M NaH2PO4 + 0.04M Na2HPO4 solutions exhibited a similar shape at all the tested temperatures. No localized or generalized corrosion was detected on the metallic surface after polarization. The results obtained in chloride plus bicarbonate and chloride plus phosphate mixtures showed that the pitting potential of alloy 800 in chloride solutions was increased by the presence of bicarbonate or phosphate ions. In those solutions where the inhibitor concentration in the mixture is equal to or higher than the chloride concentration, the behaviour of the alloy is similar to the one observed in the absence of chlorides. Changes in pitting morphology were found in phosphate containing solutions, while the pits found in bicarbonate containing solutions were similar to those found in pure chloride solutions. DOE

N95-24067# Los Alamos National Lab., NM.
DEFORMATION OF C15 LAVES PHASE ALLOYS
F. Chu and D. P. Pope 1995 13 p Presented at the 1994 Fall Meeting of the Materials Research Society (MRS), Boston, MA, 28 Nov. - 2 Dec. 1994
(Contract W-7405-eng-36)
(DE95-003636; LA-UR-94-4084; CONF-941144-2) Avail: CASI HC A03/MF A01

Details of the structure and previous work on the deformation of C Laves phases are reviewed. The phase diagram of the Hf-V-Nb system, some metallurgical and physical properties, mechanical behavior, and the deformation mechanisms of HfV2+Nb (C15 HfV2+Nb and V-rich bcc solution) are presented based on our previous work. Theoretical approaches to understanding the results of these studies are discussed. DOE

N95-24140# Carnegie-Mellon Univ., Pittsburgh, PA.
THE EFFECT OF ELASTIC STRESS ON OSTWALD RIPENING PHENOMENA
W. C. Johnson (Virginia Univ., Charlottesville, VA.) 1994 6 p
(Contract DE-FG02-84ER-45166)
(DE95-002599; DOE/ER-45166/6) Avail: CASI HC A02/MF A01

The purpose of this research program is to understand the influence of elastic misfit strain and applied stress on the development of microstructure in two-phase coherent alloys. The long-term goal of this research is to identify those material parameters that promote microstructural stability in multiphase systems at elevated temperatures. The authors efforts have been focussed on two fronts. First, they have developed a methodology and the corresponding code to simulate the three-dimensional coarsening behavior of elastically and diffusionally interacting spherical particles in an infinite matrix. Secondly, they have completed a set of experiments using model ternary Ni-Al-Mo alloys that were designed to provide quantitative data on symmetry-conserving and symmetry-breaking precipitate shape transitions and particle coarsening kinetics for a critical check on the theory and computer simulations. DOE

N95-24144# Utah Univ., Salt Lake City, UT. Dept. of Chemistry.
THERMOCHEMISTRY OF TRANSITION METAL CLUSTERS
P. B. Armentrout 1994 11 p
(Contract DE-FG02-91ER-14193)
(DE95-003144; DOE/ER-14193/T1) Avail: CASI HC A03/MF A01

The objective of this project was to obtain information regarding the thermodynamic properties of transition metal clusters, their binding energies to various ligands, and their reactions by using a metal cluster guided ion beam mass spectrometer and a cluster ion photodissociation spectrometer. The work performed falls into three main categories: collision-induced dissociation studies, reaction studies, photodissociation studies. The first two utilized a guided ion beam mass spectrometer and the latter, the photodissociation spectrometer. DOE

N95-24153# Argonne National Lab., IL.
EFFECT OF DYNAMICALLY CHARGED HELIUM ON MECHANICAL PROPERTIES OF VANADIUM-BASE ALLOYS
H. M. Chung, B. A. Loomis, and D. L. Smith Aug. 1994 14 p Presented at the 17th Symposium on Effects of Radiation on Materials, Sun Valley, ID, 20-23 Jun. 1994
(Contract W-31-109-eng-38)
(DE95-004613; ANL/ET/CP-82008; CONF-940657-7) Avail: CASI HC A03/MF A01

One property of the vanadium-based alloys that is not well understood for the purpose of application as fusion reactor structural material is the effect of simultaneous generation of helium and neutron damage under conditions relevant to fusion-reactor operation. In the present dynamic helium charging experiment (DHCE), helium was produced uniformly in the specimen at linear rates ranging from approximately 0.4 to 4.2 appm helium/dpa by the decay of tritium during irradiation to 18-31 dpa at 425-600 C in the Li-filled DHCE capsules in the Fast Flux Test Facility. This paper presents results of postirradiation tests of mechanical properties of V-4Cr-4Ti alloy which has been identified as the most promising candidate alloy on the basis of its superior baseline and irradiation properties. Effects of helium on tensile strength and ductility were insignificant for test temperatures greater than 420 C. However, room-temperature ductiilities of the DHCE specimens were higher than those of the non-DHCE specimens (negligible helium generation) whereas strengths were lower, indicating that different types of hardening centers are produced during the DHCE and non-DHCE irradiation. Ductile-brittle transition behavior of the DHCE specimens was also determined from bend tests on TEM disks and broken tensile specimens. No brittle behavior was observed at temperatures greater than 150 C for DHCE specimens. Predominantly brittle-cleavage fracture morphologies were observed only at -196 C in some specimens that were irradiated to 31 dpa at 425 C during DHCE. In strong contrast to tritium-trick experiments in which a large amount of helium is produced in absence of displacement damage, no intergranular fracture was observed in any tensile or bend-tested specimens that were irradiated in the DHCE. DOE

N95-23820*# National Aeronautics and Space Administration. Marshall Space Flight Center, Huntsville, AL.
Be-10 IN TERRESTRIAL BAUXITE AND INDUSTRIAL ALUMINUM: AN LDEF FALLOUT
J. C. Gregory (Alabama Univ., Huntsville, AL.), A. Albrecht (Rutgers Univ., New Brunswick, NJ.), G. Herzog (Rutgers Univ., New Brunswick, NJ.), J. Klein (Pennsylvania Univ., Philadelphia, PA.), R. Middleton (Pennsylvania Univ., Philadelphia, PA.), B. A. Harmon, and T. A. Parnell *In* NASA. Langley Research Center, LDEF: 69 Months in Space. Third Post-Retrieval Symposium, Part 1 Feb. 1995 p 227-230 (For primary document see N95-23796 07-99)
Avail: CASI HC A01/MF A04

N95-23905*# Boeing Defense and Space Group, Seattle, WA.
COLLECTION AND REVIEW OF METALS DATA OBTAINED FROM LDEF EXPERIMENT SPECIMENS AND SUPPORT HARDWARE
Roger Bourassa and H. Gary Pippin *In* NASA. Langley Research Center, LDEF: 69 Months in Space. Third Post-Retrieval Symposium, Part 2 Feb. 1995 p 667-688 (For primary document see N95-23896 07-99)
(Contract NAS1-19247)
Avail: CASI HC A03/MF A03

27 NONMETALLIC MATERIALS

Includes physical, chemical, and mechanical properties of plastics, elastomers, lubricants, polymers, textiles, adhesives, and ceramic materials.

For composite materials see *24 Composite Materials*.

N95-22553# Los Alamos National Lab., NM.
NEUTRON SCATTERING ANALYSIS OF RUBBER CARBON BLACK COMPOSITE STRUCTURE
Rex P. Hjelm, Jr., Wesley A. Wampler (Sid Richardson Carbon Co., Forth Worth, TX.), and Michel Gerspacher (Sid Richardson Carbon Co., Forth Worth, TX.) 1994 16 p Presented at the American Chemical Society Conference, Pittsburgh, PA, 11-14 Oct. 1994

(Contract W-7405-eng-36)
(DE95-002735; LA-UR-94-3523; CONF-9410239-1) Avail: CASI HC A03/MF A01

We explore the uses of small-angle neutron scattering to dissect component form, structure and distribution in carbon black-reinforced rubber by varying the contrast of the system relative to some fluid by changing the fluid scattering-length density. This is the method of contrast variation. Contrast variation allows us to separate scattering contributions from the different components. Here, we extend our studies on high surface area (HSA) carbon black suspended in cyclohexane/deuterocyclohexane to HSA mixed with polyisoprene as a gel of 'bound' rubber swollen with the same solvent mixtures. Contrast variation of swollen composite gels shows that there are two length scales in the gel structure. Above 1 nm fluctuations in the carbon black predominate. Interactions with elastomer hold the HSA aggregates apart. Below 1 nm the scattering is largely from the elastomer. The smooth surface structure of the carbon black is unaltered by the interactions with elastomer and appears smooth over length scales above about 1 nm. These results show that contrast variation can provide information on composite structure that is not available by other means. This information relates to the reinforcement mechanism of elastomers by carbon blacks. DOE

N95-22558* National Aeronautics and Space Administration. Marshall Space Flight Center, Huntsville, AL.
VACUUM VAPOR DEPOSITION Patent
Richard M. Poorman, inventor (to NASA) and Jack L. Weeks, inventor (to NASA) 10 Jan. 1995 6 p Filed 3 Feb. 1994 Supersedes N94-29446 (32 - 8, p 3215)
(NASA-Case-MFS-28652-1; US-Patent-5,380,415;
US-Patent-Appl-SN-191309; US-Patent-Class-204-192.38;
US-Patent-Class-427-580; US-Patent-Class-118-723VE;
US-Patent-Class-204-298.41; Int-Patent-Class-C23C-14/00) Avail: US Patent and Trademark Office

A method and apparatus is described for vapor deposition of a thin metallic film utilizing an ionized gas arc directed onto a source material spaced from a substrate to be coated in a substantial vacuum while providing a pressure differential between the source and the substrate so that, as a portion of the source is vaporized, the vapors are carried to the substrate. The apparatus includes a modified tungsten arc welding torch having a hollow electrode through which a gas, preferably inert, flows and an arc is struck between the electrode and the source. The torch, source, and substrate are confined within a chamber within which a vacuum is drawn. When the arc is struck, a portion of the source is vaporized and the vapors flow rapidly toward the substrate. A reflecting shield is positioned about the torch above the electrode and the source to ensure that the arc is struck between the electrode and the source at startup. The electrode and the source may be confined within a vapor guide housing having a duct opening toward the substrate for directing the vapors onto the substrate. Official Gazette of the U.S. Patent and Trademark Office

N95-22610# International Centre for Theoretical Physics, Trieste (Italy).
A STUDY OF CERAMIC COMPOSITE OF FERROELECTRIC BaTiO3 CERAMIC AND SUPERCONDUCTOR YBa2Cu3O(6+DELTA) CERAMIC
Ang Chen, Yu Zhi (Zhejiang Univ., China.), Yahua Bao (Zhejiang Univ., China.), and Xi Dai (Zhejiang Univ., China.) Nov. 1993 15 p
(DE94-627563; IC-93/385) Avail: CASI HC A03/MF A01 (US Sales Only)

A class of ceramic composite prepared with two kinds of oxide ceramics of ferroelectric BaTiO3 and superconducting YBa2Cu3O(6+delta) was reported, and the phase structure and electrical transport properties of the samples were investigated. The results show that the main phases varied in different composition regions. For low nominal YBa2Cu3O(6+delta) content, the conductive characteristics of the two phase (BaTiO3 and YBa3Ti2O(8.5)) composite follow the three-dimensional percolation model, while for high nominal YBa2Cu3O(6+delta) contents, superconductivity was observed. DOE

N95-22611# International Centre for Theoretical Physics, Trieste (Italy).
A SPECIAL PERCOLATION PROBLEM IN CERAMIC COMPOSITES
Ang Chen, Xi Dai (Zhejiang Univ., China.), Yu Zhi (Zhejiang Univ., China.), and Yahua Bao (Zhejiang Univ., China.) Nov. 1993 11 p
(DE94-627641; IC-93/386) Avail: CASI HC A03/MF A01 (US Sales Only)

The interface effect is taken into consideration, and a special percolation model is proposed for a two-phase metal/ceramic composite. The computer simulation shows that the percolation threshold of this interface-controlled percolation behavior is 4.5% in the three dimensional f.c.c. lattices, which is in good agreement with the experimental data. DOE

N95-22647# Westinghouse Hanford Co., Richland, WA.
GLASS SCIENCE TUTORIAL: LECTURE 1, CHEMISTRY AND PROPERTIES OF OXIDE GLASSES
Albert A. Kruger Oct. 1994 162 p
(Contract DE-AC06-87RL-10930)
(DE95-002963; WHC-MR-0479) Avail: CASI HC A08/MF A02

The tutorial covers the following topics: Definitions and terminology; Introduction to glass structure and properties; The glass transition; Structure/property relationships in oxide glasses; Generalized models for predicting structure/properties; Glass surfaces; Chemical durability; and Mechanical properties. DOE

N95-22648# Westinghouse Hanford Co., Richland, WA.
GLASS SCIENCE TUTORIAL: LECTURE 2, OPERATING ELECTRIC GLASS MELTERS
Albert A. Kruger Oct. 1994 107 p
(Contract DE-AC06-87RL-10930)
(DE95-002965; WHC-MR-0480) Avail: CASI HC A06/MF A02

This report contains basic information on electric furnaces used for glass melting and on the properties of glass useful for the stabilization of radioactive wastes. Furnace nomenclature, furnace types, typical silicate glass composition and properties, thermal conductivity information, kinetics of the melting process, glass furnace refractory materials composition and thermal conductivity, and equations required for the operation of glass melters are included. DOE

N95-22688# Oak Ridge National Lab., TN.
TRANSFORMATION BEHAVIOR IN Al2O3-ZrO2 CERAAMIC COMPOSITES
X. L. Wang, J. A. Fernandez-Baca, C. R. Hubbard, K. B. Alexander, and P. F. Becher 15 Aug. 1994 10 p Presented at the Neutron Scattering, Sendai, Japan, 11-14 Oct. 1994
(Contract DE-AC05-84OR-21400)
(DE95-001359; CONF-9410165-7) Avail: CASI HC A02/MF A01

Neutron powder diffraction was used to investigate the tetragonal to monoclinic transformation of ZrO2 in a Al2O3-ZrO2 ceramic composite containing 40 vol % tetragonal ZrO2. The neutron diffraction data were analyzed using the Rietveld refinement technique, which allowed to determine the extent of the transformation as a function of temperature. The onset transformation temperature determined for this sample was 130 K. Below this temperature, the fraction of the monoclinic phase continued to increase to about 9 vol % at 80 K and remained constant for temperatures below 80 K. The calculated thermal expansion, using the refined lattice parameters, was found in excellent agreement with dilatometry data, confirming that the sharp increase in the thermal expansion upon cooling resulted from the tetragonal to monoclinic phase transformation in ZrO2. DOE

N95-22689# Oak Ridge National Lab., TN.
EVOLUTION OF OXIDATION AND CREEP DAMAGE MECHANISMS IN HIPed SILICON NITRIDE MATERIALS
A. A. Wereszczak, M. K. Ferber, T. P. Kirkland, and K. L. More 1994 14 p Presented at the Conference on Plastic Deformation of Ceramics, Snowbird, UT, 7-12 Aug. 1994
(Contract DE-AC05-84OR-21400)
(DE95-001360; CONF-940865-4) Avail: CASI HC A03/MF A01

Several yttria-fluxed, hot-isostatically pressed (HIPed) silicon nitrides have been tensile creep tested at temperatures representative of gas turbine engines. Creep and oxidation assisted damage mechanisms concurrently evolve when these materials are tested at high temperatures and low stresses (i.e., long exposure times at temperature). Atmospheric creep testing results in creation of oxygen and yttrium gradients across the radial dimension. High concentrations of oxygen and yttrium coincide with dense populations of lenticular-shaped cavities near the surface of crept specimens. The center of the tensile specimens was devoid of oxygen or yttrium; in

addition, lenticular cavities were rare. The gradient in lenticular-cavity concentration is coincident with the oxygen and yttrium gradients. Stress corrosion cracking (SCC) also occurs in these HIPed silicon nitrides when they are subjected to stress at high temperatures in ambient air. The size of this damage zone increases when the temperature is higher and/or the applied stress is lower. Stress-corrosion cracking initiates at the surface of the tensile specimen and advances radially inwards. What nucleates SCC has not yet been identified, but it is believed to result from a stress-concentrator (e.g., machining damage) at the surface and its growth is a result of coalescence of microcracks and cavities. The higher concentration of oxygen and yttrium in the grain boundaries near the specimen's surface lessens the local high temperature mechanical integrity; this is believed to be associated with the growth of the SCC zone. This SCC zone continues to grow in size during tensile loading until it reaches a critical size which causes fracture. DOE

N95-22882*# National Aeronautics and Space Administration. Langley Research Center, Hampton, VA.

TOUGH, SOLUBLE, AROMATIC, THERMOPLASTIC COPOLYIMIDES Patent Application

Robert G. Bryant, inventor (to NASA) 16 Dec. 1994 27 p

(NASA-Case-LAR-15205-1; NAS 1.71:LAR-15205-1; US-Patent-Appl-SN-359752) Avail: CASI HC A03/MF A01

Tough, soluble, aromatic, thermoplastic copolyimides were prepared by reacting 4,4'-oxydiphthalic anhydride, 3,4,3',4'-biphenyltetracarboxylic dianhydride and 3,4'-oxydianiline. These copolyimides were found to be soluble in common amide solvents such as acetamide, Nmethylpyrrolidinone, and dimethylformamide allowing them to be applied as the fully imidized copolymer and to be used to prepare a wide range of articles. NASA

N95-22883*# Clemson Univ., SC. Dept. of Ceramic Engineering.

SUPERCONDUCTIVITY DEVICES: COMMERCIAL USE OF SPACE Annual Report, 2 Jul. 1993 - 31 Jan. 1995

Gene Haertling, Eugene Furman, and Guang Li 17 Mar. 1995 176 p Original contains color illustrations

(Grant NAG1-1301)

(NASA-CR-197885; NAS 1.26:197885) Avail: CASI HC A09/MF A02; 1 functional color page

The work described in this report covers various aspects of the Rainbow solid-state actuator technology. It is presented in six parts dealing with materials, processing, fabrication, properties and associated phenomena. The Rainbow actuator technology is a relatively new materials development which had its inception in 1992. It consists of a new processing technology for preparing piezoelectric and electrostrictive ceramic materials. It involves a high temperature chemical reduction process which leads to an internal pre-stressing of the oxide wafer, thus the name Rainbow, an acronym for Reduced And INternally Biased Oxide Wafer. Ceramics fabricated by this method produce bending-mode actuator devices which possess several times more displacement and load bearing capacity than present-day benders (unimorphs, bimorphs). It is anticipated that these solid-state, electromechanical actuators which can be used in a number of applications in space such as cryopump motors, anti-vibration active structures, autoleveling platforms, telescope mirror correctors and autofocusing devices. When considering any of these applications, the key to the development of a successful device is the successful development of a ceramic material which can produce maximum displacement per volt input; hence, this initiative involving a solid-state means for achieving unusually high electromechanical displacement can be significant and far reaching. An additional benefit obtained from employing the piezoelectric effect in these actuator devices is the ability to also utilize them as sensors; and, indeed, they can be used as both motor (actuator) and generator (sensor) in multifunction devices. Author

N95-23128 Technische Univ., Twente (Netherlands). Dept. of Computer Science.

PLINIUS INTERMEDIATE REPORT

P. E. vanderVet, H. deJong, N. J. I. Mars, P. H. Speel, and W. G. terStal 1 Jul. 1994 101 p

(PB95-135216; Memo-INF-94-35) Copyright Avail: Issuing Activity (National Technical Information Service (NTIS))

The Plinius project aims to develop a system able to acquire knowledge semi-automatically from natural-language abstracts about the mechanical properties of ceramics. The project also serves as an agenda for scientific research. In tracing the prehistory and history of Plinius, we concentrate on the first aspect. It is an answer to the well-known knowledge acquisition bottleneck. Knowledge-based programs will have to store large amounts of knowledge in their knowledge bases if they are to perform interesting tasks. The costs of hand-coding large knowledge bases prevent widespread use of knowledge-based systems, so that fully or at least partially automated ways of acquiring knowledge are needed. Informative texts written in natural language and stored in a machine-readable format constitute an attractive source for (semi)automated knowledge acquisition. What is needed is a system able to translate natural language into a language fit for machine reasoning (a knowledge representation language). This kind of task has become known as knowledge extraction, a term we will use here, too. NTIS

N95-23145# Technische Univ., Eindhoven (Netherlands). Dept. of Mathematics and Computing Science.

BEM SOLUTION TO SIMULATE THE CURVATURE DRIVEN DEFORMATION OF A PROFILE THAT IS PRESSED INTO A PLATE OF HOT GLASS

G. A. L. vandeVorst Apr. 1994 14 p

(PB95-138913; RANA-94-03) Avail: CASI HC A03/MF A01

In the paper the authors describe a numerical method to simulate the deformation of a particular morphology arising from a mold pressed into the surface of a plate of hot glass. The deformation is driven solely by surface tension. This problem occurs, for example, during the production of cathode ray tubes (CRT). One is typically interested in the relation between the obtained morphology in the finally cooled down glass and the originally pressed morphology by the mold. In the paper a first approach is described to tackle this problem by modeling the fluid as a temperature independent flow. Such a simplified flow can be described by the Stokes equations. The numerical simulation is carried out by solving these Stokes equations for a fixed halfspace through a Boundary Element Method (BEM). The resulting velocity field then determines an approximate geometry of the surface of the halfspace at a next time level by employing a variable step, variable order Backward Differences Formulae (BDF) method. This numerical algorithm is demonstrated for the deformation of a Gaussian distribution in both the two-dimensional and axisymmetric case. NTIS

N95-23179*# Virginia Polytechnic Inst., Blacksburg, VA. Dept. of Engineering Science and Mechanics.

DEVELOPMENT AND VERIFICATION OF A RESIN FILM INFUSION/RESIN TRANSFER MOLDING SIMULATION MODEL FOR FABRICATION OF ADVANCED TEXTILE COMPOSITES Interim Report 99, Jan 1992 - Dec. 1994

John Douglas MacRae, Alfred C. Loos, H. Benson Dexter (National Aeronautics and Space Administration. Langley Research Center, Hampton, VA.), Jerry W. Deaton (National Aeronautics and Space Administration. Langley Research Center, Hampton, VA.), and Grogory H. Hasko (Lockheed Engineering and Sciences Co., Hampton, VA.) Dec. 1994 176 p

(Grant NAG1-343)

(NASA-CR-197439; NAS 1.26:197439; CCMS-95-01; VPI-E-94-09) Avail: CASI HC A09/MF A02

The objective of this study was to develop a two-dimensional computer model for the simulation of the resin transfer molding/resin film infusion processing of advanced composite materials. This computer simulation model is designed to provide aircraft structure and tool designers with a method of predicting the infiltration and curing behavior of a composite material component. For a given specified cure cycle, the computer model can be used to calculate the resin infiltration, resin viscosity, resin advancement, heat transfer within the component/tool assembly during processing and preform compaction. Formulations of the resin flow problem are given using the finite element/control volume technique based on Darcy's Law of flow through porous media. This technique allows for the efficient numerical calculation of the advancing resin front within the preform materials. The heat transfer in the fabric preform and tooling is analyzed using a transient finite element method which included the effects of convection on the tooling surfaces. Compaction behavior of the tooling assembly is analyzed using a simplified isotropic form of the plane elasticity equations. All of these solutions were coupled together in a quasi-steady state non-linear fashion inside the computer code. Simulation model verifications were carried out on individual components of the computer

model. A verification of the flow model is carried out by a comparison with experiments reported in literature as well as two dimensional visualization studies performed for a center-port injection of a flat plate. The heat transfer model was verified using the experimental results of a thick section composite laminate processing. Verification of the compaction model were limited to the comparison of the final part dimensions. Two computer simulations were performed on two resin infusion cycles of a single blade-stiffened composite panel. The simulation model results of the two cycles were used to assist in the development of an alternative cycle for the composite manufacturing of a three blade stiffened panel. The results demonstrated the importance of a sufficient minimum viscosity region in the cycle in order to allow the resin to completely infiltrate the fabric preform of the structure. Predictions of the viscosities and degree of cure profiles wthin the single blade stiffened panel illustrated the uniformity of these parameters during the curing cycle. Author

N95-23253* National Aeronautics and Space Administration. Langley Research Center, Hampton, VA.

POLYAZOMETHINES CONTAINING TRIFLUOROMETHYLBENZENE UNITS Patent

Robert G. Bryant, inventor (to NASA) 3 Jan. 1995 9 p Filed 30 Jul. 1993

(NASA-Case-LAR-14896-1; US-Patent-5,378,795;
US-Patent-Appl-SN-105251; US-Patent-Class-528-244;
US-Patent-Class-528-230; US-Patent-Class-528-232;
US-Patent-Class-528-243; US-Patent-Class-528-266;
Int-Patent-Class-C08G-10/02) Avail: US Patent and Trademark Office

Soluble, amorphous, aromatic polyazomethine polymers and copolymers were prepared by reacting a dialdehyde monomer with a diamine monomer containing trifluoromethylbenzene and various combinations thereof in a solvent, such as N,N-dimethylacetamide. The reaction was heated to reflux yielding a polyazomethine which, after cooling to room temperature, was precipitated. These polymers and copolymers may be used to make films, coatings, composites and adhesives.

Official Gazette of the U.S. Patent and Trademark Office

N95-23254* National Aeronautics and Space Administration. Langley Research Center, Hampton, VA.

PROCESS FOR PREPARING AN ASSEMBLY OF AN ARTICLE AND A POLYIMIDE WHICH RESISTS DIMENSIONAL CHANGE, DELAMINATION AND DEBONDING WHEN EXPOSED TO CHANGES IN TEMPERATURE Patent

Diane M. Stoakley, inventor (to NASA) and Anne K. St.Clair, inventor (to NASA) 27 Dec. 1994 6 p Filed 20 Oct. 1993 Continuation of abandoned US-Patent-Appl-SN-736880, filed 26 Jul. 1991

(NASA-Case-LAR-14538-2; US-Patent-5,376,209;
US-Patent-Appl-SN-141430; US-Patent-Appl-SN-736880;
US-Patent-Class-156-330.9; US-Patent-Class-427-96;
US-Patent-Class-427-207.1; US-Patent-Class-427-430.1;
US-Patent-Class-156-60; Int-Patent-Class-C09J-5/00) Avail: US Patent and Trademark Office

An assembly of an article and a polyimide composition is prepared. The assembly resists dimensional change, delamination, or debonding when exposed to changes in temperature. An article is provided. A polyamic acid solution which yields a polyimide having a low coefficient of thermal expansion (CTE) was prepared. Equimolar quantities of an aromatic diamine and an aromatic dianhydride were reacted in a solvent medium to form a polyamic acid solution. A metal ion-containing additive was added to the solution. Examples of this additive are: TbCl3, DyCl3, ErCl3, TmCl3, Al(C5H7O2)3, and Er2S3. The polyamic acid solution was imidized and is combined with the article to form the assembly.

Official Gazette of the U.S. Patent and Trademark Office

N95-23268# Los Alamos National Lab., NM.

VAPOR DEPOSITION OF THIN-FILM Y-DOPED ZrO2 FOR ELECTROCHEMICAL DEVICE APPLICATIONS

B. W. Chung, E. L. Brosha, D. R. Brown, and F. H. Garzon 1994 6 p Presented at the 1994 Fall Meeting of the Materials Research Society (MRS), Boston, MA, 28 Nov. - 2 Dec. 1994

(Contract W-7405-eng-36)
(DE95-003705; LA-UR-94-3935; CONF-941144-13) Avail: CASI HC A02/MF A01

Solid oxide electrolytes based on yttria-stabilized zirconia (YSZ) are widely used in applications such as oxygen sensors, solid oxide fuel cells, oxygen pumps, electrocatalytic reactors, and electrochemically driven oxygen separation membranes. However, bulk YSZ is used in these applications. This requires high operating temperatures in order to minimize ohmic loss. One alternative of overcoming this problem is to use a thin film of the electrolyte. The authors have grown polycrystalline thin films of fully stabilized Y-ZrO2 on thick porous Al2O3 substrates in multilayer La(1-x)Sr(x)MEO3YSZ / La(1-x)Sr(x)MEO3 (ME = Mn, Co) configurations using a combination of single-target RF magnetron sputtering and electron beam physical vapor deposition techniques. The structure and morphology of these films have been studied using x-ray diffraction and scanning electron microscopy techniques. The ionic conductivity of the thin films has been measured using AC impedance analysis. DOE

N95-23356# Nebraska Univ., Lincoln, NE.

PROGRESS REPORT ON CONDUCTIVE PAINTS, SEPTEMBER 1, 1994-NOVEMBER 30, 1994

R. J. Soukup and N. J. Ianno 1995 7 p

(Contract DE-FG01-92CE-15974)
(DE95-004297; DOE/CE-15974/T9) Avail: CASI HC A02/MF A01

This progress report describes testing of the electric and thermal conducting properties of conductive metallic paints. The apparatus constructed for these measurements is described. DOE

N95-23394* National Aeronautics and Space Administration. Ames Research Center, Moffett Field, CA.

PROTECTIVE COATING FOR CERAMIC MATERIALS Patent

Demetrius A. Kourtides, inventor (to NASA), Rex A. Churchward, inventor (to NASA), and David M. Lowe, inventor (to NASA) 22 Mar. 1994 13 p Filed 9 Apr. 1992

(NASA-Case-ARC-11969-1-CU; US-Patent-5,296,288;
US-Patent-Appl-SN-865535; US-Patent-Class-428-262;
US-Patent-Class-428-268; US-Patent-Class-428-289;
US-Patent-Class-428-325; US-Patent-Class-428-331;
US-Patent-Class-428-469; Int-Patent-Class-B32B-18/00) Avail: US Patent and Trademark Office

A protective coating for ceramic materials such as those made of silicon carbide, aluminum oxide, zirconium oxide, aluminoborosilicate and silicon dioxide, and a thermal control structure comprising a ceramic material having coated thereon the protective coating. The protective coating contains, in admixture, silicon dioxide powder, colloidal silicon dioxide, water, and one or more emittance agents selected from silicon tetraboride, silicon hexaboride, silicon carbide, molybdenum disilicide, tungsten disilicide and zirconium diboride. In another aspect, the protective coating is coated on a flexible ceramic fabric which is the outer cover of a composite insulation. In yet another aspect, a metallic foil is bonded to the outer surface of a ceramic fabric outer cover of a composite insulation via the protective coating. A primary application of this invention is as a protective coating for ceramic materials used in a heat shield for space vehicles subjected to very high aero-convective heating environments.

Official Gazette of the U.S. Patent and Trademark Office

N95-23568# Los Alamos National Lab., NM.

REFLECTIVITY STUDIES ON ADSORBED BLOCK COPOLYMERS UNDER SHEAR

G. S. Smith, S. Wages, S. M. Baker (Harvey Mudd Coll., Claremont, CA.), C. Toprakcioglu (Patras Univ., Greece.), and G. Hadziioannou (Groningen Rijksuniv., Netherlands.) 1994 7 p Presented at the 1994 Fall Meeting of the Materials Research Society (MRS), Boston, MA, 28 Nov. - 2 Dec. 1994

(Contract W-7405-eng-36)
(DE95-003676; LA-UR-94-3999; CONF-941144-12) Avail: CASI HC A02/MF A01

The authors report neutron reflectivity data on (poly)styrene-(poly)ethylene oxide (PS-PEO) diblock copolymers adsorbed onto quartz from the selective solvent cyclohexane (a non-solvent for PEO and a poor solvent for PS). The PEO 'anchor block' adsorbs strongly to form a thin layer on the quartz substrate, while the deuterated PS chains dangle into the solvent. They find that under static conditions the density profile of the PS block in a poor solvent can be well described by a Schultz function which is indicative of a polymer 'mushroom'. Furthermore, they have studied the

same system under shear at shear rates from 0-400/s. They find that there is a dramatic increase in the thickness of the PS layer under shear in cyclohexane and that the relaxation time from the shear-on profile back to the static profile is on the order of several days. DOE

N95-23577# Sandia National Labs., Albuquerque, NM.
HIGH SURFACE AREA, HIGH PERMEABILITY CARBON MONOLITHS
R. R. Lagasse and J. L. Schroeder 1994 7 p Presented at the 1994 Fall Meeting of the Materials Research Society (MRS), Boston, MA, 28 Nov. - 2 Dec. 1994
(Contract DE-AC04-94AL-85000)
(DE95-004555; SAND-94-1692C; CONF-941144-23) Avail: CASI HC A02/MF A01

The goal of this work is to prepare carbon monoliths having precisely tailored pore size distribution. Prior studies have demonstrated that poly(acrylonitrile) can be processed into a precursor having tailored macropore structure. Since the macropores were preserved during pyrolysis, this synthetic process provided a route to porous carbon having macropores with size =0.1 to 10 micrometers. No micropores of sizeless than 2 nm could be detected in the carbon, however, by nitrogen adsorption. In the present work, the authors have processed a different polymer, poly(vinylidene chloride) into a macroporous precursor, Pyrolysis produced carbon monoliths having macropores derived from the polymer precursor as well as extensive microporosity produced during the pyrolysis of the polymer. One of these carbons had BET surface area of 1,050 sq m/g and about 1.2 cc/g total pore volume, with about 1/3 of the total pore volume in micropores and the remainder in 1 micrometer macropores. No mesopores in the intermediate size range could be detected by nitrogen adsorption. Carbon materials having high surface area as well as micron size pores have potential applications as electrodes for double layer supercapacitors containing liquid electrolyte, or as efficient media for performing chemical separations. DOE

N95-23932# Wichita State Univ., Wichita, KS. National Inst. for Aviation Research.
ASSESSMENT OF RESIN TRANSFER MOLDING PROCESS FOR THE XM6 DISCHARGER, ERDEC SSP 93-64 Final Report
G. E. Brinkman and A. J. Arnold Apr. 1994 20 p
(NIAR-94-2) Avail: CASI HC A03/MF A01

The U.S. Army Edgewood Research, Development and Engineering Center (ERDEC)-sponsored short term analysis service (STAS) contract was established to provide an independent expert assessment of the XM6 discharger technical data package and prototype production process. ERDEC had requested an independent assessment of the XM6 discharger because of their ongoing concerns with dimensional control of the discharger bore diameters and overall discharger quality. The National Institute for Aviation Research (NIAR) was provided with a full set of appropriate engineering documents and three dischargers to evaluate. The dischargers were dissected and evaluated for defects. Requests were submitted to alter the core material and the resin transfer molding (RTM) resin curing agent. NIAR had concern that the lower temperature curing agent would not hold up well over long term environmental conditions, so elevated temperature mechanical and environmental conditioning (temperature and humidity) tests were performed with acceptable results. Observations of and recommendations for RTM processing are included. It is concluded that the RTM process observed was not a repeatable process. CASI

N95-23981# Oak Ridge National Lab., TN.
Cu DEPOSITION USING A PERMANENT MAGNET ELECTRON CYCLOTRON RESONANCE MICROWAVE PLASMA SOURCE
L. A. Berry, S. M. Gorbatkin, and R. L. Rhoades 1994 14 p Presented at the International Conference on Metallurgical Coatings and Thin Films, San Diego, CA, 25-29 Apr. 1994
(Contract DE-AC05-84OR-21400)
(DE94-017768; CONF-940440-5) Avail: CASI HC A03/MF A01

An electron cyclotron resonance (ECR) plasma has been used in conjunction with a solid metal sputter target for Cu deposition over 200-mm diameters. The goal is to develop a deposition process suitable for filling submicron, high aspect ratio features used for ultralarge scale integration. The system uses a permanent magnet for creation of the magnetic field necessary for ECR and is significantly more compact than systems equipped with electromagnets. A custom launcher design allows remote microwave injection with the microwave entrance window shielded from the Cu flux. Cu deposition rates up to 100 nm/min were observed and film resistivities were typically in the low to mid 2 micro-ohm-cm range. Based on deposition rate measurements at two radial sample position, uniformities of a few percent over 200-mm diameters should be attainable. DOE

N95-24159# Sandia National Labs., Albuquerque, NM.
MICROPOROUS POLYIMIDE FILMS FOR REDUCED DIELECTRIC APPLICATIONS
R. S. Saunders, J. H. Aubert, and W. F. McNamara 1995 11 p Presented at the American Society of Mechanical Engineers' Winter Annual Meeting, Chicago, IL, 9-11 Nov. 1994
(Contract DE-AC04-94AL-85000)
(DE95-004543; SAND-94-2831C; CONF-941142-27) Avail: CASI HC A03/MF A01

With all the advances in the microelectronics industry, a limiting factor to computer chip speed and size is becoming the dielectric constant of the interlayer insulating materials. Dielectric constants of these layers have been reduced in going from inorganic to organic type materials. A further reduction in dielectric constant, coupled with better mechanical properties are still required for these types of materials. The authors have developed a technique involving spincoating in conjunction with a thermodynamic process called 'Non-solvent Induced Phase Separation' (NSIPS) to create microporous polyimide films that exhibit both a lower dielectric constant and better stress reduction properties compared to their solid film counterparts. In this technique, the authors spincoat a soluble polyimide solution in 1,3-dimethoxybenzene solvent onto a silicon wafer, and then immediately submerse the 'wet' polymer film into a non-solvent bath, typically toluene. Phase separation of the polymer occurs on a micron size scale and the resulting microporous structure becomes locked in by the high glass transition temperature of the polyimide. The authors have determined the factors affecting the film morphology, thickness, pore size, and percent porosity; these factors include the polymer concentration, spin speed, and the type of non-solvent used. The different morphologies obtained for the varying non-solvents are explained in terms of thermodynamics and kinetics of phase separation and diffusion, using an idealized ternary phase diagram. One particular film having a porosity of 68%, thickness of 22 microns and pore size of 1.4 microns had a measured dielectric constant of 1.88 and dielectric loss of 0.002. Stress measurements indicated that the microporous film reduced surface stress on the wafer by more than a factor of 10 when compared to the analogous solid polyimide film. DOE

N95-24187*# National Aeronautics and Space Administration. Lewis Research Center, Cleveland, OH.
ATOMIC OXYGEN TEXTURED POLYMERS
Bruce A. Banks, Sharon K. Rutledge, Jason D. Hunt (Ohio Aerospace Inst., Cleveland, OH.), Erin Drobotij (Ohio Aerospace Inst., Cleveland, OH.), Michael R. Cales (Cleveland State Univ., OH.), and Gidget Cantrell (Cleveland State Univ., OH.) Apr. 1995 21 p Presented at the 1995 Spring Meeting, San Francisco, CA, 17-21 Apr. 1995; sponsored by Materials Research Society
(RTOP 243-30-0A)
(NASA-TM-106769; E-9217; NAS 1.15:106769) Avail: CASI HC A03/MF A01

Atomic oxygen can be used to microscopically alter the surface morphology of polymeric materials in space or in ground laboratory facilities. For polymeric materials whose sole oxidation products are volatile species, directed atomic oxygen reactions produce surfaces of microscopic cones. However, isotropic atomic oxygen exposure results in polymer surfaces covered with lower aspect ratio sharp-edged craters. Isotropic atomic oxygen plasma exposure of polymers typically causes a significant decrease in water contact angle as well as altered coefficient of static friction. Such surface alterations may be of benefit for industrial and biomedical applications. The results of atomic oxygen plasma exposure of thirty-three (33) different polymers are presented, including typical morphology changes, effects on water contact angle, and coefficient of static friction. Author

N95-23291*# Air Force Academy, CO. Dept. of Chemistry.
METHOD DEVELOPMENT FOR COMPENSATING TEMPERATURE EFFECTS IN PRESSURE SENSITIVE PAINT MEASUREMENTS Abstract Only
Carlo Greg N. Demandante *In* Hampton Univ., 1994 NASA-HU American

Society for Engineering Education (ASEE) Summer Faculty Fellowship Program Dec. 1994 p 72 (For primary document see N95-23276 07-99)
Avail: CASI HC A01/MF A02

N95-23513# Air Products and Chemicals, Inc., Allentown, PA.
ORGANIC COATING TECHNOLOGY FOR THE PROTECTION OF AIRCRAFT AGAINST CORROSION
Charles R. Hegedus, Stephen J. Spadafora, and Anthony T. Eng (Naval Air Warfare Center, Warminster, PA.) *In* AGARD, Corrosion Detection and Management of Advanced Airframe Materials Jan. 1995 12 p Original contains color illustrations (For primary document see N95-23496 07-26)
Copyright Avail: CASI HC A03/MF A03

N95-23802*# National Aeronautics and Space Administration. Lewis Research Center, Cleveland, OH.
PERFORMANCE CHARACTERIZATION OF EURECA RETROREFLECTORS WITH FLUOROPOLYMER-FILLED SiO(x) PROTECTIVE COATINGS
Bruce A. Banks, Sharon K. Rutledge, and Michael Cales (Cleveland State Univ., OH.) *In* NASA. Langley Research Center, LDEF: 69 Months in Space. Third Post-Retrieval Symposium, Part 1 Feb. 1995 p 51-63 (For primary document see N95-23796 07-99)
Avail: CASI HC A03/MF A04

N95-23899*# National Aeronautics and Space Administration. Langley Research Center, Hampton, VA.
LDEF POLYMERIC MATERIALS: A SUMMARY OF LANGLEY CHARACTERIZATION
Philip R. Young, Wayne S. Slemp, Karen S. Whitley, Carol R. Kalil (Analytical Services and Materials, Inc., Hampton, VA.), Emilie J. Siochi (Lockheed Engineering and Sciences Co., Hampton, VA.), James Y. Shen (Lockheed Engineering and Sciences Co., Hampton, VA.), and A. C. Chang (Lockheed Engineering and Sciences Co., Hampton, VA.) *In its* LDEF: 69 Months in Space. Third Post-Retrieval Symposium, Part 2 Feb. 1995 p 567-599 (For primary document see N95-23896 07-99)
Avail: CASI HC A03/MF A03

N95-23901*# Toronto Univ., North York (Ontario). Inst. for Aerospace Studies.
SPACE ENVIRONMENTAL EFFECTS ON POLYMER MATRIX COMPOSITES AS A FUNCTION OF SAMPLE LOCATION ON LDEF
R. C. Tennyson, G. R. Cool, and D. G. Zimcik (Canadian Space Agency, Ottawa, Ontario.) *In* NASA. Langley Research Center, LDEF: 69 Months in Space. Third Post-Retrieval Symposium, Part 2 Feb. 1995 p 613-629 (For primary document see N95-23896 07-99)
Avail: CASI HC A03/MF A03

N95-23902*# Texas A&M Univ., College Station, TX. Dept. of Aerospace Engineering.
NONLINEAR VISCOELASTIC CHARACTERIZATION OF POLYMER MATERIALS USING A DYNAMIC-MECHANICAL METHODOLOGY
Thomas W. Strganac, Debbie Flowers Payne, Bruce A. Biskup, and Alan Letton *In* NASA. Langley Research Center, LDEF: 69 Months in Space. Third Post-Retrieval Symposium, Part 2 Feb. 1995 p 631-644 (For primary document see N95-23896 07-99)
(Grant NAG5-673)
Avail: CASI HC A03/MF A03

N95-23903*# Queensland Univ., Brisbane (Australia). Polymer Materials and Radiation Group.
THE EFFECT OF SIMULATED LOW EARTH ORBIT RADIATION ON POLYIMIDES (UV DEGRADATION STUDY)
John S. Forsythe, Graeme A. George, David J. T. Hill, James H. ODonnell, Peter J. Pomery, and Firas A. Rasoul *In* NASA. Langley Research Center, LDEF: 69 Months in Space. Third Post-Retrieval Symposium, Part 2 Feb. 1995 p 645-656 (For primary document see N95-23896 07-99)
Avail: CASI HC A03/MF A03

N95-23904*# Queensland Univ., Brisbane (Australia). Polymer Materials and Radiation Group.
THE SURFACE PROPERTIES OF FLUORINATED POLYIMIDES EXPOSED TO VUV AND ATOMIC OXYGEN
John S. Forsythe, Graeme A. George, David J. T. Hill, James H. ODonnell, Peter J. Pomery, and Firas A. Rasoul *In* NASA. Langley Research Center, LDEF: 69 Months in Space. Third Post-Retrieval Symposium, Part 2 Feb. 1995 p 657-665 (For primary document see N95-23896 07-99)
Avail: CASI HC A02/MF A03

N95-23906*# National Aeronautics and Space Administration. Marshall Space Flight Center, Huntsville, AL.
MEASUREMENTS OF THE OPTICAL PROPERTIES OF THIN FILMS OF SILVER AND SILVER OXIDE
Palmer N. Peters, Robert C. Sisk, Yolanda Brown, John C. Gregory (Alabama Univ., Huntsville, AL.), Pallob K. Nag (Alabama Univ., Huntsville, AL.), and Ligia Christl (Alabama Univ., Huntsville, AL.) *In* NASA. Langley Research Center, LDEF: 69 Months in Space. Third Post-Retrieval Symposium, Part 2 Feb. 1995 p 689-701 (For primary document see N95-23896 07-99)
Avail: CASI HC A03/MF A03

N95-23907*# National Aeronautics and Space Administration. Marshall Space Flight Center, Huntsville, AL.
CHANGES IN CHEMICAL AND OPTICAL PROPERTIES OF THIN FILM METAL MIRRORS ON LDEF
Palmer N. Peters, James M. Zwiener, John C. Gregory (Alabama Univ., Huntsville, AL.), Ganesh N. Raikar (Alabama Univ., Huntsville, AL.), Ligia C. Christl (Alabama Univ., Huntsville, AL.), and Donald R. Wilkes (AZ Technology, Huntsville, AL.) *In* NASA. Langley Research Center, LDEF: 69 Months in Space. Third Post-Retrieval Symposium, Part 2 Feb. 1995 p 703-725 (For primary document see N95-23896 07-99)
Avail: CASI HC A03/MF A03

N95-23908*# National Aeronautics and Space Administration. Marshall Space Flight Center, Huntsville, AL.
FURTHER INVESTIGATIONS OF EXPERIMENT A0034 ATOMIC OXYGEN STIMULATED OUTGASSING
Roger C. Linton, Miria M. Finckenor, and Rachel R. Kamenetzky *In* NASA. Langley Research Center, LDEF: 69 Months in Space. Third Post-Retrieval Symposium, Part 2 Feb. 1995 p 727-736 (For primary document see N95-23896 07-99)
(Contract NAS8-39924)
Avail: CASI HC A02/MF A03

N95-23911*# National Aeronautics and Space Administration. Marshall Space Flight Center, Huntsville, AL.
WHISKER/CONE GROWTH ON THE THERMAL CONTROL SURFACES EXPERIMENT NO. S0069
James M. Zwiener, James E. Coston, Jr., Edgar R. Miller (AZ Technology, Huntsville, AL.), Richard J. Mell (AZ Technology, Huntsville, AL.), and Donald R. Wilkes (AZ Technology, Huntsville, AL.) *In* NASA. Langley Research Center, LDEF: 69 Months in Space. Third Post-Retrieval Symposium, Part 2 Feb. 1995 p 771-790 (For primary document see N95-23896 07-99)
Avail: CASI HC A03/MF A03

N95-23912*# National Aeronautics and Space Administration. Marshall Space Flight Center, Huntsville, AL.
DURABILITY OF REFLECTOR MATERIALS IN THE SPACE ENVIRONMENT
Ann F. Whitaker, Miria M. Finckenor, David Edwards, Rachel R. Kamenetzky, and Roger C. Linton *In* NASA. Langley Research Center, LDEF: 69 Months in Space. Third Post-Retrieval Symposium, Part 2 Feb. 1995 p 791-802 (For primary document see N95-23896 07-99)
Avail: CASI HC A03/MF A03

N95-23913*# National Aeronautics and Space Administration. Goddard Space Flight Center, Greenbelt, MD.
FOUR SPACE APPLICATION MATERIAL COATINGS ON THE LONG-DURATION EXPOSURE FACILITY (LDEF)

John J. Scialdone and Carroll Clatterbuck *In* NASA. Langley Research Center, LDEF: 69 Months in Space. Third Post-Retrieval Symposium, Part 2 Feb. 1995 p 803-823 (For primary document see N95-23896 07-99)
Avail: CASI HC A03/MF A03

N95-23915*# Altai State Univ., Barnaul (USSR).
STRUCTURE AND PROPERTIES OF POLYMERIC COMPOSITE MATERIALS DURING 1501 DAYS OUTER SPACE EXPOSURE AT SALYUT-7 ORBITAL STATION
Oleg V. Startsev and Eugene F. Nikishin (Salyut Design Office 18, Moscow, Russia.) *In* NASA. Langley Research Center, LDEF: 69 Months in Space. Third Post-Retrieval Symposium, Part 2 Feb. 1995 p 843-857 (For primary document see N95-23896 07-99)
Avail: CASI HC A03/MF A03

N95-24124*# Sony Corp., Tagajyo (Japan).
A KINETIC STUDY OF HYDROLYSIS OF POLYESTER ELASTOMER IN MAGNETIC TAPE
K. Yamamoto and H. Watanabe *In* NASA. Goddard Space Flight Center, Fourth NASA Goddard Conference on Mass Storage Systems and Technologies 203-210 (SEE N95-24108 07-82) Mar. 1994 (For primary document see N95-24108 07-82)
Avail: CASI HC A02/MF A04

28 PROPELLANTS AND FUELS

Includes rocket propellants, igniters, and oxidizers; their storage and handling procedures; and aircraft fuels.

For related information see also *07 Aircraft Propulsion and Power, 20 Spacecraft Propulsion and Power,* and *44 Energy Production and Conversion.*

N95-22506# Army Research Lab., Aberdeen Proving Ground, MD.
MORPHOLOGY OF EXTINGUISHED MONOLITHIC JA2 GRAINS FIRED IN A 30-mm SOLID PROPELLANT ELECTROTHERMAL CHEMICAL (SPETC) GUN Final Report, Sep. 1993 - Jan. 1994
Robert J. Lieb and Christopher J. Gillich Nov. 1994 33 p
(AD-A285792; ARL-TR-606) Avail: CASI HC A03/MF A01

Monolithic grains of JA2 were fired in a 30-mm solid propellant electrothermal-chemical (SPETC) gun and were recovered after self-extinguishing because of depressurization. A morphological investigation was performed on these grains to gain insight into the interaction between the plasma and the propellant. Scanning electron microscopy (SEM) was used to characterize the morphology of the combustion surface and bulk of the propellant. Results show that the propellant burning surface was pitted and showed evidence of both brittle fracture and plastic flow. These features were the results of rapid pressurization within the single perforated grain caused by the plasma injection and the subsequent burning. Regions within the propellant showed evidence of augmented mass generation when compared with conventional propellant combustion. Mechanisms causing this accelerated burning are conjectured; they included erosive burning, fracture-generated tunneling, and in-depth burning. Micrographs are presented to support these findings and proposals are made to exploit these enhanced burning processes. DTIC

N95-22587# Oak Ridge National Lab., TN. Chemical Technology Div.
DESIGN AND DEMONSTRATION OF AN IMMOBILIZED-CELL FLUIDIZED-BED REACTOR FOR THE EFFICIENT PRODUCTION OF ETHANOL
O. F. Webb, T. C. Scott, B. H. Davison, and C. D. Scott 1994 13 p Presented at the 16th Symposium on Biotechnology for Fuels and Chemicals, Gatlinburg, TN, 9-13 May 1994
(Contract DE-AC05-84OR-21400)
(DE94-014023; CONF-940526-5) Avail: CASI HC A03/MF A01

Initial studies have been carried out using a 4 inch ID fluidized bed reactor (FBR). This medium scale FBR was designed for scale-up. Present performance was compared with results from experiments using smaller FBR's. On-line and off-line measurement systems are also described. Zymomonas mobilis was immobilized in kappa-carrageenan at cell loadings of 15-50 g (dry weight) L(exp -1). The system is designed for determining optimal operation with high conversion and productivity for a variety of conditions including feedstocks, temperature, flow rate, and column sizes (from 2 to 5 meters tall). The demonstration used nonsterile feedstocks containing either industrial (light steep water) or synthetic nutrients and dextrose. DOE

N95-22672*# National Aeronautics and Space Administration. Marshall Space Flight Center, Huntsville, AL.
ADVANCED LIQUID OXYGEN (LO2) PROPELLANT CONDITIONING CONCEPT TESTING
G. L. E. Perry, J. D. Suter, and S. G. Turner Washington Jan. 1995 23 p
(NASA-TM-108477; NAS 1.15:108477) Avail: CASI HC A03/MF A01

Advanced methods of liquid oxygen (LO2) propellant conditioning were studied as part of an effort for increasing reliability and operability while reducing cost of future heavy lift launch vehicles. The most promising conditioning concept evaluated was no-bleed (passive recirculation) followed by low-bleed, helium injection, and use of a recirculation line. Full-scale cryogenic testing was performed with a sloped feedline test article to validate models of behavior of LO2 in the feedline and to prove no-bleed feasibility. Test data are also intended to help generate design guidelines for the development of a main propulsion system feed duct. A design-of-experiments matrix of over 100 tests was developed to test all four propellant conditioning concepts and the impact of design parameters on the concepts. Liquid nitrogen was used as the test fluid. The work for this project was conducted from October 1992 through January 1994 at the hydrogen cold flow facility of the west test area of MSFC. Test data have shown that satisfactory temperatures are being obtained for the no-bleed conditioning concept. Author

N95-22721# Sandia National Labs., Livermore, CA.
COMPUTER MODELING OF DETONATORS
Carlton M. Furnberg 1994 4 p Presented at the 37th Midwest Symposium on Circuits and Systems, Lafayette, LA, 2-5 Aug. 1994
(Contract DE-AC04-94AL-85000)
(DE95-003031; SAND-94-8725C; CONF-9408126-5) Avail: CASI HC A01/MF A01

A mathematical model of detonators which describes the resistance of the exploding bridgewire or exploding foil initiator as a function of energy deposition is described. This model includes many parameters that can be adjusted to obtain a close fit to experimental data. This is demonstrated using recent experimental data taken within Sandia National Laboratories. DOE

N95-22838# Sandia National Labs., Albuquerque, NM.
DECOMPOSITION MECHANISMS IN THERMALLY-AGED THIN-FILM EXPLOSIVES
K. L. Erickson, W. M. Trott, and A. M. Renlund 1994 12 p Presented at the 1994 Joint Army, Navy, NASA, Air Force (JANNAF) Propulsion Systems Hazards Meeting, San Diego, CA, 1-5 Aug. 1994
(Contract DE-AC04-94AL-85000)
(DE95-000741; SAND-94-0468C; CONF-9408123-3) Avail: CASI HC A03/MF A01

The isothermal decomposition of nitrocellulose (NC) has been examined using two substantially different experimental techniques, involving both confined and unconfined samples. The confined isothermal aging technique involved confined thin-film samples heated to temperatures of 150 to 170 C, for 1 to 72 hours. Condensed-phase chemistry was monitored real-time using FTIR. Results indicated that the first step in decomposition was scission of the O-NO2 bond and subsequent formation of carbonyl and hydroxyl products. Scission of the O-NO2 bond appeared to occur by a first order reaction. The Arrhenius expression for the first order reaction rate constant was evaluated from the experimental data. The unconfined rapid isothermal decomposition technique involved both high speed photography and time-of-flight mass spectrometry (TOFMS). Mass spectra obtained from experiments at 420 C indicated that NO2 formation and, therefore, scission of the O-NO2 bond occurred by a first order reaction, the rate constant for which was evaluated from the experimental data. The rate constant for global pseudo first order decomposition of NC at 450 C was also estimated from high speed photography results. Rate constants at 420 and 450 C were predicted using the Arrhenius expression developed from the confined isothermal aging results and were in good

agreement with the rate constants obtained at those temperatures in the unconfined rapid decomposition experiments using TOFMS and high-speed photography. Results from these substantially different measurements gave consistent results over a temperature range of about 300 C, in which reaction rates vary by nine orders of magnitude, and indicate that the two experimental techniques being developed have good potential for studying condensed-phase decomposition of energetic materials. DOE

N95-23668 Defence Science and Technology Organization, Melbourne (Australia). Airframes and Engines Div.
SIMULATION OF COOKOFF RESULTS IN A SMALL SCALE TEST
David A. Jones and Robert P. Parker Oct. 1994 37 p
(DSTO-TR-0090; AR-008-959) Copyright Avail: Issuing Activity (DSTO Aeronautical and Maritime Research Lab., GPO Box 4331, Melbourne, Victoria 3001, Australia)

The fast and slow cookoff behavior of two series of candidate insensitive booster compositions based on RDX/Elvax 210, and incorporating various amounts of PETN and TATB, has been numerically simulated using a one-dimensional finite difference code. The model solves a cylindrically symmetric heat flow equation for a mixture of two energetic materials with a time dependent boundary temperature. The temperature dependence of the thermal conductivity and specific heat of each of the explosives is included, as well as the effect of melting, and the effect of different kinetic schemes for the decomposition of the RDX. The simulations accurately reproduce the time to explosion and surface temperature at explosion for varying PETN concentration at both fast and slow heating rates, and also provide good agreement with experiment for varying TATB levels at the slow heating rate. However at the fast heating rate there is a divergence between the simulated results and experiment. The calculations clearly illustrate the need to include the temperature dependence of the thermal properties of the material, and a kinetic decomposition scheme appropriate to the degree of confinement, before good agreement between simulated and experimental results can be obtained. Author

N95-24186*# National Aeronautics and Space Administration. Lewis Research Center, Cleveland, OH.
A SUMMARY OF THE SLUSH HYDROGEN TECHNOLOGY PROGRAM FOR THE NATIONAL AERO-SPACE PLANE
Nancy B. McNelis, Terry L. Hardy, Margaret V. Whalen, Maureen T. Kudlac, Matthew E. Moran, Thomas M. Tomsik, and Mark S. Haberbusch (Ohio Aerospace Inst., Brook Park, OH.) Apr. 1995 12 p Presented at the Hypersonics Technologies Conference, Chattanooga, TN, 3-7 Apr. 1995; sponsored by AIAA
(RTOP 763-22-21)
(NASA-TM-106863; E-9469; NAS 1.15:106863; AIAA Paper 95-6056)
Avail: CASI HC A03/MF A01

Slush hydrogen, a mixture of solid and liquid hydrogen, offers advantages of higher density (16 percent) and higher heat capacity (18 percent) than normal boiling point hydrogen. The combination of increased density and heat capacity of slush hydrogen provided a potential to decrease the gross takeoff weight of the National Aero-Space Plane (NASP) and therefore slush hydrogen was selected as the propellant. However, no large-scale data was available on the production, transfer and tank pressure control characteristics required to use slush hydrogen as a fuel. Extensive testing has been performed at the NASA Lewis Research Center K-Site and Small Scale Hydrogen Test Facility between 1990 and the present to provide a database for the use of slush hydrogen. This paper summarizes the results of this testing. Author

29 MATERIALS PROCESSING

Includes space-based development of products and processes for commercial applications.

For biological materials see *55 Space Biology*.

N95-23204*# Universities Space Research Association, Huntsville, AL.
MICROGRAVITY SCIENCES APPLICATION VISITING SCIENTIST PROGRAM Final Progress Report, 20 Dec. 1991 - 3 Feb. 1995
Martin Glicksman (Rensselaer Polytechnic Inst., Troy, NY.) and James VanAlstine (Alabama Univ., Huntsville, AL.) 28 Feb. 1995 48 p
(Contract NAS8-38785)
(NASA-CR-197854; NAS 1.26:197854) Avail: CASI HC A03/MF A01

Marshall Space Flight Center pursues scientific research in the area of low-gravity effects on materials and processes. To facilitate these Government performed research responsibilities, a number of supplementary research tasks were accomplished by a group of specialized visiting scientists. They participated in work on contemporary research problems with specific objectives related to current or future space flight experiments and defined and established independent programs of research which were based on scientific peer review and the relevance of the defined research to NASA microgravity for implementing a portion of the national program. The programs included research in the following areas: protein crystal growth, X-ray crystallography and computer analysis of protein crystal structure, optimization and analysis of protein crystal growth techniques, and design and testing of flight hardware. Author

N95-23552*# Alabama Univ., Huntsville, AL. Center for Microgravity and Materials Research.
USML-1 MICROGRAVITY GLOVEBOX EXPERIMENT NO. 1 PASSIVE ACCELEROMETER SYSTEM Final Report, 1 Sep. 1990 - 4 Sep. 1993
J. Iwan D. Alexander and Melissa J. B. Rogers 1995 13 p
(Contract NAS8-38773)
(NASA-CR-196575; NAS 1.26:196575) Avail: CASI HC A03/MF A01

The passive accelerometer system (PAS) is a simple moving ball accelerometer capable of measuring the small magnitude steady relative acceleration that occurs in a low earth orbit spacecraft due to atmospheric drag and the earth's gravity gradient. The accelerometer can be used when the spacecraft continuously rotates during the orbit such that some line of reference in the craft always points along the vector connecting the earth's mass center with the spacecraft mass center. PAS was used successfully on the first United States Microgravity Laboratory (USML-1). Author

N95-24028*# Alabama Univ., Huntsville, AL.
USML-1 GLOVEBOX EXPERIMENTS Final Report
Robert J. Naumann 31 Jan. 1995 60 p
(Contract NAS8-38773)
(NASA-CR-196574; NAS 1.26:196574) Avail: CASI HC A04/MF A01

This report covers the development of and results from three experiments that were flown in the Materials Science Glovebox on USML-1: Marangoni convection in Closed Containers (MCCC), Double Float Zone (DFZ), and Fiber Pulling in Microgravity (FPM). The Glovebox provided a convenient, low cost method for doing simple 'try and see' experiments that could test new concepts or elucidate microgravity phenomena. Since the Glovebox provided essentially one (or possibly two levels of confinement, many of the stringent verification and test requirements on the experiment apparatus could be relaxed and a streamlined test and verification plan for flight qualification could be implemented. Furthermore, the experiments were contained in their own carrying cases whose external configurations could be identified early in the integration sequence for stowage considerations while delivery of the actual experiment apparatus could be postponed until only a few months before flight. This minimized the time fluids must be contained and reduced the possibility of corrosive reactions that could ruin the experiment. In many respects, this exercise was as much about developing a simpler, cheaper way of doing crew-assisted science as it was about the actual scientific accomplishments of the individual experiments. The Marangoni Convection in Closed Containers experiment was designed to study the effects of a void space in a simulated Bridgman crystal growth configuration and to determine if surface tension driven convective flows that may result from thermal gradients along any free surfaces could affect the solidification process. The Fiber Pulling in Microgravity experiment sought to separate the role of gravity drainage from capillarity effects in the break-up of slender cylindrical liquid columns. The Stability of a Double Float Zone experiment explored the feasibility of a quasi-containerless process in which a solidifying material is suspended by two liquid bridges of its own melt. Author

31 ENGINEERING (GENERAL)

Includes vacuum technology; control engineering; display engineering; cryogenics; and fire prevention.

N95-22678# Los Alamos National Lab., NM.
ASPECTS OF SURFACE GENERATION IN ORTHOGONAL ULTRAPRECISION MACHINING
D. A. Lucca (Oklahoma State Univ., Stillwater, OK.), Y. W. Seo (Oklahoma State Univ., Stillwater, OK.), and R. L. Rhorer 1994 5 p Presented at the 1994 CIRP General Assembly, Singapore, Singapore, 21-27 Aug. 1994
(Contract W-7405-eng-36)
(DE95-000922; LA-UR-94-3166; CONF-940854-2) Avail: CASI HC A01/MF A01

The depth of the plastically deformed layer at the workpiece surface which resulted in the orthogonal ultraprecision machining of Cu over the range of uncut chip thicknesses of 0.01-10 micrometers was investigated. Two tools with the same nominal geometry but with differing edge geometries were used to machine both Te-Cu and fine grain Cu. Tool edge geometries were characterized by atomic force microscopy, taking into account the AFM cantilever tip radius. Magnitudes of the measured depths appear to be consistent with values reported in the literature and those arrived at by simple analyses. DOE

N95-22692# Pacific Northwest Lab., Richland, WA.
TECHNOLOGY MATURATION PROJECT ON OPTIMIZATION OF SHEET METAL FORMING OF ALUMINUM FOR USE IN TRANSPORTATION SYSTEMS Final Report
Ken I. Johnson, Mark T. Smith, Curt A. Lavender, and Mohammad A. Khalell Oct. 1994 51 p
(Contract DE-AC06-76RL-01830)
(DE95-003005; PNL-10165) Avail: CASI HC A04/MF A01

Using aluminum instead of steel in transportation systems could dramatically reduce the weight of vehicles, an effective way of decreasing energy consumption and emissions. The current cost of sheet metal formed (SMF) aluminum alloys (about $4 per pound) and the relatively long forming times of current materials are serious drawbacks to the widespread use of SMF in industry. The interdependence of materials testing and model development is critical to optimizing SMF since the current process is conducted in a heated, pressurized die where direct measurement of critical SMF parameters is extremely difficult. Numerical models provide a means of tracking the forming process, allowing the applied gas pressure to be adjusted to maintain the optimum SMF behavior throughout the forming process. Thus, models can help produce the optimum SMF component in the least amount of time. The Pacific Northwest Laboratory is integrating SMF model development with research in improved aluminum alloys for SMF. The objectives of this research are: develop and characterize competitively priced aluminum alloys for SMF applications in industry; improve numerical models to accurately predict the optimum forming cycle for reduced forming time and improved quality; and verify alloy performance and model accuracy with forming tests conducted in PNL's Superplastic Forming User Facility. The activities performed in this technology maturation project represent a critical first step in achieving these objectives through cooperative research among industry, PNL, and universities. DOE

N95-22804*# National Aeronautics and Space Administration. Ames Research Center, Moffett Field, CA.
NONLINEAR SYSTEM GUIDANCE IN THE PRESENCE OF TRANSMISSION ZERO DYNAMICS
G. Meyer, L. R. Hunt, and R. Su Jan. 1995 42 p
(RTOP 505-64-52)
(NASA-TM-4661; A-95014; NAS 1.15:4661) Avail: CASI HC A03/MF A01

An iterative procedure is proposed for computing the commanded state trajectories and controls that guide a possibly multiaxis, time-varying, nonlinear system with transmission zero dynamics through a given arbitrary sequence of control points. The procedure is initialized by the system inverse with the transmission zero effects nulled out. Then the 'steady state' solution of the perturbation model with the transmission zero dynamics intact is computed and used to correct the initial zero-free solution. Both time domain and frequency domain methods are presented for computing the steady state solutions of the possibly nonminimum phase transmission zero dynamics. The procedure is illustrated by means of linear and nonlinear examples. Author

N95-23195*# Pennsylvania State Univ., University Park, PA. Dept. of Mechanical Engineering.
DAMAGE-MITIGATING CONTROL OF A REUSABLE ROCKET ENGINE FOR HIGH PERFORMANCE AND EXTENDED LIFE Final Report
Asok Ray and Xiaowen Dai Cleveland, OH NASA Jan. 1995 94 p
(Grant NAG3-1240; RTOP 505-62-50)
(NASA-CR-4640; E-9336; NAS 1.26:4640) Avail: CASI HC A05/MF A01

The goal of damage mitigating control in reusable rocket engines is to achieve high performance with increased durability of mechanical structures such that functional lives of the critical components are increased. The major benefit is an increase in structural durability with no significant loss of performance. This report investigates the feasibility of damage mitigating control of reusable rocket engines. Phenomenological models of creep and thermo-mechanical fatigue damage have been formulated in the state-variable setting such that these models can be combined with the plant model of a reusable rocket engine, such as the Space Shuttle Main Engine (SSME), for synthesizing an optimal control policy. Specifically, a creep damage model of the main thrust chamber wall is analytically derived based on the theories of sandwich beam and viscoplasticity. This model characterizes progressive bulging-out and incremental thinning of the coolant channel ligament leading to its eventual failure by tensile rupture. The objective is to generate a closed form solution of the wall thin-out phenomenon in real time where the ligament geometry is continuously updated to account for the resulting deformation. The results are in agreement with those obtained from the finite element analyses and experimental observation for both Oxygen Free High Conductivity (OFHC) copper and a copper-zerconium-silver alloy called NARloy-Z. Due to its computational efficiency, this damage model is suitable for on-line applications of life prediction and damage mitigating control, and also permits parametric studies for off-line synthesis of damage mitigating control systems. The results are presented to demonstrate the potential of life extension of reusable rocket engines via damage mitigating control. The control system has also been simulated on a testbed to observe how the damage at different critical points can be traded off without any significant loss of engine performance. The research work reported here is built upon concepts derived from the disciplines of Controls, Thermo-fluids, Structures, and Materials. The concept of damage mitigation, as presented in this report, is not restricted to control of rocket engines. It can be applied to any system where structural durability is an important issue. Author

N95-24045 British Broadcasting Corp., Tadworth (England). Research and Development Dept.
THE SOUND INSULATIONS OF STUDIO DOORS. PART 2: DOOR SEALS
G. D. Plumb and R. Clark 1994 14 p
(BBC-RD-1994/15) Copyright Avail: Issuing Activity (BBC, Kingswood Warren, Tadworth, Surrey, England)

The acoustic performances of a range of proprietary acoustic door seals were measured in the Transmission Suite. The seals were fitted to a standard BBC lead-cored door hung in a purpose-built blockwork wall. As a result of the work, suitable plant-on magnetic perimeter seals and drop-down threshold seals are recommended. The use of these seals will simplify the existing door frame design and should reduce costs without compromising the acoustic performances. The sound insulations were also measured of a range of door blanks with the intention of improving the performances. This work is documented in a companion Report (BBC RD 1994/14). Author

N95-24093 British Broadcasting Corp., Tadworth (England). Research and Development Dept.
THE SOUND INSULATIONS OF STUDIO DOORS. PART 1: DOOR BLANKS
G. D. Plumb and R. Clark 1994 18 p
(BBC-RD-1994/14) Copyright Avail: Issuing Activity (BBC, Kingswood Warren, Tadworth, Surrey, England)

The sound insulations of a range of different door blanks were measured. The results were compared with the sound insulations of existing BBC

door blanks. The new doors were made from medium density fiberboard (MDF) which is more stable than the blockboard used in existing studio doors. Consequently, they should require less maintenance and adjustment and should have a longer lifespan. The doors had higher sound insulations for their weight than existing designs, which might permit savings in the costs of the surrounding building structures. Overall construction costs of the door blanks themselves are likely to be similar to those of existing designs. A companion Report (BBC RD 1994/15) describes sound insulation measurements made on plant-on door seals. The intention of this work was to simplify the construction of the door frame and the fitting of the seals to reduce costs. Author

32 COMMUNICATIONS AND RADAR

Includes radar; land and global communications; communications theory; and optical communications.

For related information see also *04 Aircraft Communications and Navigation* and *17 Space Communications, Spacecraft Communications, Command and Tracking.* For search and rescue see *03 Air Transportation and Safety,* and *16 Space Transportation.*

N95-22505# Naval Postgraduate School, Monterey, CA. Dept. of Electrical and Computer Engineering.

WAVELET TIME-FREQUENCY ANALYSIS OF PHASE-SHIFT-KEY MODULATED SIGNALS Final Report, 1 Oct. 1993 - 30 Sep. 1994

Alex W. Lam 29 Sep. 1994 64 p

(AD-A285791; NPSEC-94-013) Avail: CASI HC A04/MF A01

Continuous and discrete wavelet transforms are discussed. Recursive Generations of compactly supported wavelet time functions are described. Haar, Daubechies, and complex modulated Gaussian wavelets are utilized to analyze phase shifts in signals with noise. DTIC

N95-22636 Institute for Telecommunication Sciences, Boulder, CO.

INVESTIGATION OF FEDERAL STANDARD 1045 HIGH-FREQUENCY ALE RADIO PERFORMANCE IN THE SOUTHERN TRANS-AURORAL ZONE

P. C. Smith, R. T. Adair, and D. F. Peach Mar. 1994 96 p Sponsored by Naval Undersea Warfare Center Div. Prepared for NSF, Washington, DC Limited Reproducibility: More than 20% of this document may be affected by microfiche quality

(PB94-204831; NTIA-94-304) Avail: Issuing Activity (National Technical Information Service (NTIS))

This report presents the results of two weeks of bidirectional high-frequency radio path soundings in a trans-auroral environment between Christchurch, New Zealand, and the U.S. station, McMurdo (Black Island), Antarctica, during mid-January 1992. This investigation demonstrated the value of automatic link establishment (ALE) adaptive radio systems as a real-time frequency management tool. Based on the results observed, the authors recommended that the National Science Foundation (NSF) consider the acquisition of a 1-kW ALE radio system to be used, primarily as an oblique ionospheric channel sounder, with their existing communications system. This addition would provide significant improvement to the NSF frequency management capability. NTIS

N95-22746# International Centre for Theoretical Physics, Trieste (Italy).

UNIFICATION OF ELECTROMAGNETIC, STRONG AND WEAK INTERACTION

Duong Van Phi and Duong Anh Duc (Ho Chi Minh City Univ., Ho Chi Minh, Viet Nam.) Sep. 1993 13 p

(DE94-628570; IC-93/311) Avail: CASI HC A03/MF A01 (US Sales Only)

The Unification of Electromagnetic, Strong and Weak Interactions is realized in the framework of the Quantum Field Theory, established in an 8-dimensional Unified Space. Two fundamental, spinor and vector field equations are considered. The first of the matter particles and the second is of the gauge particles. Interaction Lagrangians are formed from the external and internal currents and the external and internal vector field operators. Generators of the local gauge transformations are the combinations of the matrices of the first field equation. DOE

N95-22813*# Jet Propulsion Lab., California Inst. of Tech., Pasadena, CA.

ADDENDUM TO THE PROCEEDINGS OF THE THIRD INTERNATIONAL MOBILE SATELLITE CONFERENCE (IMSC 1993)

Robert Kwan, comp., Jack Rigley, comp. (Communications Research Centre, Ottawa, Ontario.), and Randy Cassingham, ed. 1993 52 p Conference held in Pasadena, CA, 16-18 Jun. 1993 Prepared in cooperation with Communications Research Centre, Ottawa, Ontario

(Contract NAS7-918; RTOP 669-00-00)

(NASA-CR-197343; JPL-Publ-93-009-Add; NAS 1.26:197343) Avail: CASI HC A04/MF A01

Satellite-based mobile communications systems provide voice and data communications to users over a vast geographic area. The users may communicate via mobile or hand-held terminals, which may also provide access to terrestrial cellular communications services. This Third IMSC focuses on the increasing worldwide commercial activities in Mobile Satellite Services, along with technical advances in the field. Because of the large service areas provided by such systems, it is important to consider political and regulatory issues in addition to technical and user requirements issues. The official Proceedings presented in 11 sessions include: direct broadcast of audio programming from satellites; spacecraft technology; regulatory and policy considerations; hybrid networks for personal and mobile applications; advanced system concepts and analysis; propagation; and mobile terminal technology; and mobile antenna technology. For individual titles, see N95-22814 through N95-22819.

N95-22814*# National Aeronautics and Space Administration. Lewis Research Center, Cleveland, OH.

UTILIZING A TDRS SATELLITE FOR DIRECT BROADCAST SATELLITE-RADIO PROPAGATION EXPERIMENTS AND DEMONSTRATIONS **c18**

James E. Hollansworth *In* JPL, Addendum to the Proceedings of the Third International Mobile Satellite Conference (IMSC 1993) 1993 p 13-18 (For primary document see N95-22813 07-32)

Avail: CASI HC A02/MF A01

The NASA/VOA Direct Broadcast Satellite - Radio (DBS-R) Program will be using a NASA Tracking Data Relay Satellite (TDRS) satellite at 62 deg West longitude to conduct live satellite S-band propagation experiments and demonstrations of satellite sound broadcasting over the next two years (1993-1994). The NASA/VOA DBS-R program has applied intensive effort to garner domestic and international support for the DBS-R concept. An S-band DBS-R allocation was achieved for Region 2 at WARC-92 held in Spain. With this allocation, the DBS-R program now needs to conduct S-band propagation experiments and systems demonstrations that will assist in the development of planning approaches for the use of Broadcast Satellite Service (Sound) frequency bands prior to the planning conference called for by WARC-92. These activities will also support receiver concept development applied to qualities ranging from AM to Monophonic FM, Stereophonic FM, Monophonic CD, and Stereophonic CD quality. Author

N95-22815*# European Space Agency. European Space Research and Technology Center, ESTEC, Noordwijk (Netherlands). Communications Satellites Dept.

ADAPTIVE BEAMFORMING IN A CDMA MOBILE SATELLITE COMMUNICATIONS SYSTEM

Samuel G. Munoz-Garcia *In* JPL, Addendum to the Proceedings of the Third International Mobile Satellite Conference (IMSC 1993) 1993 p 19-24 Presented at the ERA Conference on DSP: The Enabling Technology for Communications, Amsterdam, Netherlands, 9-10 Mar. 1993 (For primary document see N95-22813 07-32)

Avail: CASI HC A02/MF A01

Code-Division Multiple-Access (CDMA) stands out as a strong contender for the choice of multiple access scheme in these future mobile communication systems. This is due to a variety of reasons such as the excellent performance in multipath environments, high scope for frequency reuse and graceful degradation near saturation. However, the capacity of CDMA is limited by the self-interference between the transmissions of the different users in the network. Moreover, the disparity between the received power levels gives rise to the near-far problem, this is, weak signals are severely degraded by the transmissions from other users. In this paper, the use of time-reference adaptive digital beamforming on board the satellite is proposed as a means to overcome the problems associated with CDMA.

This technique enables a high number of independently steered beams to be generated from a single phased array antenna, which automatically track the desired user signal and null the unwanted interference sources. Since CDMA is interference limited, the interference protection provided by the antenna converts directly and linearly into an increase in capacity. Furthermore, the proposed concept allows the near-far effect to be mitigated without requiring a tight coordination of the users in terms of power control. A payload architecture will be presented that illustrates the practical implementation of this concept. This digital payload architecture shows that with the advent of high performance CMOS digital processing, the on-board implementation of complex DSP techniques -in particular digital beamforming- has become possible, being most attractive for Mobile Satellite Communications. Derived from text

N95-22816*# Harris Corp., Melbourne, FL.
PASSIVE INTERMODULATION GENERATION IN WIRE MESH DEPLOYABLE REFLECTOR ANTENNAS
Gregory M. Turner *In* JPL, Addendum to the Proceedings of the Third International Mobile Satellite Conference (IMSC 1993) 1993 p 25-30 (For primary document see N95-22813 07-32)
Avail: CASI HC A02/MF A01

Deployable reflector antennas represent a proven technology with obvious benefits for mobile satellite applications. Harris Corporation has provided deployable reflector antennas for NASA's Tracking and Data Relay Satellite System (TDRSS). These antennas utilize a rigid, radial rib unfurlable reflector with a wire mesh surface. This type of mesh has been identified as a potential design risk for multichannel communications applications based on the potential for generation of Passive Intermodulation (PIM). These concerns are based on the existence of numerous, nonpermanent metal to metal contacts that are inherent to the mesh design. To address this issue, Harris has an ongoing IR&D program to characterize mesh PIM performance. This paper presents the results of the investigation into mesh PIM performance to date and provides background information on the design and performance of the Harris radial rib deployable reflector. Author

N95-22817*# European Space Agency. European Space Research and Technology Center, ESTEC, Noordwijk (Netherlands).
THE POSSIBILITIES FOR MOBILE AND FIXED SERVICES UP TO THE 20/30 GHz FREQUENCY BANDS
Clifford D. Hughes, F. Feliciani, and J. Spiller (MATRA Marconi Space Portsmouth, Hampshire, England.) *In* JPL, Addendum to the Proceedings of the Third International Mobile Satellite Conference (IMSC 1993) 1993 p 31-36 (For primary document see N95-22813 07-32)
Avail: CASI HC A02/MF A01

Satellite Communications and broadcasting is presently in a period of considerable change. In the fixed service there is strong competition from terrestrial fiber optic systems which have virtually arrested the growth of the traditional satellite market for long distance high capacity communications. The satellite has however made considerable progress in areas where it has unique advantages; for example, in point to multipoint (broadcasting), multipoint to point (data collection) and generally in small terminal system applications where flexibility of deployment coupled with ease of installation are of importance. In the mobile service, in addition to the already established geostationary systems, there are numerous proposals for HEO, MEO and LEO systems. There are also several new frequency allocations as a result of the WARC 92 to be taken into account. At one extreme there are researchers working on Ka band 20/30 GHz mobile systems and there are other groups who foresee no future above the L-band frequency allocations. Amongst all these inputs it is difficult to see the direction in which development activities both for satellites and for earth segment should be focused. However, as an aid to understanding, this paper seeks to find some underlying relationships and to clarify some of the variables. Derived from text

N95-22818*# Nauchno-Proizvodstvennoe Obedinenie Precision Instruments, Moscow (Russia).
GEOLOCATION APPLICATIONS OF THE GONETS LEO MESSAGING SATELLITES
Vladimir N. Vlasov and Javad M. Ashjaee (Ashtech, Inc., Sunnyvale, CA.) *In* JPL, Addendum to the Proceedings of the Third International Mobile Satellite Conference (IMSC 1993) 1993 p 37-42 (For primary document see N95-22813 07-32)
Avail: CASI HC A02/MF A01

Geostationary satellites carry a majority of the international telecommunications traffic not carried by transoceanic cable. However, because the radio path links to and from geostationary satellites total at least 70,000 km and because of inherent on-board spacecraft power limitations, earth stations used in conjunction with geostationary satellites are usually large and expensive. This limits their installation to areas with a well-developed industrial and economic infrastructure. This reality helps perpetuate a chicken egg dilemma for the developing countries and isolated regions. Economic integration with the developed world requires being 'networked'. But for many developing entities, even the initial price of entry exceeds their modest resources. Exclusion from the global information highways virtually assures retardation of economic growth for developing nations, remote and isolated areas. Very Small Aperture Terminal (VSAT) earth stations are often thought of as a solution for networking developing regions. But economic considerations often forecloses this option. If VSAT size and cost is to be minimized, powerful spot beams from the satellite need to be focused on relatively small regions. This is not often feasible because of the high cost of the satellite itself. To dedicate a high power spot beam to a small region is usually not economically feasible. Derived from text

N95-22819*# Bradford Univ. (England). Dept. of Electronic and Electrical Engineering.
LOW EARTH ORBIT SATELLITE/TERRESTRIAL MOBILE SERVICE COMPATIBILITY
Ray E. Sheriff and John G. Gardiner *In* JPL, Addendum to the Proceedings of the Third International Mobile Satellite Conference (IMSC 1993) 1993 p 43-48 (For primary document see N95-22813 07-32)
Avail: CASI HC A02/MF A01

Currently the geostationary type of satellite is the only one used to provide commercial mobile-satellite communication services. Low earth orbit (LEO) satellite systems are now being proposed as a future alternative. By the implementation of LEO satellite systems, predicted at between 5 and 8 years time, mobile space/terrestrial technology will have progressed to the third generation stage of development. This paper considers the system issues that will need to be addressed when developing a dual mode terminal, enabling access to both terrestrial and LEO satellite systems. Author

N95-22841 International Centre for Theoretical Physics, Trieste (Italy).
GENERALIZED PHASE TRANSFORMATIONS OF SPINOR FIELDS
S. G. Mikhov Sep. 1993 18 p Limited Reproducibility: More than 20% of this document may be affected by microfiche quality
(DE94-628505; IC-93/320) Avail: Issuing Activity (Department of Energy (DOE)) (US Sales Only)

In this paper some generalized four parameter phase transformations of a Dirac spinor are considered. It is shown that a corresponding compensating transformation of the electromagnetic field which restores the invariance of the Dirac-Maxwell equation might exist, provided some consistency conditions are satisfied by the parameters of the transformations. These transformations are used further to consider the Maxwell equations under the assumption that a Bosonization takes place. Only one of the considered cases proves to have a solution (the other cases show to be trivial) which although unphysical is obtained explicitly. DOE

N95-22852*# Jet Propulsion Lab., California Inst. of Tech., Pasadena, CA.
SYNTHESIS OF A LARGE COMMUNICATIONS APERTURE USING SMALL ANTENNAS
George M. Resch, T. W. Cwik, V. Jamnejad, R. T. Logan, R. B. Miller, and Dave H. Rogstad 1 Jul. 1994 130 p
(Contract NAS7-918; RTOP 315-91-60-10-07)
(NASA-CR-197330; JPL-Publ-94-15; NAS 1.26:197330) Avail: CASI HC A07/MF A02

In this report we compare the cost of an array of small antennas to that of a single large antenna assuming both the array and single large antenna have equal performance and availability. The single large antenna is taken to be one of the 70-m antennas of the Deep Space Network. The cost of the array is estimated as a function of the array element

diameter for three different values of system noise temperature corresponding to three different packaging schemes for the first amplifier. Array elements are taken to be fully steerable paraboloids and their cost estimates were obtained from commercial vendors. Array loss mechanisms and calibration problems are discussed. For array elements in the range 3 - 35 m there is no minimum in the cost versus diameter curve for the three system temperatures that were studied. Author

N95-22944*# New Mexico State Univ., Las Cruces, NM. Center for Space Telemetering and Telecommunications Systems.
IMPROVED SMALL SATELLITE ACCESS OF THE SPACE NETWORK Report, Jun. - Dec. 1994
Stephen Horan, William P. Osborne, and Timothy Minnix 14 Dec. 1994 128 p
(Grant NAG5-1491)
(NASA-CR-197863; NAS 1.26:197863) Avail: CASI HC A07/MF A02

This report contains the results of a study performed under the sponsorship of the National Aeronautics and Space Administration (NASA) made as a grant to the Center for Space Telemetering and Telecommunication Systems at New Mexico State University. The purpose of this phase of the grant is to increase user access to the Space Network (SN) run by NASA for supplying space-to-ground communications for satellites and associated control centers. The identified need is to bring more users into the community of those accessing the SN, especially those in the small satellite class of users. The initial phase of the study concerned the potential for modifications to the standard transponder used in the SN. The results of that investigation are summarized in Section 4. As the hardware modifications were being investigated, a second option was developed, namely to consider changes to the operational mode for the small satellites. This operational concept was to use a single, fixed-pointing antenna in a spin-stabilized satellite and let the antenna pattern sweep past the Tracking and Data Relay Satellites (TDRS) in the SN. The question to be answered by this phase of the study was twofold: could enough contact time per day be made available using this simple operating mode and could the data rate be high enough to allow for sufficient data throughput to satisfy the user community using existing components. Section 2 outlines the methodology and simulation results to answer these questions. Section 3 contains a summary of an operational simulation of a simple satellite payload using these contact scenarios. The simulation is not all inclusive but shows how a payload simulation could be configured to utilize variable contact times. The answer to both of the questions desired to be answered is affirmative. By carefully choosing the correct system transmission power and antenna pattern, the system will allow support to the 50th percentile of expected systems. It is recommended that based on this initial study, further work be done to quantify the exact parameters for transmission through the space network and to optimize usage of the contact time to maximize throughput. Author

N95-23023# Naval Research Lab., Washington, DC.
EFFECTS OF MODULATION INDEX ON TELECOMMUNICATIONS
Junho Choi and Porter Lyon 26 Sep. 1994 53 p
(AD-A286018; NRL/FR/8140-94-9739) Avail: CASI HC A04/MF A01

The relationship between modulation index and telecommunication link was studied for the Deep Space Program Science Experiment. Analytical aspects of modulation index are presented with a brief overview of modulation process in the relational format. Relations of modulation index with bandwidth, ranging/command/telemetry/carrier power losses, bit error rate, signal-to-noise ratio, and hardware simulation results of DSPSE communication links have been investigated with samples of graphical analysis to show optimum ranges of modulation indexes. It is noted that the influence of modulation indexes should not be overlooked in space communication link analysis. DTIC

N95-23075# Oak Ridge National Lab., TN.
A DRAFT STANDARD FOR MESSAGE PASSING IN A DISTRIBUTED MEMORY ENVIRONMENT
J. J. Dongarra (Tennessee Univ., Knoxville, TN.), R. Hempel (Gesellschaft fuer Mathematik und Datenverarbeitung, Saint Augustin, Germany.), A. J. G. Hey (Southampton Univ., England.), and David W. Walker 1994 18 p Presented at the 5th ECMWF Workshop on Parallel Processing in Meteorology, Reading, England, 23-27 Nov. 1992
(Contract DE-AC05-84OR-21400)
(DE94-019159; CONF-9211198-4) Avail: CASI HC A03/MF A01

This paper describes Message Passing Interface 1 (MPI1), a proposed library interface standard for supporting point-to-point message passing. The intended standard will be provided with Fortran 77 and C interfaces, and will form the basis of a standard high level communication environment featuring collective communication and data distribution transformations. The standard proposed here provides blocking and nonblocking message passing between pairs of processes, with message selectivity by source process and message type. Provision is made for noncontiguous messages. Context control provides a convenient means of avoiding message selectivity conflicts between different phases of an application. The ability to form and manipulate process groups permits task parallelism to be exploited. DOE

N95-23151# Technische Univ., Eindhoven (Netherlands). Dept. of Mathematics and Computing Science.
ALGEBRAIC SEMANTICS OF BASIC MESSAGE SEQUENCE CHARTS
S. Mauw and M. A. Reniers Apr. 1994 19 p See also PB95-110581
(PB95-138970) Avail: CASI HC A03/MF A01

Message Sequence Charts are a widely used technique for the visualization of communications between system components. We present a formal semantics of Basic Message Sequence Charts, exploiting techniques from process algebra. This semantics is based on the semantics of the full language as proposed for standardization in the International Telecommunication Union. NTIS

N95-23391*# Ohio State Univ., Columbus, OH. ElectroScience Lab.
A UNIFORM GEOMETRICAL OPTICS AND AN EXTENDED UNIFORM GEOMETRICAL THEORY OF DIFFRACTION FOR EVALUATING HIGH FREQUENCY EM FIELDS NEAR SMOOTH CAUSTICS AND COMPOSITE SHADOW BOUNDARIES Final Report
E. D. Constantinides and R. J. Marhefka Oct. 1994 215 p
(Grant NsG-1498)
(NASA-CR-197934; NAS 1.26:197934; Rept-725311-3) Avail: CASI HC A10/MF A03

A uniform geometrical optics (UGO) and an extended uniform geometrical theory of diffraction (EUTD) are developed for evaluating high frequency electromagnetic (EM) fields within transition regions associated with a two and three dimensional smooth caustic of reflected rays and a composite shadow boundary formed by the caustic termination or the confluence of the caustic with the reflection shadow boundary (RSB). The UGO is a uniform version of the classic geometrical optics (GO). It retains the simple ray optical expressions of classic GO and employs a new set of uniform reflection coefficients. The UGO also includes a uniform version of the complex GO ray field that exists on the dark side of the smooth caustic. The EUTD is an extension of the classic uniform geometrical theory of diffraction (UTD) and accounts for the non-ray optical behavior of the UGO reflected field near caustics by using a two-variable transition function in the expressions for the edge diffraction coefficients. It also uniformly recovers the classic UTD behavior of the edge diffracted field outside the composite shadow boundary transition region. The approach employed for constructing the UGO/EUTD solution is based on a spatial domain physical optics (PO) radiation integral representation for the fields which is then reduced using uniform asymptotic procedures. The UGO/EUTD analysis is also employed to investigate the far-zone RCS problem of plane wave scattering from two and three dimensional polynomial defined surfaces, and uniform reflection, zero-curvature, and edge diffraction coefficients are derived. Numerical results for the scattering and diffraction from cubic and fourth order polynomial strips are also shown and the UGO/EUTD solution is validated by comparison to an independent moment method (MM) solution. The UGO/EUTD solution is also compared with the classic GO/UTD solution. The failure of the classic techniques near caustics and composite shadow boundaries is clearly demonstrated and it is shown that the UGO/EUTD results remain valid and uniformly reduce to the classic results away from the transition regions. Mathematical details on the asymptotic properties and efficient numerical evaluation of the canonical functions involved in the UGO/EUTD expressions are also provided. Author

N95-23670*# Clemson Univ., SC. Radar Systems Lab.
MAXIMUM-LIKELIHOOD SPECTRAL ESTIMATION AND ADAPTIVE FILTERING TECHNIQUES WITH APPLICATION TO AIRBORNE DOPPLER WEATHER RADAR Thesis Technical Report No. 20
Jonathan Y. Lai 28 Nov. 1994 88 p
(Grant NAG1-928)
(NASA-CR-197699; NAS 1.26:197699; TR-112894-3570P) Avail: CASI HC A05/MF A01

This dissertation focuses on the signal processing problems associated with the detection of hazardous windshears using airborne Doppler radar when weak weather returns are in the presence of strong clutter returns. In light of the frequent inadequacy of spectral-processing oriented clutter suppression methods, we model a clutter signal as multiple sinusoids plus Gaussian noise, and propose adaptive filtering approaches that better capture the temporal characteristics of the signal process. This idea leads to two research topics in signal processing: (1) signal modeling and parameter estimation, and (2) adaptive filtering in this particular signal environment. A high-resolution, low SNR threshold maximum likelihood (ML) frequency estimation and signal modeling algorithm is devised and proves capable of delineating both the spectral and temporal nature of the clutter return. Furthermore, the Least Mean Square (LMS) -based adaptive filter's performance for the proposed signal model is investigated, and promising simulation results have testified to its potential for clutter rejection leading to more accurate estimation of windspeed thus obtaining a better assessment of the windshear hazard. Author

N95-23772# Los Alamos National Lab., NM.
NETWORK EVENT RECORDING DEVICE: AN AUTOMATED SYSTEM FOR NETWORK ANOMALY DETECTION, AND NOTIFICATION
D. G. Simmons and R. Wilkins 1994 28 p Presented at the Internet Society Symposium, San Diego, CA, 16-27 Feb. 1995
(Contract W-7405-eng-36)
(DE94-018274; LA-UR-94-2790; CONF-950233-1) Avail: CASI HC A03/MF A01

The goal of the Network Event Recording Device (NERD) is to provide a flexible autonomous system for network logging and notification when significant network anomalies occur. The NERD is also charged with increasing the efficiency and effectiveness of currently implemented network security procedures. While it has always been possible for network and security managers to review log files for evidence of network irregularities, the NERD provides real-time display of network activity, as well as constant monitoring and notification services for managers. Similarly, real-time display and notification of possible security breaches will provide improved effectiveness in combating resource infiltration from both inside and outside the immediate network environment. DOE

N95-23794# Rochester Univ., NY. Dept. of Computer Science.
REEVALUATION OF THE SIGNIFICANCE OF SEQUENCE INFORMATION FOR SPEECH RECOGNITION
Ramesh R. Sarukkai and Dana H. Ballard Dec. 1994 21 p
(Grants NSF IRI-89-03592; PHS-1-R24-RR-06853-02)
(TR-555) Avail: CASI HC A03/MF A01

A central difficulty with automatic speech recognition is the temporally inaccurate nature of the speech signal. Despite this, speech has been traditionally modeled as a purely sequential (albeit probabilistic) process. The usefulness of accurate sequence information is reevaluated in this paper, both at the acoustic and lexical levels for the task of speech recognition. At the acoustic level, speech segments are quantized into discrete vectors, and converted into set representations as opposed to accurate sequences. Recognition of the quantized vector sets dramatically improved performance as contrasted with the corresponding vector sequence representations. At the lexical level, our study suggests that accurate sequence information is, again, not crucial. In fact locally discarding phoneme sequence information may be useful for coping with errors (such as insertion, substitution). Based on the idea of phone set indexing, a lexical access algorithm is developed. Thus, this work questions the traditional approach of modeling speech as a purely sequential process, and suggests that discarding local sequential information may be a good idea. As an alternative to a purely sequential representation, a set representation seems to be a viable option. Author

N95-23937# Rochester Univ., NY. Dept. of Computer Science.
SPOKEN DIALOGUE UNDERSTANDING AND LOCAL CONTEXT
Peter A. Heeman Jul. 1994 53 p Sponsored by Natural Sciences and Engineering Research Council of Canada
(Contract NSF IRI-90-13160; N00014-92-J-1512)
(TR-523) Avail: CASI HC A04/MF A01

Spoken dialogue poses many new problems to researchers in the field of computational linguistics. In particular, conversants must detect and correct speech repairs, segment a turn into individual utterances, and identify discourse markers. These problems are interrelated. For instance, there are some lexical items whose role in an utterance can be ambiguous: they can act as discourse markers, signal as speech repair, or even be part of the content of an utterance unit. So, these issues must be addressed together. The resolution of these problems will allow a basic understanding of how a speaker's turn can be broken down into individual contributions to the dialogue. We propose that this resolution must be and can be done using local context. They do not require a full understanding of the dialogue so far, nor, in most cases, a deep understanding of the current turn. Resolving these issues locally also means they can be resolved for the most part before later processing, and so will make a natural language understanding system more robust and able to deal with the unconstrained nature of spoken dialogue. Author

N95-24015# Los Alamos National Lab., NM.
TRACKER: A THREE-DIMENSIONAL RAYTRACING PROGRAM FOR IONOSPHERIC RADIO PROPAGATION
P. E. Argo, D. DeLapp, C. D. Sutherland, and R. G. Farrer 1994 1746 p
(Contract W-7405-eng-36)
(DE95-003510; LA-UR-94-3706) Avail: CASI HC A99/MF A10

TRACKER is an extension of a three-dimensional Hamiltonian raytrace code developed some thirty years ago by R. Michael Jones. Subsequent modifications to this code, which is commonly called the 'Jones Code' were documented by Jones and Stephensen (1975). TRACKER incorporates an interactive user's interface, modern differential equation integrators, graphical outputs, homing algorithms, and the Ionospheric Conductivity and Electron Density (ICED) ionosphere. TRACKER predicts the three-dimensional paths of radio waves through model ionospheres by numerically integrating Hamilton's equations, which are a differential expression of Fermat's principle of least time. By using continuous models, the Hamiltonian method avoids false caustics and discontinuous raypath properties often encountered in other raytracing methods. In addition to computing the raypath, TRACKER also calculates the group path (or pulse travel time), the phase path, the geometrical (or 'real') pathlength, and the Doppler shift (if the time variation of the ionosphere is explicitly included). Computational speed can be traded for accuracy by specifying the maximum allowable integration error per step in the integration. Only geometrical optics are included in the main raytrace code; no partial reflections or diffraction effects are taken into account. In addition, TRACKER does not lend itself to statistical descriptions of propagation -- it requires a deterministic model of the ionosphere. DOE

N95-24039# Rochester Univ., NY. Dept. of Computer Science.
PHONETIC SET HASHING: A NOVEL SCHEME FOR TRANSFORMING PHONE SEQUENCES TO WORDS
Ramesh R. Sarukkai and Dana H. Ballard Nov. 1994 21 p
(Grants NSF IRI-89-03582; PHS-1-R24-RR-06853-02)
(TR-538) Avail: CASI HC A03/MF A01

The usefulness of accurate sequence information is re-evaluated in this paper. A novel idea, called phonetic set hashing, for transforming phone sequences to words is then suggested. Phone sequences are mapped onto the corresponding phone sets, and the latter used as keys for indexing appropriate words. By using data-driven training strategies, the problem of word segmentation has been alleviated. The robustness of phone set hashing towards insertion, deletion, and substitution errors has also been studied. Experiments with subsets of the TIMIT database indicate that phone set hashing is a simple, fast scheme for word pre-selection. Author

N95-24044 British Broadcasting Corp., Tadworth (England). Research and Development Dept.
DRACULA: DYNAMIC RANGE CONTROL FOR BROADCASTING AND OTHER APPLICATIONS

N. H. C. Gilchrist 1994 13 p
(BBC-RD-1994/13) Copyright Avail: Issuing Activity (BBC, Kingswood Warren, Tadworth, Surrey, England)

The BBC has developed a digital processor which is capable of reducing the dynamic range of audio in an unobtrusive manner. It is ideally suited to the task of controlling the level of musical programs. Operating as a self-contained dynamic range controller, the processor is suitable for controlling levels in conventional AM or FM broadcasting, or for applications such as the compression of program material for in-flight entertainment. It can, alternatively, be used to provide a supplementary signal in DAB (digital audio broadcasting) for optional dynamic compression in the receiver.

Author

N95-24193# Rochester Univ., NY. Dept. of Computer Science.
THE TRAINS PROJECT: A CASE STUDY IN BUILDING A CONVERSATIONAL PLANNING AGENT
James F. Allen, Lenhart K. Schubert, George Ferguson, Peter Heeman, Chung Hee Hwang, Tsuneaki Kato (Nippon Electric Co. Ltd., Kanagawa, Japan.), Marc Light, Nathaniel G. Martin, Bradford W. Miller, and Massimo Poesio (Edinburgh Univ., Scotland.) et al Sep. 1994 60 p Submitted for publication
(Contracts F30602-91-C-0010; N00014-92-J-1512; NSF IRI-90-13160)
(TR-532; TN-94-3) Avail: CASI HC A04/MF A01

The TRAINS project is an effort to build a conversationally proficient planning assistant. A key part of the project is the construction of the TRAINS system, which provides the research platform for a wide range of issues in natural language understanding, mixed-initiative planning systems, and representing and reasoning about time, actions and events. Four years have not passed since the beginning of the project. Each year, we produced a demonstration system that focused on a dialog that illustrated particular aspects of our research. The commitment to building complete integrated systems is a significant overhead on the research, but we feel it is essential to guarantee that the results constitute real progress in the field. This paper describes the goals of the project, and our experience with the effort so far.

Author

N95-23682*# National Aeronautics and Space Administration. Lyndon B. Johnson Space Center, Houston, TX.
TOWARD AN AUTOMATED SIGNATURE RECOGNITION TOOLKIT FOR MISSION OPERATIONS
T. Cleghorn, P Laird (National Aeronautics and Space Administration. Ames Research Center, Moffett Field, CA.), L. Perrine, C. Culbert, M. Macha, R. Saul (RECOM Technologies, Inc., Moffett Field, CA.), D. Hammen (Mitre Corp., Houston, TX.), T. Moebes (Science Applications International Corp., Houston, TX.), and R. Shelton *In* JPL, Third International Symposium on Artificial Intelligence, Robotics, and Automation for Space 1994 Oct. 1994 p 53-56 (For primary document see N95-23672 07-63)
Avail: CASI HC A01/MF A03

N95-23710*# Communications Research Lab., Koganei (Japan).
ROBUST CONTROL OF MULTI-JOINTED ARM WITH A DECENTRALIZED AUTONOMOUS CONTROL MECHANISM
Shinichi Kimura, Ken Miyazaki, and Yoshiaki Suzuki *In* JPL, Third International Symposium on Artificial Intelligence, Robotics, and Automation for Space 1994 191-195 (SEE N95-23672 07-63) Oct. 1994 (For primary document see N95-23672 07-63)
Avail: CASI HC A02/MF A03

33 ELECTRONICS AND ELECTRICAL ENGINEERING

Includes test equipment and maintainability; components, e.g., tunnel diodes and transistors; microminiaturization; and integrated circuitry.

For related information see also *60 Computer Operations and Hardware* and *76 Solid-State Physics.*

N95-22504# Lawrence Livermore National Lab., Livermore, CA.
A HIGH-POWER SWITCH-MODE DC POWER SUPPLY FOR DYNAMIC LOADS
D. W. Shimer, A. C. Lange, and J. N. Bombay (Kaiser Engineers, Oakland, CA.) 23 Jun. 1994 9 p Presented at the 1994 Institute for Electrical and Electronics Engineers (IEEE) Industry Applications Annual Meeting, Denver, CO, 2-7 Oct. 1994
(Contract W-7405-eng-48)
(DE94-016714; UCRL-JC-115595; CONF-9410168-1) Avail: CASI HC A02/MF A01

High-voltage dc power supplies are often required to operate with highly dynamic loads, such as arcs. A switch-mode dc power supply can offer significant advantages over conventional thyristor-based dc power supplies under such conditions. It can quickly turn off the supply to extinguish the arc, and it can quickly recover after the arc. It has a relatively small output filter capacitance, which results in small stored energy available to the arc. A 400-kW, 50-kV switch-mode dc power supply for an electron-beam gun that exploits these advantages was designed and tested. It uses four 100-kW, current-source-type dc-dc converters with inputs in parallel and outputs in series. The dc-dc converters operate at 20 kHz in the voltage regulator part and 10 kHz in the inverter, transformer, and output rectifier part of the circuit. Insulated gate bipolar transistors (IGBT's) are used as the power switches. Special techniques are used to protect the power supply and load against arcs and hard shorts. The power supply has an efficiency of 93%, an output voltage ripple of 1%, and fast dynamic response. In addition, it is nearly one-third the size of conventional power supplies.

DOE

N95-22507 Illinois Univ., Urbana, IL. Coordinated Science Lab.
CURRENT ESTIMATION FOR ELECTROMIGRATION, HOT CARRIERS, AND VOLTAGE DROP Final Report, Aug. 1992 - 1993
Ibrahim N. Hajj, George Stamoulis, Ping-Chung Li, Harish Kriplani, and Gautham Kamath Sep. 1994 167 p Limited Reproducibility: More than 20% of this document may be affected by microfiche quality
(Contract F30602-92-C-0059)
(AD-A285794; RL-TR-94-124) Avail: CASI HC A08

This report summarizes work in reliability analysis in VLSI CMOS circuits, particularly electromigration in metal lines, power busses and signal lines, hot carrier effects in devices, and voltage drop in power busses. In addition to process parameters, all of these effects can be shown to depend on current flow in the circuit. More specifically, electromigration and hot carrier induced degradation are both long-term effects and are related to the average current flow over time under all possible input signals that the design experiences. Maximum voltage drop, on the other hand, depends on finding the maximum current flow in the power busses, caused by a specific few inputs. Thus, our emphasis in this work is on developing fast and reliable methods for estimating average and maximum currents. In addition, we have also improved on our bus extractor to extract accurate RC models of power busses from layout information for electromigration and voltage drop estimation. This work is part of our goal of developing CAD tools for estimating physical reliability effects in VLSI designs, and to automatically modify the design, or at least suggest design changes, in order to improve the short and long term reliability of the design under realistic operating conditions.

DTIC

N95-22549# Sandia National Labs., Albuquerque, NM.
HIGH GAIN GaAs PHOTOCONDUCTIVE SEMICONDUCTOR SWITCHES FOR IMPULSE SOURCES
G. M. Loubriel, F. J. Zutavern, M. W. OMalley, and W. D. Helgeson 1994 8 p Presented at the Brittle Fracture Safety Assessment, Krefeld, Germany, Oct. 1994
(Contract DE-AC04-94AL-85000)
(DE95-001885; SAND-94-0882C; CONF-9410134-3) Avail: CASI HC A02/MF A01

A high peak power impulse pulser that is controlled with high gain, optically triggered GaAs Photoconductive Semiconductor Switches (PCSS) has been constructed and tested. The system has a short 50 Omega line that is charged to 100 kV and discharged through the switch when the switch is triggered with as little as 90 nJ of laser energy. We have demonstrated that the GaAs switches can be used to produce either a monocycle or a monopulse with a period or total duration of about 3 ns. For the monopulse, the voltage switched was above 100 kV, producing a peak power of about 48 MW to the 30 Omega load at a burst repetition rate of 1 kHz. The laser that is used is a small laser diode array whose output is delivered through a fiber to the switch. The current in the system

has rise times of 430 ps and a pulse width of 1.4 ns when two laser diode arrays are used to trigger the switch. The small trigger energy and switch jitter are due to a high gain switching mechanism in GaAs. DOE

N95-22569# Argonne National Lab., IL.
CONCEPTUAL DESIGN OF A 20-kA CURRENT LEAD USING FORCED-FLOW COOLING AND Ag-ALLOY-SHEATHED Bi-2223 HIGH-TEMPERATURE SUPERCONDUCTORS
Reinhard Heller (Kernforschungszentrum G.m.b.H., Karlsruhe, Germany.) and John R. Hull 1994 5 p Presented at the Applied Superconductivity Conference, Boston, MA, 16-21 Oct. 1994
(Contract W-31-109-eng-38)
(DE95-002916; ANL/ET/CP-82300; CONF-941013-10) Avail: CASI HC A01/MF A01

High-temperature superconductors (HTS's), consisting of Bi-2223 HTS tapes sheathed with Ag alloys are proposed for a 20-kA current lead for the planned stellarator WENDELSTEIN 7-X. Forced-flow He cooling is used, and 4-K He cooling of the whole lead as well as 60-K He cooling of the copper part of the lead, is discussed. Power consumption and behavior in case of loss of He flow are given. DOE

N95-22586# National Renewable Energy Lab., Golden, CO.
RESEARCH ON DEFECTS AND TRANSPORT IN AMORPHOUS-SILICON-BASED SEMICONDUCTORS Final Subcontractor Report, 20 Feb. 1991 - 19 Apr. 1994
E. A. Schiff, H. Antoniadis, Q. Gu, J. K. Lee, Q. Wang, and S. Zafar Sep. 1994 28 p
(Contract DE-AC36-83CH-10093)
(DE94-011888; NREL/TP-451-7164) Avail: CASI HC A03/MF A01

This report describes work on three individual tasks as follows. (1) Electron and hole drift measurements in a-Si(1-x)Ge(x):H and a-Si(1-x)C(x):H p-i-n solar cells: Multijunction solar cells incorporating modified band gap a-Si:H in a triple-junction structure are generally viewed as the most promising avenue for achieving an amorphous silicon-based solar cell with 15% stabilized conversion efficiency. The specific objective of this task was to document the mobilities and deep-trapping mobility-lifetime products for electrons and holes in a-Si(1-x)Ge(x):H and a-Si(1-x)C(x):H alloys materials. (2) Electroabsorption measurements and built-in potential (V(sub bi)) in solar cells: V(sub bi) in a p-i-n solar cell may be limiting the open-circuit voltage (V(sub oc)) in wide-band-gap cells (E(sub g) greater than 1.8 eV) currently under investigation as the top cell for 15% triple junction devices. The research addressed four issues that need to be resolved before the method can yield an error less than 0.1 V for V(sub bi). (3) Defect relaxation and Shockley-Read kinetics in a-Si:H: Quantitative modeling of solar cells is usually based on Shockley-Read kinetics. An important assumption of this approach is that the rate of emission of a photocarrier trapped on a defect is independent of quasi-Fermi level location. DOE

N95-22591# International Centre for Theoretical Physics, Trieste (Italy).
METALLIZATION AND INCOMPLETE MELTING OF A SEMICONDUCTOR SURFACE AT HIGH TEMPERATURE
Noboru Takeuchi, E. Tosatti (International School for Advanced Studies, Trieste, Italy.), and A. Selloni Oct. 1993 15 p
(DE94-627342; IC-93/365) Avail: CASI HC A03/MF A01 (US Sales Only)

We present a first microscopic study of the state of a semiconductor surface, clean Ge(111), close to the bulk melting temperature. Both electronic states and ionic motions are fully treated via first-principles molecular dynamics. Results indicate a clear dynamical disordering, however confined to the first atomic bilayer. This region acquires a liquid-like diffusion, and is metallic. Lack of melting of the second and deeper bilayers, found to be in good quantitative agreement with recent x-ray data, indicates an incomplete wetting of the semiconducting solid by its own metallic melt. Previously conflicting data on Ge(111) are also reconciled within this picture. DOE

N95-22593# Argonne National Lab., IL. Chemistry and Material Science Div.
SURFACE IMPEDANCE STUDIES ON THE ELECTRODYNAMICAL RESPONSE OF ORGANIC SUPERCONDUCTORS
M. Dressel, O. Klein, S. Bruder, G. Gruener, K. D. Carlson (California Univ., Los Angeles, CA.), H. H. Wang (California Univ., Los Angeles, CA.), and J. M. Williams (California Univ., Los Angeles, CA.) 1994 4 p Presented at the International Conference on Science and Technology of Synthetic Metals, Seoul, Republic of Korea, 24-29 Jul. 1994
(Contract W-31-109-eng-38)
(DE95-002986; ANL/CHM/CP-84364; CONF-9407117-5) Avail: CASI HC A01/MF A01

The authors have performed detailed measurements of the surface impedance in the normal and superconducting state of kappa-(BEDT-TTF)2Cu(NCS)2 in the millimeter wave frequency range (1 cm(exp -1) to 3 cm(exp -1)), and have evaluated the complex conductivity for different crystallographic orientations. Above the transition temperature, the material behaves like a metal with a scattering rate of approximately 20 cm(exp -1). In the superconducting state the electrodynamics of both materials is in good agreement with calculations based on a BCS ground state: the penetration depth is temperature independent for T approaches 0; while the penetration depth and the coherence length are strongly anisotropic, the superconducting energy gap shows no indications of line nodes. DOE

N95-22708 Department of the Navy, Washington, DC.
LIMITED BANDWIDTH MICROWAVE FILTER Patent
Christen Rauscher, inventor (to Navy) 16 Aug. 1994 15 p Filed 26 Feb. 1993 Supersedes AD-D015744
(AD-D016553; US-Patent-5,339,057; US-Patent-Appl-SN-025210; US-Patent-Class-333-166) Avail: US Patent and Trademark Office

A limited-bandwidth microwave transversal or recursive, filter, compatible with microwave monolithic integrated circuit (MMIC) design requirements is described in this invention. The device comprises a means to split an incident signal into multiple parts for distribution among a plurality of input ports of frequency-selective feedforward and feedback network branches comprising filter elements and active devices so designed as to provide a desired degree and type of signal filtration. After filtration, the resulting signals from these branches are combined to form a composite filter output signal. DTIC

N95-22709 Department of the Navy, Washington, DC.
METHOD AND SYSTEM FOR ELECTRON BEAM LITHOGRAPHY Patent
Elizabeth A. Dobisz, inventor (to Navy), Christie R. Marrian, inventor (to Navy), Martin C. Peckerar, inventor (to Navy), and Kee W. Rhee, inventor (to Navy) 9 Aug. 1994 8 p Filed 13 May 1992 Supersedes AD-D015397
(AD-D016554; US-Patent-5,336,892; US-Patent-Appl-SN-882230; US-Patent-Class-250-492.2) Avail: US Patent and Trademark Office

Improvement of resolution in terms of reducing minimum feature sizes and proximity effects on bulk substrates in high voltage electron beam lithography as applied to manufacture of electronic circuits from coated semiconductors involves the use of a dielectric layer interposed between an electrically semiconducting substrate and a resist layer. The dielectric layer functions to reduce the resist exposure resulting from the backscattered electrons coming from the substrate into the resist layer. DTIC

N95-22716# Brookhaven National Lab., Upton, NY. Magnet Div.
GAS COOLED LEADS. PART 1: THEORETICAL STUDY. PART 2: FROST FREE LEAD OPTIMIZED FOR A SPECIFIC CURRENT. PART 3: FROST FREE LEAD OPTIMIZED FOR A LARGE CURRENT RANGE
R. P. Shutt, M. L. Rehak, and K. E. Hornik Dec. 1993 127 p
(Contract DE-AC02-76CH-00016)
(DE95-002657; BNL-52424-Rev-9/94-Pt-1-3) Avail: CASI HC A07/MF A02

The intent of this paper is to cover as completely as possible and in sufficient detail the topics relevant to lead design. The first part identifies the problems associated with lead design, states the mathematical formulation, and shows the results of numerical and analytical solutions. The second part presents the results of a parametric study whose object is to determine the best choice for cooling method, material, and geometry. These findings are applied in a third part to the design of high-current leads whose end temperatures are determined from the surrounding equipment. It is found that cooling method or improved heat transfer are not critical once good heat exchange is established. The range 5 less than RRR less than 100 is found to be acceptable for the relative resistivity ratio of the material. Use of high transition temperature super conductor materials is not warranted for this application. The optimal geometry

(L:Length, A:cross-section) for a given current (I) follows the relation LI/A = 2 x 105 but extends over a large range of values. Mass flow needed to prevent thermal runaway varies linearly with current above a given threshold. Below that value, the mass flow is constant with current. Transient analysis shows no evidence of hysteresis. If cooling is interrupted, the mass flow needed to restore the lead to its initially cooled state grows exponentially with the time that the lead was left without cooling. DOE

N95-22733# Virginia Polytechnic Inst. and State Univ., Blacksburg, VA.
ANALYSES, ALGORITHMS, AND COMPUTATIONS FOR MODELS OF HIGH-TEMPERATURE SUPERCONDUCTIVITY Progress Report
M. D. Gunzburger and J. S. Peterson 1994 19 p
(Contract DE-FG05-93ER-25175)
(DE95-003290; DOE/ER-25175/1) Avail: CASI HC A03/MF A01

Under the sponsorship of the Department of Energy, we have achieved significant progress in the modeling, analysis, and computation of superconducting phenomena. Our work so far has focused on mezoscale models as typified by the celebrated Ginzburg-Landau equations; these models are intermediate between the microscopic models (that can be used to understand the basic structure of superconductors and of the atomic and subatomic behavior of these materials) and the macroscale, or homogenized, models (that can be of use for the design of devices). The models we have considered include a time dependent Ginzburg-Landau model, a variable thickness thin film model, models for high values of the Ginzburg-Landau parameter, models that account for normal inclusions and fluctuations and Josephson effects, and the anisotropic Ginzburg-Landau and Lawrence-Doniach models for layered superconductors, including those with high critical temperatures. In each case, we have developed or refined the models, derived rigorous mathematical results that enhance the state of understanding of the models and their solutions, and developed, analyzed, and implemented finite element algorithms for the approximate solution of the model equations. DOE

N95-22799# Westinghouse Hanford Co., Richland, WA.
RADIOISOTOPE THERMOELECTRIC GENERATOR LICENSED HARDWARE PACKAGE AND CERTIFICATION TESTS
L. H. Goldmann and H. S. Averette 30 Sep. 1994 8 p Presented at the 12th Symposium on Space Nuclear Power and Propulsion, Albuquerque, NM, 8-12 Jan. 1995
(Contract DE-AC06-87RL-10930)
(DE95-003039; WHC-SA-2614; CONF-950110-14) Avail: CASI HC A02/MF A01

This paper presents the Licensed Hardware package and the Certification Test portions of the Radioisotope Thermoelectric Generator Transportation System. This package has been designed to meet those portions of the Code of Federal Regulations (10 CFR 71) relating to 'Type B' shipments of radioactive materials. The detailed information for the anticipated license is presented in the safety analysis report for packaging, which is now in process and undergoing necessary reviews. As part of the licensing process, a full-size Certification Test Article unit, which has modifications slightly different than the Licensed Hardware or production shipping units, is used for testing. Dimensional checks of the Certification Test Article were made at the manufacturing facility. Leak testing and drop testing were done at the 300 Area of the US Department of Energy's Hanford Site near Richland, Washington. The hardware includes independent double containments to prevent the environmental spread of Pu-238, impact limiting devices to protect portions of the package from impacts, and thermal insulation to protect the seal areas from excess heat during accident conditions. The package also features electronic feed-throughs to monitor the Radioisotope Thermoelectric Generator's temperature inside the containment during the shipment cycle. This package is designed to safely dissipate the typical 4500 thermal watts produced in the largest Radioisotope Thermoelectric Generators. The package also contains provisions to ensure leak tightness when radioactive materials, such as a Radioisotope Thermoelectric Generator for the Cassini Mission, planned for 1997 by the National Aeronautics and Space Administration, are being prepared for shipment. These provisions include test ports used in conjunction with helium mass spectrometers to determine seal leakage rates of each containment during the assembly process. DOE

N95-22844# Sandia National Labs., Albuquerque, NM.
HIGH GAIN GaAs PHOTOCONDUCTIVE SEMICONDUCTOR SWITCHES: MEASUREMENT OF FILAMENT VELOCITY AND REDUCED TRIGGER ENERGY
G. M. Loubriel, F. J. Zutavern, M. W. OMalley, and W. D. Helgeson 1994 12 p Presented at the SPIE International Symposium on Photonic Sensors and Controls for Commercial Applications, Boston, MA, 31 Oct. - 4 Nov. 1994
(Contract DE-AC04-94AL-85000)
(DE95-001884; SAND-94-0883C; CONF-9410154-4) Avail: CASI HC A03/MF A01

The time evolution of the current filaments in an optically triggered, high gain GaAs switch was studied by recording the infrared photoluminescence from the filaments. When the switch is triggered with two laser diode arrays (through a fiber optic) that are activated within 1 ns of each other, two current filaments are observed, each one emanating from the point of illumination. By delaying one laser with respect to the other, the evolution of the filament was recorded in a time resolved fashion. The first filament that is triggered crosses the switch, the voltage drops and the other filament ceases to grow. By varying the delay between the trigger lasers, the tip velocity is measured to be up to 5.9 +/- (1 x 10(exp 9)) cm/s. This speed is 600 times larger than the peak drift velocity of carriers in GaAs. This observation supports switching models that rely on carrier generation at the tip of the filament. The filaments speed up as they cross the switch: for one voltage range initial speeds were 0.7 +/- (1 x 10(exp 9)) cm/s and final speeds (the last 100 ps of motion) exceed 5.5 +/- (1 x 10(exp 9)) cm/s. This experiment also shows a relationship between the rise time of the voltage across the switch and the required trigger energy and switch jitter. DOE

N95-22896# Sandia National Labs., Albuquerque, NM. Custom Magnetics/Capacitors/Interconnections Dept.
PLANAR MAGNETIC COMPONENT DEVELOPMENT
Robert L. Nagel and Michael E. Partridge Sep. 1994 39 p
(Contract DE-AC04-94AL-85000)
(DE95-003311; SAND-94-2246) Avail: CASI HC A03/MF A01

Although planar magnetic components are relatively new, the technology offers several advantages. Component properties show less variation because the construction technique keeps the winding in the same relative position each time, and batch processes can be used if the components are all formed on one printed circuit board panel. Assembly is simplified, and labor is reduced. If the component windings are integrated within the same printed circuit board as other circuitry for the design, assembly steps and chemical waste are reduced as well. These advantages could easily translate into cost savings. The steps used to design planar magnetic versions of a current-viewing transformer and a power converter flyback transformer have been detailed in this report, and include special considerations associated with planar techniques. Finally, the authors have demonstrated the use of planar components in a circuit. DOE

N95-23046# International Centre for Theoretical Physics, Trieste (Italy).
EFFECT OF CRITICAL FIELD ON SCREENED DIELECTRIC BREAKDOWN GROWTH
Wei Wang Oct. 1993 13 p
(DE94-628482; IC-93/363) Avail: CASI HC A03/MF A01 (US Sales Only)

In this paper we have shown that due to a critical field, the patterns growing in the screened Laplacian field will be affected. When the critical field is zero, there is a transition from a dense growing to single branch of aggregate. At a higher critical field, the pattern shows a spiky-type aggregate, and for a small critical field the transition is cut. For an intermediate critical field, the result shows that below the transition, there no dense structure. DOE

N95-23080# Lawrence Livermore National Lab., Livermore, CA.
TPX MAGNET SYSTEM STATUS
R. H. Bulmer, M. R. Chaplin, and D. D. Lang 17 Aug. 1994 6 p Presented at the 18th European Symposium on Fusion Technology, Karlsruhe, Germany, 22-26 Aug. 1994
(Contracts W-7405-eng-48; DE-AC02-76CH-03073)
(DE95-002389; UCRL-JC-116947; CONF-940843-9) Avail: CASI HC A02/MF A01

We present a status report on the magnet system for the Tokamak Physics eXperiment (TPX), a machine with a major radius of 2.25 m and a minor radius of 0.5 m to be built at the Princeton Plasma Physics Laboratory, in which all main coils will use cable-in-conduit superconductors. The 16-coil toroidal field system must produce a 4T field at the plasma center (8.4 T peak field) and accommodate about 5 kW of steady-state heating from nuclear heating, eddy currents, and thermal radiation in the windings. The poloidal system provides a plasma initiation voltage of 20 V and a total flux swing of 18 Wb to ramp the plasma current to 2 MA and provide a short flat-top. The poloidal system consists of 14 individual coils arranged symmetrically above and below the machine midplane, connected to allow either double-null or single-null plasma configurations. DOE

N95-23117# Army Construction Engineering Research Lab., Champaign, IL.

CORROSION CONTROL ACCEPTANCE CRITERIA FOR SACRIFICIAL ANODE TYPE, CATHODIC PROTECTION SYSTEMS (USER GUIDE)

Vincent F. Hock, Michael Noble, and Malcolm E. McLeod Jul. 1994 28 p

(AD-A285275; CERL-FEAP-UG-FM-94/10) Avail: CASI HC A03/MF A01

The Army currently operates and maintains more than 20,000 underground storage tanks and over 3000 miles of underground gas pipelines, all of which require some form of corrosion control. Cathodic protection is one method of corrosion control used to prevent corrosion-induced leaks when a steel structure is exposed to an aggressive soil. The corrosion control acceptance criteria for sacrificial anode type CP systems provides guidelines for the DEH/DPW cathodic protection installation inspectors whose responsibilities are to ensure that the materials and equipment specified are delivered to the job site and subsequently installed in accordance with the engineering drawings and specifications. The sacrificial anode CP acceptance criteria includes all components for the sacrificial anode system such as insulated conductors, anodes, anode backfills, and auxiliary equipment. The sacrificial anode CP acceptance criteria is composed of a checklist that lists each component and that contains a space for the inspector to either check 'yes' or 'no' to indicate whether the component complies with the job specifications. In some cases, the inspector must measure and record physical dimensions or electrical output and compare the measurements to standards shown in attached tables. Author (DTIC)

N95-23219*# National Aeronautics and Space Administration. Lewis Research Center, Cleveland, OH.

LIQUID NITROGEN TEMPERATURE OPERATION OF A SWITCHING POWER CONVERTER

Biswajit Ray, Scott S. Gerber (NYMA, Inc., Brook Park, OH.), Richard L. Patterson, and Ira T. Myers Mar. 1995 10 p Presented at the Low Temperature Electronics and High Temperature Superconductivity Symposium, Reno, NV, 21-26 May 1995; sponsored by The Electrochemical Society

(Contract NAS3-27186; RTOP 233-02-0C)

(NASA-TM-106867; E-9482; NAS 1.15:106867) Avail: CASI HC A02/MF A01

The performance of a 42/28 V, 175 W, 50 kHz pulse-width modulated buck dc/dc switching power converter at liquid nitrogen temperature (LNT) is compared with room temperature operation. The power circuit as well as the control circuit of the converter, designed with commercially available components, were operated at LNT and resulted in a slight improvement in converter efficiency. The improvement in power MOSFET operation was offset by deteriorating performance of the output diode rectifier at LNT. Performance of the converter could be further improved at low temperatures by using only power MOSFET's as switches. The use of a resonant topology will further improve the circuit performance by reducing the switching noise and loss. Author

N95-23241 Department of the Navy, Washington, DC.

METHOD OF MAKING A SEMICONDUCTOR DEVICE USING A NANOCHANNEL GLASS MATRIX Patent

Ronald J. Tonucci, inventor (to Navy) and Brian L. Justus, inventor (to Navy) 26 Apr. 1994 21 p Filed 29 Apr. 1993

(AD-D016383; US-Patent-5,306,661; US-Patent-Appl-SN-053752; US-Patent-Class-437-90) Avail: US Patent and Trademark Office

The present invention provides a method of forming a semiconductor device comprising the steps of: (1) forming a glass block of an acid inert glass having acid etchable glass rods extending therethrough, the acid etchable glass rods having an average diameter of less than 1 micron; (2) partially etching one end of the acid etchable rods surface of the glass block to form cavities in the glass block, on one surface thereof having an average diameter of less than 1 micron; (3) depositing material(s) in the cavities to form a semiconductor device in which the acid etchable glass rods are completely etched and the deposition material(s) is deposited to fill the nanochannels formed by the etching. The present invention also provides semiconductor devices made by these methods. Author

N95-23334# Lawrence Livermore National Lab., Livermore, CA.

A HYBRID VEHICLE EVALUATION CODE AND ITS APPLICATION TO VEHICLE DESIGN

S. M. Aceves and J. R. Smith 15 Jul. 1994 26 p Presented at the Society of Automotive Engineers International Congress and Exposition, Detroit, MI, 27 Feb. - 2 Mar. 1995

(Contract W-7405-eng-48)

(DE95-004205; UCRL-JC-117918; CONF-950256-1) Avail: CASI HC A03/MF A01

This report describes a hybrid vehicle simulation model, which can be applied to many of the vehicles currently being considered for low pollution and high fuel economy. The code operates interactively, with all the vehicle information stored in data files. The code calculates fuel economy for three driving schedules, time for 0-96 km/h at maximum acceleration, hill climbing performance, power train dimensions, and pollution generation rates. This report also documents the application of the code to a hybrid vehicle that operates with a hydrogen internal combustion engine. The simulation model is used for parametric studies of the vehicle. The results show the fuel economy of the vehicle as a function of vehicle mass, aerodynamic drag, engine-generator efficiency, flywheel efficiency, and flywheel energy and power capacities. DOE

N95-23351# Westinghouse Hanford Co., Richland, WA.

RADIOISOTOPE THERMOELECTRIC GENERATOR TRANSPORTATION SYSTEM SUBSYSTEM 143 SOFTWARE DEVELOPMENT PLAN

D. A. King 10 Nov. 1994 22 p

(Contract DE-AC06-87RL-10930)

(DE95-003774; WHC-SD-RTG-SDP-001) Avail: CASI HC A03/MF A01

This plan describes the activities to be performed and the controls to be applied to the process of specifying, developing, and qualifying the data acquisition software for the Radioisotope Thermoelectric Generator (RTG) Transportation System Subsystem 143 Instrumentation and Data Acquisition System (IDAS). This plan will serve as a software quality assurance plan, a verification and validation (V and V) plan, and a configuration management plan. DOE

N95-23355# Argonne National Lab., IL.

DESIGN AND PRODUCTION OF EFFICIENT CURRENT LEADS FOR 1500-A, 50-Hz SERVICE IN A 77-4 K TEMPERATURE GRADIENT

U. Balachandran, C. A. Youngdahl, and M. T. Lanagan Oct. 1994 5 p Presented at the 7th International Symposium on Superconductivity, Kita Kiyushu, Japan, 8-11 Nov. 1994

(Contract W-31-109-eng-38)

(DE95-004121; ANL/ET/CP-83629; CONF-941176-1) Avail: CASI HC A01/MF A01

Two arrays of BSCCO 2223 bars were designed and produced for use in current leads for a power utility fault-current limiter operating at 4 K. Each conduction-cooled array, consisting of four parallel bars arranged within a 100-mm-diameter boundary, delivered 1,500 A peak, 50-Hz AC through a 77-4 K temperature gradient while dissipating less than 0.2 W. The sinter-forged bars displayed DC critical current densities of 950-1,300 A/sq cm at 77 K and greater than 5,000 A/sq cm at 4 K. Magnetic field sensitivity was relatively low. Thermal conductivity tests showed values higher than literature values for polycrystalline BSCCO 2223 made by other processes. DOE

N95-23368# Los Alamos National Lab., NM.

HTS CURRENT LEAD USING A COMPOSITE HEAT PIPE

M. A. Daugherty, F. C. Prenger, D. D. Hill, D. E. Daney, and K. A. Woloshun 1995 5 p Presented at the Applied Superconductivity

Conference, Boston, MA, 16-21 Oct. 1994
(Contract W-7405-eng-36)
(DE95-003718; LA-UR-94-3725; CONF-941013-14) Avail: CASI HC A01/MF A01

The design and fabrication of HTS current leads being built by Los Alamos to supply power to a demonstration HTS coil which will operate in a vacuum cooled by a cryocooler is discussed. Because vapor cooling is not an option for this application, the leads must be entirely conductively cooled. In the design of HTS current leads for this type of application, it is desirable to intercept part of the heat load at an intermediate temperature. This thermal intercept or connection must be electrically insulating but thermally conductive, two mutually exclusive properties of most candidate solid materials. To achieve this end we incorporate a composite nitrogen heat pipe, constructed of conducting and non-conducting materials, to provide efficient thermal communication and simultaneously, electrical isolation between the lead and the intermediate temperature heat sink. Another important feature of the current lead design is the use of high Jc thick film superconductors deposited on a non-conducting substrate to reduce the conductive heat leak through the lower portion of the lead. Two flexible electrical conductors are incorporated to accommodate handling, assembly and the dissimilar expansion coefficients of the various materials. DOE

N95-23405# Fermi National Accelerator Lab., Batavia, IL.
OPERATION AND TESTS OF A DDC101 A/D
H. Nguyen Nov. 1994 14 p
(Contract DE-AC02-76CH-03000)
(DE95-003747; FNAL-TM-1913) Avail: CASI HC A03/MF A01

For the KTeV PMT laser monitoring system, one needs a high resolution device with a large dynamic range to be used for digitizing PIN photodiodes. The dynamic range should be wider than or comparable to the KTeV digitizer (17-bits). The Burr-Brown DDC101 is a precision, wide dynamic range, charge digitizing A/D converter with 20-bit resolution, packaged in a 28-pin plastic, double-wide DP. Low level current output devices such as photosensors can be directly connected to its input. The digital output can be clocked-out serially from the pins. For typical operations, a relatively wide gate of 1 msec should be used. The full scale charge is 500 pC for unipolar mode. The bipolar mode scale is +/- 250 pC. The advertised integral nonlinearity is 0.003% of FSR. This document describes only the basic DDC101 operations since full detail can be found in the DDC101 manual. Tests results are given in section 3. DOE

N95-23479# Los Alamos National Lab., NM.
USER'S GUIDE AND PHYSICS MANUAL FOR THE SCATPLUS CIRCUIT CODE
M. L. Yapuncich, W. J. Deninger, and R. F. Gribble May 1994 120 p
(Contract W-7405-eng-36)
(DE95-003755; LA-UR-94-1947) Avail: CASI HC A06/MF A02

ScatPlus is a user friendly circuit code and an expandable library of circuit models for electrical components and devices; it can be used to predict the transient behavior in electric circuits. The heart of ScatPlus is the transient circuit solver SCAT written in 1986 by R.F. Gribble. This manual includes system requirements, physics manual, ScatPlus component library, tutorial, ScatPlus screen, menus and toolbar, ScatPlus tool bar, procedures. DOE

N95-23494# California Univ., Berkeley. Lawrence Berkeley Lab, CA.
THERMAL MODELING OF THE LITHIUM/POLYMER BATTERY Ph.D. Thesis
C. R. Pals Oct. 1994 144 p
(Contract DE-AC03-76SF-00098)
(DE95-004680; LBL-36293) Avail: CASI HC A07/MF A02

Research in the area of advanced batteries for electric-vehicle applications has increased steadily since the 1990 zero-emission-vehicle mandate of the California Air Resources Board. Due to their design flexibility and potentially high energy and power densities, lithium/polymer batteries are an emerging technology for electric-vehicle applications. Thermal modeling of lithium/polymer batteries is particularly important because the transport properties of the system depend exponentially on temperature. Two models have been presented for assessment of the thermal behavior of lithium/polymer batteries. The one-cell model predicts the cell potential, the concentration profiles, and the heat-generation rate during discharge. The cell-stack model predicts temperature profiles and heat transfer limitations of the battery. Due to the variation of ionic conductivity and salt diffusion coefficient with temperature, the performance of the lithium/polymer battery is greatly affected by temperature. Because of this variation, it is important to optimize the cell operating temperature and design a thermal management system for the battery. Since the thermal conductivity of the polymer electrolyte is very low, heat is not easily conducted in the direction perpendicular to cell layers. Temperature profiles in the cells are not as significant as expected because heat-generation rates in warmer areas of the cell stack are lower than heat-generation rates in cooler areas of the stack. This nonuniform heat-generation rate flattens the temperature profile. Temperature profiles as calculated by this model are not as steep as those calculated by previous models that assume a uniform heat-generation rate. DOE

N95-23779# Sandia National Labs., Albuquerque, NM.
MICRO HEAT SPREADER ENHANCED HEAT TRANSFER IN MCM'S
D. S. Shen, R. T. Mitchell, D. Dobranich, D. R. Adkins, and M. R. Tuck 1994 6 p Presented at the Multi Chip Module Conference, Santa Cruz, CA, 31 Jan. - 2 Feb. 1995
(Contract DE-AC04-94AL-85000)
(DE95-004520; SAND-94-2922C; CONF-950154-1) Avail: CASI HC A02/MF A01

The peak thermal power generated in microelectronics assemblies has risen from less than 1 W/sq cm in 1980 to greater than 40 W/sq cm today, due primarily to increasing densities at both the IC and packaging levels. The authors have demonstrated enhanced heat transfer in a prototype Si substrate with a backside micro heat channel structure. Unlike conventional micro heat pipes, these channels are biaxial with a greater capacity for fluid transfer. Thermal modeling and preliminary experiments have shown an equivalent increase in substrate thermal conductivity to over 500 W/m(center dot)K, or a four times improvement. Optimization of the structure and alternative liquids will further increase the thermal conductivity of the micro heat channel substrate with the objective being polycrystalline diamond, or about 1,200 W/m(center dot)K. The crucial design parameters for the micro heat channel system and the thermal characteristics of the system will be covered. DOE

N95-23783# California Univ., Los Angeles, CA.
VLSI FOR HIGH-SPEED DIGITAL SIGNAL PROCESSING Final Report, 1 Jul. 1991 - 30 Sep. 1994
Alan N. Wilson, Jr. 30 Sep. 1994 117 p
(Contract N00014-91-J-1852)
(AD-A285643) Avail: CASI HC A06/MF A02

The research supported by this ONR grant has investigated modern high-speed signal processing system design. It has encompassed a complete spectrum of activities, starting with the discovery of new signal processing algorithms, and continuing through the development of the most appropriate methods for their realization, including, in particular, the design, layout and fabrication of integrated circuits. The primary project for this grant has been the design and implementation of a new type of programmable general purpose digital filter IC. It employs multiple processing units on a single integrated circuit. The multiple processors operate in parallel and communicate with one another through on-chip dual-access storage register blocks, thereby incurring no operating speed penalties as would result if it were necessary to read and write to off-chip RAM. The system's topology has the processors arranged in a ring, with locally-shared register blocks between each adjacent pair of processors. Our prototype IC has five processors, and it is capable of realizing a rich variety of filter structures that operate at the maximum instruction execution rate possible for any custom parallel implementation. DTIC

N95-24048*# National Aeronautics and Space Administration. Langley Research Center, Hampton, VA.
CIRCULAR ELECTRODE GEOMETRY METAL-SEMICONDUCTOR-METAL PHOTODETECTORS Patent Application
James A. McAddo, inventor (to NASA), Elias Towe, inventor (to NASA) (Virginia Univ., Charlottesville, VA.), William L. Bishop, inventor (to NASA) (Bishop, William L., Charlottesville, VA.), and Liang-Guo Wang, inventor (to NASA) (Wang, Liang-Guo, Hampton, VA.) 5 Jan. 1994 17 p
(Grant NAG1-1434)

(NASA-Case-LAR-15172-1-CU; NAS 1.71:LAR-15172-1-CU; US-Patent-Appl-SN-179598) Avail: CASI HC A03/MF A01

The invention comprises a high speed, metal-semiconductor-metal photodetector which comprises a pair of generally circular, electrically conductive electrodes formed on an optically active semiconductor layer. Various embodiments of the invention include a spiral, intercoiled electrode geometry and an electrode geometry comprised of substantially circular, concentric electrodes which are interposed. These electrode geometries result in photodetectors with lower capacitances, dark currents and lower inductance which reduces the ringing seen in the optical pulse response. Author

N95-24070# Argonne National Lab., IL.
ENERGY EFFICIENCY OF ELECTRIC VEHICLES AT THE 1994 AMERICAN TOUR DE SOL
S. Quong, M. Duoba, C. Buitrago, N. LeBlanc, and R. Larsen 1994 5 p Presented at the Solar and Electric Vehicles '94, Providence, RI, 3-5 Oct. 1994
(Contract W-31-109-eng-38)
(DE95-002905; ANL/ES/CP-84138; CONF-9410241-1) Avail: CASI HC A01/MF A01

In 1994, the US Department of Energy, through Argonne National Laboratory's Center for Transportation Research, sponsored energy-efficiency data collection from student, private, and professional electric vehicles during the American Tour de Sol (ATDS). The ATDS is a multiple-day road rally event, from New York City to Philadelphia. During each leg of the event, kilowatt-hour meters measured the efficiency of the electric vehicles (EV's), which averaged from 5.68 to 65.74 km/kWh. In addition to daily energy-usage measurements, some vehicles used a data-acquisition unit to collect second-by-second information. This showed, in one case, that 21% of the total energy was captured in regenerative braking. Some of the vehicles were also tested on a dynamometer for energy-efficiency, acceleration, and steady-state power ratings. This paper also compares the energy efficiency of the vehicles during the road rally to the dynamometer results. In almost all vehicles, there was an increase in energy efficiency when the vehicle was traveling over the road, due to the non-transient duty cycle and efficient driving techniques. The dynamometer testing also showed that some EV's are equal to or better than gasoline vehicles in performance and efficiency. DOE

N95-24081# Fermi National Accelerator Lab., Batavia, IL.
A HIGH SPEED DIGITIZING PHOTOMULTIPLIER TUBE BASE FOR THE KTeV CsI CALORIMETER
J. Whitmore Nov. 1994 9 p Presented at the 5th International Conference on Calorimetry in High Energy Physics, Upton, NY, 25 Sep. - 1 Oct. 1994
(Contract DE-AC02-76CH-03000)
(DE95-003739; FNAL/C-94/372; CONF-9409268-1) Avail: CASI HC A02/MF A01

A circuit has been designed to digitize PMT signals over an 18-bit dynamic range with 8-bits of resolution. The crucial element of the circuit is the custom charge integrating and encoding (QIE) ASIC. This chip is designed to operate at rates up to 53 MHz, and, in conjunction with an 8-bit FADC, generates 12-bit floating point output. Bench tests of a 17-bit version of the digital base demonstrated excellent noise performance, linearity and pedestal and gain stability. Twenty-five channels of digitizing PMT bases have been built and used for readout of a CsI array in a test beam at CERN. Performance of these devices in a beam environment is discussed. DOE

N95-24149# Sandia National Labs., Albuquerque, NM.
SOLDERABILITY PRESERVATION THROUGH THE USE OF ORGANIC INHIBITORS
N. R. Sorensen and F. M. Hosking 1994 5 p Presented at the InterPack '95: International Electronic Packaging Conference, Maui, HI, 26-30 Mar. 1995
(Contract DE-AC04-94AL-85000)
(DE95-003633; SAND-94-2749C; CONF-950344-4) Avail: CASI HC A01/MF A01

Organic inhibitors can be used to prevent corrosion of metals and have application in the electronics industry as solderability preservatives. We have developed a model to describe the action of two inhibitors (benzotriazole and imidazole) during the environmental aging and soldering process. The inhibitors bond with the metal surface and form a barrier that prevents or retards oxidation. At soldering temperatures, the metal-organic complex breaks down leaving an oxide-free metal surface that allows excellent wetting by molten solder. The presence of the inhibitor retards the wetting rate relative to clean copper, but provides a vast improvement relative to oxidized copper. DOE

N95-24163# Argonne National Lab., IL.
DESIGN OF A HIGH-TEMPERATURE SUPERCONDUCTOR CURRENT LEAD FOR ELECTRIC UTILITY SMES
R. C. Niemann, Y. S. Cha, J. R. Hull, C. M. Rey (Babcock and Wilcox Co., Lynchburg, VA.), and K. D. Dixon (Babcock and Wilcox Co., Lynchburg, VA.) 1995 5 p Presented at the Applied Superconductivity Conference, Boston, MA, 16-21 Oct. 1994
(Contract W-31-109-eng-38)
(DE95-004604; ANL/ET/CP-82120; CONF-941013-18) Avail: CASI HC A01/MF A01

Current leads that rely on high-temperature superconductors (HTS's) to deliver power to devices operating at liquid helium temperature have the potential to reduce refrigeration requirements to levels significantly below those achievable with conventional leads. The design of HTS current leads suitable for use in near-term superconducting magnetic energy storage (SMES) is in progress. The SMES system has an 0.5 MWh energy capacity and a discharge power of 30 MW. Lead-design considerations include safety and reliability, electrical and thermal performance, structural integrity, manufacturability, and cost. Available details of the design, including materials, configuration, and performance predictions, are presented. DOE

N95-24164# Argonne National Lab., IL.
ULTRAFAST, HIGH PRECISION GATED INTEGRATOR
X. Wang 1995 8 p Presented at the Beam Instrumentation Workshop, Vancouver, Canada, 2-6 Oct. 1994
(Contract W-31-109-eng-38)
(DE95-004616; ANL/ASD/CP-83682; CONF-9410219-23) Avail: CASI HC A02/MF A01

An ultrafast, high precision gated integrator has been developed by introducing new design approaches that overcome the problems associated with earlier gated integrator circuits. The very high speed is evidenced by the output settling time of less than 50 ns and 20 MHz input pulse rate. The very high precision is demonstrated by the total output offset error of less than 0.2mV and the output droop rate of less than 10 micro volts/micro seconds. This paper describes the theory of this new gated integrator circuit operation. The completed circuit test results are presented. DOE

N95-23322*# Christopher Newport Coll., Newport News, VA. Dept. of Physics and Computer Science.
POTENTIAL AEROSPACE APPLICATIONS OF HIGH TEMPERATURE SUPERCONDUCTORS Abstract Only
Raouf Selim *In* Hampton Univ., 1994 NASA-HU American Society for Engineering Education (ASEE) Summer Faculty Fellowship Program Dec. 1994 p 104 (For primary document see N95-23276 07-99)
Avail: CASI HC A01/MF A02

34 FLUID MECHANICS AND HEAT TRANSFER

Includes boundary layers; hydrodynamics; fluidics; mass transfer; and ablation cooling.

For related information see also *02 Aerodynamics* and *77 Thermodynamics and Statistical Physics.*

N95-22481*# Eloret Corp., Palo Alto, CA.
PARTICLE KINETIC SIMULATION OF HIGH ALTITUDE HYPERVELOCITY FLIGHT Report, 1 Jan. 1989 - 31 Jan. 1994
Iain Boyd and Brian L. Haas 19 Apr. 1994 9 p
(Contract NCC2-582)
(NASA-CR-197383; NAS 1.26:197383) Avail: CASI HC A02/MF A01

Rarefied flows about hypersonic vehicles entering the upper atmosphere or through nozzles expanding into a near vacuum may only be simulated accurately with a direct simulation Monte Carlo (DSMC) method. Under

this grant, researchers enhanced the models employed in the DSMC method and performed simulations in support of existing NASA projects or missions. DSMC models were developed and validated for simulating rotational, vibrational, and chemical relaxation in high-temperature flows, including effects of quantized anharmonic oscillators and temperature-dependent relaxation rates. State-of-the-art advancements were made in simulating coupled vibration - dissociation - recombination for post-shock flows. Models were also developed to compute vehicle surface temperatures directly in the code rather than requiring isothermal estimates. These codes were instrumental in simulating aerobraking of NASA's Magellan spacecraft during orbital maneuvers to assess heat transfer and aerodynamic properties of the delicate satellite. NASA also depended upon simulations of entry of the Galileo probe into the atmosphere of Jupiter to provide drag and flow field information essential for accurate interpretation of an onboard experiment. Finally, the codes have been used extensively to simulate expanding nozzle flows in low-power thrusters in support of propulsion activities at NASA-Lewis. Detailed comparisons between continuum calculations and DSMC results helped to quantify the limitations of continuum CFD codes in rarefied applications. Author

N95-22491# Lawrence Livermore National Lab., Livermore, CA.
AN ADAPTIVE PROJECTION METHOD FOR THE INCOMPRESSIBLE NAVIER-STOKES EQUATIONS
A. S. Almgren, J. B. Bell, L. H. Howell, and P. Colella (California Univ., Berkeley, CA.) May 1994 6 p Presented at the World Congress on Computational and Applied Mathematics, Atlanta, GA, 11-15 Jul. 1994
(Contracts W-7405-eng-48; DE-FG03-92ER-25140)
(DE94-019049; UCRL-JC-112328; CONF-940719-7) Avail: CASI HC A02/MF A01

In this paper the authors present a method for solving the time-dependent incompressible Navier-Stokes equations on an adaptive grid. The method is based on a projection formulation in which they first solve convection-diffusion equations to predict intermediate velocities, and then project these velocities onto a space of approximately divergence-free vector fields. Their treatment of convection uses a specialized second-order upwind method for differencing the nonlinear convection terms that provide a robust treatment of these terms suitable for high Reynolds number flows. Their approach to adaptive refinement uses a nested hierarchy of grids with simultaneous refinement of the grids in both space and time. The integration algorithm on the grid hierarchy is a recursive procedure in which coarse grids are advanced, fine grids are advanced multiple steps to reach the same time as the coarse grids, and the grid levels are then synchronized. DOE

N95-22585 Paris VI Univ. (France). Lab. de Modelisation en Mecanique
STUDY OF THE PRESSURE FIELD IN ROTATING HOMOGENEOUS TURBULENT FLOWS Final Report
H. Makroum May 1993 52 p Prepared in cooperation with Direction des Recherches, Etudes et Techniques, Paris, France
(PB94-189107) Avail: Issuing Activity (National Technical Information Service (NTIS))

The first section of the study to identify pressure field properties in a homogeneous rotating flow looks at the pressure spectrum. The author shows that the EDQNM (eddy-damped quasi-normal markovian) closure method applied to the fourth-order moments reflecting turbulence/turbulence interactions is equivalent to the quasi-normal closure hypothesis. He also shows that the two terms corresponding to second-order and fourth-order moments are independent of the flow's helicity. The author and his team then demonstrate that the pressure spectrum component determined by second-order moments correlates with the flow's tendency to be two dimensional, while that associated with fourth-order moments expressed a tendency toward three dimensionality. Finally, the relative importance of the different terms that determine the pressure spectrum are analyzed as a function of the k wave vector module and its orientation. The second part of the report details a similar investigation for the tensor of pressure-strain correlations. NTIS

N95-22638# Wageningen Agricultural Univ. (Netherlands).
FLOW MEASURING STRUCTURES
W. Boiten Nov. 1993 36 p
(PB95-127254) Avail: CASI HC A03/MF A01

The use of flow measuring structures is one of the various methods for the continuous measurement of discharges in open channels. In this report a brief summary of these methods is presented to get some insight in the selection of the most appropriate method. Then the distinct functions of water control structures are described. The flow measuring structures are classified according to international rules. The fields of application are dealt with and the definitions of weir flow are given. Much attention is paid to the aspects of how to select the most suitable flow measuring structure. The accuracy in the evaluation of the discharge has been related to the different error sources. A review of international standards on flow measuring structures concludes the report. NTIS

N95-22669*# National Aeronautics and Space Administration. Lewis Research Center, Cleveland, OH.
ADDITIONAL IMPROVEMENTS TO THE NASA LEWIS ICE ACCRETION CODE LEWICE
William B. Wright (NYMA, Inc., Brook Park, OH.) and Colin S. Bidwell Mar. 1995 14 p Presented at the 33rd Aerospace Sciences Meeting and Exhibit, Reno, NV, 9-12 Jan. 1995; sponsored byAIAA
(Contract NAS3-27186; RTOP 505-68-10)
(NASA-TM-106849; E-9425; NAS 1.15:106849; AIAA Paper 95-0752)
Avail: CASI HC A03/MF A01

Due to the feedback of the user community, three major features have been added to the NASA Lewis ice accretion code LEWICE. These features include: first, further improvements to the numerics of the code so that more time steps can be run and so that the code is more stable; second, inclusion and refinement of the roughness prediction model described in an earlier paper; third, inclusion of multi-element trajectory and ice accretion capabilities to LEWICE. This paper will describe each of these advancements in full and make comparisons with the experimental data available. Further refinement of these features and inclusion of additional features will be performed as more feedback is received. Author

N95-22767 Ecole Polytechnique, Palaiseau (France).
EXPERIMENTAL STUDY OF VORTEX BREAKDOWN IN A SWIRLING WATER JET Final Report [ESTUDE EXPERIMENTALE DE L'ECLATEMENT TOURBILLONNAIRE ET INSTABILITES HYDRODYNAMIQUES]
M. M. Wu, P. Huerre, and J. M. Chomaz Feb. 1993 29 p Prepared in cooperation with Direction des Recherches, Etudes et Techniques, Paris, France
(PB95-130407) Avail: Issuing Activity (National Technical Information Service (NTIS))

A swirling water jet has been designed and constructed with well-controlled axial and azimuthal velocities. The effects of swirl motion on the jet flow have been studied using both laser induced fluorescence (LIF) visualization technique and laser doppler velocimetry (LDV) measurements. A new inverse fluorescence visualization technique coupled with suitable image processing has provided quantitative information on the increase of the mixing layer thickness with swirl number S. Single fluorescence line visualizations in the middle of the jet reproduce the classical S-type vortex breakdown. The breakdown point is observed to approach the jet nozzle exit as the swirl number increases. The average velocity at one point in the middle of the jet was measured by LDV velocimetry. The results show that average velocity approaches zero as the swirling number reaches a certain threshold. This is consistent with visualization results: when mixing layer thickness is used as an order parameter, it undergoes a transition as S exceeds a threshold value. The onset of vortex breakdown is apparently non-hysteretic, but this result remains to be interpreted in light of the recent paper of Chomaz. NTIS

N95-22771# International Centre for Theoretical Physics, Trieste (Italy).
SULLIVAN MODEL FOR WETTING TRANSITION IN CLOSED SYSTEM
E. J. Ding Sep. 1993 18 p
(DE94-628472; IC-93/317) Avail: CASI HC A03/MF A01 (US Sales Only)

The wetting transition in a closed system is analytically discussed based on the Sullivan model. In order to have a wetting transition in the system the wall potential must have intermediate strength. The wetting transition is first order for the finite system, while it becomes of second order for the infinite one. In addition, the temperature T(sub W) of the wetting transition becomes lower as the separation of the two walls decreases. DOE

N95-22901# Los Alamos National Lab., NM.
LEVEL SET TECHNIQUES APPLIED TO UNSTEADY DETONATION PROPAGATION
D. S. Stewart (Illinois Univ., Urbana, IL.), T. Aslam (Illinois Univ., Urbana, IL.), Jin Yao (Illinois Univ., Urbana, IL.), and J. B. Bdzil 1994 18 p Presented at the Mathematical Modeling and Combustion Science, Kauai, HI, 18-22 Jul. 1994
(Contract W-7405-eng-36)
(DE95-002741; LA-UR-94-3546; CONF-9407146-1) Avail: CASI HC A03/MF A01

Here we are concerned with describing the dynamics of multidimensional detonation as a self-propagating surface. The detonation shock surface has been shown under certain circumstance to be governed by an intrinsic relation between the normal shock velocity and the local curvature, obtaining a D(sub n) - (kappa) relation. Once the initial shock position is given, then subsequently the motion of the shock can be determined by solving a scalar partial differential equation for the shock position. One can think that in principle, the D(sub n) - (kappa) relation is determined by some means, theory or experiment, and then once prescribed, predictions of the physical system further depend wholly on the initial configuration. Thus we are also concerned about an efficient numerical solution of this equation in three-dimensions, with possibly multiply connected and disjoint shock surfaces. This has led us to consider the level-set techniques of Osher and Sethian, which are naturally suited to these problems. In what follows, we discuss examples of propagating surfaces, from formulations in combustion and heat transfer to which level-set methods apply. We discuss the specific example from detonation theory. We briefly explain the derivation of the D(sub n) - (kappa) relation, in the context of detonation and mention some recent extensions of the theory, that includes shock acceleration terms and the possibility of extinction for reaction rates that have large activation energies. These new results can all be summarized as an extension of the D(sub n) - (kappa) relation. Importantly, the resulting equation is hyperbolic in character as opposed to parabolic, for a simple D(sub n) - (kappa). relation. Finally we indicate the interesting new features of the dynamics that can be observed in the detonation shock surface evolution, and speculate on their relevance to formation of sustained detonation cells. DOE

N95-22902# Los Alamos National Lab., NM.
THE EFFECT OF A NON-ZERO SHOCK WIDTH ON WAVE PROPAGATION IN MULTI-DIMENSIONS
R. Menikoff, K. S. Lackner, and B. G. Bukiet (New Jersey Inst. of Tech., Newark, NJ.) 1994 7 p Presented at the 5th International Conference on Hyperbolic Problems, Stony Brook, NY, Jun. 1994
(Contract W-7405-eng-36)
(DE95-002748; LA-UR-94-3585; CONF-9406279-1) Avail: CASI HC A02/MF A01

It is known that a numerical shock width in one dimension can lead to a localized entropy error when waves interact . In multi-dimensions the wave width, either numerical or physical, can also affect the propagation of the wave, and thus have a global effect on fluid flow. A well known physical example is the diameter effect for detonation waves. This effect is due to reaction zone dynamics; the competition between a source term for the release of chemical energy and a geometric source term due to front curvature. When the reaction zone is underresolved, the effective reaction zone dynamics leads to mesh dependent numerical results. The mesh dependence is due to an artificial numerical curvature effect. An explanation of this effect is given based on the conservation laws. Because of the non-zero wave width, the standard Hugoniot jump conditions must be modified. Correction terms are proportional to the wave width. It follows when the width is proportional to the cell size, as occurs in shock capturing schemes, that the curvature effect is mesh dependent. A similar modification of the jump conditions can be expected whenever there are multiple length scales determining the dissipation which gives rise to the wave width. As a consequence, the wave curve depends on the local front curvature and the divergence of the velocity field in the tangent plane in addition to the usual state variables. In computations, the length scales affecting the wave curve may either be physical or artificial in nature. Artificial length scales lead to numerical errors which may not vanish under mesh refinement. DOE

N95-22906*# National Aeronautics and Space Administration. Langley Research Center, Hampton, VA.
MICRO-SENSOR THIN-FILM ANEMOMETER Patent Application
Mark Sheplak, inventor (to NASA) (Syracuse Univ., NY.), Catherine B. McGinley, inventor (to NASA), Eric F. Spina, inventor (to NASA) (Syracuse Univ., NY.), Ralph M. Stephens, inventor (to NASA), Purnell Hopson, Jr., inventor (to NASA), and Vincent B. Cruz, inventor (to NASA) 24 Nov. 1994 14 p
(Grant NAG1-1400)
(NASA-Case-LAR-15112-1-CU; NAS 1.71:LAR-15112-1-CU; US-Patent-Appl-SN-361601) Avail: CASI HC A03/MF A01

A device for measuring turbulence in high-speed flows is provided which includes a micro-sensor thin-film probe. The probe is formed from a single crystal of aluminum oxide having a 14 deg half-wedge shaped portion. The tip of the half-wedge is rounded and has a thin-film sensor attached along the stagnation line. The bottom surface of the half-wedge is tilted upward to relieve shock induced disturbances created by the curved tip of the half-wedge. The sensor is applied using a microphotolithography technique. NASA

N95-22914# Sandia Labs., Albuquerque, NM.
COYOTE 2: A FINITE ELEMENT COMPUTER PROGRAM FOR NOONLINEAR HEAT CONDUCTION PROBLEMS
D. K. Gartling and R. E. Hogan Oct. 1994 138 p
(Contract DE-AC04-94AL-85000)
(DE95-002848; SAND-94-1179) Avail: CASI HC A07/MF A02

User instructions are given for the finite element computer program, COYOTE 2. COYOTE 2 is designed for the multi-dimensional analysis of nonlinear heat conduction problems including the effects of enclosure radiation and chemical reaction. The theoretical background and numerical methods used in the program are documented in SAND94-1173. Examples of the use of the code are presented in SAND94-1180. DOE

N95-23015*# National Aeronautics and Space Administration. Langley Research Center, Hampton, VA.
MACH 10 COMPUTATIONAL STUDY OF A THREE-DIMENSIONAL SCRAMJET INLET FLOW FIELD
Scott D. Holland Mar. 1995 32 p
(RTOP 506-40-41-02)
(NASA-TM-4602; L-17348; NAS 1.15:4602) Avail: CASI HC A03/MF A01

The present work documents the computational results for a combined computational and experimental parametric study of the internal aerodynamics of a generic three-dimensional sidewall-compression scramjet inlet configuration at Mach 10. The three-dimensional Navier-Stokes code SCRAMIN was chosen for the computational portion of the study because it uses a well-known and well-proven numerical scheme and has shown favorable comparison with experiment at Mach numbers between 2 and 6. One advantage of CFD was that it provided flow field data for a detailed examination of the internal flow characteristics in addition to the surface properties. The experimental test matrix at mach 10 included three geometric contraction ratios (3, 5, and 9), three Reynolds numbers (0.55 x 10(exp 6) per foot, 1.14 x 10(exp 6) per foot, and 2.15 x 10(exp 6) per foot), and three cowl positions (at the throat and two forward positions). Computational data for two of these configurations (the contraction ratio of 3, Re = 2.15 x 10 (exp 6) per foot, at two cowl positions) are presented along with a detailed analysis of the flow interactions in successive computational planes. Author

N95-23081# Sandia National Labs., Albuquerque, NM.
THE PROBABILISTIC STRUCTURE OF SPRAYS: IMPLICATIONS FOR MEASUREMENTS BY IN SITE PARTICLE COUNTERS
C. F. Edwards 1994 11 p Presented at the International Symposium on Advanced Spray Combustion, Hiroshima, Japan, 6-7 Jul. 1994
(Contract DE-AC04-76DP-00789)
(DE95-002483; SAND-94-8643C; CONF-9407141-1) Avail: CASI HC A03/MF A01

An overview of recent progress in the understanding of sprays and spray measurements based on a stochastic process view is given. The temporal probabilistic structure of a spray is discussed and a specific model, the ideal spray, is used to lend rigor to the analysis. Results from

studies using this model are reported for both single- and multi-point statistics of sprays. DOE

N95-23144# Technische Univ., Eindhoven (Netherlands). Dept. of Mathematics and Computing Science.

BEM-BDF SCHEME FOR CURVATURE DRIVEN MOVING STOKES FLOWS

G. A. L. vandeVorst and R. M. M. Mattheij May 1994 29 p

(PB95-138905; RANA-94-05) Avail: CASI HC A03/MF A01

A Backward Differences Formulae (BDF) scheme, is proposed to simulate the deformation of a viscous incompressible Newtonian fluid domain in time, which is driven solely by the boundary curvature. The boundary velocity field of the fluid domain is obtained by writing the governing Stokes equations in terms of an integral formulation that is solved by a Boundary Element Method (BEM). The motion of the boundary is modeled by considering the boundary curve as material points. The trajectories of those points are followed by applying the Lagrangian representation for the velocity. Substituting this representation into the discretized version of the integral equation yields a system of non linear Ordinary Differential Equations (ODEs). Here the numerical integration of this system of ODEs is outlined. It is shown that, depending on the geometrical shape, the system can be stiff. Hence, a BDF-scheme is applied to solve those equations. Some important features with respect to the numerical implementation of this method are high-lighted, like the approximation of the Jacobian matrix and the continuation of integration after a mesh redistribution. The usefulness of the method for both two-dimensional and axisymmetric problems is demonstrated. NTIS

N95-23172# Technische Univ., Eindhoven (Netherlands). Dept. of Mathematics and Computing Science.

QUASISTATIC MODEL FOR THE MOTION OF A VISCOUS CAPILLARY LIQUID DROP

G. Prokert Nov. 1993 24 p

(PB95-138848; RANA-93-16) Avail: CASI HC A03/MF A01

In the modeling of a very viscous drop that moves freely under the influence of surface tension it may be convenient to omit the inertial terms. Thus, a quasistatic model is obtained for which an exact statement is given using Lagrange coordinates. At any time the velocity and pressure field fulfill the Stokes equations with natural boundary conditions of Neumann type. It is shown that the solution of this problem for fixed time exists and is defined up to rigid body motions. For the investigation of the time-dependent problem a result on global invertibility of small C(sup 2)-deformations is proved and the dependence of the solution on such deformations is investigated. A condition concerning this dependence is formulated under which the time-dependent problem has a unique solution on a short interval of time. Finally, a study of the asymptotic behavior of globally existing solutions shows that (under resonable regularity presumptions) our model resembles the fact that the drop approaches the state of a ball of resting liquid. NTIS

N95-23175# Technische Univ., Eindhoven (Netherlands). Dept. of Mathematics and Computing Science.

NUMERICAL SIMULATION OF AXISYMMETRIC VISCOUS SINTERING

G. A. L. vandeVorst May 1994 26 p See also PB93-237717 Sponsored by Stichting voor de Technische Wetenschappen

(PB95-138889; RANA-94-06) Avail: CASI HC A03/MF A01

We describe a numerical method to simulate particular axisymmetric viscous sintering problems. In these problems the material transport is modeled as a viscous incompressible Newtonian volume flow driven solely by surface tension. The numerical simulation is carried out by solving the governing Stokes equations for a fixed domain through a boundary element method (BEM). The resulting velocity field then determines an approximate geometry at a next time level by employing a variable step, variable order backward differences formulae (BDF) method. This numerical algorithm is demonstrated for several simply connected sintering domains, including two coalescing spheres. Furthermore, by considering the movement of a particular fluid region some discrepancies between modeling it as a two-dimensional fluid and as an axisymmetric problem are demonstrated. NTIS

N95-23183*# Tennessee Univ., Tullahoma, TN. Center for Space Transportation and Applied Research.

A WALL INTERFERENCE ASSESSMENT/CORRECTION SYSTEM Final Report, Jun. 1991 - Jun. 1994

C. F. Lo Jun. 1994 10 p

(Grant NAG2-733)

(NASA-CR-197421; NAS 1.26:197421) Avail: CASI HC A02/MF A01

A Wall Signature method originally developed by Hackett has been selected to be adapted for the Ames 12-ft Wind Tunnel WIAC system in the project. This method uses limited measurements of the static pressure at the wall, in conjunction with the solid wall boundary condition, to determine the strength and distribution of singularities representing the test article. The singularities are used in turn for estimating wall interference at the model location. The development and implementation of a working prototype will be completed, delivered and documented with a software manual. The WIAC code will be validated by conducting numerically simulated experiments rather than actual wind tunnel experiments. The simulations will be used to generate both free-air and confined wind-tunnel flow fields for each of the test articles over a range of test configurations. Specifically, the pressure signature at the test section wall will be computed for the tunnel case to provide the simulated 'measured' data. These data will serve as the input for the WIAC method--Wall Signature method. The performance of the WIAC method then may be evaluated by comparing the corrected parameters with those for the free-air simulation. The following two additional tasks are included: (1) On-line wall interference calculation: The developed wall signature method (modified Hackett's method) for Ames 12-ft Tunnel will be the pre-computed coefficients which facilitate the on-line calculation of wall interference, and (2) Support system effects estimation: The effects on the wall pressure measurements due to the presence of the model support systems will be evaluated. Author

N95-23207*# Institute for Computer Applications in Science and Engineering, Hampton, VA.

THE INITIAL-VALUE PROBLEM FOR VISCOUS CHANNEL FLOWS Final Report

W. O. Criminale (Washington Univ., Seattle, WA.), T. L. Jackson, and D. G. Lasseigne (Old Dominion Univ., Norfolk, VA.) Feb. 1995 30 p

(Contract NAS1-19480; RTOP 505-90-52-01)

(NASA-CR-195034; NAS 1.26:195034; ICASE-95-6) Avail: CASI HC A03/MF A01

Plane viscous channel flows are perturbed and the ensuing initial-value problems are investigated in detail. Unlike traditional methods where traveling wave normal modes are assumed for solution, this works offers a means whereby completely arbitrary initial input can be specified without having to resort to eigenfunction expansions. The full temporal behavior, including both early time transients and the long time asymptotics, can be determined for any initial disturbance. Effects of three-dimensionality can be assessed. The bases for the analysis are: (a) linearization of the governing equations; (b) Fourier decomposition in the spanwise and streamwise directions of the flow; and (c) direct numerical integration of the resulting partial differential equations. All of the stability data that are known for such flows can be reproduced. Also, the optimal initial condition can be determined in a straight forward manner and such optimal conditions clearly reflect transient growth data that is easily determined by a rational choice of a basis for the initial conditions. Although there can be significant transient growth for subcritical values of the Reynolds number using this approach it does not appear possible that arbitrary initial conditions will lead to the exceptionally large transient amplitudes that have been determined by optimization of normal modes. The approach is general and can be applied to other classes of problems where only a finite discrete spectrum exists, such as the boundary layer for example. Author

N95-23210*# National Aeronautics and Space Administration. Langley Research Center, Hampton, VA.

MACH 10 COMPUTATIONAL STUDY OF A THREE-DIMENSIONAL SCRAMJET INLET FLOW FIELD

Scott D. Holland Mar. 1995 30 p

(RTOP 506-40-41-02)

(NASA-TM-4602; L-17348; NAS 1.15:4602) Avail: CASI HC A03/MF A01

The present work documents the computational results for a combined computational and experimental parametric study of the internal

aerodynamics of a generic three-dimensional sidewall-compression scramjet inlet configuration at Mach 10. The three-dimensional Navier-Stokes code SCRAMIN was chosen for the computational portion of the study because it uses a well-known and well-proven numerical scheme and has shown favorable comparison with experiment at Mach numbers between 2 and 6. One advantage of CFD was that it provided flow field data for a detailed examination of the internal flow characteristics in addition to the surface properties. The experimental test matrix at Mach 10 included three geometric contraction ratios (3, 5, and 9), three Reynolds numbers (0.55 x 10(exp 6) per foot, 1.14 x 10(exp 6) per foot, and 2.15 x 10(exp 6) per foot), and three cowl positions (at the throat and two forward positions). Computational data for two of these configurations (the contraction ratio of 3, Re = 2.15 x 10(exp 6) per foot, at two cowl positions) are presented along with a detailed analysis of the flow interactions in successive computational planes. Author

N95-23220*# National Aeronautics and Space Administration. Lewis Research Center, Cleveland, OH.

THREE-DIMENSIONAL STRUCTURE IN A SUPERSONIC JET: BEHAVIOR NEAR CENTERLINE

S. H. Shih, R. Hixon, and Reda R. Mankbadi Mar. 1995 12 p Presented at the 33rd Aerospace Meeting and Exhibit, Reno, NV, 9-12 Jan. 1995; sponsored by AIAA Original contains color illustrations

(Contract NCC3-370; RTOP 505-50-5K)

(NASA-TM-106869; ICOMP-95-5; E-9487; NAS 1.15:106869; AIAA Paper 95-0681) Avail: CASI HC A03/MF A01; 1 functional color page

The unsteady structure of a supersonic jet is highly three dimensional, though the mean flow is axisymmetric. In simulating a circular jet, the centerline represents a computational boundary. As such, spurious modes can be generated near centerline, unless special attention is given to the behavior of the 3D structure near the centerline. Improper treatment of the dependent variables near the centerline results in the solution diverging or being suitable only for small amplitude excitation. With a careful treatment of the centerline formation, no spurious mode is generated. The results show that a near-linear disturbance growth is obtained, as the linear stability theory indicates. At high levels of excitation, nonlinear development of disturbances is evident and saturation is reached downstream. Author

N95-23248*# National Aeronautics and Space Administration. Lewis Research Center, Cleveland, OH.

EXPERIMENTAL TECHNIQUE AND ASSESSMENT FOR MEASURING THE CONVECTIVE HEAT TRANSFER COEFFICIENT FROM NATURAL ICE ACCRETIONS

K. Cyril Masiulaniec (Toledo Univ., OH.), G. James VanFossen, Jr., Kenneth J. DeWitt (Toledo Univ., OH.), and Nihad Dukhan (Toledo Univ., OH.) Mar. 1995 26 p Presented at the 33rd Aerospace Sciences Meeting and Exhibit, Reno, NV, 9-12 Jan. 1995; sponsored by AIAA

(Grant NAG3-72; RTOP 505-68-10)

(NASA-TM-106864; E-9476; NAS 1.15:106864; AIAA Paper 95-0537) Avail: CASI HC A03/MF A01

A technique was developed to cast frozen ice shapes that had been grown on a metal surface. This technique was applied to a series of ice shapes that were grown in the NASA Lewis Icing Research Tunnel on flat plates. Nine flat plates, 18 inches square, were obtained from which aluminum castings were made that gave good ice shape characterizations. Test strips taken from these plates were outfitted with heat flux gages, such that when placed in a dry wind tunnel, can be used to experimentally map out the convective heat transfer coefficient in the direction of flow from the roughened surfaces. The effects on the heat transfer coefficient for both parallel and accelerating flow will be studied. The smooth plate model verification baseline data as well as one ice roughened test case are presented. Author

N95-23257*# Vigyan Research Associates, Inc., Hampton, VA.

PERFORMANCE OF THE 0.3-METER TRANSONIC CRYOGENIC TUNNEL WITH AIR, NITROGEN, AND SULFUR HEXAFLUORIDE MEDIA UNDER CLOSED LOOP AUTOMATIC CONTROL

S. Balakrishna and W. Allen Kilgore Jan. 1995 35 p

(Contract NAS1-19672; RTOP 505-59-50-02)

(NASA-CR-195052; NAS 1.26:195052) Avail: CASI HC A03/MF A01

The NASA Langley 0.3-m Transonic Cryogenic Tunnel was modified in 1994, to operate with any one of the three test gas media viz., air, cryogenic nitrogen gas, or sulfur hexafluoride gas. This document provides the initial test results with respect to the tunnel performance and tunnel control, as a part of the commissioning activities on the microcomputer based controller. The tunnel can provide precise and stable control of temperature to less than or equal to +/- 0.3 K in the range 80-320 K in cyro mode or 300-320 K in air/SF6 mode, pressure to +/- 0.01 psia in the range 15-88 psia and Mach number to +/- O.0015 in the range 0.150 to transonic Mach numbers up to 1.000. A new heat exchanger has been included in the tunnel circuit and is performing adequately. The tunnel airfoil testing benefits considerably by precise control of tunnel states and helps in generating high quality aerodynamic test data from the 0.3-m TCT. Author

N95-23372# Oak Ridge National Lab., TN.

MPI IMPLEMENTATION OF CFD PROGRAM PHOENICS

S. Simunovic and T. Zacharia 26 Oct. 1994 11 p

(Contract DE-AC05-84OR-21400)

(DE95-003896; ORNL/M-3986) Avail: CASI HC A03/MF A01

This document describes the work on Message Passing Interface (MPI) standard implementation of the parallel version of the solver EARTH for the Computational Fluid Dynamics (CFD) program PHOENICS. The Intel Paragon NX and MPI versions of the program have been developed and tested on massively parallel (MP) supercomputers Intel Paragon XP/S 5, XP/S 35, and Kendall Square Research (KSR) supercomputers at Oak Ridge National Laboratory (ORNL). The preliminary testing results of the developed program have shown scalable performance for reasonably sized computational domains. DOE

N95-23412*# National Aeronautics and Space Administration. Marshall Space Flight Center, Huntsville, AL.

ELEVENTH WORKSHOP FOR COMPUTATIONAL FLUID DYNAMIC APPLICATIONS IN ROCKET PROPULSION

R. W. Williams, comp. Washington Jul. 1993 937 p Workshop held in Huntsville, AL, 20-22 Apr. 1993

(NASA-CP-3221-Pt-2; M-726-Pt-2; NAS 1.55:3221-Pt-2) Avail: CASI HC A99/MF A10

Conference publication includes 79 abstracts and presentations and 3 invited presentations given at the Eleventh Workshop for Computational Fluid Dynamic Applications in Rocket Propulsion held at George C. Marshall Space Flight Center, April 20-22, 1993. The purpose of the workshop is to discuss experimental and computational fluid dynamic activities in rocket propulsion. The workshop is an open meeting for government, industry, and academia. A broad number of topics are discussed including computational fluid dynamic methodology, liquid and solid rocket propulsion, turbomachinery, combustion, heat transfer, and grid generation. For individual titles, see N95-23413 through N95-23448.

N95-23413*# SECA, Inc., Huntsville, AL.

HEAT TRANSFER IN ROCKET ENGINE COMBUSTION CHAMBERS AND NOZZLES

P. G. Anderson, G. C. Cheng, and R. C. Farmer *In* NASA. Marshall Space Flight Center, Eleventh Workshop for Computational Fluid Dynamic Applications in Rocket Propulsion Jul. 1993 p 963-990 (For primary document see N95-23412 07-34)

Avail: CASI HC A03/MF A10

Complexities of liquid rocket engine heat transfer which involve the injector faceplate and regeneratively and film cooled walls are being investigated by computational analysis. A conjugate heat transfer analysis will be used to describe localized heating phenomena associated with particular injector configurations and coolant channels and film coolant dumps. These components are being analyzed, and the analyses verified with appropriate test data. Finally, the component analyses will be synthesized into an overall flowfield/heat transfer model. The FDNS code is being used to make the component analyses. Particular attention is being given to the representation of the thermodynamic properties of the fluid streams and to the method of combining the detailed models to represent overall heating. Unit flow models of specific coaxial injector elements have been developed and will be described. Since test data from the NLS development program are not available, new validation heat transfer data have been sought. Suitable data were obtained from a Rocketdyne test program on a model hydrocarbon/oxygen engine. Simulations of these test data will be presented. Recent interest in the

hybrid motor have established the need for analyses of ablating solid fuels in the combustion chamber. Analysis of a simplified hybrid motor will also be presented. Author

N95-23414*# SECA, Inc., Huntsville, AL.
RADIATION/CONVECTION COUPLING IN ROCKET MOTORS AND PLUMES
R. C. Farmer and A. J. Saladino *In* NASA. Marshall Space Flight Center, Eleventh Workshop for Computational Fluid Dynamic Applications in Rocket Propulsion Jul. 1993 p 991-1019 (For primary document see N95-23412 07-34)
Avail: CASI HC A03/MF A10

The three commonly used propellant systems - H2/O2, RP-1/O2, and solid propellants - primarily radiate as molecular emitters, non-scattering small particles, and scattering larger particles, respectively. Present technology has accepted the uncoupling of the radiation analysis from that of the flowfield. This approximation becomes increasingly inaccurate as one considers plumes, interior rocket chambers, and nuclear rocket propulsion devices. This study will develop a hierarchy of methods which will address radiation/convection coupling in all of the aforementioned propulsion systems. The nature of the radiation/convection coupled problem is that the divergence of the radiative heat flux must be included in the energy equation and that the local, volume-averaged intensity of the radiation must be determined by a solution of the radiative transfer equation (RTE). The intensity is approximated by solving the RTE along several lines of sight (LOS) for each point in the flowfield. Such a procedure is extremely costly; therefore, further approximations are needed. Modified differential approximations are being developed for this purpose. It is not obvious which order of approximations are required for a given rocket motor analysis. Therefore, LOS calculations have been made for typical rocket motor operating conditions in order to select the type approximations required. The results of these radiation calculations, and the interpretation of these intensity predictions are presented herein. Author

N95-23415*# Mississippi State Univ., Mississippi State, MS.
IGES TRANSFORMER AND NURBS IN GRID GENERATION **c61**
Tzu-Yi Yu and Bharat K. Soni *In* NASA. Marshall Space Flight Center, Eleventh Workshop for Computational Fluid Dynamic Applications in Rocket Propulsion Jul. 1993 p 1021-1053 (For primary document see N95-23412 07-34)
Avail: CASI HC A03/MF A10

In the field of Grid Generation and the CAD/CAM, there are numerous geometry output formats which require the designer to spend a great deal of time manipulating geometrical entities in order to achieve a useful sculptured geometrical description for grid generation. Also in this process, there is a danger of losing fidelity of the geometry under consideration. This stresses the importance of a standard geometry definition for the communication link between varying CAD/CAM and grid system. The IGES (Initial Graphics Exchange Specification) file is a widely used communication between CAD/CAM and the analysis tools. The scientists at NASA Research Centers - including NASA Ames, NASA Langley, NASA Lewis, NASA Marshall - have recognized this importance and, therefore, in 1992 they formed the committee of the 'NASA-IGES' which is the subset of the standard IGES. This committee stresses the importance and encourages the CFD community to use the standard IGES file for the interface between the CAD/CAM and CFD analysis. Also, two of the IGES entities -- the NURBS Curve (Entity 126) and NURBS Surface (Entity 128) -- which have many useful geometric properties -- like the convex hull property, local control property and affine invariance, also widely utilized analytical geometries can be accurately represented using NURBS. This is important in today grid generation tools because of the emphasis of the interactive design. To satisfy the geometry transformation between the CAD/CAM system and Grid Generation field, the CAGI (Computer Aided Geometry Design) developed, which include the Geometry Transformation, Geometry Manipulation and Geometry Generation as well as the user interface. This paper will present the successful development IGES file transformer and application of NURBS definition in the grid generation. Author

N95-23416*# Rockwell International Corp., Canoga Park, CA. Rocketdyne Div.
CRITERIA FOR EVALUATION OF GRID GENERATION SYSTEMS **c61**
Edward P. Ascoli, Steven L. Barson, Michele E. DeCroix, and Wayne W. Hsu *In* NASA. Marshall Space Flight Center, Eleventh Workshop for Computational Fluid Dynamic Applications in Rocket Propulsion Jul. 1993 p 1055-1090 (For primary document see N95-23412 07-34)
Avail: CASI HC A03/MF A10

Many CFD grid generation systems are in use nationally, but few comparative studies have been performed to quantify their relative merits. A study was undertaken to systematically evaluate and select the best CFD grid generation codes available. Detailed evaluation criteria were established as the basis for the evaluation conducted. Descriptions of thirty-four separate criteria, grouped into eight general categories are provided. Benchmark test cases, developed to test basic features of selected codes, are described in detail. Scoring guidelines were generated to establish standards for measuring code capabilities, ensuring uniformity of ratings, and minimizing personal bias among the three code evaluators. Ten candidate codes were identified from government, industry, universities, and commercial software companies. A three phase evaluation was conducted. In Phase 1, ten codes identified were screened through conversations with code authors and other industry experts. Seven codes were carried forward into a Phase 2 evaluation in which all codes were scored according to the predefined criteria. Two codes emerged as being significantly better than the others: RAGGS and GRIDGEN. Finally, these two codes were carried forward into a Phase 3 evaluation in which complex 3-D multizone grids were generated to verify capability. Author

N95-23417*# Mississippi State Univ., Mississippi State, MS.
STRUCTURED ADAPTIVE GRID GENERATION USING ALGEBRAIC METHODS **c64**
Jiann-Cherng Yang, Bharat K. Soni, R. P. Roger (Teledyne Brown Engineering, Huntsville, AL.), and Stephen C. Chan (Teledyne Brown Engineering, Huntsville, AL.) *In* NASA. Marshall Space Flight Center, Eleventh Workshop for Computational Fluid Dynamic Applications in Rocket Propulsion Jul. 1993 p 1091-1128 (For primary document see N95-23412 07-34)
Avail: CASI HC A03/MF A10

The accuracy of the numerical algorithm depends not only on the formal order of approximation but also on the distribution of grid points in the computational domain. Grid adaptation is a procedure which allows optimal grid redistribution as the solution progresses. It offers the prospect of accurate flow field simulations without the use of an excessively timely, computationally expensive, grid. Grid adaptive schemes are divided into two basic categories: differential and algebraic. The differential method is based on a variational approach where a function which contains a measure of grid smoothness, orthogonality and volume variation is minimized by using a variational principle. This approach provided a solid mathematical basis for the adaptive method, but the Euler-Lagrange equations must be solved in addition to the original governing equations. On the other hand, the algebraic method requires much less computational effort, but the grid may not be smooth. The algebraic techniques are based on devising an algorithm where the grid movement is governed by estimates of the local error in the numerical solution. This is achieved by requiring the points in the large error regions to attract other points and points in the low error region to repel other points. The development of a fast, efficient, and robust algebraic adaptive algorithm for structured flow simulation applications is presented. This development is accomplished in a three step process. The first step is to define an adaptive weighting mesh (distribution mesh) on the basis of the equidistribution law applied to the flow field solution. The second, and probably the most crucial step, is to redistribute grid points in the computational domain according to the aforementioned weighting mesh. The third and the last step is to reevaluate the flow property by an appropriate search/interpolate scheme at the new grid locations. The adaptive weighting mesh provides the information on the desired concentration of points to the grid redistribution scheme. The evaluation of the weighting mesh is accomplished by utilizing the weight function representing the solution variation and the equidistribution law. The selection of the weight function plays a key role in grid adaptation. A new weight function utilizing a properly weighted boolean sum of various flowfield characteristics is defined. The redistribution scheme is developed utilizing Non-Uniform Rational B-Splines (NURBS) representation. The application of NURBS representation results in a well distributed smooth grid by maintaining the fidelity of the geometry associated with boundary curves. Several algebraic methods are applied to smooth and/or nearly

orthogonalize the grid lines. An elliptic solver is utilized to smooth the grid lines if there are grid crossings. Various computational examples of practical interest are presented to demonstrate the success of these methods.
Author

N95-23418*# National Aeronautics and Space Administration. Marshall Space Flight Center, Huntsville, AL.
A GENERIC EFFICIENT ADAPTIVE GRID SCHEME FOR ROCKET PROPULSION MODELING **c61**
J. D. Mo and Alan S. Chow *In its* Eleventh Workshop for Computational Fluid Dynamic Applications in Rocket Propulsion Jul. 1993 p 1129-1148 (For primary document see N95-23412 07-34)
Avail: CASI HC A03/MF A10

The objective of this research is to develop an efficient, time-accurate numerical algorithm to discretize the Navier-Stokes equations for the predictions of internal one-, two-dimensional and axisymmetric flows. A generic, efficient, elliptic adaptive grid generator is implicitly coupled with the Lower-Upper factorization scheme in the development of ALUNS computer code. The calculations of one-dimensional shock tube wave propagation and two-dimensional shock wave capture, wave-wave interactions, shock wave-boundary interactions show that the developed scheme is stable, accurate and extremely robust. The adaptive grid generator produced a very favorable grid network by a grid speed technique. This generic adaptive grid generator is also applied in the PARC and FDNS codes and the computational results for solid rocket nozzle flowfield and crystal growth modeling by those codes will be presented in the conference, too. This research work is being supported by NASA/MSFC. Author

N95-23419*# Mississippi State Univ., Mississippi State, MS. Center for Computational Field Simulation.
TIGER: A USER-FRIENDLY INTERACTIVE GRID GENERATION SYSTEM FOR COMPLICATED TURBOMACHINERY AND AXIS-SYMMETRIC CONFIGURATIONS **c61**
Ming H. Shih and Bharat K. Soni *In* NASA. Marshall Space Flight Center, Eleventh Workshop for Computational Fluid Dynamic Applications in Rocket Propulsion Jul. 1993 p 1149-1161 Sponsored by NASA. Lewis Research Center (For primary document see N95-23412 07-34)
Avail: CASI HC A03/MF A10

The issue of time efficiency in grid generation is addressed by developing a user friendly graphical interface for interactive/automatic construction of structured grids around complex turbomachinery/axis-symmetric configurations. The accuracy of geometry modeling and its fidelity is accomplished by adapting the nonuniform rational b-spline (NURBS) representation. A customized interactive grid generation code, TIGER, has been developed to facilitate the grid generation process for complicated internal, external, and internal-external turbomachinery fields simulations. The FORMS Library is utilized to build user-friendly graphical interface. The algorithm allows a user to redistribute grid points interactively on curves/surfaces using NURBS formulation with accurate geometric definition. TIGER's features include multiblock, multiduct/shroud, multiblade row, uneven blade count, and patched/overlapping block interfaces. It has been applied to generate grids for various complicated turbomachinery geometries, as well as rocket and missile configurations. Author (revised)

N95-23420*# Aerosoft, Inc., Blacksburg, VA.
TOWARDS A GENERALIZED COMPUTATIONAL FLUID DYNAMICS TECHNIQUE FOR ALL MACH NUMBERS
R. W. Walters, D. C. Slack, and A. G. Godfrey *In* NASA. Marshall Space Flight Center, Eleventh Workshop for Computational Fluid Dynamic Applications in Rocket Propulsion Jul. 1993 p 1163-1195 (For primary document see N95-23412 07-34)
Avail: CASI HC A03/MF A10

Currently there exists no single unified approach for efficiently and accurately solving computational fluid dynamics (CFD) problems across the Mach number regime, from truly low speed incompressible flows to hypersonic speeds. There are several CFD codes that have evolved into sophisticated prediction tools with a wide variety of features including multiblock capabilities, generalized chemistry and thermodynamics models among other features. However, as these codes evolve, the demand placed on the end user also increases simply because of the myriad of features that are incorporated into these codes. In order for a user to be able to solve a wide range of problems, several codes may be needed requiring the user to be familiar with the intricacies of each code and their rather complicated input files. Moreover, the cost of training users and maintaining several codes becomes prohibitive. The objective of the current work is to extend the compressible, characteristic-based, thermochemical nonequilibrium Navier-Stokes code GASP to very low speed flows and simultaneously improve convergence at all speeds. Before this work began, the practical speed range of GASP was Mach numbers on the order of 0.1 and higher. In addition, a number of new techniques have been developed for more accurate physical and numerical modeling. The primary focus has been on the development of optimal preconditioning techniques for the Euler and the Navier-Stokes equations with general finite-rate chemistry models and both equilibrium and nonequilibrium thermodynamics models. We began with the work of Van Leer, Lee, and Roe for inviscid, one-dimensional perfect gases and extended their approach to include three-dimensional reacting flows. The basic steps required to accomplish this task were a transformation to stream-aligned coordinates, the formulation of the preconditioning matrix, incorporation into both explicit and implicit temporal integration schemes, and modification of the numerical flux formulae. In addition, we improved the convergence rate of the implicit time integration schemes in GASP through the use of inner iteration strategies and the use of the GMRES (General Minimized Resisual) which belongs to the class of algorithms referred to as Krylov subspace iteration. Finally, we significantly improved the practical utility of GASP through the addition of mesh sequencing, a technique in which computations begin on a coarse grid and get interpolated onto successively finer grids. The fluid dynamic problems of interest to the propulsion community involve complex flow physics spanning different velocity regimes and possibly involving chemical reactions. This class of problems results in widely disparate time scales causing numerical stiffness. Even in the absence of chemical reactions, eigenvalue stiffness manifests itself at transonic and very low speed flows which can be quantified by the large condition number of the system and evidenced by slow convergence rates. This results in the need for thorough numerical analysis and subsequent implementation of sophisticated numerical techniques for these difficult yet practical problems. As a result of this work, we have been able to extend the range of applicability of compressible codes to very low speed inviscid flows (M = .001) and reacting flows.
Derived from text

N95-23421*# Aero Thermo Technology, Inc., Huntsville, AL.
PRECONDITIONING FOR THE NAVIER-STOKES EQUATIONS WITH FINITE-RATE CHEMISTRY
Andrew G. Godfrey *In* NASA. Marshall Space Flight Center, Eleventh Workshop for Computational Fluid Dynamic Applications in Rocket Propulsion Jul. 1993 p 1197-1211 (For primary document see N95-23412 07-34)
Avail: CASI HC A03/MF A10

The extension of Van Leer's preconditioning procedure to generalized finite-rate chemistry is discussed. Application to viscous flow is begun with the proper preconditioning matrix for the one-dimensional Navier-Stokes equations. Eigenvalue stiffness is resolved and convergence-rate acceleration is demonstrated over the entire Mach-number range from nearly stagnant flow to hypersonic. Specific benefits are realized at the low and transonic flow speeds typical of complete propulsion-system simulations. The extended preconditioning matrix necessarily accounts for both thermal and chemical nonequilibrium. Numerical analysis reveals the possible theoretical improvements from using a preconditioner for all Mach number regimes. Numerical resuits confirm the expectations from the numerical analysis. Representative test cases include flows with previously troublesome embedded high-condition-number areas. Van Leer, Lee, and Roe recently developed an optimal, analytic preconditioning technique to reduce eigenvalue stiffness over the full Mach-number range. By multiplying the flux-balance residual with the preconditioning matrix, the acoustic wave speeds are scaled so that all waves propagate at the same rate, an essential property to eliminate inherent eigenvalue stiffness. This session discusses a synthesis of the thermochemical nonequilibrium flux-splitting developed by Grossman and Cinnella and the characteristic wave preconditioning of Van Leer into a powerful tool for implicitly solving two and three-dimensional flows with generalized finite-rate chemistry. For finite-rate chemistry, the state vector of unknowns is variable in length. Therefore, the preconditioning matrix extended to generalized finite-rate chemistry must accommodate a flexible system of moving waves. Fortunately,

no new kind of wave appears in the system. The only existing waves are entropy and vorticity waves, which move with the fluid, and acoustic waves, which propagate in Mach number dependent directions. The nonequilibrium vibrational energies and species densities in the unknown state vector act strictly as convective waves. The essential concept for extending the preconditioning to generalized chemistry models is determining the differential variables which symmetrize the flux Jacobians. The extension is then straight-forward. This algorithm research effort will be released in a future version of the production level computational code coined the General Aerodynamic Simulation Program (GASP), developed by Walters, Slack, and McGrory. Author

N95-23422*# National Aeronautics and Space Administration. Marshall Space Flight Center, Huntsville, AL.

A NUMERICAL PROCEDURE FOR ANALYSIS OF FINITE RATE REACTING FLOWS

H. M. Shang (Engineering Sciences, Inc., Huntsville, AL.), Y. S. Chen (Engineering Sciences, Inc., Huntsville, AL.), Z. J. Chen (Alabama Univ., Huntsville, AL.), C. P. Chen (Alabama Univ., Huntsville, AL.), and T. S. Wang *In its* Eleventh Workshop for Computational Fluid Dynamic Applications in Rocket Propulsion Jul. 1993 p 1213-1238 (For primary document see N95-23412 07-34)

Avail: CASI HC A03/MF A10

Combustion processes in rocket propulsion systems are characterized by the existence of multiple, vastly differing time and length scales, as well as flow-speeds at wide variation of Mach numbers. The chemical kinetics processes in the highly active reaction zone are characterized by much smaller scales compared to fluid convective and diffusive time scales. An operator splitting procedure for transient finite rate chemistry problems has been developed using a pressure based method, which can be applied to all speed flows without difficulties. The splitting of chemical kinetics terms formed the fluid-mechanical terms of the species equation ameliorated the difficulties associated with the disparate time scales and stiffness in the set of equations which describes highly exothermic combustion. A combined efficient ordinary differential equations (ODE) solver was used to integrate the effective chemical source terms over the residence time at each grid cell. One and two dimensional reacting flow situations were carried out to demonstrate and verify the current procedure. Different chemical kinetics with different degrees of nonlinearity have also been incorporated to test the robustness and generality of the proposed method. Author

N95-23423*# Sverdrup Technology, Inc., Brook Park, OH.

THREE-DIMENSIONAL NAVIER-STOKES ANALYSIS AND REDESIGN OF AN IMBEDDED BELLMOUTH NOZZLE IN A TURBINE CASCADE INLET SECTION

P. W. Giel and J. R. Sirbaugh *In* NASA. Marshall Space Flight Center, Eleventh Workshop for Computational Fluid Dynamic Applications in Rocket Propulsion Jul. 1993 p 1239-1257 (For primary document see N95-23412 07-34)

Avail: CASI HC A03/MF A10

Verification of proposed turbopump blading performance will involve evaluation of candidate blades in cascade test facilities. It is necessary to be able to predict the flow fields within these cascades for the results to be applicable to actual engine environments. This work presents the results of a study to predict the flow field for the NASA Lewis Transonic Turbine Blade Cascade Facility, which is similar to those used to evaluate rocket propulsion turbines. A pitchwise nonuniform total pressure distribution was observed at the blade row leading edge plane. A CFD analysis was used to show that the cause of the flow nonuniformity was a pair of vortices that originated in an embedded bellmouth inlet. Further CFD analysis was used to verify that a redesigned inlet section resulted in a flow with acceptable uniformity. A computational analysis was chosen because physical accessibility to the inlet section was limited, and because a computational approach also allows one to examine design changes cheaper and more quickly than an experimental approach would. The PARC code, a general purpose, three-dimensional, Navier-Stokes code with multiblock solution capability, was chosen for the present study. Results are presented detailing the computational requirements needed to accurately predict flows of this nature. Calculations of the original geometry showed total pressure loss regions consistent in strength and in location to experimental measurements. An examination of the results shows that the distortions are caused by a pair of vortices that originate as a result of the interaction of the flow with the imbedded bellmouth. Computations were performed for an inlet geometry which eliminated the imbedded bellmouth by bridging the region between it and the upstream wall. This analysis indicated that eliminating the imbedded bellmouth eliminates the troublesome pair of vortices, resulting in a flow with much greater pitchwise uniformity. Author

N95-23424*# National Aeronautics and Space Administration. Lewis Research Center, Cleveland, OH.

PREDICTION OF INCIDENCE AND SURFACE ROUGHNESS EFFECTS ON TURBINE PERFORMANCE

R. J. Boyle *In* NASA. Marshall Space Flight Center, Eleventh Workshop for Computational Fluid Dynamic Applications in Rocket Propulsion Jul. 1993 p 1259-1285 (For primary document see N95-23412 07-34)

Avail: CASI HC A03/MF A10

The results of a Navier-Stokes analysis for predicting the change in turbine efficiency due to a change in either incidence or surface roughness is discussed. It was experimentally determined by Boynton, Tabibzadeh, and Hudson that polishing the SSME high pressure fuel turbine blades improved turbine efficiency by about 2 points over a wide range of operating conditions. These conditions encompassed the range of incidence seen by the turbine blading during flight. It is also necessary to be able to predict turbine performance at various operating points for future rocket turbopump applications. The code RVCQ3D, developed by Rod Chima, was used to determine the effects of changes in incidence angle on turbine blade row efficiency. The midspan Navier-Stokes results were used in conjunction with an inviscid flow analysis code to predict the efficiency of the two stage SSME over a wide range of operating conditions for smooth and rough turbine blades. The use of the Navier-Stokes analysis to predict changes in turbine efficiency due to variation in incidence angles was found to be superior to other incidence loss correlations available in the literature. The sensitivity of the Navier-Stokes results to grid parameters is discussed. The effects of the surface roughness were accounted for using the Cebeci-Chang rough wall turbulence model. This model was implemented in the code RVCQ3D. The implementation of this model for predicting the change in efficiency is also discussed. Author

N95-23425*# MCAT Inst., Moffett Field, CA.

THREE-DIMENSIONAL UNSTEADY FLOW CALCULATIONS IN AN ADVANCED GAS GENERATOR TURBINE

Akil A. Rangwalla *In* NASA. Marshall Space Flight Center, Eleventh Workshop for Computational Fluid Dynamic Applications in Rocket Propulsion Jul. 1993 p 1287-1320 (For primary document see N95-23412 07-34)

Avail: CASI HC A03/MF A10

This paper deals with the application of a three-dimensional, unsteady Navier-Stokes code for predicting the unsteady flow in a single stage of an advanced gas generator turbine. The numerical method solves the three-dimensional thin-layer Navier-Stokes equations, using a system of overlaid grids, which allow for relative motion between the rotor and stator airfoils. Results in the form of time averaged pressures and pressure amplitudes on the airfoil surfaces will be shown. In addition, instantaneous contours of pressure, Mach number, etc. will be presented in order to provide a greater understanding of the inviscid as well as the viscous aspects of the flowfield. Also, relevant secondary flow features such as cross-plane velocity vectors and total pressure contours will be presented. Prior work in two-dimensions has indicated that for the advanced designs, the unsteady interactions can play a significant role in turbine performance. These interactions affect not only the stage efficiency but can substantially alter the time-averaged features of the flow. This work is a natural extension of the work done in two-dimensions and hopes to address some of the issues raised by the two-dimensional calculations. These calculations are being performed as an integral part of an actual design process and demonstrate the value of unsteady rotor-stator interaction calculations in the design of turbomachines. Author

N95-23426*# Pennsylvania State Univ., University Park, PA. Dept. of Aerospace Engineering.

NUMERICAL SIMULATION OF STEADY AND UNSTEADY VISCOUS FLOW IN TURBOMACHINERY USING PRESSURE BASED ALGORITHM

B. Lakshminarayana, Y. Ho, and A. Basson *In* NASA. Marshall Space Flight Center, Eleventh Workshop for Computational Fluid Dynamic

Applications in Rocket Propulsion Jul. 1993 p 1321-1357 (For primary document see N95-23412 07-34)
Avail: CASI HC A03/MF A10

The objective of this research is to simulate steady and unsteady viscous flows, including rotor/stator interaction and tip clearance effects in turbomachinery. The numerical formulation for steady flow developed here includes an efficient grid generation scheme, particularly suited to computational grids for the analysis of turbulent turbomachinery flows and tip clearance flows, and a semi-implicit, pressure-based computational fluid dynamics scheme that directly includes artificial dissipation, and is applicable to both viscous and inviscid flows. The values of these artificial dissipation is optimized to achieve accuracy and convergency in the solution. The numerical model is used to investigate the structure of tip clearance flows in a turbine nozzle. The structure of leakage flow is captured accurately, including blade-to-blade variation of all three velocity components, pitch and yaw angles, losses and blade static pressures in the tip clearance region. The simulation also includes evaluation of such quantities of leakage mass flow, vortex strength, losses, dominant leakage flow regions and the spanwise extent affected by the leakage flow. It is demonstrated, through optimization of grid size and artificial dissipation, that the tip clearance flow field can be captured accurately. The above numerical formulation was modified to incorporate time accurate solutions. An inner loop iteration scheme is used at each time step to account for the non-linear effects. The computation of unsteady flow through a flat plate cascade subjected to a transverse gust reveals that the choice of grid spacing and the amount of artificial dissipation is critical for accurate prediction of unsteady phenomena. The rotor-stator interaction problem is simulated by starting the computation upstream of the stator, and the upstream rotor wake is specified from the experimental data. The results show that the stator potential effects have appreciable influence on the upstream rotor wake. The predicted unsteady wake profiles are compared with the available experimental data and the agreement is good. The numerical results are interpreted to draw conclusions on the unsteady wake transport mechanism in the blade passage. Author

N95-23427*# Aerojet-General Corp., Sacramento, CA. Propulsion Div.
GGOT TOTAL PRESSURE LOSS CONTROL CONCEPT EVALUATION
R. F. Blumenthal *In* NASA. Marshall Space Flight Center, Eleventh Workshop for Computational Fluid Dynamic Applications in Rocket Propulsion Jul. 1993 p 1359-1396 (For primary document see N95-23412 07-34)
Avail: CASI HC A03/MF A10

Total pressure loss is one of the most important parameters in the design of a turbine. This parameter effects not only the turbine performance, but consequently the engine power balance and engine performance. Computational Fluid Dynamics (CFD) can be an effective tool in predicting turbine total pressure loss, and also for performing sensitivity studies to achieve an optimal design with respect to pressure loss. In the present study, the AEROVISC code was used to predict the total pressure loss in the Turbine Technology Team Gas Generator Oxidizer Turbine (GGOT). The objectives in this study are two-fold. It is first necessary to determine an optimal methodology in predicting total pressure loss. The type of grid, grid density and distribution are parameters which may affect the loss prediction. Also, the effect of using a standard K-epsilon turbulence model with wall functions versus a two-layer turbulence model needs to be investigated. The use of grid embedding to resolve areas with high flow gradients needs to be explored. The second objective of the study is to apply the optimal methodology toward evaluating different tip leakage control concepts. Author

N95-23428*# Scientific Research Associates, Inc., Glastonbury, CT.
NAVIER-STOKES ANALYSIS OF AN OXIDIZER TURBINE BLADE WITH TIP CLEARANCE WITH AND WITHOUT A MINI-SHROUD
Tony Chan and Frederik J. deJong *In* NASA. Marshall Space Flight Center, Eleventh Workshop for Computational Fluid Dynamic Applications in Rocket Propulsion Jul. 1993 p 1397-1422 (For primary document see N95-23412 07-34)
(Contract NAS8-38865)
Avail: CASI HC A03/MF A10

The Gas Generator Oxidizer Turbine (GGOT) Blade is being analyzed by various investigators under the NASA MSFC-sponsored Turbine Stage Technology Team design effort. The present work concentrates on the tip clearance region flow and associated losses; however, flow details for the passage region are also obtained in the simulations. The present calculations simulate the rotor blade row in a rotating reference frame with the appropriate coriolis and centrifugal acceleration term included in the momentum equations. The upstream computational boundary is located about one axial chord from the blade leading edge. The boundary conditions at this location have been determined by Pratt & Whitney using an Euler analysis without the vanes to obtain approximately the same flow profiles at the rotor as were obtained with the Euler stage analysis including the vanes. Inflow boundary layer profiles are then constructed assuming the skin friction coefficient at both the hub and the casing. The downstream computational boundary is located about one axial chord from the blade trailing edge, and the circumferentially averaged static pressure at this location was also obtained from the P&W Euler analysis. Results obtained for the 3-D baseline GGOT geometry at the full scale design Reynolds number show a region of high loss in the region near the casing. Particle traces in the near tip region show vortical flow behavior of the fluid which passes through the clearance region and exits at the downstream edge of the gap. In an effort to reduce clearance flow losses, the mini-shroud concept was proposed by the Pratt & Whitney design team. Calculations were performed on the GGO geometry with the mini-shroud. Results of these calculations indicate that the mini-shroud does not significantly affect the flow in the passage region, and although the tip clearance flow is different, the mini-shroud does not seem to prevent the above-mentioned vortical flow behavior. Since both flow distortion and total pressure losses are similar for both geometries, the addition of the mini-shroud does not seem to reduce the tip clearance flow effects. Author

N95-23429*# Virginia Polytechnic Inst. and State Univ., Blacksburg, VA. Dept. of Mechanical Engineering.
SUPERSONIC FLOW AND SHOCK FORMATION IN TURBINE TIP GAPS
John Moore *In* NASA. Marshall Space Flight Center, Eleventh Workshop for Computational Fluid Dynamic Applications in Rocket Propulsion Jul. 1993 p 1423-1433 (For primary document see N95-23412 07-34)
Avail: CASI HC A03/MF A10

Shock formation due to overexpansion of supersonic flow at the inlet to the tip clearance gap of a turbomachine has been studied. As the flow enters the tip gap, it accelerates around the blade pressure-side corner creating a region of minimum static pressure. The 'free streamline' separates from the wall at the corner; and, for Mach numbers greater than about 1.3, it curves back to intersect the blade tip. At this point, the freestream flow is abruptly turned parallel to the surface, giving rise to an oblique shock. The results are consistent with compressible sharp-edged orifice flow calculations found in the literature and with the theory of oblique shock wave formation in supersonic flow over a wedge. For freestream Mach numbers of 1.4 to 1.8, wave angles are 43 to 54 deg, and turning angles are 9 to 20 deg; as the Mach number increases, the angle of turn also increases. It appears that in a turbine, after separating from the inlet corner, the flow reattaches on the blade tip and an oblique shock is formed at 0.4-1.4 tip gap heights into the clearance gap. The resulting shock-boundary layer interaction may contribute to further enhancement of already high heat transfer to the blade tip in this region. This in turn could lead to higher blade temperatures and adversely affect blade life and turbine efficiency. Author

N95-23430*# National Aeronautics and Space Administration. Marshall Space Flight Center, Huntsville, AL.
AXISYMMETRIC COMPUTATIONAL FLUID DYNAMICS ANALYSIS OF SATURN V/S1-C/F1 NOZZLE AND PLUME
Joseph H. Ruf *In its* Eleventh Workshop for Computational Fluid Dynamic Applications in Rocket Propulsion Jul. 1993 p 1435-1455 (For primary document see N95-23412 07-34)
Avail: CASI HC A03/MF A10

An axisymmetric single engine Computational Fluid Dynamics calculation of the Saturn V/S 1-C vehicle base region and F1 engine plume is described. There were two objectives of this work, the first was to calculate an axisymmetric approximation of the nozzle, plume and base region flow fields of S1-C/F1, relate/scale this to flight data and apply this scaling factor to a NLS/STME axisymmetric calculations from a parallel effort. The second was to assess the differences in F1 and STME plume shear layer development and concentration of combustible gases. This second piece of information was to be input/supporting data for assumptions made in

NLS2 base temperature scaling methodology from which the vehicle base thermal environments were being generated. The F1 calculations started at the main combustion chamber faceplate and incorporated the turbine exhaust dump/nozzle film coolant. The plume and base region calculations were made for ten thousand feet and 57 thousand feet altitude at vehicle flight velocity and in stagnant freestream. FDNS was implemented with a 14 species, 28 reaction finite rate chemistry model plus a soot burning model for the RP-1/LOX chemistry. Nozzle and plume flow fields are shown, the plume shear layer constituents are compared to a STME plume. Conclusions are made about the validity and status of the analysis and NLS2 vehicle base thermal environment definition methodology. Author

N95-23431*# National Aeronautics and Space Administration. Marshall Space Flight Center, Huntsville, AL.

COMPUTATIONAL FLUID DYNAMIC (CFD) ANALYSIS OF AXISYMMETRIC PLUME AND BASE FLOW OF FILM/DUMP COOLED ROCKET NOZZLE

P. K. Tucker and S. A. Warsi (Sverdrup Technology, Inc., Huntsville, AL.) *In its* Eleventh Workshop for Computational Fluid Dynamic Applications in Rocket Propulsion Jul. 1993 p 1457-1472 (For primary document see N95-23412 07-34)

Avail: CASI HC A03/MF A10

Film/dump cooling a rocket nozzle with fuel rich gas, as in the National Launch System (NLS) Space Transportation Main Engine (STME), adds potential complexities for integrating the engine with the vehicle. The chief concern is that once the film coolant is exhausted from the nozzle, conditions may exist during flight for the fuel-rich film gases to be recirculated to the vehicle base region. The result could be significantly higher base temperatures than would be expected from a regeneratively cooled nozzle. CFD analyses were conduced to augment classical scaling techniques for vehicle base environments. The FDNS code with finite rate chemistry was used to simulate a single, axisymmetric STME plume and the NLS base area. Parallel calculations were made of the Saturn V S-1 C/F1 plume base area flows. The objective was to characterize the plume/freestream shear layer for both vehicles as inputs for scaling the S-C/F1 flight data to NLS/STME conditions. The code was validated on high speed flows with relevant physics. This paper contains the calculations for the NLS/STME plume for the baseline nozzle and a modified nozzle. The modified nozzle was intended to reduce the fuel available for recirculation to the vehicle base region. Plumes for both nozzles were calculated at 10kFT and 50kFT. Author

N95-23432*# Rockwell International Corp., Canoga Park, CA. Rocketdyne Div.

NLS BASE HEATING CFD ANALYSIS

Edward P. Ascoli, Adel H. Heiba, Yann-Fu Hsu, Ronald R. Lagnado, and Edward D. Lynch *In* NASA. Marshall Space Flight Center, Eleventh Workshop for Computational Fluid Dynamic Applications in Rocket Propulsion Jul. 1993 p 1475-1509 (For primary document see N95-23412 07-34)

Avail: CASI HC A03/MF A10

Concerns raised over possible base heating effects on the National Launch System (NLS) 1.5 stage reference vehicle resulted in the use of CFD as a predictive analysis tool. The objective established was to obtain good engineering solutions to describe the base region flowfields at 10,000 ft and 50,000 ft altitudes. The Rockwell USA CFD code was employed with a zero-equation turbulence model and a four species, 1 step chemical kinetics package. Three solutions were generated for the specified altitudes on coarse and fine grids. CFD results show the base region flowfields to be highly three dimensional in character. At the 10,000 ft altitude, plumes contract soon after exiting the nozzles and do not interact with each other. No mechanism was identified for driving hot gas back into the base region and no significant amounts of hydrogen or water were found in the base region. Consequently, surface temperatures were all near the ambient level. At 50,000 ft, the nozzle exhaust plumes begin to interact, particularly those of the two inboard engines which are closer together. A small amount of hot gas is recirculated between the inboard nozzles near the nozzle exit plane. As a result, base region surface temperatures are slightly elevated, but still remain well within the design guideline of 1000 R.

Author

N95-23433*# McDonnell-Douglas Aerospace, Huntington Beach, CA. Transportation Div.

CFD FLOWFIELD SIMULATION OF DELTA LAUNCH VEHICLES IN A POWER-ON CONFIGURATION

D. L. Pavish, T. P. Gielda, B. K. Soni (Mississippi State Univ., Starkville, MS.), J. E. Deese (McDonnell-Douglas Aerospace, Saint Louis, MO.), and R. K. Agarwal (Mississippi State Univ., Starkville, MS.) *In* NASA. Marshall Space Flight Center, Eleventh Workshop for Computational Fluid Dynamic Applications in Rocket Propulsion Jul. 1993 p 1511-1529 (For primary document see N95-23412 07-34)

Avail: CASI HC A03/MF A10

This paper summarizes recent work at McDonnell Douglas Aerospace (MDA) to develop and validate computational fluid dynamic (CFD) simulations of under expanded rocket plume external flowfields for multibody expendable launch vehicles (ELVs). Multi engine reacting gas flowfield predictions of ELV base pressures are needed to define vehicle base drag and base heating rates for sizing external nozzle and base region insulation thicknesses. Previous ELV design programs used expensive multibody power-on wind tunnel tests that employed chamber/nozzle injected high pressure cold or hot-air. Base heating and pressure measurements were belatedly made during the first flights of past ELV's to correct estimates from semi-empirical engineering models or scale model tests. Presently, CFD methods for use in ELV design are being jointly developed at the Space Transportation Division (MDA-STD) and New Aircraft Missiles Division (MDA-NAMD). An explicit three dimensional, zonal, finite-volume, full Navier-Stokes (FNS) solver with finite rate hydrocarbon/air and aluminum combustion kinetics was developed to accurately compute ELV power-on flowfields. Mississippi State University's GENIE++ general purpose interactive grid generation code was chosen to create zonal, finite volume viscous grids. Axisymmetric, time dependent, turbulent CFD simulations of a Delta DSV-2A vehicle with a MB-3 liquid main engine burning RJ-1/LOX were first completed. Hydrocarbon chemical kinetics and a k-epsilon turbulence model were employed and predictions were validated with flight measurements of base pressure and temperature. Zonal internal/external grids were created for a Delta DSV-2C vehicle with a MB-3 and three Castor-1 solid motors burning and a Delta-2 with an RS-27 main engine (LOX/RP-1) and 9 GEM's attached/6 burning. Cold air, time dependent FNS calculations were performed for DSV-2C during 1992. Single phase simulations that employ finite rate hydrocarbon and aluminum (solid fuel) combustion chemistry are currently in progress. Reliable and efficient Eulerian algorithms are needed to model two phase (solid-gas) momentum and energy transfer mechanisms for solid motor fuel combustion products.

Author

N95-23434*# National Aeronautics and Space Administration. Marshall Space Flight Center, Huntsville, AL.

NUMERICAL STUDY OF THE SSME NOZZLE FLOW FIELDS DURING TRANSIENT OPERATIONS: A COMPARISON OF THE ANIMATED RESULTS WITH TEST

Ten-See Wang and Catherine Dumas (Sverdrup Technology, Inc., Huntsville, AL.) *In its* Eleventh Workshop for Computational Fluid Dynamic Applications in Rocket Propulsion Jul. 1993 p 1529-1533 (For primary document see N95-23412 07-34)

Avail: CASI HC A01/MF A10

A computational fluid dynamics (CFD) model has been applied to study the transient flow phenomena of the nozzle and exhaust plume of the Space Shuttle Main Engine (SSME), fired at sea level. The CFD model is a time accurate, pressure based, reactive flow solver. A six-species hydrogen/oxygen equilibrium chemistry is used to describe the chemical-thermodynamics. An adaptive upwinding scheme is employed for the spatial discretization, and a predictor, multiple corrector method is used for the temporal solution. Both engine start-up and shut-down processes were simulated. The elapse time is approximately five seconds for both cases. The computed results were animated and compared with the test. The images for the animation were created with PLOT3D and FAST and then animated with ABEKAS. The hysteresis effects, and the issues of free-shock separation, restricted-shock separation and the end-effects were addressed. Author

N95-23435*# Pratt and Whitney Aircraft, West Palm Beach, FL.

AERODYNAMIC DESIGN AND ANALYSIS OF A HIGHLY LOADED TURBINE EXHAUST

F. W. Huber, X. A. Montesdeoca, and R. J. Rowey *In* NASA. Marshall Space Flight Center, Eleventh Workshop for Computational Fluid Dynamic Applications in Rocket Propulsion Jul. 1993 p 1535-1553 (For primary document see N95-23412 07-34)
Avail: CASI HC A03/MF A10

The aerodynamic design and analysis of a turbine exhaust volute manifold is described. This turbine exhaust system will be used with an advanced gas generator oxidizer turbine designed for very high specific work. The elevated turbine stage loading results in increased discharge Mach number and swirl velocity which, along with the need for minimal circumferential variation of fluid properties at the turbine exit, represent challenging volute design requirements. The design approach, candidate geometries analyzed, and steady state/unsteady CFD analysis results are presented. Author

N95-23436*# Rockwell International Corp., Canoga Park, CA. Rocketdyne Div.
CFD ANALYSIS OF TURBOPUMP VOLUTES
Edward P. Ascoli, Daniel C. Chan, Armen Darian, Wayne W. Hsu, and Ken Tran *In* NASA. Marshall Space Flight Center, Eleventh Workshop for Computational Fluid Dynamic Applications in Rocket Propulsion Jul. 1993 p 1555-1578 (For primary document see N95-23412 07-34)
Avail: CASI HC A03/MF A10

An effort is underway to develop a procedure for the regular use of CFD analysis in the design of turbopump volutes. Airflow data to be taken at NASA Marshall will be used to validate the CFD code and overall procedure. Initial focus has been on preprocessing (geometry creation, translation, and grid generation). Volute geometries have been acquired electronically and imported into the CATIA CAD system and RAGGS (Rockwell Automated Grid Generation System) via the IGES standard. An initial grid topology has been identified and grids have been constructed for turbine inlet and discharge volutes. For CFD analysis of volutes to be used regularly, a procedure must be defined to meet engineering design needs in a timely manner. Thus, a compromise must be established between making geometric approximations, the selection of grid topologies, and possible CFD code enhancements. While the initial grid developed approximated the volute tongue with a zero thickness, final computations should more accurately account for the geometry in this region. Additionally, grid topologies will be explored to minimize skewness and high aspect ratio cells that can affect solution accuracy and slow code convergence. Finally, as appropriate, code modifications will be made to allow for new grid topologies in an effort to expedite the overall CFD analysis process. Author

N95-23437*# National Aeronautics and Space Administration. Lewis Research Center, Cleveland, OH.
THREE-DIMENSIONAL VISCOUS FLOW ANALYSIS INSIDE A TURBINE VOLUTE
C. Hah, J. Loellbach, D. A. Greenwald, L. Griffin (National Aeronautics and Space Administration. Marshall Space Flight Center, Huntsville, AL.), and J. Ruf (National Aeronautics and Space Administration. Marshall Space Flight Center, Huntsville, AL.) *In* NASA. Marshall Space Flight Center, Eleventh Workshop for Computational Fluid Dynamic Applications in Rocket Propulsion Jul. 1993 p 1579-1606 (For primary document see N95-23412 07-34)
Avail: CASI HC A03/MF A10

A three-dimensional numerical method has been developed to analyze the complex flow field inside a turbine volute. Comparisons are made between solutions with different boundary conditions. Author

N95-23438*# Pratt and Whitney Aircraft, West Palm Beach, FL.
PHASE 2: HGM AIR FLOW TESTS IN SUPPORT OF HEX VANE INVESTIGATION
G. B. Cox, Jr., L. L. Steele, and D. W. Eisenhart *In* NASA. Marshall Space Flight Center, Eleventh Workshop for Computational Fluid Dynamic Applications in Rocket Propulsion Jul. 1993 p 1607-1618 (For primary document see N95-23412 07-34)
(Contract NAS8-36801)
Avail: CASI HC A03/MF A10

Following the start of SSME certification testing for the Pratt and Whitney Alternate Turbopump Development (ATD) High Pressure Oxidizer Turbopump (HPOTP), cracking of the leading edge of the inner HEX vane was experienced. The HEX vane, at the inlet of the oxidizer bowl in the Hot Gas Manifold (HGM), accepts the HPOTP turbine discharge flow and turns it toward the Gaseous Oxidizer Heat Exchanger (GOX HEX) coil. The cracking consistently initiated over a specific circumferential region of the hex vane, with other circumferential locations appearing with increased run time. Since cracking had not to date been seen with the baseline HPOTP, a fluid-structural interaction involving the ATD HPOTP turbine exit flowfield and the HEX inner vane was suspected. As part of NASA contract NAS8-36801, Pratt and Whitney conducted air flow tests of the ATD HPOTP turbine turnaround duct flowpath in the MSFC Phase 2 HGM air flow model. These tests included HEX vane strain gages and additional fluctuating pressure gages in the turnaround duct and HEX vane flowpath area. Three-dimensional flow probe measurements at two stations downstream of the turbine simulator exit plane were also made. Modifications to the HPOTP turbine simulator investigated the effects on turbine exit flow profile and velocity components, with the objective of reproducing flow conditions calculated for the actual ATD HPOTP hardware. Testing was done at the MSFC SSME Dynamic Fluid Air Flow (Dual-Leg) Facility, at air supply pressures between 50 and 250 psia. Combinations of turbine exit Mach number and pressure level were run to investigate the effect of flow regime. Information presented includes: (1) Descriptions of turbine simulator modifications to produce the desired flow environment; (2) Types and locations for instrumentation added to the flow model for improved diagnostic capability; (3) Evaluation of the effect of changes to the turbine simulator flowpath on the turbine exit flow environment; and (4) Comparison of the experimental turbine exit flow environment to the environment calculated for the ATD HPOTP. Author

N95-23439*# Rockwell International Corp., Canoga Park, CA. Rocketdyne Div.
NON-INTRUSIVE MEASUREMENTS IN A ROCKET ENGINE COMBUSTOR **c20**
S. Farhangi, V. T. Gylys, and R. J. Jensen *In* NASA. Marshall Space Flight Center, Eleventh Workshop for Computational Fluid Dynamic Applications in Rocket Propulsion Jul. 1993 p 1619-1634 (For primary document see N95-23412 07-34)
Avail: CASI HC A03/MF A10

In recent years analytical tools to characterize combustor flow have been developed in order to support design. To facilitate anchoring of combustion related physical models and the CFD codes in which they are incorporated, considerable development and application of non-intrusive combustion diagnostic capabilities has occurred. Raman spectroscopy can be used to simultaneously detect all polyatomic molecules present in significant concentrations and to determine gas temperature. This is because all molecules possess a distinct temperature dependent Raman spectrum. A multi-point diagnostic system for non-intrusive temperature and species profiling in rocket engines has been developed at Rocketdyne. In the present effort, the system has been undergoing validation for application to rocket engine component testing. A 4 inch diameter windowed combustor with a coaxial gas-gas injector was chosen for this series of validation experiments. Initially an excimer-pumped tunable dye laser and later a solid state Nd-Yag laser served as excitation sources. The Raman signal was dispersed by a monochromator and detected by a gated, intensified Charged Coupled Device (CCD) array. Experiments were carried out prior to each series of hot fire tests to ensure that the Raman signal detected was due to a spontaneous rather than a stimulated Raman emission process. Over sixty hot fire tests were conducted during the first series of tests with the excimer/dye laser. All hot fire testing was at a mixture ratio of 0.5 and chamber pressures of approximately 100 and approximately 300 psia. The Raman spectra of hydrogen, water vapor and oxygen recorded during single element hot fire tests were reduced and analyzed. A significant achievement was the attainment of single shot Raman spectra in cold flow tests. Unfortunately, the single shot signal-to-noise ratio deteriorated to an unacceptable level during the hot fire testing. Attempts to obtain temperature data from the hydrogen Q1-branch profiles obtained in hot fire tests suggest that potentially complicating factors may render the approach of averaging data on the photodiode array invalid. A second series of hot fire tests was conducted with a 4 element coaxial injector using the Nd-Yag laser. A very compact and portable diagnostics set up was assembled for ease of alignment, relocation and flexibility. Measurements were made at several regions in the chamber in order to map concentration profiles. High spatial

resolution and improved signal to noise characteristics were demonstrated.
Author

N95-23440*# Rockwell International Corp., Canoga Park, CA. Rocketdyne Div.

IMPELLER FLOW FIELD CHARACTERIZATION WITH A LASER TWO-FOCUS VELOCIMETER

L. A. Brozowski, T. V. Ferguson, and L. Rojas *In* NASA. Marshall Space Flight Center, Eleventh Workshop for Computational Fluid Dynamic Applications in Rocket Propulsion Jul. 1993 p 1635-1688 (For primary document see N95-23412 07-34)
(Contract NAS8-38864)
Avail: CASI HC A04/MF A10

Use of Computational Fluid Dynamics (CFD) codes, prevalent in the rocket engine turbomachinery industry, necessitates data of sufficient quality and quantity to benchmark computational codes. Existing data bases for typical rocket engine configurations, in particular impellers, are limited. In addition, traditional data acquisition methods have several limitations: typically transducer uncertainties are 0.5% of transducer full scale and traditional pressure probes are unable to provide flow characteristics in the circumferential (blade-to-blade) direction. Laser velocimetry circumvents these limitations by providing +0.5% uncertainty in flow velocity and +0.5% uncertainty in flow angle. The percent of uncertainty in flow velocity is based on the measured value, not full range capability. The laser electronics multiple partitioning capability allows data acquired between blades as the impeller rotates, to be analyzed separately, thus providing blade-to-blade flow characterization. Unlike some probes, the non-intrusive measurements made with the laser velocimeter does not disturb the flow. To this end,, and under Contract (NAS8-38864) to the National Aeronautics and Space Administration (NASA) at Marshall Space Flight Center (MSFC), an extensive test program was undertaken at Rocketdyne. Impellers from two different generic rocket engine pump configurations were examined. The impellers represent different spectrums of pump design: the Space Shuttle Main Engine (SSME) high pressure fuel turbopump (HPFTP) impeller was designed in the 1 1970's the Consortium for CFD application in Propulsion Technology Pump Stage Technology Team (Pump Consortium) optimized impeller was designed with the aid of modern computing techniques. The tester configuration for each of the impellers consisted of an axial inlet, an inducer, a diffuser, and a crossover discharge. While the tested configurations were carefully chosen to be representative of generic rocket engine pumps, several features of both testers were intentionally atypical. A crossover discharge, downstream of the impeller, rather than a volute discharge was used to minimize asymmetric flow conditions that might be reflected in the impeller discharge flow data. Impeller shroud wear ring radial clearances were purposely close to minimize leakage flow, thus increasing confidence in using the inlet data as an input to CFD programs. The empirical study extensively examined the flow fields of the two impellers via performance of laser two-focus velocimeter surveys in an axial plane upstream of the impellers and in multiple radial planes downstream of the impellers. Both studies were performed at the impeller design flow coefficients. Inlet laser surveys that provide CFD code inlet boundary conditions were performed in one axial plane, with ten radial locations surveyed. Three wall static pressures, positioned circumferentially around the impeller inlet, were used to identify asymmetrical pressure distributions in the inlet survey plane. The impeller discharge flow characterization consisted of three radial planes for the SSME HPFTP impeller and two radial planes for the Pump Consortium optimized impeller. Housing wall static pressures were placed to correspond to the radial locations surveyed with the laser velocimeter. Between five and thirteen axial stations across the discharge channel width were examined in each radial plane during the extensive flow mapping. The largely successful empirical flow characterization of two different impellers resulted in a substantial contribution to the limited existing data base, and yielded accurate data for CFD code benchmarking.
Author

N95-23441*# National Aeronautics and Space Administration. Marshall Space Flight Center, Huntsville, AL.

DETAILED MEASUREMENTS IN THE SSME HIGH PRESSURE FUEL TURBINE WITH SMOOTH ROTOR BLADES **c37**

Susan T. Hudson *In its* Eleventh Workshop for Computational Fluid Dynamic Applications in Rocket Propulsion Jul. 1993 p 1689-1712 (For primary document see N95-23412 07-34)
Avail: CASI HC A03/MF A10

Several tests of the Rocketdyne configuration of the Space Shuttle Main Engine (SSME) High Pressure Fuel Turbopump (HPFTP) Turbine have been completed in the Turbine Test Equipment (TTE) at Marshall Space Flight Center. The tests involved using scaled performance parameters and model measurements to predict the performance of the turbine. The overall performance has been the primary objective of the tests to date, but more detailed measurements are also of interest. During the most recent test of the Rocketdyne configuration of the HPFTP turbine with smooth rotor blades, several different measurement techniques were used to study the turbine inlet and exit velocity profiles, boundary layer thicknesses, turbulence intensities, etc. Data has been obtained using various hot film probes and three-hole cobra probes. Laser Velocimeter measurements were also made. The test plan and test data will be presented and discussed as well as lessons learned on how to obtain the various types of data.
Author

N95-23442*# Alabama Univ., Huntsville, AL. Dept. of Chemical Engineering.

DEVELOPMENT OF AN ALGEBRAIC STRESS/TWO-LAYER MODEL FOR CALCULATING THRUST CHAMBER FLOW FIELDS

C. P. Chen, H. M. Shang, and J. Huang *In* NASA. Marshall Space Flight Center, Eleventh Workshop for Computational Fluid Dynamic Applications in Rocket Propulsion Jul. 1993 p 1713-1748 (For primary document see N95-23412 07-34)
Avail: CASI HC A03/MF A10

Following the consensus of a workshop in Turbulence Modeling for Liquid Rocket Thrust Chambers, the current effort was undertaken to study the effects of second-order closure on the predictions of thermochemical flow fields. To reduce the instability and computational intensity of the full second-order Reynolds Stress Model, an Algebraic Stress Model (ASM) coupled with a two-layer near wall treatment was developed. Various test problems, including the compressible boundary layer with adiabatic and cooled walls, recirculating flows, swirling flows and the entire SSME nozzle flow were studied to assess the performance of the current model. Detailed calculations for the SSME exit wall flow around the nozzle manifold were executed. As to the overall flow predictions, the ASM removes another assumption for appropriate comparison with experimental data, to account for the non-isotropic turbulence effects.
Author

N95-23443*# Rockwell International Corp., Canoga Park, CA. Rocketdyne Div.

ADVANCED TURBULENCE MODELS FOR TURBOMACHINERY

Ali H. Hadid, Michele E. DeCroix, and Munir M. Sindir *In* NASA. Marshall Space Flight Center, Eleventh Workshop for Computational Fluid Dynamic Applications in Rocket Propulsion Jul. 1993 p 1749-1771 (For primary document see N95-23412 07-34)
Avail: CASI HC A03/MF A10

Development and assessment of the single-time-scale k-epsilon turbulence model with different near-wall treatments and the multi-scale turbulence model for rotating flows are presented. These turbulence models are coded as self contained module decks that can be interfaced with a number of CFD main flow solvers. For each model, a stand-alone module deck with its own formulation, discretization scheme, solver and boundary condition implementations is presented. These satellite decks will take as input (from a main flow solver) the velocity field, grid, boundary condition specifications and will deliver turbulent quantities as output. These modules were tested as separate entities and, although many logical and programming problems were overcome, only wider use and further testing can render the modules sufficiently 'fool proof'.
Author

N95-23444*# Pennsylvania State Univ., University Park, PA. Dept. of Aerospace Engineering.

NUMERICAL COMPUTATION OF AERODYNAMICS AND HEAT TRANSFER IN A TURBINE CASCADE AND A TURN-AROUND DUCT USING ADVANCED TURBULENCE MODELS

B. Lakshminarayana and J. Luo *In* NASA. Marshall Space Flight Center, Eleventh Workshop for Computational Fluid Dynamic Applications in Rocket Propulsion Jul. 1993 p 1773-1806 (For primary document see N95-23412 07-34)
Avail: CASI HC A03/MF A10

The objective of this research is to develop turbulence models to predict the flow and heat transfer fields dominated by the curvature effect

such as those encountered in turbine cascades and turn-around ducts. A Navier-Stokes code has been developed using an explicit Runge-Kutta method with a two layer k-epsilon/ARSM (Algebraic Reynolds Stress Model), Chien's Low Reynolds Number (LRN) k-epsilon model and Coakley's LRN q-omega model. The near wall pressure strain correlation term was included in the ARSM. The formulation is applied to Favre-averaged N-S equations and no thin-layer approximations are made in either the mean flow or turbulence transport equations. Anisotropic scaling of artificial dissipation terms was used. Locally variable timestep was also used to improve convergence. Detailed comparisons were made between computations and data measured in a turbine cascade by Arts et al. at Von Karman Institute. The surface pressure distributions and wake profiles were predicted well by all the models. The blade heat transfer is predicted well by k-epsilon/ARSM model, as well as the k-epsilon model. It's found that the onset of boundary layer transition on both surfaces is highly dependent upon the level of local freestream turbulence intensity, which is strongly influenced by the streamline curvature. Detailed computation of the flow in the turn around duct has been carried out and validated against the data by Monson as well as Sandborn. The computed results at various streamwise locations both on the concave and convex sides are compared with flow and turbulence data including the separation zone on the inner well. The k-epsilon/ARSM model yielded relatively better results than the two-equation turbulence models. A detailed assessment of the turbulence models has been made with regard to their applicability to curved flows. Author

N95-23445*# National Aeronautics and Space Administration. Marshall Space Flight Center, Huntsville, AL.

LIQUID PROPELLANT ROCKET ENGINE COMBUSTION SIMULATION WITH A TIME-ACCURATE CFD METHOD

Y. S. Chen (Engineering Sciences, Inc., Huntsville, AL.), H. M. Shang (Engineering Sciences, Inc., Huntsville, AL.), Paul Liaw (Engineering Sciences, Inc., Huntsville, AL.), and J. Hutt *In its* Eleventh Workshop for Computational Fluid Dynamic Applications in Rocket Propulsion Jul. 1993 p 1807-1827 (For primary document see N95-23412 07-34)

Avail: CASI HC A03/MF A10

Time-accurate computational fluid dynamics (CFD) algorithms are among the basic requirements as an engineering or research tool for realistic simulations of transient combustion phenomena, such as combustion instability, transient start-up, etc., inside the rocket engine combustion chamber. A time-accurate pressure based method is employed in the FDNS code for combustion model development. This is in connection with other program development activities such as spray combustion model development and efficient finite-rate chemistry solution method implementation. In the present study, a second-order time-accurate time-marching scheme is employed. For better spatial resolutions near discontinuities (e.g., shocks, contact discontinuities), a 3rd-order accurate TVD scheme for modeling the convection terms is implemented in the FDNS code. Necessary modification to the predictor/multi-corrector solution algorithm in order to maintain time-accurate wave propagation is also investigated. Benchmark 1-D and multidimensional test cases, which include the classical shock tube wave propagation problems, resonant pipe test case, unsteady flow development of a blast tube test case, and H2/O2 rocket engine chamber combustion start-up transient simulation, etc., are investigated to validate and demonstrate the accuracy and robustness of the present numerical scheme and solution algorithm. Author

N95-23446*# Pennsylvania State Univ., University Park, PA. Propulsion Engineering Research Center.

CONVERGENCE ACCELERATION OF IMPLICIT SCHEMES IN THE PRESENCE OF HIGH ASPECT RATIO GRID CELLS

B. E. O. Buelow, S. Venkateswaran, and C. L. Merkle *In* NASA. Marshall Space Flight Center, Eleventh Workshop for Computational Fluid Dynamic Applications in Rocket Propulsion Jul. 1993 p 1829-1855 (For primary document see N95-23412 07-34)

Avail: CASI HC A03/MF A10

The performance of Navier-Stokes codes are influenced by several phenomena. For example, the robustness of the code may be compromised by the lack of grid resolution, by a need for more precise initial conditions or because all or part of the flowfield lies outside the flow regime in which the algorithm converges efficiently. A primary example of the latter effect is the presence of extended low Mach number and/or low Reynolds number regions which cause convergence deterioration of time marching algorithms. Recent research into this problem by several workers including the present authors has largely negated this difficulty through the introduction of time-derivative preconditioning. In the present paper, we employ the preconditioned algorithm to address convergence difficulties arising from sensitivity to grid stretching and high aspect ratio grid cells. Strong grid stretching is particularly characteristic of turbulent flow calculations where the grid must be refined very tightly in the dimension normal to the wall, without a similar refinement in the tangential direction. High aspect ratio grid cells also arise in problems that involve high aspect ratio domains such as combustor coolant channels. In both situations, the high aspect ratio cells can lead to extreme deterioration in convergence. It is the purpose of the present paper to address the reasons for this adverse response to grid stretching and to suggest methods for enhancing convergence under such circumstances. Numerical algorithms typically possess a maximum allowable or optimum value for the time step size, expressed in non-dimensional terms as a CFL number or vonNeumann number (VNN). In the presence of high aspect ratio cells, the smallest dimension of the grid cell controls the time step size causing it to be extremely small, which in turn results in the deterioration of convergence behavior. For explicit schemes, this time step limitation cannot be exceeded without violating stability restrictions of the scheme. On the other hand, for implicit schemes, which are typically unconditionally stable, there appears to be room for improvement through careful tailoring of the time step definition based on results of linear stability analyses. In the present paper, we focus on the central-differenced alternating direction implicit (ADI) scheme. The understanding garnered from this analyses can then be applied to other implicit schemes. In order to systematically study the effects of aspect ratio and the methods of mitigating the associated problems, we use a two pronged approach. We use stability analyses as a tool for predicting numerical convergence behavior and numerical experiments on simple model problems to verify predicted trends. Based on these analyses, we determine that efficient convergence may be obtained at all aspect ratios by getting a combination of things right. Primary among these are the proper definition of the time step size, proper selection of viscous preconditioner and the precise treatment of boundary conditions. These algorithmic improvements are then applied to a variety of test cases to demonstrate uniform convergence at all aspect ratios. Author

N95-23447*# National Aeronautics and Space Administration. Lewis Research Center, Cleveland, OH.

A TIME-ACCURATE FINITE VOLUME METHOD VALID AT ALL FLOW VELOCITIES

S.-W. Kim *In* NASA. Marshall Space Flight Center, Eleventh Workshop for Computational Fluid Dynamic Applications in Rocket Propulsion Jul. 1993 p 1857-1887 (For primary document see N95-23412 07-34)

Avail: CASI HC A03/MF A10

A finite volume method to solve the Navier-Stokes equations at all flow velocities (e.g., incompressible, subsonic, transonic, supersonic and hypersonic flows) is presented. The numerical method is based on a finite volume method that incorporates a pressure-staggered mesh and an incremental pressure equation for the conservation of mass. Comparison of three generally accepted time-advancing schemes, i.e., Simplified Marker-and-Cell (SMAC), Pressure-Implicit-Splitting of Operators (PISO), and Iterative-Time-Advancing (ITA) scheme, are made by solving a lid-driven polar cavity flow and self-sustained oscillatory flows over circular and square cylinders. Calculated results show that the ITA is the most stable numerically and yields the most accurate results. The SMAC is the most efficient computationally and is as stable as the ITA. It is shown that the PISO is the most weakly convergent and it exhibits an undesirable strong dependence on the time-step size. The degenerated numerical results obtained using the PISO are attributed to its second corrector step that cause the numerical results to deviate further from a divergence free velocity field. The accurate numerical results obtained using the ITA is attributed to its capability to resolve the nonlinearity of the Navier-Stokes equations. The present numerical method that incorporates the ITA is used to solve an unsteady transitional flow over an oscillating airfoil and a chemically reacting flow of hydrogen in a vitiated supersonic airstream. The turbulence fields in these flow cases are described using multiple-time-scale turbulence equations. For the unsteady transitional over an oscillating airfoil, the fluid flow is described using ensemble-averaged Navier-Stokes equations defined on the Lagrangian-Eulerian coordinates. It

is shown that the numerical method successfully predicts the large dynamic stall vortex (DSV) and the trailing edge vortex (TEV) that are periodically generated by the oscillating airfoil. The calculated streaklines are in very good comparison with the experimentally obtained smoke picture. The calculated turbulent viscosity contours show that the transition from laminar to turbulent state and the relaminarization occur widely in space as well as in time. The ensemble-averaged velocity profiles are also in good agreement with the measured data and the good comparison indicates that the numerical method as well as the multipletime-scale turbulence equations successfully predict the unsteady transitional turbulence field. The chemical reactions for the hydrogen in the vitiated supersonic airstream are described using 9 chemical species and 48 reaction-steps. Consider that a fast chemistry can not be used to describe the fine details (such as the instability) of chemically reacting flows while a reduced chemical kinetics can not be used confidently due to the uncertainty contained in the reaction mechanisms. However, the use of a detailed finite rate chemistry may make it difficult to obtain a fully converged solution due to the coupling between the large number of flow, turbulence, and chemical equations. The numerical results obtained in the present study are in good agreement with the measured data. The good comparison is attributed to the numerical method that can yield strongly converged results for the reacting flow and to the use of the multiple-time-scale turbulence equations that can accurately describe the mixing of the fuel and the oxidant. Author

N95-23448*# National Aeronautics and Space Administration. Marshall Space Flight Center, Huntsville, AL.

A CONTROLLED VARIATION SCHEME FOR CONVECTION TREATMENT IN PRESSURE-BASED ALGORITHM

Wei Shyy (Florida Univ., Gainesville, FL.), Siddharth Thakur (Florida Univ., Gainesville, FL.), and Kevin Tucker (Florida Univ., Gainesville, FL.) *In its* Eleventh Workshop for Computational Fluid Dynamic Applications in Rocket Propulsion Jul. 1993 p 1889-1908 (For primary document see N95-23412 07-34)

Avail: CASI HC A03/MF A10

Convection effect and source terms are two primary sources of difficulties in computing turbulent reacting flows typically encountered in propulsion devices. The present work intends to elucidate the individual as well as the collective roles of convection and source terms in the fluid flow equations, and to devise appropriate treatments and implementations to improve our current capability of predicting such flows. A controlled variation scheme (CVS) has been under development in the context of a pressure-based algorithm, which has the characteristics of adaptively regulating the amount of numerical diffusivity, relative to central difference scheme, according to the variation in local flow field. Both the basic concepts and a pragmatic assessment will be presented to highlight the status of this work. Author

N95-23451*# Florida Univ., Gainesville, FL. Dept. of Aerospace Engineering, Mechanics and Engineering Science.

ON THE CONSERVATIVE INTERFACE TREATMENT FOR MULTI-BLOCK VISCOUS FLOW COMPUTATIONS

J. Liu and W. Shyy (National Aeronautics and Space Administration. Lewis Research Center, Cleveland, OH.) Mar. 1995 35 p

(Contract NCC3-370; RTOP 505-90-5K)

(NASA-CR-195442; E-9485; NAS 1.26:195442; ICOMP-95-4) Avail: CASI HC A03/MF A01

A pressure-based multi-block computational method is developed for solving the incompressible Navier-Stokes equations in general curvilinear grid systems. The scheme is based on the semi-implicit type flow solver with the staggered grid. Issues concerning the mass and momentum flux treatments at the discontinuous grid interface are addressed. Systematic numerical experiments for different interface treatments involving (1) straightforward interpolation, (2) globally conservative scheme, and (3) locally conservative scheme have been conducted. It is demonstrated that mass conservation has to be maintained locally, at the grid interface, with accuracy compatible with that of the scheme used in interior domain. Direct interpolation or globally conservative interface treatment of mass flux can not yield solutions with desirable accuracy. Author

N95-23464*# National Aeronautics and Space Administration. Lewis Research Center, Cleveland, OH.

INSTITUTE FOR COMPUTATIONAL MECHANICS IN PROPULSION (ICOMP) Annual Report No. 9, 1994

Charles E. Feiler, ed. Mar. 1995 53 p

(Contract NCC3-370; RTOP 505-90-5K)

(NASA-TM-106884; ICOMP-95-01; E-9520; NAS 1.15:106884) Avail: CASI HC A04/MF A01

The Institute for Computational Mechanics in Propulsion (ICOMP) is operated by the Ohio Aerospace Institute (OAI) and funded under a cooperative agreement by the NASA Lewis Research Center in Cleveland, Ohio. The purpose of ICOMP is to develop techniques to improve problem-solving capabilities in all aspects of computational mechanics related to propulsion. This report describes the activities at ICOMP during 1994. Author

N95-23466*# Institute for Computer Applications in Science and Engineering, Hampton, VA.

A STUDY OF THE VORTEX FLOW OVER 76/40-DEG DOUBLE-DELTA WING Final Report

N. G. Verhaagen (Technische Hogeschool, Delft, Netherlands.), L. N. Jenkins (National Aeronautics and Space Administration. Langley Research Center, Hampton, VA.), S. B. Kern (Naval Air Warfare Center, Warminster, PA.), and A. E. Washburn (Vigyan Research Associates, Inc., Hampton, VA.) NASA Feb. 1995 34 p

(Contract NAS1-19480; RTOP 505-90-52-01)

(NASA-CR-195032; NAS 1.26:195032; ICASE-95-5; AIAA Paper 95-0560) Avail: CASI HC A03/MF A01

A low-speed wind-tunnel study of the flow about a 76/40-deg double-delta wing is described for angles of attack ranging from -10 to 25 deg and Reynolds numbers ranging from 0.5 to 1.5 Million. The study was conducted to provide data for the purpose of understanding the vortical flow behavior and for validating Computational Fluid Dynamics methods. Flow visualization tests have provided insight into the effect of the angle of attack and Reynolds number of the vortex-dominated flow both on and off of the surface of the double-delta wing. Upper surface pressure recordings from pressure orifices and Pressure Sensitive Paint have provided data on the pressures induced by the vortices. Flowfield surveys were carried out at an angle of attack of 10 deg by using a thin 5-hole probe. Numerical solutions of the compressible thin-layer Navier-Stokes equations were conducted and compared to the experimental data. Author

N95-23483# Texas Univ., Austin, TX.

A WAVENUMBER-PARTITIONING SCHEME FOR TWO-DIMENSIONAL STATISTICAL CLOSURES

J. C. Bowman Nov. 1994 50 p

(Contract DE-FG05-80ET-53088)

(DE95-004514; DOE/ET-53088/670; IFSR-670) Avail: CASI HC A03/MF A01

One of the principal advantages of statistical closure approximations for fluid turbulence is that they involve smoothly varying functions of wavenumber. This suggests the possibility of modeling a flow by following the evolution of only a few representative wavenumbers. This work presents two new techniques for the implementation of two-dimensional isotropic statistical closures that for the first time allows the inertial-range scalings of these approximation to be numerically demonstrated. A technique of wavenumber partitioning that conserves both energy and enstrophy is developed for two-dimensional statistical closures. Coupled with a new time-stepping scheme based on a variable integrating factor, this advance facilitates the computation of energy spectra over seven wavenumber decades, a task that will clearly remain outside the realm of conventional numerical simulations for the foreseeable future. Within the context of the test-field model, the method is used to demonstrate Kraichnan's logarithmically-corrected scaling for the enstrophy inertial range and to make a quantitative assessment of the effect of replacing the physical Laplacian viscosity with an enhanced hyperviscosity. DOE

N95-23484# Texas Univ., Austin, TX.

ON INERTIAL RANGE SCALING LAWS

J. C. Bowman Dec. 1994 29 p

(Contract DE-FG05-80ET-53088)

(DE95-004515; DOE/ET-53088/685; IFSR-685) Avail: CASI HC A03/MF A01

Inertial-range scaling laws for two- and three-dimensional turbulence are re-examined within a unified framework. A new correction to Kolmogorov's k(sup -5/3) scaling is derived for the energy inertial range. A

related modification is found to Kraichnan's logarithmically corrected two-dimensional enstrophy cascade law that removes its unexpected divergence at the injection wavenumber. The significance of these corrections is illustrated with steady-state energy spectra from recent high-resolution closure computations. The results also underscore the asymptotic nature of inertial-range scaling laws. Implications for conventional numerical simulations are discussed. DOE

N95-23544*# Institute for Computer Applications in Science and Engineering, Hampton, VA.

ON THE BREAKUP OF VISCOUS LIQUID THREADS Final Report

Demetrios T. Papageorgiou (New Jersey Inst. of Tech., Newark, NJ.) Jan. 1995 50 p Sponsored in cooperation with NSF Submitted for publication

(Contracts NAS1-19480; RTOP 505-90-52-01; F49620-94-1-0242)

(NASA-CR-195023; NAS 1.26:195023; ICASE-95-1) Avail: CASI HC A03/MF A01

A one-dimensional model evolution equation is used to describe the nonlinear dynamics that can lead to the breakup of a cylindrical thread of Newtonian fluid when capillary forces drive the motion. The model is derived from the Stokes equations by use of rational asymptotic expansions and under a slender jet approximation. The equations are solved numerically and the jet radius is found to vanish after a finite time yielding breakup. The slender jet approximation is valid throughout the evolution leading to pinching. The model admits self-similar pinching solutions which yield symmetric shapes at breakup. These solutions are shown to be the ones selected by the initial boundary value problem, for general initial conditions. Further more, the terminal state of the model equation is shown to be identical to that predicted by a theory which looks for singular pinching solutions directly from the Stokes equations without invoking the slender jet approximation throughout the evolution. It is shown quantitatively, therefore, that the one-dimensional model gives a consistent terminal state with the jet shape being locally symmetric at breakup. The asymptotic expansion scheme is also extended to include unsteady and inerticial forces in the momentum equations to derive an evolution system modelling the breakup of Navier-Stokes jets. The model is employed in extensive simulations to compute breakup times for different initial conditions; satellite drop formation is also supported by the model and the dependence of satellite drop volumes on initial conditions is studied. Author

N95-23596*# Institute for Computer Applications in Science and Engineering, Hampton, VA.

ENTROPY JUMP ACROSS AN INVISCID SHOCK WAVE Final Report

Manuel D. Salas (National Aeronautics and Space Administration. Langley Research Center, Hampton, VA.) and Angelo Iollo (Politecnico di Torino, Torino, Italy.) NASA Feb. 1995 17 p Submitted for publication

(Contract NAS1-19480; RTOP 505-90-52-01)

(NASA-CR-195046; NAS 1.26:195046; ICASE-95-12) Avail: CASI HC A03/MF A01

The shock jump conditions for the Euler equations in their primitive form are derived by using generalized functions. The shock profiles for specific volume, speed, and pressure are shown to be the same, however density has a different shock profile. Careful study of the equations that govern the entropy shows that the inviscid entropy profile has a local maximum within the shock layer. We demonstrate that because of this phenomenon, the entropy, propagation equation cannot be used as a conservation law. Author

N95-23615*# National Aeronautics and Space Administration. Marshall Space Flight Center, Huntsville, AL.

ELEVENTH WORKSHOP FOR COMPUTATIONAL FLUID DYNAMIC APPLICATIONS IN ROCKET PROPULSION, PART 1

Robert W. Williams, comp. Washington Jul. 1993 942 p Workshop held in Huntsville, AL, 20-22 Apr. 1993

(NASA-CP-3221-Pt-1; M-726-Pt-1; NAS 1.55:3221-Pt-1) Avail: CASI HC A99/MF A10

Conference publication includes 79 abstracts and presentations given at the Eleventh Workshop for Computational Fluid Dynamic Applications in Rocket Propulsion held at the George C. Marshall Space Flight Center, April 20-22, 1993. The purpose of this workshop is to discuss experimental and computational fluid dynamic activities in rocket propulsion. The workshop is an open meeting for government, industry, and academia. A broad number of topics are discussed including computational fluid dynamic methodology, liquid and solid rocket propulsion, turbomachinery, combustion, heat transfer, and grid generation. For individual titles, see N95-23616 through N95-23655.

N95-23616*# Rockwell International Corp., Canoga Park, CA. Rocketdyne Div.

THREE-D CFD ANALYSIS OF HYDROSTATIC BEARINGS **c37**

Shyi-Jang Lin and Robert I. Hibbs, Jr. *In* NASA. Marshall Space Flight Center, Eleventh Workshop for Computational Fluid Dynamic Applications in Rocket Propulsion, Part 1 Jul. 1993 p 37-55 (For primary document see N95-23615 07-34)

Avail: CASI HC A03/MF A10

The hydrostatic bearing promises life and speed characteristics currently unachievable with rolling element bearings alone. In order to achieve the speed and life requirements of the next generation of rocket engines, turbopump manufacturers are proposing hydrostatic bearings to be used in place of, or in series with, rolling element bearings. The design of a hydrostatic bearing is dependent on accurate pressure in the bearing. The stiffness and damping of the hydrostatic bearing is very sensitive to the bearing recess pressure ratio. In the conventional approach, usually ad hoc assumptions were made in determining the bearing pressure of this approach is inherently incorrect. In the present paper, a more elaborate approach to obtain bearing pressure is used. The bearing pressure and complete flow features of the bearing are directly computed by solving the complete 3-D Navier Stokes equation. The code used in the present calculation is a modified version of REACT3D code. Several calculations have been performed for the hydrostatic bearing designed and tested at Texas A&M. Good agreement has been obtained between computed and test results. Detailed flow features in the bearing will also be described and discussed. Author

N95-23617*# National Aeronautics and Space Administration. Marshall Space Flight Center, Huntsville, AL.

FINITE-DIFFERENCE SOLUTIONS OF THE ALTERNATE TURBOPUMP DEVELOPMENT HIGH-PRESSURE OXIDIZER TURBOPUMP PUMP-END BALL-BEARING CAVITY FLOWS

Theodore G. Benjamin, Roberto Garcia, Paul K. McConnaughey, Ten-See Wang, Bruce T. Vu, and Youssef Dakhoul (Sverdrup Technology, Inc., Huntsville, AL.) *In its* Eleventh Workshop for Computational Fluid Dynamic Applications in Rocket Propulsion, Part 1 Jul. 1993 p 57-74 (For primary document see N95-23615 07-34)

Avail: CASI HC A03/MF A10

These analyses were undertaken to aid in the understanding of flow phenomena in the Alternate Turbopump Development (ATD) High-pressure Oxidizer Turbopump (HPOTP) Pump-end ball bearing (PEBB) cavities and their roles in turbopump vibration initiation and bearing distress. This effort was being performed to provide timely support to the program in a decision as to whether or not the program should be continued. In the first case, it was determined that a change in bearing through flow had no significant effect on axial preload. This was a follow-on to a previous study which had resulted in a redesign of the bearing exit cavity which virtually eliminated bearing axial loading. In the second case, a three-dimensional analysis of the inner-race-guided cage configuration was performed so as to determine the pressure distribution on the outer race when the shaft is 0.0002 inches off-center. The results indicate that there is virtually no circumferential pressure difference caused by the offset to contribute to bearing tilt. In the third case, axisymmetric analyses were performed on an outer-race guided cage configuration to determine the magnitude of tangential flow entering the bearing. The removed-shoulder case was analyzed as was the static diverter case. A third analysis where the preload spring was shielded by a sheet of metal for the baseline case was also performed. It was determined that the swirl entering the bearing was acceptable and the project decided to use the outer-race-guided cage configuration. In the fourth case, more bearing configurations were analyzed. These analyses included thermal modeling so as to determine the added benefit of injecting colder fluid directly onto the bearing inner-race contact area. The results of these analyses contributed to a programmatic decision to include coolant injection in the design. Author

N95-23618*# National Aeronautics and Space Administration. Marshall Space Flight Center, Huntsville, AL.

NAVIER-STOKES FLOW FIELD ANALYSIS OF COMPRESSIBLE FLOW IN A PRESSURE RELIEF VALVE

Bruce T. Vu, Ten-See Wang, Ming-Hsin Shih (Mississippi State Univ., Mississippi State, MS.), and Bharat K. Soni (Mississippi State Univ., Mississippi State, MS.) *In its* Eleventh Workshop for Computational Fluid Dynamic Applications in Rocket Propulsion, Part 1 Jul. 1993 p 75-97 (For primary document see N95-23615 07-34)

Avail: CASI HC A03/MF A10

The present study was motivated to analyze the complex flow field involving gaseous oxygen (GOX) flow in a relief valve (RV). The 9391 RV, pictured in Figure 1, was combined with the pilot valve to regulate the actuation pressure of the main valve system. During a high-pressure flow test at Marshall Space Flight Center (MSFC) the valve system developed a resonance chatter, which destroyed most of the valve body. Figures 2-4 show the valve body before and after accident. It was understood that the subject RV has never been operated at 5500 psia. In order to fully understand the flow behavior in the RV, a computational fluid dynamics (CFD) analysis is carried out to investigate the side load across the piston sleeve and the erosion patterns resulting from flow distribution around piston/nozzle interface. Author

N95-23619*# National Aeronautics and Space Administration. Marshall Space Flight Center, Huntsville, AL.

COMPUTATIONAL FLUID DYNAMICS (CFD) ANALYSES IN SUPPORT OF SPACE SHUTTLE MAIN ENGINE (SSME) HEAT EXCHANGER (HX) VANE CRACKING INVESTIGATION

Roberto Garcia, Theodore G. Benjamin, J. Cornelison, and A. J. Fredmonski (Pratt and Whitney Aircraft, West Palm Beach, FL.) *In its* Eleventh Workshop for Computational Fluid Dynamic Applications in Rocket Propulsion, Part 1 Jul. 1993 p 99-122 (For primary document see N95-23615 07-34)

Avail: CASI HC A03/MF A10

Integration issues involved with installing the alternate turbopump (ATP) High Pressure Oxygen Turbopump (HPOTP) into the SSME have raised questions regarding the flow in the HPOTP turnaround duct (TAD). Steady-state Navier-Stokes CFD analyses have been performed by NASA and Pratt & Whitney (P&W) to address these questions. The analyses have consisted of two-dimensional axisymmetric calculations done at Marshall Space Flight Center and three-dimensional calculations performed at P&W. These analyses have identified flowfield differences between the baseline ATP and the Rocketdyne configurations. The results show that the baseline ATP configuration represents a more severe environment to the inner HX guide vane. This vane has limited life when tested in conjunction with the ATP but infinite life when tested with the current SSME HPOTP. The CFD results have helped interpret test results and have been used to assess proposed redesigns. This paper includes details of the axisymmetric model, its results, and its contribution towards resolving the problem. Author

N95-23620*# Pratt and Whitney Aircraft, West Palm Beach, FL. Government Engines and Space Propulsion Div.

THREE-D FLOW ANALYSIS OF THE ALTERNATE SSME HPOT TAD

Cheryl A. Kubinski *In* NASA. Marshall Space Flight Center, Eleventh Workshop for Computational Fluid Dynamic Applications in Rocket Propulsion, Part 1 Jul. 1993 p 123-147 (For primary document see N95-23615 07-34)

Avail: CASI HC A03/MF A10

This paper describes the results of numerical flow analyses performed in support of design development of the Space Shuttle Main Engine Alternate High Pressure Oxidizer Turbine Turn-around duct (TAD). The flow domain has been modeled using a 3D, Navier-Stokes, general purpose flow solver. The goal of this effort is to achieve an alternate TAD exit flow distribution which closely matches that of the baseline configuration. 3D Navier Stokes CFD analyses were employed to evaluate numerous candidate geometry modifications to the TAD flowpath in order to achieve this goal. The design iterations are summarized, as well as a description of the computational model, numerical results and the conclusions based on these calculations. Author

N95-23621*# National Aeronautics and Space Administration. Marshall Space Flight Center, Huntsville, AL.

UNSTEADY FLOW SIMULATIONS IN SUPPORT OF THE SSME HEX TURNING VANE CRACKING INVESTIGATION WITH THE ATD HPOTP

N. S. Dougherty (Rockwell International Corp., Huntsville, AL.), D. W. Burnette (Rockwell International Corp., Huntsville, AL.), J. B. Holt (Rockwell International Corp., Huntsville, AL.), and T. Nesman *In its* Eleventh Workshop for Computational Fluid Dynamic Applications in Rocket Propulsion, Part 1 Jul. 1993 p 149-169 (For primary document see N95-23615 07-34)

Avail: CASI HC A03/MF A10

Unsteady flow computations are being performed with the P&W (ATD) and the Rocketdyne baseline configurations of the SSME LO2 turbine turnaround duct (TAD) and heat exchanger (HEX). The work is in support of the HEX inner turning vane cracking investigation. Fatigue cracking has occurred during hot firings with the P&W configuration on the HEX inner vane, and it appears the fix will involve changes to the TAD splitter vane position and to the TAD inner wall curvature to reduce the dynamic loading on the inner vane. Unsteady flow computations on the P&W baseline and fix and on the Rocketdyne baseline reference follow steady-flow screening computations done by MSFC/ED32 on several trial configurations arriving at the fix. The P&W TAD inlet velocity profile has a strong radial velocity component that directs the flow toward the inner wall and raises the local velocity a factor of two and the dynamic pressure a factor, of four. The fix is intended to redistribute the flow more evenly across the HEX inner and outer vanes like the Rocketdyne baseline reference. Vane buffeting at frequencies around 4,000 Hz is the leading suspected cause of the problem. Our simulations (work in progress) are being done with the USA 2D axisymmetric code approximating the flow as axisymmetric u+v 2D (axial, u, and radial, v, components only). The HEX coils are included in the model to make sure the fix does not adversely affect the HEX environment. Turbulent kinetic energy, k, levels where k = 1/2 v' rms2 are locally as high as 10,000 ft2/sec2 for the P&W baseline at the engine interface (between the TAD and HEX) at the HEX inner vane location. However, k is less than 8,000 on the HEX outer vane and only about 4,500 on the HEX inner vane for the Rocketdyne baseline. Unsteady turbulence intensity, v'rms/v, and pressure, p', are being computed in the present computations to compare with steady-flow Reynolds-averaged computations where p'rms = const (pk) for overall rms random turbulence from 0.1 to 12,000 Hz frequency. Random overall static, p'rms fluctuations as large as 1.7 psi are estimated from k on the HEX inner vane for the P&W baseline configuration but only about 0.7 psi for the Rocketdyne configuration. Author

N95-23622*# Advanced Scientific Computing Corp., El Dorado Hills, CA.

COMPARISON BETWEEN PREDICTED AND EXPERIMENTALLY MEASURED FLOW FIELDS AT THE EXIT OF THE SSME HPFTP IMPELLER

George Bache *In* NASA. Marshall Space Flight Center, Eleventh Workshop for Computational Fluid Dynamic Applications in Rocket Propulsion, Part 1 Jul. 1993 p 171-194 (For primary document see N95-23615 07-34)

Avail: CASI HC A03/MF A10

Validation of CFD codes is a critical first step in the process of developing CFD design capability. The MSFC Pump Technology Team has recognized the importance of validation and has thus funded several experimental programs designed to obtain CFD quality validation data. The first data set to become available is for the SSME High Pressure Fuel Turbopump Impeller. LDV Data was taken at the impeller inlet (to obtain a reliable inlet boundary condition) and three radial positions at the impeller discharge. Our CFD code, TASCflow, is used within the Propulsion and Commercial Pump industry as a tool for pump design. The objective of this work, therefore, is to further validate TASCflow for application in pump design. TASCflow was used to predict flow at the impeller discharge for flowrates of 80, 100 and 115 percent of design flow. Comparison to data has been made with encouraging results. Author

N95-23623*# National Aeronautics and Space Administration. Lewis Research Center, Cleveland, OH.

THREE-DIMENSIONAL FLOW ANALYSIS INSIDE CONSORTIUM IMPELLER AT DESIGN AND OFF-DESIGN CONDITIONS

C. Hah, J. Loellbach, F.-L. Tsung, D. A. Greenwald, and Roberto Garcia (National Aeronautics and Space Administration. Marshall Space Flight

Center, Huntsville, AL.) *In* NASA. Marshall Space Flight Center, Eleventh Workshop for Computational Fluid Dynamic Applications in Rocket Propulsion, Part 1 Jul. 1993 p 195-217 (For primary document see N95-23615 07-34)
Avail: CASI HC A03/MF A10

Three-dimensional flow fields inside the Consortium impeller were analyzed with a Navier-Stokes code. The numerical results at the design and off-design conditions are compared with the experimental data.

Author

N95-23624*# National Aeronautics and Space Administration. Marshall Space Flight Center, Huntsville, AL.

OPTIMIZATION OF A CENTRIFUGAL IMPELLER DESIGN THROUGH CFD ANALYSIS

W. C. Chen (Rockwell International Corp., Canoga Park, CA.), A. H. Eastland (Rockwell International Corp., Canoga Park, CA.), D. C. Chan (Rockwell International Corp., Canoga Park, CA.), and Roberto Garcia *In its* Eleventh Workshop for Computational Fluid Dynamic Applications in Rocket Propulsion, Part 1 Jul. 1993 p 219-249 (For primary document see N95-23615 07-34)
Avail: CASI HC A03/MF A10

This paper discusses the procedure, approach and Rocketdyne CFD results for the optimization of the NASA consortium impeller design. Two different approaches have been investigated. The first one is to use a tandem blade arrangement, the main impeller blade is split into two separate rows with the second blade row offset circumferentially with respect to the first row. The second approach is to control the high losses related to secondary flows within the impeller passage. Many key parameters have been identified and each consortium team member involved will optimize a specific parameter using 3-D CFD analysis. Rocketdyne has provided a series of CFD grids for the consortium team members. SECA will complete the tandem blade study, SRA will study the effect of the splitter blade solidity change, NASA LeRC will evaluate the effect of circumferential position of the splitter blade, VPI will work on the hub to shroud blade loading distribution, NASA Ames will examine the impeller discharge leakage flow impacts and Rocketdyne will continue to work on the meridional contour and the blade leading to trailing edge work distribution. This paper will also present Rocketdyne results from the tandem blade study and from the blade loading distribution study. It is the ultimate goal of this consortium team to integrate the available CFD analysis to design an advanced technology impeller that is suitable for use in the NASA Space Transportation Main Engine (STME) fuel turbopump. Author

N95-23625*# Virginia Polytechnic Inst. and State Univ., Blacksburg, VA. Dept. of Mechanical Engineering.

USE OF BLADE LEAN IN TURBOMACHINERY REDESIGN

John Moore, Joan G. Moore, and Alex Lupi *In* NASA. Marshall Space Flight Center, Eleventh Workshop for Computational Fluid Dynamic Applications in Rocket Propulsion, Part 1 Jul. 1993 p 251-269 (For primary document see N95-23615 07-34)
Avail: CASI HC A03/MF A10

Blade lean is used to improve the uniformity of exit flow distributions from turbomachinery blading. In turbines, it has been used to control secondary flows by tailoring blade turning to reduce flow overturning and underturning and to create more uniform loss distributions from hub to shroud. In the present study, the Pump Consortium centrifugal impeller has been redesigned using blade lean. The flow at the exit of the baseline impeller had large blade-to-blade variations, creating a highly unsteady flow for the downstream diffuser. Blade lean is used to redesign the flow to move the high loss fluid from the suction side to the hub, significantly reducing blade-toblade variations at the exit. Author

N95-23626*# National Aeronautics and Space Administration. Marshall Space Flight Center, Huntsville, AL.

CFD PARAMETRIC STUDY OF CONSORTIUM IMPELLER

Gary C. Cheng (SECA, Inc., Huntsville, AL.), Y. S. Chen (Engineering Sciences, Inc., Huntsville, AL.), Roberto Garcia, and Robert W. Williams *In its* Eleventh Workshop for Computational Fluid Dynamic Applications in Rocket Propulsion, Part 1 Jul. 1993 p 271-303 (For primary document see N95-23615 07-34)
Avail: CASI HC A03/MF A10

Current design of high performance turbopumps for rocket engines requires effective and robust analytical tools to provide design impact in a productive manner. The main goal of this study is to develop a robust and effective computational fluid dynamics (CFD) pump model for general turbopump design and analysis applications. A Finite Difference Navier-Stokes flow solver, FDNS, which includes the extended k-epsilon turbulence model and appropriate moving interface boundary conditions, was developed to analyze turbulent flows in turbomachinery devices. A second-order central difference scheme plus adaptive dissipation terms was employed in the FDNS code, along with a predictor plus multi-corrector pressure-based solution procedure. The multi-zone, multi-block capability allows the FDNS code to efficiently solve flow fields with complicated geometry. The FDNS code has been benchmarked by analyzing the pump consortium inducer, and it provided satisfactory results. In the present study, a CFD parametric study of the pump consortium impeller was conducted using the FDNS code. The pump consortium impeller, with partial blades, is a new design concept of the advanced rocket engines. The parametric study was to analyze the baseline design of the consortium impeller and its modification which utilizes TANDEM blades. In the present study, the TANDEM blade configuration of the consortium impeller considers cut full blades for about one quarter chord length from the leading edge and clocks the leading edge portion with an angle of 7.5 or 22.5 degrees. The purpose of the present study is to investigate the effect and trend of the TANDEM blade modification and provide the result as a design guideline. A 3-D flow analysis, with a 103 x 23 x 30 mesh grid system and with the inlet flow conditions measured by Rocketdyne, was performed for the baseline consortium impeller. The numerical result shows that the mass flow rate splits through various blade passages are relatively uniform. Due to the complexity of blade geometries, the TANDEM blade configurations were analyzed with the multi-zone grid structure. Both the 7.5 deg- and the 22.5 deg-clocking TANDEM blade cases utilized a 80K mesh system. The numerical result of two TANDEM blade modifications indicates the efficiency and the head are worse than those of the baseline case due to larger flow distortion. The gap between the TANDEM blade and the full blade allows the flow passes through and heavily loads the pressure side of the partial blade such that flow reversal occurs near the suction side of the splitter. The flow split at the exit of impeller blades is very non-uniform for TANDEM blade cases, and this will greatly induce the side load on the diffuser. Therefore, the TANDEM blade modification in the present CFD analysis does not improve the performance of the consortium impeller.

Author

N95-23627*# National Aeronautics and Space Administration. Ames Research Center, Moffett Field, CA.

INCOMPRESSIBLE NAVIER-STOKES CALCULATIONS IN PUMP FLOWS

Cetin Kiris (MCAT Inst., Moffett Field, CA.), Leon Chang (MCAT Inst., Moffett Field, CA.), and Dochan Kwak *In* NASA. Marshall Space Flight Center, Eleventh Workshop for Computational Fluid Dynamic Applications in Rocket Propulsion, Part 1 Jul. 1993 p 305-338 (For primary document see N95-23615 07-34)
Avail: CASI HC A03/MF A10

Flow through pump components, such as the SSME-HPFTP Impeller and an advanced rocket pump impeller, is efficiently simulated by solving the incompressible Navier-Stokes equations. The solution method is based on the pseudo compressibility approach and uses an implicit-upwind differencing scheme together with the Gauss-Seidel line relaxation method. The equations are solved in steadily rotating reference frames and the centrifugal force and the Coriolis force are added to the equation of motion. Current computations use one-equation Baldwin-Barth turbulence model which is derived from a simplified form of the standard k-epsilon model equations. The resulting computer code is applied to the flow analysis inside an 11-inch SSME High Pressure Fuel Turbopump impeller, and an advanced rocket pump impeller. Numerical results of SSME-HPFTP impeller flow are compared with experimental measurements. In the advanced pump impeller, the effects of exit and shroud cavities are investigated. Flow analyses at design conditions will be presented. Author

N95-23628*# California Inst. of Tech., Pasadena, CA. Div. of Engineering and Applied Science.

THE INFLUENCE OF SWIRL BRAKES AND A TIP DISCHARGE ORIFICE ON THE ROTORDYNAMIC FORCES GENERATED BY DISCHARGE-TO-SUCTION LEAKAGE FLOWS IN SHROUDED CENTRIFUGAL PUMPS

Joseph M. Sivo, A. J. Acosta, C. E. Brennen, and T. K. Caughey *In* NASA. Marshall Space Flight Center, Eleventh Workshop for Computational Fluid Dynamic Applications in Rocket Propulsion, Part 1 Jul. 1993 p 339-361 (For primary document see N95-23615 07-34)
Avail: CASI HC A03/MF A10

Recent experiments conducted in the Rotor Force Test Facility at the California Institute of Technology have examined the effects of a tip leakage restriction and swirl brakes on the rotordynamic forces due to leakage flows on an impeller undergoing a prescribed circular whirl. The experiments simulate the leakage flow conditions and geometry of the Alternate Turbopump Design (ATD) of the Space Shuttle High Pressure Oxygen Turbopump and are critical to evaluating the pump's rotordynamic instability problems. Previous experimental and analytical results have shown that discharge-to-suction leakage flows in the annulus of a shrouded centrifugal pump contribute substantially to the fluid induced rotordynamic forces. Also, previous experiments have shown that leakage inlet (pump discharge) swirl can increase the cross-coupled stiffness coefficient and hence increase the range of positive whirl for which the tangential force is destabilizing. In recent experimental work, the present authors demonstrated that when the swirl velocity within the leakage path is reduced by the introduction of ribs or swirl brakes, then a substantial decrease in both the destabilizing normal and tangential forces could be achieved. Motivation for the present research is that previous experiments have shown that restrictions such as wear rings or orifices at pump inlets affect the leakage forces. Recent pump designs such as the Space Shuttle Alternate Turbopump Design (ATD) utilize tip orifices at discharge for the purpose of establishing axial thrust balance. The ATD has experienced rotordynamic instability problems and one may surmise that these tip discharge orifices may also have an important effect on the normal and tangential forces in the plane of impeller rotation. The present study determines if such tip leakage restrictions contribute to undesirable rotordynamic forces. Additional motivation for the present study is that the widening of the leakage path annular clearance and the installation of swirl brakes in the ATD has been proposed to solve its instability problems. The present study assesses the effect of such a design modification on the rotordynamic forces. The experimental apparatus consists of a solid or dummy impeller, a housing instrumented for pressure measurements, a rotating dynamometer and an eccentric whirl mechanism. The solid impeller is used so that leakage flow contributions to the forces are measured, but the main throughflow contributions are not experienced. The inner surface of the housing has been modified to accommodate meridional ribs or swirl brakes within the leakage annulus. In addition, the housing has been modified to accommodate a discharge orifice that qualitatively simulates one side of the balance piston orifice of the Space Shuttle ATD. Results indicate the detrimental effects of a discharge orifice and the beneficial effects of brakes. Plots of the tangential and normal forces versus whirl ratio show a substantial increase in these forces along with destabilizing resonances at some positive whirl ratios when a discharge orifice is added. When brakes are added, some of the detrimental effects of the orifice are reduced. For the tangential force, a plot versus whirl ratio shows a significant reduction and a destabilizing resonance appears to be eliminated. For the normal force, although the overall force is not reduced, again a destabilizing resonance appears to be eliminated.

Author

N95-23629*# Rockwell International Corp., Canoga Park, CA. Rocketdyne Div.

ADAPTATION OF THE ADVANCED SPRAY COMBUSTION CODE TO CAVITATING FLOW PROBLEMS

Pak-Yan Liang *In* NASA. Marshall Space Flight Center, Eleventh Workshop for Computational Fluid Dynamic Applications in Rocket Propulsion, Part 1 Jul. 1993 p 363-376 (For primary document see N95-23615 07-34)
Avail: CASI HC A03/MF A10

A very important consideration in turbopump design is the prediction and prevention of cavitation. Thus far conventional CFD codes have not been generally applicable to the treatment of cavitating flows. Taking advantage of its two-phase capability, the Advanced Spray Combustion Code is being modified to handle flows with transient as well as steady-state cavitation bubbles. The volume-of-fluid approach incorporated into the code is extended and augmented with a liquid phase energy equation and a simple evaporation model. The strategy adopted also successfully deals with the cavity closure issue. Simple test cases will be presented and remaining technical challenges will be discussed.

Author

N95-23630*# Pennsylvania State Univ., State College, PA. Propulsion Engineering Research Center.

CAVITATION MODELING IN EULER AND NAVIER-STOKES CODES

Manish Deshpande, Jinzhang Feng, and Charles L. Merkle *In* NASA. Marshall Space Flight Center, Eleventh Workshop for Computational Fluid Dynamic Applications in Rocket Propulsion, Part 1 Jul. 1993 p 377-401 (For primary document see N95-23615 07-34)
Avail: CASI HC A03/MF A10

Many previous researchers have modeled sheet cavitation by means of a constant pressure solution in the cavity region coupled with a velocity potential formulation for the outer flow. The present paper discusses the issues involved in extending these cavitation models to Euler or Navier-Stokes codes. The approach taken is to start from a velocity potential model to ensure our results are compatible with those of previous researchers and available experimental data, and then to implement this model in both Euler and Navier-Stokes codes. The model is then augmented in the Navier-Stokes code by the inclusion of the energy equation which allows the effect of subcooling in the vicinity of the cavity interface to be modeled to take into account the experimentally observed reduction in cavity pressures that occurs in cryogenic fluids such as liquid hydrogen. Although our goal is to assess the practicality of implementing these cavitation models in existing three-dimensional, turbomachinery codes, the emphasis in the present paper will center on two-dimensional computations, most specifically isolated airfoils and cascades. Comparisons between velocity potential, Euler and Navier-Stokes implementations indicate they all produce consistent predictions. Comparisons with experimental results also indicate that the predictions are qualitatively correct and give a reasonable first estimate of sheet cavitation effects in both cryogenic and non-cryogenic fluids. The impact on CPU time and the code modifications required suggests that these models are appropriate for incorporation in current generation turbomachinery codes.

Author

N95-23631*# Pratt and Whitney Aircraft, West Palm Beach, FL. Government Engines and Space Propulsion Div.

AN INDUCER CFD SOLUTION AND EFFECTS ASSOCIATED WITH CAVITATION

Mehtab M. Pervaiz, J. Garrett, and J. Kuryla *In* NASA. Marshall Space Flight Center, Eleventh Workshop for Computational Fluid Dynamic Applications in Rocket Propulsion, Part 1 Jul. 1993 p 403-422 (For primary document see N95-23615 07-34)
Avail: CASI HC A03/MF A10

This presentation describes a CFD analysis for an Alternate Turbopump Development (ATD) configuration. The analysis consists of a coupled configuration of the inducer and impeller. The work presented here is a joint collaboration of J. Garrett, J. Kuryla and myself.

Author

N95-23632*# CFD Research Corp., Huntsville, AL.

CURRENT STATUS IN CAVITATION MODELING

Ashok K. Singhal and Ram K. Avva *In* NASA. Marshall Space Flight Center, Eleventh Workshop for Computational Fluid Dynamic Applications in Rocket Propulsion, Part 1 Jul. 1993 p 423-435 (For primary document see N95-23615 07-34)
Avail: CASI HC A03/MF A10

Cavitation is a common problem for many engineering devices in which the main working fluid is in liquid state. In turbomachinery applications, cavitation generally occurs on the inlet side of pumps. The deleterious effects of cavitation include: lowered performance, load asymmetry, erosion and pitting of blade surfaces, vibration and noise, and reduction of the overall machine life. Cavitation models in use today range from rather crude approximations to sophisticated bubble dynamics models. Details about bubble inception, growth and collapse are relevant to the prediction of blade erosion, but are not necessary to predict the performance of pumps. An engineering model of cavitation is proposed to predict the extent of cavitation and performance. The vapor volume fraction is used as an indicator variable to quantify cavitation. A two-phase flow approach is employed with the assumption of the thermal equilibrium between liquid and vapor. At present velocity slip between the two phases is selected. Preliminary analyses of 2D flows shows qualitatively correct results.

Author

N95-23633*# Scientific Research Associates, Inc., Glastonbury, CT.
A GENERALIZED EULERIAN-LAGRANGIAN ANALYSIS, WITH APPLICATION TO LIQUID FLOWS WITH VAPOR BUBBLES
Frederik J. deJong and Meyya Meyyappan *In* NASA. Marshall Space Flight Center, Eleventh Workshop for Computational Fluid Dynamic Applications in Rocket Propulsion, Part 1 Jul. 1993 p 437-448 (For primary document see N95-23615 07-34)
(Contract NAS8-38959)
Avail: CASI HC A03/MF A10

Under a NASA MSFC SBIR Phase 2 effort an analysis has been developed for liquid flows with vapor bubbles such as those in liquid rocket engine components. The analysis is based on a combined Eulerian-Lagrangian technique, in which Eulerian conservation equations are solved for the liquid phase, while Lagrangian equations of motion are integrated in computational coordinates for the vapor phase. The novel aspect of the Lagrangian analysis developed under this effort is that it combines features of the so-called particle distribution approach with those of the so-called particle trajectory approach and can, in fact, be considered as a generalization of both of those traditional methods. The result of this generalization is a reduction in CPU time and memory requirements. Particle time step (stability) limitations have been eliminated by semi-implicit integration of the particle equations of motion (and, for certain applications, the particle temperature equation), although practical limitations remain in effect for reasons of accuracy. The analysis has been applied to the simulation of cavitating flow through a single-bladed section of a labyrinth seal. Models for the simulation of bubble formation and growth have been included, as well as models for bubble drag and heat transfer. The results indicate that bubble formation is more or less 'explosive'. for a given flow field, the number density of bubble nucleation sites is very sensitive to the vapor properties and the surface tension. The bubble motion, on the other hand, is much less sensitive to the properties, but is affected strongly by the local pressure gradients in the flow field. In situations where either the material properties or the flow field are not known with sufficient accuracy, parametric studies can be carried out rapidly to assess the effect of the important variables. Future work will include application of the analysis to cavitation in inducer flow fields. Author

N95-23634*# Pratt and Whitney Aircraft, West Palm Beach, FL.
ON THE ACCURACY OF CFD-BASED PRESSURE DROP PREDICTIONS FOR RIGHT-ANGLE DUCTS
Andreja Brankovic *In* NASA. Marshall Space Flight Center, Eleventh Workshop for Computational Fluid Dynamic Applications in Rocket Propulsion, Part 1 Jul. 1993 p 449-461 (For primary document see N95-23615 07-34)
Avail: CASI HC A03/MF A10

The predictive capability of computational fluid dynamics (CFD) codes for turbulent flow through curved ducts is of significant importance to the design and performance analysis of modern rocket engine flowpaths. Code calibration and validation studies for this class of flow are desireable to estimate the performance margin and operating range of components designed using Navier-Stokes methods. Parametric experimental studies such as that of Weske (NACA ARR W-39) provided a wealth of performance data for the design of single- and compound elbow configurations with various cross-sections, curvature and aspect ratios at varying Reynolds numbers. In that work, the majority of data is presented in the form of loss coefficients, characterizing pressure losses due to duct curvature, and including losses due to wall friction. Using measured friction coefficients, losses of equivalent straight lengths of duct are subtracted, resulting in performance curves useful for design computations. These data are currently used in a CFD-based parametric study covering a broad range of operating conditions. Of particular interest for the accuracy of CFD predictions are the effects on pressure loss due to inlet boundary layer thickness (dependent on upstream development length), and the wall treatment for the turbulence equations (conventional wall functions vs. wall integration using a two-layer model). The experimental data are reassessed in the form of an error analysis, and are compared with CFD predictions for 18 computational cases. Grid-independence, grid spacing, and convergence requirements of the cases are discussed. Conclusions regarding the relative importance of the parametric variables will be presented. Author

N95-23635*# Rockwell International Corp., Canoga Park, CA. Rocketdyne Div.
CFD MODELING OF TURBULENT DUCT FLOWS FOR COOLANT CHANNEL ANALYSIS
Ronald J. Ungewitter and Daniel C. Chan *In* NASA. Marshall Space Flight Center, Eleventh Workshop for Computational Fluid Dynamic Applications in Rocket Propulsion, Part 1 Jul. 1993 p 463-481 (For primary document see N95-23615 07-34)
Avail: CASI HC A03/MF A10

The design of modern liquid rocket engines requires the analysis of chamber coolant channels to maximize the heat transfer while minimizing the coolant flow. Coolant channels often do not remain at a constant cross section or at uniform curvature. New designs require higher aspect ratio coolant channels than previously used. To broaden the analysis capability and to complement standard analysis tools an investigation on the accuracy of CFD predictions for coolant channel flow has been initiated. Validation of CFD capabilities for coolant channel analysis will enhance the capabilities for optimizing design parameters without resorting to extensive experimental testing. The eventual goal is to use CFD to determine the flow fields of unique coolant channel designs and therefore determine critical heat transfer coefficients. In this presentation the accuracy of a particular CFD code is evaluated for turbulent flows. The first part of the presentation is a comparison of numerical results to existing cold flow data for square curved ducts (NASA CR-3367, 'Measurements of Laminar and Turbulent Flow in a Curved Duct with Thin Inlet Boundary Layers'). The results of this comparison show good agreement with the relatively coarse experimental data. The second part of the presentation compares two cases of higher aspect ratio channels (AR=2.5,10) to show changes in axial and secondary flow strength. These cases match experimental work presently in progress and will be used for future validation. The comparison shows increased secondary flow strength of the higher aspect ratio case due to the change in radius of curvature. The presentation includes a test case with a heated wall to demonstrate the program's capability. The presentation concludes with an outline of the procedure used to validate the CFD code for future design analysis. Author

N95-23636*# National Aeronautics and Space Administration. Marshall Space Flight Center, Huntsville, AL.
FLOW AND HEAT TRANSFER IN 180-DEGREE TURN SQUARE DUCTS: EFFECTS OF TURNING CONFIGURATION AND SYSTEM ROTATION
Ten-See Wang and Ming-King Chyu (Carnegie-Mellon Univ., Pittsburgh, PA.) *In its* Eleventh Workshop for Computational Fluid Dynamic Applications in Rocket Propulsion, Part 1 Jul. 1993 p 483-501 (For primary document see N95-23615 07-34)
Avail: CASI HC A03/MF A10

Forced flow through channels connected by sharp bends is frequently encountered in various rocket and gas turbine engines. For example, the transfer ducts, the coolant channels surround the combustion chamber, the internal cooling passage in a blade or vane, the flow path in the fuel element of a nuclear rocket engine, the flow around a pressure relieve valve piston, and the recirculated base flow of multiple engine clustered nozzles. Transport phenomena involved in such a flow passage are complex and considered to be very different from those of conventional turning flow with relatively mild radii of curvature. While previous research pertaining to this subject has been focused primarily on the experimental heat transfer, very little analytical work is directed to understanding the flowfield and energy transport in the passage. Therefore, the primary goal of this paper is to benchmark the predicted wall heat fluxes using a state-of-the-art computational fluid dynamics (CFD) formulation against those of measurement for a rectangular turn duct. Other secondary goals include studying the effects of turning configurations, e.g., the semi-circular turn, and the rounded-corner turn, and the effect of system rotation. The computed heat fluxes for the rectangular turn duct compared favorably with those of the experimental data. The results show that the flow pattern, pressure drop, and heat transfer characteristics are different among the three turning configurations, and are substantially different with system rotation. Also demonstrated in this work is that the present computational approach is quite effective and efficient and will be suitable for flow and thermal modeling in rocket and turbine engine applications. Author

N95-23637*# Pratt and Whitney Aircraft, West Palm Beach, FL.
METHODOLOGY FOR CFD DESIGN ANALYSIS OF NATIONAL LAUNCH SYSTEM NOZZLE MANIFOLD
Scot L. Haire *In* NASA. Marshall Space Flight Center, Eleventh Workshop for Computational Fluid Dynamic Applications in Rocket Propulsion, Part 1 Jul. 1993 p 503-523 (For primary document see N95-23615 07-34)
Avail: CASI HC A03/MF A10

The current design environment dictates that high technology CFD (Computational Fluid Dynamics) analysis produce quality results in a timely manner if it is to be integrated into the design process. The design methodology outlined describes the CFD analysis of an NLS (National Launch System) nozzle film cooling manifold. The objective of the analysis was to obtain a qualitative estimate for the flow distribution within the manifold. A complex, 3D, multiple zone, structured grid was generated from a 3D CAD file of the geometry. A Euler solution was computed with a fully implicit compressible flow solver. Post processing consisted of full 3D color graphics and mass averaged performance. The result was a qualitative CFD solution that provided the design team with relevant information concerning the flow distribution in and performance characteristics of the film cooling manifold within an effective time frame. Also, this design methodology was the foundation for a quick turnaround CFD analysis of the next iteration in the manifold design. Author

N95-23638*# National Aeronautics and Space Administration. Marshall Space Flight Center, Huntsville, AL.
ADVANCED MULTI-PHASE FLOW CFD MODEL DEVELOPMENT FOR SOLID ROCKET MOTOR FLOWFIELD ANALYSIS
Paul Liaw (Engineering Sciences, Inc., Huntsville, AL.), Y. S. Chen (Engineering Sciences, Inc., Huntsville, AL.), H. M. Shang (Engineering Sciences, Inc., Huntsville, AL.), and Denise Doran *In its* Eleventh Workshop for Computational Fluid Dynamic Applications in Rocket Propulsion, Part 1 Jul. 1993 p 525-550 (For primary document see N95-23615 07-34)
(Contract NAS8-39398)
Avail: CASI HC A03/MF A10

It is known that the simulations of solid rocket motor internal flow field with AL-based propellants require complex multi-phase turbulent flow model. The objective of this study is to develop an advanced particulate multi-phase flow model which includes the effects of particle dynamics, chemical reaction and hot gas flow turbulence. The inclusion of particle agglomeration, particle/gas reaction and mass transfer, particle collision, coalescence and breakup mechanisms in modeling the particle dynamics will allow the proposed model to realistically simulate the flowfield inside a solid rocket motor. The Finite Difference Navier-Stokes numerical code FDNS is used to simulate the steady-state multi-phase particulate flow field for a 3-zone 2-D axisymmetric ASRM model and a 6-zone 3-D ASRM model at launch conditions. The 2-D model includes aft-end cavity and submerged nozzle. The 3-D model represents the whole ASRM geometry, including additional grain port area in the gas cavity and two inhibitors. FDNS is a pressure based finite difference Navier-Stokes flow solver with time-accurate adaptive second-order upwind schemes, standard and extended k-epsilon models with compressibility corrections, multi zone body-fitted formulations, and turbulence particle interaction model. Eulerian/Lagrangian multi-phase solution method is applied for multi-zone mesh. To simulate the chemical reaction, penalty function corrected efficient finite-rate chemistry integration method is used in FDNS. For the AL particle combustion rate, the Hermsen correlation is employed. To simulate the turbulent dispersion of particles, the Gaussian probability distribution with standard deviation equal to (2k/3)(exp 1/2) is used for the random turbulent velocity components. The computational results reveal that the flow field near the juncture of aft-end cavity and the submerged nozzle is very complex. The effects of the turbulent particles affect the flow field significantly and provide better prediction of the ASRM performance. The multi-phase flow analysis using the FDNS code in the present research can be used as a design tool for solid rocket motor applications. Author

N95-23639*# National Aeronautics and Space Administration. Marshall Space Flight Center, Huntsville, AL.
ASRM MULTI-PORT IGNITER FLOW FIELD ANALYSIS
Lee Kania (Sverdrup Technology, Inc., Huntsville, AL.), Catherine Dumas (Sverdrup Technology, Inc., Huntsville, AL.), and Denise Doran *In its* Eleventh Workshop for Computational Fluid Dynamic Applications in Rocket Propulsion, Part 1 Jul. 1993 p 551-569 (For primary document see N95-23615 07-34)
Avail: CASI HC A03/MF A10

The Advanced Solid Rocket Motor (ASRM) program was initiated by NASA in response to the need for a new generation rocket motor capable of providing increased thrust levels over the existing Redesigned Solid Rocket Motor (RSRM) and thus augment the lifting capacity of the space shuttle orbiter. To achieve these higher thrust levels and improve motor reliability, advanced motor design concepts were employed. In the head end of the motor, for instance, the propellent cast has been changed from the conventional annular configuration to a 'multi-slot' configuration in order to increase the burn surface area and guarantee rapid motor ignition. In addition, the igniter itself has been redesigned and currently features 12 exhaust ports in order to channel hot igniter combustion gases into the circumferential propellent slots. Due to the close proximity of the igniter ports to the propellent surfaces, new concerns over possible propellent deformation and erosive burning have arisen. The following documents the effort undertaken using computational fluid dynamics to perform a flow field analysis in the top end of the ASRM motor to determine flow field properties necessary to permit a subsequent propellent fin deformation analysis due to pressure loading and an assessment of the extent of erosive burning. Author

N95-23640*# Auburn Univ., AL. Dept. of Aerospace Engineering.
IGNITION TRANSIENT CALCULATIONS IN THE SPACE SHUTTLE SOLID ROCKET MOTOR **c20**
Rhonald M. Jenkins and Winfred A. Foster, Jr. *In* NASA. Marshall Space Flight Center, Eleventh Workshop for Computational Fluid Dynamic Applications in Rocket Propulsion, Part 1 Jul. 1993 p 571-595 (For primary document see N95-23615 07-34)
Avail: CASI HC A03/MF A10

The work presented is part of an effort to develop a multidimensional ignition transient model for large solid propellant rocket motors. On the Space Shuttle, the ignition transient in the slot is induced when the igniter, itself a small rocket motor, is fired into the head-end portion of the main rocket motor. The computational results presented in this paper consider two different igniter configurations. The first configuration is a simulated Space Shuttle RSRM igniter which has one central nozzle that is parallel to the centerline of the motor. The second igniter configuration has a nozzle which is canted at an angle of 45 deg from the centerline of the motor. This paper presents a computational fluid dynamic (CFD) analyses of certain flow field characteristics inside the solid propellant star grain slot of the Space Shuttle during the ignition transient period of operation for each igniter configuration. The majority of studies made to date regarding ignition transient performance in solid rocket motors have concluded that the key parameter to be determined is the heat transfer rate to the propellant surface and hence the heat transfer coefficient between the gas and the propellant. In this paper the heat transfer coefficients, pressure and velocity distributions are calculated in the star slot. In order to validate the computational method and to attempt to establish a correlation between the flow field characteristics and the heat transfer rates a series of cold flow experimental investigations were conducted. The results of these experiments show excellent qualitative and quantitative agreement with the pressure and velocity distributions obtained from the CFD analysis. The CFD analysis utilized a classical pipe flow type correlation for the heat transfer rates. The experimental results provide an excellent qualitative comparison with regard to spatial distribution of the heat transfer rates as a function of nozzle configuration and igniter pressure. The results indicate that from a quantitative point of view that the pipe flow correlation gives reasonably good results. Furthermore, there appears to be a direct correlation between igniter pressure and an average Reynolds number in the star grain slot. This may lead to a simple method for modifying the convection heat transfer correlation. Calculated results of pressure-vs-time for the first 200 msec of motor firing of the Space Shuttle RSRM support the trends shown for the heat transfer rate comparisons between the cold flow CFD and experimental data. Author

N95-23641*# Scientific Research Associates, Inc., Glastonbury, CT.
AN INTERACTIVE TOOL FOR DISCRETE PHASE ANALYSIS IN TWO-PHASE FLOWS
Frederik J. deJong and Stephen J. Thoren *In* NASA. Marshall Space Flight Center, Eleventh Workshop for Computational Fluid Dynamic

Applications in Rocket Propulsion, Part 1 Jul. 1993 p 597-612 (For primary document see N95-23615 07-34)
Avail: CASI HC A03/MF A10

Under a NASA MSFC SBIR Phase 1 effort an interactive software package has been developed for the analysis of discrete (particulate) phase dynamics in two-phase flows in which the discrete phase does not significantly affect the continuous phase. This package contains a Graphical User Interface (based on the X Window system and the Motif tool kit) coupled to a particle tracing program, which allows the user to interactively set up and run a case for which a continuous phase grid and flow field are available. The software has been applied to a solid rocket motor problem, to demonstrate its ease of use and its suitability for problems of engineering interest, and has been delivered to NASA Marshall Space Flight Center. Author

N95-23642*# Pennsylvania State Univ., University Park, PA. Propulsion Engineering Research Center.
FLOWFIELD CHARACTERIZATION IN A LOX/GH2 PROPELLANT ROCKET
S. Pal, M. D. Moser, H. M. Ryan, M. J. Foust, and R. J. Santoro *In* NASA. Marshall Space Flight Center, Eleventh Workshop for Computational Fluid Dynamic Applications in Rocket Propulsion, Part 1 Jul. 1993 p 613-644 (For primary document see N95-23615 07-34)
(Contract NAS8-38862; NAGw-1356)
Avail: CASI HC A03/MF A10

The objective of the current work is to experimentally characterize the flowfield associated with an uni-element shear coaxial injector burning liquid oxygen/gaseous hydrogen (LOX/GH2) propellants. These experiments were carried out in an optically-accessible rocket chamber operating at a high pressure (approximately 400 psia). Quantitative measurements of drop size and velocity were obtained along with qualitative measurements of the disintegrating jet. Derived from text

N95-23643*# National Aeronautics and Space Administration. Lewis Research Center, Cleveland, OH.
SPRAY COMBUSTION EXPERIMENTS AND NUMERICAL PREDICTIONS **c25**
Edward J. Mularz (Army Research Lab., Cleveland, OH.), Daniel L. Bulzan, and Kuo-Huey Chen (Toledo Univ., OH.) *In* NASA. Marshall Space Flight Center, Eleventh Workshop for Computational Fluid Dynamic Applications in Rocket Propulsion, Part 1 Jul. 1993 p 645-665 (For primary document see N95-23615 07-34)
Avail: CASI HC A03/MF A10

The next generation of commercial aircraft will include turbofan engines with performances significantly better than those in the current fleet. Control of particulate and gaseous emissions will also be an integral part of the engine design criteria. These performance and emission requirements present a technical challenge for the combustor: control of the fuel and air mixing and control of the local stoichiometry will have to be maintained much more rigorously than combustors in current production. A better understanding of the flow physics of liquid fuel spray combustion is necessary. This presentation describes recent experiments on spray combustion where detailed measurements of the spray characteristics were made, including local drop-size distributions and velocities. In addition, an advanced combustor CFD code has been under development and predictions from this code are presented and compared with measurements. Studies such as these will provide information to the advanced combustor designer on fuel spray quality and mixing effectiveness. Validation of new fast, robust, and efficient CFD codes will also enable the combustor designer to use them as valuable design tools for optimization of combustor concepts for the next generation of aircraft engines. Author

N95-23644*# Rockwell International Corp., Canoga Park, CA. Rocketdyne Div.
PROGRESS IN ADVANCED SPRAY COMBUSTION CODE INTEGRATION **c25**
Pak-Yan Liang *In* NASA. Marshall Space Flight Center, Eleventh Workshop for Computational Fluid Dynamic Applications in Rocket Propulsion, Part 1 Jul. 1993 p 667-687 (For primary document see N95-23615 07-34)
Avail: CASI HC A03/MF A10

A multiyear project to assemble a robust, muitiphase spray combustion code is now underway and gradually building up to full speed. The overall effort involves several university and government research teams as well as Rocketdyne. The first part of this paper will give an overview of the respective roles of the different participants involved, the master strategy, the evolutionary milestones, and an assessment of the state-of-the-art of various key components. The second half of this paper will highlight the progress made to date in extending the baseline Navier-Stokes solver to handle multiphase, multispecies, chemically reactive sub- to supersonic flows. The major hurdles to overcome in order to achieve significant speed ups are delineated and the approaches to overcoming them will be discussed. Author

N95-23645*# National Aeronautics and Space Administration. Marshall Space Flight Center, Huntsville, AL.
CFD ANALYSIS OF SPRAY COMBUSTION AND RADIATION IN OMV THRUST CHAMBER **c25**
M. G. Giridharan (CFD Research Corp., Huntsville, AL.), A. Krishnan (CFD Research Corp., Huntsville, AL.), A. J. Przekwas (CFD Research Corp., Huntsville, AL.), and K. Gross *In its* Eleventh Workshop for Computational Fluid Dynamic Applications in Rocket Propulsion, Part 1 Jul. 1993 p 689-715 (For primary document see N95-23615 07-34)
Avail: CASI HC A03/MF A10

The Variable Thrust Engine (VTE), developed by TRW, for the Orbit Maneuvering Vehicle (OMV) uses a hypergolic propellant combination of Monomethyl Hydrazine (MMH) and Nitrogen Tetroxide (NTO) as fuel and oxidizer, respectively. The propellants are pressure fed into the combustion chamber through a single pintle injection element. The performance of this engine is dependent on the pintle geometry and a number of complex physical phenomena and their mutual interactions. The most important among these are (1) atomization of the liquid jets into fine droplets; (2) the motion of these droplets in the gas field; (3) vaporization of the droplets (4) turbulent mixing of the fuel and oxidizer; and (5) hypergolic reaction between MMH and NTO. Each of the above phenomena by itself poses a considerable challenge to the technical community. In a reactive flow field of the kind occurring inside the VTE, the mutual interactions between these physical processes tend to further complicate the analysis. The objective of this work is to develop a comprehensive mathematical modeling methodology to analyze the flow field within the VTE. Using this model, the effect of flow parameters on various physical processes such as atomization, spray dynamics, combustion, and radiation is studied. This information can then be used to optimize design parameters and thus improve the performance of the engine. The REFLEQS CFD Code is used for solving the fluid dynamic equations. The spray dynamics is modeled using the Eulerian-Lagrangian approach. The discrete ordinate method with 12 ordinate directions is used to predict the radiative heat transfer in the OMV combustion chamber, nozzle, and the heat shield. The hypergolic reaction between MMH and NTO is predicted using an equilibrium chemistry model with 13 species. The results indicate that mixing and combustion is very sensitive to the droplet size. Smaller droplets evaporate faster than bigger droplets, leading to a well mixed zone in the combustion chamber. The radiative heat flux at combustion chamber and nozzle walls are an order of negligible less than the conductive heat flux. Simulations performed with the heat shield show that a negligible amount of fluid is entrained into the heat shield region. However, the heat shield is shown to be effective in protecting the OMV structure surrounding the engine from the radiated heat. Author

N95-23646*# Alabama Univ., Huntsville, AL. Dept. of Chemical Engineering.
DEVELOPMENT OF AN ATOMIZATION METHODOLOGY FOR SPRAY COMBUSTION **c25**
S. P. Seung, C. P. Chen, and Y. S. Chen (Engineering Sciences, Inc., Huntsville, AL.) *In* NASA. Marshall Space Flight Center, Eleventh Workshop for Computational Fluid Dynamic Applications in Rocket Propulsion, Part 1 Jul. 1993 p 717-747 (For primary document see N95-23615 07-34)
Avail: CASI HC A03/MF A10

In liquid rocket propulsion, the knowledge and the understanding of liquid-gas interfacial phenomena are very important. This is important for predicting the onset of cavitation occurring in swirl injection elements used in STME, as well as atomization processes in shear-induced injectors (co-axial) and impinging injector elements. From the fact that all the physical processes including droplet size distribution, droplet dispersion, mixing and combustion are controlled by atomization processes, it is expected that

the successful incorporation of the volume of fraction (VOF) will greatly enhance the analytical capability of predicting spray combustion processes in liquid-fueled engines. In this paper, a methodology is developed to define and track interfaces between two fluids in non-orthogonal, body-fitted grids using a single fractional volume of fluid (VOF) variable to describe the distribution of the liquid phase in a gas-liquid flow field. This method was implemented in a mature CFD code MAST (Multiphase All-Speed Transient) utilizing the general PISO-C algorithm. For the preliminary study on the analysis of spray combustion and tracking of the interface between two phases, we will report on the progress of the simulation of the instability on the liquid column; the surface wave instability and the droplet breakup from the liquid surface. Derived from text

N95-23647*# National Aeronautics and Space Administration. Marshall Space Flight Center, Huntsville, AL.

MODELING OF NON-SPHERICAL DROPLET DYNAMICS

Zheng-Tao Deng (Alabama A & M Univ., Huntsville, AL.), Goang-Shin Liaw (Alabama A & M Univ., Huntsville, AL.), and Lynn C. Chou *In its* Eleventh Workshop for Computational Fluid Dynamic Applications in Rocket Propulsion, Part 1 Jul. 1993 p 749-768 (For primary document see N95-23615 07-34)

Avail: CASI HC A03/MF A10

A two-dimensional time-dependent computer code based on the modified Arbitrary Lagrangian Eulerian (ALE) technique, has been developed to simulate non-spherical droplet dynamics and evaporation under convective flows at real rocket combustion chamber conditions. The equations of mass, momentum, energy and species are simultaneously solved for both liquid and gas phases with an accurate dynamic interface tracking. The jump boundary conditions across the deforming droplet surface are obtained by applying the integral forms of conservation of mass, momentum, and energy. At each time step, the interface geometry and flow properties at the droplet surface are implicitly solved by satisfying the interface boundary conditions. A Lagrangian technique was developed to track the arbitrarily moving interface between the liquid droplet and the external gas. An elliptic grid generator is adopted to dynamically reconstruct grids both inside and outside the droplet surface. This code has been used to study droplet oscillation, droplet deformation/breakup, nonspherical droplet evaporation in both low and high pressure convective flows. This presentation briefly describes the numerical algorithm for modeling of the nonspherical droplet dynamics and demonstrates the representative simulation results of nonspherical droplet evaporation at low and high pressure convective flows. Potential applications of this code to rocket combustor design and performance predictions are discussed. Author

N95-23648*# National Aeronautics and Space Administration. Marshall Space Flight Center, Huntsville, AL.

A FINE-GRID MODEL FOR THE ASRM AFT SEGMENT WITH GIMBALLED NOZZLE

Edward J. Reske *In its* Eleventh Workshop for Computational Fluid Dynamic Applications in Rocket Propulsion, Part 1 Jul. 1993 p 769-792 (For primary document see N95-23615 07-34)

Avail: CASI HC A03/MF A10

Results from computational fluid dynamic analyses for complex three-dimensional internal flows in the Advanced Solid Rocket Motor (ASRM) are presented. In particular, flow visualization and tabulated results from a fine-grid model consisting of 1.5 M grid points for the ASRM Aft Segment at the l9-second burn time with an 8-degree nozzle gimbal angle are shown. The results from this model will enable characterization of various aspects of the ASRM internal environment, and in particular will allow an assessment of the heat transfer and stresses exerted on the submerged nozzle, casing insulation, and nozzle case joint. Author

N95-23649*# Engineering Research and Consulting, Inc., Huntsville, AL.

APPLICATION OF CFD ANALYSIS TO DESIGN SUPPORT AND PROBLEM RESOLUTION FOR ASRM AND RSRM

Richard A. Dill and R. Harold Whitesides *In* NASA. Marshall Space Flight Center, Eleventh Workshop for Computational Fluid Dynamic Applications in Rocket Propulsion, Part 1 Jul. 1993 p 793-835 (For primary document see N95-23615 07-34)

Avail: CASI HC A03/MF A10

The use of Navier-Stokes CFD codes to predict the internal flow field environment in a solid rocket motor is a very important analysis element during the design phase of a motor development program. These computational flow field solutions uncover a variety of potential problems associated with motor performance as well as suggesting solutions to these problems. CFD codes have also proven to be of great benefit in explaining problems associated with operational motors such as in the case of the pressure spike problem with the STS-54B flight motor. This paper presents results from analyses involving both motor design support and problem resolution. The issues discussed include the fluid dynamic/mechanical stress coupling at field joints relative to significant propellant deformations, the prediction of axial and radial pressure gradients in the motor associated with motor performance and propellant mechanical loading, the prediction of transition of the internal flow in the motor associated with erosive burning, the accumulation of slag at the field joints and in the submerged nozzle region, impingement of flow on the nozzle nose, and pressure gradients in the nozzle region of the motor. The analyses presented in this paper have been performed using a two-dimensional axisymmetric model. Fluent/BFC, a three dimensional Navier-Stokes flow field code, has been used to make the numerical calculations. This code utilizes a staggered grid formulation along with the SIMPLER numerical pressure-velocity coupling algorithm. Wall functions are used to represent the character of the viscous sub-layer flow, and an adjusted k-epsilon turbulence model especially configured for mass injection internal flows, is used to model the growth of turbulence in the motor port. Conclusions discussed in this paper consider flow field effects on the forward, center, and aft propellant grains except for the head end star grain region of the forward propellant segment. The field joints and the submerged nozzle are discussed as well. Conclusions relative to both the design evaluation of the ASRM and the RSRM scenarios explaining the pressure spikes were based on the flow field solutions presented in this paper. Derived from text

N95-23650*# National Aeronautics and Space Administration. Marshall Space Flight Center, Huntsville, AL.

TIME-ACCURATE UNSTEADY FLOW SIMULATIONS SUPPORTING THE SRM T+68-SECOND PRESSURE SPIKE ANOMALY INVESTIGATION (STS-54B)

N. S. Dougherty (Rockwell International Corp., Huntsville, AL.), D. W. Burnette (Rockwell International Corp., Huntsville, AL.), J. B. Holt (Rockwell International Corp., Huntsville, AL.), and Jose Matienzo *In its* Eleventh Workshop for Computational Fluid Dynamic Applications in Rocket Propulsion, Part 1 Jul. 1993 p 837-863 (For primary document see N95-23615 07-34)

Avail: CASI HC A03/MF A10

Time-accurate unsteady flow simulations are being performed supporting the SRM T+68sec pressure 'spike' anomaly investigation. The anomaly occurred in the RH SRM during the STS-54 flight (STS-54B) but not in the LH SRM (STS-54A) causing a momentary thrust mismatch approaching the allowable limit at that time into the flight. Full-motor internal flow simulations using the USA-2D axisymmetric code are in progress for the nominal propellant burn-back geometry and flow conditions at T+68-sec--Pc = 630 psi, gamma = 1.1381, T(sub c) = 6200 R, perfect gas without aluminum particulate. In a cooperative effort with other investigation team members, CFD-derived pressure loading on the NBR and castable inhibitors was used iteratively to obtain nominal deformed geometry of each inhibitor, and the deformed (bent back) inhibitor geometry was entered into this model. Deformed geometry was computed using structural finite-element models. A solution for the unsteady flow has been obtained for the nominal flow conditions (existing prior to the occurrence of the anomaly) showing sustained standing pressure oscillations at nominally 14.5 Hz in the motor IL acoustic mode that flight and static test data confirm to be normally present at this time. Average mass flow discharged from the nozzle was confirmed to be the nominal expected (9550 lbm/sec). The local inlet boundary condition is being perturbed at the location of the presumed reconstructed anomaly as identified by interior ballistics performance specialist team members. A time variation in local mass flow is used to simulate sudden increase in burning area due to localized propellant grain cracks. The solution will proceed to develop a pressure rise (proportional to total mass flow rate change squared). The volume-filling time constant (equivalent to 0.5 Hz) comes into play in shaping the rise rate of the developing pressure 'spike' as it propagates at the speed of sound in both directions to the motor head end and nozzle. The objectives of the present analysis are to: (1) capture the dynamic responses of the motor combustion

gas flow to correlate with available low-frequency (less than 12.5 sample/sec) data and (2) observe the high-frequency (up to 50 Hz) characteristics of the response to determine any potentials for dynamic coupling. Author

N95-23651*# National Aeronautics and Space Administration. Marshall Space Flight Center, Huntsville, AL.

STATUS OF AXISYMMETRIC CFD OF AN ELEVEN INCH DIAMETER HYBRID ROCKET MOTOR

Joseph Ruf, Matthew R. Sullivan, and Ten See Wang *In its* Eleventh Workshop for Computational Fluid Dynamic Applications in Rocket Propulsion, Part 1 Jul. 1993 p 865-878 (For primary document see N95-23615 07-34)

Avail: CASI HC A03/MF A10

Current status of a steady state, axisymmetric analysis of an experimental 11 inch diameter hybrid rocket motor internal flow field is given. The objective of this effort is to develop a steady state axisymmetric model of the 11 inch hybrid rocket motor which can be used as a design and/or analytical tool. A test hardware description, modeling approach, and future plans are given. The analysis was performed with FDNS implementing several finite rate chemistry sets. A converged solution for a two equation and five species set on a 'fine' grid is shown. Author

N95-23652*# National Aeronautics and Space Administration. Marshall Space Flight Center, Huntsville, AL.

VALIDATION OF A COMPUTATIONAL FLUID DYNAMICS (CFD) CODE FOR SUPERSONIC AXISYMMETRIC BASE FLOW

P. Kevin Tucker *In its* Eleventh Workshop for Computational Fluid Dynamic Applications in Rocket Propulsion, Part 1 Jul. 1993 p 879-901 (For primary document see N95-23615 07-34)

Avail: CASI HC A03/MF A10

The ability to accurately and efficiently calculate the flow structure in the base region of bodies of revolution in supersonic flight is a significant step in CFD code validation for applications ranging from base heating for rockets to drag for protectives. The FDNS code is used to compute such a flow and the results are compared to benchmark quality experimental data. Flowfield calculations are presented for a cylindrical afterbody at M = 2.46 and angle of attack a = O. Grid independent solutions are compared to mean velocity profiles in the separated wake area and downstream of the reattachment point. Additionally, quantities such as turbulent kinetic energy and shear layer growth rates are compared to the data. Finally, the computed base pressures are compared to the measured values. An effort is made to elucidate the role of turbulence models in the flowfield predictions. The level of turbulent eddy viscosity, and its origin, are used to contrast the various turbulence models and compare the results to the experimental data. Author

N95-23653*# Rockwell International Corp., Canoga Park, CA. Rocketdyne Div.

CODE VALIDATION STUDY FOR BASE FLOWS

Edward P. Ascoli, Adel H. Heiba, Ronald R. Lagnado, Ronald J. Ungewitter, and Morgan Williams *In* NASA. Marshall Space Flight Center, Eleventh Workshop for Computational Fluid Dynamic Applications in Rocket Propulsion, Part 1 Jul. 1993 p 903-919 (For primary document see N95-23615 07-34)

Avail: CASI HC A03/MF A10

New and old rocket launch concepts recommend the clustering of motors for improved lift capability. The flowfield of the base region of the rocket is very complex and can contain high temperature plume gases. These hot gases can cause catastrophic problems if not adequately designed for. To assess the base region characteristics, advanced computational fluid dynamics (CFD) is being used. As a precursor to these calculations the CFD code requires validation on base flows. The primary objective of this code validation study was to establish a high level of confidence in predicting base flows with the USA CFD code. USA has been extensively validated for fundamental flows and other applications. However, base heating flows have a number of unique characteristics so it was necessary to extend the existing validation for this class of problems. In preparation for the planned NLS 1.5 Stage base heating analysis, six case sets were studied to extend the USA code validation data base. This presentation gives a cursive review of three of these cases. The cases presented include a 2D axi-symmetric study, a 3D real nozzle study, and a 3D multi-species study. The results of all the studies show good general agreement with data with no adjustments to the base numerical algorithms or physical models in the code. The study proved the capability of the USA code for modeling base flows within the accuracy of available data. Author

N95-23654*# Rockwell International Corp., Huntsville, AL. Space Systems Div.

FOUR-NOZZLE BENCHMARK WIND TUNNEL MODEL USA CODE SOLUTIONS FOR SIMULATION OF MULTIPLE ROCKET BASE FLOW RECIRCULATION AT 145,000 FEET ALTITUDE

N. S. Dougherty and S. L. Johnson *In* NASA. Marshall Space Flight Center, Eleventh Workshop for Computational Fluid Dynamic Applications in Rocket Propulsion, Part 1 Jul. 1993 p 921-940 (For primary document see N95-23615 07-34)

Avail: CASI HC A03/MF A10

Multiple rocket exhaust plume interactions at high altitudes can produce base flow recirculation with attendant alteration of the base pressure coefficient and increased base heating. A search for a good wind tunnel benchmark problem to check grid clustering technique and turbulence modeling turned up the experiment done at AEDC in 1961 by Goethert and Matz on a 4.25-in. diameter domed missile base model with four rocket nozzles. This wind tunnel model with varied external bleed air flow for the base flow wake produced measured p/p(sub ref) at the center of the base as high as 3.3 due to plume flow recirculation back onto the base. At that time in 1961, relatively inexpensive experimentation with air at gamma = 1.4 and nozzle A(sub e)/A of 10.6 and theta(sub n) = 7.55 deg with P(sub c) = 155 psia simulated a LO2/LH2 rocket exhaust plume with gamma = 1.20, A(sub e)/A of 78 and P(sub c) about 1,000 psia. An array of base pressure taps on the aft dome gave a clear measurement of the plume recirculation effects at p(infinity) = 4.76 psfa corresponding to 145,000 ft altitude. Our CFD computations of the flow field with direct comparison of computed-versus-measured base pressure distribution (across the dome) provide detailed information on velocities and particle traces as well eddy viscosity in the base and nozzle region. The solution was obtained using a six-zone mesh with 284,000 grid points for one quadrant taking advantage of symmetry. Results are compared using a zero-equation algebraic and a one-equation pointwise R(sub t) turbulence model (work in progress). Good agreement with the experimental pressure data was obtained with both; and this benchmark showed the importance of: (1) proper grid clustering and (2) proper choice of turbulence modeling for rocket plume problems/recirculation at high altitude. Author

N95-23655*# National Aeronautics and Space Administration. Marshall Space Flight Center, Huntsville, AL.

NUMERICAL STUDY OF BASE PRESSURE CHARACTERISTIC CURVE FOR A FOUR-ENGINE CLUSTERED NOZZLE CONFIGURATION **c20**

Ten-See Wang *In its* Eleventh Workshop for Computational Fluid Dynamic Applications in Rocket Propulsion, Part 1 Jul. 1993 p 941-961 (For primary document see N95-23615 07-34)

Avail: CASI HC A03/MF A10

Excessive base heating has been a problem for many launch vehicles. For certain designs such as the direct dump of turbine exhaust in the nozzle section and at the nozzle lip of the Space Transportation Systems Engine (STME), the potential burning of the turbine exhaust in the base region has caused tremendous concern. Two conventional approaches have been considered for predicting the base environment: (1) empirical approach, and (2) experimental approach. The empirical approach uses a combination of data correlations and semi-theoretical calculations. It works best for linear problems, simple physics and geometry. However, it is highly suspicious when complex geometry and flow physics are involved, especially when the subject is out of historical database. The experimental approach is often used to establish database for engineering analysis. However, it is qualitative at best for base flow problems. Other criticisms include the inability to simulate forebody boundary layer correctly, the interference effect from tunnel walls, and the inability to scale all pertinent parameters. Furthermore, there is a contention that the information extrapolated from subscale tests with combustion is not conservative. One potential alternative to the conventional methods is computational fluid dynamics (CFD), which has none of the above restrictions and is becoming more feasible due to maturing algorithms and advancing computer technology. It provides more details of the flowfield and is only limited by computer resources. However, it has its share of criticisms as a predictive tool for base environment.

One major concern is that CFD has not been extensively tested for base flow problems. It is therefore imperative that CFD be assessed and benchmarked satisfactorily for base flows. In this study, the turbulent base flowfield of a experimental investigation for a four-engine clustered nozzle is numerically benchmarked using a pressure based CFD method. Since the cold air was the medium, accurate prediction of the base pressure distributions at high altitudes is the primary goal. Other factors which may influence the numerical results such as the effects of grid density, turbulence model, differencing scheme, and boundary conditions are also being addressed. Preliminary results of the computed base pressure agreed reasonably well with that of the measurement. Basic base flow features such as the reverse jet, wall jet, recompression shock, and static pressure field in plane of impingement have been captured. Author

N95-24022*# Cleveland State Univ., OH. Dept. of Chemical Engineering.
FLOW DIAGNOSTICS, CHEMICALLY REACTING TURBULENT FLOW MODELING AND TURBULENT MIXING: A SUMMARY OF PROJECT STUDIES IN COMBUSTION
Bahman Ghorashi 1995 130 p
(Grant NAG3-1010)
(NASA-CR-197348; NAS 1.26:197348) Avail: CASI HC A07/MF A02

This report includes copies of relevant publications, including conference proceedings, resulting from studies funded by NAG3-1010. Topics include flow visualization, LDV (laser doppler velocimeter), straight and curved simulations, and kinetics modeling of nitrogen oxides, including a turbulent mixing model for O2 and a maximum mixedness model. CASI

N95-24051# National Aerospace Lab., Tokyo (Japan).
A COMPUTER MODEL IN GENERAL 3-D CURVILINEAR COORDINATES FOR THE PREDICTION OF THE TURBULENT FLOW FIELD IN A JET INDUCED RAM COMBUSTOR
Sanjiv Kumar Jun. 1994 19 p Sponsored by Science and Technology Agency of Japan
(ISSN 0389-4010)
(NAL-TR-1240T) Avail: CASI HC A03/MF A01

A three-dimensional computer code, in arbitrary coordinates, for the simulation of the isothermal flow pattern in a jet induced ram combustor is developed. The Navier-Stokes equation and the equations for a low Reynolds number k-epsilon model are solved using the Semi-Implicit Method for Pressure Linked Equations Revised (SIMPLER). The code is used to compute the steady state flow field in the combustor. Computed results showing the formation of vortices, velocity field and pressure distribution are presented. Author

N95-24082# National Aerospace Lab., Tokyo (Japan).
MONTE CARLO SIMULATION OF RAREFIED NITROGEN GASES CONTAINED BETWEEN PARALLEL PLATES USING THE STATISTICAL INELASTIC CROSS-SECTION MODEL
Katsuhisa Koura Mar. 1994 8 p
(ISSN 0389-4010)
(NAL-TR-1229T) Avail: CASI HC A02/MF A01

The statistical inelastic cross-section (SICS(D)) model for molecules with discrete rotational energy is used for the Monte Carlo simulation of rarefied nitrogen gases contained between two parallel plates at a large temperature difference with the null-collision direct-simulation Monte Carlo method to compare with the density distributions measured by Alofs et al. Good agreement is found between the experimental and Monte Carlo results for the fully diffuse reflection plates. The rotational distribution near the cold plate indicates the bimodal form represented approximately by the merging of two Boltzmann distributions at the cold and hot plate temperatures. Author

N95-23289*# Pennsylvania State Univ., University Park, PA. Dept. of Mechanical Engineering.
DIRECT NUMERICAL SIMULATIONS AND MODELING OF A SPATIALLY-EVOLVING TURBULENT WAKE Abstract Only
John M. Cimbala *In* Hampton Univ., 1994 NASA-HU American Society for Engineering Education (ASEE) Summer Faculty Fellowship Program Dec. 1994 p 70 (For primary document see N95-23276 07-99)
Avail: CASI HC A01/MF A02

N95-23296*# Tuskegee Inst., AL. Dept. of Aerospace Science Engineering.
DIRECT NUMERICAL SIMULATION OF SHEARED TURBULENT FLOW Abstract Only
Vascar G. Harris *In* Hampton Univ., 1994 NASA-HU American Society for Engineering Education (ASEE) Summer Faculty Fellowship Program Dec. 1994 p 78 (For primary document see N95-23276 07-99)
Avail: CASI HC A01/MF A02

N95-23307*# Old Dominion Coll., Norfolk, VA. Dept. of Electrical and Computer Engineering.
ACCELERATED PANEL METHODS USING THE FAST MULTIPOLE METHOD Abstract Only
James F. Leathrum, Jr. *In* Hampton Univ., 1994 NASA-HU American Society for Engineering Education (ASEE) Summer Faculty Fellowship Program Dec. 1994 p 89 (For primary document see N95-23276 07-99)
Avail: CASI HC A01/MF A02

35 INSTRUMENTATION AND PHOTOGRAPHY

Includes remote sensors; measuring instruments and gages; detectors; cameras and photographic supplies; and holography.

For aerial photography see *43 Earth Resources and Remote Sensing*. For related information see also *06 Aircraft Instrumentation*, and *19 Spacecraft Instrumentation*.

N95-22536# Technische Univ., Eindhoven (Netherlands).
PRECISE CLOCK SYNCHRONIZATION PROTOCOL
E. J. Luit and J. M. M. Martin Dec. 1993 44 p
(PB95-127247) Avail: CASI HC A03/MF A01

A distributed clock synchronization protocol is presented which achieves a very high precision without the need for very frequent resynchronizations. The protocol tolerates failures of the clocks: clocks may be too slow or too fast, exhibit omission failures and report inconsistent values. Synchronization takes place in synchronization rounds as in many other synchronization protocols. At the end of each round, clock times are exchanged between the clocks. Each clock applies a convergence function (CF) to the values obtained. This function estimates the difference between its clock and an average clock and corrects its clock accordingly. Clocks are corrected for drift relative to this average clock during the next synchronization round. The protocol is based on the assumption that clock reading errors are small with respect to the required precision of synchronization. It is shown that the CF resynchronizes the clocks with high precision even when relatively large clock drifts are possible. It is also shown that the drift-corrected clocks remain synchronized until the end of the next synchronization round. The stability of the protocol is proven. NTIS

N95-22682# SRI International Corp., Menlo Park, CA.
NOVEL MASS SPECTROMETRIC INSTRUMENT FOR GASEOUS AND PARTICULATE CHARACTERIZATION AND MONITORING
M. J. Coggiola Jul. 1994 23 p
(Contract DE-AC21-92MC-29116)
(DE95-001135; DOE/MC-29116/3913) Avail: CASI HC A03/MF A01

Purpose of the instrument is for real-time (less than 1 min), ppB analysis of gaseous/particulate pollutants (VOC's, PAH's, heavy metals, transuranics) from DOE waste cleanup. It will consist of an isokinetic sampler, a pressure transition and sampling region for parallel analyses, two small mass spectrometers (one for organic analysis using field ionization, one 'ion trap' for particulates using pyrolysis and electron-impact ionization), and a personal computer. A dimethylsilicone membrane will be used for the organic vapors. A forward-backward coincidence method will be used in the laser scattering particle detector. The instrument will be easily transportable to DOE waste sites, such as waste storage tanks. DOE

N95-22706 Department of the Navy, Washington, DC.
CORROSIVITY SENSOR Patent
Vinoid S. Agarwala, inventor (to Navy) and Fred Pearlstein, inventor (to Navy) 16 Aug. 1994 7 p Filed 30 Jun. 1993 Supersedes

AD-D016207
(AD-D016549; US-Patent-5,338,432; US-Patent-Appl-SN-087237;
US-Patent-Class-205-118) Avail: US Patent and Trademark Office

A lightweight corrosivity sensor is provided which is thin enough to be embedded between the layers of a composite structure or placed on a surface beneath a coating. It comprises a thin non-conductive base and two electrically isolated conductive elements fixed to the surface thereof. Each conductive element comprises a bus bar and a plurality of strips extending from the bus bar and interdigitated with the strips of the other conductive element. The corrosivity sensor is connectable to a current measuring means for measuring the current across the two conductive elements as an indicator of the presence of a corrosive environment. A masking method of manufacturing such a sensor is also provided. DTIC

N95-23012*# National Aeronautics and Space Administration. Langley Research Center, Hampton, VA.
SUMMARY OF OARE FLIGHT CALIBRATION MEASUREMENTS
Robert C. Blanchard and John Y. Nicholson (Vigyan Research Associates, Inc., Hampton, VA.) Jan. 1995 64 p
(RTOP 242-80-01-01)
(NASA-TM-109159; NAS 1.15:109159) Avail: CASI HC A04/MF A01

To date, the Orbital Acceleration Research Experiment (OARE) has flown on the shuttle orbiter for five missions; namely, STS-40, STS-50, STS-58, STS-62, and STS-65. The OARE instrument system contains a three-axis accelerometer which can resolve accelerations to the nano-g (10(exp -9) g) level and a full calibration station to permit in situ bias and scale factor calibration measurements. This calibration capability eliminates the large uncertainty encountered with accelerometers flown in the past on the orbiter which use ground-based calibrations to provide absolute acceleration measurements. A detailed flight data report presentation is given for the OARE calibration measurements from all missions, along with an estimate of the calibration errors. The main aim is to collect, process, and present the calibration data in one archival report. These calibration data are the necessary key ingredient to produce the absolute acceleration levels from the OARE acceleration flight data. Author

N95-23087*# Lockheed Missiles and Space Co., Palo Alto, CA. Space Science Lab.
TIMED IMAGING PHOTOMETER EXPERIMENT (TIPE) Final Reoprt, 31 Dec. 1994
Stephen B. Mende, D. C. Fritts (Colorado Univ., Boulder, CO.), James H. Hecht (Aerospace Corp., Los Angeles, CA.), T. L. Killeen (Michigan Univ., Ann Arbor, MI.), Edward J. Llewellyn (Saskatchewan Univ., Saskatoon, Saskatchewan, Canada.), Robert P. Lowe (University of Western Ontario, London, Ontario.), Ian C. McDade (Saskatchewan Univ., Saskatoon, Saskatchewan, Canada.), Martin N. Ross (Aerospace Corp., Los Angeles, CA.), Gary R. Swenson, and David N. Turnbull (University of Western Ontario, London, Ontario.) et al 31 Dec. 1994 10 p
(Contract NAS5-32573)
(NASA-CR-197431; NAS 1.26:197431) Avail: CASI HC A02/MF A01

This document contains a summary of the TIMED Imaging Photometer Experiment (TIPE) instrument study at the time of the termination of project due to TIPE being de-selected from the Thermosphere, Ionosphere and Mesosphere Energetics and Dynamics (TIMED) mission. Author

N95-23263* National Aeronautics and Space Administration. Ames Research Center, Moffett Field, CA.
METHOD AND APPARATUS FOR MEASURING THE STRAIN DEVELOPED IN A COATED SURFACE Patent
Sheldon M. Smith, inventor (to NASA) and Clement C. Hiel, inventor (to NASA) 6 Apr. 1993 5 p Filed 21 Oct. 1991
(NASA-Case-ARC-11938-1-C; US-Patent-5,199,305;
US-Patent-Appl-SN-779672; US-Patent-Class-73-851;
US-Patent-Class-73-150A; US-Patent-Class-73-827;
Int-Patent-Class-G01N-3/20) Avail: US Patent and Trademark Office

A method and apparatus are provided for determining the strain developed in a coated surface. A beam with a coating on a surface thereof is mounted as a cantilever and a force is applied to the free end of the beam to cause deflection of the beam until the coating on the beam fails. The strain in the beam, and hence in the coating at the point of failure, is determined based on the dimensions of the beam, the point along the beam where failure of the coating occurs and the amount of deflection of the beam, and this determination is made independently of the temperature of the beam and the material from which the beam is made. The determination is made based on the equation E= 1.5hdx/l(exp 3), where E is strain, h is the beam thickness, d is the beam deflection, x is the distance from the free end of the beam to the point where failure of the coating occurred, and l is the length of the beam.
Official Gazette of the U.S. Patent and Trademark Office

N95-23377* National Aeronautics and Space Administration. Ames Research Center, Moffett Field, CA.
SYSTEM FOR DETERMINING AERODYNAMIC IMBALANCE Patent
Gary B. Churchill, inventor (to NASA) and Benny K. Cheung, inventor (to NASA) 4 Oct. 1994 7 p Filed 7 Aug. 1992
(NASA-Case-ARC-11913-1; US-Patent-5,352,090;
US-Patent-Appl-SN-926117; US-Patent-Class-416-61;
US-Patent-Class-416-34; Int-Patent-Class-B64C-11/00) Avail: US Patent and Trademark Office

A system is provided for determining tracking error in a propeller or rotor driven aircraft by determining differences in the aerodynamic loading on the propeller or rotor blades of the aircraft. The system includes a microphone disposed relative to the blades during the rotation thereof so as to receive separate pressure pulses produced by each of the blades during the passage thereof by the microphone. A low pass filter filters the output signal produced by the microphone, the low pass filter having an upper cut-off frequency set below the frequency at which the blades pass by the microphone. A sensor produces an output signal after each complete revolution of the blades, and a recording display device displays the outputs of the low pass filter and sensor so as to enable evaluation of the relative magnitudes of the pressure pulses produced by passage of the blades by the microphone during each complete revolution of the blades.
Official Gazette of the U.S. Patent and Trademark Office

N95-23461*# National Aeronautics and Space Administration. Lewis Research Center, Cleveland, OH.
INSTANTANEOUS 2D VELOCITY AND TEMPERATURE MEASUREMENTS IN HIGH SPEED FLOWS BASED ON SPECTRALLY RESOLVED MOLECULAR RAYLEIGH SCATTERING
Richard G. Seasholtz Mar. 1995 11 p Presented at the 33rd Aerospace Sciences Meeting and Exhibit, Reno, NV, 9-12 Jan. 1995; sponsored by AIAA
(RTOP 505-62-50)
(NASA-TM-106883; E-9481; NAS 1.15:106883; AIAA Paper 95-0300)
Avail: CASI HC A03/MF A01

A Rayleigh scattering diagnostic for high speed flows is described for the simultaneous, instantaneous measurement of gas temperature and velocity at a number (up to about one hundred) of locations in a plane illuminated by an injection-seeded, frequency doubled Nd:YAG laser. Molecular Rayleigh scattered light is collected and passed through a planar mirror Fabry-Perot interferometer. The resulting image is analyzed to determine the gas temperature and bulk velocity at each of the regions. The Cramer Rao lower bound for measurement uncertainty is calculated. Experimental data is presented for a free jet and for preliminary measurements in the Lewis 4 inch by 10 inch supersonic wind tunnel.
Author

N95-23492# Argonne National Lab., IL.
THERMAL EFFECTS ON THE STAR ELECTROMAGNETIC CALORIMETER
T. Fornek, V. Guarino, H. Spinka, and D. Underwood 19 Jul. 1994 38 p
(Contract W-31-109-eng-38)
(DE95-004663; ANL-HEP-TR-94-42) Avail: CASI HC A03/MF A01

The STAR detector for the RHIC colliding beam accelerator is under construction at Brookhaven National Laboratory. This detector will consist of a number of subsystems. These include a silicon vertex detector (SVT) for charged particle tracks near the interaction region, a time projection chamber (TPC) for charged particle tracking, an array of plastic scintillation counters (CTB) in a layer around the TPC for triggering on charged particles, a conventional solenoidal magnet, and some additional small triggering detectors along the beam-line. An electromagnetic calorimeter (EMC) is an upgrade to the 'baseline' detector configuration above. The conventional magnet and numerous electronic channels for the SVT and TPC subsystems

will generate a considerable amount of heat during the operation of STAR. However, it is possible that a chiller for the magnet cooling water will not be available during some of the early STAR runs. As a result, the average magnet temperature may vary considerably between winter and summer. This note summarizes calculations and measurements performed to evaluate the effects of an elevated magnet temperature on the performance of the electromagnetic calorimeter. DOE

N95-23520# Fermi National Accelerator Lab., Batavia, IL.
MECHANICAL DESIGN OF THE CDF SVX 2 SILICON VERTEX DETECTOR
J. E. Skarha (Johns Hopkins Univ., Baltimore, MD.) Aug. 1994 6 p Presented at the Meeting of the Division of Particles and Fields of the American Physical Society, Albuquerque, NM, 2-6 Aug. 1994
(Contract DE-AC02-76CH-03000)
(DE94-018985; FNAL/C-94/242-E; CONF-940816-11) Avail: CASI HC A02/MF A01

A next generation silicon vertex detector is planned at CDF for the 1998 Tevatron collider run with the Main Injector. The SVX 2 silicon vertex detector will allow high luminosity data-taking, enable online triggering of secondary vertex production, and greatly increase the acceptance for heavy flavor physics at CDF. The design specifications, geometric layout, and early mechanical prototyping work for this detector are discussed. DOE

N95-23521# Fermi National Accelerator Lab., Batavia, IL.
SVX(PRIME), THE NEW CDF SILICON VERTEX DETECTOR
S. Cihangir, G. Gillespie, and H. Gonzalez et al 26 Aug. 1994 12 p Presented at the 6th Pisa Meeting on Advanced Detectors, Elba, Italy, 22-28 May 1994
(Contract DE-AC02-76CH-03000)
(DE94-018986; FNAL/C-94/205-E; CONF-9405168-6) Avail: CASI HC A03/MF A01

The Collider Detector at Fermilab (CDF) radiation hardened silicon vertex detector (SVX') is described. The new detector has several improvements over its predecessor, such as better signal to noise and higher efficiency. It's expected to have a radiation tolerance in excess of 1 Mrad. It has been taking data for several months and some preliminary results are shown. DOE

N95-23583# Argonne National Lab., IL.
THE STAR EM CALORIMETER DESIGN AND SMALL PROTOTYPE TEST RESULTS
D. G. Underwood 1995 7 p Presented at the 5th International Conference on Calorimetry in High Energy Physics, Upton, NY, 25 Sep. - 1 Oct. 1994
(Contract W-31-109-eng-38)
(DE95-004592; ANL-HEP-CP-94-78; CONF-9409268-3) Avail: CASI HC A02/MF A01

The basis for several design features of The STAR Electromagnetic Calorimeter and Shower Maximum Detector is presented. This includes some of the tile-fiber optical design. The authors describe both the barrel and the end cap. Some preliminary analysis of electron acceptance vs pion rejection in test beam data is also discussed. DOE

N95-23789*# Dimension Technologies, Inc., Rochester, NY.
FULL RESOLUTION HOLOGRAM-LIKE AUTOSTEREOSCOPIC DISPLAY Final
Jesse B. Eichenlaub and Jamie Hutchins Mar. 1995 39 p
(Contract NAS2-13642)
(NASA-CR-197913; NAS 1.26:197913; DTI/FR-95/2014) Avail: CASI HC A03/MF A01

Under this program, Dimension Technologies Inc. (DTI) developed a prototype display that uses a proprietary illumination technique to create autostereoscopic hologram-like full resolution images on an LCD operating at 180 fps. The resulting 3D image possesses a resolution equal to that of the LCD along with properties normally associated with holograms, including change of perspective with observer position and lack of viewing position restrictions. Furthermore, this autostereoscopic technique eliminates the need to wear special glasses to achieve the parallax effect. Under the program a prototype display was developed which demonstrates the hologram-like full resolution concept. To implement such a system, DTI explored various concept designs and enabling technologies required to support those designs. Specifically required were: a parallax illumination system with sufficient brightness and control; an LCD with rapid address and pixel response; and an interface to an image generation system for creation of computer graphics. Of the possible parallax illumination system designs, we chose a design which utilizes an array of fluorescent lamps. This system creates six sets of illumination areas to be imaged behind an LCD. This controlled illumination array is interfaced to a lenticular lens assembly which images the light segments into thin vertical light lines to achieve the parallax effect. This light line formation is the foundation of DTI's autostereoscopic technique. The David Sarnoff Research Center (Sarnoff) was subcontracted to develop an LCD that would operate with a fast scan rate and pixel response. Sarnoff chose a surface mode cell technique and produced the world's first large area pi-cell active matrix TFT LCD. The device provided adequate performance to evaluate five different perspective stereo viewing zones. A Silicon Graphics' Iris Indigo system was used for image generation which allowed for static and dynamic multiple perspective image rendering. During the development of the prototype display, we identified many critical issues associated with implementing such a technology. Testing and evaluation enabled us to prove that this illumination technique provides autostereoscopic 3D multi perspective images with a wide range of view, smooth transition, and flickerless operation given suitable enabling technologies. Author

N95-23795*# United Technologies Corp., East Hartford, CT.
DEVELOPMENT OF SENSORS FOR CERAMIC COMPONENTS IN ADVANCED PROPULSION SYSTEMS Final Report
William H. Atkinson, M. A. Cyr, and R. R. Strange Oct. 1994 43 p
(Contract NAS3-25141; RTOP 505-62-50)
(NASA-CR-195324; E-8773; NAS 1.26:195324; PWA-6113-73) Avail: CASI HC A03/MF A01

The 'Development of Sensors for Ceramics Components in Advanced Propulsion Systems' program was divided into two phases. The objectives of Phase 1 were to analyze, evaluate and recommend sensor concepts for the measurement of surface temperature, strain and heat flux on ceramic components for advanced propulsion systems. The results of this effort were previously published in NASA CR-182111. As a result of Phase 1, three approaches were recommended for further development: pyrometry, thin-film sensors, and thermographic phosphors. The objectives of Phase 2 were to fabricate and conduct laboratory demonstration tests of these systems. A summary report of the Phase 2 effort, together with conclusions and recommendations for each of the categories evaluated, has been submitted to NASA. Emittance tests were performed on six materials furnished by NASA Lewis Research Center. Measurements were made of various surfaces at high temperature using a Thermogage emissometer. This report describes the emittance test program and presents a summary of the results. Author

N95-24069# Los Alamos National Lab., NM.
COLOR ORTHOPHOTOGRAPHY: TO SCAN OR NOT
J. L. Benson 1994 8 p Presented at the 1994 ASPRS/ACSM Technical Program, Bethesda, MD, 2 Mar. 1995
(Contract W-7405-eng-36)
(DE95-002749; LA-UR-94-3653; CONF-950364-1) Avail: CASI HC A02/MF A01

A picture is worth a thousand words, which explains why digital orthophotographs have become such a popular item. Today, most procurement of orthophotographs result in a digital product. However, if one already has hard copy orthophotography, should one scan them, or have them produced as true digital orthophotographs? What are the advantages and disadvantages of each methodology? This paper examines the procedure the Facility for Information Management, Analysis, and Display (FIMAD) at Los Alamos National Laboratory (LANL) uses to determine the appropriate product based on our needs. The scanned product is compared to a digitally produced orthophotograph, procured through a vendor. Comparison is performed on the screen, on hard copy output, and by spectral analysis in the red, green and blue bands. Full screen sized images look fairly good, but when enlarged, the scanned image appeared blocky and fuzzy. Hard copy output from the electrostatic plotter produces colors similar to the screen for the demo image, but renders poor color matching with the scanned image. Histograms of each band of the scanned image show a high count at the low end of the curve. These findings

confirm that the images are different, and that the differences are not just in the eyes of the beholder. It was concluded true digital orthophotographs are needed. DOE

N95-24107# Japan Broadcasting Corp., Tokyo (Japan). Image Devices Research Div.
AMPLIFIED MOS IMAGER
Fumihiko Andoh, Junichi Yamazaki, Masayuki Sugawara, and Yoshihiro Fujita Jan. 1995 9 p
(ISSN 0027-657X)
(NHK-Labs-Note-432) Avail: CASI HC A02/MF A01

We have developed a new Amplified MOS Imager (AMI) equipped with three horizontally aligned output lines for use in high-speed TV cameras. A TV camera using the AMI can take images 6 times as quickly as ordinary cameras. We have also developed a modified AMI with a photoconductive amorphous selenium surface. Four point two times the signal value can be obtained in blue light. Author

N95-23287*# Illinois Univ., Chicago, IL.
HOLOGRAPHIC INTERFEROMETRIC TOMOGRAPHY FOR RECONSTRUCTING FLOW FIELDS Abstract Only
Soyoung S. Cha *In* Hampton Univ., 1994 NASA-HU American Society for Engineering Education (ASEE) Summer Faculty Fellowship Program Dec. 1994 p 68 (For primary document see N95-23276 07-99)
Avail: CASI HC A01/MF A02

N95-23290*# Rochester Univ., NY. Dept. of Imaging and Photographic Technology.
SCIENTIFIC AND TECHNICAL PHOTOGRAPHY AT NASA LANGLEY RESEARCH CENTER Abstract Only
Andrew Davidhazy *In* Hampton Univ., 1994 NASA-HU American Society for Engineering Education (ASEE) Summer Faculty Fellowship Program (SEE N95-23276 07-99) Dec. 1994 (For primary document see N95-23276 07-99)
Avail: CASI HC A01/MF A02

N95-23298*# Rochester Univ., NY.
ELECTRONIC PHOTOGRAPHY AT NASA LANGLEY RESEARCH CENTER Abstract Only
Jack M. Holm *In* Hampton Univ., 1994 NASA-HU American Society for Engineering Education (ASEE) Summer Faculty Fellowship Program Dec. 1994 p 80 (For primary document see N95-23276 07-99)
Avail: CASI HC A01/MF A02

N95-23674*# National Space Development Agency, Tsukuba (Japan).
A NEW CONTAINERLESS IMAGE FURNACE WITH ELECTRO-STATIC POSITIONING DEVICE
Toshihiko Yamawaki, Chihiro Tsukishima (Mitsubishi Electric Corp., Amagasaki, Japan.), Toshio Abe (Mitsubishi Electric Corp., Kamakura, Japan.), and Atsuko Kaneko (Mitsubishi Electric Corp., Kamakura, Japan.) *In* JPL, Third International Symposium on Artificial Intelligence, Robotics, and Automation for Space 1994 Oct. 1994 p 15-18 (For primary document see N95-23672 07-63)
Avail: CASI HC A01/MF A03

N95-23852*# Jet Propulsion Lab., California Inst. of Tech., Pasadena, CA.
AIRBORNE VISIBLE/INFRARED IMAGING SPECTROMETER (AVIRIS): RECENT IMPROVEMENTS TO THE SENSOR
Thomas G. Chrien, Robert O. Green, Charles M. Sarture, Christopher Chovit, Michael L. Eastwood, and Bjorn T. Eng *In its* Summaries of the 4th Annual JPL Airborne Geoscience Workshop. Volume 1: AVIRIS Workshop 25 Oct. 1993 p 27-30 (For primary document see N95-23844 07-42)
Avail: CASI HC A01/MF A03

N95-23862*# Jet Propulsion Lab., California Inst. of Tech., Pasadena, CA.
INFLIGHT CALIBRATION OF AVIRIS IN 1992 AND 1993
Robert O. Green, James E. Conel, Mark Helmlinger, Jeannette vandenBosch, Chris Chovit, and Tom Chrien *In its* Summaries of the 4th Annual JPL Airborne Geoscience Workshop. Volume 1: AVIRIS Workshop 25 Oct. 1993 p 69-72 (For primary document see N95-23844 07-42)
Avail: CASI HC A01/MF A03

N95-24118*# Massachusetts Inst. of Tech., Westford, MA. Haystack Observatory.
HIGH DATA RATE RECORDER DEVELOPMENT AT MIT HAYSTACK OBSERVATORY
H. F. Hinteregger *In* NASA. Goddard Space Flight Center, Fourth NASA Goddard Conference on Mass Storage Systems and Technologies Mar. 1994 p 115-121 (For primary document see N95-24108 07-82)
Avail: CASI HC A02/MF A04

N95-24122*# Run Length Ltd., Burghfield (England).
A COMPARISON OF ROTARY- AND STATIONARY-HEAD TAPE RECORDERS
John R. Watkinson *In* NASA. Goddard Space Flight Center, Fourth NASA Goddard Conference on Mass Storage Systems and Technologies Mar. 1994 p 177-183 (For primary document see N95-24108 07-82)
Avail: CASI HC A02/MF A04

N95-24127*# International Business Machines Corp., Tucson, AZ.
INFLUENCE OF TECHNOLOGY ON MAGNETIC TAPE STORAGE DEVICE CHARACTERISTICS
John J. Gniewek and Stephen M. Vogel *In* NASA. Goddard Space Flight Center, Fourth NASA Goddard Conference on Mass Storage Systems and Technologies Mar. 1994 p 237-251 (For primary document see N95-24108 07-82)
Avail: CASI HC A03/MF A04

N95-24128*# Carnegie-Mellon Univ., Pittsburgh, PA. Engineering Research Center and Data Storage Systems.
APPROACHES TO 100 Gbit/SQ. IN. RECORDING DENSITY
Mark H. Kryder *In* NASA. Goddard Space Flight Center, Fourth NASA Goddard Conference on Mass Storage Systems and Technologies Mar. 1994 p 253-254 (For primary document see N95-24108 07-82)
Avail: CASI HC A01/MF A04

N95-24129*# Carnegie-Mellon Univ., Pittsburgh, PA. Dept. of Chemical Engineering.
REPRODUCIBLE DIRECT EXPOSURE ENVIRONMENTAL TESTING OF METAL-BASED MAGNETIC MEDIA
Paul J. Sides *In* NASA. Goddard Space Flight Center, Fourth NASA Goddard Conference on Mass Storage Systems and Technologies Mar. 1994 p 255-264 (For primary document see N95-24108 07-82)
Avail: CASI HC A02/MF A04

N95-24139*# Interferometrics, Inc., Vienna, VA.
A TERABYTE LINEAR TAPE RECORDER
John C. Webber *In* NASA. Goddard Space Flight Center, Fourth NASA Goddard Conference on Mass Storage Systems and Technologies Mar. 1994 p 393-397 (For primary document see N95-24108 07-82)
Avail: CASI HC A01/MF A04

36 LASERS AND MASERS

Includes parametric amplifiers.
For related information see also *76 Solid-State Physics.*

N95-22595# Lawrence Livermore National Lab., Livermore, CA.
PRODUCTION OF HIGH CONTRAST ULTRASHORT LASER PULSES FOR SHORT SCALE LENGTH PLASMA EXPERIMENTS
W. E. White, A. Sullivan, D. F. Price, R. Trebino (Sandia National Labs., Albuquerque, NM.), K. DeLong (Sandia National Labs., Albuquerque, NM.), and J. Heritage (California Univ., Davis, CA.) Jul. 1994 5 p *Presented* at the Optical Society of America Conference on High Field Interactions, Saint Malo, France, 21-25 Aug. 1994
(Contract W-7405-eng-48)
(DE95-003640; UCRL-JC-117858; CONF-9408121-3) Avail: CASI HC A01/MF A01

The production of hot, high energy plasmas has been one of the many proposed uses of high intensity ultrashort pulse laser systems since their

development began with the introduction of chirped pulse amplification (CPA). A design for a stretcher is presented that provides continuous, independent adjustment of the second, third, and fourth order frequency dependent phase. The design is based on the now standard single grating, single lens stretcher with the lens replaced by an air spaced doublet lens. Experimental and numerical results indicate that high fidelity transform limited pulses can be produced by this CPA system. It should be noted that while the results demonstrate the effectiveness of this stretcher design in producing high fidelity 100 fs pulses, the stretcher can easily be extended to shorter pulses. DOE

N95-22670*# National Aeronautics and Space Administration. Lewis Research Center, Cleveland, OH.

GROUND-BASED AND SPACE-BASED LASER BEAM POWER APPLICATIONS

John M. Bozek Feb. 1995 12 p

(RTOP 233-01-05)

(NASA-TM-106744; E-9156; NAS 1.15:106744) Avail: CASI HC A03/MF A01

A space power system based on laser beam power is sized to reduce mass, increase operational capabilities, and reduce complexity. The advantages of laser systems over solar-based systems are compared as a function of application. Power produced from the conversion of a laser beam that has been generated on the Earth's surface and beamed into cislunar space resulted in decreased round-trip time for Earth satellite electric propulsion tugs and a substantial landed mass savings for a lunar surface mission. The mass of a space-based laser system (generator in space and receiver near user) that beams down to an extraterrestrial airplane, orbiting spacecraft, surface outpost, or rover is calculated and compared to a solar system. In general, the advantage of low mass for these space-based laser systems is limited to high solar eclipse time missions at distances inside Jupiter. The power system mass is less in a continuously moving Mars rover or surface outpost using space-based laser technology than in a comparable solar-based power system, but only during dust storm conditions. Even at large distances for the Sun, the user-site portion of a space-based laser power system (e.g., the laser receiver component) is substantially less massive than a solar-based system with requisite on-board electrochemical energy storage. Author

N95-22704# Stanford Linear Accelerator Center, CA.

ELECTRON BEAM ACCELERATION AND COMPRESSION FOR SHORT WAVELENGTH FELs

T. O. Raubenheimer Nov. 1994 6 p Presented at the 16th International Free Electron Laser Conference, Stanford, CA, 21-26 Aug. 1994

(Contract DE-AC03-76SF-00515)

(DE95-003371; SU-SLAC-PUB-6709; CONF-9408146-13) Avail: CASI HC A02/MF A01

A single pass UV or x-ray free electron laser (FEL) will require a low emittance electron beam with high peak current and relatively high beam energy, a few hundred MeV to many GeV. To achieve the necessary peak current and beam energy, the beams must be bunch compressed and they must be accelerated in long transport lines where dispersive and wakefield emittance dilutions are important. We describe the sources and significance of the dilutions during acceleration, bunch compression, and transport through the undulator. In addition, we discuss sources of jitter, especially effects arising from the bunch compressions, and the possible cancellation techniques. DOE

N95-22748# Louisiana State Univ., Baton Rouge, LA.

OPTOGALVANIC MONITORING OF COLLISIONAL TRANSFER OF LASER EXCITATION ENERGY IN A NEON RF PLASMA

Thomas D. Armstrong 12 Aug. 1994 17 p

(Contract DE-FG05-87ER-60503)

(DE95-003103; DOE/ER-60503/367) Avail: CASI HC A03/MF A01

The optogalvanic signals produced by pulsed laser excitation of 1s5-2p8 and 1s5-2p9 (Paschen notation) transition by an approximately 29 MHz radiofrequency (rf) discharge at approximately 5 torr have been investigated. The optogalvanic signal produced by 1s5-2p9 excitations indicates that there is transfer of energy from the 2p9 state to some other state. The state to which this energy is transferred is believed to be mainly the 2p8 state because of the very small energy gap between the 2p9 and 2p8 states. To verify this transfer, the 1s5-2p8 transition was investigated. The similarity of the temporal profiles of the optogalvanic signals in both excitations confirms the collisional transfer of laser excitation energy from 2p9 to 2p8. DOE

N95-22937# Ohio Wesleyan Univ., Delaware, DE. Vision Lab.

LASER IRRADIATION EFFECTS: A FUNCTIONAL ASSESSMENT

Technical Midterm Report, 30 Sep. 1992 - 31 Jul. 1994

David O. Robbins Aug. 1994 27 p

(Contract DAMD17-92-C-2096)

(AD-A285100) Avail: CASI HC A03/MF A01

Specification of damage criteria and establishment of morphological data resulting from laser exposure has been an important mission for biomedical researchers and strategic planners. Equally important, however, from a military standpoint is the impact that this alteration, whether temporary or permanent, has on the ability of a soldier to complete a visually guided mission. Furthermore, while permanent visual loss associated with distinct morphological damage is of course serious it must also be recognized that temporary shifts in visual acuity or contrast sensitivity can occur at energy densities below those associated with distinct tissue damage. These temporary visual performance shifts could themselves be life threatening and may be the result of reversible or minute physical changes that are undetectable using current damage criteria. Our result suggests that significant shifts in visual sensitivity does occur at or below the ED50 level and that these shifts can be long lasting. Using a behavioral technique to measure on-going visual acuity, we have exposed awake, task-oriented rhesus monkeys to a variety of laser exposures which vary in energy density and temporal and spatial distribution on the retina. Our preliminary results in this project are consistent with the results of our previous studies and have extended the various exposure and performance criteria already established. DTIC

N95-23118# Technical Univ. of Lisbon (Portugal).

7TH INTERNATIONAL SYMPOSIUM ON APPLICATIONS OF LASER TECHNIQUES TO FLUID MECHANICS, VOLUME 1

14 Jul. 1994 512 p Symposium held in Lisbon, Portugal, 11-14 Jul. 1994

(Contract N68171-94-M-6048)

(AD-A285647; R/D-7414-AN-02-Vol-1) Avail: CASI HC A22/MF A04

The proceedings volumes 1 and 2 comprise the papers that were accepted for presentation at the Seventh International Symposium on Applications of Laser Techniques to Fluid Mechanics held at The Calouste Gulbenkian Foundation in Lisbon, during the period of July 11 to 14, 1994. The prime objective of this Seventh Symposium is to provide a forum for the presentation of the most advanced research on laser techniques for flow measurements, and reveal significant results to fluid mechanics. The applications of laser techniques to scientific and engineering fluid flow research is emphasized, but contributions to the theory and practice of laser methods are also considered where they facilitate new improved fluid mechanics research. Attention is focused on laser-Doppler anemometry, particle sizing and other methods for the measurement of velocity and scalars such as particle image velocimetry and laser induced fluorescence. DTIC

N95-23411*# National Aeronautics and Space Administration. Langley Research Center, Hampton, VA.

REDUCED DIMER PRODUCTION IN SOLAR-SIMULATOR-PUMPED CONTINUOUS WAVE IODINE LASERS BASED ON MODEL SIMULATIONS AND SCALING AND PUMPING STUDIES

Robert C. Costen, John H. Heinbockel (Old Dominion Univ., Norfolk, VA.), Gilda A. Miner, Willard E. Meador, Jr., Bagher M. Tabibi (Hampton Univ., VA.), Ja H. Lee, and Michael D. Williams Mar. 1995 69 p

(RTOP 232-01-04-04)

(NASA-TP-3486; L-17391; NAS 1.60:3486) Avail: CASI HC A04/MF A01

A numerical rate equation model for a continuous wave iodine laser with longitudinally flowing gaseous lasant is validated by approximating two experiments that compare the perfluoroalkyl iodine lasants n-C3F7I and t-C4F9I. The salient feature of the simulations is that the production rate of the dimer (C4F9)2 is reduced by one order of magnitude relative to the dimer (C3F7)2. The model is then used to investigate the kinetic effects of this reduced dimer production, especially how it improves output power. Related parametric and scaling studies are also presented. When dimer

production is reduced, more monomer radicals (t-C4F9) are available to combine with iodine ions, thus enhancing depletion of the laser lower level and reducing buildup of the principal quencher, molecular iodine. Fewer iodine molecules result in fewer downward transitions from quenching and more transitions from stimulated emission of lasing photons. Enhanced depletion of the lower level reduces the absorption of lasing photons. The combined result is more lasing photons and proportionally increased output power. Author

N95-23487# California Univ., Berkeley. Lawrence Berkeley Lab, CA.
UNDULATORS FOR SHORT WAVELENGTH FEL AMPLIFIERS
R. Schlueter Aug. 1994 10 p Presented at the 16th International Free Electron Laser Conference, Stanford, CA, 21-26 Aug. 1994
(Contract DE-AC03-76SF-00098)
(DE95-004690; LBL-36055; CONF-9408146-14) Avail: CASI HC A02/MF A01

Issues critical to the design of undulators for use in short wavelength FEL amplifiers, such as attainable on-axis field strength, device compactness, field quality, required magnetic gap, and strong focusing schemes, are discussed. The relative strength of various undulator technologies, including pure permanent magnet, hybrid, warm electromagnetic, pulsed, and superconducting electromagnetic devices in both helical and planar configurations are reviewed. Favored design options for proposed short wavelength FEL's, such as the Linac Coherent Light Source at SLAC and the DUV Free-Electron Laser at BNL, are presented. DOE

N95-23657# Academy of Sciences (USSR), Novosibirsk (USSR).
THE PROJECT OF HIGH FREE ELECTRON LASER USING RACE-TRACK MICROTRON-RECUPERATOR
G. I. Erg, N. G. Gavrilov, and E. I. Gorniker 1993 18 p
(DE94-634034; BUDKERINP-93-75; IYaF-93-75) Avail: CASI HC A03/MF A01 (US Sales Only)

The high power free electron laser (FEL) is under construction in the Novosibirst. The goal of this project is to provide the user facility for photochemical research. DOE

N95-24072# Los Alamos National Lab., NM.
ADVANCED TECHNOLOGIES FOR A COMPACT RF LINAC FEL
D. C. Nguyen 1995 10 p Presented at the FEL '94: Nuclear Instrument Methods, Stanford, CA, 21-26 Aug. 1994
(Contract W-7405-eng-36)
(DE95-003674; LA-UR-94-3985; CONF-9408196-1) Avail: CASI HC A02/MF A01

Advanced technologies such as the photoinjector, the short-period microwigglers, and harmonic lasing enable free-electron-laser operation in the infrared with a low-energy (approximately 10 MeV) electron beam and thus reduce the size and cost of FEL's. The next-generation, RF-linac FEL will fit in a small laboratory and produce high-power, picosecond infrared. DOE

N95-23001*# Open Univ., Milton Keynes (England). Dept. of Mathematics nad Computing.
REAL LASERS AND OTHER DEFORMED OBJECTS
Allan I. Solomon *In* NASA. Goddard Space Flight Center, Second International Workshop on Harmonic Oscillators Jan. 1995 p 363-373 (For primary document see N95-22957 07-74)
Avail: CASI HC A03/MF A04

N95-23303*# Elizabeth City State Univ., NC. Dept. of Physical Sciences.
RAMAN-SHIFTING AN ArF EXCIMER LASER TO GENERATE NEW LINES FOR OBTAINING OPTICAL DIAGNOSTIC BASED INFORMATION IN FLOW FIELDS Abstract Only
Edmond B. Koker *In* Hampton Univ., 1994 NASA-HU American Society for Engineering Education (ASEE) Summer Faculty Fellowship Program Dec. 1994 p 85 (For primary document see N95-23276 07-99)
Avail: CASI HC A01/MF A02

N95-23326*# Montana State Univ., Bozeman, MT. Dept. of Chemistry.
COMPUTATIONAL MODELLING OF Er(3+): GARNET LASER MATERIALS Abstract Only
Lee H. Spangler *In* Hampton Univ., 1994 NASA-HU American Society for Engineering Education (ASEE) Summer Faculty Fellowship Program Dec. 1994 p 108 (For primary document see N95-23276 07-99)
Avail: CASI HC A01/MF A02

N95-23330*# Sage Junior Coll. of Albany, Albany, NY. Math/Science Div.
COMPUTER MODELING OF THE SENSITIVITY OF A LASER WATER VAPOR SENSOR TO VARIATIONS IN TEMPERATURE AND AIR SPEED Abstract Only
George F. Tucker *In* Hampton Univ., 1994 NASA-HU American Society for Engineering Education (ASEE) Summer Faculty Fellowship Program Dec. 1994 p 112 (For primary document see N95-23276 07-99)
Avail: CASI HC A01/MF A02

N95-23712*# National Space Development Agency, Tsukuba (Japan). Space Center.
SMALL IMAGE LASER RANGE FINDER FOR PLANETARY ROVER
Yasufumi Wakabayashi, Masahisa Honda, Tadashi Adachi, and Takahiko Iijima *In* JPL, Third International Symposium on Artificial Intelligence, Robotics, and Automation for Space 1994 Oct. 1994 p 201-204 (For primary document see N95-23672 07-63)
Avail: CASI HC A01/MF A03

37 MECHANICAL ENGINEERING

Includes auxiliary systems (nonpower); machine elements and processes; and mechanical equipment.

N95-22543*# National Aeronautics and Space Administration. Pasadena Office, CA.
CONTROLLING UNDER-ACTUATED ROBOT ARMS USING A HIGH SPEED DYNAMICS PROCESS Patent
Abhinandan Jain, inventor (to NASA) (Jet Propulsion Lab., California Inst. of Tech., Pasadena, CA.) and Guillermo Rodriguez, inventor (to NASA) (Jet Propulsion Lab., California Inst. of Tech., Pasadena, CA.) 27 Dec. 1994 25 p Filed 3 Apr. 1992 Supersedes N92-24043 (30 - 14, p 2385
(Contract NAS7-918)
(NASA-Case-NPO-18498-1-CU; US-Patent-5,377,310;
US-Patent-Appl-SN-866779; US-Patent-Class-395-95;
US-Patent-Class-395-97; US-Patent-Class-395-98;
Int-Patent-Class-G06F-15/00) Avail: US Patent and Trademark Office

The invention controls an under-actuated manipulator by first obtaining predetermined active joint accelerations of the active joints and the passive joint friction forces of the passive joints, then computing articulated body qualities for each of the joints from the current positions of the links, and finally computing from the articulated body qualities and from the active joint accelerations and the passive joint forces, active joint forces of the active joints. Ultimately, the invention transmits servo commands to the active joint forces thus computed to the respective ones of the joint servos. The computation of the active joint forces is accomplished using a recursive dynamics algorithm. In this computation, an inward recursion is first carried out for each link, beginning with the outermost link in order to compute the residual link force of each link from the active joint acceleration if the corresponding joint is active, or from the known passive joint force if the corresponding joint is passive. Then, an outward recursion is carried out for each link in which the active joint force is computed from the residual link force if the corresponding joint is active or the passive joint acceleration is computed from the residual link force if the corresponding joint is passive. Official Gazette of the U.S. Patent and Trademark Office

N95-22556# Argonne National Lab., IL.
THE INFLUENCE OF HIGH-OCTANE FUEL BLENDS ON THE PERFORMANCE OF A TWO-STROKE SI ENGINE WITH KNOCK-LIMITED-COMPRESSION RATIO
Ramesh B. Poola, T. Bhasker (Indian Inst. of Tech., Madras.), B. Nagalingam (Indian Inst. of Tech., Madras.), and K. V. Gopalakrishnan (Indian Inst. of Tech., Madras.) 1994 12 p Presented at the SAE International Fuels and Lubricants Meeting and Exposition: Fuels and Lubricants Needs - Charting A Course for the Future, Baltimore, MD, 17-20 Oct. 1994

(Contract W-31-109-eng-38)
(DE95-002902; ANL/ES/CP-84174; CONF-9410173-3) Avail: CASI HC A03/MF A01

The use of alcohol-gasoline blends enables the favorable features of alcohols to be utilized in spark ignition (SI) engines while avoiding the shortcomings of their application as straight fuels. Eucalyptus and orange oils possess high octane values and are also good potential alternative fuels for SI engines. The high octane value of these fuels can enhance the octane value of the fuel when it is blended with low-octane gasoline. In the present work, 20 percent by volume of orange oil, eucalyptus oil, methanol and ethanol were blended separately with gasoline, and the performance, combustion and exhaust emission characteristics were evaluated at two different compression ratios. The phase separation problems arising from the alcohol-gasoline blends were minimized by adding eucalyptus oil as a cosolvent. Test results indicate that the compression ratio can be raised from 7.4 to 9 without any detrimental effect, due to the higher octane rating of the fuel blends. Knock-limited maximum brake output also increases due to extension of the knock limit. The knock limit is extended by methanol-eucalyptus-ethanol-orange oil blends, in descending order. DOE

N95-22557# Argonne National Lab., IL.
PERFORMANCE OF THIN-CERAMIC-COATED COMBUSTION CHAMBER WITH GASOLINE AND METHANOL AS FUELS IN A TWO-STROKE SI ENGINE
Ramesh B. Poola, B. Nagalingam (Indian Inst. of Tech., Madras.), and K. V. Gopalakrishnan (Indian Inst. of Tech., Madras.) 1994 14 p Presented at the SAE International Fuels and Lubricants Meeting and Exposition: Fuels and Lubricants Needs - Charting A Course for the Future, Baltimore, MD, 17-20 Oct. 1994
(Contract W-31-109-eng-38)
(DE95-002903; ANL/ES/CP-83720; CONF-9410173-2) Avail: CASI HC A03/MF A01

The performance of a conventional, carbureted, two-stroke spark-ignition (SI) engine can be improved by providing moderate thermal insulation in the combustion chamber. This will help to improve the vaporization characteristics in particular at part load and medium loads with gasoline fuel and high-latent-heat fuels such as methanol. In the present investigation, the combustion chamber surface was coated with a 0.5-mm thickness of partially stabilized zirconia, and experiments were carried out in a single-cylinder, two-stroke SI engine with gasoline and methanol as fuels. Test results indicate that with gasoline as a fuel, the thin ceramic-coated combustion chamber improves the part load to medium load operation considerably, but it affects the performance at higher speeds and at higher loads to the extent of knock and loss of brake power by about 18%. However, with methanol as a fuel, the performance is better under most of the operating range and free from knock. Carbon monoxide (CO) emissions are significantly reduced, by about 3 to 4% volume, for both gasoline and methanol fuels due to relatively lean operation and more complete combustion. NO(x) emissions were not measured. The results show that moderate thermal insulation of the two-stroke SI engine's combustion chamber is better suited to methanol fuel with respect to thermal efficiency, CO emissions, and knock-free operation compared to gasoline fuel. DOE

N95-22707 Department of the Navy, Washington, DC.
VIBRATION-DAMPING STRUCTURAL COMPONENT Patent
David J. Barrett, inventor (to Navy) 16 Aug. 1994 3 p Filed 26 Nov. 1991 Supersedes AD-D016226
(AD-D016550; US-Patent-5,338,599; US-Patent-Appl-SN-800902) Avail: US Patent and Trademark Office

A laminated structural component with superior resistance to flexural vibrations is provided comprising two load-bearing layers and a viscoelastic damping layer sandwiched there between. Each of the load-bearing layers comprises an outer stiffness sublayer and an inner compliant sublayer, the compliant sublayer being positioned between the outer stiffness sublayer and the viscoelastic damping layer. The compliant sublayers have an extensional elastic modulus which is less than that of the stiffness sublayers, and greater than that of the viscoelastic damping layer. The laminated structural component experiences greater relative in-plane displacements between the load-bearing layers, and preserves transverse static stiffness. DTIC

N95-22796# General Atomics Co., San Diego, CA.
THE DIII-D DIVERTOR CRYOPUMP SYSTEM: DESIGN AND OPERATIONAL EXPERIENCE
K. M. Schaubel, J. P. Smith, G. J. Laughon, C. B. Baxi, G. L. Campbell, M. A. Mahdavi, M. J. Schaffer, R. Maingi (Oak Ridge National Lab., TN.), M. M. Meneon (Oak Ridge National Lab., TN.), and R. D. Stambaugh (Oak Ridge National Lab., TN.) Oct. 1994 4 p Presented at the 18th European Symposium on Fusion Technology, Karlsruhe, Germany, 22-26 Aug. 1994
(Contracts DE-AC03-89ER-51114; DE-AC05-84OR-21400)
(DE95-003007; GA-A-21787; CONF-940843-10) Avail: CASI HC A01/MF A01

A high throughput cryocondensation pump has been installed inside the DIII-D plasma chamber as part of the Advanced Divertor Program. During normal plasma discharges the pumping surface temperature must remain sufficiently low (less than 6.3 K) to pump deuterium while the pump is subjected to transient Joule heating induced by the Ohmic heating coils as well as energetic particles from the plasma. A cryogenic cooling system was specifically designed to handle pulsed heat loads up to 100 W lasting for 10 S. Prototype testing was carried out to verify and develop pulsed capability. During characterization tests, deuterium pumping speeds of 42,000 (ell)/s at 0.66 Pa pressure were achieved. This speed was maintained during 300 W, 8 s long test heat pulses. Physics experiments with the cryopump have been very successful showing a 50% plasma density reduction during H-mode. The design of the advanced divertor cryosystem and cryosystem operational experience are presented. DOE

N95-22798# General Atomics Co., San Diego, CA.
ENGINEERING DESIGN OF A RADIATIVE DIVERTOR FOR DIII-D
J. P. Smith, P. M. Anderson, C. B. Baxi, E. Chin, M. A. Hollerbach, A. W. Hyatt, R. Junge, M. A. Mahdavi, K. Redler, and E. E. Reis et al Oct. 1994 4 p Presented at the 18th European Symposium on Fusion Technology, Karlsruhe, Germany, 22-26 Aug. 1994
(Contracts DE-AC03-89ER-51114; W-7405-eng-48)
(DE95-003008; GA-A-21788; CONF-940843-11) Avail: CASI HC A01/MF A01

A new divertor called the Radiative Divertor is presently being designed for the DIII-D tokamak. Input from tokamak experiments and modeling form the basis for the new design. The Radiative Divertor is intended to reduce the heat flux on the divertor plates by dispersing the power with radiation. Gas puffing experiments in the current open divertor have shown a reduction of the divertor heat flux with either deuterium or impurity puffing. However, either the plasma density (D(sub 2)) or the core Z(sub eff) (impurities) increases in these experiments. The radiative divertor uses a slot structure to isolate the divertor plasma region from the area surrounding the core plasma. Modeling has shown that the Radiative Divertor hardware will provide better baffling and particle control and thereby minimize the effect of the gas puffing in the divertor region on the plasma core. In addition, the Radiative Divertor structure will allow density control in plasma shapes with high triangularity (greater than 0.8) required for advanced tokamak operation. The divertor structure allows for operation in either double or single-null plasma configurations. Four independently controlled divertor cryopumps will enable pumping at either the inboard (upper and lower) or the outboard (upper and lower) divertor plates. Biasing is an integral part of the design and is based on experience at the Tokamak de Varennes (TdeV) and DIII-D. Boron nitride tiles electrically insulate the inner and outer strike points and a low current electrode is used to apply a radial electric field to the scrape-off layer. TdeV has shown that biasing can provide particle and impurity control. The design is extremely flexible, and will allow physics studies of the effect of slot width and height. This is extremely important as the amount of chamber volume needed for the divertor in future machines such as International Thermonuclear Experiment Reactor (ITER) and Tokamak Physics Experiment (TPX) must be determined. DOE

N95-22880# National Aeronautics and Space Administration. Lewis Research Center, Cleveland, OH.
ADVANCED TURBINE TECHNOLOGY APPLICATIONS PROJECT (ATTAP) 1993 ANNUAL REPORT
Jul. 1994 48 p
(DE95-003198; DOE/NASA-0335/6) Avail: CASI HC A03/MF A01

This report summarizes work performed by AlliedSignal Engines, a unit

of AlliedSignal Aerospace Company, during calendar year 1993, toward development and demonstration of structural ceramic technology for automotive gas turbine engines. This work was performed for the U.S. Department of Energy (DOE) under National Aeronautics and Space Administration (NASA) Contract DEN3-335, Advanced Turbine Technology Applications Project (ATFAP). During 1993, the test bed used to demonstrate ceramic technology was changed from the AlliedSignal Engines/Garrett Model AGT101 regenerated gas turbine engine to the Model 331-200(CT) engine. The 331-200(CT) ceramic demonstrator is a fully-developed test platform based on the existing production AlliedSignal 331-200(ER) gas turbine auxiliary power unit (APU), and is well suited to evaluating ceramic turbine blades and nozzles. In addition, commonality of the 331-200(CT) engine with existing gas turbine APU's in commercial service provides the potential for field testing of ceramic components. The 1993 ATTAP activities emphasized design modifications of the 331-200 engine test bed to accommodate ceramic first-stage turbine nozzles and blades, fabrication of the ceramic components, ceramic component proof and rig tests, operational tests of the test bed equipped with the ceramic components, and refinement of critical ceramic design technologies. DOE

N95-22892*# National Aeronautics and Space Administration. Lyndon B. Johnson Space Center, Houston, TX.

PRESSURIZED FLUID TORQUE DRIVER CONTROL AND METHOD Patent Application

Joseph S. Cook, Jr., inventor (to NASA) 10 Aug. 1994 45 p

(NASA-Case-MSC-22385-1; NAS 1.17:MSC-22385-1; US-Patent-Appl-SN-288114) Avail: CASI HC A03/MF A01

Methods and apparatus are provided for a torque driver including a displaceable gear to limit torque transfer to a fastener at a precisely controlled torque limit. A biasing assembly biases a first gear into engagement with a second gear for torque transfer between the first and second gear. The biasing assembly includes a pressurized cylinder controlled at a constant pressure that corresponds to a torque limit. A calibrated gage and valve is used to set the desired torque limit. One or more coiled output linkages connect the first gear with the fastener adaptor which may be a socket for a nut. A gear tooth profile provides a separation force that overcomes the bias to limit torque at the desired torque limit. Multiple fasteners may be rotated simultaneously to a desired torque limit if additional output spur gears are provided. The torque limit is adjustable and may be different for fasteners within the same fastener configuration. NASA

N95-22909*# Alabama Univ., Tuscaloosa, AL. Dept. of Electrical Engineering.

DESIGN AND APPLICATION OF ELECTROMECHANICAL ACTUATORS FOR DEEP SPACE MISSIONS Semiannual Report No. 3, 16 Aug. 1994 - 15 Feb. 1995

Tim A. Haskew and John Wander Mar. 1995 36 p

(Grant NAG8-240)

(NASA-CR-197957; NAS 1.26:197957; BER-620-163) Avail: CASI HC A03/MF A01

This third semi-annual progress report covers the reporting period from August 16, 1994 through February 15, 1995 on NASA Grant NAG8-240, 'Design and Application of Electromechanical Actuators for Deep Space Missions'. There are two major report sections: Motor Control Status/Electrical Experiment Planning and Experiment Planning and Initial Results. The primary emphasis of our efforts during the reporting period has been final construction and testing of the laboratory facilities. As a result, this report is dedicated to that topic. Author

N95-22923# National Renewable Energy Lab., Golden, CO.

APPLICATION REQUIREMENTS FOR WIND TURBINE GEARBOXES

Robert Errichello (GEARTECH, Albany, CA.) and Jane Muller (GEARTECH, Albany, CA.) Sep. 1994 162 p

(Contract DE-AC36-83CH-10093)

(DE94-011883; NREL/TP-442-7076) Avail: CASI HC A08/MF A02

This report is a technical guide which documents the wind turbine gearbox experience of the GEARTECH consulting firm. The report provides a reference on wind turbine gearbox applications for the gear industry, wind turbine designers, and wind turbine operators. This report will assist in selecting, designing, manufacturing, procuring, operating, and maintaining gearboxes for use on wind turbines. DOE

N95-23056# Sandia National Labs., Albuquerque, NM.

THE SPECTRAL CONTENT OF THE TORQUE LOADS ON A TURBINE GEAR TOOTH

H. J. Sutherland and D. P. Burwinkle (New Mexico Univ., Albuquerque, NM.) 1994 7 p Presented at the American Society of Mechanical Engineers Energy Technology Conference and Exhibition, Houston, TX, 29 Jan. - 1 Feb. 1995

(Contract DE-AC04-94AL-85000)

(DE95-002188; SAND-94-2333C; CONF-950116-3) Avail: CASI HC A02/MF A01

The torque loads on two classes of wind turbine gearboxes are analyzed using a time-at-torque technique and a rainflow counting technique to determine the cyclic loads on the gear teeth. The two techniques are compared and contrasted to one another using representative samples of the time histograms from a Micon 65 and the Sandia/DOE Test Bed wind turbines. To place these differences in perspective, Miner's Rule is used to determine the damage produced by each of the distributions. The damage analyses illustrate that the differences in the distributions are minimal. DOE

N95-23065# Sandia National Labs., Albuquerque, NM.

ROBOTIC ALL-TERRAIN LUNAR EXPLORATION ROVER (RATLER) FY93 PROGRAM STATUS REPORT

W. A. Amai, P. R. Klarer, J. B. Pletta, J. W. Purvis, and R. P. Case (Technadyne Engineering Consultants, Albuquerque, NM.) Oct. 1994 70 p

(Contract DE-AC04-94AL-85000)

(DE95-003589; SAND-94-1706) Avail: CASI HC A04/MF A01

The development of a Robotic All-Terrain Lunar Exploration Rover (RATLER) prototype is described. The RATLER Laboratory-Directed Research and Development (LDRD) project was initiated in Fiscal Year 1993 (FY93) for a period of two years. This document reports on the project's activities during the first year of development and briefly discusses plans for the second year's work. Details include analysis of the rover's performance requirements for expected lunar conditions and a description of a point design selected as being representative for an actual rover. Technical information regarding several prototypes constructed and tested during FY93 is included, as is a discussion of weaknesses in the current RATLER design. Plans for addressing these weaknesses in the project's second year are outlined and briefly discussed. DOE

N95-23190*# Auburn Univ., AL. Dept. of Mechanical Engineering.

INFLUENCE OF BACKUP BEARINGS AND SUPPORT STRUCTURE DYNAMICS ON THE BEHAVIOR OF ROTORS WITH ACTIVE SUPPORTS Semiannual Status Report

George T. Flowers Feb. 1995 5 p

(Grant NAG3-1507)

(NASA-CR-197438; NAS 1.26:197438) Avail: CASI HC A01/MF A01

This semiannual status report lists specific accomplishments made on the research of the influence of backup bearings and support structure dynamics on the behavior of rotors with active supports. Papers have been presented representing work done on the T-501 engine model; an experimental/simulation study of auxiliary bearing rotordynamics; and a description of a rotordynamical model for a magnetic bearing supported rotor system, including auxiliary bearing effects. A finite element model for a foil bearing has been developed. Additional studies of rotor/bearing/housing dynamics are currently being performed as are studies of the effects of sideloading on auxiliary bearing rotordynamics using the magnetic bearing supported rotor model. Derived from text

N95-23213*# Auburn Univ., AL.

DYNAMIC MODELLING AND RESPONSE CHARACTERISTICS OF A MAGNETIC BEARING ROTOR SYSTEM INCLUDING AUXILIARY BEARINGS

April M. Free, George T. Flowers, and Victor S. Trent [1993] 9 p

(Grant NAG3-1507)

(NASA-CR-197859; NAS 1.26:197859) Avail: CASI HC A02/MF A01

Auxiliary bearings are a critical feature of any magnetic bearing system. They protect the soft iron core of the magnetic bearing during an overload or failure. An auxiliary bearing typically consists of a rolling element bearing or bushing with a clearance gap between the rotor and the inner race of the support. The dynamics of such systems can be quite complex. It is

desired to develop a rotor-dynamic model and assess the dynamic behavior of a magnetic bearing rotor system which includes the effects of auxiliary bearings. Of particular interest is the effects of introducing sideloading into such a system during failure of the magnetic bearing. A model is developed from an experimental test facility and a number of simulation studies are performed. These results are presented and discussed. Author

N95-23214*# Auburn Univ., AL.
SYNCHRONOUS DYNAMICS OF A COUPLED SHAFT/BEARING/HOUSING SYSTEM WITH AUXILIARY SUPPORT FROM A CLEARANCE BEARING: ANALYSIS AND EXPERIMENT
James Lawen, Jr. and George T. Flowers [1992] 8 p
(Grants NAG3-1507; NGT-70312)
(NASA-CR-197858; NAS 1.26:197858) Avail: CASI HC A02/MF A01

This study examines the response of a flexible rotor supported by load sharing between linear bearings and an auxiliary clearance bearing. The objective of the work is to develop a better understanding of the dynamical behavior of a magnetic bearing supported rotor system interacting with auxiliary bearings during a critical operating condition. Of particular interest is the effect of coupling between the bearing/housing and shaft vibration on the rotordynamical responses. A simulation model is developed and a number of studies are performed for various parametric configurations. An experimental investigation is also conducted to compare and verify the rotordynamic behavior predicted by the simulation studies. A strategy for reducing synchronous shaft vibration through appropriate design of coupled shaft/bearing/housing vibration modes is identified. The results are presented and discussed. Author

N95-23342# Texas Univ., Austin, TX.
THE RAILPLUG: DEVELOPMENT OF A NEW IGNITOR FOR INTERNAL COMBUSTION ENGINES Final Report
R. D. Matthews, S. P. Nichols, and W. F. Weldon 29 Nov. 1994 70 p
(Contract DE-FG05-91ER-12115)
(DE95-004375; DOE/ER-12115/T1) Avail: CASI HC A04/MF A01

A three year investigation of a new type of ignitor for internal combustion engines has been performed using funds from the Advanced Energy Projects Program of The Basic Energy Sciences Division of the U.S. Department of Energy and with matching funding from Research Applications, Inc. This project was a spin-off of 'Star Wars' defense technology, specifically the railgun. The 'railplug' is a miniaturized railgun which produces a high velocity plume of plasma that is injected into the combustion chamber of an engine. Unlike other types of alternative ignitors, such as plasma jet ignitors, electromagnetic forces enhance the acceleration of the plasma generated by a railplug. Thus, for a railplug, the combined effects of electromagnetic and thermodynamic forces drive the plasma into the combustion chamber. Several engine operating conditions or configurations can be identified that traditionally present ignition problems, and might benefit from enhanced ignition systems. One of these is ultra-lean combustion in spark ignition (SI) engines. This concept has the potential for lowering emissions of NO(x) while simultaneously improving thermal efficiency. Unfortunately, current lean burn engines cannot be operated sufficiently lean before ignition related problems are encountered to offer any benefits. High EGR engines have similar potential for emissions improvement, but also experience similar ignition problems, particularly at idle. Other potential applications include diesel cold start, alcohol and dual fuel engines, and high altitude relight of gas turbines. The railplug may find application for any of the above. This project focused on three of these potential applications: lean burn SI engines, high EGR SI engines, and diesel cold start. DOE

N95-23343# Allied-Signal Aerospace Co., Kansas City, MO.
PROGRESS REPORT ON A FULLY AUTOMATIC GAS TUNGSTEN ARC WELDING (GTAW) SYSTEM DEVELOPMENT
G. J. Daumeyer, III Dec. 1994 31 p
(Contract DE-AC04-76DP-00613)
(DE95-004397; KCP-613-4884) Avail: CASI HC A03/MF A01

A plan to develop a fully automatic gas tungsten arc welding (GTAW) system that will utilize a vision-sensing computer (which will provide in-process feedback control) is presently in work. Evaluations of different technological aspects and system design requirements continue. This report summaries major activities in the plan's successful progress. The technological feasibility of producing the fully automated GTAW system has been proven. The goal of this process development project is to provide a production-ready system within the shortest reasonable time frame. DOE

N95-23358# Lawrence Livermore National Lab., Livermore, CA.
LOAD CALCULATION AND SYSTEM EVALUATION FOR ELECTRIC VEHICLE CLIMATE CONTROL
S. M. Aceves and W. J. Comfort, III 12 Sep. 1994 25 p Presented at the Society of Automotive Engineers International Congress and Exposition, Detroit, MI, 27 Feb. - 2 Mar. 1995
(Contract W-7405-eng-48)
(DE95-004350; UCRL-JC-116834; CONF-950256-2) Avail: CASI HC A03/MF A01

This paper presents an analysis of the applicability of alternative systems for electric vehicle (EV) heating and air conditioning (HVAC). The paper consists of two parts. The first part is a cooling and heating load calculation for electric vehicles. The second part is an evaluation of several systems that can provide the desired cooling and heating in EV's. These systems are ranked according to their overall weight. Theoverall weight is calculated by adding the system weight and the weight of the battery necessary to provide energy for system operation. The system with the minimum overall weight is considered to be the best, because minimum vehicle weight decreases the energy required for propulsion, and therefore increases the vehicle range. Three systems are considered as the best choices for EV HVAC. These are, vapor compression, ice storage and adsorption systems. These systems are evaluated, including calculations of system weight, system volume, and COP. The paper also includes a calculation on how the battery energy storage capacity affects the overall system weights and the selection of the optimum system. The results indicate that, at the conditions analyzed in this paper, an ice storage system has the minimum weight of all the systems considered. Vapor compression air conditioners become the system with the minimum weight for battery storage capacities above 230 kJ/kg. DOE

N95-23373# Allied-Signal Aerospace Co., Kansas City, MO.
VISION-SENSING IMAGE ANALYSIS FOR GTAW PROCESS CONTROL
D. D. Long Nov. 1994 54 p
(Contract DE-AC04-76DP-00613)
(DE95-003936; KCP-613-5302) Avail: CASI HC A04/MF A01

Image analysis of a gas tungsten arc welding (GTAW) process was completed using video images from a charge coupled device (CCD) camera inside a specially designed coaxial (GTAW) electrode holder. Video data was obtained from filtered and unfiltered images, with and without the GTAW arc present, showing weld joint features and locations. Data Translation image processing boards, installed in an IBM PC AT 386 compatible computer, and Media Cybernetics image processing software were used to investigate edge flange weld joint geometry for image analysis. DOE

N95-23374# Allied-Signal Aerospace Co., Kansas City, MO.
INVESTIGATION OF ARC LENGTH VERSUS FLANGE THICKNESS WHILE USING AN ARC VOLTAGE CONTROLLER
G. J. Daumeyer Nov. 1994 22 p
(Contract DE-AC04-76DP-00613)
(DE95-003937; KCP-613-4808) Avail: CASI HC A03/MF A01

An arc voltage controller (AVC) for gas tungsten arc welding will change arc length when flange thickness changes while all other variables, including AVC setting, are held constant. A procedure for calibrating an LVDT (linear variable displacement transducer) used for electrode assembly motion monitoring was proven for laboratory setups and special investigations. A partial characterization on the deadband and sensitivity control settings of the Cyclomatic AVC was completed. DOE

N95-23376* National Aeronautics and Space Administration. Ames Research Center, Moffett Field, CA.
QUICK CONNECT COUPLING Patent
Curtis Lomax, inventor (to NASA) and Bruce Webbon, inventor (to NASA) 28 Feb. 1995 11 p Filed 16 Aug. 1993 Division of US-Patent-Appl-SN-703649, filed 21 May 1991, US-Patent-5,261,482
(NASA-Case-ARC-11921-2; US-Patent-5,392,844;
US-Patent-Appl-SN-106865; US-Patent-Appl-SN-703649;
US-Patent-Class-165-10; US-Patent-Class-62-250.3;

US-Patent-Class-62-299; US-Patent-Class-137-614.04; US-Patent-Class-165-104.17; Int-Patent-Class-F28D-17/00) Avail: US Patent and Trademark Office

A cooling apparatus includes a container filled with a quantity of coolant fluid initially cooled to a solid phase, a cooling loop disposed between a heat load and the container, a pump for circulating a quantity of the same type of coolant fluid in a liquid phase through the cooling loop, and a pair of couplings for communicating the liquid phase coolant fluid into the container in a direct interface with the solid phase coolant fluid.
Official Gazette of the U.S. Patent and Trademark Office

N95-23397# Argonne National Lab., IL.
EXPLOSIVE BONDING AND ITS APPLICATION IN THE ADVANCED PHOTON SOURCE FRONT-END AND BEAMLINE COMPONENTS DESIGN
D. Shu, Y. Li, D. Ryding, T. M. Kuzay, and D. Brasher (Northwest Technical Industries, Inc., Sequim, WA.) 1994 16 p Presented at the International Meeting on Synchrotron Radiation Instrumentation, Stony Brook, NY, 18-22 Jul. 1994
(Contract W-31-109-eng-38)
(DE95-004132; ANL/XFD/CP-82946; CONF-940714-45) Avail: CASI HC A03/MF A01

Explosive bonding is a bonding method in which the controlled energy of a detonating explosive is used to create a metallurgical bonding between two or more similar or dissimilar materials. Since 1991, a number of explosive-bonding joints have been designed for high-thermal-load ultrahigh-vacuum (UHV) compatible components in the Advanced Photon Source. A series of standardized explosive bonded joint units has also been designed and tested, such as: oxygen-free copper (OFHC) to stainless-steel vacuum joints for slits and shutters, GlidCop to stainless-steel vacuum joints for fixed masks, and GlidCop to OFHC thermal and mechanical joints for shutter face-plates, etc. The design and test results for the explosive bonding units to be used in the Advanced Photon Source front ends and beamlines will be discussed in this paper. DOE

N95-23409*# North Carolina Agricultural and Technical State Univ., Greensboro, NC. Mars Mission Research Center.
A MICROCONTROLLER-BASED THREE DEGREE-OF-FREEDOM MANIPULATOR TESTBED M.S. Thesis
Robert Michael Brown, Jr. 1995 125 p
(Grant NAG1-1283)
(NASA-CR-197423; NAS 1.26:197423) Avail: CASI HC A06/MF A02

A wheeled exploratory vehicle is under construction at the Mars Mission Research Center at North Carolina State University. In order to serve as more than an inspection tool, this vehicle requires the ability to interact with its surroundings. A crane-type manipulator, as well as the necessary control hardware and software, has been developed for use as a sample gathering tool on this vehicle. The system is controlled by a network of four Motorola M68HC11 microcontrollers. Control hardware and software were developed in a modular fashion so that the system can be used to test future control algorithms and hardware. Actuators include three stepper motors and one solenoid. Sensors include three optical encoders and one cable tensiometer. The vehicle supervisor computer provides the manipulator system with the approximate coordinates of the target object. This system maps the workspace surrounding the given location by lowering the claw, along a set of evenly spaced vertical lines, until contact occurs. Based on this measured height information and prior knowledge of the target object size, the system determines if the object exists in the searched area. The system can find and retrieve a 1.25 in. diameter by 1.25 in. tall cylinder placed within the 47.5 sq in search area in less than 12 minutes. This manipulator hardware may be used for future control algorithm verification and serves as a prototype for other manipulator hardware. Author

N95-23792*# Technology Integration and Development Group, Inc., Bedford, MA.
GEARBOX VIBRATION DIAGNOSTIC ANALYZER Final Report
Cleveland, OH NASA Apr. 1992 19 p
(Contract NAS3-26134; RTOP 505-63-36)
(NASA-CR-189141; E-9589; NAS 1.26:189141; TII-R9201-001-RD) Avail: CASI HC A03/MF A01

This report describes the Gearbox Vibration Diagnostic Analyzer installed in the NASA Lewis Research Center's 500 HP Helicopter Transmission Test Stand to monitor gearbox testing. The vibration of the gearbox is analyzed using diagnostic algorithms to calculate a parameter indicating damaged components. Author

N95-24064*# Rockwell International Corp., Canoga Park, CA. Rocketdyne Div.
VACCUM GAS TUNGSTEN ARC WELDING, PHASE 1 Technical Report, Oct. 1993 - Mar. 1995
J. L. Weeks, P. D. Krotz, D. T. Todd, and Y. K. Liaw Mar. 1995 34 p
(Contract NAS8-39932)
(NASA-CR-197979; NAS 1.26:197979; RI/RD95-146) Avail: CASI HC A03/MF A01

This two year program will investigate Vacuum Gas Tungsten Arc Welding (VGTAW) as a method to modify or improve the weldability of normally difficult-to-weld materials. VGTAW appears to offer a significant improvement in weldability because of the clean environment and lower heat input needed. The overall objective of the program is to develop the VGTAW technology and implement it into a manufacturing environment that will result in lower cost, better quality and higher reliability aerospace components for the space shuttle and other NASA space systems. Phase 1 of this program was aimed at demonstrating the process's ability to weld normally difficult-to-weld materials. Phase 2 will focus on further evaluation, a hardware demonstration and a plan to implement VGTAW technology into a manufacturing environment. During Phase 1, the following tasks were performed: (1) Task 11000 Facility Modification - an existing vacuum chamber was modified and adapted to a GTAW power supply; (2) Task 12000 Materials Selection - four difficult-to-weld materials typically used in the construction of aerospace hardware were chosen for study; (3) Task 13000 VGTAW Experiments - welding experiments were conducted under vacuum using the hollow tungsten electrode and evaluation. As a result of this effort, two materials, NARloy Z and Incoloy 903, were downselected for further characterization in Phase 2; and (4) Task 13100 Aluminum-Lithium Weld Studies - this task was added to the original work statement to investigate the effects of vacuum welding and weld pool vibration on aluminum-lithium alloys. Author

N95-24141# Lehigh Univ., Bethlehem, PA.
ROBOTIC WELD OVERLAY COATINGS FOR EROSION CONTROL
1994 7 p
(Contract DE-FG22-92PC-92542)
(DE95-002624; DOE/PC-92542/T7) Avail: CASI HC A02/MF A01

The erosion of materials by the impact of solid particles has received increasing attention during the past twenty years. Recently, research has been initiated with the event of advanced coal conversion processes in which erosion plays an important role. The resulting damage, termed Solid Particle Erosion (SPE), is of concern primarily because of the significantly increased operating costs which result in material failures. Reduced power plant efficiency due to solid particle erosion of boiler tubes and waterfalls has led to various methods to combat SPE. One method is to apply coatings to the components subjected to erosive environments. Protective weld overlay coatings are particularly advantageous in terms of coating quality. The weld overlay coatings are essentially immune to spallation due to a strong metallurgical bond with the substrate material. By using powder mixtures, multiple alloys can be mixed in order to achieve the best performance in an erosive environment. However, a review of the literature revealed a lack of information on weld overlay coating performance in erosive environments which makes the selection of weld overlay alloys a difficult task. The objective of this project is to determine the effects of weld overlay coating composition and microstructure on erosion resistance. These results will lead to a better understanding of erosion mitigation in CFB's. DOE

N95-23441*# National Aeronautics and Space Administration. Marshall Space Flight Center, Huntsville, AL.
DETAILED MEASUREMENTS IN THE SSME HIGH PRESSURE FUEL TURBINE WITH SMOOTH ROTOR BLADES
Susan T. Hudson *In its* Eleventh Workshop for Computational Fluid Dynamic Applications in Rocket Propulsion Jul. 1993 p 1689-1712
(For primary document see N95-23412 07-34)
Avail: CASI HC A03/MF A10

N95-23616*# Rockwell International Corp., Canoga Park, CA. Rocketdyne Div.
THREE-D CFD ANALYSIS OF HYDROSTATIC BEARINGS
Shyi-Jang Lin and Robert I. Hibbs, Jr. *In* NASA. Marshall Space Flight Center, Eleventh Workshop for Computational Fluid Dynamic Applications in Rocket Propulsion, Part 1 Jul. 1993 p 37-55 (For primary document see N95-23615 07-34)
Avail: CASI HC A03/MF A10

N95-23694*# Carnegie-Mellon Univ., Pittsburgh, PA. Robotics Inst.
LUNAR ROVER TECHNOLOGY DEMONSTRATIONS WITH DANTE AND RATLER
Eric Krotkov, John Bares, Lalitesh Katragadda, Reid Simmons, and Red Whittaker *In* JPL, Third International Symposium on Artificial Intelligence, Robotics, and Automation for Space 1994 Oct. 1994 p 113-116 (For primary document see N95-23672 07-63)
Avail: CASI HC A01/MF A03

N95-23695*# Tokyo Inst. of Tech. (Japan). Dept. of Mechano-Aerospace Engineering.
A PERSPECTIVE ON SPACE ROBOTICS IN JAPAN
Yoshiaki Ohkami, Ichiro Nakatani, Yasufumi Wakabayashi (National Space Development Agency, Tsukuba, Japan.), and Tsutomu Iwata (National Space Development Agency, Tsukuba, Japan.) *In* JPL, Third International Symposium on Artificial Intelligence, Robotics, and Automation for Space 1994 Oct. 1994 p 119-124 (For primary document see N95-23672 07-63)
Avail: CASI HC A02/MF A03

N95-23696*# Italian Space Agency, Rome.
ASI'S SPACE AUTOMATION AND ROBOTICS PROGRAMS: THE SECOND STEP
Simonetta DiPippo *In* JPL, Third International Symposium on Artificial Intelligence, Robotics, and Automation for Space 1994 Oct. 1994 p 125-130 (For primary document see N95-23672 07-63)
Avail: CASI HC A02/MF A03

N95-23697*# Jet Propulsion Lab., California Inst. of Tech., Pasadena, CA.
JPL SPACE ROBOTICS: PRESENT ACCOMPLISHMENTS AND FUTURE THRUSTS
C. R. Weisbin, S. A. Hayati, and G. Rodriguez *In its* Third International Symposium on Artificial Intelligence, Robotics, and Automation for Space 1994 Oct. 1994 p 131-134 (For primary document see N95-23672 07-63)
Avail: CASI HC A01/MF A03

N95-23701*# National Space Development Agency, Tsukuba (Japan).
SPACE ROBOTIC EXPERIMENT IN JEM FLIGHT DEMONSTRATION
Masanori Nagatomo, Masaki Tanaka (Toshiba Corp., Kawasaki, Japan.), Kazuyuki Nakamura (Toshiba Corp., Kawasaki, Japan.), and Shinichi Tsuda (Toshiba Corp., Kawasaki, Japan.) *In* JPL, Third International Symposium on Artificial Intelligence, Robotics, and Automation for Space 1994 Oct. 1994 p 149-152 (For primary document see N95-23672 07-63)
Avail: CASI HC A01/MF A03

N95-23703*# McDonnell-Douglas Aerospace, Houston, TX.
THE CHARLOTTE (TM) INTRA-VEHICULAR ROBOT
Patrick L. Swaim, Clark J. Thompson, and Perry D. Campbell *In* JPL, Third International Symposium on Artificial Intelligence, Robotics, and Automation for Space 1994 Oct. 1994 p 157-162 (For primary document see N95-23672 07-63)
Avail: CASI HC A02/MF A03

N95-23706*# Rockwell International Corp., Downey, CA. Space Systems Div.
HARDWARE INTERFACE UNIT FOR CONTROL OF SHUTTLE RMS VIBRATIONS
Thomas S. Lindsay, Joseph M. Hansen, Davoud Manouchehri, and Kamran Forouhar *In* JPL, Third International Symposium on Artificial Intelligence, Robotics, and Automation for Space 1994 Oct. 1994 p 173-176 (For primary document see N95-23672 07-63)
(Contract NAS1-19243)
Avail: CASI HC A01/MF A03

N95-23722*# National Space Development Agency, Tsukuba (Japan).
ROBOTIC SERVICING SYSTEM FOR SPACE MATERIAL EXPERIMENT
Toshihiko Yamawaki, Haruhiko Shimoji (Mitsubishi Electric Corp., Amagasaki, Japan.), and Toshio Abe (Mitsubishi Electric Corp., Kamakura, Japan.) *In* JPL, Third International Symposium on Artificial Intelligence, Robotics, and Automation for Space 1994 Oct. 1994 p 253-256 (For primary document see N95-23672 07-63)
Avail: CASI HC A01/MF A03

N95-23724*# National Aeronautics and Space Administration. John F. Kennedy Space Center, Cocoa Beach, FL.
ROBOTIC SYSTEM FOR THE SERVICING OF THE ORBITER THERMAL PROTECTION SYSTEM
Todd Graham, Richard Bennett, Kevin Dowling, Davoud Manouchehri, Eric Cooper, and Cregg Cowan *In* JPL, Third International Symposium on Artificial Intelligence, Robotics, and Automation for Space 1994 Oct. 1994 p 263-266 (For primary document see N95-23672 07-63)
Avail: CASI HC A01/MF A03

38 QUALITY ASSURANCE AND RELIABILITY

Includes product sampling procedures and techniques; and quality control.

N95-23602# Advisory Group for Aeronautical Research and Development, Oxford (England). Structures and Materials Panel.
POD ASSESSMENT OF NDI PROCEDURES USING A ROUND ROBIN TEST [LES TESTS COMPARATIFS INTER-LABORATOIRES POUR L'EVALUATION DE LA PROBABILITE DE DETECTION (POD) DES PROCEDURES NDI]
Jan. 1995 40 p
(AGARD-R-809; ISBN-92-836-1010-5) Copyright Avail: CASI HC A03/MF A01

Under the auspices of the AGARD Structures and Materials Panel R&D Cooperation Program, a round-robin NDI demonstration has been carried out. Six laboratories in four NATO countries participated in the project. The aim of the project was to determine the sensitivity and reliability of NDI procedures presently employed by the participating laboratories and to establish whether or not the procedures would be adequate for the implementation of a damage-tolerance based maintenance approach or whether improved methods are required. Author

N95-24106*# Nichols Research Corp., Huntsville, AL.
FRACTURE MECHANICS LIFE ANALYTICAL METHODS VERIFICATION TESTING Final Report, 1 Sept. 1991 - 12 Sept. 1994
J. A. Favenesi, T. G. Clemons, W. T. Riddell, A. R. Ingraffea, and P. A. Wawrzynek 16 Sep. 1994 274 p Prepared in cooperation with Cornell Univ., Ithaca, NY and Fracture Analysis Consultatns, Ithaca, NY
(Contract NAS8-38103)
(NASA-CR-196555; NAS 1.26:196555) Avail: CASI HC A12/MF A03

The objective was to evaluate NASCRAC (trademark) version 2.0, a second generation fracture analysis code, for verification and validity. NASCRAC was evaluated using a combination of comparisons to the literature, closed-form solutions, numerical analyses, and tests. Several limitations and minor errors were detected. Additionally, a number of major flaws were discovered. These major flaws were generally due to application of a specific method or theory, not due to programming logic. Results are presented for the following program capabilities: K versus a, J versus a, crack opening area, life calculation due to fatigue crack growth, tolerable crack size, proof test logic, tearing instability, creep crack growth, crack transitioning, crack retardation due to overloads, and elastic-plastic stress redistribution. It is concluded that the code is an acceptable fracture tool for K solutions of simplified geometries, for a limited number of J and crack opening area solutions, and for fatigue crack propagation with the Paris equation and constant amplitude loads when the Paris equation is applicable. Author (revised)

N95-23293*# Norfolk State Univ., VA. Dept. of Physics.
NONDESTRUCTIVE EVALUATION OF FATIGUE DAMAGE IN ALUMINUM 2024 BY X-RAY DIFFRACTION Abstract Only
Milton W. Ferguson *In* Hampton Univ., 1994 NASA-HU American Society for Engineering Education (ASEE) Summer Faculty Fellowship Program Dec. 1994 p 74 (For primary document see N95-23276 07-99)
Avail: CASI HC A01/MF A02

N95-23302*# Thomas Nelson Community Coll., Hampton, VA. Dept. of Engineering and Technology.
RELIABILITY ANALYSIS IN THE OFFICE OF SAFETY, ENVIRONMENTAL, AND MISSION ASSURANCE (OSEMA) Abstract Only
Paul J. Kauffmann *In* Hampton Univ., 1994 NASA-HU American Society for Engineering Education (ASEE) Summer Faculty Fellowship Program Dec. 1994 p 84 (For primary document see N95-23276 07-99)
Avail: CASI HC A01/MF A02

N95-23505# Defence Research Agency, Farnborough, Hampshire (England). Structural Materials Centre.
NON-DESTRUCTIVE DETECTION OF CORROSION FOR LIFE MANAGEMENT
David A. Bruce *In* AGARD, Corrosion Detection and Management of Advanced Airframe Materials Jan. 1995 8 p (For primary document see N95-23496 07-26)
Copyright Avail: CASI HC A02/MF A03

N95-23507# National Aerospace Lab., Amsterdam (Netherlands).
EDDY CURRENT DETECTION OF PITTING CORROSION AROUND FASTENER HOLES
J. H. Heida and W. G. J. tHart *In* AGARD, Corrosion Detection and Management of Advanced Airframe Materials Jan. 1995 10 p Sponsored by Royal Netherlands Air Force (For primary document see N95-23496 07-26)
Copyright Avail: CASI HC A02/MF A03

N95-23512# National Aeronautics and Space Administration. Langley Research Center, Hampton, VA.
NEW NONDESTRUCTIVE TECHNIQUES FOR THE DETECTION AND QUANTIFICATION OF CORROSION IN AIRCRAFT STRUCTURES
W. P. Winfree, K. E. Cramer, P. H. Johnston, and M. Namkung *In* AGARD, Corrosion Detection and Management of Advanced Airframe Materials Jan. 1995 6 p (For primary document see N95-23496 07-26)
Copyright Avail: CASI HC A02/MF A03

N95-23514# KOMPOZIT Corp., Kaliningrad (Russia).
PROBLEMS OF PREDICTING MATERIAL PROPERTY RETENTION DURING LONG TERM SERVICE
Yu. P. Gordeev and A. M. Khomutov *In* AGARD, Corrosion Detection and Management of Advanced Airframe Materials Jan. 1995 6 p (For primary document see N95-23496 07-26)
Copyright Avail: CASI HC A02/MF A03

39 STRUCTURAL MECHANICS

Includes structural element design and weight analysis; fatigue; and thermal stress.

For applications see *05 Aircraft Design, Testing and Performance* and *18 Spacecraft Design, Testing and Performance.*

N95-22500# Sandia National Labs., Albuquerque, NM.
HIGH-VELOCITY PENETRATORS
Ronald G. Lundgren 1994 6 p Presented at the American Institute of Aeronautics and Astronautics Missile Sciences Conference, Monterey, CA, 7-9 Nov. 1994
(Contract DE-AC04-94AL-85000)
(DE95-001886; SAND-94-2724C; CONF-9411142-1) Avail: CASI HC A02/MF A01

This paper summarizes the results of studies, coupled with a series of tests, that investigated rigid-body projectiles (penetrators) at high (up to 5500 ft/sec) velocities. Before these studies, it had been hypothesized that a velocity limit would be reached at which increasing the velocity would not commensurately increase depth of penetration into a target. It was further inferred that a given velocity/ penetration depth curve would avalanche into the hydrodynamic regime; that is, increasing the velocity past a certain point would decrease penetration performance. The test series utilized 1/2-in., 3-in., and 5 1/2-in. diameter, ogive-nose steel projectiles and grout and concrete targets. The tests confirmed that penetration depth increased as striking velocity increased to 4000 ft/sec. However, beyond striking velocities of 4000 ft/sec, asymmetric erosion and indentation of the projectile nose from the aggregate caused the projectile trajectories to deviate severely from the target centerline. These trajectory deviations caused the projectile to exit the side of the target, severely bend, break, or exhibit decreased penetration performance, confirming the hypothesis. Clearly, these results were dependent on the specific material and geometric parameters. The projectiles had 3.0 and 4.25 CRH (Caliber-Radius-Head) nose shapes and were heat-treated to R(sub c) 38-40. The grout targets had a maximum aggregate diameter of 3/16 in. and a nominal unconfined compressive strength of 2.5 ksi. The concrete targets had a maximum aggregate diameter of 3/4 in. and unconfined compressive strength of 5.5 ksi. DOE

N95-22726# Sandia National Labs., Albuquerque, NM. Security and Survivability Dept.
PROJECTILE PENETRATION INTO REPRESENTATIVE TARGETS
George W. Stone Oct. 1994 25 p
(Contract DE-AC04-94AL-85000)
(DE95-003089; SAND-94-1490) Avail: CASI HC A03/MF A01

The differential equation representing the penetration of a 'hard' projectile into semi-infinite, homogeneous target materials is solved for several generic combinations of the target material/projectile characteristics. A 'hard' projectile is defined as one that does not change size or shape and does not lose mass during the penetration process. The target materials evaluated range from the structurally 'soft' materials (liquids) to structurally 'hard' materials (armor plate) with viscous and fluid dynamic drag considered. The solutions to the differential equation(s) are expanded in series form to demonstrate the underlying parameters governing projectile penetration and the way they interact to limit penetration in a given target material. It is shown that the fundamental parameter governing projectile penetration into structurally 'firm' materials is the initial kinetic energy of the projectile divided by the frontal area of the projectile and the inherent structural characteristic of the target. Experimental data on the penetration of steel spheres into ballistic gelatin and for armor piercing bullets into armor plate materials are used to verify the characteristics of the solutions to the equation of motion for the projectile and to demonstrate how penetration can vary with projectile size and target characteristics. The penetration equation for a single 'hard' target material is used to develop a solution for the penetration of multilayered 'hard' target materials. DOE

N95-22773# International Centre for Theoretical Physics, Trieste (Italy).
FLEXURAL VIBRATION OF THIN PIEZOELECTRIC LAMINATE CIRCULAR CYLINDER OF HEXAGONAL SYMMETRY
R. R. Rodriguez and H. S. Camacho Sep. 1993 7 p
(DE94-628474; IC-93/321) Avail: CASI HC A02/MF A01 (US Sales Only)

This paper describes a procedure for calculating the free vibration of thin piezoelectric laminate circular cylinder of hexagonal symmetry for free boundary condition. The vibration is assumed to be governed by the Poisson-Kirchoff theory of flexure, omitting the effects of transverse shear deformation. The frequency equation has been obtained. DOE

N95-22805*# National Aeronautics and Space Administration. Lewis Research Center, Cleveland, OH.
WEIGHT MINIMIZATION OF STRUCTURAL COMPONENTS FOR LAUNCH IN SPACE SHUTTLE
Surya N. Patnaik (Ohio Aerospace Inst., Brook Park, OH.), Atef S. Gendy (Akron Univ., Akron, OH.), Dale A. Hopkins, and Laszlo Berke Nov. 1994 25 p Original contains color illustrations
(Grant NAG3-1350; RTOP 474-46-10)
(NASA-TM-4586; E-8713; NAS 1.15:4586) Avail: CASI HC A03/MF A01; 4 functional color pages

Minimizing the weight of structural components of the space station

launched into orbit in a space shuttle can save cost, reduce the number of space shuttle missions, and facilitate on-orbit fabrication. Traditional manual design of such components, although feasible, cannot represent a minimum weight condition. At NASA Lewis Research Center, a design capability called CometBoards (Comparative Evaluation Test Bed of Optimization and Analysis Routines for the Design of Structures) has been developed especially for the design optimization of such flight components. Two components of the space station - a spacer structure and a support system - illustrate the capability of CometBoards. These components are designed for loads and behavior constraints that arise from a variety of flight accelerations and maneuvers. The optimization process using CometBoards reduced the weights of the components by one third from those obtained with traditional manual design. This paper presents a brief overview of the design code CometBoards and a description of the space station components, their design environments, behavior limitations, and attributes of their optimum designs. Author

N95-22950*# National Aeronautics and Space Administration. Marshall Space Flight Center, Huntsville, AL.

STATISTICALLY GENERATED WEIGHTED CURVE FIT OF RESIDUAL FUNCTIONS FOR MODAL ANALYSIS OF STRUCTURES

P. S. Bookout Washington, DC Feb. 1995 61 p

(NASA-TM-108481; NAS 1.15:108481) Avail: CASI HC A04/MF A01

A statistically generated weighting function for a second-order polynomial curve fit of residual functions has been developed. The residual flexibility test method, from which a residual function is generated, is a procedure for modal testing large structures in an external constraint-free environment to measure the effects of higher order modes and interface stiffness. This test method is applicable to structures with distinct degree-of-freedom interfaces to other system components. A theoretical residual function in the displacement/force domain has the characteristics of a relatively flat line in the lower frequencies and a slight upward curvature in the higher frequency range. In the test residual function, the above-mentioned characteristics can be seen in the data, but due to the present limitations in the modal parameter evaluation (natural frequencies and mode shapes) of test data, the residual function has regions of ragged data. A second order polynomial curve fit is required to obtain the residual flexibility term. A weighting function of the data is generated by examining the variances between neighboring data points. From a weighted second-order polynomial curve fit, an accurate residual flexibility value can be obtained. The residual flexibility value and free-free modes from testing are used to improve a mathematical model of the structure. The residual flexibility modal test method is applied to a straight beam with a trunnion appendage and a space shuttle payload pallet simulator. Author

N95-22952 Defence Science and Technology Organization, Melbourne (Australia). Aeronautical and Maritime Research Lab.

STRESS INTENSITY FACTORS AND CRACK MOUTH OPENINGS FOR BRIDGED CRACKS EMANATING FROM CIRCULAR HOLES

Colin R. Pickthall Jul. 1994 67 p

(AR-008-408; DSTO-RR-0005) Copyright Avail: Issuing Activity (DSTO Aeronautical and Maritime Research Lab., GPO Box 4331, Melbourne, Victoria 3001, Australia)

Muskhelishvili's method of complex potentials has been applied to the problems of one crack, and two diametrically opposed (symmetrical) cracks emanating from a circular hole of radius R, subjected to a biaxial load. The cracks of length a, are orthogonal to the principal applied stress sigma(sub yy)(infinity), with transverse stress sigma(sub xx)(infinity) = lambda sigma(sub yy)(infinity). This work extends previous work through the inclusion of linear springs with spring constant k bridging the crack opening. Analysis focussed on the (normalized) design parameters of crack tip stress intensity factor F(sub n) and crack mouth opening V(sub n). Their dependencies on biaxiality lambda, normalized spring stiffness ka, and the geometry specified by a(sub n) = a/(a + R), were investigated. Interpolation formulae with parameters depending on a(sub n) were fitted to the high and low ka limits of F(sub n) and V(sub n). These provided a simple means for calculating F(sub n) and V(sub n), in most cases to within a few percent of the numerically calculated values. An interesting comparison of the symmetrically cracked hole to the partially bridged center crack, showed that the latter had a lower stress intensity factor in all but the very short crack cases. Author

N95-23662# Technion - Israel Inst. of Tech., Haifa (Israel). Faculty of Aerospace Engineering.

REVIEW OF SOME RESULTS OF THE AUTHOR'S FATIGUE INVESTIGATIONS WITH APPLICATIONS IN ENGINEERING AND MATERIAL SCIENCE

A. Buch Apr. 1994 61 p

(TAE-698) Avail: CASI HC A04/MF A01

This document deals with research results mainly connected with the problem of fatigue calculations and various aspects of fatigue. It contains the following topics: Correlation between fatigue limits and ultimate tensile strength, Fatigue properties of pure metals, Analytical approach to notch-size effects in fatigue of aircraft sheet materials, Torsional fatigue life of axle shafts under program loading, Fatigue properties of aircraft lugs with interference fit, Comparison of various aircraft loading test results with the aid of Relative-Miner-Rule, The Relative Method in the case of Local-Strain-Approach, and Prediction of fatigue life. CASI

N95-23923# Technion - Israel Inst. of Tech., Haifa (Israel). Faculty of Aerospace Engineering.

THE DEVELOPMENT OF SHELL IMPERFECTION MEASUREMENT TECHNIQUES

Josef Singer and Haim Abramovich Apr. 1994 42 p Sponsored in part by the Lena and Ben Fohrman Aerospace Structures Research Fund

(TAE-712) Avail: CASI HC A03/MF A01

The development of the techniques for measurement of geometric imperfections is traced from the sixties to the present. First, the early laboratory experiments which initiated the concepts and developed the basic techniques are outlined. Imperfection measurements of large and full scale shells are then considered, including those performed in industry. Modern, more sophisticated, semi-automated measurement techniques as well as imperfection data banks are discussed. Finally, a design methodology which includes the correlation of realistic imperfections with manufacturing techniques is outlined, and ways are indicated for inclusion of the relevant imperfection data in design methods and recommendations. Author

N95-24055*# National Aeronautics and Space Administration. Lewis Research Center, Cleveland, OH.

THERMOELASTIC THEORY FOR THE RESPONSE OF MATERIALS FUNCTIONALLY GRADED IN TWO DIRECTIONS WITH APPLICATIONS TO THE FREE-EDGE PROBLEM

Jacob Aboudi (Virginia Univ. Hospital, Charlottesville, VA.), Marek-Jerzy Pindera (Virginia Univ. Hospital, Charlottesville, VA.), and Steven M. Arnold Mar. 1995 60 p

(Grant NAG3-1377; RTOP 505-63-12)

(NASA-TM-106882; E-9518; NAS 1.15:106882) Avail: CASI HC A04/MF A01

A recently developed micromechanical theory for the thermoelastic response of functionally graded composites with nonuniform fiber spacing in the through-thickness direction is further extended to enable analysis of material architectures characterized by arbitrarily nonuniform fiber spacing in two directions. In contrast to currently employed micromechanical approaches applied to functionally graded materials, which decouple the local and global effects by assuming the existence of a representative volume element at every point within the composite, the new theory explicitly couples the local and global effects. The analytical development is based on volumetric averaging of the various field quantities, together with imposition of boundary and interfacial conditions in an average sense. Results are presented that illustrate the capability of the derived theory to capture local stress gradients at the free edge of a laminated composite plate due to the application of a uniform temperature change. It is further shown that it is possible to reduce the magnitude of these stress concentrations by a proper management of the microstructure of the composite plies near the free edge. Thus by an appropriate tailoring of the microstructure it is possible to reduce or prevent the likelihood of delamination at free edges of standard composite laminates. Author

N95-24189*# Toledo Univ., OH. Dept. of Mechanical Engineering.

USER'S GUIDE FOR ECAP2D: AN EULER UNSTEADY AERODYNAMIC AND AEROELASTIC ANALYSIS PROGRAM FOR TWO DIMENSIONAL OSCILLATING CASCADES, VERSION 1.0

T. S. R. Reddy Cleveland, OH NASA Apr. 1995 71 p

(Grant NAG3-1137; RTOP 538-06-13)
(NASA-CR-189146; E-9552; NAS 1.26:189146) Avail: CASI HC A04/MF A01

This guide describes the input data required for using ECAP2D (Euler Cascade Aeroelastic Program-Two Dimensional). ECAP2D can be used for steady or unsteady aerodynamic and aeroelastic analysis of two dimensional cascades. Euler equations are used to obtain aerodynamic forces. The structural dynamic equations are written for a rigid typical section undergoing pitching (torsion) and plunging (bending) motion. The solution methods include harmonic oscillation method, influence coefficient method, pulse response method, and time integration method. For harmonic oscillation method, example inputs and outputs are provided for pitching motion and plunging motion. For the rest of the methods, input and output for pitching motion only are given. Author

N95-23280*# Hampton Univ., VA.
INFINITE POSSIBILITIES: COMPUTATIONAL STRUCTURES TECHNOLOGY Abstract Only
Sherilee F. Beam *In its* 1994 NASA-HU American Society for Engineering Education (ASEE) Summer Faculty Fellowship Program Dec. 1994 p 60 (For primary document see N95-23276 07-99)
Avail: CASI HC A01/MF A02

N95-23281*# Carnegie-Mellon Univ., Pittsburgh, PA. Dept. of Mechanical Engineering.
SEPARATION OF CRACK EXTENSION MODES IN COMPOSITE DELAMINATION PROBLEMS Abstract Only
Jack L. Beuth *In* Hampton Univ., 1994 NASA-HU American Society for Engineering Education (ASEE) Summer Faculty Fellowship Program Dec. 1994 p 61 (For primary document see N95-23276 07-99)
Avail: CASI HC A01/MF A02

N95-23310*# Memphis Univ., Memphis, TN. Dept. of Mechanical Engineering.
DEFLECTIONS OF ANISOTROPIC SANDWICH BEAMS WITH VARIABLE FACE SHEETS AND CORE THICKNESSES Abstract Only
Chu-Ho Lu *In* Hampton Univ., 1994 NASA-HU American Society for Engineering Education (ASEE) Summer Faculty Fellowship Program Dec. 1994 p 92 (For primary document see N95-23276 07-99)
Avail: CASI HC A01/MF A02

N95-23311*# Arizona Univ., Tucson, AZ. Dept. of Aerospace and Mechanical Engineering.
RESIDUAL STRENGTH OF THIN PANELS WITH CRACKS Abstract Only
Erdogan Madenci *In* Hampton Univ., 1994 NASA-HU American Society for Engineering Education (ASEE) Summer Faculty Fellowship Program Dec. 1994 p 93 (For primary document see N95-23276 07-99)
Avail: CASI HC A01/MF A02

N95-23321*# Virginia Polytechnic Inst. and State Univ., Blacksburg, VA. Dept. of Mechanical Engineering.
ASSOCIATED WITH AEROSPACE VEHICLES DEVELOPMENT OF METHODOLOGIES FOR THE ESTIMATION OF THERMAL PROPERTIES Abstract Only
Elaine P. Scott *In* Hampton Univ., 1994 NASA-HU American Society for Engineering Education (ASEE) Summer Faculty Fellowship Program Dec. 1994 p 103 (For primary document see N95-23276 07-99)
Avail: CASI HC A01/MF A02

N95-23327*# Oklahoma Univ., Norman, OK. School of Aerospace and Mechanical Engineering.
A NEW LOOK AT THE SIMULTANEOUS ANALYSIS AND DESIGN OF STRUCTURES Abstract Only
Alfred G. Striz *In* Hampton Univ., 1994 NASA-HU American Society for Engineering Education (ASEE) Summer Faculty Fellowship Program Dec. 1994 p 109 (For primary document see N95-23276 07-99)
Avail: CASI HC A01/MF A02

N95-23831*# National Aeronautics and Space Administration. Ames Research Center, Moffett Field, CA.
HYPERVELOCITY IMPACT SURVIVABILITY EXPERIMENTS FOR CARBONACEOUS IMPACTORS, PART 2
T. E. Bunch, Julie M. Paque (Search for Extraterrestrial Intelligence Inst., Mountain View, CA.), Luann Becker (Scripps Institution of Oceanography, La Jolla, CA.), James F. Vedder, and Jozef Erlichman (TMA/Norcal, Richmond, CA.) *In* NASA. Langley Research Center, LDEF: 69 Months in Space. Third Post-Retrieval Symposium, Part 1 Feb. 1995 p 385-399 (For primary document see N95-23796 07-99)
Avail: CASI HC A03/MF A04

N95-23838*# National Aeronautics and Space Administration. Ames Research Center, Moffett Field, CA.
IMAGE AND COMPOSITIONAL CHARACTERISTICS OF THE LDEF BIG GUY IMPACT CRATER
T. E. Bunch, Julie M. Paque (Search for Extraterrestrial Intelligence Inst., Mountain View, CA.), and Michael Zolensky (National Aeronautics and Space Administration. Lyndon B. Johnson Space Center, Houston, TX.) *In* NASA. Langley Research Center, LDEF: 69 Months in Space. Third Post-Retrieval Symposium, Part 1 Feb. 1995 p 475-481 (For primary document see N95-23796 07-99)
Avail: CASI HC A02/MF A04

N95-23839*# Auburn Univ., AL. Space Power Inst.
THE EFFECT OF IMPACT ANGLE ON CRATERS FORMED BY HYPERVELOCITY PARTICLES
David C. Hill, M. Frank Rose, Steve R. Best, Michael S. Crumpler, Gary D. Crawford, Ralph H.-C. Zee, and Michael J. Bozack *In* NASA. Langley Research Center, LDEF: 69 Months in Space. Third Post-Retrieval Symposium, Part 1 Feb. 1995 p 483-498 (For primary document see N95-23796 07-99)
(Grant NAG1-1329)
Avail: CASI HC A03/MF A04

N95-23840*# Kent Univ., Canterbury (England). Unit for Space Sciences.
EXPERIMENTAL INVESTIGATION OF THE RELATIONSHIP BETWEEN IMPACT CRATER MORPHOLOGY AND IMPACTING PARTICLE VELOCITY AND DIRECTION
N. G. Mackay, S. F. Green, D. J. Gardner, and J. A. M. McDonnell *In* NASA. Langley Research Center, LDEF: 69 Months in Space. Third Post-Retrieval Symposium, Part 1 Feb. 1995 p 499-508 (For primary document see N95-23796 07-99)
Avail: CASI HC A02/MF A04

N95-23841*# Technische Univ., Munich (Germany). Lehrstuhl fuer Raumfahrttechnik.
DETERMINING ORBITAL PARTICLE PARAMETERS OF IMPACTS INTO GERMANIUM USING MORPHOLOGY ANALYSIS AND CALIBRATION DATA FROM HYPERVELOCITY IMPACT EXPERIMENTS IN THE LABORATORY
Klaus G. Paul *In* NASA. Langley Research Center, LDEF: 69 Months in Space. Third Post-Retrieval Symposium, Part 1 Feb. 1995 p 509-520 (For primary document see N95-23796 07-99)
(Contract DARA-50-QV-9194-0)
Avail: CASI HC A03/MF A04

N95-23842*# National Aeronautics and Space Administration. Lyndon B. Johnson Space Center, Houston, TX.
CRATERING AND PENETRATION EXPERIMENTS IN TEFLON TARGETS AT VELOCITIES FROM 1 TO 7 km/s Abstract Only
Friedrich Hoerz, Ronald P. Bernhard (Lockheed Engineering and Sciences Co., Houston, TX.), Mark J. Cintala, and Thomas H. See (Lockheed Engineering and Sciences Co., Houston, TX.) *In* NASA. Langley Research Center, LDEF: 69 Months in Space. Third Post-Retrieval Symposium, Part 1 Feb. 1995 p 521 (For primary document see N95-23796 07-99)
Avail: CASI HC A01/MF A04

42 GEOSCIENCES (GENERAL)

N95-22639# Wageningen Agricultural Univ. (Netherlands).
HAPEX-SAHEL: BASIC DESCRIPTION OF METHODS AND DATA SETS
M. Soet, P. Droogers, M. N. Jaarsma, C. P. Kim, and J. F. Monincx Dec. 1993 80 p Sponsored by Commission of the European Communities, Brussels, Belgium
(PB95-127262) Avail: CASI HC A05/MF A01

The Hydrological Atmospheric Pilot EXperiment in the Sahel (HAPEX-Sahel) is developed to improve the understanding of interactions between the land surface and the atmosphere in semi-arid areas. HAPEX-Sahel includes an intensive field experiment from August 15 to October 9, 1992 (Special Observation Period, SOP) and longterm extensive monitoring of soil and weather characteristics as rainfall and soil moisture. This report documents the field-activities and the resulting datasets. For that reason, the depicted results are hardly analyses. The first part of this report describes the set-up and methods used to determine the different characteristics. In the second part the data are described and some preliminary results are given. All data-sets, described in appendix 2, are also available on diskette. In addition to this report, slides and photographs from the SOP are available. NTIS

N95-23844*# Jet Propulsion Lab., California Inst. of Tech., Pasadena, CA.
SUMMARIES OF THE 4TH ANNUAL JPL AIRBORNE GEOSCIENCE WORKSHOP. VOLUME 1: AVIRIS WORKSHOP
Robert O. Green, ed. 25 Oct. 1993 219 p Workshop held in Washington, DC, 25-29 Oct. 1993 Contains 35mm slides as supplement
(Contract NAS7-918; RTOP 465-01-00)
(NASA-CR-197877-Vol-1; JPL-Publ-93-26-Vol-1; NAS 1.26:197877-Vol-1)
Avail: CASI HC A10/MF A03

This publication contains the summaries for the Fourth Annual JPL Airborne Geoscience Workshop, held in Washington, D. C. October 25-29, 1993 The main workshop is divided into three smaller workshops as follows: The Airborne Visible/Infrared Imaging Spectrometer (AVIRIS) workshop, October 25-26 (the summaries for this workshop appear in this volume, Volume 1); The Thermal Infrared Multispectral Scanner (TMIS) workshop, on October 27 (the summaries for this workshop appear in Volume 2); and The Airborne Synthetic Aperture Radar (AIRSAR) workshop, October 28-29 (the summaries for this workshop appear in Volume 3). For individual titles, see N95-23845 through N95-23895.

N95-23845*# National Aeronautics and Space Administration. Ames Research Center, Moffett Field, CA.
USE OF SPECTRAL ANALOGY TO EVALUATE CANOPY REFLECTANCE SENSITIVITY TO LEAF OPTICAL PROPERTY Abstract Only **c43**
Frederic Baret (Institut National de la Recherche Agronomique, Montfavet, France.), Vern C. Vanderbilt, Michael D. Steven (Nottingham Univ., England.), and Stephane Jacquemoud (Joint Research Centre of the European Communities, Ispra, Italy.) *In* JPL, Summaries of the 4th Annual JPL Airborne Geoscience Workshop. Volume 1: AVIRIS Workshop 25 Oct. 1993 p 1 (For primary document see N95-23844 07-42)
Avail: CASI HC A01/MF A03

The spectral variation of canopy reflectance is mostly governed by the absorption properties of the elements, hence the leaves, since their intrinsic scattering properties show very little spectral variation. The relationship between canopy reflectance and leaf reflectance measured at the red edge over sugar beet canopies was used to simulate canopy reflectance from leaf reflectance spectra measured over the whole spectral domain. The results show that the spectral analogies found allows accurate reconstruction of canopy reflectance spectra. Explicit assumptions about the very low spectral variation of leaf intrinsic scattering properties are thus indirectly justified. The sensitivity of canopy reflectance (rho(sub c)) to leaf optical properties can then be investigated from concurrent spectral variations of canopy (delta rho(sub c)/delta lambda) and leaf reflectance (delta rho(sub l)/delta lambda): (delta rho(sub c))/(delta rho(sub l)) = ((delta rho(sub c))/(delta lambda) ((delta rho(sub l))/(delta lambda))(sup -1)). This expression is strictly valid only when the optical properties of the soil background or the other vegetation elements such as bark are either spectrally flat or do not contribute significantly to canopy reflectance. Simulations using the SAIL and PROSPECT models demonstrate that the sensitivity of canopy reflectance to leaf reflectance is significant for large vegetation cover fractions in spectral domains where absorption is low. In these conditions, multiple, scattering enhances the leaf absorption features by a factor that can be greater than 2.0. To override the limitations of the SAIL model for the description of the canopy architecture, we tested the previous findings on experimental data. Concurrent canopy and leaf reflectance spectra were measured for a range of sugar beet canopies. The results show good agreement with the theoretical findings. Conclusions are drawn about the applicability of these findings, with particular attention to the potential detectability of leaf biochemical composition from canopy reflectance sensed from space. Author

N95-23846*# Colorado Univ., Boulder, CO. Center for Study of Earth from Space.
A TOOL FOR MANUAL ENDMEMBER SELECTION AND SPECTRAL UNMIXING **c43**
C. Ann Bateson and Brian Curtiss *In* JPL, Summaries of the 4th Annual JPL Airborne Geoscience Workshop. Volume 1: AVIRIS Workshop 25 Oct. 1993 p 3-6 (For primary document see N95-23844 07-42)
Avail: CASI HC A01/MF A03

Sampling a continuous radiance spectrum in many narrow contiguous spectral bands results in a high covariance between the bands. Hence, the true dimensionality of imaging spectrometer data is not determined by the number of spectral bands, but by the number of spectrally unique signatures whose mixtures reproduce the spectral variance observed in an image. Methods to unmix high dimensional multispectral data use principal components analysis to reduce the dimensionality. The variance of the spectral data is modeled as a linear combination of a finite set of endmembers in the space of the eigen-vectors that account for most of the variance. The number and characteristics of these endmembers are determined not only by the number and characteristics of the spectrally unique materials on the surface but also by processes (e.g., illumination, atmospheric scattering and absorption) affecting the signal received by the sensor. Selection of endmember spectra has typically been from a library. However, since most libraries are incomplete and do not account for the processes mentioned above, we have devised a computer display that allows researchers to explore interactively the eigenvector space of a representative and mean-corrected subset of the image data in search of extreme spectra to designate as endmembers. This display, which is based on parallel coordinates, is unique in the area of multidimensional visualization in that it includes not only a passive view of higher dimensional data but also the capability to interact and move geometrical objects in higher dimensional spaces. Author

N95-23847*# Jet Propulsion Lab., California Inst. of Tech., Pasadena, CA. Dept. of Geology and Planetary Science.
LITHOLOGIC DISCRIMINATION AND ALTERATION MAPPING FROM AVIRIS DATA, SOCORRO, NEW MEXICO **c43**
K. K. Beratan (Pittsburgh Univ., Pittsburgh, PA.), N. DeLillo (Pittsburgh Univ., Pittsburgh, PA.), A. Jacobson, R. Blom, and C. E. Chapin (New Mexico Inst. of Mining and Technology, Socorro, NM.) *In its* Summaries of the 4th Annual JPL Airborne Geoscience Workshop. Volume 1: AVIRIS Workshop 25 Oct. 1993 p 7-10 (For primary document see N95-23844 07-42)
Avail: CASI HC A01/MF A03

Geologic maps are, by their very nature, interpretive documents. In contrasts, images prepared from AVIRIS data can be used as uninterpreted, and thus unbiased, geologic maps. We are having significant success applying AVIRIS data in this non-quantitative manner to geologic problems. Much of our success has come from the power of the Linked Windows Interactive Data System. LinkWinds is a visual data analysis and exploration system under development at JPL which is designed to rapidly and interactively investigate large multivariate data sets. In this paper, we present information on the analysis technique, and preliminary results from research on potassium metasomatism, a distinctive and structurally significant type of alteration associated with crustal extension. Author

N95-23848*# Colorado Univ., Boulder, CO. Center for the Study of Earth from Space.

AUTOMATING SPECTRAL UNMIXING OF AVIRIS DATA USING CONVEX GEOMETRY CONCEPTS **c82**

Joseph W. Boardman *In* JPL, Summaries of the 4th Annual JPL Airborne Geoscience Workshop. Volume 1: AVIRIS Workshop 25 Oct. 1993 p 11-14 (For primary document see N95-23844 07-42)
(Contract NAS5-31711)
Avail: CASI HC A01/MF A03

Spectral mixture analysis, or unmixing, has proven to be a useful tool in the semi-quantitative interpretation of AVIRIS data. Using a linear mixing model and a set of hypothesized endmember spectra, unmixing seeks to estimate the fractional abundance patterns of the various materials occurring within the imaged area. However, the validity and accuracy of the unmixing rest heavily on the 'user-supplied' set of endmember spectra. Current methods for emdmember determination are the weak link in the unmixing chain. Author

N95-23849*# University of South Florida, Saint Petersburg, FL. Dept. of Marine Science.

AVIRIS CALIBRATION USING THE CLOUD-SHADOW METHOD **c82**

K. L. Carder, P. Reinersman, and R. F. Chen *In* JPL, Summaries of the 4th Annual JPL Airborne Geoscience Workshop. Volume 1: AVIRIS Workshop 25 Oct. 1993 p 15-18 (For primary document see N95-23844 07-42)
Avail: CASI HC A01/MF A03

More than 90 percent of the signal at an ocean-viewing, satellite sensor is due to the atmosphere, so a 5 percent sensor-calibration error viewing a target that contributes but 10 percent of the signal received at the sensor may result in a target-reflectance error of more than 50 percent. Since prelaunch calibration accuracies of 5 percent are typical of space-sensor requirements, recalibration of the sensor using ground-base methods is required for low-signal target. Known target reflectance or water-leaving radiance spectra and atmospheric correction parameters are required. In this article we describe an atmospheric-correction method that uses cloud shadowed pixels in combination with pixels in a neighborhood region of similar optical properties to remove atmospheric effects from ocean scenes. These neighboring pixels can then be used as known reflectance targets for validation of the sensor calibration and atmospheric correction. The method uses the difference between water-leaving radiance values for these two regions. This allows nearly identical optical contributions to the two signals (e.g., path radiance and Fresnel-reflected skylight) to be removed, leaving mostly solar photons backscattered from beneath the sea to dominate the residual signal. Normalization by incident solar irradiance reaching the sea surface provides the remote-sensing reflectance of the ocean at the location of the neighbor region. Author

N95-23850*# Jet Propulsion Lab., California Inst. of Tech., Pasadena, CA.

FIELD OBSERVATIONS USING AN AOTF POLARIMETRIC IMAGING SPECTROMETER **c43**

Li-Jen Cheng, Mike Hamilton, Colin Mahoney, and George Reyes *In its* Summaries of the 4th Annual JPL Airborne Geoscience Workshop. Volume 1: AVIRIS Workshop 25 Oct. 1993 p 19-22 (For primary document see N95-23844 07-42)
Avail: CASI HC A01/MF A03

This paper reports preliminary results of recent field observations using a prototype acousto-optic tunable filter (AOTF) polarimetric imaging spectrometer. The data illustrate application potentials for geoscience. The operation principle of this instrument is different from that of current airborne multispectral imaging instruments, such as AVIRIS. The AOTF instrument takes two orthogonally polarized images at a desired wavelength at one time, whereas AVIRIS takes a spectrum over a predetermined wavelength range at one pixel at a time and the image is constructed later. AVIRIS does not have any polarization measuring capability. The AOTF instrument could be a complement tool to AVIRIS. Polarization measurement is a desired capability for many applications in remote sensing. It is well know that natural light is often polarized due to various scattering phenomena in the atmosphere. Also, scattered light from canopies is reported to have a polarized component. To characterize objects of interest correctly requires a remote sensing imaging spectrometer capable of measuring object signal and background radiation in both intensity and polarization so that the characteristics of the object can be determined. The AORF instrument has the capability to do so. The AOTF instrument has other unique properties. For example, it can provide spectral images immediately after the observation. The instrument can also allow observations to be tailored in real time to perform the desired experiments and to collect only required data. Consequently, the performance in each mission can be increased with minimal resources. The prototype instrument was completed in the beginning of this year. A number of outdoor field experiments were performed with the objective to evaluate the capability of this new technology for remote sensing applications and to determine issues for further improvements. Author

N95-23851*# Jet Propulsion Lab., California Inst. of Tech., Pasadena, CA.

INSTANTANEOUS FIELD OF VIEW AND SPATIAL SAMPLING OF THE AIRBORNE VISIBLE/INFRARED IMAGING SPECTROMETER (AVIRIS) **c43**

Thomas G. Chrien and Robert O. Green *In its* Summaries of the 4th Annual JPL Airborne Geoscience Workshop. Volume 1: AVIRIS Workshop 25 Oct. 1993 p 23-26 (For primary document see N95-23844 07-42)
Avail: CASI HC A01/MF A03

The Airborne Visible/Infrared Imaging Spectrometer (AVIRIS) measures the upwelling radiance in 224 spectral bands. These data are required as images of approximately 11 by up to 100 km in extent at nominally 20 by 20 meter spatial resolution. In this paper we describe the underlying spatial sampling and spatial response characteristics of AVIRIS. Author

N95-23852*# Jet Propulsion Lab., California Inst. of Tech., Pasadena, CA.

AIRBORNE VISIBLE/INFRARED IMAGING SPECTROMETER (AVIRIS): RECENT IMPROVEMENTS TO THE SENSOR **c35**

Thomas G. Chrien, Robert O. Green, Charles M. Sarture, Christopher Chovit, Michael L. Eastwood, and Bjorn T. Eng *In its* Summaries of the 4th Annual JPL Airborne Geoscience Workshop. Volume 1: AVIRIS Workshop 25 Oct. 1993 p 27-30 (For primary document see N95-23844 07-42)
Avail: CASI HC A01/MF A03

AVIRIS is a NASA-sponsored Earth-looking imaging spectrometer designed, built and operated by the Jet Propulsion Laboratory. Spectral, radiometric and geometric characteristics of the data acquired by AVIRIS are given in Table 1. AVIRIS has been operational since 1989, however in each year since 1989 major improvements have been completed in most of the subsystems of the sensor. As a consequence of these efforts, the capabilities of AVIRIS to acquire and deliver calibrated imaging spectrometer data of high quality have improved significantly over those in 1989. Improvements to AVIRIS prior to 1992 have been described previously (Porter et al., 1990, Chrien et al., 1991, & Chrien et al., 1992). In the following sections of this paper we describe recent and planned improvements to AVIRIS in the sensor task. Author

N95-23853*# Geological Survey, Denver, CO.

COMPARISON OF THREE METHODS FOR MATERIALS IDENTIFICATION AND MAPPING WITH IMAGING SPECTROSCOPY **c43**

Roger N. Clark, Gregg Swayze (Colorado Univ., Boulder, CO.), Joe Boardman (Colorado Univ., Boulder, CO.), and Fred Kruse (Colorado Univ., Boulder, CO.) *In* JPL, Summaries of the 4th Annual JPL Airborne Geoscience Workshop. Volume 1: AVIRIS Workshop 25 Oct. 1993 p 31-33 (For primary document see N95-23844 07-42)
Avail: CASI HC A01/MF A03

We are comparing three methods of mapping analysis tools for imaging spectroscopy data. The purpose of this comparison is to understand the advantages and disadvantages of each algorithm so others would be better able to choose the best algorithm or combinations of algorithms for a particular problem. The three algorithms are: (1) the spectralfeature modified least squares mapping algorithm of Clark et al (1990, 1991): programs mbandmap and tricorder; (2) the Spectral Angle Mapper Algorithm(Boardman, 1993) found in the CU CSES SIPS package; and (3) the Expert System of Kruse et al. (1993). The comparison uses a ground-calibrated 1990 AVIRIS scene of 400 by 410 pixels over Cuprite, Nevada. Along with the test data set is a spectral library of 38 minerals. Each algorithm is tested with the same AVIRIS data set and spectral library. Field work has confirmed the

presence of many of these minerals in the AVIRIS scene (Swayze et al. 1992). Author

N95-23854*# Jet Propulsion Lab., California Inst. of Tech., Pasadena, CA.

COMPARISON OF METHODS FOR CALIBRATING AVIRIS DATA TO GROUND REFLECTANCE **c82**

Roger N. Clark (Geological Survey, Denver, CO.), Gregg Swayze (Geological Survey, Denver, CO.), Kathy Heidebrecht (Colorado Univ., Boulder, CO.), Alexander F. H. Goetz (Colorado Univ., Boulder, CO.), and Robert O. Green *In its* Summaries of the 4th Annual JPL Airborne Geoscience Workshop. Volume 1: AVIRIS Workshop 25 Oct. 1993 p 35-36 (For primary document see N95-23844 07-42)

Avail: CASI HC A01/MF A03

We are comparing three basic methods of calibrating AVIRIS data to ground reflectance: (1) atmospheric radiative transfer models with the solar flux can be used to calibrate AVIRIS radiance data (Specific methods include the University of Colorado CSES ARP and ATREM algorithms); (2) Robert Green's modified MODTRAN and AVIRIS radiance model (This method is similar to 1 but differs in that the solar radiance is bypassed, so any errors in the solar flux are canceled, too); and (3) ground calibration using known sites in the AVIRIS scene. We are using 1992AVIRIS data over Cuprite, Nevada, and Blackhawk Island, Wisconsin, as our test scenes. Both these sites have extensive field measurements. The Cuprite site had a very clear atmosphere, thus path radiance was dominated by Rayleigh scattering with little or no flux beyond 1 micron. The Blackhawk site has more aerosols, with significant path radiance flux beyond 2 micron.

Author

N95-23855*# Geological Survey, Denver, CO.

THE US GEOLOGICAL SURVEY, DIGITAL SPECTRAL REFLECTANCE LIBRARY: VERSION 1: 0.2 TO 3.0 MICRONS Abstract Only **c82**

Roger N. Clark, Gregg A. Swayze, Trude V. V. King, Andrea J. Gallagher, and Wendy M. Calvin (Geological Survey, Flagstaff, AZ.) *In* JPL, Summaries of the 4th Annual JPL Airborne Geoscience Workshop. Volume 1: AVIRIS Workshop 25 Oct. 1993 p 3 (For primary document see N95-23844 07-42)

Avail: CASI HC A01/MF A03

We have developed a digital reflectance spectral library, with management and spectral analysis software. The library includes 500 spectra of 447 samples (some samples include a series of grain sizes) measured from approximately 0.2 to 3.0 microns. The spectral resolution (Full Width Half Maximum) of the reflectance data is less than or equal to 4 nm in the visible (0.2-0.8 microns) and less than or equal 10 nm in the NIR (0.8-2.35 microns). All spectra were corrected to absolute reflectance using an NBS Halon standard. Library management software lets users search on parameters (e.g. chemical formulae, chemical analyses, purity of samples, mineral groups, etc.) as well as spectral features. Minerals from sulfide, oxide, hydroxide, halide, carbonate, nitrate, borate, phosphate, and silicate groups are represented. X-ray and chemical analyses are tabulated for many of the entries, and all samples have been evaluated for spectral purity. The library also contains end and intermediate members for the olivine, garnet, scapolite, montmorillonite, muscovite, jarosite, and alunite solid-solution series. We have included representative spectra of H2O ice, kerogen, ammonium-bearing minerals, rare-earth oxides, desert varnish coatings, kaolinite crystallinity series, kaolinite-smectite series, zeolite series, and an extensive evaporite series. Because of the importance of vegetation to climate-change studies we have include 17 spectra of tree leaves, bushes, and grasses. Author

N95-23856*# Jet Propulsion Lab., California Inst. of Tech., Pasadena, CA.

APPLICATION OF A TWO-STREAM RADIATIVE TRANSFER MODEL FOR LEAF LIGNIN AND CELLULOSE CONCENTRATIONS FROM SPECTRAL REFLECTANCE MEASUREMENTS, PART 1 **c43**

James E. Conel, Jeannette vandenBosch, and Cindy I. Grove *In its* Summaries of the 4th Annual JPL Airborne Geoscience Workshop. Volume 1: AVIRIS Workshop 25 Oct. 1993 p 39-44 (For primary document see N95-23844 07-42)

Avail: CASI HC A01/MF A03

Lignin and nitrogen contents of leaves constitute the primary rate-limiting parameters for the decomposition of forest litter, and are determinants of nutrient- and carbon-cyclic rates in forest ecosystems (Melillo et al., 1982). Wessman et al. (1988a) developed empirical multivariate relationships between forest canopy lignin amount and the (first-difference) AIS spectral response in three bands spread over the wavelength interval 1256-1555 nm. Wessman et al. (1988b) and McLellan et al. (1991) developed similar regression relationships from laboratory reflectance measurements on dried samples prepared in a standard fashion. They used four to six infrared bands for analysis of nitrogen, lignin and cellulose content of foliage in forest and prairie species. In the present article (Parts 1 and 2) the feasibility of compositional determinations is explored using positions of composite absorption bands that originate from mixtures of lignin, cellulose, and possibly other chemical constituents in the spectral reflectance of green leaves. To carry out this program, we employ full-spectral-resolution single-leaf diffuse reflectance measurements made with a laboratory spectrometer and integrating sphere. The leaf and other chemical reflectance data compiled by Elvidge (1990) have also been utilized extensively. Author

N95-23857*# Jet Propulsion Lab., California Inst. of Tech., Pasadena, CA.

APPLICATION OF A TWO-STREAM RADIATIVE TRANSFER MODEL FOR LEAF LIGNIN AND CELLULOSE CONCENTRATIONS FROM SPECTRAL REFLECTANCE MEASUREMENTS, PART 2 **c43**

James E. Conel, Jeannette vandenBosch, and Cindy I. Grove *In its* Summaries of the 4th Annual JPL Airborne Geoscience Workshop. Volume 1: AVIRIS Workshop 25 Oct. 1993 p 45-51 (For primary document see N95-23844 07-42)

Avail: CASI HC A02/MF A03

We used the Kubelka-Munk theory of diffuse spectral reflectance in layers to analyze influences of multiple chemical components in leaves. As opposed to empirical approaches to estimation of plant chemistry, the full spectral resolution of laboratory reflectance data was retained in an attempt to estimate lignin or other constituent concentrations from spectral band positions. A leaf water reflectance spectrum was derived from theoretical mixing rules, reflectance observations, and calculations from theory of intrinsic k- and s-functions. Residual reflectance bands were then isolated from spectra of fresh green leaves. These proved hard to interpret for composition in terms of simple two component mixtures such as lignin and cellulose. We next investigated spectral and dilution influences of other possible components (starch, protein). These components, among others, added to cellulose in hypothetical mixtures, produce band displacements similar to lignin, but will disguise by dilution the actual abundance of lignin present in a multicomponent system. This renders interpretation of band positions problematical. Knowledge of end-members and their spectra, and a more elaborate mixture analysis procedure may be called for. Good observational atmospheric and instrumental conditions and knowledge thereof are required for retrieval of expected subtle reflectance variations present in spectra of green vegetation. Author

N95-23858*# Naval Research Lab., Washington, DC. HYDICE Project Office.

DISCRIMINATION OF POORLY EXPOSED LITHOLOGIES IN AVIRIS DATA **c82**

William H. Farrand and Joseph C. Harsanyi *In* JPL, Summaries of the 4th Annual JPL Airborne Geoscience Workshop. Volume 1: AVIRIS Workshop 25 Oct. 1993 p 53-56 (For primary document see N95-23844 07-42)

Avail: CASI HC A01/MF A03

One of the advantages afforded by imaging spectrometers such as AVIRIS is the capability to detect target materials at a sub-pixel scale. This paper presents several examples of the identification of poorly exposed geologic materials - materials which are either subpixel in scale or which, while having some surface expression over several pixels, are partially covered by vegetation or other materials. Sabol et al. (1992) noted that a primary factor in the ability to distinguish sub-pixel targets is the spectral contrast between the target and its surroundings. In most cases, this contrast is best expressed as an absorption feature or features present in the target but absent in the surroundings. Under such circumstances, techniques such as band depth mapping (Clark et al., 1992) are feasible. However, the only difference between a target material and its surroundings is often expressed solely in the continuum. We define the 'continuum' as the reflectance or radiance spanning spectral space between spectral features. Differences in continuum slope and shape can only be determined

by reduction techniques which considers the entire spectral range; i.e., techniques such as spectral mixture analysis (Adams et al., 1989) and recently developed techniques which utilize an orthogonal subspace projection operator (Harsanyi, 1993). Two of the three examples considered herein deal with cases where the target material differs from its surroundings only by such a subtle continuum change. Author

N95-23859*# Geological Survey, Flagstaff, AZ.
SPECTRAL DECOMPOSITION OF AVIRIS DATA **c82**
Lisa Gaddis, Laurence Soderblom, Hugh Kieffer, Kris Becker, Jim Torson, and Kevin Mullins *In* JPL, Summaries of the 4th Annual JPL Airborne Geoscience Workshop. Volume 1: AVIRIS Workshop 25 Oct. 1993 p 57-60 (For primary document see N95-23844 07-42)
Avail: CASI HC A01/MF A03

A set of techniques is presented that uses only information contained within a raw Airborne Visible/Infrared Imaging Spectrometer (AVIRIS) scene to estimate and to remove additive components such as multiple scattering and instrument dark current. Multiplicative components (instrument gain, topographic modulation of brightness, atmospheric transmission) can then be normalized, permitting enhancement, extraction, and identification of relative reflectance information related to surface composition and mineralogy. The technique for derivation of additive-component spectra from a raw AVIRIS scene is an adaption of the 'regression intersection method' of Crippen. This method uses two surface units that are spatially extensive, and located in rugged terrain. For a given wavelength pair, subtraction of the derived additive component from individual band values will remove topography in both regions in a band/band ratio image. Normalization of all spectra in the scene to the average scene spectrum then results in cancellation of multiplicative components and production of a relative-reflectance scene. The resulting AVIRIS product contains relative-reflectance features due to mineral absorption that depart from the average spectrum. These features commonly are extremely weak and difficult to recognize, but they can be enhanced by using two simple 3-D image-processing tools. The validity of these techniques will be demonstrated by comparisons between relative-reflectance AVIRIS spectra and those derived by using JPL standard calibrations. The AVIRIS data used in this analysis were acquired over the Kelso Dunes area (34 deg 55' N, 115 deg 43' W) of the eastern Mojave Desert, CA (in 1987) and the Upheaval Dome area (38 deg 27' N, 109 deg 55' W) of the Canyonlands National Park, UT (in 1991). Derived from text

N95-23860*# Jet Propulsion Lab., California Inst. of Tech., Pasadena, CA.
REMOTE SENSING OF SMOKE, CLOUDS, AND FIRE USING AVIRIS DATA **c43**
Bo-Cai Gao (Universities Space Research Association, Greenbelt, MD.), Yorman J. Kaufman (National Aeronautics and Space Administration. Goddard Space Flight Center, Greenbelt, MD.), and Robert O. Green *In its* Summaries of the 4th Annual JPL Airborne Geoscience Workshop. Volume 1: AVIRIS Workshop 25 Oct. 1993 p 61-64 (For primary document see N95-23844 07-42)
Avail: CASI HC A01/MF A03

Clouds remain the greatest element of uncertainty in predicting global climate change. During deforestation and biomass burning processes, a variety of atmospheric gases, including CO2 and SO2, and smoke particles are released into the atmosphere. The smoke particles can have important effects on the formation of clouds because of the increased concentration of cloud condensation nuclei. They can also affect cloud albedo through changes in cloud microphysical properties. Recently, great interest has arisen in understanding the interaction between smoke particles and clouds. We describe our studies of smoke, clouds, and fire using the high spatial and spectral resolution data acquired with the NASA/JPL Airborne Visible/Infrared Imaging Spectrometer (AVIRIS). Derived from text

N95-23861*# Jet Propulsion Lab., California Inst. of Tech., Pasadena, CA.
USE OF DATA FROM THE AVIRIS ONBOARD CALIBRATOR **c82**
Robert O. Green *In its* Summaries of the 4th Annual JPL Airborne Geoscience Workshop. Volume 1: AVIRIS Workshop 25 Oct. 1993 p 65-68 (For primary document see N95-23844 07-42)
Avail: CASI HC A01/MF A03

The AVIRIS onboard calibrator became operational in 1992. This subsystem on the AVIRIS sensor has operated nominally throughout the 1992 and 1993 flight season. This paper describes the data measured by the onboard calibration and the two primary uses of these data. First, the data may be used to optimize the tractability of the calibration of the delivered AVIRIS data to the laboratory radiometric calibration standard. Second, these data may be used to monitor and normalize the inflight radiometric performance of AVIRIS through the flight season. Author (revised)

N95-23862*# Jet Propulsion Lab., California Inst. of Tech., Pasadena, CA.
INFLIGHT CALIBRATION OF AVIRIS IN 1992 AND 1993 **c35**
Robert O. Green, James E. Conel, Mark Helmlinger, Jeannette vandenBosch, Chris Chovit, and Tom Chrien *In its* Summaries of the 4th Annual JPL Airborne Geoscience Workshop. Volume 1: AVIRIS Workshop 25 Oct. 1993 p 69-72 (For primary document see N95-23844 07-42)
Avail: CASI HC A01/MF A03

In order to pursue the quantitative research objective of AVIRIS, the spectral, radiometric characteristic of the sensor must be known at the time of flight data acquisition. AVIRIS is rigorously calibrated in the laboratory. In addition, three times each year these characteristics of AVIRIS are validated through an inflight calibration experiment. Absolute radiometric calibration and signal-to-noise results are present for the inflight calibration experiment orchestrated in 1992 and 1993. Author

N95-23863*# Jet Propulsion Lab., California Inst. of Tech., Pasadena, CA.
ESTIMATION OF AEROSOL OPTICAL DEPTH AND ADDITIONAL ATMOSPHERIC PARAMETERS FOR THE CALCULATION OF APPARENT REFLECTANCE FROM RADIANCE MEASURED BY THE AIRBORNE VISIBLE/INFRARED IMAGING SPECTROMETER **c43**
Robert O. Green, James E. Conel, and Dar A. Roberts (Washington Univ., Seattle, WA.) *In its* Summaries of the 4th Annual JPL Airborne Geoscience Workshop. Volume 1: AVIRIS Workshop 25 Oct. 1993 p 73-76 (For primary document see N95-23844 07-42)
Avail: CASI HC A01/MF A03

The Airborne Visible/Infrared Imaging Spectrometer (AVIRIS) measures spatial images of the total upwelling spectral radiance from 400 to 2500 nm through 10 nm spectral channels. Quantitative research and application objectives for surface investigations require inversion of the measured radiance of surface reflectance or surface leaving radiance. To calculate apparent surface reflectance, estimates of atmospheric water vapor abundance, cirrus cloud effects, surface pressure elevation, and aerosol optical depth are required. Algorithms for the estimation of these atmospheric parameters from the AVIRIS data themselves are described. From these atmospheric parameters we show an example of the calculation of apparent surface reflectance from the AVIRIS-measured radiance using a radiative transfer code. Author

N95-23864*# Jet Propulsion Lab., California Inst. of Tech., Pasadena, CA.
USE OF THE AIRBORNE VISIBLE/INFRARED IMAGING SPECTROMETER TO CALIBRATE THE OPTICAL SENSOR ON BOARD THE JAPANESE EARTH RESOURCES SATELLITE-1 **c19**
Robert O. Green, James E. Conel, Jeannette vandenBosch, and Masanobu Shimada (National Space Development Agency, Ohashi, Japan.) *In its* Summaries of the 4th Annual JPL Airborne Geoscience Workshop. Volume 1: AVIRIS Workshop 25 Oct. 1993 p 77-80 Sponsored by NASDA (For primary document see N95-23844 07-42)
Avail: CASI HC A01/MF A03

We describe an experiment to calibrate the optical sensor (OPS) on board the Japanese Earth Resources Satellite-1 with data acquired by the Airborne Visible/Infrared Imaging Spectrometer (AVIRIS). On 27 Aug. 1992 both the OPS and AVIRIS acquired data concurrently over a calibration target on the surface of Rogers Dry Lake, California. The high spectral resolution measurements of AVIRIS have been convolved to the spectral response curves of the OPS. These data in conjunction with the corresponding OPS digitized numbers have been used to generate the radiometric calibration coefficients for the eight OPS bands. This experiment establishes the suitability of AVIRIS for the calibration of spaceborne sensors in the 400 to 2500 nm spectral region. Author

N95-23865*# Jet Propulsion Lab., California Inst. of Tech., Pasadena, CA.

A PROPOSED UPDATE TO THE SOLAR IRRADIANCE SPECTRUM USED IN LOWTRAN AND MODTRAN **c92**

Robert O. Green and Bo-Cai Gao (National Aeronautics and Space Administration. Goddard Space Flight Center, Greenbelt, MD.) *In its* Summaries of the 4th Annual JPL Airborne Geoscience Workshop. Volume 1: AVIRIS Workshop 25 Oct. 1993 p 81-84 (For primary document see N95-23844 07-42)

Avail: CASI HC A01/MF A03

The calibrated upwelling radiance spectra measured by AVIRIS are increasingly being analyzed with radiative transfer codes. Analysis of AVIRIS data with the LOWTRAN and MODTRAN radiative transfer codes has led to indications of an error in the solar irradiance spectra used by these codes. This paper presents evidence for the error and proposed update to the solar irradiance spectra used by LOWTRAN and MODTRAN. Author

N95-23866*# Jet Propulsion Lab., California Inst. of Tech., Pasadena, CA.

A ROLE FOR AVIRIS IN THE LANDSAT AND ADVANCED LAND REMOTE SENSING SYSTEMS PROGRAM **c43**

Robert O. Green and John J. Simmonds *In its* Summaries of the 4th Annual JPL Airborne Geoscience Workshop. Volume 1: AVIRIS Workshop 25 Oct. 1993 p 85-88 (For primary document see N95-23844 07-42)

Avail: CASI HC A01/MF A03

As a calibrated imaging spectrometer flying at a 20 km altitude, AVIRIS may contribute to the Landsat and the Advanced Land Remote Sensing System efforts. These contributions come in the areas of: (1) on-orbit calibration, (2) specification of new spectral bands, (3) validation of algorithms, and (4) investigation of an imaging spectrometer of the Advanced Land Remote Sensing System. Author

N95-23867*# California Univ., Davis, CA. Dept. of Land, Air, and Water Resources.

ESTIMATING DRY GRASS RESIDUES USING LANDSCAPE INTEGRATION ANALYSIS **c43**

Quinn J. Hart, Susan L. Ustin, Lian Duan, and George Scheer *In* JPL, Summaries of the 4th Annual JPL Airborne Geoscience Workshop. Volume 1: AVIRIS Workshop 25 Oct. 1993 p 89-92 (For primary document see N95-23844 07-42)

Avail: CASI HC A02/MF A03

The acreage of grassland and grassland-savannah is extensive in California, making direct measurement and assessment logistically impossible. Grasslands cover the entire Central Valley up to about 1200 m elevation in the Coast Range and Sierra Nevada Range. Kuchler's map shows 5.35 M ha grassland with an additional 3.87 M ha in Oak savannah. The goal of this study was to examine the use of high spectral resolution sensors to distinguish between dry grass and soil in remotely sensed images. Spectral features that distinguish soils and dry plant material in the shortwave infrared (SWIR) region are thought to be primarily caused by cellulose and lignin, biochemicals which are absent from soils or occur as breakdown products in humid substances that lack the narrow-band features. We have used spectral mixing analysis (SMA) combined with Geographic Information Systems (GIS) analysis to characterize plant communities and dry grass biomass. The GIS was used to overlay elevation maps, and vegetation maps, with the SMA results. The advantage of non-image data is that it provides an independent source of information for the community classification. Derived from text

N95-23868*# Purdue Univ., West Lafayette, IN. School of Electrical Engineering.

CLASSIFICATION OF HIGH DIMENSIONAL MULTISPECTRAL IMAGE DATA **c82**

Joseph P. Hoffbeck and David A. Landgrebe *In* JPL, Summaries of the 4th Annual JPL Airborne Geoscience Workshop. Volume 1: AVIRIS Workshop 25 Oct. 1993 p 93-96 (For primary document see N95-23844 07-42)

(Grant NAGw-925)

Avail: CASI HC A01/MF A03

A method for classifying high dimensional remote sensing data is described. The technique uses a radiometric adjustment to allow a human operator to identify and label training pixels by visually comparing the remotely sensed spectra to laboratory reflectance spectra. Training pixels for material without obvious spectral features are identified by traditional means. Features which are effective for discriminating between the classes are then derived from the original radiance data and used to classify the scene. This technique is applied to Airborne Visible/Infrared Imaging Spectrometer (AVIRIS) data taken over Cuprite, Nevada in 1992, and the results are compared to an existing geologic map. This technique performed well even with noisy data and the fact that some of the materials in the scene lack absorption features. No adjustment for the atmosphere or other scene variables was made to the data classified. While the experimental results compare favorably with an existing geologic map, the primary purpose of this research was to demonstrate the classification method, as compared to the geology of the Cuprite scene. Derived from text

N95-23869*# Aerospace Corp., Los Angeles, CA.

SIMULATION OF LANDSAT THEMATIC MAPPER IMAGERY USING AVIRIS HYPERSPECTRAL IMAGERY **c82**

Linda S. Kalman and Gerard R. Peltzer *In* JPL, Summaries of the 4th Annual JPL Airborne Geoscience Workshop. Volume 1: AVIRIS Workshop 25 Oct. 1993 p 97-100 Sponsored by Aerospace Sponsored Research program (For primary document see N95-23844 07-42)

Avail: CASI HC A01/MF A03

In this paper we present a methodology for simulating multispectral imagery (MSI) using hyperspectral imagery (HSI), and present a validation of the technique using one nearly coincident Landsat TM and AVIRIS data set. Generation of MSI from HSI supports several investigations including selection of multispectral sensor band edges, and engineering trade studies related to on-board or ground-based aggregation of HSI to simulate MSI. In addition, the utility of this technique as a potential procedure for monitoring calibration changes in spaceborne instrument is also addressed. Author

N95-23870*# Colorado Univ., Boulder, CO. Center for the Study of Earth from Space.

THE EFFECTS OF AVIRIS ATMOSPHERIC CALIBRATION METHODOLOGY ON IDENTIFICATION AND QUANTITATIVE MAPPING OF SURFACE MINERALOGY, DRUM MOUNTAINS, UTAH **c43**

Fred A. Kruse and John L. Dwyer *In* JPL, Summaries of the 4th Annual JPL Airborne Geoscience Workshop. Volume 1: AVIRIS Workshop 25 Oct. 1993 p 101-104 (For primary document see N95-23844 07-42)

(Contract GS-14-08-0001-A-0746)

Avail: CASI HC A01/MF A03

The Airborne Visible/Infrared Imaging Spectrometer (AVIRIS) measures reflected light in 224 contiguous spectra bands in the 0.4 to 2.45 micron region of the electromagnetic spectrum. Numerous studies have used these data for mineralogic identification and mapping based on the presence of diagnostic spectral features. Quantitative mapping requires conversion of the AVIRIS data to physical units (usually reflectance) so that analysis results can be compared and validated with field and laboratory measurements. This study evaluated two different AVIRIS calibration techniques to ground reflectance: an empirically-based method and an atmospheric model based method to determine their effects on quantitative scientific analyses. Expert system analysis and linear spectral unmixing were applied to both calibrated data sets to determine the effect of the calibration on the mineral identification and quantitative mapping results. Comparison of the image-map results and image reflectance spectra indicate that the model-based calibrated data can be used with automated mapping techniques to produce accurate maps showing the spatial distribution and abundance of surface mineralogy. This has positive implications for future operational mapping using AVIRIS or similar imaging spectrometer data sets without requiring a priori knowledge. Author

N95-23871*# University Coll. of Swansea (Wales). Dept. of Geography.

AVIRIS SPECTRA CORRELATED WITH THE CHLOROPHYLL CONCENTRATION OF A FOREST CANOPY **c43**

John Kupiec, Geoffrey M. Smith, and Paul J. Curran (Southampton Univ., England.) *In* JPL, Summaries of the 4th Annual JPL Airborne Geoscience Workshop. Volume 1: AVIRIS Workshop 25 Oct. 1993 p 105-108 Sponsored by NSF and NERC (UK) (For primary document see N95-23844 07-42)

Avail: CASI HC A01/MF A03

Imaging spectrometers have many potential applications in the environmental sciences. One of the more promising applications is that of

estimating the biochemical concentrations of key foliar biochemicals in forest canopies. These estimates are based on spectroscopic theory developed in agriculture and could be used to provide the spatial inputs necessary for the modeling of forest ecosystem dynamics and productivity. Several foliar biochemicals are currently under investigation ranging from those with primary absorption features in visible to middle infrared wavelengths (e.g., water, chlorophyll) to those with secondary to tertiary absorption features in this part of the spectrum (e.g., nitrogen, lignin). The foliar chemical of interest in this paper is chlorophyll; this is a photoreceptor and catalyst for the conversion of sunlight into chemical energy and as such plays a vital role in the photochemical synthesis of carbohydrates in plants. The aim of the research reported here was to determine if the chlorophyll concentration of a forest canopy could be correlated with the reflectance spectra recorded by the Airborne Visible/Infrared Imaging Spectrometer (AVIRIS). Author

N95-23872*# National Aeronautics and Space Administration. Ames Research Center, Moffett Field, CA.

AVIRIS AND TIMS DATA PROCESSING AND DISTRIBUTION AT THE LAND PROCESSES DISTRIBUTED ACTIVE ARCHIVE CENTER **c82**

G. R. Mah and J. Myers *In* JPL, Summaries of the 4th Annual JPL Airborne Geoscience Workshop. Volume 1: AVIRIS Workshop 25 Oct. 1993 p 109-112 (For primary document see N95-23844 07-42)

Avail: CASI HC A01/MF A03

The U.S. Government has initiated the Global Change Research program, a systematic study of the Earth as a complete system. NASA's contribution of the Global Change Research Program is the Earth Observing System (EOS), a series of orbital sensor platforms and an associated data processing and distribution system. The EOS Data and Information System (EOSDIS) is the archiving, production, and distribution system for data collected by the EOS space segment and uses a multilayer architecture for processing, archiving, and distributing EOS data. The first layer consists of the spacecraft ground stations and processing facilities that receive the raw data from the orbiting platforms and then separate the data by individual sensors. The second layer consists of Distributed Active Archive Centers (DAAC) that process, distribute, and archive the sensor data. The third layer consists of a user science processing network. The EOSDIS is being developed in a phased implementation. The initial phase, Version 0, is a prototype of the operational system. Version 0 activities are based upon existing systems and are designed to provide an EOSDIS-like capability for information management and distribution. An important science support task is the creation of simulated data sets for EOS instruments from precursor aircraft or satellite data. The Land Processes DAAC, at the EROS Data Center (EDC), is responsible for archiving and processing EOS precursor data from airborne instruments such as the Thermal Infrared Multispectral Scanner (TIMS), the Thematic Mapper Simulator (TMS), and Airborne Visible and Infrared Imaging Spectrometer (AVIRIS). AVIRIS, TIMS, and TMS are flown by the NASA-Ames Research Center ARC) on an ER-2. The ER-2 flies at 65000 feet and can carry up to three sensors simultaneously. Most jointly collected data sets are somewhat boresighted and roughly registered. The instrument data are being used to construct data sets that simulate the spectral and spatial characteristics of the Advanced Spaceborne Thermal Emission and Reflection Radiometer (ASTER) instrument scheduled to be flown on the first EOS-AM spacecraft. The ASTER is designed to acquire 14 channels of land science data in the visible and near-IR (VNIR), shortwave-IR (SWIR), and thermal-IR (TIR) regions from 0.52 micron to 11.65 micron at high spatial resolutions of 15 m to 90 m. Stereo data will also be acquired in the VNIR region in a single band. The AVIRIS and TMS cover the ASTER VNIR and SWIR bands, and the TIMS covers the TIR bands. Simulated ASTER data sets have been generated over Death Valley, California, Cuprite, Nevada, and the Drum Mountains, Utah using a combination of AVIRIS, TIMS, amd TMS data, and existing digital elevation models (DEM) for the topographic information. Author

N95-23873*# New Hampshire Univ., Durham, NH. Complex Systems Research Center.

MEASUREMENTS OF CANOPY CHEMISTRY WITH 1992 AVIRIS DATA AT BLACKHAWK ISLAND AND HARVARD FOREST **c43**

Mary E. Martin and John D. Aber *In* JPL, Summaries of the 4th Annual JPL Airborne Geoscience Workshop. Volume 1: AVIRIS Workshop 25 Oct. 1993 p 113-116 (For primary document see N95-23844 07-42)

Avail: CASI HC A01/MF A03

The research described in this paper was designed to determine if high spectral resolution imaging spectrometer data can be used to measure the chemical composition of forest foliage, specifically nitrogen and lignin concentration. Information about the chemical composition of forest canopies can be used to determine nutrient cycling rates and carbon balances in forest ecosystems. This paper will describe the results relating data from the Airborne Visible/Infrared Imaging Spectrometer (AVIRIS) to field measured canopy chemistry at Blackhawk Island, WI and Harvard Forest, MA. Author

N95-23874*# Arizona Univ., Tucson, AZ.

CLASSIFICATION OF THE LCVF AVIRIS TEST SITE WITH A KOHONEN ARTIFICIAL NEURAL NETWORK **c63**

Erzsebet Merenyi, Robert B. Singer, and William H. Farrand (Science Applications International Corp., Falls Church, VA.) *In* JPL, Summaries of the 4th Annual JPL Airborne Geoscience Workshop. Volume 1: AVIRIS Workshop 25 Oct. 1993 p 117-120 (For primary document see N95-23844 07-42)

Avail: CASI HC A01/MF A03

We present a classification of an AVIRIS spectral image of the Lunar Crater Volcanic Field (LCVF). Geologic mapping from such data is made possible by distinctive mineral signatures: absorption features and the shape of the spectral continuum. The subtle spectral shape differences between some of the geological units in this scene along with the high dimensionality of the spectral presents a challenging pattern recognition task. We found an artificial neural network powerful in separating 13 geological units based on the full spectral resolution. The LCVF, in northern Nye County, Nevada, was the primary focus of the NASA-sponsored Geologic Remote Sensing Field Experiment in the summer of 1989. It consists of over 100 square miles of Quaternary basaltic pyroclastic and flow deposits. These deposits lie atop ignimbrites and silicic lava flows of Tertiary age and in turn are overlain by Quaternary alluvial and playa deposits. This AVIRIS image was collected on September 29, 1989 at 11:44 at 11:44 PDT. The 256-by-256 pixel subsection in this study contains oxidized basaltic cinder deposits, the southern half of the Lunar Lake playa, and outcrops of the Rhyollite of Big Sand Spring Valley. Vegetation in LCVF is sparse, but locally abundant within washes and near springs. Author

N95-23875*# Jet Propulsion Lab., California Inst. of Tech., Pasadena, CA.

EXTRACTION OF AUXILIARY DATA FROM AVIRIS DISTRIBUTION TAPE FOR SPECTRAL, RADIOMETRIC, AND GEOMETRIC QUALITY ASSESSMENT **c82**

Peter Meyer, Robert O. Green, and Thomas G. Chrien *In its* Summaries of the 4th Annual JPL Airborne Geoscience Workshop. Volume 1: AVIRIS Workshop 25 Oct. 1993 p 121-125 (For primary document see N95-23844 07-42)

Avail: CASI HC A01/MF A03

Remotely sensed data are affected by system (sensor and platform), and scene related effects. For quantitative investigations the spectral, radiometric characteristics of the system and scene have to be known. The relevant effects and their possible influence on an image have to be specifically determined for every remote sensing system and adequate description parameters need to be updated and reported on a regular basis as they are carried out, e.g., for the AVIRIS system. It is evident that the strength of the influence of similar effects in very dependent on the accessibility of auxiliary information about such sensor systems. Degradation in a spaceborne system can normally be just reported and cannot be corrected. In contrast, an airborne sensor can be evaluated, maintained and improved periodically. Such maintenance efforts are particularly important because airborne systems are exposed to extreme and changing environments. These include tens of takeoffs and landing each year as well as extreme changes in temperature and humidity on the tarmac and in flight. For the AVIRIS system there are environmental stresses such as changes in temperature, air pressure, humidity, vibration of the platform or scene-related reasons like atmospheric conditions, and topography. The information contained in the auxiliary files included with the AVIRIS data can be used to assess these effects and compensate for them. In addition the spectral, radiometer and geometric calibration data contained in the auxiliary file are required for quantitative analysis of the data. The paper describes tools to access the auxiliary information that characterizes the AVIRIS system. These tools allow the examination of

parameters that may impact the quality of the measured AVIRIS image. An example of the use of this auxiliary data was carried out with regard to a parametric geocoding approach. Emphasis is placed on the reported auxiliary information that describes the geometric character of the AVIRIS data in 1991. Results are presented using data from the AVIRIS flight #910705, run 6 and 7 of the NASA MAC Europe 1991 campaign in a test site in Central Switzerland. Author

N95-23876*# Jet Propulsion Lab., California Inst. of Tech., Pasadena, CA.

PREPROCESSING: GEOCODING OF AVIRIS DATA USING NAVIGATION, ENGINEERING, DEM, AND RADAR TRACKING SYSTEM DATA **c82**

Peter Meyer, Steven A. Larson, Earl G. Hansen, and Klaus I. Itten *In its* Summaries of the 4th Annual JPL Airborne Geoscience Workshop. Volume 1: AVIRIS Workshop 25 Oct. 1993 p 127-132 Sponsored by NASA, Ames Research Center and Litton Aero Products (For primary document see N95-23844 07-42)

(SNSF Proj. 82-20332.90)

Avail: CASI HC A02/MF A03

Remotely sensed data have geometric characteristics and representation which depend on the type of the acquisition system used. To correlate such data over large regions with other real world representation tools like conventional maps or Geographic Information System (GIS) for verification purposes, or for further treatment within different data sets, a coregistration has to be performed. In addition to the geometric characteristics of the sensor there are two other dominating factors which affect the geometry: the stability of the platform and the topography. There are two basic approaches for a geometric correction on a pixel-by-pixel basis: (1) A parametric approach using the location of the airplane and inertial navigation system data to simulate the observation geometry; and (2) a non-parametric approach using tie points or ground control points. It is well known that the non-parametric approach is not reliable enough for the unstable flight conditions of airborne systems, and is not satisfying in areas with significant topography, e.g. mountains and hills. The present work describes a parametric preprocessing procedure which corrects effects of flight line and attitude variation as well as topographic influences and is described in more detail by Meyer. Author

N95-23877*# Jet Propulsion Lab., California Inst. of Tech., Pasadena, CA.

THE DATA FACILITY OF THE AIRBORNE VISIBLE/INFRARED IMAGING SPECTROMETER (AVIRIS) **c82**

Pia J. Nielsen, Robert O. Green, Alex T. Murray, Bjorn T. Eng, H. Ian Novack, Manuel Solis, and Martin Olah *In its* Summaries of the 4th Annual JPL Airborne Geoscience Workshop. Volume 1: AVIRIS Workshop p133-136 (SEE N95-23844 07-42) 25 Oct. 1993 (For primary document see N95-23844 07-42)

Avail: CASI HC A01/MF A03

AVIRIS operations at the Jet Propulsion Laboratory include a significant data task. The AVIRIS data facility is responsible for data archiving, data calibration, quality monitoring and distribution. Since 1987, the data facility has archived over one terabyte of AVIRIS data and distributed these data to science investigators as requested. In this paper we describe recent improvements in the AVIRIS data facility. Author

N95-23878*# Centre National de la Recherche Scientifique, Toulouse (France).

MAPPING OF THE RONDA PERIDOTITE MASSIF (SPAIN) FROM AVIRIS SPECTRO-IMAGING SURVEY: A FIRST ATTEMPT **c43**

P. C. Pinet, S. Chabrillat, and G. Ceuleneer *In* JPL, Summaries of the 4th Annual JPL Airborne Geoscience Workshop. Volume 1: AVIRIS Workshop 25 Oct. 1993 p 137-140 (For primary document see N95-23844 07-42)

Avail: CASI HC A01/MF A03

In both AVIRIS and ISM data, through the use of mixing models, geological boundaries of the Ronda massif are identified with respect to the surrounding rocks. We can also yield first-order vegetation maps. ISM and AVIRIS instruments give consistent results. On the basis of endmember fraction images, it is then possible to discard areas highly vegetated or not belonging to the peridotite massif. Within the remaining part of the mosaic, spectro-mixing analysis reveals spectral variations in the peridotite massif between the well-exposed areas. Spatially organized units are depicted, related to differences in the relative depth of the absorption band at 1 micron, and it may be due to a different pyroxene content. At this stage, it is worth noting that, although mineralogical variations observed in the rocks are at a sub-pixel scale for the airborne analysis, we see an emerging spatial pattern in the distribution of spectral variations across the massif which might be prevailingly related to mineralogy. Although it is known from fieldwork that the Ronda peridotite massif exhibits mineralogical variations at local scale in the content of pyroxene, and at regional scale in different mineral facies, ranging from garnet-, to spinel- to plagioclase-lherzolites, no attempt has been done yet to produce a synoptic map relating the two scales of analysis. The present work is a first attempt to reach this objective, though a lot more work is still required. In particular, for the purpose of mineralogical interpretation, it is critical to relate the airborne observation to field work and laboratory spectra of Ronda rocks already obtained, with the use of image endmembers and associated reference endmembers. Also, the pretty rough linear mixing model used here is taken as a 'black-box' process which does not necessarily apply correctly to the physical situation at the sub-pixel level. One may think of using the ground-truth observations bearing on the sub-pixel statistical characteristics (texture, structural pattern, surface distribution and vegetation contribution (grass,..)) to produce a more advanced mixing model, physically appropriate to the geologic and environmental contexts. Author

N95-23879*# Agricultural Research Service, Beltsville, MD.

SPECTRAL VARIATIONS IN A COLLECTION OF AVIRIS IMAGERY **c43**

John C. Price *In* JPL, Summaries of the 4th Annual JPL Airborne Geoscience Workshop. Volume 1: AVIRIS Workshop 25 Oct. 1993 p 141-144 (For primary document see N95-23844 07-42)

Avail: CASI HC A01/MF A03

The advent of AVIRIS presents to the scientific community the first opportunity to examine high quality hyperspectral data over areas of interest, while recent developments promise even better data in the future. With these data we may address questions such as: (1) Is such high spectral resolution (0.01 micron) necessary?; and (2) How can we take advantage of the AVIRIS experience in specifying an improved future Landsat satellite? In this paper we describe the use of relatively broadband measurements (20-50 nm) to represent spectral variability. The problem of generality is addressed through consideration of 28 AVIRIS scenes, although analysis of additional areas is clearly desirable. Section 2 defines the expansion of spectra in terms of basis functions, section 3 describes the application to AVIRIS data, and the conclusion, section 4, relates these preliminary results to possible future remote sensing instrumentation such as the planned Landsat 8. Author

N95-23880*# Jet Propulsion Lab., California Inst. of Tech., Pasadena, CA.

MONITORING LAND USE AND DEGRADATION USING SATELLITE AND AIRBORNE DATA **c43**

Terrill W. Ray (California Inst. of Tech., Pasadena, CA.), Thomas G. Farr, Ronald G. Blom, and Robert E. Crippen *In its* Summaries of the 4th Annual JPL Airborne Geoscience Workshop. Volume 1: AVIRIS Workshop 25 Oct. 1993 p 145-148 (For primary document see N95-23844 07-42)

Avail: CASI HC A01/MF A03

In July 1990 AVIRIS and AIRSAR data were collected over the Manix Basin Area of the Mojave Desert to study land degradation in an arid area where centerpivot irrigation had been in use. The Manix Basin is located NE of Barstow, California, along Interstate-15 at 34 deg 57 min N 116 deg 35 min W. This region was covered by a series of lakes during the Late Pleistocence and Early Holocene. Beginning in the 1960's, areas were cleared of the native creosote bush-dominated plant community to be used for agricultural purposes. Starting in 1972 fields have been abandoned due to the increased cost of electricity needed to pump the irrigation water, with some fields abandoned as recently as 1988 and 1992. These circumstances provide a time series of abandoned fields which provide the possibility of studying the processes which act on agricultural fields in arid regions when they are abandoned. Ray et al. reported that polarimetric SAR (AIRSAR) could detect that the concentric circular planting furrows plowed on these fields persists for a few years after abandonment and then disappear over time and that wind ripples which form on these fields

over time due to wind erosion can be detected with polarimetric radar. Ray et al. used Landsat Thematic Mapper (TM) bandpasses to generate NDVI images of the Manix Basin which showed that the fields abandoned for only a few years had higher NDVI's than the undisturbed desert while the fields abandoned for a longer time had NDVI levels lower than that of the undisturbed desert. The purpose of this study is to use a fusion of a time series of satellite data with airborne data to provide a context for the airborne data. The satellite data time series will additionally help to validate the observation and analysis of time-dependent processes observed in the single AVIRIS image of fields abandoned for different periods of time.

Author

N95-23881*# Jet Propulsion Lab., California Inst. of Tech., Pasadena, CA.

THE RED EDGE IN ARID REGION VEGETATION: 340-1060 NM SPECTRA **c43**

Terrill W. Ray, Bruce C. Murray, A. Chehbouni, and Eni Njoku *In its* Summaries of the 4th Annual JPL Airborne Geoscience Workshop. Volume 1: AVIRIS Workshop 25 Oct. 1993 p 249-152 (For primary document see N95-23844 07-42)

Avail: CASI HC A01/MF A03

The remote sensing study of vegetated regions of the world has typically been focused on the use of broad-band vegetation indices such as NDVI. Various modifications of these indices have been developed in attempts to minimize the effect of soil background, e.g., SAVI, or to reduce the effect of the atmosphere, e.g., ARVI. Most of these indices depend on the so-called 'red edge,' the sharp transition between the strong absorption of chlorophyll pigment in visible wavelengths and the strong scattering in the near-infrared from the cellular structure of leaves. These broadband indices tend to become highly inaccurate as the green canopy cover becomes sparse. The advent of high spectral resolution remote sensing instrument such as the Airborne Visible and Infrared Imaging Spectrometer (AVIRIS) has allowed the detection of narrow spectral features in vegetation and there are reports of detection of the red edge even for pixels with very low levels of green vegetation cover by Vane et al. and Elvidge et al., and to characterize algal biomass in coastal areas. Spectral mixing approaches similar to those of Smith et al. can be extended into the high spectral resolution domain allowing for the analysis of more endmembers, and potentially, discrimination between material with narrow spectral differences. Vegetation in arid regions tends to be sparse, often with small leaves such as the creosote bush. Many types of arid region vegetation spend much of the year with their leaves in a senescent state, i.e., yellow, with lowered chlorophyll pigmentation. The sparseness of the leaves of many arid region plants has the dual effect of lowering the green leaf area which can be observed and of allowing more of the sub-shrub soil to be visible which further complicates the spectrum of a region covered with arid region vegetation. Elvidge examined the spectral characteristics of dry plant materials showing significant differences in the region of the red edge and the diagnostic ligno-cellulose absorptions at 2090 nm and 2300 nm. Ray et al. detected absorption at 2100 nm in AVIRIS spectra of an abandoned field known to be covered by a great deal of dead plant litter. In order to better study arid region vegetation remote sensing data, it is necessary to better characterize the reflectance spectra of in situ, living, arid region plants.

Author

N95-23882*# Jet Propulsion Lab., California Inst. of Tech., Pasadena, CA.

TEMPORAL CHANGES IN ENDMEMBER ABUNDANCES, LIQUID WATER AND WATER VAPOR OVER VEGETATION AT JASPER RIDGE **c43**

Dar A. Roberts (Washington Univ., Seattle, WA.), Robert O. Green, Donald E. Sabol (Washington Univ., Seattle, WA.), and John B. Adams (Washington Univ., Seattle, WA.) *In its* Summaries of the 4th Annual JPL Airborne Geoscience Workshop. Volume 1: AVIRIS Workshop 25 Oct. 1993 p 153-156 (For primary document see N95-23844 07-42)

Avail: CASI HC A01/MF A03

Imaging spectrometry offers a new way of deriving ecological information about vegetation communities from remote sensing. Applications include derivation of canopy chemistry, measurement of column atmospheric water vapor and liquid water, improved detectability of materials, more accurate estimation of green vegetation cover and discrimination of spectrally distinct green leaf, non-photosynthetic vegetation (NPV: litter, wood, bark, etc.) and shade spectra associated with different vegetation communities. Much of our emphasis has been on interpreting Airborne Visible/Infrared Imaging Spectrometry (AVIRIS) data spectral mixtures. Two approaches have been used, simple models, where the data are treated as a mixture of 3 to 4 laboratory/field measured spectra, known as reference endmembers (EM's), applied uniformly to the whole image, to more complex models where both the number of EM's and the types of EM's vary on a per-pixel basis. Where simple models are applied, materials, such as NPV, which are spectrally similar to soils, can be discriminated on the basis of residual spectra. One key aspect is that the data are calibrated to reflectance and modeled as mixtures of reference EM's, permitting temporal comparison of EM fractions, independent of scene location or data type. In previous studies the calibration was performed using a modified-empirical line calibration, assuming a uniform atmosphere across the scene. In this study, a Modtran-based calibration approach was used to map liquid water and atmospheric water vapor and retrieve surface reflectance from three AVIRIS scenes acquired in 1992 over the Jasper Ridge Biological Preserve. The data were acquired on June 2nd, September 4th and October 6th. Reflectance images were analyzed as spectral mixtures of reference EM's using a simple 4 EM model. Atmospheric water vapor derived from Modtran was compared to elevation, and community type. Liquid water was compare to the abundance of NPV, Shade and Green Vegetation (VG) for select sites to determine whether a relationship existed, and under what conditions the relationship broke down. Temporal trends in endmember fractions, liquid water and atmospheric water vapor were investigated also. The combination of spectral mixture analysis and the Modtran based atmospheric/liquid water models was used to develop a unique vegetation community description.

Author

N95-23883*# Washington Univ., Seattle, WA. Dept. of Geological Sciences.

MAPPING AND MONITORING CHANGES IN VEGETATION COMMUNITIES OF JASPER RIDGE, CA, USING SPECTRAL FRACTIONS DERIVED FROM AVIRIS IMAGES **c43**

Donald E. Sabol, Jr., Dar A. Roberts, John B. Adams, and Milton O. Smith *In* JPL, Summaries of the 4th Annual JPL Airborne Geoscience Workshop. Volume 1: AVIRIS Workshop 25 Oct. 1993 p 157-160 (For primary document see N95-23844 07-42)

Avail: CASI HC A01/MF A03

An important application of remote sensing is to map and monitor changes over large areas of the land surface. This is particularly significant with the current interest in monitoring vegetation communities. Most of traditional methods for mapping different types of plant communities are based upon statistical classification techniques (i.e., parallel piped, nearest-neighbor, etc.) applied to uncalibrated multispectral data. Classes from these techniques are typically difficult to interpret (particularly to a field ecologist/botanist). Also, classes derived for one image can be very different from those derived from another image of the same area, making interpretation of observed temporal changes nearly impossible. More recently, neural networks have been applied to classification. Neural network classification, based upon spectral matching, is weak in dealing with spectral mixtures (a condition prevalent in images of natural surfaces). Another approach to mapping vegetation communities is based on spectral mixture analysis, which can provide a consistent framework for image interpretation. Roberts et al. (1990) mapped vegetation using the band residuals from a simple mixing model (the same spectral endmembers applied to all image pixels). Sabol et al. (1992b) and Roberts et al. (1992) used different methods to apply the most appropriate spectral endmembers to each image pixel, thereby allowing mapping of vegetation based upon the the different endmember spectra. In this paper, we describe a new approach to classification of vegetation communities based upon the spectra fractions derived from spectral mixture analysis. This approach was applied to three 1992 AVIRIS images of Jasper Ridge, California to observe seasonal changes in surface composition.

Author

N95-23884*# University Coll. of Swansea (Wales). Dept. of Geography.

THE EFFECT OF SIGNAL NOISE ON THE REMOTE SENSING OF FOLIAR BIOCHEMICAL CONCENTRATION **c43**

Geoffrey M. Smith and Paul J. Curran (Southampton Univ., England.) *In* JPL, Summaries of the 4th Annual JPL Airborne Geoscience Workshop. Volume 1: AVIRIS Workshop 25 Oct. 1993 p 161-164 (For primary

document see N95-23844 07-42)
Avail: CASI HC A01/MF A03

Spectral measurements made using an imaging spectrometer contain systematic and random noise, while the former can be corrected the latter remains a source of error in the remotely sensed signal. A number of investigators have tried to determine the signal-to-noise-ratio (SNR) of the instrument, or the resultant imagery. However, the level of noise at which spectra are too noisy to be useful is not usually determined. The first attempt was by Goetz and Calvin, who suggested that the depth of the absorption feature should be at least an order of magnitude greater than the noise and more recently Dekker suggested a SNR of around 600:1 was required in visible/near infrared wavelengths to measure a 1/gl change in chlorophyll a concentration water. The wide range of applications of imaging spectroscopy make it difficult to set SNR specifications as they are dependent on a number of factors, one of the most important being reflectance of a particular target. For example, the SNR of imagery for vegetated targets is relatively low simply because vegetation has a relatively low level of reflectance. The Airborne Visible/Infrared Imaging Spectrometer (AVIRIS) is being used to estimate the concentration of biochemicals within vegetation canopies. This paper reports a study undertaken to identify first, wavebands that were highly correlated with foliar biochemical concentration and second, to determine how sensitive these correlations were to sensor noise. Author

N95-23885*# Ludwig-Maximilians-Univ., Munich (Germany). Inst. for General and Applied Geology.
APPLICATION OF MAC-EUROPE AVIRIS DATA TO THE ANALYSIS OF VARIOUS ALTERATION STAGES IN THE LANDDMANNALAUGER HYDROTHERMAL AREA (SOUTH ICELAND) **c43**
S. Sommer, G. Loercher, and S. Endres *In* JPL, Summaries of the 4th Annual JPL Airborne Geoscience Workshop. Volume 1: AVIRIS Workshop 25 Oct. 1993 p 165-168 (For primary document see N95-23844 07-42)
Avail: CASI HC A01/MF A03

In June 1991 extensive airborne remote sensing data-sets have been acquired over Iceland in the framework of the joint NASA/ESA Multisensor Airborne Campaign Europe (MAC-Europe). The study area is located within the Torfajokull central volcanic complex in South Iceland. This complex is composed by anomalously abundant rhyolitic acid volcanics, which underwent intensive hydrothermal alteration. Detailed studies of surface alteration of rhyolitic rocks in the area showed that all the major elements are leached as the rock is affected by complex mineralogical changes. Montmorillonite appears during the earliest stages of alteration. In the ultimate alteration product montmorillonite is absent and the rock consists mostly of amorphous silica, anatase, up to a volume of 50% kaolinite and variable amounts of native sulphur and pyrite. The case study presented shall endeavor to assess the potential of MAC-Europe AVIRIS and TMS data in determining a possible zonation of hydrothermal alteration in relationship to the active geo-thermal fields and structural features. To this end, the airborne data is analysed in comparison with laboratory spectral measurements of characteristics rock, soil, and vegetation samples collected in the study areaduring the summer of 1992. Various spectral mapping algorithms as well as unmixing approaches are tested and evaluated. Detailed geological and structural mapping as well as geochemical analysis of the main rock and soil types were performed to underpin the analysis of the airborne data. Author

N95-23886*# Canada Centre for Remote Sensing, Ottawa (Ontario).
ESTIMATION OF CROWN CLOSURE FROM AVIRIS DATA USING REGRESSION ANALYSIS **c43**
K. Staenz, D. J. Williams (MacDonald, Dettwiler and Associates Ltd., Richmond, British Columbia.), M. Truchon, and R. Fritz (Freiburg Univ., Germany.) *In* JPL, Summaries of the 4th Annual JPL Airborne Geoscience Workshop. Volume 1: AVIRIS Workshop 25 Oct. 1993 p 169-172 (For primary document see N95-23844 07-42)
Avail: CASI HC A01/MF A03

Crown closure is one of the input parameters used for forest growth and yield modelling. Preliminary work by Staenz et al. indicates that imaging spectrometer data acquired with sensors such as the Airborne Visible/Infrared Imaging Spectrometer (AVIRIS) have some potential for estimating crown closure on a stand level. The objectives of this paper are: (1) to establish a relationship between AVIRIS data and the crown closure derived from aerial photography of a forested test site within the Interior Douglas Fir biogeoclimatic zone in British Columbia, Canada; (2) to investigate the impact of atmospheric effects and the forest background on the correlation between AVIRIS data and crown closure estimates; and (3) to improve this relationship using multiple regression analysis. Author

N95-23887*# Electromagnetic Systems Labs., Inc., Sunnyvale, CA.
OPTIMAL BAND SELECTION FOR DIMENSIONALITY REDUCTION OF HYPERSPECTRAL IMAGERY **c43**
Stephen D. Stearns, Bruce E. Wilson, and James R. Peterson *In* JPL, Summaries of the 4th Annual JPL Airborne Geoscience Workshop. Volume 1: AVIRIS Workshop 25 Oct. 1993 p 173-176 (For primary document see N95-23844 07-42)
Avail: CASI HC A01/MF A03

Hyperspectral images have many bands requiring significant computational power for machine interpretation. During image pre-processing, regions of interest that warrant full examination need to be identified quickly. One technique for speeding up the processing is to use only a small subset of bands to determine the 'interesting' regions. The problem addressed here is how to determine the fewest bands required to achieve a specified performance goal for pixel classification. The band selection problem has been addressed previously Chen et al., Ghassemian et al., Henderson et al., and Kim et al.. Some popular techniques for reducing the dimensionality of a feature space, such as principal components analysis, reduce dimensionality by computing new features that are linear combinations of the original features. However, such approaches require measuring and processing all the available bands before the dimensionality is reduced. Our approach, adapted from previous multidimensional signal analysis research, is simpler and achieves dimensionality reduction by selecting bands. Feature selection algorithms are used to determine which combination of bands has the lowest probability of pixel misclassification. Two elements required by this approach are a choice of objective function and a choice of search strategy. Author

N95-23888*# Brown Univ., Providence, RI. Dept. Geological Science.
OBJECTIVE DETERMINATION OF IMAGE END-MEMBERS IN SPECTRAL MIXTURE ANALYSIS OF AVIRIS DATA **c43**
Stefanie Tompkins, John F. Mustard, Carle M. Pieters, and Donald W. Forsyth *In* JPL, Summaries of the 4th Annual JPL Airborne Geoscience Workshop. Volume 1: AVIRIS Workshop 25 Oct. 1993 p 177-180 (For primary document see N95-23844 07-42)
Avail: CASI HC A01/MF A03

Spectral mixture analysis has been shown to be a powerful, multifaceted tool for analysis of multi- and hyper-spectral data. Applications of AVIRIS data have ranged from mapping soils and bedrock to ecosystem studies. During the first phase of the approach, a set of end-members are selected from an image cube (image end-members) that best account for its spectral variance within a constrained, linear least squares mixing model. These image end-members are usually selected using a priori knowledge and successive trial and error solutions to refine the total number and physical location of the end-members. However, in many situations a more objective method of determining these essential components is desired. We approach the problem of image end-member determination objectively by using the inherent variance of the data. Unlike purely statistical methods such as factor analysis, this approach derives solutions that conform to a physically realistic model. Author

N95-23889*# California Univ., Davis, CA. Dept. of Land, Air, and Water Resources.
RELATIONSHIPS BETWEEN PIGMENT COMPOSITION VARIATION AND REFLECTANCE FOR PLANT SPECIES FROM A COASTAL SAVANNAH IN CALIFORNIA **c43**
Susan L. Ustin, Eric W. Sanderson, Yaffa Grossman, and Quinn J. Hart *In* JPL, Summaries of the 4th Annual JPL Airborne Geoscience Workshop. Volume 1: AVIRIS Workshop 25 Oct. 1993 p 181-184 (For primary document see N95-23844 07-42)
Avail: CASI HC A01/MF A03

Advances in imaging spectroscopy have indicated that remotely sensed reflectance measurements of the plant canopy may be used to identify and qualify some classes of canopy biochemicals; however, the manner in which differences in biochemical compositions translate into differences is not well understood. Most frequently, multiple linear regression routines

have been used to correlate narrow band reflectance values with measured biochemical concentrations. Although some success has been achieved with such methods for given data sets, the bands selected by multiple regression are not consistent between data sets, nor is it always clear what physical or biological basis underlies the correlation. To examine the relationship between biochemical concentration and leaf reflectance signal we chose to focus on the visible spectrum where the primary biochemical absorbances are due to photosynthetic pigments. Pigments provide a range of absorbance features, occur over a range of concentrations in natural samples, and are ecophysiologically important. Concentrations of chlorophyll, for example, have been strongly correlated to foliar nitrogen levels within a species and to photosynthetic capacity across many species. In addition pigments effectively absorb most of the photosynthetically active radiation between 400-700 nm, a spectral region for which silicon detectors have good signal/noise characteristics. Our strategy has been to sample a variety of naturally occurring species to measure leaf reflectance and pigment compositions. We hope to extend our understanding of pigment reflectance effects to interpret small overlapping absorbances of other biochemicals in the infrared region. For this reason, selected samples were also tested to determine total nitrogen, crude protein, cellulose, and lignin levels. Leaf reflectance spectra measured with AVIRIS bandwidths and wavelengths were compared between species and within species and for differences between seasons, for changes in the the shape of the spectra. We attempt to statistically correlate these shape changes with differences in pigment compositions. In parallel with our comparisons of pigment composition and leaf reflectance, we have modified the PROSPECT leaf reflectance model to test the contributions of pigments or pigment group concentrations. PROSPECT considers a leaf as a multi-layer dielectric plane with an uneven surface. Jacquemoud adapted the basic analysis of Allen for surface effects, a leaf thickness factor, and the absorption of water and chlorophyll (actually all pigments) and the plant matrix. Our modifications to PROSPECT in the forward direction include breaking out the pigment concentration parameter into separate components for chlorophyll a and b and a number of xanthophylls and carotenes, and introducing a shift and convolution function to model the spread and shift from their in vitro measurements to their in vivo state. Further, we have considered how the matrix elements (i.e., all biochemicals and structural effects not modeled explicity) vary with species. Author

N95-23890*# Jet Propulsion Lab., California Inst. of Tech., Pasadena, CA.

ATMOSPHERIC CORRECTION OF AVIRIS DATA OF MONTEREY BAY CONTAMINATED BY THIN CIRRUS CLOUDS **c43**

Jeannette vandenBosch, Curtiss O. Davis, Curtis D. Mobley, and W. Joseph Rhea *In its* Summaries of the 4th Annual JPL Airborne Geoscience Workshop. Volume 1: AVIRIS Workshop 25 Oct. 1993 p 185-188 (For primary document see N95-23844 07-42)

Avail: CASI HC A01/MF A03

Point source measurements (e.g. sun photometer data, weather station observations) are often used to constrain radiative transfer models such as MODTRAN/LOWTRAN7 when atmospherically correcting AVIRIS imagery. The basic assumption is that the atmosphere is horizontally homogeneous throughout the entire area. If the target area of interest is isolated a distance away from the point measurement position, the calculated visibility and atmospheric profiles may not be characteristic of the atmosphere over the target. AVIRIS scenes are often rejected when cloud cover exceeds 10%. However, if the cloud cover is determined to be primarily cirrus rather than cumulus, in-water optical properties may still be extracted over open ocean. High altitude cirrus clouds are non-absorbing at 744 nm. If the optical properties of the AVIRIS scene can be determined from the 744 nm band itself, the atmospheric conditions during the overflight may be deduced. Author

N95-23891*# Commission of the European Communities, Ispra (Italy). Inst. for Remote Sensing Applications.

INVESTIGATIONS ON THE 1.7 MICRON RESIDUAL ABSORPTION FEATURE IN THE VEGETATION REFLECTION SPECTRUM **c43**

J. Verdebout, S. Jacquemoud, G. Andreoli, B. Hosgood, and A. Sieber *In* JPL, Summaries of the 4th Annual JPL Airborne Geoscience Workshop. Volume 1: AVIRIS Workshop 25 Oct. 1993 p 189-192 (For primary document see N95-23844 07-42)

Avail: CASI HC A01/MF A03

The detection and interpretation of the weak absorption features associated with the biochemical components of vegetation is of great potential interest to a variety of applications ranging from classification to global change studies. This recent subject is also challenging because the spectral signature of the biochemicals is only detectable as a small distortion of the infrared spectrum which is mainly governed by water. Furthermore, the interpretation is complicated by complexity of the molecules (lignin, cellulose, starch, proteins) which contain a large number of different and common chemical bonds. In this paper, we present investigations on the absorption feature centered at 1.7 micron; these were conducted both on AVIRIS data and laboratory reflectance spectra of leaves. Author

N95-23892*# Brown Univ., Providence, RI. Dept. of Environmental, Population and Organismic Biology.

A COMPARISON OF SPECTRAL MIXTURE ANALYSIS AN NDVI FOR ASCERTAINING ECOLOGICAL VARIABLES **c43**

Carol A. Wessman, C. Ann Bateson, Brian Curtiss, and Tracy L. Benning *In* JPL, Summaries of the 4th Annual JPL Airborne Geoscience Workshop. Volume 1: AVIRIS Workshop 25 Oct. 1993 p 193-196 (For primary document see N95-23844 07-42)

Avail: CASI HC A01/MF A03

In this study, we compare the performance of spectral mixture analysis to the Normalized Difference Vegetation Index (NDVI) in detecting change in a grassland across topographically-induced nutrient gradients and different management schemes. The Konza Prairie Research Natural Area, Kansas, is a relatively homogeneous tallgrass prairie in which change in vegetation productivity occurs with respect to topographic positions in each watershed. The area is the site of long-term studies of the influence of fire and grazing on tallgrass production and was the site of the First ISLSCP (International Satellite Land Surface Climatology Project) Field Experiment (FIFE) from 1987 to 1989. Vegetation indices such as NDVI are commonly used with imagery collected in few (less than 10) spectral bands. However, the use of only two bands (e.g. NDVI) does not adequately account for the complex of signals making up most surface reflectance. Influences from background spectral variation and spatial heterogeneity may confound the direct relationship with biological or biophysical variables. High dimensional multispectral data allows for the application position of techniques such as derivative analysis and spectral curve fitting, thereby increasing the probability of successfully modeling the reflectance from mixed surfaces. The higher number of bands permits unmixing of a greater number of surface components, separating the vegetation signal for further analyses relevant to biological variables. Author

N95-23893*# Littoral Univ., Wimereux (France). d'Optique Atmospherique Lab.

USING AVIRIS FOR IN-FLIGHT CALIBRATION OF THE SPECTRAL SHIFTS OF SPOT-HRV AND OF AVHRR? **c43**

Veronique Willart-Soufflet and Richard Santer *In* JPL, Summaries of the 4th Annual JPL Airborne Geoscience Workshop. Volume 1: AVIRIS Workshop 25 Oct. 1993 p 197-200 (For primary document see N95-23844 07-42)

Avail: CASI HC A01/MF A03

The response of a satellite sensor varies during its lifetime; internal calibration devices can be used to follow the sensor degradation or in-flight calibrations are conducted from estimates of the radiance at satellite level for well predictable situations. Changes in gain are evaluated assuming that the spectral response of the sensor is stable with time; i.e., that the filter response as well as the optics or the electronics are not modified since the prelaunch determinations. Nevertheless, there is some evidence that the SPOT interferometer filters are affected by outgassing effects during the launch. Tests in vacuum chambers indicated a narrowing of the filters with a shift of the upper side towards the blue of about 10 nm which is more over consistant with the loss of gain observed during the launch. Also, during the lifetime of SPOT, the relationship between the loss of sensitivity and the filter bandwidth may correspond to this effect. On the other hand, the inconsistancy of the NOAA7 calibration between two methods (desert and ocean) having a different spectral sensitivity may indicate a spectral problem with a shift of the central wavelength of -20 nm. The basic idea here is to take advantage of the good spectral definition of AVIRIS to monitor these potential spectral degradations with an experimental opportunity provided by a field campaign held in La Crau

(S.E. of France) in June 1991 which associated ground-based measurements and AVIRIS, SPOT2, NOAA-11 overpasses over both the calibration site of La Crau and an agricultural area. Author

N95-23894*# Arizona State Univ., Tempe, AZ. Dept. of Geology.
LABORATORY SPECTRA OF FIELD SAMPLES AS A CHECK ON TWO ATMOSPHERIC CORRECTION METHODS **c82**
Pung Xu and Ronald Greeley *In* JPL, Summaries of the 4th Annual JPL Airborne Geoscience Workshop. Volume 1: AVIRIS Workshop 25 Oct. 1993 p 201-204 (For primary document see N95-23844 07-42)
Avail: CASI HC A01/MF A03

Atmospheric correction is the first step toward quantitative analysis of imaging spectroscopy data. Two methods, MODTRAN model and the empirical line, were used to convert AVIRIS radiance values to reflectance values. A set of laboratory spectra of field samples corresponding to AVIRIS coverage was used to assess these methods. This will also serve to select bands for future quantative analyses. Author

N95-23895*# Colorado Univ., Boulder, CO. Center for the Study of Earth from Space.
DETERMINATION OF SEMI-ARID LANDSCAPE ENDMEMBERS AND SEASONAL TRENDS USING CONVEX GEOMETRY SPECTRAL UNMIXING TECHNIQUES **c43**
Roberta H. Yuhas, Joseph W. Boardman, and Alexander F. H. Goetz *In* JPL, Summaries of the 4th Annual JPL Airborne Geoscience Workshop. Volume 1: AVIRIS Workshop 25 Oct. 1993 p 205-208 (For primary document see N95-23844 07-42)
(Contract NAS5-30552; NAGw-2070)
Avail: CASI HC A01/MF A03

Airborne Visible/Infrared Imaging Spectrometer (AVIRIS) data were acquired during three consecutive growing seasons (26 September 1989, 22 March 1990, and 7 August 1990) over an area of the High Plains east of Greeley, Colorado (40 deg 20 min N and 104 deg 16 min W). A repeat visit to assess vegetation at its peak growth was flown on 6 June 1993. This region contains extensive eolian deposits in the form of stabilized dune complexes (small scale parabolic dunes superimposed on large scale longitudinal and parabolic dunes). Due to the dunes' large scale (2-10 km) and low relief (1-5 m), the scaling and morphological relationships that contribute to the evolution of this landscape are nearly impossible to understand without the use of remote sensing. Additionally, this area and regions similarly situated could be the first to experience the effects caused by global climate change. During the past 10,000 years there were at least four periods of extensive sand activity due to climate change, followed by periods of landscape stability, as shown in the stratigraphic record of this area. Author

N95-23917*# Jet Propulsion Lab., California Inst. of Tech., Pasadena, CA.
SUMMARIES OF THE 4TH ANNUAL JPL AIRBORNE GEOSCIENCE WORKSHOP. VOLUME 2: TIMS WORKSHOP
Vincent J. Realmuto, ed. 25 Oct. 1993 29 p Workshop held in Washington, DC, 25-29 Oct. 1993
(Contract NAS7-918; RTOP 465-66-00-01)
(NASA-CR-197876-Vol-2; JPL-Publ-93-26-Vol-2; NAS 1.26:197876-Vol-2)
Avail: CASI HC A03/MF A01

This is volume 2 of a three volume set of publications that contain the summaries for the Fourth Annual JPL Airborne Geoscience Workshop, held in Washington, D.C. on October 25-29, 1993. The main workshop is divided into three smaller workshops as follows: The Airborne Visible/Infrared Imaging Spectrometer (AVIRIS) workshop, on October 25-26. The summaries for this workshop appear in Volume 1. The Thermal Infrared Multispectral Scanner (TIMS) workshop, on October 27. The summaries for this workshop appear in Volume 2. The Airborne Synthetic Aperture Radar (AIRSAR) workshop, on October 28-29. The summaries for this workshop appear in Volume 3. For individual titles, see N95-23918 through N95-23921.

N95-23918*# Environmental Research Inst. of Michigan, Ann Arbor, MI.
ESTIMATION OF SPECTRAL EMISSIVITY IN THE THERMAL INFRARED **c43**
David Kryskowski and J. R. Maxwell *In* JPL, Summaries of the 4th Annual JPL Airborne Geoscience Workshop. Volume 2: TIMS Workshop 25 Oct. 1993 p 1-4 (For primary document see N95-23917 07-42)
Avail: CASI HC A01/MF A01

A number of algorithms are available in the literature that attempt to remove most of the effects of temperature from thermal multispectral data where the final goal is to extract emissivity differences. Early approaches include adjacent spectral band ratioing, broad band radiance normalization and the use of one band where emissivities are generally high (e.g., 11 to 12 micrometers) to determine the temperature. More recent work has produced two techniques that use data averaging to extract temperature to leave a quantity related to emissivity changes. These two techniques have been investigated and compared and appear to provide reasonable results. The analysis presented in this paper develops a thermal IR multispectral temperature/emissivity estimation procedure based on formal estimation theory, Gaussian statistics, and a stochastic radiance signal model including the effects of both temperature and emissivity. The importance of this work is that this is an optimal estimation procedure which will provide minimum variance estimates of temperature and emissivity changes directly. Section 2 discusses optimal linear spectral emissivity estimation and Section 3 is a summary. Author

N95-23919*# Geological Survey of Japan, Kawasaki (Japan). Geophysics Dept.
THE DIFFERENCE BETWEEN LABORATORY AND IN-SITU PIXEL-AVERAGED EMISSIVITY: THE EFFECTS ON TEMPERATURE-EMISSIVITY SEPARATION **c43**
Tsuneo Matsunaga *In* JPL, Summaries of the 4th Annual JPL Airborne Geoscience Workshop. Volume 2: TIMS Workshop 25 Oct. 1993 p 5-8 (For primary document see N95-23917 07-42)
Avail: CASI HC A01/MF A01

Advanced Spaceborne Thermal Emission and Reflection Radiometer (ASTER) is a Japanese future imaging sensor which has five channels in thermal infrared (TIR) region. To extract spectral emissivity information from ASTER and/or TIMS data, various temperature-emissivity (T-E) separation methods have been developed to date. Most of them require assumptions on surface emissivity, in which emissivity measured in a laboratory is often used instead of in-situ pixel-averaged emissivity. But if these two emissivities are different, accuracies of separated emissivity and surface temperature are reduced. In this study, the difference between laboratory and in-situ pixel-averaged emissivity and its effect on T-E separation are discussed. TIMS data of an area containing both rocks and vegetation were also processed to retrieve emissivity spectra using two T-E separation methods. Author

N95-23920*# Arizona State Univ., Tempe, AZ. Dept. of Geology.
MINERALOGIC VARIABILITY OF THE KELSO DUNES, MOJAVE DESERT, CALIFORNIA DERIVED FROM THERMAL INFRARED MULTISPECTRAL SCANNER (TIMS) DATA **c43**
Michael S. Ramsey, Douglas A. Howard, Philip R. Christensen, and Nicholas Lancaster (Desert Research Inst., Reno, NV.) *In* JPL, Summaries of the 4th Annual JPL Airborne Geoscience Workshop. Volume 2: TIMS Workshop 25 Oct. 1993 p 9-1 (For primary document see N95-23917 07-42)
Avail: CASI HC A01/MF A01

Mineral identification and mapping of alluvial material using thermal infrared (TIR) remote sensing is extremely useful for tracking sediment transport, assessing the degree of weathering and locating sediment sources. As a result of the linear relation between a mineral's percentage in a given area (image pixel) and the depth of its diagnostic spectral features, TIR spectra can be deconvolved in order to ascertain mineralogic percentages. Typical complications such as vegetation, particle size and thermal shadowing are minimized upon examination of dunes. Actively saltating dunes contain little to no vegetation, are very well sorted and lack the thermal shadows that arise from rocky terrain. The primary focus of this work was to use the Kelso Dunes as a test location for an accuracy analysis of temperature/emissivity separation and linear unmixing algorithms. Accurate determination of ground temperature and component discrimination will become key products of future ASTER data. A decorrelation stretch of the TIMS image showed clear color variations within the active dunes. Samples collected from these color units were analyzed for mineralogy, grain size, and separated into endmembers. This analysis not only revealed that the dunes contained significant mineralogic variation, but were more immature (low quartz percentage) than previously reported. Unmixing of

the TIMS data using the primary mineral endmembers produced unique variations within the dunes and may indicate near, rather than far, source locales for the dunes. The Kelso Dunes lie in the eastern Mojave Desert, California, approximately 95 km west of the Colorado River. The primary dune field is contained within a topographic basin bounded by the Providence, Granite Mountains, with the active region marked by three northeast trending linear ridges. Although active, the dunes appear to lie at an opposing regional wind boundary which produces little net movement of the crests. Previous studies have estimated the dunes range from 70% to 90% quartz mainly derived from a source 40 km to the west. The dune field is assumed to have formed in a much more arid climate than present, with the age of the deposit estimated at greater than 100,000 years. Author

N95-23921*# Forest Service, Atlanta, GA. Engineering Unit.

REMOTE IDENTIFICATION OF A GRAVEL LADEN PLEISTOCENE RIVER BED **c43**

Douglas E. Scholen *In* JPL, Summaries of the 4th Annual JPL Airborne Geoscience Workshop. Volume 2: TIMS Workshop 25 Oct. 1993 p 13-16 (For primary document see N95-23917 07-42)

Avail: CASI HC A01/MF A01

The abundance of gravel deposits is well known in certain areas across the Gulf of Mexico coastal plain, including lands within several National Forests. These Pleistocene gravels were deposited following periods of glacial buildup when ocean levels were down and the main river channels had cut deep gorges, leaving the subsidiary streams with increased gradients to reach the main channels. During the warm interglacial periods that followed each glaciation, melting ice brought heavy rainfall and torrents of runoff carrying huge sediment loads that separated into gravel banks below these steeper reaches where abraiding streams, developed. As the oceans rose again, filling in the main channels, these abraiding areas were gradually flattened and covered over by progressively finer material. Older terraces were uplifted by tectonic movements associated with the Gulf Coastal Plain, and the subsequent erosional processes gradually brought the gravels closer to the surface. The study area is located on the Kisatchie National Forest, in central Louisiana, near Alexandria. Details of the full study have been discussed elsewhere. The nearest source of chert is in the Ouachita Mountains located to the northeast. The Ouachita River flows south, out of these mountains, and in Pleistocene times probably carried these chert gravels into the vicinity of the present day Little River Basin which lies along the eastern boundary of the National Forest. Current day drainages cross the National Forest from west to east, emptying into the Little River on the east side. However, a north-south oriented ridge of hills along the west side of the Forest appears to be a recent uplift associated with the hinge line of the Mississippi River depositional basin further to the east, and 800,000 years ago, when these gravels were first deposited during the Williana interglacial period, the streams probably flowed east to west, from the Little River basin to the Red River basin on the west side of the Forest. Within the National Forest and north of Alexandria, along Fish Creek, and east and west of an area known as Breezy Hill, exist several small, worked out gravel pits on privately owned blocks of land, formerly used by the state and county road departments. The pattern presented by these pits gives the impression of a series of north-south drainages lacing through the Forest, probable tributaries to Fish Creek which flows south of east from the west side of the Forest to empty into the Little River. Because of this predominant north-south pattern, no consideration was given to areas between these drainages during early gravel exploration efforts. Author

N95-23938*# Jet Propulsion Lab., California Inst. of Tech., Pasadena, CA.

SUMMARIES OF THE 4TH ANNUAL JPL AIRBORNE GEOSCIENCE WORKSHOP. VOLUME 3: AIRSAR WORKSHOP

Jakob vanZyl, ed. 25 Oct. 1993 106 p Workshop held in Washington, DC, 25-29 Oct. 1993 Contains 35mm color slides as supplement

(Contract NAS7-918; RTOP 666-31-00)

(NASA-CR-197354-Vol-3; JPL-Publ-93-26-Vol-3; NAS 1.26:197354-Vol-3)

Avail: CASI HC A06/MF A02

This publication contains the summaries for the Fourth Annual JPL Airborne Geoscience Workshop, held in Washington, D.C. on October 25-29, 1993. The main workshop is divided into three smaller workshops as follows: The Airborne Visible/Infrared Spectrometer (AVIRIS) workshop, on October 25-26, whose summaries appear in Volume 1; The Thermal Infrared Multispectral Scanner (TIMS) workshop, on October 27, whose summaries appear in Volume 2; and The Airborne Synthetic Aperture Radar (AIRSAR) workshop, on October 28-29, whose summaries appear in this volume, Volume 3. For individual titles, see N95-23939 through N95-23961.

N95-23939*# Jet Propulsion Lab., California Inst. of Tech., Pasadena, CA.

INTERFEROMETRIC SYNTHETIC APERTURE RADAR IMAGERY OF THE GULF STREAM **c48**

T. L. Ainsworth (Naval Research Lab., Washington, DC.), M. E. Cannella (Naval Research Lab., Washington, DC.), R. W. Jansen (Naval Research Lab., Washington, DC.), S. R. Chubb (Naval Research Lab., Washington, DC.), R. E. Carande, E. W. Foley (Naval Surface Warfare Center, Bethesda, MD.), R. M. Goldstein, and G. R. Valenzuela (Naval Research Lab., Washington, DC.) *In its* Summaries of the 4th Annual JPL Airborne Geoscience Workshop. Volume 3: AIRSAR Workshop 25 Oct. 1993 p 1- (For primary document see N95-23938 07-42)

Avail: CASI HC A01/MF A01

The advent of interferometric synthetic aperture radar (INSAR) imagery brought to the ocean remote sensing field techniques used in radio astronomy. Whilst details of the interferometry differ between the two fields, the basic idea is the same: Use the phase information arising from positional differences of the radar receivers and/or transmitters to probe remote structures. The interferometric image is formed from two complex synthetic aperture radar (SAR) images. These two images are of the same area but separated in time. Typically the time between these images is very short -- approximately 50 msec for the L-band AIRSAR (Airborne SAR). During this short period the radar scatterers on the ocean surface do not have time to significantly decorrelate. Hence the two SAR images will have the same amplitude, since both obtain the radar backscatter from essentially the same object. Although the ocean surface structure does not significantly decorrelate in 50 msec, surface features do have time to move. It is precisely the translation of scattering features across the ocean surface which gives rise to phase differences between the two SAR images. This phase difference is directly proportional to the range velocity of surface scatterers. The constant of proportionality is dependent upon the interferometric mode of operation. Derived from text

N95-23940*# Consiglio Nazionale delle Ricerche, Rome (Italy).

MAX-91: POLARIMETRIC SAR RESULTS ON MONTESPERTOLI SITE **c43**

S. Baronti, S. Luciani (Tor Vergata Univ., Rome, Italy.), S. Moretti (Florence Univ., Italy.), S. Paloscia, G. Schiavon (Tor Vergata Univ., Rome, Italy.), and S. Sigismondi (Florence Univ., Italy.) *In* JPL, Summaries of the 4th Annual JPL Airborne Geoscience Workshop. Volume 3: AIRSAR Workshop 25 Oct. 1993 p 5-8 Sponsored by Italian Space Agency (For primary document see N95-23938 07-42)

Avail: CASI HC A01/MF A01

The polarimetric Synthetic Aperture Radar (SAR) is a powerful sensor for high resolution ocean and land mapping and particularly for monitoring hydrological parameters in large watersheds. There is currently much research in progress to assess the SAR operational capability as well as to estimate the accuracy achievable in the measurements of geophysical parameters with the presently available airborne and spaceborne sensors. An important goal of this research is to improve our understanding of the basic mechanisms that control the interaction of electro-magnetic waves with soil and vegetation. This can be done both by developing electromagnetic models and by analyzing statistical relations between backscattering and ground truth data. A systematic investigation, which aims at a better understanding of the information obtainable from the multi-frequency polarimetric SAR to be used in agro-hydrology, is in progress by our groups within the framework of SIR-C/X-SAR Project and has achieved a most significant milestone with the NASA/JPL Aircraft Campaign named MAC-91. Indeed this experiment allowed us to collect a large and meaningful data set including multi-temporal multi-frequency polarimetric SAR measurements and ground truth. This paper presents some significant results obtained over an agricultural flat area within the Montespertoli site, where intensive ground measurements were carried out. The results are critically discussed with special regard to the information associated with polarimetric data. Author

N95-23941*# Arizona State Univ., Tempe, AZ. Dept. of Geology.
AIRSAR VIEWS OF AEROLIAN TERRAIN **c43**
Dan G. Blumberg and Ronald Greeley *In* JPL, Summaries of the 4th Annual JPL Airborne Geoscience Workshop. Volume 3: AIRSAR Workshop 25 Oct. 1993 p 9-12 (For primary document see N95-23938 07-42)
Avail: CASI HC A01/MF A01

The Stovepipe Wells Dune Field provides a unique opportunity to observe several dune forms in one scene. These forms include reverse dunes, star dunes, transverse, and linear dunes. A sand mantle surrounds the dune field and can also be observed in the radar image. Dune types were discriminated best in co-polarized channels. Three major wind directions are responsible for the various dune forms. Winds from the north and south are responsible for the reverse dunes, winds from north for the transverse dunes, and the north - south and westerly winds for the star dunes. The winds also reflect the topographic configuration of this part of Death Valley. Vegetation over the dunes was most pronounced in the cross-polarized images. Lancaster et al. (1992) find that cross-polarized images are most useful in differentiating active from inactive dunes. This is because the vegetation backscatter signature is present over inactive dunes. Future studies should include multiple look and incidence angles to determine if the dune forms can still be seen at other angles. Derived from text

N95-23942*# Cornell Univ., Ithaca, NY. Dept. of Geological Sciences.
GLACIOLOGICAL STUDIES IN THE CENTRAL ANDES USING AIRSAR/TOPSAR **c43**
Richard R. Forster, Andrew G. Klein, Troy A. Blodgett, and Bryan L. Isacks *In* JPL, Summaries of the 4th Annual JPL Airborne Geoscience Workshop. Volume 3: AIRSAR Workshop 25 Oct. 1993 p 13-15 (For primary document see N95-23938 07-42)
Avail: CASI HC A01/MF A01

The interaction of climate and topography in mountainous regions is dramatically expressed in the spatial distribution of glaciers and snowcover. Monitoring existing alpine glaciers and snow extent provides insight into the present mountain climate system and how it is changing, while mapping the positions of former glaciers as recorded in landforms such as cirques and moraines provide a record of the large past climate change associated with the last glacial maximum. The Andes are an ideal mountain range in which to study the response of snow and ice to past and present climate change. Their expansive latitudinal extent offers the opportunity to study glaciers in diverse climate settings from the tropical glaciers of Peru and Bolivia to the ice caps and tide-water glaciers of sub-polar Patagonia. SAR has advantages over traditional passive remote sensing instruments for monitoring present snow and ice and differentiating moraine relative ages. The cloud penetrating ability of SAR is indispensable for perennially cloud covered mountains. Snow and ice facies can be distinguished from SAR's response to surface roughness, liquid water content and grain size distribution. The combination of SAR with a coregestered high-resolution DEM (TOPSAR) provides a promising tool for measuring glacier change in three dimensions, thus allowing ice volume change to be measured directly. The change in moraine surface roughness over time enables SAR to differentiate older from younger moraines. Polarimetric SAR data have been used to distinguish snow and ice facies and relatively date moraines. However, both algorithms are still experimental and require ground truth verification. We plan to extend the SAR classification of snow and ice facies and moraine age beyond the ground truth sites to throughout the Cordillera Real to provide a regional view of past and present snow and ice. The high resolution DEM will enhance the SAR moraine dating technique by discriminating relative ages based on moraine slope degradation.
Author

N95-23943*# University Coll. of Swansea (Wales). Dept. of Geography.
ESTIMATION OF BIOPHYSICAL PROPERTIES OF UPLAND SITKA SPRUCE (PICEA SITCHENSIS) PLANTATIONS **c43**
Robert M. Green *In* JPL, Summaries of the 4th Annual JPL Airborne Geoscience Workshop. Volume 3: AIRSAR Workshop 25 Oct. 1993 p 17-20 (For primary document see N95-23938 07-42)
(Contract NERC-GT4/91/TLS/62)
Avail: CASI HC A01/MF A01

It is widely accepted that estimates of forest above-ground biomass are required as inputs to forest ecosystem models, and that SAR data have the potential to provide such information. This study describes relationships between polarimetric radar backscatter and key biophysical properties of a coniferous plantation in upland central Wales, U.K. Over the test site, topography was relatively complex and was expected to influence the amount of radar backscatter.
Author

N95-23944*# Deutsche Forschungsanstalt fuer Luft- und Raumfahrt, Oberpfaffenhofen (Germany).
FOREST INVESTIGATIONS BY POLARIMETRIC AIRSAR DATA IN THE HARZ MOUNTAINS **c43**
M. Keil, D. Poll, J. Raupenstrauch, T. Tares (Helsinki Univ. of Technology, Espoo, Finland.), and R. Winter *In* JPL, Summaries of the 4th Annual JPL Airborne Geoscience Workshop. Volume 3: AIRSAR Workshop 25 Oct. 1993 p 21-24 (For primary document see N95-23938 07-42)
Avail: CASI HC A01/MF A01

The Harz Mountains in the North of Germany have been a study site for several remote sensing investigations since 1985, as the mountainous area is one of the forest regions in Germany heavily affected by forest decline, especially in the high altitudes above 800 m. In a research program at the University of Berlin, methods are developed for improving remote sensing assessment of forest structure and forest state by additional GIS information, using several datasets for establishing a forest information system. The Harz has been defined as a test site for the SIR-C/X-SAR mission which is going to deliver multifrequency and multipolarizational SAR data from orbit. In a pilot project let by DLR-DFD, these data are to be investigated for forestry and ecology purposes. In preparing a flight campaign to the SIR-C / X-SAR mission, 'MAC EUROPE 1991', performed by NASA/JPL, an area of about 12 km in the Northern Harz was covered with multipolarizational AIRSAR data in the C-, L- and P-band, including the Brocken, the highest mountain of the Harz, with an altitude of 1142 m. The multiparameter AIRSAR data are investigated for their information content on the forest state, regarding the following questions: (1) information on forest stand parameters like forest types, age classes and crown density, especially for the separation of deciduous and coniferous forest; (2) information on the storm damages (since 1972) and the status of regeneration; (3) information on the status of forest destruction because of forest decline; and (4) influence of topography, local incidence angle and soil moisture on the SAR data. Within the project various methods and tools have been developed for the investigation of multipolarimetric radar backscatter responses and for discrimination purposes, in order to use the multipolarization information of the compressed Stokes matrix delivered by JPL.
Author

N95-23945*# Colorado Univ., Boulder, CO. Center for the Study of Earth from Space.
COMPARISON OF INVERSION MODELS USING AIRSAR DATA FOR DEATH VALLEY, CALIFORNIA **c43**
Kathryn S. Kierein-Young *In* JPL, Summaries of the 4th Annual JPL Airborne Geoscience Workshop. Volume 3: AIRSAR Workshop 25 Oct. 1993 p 25-28 (For primary document see N95-23938 07-42)
(Contract JPL-958456; NGT-50728)
Avail: CASI HC A01/MF A01

Polarimetric Airborne Synthetic Aperture Radar (AIRSAR) data were collected for the Geologic Remote Sensing Field Experiment (GRSFE) over Death Valley, California, USA, in September 1989. AIRSAR is a four-look, quid-polarizaiton, three frequency instrument. It collects measurements at C-band (5.66 cm), L-band (23.98 cm), and P-band (68.13 cm), and has a GIFOV of 10 meters and a swath width of 12 kilometers. Because the radar measures at three wavelengths, different scales of surface roughness are measured. Also, dielectric constants can be calculated from the data. The scene used in this study is in Death Valley, California and is located over Trail Canyon alluvial fan, the valley floor, and Artists Drive alluvial fan. The fans are very different in mineralogic makeup, size, and surface roughness. Trail Canyon fan is located on the west side of the valley at the base of the Panamint Range and is a large fan with older areas of desert pavement and younger active channels. The source for the material on southern part of the fan is mostly quartzites and there is an area of carbonate source on the northern part of the fan. Artists Drive fan is located at the base of the Black Mountains on the east side of the valley and is a smaller, young fan with its source mostly from volcanic rocks. The valley floor contains playa and salt deposits that range from smooth to Devil's Golf course type salt pinnacles.
Author

N95-23946*# Colorado Univ., Boulder, CO. Center for Study of Earth from Space.

GEOLOGIC MAPPING USING INTEGRATED AIRSAR, AVIRIS, AND TIMS DATA **c43**

Fred A. Kruse *In* JPL, Summaries of the 4th Annual JPL Airborne Geoscience Workshop. Volume 3: AIRSAR Workshop 25 Oct. 1993 p 29-32 (For primary document see N95-23938 07-42)

(Contract JPL-958456; NAGw-1143; NAGw-1601)

Avail: CASI HC A01/MF A01

The multi-sensor aircraft campaign called the 'Geologic Remote Sensing Field Experiment' (GRSFE), conducted during 1989 in the southwestern United States, collected multiple airborne remote sensing data sets and associated field and laboratory measurements. The GRSFE airborne data sets used in this study include the airborne Synthetic Aperture Radar (AIRSAR), the Airborne Visible/Infrared Imaging Spectrometer (AVIRIS), and the Thermal Infrared Multispectral Scanner (TIMS). Each sensor's unique characteristics were used for this study in a combined analysis scheme for geologic mapping. AIRSAR was used to map structures and landforms, AVIRIS was used to map mineralogy, and TIMS was used to map lithology. Visual data integration using IHS transforms and combined numerical analysis using derived geophysical and geologic parameters with 'multispectral' techniques resulted in improved geologic mapping over that possible using each data set individually. Derived from text

N95-23947*# Naval Research Lab., Washington, DC. Remote Sensing Div.

STATISTICS OF MULTI-LOOK AIRSAR IMAGERY: A COMPARISON OF THEORY WITH MEASUREMENTS **c43**

J. S. Lee, K. W. Hoppel, and S. A. Mango *In* JPL, Summaries of the 4th Annual JPL Airborne Geoscience Workshop. Volume 3: AIRSAR Workshop 25 Oct. 1993 p 33-36 (For primary document see N95-23938 07-42)

Avail: CASI HC A01/MF A01

The intensity and amplitude statistics of SAR images, such as L-Band HH for SEASAT and SIR-B, and C-Band VV for ERS-1 have been extensively investigated for various terrain, ground cover and ocean surfaces. Less well-known are the statistics between multiple channels of polarimetric of interferometric SAR's, especially for the multi-look processed data. In this paper, we investigate the probability density functions (PDF's) of phase differences, the magnitude of complex products and the amplitude ratios, between polarization channels (i.e. HH, HV, and VV) using 1-look and 4-look AIRSAR polarimetric data. Measured histograms are compared with theoretical PDF's which were recently derived based on a complex Gaussian model. Author

N95-23948*# New South Wales Univ., Kensington (Australia). Center for Remote Sensing and GIS.

AIRSAR DEPLOYMENT IN AUSTRALIA, SEPTEMBER 1993: MANAGEMENT AND OBJECTIVES **c43**

A. K. Milne and I. J. Tapley (Commonwealth Scientific and Industrial Research Organization, Wembley, Australia.) *In* JPL, Summaries of the 4th Annual JPL Airborne Geoscience Workshop. Volume 3: AIRSAR Workshop 25 Oct. 1993 p 37-40 (For primary document see N95-23938 07-42)

Avail: CASI HC A01/MF A01

Past co-operation between the NASA Earth Science and Applications Division and the CSIRO and Australian university researchers has led to a number of mutually beneficial activities. These include the deployment of the C-130 aircraft with TIMS, AIS, and NS001 sensors in Australia in 1985; collaboration between scientists from the USA and Australia in soils research which has extended for the past decade; and in the development of imaging spectroscopy where DSIRO and NASA have worked closely together and regularly exchanged visiting scientists. In May this year TIMS was flown in eastern Australia on board a CSIRO-owned aircraft together with a CSIRO-designed CO2 laser spectrometer. The Science Investigation Team for the Shuttle Imaging Radar (SIRC-C) Program includes one Australian Principal Investigator and ten Australian co-investigators who will work on nine projects related to studying land and near-shore surfaces after the Shuttle flight scheduled for April 1994. This long-term continued joint collaboration was progressed further with the deployment of AIRSAR downunder in September 1993. During a five week period, the DC-8 aircraft flew in all Australian states and collected data from some 65 individual test sites. Derived from text

N95-23949*# Hawaii Univ., Honolulu, HI. Planetary Geosciences.

CURRENT AND FUTURE USE OF TOPSAR DIGITAL TOPOGRAPHIC DATA FOR VOLCANOLOGICAL RESEARCH **c43**

Peter J. Mouginis-Mark, Scott K. Rowland, and Harold Garbeil *In* JPL, Summaries of the 4th Annual JPL Airborne Geoscience Workshop. Volume 3: AIRSAR Workshop 25 Oct. 1993 p 41-44 (For primary document see N95-23938 07-42)

(Grants NAGw-1162; NAGw-2468)

Avail: CASI HC A01/MF A01

In several investigations of volcanoes, high quality digital elevation models (DEM's) are required to study either the geometry of the volcano or to investigate temporal changes in relief due to eruptions. Examples include the analysis of volume changes of a volcanic dome, the prediction of flow paths for pyroclastic flows, and the quantitative investigation of the geometry of valleys carved by volcanic mudflows. Additionally, to provide input data for models of lava flow emplacement, accurate measurements are needed of the thickness of lava flows as a function of distance from the vent and local slope. Visualization of volcano morphology is also aided by the ability to view a DEM from oblique perspectives. Until recently, the generation of these DEM's has required either high resolution stereo air photographs or extensive field surveying using the Global Positioning System (GPS) and other field techniques. Through the use of data collected by the NASA/JPL TOPSAR system, it is now possible to remotely measure the topography of volcanoes using airborne radar interferometry. TOPSAR data can be collected day or night under any weather conditions, thereby avoiding the problems associated with the derivation of DEM's from air photographs that may often contain clouds. Here we describe some of our initial work on volcanoes using TOPSAR data for Mt. Hekla (Iceland) and Vesuvius (Italy). We also outline various TOPSAR topographic studies of volcanoes in the Galapagos and Hawaii that will be conducted in the near future, describe how TOPSAR complements the volcanology investigations to be conducted with orbital radars (SIR-C/X-SAR, JERS-1 and ERS-1), and place these studies into the broader context of NASA's Global Change Program. Author

N95-23950*# National Aeronautics and Space Administration. Goddard Space Flight Center, Greenbelt, MD.

PRELIMINARY ANALYSIS OF THE SENSITIVITY OF AIRSAR IMAGES TO SOIL MOISTURE VARIATIONS **c43**

Rajan Pardipuram (Hughes STX, Inc., Lanham, MD.), William L. Teng (Hughes STX, Inc., Lanham, MD.), James R. Wang, and Edwin T. Engman *In* JPL, Summaries of the 4th Annual JPL Airborne Geoscience Workshop. Volume 3: AIRSAR Workshop 25 Oct. 1993 p 45-48 (For primary document see N95-23938 07-42)

Avail: CASI HC A01/MF A01

Synthetic Aperture Radar (SAR) images acquired from various sources such as Shuttle Imaging Radar B (SIR-B) and airborne SAR (AIRSAR) have been analyzed for signatures of soil moisture. The SIR-B measurements have shown a strong correlation between measurements of surface soil moisture (0-5 cm) and the radar backscattering coefficient sigma(sup o). The AIRSAR measurements, however, indicated a lower sensitivity. In this study, an attempt has been made to investigate the causes for this reduced sensitivity. Author

N95-23951*# Jet Propulsion Lab., California Inst. of Tech., Pasadena, CA.

UNUSUAL RADAR ECHOES FROM THE GREENLAND ICE SHEET **c43**

E. J. Rignot, J. J. vanZyl, S. J. Ostro, and K. C. Jezek (Ohio State Univ., Columbus, OH.) *In its* Summaries of the 4th Annual JPL Airborne Geoscience Workshop. Volume 3: AIRSAR Workshop 25 Oct. 1993 p 49-52 (For primary document see N95-23938 07-42)

Avail: CASI HC A01/MF A01

In June 1991, the NASA/Jet Propulsion Laboratory airborne synthetic-aperture radar (AIRSAR) instrument collected the first calibrated data set of multifrequency, polarimetric, radar observations of the Greenland ice sheet. At the time of the AIRSAR overflight, ground teams recorded the snow and firn (old snow) stratigraphy, grain size, density, and temperature at ice camps in three of the four snow zones identified by glaciologists to characterize four different degrees of summer melting of the Greenland ice sheet. The four snow zones are: (1) the dry-snow zone, at high elevation, where melting rarely occurs; (2) the percolation zone, where summer melting generates water that percolates down through the cold, porous, dry snow

and then refreezes in place to form massive layers and pipes of solid ice; (3) the soaked-snow zone where melting saturates the snow with liquid water and forms standing lakes; and (4) the ablation zone, at the lowest elevations, where melting is vigorous enough to remove the seasonal snow cover and ablate the glacier ice. There is interest in mapping the spatial extent and temporal variability of these different snow zones repeatedly by using remote sensing techniques. The objectives of the 1991 experiment were to study changes in radar scattering properties across the different melting zones of the Greenland ice sheet, and relate the radar properties of the ice sheet to the snow and firn physical properties via relevant scattering mechanisms. Here, we present an analysis of the unusual radar echoes measured from the percolation zone. Derived from text

N95-23952*# Telespazio S.p.A., Rome (Italy).
MAC EUROPE 1991 CAMPAIGN: AIRSAR/AVIRIS DATA INTEGRATION FOR AGRICULTURAL TEST SITE CLASSIFICATION **c82**
S. Sangiovanni, M. F. Buongiorno, M. Ferrarini (La Sapienza Univ., Rome, Italy.), and A. Fiumara *In* JPL, Summaries of the 4th Annual JPL Airborne Geoscience Workshop. Volume 3: AIRSAR Workshop 25 Oct. 1993 p 53-56 (For primary document see N95-23938 07-42)
Avail: CASI HC A01/MF A01

During summer 1991, multi-sensor data were acquired over the Italian test site 'Otrepo Pavese', an agricultural flat area in Northern Italy. This area has been the Telespazio pilot test site for experimental activities related to agriculture applications. The aim of the investigation described in the following paper is to assess the amount of information contained in the AIRSAR (Airborne Synthetic Aperture Radar) and AVIRIS (Airborne Visible/Infrared Imaging Spectrometer) data, and to evaluate classification results obtained from each sensor data separately and from the combined dataset. All classifications are examined by means of the resulting confusion matrices and Khat coefficients. Improvements of the classification results obtained by using the integrated dataset are finally evaluated. Author

N95-23953*# Naval Research Lab., Washington, DC. Remote Sensing Div.
MEASUREMENT OF OCEAN WAVE SPECTRA USING POLARIMETRIC AIRSAR DATA **c48**
D. L. Schuler *In* JPL, Summaries of the 4th Annual JPL Airborne Geoscience Workshop. Volume 3: AIRSAR Workshop 25 Oct. 1993 p 57-60 (For primary document see N95-23938 07-42)
Avail: CASI HC A01/MF A01

A polarimetric technique for improving the visibility of waves, whose propagation direction has an azimuthal component, in RAR (real aperture radar) or SAR (synthetic aperture radar) images has been investigated. The technique shows promise as a means of producing more accurate 2-D polarimetric RAR ocean wave spectra. For SAR applications domination by velocity-bunching effects may limit its usefulness to long ocean swell. A modification of this technique involving measurement of polarization signature modulations in the image is useful for detecting waves in SAR images and, potentially, estimating RMS wave slopes. Author

N95-23954*# California Univ., Santa Barbara, CA. Center for Remote Sensing and Environmental Optics.
AN IMPROVED ALGORITHM FOR RETRIEVAL OF SNOW WETNESS USING C-BAND AIRSAR **c43**
Jiancheng Shi (Innsbruck Univ., Austria.), Jeff Dozier (Innsbruck Univ., Austria.), and Helmut Rott (Innsbruck Univ., Austria.) *In* JPL, Summaries of the 4th Annual JPL Airborne Geoscience Workshop. Volume 3: AIRSAR Workshop 25 Oct. 1993 p 61-64 (For primary document see N95-23938 07-42)
Avail: CASI HC A01/MF A01

This study shows recent results of our efforts to develop and verify an algorithm for snow wetness retrieval from a polarimetric SAR (Synthetic Aperture Radar). Our algorithm is based on the first-order scattering model with consideration of both surface and volume scattering. It operates at C-band and requires only rough information about the ice volume fraction in snowpack. Comparing ground measurements and inferred from JPL AIRSAR data, the results showed that the relative error inferred from SAR imagery was within 25 percent. The inferred snow wetness from different looking geometries (two flight passes) provided consistent results within 2 percent. Both regional and point measurement comparisons between the ground and SAR derived snow wetness indicates that the inversion algorithm performs well using AIRSAR (Airborne Synthetic Aperture Radar) data and should prove useful for routine and large-area snow wetness (in top layer of a snowpack) measurements. Derived from text

N95-23955*# National Aeronautics and Space Administration. Goddard Space Flight Center, Greenbelt, MD.
POLARIMETRIC RADAR DATA DECOMPOSITION AND INTERPRETATION **c82**
Guoqing Sun (Science Systems and Applications, Inc., Lanham, MD.) and K. Jon Ranson *In* JPL, Summaries of the 4th Annual JPL Airborne Geoscience Workshop. Volume 3: AIRSAR Workshop 25 Oct. 1993 p 65-68 (For primary document see N95-23938 07-42)
Avail: CASI HC A01/MF A01

Significant efforts have been made to decompose polarimetric radar data into several simple scattering components. The components which are selected because of their physical significance can be used to classify SAR (Synthetic Aperture Radar) image data. If particular components can be related to forest parameters, inversion procedures may be developed to estimate these parameters from the scattering components. Several methods have been used to decompose an averaged Stoke's matrix or covariance matrix into three components representing odd (surface), even (double-bounce) and diffuse (volume) scatterings. With these decomposition techniques, phenomena, such as canopy-ground interactions, randomness of orientation, and size of scatters can be examined from SAR data. In this study we applied the method recently reported by van Zyl (1992) to decompose averaged backscattering covariance matrices extracted from JPL SAR images over forest stands in Maine, USA. These stands are mostly mixed stands of coniferous and deciduous trees. Biomass data have been derived from field measurements of DBH and tree density using allometric equations. The interpretation of the decompositions and relationships with measured stand biomass are presented in this paper. Derived from text

N95-23956*# Centre de Recherches en Physique de l'Environnement Terrestre et Planetaire, Orleans (France).
SYNERGY BETWEEN OPTICAL AND MICROWAVE REMOTE SENSING TO DERIVE SOIL AND VEGETATION PARAMETERS FROM MAC EUROPE 1991 EXPERIMENT **c43**
O. Taconet, M. Benallegue (Centre Machinisme Agricole Genie Rural Eaux Forets, Antony, France.), A. Vidal (Centre Machinisme Agricole Genie Rural Eaux Forets, Montpellier, France.), D. Vidal-Madjar, L. Prevot (Institut National de la Recherche Agronomique, Montfavet, France.), and M. Normand (Centre Machinisme Agricole Genie Rural Eaux Forets, Antony, France.) *In* JPL, Summaries of the 4th Annual JPL Airborne Geoscience Workshop. Volume 3: AIRSAR Workshop 25 Oct. 1993 p 69-72 (For primary document see N95-23938 07-42)
Avail: CASI HC A01/MF A01

The ability of remote sensing for monitoring vegetation density and soil moisture for agricultural applications is extensively studied. In optical bands, vegetation indices (NDVI, WDVI) in visible and near infrared reflectances are related to biophysical quantities as the leaf area index, the biomass. In active microwave bands, the quantitative assessment of crop parameters and soil moisture over agricultural areas by radar multiconfiguration algorithms remains prospective. Furthermore the main results are mostly validated on small test sites, but have still to be demonstrated in an operational way at a regional scale. In this study, a large data set of radar backscattering has been achieved at a regional scale on a French pilot watershed, the Orgeval, along two growing seasons in 1988 and 1989 (mainly wheat and corn). The radar backscattering was provided by the airborne scatterometer ERASME, designed at CRPE, (C and X bands and HH and VV polarizations). Empirical relationships to estimate water crop and soil moisture over wheat in CHH band under actual field conditions and at a watershed scale are investigated. Therefore, the algorithms developed in CHH band are applied for mapping the surface conditions over wheat fields using the AIRSAR and TMS images collected during the MAC EUROPE 1991 experiment. The synergy between optical and microwave bands is analyzed. Author

N95-23957*# Michigan Univ., Ann Arbor, MI. Radiation Lab.
SAR TERRAIN CLASSIFIER AND MAPPER OF BIOPHYSICAL ATTRIBUTES **c43**
Fawwaz T. Ulaby, M. Craig Dobson, Leland Pierce, and Kamal Sarabandi

In JPL, Summaries of the 4th Annual JPL Airborne Geoscience Workshop. Volume 3: AIRSAR Workshop 25 Oct. 1993 p 73-76 (For primary document see N95-23938 07-42)
Avail: CASI HC A01/MF A01

In preparation for the launch of SIR-C/X-SAR and design studies for future orbital SAR, a program has made considerable progress in the development of an SAR terrain classifier and algorithms for quantification of biophysical attributes. The goal of this program is to produce a generalized software package for terrain classification and estimation of biophysical attributes and to make this package available to the larger scientific community. The basic elements of the SAR (Synthetic Aperture Radar) terrain classifier are outlined. An SAR image is calibrated with respect to known system and processor gains and external targets (if available). A Level 1 classifier operates on the data to differentiate: urban features, surfaces and tall and short vegetation. Level 2 classifiers further subdivide these classes on the basis of structure. Finally, biophysical and geophysical inversions are applied to each class to estimate attributes of interest. The process used to develop the classifiers and inversions is shown. Radar scattering models developed from theory and from empirical data obtained by truck-mounted polarimeters and the JPL AirSAR are validated. The validated models are used in sensitivity studies to understand the roles of various scattering sources (i.e., surface trunk, branches, etc.) in determining net backscatter. Model simulations of sigma (sup o) as functions of the wave parameters (lambda, polarization and angle of incidence) and the geophysical and biophysical attributes are used to develop robust classifiers. The classifiers are validated using available AirSAR data sets. Specific estimators are developed for each class on the basis of the scattering models and empirical data sets. The candidate algorithms are tested with the AirSAR data sets. The attributes of interest include: total above ground biomass, woody biomass, soil moisture and soil roughness.

Derived from text

N95-23958*# Organisatie voor Toegepast Natuurwetenschappelijk Onderzoek, The Hague (Netherlands). Physics and Electronics Lab.

CLASSIFICATION AND SOIL MOISTURE DETERMINATION OF AGRICULTURAL FIELDS **c43**

A. C. vandenBroek and J. S. Groot *In* JPL, Summaries of the 4th Annual JPL Airborne Geoscience Workshop. Volume 3: AIRSAR Workshop 25 Oct. 1993 p 77-80 (For primary document see N95-23938 07-42)
Avail: CASI HC A01/MF A01

During the Mac-Europe campaign of 1991 several SAR (Synthetic Aperature Radar) experiments were carried out in the Flevoland test area in the Netherlands. The test site consists of a forested and an agricultural area with more than 15 different crop types. The experiments took place in June and July (mid to late growing season). The area was monitored by the spaceborne C-band VV polarized ERS-1, the Dutch airborne PHARS with similar frequency and polarization and the three-frequency PP-, L-, and C-band) polarimetric AIRSAR system of NASA/JPL. The last system passed over on June 15, 3, 12, and 28. The last two dates coincided with the overpasses of the PHARS and the ERS-1. Comparison of the results showed that backscattering coefficients from the three systems agree quite well. In this paper we present the results of a study of crop type classification (section 2) and soil moisture determination in the agricultural area (section 3). For these studies we used field averaged Stokes matrices extracted from the AIRSAR data (processor version 3.55 or 3.56).

Derived from text

N95-23959*# California Univ., Santa Barbara, CA. Center for Remote Sensing and Environmental Optics.

RELATING P-BAND AIRSAR BACKSCATTER TO FOREST STAND PARAMETERS **c43**

Yong Wang, John M. Melack, Frank W. Davis, Eric S. Kasischke (Duke Univ., Durham, NC.), and Norman L. Christensen, Jr. (Duke Univ., Durham, NC.) *In* JPL, Summaries of the 4th Annual JPL Airborne Geoscience Workshop. Volume 3: AIRSAR Workshop 25 Oct. 1993 p 81-84 (For primary document see N95-23938 07-42)
Avail: CASI HC A01/MF A01

As part of research on forest ecosystems, the Jet Propulsion Laboratory (JPL) and collaborating research teams have conducted multi-season airborne synthetic aperture radar (AIRSAR) experiments in three forest ecosystems including temperate pine forest (Duke, Forest, North Carolina), boreal forest (Bonanza Creek Experimental Forest, Alaska), and northern mixed hardwood-conifer forest (Michigan Biological Station, Michigan). The major research goals were to improve understanding of the relationships between radar backscatter and phenological variables (e.g. stand density, tree size, etc.), to improve radar backscatter models of tree canopy properties, and to develop a radar-based scheme for monitoring forest phenological changes. In September 1989, AIRSAR backscatter data were acquired over the Duke Forest. As the aboveground biomass of the loblolly pine forest stands at Duke Forest increased, the SAR backscatter at C-, L-, and P-bands increased and saturated at different biomass levels for the C-band, L-band, and P-band data. We only use the P-band backscatter data and ground measurements here to study the relationships between the backscatter and stand density, the backscatter and mean trunk dbh (diameter at breast height) of trees in the stands, and the backscatter and stand basal area.

Derived from text

N95-23960*# Technische Univ., Munich (Germany). Dept. of General and Applied Geology.

SOIL MOISTURE RETRIEVAL IN THE OBERPFAFFENHOFEN TESTSITE USING MAC EUROPE AIRSAR DATA **c43**

Tobias Wever and Jochen Henkel *In* JPL, Summaries of the 4th Annual JPL Airborne Geoscience Workshop. Volume 3: AIRSAR Workshop 25 Oct. 1993 p 85-88 (For primary document see N95-23938 07-42)
Avail: CASI HC A01/MF A01

Soil moisture content is an important parameter in many disciplines of science like hydrology, meteorology, agriculture and others. Microwave remote sensing technique has a high potential in measuring the dielectric constant of soils, which is strongly governed by the soil moisture. Much excellent work has been done on investigating the relationship between backscattering coefficient and soil moisture. Most of these studies are measured in a laboratory or are carried out with a multitemporal data set. This means, that the variation in the backscattering coefficient is only related to the soil moisture because all other parameters influencing the backscattering like surface roughness, vegetation cover, plant geometry, phenology of plants and row direction are kept constant. In this study the sensitivity of the backscattering coefficient to soil moisture of corn fields is investigated. In the framework of the MAC-Europe Campaign in June 1991, the NASA/JPL three-frequency polarimetric AIRSAR system collected data over the test site Oberpfaffenhofen. The AIRSAR campaign in Oberpfaffenhofen was complemented with intensive ground truth measurements. The sampled corn fields are nearly in the range of the same incidence angle (approximately 20 deg) and belong to different soil types. The evaluation was carried out at a single data set. The results show that the backscattering, measured at P-band, can be described with only two parameters very well. The main parameter influencing the backscattering is the soil moisture content; the second subordinated parameter is the row direction.

Author

N95-23961*# Canada Centre for Remote Sensing, Ottawa (Ontario).

MICROWAVE DIELECTRIC PROPERTIES OF BOREAL FOREST TREES **c43**

G. Xu, F. Ahern, and J. Brown (Dendron Resource Surveys Ltd., Ottawa, Ontario.) *In* JPL, Summaries of the 4th Annual JPL Airborne Geoscience Workshop. Volume 3: AIRSAR Workshop 25 Oct. 1993 p 89-92 (For primary document see N95-23938 07-42)
Avail: CASI HC A01/MF A01

The knowledge of vegetation dielectric behavior is important in studying the scattering properties of the vegetation canopy and radar backscatter modelling. Until now, a limited number of studies have been published on the dielectric properties in the boreal forest context. This paper presents the results of the dielectric constant as a function of depth in the trunks of two common boreal forest species: black spruce and trembling aspen, obtained from field measurements. The microwave penetration depth for the two species is estimated at C, L, and P bands and used to derive the equivalent dielectric constant for the trunk as a whole. The backscatter modelling is carried out in the case of black spruce and the results are compared with the JPL AIRSAR data. The sensitivity of the backscatter coefficient to the dielectric constant is also examined.

Author

43 EARTH RESOURCES AND REMOTE SENSING

Includes remote sensing of earth resources by aircraft and spacecraft; photogrammetry; and aerial photography.

For instrumentation see *35 Instrumentation and Photography.*

N95-22503# Idaho National Engineering Lab., Idaho Falls, ID.
A MULTISPECTRAL SCANNER SURVEY OF THE TONOPAH TEST RANGE, NEVADA. DATE OF SURVEY: AUGUST 1993
S. B. Brewster, Jr., M. E. Howard, and J. E. Shines Aug. 1994 45 p
(Contract DE-AC08-93NV-11265)
(DE95-003920; EGG-11265-1092) Avail: CASI HC A03/MF A01

The Multispectral Remote Sensing Department of the Remote Sensing Laboratory conducted an airborne multispectral scanner survey of a portion of the Tonopah Test Range, Nevada. The survey was conducted on August 21 and 22, 1993, using a Daedalus AADS1268 scanner and coincident aerial color photography. Flight altitudes were 5,000 feet (1,524 meters) above ground level for systematic coverage and 1,000 feet (304 meters) for selected areas of special interest. The multispectral scanner survey was initiated as part of an interim and limited investigation conducted to gather preliminary information regarding historical hazardous material release sites which could have environmental impacts. The overall investigation also includes an inventory of environmental restoration sites, a ground-based geophysical survey, and an aerial radiological survey. The multispectral scanner imagery and coincident aerial photography were analyzed for the detection, identification, and mapping of man-made soil disturbances. Several standard image enhancement techniques were applied to the data to assist image interpretation. A geologic ratio enhancement and a color composite consisting of AADS1268 channels 10, 7, and 9 (mid-infrared, red, and near-infrared spectral bands) proved most useful for detecting soil disturbances. A total of 358 disturbance sites were identified on the imagery and mapped using a geographic information system. Of these sites, 326 were located within the Tonopah Test Range while the remaining sites were present on the imagery but outside the site boundary. The mapped site locations are being used to support ongoing field investigations. DOE

N95-22537# Wageningen Agricultural Univ. (Netherlands).
EFFECTS OF WIND ON RAINFALL SIMULATION. SPATIAL DISTRIBUTION OF WATER APPLICATION, KINETIC ENERGY, AND OVERLAND FLOW UNDER SINGLE FULL-CONE NOZZLE SPRAYS
J. L. M. P. deLima (Coimbra Univ., Portugal.) and P. J. J. Torfs Aug. 1993 101 p Prepared in cooperation with Coimbra Univ.
(PB95-127304) Avail: CASI HC A06/MF A02

Portable rainfall simulators used in small plots give sufficient flexibility to study a wide variety of processes (e.g. infiltration, interrill erosion, water quality) on different soils and slopes for a wide range of land uses. They also allow a number of repetitions in a short period of time. In conducting these studies, it is important to measure the characteristics of the simulated rainfall applied to the test surface. It is unquestionable that wind affects field experiments that make use of rainfall simulators. Water-drop trajectories and velocities are altered, affecting water application, kinetic energy distributions, and the hydraulics of underlying overland flow, namely water depths and velocities. The mathematical model presented in this paper should facilitate the selection of single full-cone spray-nozzles (spray angles, ejection velocities, and drop-size distribution) and of the size and configuration of the spray area for expected field situations (rainfall characteristics, wind conditions, slope of terrain, and plot size). It provides a simple way of visualizing spray patterns and overland flow on different sloping surfaces and for different wind conditions. NTIS

N95-22538# Wageningen Agricultural Univ. (Netherlands).
COMBINING OPTICAL AND MICROWAVE REMOTE SENSING DATA OF FOREST VEGETATION: MAC EUROPE 1991
G. vanMaren and C. Varekamp Feb. 1993 89 p
(PB95-127312) Avail: CASI HC A05/MF A01

In the study the possibilities for a combined (synergic) use of optical and microwave remote sensing data of forest vegetation were examined. Within the framework of the MAC Europe campaign, airborne TMS (Thematic Mapper Simulator) and airborne C-L-P band SAR (Synthetic Aperture Radar) data over two forest areas in the Netherlands were registered. First variance analysis, signature analysis and discriminant analysis were performed in order to assess the usefulness of each band and combinations of bands for discriminating forest classes. Combining optical and microwave data improved forest classification results in most cases. Next the empirical relationships between optical/microwave data and forest parameters were examined. Microwave P-band data gave some relationships with forest parameters for all stands independent of forest class. Optical data were highly correlated with forest parameters but for Fagus sylvatica only. NTIS

N95-22713# Office of Technology Assessment, Washington, DC.
CIVILIAN SATELLITE REMOTE SENSING: A STRATEGIC APPROACH
Sep. 1994 181 p
(PB95-109633; OTA-ISS-607; ISBN-0-16-045310-0) Avail: CASI HC A09/MF A02

The report analyzes the case for developing a long-term, comprehensive strategic plan for civilian satellite remote sensing, and explores the elements of such a plan, if it were adopted. The report also enumerates many of the congressional decisions needed to ensure that future data needs will be satisfied. NTIS

N95-22832*# Massachusetts Inst. of Tech., Cambridge, MA. Dept. of Earth, Atmospheric, and Planetary Sciences.
GPS SURVEY OF THE WESTERN TIEN SHAN Semiannual Report, 15 Mar. 1994 - 14 Mar. 1995
Bradford H. Hager, Peter H. Molnar, Michael W. Hamburger (Indiana Univ., Bloomington, IN.), and Robert E. Reilinger 14 Mar. 1995 17 p
(Grants NAG5-1947; NAG5-1941; NSF EAR-91-17889; NSF EAR-91-15159; MIT Proj. OSP-8129)
(NASA-CR-197901; NAS 1.26:197901) Avail: CASI HC A03/MF A01

There were two major developments in 1994 in our collaborative GPS experiment in the Tien Shan of the Former Soviet Union (FSU). Both were motivated by our expectation that we will ultimately obtain better science at lower cost if we involve our colleagues in the FSU more deeply in (1) the collection and (2) the analysis of data. As an experimental test of the concept of having our local collaborators carry out the field work semi-autonomously, we sent 6 MIT receivers to the Tien Shan for a period of 3 months. To enable our collaborators to have the capability for data analysis, we provided computers for two data analysis centers and organized a two-week training session. This report emphasizes the rationale for deeper involvement of FSU scientists, describes the training sessions, discusses the data collection, and presents the results. We also discuss future plans. More detailed discussion of background, general scientific objectives, discussions with collaborators, and results for the campaigns in 1992 and 1993 have been given in previous reports. Author

N95-22916*# Miami Univ., Coral Gables, FL. Dept. of Physics.
OCEAN OBSERVATIONS WITH EOS/MODIS: ALGORITHM DEVELOPMENT AND POST LAUNCH STUDIES Semiannual Report, 1 Jan. - 30 Jun. 1994
Howard R. Gordon 15 Jul. 1994 16 p
(Contract NAS5-31363)
(NASA-CR-197402; NAS 1.26:197402) Avail: CASI HC A03/MF A01

During CY 1994 there are five objectives under this task: (1) investigate the effects of stratospheric aerosol on the proposed correction algorithm, and investigate the use of the 1380 nm MODIS band to remove the stratospheric aerosol perturbation; (2) investigate the effect of vertical structure in aerosol concentration and type on the behavior of the proposed correction algorithm; (3) investigate the effects of polarization on the accuracy of the algorithm; (4) improve the accuracy and speed of the existing algorithm; and (5) investigate removal of the O2 'A' absorption band at 762 nm from the 765 nm SeaWiFS band so the latter can be used in atmospheric correction of SeaWiFS. The importance of this to MODIS is that SeaWiFS data will be used extensively to test and improve the MODIS algorithm. Thus it is essential that the O2 absorption be adequately dealt with for SeaWiFS. Author

N95-23191*# California Univ., Santa Barbara, CA. Center for Remote Sensing and Environmental Optics.
LAND SURFACE TEMPERATURE MEASUREMENTS FOR EOS MODIS DATA Semiannual Report, Jan. - Jun. 1994
Zhengming Wan Jun. 1994 15 p
(Contract NAS5-31370)
(NASA-CR-197443; NAS 1.26:197443) Avail: CASI HC A03/MF A01

Work accomplished includes: Beta delivery 1 of the MODIS LST product; the first version of MODIS LST ATBD; update of the atmospheric radiative transfer code ATRAD; the development of a new approach look-up table method; and improvement of the TIR spectrometer. Preliminary feasibility analysis of the look-up table approach is presented in terms of showing the effects on the TIR radiance at the top of the atmosphere of the stratospheric and upper atmospheric temperature profiles, the surface emissivity and temperature, the lower atmospheric temperature and water vapor profiles, and the viewing angle. Derived from text

N95-23469# State Agricultural Univ., Wageningen (Netherlands).
REVITALIZATION OF THE GEMENC-AREA, BAJA, HUNGARY. 1: A STUDY ON HYDROLOGICAL POSSIBILITIES TO REVITALISE THE ECOSYSTEM IN THE KESELYUES-AREA. 2: TOWARDS THE RESTORATION OF THE GYUERUESALJ FLOODPLAIN
T. Rosmalen, L. Stalpers, and I. Zsuffa Apr. 1994 216 p Sponsored by Commission of the European Communities
(PB95-139283) Avail: CASI HC A10/MF A03

This publication is the result of two studies made in the framework of TEMPUS (Trans European Mobility Scheme for University Studies). Both studies concern the Gemenc-area, a floodplain of the Danube near the town of Baja in the South of Hungary. The water regime of the Danube has a main influence on the abiotic conditions of this area and therefore also a very important influence on its ecological development. Nowadays, the Gemenc is exposed to serious degradation mainly due to changes in the water regime of the Danube. The most harmful change is the lowering of the water levels of the river, caused by the regulation works. This process has resulted in desiccation in the area and degradation of the forest. The common goal of both studies is to find methods for restoration of the water regime on the floodplain for the benefit of the ecosystem. NTIS

N95-23471 National Aerospace Lab., Amsterdam (Netherlands).
FAME: A FOREST ASSESSMENT AND MONITORING ENVIRONMENT SCENARIO
W. J. Looyen, F. O. Zeppenfeldt, J. C. Venema, and G. vanderBurg 26 Feb. 1993 18 p See also PB95-139192 Prepared in cooperation with State Agricultural Univ. Limited Reproducibility: More than 20% of this document may be affected by microfiche quality
(PB95-139309; NLR-TP-93047-U) Avail: CASI HC A03

The report includes effective management of forest resources which requires suitable for, up-to-date information on the state, extent and distribution of forest. Remote Sensing data can provide this information. FAO has initiated a feasibility study on a global operational forest cover monitoring network using satellite remote sensing data within the framework of the Tropical Forestry Action Plan. The study indicates that the use of remote sensing data for global forest cover monitoring is of great importance. To enable this, provisions are required to allow operational pre-processing of remote sensing data to well defined and standardized products. A scenario for the development of a Forest Assessment and Monitoring Environment (FAME) is presented. Firstly, Pilot FAME is developed, aiming at providing a suitable infrastructure for forest management using satellite remote sensing data to compile information on global forests. Secondly, PFAME is upgraded to improve its functionality and to introduce Forest Management Systems. Thirdly, PFAME is extended by introducing remote sensing data from other newly launched sensors. NTIS

N95-23473*# Miami Univ., Coral Gables, FL. Dept. of Physics.
OCEAN OBSERVATIONS WITH EOS/MODIS: ALGORITHM DEVELOPMENT AND POST LAUNCH STUDIES Semiannual Report, 1 Jul. - 31 Dec. 1994
Howard R. Gordon 13 Jan. 1995 83 p
(Contract NAS5-31363)
(NASA-CR-197894; NAS 1.26:197894) Avail: CASI HC A05/MF A01

Several significant accomplishments were made during the present reporting period. (1) Initial simulations to understand the applicability of the MODerate Resolution Imaging Spectrometer (MODIS) 1380 nm band for removing the effects of stratospheric aerosols and thin cirrus clouds were completed using a model for an aged volcanic aerosol. The results suggest that very simple procedures requiring no a priori knowledge of the optical properties of the stratospheric aerosol may be as effective as complex procedures requiring full knowledge of the aerosol properties, except the concentration which is estimated from the reflectance at 1380 nm. The limitations of this conclusion will be examined in the next reporting period; (2) The lookup tables employed in the implementation of the atmospheric correction algorithm have been modified in several ways intended to improve the accuracy and/or speed of processing. These have been delivered to R. Evans for implementation into the MODIS prototype processing algorithm for testing; (3) A method was developed for removal of the effects of the O2 'A' absorption band from SeaWiFS band 7 (745-785 nm). This is important in that SeaWiFS imagery will be used as a test data set for the MODIS atmospheric correction algorithm over the oceans; and (4) Construction of a radiometer, and associated deployment boom, for studying the spectral reflectance of oceanic whitecaps at sea was completed. The system was successfully tested on a cruise off Hawaii on which whitecaps were plentiful during October-November. This data set is now under analysis. Author

N95-23597 Commonwealth Scientific and Industrial Research Organization, Mordialoc (Australia). Div. of Atmospheric Research
VALIDATION DATA FOR LAND SURFACE TEMPERATURE DETERMINATION FROM SATELLITES
A. J. Prata 1994 40 p
(CSIRO-TR-33; ISBN-0-643-05600-9) Copyright Avail: Issuing Activity (CSIRO, Div. of Atmospheric Research, Private Bag 1, Mordialloc, Victoria 3195, Australia)

There has been a paucity of appropriate ground-truth data for validating satellite estimates of land surface temperatures, due mostly to the difficulties associated with obtaining representative surface temperatures over an area comparable in size to that from a satellite measurement (typically about 1 sq km in area). For the express purpose of obtaining ground-truth data, field experiments were set up in two semi-arid regions of Australia. The data from these field experiments are reported here in the form of tables. The tables contain ground-truth surface temperatures, satellite brightness temperatures, and the relevant satellite and solar geometries. A description of the sites, the measurement techniques and accuracies, and some climatological variables are also provided. Author

N95-24026 Commonwealth Scientific and Industrial Research Organization, Mordialoc (Australia). Div. of Atmospheric Research.
IMPROVED AVHRR DATA NAVIGATION USING AUTOMATED LAND FEATURE RECOGNITION TO CORRECT A SATELLITE ORBITAL MODEL
A. C. Dilley and C. C. Elsum 1994 28 p
(CSIRO-TR-34; ISBN-0-643-05601-7) Copyright Avail: Issuing Activity (CSIRO, Div. of Atmospheric Research, Private Bag 1, Mordialloc, Victoria 3195, Australia)

An operational procedure for the automatic navigation of daytime image data from the Advanced Very High Resolution Radiometer (AVHRR) is described. The procedure achieves greater accuracy than methods which rely solely on models of satellite orbit and attitude. It applies a land feature recognition technique to determine the errors generated across an image using the Brouwer-Lyddane model of satellite orbit and assuming zero error in satellite attitude and radiometer alignment. It then uses a non-linear least-squares regression technique to determine corrections which need to be applied to the satellite position in order to minimize residual errors across the image. Corrections to the model-predicted satellite position and attitude in terms of satellite heights, cross-track position, along-track position and yaw are derived as a linear function of image line number. Related coefficients are recorded in the header of each processed image data file whence they are accessed and used by image navigation algorithms to provide line-by-line corrections to model-predicted position and attitude. Some of the corrections show a consistent bias -- a cross-track correction for the NOAA-11 satellite and a cross-track and yaw correction for the NOAA-12 satellite -- suggesting a mechanical misalignment of instruments and/or a permanent bias in the satellites' attitude control systems. Under conditions where the number and distribution of identified land features is sufficient to allow full analysis (approximately 60-70% of daytime overpasses using the current implementation), the method provides navigation to an accuracy of approximately +/- 1 pixel/line for pixels which lie within +/- 800 pixels of the center of the swath. Under operational conditions, this performance is only marginally reduced. Author

N95-24094*# Oregon State Univ., Corvallis, OR. Environmental Remote Sensing Applications Lab.

GEOGRAPHIC INFORMATION ANALYSIS: AN ECOLOGICAL APPROACH FOR THE MANAGEMENT OF WILDLIFE ON THE FOREST LANDSCAPE Final Technical Report, 1 Jul. 1988 - 20 Sep. 1992

William J. Ripple 1995 83 p Original contains color illustrations (Grant NAGw-1460)

(NASA-CR-197941; NAS 1.26:197941) Copyright Avail: CASI HC A05/MF A01; 4 functional color pages

This document is a summary of the project funded by NAGw-1460 as part of the Earth Observation Commericalization/Applications Program (EOCAP) directed by NASA's Earth Science and Applications Division. The goal was to work with several agencies to focus on forest structure and landscape characterizations for wildlife habitat applications. New analysis techniques were used in remote sensing and landscape ecology with geographic information systems (GIS). The development of GIS and the emergence of the discipline of landscape ecology provided us with an opportunity to study forest and wildlife habitat resources from a new perspective. New techniques were developed to measure forest structure across scales from the canopy to the regional level. This paper describes the project team, technical advances, and technology adoption process that was used. Reprints of related refereed journal articles are in the Appendix. For individual titles, see N95-24095 through N95-24104.

N95-24095*# Oregon State Univ., Corvallis, OR. Environmental Remote Sensing Applications Lab.

COMPARISON OF 7.5-MINUTE AND 1-DEGREE DIGITAL ELEVATION MODELS

Dennis L. Isaacson and William J. Ripple *In its* Geographic Information Analysis: An Ecological Approach for the Management of Wildlife on theForest Landscape 1995 6 p Repr. from Photogrammetric Engineering and Remote Sensing (American Society for Photogrammetry and Remote Sensing), v. 56, no. 11, Nov. 1990 p 1523-1527 Original contains color illustrations (For primary document see N95-24094 07-43)

(ISSN 0099-1112; ISSN 5611-1523)

Copyright Avail: CASI HC A02/MF A01; 4 functional color pages

We compared two digital elevation models (DEM's) for the Echo Mountain SE quadrangle in the Cascade Mountains of Oregon. Comparisons were made between 7.5-minute (1:24,000-scale) and 1-degree (1:250,000-scale) images using the variables of elevation, slope aspect, and slope gradient. Both visual and statistical differences are presented. Author

N95-24096*# Oregon State Univ., Corvallis, OR. Environmental Remote Sensing Applications Lab.

MEASURING FOREST LANDSCAPE PATTERNS IN THE CASCADE RANGE OF OREGON, USA

William J. Ripple, G. A. Bradshaw, and Thomas A. Spies (Pacific Northwest Environmental Research Lab., Corvallis, OR.) *In its* Geographic Information Analysis: An Ecological Approach for the Management of Wildlife on the Forest Landscape 1995 16 p Repr. from Biological Conservation (Elsevier Science Publishers Ltd. England), v. 57, 1991 p 73-88 (For primary document see N95-24094 07-43)

(ISSN 0006-3207)

Copyright Avail: CASI HC A03/MF A01; 4 functional color pages

This paper describes the use of a set of spatial statistics to quantify the landscape pattern caused by the patchwork of clearcuts made over a 15-year period in the western Cascades of Oregon. Fifteen areas were selected at random to represent a diversity of landscape fragmentation patterns. Managed forest stands (patches) were digitized and analyzed to produce both tabular and mapped information describing patch size, shape, abundance and spacing, and matrix characteristics of a given area. In addition, a GIS fragmentation index was developed which was found to be sensitive to patch abundance and to the spatial distribution of patches. Use of the GIS-derived index provides an automated method of determining the level of forest fragmentation and can be used to facilitate spatial analysis of the landscape for later coordination with field and remotely sensed data. A comparison of the spatial statistics calculated for the two years indicates an increase in forest fragmentation as characterized by an increase in mean patch abundance and a decrease in interpatch distance, amount of interior natural forest habitat, and the GIS fragmentation index. Such statistics capable of quantifying patch shape and spatial distribution may prove important in the evaluation of the changing character of interior and edge habitats for wildlife. Author

N95-24097*# Oregon State Univ., Corvallis, OR. Environmental Remote Sensing Applicaitons Lab.

A PRELIMINARY COMPARISON OF LANDSAT THEMATIC MAPPER AND SPOT-1 HRV MULTISPECTRAL DATA FOR ESTIMATING CONIFEROUS FOREST VOLUME

William J. Ripple, S. Wang, Dennis L. Isaacson, and D. P. Paine *In its* Geographic Information Analysis: An Ecological Approach for the Management of Wildlife on theForest Landscape 1995 7 p Repr. from Int. J. Remote Sensing (Taylor and Fra ncis Ltd.), v. 12, no. 9, 1991 p 1971-1977 (For primary document see N95-24094 07-43)

Copyright Avail: CASI HC A02/MF A01; 4 functional color pages

Digital Landsat Thematic Mapper (TM) and Satellite Probatoire d'Observation de la Terre (SPOT) High Resolution Visible (HRV) images of coniferous forest canopies were compared in their relationship to forest wood volume using correlation and regression analyses. Significant inverse relationships were found between softwood volume and the spectral bands from both sensors (P less than 0.01). The highest correlations were between the log of softwood volume and the near-infrared bands (HRV band 3, r = -0.89; TM band 4, r = -0.83). Author

N95-24098*# Oregon State Univ., Corvallis, OR. Environmental Remote Sensing Applications Lab.

OLD-GROWTH AND MATURE FORESTS NEAR SPOTTED OWL NESTS IN WESTERN OREGON

William J. Ripple, David H. Johnson, K. T. Hershey, and E. Charles Meslow *In its* Geographic Information Analysis: An Ecological Approach for the Management of Wildlife on theForest Landscape 1995 3 p Repr. from J. Wildl. Manage., v. 55, no. 2 p 316-318 (For primary document see N95-24094 07-43)

Avail: CASI HC A01/MF A01; 4 functional color pages

We investigated how the amount of old-growth and mature forest influences the selection of nest sites by northern spotted owls (Strix occidentalis caurina) in the Central Cascade Mountains of Oregon. We used 7 different plot sizes to compare the proportion of mature and old-growth forest between 30 nest sites and 30 random sites. The proportion of old-growth and mature forest was significantly greater at nests sites than at random sites for all plot sizes (P less than or equal to 0.01). Thus, management of the spotted owl might require setting the percentage of old-growth and mature forest retained from harvesting at least 1 standard deviation above the mean for the 30 nest sites we examined. Author

N95-24099*# Oregon State Univ., Corvallis, OR.

HIERARCHICAL ANALYSIS OF SPATIAL PATTERN AND PROCESSES OF DOUGLAS-FIR FORESTS Ph.D. Thesis, 10 Sep. 1991 Abstract Only

G. A. Bradshaw *In its* Geographic Information Analysis: An Ecological Approach for the Management of Wildlife on theForest Landscape 1995 2 p (For primary document see N95-24094 07-43)

Avail: CASI HC A01/MF A01; 4 functional color pages

There has been an increased interest in the quantification of pattern in ecological systems over the past years. This interest is motivated by the desire to construct valid models which extend across many scales. Spatial methods must quantify pattern, discriminate types of pattern, and relate hierarchical phenomena across scales. Wavelet analysis is introduced as a method to identify spatial structure in ecological transect data. The main advantage of the wavelet transform over other methods is its ability to preserve and display hierarchical information while allowing for pattern decomposition. Two applications of wavelet analysis are illustrated, as a means to: (1) quantify known spatial patterns in Douglas-fir forests at several scales, and (2) construct spatially-explicit hypotheses regarding pattern generating mechanisms. Application of the wavelet variance, derived from the wavelet transform, is developed for forest ecosystem analysis to obtain additional insight into spatially-explicit data. Specifically, the resolution capabilities of the wavelet variance are compared to the semi-variogram and Fourier power spectra for the description of spatial data using a set of one-dimensional stationary and non-stationary processes. The wavelet cross-covariance function is derived from the wavelet transform and introduced as a alternative method for the analysis of multivariate spatial

data of understory vegetation and canopy in Douglas-fir forests of the western Cascades of Oregon. Author

N95-24100*# Oregon State Univ., Corvallis, OR.
FOREST AND WILDLIFE HABITAT ANALYSIS USING REMOTE SENSING AND GEOGRAPHIC INFORMATION SYSTEMS M.S. Thesis, 26 May 1992 Abstract Only
Maria Fiorella *In its* Geographic Information Analysis: An Ecological Approach for the Management of Wildlife on theForest Landscape 1995 2 p (For primary document see N95-24094 07-43)
Avail: CASI HC A01/MF A01; 4 functional color pages

Forest and wildlife habitat analyses were conducted at the H.J. Andrews Experimental Forest in the Central Cascade Mountains of Oregon using remotely sensed data and a geographic information system (GIS). Landsat Thematic Mapper (TM) data were used to determine forest successional stages, and to analyze the structure of both old and young conifer forests. Two successional stage maps were developed. One was developed from six TM spectral bands alone, and the second was developed from six TM spectral bands and a relative sun incidence band. Including the sun incidence band in the classification improved the mapping accuracy in the two youngest successional stages, but did not improve overall accuracy or accuracy of the two oldest successional stages. Mean spectral values for old-growth and mature stands were compared in seven TM bands and seven band transformations. Differences between mature and old-growth successional stages were greatest for the band ratio of TM 4/5 (P = 0.00005) and the multiband transformation of wetness (P = 0.00003). The age of young conifer stands had the highest correlation to TM 4/5 values (r = 0.9559) of any of the TM band or band transformations used. TM 4/5 ratio values of poorly regenerated conifer stands were significantly different from well regenerated conifer stands after age 15 (P = 0.0000). TM 4/5 was named a 'Successional Stage Index' (SSI) because of its ability to distinguish forest successional stages. The forest successional stage map was used as input into a vertebrate richness model using GIS. The three variables of (1) successional stage, (2) elevation, and (3) site moisture were used in the GIS to predict the spatial occurrence of small mammal, amphibian, and reptile species based on primary and secondary habitat requirements. These occurrence or habitat maps were overlayed to tally the predicted number of vertebrate at any given point in the study area. Overall, sixty-three and sixty-seven percent of the model predictions for vertebrate occurrence matched the vertebrates that were trapped in the field in eight forested stands. Of the three model variables, site moisture appeared to have the greatest influence on the pattern of high vertebrate richness in all vertebrate classes. Author

N95-24101*# Oregon State Univ., Corvallis, OR. Environmental Remote Sensing Applications Lab.
ANALYSIS OF CONIFER FOREST REGENERATION USING LANDSAT THEMATIC MAPPER DATA
Maria Fiorella and William J. Ripple *In its* Geographic Information Analysis: An Ecological Approach for the Management of Wildlife on theForest Landscape 1995 6 p Repr. from Photogrammetric Engineering and Remote Sensing (American Society for Photogrammetry and Remote Sensing), v. 59, no. 9, Sep. 1993 p 1383-1388 (For primary document see N95-24094 07-43)
(ISSN 0099-1112; ISSN 5909-1383)
Copyright Avail: CASI HC A02/MF A01; 4 functional color pages

Landsat Thematic Mapper (TM) data were used to evaluate young conifer stands in the western Cascade Mountains of Oregon. Regression and correlation analyses were used to describe the relationships between TM band values and age of young Douglas-fir stands (2 to 35 years old). Spectral data from well regenerated Douglas-fir stands were compared to those of poorly regenerated conifer stands. TM bands 1, 2, 3, 5, 6, and 7 were inversely correlated with the age (r greater than or equal to -0.80) of well regenerated Douglas-fir stands. Overall, the 'structural index' (TM 4/5 ratio) had the highest correlation to age of Douglas-fir stands (r = 0.96). Poorly regenerated stands were spectrally distinct from well regenerated Douglas-fir stands after the stands reached an age of approximately 15 years. Author

N95-24102*# Oregon State Univ., Corvallis, OR. Environmental Remote Sensing Applications Lab.
DETERMINING SUCCESSIONAL STAGE OF TEMPERATE CONIFEROUS FORESTS WITH LANDSAT SATELLITE DATA
Maria Fiorella and William J. Ripple *In its* Geographic Information Analysis: An Ecological Approach for the Management of Wildlife on theForest Landscape 1995 8 p Repr. from Photogrammetric Engineering and Remote Sensing (American Society for Photogrammetry and Remote Sensing), v. 59, no. 2, Feb. 1993 p 239-246 (For primary document see N95-24094 07-43)
(ISSN 0099-1112)
Copyright Avail: CASI HC A02/MF A01; 4 functional color pages

Thematic Mapper (TM) digital imagery was used to map forest successional stages and to evaluate spectral differences between old-growth and mature forests in the central Cascade Range of Oregon. Relative sun incidence values were incorporated into the successional stage classification to compensate for topographic induced variation. Relative sun incidence improved the classification accuracy of young successional stages, but did not improve the classification accuracy of older, closed canopy forest classes or overall accuracy. TM bands 1, 2, and 4; the normalized difference vegetation index (NDVI); and TM 4/3, 4/5, and 4/7 band ratio values for old-growth forests were found to be significantly lower than the values of mature forests (P less than or equal to 0.010). Wetness and the TM 4/5 and 4/7 band ratios all had low correlations to relative sun incidence (r(exp 2) less than or equal to 0.16). The TM 4/5 band ratio was named the 'structural index' (SI) because of its ability to distinguish between mature and old-growth forests and its simplicity. Author

N95-24103*# Oregon State Univ., Corvallis, OR. Environmental Remote Sensing Applications Lab.
DETERMINING CONIFEROUS FOREST COVER AND FOREST FRAGMENTATION WITH NOAA-9 ADVANCED VERY HIGH RESOLUTION RADIOMETER DATA
William J. Ripple *In its* Geographic Information Analysis: An Ecological Approach for the Management of Wildlife on the Forest Landscape 1995 8 p Repr. from Photogrammetric Engineering and Remote Sensing (American Society for Photogrammetry and Remote Sensing), v. 60, no. 5, May 1994 p 533-540 Original contains color illustrations (For primary document see N95-24094 07-43)
(ISSN 0099-1112)
Copyright Avail: CASI HC A02/MF A01; 4 functional color pages

NOAA-9 satellite data from the Advanced Very High Resolution Radiometer (AVHRR) were used in conjunction with Landsat Multispectral Scanner (MSS) data to determine the proportion of closed canopy conifer forest cover in the Cascade Range of Oregon. A closed canopy conifer map, as determined from the MSS, was registered with AVHRR pixels. Regression was used to relate closed canopy conifer forest cover to AVHRR spectral data. A two-variable (band) regression model accounted for more variance in conifer cover than the Normalized Difference Vegetation Index (NDVI). The spectral signatures of various conifer successional stages were also examined. A map of Oregon was produced showing the proportion of closed canopy conifer cover for each AVHRR pixel. The AVHRR was responsive to both the percentage of closed canopy conifer cover and the successional stage in these temperate coniferous forests in this experiment. Author

N95-24104*# Pacific Northwest Environmental Research Lab., Corvallis, OR.
DYNAMICS AND PATTERN OF A MANAGED CONIFEROUS FOREST LANDSCAPE IN OREGON
Thomas A. Spies, William J. Ripple (Oregon State Univ., Corvallis, OR.), and G. A. Bradshaw (Oregon State Univ., Corvallis, OR.) *In* Oregon State Univ., Geographic Information Analysis: An Ecological Approach for the Management of Wildlife on the Forest Landscape 1995 14 p Repr. from Ecological Applications (Ecological Society of America), v. 4, no. 3, 1994 p 555-568 Original contains color illustrations (For primary document see N95-24094 07-43)
Avail: CASI HC A03/MF A01; 4 functional color pages

We examined the process of fragmentation in a managed forest landscape by comparing rates and patterns of disturbance (primarily clear-cutting) and regrowth between 1972 and 1988 using Landsat imagery. A 2589-km(exp 2) managed forest landscape in western Oregon was

classified into two forest types, closed-canopy conifer forest (CF) (typically, greater than 60% conifer cover) and other forest and nonforest types (OT) (typically, less than 40 yr old or deciduous forest). The percentage of CF declined from 71 to 58% between 1972 and 1988. Declines were greatest on private land, least in wilderness, and intermediate in public nonwilderness. High elevations (greater than 914 m) maintained a greater percentage of CF than lower elevations (less than 914 m). The percentage of the area at the edge of the two cover types increased on all ownerships and in both elevational zones, whereas the amount of interior habitat (defined as CF at least 100 m from OT) decreased on all ownerships and elevational zones. By 1988 public lands contained approximately 45% interior habitat while private lands had 12% interior habitat. Mean interior patch area declined from 160 to 62 ha. The annual rate of disturbance (primarily clear-cutting) for the entire area including the wilderness was 1.19%, which corresponds to a cutting rotation of 84 yr. The forest landscape was not in a steady state or regulated condition which is not projected to occur for at least 40 yr under current forest plans. Variability in cutting rates within ownerships was higher on private land than on nonreserve public land. However, despite the use of dispersed cutting patterns on public land, spatial patterns of cutting and remnant forest patches were nonuniform across the entire public ownership. Large remaining patches (less than 5000 ha) of contiguous interior forest were restricted to public lands designated for uses other than timber production such as wilderness areas and research natural areas. Author

N95-24148# EG and G Energy Measurements, Inc., Las Vegas, NV.
THERMAL RADIANT EXITANCE MODEL PERFORMANCE: SOILS AND FORESTS
L. K. Balick and J. A. Smith 1995 12 p Presented at the European Symposium on Satellite Remote Sensing, Rome, Italy, 26-30 Sep. 1994
(Contract DE-AC08-93NV-11265)
(DE95-003619; EGG-11265-1075; CONF-9409265-1) Avail: CASI HC A03/MF A01

Models of surface temperatures of two land surface types based on their energy budgets were developed to simulate the effects of environmental factors on thermal radiant exitance. The performance of these models is examined in detail. One model solves the non-linear differential equation for heat diffusion in solids using a set of submodels for surface energy budget components. The model performance is examined under three desert conditions thought to be a strong test of the submodels. The accuracy of the temperature predictions and submodels is described. The accuracy of the model is generally good but some discrepancies between some of the submodels and measurements are noted. The sensitivity of the submodels is examined and is seen to be strongly controlled by interaction and feedback among energy components that are a function of surface temperature. The second model simulates vegetation canopies with detailed effects of surface geometry on radiant transfer in the canopy. Foliage solar absorption coefficients are calculated using a radiosity approach for a three layer canopy and long wave fluxes are modeled using a view factor matrix. Sensible and latent heat transfer through the canopy are also simulated using, nearby meteorological data but heat storage in the canopy is not included. Simulations for a coniferous forest canopy are presented and the sensitivity of the model to environmental inputs is discussed. DOE

N95-24190*# California Univ., Santa Barbara, CA. Inst. for Computational Earth System Science.
LAND SURFACE TEMPERATURE MEASUREMENTS FROM EOS MODIS DATA Semiannual Report, Jul. - Dec. 1994
Zhengming Wan Dec. 1994 29 p
(Contract NAS5-31370)
(NASA-CR-197969; NAS 1.26:197969) Avail: CASI HC A03/MF A01

A generalized split-window method for retrieving land-surface temperature (LST) from AVHRR and MODIS data has been developed. Accurate radiative transfer simulations show that the coefficients in the split-window algorithm for LST must depend on the viewing angle, if we are to achieve a LST accuracy of about 1 K for the whole scan swath range (+/-55.4 deg and +/-55 deg from nadir for AVHRR and MODIS, respectively) and for the ranges of surface temperature and atmospheric conditions over land, which are much wider than those over oceans. We obtain these coefficients from regression analysis of radiative transfer simulations, and we analyze sensitivity and error by using results from systematic radiative transfer simulations over wide ranges of surface temperatures and emissivities, and atmospheric water vapor abundance and temperatures. Simulations indicated that as atmospheric column water vapor increases and viewing angle is larger than 45 deg it is necessary to optimize the split-window method by separating the ranges of the atmospheric column water vapor and lower boundary temperature, and the surface temperature into tractable sub-ranges. The atmospheric lower boundary temperature and (vertical) column water vapor values retrieved from HIRS/2 or MODIS atmospheric sounding channels can be used to determine the range where the optimum coefficients of the split-window method are given. This new LST algorithm not only retrieves LST more accurately but also is less sensitive than viewing-angle independent LST algorithms to the uncertainty in the band emissivities of the land-surface in the split-window and to the instrument noise. Author

N95-24192 Commonwealth Scientific and Industrial Research Organization, Mordialoc (Australia). Div. of Atmospheric Research
IMPLEMENTATION OF A SOIL-CANOPY SCHEME INTO THE CSIRO GCM: REGIONAL ASPECTS OF THE MODEL RESPONSE
E. A. Kowalczyk, J. R. Garratt, and P. B. Krummel 1994 65 p
(CSIRO-TR-32; ISBN-0-643-05257-7) Copyright Avail: Issuing Activity (CSIRO, Div. of Atmospheric Research, Private Bag 1, Mordialloc, Victoria 3195, Australia)

We have assessed the impact of a new soil-canopy scheme on aspects of the regional surface energy and water balances as simulated in the Commonwealth Scientific and Industrial Research Organization (CSIRO) 9-level General Circulation Models (GCM). Attention has been given to mean monthly statistics of rainfall, evaporation, soil moisture, net radiation and air temperature, both from a modelling and observational viewpoint. Five regions in Africa, Amazonia, Australia, Eurasia and North America were selected for study, with additional sites chosen for validation of the mean monthly diurnal cycle in air temperature, net radiation, sensible heat flux and evaporation simulated in the GCM. Each of these sites had comprehensive hourly observations of these quantities. Overall, we believe significant improvements to model simulations have resulted from implementation of the surface scheme discussed previously. Author

N95-23295*# Moravian Coll., Bethlehem, PA. Dept. of Computer Science.
LOCATING BUILDINGS IN AERIAL PHOTOS Abstract Only
James S. Green *In* Hampton Univ., 1994 NASA-HU American Society for Engineering Education (ASEE) Summer Faculty Fellowship Program Dec. 1994 p 77 (For primary document see N95-23276 07-99)
Avail: CASI HC A01/MF A02

N95-23675*# Lockheed Missiles and Space Co., Palo Alto, CA. Artificial Intelligence Center.
SOFTWARE AGENTS FOR THE DISSEMINATION OF REMOTE TERRESTRIAL SENSING DATA
Christopher N. Toomey, Evangelos Simoudis, Raymond W. Johnson, and William S. Mark *In* JPL, Third International Symposium on Artificial Intelligence, Robotics, and Automation for Space 1994 Oct. 1994 p 19-22 (For primary document see N95-23672 07-63)
Avail: CASI HC A01/MF A03

N95-23765*# Alcatel Espace, Toulouse (France).
TERRAIN MODELLING AND MOTION PLANNING FOR AN AUTONOMOUS EXPLORATION ROVER
F. Richard, S. Benoliel (Alcatel Alsthom Recherche, Marcoussis, France.), O. Faugeras (Institut National de Recherche d'Informatique et d'Automatique, Sophia Antipolis, France.), P. Grandjean (Centre National d'Etudes Spatiales, Toulouse, France.), M. Hayard, and T. Simeon (Centre National d'Etudes Spatiales, Toulouse, France.) *In* JPL, Third International Symposium on Artificial Intelligence, Robotics, and Automation for Space 1994 Oct. 1994 p 95-98 (For primary document see N95-23672 07-63)
Avail: CASI HC A01/MF A03

N95-23845*# National Aeronautics and Space Administration. Ames Research Center, Moffett Field, CA.
USE OF SPECTRAL ANALOGY TO EVALUATE CANOPY REFLECTANCE SENSITIVITY TO LEAF OPTICAL PROPERTY Abstract Only
Frederic Baret (Institut National de la Recherche Agronomique, Montfavet,

France.), Vern C. Vanderbilt, Michael D. Steven (Nottingham Univ., England.), and Stephane Jacquemoud (Joint Research Centre of the European Communities, Ispra, Italy.) *In* JPL, Summaries of the 4th Annual JPL Airborne Geoscience Workshop. Volume 1: AVIRIS Workshop 25 Oct. 1993 p 1 (For primary document see N95-23844 07-42)
Avail: CASI HC A01/MF A03

N95-23846*# Colorado Univ., Boulder, CO. Center for Study of Earth from Space.
A TOOL FOR MANUAL ENDMEMBER SELECTION AND SPECTRAL UNMIXING
C. Ann Bateson and Brian Curtiss *In* JPL, Summaries of the 4th Annual JPL Airborne Geoscience Workshop. Volume 1: AVIRIS Workshop 25 Oct. 1993 p 3-6 (For primary document see N95-23844 07-42)
Avail: CASI HC A01/MF A03

N95-23847*# Jet Propulsion Lab., California Inst. of Tech., Pasadena, CA. Dept. of Geology and Planetary Science.
LITHOLOGIC DISCRIMINATION AND ALTERATION MAPPING FROM AVIRIS DATA, SOCORRO, NEW MEXICO
K. K. Beratan (Pittsburgh Univ., Pittsburgh, PA.), N. DeLillo (Pittsburgh Univ., Pittsburgh, PA.), A. Jacobson, R. Blom, and C. E. Chapin (New Mexico Inst. of Mining and Technology, Socorro, NM.) *In its* Summaries of the 4th Annual JPL Airborne Geoscience Workshop. Volume 1: AVIRIS Workshop 25 Oct. 1993 p 7-10 (For primary document see N95-23844 07-42)
Avail: CASI HC A01/MF A03

N95-23850*# Jet Propulsion Lab., California Inst. of Tech., Pasadena, CA.
FIELD OBSERVATIONS USING AN AOTF POLARIMETRIC IMAGING SPECTROMETER
Li-Jen Cheng, Mike Hamilton, Colin Mahoney, and George Reyes *In its* Summaries of the 4th Annual JPL Airborne Geoscience Workshop. Volume 1: AVIRIS Workshop 25 Oct. 1993 p 19-22 (For primary document see N95-23844 07-42)
Avail: CASI HC A01/MF A03

N95-23851*# Jet Propulsion Lab., California Inst. of Tech., Pasadena, CA.
INSTANTANEOUS FIELD OF VIEW AND SPATIAL SAMPLING OF THE AIRBORNE VISIBLE/INFRARED IMAGING SPECTROMETER (AVIRIS)
Thomas G. Chrien and Robert O. Green *In its* Summaries of the 4th Annual JPL Airborne Geoscience Workshop. Volume 1: AVIRIS Workshop 25 Oct. 1993 p 23-26 (For primary document see N95-23844 07-42)
Avail: CASI HC A01/MF A03

N95-23853*# Geological Survey, Denver, CO.
COMPARISON OF THREE METHODS FOR MATERIALS IDENTIFICATION AND MAPPING WITH IMAGING SPECTROSCOPY
Roger N. Clark, Gregg Swayze (Colorado Univ., Boulder, CO.), Joe Boardman (Colorado Univ., Boulder, CO.), and Fred Kruse (Colorado Univ., Boulder, CO.) *In* JPL, Summaries of the 4th Annual JPL Airborne Geoscience Workshop. Volume 1: AVIRIS Workshop 25 Oct. 1993 p 31-33 (For primary document see N95-23844 07-42)
Avail: CASI HC A01/MF A03

N95-23856*# Jet Propulsion Lab., California Inst. of Tech., Pasadena, CA.
APPLICATION OF A TWO-STREAM RADIATIVE TRANSFER MODEL FOR LEAF LIGNIN AND CELLULOSE CONCENTRATIONS FROM SPECTRAL REFLECTANCE MEASUREMENTS, PART 1
James E. Conel, Jeannette vandenBosch, and Cindy I. Grove *In its* Summaries of the 4th Annual JPL Airborne Geoscience Workshop. Volume 1: AVIRIS Workshop 25 Oct. 1993 p 39-44 (For primary document see N95-23844 07-42)
Avail: CASI HC A01/MF A03

N95-23857*# Jet Propulsion Lab., California Inst. of Tech., Pasadena, CA.
APPLICATION OF A TWO-STREAM RADIATIVE TRANSFER MODEL FOR LEAF LIGNIN AND CELLULOSE CONCENTRATIONS FROM SPECTRAL REFLECTANCE MEASUREMENTS, PART 2
James E. Conel, Jeannette vandenBosch, and Cindy I. Grove *In its* Summaries of the 4th Annual JPL Airborne Geoscience Workshop. Volume 1: AVIRIS Workshop 25 Oct. 1993 p 45-51 (For primary document see N95-23844 07-42)
Avail: CASI HC A02/MF A03

N95-23860*# Jet Propulsion Lab., California Inst. of Tech., Pasadena, CA.
REMOTE SENSING OF SMOKE, CLOUDS, AND FIRE USING AVIRIS DATA
Bo-Cai Gao (Universities Space Research Association, Greenbelt, MD.), Yorman J. Kaufman (National Aeronautics and Space Administration. Goddard Space Flight Center, Greenbelt, MD.), and Robert O. Green *In its* Summaries of the 4th Annual JPL Airborne Geoscience Workshop. Volume 1: AVIRIS Workshop 25 Oct. 1993 p 61-64 (For primary document see N95-23844 07-42)
Avail: CASI HC A01/MF A03

N95-23863*# Jet Propulsion Lab., California Inst. of Tech., Pasadena, CA.
ESTIMATION OF AEROSOL OPTICAL DEPTH AND ADDITIONAL ATMOSPHERIC PARAMETERS FOR THE CALCULATION OF APPARENT REFLECTANCE FROM RADIANCE MEASURED BY THE AIRBORNE VISIBLE/INFRARED IMAGING SPECTROMETER
Robert O. Green, James E. Conel, and Dar A. Roberts (Washington Univ., Seattle, WA.) *In its* Summaries of the 4th Annual JPL Airborne Geoscience Workshop. Volume 1: AVIRIS Workshop 25 Oct. 1993 p 73-76 (For primary document see N95-23844 07-42)
Avail: CASI HC A01/MF A03

N95-23866*# Jet Propulsion Lab., California Inst. of Tech., Pasadena, CA.
A ROLE FOR AVIRIS IN THE LANDSAT AND ADVANCED LAND REMOTE SENSING SYSTEMS PROGRAM
Robert O. Green and John J. Simmonds *In its* Summaries of the 4th Annual JPL Airborne Geoscience Workshop. Volume 1: AVIRIS Workshop 25 Oct. 1993 p 85-88 (For primary document see N95-23844 07-42)
Avail: CASI HC A01/MF A03

N95-23867*# California Univ., Davis, CA. Dept. of Land, Air, and Water Resources.
ESTIMATING DRY GRASS RESIDUES USING LANDSCAPE INTEGRATION ANALYSIS
Quinn J. Hart, Susan L. Ustin, Lian Duan, and George Scheer *In* JPL, Summaries of the 4th Annual JPL Airborne Geoscience Workshop. Volume 1: AVIRIS Workshop 25 Oct. 1993 p 89-92 (For primary document see N95-23844 07-42)
Avail: CASI HC A02/MF A03

N95-23870*# Colorado Univ., Boulder, CO. Center for the Study of Earth from Space.
THE EFFECTS OF AVIRIS ATMOSPHERIC CALIBRATION METHODOLOGY ON IDENTIFICATION AND QUANTITATIVE MAPPING OF SURFACE MINERALOGY, DRUM MOUNTAINS, UTAH
Fred A. Kruse and John L. Dwyer *In* JPL, Summaries of the 4th Annual JPL Airborne Geoscience Workshop. Volume 1: AVIRIS Workshop 25 Oct. 1993 p 101-104 (For primary document see N95-23844 07-42)
(Contract GS-14-08-0001-A-0746)
Avail: CASI HC A01/MF A03

N95-23871*# University Coll. of Swansea (Wales). Dept. of Geography.
AVIRIS SPECTRA CORRELATED WITH THE CHLOROPHYLL CONCENTRATION OF A FOREST CANOPY
John Kupiec, Geoffrey M. Smith, and Paul J. Curran (Southampton Univ., England.) *In* JPL, Summaries of the 4th Annual JPL Airborne Geoscience Workshop. Volume 1: AVIRIS Workshop 25 Oct. 1993 p 105-108

Sponsored by NSF and NERC (UK) (For primary document see N95-23844 07-42)
Avail: CASI HC A01/MF A03

N95-23873*# New Hampshire Univ., Durham, NH. Complex Systems Research Center.
MEASUREMENTS OF CANOPY CHEMISTRY WITH 1992 AVIRIS DATA AT BLACKHAWK ISLAND AND HARVARD FOREST
Mary E. Martin and John D. Aber *In* JPL, Summaries of the 4th Annual JPL Airborne Geoscience Workshop. Volume 1: AVIRIS Workshop 25 Oct. 1993 p 113-116 (For primary document see N95-23844 07-42)
Avail: CASI HC A01/MF A03

N95-23878*# Centre National de la Recherche Scientifique, Toulouse (France).
MAPPING OF THE RONDA PERIDOTITE MASSIF (SPAIN) FROM AVIRIS SPECTRO-IMAGING SURVEY: A FIRST ATTEMPT
P. C. Pinet, S. Chabrillat, and G. Ceuleneer *In* JPL, Summaries of the 4th Annual JPL Airborne Geoscience Workshop. Volume 1: AVIRIS Workshop 25 Oct. 1993 p 137-140 (For primary document see N95-23844 07-42)
Avail: CASI HC A01/MF A03

N95-23879*# Agricultural Research Service, Beltsville, MD.
SPECTRAL VARIATIONS IN A COLLECTION OF AVIRIS IMAGERY
John C. Price *In* JPL, Summaries of the 4th Annual JPL Airborne Geoscience Workshop. Volume 1: AVIRIS Workshop 25 Oct. 1993 p 141-144 (For primary document see N95-23844 07-42)
Avail: CASI HC A01/MF A03

N95-23880*# Jet Propulsion Lab., California Inst. of Tech., Pasadena, CA.
MONITORING LAND USE AND DEGRADATION USING SATELLITE AND AIRBORNE DATA
Terrill W. Ray (California Inst. of Tech., Pasadena, CA.), Thomas G. Farr, Ronald G. Blom, and Robert E. Crippen *In its* Summaries of the 4th Annual JPL Airborne Geoscience Workshop. Volume 1: AVIRIS Workshop 25 Oct. 1993 p 145-148 (For primary document see N95-23844 07-42)
Avail: CASI HC A01/MF A03

N95-23881*# Jet Propulsion Lab., California Inst. of Tech., Pasadena, CA.
THE RED EDGE IN ARID REGION VEGETATION: 340-1060 NM SPECTRA
Terrill W. Ray, Bruce C. Murray, A. Chehbouni, and Eni Njoku *In its* Summaries of the 4th Annual JPL Airborne Geoscience Workshop. Volume 1: AVIRIS Workshop 25 Oct. 1993 p 249-152 (For primary document see N95-23844 07-42)
Avail: CASI HC A01/MF A03

N95-23882*# Jet Propulsion Lab., California Inst. of Tech., Pasadena, CA.
TEMPORAL CHANGES IN ENDMEMBER ABUNDANCES, LIQUID WATER AND WATER VAPOR OVER VEGETATION AT JASPER RIDGE
Dar A. Roberts (Washington Univ., Seattle, WA.), Robert O. Green, Donald E. Sabol (Washington Univ., Seattle, WA.), and John B. Adams (Washington Univ., Seattle, WA.) *In its* Summaries of the 4th Annual JPL Airborne Geoscience Workshop. Volume 1: AVIRIS Workshop 25 Oct. 1993 p 153-156 (For primary document see N95-23844 07-42)
Avail: CASI HC A01/MF A03

N95-23883*# Washington Univ., Seattle, WA. Dept. of Geological Sciences.
MAPPING AND MONITORING CHANGES IN VEGETATION COMMUNITIES OF JASPER RIDGE, CA, USING SPECTRAL FRACTIONS DERIVED FROM AVIRIS IMAGES
Donald E. Sabol, Jr., Dar A. Roberts, John B. Adams, and Milton O. Smith *In* JPL, Summaries of the 4th Annual JPL Airborne Geoscience Workshop. Volume 1: AVIRIS Workshop 25 Oct. 1993 p 157-160 (For primary document see N95-23844 07-42)
Avail: CASI HC A01/MF A03

N95-23884*# University Coll. of Swansea (Wales). Dept. of Geography.
THE EFFECT OF SIGNAL NOISE ON THE REMOTE SENSING OF FOLIAR BIOCHEMICAL CONCENTRATION
Geoffrey M. Smith and Paul J. Curran (Southampton Univ., England.) *In* JPL, Summaries of the 4th Annual JPL Airborne Geoscience Workshop. Volume 1: AVIRIS Workshop 25 Oct. 1993 p 161-164 (For primary document see N95-23844 07-42)
Avail: CASI HC A01/MF A03

N95-23885*# Ludwig-Maximilians-Univ., Munich (Germany). Inst. for General and Applied Geology.
APPLICATION OF MAC-EUROPE AVIRIS DATA TO THE ANALYSIS OF VARIOUS ALTERATION STAGES IN THE LANDDMANNALAUGER HYDROTHERMAL AREA (SOUTH ICELAND)
S. Sommer, G. Loercher, and S. Endres *In* JPL, Summaries of the 4th Annual JPL Airborne Geoscience Workshop. Volume 1: AVIRIS Workshop 25 Oct. 1993 p 165-168 (For primary document see N95-23844 07-42)
Avail: CASI HC A01/MF A03

N95-23886*# Canada Centre for Remote Sensing, Ottawa (Ontario).
ESTIMATION OF CROWN CLOSURE FROM AVIRIS DATA USING REGRESSION ANALYSIS
K. Staenz, D. J. Williams (MacDonald, Dettwiler and Associates Ltd., Richmond, British Columbia.), M. Truchon, and R. Fritz (Freiburg Univ., Germany.) *In* JPL, Summaries of the 4th Annual JPL Airborne Geoscience Workshop. Volume 1: AVIRIS Workshop 25 Oct. 1993 p 169-172 (For primary document see N95-23844 07-42)
Avail: CASI HC A01/MF A03

N95-23887*# Electromagnetic Systems Labs., Inc., Sunnyvale, CA.
OPTIMAL BAND SELECTION FOR DIMENSIONALITY REDUCTION OF HYPERSPECTRAL IMAGERY
Stephen D. Stearns, Bruce E. Wilson, and James R. Peterson *In* JPL, Summaries of the 4th Annual JPL Airborne Geoscience Workshop. Volume 1: AVIRIS Workshop 25 Oct. 1993 p 173-176 (For primary document see N95-23844 07-42)
Avail: CASI HC A01/MF A03

N95-23888*# Brown Univ., Providence, RI. Dept. Geological Science.
OBJECTIVE DETERMINATION OF IMAGE END-MEMBERS IN SPECTRAL MIXTURE ANALYSIS OF AVIRIS DATA
Stefanie Tompkins, John F. Mustard, Carle M. Pieters, and Donald W. Forsyth *In* JPL, Summaries of the 4th Annual JPL Airborne Geoscience Workshop. Volume 1: AVIRIS Workshop 25 Oct. 1993 p 177-180 (For primary document see N95-23844 07-42)
Avail: CASI HC A01/MF A03

N95-23889*# California Univ., Davis, CA. Dept. of Land, Air, and Water Resources.
RELATIONSHIPS BETWEEN PIGMENT COMPOSITION VARIATION AND REFLECTANCE FOR PLANT SPECIES FROM A COASTAL SAVANNAH IN CALIFORNIA
Susan L. Ustin, Eric W. Sanderson, Yaffa Grossman, and Quinn J. Hart *In* JPL, Summaries of the 4th Annual JPL Airborne Geoscience Workshop. Volume 1: AVIRIS Workshop 25 Oct. 1993 p 181-184 (For primary document see N95-23844 07-42)
Avail: CASI HC A01/MF A03

N95-23890*# Jet Propulsion Lab., California Inst. of Tech., Pasadena, CA.
ATMOSPHERIC CORRECTION OF AVIRIS DATA OF MONTEREY BAY CONTAMINATED BY THIN CIRRUS CLOUDS
Jeannette vandenBosch, Curtiss O. Davis, Curtis D. Mobley, and W. Joseph Rhea *In its* Summaries of the 4th Annual JPL Airborne Geoscience Workshop. Volume 1: AVIRIS Workshop 25 Oct. 1993 p 185-188 (For primary document see N95-23844 07-42)
Avail: CASI HC A01/MF A03

N95-23891*# Commission of the European Communities, Ispra (Italy). Inst. for Remote Sensing Applications.
INVESTIGATIONS ON THE 1.7 MICRON RESIDUAL ABSORPTION FEATURE IN THE VEGETATION REFLECTION SPECTRUM
J. Verdebout, S. Jacquemoud, G. Andreoli, B. Hosgood, and A. Sieber *In* JPL, Summaries of the 4th Annual JPL Airborne Geoscience Workshop. Volume 1: AVIRIS Workshop 25 Oct. 1993 p 189-192 (For primary document see N95-23844 07-42)
Avail: CASI HC A01/MF A03

N95-23892*# Brown Univ., Providence, RI. Dept. of Environmental, Population and Organismic Biology.
A COMPARISON OF SPECTRAL MIXTURE ANALYSIS AN NDVI FOR ASCERTAINING ECOLOGICAL VARIABLES
Carol A. Wessman, C. Ann Bateson, Brian Curtiss, and Tracy L. Benning *In* JPL, Summaries of the 4th Annual JPL Airborne Geoscience Workshop. Volume 1: AVIRIS Workshop 25 Oct. 1993 p 193-196 (For primary document see N95-23844 07-42)
Avail: CASI HC A01/MF A03

N95-23893*# Littoral Univ., Wimereux (France). d'Optique Atmospherique Lab.
USING AVIRIS FOR IN-FLIGHT CALIBRATION OF THE SPECTRAL SHIFTS OF SPOT-HRV AND OF AVHRR?
Veronique Willart-Soufflet and Richard Santer *In* JPL, Summaries of the 4th Annual JPL Airborne Geoscience Workshop. Volume 1: AVIRIS Workshop 25 Oct. 1993 p 197-200 (For primary document see N95-23844 07-42)
Avail: CASI HC A01/MF A03

N95-23895*# Colorado Univ., Boulder, CO. Center for the Study of Earth from Space.
DETERMINATION OF SEMI-ARID LANDSCAPE ENDMEMBERS AND SEASONAL TRENDS USING CONVEX GEOMETRY SPECTRAL UNMIXING TECHNIQUES
Roberta H. Yuhas, Joseph W. Boardman, and Alexander F. H. Goetz *In* JPL, Summaries of the 4th Annual JPL Airborne Geoscience Workshop. Volume 1: AVIRIS Workshop 25 Oct. 1993 p 205-208 (For primary document see N95-23844 07-42)
(Contract NAS5-30552; NAGw-2070)
Avail: CASI HC A01/MF A03

N95-23918*# Environmental Research Inst. of Michigan, Ann Arbor, MI.
ESTIMATION OF SPECTRAL EMISSIVITY IN THE THERMAL INFRARED
David Kryskowski and J. R. Maxwell *In* JPL, Summaries of the 4th Annual JPL Airborne Geoscience Workshop. Volume 2: TIMS Workshop 25 Oct. 1993 p 1-4 (For primary document see N95-23917 07-42)
Avail: CASI HC A01/MF A01

N95-23919*# Geological Survey of Japan, Kawasaki (Japan). Geophysics Dept.
THE DIFFERENCE BETWEEN LABORATORY AND IN-SITU PIXEL-AVERAGED EMISSIVITY: THE EFFECTS ON TEMPERATURE-EMISSIVITY SEPARATION
Tsuneo Matsunaga *In* JPL, Summaries of the 4th Annual JPL Airborne Geoscience Workshop. Volume 2: TIMS Workshop 25 Oct. 1993 p 5-8 (For primary document see N95-23917 07-42)
Avail: CASI HC A01/MF A01

N95-23920*# Arizona State Univ., Tempe, AZ. Dept. of Geology.
MINERALOGIC VARIABILITY OF THE KELSO DUNES, MOJAVE DESERT, CALIFORNIA DERIVED FROM THERMAL INFRARED MULTISPECTRAL SCANNER (TIMS) DATA
Michael S. Ramsey, Douglas A. Howard, Philip R. Christensen, and Nicholas Lancaster (Desert Research Inst., Reno, NV.) *In* JPL, Summaries of the 4th Annual JPL Airborne Geoscience Workshop. Volume 2: TIMS Workshop 25 Oct. 1993 p 9-1 (For primary document see N95-23917 07-42)
Avail: CASI HC A01/MF A01

N95-23921*# Forest Service, Atlanta, GA. Engineering Unit.
REMOTE IDENTIFICATION OF A GRAVEL LADEN PLEISTOCENE RIVER BED
Douglas E. Scholen *In* JPL, Summaries of the 4th Annual JPL Airborne Geoscience Workshop. Volume 2: TIMS Workshop 25 Oct. 1993 p 13-16 (For primary document see N95-23917 07-42)
Avail: CASI HC A01/MF A01

N95-23940*# Consiglio Nazionale delle Ricerche, Rome (Italy).
MAX-91: POLARIMETRIC SAR RESULTS ON MONTESPERTOLI SITE
S. Baronti, S. Luciani (Tor Vergata Univ., Rome, Italy.), S. Moretti (Florence Univ., Italy.), S. Paloscia, G. Schiavon (Tor Vergata Univ., Rome, Italy.), and S. Sigismondi (Florence Univ., Italy.) *In* JPL, Summaries of the 4th Annual JPL Airborne Geoscience Workshop. Volume 3: AIRSAR Workshop 25 Oct. 1993 p 5-8 Sponsored by Italian Space Agency (For primary document see N95-23938 07-42)
Avail: CASI HC A01/MF A01

N95-23941*# Arizona State Univ., Tempe, AZ. Dept. of Geology.
AIRSAR VIEWS OF AEROLIAN TERRAIN
Dan G. Blumberg and Ronald Greeley *In* JPL, Summaries of the 4th Annual JPL Airborne Geoscience Workshop. Volume 3: AIRSAR Workshop 25 Oct. 1993 p 9-12 (For primary document see N95-23938 07-42)
Avail: CASI HC A01/MF A01

N95-23942*# Cornell Univ., Ithaca, NY. Dept. of Geological Sciences.
GLACIOLOGICAL STUDIES IN THE CENTRAL ANDES USING AIRSAR/TOPSAR
Richard R. Forster, Andrew G. Klein, Troy A. Blodgett, and Bryan L. Isacks *In* JPL, Summaries of the 4th Annual JPL Airborne Geoscience Workshop. Volume 3: AIRSAR Workshop 25 Oct. 1993 p 13-15 (For primary document see N95-23938 07-42)
Avail: CASI HC A01/MF A01

N95-23943*# University Coll. of Swansea (Wales). Dept. of Geography.
ESTIMATION OF BIOPHYSICAL PROPERTIES OF UPLAND SITKA SPRUCE (PICEA SITCHENSIS) PLANTATIONS
Robert M. Green *In* JPL, Summaries of the 4th Annual JPL Airborne Geoscience Workshop. Volume 3: AIRSAR Workshop 25 Oct. 1993 p 17-20 (For primary document see N95-23938 07-42)
(Contract NERC-GT4/91/TLS/62)
Avail: CASI HC A01/MF A01

N95-23944*# Deutsche Forschungsanstalt fuer Luft- und Raumfahrt, Oberpfaffenhofen (Germany).
FOREST INVESTIGATIONS BY POLARIMETRIC AIRSAR DATA IN THE HARZ MOUNTAINS
M. Keil, D. Poll, J. Raupenstrauch, T. Tares (Helsinki Univ. of Technology, Espoo, Finland.), and R. Winter *In* JPL, Summaries of the 4th Annual JPL Airborne Geoscience Workshop. Volume 3: AIRSAR Workshop 25 Oct. 1993 p 21-24 (For primary document see N95-23938 07-42)
Avail: CASI HC A01/MF A01

N95-23945*# Colorado Univ., Boulder, CO. Center for the Study of Earth from Space.
COMPARISON OF INVERSION MODELS USING AIRSAR DATA FOR DEATH VALLEY, CALIFORNIA
Kathryn S. Kierein-Young *In* JPL, Summaries of the 4th Annual JPL Airborne Geoscience Workshop. Volume 3: AIRSAR Workshop 25 Oct. 1993 p 25-28 (For primary document see N95-23938 07-42)
(Contract JPL-958456; NGT-50728)
Avail: CASI HC A01/MF A01

N95-23946*# Colorado Univ., Boulder, CO. Center for Study of Earth from Space.
GEOLOGIC MAPPING USING INTEGRATED AIRSAR, AVIRIS, AND TIMS DATA
Fred A. Kruse *In* JPL, Summaries of the 4th Annual JPL Airborne Geoscience Workshop. Volume 3: AIRSAR Workshop 25 Oct. 1993 p 29-32 (For primary document see N95-23938 07-42)
(Contract JPL-958456; NAGw-1143; NAGw-1601)
Avail: CASI HC A01/MF A01

N95-23947*# Naval Research Lab., Washington, DC. Remote Sensing Div.
STATISTICS OF MULTI-LOOK AIRSAR IMAGERY: A COMPARISON OF THEORY WITH MEASUREMENTS
J. S. Lee, K. W. Hoppel, and S. A. Mango *In* JPL, Summaries of the 4th Annual JPL Airborne Geoscience Workshop. Volume 3: AIRSAR Workshop 25 Oct. 1993 p 33-36 (For primary document see N95-23938 07-42)
Avail: CASI HC A01/MF A01

N95-23948*# New South Wales Univ., Kensington (Australia). Center for Remote Sensing and GIS.
AIRSAR DEPLOYMENT IN AUSTRALIA, SEPTEMBER 1993: MANAGEMENT AND OBJECTIVES
A. K. Milne and I. J. Tapley (Commonwealth Scientific and Industrial Research Organization, Wembley, Australia.) *In* JPL, Summaries of the 4th Annual JPL Airborne Geoscience Workshop. Volume 3: AIRSAR Workshop 25 Oct. 1993 p 37-40 (For primary document see N95-23938 07-42)
Avail: CASI HC A01/MF A01

N95-23949*# Hawaii Univ., Honolulu, HI. Planetary Geosciences.
CURRENT AND FUTURE USE OF TOPSAR DIGITAL TOPOGRAPHIC DATA FOR VOLCANOLOGICAL RESEARCH
Peter J. Mouginis-Mark, Scott K. Rowland, and Harold Garbeil *In* JPL, Summaries of the 4th Annual JPL Airborne Geoscience Workshop. Volume 3: AIRSAR Workshop 25 Oct. 1993 p 41-44 (For primary document see N95-23938 07-42)
(Grants NAGw-1162; NAGw-2468)
Avail: CASI HC A01/MF A01

N95-23950*# National Aeronautics and Space Administration. Goddard Space Flight Center, Greenbelt, MD.
PRELIMINARY ANALYSIS OF THE SENSITIVITY OF AIRSAR IMAGES TO SOIL MOISTURE VARIATIONS
Rajan Pardipuram (Hughes STX, Inc., Lanham, MD.), William L. Teng (Hughes STX, Inc., Lanham, MD.), James R. Wang, and Edwin T. Engman *In* JPL, Summaries of the 4th Annual JPL Airborne Geoscience Workshop. Volume 3: AIRSAR Workshop 25 Oct. 1993 p 45-48 (For primary document see N95-23938 07-42)
Avail: CASI HC A01/MF A01

N95-23951*# Jet Propulsion Lab., California Inst. of Tech., Pasadena, CA.
UNUSUAL RADAR ECHOES FROM THE GREENLAND ICE SHEET
E. J. Rignot, J. J. vanZyl, S. J. Ostro, and K. C. Jezek (Ohio State Univ., Columbus, OH.) *In its* Summaries of the 4th Annual JPL Airborne Geoscience Workshop. Volume 3: AIRSAR Workshop 25 Oct. 1993 p 49-52 (For primary document see N95-23938 07-42)
Avail: CASI HC A01/MF A01

N95-23954*# California Univ., Santa Barbara, CA. Center for Remote Sensing and Environmental Optics.
AN IMPROVED ALGORITHM FOR RETRIEVAL OF SNOW WETNESS USING C-BAND AIRSAR
Jiancheng Shi (Innsbruck Univ., Austria.), Jeff Dozier (Innsbruck Univ., Austria.), and Helmut Rott (Innsbruck Univ., Austria.) *In* JPL, Summaries of the 4th Annual JPL Airborne Geoscience Workshop. Volume 3: AIRSAR Workshop 25 Oct. 1993 p 61-64 (For primary document see N95-23938 07-42)
Avail: CASI HC A01/MF A01

N95-23956*# Centre de Recherches en Physique de l'Environnement Terrestre et Planetaire, Orleans (France).
SYNERGY BETWEEN OPTICAL AND MICROWAVE REMOTE SENSING TO DERIVE SOIL AND VEGETATION PARAMETERS FROM MAC EUROPE 1991 EXPERIMENT
O. Taconet, M. Benallegue (Centre Machinisme Agricole Genie Rural Eaux Forets, Antony, France.), A. Vidal (Centre Machinisme Agricole Genie Rural Eaux Forets, Montpellier, France.), D. Vidal-Madjar, L. Prevot (Institut National de la Recherche Agronomique, Montfavet, France.), and M. Normand (Centre Machinisme Agricole Genie Rural Eaux Forets, Antony, France.) *In* JPL, Summaries of the 4th Annual JPL Airborne Geoscience Workshop. Volume 3: AIRSAR Workshop 25 Oct. 1993 p 69-72 (For primary document see N95-23938 07-42)
Avail: CASI HC A01/MF A01

N95-23957*# Michigan Univ., Ann Arbor, MI. Radiation Lab.
SAR TERRAIN CLASSIFIER AND MAPPER OF BIOPHYSICAL ATTRIBUTES
Fawwaz T. Ulaby, M. Craig Dobson, Leland Pierce, and Kamal Sarabandi *In* JPL, Summaries of the 4th Annual JPL Airborne Geoscience Workshop. Volume 3: AIRSAR Workshop 25 Oct. 1993 p 73-76 (For primary document see N95-23938 07-42)
Avail: CASI HC A01/MF A01

N95-23958*# Organisatie voor Toegepast Natuurwetenschappelijk Onderzoek, The Hague (Netherlands). Physics and Electronics Lab.
CLASSIFICATION AND SOIL MOISTURE DETERMINATION OF AGRICULTURAL FIELDS
A. C. vandenBroek and J. S. Groot *In* JPL, Summaries of the 4th Annual JPL Airborne Geoscience Workshop. Volume 3: AIRSAR Workshop 25 Oct. 1993 p 77-80 (For primary document see N95-23938 07-42)
Avail: CASI HC A01/MF A01

N95-23959*# California Univ., Santa Barbara, CA. Center for Remote Sensing and Environmental Optics.
RELATING P-BAND AIRSAR BACKSCATTER TO FOREST STAND PARAMETERS
Yong Wang, John M. Melack, Frank W. Davis, Eric S. Kasischke (Duke Univ., Durham, NC.), and Norman L. Christensen, Jr. (Duke Univ., Durham, NC.) *In* JPL, Summaries of the 4th Annual JPL Airborne Geoscience Workshop. Volume 3: AIRSAR Workshop 25 Oct. 1993 p 81-84 (For primary document see N95-23938 07-42)
Avail: CASI HC A01/MF A01

N95-23960*# Technische Univ., Munich (Germany). Dept. of General and Applied Geology.
SOIL MOISTURE RETRIEVAL IN THE OBERPFAFFENHOFEN TESTSITE USING MAC EUROPE AIRSAR DATA
Tobias Wever and Jochen Henkel *In* JPL, Summaries of the 4th Annual JPL Airborne Geoscience Workshop. Volume 3: AIRSAR Workshop 25 Oct. 1993 p 85-88 (For primary document see N95-23938 07-42)
Avail: CASI HC A01/MF A01

N95-23961*# Canada Centre for Remote Sensing, Ottawa (Ontario).
MICROWAVE DIELECTRIC PROPERTIES OF BOREAL FOREST TREES
G. Xu, F. Ahern, and J. Brown (Dendron Resource Surveys Ltd., Ottawa, Ontario.) *In* JPL, Summaries of the 4th Annual JPL Airborne Geoscience Workshop. Volume 3: AIRSAR Workshop 25 Oct. 1993 p 89-92 (For primary document see N95-23938 07-42)
Avail: CASI HC A01/MF A01

44 ENERGY PRODUCTION AND CONVERSION

Includes specific energy conversion systems, e.g., fuel cells; global sources of energy; geophysical conversion; and windpower.

For related information see also *07 Aircraft Propulsion and Power, 20 Spacecraft Propulsion and Power,* and *28 Propellants and Fuels.*

N95-22501# California Univ., Berkeley. Lawrence Berkeley Lab, CA.
ENERGY CONVERSION AND STORAGE PROGRAM Annual Report, 1993
E. J. Cairns Jun. 1994 22 p
(Contract DE-AC03-76SF-00098)
(DE95-003796; LBL-35242) Avail: CASI HC A03/MF A01

The Energy Conversion and Storage Program applies chemistry and materials science principles to solve problems in: production of new synthetic fuels; development of high-performance rechargeable batteries and fuel cells; development of high-efficiency thermochemical processes for energy conversion; characterization of complex chemical processes and chemical species; and the study and application of novel materials for energy conversion and transmission. Projects focus on transport-process principles,

chemical kinetics, thermodynamics, separation processes, organic and physical chemistry, novel materials, and advanced methods of analysis.
DOE

N95-22502# Sandia National Labs., Albuquerque, NM.
EVALUATING PHOTOVOLTAIC APPLICATIONS: A GUIDE FOR UTILITIES
M. Reineke 1994 11 p
(Contract DE-AC04-94AL-85000)
(DE95-003807; SAND-93-0120) Avail: CASI HC A03/MF A01

For many applications on utility systems today, photovoltaics provides a cost-effective energy source for serving low power loads. In certain applications, photovoltaics can be utilized as a cost-effective alternative to distribution line extensions or step-down transformers. This guide was written primarily for utility personnel to use in determining whether photovoltaics compares favorably with the cost of extending the utility line. The applications listed at the end of this pamphlet are limited to those that have immediate payback - systems for which photovoltaics is a less expensive option than conventional service would be. Scores of applications exist today for photovoltaic systems within utility companies; this publication suggests only a few of the many possibilities. Sandia National Laboratories Photovoltaic Design Assistance Center is a resource for utilities and agencies, providing contact among potential users of photovoltaic systems, suppliers of systems and components, and qualified engineers who evaluate needs and available equipment.
DOE

N95-22518# Florida Solar Energy Center, Cape Canaveral, FL.
SOUTHEAST REGIONAL EXPERIMENT STATION
Aug. 1994 15 p
(Contract DE-FC04-82AL-20729)
(DE95-000903; DOE/AL-20729/T2) Avail: CASI HC A03/MF A01

This is the final report of the Southeast Regional Experiment Station project. The Florida Solar Energy Center (FSEC), a research institute of the University of Central Florida (UCF), has operated the Southeast Regional Experiment Station (SE RES) for the US Department of Energy (DOE) since September 1982. Sandia National Laboratories, Albuquerque (SNLA) provides technical program direction for both the SE RES and the Southwest Regional Experiment Station (SW RES) located at the Southwest Technology Development Institute at Las Cruces, New Mexico. This cooperative effort serves a critical role in the national photovoltaic program by conducting system evaluations, design assistance and technology transfer to enhance the cost-effective utilization and development of photovoltaic technology. Initially, the research focus of the SE RES program centered on utility-connected PV systems and associated issues. In 1987, the SE RES began evaluating amorphous silicon (a-Si) thin-film PV modules for application in utility-interactive systems. Stand-alone PV systems began receiving increased emphasis at the SE RES in 1986. Research projects were initiated that involved evaluation of vaccine refrigeration, water pumping and other stand-alone power systems. The results of this work have led to design optimization techniques and procedures for the sizing and modeling of PV water pumping systems. Later recent research at the SE RES included test and evaluation of batteries and charge controllers for stand-alone PV system applications. The SE RES project provided the foundation on which FSEC achieved national recognition for its expertise in PV systems research and related technology transfer programs. These synergistic products of the SE RES illustrate the high visibility and contributions the FSEC PV program offers to the DOE.
DOE

N95-22546# National Renewable Energy Lab., Golden, CO.
LARGE-AREA TRIPLE-JUNCTION a-Si ALLOY PRODUCTION SCALEUP
Annual Subcontract Report, 17 Mar. 1993 - 18 Mar. 1994
R. Oswald (Solarex Corp., Newtown, PA.) and J. Morris (Solarex Corp., Newtown, PA.) Nov. 1994 57 p
(Contract DE-AC36-83CH-10093)
(DE95-000245; NREL/TP-411-7350) Avail: CASI HC A04/MF A01

The objective of this subcontract over its three-year duration is to advance Solarex's photovoltaic manufacturing technologies, reduce its a-Si:H module production costs, increase module performance and expand the Solarex commercial production capacity. Solarex shall meet these objectives by improving the deposition and quality of the transparent front contact, by optimizing the laser patterning process, scaling-up the semiconductor deposition process, improving the back contact deposition, scaling-up and improving the encapsulation and testing of its a-Si:H modules. In the Phase 2 portion of this subcontract, Solarex focused on improving deposition of the front contact, investigating alternate feed stocks for the front contact, maximizing throughput and area utilization for all laser scribes, optimizing a-Si:H deposition equipment to achieve uniform deposition over large-areas, optimizing the triple-junction module fabrication process, evaluating the materials to deposit the rear contact, and optimizing the combination of isolation scribe and encapsulant to pass the wet high potential test. Progress is reported on the following: Front contact development; Laser scribe process development; Amorphous silicon based semiconductor deposition; Rear contact deposition process; Frit/bus/wire/frame; Materials handling; and Environmental test, yield and performance analysis.
DOE

N95-22547# National Renewable Energy Lab., Golden, CO.
ADVANCED REFLECTOR MATERIALS FOR SOLAR CONCENTRATORS
Gary Jorgensen, Tom Williams, and Tim Wendelin Oct. 1994 9 p Presented at the 7th International Symposium on Solar Thermal Concentrating Technologies, Moscow, Russia, 26-30 Sep. 1994
(Contract DE-AC36-83CH-10093)
(DE95-000248; NREL/TP-471-7018; CONF-940970-6) Avail: CASI HC A02/MF A01

This paper describes the research and development at the US National Renewable Energy Laboratory (NREL) in advanced reflector materials for solar concentrators. NREL's research thrust is to develop solar reflector materials that maintain high specular reflectance for extended lifetimes under outdoor service conditions and whose cost is significantly lower than existing products. Much of this work has been in collaboration with private-sector companies that have extensive expertise in vacuum-coating and polymer-film technologies. Significant progress and other promising developments will be discussed. These are expected to lead to additional improvements needed to commercialize solar thermal concentration systems and make them economically attractive to the solar manufacturing industry. To explicitly demonstrate the optical durability of candidate reflector materials in real-world service conditions, a network of instrumented outdoor exposure sites has been activated.
DOE

N95-22554# Sandia National Labs., Albuquerque, NM.
TWELVE MONTH PERFORMANCE EVALUATION FOR THE ROTATING SHADOWBAND RADIOMETER
Andrew L. Rosenthal (New Mexico State Univ., Las Cruces, NM.) and Jeffrey M. Roberg (New Mexico State Univ., Las Cruces, NM.) Sep. 1994 33 p
(Contract DE-AC04-94AL-85000)
(DE95-002847; SAND-94-1248) Avail: CASI HC A03/MF A01

The Southwest Technology Development institute staff compared twelve months of 10-minute average data from a rotating shadowband radiometer (RSR) with data from three thermopile-based reference radiometers. Particular attention was focused on determining the accuracy of the direct normal irradiance data reported by the RSR. Accurate measurement of direct normal irradiance is the most critical requirement of the RSR when used for performance assessment of concentrating solar thermal collectors. Evaluation of three different methods of post-collection data processing was also performed.
DOE

N95-22568# Argonne National Lab., IL. Electrochemical Technology Program.
SUPPORT RESEARCH FOR SOLID OXIDE FUEL CELLS
M. Krumpelt and T. W. Kueper 1994 6 p Presented at the Fuel Cells 1994, Morgantown, WV, 17-19 Aug. 1994
(Contract W-31-109-eng-38)
(DE95-002910; ANL/CMT/CP-83648; CONF-940883-7) Avail: CASI HC A02/MF A01

The purpose of this work is to develop technology for a planar Solid Oxide Fuel Cell (SOFC) which uses a thin electrolyte and operates at about 800 C. The two major tasks of this effort are: (1) develop a conductive bond layer between the electrodes and the interconnect and (2) integrate a metallic interconnect into the stack which is well matched with the other cell components with regard to thermal expansion and is adequately protected from corrosion. Initial experiments tested the concept of a metallic slurry as a bond layer. Thermal expansion and oxidation resistance were tested for three candidate materials for the metal interconnect: a bipolar plate material, a YSZ trilayer, and Inconel 825.
DOE

N95-22574# Lawrence Livermore National Lab., Livermore, CA.
ELECTROMECHANICAL BATTERY PROGRAM AT THE LAWRENCE LIVERMORE NATIONAL LABORATORY
R. F. Post, D. A. Bender, and B. T. Merritt 31 May 1994 12 p Presented at the 29th Intersociety Energy Conversion Engineering Conference, Monterey, CA, 7-12 Aug. 1994
(Contract W-7405-eng-48)
(DE95-003657; UCRL-JC-117506; CONF-940812-24) Avail: CASI HC A03/MF A01

New materials and new design concepts are being incorporated in a new approach to an old idea - flywheel energy storage - to create an important alternative to the electrochemical storage battery for use in electric vehicles or for stationary applications, such as computer back-up power or utility load-leveling. We visualize such EMB's (electromechanical batteries) as being modular in character, with small (1-5 kWh) modules being used for power-conditioning and for vehicular use, and paralleled 25 kWh modules being used for bulk storage, i.e., load-leveling, applications. In a funded program at the Laboratory two fractional kWh, 200 kW (design peak power) modules have been constructed and subjected to shake-down testing. Their design for high peak power was prompted by awareness of a particular commercial need, as a component in a power-line conditioning device. In addition to such stationary applications, the high power capability of our EMB designs makes them attractive for use in hybrid-electric vehicles. Important elements of the LLNL program include the development of passive magnetic bearings and the application of new high-efficiency permanent magnet arrays to an ironless generator/motor. Use of these particular elements, together with a multi-ring design for the flywheel rotor, is particularly conducive to a systemic approach to the design of an EMB module. These particular design developments have been motivated by the economic issues of simplification, lowered cost, and extended maintenance-free service life. DOE

N95-22650# Sandia National Labs., Albuquerque, NM.
WORLD'S FIRST 15%-EFFICIENT MULTICRYSTALLINE SILICON MODULES
D. L. King, W. K. Schubert, and T. D. Hund 1994 4 p Presented at the 1st World Conference on Photovoltaic Energy Conversion, Waikoloa, HI, 5-9 Dec. 1994
(Contract DE-AC04-94AL-85000)
(DE95-002604; SAND-94-2777C; CONF-941203-7) Avail: CASI HC A01/MF A01

This paper describes the result of a team effort at Sandia to demonstrate the near-term performance potential for multicrystalline silicon modules using commercial mc-Si material and improved cell fabrication processes. Large-area high-performance mc-Si cells were fabricated, prototype modules were built, and world-record module efficiency was confirmed by outdoor testing at over 15% for standard test conditions. DOE

N95-22842# National Renewable Energy Lab., Golden, CO.
POLYCRYSTALLINE CuInSe2 AND CdTePV SOLAR CELLS Annual Subcontract Report, 15 Apr. 1993 - 14 Apr. 1994
N. G. Dhere (Florida Solar Energy Center, Cape Canaveral, FL.) Nov. 1994 35 p
(Contract DE-AC36-83CH-10093)
(DE95-000244; NREL/TP-451-7189) Avail: CASI HC A03/MF A01

This is an annual technical report on the Phase 2 of a three-year phased research program. The principal objective of the research project is to develop novel and low-cost processes for the fabrication of stable and efficient CuIn(1-x) Ga(x)Se2 and CdTe polycrystalline-thin-film solar cells using reliable techniques amenable to scale-up for economic, large-scale manufacture. The aims are to develop a process for the non-toxic selenization so as to avoid the use of extremely toxic H2Se in the fabrication of CuIn(1-x)Ga(x)Se2 thin-film solar cells; to optimize selenization parameters; to develop a process for the fabrication of CdTe solar cells using Cd and Te layers sputtered from elemental targets; to develop an integrated process for promoting the interdiffusion between Cd/Te layers, CdTe phase formation, grain growth, type conversion, and junction formation; to improve adhesion; to minimize residual stresses; to improve the metallic back-contact; to improve the uniformity, stoichiometry, and morphology of CuIn(1-x)Ga(x)Se2 and CdTe thin films; and to improve the efficiency of CuIn(1-x)Ga(x)Se2 and CdTe solar cells. DOE

N95-22855# Czechoslovak Solar Energy Society, Prague.
RENEWABLE ENERGY SOURCES BRNO 1993 [OBNOVITELNE ZDROJE ENERGIE BRNO 1993]
1993 102 p In CZECH Conference held in Brno, Czechoslovakia, 30 Aug. 1993 Prepared in cooperation with Technical Univ. of Brno, Czechoslovakia
(DE94-633975; INIS-mf-13868; CONF-9308231) Avail: CASI HC A06/MF A02 (US Sales Only)

The proceedings contain 27 contributions dealing with unconventional energy sources. The numbers of contributions in the individual classes of topics indicate that interest has mostly concentrated on the direct utilization of solar energy, whereas wind energy, hydroelectric energy and geothermal energy receive less attention and the use of biomass is at the margin of interest. DOE

N95-22861# Little (Arthur D.), Inc., Cambridge, MA.
MULTI-FUEL REFORMERS FOR FUEL CELLS USED IN TRANSPORTATION: ASSESSMENT OF HYDROGEN STORAGE TECHNOLOGIES
Mar. 1994 41 p
(Contracts DE-AC02-92CE-50343; W-31-109-eng-38)
(DE94-017655; DOE/CE-50343/1) Avail: CASI HC A03/MF A01

This report documents a portion of the work performed on Multi-fuel Reformers for Fuel Cells Used in Transportation. One objective of this program is to develop advanced fuel processing systems to reform methanol, ethanol, natural gas, and other hydrocarbons into hydrogen for use in transportation fuel cell systems, while a second objective is to develop better systems for on-board hydrogen storage. This report examines techniques and technology available for storage of pure hydrogen on board a vehicle as pure hydrogen of hydrides. The report focuses separately on near and far-term technologies, with particular emphasis on the former. Development of lighter, more compact near-term storage systems is recommended to enhance competitiveness and simplify fuel cell design. The far-term storage technologies require substantial applied research in order to become serious contenders. DOE

N95-22888# Institute of Gas Technology, Chicago, IL.
DEVELOPMENT OF THE IGT RENUGAS(REG SIGN) PROCESS
Francis S. Lau, Ronald H. Carty, Michael Onischak, and Richard L. Bain (National Renewable Energy Lab., Golden, CO.) 1993 15 p Presented at the Strategic Benefits of Biomass and Waste Fuels Conference, Washington, DC, 30 Mar. - 1 Apr. 1993
(Contracts DE-AC02-80CS-83004; DE-FC02-91CH-10407)
(DE94-017652; CONF-9303301-1) Avail: CASI HC A03/MF A01

The development of the IGT RENUGAS(reg sign) process from a concept in 1977 to the design of a 91 metric ton per day demonstration gasifier planned for Hawaii is described. The RENUGAS(reg sign) process was specifically developed for pressurized fluidized bed gasification of biomass to produce either an industrial fuel gas or a chemical synthesis gas depending on air- or oxygen-blown operation. The RENUGAS(reg sign) gasifier is a single-stage fluidized bed reactor with a deep bed of inert fluidization solids that provide stable fluidization behavior and needed heat capacity for efficient transfer of energy released by the combustion to the endothermic devolatilization and gasification reactions. The use of a deep single-stage bed of inert solids yields high carbon conversion and low production of oils and tars. The 10.9 metric ton per day RENUGAS(reg sign) process development unit built at IGT under a USDOE program, has been tested under various operating conditions, processing over 81 metric tons of biomass feedstocks in over 220 hours of steady-state tests. Initial parameter variation tests were conducted to determine the optimum gasification conditions of temperature, pressure, steam input, and feedstock moisture and different feedstocks. Currently, the PDU is being used to test hot gas cleanup for power turbines in support of the Hawaii demonstration gasifier. DOE

N95-22904*# Auburn Univ., AL. Space Power Inst.
SUMMARY OF SOLAR CELL DATA FROM THE LONG DURATION EXPOSURE FACILITY (LDEF) Final Report, 21 Jul. 1993 - 19 Aug. 1994
David C. Hill and M. Frank Rose 21 Oct. 1994 62 p
(Contract NAS8-39131)
(NASA-CR-196539; NAS 1.26:196539) Avail: CASI HC A04/MF A01

The contractor has obtained and reviewed data relating solar cells assemblies (SCA's) flown as part of the following LDEF experiments: the Advanced Photovoltaic Experiment (S0014); the Solar Array Materials Passive LDEF Experiment (A0171); the Advanced Solar Cell and Coverglass Analysis Experiment (M0003-4); the LDEF Heat Pipe Experiment (S1001); the Evaluation of Thermal Control Coatings Y Solar Cells Experiment (S1002); and the Space Plasma-High Voltage Drainage Experiment (A0054). Where possible, electrical data have been tabulated and correlated with various environmental effects, including meteoroid and debris impacts, radiation exposure, atomic oxygen exposure, contamination, UV radiation exposure, and thermal cycling. The type, configuration, and location of all SCA's are documented here. By gathering all data and results together, a comparison of the survivability of the various types and configurations can be made. Author

N95-23061# National Renewable Energy Lab., Golden, CO.
CONTINUOUS ROLL-TO-ROLL AMORPHOUS-SILICON PHOTOVOLTAIC MANUFACTURING TECHNOLOGY Annual Subcontract Report, 8 Apr. 1993 - 7 Apr. 1994
M. Izu (Energy Conversion Devices, Inc., Troy, MI.) Nov. 1994 92 p
(Contract DE-AC36-83CH-10093)
(DE95-000243; NREL/TP-411-7188) Avail: CASI HC A05/MF A01

This report describes work done in Phase 2 of a 3-year project to advance Energy Conversion Devices, Inc. (ECD), roll-to-roll, triple-junction photovoltaic manufacturing technologies, to reduce the module production costs, to increase the stabilized module performance, and to expand the commercial capacity utilizing ECD technology. Major accomplishments in Phase 2 include: (1) designing, constructing and completing the initial optimization of a 200-kW multi-purpose continuous roll-to-roll amorphous silicon (a-Si) alloy solar cell deposition machine; (2) designing and constructing a serpentine deposition chamber that will be used to demonstrate a compact, low-cost deposition machine design with improved throughput and gas utilization factor; (3) demonstrating greater than or equal to 8.3% initial small-area efficiency a-Si-alloy devices with an intrinsic a-Si layer deposited using serpentine technology in the initial start-up experiment; (4) developing a new back-reflector evaluation technique using Photothermal Defection Spectroscopy (PDS) to analyze the optical losses of textured back-reflector; (5) developing an improved textured Ag/ZnO back-reflector system demonstrating a 26% gain in short-circuit current density over the previous textured Al back-reflector system; (6) demonstrating the long-term stability of ECD's 0.3 m x 1.2 m (1 ft x 4 ft) production module; (7) developing a new grid/bus-bar design utilizing thin wire grids to improve the efficiency by approximately 3% to 4% and reduce the grid/bus-bar cost by about 50%; and (8) achieving accumulative material cost reduction of 56%. DOE

N95-23062# National Renewable Energy Lab., Golden, CO.
ADVANCED DEVELOPMENT OF PV ENCAPSULANTS Annual Subcontract Report, 30 Dec. 1992 - 31 Mar. 1994
W. Holley, S. Agro, J. Galica, L. Thoma, R. White, and R. Yorgensen (Springborn Labs., Inc., Enfield, CT.) Nov. 1994 81 p
(Contract DE-AC36-83CH-10093)
(DE95-000246; NREL/TP-411-7352) Avail: CASI HC A05/MF A01

This report describes work under Phase 2 of a Photovoltaic Manufacturing Technology project to conduct laboratory problem definition with an emphasis on controlled aging studies to evaluate the influence of various compositional, processing, and operating parameters on ethylene vinyl acetate (EVA) discoloration. In support of future accelerated UV aging studies (AAS) of coupon-sized EVA laminates, an Atlas xenon arc Ci35A Weather-Ometer was procured, installed, and calibrated for temperature and irradiance. In preparing for the AAS studies, UV-visible spectroscopy measurements were performed on various types of low-iron glass, representative of materials used for module superstrates. It was discovered that the transmission spectra of some of the grades in the UV region from 250 to 400 nm was significantly different. Older grades of Solatex and Solite, and StarPhire 'cut off' well below 290 nm, while newer grades of Solatex and Solite, and StarPhire and Airphire greatly reduce the UV transmittance between 280 and 330 nm. Controlled aging studies are presently underway at 0.55 W/m(exp 2), 340 nm, and 100 C, and we expect comparative data on yellowing to be available soon. DOE

N95-23133# Brookhaven National Lab., Upton, NY.
NET ENERGY ANALYSIS: POWERFUL TOOL FOR SELECTING ELECTRIC POWER OPTIONS
S. Baron 1994 9 p Presented at the Energy and Environment: Transitions in East Central Europe, Prague, Czechoslovakia, 1-5 Nov. 1994
(Contract DE-AC02-76CH-00016)
(DE95-002516; BNL-60058; CONF-941117-2) Avail: CASI HC A02/MF A01

A number of net energy analysis studies have been conducted in recent years for electric power production from coal, oil and uranium fuels; synthetic fuels from coal and oil shale; and heat and electric power from solar energy. This technique is an excellent indicator of investment costs, environmental impact and potential economic competitiveness of alternative electric power systems for energy planners from the Eastern European countries considering future options. Energy conservation is also important to energy planners and the net energy analysis technique is an excellent accounting system on the extent of energy resource conservation. The author proposes to discuss the technique and to present the results of his studies and others in the field. The information supplied to the attendees will serve as a powerful tool to the energy planners considering their electric power options in the future. DOE

N95-23162# Morgantown Technology Center, WV.
THE US MOLTEN CARBONATE FUEL-CELL DEVELOPMENT AND COMMERCIALIZATION EFFORT
M. C. Williams, E. L. Parsons, Jr., and M. J. Mayfield 1994 7 p Presented at the 29th Intersociety Energy Conversion Engineering Conference, Monterey, CA, 7-12 Aug. 1994
(DE94-019096; DOE/METC-C/94/7134; CONF-940812-22) Avail: CASI HC A02/MF A01

The authors discuss the status of molten carbonate fuel-cell (MCFC) development in the U.S., including the role of the U.S. Department of Energy (DOE) in commercializing MCFC power-plant products for use by gas utility and electric power industries. They describe major fundamental stack research issues, as well as MCF power-plant network and system issues, that need to be resolved before MCFC technology can be commercialized. A significant initiative in MCFC research is the spatial configuration of MCFC stacks into networks in a fuel-cell power plant. DOE

N95-23259*# National Aeronautics and Space Administration. Lewis Research Center, Cleveland, OH.
DESIGN OF A GaAs/Ge SOLAR ARRAY FOR UNMANNED AERIAL VEHICLES
David A. Scheiman (NYMA, Inc., Brook Park, OH.), David J. Brinker, David J. Bents, and Anthony J. Colozza (NYMA, Inc., Brook Park, OH.) Mar. 1995 6 p Presented at the First World Conference on Photovoltaic Energy Conversion, Waikoloa, HI, 5-9 Dec. 1994; cosponsored by IEEE, PVSEC-Japan, and PVSEC-Europe
(Contract NAS3-27186; RTOP 233-02-0A)
(NASA-TM-106870; E-9489; NAS 1.15:106870) Avail: CASI HC A02/MF A01

Unmanned Aerial Vehicles (UAV) are being proposed for many applications including surveillance, mapping and atmospheric studies. These applications require a lightweight, low speed, medium to long duration airplane. Due to the weight, speed, and altitude constraints imposed on such aircraft, solar array generated electric power is a viable alternative to air-breathing engines. Development of such aircraft is currently being funded under the Environmental Research Aircraft and Sensor Technology (ERAST) program. NASA Lewis Research Center (LeRC) is currently building a Solar Electric Airplane to demonstrate UAV technology. This aircraft utilizes high efficiency Applied Solar Energy Corporation (ASEC) GaAs/Ge space solar cells. The cells have been provided by the Air Force through the ManTech Office. Expected completion of the plane is early 1995, with the airplane currently undergoing flight testing using battery power. Author

N95-23344# Department of Energy, Washington, DC. Div. of Electric Energy Systems.
THE LOUISIANA STATE UNIVERSITY WASTE-TO-ENERGY INCINERATOR
26 Oct. 1994 68 p
(DE95-004417; DOE/EA-0952) Avail: CASI HC A04/MF A01

This proposed action is for cost-shared construction of an incinerator/steam-generation facility at Louisiana State University under the State Energy Conservation Program (SECP). The SECP, created by the Energy Policy and Conservation Act, calls upon DOE to encourage energy conservation, renewable energy, and energy efficiency by providing Federal technical and financial assistance in developing and implementing comprehensive state energy conservation plans and projects. Currently, LSU runs a campus-wide recycling program in order to reduce the quantity of solid waste requiring disposal. This program has removed recyclable paper from the waste stream; however, a considerable quantity of other non-recyclable combustible wastes are produced on campus. Until recently, these wastes were disposed of in the Devil's Swamp landfill (also known as the East Baton Rouge Parish landfill). When this facility reached its capacity, a new landfill was opened a short distance away, and this new site is now used for disposal of the University's non-recyclable wastes. While this new landfill has enough capacity to last for at least 20 years (from 1994), the University has identified the need for a more efficient and effective manner of waste disposal than landfilling. The University also has non-renderable biological and potentially infectious waste materials from the School of Veterinary Medicine and the Student Health Center, primarily the former, whose wastes include animal carcasses and bedding materials. Renderable animal wastes from the School of Veterinary Medicine are sent to a rendering plant. Non-renderable, non-infectious animal wastes currently are disposed of in an existing on-campus incinerator near the School of Veterinary Medicine building. DOE

N95-23361# Arizona Univ., Tucson, AZ.
PHOTOCHEMICAL ENERGY CONVERSION BY MEMBRANE-BOUND PHOTOREDOX SYSTEMS Final Report
G. Tollin 16 Jun. 1994 10 p
(Contract DE-FG02-86ER-13631)
(DE95-004405; DOE/ER-13631/T2) Avail: CASI HC A02/MF A01

This project has received DOE support since July 1, 1978. During this period, 40 papers have been published dealing predominantly with chlorophyll-photosensitized electron transfer reactions in a variety of media (solutions, polymer films, lipid bilayer membranes). The overall theme of this work has been to develop mechanistic strategies for photochemical energy storage via chlorophyll, using the green plant photosynthetic system as a paradigm for designing in vitro systems. Microheterogeneous lipid vesicle suspensions allow ready application of time-resolved optical spectroscopy to follow the course of light-induced electron transfer processes. Both the yields and the lifetimes of electron transfer products were markedly improved in the vesicle systems. In subsequent studies, this compartmentalization was favorably manipulated by controlling the electrical charge on the membrane surface, by controlling the solubility properties of the acceptors, by varying the lipid composition, by using mediators to create a concentration gradient to carry electrons from within the bilayer to the aqueous medium, and by incorporating secondary electron acceptors into the aqueous phase. DOE

N95-23382# Helsinki Univ. of Technology, Otaniemi (Finland).
HYDROGEN AND FUEL CELLS FOR ENERGY STORAGE
P. Lund, ed. 1993 166 p Presented at the 1st Nordic Symposium on Hydrogen and Fuel Cells for Energy Storage, Espoo, 11-12 Mar. 1993
(DE95-723907; NEI-FI-248; CONF-9303322) Avail: CASI HC A08/MF A02

The first Nordic Symposium on Hydrogen and Fuel Cells for Energy Storage was held on March 11-12, 1993 at the premises of the Helsinki University of Technology in Espoo-Otaniemi. The initiator and main sponsor of this Symposium was the Nordic Energy Research Program and its Committee for Fuel Cells. The major objective of the seminar was to present recent developments and research activities on the use of hydrogen and fuel cells for energy storage purposes. Emphasis was laid on smaller systems applicable, e.g., for autonomous energy production. Hydrogen storage, conversion of hydrogen into final energy, and on-site production of hydrogen, e.g., by renewable energy sources were considered. Besides basic scientific issues and components; system technology aspects were also discussed. New areas for further Nordic cooperation were identified during the symposium. The seminar was attended by almost 60 persons from all Nordic countries. Furthermore, three world-known scientists gave their overview on the status and trends of the hydrogen technology. This proceeding comprises the papers presented at the symposium. DOE

N95-23383# National Renewable Energy Lab., Golden, CO.
GPP: A GENERAL-PURPOSE POST PROCESSOR FOR WIND TURBINE DATA ANALYSIS
M. L. Buhl, Jr., N. D. Kelley, and D. A. Simms Oct. 1994 8 p Presented at the American Society of Mechanical Engineers Energy Technology Conference and Exhibition, Houston, TX, 29 Jan. - 1 Feb. 1995
(Contract DE-AC36-83CH-10093)
(DE95-000223; NREL/TP-442-7112; CONF-950116-2) Avail: CASI HC A02/MF A01

GPP (pronounced 'jeep') is a General-Purpose Post Processor for wind turbine data analysis. Engineers in the Wind Technology Division (WTD) of the National Renewable Energy Laboratory (NREL) developed it to postprocess test data and simulation predictions. GPP reads data into large arrays and allows you to run many types of analyses on the data in memory. GPP runs on inexpensive computers commonly used in the wind industry. You can even use it on a laptop computer in the field. We wrote the program in such a way as to make it easy to add new types of analyses and to port it to many types of computers. Although GPP is very powerful and feature-rich, it is still very easy to learn and use. Exhaustive error trapping prevents you from losing valuable work due to input errors. GPP should make a significant impact on engineering productivity in the wind industry. DOE

N95-23478# National Renewable Energy Lab., Golden, CO.
AMORPHOUS SILICON PHOTOVOLTAIC MANUFACTURING TECHNOLOGY, PHASE 2A Annual Subcontract Report, 1 May 1993 - 30 Apr. 1994
G. Duran, K. Mackamul, and D. Metcalf (Utility Power Group, Chatsworth, CA.) Jan. 1995 79 p
(Contract DE-AC36-83CH-10093)
(DE95-000298; NREL/TP-411-7472) Avail: CASI HC A05/MF A01

Utility Power Group (UPG), and its lower-tier subcontractor, Advanced Photovoltaic Systems, Inc. (APS) have conducted efforts in developing their manufacturing lines. UPG has focused on the automation of encapsulation and termination processes developed in Phase 1. APS has focused on completion of the encapsulation and module design tasks, while continuing the process and quality control and automation projects. The goal is to produce 55 watt (stabilized) EP50 modules in a new facility. In the APS Trenton EUREKA manufacturing facility, APS has: (1) Developed high throughput lamination procedures; (2) Optimized existing module designs; (3) Developed new module designs for architectural applications; (4) Developed enhanced deposition parameter control; (5) Designed equipment required to manufacture new EUREKA modules developed during Phase II; (6) Improved uniformity of thin-film materials deposition; and (7) Improved the stabilized power output of the APS EP50 EUREKA module to 55 watts. In the APS Fairfield EUREKA manufacturing facility, APS has: (1) Introduced the new products developed under Phase 1 into the APS Fairfield EUREKA module production line; (2) Increased the extent of automation in the production line; (3) Introduced Statistical Process Control to the module production line; and (4) Transferred-progress made in the APS Trenton facility into the APS Fairfield facility. DOE

N95-23482# Little (Arthur D.), Inc., Cambridge, MA.
MULTI-FUEL REFORMERS FOR FUEL CELLS USED IN TRANSPORTATION. PHASE 1: MULTI-FUEL REFORMERS Final Report
May 1994 207 p
(Contract DE-AC02-92CE-50343)
(DE95-004215; DOE/CE-50343/2) Avail: CASI HC A10/MF A03

DOE has established the goal, through the Fuel Cells in Transportation Program, of fostering the rapid development and commercialization of fuel cells as economic competitors for the internal combustion engine. Central to this goal is a safe feasible means of supplying hydrogen of the required purity to the vehicular fuel cell system. Two basic strategies are being considered: (1) on-board fuel processing whereby alternative fuels such as methanol, ethanol or natural gas stored on the vehicle undergo reformation and subsequent processing to produce hydrogen, and (2) on-board storage of pure hydrogen provided by stationary fuel processing plants. This report analyzes fuel processor technologies, types of fuel and fuel cell options for on-board reformation. As the Phase 1 of a multi-phased program to develop a prototype multi-fuel reformer system for a fuel cell powered vehicle, the objective of this program was to evaluate the feasibility of a

multi-fuel reformer concept and to select a reforming technology for further development in the Phase 2 program, with the ultimate goal of integration with a DOE-designated fuel cell and vehicle configuration. The basic reformer processes examined in this study included catalytic steam reforming (SR), non-catalytic partial oxidation (POX) and catalytic partial oxidation (also known as Autothermal Reforming, or ATR). Fuels under consideration in this study included methanol, ethanol, and natural gas. A systematic evaluation of reforming technologies, fuels, and transportation fuel cell applications was conducted for the purpose of selecting a suitable multi-fuel processor for further development and demonstration in a transportation application. DOE

N95-23489# Sandia National Labs., Albuquerque, NM.
RAPID THERMAL PROCESSING OF HIGH-EFFICIENCY SILICON SOLAR CELLS WITH CONTROLLED IN-SITU ANNEALING
P. Doshi, A. Rohatgi, M. Ropp, Z. Chen, and D. Ruby 1995 5 p Presented at the 1st World Conference on Photovoltaic Energy Conversion, Waikoloa, HI, 5-9 Dec. 1994
(Contract DE-AC04-94AL-85000)
(DE95-004729; SAND-94-3077C; CONF-941203-12) Avail: CASI HC A01/MF A01

Silicon solar cell efficiencies of 17.1%, 16.4%, 14.8%, and 14.9% have been achieved on FZ, Cz, multicrystalline (mc-Si), and dendritic web (DW) silicon, respectively, using simplified, cost-effective rapid thermal processing (RTP). These represent the highest reported efficiencies for solar cells processed with simultaneous front and back diffusion with no conventional high-temperature furnace steps. Appropriate diffusion temperature coupled with the added in-situ anneal resulted in suitable minority-carrier lifetime and diffusion profiles for high-efficiency cells. The cooling rate associated with the in-situ anneal can improve the lifetime and lower the reverse saturation current density (J(sub 0)), however, this effect is material and base resistivity specific. PECVD antireflection (AR) coatings provided low reflectance and efficient front surface and bulk defect passivation. Conventional cells fabricated on FZ silicon by furnace diffusions and oxidations gave an efficiency of 18.8% due to greater short wavelength response and lower J(sub 0). DOE

N95-23582# Argonne National Lab., IL.
ADVANCES IN RESEARCH FOR SOLID OXIDE FUEL CELLS
M. Krumpelt, T. W. Kueper, and R. Doshi 1994 4 p Presented at the Fuel Cells '94, Morgantown, WV, 17-19 1994
(Contract W-31-109-eng-38)
(DE95-004590; ANL/CMT/CP-83639; CONF-940883-8) Avail: CASI HC A01/MF A01

Solid oxide fuel cells are attracting considerable interest among industrial organizations wanting to position themselves in a potentially important technology of the future. More than a dozen new organizations worldwide have begun SOFC development in the last few years. Most of this R and D activity is in the planar technology, because it represents a good compromise between the proven but IR-limited tubular configuration and the high-performance but difficult-to-fabricate monolithic structure. The challenges of developing the planar cell configurations are finding high-temperature edge and manifold seal materials that will make very flat ceramic trilayers of sufficiently large area, and minimize contact resistances in stacks of cells. Also, decreasing the operating temperature requires development of reliable thin-film fabrication methods for the electrolyte, and finding a metal with good oxidation resistance and a thermal expansion coefficient well matched with the different cell components. Finally, toughness and a thermal stress tolerance of stacks need to be improved. DOE

N95-23605# Oak Ridge National Lab., TN.
OAK RIDGE NATIONAL LABORATORY ENERGY EFFICIENCY AND RENEWABLE ENERGY PROGRAM BIBLIOGRAPHY: 1994 EDITION
K. H. Vaughan Oct. 1994 148 p
(Contract DE-AC05-84OR-21400)
(DE95-002296; ORNL/CON-394) Avail: CASI HC A07/MF A02

The bibliography contains listings of publicly available technical reports, journal articles, and conference papers resulting from Oak Ridge National Laboratory research and development projects sponsored by the Department of Energy, Office of Energy Efficiency and Renewable Energy, and published between 1989 and mid-1994. Over 200 citations have been added since the last edition. DOE

N95-23776# National Renewable Energy Lab., Golden, CO.
GPP USER'S GUIDE: A GENERAL-PURPOSE POSTPROCESSOR FOR WIND TURBINE DATA ANALYSIS
M. L. Buhl, Jr. Jan. 1995 39 p
(Contract DE-AC36-83CH-10093)
(DE95-000293; NREL/TP-442-7111) Avail: CASI HC A03/MF A01

GPP is a General-Purpose Postprocessor for wind turbine data analysis. The author, a member of the Wind Technology Division (WTD) of the National Renewable Energy Laboratory (NREL), developed GPP to postprocess test data and simulation predictions. GPP reads data into large arrays and allows the user to run many types of analyses on the data stored in memory. It runs on inexpensive computers common in the wind industry. One can even use it on a laptop in the field. The author wrote the program in such a way as to make it easy to add new types of analyses and to port it to many types of computers. Although GPP is very powerful and feature-rich, it is still very easy to learn and to use. Exhaustive error trapping prevents one from losing valuable work due to input errors. GPP will, hopefully, make a significant impact on engineering productivity in the wind industry. DOE

N95-23777# National Renewable Energy Lab., Golden, CO.
AUTOMATED SOLAR CELL ASSEMBLY TEAMED PROCESS RESEARCH Semiannual Subcontract Report, 6 Dec. 1993 - 30 Jun. 1994
M. Nowlan (Spire Corp., Bedford, MA.) Jan. 1995 27 p
(Contract DE-AC36-83CH-10093)
(DE95-000299; NREL/TP-411-7473) Avail: CASI HC A03/MF A01

This report describes the work done on Phase 2 of the program in the period from December 6, 1993 to June 30, 1994. Spire's objective in this program is to develop high throughput (5 MW/yr) automated processes for interconnecting thin (200 micrometers) silicon solar cells. High yield will be achieved with these fragile cells through the development of low mechanical stress and low thermal stress processes. For example, a machine vision system is being developed for cell alignment without mechanically contacting the cell edges, while a new soldering process is being developed to solder metal interconnect ribbons simultaneously to a cells' front and back contacts, eliminating one of the two heating steps normally used for soldering each cell. DOE

N95-23778# National Renewable Energy Lab., Golden, CO.
SOLAR PHOTOCHEMISTRY: TWENTY YEARS OF PROGRESS, WHAT'S BEEN ACCOMPLISHED, AND WHERE DOES IT LEAD?
D. M. Blake Jan. 1995 10 p
(Contract DE-AC36-83CH-10093)
(DE95-004007; NREL/TP-433-7209) Avail: CASI HC A02/MF A01

It has been more than 20 years since the first oil embargo. That event created an awareness of the need for alternative sources of energy and renewed interest in combining sunlight and chemistry to produce the chemicals and materials required by industry. This paper will review approaches that have been taken, progress that has been made, and gives some projections for the near and longer term prospects for commercialization of solar photochemistry. DOE

N95-23977# Department of Energy, Washington, DC.
PROCEEDINGS OF THE FUEL CELLS 1994 CONTRACTORS REVIEW MEETING
C. P. Carpenter, II, ed. and M. J. Mayfield, ed. Aug. 1994 191 p Presented at the Fuel Cells '94, Morgantown, WV, 17-19 Aug. 1994
(DE94-012285; DOE/METC-94-1010; CONF-940883) Avail: CASI HC A09/MF A02

METC annually sponsors this conference to provide a forum for energy executives, engineers, etc. to discuss advances in fuel cell research and development projects, to exchange ideas with private sector attendees, and to review relevant results in fuel cell technology programs. Two hundred and three people from industry, academia, and Government attended. The conference attempts to showcase the partnerships with the Government and with industry, by seeking activity participation and involvement from the Office of Energy Efficiency and Renewable Energy, EPRI, GRI, and APRA. In addition to sessions on fuel cells (solid oxide, molten carbonate,

etc.) for stationary electric power generation, sessions on US DOE's Fuel Cell Transportation Program and on DOD/APRA's fuel cell logistic fuel program were presented. In addition to the 29 technical papers, an abstract of an overview of international fuel cell development and commercialization plans in Europe and Japan is included. Selected papers were indexed separately for inclusion in the Energy Science and Technology Database.
DOE

N95-24090# Sandia National Labs., Albuquerque, NM.
SILICON SURFACE AND BULK DEFECT PASSIVATION BY LOW TEMPERATURE PECVD OXIDES AND NITRIDES
Z. Chen, A. Rohatgi, and D. Ruby 1995 5 p Presented at the 1st World Conference on Photovoltaic Energy Conversion, Waikoloa, HI, 5-9 Dec. 1994
(Contract DE-AC04-94AL-85000)
(DE95-004531; SAND-94-1546C; CONF-941203-8) Avail: CASI HC A01/MF A01

The effectiveness of PECVD passivation of surface and bulk defects in Si, as well as phosphorus diffused emitters, is investigated and quantified. Significant hydrogen incorporation coupled with high positive charge density in the PECVD SiN layer is found to play an important role in bulk and surface passivation. It is shown that photo-assisted annealing in a forming gas ambient after PECVD depositions significantly improves the passivation of emitter and bulk defects. PECVD passivation of phosphorus doped emitters and boron doped bare Si surfaces is found to be a strong function of doping concentration. Surface recombination velocity of less than 200 cm/s for 0.2 Ohm-cm and less than 1 cm/s for high resistivity substrates (approximately Ohm-cm) were achieved. PECVD passivation improved bulk lifetime in the range of 30 to 70% in multicrystalline Si materials. However, the degree of the passivation was found to be highly material specific. Depending upon the passivation scheme, emitter saturation current density (J(sub oe)) can be reduced by a factor of 3 to 9. Finally, the stability of PECVD oxide/nitride passivation under prolonged UV exposure is established.
DOE

N95-24155# Sandia National Labs., Albuquerque, NM.
REFLECTANCE CONTROL FOR MULTICRYSTALLINE-SILICON PHOTOVOLTAIC MODULES USING TEXTURED-DIELECTRIC COATINGS
J. M. Gee, H. L. Tardy, T. D. Hund, R. Gordon (Harvard Univ., Cambridge, MA.), and H. Liang (Harvard Univ., Cambridge, MA.) 1995 4 p Presented at the 1st World Conference on Photovoltaic Energy Conversion, Waikoloa, HI, 5-9 Dec. 1994
(Contract DE-AC04-94AL-85000)
(DE95-004532; SAND-94-1570C; CONF-941203-1) Avail: CASI HC A01/MF A01

The authors describe a new approach for controlling the reflectance of photovoltaic modules with planar-surface solar cells. The new approach uses an optically thick, dielectric coating with a large refractive index and a textured surface; this dielectric coating is deposited on the planar-surface solar cell. The textured-dielectric coating works optically with the module encapsulation to promote optical confinement of rays inside the module encapsulation structure, which reduces the net reflectance of the photovoltaic module. The advantage of this approach is that deposition of a textured-dielectric film may be less costly and less intrusive on the cell manufacturing process than texturing multicrystalline-silicon substrates. The authors present detailed optical models and experimental confirmation of the new approach.
DOE

N95-24157# Sandia National Labs., Albuquerque, NM.
CRYSTALLINE-SILICON PHOTOVOLTAICS: NECESSARY AND SUFFICIENT
P. A. Basore and J. M. Gee 1995 10 p Presented at the 1st World Conference on Photovoltaic Energy Conversion, Waikoloa, HI, 5-9 Dec. 1994
(Contract DE-AC04-94AL-85000)
(DE95-004540; SAND-94-1562C; CONF-941203-9) Avail: CASI HC A02/MF A01

Photovoltaic (PV) energy systems have always been dominated by crystalline-silicon (c-Si) technology, and recent developments persuasively suggest that c-Si will continue to be the dominant technology well into the next century. The authors explain why c-Si technology is fairing much better than previously expected, and discuss the impact of improvements currently under development. They use a ground-up, engineering-based approach to predict the expected evolution of this type of PV system, and argue that c-Si PV will be in a position to compete for the US residential power market starting in about the year 2010. This market alone will provide the opportunity for PV to supply several percent of the electrical energy used in the United States. Crystalline-silicon technology is therefore not just necessary for building a near-term PV industry; it also offers a low-risk approach to meeting long-term goals for PV energy systems.
DOE

45 ENVIRONMENT POLLUTION

Includes atmospheric, noise, thermal, and water pollution.

N95-22673*# Oregon Graduate Inst. of Science and Technology, Portland, OR. Dept. of Environmental Science and Engineering.
THE ATMOSPHERIC LIFETIME EXPERIMENT AND THE GLOBAL ATMOSPHERIC GAS EXPERIMENT (ALE/GAGE) Final Report, 1 Apr. 1988 - 31 Jan. 1991
R. A. Rasmussen and M. Aslam K. Khalil Jan. 1995 260 p Original contains color illustrations
(Grant NAGw-1348)
(NASA-CR-197400; NAS 1.26:197400) Avail: CASI HC A12/MF A03; 19 functional color pages

The ALE/GAGE project was designed to determine the global atmospheric lifetimes of the chlorofluorocarbons CCl3F and CCl2F2 (F-11 and F-12), which had been identified as the main gases that cause stratospheric ozone depletion. The experimental procedures also provided the concentrations of CH3CCl3, CCl4 and N2O. The extended role of the project was to evaluate the mass balances of these gases as well. Methylchloroform (CH3CCl3) serves as a tracer of average atmospheric OH concentrations and hence the oxidizing capacity of the atmosphere. Nitrous oxide (N2O) is a potent greenhouse gas and can also deplete the ozone layer. Measurements of these gases were taken with optimized instruments in the field at a frequency of about 1 sample/hr. Toward the end of the present project methane measurements were added to the program. The final report deals with the research of the Oregon Graduate Institute (OGI) as part of the ALE/GAGE program between 4/1/1988 and 1/31/1991. The report defines the scope of the OGI project, the approach, and the results.
Author

N95-22691# Energy Information Administration, Washington, DC.
EMISSIONS OF GREENHOUSE GASES IN THE UNITED STATES, 1987-1992
Nov. 1994 125 p
(DE95-003001; DOE/EIA-0573(11-94)) Avail: CASI HC A06/MF A02

This is the second annual Energy Information Administration (EIA) report on US emissions of greenhouse gases. This report presents estimates of US anthropogenic (human-caused) emissions of carbon dioxide, methane, nitrous oxide, and several other greenhouse gases for the period 1987 to 1992. Estimates of 1993 carbon dioxide emissions are also provided, although complete 1993 estimates for other gases are not yet available. Many of the estimates in this report have been revised from the first EIA report. Estimates of carbon dioxide emissions were revised upward by about 25 million metric tons of carbon dioxide (0.5 percent) for each year as a result of revised emissions coefficients and revised estimates of nonfuel use of fossil fuels. Methane emissions estimates were revised downward by about 2 million metric tons (6.6 percent) for each year as a result of changes in estimation methods.
DOE

N95-22725# Oak Ridge National Lab., TN. Environmental Sciences Div.
DIRECT EFFECTS OF ATMOSPHERIC CO2 ENRICHMENT ON PLANTS AND ECOSYSTEMS: AN UPDATED BIBLIOGRAPHIC DATA BASE
Boyd R. Strain, ed. (Duke Univ., Durham, NC.), Jennifer D. Cure, ed. (Duke Univ., Durham, NC.), and Robert M. Cushman, comp. Jun. 1994 293 p
(Contract DE-AC05-84OR-21400)
(DE95-003060; ORNL/CDIAC-70) Avail: CASI HC A13/MF A03

This publication provides bibliographic citations and abstracts on recent literature concerning the direct effects of elevated atmospheric

concentrations of carbon dioxide (CO2) on plants and ecosystems. This report is an update to Direct Effects of Atmospheric CO2 Enrichment on Plants and Ecosystems: A Bibliography with Abstracts (ORNL/CDIC-13), which was published in 1986. The updated bibliography provides complete bibliographic citations, abstracts, keywords, and common and scientific plant names for approximately 800 references published between 1980 and 1994 (half the cited references were published in 1990 or later). Many of the papers included in this volume, particularly papers from Europe, reflect a renewed interest in growth analysis as a way of studying allocation of mass and energy to the various organ systems. A large proportion of the recent research has focused at a level of organization beyond the individual organism. DOE

N95-22781# Pacific Northwest Lab., Richland, WA.
P2INFO RESOURCE CENTER: LINKING THE DOE POLLUTION PREVENTION COMMUNITY
E. L. Edwards Oct. 1994 8 p Presented at the Office of Scientific and Technical Information INFOTECH '94, Oak Ridge, TN, 25-26 Oct. 1994
(Contract DE-AC06-76RL-01830)
(DE95-003133; PNL-SA-24515; CONF-9410141-5) Avail: CASI HC A02/MF A01

At Pacific Northwest Laboratory, researchers and information specialist are teaming to connect DOE's Pollution Prevention (P2) community. Through the P2Info Resource Center, multiple levels of information needs are fulfilled, First, engineers and researchers staff a hotline offering direct technical or programmatic assistance. Commercial and locally produced databases offer information retrieval for specific queries and current awareness. Finally, filtered information will be disseminated through electronic systems such as DOE's EPIC (Pollution Prevention Information Clearinghouse). P2Info's connections model our electronic future. DOE

N95-22834# Southwest Research Inst., San Antonio, TX.
DIESEL FUEL COMPONENT CONTRIBUTIONS TO ENGINE EMISSIONS AND PERFORMANCE: CLEAN FUEL STUDY
J. Erwin, T. W. Ryan, III, and D. S. Moulten Aug. 1994 49 p Prepared for National Renewable Energy Lab., Golden, CO
(Contract DE-AC36-83CH-10093)
(DE94-011868; NREL/TP-425-6355) Avail: CASI HC A03/MF A01

The emissions characteristics of diesel engines are dominated by current engine design parameters as long as the fuels conform to the current industry-accepted specifications. The current and future emissions standard, are low enough that the fuel properties and compositions are starting to play a more significant role in meeting the emerging standards. The potential role of the fuel composition has been recognized by state and federal government agencies, and for the first time, fuel specifications have become part of the emissions control legislation. In this work, five different fuel feed and blend stocks were hydrotreated to two levels of sulfur and aromatic content. These materials were then each distilled to seven or eight fractions of congruent boiling points. After this, the raw materials and all of the fractions were characterized by a complement of tests from American Society for Testing and Materials and by hydrocarbon-type analyses. The sample matrix was subjected to a series of combustion bomb and engine tests to determine the ignition, combustion, and emissions characteristics of each of the 80 test materials. DOE

N95-22856# General Atomics Co., San Diego, CA.
ENVIRONMENTAL SYSTEMS MANAGEMENT ANALYSIS AND REPORTING NETWORK (E-SMART) Final Technical Report, Sep. 1991 - May 1993
J. S. Leffler Aug. 1993 167 p
(Contract F08635-91-C-0224)
(AD-A279766; GA-C21601; AL/EQ-TR-1993-0027) Avail: CASI HC A08/MF A02

The Environmental Systems Management, Analysis, and Reporting Network (E-SMART) project has the goal of developing a standard for interconnecting microprocessor-controlled, smart sensors or actuators into environmental monitoring and control networks that collect, manage, and analyze the resulting sensor data. A bench-scale proof-of-concept demonstration was completed. E-SMART integrates diverse on-line monitoring and control technologies via a modular design approach and standards that enhance data quality, allow flexible system configuration and operation, and provide for straight-forward, graphically-based user interfaces. Tens of thousands of smart sensors or actuators can function within a single monitoring network. Each smart sensor or actuator device contains its own microprocessor brain which enables it to store calibration data and individual control programs. Standard communication protocols and electrical interfaces for the network will allow multiple vendors to produce sensors which meet the same network communication provides protection against single-point failures. By defining a standard, modular methodology for constructing monitoring and controlling networks, E-SMART eliminates the incompatibilities suffered by conventional monitoring systems and will promote the acceptance of in situ environmental monitoring. DTIC

N95-22865# Radian Corp., Research Triangle Park, NC.
PRELIMINARY ASSESSMENT OF AIR TOXIC EMISSIONS IN THE NATURAL GAS INDUSTRY, PHASE 1 Topical Report, Sep. 1991 - Apr. 1993
Lisa M. Campbell, Kathy R. Ferry, and Gunseli Sagun Shareef Aug. 1994 157 p See also PB91-178962, PB93-141943 and PB93-158582 Prepared for Gas Research Inst., Chicago, IL
(Contract GRI-5091-254-2293)
(PB95-135547; RC-275-114; GRI-94/0268) Avail: CASI HC A08/MF A02

This report presents the results of an initial research effort to identify potentially significant sources of air toxics emissions within the natural gas industry. Phase 1 activities focused on characterizing the gas industry from available information collected from literature searches, other Gas Research Institute (GRI) programs, industry representatives, EPA databases, state agencies, and trade organizations. This characterization included potential air toxics emissions sources and individual species from each source, where available. Process flow diagrams were developed for each industry segment, and within each segment, process operations were identified with potential emissions sources indicated. A database was designed and constructed to store the information collected. The available emissions data identified in the current study are very limited and represent four types of emission sources: (1) glycol dehydrator units; (2) internal combustion (IC) engines; (3) gas turbines; and (4) utility boilers. NTIS

N95-22898# Lawrence Livermore National Lab., Livermore, CA.
ANALYTICAL BOLTZMANN MOMENTS FOR ELECTRONS IN N2-O2-H2O GAS MIXTURES
Manuel Garcia and Britton Chang Apr. 1994 33 p
(Contract W-7405-eng-48)
(DE95-003474; UCRL-ID-117124) Avail: CASI HC A03/MF A01

Non-equilibrium gas plasmas are under study today as sources of electrically powered chemistry for the elimination of volatile organic vapors and combustion exhaust pollutants. The aim of these research efforts is to develop either non-catalytic oxidation to acids which can be 'scrubbed' out of ga s flows as salts, or non-catalytic reduction, specifically of NO(x) to N2 and O2. This work is an effort to simplify the electron kinetics so as to enable a convenient study of a wide range of mixtures and Townsend parameters, and for a reasonable sacrifice in precision. Key insights gained in this way can be honed by more accurate numerical computation as needed. In this report they present a brief description of the approximate analytical solution of the Boltzmann equation, then additional modeling of electron-molecule cross sections which simplifies the expressions for moments, and finally a number of examples and comparisons to experiment and published results. DOE

N95-22930*# Stanford Univ., CA. Dept. of Chemistry.
DIMETHYLSULFIDE OXIDATION OVER THE TROPICAL SOUTH ATLANTIC: OH AND OTHER OXIDANTS Final Report
Brooke L. Hemming, John A. Vastano (National Aeronautics and Space Administration. Ames Research Center, Moffett Field, CA.), Robert B. Chatfield (National Aeronautics and Space Administration. Ames Research Center, Moffett Field, CA.), Meinrat O. Andreae (Max-Planck-Inst. fuer Chemie, Mainz, Germany.), and Lynn M. Hildemann [1994] 45 p
(Contract NCC2-5023)
(NASA-CR-197417; NAS 1.26:197417) Avail: CASI HC A03/MF A01

The general course of events in the formation of a marine cloud begins with the emission of species which can eventually serve as nuclei around which water can condense to form a cloud droplet. In remote

marine regions, cloud condensation nuclei (CCN) are primarily composed of sulfate, in either its acid or ammonium salt form. Most sulfate in these regions is the product of atmospheric oxidation of dimethyl sulfide (DMS), a reduced sulfur gas that is released by phytoplankton at the ocean surface. Therefore, in order to effectively quantify the links in the cloud-formation cycle, one must begin with a well-defined description of the atmospheric chemistry of DMS. The intent of this project has been to initiate development of a comprehensive model of the chemistry and dynamics responsible for the formation of clouds in the remote marine boundary layer. The primary tool in this work has been the Global/Regional Atmospheric Chemistry Event Simulator (GRACES), a global atmospheric chemistry model, which is under development within the Atmospheric Chemistry and Dynamics Branch of NASA-Ames Research Center. In this effort, GRACES was used to explore the first chemical link between DMS and sulfate by modeling the diurnal variation of DMS. Author

N95-23009*# National Aeronautics and Space Administration. Langley Research Center, Hampton, VA.
COMPENDIUM OF NASA DATA BASE FOR THE GLOBAL TROPOSPHERIC EXPERIMENT'S PACIFIC EXPLORATORY MISSION WEST-A (PEM WEST-A)
G. L. Gregory and A. D. Scott, Jr. Feb. 1995 140 p
(RTOP 464-54-03-70)
(NASA-TM-109177; NAS 1.15:109177) Avail: CASI HC A07/MF A02

This compendium describes aircraft data that are available from NASA's Pacific Exploratory Mission West-A (PEM West-A). PEM West is a component of the International Global Atmospheric Chemistry's (IGAC) East Asia/North Pacific Regional Study (APARE) project. The PEM- West program encompassed two expeditions to study contrasting meteorological regimes in the Pacific. Objectives of PEM West are to investigate the atmospheric chemistry of ozone over the northwest Pacific -- natural budgets and the impact of anthropogenic sources; and to investigate sulfur chemistry -- continental versus marine sulfur sources. PEM West-A was conducted in September 1991 during which the predominance of tropospheric air is from the mid-Pacific (marine) regions, but (at times) is modified/mixed with Asian continental outflow. PEM West-B was conducted during February 1994, a period characterized by maximum continental outflow. PEM-B data (not included) will become public domain during the Summer of 1995. PEM West-A flight experiments were based at Japan, Hong Kong, and Guam. This document provides a representation of NASA DC-8 aircraft data that are available from NASA Langley's Distributed Active Archive Center (DAAC), which include numerous data such as meteorological observations, modeling products, results from surface studies, satellite observations, and sonde releases. Author

N95-23067# Rijksinstituut voor de Volksgezondheid, Bilthoven (Netherlands).
OUTLINE FOR A GLOBAL ENVIRONMENTAL STRATEGIC PLANNING EXERCISE (GESPE-PROJECT)
H. J. M. deVries, T. Fiddaman (Massachusetts Inst. of Tech., Cambridge, MA.), and R. Janssen (Vrije Univ., Amsterdam, Netherlands.) May 1993 66 p
(PB95-133773; GLOBO-2) Avail: CASI HC A04/MF A01

The report describes the results of the first phase of the Greenhouse Gas Policy Exercise project. It provides the terms of reference for the project, comprising a description of the simulation models to be used as well as a theoretical design and an indication of clients and set-up of the policy exercise. NTIS

N95-23123# Lawrence Livermore National Lab., Livermore, CA.
RAS DIVISION MODEL EVALUATION DATABASE TOOLS
K. T. Foster Sep. 1994 16 p
(Contract W-7405-eng-48)
(DE95-003480; UCRL-ID-118630) Avail: CASI HC A03/MF A01

Recently the RAS Division Model Evaluation Database (MEDb) was implemented. This database is primarily designed to hold atmospheric and tracer concentration data collected as part of various atmospheric field experiments. To allow users of this data to interface with the MEDb a series of computer tools have been developed. This document contains a discussion of these tools as they currently exist. First a discussion is presented on initiating the MEDb tools, followed by a description of common user interaction for all MEDb Motif forms. The remaining sections contain a detailed description of the MEDb editing interface and generation of MEDb hard copy. DOE

N95-23124# Lawrence Livermore National Lab., Livermore, CA.
RAS DIVISION MODEL EVALUATION DATABASE DESCRIPTION
K. T. Foster Sep. 1994 20 p
(Contract W-7405-eng-48)
(DE95-003481; UCRL-ID-118631) Avail: CASI HC A03/MF A01

Over the past several years what is now the Regional Atmospheric Sciences (RAS) Division conducted several atmospheric model evaluation studies. Recently, planning has begun for the potential development of a set of 'model evaluation' tools for the division's use. The primary function of these tools will be to facilitate comparison of model calculations with measurements of both atmospheric variables (e.g. wind velocity, temperatures, etc.) and the atmosphere's transport and dispersion effects on the concentration of atmospheric tracers. To supply these tools with the necessary atmospheric measurements, and to create a relatively more permanent archive of field experiment data, a Model Evaluation Data based (MEDb) has been designed and implemented. This document contains a description of the contents and current structure of the MEDb, and provides guidance on determining appropriate database entries. DOE

N95-23125 Nederlands Inst. voor Onderzoek der Zee, Texel (Netherlands).
STUDY ON POSSIBLE ENVIRONMENTAL EFFECTS OF A WBM CUTTING DISCHARGE IN THE NORTH SEA, ONE YEAR AFTER TERMINATION OF DRILLING
R. Daan and M. Mulder 1993 22 p
(PB95-133740; NIOZ-1993-16) Copyright Avail: Issuing Activity (National Technical Information Service (NTIS))

In 1991 and 1992, a 2-phase field monitoring program has been carried out, aimed to assess possible environmental effects of discharges of drill cuttings drilled with water based muds (WBM). The results and conclusions of the WBM study in the Frisian Front area may be summarized as follows: (1) During the 1991 survey at L3-3, 2 months after dumping of WBM cuttings, adverse effects on the benthic community were not observed; (2) The 1992 survey at L3-3, 1 year after dumping of WBM cuttings, also revealed no adverse effects on the benthic community, not even at a distance as close as 25 m from the former discharge site; and (3) The results suggest that dumping of cuttings drilled with WBM with a chemical composition like used at L3-3 has no detectable effect on the benthic community. NTIS

N95-23126 Rijksinstituut voor de Volksgezondheid, Bilthoven (Netherlands).
CO2 AND WASTE POLICY: MONITORING RESULTS 1991/1992 AND MAIN PROBLEMS [CO2 EN AFVALBELEID: RESULTATEN MONITORING 1991/1992 EN KNELPUNTEN]
K. M. M. Oh, J. M. Joosten, and W. G. Martens Mar. 1994 41 p In DUTCH
(PB95-133799; RIVM-776201007) Avail: Issuing Activity (National Technical Information Service (NTIS))

In the Dutch National Environmental Policy Plans specific targets have been formulated concerning the reduction of carbon dioxide emissions. With respect to waste policy a contribution of 1,5 million tons CO2 reduction in 1995 and 3,5 million tons in 2000 has been formulated. In this report the situation of the following waste streams will be described for the years 1991 and 1992: natural materials (organic fraction of household waste, wood and manure); synthetic materials (plastics); and energy-intensive materials (aluminum). These waste streams can give a major contribution in reaching the targets for CO2 emissions. The monitoring results presented in this study will be used in further research, in which the actual effects of waste policy on reduction targets of CO2-emission will be calculated. NTIS

N95-23362# State Univ. of New York, Old Westbury, NY.
ATMOSPHERIC PEROXIDES Technical Progress Report
J. Weinstein-Lloyd Aug. 1994 12 p
(Contract DE-FG02-91ER-61206)
(DE95-004435; DOE/ER-61206/3) Avail: CASI HC A03/MF A01

The research conducted in this program has furthered the development

of a method for real-time analysis of hydrogen peroxide, methyl hydroperoxide, and hydroxymethyl hydroperoxide, the most abundant peroxides in the atmosphere. The Fenton method was used in a number of major field studies and the results used to test models of atmospheric photochemistry and observed diurnal profiles have shed light on the mechanism of formation of H2O2 and organic peroxides. The technique has also been adapted for analysis of peroxides in precipitation in an undergraduate analytical chemistry/instrumental analysis course. DOE

N95-23384# EG and G Rocky Flats, Inc., Golden, CO.
OU3 SEDIMENT DATING AND SEDIMENTATION RATES
R. B. Blair, ed. 12 Aug. 1994 37 p
(Contract DE-AC34-90DP-62349)
(DE95-001891; RFP-4882) Avail: CASI HC A03/MF A01

Environmental Technologies at Rocky Flats Environmental Technology Site (RFS) investigated the sediment history of Standley Lake, Great Western Reservoir, and Mower Reservoir using Cs(sup 137) and Pu(sup 239), Pu(sup 240) global fall-out as dating indicators. These Colorado Front Range reservoirs have been the subject of study by various city, state and national agencies due to suspected Department of Energy Rocky Flats Plant impacts. We performed sediment dating as part of the RCRA Facility Investigation/Remedial Investigation Report for Operable Unit 3. A sediment chronology profile assists scientist in determining the year of sedimentation for a particular peak concentration of contaminants. Radioisotope sediment dating for the three reservoirs indicated sedimentation rates of 0.7 to 0.8 in./yr. for Standley Lake (SL), 0.9 in./yr. for Great Western Reservoir (GWR), and 0.3 in./yr. in Mower Reservoir (MR). RFS sediment dating for Operable Unit 3 compared favorably with the Hardy, Livingston, Burke, and Volchok Standley Lake study. This report describes the cesium/plutonium sediment dating method, estimates sedimentation rates for Operable Unit 3 reservoirs, and compares these results to previous investigations. DOE

N95-23460*# American Chemical Society, Washington, DC. Dept. of Meetings and Divisional Activities.
OXIDANTS AND OXIDATION IN THE EARTH'S ATMOSPHERE Final Technical Report, 1 Jun. 1994 - 30 May 1995
2 Feb. 1995 17 p Presented at the 1994 BOC Priestley Conference, Lewisburg, PA, 24-27 Jun. 1994
(Grant NAGw-4209)
(NASA-CR-197945; NAS 1.26:197945) Avail: CASI HC A03/MF A01

The 1994 BOC Priestley Conference was held at Bucknell University in Lewisburg, Pennsylvania, from June 24 through June 27, 1994. This conference, managed by the American Chemical Society (ACS), was a joint celebration with the Royal Society of Chemistry (RSC) commemorating Joseph Priestley's arrival in the U.S. and his discovery of oxygen. The basic theme of the conference was 'Oxidants and Oxidation in the Earth's Atmosphere,' with a keynote lecture on the history of ozone. A distinguished group of U.S. and international atmospheric chemists addressed the issues dominating current research and policy agendas. Topics crucial to the atmospheric chemistry of global change and local and regional air pollution were discussed. The program for the conference included four technical sessions on the following topics: (1) Oxidative Fate of Atmospheric Pollutants; (2) Photochemical Smog and Ozone; (3) Stratospheric Ozone; and (4) Global Tropospheric Ozone. Author

N95-23480# National Renewable Energy Lab., Golden, CO.
REVIEW OF RESEARCH RESULTS FOR THE PHOTOCATALYTIC OXIDATION OF HAZARDOUS WASTES IN AIR
M. R. Nimlos, E. J. Wolfrum, D. A. Gratson, A. S. Watt, W. A. Jacoby, and C. Turchi Jan. 1995 53 p
(Contract DE-AC36-83CH-10093)
(DE95-004004; NREL/TP-433-6943) Avail: CASI HC A04/MF A01

Laboratory experiments of gas-phase photocatalytic oxidation (PCO) at NREL have focused on measurements that can help commercialize this technology for treating gaseous air streams. This effort proceeds earlier NREL work and studies conducted elsewhere which demonstrated the general applicability of PCO. The more recent work has concentrated on: (1) the kinetics of the PCO process; (2) the formation and destruction of intermediates; and (3) possible enhancements to improve the destruction rates. The results from these studies will be used to help design large scale PCO equipment and they will be used to evaluate the economics of the PCO process. For trichloroethylene and ethanol, extensive studies of the rates of destruction have yielded kinetic parameters for the destruction of intermediates as well as the substrate. The kinetics of intermediates is essential for sizing a large scale reactor, as complete conversion to carbon dioxide is often desired. The kinetic data from these laboratory studies has been used for analyzing IT's pilot PCO reactor and has been used to suggest modifications to this unit. For compounds that are more difficult to destroy (such as the components of BTEX), rate enhancement experiments have been conducted. These compounds represent a very large market for this technology and improvement of the rate of the process should make it competitive. Towards this goal, the enhancement of the destruction of BTEX components have been studied. Experiments have demonstrated that there is a significant increase in the rates of destruction of BTEX with the addition of ozone. Preliminary economic assessments have shown that PCO with ozone may be cost competitive. Future laboratory experiments of PCO will focus on refinements of what has been learned. Rate measurements will also be expanded to include other compounds representing significant markets for the PCO technology. DOE

N95-23541# International Atomic Energy Agency, Vienna (Austria).
THE SIGNIFICANCE OF HAIR MINERAL ANALYSIS AS A MEANS FOR ASSESSING INTERNAL BODY BURDENS OF ENVIRONMENTAL POLLUTANTS
1993 315 p
(DE94-633512; NAHRES-18) Avail: CASI HC A14/MF A03 (US Sales Only)

In recent years there has been a considerable growth of interest in problems of environmental pollution from industrial and agricultural substances and the harmful impact of such pollution on human health. There has been an increasing interest in using hair mineral analysis for biological monitoring of human population exposure to environmental mineral pollutants. This is because hair has some ideal attributes for such purposes. It can be collected by simple, non-invasive methods, and is easily sampled and stored. Concentrations of most of the toxic trace elements, i.e. mercury and lead, in scalp hair are at least an order of magnitude higher than those in body fluids or other easily accessible tissues. In addition, mineral elements in hair can easily be determined with good precision and sensitivity by nuclear as well as conventional methods of chemical analysis. Despite these apparent advantages of using hair as a biomonitor, serious uncertainty existed, and to some extent still exist, as to the meaningful interpretation of human hair mineral data in environmental health studies. The Co-ordinated Research Programme (CRP), which is the subject of this report, has attempted to tackle this problem by promoting a variety of studies (as distinct from routine monitoring) to investigate the quantitative relationships between internal body burdens of a number of elements of environmental health significance and their respective concentrations in hair. DOE

N95-23542# International Atomic Energy Agency, Vienna (Austria).
APPLIED RESEARCH ON AIR POLLUTION USING NUCLEAR-RELATED ANALYTICAL TECHNIQUES
1994 278 p Presented at the 1st Research Co-ordination Meeting on Applied Research on Air Pollution Using Nuclear-related Analytical Techniques, Vienna, Austria, 30 Mar. - 2 Apr. 1993
(DE94-633513; NAHRES-19; CONF-9303296) Avail: CASI HC A13/MF A03 (US Sales Only)

A co-ordinated research program (CRP) on applied research on air pollution using nuclear-related techniques is a global CRP which will run from 1992-1996, and will build upon the experience gained by the Agency from the laboratory support that it has been providing for several years to BAPMoN - the Background Air Pollution Monitoring Network program organized under the auspices of the World Meteorological Organization. The purpose of this CRP is to promote the use of nuclear analytical techniques in air pollution studies, e.g. NAA, XFR, and PIXE for the analysis of toxic and other trace elements in suspended particulate matter (including air filter samples), rainwater and fog-water samples, and in biological indicators of air pollution (e.g. lichens and mosses). The main purposes of the core program are: (1) to support the use of nuclear and nuclear-related analytical techniques for practically-oriented research and monitoring studies on air pollution; (2) to identify major sources of air pollution affecting each of the participating countries with particular reference to toxic heavy metals; and (3) to obtain comparative data on pollution levels in areas of high pollution (e.g. a city centre or a populated area downwind of a large

pollution source) and low pollution (e.g. rural areas). This document reports the discussions held during the first Research Co-ordination Meeting (RCM) for the CRP which took place at the IAEA Headquarters in Vienna. DOE

N95-23580# Pacific Northwest Lab., Richland, WA.
EXTRACTION AND DETECTION OF PESTICIDE RESIDUES FROM AIR FILTER INSERTS USING SUPERCRITICAL CARBON DIOXIDE
T. S. Zemanian, W. H. Robins, R. N. Lee, and B. W. Wright Oct. 1994 7 p Presented at the 3rd International Symposium on Supercritical Fluids, Strasbourg, France, 17-19 Oct. 1994
(Contract DE-AC06-76RL-01830)
(DE95-004579; PNL-SA-24394; CONF-9410114-5) Avail: CASI HC A02/MF A01

Trace quantities of airborne herbicide residues were collected on adsorbent bed cartridges and were subsequently extracted from the adsorbent using supercritical carbon dioxide. An apparatus was constructed to facilitate the extraction and recovery of the desired analytes. The resulting extracts were analyzed using gas chromatography/mass spectrometry (GC/MS) or high performance liquid chromatography (HPLC) techniques. Results are presented for a series of analytes representative of common commercial pesticides or herbicides. DOE

N95-24018# Lawrence Livermore National Lab., Livermore, CA.
REMOTE SENSOR TEST RANGE UPDATE
D. Slaughter Jul. 1994 13 p Presented at the 1994 Chemical Analysis By Laser Interrogation of Proliferation Effluents (CALIOPE ITR) Interim Technical Review, Livermore, CA, 26-28 Apr. 1994
(Contract W-7405-eng-48)
(DE95-003629; UCRL-JC-118477; CONF-9404162-15) Avail: CASI HC A03/MF A01

It has been recognized since the beginning of the CALIOPE remote sensor development program that performance criteria must be developed to measure progress and efficacy, then prototype sensors must be evaluated against them. Much of the early evaluation may be carried out cost effectively in the laboratory and at field ranges located near each of the participating national laboratories. However, sensor performance is expected to be degraded by many factors in the field at remote sites and the extent of that degradation must be quantified before instruments can be designed and constructed for international deployment. LLNL proposed a series of field tests for this purpose at the Remote Sensor Test Range (RSTR) located at the Nevada Test Site (NTS). Well-controlled gas plumes containing mixtures of important species at known concentration would be released to the open atmosphere and used as targets for the prototype remote sensors. The plume dimensions and gas concentrations will be well diagnosed to provide 'ground truth'. Gases selected as targets will, in the beginning, be chosen to optimize instrument performance in the field and identifying those factors that limit performance. The initial experiments will use ground based-instruments observing the target plumes from relatively close range. Field tests will evolve toward gases identified by the 'signatures study' as relevant to proliferant activity. Target concentrations will be reduced to those expected in proliferant scenarios and may be modulated in time. Observation range will be increased, and elevated or airborne sensor platforms will be introduced. DOE

N95-24057# General Accounting Office, Washington, DC. National Security and International Affairs Div.
MILITARY BASES: ENVIRONMENTAL IMPACT AT CLOSING INSTALLATIONS. REPORT TO CONGRESSIONAL REQUESTERS
Feb. 1995 49 p
(GAO/NSIAD-95-70; B-256333) Avail: CASI HC A03/MF A01

This GAO (General Accounting Office) report addresses concerns that the environmental cleanup at closing military bases is costly and is significantly affecting the DOD's ability to transfer property to nonfederal users. This report summarizes investigative results, such as: (1) cleanup costs; (2) transferability and reuse of property; and (3) progress, difficulties, and plans to address these problems. Derived from text

N95-24146# Pacific Northwest Lab., Richland, WA.
ASSESSING THE RELATIVE CONTRIBUTION OF BIOGENIC AND FOSSIL PROCESSES TO VISIBILITY SCATTERING AEROSOLS FOUND IN REMOTE AREAS: NEAR-TERM ORGANIC RESEARCH PROGRAM
N. Laulainen and E. Trexler (Department of Energy, Washington, DC.) Sep. 1994 5 p Presented at the Conference on Aerosols and Atmospheric Optics: Radiation Balance and Visual Air Quality, Snowbird, UT, 25-30 Sep. 1994
(Contract DE-AC06-76RL-01830)
(DE95-003149; PNL-SA-24038; CONF-9409255-1) Avail: CASI HC A01/MF A01

Organic carbon aerosols are a major component of aerosols that impair visibility in remote areas across the country. They are particularly important in western areas of the U.S. and contribute roughly equally with sulfate aerosols and dust to the total extinction budget. Potential visibility enhancement resulting from various emissions-control and/or fuel-switching strategies, aimed at reducing volatile organic carbon (VOC) and particulate material emissions from fossil-energy-related processes, hinges on the relative contribution of the fossil-fuel-derived organic component. Moreover, additional information is needed on the relative humidity response function of organic carbon aerosols, especially at high relative humidities. The purpose of this paper is to describe a proposed interagency/private sector research program designed to address the major uncertainties of biogenic (live) and fossil-fuel (dead) carbon contributions to the fine-particle extinction budget and visibility impairment. In addition, the use of a relative humidity-controlled integrating nephelometer to evaluate the high humidity behavior of organic carbon aerosols is discussed. DOE

N95-24147# California State Univ., Fullerton, CA.
LABORATORY STUDIES OF THE SENSITIVITY OF TROPOSPHERIC OZONE TO THE CHEMISTRY OF SEA SALT AEROSOL Final Report, 15 Sep. 1993 - 14 Sep. 1994
B. J. Finlayson-Pitts 15 Nov. 1994 15 p
(Contract DE-FG03-93ER-61728)
(DE95-003607; DOE/ER-61728/T1) Avail: CASI HC A03/MF A01

Ozone plays a critical role in both the chemistry and radiation balance of the troposphere. Understanding the factors controlling tropospheric ozone levels is critical to our understanding of a variety of issues in global chemistry and climate change. Chlorine atoms have the potential to contribute significantly to the ozone balance in the free troposphere. They can react directly with ozone or alternately, with organics and may actually lead to the formation of ozone in the presence of sufficient NO. Reactions of alkali halides in sea salt particles are a potential source of atomic chlorine, hence reactions of these alkali halides, especially those producing precursors to atomic chlorine, are of great interest. Finally, the mechanisms, intermediates and products of the Cl-biogenic reactions are unknown; these could serve as unique markers of chlorine atom chemistry in the troposphere, and hence are important to define. DOE

46 GEOPHYSICS

Includes aeronomy; upper and lower atmosphere studies; ionospheric and magnetospheric physics; and geomagnetism.

For space radiation see *93 Space Radiation*.

N95-22482*# Smithsonian Institution, Cambridge, MA.
MEASUREMENT OF HO2 AND OTHER TRACE GASES IN THE STRATOSPHERE USING A HIGH RESOLUTION FAR-INFRARED SPECTROMETER Annual Status Report No. 34, 1 Jan. - 31 Dec. 19944
Wesley A. Traub, Kelly V. Chance, David G. Johnson, Kenneth W. Jucks, Ross J. Salawitch, Jim Changqin Xue, and Paola Ciarpallini Jan. 1995 54 p
(Grant NsG-5175)
(NASA-CR-197368; NAS 1.26:197368) Avail: CASI HC A04/MF A01

This report covers the time period 1 January 1994 to 31 December 1994. During this reporting period we had our fourth Upper Atmosphere Research Satellite (UARS) correlative balloon flight; the data from this flight have been reduced and submitted to the UARS CDHF. We have spent most of the past year analyzing data from this and past flights. For example, using data from our September 1989 balloon flight we have demonstrated for the first time ever that the rates of production and loss of ozone are in balance in the upper stratosphere. As part of this analysis, we have completed the most detailed study to date of radical partitioning throughout the stratosphere. We have also produced the first measurement of HBr and HOBr mixing ratio profiles over a full diurnal cycle. Author

N95-22612# International Centre for Theoretical Physics, Trieste (Italy).
INTERMEDIATE-TERM EARTHQUAKE PREDICTION AND SEISMIC ZONING IN NORTHERN ITALY
Giuliano F. Panza, Ivanka Orozova-Stanishkova (Trieste Univ., Italy.), Giovani Costa (Trieste Univ., Italy.), Franco Vaccari (Trieste Univ., Italy.), and Ira Rotwain (International Inst. for Earthquake Prediction Theory and Mathematical Geophysics, Moscow, Russia.) Dec. 1993 15 p
(DE94-627689; IC-93/414) Avail: CASI HC A03/MF A01 (US Sales Only)

The algorithm CN for intermediate earthquake prediction has been applied to an area in Northern Italy, which has been chosen according to a recently proposed seismotectonic model. Earthquakes with magnitude greater than or equal to 5.4 occur in the area with a relevant frequency and their occurrence is predicted by algorithm CN. Therefore a seismic hazard analysis has been performed using a deterministic procedure, based on the computation of complete synthetic seismograms. The results are summarized in a map giving the distribution of peak ground acceleration, but the complete time series are available, which can be used by civil engineers in the design of new seismo-resistant constructions and in the retrofitting of the existing ones. This risk reduction action should be intensified in connection with warnings issued on the basis of the forward predictions made by CN. DOE

N95-22613# International Centre for Theoretical Physics, Trieste (Italy).
A COMPARISON OF IONOSPHERIC F2-LAYER IRI MODEL WITH EXPERIMENTAL DATA FOR IBADAN GEOG. LAT. 7.4 DEG N
J. O. Adeniyi and I. A. Adimula (Ilorin Univ., Nigeria.) Oct. 1993 5 p
(DE94-627710; IC-93/368) Avail: CASI HC A01/MF A01 (US Sales Only)

IRI-90 model of F2 layer was compared with experimental data at Ibadan (Geog. Lat. 7.4 deg. N), using N(sub m)F2 and h(sub m)F2. The study was done for both high and low solar activity periods. The N(sub m)F2 model generally agrees with observed values during the morning hours, 0500 to about 0900 hours local time. The best agreement at other hours of the day occurs during the June solstice of the period of low solar activity. During period of high solar activity, good agreement occurs, between the hours of 0500 to about 1800 hours for December solstice period. At other seasons, and apart from the periods mentioned above, departures from experimental values of N(sub m)F2 exist. The magnitude of IRI-h(sub m)F2 is higher during the daytime at low solar activity period. There is a close agreement during the period of high solar activity. The usual post sunset peak normally observed in equatorial h(sub m)F2 is not present in the IRI model for the whole solar cycle period. DOE

N95-22843# Westinghouse Hanford Co., Richland, WA.
GEOPHYSICAL INVESTIGATIONS IN THE 100 AREAS: FISCAL YEAR 1991 THROUGH DECEMBER 1993
T. H. Mitchell 23 Sep. 1994 24 p
(Contract DE-AC06-87RL-10930)
(DE95-001573; WHC-SD-EN-TI-247) Avail: CASI HC A03/MF A01

The geophysical investigations identified in this document were conducted by the Westinghouse Hanford Company (WHC) Surface Geophysics Team, Geophysics Group, between October, 1991 and December, 1993. The investigations supported 100-Area activities for the Resource Conservation and Recovery Act of 1976 (RCRA) and the Comprehensive Environmental Response, Compensations and Liability Act of 1980 (CERCLA). The primary intent of this document is to provide a general map location and the associated document number for investigations that have been conducted as of December, 1993. The results of the individual investigations are not included here. The results of all of these investigations have been previously reported individually in WHC supporting documents. The investigations conducted during Fiscal Year (FY) 1992 are summarized in a single WHC document, WHC-SD-EN-TI-204, Rev. O. A brief summary of some of the successful applications of geophysics in the 100-Areas is included. DOE

N95-22850# Los Alamos National Lab., NM.
HOT PROTON ANISOTROPIES AND COOL PROTON TEMPERATURES IN THE OUTER MAGNETOSPHERE
S. Peter Gary, Mark B. Moldwin, Michelle F. Thomsen, Dan Winske, and David J. McComas 1994 16 p Presented at the 10th Taos Workshop on the Earth's Trapped Particle Environment, Taos, NM, Aug. 1994
(Contract W-7405-eng-36)
(DE95-002719; LA-UR-94-3493; CONF-9408182-3) Avail: CASI HC A03/MF A01

The plasma sheet and ring current ions of the outer magnetosphere typically exhibit an anisotropy such that the perpendicular temperature is greater than the parallel temperature. If such an anisotropy is sufficiently large, the electromagnetic proton cyclotron instability will be excited. This instability is studied using linear Vlasov theory and one-dimensional hybrid simulations for a homogeneous plasma model representative of conditions in the outer magnetosphere. The model includes a hot anisotropic proton component and a cool, initially isotropic proton component. Theory and simulations both predict that there is a threshold hot proton anisotropy for this instability which depends inversely on the parallel (beta) of the hot component. The simulations are also used to examine the nonlinear response of the cool protons to the proton cyclotron instability; the late-time temperature of the cool protons is found to increase as the relative hot proton density increases. Analysis of plasma observations obtained by the Los Alamos magnetospheric plasma analyzer in geosynchronous orbit finds that the hot ion anisotropy is indeed bounded by the predicted (beta)-independent threshold. DOE

N95-22867*# Georgia Inst. of Tech., Atlanta, GA. School of Computer and Electrical Engineering.
TOGA/COARE AMMR 1992 DATA PROCESSING
D. B. Kunkee 6 May 1994 4 p
(Grant NAG5-1490)
(NASA-CR-197289; NAS 1.26:197289) Avail: CASI HC A01/MF A01

The complete set of Tropical Ocean and Global Atmosphere (TOGA)/Coupled Ocean Atmosphere Response Experiment (COARE) flight data for the 91.65 GHz Airborne Meteorological Radiometer (AMMR92) contains data from nineteen flights: two test flights, four transit flights, and thirteen experimental flights. The data flight occurred between December 16, 1992 and February 28, 1993. Data collection from the AMMR92 during the first ten flights of TOGA/COARE was performed using the executable code TSK30041. These are IBM PC/XT programs used by the NASA Goddard Space Flight Center (GSFC). During one flight, inconsistencies were found during the operation of the AMMR92 using the GSFC data acquisition system. Consequently, the Georgia Tech (GT) data acquisition system was used during all successive TOGA/COARE flights. These inconsistencies were found during the data processing to affect the recorded data as well. Errors are caused by an insufficient pre- and post-calibration setting period for the splash-plate mechanism. The splash-plate operates asynchronusly with the data acquisition system (there is no position feedback to the GSFC or GT data system). This condition caused both the calibration and the post-calibration scene measurement to be corrupted on a randomly occurring basis when the GSFC system was used. This problem did not occur with the GT data acquisition system due to sufficient allowance for splash-plate settling. After TOGA/COARE it was determined that calibration of the instrument was a function of the scene brightness temperature. Therefore, the orientation error in the main antenna beam of the AMMR92 is hypothesized to be caused by misalignment of the internal 'splash-plate' responsible for directing the antenna beam toward the scene or toward the calibration loads. Misalignment of the splash-plate is responsible for 'scene feedthrough' during calibration. Laboratory investigation at Georgia Tech found that each polarization is affected differently by the splash-plate alignment error. This is likely to cause significant and unique errors in the absolute calibration of each channel. Derived from text

N95-22879# Colorado State Univ., Fort Collins, CO. Dept. of Atmospheric Science.
DEVELOPMENT OF AN ADVANCED FINITE DIFFERENCE ATMOSPHERIC GENERAL CIRCULATION MODEL
D. A. Randall Nov. 1994 16 p
(Contract DE-FG02-91ER-61218)
(DE95-003187; DOE/ER-61218/4) Avail: CASI HC A03/MF A01

The essence of this research is further development of the Colorado State University (CSU) atmospheric general circulation model (AGCM). Although the CSU AGCM is currently evolving rapidly, is also being used in a variety of 'applications' in which the results of simulation performed with the model are analyzed to gain better understanding of the climate system. In parallel, a GCM development effort is also under way at UCLA. The CSU GCM was derived from the UCLA GCM of 1982, but has evolved

to the point that the two models are now really quite distinct. The key distinguishing elements of the CSU model are briefly summarized. The goal of CHAMMP is 'to accelerate the development of more accurate and useful climate prediction capabilities to forecast climate change on sub-continental and smaller scales over time periods ranging from a decade to several centuries'. DOE

N95-22903# Los Alamos National Lab., NM.
AN UPPER BOUND FOR THE PROTON TEMPERATURE ANISOTROPHY
S. P. Gary 1994 20 p Presented at the Workshop on Coupling of Micro- and Mesoscale Processes in Space Plasma Transport, Guntersville, AL, Oct. 1994
(Contract W-7405-eng-36)
(DE95-002752; LA-UR-94-3658; CONF-9410243-1) Avail: CASI HC A03/MF A01

This tutorial describes recent research concerning the upper bound on the hot proton temperature anisotropy imposed by wave-particle scattering due to enhanced fluctuations from the electromagnetic proton cyclotron anisotropy instability. This upper bound, which has been observed in both the magnetosheath and the outer magnetosphere, represents a limited closure relation for the equations of anisotropic magnetohydrodynamics. Such a closure relation has the potential to improve the predictive capability of large-scale anisotropic models of the magnetosphere. DOE

N95-22924# Geological Survey, Menlo Park, CA.
SEISMIC HAZARDS AT KILAUEA AND MAUNA LOA VOLCANOES, HAWAII
Fred W. Klein 22 Apr. 1994 97 p
(Contract DE-AI05-93OR-22089)
(DE94-012109; DOE/OR-22089/3D; USGS-OFR-94-216) Avail: CASI HC A05/MF A02

A significant seismic hazard exists in south Hawaii from large tectonic earthquakes that can reach magnitude 8 and intensity XII. This paper quantifies the hazard by estimating the horizontal peak ground acceleration (PGA) in south Hawaii which occurs with a 90% probability of not being exceeded during exposure times from 10 to 250 years. The largest earthquakes occur beneath active, unbuttressed and mobile flanks of volcanos in their shield building stage. The flanks are compressed and pushed laterally by rift zone intrusions. The largest earthquakes are thus not directly caused by volcanic activity. Historic earthquakes (since 1823) and the best Hawaiian Volcano Observatory catalog (since 1970) under the south side of the island define linear frequency-magnitude distributions that imply average recurrence intervals for M greater than 5.5 earthquakes of 3.4-5 years, for M greater than 7 events of 29-44 years, and for M greater than 8 earthquakes of 120-190 years. These estimated recurrences are compatable with the 107 year interval between the two major April 2, 1868 (M(approximately)7.9) and November 29, 1975 (M=7.2) earthquakes. Frequency-magnitude distributions define the activity levels of 19 different seismic source zones for probabilistic ground motion estimations. The available measurements of PGA (33 from 7 moderate earthquakes) are insufficient to define a new attenuation curve. We use the Boore et al. (1993) curve shifted upward by a factor of 1.2 to fit Hawaiian data. Amplification of sites on volcanic ash or unconsolidated soil are about two times those of hard lava sites. On a map for a 50 year exposure time with a 90% probability of not being exceeded, the peak ground accelerations are 1.0 g Kilauea's and Mauna Loa's mobile south flanks and 0.9 g in the Kaoiki seismic zone. This hazard from strong ground shaking is comparable to that near the San Andreas Fault in California or the subduction zone in the Gulf of Alaska. DOE

N95-22945*# Maryland Univ. Baltimore County, Catonsville, MD.
GLOBAL ELECTRIC FIELD DETERMINATION IN THE EARTH'S OUTER MAGNETOSPHERE USING ENERGETIC CHARGED PARTICLES Final Report
Timothy E. Eastman, R. Sheldon, and D. Hamilton 14 Feb. 1995 34 p
(Grant NAG5-1558)
(NASA-CR-197392; NAS 1.26:197392) Avail: CASI HC A03/MF A01

Although many properties of the Earth's magnetosphere have been measured and quantified in the past 30 years since it was discovered, one fundamental measurement (for zeroth order MHD equilibrium) has been made infrequently and with poor spatial coverage - the global electric field. This oversight is due in part to the neglect of theorists. However, there is renewed interest in the convection electric field because it is now realized to be central to many magnetospheric processes, including the global MHD equilibrium, reconnection rates, Region 2 Birkeland currents, magnetosphere ionosphere coupling, ring current and radiation belt transport, substorm injections, and several acceleration mechanisms. Unfortunately the standard experimental methods have not been able to synthesize a global field (excepting the pioneering work of McIlwain's geostationary models) and we are left with an overly simplistic theoretical field, the Volland-Stern electric field model. Single point measurements of the plasmapause were used to infer the appropriate amplitudes of this model, parameterized by K(sub p). Although this result was never intended to be the definitive electric field model, it has gone nearly unchanged for 20 years. The analysis of current data sets requires a great deal more accuracy than can be provided by the Volland-Stern model. The variability of electric field shielding has not been properly addressed although effects of penetrating magnetospheric electric fields has been seen in mid-and low-latitude ionospheric data sets. The growing interest in substorm dynamics also requires a much better assessment of the electric fields responsible for particle injections. Thus we proposed and developed algorithms for extracting electric fields from particle data taken in the Earth's magnetosphere. As a test of the effectiveness of these new techniques, we analyzed data taken by the AMPTE/CCE spacecraft in equatorial orbit from 1984 to 1989. Derived from text

N95-22951# Michigan Univ., Ann Arbor, MI. Space Physics Research Lab.
CONTINUED STUDIES OF POLAR CAP THERMOSPHERIC DYNAMICS Final Report, 23 Oct. 1989 - 23 Jan. 1993
T. L. Killeen and R. J. Niciejewski Mar. 1994 53 p
(Contract F19628-89-K-0047; AF Proj. 2310)
(PL-TR-94-2076) Avail: CASI HC A04/MF A01

The primary scientific goal for the Thule Greenland optical facility was to acquire measurements of upper thermospheric winds and temperatures during the dark optical observing season. The data acquired by the Fabry-Perot interferometer has been used to extend the thermospheric database coverage for Thule from the initial December 1985 period to the conclusion of the 1990/91 observing season. The initial observations have been used in concert with the NCAR Thermospheric General Circulation Model to improve the understanding of the thermodynamics of the polar cap ionosphere. The airglow facility at Thule AB is the high latitude anchor of a latitudinal chain of Fabre Perot interferometer stations devoted to observing the OI (6300A) emission feature. Thus, the F region measurements obtained at Thule AB provide valuable data in a global effort at improving our understanding of the dynamic state of the upper atmosphere. Author

N95-22956*# Alabama Univ., Huntsville, AL. Dept. of Physics.
THE HIGH LATITUDE IONOSPHERE-MAGNETOSPHERE TRANSITION REGION: SIMULATION AND DATA COMPARISON Annual Progress Report, Mar. 1994 - Feb. 1995
Gordon R. Wilson and James L. Horwitz Feb. 1995 28 p
(Grant NAGw-3470)
(NASA-CR-197404; NAS 1.26:197404) Avail: CASI HC A03/MF A01

A brief description of the major activities pursued during the last year (March 1994 - February 1995) of this grant are: (1) the development of a 200 km to 1 Re, O(+) H(+) Model; (2) the extension of the E x B convection heating study to include centrifugal effects; (3) the study of electron precipitation effects; (4) the study of wave heating of O(+); and (5) the polar wind acceleration study. A list of both papers published and papers submitted, along with a proposal for next year's study and a copy of the published paper is included. Derived from text

N95-23063# Lawrence Livermore National Lab., Livermore, CA.
FORMAT( )MEDIC( )INPUT
K. Foster Sep. 1994 25 p
(Contract W-7405-eng-48)
(DE95-003482; UCRL-ID-118632) Avail: CASI HC A03/MF A01

This document is a description of a computer program called Format( )MEDIC( )Input. The purpose of this program is to allow the user to quickly reformat wind velocity data in the Model Evaluation Database (MEDb) into a reasonable 'first cut' set of MEDIC input files (MEDIC.nml, StnLoc.Met, and Observ.Met). The user is cautioned that these resulting input files must be reviewed for correctness and completeness. This program will not

format MEDb data into a Problem Station Library or Problem Metdata File. A description of how the program reformats the data is provided, along with a description of the required and optional user input and a description of the resulting output files. A description of the MEDb is not provided here but can be found in the RAS Division Model Evaluation Database Description document. DOE

N95-23090*# SRI International Corp., Menlo Park, CA. Geoscience and Engineering Center.

MODELING OF THE COUPLED MAGNETOSPHERIC AND NEUTRAL WIND DYNAMOS Annual Technical Status Report No. 2, 1 Apr. 1994 - 30 Mar. 1995

J. P. Thayer, J. F. Vickrey, R. A. Heelis (Texas Univ. at Dallas, Richardson, TX.), and J. B. Gary (Texas Univ. at Dallas, Richardson, TX.) 8 Mar. 1995 60 p Submitted for publication Original contains color illustrations

(Grant NAGw-3508)

(NASA-CR-197861; NAS 1.26:197861; SRI Proj. ESU-4604) Avail: CASI HC A04/MF A01; 3 functional color pages

Work at SRI involved modeling the exchange of electromagnetic energy between the ionosphere and magnetosphere to help interpret the DE-B Poynting flux observations. To describe the electrical properties of the high-latitude ionosphere, we constructed a numerical model, from the framework provided by the Vector Spherical Harmonic (VSH) model, that determines the ionospheric currents, conductivities, and electric fields including both magnetospheric inputs and neutral wind dynamo effects. This model development grew from the earlier question of whether an electrical energy source in the ionosphere was capable of providing an upward Poynting flux. The model solves the steady-state neutral wind dynamo equations and the Poynting flux equation to provide insight into the electrodynamic role of the neutral winds. The modeling effort to determine the high-latitude energy flux has been able to reproduce many of the large-scale features observed in the Poynting flux measurements made by DE-2. Because the Poynting flux measurement is an integrated result of energy flux into or out of the ionosphere, we investigated the ionospheric properties that may contribute to the observed flux of energy measured by the spacecraft. During steady state the electromagnetic energy flux, or DC Poynting flux, is equal to the Joule heating rate and the mechanical energy transfer rate in the high-latitude ionosphere. Although the Joule heating rate acts as an energy sink, transforming electromagnetic energy into thermal or internal energy of the gas, the mechanical energy transfer rate may be either a sink or source of electromagnetic energy. In the steady state, it is only the mechanical energy transfer rate that can generate electromagnetic energy and result in a DC Poynating flux that is directed out of the ionosphere. Author

N95-23116*# National Aeronautics and Space Administration. Lewis Research Center, Cleveland, OH.

ELECTROMAGNETIC RADIATION IN THE PLASMA ENVIRONMENT AROUND THE SHUTTLE

Boris V. Vayner and Dale C. Ferguson Mar. 1995 21 p Presented at the Chapman Conference on Measurement Techniques for Space Plasma, Santa Fe, NM, 3-7 Apr. 1995; sponsored by the American Geophysical Union

(RTOP 233-01-0E)

(NASA-TM-106891; E-9533; NAS 1.15:106891) Avail: CASI HC A03/MF A01

As part of the SAMPIE (The Solar Array Module Plasma Interaction Experiment) program, the Langmuir probe (LP) was employed to measure plasma characteristics during the flight STS-62. The whole set of data could be divided into two parts: (1) low frequency sweeps to determine voltage-current characteristics and to find electron temperature and number density; (2) high frequency turbulence (HFT dwells) data caused by electromagnetic noise around the shuttle. The broadband noise was observed at frequencies 250-20,000 Hz. Measurements were performed in ram conditions; thus, it seems reasonable to believe that the influence of spacecraft operations on plasma parameters was minimized. The average spectrum of fluctuations is in agreement with theoretical predictions. According to purposes of SAMPIE, the samples of solar cells were placed in the cargo bay of the shuttle, and high negative bias voltages were applied to them to initiate arcing between these cells and surrounding plasma. The arcing onset was registered by special counters, and data were obtained that included the amplitudes of current, duration of each arc, and the number of arcs per one experiment. The LP data were analyzed for two different situations: with arcing and without arcing. Electrostatic noise spectra for both situations and theoretical explanation of the observed features are presented in this report. Author

N95-23143# Lawrence Livermore National Lab., Livermore, CA.

CONJUGATE GRADIENT MATHEW

G. Sugiyama, R. L. Lee, and H. Walker Sep. 1994 29 p

(Contract W-7405-eng-48)

(DE95-003479; UCRL-ID-118629) Avail: CASI HC A03/MF A01

MATHEW generates mass-consistent winds by minimal adjustment of input fields derived from observational, analyzed, or model data. The adjustment is performed by a constrained variational minimization using finite-difference methods and a conjugate gradient solution. Generalized symmetric boundary conditions are implemented, which allow control of the relative amounts of normal and tangential adjustment at the lateral and terrain surfaces. The authors discuss in detail the derivation of the Euler-Lagrange equations, the MATHEW boundary conditions, the finite-difference stencil for the Poisson equation, and the conjugate-gradient algorithm. MATHEW results are then compared with potential flow solution for simple geometries. They also give examples of the use of boundary conditions to create different kinds of flow fields, to prevent speed reductions, and to eliminate flow artifacts caused by complex terrain. The present MATHEW code is twice as fast as the original successive over relaxation algorithm and can be straightforwardly generalized from block to continuous terrain representations. DOE

N95-23184*# Maryland Univ. Baltimore County, Catonsville, MD.

OBSERVATIONS OF THE MAGNETOPAUSE CURRENT LAYER: CASES WITH NO BOUNDARY LAYER AND TESTS OF RECENT MODELS Final Report, 20 Jan. 1995

Timothy E. Eastman 20 Jan. 1995 32 p

(Grant NAGw-1848)

(NASA-CR-197391; NAS 1.26:197391) Avail: CASI HC A03/MF A01

Evidence for the probable existence of magnetospheric boundary layers was first presented by Hones, et al. (1972), based on VELA satellite plasma observations (no magnetic field measurements were obtained). This magnetotail boundary layer is now known to be the tailward extension of the high-latitude boundary layer or plasma mantle (first uniquely identified using HEOS 2 plasma and field observations by Rosenbauer et al., 1975) and the low-latitude boundary layer (first uniquely identified using IMP 6 plasma and field observations by Eastman et al., 1976). The magnetospheric boundary layer is the region of magnetosheath-like plasma located Earthward of, but generally contiguous with the magnetopause. This boundary layer is typically identified by comparing low-energy (less than 10 keV) ion spectra across the magnetopause. Low-energy electron measurements are also useful for identifying the boundary layer because the shocked solar wind or magnetosheath has a characteristic spectral signature for electrons as well. However, there are magnetopause crossings where low-energy electrons might suggest a depletion layer outside the magnetopause even though the traditional field-rotation signature indicates that this same region is a boundary layer Earthward of the current layer. Our analyses avoided crossings which exhibit such ambiguities. Pristine magnetopause crossings are magnetopause crossings for which the current layer is well defined and for which there is no adjoining magnetospheric boundary layer as defined above. Although most magnetopause models to date apply to such crossings, few comparisons between such theory and observations of pristine magnetopause crossings have been made because most crossings have an associated magnetospheric boundary layer which significantly affects the applicable boundary conditions for the magnetopause current layer. Furthermore, almost no observational studies of magnetopause microstructure have been done even though key theoretical issues have been discussed for over two decades. This is because plasma instruments deployed prior to the ISEE and AMPTE missions did not have the required time resolution and most ISEE investigations to-date have focused on tests of MHD plasma models, especially reconnection. More recently, many phenomenological and theoretical models have been developed to explain the existence and characteristics of the magnetospheric boundary layers with only limited success to date. The cases with no boundary layer treated in this study provide a contrary set of conditions to those observed with a boundary layer. For the measured parameters of such cases, a successful

boundary layer model should predict no plasma penetration across the magnetopause. Thus, this research project provides the first direct observational tests of magnetopause models using pristine magnetopause crossings and provides important new results on magnetopause microstructure and associated kinetic processes. Author

N95-23244# Los Alamos National Lab., NM.
DESIGN OF A DIFFERENTIAL RADIOMETER FOR ATMOSPHERIC RADIATIVE FLUX MEASUREMENTS
P. C. LaDelfe, P. G. Weber, and C. W. Rodriguez 1994 6 p Presented at the Optical Sensing for Environmental and Process Monitoring, McLean, VA, 7-10 Nov. 1994
(Contract W-7405-eng-36)
(DE95-002701; LA-UR-94-3406; CONF-9411144-2) Avail: CASI HC A02/MF A01

The Hemispherical Optimized NEt Radiometer (HONER) is an instrument under development at the Los Alamos National Laboratory for deployment on an unmanned aerospace vehicle as part of the Atmospheric Radiation Measurements (ARM/UAV) program. HONER is a differential radiometer which will measure the difference between the total upwelling and downwelling fluxes and is intended to provide a means of measuring the atmospheric radiative flux divergence. Unlike existing instruments which measure the upwelling and downwelling fluxes separately, HONER will achieve an optical difference by chopping the two fluxes alternately onto a common pyroelectric detector. HONER will provide data resolved into two spectral bands; one covering the solar dominated region from less than 0.4 micrometer to approximately 4.5 micrometers and the other covering the region from approximately 4.5 micrometers to greater than 50 micrometers, dominated by thermal radiation. The means of separating the spectral regions guarantees seamless summation to calculate the total flux. The fields-of-view are near-hemispherical, upward and downward. The instrument can be converted, in flight, from the differential mode to absolute mode, measuring the upwelling and downwelling fluxes separately and simultaneously. The instrument also features continuous calibration from on-board sources. We will describe the design and operation of the sensor head and the on-board reference sources as well as the means of deployment. DOE

N95-23247 Weston Observatory, MA.
TOMOGRAPHIC ANALYSIS OF THE THREE-DIMENSIONAL VARIATION OF THE SEISMIC VELOCITY STRUCTURE OF THE SHALLOW CRUST UNDERLYING SOUTHERN NEW ENGLAND
A. K. Bowers and A. L. Kafka 30 Sep. 1993 156 p Limited Reproducibility: More than 20% of this document may be affected by microfiche quality
(Contract F19628-90-K-0035)
(AD-A279406; PL-TR-93-2201; AD-E201924; SR-3) Avail: Issuing Activity (Defense Technical Information Center (DTIC))

This report describes a study in which tomographic inversion was used to investigate the three-dimensional variation of the seismic velocity structure of the shallow crust underlying southern New England (SNE). Group velocity dispersion curves for Rg waves with periods between 0.5 and 2.0 sec have been published for SNE. Dispersion curves from these studies and from our own analyses were converted to travel time data. Two dimensional tomography was then used to estimate group velocities for blocks into which study areas in SNE tomography was then used to estimate group velocities for blocks into which study areas in SNE were divided. Lateral variation in group velocity across SNE is estimated from these results. A combination of the maximum likelihood inverse and forward modelling is used to determine the vertical velocity structure beneath some of these blocks and for other subregions of SNE. DTIC

N95-23256# Los Alamos National Lab., NM.
THEORY OF HF INDUCED TURBULENCE IN THE IONOSPHERE: STATUS AND CHALLENGES
D. F. DuBois 1994 32 p Presented at the 4th Suzdal URSI Symposium on Artificial Modification of the Ionosphere, Uppsala, Sweden, 14-20 Aug. 1994
(Contract W-7405-eng-36)
(DE95-002705; LA-UR-94-3445; CONF-9408181-1) Avail: CASI HC A03/MF A01

In the past five years the combination of new theoretical concepts and computer simulations along with dramatically improved observational diagnostics appear to have led to a detailed, quantitative, understanding of the properties of the Langmuir turbulence induced in the unpreconditioned ionosphere at Arecibo during the first tens of milliseconds following the turn-on of the HF heater. This is the only observational regime in which the initial ionospheric conditions are known to a high level of confidence. The so called strong Langmuir turbulence (SLT) theory predicts observed features in this early time heating which are completely at odds with the prediction of the traditional weak turbulence approximation. The understanding of the observed signatures for times greater than say 30-50 ms following the onset of heating at Arecibo is still incomplete. The same is apparently true for the observations at Tromso where the unique predictions of SLT theory are not so clearly observed. Density irregularities, induced by heating at Arecibo and perhaps present in the ambient ionosphere at Tromso, appear to control the properties of the turbulence. The proper description of the coexistence of Langmuir turbulence with various density irregularities and accounting for the turbulent modification of the electron velocity distribution are challenges for the theory. In this paper the author reviews, starting from the Vlasov-Poisson equations, the fundamental basis of the reduced models used to describe SLT and suggest improvements to the standard model including a new local quasi linear theory for the treatment of hot electron acceleration and transit time damping or burnout of collapsing Langmuir cavitons. DOE

N95-23271*# Iowa Univ., Iowa City, IA. Dept. of Physics and Astronomy.
PHYSICS OF MAGNETOSPHERIC BOUNDARY LAYERS Final Report, 15 Dec. 1990 - 31 Dec. 1994
Iver H. Cairns 18 Jan. 1995 12 p
(Grant NAGw-1483)
(NASA-CR-197920; NAS 1.26:197920) Avail: CASI HC A03/MF A01

This final report was concerned with the ideas that: (1) magnetospheric boundary layers link disparate regions of the magnetosphere-solar wind system together; and (2) global behavior of the magnetosphere can be understood only by understanding its internal linking mechanisms and those with the solar wind. The research project involved simultaneous research on the global-, meso-, and micro-scale physics of the magnetosphere and its boundary layers, which included the bow shock, the magnetosheath, the plasma sheet boundary layer, and the ionosphere. Analytic, numerical, and simulation projects were performed on these subjects, as well as comparisons of theoretical results with observational data. Other related activity included in the research included: (1) prediction of geomagnetic activity; (2) global MHD (magnetohydrodynamic) simulations; (3) Alfven resonance heating; and (4) Critical Ionization Velocity (CIV) effect. In the appendixes are list of personnel involved, list of papers published; and reprints or photocopies of papers produced for this report.
Derived from text

N95-23272*# Texas Univ. at Dallas, Richardson, TX. Center for Space Sciences Physics Program.
INVESTIGATION OF THE ROLE OF GRAVITY WAVES IN THE GENERATION OF EQUATORIAL BUBBLES Technical Progress Report, 1 May 1994 - 28 Feb. 1995
Francis S. Johnson and William R. Coley 28 Feb. 1995 6 p
(Grant NAGw-4002)
(NASA-CR-197962; NAS 1.26:197962) Avail: CASI HC A02/MF A01

The following areas of interest in this progress report are: (1) the continuation of software development in the examination of F-region gravity-wave power using in-situ data from the Atmosphere Explorer (AE-E); (2) the inquiry into the use of the San Marco data for the study of the initiation and growth of bubbles, particularly when the satellite passes through the early evening hours at relatively high altitudes, and the development of bubbles using not only the San Marco data but includes the use of airglow observations made in Hawaii; and (3) the promising development in the observation of distinct well formed waves at about 400 km altitude in the equatorial region. These waves look very much like waves seen over the polar cap that are attributed to internal gravity waves in the neutral atmosphere driving ionization up and down the magnetic field lines. These equatorial waves show no modulation of the total ion concentration.
Derived from text

N95-23386# EG and G Energy Measurements, Inc., Idaho Falls, ID.
SEISMIC EVIDENCE OF CONJUGATE NORMAL FAULTING: THE 1994 DEVIL CANYON EARTHQUAKE SEQUENCE NEAR CHALLIS, IDAHO Ph.D. Thesis
S. M. Jackson Aug. 1994 156 p
(Contract DE-AC07-76ID-01570)
(DE95-002052; EGG-EES-11478) Avail: CASI HC A08/MF A02

In this study, the term 'conjugate' refers to faults that occur in two intersecting sets and coordinated kinematically, with each set being distinctive in both orientation and sense of shear (Davis, 1984). Contemporaneous activity along the conjugate faults is defined as occurring within the time frame of the mainshock-aftershock sequence (three weeks for this sequence and generally less than one month in other observed cases). Detailed recordings of microearthquakes from a dense array of temporary analog seismic stations are analyzed. The focal mechanisms and hypocenter spatial and temporal characteristics are combined with geological information to assess the style, geometry, timing, kinematics, and mechanics of conjugate normal faulting. The characteristics of conjugate normal faulting observed in the Devil Canyon sequence are compared to other conjugate normal faulting sequences, and strike-slip and thrust conjugate sequences worldwide. DOE

N95-23470# State Agricultural Univ., Wageningen (Netherlands).
BASIC DATA SETS DESCRIPTION AND PRELIMINARY RESULTS OF EFEDA-SPAIN
P. Droogers, G. D. v. d. Abeele, J. Cobbaert, C. P. Kim, and R. Roesslerova Jul. 1993 211 p
(PB95-139291) Avail: CASI HC A10/MF A03

To improve the understanding of the interaction between soil, vegetation and atmosphere, ECHIVAL (European International Project on Climatic and Hydrological Interactions between the Vegetation, the Atmosphere and the Land-surface) has been established. The first phase in this research program is EFEDA (ECHIVAL Field Experiment in a Desertification-threatened Area). EFEDA was started with an extensive field experiment in the area of Castilla - La Mancha in Spain aimed at the measurement of the energy and water fluxes during the month of June, 1991. This report consists of two parts. The first part describes methods and materials; the second part gives an overview of the data that have been checked. As much as possible, data are listed in separate appendices. All data described in this report is also available on diskette. A full description of the energy balance measurements is given in Moors (1993) and will not be described here. NTIS

N95-23529*# National Aeronautics and Space Administration. Goddard Space Flight Center, Greenbelt, MD.
TECHNICAL REPORT SERIES ON GLOBAL MODELING AND DATA ASSIMILATION. VOLUME 4: DOCUMENTATION OF THE GODDARD EARTH OBSERVING SYSTEM (GEOS) DATA ASSIMILATION SYSTEM, VERSION 1
Max J. Suarez, ed., James Pfaendtner, Stephen Bloom (General Sciences Corp., Laurel, MD.), David Lamich (General Sciences Corp., Laurel, MD.), Michael Seablom (General Sciences Corp., Laurel, MD.), Meta Sienkiewicz (General Sciences Corp., Laurel, MD.), James Stobie (General Sciences Corp., Laurel, MD.), and Arlindo daSilva Jan. 1995 50 p
(Contract NAS5-32332)
(NASA-TM-104606-Vol-4; Rept-95B00040-Vol-4; NAS 1.15:104606-Vol-4)
Avail: CASI HC A03/MF A01

This report describes the analysis component of the Goddard Earth Observing System, Data Assimilation System, Version 1 (GEOS-1 DAS). The general features of the data assimilation system are outlined, followed by a thorough description of the statistical interpolation algorithm, including specification of error covariances and quality control of observations. We conclude with a discussion of the current status of development of the GEOS data assimilation system. The main components of GEOS-1 DAS are an atmospheric general circulation model and an Optimal Interpolation algorithm. The system is cycled using the Incremental Analysis Update (IAU) technique in which analysis increments are introduced as time independent forcing terms in a forecast model integration. The system is capable of producing dynamically balanced states without the explicit use of initialization, as well as a time-continuous representation of non-observables such as precipitation and radiational fluxes. This version of the data assimilation system was used in the five-year reanalysis project completed in April 1994 by Goddard's Data Assimilation Office (DAO) Data from this reanalysis are available from the Goddard Distributed Active Center (DAAC), which is part of NASA's Earth Observing System Data and Information System (EOSDIS). For information on how to obtain these data sets, contact the Goddard DAAC at (301) 286-3209, EMAIL daac@gsfc.nasa.gov. Author

N95-23663* National Aeronautics and Space Administration. Lyndon B. Johnson Space Center, Houston, TX.
THE ATMOSPHERE BELOW (Videotape)
1992 *Its* Liftoff to Learning Series Videotape: 16 min. playing time, in color, with sound
(NASA-TM-110538; NONP-NASA-VT-95-43941) Avail: CASI VHS A02/BETA A22

In this educational 'Liftoff to Learning' video series, astronauts from the STS-45 Space Shuttle Mission (Kathy Sullivan, Byron Lichtenberg, Brian Duffy, Mike Foale, David Leestma, Charlie Bolden, and Dirk Frimont) explain and discuss the Earths atmosphere, its needs, the changes occurring within it, the importance of ozone, and some of the reasons behind the ozone depletion in the Earths atmosphere. The questions of: (1) what is ozone; (2) what has happened to the ozone layer in the atmosphere; and (3) what exactly does ozone do in the atmosphere, are answered. Different chemicals and their reactions with ozone are discussed. Computer animation and graphics show how these chemical reactions affect the atmosphere and how the ozone hole looks and develops at the south pole during its winter season appearance. CASI

N95-23933# Aerospace Corp., El Segundo, CA. Space and Environment Technology Center.
AN EXPLANATION FOR TAILWARD FLOWS WITH POSITIVE B(SUB z) IN THE DISTANT TAIL NEUTRAL SHEET DURING QUITE TIMES
L. R. Lyons and D. C. Pridmore-Brown 6 Mar. 1995 7 p
(Grant NSF ATM-91-20072)
(ATR-95(7270)-1) Avail: CASI HC A02/MF A01

ISEE-3 and GEOTAIL observations have revealed that at x = -210 to -220 R(sub E), the z-component of magnetic field across the tail neutral sheet is positive, and the plasma flow is tailward during geomagnetically quiet times. Observations have also shown that the y- and z-components of the interplanetary magnetic field (IMF) partially penetrate into the magnetotail for both positive and negative IMF B(sub z). We have evaluated the topology of the magnetospheric magnetic field expected from a partial penetration of the IMF when it has a positive z-component. We find that, in addition to the closed and purely IMF field lines that are generally acknowledged to exist for a southward IMF B(sub z), there is a region at intermediate radial distances of open field lines that cross the tail neutral sheet before exiting the magnetosphere. This region lies between x approx. -150 R(sub E) and x approx. -325 R(sub E) for the representative IMF orientation and model that we have used. We suggest that the quiet-time observations from ISEE-3 and GEOTAIL of tailward flow and positive B(sub z) across the distant tail neutral sheet were obtained during positive IMF B(sub z) conditions and in the region of open field lines. Such an explanation would also account for the GEOTAIL observation that magnetosheath-like plasma associated with positive B(sub z) is common in the distant tail plasma sheet beyond 150 R(sub E) but not closer to Earth. Author

N95-24008# Sandia National Labs., Albuquerque, NM.
AXIAL FOCUSING OF ENERGY FROM A HYPERVELOCITY IMPACT ON EARTH
M. B. Boslough, E. P. Chael, T. G. Trucano, and D. A. Crawford 1994 10 p Presented at the 1994 Hypervelocity Impact Symposium, Santa Fe, NM, 16-20 Oct. 1994
(Contract DE-AC04-94AL-85000)
(DE95-003347; SAND-94-1816C; CONF-9410131-11) Avail: CASI HC A02/MF A01

We have performed computational simulations to determine how energy from a large hypervelocity impact on the Earth's surface would couple to its interior. Because of the first-order axial symmetry of both the impact energy source and the stress-wave velocity structure of the Earth, a disproportionate amount of energy is dissipated along the axis defined by the impact point and its antipode (point opposite the impact). For a symmetric and homogeneous Earth model, all the impact energy that is radiated as seismic waves into the Earth at a given takeoff angle (ray parameter),

independent of azimuthal direction, is refocused (minus attenuation) on the axis of symmetry, regardless of the number of reflections and refractions it has experienced. Material on or near the axis of symmetry experiences more strain cycles with much greater amplitude than elsewhere, and therefore experiences more irreversible heating. The focusing is most intense in the upper mantle, within the asthenosphere, where seismic energy is most effectively converted to heat. For a sufficiently energetic impact, this mechanism might generate enough local heating to create an isostatic instability leading to uplift, possibly resulting in rifting, volcanism, or other rearrangement of the interior dynamics of the planet. These simulations demonstrate how hypervelocity impact energy can be transported to the Earth's interior, supporting the possibility of a causal link between large impacts on Earth and major internally-driven geophysical processes. DOE

N95-24009# Sandia National Labs., Albuquerque, NM.
AXIAL FOCUSING OF IMPACT ENERGY IN THE EARTH'S INTERIOR: A POSSIBLE LINK TO FLOOD BASALTS AND HOTSPOTS
M. B. Boslough, E. P. Chael, T. G. Trucano, D. A. Crawford, and D. L. Campbell 1994 32 p Presented at the New Developments Regarding the KT Event and Other Catastrophes in Earth History, Houston, TX, 9-12 Feb. 1994
(Contract DE-AC04-94AL-85000)
(DE95-003357; SAND-93-2557C; CONF-940285-1) Avail: CASI HC A03/MF A01

We present the results of shock physics and seismological computational simulations that show how energy from a large impact can be coupled to the interior of the Earth. The radially-diverging shock wave generated by the impact decays to linearly elastic seismic waves. These waves reconverge (minus attenuation) along the axis of symmetry between the impact and its antipode. The locations that experience the most strain cycles with the largest amplitudes will dissipate the most energy and have the largest increases in temperature (for a given attenuation efficiency). We have shown that the focus of maximum energy deposition in the mantle lies along the impact axis. Moreover, the most intense focusing is within the asthenosphere at the antipode, within the range of depths where mechanical energy is most readily converted to heat. We propose that if large impacts on the Earth leave geological evidence anywhere other than the impact site itself, it will be at the antipode. We suggest that the most likely result of the focusing for a sufficiently large impact, consistent with features observed in the geological record, would be a flood basalt eruption at the antipode followed by hotspot volcanism. A direct prediction of this model would be the existence of undiscovered impact structures whose reconstructed locations would be antipodal to flood basalt provinces. One such structure would be in the Indian Ocean, associated with the Columbia River Basalts and Yellowstone; another would be a second K/T impact structure in the Pacific Ocean, associated with the Deccan Traps and Reunion. DOE

N95-24041*# Stanford Univ., CA. High Temperature Gasdynamics Lab.
INVESTIGATION OF INFRA-RED AND NONEQUILIBRIUM AIR RADIATION Annual Technical Report, 1 May 1994 - 28 Feb. 1995
Charles H. Kruger 28 Feb. 1995 15 p
(Grant NAG2-910)
(NASA-CR-197977; NAS 1.26:197977) Avail: CASI HC A03/MF A01

This report describes progress on the first year of a research program on the infrared radiation of air plasmas conducted in the High Temperature Gasdynamics Laboratory at Stanford University. This program is intended to investigate the masking of infrared signatures by the air plasma formed behind the bow shock of high velocity missiles. To this date, the radiative emission of air plasmas in the infrared has been the object of few experimental investigations, and although several infrared systems are already modeled in radiation codes such as NEQAIR, measurements are required to validate numerical predictions and indicate whether all transitions of importance are accounted for. The present program is motivated by the fact that 9 excited states (A, B, C, D, B', F, H, and H') of NO radiate in the infrared, especially between 1 and 1.5 microns where at least 9 transitions involving can be observed. Because these IR transitions are relatively well separated from each other, excited NO states concentrations can be easily measured, thus providing essential information on excited-state chemistry for use in optical diagnostics or in electronic excitation model validation. Developing accurate collisional-radiative models for these excited NO states is of importance as the UV-VUV transitions of NO (beta, gamma, epsilon, beta prime, gamma prime) produce a major, if not dominant, fraction of the radiation emitted by air plasmas. During the first year of the program, research has focused on the spectral range 1.0 to 1.5 microns, as detailed in Section 2 of this report. The measurements, conducted in a 50 kW radio-frequency inductively coupled plasma torch operating on air at atmospheric pressure, extend previous shock tube investigations by Wray to a wider spectral range (1.0 to 1.5 microns vs 0.9 to 1.2 microns) and higher temperatures (7600 K in the plasma torch versus 6700 K in the shock-tube). These higher temperatures in the present experiment have made it possible to observe high-lying excited NO states that were previously undetectable. These measurements are currently being extended up to 5 microns, with particular attention paid to the rovibronic bands of ground state NO, molecular continua, CO transitions, and other systems of importance. Publications and presentations resulting from or related to this work are cited in Section 3, and Section 4 lists the personnel who contributed to this report. Derived from text

N95-24078# Los Alamos National Lab., NM.
BURSTING IN THE NEAR-SURFACE BOUNDARY LAYER: COMPARISONS BETWEEN REALISTIC MODELS AND OBSERVATIONS
D. O. ReVelle and R. C. Coulter 1995 5 p Presented at the American Meteorological Society Conference on Boundary Layers and Turbulence, Charlotte, NC, 27-31 Mar. 1994
(Contract W-7405-eng-36)
(DE95-003714; LA-UR-94-2956; CONF-9403185-1) Avail: CASI HC A01/MF A01

In this paper, the authors examine the stable, nocturnal boundary layer, bursting phenomena. Bursting (or intermittent breakdowns from turbulent to laminar flow) can occur if the critical Richardson number, Ri(sub c), is exceeded. During the bursting process, which occurs at irregular, chaotic intervals, periods of active turbulence (large sudden changes in u*) are followed by calm periods when the air temperatures near the ground can drop rapidly. During the turbulent periods, air temperatures can also rise considerably. DOE

N95-23278*# South Dakota State Univ., Brookings, SD. Dept. of Electrical Engineering.
STUDY OF ATMOSPHERIC PARAMETERS MEASUREMENTS USING MM-WAVE RADAR IN SYNERGY WITH LITE-2 Abstract Only
Madeleine Y. Andrawis *In* Hampton Univ., 1994 NASA-HU American Society for Engineering Education (ASEE) Summer Faculty Fellowship Program Dec. 1994 p 58 (For primary document see N95-23276 07-99)
Avail: CASI HC A01/MF A02

N95-23329*# Alabama Univ., Tuscaloosa, AL. Dept. of Physics and Astronomy.
THEORETICAL STUDIES OF SPECTROSCOPIC PROBLEMS OF IMPORTANCE FOR ATMOSPHERIC RADIATION MEASUREMENTS Abstract Only
Richard H. Tipping *In* Hampton Univ., 1994 NASA-HU American Society for Engineering Education (ASEE) Summer Faculty Fellowship Program Dec. 1994 p 111 (For primary document see N95-23276 07-99)
Avail: CASI HC A01/MF A02

47 METEOROLOGY AND CLIMATOLOGY

Includes weather forecasting and modification.

N95-22640# Wageningen Agricultural Univ. (Netherlands).
ACCURACY OF RADAR RAINFALL ESTIMATES COMPARED TO RAINGAUGE MEASUREMENTS AND A HYDROLOGICAL APPLICATION
H. A. M. Hakvoort, R. Uijlenhoet, and J. N. M. Stricker Nov. 1993 79 p Sponsored by Commission of the European Communities, Brussels, Belgium
(Contract CEC-EV5V-CT92-0182)
(PB95-127296) Avail: CASI HC A05/MF A01

Since it is possible to estimate rainfall intensities using a weather radar, it is interesting to know the accuracy of such rainfall estimates as compared to raingauges. Moreover, there are various procedures to adjust radar rainfall estimates using raingauge measurements in order to reduce their

bias error. The report deals with the accuracy of unadjusted and adjusted radar rainfall estimates. In addition, the accuracy of radar rainfall estimates for hydrological purposes has been investigated. NTIS

N95-22651 National Weather Service, Fort Worth, TX. Southern Region.
SWIFT BOAT 1994: USING A FAST CHASE BOAT TO INVESTIGATE OFFSHORE WEATHER FEATURES IN CONJUNCTION WITH WSR-88D OBSERVATIONS
B. K. Choy and M. Trexler Aug. 1994 20 p Limited Reproducibility: More than 20% of this document may be affected by microfiche quality
(PB94-195146; NOAA-TM-NWS-SR-159) Avail: Issuing Activity (National Technical Information Service (NTIS))

The National Weather Service (NWS) is modernizing offices, equipment, and products, and enhancing the training of its employees in order to heighten services it provides to the nation. A cornerstone of the modernization is the WSR-88D (Weather Surveillance Radar-1988 Doppler). The national network of WSR-88D radars will provide nearly complete coverage of the United States and the adjacent coastal waters. Melbourne forecasters recognized the need for additional offshore data in order to better interpret the mechanisms producing the observed features and the resulting conditions. Consequently, a research project was designed to look at meteorological features in the coastal waters with both the Melbourne WSR-88D and marine observations from an instrumented vessel. Observations made from the chase vessel would supplement Surface Aviation Observations (SAO), Cape Canaveral tower wind instruments, weather buoy observations, and ship observations to provide a more complete surface observation network from which to analyze radar observed features. This project was designated SWIFT BOAT (Subtropical Weather Investigation and Forecaster Training using Boat Observations and Atmospheric sampling to marine Truth and WSR-88D). Author

N95-22701# Stanford Linear Accelerator Center, CA.
A MODEL FOR BALL LIGHTNING
D. Fryberger Oct. 1994 41 p Presented at the 1st International Workshop on the Unidentified Atmospheric Light Phenomena in Hessdalen, Hessdalen, Norway, 23-27 Mar. 1994
(Contract DE-AC03-76SF-00515)
(DE95-003366; SU-SLAC-PUB-6473; CONF-9403180-1) Avail: CASI HC A03/MF A01

A model for ball lightning (BL) is described. It is based upon the vorton model for elementary particles, which exploits the symmetry between electricity and magnetism. The core, or driving engine, of BL in this model is comprised of a vorton-antivorton plasma. The energy of BL, which derives from nucleon decay catalyzed by this plasma, leads, through various mechanisms, to BL luminosity as well as to other BL features. It is argued that this model could also be a suitable explanation for other luminous phenomena, such as the unidentified atmospheric light phenomena seen at Hessdalen. It is predicted that BL and similar atmospheric luminous phenomena should manifest certain features unique to this model, which would be observable with suitable instrumentation. DOE

N95-23010*# National Aeronautics and Space Administration. John F. Kennedy Space Center, Cocoa Beach, FL.
THE EFFECT OF SENSOR SPACING ON WIND MEASUREMENTS AT THE SHUTTLE LANDING FACILITY Final Report, 1 Jan. 1993 - 30 Dec. 1994
Francis J. Merceret Jan. 1995 54 p
(NASA-TP-3529; NAS 1.60:3529) Avail: CASI HC A04/MF A01

This document presents results of a field study of the effect of sensor spacing on the validity of wind measurements at the Space Shuttle landing Facility (SLF). Standard measurements are made at one second intervals from 30 foot (9.1m) towers located 500 feet (152m) from the SLF centerline. The centerline winds are not exactly the same as those measured by the towers. This study quantifies the differences as a function of statistics of the observed winds and distance between the measurements and points of interest. The field program used logarithmically spaced portable wind towers to measure wind speed and direction over a range of conditions. Correlations, spectra, moments, and structure functions were computed. A universal normalization for structure functions was devised. The normalized structure functions increase as the 2/3 power of separation distance until an asymptotic value is approached. This occurs at spacings of several hundred feet (about 100m). At larger spacings, the structure functions are bounded by the asymptote. This enables quantitative estimates of the expected differences between the winds at the measurement point and the points of interest to be made from the measured wind statistics. A procedure is provided for making these estimates. Author

N95-23208*# Georgia Inst. of Tech., Atlanta, GA.
UPGRADE OF THE 92 GHz AIRBORNE MULTI-CHANNEL METEOROLOGICAL RADIOMETER (AMMR)
D. B. Kunkee and A. J. Gasiewski 6 May 1994 3 p
(Grant NAG5-1490)
(NASA-CR-197875; NAS 1.26:197875) Avail: CASI HC A01/MF A01

The AMMR 92 GHz dual polarized radiometer (AMMR-92) has been used to perform experiments in the Laboratory for Radioscience and Remote Sensing at Georgia Tech during two periods, the first period was from March 1991 to November 1992, and the second period was from March 1993 to September 1993. Early in the first period a polarization correlation channel was added to the radiometer. This new channel can be configured to measure the third (Re(E(sub v)E(sub h)(sup *)) or fourth (Im(E(sub v)E(sub h)(sup *)) Stokes parameter in the radiometer's feedhorn polarization basis. Operation of the instrument as a polarization correlating radiometer is does not affect its originally intended operation as a dual-polarized radiometer. Investigations with the AMMR-92 at Georgia Tech have uncovered some problems which may compromise the accuracy of the instrument. These problems are not related to the installation of the new cross-correlating channel but are inherent in the original design. This report discusses the following topics: (1) Splash-plate alignment; (2) Replacement of calibration load with pyramidal type; (3) Mixer upgrade; and (4) Installation of a video blanking circuit. Derived from text

N95-23255# Naval Oceanography Command Center/Joint Typhoon Warning Center, FPO San Francisco, CA.
ANNUAL TROPICAL CYCLONE REPORT, 1993
James F. Etro and Peter A. Morse 1993 251 p
(Contract N00014-91-J-1721)
(AD-A285097) Avail: CASI HC A12/MF A03

The Joint Typhoon Warning Center (JTWC) provides a variety of routine products and services to the organizations within its area of responsibility including: (1) significant tropical weather advisory; (2) tropical cyclone formation and depression alert; (3) prognostic reasoning message; (4) computer products; (5) satellite, radar and aircraft reconnaissance; (6) drifting meteorological buoys and automated meteorological observing stations (AMOS). The mission and operational procedures of the (JTWC) are discussed. Derived from text

N95-23385# Department of Energy, Las Vegas, NV.
STREAMFLOW AND SELECTED PRECIPITATION DATA FOR YUCCA MOUNTAIN REGION, SOUTHERN NEVADA AND EASTERN CALIFORNIA, WATER YEARS 1986-90
T. G. Kane, III, D. J. Bauer, and C. M. Martinez 1994 122 p
(Contract DE-AI08-92NV-10874)
(DE95-001893; USGS-OFR-94-312) Avail: CASI HC A06/MF A02

Streamflow and precipitation data collected at and near Yucca Mountain, Nevada, during water years 1986-90 are presented in this report. The data were collected and compiled as part of the studies by the US Geological Survey, in cooperation with the US Department of Energy, to characterize surface-water hydrology in the Yucca Mountain area. Streamflow data include daily-mean discharges and peak discharges at 5 continuous-record gaging stations, and peak discharges at 10 crest-stage, partial-record stations and 2 miscellaneous sites. Precipitation data include cumulative totals at 20 stations maintained by the US Geological Survey and daily totals at 15 stations maintained by the Weather Service Nuclear Support Office, National Oceanic and Atmospheric Administration. DOE

48 OCEANOGRAPHY

Includes biological, dynamic, and physical oceanography; and marine resources.

For related information see also *43 Earth Resources and Remote Sensing.*

N95-22671*# National Aeronautics and Space Administration. Goddard Space Flight Center, Greenbelt, MD.

SeaWiFS TECHNICAL REPORT SERIES. VOLUME 25: OCEAN OPTICS PROTOCOLS FOR SeaWiFS VALIDATION, REVISION 1

Stanford B. Hooker, ed., Elaine R. Firestone, ed. (General Sciences Corp., Laurel, MD.), James G. Acker, ed. (Hughes STX, Inc., Lanham, MD.), James L. Mueller (San Diego State Univ., San Diego, CA.), and Roswell W. Austin (San Diego State Univ., San Diego, CA.) Feb. 1995 75 p

(NASA-TM-104566-Vol-25-Rev-1; Rept-95B00043-Vol-25-Rev-1; NAS 1.15:104566-Vol-25-Rev-1) Avail: CASI HC A04/MF A01

This report presents protocols for measuring optical properties, and other environmental variables, to validate the radiometric performance of the Sea-viewing Wide Field-of-view Sensor (SeaWiFS), and to develop and validate bio-optical algorithms for use with SeaWiFS data. The protocols are intended to establish foundations for a measurement strategy to verify the challenging SeaWiFS uncertainty goals of 5 percent in water-leaving radiances and 35 percent in chlorophyll alpha concentration. The protocols first specify the variables which must be measured, and briefly review the rationale for measuring each variable. Subsequent chapters cover detailed protocols for instrument performance specifications, characterizing and calibrating instruments, methods of making measurements in the field, and methods of data analysis. These protocols were developed at a workshop sponsored by the SeaWiFS Project Office (SPO) and held at the Naval Postgraduate School in Monterey, California (9-12 April 1991). This report began as the proceedings of the workshop, as interpreted and expanded by the authors and reviewed by workshop participants and other members of the bio-optical research community. The protocols are an evolving prescription to allow the research community to approach the unprecedented measurement uncertainties implied by the SeaWiFS goals; research and development are needed to improve the state-of-the-art in specific areas. These protocols should be periodically revised to reflect technical advances during the SeaWiFS Project cycle. The present edition (Revision 1) incorporates new protocols in several areas, including expanded protocol descriptions for Case-2 waters and other improvements, as contributed by several members of the SeaWiFS Science Team. Author

N95-22695# Texas Univ., Austin, TX.

ENERGY FLUX AND HYDROGEOLOGY OF THERMAL ANOMALIES IN THE GULF OF MEXICO BASIN - SOUTH TEXAS EXAMPLE Progress Report, Sep. 1993 - Aug. 1994

J. M. Sharp, Jr. Oct. 1994 12 p

(Contract DE-FG05-92ER-14278)

(DE95-003341; DOE/ER-14278/4) Avail: CASI HC A03/MF A01

This report covers the period from 1 September 1993 through 31 August 1994. In this period, we have focused our efforts on the following activities: (1) finalizing collection of radiogenic heat production data and evaluating results; (2) evaluating petrographic controls on thermal conductivity; (3) preparing paper on petrographic controls on thermal conductivity; (4) modeling one-dimensional heat conduction with sources; (5) completing base geologic cross-section; (6) acquiring pressure data to augment data base; (7) putting map and well data into digital format for analysis; (8) analyzing salinity, temperature, and fluid potential data for propensity of free convection; (9) finalizing preliminary investigation into depressurization of reservoirs; (10) presenting results at the Geological Society of America Annual Meeting in Boston, MA (October 1993); (11) presenting results at the Annual Meeting of the American Association of Petroleum Geologists in Denver, Colorado (June 1994); (12) preparing talk for the Geological Society of America Annual Meeting in Seattle, WA (October 1994); (13) collaborating with project members of the DOE funded Global Basins Research Network who are working on a similar project in the Eugene Island Block in offshore Louisiana; and (14) collaborating with others working on research in the Gulf of Mexico Basin or similar projects elsewhere. DOE

N95-22878# Ohio State Univ., Columbus, OH. Research Foundation.

REGULATION OF PHOTOSYNTHETIC CARBON FIXATION ON THE OCEAN MARGINS

J. H. Paul and F. R. Tabita 3 May 1994 5 p

(Contract DE-FG02-93ER-61700)

(DE95-003185; DOE/ER-61700/1) Avail: CASI HC A01/MF A01

The goals of our DOE OMP project are to: (1) understand regulation of ribulose bisphosphate carboxylase (RubisCO) in phytoplankton cultures in response to light regime; (2) determine regulation of RubisCO in response to light during nutrient limitation in these cultures; (3) to determine mechanisms of RubisCO regulation in natural populations of phytoplankton on the ocean margins in the Gulf of Mexico; and (4) to measure regulation of RubisCO in phytoplankton of the Hatteras System. Two goals are laboratory-based, and two are ship-based. DOE

N95-23074# Naval Postgraduate School, Monterey, CA.

A NUMERICAL STUDY OF INTERANNUAL WIND FORCING EFFECTS ON THE CALIFORNIA CURRENT SYSTEM, 1980-1983 M.S. Thesis

Robert T. Haines Sep. 1994 138 p

(AD-A286023) Avail: CASI HC A07/MF A02

A high resolution, multi-level, primitive equation ocean model is used to examine the response of an idealized, flat-bottomed, eastern boundary oceanic regime on a beta-plane to climatological average (1980-1989) and individual yearly (1980-1983) wind forcing. The focus of this study is the California Current System (CCS) along the coastal region, from 35 deg N to 47.5 deg N, of the Western United States. Five experiments were initialized from a state of rest and two from the fields remaining at day 360 from the climatological average wind forcing. With the climatological average wind forcing, a surface equatorward jet and poleward undercurrent are generated. Eddies form along the entire eastern boundary and a field of cyclonic eddies approximately 200 km in diameter remain at day 360. Results for the non-El Nino (1980-1981) years are very similar to the results for the climatological average wind forcing. Early in the year, the El Nino wind fields for 1983 are more intense than the average and 1980-1982 winds, and they have a much stronger poleward component. A surface poleward current develops over an equatorward undercurrent. DTIC

N95-23212*# Miami Univ., FL.

INFRARED ALGORITHM DEVELOPMENT FOR OCEAN OBSERVATIONS WITH EOS/MODIS Semiannual Report, Jul. - Dec. 1994

Otis B. Brown Dec. 1994 17 p

(Contract NAS5-31361)

(NASA-CR-197851; NAS 1.26:197851) Avail: CASI HC A03/MF A01

Efforts continue under this contract to develop algorithms for the computation of sea surface temperature (SST) from MODIS infrared retrievals. This effort includes radiative transfer modeling, comparison of in situ and satellite observations, development and evaluation of processing and networking methodologies for algorithm computation and data accession, evaluation of surface validation approaches for IR radiances, and participation in MODIS (project) related activities. Efforts in this contract period have focused on radiative transfer modeling and evaluation of atmospheric path radiance efforts on SST estimation, exploration of involvement in ongoing field studies, evaluation of new computer networking strategies, and objective analysis approaches. Author

N95-23667 Defence Science and Technology Organization, Melbourne (Australia). Maritime Operations Div.

THEORETICAL ESTIMATES OF HIGH FREQUENCY ACOUSTIC ATTENUATION AND BACKSCATTERING FROM SUSPENDED SAND PARTICLES IN THE OCEAN AND IN AN ESTUARY

R. A. Thuraisingham Nov. 1994 25 p

(DSTO-TR-0078; AR-008-946) Copyright Avail: Issuing Activity (DSTO Aeronautical and Maritime Research Lab., GPO Box 4331, Melbourne, Victoria 3001, Australia)

Theoretical estimates of high frequency sound attenuation and backscattering strengths from suspended sand particles in the ocean and in an estuary are given. The estimates are obtained using the measured volume concentrations of suspended particle in the upper layers of the ocean, from the particle size spectra near the clear water minimum, and from measurements of suspended sediments at different depths from the bottom of an estuary. Estimates are given for frequencies in the 1-10 MHz region. Contributions to acoustic attenuation from scattering, viscous drag

and thermal conduction are evaluated separately using existing theoretical models. Contribution to attenuation from thermal conduction is negligible at the frequencies used. For particles in the sub micrometer to 10 micron range attenuation is predominantly due to viscous drag. For large particles scattering is the main cause of attenuation. Estimates reveal attenuation and backscattering near the bottom of the estuary is quite high. At 5 MHz, attenuation at a depth of 80 cm and 10 cm from the bottom are approximately 0.1 dB/m and 10 dB/m respectively. At this frequency backscattering strength at 80 cm and 10 cm depths from the bottom, are approximately minus 25 dB and minus 5 dB respectively. Author

N95-23766* Woods Hole Oceanographic Inst., MA. Dept. of Applied Ocean Physics and Engineering.

ASSIMILATION OF ALTIMETER DATA IN A QUASI-GEOSTROPHIC MODEL OF THE GULF STREAM SYSTEM: A DYNAMICAL PERSPECTIVE Ph.D. Thesis - MIT

Antonietta Capotondi Jun. 1993 243 p Limited Reproducibility: More than 20% of this document may be affected by microfiche quality
(Contract JPL-958208)
(NASA-CR-196313; NAS 1.26:196313; AD-A279436; WHOI-93-29) Avail: Issuing Activity (Defense Technical Information Center (DTIC))

The dynamical aspects involved in the assimilation of altimeter data in a numerical ocean model have been investigated. The model used for this study is a quasi-geostrophic model of the Gulf Stream region. The data that have been assimilated are maps of sea surface height which have been obtained as the superposition of sea surface height variability deduced from the Geosat altimeter measurements and a mean field constructed from historical hydrographic data. The method used for assimilating the data is the nudging technique. Nudging has been implemented in such a way as to achieve a high degree of convergence of the surface model fields toward the observations. We have analyzed the mechanisms of the model adjustment, and the final statistical equilibrium characteristics of the model simulation when the surface data are assimilated. Since the surface data are the superposition of a mean component and an eddy component, in order to understand the relative role of these two components in determining the characteristics of the final statistical steady state, we have considered two different experiments: in the first experiment only the climatological mean field is assimilated, while in the second experiment the total surface streamfunction field (mean + eddies) has been used. We have found that the mean component of the surface data determines, to a large extent, the structure of the flow field in the subsurface layers, while the eddy field, as well as the inflow/outflow conditions at the open boundaries, affect its intensity. In particular, if surface eddies are not assimilated only a weak flow develops in the two deeper model layers where no inflow/outflow is prescribed at the boundaries. DTIC

N95-23939*# Jet Propulsion Lab., California Inst. of Tech., Pasadena, CA.

INTERFEROMETRIC SYNTHETIC APERTURE RADAR IMAGERY OF THE GULF STREAM

T. L. Ainsworth (Naval Research Lab., Washington, DC.), M. E. Cannella (Naval Research Lab., Washington, DC.), R. W. Jansen (Naval Research Lab., Washington, DC.), S. R. Chubb (Naval Research Lab., Washington, DC.), R. E. Carande, E. W. Foley (Naval Surface Warfare Center, Bethesda, MD.), R. M. Goldstein, and G. R. Valenzuela (Naval Research Lab., Washington, DC.) *In its* Summaries of the 4th Annual JPL Airborne Geoscience Workshop. Volume 3: AIRSAR Workshop 25 Oct. 1993 p 1- (For primary document see N95-23938 07-42)
Avail: CASI HC A01/MF A01

N95-23953*# Naval Research Lab., Washington, DC. Remote Sensing Div.

MEASUREMENT OF OCEAN WAVE SPECTRA USING POLARIMETRIC AIRSAR DATA

D. L. Schuler *In* JPL, Summaries of the 4th Annual JPL Airborne Geoscience Workshop. Volume 3: AIRSAR Workshop 25 Oct. 1993 p 57-60 (For primary document see N95-23938 07-42)
Avail: CASI HC A01/MF A01

51 LIFE SCIENCES (GENERAL)

N95-22493# Iowa State Univ. of Science and Technology, Ames, IA.

DEVELOPMENT OF NOVEL SEPARATION TECHNIQUES FOR BIOLOGICAL SAMPLES IN CAPILLARY ELECTROPHORESIS Ph.D. Thesis

Huan-Tsung Chang 27 Jul. 1994 267 p
(Contract W-7405-eng-82)
(DE95-001672; IS-T-1710) Avail: CASI HC A12/MF A03

This dissertation includes three different topics: general introduction of capillary electrophoresis (CE); gradient in CE and CE in biological separations; and capillary gel electrophoresis (CGE) for DNA separation. Factors such as temperature, viscosity, pH, and the surface of capillary walls affecting the separation performance are demonstrated. A pH gradient between 3.0 and 5.2 is useful to improve the resolution among eight different organic acids. A flow gradient due to the change in the concentration of surfactant, which is able to coat to the capillary wall to change the flow rate and its direction, is also shown as a good way to improve the resolution for organic compounds. A temperature gradient caused by joule heat is shown by voltage programming to enhance the resolution and shorten the separation time for several phenolic compounds. The author also shows that self-regulating dynamic control of electroosmotic flow in CE by simply running separation in different concentrations of surfactant has less matrix effect on the separation performance. One of the most important demonstrations in this dissertation is that the author proposes on-column reaction which gives several advantages including the use of a small amount of sample, low risk of contamination, and time saving and kinetic features. The author uses this idea with laser induced fluorescence (LIF) as a detection mode to detect an on-column digestion of sub-ng of protein. This technique also is applied to single cell analysis in the group. DOE

N95-22588# Oak Ridge National Lab., TN. Bioprocessing Research and Development Center.

CONTINUOUS PRODUCTION OF CELLULASE IN A FLUIDIZED-BED REACTOR BY PSEUDONOMAS FLUORESCENS IMMOBILIZED IN HYDROGEL BEADS

John M. Cosgrove, T. C. Scott, C. D. Scott, and H. C. Dees 1994 13 p Presented at the 16th Symposium on Biotechnology for Fuels and Chemicals, Gatlinburg, TN, 9-13 May 1994
(Contract DE-AC05-84OR-21400)
(DE94-014105; CONF-940526-6) Avail: CASI HC A03/MF A01

At present, the most widely used microorganism for commercial production of cellulase is probably the filamentous fungus Trichoderma reesei. The T. reesei cellulase system is typically complete and highly productive but the solid-state culture involves complex media and substrate and an inducer which add to the production costs. There is considerable interest in isolating bacteria that produce cellulase enzymes which are more stable, have higher temperature optima, and broader pH optima. Bacterial cellulases may also exhibit greater substrate specificity and more favorable reaction kinetics. We feel that enzyme production could be significantly enhanced by increasing the concentration of active biomass in the reactor, and using organisms that take advantage of simpler media or do not require inducers for enzyme production. Our efforts to develop a more effective cellulase production system have focused on a modified bacterium and on immobilization and utilization of the microorganism in a high-productivity fluidized-bed reactor. The approach is to use a proprietary, cellulase-producing pseudomonad-like bacterium under development at Oak Ridge National Laboratory. The cellulase is constitutively produced and excreted by the bacterium in a minimal media with no requirement for inducers or special chemicals. This bacterium is then immobilized in a hydrogel bead that is used in a continuous fluidized-bed bioreactor. The cellulase can be recovered in downstream processing of the bioreactor effluent. DOE

N95-22589# Department of Energy, Washington, DC. Office of Environment, Safety, and Health.

THE DEVELOPMENT AND APPLICATIONS OF BIOMARKERS

Janet Normandy, ed. and John Peeters, ed. 15 Apr. 1994 79 p Presented at the Workshop on Development and Application of Biomarkers,

Santa Fe, NM, 26-29 Apr. 1994
(DE94-014249; DOE/EH-0377T; CONF-9404178-Absts) Avail: CASI HC A05/MF A01

This report is a compilation of submitted abstracts of scientific papers presented at the second Department of Energy-supported workshop on the use and applications of biomarkers held in Santa Fe, New Mexico, from April 26-29, 1994. The abstracts present a synopsis of the latest scientific developments in biomarker research and how these developments meet with the practical needs of the occupational physician as well as the industrial hygienist and the health physicist. In addition to considering the practical applications and potential benefits of this promising technology, the potential ethical and legal ramifications of using biomarkers to monitor workers are discussed. The abstracts further present insights on the present benefits that can be derived from using biomarkers as well as a perspective on what further research is required to fully meet the needs of the medical community. DOE

N95-22590# California Univ., Berkeley. Lawrence Berkeley Lab, CA. Structural Biology Div.
COMPARISON OF THE RATE CONSTANTS FOR ENERGY TRANSFER IN THE LIGHT-HARVESTING PROTEIN, C-PHYCOCYANIN, CALCULATED FROM FOERSTER'S THEORY AND EXPERIMENTALLY MEASURED BY TIME-RESOLVED FLUORESCENCE SPECTROSCOPY Ph.D. Thesis
Martin Paul Debreczeny May 1994 168 p
(Contract DE-AC03-76SF-00098)
(DE94-014961; LBL-35672) Avail: CASI HC A08/MF A02

We have measured and assigned rate constants for energy transfer between chromophores in the light-harvesting protein C-phycocyanin (PC), in the monomeric and trimeric aggregation states, isolated from Synechococcus sp. PCC 7002. In order to compare the measured rate constants with those predicted by Foerster's theory of inductive resonance in the weak coupling limit, we have experimentally resolved several properties of the three chromophore types (beta(sub 155), alpha(sub 84), beta(sub 84)) found in PC monomers, including absorption and fluorescence spectra, extinction coefficients, fluorescence quantum yields, and fluorescence lifetimes. The cpcB/C155S mutant, whose PC is missing the beta(sub 155) chromophore, was useful in effecting the resolution of the chromophore properties and in assigning the experimentally observed rate constants for energy transfer to specific pathways. DOE

N95-22801*# Washington State Univ., Pullman, WA. Inst. of Biological Chemistry.
PLANT METABOLISM AND CELL WALL FORMATION IN SPACE (MICROGRAVITY) AND ON EARTH Progress Report
Norman G. Lewis [1994] 5 p
(Grant NAGw-3672)
(NASA-CR-197618; NAS 1.26:197618) Avail: CASI HC A01/MF A01

Variations in cell wall chemistry provide vascular plants with the ability to withstand gravitational forces, as well as providing facile mechanisms for correctional responses to various gravitational stimuli, e.g., in reaction wood formation. A principal focus of our current research is to precisely and systematically dissect the essentially unknown mechanism(s) of vascular plant cell wall assembly, particularly with respect to formation of its phenolic constituents, i.e., lignins and suberins, and how gravity impacts upon these processes. Formation of these phenolic polymers is of particular interest, since it appears that elaboration of their biochemical pathways was essential for successful land adaptation. By extrapolation, we are also greatly intrigued as to how the microgravity environment impacts upon 'normal' cell wall assembly mechanisms/metabolism. Derived from text

N95-22866# Telluride Summer Research Center, Telluride, CO.
OPEN PROBLEMS OF COMPUTATIONAL MOLECULAR BIOLOGY
1993 68 p Presented at the 3d Computational Molecular Biology International Workshop, Telluride, CO, 11-25 Jul. 1993
(Contract DE-FG03-93ER-61638)
(DE95-000895; CONF-9307199-Extd-Absts) Avail: CASI HC A04/MF A01 (US Sales Only)

This volume contains short papers and abstracts provided by session leaders of the Third International Workshop on Open Problems of Computational Molecular Biology held in Telluride, Colorado July 11 - 25, 1993. Individual contributions are abstracted and indexed for the database. DOE

N95-22872# Michigan Univ., Ann Arbor, MI. Dept. of Chemical Engineering.
BIOLOGICAL DETERMINANTS OF PHOTOBIOREACTOR DESIGN Quarterly Report No. 3, 1 Mar. - 31 May 1994
Bernhard O. Palsson and G. G. Brown 1994 8 p
(Contract DE-FG22-93PC-93212)
(DE94-016032; DOE/PC-93212/T3) Avail: CASI HC A02/MF A01

Proper mixing is very important for achieving high concentration photosynthetic cultures. Good mixing can keep the cells in suspension, eliminate thermal stratification, help nutrient distribution, and improve gas exchange. We have tested various configurations of photobioreactors and found a PBR with a vertical rectangular slab-shaped illumination chamber to be the best. This shape meets all the criteria of a successful photobioreactor and could support Chlorella vulgaris up to 10(exp 8) cells/ml. DOE

N95-22873# Ohio State Univ., Columbus, OH. Dept. of Microbiology.
TRANSMETHYLATION REACTIONS DURING METHANOGENESIS FROM ACETATE IN METHANOSARCINA BARKERI Annual Technical Progress Report, Aug. 1993 - Jul. 1994
Joseph A. Krzycki 1994 22 p
(Contract DE-FG02-91ER-20042)
(DE94-016222; DOE/ER-20042/2) Avail: CASI HC A03/MF A01

Catabolic production of methane by methanogenic archaebacteria is a unique biochemical process, employing several unusual cofactors and a variety of unusual enzymes. Methanosarcina barkeri MS (DSM 800) metabolizes H2/CO2, methanol, monomethylamine (MMA), dimethylamine (DMA), and trimethylamine (TMA), and acetate. M. barkeri possesses multiple methyltransferases which convert methylated substrates to methylated cofactors or proteins prior to their reduction to methane. Methylated substrates are also oxidized to CO2 to provide reducing equivalents for reduction to methane or for biosynthesis. This short review focuses on methyltransferase reactions leading to methane formation in Methanosarcina. DOE

N95-22874# University of Southern Illinois, Carbondale, IL. Dept. of Microbiology.
REGULATION OF ALCOHOL FERMENTATION IN ESCHERICHIA COLI Progress Report, Jul. 1991 - Jun. 1994
David P. Clark 1994 7 p
(Contract DE-FG02-88ER-13941)
(DE94-016227; DOE/ER-13941/5) Avail: CASI HC A02/MF A01

This report describes progress in sections entitled (1) Regulation of the adhE gene, (2) Molecular Analysis of the adhE Promoter Region, (3) The adhR Regulatory System, (4) The Molecular Biology of the AdhE Protein, (5) The Fermentative Lactate Dehydrogenase, (6) A Novel Secondary ADH from Salmonella, (7) Regulation of the cadA gene, and (8) Side Issues. DOE

N95-22884# Wisconsin Univ., Madison, WI.
ANALYSIS OF STRUCTURAL DOMAINS REQUIRED FOR PHYTOCHROME FUNCTION BY IN VITRO MUTAGENESIS Progress Report, 1993 - - 1994
Richard D. Vierstra 1994 3 p
(Contract DE-FG02-88ER-13968)
(DE94-016230; DOE/ER-13968/3) Avail: CASI HC A01/MF A01

We have successfully expressed in tobacco a series of 8 nested deletions of phytochrome A that involved the removal of both amino- and carboxy-terminal sequences. From examination of the encoded proteins synthesized in plants, we have identify several domains important for phytochrome structure and function. Sequences necessary for chromophore attachment in vivo were localized to the amino-terminal 398 residues because mutant proteins this small had covalently bound chromophore. Deletion mutants from the carboxy terminus to residue 653 were spectrally indistinguishable from the full-length chromoprotein. In contrast, further truncation to residue 399 resulted in a chromoprotein with a bleached Pfr absorbance spectrum; Pr and Pfr absorbance maxima shifted toward shorter wavelengths; and reduced Pfr to Pr phototransformation efficiency. These results identified residues between 399 and 652 as essential for spectral

integrity, but are not essential for chromophore attachment. Sequence(s) between residues 919 and 1093 appear to be necessary for dimerization. Carboxy-terminal mutants containing this region behaved as dimers under nondenaturing conditions in-vitro, whereas truncations without this region behaved as monomers. DOE

N95-22890# Oak Ridge National Lab., TN. Informatics Group.
AN IMPROVED SYSTEM FOR EXON RECOGNITION AND GENE MODELING IN HUMAN DNA SEQUENCES
Ying Xu, J. Ralph Einstein, R. J. Mural, Manesh Shah, and E. C. Uberbacher 1994 14 p Presented at the 2nd International Conference on Intelligent Systems for Molecular Biology, Stanford, CA, 15-17 Aug. 1994
(Contract DE-AC05-84OR-21400)
(DE94-017863; CONF-9408117-3) Avail: CASI HC A03/MF A01

A new version of the GRAIL system called GRAIL II, has recently been developed. GRAIL II is a hybrid artificial intelligence system that supports a number of DNA sequence analysis tools including protein-coding region recognition. PolyA site and transcription promoter recognition, gene model construction, translation to protein, and DNA/protein database searching capabilities. This paper describes the core of GRAIL II, the coding exon recognition and gene model construction algorithms. The exon recognition algorithm recognizes coding exons by combining coding feature analysis and edge-signal (acceptor/donor/translation-start sites) detection. Unlike the original GRAIL system, this algorithm uses variable-length windows tailored to each potential exon candidate, making its performance almost exon length-independent. In this algorithm, the recognition process is divided into four steps. Initially a large number of possible coding exon candidates are generated. Then a rule-based prescreening algorithm eliminates the majority of the improbable candidates. As the kernel of the recognition algorithm, three neural networks are trained to evaluate the remaining candidates. The outputs of the neural networks are then divided into clusters of candidates, corresponding to presumed exons. The algorithm makes its final prediction by picking the best candidate from each cluster. The gene construction algorithm uses a dynamic programming approach to build gene models by using as input the clusters predicted by the exon recognition algorithm. DOE

N95-22897# Stanford Linear Accelerator Center, CA.
PROTEIN FOLDING AND PROTEIN METALLOCLUSTER STUDIES USING SYNCHROTRON SMALL ANGLER X RAY SCATTERING Ph.D. Thesis
David Eliezer Jun. 1994 162 p
(Contract DE-AC03-76SF-00515)
(DE95-003339; SU-SLAC-448) Avail: CASI HC A08/MF A02

Proteins, biological macromolecules composed of amino-acid building blocks, possess unique three dimensional shapes or conformations which are intimately related to their biological function. All of the information necessary to determine this conformation is stored in a protein's amino acid sequence. The problem of understanding the process by which nature maps protein amino-acid sequences to three-dimensional conformations is known as the protein folding problem, and is one of the central unsolved problems in biophysics today. The possible applications of a solution are broad, ranging from the elucidation of thousands of protein structures to the rational modification and design of protein-based drugs. The scattering of x rays by matter has long been useful as a tool for the characterization of physical properties of materials, including biological samples. The high photon flux available at synchrotron x ray sources allows for the measurement of scattering cross-sections of dilute and/or disordered samples. Such measurements do not yield the detailed geometrical information available from crystalline samples, but do allow for lower resolution studies of dynamical processes not observable in the crystalline state. The main focus of the work described here has been the study of the protein folding process using time-resolved small-angle x ray scattering measurements. The original intention was to observe the decrease in overall size which must accompany the folding of a protein from an extended conformation to its compact native state. Although this process proved too fast for the current time-resolution of the technique, upper bounds were set on the probable compaction times of several small proteins. In addition, an interesting and unexpected process was detected, in which the folding protein passes through an intermediate state which shows a tendency to associate. This state is proposed to be a kinetic molten globule folding intermediate. DOE

N95-22911*# Alabama A & M Univ., Normal, AL. Dept. of Biology.
GENETIC EFFECTS ON HEAVY IONS IN DROSOPHILA Final Technical Report
P. G. Kale [1986] 22 p
(Grant NAG9-246)
(NASA-CR-197916; NAS 1.26:197916) Avail: CASI HC A03/MF A01

Drosophila sex-linked recessive lethal mutation test was used to study the dose response relation and relative biological effectiveness of heavy ions. The experiments were performed using the heavy ion beams at BEVALAC of Lawrence Berkeley Laboratory. These experiments were undertaken according to the proposed milestones and included Ne-20, A-40 and Fe-65 ions with respective energies of 600 MeV, 840 MeV and 850 MeV. At these energies several doses of these radiations ranging from 20 to 1280 R were used. Space radiation exposure to astronauts is supposed to be quite low and therefore very low dose experiments i.e., 20 R, were also performed for the three ions. The mutation response was measured in all germ cell types i.e., spermatozoa, spermatids, spermatocytes and spermatogonia of treated Drosophila males. A linear dose frequency relation was observed for most of the range except at high doses where the saturation effect was observed. Also, a very significant difference was observed among the sensitivity of the four germ cell stages where spermatozoa and spermatids were more sensitive. At the higher doses of this range, most of the spermatogonia and spermatocytes were killed. Although comparative and identical experiments with X-rays or neutrons have not been performed, the compassion of our data with the ones available in literature suggest that the heavy ions have a high rbe and that they are several times more effective than low LET X-rays. The rbe compared to neutrons however appears to be only slightly higher. Author

N95-22912# Argonne National Lab., IL. Biological and Medical Research Div.
ACTIVATION OF THE JUN-D GENE IN HUMAN MYELOID CELLS BY 1-(BETA)-D-ARABINOFURANOSYLCYTOSINE
Surender Kharbanda (Harvard Medical School, Boston, MA.), Donald Kufe (Harvard Medical School, Boston, MA.), and Eliezer Huberman (Harvard Medical School, Boston, MA.) 1994 21 p
(Contract W-31-109-eng-38)
(DE94-016591; ANL/BIM/PP-76678) Avail: CASI HC A03/MF A01

The-transcription factor AP-1 binds to a DNA consensus sequence TGA(sup G)/(sub C)TCA (TRE) that regulates the activation of genes responsive to phorbol esters. This factor is a complex composed of proteins encoded by different members of the jun and fos gene family. The c-jun gene, which is induced as an immediate early event by phorbol esters, as well as serum and growth factors, codes for a major form of AP-1. The c-jun, jun-B and jun-D genes are differentially expressed in mouse tissues. jun-D mRNA is more abundant than c-jun and, while jun-B and jun-D expression is similar in most tissues, jun-B mRNA levels are higher than that for jun-D in testis and ovary. Levels of jun-D expression are also higher compared to c-jun and jun-B in quiescent 3T3 cells. Moreover, while c-jun and jun-B transcription is stimulated by phorbol esters and, serum, similar conditions have minimal effects on jun-D expression. These findings have suggested that the jun-D gene has a distinct role in control of gene activity. The treatment of human myeloid leukemia cells with ara-C is associated with transient increases in c-jun and jun-B gene expression. However, transcriptional activation of the c-jun and jun-B genes and the mechanisms responsible for these effects remain unclear. The present studies extend these findings to the jun-D gene. The results demonstrate that ara-C increases jun-D expression by both transcriptional and posttranscriptional mechanisms. We also demonstrate that this agent has little effect on expression of genes coding for proteins that bind. to the related cAMP-responsive consensus sequence. DOE

N95-22913# Argonne National Lab., IL. Center for Mechanistic Biology and Biotechnology.
REARRANGEMENT OF RAG-1 RECOMBINASE GENE IN RADIATION-SENSITIVE WASTED MICE
Gayle E. Woloschak, Claudia R. Libertin (Loyola Univ., Chicago, IL.), Paul Weaver, Mark Churchill, and Chin-Mei Chang-Liu 1994 22 p

(Contract W-31-109-eng-38)
(DE94-017083; ANL/CMB/PP-82201) Avail: CASI HC A03/MF A01

The recent cloning and characterization of recombinase genes (RAG-1/RAG-2) expressed in lymphoid and possibly central nervous system tissues prompted us to examine expression of these genes in DNA repair-deficient/immunodeficient wasted mice (wst). Our results revealed expression of RAG-1 mRNA was detected in spinal cord or brain from wst/wst mice or their normal littermates (wst/(sm bullet)mice). In thymus tissue, a small RAG-1 transcript was detected in wst/wst mice that was not evident in thymus from control mice. In wst/(lg bullet) mice, a two-fold increase in RAG-1 mRNA was evident in thymus tissue. RAG-2 mRNA could only be detected in thymus tissue from wst/(sm bullet) and not from wst;/wst or parental control BCF(sub 1) mice. Southern blots revealed a rearrangement/deletion within the RAG-1 gene of affected wasted mice, not evident in known strain-specific parental or littermate controls. These results support the idea that the RAG-1 gene may map at or near the locus for the wasted mutation. In addition, they suggest the importance of recombinase function in normal immune and central nervous system development as well as the potential contribution of this gene family to the normal repair of radiation-induced DNA damage. DOE

N95-23050# International Centre for Theoretical Physics, Trieste (Italy).
MEMBRANE PHASE SEPARATIONS, ASYMMETRY AND IMPLICATIONS IN THE ORIGIN OF LIFE
M. O. Eze Nov. 1993 8 p
(DE94-628486; IC-93/381) Avail: CASI HC A02/MF A01 (US Sales Only)

Membrane lipids, by affecting membrane physical state, influence solute transport as in Escherichia coli, and play a prominent role in homeoviscous (homeophasic) adaptation whereby cells adapt to varying temperatures. Thus, on prebiotic earth, lipid-doped precells were possibly stabilized. Studies to investigate this hypothesis are advocated. DOE

N95-23053# International Centre for Theoretical Physics, Trieste (Italy).
ENHANCEMENT OF BIOMEMBRANE FUNCTIONS UNDER PHASE-SEPARATED CONDITIONS: A SELF-ORGANIZED CRITICALITY PHENOMENON?
M. O. Eze and J. ChelaFlores Dec. 1993 8 p
(DE94-628489; IC-93/398) Avail: CASI HC A02/MF A01 (US Sales Only)

Self-organized criticality (SOC) is hereby proposed as a possible physical basis for explaining observations in the temperature-dependence of the rates of biological membrane-associated events. The biomembrane undergoes a reversible, cooperative, thermotropic gel-to-liquid crystalline phase transition which is broad, and involves lateral phase separation. The lateral phase separated (rather than the totally gel-, or the totally liquid crystalline-) membrane state has been observed to be the state in which vital membrane functions are facilitated. The membrane in this unique state is viewed, for our purposes here, as a dynamical, extended dissipative system with spatial and temporal degrees of freedom, exhibiting power law behavior, typical of the self-organized critical state. Experiments are suggested for verifying this hypothesis. DOE

N95-23058# International Centre for Theoretical Physics, Trieste (Italy).
THE ORIGIN OF CHIRALITY IN PROTEIN AMINO ACIDS
J. ChelaFlores Mar. 1994 13 p
(DE94-628491; IC-94/59) Avail: CASI HC A03/MF A01 (US Sales Only)

We discuss the origin of the chirality of protein amino acids from the point of view of a phase transition from a racemic mixture into an optically pure state. We assume that Bose-Einstein condensation may act as an amplification mechanism. The originals theory is due to Salam. We suggest a new role for the phase transition. Following Quack we distinguish parity violation of two kinds (de facto and de lege symmetry breaking). While the Salam phase transition corresponds to parity violation of the second kind (de lege), the phase transition we discuss in this work corresponds to parity violation of what we may call a third kind. This is suggested by recent experimental phenomena which correlate chiral symmetry breaking and pattern formation (spontaneous symmetry breaking that separates an initial racemic mixture into right- and left-handed space domains by means of a substrate). Tentative comments are given on the eventual design of possible experiments that may test this new hypothesis. DOE

N95-23060# International Centre for Theoretical Physics, Trieste (Italy).
MOLECULAR RELICS FROM CHEMICAL EVOLUTION AND THE ORIGIN OF LIFE
J. ChelaFlores Apr. 1994 16 p
(DE94-628493; IC-94/75) Avail: CASI HC A03/MF A01 (US Sales Only)

The main hypothesis proposed in this work intends to remove the difficulty that arises from the conjecture that the RNA world may have left molecular relics that may still be extant in the angiosperms. We discuss whether it is possible to envisage a possible evolutionary pathway of the RNA replicators spanning the vast time span separating the first appearance of the angiosperms, late in the Mesozoic era (the Lower Cretaceous), from the most likely suberas in which the RNA world may have occurred, namely the Hadean/Early Archean. In order to address this question we suggest that through horizontal gene transfer, as well as through a series of symbiosis of the precursor cell of the land plants, the genes of the replicases (RNA-directed RNA polymerases) associated with putative DNA-independent RNA replicators may have been transferred vertically, eventually becoming specific to the angiosperms. DOE

N95-23177*# National Aeronautics and Space Administration. Lewis Research Center, Cleveland, OH.
NASA ADVANCED REFRIGERATOR/FREEZER TECHNOLOGY DEVELOPMENT PROJECT OVERVIEW
J. E. Cairelli Mar. 1995 10 p Presented at the 8th International Cryocooler Conference, Vail, CO, 28-30 Jun. 1994; sponsored by the ICC Conference Committee
(RTOP 233-03-0A)
(NASA-TM-106309; E-9204; NAS 1.15:106309) Avail: CASI HC A02/MF A01

NASA Lewis Research Center (LeRC) has recently initiated a three-year project to develop the advanced refrigerator/freezer (R/F) technologies needed to support future life and biomedical sciences space experiments. Refrigerator/freezer laboratory equipment, most of which needs to be developed, is enabling to about 75 percent of the planned space station life and biomedical science experiments. These experiments will require five different classes of equipment; three storage freezers operating at -20 C, -70 C and less than 183 C, a -70 C freeze-dryer, and a cryogenic (less than 183 C) quick/snap freezer. This project is in response to a survey of cooling system technologies, performed by a team of NASA scientists and engineers. The team found that the technologies, required for future R/F systems to support life and biomedical sciences spaceflight experiments, do not exist at an adequate state of development and concluded that a program to develop the advanced R/F technologies is needed. Limitations on spaceflight system size, mass, and power consumption present a significant challenge in developing these systems. This paper presents some background and a description of the Advanced R/F Technology Development Project, project approach and schedule, general description of the R/F systems, and a review of the major R/F equipment requirements. Author

N95-23251 Army Natick Labs., MA.
EFFECT OF HYPERBARIC CARBON DIOXIDE ON SPORES AND VEGETATIVE CELLS OF BACILLUS STEAROTHERMOPHILUS Final Report, 30 Mar. - 30 Sep. 1992
Chester T. Roskey and Anthony Sikes May 1994 36 p Limited Reproducibility: More than 20% of this document may be affected by microfiche quality
(AD-A280115; NATICK/TR-94/019) Avail: CASI HC A03

Spore suspensions in water, 0.05M pH 7 phosphate buffer, 0.05M pH 4.5 and 0.05M pH 4.0 acetate buffer, and antibiotic assay media supplement broth (AAMS) were subjected to 50 psi to 1100 psi carbon dioxide at various temperatures in Parr bombs for up to 96 hours. Spores were resistant to high pressure carbon dioxide treatment at each pH and at both high and low temperatures. Spore suspensions that were first heat activated and then incubated at 550C for a short time increased sensitivity to destruction by CO2. Although spores were resistant to destruction by hyperboric CO2 low pressure (50 psi) CO2 was seen to completely inhibit spore germination and outgrowth. Inhibition to germination was found to be reversible. Spore germination was found to be impaired in carbonated AAMS broth. However, the addition of 50 mM NaHCO3 to AAMS enhanced germination and outgrowth. DTIC

N95-23771# Argonne National Lab., IL. Biological and Medical Research Div.

A COMPARATIVE STUDY OF THE EFFECTS OF CLOFIBRATE, CIPROFIBRATE, WY-14,643, AND DI-(2-ETHYLHEXYL)-PHTHALATE ON LIVER PROTEIN EXPRESSION IN MICE

Carol S. Giometti, John Taylor, M. Anne Gemmell, Sandra L. Tollaksen, Narendra D. Lalwani (Northwestern Univ., Chicago, IL.), and Janardan K. Reddy (Northwestern Univ., Chicago, IL.) 1994 17 p

(Contract W-31-109-eng-38)

(DE94-016587; ANL/BIM/PP-71687) Avail: CASI HC A03/MF A01

A comparative study of the effects of clofibrate, ciprofibrate, WY-14,643, and di-(2-ethylhexyl)-phthalate on liver protein expression in mice is described. Two-dimensional gel electrophoresis (2DE) coupled with computer-assisted data analysis was used to examine liver protein expression in untreated mice and in mice exposed to 0.25% clofibrate, 0.025% ciprofibrate, 0.1% (4-chloro-6(2,3-xylidino)-2-pyrimidinylthio)acetic acid (Wy-14,643), or 2.0% di-(2-ethylhexyl)-phthalate (DEHP). To determine the subcellular distribution of the proteins seen in 2DE patterns of liver, preparations of mitochondria, microsomes, peroxisomes, and cytosol were also analyzed by 2DE. At the doses administered, all of these chemicals are known to cause comparable levels of peroxisome proliferation accompanied by an increase in betaoxidation of lipids, and upon prolonged administration, hepatocellular carcinoma. The similarities in biological effects suggest a pleiotropic biochemical response to this group of chemicals. Analysis of 2DE patterns of liver proteins showed that 260 proteins out of a total of approximately 400 were changed in abundance by at least one of the four treatments used. Out of these 260 quantitative protein changes, 45 were comparable in magnitude and direction for all four treatments while the remainder showed treatment-related variability in either magnitude or direction of response. These results indicate, therefore, that against a background of protein changes that are characteristic of the individual chemicals, there is a set of pleiotropic protein changes common to the peroxisome proliferators. The subcellular location of the proteins involved in this pleiotropic response does not appear to be restricted to the peroxisome fraction. DOE

N95-24047*# Rhode Island Univ., Kingston, RI.

THE 1993 GORDON RESEARCH CONFERENCE ON CHRONOBIOLOGY Final Report

William J. Schwartz 1993 41 p Conference held in New London, NH, 9-13 Aug. 1993

(Grant NAGw-3645)

(NASA-CR-197990; NAS 1.26:197990) Avail: CASI HC A03/MF A01

The study of biological timekeeping is now at a particularly fertile stage, encompassing multiple levels of biological organization, recruiting a wide array of disciplines and methodologies and uniting a host of investigators. This report summarizes a research conference on Chronobiology. Some of the topics focused on transcriptional and translational mechanisms of circadian rhythmicity, with discussions of putative 'clock genes' in cyanobacteria, algae, fungi, fruitflies, and hamsters. Cellular analysis, with emphasis on photoreceptors in frogs, neurons in molluscs, and testis in moths was addressed. New methods for investigating the circadian clock in the suprachiasmatic nucleus were introduced. Derived from text

N95-24075# Georgia Univ., Athens, GA.

STRUCTURAL STUDIES OF COMPLEX CARBOHYDRATES OF PLANT CELL WALLS Final Report, 15 Dec. 1989 - 14 Jun. 1993

A. G. Darvill Oct. 1994 16 p

(Contract DE-FG09-85ER-13426)

(DE95-003099; DOE/ER-13426/T3) Avail: CASI HC A03/MF A01

Characterizing the polysaccharides that constitute the primary cell walls of plants and developing the methods for these characterizations has been a major research goal of our laboratory for many years. We have made considerable progress in both of these areas during the past three years. The cell walls of a plant determine the plant's structure and morphology and act as a barrier to pests. Cell walls also control the rate of growth of plant cells and are a source of complex carbohydrates with biological regulatory properties (oligosaccharins). The research projects supported by this grant concentrate on the isolation and structural characterization of the complex carbohydrates that account for approximately 70-80% of the primary cell walls of dicotyledons and non-graminaceous monocotyledons. Abstracts of papers published, in press, or in preparation reporting work supported by this grant during the past three years follow and summarize more fully the progress made in this research project. DOE

N95-22963*# Universidade Estadual de Paulista, Sao Paulo (Brazil).

A SUPERSYMMETRIC FAMILY OF HARMONIC OSCILLATORS SIMULATING H-BONDS IN DNA

Elso Drigo Filho and Jose R. Ruggiero *In* NASA. Goddard Space Flight Center, Second International Workshop on Harmonic Oscillators Jan. 1995 p 45-49 Sponsored by CNPq and FAPESP (For primary document see N95-22957 07-74)

Avail: CASI HC A01/MF A04

N95-23821*# Morgan State Univ., Baltimore, MD.

GERMINATION, GROWTH RATES, AND ELECTRON MICROSCOPE ANALYSIS OF TOMATO SEEDS FLOWN ON THE LDEF

Ernest C. Hammond, Jr., Kevin Bridgers, and Cecelia Wright Brown *In* NASA. Langley Research Center, LDEF: 69 Months in Space. Third Post-Retrieval Symposium, Part 1 Feb. 1995 p 231-252 (For primary document see N95-23796 07-99)

Avail: CASI HC A03/MF A04

52 AEROSPACE MEDICINE

Includes physiological factors; biological effects of radiation; and effects of weightlessness on man and animals.

N95-22770 Institut National de la Sante et de la Research Medicale, Bordeaux (France).

INTERRELATIONS BETWEEN NERVOUS SYSTEM AND IMMUNE SYSTEM IN STRESS SITUATIONS Final Report, 1 Jan. 1991 - 31 Dec. 1992 [INTER-RELATIONS ENTRE SYSTEME NERVEUX ET SYSTEME IMMUNITAIRE DANS LES SITUATIONS DE STRESS]

R. Dantzer and G. Simonnet 25 Mar. 1994 21 p In FRENCH

(PB95-135521) Avail: Issuing Activity (National Technical Information Service (NTIS))

Designed to define the interrelations between the nervous system and the immune system in stress situations, the research covered by the contract involved a study of the behavioral and physic effects of the cytokines released by immune cells during infection and inflammation, and of the role of anti-morphinic peptides in maintaining homeostasis in disrupted situations. The results obtained show the importance of functional peptide/antipeptide couples in regulating the various phases of adjustment to stress (defense and recovery). NTIS

N95-22875# New England Medical Center Hospitals, Boston, MA.

CONTINUATION OF BNCT RESEARCH PROGRAM AT NEMC AND MIT Technical Progress Report, 1 Jun. 1993 - 31 May 1994

Robert G. Zamenhof (Massachusetts Inst. of Tech., Cambridge, MA.) 1 Jul. 1994 13 p

(Contract DE-FG02-87ER-60600)

(DE94-016228; DOE/ER-60600/4) Avail: CASI HC A03/MF A01

We report on a complete state of readiness for initiating clinical trials of boron neutron capture therapy (BNCT). We present a summary of the status of our program in the context of our being the first research group in the US to have achieved a state of readiness to initiate clinical trials of BNCT. Topics covered in this summary includes: High-Resolution Alpha-Autoradiography; Design of a Final Optimized Epithermal Neutron Beam for Clinical Studies; Preliminary Design of a Fission Converter Epithermal Beam; Dosimetry and Treatment Planning Using Monte Carlo; Microdosimetry of the B-10 Reaction; Prompt-Gamma B-10 Analysis Facility; Experimental in-Phantom Dosimetry; Development of a Dose Control System in the Medical Room Development of Patient Support System in Medical Room; Development of Patient Positioning System in Medical Room; General Upgrades to Medical Therapy Room; Evaluation of Collateral Dose to Irradiated Patients; Design of Clinical Phase-I Melanoma and Glioblastoma Study; Approvals for Phase-I Melanoma and Glioblastoma Studies; Other Research Activities in Neutron Capture Therapy; and Training of NEMC and MIT Staff for Clinical Studies. DOE

N95-23142# Lawrence Livermore National Lab., Livermore, CA.
HOW HEALTH RISK FROM RADIATION IS ASSESSED
L. Rahm-Crites Jul. 1994 7 p
(Contract W-7405-eng-48)
(DE95-003477; UCRL-ID-118487) Avail: CASI HC A02/MF A01

The likelihood that a dose of radiation will result in death from cancer at some future time can be estimated by multiplying the dose equivalent by a risk factor, or dose-to-risk conversion factor. Conversion factors, which are based on studies of atomic bomb survivors and others, provide approximate predictions of the health effects to be expected from a given radiological exposure. Following recommendations of the Nuclear Regulatory Commission, the Department of Energy currently uses risk conversion factors of 4 x 10(exp -4) (0.0004 LCF's) per person-rem for workers and 5 x 10(exp -4) (0.0005 LCF's) per person-rem for the general public (NRC 1991; DOE 1993). The conversion factor for general public is slightly higher than that for workers because the general public includes infants and children, who are more susceptible to cancer. The current overall death rate from cancer in the United States is between 20 and 25 percent, in other words, cancer accounts for one out of nearly every four deaths. An action affecting a population of 20,000 people, with the estimated potential to induce one latent cancer fatality, should therefore be understood as adding one death from cancer to a normally expected total of 4500. Studies dedicated to improving their ability to predict radiation health effects are constantly in progress, nationally and internationally, and risk conversion factors are periodically revised to incorporate new experimental and epidemiological information. DOE

N95-23780# Stanford Univ., CA.
CELLULAR INTERACTIONS IN THE SUPRACHIASMATIC NUCLEUS Annual Report, 1 May 1993 - 30 Apr. 1994
Anthony N. VandenPol May 1994 12 p
(Contract F49620-93-1-0283)
(AD-A285639; AFOSR-94-0641TR) Avail: CASI HC A03/MF A01

The technical report examines the progress made in the last year relating to our work on the suprachiasmatic nucleus, the circadian clock in the mammalian hypothalamus. Much of the work examines different aspects of glutamate neurotransmission. Glutamate is probably the transmitter of the retinohypothalamic pathway, and therefore plays an important role in entrainment of circadian rhythms. DTIC

N95-24145# Pacific Northwest Lab., Richland, WA.
BIOLOGICAL INTERACTIONS AND HUMAN HEALTH EFFECTS OF STATIC MAGNETIC FIELDS
T. S. Tenforde Sep. 1994 3 p Presented at the Occupational Exposure Limits To Electromagnetic Fields Conference, Stockholm, Sweden, 22-23 Sep. 1994
(Contract DE-AC06-76RL-01830)
(DE95-003147; PNL-SA-24931; CONF-9409253-1) Avail: CASI HC A01/MF A01

Mechanisms through which static magnetic fields interact with living systems will be described and illustrated by selected experimental observations. These mechanisms include electrodynamic interactions with moving ionic charges (blood flow and nerve impulse conduction), magnetomechanical interactions (orientation and translation of molecular structures and magnetic particles), and interactions with electronic spin states in charge transfer reactions (photo-induced electron transfer in photosynthesis). A general summary will also be presented of the biological effects of static magnetic fields studied in the laboratory and in natural settings. One aspect of magnetic field effects that merits special concern is their influence on implanted medical electronic devices such as cardiac pacemakers. Several extensive studies have demonstrated closure of the reed switch in pacemakers exposed to relatively weak static magnetic fields, thereby causing them to revert to an asynchronous mode of operation that is potentially hazardous. Recommendations for human exposure limits are provided. DOE

N95-22987*# Universidad Nacional Autonoma de Mexico, Cuernavaca (Mexico). Lab. de Cibernetica.
NEURODYNAMIC OSCILLATORS
Ismael Espinosa, Hortensia Gonzalez, Jorge Quiza, J. Jesus Gonazalez, Ruben Arroyo, and Ritaluz Lara (Instituto Politecnico Nacional, Mexico City, Mexico.) *In* NASA. Goddard Space Flight Center, Second International Workshop on Harmonic Oscillators Jan. 1995 p 255-262 Sponsored by Direccion General de Asuntos del Personal Academico (For primary document see N95-22957 07-74)
Avail: CASI HC A02/MF A04

53 BEHAVIORAL SCIENCES

Includes psychological factors; individual and group behavior; crew training and evaluation; and psychiatric research.

N95-22579* National Aeronautics and Space Administration. Langley Research Center, Hampton, VA.
METHOD OF ENCOURAGING ATTENTION BY CORRELATING VIDEO GAME DIFFICULTY WITH ATTENTION LEVEL Patent
Alan T. Pope, inventor (to NASA) and Edward H. Bogart, inventor (to NASA) (Lockheed Engineering and Sciences Co., Hampton, VA.) 27 Dec. 1994 13 p Filed 8 Mar. 1993 Supersedes N93-28128 (31 - 10, p 3085)
(NASA-Case-LAR-15022-1; US-Patent-5,377,100;
US-Patent-Appl-SN-029808; US-Patent-Class-364-410;
Int-Patent-Class-G06F-15/44) Avail: US Patent and Trademark Office

A method of encouraging attention in persons such as those suffering from Attention Deficit Disorder is provided by correlating the level of difficulty of a video game with the level of attention in a subject. A conventional video game comprises a video display which depicts objects for interaction with a player and a difficulty adjuster which increases the difficulty level, e.g., action speed and/or evasiveness of the depicted object, in a predetermined manner. The electrical activity of the brain is measured at selected sites to determine levels of awareness, e.g., activity in the beta, theta, and alpha states. A value is generated based on this measured electrical signal which is indicative of the level of awareness. The difficulty level of the game is increased as the awareness level value decreases and is decreased as this awareness level value increases.
Official Gazette of the U.S. Patent and Trademark Office

N95-23788# Civil Aeromedical Inst., Oklahoma City, OK.
SOME PERFORMANCE EFFECTS OF AGE AND LOW BLOOD ALCOHOL LEVELS ON A COMPUTERIZED NEUROPSYCHOLOGICAL TEST Final Report
David J. Schroeder, Howard C. Harris, Jr., William E. Collins, and Thomas E. Nesthus Feb. 1995 38 p
(DOT/FAA/AM-95/7) Avail: CASI HC A03/MF A01

COGSCREEN is a computerized test battery developed for the Federal Aviation Administration as an airman neuropsychological screening instrument for cognitive functioning. This study explored a multifaceted application of the sensitivity of the battery to potential differences in performance capabilities, current civil aviation interest in the performance effects of low levels of blood alcohol, and the potential significance of age on cognitive performance. Nine of 11 basic COGSCREEN tests were used with 60 subjects divided into three age groups, 27-32, 42-47, and 57-62 years. Twelve subjects within each age category (N=36) comprised an alcohol group, 8 subjects within each age category (N=24) comprised a control group. Subjects were given four 30-minute sessions of training on the task battery during one afternoon and participated in experimental sessions on the next afternoon. Experimental sessions comprised a pre-drinking (baseline) and three post-drinking sessions targeted to breath alcohol (BrAC) levels of 0.04, 0.027, and 0.014 percent for the alcohol group; each control subject received a placebo. The results yielded statistically significant age effects on 20 of 25 measures of performance across the 9 tasks for the pre-drinking sessions favoring the younger age group, using the entire subject population (N=60). An analysis using only the control subject found significant age effects on 18 of the 25 measures of performance on both the baseline and the post-baseline sessions; whereas, the analysis of the alcohol subjects (N=36) found significant age differences on 15 of 25 scores for the pre-drinking session and only 13, 11, and 10 of 25 on the post-drinking sessions respectively. Results of the analyses for age and alcohol session effects revealed statistically significant interactions for 3 measures: mean reaction time of visual comparisons during dual task, and the symbol-digit delayed recall task, as well as the number of correct symbol-digit pairings of the delayed recall task. These data indicate that the COGSCREEN test battery is sensitive to decremental

effects on information processing time and cognitive reductions associated with aging. Generally, the results of this study do not support a typical alcohol effect. The simple effects tests yielded results that failed to show sessional patterns consistent with BrAC levels. However, the alcohol sessions may have reduced differences between the age groups. Author

N95-23934# Civil Aeromedical Inst., Oklahoma City, OK.
EFFECTS OF AGE AND LOW DOSES OF ALCOHOL ON COMPENSATORY TRACKING DURING ANGULAR ACCELERATION Final Report
Howard C. Harris, Jr., David J. Schroeder, and William E. Collins Jan. 1995 22 p
(DOT/FAA/AM-95/3) Avail: CASI HC A03/MF A01

Heightened interest in existing FAA regulations regarding alcohol and flying, with emphasis on the potential effects of low blood alcohol levels on performance, indicated a need for research to help define effects of low doses of alcohol on performance. This study was designed to assess the effects of age and three breath alcohol levels (0.04, 0.027, and 0.014 percent). Performance was assessed while subjects experienced mild angular stimulation. On the day prior to drinking, 48 subjects drawn from three age categories (27-32, 42-47, and 57-62 years) completed four training sessions on a compensatory tracking task (a localizer/glide slope instrument that required compensatory tracking of both a horizontal and a vertical needle) with and without a secondary auditory recognition task, under 1.0 ft L. and 0.1 ft L. illumination conditions. The test day consisted of a pre-drinking session and three experimental alcohol measurements. Mean performance scores for the three age groups were compared across the four sessions, (pre-drinking and three levels of alcohol). A Mutivariate Analysis of Variance (MANOVA) test yielded a significant interaction and a significant mean effect (age and session) for the combined needle errors under the 0.1 ft L. illumination level with the secondary task. The resulting simple effects tests revealed age differences at all post-drinking sessions favoring younger over older subjects, and poorer performance for the older age subjects at the 0.04 percent BrAC level. When testing individual needle errors, MANOVA tests yielded a significant interaction and main effects in the high illumination condition both with and without the secondary task for vertical needle errors. Resulting simple effects Analysis of Variance tests yielded significant age and alcohol effects for the older age subjects. The 0.04 percent level accounted for the alcohol effects. The alcohol and age interaction was accounted for by the older age group at the 0.04 percent BrAC level. This study showed no evidence of performance decrement associated with BrAC's below 0.04 percent. Author

N95-24088# Civil Aeromedical Inst., Oklahoma City, OK.
FUNCTIONS OF EXTERNAL CUES IN PROSPECTIVE MEMORY Final Report
O. U. Vortac (Oklahoma Univ., Norman, OK.), Mark B. Edwards (Oklahoma Univ., Norman, OK.), and Carol A. Manning Feb. 1995 16 p
(Contract DTFA02-91-C-91089)
(DOT/FAA/AM-95/9) Avail: CASI HC A03/MF A01

A simulation of an air traffic control task was the setting for an investigation of the functions of external cues in prospective memory. External cues can support the triggering of an action or memory for the content of the action. We focused on memory of the content and manipulated the temporal characteristics of the external cue to disentangle two possible functions the cue can support: (1) An external cue visible during a retention interval could support rehearsal of the to-be-performed action; and (2) An external cue visible at the end of a retention interval could support retrieval of the to-be-performed action. Two experiments were conducted that converge on the same conclusion: the primary function of an external cue was to support retrieval. Implications for the design of a computer interface to present prospective cues are discussed. Author

54 MAN/SYSTEM TECHNOLOGY AND LIFE SUPPORT

Includes human engineering; biotechnology; and space suits and protective clothing.

For related information see also *16 Space Transportation*.

N95-22513# Dayton Univ. Research Inst., OH.
AVIATOR'S NIGHT VISION IMAGING SYSTEM PREFLIGHT ADJUSTMENT/ASSESSMENT PROCEDURES Final Technical Report, Oct. - Dec. 1993
Joseph C. Antonio, DeForest Q. Joralmon, George M. Fiedler, and William E. Berkley Sep. 1994 23 p
(Contract F33615-90-C-0005)
(AD-A285829; AL/HR-TR-1994-0111) Avail: CASI HC A03/MF A01

Night vision goggles (NVG's) have been employed in a variety of aircraft for over 20 years. However, only recently has their application begun in fixed-wing fast movers. Research accomplished by the Aircrew Training Research Division of the USAF Armstrong Laboratory demonstrated the loss of NVG performance resulting from improper adjustments. This report describes correct adjustment procedures for the Aviator's Night Vision Imaging System, or ANVIS. The procedures described were developed so aircrews could take advantage of the adjustments available on the NVG's. Additionally, image descriptions are given to help aircrews evaluate NVG performance. Information on the proper equipment/space needed for proper evaluation is also included. DTIC

N95-22766* National Aeronautics and Space Administration. Lyndon B. Johnson Space Center, Houston, TX.
METHOD FOR FORMING A GLOVE ATTACHMENT Patent
Frederic S. Dawn, inventor (to NASA), Walter W. Guy, inventor (to NASA), Joseph Kosmo, inventor (to NASA), Arthur P. Drennan, inventor (to NASA), and Richard P. Tschirch, inventor (to NASA) 24 Jan. 1995 6 p Filed 14 Aug. 1992 Supersedes N92-34210 (30 - 24, p 4222)
(NASA-Case-MSC-21632-1; US-Patent-5,384,083;
US-Patent-Appl-SN-929556; US-Patent-Class-264-130;
US-Patent-Class-264-135; US-Patent-Class-264-137;
US-Patent-Class-264-257; Int-Patent-Class-B29C-39/12;
Int-Patent-Class-B29C-67/14) Avail: US Patent and Trademark Office

An attachment principally for the palm of an astronaut glove to enhance the gripping area of the palm without detracting from the flexibility and utility of the glove is presented. The attachment is a composite construction formed from a layer of silicone rubber having an outer surface with a friction configuration and another layer of silicone rubber in which a Nomex Aramid mesh fabric is embedded prior to curing. The method of construction involves the use of a mold with a friction configuration surface. A first layer of silicone rubber or sealant is disposed in the mold and allowed to set for an hour. A second layer of silicone rubber or sealant is layered over the first layer and leveled. A Nomex Aramid mesh fabric is embedded into the second layer and the composite is permitted to cure. When cured, a configured area of the composite construction is glued or stitched to the palm area of the glove.
Official Gazette of the U.S. Patent and Trademark Office

N95-22797*# Georgia Inst. of Tech., Atlanta, GA. Center for Human-Machine Systems Research.
HUMAN-CENTERED DESIGN OF HUMAN-COMPUTER-HUMAN DIALOGS IN AEROSPACE SYSTEMS Semiannual Report No. 2, 1 Feb. - 31 Jul. 1994
Christine M. Mitchell 31 Jul. 1994 13 p
(Contract NCC2-824)
(NASA-CR-197379; NAS 1.26:197379; E-24-X30) Avail: CASI HC A03/MF A01

The second six months of this grant saw further development of GT-CATS, the Georgia Tech Crew Activity Tracking System, and progress on research exploring tutoring concepts for tutors for mode management. The latter included data analysis and a preliminary paper summarizing the development and evaluation of the VNAV Tutor. A follow-on to the VNAV Tutor is planned. Research in this direction will examine the use of OFMspert and GT-CATS to create an 'intelligent' tutor for mode management, a more extensive domain of application than only vertical navigation, and

alternative pedagogy, such as substituting focused 'cases' of reported mode management situations rather than lessons defined by full LOFT scenarios.
Derived from text

N95-23194*# Jet Propulsion Lab., California Inst. of Tech., Pasadena, CA.
LIFE SUPPORT SYSTEMS ANALYSIS AND TECHNICAL TRADES FOR A LUNAR OUTPOST Report, Oct. 1993
J. F. Ferrall, G. B. Ganapathi, N. K. Rohatgi, and P. K. Seshan Dec. 1994 109 p
(NASA-TM-109927; NAS 1.15:109927) Avail: CASI HC A06/MF A02

The NASA/JPL life support systems analysis (LISSA) software tool was used to perform life support system analysis and technology trades for a Lunar Outpost. The life support system was modeled using a chemical process simulation program on a steady-state, one-person, daily basis. Inputs to the LiSSA model include metabolic balance load data, hygiene load data, technology selection, process operational assumptions and mission parameter assumptions. A baseline set of technologies has been used against which comparisons have been made by running twenty-two cases with technology substitutions. System, subsystem, and technology weights and powers are compared for a crew of 4 and missions of 90 and 600 days. By assigning a weight value to power, equivalent system weights are compared. Several less-developed technologies show potential advantages over the baseline. Solid waste treatment technologies show weight and power disadvantages but one could have benefits associated with the reduction of hazardous wastes and very long missions. Technology development towards reducing the weight of resupplies and lighter materials of construction was recommended. It was also recommended that as technologies are funded for development, contractors should be required to generate and report data useful for quantitative technology comparisons.
Author

N95-23264* National Aeronautics and Space Administration. Ames Research Center, Moffett Field, CA.
SELF-GENERATING OSCILLATING PRESSURE EXERCISE DEVICE Patent
Donald E. Watenpaugh, inventor (to NASA) 18 Oct. 1994 8 p Filed 13 May 1993
(NASA-Case-ARC-12000-1; US-Patent-5,356,361;
US-Patent-Appl-SN-061401; US-Patent-Class-482-111;
US-Patent-Class-601-23; Int-Patent-Class-A63B-21/008) Avail: US Patent and Trademark Office

An exercise device, especially suitable for zero gravity workouts, has a collapsible chamber which generates negative pressure on the lower portion of a body situated therein. The negative pressure is generated by virtue of leg, hand and shoulder interaction which contracts and expands the chamber about the person and by virtue of air flow regulation by valve action.
Official Gazette of the U.S. Patent and Trademark Office

N95-23274* National Aeronautics and Space Administration. Lyndon B. Johnson Space Center, Houston, TX.
LIVING IN SPACE (Videotape)
Ray Brown, ed. 1993 *Its* Liftoff to Learning Series Videotape: 9 min. 45 sec. playing time, in color, with sound
(NASA-TM-110536; NONP-NASA-VT-95-43939) Avail: CASI VHS A02/BETA A22

In this educational video from the 'Liftoff to Learning' series, astronauts from the STS-56 Mission (Ken Cockell, Mike Foale, Ellen Ochoa, Steve Oswald, and Ken Cameron) explain and show through demonstrations how microgravity affects the way astronauts live onboard the Space Shuttle, and how these same daily habits or processes differ on Earth. A tour of the Space Shuttle is given, including the sleeping compartments, the kitchen area, the storage compartments, and the Waste Collection System (or WCS, as they call it). Daily habits (brushing teeth, shampooing hair and bathing, eating,...) are explained and actively illustrated, along with reasons of how these applications differ from their employment on Earth
CASI

N95-23474*# Lamar Univ., Beaumont, TX. Dept. of Chemical Engineering.
RESOURCE RECOVERY AND EPIDEMIOLOGY OF ANAEROBIC WASTEWATER TREATMENT PROCESS IN A CONTROLLED ECOLOGICAL LIFE SUPPORT SYSTEM Final Report
Ku-Yen Li and Madelyn D. Hunt 27 Feb. 1995 121 p
(Grant NAG9-696)
(NASA-CR-197930; NAS 1.26:197930) Avail: CASI HC A06/MF A02

The results of work accomplished under two different areas: (1) Resource Recovery of an Anaerobic Wastewater Treatment process, and (2) Epidemiological Study of an Anaerobic Wastewater Treatment Process are documented. The first part of the work was to set up and test three anaerobic digesters and then run these three digesters with a NASA-simulated wastewater. The second part of the work was to use a multi-drug resistant strain of Salmonella choleraesuis as the indicator bacteria for the epidemiological study. Details of these two parts can be found in two master's theses and are described in Sections 3 and 4 of this report. Several important results condensed from these two parts are summarized in Section 2.
Author

N95-23601# Advisory Group for Aerospace Research and Development, Neuilly-Sur-Seine (France). Guidance and Control Panel.
KNOWLEDGE-BASED GUIDANCE AND CONTROL FUNCTIONS [APPLICATION DES SYSTEMES EXPERTS POUR LE GUIDAGE ET LE PILOTAGE]
Jan. 1995 183 p
(AGARD-AR-325; ISBN-92-836-1009-1) Copyright Avail: CASI HC A09/MF A02

This report summarizes the deliberations of Working Group 11 of the Guidance and Control Panel of AGARD. The objectives of the Working Group are: (1) analyze the structure of knowledge-based guidance and control functions related to aircraft, missions, and the battlefield and identify their potential for automation; (2) analyze the structure of knowledge-based guidance and control functions related to the life cycle of guidance and control systems, and identify their potential for automation; (3) review the state-of-the-art of those software and hardware oriented technologies required for the transfer of the knowledge-based G&C functions to automatic systems; (4) review existing programs; and (5) make recommendations for future work.
Author

N95-24021# Wichita State Univ., Wichita, KS. National Inst. for Aviation Research.
DESIGN OF A CERVICAL SPINE GROSS MOTION SIMULATOR FOR STANDARD SIZE HUMAN AND ANTHROPOMORPHIC DUMMY ADULT AND CHILD
Srinivas Reddy Malapati Sep. 1994 161 p
(NIAR-94-16) Avail: CASI HC A08/MF A02

In the field of automotive and aircraft safety research, simulation of crashes to study the effect on the human body is vital in order to evaluate and improve crash safety devices and occupant environment. Realistic simulation of the neck response in a dummy is of vital importance to get a human-like dynamical behavior of the head. Trajectories of the head and the nature of the head contact with vehicle interior or exterior are critically dependent on the dummy's neck design. Most of this work is done by way of experiments, using instrumented dummies, cadavers, and occasionally animals or volunteers. In the sixties, fast digital computers together with advanced mathematical techniques led to a new method of simulations with mathematical models. These models have the advantage that a great number of simulation results can be obtained easily, without any measurement problems as occur with experiments. This thesis describes the development and validation of two-dimensional, nine degree-of-freedom mathematical models which simulate the dynamic responses of the head-neck assembly of a 50th percentile male human and a three-year-old child. The validation of the three-year-old child head-neck model is made by comparing the results with the simple single hinge-type head-neck model of a three-year-old child dummy in the code MADYMO frequently used by the automobile industries for prediction of potential injuries to vehicle occupants as a result of crash. Sensitivity studies are conducted and model performances are evaluated. Comparison between child and adult responses were made and significant differences were noticed. Numerous similarities between the model response and experimental performance suggest that the models have considerable potential as a design tool.
Author

N95-23704*# Ministry of International Trade and Industry, Tsukuba (Japan). Electromechanical Lab.
DEVELOPMENT OF ADVANCED ROBOTIC HAND SYSTEM FOR SPACE APPLICATION
Kazuo Machida, Kenzo Akita (Institute for Unmanned Space Experiments Free Flyer, Tokyo, Japan.), Tatsuo Mikami (Fujitsu Ltd., Kawasaki, Japan.), and Satoru Komada (Fujitsu Ltd., Kawasaki, Japan.) *In* JPL, Third International Symposium on Artificial Intelligence, Robotics, and Automation for Space 1994 Oct. 1994 p 165-168 (For primary document see N95-23672 07-63)
Avail: CASI HC A01/MF A03

N95-23705*# Fujitsu Ltd., Kawasaki (Japan).
A THREE-FINGER MULTISENSORY HAND FOR DEXTEROUS SPACE ROBOTIC TASKS
Yuichi Murase, Satoru Komada, Takashi Uchiyama, Kazuo Machida (Ministry of International Trade and Industry, Tsukuba, Japan.), and Kenzo Akita (Institute for Unmanned Space Experiments Free Flyer, Tokyo, Japan.) *In* JPL, Third International Symposium on Artificial Intelligence, Robotics, and Automation for Space 1994 Oct. 1994 p 169-172 (For primary document see N95-23672 07-63)
Avail: CASI HC A01/MF A03

N95-23707*# Centre National d'Etudes Spatiales, Toulouse (France).
ROBOTIC EXPERIMENT WITH A FORCE REFLECTING HANDCONTROLLER ONBOARD MIR SPACE STATION
M. Delpech and Y. Matzakis (MATRA Marconi Space, Toulouse, France.) *In* JPL, Third International Symposium on Artificial Intelligence, Robotics, and Automation for Space 1994 Oct. 1994 p 177-181 (For primary document see N95-23672 07-63)
Avail: CASI HC A01/MF A03

N95-23708*# National Space Development Agency, Tsukuba (Japan). Space Station Dept.
DEVELOPMENT OF JAPANESE EXPERIMENT MODULE REMOTE MANIPULATOR SYSTEM
Tatsuo Matsueda, Fumihiro Kuwao (Toshiba Corp., Kawasaki, Japan.), Shoichi Motohasi (Toshiba Corp., Kawasaki, Japan.), and Ryo Okamura (Toshiba Corp., Kawasaki, Japan.) *In* JPL, Third International Symposium on Artificial Intelligence, Robotics, and Automation for Space 1994 Oct. 1994 p 183-186 (For primary document see N95-23672 07-63)
Avail: CASI HC A01/MF A03

N95-23709*# Toshiba Corp., Kawasaki (Japan). Space Systems Engineering Dept.
ROBOT ARM SYSTEM FOR AUTOMATIC SATELLITE CAPTURE AND BERTHING
Shinichiro Nishida, Hidetoshi Toriu, Masato Hayashi, Tomoaki Kubo, and Makoto Miyata *In* JPL, Third International Symposium on Artificial Intelligence, Robotics, and Automation for Space 1994 Oct. 1994 p 187-190 (For primary document see N95-23672 07-63)
Avail: CASI HC A01/MF A03

N95-23714*# Organisatie voor Toegepast Natuurwetenschappelijk Onderzoek, The Hague (Netherlands). Physics and electronics Lab.
POINTER: PORTABLE INTELLIGENT TRAINER FOR EXTERNAL ROBOTICS
Hilbert Kuiper and Patrick J. Rikken *In* JPL, Third International Symposium on Artificial Intelligence, Robotics, and Automation for Space 1994 Oct. 1994 p 209-212 (For primary document see N95-23672 07-63)
Avail: CASI HC A01/MF A03

N95-23715*# National Space Development Agency, Tsukuba (Japan). Space Experiment Dept.
AUTOMATION AND CREW TIME SAVING IN THE SPACE EXPERIMENT
Kohtaro Matsumoto, Tsuyoshi Suzuki, Kouichi Funaya (NEC Corp., Kawasaki, Japan.), Takeya Kawamura (Mitsubishi Heavy Industries Ltd., Wadasaki, Japan.), and Masayoshi Sonobe (Hitachi Ltd., Japan.) *In* JPL, Third International Symposium on Artificial Intelligence, Robotics, and Automation for Space 1994 Oct. 1994 p 215-218 (For primary document see N95-23672 07-63)
Avail: CASI HC A01/MF A03

N95-23720*# MATRA Marconi Space, Toulouse (France).
FORMALIZING PROCEDURES FOR OPERATIONS AUTOMATION, OPERATOR TRAINING AND SPACECRAFT AUTONOMY
Francois Lecouat and Arnaud DeSaintVincent *In* JPL, Third International Symposium on Artificial Intelligence, Robotics, and Automation for Space 1994 Oct. 1994 p 239-242 (For primary document see N95-23672 07-63)
Avail: CASI HC A01/MF A03

N95-23723*# National Aeronautics and Space Administration. Lyndon B. Johnson Space Center, Houston, TX.
DEXTEROUS ORBITAL SERVICING SYSTEM (DOSS)
Charles R. Price, Reginald B. Berka, and John T. Chladek *In* JPL, Third International Symposium on Artificial Intelligence, Robotics, and Automation for Space 1994 Oct. 1994 p 257-260 (For primary document see N95-23672 07-63)
Avail: CASI HC A01/MF A03

N95-23732*# Italian Space Agency, Rome.
PLANETARY STATIONS AND ABYSSAL BENTHIC LABORATORIES: AN OVERVIEW OF PARALLEL APPROACHES FOR LONG-TERM INVESTIGATION IN EXTREME ENVIRONMENTS
S. DiPippo, W. Prendin (Tecnomare S.p.A., Italy.), and F. Gasparoni (Tecnomare S.p.A., Italy.) *In* JPL, Third International Symposium on Artificial Intelligence, Robotics, and Automation for Space 1994 Oct. 1994 p 301-304 (For primary document see N95-23672 07-63)
Avail: CASI HC A01/MF A03

N95-23735*# National Aeronautics and Space Administration. Lyndon B. Johnson Space Center, Houston, TX.
TELEPRESENCE CONTROL OF A DUAL-ARM DEXTEROUS ROBOT
Larry Li, Brian Cox (Lockheed Engineering and Sciences Co., Houston, TX.), Susan Shelton (Lockheed Engineering and Sciences Co., Houston, TX.), and Myron Diftler (Lockheed Engineering and Sciences Co., Houston, TX.) *In* JPL, Third International Symposium on Artificial Intelligence, Robotics, and Automation for Space 1994 Oct. 1994 p 313-316 (For primary document see N95-23672 07-63)
Avail: CASI HC A01/MF A03

55 SPACE BIOLOGY

Includes exobiology; planetary biology; and extraterrestrial life.

No abstracts in this category.

59 MATHEMATICAL AND COMPUTER SCIENCES (GENERAL)

No abstracts in this category.

60 COMPUTER OPERATIONS AND HARDWARE

Includes hardware for computer graphics, firmware, and data processing.

For components see *33 Electronics and Electrical Engineering.*

N95-23153# Technische Univ., Eindhoven (Netherlands). Dept. of Mathematics and Computing Science.
VERIFYING SEQUENTIALLY CONSISTENT MEMORY USING INTERFACE REFINEMENT
R. Gerth Dec. 1993 29 p
(PB95-139002) Avail: CASI HC A03/MF A01

In large multiprocessor architectures the design of efficient shared memory systems is important because the latency imposed on the processors when reading or writing should be kept at a minimum. The challenge that sequentially correct memory poses is not so much the verification of yet another complex protocol but rather the fact that sequential consistency does not comfortably fit the patterns of standard refinement strategies (trace inclusion, failure or ready trace equivalence, testing pre order, bisimulation, etc.). The aim of this paper is to show how sequential consistency can be interpreted as an instance of interface refinement and to verify a sequentially consistent memory protocol--the lazy caching protocol. Section 2 explains and defines sequential consistency. The lazy caching protocol is introduced in Section 3. The heart of the paper is formed by Section 3 and 4. The latter contains the proof of sequential correctness of the protocol. Section 3 gives an overview of the verification methodology. Investigating sequential consistency made us realize that the methodology to prove interface refinement can be considerably simplified. Accordingly, this Section is also of independent interest. In Section 5 some conclusions are drawn. NTIS

N95-23962# Bhabha Atomic Research Centre, Bombay (India).
VIDEO FRAME PROCESSOR
V. M. Joshi, Alok Agashe, and B. R. Bairi 1993 46 p
(DE94-635414; BARC-1993/E/031) Avail: CASI HC A03/MF A01 (US Sales Only)

This report provides a description of the Video Frame Processor (VFP) developed at Bhabha Atomic Research Center. The instrument captures video images available in CCIR format. Two memory planes each with a capacity of 512 x 512 x 8 bit data enable storage of two video image frames. The stored image can be processed on-line, and on-line image subtraction can also be carried out for image comparisons. The VFP is a PC Add-on board and is I/O mapped within the host IBM PC/AT compatible computer. DOE

N95-24177# Rochester Univ., NY. Dept. of Computer Science.
USING SIMPLE PAGE PLACEMENT POLICIES TO REDUCE THE COST OF CACHE FILLS IN COHERENT SHARED-MEMORY SYSTEMS
Michael Marchetti, Leonidas Kontothanassis, Ricardo Bianchini, and Michael L. Scott Sep. 1994 14 p
(Contract N00014-92-J-1801; NSF CDA-88-22724; ARPA Order 8930)
(TR-535) Avail: CASI HC A03/MF A01

The cost of a cache miss depends heavily on the location of the main memory that backs the missing line. For certain applications, this cost is a major factor in overall performance. We report on the utility of OS-based page placement as a mechanism to increase the frequency with which cache fills access local memory in a distributed shared memory multiprocessor. Even with the very simple policy of first-use placement, we find significant improvements over round-robin placement for many applications on both hardware and software-coherent systems. For most of our applications, dynamic placement allows 35 to 75% of cache fills to be performed locally, resulting in performance improvements of 20 to 40%. We have also investigated the performance impact of more sophisticated policies including hardware support for page placement, dynamic page migration, and page replication. We were surprised to find no performance advantage for the more sophisticated policies; in fact in most cases performance of our applications suffered. Author

N95-23301*# Alabama Univ., Huntsville, AL. Dept. of Electrical and Computer Engineering.
TASK SCHEDULING IN DATAFLOW COMPUTER ARCHITECTURES Abstract Only
Constantine Katsinis *In* Hampton Univ., 1994 NASA-HU American Society for Engineering Education (ASEE) Summer Faculty Fellowship Program Dec. 1994 p 83 (For primary document see N95-23276 07-99)
Avail: CASI HC A01/MF A02

N95-24114*# Minnesota Univ., Minneapolis, MN. Graphics and Visualization Lab.
A 500 MEGABYTE/SECOND DISK ARRAY
Thomas M. Ruwart and Matthew T. OKeefe *In* NASA. Goddard Space Flight Center, Fourth NASA Goddard Conference on Mass Storage Systems and Technologies Mar. 1994 p 75-90 Sponsored by Army (For primary document see N95-24108 07-82)
(Contract USRA-C-5555-23)
Avail: CASI HC A03/MF A04

N95-24119*# Primelink Technologies, Inc., Edmonton (Alberta).
PETABYTE MASS MEMORY SYSTEM USING THE NEWELL OPTICEL(TM)
Chester W. Newell *In* NASA. Goddard Space Flight Center, Fourth NASA Goddard Conference on Mass Storage Systems and Tecnologies Mar. 1994 p 123-136 (For primary document see N95-24108 07-82)
Avail: CASI HC A03/MF A04

N95-24125*# Quantum Corp., Shrewbury, MA.
DIGITAL LINEAR TAPE (DLT) TECHNOLOGY AND PRODUCT FAMILY OVERVIEW
Demetrios Lignos *In* NASA. Goddard Space Flight Center, Fourth NASA Goddard Conference on Mass Storage Systems and Technologies Mar. 1994 p 211-231 (For primary document see N95-24108 07-82)
Avail: CASI HC A03/MF A04

N95-24126*# Exabyte Corp., Boulder, CO.
THE MAMMOTH PROJECT
Tim Gerchar *In* NASA. Goddard Space Flight Center, Fourth NASA Goddard Conference on Mass Storage Systems and Technologies Mar. 1994 p 233-236 (For primary document see N95-24108 07-82)
Avail: CASI HC A01/MF A04

61 COMPUTER PROGRAMMING AND SOFTWARE

Includes computer programs, routines, alogorithms, and specific applications, e.g., CAD/CAM.

N95-22479*# National Aeronautics and Space Administration. Langley Research Center, Hampton, VA.
HiRel: HYBRID AUTOMATED RELIABILITY PREDICTOR (HARP) INTEGRATED RELIABILITY TOOL SYSTEM, (VERSION 7.0). VOLUME 3: HARP GRAPHICS ORIENTED (GO) INPUT USER'S GUIDE
Salvatore J. Bavuso, Elizabeth Rothmann (Duke Univ., Durham, NC.), Nitin Mittal (Duke Univ., Durham, NC.), and Sandra Howell Koppen (Lockheed Engineering and Sciences Co., Hampton, VA.) Nov. 1994 , 39 p
(RTOP 505-66-21-02)
(NASA-TP-3452-Vol-3; L-16553C-Vol-3; NAS 1.60:3452-Vol-3) Avail: CASI HC A03/MF A01

The Hybrid Automated Reliability Predictor (HARP) integrated Reliability (HiRel) tool system for reliability/availability prediction offers a toolbox of integrated reliability/availability programs that can be used to customize the user's application in a workstation or nonworkstation environment. HiRel consists of interactive graphical input/output programs and four reliability/availability modeling engines that provide analytical and simulative solutions to a wide host of highly reliable fault-tolerant system architectures and is also applicable to electronic systems in general. The tool system was designed at the outset to be compatible with most computing platforms and operating systems, and some programs have been beta tested within the aerospace community for over 8 years. This document is a user's guide for the HiRel graphical preprocessor Graphics Oriented (GO) program. GO is a graphical user interface for the HARP engine that enables the drawing of reliability/availability models on a monitor. A mouse is used to select fault tree gates or Markov graphical symbols from a menu for drawing. Author

N95-22480*# Michigan Univ., Ann Arbor, MI. Architecture Planning Research Lab.
[THE VIABILITY OF ESTABLISHING COLLABORATIVE, RECONFIGURABLE RESEARCH ENVIRONMENTS FOR THE HUMAN PERFORMANCE RESEARCH LABORATORY AT NASA AMES] Final Technical Report, 1987-1992
Colin Clipson Nov. 1994 20 p

(Grant NAG2-635)
(NASA-CR-197384; NAS 1.26:197384) Avail: CASI HC A03/MF A01

This paper will review and summarize research initiatives conducted between 1987 and 1992 at NASA Ames Research Center by a research team from the University of Michigan Architecture Research Laboratory. These research initiatives, funded by a NASA grant NAG2-635, examined the viability of establishing collaborative, reconfigurable research environments for the Human Performance Research Laboratory at NASA Ames in California. Collaborative Research Environments are envisioned as a way of enhancing the work of NASA research teams, optimizing the use of shared resources, and providing superior environments for housing research activities. The Integrated Simulation Project at NASA, Ames Human Performance Research Laboratory is one of the current realizations of this initiative. Author

N95-22522# Vrije Univ., Amsterdam (Netherlands).
ROLES AND DYNAMIC SUBCLASSES: A MODAL LOGIC APPROACH
R. J. Wieringa, W. deJonge, and P. Spruit Dec. 1993 26 p
(PB95-127320) Avail: CASI HC A03/MF A01

In the paper, the authors argue that object-oriented models must be able to represent three kinds of taxonomic structures: static subclasses, dynamic subclasses and role classes. If CAR is a static subclass of VEHICLE, then a vehicle that is not a car can never migrate to the CAR subclass. If EMPloyee is a dynamic subclass of PERSON, then a PERSON that is not an employee may migrate to EMP. In both cases, an instance of the subclass is identical to an instance of the superclass. Finally, if EMP is modeled as a role class of PERSON every employee differs from every person, but a PERSON instance can acquire one or more EMP instances as roles. The authors outline an approach to formalizing these taxonomic structures in order-sorted dynamic logic with equality. NTIS

N95-22529# Vrije Univ., Amsterdam (Netherlands).
COMPARING DATA SYNCHRONIZATION IN Ada 9X AND ORCA
H. E. Bal Dec. 1993 15 p See also PB93-142594 Sponsored by Nederlandse Organisatie voor Wetenschappelijk Onderzoek, The Hague
(PB95-127999) Avail: CASI HC A03/MF A01

Protected record types are one of three major extensions to Ada 83 proposed by Ada 9X. This language feature is intended for light-weight data synchronization between tasks. The Orca parallel programming language has a very similar construct, the shared data-object, with which we have over five years of experience, both in usage and implementation. This paper compares protected records and shared data-objects, with regard to design, usage, and implementation. NTIS

N95-22548# Sandia National Labs., Albuquerque, NM.
LAYERED ELECTRICAL PRODUCT APPLICATION PROTOCOL (AP)
1 Sep. 1994 228 p
(Contract DE-AC04-94AL-85000)
(DE95-001524; SAND-94-2375C) Avail: CASI HC A11/MF A03

An application protocol is an information systems engineering view of a specific product. The view represents an agreement on the generic activities needed to design and fabricate the product, the agreement on the information needed to support those activities, and the specific constructs of a product data standard for use in transferring some or all of the information required. This applications protocol describes the data for electrical and electronic products in terms of a product description standard called the Initial Graphics Exchange Specification (IGES). More specifically, the Layered Electrical Product IGES Application Protocol (AP) specifies the mechanisms for defining and exchanging computer-models and their associated data for those products which have been designed in two dimensional geometry so as to be produced as a series of layers in IGES format. The AP defines the appropriateness of the data items for describing the geometry of the various parts of a product (shape and location), the connectivity, and the processing and material characteristics. Excluded is the behavioral requirements which the product was intended to satisfy, except as those requirements have been recorded as design rules or product testing requirements. DOE

N95-22570# Argonne National Lab., IL.
A WORST-CASE EXAMPLE USING LINESEARCH METHODS FOR NUMERICAL OPTIMIZATION WITH INEXACT GRADIENT EVALUATIONS
Richard G. Carter (Minnesota Univ., Minneapolis, MN.) 1994 7 p
(Contracts W-31-109-eng-38; DAAL03-89-C-0038)
(DE95-002917; ANL/MCS/PP-75185) Avail: CASI HC A02/MF A01

Two approaches often used to improve the robustness of numerical optimization algorithms are linesearch and trust region methods. Trust region methods have previously been shown to be extremely forgiving of high levels of noise and inaccuracy in gradient evaluations. The authors present a worst-case example demonstrating that linesearch methods can be very fragile with respect to such noise. DOE

N95-22577* National Aeronautics and Space Administration. Pasadena Office, CA.
MAPPINGS BETWEEN CODEWORDS OF TWO DISTINCT (N,K) REED-SOLOMON CODES OVER GF(2(SUP J)) Patent
Marvin Perlman, inventor (to NASA) (Jet Propulsion Lab., California Inst. of Tech., Pasadena, CA.) 27 Dec. 1994 32 p Filed 3 Sep. 1992 Supersedes N93-11664 (31 - 2, p 412)
(Contract NAS7-918)
(NASA-Case-NPO-18771-1-CU; US-Patent-5,377,207;
US-Patent-Appl-SN-942500; US-Patent-Class-371-37.1;
Int-Patent-Class-G06F-11/10; Int-Patent-Class-H03M-13/00) Avail: US Patent and Trademark Office

A process for realizing mappings between code-words of two distinct (N,K) Reed-Solomon (RS) codes over GF(2 sup J) having selected two independent parameters: J, specifying the number of bits per symbol; and E, the symbol error correction capability of the code, wherein said independent parameters J and E yield the following: N = 2(sup J)-1 total number of symbols per codeword; 2E, the number of symbols assigned a role of check symbols; and K = N-2E, the number of code symbols representing information, all within a codeword of an (N,K) RS code over GF(2 sup J), and having selected said parameters for encoding, the implementation of a decoder is governed by: 2(sup J) field elements defined by a degree J primitive polynomial over GF(2) denoted by F(x); a code generator polynomial of degree 2E containing 2E consecutive roots of a primitive element defined by F(x); and, in a Berlekamp RS code, the basis in which the RS information and check symbols are represented. The process includes separate transformation steps for symbol-by-symbol conversion for a first RS code to ultimately a second conventional RS code capable of being corrected by a conventional RS decoder, followed by a reverse sequence of the inverse of the first set of steps to arrive at codewords having connected information symbols, at which time check symbols of the RS code may be discarded.
Official Gazette of the U.S. Patent and Trademark Office

N95-22603*# National Aeronautics and Space Administration. Langley Research Center, Hampton, VA.
HiRel: HYBRID AUTOMATED RELIABILITY PREDICTOR (HARP) INTEGRATED RELIABILITY TOOL SYSTEM, (VERSION 7.0). VOLUME 1: HARP INTRODUCTION AND USER'S GUIDE
Salvatore J. Bavuso, Elizabeth Rothmann (Duke Univ., Durham, NC.), Joanne Bechta Dugan (Duke Univ., Durham, NC.), Kishor S. Trivedi (Duke Univ., Durham, NC.), Nitin Mittal (Duke Univ., Durham, NC.), Mark A. Boyd (Duke Univ., Durham, NC.), Robert M. Geist (Clemson Univ., SC.), and Mark D. Smotherman (Clemson Univ., SC.) Nov. 1994 147 p
(RTOP 505-66-21-02)
(NASA-TP-3452-Vol-1; L-16553A-Vol-1; NAS 1.60:3452-Vol-1) Avail: CASI HC A07/MF A02

The Hybrid Automated Reliability Predictor (HARP) integrated Reliability (HiRel) tool system for reliability/availability prediction offers a toolbox of integrated reliability/availability programs that can be used to customize the user's application in a workstation or nonworkstation environment. HiRel consists of interactive graphical input/output programs and four reliability/availability modeling engines that provide analytical and simulative solutions to a wide host of reliable fault-tolerant system architectures and is also applicable to electronic systems in general. The tool system was designed to be compatible with most computing platforms and operating systems, and some programs have been beta tested, within the aerospace community for over 8 years. Volume 1 provides an introduction to the HARP program. Comprehensive information on HARP mathematical models can be found in the references. Author

N95-22604*# National Aeronautics and Space Administration. Langley Research Center, Hampton, VA.
HiRel: HYBRID AUTOMATED RELIABILITY PREDICTOR (HARP) INTEGRATED RELIABILITY TOOL SYSTEM, (VERSION 7.0). VOLUME 2: HARP TUTORIAL
Elizabeth Rothmann (Duke Univ., Durham, NC.), Joanne Bechta Dugan (Duke Univ., Durham, NC.), Kishor S. Trivedi (Duke Univ., Durham, NC.), Nitin Mittal (Duke Univ., Durham, NC.), and Salvatore J. Bavuso Nov. 1994 132 p
(RTOP 505-66-21-02)
(NASA-TP-3452-Vol-2; L-16553B-Vol-2; NAS 1.60:3452-Vol-2) Avail: CASI HC A07/MF A02

The Hybrid Automated Reliability Predictor (HARP) integrated Reliability (HiRel) tool system for reliability/availability prediction offers a toolbox of integrated reliability/availability programs that can be used to customize the user's application in a workstation or nonworkstation environment. The Hybrid Automated Reliability Predictor (HARP) tutorial provides insight into HARP modeling techniques and the interactive textual prompting input language via a step-by-step explanation and demonstration of HARP's fault occurrence/repair model and the fault/error handling models. Example applications are worked in their entirety and the HARP tabular output data are presented for each. Simple models are presented at first with each succeeding example demonstrating greater modeling power and complexity. This document is not intended to present the theoretical and mathematical basis for HARP. Author

N95-22605*# National Aeronautics and Space Administration. Langley Research Center, Hampton, VA.
HiRel: HYBRID AUTOMATED RELIABILITY PREDICTOR (HARP) INTEGRATED RELIABILITY TOOL SYSTEM, (VERSION 7.0). VOLUME 4: HARP OUTPUT (HARPO) GRAPHICS DISPLAY USER'S GUIDE
Darrell W. Sproles (Computer Sciences Corp., Hampton, VA.) and Salvatore J. Bavuso Nov. 1994 55 p
(RTOP 505-66-21-02)
(NASA-TP-3452-Vol-4; L-16553D-Vol-4; NAS 1.60:3452-Vol-4) Avail: CASI HC A04/MF A01

The Hybrid Automated Reliability Predictor (HARP) integrated Reliability (HiRel) tool system for reliability/availability prediction offers a toolbox of integrated reliability/availability programs that can be used to customize the user's application in a workstation or nonworkstation environment. HiRel consists of interactive graphical input/output programs and four reliability/availability modeling engines that provide analytical and simulative solutions to a wide host of highly reliable fault-tolerant system architectures and is also applicable to electronic systems in general. The tool system was designed at the outset to be compatible with most computing platforms and operating systems and some programs have been beta tested within the aerospace community for over 8 years. This document is a user's guide for the HiRel graphical postprocessor program HARPO (HARP Output). HARPO reads ASCII files generated by HARP. It provides an interactive plotting capability that can be used to display alternate model data for trade-off analyses. File data can also be imported to other commercial software programs. Author

N95-22616# International Centre for Theoretical Physics, Trieste (Italy).
FUZZINESS AND RANDOMNESS IN AN OPTIMIZATION FRAMEWORK
M. K. Luhandjula Mar. 1994 12 p
(DE94-628383; IC-94/45) Avail: CASI HC A03/MF A01 (US Sales Only)

This paper presents a semi-infinite approach for linear programming in the presence of fuzzy random variable coefficients. As a byproduct a way for dealing with optimization problems including both fuzzy and random data is obtained. Numerical examples are provided for the sake of illustration. DOE

N95-22637 National Inst. of Standards and Technology, Gaithersburg, MD. Robot Systems Div.
A CERTAINTY GRID TO OBJECT BOUNDARY ALGORITHM
John Albert Horst, Hui-Min Huang, and Tsung-Ming Tsai Jun. 1994 16 p Limited Reproducibility: More than 20% of this document may be affected by microfiche quality
(PB94-203510; NISTIR-5447) Avail: Issuing Activity (National Technical Information Service (NTIS))

An edge linking algorithm is modified for a mobile robot map representation application. Certainly grid 'images' are transformed to an appropriate set of object boundary curves. The latter are expressed as oriented piecewise linear segments. Image processing techniques, such as edge detection, thinning, curve tracing, and linear approximation are employed with various modifications. The most significant modification is a new method for linear curve approximation that is simple, accurate, and efficient. The method monitors chord and arc length and its excellent performance is demonstrated against similar algorithms. The certainty grid to object boundary algorithm is tested against simulated noisy certainty grid maps. NTIS

N95-22652# Vrije Univ., Amsterdam (Netherlands).
LCM 3.0: A LANGUAGE FOR DESCRIBING CONCEPTUAL MODELS. SYNTAX DEFINITION
R. J. Wieringa and R. B. Feenstra Dec. 1993 80 p See also PB95-127957 Sponsored by Nederlandse Organisatie voor Wetenschappelijk Onderzoek, The Hague
(PB95-128005) Avail: CASI HC A05/MF A01

LCM (Language for Conceptual Modeling) is a specification language with which conceptual models (CM's) can be specified. The authors assume that the CM's specified in LCM are used to represent some part of reality that is to be represented by a database system (DBS). A subset of LCM is intended to be executable. Version 3.0 of the LCM specification language is a revision of version 2 of the language, formerly known as CMSL (Conceptual Model Specification Language). The document intended to serve as a reference for the specifier int he area of syntactic issues of LCM 3.0. Although the text and examples in the document suggest informally a meaning of the specifications, the formal semantics of LCM 3.0 is not given. NTIS

N95-22690# Argonne National Lab., IL. Mathematics and Computer Science Div.
SOFTWARE FOR THE GENERALIZED EIGENPROBLEM ON DISTRIBUTED MEMORY ARCHITECTURES
Mark T. Jones and Paul E. Plassmann 1993 3 p Presented at the Lanczos Centenary Conference, Raleigh, NC, 12-17 Dec. 1993
(Contract W-31-109-eng-38)
(DE95-002999; ANL/MCS/CP-84113; CONF-931260-2) Avail: CASI HC A01/MF A01

The generalized eigenproblem is of significant importance in several fields. Generalized eigenproblems can be very large with matrices of order greater than one million for problems arising from three-dimensional finite element models. To solve such problems we are proposing a flexible software system for parallel distributed memory architectures. This software is based on the Lanczos algorithm with a shift-and-invert transformation. We briefly describe the prototype version of the software, present computational results, and indicate the status of the project. DOE

N95-22718# Westinghouse Hanford Co., Richland, WA.
CDMS-CAD DATA SET MANAGEMENT SYSTEM TEST PLAN
E. L. Gray 1994 21 p
(Contract DE-AC06-87RL-10930)
(DE95-003219; WHC-SD-GN-CSWD-30076) Avail: CASI HC A03/MF A01

This document defines the system test plan for the necessary modifications made to a commercial software product that manages and controls engineering drawings. Modifications include the ability to interface with the final plotting of CAD data sets. DOE

N95-22769 Rutherford Appleton Lab., Oxford (England).
PRISMA GENIE DATA ANALYSIS MANUAL
M. Hagen Aug. 1994 20 p See also PB95-130498 Prepared in cooperation with Keele Univ.
(PB95-130464; RAL-94-086) Avail: Issuing Activity (National Technical Information Service (NTIS))

The GENIE program provides the basic means for analyzing data taken on ISIS instruments. In this manual, various GENIE macros and some FORTRAN programs which are customized for the analysis of PRISMA data are described. These macros/programs are available to a user who has executed the PRISMA GENIE SETUP.COM file and the various two or three letter abbreviations should appear when the user starts GENIE. A

point to remember is that as some of these macros create files of their own during data processing, it is not wise (safe) for the GENIE program using these macros to be simultaneously run by more than one user in the same subdirectory, otherwise conflicts may occur. The macros listed in the document and the FORTRAN programs are described in more detail in the following report. NTIS

N95-22853*# Jet Propulsion Lab., California Inst. of Tech., Pasadena, CA.

OBSERVATION MODEL AND PARAMETER PARTIALS FOR THE JPL VLBI PARAMETER ESTIMATION SOFTWARE MODEST, 19 94

O. J. Sovers and C. S. Jacobs Aug. 1994 121 p Revised

(Contract NAS7-918; RTOP 314-40-31-30-26D)

(NASA-CR-197328; JPL-Publ-83-39-Rev-5; NAS 1.26:197328) Avail: CASI HC A06/MF A02

This report is a revision of the document Observation Model and Parameter Partials for the JPL VLBI Parameter Estimation Software 'MODEST'—1991, dated August 1, 1991. It supersedes that document and its four previous versions (1983, 1985, 1986, and 1987). A number of aspects of the very long baseline interferometry (VLBI) model were improved from 1991 to 1994. Treatment of tidal effects is extended to model the effects of ocean tides on universal time and polar motion (UTPM), including a default model for nearly diurnal and semidiurnal ocean tidal UTPM variations, and partial derivatives for all (solid and ocean) tidal UTPM amplitudes. The time-honored 'K(sub 1) correction' for solid earth tides has been extended to include analogous frequency-dependent response of five tidal components. Partials of ocean loading amplitudes are now supplied. The Zhu-Mathews-Oceans-Anisotropy (ZMOA) 1990-2 and Kinoshita-Souchay models of nutation are now two of the modeling choices to replace the increasingly inadequate 1980 International Astronomical Union (IAU) nutation series. A rudimentary model of antenna thermal expansion is provided. Two more troposphere mapping functions have been added to the repertoire. Finally, corrections among VLBI observations via the model of Treuhaft and Ianyi improve modeling of the dynamic troposphere. A number of minor misprints in Rev. 4 have been corrected. Author

N95-22894# Westinghouse Hanford Co., Richland, WA.

CDMS: CAD DATA SET SYSTEM DESIGN DESCRIPTION

E. L. Gray 25 Oct. 1994 107 p

(Contract DE-AC06-87RL-10930)

(DE95-003218; WHC-SD-GN-SDD-30007-Rev-1) Avail: CASI HC A06/MF A02

This document is intended to formalize the program design of the CAD Data Set Management System (CDMS) and to be the vehicle to communicate the design to the Engineering, Design Services, and Configuration Management organizations and the WHC IRM Analysts/Programmers. The SDD shows how the software system will be structured to satisfy the requirements identified in the WHC-SD-GN-CSRS-30005 CDMS Software Requirement Specification (SRS). It is a description of the software structure, software components, interfaces, and data that make up the CDMS System. The design descriptions contained within this document will describe in detail the software product that will be developed to assist the aforementioned organizations for the express purpose of managing CAD data sets associated with released drawings, replacing the existing locally developed system and laying the foundation for automating the configuration management. DOE

N95-23017*# Virginia Univ. Hospital, Charlottesville, VA. Dept. of Computer Science.

ALGORITHMS FOR PARALLEL AND VECTOR COMPUTATIONS Final Report, 1 Mar. 1990 - 28 Feb. 1995

James M. Ortega Mar. 1995 9 p

(Grant NAG1-1112)

(NASA-CR-197394; UVA/528340/CS95/108; NAS 1.26:197394) Avail: CASI HC A02/MF A01

This is a final report on work performed under NASA grant NAG-1-1112-FOP during the period March, 1990 through February 1995. Four major topics are covered: (1) solution of nonlinear poisson-type equations; (2) parallel reduced system conjugate gradient method; (3) orderings for conjugate gradient preconditioners, and (4) SOR as a preconditioner. Derived from text

N95-23071# Technische Univ., Twente (Netherlands). Dept. of Computer Science.

OVERVIEW OF PH.D. THESES AND MEMORANDA, 1993

May 1994 44 p See also report for 1992, PB94-149598

(PB95-135190; Memo-INF-94-01) Copyright Avail: CASI HC A03/MF A01

This memorandum gives an overview of the PhD theses and Memoranda Informatica (Technical Reports) of 1993 published by members of the Department of Computer Science of the University of Twente. NTIS

N95-23079# California Univ., Berkeley. Lawrence Berkeley Lab, CA.

GHOST IMAGES AND FEASIBILITY OF RECONSTRUCTIONS WITH THE RICHARDSON-LUCY ALGORITHM

J. Llacer and J. Nunez (Barcelona Univ., Spain.) Jul. 1994 15 p Presented at the Annual Meeting of the Society of Photo-Optical Instrumentation Engineers, San Diego, CA, 24-29 Jul. 1994

(Contract DE-AC03-76SF-00098)

(DE95-002351; LBL-35841; CONF-940723-30) Avail: CASI HC A03/MF A01

This paper is the result of a question that was raised at the recent workshop on 'The Restoration of HST Images and Spectra II', that took place at the Space Telescope Science Institute in November 1993, for which there was no forthcoming answer at that time. The question was: What is the null space (ghost images) of the Richardson-Lucy (RL) algorithm?. Another question that came up for which there is a straight-forward answer was: What does the MLE algorithm really do?. In this paper we attempt to answer both questions. This paper will begin with a brief description of the null space of an imaging system, with particular emphasis on the Hubble telescope. The imaging conditions under which there is a possibly damaging null space will be described in terms of linear methods of reconstruction. For the uncorrected Hubble telescope, it is shown that for a PSF computed by TIN on a 512 x 512 dimension, there is no null space. We introduce the concept of a 'nearly null' space, with an unsharp distinction between the 'measurement' and the 'null' components of an image and generate a reduced resolution Hubble Point Spread Function (PSF) that has that nearly null space. We then study the propagation characteristics of null images in the Maximum Likelihood Estimator (MLE), or Richardson-Lucy algorithm, and the nature of its possible effects, but we find in computer simulations that the algorithm is very robust to those effects: if they exist, the effects are local and tend to disappear with increasing iteration numbers. We then demonstrate how a PSF that has small components in frequency domain results in noise magnification, just as one would expect in linear reconstruction. The answer to the second question is given in terms of the residuals of a reconstruction and the concept of feasibility. DOE

N95-23131# Technische Univ., Eindhoven (Netherlands). Dept. of Mathematics and Computing Science.

TAXONOMY OF FINITE AUTOMATA MINIMIZATION ALGORITHMS

B. W. Watson Dec. 1993 35 p See also PB95-139234

(PB95-139226) Avail: CASI HC A03/MF A01

The paper presents a taxonomy of finite automata minimization algorithms. Brzozowski's elegant minimization algorithm differs from all other known minimization algorithms, and is derived separately. All of the remaining algorithms depend upon computing an equivalence relation on states. The authors define the equivalence relation, the partition that it induces, and its complement. Additionally, some useful properties are derived. It is shown that the equivalence relation is the greatest fixed point of an equation, providing a useful characterization of the required computation. The authors derive an upperbound on the number of approximation steps required to compute the fixed point. Algorithms computing the equivalence relation (or the partition, or its complement) are derived systematically in the same framework. NTIS

N95-23150# Technische Univ., Eindhoven (Netherlands). Dept. of Mathematics and Computing Science.

PERFORMANCE OF SINGLE-KEYWORD AND MULTIPLE-KEYWORD PATTERN MATCHING ALGORITHMS

B. W. Watson 21 Apr. 1994 58 p See also PB93-225225

(PB95-138954) Avail: CASI HC A04/MF A01

The paper presents a toolkit of pattern matching algorithms, performance data on the algorithms, and recommendations for the selection of an

algorithm (given a particular application). The pattern matching problem is: given a finite non-empty set of keywords and an input string, find all occurrences of any of the keywords in the input string. The pattern matching toolkit contains implementation of the Knuth-Morris-Pratt, Boyer-Moore, Aho-Corasick, and Commentax-Walter algorithms. The performance of all of the algorithms (running on a variety of workstation hardware) was measured on two types of input: English text and genetic sequences. The Knuth-Morris-Pratt and Aho-Corasick algorithms performed linearly and consistently (on widely varying keyword sets), as their theoretical running time predicts. The Commentz-Walter algorithm (and its variants) displayed more interesting behavior, greatly out-performing even the best Aho-Corasick variant on a large portion of the input data. The recommendations section of the paper details the conditions under which a particular algorithm should be chosen. NTIS

N95-23152# Technische Univ., Eindhoven (Netherlands). Dept. of Mathematics and Computing Science.
TEMPORAL OPERATORS VIEWED AS PREDICATE TRANSFORMERS
A. Bijlsma Nov. 1993 20 p
(PB95-138996) Avail: CASI HC A03/MF A01

In this paper we present a calculus of temporal operators that is intended as an alternative to temporal logic in program verification. Temporal logic is a form of modal logic, designed for the description of time-dependent phenomena. Several different kinds of temporal logic have been proposed, but in the present paper only the linear time version is treated. In section 2 we define the concept of a shift operator, and in section 3 we show how a shift operator can be used to construct a predicate-transformer model for the axioms of temporal logic. In section 4 we prove that, in fact, every such model can be obtained from a shift operator, which establishes the equivalence of both approaches. Finally, in section 5, examples demonstrate that reasoning with shift operators often leads to proofs that are considerably shorter than those of temporal logic. NTIS

N95-23180*# University of Southern California, Marina del Rey, CA. Dept. of Contracts and Grants.
Distributed VIRtual System (DIVIRS) PROJECT Semiannual Progress Report No. 13, 1 May - 30 Nov. 1994
Herbert Schorr and Clifford B. Neuman Mar. 1995 15 p
(Contract NCC2-539)
(NASA-CR-197855; NAS 1.26:197855) Avail: CASI HC A03/MF A01

As outlined in our continuation proposal 92-ISI-50R (revised) on NASA cooperative agreement NCC2-539, we are (1) developing software, including a system manager and a job manager, that will manage available resources and that will enable programmers to develop and execute parallel applications in terms of a virtual configuration of processors, hiding the mapping to physical nodes; (2) developing communications routines that support the abstractions implemented in item one; (3) continuing the development of file and information systems based on the Virtual System Model; and (4) incorporating appropriate security measures to allow the mechanisms developed in items 1 through 3 to be used on an open network. The goal throughout our work is to provide a uniform model that can be applied to both parallel and distributed systems. We believe that multiprocessor systems should exist in the context of distributed systems, allowing them to be more easily shared by those that need them. Our work provides the mechanisms through which nodes on multiprocessors are allocated to jobs running within the distributed system and the mechanisms through which files needed by those jobs can be located and accessed. Author

N95-23232# Technische Univ., Twente (Netherlands). Faculty of Applied Mathematics.
CHARACTERIZATION OF NON-NEGATIVE GREEDY MATRICES
U. Faigle and W. Kern Nov. 1993 14 p See also N83-18401
(PB95-139366) Avail: CASI HC A03/MF A01

Given an ordering of the variables according to non-increasing coefficients of the objective function c(sup T)x, the non-negative matrix A is said to be greedy if, under arbitrary non-negative constraint vectors b and h, the greedy algorithm maximizes C(sup T)x subject to Ax less than or = b, 0 less than or = x less than or = h. Extending a result of Hoffman, Kolen and Sakarovaitch for (0,1)-matrices, we characterize greedy matrices in terms of forbidden submatrices. NTIS

N95-23238# Technische Univ., Twente (Netherlands). Dept. of Applied Mathematics.
SOME RECENT RESULTS IN THE ANALYSIS OF GREEDY ALGORITHMS FOR ASSIGNMENT PROBLEMS
U. Faigle Sep. 1993 28 p
(PB95-140620; MEMO-1160) Avail: CASI HC A03/MF A01

We survey some recent developments in the analysis of greedy algorithms for assignment problems. We focus on the linear programming model for matroids and linear assignment problems with Monge property, on general linear programs, probabilistic analysis for linear assignment and makespan minimization, and on-line algorithms for linear and non-linear assignment problems. NTIS

N95-23337# Sandia National Labs., Albuquerque, NM.
APPLICATION PROTOCOL, INITIAL GRAPHICS EXCHANGE SPECIFICATION (IGES), LAYERED ELECTRICAL PRODUCT
L. J. OConnell, ed. Dec. 1994 261 p
(Contract DE-AC04-94AL-85000)
(DE95-004266; SAND-94-2375) Avail: CASI HC A12/MF A03

An application protocol is an information systems engineering view of a specific product. The view represents an agreement on the generic activities needed to design and fabricate the product, the agreement on the information needed to support those activities, and the specific constructs of a product data standard for use in transferring some or all of the information required. This application protocol describes the data for electrical and electronic products in terms of a product description standard called the Initial Graphics Exchange Specification (IGES). More specifically, the Layered Electrical Product IGES Application Protocol (AP) specifies the mechanisms for defining and exchanging computer-models and their associated data for those products which have been designed in two dimensional geometry so as to be produced as a series of layers in IGES format The AP defines the appropriateness of the data items for describing the geometry of the various parts of a product (shape and location), the connectivity, and the processing and material characteristics. Excluded is the behavioral requirements which the product was intended to satisfy, except as those requirements have been recorded as design rules or product testing requirements. DOE

N95-23346# Wisconsin Univ., Madison, WI.
VERIFICATION AND VALIDATION OF DECISION SUPPORT SOFTWARE: EXPERT CHOICE(TRADEMARK) AND PCM(TRADEMARK)
Q. H. Nguyen and J. D. Martin Nov. 1994 63 p
(Contract DE-AC06-87RL-10930)
(DE95-004469; WHC-SD-GN-ER-30033) Avail: CASI HC A04/MF A01

This report documents the verification and validation of two decision support programs: EXPERT CHOICE(trademark) and PCM(trademark). Both programs use the Analytic Hierarchy Process (AHP) -- or pairwise comparison technique -- developed by Dr. Thomas L. Saaty. In order to provide an independent method for validating the two programs, the pairwise comparison algorithm was developed for a standard mathematical program. A standard data set -- selecting a car to purchase -- was used with each of the three programs for validation. The results show that both commercial programs performed correctly. DOE

N95-23388*# Texas A&M Univ., College Station, TX. Dept. of Mechanical Enagineering.
LONG RANGE TARGETING FOR SPACE BASED RENDEZVOUS Final Report
Louis J. Everett and R. C. Redfield 20 Mar. 1995 236 p
(Grant NAG9-566)
(NASA-CR-197890; NAS 1.26:197890) Avail: CASI HC A11/MF A03

The work performed under this grant supported the Dexterous Flight Experiment one STS-62 The project required developing hardware and software for automating a TRAC sensor on orbit. The hardware developed by for the flight has been documented through standard NASA channels since it has to pass safety, environmental, and other issues. The software has not been documented previously, therefore, this report provides a software manual for the TRAC code developed for the grant. Author

N95-23467# Vrije Univ., Amsterdam (Netherlands).
RELATING MULTIFUNCTIONS AND PREDICATE TRANSFORMERS THROUGH CLOSURE OPERATORS

M. Bonsangue and J. N. Kok (Utrecht State Univ., Netherlands.) Jan. 1994 24 p
(PB95-135646) Avail: CASI HC A03/MF A01

Relations between predicate transformers and multifunctions in a topological setting based on closure operators are studied. Topological definitions of safety and liveness predicates are given and using these predicates predicate transformers are defined. State transformers are multifunctions with values in the collection of fixed points of a closure operator. Several isomorphisms between predicate transformers and multifunctions are defined. By choosing different closure operators the authors obtain multifunctions based on the usual power set construction, on the Hoare, Smyth and Plotkin power domains, and based on the compact and closed metric power constructions. Moreover, they are all related by isomorphisms to the predicate transformers. NTIS

N95-23553 Gesellschaft fuer Mathematik und Datenverarbeitung, Saint Augustin (Germany).
PROCEEDINGS OF THE WORKSHOP ON DEDUCTIVE DATABASES AND LOGIC PROGRAMMING
U. Geske and D. Seipel Jun. 1994 172 p Conference held in Santa Margherita Ligure, Italy, 17 Jun. 1994 Limited Reproducibility: More than 20% of this document may be affected by microfiche quality
(PB95-139382; GMD-231) Copyright Avail: Issuing Activity (National Technical Information Service (NTIS))

The following topics are discussed: (1) a simple model for active rules and their behavior in deductive databases; (2) expressive power of non-deterministic operators for logic-based languages; (3) representing objects as modules in deductive databases; (4) static analysis of transactional intensional databases; (5) determining correct view update translations via query containment; (6) on expressing stratified datalog; (7) constraint stratification in deductive databases; (8) dynamic argument reduction for in-memory data queries; (9) one-phase magic-sets transformation; (10) a deductive database solution to the preferential vote counting problem; and (11) constraint-based reasoning in geographic databases: the case of symbolic arrays. NTIS

N95-23567# Los Alamos National Lab., NM.
TAYLOR SERIES EXPANSION AND MODIFIED EXTENDED PRONY ANALYSIS FOR LOCALIZATION
J. C. Mosher and P. S. Lewis 1994 5 p Presented at the 28th Annual Asilomar Conference on Signals, Systems, and Computers, Pacific Grove, CA, 31 Oct. - 2 Nov. 1994
(Contract W-7405-eng-36)
(DE95-003671; LA-UR-94-3978; CONF-9410156-3) Avail: CASI HC A01/MF A01

In the multiple source localization problem, many inverse routines use a rooting of a polynomial to determine the source locations. The authors present a rooting algorithm for locating an unknown number of three-dimensional, near-field, static sources from measurements at an arbitrarily spaced three-dimensional array. Since the sources are near-field and static, the spatial covariance matrix is always rank one, and spatial smoothing approaches are inappropriate due to the spatial diversity. The authors approach the solution through spherical harmonics, essentially replacing the point source function with its Taylor series expansion. They then perform a modified extended Prony analysis of the expansion coefficients to determine the number and location of the sources. The full inverse method is typically ill-conditioned, but a portion of the algorithm is suitable for synthesis analysis. They present a simulation for simplifying point charges limited to a spherical region, using an array of voltage potential measurements made outside the region. Future efforts of this work will focus on adapting the analysis to the electroencephalography and magnetoencephalography. DOE

N95-23603# Civil Aeromedical Inst., Oklahoma City, OK.
DEVELOPMENT OF QUALIFICATION GUIDELINES FOR PERSONAL COMPUTER-BASED AVIATION TRAINING DEVICES Final Report
Kevin W. Williams and Robert E. Blanchard Feb. 1995 28 p
(DOT/FAA/AM-95/6) Avail: CASI HC A03/MF A01

Recent advances in the capabilities of personal computers have resulted in an increase in the number of flight simulation programs made available as Personal Computer-Based Aviation Training Devices (PCATD's). The potential benefits of PCATD's have been recognized by researchers and software/hardware developers alike. The purpose of this report is twofold: (1) present a conceptual approach based upon human learning principles and available flight training data for use in the development and evaluation of PCATD's; and (2) provide a detailed technical plan for an initial effort to develop and test guidelines for assessing the use of PCATD's in a training curriculum of a flight school conducted in accordance with the regulations stated in FAR Part 141. Author

N95-23606 Technische Univ., Eindhoven (Netherlands). Dept. of Mathematics and Computing Science.
TAXONOMY OF FINITE AUTOMATA CONSTRUCTION ALGORITHMS
B. W. Watson Dec. 1993 98 p See also PB95-139226 Limited Reproducibility: More than 20% of this document may be affected by microfiche quality
(PB95-139234) Avail: CASI HC A05

The paper presents a taxonomy of finite automata construction algorithms. Each algorithm is classified into one of two families: those based upon the structure of regular expressions, and those based upon the automata-theoretic work of Myhill and Nerode. Many of the algorithms appearing in the literature are based upon the structure of regular expressions. In this paper, the authors make this term precise by defining regular expressions as a Sigma-term algebra, and automata constructions as various Sigma-algebras of automata. Each construction algorithm is then presented as the unique natural homomorphism from the Sigma-term algebra of regular expressions to the appropriate Sigma-algebra of automata. The concept of duality is introduced and used to derive more practical construction algorithms. In addition to classifying the algorithms, the authors identify (and abstract from) the coding tricks and implementation details present in many of the published algorithms. The paper also presents an introduction to finite automata, Sigma-algebras, and their properties. NTIS

N95-23608 Technische Univ., Twente (Netherlands). Faculty of Applied Mathematics.
SUBMODULAR LINEAR PROGRAMS ON FORESTS Memorandum Report
U. Faigle and W. Kern Sep. 1993 18 p Limited Reproducibility: More than 20% of this document may be affected by microfiche quality
(PB95-139820; MEMO-1163) Avail: Issuing Activity (National Technical Information Service (NTIS))

A general linear programming model for an order-theoretic analysis of both Edmond's greedy algorithm for matroids and Hoffman's greedy algorithm for transportation problems with Monge costs is introduced. This approach includes the model of Queyranne, Spieksma and Tardella as a special case. We solve the problem by optimal greedy algorithms for rooted forests as underlying structures. Other solvable cases are also discussed. NTIS

N95-23610*# Research Inst. for Advanced Computer Science, Moffett Field, CA.
UNSTRUCTURED GRIDS ON SIMD TORUS MACHINES
Petter E. Bjorstad (Bergen Univ., Norway.) and Robert Schreiber Mar. 1994 10 p Presented at the 1994 Scalable High Performance Computer Conference, Knoxville, TN, May 1994 Submitted for publication
(Contract NAS2-13721)
(NASA-CR-197954; NAS 1.26:197954; RIACS-TR-94-05) Avail: CASI HC A02/MF A01

Unstructured grids lead to unstructured communication on distributed memory parallel computers, a problem that has been considered difficult. Here, we consider adaptive, offline communication routing for a SIMD processor grid. Our approach is empirical. We use large data sets drawn from supercomputing applications instead of an analytic model of communication load. The chief contribution of this paper is an experimental demonstration of the effectiveness of certain routing heuristics. Our routing algorithm is adaptive, nonminimal, and is generally designed to exploit locality. We have a parallel implementation of the router, and we report on its performance. Author

N95-23613*# Institute for Computer Applications in Science and Engineering, Hampton, VA.
DISCRETE-TIME MARKOVIAN STOCHASTIC PETRI NETS Final Report
Gianfranco Ciardo (College of William and Mary, Williamsburg, VA.) NASA Feb. 1995 21 p Submitted for publication

(Contract NAS1-19480; RTOP 505-90-52-01)
(NASA-CR-195039; NAS 1.26:195039; ICASE-95-9) Avail: CASI HC A03/MF A01

We revisit and extend the original definition of discrete-time stochastic Petri nets, by allowing the firing times to have a 'defective discrete phase distribution'. We show that this formalism still corresponds to an underlying discrete-time Markov chain. The structure of the state for this process describes both the marking of the Petri net and the phase of the firing time for each transition, resulting in a large state space. We then modify the well-known power method to perform a transient analysis even when the state space is infinite, subject to the condition that only a finite number of states can be reached in a finite amount of time. Since the memory requirements might still be excessive, we suggest a bounding technique based on truncation. Author

N95-23928# Rochester Univ., NY. Dept. of Computer Science.
ALGORITHMS FOR CATEGORIZING MULTIPROCESSOR COMMUNICATION UNDER INVALIDATE AND UPDATE-BASED COHERENCE PROTOCOLS
R. Bianchini and L. I. Kontothanassis Feb. 1995 17 p Revised Sponsored by Brazilian CAPES and NUTES/UFRJ fellowships
(Contract NSF CDA-88-22724; N00014-92-J-1801; ARPA Order 8930)
(TR-533-Rev) Avail: CASI HC A03/MF A01

In this paper we present simulation algorithms that characterize the main sources of communication generated by parallel applications under both invalidate and update-based cache coherence protocols. The algorithms provide insight into the reference and sharing patterns of parallel programs and to the amount of useless traffic entailed by each coherence protocol. Under an invalidate-based protocol, our algorithms classify the data traffic caused by the different types of cache misses. Under an update-based protocol, our algorithms not only categorize the data traffic, but also classify update transactions with respect to the sharing patterns that caused them. Although our algorithms deal with numerous hardware features, our categorization is widely applicable and can be easily simplified for use in less detailed simulators. Author

N95-23935# Rochester Univ., NY. Dept. of Computer Science.
ON HELPING BY PARITY-LIKE LANGUAGES
Mitsunori Ogihara Dec. 1994 7 p
(Grants NSF INT-91-16781; JSPS-ENG-207)
(TR-553) Avail: CASI HC A02/MF A01

A deterministic oracle Turing machine M is robust if for every oracle X, M(sup X) and M(sup 0) accept the same language. A language H is said to P-help a robust oracle machine M if there exists a polynomial p such that for every x, M(sup H) on input x runs for at most p(absolute value of x) steps. Such H is called a P-helper for M. For a language H, let P(sub help)(H) denote the class of languages recognized by robust machines for which H behaves as a P-helper and, for a language class C, let P(sub help)(C) denote the union of (H belonging to C)P(sub help)(H). Schoening showed that a language is accepted by a robust machine with a P-helper if and only if it is accepted by a robust machine with a P-helper in NP if and only if it is in NP intersection coNP; that is, NP intersection coNP = P(sub help)(2 sup Sigma*) = P(sub help)(NP). Given this characterization, it is natural to ask, for a language L belonging to NP intersection coNP, what is the lower bound on the complexity of P-helpers for robust machines accepting L. A partial answer is given in terms of a proof of the following theorem: for every prime power k, MODZ(sub k)P intersection co-MODZ(sub k)P = P(sub help)(MOD(sub k)P). Derived from text

N95-23963# Comision Nacional de Energia Atomica, Buenos Aires (Argentina).
PCLOOK: AN INTERACTIVE CODE FOR SPECTRAL ANALYSIS
A. O. Macchiavelli and D. Tomasi 1993 17 p Presented at the 4th Academical Meeting on Technology, Resistencia, Argentina, 22-24 Sep. 1993
(DE94-635415; INIS-AR-073; CONF-9309407) Avail: CASI HC A03/MF A01 (US Sales Only)

The present work describes an interactive program for the analysis of spectra developed to run in a PC platform. PCLOOK has a graphic interface that allows the user to get access to different functions using the mouse or directly typing commands. In this way one can switch to a suitable required environment to manage the histograms, reassembling in this way a spectrum calculator. The PCLOOK program was mainly developed to be used in nuclear physics applications, but it is also possible to modify it with little effort, making it adaptable to other applications. It was written in Microsoft's BASIC 7.1 installed in a 33MHz 486 Everex PC. For a proper operation an ordinary VGA display and mouse are needed. The memory requirements depend on the size and number of the user defined spectra; for instance, for twenty 2048 channels spectra the available memory space must be 320 KBytes. DOE

N95-24006 Westinghouse Hanford Co., Richland, WA.
COMPUTER SOFTWARE DESIGN DESCRIPTION FOR THE TREATED EFFLUENT DISPOSAL FACILITY (TEDF), PROJECT L-045H, OPERATOR TRAINING STATION (OTS)
R. L. Carter, Jr. Nov. 1994 278 p Limited Reproducibility: More than 20% of this document may be affected by microfiche quality
(Contract DE-AC06-87RL-10930)
(DE95-003065; WHC-SD-L045H-CSDD-001) Avail: CASI HC A13

The Treated Effluent Disposal Facility (TEDF) Operator Training Station (OTS) is a computer-based training tool designed to aid plant operations and engineering staff in familiarizing themselves with the TEDF Central Control System (CCS). DOE

N95-24020# Sandia National Labs., Albuquerque, NM.
A MODAL TEST DESIGN STRATEGY FOR MODEL CORRELATION
T. G. Carne and C. R. Dohrmann 1994 7 p Presented at the International Modal Analysis Conference, Nashville, TN, 13-16 Feb. 1995
(Contract DE-AC04-94AL-85000)
(DE95-003631; SAND-94-2702C; CONF-950240-4) Avail: CASI HC A02/MF A01

When a modal test is to be performed for purposes of correlation with a finite element model, one needs to design the test so that the resulting measurements will provide the data needed for the correlation. There are numerous issues to consider in the design of a modal test; two important ones are the number and location of response sensors, and the number, location, and orientation of input excitation. From a model correlation perspective, one would like to select the response locations to allow a definitive, one-to-one correspondence between the measured modes and the predicted modes. Further, the excitation must be designed to excite all the modes of interest at a sufficiently high level so that the modal estimation algorithms can accurately extract the modal parameters. In this paper these two issues are examined in the context of model correlation with methodologies presented for obtaining an experiment design. DOE

N95-24033# Rochester Univ., NY. Dept. of Computer Science.
AN EFFICIENT ALGORITHM FOR CONCURRENT PRIORITY QUEUE HEAPS
Galen C. Hunt, Maged M. Michael, Srinivasan Parthasarathy, and Michael L. Scott Dec. 1994 12 p
(Contract NSF CDA-88-22724; NSF CCR-93-19445; N00014-92-J-1801; ARPA Order 8930)
(TR-560) Avail: CASI HC A03/MF A01

We present a new algorithm for concurrent access to array-based priority queue heaps. Deletions proceed top-down as they do in a previous algorithm due to Rao and Kumar, but insertions proceed bottom-up, and consecutive insertions use a bit-reversal technique to scatter accesses across the fringe of the tree, to reduce contention. Because insertions do not have to traverse the entire height of the tree (as they do in previous work), as many as O(M) operations can proceed in parallel, rather than O(log M) on a heap of size M. Experimental results on a Silicon Graphics Challenge multiprocessor demonstrate good overall performance for the new algorithm on small heaps, and significant performance improvements over known alternatives on large heaps with mixed insertion/deletion workloads. Author

N95-24052*# National Aeronautics and Space Administration. Ames Research Center, Moffett Field, CA.
TRANSFERRING ECOSYSTEM SIMULATION CODES TO SUPERCOMPUTERS
J. W. Skiles and C. H. Schulbach (Johnson Controls World Services, Cape Canaveral, FL.) Feb. 1995 40 p
(RTOP 233-01-03-05)

(NASA-TM-4662; A-94142; NAS 1.15:4662) Avail: CASI HC A03/MF A01

Many ecosystem simulation computer codes have been developed in the last twenty-five years. This development took place initially on main-frame computers, then mini-computers, and more recently, on micro-computers and workstations. Supercomputing platforms (both parallel and distributed systems) have been largely unused, however, because of the perceived difficulty in accessing and using the machines. Also, significant differences in the system architectures of sequential, scalar computers and parallel and/or vector supercomputers must be considered. We have transferred a grassland simulation model (developed on a VAX) to a Cray Y-MP/C90. We describe porting the model to the Cray and the changes we made to exploit the parallelism in the application and improve code execution. The Cray executed the model 30 times faster than the VAX and 10 times faster than a Unix workstation. We achieved an additional speedup of 30 percent by using the compiler's vectoring and 'in-line' capabilities. The code runs at only about 5 percent of the Cray's peak speed because it ineffectively uses the vector and parallel processing capabilities of the Cray. We expect that by restructuring the code, it could execute an additional six to ten times faster. Author

N95-24056# Rochester Univ., NY. Dept. of Computer Science.
PROPERTIES OF PROBABILISTIC PUSHDOWN AUTOMATA
Ioan I. Macarie and Mitsunori Ogihara Dec. 1994 18 p
(TR-554) Avail: CASI HC A03/MF A01

Properties of probabilistic as well as 'probabilistic plus nondeterministic' pushdown automata and auxiliary pushdown automata are studied. These models are analogous to their counterparts with nondeterministic and alternating states. Complete characterizations in terms of well-known complexity classes are given for the classes of languages recognized by polynomial time-bounded, logarithmic space-bounded auxiliary pushdown automata with probabilistic states and with 'probabilistic plus nondeterministic' states. Also, complexity lower bounds are given for the classes of languages recognized by these automata with unlimited running time. It follows that, by fixing an appropriate mode of computation, the difference between classes of languages such as P and PSPACE, NL and SAC, PL and Diff (greater than) (#SAC) is characterized as the difference between the number of stack symbols; that is, whether the stack alphabet contains one versus two distinct symbols. Author

N95-24058# Rochester Univ., NY. Dept. of Computer Science.
A COMPUTATIONAL THEORY OF GROUNDING IN NATURAL LANGUAGE CONVERSATION Ph.D. Thesis
David Rood Traum Dec. 1994 103 p
(Contracts N00014-92-J-1512; N00014-90-J-1811; NSF IRI-90-03841)
(TR-545) Avail: CASI HC A06/MF A02

The process of adding to the common ground between conversational participants (called grounding) has previously been either oversimplified or studied in an off-line manner. This dissertation presents a computational theory, in which a protocol is presented which can be used to determine, for any given state of the conversation, whether the material has been grounded or what it would take to ground the material. This prototype is related to the mental states of participating agents, showing the motivations for performing particular grounding acts and what their effects will be. We extend speech act theory to account for levels of action both above and below the sentence level, including the level of grounding acts described above. Traditional illocutionary acts are now seen to be multi-agent acts which must be grounded to have their usual effects. A conversational agent model is provided, showing how grounding fits in naturally with the other functions that an agency must perform in engaging in conversation. These ideas are implemented within the TRAINS conversation system. Also presented is a situation-theoretic model of plan execution relations, giving definitions of what is meant for an action to begin, continue, complete, or repair the execution of a plan. This framework is then used to provide precise definitions of the grounding acts in terms of agents executing a general communication plan in which one agent must present the content and another acknowledge it. Author

N95-24059# Rochester Univ., NY. Dept. of Computer Science.
LOGSPACE REDUCIBILITY AND SELF-REDUCIBILITY: MODELS AND EQUIVALENCES
Lane A. Hemaspaandra and Zhigen Jiang Nov. 1994 17 p Sponsored by Chinese Academy of Sciences
(Grants NSF CCR-89-57604; NSF INT-91-16781; JSPS-ENG-207; NSF CCR-93-22513)
(TR-544) Avail: CASI HC A03/MF A01

We study the relative computational power of logspace reduction models. In particular, we study the relationships between one-way and two-way oracle tapes, resetting of the oracle head, and blanking of the oracle tape. We show that oracle models letting information persist between queries can be quite powerful, even if the information is not readable by the querying machine. We show that logspace f(n)-Turing reductions are stronger than polynominal-time f(n)-Turing reductions when f(n) = omega (log n), and that this is optimal if P = L. We also study the structure of self-reducible degrees. Author

N95-24092# Rochester Univ., NY. Dept. of Computer Science.
SEMI-MEMBERSHIP ALGORITHMS: SOME RECENT ADVANCES
Derek Denny-Brown, Yenjo Han, Lane A. Hemaspaandra, and L. Torenvliet Jul. 1994 16 p Submitted for publication Sponsored by HC andM
(Grants NSF CCR-89-57604; NSF INT-91-16781; JSPS-ENGR-207)
(TR-526) Avail: CASI HC A03/MF A01

A semi-membership algorithm for a set A is, informally, a program that when given any two strings determines which is logically more likely to be in A. A flurry of interest in this topic in the late seventies and early eighties was followed by a relatively quiescent half-decade. However, in the 1990's there has been a resurgence of interest in this topic. We survey recent work on the theory of semi-memberhsip algorithms. Author

N95-24176# Intellicorp, Mountain View, CA.
OPUS: A NEW GENERATION KNOWLEDGE ENGINEERING ENVIRONMENT Final Report
Richard Fikes, Robert Nado, Robert Filman, Philip McBride, Paul Morris, Anne Paulson, Richard Treitel, and Martin Yonke Jul. 1987 87 p
(Contract F30602-85-C-0065)
Avail: CASI HC A05/MF A01

This document is the final report of the results of IntelliCorp's activities during phase 1 of its participation in the knowledge systems technology base of the DARPA-sponsored Strategic Computing Program (SCP). Knowledge system developers now have available to them well engineered software environments (e.g., IntelliCorp's Knowledge Engineering Environment (KEE)) that provide integrated collections of 'power tools' to support and accelerate their work. These environments provide tools for knowledge acquisition, knowledge representation, reasoning, and user interface construction. A fundamental goal of the SCP knowledge systems technology base is to produce a new generation of such tool environments that make knowledge system development easier and faster, reduce the expertise in artificial intelligence techniques needed to develop such systems, and broaden the class of problems to which the technology can be effectively applied. IntelliCorp's goals in the SCP are to: (1) provide to the program's contractors a common tool base for development of both knowledge system component technology and applications; and (2) evolve that tool base into a new generation knowledge system development environment by developing new knowledge system technology (e.g., inheritance and default reasoning algorithms), and integrating existing knowledge system technology (e.g., truth maintenance and frame-based representation) so that multiple tools can be coherently applied to a given application problem. Our methodology is to encourage use of the KEE system family of products by SCP contractors as a common tool base and to evolve the new generation system from that base. Author

N95-22985*# Saint Louis Univ., Cahokia, IL.
AN ALGORITHM FOR THE BASIS OF THE FINITE FOURIER TRANSFORM
Thalanayar S. Santhanam *In* NASA. Goddard Space Flight Center, Second International Workshop on Harmonic Oscillators Jan. 1995 p 239-248 (For primary document see N95-22957 07-74)
Avail: CASI HC A02/MF A04

N95-23415*# Mississippi State Univ., Mississippi State, MS.
IGES TRANSFORMER AND NURBS IN GRID GENERATION
Tzu-Yi Yu and Bharat K. Soni *In* NASA. Marshall Space Flight Center, Eleventh Workshop for Computational Fluid Dynamic Applications in Rocket

Propulsion Jul. 1993 p 1021-1053 (For primary document see N95-23412 07-34)
Avail: CASI HC A03/MF A10

N95-23416*# Rockwell International Corp., Canoga Park, CA. Rocketdyne Div.
CRITERIA FOR EVALUATION OF GRID GENERATION SYSTEMS
Edward P. Ascoli, Steven L. Barson, Michele E. DeCroix, and Wayne W. Hsu *In* NASA. Marshall Space Flight Center, Eleventh Workshop for Computational Fluid Dynamic Applications in Rocket Propulsion Jul. 1993 p 1055-1090 (For primary document see N95-23412 07-34)
Avail: CASI HC A03/MF A10

N95-23418*# National Aeronautics and Space Administration. Marshall Space Flight Center, Huntsville, AL.
A GENERIC EFFICIENT ADAPTIVE GRID SCHEME FOR ROCKET PROPULSION MODELING
J. D. Mo and Alan S. Chow *In its* Eleventh Workshop for Computational Fluid Dynamic Applications in Rocket Propulsion Jul. 1993 p 1129-1148 (For primary document see N95-23412 07-34)
Avail: CASI HC A03/MF A10

N95-23419*# Mississippi State Univ., Mississippi State, MS. Center for Computational Field Simulation.
TIGER: A USER-FRIENDLY INTERACTIVE GRID GENERATION SYSTEM FOR COMPLICATED TURBOMACHINERY AND AXIS-SYMMETRIC CONFIGURATIONS
Ming H. Shih and Bharat K. Soni *In* NASA. Marshall Space Flight Center, Eleventh Workshop for Computational Fluid Dynamic Applications in Rocket Propulsion Jul. 1993 p 1149-1161 Sponsored by NASA. Lewis Research Center (For primary document see N95-23412 07-34)
Avail: CASI HC A03/MF A10

N95-23680*# RECOM Technologies, Inc., Moffett Field, CA. AI Research Branch.
AMPHION: SPECIFICATION-BASED PROGRAMMING FOR SCIENTIFIC SUBROUTINE LIBRARIES
Michael Lowry, Andrew Philpot, Thomas Pressburger, Ian Underwood, Richard Waldinger (SRI International Corp., Menlo Park, CA.), and Mark Stickel (SRI International Corp., Menlo Park, CA.) *In* JPL, Third International Symposium on Artificial Intelligence, Robotics, and Automation for Space 1994 Oct. 1994 p 41-44 (For primary document see N95-23672 07-63)
Avail: CASI HC A01/MF A03

N95-23688*# Jet Propulsion Lab., California Inst. of Tech., Pasadena, CA.
PERFORMANCE RESULTS OF COOPERATING EXPERT SYSTEMS IN A DISTRIBUTED REAL-TIME MONITORING SYSTEM
U. M. Schwuttke, J. R. Veregge, and A. G. Quan *In its* Third International Symposium on Artificial Intelligence, Robotics, and Automation for Space 1994 Oct. 1994 p 79-83 (For primary document see N95-23672 07-63)
Avail: CASI HC A01/MF A03

N95-23746*# National Aeronautics and Space Administration. Marshall Space Flight Center, Huntsville, AL.
GRAPHICAL TIMELINE EDITING
Patrick E. Meyer and John P. Jaap *In* JPL, Third International Symposium on Artificial Intelligence, Robotics, and Automation for Space 1994 Oct. 1994 p 368 (For primary document see N95-23672 07-63)
Avail: CASI HC A01/MF A03

N95-23748*# RECOM Technologies, Inc., Moffett Field, CA.
A DATA ANALYSIS ASSISTANT
Amy L. Lansky *In* JPL, Third International Symposium on Artificial Intelligence, Robotics, and Automation for Space 1994 Oct. 1994 p 373-376 (For primary document see N95-23672 07-63)
Avail: CASI HC A01/MF A03

N95-23749*# Symbiotics, Inc., Cambridge, MA.
COORDINATING COMPLEX DECISION SUPPORT ACTIVITIES ACROSS DISTRIBUTED APPLICATIONS
Richard M. Adler *In* JPL, Third International Symposium on Artificial Intelligence, Robotics, and Automation for Space 1994 Oct. 1994 p 379-381 (For primary document see N95-23672 07-63)
(Contracts NAS10-11606; NAS10-11882; NAS5-31920; NAS8-399905; DAAB10-87-C-0053)
Avail: CASI HC A01/MF A03

N95-23762*# Boeing Co., Huntsville, AL.
SCHEDULING WITH GENETIC ALGORITHMS
Theron R. Fennel, A. J. Underbrink, Jr., and George P. W. Williams, Jr. *In* JPL, Third International Symposium on Artificial Intelligence, Robotics, and Automation for Space 1994 Oct. 1994 p 435-438 (For primary document see N95-23672 07-63)
Avail: CASI HC A01/MF A03

N95-24116*# Mega Drive Systems, Inc., Beverly Hills, CA.
OPTIMIZING RAID PERFORMANCE WITH CACHE
Alex Bouzari *In* NASA. Goddard Space Flight Center, Fourth NASA Goddard Conference on Mass Storage Systems and Technologies Mar. 1994 p 99-103 (For primary document see N95-24108 07-82)
Avail: CASI HC A01/MF A04

N95-24117*# National Library of Medicine, Bethesda, MD. National Center for Biomedical Communications.
DOCUMENT IMAGE ARCHIVE TRANSFER FROM DOS TO UNIX
Susan E. Hauser, Michael J. Gill, and George R. Thoma *In* NASA. Goddard Space Flight Center, Fourth NASA Goddard Conference on Mass Storage Systems and Technologies Mar. 1994 p 105-113 (For primary document see N95-24108 07-82)
Avail: CASI HC A02/MF A04

N95-24120*# CONVEX Computer Corp., Richardson, TX.
INTEGRATING UniTree WITH THE DATA MIGRATION API
David G. Schrodel *In* NASA. Goddard Space Flight Center, Fourth NASA Goddard Conference on Mass Storage Systems and Technologies Mar. 1994 p 137-155 (For primary document see N95-24108 07-82)
Avail: CASI HC A03/MF A04

N95-24123*# Maximum Strategy, Inc., Milpitas, CA.
CLIENT/SERVER DATA SERVING FOR HIGH PERFORMANCE COMPUTING
Chris Wood *In* NASA. Goddard Space Flight Center, Fourth NASA Goddard Conference on Mass Storage Systems and Technologies Mar. 1994 p 185-201 (For primary document see N95-24108 07-82)
Avail: CASI HC A03/MF A04

62 COMPUTER SYSTEMS

Includes computer networks and special application computer systems.

N95-22478*# Jet Propulsion Lab., California Inst. of Tech., Pasadena, CA.
PARALLEL DIGITAL MODEM USING MULTIRATE DIGITAL FILTER BANKS
Ramin Sadr, P. P. Vaidyanathan, Dan Raphaeli, and Sami Hinedi 15 Aug. 1994 116 p
(Contract NAS7-918; RTOP 315-91-40-20)
(NASA-CR-197331; JPL-Publ-94-20; NAS 1.26:197331) Avail: CASI HC A06/MF A02

A new class of architectures for an all-digital modem is presented in this report. This architecture, referred to as the parallel receiver (PRX), is based on employing multirate digital filter banks (DFB's) to demodulate, track, and detect the received symbol stream. The resulting architecture is derived, and specifications are outlined for designing the DFB for the PRX. The key feature of this approach is a lower processing rate then either the Nyquist rate or the symbol rate, without any degradation in the symbol error rate. Due to the freedom in choosing the processing rate, the designer

is able to arbitrarily select and use digital components, independent of the speed of the integrated circuit technology. PRX architecture is particularly suited for high data rate applications, and due to the modular structure of the parallel signal path, expansion to even higher data rates is accommodated with each. Applications of the PRX would include gigabit satellite channels, multiple spacecraft, optical links, interactive cable-TV, telemedicine, code division multiple access (CDMA) communications, and others. Author

N95-22509# Army Research Lab., Watertown, MA. Materials Directorate.

EVALUATION OF A MULTIPLE INSTRUCTION/MULTIPLE DATA (MIMD) PARALLEL COMPUTER FOR CFD APPLICATIONS Final Report, Apr. 1991 - Nov. 1992

Stephen J. Schraml Oct. 1994 30 p

(AD-A285796; ARL-TR-589) Avail: CASI HC A03/MF A01

In an attempt to evaluate the merits of massively parallel processing computers for the numerical simulation of blast phenomena, the U.S. Army Research Laboratory (ARL) has adapted one of its blast modeling tools to several unique parallel architectures. This report describes the adaptation of the BRL-QID code, a quasi-one-dimensional, finite difference Euler solver, to the Intel iPSC/860 parallel supercomputer. The code was reconfigured for the iPSC/860 using FORTRAN 77 and the Intel iPSC/860 message-passing library. The performance of the code was measured on the iPSC/860 for a variety of problem sizes and processor configurations. The performance was found to be highly dependent on the size of the problem. This problem size dependency was most noticeable when fewer processors were employed. Results of scalability tests indicate that the code performance scales in a roughly linear fashion about extrapolated lines of ideal performance. DTIC

N95-22564* National Aeronautics and Space Administration. Pasadena Office, CA.

NON-BLOCKING CROSSBAR PERMUTATION ENGINE WITH CONSTANT ROUTING LATENCY Patent

Steve P. Monacos, inventor (to NASA) (Jet Propulsion Lab., California Inst. of Tech., Pasadena, CA.) 27 Dec. 1994 30 p Filed 18 Aug. 1993

Supersedes N94-17328 (32 - 3, p 1161)

(Contract NAS7-918)

(NASA-Case-NPO-18864-1-CU; US-Patent-5,377,182; US-Patent-Appl-SN-111318; US-Patent-Class-370-16; US-Patent-Class-370-58.3; US-Patent-Class-370-60; US-Patent-Class-370-94.1; US-Patent-Class-340-827; US-Patent-Class-340-825.8; US-Patent-Class-379-221) Avail: US Patent and Trademark Office

The invention is embodied in an N x N crossbar for routing packets from a set of N input ports to a set of N output ports, each packet having a header identifying one of the output ports as its destination, including a plurality of individual links which carry individual packets. Each link has a link input end and a link output end, a plurality of switches. Each of the switches has at least top and bottom switch inputs connected to a corresponding pair of the link output ends and top and bottom switch outputs connected to a corresponding pair of link input ends, whereby each switch is connected to four different links. Each of the switches has an exchange state which routes packets from the top and bottom switch inputs to the bottom and top switch outputs, respectively, and a bypass state which routes packets from the top and bottom switch inputs to the top and bottom switch outputs, respectively. A plurality of individual controller devices governing respective switches for sensing from a header of a packet at each switch input for the identity of the destination output port of the packet and selecting one of the exchange and bypass states in accordance with the identity of the destination output port and with the location of the corresponding switch relative to the destination output port. Official Gazette of the U.S. Patent and Trademark Office

N95-22668*# National Aeronautics and Space Administration. Lewis Research Center, Cleveland, OH.

DESCRIPTION OF A MIL-STD-1553B DATA BUS Ada DRIVER FOR THE LeRC EPS TESTBED

Michael A. Mackin Feb. 1995 39 p

(RTOP 478-29-10)

(NASA-TM-106866; E-9478; NAS 1.15:106866) Avail: CASI HC A03/MF A01

This document describes the software designed to provide communication between control computers in the NASA Lewis Research Center Electrical Power System Testbed using MIL-STD-1553B. The software drivers are coded in the Ada programming language and were developed on a MSDOS-based computer workstation. The Electrical Power System (EPS) Testbed is a reduced-scale prototype space station electrical power system. The power system manages and distributes electrical power from the sources (batteries or photovoltaic arrays) to the end-user loads. The electrical system primary operates at 120 volts DC, and the secondary system operates at 28 volts DC. The devices which direct the flow of electrical power are controlled by a network of six control computers. Data and control messages are passed between the computers using the MIL-STD-1553B network. One of the computers, the Power Management Controller (PMC), controls the primary power distribution and another, the Load Management Controller (LMC), controls the secondary power distribution. Each of these computers communicates with two other computers which act as subsidiary controllers. These subsidiary controllers are, in turn, connected to the devices which directly control the flow of electrical power. Author

N95-22679# Los Alamos National Lab., NM.

ACCEPTING THE T3D

D. O. Rich, S. C. Pope, and J. G. DeLapp 1994 9 p Presented at the Cray User's Group Conference, Tours, France, 10-14 Oct. 1994

(Contract W-7405-eng-36)

(DE95-000924, LA-UR-94-3374; CONF-9410212-1) Avail: CASI HC A02/MF A01

In April, a 128 PE Cray T3D was installed at Los Alamos National Laboratory's Advanced Computing Laboratory as part of the DOE's High-Performance Parallel Processor Program (H4P). In conjunction with CRI, the authors implemented a 30 day acceptance test. The test was constructed in part to help them understand the strengths and weaknesses of the T3D. In this paper, they briefly describe the H4P and its goals. They discuss the design and implementation of the T3D acceptance test and detail issues that arose during the test. They conclude with a set of system requirements that must be addressed as the T3D system evolves. DOE

N95-22680# Los Alamos National Lab., NM.

AN AUTOMATED COMPUTER MISUSE DETECTION SYSTEM FOR UNICOS

K. A. Jackson, M. C. Neuman, D. D. Simmonds, C. A. Stallings, J. L. Thompson, and G. G. Christoph 27 Sep. 1994 17 p Presented at the Cray User's Group Conference, Tours, France, 10-14 Oct. 1994

(Contract W-7405-eng-36)

(DE95-000929; LA-UR-94-3385; CONF-9410212-2) Avail: CASI HC A03/MF A01

An effective method for detecting computer misuse is the automatic monitoring and analysis of on-line user activity. This activity is reflected in the system audit record, in the system vulnerability posture, and in other evidence found through active testing of the system. During the last several years we have implemented an automatic misuse detection system at Los Alamos. This is the Network Anomaly Detection and Intrusion Reporter (NADIR). We are currently expanding NADIR to include processing of the Cray UNICOS operating system. This new component is called the UNICOS Realtime NADIR, or UNICORN. UNICORN summarizes user activity and system configuration in statistical profiles. It compares these profiles to expert rules that define security policy and improper or suspicious behavior. It reports suspicious behavior to security auditors and provides tools to aid in follow-up investigations. The first phase of UNICORN development is nearing completion, and will be operational in late 1994. DOE

N95-22830*# Computational Logic, Inc., Austin, TX.

SPECIFICATION AND VERIFICATION OF GATE-LEVEL VHDL MODELS OF SYNCHRONOUS AND ASYNCHRONOUS CIRCUITS Final Report

David M. Russinoff Jan. 1995 138 p

(Contract NAS1-18878; RTOP 506-64-10-13)

(NASA-CR-191608; NAS 1.26:191608) Avail: CASI HC A07/MF A02

We present a mathematical definition of hardware description language (HDL) that admits a semantics-preserving translation to a subset of VHDL.

Our HDL includes the basic VHDL propagation delay mechanisms and gate-level circuit descriptions. We also develop formal procedures for deriving and verifying concise behavioral specifications of combinational and sequential devices. The HDL and the specification procedures have been formally encoded in the computational logic of Boyer and Moore, which provides a LISP implementation as well as a facility for mechanical proof-checking. As an application, we design, specify, and verify a circuit that achieves asynchronous communication by means of the biphase mark protocol. Author

N95-22858# Lawrence Livermore National Lab., Livermore, CA.
REALIZING PARALLEL REDUCTION OPERATION IN SISAL 1.2
S. M. Denton, J. T. Feo, and P. J. Miller Aug. 1994 12 p Presented at the Working Conference on Parallel Architectures and Compilation Techniques, Montreal, Quebec, 24-26 Aug. 1994 Revised
(Contract W-7405-eng-48)
(DE94-017524; UCRL-JC-116015-Rev-1; CONF-9408147-1-Rev-1) Avail: CASI HC A03/MF A01

Often the tasks of a parallel job are to compute sets of values that are reduced to a single value or gathered to build an aggregate structure. Since reductions may introduce dependencies, most languages separate computation and reduction. For example, Fortran 90 and HPF provide a rich set of predefined reduction functions but only for extant arrays. Sisal 1.2 is unique in that it supports seven reduction operations as a natural consequence of loop expressions. These reductions are limited and cannot express the variety of reduction operations found in parallel programs. In this paper, the authors present compilation techniques that recognize pairs of computation-reduction expressions in Sisal 1.2 and fuse them into single parallel loops. This optimization overlaps computation and reduction, reduces runtime overhead, and reduces storage requirements. They describe an implementation and they present performance numbers that demonstrate the utility of their techniques. DOE

N95-22859# Lawrence Livermore National Lab., Livermore, CA.
REALIZING PARALLEL REDUCTION OPERATIONS IN SISAL 1.2
S. M. Denton, J. T. Feo, and P. J. Miller Feb. 1994 11 p Presented at the Working Conference on Parallel Architectures and Compilation Techniques, Montreal, Quebec, 24-26 Aug. 1994
(Contract W-7405-eng-48)
(DE94-017525; UCRL-JC-116015; CONF-9408147-1) Avail: CASI HC A03/MF A01

A parallel job consists of sets of concurrent and sequential tasks. Often the tasks compute sets of values that are reduced to a single value or gathered to build an aggregate structure. Since reductions may introduce dependencies, most languages separate computation and reduction. For example, Fortran 90 and HPF provide a rich set of predefined reduction functions, but only for extant arrays. Sisal 1.2 is unique in that reduction is a natural consequence of loop expressions. Unfortunately, the language supports only seven reduction operations. In this paper, the authors present compilation techniques that recognize pairs of for expressions in Sisal 1.2 as computation-reduction expressions. The techniques work without any language or intermediate form extensions; however, they recognize only certain forms. They describe how they implement pairs of computation-reduction expressions as single parallel loops, and they present performance numbers that demonstrate the utility of their techniques. DOE

N95-23129# Technische Univ., Eindhoven (Netherlands). Dept. of Mathematics and Computing Science.
HIERARCHICAL MEMBERSHIP PROTOCOL FOR SYNCHRONOUS DISTRIBUTED SYSTEMS
P. vanderStok, M. Claessen, and D. Alstein 22 Nov. 1993 53 p
(PB95-138947) Avail: CASI HC A04/MF A01

A membership service for a synchronous distributed computer system is described. The system is assumed to be composed of groups in which a relatively frequent message exchange occurs. A hierarchy of connected groups constitutes a connected network. The membership service protocol reflects this hierarchical structure. Time-bounds are specified in which additions (removals) of processors to (from) the system are known to all participating processors. NTIS

N95-23166# Groningen Rijksuniv. (Netherlands).
DUALITY: A SIMPLE FORMALISM FOR THE ANALYSIS OF UNITY Scientific Report
R. M. Dijkstra 1994 50 p
(PB95-135703; CS-R9404) Avail: CASI HC A03/MF A01

The authors present the programming language DUALITY and demonstrate its utility for the analysis of UNITY. DUALITY is a simple language supporting demonic and angelic choice and two forms of tail-recursion. Starting from the predicate transformer approach to the semantics of parallel programs, they show that, given a UNITY program, they can write a program in DUALITY that has the same formal characteristics. This they use to reformulate and reprove some important theorems from the UNITY theory, viz. the 'PSP-rule' and the 'completion rule'. Finally the authors show that the conjunctive predicate transformers for reasoning about concurrent computation also fit nicely within this framework. NTIS

N95-23243# Lawrence Livermore National Lab., Livermore, CA.
TWO PORTABLE PARALLEL TRIDIAGONAL SOLVERS
P. G. Eltgroth 15 Jul. 1994 9 p Presented at the 4th CHAMMP Workshop for the Numerical Solution of the PDE's in Spherical Geometry, Chicago, IL, 24-26 Aug. 1994
(Contract W-7405-eng-48)
(DE94-019044; UCRL-JC-118017; CONF-940875-1) Avail: CASI HC A02/MF A01

Many scientific computer codes involve linear systems of equations which are coupled only between nearest neighbors in a single dimension. The most common situation can be formulated as a tridiagonal matrix relating source terms and unknowns. This system of equations is commonly solved using simple forward and back substitution. The usual algorithm is spectacularly ill suited for parallel processing with distributed data, since information must be sequentially communicated across all domains. Two new tridiagonal algorithms have been implemented in FORTRAN 77. The two algorithms differ only in the form of the unknown which is to be found. The first and simplest algorithm solves for a scalar quantity evaluated at each point along the single dimension being considered. The second algorithm solves for a vector quantity evaluated at each point. The solution method is related to other recently published approaches, such as that of Bondeli. An alternative parallel tridiagonal solver, used as part of an Alternating Direction Implicit (ADI) scheme, has recently been developed at LLNL by Lambert. For a discussion of useful parallel tridiagonal solvers, see the work of Mattor, et al. Previous work appears to be concerned only with scalar unknowns. This paper presents a new technique which treats both scalar and vector unknowns. There is no restriction upon the sizes of the subdomains. Even though the usual tridiagonal formulation may not be theoretically optimal when used iteratively, it is used in so many computer codes that it appears reasonable to write a direct substitute for it. The new tridiagonal code can be used on parallel machines with a minimum of disruption to pre-existing programming. As tested on various parallel computers, the parallel code shows efficiency greater than 50% (that is, more than half of the available computer operations are used to advance the calculation) when each processor is given at least 100 unknowns for which to solve. DOE

N95-23486# California Univ., Berkeley. Lawrence Berkeley Lab, CA.
PARALLEL COMPUTATION OF AUTOMATIC DIFFERENTIATION APPLIED TO MAGNETIC FIELD CALCULATIONS
R. L. Hinkins Sep. 1994 26 p
(Contract DE-AC03-76SF-00098)
(DE95-004689; LBL-36024) Avail: CASI HC A03/MF A01

The author presents a parallelization of an accelerator physics application to simulate magnetic field in three dimensions. The problem involves the evaluation of high order derivatives with respect to two variables of a multivariate function. Automatic differentiation software had been used with some success, but the computation time was prohibitive. The implementation runs on several platforms, including a network of workstations using PVM, a MasPar using MPFortran, and a CM-5 using CMFortran. A careful examination of the code led to several optimizations that improved its serial performance by a factor of 8.7. The parallelization produced further improvements, especially on the MasPar with a speedup factor of 620. As a result a problem that took six days on a SPARC 10/41 now runs in

minutes on the MasPar, making it feasible for physicists at Lawrence Berkeley Laboratory to simulate larger magnets. DOE

N95-23538# Helsinki Univ. of Technology, Espoo (Finland). Digital Systems Lab.

MODELLING AND ANALYSIS OF A HIGH SPEED DATA BUS WITH PREDICATE/TRANSITION NETS Research Report

T. Pyssysalo Mar. 1994 79 p

(PB95-140695; ISBN-951-22-2028-8) Avail: CASI HC A05/MF A01

In this work predicate/transition nets (Pr/T-nets) are used in the modeling and analysis of the medium access control algorithm of a parallel high speed data bus, Frame Synchronized Ring (FSR-bus). Two Pr/T-net models of the bus are presented. One models the basic operation of the control algorithm. The other is an extended model, in which nodes can send longer frames and the reception of a frame can fail. The analysis of the nets is based on the reachability analysis, which is made by a highly advanced Pr/T-net reachability analysis tool, PROD. The state space of the reachability graph grows very fast with respect to the number of nodes in the ring. The state space explosion is tried to be reduced with the stubborn set and symmetry methods. The stubborn set method reduces the number of reachable states almost 70%. The symmetry method is not so efficient. These results show how effective these methods can be. NTIS

N95-23594*# Research Inst. for Advanced Computer Science, Moffett Field, CA.

TOWARDS THE TERAFLOP CFD

Robert Schreiber and Horst D. Simon (Computer Sciences Corp., Moffett Field, CA.) 1 May 1992 35 p Submitted for publication Sponsored in cooperation with NAS Systems Division

(Contract NCC2-387)

(NASA-CR-197947; NAS 1.26:197947; RIACS-TR-92-12) Avail: CASI HC A03/MF A01

We are surveying current projects in the area of parallel supercomputers. The machines considered here will become commercially available in the 1990 - 1992 time frame. All are suitable for exploring the critical issues in applying parallel processors to large scale scientific computations, in particular CFD calculations. This chapter presents an overview of the surveyed machines, and a detailed analysis of the various architectural and technology approaches taken. Particular emphasis is placed on the feasibility of a Teraflops capability following the paths proposed by various developers. Author

N95-23599# Illinois Univ., Urbana-Champaign, IL. Center for Superconducting Research and Development.

WHAMS3D PROJECT: PARALLEL IMPLEMENTATIONS OF WHAMS3D ON TWO SHARED-MEMORY MULTIPROCESSORS Progress Report No. 3

H. Chen, H. Gao, and G. Lai Jul. 1992 23 p Sponsored by Illinois Dept. of Commerce and Community Affairs and State of Illinois Technology Challenge

(WHAMS3D Proj.)

(CSRD-1248) Avail: CASI HC A03/MF A01

The third phase of the WHAMS3D project has been completed. The main tasks during this phase were the parallelization of the code on both the Cray T0MP4/464 and the Alliant FX/80 multiprocessor, the collection of performance results from the parallelized code using the four data sets provided by Argonne National Laboratory, and the comparison of the performance data. Author

N95-23930# Rochester Univ., NY. Dept. of Computer Science.

SCALABILITY OF ATOMIC PRIMITIVES ON DISTRIBUTED SHARED MEMORY MULTIPROCESSORS

Maged M. Michael and Michael L. Scott Jul. 1994 20 p

(Contract NSF CDA-88-22724; NSF CCR-93-19445; N00014-92-J-1801; ARPA Order 8930)

(TR-528) Avail: CASI HC A03/MF A01

Many hardware primitives have been proposed for synchronization and atomic memory update on shared-memory multiprocessors. In this paper, we focus on general-purpose primitives that have proven popular on small-scale bus-based machines, but have yet to become widely available on large-scale, distributed-memory machines. Specifically, we propose several alternative implementations of fetch and Phi, compare and swap, and load linked/store conditional. We then analyze the performance of these implementations for various data sharing patterns, in both real and synthetic applications. Our results indicate that good overall performance can be obtained by implementing compare and swap in a multiprocessor's cache controllers, and by providing an additional instruction to load an exclusive copy of a line. Author

N95-23936# Rochester Univ., NY. Dept. of Computer Science.

LOOP SCHEDULING FOR HETEROGENEITY

Michal J. Cierniak, Wei Li, and Mohammed Javeed Zaki Oct. 1994 26 p

(Contract F19628-94-C-0057)

(TR-540) Avail: CASI HC A03/MF A01

The problem of scheduling parallel loops at compile-time for a heterogeneous network of machines is studied. We consider heterogeneity in three aspects of parallel programming: program, processor and network. A heterogeneous program has parallel loops with different amounts of work in each iteration; heterogeneous processors have different speeds; and a heterogeneous network has different costs of communication between processors. We propose a simple yet comprehensive model for use in compiling for a network of processors, and develop compiler algorithms for generating optimal and sub-optimal schedules of loops for load balancing, communication optimizations and network contention. Experiments show that significant improvement of performance is achieved using our techniques. Author

N95-24023*# Research Inst. for Advanced Computer Science, Moffett Field, CA.

USING HIGH-PERFORMANCE NETWORKS TO ENABLE COMPUTATIONAL AEROSCIENCES APPLICATIONS

Marjory J. Johnson Jan. 1992 18 p Submitted for publication Sponsored in part by DARPA

(Contract NCC2-387)

(NASA-CR-197951; NAS 1.26:197951; RIACS-TR-92-01) Avail: CASI HC A03/MF A01

One component of the U.S. Federal High Performance Computing and Communications Program (HPCCP) is the establishment of a gigabit network to provide a communications infrastructure for researchers across the nation. This gigabit network will provide new services and capabilities, in addition to increased bandwidth, to enable future applications. An understanding of these applications is necessary to guide the development of the gigabit network and other high-performance networks of the future. In this paper we focus on computational aerosciences applications run remotely using the Numerical Aerodynamic Simulation (NAS) facility located at NASA Ames Research Center. We characterize these applications in terms of network-related parameters and relate user experiences that reveal limitations imposed by the current wide-area networking infrastructure. Then we investigate how the development of a nationwide gigabit network would enable users of the NAS facility to work in new, more productive ways. Author

N95-24037# Rochester Univ., NY. Dept. of Computer Science.

ELIMINATING USELESS MESSAGES IN WRITE-UPDATE PROTOCOLS ON SCALABLE MULTIPROCESSORS

Ricardo Bianchini, Thomas J. LeBlanc, and Jack E. Veenstra Nov. 1994 32 p Sponsored by Brazilian CAPES and NUTES/UFRJ fellowships

(Contract N00014-92-J-1801; NSF CDA-88-22724; ARPA Order 8930)

(TR-539) Avail: CASI HC A03/MF A01

Cache coherence protocols for shared-memory multiprocessors are invalidations or updates to maintain coherence across processors. Although invalidation protocols usually produce higher miss rates, update protocols typically perform worse. Detailed simulations of these two classes of protocol show that the excessive network traffic caused by update protocols significantly degrades performance, even with infinite bandwidth. Motivated by this observation, we categorize the coherence traffic in update-based protocols and show that, for most applications, more than 90% of all updates generated by the protocol are unnecessary. We identify application characteristics that generate useless update traffic, and compare the isolated and combined effects of several software and hardware techniques for eliminating useless updates. These techniques include dynamic and static hybrid protocols, false sharing elimination strategies, and coalescing write

buffers. Our simulations show that software caching (where coherence is managed under programmer or compiler control) and the dynamic hybrid protocol reduce useless updates the most, but coalescing write buffers produce fewer, albeit larger, coherence messages. As a result, coalescing write buffers usually produce the best running time, except when the block size is large or the bandwidth is limited. Finally, based on the observation that the techniques we consider are unable to eliminate a large number of useless updates, we suggest directions for further reducing the useless traffic in update-based protocols. Author

N95-24061# Rochester Univ., NY. Dept. of Computer Science.
UNIFYING DATA AND CONTROL TRANSFORMATIONS FOR DISTRIBUTED SHARED-MEMORY MACHINES
Michal Cierniak and Wei Li Nov. 1994 25 p
(Contract F19628-94-C-0057; NSF CCR-94-09120)
(TR-542) Avail: CASI HC A03/MF A01

We present a unified approach to locality optimization that employs both data and control transformations. Data transformations include changing the array layout in memory. Control transformations involve changing the execution order of programs. We have developed new techniques for compiler optimizations for distributed shared-memory machines, although the same techniques can be used for sequential machines with a memory hierarchy. Our compiler optimizations are based on an algebraic representation of data mappings and a new data locality model. We present a pure data transformation algorithm and an algorithm unifying data and control transformations. While there has been much work on control transformations, the opportunities for data transformations have been largely neglected. In fact, data transformations have the advantage of being applicable to programs that cannot be optimized with control transformations. The unified algorithm, which performs data and control transformations simultaneously, offers improvement over optimizations obtained by applying data and control transformations separately. The experimental results using a set of applications on a parallel machine show that the new optimizations improve performance significantly. These results are further analyzed using locality metrics with instrumentation and simulation. Author

N95-24074# Los Alamos National Lab., NM.
A NETWORK-BASED DISTRIBUTED, MEDIA-RICH COMPUTING AND INFORMATION ENVIRONMENT
R. L. Phillips 1995 13 p Presented at the Supercomputing '94 Meeting; Digital Media and Electronic Publishing Conference, Washington, DC; Leeds, England, 14-18 Nov. 1994; 6-8 Dec. 1994
(Contract W-7405-eng-36)
(DE95-003696; LA-UR-94-3835; CONF-941118-9; CONF-941243-1) Avail: CASI HC A03/MF A01

Sunrise is a Los Alamos National Laboratory (LANL) project started in October 1993. It is intended to be a prototype National Information Infrastructure development project. A main focus of Sunrise is to tie together enabling technologies (networking, object-oriented distributed computing, graphical interfaces, security, multi-media technologies, and data-mining technologies) with several specific applications. A diverse set of application areas was chosen to ensure that the solutions developed in the project are as generic as possible. Some of the application areas are materials modeling, medical records and image analysis, transportation simulations, and K-12 education. This paper provides a description of Sunrise and a view of the architecture and objectives of this evolving project. The primary objectives of Sunrise are three-fold: (1) To develop common information-enabling tools for advanced scientific research and its applications to industry; (2) To enhance the capabilities of important research programs at the Laboratory; and (3) To define a new way of collaboration between computer science and industrially-relevant research. DOE

N95-24172# Argonne National Lab., IL.
SCALABLE, EXTENSIBLE, AND PORTABLE NUMERICAL LIBRARIES
W. Gropp and B. Smith 1995 8 p Presented at the Institute of Electrical and Electronic Engineers (IEEE) Meeting on Scalable Parallel Libraries, Starkville, MS, 6-8 Oct. 1993
(Contract W-31-109-eng-38)
(DE95-004643; ANL/MCS/CP-85098; CONF-9310220-7) Avail: CASI HC A02/MF A01

Designing a scalable and portable numerical library requires consideration of many factors, including choice of parallel communication technology, data structures, and user interfaces. The PETSc library (Portable Extensible Tools for Scientific computing) makes use of modern software technology to provide a flexible and portable implementation. This talk will discuss the use of a meta-communication layer (allowing the user to choose different transport layers such as MPI, p4, pvm, or vendor-specific libraries) for portability, an aggressive data-structure-neutral implementation that minimizes dependence on particular data structures (even vectors), permitting the library to adapt to the user rather than the other way around, and the separation of implementation language from user-interface language. Examples are presented. DOE

N95-24183# Rochester Univ., NY. Dept. of Computer Science.
SCHEDULER-CONSCIOUS SYNCHRONIZATION
Leonidas I. Kontothanassis, Robert W. Wisniewski, and Michael L. Scott Dec. 1994 49 p Sponsored by Univ. of Maryland, New York State, NIH, IBM Corp., and Center's Corporate Research Institute
(Contracts N00014-92-J-1801; MDA972-92-J-1012; NSF CCR-93-19445; NSF CDA-88-22724; ARPA Order 8930)
(TR-550) Avail: CASI HC A03/MF A01

Efficient synchronization is important for achieving good performance in parallel programs, especially on large-scale multiprocessors. Most synchronization algorithms have been designed to run on a dedicated machine, with one application process per processor, and can suffer serious performance degradation in the presence of multiprogramming. Problems arise when running processes block or, worse, busy-wait for action on the part of a process that the scheduler has chosen not to run. In this paper we describe and evaluate a set of scheduler-conscious synchronization algorithms that perform well in the presence of multiprogramming while maintaining good performance on dedicated machines. We consider both large and small machines, with a particular focus on scalability, and examine mutual-exclusion locks, reader-writer locks, and barriers. The algorithms we study fall into two classes: those that heuristically determine appropriate behavior and those that use scheduler information to guide their behavior. We show that while in some cases either method is sufficient, in general sharing information across the kernel-user interface both eases the design of synchronization algorithms and improves their performance. Author

N95-24184# Rochester Univ., NY. Dept. of Computer Science.
LAZY RELEASE CONSISTENCY FOR HARDWARE-COHERENT MULTIPROCESSORS
Leonidas I. Kontothanassis, Michael L. Scott, and Ricardo Bianchini Dec. 1994 18 p Sponsored by Brazilian CAPES and NUTES/UFRJ fellowships
(Contract NSF CDA-88-22724; N00014-92-J-1801; ARPA Order 8930)
(TR-547) Avail: CASI HC A03/MF A01

Release consistency is a widely accepted memory model for distributed shared memory systems. It provides significant opportunities for a coherence protocol to improve performance by delaying and buffering coherence operations. Different protocol implementations exploit these opportunities to different extents. Eager release consistency represents the state of the art for hardware-coherent multiprocessors, while lazy release consistency has been shown to provide better performance for software distributed shared memory (DSM). Several of the optimizations performed by lazy protocols have the potential to improve the performance of hardware-coherent multiprocessors, but their complexity has precluded a hardware implementation. With the advent of programmable protocol processors it may become possible to use them after all. We present and evaluate a lazy release-consistent protocol suitable for machines with dedicated protocol processors. This protocol admits multiple concurrent writers, sends write notices concurrently with omputation, and delays invalidations until acquire operations. We also consider a lazier protocol that delays sending write notices until release operations. Our results indicate that the first protocol outperforms eager release consistency by as much as 20% across a variety of applications. The lazier protocol, on the other hand, is unable to recoup its high synchronization overhead. This represents a qualitative shift from the DSM world, where lazier protocols always yield performance improvements. We also study protocol performance under a variety of architectural settings and show that the performance gap between lazy and eager implementations of release consistency will increase on future machines. Based on our results, we conclude that machines with flexible hardware support for coherence should use protocols based on

lazy release consistency, but in a less 'aggressively lazy' form than is appropriate for DSM. Author

63 CYBERNETICS

Includes feedback and control theory, artificial intelligence, robotics and expert systems.

For related information see also *54 Man/System Technology and Life Support.*

N95-22512# University of Southern California, Marina del Rey, CA. Information Sciences Inst.
TOWARDS METHOD-INDEPENDENT KNOWLEDGE ACQUISITION
Yolanda Gil and Cecile Paris Jun. 1994 21 p
(Contract DABT63-91-C-0025)
(AD-A285823; ISI/RR-94-377) Avail: CASI HC A03/MF A01

Rapid prototyping and tool reusability have pushed knowledge acquisition research to investigate method-specific knowledge acquisition tools appropriate for predetermined problem-solving methods. We believe that method-dependent knowledge acquisition is not the only approach. The aim of our research is to develop powerful yet versatile machine learning mechanisms that can be incorporated into general-purpose but practical knowledge acquisition tools. This paper shows through examples the practical advantages of this approach. In particular, we illustrate how existing knowledge can be used to facilitate knowledge acquisition through analogy mechanisms within a domain and across domains. Our sample knowledge acquisition dialogues with a domain expert illustrate which parts of the process are addressed by the human and which parts are automated by the tool, in a synergistic cooperation for knowledge-base extension and refinement. The paper also describes briefly the EXPECT problem-solving architecture that facilitates this approach to knowledge acquisition. DTIC

N95-22524# Vrije Univ., Amsterdam (Netherlands).
TEMPORAL MODEL THEORY FOR DEFAULT LOGIC
J. Engelfriet and J. Treur Sep. 1993 42 p
(PB95-127346) Avail: CASI HC A03/MF A01

When reasoning about complex domains, where information available is usually only partial, nonmonotonic reasoning can be an important tool. One of the formalisms introduced in this area is Reiter's Default Logic. For this logic, several semantics have been proposed, which in our view lack a clear intuitive motivation. We propose a temporal semantics, in which a model reflects the reasoning process leading to the conclusions, as the conclusions in Default Logic depend on choices made during the reasoning process. Because the knowledge about the domain remains partial during the reasoning, partial temporal models can be used. In this paper we introduce a temporal partial logic, which is then used to describe the models of a theory in Default Logic. It will be shown that our approach gives an intuitive and valid semantics to Reiter's Default Logic. A comparison between the various semantics for Default Logic will show the differences and similarities of these approaches. NTIS

N95-22614# Joint Inst. for Nuclear Research, Dubna (USSR).
A NEWTON-TYPE NEURAL NETWORK LEARNING ALGORITHM
V. V. Ivanov, I. V. Puzynin, and B. Purehvdorzh 1993 7 p
(DE94-628371; JINR-D-11-93-317) Avail: CASI HC A02/MF A01 (US Sales Only)

First- and second-order learning methods for feed-forward multilayer networks are considered. A Newton-type algorithm is proposed and compared with the common back-propagation algorithm. It is shown that the proposed algorithm provides better learning quality. Some recommendations for their usage are given. DOE

N95-22705 Department of the Navy, Washington, DC.
NEURAL NETWORK FOR DETECTION AND CORRECTION OF LOCAL BOUNDARY MISALIGNMENTS BETWEEN IMAGES Patent
George W. Rogers, inventor (to Navy), Jeffrey L. Solka, inventor (to Navy), Donald Vermillion, inventor (to Navy), Carey E. Priebe, inventor (to Navy), and Wendy L. Poston, inventor (to Navy) 27 Sep. 1994 10 p Filed 28 Jul. 1992
(AD-D016539; US-Patent-5,351,311; US-Patent-Appl-SN-920700; US-Patent-Class-382-415) Avail: US Patent and Trademark Office

A network is provided for the detection and correction of local boundary misalignments in a two-dimensional pixel space between a reference and transformed image. An input layer has input layer sections, each of which contains a plurality of input nodes associated with a cell. The cell is centered on a pixel and divided along a straightline orientation into first and second cell sections. Each of the input nodes outputs a digital signal indicative of the presence or absence of a contrast gradient as measured by the two cell sections. A second layer has a plurality of second layer sections, each of which is associated with one of the input layer sections and contains a plurality of second layer nodes. Each second layer node is responsive to a combination of input nodes to indicate the presence or absence of a boundary misalignment between the reference and transformed images. Presence of a contrast gradient at the combination of nodes defines a local boundary misalignment. DTIC

N95-22831*# Georgia Inst. of Tech., Atlanta, GA. School of Aerospace Engineering.
DEVELOPMENT OF AN ADAPTIVE hp-VERSION FINITE ELEMENT METHOD FOR COMPUTATIONAL OPTIMAL CONTROL Final Report, 22 Apr. 1992 - 30 Nov. 1994
Dewey H. Hodges and Michael S. Warner 30 Nov. 1994 38 p
(Grant NAG1-1435)
(NASA-CR-197898; NAS 1.26:197898) Avail: CASI HC A03/MF A01

In this research effort, the usefulness of hp-version finite elements and adaptive solution-refinement techniques in generating numerical solutions to optimal control problems has been investigated. Under NAG-939, a general FORTRAN code was developed which approximated solutions to optimal control problems with control constraints and state constraints. Within that methodology, to get high-order accuracy in solutions, the finite element mesh would have to be refined repeatedly through bisection of the entire mesh in a given phase. In the current research effort, the order of the shape functions in each element has been made a variable, giving more flexibility in error reduction and smoothing. Similarly, individual elements can each be subdivided into many pieces, depending on the local error indicator, while other parts of the mesh remain coarsely discretized. The problem remains to reduce and smooth the error while still keeping computational effort reasonable enough to calculate time histories in a short enough time for on-board applications. Derived from text

N95-23078# Lawrence Livermore National Lab., Livermore, CA.
SIMULATION AND OFF-LINE PROGRAMMING SYSTEMS COMPARISON
M. A. Holliday May 1994 8 p Presented at the European Simulation Multiconference, Barcelona, Spain, 1-3 Jun. 1994
(Contract W-7405-eng-48)
(DE95-002267; UCRL-JC-117308; CONF-9406276-1) Avail: CASI HC A02/MF A01

Off-line programs systems (OLP's) are presently being used to conceptualize, design, simulate and now control automated robotic work cells. Currently available systems by Deneb, Silma, and Cimetrix Inc. are being used at the Lawrence Livermore National Laboratory (LLNL) to simulate and control automated robotic systems for radioactive material processing and hazardous waste sorting. The latest improvements and new feature additions in system architectures, workcell and robot calibration procedures, interface and graphical output capability of each will be discussed. The relative strengths and weaknesses of these attributes will be discussed as they relate to varying applications in robotic workcell development and control. These systems are constantly evolving and each have their own strengths and weaknesses relative to different applications in robotic control and simulation. Therefore system comparisons become problematic when one system, by design, excels in one area and is lacking, by design, in other areas. Due to the limited length of this paper only new and enhanced features will be discussed with a complete categorical comparison of all attributes being done at a later date. DOE

N95-23134# Sandia National Labs., Albuquerque, NM.
SEGREGATED RIGID AND STRUCTURAL CONTROL FOR A PHOTOLITHOGRAPHY POSITIONING SYSTEM
J. Redmond, J. Dohner, G. Parker, and G. Reese 1994 10 p Presented at the 5th International Conference on Adaptive Structures, Sendai, Japan, 5-7 Dec. 1994
(Contract DE-AC04-94AL-85000)

(DE95-002603; SAND-94-2827C; CONF-941220-1) Avail: CASI HC A02/MF A01

This paper presents a conceptual design of a supplemental flexible body control system for a magnetically levitated platen used in the manufacture of integrated circuits. Structural resonances currently limit system performance and are not easily handled using conventional control methodologies due to the complexities of the electromagnetic actuators. A technique for active vibration damping using Rush mounted PZT stack actuators on the platen surface is presented. Preliminary results obtained from a computer simulation indicate that this approach provides ample vibration attenuation and has the potential for significantly increasing rigid body positioning speed. DOE

N95-23199# Technische Univ., Twente (Netherlands).

ADAPTIVE CONTROL OF LINEAR SYSTEMS BASED ON APPROXIMATE MODELS

K. Arent, I. M. Y. Mareels, and J. W. Polderman Nov. 1993 17 p Prepared in cooperation with Australian National Univ.

(PB95-139333) Avail: CASI HC A03/MF A01

In the context of a restricted class of linear time invariant SISO discrete time dynamical systems, we propose an indirect adaptive regulation method capable of avoiding the so called pole-zero cancellation problem. The key idea is to use an approximate model for which the problem is nonexistent. The development of the adaptive algorithm proceeds from an identification perspective and relies on the concept of unfalsified model. NTIS

N95-23387* National Aeronautics and Space Administration. Ames Research Center, Moffett Field, CA.

METHOD AND SYSTEM FOR PATTERN ANALYSIS USING A COARSE-CODED NEURAL NETWORK Patent

Liljana Spirkovska, inventor (to NASA) and Max B. Reid, inventor (to NASA) 26 Jul. 1994 20 p Filed 2 Jul. 1992

(NASA-Case-ARC-11961-1; US-Patent-5,333,210;

US-Patent-Appl-SN-908141; US-Patent-Class-382-15;

US-Patent-Class-382-27; Int-Patent-Class-G06K-9/46) Avail: US Patent and Trademark Office

A method and system for performing pattern analysis with a neural network coarse-coding a pattern to be analyzed so as to form a plurality of sub-patterns collectively defined by data. Each of the sub-patterns comprises sets of pattern data. The neural network includes a plurality fields, each field being associated with one of the sub-patterns so as to receive the sub-pattern data therefrom. Training and testing by the neural network then proceeds in the usual way, with one modification: the transfer function thresholds the value obtained from summing the weighted products of each field over all sub-patterns associated with each pattern being analyzed by the system.

Official Gazette of the U.S. Patent and Trademark Office

N95-23556 Technische Univ., Twente (Netherlands). Faculty of Applied Mathematics.

LIGHT-TRAFFIC ANALYSIS FOR QUEUES WITH SPATIALLY DISTRIBUTED ARRIVALS

D. P. Kroese and V. Schmidt 26 Jul. 1993 30 p See also N92-14750 and PB94-126638 Prepared in cooperation with Ulm Univ. Limited Reproducibility: More than 20% of this document may be affected by microfiche quality

(PB95-140802) Avail: CASI HC A03

We consider the following continuous polling system: Customers arrive according to a homogeneous Poisson process (or a more general stationary point process) and wait on a circle in order to be served by a single server. The server is 'greedy', in the sense that he always moves (with constant speed) towards the nearest customer. The customers are served according to an arbitrary service time distribution, in the order in which they are encountered by the server. First-order and second-order Taylor-expansions are found for the expected configuration of customers, for the mean queue length, and for expectation and distribution function of the workload. It is shown that under light traffic conditions the greedy server works more efficiently than the cyclically polling server. NTIS

N95-23557# Technische Univ., Twente (Netherlands). Faculty of Applied Mathematics.

NORMALIZED COPRIME FACTORIZATIONS AND BALANCING FOR UNSTABLE NONLINEAR SYSTEMS Memorandum Report

J. M. A. Scherpen and A. J. vanderSchaft 26 Aug. 1993 33 p See also N94-10273

(PB95-141222; MEMO-1155) Avail: CASI HC A03/MF A01

In this paper we first study the normalized right and left coprime factorizations of a nonlinear system from a state space point of view. In order to do so, we introduce the notion of inner and co-inner nonlinear systems. Secondly we deal with balancing for unstable nonlinear systems. For linear systems there are several ways to approach this problem, and we generalize the ideas of balancing the normalized coprime factorization and of Linear Quadratic Gaussian (LQG) balancing to the nonlinear case. LQG balancing can be seen as measuring the influence of a state component on a certain future and past energy function. We extend this interpretation to the nonlinear case. Furthermore we use the normalized coprime factorization to give another way of balancing the unstable nonlinear system. We give the relation between these two methods of balancing, which is similar to the relation in the linear case. NTIS

N95-23558 Technische Univ., Twente (Netherlands). Faculty of Applied Mathematics.

DYNAMIC DISTURBANCE DECOUPLING OF NONLINEAR SYSTEMS AND LINEARIZATION Memorandum Report

H. J. C. Huiberts and H. Nijmeijer Sep. 1993 20 p See also PB91-142083 Prepared in cooperation with Technische Univ. Limited Reproducibility: More than 20% of this document may be affected by microfiche quality

(PB95-141248; MEMO-1157) Avail: Issuing Activity (National Technical Information Service (NTIS))

In this paper we investigate the connections between the solvability of the dynamic disturbance decoupling problem with exponential stability (DDDPes) for a nonlinear system and the solvability of the same problem for its linearization around an equilibrium point. It is shown that under generic conditions the nonlinear DDDPes is solvable for a nonlinear system if and only if the static disturbance decoupling problem with stability (DDPs) is solvable for its linearization around an equilibrium point. NTIS

N95-23578# Pacific Northwest Lab., Richland, WA.

ALPHA SPECTRAL ANALYSIS VIA ARTIFICIAL NEURAL NETWORKS

L. J. Kangas, S. Hashem, P. E. Keller, R. T. Kouzes, and G. L. Troyer (Westinghouse Hanford Co., Richland, WA.) Oct. 1994 5 p Presented at the Nuclear Science Symposium: Medical Imaging Conference, Norfolk, VA, 30 Oct. - 5 Nov. 1994

(Contract DE-AC06-76RL-01830)

(DE95-004567; PNL-SA-24176; CONF-941061-13) Avail: CASI HC A01/MF A01

An artificial neural network system that assigns quality factors to alpha particle energy spectra is discussed. The alpha energy spectra are used to detect plutonium contamination in the work environment. The quality factors represent the levels of spectral degradation caused by miscalibration and foreign matter affecting the instruments. A set of spectra was labeled with a quality factor by an expert and used in training the artificial neural network expert system. The investigation shows that the expert knowledge of alpha spectra quality factors can be transferred to an ANN system. DOE

N95-23672*# Jet Propulsion Lab., California Inst. of Tech., Pasadena, CA.

THIRD INTERNATIONAL SYMPOSIUM ON ARTIFICIAL INTELLIGENCE, ROBOTICS, AND AUTOMATION FOR SPACE 1994

Oct. 1994 457 p Symposium held in Pasadena, CA, 18-20 Oct. 1994

(Contract NAS7-918; RTOP 233-03-04-00-00)

(NASA-CR-197340; JPL-Publ-94-23; NAS 1.26:197340) Avail: CASI HC A15/MF A03

The Third International Symposium on Artificial Intelligence, Robotics, and Automation for Space (i-SAIRAS 94), held October 18-20, 1994, in Pasadena, California, was jointly sponsored by NASA, ESA, and Japan's National Space Development Agency, and was hosted by the Jet Propulsion Laboratory (JPL) of the California Institute of Technology. i-SAIRAS 94 featured presentations covering a variety of technical and programmatic

topics, ranging from underlying basic technology to specific applications of artificial intelligence and robotics to space missions. i-SAIRAS 94 featured a special workshop on planning and scheduling and provided scientists, engineers, and managers with the opportunity to exchange theoretical ideas, practical results, and program plans in such areas as space mission control, space vehicle processing, data analysis, autonomous spacecraft, space robots and rovers, satellite servicing, and intelligent instruments. For individual titles, see N95-23673 through N95-23765.

N95-23673*# National Aeronautics and Space Administration, Washington, DC.

THE NEXT DECADE OF SPACE ROBOTICS

Dave Lavery and Charles Weisbin (Jet Propulsion Lab., California Inst. of Tech., Pasadena, CA.) *In* JPL, Third International Symposium on Artificial Intelligence, Robotics, and Automation for Space 1994 Oct. 1994 p 9-12 (For primary document see N95-23672 07-63)

Avail: CASI HC A01/MF A03

In the same way that the launch of Yuri Gagarin in April 1961 announced the beginning of human space flight, last year's flight of the German ROTEX robot flight experiment is heralding the start of a new era of space robotics. After a gap of twelve years since the introduction of a new capability in space remote manipulation, ROTEX is the first of at least ten new robotic systems and experiments which will fly before the year 2000. Author

N95-23674*# National Space Development Agency, Tsukuba (Japan).

A NEW CONTAINERLESS IMAGE FURNACE WITH ELECTRO-STATIC POSITIONING DEVICE **c35**

Toshihiko Yamawaki, Chihiro Tsukishima (Mitsubishi Electric Corp., Amagasaki, Japan.), Toshio Abe (Mitsubishi Electric Corp., Kamakura, Japan.), and Atsuko Kaneko (Mitsubishi Electric Corp., Kamakura, Japan.) *In* JPL, Third International Symposium on Artificial Intelligence, Robotics, and Automation for Space 1994 Oct. 1994 p 15-18 (For primary document see N95-23672 07-63)

Avail: CASI HC A01/MF A03

A new containerless image furnace with a microwave discharge plasma lamp and electrostatic positioning device was developed for the use of the microgravity experiment on the Japanese experimental module (JEM). The electrostatic positioning system was tested under the reduced gravity environment in the MU-300 aircraft. Solid specimens (maximum weight is 1.3 gr and 10 mm in diameter) and water drops (maximum weight is 0.11 gr and 6 mm in diameter) were successfully controlled under the 0.02G environment. Rotation control of the dielectric specimen was also possible by means of supplying a rotating electric field while the specimen is levitating. The measured rotation speed of the glass shell specimen (0.08 gr, 10 mm) was up to 110 rpm, when the rotating field frequency was 6Hz. Author

N95-23675*# Lockheed Missiles and Space Co., Palo Alto, CA. Artificial Intelligence Center.

SOFTWARE AGENTS FOR THE DISSEMINATION OF REMOTE TERRESTRIAL SENSING DATA **c43**

Christopher N. Toomey, Evangelos Simoudis, Raymond W. Johnson, and William S. Mark *In* JPL, Third International Symposium on Artificial Intelligence, Robotics, and Automation for Space 1994 Oct. 1994 p 19-22 (For primary document see N95-23672 07-63)

Avail: CASI HC A01/MF A03

Remote terrestrial sensing (RTS) data is constantly being collected from a variety of space-based and earth-based sensors. The collected data, and especially 'value-added' analyses of the data, are finding growing application for commercial, government, and scientific purposes. The scale of this data collection and analysis is truly enormous; e.g., by 1995, the amount of data available in just one sector, NASA space science, will reach 5 petabytes. Moreover, the amount of data, and the value of analyzing the data, are expected to increase dramatically as new satellites and sensors become available (e.g., NASA's Earth Observing System satellites). Lockheed and other companies are beginning to provide data and analysis commercially. A critical issue for the exploitation of collected data is the dissemination of data and value-added analyses to a diverse and widely distributed customer base. Customers must be able to use their computational environment (eventually the National Information Infrastructure) to obtain timely and complete information, without having to know the details of where the relevant data resides and how it is accessed. Customers must be able to routinely use standard, widely available (and, therefore, low cost) analyses, while also being able to readily create on demand highly customized analyses to make crucial decisions. The diversity of user needs creates a difficult software problem: how can users easily state their needs, while the computational environment assumes the responsibility of finding (or creating) relevant information, and then delivering the results in a form that users understand? A software agent is a self-contained, active software module that contains an explicit representation of its operational knowledge. This explicit representation allows agents to examine their own capabilities in order to modify their goals to meet changing needs and to take advantage of dynamic opportunities. In addition, the explicit representation allows agents to advertize their capabilities and results to other agents, thereby allowing the collection of agents to reuse each others work. Author

N95-23676*# Jet Propulsion Lab., California Inst. of Tech., Pasadena, CA.

COMMERCIALIZATION OF JPL VIRTUAL REALITY CALIBRATION AND REDUNDANT MANIPULATOR CONTROL TECHNOLOGIES

Won S. Kim, Homayoun Seraji, Paolo Fiorini, Robert Brown (Deneb Robotics, Inc., Auburn Hills, MI.), Brian Christensen (Deneb Robotics, Inc., Auburn Hills, MI.), Chris Beale (Deneb Robotics, Inc., Auburn Hills, MI.), James Karlen (Robotics Research Corp., Amelia, OH.), and Paul Eismann (Robotics Research Corp., Amelia, OH.) *In its* Third International Symposium on Artificial Intelligence, Robotics, and Automation for Space 1994 Oct. 1994 p 23-26 (For primary document see N95-23672 07-63)

Avail: CASI HC A01/MF A03

Within NASA's recent thrust for industrial collaboration, JPL (Jet Propulsion Laboratory) has recently established two technology cooperation agreements in the robotics area: one on virtual reality (VR) calibration with Deneb Robotics, Inc., and the other on redundant manipulator control with Robotics Research Corporation (RRC). These technology transfer cooperation tasks will enable both Deneb and RRC to commercialize enhanced versions of their products that will greatly benefit both space and terrestrial telerobotic applications. Derived from text

N95-23677*# Siemens A.G., Vienna (Austria).

UTILIZING INHERITANCE IN REQUIREMENTS ENGINEERING **c81**

Hermann Kaindl *In* JPL, Third International Symposium on Artificial Intelligence, Robotics, and Automation for Space 1994 Oct. 1994 p 29-31 Sponsored by ESA and Innovation- und Technologiefonds (For primary document see N95-23672 07-63)

Avail: CASI HC A01/MF A03

The scope of this paper is the utilization of inheritance for requirements specification, i.e., the tasks of analyzing and modeling the domain, as well as forming and defining requirements. Our approach and the tool supporting it are named RETH (Requirements Engineering Through Hypertext). Actually, RETH uses a combination of various technologies, including object-oriented approaches and artificial intelligence (in particular frames). We do not attempt to exclude or replace formal representations, but try to complement and provide means for gradually developing them. Among others, RETH has been applied in the CERN (Conseil Europeen pour la Rechereche Nucleaire) Cortex project. While it would be impossible to explain this project in detail here, it should be sufficient to know that it deals with a generic distributed control system. Since this project is not finished yet, it is difficult to state its size precisely. In order to give an idea, its final goal is to substitute the many existing similar control systems at CERN by this generic approach. Currently, RETH is also tested using real-world requirements for the Pastel Mission Planning System at ESOC in Darmstadt. First, we outline how hypertext is integrated into a frame system in our approach. Moreover, the usefulness of inheritance is demonstrated as performed by the tool RETH. We then summarize our experiences of utilizing inheritance in the Cortex project. Lastly, RETH will be related to existing work. Derived from text

N95-23678*# National Aeronautics and Space Administration. Ames Research Center, Moffett Field, CA.

USING DEDAL TO SHARE AND REUSE DISTRIBUTED ENGINEERING DESIGN INFORMATION **c82**

Vinod Baya (Stanford Univ., CA.), Catherine Baudin, Ade Mabogunje (Stanford Univ., CA.), Aseem Das, David M. Cannon (Stanford Univ., CA.), and Larry J. Leifer (Stanford Univ., CA.) *In* JPL, Third International

Symposium on Artificial Intelligence, Robotics, and Automation for Space 1994 Oct. 1994 p 33-36 (For primary document see N95-23672 07-63)
Avail: CASI HC A01/MF A03

The overall goal of the project is to facilitate the reuse of previous design experience for the maintenance, repair and redesign of artifacts in the electromechanical engineering domain. An engineering team creates information in the form of meeting summaries, project memos, progress reports, engineering notes, spreadsheet calculations and CAD drawings. Design information captured in these media is difficult to reuse because the way design concepts are referred to evolve over the life of a project and because decisions, requirements and structure are interrelated but rarely explicitly linked. Based on protocol analysis of the information seeking behavior of designer's, we defined a language to describe the content and the form of design records and implemented this language in Dedal, a tool for indexing, modeling and retrieving design information. We first describe the approach to indexing and retrieval in Dedal. Next we describe ongoing work in extending Dedal's capabilities to a distributed environment by integrating it with World Wide Web. This will enable members of a design team who are not co-located to share and reuse information.

Derived from text

N95-23679*# Siemens A.G., Vienna (Austria). Knowledge Systems Lab.
OPERATOR PROCEDURE VERIFICATION WITH A RAPIDLY RECONFIGURABLE SIMULATOR **c14**
Yumi Iwasaki, Robert Engelmore, Gary Fehr, and Richard Fikes *In* JPL, Third International Symposium on Artificial Intelligence, Robotics, and Automation for Space 1994 Oct. 1994 p 37-40 (For primary document see N95-23672 07-63)
(Contract NCC2-537; NAG2-581; ARPA Order 8607)
Avail: CASI HC A01/MF A03

Generating and testing procedures for controlling spacecraft subsystems composed of electro-mechanical and computationally realized elements has become a very difficult task. Before a spacecraft can be flown, mission controllers must envision a great variety of situations the flight crew may encounter during a mission and carefully construct procedures for operating the spacecraft in each possible situation. If, despite extensive pre-compilation of control procedures, an unforeseen situation arises during a mission, the mission controller must generate a new procedure for the flight crew in a limited amount of time. In such situations, the mission controller cannot systematically consider and test alternative procedures against models of the system being controlled, because the available simulator is too large and complex to reconfigure, run, and analyze quickly. A rapidly reconfigurable simulation environment that can execute a control procedure and show its effects on system behavior would greatly facilitate generation and testing of control procedures both before and during a mission. The How Things Work project at Stanford University has developed a system called DME (Device Modeling Environment) for modeling and simulating the behavior of electromechanical devices. DME was designed to facilitate model formulation and behavior simulation of device behavior including both continuous and discrete phenomena. We are currently extending DME for use in testing operator procedures, and we have built a knowledge base for modeling the Reaction Control System (RCS) of the space shuttle as a testbed. We believe that DME can facilitate design of operator procedures by providing mission controllers with a simulation environment that meets all these requirements.

Derived from text

N95-23680*# RECOM Technologies, Inc., Moffett Field, CA. AI Research Branch.
AMPHION: SPECIFICATION-BASED PROGRAMMING FOR SCIENTIFIC SUBROUTINE LIBRARIES **c61**
Michael Lowry, Andrew Philpot, Thomas Pressburger, Ian Underwood, Richard Waldinger (SRI International Corp., Menlo Park, CA.), and Mark Stickel (SRI International Corp., Menlo Park, CA.) *In* JPL, Third International Symposium on Artificial Intelligence, Robotics, and Automation for Space 1994 Oct. 1994 p 41-44 (For primary document see N95-23672 07-63)
Avail: CASI HC A01/MF A03

AMPHION is a knowledge-based software engineering (KBSE) system that guides a user in developing a diagram representing a formal problem specification. It then automatically implements a solution to this specification as a program consisting of calls to subroutines from a library. The diagram provides an intuitive domain oriented notation for creating a specification that also facilitates reuse and modification. AMPHION'S architecture is domain independent. AMPHION is specialized to an application domain by developing a declarative domain theory. Creating a domain theory is an iterative process that currently requires the joint expertise of domain experts and experts in automated formal methods for software development.

Derived from text

N95-23681*# Entwicklungsring Nord, Bremen (Germany).
AN INTELLIGENT GROUND OPERATOR SUPPORT SYSTEM
Thomas Goerlach, Gerhard Ohlendorf, Frank Plassmeier, and Uwe Bruege *In* JPL, Third International Symposium on Artificial Intelligence, Robotics, and Automation for Space 1994 Oct. 1994 p 47-51 (For primary document see N95-23672 07-63)
Avail: CASI HC A01/MF A03

This paper presents first results of the project 'Technologien fuer die intelligente Kontrolle von Raumfahrzeugen' (TIKON). The TIKON objective was the demonstration of feasibility and profit of the application of artificial intelligence in the space business. For that purpose a prototype system has been developed and implemented for the operation support of the Roentgen Satellite (ROSAT), a scientific spacecraft designed to perform the first all-sky survey with a high-resolution X-ray telescope and to investigate the emission of specific celestial sources. The prototype integrates a scheduler and a diagnosis tool both based on artificial intelligence techniques. The user interface is menu driven and provides synoptic displays for the visualization of the system status. The prototype has been used and tested in parallel to an already existing operational system.

Author (revised)

N95-23682*# National Aeronautics and Space Administration. Lyndon B. Johnson Space Center, Houston, TX.
TOWARD AN AUTOMATED SIGNATURE RECOGNITION TOOLKIT FOR MISSION OPERATIONS **c32**
T. Cleghorn, P Laird (National Aeronautics and Space Administration. Ames Research Center, Moffett Field, CA.), L. Perrine, C. Culbert, M. Macha, R. Saul (RECOM Technologies, Inc., Moffett Field, CA.), D. Hammen (Mitre Corp., Houston, TX.), T. Moebes (Science Applications International Corp., Houston, TX.), and R. Shelton *In* JPL, Third International Symposium on Artificial Intelligence, Robotics, and Automation for Space 1994 Oct. 1994 p 53-56 (For primary document see N95-23672 07-63)
Avail: CASI HC A01/MF A03

Signature recognition is the problem of identifying an event or events from its time series. The generic problem has numerous applications to science and engineering. At NASA's Johnson Space Center, for example, mission control personnel, using electronic displays and strip chart recorders, monitor telemetry data from three-phase electrical buses on the Space Shuttle and maintain records of device activation and deactivation. Since few electrical devices have sensors to indicate their actual status, changes of state are inferred from characteristic current and voltage fluctuations. Controllers recognize these events both by examining the waveform signatures and by listening to audio channels between ground and crew. Recently the authors have developed a prototype system that identifies major electrical events from the telemetry and displays them on a workstation. Eventually the system will be able to identify accurately the signatures of over fifty distinct events in real time, while contending with noise, intermittent loss of signal, overlapping events, and other complications. This system is just one of many possible signature recognition applications in Mission Control. While much of the technology underlying these applications is the same, each application has unique data characteristics, and every control position has its own interface and performance requirements. There is a need, therefore, for CASE tools that can reduce the time to implement a running signature recognition application from months to weeks or days. This paper describes our work to date and our future plans.

Derived from text

N95-23683*# Jet Propulsion Lab., California Inst. of Tech., Pasadena, CA.
ATTENTION FOCUSING AND ANOMALY DETECTION IN SYSTEMS MONITORING
Richard J. Doyle *In its* Third International Symposium on Artificial Intelligence, Robotics, and Automation for Space 1994 Oct. 1994

p 57-60 (For primary document see N95-23672 07-63)
Avail: CASI HC A01/MF A03

Any attempt to introduce automation into the monitoring of complex physical systems must start from a robust anomaly detection capability. This task is far from straightforward, for a single definition of what constitutes an anomaly is difficult to come by. In addition, to make the monitoring process efficient, and to avoid the potential for information overload on human operators, attention focusing must also be addressed. When an anomaly occurs, more often than not several sensors are affected, and the partially redundant information they provide can be confusing, particularly in a crisis situation where a response is needed quickly. The focus of this paper is a new technique for attention focusing. The technique involves reasoning about the distance between two frequency distributions, and is used to detect both anomalous system parameters and 'broken' causal dependencies. These two forms of information together isolate the locus of anomalous behavior in the system being monitored. Author

N95-23684*# National Aeronautics and Space Administration. Goddard Space Flight Center, Greenbelt, MD.
AN EXPERT SYSTEM FOR DIAGNOSING ANOMALIES OF SPACECRAFT
Michael Lauriente, Rick Durand (University Research Foundation, Greenbelt, MD.), Al Vampola (University Research Foundation, Greenbelt, MD.), Harry C. Koons (Aerospace Corp., Los Angeles, CA.), and David Gorney (Aerospace Corp., Los Angeles, CA.) *In* JPL, Third International Symposium on Artificial Intelligence, Robotics, and Automation for Space 1994 Oct. 1994 p 63-66 (For primary document see N95-23672 07-63)
Avail: CASI HC A01/MF A03

Although the analysis of anomalous behavior of satellites is difficult because it is a very complex process, it is important to be able to make an accurate assessment in a timely manner when the anomaly is observed. Spacecraft operators may have to take corrective action or to 'safe' the spacecraft; space-environment forecasters may have to assess the environmental situation and issue warnings and alerts regarding hazardous conditions, and scientists and engineers may want to gain knowledge for future designs to mitigate the problems. Anomalies can be hardware problems, software errors, environmentally induced, or even the cause of workmanship. Spacecraft anomalies attributable to electrostatic discharges have been known to cause command errors. A goal is to develop an automated system based on this concept to reduce the number of personnel required to operate large programs or missions such as Hubble Space Telescope (HST) and Mission to Planet Earth (MTPE). Although expert systems to detect anomalous behavior of satellites during operations are established, diagnosis of the anomaly is a complex procedure and is a new development. Derived from text

N95-23685*# CRI Space, (Denmark).
DISTRIBUTED INTELLIGENCE FOR GROUND/SPACE SYSTEMS
Mads Aarup, Klaus Heje Munch, Joachim Fuchs (European Space Agency. European Space Research and Technology Center, ESTEC, Noordwijk, Netherlands.), Ralf Hartmann (Dornier Luftfahrt G.m.b.H., Friedrichshafen, Germany.), and Tim Baud (Cray Systems, Bristol, England.) *In* JPL, Third International Symposium on Artificial Intelligence, Robotics, and Automation for Space 1994 Oct. 1994 p 67-70 (For primary document see N95-23672 07-63)
Avail: CASI HC A01/MF A03

DI is short for Distributed Intelligence for Ground/Space Systems and the DI Study is one in a series of ESA projects concerned with the development of new concepts and architectures for future autonomous spacecraft systems. The kick-off of DI was in January 1994 and the planned duration is three years. The background of DI is the desire to design future ground/space systems with a higher degree of autonomy than seen in today's missions. The aim of introducing autonomy in spacecraft systems is to: (1) lift the role of the spacecraft operators from routine work and basic troubleshooting to supervision; (2) ease access to and increase availability of spacecraft resources; (3) carry out basic mission planning for users; (4) enable missions which have not yet been feasible due to eg. propagation delays, insufficient ground station coverage etc.; and (5) possibly reduce mission cost. The study serves to identify the feasibility of using state-of-the-art technologies in the area of planning, scheduling, fault detection using model-based diagnosis and knowledge processing to obtain a higher level of autonomy in ground/space systems. Derived from text

N95-23686*# Vanderbilt Univ., Nashville, TN. Dept. of Computer Science.
LEARNING TIME SERIES FOR INTELLIGENT MONITORING
Stefanos Manganaris and Doug Fisher *In* JPL, Third International Symposium on Artificial Intelligence, Robotics, and Automation for Space 1994 Oct. 1994 p 71-74 (For primary document see N95-23672 07-63)
(Grant NAG2-834)
Avail: CASI HC A01/MF A03

We address the problem of classifying time series according to their morphological features in the time domain. In a supervised machine-learning framework, we induce a classification procedure from a set of preclassified examples. For each class, we infer a model that captures its morphological features using Bayesian model induction and the minimum message length approach to assign priors. In the performance task, we classify a time series in one of the learned classes when there is enough evidence to support that decision. Time series with sufficiently novel features, belonging to classes not present in the training set, are recognized as such. We report results from experiments in a monitoring domain of interest to NASA. Author

N95-23687*# National Aeronautics and Space Administration. Ames Research Center, Moffett Field, CA.
AN OPERATIONS AND COMMAND SYSTEMS FOR THE EXTREME ULTRAVIOLET EXPLORER
Nicola Muscettola, David J. Korsmeyer, Eric C. Olson (California Univ., Berkeley, CA.), and Gary Wong (California Univ., Berkeley, CA.) *In* JPL, Third International Symposium on Artificial Intelligence, Robotics, and Automation for Space 1994 Oct. 1994 p 75-78 (For primary document see N95-23672 07-63)
Avail: CASI HC A01/MF A03

About 40% of the budget of a scientific spacecraft mission is usually consumed by Mission Operations & Data Analysis (MO&DA) with MO driving these costs. In the current practice, MO is separated from spacecraft design and comes in focus relatively late in the mission life cycle. As a result, spacecraft may be designed that are very difficult to operate. NASA centers have extensive MO expertise but often lessons learned in one mission are not exploited for other parallel or future missions. A significant reduction of MO costs is essential to ensure a continuing and growing access to space for the scientific community. We are addressing some of these issues with a highly automated payload operations and command system for an existing mission, the Extreme Ultraviolet Explorer (EUVE). EUVE is currently operated jointly by the Goddard Space Flight Center (GSFC), responsible for spacecraft operations, and the Center for Extreme Ultraviolet Astrophysics (CEA) of the University of California, Berkeley, which controls the telescopes and scientific instruments aboard the satellite. The new automated system is being developed by a team including personnel from the NASA Ames Research Center (ARC), the Jet Propulsion Laboratory (JPL) and the Center for EUV Astrophysics (CEA). An important goal of the project is to provide AI-based technology that can be easily operated by nonspecialists in AI. Another important goal is the reusability of the techniques for other missions. Models of the EUVE spacecraft need to be built both for planning/scheduling and for monitoring. In both cases, our modeling tools allow the assembly of a spacecraft model from separate sub-models of the various spacecraft subsystems. These sub-models are reusable; therefore, building mission operations systems for another small satellite mission will require choosing pre-existing modules, reparametrizing them with respect to the actual satellite telemetry information, and reassembling them in a new model. We briefly describe the EUVE mission and indicate why it is particularly suitable for the task. Then we briefly outline our current work in mission planning/scheduling and spacecraft and instrument health monitoring. Derived from text

N95-23688*# Jet Propulsion Lab., California Inst. of Tech., Pasadena, CA.
PERFORMANCE RESULTS OF COOPERATING EXPERT SYSTEMS IN A DISTRIBUTED REAL-TIME MONITORING SYSTEM **c61**
U. M. Schwuttke, J. R. Veregge, and A. G. Quan *In its* Third International Symposium on Artificial Intelligence, Robotics, and Automation for Space 1994 Oct. 1994 p 79-83 (For primary document see N95-23672 07-63)
Avail: CASI HC A01/MF A03

There are numerous definitions for real-time systems, the most stringent of which involve guaranteeing correct system response within a domain-dependent or situationally defined period of time. For applications such as diagnosis, in which the time required to produce a solution can be non-deterministic, this requirement poses a unique set of challenges in dynamic modification of solution strategy that conforms with maximum possible latencies. However, another definition of real time is relevant in the case of monitoring systems where failure to supply a response in the proper (and often infinitesimal) amount of time allowed does not make the solution less useful (or, in the extreme example of a monitoring system responsible for detecting and deflecting enemy missiles, completely irrelevant). This more casual definition involves responding to data at the same rate at which it is produced, and is more appropriate for monitoring applications with softer real-time constraints, such as interplanetary exploration, which results in massive quantities of data transmitted at the speed of light for a number of hours before it even reaches the monitoring system. The latter definition of real time has been applied to the MARVEL system for automated monitoring and diagnosis of spacecraft telemetry. An early version of this system has been in continuous operational use since it was first deployed in 1989 for the Voyager encounter with Neptune. This system remained under incremental development until 1991 and has been under routine maintenance in operations since then, while continuing to serve as an artificial intelligence (AI) testbed in the laboratory. The system architecture has been designed to facilitate concurrent and cooperative processing by multiple diagnostic expert systems in a hierarchical organization. The diagnostic modules adhere to concepts of data-driven reasoning, constrained but complete nonoverlapping domains, metaknowledge of global consequences of anomalous data, hierarchical reporting of problems that extend beyond a single domain, and shared responsibility for problems that overlap domains. The system enables efficient diagnosis of complex system failures in real-time environments with high data volumes and moderate failure rates, as indicated by extensive performance measurements. Derived from text

N95-23689*# Tokyo Univ., Sagamihara (Japan).
PATH PLANNING FOR PLANETARY ROVER USING EXTENDED ELEVATION MAP **c91**
Ichiro Nakatani, Takashi Kubota, and Tetsuo Yoshimitsu *In* JPL, Third International Symposium on Artificial Intelligence, Robotics, and Automation for Space 1994 Oct. 1994 p 87-90 (For primary document see N95-23672 07-63)
Avail: CASI HC A01/MF A03

This paper describes a path planning method for planetary rovers to search for paths on planetary surfaces. The planetary rover is required to travel safely over a long distance for many days over unfamiliar terrain. Hence it is very important how planetary rovers process sensory information in order to understand the planetary environment and to make decisions based on that information. As a new data structure for informational mapping, an extended elevation map (EEM) has been introduced, which includes the effect of the size of the rover. The proposed path planning can be conducted in such a way as if the rover were a point while the size of the rover is automatically taken into account. The validity of the proposed methods is verified by computer simulations. Author (revised)

N95-23690*# Tokyo Univ. (Japan). Dept. of Aeronautics and and Astronautics.
SUBSUMPTION-BASED ARCHITECTURE FOR AUTONOMOUS MOVEMENT PLANNING FOR PLANETARY ROVERS
Shinichi Nakasuka and Seikoh Shirasaka *In* JPL, Third International Symposium on Artificial Intelligence, Robotics, and Automation for Space 1994 Oct. 1994 p 91-94 (For primary document see N95-23672 07-63)
Avail: CASI HC A01/MF A03

The paper proposes a new architecture for autonomously generating and managing movement plans of planetary rovers. The system utilizes the uniform representation of the instantaneous subgoals in the form of virtual sensor states and the autonomous generation of the subsumption type plan network, which are expected to lead to the capability to pursue the overall goal while efficiently managing various unpredicted anomalies in a partially unknown, ill-structured environment such as a planetary surface. Author

N95-23691*# Minnesota Univ., Minneapolis, MN. Dept. of Computer Science.
VERY FAST MOTION PLANNING FOR HIGHLY DEXTEROUS-ARTICULATED ROBOTS
Daniel J. Challou, Maria Gini, and Vipin Kumar *In* JPL, Third International Symposium on Artificial Intelligence, Robotics, and Automation for Space 1994 Oct. 1994 p 99-102 (For primary document see N95-23672 07-63)
(Contracts DAAL03-89-C-0038; DAAH04-96-G-0800; NSF CDA-90-22509; NSF IRI-92-16941)
Avail: CASI HC A01/MF A03

Due to the inherent danger of space exploration, the need for greater use of teleoperated and autonomous robotic systems in space-based applications has long been apparent. Autonomous and semi-autonomous robotic devices have been proposed for carrying out routine functions associated with scientific experiments aboard the shuttle and space station. Finally, research into the use of such devices for planetary exploration continues. To accomplish their assigned tasks, all such autonomous and semi-autonomous devices will require the ability to move themselves through space without hitting themselves or the objects which surround them. In space it is important to execute the necessary motions correctly when they are first attempted because repositioning is expensive in terms of both time and resources (e.g., fuel). Finally, such devices will have to function in a variety of different environments. Given these constraints, a means for fast motion planning to insure the correct movement of robotic devices would be ideal. Unfortunately, motion planning algorithms are rarely used in practice because of their computational complexity. Fast methods have been developed for detecting imminent collisions, but the more general problem of motion planning remains computationally intractable. However, in this paper we show how the use of multicomputers and appropriate parallel algorithms can substantially reduce the time required to synthesize paths for dexterous articulated robots with a large number of joints. We have developed a parallel formulation of the Randomized Path Planner proposed by Barraquand and Latombe. We have shown that our parallel formulation is capable of formulating plans in a few seconds or less on various parallel architectures including: the nCUBE2 multicomputer with up to 1024 processors (nCUBE2 is a registered trademark of the nCUBE corporation), and a network of workstations. Derived from text

N95-23692*# Tokyo Univ., Sagamihara (Japan).
CONTROL TECHNIQUE FOR PLANETARY ROVER
Ichiro Nakatani, Takashi Kubota, Tadashi Adachi (Nissan Motor Co. Ltd., Kawagoe, Japan.), Hiroaki Saitou (Nissan Motor Co. Ltd., Kawagoe, Japan.), and Sinya Okamoto (Nissan Motor Co. Ltd., Kawagoe, Japan.) *In* JPL, Third International Symposium on Artificial Intelligence, Robotics, and Automation for Space 1994 Oct. 1994 p 103-106 (For primary document see N95-23672 07-63)
Avail: CASI HC A01/MF A03

Beginning next century, several schemes for sending a planetary rover to the moon or Mars are being planned. As part of the development program, autonomous navigation technology is being studied to allow the rover the ability to move autonomously over a long range of unknown planetary surface. In the previous study, we ran the autonomous navigation experiment on an outdoor test terrain by using a rover test-bed that was controlled by a conventional sense-plan-act method. In some cases during the experiment, a problem occurred with the rover moving into untraversable areas. To improve this situation, a new control technique has been developed that gives the rover the ability of reacting to the outputs of the proximity sensors, a reaction behavior if you will. We have developed a new rover test-bed system on which an autonomous navigation experiment was performed using the newly developed control technique. In this outdoor experiment, the new control technique effectively produced the control command for the rover to avoid obstacles and be guided to the goal point safely. Author (revised)

N95-23693*# Centre National d'Etudes Spatiales, Toulouse (France).
AUTONOMOUS NAVIGATION SYSTEM FOR THE MARSOKHOD ROVER PROJECT
C. Proy, M. Lamboley, and L. Rastel *In* JPL, Third International Symposium on Artificial Intelligence, Robotics, and Automation for Space 1994 Oct. 1994 p 107-110 (For primary document see N95-23672 07-63)
Avail: CASI HC A01/MF A03

This paper presents a general overview of the Marsokhod rover mission. The autonomous navigation for a Mars exploration rover is controlled by a vision system which has been developed on the basis of two CCD cameras, stereovision and path planning algorithms. Its performances have been tested on a Mars-like experimentation site. Author

N95-23694*# Carnegie-Mellon Univ., Pittsburgh, PA. Robotics Inst.
LUNAR ROVER TECHNOLOGY DEMONSTRATIONS WITH DANTE AND RATLER **c37**
Eric Krotkov, John Bares, Lalitesh Katragadda, Reid Simmons, and Red Whittaker *In* JPL, Third International Symposium on Artificial Intelligence, Robotics, and Automation for Space 1994 Oct. 1994 p 113-116 (For primary document see N95-23672 07-63)
Avail: CASI HC A01/MF A03

Carnegie Mellon University has undertaken a research, development, and demonstration program to enable a robotic lunar mission. The two-year mission scenario is to traverse 1,000 kilometers, revisiting the historic sites of Apollo 11, Surveyor 5, Ranger 8, Apollo 17, and Lunokhod 2, and to return continuous live video amounting to more than 11 terabytes of data. Our vision blends autonomously safeguarded user driving with autonomous operation augmented with rich visual feedback, in order to enable facile interaction and exploration. The resulting experience is intended to attract mass participation and evoke strong public interest in lunar exploration. The encompassing program that forwards this work is the Lunar Rover Initiative (LRI). Two concrete technology demonstration projects currently advancing the Lunar Rover Initiative are: (1) The Dante/Mt. Spurr project, which, at the time of this writing, is sending the walking robot Dante to explore the Mt. Spurr volcano, in rough terrain that is a realistic planetary analogue. This project will generate insights into robot system robustness in harsh environments, and into remote operation by novices; and (2) The Lunar Rover Demonstration project, which is developing and evaluating key technologies for navigation, teleoperation, and user interfaces in terrestrial demonstrations. The project timetable calls for a number of terrestrial traverses incorporating teleoperation and autonomy including natural terrain this year, 10 km in 1995. and 100 km in 1996. This paper will discuss the goals of the Lunar Rover Initiative and then focus on the present state of the Dante/Mt. Spurr and Lunar Rover Demonstration projects. Derived from text

N95-23695*# Tokyo Inst. of Tech. (Japan). Dept. of Mechano-Aerospace Engineering.
A PERSPECTIVE ON SPACE ROBOTICS IN JAPAN **c37**
Yoshiaki Ohkami, Ichiro Nakatani, Yasufumi Wakabayashi (National Space Development Agency, Tsukuba, Japan.), and Tsutomu Iwata (National Space Development Agency, Tsukuba, Japan.) *In* JPL, Third International Symposium on Artificial Intelligence, Robotics, and Automation for Space 1994 Oct. 1994 p 119-124 (For primary document see N95-23672 07-63)
Avail: CASI HC A02/MF A03

This report summarizes the research and development status and perspective on space robotics in Japan. The R & D status emphasizes the current on-going projects at NASDA including the JEM Remote Manipulator System (JEMRMS) to be used on Space Station Freedom and the robotics experiments on Engineering Satellite 7 (ETS-7). As a future perspective, not only NASDA, but also ISAS and other government institutes have been promoting their own research in space robotics in order to support wide spread space activities in the future. Included in this future research is an autonomous satellite retrieval experiment, a dexterous robot experiment, an on-orbit servicing platform, an IVA robot, and several moon/planetary rovers proposed by NASDA or ISAS and other organizations. Author (revised)

N95-23696*# Italian Space Agency, Rome.
ASI'S SPACE AUTOMATION AND ROBOTICS PROGRAMS: THE SECOND STEP **c37**
Simonetta DiPippo *In* JPL, Third International Symposium on Artificial Intelligence, Robotics, and Automation for Space 1994 Oct. 1994 p 125-130 (For primary document see N95-23672 07-63)
Avail: CASI HC A02/MF A03

The strategic decisions taken by ASI in the last few years in building up the overall A&R program, represent the technological drivers for other applications (i.e., internal automation of the Columbus Orbital Facility in the ESA Manned Space program, applications to mobile robots both in space and non-space environments, etc...). In this context, the main area of application now emerging is the scientific missions domain. Due to the broad range of applications of the developed technologies, both in the in-orbit servicing and maintenance of space structures and scientific missions, ASI foresaw the need to have a common technological development path, mainly focusing on: (1) control; (2) manipulation; (3) on-board computing; (4) sensors; and (5) teleoperation. Before entering into new applications in the scientific missions field, a brief overview of the status of the SPIDER related projects is given, underlining also the possible new applications for the LEO/GEO space structures. Derived from text

N95-23697*# Jet Propulsion Lab., California Inst. of Tech., Pasadena, CA.
JPL SPACE ROBOTICS: PRESENT ACCOMPLISHMENTS AND FUTURE THRUSTS **c37**
C. R. Weisbin, S. A. Hayati, and G. Rodriguez *In its* Third International Symposium on Artificial Intelligence, Robotics, and Automation for Space 1994 Oct. 1994 p 131-134 (For primary document see N95-23672 07-63)
Avail: CASI HC A01/MF A03

Complex missions require routine and unscheduled inspection for safe operation. The purpose of research in this task is to facilitate structural inspection of the planned Space Station while mitigating the need for extravehicular activity (EVA), and giving the operator supervisory control over detailed and somewhat mundane, but important tasks. The telerobotic system enables inspection relative to a given reference (e.g., the status of the facility at the time of the last inspection) and alerts the operator to potential anomalies for verification and action. There are two primary objectives of this project: (1) To develop technologies that enable well-integrated NASA ground-to-orbit telerobotics operations, and (2) to develop a prototype common architecture workstation which implements these capabilities for other NASA technology projects and planned NASA flight applications. This task develops and supports three telerobot control modes which are applicable to time delay operation: Preview teleoperation, teleprogramming, and supervised autonomy. Derived from text

N95-23698*# Jet Propulsion Lab., California Inst. of Tech., Pasadena, CA.
A US-JAPAN COLLABORATIVE ROBOTICS RESEARCH PROGRAM
Paul S. Schenker and Shigeoki Hirai (Ministry of International Trade and Industry, Tsukuba, Japan.) *In its* Third International Symposium on Artificial Intelligence, Robotics, and Automation for Space 1994 Oct. 1994 p 135-138 (For primary document see N95-23672 07-63)
Avail: CASI HC A01/MF A03

The Jet Propulsion Laboratory (JPL) and the Electrotechnical Laboratory (ETL) have recently initiated a cooperative R&D effort in telerobotics. This new effort, sponsored by the U.S. National Aeronautics and Space Administration (NASA) and Japan's Ministry of International Trade and Industry (MITI), has two major themes. First, our work broadens the outreach of space telerobotics R&D to international technical collaboration and facilities usage in the United States and Japan. Second, our work fosters development and demonstration of new operator interface technologies to improve the flexibility and reliability of ground-to-orbit telerobotic operations. This new technology is important, given the continuing imperatives to off-load platform maintenance from the extravehicular activity/intravehicular activity (EVA/IVA) crew to on-board robot assists under direct ground mission control. Derived from text

N95-23699*# Canadian Space Agency, Saint Hubert (Quebec).
ROBOTICS RESEARCH AT CANADIAN SPACE AGENCY
Raymond Hui *In* JPL, Third International Symposium on Artificial Intelligence, Robotics, and Automation for Space 1994 Oct. 1994 p 139-142 (For primary document see N95-23672 07-63)
Avail: CASI HC A01/MF A03

In addition to major crown projects such as the Mobile Servicing System for Space Station, the Canadian Space Agency is also engaged in internal, industrial and academic research and development activities in robotics and other space-related areas of science and technology. These activities support current and future space projects, and lead to technology development which can be spun off to terrestrial applications, thus satisfying

the Agency's objective of providing economic benefits to the public at large through its space-related work. Author

N95-23700*# National Space Development Agency, Tokyo (Japan).
DESIGN AND DEVELOPMENT STATUS OF ETS-7, AN RVD AND SPACE ROBOT EXPERIMENT SATELLITE **c18**
M. Oda, T. Inagaki, M. Nishida, K. Kibe, and F. Yamagata *In* JPL, Third International Symposium on Artificial Intelligence, Robotics, and Automation for Space 1994 Oct. 1994 p 143-147 (For primary document see N95-23672 07-63)
Avail: CASI HC A01/MF A03

ETS-7 (Engineering Test Satellite #7) is an experimental satellite for the in-orbit experiment of the Rendezvous Docking (RVD) and the space robot (RBT) technologies. ETS-7 is a set of two satellites, a chaser satellite and a target satellite. Both satellites will be launched together by NASDA's H-2 rocket into a low earth orbit. Development of ETS-7 started in 1990. Basic design and EM (Engineering Model) development are in progress now in 1994. The satellite will be launched in mid 1997 and the above in-orbit experiments will be conducted for 1.5 years. Design of ETS-7 RBT experiment system and development status are described in this paper. Author

N95-23701*# National Space Development Agency, Tsukuba (Japan).
SPACE ROBOTIC EXPERIMENT IN JEM FLIGHT DEMONSTRATION **c37**
Masanori Nagatomo, Masaki Tanaka (Toshiba Corp., Kawasaki, Japan.), Kazuyuki Nakamura (Toshiba Corp., Kawasaki, Japan.), and Shinichi Tsuda (Toshiba Corp., Kawasaki, Japan.) *In* JPL, Third International Symposium on Artificial Intelligence, Robotics, and Automation for Space 1994 Oct. 1994 p 149-152 (For primary document see N95-23672 07-63)
Avail: CASI HC A01/MF A03

Japan is collaborating on the multinational space station program. The JEM, Japanese Experiment Module, has both a pressurized module and an Exposed Facility (EF). JEM Remote Manipulator System (JEMRMS) will play a dominant role in handling/servicing payloads and the maintenance of the EF, and consists of two robotic arms, a main arm and a small fine arm. JEM Flight Demonstration (JFD) is a space robotics experiment using the prototype small fine arm to demonstrate its capability, prior to the Space Station operation. The small fine arm will be installed in the Space Shuttle cargo bay and operated by a crew from a dedicated workstation in the Aft Flight Deck of the orbiter. Author

N95-23702*# National Aerospace Lab., Tokyo (Japan).
CONCEPT VERIFICATION OF THREE DIMENSIONAL FREE MOTION SIMULATOR FOR SPACE ROBOT **c14**
Osamu Okamoto, Teruomi Nakaya, and Brett Pokines (Virginia Polytechnic Inst. and State Univ., Blacksburg, VA.) *In* JPL, Third International Symposium on Artificial Intelligence, Robotics, and Automation for Space 1994 Oct. 1994 p 153-156 (For primary document see N95-23672 07-63)
Avail: CASI HC A01/MF A03

In the development of automatic assembling technologies for space structures, it is an indispensable matter to investigate and simulate the movements of robot satellites concerned with mission operation. The movement investigation and simulation on the ground will be effectively realized by a free motion simulator. Various types of ground systems for simulating free motion have been proposed and utilized. Some of these methods are a neutral buoyancy system, an air or magnetic suspension system, a passive suspension balance system, and a free flying aircraft or drop tower system. In addition, systems can be simulated by computers using an analytical model. Each free motion simulation method has limitations and well known problems, specifically, disturbance by water viscosity, limited number of degrees-of-freedom, complex dynamics induced by the attachment of the simulation system, short experiment time, and the lack of high speed super-computer simulation systems, respectively. The basic idea presented here is to realize 3-dimensional free motion. This is achieved by combining a spherical air bearing, a cylindrical air bearing, and a flat air bearing. A conventional air bearing system has difficulty realizing free vertical motion suspension. The idea of free vertical suspension is that a cylindrical air bearing and counter balance weight realize vertical free motion. This paper presents a design concept, configuration, and basic performance characteristics of an innovative free motion simulator. A prototype simulator verifies the feasibility of 3-dimensional free motion simulation. Derived from text

N95-23703*# McDonnell-Douglas Aerospace, Houston, TX.
THE CHARLOTTE (TM) INTRA-VEHICULAR ROBOT **c37**
Patrick L. Swaim, Clark J. Thompson, and Perry D. Campbell *In* JPL, Third International Symposium on Artificial Intelligence, Robotics, and Automation for Space 1994 Oct. 1994 p 157-162 (For primary document see N95-23672 07-63)
Avail: CASI HC A02/MF A03

NASA has identified telerobotics and telescience as essential technologies to reduce the crew extra-vehicular activity (EVA) and intra-vehicular activity (IVA) workloads. Under this project, we are developing and flight testing a novel IVA robot to relieve the crew of tedious and routine tasks. Through ground telerobotic control of this robot, we will enable ground researchers to routinely interact with experiments in space. Our approach is to develop an IVA robot system incrementally by employing a series of flight tests with increasing complexity. This approach has the advantages of providing an early IVA capability that can assist the crew, demonstrate capabilities that ground researchers can be confident of in planning for future experiments, and allow incremental refinement of system capabilities and insertion of new technology. In parallel with this approach to flight testing, we seek to establish ground test beds, in which the requirements of payload experimenters can be further investigated. In 1993 we reviewed manifested SpaceHab experiments and defined IVA robot requirements to assist in their operation. We also examined previous IVA robot designs and assessed them against flight requirements. We rejected previous design concepts on the basis of threat to crew safety, operability, and maintainability. Based on this insight, we developed an entirely new concept for IVA robotics, the CHARLOTTE robot system. Ground based testing of a prototype version of the system has already proven its ability to perform most common tasks demanded of the crew, including operation of switches, buttons, knobs, dials, and performing video surveys of experiments and switch panels. Derived from text

N95-23704*# Ministry of International Trade and Industry, Tsukuba (Japan). Electromechanical Lab.
DEVELOPMENT OF ADVANCED ROBOTIC HAND SYSTEM FOR SPACE APPLICATION **c54**
Kazuo Machida, Kenzo Akita (Institute for Unmanned Space Experiments Free Flyer, Tokyo, Japan.), Tatsuo Mikami (Fujitsu Ltd., Kawasaki, Japan.), and Satoru Komada (Fujitsu Ltd., Kawasaki, Japan.) *In* JPL, Third International Symposium on Artificial Intelligence, Robotics, and Automation for Space 1994 Oct. 1994 p 165-168 (For primary document see N95-23672 07-63)
Avail: CASI HC A01/MF A03

The Advanced Robotic Hand System (ARH) is a precise telerobotics system with a semi dexterous hand for future space application. The ARH will be tested in space as one of the missions of the Engineering Tests Satellite 7 (ETS-7) which will be launched in 1997. The objectives of the ARH development are to evaluate the capability of a possible robot hand for precise and delicate tasks and to validate the related technologies implemented in the system. The ARH is designed to be controlled both from ground as a teleoperation and by locally autonomous control. This paper presents the overall system design and the functional capabilities of the ARH as well as its mission outline as the preliminary design has been completed. Author

N95-23705*# Fujitsu Ltd., Kawasaki (Japan).
A THREE-FINGER MULTISENSORY HAND FOR DEXTEROUS SPACE ROBOTIC TASKS **c54**
Yuichi Murase, Satoru Komada, Takashi Uchiyama, Kazuo Machida (Ministry of International Trade and Industry, Tsukuba, Japan.), and Kenzo Akita (Institute for Unmanned Space Experiments Free Flyer, Tokyo, Japan.) *In* JPL, Third International Symposium on Artificial Intelligence, Robotics, and Automation for Space 1994 Oct. 1994 p 169-172 (For primary document see N95-23672 07-63)
Avail: CASI HC A01/MF A03

The National Space Development Agency of Japan will launch ETS-7 in 1997, as a test bed for next generation space technology of RV&D and space robot. MITI has been developing a three-finger multisensory hand

for complex space robotic tasks. The hand can be operated under remote control or autonomously. This paper describes the design and development of the hand and the performance of a breadboard model. Author

N95-23706*# Rockwell International Corp., Downey, CA. Space Systems Div.

HARDWARE INTERFACE UNIT FOR CONTROL OF SHUTTLE RMS VIBRATIONS **c37**

Thomas S. Lindsay, Joseph M. Hansen, Davoud Manouchehri, and Kamran Forouhar *In* JPL, Third International Symposium on Artificial Intelligence, Robotics, and Automation for Space 1994 Oct. 1994 p 173-176 (For primary document see N95-23672 07-63)

(Contract NAS1-19243)

Avail: CASI HC A01/MF A03

Vibration of the Shuttle Remote Manipulator System (RMS) increases the time for task completion and reduces task safety for manipulator-assisted operations. If the dynamics of the manipulator and the payload can be physically isolated, performance should improve. Rockwell has developed a self contained hardware unit which interfaces between a manipulator arm and payload. The End Point Control Unit (EPCU) is built and is being tested at Rockwell and at the Langley/Marshall Coupled, Multibody Spacecraft Control Research Facility in NASA's Marshall Space Flight Center in Huntsville, Alabama. Author

N95-23707*# Centre National d'Etudes Spatiales, Toulouse (France).

ROBOTIC EXPERIMENT WITH A FORCE REFLECTING HANDCONTROLLER ONBOARD MIR SPACE STATION **c54**

M. Delpech and Y. Matzakis (MATRA Marconi Space, Toulouse, France.) *In* JPL, Third International Symposium on Artificial Intelligence, Robotics, and Automation for Space 1994 Oct. 1994 p 177-181 (For primary document see N95-23672 07-63)

Avail: CASI HC A01/MF A03

During the French CASSIOPEE mission that will fly onboard MIR space station in 1996, ergonomic evaluations of a force reflecting handcontroller will be performed on a simulated robotic task. This handcontroller is a part of the COGNILAB payload that will be used also for experiments in neurophysiology. The purpose of the robotic experiment is the validation of a new control and design concept that would enhance the task performances for telemanipulating space robots. Besides the handcontroller and its control unit, the experimental system includes a simulator of the slave robot dynamics for both free and constrained motions, a flat display screen and a seat with special fixtures for holding the astronaut. Author

N95-23708*# National Space Development Agency, Tsukuba (Japan). Space Station Dept.

DEVELOPMENT OF JAPANESE EXPERIMENT MODULE REMOTE MANIPULATOR SYSTEM **c54**

Tatsuo Matsueda, Fumihiro Kuwao (Toshiba Corp., Kawasaki, Japan.), Shoichi Motohasi (Toshiba Corp., Kawasaki, Japan.), and Ryo Okamura (Toshiba Corp., Kawasaki, Japan.) *In* JPL, Third International Symposium on Artificial Intelligence, Robotics, and Automation for Space 1994 Oct. 1994 p 183-186 (For primary document see N95-23672 07-63)

Avail: CASI HC A01/MF A03

National Space Development Agency of Japan (NASDA) is developing the Japanese Experiment Module (JEM), as its contribution to the International Space Station. The JEM consists of the pressurized module (PM), the exposed facility (EF), the experiment logistics module pressurized section (ELM-PS), the experiment logistics module exposed section (ELM-ES) and the Remote Manipulator System (RMS). The JEMRMS services for the JEM EF, which is a space experiment platform, consists of the Main Arm (MA), the Small Fine Arm (SFA) and the RMS console. The MA handles the JEM EF payloads, the SFA and the JEM element, such as ELM-ES. Derived from text

N95-23709*# Toshiba Corp., Kawasaki (Japan). Space Systems Engineering Dept.

ROBOT ARM SYSTEM FOR AUTOMATIC SATELLITE CAPTURE AND BERTHING **c54**

Shinichiro Nishida, Hidetoshi Toriu, Masato Hayashi, Tomoaki Kubo, and Makoto Miyata *In* JPL, Third International Symposium on Artificial Intelligence, Robotics, and Automation for Space 1994 Oct. 1994 p 187-190 (For primary document see N95-23672 07-63)

Avail: CASI HC A01/MF A03

Load control is one of the most important technologies for capturing and berthing free flying satellites by a space robot arm because free flying satellites have different motion rates. The performance of active compliance control techniques depend on the location of the force sensor and the arm's structural compliance. A compliance control technique for the robot arm's structural elasticity and a consideration for an end-effector appropriate for it are presented in this paper. Author

N95-23710*# Communications Research Lab., Koganei (Japan).

ROBUST CONTROL OF MULTI-JOINTED ARM WITH A DECENTRALIZED AUTONOMOUS CONTROL MECHANISM **c32**

Shinichi Kimura, Ken Miyazaki, and Yoshiaki Suzuki *In* JPL, Third International Symposium on Artificial Intelligence, Robotics, and Automation for Space 1994 191-195 (SEE N95-23672 07-63) Oct. 1994 (For primary document see N95-23672 07-63)

Avail: CASI HC A02/MF A03

A decentralized autonomous control mechanism applied to the control of three dimensional manipulators and its robustness to partial damage was assessed by computer simulation. Decentralized control structures are believed to be quite robust to time delay between the operator and the target system. A 10-jointed manipulator based on our control mechanism was able to continue its positioning task in three-dimensional space without revision of the control program, even after some of its joints were damaged. These results suggest that this control mechanism can be effectively applied to space telerobots, which are associated with serious time delay between the operator and the target system, and which cannot be easily repaired after being partially damaged. Author

N95-23711*# Tokyo Inst. of Tech. (Japan). Dept. of Mechano-Aerospace Engineering.

DEVELOPMENT OF THE DYNAMIC MOTION SIMULATOR OF 3D MICRO-GRAVITY WITH A COMBINED PASSIVE/ACTIVE SUSPENSION SYSTEM **c14**

Kazuya Yoshida, Shigeo Hirose, and Tadashi Ogawa *In* JPL, Third International Symposium on Artificial Intelligence, Robotics, and Automation for Space 1994 Oct. 1994 p 197-200 (For primary document see N95-23672 07-63)

Avail: CASI HC A01/MF A03

The establishment of those in-orbit operations like 'Rendez-Vous/Docking' and 'Manipulator Berthing' with the assistance of robotics or autonomous control technology, is essential for the near future space programs. In order to study the control methods, develop the flight models, and verify how the system works, we need a tool or a testbed which enables us to simulate mechanically the micro-gravity environment. There have been many attempts to develop the micro-gravity testbeds, but once the simulation goes into the docking and berthing operation that involves mechanical contacts among multi bodies, the requirement becomes critical. A group at the Tokyo Institute of Technology has proposed a method that can simulate the 3D micro-gravity producing a smooth response to the impact phenomena with relatively simple apparatus. Recently the group carried out basic experiments successfully using a prototype hardware model of the testbed. This paper will present our idea of the 3D micro-gravity simulator and report the results of our initial experiments.

Derived from text

N95-23712*# National Space Development Agency, Tsukuba (Japan). Space Center.

SMALL IMAGE LASER RANGE FINDER FOR PLANETARY ROVER **c36**

Yasufumi Wakabayashi, Masahisa Honda, Tadashi Adachi, and Takahiko Iijima *In* JPL, Third International Symposium on Artificial Intelligence, Robotics, and Automation for Space 1994 Oct. 1994 p 201-204 (For primary document see N95-23672 07-63)

Avail: CASI HC A01/MF A03

A variety of technical subjects need to be solved before planetary rover navigation could be a part of future missions. The sensors which will perceive terrain environment around the rover will require critical development efforts. The image laser range finder (ILRF) discussed here is one of the candidate sensors because of its advantage in providing range data required for its navigation. The authors developed a new compact-sized ILRF which is a quarter of the size of conventional ones. Instead of the current two

directional scanning system which is comprised of nodding and polygon mirrors, the new ILRF is equipped with the new concept of a direct polygon mirror driving system, which successfully made its size compact to accommodate the design requirements. The paper reports on the design concept and preliminary technical specifications established in the current development phase. Author

N95-23713*# National Space Development Agency, Tsukuba (Japan). Systems Engineering Dept.

AUTOMATIC SATELLITE CAPTURE AND BERTHING WITH ROBOT ARM (ASCABRA) **c18**

Noriyasu Inaba, Yasufumi Wakabayashi, and Takahiko Iijima *In* JPL, Third International Symposium on Artificial Intelligence, Robotics, and Automation for Space 1994 Oct. 1994 p 205-208 (For primary document see N95-23672 07-63)

Avail: CASI HC A01/MF A03

The NASDA office of R&D is studying an automatic technique to capture and berth free-floating satellites using a robot arm on another satellite. A demonstration experiment plan with the Japanese engineering test satellite ETS-7 is being developed based on the basic research on the ground. The overview and key technologies of this experiment plan are presented, and future applications of the automatic capture technique are also reviewed. Author

N95-23714*# Organisatie voor Toegepast Natuurwetenschappelijk Onderzoek, The Hague (Netherlands). Physics and electronics Lab.

POINTER: PORTABLE INTELLIGENT TRAINER FOR EXTERNAL ROBOTICS **c54**

Hilbert Kuiper and Patrick J. Rikken *In* JPL, Third International Symposium on Artificial Intelligence, Robotics, and Automation for Space 1994 Oct. 1994 p 209-212 (For primary document see N95-23672 07-63)

Avail: CASI HC A01/MF A03

Intelligent tutoring systems (ITS's) play an increasing role in training and education of people with different levels of skill and knowledge. As compared to conventional computer based training (CBT) an ITS provides more tailored instruction by trying to mimic the teaching behavior of a human instructor as much as possible and is therefore much more flexible. This paper starts with an introduction to ITS's, followed by the description of an ITS for training of an (astronaut) operator in monitoring and controlling robotic arm procedures. The robotic arm will be used for exchange of equipment between a space station and a space plane involving critical and accurate movements of the robotic arm. The ITS for this application, called Pointer, is developed by TNO Physics and Electronics Laboratory and is based upon an existing ITS that includes procedural training. Pointer has been developed on a workstation whereas the target platform was a portable computer. Therefore, a lot of attention had to be paid to scaling effects and keeping up with user friendliness of the much smaller user interface. Although the learning domain was the control of a robotic arm, it is clear that use of intelligent training technologies on a portable computer has many other applications (payload operations, operation control rooms, etc.). Training can occur at any time and place in an attractive and cost effective way. Author

N95-23715*# National Space Development Agency, Tsukuba (Japan). Space Experiment Dept.

AUTOMATION AND CREW TIME SAVING IN THE SPACE EXPERIMENT **c54**

Kohtaro Matsumoto, Tsuyoshi Suzuki, Kouichi Funaya (NEC Corp., Kawasaki, Japan.), Takeya Kawamura (Mitsubishi Heavy Industries Ltd., Wadasaki, Japan.), and Masayoshi Sonobe (Hitachi Ltd., Japan.) *In* JPL, Third International Symposium on Artificial Intelligence, Robotics, and Automation for Space 1994 Oct. 1994 p 215-218 (For primary document see N95-23672 07-63)

Avail: CASI HC A01/MF A03

We describe preliminary results of the feasibility study of automation and crew workload saving in space experiments on the space station. Some functions have been studied that can be automated within a single rack and without major impact to the development process and costs. In addition, we assume the following premises: (1) applicable as the second generation apparatuses; (2) maximum reduction of the crew workload; and (3) automation between racks including storage. Four apparatuses have been selected as the study case; results for three are summarized. Derived from text

N95-23716*# Rutgers - The State Univ., Piscataway, NJ. Dept. of Computer Science.

A TOOLBOX AND RECORD FOR SCIENTIFIC MODELS

Thomas Ellman *In* JPL, Third International Symposium on Artificial Intelligence, Robotics, and Automation for Space 1994 Oct. 1994 p 219-222 (For primary document see N95-23672 07-63)

(Contract NCC2-802)

Avail: CASI HC A01/MF A03

Computational science presents a host of challenges for the field of knowledge-based software design. Scientific computation models are difficult to construct. Models constructed by one scientist are easily misapplied by other scientists to problems for which they are not well-suited. Finally, models constructed by one scientist are difficult for others to modify or extend to handle new types of problems. Construction of scientific models actually involves much more than the mechanics of building a single computational model. In the course of developing a model, a scientist will often test a candidate model against experimental data or against a priori expectations. Test results often lead to revisions of the model and a consequent need for additional testing. During a single model development session, a scientist typically examines a whole series of alternative models, each using different simplifying assumptions or modeling techniques. A useful scientific software design tool must support these aspects of the model development process as well. In particular, it should propose and carry out tests of candidate models. It should analyze test results and identify models and parts of models that must be changed. It should determine what types of changes can potentially cure a given negative test result. It should organize candidate models, test data, and test results into a coherent record of the development process. Finally, it should exploit the development record for two purposes: (1) automatically determining the applicability of a scientific model to a given problem; (2) supporting revision of a scientific model to handle a new type of problem. Existing knowledge-based software design tools must be extended in order to provide these facilities. Derived from text

N95-23717*# Jet Propulsion Lab., California Inst. of Tech., Pasadena, CA.

A NEW GENERATION OF INTELLIGENT TRAINABLE TOOLS FOR ANALYZING LARGE SCIENTIFIC IMAGE DATABASES

Usama M. Fayyad, Padhraic Smyth, and David J. Atkinson *In its* Third International Symposium on Artificial Intelligence, Robotics, and Automation for Space 1994 Oct. 1994 p 223-227 (For primary document see N95-23672 07-63)

Avail: CASI HC A01/MF A03

The focus of this paper is on the detection of natural, as opposed to human-made, objects. The distinction is important because, in the context of image analysis, natural objects tend to possess much greater variability in appearance than human-made objects. Hence, we shall focus primarily on the use of algorithms that 'learn by example' as the basis for image exploration. The 'learn by example' approach is potentially more generally applicable compared to model-based vision methods since domain scientists find it relatively easier to provide examples of what they are searching for versus describing a model. Derived from text

N95-23718*# National Aeronautics and Space Administration. Ames Research Center, Moffett Field, CA. Artificial Intelligence Research Branch.

SPACE SCIENCE EXPERIMENTATION AUTOMATION AND SUPPORT

Richard J. Frainier, Nicolas Groleau, and Jeff C. Shapiro *In* JPL, Third International Symposium on Artificial Intelligence, Robotics, and Automation for Space 1994 Oct. 1994 p 229-232 (For primary document see N95-23672 07-63)

Avail: CASI HC A01/MF A03

This paper outlines recent work done at the NASA Ames Artificial Intelligence Research Laboratory on automation and support of science experiments on the US Space Shuttle in low earth orbit. Three approaches to increasing the science return of these experiments using emerging automation technologies are described: remote control (telescience), science advisors for astronaut operators, and fully autonomous experiments. The

capabilities and limitations of these approaches are reviewed.
Derived from text

N95-23719*# Hitachi Ltd., Kawasaki (Japan). Systems Development Lab.
AUTONOMOUS SPACECRAFT EXECUTIVE AND ITS APPLICATION TO RENDEZVOUS AND DOCKING **c18**
Fuminobu Komura, Masatoshi Furuya, Toshiro Sasaki, Robert L. Anderson (TRW Systems Group, Redondo Beach, CA.), and Roy K. Tsugawa (TRW Systems Group, Redondo Beach, CA.) *In* JPL, Third International Symposium on Artificial Intelligence, Robotics, and Automation for Space 1994 Oct. 1994 p 235-238 (For primary document see N95-23672 07-63)
Avail: CASI HC A01/MF A03

Autonomy is needed for future spacecraft to solve the problems of human operator overload and transmission delay. This paper describes the autonomous spacecraft executive for rendezvous and docking. It is an onboard expert system and has decision making capability for mission planning of nominal and contingency cases. The executive has been developed and verified using a hardware motion based simulator. Author

N95-23720*# MATRA Marconi Space, Toulouse (France).
FORMALIZING PROCEDURES FOR OPERATIONS AUTOMATION, OPERATOR TRAINING AND SPACECRAFT AUTONOMY **c54**
Francois Lecouat and Arnaud DeSaintVincent *In* JPL, Third International Symposium on Artificial Intelligence, Robotics, and Automation for Space 1994 Oct. 1994 p 239-242 (For primary document see N95-23672 07-63)
Avail: CASI HC A01/MF A03

The generation and validation of operations procedures is a key task of mission preparation that is quite complex and costly. This has motivated the development of software applications providing support for procedures preparation. Several applications have been developed at MATRA MARCONI SPACE (MMS) over the last five years. They are presented in the first section of this paper. The main idea is that if procedures are represented in a formal language, they can be managed more easily with a computer tool and some automatic verifications can be performed. One difficulty is to define a formal language that is easy to use for operators and operations engineers. From the experience of the various procedures management tools developed in the last five years (including the POM, EOA, and CSS projects), MMS has derived OPSMAKER, a generic tool for procedure elaboration and validation. It has been applied to quite different types of missions, ranging from crew procedures (PREVISE system), ground control centers management procedures (PROCSU system), and - most relevant to the present paper - satellite operation procedures (PROCSAT developed for CNES, to support the preparation and verification of SPOT 4 operation procedures, and OPSAT for MMS telecom satellites operation procedures).
Derived from text

N95-23721*# Hughes Information Technology Corp., Aurora, IL.
THE STARPICKER EXPERT SYSTEM: A PROBLEM IN EXPERTISE CAPTURE **c18**
David Smith and G. Martin Hudson *In* JPL, Third International Symposium on Artificial Intelligence, Robotics, and Automation for Space 1994 Oct. 1994 p 245-248 (For primary document see N95-23672 07-63)
Avail: CASI HC A01/MF A03

This paper describes the Starpicker expert system, a tool for spacecraft operations planning. Both programmatic and technical aspects are discussed. Author

N95-23722*# National Space Development Agency, Tsukuba (Japan).
ROBOTIC SERVICING SYSTEM FOR SPACE MATERIAL EXPERIMENT **c37**
Toshihiko Yamawaki, Haruhiko Shimoji (Mitsubishi Electric Corp., Amagasaki, Japan.), and Toshio Abe (Mitsubishi Electric Corp., Kamakura, Japan.) *In* JPL, Third International Symposium on Artificial Intelligence, Robotics, and Automation for Space 1994 Oct. 1994 p 253-256 (For primary document see N95-23672 07-63)
Avail: CASI HC A01/MF A03

A containerless image furnace with an electrostatic positioning device has been developed as one of the material experiment facilities on the Japanese experimental module (JEM). It is characterized by heating/melting/cooling the sample whose position is kept without any contacts by actively controlled electrostatic force exerted between the sample and a set of electrodes. The experiment using the image furnace requires various servicing operations. We have been developing a robotic servicing system with an internal robot accommodated in the rack as an alternative to the crew. It aims to reduce the load on the crew by automating regular tasks and to increase the flexibility applicable to simple irregular tasks by introducing a remote teleoperation scheme. The present robot has poor capability to replace the crew. In order to compensate it, introducing of the concept of the robot friendliness and improving the controllability of the teleoperation by the ground operator aids are essential. In this paper, we identify the tasks to be performed by the robotic servicing system and discuss the way to compensate the capability of the robot. In addition we describe the evaluation tests using an experimental model.
Derived from text

N95-23723*# National Aeronautics and Space Administration. Lyndon B. Johnson Space Center, Houston, TX.
DEXTEROUS ORBITAL SERVICING SYSTEM (DOSS) **c54**
Charles R. Price, Reginald B. Berka, and John T. Chladek *In* JPL, Third International Symposium on Artificial Intelligence, Robotics, and Automation for Space 1994 Oct. 1994 p 257-260 (For primary document see N95-23672 07-63)
Avail: CASI HC A01/MF A03

The Dexterous Orbiter Servicing System (DOSS) is a dexterous robotic spaceflight system that is based on the manipulator designed as part of the Flight Telerobotics Servicer program for the Space Station Freedom and built during a 'technology capture' effort that was commissioned when the FTS was cancelled from the Space Station Freedom program. The FTS technology capture effort yielded one flight manipulator and the 1 g hydraulic simulator that had been designed as an integrated test tool and crew trainer. The DOSS concept was developed to satisfy needs of the telerobotics research community, the space shuttle, and the space station. As a flight testbed, DOSS would serve as a baseline reference for testing the performance of advanced telerobotics and intelligent robotics components. For shuttle, the DOSS, configured as a movable dexterous tool, would be used to provide operational flexibility for payload operations and contingency operations. As a risk mitigation flight demonstration, the DOSS would serve the International Space Station to characterize the end to end system performance of the Special Purpose Dexterous Manipulator performing assembly and maintenance tasks with actual ISSA orbital replacement units. Currently, the most likely entrance of the DOSS into spaceflight is a risk mitigation flight experiment for the International Space Station. Author

N95-23724*# National Aeronautics and Space Administration. John F. Kennedy Space Center, Cocoa Beach, FL.
ROBOTIC SYSTEM FOR THE SERVICING OF THE ORBITER THERMAL PROTECTION SYSTEM **c37**
Todd Graham, Richard Bennett, Kevin Dowling, Davoud Manouchehri, Eric Cooper, and Cregg Cowan *In* JPL, Third International Symposium on Artificial Intelligence, Robotics, and Automation for Space 1994 Oct. 1994 p 263-266 (For primary document see N95-23672 07-63)
Avail: CASI HC A01/MF A03

This paper describes the design and development of a mobile robotic system to process orbiter thermal protection system (TPS) tiles. This work was justified by a TPS automation study which identified tile rewaterproofing and visual inspection as excellent applications for robotic automation.
Derived from text

N95-23725*# Canadian Space Agency, Saint Hubert (Quebec).
ROBOTICS AND TELEPRESENCE FOR MOON MISSIONS **c91**
Christian Sallaberger *In* JPL, Third International Symposium on Artificial Intelligence, Robotics, and Automation for Space 1994 Oct. 1994 p 269-273 (For primary document see N95-23672 07-63)
Avail: CASI HC A01/MF A03

An integrated moon program has often been proposed as a logical next step for today's space efforts. In the context of preparing for the possibility of launching a moon program, the European Space Agency is currently conducting an internal study effort which is focusing on the assessment of key technologies. Current thinking has this moon program organized into four phases. Phase 1 will deal with lunar resource exploration.

The goal would be to produce a complete chemical inventory of the moon, including oxygen, water, other volatiles, carbon, silicon, and other resources. Phase 2 will establish a permanent robotic presence on the moon via a number of landers and surface rovers. Phase 3 will extend the second phase and concentrate on the use and exploitation of local lunar resources. Phase 4 will be the establishment of a first human outpost. Some preliminary work such as the building of the outpost and the installation of scientific equipment will be done by unmanned systems before a human crew is sent to the moon. Derived from text

N95-23726*# National Aerospace Lab., Tokyo (Japan).
TRUSS STRUCTURE TELE-MANIPULATION EXPERIMENT USING ETS-7 **c18**

Kohtaro Matsumoto, Seishiroh Kibe, Isao Yamaguchi, Takashi Kida, Sachiko Wakabayashi, Hiroshi Ueno (Shimizu Corp., Japan.), Hitoshi Sato (Shimizu Corp., Japan.), Shigeru Aoki (Shimizu Corp., Japan.), and Tetsuji Yoshida (Shimizu Corp., Japan.) *In* JPL, Third International Symposium on Artificial Intelligence, Robotics, and Automation for Space 1994 Oct. 1994 p 275-278 (For primary document see N95-23672 07-63)
Avail: CASI HC A01/MF A03

A robot experiment concept of space truss telemanipulation by National Aerospace Laboratory (NAL) is described in its flight model development. The experiment will be carried out on the Engineering Test Satellite No. 7 (ETS-7) using its robot arm. The satellite is scheduled to be launched in 1997 by National Space Development Agency of Japan (NASDA). The truss flight model is composed of deployable truss system and assemble truss joint. Those truss components will be manipulated by the ETS-7 robot arm using its small grapple fixture type-N (GPF-N), and the experimental task operation will be executed from the ground control station. Author (revised)

N95-23727*# Communications Research Lab., Koganei (Japan).
ANTENNA-ASSEMBLING MECHANISM TEST ON ETS-7 **c18**

Yoshiaki Suzuki, Shinichi Kimura, Tetsuo Takahashi, Kazuo Nakamura (NEC Corp., Ikebe, Japan.), and Hajime Morikawa (NEC Corp., Ikebe, Japan.) *In* JPL, Third International Symposium on Artificial Intelligence, Robotics, and Automation for Space 1994 Oct. 1994 p 279-284 (For primary document see N95-23672 07-63)
Avail: CASI HC A02/MF A03

The Communications Research Laboratory plans to test an antenna-assembling mechanism on the Engineering Test Satellite 7. The test is one of the application missions for the space robotics experiments that will be conducted mainly by the National Space Development Agency of Japan (NASDA). The purpose of the test is to verify the ability of the antenna assembling mechanism to function in space and to experiment on the teleoperation of a space robot to develop antenna-assembling technology. We present the test experiment plans and the outline of the onboard assembling mechanism. Author (revised)

N95-23728*# Electrotechnical Lab., Tsukuba (Japan).
INTELLIGENT MONITORING SYSTEM APPLIED TO SUPER LONG DISTANCE TELEROBOTIC TASKS

Yujin Wakita, Shigeoki Hirai, and Kazuo Machida *In* JPL, Third International Symposium on Artificial Intelligence, Robotics, and Automation for Space 1994 Oct. 1994 p 285-288 (For primary document see N95-23672 07-63)
Avail: CASI HC A01/MF A03

Time delay and small capacity of communication are the primary constraint in super long distance telerobotic systems such as astronautical robotic tasks. Intelligent telerobotics is thought to break this constraint. We aim to realize this super long distance telerobotic system with object handling knowledge base and intelligent monitoring. We will discuss physical and technical factors for this purpose. Author

N95-23729*# Ministry of International Trade and Industry, Tsukuba (Japan). Mechanical Engineering Lab.
MANIPULATING FLEXIBLE PARTS USING A TELEOPERATED SYSTEM WITH TIME DELAY: AN EXPERIMENT

T. Kotoku, K. Takamune, K. Tanie, K. Komoriya, N. Matsuhira (Toshiba Corp., Kawasaki, Japan.), M. Asakura (Toshiba Corp., Kawasaki, Japan.), and H. Bamba (Toshiba Corp., Kawasaki, Japan.) *In* JPL, Third International Symposium on Artificial Intelligence, Robotics, and Automation for Space 1994 Oct. 1994 p 289-292 (For primary document see N95-23672 07-63)
Avail: CASI HC A01/MF A03

This paper reports experiments involving the handling of flexible parts (e.g. wires) when using a teleoperated system with time delay. The task is principally a peg-in-hole task involving the wrapping of a wire around two posts on the task-board. It is difficult to estimate the effects of the flexible parts; therefore, on-line teleoperation is indispensable for this class of unpredictable task. We first propose a teleoperation system based on the predictive image display, then describe an experimental teleoperation testbed with a four second transmission time delay. Finally, we report on wire handling operations that were performed to evaluate the performance of this system. Those experiments will contribute to future advanced experiments for the MITI ETS-7 mission. Author

N95-23730*# Deutsche Aerospace A.G., Bremen (Germany).
INTERACTIVE AUTONOMY AND ROBOTIC SKILLS

A. Kellner and B. Maediger *In* JPL, Third International Symposium on Artificial Intelligence, Robotics, and Automation for Space 1994 Oct. 1994 p 293-295 (For primary document see N95-23672 07-63)
Avail: CASI HC A01/MF A03

Current concepts of robot-supported operations for space laboratories (payload servicing, inspection, repair, and ORU exchange) are mainly based on the concept of 'interactive autonomy' which implies autonomous behavior of the robot according to predefined timelines, predefined sequences of elementary robot operations and within predefined world models supplying geometrical and other information for parameter instantiation on the one hand, and the ability to override and change the predefined course of activities by human intervention on the other hand. Although in principle a very powerful and useful concept, in practice the confinement of the robot to the abstract world models and predefined activities appears to reduce the robot's stability within real world uncertainties and its applicability to non-predefined parts of the world, calling for frequent corrective interaction by the operator, which in itself may be tedious and time-consuming. Methods are presented to improve this situation by incorporating 'robotic skills' into the concept of interactive autonomy. Derived from text

N95-23731*# Centre National de la Recherche Scientifique, Toulouse (France).
VISUALLY GUIDED GRASPING TO STUDY TELEPROGRAMMATION WITHIN THE BAROCO TESTBED

M. Devy, V. Garric, M. Delpech (Centre National d'Etudes Spatiales, Toulouse, France.), and C. Proy (Centre National d'Etudes Spatiales, Toulouse, France.) *In* JPL, Third International Symposium on Artificial Intelligence, Robotics, and Automation for Space 1994 Oct. 1994 p 297-300 (For primary document see N95-23672 07-63)
Avail: CASI HC A01/MF A03

This paper describes vision functionalities required in future orbital laboratories; in such systems, robots will be needed in order to execute the on-board scientific experiments or servicing and maintenance tasks under the remote control of ground operators. For this sake, ESA has proposed a robotic configuration called EMATS; a testbed has been developed by ESTEC in order to evaluate the potentialities of EMATS-like robot to execute scientific tasks in automatic mode. For the same context, CNES develops the BAROCO testbed to investigate remote control and teleprogrammation, in which high level primitives like 'Pick Object A' are provided as basic primitives. In nominal situations, the system has an a priori knowledge about the position of all objects. These positions are not very accurate, but this knowledge is sufficient in order to predict the position of the object which must be grasped, with respect to the manipulator frame. Vision is required in order to insure a correct grasping and to guarantee a good accuracy for the following operations. We describe our results about a visually guided grasping of static objects. It seems to be a very classical problem, and a lot of results are available. But, in many cases, it lacks a realistic evaluation of the accuracy, because such an evaluation requires tedious experiments. We propose several results about calibration of the experimental testbed, recognition algorithms required to locate a 3D polyhedral object, and the grasping itself. Derived from text

N95-23732*# Italian Space Agency, Rome.
PLANETARY STATIONS AND ABYSSAL BENTHIC LABORATORIES: AN OVERVIEW OF PARALLEL APPROACHES FOR LONG-TERM INVESTIGATION IN EXTREME ENVIRONMENTS **c54**
S. DiPippo, W. Prendin (Tecnomare S.p.A., Italy.), and F. Gasparoni (Tecnomare S.p.A., Italy.) *In* JPL, Third International Symposium on Artificial Intelligence, Robotics, and Automation for Space 1994 Oct. 1994 p 301-304 (For primary document see N95-23672 07-63)
Avail: CASI HC A01/MF A03

In spite of the apparent great differences between deep ocean and space environment, significant similarities can be recognized when considering the possible solutions and technologies enabling the development of remote automatic stations supporting the execution of scientific activities. In this sense it is believed that mutual benefits shall be derived from the exchange of experiences and results between people and organizations involved in research and engineering activities for hostile environments, such as space, deep sea, and polar areas. A significant example of possible technology transfer and common systematic approach is given, which describes in some detail how the solutions and the enabling technologies identified for an Abyssal Benthic Laboratory can be applied for the case of a lunar or planetary station. Author

N95-23733*# Fujitsu Ltd., Kawasaki (Japan).
DESIGN OF TELEOPERATION SYSTEM WITH A FORCE-REFLECTING REAL-TIME SIMULATOR
Mitsunori Hirata, Yuichi Sato, Fumio Nagashima, and Tsugito Maruyama *In* JPL, Third International Symposium on Artificial Intelligence, Robotics, and Automation for Space 1994 Oct. 1994 p 305-308 (For primary document see N95-23672 07-63)
Avail: CASI HC A01/MF A03

We developed a force-reflecting teleoperation system that uses a real-time graphic simulator. This system eliminates the effects of communication time delays in remote robot manipulation. The simulator provides the operator with predictive display and feedback of computed contact forces through a six-degree of freedom (6-DOF) master arm on a real-time basis. With this system, peg-in-hole tasks involving round-trip communication time delays of up to a few seconds were performed at three support levels: a real image alone, a predictive display with a real image, and a real-time graphic simulator with computed-contact-force reflection and a predictive display. The experimental results indicate the best teleoperation efficiency was achieved by using the force-reflecting simulator with two images. The shortest work time, lowest sensor maximum, and a 100 percent success rate were obtained. These results demonstrate the effectiveness of simulated-force-reflecting teleoperation efficiency. Author

N95-23734*# Kawasaki Heavy Industries Ltd., Kakamigahara (Japan). Space Systems Engineering Div.
TELEROBOTICS TEST BED FOR SPACE STRUCTURE ASSEMBLY **c14**
M. Kitami, K. Ogimoto, F. Yasumoto (Kawasaki Heavy Industries Ltd., Akashi, Japan.), T. Katsuragawa (Kawasaki Heavy Industries Ltd., Akashi, Japan.), T. Itoko (Kawasaki Heavy Industries Ltd., Akashi, Japan.), Y. Kurosaki (Kawasaki Heavy Industries Ltd., Akashi, Japan.), S. Hirai (Ministry of International Trade and Industry, Tsukuba, Japan.), and K. Machida (Ministry of International Trade and Industry, Tsukuba, Japan.) *In* JPL, Third International Symposium on Artificial Intelligence, Robotics, and Automation for Space 1994 Oct. 1994 p 309-312 (For primary document see N95-23672 07-63)
Avail: CASI HC A01/MF A03

A cooperative research on super long distance space telerobotics is now in progress both in Japan and USA. In this program. several key features will be tested, which can be applicable to the control of space robots as well as to terrestrial robots. Local (control) and remote (work) sites will be shared between Electrotechnical Lab (ETL) of MITI in Japan and Jet Propulsion Lab (JPL) in USA. The details of a test bed for this international program are discussed in this report. Derived from text

N95-23735*# National Aeronautics and Space Administration. Lyndon B. Johnson Space Center, Houston, TX.
TELEPRESENCE CONTROL OF A DUAL-ARM DEXTEROUS ROBOT **c54**
Larry Li, Brian Cox (Lockheed Engineering and Sciences Co., Houston, TX.), Susan Shelton (Lockheed Engineering and Sciences Co., Houston, TX.), and Myron Diftler (Lockheed Engineering and Sciences Co., Houston, TX.) *In* JPL, Third International Symposium on Artificial Intelligence, Robotics, and Automation for Space 1994 Oct. 1994 p 313-316 (For primary document see N95-23672 07-63)
Avail: CASI HC A01/MF A03

Telepresence is an approach to teleoperation that provides egocentric, intuitive interactions between an operator and a remote environment. This approach takes advantage of the natural cognitive and sensory-motor skills of an on-orbit crew and effectively transfers them to a slave robot. A dual-arm dexterous robot operating under telepresence control has been developed and is being evaluated. Preliminary evaluation revealed several important observations that suggest the directions of future enhancement. Author

N95-23736*# Fujitsu Ltd., Kawasaki (Japan).
MARK TRACKING: POSITION/ORIENTATION MEASUREMENTS USING 4-CIRCLE MARK AND ITS TRACKING EXPERIMENTS
Shinji Kanda, Keijyu Okabayashi, Tsugito Maruyama, and Takashi Uchiyama *In* JPL, Third International Symposium on Artificial Intelligence, Robotics, and Automation for Space 1994 Oct. 1994 p 319-322 (For primary document see N95-23672 07-63)
Avail: CASI HC A01/MF A03

Future space robots require position and orientation tracking with visual feedback control to track and capture floating objects and satellites. We developed a four-circle mark that is useful for this purpose. With this mark, four geometric center positions as feature points can be extracted from the mark by simple image processing. We also developed a position and orientation measurement method that uses the four feature points in our mark. The mark gave good enough image measurement accuracy to let space robots approach and contact objects. A visual feedback control system using this mark enabled a robot arm to track a target object accurately. The control system was able to tolerate a time delay of 2 seconds. Author

N95-23737*# National Aerospace Lab., Tokyo (Japan).
A FUZZY STRUCTURAL MATCHING SCHEME FOR SPACE ROBOTICS VISION
Masao Naka, Hiromichi Yamamoto, Khozo Homma, and Yoshitaka Iwata (Fujitsu F.I.P., Inc., Sibuya, Japan.) *In* JPL, Third International Symposium on Artificial Intelligence, Robotics, and Automation for Space 1994 Oct. 1994 p 323-326 (For primary document see N95-23672 07-63)
Avail: CASI HC A01/MF A03

In this paper, we propose a new fuzzy structural matching scheme for space stereo vision which is based on the fuzzy properties of regions of images and effectively reduces the computational burden in the following low level matching process. Three dimensional distance images of a space truss structural model are estimated using this scheme from stereo images sensed by Charge Coupled Device (CCD) TV cameras. Author

N95-23738*# Dassault Aviation, Saint-Cloud (France).
ACTIVE VISION IN SATELLITE SCENE ANALYSIS
Martine Naillon *In* JPL, Third International Symposium on Artificial Intelligence, Robotics, and Automation for Space 1994 Oct. 1994 p 327-330 (For primary document see N95-23672 07-63)
Avail: CASI HC A01/MF A03

In earth observation or planetary exploration it is necessary to have more and, more autonomous systems, able to adapt to unpredictable situations. This imposes the use, in artificial systems, of new concepts in cognition, based on the fact that perception should not be separated from recognition and decision making levels. This means that low level signal processing (perception level) should interact with symbolic and high level processing (decision level). This paper is going to describe the new concept of active vision, implemented in Distributed Artificial Intelligence by Dassault Aviation following a 'structuralist' principle. An application to spatial image interpretation is given, oriented toward flexible robotics. Derived from text

N95-23739*# Teleos Research, Palo Alto, CA.
REAL-TIME TRACKING USING STEREO AND MOTION: VISUAL PERCEPTION FOR SPACE ROBOTICS
H. Keith Nishihara, Hans Thomas, Eric Huber (Mitre Corp., Houston, TX.), and C. Ann Reid *In* JPL, Third International Symposium on Artificial

Intelligence, Robotics, and Automation for Space 1994 Oct. 1994 p 331-334 (For primary document see N95-23672 07-63)
Avail: CASI HC A01/MF A03

The state-of-the-art in computing technology is rapidly attaining the performance necessary to implement many early vision algorithms at real-time rates. This new capability is helping to accelerate progress in vision research by improving our ability to evaluate the performance of algorithms in dynamic environments. In particular, we are becoming much more aware of the relative stability of various visual measurements in the presence of camera motion and system noise. This new processing speed is also allowing us to raise our sights toward accomplishing much higher-level processing tasks, such as figure-ground separation and active object tracking, in real-time. This paper describes a methodology for using early visual measurements to accomplish higher-level tasks; it then presents an overview of the high-speed accelerators developed at Teleos to support early visual measurements. The final section describes the successful deployment of a real-time vision system to provide visual perception for the Extravehicular Activity Helper/Retriever robotic system in tests aboard NASA's KC135 reduced gravity aircraft. Derived from text

N95-23740*# Space Telescope Science Inst., Baltimore, MD.
PLANNING AND SCHEDULING THE HUBBLE SPACE TELESCOPE: PRACTICAL APPLICATION OF ADVANCED TECHNIQUES **c89**
Glenn E. Miller *In* JPL, Third International Symposium on Artificial Intelligence, Robotics, and Automation for Space 1994 Oct. 1994 p 339-343 (For primary document see N95-23672 07-63)
Avail: CASI HC A01/MF A03

NASA's Hubble Space Telescope (HST) is a major astronomical facility that was launched in April, 1990. In late 1993, the first of several planned servicing missions refurbished the telescope, including corrections for a manufacturing flaw in the primary mirror. Orbiting above the distorting effects of the Earth's atmosphere, the HST provides an unrivaled combination of sensitivity, spectral coverage and angular resolution. The HST is arguably the most complex scientific observatory ever constructed and effective use of this valuable resource required novel approaches to astronomical observation and the development of advanced software systems including techniques to represent scheduling preferences and constraints, a constraint satisfaction problem (CSP) based scheduler and a rule based planning system. This paper presents a discussion of these systems and the lessons learned from operational experience. Derived from text

N95-23741*# Computer Sciences Corp., Greenbelt, MD. Science Programs.
A CONSTRAINT-LOGIC BASED IMPLEMENTATION OF THE COARSE-GRAINED APPROACH TO DATA ACQUISITION SCHEDULING OF THE INTERNATIONAL ULTRAVIOLET EXPLORER ORBITING OBSERVATORY **c89**
Bruce McCollum and Mark Graves (Baylor Coll. of Medicine, Houston, TX.) *In* JPL, Third International Symposium on Artificial Intelligence, Robotics, and Automation for Space 1994 Oct. 1994 p 343-346 (For primary document see N95-23672 07-63)
Avail: CASI HC A01/MF A03

The International Ultraviolet Explorer (IUE) satellite observatory has been in operation continuously since 1978. It typically carries out several thousand observations per year for over a hundred different science projects. These observations, which can occur in one of four different data-taking modes, fall under several satellite-related constraints and many other constraints which derive from the science goals of the projects being undertaken. One strategy which has made the scheduling problem tractable has been that of 'coarse-graining' the time into discrete blocks of equal size (8 hours), each of which is devoted to a single science program, and each of which is sufficiently long for several observations to be carried out. We call it 'coarse-graining' because the schedule is done at a 'coarse' level which ignores fine structure; i.e., no attempt is made to plan the sequence of observations occurring within each time block. We have incorporated the IUE's coarse-grained approach in new software which examines the science needs of the observations and produces a limited set of alternative schedules which meet all of the instrument and science-related constraints. With this algorithm, the IUE can still be scheduled by a single person using a standard workstation, as it has been. We believe that this software could could be adapted to a more complex mission while retaining the IUE's high flexibility and efficiency and scientific return of future satellite missions. Derived from text

N95-23742*# National Aeronautics and Space Administration. Ames Research Center, Moffett Field, CA.
ROBUST TELESCOPE SCHEDULING **c89**
Keith Swanson, John Bresina (RECOM Technologies, Inc., Moffett Field, CA.), and Mark Drummond (RECOM Technologies, Inc., Moffett Field, CA.) *In* JPL, Third International Symposium on Artificial Intelligence, Robotics, and Automation for Space 1994 Oct. 1994 p 347-350 (For primary document see N95-23672 07-63)
Avail: CASI HC A01/MF A03

This paper presents a technique for building robust telescope schedules that tend not to break. The technique is called Just-In-Case (JIC) scheduling and it implements the common sense idea of being prepared for likely errors, just in case they should occur. The JIC algorithm analyzes a given schedule, determines where it is likely to break, reinvokes a scheduler to generate a contingent schedule for each highly probable break case, and produces a 'multiply contingent' schedule. The technique was developed for an automatic telescope scheduling problem, and the paper presents empirical results showing that Just-In-Case scheduling performs extremely well for this problem. Author

N95-23743*# RECOM Technologies, Inc., Moffett Field, CA.
THE ASSOCIATE PRINCIPAL ASTRONOMER TELESCOPE OPERATIONS MODEL **c89**
Mark Drummond, John Bresina, Keith Swanson, Will Edgington, and Greg Henry (Tennessee State Univ., Nashville, TN.) *In* JPL, Third International Symposium on Artificial Intelligence, Robotics, and Automation for Space 1994 Oct. 1994 p 351-354 (For primary document see N95-23672 07-63)
Avail: CASI HC A01/MF A03

This paper outlines a new telescope operations model that is intended to achieve low operating costs with high operating efficiency and high scientific productivity. The model is based on the existing Principal Astronomer approach used in conjunction with ATIS, a language for commanding remotely located automatic telescopes. This paper introduces the notion of an Associate Principal Astronomer, or APA. At the heart of the APA is automatic observation loading and scheduling software, and it is this software that is expected to help achieve efficient and productive telescope operations. The purpose of the APA system is to make it possible for astronomers to submit observation requests to and obtain resulting data from remote automatic telescopes, via the Internet, in a highly-automated way that minimizes human interaction with the system and maximizes the scientific return from observing time. Author

N95-23744*# Heuristicrats Research, Inc., Berkeley, CA.
DTS: BUILDING CUSTOM, INTELLIGENT SCHEDULERS
Othar Hansson and Andrew Mayer *In* JPL, Third International Symposium on Artificial Intelligence, Robotics, and Automation for Space 1994 Oct. 1994 p 357-360 (For primary document see N95-23672 07-63)
Avail: CASI HC A01/MF A03

DTS is a decision-theoretic scheduler, built on top of a flexible toolkit -- this paper focuses on how the toolkit might be reused in future NASA mission schedulers. The toolkit includes a user-customizable scheduling interface, and a 'Just-For-You' optimization engine. The customizable interface is built on two metaphors: objects and dynamic graphs. Objects help to structure problem specifications and related data, while dynamic graphs simplify the specification of graphical schedule editors (such as Gantt charts). The interface can be used with any 'back-end' scheduler, through dynamically-loaded code, interprocess communication, or a shared database. The 'Just-For-You' optimization engine includes user-specific utility functions, automatically compiled heuristic evaluations, and a postprocessing facility for enforcing scheduling policies. The optimization engine is based on BPS, the Bayesian Problem-Solver (1,2), which introduced a similar approach to solving single-agent and adversarial graph search problems. Author

N95-23745*# Jet Propulsion Lab., California Inst. of Tech., Pasadena, CA.
AUTOMATED SYNTHESIS OF IMAGE PROCESSING PROCEDURES USING AI PLANNING TECHNIQUES

Steve Chien and Helen Mortensen *In its* Third International Symposium on Artificial Intelligence, Robotics, and Automation for Space 1994 Oct. 1994 p 361-364 (For primary document see N95-23672 07-63)
Avail: CASI HC A01/MF A03

This paper describes the Multimission VICAR (Video Image Communication and Retrieval) Planner (MVP) (Chien 1994) system, which uses artificial intelligence planning techniques (Iwasaki & Friedland, 1985, Pemberthy & Weld, 1992, Stefik, 1981) to automatically construct executable complex image processing procedures (using models of the smaller constituent image processing subprograms) in response to image processing requests made to the JPL Multimission Image Processing Laboratory (MIPL). The MVP system allows the user to specify the image processing requirements in terms of the various types of correction required. Given this information, MVP derives unspecified required processing steps and determines appropriate image processing programs and parameters to achieve the specified image processing goals. This information is output as an executable image processing program which can then be executed to fill the processing request. Author

N95-23746*# National Aeronautics and Space Administration. Marshall Space Flight Center, Huntsville, AL.
GRAPHICAL TIMELINE EDITING c61
Patrick E. Meyer and John P. Jaap *In* JPL, Third International Symposium on Artificial Intelligence, Robotics, and Automation for Space 1994 Oct. 1994 p 368 (For primary document see N95-23672 07-63)
Avail: CASI HC A01/MF A03

NASA's Experiment Scheduling Program (ESP), which has been used for approximately 12 Spacelab missions, is being enhanced with the addition of a Graphical Timeline Editor. The GTE Clipboard, as it is called, was developed to demonstrate new technology which will lead the development of International Space Station Alpha's Payload Planning System and support the remaining Spacelab missions. ESP's GTE Clipboard is developed in C using MIT's X Windows System X11R5 and follows OSF/Motif Style Guide Revision 1.2. Author

N95-23747*# National Aeronautics and Space Administration. Marshall Space Flight Center, Huntsville, AL.
A FORMAT FOR THE INTERCHANGE OF SCHEDULING MODELS c81
John P. Jaap and Elizabeth K. Davis *In* JPL, Third International Symposium on Artificial Intelligence, Robotics, and Automation for Space 1994 Oct. 1994 p 369-372 (For primary document see N95-23672 07-63)
Avail: CASI HC A01/MF A03

In recent years a variety of space-activity schedulers have been developed within the aerospace community. Space-activity schedulers are characterized by their need to handle large numbers of activities which are time-window constrained and make high demands on many scarce resources, but are minimally constrained by predecessor/successor requirements or critical paths. Two needs to exchange data between these schedulers have materialized. First, there is significant interest in comparing and evaluating the different scheduling engines to ensure that the best technology is applied to each scheduling endeavor. Second, there is a developing requirement to divide a single scheduling task among different sites, each using a different scheduler. In fact, the scheduling task for International Space Station Alpha (ISSA) will be distributed among NASA centers and among the international partners. The format used to interchange scheduling data for ISSA will likely use a growth version of the format discussed in this paper. The model interchange format (or MIF, pronounced as one syllable) discussed in this paper is a robust solution to the need to interchange scheduling requirements for space activities. It is highly extensible, human-readable, and can be generated or edited with common text editors. It also serves well the need to support a 'benchmark' data case which can be delivered on any computer platform. Author

N95-23748*# RECOM Technologies, Inc., Moffett Field, CA.
A DATA ANALYSIS ASSISTANT c61
Amy L. Lansky *In* JPL, Third International Symposium on Artificial Intelligence, Robotics, and Automation for Space 1994 Oct. 1994 p 373-376 (For primary document see N95-23672 07-63)
Avail: CASI HC A01/MF A03

This paper discusses the use of a domain-independent planner, COLLAGE, as a software assistant to Earth scientists working with remotely-sensed and ground based data sets. The planner can be viewed as an advisory agent that helps scientists select appropriate data and creates a suitable plan for data-processing that meets stated scientific requirements. Author

N95-23749*# Symbiotics, Inc., Cambridge, MA.
COORDINATING COMPLEX DECISION SUPPORT ACTIVITIES ACROSS DISTRIBUTED APPLICATIONS c61
Richard M. Adler *In* JPL, Third International Symposium on Artificial Intelligence, Robotics, and Automation for Space 1994 Oct. 1994 p 379-381 (For primary document see N95-23672 07-63)
(Contracts NAS10-11606; NAS10-11882; NAS5-31920; NAS8-399905; DAAB10-87-C-0053)
Avail: CASI HC A01/MF A03

Knowledge-based technologies have been applied successfully to automate planning and scheduling in many problem domains. Automation of decision support can be increased further by integrating task-specific applications with supporting database systems, and by coordinating interactions between such tools to facilitate collaborative activities. Unfortunately, the technical obstacles that must be overcome to achieve this vision of transparent, cooperative problem-solving are daunting. Intelligent decision support tools are typically developed for standalone use, rely on incompatible, task-specific representational models and application programming interfaces (API's), and run on heterogeneous computing platforms. Getting such applications to interact freely calls for platform independent capabilities for distributed communication, as well as tools for mapping information across disparate representations. Symbiotics is developing a layered set of software tools (called NetWorks! for integrating and coordinating heterogeneous distributed applications. he top layer of tools consists of an extensible set of generic, programmable coordination services. Developers access these services via high-level API's to implement the desired interactions between distributed applications. Author

N95-23750*# National Aeronautics and Space Administration. Lyndon B. Johnson Space Center, Houston, TX.
MODELING ACTIONS AND OPERATIONS TO SUPPORT MISSION PREPARATION c12
Jane T. Malin, D. P. Ryan (Metrica, Inc., Houston, TX.), and D. L. Schreckenghost (Metrica, Inc., Houston, TX.) *In* JPL, Third International Symposium on Artificial Intelligence, Robotics, and Automation for Space 1994 Oct. 1994 p 385-388 (For primary document see N95-23672 07-63)
Avail: CASI HC A01/MF A03

This paper describes two linked technology development projects to support Space Shuttle ground operations personnel, both during mission preparation analysis and related analyses in missions. The Space Propulsion Robust Analysis Tool (SPRAT) will provide intelligent support and automation for mission analysis setup, interpretation, reporting and documentation. SPRAT models the actions taken by flight support personnel during mission preparation and uses this model to generate an action plan. CONFIG will provide intelligent automation for procedure analyses and failure impact analyses, by simulating the interactions between operations and systems with embedded failures. CONFIG models the actions taken by crew during space vehicle malfunctions and simulates how the planned action sequences in procedures affect a device model. Jointly the SPRAT and CONFIG projects provide an opportunity to investigate how the nature of a task affects the representation of actions, and to determine a more general action representation supporting a broad range of tasks. This paper describes the problems in representing actions for mission preparation and their relation to planning and scheduling. Author

N95-23751*# CRI Space, (Denmark).
CRI PLANNING AND SCHEDULING FOR SPACE c12
Mads Aarup *In* JPL, Third International Symposium on Artificial Intelligence, Robotics, and Automation for Space 1994 Oct. 1994 p 289-392 (For primary document see N95-23672 07-63)
Avail: CASI HC A01/MF A03

Computer Resources International (CRI) has many years of experience in developing space planning and scheduling systems for the European Space Agency. Activities range from AIT/AIV planning over mission planning to research in on-board autonomy using advanced planning and scheduling technologies in conjunction with model based diagnostics. This article presents four projects carried out for ESA by CRI with various subcontractors:

(1) DI, Distributed Intelligence for Ground/Space Systems is an on-going research project; (2) GMPT, Generic Mission Planning Toolset, a feasibility study concluded in 1993; (3) OPTIMUM-AIV, Open Planning Tool for AIV, development of a knowledge based AIV planning and scheduling tool ended in 1992; and (4) PlanERS-1, development of an AI and knowledge-based mission planning prototype for the ERS-1 earth observation spacecraft ended in 1991. Derived from text

N95-23752*# MATRA Marconi Space, Toulouse (France).
BENEFITS OF ADVANCED SOFTWARE TECHNIQUES FOR MISSION PLANNING SYSTEMS **c12**
A. Gasquet, Y. Parrod, and A. DeSaintVincent *In* JPL, Third International Symposium on Artificial Intelligence, Robotics, and Automation for Space 1994 Oct. 1994 p 393-396 (For primary document see N95-23672 07-63)
Avail: CASI HC A01/MF A03

The increasing complexity of modern spacecraft, and the stringent requirement for maximizing their mission return, call for a new generation of Mission Planning Systems (MPS). In this paper, we discuss the requirements for the Space Mission Planning and the benefits which can be expected from Artificial Intelligence techniques through examples of applications developed by Matra Marconi Space. Author

N95-23753*# Tokyo Univ., Sagamihara (Japan).
A SCHEDULING AND DIAGNOSTIC SYSTEM FOR SCIENTIFIC SATELLITE GEOTAIL USING EXPERT SYSTEM
I Nakatani, M. Hashimoto, T. Mukai, T. Obara, and N. Nishigori (Fujitsu Ltd., Chiba, Japan.) *In* JPL, Third International Symposium on Artificial Intelligence, Robotics, and Automation for Space 1994 Oct. 1994 p 397-400 (For primary document see N95-23672 07-63)
Avail: CASI HC A01/MF A03

The Intelligent Satellite Control Software (ISACS) for the geoMagnetic tail observation satellite named GEOTAIL (launched in July 1992) has been successfully developed. ISACS has made it possible by applying Artificial Intelligence (AI) technology including an expert system to autonomously generate a tracking schedule, which originally used to be conducted manually. Using ISACS, a satellite operator can generate a maximum four day period of stored command stream autonomously and can easily confirm its safety. The ISACS system has another function -- to diagnose satellite troubles and to suggest necessary remedies. The workload of satellite operators has drastically been reduced since ISACS has been introduced into the operations of GEOTAIL. Author

N95-23754*# Malin Space Science Systems, San Diego, CA.
AUTOMATIC COMMANDING OF THE MARS OBSERVER CAMERA **c17**
Michael Caplinger *In* JPL, Third International Symposium on Artificial Intelligence, Robotics, and Automation for Space 1994 Oct. 1994 p 401-404 (For primary document see N95-23672 07-63)
(Contract JPL-959060)
Avail: CASI HC A01/MF A03

Mars Observer, launched in September 1992, was intended to be a 'survey-type' mission that acquired global coverage of Mars from a low, circular, near-polar orbit during an entire Martian year. As such, most of its instruments had fixed data rates, wide fields of view, and relatively low resolution, with fairly limited requirements for commanding. An exception is the Mars Observer Camera, or MOC. The MOC consists of a two-color Wide Angle (WA) system that can acquire both global images at low resolution (7.5 km/pixel) and regional images at commandable resolutions up to 250 m/pixel. Complementing the WA is the Narrow Angle (NA) system, that can acquire images at 8 resolutions from 12 m/pixel to 1.5 m/pixel, with a maximum crosstrack dimension of 3 km. The MOC also provides various forms of data compression (both lossless and lossy), and is designed to work at data rates from 700 bits per second (bps) to over 80k bps. Because of this flexibility, developing MOC command sequences is much more difficult than the routine mode-changing that characterizes other instrument operations. Although the MOC cannot be pointed (the spacecraft is fixed nadir-pointing and has no scan platform), the timing, downlink stream allocation, compression type and parameters, and image dimensions of each image must be commanded from the ground, subject to the constraints inherent in the MOC and the spacecraft. To minimize the need for a large operations staff, the entire command generation process has been automated within the MOC Ground Data System. Following the loss of the Mars Observer spacecraft in August 1993, NASA intends to launch a new spacecraft, Mars Global Surveyor (MGS), in late 1996. This spacecraft will carry the MOC flight spare (MOC 2). The MOC 2 operations plan will be largely identical to that developed for MOC, and all of the algorithms described here are applicable to it. Derived from text

N95-23755*# Stottler Henke Associates, Inc., Belmont, CA.
ARTIFICIAL INTELLIGENCE TECHNIQUES FOR SCHEDULING SPACE SHUTTLE MISSIONS
Andrea L. Henke and Richard H. Stottler *In* JPL, Third International Symposium on Artificial Intelligence, Robotics, and Automation for Space 1994 Oct. 1994 p 405-408 (For primary document see N95-23672 07-63)
Avail: CASI HC A01/MF A03

Planning and scheduling of NASA Space Shuttle missions is a complex, labor-intensive process requiring the expertise of experienced mission planners. We have developed a planning and scheduling system using combinations of artificial intelligence knowledge representations and planning techniques to capture mission planning knowledge and automate the multi-mission planning process. Our integrated object oriented and rule-based approach reduces planning time by orders of magnitude and provides planners with the flexibility to easily modify planning knowledge and constraints without requiring programming expertise. Author

N95-23756*# NYMA, Inc., Cleveland, OH.
DESIGN AND IMPLEMENTATION OF AN EXPERIMENT SCHEDULING SYSTEM FOR THE ACTS SATELLITE **c17**
Mark J. Ringer *In* JPL, Third International Symposium on Artificial Intelligence, Robotics, and Automation for Space 1994 Oct. 1994 p 409-412 (For primary document see N95-23672 07-63)
Avail: CASI HC A01/MF A03

The Advanced Communication Technology Satellite (ACTS) was launched on the 12th of September 1993 aboard STS-51. All events since that time have proceeded as planned with user operations commencing on December 6th, 1993. ACTS is a geosynchronous satellite designed to extend the state of the art in communication satellite design and is available to experimenters on a 'time/bandwidth available' basis. The ACTS satellite requires the advance scheduling of experimental activities based upon a complex set of resource, state, and activity constraints in order to ensure smooth operations. This paper describes the software system developed to schedule experiments for ACTS. Author

N95-23757*# RECOM Technologies, Inc., Moffett Field, CA.
TELESCOPE LOADING: A PROBLEM REDUCTION APPROACH **c89**
John L. Bresina *In* JPL, Third International Symposium on Artificial Intelligence, Robotics, and Automation for Space 1994 Oct. 1994 p 415-418 (For primary document see N95-23672 07-63)
Avail: CASI HC A01/MF A03

This paper presents a problem reduction approach to telescope loading. To study time-varying celestial behavior, astronomers submit periodic observation campaigns which involve a sequence of observations at a given sampling frequency over months or years. The loader's task is to generate an assignment of observation tasks to each night in the time window such that resource demand does not exceed resource capacity and such that the observations usefully contribute to the campaigns' scientific purposes, in a manner that is fair to all participating astronomers. Author

N95-23758*# Carnegie-Mellon Univ., Pittsburgh, PA. The Robotics Inst.
HIGH PERFORMANCE TECHNIQUES FOR SPACE MISSION SCHEDULING **c12**
Stephen F. Smith *In* JPL, Third International Symposium on Artificial Intelligence, Robotics, and Automation for Space 1994 Oct. 1994 p 419-422 (For primary document see N95-23672 07-63)
(Contracts NCC2-531; F30602-90-C-0119)
Avail: CASI HC A01/MF A03

In this paper, we summarize current research at Carnegie Mellon University aimed at development of high performance techniques and tools for space mission scheduling. Similar to prior research in opportunistic scheduling, our approach assumes the use of dynamic analysis of problem constraints as a basis for heuristic focusing of problem solving search. This methodology, however, is grounded in representational assumptions more akin to those adopted in recent temporal planning research, and in a

problem solving framework which similarly emphasizes constraint posting in an explicitly maintained solution constraint network. These more general representational assumptions are necessitated by the predominance of state-dependent constraints in space mission planning domains, and the consequent need to integrate resource allocation and plan synthesis processes. First, we review the space mission problems we have considered to date and indicate the results obtained in these application domains. Next, we summarize recent work in constraint posting scheduling procedures, which offer the promise of better future solutions to this class of problems. Author

N95-23759*# Tokyo Univ. (Japan). Dept. of Aeronautics an Astronautics.

APPLICATIONS OF DYNAMIC SCHEDULING TECHNIQUE TO SPACE RELATED PROBLEMS: SOME CASE STUDIES **c12**

Shinichi Nakasuka and Tetsujiro Ninomiya *In* JPL, Third International Symposium on Artificial Intelligence, Robotics, and Automation for Space 1994 Oct. 1994 p 423-426 (For primary document see N95-23672 07-63)

Avail: CASI HC A01/MF A03

The paper discusses the applications of 'Dynamic Scheduling' technique, which has been invented for the scheduling of Flexible Manufacturing System, to two space related scheduling problems: operation scheduling of a future space transportation system, and resource allocation in a space system with limited resources such as space station or space shuttle. Author

N95-23760*# Office National d'Etudes et de Recherches Aerospatiales, Toulouse (France).

SOLUTION AND REASONING REUSE IN SPACE PLANNING AND SCHEDULING APPLICATIONS **c12**

Gerard Verfaillie and Thomas Schiex *In* JPL, Third International Symposium on Artificial Intelligence, Robotics, and Automation for Space 1994 Oct. 1994 p 427-430 (For primary document see N95-23672 07-63)

Avail: CASI HC A01/MF A03

In the space domain, as in other domains, the CSP (Constraint Satisfaction Problems) techniques are increasingly used to represent and solve planning and scheduling problems. But these techniques have been developed to solve CSP's which are composed of fixed sets of variables and constraints, whereas many planning and scheduling problems are dynamic. It is therefore important to develop methods which allow a new solution to be rapidly found, as close as possible to the previous one, when some variables or constraints are added or removed. After presenting some existing approaches, this paper proposes a simple and efficient method, which has been developed on the basis of the dynamic backtracking algorithm. This method allows previous solution and reasoning to be reused in the framework of a CSP which is close to the previous one. Some experimental results on general random CSPs and on operation scheduling problems for remote sensing satellites are given. Author

N95-23761*# Honeywell Technology Center, Minneapolis, MN.

EMPIRICAL RESULTS ON SCHEDULING AND DYNAMIC BACKTRACKING **c12**

Mark S. Boddy and Robert P. Goldman *In* JPL, Third International Symposium on Artificial Intelligence, Robotics, and Automation for Space 1994 Oct. 1994 p 431-434 (For primary document see N95-23672 07-63)

Avail: CASI HC A01/MF A03

At the Honeywell Technology Center (HTC), we have been working on a scheduling problem related to commercial avionics. This application is large, complex, and hard to solve. To be a little more concrete: 'large' means almost 20,000 activities, 'complex' means several activity types, periodic behavior, and assorted types of temporal constraints, and 'hard to solve' means that we have been unable to eliminate backtracking through the use of search heuristics. At this point, we can generate solutions, where solutions exist, or report failure and sometimes why the system failed. To the best of our knowledge, this is among the largest and most complex scheduling problems to have been solved as a constraint satisfaction problem, at least that has appeared in the published literature. This abstract is a preliminary report on what we have done and how. In the next section, we present our approach to treating scheduling as a constraint satisfaction problem. The following sections present the application in more detail and describe how we solve scheduling problems in the application domain. The implemented system makes use of Ginsberg's Dynamic Backtracking algorithm, with some minor extensions to improve its utility for scheduling. We describe those extensions and the performance of the resulting system. The paper concludes with some general remarks, open questions and plans for future work. Derived from text

N95-23762*# Boeing Co., Huntsville, AL.

SCHEDULING WITH GENETIC ALGORITHMS **c61**

Theron R. Fennel, A. J. Underbrink, Jr., and George P. W. Williams, Jr. *In* JPL, Third International Symposium on Artificial Intelligence, Robotics, and Automation for Space 1994 Oct. 1994 p 435-438 (For primary document see N95-23672 07-63)

Avail: CASI HC A01/MF A03

In many domains, scheduling a sequence of jobs is an important function contributing to the overall efficiency of the operation. At Boeing, we develop schedules for many different domains, including assembly of military and commercial aircraft, weapons systems, and space vehicles. Boeing is under contract to develop scheduling systems for the Space Station Payload Planning System (PPS) and Payload Operations and Integration Center (POIC). These applications require that we respect certain sequencing restrictions among the jobs to be scheduled while at the same time assigning resources to the jobs. We call this general problem scheduling and resource allocation. Genetic algorithms (GA's) offer a search method that uses a population of solutions and benefits from intrinsic parallelism to search the problem space rapidly, producing near-optimal solutions. Good intermediate solutions are probabalistically recombined to produce better offspring (based upon some application specific measure of solution fitness, e.g., minimum flowtime, or schedule completeness). Also, at any point in the search, any intermediate solution can be accepted as a final solution; allowing the search to proceed longer usually produces a better solution while terminating the search at virtually any time may yield an acceptable solution. Many processes are constrained by restrictions of sequence among the individual jobs. For a specific job, other jobs must be completed beforehand. While there are obviously many other constraints on processes, it is these on which we focussed for this research: how to allocate crews to jobs while satisfying job precedence requirements and personnel, and tooling and fixture (or, more generally, resource) requirements. Derived from text

N95-23763*# SRI International Corp., Menlo Park, CA. Artificial Intelligence Center.

INTEGRATING PLANNING AND REACTIVE CONTROL **c12**

David E. Wilkins and Karen L. Myers *In* JPL, Third International Symposium on Artificial Intelligence, Robotics, and Automation for Space 1994 Oct. 1994 p 435-442 (For primary document see N95-23672 07-63)

(Contract F30602-90-C-0086)

Avail: CASI HC A01/MF A03

Our research is developing persistent agents that can achieve complex tasks in dynamic and uncertain environments. We refer to such agents as taskable, reactive agents. An agent of this type requires a number of capabilities. The ability to execute complex tasks necessitates the use of strategic plans for accomplishing tasks; hence, the agent must be able to synthesize new plans at run time. The dynamic nature of the environment requires that the agent be able to deal with unpredictable changes in its world. As such, agents must be able to react to unanticipated events by taking appropriate actions in a timely manner, while continuing activities that support current goals. The unpredictability of the world could lead to failure of plans generated for individual tasks. Agents must have the ability to recover from failures by adapting their activities to the new situation, or replanning if the world changes sufficiently. Finally, the agent should be able to perform in the face of uncertainty. The Cypress system, described here, provides a framework for creating taskable, reactive agents. Several features distinguish our approach: (1) the generation and execution of complex plans with parallel actions; (2) the integration of goal-driven and event driven activities during execution; (3) the use of evidential reasoning for dealing with uncertainty; and (4) the use of replanning to handle run-time execution problems. Our model for a taskable, reactive agent has two main intelligent components, an executor and a planner. The two components share a library of possible actions that the system can take. The library encompasses a full range of action representations, including plans, planning

operators, and executable procedures such as predefined standard operating procedures (SOP's). These three classes of actions span multiple levels of abstraction. Derived from text

N95-23764*# Florida Inst. of Tech., Melbourne, FL. Computer Science Program.

AUTOMATIC GENERATION OF EFFICIENT ORDERINGS OF EVENTS FOR SCHEDULING APPLICATIONS **c12**

Robert A. Morris *In* JPL, Third International Symposium on Artificial Intelligence, Robotics, and Automation for Space 1994 Oct. 1994 p 443-447 (For primary document see N95-23672 07-63)
Avail: CASI HC A01/MF A03

In scheduling a set of tasks, it is often not known with certainty how long a given event will take. We call this duration uncertainty. Duration uncertainty is a primary obstacle to the successful completion of a schedule. If a duration of one task is longer than expected, the remaining tasks are delayed. The delay may result in the abandonment of the schedule itself, a phenomenon known as schedule breakage. One response to schedule breakage is on-line, dynamic rescheduling. A more recent alternative is called proactive rescheduling. This method uses statistical data about the durations of events in order to anticipate the locations in the schedule where breakage is likely prior to the execution of the schedule. It generates alternative schedules at such sensitive points, which can be then applied by the scheduler at execution time, without the delay incurred by dynamic rescheduling. This paper proposes a technique for making proactive error management more effective. The technique is based on applying a similarity-based method of clustering to the problem of identifying similar events in a set of events. Derived from text

N95-23765*# Alcatel Espace, Toulouse (France).

TERRAIN MODELLING AND MOTION PLANNING FOR AN AUTONOMOUS EXPLORATION ROVER **c43**

F. Richard, S. Benoliel (Alcatel Alsthom Recherche, Marcoussis, France.), O. Faugeras (Institut National de Recherche d'Informatique et d'Automatique, Sophia Antipolis, France.), P. Grandjean (Centre National d'Etudes Spatiales, Toulouse, France.), M. Hayard, and T. Simeon (Centre National d'Etudes Spatiales, Toulouse, France.) *In* JPL, Third International Symposium on Artificial Intelligence, Robotics, and Automation for Space 1994 Oct. 1994 p 95-98 (For primary document see N95-23672 07-63)
Avail: CASI HC A01/MF A03

To assess the feasibility of planetary exploration missions using rovers, the French national agency CNES, with a consortium of European laboratories and industrial concerns, has initiated the Eureka project, 'Illustration of an Autonomous Robot for the Exploration of Space' (IARES). IARES is a demonstrator composed of a rover and a ground station, linked by telemetry and telecommand. It is aimed at verifying, on earth, robotic concepts developed by the RISP group of French laboratories (LAAS, INRIA, CERT, LETI) to perform scientific missions such as autonomous terrain sample collecting over large areas. To cope with the actual needs of planet exploration, IARES suitability is assessed through constraints on limited bandwidth, time delay and on-board resources. This autonomy relies heavily on robust onboard trajectory generation capabilities. This paper presents the main functions of the IARES navigation sub-system and shows how they are combined to allow movement in Mars-like environments. Section 2 gives an overall description of the IARES system. Section 3 details the functions of the Navigation sub-system, and finally, section 4 illustrates with a simple example the use of these functions. Author (revised)

N95-24001# Rochester Univ., NY. Dept. of Computer Science.

REAL-WORLD SHEPHERDING: COMBINING VISION, MANIPULATION, AND PLANNING IN REAL TIME

Peter vonKaenel and Robert W. Wisniewski Aug. 1994 28 p
(Contracts NSF IRI-89-03582; NSF CDA-88-22724; MDA972-92-J-1012; N00014-93-1-0221)
(TR-530) Avail: CASI HC A03/MF A01

Designing real-world applications can involve coordinating many pieces of hardware and integrating multiple software components. Increased processing power has allowed complex real-world applications to be designed, and there has been increasing interest in the issues involved in designing both the applications and their support. In this paper we describe the issue involved in designing the application. The shepherding application we have chosen is representative of many real-world applications. This report focuses on technical details. We describe the underlying hardware, including the camera, vision processing boards, processors, and puma robot arm. We then discuss the software components we designed to integrate the hardware components in real-time. At each stage we describe the trade-offs between the different possibilities and why the ones chosen were best suited for our environment. We also present results supporting our selection. At appropriate points we indicate underlying support that would have eased and improved our implementation. Author

N95-24031# Rochester Univ., NY. Dept. of Computer Science.

KNOWLEDGE REPRESENTATION AND REASONING FOR MIXED-INITIATIVE PLANNING Ph.D. Thesis

George M. Ferguson Jan. 1995 194 p
(Contracts F30602-91-C-0010; NSF IRI-90-03841; N00014-92-J-1512)
(TR-562) Avail: CASI HC A09/MF A03

This dissertation describes the formal foundations and implementation of a common-sense, mixed-initiative plan reasoning system. By 'plan reasoning' I mean the complete range of cognitive tasks that people perform with plans including, for example, plan construction (planning), plan recognition, plan evaluation and comparison, and plan repair (replanning), among other things. 'Mixed-initiative' means that several participants can each make contributions to the plan under development through some form of communication. 'Commonsense' means that the system represents plans and their constituents at a level that is 'natural' to us in the sense that they can be described and discussed in language. In addition, the reasoning that the system performs includes those conclusions that we would take to be sanctioned by common sense, including especially those conclusions that are defeasible given additional knowledge or time spent reasoning. The main theses of this dissertation are the following: (1) any representation of plans sufficient for commonsense plan reasoning must be based on an expressive and natural representation such underlying phenomena as time, properties, events, and actions; and (2) for mixed-initiative planning, plans should be viewed as arguments that a certain course of action under certain conditions will achieve certain goals. These theses are defended by presenting, first, a representation of events and actions based on interval temporal logic and, second, a representation of plans as arguments in a formal system of defeasible reasoning that explicitly constructs arguments. These two aspects of commonsense plan reasoning are combined and implemented in the TRAINS domain plan reasoner, which is also described in detail. Author

N95-24036# Rochester Univ., NY.

MORPHING HANDS AND VIRTUAL TOOLS (OR WHAT GOOD IS AN EXTRA DEGREE OF FREEDOM?)

Olac Fuentes and Randal C. Nelson Dec. 1994 28 p
(Contracts MDA972-92-J-1012; N00014-93-1-0221)
(TR-551) Avail: CASI HC A03/MF A01

Manipulators with large numbers of degrees of freedom, from the human hand to the trunk of an elephant, are common in the biological world. These freedoms allow highly flexible and robust performance of complex tasks. However, progress in developing and controlling artificial high-degree-of-freedom manipulators has been slow. The main problem is that traditional robotics has focussed on the solution of systems of kinematic equations where there is a unique solution. Such approaches tend not to generalize well to situations with a high-dimensional solution space, and controlling redundant systems has acquired a reputation as a hard problem. However, this need not be the case. In this paper, we describe a behavioral method for using extra degrees of freedom to simplify rather than complicate manipulation problems, while at the same time obtaining more flexibility than would be available with a simpler system. The method is developed in the context of a high DOF robot hand, but it has the potential to generalize to other sorts of manipulators. The basic idea is based on the observation that, for a particular task, using a custom-designed fitting can greatly simplify the control problem. Using a wrench sized for a particular nut is an extreme example. We use the extra degrees of freedom to dynamically configure or 'tailor' the manipulator to match the particular object and task at hand. This creates a virtual tool. The tailoring is accomplished by imposing low-level, task-specific constraints on the degrees of freedom. These constraints are selected dynamically from a large set of potential constraints in response to the demands of the current task. The process of smoothly transitioning from one virtual tool to another in the

course of task execution is referred to as morphing. We apply the technique to the control of a 16-DOF Utah/MIT hand, and perform fine manipulations on a range of objects using virtual tools that are dynamically instantiated on the basis of sensory information. Author

N95-24038# Rochester Univ., NY. Dept. of Computer Science.
ROBOT SKILL LEARNING THROUGH INTELLIGENT EXPERIMENTATION Ph.D. Thesis
Jeff G. Schneider Jan. 1995 113 p
(Contracts MDA972-92-J-1012; N00014-93-1-0221; AF-AFOSR-0288-91; NSF IRI-93-06454)
(TR-567) Avail: CASI HC A06/MF A02

In robot skill learning the robot must obtain data for training by executing expensive practice trials and recording their results. The thesis is that the high cost of acquiring training data is the limiting factor in the performance of skill learners. Since the data is obtained from practice trials, it is important that the system make intelligent choices about what actions to attempt while practicing. In this dissertation we present several algorithms for intelligent experimentation in skill learning. In open-loop skills the execution goal is presented and the controller must then choose all the control signals for the duration of the task. Learning is a high-dimensional search problem. The system must associate a sequence of actions with each commandable goal. We propose an algorithm that selects practice actions most likely to improve performance by making use of information gained on previous trials. On the problem of learning to throw a ball using a robot with a flexible link, the algorithm takes only 100 trials to find a 'whipping' motion for long throws. Most closed loop learners improve their performance by gradient descent on a cost function. The main drawback of this method is convergence to nonoptimal local minima. We introduce the concept of cooperation as a means of escaping these local minima. We assume the existence of several coaches that each improve some aspect of the controller's performance. Switching training between coaches can help the controller avoid locally minimal solutions. On the task of curve tracing with an inverted pendulum the cooperative algorithm learns to track faster than with a traditional method. In an integrated system with scarce sensor resources it is preferable to perform tasks without sensing. We observe that closed loop learning can function as an efficient search technique for open-loop control. Our system starts with closed loop learning. As it improves its ability to control the plant, it replaces sensor information with estimates. The result is a controller that tracks long segments of a reference curve open loop. Author

N95-24040# Rochester Univ., NY. Dept. of Computer Science.
UNSUPERVISED CLASSIFICATION LEARNING FROM CROSS-MODAL ENVIRONMENTAL STRUCTURE Ph.D. Thesis
Virginia Ruth deSa Nov. 1994 102 p Sponsored by Canadian NSERC Science and Engineering Scholarship and Human Science Frontiers Program
(Grants NSF IRI-89-03582; PHS-1-R24-RR-06853-02)
(TR-536) Avail: CASI HC A06/MF A02

This dissertation addresses the problem of unsupervised learning or pattern classification or category learning. A model that is based on gross cortical anatomy and implements biologically plausible computations is developed and shown to have classification power approaching that of a supervised discriminant algorithm. The advantage of supervised learning is that the final error metric is available during training. Unfortunately, when modeling human category learning, or in constructing classifiers for autonomous robots, one must deal with not having an omniscient entity labeling all incoming sensory patterns. We show that we can substitute for the labels by making use of structure between the pattern distributions to different sensory modalities. For example the co-occurrence of a visual image of a cow with a 'moo' sound can be used to simultaneously develop appropriate visual features for distinguishing the cow image and appropriate auditory features for recognizing the moo. We model human category learning as a process of minimizing the disagreement between outputs of sensory modalities processing temporally coincident patterns. We relate this mathematically to the optimal goal of minimizing the number of misclassifications in each modality and apply the idea to derive an algorithm for piecewise linear classifiers in which each network uses the output of the other networks as a supervisory signal. Using the Peterson-Barney vowel dataset we show that the algorithm finds appropriate placement for the classification boundaries. The algorithm is then demonstrated on the task of learning to recognize acoustic and visual speech from images of lips and their emanating sounds. performance on these tasks is within 1-7% of the related supervised algorithm (LVQ2.1). Finally, we compare the algorithm to Becker's IMAX algorithm and give suggestions as to how the algorithm may be implemented in the brain using physiological results concerning the relationship between two types of neural plasticity, LTP and LTD, observed in visual cortical cells. We also show how the algorithm can be used as an efficient method for dealing with learning from data with missing values. Author

N95-24060# Rochester Univ., NY. Dept. of Computer Science.
TEACHING COMPUTATIONAL COMPLEXITY: RESOURCES TO TREASURE
Lane A. Hemaspaandra Nov. 1994 13 p Submitted for publication
(Grants NSF INT-91-16781; JSPS-ENG-207; NSF CCR-93-22513)
(TR-543) Avail: CASI HC A03/MF A01

This note describes and discusses textbooks, monographs, and collections that are excellent from which to teach courses on computational complexity theory. Author

N95-24185# Rochester Univ., NY. Dept. of Computer Science.
VISION-BASED PLANNING AND EXECUTION OF PRECISION GRASPS
Olac Fuentes, Hilcea F. Marengoni, and Randal C. Nelson Dec. 1994 25 p Sponsored by Brazilian CNPq/RHAE
(Contracts MDA972-92-J-1012; N00014-93-1-0221)
(TR-546) Avail: CASI HC A03/MF A01

A system for vision-based planning and execution of fingertip grasps using a four-fingered dextrous hand is presented. Our system does not rely on prior models of the objects to be grasped; it obtains all the information it needs from vision and from tactile sensors located at the fingertips of the hand. The grasp planner is based on a genetic algorithm modified to allow the use of real numbers as the basic representation unit. The grasp executer is based on differential visual feedback, which allows the system to specify goals and monitor progress in image space without needing absolute calibration between the camera and the hand. We present experimental results showing the application of the system to grasping unknown objects with the Utah/MIT hand. Author

N95-22988*# Universidad Nacional Autonoma de Mexico, Cuernavaca (Mexico). Lab. de Cibernetica.
LYAPUNOV EXPONENTS FROM CHUA'S CIRCUIT TIME SERIES USING ARTIFICIAL NEURAL NETWORKS
J. Jesus Gonzalez, Ismael E. Espinosa, and Alberto M. Fuentes *In* NASA. Goddard Space Flight Center, Second International Workshop on Harmonic Oscillators Jan. 1995 p 263-269 Sponsored by CONACYT
(For primary document see N95-22957 07-74)
(DGAPA Proj-IN100593-UNAM)
Avail: CASI HC A03/MF A04

N95-23308*# Kansas Univ., Lawrence, KS. Dept. of Aerospace Engineering.
ON-LINE, ADAPTIVE STATE ESTIMATOR FOR ACTIVE NOISE CONTROL Abstract Only
Tae W. Lim *In* Hampton Univ., 1994 NASA-HU American Society for Engineering Education (ASEE) Summer Faculty Fellowship Program Dec. 1994 p 90 (For primary document see N95-23276 07-99)
Avail: CASI HC A01/MF A02

N95-23874*# Arizona Univ., Tucson, AZ.
CLASSIFICATION OF THE LCVF AVIRIS TEST SITE WITH A KOHONEN ARTIFICIAL NEURAL NETWORK
Erzsebet Merenyi, Robert B. Singer, and William H. Farrand (Science Applications International Corp., Falls Church, VA.) *In* JPL, Summaries of the 4th Annual JPL Airborne Geoscience Workshop. Volume 1: AVIRIS Workshop 25 Oct. 1993 p 117-120 (For primary document see N95-23844 07-42)
Avail: CASI HC A01/MF A03

64 NUMERICAL ANALYSIS

Includes iteration, difference equations, and numerical approximation.

N95-22528# Vrije Univ., Amsterdam (Netherlands).
IS OMEGA* - (MU) ABSOLUTELY COUNTABLY COMPACT?
J. vanMill and J. E. Vaughan Sep. 1993 7 p Prepared in cooperation with North Carolina Univ.
(PB95-127981) Avail: CASI HC A02/MF A01

The authors construct an ultrafilter (mu)(a member of)omega(star) = (beta)(omega) - omega such that the subspace omega(star)-(mu) is not absolutely countably compact, and the authors show that under the continuum hypothesis, for every (mu)(a member of)(beta)(omega) - omega, the subspace omega(star)-(mu) is not absolutely countably compact. NTIS

N95-22533# Vrije Univ., Amsterdam (Netherlands).
COUNTABLE SPACE WITH A CLOSED SUBSPACE WITHOUT CONTINUOUS EXTENDER
J. vanMill and R. Pol Oct. 1993 8 p
(PB95-127973) Avail: CASI HC A02/MF A01

We construct an example of a countable space Delta having a closed subspace Alpha such that no extender e: C(sub p)(Alpha) approaches C(sub p)(Delta) is continuous. This answers a question of Arhangelskii. NTIS

N95-22535# Technische Univ., Eindhoven (Netherlands).
TREEWIDTH AND PATHWIDTH OF COCOMPARABILITY GRAPHS OF BOUNDED DIMENSION
T. Kloks, D. Kratsch (Institut de Recherche en Informatique et Systemes Aleatoires, Rennes, France.), and J. Spinrad (Vanderbilt Univ., Nashville, TN.) 1994 26 p See also N93-27305 Prepared in cooperation with Institut de Recherche en Informatique et Systemes Aleatoires
(PB95-127239) Avail: CASI HC A03/MF A01

In this paper we describe a polynomial time algorithm computing the treewidth of a cocomparability graph of bounded dimension. We do not assume that an intersection model of the graph is part of the input. NTIS

N95-22544# Rutherford Appleton Lab., Oxford (England). Mathematical Software Group.
PARTITIONING METHODS FOR UNSTRUCTURED FINITE ELEMENT MESHES
C. Greenough and R. F. Fowler Aug. 1994 19 p Sponsored by European Strategic Program for Research and Development in Information Technology
(PB95-130555; RAL-94-092) Avail: CASI HC A03/MF A01

In this paper we review and compare a range of basic methods which can be used to partition finite element meshes. These have been implemented within a software tool called ralpar and tests made on a small set of 3D meshes. The comparisons are made in terms of the basic attributes of the partitions such as number of neighbors, number of interface nodes and number of cut edges in the underlying graph. We also describe some of the extensions to these methods we have made and compare these with existing techniques together with some ideas of partition assessment based on software and architectural models. NTIS

N95-22618# International Centre for Theoretical Physics, Trieste (Italy).
DIFFUSION TERMS IN SYSTEMS OF REACTION DIFFUSION EQUATIONS CAN LEAD TO BLOW UP
M. Kirane and A. DiLiddo Jan. 1994 5 p
(DE94-628408; IC-93/128) Avail: CASI HC A01/MF A01 (US Sales Only)

We present a system of reaction diffusion equations posed in R in which the diffusion terms are responsible for the finite time breakdown of its solutions. DOE

N95-22619# International Centre for Theoretical Physics, Trieste (Italy).
LECTURES ON HOMOLOGY WITH INTERNAL SYMMETRIES
Yu. Solovyov Sep. 1993 76 p
(DE94-628409; IC-93/295) Avail: CASI HC A05/MF A01 (US Sales Only)

Homology with internal symmetries is a natural generalization of cyclic homology introduced, independently, by Connes and Tsygan, which has turned out to be a very useful tool in a number of problems of algebra, geometry topology, analysis, and mathematical physics. It suffices to say cycling homology and cohomology are successfully applied in the index theory of elliptic operators on foliations, in the description of the homotopy type of pseudoisotopy spaces, and in the theory of characteristic classes in algebraic K-theory. They are also applied in noncommutative differential geometry and in the cohomology of Lie algebras, the branches of mathematics which brought them to life in the first place. Essentially, we consider dihedral homology, which was successfully applied for the description of the homology type of groups of homeomorphisms and diffeomorphisms of simply connected manifolds. DOE

N95-22624# International Centre for Theoretical Physics, Trieste (Italy).
REMARKS ON MULTIPLE SOLUTIONS FOR ASYMPTOTICALLY LINEAR ELLIPTIC BOUNDARY VALUE PROBLEMS
Chang Kung Ching, Li Shujie, and Liu Jiaquan Oct. 1993 8 p
(DE94-628416; IC-93/344) Avail: CASI HC A02/MF A01 (US Sales Only)

Some new results on the existence of multiple solutions for asymptotically linear elliptic boundary value problems via critical groups are obtained. DOE

N95-22625# International Centre for Theoretical Physics, Trieste (Italy).
EXISTENCE OF SOLUTIONS FOR SOME SUPERLINEAR OR SUBLINEAR ELLIPTIC SYSTEMS ON R(SUP N)
Ying Yanheng (Academia Sinica, Beijing, China.) and Li Shujie Oct. 1993 17 p
(DE94-628417; IC-93/349) Avail: CASI HC A03/MF A01 (US Sales Only)

The existence of solutions for some superlinear or sublinear elliptic systems on R(sup N) is demonstrated using a compact embedding lemma which enables the application of standard critical theory for such problems. DOE

N95-22626# International Centre for Theoretical Physics, Trieste (Italy).
THE EULER SERIES OF RESTRICTED CHOW VARIETIES
J. Elizondo Oct. 1993 15 p
(DE94-628418; IC-93/351) Avail: CASI HC A03/MF A01 (US Sales Only)

The 'restricted' Chow variety C(sub lambda)(X) of a projective algebraic variety X is the space consisting of all effective cycles with a given homology class lambda. This space is a subvariety of the usual Chow variety and has the advantage of not depending on the projective embedding of X. The main purpose of this paper is to calculate the Euler characteristic of C(sub lambda)(X), when X admits a linear action of an algebraic torus, for which there are only finitely many irreducible invariant subvarieties. An important class of such varieties are the projective toric varieties. DOE

N95-22627# International Centre for Theoretical Physics, Trieste (Italy).
A NEW METHOD OF CONSTRUCTING SCALAR-FLAT KAEHLER SURFACES
Jongsu Kim and M. Pontecorvo (International School for Advanced Studies, Trieste, Italy.) Oct. 1993 24 p
(DE94-628419; IC-93/358) Avail: CASI HC A03/MF A01 (US Sales Only)

Building on the work of Donaldson-Friedman we present a geometric way of constructing anti-self-dual hermitian metrics on compact complex surfaces which is based on the relative complex deformations of singular 3-folds with divisors. Some of the consequences are that under a mild condition, fully described by LeBrun-Singer, any blow up of a scalar-flat Kaehler surface admits scalar-flat Kaehler metrics; this is used to prove that such extremal Kaehler metrics exists on an open dense subset of the moduli space of non-minimal ruled surfaces of genus g greater than or equal to 2. Related results have been obtained by LeBrun-Singer. DOE

N95-22628# International Centre for Theoretical Physics, Trieste (Italy).
HAUSDORFF DIMENSION OF JULIA SETS OF COMPLEX HENON MAPPINGS
A. Verjovsky and H. Wu Nov. 1993 17 p

(DE94-628420; IC-93/380) Avail: CASI HC A03/MF A01 (US Sales Only)

The Hausdorff dimension of closed invariant sets under diffeomorphism is an interesting concept as it is a measure of their complexity. The theory of holomorphic dynamical systems provides us with many examples of fractal sets, and in particular, a theorem of Ruelle shows that the Hausdorff dimension of the Julia set depends real analytically on f if f is a rational function of C and the Julia set of J of f is hyperbolic. In this paper we generalize Ruelle's result for complex dimensional 2 and show the real analytic dependence of the Hausdorff dimension of the corresponding Julia sets of hyperbolic Henon mappings. DOE

N95-22629# International Centre for Theoretical Physics, Trieste (Italy).
ON OSCILLATIONS OF HIGHER ORDER NEUTRAL DIFFERENTIAL EQUATIONS
N. Parhi Nov. 1993 9 p
(DE94-628421; IC-93/392) Avail: CASI HC A02/MF A01 (US Sales Only)

In this paper, sufficient conditions have been obtained for oscillations of solutions of a class of nth order linear homogeneous neutral delay differential equations with variable coefficients and several constant delays. DOE

N95-22631# International Centre for Theoretical Physics, Trieste (Italy).
BETHE ANSATZ AND QUANTUM DAVEY-STEWARTSON 1 SYSTEM WITH MULTICOMPONENT IN TWO DIMENSIONS
Yi Cheng, Mu-Lin Yan, and Bao-Heng Zhao Jan. 1994 8 p
(DE94-628423; IC-94/35) Avail: CASI HC A02/MF A01 (US Sales Only)

The quantum 2-component DS1 system was reduced to two 1D many-body problems with (delta)-function interactions, which were solved by Bethe ansatz. Using the ansatz of Pang, Pu and Zhao and introducing symmetric and antisymmetric Young operators of the permutation group, we obtain the exact solutions for the system. DOE

N95-22633# International Centre for Theoretical Physics, Trieste (Italy).
SOLUTIONS FOR THE VECTOR k-CONSTRAINED KP HIERARCHY
You Jin Zhang and Yi Cheng Mar. 1994 19 p
(DE94-628431; IC-94/61) Avail: CASI HC A03/MF A01 (US Sales Only)

We study a class of integrable systems in $1+1$-dimension which are constrained from the KP hierarchy. We first show the bilinear equations of these integrable systems, then by using the free fermion operators we obtain their rational and soliton solutions which are closely related to the (tau)-functions of the KP hierarchy. Our result implies that a large family of solutions of the $2+1$-dimensional KP hierarchy can be obtained by solving these $1+1$-dimensional integrable systems, in particular, the N-soliton solutions of the KP hierarchy can be deduced from the soliton solutions of these $1+1$-dimensional integrable systems. DOE

N95-22634# International Centre for Theoretical Physics, Trieste (Italy).
ITERATIVE SOLUTIONS OF NONLINEAR EQUATIONS WITH STRONGLY ACCRETIVE OR STRONGLY PSEUDOCONTRACTIVE MAPS
C. E. Chidume Mar. 1994 13 p
(DE94-628432; IC-94/66) Avail: CASI HC A03/MF A01 (US Sales Only)

Let E be a real q-uniformly smooth Banach space. Suppose T is a strongly pseudo-contractive map with open domain D(T) in E. Suppose further that T has a fixed point in D(T). Under various continuity assumptions on T it is proved that each of the Mann iteration process or the Ishikawa iteration method converges strongly to the unique fixed point of T. Related results deal with iterative solutions of nonlinear operator equations involving strongly accretive maps. Explicit error estimates are also provided. DOE

N95-22641# Tilburg Univ. (Netherlands).
CAPACITATED FACILITY LOCATION: VALID INEQUALITIES AND FACETS (REVISED) Research Memo
K. Aardal, Y. Pochet, and L. A. Wolsey Feb. 1994 40 p Prepared in cooperation with Universite Catholique de Louvain, Louvain-la-Neuve, Belgium
(PB95-130225; FEW-644) Avail: CASI HC A03/MF A01

We examine the polyhedral structure of the convex hull of feasible solutions of the capacitated facility location problem. In particular we derive necessary and sufficient conditions for a family of 'effective capacity' inequalities to be facet-defining, and further results on a more general family called 'submodular' inequalities. NTIS

N95-22642# International Centre for Theoretical Physics, Trieste (Italy).
ON THE THEORY OF SMOOTH STRUCTURES 3
A. ShafeiDehAbad and F. KamaliKhamseh Sep. 1993 14 p
(DE94-628411; IC-93/308) Avail: CASI HC A03/MF A01 (US Sales Only)

In this paper after some elementary differential calculus we give some criteria for smoothness and sufficient conditions for compatibility of two smooth algebras. After which we give the definition of a new product of smooth algebras over integral domains which are not fields and prove its existence. DOE

N95-22696# Argonne National Lab., IL.
EXTENSIBLE PDE SOLVERS PACKAGE USERS MANUAL
B. Smith Sep. 1994 38 p
(Contract W-31-109-eng-38)
(DE95-003333; ANL-94/40) Avail: CASI HC A03/MF A01

This manual describes the design and use of the Extensible PDE Solvers package for the solution of elliptic PDE's. At this time, the package provides support for the solution of elliptic PDE's using either finite elements or finite differences in two or three dimensions on either structured or unstructured grids. The package is designed to be easily extended to new discretizations or classes of PDE's. Several classical direct and iterative methods, as well as several multigrid variants, may be used to solve the resulting linear systems. The package is intended as a prototype, working implementation to demonstrate, and learn, how such packages may be organized. Many important features for particular problems are lacking; future versions of the package may add increased functionality. The software described is purely experimental; its structure and organization may change significantly at any time. There is no explicit support for parallel computing in the Extensible PDE Solvers package. DOE

N95-22711# Institut des Hautes Etudes Scientifiques, Bures-sur-Yvette (France).
DETERMINANTS OF ELLIPTIC PSEUDO-DIFFERENTIAL OPERATORS
Maxim Kontsevich and Simeon Vishik Apr. 1994 157 p
(PB95-109062; IHES/M/94/30) Avail: CASI HC A08/MF A02

Determinants of invertible pseudo-differential operators (PDO's) close to positive self-adjoint ones are defined through the zeta-function regularization. We define a multiplicative anomaly as the ratio $\det(AB)/(\det(A)\det(B))$ considered as a function on pairs of elliptic PDO's. We obtained an explicit formula for the multiplicative anomaly in terms of symbols of operators. For a certain natural class of PDO's on odd-dimensional manifolds generalizing the class of elliptic differential operators, the multiplicative anomaly is identically 1. For elliptic PDO's from this class a holomorphic determinant and determinant for zero order PDO's are introduced. Using various algebraic, analytic, and topological tools, we study local and global properties of the multiplicative anomaly and of the determinant Lie group closely related with it. The Lie algebra for the determinant Lie group has a description in terms of symbols only. Our main discovery is that there is a quadratic non-linearity hidden in the definition of determinants of PDO's through zeta-functions. NTIS

N95-22714# Technische Hogeschool, Eindhoven (Netherlands). Dept. of Mathematics and Computing Science.
GRAPH ISOMORPHISM MODELS FOR NON INTERLEAVING PROCESS ALGEBRA
J. C. M. Baeten and J. A. Bergstra (Amsterdam Univ., Netherlands.) Jan. 1994 29 p See also PB95-110607
(ISSN 0926-4515)
(PB95-110490) Avail: CASI HC A03/MF A01

We present a simple and intuitive model for the syntax of the Algebra of Communicating Processes (ACP) based on graph isomorphism. We prove an expressivity result and use the model to determine the number of states of a process. NTIS

N95-22715# Institut des Hautes Etudes Scientifiques, Bures-sur-Yvette (France).
CLASSIFICATION OF SU(3) MODULAR INVARIANTS REVISITED
Terry Gannon Apr. 1994 35 p See also PB94-217247 and PB95-111118
(PB95-110771; IHES/P/94/32) Avail: CASI HC A03/MF A01

The SU(3) modular invariant partition functions were first completely classified in another paper by the author (1994). The purpose of these notes is four-fold: (1) Here the authors accomplish the SU(3) classification using only the most basic facts: modular invariance; M(sub lambda mu) is a member of Z(sub = or greater than); and M(sub 00) = 1. In that other paper they made use of less elementary results from Moore-Seiberg, in addition to these 3 basic facts. (2) That other paper was completed well over a year ago. Since then they have found a number of significant simplications to the general argument. They are all included here. (3) A number of people have complained that some of the arguments in that other paper were hard to follow. They have tried here to be as explicit and as clear as possible. (4) Hidden in that other paper were a number of smaller results which should be of independent value. These are explicitly mentioned here. NTIS

N95-22717 Center for Mathematics and Computer Science, Amsterdam (Netherlands). Dept. of Numerical Mathematics.
PARALLAL ARNOLDI METHOD FOR THE CONSTRUCTION OF A KRYLOV SUBSPACE BASIS: AN APPLICATION IN MAGNETOHYDRODYNAMICS
J. G. L. Booten, P. M. Meijer (Mason Hanger Pantex Plant, Amarillo, TX.), H. J. J. teRiele, and H. A. vanderVorst (Utsunomiya Univ., Japan.) Mar. 1994 10 p
(ISSN 0169-0388)
(PB95-135786; CWI-NM-R9406) Copyright Avail: Issuing Activity (National Technical Information Service (NTIS))

In a recent article by Paige et al, a new method was proposed for computing internal eigenvalues of symmetric matrices. In the present paper, we extend these ideas to non-hermitian eigenvalue problems and apply them to a practical example from the field of magnetohydrodynamics (MHD). The method is very suitable for an efficient parallel implementation. We give some results for the time-consuming kernels of the underlying orthogonalization process, the Arnoldi method, obtained for an MHD problem on a distributed memory multiprocessor. NTIS

N95-22750# International Centre for Theoretical Physics, Trieste (Italy).
A PRESCRIBING GEODESIC CURVATURE PROBLEM
K. C. Chang and J. Q. Liu Sep. 1993 22 p
(DE94-628503; IC-93/285) Avail: CASI HC A03/MF A01 (US Sales Only)

Let D be the unit disk and k be a function on S(sup 1) = (delta)D. Find a flat metric which is pointwise conformal to the standard metric and has k as the geodesic curvature of S(sup 1). A sufficient condition for the existence of such a metric is that the harmonic extension of k in D has saddle points. DOE

N95-22768 Newcastle-upon-Tyne Univ., Newcastle (England). Dept. of Computing Science.
ALGEBRA OF LINES AND BOXES
C. M. Holt Jun. 1994 11 p
(PB95-130456; TRS-483) Copyright Avail: Issuing Activity (National Technical Information Service (NTIS))

Visual language design is driven by interaction between syntax and semantics: changing the way a concept is represented affects the ease with which it can be understood and related to other concepts. The use of lines, boxes, and icons to augment text affects intuitions about operations and properties. The paper is concerned with characterizing syntax by developing a natural algebra that tries to reflect it. The nature of boxes gives rise to two kinds of operations, enclosure and adjointness, that can be related to form a ring, which can be embedded in a vector space. Lines connecting boxes can represent an operation that is related to adjointness, but which is more general in arity and the orientations of the edges that can be linked. The decoration of lines and boxes with emblems provides a facility for representing higher-order operations. NTIS

N95-22772# International Centre for Theoretical Physics, Trieste (Italy).
THE PROPAGATION OF TRAVELLING WAVES FOR STOCHASTIC GENERALIZED KPP EQUATIONS
K. D. Elworthy and H. Z. Zhao Sep. 1993 39 p
(DE94-628473; IC-93/318) Avail: CASI HC A03/MF A01 (US Sales Only)

We study the existence and propagation of approximate travelling waves of generalized KPP equations with seasonal multiplicative white noise perturbations of Ito type. Three regimes of perturbation are considered: weak, mild, and strong. We show that weak perturbations have little effect on the wave like solutions of the unperturbed equations while strong perturbations essentially destroy the wave and force the solutions to die down. For mild perturbations we show that there is a residual wave form but propagating at a different speed to that of the unperturbed equation. In the appendix J.G. Gaines illustrates these different regimes by computer simulations. DOE

N95-22777# International Centre for Theoretical Physics, Trieste (Italy).
NAHM'S PRODUCT AND W-ALGEBRA
Pei Wang Sep. 1993 11 p
(DE94-628504; IC-93/297) Avail: CASI HC A03/MF A01 (US Sales Only)

We apply Nahm's normal ordered product to the Z(sub k) parafermion and prove (up to the level k = 4) that different orders of the product of generating parafermion with its conjugate, except a normalization constant, can be identified with the generators in a W(sub k) is equivalent to W (2, 3,..., K) algebra. The scheme we describe is also an illustration of how to enlarge an algebra. W(sub k) to W(sub k+1). DOE

N95-22794# International Centre for Theoretical Physics, Trieste (Italy).
IDEMPOTENTS IN BANACH ALGEBRA [IDEMPOTENTS DANS LAS ALGEBRES DE BANACH]
M. Berkani Mar. 1994 4 p In ITALIAN
(DE94-628429; IC-94/57) Avail: CASI HC A01/MF A01 (US Sales Only)

Using the holomorphic functional calculus we give a characterization of idempotent elements commuting with a given element in a Banach algebra. DOE

N95-22809# International Centre for Theoretical Physics, Trieste (Italy).
TRISECANT CURVE ASSOCIATED TO A SMOOTH CURVE IN P(SUB 3) OF DEGREE D GREATER THAN G+2
F. Laytimi and D. S. Nagaraj Mar. 1994 10 p
(DE94-628425; IC-94/44) Avail: CASI HC A02/MF A01

Let C be a smooth irreducible curve imbedded in P(sub 3) by the line bundle L on C of degree d (d greater than or equal to 4), and C(sub 3) the third symmetric product of C. The trisecant variety of C, T(sub C) included in C(sub 3) is a curve. The problem studied here is the connectedness of T(sub C). DOE

N95-22836# Institut des Hautes Etudes Scientifiques, Bures-sur-Yvette (France).
ENTROPY OF Z(SUP d) SUBSHIFTS OF FINITE TYPE
Shmuel Friedland (Illinois Univ., Chicago, IL.) 20 Jun. 1994 16 p
(PB95-108072; IHES/M/94/37) Avail: CASI HC A03/MF A01

In this paper we study the entropy of Z(sup d) subshift of finite type (SFT) for d greater than 1. In section 1 we prove the results (0.1) - (0.3). In section 2 we prove the analogous results for Z(sup d)-SFT for d greater than 2. In the last section we generalize the concept of nontransient states for Z(sup d)-SFT. We discuss some open problems and we show the equivalence of our definition of Z(sup d)-SFT to the standard definition. NTIS

N95-22837 Institut des Hautes Etudes Scientifiques, Bures-sur-Yvette (France).
ANALYTIC SETS AND GAMES IN BANACH SPACES
W. T. Gowers Jul. 1994 27 p Limited Reproducibility: More than 20% of this document may be affected by microfiche quality
(PB95-108080; IHES/M/94/42) Avail: CASI HC A03

A Ramsey-type lemma from a preprint by the present author is generalized from sets of finite sequences to analytic sets of infinite sequences. The

method is related to methods of Galvin and Prikry and Ellentuck. The authors give consequences for the structure of infinite-dimensional Banach spaces. NTIS

N95-22922 International Centre for Theoretical Physics, Trieste (Italy).
SEMI-SYMMETRIC MANIFOLDS SATISFYING CERTAIN CURVATURE CONDITIONS
M. S. Rahman Sep. 1993 9 p Limited Reproducibility: More than 20% of this document may be affected by microfiche quality
(DE94-628414; IC-93/319) Avail: Issuing Activity (Department of Energy (DOE)) (US Sales Only)

Use is made of the conditions R(X,Y).C = 0,C not equal to 0 on an (M,g) to show how it becomes a semi-symmetric manifold. On projecting a semi-symmetric manifold (M,g) in local coordinates with curvature conditions S(sub hijk) = 0, R not equal to 0; nabla(sub l)R(sub ij) = a(sub l)R(sub ij); nabla (sub l)E(sup i, sub j) = k(sub l) E(sup i, sub j) and nabla(sub l)C(sub hijk) = a(sub l)C(sub hijk), C not equal to 0 a chain of theorems are presented. An expression for the Laplacian in spirit to semi-symmetric manifold is also given. On semi-symmetric (M,g) admitting special metric connection the symmetry property of the (0,2)-type tensor T on the tangent bundle and of the expression (nabla(sub (chi))(pi))Y are then shown. DOE

N95-22931*# Institute for Computer Applications in Science and Engineering, Hampton, VA.
A PERSPECTIVE ON UNSTRUCTURED GRID FLOW SOLVERS Final Report
V. Venkatakrishnan Feb. 1995 40 p Submitted for publication
(Contract NAS1-19480; RTOP 505-90-52-01)
(NASA-CR-195025; NAS 1.26:195025; ICASE-95-3) Avail: CASI HC A03/MF A01

This survey paper assesses the status of compressible Euler and Navier-Stokes solvers on unstructured grids. Different spatial and temporal discretization options for steady and unsteady flows are discussed. The integration of these components into an overall framework to solve practical problems is addressed. Issues such as grid adaptation, higher order methods, hybrid discretizations and parallel computing are briefly discussed. Finally, some outstanding issues and future research directions are presented. Author

N95-22932# Technische Univ., Delft (Netherlands).
TIME-PERIODIC SOLUTIONS OF SOME FORCED NONLINEAR WAVE EQUATIONS: ANALYSIS, APPROXIMATIONS AND APPLICATIONS Ph.D. Thesis
Caspar Jacobus Blom 31 May 1994 166 p
(PB95-135083) Avail: CASI HC A08/MF A02

The partial differential equations we consider here form a sequence of increasing degree of complexity. We start with a relatively innocuous looking perturbed wave equation. For this wave equation there exists a unique time-periodic solution. A linear term is added and the problem immediately becomes more complex. Uniqueness of the time-periodic solution is now no longer guaranteed. Changing the forcing term in this equation in a continuous way (the amplitude more specifically) can cause a given periodic solution to disappear. This problem is made considerably more difficult by allowing the frequency of the forcing term to be in a neighborhood of the basic eigenfrequency of the system. This we call the near-resonance case. We then proceed to study coupled systems near-resonance. In the last chapter we examine a coupled system near-resonance with several solutions. Main topic headings are as follows: The Methods; A Simple Nonlinear Wave Equation; Resonance and Near-Resonance for a Nonlinear Wage Equation which Models the Oscillations of Overhead Transmission Lines; Exciting a String. NTIS

N95-23051# International Centre for Theoretical Physics, Trieste (Italy).
CUMULANT APPROACH TO DYNAMICAL CORRELATION FUNCTIONS AT FINITE TEMPERATURES
Tran MinhTien Nov. 1993 7 p
(DE94-628487; IC-93/389) Avail: CASI HC A02/MF A01 (US Sales Only)

A new theoretical approach, based on the introduction of cumulants, to calculate thermodynamic averages and dynamical correlation functions at finite temperatures is developed. The method is formulated in Liouville instead of Hilbert space and can be applied to operators which do not require to satisfy fermion or boson commutation relations. The application of the partitioning and projection methods for the dynamical correlation functions is discussed. The present method can be applied to weakly as well as to strongly correlated systems. DOE

N95-23068# Tilburg Univ. (Netherlands).
REGULAR GRAPHS WITH FOUR EIGENVALUES Research Memo
E. R. vanDam 1994 19 p
(PB95-135141; FEW-659) Avail: CASI HC A03/MF A01

The authors study the connected regular graphs with four distinct eigenvalues. Properties and feasibility conditions of the eigenvalues are found. Several examples, constructions and characterizations are given, as well as some uniqueness and nonexistence results. NTIS

N95-23069# Tilburg Univ. (Netherlands).
SECOND DERIVATIVE OF THE LIKELIHOOD OF AN EXACT ARMA MODEL Research Memo
J. vanderLeeuw 1994 34 p
(PB95-135158; FEW-661) Avail: CASI HC A03/MF A01

The likelihood of an exact Autoregressive Moving Average (ARMA) model under the assumption of normality is investigated. Using a closed form expression of the covariance matrix the elements of the matrix of second derivatives of the concentrated likelihood function are derived. These elements consist in general of four or five terms. Two terms come from the determinant, one of them belonging to the information matrix. These terms are sums of the elements of the covariance matrix or its inverse. The next two terms are quadratic forms of the error vector. The last term is based on the matrix of independent variables, and thus only present in a regression model and not in the pure time series model. The general form of second derivative does not permit conclusions about the existence of global maximum of the likelihood function. NTIS

N95-23070# Tilburg Univ. (Netherlands).
ASYMPTOTIC JUSTIFICATION FOR A MODIFIED GLS PROCEDURE TO ESTIMATE ARMA PARAMETERS Research Memo
J. vanderLeeuw and H. Tigelaar 1994 25 p
(PB95-135166; FEW-662) Avail: CASI HC A03/MF A01

The asymptotic form of the concentrated likelihood function of a stationary Autoregressive Moving Average (ARMA) model is investigated. Basis for the analysis is the closed form formula for the exact covariance matrix. GLS estimates of regression coefficients can be based on a simple and widely used adjusted form of the covariance matrix. However, Maximum Likelihood (ML)-estimates of the ARMA parameters become more complicated, as they depend on the limit of the determinant of the covariance matrix. NTIS

N95-23076# Institut des Hautes Etudes Scientifiques, Bures-sur-Yvette (France).
ALGEBRAIC DESCRIPTION OF THE ELLIPTIC COHOMOLOGY OF CLASSIFYING SPACES
Jorge A. Devoto 13 Jul. 1994 17 p
(PB95-110797; IHES/M/94/40) Avail: CASI HC A03/MF A01

Let G be a finite group of order (the absolute value of G) odd and let Ell(exp *)(-)(circle multiply) Z(1/(the absolute value of Ge)) denote elliptic cohomology tensored by Z(1/(the absolute value of G)). Then the authors give a description of Ell(sub *)(E(N,G) x(sub N)X) (circle multiply)(Z(1/(the absolute value of G)), where N is a normal subgroup of G, E(N,G) is the universal N-free G space and X is any finite G-CW complex where N acts freely. The authors explain how some of the results of Hopkins-Kuhn-Ravenel can be recovered for their results. NTIS

N95-23130# Technische Univ., Eindhoven (Netherlands). Dept. of Mathematics and Computing Science.
CANONICAL TYPING AND PI-CONVERSION
F. Kamareddine and R. P. Nederpelt Jan. 1994 62 p Prepared in cooperation with Glasgow Univ.
(PB95-139218) Avail: CASI HC A04/MF A01

The authors present a lambda-calculus in which the conversion rules apply to types as well as terms. Abstraction and application, moreover, range over both types and terms. They extend the calculus with a canonical type operator tau in order to associate types to terms. The type of fa will then be Fa, where F is the tyPe of f and the statement Gamma typed t :

sigma from usual type theory is split in two statements in the system: Gamma types t and tau (Gamma,t) = sigma. Such a splitting enables one to discuss the two questions of the typability of a term and of what is its type separately. Again the authors believe that this splitting is important and should be usually considered. As a demonstration of what the authors can do with their calculus, they interpret Church's lambda arrow-type in the calculus. This enables them to view their approach as an attempt to extend lambda arrow-type with a unified treatment for type and term substitution and conversion and at splitting Gamma types t : sigma in the two statements: Gamma types t and tau (Gamma,t) = beta sigma. Such an approach should eventually be used to deal with the Barendregt cube and the Pure Type Systems. NTIS

N95-23146# Technische Univ., Eindhoven (Netherlands). Dept. of Mathematics and Computing Science.

AUTOMATIC VERIFICATION OF REGULAR PROTOCOLS IN P/T NETS

P. M. P. Rambags Dec. 1993 30 p

(PB95-138921) Avail: CASI HC A03/MF A01

In this article, we present two algorithms to determine whether a given place/transition (P/T) net N with transitions T satisfies a given protocol II, where II consists of an alphabet A is contained in or equal to T and a regular language over A. The first algorithm checks whether N cannot do more than II allows (trace-safety). The second one verifies whether N does not stop too early (weak progress). NTIS

N95-23149# Technische Univ., Eindhoven (Netherlands). Dept. of Mathematics and Computing Science.

AR-DESCRIPTIONS IN TRANSLATABLE FRECHET SPACES

M. M. A. deRijcke Dec. 1993 65 p

(PB95-138855; RANA-93-19) Avail: CASI HC A04/MF A01

C sub 0 groups on (pre-) Frechet spaces are studied. For arbitrary c sub 0 groups (alpha sub t) sub(t is an element of R) on arbitrary Frechet spaces F the authors introduce a class of 'convolution' operators. These classes of operators are used to obtain results on closed, (alpha sub t)-invariant subspaces of F and (alpha sub t)-invariant, closed, linear operators on F. Furthermore, a class of Frechet spaces F is constructed, such that each F is in duality with D(Real number) and the dual of the translation group on D(Real number) is a c sub 0 group on F. Complete characterizations of closed, translation invariant subspaces and operators are given based on earlier work of Kahane and Schwartz. These results will be applied in fundamental system theory. A characterization of dynamical systems described by an AR-relation is presented, based on earlier work of Soethoudt. NTIS

N95-23167 Center for Mathematics and Computer Science, Amsterdam (Netherlands). Dept. of Numerical Mathematics.

VLUGR2: A VECTORIZABLE ADAPTIVE GRID SOLVER FOR PDES IN 2D

J. G. Blom, R. A. Trompert, and J. G. Verwer Feb. 1994 27 p See also N94-26772

(PB95-136008; CWI-NM-R9403) Copyright Avail: Issuing Activity (National Technical Information Service (NTIS))

This paper deals with an adaptive-grid finite-difference solver for time-dependent two-dimensional systems of partial differential equations. It describes the ANSI FORTRAN 77 code, VLUGR2, auto-vectorizable on the Cray Y-MP, that is based on this method. The robustness and the efficiency of the solver, both for vector and scalar processors, is illustrated by the application of the code to two example problems arising from a groundwater-flow model. NTIS

N95-23169 Technische Univ., Eindhoven (Netherlands). Dept. of Mathematics and Computing Science.

OPTIMALLY SCALED SYSTEMS FOR SECOND ORDER SCALAR SINGULARITY PERTURBED PROBLEMS

L. V. Kalachev and R. M. M. Mattheij Sep. 1993 25 p Prepared in cooperation with Montana Univ.

(PB95-138814; RANA-93-14) Avail: Issuing Activity (National Technical Information Service (NTIS))

The conditioning of a singularly perturbed scalar Dirichlet problem is considered. It is shown how this is related to the conditioning of an appropriate associated first order system. Through this, the dichotomy of the solution space (a concept that only make sense in a vectorial setting) can be investigated. Two typical equations are studied in more detail, one with possible boundary layers on both sides of the interval and one with an internal layer (i.e. the turning point case). The results are applied to obtain estimates of global discretization errors for difference methods. Several examples illustrate the analysis. NTIS

N95-23171# Technische Univ., Eindhoven (Netherlands). Dept. of Mathematics and Computing Science.

TRANSLATION INVARIANT FRECHET SUBSPACES OF DISTRIBUTIONS

S. J. L. vanEijndhoven Oct. 1993 44 p

(PB95-138830; RANA-93-15) Avail: CASI HC A03/MF A01

This paper is about translation invariant subspaces F of the classical distribution space D'(IR) of Schwartz which admit a Frechet linear topology such that the translation group is strongly continuous on F. If C (sup infinity) (IR) is contained in F, then complete characterizations of the closed translation invariant subspaces of F are derived on the basis of earlier work of Kahane and Schwartz. The first part of the paper is preparatory and devoted to c(sub 0)- groups on Frechet spaces in general. NTIS

N95-23173# Technische Univ., Eindhoven (Netherlands). Dept. of Mathematics and Computing Science.

STABILITY AND EFFICIENCY OF WAVEFORM RELAXATION METHODS

J. K. M. Jansen, R. M. M. Mattheij, M. T. M. Penders, and W. H. A. Schilders Dec. 1993 22 p Prepared in cooperation with Philips Research Labs.

(PB95-138863; RANA-93-17) Avail: CASI HC A03/MF A01

We investigate the behavior of waveform relaxation (WR) methods for some model problems. First it is shown how convergence (of the iteration) is related to stability of some one-step integration schemes. Then we investigate the computational complexity of a 1-D and 2-D heat equation when WR is used in combination with nested iteration and assess its efficiency, in particular compared to straightforward methods based on Gaussian elimination. Finally we present some results, showing the performance of WR. NTIS

N95-23174# Technische Univ., Eindhoven (Netherlands). Dept. of Mathematics and Computing Science.

DEGENERATE HAMILTONIAN HOPF BIFURCATIONS

J. C. vanderMeer Dec. 1993 20 p

(PB95-138871; RANA-93-18) Avail: CASI HC A03/MF A01

We give an outline of the qualitative analysis of degenerate Hamiltonian Hopf bifurcations along the lines of Van der Meer. Basically the approach consists of four steps: (1) normal form theory for (Hamiltonian) vector fields, (2) Weinstein-Moser reduction, (3) singularity theory, and (4) analysis of the singularity (bifurcation) theoretic normal form. NTIS

N95-23176# Technische Univ., Eindhoven (Netherlands). Dept. of Mathematics and Computing Science.

NEW ROBUST MULTIGRID METHOD FOR 2D CONVECTION-DIFFUSION PROBLEMS

A. A. Reusken Apr. 1994 16 p See also PB95-110821

(PB95-138897; RANA-94-04) Avail: CASI HC A03/MF A01

We introduce a new multigrid approach for solving 2D convection-diffusion problems. As in the hierarchical basis multigrid method, we use a transformed matrix with a relatively low generalized condition number. The transformation we use is not based on the nesting of the coarse and fine grid only, but uses more information from the matrix. After transforming back to the original matrix, this results in a robust multigrid algorithm with matrix-dependent prolongations and restrictions. NTIS

N95-23200# Technische Univ., Twente (Netherlands). Faculty of Applied Mathematics.

STOERMER-COWELL: STRAIGHT, SUMMED AND SPLIT. AN OVERVIEW

J. F. Frankena Nov. 1993 28 p See also PB93-192060 and N92-14714

(PB95-139341) Avail: CASI HC A03/MF A01

In the paper the authors consider the relationship between some (forms of) specific numerical methods for (second order) initial value problems. In particular, the Stormer-Cowell method in second sum form is shown to be the Gauss-Jackson method (and analogously, for the sake of completeness,

the authors relate Adams-Bashforth-Moulton methods to their first-sum forms). Furthermore, they consider the split form of the Stormer-Cowell method. The reason for this consideration is the fact that these summed and split forms exhibit a better behavior with respect to rounding errors than the original method (whether in difference or in ordinate notation). Numerical evidence will support the formal proofs that have been given elsewhere. NTIS

N95-23231# Technische Univ., Twente (Netherlands). Faculty of Applied Mathematics.
NOTE ON THE COMPUTATIONAL COMPLEXITY OF j-RADII OF POLYTOPES IN (R SUP n)
U. Faigle, W. Kern, and M. Streng Nov. 1993 8 p See also N92-30147
(PB95-139358) Avail: CASI HC A02/MF A01

We show that, for fixed dimension n, the approximation of inner and outer j-radii of polytopes in R(sup n), endowed with the Euclidean norm, is in P. NTIS

N95-23233# Technische Univ., Twente (Netherlands). Faculty of Applied Mathematics.
PUZZLES 4: SPERNER COLLECTIONS AND THE KEYS PUZZLE
F. Goebel Oct. 1993 10 p See also PB92-223742
(PB95-139374) Avail: CASI HC A02/MF A01

The well-known keys puzzle and its solution are generalized to the case where the collection of minimal sets of persons who have access to the safe is an arbitrary Sperner collection. When all such minimal sets have 2 elements, the solution is given in graph-theoretic terms. NTIS

N95-23235# Technische Univ., Twente (Netherlands). Faculty of Applied Mathematics.
PARTITION OF REAL SYMMETRIC MATRICES ACCORDING TO THE MULTIPLICITIES OF THEIR EIGENVALUES Memorandum Report
P. Jonker, G. Still, and F. Twilt Oct. 1993 20 p See also N86-29596
(PB95-139846; MEMO-1166) Avail: CASI HC A03/MF A01

In this paper we will be concerned with a partition of the set of all real symmetric n x n-matrices into strata corresponding to the multiplicities of the eigenvalues. It will be shown that this stratification is Whitney Regular. Moreover, we derive an explicit formula for the codimension of the strata in terms of the multiplicities involved. The transversality theory of R. Thom leads to generic perturbation results for the eigenvalues of one-parameter families of real symmetric matrices. The connections with sensitivity results in parametric optimization are investigated. NTIS

N95-23236# Technische Univ., Twente (Netherlands). Faculty of Applied Mathematics.
TREES ARE GRACEFUL IF AND ONLY IF TREES WITH A PERFECT MATCHING ARE STRONGLY GRACEFUL Memorandum Report
H. J. Broersma and C. Hoede 19 Oct. 1993 11 p
(PB95-139853; MEMO-1167) Avail: CASI HC A03/MF A01

Let T = (V,E) be a tree on V = n vertices. T is graceful if there exists a bijection f:V to (0,1, ...,n-1) such that (f(u)-f(v) where uv is an element of E) = (1,2,...,n-1). If, moreover, T contains a perfect matching M and f can be chosen in such a way that f(u) + f(v) = n-1 for every edge uv is an element of M, then T is called strongly graceful. We show that the well-known conjecture that all trees are graceful is equivalent to the conjecture that all trees containing a perfect matching are strongly graceful. We also give some applications of this result. NTIS

N95-23237# Technische Univ., Twente (Netherlands). Faculty of Applied Mathematics.
ORDERS OF PREDICTOR-CORRECTOR PAIRS FOR SECOND-ORDER ODE'S
J. F. Frankena Sep. 1993 15 p See also PB93-192060 and N92-14714
(PB95-140612; MEMO-1159) Avail: CASI HC A03/MF A01

For first-order ordinary differential equations (ODE's), there is a general description of the order of predictor-corrector pairs. In this paper, a generalization to predictor-corrector methods for second-order ODE's is presented, in relation to the number of iterations. The theoretical results are verified with the Stormer-Cowell method and several related predictor-corrector methods, using constant step size. This leads to a comparison of the performances of these methods with respect to the order. NTIS

N95-23455# International Centre for Theoretical Physics, Trieste (Italy).
ITERATIVE SOLUTIONS OF NONLINEAR EQUATIONS IN SMOOTH BANACH SPACES
C. E. Chidume May 1994 14 p
(DE94-634287; IC-94/96) Avail: CASI HC A03/MF A01 (US Sales Only)

Let E be a smooth Banach space over the real field, phi does not equal K is contained in E closed convex and bounded, T:K approaches K uniformly continuous and strongly pseudo-contractive. It is proved that the Ishikawa iteration process converges strongly to the unique fixed point of T. Applications of this result to the operator equations Au = f or u + Au = f where A is a strongly accretive mapping of E into itself and under various continuity assumptions on A are also given. DOE

N95-23457# International Centre for Theoretical Physics, Trieste (Italy).
LINEARIZING W-ALGEBRAS
S. O. Krivonos and A. S. Sorin Jun. 1994 8 p
(DE94-634324; IC-94/112; HEP-TH-9406005) Avail: CASI HC A02/MF A01 (US Sales Only)

We show that the Zamolodchikov's and Polyakov-Bershadsky nonlinear algebras W(sub 3) and W(exp (2))(sub 3) can be embedded as subalgebras into some linear algebras with finite set of currents. Using these linear algebras we find new field realizations of W(exp (2))(sub 3) and W(sub 3) which could be a starting point for constructing new versions of W-string theories. We also reveal a number of hidden relationships between W(sub 3) and W(exp (2))(sub 3). We conjecture that similar linear algebras can exist for other W-algebra as well. DOE

N95-23465*# Institute for Computer Applications in Science and Engineering, Hampton, VA.
UNIFICATION OF SOME ADVECTION SCHEMES IN TWO DIMENSIONS Final Report
D. Sidilkover and P. L. Roe (Michigan Univ., Ann Arbor, MI.) NASA Feb. 1995 28 p Submitted for publication
(Contracts NAS1-19480; RTOP 505-90-52-01; DE-FG02-92ER-25139)
(NASA-CR-195044; NAS 1.26:195044; ICASE-95-10) Avail: CASI HC A03/MF A01

The relationship between two approaches towards construction of genuinely two-dimensional upwind advection schemes is established. One of these approaches is of the control volume type applicable on structured cartesian meshes. It resulted in the compact high resolution schemes capable of maintaining second order accuracy in both homogeneous and inhomogeneous cases. Another one is the fluctuation splitting approach, which is well suited for triangular (and possibly) unstructured meshes. Understanding the relationship between these two approaches allows us to formulate here a new fluctuation splitting high resolution (i.e. possible use of artificial compression, while maintaining positivity property) scheme. This scheme is shown to be linearity preserving in inhomogeneous as well as homogeneous cases. Author

N95-23536# Lawrence Livermore National Lab., Livermore, CA.
SCHWARZ-CHRISTOFFEL METHODS FOR MULTIPLY-ELONGATED REGIONS
L. H. Howell May 1994 6 p Presented at the World Congress on Computational and Applied Mathematics, Atlanta, GA, 11-15 Jul. 1994
(Contract W-7405-eng-48)
(DE94-019048; UCRL-JC-116614; CONF-940719-8) Avail: CASI HC A02/MF A01

Previous solutions to the crowding problem in Schwarz-Christoffel maps utilized an infinite strip as a standard domain in order to map onto highly elongated regions. This paper presents transformations onto polygons which are elongated in more than one direction. Infinite strips with one or two cuts are the standard domains for these mapping functions, which are well-conditioned for numerical computations. DOE

N95-23547*# Research Inst. for Advanced Computer Science, Moffett Field, CA.

ON ADAPTIVE WEIGHTED POLYNOMIAL PRECONDITIONING FOR HERMITIAN POSITIVE DEFINITE MATRICES

Bernd Fischer (Hamburg Univ., Germany.) and Roland W. Freund Mar. 1992 14 p Presented at the Copper Mountain Conference on Iterative Methods, 1992 Submitted for publication
(Contract NCC2-387)
(NASA-CR-197946; NAS 1.26:197946; RIACS-TR-92-09) Avail: CASI HC A03/MF A01

The conjugate gradient algorithm for solving Hermitian positive definite linear systems is usually combined with preconditioning in order to speed up convergence. In recent years, there has been a revival of polynomial preconditioning, motivated by the attractive features of the method on modern architectures. Standard techniques for choosing the preconditioning polynomial are based only on bounds for the extreme eigenvalues. Here a different approach is proposed, which aims at adapting the preconditioner to the eigenvalue distribution of the coefficient matrix. The technique is based on the observation that good estimates for the eigenvalue distribution can be derived after only a few steps of the Lanczos process. This information is then used to construct a weight function for a suitable Chebyshev approximation problem. The solution of this problem yields the polynomial preconditioner. In particular, we investigate the use of Bernstein-Szego weights. Author

N95-23548*# Research Inst. for Advanced Computer Science, Moffett Field, CA.

FOURTH ORDER DIFFERENCE METHODS FOR HYPERBOLIC IBVP'S

Bertil Gustafsson and Pelle Olsson Mar. 1994 38 p
(Contract NAS2-13721)
(NASA-CR-197955; NAS 1.26:197955; RIACS-TR-94-04) Avail: CASI HC A03/MF A01

Fourth order difference approximations of initial-boundary value problems for hyperbolic partial differential equations are considered. We use the method of lines approach with both explicit and compact implicit difference operators in space. The explicit operator satisfies an energy estimate leading to strict stability. For the implicit operator we develop boundary conditions and give a complete proof of strong stability using the Laplace transform technique. We also present numerical experiments for the linear advection equation and Burgers' equation with discontinuities in the solution or in its derivative. The first equation is used for modeling contact discontinuities in fluid dynamics, the second one for modeling shocks and rarefaction waves. The time discretization is done with a third order Runge-Kutta TVD method. For solutions with discontinuities in the solution itself we add a filter based on second order viscosity. In case of the non-linear Burger's equation we use a flux splitting technique that results in an energy estimate for certain different approximations, in which case also an entropy condition is fulfilled. In particular we shall demonstrate that the unsplit conservative form produces a non-physical shock instead of the physically correct rarefaction wave. In the numerical experiments we compare our fourth order methods with a standard second order one and with a third order TVD-method. The results show that the fourth order methods are the only ones that give good results for all the considered test problems. Author

N95-23592*# Research Inst. for Advanced Computer Science, Moffett Field, CA.

BLOCK LU FACTORIZATION

James W. Demmel (California Univ., Berkeley, CA.), Nicholas J. Higham (Manchester Univ., England.), and Robert S. Schreiber 16 Feb. 1992 25 p Submitted for publication Sponsored in part by NSF and DARPA
(Contracts NCC2-387; DAAL03-91-C-0047; NSF ASC-90-05933)
(NASA-CR-197949; NAS 1.26:197949; RIACS-TR-92-03) Avail: CASI HC A03/MF A01

Many of the currently popular 'block algorithms' are scalar algorithms in which the operations have been grouped and reordered into matrix operations. One genuine block algorithm in practical use is block LU factorization, and this has recently been shown by Demmel and Higham to be unstable in general. It is shown here that block LU factorization is stable if A is block diagonally dominant by columns. Moreover, for a general matrix the level of instability in block LU factorization can be founded in terms of the condition number kappa(A) and the growth factor for Gaussian elimination without pivoting. A consequence is that block LU factorization is stable for a matrix A that is symmetric positive definite or point diagonally dominant by rows or columns as long as A is well-conditioned. Author

N95-23593*# Research Inst. for Advanced Computer Science, Moffett Field, CA.

QUASI-KERNEL POLYNOMIALS AND CONVERGENCE RESULTS FOR QUASI-MINIMAL RESIDUAL ITERATIONS

Roland W. Freund Mar. 1992 17 p Submitted for publication
(Contract NCC2-387)
(NASA-CR-197948; NAS 1.26:197948; RIACS-TR-92-07) Avail: CASI HC A03/MF A01

Recently, Freund and Nachtigal have proposed a novel polynominal-based iteration, the quasi-minimal residual algorithm (QMR), for solving general nonsingular non-Hermitian linear systems. Motivated by the QMR method, we have introduced the general concept of quasi-kernel polynomials, and we have shown that the QMR algorithm is based on a particular instance of quasi-kernel polynomials. In this paper, we continue our study of quasi-kernel polynomials. In particular, we derive bounds for the norms of quasi-kernel polynomials. These results are then applied to obtain convergence theorems both for the QMR method and for a transpose-free variant of QMR, the TFQMR algorithm. Author

N95-23600# Illinois Univ., Urbana-Champaign, IL. Center for Superconducting Research and Development.

MICROARCHITECTURE SUPPORT FOR DYNAMIC SCHEDULING OF ACYCLIC TASK GRAPHS

Carl J. Beckmann and Constantine D. Polychronopoulos Aug. 1992 39 p Sponsored by Shell Doctoral Fellowship
(Contract DE-FG02-85ER-25001; NSF CCR-89-57310)
(CSRD-1207) Avail: CASI HC A03/MF A01

It can be shown that any program can be broken into its loop structure, plus acyclic dependence graphs representing the body of each loop or subroutine. The parallelism inherent in these acyclic graphs augments the loop-level parallelism available in the program. This paper presents two algorithms for dynamic scheduling of such acyclic task graphs containing both data and control dependencies, and describes a microarchitecture which implements these algorithms efficiently. Author

N95-23611*# Research Inst. for Advanced Computer Science, Moffett Field, CA.

RECENT ADVANCES IN LANCZOS-BASED ITERATIVE METHODS FOR NONSYMMETRIC LINEAR SYSTEMS

Roland W. Freund, Gene H. Golub (Stanford Univ., CA.), and Noel M. Nachtigal Jan. 1992 20 p Submitted for publication
(Contract NCC2-387; NSF CCR-88-21078)
(NASA-CR-197950; NAS 1.26:197950; RIACS-TR-92-02) Avail: CASI HC A03/MF A01

In recent years, there has been a true revival of the nonsymmetric Lanczos method. On the one hand, the possible breakdowns in the classical algorithm are now better understood, and so-called look-ahead variants of the Lanczos process have been developed, which remedy this problem. On the other hand, various new Lanczos-based iterative schemes for solving nonsymmetric linear systems have been proposed. This paper gives a survey of some of these recent developments. Author

N95-23612*# Research Inst. for Advanced Computer Science, Moffett Field, CA.

AN IMPLEMENTATION OF THE QMR METHOD BASED ON COUPLED TWO-TERM RECURRENCES

Roland W. Freund (Bell Telephone Labs., Inc., Murray Hill, NJ.) and Noeel M. Nachtigal Jun. 1992 33 p Sponsored in cooperation with DARPA
(Contract NCC2-387)
(NASA-CR-197956; NAS 1.26:197956; RIACS-TR-92-15) Avail: CASI HC A03/MF A01

The authors have proposed a new Krylov subspace iteration, the quasi-minimal residual algorithm (QMR), for solving non-Hermitian linear systems. In the original implementation of the QMR method, the Lanczos process with look-ahead is used to generate basis vectors for the underlying Krylov subspaces. In the Lanczos algorithm, these basis vectors are computed by means of three-term recurrences. It has been observed that, in finite precision arithmetic, vector iterations based on three-term recursions

are usually less robust than mathematically equivalent coupled two-term vector recurrences. This paper presents a look-ahead algorithm that constructs the Lanczos basis vectors by means of coupled two-term recursions. Implementation details are given, and the look-ahead strategy is described. A new implementation of the QMR method, based on this coupled two-term algorithm, is described. A simplified version of the QMR algorithm without look-ahead is also presented, and the special case of QMR for complex symmetric linear systems is considered. Results of numerical experiments comparing the original and the new implementations of the QMR method are reported. Author

N95-23614*# National Aeronautics and Space Administration. Lewis Research Center, Cleveland, OH.
COMBINING COMPARISON FUNCTIONS AND FINITE ELEMENT APPROXIMATIONS IN CFD
Kenneth J. Baumeister and Joseph F. Baumeister Mar. 1995 25 p
(RTOP 505-62-52)
(NASA-TM-106851; E-9440; NAS 1.15:106851) Avail: CASI HC A03/MF A01

In a variety of potential flow applications, the modal element method has been shown to significantly reduce the numerical grid, employ a more precise grid termination boundary condition, and give theoretical insight to the flow physics. The method employs eigenfunctions to replace the numerical grid over significant portions of the flow field. Generally, a numerical grid is employed around obstacles with complex geometry while eigenfunctions are applied to regions in the flow field where the boundary conditions can easily be satisfied. To handle a wider class of computational fluid dynamics (CFD) problems, the present paper extends the modal element to include function approximations which do not satisfy the governing differential equation. To accomplish this task, a double modal series approximation and weighted residual constraints are developed to force the comparison functions to satisfy the governing differential equation and to interface properly with the finite element solution. As an example, the method is applied to the problem of potential flow in a channel with two-dimensional cylindrical like obstacles. The calculated flow fields are in excellent agreement with exact analytical solutions. Author

N95-23658# International Centre for Theoretical Physics, Trieste (Italy).
ISHIKAWA ITERATION PROCESS FOR NONLINEAR LIPSCHITZ STRONGLY ACCRETIVE MAPPINGS
C. E. Chidume and M. O. Osilike (Nigeria Univ., Nsukka, Nigeria.) May 1994 16 p
(DE94-634284; IC-94/91) Avail: CASI HC A03/MF A01 (US Sales Only)

Let E = L(sub p), p greater than or equal to 2 and let T:E (yields) E be a Lipschitzian and strongly accretive mapping. Let S:E (yields) E be defined by Sx = f-Tx+x. It is proved that under suitable conditions on the real sequences ((alpha) (sub n))(sup (infinity))(sub n=0) and ((beta)(sub n))(sup (infinity))(sub n=0), the iteration process, x(sub 0) is an element of E, x(sub n+1)=(1-(alpha)(sub n)) x(sub n)+(alpha)(sub n) S(1-(beta)(sub n)) x(sub n)+(beta)(sub n) Sx(sub n), n greater than or equal to 0, converges strongly to the unique solution of Tx=f. A related result deals with the iterative approximation of fixed points for Lipschitz strongly pseudocontractive mappings in E. A consequence of our results gives an affirmative answer to a problem posed by one of the authors in 1990. DOE

N95-23659# International Centre for Theoretical Physics, Trieste (Italy).
SINGULAR MODULI AND ARAKELOV INTERSECTION
Lin Weng May 1994 14 p
(DE94-634286; IC-94/94) Avail: CASI HC A03/MF A01 (US Sales Only)

The value of the modular function j((tau)) at imaginary quadratic arguments (tau) in the upper half plane is usually called singular moduli. In this paper, we use Arakelov intersection to give the prime factorizations of a certain combination of singular moduli, coming from the Hecke correspondence. Such a result may be considered as the degenerate one of Gross and Zagier on Heegner points and derivatives of L-series in their paper (GZ1), and is parallel to the result in (GZ2). DOE

N95-23793# Rochester Univ., NY. Dept. of Computer Science.
COMBINATORIAL SEMANTICS
Henry E. Kyburg, Jr. Jan. 1995 59 p
(Grant NSF IRI-90-02659)
(TR-563) Avail: CASI HC A04/MF A01

In ordinary first order logic, a valid inference in a language L is one in which the conclusion is true in every model of the language in which the premises are true. To accommodate inductive / uncertain / probabilistic / nonmonotonic inference, we weaken that demand to the demand that the conclusion be true in a large proportion of the models in which the relevant premises are true. More generally, we say that an inference is (p,q) valid if its conclusion is true in a proportion lying between p and q of those models in which the relevant premises are true. If we include a statistical variable binding operator '%' in our language, there are many quite general (and useful) things we can say about uncertain validity. A surprising result is that some of these things may conflict with Bayesian conditionalization. Author

N95-23929# Rochester Univ., NY.
EFFECTIVE CATEGORY AND MEASURE IN ABSTRACT COMPLEXITY THEORY
Cristian Calude and Marius Zimand (Auckland Univ., New Zealand.) Aug. 1994 18 p Sponsored by Auckland Univ. and Romanian Dept. of Education and Science
(Grant NSF CCR-89-57604)
(TR-529) Avail: CASI HC A03/MF A01

Strong variants of the Operator Speed-up Theorem, Operator Gap Theorem and Compression Theorem are obtained using an effective version of Baire Category Theorem. It is also shown that all complexity classes of recursive predicates have effective measure zero in the space of recursive predicates and, on the other hand, the class of predicates with almost everywhere complexity above an arbitrary recursive threshold has recursive measure one in the class of recursive predicates. Author

N95-23931# Rochester Univ., NY. Dept. of Computer Science.
OPTIMAL ADVICE
Lane A. Hemaspaandra and Leen Torenvliet (Amsterdam Univ., Netherlands.) Jul. 1994 12 p Sponsored by HC and M
(Grants NSF CCR-89-57604; NSF INT-91-16781; JSPS-ENGR-207)
(TR-527) Avail: CASI HC A03/MF A01

Ko (Ko83) proved that the P-selective sets are in the advice class P/quadratic. We prove that the P-selective sets are in the intersection of NP/linear intersecting coNP/linear. We show this to be optimal in terms of the amount of advice needed. Author

N95-23971# International Centre for Theoretical Physics, Trieste (Italy).
THE EXCHANGE ALGEBRA FOR LIOUVILLE FIELD ON RIEMANN SURFACES WITH h GREATER THAN 1 GENUS
Jianmin Shen, Zhengmao Sheng (Zhejiang Univ., China.), and Zhonghua Wang (International School for Advanced Studies, Trieste, Italy.) Apr. 1994 10 p
(DE94-635446; IC-94/86) Avail: CASI HC A02/MF A01 (US Sales Only)

We consider in this paper the classical Liouville field theory on the Riemann surface with h greater than 1 genus. In terms of the uniformization theorem of Riemann surface, we show explicitly the classical exchange algebra (CEA) for the chiral components of the solution of the Liouville equation. We find that this classical exchange algebra is just the same as that on a Riemann sphere with 2h punctures. DOE

N95-24002# Rochester Univ., NY. Dept. of Computer Science.
REDUCIBILITY CLASSES OF P-SELECTIVE SETS
Lane A. Hemaspaandra, Albrecht Hoene (Technische Univ., Berlin, Germany.), and Mitsunori Ogihara 18 Jul. 1994 18 p Sponsored by DFG Postdoctoral Fellowship
(Grants NSF CCR-89-57604; NSF INT-91-16781; JSPS-ENG-207; NSF CCR-90-02292)
(TR-524) Avail: CASI HC A03/MF A01

A set is P-selective if there is a polynomial-time semi-decision algorithm for the set--an algorithm that given any two strings decides which is 'more likely' to be in the set. This paper establishes a strict hierarchy among the various reductions and equivalences to P-selective sets. Author

N95-24003# Rochester Univ., NY. Dept. of Computer Science.
WITNESS-ISOMORPHIC REDUCTIONS AND THE LOCAL SEARCH PROBLEM
Sophie Fischer (Amsterdam Univ., Netherlands.), Lane A. Hemaspaandra, and Leon Torenvliet (Amsterdam Univ., Netherlands.) Jul. 1994 43 p
(Grants NSF CCR-89-57604; NSF INT-91-16781; JSPS-ENGR-207)
(TR-522) Avail: CASI HC A03/MF A01

We study witness-isomorphic reductions, a type of structure-preserving reduction between NP decision problems. We show that witness-isomorphic reductions can be used in a uniform approach to the local search problem. Author

N95-24034# Rochester Univ., NY. Dept. of Computer Science.
ON THE SIZE OF SETS WITH WEAK MEMBERSHIP PROPERTIES
Marius Zimand Dec. 1994 12 p
(Grants NSF CCR-89-57604; JSPS-ENG-207; NSF INT-91-16781; NSF CCR-93-22513)
(TR-557) Avail: CASI HC A03/MF A01

It is shown that the following classes have measure 0 in E: the class of P-selective sets, the class of P-multiselective sets, the class of cheatable sets, the class of easily countable sets, the class of easily approximable sets, the class of near-testable sets, the class of nearly near-testable sets, the class of sets that are not P-bi-immune. These are corollaries of a more general result stating that the class of sets that are p-isomorphic to P-quasi-approximable sets has measure O in E. By considering the recent approach of Allender and Strauss for measuring in subexponential classes, we cbtain similar results with respect to P for classes having weak logarithmic time membership properties. Author

N95-24042# Rochester Univ., NY. Dept. of Computer Science.
TUTORIAL ON FILTERING, RESTORATION, AND STATE ESTIMATION
Christopher M. Brown, ed. Sep. 1994 43 p
(TR-534) Avail: CASI HC A03/MF A01

This tutorial is dedicated to our long-suffering 442 students, and to the excellent authors from whom I shamelessly cribbed this work. It is a pure cut-and-paste job from my favorite sources on this material. This is not my own work - think of me as an editor working without his authors' permissions. Readers should know that original authors are usually easier to understand than rehashed versions. If this representation helps you, good. If not it at least helped me to sort a few things out. I assume knowledge of all necessary linear systems theory, differential equations, statistics, control theory, etc. We start with the ideas of filtering, smoothing, prediction, and state estimation. Wiener filtering and its associated intellectual framework follows, with a brief foray into ARMA filtering. The idea of recursive estimation is introduced to give some motivation for the slog ahead, and then we start with basic concepts in maximum likelihood, maximum a posteriori, and least-squares estimation. The strategy is to work toward the Kalman Filtering equations by showing how they are simply related to general least-squares estimation. After Kalman filtering, some simpler versions of recursive filters are presented. There are appendices on the orthogonality principle, the matrix inversion lemma, singular value decomposition, partial C and LISP code, and a worked example. Author

N95-24182# Rochester Univ., NY. Dept. of Computer Science.
POLYNOMIAL-TIME MEMBERSHIP COMPARABLE SETS
Mitsunori Ogihara Dec. 1994 26 p
(Grants NSF INT-91-16781; JSPS-ENG-207)
(TR-552) Avail: CASI HC A03/MF A01

This paper studies a notion called polynomial-time membership comparable sets. For a function g, a set A is polynomial-time g-membership comparable if there is a polynomial-time computable function f such that for any x(sub 1),..., x(sub m) with m greater than or equal to g(max (absolute value of x(sub 1),..., absolute value of x(sub m)), outputs b a member of the set (0, 1)(sup m) such that (A(x(sub 1)),...,A(x(sub m))) does not equal b. The following is a list of major results proven in the paper: (1) Polynomial-time membership comparable sets construct a proper hierarchy according to the bound on the number of arguments. (2) Polynomial-time membership comparable sets have polynomial-size circuits. (3) For any function f and for any constant c greater than 0, if a set is less than or equal to (sup p, sub f(n)-tt)-reducible to a P-selective set, then the set is polynomial-time (1+c) log f(n)-membership comparable. And (4) for any C chosen from the set (PSPACE, UP, FewP, NP, C(sub =)P, PP, MOD(sub 2)P, MOD(sub 3)P,...), if C is contained in P-mc(c log n) for some c less than 1, then C = P. As a corollary of the last two results, it is shown that if there is some constant c less than 1 such that all of C are polynomial-time n(sup c)-truth table reducible to some P-selective sets, then C = P, which resolves a question that has been left open for a long time. Author (revised)

N95-24194# Rochester Univ., NY. Dept. of Computer Science.
THE SATANIC NOTATIONS: COUNTING CLASSES BEYOND #P AND OTHER DEFINITIONAL ADVENTURES
Lane A. Hemaspaandra and Heribert Vollmer (California Univ., Santa Barbara, CA.) Dec. 1994 18 p Sponsored by Alexander von Humboldt fellowship
(Grants NSF CCR-89-57604; NSF INT-91-16781; JSPS-ENGR-207; NSF CCR-93-22513; NSF CCR-93-02057)
(TR-561) Avail: CASI HC A03/MF A01

We explore the potentially 'off-by-one' nature of the definitions of counting (#P versus #NP), difference (DP versus DNP), and unambiguous (UP versus UNP; FewP versus FewNP) classes, and make suggestions as to logical approaches in each case. We discuss the strangely differing representations that oracle and predicate models give for counting classes, and we survey the properties of counting classes beyond #P. We ask whether subtracting a #P function from a P function it is no greater than necessarily yields a #P function. Author

N95-23417*# Mississippi State Univ., Mississippi State, MS.
STRUCTURED ADAPTIVE GRID GENERATION USING ALGEBRAIC METHODS
Jiann-Cherng Yang, Bharat K. Soni, R. P. Roger (Teledyne Brown Engineering, Huntsville, AL.), and Stephen C. Chan (Teledyne Brown Engineering, Huntsville, AL.) *In* NASA. Marshall Space Flight Center, Eleventh Workshop for Computational Fluid Dynamic Applications in Rocket Propulsion Jul. 1993 p 1091-1128 (For primary document see N95-23412 07-34)
Avail: CASI HC A03/MF A10

65 STATISTICS AND PROBABILITY

Includes data sampling and smoothing; Monte Carlo method; and stochastic processes.

N95-22527# Vrije Univ., Amsterdam (Netherlands).
NONPARAMETRIC MEASURE OF SPATIAL INTERACTION IN POINT PATTERNS
A. J. Baddeley and M. N. M. vanLieshout Dec. 1993 20 p Prepared in cooperation with Western Australia Univ., Nedlands. Dept. of Mathematics., Leiden Rijksuniversiteit (Netherlands). Dept. of Mathematics and Computer Science, and Centrum voor Wiskunde en Informatica, Amsterdam (Netherlands)
(PB95-127965) Avail: CASI HC A03/MF A01

The strength and range of interpoint interactions in a spatial point process can be quantified by the function J = (1-G)/(1-F), where G is the nearest-neighbor distance distribution function and F the empty space function of the process. J(r) is identically equal to 1 for a Poisson process; values of J(r) smaller or larger than 1 indicate clustering or regularity, respectively. The authors show that, for a large class of point processes, J(r) is constant for distances r greater than the range of spatial interaction. Hence both the range and type of interaction can be inferred from J without parametric model assumptions. It is also possible to evaluate J(r) explicitly for many point process models, so that J is also useful for parameter estimation. Various properties are derived, including the fact that the J function of the superposition of independent point processes is a weighted mean of the J functions of the individual processes. Estimators of J can be constructed from standard estimators of F and G. The authors compute estimates of J for several standard point pattern datasets and conclude that it is a useful indicator of spatial interaction. NTIS

N95-22550# Idaho National Engineering Lab., Idaho Falls, ID.
COLLECTING OPERATIONAL EVENT DATA FOR STATISTICAL ANALYSIS

C. L. Atwood Sep. 1994 33 p
(Contract DE-AC07-76ID-01570)
(DE95-002020; EGG-RAAM-11086) Avail: CASI HC A03/MF A01

This report gives guidance for collecting operational data to be used for statistical analysis, especially analysis of event counts. It discusses how to define the purpose of the study, the unit (system, component, etc.) to be studied, events to be counted, and demand or exposure time. Examples are given of classification systems for events in the data sources. A checklist summarizes the essential steps in data collection for statistical analysis. DOE

N95-23019# International Centre for Theoretical Physics, Trieste (Italy).
STATIC PARAMETRIC FLUCTUATIONS GIVE NONSTATISTICAL BEHAVIOUR IN UNCOUPLED CHAOTIC SYSTEMS
G. Perez and H. A. Cerdeira Oct. 1993 14 p
(DE94-628478; IC-93/337) Avail: CASI HC A03/MF A01 (US Sales Only)

We show that an ensemble of logistic maps, with parameters distributed in some range inside a chaotic region, cannot be statistical. This is so because any parameter range for this map includes periodic windows. The effects of this periodicity in the averages of the system can be estimated, and are also apparent in the power spectra of average values. As a counterexample, we show that the behavior for tent maps, where chaotic regions do not include periodic windows, is statistical. DOE

N95-23066# Sandia National Labs., Albuquerque, NM.
SIMULTANEOUS INFERENCE IN MULTIVARIATE CALIBRATION
E. V. Thomas Nov. 1994 28 p
(Contract DE-AC04-94AL-85000)
(DE95-003592; SAND-94-2642) Avail: CASI HC A03/MF A01

A set of q responses, y = (y(sub 1), y(sub 2), ..., y(sub q))(sup T), is related to a set of p explanatory variables, x = (x(sub 1), x(sub 2), ..., x(sub p))(sup T), through the classical linear model, y(sup T) = a + x(sup T)B + e(sup T). The parameters, a and B, are estimated during calibration using a training set. The fitted calibration model that follows is then used repeatedly on a number of new observations where y is observed and x is to be inferred. This procedure is often referred to as prediction (or inverse prediction). The prediction procedure can be viewed as parameter estimation in errors-in-variables regression. By using the errors-in-variables connection and assuming normally distributed measurement errors, the maximum likelihood estimates of the new x's can be obtained either individually or jointly. The limiting (q (yields) (infinity)) normal distribution of the maximum likelihood estimates of the new x's, obtained jointly, can be used to construct approximate simultaneous confidence regions for the new x's. In situations where the new observations are numerous and well dispersed from the center of the training set, the uncertainty in a and B is substantial, and the specificity of the responses is poor, joint estimation can improve significantly on individual estimation, which is the traditional approach. DOE

N95-23349# Los Alamos National Lab., NM.
(PHI)(SUP 4) KINKS: STATISTICAL MECHANICS
S. Habib 1995 13 p Presented at the NEEDS '94, Los Alamos, NM, 12-16 Sep. 1994
(Contract W-7405-eng-36)
(DE95-003693; LA-UR-94-3816; CONF-9409241-4) Avail: CASI HC A03/MF A01

Some recent investigations of the thermal equilibrium properties of kinks in a 1+1-dimensional, classical (phi)(sup 4) field theory are reviewed. The distribution function, kink density, correlation function, and certain thermodynamic quantities are studied both theoretically and via large scale simulations. A simple double Gaussian variational approach within the transfer operator formalism is shown to give good results in the intermediate temperature range where the dilute gas theory is known to fail. DOE

N95-23559# Technische Univ., Twente (Netherlands). Faculty of Applied Mathematics.
CONSISTENCY AND MONTE CARLO SIMULATION OF A DATA DRIVEN VERSION OF SMOOTH GOODNESS-OF-FIT TESTS
Memorandum Report
W. C. M. Kallenberg and T. Ledwina Sep. 1993 35 p See also PB85-202166 Prepared in cooperation with Wroclaw Technical Univ.
(PB95-141255; MEMO-1158) Avail: CASI HC A03/MF A01

The data driven method of selecting the number of components in Neyman's smooth test for uniformity is extended. The resulting tests consist of a combination of Schwarz's BIC procedure and smooth tests. The upper bound of the dimension of the exponential families in applying Schwarz's rule is allowed to grow with the number of observations to infinity. Simulation results show that the data driven version of Neyman's test performs very well for a wide range of alternatives, and is competitive with other recently introduced (data driven) procedures. It is shown that the data driven smooth tests are consistent against essentially all alternatives. In proving consistency new results on Schwarz's selection rule are derived, which may be of independent interest. NTIS

N95-23927# Rochester Univ., NY. Dept. of Computer Science.
PLOXOMA: TESTBED FOR UNCERTAIN INFERENCE
Hannah Blau and Henry E. Kyburg, Jr. Dec. 1994 25 p
(TR-537) Avail: CASI HC A03/MF A01

This report compares two formalisms for uncertain inference, Combinatorial Semantics and Dempster-Shafer belief function theory, on the basis of an example from the domain of medical diagnosis. We review Shafer's example about the imaginary disease ploxoma and show how it would be represented in Combinatorial Semantics. We conclude that belief function theory has a qualitative advantage because it offers greater flexibility of expression, and provides results about more specific classes of patients. Nevertheless, a quantitative comparison reveals that the inferences sanctioned by Combinatorial Semantics are more reliable than those of belief function theory. Author

N95-23972# Joint Inst. for Nuclear Research, Dubna (USSR).
INDEPENDENT PRODUCTION AND POISSON DISTRIBUTION
A. I. Golokhvastov 1994 7 p
(DE94-635632; JINR-E-2-94-43) Avail: CASI HC A02/MF A01 (US Sales Only)

The well-known statement of factorization of inclusive cross-sections in the case of independent production of particles (or clusters, jets etc.) and the conclusion of Poisson distribution over their multiplicity arising from it do not follow from the probability theory in any way. Using accurately the theorem of the product of independent probabilities, quite different equations are obtained and no consequences relative to multiplicity distributions are obtained. DOE

66 SYSTEMS ANALYSIS

Includes mathematical modeling; network analysis; and operations research.

N95-23239# Technische Univ., Twente (Netherlands). Dept. of Applied Mathematics.
MARGINALISTIC VALUE FOR MONOTONIC SET GAMES
H. F. M. Aarts, Y. Funaki, and C. Hoede Sep. 1993 17 p See also N93-28074 Prepared in cooperation with Tokyo Univ.
(PB95-140646; MEMO-1162) Avail: CASI HC A03/MF A01

In this paper we characterize a value for monotonic set games which can be considered as the analog of the Shapley value for TU-games. NTIS

N95-23539# Technische Univ., Twente (Netherlands). Faculty of Applied Mathematics.
SET GAMES
H. F. M. Aarts, Y. Funaki, and C. Hoede Jul. 1993 18 p See also N93-28074 Prepared in cooperation with Toyo Univ.
(PB95-140786) Avail: CASI HC A03/MF A01

In this paper a new type of cooperative games in characteristic function form (called set games) is introduced. In a set game, the worth of a coalition is expressed by a set instead of a real number. For this class of games we will define the notion of value, being a solution concept and also several axioms. Furthermore we will study values for set games that satisfy the so-called additivity axiom which is the analog of the additivity axiom of the Shapley value. NTIS

N95-23555# Tilburg Univ. (Netherlands). Dept. of Economics.
NOTE ON THE TAU-VALUE AND TAU-RELATED SOLUTION CONCEPTS Research Memo
R. vandenBrink Apr. 1994 16 p Sponsored by Nederlandse Organisatie voor Wetenschappelijk Onderzoek
(PB95-140752; FEW-652) Avail: CASI HC A03/MF A01

The tau-value is a solution concept for a special class of cooperative games with transferable utilities (TU-games). Other solution concepts can be defined and axiomatized in a similar way as the tau-value. We discuss an example of such a tau-related solution concept which is defined for all TU-games. NTIS

67 THEORETICAL MATHEMATICS

Includes topology and number theory.

N95-22617# International Centre for Theoretical Physics, Trieste (Italy).
LECTURES ON FERMAT'S LAST THEOREM
B. Sury Sep. 1993 15 p
(DE94-628392; IC-93/326) Avail: CASI HC A03/MF A01 (US Sales Only)

The report presents the main ideas involved in the approach towards the so-called Fermat's last theorem (FLT). The discussion leads to the point where recent work of A. Wiles starts and his work is not discussed. After a short history of the FLT and of the present approach, discussed are the elliptic curves and the modular forms with their relations, the Taniyama-Shimura-Well conjecture and the FLT. DOE

N95-22623# International Centre for Theoretical Physics, Trieste (Italy).
GEOMETRY OF MOISHEZON AND 1-CONVEX SPACES 2: PROJECTIVITY OF MOISHEZON SPACES AND ITS NON-COMPACT VERSION
M. Sitaramayya Nov. 1993 39 p
(DE94-628415; IC-93/333) Avail: CASI HC A03/MF A01 (US Sales Only)

After a brief review of the geometry of Moishezon spaces, their relation with l-convex spaces and a reasonable and up to date understanding of the obstructions for projectivity of Moishezon objects both in singular and non-singular case is given. The geometry of l-convex manifolds and with l-dimensional exceptional set is studied and some problems and conjectures are stated. The tools of cohomology vanishing theorems important for the subject are briefly sketched. Compactifications of C(sup 3) and Stein spaces are finally outlined. DOE

N95-22630# International Centre for Theoretical Physics, Trieste (Italy).
VECTOR BUNDLES AS DIRECT IMAGES OF LINE BUNDLES
A. Hirschowitz (Nice Univ., France.) and M. S. Narasimhan Dec. 1993 13 p
(DE94-628422; IC-93/426) Avail: CASI HC A03/MF A01 (US Sales Only)

Considering X a smooth irreducible projective variety over an algebraically closed field and E a vector bundle on X, it is proved that, if dim X greater than or equal to 1, E is the direct image of a line bundle L on a smooth irreducible projective variety Z by a morphism f:Z approaches X which is finite outside an algebraic subset of codimension greater than or equal to 3 in X. In the second part of the paper the case when X is a curve is considered. DOE

N95-22632# International Centre for Theoretical Physics, Trieste (Italy).
SPECTRAL APPLICATION OF THE THEOREM FOR THE ESSENTIAL QUASI-FREDHOLM SPECTRUM
M. Berkani and A. Ouahab Mar. 1994 11 p
(DE94-628430; IC-94/58) Avail: CASI HC A03/MF A01 (US Sales Only)

In 1958, T. Kato has proved that a closed semi-Fredholm operator A in Banach space can be written A=A(sub 1) + A(sub 0) where A(sub 0) is a nilpotent operator and A(sub 1) is a regular one. In J.P. Labrousse has defined and studied quasi-Fredholm operators which are an extension of semi-Fredholm operators. He has also defined the essential quasi-Fredholm spectrum. In this paper we prove the mapping spectral theorem for the essential quasi-Fredholm spectrum concerning bounded operators in Hilbert spaces. DOE

N95-22654# Brookhaven National Lab., Upton, NY.
SYMPLECTIC COMPUTATION OF LYAPUNOV EXPONENTS
Salman Habib and Robert D. Ryne 1994 12 p Presented at the NEEDS 1994 Conference, Los Alamos, NM, 12-16 Sep. 1994
(Contract W-7405-eng-36)
(DE95-002732; LA-UR-94-3641; CONF-9409241-3) Avail: CASI HC A03/MF A01

A recently developed method for the calculation of Lyapunov exponents of dynamical systems is described. The method is applicable whenever the linearized dynamics is Hamiltonian. By utilizing the exponential representation of symplectic matrices, this approach avoids the renormalization and reorthogonalization procedures necessary in usual techniques. It is also easily extendible to damped systems. The method is illustrated by considering two examples of physical interest: a model system that describes the beam halo in charged particle beams and the driven van der Pol oscillator. DOE

N95-22712# Institut des Hautes Etudes Scientifiques, Bures-sur-Yvette (France).
GRASSMAN AND HYPERKAEHLER STRUCTURES ON SOME SPACES OF SECTIONS OF HOLOMORPHIC BUNDLES
D. V. Alekseevsky and M. M. Graev Apr. 1994 17 p Sponsored by IHES
(PB95-109104; IHES/M/94/31) Avail: CASI HC A03/MF A01

A holomorphic submersion pi: Z yields C(P(sup 1)) over projective line is considered. On an open submanifold M of the complex manifold of sections, a right flat Grassman structure is defined, that is an isomorphism TM congruent E (center dot) H of the holomorphic tangent bundle TM onto tensor product of a holomorphic vector bundle E and the trivial bundle H congruent C(sup l). If a conformal sympletic structure (omega) which depends holomorphically on a fiber is given, then the Grassman structure reduces to Sp(sub k) (center dot) id(sub H)-structure. For l = 2 it admits unique torsionless connection and is identified with a complex hyperKahler structure. This construction is applied to the case when a fiber of the submersion pi is an adjoint orbit of a complex semisimple Lie group G of automorphisms of pi. With the help of the momentum mapping, such submersions are described as submersion associated with polynomials with coefficients from the Lie algebra of G. The generalized hyperKahler structure on the corresponding space of sections are described. NTIS

N95-22734# Sandia National Labs., Albuquerque, NM.
NONLINEAR GENERALIZED FUNCTIONS AND NONCONSERVATIVE SHOCK SIMULATIONS
R. S. Baty Sep. 1994 63 p
(Contract DE-AC04-94AL-85000)
(DE95-003307; SAND-94-2258) Avail: CASI HC A04/MF A01

New mathematical techniques from the theory of nonlinear generalized functions were applied to compute solutions of nonlinear hyperbolic field equations in nonconservative form. Nonconservative field equations contain products of generalized functions which are not defined in classical mathematics. Because of these products, traditional computational schemes are very difficult to apply and can produce erroneous numerical results. In the present work, existing first-order computational schemes based on results from the theory of nonlinear generalized functions were applied to simulate numerically two model problems cast in nonconservative form. From the results of these computational experiments, a higher-order Godunov scheme based on the piecewise parabolic method was proposed and tested. The numerical results obtained for the model problems are encouraging and suggest that the theory of nonlinear generalized functions provides a powerful tool for studying the complicated behavior of nonlinear hyperbolic field equations. DOE

N95-22736# International Centre for Theoretical Physics, Trieste (Italy).
ASPECTS OF SIGMA MODELS
S. RandjbarDaemi and J. Strathdee Nov. 1993 15 p
(DE94-628511; IC-93/399) Avail: CASI HC A03/MF A01 (US Sales Only)

Some aspects and applications of the sigma-models in particle and condensed matter physics are briefly reviewed. DOE

N95-22737# International Centre for Theoretical Physics, Trieste (Italy).
POSSIBILITY OF EXTENDING SPACE-TIME COORDINATES
Yongcheng Wang Nov. 1993 7 p
(DE94-628512; IC-93/402) Avail: CASI HC A02/MF A01 (US Sales Only)

It has been shown that one coordinate system can describe a whole space-time region except some supersurfaces on which there are coordinate singularities. The conditions of extending a coordinate from real field to complex field are studied. It has been shown that many-valued coordinate transformations may help us to extend space-time regions and many-valued metric functions may make one coordinate region to describe more than one space-time regions. DOE

N95-22740# International Centre for Theoretical Physics, Trieste (Italy).
ON DIAGONALIZATION IN MAP (M,G)
M. Blau and G. Thompson Jan. 1994 41 p
(DE94-628515; IC-94/37) Avail: CASI HC A03/MF A01 (US Sales Only)

Motivated by some questions in the path integral approach to (topological) gauge theories, we are led to address the following question: given a smooth map from a manifold M to a compact group G, is it possible to smoothly 'diagonalize' it, i.e. conjugate it into a map to a maximal torus T of G? We analyze the local and global obstructions and give a complete solution to the problem for regular maps. We establish that these can always be smoothly diagonalized locally and that the obstructions to doing this globally are non-trivial Weyl group and torus bundles on M. We show how the patching of local diagonalizing maps gives rise to non-trivial T-bundles, explain the relation to winding numbers of maps into G/T and restrictions of the structure group and examine the behaviour of gauge fields under this diagonalization. We also discuss the complications that arise for non-regular maps and in the presence of non-trivial G-bundles. In particular, we establish a relation between the existence of regular sections of a non-trivial adjoint bundle and restrictions of the structure group of a principal G-bundle to T. We use these results to justify a Weyl integral formula for functional integrals which, as a novel feature not seen in the finite-dimensional case, contains a summation over all those topological T-sectors which arise as restrictions of a trivial principal G bundle and which was used previously to solve completely Yang-Mills theory and the G/G model in two dimensions. DOE

N95-22741# International Centre for Theoretical Physics, Trieste (Italy).
ON THE SCALAR CURVATURE OF MINIMAL HYPERSURFACES
Quing-Ming Cheng Mar. 1994 7 p
(DE94-628516; IC-94/52) Avail: CASI HC A02/MF A01 (US Sales Only)

In this paper, we prove that if M is an n-dimensional closed minimal hypersurface in a unit sphere S(sup n+1)(1) with constant scalar curvature, then S=0, or S=n or S is greater than or equal to 2n - 6n/n(n+4)+6, where S is the squared norm of the second fundamental form of M. Our theorem indicates that the conjecture proposed by Chern and Peng-Terng would be solved affirmatively. DOE

N95-22751# International Centre for Theoretical Physics, Trieste (Italy).
ONE LOOP RENORMALIZATION OF CHERN-SIMONS FIELD THEORY IN OPERATOR REGULARIZATION
W. F. Chen and Z. Y. Zhu (Academia Sinica, Beijing, China.) Oct. 1993 7 p
(DE94-628508; IC-93/353) Avail: CASI HC A02/MF A01 (US Sales Only)

Operator regularization together with the background field method is used to calculate one loop renormalization constant of the Chern-Simons field theory. The result shows the existence of the famous k shift, i.e. k yields k + sgn(k)C(sub v). DOE

N95-22788# International Centre for Theoretical Physics, Trieste (Italy).
DIRAC CANONICAL QUANTIZATION AND FADDEEV-JACKIW SYMPLECTIC QUANTIZATION OF HIGHER ORDER LAGRANGIANS
M. S. Rashid Mar. 1994 10 p
(DE94-628428; IC-94/51) Avail: CASI HC A02/MF A01 (US Sales Only)

Higher order Lagrangians are canonically quantized by two different methods. The first is the pioneering method of Dirac. A Schroedinger equation is obtained and it turns out that the higher order velocities contribute nontrivially to this equation. The second is the recent symplectic method due to Faddeev-Jackiw, as expected the two methods are equivalent and produce the same value for the generalized brackets (Dirac brackets). DOE

N95-22808# International Centre for Theoretical Physics, Trieste (Italy).
JACOBSON RADICALS IN MATRIX NEAR RINGS
S. J. Abbasi Jan. 1994 5 p
(DE94-628424; IC-94/39) Avail: CASI HC A01/MF A01 (US Sales Only)

This paper was motivated by the question: Does, like the ring case, the process of taking Jacobson Radicals and constructing matrix near rings coincide? We present here, for the class of weakly distributive d.g. near rings, a conditionally affirmative answer to this question. Our main result is as follows: Let R be a weakly distributive d.g. near ring with identity. If J(R) is contained (delta)(sub 1)M(sub n)(R), the derived group of M(sub n)(R), then J(R) = J(M(sub n)(R)) where I-bar is defined as a subnear ring of M(sub n)(R) generated by (I brace)f(sup a)(sub ij); a is an element of I, 1 less than or equal to i, j less than or equal to n(r brace). DOE

N95-22900# Los Alamos National Lab., NM.
THE ROLE OF SU(2) 3n-j COEFFICIENTS IN SU(3)
W. Y. C. Chen, J. D. Louck, L. C. Biedenharn (Texas Univ., Austin, TX.), and M. A. Lohe (Texas Univ., Austin, TX.) 1994 33 p Presented at the Symmetry and Structural Properties Conference, Pozana, Poland, Sep. 1994
(Contract W-7405-eng-36)
(DE95-002726; LA-UR-94-3622; CONF-9409246-1) Avail: CASI HC A03/MF A01

The irreducible representations of the group SU(3) may be given completely in terms of the 3-j, 6-j, and 9-j coefficients of SU(2). More remarkably these same coefficients, and the 12-j coefficients as well, enter into the description of a large class of Clebsch-Gordan (C-G) coefficients for the group SU(3), this occurrence going beyond that in the well-known group-subgroup reduction SU(3)(down arrow)U(2). The problem of determining the SU(3) irreducible representations and its C-G coefficients is reviewed, and it is shown how the SU(2) quantities enter into the SU(3) problem in special cases. DOE

N95-22933# International Centre for Theoretical Physics, Trieste (Italy).
THE FUNDAMENTAL GROUP OF COMPLEX HYPERPLANES ARRANGEMENTS
Nguyen Viet Dung and Huy Vui Ha (Institute of Mathematics, Hanoi, Viet Nam.) Mar. 1994 8 p
(DE94-628426; IC-94/47) Avail: CASI HC A02/MF A01 (US Sales Only)

In this paper we suggest a new method to compute the fundamental group of the complemented of any complex hyperplanes arrangements. Our computation is based on a construction called labyrinth of an arrangement of complex lines. The method can be generalized for the case of an arbitrary affine curve. DOE

N95-23052# International Centre for Theoretical Physics, Trieste (Italy).
AN EXTENSION OF FREEDMAN'S RESULTS ON A MODEL OF PREDATOR-PREY DYNAMICS AS MODIFIED BY THE ACTION OF A PARASITE
Tran VanNhung Nov. 1993 18 p
(DE94-628488; IC-93/391) Avail: CASI HC A03/MF A01 (US Sales Only)

In this paper we consider a model of predator-prey populations with parasitic infection in which each individual of prey or predator can be invaded by a parasite. This is a generalization of the model studied by H.I. Freedman. Our situation is described by system of four autonomous ordinary differential equations. Conditions for persistence of all populations are given. A discussion of the stability of the interior equilibrium is also given. DOE

N95-23660# International Centre for Theoretical Physics, Trieste (Italy).
UNIVERSAL HODGE BUNDLE AND MUMFORD ISOMORPHISMS ON THE ABELIAN INDUCTIVE LIMIT OF TEICHMUELLER SPACES
I. Biswas, S. Nag (Institute of Mathematical Science, Madras, India.), and D. Sullivan (Institut des Hautes Etudes Scientifiques, Bures-sur-Yvette,

France.) Jun. 1994 34 p
(DE94-634325; IC-94/115) Avail: CASI HC A03/MF A01 (US Sales Only)

Let M(sub g) denote the moduli space of compact Riemann surfaces of genus g. Mumford had proved, for each fixed genus g, that there are isomorphisms asserting that certain higher DET bundles over M(sub g) are certain fixed (genus-independent) tensor power of the Hodge line bundle on M(sub g). We obtain a coherent, genus-independent description of the Mumford isomorphisms over certain infinite-dimensional 'universal' parameter spaces of compact Riemann surfaces (with or without marked points). We work with an inductive limit of Teichmueller spaces comprising complex structures on a certain 'solenoidal Riemann surface', H(sub (infinity),ab), which appears as the inverse limit of an inverse system of surfaces of different general connected by abelian covering maps. We construct the universal Hodge and higher DET line bundles on this direct limit of Teichmueller spaces (in the sense of Shafarevich). The main result shows how such DET line bundles on the direct limit carry coherently-glued Quillen metrics and are related by the appropriate Mumford isomorphisms. Our work can be viewed as a contribution to a non-perturbative formulation of the Polyakov measure structure in a genus-independent fashion. DOE

N95-23661# International Centre for Theoretical Physics, Trieste (Italy).
ON CERTAIN N-SHEETED COVERINGS OF CURVES AND SYMMETRIC NUMERICAL SEMIGROUPS WHICH CANNOT BE REALIZED AS WEIERSTRASS SEMIGROUPS
F. Torres Apr. 1994 10 p
(DE94-634328; IC-94/80) Avail: CASI HC A02/MF A01 (US Sales Only)

A curve X is said to be of type (N, (gamma)) if it is an N-sheeted covering of a curve of genus (gamma) with at least one totally ramified point. A numerical subsemigroup H of (N, +) is said to be of type (N, (gamma)) if the first (gamma) positive terms m(sub 1),...,m(sub (gamma)) are multiples of N; m(sub (gamma))=2N(sub (gamma)) and (2(sub (gamma))+1) N is an element of H. If the genus of X is large enough and if N and (gamma) satisfy certain arithmetical conditions then X is of type (N,(gamma)) if and only if there is a point P is an element of X such that the Weierstrass semigroup at P is of type (N,(gamma)). (This is a generalization of the (gamma)-hyperelliptic situation). This result implies the existence of symmetric numerical semigroups which cannot be realized as Weierstrass semigroups. DOE

N95-23965# Joint Inst. for Nuclear Research, Dubna (USSR).
SCATTERING PROBLEM FOR QUANTUM SYSTEM WITH TIME-DEPENDENT PERIODIC HAMILTONIAN
A. A. Skoblin 1994 11 p
(DE94-635421; JINR-R-4-94-63) Avail: CASI HC A03/MF A01 (US Sales Only)

Scattering theory for quantum systems located in time-dependent periodic strong field is considered. Scattering matrix is constructed in the quasi-energy states basis. Transition operators are introduced, perturbation series is constructed, interstates transition rate is calculated. Optical theorem is generalized in case of periodic field. DOE

N95-23966# Joint Inst. for Nuclear Research, Dubna (USSR).
THE KINETICS OF QUANTUM SYSTEM WITH TIME-DEPENDENT PERIODIC HAMILTONIAN
A. A. Skoblin 1994 7 p
(DE94-635422; JINR-R-4-94-65) Avail: CASI HC A02/MF A01 (US Sales Only)

The kinetics of faintly non-ideal quantum systems located in time-dependent periodic strong fields are considered. Quasi-energy states constructed with neglect to the inter system interaction are introduced. It is shown that in the indicated basis one can describe the system using the kinetic equation, that generalized the well-known Pauli equation. The system-thermostat interaction is taken into account. Possible types of system equilibrium are considered. DOE

N95-24029# Rochester Univ., NY. Dept. of Computer Science.
LARGE SETS IN AC(EXP 0): A KOLMOGOROV COMPLEXITY RELATED PROPERTY AND SOME APPLICATIONS
Marius Zimand Dec. 1994 10 p
(Grants NSF CCR-89-57604; NSF INT-91-16781; JSPS-ENG-207; NSF CCR-93-22513)
(TR-556) Avail: CASI HC A02/MF A01

If A is a set in AC(exp 0) such that for some q greater than 0 and infinitely many n, absolute value of (A(exp n)) is greater than 2(exp(n-log(sup q)n)), then A contains more than quasipolynomially many strings with polynomial-time bounded length-conditioned Kolmogorov complexity below n(exp epsilon), for arbitrary epsilon greater than 0, at each length n where A satisfies the above density condition. As a consequence, we exhibit a set in NP that is bi-immune to sets in AC(exp 0) that satisfy the above density condition. Author

N95-24063# Rochester Univ., NY. Dept. of Computer Science.
MARTIN-LOF TESTS CAN HELP TOO
Marius Zimand Nov. 1994 14 p
(Grants NSF CCR-89-57604; NSF INT-91-16781; JSPS-ENG-207; NSF CCR-93-22513)
(TR-541) Avail: CASI HC A03/MF A01

The authors argue that Martin-Lof tests provide useful techniques in proofs involving Kolmogorov complexity. Our examples cover more areas: (1) logical definability; we prove an analogue of the 0-1 Law for various logics in terms of structures with high Kolmogorov complexity; (2) probabilistic computation: we display a relation between the Kolmogorov complexity of the random strings on which a probabilistic algorithm errs and the probability error of the algorithm as well as a trade-off relation between the error probability, the length of the random bits, the number of provers and the length of the provers' answers in one-round multiprover interactive proof systems for NP; and (3) convergence rates of probability asymptotics; we find a general lower bound on the convergence rate of such probabilities in terms of Kolmogorov complexity and provide a concrete example for the probability that a random graph with n vertices is connected. Author

N95-22975*# Universidad Nacional Autonoma de Mexico, Cuernavaca (Mexico). Inst. de Investigaciones en Matematicas Aplicadas y en Sistemas.
A RAMANUJAN-TYPE MEASURE FOR THE ASKEY-WILSON POLYNOMIALS
Natig M. Atakishiyev *In* NASA. Goddard Space Flight Center, Second International Workshop on Harmonic Oscillators Jan. 1995 p 153-164 Sponsored by Direccion General de Asuntos del Persona Academico (For primary document see N95-22957 07-74)
Avail: CASI HC A03/MF A04

N95-22978*# Brussels Univ. (Belgium). Physique Nucleaire Theorique et physique Mathematique.
COVARIANT DEFORMED OSCILLATOR ALGEBRAS
Christiane Quesne *In* NASA. Goddard Space Flight Center, Second International Workshop on Harmonic Oscillators Jan. 1995 p 181-188 (For primary document see N95-22957 07-74)
Avail: CASI HC A02/MF A04

N95-22986*# Georgia Inst. of Tech., Atlanta, GA. School of Electrical Engineering.
A NOTE ON THE ANGULAR FOURIER TRANSFORMATION
Balu Santhanam and Thalanayar S. Santhanam (Saint Louis Univ., Cahokia, IL.) *In* NASA. Goddard Space Flight Center, Second International Workshop on Harmonic Oscillators Jan. 1995 p 249-254 (For primary document see N95-22957 07-74)
Avail: CASI HC A02/MF A04

N95-22989*# Costa Rica National Univ., Heredia (Costa Rica). Dept. de Fisica.
A METHOD OF SOLVING SIMPLE HARMONIC OSCILLATOR SCHROEDINGER EQUATION
Juan Carlos F. Maury *In* NASA. Goddard Space Flight Center, Second International Workshop on Harmonic Oscillators Jan. 1995 p 271-273 (For primary document see N95-22957 07-74)
Avail: CASI HC A01/MF A04

N95-22990*# Academia R. P. R., Bucharest (Romania). Dept. of Theoretical Physics.
WIGNER DISTRIBUTION FUNCTION AND ENTROPY OF THE DAMPED HARMONIC OSCILLATOR WITHIN THE THEORY OF THE OPEN QUANTUM SYSTEMS
Aurelian Isar *In* NASA. Goddard Space Flight Center, Second International Workshop on Harmonic Oscillators Jan. 1995 p 275-282 (For primary document see N95-22957 07-74)
Avail: CASI HC A02/MF A04

N95-23006*# Universidad Nacional Autonoma de Mexico, Cuernavaca (Mexico). Inst. de Investigaciones en Matematicas Aplicadas y en Sistemas
KRAVCHUK FUNCTIONS FOR THE FINITE OSCILLATOR APPROXIMATION
Natig M. Atakishiyev and Kurt Bernardo Wolf *In* NASA. Goddard Space Flight Center, Second International Workshop on Harmonic Oscillators Jan. 1995 p 403-408 Sponsored by Direccion General de Asuntos del Personal Academico (For primary document see N95-22957 07-74)
(Proj UNAM-DGAPA IN1042-93)
Avail: CASI HC A02/MF A04

70 PHYSICS (GENERAL)

For precision time and time interval (PTTI) see *35 Instrumentation and Photography;* for geophysics, astrophysics or solar physics see *46 Geophysics, 90 Astrophysics,* or *92 Solar Physics.*

N95-22497# International Centre for Theoretical Physics, Trieste (Italy).
RESONANT SHALLOW DONOR MAGNETOPOLARON EFFECT IN A GaAs/AlGaAs QUANTUM DOT IN HIGH MAGNETIC FIELDS
Ka-Di Zhu Nov. 1993 13 p
(DE94-629039; IC-93/394) Avail: CASI HC A03/MF A01 (US Sales Only)

Resonant shallow donor magnetopolaron effect in a GaAs/AlGaAs quantum dot in high magnetic fields is investigated by the variational treatment. It is shown that both the cyclotron resonant frequency omega(sup *)(sub c+) due to the 1s-p(sup +) hydrogenic transition and the cyclotron resonant frequency omega(sup *)(sub c-)due to the 1s-p(sup -) hydrogenic transition increase with the decrease of the dot size. The cyclotron resonant frequency omega(sup *)(sub c+) is always larger than the bulk LO-phonon frequency omega(sub LO), while the cyclotron resonant frequency omega(sup *)(sub c-) is lower than omega(sub LO) for larger quantum dots (l(sub 0)is greater than 2.0.r(sub 0), r(sub 0) is the polaron radius). The results also show that the Coulomb interaction effect on the resonant frequencies is significant. DOE

N95-22552# Los Alamos National Lab., NM.
HIGH MAGNETIC FIELDS IN THE USA
Laurence J. Campbell, Don E. Parkin, Jack E. Crow (Florida State Univ., Tallahassee, FL.), Hans J. Schneider-Muntau (Florida State Univ., Tallahassee, FL.), and Neil S. Sullivan (Florida Univ., Gainesville, FL.) 1994 10 p Presented at the 2nd European Workshop on Science in 100, Leuven, Belgium, 30 Sep. - 1 Oct. 1994
(Contract W-7405-eng-36)
(DE95-002716; LA-UR-94-3486; CONF-9409243-1) Avail: CASI HC A02/MF A01

During the past thirty years research using high magnetic fields has technically evolved in the manner, but not the magnitude, of the so-called big science areas of particle physics, plasma physics, neutron scattering, synchrotron light scattering, and astronomy. Starting from the laboratories of individual researchers it moved to a few larger universities, then to centralized national facilities with research and maintenance staffs, and, finally, to joint international ventures to build unique facilities, as illustrated by the subject of this conference. To better understand the nature of this type of research and its societal justification it is helpful to compare it, in general terms, with the aforementioned big-science fields. High magnetic field research differs from particle physics, plasma physics, and astronomy in three respects: (1) it is generic research that cuts across a wide range of scientific disciplines in physics, chemistry, biology, medicine, and engineering; (2) it studies materials and processes that are relevant for a variety of technological applications and it gives insight into biological processes; (3) it has produced, at least, comparably significant results with incomparably smaller resources. Unlike neutron and synchrotron light scattering, which probe matter, high magnetic fields change the thermodynamic state of matter. This change of state is fundamental and independent of other state variables, such as pressure and temperature. After the magnetic field is applied, various techniques are then used to study the new state. DOE

N95-22895# Argonne National Lab., IL. Center for Transportation Research.
COMPUTATION OF MAGNETIC FORCES ON MOVING CONDUCTORS BY USING ELEKTRA AND OTHER 3-D COMPUTER CODES
Z. Wang, H. T. Coffey, and T. Mulcahy Aug. 1994 68 p
(Contract W-31-109-eng-38)
(DE95-003308; ANL/ESD/TM-72) Avail: CASI HC A04/MF A01

The finite-element computer code ELEKTRA is the only publicly available code known to the authors that is capable of solving 3-D eddy-current problems that entail the use of moving electrical conductors having finite dimensions. It is, therefore, expected to become a standard tool for the analysis of magnetic levitation (maglev) systems using sheet guideways. This study systematically evaluates the ELEKTRA code by comparing it with experimental data and 'benchmark' solutions, as appropriate. In addition, alternatives to ELEKTRA were investigated, and a new computer code, based on an extension of the double-Fourier series analysis, was developed. DOE

N95-23083# Miami Univ., FL.
MAGNETIC MULTILAYER PHYSICS Technical Progress Report, 1 Jan. 1994 - 31 Dec. 1994
M. J. Pechan 23 Sep. 1994 4 p
(Contract DE-FG02-86ER-45281)
(DE95-003408; DOE/ER-45281/T1) Avail: CASI HC A01/MF A01

Microscopic magnetic systems, and especially multilayer structures, are providing a wealth of novel phenomena in condensed matter magnetism. Of particular significance are interfacial and interlayer effects. The interface between two magnetically dissimilar materials can significantly alter the bulk magnetic properties of either constituent material; and coupling of magnetic layers across relatively thick nonmagnetic interlayers are observed to have unexpectedly large impact upon electronic transport properties. The PI proposes to determine the source of magnetic interface anisotropy in transition metal multilayer systems by varying elemental constituents, magnetic and nonmagnetic layer thickness and temperature. Also both static and dynamic effects associated with multilayer interlayer coupling will be investigated using torque and FMR techniques. In particular, the highest frequency 'optical' modes of interacting magnetic layers will be examined. A tristable magnetic system is predicted and experimental verification proposed. Enhancements of a novel torque magnetometer are planned. DOE

N95-23127 Rutherford Appleton Lab., Oxford (England).
DYNAMICAL PROPERTIES OF CRITICAL AND PARAMAGNETIC SPIN FLUCTUATIONS IN ANISOTROPIC HEISENBERG MAGNETS
S. W. Lovesey and E. Balcar Sep. 1994 46 p Prepared in cooperation with Atominstitut der Oesterreichischen Univ.
(PB95-134623; RAL-94-098) Avail: Issuing Activity (National Technical Information Service (NTIS))

Decay rates for long wavelength spin fluctuations in the standard x-y model, and a second model described by the sum of the full Heisenberg exchange interaction and a single-site anisotropy are calculated on the basis of a coupled-mode theory in which the isothermal susceptibilities are consistent with corresponding spherical models (in consequence, quantum fluctuations are absent). Results for the decay rates are provided for two and three dimensional lattices, and ferromagnetic and antiferromagnetic exchange interactions. Their dependence on the wave vector, q, and the inverse correlation lengths are derived from integral equations that admit homogeneous functions as solutions. The decay rates may thus be expressed as q(sup d/2)R(sub 1)(q/Kappa(sub 0)) and q(sup (d+2)/2)R(sub 2)(q/Kappa, q/Kappa(sub 0)) where R(sub 1) and R(sub 2) are, respectively, scaling functions for the x-y and ferromagnetic single-site anisotropy models, d is the spatial dimension, and Kappa(Kappa(sub 0)) is the out-of-plane

(in-plane) inverse correlation length. Analytical and numerical values of the scaling functions are presented for the limits of main physical interest. NTIS

N95-23155 Rutherford Appleton Lab., Chilton (England).
STUDY OF FRUSTRATED SYSTEMS VIA DISSIPATIVE MAPS
G. S. Canright and G. I. Watson May 1994 9 p Prepared in cooperation with Tennessee Univ.
(Contract DE-AC05-84OR-21400)
(PB95-139093; RAL-94-037) Avail: Issuing Activity (National Technical Information Service (NTIS))

We wish to consider 'frustrated' problems in classical equilibrium statistical mechanics. We briefly describe a method for finding complex metastable states for frustrated classical systems, using a dissipative dynamical map. We show by example that this technique can give states which are very competitive in energy with the ground state, and with other, simpler states which are found by exhaustive search. NTIS

N95-23273* National Aeronautics and Space Administration. Lyndon B. Johnson Space Center, Houston, TX.
NEWTON IN SPACE (Videotape)
Dexter Herbert, ed. 4 Mar. 1992 *Its* Liftoff to Learning Series Videotape: 12 min. 35 sec. playing time, in color, with sound
(NASA-TM-110535; NONP-NASA-VT-95-43938) Avail: CASI VHS A02/BETA A22

In this 'Liftoff to Learning' series video, astronauts (Charles Veach, Gregory Harbaugh, Donald McMonagle, Michael Coats, L. Blaine Hammond, Guion Bluford, Richard Hieb) from the STS-39 Mission use physical experiments and computer animation to explain how weightlessness and gravity affects everything and everyone onboard the Space Shuttle. The physics behind the differences between weight and mass, and the concepts of 'free fall', are demonstrated along with explanations and experiments of Sir Issac Newton's three laws of motion. CASI

N95-23379# Sandia National Labs., Livermore, CA.
DYNAMIC RESPONSE OF A TRANSDUCER MOUNTED AT ONE END OF AN ACOUSTICAL CAVITY WHICH IS SUBJECTED TO A SPECIFIED PRESSURE AT THE OPEN END OF THE CAVITY
G. A. Benedetti and J. Z. Benson Nov. 1994 111 p
(Contract DE-AC04-94AL-85000)
(DE95-004192; SAND-95-8200) Avail: CASI HC A06/MF A02

The purpose of this report is to develop a mathematical model for a pressure transducer mounted in a fluid filled cavity (a system) and examine the pressure 'measurement' error of the cavity and transducer by computing the dynamic response (output pressure) of the system to a specified pressure time history (input pressure). The 'measurement' error is determined by comparing the calculated output pressure to the specified input pressure. The dynamic response of a transducer mounted at one end of a one-dimensional acoustical cavity is determined. The cavity is filled with a compressible isentropic fluid, and the fluid at the open end of the cavity (i.e., the boundary at $x = 0$) is subjected to a specified uniform axial input pressure. At the other end of the cavity the transducer is represented as a mass, spring, and damper system. Consequently, the boundary condition at $x = (ell)$ is also time dependent. The general solution to the boundary value problem, as well as the steady state solution for periodic excitation, is obtained by integrating a coupled set of ordinary differential equations. DOE

N95-23979# Los Alamos National Lab., NM.
A THEORY FOR THE MORPHOLOGY OF LAPLACIAN GROWTH FROM STATISTICS OF EQUIVALENT MANY-BODY HAMILTONIAN SYSTEMS
R. Blumenfeld 1994 14 p Presented at the 3rd International Working Conference on Fractals in the Natural and Applied Sciences, Marseille, 7-10 Feb. 1995
(Contract W-7405-eng-36)
(DE94-014473; LA-UR-94-2077; CONF-950221-1) Avail: CASI HC A03/MF A01

The evolution of two dimensional interfaces in a Laplacian field is discussed. By mapping the growing region conformally onto the unit disk, the problem is converted to the dynamics of a many-body system and is shown to be Hamiltonian. An extension of the many body approach to a continuous density is discussed. The Hamiltonian structure allows introduction of surface effects as an external field. These results are used to formulate a first-principles statistical theory for the morphology of the interface using statistical mechanics for the many-body system. DOE

71 ACOUSTICS

Includes sound generation, transmission and attenuation.
For noise pollution see *45 Environmental Pollution.*

N95-22675*# Cambridge Acoustical Associates, Inc., Cambridge, MA.
THE USE OF COWL CAMBER AND TAPER TO REDUCE ROTOR/STATOR INTERACTION NOISE Final Report
R. Martinez Cleveland, OH NASA Feb. 1995 89 p
(Contract NAS3-27229; RTOP 535-03-10)
(NASA-CR-195421; E-9364; NAS 1.26:195421) Avail: CASI HC A05/MF A01

The project had two specific technical objectives: (1) to develop a realistic three-dimensional model of tonal noise due to rotor/stator interaction, as the input field for predictions of diffraction and dissipation by a lined cowl; and (2) to determine whether the generator curve of that cowl, or duct, could be 'steered' to yield substantially lower values of propulsor noise along the engine's fore and aft open sectors. The more general and important aim of their research is to provide the commercial aircraft industry with a useful predictive tool to help it meet its noise-reduction goals. The work has produced a tractable and yet realistic model of rotor/stator interaction noise. The blades in the fan stage are radially divergent, twisted, and of realistically wide chords to match the high frequencies and speeds of the sound-production process. The resulting three-dimensional acoustic nearfield insonifies the interior wall of the diffracting cowl, whose shape, incidentally, does not affect fore or aft noise significantly (but other factors do). Author

N95-22863 Department of the Navy, Washington, DC.
PITCH SENSOR SYSTEM Patent Application
Foster Striffler, inventor (to Navy) 24 Mar. 1994 15 p Limited Reproducibility: More than 20% of this document may be affected by microfiche quality
(AD-D016488; US-Patent-Appl-SN-217511) Avail: Issuing Activity (Defense Technical Information Center (DTIC))

A very small pitch sensor which accurately measures angular rotation about the pitch axis while being substantially insensitive to angular rotations about the roll or yaw axes. The pitch sensor comprises a spherical cavity that is fluid filled. The fluid fill further comprises one half conductive fluid and one half dielectric fluid. The fluids are selected to be immiscible and of different densities. The inside of the spherical cavity is segmented into three surface areas for connection to an electronic circuit. The electronic circuit measures voltage differentials between the segmented surface areas which vary with the conductive fluid surface in contact with the respective segmented areas. The conductive fluid surface contact area varies with the angular rotation of the cavity and about the pitch axis. DTIC

N95-22921*# National Aeronautics and Space Administration. Langley Research Center, Hampton, VA.
CAPACITIVE ACOUSTIC WAVE DETECTOR AND METHOD OF USING SAME Patent Application
William T. Yost, inventor (to NASA) 27 Sep. 1994 18 p
(NASA-Case-LAR-13890-1; NAS 1.71:LAR-13890-1; US-Patent-Appl-SN-317491) Avail: CASI HC A03/MF A01

A capacitor having two substantially parallel conductive faces is acoustically coupled to a conductive sample end such that the sample face is one end of the capacitor. A non-contacting dielectric may serve as a spacer between the two conductive plates. The formed capacitor is connected to an LC oscillator circuit such as a Hartley oscillator circuit producing an output frequency which is a function of the capacitor spacing. This capacitance oscillates as the sample end coating is oscillated by an acoustic wave generated in the sample by a transmitting transducer. The electrical output can serve as an absolute indicator of acoustic wave displacement. NASA

N95-23018# International Centre for Theoretical Physics, Trieste (Italy).
PROPAGATION OF WAVES AT THE LOOSELY BONDED INTERFACE OF TWO POROUS ELASTIC HALF-SPACES
M. Tajuddin Oct. 1993 5 p
(DE94-628477; IC-93/335) Avail: CASI HC A01/MF A01 (US Sales Only)

Employing Biot's theory for wave propagation in porous solids, the propagation of waves at the loosely bonded interface between two poroelastic half-spaces is examined theoretically. The analogous study of Stoneley waves for smooth interface and bonded interface form a limiting case. The results due to classical theory are shown as a special case. DOE

N95-23073 Department of the Navy, Washington, DC.
MATERIAL CHARACTERIZATION SYSTEM Patent
Gilbert F. Lee, inventor (to Navy) and Bruce Hartmann, inventor (to Navy) 13 Sep. 1994 10 p Filed 8 Feb. 1991 Supersedes AD-D014915
(AD-D016536; US-Patent-5,345,825; US-Patent-Appl-SN-652821; US-Patent-Class-73-574) Avail: US Patent and Trademark Office

A plurality of elongated test specimens undergo vibrations induced by random noise within an acoustical frequency range establishing standing waves therein having resonant frequencies at which the collection of measurement data through accelerometers mounted at the ends of the specimens provides for calculation of physical material properties. The processing of the data during collection, analysis and calculation is automated by programmed computer control. DTIC

N95-23178*# National Aeronautics and Space Administration. Lewis Research Center, Cleveland, OH.
SUPERSONIC JET NOISE REDUCTIONS PREDICTED WITH INCREASED JET SPREADING RATE
Milo D. Dahl and Philip J. Morris (Pennsylvania State Univ., University Park, PA.) Mar. 1995 8 p Presented at the Joint Fluids Engineering Conference, Hilton Head, SC, 13-18 Aug. 1995; cosponsored by the ASME and the Japan Society of Mechanical Engineers
(RTOP 505-62-52)
(NASA-TM-106872; E-9491; NAS 1.15:106872) Avail: CASI HC A02/MF A01

In this paper, predictions are made of noise radiation from single, supersonic, axisymmetric jets. We examine the effects of changes in operating conditions and the effects of simulated enhanced mixing that would increase the spreading rate of the jet shear layer on radiated noise levels. The radiated noise in the downstream direction is dominated by mixing noise and it is well described by the instability wave noise radiation analysis. A numerical prediction scheme is used for the mean flow providing an efficient method to obtain the mean flow development for various operating conditions and to simulate the enhanced mixing. Using far field radiated noise measurements as a reference, the calculations predict that enhanced jet spreading results in a reduction of radiated noise. Author

N95-23375# Allied-Signal Aerospace Co., Kansas City, MO.
CALORIMETRIC MEASUREMENT OF ENERGY OF ULTRASONIC CLEANERS
W. B. Harding Nov. 1994 5 p
(Contract DE-AC04-76DP-00613)
(DE95-003938; KCP-613-4805) Avail: CASI HC A01/MF A01

The development of a calorimeter that measured the power within an ultrasonic cleaning tank is presented. The principle involved is explained. Several types of calorimeter that were tested are described. Measurement of the power in an ultrasonic cleaner permits: (1) comparing different ultrasonic cleaners; (2) monitoring the performance of a specific cleaner; (3) measuring the distribution of power in a cleaning tank, and (4) evaluating the effects of process variables on the power. DOE

N95-23782# Boston Univ., MA. Center for Adaptive Systems.
A SELF-ORGANIZING NEURAL NETWORK ARCHITECTURE FOR AUDITORY AND SPEECH PERCEPTION WITH APPLICATIONS TO ACOUSTIC AND OTHER TEMPORAL PREDICTION PROBLEMS Annual Technical Report, 1 May 1993 - 30 Apr. 1994
Michael Cohen and Stephen Grossberg 28 Sep. 1994 25 p
(Contract F49620-92-J-0225)
(AD-A285640; AFOSR-94-0647TR) Avail: CASI HC A03/MF A01

This project is developing autonomous neural network models for the real-time perception and production of acoustic and speech signals. Our SPINET pitch model was developed to take realtime acoustic input and to simulate the key pitch data. SPINET was embedded into a model for auditory scene analysis, or how the auditory system separates sound sources in environments with multiple sources. The model groups frequency components based on pitch and spatial location cues and resonantly binds them within different streams. The model simulates psychophysical grouping data, such as how an ascending, tone groups with a descending tone even if noise exists at the intersection point, and how a tone before and after a noise burst is perceived to continue through the noise. These resonant streams input to working memories, wherein phonetic percepts adapt to global speech rate. Computer simulations quantitatively generate the experimentally observed category boundary shifts for voiced stop pairs that have the same or different place of articulation, including why the interval to hear a double (geminate) stop is twice as long as that to hear two different stops. This model also uses resonant feedback, here between list categories and working memory. DTIC

N95-23313*# Christopher Newport Coll., Newport News, VA. Dept. of Mathematics.
AEROACOUSTIC COMPUTATION OF GUST-BLADE INTERACTION Abstract Only
James E. Martin *In* Hampton Univ., 1994 NASA-HU American Society for Engineering Education (ASEE) Summer Faculty Fellowship Program Dec. 1994 p 95 (For primary document see N95-23276 07-99)
Avail: CASI HC A01/MF A02

N95-23315*# Pembroke State Univ., NC.
BENCHMARK PROBLEMS IN COMPUTATIONAL AEROACOUSTICS Abstract Only
Freda Porter-Locklear *In* Hampton Univ., 1994 NASA-HU American Society for Engineering Education (ASEE) Summer Faculty Fellowship Program Dec. 1994 p 97 (For primary document see N95-23276 07-99)
Avail: CASI HC A01/MF A02

72 ATOMIC AND MOLECULAR PHYSICS

Includes atomic structure, electron properties, and molecular spectra.

N95-22495# International Centre for Theoretical Physics, Trieste (Italy).
FERMION-SPIN TRANSFORMATION TO IMPLEMENT THE CHARGE-SPIN SEPARATION
S. Feng, Z. B. Su, and L. Yu Oct. 1993 49 p
(DE94-629035; IC-93/354) Avail: CASI HC A03/MF A01 (US Sales Only)

A novel approach, the fermion-spin transformation implement the charge-spin separation, is developed to study the low-dimensional t - J model. In this approach, the charge and spin degrees of freedom of the physical electron are separated, and the charge degree of freedom is represented by a spinless fermion while the spin degree of freedom is represented by a hard-core boson. The on-site local constraint for single occupancy is satisfied even in the mean-field approximation and the sum rule for the physical electron is obeyed. This approach can be applied to both one and two-dimensional systems. In the one-dimensional case, the spinon as well as the physical electron behaves like Luttinger liquids. We have obtained a gapless charge and spin excitation spectrum, a good ground state energy, and a reasonable electron-momentum distribution within the mean-field approximation. The correct exponents of the correlation functions and momentum distribution are also obtained it the squeezing effect and rearrangement of the spin configurations are taken into account. In the two-dimensional case, within the mean-field approximation the magnetized flux state with gap in the spinon spectrum has the lowest energy at half-filling. The antiferromagnetic long-range order is destroyed by hole doping of the order approx. 10/15% for t - J = 3/5 and a disordered flux state with gapless spinon spectrum becomes stable. The calculated specific heat is roughly consistent with observed results on copper oxide superconductors. The possible phase separation is also discussed at the mean-field level. DOE

N95-22498# International Centre for Theoretical Physics, Trieste (Italy).
ASYMPTOTICALLY EXACT SOLUTION OF THE MULTI-CHANNEL RESONANT-LEVEL MODEL
Guangming Zhang, Zhaobin Su, and Lu Yu Jan. 1994 11 p
(DE94-629040; IC-94/19) Avail: CASI HC A03/MF A01 (US Sales Only)

An asymptotically exact partition function of the multi-channel resonant-level model is obtained through Tomonaga-Luttinger bosonization. A Fermi-liquid vs. non-Fermi-liquid transition, resulting from a competition between the Kondo and X-ray edge physics, is elucidated explicitly via the renormalization group theory. In the strong-coupling limit, the model is renormalized to the Toulouse limit. DOE

N95-22521# Stanford Linear Accelerator Center, CA.
EXPERIMENTAL RESULTS ON POLARIZED STRUCTURE FUNCTIONS IN DEEP INELASTIC LEPTON-NUCLEON SCATTERING
L. Stuart Aug. 1994 6 p Presented at the Tennessee International Symposium on Radiative Corrections, Gatlinburg, TN, 27 Jun. - 1 Jul. 1994
(Contract DE-AC03-76SF-00515)
(DE95-002782; SLAC-PUB-6638; CONF-9406273-3) Avail: CASI HC A02/MF A01

A summary is given of experimental results on spin structure functions of the proton g(sub 1, sup p)(x,Q(exp 2)), deuteron g(sub 1, sup d)(x,Q(exp 2)), and neutron g(sub 1, sup n)(x,Q(exp 2)) as measured in deep inelastic scattering of polarized leptons from a polarized target. All results are consistent with the Bjorken sum rule predictions at the Q(exp 2) of each experiment. The data does not support the Ellis-Jaffe sum rule prediction for the proton which implies that the helicity carried by the strange quark may be nonzero and that the net quark helicity is smaller than expected from simple quark models. DOE

N95-22551# Los Alamos National Lab., NM.
DIMUON PRODUCTION IN PROTON-NUCLEUS INTERACTIONS
J. C. Peng 1994 16 p Presented at the International Symposium on Medium Energy Physics, Beijing, China, 22-26 Aug. 1994
(Contract W-7405-eng-36)
(DE95-002613; LA-UR-94-3650; CONF-9408185-1) Avail: CASI HC A03/MF A01

Results from the Fermilab experiments E772 and E789 on the Drell-Yan cross sections, quarkonia production, and open-charm production are presented. These data provide information on the parton distributions in the nucleons and nuclei. They also shed light on the origin of the J/(Psi) suppression observed in heavy ion collisions. The physics motivation and the proposed measurements for a new experiment to probe the sea quark distributions in the proton are also discussed. DOE

N95-22573# Argonne National Lab., IL.
NEUTRINO OSCILLATION EXPERIMENTS WITH ATMOSPHERIC NEUTRINOS
Tom Gaisser (Delaware Univ., Newark, DE.) and Maury Goodman 1994 5 p Presented at the Snowmass 1994: Particle and Astrophysics in the Next Millenium, Snowmass, CO, 29 Jun. - 14 Jul. 1994
(Contract W-31-109-eng-38)
(DE95-002994; ANL-HEP-CP-94-72; CONF-9406269-2) Avail: CASI HC A01/MF A01

The possible atmospheric neutrino deficit is reviewed with an emphasis on recent data. The regions of (Delta)m(exp 2) implied by a neutrino oscillation hypothesis are considered. DOE

N95-22583# Brookhaven National Lab., Upton, NY.
LIMIT ON THE MUON NEUTRINO MASS FROM K(EXP 0)MUON 3 DECAY SPECTRA
M. Diwan 1994 4 p Presented at the Snowmass 1994: Particle and Astrophysics in the Next Millenium, Snowmass, CO, 29 Jun. - 14 Jul. 1994
(Contract DE-AC02-76CH-00016)
(DE95-000816; BNL-60843; CONF-9406269-1) Avail: CASI HC A01/MF A01

The statistics and the resolution needed to improve the limit on the muon neutrino mass using k(sub L)(sup 0) yields pi(+/-) mu(-/+) nu(sub mu) decays are considered. The method relies on the shape of the invariant mass distribution of the pion and the muon, m(sub pi mu), near the end point where the neutrino energy is low in the center of mass. The use of simultaneously detected k(sub L)(sup 0) yields pi(+) pi(-) events to calibrate the mass scale and understand the resolution of the spectrometer reduces the sensitivity of this method to previously measured particle masses and to the magnetic field in the spectrometer. An additional check on the experimental method can be obtained by measuring the endpoint of k(sub L)(sup 0) yields pi(+/-) e(-/+) nu(sub e) decays in which one does not expect to observe a nonzero neutrino mass at the sensitivity level of this experiment. Finally, by comparing the end point spectra for neutrinos and antineutrinos one can obtain the most stringent limit on a neutrino-antineutrino mass difference, a nonzero value of which would violate CPT invariance. DOE

N95-22643# International Centre for Theoretical Physics, Trieste (Italy).
MORE ABOUT THE q-DEFORMED H-ATOM WAVE FUNCTIONS: NORMAL AND ABNORMAL SERIES
Xing-Chang Song and Li Liao Jan. 1994 10 p
(DE94-628434; IC-94/8) Avail: CASI HC A02/MF A01 (US Sales Only)

The 3-dim quantum Euclidean space and the q-deformed Schroedinger equation are further investigated. The reality condition is taken into account by introducing the right derivatives as well as the left ones. It seems that from the properties of the q-derivatives, corresponding to a fixed 'energy level' there are infinitive numbers of q deformed wave functions. Among them only one belongs to the normal series, its radial wave function (rwf) has the same number of nodes as that of its classical counterpart. All others have more nodes in their rwf's, and then fall into the abnormal series. This is illustrated by solving the q-Schroedinger equation explicitly for the s-wave solutions. DOE

N95-22646# Fermi National Accelerator Lab., Batavia, IL.
NEW PRELIMINARY RESULTS ON THE PHYSICS OF CHARM HADROPRODUCTION SUBPROCESSES
Jeffrey A. Appel Oct. 1994 5 p Presented at the ICHEP 1994, Glasgow, Scotland, 20-27 Jul. 1994
(Contract DE-AC02-76CH-03000)
(DE95-002530; FNAL/C-94/347-E; CONF-9407142-1) Avail: CASI HC A01/MF A01

This paper reviews the results and physics of two contributed papers to ICHEP94. Both papers relate to charm meson hadroproduction at Fermilab fixed target energies. The first (from E769) addresses the total forward cross section for charm mesons D(sup +/-) and D(sub s, sup +/-) produced by (pi)(sup +/-), K(sup+/-), and proton beams. The second paper (from E791) deals with the asymmetries in the differential cross sections for charged D mesons produced in the forward direction by (pi)(sup -) beam. The physics most directly related to the results of the E769 paper are the gluon distributions in the incident hadrons as well as perturbative QCD calculations of charm quark production and the charm quark mass. The E791 results address the details of the hadronization process after production of the charm quarks. DOE

N95-22656# Brookhaven National Lab., Upton, NY. Dept. of Physics.
(PI)N CORRELATIONS AT AGS
Flemming Videbaek 1994 7 p Presented at the CORINNE 2: International Conference on Multiparticles Correlation and Particle Production in Nucleus-nucleus Collisions, Nantes, France, 5-9 Sep. 1994
(Contract DE-AC02-76CH-00016)
(DE95-002933; BNL-60958; CONF-9409242-1) Avail: CASI HC A02/MF A01

The importance of (delta) at Alternating Gradient Synchrotron (AGS) energies in relativistic heavy ion reactions have long been recognized on theoretical grounds. This paper reviews some of the experimental evidence as observed through the low p(sub t) (pi) spectra and by the direct observation of (delta)(sup ++) by the (pi)(sup +)p correlation measurements. DOE

N95-22685# Fermi National Accelerator Lab., Batavia, IL.
BOTTOM-QUARK PRODUCTION FROM MUON-JET AND DIMUON EVENTS IN p(BAR p)-INTERACTIONS AT THE SQUARE ROOT OF s = 1.8 TeV
T. Huehn (California Univ., Riverside, CA.) Sep. 1994 7 p Presented at the Meeting of the Division of Particles and Fields of the American Physical Society, Albuquerque, NM, 2-6 Aug. 1994

(Contract DE-AC02-76CH-03000)
(DE95-001286; FNAL/C-94/319E; CONF-940816-36) Avail: CASI HC A02/MF A01

Bottom quark production in p(bar p)-interactions has been measured in the rapidity range (vert bar) y(sup b) (vert bar)less than 1 with the DO detector at the Fermilab Tevatron collider. The cross section is determined from events containing a muon and jets as well as from dimuon events. Preliminary results are presented based on 197 nb(sup -1) and 6.4 pb(sup -1) of data for the muon-jets and dimuon analysis, respectively, and are compared to next-to-leading order QCD predictions. The measurements are consistent within errors and are in reasonable agreement with QCD predictions. DOE

N95-22697# Stanford Linear Accelerator Center, CA.
THE FIRST MEASUREMENT OF THE LEFT-RIGHT CROSS SECTION ASYMMETRY IN Z(SUP 0) BOSON PRODUCTION Ph.D. Thesis
R. J. Ben-David May 1994 118 p
(Contract DE-AC03-76SF-00515)
(DE95-003335; SU-SLAC-422) Avail: CASI HC A06/MF A02

The first measurement of the left-right cross section asymmetry (A(sub LR)) in Z(sup 0) boson production has been made with the SLAC Large Detector (SLD) at the SLAC Linear Collider (SLC). The measurement was performed at a center-of-mass energy (E(sub cm)) of 91.55 GeV with a longitudinally polarized electron beam. The average beam polarization was (22.4 +/- 0.6)%. Using a sample of 10,224 Z(sup 0) decays, A(sub LR) is measured to be 0.102 +/- 0.044(stat) +/- 0.003(syst), which determines the effective electroweak mixing angle to be sin(exp 2) theta(sub W)(sup eff) = 0.2375 +/- 0.0056(stat) +/- 0.0004(syst). DOE

N95-22699# Stanford Linear Accelerator Center, CA.
MEASUREMENT OF THE LEFT-RIGHT ASYMMETRY IN Z BOSON PRODUCTION BY ELECTRON-POSITRON COLLISIONS Ph.D. Thesis
R. D. Elia Apr. 1994 144 p
(Contract DE-AC03-76SF-00515)
(DE95-003337; SU-SLAC-429) Avail: CASI HC A07/MF A02

We present the first measurement of the left-right cross-section asymmetry (A(sub LR)) in Z boson production at the SLAC Linear Collider. The left-right asymmetry provides a direct measurement of the e(-)-Z coupling and thus of the effective weak mixing angle; in addition, A(sub LR) is sensitive to the unknown top-quark and Higgs-boson masses. In 1992 the SLD detector recorded 10,224 Z events produced by the collision of longitudinally polarized electrons with an unpolarized positron beam at a center-of-mass energy of 91.55 GeV. The average electron beam polarization during the run was (22.4 +/- 0.6)%. We measure A(sub LR) to be 0.101 +/- 0.044 (stat.) +/- 0.004 (syst.), which determines the effective weak mixing angle to be sin(exp 2) theta(sup eff)(sub W) = 0.2377 +/- 0.0056 (stat.) +/- 0.0005 (syst.). This measurement of A(sub LR) is in agreement with comparable measurements and is consistent with Standard-Model predictions for allowed top and Higgs masses. DOE

N95-22700# Clark-Atlanta Univ., GA.
STUDIES OF PHOTON AND ELECTRON INTERACTIONS WITH ATOMS AND IONS Progress Report, 1 Jun. 1993 - 30 Jun. 1994
A. Z. Msezane 1994 7 p
(Contract DE-FG05-84ER-13266)
(DE95-003340; DOE/ER-13266/T5) Avail: CASI HC A02/MF A01

This report discusses electron collisions at small scattering angles, atomic ionization, and photoionization of inner-shell of sodium. DOE

N95-22703# Stanford Linear Accelerator Center, CA.
THE CHARM PHYSICS POTENTIAL OF A TAU-CHARM FACTORY
J. L. Hewett Oct. 1994 13 p Presented at the Tau-Charm Factory in the Era of B-factories and CESR Conference, Stanford, CA, 15-16 Aug. 1994
(Contract DE-AC03-76SF-00515)
(DE95-003369; SU-SLAC-PUB-6695; CONF-9408190-1) Avail: CASI HC A03/MF A01

The charm physics program accessible to a Tau-Charm Factory is summarized. Semileptonic, leptonic, hadronic, rare, and forbidden charm decay modes are discussed, as well as D(sup 0) - bar-D(sup 0) mixing and CP violation in the charm sector. The theoretical expectations in the Standard Model and beyond as well as the experimental capabilities of a Tau-Charm Factory are examined for each of the above processes. DOE

N95-22720# International Centre for Theoretical Physics, Trieste (Italy).
QCD IMPROVED EXCLUSIVE RARE B-DECAYS AT THE HEAVY b-QUARK LIMIT
Dongsheng Liu Sep. 1993 15 p
(DE94-628609; IC-93/323) Avail: CASI HC A03/MF A01 (US Sales Only)

The renormalization effects from the b-quark scale down to the non-perturbative QCD regime are studied for rare B-decays at the heavy b-quark limit. Phenomenological consequences of these effects are investigated. We find that the anomalous scaling behaviour plays a positive role in making non-perturbative model calculations consistent with recent CLEO measurements of B yields K*gamma. DOE

N95-22727# Brookhaven National Lab., Upton, NY.
SEARCHES FOR THE H-DIBARYON AT THE AGS
B. Quinn, A. Berdoz, G. Franklin, R. Magahiz, R. McCrady, F. Merrill, C. Meyer, R. Schumacher, R. Sukaton, and V. Zeps (Carnegie-Mellon Univ., Pittsburgh, PA.) 1994 6 p Presented at the Intersections of Particle and Nuclear Physics, St. Petersburg, FL, 31 May - 6 Jun. 1994
(Contract DE-AC02-76CH-00016)
(DE95-003091; BNL-61018; CONF-940514-15) Avail: CASI HC A02/MF A01

A review is made of those past, present, and planned experiments at the AGS whose primary purpose is to determine whether the H-dibaryon exists. Preliminary results are given for experiment E813, based on partially-completed analysis. DOE

N95-22729# Washington Univ., Seattle, WA.
NEUTRINO OVERVIEW
W. C. Haxton 1994 8 p Presented at the Workshop on Nuclear and Particle Astrophysics and Cosmology in the Next Millenium, Snowmass, CO, Jul. 1994
(Contract DE-FG06-90ER-40561)
(DE95-003201; DOE/ER-40561/161; CONF-9407151-1) Avail: CASI HC A02/MF A01

The author discusses some of the open issues in neutrino physics, emphasizing areas of intersection with astrophysics, that occupied the participants of the Snowmass Workshop on Nuclear and Particle Astrophysics and Cosmology in the Next Millenium. DOE

N95-22730# Washington Univ., Seattle, WA.
OUTLOOK FROM THE INTERSECTIONS
W. C. Haxton 1994 16 p Presented at the Intersections of Particle and Nuclear Physics, St. Petersburg, FL, 31 May - 6 Jun. 1994
(Contract DE-FG06-90ER-40561)
(DE95-003202; DOE/ER-40561/162; CONF-940514-17) Avail: CASI HC A03/MF A01

The author reviews a number of the physics themes of the Fifth Conference on the Intersections of Particle and Nuclear Physics, discussing the significance and promise of current work at the interface of these fields. Some of the themes are: pattern of quark and boson masses; solar neutrino problem; lepton flavor violation tests; atomic dipole moments studies; Delta s = 0 weak interaction between nucleons; and strongly-interacting many-body problems. DOE

N95-22731# Washington Univ., Seattle, WA.
A MODEL OF MESONS BASED ON CHI SB IN THE LIGHT-FRONT FRAME
L. Susskind and M. Burkardt 1994 10 p
(Contract DE-FG06-90ER-40561)
(DE95-003203; DOE/ER-40561/163) Avail: CASI HC A02/MF A01

Spontaneous breaking of chiral symmetry is discussed in the light-cone framework. The essential ingredient is an infinite number of constituents near zero light-cone momentum. These high (light-cone) energy degrees of freedom freeze out and leave behind some explicit symmetry breaking in the low (light-cone) energy effective Hamiltonian. Connections with Regge theory and soft pion theorems are discussed. Taking the order parameter to be the fourth component of a chiral 4-vector, the effect of the spontaneous

symmetry breaking on meson masses and decay width is calculated and compared with experimental data. DOE

N95-22747# Louisiana State Univ., Baton Rouge, LA. Dept. of Chemistry.
PRESSURE SHIFTS AND ELECTRON SCATTERING IN ATOMIC AND MOLECULAR GASES
K. Rupnik, S. P. McGlynn, and U. Asaf (Hebrew Univ., Jerusalem, Israel.) 1994 7 p
(Contract DE-FG05-87ER-60503)
(DE95-003102; DOE/ER-60503/365) Avail: CASI HC A02/MF A01

The authors focus on one aspect of Rydberg electron scattering, namely number density effects in molecular gases. The recent study of Rydberg states of CH3I and C6H6 perturbed by H2 is the first attempt to investigate number density effects of a molecular perturber on Rydberg electrons. Highly excited Rydberg states, because of their 'large orbital' nature, are very sensitive to the surrounding medium. Photoabsorption or photoionization spectra of CH3I have also been measured as a function of perturber pressure in 11 different binary gas mixtures consisting of CH3I and each one of eleven different gaseous perturbers. Five of the perturbers were rare gases (He, Ne, Ar, Kr, Xe) and six were non-dipolar molecules (H2, CH4, N2, C2H6, C3H8). The goal of this work is to underline similarities and differences between atomic and molecular perturbers. The authors first list some results of the molecular study. DOE

N95-22749# Institute for Advanced Study, Princeton, NJ.
PROBLEMS IN PARTICLE THEORY
Stephen L. Adler and Frank Wilczek Oct. 1994 24 p
(Contract DE-FG02-90ER-40542)
(DE95-003106; DOE/ER-40542/89) Avail: CASI HC A03/MF A01

This report is a progress report on the work of two principal investigators in the broad area of particle physics theory, covering their personal work, that of their coworkers, and their proposed work for the future. One author has worked in the past on various topics in field theory and particle physics, among them current algebras, the physics of neutrino induced reactions, quantum electrodynamics (including strong magnetic field processes), the theory of the axial-vector current anomaly, topics in quantum gravity, and nonlinear models for quark confinement. While much of his work has been analytical, all of the projects listed above (except for the work on gravity) had phases which required considerable computer work as well. Over the next several years, he proposes to continue or initiate research on the following problems: (1) acceleration algorithms for the Monte Carlo analysis of lattice field and gauge theories, and more generally, new research in computational neuroscience and pattern recognition; (2) construction of quaternionic generalizations of complex quantum mechanics and field theory, and their application to composite models of quarks and leptons, and to the problem of unifying quantum theories of matter with general relativity. One author has worked on problems in exotic quantum statistics and its applications to condensed matter systems. His work has also continued on the quantum theory of black holes. This has evolved toward understanding properties of quantum field theory and string theory in incomplete regions of flat space. DOE

N95-22754# International Centre for Theoretical Physics, Trieste (Italy).
ON THE D YIELDS K-BAR(SUP *)e(SUP +)(NU)(SUB e) FORM FACTORS
F. Hussain, A. N. Ivanov, and N. I. Troitskaya Jan. 1994 6 p
(DE94-628614; IC-94/31) Avail: CASI HC A02/MF A01 (US Sales Only)

The infinite mass effective theory, when a heavy quark mass goes to infinity, and chiral perturbation theory at the quark level, based on the extended Nambu-Jona-Lasinio model, are applied for the calculation of the D yields K-bar(sup *)e(sup +) nu(sub e) decay form factors. The theoretical results agree with experimental data. DOE

N95-22755# International Centre for Theoretical Physics, Trieste (Italy).
TO THE PROBLEM OF D-MESON LEPTONIC AND SEMILEPTONIC DECAYS
A. N. Ivanov, N. I. Troitskaya, and M. Nagy (Slovak Academy of Sciences, Bratislava, Czechoslovakia.) Jan. 1994 8 p
(DE94-628615; IC-94/9) Avail: CASI HC A02/MF A01 (US Sales Only)

The infinite mass effective theory, when a heavy quark mass goes to infinity, and chiral perturbation theory at the quark level, based on the extended Nambu-Jona-Lasinio model, are applied for the description of form factors of semileptonic decay D (yields) K-bare(sup +)(nu)(sub e) and leptonic constant F(sub D) of D-mesons. There is derived the relation, connecting the form factor f(sub +)(0) with the ratio F(sub D)/F(sub (pi)), which gives the estimate F(sub D)/F(sub pi) approx. equal to 1.20 +/- 0.17. The slope parameter of the f(sub +) -form factor is calculated in agreement with experimental data. DOE

N95-22756# International Centre for Theoretical Physics, Trieste (Italy).
NEUTRINOS WITH ZEE-MASS MATRIX IN VACUUM AND MATTER
A. Yu. Smirnov and Zhijian Tao Mar. 1994 27 p
(DE94-628635; IC-94/42) Avail: CASI HC A03/MF A01 (US Sales Only)

Neutrino mass matrix generated by the Zee (radiative) mechanism has zero (in general, small) diagonal elements and a natural hierarchy of the nondiagonal elements. It can be considered as an alternative (with strong predictive power) to the matrices generated by the see-saw mechanism. The propagation in medium of the neutrinos with the Zee-mass matrix is studied. The flavor neutrino transitions are described analytically. In the physically interesting cases the probabilities of transitions as functions of neutrino energy can be represented as two-neutrino probabilities modulated by the effect of vacuum oscillations related to the small mass splitting. Possible applications of the results to the solar, supernova, atmospheric and relic neutrinos are discussed. A set of the predictions is found which could allow to identify the Zee-mass matrix and therefore the corresponding mechanism of mass generation. DOE

N95-22758# International Centre for Theoretical Physics, Trieste (Italy).
STRONG COLLISION APPROACH TO CALCULATION OF DEPOLARIZATION FUNCTION FOR NEUTRON BEAM PASSING THROUGH FERROMAGNETIC BULK DOMAINS
E. Kornilov and V. Pomjakushin (Joint Inst. for Nuclear Research, Dubna, USSR.) Nov. 1993 8 p
(DE94-628847; IC-93/384) Avail: CASI HC A02/MF A01 (US Sales Only)

We propose the Markovian random walk approach for calculation of the depolarization function of the polarized neutron beam transmitted through a magnetic medium. This approach allows one to obtain exact analytical results for the depolarization function P(lambda) which is valid for any wavelength lambda. Two magnetic configurations were considered in the present work: random ferromagnetic domains, and staggered ferromagnetic domains. DOE

N95-22763# Brookhaven National Lab., Upton, NY.
DO NARROW SIGMA HYPERNUCLEAR STATES EXIST?
R. Sawafta 1994 6 p Presented at the International Conference on Hypernuclear and Strange Particle Physics, Vancouver, Canada, 4-8 Jul. 1994
(Contract DE-AC02-76CH-00016)
(DE95-002930; BNL-60835; CONF-940725-4) Avail: CASI HC A02/MF A01

The Sigma hypernuclear problem has been the subject of intense experimental and theoretical debate for more than 15 years. Despite these efforts, the Sigma-nucleus interaction is not well understood. Experimental data have been taken on different targets at different momenta and at different conditions. These data suffer from poor resolution and insufficient statistics. Contradictions among the different sets of data often resulted more in clouding the issues than clarifying them. This paper aims at clearing up this long-standing problem. Hypernuclear mass spectra for in-flight (K(-),pi(+/-)) reactions from H-1, H-2, Li-6 and Be-9 have been measured. Preliminary results based on analysis of the (K(-) ,pi(+/-)) spectra from Be-9 are discussed. DOE

N95-22778# International Centre for Theoretical Physics, Trieste (Italy).
RELATIVISTIC PARTICLE WITH TORSION AND CHARGED PARTICLE IN A CONSTANT ELECTROMAGNETIC FIELD: IDENTITY OF EVOLUTION
M. S. Plyushchay Sep. 1993 6 p
(DE94-628506; IC-93/327) Avail: CASI HC A02/MF A01 (US Sales Only)

The identity of classical motion is established for two physically different

models, one of which is the relativistic particle with torsion, whose action contains higher derivatives and which is the effective system for the statistically charged particle interacting with the Chern-Simons U(1) gauge field, and another is the (2+1)-dimensional relativistic charged particle in external constant electromagnetic field. DOE

N95-22786# International Centre for Theoretical Physics, Trieste (Italy).
BARYON NUMBER FLUCTUATIONS IN A QUARK-HADRON PHASE TRANSITION
C. P. Singh (Banaras Hindu Univ., Varanasi, India.), B. K. Patra (Banaras Hindu Univ., Varanasi, India.), and S. Uddin Jan. 1994 19 p
(DE94-628585; IC-94/15) Avail: CASI HC A03/MF A01 (US Sales Only)

Isothermal baryon number fluctuations arising from a first-order quark-hadron phase transition in the early universe are obtained by including the quark-gluon interactions up to the order g(sup 3)(sub s) in the perturbative QCD coupling constant in the quark-gluon plasma (QGP) phase and the finite size volume corrections for the hadrons in the hadron-resonance gas (HRG) and their effects on the primordial nucleosynthesis (PNS) are analyzed. The ratio of the baryon-number densities in the QGP and HRG phases at the critical temperature T(sub c) is larger than one in the range 150 MeV less than T(sub c) less than 260 MeV. However, it is far larger than one even when T(sub c) is outside this range thus affecting primordial nucleosynthesis significantly. DOE

N95-22787# Joint Inst. for Nuclear Research, Dubna (USSR).
THE U(3) X U(3) NAMBU - JONA-LASINIO MODEL WITH THE GLUON CONDENSATE AND AXIAL ANOMALY AT FINITE TEMPERATURE
Yu. L. Kalinovskij and M. K. Volkov 1993 18 p
(DE94-628588; JINR-E-2-93-38) Avail: CASI HC A03/MF A01 (US Sales Only)

The U(3) x U(3) Nambu - Jona-Lasinio model with the gluon condensate and axial anomaly ((sup ')t Hooft determinant) is investigated at finite temperature. The behaviour of the constituent quark masses, quark condensates, meson masses, coupling constants as functions of temperature is studied. It is shown that the gluon condensate plays a stabilizing role for the behavior of physical quantities when temperature changes. This influence is more visible for the light quarks (up and down). The axial anomaly and the mixing angle ((eta) - (eta)(sup ')) decrease with increasing temperature. DOE

N95-22789# International Centre for Theoretical Physics, Trieste (Italy).
HADRONS OF ARBITRARY SPIN AND HEAVY QUARK SYMMETRY
F. Hussain, G. Thompson, and J. G. Koerner (Mainz Univ., Germany.) Nov. 1993 69 p
(DE94-628597; IC-93/314; MZ-TH-93-23) Avail: CASI HC A04/MF A01 (US Sales Only)

We present a general construction of the spin content of the Bethe-Salpeter amplitudes (covariant wave functions) for heavy hadrons with arbitrary orbital excitations, using representations of 1 x 0(3, 1). These wave functions incorporate the symmetries manifest in the heavy quark limit. In the baryonic sector we clearly differentiate between the (Lambda) and (Sigma)-type excited baryons. We then use the trace formalism to evaluate the weak transitions of ground state heavy hadrons to arbitrary excited heavy hadrons. The contributions of excited states to the Bjorken sum rule are also worked out in detail. DOE

N95-22790# International Centre for Theoretical Physics, Trieste (Italy).
RESULTS FROM NEUTRINO EXPERIMENTS
A. Yu. Smirnov Nov. 1993 36 p
(DE94-628604; IC-93/388; HEP-PH-9311359) Avail: CASI HC A03/MF A01 (US Sales Only)

Recent (first or/and the best) results from the neutrino experiments are reviewed and their implications for the theory are discussed. The sense of the experiments is the searching for neutrino masses, mixing and interactions beyond the standard model. Present laboratory experiments give upper bounds on the masses and the mixing which are at the level of predictions of the 'electroweak see-saw'. Positive indications of nonzero lepton mixing follow from studies of the solar and atmospheric neutrinos. DOE

N95-22791# International Centre for Theoretical Physics, Trieste (Italy).
LONG RANGE POTENTIALS AND MULTIPLE SCATTERING THEORY IN COMPLEX SYSTEMS
L. Fonda Dec. 1993 12 p
(DE94-628881; IC-93/423) Avail: CASI HC A03/MF A01 (US Sales Only)

In this paper consideration is given to EXAFS and Photoelectron Diffraction in the case of incomplete screening of the core hole charge. The relevant multiple-scattering formulas are obtained in the framework of the Green's operator approach. DOE

N95-22792# Argonne National Lab., IL.
COMPUTER SIMULATION OF THE STRUCTURE OF IONIC SURFACES AND INTERFACES
D. Wolf Sep. 1994 7 p Presented at the 8th Latin American Congress on Surface Science: Interfacial Phenomena in Biomaterials Symposium, Cancun, 19-23 Sep. 1994
(Contract W-31-109-eng-38)
(DE95-002991; ANL/MSD/CP-84182; CONF-9409248-1) Avail: CASI HC A02/MF A01

The classic Madelung problem, i.e., the divergence associated with the r(sup -1) term in the Coulomb potential of condensed ionic systems, was recently cast into an absolutely convergent form that is readily evaluated by direct lattice summation, revealing a net r(sup -5) range of this potential. This realization that Coulomb interactions in condensed systems can actually be rather short ranged (if the system is overall neutral) permits novel physical insights into their structure and energetics to be gained. As an example, the authors demonstrate that an understanding of the range and the nature of the convergence of the Coulomb potential leads naturally to the prediction, verified here by computer simulations for rocksalt-structured surfaces, that all surfaces in predominantly ionic materials should be fundamentally reconstructed. The work also provides a conceptual framework for the theoretical treatment of polar surfaces and interfaces, as demonstrated here for the case of the (111) stacking fault and of the (111) twin boundary in the rocksalt structure. DOE

N95-22810# International Centre for Theoretical Physics, Trieste (Italy).
THE DECAYS OF D(SUP *)-MESONS
M. P. Khanna and M. K. Volkov Oct. 1993 7 p
(DE94-628610; IC-93/355) Avail: CASI HC A02/MF A01 (US Sales Only)

The strong and radiative decays of the D(sup *)-mesons are studied with the effective Lagrangian in a model of the Nambu-Jona-Lasinio type. DOE

N95-22811# International Centre for Theoretical Physics, Trieste (Italy).
(PI)- AND a(SUB 1)-MESON PHYSICS IN CURRENT ALGEBRA AT THE QUARK LEVEL
A. N. Ivanov and N. I. Troitskaya Jan. 1994 12 p
(DE94-628611; IC-94/10) Avail: CASI HC A03/MF A01 (US Sales Only)

The a(sub 1) yields pi(pi pi) S-wave decay and the low-energy pi pi-scattering are considered within current algebra at the quark level (CA)(sub q) and Chiral perturbation theory at the quark level (CHPT)(sub q) based on the Extended Nambu-Jona-Lasinio model with linear realization of chiral U(3) X U(3) symmetry. It is shown that low-energy interactions of a new kind, produced by convergent constituent-quark diagrams and being very useful for the theoretical understanding of experimental data on the processes under consideration, are very good blending with (CA)(sub q) and (CHPT)(sub q). The contribution of these interactions is caused by the application of ordinary rules of quantum field theory. DOE

N95-22847# Academy of Sciences (USSR), Novosibirsk (USSR).
ONCE MORE ABOUT THE OMEGA APPROACHES 3(PI) CONTACT TERM
E. A. Kuraev and Z. K. Siagadze 1993 26 p
(DE94-633202; BUDKERINP-93-52; IYaF-93-52) Avail: CASI HC A03/MF A01 (US Sales Only)

The manifestations of the (omega) approaches 3(pi) contact term and its unitary partners are investigated in the framework of the chiral effective Lagrangian theory with vector mesons. DOE

N95-22870# Niigata Univ. (Japan).
IONIC CORE EFFECTS ON THE MIE RESONANCE IN LITHIUM CLUSTERS
K. Yabana and G. F. Bertsch (Washington Univ., Saint Louis, MO.) 1994 29 p
(Contract DE-FG06-90ER-40561)
(DE94-014974; DOE/ER-40561/144) Avail: CASI HC A03/MF A01

We investigate effects of atomic cores on the Mie resonance in lithium metal clusters, perturbing a helium Hamiltonian with zero-range pseudopotentials. The resonance is red-shifted with respect to the classical formula by core effects, most important of which is the increased effective mass due to the core potentials. Much of the large shift seen in lithium clusters is thereby explained if the strength of the Pseudopotentials is taken from band structure calculations. However, such pseudopotentials cause the resonance to be greatly broadened, contrary to observation. DOE

N95-22881# Wyoming Univ., Laramie, WY.
EXOTIC ATOMS Technical Progress Report
R. Kunselman 1994 6 p
(Contract DE-FG02-87ER-40333)
(DE95-003199; DOE/ER-40333/147) Avail: CASI HC A02/MF A01

The experiments use a variety of hydrogen isotopic mixtures to form solid targets for muons to produce muonic hydrogen isotope atoms that escape into vacuum. The method relies on transfer of the muon from a proton to either a deuteron or a triton. The resulting muonic deuterium or muonic tritium will not immediately thermalize because of the very low elastic cross sections (RT effect), and are emitted from the surface of the layer. A second solid hydrogen isotopic target is produced downstream on which the muonic hydrogen atom can react. Measurements which detect decay electrons, muonic x-rays, and fusion products have been used to study the processes of energy dependence of transfer, production rates, and muon molecular formation. The processes include muon catalyzed fusion of muonic tritium with deuterium which is the most possible candidate for energy production fusion. Our interest is the nuclear physics reaction rates and to use the muonic hydrogen isotopes in vacuum for energy level measurements. The method uses time of flight and is reminiscent of double scattering experiments. Two other experiments are in the development stages. First to measure the energy dependence of the Ramsauer-Townsend cross section in tritium where it has not been measured. The measurements would be compared to deuterium and calculations. Second, kaonic atoms, hypernuclei, and kaon-nucleon scattering at DAPHNE. DOE

N95-22889# Oak Ridge National Lab., TN. Health Sciences Research Div.
THE TORSION SPACE NUCLEIC ACIDS MOLECULAR MECHANICS PROGRAM DUPLEX: SURVEYING CONFORMATION SPACE BY POTENTIAL ENERGY MINIMIZATION Progress Report
Brian E. Hingerty and Suse Broyde (New York Univ., New York, NY.) 1993 5 p Presented at the Structural Biology: the State of the Art: 8th Conversation, Albany, NY, 22-26 Jun. 1993
(Contracts DE-AC05-84OR-21400; DE-FG02-90ER-60931)
(DE94-017707; CONF-9306364-1) Avail: CASI HC A01/MF A01

The molecular mechanics program DUPLE-X has proven useful in surveying the conformation space of unmodified DNA's and RNA's, and covalently damaged DNA's, by potential energy minimization. The reduced variable set of torsion angle space, together with search strategies that flat explore small subunits, permit location of low energy structures from high energy positions. Prediction of structure in the absence of data, though difficult is possible with large numbers of trials. With NMR data to guide the searches in first stage trials, generation of final unrestrained low energy forms that are within bounds of the data is achieved with fewer trials. DOE

N95-22925# Washington Univ., Seattle, WA. Institute for Nuclear Theory.
THE CONVERGENCE RADIUS OF THE CHIRAL EXPANSION IN THE DYSON-SCHWINGER APPROACH
T. Meissner 12 May 1994 16 p
(Contract DE-FG06-90ER-40561)
(DE94-012852; DOE/ER-40561/140) Avail: CASI HC A03/MF A01

We determine the convergence radius m(sub conv) or the expansion in the current quark mass using the Dyson-Schwinger (DS) equation of QCD in the rainbow approximation. Within a Gaussian form for the gluon propagator D(sub (mu x nu))(p) (approximately) (delta)(sub(mu x nu))chi(sup 2)e(sup -(p(sup 2)/Delta)) we find that m(sub conv) increases with decreasing width (Delta) and increasing strength (chi)(sup 2). For those values of (chi)(sup 2) and (Delta), which provide the best known description of low energy hadronic phenomena, m(sub conv) lies around 2(Lambda)(sub QCD), which is big enough, that the chiral expansion in the strange sector converges. Our analysis also explains the rather low value of m(sub conv) (approx) 50...80 MeV in the Nambu-Jona-Lasinio model, which as itself can be regarded as a special case of the rainbow DS models, where the gluon propagator is a constant in momentum space. DOE

N95-22927# Los Alamos National Lab., NM.
TRAPS FOR ANTIMATTER AND ANTIHYDROGEN PRODUCTION
M. H. Holzscheiter 1994 33 p Presented at the Traped Charged Particles and Fundamental Physics, Lyseuil, Sweden, 12-22 Aug. 1994
(Contract W-7405-eng-36)
(DE95-002814; LA-UR-94-3677; CONF-9408184-2) Avail: CASI HC A03/MF A01

Even though positrons have been captured and stored in ion traps for precision measurements, the recent trapping and cooling of antiprotons may be considered as the beginning of a new era in antimatter research. For the first time all the ingredients to produce the first atom of the antimatter world, the antihydrogen atom, are at hand, and several groups have entered an active discussion on the feasibility of producing antihydrogen as well as on the possibility to perform precision tests on CPT and gravity. At the same time, the trapping of reasonable large numbers of antiprotons has opened up the way for a variety of exciting physics with ultra-low energy antiprotons, ranging from atomic physics issues to nuclear physics and medical applications. I will describe the current status of the work on trapping antiprotons and positrons, discuss possible physics applications of this technique, and describe the two most promising routes to produce antihydrogen for precision spectroscopy. Towards the end a few comments on storing the produced antihydrogen and on utilizing antihydrogen for gravity measurements and for CPT tests are given. DOE

N95-22935# International Centre for Theoretical Physics, Trieste (Italy).
STRUCTURAL PROPERTIES OF SILICON CLUSTERS: AN EMPIRICAL POTENTIAL STUDY
X. G. Gong, Q. Q. Zheng (Academia Sinica, Hefei, China.), and Yi Zhen He (Academia Sinica, Hefei, China.) Sep. 1993 15 p
(DE94-628902; IC-93/331) Avail: CASI HC A03/MF A01 (US Sales Only)

By using our newly proposed empirical interatomic potential for silicon, the structure and some dynamical properties of silicon cluster Si(sub n) 10 (less than or equal to) n (less than or equal to) 24 have been studied. It is found that the obtained results are close to those from ab-initio methods. From present results, we can gain a new insight into the understanding of the experimental data on the Si(sub n) clusters. DOE

N95-22936# Los Alamos National Lab., NM.
A BRIEF HISTORY IN TIME OF ION TRAPS AND THEIR ACHIEVEMENTS IN SCIENCE
M. H. Holzscheiter 1994 24 p Presented at the Trapped Charged Particles and Fundamental Physics, Lyseuil, Sweden, 12-22 Aug. 1994
(Contract W-7405-eng-36)
(DE95-002815; LA-UR-94-3676; CONF-9408184-1) Avail: CASI HC A03/MF A01

A short history of the development of the ion storage technique for precision experiments is given. This is by no means meant to be a complete review of the field, but the intend is to use a few specific examples to describe how the persistence, ingenuity, and experimental skill of a few people has generated the core of a field which is now growing at an ever faster pace, spreading into new areas, developing sub fields, and allowing a view at nature, using very modest experimental equipment, which by far rivals even the most ambitious dreams of high energy physics. DOE

N95-22939# Fermi National Accelerator Lab., Batavia, IL.
SEARCH FOR SECOND GENERATION LEPTOQUARKS AT CDF
S. Park Aug. 1994 6 p Presented at the Meeting of the Division of Particles and Fields of the American Physical Society, Albuquerque, NM,

2-6 Aug. 1994
(Contract DE-AC02-76CH-03000)
(DE94-018983; FNAL/C-94/228-E; CONF-940816-19) Avail: CASI HC A02/MF A01

We present the results of a search for second generation leptoquarks S(sub 2) in p(bar-p) collisions at square root of s = 1.8 TeV at the Fermilab Tevatron. This search is based on 19.3 pb(+) of data collected during the 1992-93 CDF run. We have searched for evidence of leptoquark pairs assuming that each leptoquark decays to a muon + quark with a branching ratio beta.Two leptoquark candidate events were found with a background of 1.35 +/- 0.50. We obtained-upper limits on the production cross-section times branching ratio as a function of leptoquark mass. For pair production of second generation leptoquarks, we excluded M(sub S)(sub 2) less than 133. GeV/c(sup 2) for beta = 100% and M(sup S)(sub 2)less than 98 GeV/c(sup 2) for beta = 50% at 95% CL. DOE

N95-23054# Ohio State Univ., Columbus, OH. Research Foundation.
STRONGLY INTERACTING FERMION SYSTEMS Progress Report, 15 Nov. 1994 - 14 Nov. 1995
1994 9 p
(Contract DE-FG02-88ER-45347)
(DE95-003405; DOE/ER-45347/T3) Avail: CASI HC A02/MF A01

This paper is the progress report for the period November 15, 1993 to November 14, 1994 for a program which relates to studies of strongly interacting fermion systems. The author has made significant progress in three areas, which are discussed in the report. These are: (1) optical properties in the 'electronic structure program,' calculating optical properties of quartz and urea; (2) quasi-one-dimensional systems, discussing the tuning of the large-density-wave or Peierls distortion in transition-metal linear chain compounds and the universal subgap optical absorptance of classes of quasi-one-dimensional compounds; and (3) other strongly interacting fermion systems, emphasizing the study of the effect of many-body interactions on the low-temperature properties of metals and superconductors. DOE

N95-23055# Oak Ridge Y-12 Plant, TN.
MERCURY DETECTION WITH THERMAL NEUTRONS
Z. W. Bell 19 Sep. 1994 19 p
(Contract DE-AC05-84OS-21400)
(DE95-002061; Y/DW-1340) Avail: CASI HC A03/MF A01

This report describes the work performed to design a gauge to detect mercury concealed within walls, floors, pipes, and equipment inside a building. The project arose out of a desire to decontaminate and decommission (D&D) a building in which mercury had been used as part of a chemical process. The building contains plumbing and equipment, some with residual mercury even after draining, sumps, and hollow walls. So that releases of mercury to the environment might be minimized during D&D activities, it was considered advisable to locate pockets of mercury that may have collected in concealed spaces so that they might be drained in a controlled fashion prior to the application of the wrecking ball or sledge hammer. The detection of such pockets within a building presents some problems not ordinarily encountered in a laboratory environment. Often, only a single side of a wall or pipe is accessible. This condition disqualifies transmission gauges (such as conventional x radiography) in which a probe is sent through the volume under test (VUT) from one side and its passage or attenuation is detected on the opposite side. A robust, one-sided system was needed. DOE

N95-23077# Wisconsin Univ., Madison, WI.
ENERGY TRANSFER DYNAMICS IN ISOLATED AND IN COLLIDING HIGHLY VIBRATIONALLY EXCITED MOLECULES Annual Report No. 2, Nov. 1992 - Oct. 1993
F. F. Crim 10 May 1994 14 p
(Contract F49620-92-J-0040)
(AD-A285771; AFOSR-94-0669TR) Avail: CASI HC A03/MF A01

This process report describes studies of the collisional energy transfer in highly vibrationally excited acetylene (C2H2). It reports state-to-state vibrational and rotational energy transfer rates and pathways in acetylene. Author

N95-23082# Ohio State Univ., Columbus, OH. Dept. of Chemistry.
THE ELECTRONIC STRUCTURE OF HEAVY ELEMENT COMPLEXES Annual Report, 1 Jan. 1994 - 31 Dec. 1994
B. E. Bursten Oct. 1994 6 p
(Contract DE-FG02-86ER-13529)
(DE95-003407; DOE/ER-13529/T3) Avail: CASI HC A02/MF A01

This progress report deals with studies of the electronic structure of actinide compounds. Calculations of the electronic structure of organometallic thorium and proactinium complexes, fullerene-uranium compounds, and uranium and element 106 carbonyls were presented. DOE

N95-23137# Los Alamos National Lab., NM.
STATUS OF HELIUM-PRODUCTION REACTION STUDIES WITH A SPALLATION NEUTRON SOURCE
R. C. Haight, F. B. Bateman, and M. B. Chadwick 1994 13 p Presented at the IAEA Conference on Improvement of Measurements, Theoretical Computations, and Evaluations of Neutron-induced Helium Production Cross Sections, Beijing, China, 1-4 Nov. 1994
(Contract W-7405-eng-36)
(DE95-002816; LA-UR-94-3678; CONF-9411145-1) Avail: CASI HC A03/MF A01

Alpha-particle production cross sections and spectra are being measured at the spallation source of fast neutrons at the Los Alamos Meson Physics Facility (LAMPF). Detectors at angles of 30, 60, 90 and 135 deg are used to identify alpha particles, measure their energy spectra, and indicate the time-of-flight, and hence the energy, of the neutrons inducing the reaction. The useful neutron energy ranges from less than 1 MeV to approximately 50 MeV for the present experimental setup. Targets under study at present include C, N, O, Al-27, Si, V-51, Fe-56, Co-59, Ni-58,60, Y-89 and Nb-93. Results for Co-59 illustrate the capabilities of the approach. DOE

N95-23138# Stanford Linear Accelerator Center, CA.
HEAVY QUARK PHYSICS AT SLD: PRELIMINARY RESULTS
E. Vella Aug. 1994 10 p Presented at the Meeting on Particle Physics, Astrophysics and Cosmology, Stanford, CA, 8-12 Aug. 1994
(Contract DE-AC03-76SF-00515)
(DE95-003372; SU-SLAC-PUB-6711; CONF-9408100-2) Avail: CASI HC A02/MF A01

This report discusses SLD experiment; R(sub b) = (Gamma)(Z (yields) b(bar b))/(Gamma)(Z (yields) hadrons); B lifetime; and left-right forward-backward asymmetries A(sub b) and A(sub c). DOE

N95-23139# Stanford Linear Accelerator Center, CA.
FINAL RESULT ON THE MASS OF THE TAU LEPTON FROM THE BES COLLABORATION
E. Soderstrom Nov. 1994 4 p Presented at the Meeting on Particle Physics, Astrophysics and Cosmology; Meeting of the Division of Particles and Fields of the American Physical Society, Stanford, CA; Albuquerque, NM, 8-12 Aug. 1994; 2-6 Aug. 1994
(Contracts DE-AC03-76SF-00515; DE-FG03-92ER-40701; DE-FG03-91ER-40679; DE-FG02-91ER-40676; DE-AC02-76ER-03069; DE-AC35-89ER-40486; DE-FG05-92ER-40736)
(DE95-003466; SU-SLAC-PUB-6542; CONF-9408100-1; CONF-940816-1) Avail: CASI HC A01/MF A01

A data-driven energy scan in the immediate vicinity of tau pair production threshold has been performed using the Beijing Spectrometer (BES) at the Beijing Electron-Positron Collider (BEPC). Approximately 5 pb(sup -1) of data, distributed over twelve scan points, have been collected. An initial tau lepton mass value, obtained using only the e(mu) final state, has been published. In this paper, the final BES result on the mass measurement, based on the combined data samples of ee, e mu, e pi, eK, mu mu, mu pi, mu K, pi pi, and pi K events, is presented. A maximum likelihood fit yields the value m(sub tau) = 1776.96 (+0.18/-0.19)/(+0.20/-0.16) MeV. DOE

N95-23140# Stanford Linear Accelerator Center, CA.
MEASUREMENT OF THE LEFT-RIGHT CHARGE ASYMMETRY IN HADRONIC Z DECAYS AND A(SUB E) DETERMINATION
G. J. Baranko (Colorado Univ., Boulder, CO.) Sep. 1994 3 p Presented at the Meeting of the Division of Particles and Fields of the American Physical Society, Albuquerque, NM, 2-6 Aug. 1994
(Contract DE-AC03-76SF-00515)
(DE95-003467; SU-SLAC-PUB-6636; COLO-HEP-342; CONF-940816-52) Avail: CASI HC A01/MF A01

We present a new method for determining the electron left-right

asymmetry factor, A(sub e), by measuring the forward-backward charge flow in samples of hadronic Z events, produced in e(+) e(-) collisions, with left-handed and right-handed electron-beam polarizations. The raw, left-right charge asymmetry, Q(sub LR)(sup raw), is defined. After correction by the measured beam polarization, it provides A(sub e) with greatly reduced dependence on Monte Carlo corrections for acceptances and jet charge measurement. The Q(sub LR)(sup raw) is also combined with the raw, left-right cross section asymmetry, A(sub LR)(sup raw), to obtain A(sub e) without the use of the measured electron-beam polarization, and with half the statistical error as that obtained for A(sub e) using the polarization corrected Q(sub LR)(sup raw) alone. This method gives sin(sup 2)theta(sub W)(sup eff) = 0.2291 +/- 0.0039(stat.) +/- 0.0012(syst.). The measurement was performed at a center-of-mass energy of 91.26 GeV with the SLD detector at the SLAC Linear Collider (SLC). DOE

N95-23141# Stanford Linear Accelerator Center, CA.
MEASURING THE LEFT-RIGHT CROSS SECTION ASYMMETRY IN Z BOSON PRODUCTION BY E(+)E(-) COLLISIONS AT THE SLC
M. J. Fero Oct. 1994 4 p Presented at the ICEP '94, Glasgow, England, 20-27 Jul. 1994
(Contract DE-AC03-76SF-00515)
(DE95-003468; SU-SLAC-PUB-6679; CONF-9407142-3) Avail: CASI HC A01/MF A01

We present a precise measurement of the left-right cross section asymmetry (A(sub LR)) for Z boson production by e(+)e(-) collisions. The measurement was performed at a center-of-mass energy of 91.26 GeV with the SLD detector at the SLAC Linear Collider (SLC). The luminosity-weighted average polarization of the SLC electron beam was (63.0 +/- 1.1)%. Using a sample of 49,392 Z decays, we measure A(sub LR) to be 0.1628 +/- 0.0071(stat) +/- 0.0028(syst) which determines the effective weak mixing angle to be sin square theta(sub w)(sup eff) = 0.2292 +/- 0.0009(stat) +/- 0.0004(syst). DOE

N95-23156 Rutherford Appleton Lab., Chilton (England).
FLAVOUR DEPENDENCE OF FORM FACTORS IN HEAVY MESON DECAYS
F. E. Close and A. Wambach Apr. 1994 12 p Prepared in cooperation with Oxford Univ.
(PB95-139101; RAL-94-041) Avail: Issuing Activity (National Technical Information Service (NTIS))

Recently we have shown that due account of Wigner spin rotations is needed to match the ISGW model consistently onto HQET (Heavy Quark Effective Theory). We now discuss the flavor dependence of this procedure. We find that for finite mass 'heavy' quark the universal function xi(y = 1) nearly equal to 1 but the slope is proportional to the energy of the spectator quarks, and ratios of form factors are corrected in a way that QCD sum rules seem to require. Predictions for heavy quarks, such as in B(sub c) yields psi(eta(sub c)) and to mixed systems, such as D yields K and B yields pi show a systematic mass dependence that may be confronted with data. NTIS

N95-23157 Rutherford Appleton Lab., Chilton (England).
CLASSIFICATION OF (2,2) COMPACTIFICATIONS BY FREE FERMIONS 2
S. A. Abel and C. M. A. Scheich 3 May 1994 17 p See also PB93-211084 Prepared in cooperation with Universidad Autonoma de Madrid
(PB95-139119; RAL-94-043) Avail: Issuing Activity (National Technical Information Service (NTIS))

We present a classification of (2,2) free field compactifications with one twist in which only 95 distinct models (generations and antigenerations) are found. Models with three generations and no antigenerations are given. NTIS

N95-23158 Rutherford Appleton Lab., Chilton (England).
SINGLET QUARKS BEYOND THE TOP AT THE TEVATRON
V. Barger and R. J. N. Phillips May 1994 11 p Prepared in cooperation with Wisconsin Univ.
(Contract DE-AC04-76ER-00881)
(PB95-139127; RAL-94-045) Avail: Issuing Activity (National Technical Information Service (NTIS))

The first evidence for the top quark at the Tevatron may indicate a cross section higher than the QCD expectation. We consider the possibility that isosinglet heavy quarks may be contributing to the signal and discuss ways of testing this possibility. For example, a charge 2/3 singlet quark, approximately degenerate and mixing with the top quark, would effectively double the standard top signals. A charge -1/3 singlet quark mixing with the bottom quark would not affect top signals but would generate excess Z + multijet events with a b-tag. NTIS

N95-23159 Rutherford Appleton Lab., Chilton (England).
NEUTRON COMPTON SCATTERING
S. W. Lovesey May 1994 17 p See also PB95-130290
(PB95-139135; RAL-94-051) Avail: Issuing Activity (National Technical Information Service (NTIS))

The development of suitable instrumentation at spallation neutron sources has opened the way for easier and better use of neutron Compton scattering to measure the ground state momentum distribution of nuclei in condensed matter. In the past its main use has been in work on the He-4 aimed at measuring the condensate fraction. Recently, very good quality data has been obtained for several other systems, including H2, and compared successfully with model calculations. This article aims to serve as an introduction to the potential use of neutron Compton scattering in biology, chemistry and physics. NTIS

N95-23160 Rutherford Appleton Lab., Chilton (England).
HIGGS SEARCHES AND WW SCATTERING
R. J. N. Phillips May 1994 26 p Presented at the 3rd Workshop on High Energy Particle Physics, Madras, India, 10-22 Jan. 1994
(PB95-139143; RAL-94-048) Avail: Issuing Activity (National Technical Information Service (NTIS))

This lecture is about aspects of Electroweak Symmetry Breaking (EWSB). There are sections on Higgs searches in the Standard Model (SM), on WW, WZ and ZZ scattering as probes of EWSB, and on Higgs phenomenology in the Minimal Super-symmetric Standard Model (MSSM). NTIS

N95-23165# Stanford Linear Accelerator Center, CA.
ELECTROWEAK COUPLING MEASUREMENTS FROM POLARIZED BHABHA SCATTERING AT SLD
Kevin T. Pitts (Oregon Univ., Eugene, OR.) Sep. 1994 5 p Presented at the International Symposia on High Energy Spin Physics and Polarization Phenomena in Nuclear Physics, Bloomington, IN, 15-22 Sep. 1994
(Contracts DE-FG02-91ER-40676; DE-FG03-92ER-40701; DE-FG03-91ER-40618; DE-FG02-91ER-40672; DE-FG02-91ER-40617; DE-FG02-91ER-40661; DE-FG02-76SF-00098; DE-FG02-92ER-40715; DE-AC02-76ER-03069; DE-FG02-86ER-40224)
(DE95-003137; SU-SLAC-PUB-6699; CONF-9409103-5) Avail: CASI HC A01/MF A01

The cross section for Bhabah scattering (e(sup +)e(sup -)) (yields) e(sup +)e(sup -) with polarized electrons at the center of mass energy of the Z(sup 0) resonance has been measured with the SLD experiment at the SLAC Linear Collider (SLC) during the 1992-1993 runs. The first measurement of the left-right asymmetry in Bhabah scattering (A(sub LR, sup e+,e(sup -)) (theta)) is presented. From A(sub LR)(sup e+,e(sup -)) ((Theta)) the effective weak mixing angle is measured to be sin(exp 2)(theta)(sub W)(sup eff) = 0.2245 +/- 0.0049 +/- 0.0010. When combined with the measurement of A(sub LR), the effective electron couplings are measured to be v(sub e) = -0.0414 +/- 0.0020 and a(sub e) = -0.4977 +/- 0.0045. DOE

N95-23196# Fermi National Accelerator Lab., Batavia, IL.
TESTING QCD WITH JET PHYSICS AT CDF
E. Kovacs 28 Jul. 1994 6 p Presented at the Meeting of the Division of Particles and Fields of the American Physical Society, Albuquerque, NM, 2-6 Aug. 1994
(Contract DE-AC02-76CH-03000)
(DE94-018980; FNAL/C-94/215-E; CONF-940816-10) Avail: CASI HC A02/MF A01

We present a variety of jet cross section measurements in p(bar-p) collisions at square root of s = 1.8 TeV, using 19.5 pb(sup -1) of data collected by the Collider Detector at Fermilab during the 1992 - 93 rim of the Fermilab Tevatron. We discuss the impact of these measurements on the status of precision tests of QCD. DOE

N95-23197# Fermi National Accelerator Lab., Batavia, IL.
PROPERTIES OF JETS IN Z EVENTS FROM 1.8 TeV (BAR p)p COLLISIONS
S. A. Hauger (Duke Univ., Durham, NC.) Aug. 1994 6 p Presented at the Meeting of the Division of Particles and Fields of the American Physical Society, Albuquerque, NM, 2-6 Aug. 1994
(Contract DE-AC02-76CH-03000)
(DE94-018982; FNAL/C-94/235-E; CONF-940816-9) Avail: CASI HC A02/MF A01

We have studied the properties of Z boson events produced in 1.8 TeV p bar-p collisions using 19.3 pb(sup -1) of integrated luminosity collected by the Collider Detector at Fermilab (CDF) during the 1992 - 1993 Tevatron run. We compare the characteristics of the hadronic jets associated with the Z to leading-order QCD calculations using the VECBOS Monte Carlo program. For a subsample of events, we identify B jets and compare their rates to those expected from events with generic QCD jets. DOE

N95-23203# Fermi National Accelerator Lab., Batavia, IL.
SEARCH FOR Z' AND W' AT CDF
K. Maeshima Aug. 1994 6 p Presented at the Meeting of the Division of Particles and Fields of the American Physical Society, Albuquerque, NM, 2-6 Aug. 1994
(Contract DE-AC02-76CH-03000)
(DE94-018987; FNAL/C-94/227-E; CONF-940816-7) Avail: CASI HC A02/MF A01

We have searched for heavy neutral and charged gauge bosons via the decays Z' yields ee and W' e(nu) in bar-p p collisions at radical s = 1.8 TeV. The data were obtained using the CDF detector during 1992 - 1993 run corresponding to an integrated luminosity of 19.7 +/- 0.7 pb(sup -1). We present a 95% confidence level upper limit on the production cross section times branching ratio of Z' and W' as a function of Z' and W' mass. Assuming Standard Model coupling strengths, we exclude a Z' with mass less than 505 GeV/c(exp 2) and a W' with mass less than 652 GeV/c . We also present lower mass limits for Z' bosons from E(sub 6) models and the Alternative Left-Right Model. DOE

N95-23226# Stanford Linear Accelerator Center, CA.
A PRELIMINARY MEASUREMENT OF THE AVERAGE B HADRON LIFETIME
Steven L. Manly (Yale Univ., New Haven, CT.) Sep. 1994 10 p Presented at the ICHEP 1994, Glasgow, Scotland, 20-27 Jul. 1994
(Contracts DE-FG02-91ER-40676; DE-FG03-92ER-40701; DE-FG03-91ER-40618; DE-FG03-92ER-40689; DE-FG03-93ER-40788; DE-FG02-91ER-40672; DE-FG02-91ER-40677; DE-AC03-76SF-00098; DE-FG02-92ER-40715; DE-AC02-76ER-03069)
(DE95-003138; SU-SLAC-PUB-6668; CONF-9407142-2) Avail: CASI HC A02/MF A01

The average B hadron lifetime was measured using data collected with the SLD detector at the SLC in 1993. From a sample of (approximately)50,000 Z(sup 0) events, a sample enriched in Z(sup 0) (yields) b(bar b) was selected by applying an impact parameter tag. The lifetime was extracted from the decay length distribution of inclusive vertices reconstructed in three dimensions. A binned maximum likelihood method yielded an average B hadron lifetime of (tau)(sub B) = 1.577(+/-)0.032(stat.)(+/-)0.046(syst.) ps. DOE

N95-23242# Fermi National Accelerator Lab., Batavia, IL.
J/PSI, PSI' YIELDS MU(+)MU(-) AND B YIELDS J/PSI, PSI' CROSS SECTIONS
T. Daniels Aug. 1994 5 p Presented at the Meeting of the Division of Particles and Fields of the American Physical Society, Albuquerque, NM, 2-6 Aug. 1994
(Contract DE-AC02-76CH-03000)
(DE94-018996; FNAL/C-94/212-E; CONF-940816-13) Avail: CASI HC A01/MF A01

This paper presents a measurement of J/psi, psi' differential cross sections in p bar-p collisions at radical s = 1.8 TeV. The cross sections are measured above 4 GeV/c in the central region (absolute value of eta less than 0.6) using the dimuon decay channel. The fraction of events from B decays is measured, and used to calculate b quark cross sections and direct J/psi, psi' cross sections. The direct cross sections for the psi' are found to be more than an order of magnitude above theoretical expectations. DOE

N95-23267# Los Alamos National Lab., NM.
DISORDER-INDUCED BREAKDOWN OF SOLITON AND POLARON PARTICLES
A. R. Bishop, D. Cai, N. Gronbech-Jensen, and M. I. Salkola 1995 17 p Presented at the Fluctuation Phenomena: Disorder and Nonlinearity Conference, Madrid, 26-30 Sep. 1994
(Contract W-7405-eng-36)
(DE95-003694; LA-UR-94-3852; CONF-9409182-2) Avail: CASI HC A03/MF A01

Using examples of the perturbed (1+1) dimensional sine-Gordon, the continuous and discrete nonlinear Schroedinger systems, and a three-site quantum polaron problem, the authors briefly review some phenomena related to the fascinating interplays between nonlinearity, disorder, noise, nonadiabaticity, and lattice discreteness. The concept of competing length-scales and time-scales is emphasized as they pertain to the common concept of solitons and polarons behaving as 'particles.' DOE

N95-23336# Fermi National Accelerator Lab., Batavia, IL.
MEASUREMENT OF CORRELATED b QUARK CROSS SECTIONS AT CDF
D. Gerdes Sep. 1994 6 p Presented at the Meeting of the Division of Particles and Fields of the American Physical Society, Albuquerque, NM, 2-6 Aug. 1994
(Contract DE-AC02-76CH-03000)
(DE95-004240; FNAL/C-94/328-E; CONF-940816-67) Avail: CASI HC A02/MF A01

Using data collected during the 1992 - 93 colliderrun at Fermilab, CDF has made measurements of correlated b quark cross section where one b is detected from a muon from semileptonic decay and the second b is detected with secondary vertex techniques. We report on measurements of the cross section as a function of the momentum of the second b and as a function of the azimuthal separation of the two b quarks, for transverse momentum of the initial b quark greater than 15 GeV. Results are compared to QCD predictions. DOE

N95-23347# Fermi National Accelerator Lab., Batavia, IL.
RECENT RESULTS FROM FERMILAB E-687, CHARM PARTICLE DECAYS, LIFETIMES AND PHOTOPRODUCTION DYNAMICS: A COMPILATION RESULTS PRESENTED AT DPF 1994
Oct. 1994 27 p Presented at the Meeting of the Division of Particles and Fields of the American Physical Society, Albuquerque, NM, 2-6 Aug. 1994
(Contract DE-AC02-76CH-03000)
(DE95-004580; FNAL/C-94/365-E; CONF-940816-Pt-1) Avail: CASI HC A03/MF A01

This report contains papers on the following topics: Recent results on the semi-leptonic decay, D(sup 0) yields K(-) mu(+) nu(sub mu); charmed mesons; observation of the Decay Omega(sub c)(sup 0) Sigma(sup +)K(sup-) K(sup -) phi(+); the physics of charm lifetimes; and photoproduction of charmed hadrons. DOE

N95-23350# Westinghouse Hanford Co., Richland, WA.
TEST PROCEDURE FOR CATION EXCHANGE CHROMATOGRAPHY
T. D. Cooper 24 Aug. 1994 22 p
(Contract DE-AC06-87RL-10930)
(DE95-003770; WHC-SD-CP-TP-080) Avail: CASI HC A03/MF A01

The purpose of this test plan is to demonstrate the synthesis of inorganic antimonate ion exchangers and compare their performance against the standard organic cation exchangers. Of particular interest is the degradation rate of both inorganic and organic cation exchangers. This degradation rate will be tracked by determining the ion exchange capacity and thermal stability as a function of time, radiation dose, and chemical reaction. DOE

N95-23357# Rensselaer Polytechnic Inst., Troy, NY.
THEORETICAL ASPECTS OF ELECTROWEAK AND OTHER INTERACTIONS IN MEDIUM ENERGY NUCLEAR PHYSICS Interim Progress Report
N. C. Mukhopadhyay Dec. 1994 15 p

(Contract DE-FG02-88ER-40448)
(DE95-004341; DOE/ER-40448/T1) Avail: CASI HC A03/MF A01

Significant progress has been made in the current project year in the development of chiral soliton model and its applications to the electroweak structure of the nucleon and the Delta (1232) resonance. Further progress also has been made in the application of the perturbative QCD (pQCD) and the study of physics beyond the standard model. The postdoctoral associate and the graduate student working towards his Ph.D. degree have both made good progress. The review panel of the DOE has rated this program as a 'strong, high priority' one. A total of fifteen research communications -- eight journal papers and, conference reports and seven other communications -- have been made during the project year so far.
DOE

N95-23359# Fermi National Accelerator Lab., Batavia, IL.
ELECTRON DRIFT VELOCITIES OF Ar-CO2-CF4 GAS MIXTURES
R. Markeloff (University of Northern Illinois, De Kalb, IL.), H. Haggerty, and Y. Shao Nov. 1994 5 p Presented at the Nuclear Science Symposium: Medical Imaging Conference, Norfolk, VA, 30 Oct. - 5 Nov. 1994
(Contract DE-AC02-76CH-03000)
(DE95-004353; FNAL/C-94/399; CONF-941061-11) Avail: CASI HC A01/MF A01

The muon spectrometer for the D0 experiment at Fermi National Accelerator Laboratory uses proportional drift tubes filled with an Ar-CO2-CF4 gas mixture. Measurements of drift velocity as a function of electric field magnitude for 90%-5%-5% and 90%-4%-6% Ar-CO2-CF4 mixtures are presented, and our operational experiences with these gases at D0 is discussed.
DOE

N95-23363# Wisconsin Univ., Madison, WI.
GENERATION OF FAST ELECTRONS IN REVERSED FIELD PINCHES BY THE EQUILIBRIUM GRAD (VERT BAR)B(VERT BAR) FORCE
G. Fiksel Oct. 1994 8 p
(Contract DE-FG02-85ER-53198)
(DE95-004467; DOE/ER-53198/251) Avail: CASI HC A02/MF A01

It is shown that a decreasing magnetic field profile in reversed-field pinch plasmas leads to formation of an anisotropic electron distribution function at the plasma edge. The mechanism is the conservation of the magnetic moment and the energy of electrons that collisionlessly travel outward in a stochastic magnetic field. As a result, the electrons have high parallel energies and low perpendicular energies at the edge. The details of the distribution function correspond well to experimental results.
DOE

N95-23396# Brookhaven National Lab., Upton, NY.
INTRODUCTION TO THE PHYSICS OF HIGGS BOSONS
S. Dawson Nov. 1994 60 p Presented at the 1994 Theoretical Advanced Study Institute Conference, Boulder, CO, 30 May - 23 Jun. 1994
(Contract DE-AC02-76CH-00016)
(DE95-003965; BNL-61012; CONF-9405267-1) Avail: CASI HC A04/MF A01

A basic introduction to the physics of the Standard Model Higgs boson is given. We discuss Higgs boson production in e(+)e(-) and hadronic collisions and survey search techniques at future accelerators. The Higgs bosons of the minimal SUSY model are briefly considered. Indirect limits from triviality arguments, vacuum stability and precision measurements at LEP are also presented.
DOE

N95-23403# Los Alamos National Lab., NM.
SPIN PHYSICS IN THE NEXT DECADE
J. M. Moss 1994 10 p Presented at the International Symposia on High Energy Spin Physics and Polarization Phenomena in Nuclear Physics, Bloomington, IN, 15-22 Sep. 1994
(Contract W-7405-eng-36)
(DE95-003727; LA-UR-94-3728; CONF-9409103-8) Avail: CASI HC A02/MF A01

The author's personal opinion is that the fascinating field of nonperturbative QCD will be led by polarized beam experiments. He focuses on two developments which will surely produce a wealth of new physics within the next ten years. These are (1) polarized colliding beams and (2) polarized jet targets in conjunction with polarized beams in storage rings. In order to make the overview manageable, he covers only selected areas where the physics goals are the elucidation of nonperturbative aspects of QCD applied to nucleons and nuclei. He discusses several areas of polarized structure function physics which will be feasible in the next 5-10 years.
DOE

N95-23404# Fermi National Accelerator Lab., Batavia, IL.
SEARCH FOR NEW GAUGE BOSONS AT D(O)
Sep. 1994 6 p Presented at the Meeting of the Division of Particles and Fields of the American Physical Society, Albuquerque, NM, 2-6 Aug. 1994
(Contract DE-AC02-76CH-03000)
(DE95-003745; FNAL/C-94/289-E; CONF-940816-63) Avail: CASI HC A02/MF A01

The authors have searched for evidence of W' yields e nu and Z' yields e e in data collected with the D0 detector at the Tevatron during the 1992-1993 p(anti p) collider run at square root of s = 1.8 TeV. They exclude the existence of a W' of mass less than 600 GeV/c(exp 2) and a Z' of mass less than 480 GeV/c(exp 2) at the 95% confidence level, assuming standard model couplings to quarks and leptons.
DOE

N95-23406# Fermi National Accelerator Lab., Batavia, IL.
SEARCH FOR TOP QUARK AT CDF
Nov. 1994 12 p Presented at the Conference on High Energy Physics: Hadron Structure, Kosice, 19-23 Sep. 1994
(Contract DE-AC02-76CH-03000)
(DE95-003748; FNAL/C-94/374-E; CONF-9409134-1) Avail: CASI HC A03/MF A01

There is a vast theoretical and experimental support for idea that top quark as a weak isospin partner to b-quark should exist. Production cross section is steeply falling function of top quark mass. Therefore realistically at present only Tevatron p(anti p) collider at FNAL, with total energy 1.8 TeV in CMS system, still has a chance of top quark discovery. Dominant production mechanism for top quarks at Tevatron is pair production of t(anti t). With almost 100% probability t ((anti t)) decays in mode t yields W(+)b. Distinct features of this decay provide very good signatures of top quark production which helps to reduce otherwise very high level of background. Based on simple combinatorial arguments one can show that W should decay in 1/9 cases into W yields l + nu where l stands for lepton (e, mu, tau). Very clean signature represents case when both W's from t and (anti t) decay into e (mu) + nu. In this case experimental observation will be two isolated leptons characterized by large transverse momentum, large missing transverse energy E(sub T) and 2 b quark jets. Jets originated from b quarks can be quite frequently recognized by presence of secondary vertices associated with jets. Another feature of b-jets which can be used for their identification is frequent association of so called soft leptons with jets. Two experimental setups CDF and D0 are able to take advantage of Tevatron for top quark discovery. Recently CDF collaboration presented evidence for direct observation of t(anti t) production in 19.3 pb(sup -1) of p(anti p) collisions at square root of s = 1.8 TeV. A very brief account of these results is presented here.
DOE

N95-23407# Fermi National Accelerator Lab., Batavia, IL.
TEST PROCEDURE FOR ANION EXCHANGE CHROMATOGRAPHY
T. D. Cooper 1 Sep. 1994 33 p
(Contract DE-AC06-87RL-10930)
(DE95-003767; WHC-SD-CP-TP-079) Avail: CASI HC A03/MF A01

Plutonium from stored nitrate solutions will be sorbed onto anion exchange resins and converted to storable plutonium dioxide. Useful information will be simultaneously gained on the thermal stability and ion exchange capacity of four commercially available anion exchange resins over several years and under severe degradative conditions. This information will prove useful in predicting the safe and efficient lifetimes of these resins.
DOE

N95-23408*# Eloret Corp., Palo Alto, CA.
A MULTI-REGION RADIAL INTEGRATION SCHEME Preliminary Report
Leslie A. Barnes [1993] 12 p
(Contract NCC2-741)
(NASA-CR-197982; NAS 1.26:197982) Avail: CASI HC A03/MF A01

A multi-region radial integration is compared to the recently proposed method due to Handy, et al. Preliminary results for small systems indicate

that the new integration scheme is generally comparable to and sometimes better than that of Handy, et al., although this conclusion is by no means firm. Work for larger systems is continuing. Author

N95-23456# International Centre for Theoretical Physics, Trieste (Italy).
SPINNING PARTICLES IN THE EUCLIDEAN TAUB-NUT SPACE
D. Baleanu Apr. 1994 14 p
(DE94-634320; IC-94/83) Avail: CASI HC A03/MF A01 (US Sales Only)

The geodesic motion of pseudo-classical spinning particles in the Euclidean Taub-NUT space is analyzed. The equations of motion when Q = 0 is analyzed in the case of motion on a cone and on a plane. The general solutions corresponding to the trajectories lying on a cone are given. DOE

N95-23458# International Atomic Energy Agency, Vienna (Austria).
BROND-2.1. RUSSIAN EVALUATED NEUTRON REACTION DATA LIBRARY
V. N. Manokhin Oct. 1993 40 p
(DE94-634417; IAEA-NDS-90(Rev-7)) Avail: CASI HC A03/MF A01 (US Sales Only)

BROND-2, the computerized data library for evaluated neutron reaction data of the Russian Federation was released in 1992 and updated as BROND-2.1. Its content is summarized in this document. Upon request it is available on magnetic tape, cost free, from the IAEA Nuclear Data Section. It is also available within the IAEA online system NDIS. DOE

N95-23459*# Eloret Corp., Palo Alto, CA.
SYMMETRY BREAKING IN O4(+): AN APPLICATION OF THE BRUECKNER COUPLED-CLUSTER METHOD
Leslie A. Barnes and Roland Lindh (Lund Univ., Sweden.) [1994] 16 p Sponsored in part by Swedish Natural Research Council and IBM Sweden
(Contract NCC2-741)
(NASA-CR-197981; NAS 1.26:197981) Avail: CASI HC A03/MF A01

A recent calculation of the antisymmetric stretch frequency for the rectangular structure of quartet O4(+) using the singles and doubles quadratic configuration interaction method with a perturbational estimate of connected triple excitations (QCISD(T)) method gave a value of 3710 cm(exp -1). This anomalous frequency is shown to be a consequence of symmetry breaking effects, which occur even though the QCISD(T) solution derived from a delocalized SCF reference function lies energetically well below the two localized (symmetry-broken) solutions at the equilibrium geometry. The symmetry breaking is almost eliminated at the CCSD level of theory, but the small remaining symmetry breaking effects are magnified at the CCSD(T) level of theory so that the antisymmetric stretch frequency is still significantly in error. The use of the Brueckner coupled cluster method, however, leads to a symmetrical solution which is free of symmetry breaking effects, with an antisymmetric stretch frequency of 1322 cm(exp -1), in good agreement with our earlier calculations using the complete active space self consistent field/complete active space state interaction (CASSCF/CASSI) method. Author

N95-23475# Tokyo Univ. (Japan).
SEARCH FOR SCALAR AND VECTOR LEPTOQUARKS IN ELECTRON-PROTON COLLISIONS AT RADICAL S = 300 GeV
Masashi Hazumi Dec. 1993 175 p
(DE94-785267; INS-J-177) Avail: CASI HC A08/MF A02

A search for a resonant state coupled to an electron-quark pair has been performed using collisions of the electron beam of 26.7 GeV and the proton beam of 820 GeV. With the integrated luminosity of 26.6 +/- 1.6 nb(exp -1), scalar and vector leptoquarks have been searched for in the neutral current and charged current samples. The selected events agreed well with the prediction of the Standard Model, and no evidence has been found for production of leptoquarks decaying into e(-) + jet or nu + jet. Limits on the coupling strength of scalar (vector) leptoquarks to electron and quark have been determined for masses from 50 (40) GeV to 225 GeV. A limit on the leptoquark mass has been also obtained at the 95% confidence level assuming that either left-handed or right-handed coupling exists to the electron-quark pair with electroweak strength. The mass limit depends on the cross section determined by the choice of quantum numbers. Leptoquarks are ruled out for masses below 216 GeV with the largest cross section and below 105 GeV with the smallest cross section. DOE

N95-23488# California Univ., Berkeley. Lawrence Berkeley Lab, CA.
STUDY OF b(ANTI b) PRODUCTION IN e(+)e(-) ANNIHILATION AT RADICAL s = 29 GeV WITH THE AID OF NEURAL NETWORKS Ph.D. Thesis
D. J. Lambert Nov. 1994 157 p
(Contract DE-AC03-76SF-00098)
(DE95-004691; LBL-36353) Avail: CASI HC A08/MF A02

The author presents a measurement of sigma(b anti-b)/sigma(q anti-q) in the annihilation process e(+)e(-) yields q anti-q yields hadrons at radical s = 29 GeV. The analysis is based on 66 pb(sup -1) of data collected between 1984 and 1986 with the TPC/2 gamma detector at PEP. To identify bottom events, he uses a neural network with inputs that are computed from the 3-momenta of all of the observed charged hadrons in each event. He also presents a study of bias in techniques for measuring inclusive pi(+/-), K(+/-), and p/anti-p production in the annihilation process e(+)e(-) yields b anti-b yields hadrons at radical s = 29 GeV, using a neural network to identify bottom-quark jets. In this study, charged particles are identified by a simultaneous measurement of momentum and ionization energy loss (dE/dx). DOE

N95-23491# Argonne National Lab., IL.
TIME-RESOLVED EPR STUDIES OF THE H ATOM: A STABLE HEAVY ISOTOPE OF MUONIUM
D. M. Bartels Oct. 1994 17 p Presented at the Royal Society/CIBA Foundation Meeting on Trends in Muonium Chemistry, London, 10 Jun. 1994
(Contract W-31-109-eng-38)
(DE95-004614; ANL/CHM/CP-84392; CONF-9406294-1) Avail: CASI HC A03/MF A01

Muonium physicists and chemists, when they talk about 'primary processes,' are probably concerned mostly about end-of-track phenomena in the slowing down of a many-MeV charged particle, analogous to the proton. The author's experience is with electron accelerators and radiolysis; hence, he will comment briefly on the differences and relative advantages of electron and proton radiolysis for the study of H atoms, as opposed to muonium. Then, he will take the liberty of defining primary processes to include the recombination reactions that may occur between geminate or quasi-geminate free radicals within radiolysis spurs. DOE

N95-23522# Fermi National Accelerator Lab., Batavia, IL.
MEASUREMENT OF W AND Z BOSON PRODUCTION AND EXTRACTION OF THE W WIDTH AND BRANCHING RATIOS AT CDF
W. F. Badgett (Michigan Univ., Ann Arbor, MI.) Aug. 1994 6 p Presented at the Meeting of the Division of Particles and Fields of the American Physical Society, Albuquerque, NM, 2-6 Aug. 1994
(Contract DE-AC02-76CH-03000)
(DE94-018989; FNAL/C-94/258-E; CONF-940816-12) Avail: CASI HC A02/MF A01

We present results from W and Z boson production in proton-antiproton collisions at radical s = 1.8 TeV using the CDF detector. We measure the W and Z cross sections times lepton branching ratio, sigma(p bar-p yields W). (W yields l nu(sub l)) and sigma(p bar-p yields Z). B(Z yields k(+)l(-)) l = e, mu. We also measure the ratio: R(sub l) = sigma.B(W yields l nu(sub l))/sigma. B(Z yields ll). From R(sub l), we extract the W electron and muon branching ratios, BR(W yields l nu(sub l), and the total W width, Gamma(sub W). In addition, high transverse mass W yields e nu(sub e), candidates provide an alternate, direct measurement of Gamma(sub W). DOE

N95-23530# Fermi National Accelerator Lab., Batavia, IL.
ELECTROWEAK PHYSICS FROM THE TEVATRON
L. Nodulman (Argonne National Lab., IL.) Sep. 1994 18 p Presented at the Tennessee International Symposium on Radiative Corrections, Gatlinburg, TN, 27 Jun. - 1 Jul. 1994
(Contracts DE-AC02-76CH-03000; W-31-109-eng-38)
(DE95-002213; FNAL/C-94/317-E; ANL-HEP-CP-94-51; CONF-9406273-1) Avail: CASI HC A03/MF A01

Results from the CDF and D0 detectors at the Fermilab Tevatron collider on electroweak physics are summarized. Topics include the top quark mass, the W boson width, trilinear couplings, and the W boson mass. Electroweak radiative corrections so far provide a consistent picture,

and precision measurement constraints will continue to improve. The study of the top quark as well as diboson production is just getting started, and the W mass measurement will continue to improve. DOE

N95-23576# Sandia National Labs., Albuquerque, NM.
MASS TRANSPORT THROUGH POLYCRYSTALLINE MICROSTRUCTURES
T. P. Swiler, E. A. Holm, M. F. Young, and S. A. Wright 1994 6 p Presented at the 1994 Fall Meeting of the Materials Research Society (MRS), Boston, MA, 28 Nov. - 2 Dec. 1994
(Contract DE-AC04-94AL-85000)
(DE95-004552; SAND-94-3047C; CONF-941144-22) Avail: CASI HC A02/MF A01

Mass transport properties are important in polycrystalline materials used as protective films. Traditionally, such properties have been studied by examining model polycrystalline structures, such as a regular array of straight grain boundaries. However, these models do not account for a number of features of real grain ensembles, including the grain size distribution and variations in grain shape. In this study, a finite difference scheme is developed to study transient and steady-state mass transport through realistic two dimensional polycrystalline microstructures. Comparisons with the transport properties of traditional model microstructures provide regimes of applicability of such models. The effects of microstructural parameters such as average grain size are examined. DOE

N95-23581# Fermi National Accelerator Lab., Batavia, IL.
SEARCH FOR SUPERSYMMETRIC (TILDE W)(SUB 1) AND (TILDE Z)(SUB 2) STATES USING THE D0 DETECTOR
S. K. Blessing (Florida State Univ., Tallahassee, FL.) Sep. 1994 6 p Presented at the Meeting of the Division of Particles and Fields of the American Physical Society, Albuquerque, NM, 2-6 Aug. 1994
(Contract DE-AC02-76CH-03000)
(DE95-004581; FNAL/C-94/293-E; CONF-940816-68) Avail: CASI HC A02/MF A01

The search for signals from Supersymmetry at hadron colliders has largely been centered on the search for squark and gluino production, usually through events with large missing transverse energy (E(sub t)). A promising alternative at the Tevatron is the search for production of the lightest chargino ((tilde W)(sub 1)) and next-to-lightest neutralino ((tilde Z)(sub 2)), with the assumptions that R-parity is conserved and the lightest neutralino ((tilde Z)(sub 1)) is the lightest supersymmetric particle (LSP). Although the mass limit established by LEP experiments, (sup 2)M(sub (tilde W)1) greater than 45GeV/c(sup 2), excludes the on-shell process (anti p)p (yields) W(sup (+-)) (yields) (tilde W)(sub 1) + (tilde Z)(sub 2), the off-shell process W(sup (+-)) (yields) (tilde W)(sub 1)(tilde Z)(sub 2) can have a sizeable rate due to large WW(tilde W)(sub 1)(tilde Z)(sub 2) coupling. Here, the status of a search for the pair production of the lightest chargino and second lightest neutralino states of the minimal supersymmetric model is presented. The authors searched for four tri-lepton final states: eee, ee(mu), e(mu)(mu), and (mu)(mu)(mu), all with missing transverse energy. DOE

N95-23587# Argonne National Lab., IL.
ELECTROMAGNETIC PRODUCTION OF PIONS ON THE NUCLEON
T. S. H. Lee 1994 11 p Presented at the International Conference on Physics With GeV Particle Beams, Juelich, Germany, 22-25 Aug. 1994
(Contract W-31-109-eng-38)
(DE95-004658; ANL/PHY/CP-84618; CONF-940858-1) Avail: CASI HC A03/MF A01

The objective of this talk is to review the recent theoretical developments in the study of photo- and electro-production of pions on the nucleon. First, the author will discuss the results from the investigations in the near threshold region. The focus here is the test of pion dynamics as predicted by the theoretical models with chiral symmetry. The second subject of this talk is concerned with the deformation of the Delta (Delta) state. The central question here is how this interesting quantity is defined theoretically and related to the experiments being performed at MIT-Bates and Mainz. The author then will discuss briefly the higher energy region where the productions of higher mass nucleon resonances (N*) and two-pion states become important. The interest here is the test of (gamma)N (yields) N* matrix elements as predicted by various QCD-based models of hadrons. DOE

N95-23604# Tokyo Univ., Sagamihara (Japan).
RATE COEFFICIENTS FOR THE ELECTRON-IMPACT EXCITATION, IONIZATION AND RECOMBINATION OF He-LIKE IONS, S XV, Ca XIX AND Fe XXV, AND RELATED PROCESSES
Y. Itikawa, T. Kato (National Inst. for Fusion Science, Nagoya, Japan.), and K. Sakimoto Jan. 1995 20 p
(ISSN 0285-6808)
(ISAS-R-657) Avail: CASI HC A03/MF A01

Data on the rate coefficients for the electron-impact excitation, ionization and recombination of S XV, Ca XIX and Fe XXV ions are reviewed to recommend a comprehensive set of values. Some related processes involved in the emission from the 1s2/states of those He-like ions and its satellite lines are also considered. All the rate coefficients recommended here are expressed in an analytic form of the electron temperature. Author

N95-23769# Joint Inst. for Nuclear Research, Dubna (USSR).
NEW DETERMINATION OF V(SUB us) FROM K(SUB e3)(+) DECAY
G. V. Velev 1993 3 p
(DE94-628616; JINR-E-1-93-305) Avail: CASI HC A01/MF A01 (US Sales Only)

Using the most accurate result for the slope lambda(sub +) in the linear expansion of f(sub +)(q(sup 2)) and the value of K(sub e3)(sup +) branching ratio from Review of Particle Properties 1992 a new value of the Cabibbo-Kobayashi-Maskawa mixing matrix element V(sub us) is obtained. DOE

N95-23770# International Centre for Theoretical Physics, Trieste (Italy).
CHARM-CONSERVING STRANGENESS-CHANGING TWO BODY HADRONIC DECAYS OF CHARMED BARYONS
M. P. Khanna Oct. 1993 7 p
(DE94-628621; IC-93/350) Avail: CASI HC A02/MF A01 (US Sales Only)

The charm-conserving strangeness-changing two body hadronic decays of charmed baryons are examined in the SU(4) symmetry scheme. In addition to the 20-Hamiltonian, we consider a 15-piece of the weak Hamiltonian which may arise due to SU(4) breaking or due to some non-conventional dynamics. The numerical estimates for decay widths of some of the modes are presented. DOE

N95-23773# International Atomic Energy Agency, Vienna (Austria).
ESTAR, PSTAR, ASTAR: A PC PACKAGE FOR CALCULATING STOPPING POWERS AND RANGES OF ELECTRONS, PROTONS AND HELIUM IONS, VERSION 2
M. J. Berger (National Inst. of Standards and Technology, Gaithersburg, MD.) Dec. 1993 19 p
(DE94-634435; IAEA-NDS-144) Avail: CASI HC A03/MF A01 (US Sales Only)

A PC package is documented for calculating stopping powers and ranges of electrons, protons and helium ions in matter for energies from 1 keV up to 10 GeV. Stopping powers and ranges for electrons can be calculated for any element, compound or mixture. Stopping powers and ranges of protons and helium ions can be calculated for 74 materials (26 elements and 48 compounds and mixtures). The files are stored on two HD diskettes in compressed form. Both executable files for IBM PC and Fortran-77 source files are provided. All three programs require 5.2 Mb of disk space. This set of two diskettes with detailed documentation is available upon request, free of cost, from the IAEA Nuclear Data Section. DOE

N95-23775# Tokyo Univ. (Japan).
LARGE-SIZED AND HIGHLY RADIOACTIVE H-3 AND Cd-109 LANGMUIR-BLODGETT FILMS
S. Shibata, H. Kawakami, and S. Kato Feb. 1994 25 p
(DE94-785270; INS-1024) Avail: CASI HC A03/MF A01

A device for the deposition of a radioactive Langmuir-Blodgett (LB) film was developed with the use of: (1) a modified horizontal lifting method; (2) an extremely shallow trough; and (3) a surface pressure-generating system without piston oil. It made a precious radioactive subphase solution repeatedly usable while keeping its radioactivity concentration as high as possible. Any large-size thin film can be prepared by just changing the trough size. Two monomolecular-layers of Y-type films of cadmium (H-3) icosanoate and (Cd-109) icosanoate were built up as H-3 and Cd-109 (beta)-sources for electron spectroscopy with intensities of 1.5 GBq (40

mCi) and 7.4 MBq (200 micro Ci), respectively, and a size of 65x200 sq mm. Excellent uniformity of the distribution of deposited radioactivity was confirmed by autoradiography and photometry. DOE

N95-23784# International Centre for Theoretical Physics, Trieste (Italy).
NEUTRINO MASSES AND MIXING
A. Yu. Smirnov Oct. 1993 21 p
(DE94-628632; IC-93/359; HEP-PH-9310368) Avail: CASI HC A03/MF A01 (US Sales Only)

Restrictions on the neutrino masses and lepton mixing are reviewed. Solar, atmospheric and relic neutrinos give the indications of existence of nonzero neutrino masses and mixing. The data pick up two regions of mixing angles which are either appreciably larger or appreciably smaller than the Cabibbo angle. Some theoretical schemes with large or small lepton mixing are discussed. DOE

N95-23785# International Centre for Theoretical Physics, Trieste (Italy).
NEUTRINOLESS DOUBLE BETA DECAY AND THE SOLAR NEUTRINO PROBLEM
S. T. Petcov (International School for Advanced Studies, Trieste, Italy.) and A. Yu. Smirnov Oct. 1993 20 p
(DE94-628633; IC-93/360; SISSA-113/93/EP; HEP-PH-9311204) Avail: CASI HC A03/MF A01 (US Sales Only)

The MSW or vacuum oscillation solution of the solar neutrino problem can be reconciled with possible existence of the (beta beta)(sub 0 nu) decay with a half-line corresponding to an effective Majorana mass of the electron neutrino m(sub ee) approx. (0.1 - 1.0) eV. The phenomenological consequences of such a possibility are analyzed and the implications for the mechanisms of neutrino mass generation are considered. DOE

N95-23786# International Centre for Theoretical Physics, Trieste (Italy).
NEUTRINO MASS
G. Senjanovic Mar. 1994 7 p
(DE94-628634; IC-94/33) Avail: CASI HC A02/MF A01 (US Sales Only)

We review the issue of neutrino mass by concentrating on the minimal extensions of the standard model. In particular, we emphasize the role that gravitation may play in this regard and discuss the central aspects of the see-saw mechanism of generating neutrino mass, including the possibility of the see-saw scale being close to the electroweak scale. DOE

N95-23973# Joint Inst. for Nuclear Research, Dubna (USSR).
ENHANCED OSCILLATION OF NEUTRINOS OF DIFFERENT MASSES IN MATTER
Kh. M. Beshtoev 1994 6 p
(DE94-635648; JINR-E-2-94-46) Avail: CASI HC A02/MF A01 (US Sales Only)

The oscillation probability is estimated for neutrinos of different masses in their transition through matter of different thickness, including the Sun. DOE

N95-23974# Joint Inst. for Nuclear Research, Dubna (USSR).
INCLUSIVE RAPIDITY CORRELATIONS OF (PI)(-) MESONS IN pp-INTERACTIONS
A. I. Golokhvastov 1994 24 p
(DE94-635654; JINR-E-2-94-27) Avail: CASI HC A03/MF A01 (US Sales Only)

The simple single-parameter approximation of one-particle semi-inclusive rapidity distributions of negative particles (pi(sup -) mesons) in pp interactions at various multiplicities over the investigated range of primary momenta 6.6-400 GeV/c is presented. Assuming the lack of any kind of correlations in semi-inclusive events, a good description of experimental data on two-particle inclusive rapidity correlations (pseudo correlations), which are due to wrong normalization of the probability density functions and the multiplicity dependence of kinematic spectra, is obtained. Data on forward-backward, right-left correlations and multiplicity distributions in rapidity intervals and intervals separated by empty gaps do not contradict independent (pi)(sup -) production either. DOE

N95-23975# Joint Inst. for Nuclear Research, Dubna (USSR).
GLUON DISTRIBUTION AS FUNCTION OF F(SUB 2) AND dF(SUB 2)/dlnQ(EXP 2) AT SMALL x
A. V. Kotikov 1994 4 p
(DE94-635677; JINR-E-2-94-92) Avail: CASI HC A01/MF A01 (US Sales Only)

The paper presents a formula to extract the gluon distribution from deep inelastic structure function F(sub 2) and its derivative dF(sub 2)/dlnQ(exp 2) at small x in the leading order of perturbation theory. The detailed analysis is given for new data of H1 group from HERA. The values of gluon distribution are found at 10(exp -3) less than or equal to x less than or equal to 2 (center dot) 10(exp -2) and Q(exp 2) = 20 GeV(exp 2). DOE

N95-23976# Joint Inst. for Nuclear Research, Dubna (USSR).
LASER LIGHT INDUCED DRIFT FOR ATOMS OF RADIOACTIVE ISOTOPES Na-22 AND Na-24
Yu. P. Gangrskij, S. G. Zemlyanoj, P. Zuzaan, B. N. Markov, G. V. Myshinskij, I. Stekl, C. Hradecny, I. M. Ermolaev, J. Slovak, and T. Tethal 1994 10 p
(DE94-635759; JINR-R-15-94-47) Avail: CASI HC A02/MF A01 (US Sales Only)

The laser light induced drift for atoms of radioactive isotopes Na-22 and Na-24 in the buffer gas Kr was studied. D2-line resonance frequency for drift of Na22 and Na-24 in the opposite directions was determined. The distribution of concentration for both isotopes along the drift tube was measured at the temperatures 300 and 1000 K. The detection of (gamma)-radiation of radioactive isotopes was used for these measurements. The isotope separation factor up to 20 at the efficiency 50% and drift velocity 1.1 m/s was reached. DOE

N95-23978# Virginia Univ., Charlottesville, VA. Dept. of Physics.
STUDIES OF AUTOIONIZING STATES RELEVANT TO DIELECTRONIC RECOMBINATION Progress Report, 1 Jul. 1991 - 30 Jun. 1994
T. F. Gallagher Dec. 1993 23 p
(Contract DE-FG05-85ER-13394)
(DE94-014162; DOE/ER-13394/T3) Avail: CASI HC A03/MF A01

The goal of this research program is to study the properties of autoionizing states in order to understand in detail dielectronic recombination of ions and electrons. During the period of the present grant, July 1, 1991--June 30, 1994, we put substantial effort into the study of autoionizing states in Mg. The first topic we investigated is the angular distribution of electrons ejected from the autoionizing Mg 3-pns and 3-pnd states. Both of these measurement sets provide more stringent tests of the K matrix calculations than do those of total cross sections. The second topic is the effect of static and microwave electric fields on autoionizing states. Previous measurements in Ba states have shown the profound influence of electric fields on autoionization rates and we have made new extensive measurements in both Ba and Mg states. Electric fields are of real importance for dielectronic recombination, since they are present as macroscopic fields in beam experiments and as microfields in plasmas. In final, we began time resolved measurements. We have set up a picosecond laser system, and we have just finished the first experiment with it. Specifically we have used picosecond excitation from a bound Mg 3pnd Rydberg wave packet to the autoionizing 3pnd states to show explicitly the correlation between the spatial location of the Rydberg electron and the frequency of the exciting light. DOE

N95-23984# Joint Inst. for Nuclear Research, Dubna (USSR).
HARD e(+)e(-)-PAIR BREMSSTRAHLUNG AS A LEPTON POLARIMETER
A. V. Belitskij and A. V. Efremov 1994 6 p
(DE94-635615; JINR-E-2-94-71) Avail: CASI HC A02/MF A01 (US Sales Only)

We suggest applying a handedness concept to measure the polarization of final lepton in the reaction AB (approaches) l(sup -)l(sup +)X which is capable of probing the size of polarized gluon distribution in the nucleon. DOE

N95-23985# International Centre for Theoretical Physics, Trieste (Italy).
QUANTUM FLUCTUATIONS OF D(SUB 5d) POLARONS ON C(SUB 60) MOLECULES
Chuilin Wang, Wenzheng Wang, Yuliang Liu, Zaobin Su, and Lu Yu Jun. 1994 12 p

(DE94-635787; IC-94/126) Avail: CASI HC A03/MF A01 (US Sales Only)

The dynamic Jahn-Teller splitting of the six equivalent D(sub 5d) polarons due to quantum fluctuations is studied in the framework of the Bogoliubov-de Gennes formalism. The tunneling induced level splittings are determined to be (sup 2)T(sub 1u) + (sup 2)T(sub 2u) and (sup 1)A(sub g) + (sup 1)H(sub g) for C(sup 1-, sub 60) and C(sup -2, sub 60), respectively, which should give rise to observable effects in experiments. DOE

N95-24000# Fermi National Accelerator Lab., Batavia, IL.
W MASS MEASUREMENTS FROM D(CIRCLE SLASH) AND CDF EXPERIMENTS AT TEVATRON

Chang Kee Jung (State Univ. of New York, Stony Brook, NY.) Oct. 1994 4 p Presented at the 27th International Conference on High Energy Physics, Glasgow, England, 21-27 Jul. 1994

(Contract DE-AC02-76CH-03000)

(DE95-003497; FNAL/C-93/334-E; CONF-940722-34) Avail: CASI HC A01/MF A01

The authors present preliminary measurements of the W boson mass made by the D0 and CDF experiments using data collected at the Fermilab TeVatron (bar p)p collider operating at (radical)s = 1.8 TeV. The result from the CDF W (yields) e(nu) data analysis is M(sub W) = 80.47 +/- 0.15(stat) +/- 0.25(sys) GeV/c(exp 2) and the result from the CDF W (yields) (mu)(nu) data analysis is M(sub W) = 80.29 +/- 0.20(stat) +/- 0.24(sys) GeV/c(exp 2). The result from the D0 W (yields) e(nu) data analysis is M(sub W) = 79.86 +/- 0.16(stat) +/- 0.31(sys) GeV/c(exp 2). When combined with the previous measurements, these results yield a world average value of M(sub W), 80.23 +/- 0.18 GeV/c(exp 2). DOE

N95-24016# Fermi National Accelerator Lab., Batavia, IL.
A MEASUREMENT OF THE MASS OF THE W VECTOR BOSON AT CDF

R. M. Keup Sep. 1994 7 p Presented at the Meeting of the Division of Particles and Fields of the American Physical Society, Albuquerque, NM, 2-6 Aug. 1994

(Contract DE-AC02-76CH-03000)

(DE95-003498; FNAL/C-94/282-E; CONF-940816-58) Avail: CASI HC A02/MF A01

We present a preliminary measurement of the mass of the W vector boson using the decays W yields ev and W yields mu v. The mass of the W is an important parameter of the standard model. Through its relation to both the top quark and the higgs sector, it provides a sensitive probe of the electroweak theory. During the last run of Fermilab's Tevatron, CDF recorded p-bar p collisions at radical s = 1.8 TeV corresponding to an integrated luminosity of 19.3 pb(exp -1). An analysis of both decay channels yields a combined mass measurement of Mw = 80.38 +/- 0.23 GeV/c. DOE

N95-24046# Lawrence Livermore National Lab., Livermore, CA.
PAULI-BLOCKING EFFECTS IN NEUTRON-ALPHA REACTIONS

M. Avrigeanu (Institute of Physics and Nuclear Engineering, Bucharest, Romania.), V. Avrigeanu (Institute of Physics and Nuclear Engineering, Bucharest, Romania.), A. N. Antonov (Bulgarian Academy of Sciences, Sofia, Bulgaria.), M. B. Chadwick, P. E. Hodgson (Oxford Univ., Oxford, England.), and M. V. Stoitsov (Bulgarian Academy of Sciences, Sofia, Bulgaria.) 1 Jun. 1994 5 p Presented at the International Conference on Nuclear Data for Science and Technology, Gatlinburg, TN, 9-13 May 1994

(Contract W-7405-eng-48)

(DE94-016358; UCRL-JC-117463; CONF-940507-36) Avail: CASI HC A01/MF A01

We present a knockout model for direct (n, alpha) reactions in which the residual nucleus is left in a continuum excited state. The interaction of the neutron with a preformed alpha particle inside the nucleus is related to the free neutron-alpha scattering cross-section, with modifications to account for nuclear medium effects, including Fermi motion, Pauli-blocking, and barrier penetration. Phase space restrictions for the four nucleons of the alpha-particle after the knockout are imposed by a Pauli-blocking function. We apply this model, along with evaporation contributions, to analyze excitation functions of (n, alpha) reactions on Ti-48, V-51, Cr-52, Fe-54, Mn-55, and Co-59. Good agreement is obtained between our calculations and experimental measurements. Values for the local Fermi energy in the region from where knockout occurs indicate a surface reaction. DOE

N95-24151# Argonne National Lab., IL.
ATOMS AS MANY-BODY SYSTEMS

M. Ya. Amusia 1995 34 p Presented at the Harmony of Physics Conference, Philadelphia, PA, 8-9 May 1994

(Contract W-31-109-eng-38)

(DE95-004609; ANL/PHY/CP-84545; CONF-9405247-2) Avail: CASI HC A03/MF A01

The author presents this article in the volume, dedicated to the 70th birthday of Academician S. T. Belyaev. He has known him personally since 1961 and admires his profound contributions to the theory of Bose-liquids, to the theory of superconductivity of atomic nuclei and some other important scientific works. Belyaev is well known also as an organizer of science and education. For years he was, and is still the Chairman of the Synchrotron Radiation Commission of the Russian Academy of Science, a body which was established long ago to promote construction of high intensity light sources, and technological as well as scientific research using this light. One of the important directions of this study is investigation of photoabsorbtion by multielectron atoms in order to obtain information about their structure. DOE

N95-24166# Argonne National Lab., IL.
SCALE-INVARIANT LIPATOV KERNELS FROM t-CHANNEL UNITARITY

C. Coriano and A. R. White 10 Nov. 1994 5 p Presented at the 24th International Symposium on Multiparticle Dynamics, Vietri sul Mare, Italy, 12-19 Sep. 1994

(Contract W-31-109-eng-38)

(DE95-004625; ANL-HEP-PR-94-79; CONF-9409257-2) Avail: CASI HC A01/MF A01

The Lipatov equation can be regarded as a reggeon Bethe-Salpeter equation in which higher-order reggeon interactions give higher-order kernels. Infra-red singular contributions in a general kernel are produced by t-channel nonsense states and the allowed kinematic forms are determined by unitarity. Ward identity and infra-red finiteness gauge invariance constraints then determine the corresponding scale-invariant part of a general higher-order kernel. DOE

N95-24174# Argonne National Lab., IL.
ATOMIC PHYSICS AT HIGH BRILLIANCE SYNCHROTRON SOURCES: PROCEEDINGS

G. Berry, P. Cowan, and D. Gemmell Aug. 1994 330 p Presented at the Workshop on Atomic Physics At High Brilliance Synchrotron Sources, Argonne, IL, 23-24 Apr. 1994

(Contract W-31-109-eng-38)

(DE95-006077; ANL/APS/TM-14; CONF-9404198) Avail: CASI HC A15/MF A03

This report contains papers on the following topics: present status of Spring-8 and the atomic physics undulator beamline; recent photoabsorption measurements in the rare gases and alkalis in the 3 to 15 keV proton energy region; atomic and molecular physics at LURE; experiments on atoms, ions and small molecules using the new generation of synchrotron radiation sources; soft x-ray fluorescence spectroscopy using tunable synchrotron radiation; soft x-ray fluorescence spectroscopy excited by synchrotron radiation: Inelastic and resonant scattering near threshold; outer-shell photoionization of ions; overview of the APS BESSRC beamline development; the advanced light source: Research opportunities in atomic and molecular physics; Photoionization of the Ba(+) ion by 4d shell excitation; decay dynamics of inner-shell excited atoms and molecules; absorption of atomic Ca, Cr, Mn and Cu; High-resolution photoelectron studies of resonant molecular photoionization; radiative and radiationless resonant Raman scattering by synchrotron radiation; Auger spectrometry of atoms and molecules; some thoughts of future experiments with the new generation of storage rings; Electron spectroscopy studies of argon K-shell excitation and vacancy cascades; ionization of atoms by high energy photons; ion coincidence spectroscopy on rare gas atoms and small molecules after photoexcitation at energies of several keV; an EBIS for use with synchrotron radiation photoionization of multiply charged ions and PHOBIS; gamma-2e coincidence measurements - the wave of the future in inner-shell electron spectroscopy; recoil momentum spectroscopy in ion-atom and photon-atom collisions; a study of Compton ionization of helium; future

perspectives of photoionization studies at high photon energies; and status report on the advanced photon source. These papers have been cataloged separately elsewhere. DOE

N95-24175# Bhabha Atomic Research Centre, Bombay (India).
MODIFIED MOLECULAR SIEVES: STATIONARY PHASE FOR THE GAS CHROMATOGRAPHIC SEPARATION OF HYDROGEN ISOTOPES
K. K. Pushpa, K. AnnajiRao, and R. M. Iyer 1993 27 p
(DE94-627282; BARC-1993/E/018) Avail: CASI HC A03/MF A01 (US Sales Only)

Gas chromatographic separation of hydrogen isotopes on different molecular sieves at liquid nitrogen temperature has been investigated. Normal molecular sieves 5A, 13X and AW500 are not satisfactory for the purpose both in the partially dehydrated as well as totally dehydrated state. Molecular sieve 4A in partially dehydrated state separated H2 and D2 while H2 and HD are not well resolved. Iron exchanged or coated molecular sieves 4A, 5A, 13X and AW500 in the partially dehydrated state separated the isotopic mixtures H2, HD, D2 and H2, HT, T2. The resolution varied depending on the amount of iron content and the residual moisture in the molecular sieves. Good separations were obtained on 15% Fe coated molecular sieve 5A and 5% Fe coated molecular sieve 4A. DOE

N95-22958*# Yale Univ., New Haven, CT. Physics Lab.
ALGEBRAIC THEORY OF MOLECULES
Franco Iachello *In* NASA. Goddard Space Flight Center, Second International Workshop on Harmonic Oscillators Jan. 1995 p 1-12 (For primary document see N95-22957 07-74)
(Grant DE-FG02-91ER-40608)
Avail: CASI HC A03/MF A04

N95-22960*# Universidad Nacional Autonoma de Mexico, Mexico City (Mexico). Inst. de Ciencias Nucleares.
ALGEBRAIC APPROACH TO THE VIBRATIONAL EXCITATIONS IN METHANE
Renato Lemus and Alejandro Frank (Universidad Nacional Autonoma de Mexico, Cuernavaca, Mexico.) *In* NASA. Goddard Space Flight Center, Second International Workshop on Harmonic Oscillators Jan. 1995 p 25-30 (For primary document see N95-22957 07-74)
(Contract CONACyT-400340-5-3401E)
Avail: CASI HC A02/MF A04

N95-22961*# Universidad Nacional Autonoma de Mexico, Mexico City (Mexico). Inst. de Ciencias Nucleares.
ALGEBRAIC DESCRIPTION OF ATOM-MOLECULE INTERACTIONS
R. D. Santiago, Alejandro Frank, and Renato Lemus *In* NASA. Goddard Space Flight Center, Second International Workshop on Harmonic Oscillators Jan. 1995 p 31-38 (For primary document see N95-22957 07-74)
(Contract CONACyT-400340-5-3401E)
Avail: CASI HC A02/MF A04

N95-22962*# Karlsruhe Univ. (Germany). Inst. fuer Theoretische Physik.
FIBONACCI CHAIN POLYNOMIALS: IDENTITIES FROM SELF-SIMILARITY
Wolfdieter Lang *In* NASA. Goddard Space Flight Center, Second International Workshop on Harmonic Oscillators Jan. 1995 p 39-44 (For primary document see N95-22957 07-74)
Avail: CASI HC A02/MF A04

N95-22964*# Universidad Autonoma del Estado de Morelos, Cuernavaca (Mexico). Facultad de Ciencias.
MOLECULAR VIBRATIONAL STATES DURING A COLLISION
Jose A. Recamier and Rocio Jauregui (Universidad Nacional Autonoma de Mexico, Mexico City, Mexico.) *In* NASA. Goddard Space Flight Center, Second International Workshop on Harmonic Oscillators Jan. 1995 p 51-60 (For primary document see N95-22957 07-74)
Avail: CASI HC A02/MF A04

N95-22966*# Michigan Univ., Ann Arbor, MI. Dept. of Physics.
COHERENT STATE CONSTRUCTIONS OF BASES FOR SOME PHYSICALLY RELEVANT GROUP CHAINS
Karl T. Hecht *In* NASA. Goddard Space Flight Center, Second International Workshop on Harmonic Oscillators Jan. 1995 p 69-82 (For primary document see N95-22957 07-74)
Avail: CASI HC A03/MF A04

N95-22967*# Universidad Nacional Autonoma de Mexico, Mexico City (Mexico). Inst. de Fisica.
HARMONIC OSCILLATOR REPRESENTATION IN THE THEORY OF SCATTERING AND NUCLEAR REACTIONS
Yuri F. Smirnov, A. M. Shirokov (Moscow State Univ., Russia.), Yuri Lurie, A. (Moscow State Univ., Russia.), and S. A. Zaitsev (Moscow State Univ., Russia.) *In* NASA. Goddard Space Flight Center, Second International Workshop on Harmonic Oscillators Jan. 1995 p 83-98 (For primary document see N95-22957 07-74)
Avail: CASI HC A03/MF A04

N95-22968*# Louisiana State Univ., Baton Rouge, LA. Dept. of Physics and Astronomy.
GEOMETRICAL INTERPRETATION FOR THE OUTER SU(3) OUTER MULTIPLICITY LABEL
Jerry P. Draayer and D. Troltenier *In* NASA. Goddard Space Flight Center, Second International Workshop on Harmonic Oscillators Jan. 1995 p 99-10 Sponsored by NSF (For primary document see N95-22957 07-74)
Avail: CASI HC A02/MF A04

N95-22969*# Universidad Nacional Autonoma de Mexico, Mexico City (Mexico). Inst. de Ciencias Nucleares.
BOSON MAPPING TECHNIQUES APPLIED TO CONSTANT GAUGE FIELDS IN QCD
Peter Otto Hess and J. C. Lopez *In* NASA. Goddard Space Flight Center, Second International Workshop on Harmonic Oscillators Jan. 1995 p 107-111 Sponsored by Dept. General de Asuntos del Personal Academico (For primary document see N95-22957 07-74)
Avail: CASI HC A01/MF A04

N95-22971*# Hungarian Academy of Sciences, Debrecen. Inst. of Nuclear Research.
AN ALGEBRAIC CLUSTER MODEL BASED ON THE HARMONIC OSCILLATOR BASIS
Geza Levai and J. Cseh *In* NASA. Goddard Space Flight Center, Second International Workshop on Harmonic Oscillators Jan. 1995 p 121-127 (For primary document see N95-22957 07-74)
(Grant OTKA-3008)
Avail: CASI HC A02/MF A04

N95-22972*# Kurchatov (I. V.) Inst. of Atomic Energy, Moscow (USSR). Russian Research Center.
HARMONIC OSCILLATOR IN QUANTUM ROTATIONAL SPECTRA: MOLECULES AND NUCLEI
Igor M. Pavlichenkov *In* NASA. Goddard Space Flight Center, Second International Workshop on Harmonic Oscillators Jan. 1995 p 129-136 Sponsored by International Science Foundation (For primary document see N95-22957 07-74)
Avail: CASI HC A02/MF A04

N95-22974*# Universidad Nacional Autonoma de Mexico, Cuernavaca (Mexico). Dept. de Fisica.
SHAPES AND STABILITY OF ALGEBRAIC NUCLEAR MODELS
Enrique Lopez-Moreno and Octavio Castanos (Universidad Nacional Autonoma de Mexico, Mexico City, Mexico.) *In* NASA. Goddard Space Flight Center, Second International Workshop on Harmonic Oscillators Jan. 1995 p 145-152 (For primary document see N95-22957 07-74)
Avail: CASI HC A02/MF A04

N95-22984*# State Univ. of New York, Binghamton, NY.
q-BOSONS AND THE q-ANALOGUE QUANTIZED FIELD
Charles A. Nelson *In* NASA. Goddard Space Flight Center, Second International Workshop on Harmonic Oscillators Jan. 1995 p 231-237 (For primary document see N95-22957 07-74)
Avail: CASI HC A02/MF A04

N95-22994*# Liege Univ. (Belgium). Dept. of Theoretical and Mathematical Physics.
ON PSEUDOSUPERSYMMETRIC OSCILLATORS AND REALITY OF RELATIVISTIC ENERGIES FOR VECTOR MESONS
Jules Beckers and Nathalie Debergh *In* NASA. Goddard Space Flight Center, Second International Workshop on Harmonic Oscillators Jan. 1995 p 313-318 (For primary document see N95-22957 07-74)
Avail: CASI HC A02/MF A04

N95-22995*# Liege Univ. (Belgium). Dept. of Theoretical and Mathematical Physics.
ON PARASUPERSYMMETRIC OSCILLATORS AND RELATIVISTIC VECTOR MESONS IN CONSTANT MAGNETIC FIELDS
Nathalie Debergh and Jules Beckers *In* NASA. Goddard Space Flight Center, Second International Workshop on Harmonic Oscillators Jan. 1995 p 319-325 (For primary document see N95-22957 07-74)
Avail: CASI HC A02/MF A04

N95-22997*# Ciudad Univ., Mexico City (Mexico). Escuela de Fisica.
NOTES ON OSCILLATOR-LIKE INTERACTIONS OF VARIOUS SPIN RELATIVISTIC PARTICLES
Valeri V. Dvoeglazov and Antonio delSolMesa (Universidad Nacional Autonoma de Mexico, Mexico City, Mexico.) *In* NASA. Goddard Space Flight Center, Second International Workshop on Harmonic Oscillators Jan. 1995 p 333-340 (For primary document see N95-22957 07-74)
Avail: CASI HC A02/MF A04

N95-23328*# Hampton Univ., VA.
APPLICATION OF ELECTRON PARAMAGNETIC RESONANCE IMAGING TO THE CHARACTERIZATION OF THE ULTEM(R) EXPOSED TO 1 MeV ELECTRONS. CORRELATION OF RADICAL DENSITY DATA TO TIGER CODE CALCULATIONS Abstract Only
Naushadalli K. Suleman *In its* 1994 NASA-HU American Society for Engineering Education (ASEE) Summer Faculty Fellowship Program Dec. 1994 p 110 (For primary document see N95-23276 07-99)
Avail: CASI HC A01/MF A02

N95-23807*# George Mason Univ., Fairfax, VA. CSI Inst.
CHARACTERISTICS OF LOW ENERGY IONS IN THE HEAVY IONS IN SPACE (HIIS) EXPERIMENT
Thomas Kleis, Allan J. Tylka (Naval Research Lab., Washington, DC.), Paul R. Boberg (Naval Research Lab., Washington, DC.), James H. Adams, Jr. (Naval Research Lab., Washington, DC.), and Lorraine P. Beahm (Naval Research Lab., Washington, DC.) *In* NASA. Langley Research Center, LDEF: 69 Months in Space. Third Post-Retrieval Symposium, Part 1 Feb. 1995 p 101-112 Sponsored by ONR (For primary document see N95-23796 07-99)
(NASA Order W-18409)
Avail: CASI HC A03/MF A04

N95-23810*# National Aeronautics and Space Administration. Marshall Space Flight Center, Huntsville, AL.
ABSORBED DOSE AND LET SPECTRA MEASUREMENTS ON LDEF
E. V. Benton (San Francisco Univ., CA.), I. Csige (San Francisco Univ., CA.), A. L. Frank (San Francisco Univ., CA.), E. R. Benton (San Francisco Univ., CA.), L. A. Frigo (San Francisco Univ., CA.), T. A. Parnell, J. Watts, and A. Harmon *In* NASA. Langley Research Center, LDEF: 69 Months in Space. Third Post-Retrieval Symposium, Part 1 Feb. 1995 p 135-148 (For primary document see N95-23796 07-99)
(Grant NAG5-282)
Avail: CASI HC A03/MF A04

N95-23811*# Eril Research, Inc., San Rafael, CA.
FISSION FOIL MEASUREMENTS OF NEUTRON AND PROTON FLUENCES IN THE A0015 EXPERIMENT
A. L. Frank, E. V. Benton, T. W. Armstrong (Science Applications International Corp., Prospect, TN.), and B. L. Colborn (Science Applications International Corp., Prospect, TN.) *In* NASA. Langley Research Center, LDEF: 69 Months in Space. Third Post-Retrieval Symposium, Part 1 Feb. 1995 p 149-158 (For primary document see N95-23796 07-99)
(Contract NAS8-39610)
Avail: CASI HC A02/MF A04

N95-23812*# San Francisco Univ., CA. Physics Research Lab.
MEASUREMENT OF TRAPPED PROTON FLUENCES IN MAIN STACK OF P0006 EXPERIMENT
N. Nefedov, I. Csige, E. V. Benton, R. P. Henke, E. R. Benton, and L. A. Frigo *In* NASA. Langley Research Center, LDEF: 69 Months in Space. Third Post-Retrieval Symposium, Part 1 Feb. 1995 p 159-166 (For primary document see N95-23796 07-99)
(Grant NAG8-282)
Avail: CASI HC A02/MF A04

N95-23813*# Eril Research, Inc., San Rafael, CA.
CONTRIBUTION OF PROTON-INDUCED SHORT RANGE SECONDARIES TO THE LET SPECTRA ON LDEF
E. R. Benton, I. Csige, E. V. Benton, and L. A. Frigo *In* NASA. Langley Research Center, LDEF: 69 Months in Space. Third Post-Retrieval Symposium, Part 1 Feb. 1995 p 167-177 (For primary document see N95-23796 07-99)
(Contract NAS8-38610)
Avail: CASI HC A03/MF A04

N95-23814*# San Francisco Univ., CA. Physics Research Lab.
CHARGE, ENERGY AND LET SPECTRA OF HIGH LET PRIMARY AND SECONDARY PARTICLES IN CR-39 PLASTIC NUCLEAR TRACK DETECTORS OF THE P0006 EXPERIMENT Abstract Only
I. Csige, L. A. Frigo, E. V. Benton, and K. Oda (Kobe Univ. of Mercantile Marine, Japan.) *In* NASA. Langley Research Center, LDEF: 69 Months in Space. Third Post-Retrieval Symposium, Part 1 Feb. 1995 p 179 Sponsored by NASA. Marshall Space Flight Center (For primary document see N95-23796 07-99)
Avail: CASI HC A01/MF A04

N95-23815*# Science Applications International Corp., Prospect, TN.
PREDICTIONS OF LET SPECTRA MEASURED ON LDEF
T. W. Armstrong, B. L. Colborn, and E. V. Benton (San Francisco Univ., CA.) *In* NASA. Langley Research Center, LDEF: 69 Months in Space. Third Post-Retrieval Symposium, Part 1 Feb. 1995 p 181-188 Sponsored by NASA. Marshall Space Flight Center (For primary document see N95-23796 07-99)
Avail: CASI HC A02/MF A04

N95-23816*# California Univ., Berkeley. Lawrence Berkeley Lab, CA.
DOING PHOTONS WITH MERLIN 2 AT OROVILLE
Alan R. Smith and Donna L. Hurley *In* NASA. Langley Research Center, LDEF: 69 Months in Space. Third Post-Retrieval Symposium, Part 1 Feb. 1995 p 189-197 (For primary document see N95-23796 07-99)
(Contract NASA Order H-06815-D; DE-ACO3-76SF-00098)
Avail: CASI HC A02/MF A04

N95-23817*# National Aeronautics and Space Administration. Marshall Space Flight Center, Huntsville, AL.
STATUS OF LDEF ACTIVATION MEASUREMENTS AND ARCHIVE
B. Alan Harmon, Thomas A. Parnell, and Christopher E. Laird *In* NASA. Langley Research Center, LDEF: 69 Months in Space. Third Post-Retrieval Symposium, Part 1 Feb. 1995 p 199-201 (For primary document see N95-23796 07-99)
Avail: CASI HC A01/MF A04

N95-23818*# National Aeronautics and Space Administration. Marshall Space Flight Center, Huntsville, AL.
PREDICTIONS OF LDEF RADIOACTIVITY AND COMPARISON WITH MEASUREMENTS
T. W. Armstrong (Science Applications International Corp., Prospect, TN.), B. L. Colborn (Science Applications International Corp., Prospect, TN.), B. A. Harmon, and C. E. Laird (University of Eastern Kentucky, Richmond, KY.) *In* NASA. Langley Research Center, LDEF: 69 Months in Space. Third Post-Retrieval Symposium, Part 1 Feb. 1995 p 203-216 (For primary document see N95-23796 07-99)
Avail: CASI HC A03/MF A04

N95-23819*# National Aeronautics and Space Administration. Marshall Space Flight Center, Huntsville, AL.
STATUS OF LDEF RADIATION MODELING

John W. Watts, T. W. Armstrong (Science Applications International Corp., Prospect, TN.), and B. L. Colborn (Science Applications International Corp., Prospect, TN.) *In* NASA. Langley Research Center, LDEF: 69 Months in Space. Third Post-Retrieval Symposium, Part 1 Feb. 1995 p 217-226 (For primary document see N95-23796 07-99)
Avail: CASI HC A02/MF A04

73 NUCLEAR AND HIGH-ENERGY PHYSICS

Includes elementary and nuclear particles; and reactor theory. For space radiation see *93 Space Radiation*.

N95-22567# Stanford Linear Accelerator Center, CA.
MULTIPOLE CONTRIBUTION FROM AN OFF-AXIS ORBIT IN AN IR QUADRUPOLE AND THE CONSEQUENCES ON THE DYNAMIC APERTURE
M. Sullivan, S. Caspi (California Univ., Berkeley. Lawrence Berkeley Lab, CA.), E. Forest (California Univ., Berkeley. Lawrence Berkeley Lab, CA.), D. Robin (California Univ., Berkeley. Lawrence Berkeley Lab, CA.), A. Zholents (California Univ., Berkeley. Lawrence Berkeley Lab, CA.), Y. Cai, H. DeStaebler, M. Donald, R. Helm, and J. Irwin et al Jun. 1994 4 p Presented at the 4th European Particle Accelerator Conference, London (England), 27 Jun. - 1 Jul. 1994
(Contracts DE-AC03-76SF-00515; DE-AS03-76ER-70285; DE-AC03-76SF-00098)
(DE95-002874; SU-SLAC-PUB-6533; LBL-35911; CONF-940618-96) Avail: CASI HC A01/MF A01

The low-energy beam of the proposed PEP-II B factory enters the first quadrupole (Q1) after the interaction point off axis in order to separate the low-energy beam from the high-energy beam. The off-axis beam orbit in Q1 gives rise to significant feed-down terms from higher multipoles that originate from systematic effects and random fabrication errors. The authors study superconducting and permanent magnet designs of Q1, and look at the effect these different designs have on the dynamic aperture. Including a dipole field in a superconducting design allows one to offset the magnetic axis from the mechanical axis, thereby maintaining the separation of the beams while greatly reducing the feed-down effect. They illustrate relevant points of the discussion with tracking results for the PEP-II low-energy ring. DOE

N95-22644# Tokyo Univ., Tanashi (Japan). Inst. for Nuclear Study.
INTERDIGITAL-H LINAC FOR UNSTABLE NUCLEI AT INS
M. Tomizawa, S. Arai, M. Doi, T. Katayama, K. Niki, M. Yoshizawa, and T. Hattori May 1993 4 p
(DE94-765448; INS-981) Avail: CASI HC A01/MF A01 (US Sales Only)

In the prototype facility of the Exotic-arena at INS, unstable nuclei with a charge-to-mass ratio greater than 1/10 is accelerated from 170 to 1046 keV/u by an interdigital-H linac. Designed IH linac consists of four acceleration tanks and three sets of quadrupole triplets placed between tanks. Output energy is continuously variable by changing RF power and phase of the last operating tank. A high shunt impedance is expected from an equivalent circuit analysis. The RF measurement on the low power models is now in progress. Preliminary results of the tank-4 model shows that a resonant frequency and a shunt impedance roughly agree with the design values. DOE

N95-22684# Fermi National Accelerator Lab., Batavia, IL.
PERTURBATIVE QCD TESTS FROM THE LEP, HERA, AND TEVATRON COLLIDERS
S. Kuhlmann (Argonne National Lab., IL.) Sep. 1994 26 p Presented at the Conference on Physics in Collision, Tallahassee, FL, 15-17 Jun. 1994
(Contract DE-AC02-76CH-03000)
(DE95-001285; FNAL/C-94/310-E; CONF-940693-2) Avail: CASI HC A03/MF A01

A review of QCD tests from LEP, HERA and the TEVATRON colliders is presented. This includes jet production, quark/gluon jet separation, quark/gluon propagator spin, (alpha)(sub s) updates, photon production, and rapidity gap experiments. DOE

N95-22702# Stanford Linear Accelerator Center, CA.
PRECISION STANDARD MODEL TESTS WITH POLARIZED E(+)E(-) BEAMS
M. J. Fero Oct. 1994 10 p Presented at the Conference on Physics in Collision, Tallahassee, FL, 15-17 Jun. 1994
(Contract DE-AC03-76SF-00515)
(DE95-003367; SU-SLAC-PUB-6678; CONF-940693-4) Avail: CASI HC A02/MF A01

The advent of polarized electron beams at the Stanford Linear Collider (SLC) makes possible the new precision electroweak tests now being performed by the SLC Large Detector (SLD) experiment. One such new technique, the left-right asymmetry measurement, allows remarkably direct measurement of the effective weak mixing angle, sin(exp 2) theta(sub W)(sup eff) = 0.2292 +/- 0.0009(stat) +/- 0.0004(syst). When considered within the minimal standard model (MSM) framework, this result predicts the top mass to be m(sub t) = 240(sub -45-20)(sup +30+18) GeV where the first errors are experimental and the second reflect a range of possible Higgs mass values from 60 to 1000 GeV. DOE

N95-22785# International Centre for Theoretical Physics, Trieste (Italy).
THE PROBLEM OF PHASE TRANSITION AND THE HEAVY ION COLLISIONS AT VERY HIGH ENERGIES
A. Waheed Sep. 1993 20 p
(DE94-628584; IC-93/271) Avail: CASI HC A03/MF A01 (US Sales Only)

This paper presents a review of our current understanding of deconfined phases of strongly interacting matter at high energy densities - quark matter, or the quark-gluon plasma, likely to be produced in ultra-relativistic heavy ion collisions. Properties of the deconfined quark matter and speculations concerning the ways in which this phase transition can be explored in laboratory are discussed. Some suggestions have been put forward for the future experiments. DOE

N95-22848# Tokyo Univ., Tanashi (Japan). Inst. for Nuclear Study.
A HEAVY ION LINAC COMPLEX FOR UNSTABLE NUCLEI
S. Arai, M. Doi, Y. Hashimoto, T. Hattori, A. Imanishi, T. Katayama, H. Masuda, K. Niki, Y. Takeka, and N. Tokuda et al May 1993 4 p
(DE94-765443; INS-978) Avail: CASI HC A01/MF A01 (US Sales Only)

A heavy ion linac complex for unstable nuclei is under construction at INS. The linac complex consists of a 25.5-MHz split coaxial Radio Frequency Quadrupole (RFQ) (SCRFQ), a charge-stripper section, and a 51-MHz interdigital-H (IH) linac. The SCRFQ with modulated vanes, 0.9m in diameter and 8.6m in length, accelerates ions with a charge-to-mass ratio (q/A) greater than 1/30 from 2 to 170 keV/u. The stripper is a carbon foil. The IH linac, 1.34m in diameter and 5.54m in total length, comprises four cavities and three magnetic quadrupole triplets placed between cavities, accelerates ions with q/A greater than or equal to 1/10, and varies the output energy continuously in the range 0.17 - 1.05 MeV/u. The duty factor of the linac complex is 30% for q/A = 1/30 ions. DOE

N95-22926# Brookhaven National Lab., Upton, NY.
QUENCH PROPAGATION STUDY FOR FULL-LENGTH RHIC DIPOLE MAGNETS
J. Muratore, M. Anerella, G. Ganetis, M. Garber, A. K. Ghosh, A. Greene, R. Gupta, A. Jain, S. Kahn, and E. Kelly et al 1993 5 p Presented at the 13th International Conference on Magnet Technology, Victoria, Bristish Columbia, 20-24 Sep. 1993
(Contract DE-AC02-76CH-00016)
(DE94-014089; BNL-49323; CONF-930926-37) Avail: CASI HC A01/MF A01

Study of quench propagation velocities and MIIT's analysis of conductor hot spot temperatures during quench tests are important tools in designing quench protection strategies in superconducting accelerator magnets. Quench velocity and temperature studies have been performed on various superconducting magnets for the RHIC (Relativistic Heavy Ion Collider) project at BNL, during the research phase of magnet development there. They were done as part of an extensive test program to evaluate the mechanical and magnetic performance of RHIC magnets under varying conditions. This paper presents results for spot heater studies done on two of the full length RHIC prototype dipole magnets. DOE

N95-22929*# National Aeronautics and Space Administration. Langley Research Center, Hampton, VA.
COMPARISON OF EXACT SOLUTION WITH EIKONAL APPROXIMATION FOR ELASTIC HEAVY ION SCATTERING
Rajendra R. Dubey (Old Dominion Univ., Norfolk, VA.), Govind S. Khandelwal (Old Dominion Univ., Norfolk, VA.), Francis A. Cucinotta, and Khin Maung Maung (Hampton Univ., VA.) Feb. 1995 18 p
(RTOP 199-45-16-11)
(NASA-TP-3498; L-17428; NAS 1.60:3498) Avail: CASI HC A03/MF A01

A first-order optical potential is used to calculate the total and absorption cross sections for nucleus-nucleus scattering. The differential cross section is calculated by using a partial-wave expansion of the Lippmann-Schwinger equation in momentum space. The results are compared with solutions in the Eikonal approximation for the equivalent potential and with experimental data in the energy range from 25A to 1000A MeV. Author

N95-23148# Ohio State Univ., Columbus, OH. Research Foundation.
HIGH ENERGY THEORY: TASK B AND TASK L Progress Report
1994 30 p
(Contract DE-FG02-91ER-40690)
(DE95-003453; DOE/ER-40690/T1) Avail: CASI HC A03/MF A01

Research areas briefly covered in this report include semi-leptonic and non-leptonic B- and D-decays, CP violation, lattice gauge theory, light cone field theory, supersymmetry, fermion mass matrices, superstrings derived SUSY GUT's, neutrino physics and cosmology. DOE

N95-23245# Los Alamos National Lab., NM.
DRY CRITICAL EXPERIMENTS AND ANALYSES PERFORMED IN SUPPORT OF THE TOPAZ-2 SAFETY PROGRAM
D. B. Pelowitz, J. Sapir, E. S. Glushkov (Kurchatov, I. V. Inst. of Atomic Energy, Moscow, USSR.), N. N. Ponomarev-Stepnoi (Kurchatov, I. V. Inst. of Atomic Energy, Moscow, USSR.), V. G. Bubelev (Kurchatov, I. V. Inst. of Atomic Energy, Moscow, USSR.), G. B. Kompanietz (Kurchatov, I. V. Inst. of Atomic Energy, Moscow, USSR.), A. M. Krutov (Kurchatov, I. V. Inst. of Atomic Energy, Moscow, USSR.), D. N. Polyakov (Kurchatov, I. V. Inst. of Atomic Energy, Moscow, USSR.), and V. A. Loynstev (Kurchatov, I. V. Inst. of Atomic Energy, Moscow, USSR.) 1994 11 p Presented at the 12th Symposium on Space Nuclear Power and Propulsion, Albuquerque, NM, 8-12 Jan. 1995
(Contract W-7405-eng-36)
(DE95-002724; LA-UR-94-3326; CONF-950110-11) Avail: CASI HC A03/MF A01

In December 1991, the Strategic Defense Initiative Organization decided to investigate the possibility of launching a Russian Topaz-2 space nuclear power system. Functional safety requirements developed for the Topaz mission mandated that the reactor remain subcritical when flooded and immersed in water. Initial experiments and analyses performed in Russia and the United States indicated that the reactor could potentially become supercritical in several water- or sand-immersion scenarios. Consequently, a series of critical experiments was performed on the Narciss M-II facility at the Kurchatov Institute to measure the reactivity effects of water and sand immersion, to quantify the effectiveness of reactor modifications proposed to preclude criticality, and to benchmark the calculational methods and nuclear data used in the Topaz-2 safety analyses. In this paper we describe the Narciss M-II experimental configurations along with the associated calculational models and methods. We also present and compare the measured and calculated results for the dry experimental configurations. DOE

N95-23353# Brookhaven National Lab., Upton, NY.
A REPORT ON THE INDIANA UNIVERSITY WORKSHOP ON FUTURE U.S. HADRON FACILITIES
M. J. Syphers 1995 12 p Presented at the 4th Tamura Symposium on Accelerator Physics, Austin, TX, 14-16 Nov. 1994
(Contract DE-AC02-76CH-00016)
(DE95-003951; BNL-60963; CONF-9411120-2) Avail: CASI HC A03/MF A01

In July 1994 a workshop was held at Indiana University to study and discuss options for future hadron collider facilities in the United States, and to identify related R&D programs. The workshop was conducted under the auspices of the Accelerator Physics, Technologies, and Facilities Working Group of the DPF Long Term Planning Study. Roughly 50 participants from 17 institutions in the U.S. and Europe (CERN) were organized into six working groups to study magnets, cryogenics and vacuum, antiproton sources, injectors, interaction regions, and lattice and beam dynamics. Upgrades to existing facilities (namely, Fermilab) and a post-LHC facility were discussed at the workshop. In this paper, the discussion will focus on the post-LHC facility. One of the specific goals of the workshop was to develop a defensible parameters list for a 30 TeV x 30 TeV hadron collider with luminosity of 1 x 10(exp 34) cm(exp -2) sec(exp -1). While this accelerator would have only 50% higher energy than the SSC design, it was realized that the role of synchrotron radiation at this energy would significantly enhance the design and operation of the machine. Radiation damping times of a few hours, rather than one day, can be realized thus allowing less intense, but brighter proton beams. DOE

N95-23369# Fermi National Accelerator Lab., Batavia, IL.
D(O) UPGRADE MUON ELECTRONICS DESIGN
B. Baldin, D. Green, H. Haggerty, and S. Hansen Nov. 1994 5 p Presented at the Nuclear Science Symposium: Medical Imaging Conference, Norfolk, VA, 30 Oct. - 5 Nov. 1994
(Contract DE-AC02-76CH-03000)
(DE95-003744; FNAL/C-94/370; CONF-941061-9) Avail: CASI HC A01/MF A01

The planned luminosity for the upgrade is ten times higher than at present (L (approximately) 10(exp 32)cm(exp -2)/s) and involves a time between collisions as small as 132 ns. To operate in this environment, completely new electronics is required for the 17,500 proportional drift tubes of the system. These electronics include a deadtimeless readout, a digital TDC with about 1 ns binning for the wire signals, fast charge integrators and pipelined ADC's for digitizing the pad electrode signals, a new wire signal triggering scheme and its associated trigger logic, and high level DSP processing. Some test results of measurements performed on prototype channels and a comparison with the existing electronics are presented. DOE

N95-23485# California Univ., Berkeley. Lawrence Berkeley Lab, CA.
DESIGN STUDY OF LONGITUDINAL DYNAMICS OF THE DRIVE BEAM IN 1 TeV RELATIVISTIC KLYSTRON TWO-BEAM ACCELERATOR
H. Li, S. S. Yu, and A. M. Sessler Oct. 1994 20 p Presented at the Meeting of the Division of Plasma Physics of the American Physical Society, Minneapolis, MN, 7-11 Nov. 1994
(Contract DE-AC03-76SF-00098)
(DE95-004683; LBL-36180; CONF-941101-2) Avail: CASI HC A03/MF A01

In this paper the authors present a design study on the longitudinal dynamics of a relativistic klystron two-beam accelerator (RK-TBA) scheme which has been proposed as a power source candidate for a 1 TeV next linear collider (NLC). They address the issue of maintaining stable power output at desired level for a 300-m long TBA with 150 extraction cavities and present their simulation results to demonstrate that it can be achieved by inductively detuning the extraction cavities to counter the space charge debunching effect on the drive beam. They then carry out simulation study to show that the beam bunches desired by the RK-TBA can be efficiently obtained by first chopping an initially uniform beam of low energy into a train of beam bunches with modest longitudinal dimension and then using the 'adiabatic capture' scheme to bunch and accelerate these beam bunches into tight bunches at the operating energy of the drive beam. The authors have also examined the 'after burner' scheme which is implemented in their RK-TBA design for efficiency enhancement. DOE

N95-23493# California Univ., Berkeley. Lawrence Berkeley Lab, CA.
DESIGN STUDY OF BEAM DYNAMICS ISSUES FOR 1 TeVNEXT LINEAR COLLIDER BASED ON THE RELATIVISTIC-KLYSTRON TWO-BEAM ACCELERATOR
H. Li, N. Goffeney, E. Henestroza, A. Sessler, S. Yu, T. Houck, and G. Westenskow Nov. 1994 20 p Presented at the Advanced Accelerator Concepts Workshop, Lake Geneva, WI, 13-18 Jun. 1994
(Contract DE-AC03-76SF-00098)
(DE95-004673; LBL-36233; CONF-940681-5) Avail: CASI HC A03/MF A01

A design study has recently been conducted for exploring the feasibility of a relativistic-klystron two-beam accelerator (RK-TBA) system as a RF

power source for a 1 TeV linear collider. The author present, in this paper, the beam dynamics part of this study. They have achieved in their design study acceptable transverse and longitudinal beam stability properties for the resulting high efficiency and low cost RK-TBA. DOE

N95-23562# Department of Energy, Washington, DC. Office of Environmental Management.
CLOSING THE CIRCLE ON THE SPLITTING OF THE ATOM: THE ENVIRONMENTAL LEGACY OF NUCLEAR WEAPONS PRODUCTION IN THE UNITED STATES AND WHAT THE DEPARTMENT OF ENERGY IS DOING ABOUT IT
Jan. 1995 113 p
Avail: CASI HC A06/MF A02

This book describes environmental, safety, and health problems throughout the nuclear weapons complex and what the Department of Energy is doing to address them. Because of the secrecy that until recently surrounded nuclear weapons, many citizens today are unaware of how and where nuclear weapons were made and the resulting problems. The intention of this book it to help foster better public understanding of some of the issues concerning the nuclear legacy of the Cold War so as to help hasten progress as the DOE moves ahead on resolving these problems. Chapter 1 is an overview and a summary, including a brief history of the Department's nuclear weapons complex. Chapter 2 describes nuclear warhead production for uranium mining to final assembly to give a sense of the scale and complexity of nuclear weapons production and to characterize the sources and varieties of wastes and contamination. Chapters 3 and 4 look at the wastes and the contamination left by the Cold War and the progress and plans for solving these problems. Chapter 5 provides and international perspective on the legacy of nuclear weapons production. Chapter 6 describes the engineering and institutional challenges faced by the DOE as it embarks on new missions. Chapter 7 presents some of the long-term issues our nation faces as we come to terms with the legacy of the Cold War. The book ends with a glossary of terms and a list of books and reports that provide additional information about the nuclear weapons complex and the Department's plans for its cleanup. Derived from text

N95-24014# California Univ., Berkeley. Lawrence Berkeley Lab, CA.
HIGH CURRENT INDUCTION LINACS
W. Barletta, A. Faltens, E. Henestroza, and E. Lee Jul. 1994 10 p Presented at the International Conference on Accelerator-driven Transmutation Technologies and Applications, Las Vegas, NV, 25-28 Jul. 1994
(Contract DE-AC03-76SF-00098)
(DE95-003442; LBL-35960; HIFAN-666; CONF-9407103-32) Avail: CASI HC A02/MF A01

Induction linacs are among the most powerful accelerators in existence. They have accelerated electron bunches of several kiloamperes, and are being investigated as drivers for heavy ion driven inertial confinement fusion (HIF), which requires peak beam currents of kiloamperes and average beam powers of some tens of megawatts. The requirement for waste transmutation with an 800 MeV proton or deuteron beam with an average current of 50 mA and an average power of 40 MW lies midway between the electron machines and the heavy ion machines in overall difficulty. Much of the technology and understanding of beam physics carries over from the previous machines to the new requirements. The induction linac allows use of a very large beam aperture, which may turn out to be crucial to reducing beam loss and machine activation from the beam halo. The major issues addressed here are transport of high intensity beams, availability of sources, efficiency of acceleration, and the state of the needed technology for the waste treatment application. Because of the transformer-like action of an induction core and the accompanying magnetizing current, induction linacs make the most economic sense and have the highest efficiencies with large beam currents. Based on present understanding of beam transport limits, induction core magnetizing current requirements, and pulse modulators, the efficiencies could be very high. The study of beam transport at high intensities has been the major activity of the HIF community. Beam transport and sources are limiting at low energies but are not significant constraints at the higher energies. As will be shown, the proton beams will be space-charge-dominated, for which the emittance has only a minor effect on the overall beam diameter but does determine the density falloff at the beam edge. DOE

N95-24077# Fermi National Accelerator Lab., Batavia, IL.
STANDARDIZATION OF CDF AND D(O) REPORTED LUMINOSITIES
J. Bantly, R. Plunkett, S. Pruss, and M. Tartaglia Oct. 1994 10 p
(Contract DE-AC02-76CH-03000)
(DE95-003388; FNAL-TM-1906) Avail: CASI HC A02/MF A01

During FNAL collider store 5094, CDF- and D(O) modified the computation of their reported luminosities to utilize a standardized world average inelastic cross-section. The changes made at each experiment and in the Accelerator Division are detailed below. A net decrease was expected and was observed for the reported instantaneous luminosity from each experiment. These changes affect the estimates of instantaneous and integrated luminosities reported to the Accelerator Division for the purposes of operational coordination. DOE

N95-24084# Fermi National Accelerator Lab., Batavia, IL.
VLPC CHARACTERIZATION FOR THE DZERO UPGRADE
Sep. 1994 6 p Presented at the Meeting of the Division of Particles and Fields of the American Physical Society, Albuquerque, NM, 2-6 Aug. 1994
(Contract DE-AC02-76CH-03000)
(DE95-003742; FNAL/C-94/318-E; CONF-940816-62) Avail: CASI HC A02/MF A01

The authors have studied the performance characteristics of approximately 4,000 Visible Light Photon Counters (VLPC) over a range of operating temperatures and biases. They will describe the characterization procedure and present the measured gain, noise, and relative quantum efficiency for the devices. They will also discuss the general operation of the devices and the significant problems encountered during the characterization. DOE

N95-24160# Sandia National Labs., Albuquerque, NM.
PROGRESS IN ION BEAM POWER COUPLING AND ION-DRIVEN HOHLRAUMS ON PBFA 2
A. B. Filuk, T. A. Mehlhorn, R. G. Adams, G. O. Allshouse, J. H. Aubert, L. D. Bacon, J. E. Bailey, D. D. Bloomquist, J. Boyes, and G. A. Chandler et al 1995 9 p Presented at the International Atomic Energy Agency (IAEA) Technical Committee Meeting on Drivers for Inertial Confinement Fusion, Paris, 14-18 Nov. 1994
(Contract DE-AC04-94AL-85000)
(DE95-004544; SAND-94-1392C; CONF-9411152-2) Avail: CASI HC A02/MF A01

Light ions could provide an efficient driver for high-yield and energy applications of inertial confinement fusion. Working towards this goal, the authors have demonstrated well-diagnosed, ion-driven hohlraum targets at approximately 60 eV radiation temperature on the PBFA II accelerator, with specific power deposition of 800-1400 TW/gm. This parameter regime is of interest to both light- and heavy-ion drivers, and corresponds to the early phase of a high-yield target drive. Further increases in target temperature require increasing the ion beam driver intensity. Direct measurements of ion diode dynamics are providing insights to improve driver capability. Maximum beam intensity is obtained by both increasing the coupled lithium beam power and decreasing the beam microdivergence. The microdivergence of the beam near the ion source appears to be a major contributor early in the beam pulse. Experiments have shown that a parasitic non-lithium ion beam consumes a large fraction of the available power. Calculations indicate the coupled beam power can be increased by up to a factor of 3 by eliminating this parasitic loss. Preliminary experiments to clean the ion diode surfaces are under way. DOE

N95-24162# Argonne National Lab., IL.
SOME THOUGHTS OF FUTURE EXPERIMENTS WITH THE NEW GENERATION OF STORAGE RINGS
J. Berkowitz 1995 12 p Presented at the Workshop on Atomic Physics At High Brilliance Synchrotron Sources, Argonne, IL, 23-24 Apr. 1994
(Contract W-31-109-eng-38)
(DE95-004602; ANL/CHM/CP-84071; CONF-9404198-4) Avail: CASI HC A03/MF A01

The author presents a recounting of work he has been involved with employing vacuum ultraviolet radiation generated by laboratory sources and synchrotrons. This includes touching on early studies on the potential of synchrotron sources to generate radiation at intensities which would

allow study of transient species and very weak processes. Photoionization studies of many molecular systems are discussed, and the potential of more intense sources to allow measurement of cross sections and fragmentation reactions is discussed. DOE

74 OPTICS

Includes light phenomena; and optical devices.
For lasers see *36 Lasers and Masers.*

N95-22492 Department of the Navy, Washington, DC.
METHOD FOR MAKING FIBER-OPTIC BUNDLE COLLIMATOR ASSEMBLY Patent Application
Gregory H. Ames, inventor (to Navy) and Thomas J. Gryk, inventor (to Navy) 8 Aug. 1994 16 p Limited Reproducibility: More than 20% of this document may be affected by microfiche quality
(AD-D016491; US-Patent-Appl-SN-287028) Avail: Issuing Activity (Defense Technical Information Center (DTIC))

There is presented a method for making a fiber-optic bundle collimator assembly, comprising the steps of assembling side by side a multiplicity of first bodies of cylindrical configuration and equal diameter and applying uniform compressive force to the first bodies to force the first bodies into a predictable hexagonal pattern of minimum diameter. Additional bodies of cylindrical configuration and having diameters equal to the diameters of the first bodies are inserted on each of the sides of the bundle of first bodies with each of the additional bodies abutting two of the first bodies. A plurality of the first bodies is then removed from the bundle. Each of the removed first bodies is replaced with a pair of cylindrically-shaped second bodies having diameters equal to the diameters of the first bodies, with one of the pair protruding from the bundle on a first face thereof and another of the pair protruding from the bundle on a second face thereof. A clamp is applied to exposed portions of the second bodies at one of the bundle first and second faces, to force the second bodies into an attitude parallel to each other, the second bodies causing the first bodies to align parallel to the second bodies and parallel to each other. An outer ring of the first bodies is locked in place and a second plurality of first bodies is removed from the bundle. A plurality of optical fiber bearing ferrules is inserted in the place of the removed first bodies. DTIC

N95-22508# Accuwave Corp., Santa Monica, CA.
OPTICAL IMAGE CORRELATOR USING ORTHOGONAL DATA STORAGE Final Report, Mar. 1993 - May 1994
Koichi Sayano and George A. Rakuljic Aug. 1994 35 p
(Contract F30602-93-C-0021)
(AD-A285795; RL-TR-94-154) Avail: CASI HC A03/MF A01

A compact optical image correlator using orthogonal, wavelength multiplexed Fourier transform holograms recorded in a photorefractive crystal has been demonstrated. Cross-correlation and auto-correlation measurements were obtained using randomly selected test images against the set of reference images stored in the orthogonal data storage volume hologram. Over 40 holograms were written in the 645 to 651 nm wavelength range with greater than 2% diffraction efficiency and 1.5 A wavelength separation. A low power tunable external cavity semiconductor laser was used for readout, further demonstrating the portability of this approach. The input image translation tolerances on the correlation output and the effect of using partial images during readout were also investigated. DTIC

N95-22723# Sandia National Labs., Livermore, CA. Dept. of Materials Science and Technology.
EUV METROLOGY OF MULTILAYER OPTICS
A. K. Ray-Chaudhuri, R. H. Stulen, W. Ng (Wisconsin Univ., Madison, WI.), F. Cerrina (Wisconsin Univ., Madison, WI.), S. Spector (State Univ. of New York, Stony Brook, NY.), Z. Tan (Bell Telephone Labs., Inc., Holmdel, NJ.), J. Bjorkholm (Bell Telephone Labs., Inc., Holmdel, NJ.), and D. Tennant (Bell Telephone Labs., Inc., Holmdel, NJ.) 1994 8 p Presented at the Optical Society of America Conference on Extreme Ultraviolet Lithography, Monterey, CA, 19-21 Sep. 1994
(Contract DE-AC04-94AL-85000)
(DE95-003036; SAND-95-8422C; CONF-9409177-5) Avail: CASI HC A02/MF A01

EUV metrology is central to the successful commercialization of EUV projection lithography. Metrology carried out at the EUV wavelength of 13 nm enables a gain of approximately 50 in precision when translated from visible light wavelengths. It also uniquely measures wavefront errors due to lateral variations in the inherent phase shift upon reflection from the multilayer coating. The authors present the development of two metrology techniques: EUV Foucault and Ronchi tests. DOE

N95-22765* National Aeronautics and Space Administration. Pasadena Office, CA.
PROGRAMMABLE HYPERSPECTRAL IMAGE MAPPER WITH ON-ARRAY PROCESSING Patent
James A. Cutts, inventor (to NASA) (Jet Propulsion Lab., California Inst. of Tech., Pasadena, CA.) 3 Jan. 1995 17 p Filed 22 Jun. 1992 Supersedes N92-30104 (30 - 20, p 3553)
(Contract NAS7-918)
(NASA-Case-NPO-17794-1-CU; US-Patent-5,379,065; US-Patent-Appl-SN-904550; US-Patent-Class-348-269; US-Patent-Class-348-207; Int-Patent-Class-H04N-9/04) Avail: US Patent and Trademark Office

A hyperspectral imager includes a focal plane having an array of spaced image recording pixels receiving light from a scene moving relative to the focal plane in a longitudinal direction, the recording pixels being transportable at a controllable rate in the focal plane in the longitudinal direction, an electronic shutter for adjusting an exposure time of the focal plane, whereby recording pixels in an active area of the focal plane are removed therefrom and stored upon expiration of the exposure time, an electronic spectral filter for selecting a spectral band of light received by the focal plane from the scene during each exposure time and an electronic controller connected to the focal plane, to the electronic shutter and to the electronic spectral filter for controlling (1) the controllable rate at which the recording is transported in the longitudinal direction, (2) the exposure time, and (3) the spectral band so as to record a selected portion of the scene through M spectral bands with a respective exposure time t(sub q) for each respective spectral band q. Official Gazette of the U.S. Patent and Trademark Office

N95-22780# University of Southern Mississippi, Bay Saint Louis, MS.
DEVELOPMENT OF A MULTI-SENSOR IN SITU FIBER OPTIC FLUOROMETER Progress Report, 1 Jun. 1992 - 31 Oct. 1994
S. E. Lohrenz, V. L. Asper, M. J. Morris (Ocean Optics, Inc., Dunedin, FL.), and R. A. Walters (Ocean Optics, Inc., Dunedin, FL.) Nov. 1994 41 p
(Contract DE-FG02-92ER-61443)
(DE95-003105; DOE/ER-61443/3) Avail: CASI HC A03/MF A01

As part of the Department of Energy (DOE) Ocean Margins Program (OMP), we have developed an autonomous multi-sensor in situ fiber optic fluorometer for estimating the distribution and abundance of particulate pigment biomass. The instrument is designed to sample and store in vivo strobe-stimulated fluorescence data at multiple depths and high frequencies (1 Hz). It is unique in that it uses fiber optic technology to increase vertical resolution. The design of the instrument is such that high frequency, high vertical resolution pigment fluorescence data can be achieved at relatively low cost as compared to the deployment of multiple commercial instruments. In addition, the small size and flexibility in positioning of the fiber optic sensors permit fluorescence measurements to be made with a high degree of spatial resolution and minimal interference with other sensors. This makes the instrument particularly well suited for characterizing gradients in pigment fluorescence in the benthic boundary layer, where significant lateral transport of particulate organic matter may occur. Initial results from two separate deployments have revealed highly variable and vertically heterogeneous near-bottom pigment distributions in coastal waters of the Gulf of Mexico and the US eastern inner continental shelf near Cape Hatteras. This information will be related to measurements of the current velocity structure to enable determinations of transport of pigments in the benthic boundary layer. DOE

N95-22807* National Aeronautics and Space Administration. Langley Research Center, Hampton, VA.
OPTICAL FIBER STRAIN SENSOR WITH IMPROVED LINEARITY RANGE Patent
Claudio Oliveira Egalon, inventor (to NASA) (Analytical Services and Materials, Inc., Hampton, VA.) and Robert S. Rogowski, inventor (to NASA) 10 Jan. 1995 5 p Filed 21 Dec. 1992 Supersedes N93-19374

(31 - 6, p 1663)
(NASA-Case-LAR-14857-1-SB; US-Patent-5,381,493;
US-Patent-Appl-SN-994593; US-Patent-Class-385-13;
US-Patent-Class-385-28; US-Patent-Class-385-123;
US-Patent-Class-250-227.16; Int-Patent-Class-G02B-6/16) Avail: US Patent and Trademark Office

A strain sensor is constructed from a two mode optical fiber. When the optical fiber is surface mounted in a straight line and the object to which the optical fiber is mounted is subjected to strain within a predetermined range, the light intensity of any point at the output of the optical fiber will have a linear relationship to strain, provided the intermodal phase difference is less than 0.17 radians.

Official Gazette of the U.S. Patent and Trademark Office

N95-22864 Office of Naval Research, Arlington, VA.
A FIBER-OPTIC BUNDLE AND COLLIMATOR ASSEMBLY Patent Application
Gregory H. Ames, inventor 8 Aug. 1994 10 p Limited Reproducibility: More than 20% of this document may be affected by microfiche quality
(AD-D016500; US-Patent-Appl-SN-287029) Avail: Issuing Activity (Defense Technical Information Center (DTIC))

There is presented a fiber-optic bundle and collimator assembly comprising a plurality of bodies of cylindrical configuration and of equal diameter arranged side by side in a hexagonal close-packed configuration, a retainer for retaining the bodies in the close-packed configuration, and a potting material for locking the bodies in position. A plurality of the bodies and fiber-optic ferrules have therein a single optical fiber. A remainder of the bodies are non-optical fiber bearing ferrules in alignment width-wise of the assembly to form a collimator assembly face. The fiber-optic ferrules are each recessed from the assembly face to form a pocket. A spacer is disposed in each pocket and abuts a fiber-optic ferrule, and a spherical lens is disposed in each pocket and abuts a spacer. Each of the lenses is of the same diameter as its associated fiber-optic ferrule, and has its axis in alignment with the axis of the associated fiber-optic ferrule optical fiber.

DTIC

N95-22877# Brookhaven National Lab., Upton, NY.
PRESERVING THE HIGH SOURCE BRIGHTNESS WITH X RAY BEAM LINE OPTICS
L. E. Berman 1994 28 p Presented at the International Meeting on Synchrotron Radiation Instrumentation, Stony Brook, NY, 18-22 Jul. 1994
(Contract DE-AC02-76CH-00016)
(DE95-003172; BNL-60859; CONF-940714-39) Avail: CASI HC A03/MF A01

A first-order challenge facing developers of x-ray beam line optics at synchrotron sources lies in producing optics that faithfully deliver the brightness of the source, especially in the presence of adverse power loads. Once overcome, continued use of beam line optics in experiments often reveals a second-order challenge, that of preservation of the source brightness over time, especially as conditions such as the storage ring current change. This requires maintaining stability, with beam line optics, of the peaks, widths, and centroid positions of the various parameters that contribute to the brightness, the wavelength, position, and angle distributions of the delivered photon beam. Some ideas on the use of x-ray monochromators, mirrors, apertures, and position-sensitive monitors to sense and stabilize the brightness parameter distributions, as well as, methods to avoid or minimize transients in the first place, are presented. Examples based on experiences at the X25 wiggler beam line at the National Synchrotron Light Source (NSLS) are given.

DOE

N95-22915*# National Aeronautics and Space Administration. Lewis Research Center, Cleveland, OH.
CALCULATED COUPLING EFFICIENCY BETWEEN AN ELLIPTICAL-CORE OPTICAL FIBER AND A SILICON OXYNITRIDE RIB WAVEGUIDE
Margaret L. Tuma and Glenn Beheim Jan. 1995 15 p Presented at the 1995 International Symposium on Lasers and Applications, San Jose, CA, 4-10 Feb. 1995; sponsored by the Society of Photo-Optical Instrumentation Engineers
(RTOP 505-62-50)
(NASA-TM-106850; E-9438; NAS 1.15:106850) Avail: CASI HC A03/MF A01

The effective-index method and Marcatili's technique were utilized independently to calculate the electric field profile of a rib channel waveguide. Using the electric field profile calculated from each method, the theoretical coupling efficiency between a single-mode optical fiber and a rib waveguide was calculated using the overlap integral. Perfect alignment was assumed and the coupling efficiency calculated. The coupling efficiency calculation was then repeated for a range of transverse offsets.

Author

N95-22957*# National Aeronautics and Space Administration. Goddard Space Flight Center, Greenbelt, MD.
SECOND INTERNATIONAL WORKSHOP ON HARMONIC OSCILLATORS
Daesoo Han, ed. and Kurt Bernardo Wolf, ed. (Universidad Nacional Autonoma de Mexico, Cuernavaca, Mexico.) Jan. 1995 420 p Workshop held in Cocoyoc, Mexico, 23-25 Mar. 1994
(Contract NAS5-30376)
(NASA-CP-3286; Rept-95B00017; NAS 1.55:3286) Avail: CASI HC A18/MF A04

The Second International Workshop on Harmonic Oscillators was held at the Hotel Hacienda Cocoyoc from March 23 to 25, 1994. The Workshop gathered 67 participants; there were 10 invited lecturers, 30 plenary oral presentations, 15 posters, and plenty of discussion divided into the five sessions of this volume. The Organizing Committee was asked by the chairman of several Mexican funding agencies what exactly was meant by harmonic oscillators, and for what purpose the new research could be useful. Harmonic oscillators - as we explained - is a code name for a family of mathematical models based on the theory of Lie algebras and groups, with applications in a growing range of physical theories and technologies: molecular, atomic, nuclear and particle physics; quantum optics and communication theory. For individual titles, see N95-22958 through N95-23007.

N95-22958*# Yale Univ., New Haven, CT. Physics Lab.
ALGEBRAIC THEORY OF MOLECULES **c72**
Franco Iachello *In* NASA. Goddard Space Flight Center, Second International Workshop on Harmonic Oscillators Jan. 1995 p 1-12
(For primary document see N95-22957 07-74)
(Grant DE-FG02-91ER-40608)
Avail: CASI HC A03/MF A04

An algebraic formulation of quantum mechanics is presented. In this formulation, operators of interest are expanded onto elements of an algebra, G. For bound state problems in nu dimensions the algebra G is taken to be U(nu + 1). Applications to the structure of molecules are presented.

Author

N95-22959*# Los Alamos National Lab., NM. Theoretical Div.
EXACT, E = 0, CLASSICAL AND QUANTUM SOLUTIONS FOR GENERAL POWER-LAW OSCILLATORS **c77**
Michael Martin Nieto and Jamil Daboul (Ben Gurion Univ. of the Negev, Beersheva, Israel.) *In* NASA. Goddard Space Flight Center, Second International Workshop on Harmonic Oscillators Jan. 1995 p 13-24
See also N95-16428 (For primary document see N95-22957 07-74)
Avail: CASI HC A03/MF A04

For zero energy, E = 0, we derive exact, classical and quantum solutions for all power-law oscillators with potentials V(r) = -gamma/r(exp nu), gamma greater than 0 and -infinity less than nu less than infinity. When the angular momentum is non-zero, these solutions lead to the classical orbits (p(t) = (cos mu(phi(t) - phi(sub 0)t))(exp 1/mu) with mu = nu/2 - 1 does not equal 0. For nu greater than 2, the orbits are bound and go through the origin. We calculate the periods and precessions of these bound orbits, and graph a number of specific examples. The unbound orbits are also discussed in detail. Quantum mechanically, this system is also exactly solvable. We find that when nu is greater than 2 the solutions are normalizable (bound), as in the classical case. Further, there are normalizable discrete, yet unbound, states. They correspond to unbound classical particles which reach infinity in a finite time. Finally, the number of space dimensions of the system can determine whether or not an E = 0 state is bound. These and other interesting comparisons to the classical system will be discussed.

Author

N95-22960*# Universidad Nacional Autonoma de Mexico, Mexico City (Mexico). Inst. de Ciencias Nucleares.
ALGEBRAIC APPROACH TO THE VIBRATIONAL EXCITATIONS IN METHANE **c72**
Renato Lemus and Alejandro Frank (Universidad Nacional Autonoma de Mexico, Cuernavaca, Mexico.) *In* NASA. Goddard Space Flight Center, Second International Workshop on Harmonic Oscillators Jan. 1995 p 25-30 (For primary document see N95-22957 07-74)
(Contract CONACyT-400340-5-3401E)
Avail: CASI HC A02/MF A04

We present a description of the vibrational excitations of methane by means of an algebraic analysis of a model of coupled anharmonic oscillators. Author

N95-22961*# Universidad Nacional Autonoma de Mexico, Mexico City (Mexico). Inst. de Ciencias Nucleares.
ALGEBRAIC DESCRIPTION OF ATOM-MOLECULE INTERACTIONS **c72**
R. D. Santiago, Alejandro Frank, and Renato Lemus *In* NASA. Goddard Space Flight Center, Second International Workshop on Harmonic Oscillators Jan. 1995 p 31-38 (For primary document see N95-22957 07-74)
(Contract CONACyT-400340-5-3401E)
Avail: CASI HC A02/MF A04

We describe a new method based on algebraic techniques, which leads to a model of atom-diatom collisions. Author

N95-22962*# Karlsruhe Univ. (Germany). Inst. fuer Theoretische Physik.
FIBONACCI CHAIN POLYNOMIALS: IDENTITIES FROM SELF-SIMILARITY **c72**
Wolfdieter Lang *In* NASA. Goddard Space Flight Center, Second International Workshop on Harmonic Oscillators Jan. 1995 p 39-44 (For primary document see N95-22957 07-74)
Avail: CASI HC A02/MF A04

Fibonacci chains are special diatomic, harmonic chains with uniform nearest neighbor interaction and two kinds of atoms (mass-ratio r) arranged according to the self-similar binary Fibonacci sequence ABAABABA..., which is obtained by repeated substitution of A yields AB and B yields A. The implications of the self-similarity of this sequence for the associated orthogonal polynomial systems which govern these Fibonacci chains with fixed mass-ratio r are studied. Author

N95-22963*# Universidade Estadual de Paulista, Sao Paulo (Brazil).
A SUPERSYMMETRIC FAMILY OF HARMONIC OSCILLATORS SIMULATING H-BONDS IN DNA **c51**
Elso Drigo Filho and Jose R. Ruggiero *In* NASA. Goddard Space Flight Center, Second International Workshop on Harmonic Oscillators Jan. 1995 p 45-49 Sponsored by CNPq and FAPESP (For primary document see N95-22957 07-74)
Avail: CASI HC A01/MF A04

We test an isospectral potential from harmonic oscillator simulating H-bond interaction in DNA macromolecules. Author

N95-22964*# Universidad Autonoma del Estado de Morelos, Cuernavaca (Mexico). Facultad de Ciencias.
MOLECULAR VIBRATIONAL STATES DURING A COLLISION **c72**
Jose A. Recamier and Rocio Jauregui (Universidad Nacional Autonoma de Mexico, Mexico City, Mexico.) *In* NASA. Goddard Space Flight Center, Second International Workshop on Harmonic Oscillators Jan. 1995 p 51-60 (For primary document see N95-22957 07-74)
Avail: CASI HC A02/MF A04

Alternative algebraic techniques to approximate a given Hamiltonian by a harmonic oscillator are described both for time-independent and time-dependent systems. We apply them to the description of a one dimensional atom-diatom collision. From the resulting evolution operator, we evaluate vibrational transition probabilities as well as other time-dependent properties. As expected, the ground vibrational state becomes a squeezed state during the collision. Author

N95-22965*# Universidad Nacional Autonoma de Mexico, Mexico City (Mexico). Inst. de Fisica.
QUANTUM FIELD BETWEEN MOVING MIRRORS: A THREE DIMENSIONAL EXAMPLE **c77**
S. Hacyan, Roco Jauregui, and Carlos Villarreal *In* NASA. Goddard Space Flight Center, Second International Workshop on Harmonic Oscillators Jan. 1995 p 61-67 (For primary document see N95-22957 07-74)
Avail: CASI HC A02/MF A04

The scalar quantum field uniformly moving plates in three dimensional space is studied. Field equations for Dirichlet boundary conditions are solved exactly. Comparison of the resulting wavefunctions with their instantaneous static counterpart is performed via Bogolubov coefficients. Unlike the one dimensional problem, 'particle' creation as well as squeezing may occur. The time dependent Casimir energy is also evaluated. Author

N95-22966*# Michigan Univ., Ann Arbor, MI. Dept. of Physics.
COHERENT STATE CONSTRUCTIONS OF BASES FOR SOME PHYSICALLY RELEVANT GROUP CHAINS **c72**
Karl T. Hecht *In* NASA. Goddard Space Flight Center, Second International Workshop on Harmonic Oscillators Jan. 1995 p 69-82 (For primary document see N95-22957 07-74)
Avail: CASI HC A03/MF A04

Rotor coherent state constructions are given for the Wigner supermultiplet SU(4) contains SU(2)xSU(2) and for the special irreducible representations (N0) of the SO(5) contains SO(3) contains SO(2) group chain in exact parallel with the rotor coherent state construction for the SU(3) contains SO(3) contains SO(2) case given by Rowe, LeBlanc,, and Repka. Matrix elements of the coherent state realizations of the group generators are given in all cases by very simple expressions in terms of angular momentum Wigner coefficients involving intrinsic projection labels K. The K-matrix technique of vector coherent state theory is used to effectively elevate these K labels to the status of good quantum numbers. Analytic expressions are given for the (K K*)-matrices for many of the more important irreducible representations. Author

N95-22967*# Universidad Nacional Autonoma de Mexico, Mexico City (Mexico). Inst. de Fisica.
HARMONIC OSCILLATOR REPRESENTATION IN THE THEORY OF SCATTERING AND NUCLEAR REACTIONS **c72**
Yuri F. Smirnov, A. M. Shirokov (Moscow State Univ., Russia.), Yuri Lurie, A. (Moscow State Univ., Russia.), and S. A. Zaitsev (Moscow State Univ., Russia.) *In* NASA. Goddard Space Flight Center, Second International Workshop on Harmonic Oscillators Jan. 1995 p 83-98 (For primary document see N95-22957 07-74)
Avail: CASI HC A03/MF A04

The following questions, concerning the application of the harmonic oscillator representation (HOR) in the theory of scattering and reactions, are discussed: the formulation of the scattering theory in HOR; exact solutions of the free motion Schroedinger equation in HOR; separable expansion of the short range potentials and the calculation of the phase shifts; 'isolated states' as generalization of the Wigner-von Neumann bound states embedded in continuum; a nuclear coupled channel problem in HOR; and the description of true three body scattering in HOR. As an illustration the soft dipole mode in the (11)Li nucleus is considered in a frame of the (9)Li+n+n cluster model taking into account of three body continuum effects. Author

N95-22968*# Louisiana State Univ., Baton Rouge, LA. Dept. of Physics and Astronomy.
GEOMETRICAL INTERPRETATION FOR THE OUTER SU(3) OUTER MULTIPLICITY LABEL **c72**
Jerry P. Draayer and D. Troltenier *In* NASA. Goddard Space Flight Center, Second International Workshop on Harmonic Oscillators Jan. 1995 p 99-10 Sponsored by NSF (For primary document see N95-22957 07-74)
Avail: CASI HC A02/MF A04

A geometrical interpretation for the outer multiplicity rho that occurs in a reduction of the product of two SU(3) representations, (lambda(sub pi), mu(sub pi)) x (lambda(sub nu), mu(sub nu)) approaches sigma(sub rho)(lambda, mu)(sub rho), is introduced. This coupling of proton (pi) and neutron (nu) representations arises, for example, in both boson and fermion

descriptions of heavy deformed nuclei. Attributing a geometry to the coupling raises the possibility of introducing a simple interaction that provides a physically meaningful way for distinguishing multiple occurrences of (lambda, mu) values that can arise in such products. Author

N95-22969*# Universidad Nacional Autonoma de Mexico, Mexico City (Mexico). Inst. de Ciencias Nucleares.

BOSON MAPPING TECHNIQUES APPLIED TO CONSTANT GAUGE FIELDS IN QCD **c72**

Peter Otto Hess and J. C. Lopez *In* NASA. Goddard Space Flight Center, Second International Workshop on Harmonic Oscillators Jan. 1995 p 107-111 Sponsored by Dept. General de Asuntos del Personal Academico (For primary document see N95-22957 07-74)

Avail: CASI HC A01/MF A04

Pairs of coordinates and derivatives of the constant gluon modes are mapped to new gluon-pair fields and their derivatives. Applying this mapping to the Hamiltonian of constant gluon fields results for large coupling constants into an effective Hamiltonian which separates into one describing a scalar field and another one for a field with spin two. The ground state is dominated by pairs of gluons coupled to color and spin zero with slight admixtures of color zero and spin two pairs. As color group we used SU(2). Author

N95-22970*# Hungarian Academy of Sciences, Debrecen. Inst. of Nuclear Research.

A POSSIBLE GENERALIZATION OF THE HARMONIC OSCILLATOR POTENTIAL **c77**

Geza Levai *In* NASA. Goddard Space Flight Center, Second International Workshop on Harmonic Oscillators Jan. 1995 p 113-119 (For primary document see N95-22957 07-74)

(Grant OTKA-4303)

Avail: CASI HC A02/MF A04

A four-parameter potential is analyzed, which contains the three-dimensional harmonic oscillator as a special case. This potential is exactly solvable and retains several characteristics of the harmonic oscillator, and also of the Coulomb problem. The possibility of similar generalizations of other potentials is also pointed out. Author

N95-22971*# Hungarian Academy of Sciences, Debrecen. Inst. of Nuclear Research.

AN ALGEBRAIC CLUSTER MODEL BASED ON THE HARMONIC OSCILLATOR BASIS **c72**

Geza Levai and J. Cseh *In* NASA. Goddard Space Flight Center, Second International Workshop on Harmonic Oscillators Jan. 1995 p 121-127 (For primary document see N95-22957 07-74)

(Grant OTKA-3008)

Avail: CASI HC A02/MF A04

We discuss the semimicroscopic algebraic cluster model introduced recently, in which the internal structure of the nuclear clusters is described by the harmonic oscillator shell model, while their relative motion is accounted for by the Vibron model. The algebraic formulation of the model makes extensive use of techniques associated with harmonic oscillators and their symmetry group, SU(3). The model is applied to some cluster systems and is found to reproduce important characteristics of nuclei in the sd-shell region. An approximate SU(3) dynamical symmetry is also found to hold for the C-12 + C-12 system. Author

N95-22972*# Kurchatov (I. V.) Inst. of Atomic Energy, Moscow (USSR). Russian Research Center.

HARMONIC OSCILLATOR IN QUANTUM ROTATIONAL SPECTRA: MOLECULES AND NUCLEI **c72**

Igor M. Pavlichenkov *In* NASA. Goddard Space Flight Center, Second International Workshop on Harmonic Oscillators Jan. 1995 p 129-136 Sponsored by International Science Foundation (For primary document see N95-22957 07-74)

Avail: CASI HC A02/MF A04

The mapping of a rotational dynamics on a harmonic oscillator is considered. The method used for studying the stabilization of the rigid top rotation around the intermediate moment of inertial axix by orbiting particle is described. Author

N95-22973*# Tulane Univ., New Orleans, LA. Dept. of Physics.

GALACTIC OSCILLATOR SYMMETRY **c77**

George Rosensteel *In* NASA. Goddard Space Flight Center, Second International Workshop on Harmonic Oscillators Jan. 1995 p 137-143 (For primary document see N95-22957 07-74)

(Grant NSF PHY-92-12231)

Avail: CASI HC A02/MF A04

Riemann ellipsoids model rotating galaxies when the galactic velocity field is a linear function of the Cartesian coordinates of the galactic masses. In nuclear physics, the kinetic energy in the linear velocity field approximation is known as the collective kinetic energy. But, the linear approximation neglects intrinsic degrees of freedom associated with nonlinear velocity fields. To remove this limitation, the theory of symplectic dynamical symmetry is developed for classical systems. A classical phase space for a self-gravitating symplectic system is a co-adjoint orbit of the noncompact group SP(3,R). The degenerate co-adjoint orbit is the 12 dimensional homogeneous space Sp(3,R)/U(3), where the maximal compact subgroup U(3) is the symmetry group of the harmonic oscillator. The Hamiltonian equations of motion on each orbit form a Lax system X = (X,F), where X and F are elements of the symplectic Lie algebra. The elements of the matrix X are the generators of the symplectic Lie algebra, viz., the one-body collective quadratic functions of the positions and momenta of the galactic masses. The matrix F is composed from the self-gravitating potential energy, the angular velocity, and the hydostatic pressure. Solutions to the hamiltonian dynamical system on Sp(3,R)/U(3) are given by symplectic isospectral deformations. The Casimirs of Sp(3,R), equal to the traces of powers of X, are conserved quantities. Author

N95-22974*# Universidad Nacional Autonoma de Mexico, Cuernavaca (Mexico). Dept. de Fisica.

SHAPES AND STABILITY OF ALGEBRAIC NUCLEAR MODELS **c72**

Enrique Lopez-Moreno and Octavio Castanos (Universidad Nacional Autonoma de Mexico, Mexico City, Mexico.) *In* NASA. Goddard Space Flight Center, Second International Workshop on Harmonic Oscillators Jan. 1995 p 145-152 (For primary document see N95-22957 07-74)

Avail: CASI HC A02/MF A04

A generalization of the procedure to study shapes and stability of algebraic nuclear models introduced by Gilmore is presented. One calculates the expectation value of the Hamiltonian with respect to the coherent states of the algebraic structure of the system. Then equilibrium configurations of the resulting energy surface, which depends in general on state variables and a set of parameters, are classified through the Catastrophe theory. For one- and two-body interactions in the Hamiltonian of the interacting Boson model-1, the critical points are organized through the Cusp catastrophe. As an example, we apply this Separatrix to describe the energy surfaces associated to the Rutenium and Samarium isotopes. Author

N95-22975*# Universidad Nacional Autonoma de Mexico, Cuernavaca (Mexico). Inst. de Investigaciones en Matematicas Aplicadas y en Sistemas.

A RAMANUJAN-TYPE MEASURE FOR THE ASKEY-WILSON POLYNOMIALS **c67**

Natig M. Atakishiyev *In* NASA. Goddard Space Flight Center, Second International Workshop on Harmonic Oscillators Jan. 1995 p 153-164 Sponsored by Direccion General de Asuntos del Persona Academico (For primary document see N95-22957 07-74)

Avail: CASI HC A03/MF A04

A Ramanujan-type representation for the Askey-Wilson q-beta integral, admitting the transformation q to q(exp -1), is obtained. Orthogonality of the Askey-Wilson polynomials with respect to a measure, entering into this representation, is proved. A simple way of evaluating the Askey-Wilson q-beta integral is also given. Author

N95-22976*# Naples Univ. (Italy). Dept. di Scienze Fisiche.

NONCLASSICAL LIGHT IN INTERFEROMETRIC MEASUREMENTS

N. A. Ansari, L. DiFiore, R. Romano, S. Solimeno, F. Zaccaria, Margarita A. Manko (Academy of Sciences, USSR, Moscow, USSR.), and Vladimir I. Manko (Academy of Sciences, USSR, Moscow, USSR.) *In* NASA. Goddard Space Flight Center, Second International Workshop on Harmonic Oscillators Jan. 1995 p 165-172 (For primary document see N95-22957

07-74)
Avail: CASI HC A02/MF A04

It is shown that the even and odd coherent light and other nonclassical states of light like superposition of coherent states with different phases may replace the squeezed light in an interferometric gravitational wave detector to increase its sensitivity. Author

N95-22977*# Chile Univ., Santiago (Chile). Dept. de Fisica.
NON-NOETHERIAN SYMMETRIES FOR OSCILLATORS IN CLASSICAL MECHANICS AND IN FIELD THEORY **c77**
Sergio A. Hojman, Jamie DeLaJara, and Leda Pena *In* NASA. Goddard Space Flight Center, Second International Workshop on Harmonic Oscillators Jan. 1995 p 173-179 Sponsored by Fondo Facional de Ciencia y Tecnologia, Fundacion Andes, Comision Nacional de Investigacion Cientifica y Tecnologica-Fundacion Andes and Consejo Nacional de Ciencia y Tecnologia (For primary document see N95-22957 07-74)
Avail: CASI HC A02/MF A04

Infinitely many new conservation laws both for free fields as well as for test fields evolving on a given gravitational background are presented. The conserved currents are constructed using the field theoretical counterpart of a recently discovered non-Noetherian symmetry which gives rise to a new way of solving the classical small oscillations problem. Several examples are discussed. Author

N95-22978*# Brussels Univ. (Belgium). Physique Nucleaire Theorique et physique Mathematique.
COVARIANT DEFORMED OSCILLATOR ALGEBRAS **c67**
Christiane Quesne *In* NASA. Goddard Space Flight Center, Second International Workshop on Harmonic Oscillators Jan. 1995 p 181-188 (For primary document see N95-22957 07-74)
Avail: CASI HC A02/MF A04

The general form and associativity conditions of deformed oscillator algebras are reviewed. It is shown how the latter can be fulfilled in terms of a solution of the Yang-Baxter equation when this solution has three distinct eigenvalues and satisfies a Birman-Wenzl-Murakami condition. As an example, an SU(sub q)(n) x SU(sub q)(m)-covariant q-bosonic algebra is discussed in some detail. Author

N95-22979*# Instituto Venezolano de Investigaciones Cientificas, Caracas (Venezuela). Centro de Fisica.
LOCALIZATION IN DEFORMED QUANTUM MECHANICS **c77**
Simon Codriansky *In* NASA. Goddard Space Flight Center, Second International Workshop on Harmonic Oscillators Jan. 1995 p 189-193 Sponsored by Vicerrectorado de Investigacion y Postgrado of Universidasd Pedagogica Experimental Libertador and CONICIT (For primary document see N95-22957 07-74)
Avail: CASI HC A01/MF A04

In this talk it is shown that in one version of q-algebras there exists states-a subset of the coherent states- that have negligible dispersion in energy, position and momentum. Author

N95-22980*# Liverpool Univ. (England). Dept. of Electrical Engineering and Electronics.
NOISY BASES IN HILBERT SPACE: A NEW CLASS OF THERMAL COHERENT STATES AND THEIR PROPERTIES **c77**
A. Vourdas and R. F. Bishop (Manchester Coll. of Science and Technology, England.) *In* NASA. Goddard Space Flight Center, Second International Workshop on Harmonic Oscillators Jan. 1995 p 195-206 (For primary document see N95-22957 07-74)
Avail: CASI HC A03/MF A04

Coherent mixed states (or thermal coherent states) associated with the displaced harmonic oscillator at finite temperature, are introduced as a 'random' (or 'thermal' or 'noisy') basis in Hilbert space. A resolution of the identity for these states is proved and used to generalize the usual coherent state formalism for the finite temperature case. The Bargmann representation of an operator is introduced and its relation to the P and Q representations is studied. Generalized P and Q representations for the finite temperature case are also considered and several interesting relations among them are derived. Author

N95-22981*# Instituto Politecnico Nacional, Mexico City (Mexico). Dept de Fisica.
GEOMETRIC PHASES, EVOLUTION LOOPS AND GENERALIZED OSCILLATOR POTENTIALS **c77**
David J. Fernandez *In* NASA. Goddard Space Flight Center, Second International Workshop on Harmonic Oscillators Jan. 1995 p 207-213 Sponsored by CONACYT (For primary document see N95-22957 07-74)
Avail: CASI HC A02/MF A04

The geometric phases for dynamical processes where the evolution operator becomes the identity (evolution loops) are studied. The case of time-independent Hamiltonians with equally spaced energy levels is considered; special emphasis is made on the potentials having the same spectrum as the harmonic oscillator potential (the generalized oscillator potentials) and their recently found coherent states. Author

N95-22982*# Instituto Politecnico Nacional, Mexico City (Mexico). Dept. of Fisica.
COHERENT STATES FOR A GENERALIZATION OF THE HARMONIC OSCILLATOR **c77**
David J. Fernandez, Veronique Hussin (Montreal Univ., Quebec.), and Luis M. Nieto (Montreal Univ., Quebec.) *In* NASA. Goddard Space Flight Center, Second International Workshop on Harmonic Oscillators Jan. 1995 p 215-221 Sponsored by CONACYT, NSERC of Canada, FCAR du Gouverment du Quebec, and Ministerio de Educacion y Ciencia (For primary document see N95-22957 07-74)
Avail: CASI HC A02/MF A04

Coherent states for a family of isospectral oscillator Hamiltonians are derived from a suitable choice of annihilation and creation operators. The Fock-Bargmann representation is also obtained. Author

N95-22983*# Oklahoma Univ., Norman, OK.
FINITE-ELEMENT TIME EVOLUTION OPERATOR FOR THE ANHARMONIC OSCILLATOR **c77**
Kimball A. Milton *In* NASA. Goddard Space Flight Center, Second International Workshop on Harmonic Oscillators Jan. 1995 p 223-230 Sponsored by DOE (For primary document see N95-22957 07-74)
Avail: CASI HC A02/MF A04

The finite-element approach to lattice field theory is both highly accurate (relative errors approximately 1/N(exp 2), where N is the number of lattice points) and exactly unitary (in the sense that canonical commutation relations are exactly preserved at the lattice sites). In this talk I construct matrix elements for dynamical variables and for the time evolution operator for the anharmonic oscillator, for which the continuum Hamiltonian is H = p(exp 2)/2 + lambda q(exp 4)/4. Construction of such matrix elements does not require solving the implicit equations of motion. Low order approximations turn out to be extremely accurate. For example, the matrix element of the time evolution operator in the harmonic oscillator ground state gives a results for the anharmonic oscillator ground state energy accurate to better than 1 percent, while a two-state approximation reduces the error to less than 0.1 percent. Author

N95-22984*# State Univ. of New York, Binghamton, NY.
q-BOSONS AND THE q-ANALOGUE QUANTIZED FIELD **c72**
Charles A. Nelson *In* NASA. Goddard Space Flight Center, Second International Workshop on Harmonic Oscillators Jan. 1995 p 231-237 (For primary document see N95-22957 07-74)
Avail: CASI HC A02/MF A04

The q-analogue coherent states are used to identify physical signatures for the presence of a 1-analogue quantized radiation field in the q-CS classical limits where the absolute value of z is large. In this quantum-optics-like limit, the fractional uncertainties of most physical quantities (momentum, position, amplitude, phase) which characterize the quantum field are O(1). They only vanish as O(1/absolute value of z) when q = 1. However, for the number operator, N, and the N-Hamiltonian for a free q-boson gas, H(sub N) = h(omega)(N + 1/2), the fractional uncertainties do still approach zero. A signature for q-boson counting statistics is that (Delta N)(exp 2)/ (N) approaches 0 as the absolute value of z approaches infinity. Except for its O(1) fractional uncertainty, the q-generalization of the Hermitian phase operator of Pegg and Barnett, phi(sub q), still exhibits normal classical behavior. The standard number-phase uncertainty-relation, Delta(N) Delta phi(sub q) = 1/2, and the approximate commutation relation, (N, phi(sub q)) = i, still hold for the

single-mode q-analogue quantized field. So, N and phi(sub q) are almost canonically conjugate operators in the q-CS classical limit. The q-analogue CS's minimize this uncertainty relation for moderate (absolute value of z)(exp 2). Author

N95-22985*# Saint Louis Univ., Cahokia, IL.
AN ALGORITHM FOR THE BASIS OF THE FINITE FOURIER TRANSFORM **c61**
Thalanayar S. Santhanam *In* NASA. Goddard Space Flight Center, Second International Workshop on Harmonic Oscillators Jan. 1995 p 239-248 (For primary document see N95-22957 07-74)
Avail: CASI HC A02/MF A04

The Finite Fourier Transformation matrix (F.F.T.) plays a central role in the formulation of quantum mechanics in a finite dimensional space studied by the author over the past couple of decades. An outstanding problem which still remains open is to find a complete basis for F.F.T. In this paper we suggest a simple algorithm to find the eigenvectors of F.T.T. Author

N95-22986*# Georgia Inst. of Tech., Atlanta, GA. School of Electrical Engineering.
A NOTE ON THE ANGULAR FOURIER TRANSFORMATION **c67**
Balu Santhanam and Thalanayar S. Santhanam (Saint Louis Univ., Cahokia, IL.) *In* NASA. Goddard Space Flight Center, Second International Workshop on Harmonic Oscillators Jan. 1995 p 249-254 (For primary document see N95-22957 07-74)
Avail: CASI HC A02/MF A04

It is demonstrated that an angular Fourier transformation is obtained by making a rotation around the non-compact axis of So(2,1), the Lorentz group in three dimensions. Author

N95-22987*# Universidad Nacional Autonoma de Mexico, Cuernavaca (Mexico). Lab. de Cibernetica.
NEURODYNAMIC OSCILLATORS **c52**
Ismael Espinosa, Hortensia Gonzalez, Jorge Quiza, J. Jesus Gonazalez, Ruben Arroyo, and Ritaluz Lara (Instituto Politecnico Nacional, Mexico City, Mexico.) *In* NASA. Goddard Space Flight Center, Second International Workshop on Harmonic Oscillators Jan. 1995 p 255-262 Sponsored by Direccion General de Asuntos del Personal Academico (For primary document see N95-22957 07-74)
Avail: CASI HC A02/MF A04

Oscillation of electrical activity has been found in many nervous systems, from invertebrates to vertebrates including man. There exists experimental evidence of very simple circuits with the capability of oscillation. Neurons with intrinsic oscillation have been found and also neural circuits where oscillation is a property of the network. These two types of oscillations coexist in many instances. It is nowadays hypothesized that behind synchronization and oscillation there is a system of coupled oscillators responsible for activities that range from locomotion and feature binding in vision to control of sleep and circadian rhythms. The huge knowledge that has been acquired on oscillators from the times of Lord Rayleigh has made the simulation of neural oscillators a very active endeavor. This has been enhanced with more recent physiological findings about small neural circuits by means of intracellular and extracellular recordings as well as imaging methods. The future of this interdisciplinary field looks very promising; some researchers are going into quantum mechanics with the idea of trying to provide a quantum description of the brain. In this work we describe some simulations using neuron models by means of which we form simple neural networks that have the capability of oscillation. We analyze the oscillatory activity with root locus method, cross-correlation histograms, and phase planes. In the more complicated neural network models there is the possibility of chaotic oscillatory activity and we study that by means of Lyapunov exponents. The companion paper shows an example of that kind. Author

N95-22988*# Universidad Nacional Autonoma de Mexico, Cuernavaca (Mexico). Lab. de Cibernetica.
LYAPUNOV EXPONENTS FROM CHUA'S CIRCUIT TIME SERIES USING ARTIFICIAL NEURAL NETWORKS **c63**
J. Jesus Gonzalez, Ismael E. Espinosa, and Alberto M. Fuentes *In* NASA. Goddard Space Flight Center, Second International Workshop on Harmonic Oscillators Jan. 1995 p 263-269 Sponsored by CONACYT (For primary document see N95-22957 07-74)
(DGAPA Proj-IN100593-UNAM)
Avail: CASI HC A03/MF A04

In this paper we present the general problem of identifying if a nonlinear dynamic system has a chaotic behavior. If the answer is positive the system will be sensitive to small perturbations in the initial conditions which will imply that there is a chaotic attractor in its state space. A particular problem would be that of identifying a chaotic oscillator. We present an example of three well known different chaotic oscillators where we have knowledge of the equations that govern the dynamical systems and from there we can obtain the corresponding time series. In a similar example we assume that we only know the time series and, finally, in another example we have to take measurements in the Chua's circuit to obtain sample points of the time series. With the knowledge about the time series the phase plane portraits are plotted and from them, by visual inspection, it is concluded whether or not the system is chaotic. This method has the problem of uncertainty and subjectivity and for that reason a different approach is needed. A quantitative approach is the computation of the Lyapunov exponents. We describe several methods for obtaining them and apply a little known method of artificial neural networks to the different examples mentioned above. We end the paper discussing the importance of the Lyapunov exponents in the interpretation of the dynamic behavior of biological neurons and biological neural networks. Author

N95-22989*# Costa Rica National Univ., Heredia (Costa Rica). Dept. de Fisica.
A METHOD OF SOLVING SIMPLE HARMONIC OSCILLATOR SCHROEDINGER EQUATION **c67**
Juan Carlos F. Maury *In* NASA. Goddard Space Flight Center, Second International Workshop on Harmonic Oscillators Jan. 1995 p 271-273 (For primary document see N95-22957 07-74)
Avail: CASI HC A01/MF A04

A usual step in solving totally Schrodinger equation is to try first the case when dimensionless position independent variable w is large. In this case the Harmonic Oscillator equation takes the form (d(exp 2)/dw(exp 2) - w(exp 2))F = 0, and following W.K.B. method, it gives the intermediate corresponding solution F = exp(-w(exp 2)/2), which actually satisfies exactly another equation, (d(exp 2)/dw(exp 2) + 1 - w(exp 2))F = 0. We apply a different method, useful in anharmonic oscillator equations, similar to that of Rampal and Datta, and although it is slightly more complicated however it is also more general and systematic. Author

N95-22990*# Academia R. P. R., Bucharest (Romania). Dept. of Theoretical Physics.
WIGNER DISTRIBUTION FUNCTION AND ENTROPY OF THE DAMPED HARMONIC OSCILLATOR WITHIN THE THEORY OF THE OPEN QUANTUM SYSTEMS **c67**
Aurelian Isar *In* NASA. Goddard Space Flight Center, Second International Workshop on Harmonic Oscillators Jan. 1995 p 275-282 (For primary document see N95-22957 07-74)
Avail: CASI HC A02/MF A04

The harmonic oscillator with dissipation is studied within the framework of the Lindblad theory for open quantum systems. By using the Wang-Uhlenbeck method, the Fokker-Planck equation, obtained from the master equation for the density operator, is solved for the Wigner distribution function, subject to either the Gaussian type or the delta-function type of initial conditions. The obtained Wigner functions are two-dimensional Gaussians with different widths. Then a closed expression for the density operator is extracted. The entropy of the system is subsequently calculated and its temporal behavior shows that this quantity relaxes to its equilibrium value. Author

N95-22991*# Universidad Nacional Autonoma de Mexico, Mexico City (Mexico). Inst. de Fisica.
THE RELATIVISTIC MANY BODY PROBLEM WITH AN OSCILLATOR INTERACTION **c77**
Marcos Moshinsky *In* NASA. Goddard Space Flight Center, Second International Workshop on Harmonic Oscillators Jan. 1995 p 283-292 (For primary document see N95-22957 07-74)
Avail: CASI HC A02/MF A04

We start with the total energy E for a system of three scalar relativistic particles that, because of Einstein's relation, will have square roots of

functions of the momenta. By taking powers of this relation, we finally get a fourth degree polynomial in E(exp 2), where the square roots have disappeared, and which we can convert into a type of Schroedinger equation. To be in the center of mass frame we pass to Jocobi momenta and then replace them by creation and annihilation operators. We thus get an equation in terms of the generators of a U(2) group, which, in principle, we can solve in an elementary way. Finally, we rewrite our equation in a Poincare invariant form. Author

N95-22992*# National Aeronautics and Space Administration. Goddard Space Flight Center, Greenbelt, MD.

COVARIANT HARMONIC OSCILLATORS AND COUPLED HARMONIC OSCILLATORS **c77**

Daesoo Han, Young S. Kim (Maryland Univ., College Park, MD.), and Marilyn E. Noz (New York Univ., New York, NY.) *In its* Second International Workshop on Harmonic Oscillators Jan. 1995 p 293-304 (For primary document see N95-22957 07-74)

Avail: CASI HC A03/MF A04

It is shown that the system of two coupled harmonic oscillators shares the basic symmetry properties with the covariant harmonic oscillator formalism which provides a concise description of the basic features of relativistic hadronic features observed in high-energy laboratories. It is shown also that the coupled oscillator system has the SL(4,r) symmetry in classical mechanics, while the present formulation of quantum mechanics can accommodate only the Sp(4,r) portion of the SL(4,r) symmetry. The possible role of the SL(4,r) symmetry in quantum mechanics is discussed. Author

N95-22993*# Granada Univ. (Spain). Inst. de fisica Teorica y Computacional.

COHERENT STATES FOR THE RELATIVISTIC HARMONIC OSCILLATOR **c77**

Victor Aldaya and J. Guerrero *In* NASA. Goddard Space Flight Center, Second International Workshop on Harmonic Oscillators Jan. 1995 p 305-312 (For primary document see N95-22957 07-74)

Avail: CASI HC A02/MF A04

Recently we have obtained, on the basis of a group approach to quantization, a Bargmann-Fock-like realization of the Relativistic Harmonic Oscillator as well as a generalized Bargmann transform relating fock wave functions and a set of relativistic Hermite polynomials. Nevertheless, the relativistic creation and annihilation operators satisfy typical relativistic commutation relations of the Lie product (vector-z, vector-z(sup dagger)) approximately equals Energy (an SL(2,R) algebra). Here we find higher-order polarization operators on the SL(2,R) group, providing canonical creation and annihilation operators satisfying the Lie product (vector-a, vector-a(sup dagger)) = identity vector 1, the eigenstates of which are 'true' coherent states. Author

N95-22994*# Liege Univ. (Belgium). Dept. of Theoretical and Mathematical Physics.

ON PSEUDOSUPERSYMMETRIC OSCILLATORS AND REALITY OF RELATIVISTIC ENERGIES FOR VECTOR MESONS **c72**

Jules Beckers and Nathalie Debergh *In* NASA. Goddard Space Flight Center, Second International Workshop on Harmonic Oscillators Jan. 1995 p 313-318 (For primary document see N95-22957 07-74)

Avail: CASI HC A02/MF A04

Specific oscillators - hereafter called pseudosupersymmetric oscillators - appear as interesting nonrelativistic concepts in connection with the study of relativistic vector mesons interacting with an external constant magnetic field when the real character of the energy eigenvalues is required as expected. A new pseudosupersymmetric quantum mechanics can then be developed and the corresponding pseudosupersymmetries can be pointed out. Author

N95-22995*# Liege Univ. (Belgium). Dept. of Theoretical and Mathematical Physics.

ON PARASUPERSYMMETRIC OSCILLATORS AND RELATIVISTIC VECTOR MESONS IN CONSTANT MAGNETIC FIELDS **c72**

Nathalie Debergh and Jules Beckers *In* NASA. Goddard Space Flight Center, Second International Workshop on Harmonic Oscillators Jan. 1995 p 319-325 (For primary document see N95-22957 07-74)

Avail: CASI HC A02/MF A04

Johnson-Lippmann considerations on oscillators and their connection with the minimal coupling schemes are visited in order to introduce a new Sakata-Taketani equation describing vector mesons in interaction with a constant magnetic field. This new proposal, based on a specific parasupersymmetric oscillator-like system, is characterized by real energies as opposed to previously pointed out relativistic equations corresponding to this interacting context. Author

N95-22996*# Universidad Nacional Autonoma de Mexico, Cuernavaca (Mexico). Inst. de Fisica.

PSEUDOCLASSICAL DESCRIPTION OF THE DIRAC OSCILLATOR **c77**

Antonio DelSolMesa and R. P. MartinezyRomero *In* NASA. Goddard Space Flight Center, Second International Workshop on Harmonic Oscillators Jan. 1995 p 327-332 Sponsored by direccion General de Asuntos del Personal Academico and ESP (For primary document see N95-22957 07-74)

Avail: CASI HC A02/MF A04

In this paper we discuss the Dirac Oscillator wave equation in terms of pseudoclassical language, using Grassmann variables to describe the internal degrees of freedom of the oscillator. Regarding the original wave equation as a classical constraint, we use the theory of constrained systems, to develop a reparameterization invariant lagrangian, which is the pseudoclassical equivalent of the quantum case. The consistency of the Hamiltonian formalism and the quantization procedure are also analyzed. Author

N95-22997*# Ciudad Univ., Mexico City (Mexico). Escuela de Fisica.

NOTES ON OSCILLATOR-LIKE INTERACTIONS OF VARIOUS SPIN RELATIVISTIC PARTICLES **c72**

Valeri V. Dvoeglazov and Antonio delSolMesa (Universidad Nacional Autonoma de Mexico, Mexico City, Mexico.) *In* NASA. Goddard Space Flight Center, Second International Workshop on Harmonic Oscillators Jan. 1995 p 333-340 (For primary document see N95-22957 07-74)

Avail: CASI HC A02/MF A04

The equations for various spin particles with oscillator-like interactions are discussed in this talk. Topics discussed include: (1) comment on 'The Klein-Gordon Oscillator'; (2) the Dirac oscillator in quaternion form; (3) the Dirac-Dowker oscillator; (4) the Weinberg oscillator; and (5) note on the two-body Dirac oscillator. Author

N95-22998*# Surrey Univ., Guildford (England). Dept. of Physics.

THE DUFFIN-KEMMER-PETIAU OSCILLATOR **c77**

Youcef Nedjadi and Roger Barrett *In* NASA. Goddard Space Flight Center, Second International Workshop on Harmonic Oscillators Jan. 1995 p 341-348 (For primary document see N95-22957 07-74)

(Grant SERC GR/H53648)

Avail: CASI HC A02/MF A04

In view of current interest in relativistic spin-one systems and the recent work on the Dirac Oscillator, we introduce the Duffin-Kemmer-Petiau (DKP) equation obtained by using an external potential linear in r. Since, in the non-relativistic limit, the spin 1 representation leads to a harmonic oscillator with a spin-orbit coupling of the Thomas form, we call the equation the DKP oscillator. This oscillator is a relativistic generalization of the quantum harmonic oscillator for scalar and vector bosons. We show that it conserves total angular momentum and that it is exactly solvable. We calculate and discuss the eigenspectrum of the DKP oscillator in the spin 1 representation. Author

N95-22999*# Saint Petersburg State Univ., Saint Petersburg (Russia). Inst. of Physics.

HARMONIC OSCILLATORS AND RESONANCE SERIES GENERATED BY A PERIODIC UNSTABLE CLASSICAL ORBIT **c77**

A. K. Kazansky and Valentin N. Ostrovsky *In* NASA. Goddard Space Flight Center, Second International Workshop on Harmonic Oscillators (SEE N95-22957 07-74) Jan. 1995 Sponsored by Russian Foundation for Foundamental Researches (For primary document see N95-22957 07-74)

Avail: CASI HC A02/MF A04

The presence of an unstable periodic classical orbit allows one to introduce the decay time as a purely classical magnitude: inverse of the Lyapunov index which characterizes the orbit instability. The Uncertainty Relation gives the corresponding resonance width which is proportional to the Planck constant. The more elaborate analysis is based on the parabolic

equation method where the problem is effectively reduced to the multidimensional harmonic oscillator with the time-dependent frequency. The resonances form series in the complex energy plane which is equidistant in the direction perpendicular to the real axis. The applications of the general approach to various problems in atomic physics are briefly exposed. Author

N95-23000*# Guanajuato Univ., Guanajuato (Mexico). Inst. de Fisica.
SHANNON-WEHRL ENTROPY FOR COSMOLOGICAL AND BLACK-HOLE SQUEEZING **c90**
Haret Rosu and Marco Reyes *In* NASA. Goddard Space Flight Center, Second International Workshop on Harmonic Oscillators Jan. 1995 p 359-362 Sponsored by CONACyT (For primary document see N95-22957 07-74)
Avail: CASI HC A01/MF A04

We discuss the Shannon-Wehrl entropy within the squeezing vocabulary for the cosmological and black hole particle production. Author

N95-23001*# Open Univ., Milton Keynes (England). Dept. of Mathematics nad Computing.
REAL LASERS AND OTHER DEFORMED OBJECTS **c36**
Allan I. Solomon *In* NASA. Goddard Space Flight Center, Second International Workshop on Harmonic Oscillators Jan. 1995 p 363-373 (For primary document see N95-22957 07-74)
Avail: CASI HC A03/MF A04

In this talk we re-examine three important properties of quantum laser systems: (1) photon counting statistics; (2) squeezing; and (3) signal-to-quantum noise ratio. None of these phenomena depends on the choice of hamiltonian; indeed, we analyze them initially without restriction to any specific form of the commutation relations. Author

N95-23002*# Universidad Nacional Autonoma de Mexico, Cuernavaca (Mexico). Inst. de Investigaciones en Matematicas Aplicadas y en Sistemas.
SUPERSYMMETRIC OSCILLATOR IN OPTICS
Sergey M. Chumakov and Kurt Bernardo Wolf *In* NASA. Goddard Space Flight Center, Second International Workshop on Harmonic Oscillators Jan. 1995 p 375-379 (For primary document see N95-22957 07-74)
Avail: CASI HC A01/MF A04

We show that the supersymmetric structure (in the sense of supersymmetric quantum mechanics) appears in Helmholtz optics describing light propagation in waveguides. For the case of elliptical waveguides, with the accuracy of paraxial approximation it admits a simple physical interpretation. The supersymmetry connects light beams of different colors. The difference in light frequencies for the supersymmetric beams is determined by the transverse gradient of the refractive index. These beams have the save wavelength in the propagation direction and can form a stable interference pattern. Author

N95-23003*# Montreal Univ. (Quebec).
OSCILLATOR-LIKE COHERENT STATES FOR THE JAYNES-CUMMINGS MODEL **c77**
Y. BerubeLauziere, V. Hussin, and Michael M. Nieto *In* NASA. Goddard Space Flight Center, Second International Workshop on Harmonic Oscillators Jan. 1995 p 381-386 Sponsored by NSERC, FCAR du Gouvernement du Quebec, and Ministerio de Educacion y Ciencia (For primary document see N95-22957 07-74)
Avail: CASI HC A02/MF A04

A new way of diagonalizing the Jaynes-Cummings Hamiltonian is proposed, which allows the definition of annihilation operators and coherent states for this model. Mean values and dispersions over these states are computed and interpreted. Author

N95-23004*# Universidad de Guadalajara, Guadalajara, Jalisco (Mexico). Dept. de Fisica.
SLIGHTLY ANHARMONIC SYSTEMS IN QUANTUM OPTICS
Andrey B. Klimov and Sergey M. Chumakov *In* NASA. Goddard Space Flight Center, Second International Workshop on Harmonic Oscillators Jan. 1995 p 387-394 Sponsored by Universidad Nacional Autonoma de Mexico-Direccion General de Asuntos del Personal Academico (For primary document see N95-22957 07-74)
Avail: CASI HC A02/MF A04

We consider an arbitrary atomic system (n-level atom or many such atoms) interacting with a strong resonant quantum field. The approximate evolution operator for a quantum field case can be produced from the atomic evolution operator in an external classical field by a 'quantization prescription', passing the operator arguments to Wigner D-functions. Many important phenomena arising from the quantum nature of the field can be described by such a way. Author

N95-23005*# Academy of Sciences (USSR), Vladivostok (USSR). Pacific Oceanological Inst.
COHERENT CONTROL IN SIMPLE QUANTUM SYSTEMS **c77**
Sergey V. Prants *In* NASA. Goddard Space Flight Center, Second International Workshop on Harmonic Oscillators Jan. 1995 p 395-402 Sponsored by International Science Foundation (For primary document see N95-22957 07-74)
Avail: CASI HC A02/MF A04

Coherent dynamics of two, three, and four-level quantum systems, simultaneously driven by concurrent laser pulses of arbitrary and different forms, is treated by using a nonperturbative, group-theoretical approach. The respective evolution matrices are calculated in an explicit form. General aspects of controllability of few-level atoms by using laser fields are treated analytically. Author

N95-23006*# Universidad Nacional Autonoma de Mexico, Cuernavaca (Mexico). Inst. de Investigaciones en Matematicas Aplicadas y en Sistemas
KRAVCHUK FUNCTIONS FOR THE FINITE OSCILLATOR APPROXIMATION **c67**
Natig M. Atakishiyev and Kurt Bernardo Wolf *In* NASA. Goddard Space Flight Center, Second International Workshop on Harmonic Oscillators Jan. 1995 p 403-408 Sponsored by Direccion General de Asuntos del Personal Academico (For primary document see N95-22957 07-74)
(Proj UNAM-DGAPA IN1042-93)
Avail: CASI HC A02/MF A04

Kravchuk orthogonal functions - Kravchuk polynomials multiplied by the square root of the weight function - simplify the inversion algorithm for the analysis of discrete, finite signals in harmonic oscillator components. They can be regarded as the best approximation set. As the number of sampling points increases, the Kravchuk expansion becomes the standard oscillator expansion. Author

N95-23007*# Universidad Nacional Autonoma de Mexico, Cuernavaca (Mexico). Dept. de Ciencias.
PHASE SPACE ANALYSIS IN ANISOTROPIC OPTICAL SYSTEMS
Ana Leonor Rivera, Sergey M. Chumakov, and Kurt Bernardo Wolf *In* NASA. Goddard Space Flight Center, Second International Workshop on Harmonic Oscillators Jan. 1995 p 409-416 Sponsored by Universidad Nacional Autonoma de Mexico-Direccion General de Asuntos del Personal Academico (For primary document see N95-22957 07-74)
Avail: CASI HC A02/MF A04

From the minimal action principle follows the Hamilton equations of evolution for geometric optical rays in anisotropic media. As in classical mechanics of velocity-dependent potentials, the velocity and the canonical momentum are not parallel, but differ by an anisotropy vector potential, similar to that of linear electromagnetism. Descartes' well known diagram for refraction is generalized and a factorization theorem holds for interfaces between two anisotropic media. Author

N95-23016*# Alabama Univ., Huntsville, AL. Center for Microgravity and Materials Research.
X-RAY TRANSMISSION MICROSCOPE DEVELOPMENT Semiannual Progress Report No. 2, 1 Mar. 1994 - 28 Feb. 1995
William F. Kaukler and Franz E. Rosenberger 1 Mar. 1995 9 p
(Contract NAS8-40185)
(NASA-CR-197884; NAS 1.26:197884) Avail: CASI HC A02/MF A01

We are developing a hard x-ray microscope for direct observation of solidification dynamics in metal alloys and metal matrix composites. The Fein-Focus Inc. x-ray source was delivered in September and found to perform better than expected. Confirmed resolution of better than 2 micrometers was obtained and magnifications up to 800X were measured.

Nickel beads of 30 micrometer diameter were easily detected through 6mm of aluminum. X-ray metallography was performed on several specimens showing high resolution and clear definition of 3-dimensional structures. Prototype furnace installed and tested. Author

N95-23045* National Aeronautics and Space Administration. Pasadena Office, CA.

MOTION-SENSITIVE OPTICAL CORRELATOR USING A VANDERLUGT CORRELATOR Patent

Tsuen-Hsi Liu, inventor (to NASA) (Jet Propulsion Lab., California Inst. of Tech., Pasadena, CA.) 27 Dec. 1994 7 p Filed 7 Apr. 1993 Supersedes N93-28133 (31 - 10, p 3148)
(Contract NAS7-918)
(NASA-Case-NPO-18769-1-CU; US-Patent-5,376,807; US-Patent-Appl-SN-046331; US-Patent-Class-250-561; US-Patent-Class-359-561; US-Patent-Class-382-42; Int-Patent-Class-G06F-15/336; Int-Patent-Class-G06K-9/64) Avail: US Patent and Trademark Office

A new type of optical correlator is presented. The correlator performs motion detection or background clutter suppression and correlation simultaneously in a single photorefractive crystal. Additionally, the device is useful for moving target identification and tracking and for stationary clutter rejection. The correlation is of the VanderLugt type, and the motion detection or background clutter suppression is based on the erasing property of photorefractive crystals.

Official Gazette of the U.S. Patent and Trademark Office

N95-23089*# Massachusetts Inst. of Tech., Cambridge, MA. Dept. of Aeronautics and Astronautics.

STELLAR INTERFEROMETER TECHNOLOGY EXPERIMENT (SITE) Final Report

Edward F. Crawley, David Miller, Robert Laskin (Jet Propulsion Lab., California Inst. of Tech., Pasadena, CA.), and Michael Shao (Jet Propulsion Lab., California Inst. of Tech., Pasadena, CA.) 15 Feb. 1995 36 p Prepared in Cooperation with JPL and Payload Systems, Inc.
(Contract NASw-4886)
(NASA-CR-197856; NAS 1.26:197856) Avail: CASI HC A03/MF A01

The MIT Space Engineering Research Center and the Jet Propulsion Laboratory stand ready to advance science sensor technology for discrete-aperture astronomical instruments such as space-based optical interferometers. The objective of the Stellar Interferometer Technology Experiment (SITE) is to demonstrate system-level functionality of a space-based stellar interferometer through the use of enabling and enhancing Controlled-Structures Technologies (CST). SITE mounts to the Mission Peculiar Experiment Support System inside the Shuttle payload bay. Starlight, entering through two apertures, is steered to a combining plate where it is interferred. Interference requires 27 nanometer pathlength (phasing) and 0.29 archsecond wavefront-tilt (pointing) control. The resulting 15 milli-archsecond angular resolution exceeds that of current earth-orbiting telescopes while maintaining low cost by exploiting active optics and structural control technologies. With these technologies, unforeseen and time-varying disturbances can be rejected while relaxing reliance on ground alignment and calibration. SITE will reduce the risk and cost of advanced optical space systems by validating critical technologies in their operational environment. Moreover, these technologies are directly applicable to commercially driven applications such as precision matching, optical scanning, and vibration and noise control systems for the aerospace, medical, and automotive sectors. The SITE team consists of experienced university, government, and industry researchers, scientists, and engineers with extensive expertise in optical interferometry, nano-precision opto-mechanical control and spaceflight experimentation. The experience exists and the technology is mature. SITE will validate these technologies on a functioning interferometer science sensor in order to confirm definitely their readiness to be baselined for future science missions. Author

N95-23224*# District of Columbia Univ., Washington, DC. Dept. of Engineering and Technology.

HIGH Tc SUPERCONDUCTING BOLOMETRIC AND NONBOLOMETRIC INFRARED (IR) DETECTORS Semiannual Report, Aug. 1994 - Feb. 1995

Samuel Lakeou, M. Rajeswari, and Anuja Goyal Feb. 1995 17 p
(Grant NAG5-2348)
(NASA-CR-197868; NAS 1.26:197868) Avail: CASI HC A03/MF A01

The workplan for the period August 1994 through August 1995 includes the following: (1) expand the Applied Superconductivity Laboratory to include stand-alone optical response and noise measurement setups; (2) pursue studies of the low frequency excess electrical noise in YBCO films; and (3) enhance the academic support component of the project through increased student and faculty participation. Derived from text

N95-23378* National Aeronautics and Space Administration. Ames Research Center, Moffett Field, CA.

RESONANT INFRARED DETECTOR WITH SUBSTANTIALLY UNIT QUANTUM EFFICIENCY Patent

Jam Farhoomand, inventor (to NASA) and Robert E. McMurray, Jr., inventor (to NASA) 1 Mar. 1994 8 p Filed 28 Jan. 1992
(NASA-Case-ARC-11940-1-SB; US-Patent-5,291,055; US-Patent-Appl-SN-827177; US-Patent-Class-257-437; US-Patent-Class-257-436; US-Patent-Class-250-370.14; Int-Patent-Class-H01L-27/14; Int-Patent-Class-H01L-31/00) Avail: US Patent and Trademark Office

A resonant infrared detector includes an infrared-active layer which has first and second parallel faces and which absorbs radiation of a given wavelength. The detector also includes a first tuned reflective layer, disposed opposite the first face of the infrared-active layer, which reflects a specific portion of the radiation incident thereon and allows a specific portion of the incident radiation at the given wavelength to reach the infrared-active layer. A second reflective layer, disposed opposite the second face of the infrared-active layer, reflects back into the infrared-active layer substantially all of the radiation at the given wavelength which passes through the infrared-active layer. The reflective layers have the effect of increasing the quantum efficiency of the infrared detector relative to the quantum efficiency of the infrared-active layer alone.

Official Gazette of the U.S. Patent and Trademark Office

N95-23449# Lawrence Livermore National Lab., Livermore, CA.

LOW-COST PACKAGING OF HIGH-PERFORMANCE OPTOELECTRONIC COMPONENTS

M. Lowry, Shin-Yee Lu, M. Pocha, and O. T. Strand Aug. 1994 7 p Presented at the Annual Meeting of the Society of Photo-Optical Instrumentation Engineers, San Diego, CA), 24-29 Jul. 1994
(Contract W-7405-eng-48)
(DE95-003645; UCRL-JC-117859; CONF-940723-34) Avail: CASI HC A02/MF A01

Optoelectronic component costs are often dominated by the costs of attaching fiber optic pigtails--especially for the case of single transverse mode devices. We present early results of our program in low-cost packaging. We are employing machine-vision controlled automated positioning and silicon microbench technology to reduce the costs of optoelectronic components. Our machine vision approach to automated positioning has already attained a positional accuracy of less than 5 microns in less than 5 minutes; accuracies and times are expected to improve significantly as the development progresses. Complementing the machine vision assembly is our manufacturable approach to silicon microbench technology. We will describe our silicon microbench optoelectronic device packages that incorporate built-in heaters for solder bonding reflow. DOE

N95-23531# Brookhaven National Lab., Upton, NY.

MEASUREMENT AND ANALYSIS OF SCATTER FROM SILICON WAFERS

J. C. Stover (TMA Technologies, Inc., Bozeman, MT.), M. L. Bernt (TMA Technologies, Inc., Bozeman, MT.), E. L. Church, and P. Z. Takacs Jul. 1994 11 p Presented at the Annual Meeting of the Society of Photo-Optical Instrumentation Engineers, San Diego, CA, 24-29 Jul. 1994
(Contract DE-AC02-76CH-00016)
(DE95-002411; BNL-60899; CONF-940723-31) Avail: CASI HC A03/MF A01

The measurement of wafer surface roughness has become of increasing interest in the semiconductor industry in the last year. This interest is driven by the need to reduce background 'haze' associated with laser scanning particle counters, by the ever decreasing line width requirements and by a recent report that gate oxide breakdown voltage decreases as roughness increases. Scatter measurement offers the potential of being a

fast, non-contact method of monitoring roughness; however, the ability to accurately calculate wafer roughness via scatter depends on various wafer surface characteristics. The paper presents data taken on a number of wafers and demonstrates that bare silicon scatters almost exclusively from surface topography and is isotropic over an appropriate spatial bandwidth, thus facilitating scatter measurement. Because silicon proved to be an excellent source of topographic scatter, an experiment was undertaken to compare the one dimensional roughness measurements made with an optical profilometer to the two dimensional (area) measurements made via scatter, and these results are also reported. DOE

N95-23575# Sandia National Labs., Albuquerque, NM.
HIGH-PERFORMANCE GaAs/AlGaAs OPTICAL MODULATORS: THEIR PERFORMANCE AND PACKAGING FOR MICROWAVE PHOTONIC INTEGRATED CIRCUITS
S. H. Kravitz, V. M. Hietala, and G. A. Vawter 1994 2 p Presented at the 1994 Asia-Pacific Microwave Conference, Tokyo, 6-9 Dec. 1994
(Contract DE-AC04-94AL-85000)
(DE95-004533; SAND-94-2531C; CONF-941247-1) Avail: CASI HC A01/MF A01

The goal of this effort is to build and package photonic integrated circuits (PIC's). This infers that compact device design is very important, with all building blocks of the circuit aimed toward integration, low voltage operation, and manufacturability. With such a device, it is important that optical packaging be considered in the initial design. To this end, an advanced photonic packaging concept was designed. This concept employs vertical coupling of light both in and out of the package. This package concept is aimed at hermeticity, with no fiber penetrations through the walls of the package. This paper will describe the building blocks of this package, including output gratings, binary optics, and an automatic fiber capture device, called CLASP. DOE

N95-23767# Sandia National Labs., Albuquerque, NM.
10x REDUCTION IMAGING AT 13.4 nm
D. A. Tichenor (Sandia National Labs., Livermore, CA.), G. D. Kubiak (Sandia National Labs., Livermore, CA.), and M. E. Malinowski (Sandia National Labs., Livermore, CA.) 1994 5 p Presented at the Optical Society of America Conference on Extreme Ultraviolet Lithography, Monterey, CA, 19-21 Sep. 1994
(Contract DE-AC04-94AL-85000)
(DE94-016612; SAND-94-8602C; CONF-9409177-2) Avail: CASI HC A01/MF A01

A Schwarzschild imaging system has been designed to achieve 0.1 micro m resolution in a 0.4 mm diameter field of view when operated at a center wavelength of 13.4 nm. A decentered aperture is located on the convex primary resulting in an unobstructed numerical aperture of 0.08 and a corresponding depth of field of +/- 1 micro m. The Schwarzschild imaging objective is part of a five-reflection system containing the laser plasma source (LPS), condensing optics, turning mirror and reflection mask. Extreme ultraviolet (EUV) radiation is generated by impinging a laser beam onto a copper target. The plasma source is driven by a Lambda Physik PLX 250 KrF excimer laser emitting 0.6 Joule, 20 ns pulses at a 200 Hz maximum repetition rate. Measurements of the source indicate that the full-width-half-maximum diameter is less than 100 micro m. DOE

N95-24005# Brookhaven National Lab., Upton, NY.
PROFILING AND LIGHT SCATTERING STUDIES OF Si SURFACES
E. L. Church, P. Z. Takacs, and J. C. Stover (TMA Technologies, Inc., Bozeman, MT.) Oct. 1994 3 p Presented at the Microphysics of Surfaces: Nanoscale Processing Meeting, Santa Fe, NM, 9-11 Feb. 1995
(Contract DE-AC02-76CH-00016)
(DE95-002931; BNL-60904; CONF-950246-1) Avail: CASI HC A01/MF A01 (US Sales Only)

There is great interest in the semiconductor industry in developing light-scattering techniques for detecting 'killer particles' on Si wafer surfaces. The surface power spectral density (PSD) is important since it determines the intensity and angular dependence of the background scattering; understanding it will lead to a deeper understanding of finishing processes. Scattering measurements showed that Si wafer surfaces have the radiation-wavelength and angular dependences expected for weak topographic scattering. The data and independent profile measurements were used to deduce consistent values of the surface PSD's over the wavelength range 50 nm to 1 mm. The profile PSD's were found to consist of a sum of inverse power-law components, i.e., the surfaces are fractal-like. There is an analogy between the results and spontaneous thermodynamic roughening of solid surfaces: Below the critical roughening temperature, the surface topography is determined by the underlying crystal structure, while above it, the surface 'melts' and the roughness is determined by capillary-wave excitations of the surface. Capillary waves have the well-known 1/f(sub x) profile power spectrum. DOE

N95-24035*# Alabama Univ., Huntsville, AL.
PRISM SPECTROGRAPH OPTICAL DESIGN Final Report
Russell A. Chipman 5 Mar. 1995 41 p
(Contract NAS8-38609)
(NASA-CR-197965; NAS 1.26:197965) Avail: CASI HC A03/MF A01

The objective of this contract is to explore optical design concepts for the PRISM spectrograph and produce a preliminary optical design. An exciting optical configuration has been developed which will allow both wavelength bands to be imaged onto the same detector array. At present the optical design is only partially complete because PRISM will require a fairly elaborate optical system to meet its specification for throughput (area*solid angle). The most complex part of the design, the spectrograph camera, is complete, providing proof of principle that a feasible design is attainable. This camera requires 3 aspheric mirrors to fit inside the 20x60 cm cross-section package. A complete design with reduced throughput (1/9th) has been prepared. The design documents the optical configuration concept. A suitable dispersing prism material, CdTe, has been identified for the prism spectrograph, after a comparison of many materials.
Derived from text

N95-24068*# California Inst. of Tech., Pasadena, CA. Palomar Observatory.
NEAR INFRARED AND OPTICAL SPECTROSCOPY OF FSC10214+4724
B. T. Soifer, J. G. Cohen, L. Armus, K. Matthews, G. Neugebauer, and J. B. Oke 3 Feb. 1995 19 p Sponsored by NASA, Washington and NSF
(NASA-CR-197966; NAS 1.26:197966) Avail: CASI HC A03/MF A01

New infrared and optical spectroscopic observations, obtained with the W.M. Keck Telescope, are reported for the highly luminous infrared source FSC10214+4724. The rest frame optical spectrum shows new emission lines of (NeIII, (NeV), (OI), (OII), (SII), and He(+) while the rest frame ultraviolet spectrum shows new lines of OIV+SiIV, NII, NIV, SiII, NeIV and possibly NII and (NeIII), as well as clearly showing the L alpha is self-absorbed. The emission line spectrum is most characteristic of a Seyfert 2 nucleus. The preponderance of spectroscopic evidence strengthens the case of a dust enshrouded AGN powering much or most of the observed luminosity. The various spectral lines lead to a wide range in the inferred reddening and ionization parameter for this system, suggesting that we are viewing several environments through differing extinctions. Author

N95-24161# Sandia National Labs., Albuquerque, NM.
TRANSIENT RADIATION-INDUCED ABSORPTION IN MATERIALS FOR THE DOI LASER
P. J. Brannon Nov. 1994 23 p
(Contract DE-AC04-94AL-85000)
(DE95-004549; SAND-94-2731) Avail: CASI HC A03/MF A01

This is the final report on a series of experiments concerned with transient radiation-induced absorption in materials for a Cr,Nd:GSGG laser. Both the Sandia National Laboratories SPR III pulsed reactor and the Hermes III pulsed X-ray machine are used as radiation sources. The time dependence and the magnitude of the induced absorption in filter glasses and in doped and undoped LiNbO3 Q-switch materials have been measured. Gain has been observed in Cr,Nd:GSGG, the laser medium, when it is irradiated by X-rays. DOE

N95-23503# Institute for Aerospace Research, Ottawa (Ontario). Structures, Materials and Propulsion Lab.
DOUBLE PASS RETROREFLECTION FOR CORROSION DETECTION IN AIRCRAFT STRUCTURES
J. P. Komorowski, S. Krishnakumar, R. W. Gould, N. C. Bellinger, F. Karpala (Diffracto Ltd., Windsor, Ontario.), and O. L. Hageniers (Diffracto Ltd., Windsor, Ontario.) *In* AGARD, Corrosion Detection and Management of

Advanced Airframe Materials Jan. 1995 12 p (For primary document see N95-23496 07-26)
Copyright Avail: CASI HC A03/MF A03

N95-24130*# National Inst. of Standards and Technology, Gaithersburg, MD.
OPTICAL STORAGE MEDIA DATA INTEGRITY STUDIES
Fernando L. Podio *In* NASA. Goddard Space Flight Center, Fourth NASA Goddard Conference on Mass Storage Systems and Technologies Mar. 1994 p 265-276 (For primary document see N95-24108 07-82)
Avail: CASI HC A03/MF A04

75 PLASMA PHYSICS

Includes magnetohydrodynamics and plasma fusion.

For ionospheric plasmas see *46 Geophysics*. For space plasmas see *90 Astrophysics*.

N95-22514 Toulouse Univ. (France).
PROCEEDINGS OF NATO ADVANCED RESEARCH WORKSHOP ON THE FORMATION, TRANSPORT AND CONSEQUENCES OF PARTICLES IN PLASMAS Final Report
Jean-Pierre Boeuf 3 Sep. 1993 210 p Workshop held in Castera-Verduzan, France, 30 Aug. - 3 Sep. 1993 Limited Reproducibility: More than 20% of this document may be affected by microfiche quality
(AD-A285850) Avail: CASI HC A10

A review is presented of the phenomena associated with particles in low pressure plasmas. Dust particles which are typically micrometers in diameter have been observed by laser light scattering in various low-pressure, radiofrequency-excited plasmas. Experiments have been designed so that the origin of the dust material is unambiguous and, to some extent, quantitative. The processes involved in the appearance of the microscopic dust particles are outlined and compared with our experimental observations. The source material and its required generation rate, nucleation, charging, growth mechanisms, growth rates, and saturation mechanisms are discussed. The mutual influences of dust and plasma, particularly the role of geometric and circuit boundary conditions in laboratory plasmas, are described.
DTIC

N95-22519# Los Alamos National Lab., NM.
INNOVATIVE TECHNOLOGY FOR CONTAMINATION CONTROL IN PLASMA PROCESSING
G. S. Selwyn 1994 18 p Presented at the Cleanrooms 1994, Santa Clara, CA, 18 Oct. 1994
(Contract W-7405-eng-36)
(DE95-000913; LA-UR-94-3185; CONF-9410210-1) Avail: CASI HC A03/MF A01

The causes and contributing factors to wafer contamination during plasma processing are discussed in the context of future technologies for controlling particle contamination by tool and process design and by the development of wafer dry cleaning technology. The importance of these developments is linked with the history of technological innovation and with the continuing evolution of the cleanroom from a highly developed facility for reducing ambient particle levels to an integrated, synergistic approach involving facilities and tooling for impeding the formation and transport of particles while also actively removing particles from sensitive surfaces. The methods, strategy and requirements for innovation in contamination control for plasma processing is discussed from a diachronic viewpoint.
DOE

N95-22622# International Centre for Theoretical Physics, Trieste (Italy).
ANTI-INVARIANT SUBMANIFOLDS OF TRANS-SASAKIAN MANIFOLDS
M. HasanShahid and A. Sharfuddin Sep. 1993 10 p
(DE94-628413; IC-93/310) Avail: CASI HC A02/MF A01 (US Sales Only)

The paper presents some results obtained from the study of anti-invariant submanifolds of trans-Sasakian manifolds.
DOE

N95-22645# General Atomics Technologies Corp., San Diego, CA.
USING THE SHIELD FOR THERMAL ENERGY STORAGE IN PULSAR
G. T. Sager, C. P. C. Wong, D.-K. Sze (Argonne National Lab., IL.), C. G. Bathe (Los Alamos National Lab., NM.), J. P. Blanchard (Wisconsin Univ., Madison, WI.), C. Brimer (McDonnell-Douglas Aerospace, Saint Louis, MO.), E. T. Cheng (TSI Research, Inc., Solana Beach, CA.), L. A. El-Guebaly (McDonnell-Douglas Aerospace, Saint Louis, MO.), M. Z. Hasan (California Univ., Los Angeles, CA.), and F. Najmabadi (California Univ., San Diego, CA.) et al Apr. 1994 25 p Presented at the 3rd International Symposium on Fusion Nuclear Technology, Los Angeles, CA, 27 Jun. - 7 Jul. 1994
(Contract DE-AC03-89ER-52153)
(DE95-002457; GA-A-21671; CONF-940664-33) Avail: CASI HC A03/MF A01

The PULSAR pulsed tokamak power plant design utilizes the outboard shield for thermal energy storage to maintain full 1000 MW(e) output during the dwell period of 200 s. Thermal energy resulting from direct nuclear heating is accumulated in the shield during the 7200 s fusion power production phase. The maximum shield temperature may be much higher than that for the blanket because radiation damage is significantly reduced. During the dwell period, thermal power discharged from the shield and coolant temperature are simultaneously regulated by controlling the coolant mass flow rate at the shield inlet. This is facilitated by throttled coolant bypass. Design concepts using helium and lithium coolant have been developed. Two-dimensional, time-dependent thermal hydraulic calculations were performed to confirm performance capabilities required of the design concepts. The results indicate that the system design and performance can accommodate uncertainties in material limits or the length of the dwell period.
DOE

N95-22665# Los Alamos National Lab., NM.
DYNAMICS AND VARIABILITY OF THE PLASMASPHERE OBSERVED FROM SYNCHRONOUS ORBIT
Mark B. Moldwin, Michelle F. Thomsen, David J. McComas, and Geoff D. Reeves 1994 12 p Presented at the 10th Taos Workshop on the Earth's Trapped Particle Environment, Taos, NM, Aug. 1994
(Contract W-7405-eng-36)
(DE95-002733; LA-UR-94-3510; CONF-9408182-2) Avail: CASI HC A03/MF A01

The behavior of the cold ions in the outer plasmasphere is studied using data obtained with the magnetospheric plasma analyzers from multiple geosynchronous satellites. Dense (10-100 cm(exp -3)), cold ((approx)1 eV) regions of plasma are often observed at geosynchronous orbit; in this study the authors refer to these as plasmaspheric intervals. The duration, local time of observation, density variability, and temperature behavior within these regions often depend in a systematic way on geomagnetic and substorm activity. With increasing geomagnetic activity (as indicated by Kp) the plasmaspheric regions are generally observed over shorter durations and at earlier local times. With increasing substorm activity (as indicated by geosynchronous energetic electron injections) the density becomes increasingly variable in these regions. Occasionally, up to order-of-magnitude density variations are observed over several minute timescales corresponding to regions with physical dimensions on the order of 1000 km or less. The appearance of these short-duration, cold-plasma intervals is strongly correlated with energetic ion and electron signatures both at the spacecraft making the plasmaspheric observations and at other spacecraft observing simultaneously in the midnight region. Such energetic particle signatures are indicative of the growth and expansive phase of geomagnetic substorms. The authors conclude that the appearance of these short-duration, plasmaspheric intervals is due to a reconfiguration of the duskside magnetosphere during geomagnetic substorms.
DOE

N95-22676# Los Alamos National Lab., NM.
LASER-PLASMA INSTABILITY IN HOHLRAUMS
J. C. Fernandez, J. A. Cobble, and W. W. Hsing et al 1994 4 p Presented at the ECLIM 23: Laser Interaction with Matter, Oxford, England, 19-23 Sep. 1994
(Contract W-7405-eng-36)
(DE95-000914; LA-UR-94-3182; CONF-9409226-2) Avail: CASI HC A01/MF A01

A gas-filled hohlraum designed so as to approach plasma conditions expected in future ignition hohlraums has been fielded at the Nova laser. Radiation hydrodynamics modeling of these Nova hohlraums predicts reasonably well the measured plasma parameters. The measured reflectivity

of a probe beam by Stimulated Brillouin scattering is modest. Some observed dependencies of reflectivity on laser and plasma parameters are understood theoretically, while others are not. DOE

N95-22693# Texas Univ., Austin, TX. Inst. for Fusion Studies.
ANALYTICAL AND NUMERICAL STUDIES OF ION MOBILITY NEAR THE TOKAMAK PLASMA EDGE
H. Xiao, R. D. Hazeltine, and P. M. Valanju Nov. 1994 43 p
(Contract DE-FG05-80ET-53088)
(DE95-003019; DOE/ET-53088/681; IFSR-681) Avail: CASI HC A03/MF A01

The effects of radial electric field on charged particle motion and transport in a toroidal magnetic system have been studied both analytically and numerically. We examine the effects of radial electric field on particle orbits, allowing for the relatively large and strongly sheared field observed in some experiments. We find that ion radial mobility due to the combined effects of radial electric field and charge exchange collisions can dramatically affect the ion transport and orbit loss near the tokamak edge. These properties may help us understand the formation of transport barrier near the H mode plasma edge and explain the asymmetry between bias voltage and confinement in biased-electrode-induced H mode. DOE

N95-22694# Texas Univ., Austin, TX.
COMPARISONS OF NONLINEAR TOROIDAL TURBULENCE SIMULATIONS WITH EXPERIMENT
W. Dorland, M. Kotschenreuther, M. A. Beer (Princeton Univ., NJ.), G. W. Hammett (Princeton Univ., NJ.), R. E. Waltz (General Atomics Co., San Diego, CA.), R. R. Dominguez (General Atomics Co., San Diego, CA.), P. M. Valanju, W. H. Miner, Jr., J. Q. Dong, and W. Horton et al Oct. 1994 22 p
(Contracts DE-FG05-80ET-53088; DE-AC02-76CH-03073)
(DE95-003020; DOE/ET-53088/677; IFSR-677) Avail: CASI HC A03/MF A01

The anomalously large thermal transport observed in tokamak experiments is the outstanding physics-based obstacle in the path to a commercially viable fusion reactor. Although decades of experimental and theoretical work indicate that anomalous transport and collective instabilities in the gyrokinetic regime are linked, no widely accepted description of this transport yet exists. Here, detailed comparisons of first-principles gyrofluid and gyrokinetic simulations of tokamak microinstabilities with experimental data are presented. With no adjustable parameters, more than 50 TFTR L-mode discharges have been simulated with encouraging success. Given the local plasma parameters and the temperatures at r/a approximately equal 0.8, the simulations typically predict T(sub i)(r) and T(sub e)(r) within +/- 25% throughout the core and confinement zones. In these zones, the predicted thermal diffusivity increases with minor radius robustly. For parameters typical of r/a greater than 0.8, toroidal stability studies confirm the importance of impurity density gradients as a source of free energy potentially strong enough to explain the large edge thermal diffusivity, as first emphasized by Coppi, et al. Advanced confinement discharges have also been simulated. The dramatic increase of T(sub i)(0) observed in Supershots is recovered by our model for dozens of simulated experiments. Finally, simulations of VH and PEP mode-like plasmas show that velocity-shear stabilization of toroidal microinstabilities is quantitatively significant for realistic experimental parameters. DOE

N95-22719# General Atomics Co., San Diego, CA.
THE TEXT NEUTRAL LITHIUM BEAM EDGE DENSITY DIAGNOSTIC
A. M. Howald, J. M. McChesney, and W. P. West Jul. 1994 12 p Presented at the 10th Topical Conference on High-temperature Plasma Diagnostics, Rochester, NY, 8-12 May 1994
(Contract DE-FG03-92ER-54150)
(DE95-003256; GA-A-21711; CONF-940552-34) Avail: CASI HC A03/MF A01

A fast neutral lithium beam has been installed on the TEXT tokamak for beam emission spectroscopy (BES) studies of the edge plasma electron density profile. The diagnostic was recently upgraded from ten to twenty spatial channels, each of which has two detectors, one to measure lithium beam signal and one to monitor plasma background light. The spatial resolution is 6 mm, and the temporal resolution is designed to be as high as 10 ms for studies of transient events including plasma density fluctuations. Initial results are presented from the ten-channel system: Edge electron densities unfolded from the LiI (2 s2 S - 2 p2 P) 670.8 nm emission profile have the same general time dependence as the line-averaged density measured by microwave interferometry. DOE

N95-22757# International Atomic Energy Agency, Vienna (Austria).
REVIEW OF UNCERTAINTY FILES AND IMPROVED MULTIGROUP CROSS SECTION FILES FOR FENDL
S. Ganesan Mar. 1994 42 p Presented at the IAEA Advisory Group Meeting on Review of Uncertainty Files and Improved Multigroup Cross Section Files for FENDL, Tokai, Japan, 8-12 Nov. 1993
(DE94-628639; INDC(NDS)-297; CONF-9311217) Avail: CASI HC A03/MF A01 (US Sales Only)

The IAEA Nuclear Data Section, in co-operation with several national nuclear data centers and research groups, is creating an internationally available Fusion Evaluated Nuclear Data Library (FENDL), which will serve as a comprehensive source of processed and tested nuclear data tailored to the requirements of the Engineering and Development Activities (EDA) of the International Thermonuclear Experimental Reactor (ITER) Project and other fusion-related development projects. The FENDL project of the International Atomic Energy Agency has the task of coordination with the goal of assembling, processing and testing a comprehensive, fusion-relevant Fusion Evaluated Nuclear Data Library with unrestricted international distribution. The present report contains the summary of the IAEA Advisory Group Meeting on 'Review of Uncertainty Files and Improved Multigroup Cross Section Files for FENDL', held during 8-12 November 1993 at the Tokai Research Establishment, JAERI, Japan, organized in cooperation with the Japan Atomic Energy Research Institute. The report presents the current status of the FENDL activity and the future work plans in the form of conclusions and recommendations of the four Working Groups of the Advisory Group Meeting on: (1) experimental and calculational benchmarks; (2) preparation processed libraries for FENDL/ITER; (3) specifying procedures for improving FENDL; and (4) selection of activation libraries for FENDL. DOE

N95-22793# Michigan Univ., Ann Arbor, MI. Dept. of Geological Sciences.
RECENT DEVELOPMENTS IN INDUCTIVELY COUPLED PLASMA SOURCE MAGNETIC SECTOR MULTIPLE COLLECTOR MASS SPECTROMETRY
A. N. Halliday, Der-Chuen Lee, J. C. Christensen, C. E. Jones, C. M. Hall, Wen Yi, D. Teagle, and A. J. Walder 1994 31 p Presented at the Alfred O. Nier Symposium on Inorganic Mass Spectrometry, Durango, CO, 10-12 May 1994
(Contract DE-FG02-94ER-14412)
(DE95-003002; CONF-940556-Absts) Avail: CASI HC A03/MF A01

This paper describes advances in isotopic measurements that have been made with an inductively coupled plasma source magnetic sector multiple collector mass spectrometer and presents results of new experiments aimed at further evaluating the instrument's capability. It is shown using standard solutions that trace element ratios such as Rb/Sr can be measured precisely without isotope dilution by comparison with reference solutions of known composition. Similarly, using a new wide flight tube, Pb isotopic compositions and U/Pb ratios can be accurately measured simultaneously without isotope dilution. The effects of deliberately inducing changes in the running conditions (RF power) are shown to be significant for measuring trace element ratios but not for mass bias and interference corrected isotopic compositions. Finally, it is demonstrated that precise and accurate isotopic compositions of elements as refractory as W can be determined relatively easily by solution nebulization and even by direct laser ablation of complex silicates. Isobaric interferences in such experiments are negligible. These experiments serve to highlight the remarkable potential that this new field offers for hitherto difficult isotopic measurements in nuclear, earth, environmental and medical sciences. Isotopic measurements can be made that are reproducible at high precision through a range of running conditions, even in the presence of isobaric interferences. The ability to correct for mass discrimination accurately using a second element of similar mass, the very high sensitivity for elements that are otherwise difficult to ionize, the demonstrated capability for laser ablation work and the ability to measure through a wide mass range simultaneously give this instrument major advantages over other more traditional techniques of isotopic measurement. DOE

N95-22800# Oak Ridge National Lab., TN.
MEASUREMENTS AND MODELING OF IMPURITY SOURCE DISTRIBUTIONS FROM THE TORE SUPRA OUTBOARD PUMP LIMITER
C. C. Klepper, J. T. Hogan, R. C. Isler, S. J. Tobin, D. Guilhem, W. R. Hess, and P. Monier-Garbet Aug. 1994 19 p Presented at the 11th International Conference on Plasma Surface Interactions in Controlled Fusion Devices, Mito, Japan, 23-27 May 1994
(Contract DE-AC05-84OR-21400)
(DE95-003097; ORNL/TM-12795; CONF-940580-21) Avail: CASI HC A03/MF A01

An experiment has been carried out to study impurity generation processes on an inertial limiter on Tore Supra. It is part of a plan to assemble a more detailed integrated picture of impurity generation at the inner wall, the outboard and vertical pump limiters, and the heating and current drive antennas. A system has been implemented to permit quantitative measurement of impurity sources from the outboard limiter in Tore Supra. Data are presented for a representative case in which the limiter is isolated as much as possible from connection with other Tore Supra plasma-facing components. The data are compared with results from the Monte-Carlo SOL impurity transport code BBQ, in an attempt to identify the mechanism for impurity release. Evidence of chemical sputtering as an important impurity source is seen. DOE

N95-22849# Japan Atomic Energy Research Inst., Tokyo (Japan).
AN INVESTIGATION OF AC LOSSES IN TWO SUB-SIZE CONDUCTORS FOR THE ITER
R. J. Nelson (Massachusetts Inst. of Tech., Cambridge, MA.), Yoshikazu Takahashi, Takaaki Isono, Tomoyuki Sasaki, Kiichi Ohtsu, and Fumio Tajiri Nov. 1993 58 p
(DE94-765449; JAERI-M-93-219) Avail: CASI HC A04/MF A01 (US Sales Only)

Two second sub-size CiC conductors manufactured as models for the full-size conductors to be used in the poloidal coils of the ITER tokamak machine were tested to determine their A.C. loss characteristics. One conductor was manufactured by Furukawa (a 3x4x4 strand conductor), the other by Hitachi Cable (3x3x3). Each sub-size conductor sample, wound in a solenoid, was tested in a background magnet with zero transport current. For a single cycle ramp-up from 0 T to 1.15 T and then back to zero, hysteresis loss for the Furukawa conductor was 12.6 mJ per cubic centimeter of conductor volume (not including conduit), while the hysteresis loss for the Hitachi Cable sample was 19.9 mJ/cc. Each sample was then forced to experience an exponential decay of the background field, using different decay time constants for each trial, and the coupling loss was subsequently plotted versus the inverse of the background field decay. A 'best-estimate' value for the coupling time constant for each sample was determined based on theory; the Furukawa sample had a coupling time constant of about 27(+/-5)ms, while the Hitachi Cable sample had a coupling time constant of about 11(+/-5) ms. DOE

N95-22862# Texas Univ., Austin, TX. Fusion Research Center.
RUNAWAY ELECTRONS IN TEXT-U
M. R. Freeman 1 Aug. 1994 59 p
(Contract DE-FG03-94ER-54241)
(DE94-019218; DOE/ER-54241/133) Avail: CASI HC A04/MF A01

Runaway electrons have long been studied in tokamak plasmas. The previous results regarding runaway electrons and the detection of hard x-rays are reviewed. The hard x-ray energy on Texas EXperimental Tokamak - Upgrade(TEXT-U) is measured and the scaling of energy with electron density, n(sub e), is noted. This scaling suggests a runaway source term that scales roughly as 1 / n(sub e). The results indicate that runaways are created throughout the discharges. An upper bound for Chi(sub e) due to magnetic fluctuations was found to be .0343 sq m per sec. This is an order of magnitude too low to explain the thermal transport in TEXT, implying that electrostatic fluctuations are important in thermal transport in TEXT. DOE

N95-22899# Lawrence Livermore National Lab., Livermore, CA.
NUMERICAL TOKAMAK PROJECT CODE COMPARISON
R. E. Waltz, B. I. Cohen (General Atomics Co., San Diego, CA.), M. A. Beer (Princeton Univ., NJ.), J. A. Byers, A. M. Dimits, W. Dorland (Princeton Univ., NJ.), S. E. Parker (Princeton Univ., NJ.), A. M. Santoro (Princeton Univ., NJ.), R. D. Sydora (California Univ., Los Angeles, CA.), and H. V. Wong (Texas Univ., Austin, TX.) 21 Jun. 1994 11 p
(Contract W-7405-eng-48)
(DE95-003475; UCRL-ID-117670) Avail: CASI HC A03/MF A01

The Numerical Tokamak Project undertook a code comparison using a set of TFTR tokamak parameters. Local radial annulus codes of both gyrokinetic and gyrofluid types were compared for both slab and toroidal case limits assuming ion temperature gradient mode turbulence in a pure plasma with adiabatic electrons. The heat diffusivities were found to be in good internal agreement within (+-) 50% of the group average over five codes. DOE

N95-22948# Northeastern Univ., Boston, MA. Dept. of Electrical and Computer Engineering.
ADVANCED DETECTOR DEVELOPMENT, LABORATORY SIMULATIONS, DIAGNOSTIC DEVELOPMENT, AND DATA ANALYSIS ON WAKE PHYSICS Scientific Report No. 1
John M. Talbot and Chung Chan 30 Jun. 1994 13 p
(Contract F19628-91-K-0019; AF Proj. 2822)
(PL-TR-94-2204) Avail: CASI HC A03/MF A01

We have developed a theoretical analysis of the current scaling issues of a negatively biased probe in a plasma wake. The theoretical assumptions have been analyzed qualitatively and quantitatively by the use of the POLAR computer code. For a plasma with a constant beam energy, the analysis shows that the I-V collection characteristics are unaffected by Mach number variations for Mach numbers above a value of two. For the same case, the current was found to scale with the 3/7 power of the density. Author

N95-22955*# Alabama Univ., Huntsville, AL. Center for Space Plasma and Aeronomic Research.
MAGNETOSPHERIC SPACE PLASMA INVESTIGATIONS Semiannual Progress Report, 1 Aug. 1994 - 31 Jan. 1995
Richard H. Comfort and James L. Horwitz Feb. 1995 7 p
(Grant NAG8-239)
(NASA-CR-197405; NAS 1.26:197405) Avail: CASI HC A02/MF A01

Topics and investigations covering this period of this semiannual report period (August 1994 - January 1995) are as follows: (1) Generalized SemiKinetic (GSK) modeling of the synergistic interaction of transverse heating of ionospheric ions and magnetospheric plasma-driven electric potentials on the auroral plasma transport. Also, presentations of GSK modeling of auroral electron precipitation effects on ionospheric plasma outflows, of ExB effects on such outflow, and on warm plasma thermalization and other effects during refilling with pre-existing warm plasmas; (2) Referees' reports received on the statistical study of the latitudinal distributions of core plasmas along the L = 4.6 field line using DE-1/RIMS data. Other work is concerned in the same field, field-aligned flows and trapped ion distributions; and (3) A short study has been carried out on heating processes in low density flux tubes in the outer plasmasphere. The purpose was to determine whether the high ion temperatures observed in these flux tubes were due to heat sources operating through the thermal electrons or directly to the ions. Other investigations center along the same area of plasmasphere-ionosphere coupling. The empirical techniques and model, the listing of hardware calibrated, and/or tested, and a description of notable meetings attended is included in this report, along with a list of all present publication in submission or accepted and those reference papers that have resulted from this work thus far. CASI

N95-23008*# Alabama Univ., Huntsville, AL. Dept. of Physics.
SEMIKINETIC MODELING AND OBSERVATIONS OF HIGH-LATITUDE PLASMA OUTFLOW Annual Progress Report, 1 Jan. - 31 Dec. 1994
James L. Horwitz Jan. 1995 6 p
(Grant NAGw-1554)
(NASA-CR-197403; NAS 1.26:197403) Avail: CASI HC A02/MF A01

In one fo the most exciting areas of progress, we have now developed a dynamic semikinetic model for examining the synergistic effects of waves and magnetospheric hot plasma populations on the outflowing ionospheric plasma. We have done this by imposing hot biMaxwellian ion and electron distributions at the top of our auroral simulation flux tube (4 R(sub e)), as well as a spectrum of waves with altitude which perpendicularly heats the ionospheric ions. We have also addressed the quasi-statistical properties of out flowing O(+) through bulk parameter analysis of DE-1/RIMS observations when DE-1 was in the midaltitude polar cap magnetosphere. A very exciting paper which was both submitted and appeared during this

period in JGR concerned the centrifugal acceleration effect on the polar wind. During this year, we also developed the extension of our GSK code to include the lower ionosphere and associated processes. Finally, perhaps our most exciting project currently is a study of F-region upflows using a modification of the FLIP ionospheric fluid dynamics model of Richards and Torr to allow for the effects of soft electron precipitation ionization and convection-driven ion heating, and performed comparisons with satellite and radar data. A list of reference papers that have been published is listed. Derived from text

N95-23072# Wisconsin Univ., Madison, WI. Center for Plasma Theory and Computation.

TURBULENT TRANSPORT ACROSS INVARIANT CANONICAL FLUX SURFACES

J. B. Hollenberg and J. D. Callen Jul. 1994 27 p

(Contract DE-FG02-86ER-53218)

(DE95-000710; UW-CPTC-94-7) Avail: CASI HC A03/MF A01

Net transport due to a combination of Coulomb collisions and turbulence effects in a plasma is investigated using a fluid moment description that allows for kinetic and nonlinear effects via closure relations. The model considered allows for 'ideal' turbulent fluctuations that distort but preserve the topology of species-dependent canonical flux surfaces (psi)(sub (number sign),s) (triple bond) (integral) dF (center dot) B(sub (number sign),s) (triple bond) (gradient) x (A + (m(sub s)/q(sub s))u(sub s)) in which u(sub s) is the flow velocity of the fluid species. Equations for the net transport relative to these surfaces due to 'nonideal' dissipative processes are found for the total number of particles and total entropy enclosed by a moving canonical flux surface. The corresponding particle transport flux is calculated using a toroidal axisymmetry approximation of the ideal surfaces. The resulting Lagrangian transport flux includes classical, neoclassical-like, and anomalous contributions and shows for the first time how these various contributions should be summed to obtain the total particle transport flux. DOE

N95-23084# Wisconsin Univ., Madison, WI. Dept. of Electrical and Computer Engineering.

TFTR ION CYCLOTRON RANGE OF FREQUENCIES (ICRF) EXPERIMENTAL DATA ANALYSIS COLLABORATION Annual Progress Report, 1 Dec. 1993 - 30 Nov. 1994

J. E. Sharer, M. Bettenhausen, N. Lam, and R. Sund Aug. 1994 20 p

(Contract DE-FG02-93ER-54196)

(DE95-003409; DOE/ER-54196/2) Avail: CASI HC A03/MF A01

The research performed under this grant during the past year has concentrated on coupling, heating, and current drive issues for TFTR. The authors have developed a code and submitted for publication a '3-D' coupling analysis of the TFIR ICRF cavity-backed coil antennas to plasma edge profiles including the Faraday shield blade angle and fast wave coupling for heating and current drive. They have also carried out TFTR ICRF full-wave field solutions and heating analyses for the second harmonic tritium supershot, and the effects of fusion alpha particle and tritium ion tail populations on the ICRF absorption. They have also published a paper on the effects of alpha particle absorption on fundamental deuterium ion cyclotron absorption incorporating self-consistent deuterium tails and fusion reactivity. Research progress, publications, and conference presentations are summarized in this report. DOE

N95-23119# General Atomics Co., San Diego, CA.

DIVERTOR HEAT AND PARTICLE CONTROL EXPERIMENTS ON THE DIII-D TOKAMAK

M. A Mahdavi, D. R. Baker, S. L. Allen (Lawrence Livermore National Lab., Livermore, CA.), B. Bastasz (Sandia National Labs., Albuquerque, NM.), N. H. Brooks, D. Buchenauer (Sandia National Labs., Albuquerque, NM.), R. B. Campbell (Sandia National Labs., Albuquerque, NM.), J. W. Cuthbertson (Sandia National Labs., Albuquerque, NM.), T. E. Evans, and M. E. Fenstermacher (Lawrence Livermore National Lab., Livermore, CA.) et al May 1994 39 p Presented at the 11th International Conference on Plasma Surface Interactions in Controlled Fusion Devices, Mito, Japan, 23-27 May 1994 Submitted for publication

(Contracts DE-AC03-89ER-51114; W-7405-eng-48; DE-AC05-84OR-21400; DE-AC04-76DP-00789; DE-FG03-89ER-51121)

(DE94-017518; GA-A-21706; CONF-940580-14) Avail: CASI HC A03/MF A01

In this paper we present a summary of recent DIII-D divertor physics activity and plans for future divertor upgrades. During the past year, DIII-D experimental effort was focused on areas of active heat and particle control and divertor target erosion studies. Using the DIII-D Advanced Divertor system we have succeeded for the first time to control the plasma density and demonstrate helium exhaust in H-mode plasmas. Divertor heat flux control by means of D(sub 2) gas puffing and impurity injection were studied separately and in, both cases up to a factor of five reduction of the divertor peak heat flux was observed. Using the DiMES sample transfer system we have obtained erosion data on various material samples in well diagnosed plasmas and compared the results with predictions of numerical models. DOE

N95-23120# Cornell Univ., Ithaca, NY. Lab. of Plasma Studies.

ION RINGS FOR MAGNETIC FUSION Technical Progress Report, 1 Aug. 1993 - 1 Jun. 1994

Ravi N. Sudan 1994 8 p

(Contract DE-FG02-93ER-54221)

(DE94-017606; DOE/ER-54221/1) Avail: CASI HC A02/MF A01

In Our Proposal 'Ion Rings for Magnetic Fusion' of January 6, 1993, Stage I of our Proposed Program plan (the 12 months) consisted of the following tasks: (1) Experiments on the existing ion ring experimental system IREX to test a new magnetically-controlled anode plasma source (MAP) for the ion beam diode injector; (2) numerical simulations of ion ring formation to optimize design parameters for the field reversed ion ring experiment (FIREX) to be built and operated in Stage II; and (3) designing the power supply for the FIREX injector and the magnetic field system using results for (1) and (2). During the past 7 1/2 months our work has progressed according to the above plan. In addition to testing the MAP diode on IREX we have tested the EMFAPS (evaporating metal film anode plasma source) anode on the Sandia National Laboratories funded LION pulsed power generator. As a result of these experiments described in this paper, we have arrived at the conclusion that EMFAPS anode for the ion at present because the MAP diode beam diode injector is our preferred choice for it is still in an early stage of development. DOE

N95-23136# Texas Univ., Austin, TX.

NEURAL NET PREDICTION OF TOKAMAK PLASMA DISRUPTIONS

J. V. Hernandez, Z. Lin, W. Horton, A. Vannucci (Sao Paulo Univ., Brazil.), and S. C. McCool Oct. 1994 28 p

(Contract DE-FG05-80ET-53088)

(DE95-002616; DOE/ET-53088/676) Avail: CASI HC A03/MF A01

The computation based on neural net algorithms in predicting minor and major disruptions in TEXT tokamak discharges has been performed. Future values of the fluctuating magnetic signal are predicted based on L past values of the magnetic fluctuation signal, measured by a single Mirnov coil. The time step used (= 0.04ms) corresponds to the experimental data sampling rate. Two kinds of approaches are adopted for the task, the contiguous future prediction and the multi-timescale prediction. Results are shown for comparison. Both networks are trained through the back-propagation algorithm with inertial terms. The degree of this success indicates that the magnetic fluctuations associated with tokamak disruptions may be characterized by a relatively low-dimensional dynamical system. DOE

N95-23147# Grumman Aerospace Corp., Princeton, NJ.

HIGH BETA AND SECOND STABILITY REGION TRANSPORT AND STABILITY ANALYSIS Technical Progress Report

M. H. Hughes and M. W. Phillips Sep. 1994 12 p

(Contract DE-FG02-89ER-51124)

(DE95-003411; DOE/ER-51124/19) Avail: CASI HC A03/MF A01

This report summarizes MHD equilibrium and stability studies carried out at Grumman's Corporate Research Center during the 6 month period starting March 1, 1994. Progress is reported in both ideal and resistive MHD modeling of TFTR plasmas. The development of codes to calculate the significant effects of highly anisotropic pressure distributions is discussed along with initial results from this model. DOE

N95-23163# Oak Ridge National Lab., TN.

DYNAMICS OF L TO H BIFURCATION

B. A. Carreras, D. Newman, P. H. Diamond (California Univ., San Diego, La Jolla, CA.), Yi Ming Liang (California Univ., San Diego, La Jolla, CA.),

and V. Lebedev (California Univ., San Diego, La Jolla, CA.) 1993 10 p Presented at the IAEA Meeting on H-Mode Physics, Naka, Japan, 15-17 Nov. 1993
(Contracts DE-AC05-84OR-21400; DE-FG03-88ER-53275)
(DE94-019126; CONF-9311147-11) Avail: CASI HC A02/MF A01

A self-consistent model of the L to H transition is derived from coupled nonlinear envelope equations for the fluctuation level, radial electric field shear, E(sub r)(prime) and pressure gradient, del P(sub i). These equations exhibit a bifurcation between dual L-mode and H-mode fixed points. They show that the L to H transition has similar characteristics to a phase transition of the second kind for which the order parameter is E(sub r)(prime). The transition occurs when the turbulence drive is large enough to overcome the damping of the E x B flow. This leads to a power threshold condition for the transition P(sub crit)approx. = ((mu)nT)(sub edge) aRL(sub s). DOE

N95-23170# Technische Univ., Eindhoven (Netherlands). Dept. of Mathematics and Computing Science.
PLASMO-MAGNETOELASTIC WAVES IN A SEMICONDUCTING HETEROSTRUCTURE. 1: PLASMO-ELASTIC LONGITUDINAL MODES. 2: SH-MAGNETOELASTIC MODES
A. A. F. vandeVen and B. Maruszewski Sep. 1993 14 p Prepared in cooperation with Poznan Technical Univ.
(PB95-138822; RANA-93-13) Avail: CASI HC A03/MF A01

Wave propagation in semiconducting heterostructures is studied. Interactions of the electrical field with mechanical (elastic) and magnetic fields are considered. The first part of a 2 part document deals with longitudinal (Rayleigh-type) plasmo-elastic waves in a thin layer on a half space (substrate); both layer and substrate are semiconducting. The waves show an exponential decay with depth in the substrate; the longer the waves the more of the wave energy is transmitted through the layer. Also purely plasmonic waves can exist. These waves are dissipative, and exist only for values of the wave number exceeding a certain value. This part of the document is devoted to the analysis of propagation of the SH-magnetoelastic (Love-type) waves in an epitaxial heterostructure collected of a magnetic semiconductor layer and nonmagnetic semiconducting substrate placed into an applied constant magnetic field perpendicular to the interface of the structure. Numerical results have been obtained for ZnSe-Ge heterostructure. The first order approximation of the dispersion of SH-magnetoelastic modes comparing to the dispersion of the purely elastic SH modes has been calculated. NTIS

N95-23211*# Michigan Univ., Ann Arbor, MI. Space Physics Research Lab.
MODELING OF NONEQUILIBRIUM SPACE PLASMA FLOWS Final Technical Report, Mar. 1990 - Apr. 1994
Tamas Gombosi 15 Feb. 1995 11 p
(Grants NAG5-1500; NAGw-2162)
(NASA-CR-197432; NAS 1.26:197432) Avail: CASI HC A03/MF A01

Godunov-type numerical solution of the 20 moment plasma transport equations. One of the centerpieces of our proposal was the development of a higher order Godunov-type numerical scheme to solve the gyration dominated 20 moment transport equations. In the first step we explored some fundamental analytic properties of the 20 moment transport equations for a low b plasma, including the eigenvectors and eigenvalues of propagating disturbances. The eigenvalues correspond to wave speeds, while the eigenvectors characterize the transported physical quantities. In this paper we also explored the physically meaningful parameter range of the normalized heat flow components. In the second step a new Godunov scheme type numerical method was developed to solve the coupled set of 20 moment transport equations for a quasineutral single-ion plasma. The numerical method and the first results were presented at several national and international meetings and a paper describing the method has been published in the Journal of Computational Physics. To our knowledge this is the first numerical method which is capable of producing stable time-dependent solutions to the full 20 (or 16) moment set of transport equations, including the full heat flow equation. Previous attempts resulted in unstable (oscillating) solutions of the heat flow equations. Our group invested over two man-years into the development and implementation of the new method. The present model solves the 20 moment transport equations for an ion species and thermal electrons in 8 domain extending from a collision dominated to a collisionless region (200 km to 12,000 km). This model has been applied to study O+ acceleration due to Joule heating in the lower ionosphere. Derived from text

N95-23246# Texas Univ., Austin, TX. Fusion Research Center.
NINTH TOPICAL CONFERENCE ON ATOMIC PROCESSES IN PLASMAS
1993 187 p Presented at the 9th Biennial Topical Conference on Atomic Processes in Plasmas, San Antonio, TX, 19-23 Sep. 1993
(Contract DE-FG03-93ER-54200)
(DE95-002810; CONF-9309119-Summ-1) Avail: CASI HC A09/MF A02

This report contains abstract from the 9th topical conference on atomic processes in plasmas. The areas covered are: diagnostics and atomic data; tokamak devices; Astrophysics; atomic physics; dense plasmas; and x-ray lasers. DOE

N95-23269# Los Alamos National Lab., NM.
TRITIUM TRANSPORT, INFLUX, AND HELIUM ASH MEASUREMENTS ON TFTR DURING DT OPERATION
P. C. Efthimion, L. C. Johnson, and C. H. Skinner 1994 16 p Presented at the 15th International Conference on Plasma Physics and Controlled Nuclear Fusion Research, Seville, 26 Sep. - 1 Oct. 1994
(Contract W-7405-eng-36)
(DE95-003708; LA-UR-94-3664; CONF-940933-18) Avail: CASI HC A03/MF A01

The evolution of the tritium density profile is inferred from 14.1 MeV t(d,n)alpha and 2.5 MeV d(d,n)He-3 neutron emissivity profiles measured in a deuterium neutral beam heated plasma into which a small amount of tritium gas has been puffed. For the first time, hydrogenic ion transport coefficients in the form of a diffusivity and convective velocity are determined. The particle diffusivities of tritium and He-4 and the deuterium thermal diffusivity are of similar magnitudes, and thus are consistent with theoretically calculated ExB drift transport. The first measurements of helium ash have been made using charge exchange recombination spectroscopy (CHERS). The measured radial ash profile shape is consistent with that predicted from simulations that include calculations of the central alpha ash source and thermal ash transport. This suggests that ash transport in the plasma core will not be a fundamental limiting factor in determining helium exhaust rates in a reactor. The authors also report the first spectroscopic measurements of tritium Balmer-alpha emission which provided a measure of tritium influx from the limiter. Tritium influx persists in discharges subsequent to tritium neutral beam injection, decaying with an initial decay of 7.5 discharges, and followed by a long term decay on the order of 400 discharges. Tritium transport, influx, and helium ash transport are important issues concerning profile control, retention, and ash removal for future reactors, like ITER. DOE

N95-23338 TRW Systems Group, Redondo Beach, CA.
MHD SEED RECOVERY AND REGENERATION, PHASE 2 Final Report
Oct. 1994 384 p Limited Reproducibility: More than 20% of this document may be affected by poor print
(Contract DE-AC22-87PC-79672)
(DE95-004308; DOE/PC-79672/T9) Avail: Issuing Activity (Department of Energy (DOE))

This final report summarizes the work performed by the Space and Technology Division of the TRW Space and Electronics Group for the U.S. Department of Energy, Pittsburgh Energy Technology Center for the Econoseed process. This process involves the economical recovery and regeneration of potassium seed used in the MHD channel. The contract period of performance extended from 1987 through 1994 and was divided into two phases. The Phase II test results are the subject of this Final Report. However, the Phase I test results are presented in summary form in Section 2.3 of this Final Report. The Econoseed process involves the treatment of the potassium sulfate in spent MHD seed with an aqueous calcium formate solution in a continuously stirred reactor system to solubilize, as potassium formate, the potassium content of the seed and to precipitate and recover the sulfate as calcium sulfate. The slurry product from this reaction is centrifuged to separate the calcium sulfate and insoluble seed constituents from the potassium formate solution. The dilute solids-free potassium formate solution is then concentrated in an evaporator. The concentrated potassium formate product is a liquid which can be recycled as a spray into the MHD channel. Calcium formate is the seed regenerant used in the Econoseed process. Since calcium formate is produced in the

United States in relatively small quantities, a new route to the continuous production of large quantities of calcium formate needed to support an MHD power industry was investigated. This route involves the reaction of carbon monoxide gas with lime solids in an aqueous medium. DOE

N95-23371# General Atomics Co., San Diego, CA.
THE q PROFILE EVOLUTION AND ENHANCED CORE CONFINEMENT OF HIGH (BETA)(SUB p) PLASMAS IN D3-D
B. W. Stallard (Lawrence Livermore National Lab., Livermore, CA.), T. A. Casper (Lawrence Livermore National Lab., Livermore, CA.), M. E. Fenstermacher (Lawrence Livermore National Lab., Livermore, CA.), C. B. Forest, P. Gohil, W. W. Heidbrink (California Univ., Irvine, CA.), A. W. Hyatt, R. A. James (Lawrence Livermore National Lab., Livermore, CA.), R. A. Jong, and L. L. Lao et al Oct. 1994 8 p Presented at the 15th International Conference on Plasma Physics and Controlled Nuclear Fusion Research, Madrid, Spain, 26 Sep. - 1 Oct. 1994
(Contracts DE-AC03-89ER-51114; W-7405-eng-48)
(DE95-003878; GA-A-21799; IAEA-CN-60/A3/5-P-11; CONF-940994-3)
Avail: CASI HC A02/MF A01

In DIII-D the authors have investigated the long pulse evolution of high poloidal beta (beta(sub p)), double-null diverted H-mode discharges, which exhibit high bootstrap current fractions attractive for a reactor. At low currents I(sub p), the current profile evolved over several seconds and the on-axis safety factor (q(sub 0)) increased. When q(sub 0) increased above approximately 2, the MHD character changed from an m/n = 2/1 to an m/n = 3/1 internal kink mode, where m(n) are poloidal (toroidal) mode numbers, which then disappeared with further increases in q(sub 0). Coincident with a strong reduction of fluctuations, the authors observed enhanced core confinement, leading to strong density peaking, a further rise in beta(sub p), and a bootstrap current increasing to I(sub boot)/I(sub p) approximately 0.8, peaked within the core. Ideal MHD calculations showed access to second stability during the density rise. During the enhanced performance phase core particle lifetime (tau(sub p)) and global energy lifetime (tau(sub E)) increased by factors of 2 and 1.2 respectively. Transport analysis showed that core particle and thermal diffusivities D(sub e) and (chi)(sub eff) approached neoclassical values. During the low current experiments, large losses of fast ions (typically (approximately)50% at 0.4 MA) were observed; at higher currents these losses are much smaller. The authors have also investigated discharges with current rampdown to high (beta)(sub p). For a 5 to 6 (tau)(sub E) duration following rampdown, enhanced values of (beta)(sub p), normalized toroidal beta ((beta)(sub N)), and (tau)(sub E) were obtained at high internal inductance ((ell)(sub i)). During both the ramp and the high confinement phases, fast ion losses were low ((approximately)10%). The loss then increased, correlated with an increase in the anisotropy ratio of perpendicular and parallel plasma pressure that suggests a fast ion loss mechanism coupled to the fast ion parallel energy. DOE

N95-23523# National Inst. for Fusion Science, Nagoya (Japan).
MODIFICATION AND DAMPING OF ALFVEN WAVES IN A MAGNETIZED DUSTY PLASMA
M. Salimullah, B. Dasgupta, K. Watanabe, and T. Sato Oct. 1994 19 p Sponsored by Japan Society for Promotion of Science and Ministry of Education, Science and Culture
(ISSN 0915-633X)
(NIFS-312) Avail: CASI HC A03/MF A01

The dispersion characteristics of the circularly polarized electromagnetic waves along a homogeneous magnetic field in a dusty plasma have been investigated theoretically. The Vlasov equation has been employed to find the response of the magnetized plasma particles where the dust grains form a static background of highly charged and massive centers having certain correlations. It is found that in addition to the unusual Landau damping, which is negligible in the low temperature approximation, a novel mechanism of damping of the Alfven waves due to the dust comes into play. The modification and damping of the Alfven waves depend on the dust perturbation parameters, unequal densities of plasma particles, the average correlation length of the dust grains, temperature of the plasma and the magnetic field. Author

N95-23524# National Inst. for Fusion Science, Nagoya (Japan).
NON-TAYLOR MAGNETOHYDRODYNAMIC SELF-ORGANIZATION
Shao-Ping Zhu (Graduate Univ. for Advanced Studies, Japan.), Ritoku Horiuchi (Graduate Univ. for Advanced Studies, Japan.), Tetsuya Sato (Graduate Univ. for Advanced Studies, Japan.), K. Watanebe, T. Hayashi, Y. Todo, T.-H. Watanabe, A. Kageyama, and H. Takamaru Oct. 1994 44 p Sponsored by Japanese Ministry of Education, Science and Culture Original contains color illustrations
(ISSN 0915-633X)
(NIFS-314) Avail: CASI HC A03/MF A01

A self-organization process in a plasma with a finite pressure is investigated by means of a three-dimensional magnetohydrodynamic simulation. It is demonstrated that a non-Taylor finite Beta self-organized state is realized in which a perpendicular component of the electric current is generated and the force-free (parallel) current decreases until they reach to almost the same level. The self-organized state is described by a MHD force-balance relation, namely, j(perpendicular) = B x del(sub p)/B(center dot)B and j(parallel) = mu x B where mu is not a constant, and the pressure structure resembles the structure of the toroidal magnetic field intensity. Unless an anomalous perpendicular thermal conduction arises, the plasma cannot relax to a Taylor state but to a non-Taylor (non-force-free) self-organized state. This states becomes more prominent for a weaker resistivity condition. the non-Taylor state has a rather universal property, for example, independence of the initial Beta value. Another remarkable finding is that the Taylor's conjecture of helicity conservation is, in a strict sense, not valid. The helicity dissipation occurs and its rate slows down critically in accordance with the stepwise relaxation of the magnetic energy. It is confirmed that the driven magnetic reconnection caused by the nonlinearly excited plasma kink flows plays the leading role in all of these key features of the non-Taylor self-organization. Author

N95-23525# National Inst. for Fusion Science, Nagoya (Japan).
COLLISIONLESS MAGNETIC RECONNECTION ASSOCIATED WITH COALESCENCE OF FLUX BUNDLES
Motohiko Tanka Nov. 1994 39 p
(ISSN 0915-633X)
(NIFS-315) Avail: CASI HC A03/MF A01

The basic process of collisionless reconnection is studied in terms of coalescence of magnetized flux bundles using an implicit particle simulation of two-dimensions. The toroidal electric field that directly relates to magnetic reconnection is generated solenoidally in a region much broader than the current sheet whose width is a few electron skin depths. The reconnection flux increases linearly in time, but it is insensitive to finite Larmor radii of the ions in this Sweet-Parker regime. The toroidal electric field is controlled by a balance of transit acceleration of finite-mass electrons and their removal by sub-Alfvenic E x B drift outflow. the simulation results supports the collisionless Ohm's law E(sub t) is approximately equal to Eta(sub eq)J(sub t) with Eta(sub eq) the inertia resistivity. Author

N95-23526# National Inst. for Fusion Science, Nagoya (Japan).
MACRO-EM PARTICLE SIMULATION METHOD AND A STUDY OF COLLISIONLESS MAGNETIC RECONNECTION
Motohiko Tanaka Nov. 1994 47 p
(ISSN 0915-633X)
(NIFS-316) Avail: CASI HC A03/MF A01

A multi-dimensional electromagnetic particle simulation method which is suitable for studying low-frequency plasma phenomena is described in the first part. Its application to collisionless magnetic reconnection is shown in the second part. The present particle code efficiently deals with nonlinear kinetic processes wherein ions and electrons play their roles, since the code is implemented using the Maxwell equations and the Newton-Lorentz equations. The drift-kinetic equations are used optionally. A simulation of collisionless reconnection shows that the toroidal electric field which directly relates to reconnection is generated naturally in the kinetic study, and that a thin dissipation region is formed whose width is a few electron skin depth. Thus, collisionless reconnection is considered to proceed under the electron inertia. Author

N95-23527# National Inst. for Fusion Science, Nagoya (Japan).
SECOND ORDER FOCUSING PROPERTY OF 210 DEG CYLINDRICAL ENERGY ANALYZER
A. Fujisawa, H. Iguchi, M. Sasao, and Y. Hamada Nov. 1994 20 p
(ISSN 0915-633X)
(NIFS-317) Avail: CASI HC A03/MF A01

It was confirmed experimentally that a 210 deg cylindrical energy analyzer

with drift spaces has second order focusing. The properties of the analyzer are deeply dependent on the fringing field around the entrance and exit of the cylinders. Author

N95-23528# National Inst. for Fusion Science, Nagoya (Japan).
COMPLEXITY IN PLASMA: A GRAND VIEW OF SELF-ORGANIZATION
Tetsuya Sato, R. Horiuchi, K. Watanane, T. Hayashi, H. Amo, T. Hayashi, Y. Todo, T. H. Watanabe, A. Kageyama, and H. Takamaru et al Nov. 1994 28 p Original contains color illustrations
(ISSN 0915-633X)
(NIFS-318) Avail: CASI HC A03/MF A01

The central theme of the Complexity is the inquest of the creation of ordered structure in nature. Extensive computer simulations on plasmas have revealed that self-organization is governed by the three key processes, i.e. energy pumping, entropy expulsion and nonlinearity. A system exhibits characteristically different self-organization, depending on whether the energy pumping is instantaneous or continuous, or whether the produced entropy is expulsed or reserved. The nonlinearity acts to bring a nonequilibrium state into a bifurcation, thus resulting in a new structure along with an anomalous entropy production. Author

N95-23533# National Inst. for Fusion Science, Nagoya (Japan).
FAST POTENTIAL CHANGE IN SAWTEETH IN JIPP T-IIU TOKAMAK PLASMAS
Y. Hamada, A. Nishizawa, Y. Kawasumi, K. Kawahata, K. Itoh, A. Ejiri, K. Toi, K. Narihara, K. Sato, and T. Seki et al Dec. 1994 26 p
(ISSN 0915-633X)
(NIFS-327) Avail: CASI HC A03/MF A01

Fast changes of electric potential with different polarities are observed during sawtooth oscillation in a core region of a tokamak plasma using a heavy ion beam probe. The potential change inside the inversion radius is found to be positive. The change is negative outside the inversion radius and clearly shows a propagation nature. The observed potential can be interpreted by the mixture of the potentials of two origins. One of them drives the fast MHD plasma motion through E/B drift and the other is a barrier potential induced by the mixing of hot and cold plasmas at sawtooth crash. Author

N95-23534# National Inst. for Fusion Science, Nagoya (Japan).
PHYSICAL MECHANISM DETERMINING THE RADIAL ELECTRIC FIELD AND ITS RADIAL STRUCTURE IN A TOROIDAL PLASMA
Katsumi Ida, Yukitoshi Miura (Japan Atomic Energy Research Inst., Ibaraki, Japan.), Sanae-I. Itoh (Kyushu Univ., Fukuoka, Japan.), J. Hofmann (Okayama Univ., Japan.), Atsushi Fukuyama, Shigeru Hideuma, Heiji Sanuki, Hiroshi Idei, Hiroshi Yamada, and Harukazu Iguchi et al Oct. 1994 66 p
(ISSN 0915-663X)
(NIFS-313) Avail: CASI HC A04/MF A01

Radial structures of plasma rotation and radial electric field are experimentally studied in tokamak, heliotron/torsatron and stellarator devices. The perpendicular and parallel viscosities are measured. The parallel viscosity, which is dominant in determining the toroidal velocity in heliotron/torsatron and stellarator devices, is found to be neoclassical. On the other hand, the perpendicular viscosity, which is dominant in dictating the toroidal rotation in tokamaks, is anomalous. Even without external momentum input, both a plasma rotation and a radial electric field exist in tokamaks and heliotrons/torsatrons. The observed profiles of the radial electric field do not agree with the theoretical prediction based on neoclassical transport. This is mainly due to the existence of anomalous perpendicular viscosity. The shear of the radial electric field improves particle and heat transport both in bulk and edge plasma regimes of tokamaks. Author

N95-23535# National Inst. for Fusion Science, Nagoya (Japan).
THE NEXT LARGE HELICAL DEVICES
Atsuo Iiyoshi and Kozo Yamazaki Nov. 1994 33 p Presented at the 36th Annual Meeting of the Division of Plasma Physics American Physical Society, Minneapolis, MN, 7-11 Nov. 1994 Original contains color illustrations
(ISSN 0915-633X)
(NIFS-323) Avail: CASI HC A03/MF A01

Helical systems have strong merits of steady-state operations for fusion reactors. Two large helical devices with fully superconducting coil systems are presently under design and construction. One is the LHD (Large Helical Device, major radius = 3.9m, magnetic field = 3.4T, under construction during 1990-1997) in NIFS (National Institute for Fusion Science)-Nagoya/Toki, Japan, which provides with continuous helical coils and clean helical divertor focusing on edge configuration optimization. The other one is the W7-X (Wendelstein 7-X, major radius = 5.5m, magnetic field = 3T, under approval) in MPIPP(Max-Planck Institute for Plasma Physics)-Garching, Germany, which adopted a modular coil system after elaborate optimization studies of core plasma physics. These two programs are complementary to promote world helical fusion research and to extend the comprehensive understanding of toroidal plasmas by comparing with large tokamaks. Author

N95-23543# National Inst. for Fusion Science, Nagoya (Japan).
RECENT STUDIES OF THE LARGE HELICAL DEVICE
Atsuo Iiyoshi and Kozo Yamazaki Nov. 1994 15 p Presented at the 1994 ICPP: International Conference on Plasma Physics, Foz Do Iguacu, Brazil, 31 Oct. - 4 Nov. 1994 Original contains color illustrations
(ISSN 0915-633X)
(NIFS-322) Avail: CASI HC A03/MF A01

The Large Helical Device (LHD) is presently under construction (1990-1997) in NIFS, Japan. The magnetic configuration is chosen as an optimized heliotron with double helix coils, succeeding Heliotron-E, ATF and CHS. Target plasma parameters of the LHD with fully superconducting coil systems are; nTau(sub E)T is approximately 10(exp 20)m(exp -3)s keV, bar-Beta = 5% and steady operations with R(sub p) = 3.75m, a(sub p) = 50-65cm and BO = 3-4T. The major objectives of the LHD project are to demonstrate good plasma confinement, high beta achievement and steady-state divertor operation in the helical system. Various R&D results have been obtained on superconducting coils, negative ion source and special diagnostics for LHD. In our new site (Toki-city, Gifu-prefecture), the construction of the main experimental hall of the LHD Building was finished, and the winding of the helical coil has been started there. The construction of the LHD will be completed in 1997. Author

N95-23564# National Inst. for Fusion Science, Nagoya (Japan).
CURRENT-PROFILE FLATTENING AND HOT CORE SHIFT DUE TO THE NONLINEAR DEVELOPMENT OF RESISTIVE KINK MODE
Kunihiko Watanabe, Tetsuya Sato, and Yuichiro Nakayama (Canon Systems Globalization, Inc., Santa Clara, CA.) Oct. 1994 28 p Sponsored by Ministry of Education, Science and Culture
(ISSN 0915-633X)
(NIFS-311) Avail: CASI HC A03/MF A01

A new and interesting phenomenon showing that the toroidal current profile for the n = 0 mode, which at first exhibits a peak due to ohmic heating and later flattens around the magnetic axis, is obtained through a compressible resistive MHD simulation in a fully 3-D toroidal geometry. We conclude through a detailed analysis that the current flattening is caused by the strong excitation of a nonlinear resistive kink mode. The time-scale of the current profile flattening is of the order of the MHD time-scale. When the current profile is largely flattened, the plasma dynamic pressure due to the strongly excited kink mode pushes the hot core plasma in the radial kink flow direction and the hot core starts deviating from the magnetic surface because of the plasma compressibility and the dynamic pressure. Since the flattening of a current profile weakens the shear effect of the poloidal magnetic field in the q less than 1 region where the resistive kink mode is growing, the poloidal magnetic field reconnection is driven by the strong kink flow and leads to complete destruction of the magnetic surface within the q = 1 rational surface (minor disruption), and the poloidal magnetic field configuration recoversto an axi-symmetric profile. The effect of the thermal conduction on the evolution of such a process is also discussed. Author

N95-23566# National Inst. for Fusion Science, Nagoya (Japan).
NEW PELLET PRODUCTION AND ACCELERATION TECHNOLOGIES FOR HIGH SPEED PELLET INJECTION SYSTEM HIPEL IN LARGE HELICAL DEVICE
I. Viniar and S. Sudo Dec. 1994 27 p
(ISSN 0915-633X)
(NISF-326) Avail: CASI HC A03/MF A01

New technologies of pellet production and acceleration for fueling and diagnostics purposes in large thermonuclear reactors are proposed. The

technologies are intended to apply to the multiple-pellet injection system 'HIPEL' for Large Helical Device of NIFS in Japan. The pellet production technology has already been tested in a pipe-gun type pellet injector. It will realize the repeating pellet injection by means of decreasing of the pellet formation time into the pipe-gun barrel. The acceleration technology is based upon a new pump tube operation in two-stage gas gun and also upon a new conception of the allowable pressure acting on a pellet into a barrel. Some preliminary estimations have been made, and principles of a pump tube construction providing for a reliable long term operation in the repeating mode without any troubles from a piston are proposed. Author

N95-23569# National Inst. for Fusion Science, Nagoya (Japan).
THE ENERGY BROADENING RESULTING FROM ELECTRON STRIPPING PROCESS OF A LOW ENERGY Au(-) BEAM
Akira Taniike (Graduate Univ. for Advanced Studies, Japan.), Mamiko Sasao, Yasuji Hamada, Junji Fujita, and Motoi Wada (Doshisha Univ., Kyoto, Japan.) Dec. 1994 24 p
(ISSN 0915-633X)
(NIFS-325) Avail: CASI HC A03/MF A01

Energy loss spectra of Au(+) ions produced from Au(-) ions by electron stripping in He, Ar, Kr and Xe have been measured in the impact energy range of 24-44 keV. The energy broadening of the Au(+) beam increases as the beam energy increases, and the spectrum shows a narrower energy width for heavy target atoms. The dependence of the spectrum width upon the beam energy and that upon the target mass are well described by the calculation based on the unified potential and semi-classical internal energy transfer model of Firsov's. Author

N95-23572# National Inst. for Fusion Science, Nagoya (Japan).
QUASISYMMETRY EQUATIONS FOR CONVENTIONAL STELLARATORS
V. D. Pustovitov (Kurchatov, I. V. Inst. of Atomic Energy, Moscow, USSR.) Nov. 1994 24 p Sponsored by Russian Foundation of Fundamental Research
(ISSN 0915-633X)
(NIFS-324) Avail: CASI HC A03/MF A01

General quasisymmetry condition, which demands the independence of B(exp 2) on one of the angular Boozer coordinates, is reduced to two equations containing only geometrical characteristics and helical field of a stellarator. The analysis is performed for conventional stellarators with a planar circular axis using standard stellarator expansion. As a basis, the invariant quasisymmetry condition is used. The quasisymmetry equations for stellarators are obtained from this condition also in an invariant form. Simplified analogs of these equations are given for the case when averaged magnetic surfaces are circular shifted torii. It is shown that quasisymmetry condition can be satisfied, in principle, in a conventional stellarator by a proper choice of two satellite harmonics of the helical field in addition to the main harmonic. Besides, there appears a restriction on the shift of magnetic surfaces. Thus, in general, the problem is closely related with that of self-consistent description of a configuration. Author

N95-23589# National Inst. for Fusion Science, Nagoya (Japan).
THEORY OF PRESSURE-INDUCED ISLANDS AND SELF-HEALING IN THREE-DIMENSIONAL TOROIDAL MAGNETOHYDRODYNAMIC EQUILIBRIA
A. Bhattacharjee (Iowa Univ., Iowa City, IA.), T. Hayashi, C. C. Hegna (Wisconsin Univ., Madison, WI.), N. Nakajima, and T. Sato Nov. 1994 26 p
(Contracts DE-FG02-86ER-53222; DE-FG02-86ER-53218) (ISSN 0915-633X)
(NIFS-321) Avail: CASI HC A03/MF A01

The role of singular currents in three-dimensional toroidal equilibria and their resolution by magnetic island formation is discussed from both analytical and computational points of view. Earlier analytical results are extended to include small vacuum islands which may, in general, have different phases with respect to pressure-induced islands. In currentless stellarators, the formation of islands is shown to depend on the resistive parameter D(R) as well as the integrated effect of global Pfirsch-Schluter currents. It is demonstrated that the pressure-induced 'self-healing' effect, recently discovered computationally, is also predicted by analytical theory. Author

N95-23590# National Inst. for Fusion Science, Nagoya (Japan).
COMPUTER SIMULATION OF A MAGNETOHYDRODYNAMIC DYNAMO 2
Akira Kageyama, Tetsuya Sato, K. Watanabe, R. Horiuchi, T. Hayashi, Y. Todo, T. H. Watanabe, and H. Takamaru Nov. 1994 51 p Sponsored by Ministry of Education, Science and Culture and Graduate Univ. for Advanced Study Original contains color illustrations
(ISSN 0915-633X)
(NIFS-320) Avail: CASI HC A04/MF A01

We performed a computer simulation of a magnetohydrodynamic dynamo in a rapidly rotating spherical shell. Extensive parameter runs are carried out changing the electrical resistivity. It is found that the total magnetic energy can grow more than ten times larger than the total kinetic energy of the convection motion when the resistivity is sufficiently small. When the resistivity is relatively large and the magnetic energy is comparable or smaller than the kinetic energy, the convection motion maintains its well-organized structure. However, when the resistivity is small and the magnetic energy becomes larger than the kinetic energy, the well-organized convection motion is highly disturbed. The generated magnetic field is organized as a set of flux tubes which can be divided into two categories. The magnetic field component parallel to the rotation axis tends to be confined inside the anticyclonic columnar convection cells. On the other hand, the component perpendicular to the rotation axis is confined outside the convection cells. Author

N95-23591# National Inst. for Fusion Science, Nagoya (Japan). Theory and Computer Simulation Center.
MHD-VLASOV SIMULATION OF THE TOROIDAL ALFVEN EIGENMODE
Y. Todo, T. Sato, K. Watanabe, T. H. Watanabe, and R. Horiuchi Nov. 1994 30 p Sponsored by Ministry of Education, Science and Culture
(ISSN 0195-633X)
(NIFS-319) Avail: CASI HC A03/MF A01

A new simulation method has been developed to investigate the excitation and saturation processes of toroidal Alfven eigenmodes (TAE modes). The background plasma is described by a full-MHD fluid model, while the kinetic evolution of energetic alpha particles is followed by the drift kinetic equation. The magnetic fluctuation of n = 2 mode develops and saturates at the level of 1.8 x 10(exp -3) of the equilibrium field when the initial beta of alpha particles is 2 percent at the magnetic axis. After saturation, the TAE mode amplitude shows an oscillatory behavior with a frequency corresponding to the bounce frequency of the alpha particles trapped by the TAE mode. The decrease of the power transfer rate from the alpha particles to the TAE mode, which is due to the trapped particle effect of a finite-amplitude wave, causes the saturation. From the linear growth rate the saturation level can be estimated. Author

N95-23768# Massachusetts Inst. of Tech., Cambridge, MA.
EDGE FLUCTUATION MEASUREMENTS BY PHASE CONTRAST IMAGING ON DIII-D
S. Coda and M. Porkolab May 1994 15 p Presented at the 10th Topical Conference on High-Temperature Plasma Diagnostics, Rochester, NY, 8-12 May 1994 Prepared in cooperation with General Atomics Co., San Diego, CA
(Contracts DE-FG02-91ER-54109; DE-AC03-89ER-51114)
(DE94-016681; GA-A-21695; CONF-940552-19) Avail: CASI HC A03/MF A01

A novel CO2 laser phase contrast imaging diagnostic has been developed for the DIII-D tokamak, where it is being employed to investigate density fluctuations at the outer edge of the plasma. This system generates 16-point, 1-D images of a 7.6 cm wide region in the radial direction, and is characterized by long wavelength (7.6 cm) and high frequency (100 MHz) capability, as well as excellent sensitivity (bar-n is approximately greater than 10(exp 9) cm(sup -3)). The effects of vertical line integration have been studied in detail, both analytically and numerically with actual flux surface geometries generated by the EFITD magnetic equilibrium code. It is shown that in the present configuration the measurement is mostly sensitive to radial wave vectors. Experimental results on fluctuation suppression at the L- to H-mode transition and on the L-mode wave number spectrum are discussed briefly. Finally, future plans for extending the measurement to the core of the plasma and for investigating externally launched fast waves are presented. DOE

N95-23982# Oak Ridge National Lab., TN.
THE EFFECT OF MAGNETIC FIELD ON THE EDGE PLASMONS OF TWO-DIMENSIONAL ELECTRON GAS SYSTEMS
X. Xia (Tennessee Univ., Knoxville, TN.), X. M. Chen (Tennessee Univ., Knoxville, TN.), and J. J. Quinn (Tennessee Univ., Knoxville, TN.) Jul. 1994 5 p Presented at the Conference on the Application of High Magnetic Fields, Cambridge, MA, 8-12 Aug. 1994
(Contract DE-AC05-84OR-21400)
(DE94-018044; CONF-940847-4) Avail: CASI HC A01/MF A01

Edge magnetoplasmons of two-dimensional electron gas (2DEG) systems with density profiles that fall from their bulk value to zero in a non-abrupt manner are investigated. Higher multipole modes, which can be thought of as bulk plasmons of the low density edge region, exist as localized edge modes only for finite values of wavevector along the edge. In addition, a sequence of very low frequency edge magnetoplasmons displaying linear dispersion are found for only one direction of propagation along the edge for a given applied magnetic field. Some insight is gained from the analysis of a simple double step density profile. DOE

N95-24017# Lawrence Livermore National Lab., Livermore, CA.
GYROKINETIC AND GLOBAL FLUID SIMULATIONS OF TOKAMAK MICROTURBULENCE AND TRANSPORT
A. M. Dimits, J. A. Byers, T. J. Williams, B. I. Cohen, W. Q. Xu, R. H. Cohen, J. A. Crotinger, and A. I. Shestakov 30 Aug. 1994 7 p Presented at the 15th International Conference on Plasma Physics and Controlled Nuclear Fusion Research, Seville, 26 Sep. - 1 Oct. 1994
(Contract W-7405-eng-48)
(DE95-003628; UCRL-JC-117113; CONF-940933-17) Avail: CASI HC A02/MF A01

Results are presented from the first systematic nonlinear kinetic simulation study of the scalings and parameter dependences of toroidal ion-temperature-gradient (ITG) turbulence and transport, and from the first such study that includes sheared toroidal flows. Key results include the observation of clear gyroBohm scaling of the turbulent transport and of a surprisingly weak dependence of the transport on toroidal flow shear. Based on the simulation results, a parameterization of the transport is given that includes the dependence on all of the relevant physical parameters. The transition from local to nonlocal transport as a function of the profile scale length has been investigated using two-dimensional global fluid simulations of dissipative drift-wave turbulence. Local gyroBohm scaling is observed, except at very short profile scale lengths. DOE

N95-24083# General Atomics Co., San Diego, CA.
A 4 MW FAST WAVE CURRENT DRIVE UPGRADE FOR D3-D
R. W. Callis, W. P. Cary, F. W. Baity (Oak Ridge National Lab., TN.), D. J. Hoffman (Oak Ridge National Lab., TN.), D. J. Taylor (Oak Ridge National Lab., TN.), C. C. Petty, R. D. Phelps, R. I. Pinsker, D. B. Remsen, and R. C. Oneill et al Sep. 1994 4 p Presented at the 18th European Symposium on Fusion Technology, Karlsruhe, Germany, 22-26 Aug. 1994
(Contracts DE-AC03-89ER-51114; DE-AC05-84OR-21400; W-7405-eng-48)
(DE95-003741; GA-A-21789; CONF-940843-12) Avail: CASI HC A01/MF A01

The DIII-D program has just completed a major addition to its ion cyclotron range of frequency (ICRF) systems. This upgrade project added two new fast wave current drive (FWCD) systems, with each system consisting of a 2 MW, 30 to 120 MHz transmitter, ceramic insulated transmission lines and tuner elements, and water-cooled four-strap antenna. With this addition of 4 MW of FWCD power to the original 2 MW, 30 to 60 MHz capability, experiments can be performed that will explore advanced tokamak plasma configurations by using the centrally localized current drive to effect current profile modifications. DOE

N95-24086# General Atomics Co., San Diego, CA.
D3-D PROGRAM OVERVIEW
R. D. Stambaugh Oct. 1994 20 p Presented at the 15th International Conference on Plasma Physics and Controlled Nuclear Fusion Research, Seville, 26 Sep. - 1 Oct. 1994
(Contracts DE-AC03-89ER-51114; W-7405-eng-48; DE-AC05-84OR-21400; DE-FG03-86ER-53225; DE-AC04-94AL-85000)
(DE95-003879; GA-A-21840; CONF-940933-19) Avail: CASI HC A03/MF A01

Recent DIII-D results support the feasibility of advanced tokamak operation (H = tau(sub E)/ITER89P up to 4 and beta(sub N) equivalent to beta(sub T)/(IaB(sub T)) up to 6). Plasma rotation dynamics have been shown to be the key to the confinement improvement in H- and VH-mode, leading to the highest DIII-D fusion triple product of n(sub D)(0)tau(sub E)T(sub i)(0) = 5 x 10(exp 20) keV s/cu m. Plasma rotation, wall stabilization, and current profile control are important in exceeding nominal stability performance beta(sub N) = 3.5 and have assisted in achieving beta(sub T) = 12.5%. Excellent exhaust of deuterium and helium in ELMing H-mode was achieved in divertor operation using an in-vessel cryopump. Reduction of divertor heat loads was shown by radiative divertor operation. Achieving impurity entrainment adequate for radiative divertor operation remains an objective of a future Radiative Divertor installation. DOE

N95-24087# General Atomics Co., San Diego, CA.
EXPERIMENTAL ACHIEVEMENT OF TOROIDAL BETA BEYOND THAT PREDICTED BY 'TROYON' SCALING
T. S. Taylor Sep. 1994 16 p Presented at the ISPP Workshop on the Theory of Fusion Plasmas, Varenna, Italy, 22-26 Aug. 1994
(Contracts DE-AC03-89ER-51114; DE-AC05-84OR-21400; W-7405-eng-48)
(DE95-003880; GA-A-21821; CONF-9408176-4) Avail: CASI HC A03/MF A01

Tokamak experiments have made substantial progress toward improving the experimentally achievable beta limit beyond that predicted by Troyon scaling, beta(sub Troyon)(%) = 2.8 I/aB MA/m/T. These advances in achievable beta have come about from the modification of the plasma profiles, primarily the current density profile, and the utilization of stabilizing conducting structures. Both theory and experiment have shown that the beta limit increases with peaked current density profiles, high I(sub i), and broad pressure profiles; scaling of the beta limit beta(sub max) (%) = 4 I(sub i) I/aB has been proposed. Experiments in DIII-D, TFTR, and JT-60U have all confirmed the increase of (beta) with I(sub i), using high powered heating and negative current ramps to increase I(sub i). It is recognized that high I(sub i) is difficult to maintain at high beta(sub N) in steady-state conditions as a consequence of the profile of the bootstrap current: (beta) is limited by low n external kinks. Profiles with a negative central shear and high edge current density have been proposed that are stable to the low n external kinks provided there is a stabilizing influence from a resistive wall. Experiments from PBX-M and DIII-D provide evidence that wall stabilization is effective and recent experiments at DIII-D have resulted in beta(sub T) = 12.5% and beta(sub N) = 4.3 at I(sub i) = 0.72 and q(sub 95) = 2.5; conditions that are expected to have a lower beta limit in the absence of wall stabilization. DOE

N95-24158# Sandia National Labs., Albuquerque, NM.
PARTICLE TRANSPORT IN PLASMA REACTORS
D. J. Rader, A. S. Geller, Seung J. Choi, and M. J. Kushner (Illinois Univ., Urbana, IL.) 1995 10 p Presented at the Microcontamination '94, San Jose, CA, 5-6 Oct. 1994
(Contract DE-AC04-94AL-85000)
(DE95-004541; SAND-94-2944C; CONF-9410132-4) Avail: CASI HC A02/MF A01

SEMATECH and the Department of Energy have established a Contamination Free Manufacturing Research Center (CFMRC) located at Sandia National Laboratories. One of the programs underway at the CFMRC is directed towards defect reduction in semiconductor process reactors by the application of computational modeling. The goal is to use fluid, thermal, plasma, and particle transport models to identify process conditions and tool designs that reduce the deposition rate of particles on wafers. The program is directed toward defect reduction in specific manufacturing tools, although some model development is undertaken when needed. The need to produce quantifiable improvements in tool defect performance requires the close cooperation among Sandia, universities, SEMATECH, SEMATECH member companies, and equipment manufacturers. Currently, both plasma (e.g., etch, PECVD) and nonplasma tools (e.g., LPCVD, rinse tanks) are being worked on under this program. In this paper the authors summarize their recent efforts to reduce particle deposition on wafers during plasma-based semiconductor manufacturing. DOE

N95-24165# Argonne National Lab., IL.
BERYLLIUM IN THE ITER BLANKET
M. C. Billone 1995 31 p Presented at the Beryllium Technology Workshop, Clearwater Beach, FL, 20 Nov. 1991

(Contract W-31-109-eng-38)
(DE95-004620; ANL/EP/VU-84785; CONF-9111209-1-Vugraphs) Avail: CASI HC A03/MF A01

This paper consists of viewgraphs used in a presentation on the application of beryllium in breeding blankets for ITER and JET. The paper brings together data on the physical, thermal, mechanical, and chemical properties of beryllium and beryllium oxide for this type of application, as well as issues of compatibility with construction materials, and irradiation experience. It includes the results from testing programs carried out to arrive at some of the information, including fabrication work, irradiation experiments, and sample tests performed both in and out of the irradiation piles. DOE

N95-24167# Argonne National Lab., IL.
MODELING OF TRITIUM RECOVERY FROM LITHIUM CERAMICS
M. C. Billone 1995 27 p Presented at the 2nd Workshop on Ceramic Breeder Interaction, Clearwater, FL, 22-23 Nov. 1991
(Contract W-31-109-eng-38)
(DE95-004626; ANL/EP/SUMM-84774; CONF-9111175-2) Avail: CASI HC A03/MF A01 (US Sales Only)

The TIARA and DISPL2 codes are being developed at Argonne National Laboratory to predict tritium retention and release from lithium ceramics under steady-state and transient conditions, respectively. Emphasis has been placed on tritium behavior in Li2O because of the selection of this ceramic as a first option for the ITER driver blanket and because of the excellent materials properties data base for Li2O. In this paper, the results of validation of TIARA to tritium retention data from VOM-15H, EXOTIC-2, and CRITIC-1 are presented, along with predictions of tritium retention in BEATRIX-11. For DISPL2, results are presented for tritium release predictions vs. data for MOZART, CRITIC-1, and BEATRIX-11. DOE

76 SOLID-STATE PHYSICS

Includes superconductivity.

For related information, see also *33 Electronics and Electrical Engineering* and *36 Lasers and Masers.*

N95-22499# International Centre for Theoretical Physics, Trieste (Italy).
STRONG-COUPLING BEHAVIOUR OF TWO t-J CHAINS WITH INTERCHAIN SINGLE-ELECTRON HOPPING
Guangming Zhang, Shiping Feng, and Lu Yu Jan. 1994 11 p
(DE94-629041; IC-94/20) Avail: CASI HC A03/MF A01 (US Sales Only)

Using the fermion-spin transformation to implement spin-charge separation of constrained electrons, a model of two t - J chains with interchain single-electron hopping is studied by abelian bosonization. After spin-charge decoupling the charge dynamics can be trivially solved, while the spin dynamics is determined by a strong-coupling fixed point where the correlation functions can be calculated explicitly. This is a generalization of the Luther-Emery line for two-coupled t - J chains. The interchain single-electron hopping changes the asymptotic behaviour of the interchain spin-spin correlation functions and the electron Green function, but their exponents are independent of the coupling strength. DOE

N95-22511 State Univ. of New York, Buffalo, NY. Dept. of Physics.
HIGH POWER JOSEPHSON EFFECT SOURCES Final Report, May 1990 - Mar. 1994
James Lukens Sep. 1994 50 p Limited Reproducibility: More than 20% of this document may be affected by microfiche quality
(Contract F19628-90-K-0033)
(AD-A285808; RL-TR-94-171) Avail: CASI HC A03

Progress is reported toward the development of high power linear array Josephson effect sources for the submillimeter wave. A series biased array, fabricated at IBM, was successfully tested and demonstrated fully coherent operation with a power of over 1 microns W into 50 omega near 300 GHz. A single chip source detector was designed, fabricated (at Stony Brook) and tested. On-chip source-mixing between two small array sources operating near 300 GHz was accomplished with the IF, near 10 GHz, being coupled out of the cryostat for direct linewidth measurement. The measured linewidth agreed with theory. This chip also demonstrated a new array design in which groups of multiple, closely spaced junctions were placed at wavelength intervals. This permitted much higher density and consequently higher power per unit area from the arrays. This new design was incorporated into a 500 junction source, also fabricated at IBM, which delivered nearly 5O microns W to a load of over 50 omega near 400 GHz. The PARTS process used by IBM for this fabrication has now been set up at Stony Brook permitting on-site fabrication o even higher power sources. DTIC

N95-22520# Los Alamos National Lab., NM.
SUPERCONDUCTING TL2BA2CACU2O8 THIN FILMS PREPARED BY POST-ANNEALING IN A FLOW-THROUGH MULTIPLE-ZONE FURNACE
T. C. Pluym, R. E. Muenchausen, and P. N. Arendt 1994 5 p Presented at the Applied Superconductivity Conference, Boston, MA, 16-21 Oct. 1994
(Contract W-7405-eng-36)
(DE95-002745; LA-UR-94-3568; CONF-941013-3) Avail: CASI HC A01/MF A01

Tl2Ba2CaCu2O8 thin films were prepared for the first time by use of a multiple-zone flow-through thallination process. Thallous oxide was volatilized from condensed thallium oxide in a low temperature source zone and convectively transported to a higher temperature thallination zone in which initially amorphous Ba2CaCu2O5 precursor films were located. By careful control of the source temperature, film temperature, flow rate, anneal time, and rates of heat up and cool down, smooth Tl2Ba2CaCu2O8 thin films were prepared on (100) LaAlO3 with the following properties: inductive (Tc) of 107.6 K and 80% transition width of 1.3 K, transport J(sub c) at 75 K of 1.3 x 10(exp 5) A/sq cm, and R(sub s) at 10 GHz and 80 K of 1.3 megaohms. The scalability of the process to large area film processing was demonstrated by the preparation of Tl2Ba2CaCu2O8 thin films on LaAlO3 three-inch diameter wafers. DOE

N95-22530# Argonne National Lab., IL. Energy Technology Div.
HIGH-TEMPERATURE ULTRASONIC CHARACTERIZATION OF Ag-CLAD SUPERCONDUCTOR TAPES
M. T. Lanagan, D. S. Kupperman, G. A. Yaconi, and S. H. Kilgore 30 Sep. 1994 14 p Presented at the Applied Superconductivity Conference, Boston, MA, 16-21 Oct. 1994
(Contract W-31-109-eng-38)
(DE95-002909; ANL/ET/CP-82313; CONF-941013-6) Avail: CASI HC A03/MF A01

An ultrasonic nondestructive evaluation technique was developed to monitor liquid-phase evolution during heat treatment of high-T(sub c) superconductors. The liquid phase is important for microstructural and phase development of superconductors and is important in fabricating conductors with high critical current density, J(sub c). Tapes were fabricated by a powder-in-tube process and then placed in a controlled atmosphere furnace. During the heat treatment process, a magnetostrictive transducer launches a 140-kHz wave into the sample, and relative change in acoustic velocity is measured. A significant decrease in the velocity was seen at the incongruent melting temperatures of Bi-based superconductors. In addition, Ag-clad tapes with Al2O3 and NaCl cores were used to validate the measurement technique. Advantages of this technique over other thermal analysis methods include in-situ analysis of the final tape form, monitoring of isothermal liquid evolution, and control of volatile species such as Tl and Pb. DOE

N95-22555# North Carolina State Univ., Raleigh, NC.
ADVANCED GROWTH AND SURFACE ANALYSIS SYSTEM FOR IN SITU STUDIES OF INTERFACE FORMATION Annual Technical Report No. 1
D. E. Sayers, R. J. Nemanich, and Z. Wang 10 Oct. 1994 11 p
(Contract DE-FG05-93ER-79236)
(DE95-002850; DOE/ER-79236/1) Avail: CASI HC A03/MF A01

This is the first annual report for developing an advanced integrated in situ UHV growth/analysis system for synchrotron radiation studies of interface and surface reactions which lead to epitaxial structures on Si, Ge, and Si(1-x)Ge(x) alloys. This equipment will allow one to use techniques based on synchrotron radiation, such as photoemission, x-ray standing wave (XSW), and surface x-ray absorption spectroscopy (SXAFS) to determining the electronic states and atomic configurations of surfaces in metal-silicon, metal-germanium and metal-silicon-germanium alloys. Since the award of the contract the authors have completed a detailed design of the overall system, identified commercially available equipment which fits the

requirements and have purchased or ordered all of this equipment. They have also custom designed a considerable amount of equipment which is not available commercially because of the special requirements. This includes both of the UHV chambers, sample manipulators, and a mobile support stand. In this report, they will describe the design and purchase status of the system. An overview of the equipment purchase status is given in Appendix 1. The details of their custom designed growth and analytical chambers are given in Appendix 2. DOE

N95-22565# Los Alamos National Lab., NM.
HIGH PRESSURE NEUTRON POWDER DIFFRACTION AT LANSCE
Robert B. VonDreele 1994 11 p Presented at the International Seminar on Neutron Scattering At High Pressure, Dubna, Russia, 5-7 Oct. 1994
(Contract W-7405-eng-36)
(DE95-002703; LA-UR-94-3422; CONF-9410115-1) Avail: CASI HC A03/MF A01

By making use of the recently developed 'Paris-Edinburgh' high pressure cell, the author has successfully performed neutron powder experiments to 10GPa at ambient temperature. Results for the structural compression of the high Tc 1223-Hg superconductor to 9.2 GPa, the compression and possible hydrogen bond formation in brucite, Mg(OD)2, to 9.3 GPa, and the molecular reorientation in nitromethane to 5.5 GPa will be presented. DOE

N95-22572# Argonne National Lab., IL. Energy Technology Div.
INITIAL CRYSTALLIZATION AND GROWTH IN MELT PROCESSING OF LARGE-DOMAIN YBa2Cu3O(x) FOR MAGNETIC LEVITATION
D. Shi (Cincinnati Univ., OH.), W. Zhong, U. Welp, S. Sengupta, V. R. Todt, G. W. Crabtree, S. Dorris, and U. Balachandran Oct. 1994 5 p Presented at the Applied Superconductivity Conference, Boston, MA, 16-21 Oct. 1994
(Contracts W-31-109-eng-38; DE-FG02-90ER-45427)
(DE95-002993; ANL/ET/CP-84520; CONF-941013-9) Avail: CASI HC A01/MF A01

Crystallization temperature in YBa2Cu3O(x) (123) during peritectic reaction has been studied by differential thermal analysis (DTA) and optical microscopy. It has been found that YBa2Cu3O(x) experiences partial melting near 1,010 C during heating while crystallization takes place at a much lower temperature range upon cooling indicating a delayed nucleation process. A series of experiments have been conducted to search for the initial crystallization temperature in the Y2BaCuO(x) + liquid phase field. The authors have found that the slow-cool period (1 C/h) for the 123 grain texturing can start at as low as 960 C. This novel processing has resulted in high-quality, large-domain, strongly pinned 123 magnetic levitators. DOE

N95-22584 Paris II Univ., Orsay (France).
STUDY OF PHOTOREFRACTIVE NON-LINEARITIES IN THE 3-5 AND 2-4 SEMI-INSULATOR COMPOUNDS: THE EFFECT OF ELECTRON IRRADIATION Ph.D. Thesis
P. Delaye 6 Apr. 1993 182 p Prepared in cooperation with Direction des Recherches, Etudes et Techniques, Paris, France
(PB94-189057) Avail: Issuing Activity (National Technical Information Service (NTIS))

This manuscript presents research into the photorefractive effect in the near infrared, particularly in materials that are sensitive in the infrared wavelength range. The first section deals with existing materials synthesized for microelectronic applications: GaAs and InP. Experimental and theoretical studies shed light on their properties and limitations, notably for applications around 1.3 micrometers. Based on the results, the authors propose an electron irradiation technique to optimize GaAs performance. Irradiation induces slight variations in the Fermi level, which should favor photorefractive effect at 1.3 micrometers. The results show that the predicted effect is strongly offset by the creation of an irradiation defect at mid-gap. They also worked on II-VI compounds such as CdTe. The first crystals showed a noticeable photorefractive gain with low power beams, confirming their promise as a means of extending PR effect around 1.5 micrometers. They conclude with a technique using square AC field that amplifies photorefractive gain by one order of magnitude. NTIS

N95-22606# International Centre for Theoretical Physics, Trieste (Italy).
A FRACTAL MODEL FOR INTERGRANULAR FRACTURES IN NANOCRYSTALS
C. W. Lung, L. Y. Xiong (Academia Sinica, Shenyang, China.), and X. Z. Zhou (Academia Sinica, Shenyang, China.) Sep. 1993 15 p
(DE94-627393; IC-93/324) Avail: CASI HC A03/MF A01 (US Sales Only)

A fractal model for intergranular fractures in nanocrystals is proposed to explain the dependence of fracture toughness with grain size in this range of scale. Based on positron annihilation and internal friction experimental results, we point out that the assumption of a constant grain boundary thickness in previous models is too simplified to be true. DOE

N95-22607# International Centre for Theoretical Physics, Trieste (Italy).
THERMAL ACTIVATION OF STEADY-STATE CREEP IN POLYCRYSTALLINE COPPER
A. Ayensu, S. K. Adjepong (Cape Coast Univ., Ghana.), and G. K. Quainoo Oct. 1993 25 p
(DE94-627394; IC-93/347) Avail: CASI HC A03/MF A01 (US Sales Only)

High purity (99.9%) polycrystalline copper wires have been creep tested at atmospheric pressure and at intermediate temperatures of 573 K, 673 K, and 773 K (T/T(sub m) = 0.42-0.57), under uniaxial tensile stresses of 7.08, 14.16, and 21.24 MPa in order to determine the activation parameters of steady-state creep. The tension creep tests were conducted using a stress incremental technique (sigma(sub 1) less than sigma(sub 2) less than sigma(sub 3)). The stress exponent of the steady state creep rate n is close to 2 and the activation energy Q(sup 1)(sub c) is about 60 kJ/mol. Activation analyses of the data have been made to identify the deformation mechanism(s) and to link the external parameters with the model parameters through the operational parameters n and Q(sup 1)(sub c). The creep deformation is attributed to a boundary mechanism involving grain boundary sliding and Coble diffusion. A model is proposed for the boundary mechanism. DOE

N95-22615# International Centre for Theoretical Physics, Trieste (Italy).
A PARALLEL MOLECULAR DYNAMICS SIMULATION OF CRYSTAL GROWTH AT A CLUSTER OF WORKSTATIONS
M. J. P. Nijmeijer Jan. 1994 7 p
(DE94-628382; IC-94/36) Avail: CASI HC A02/MF A01 (US Sales Only)

To enable a simulation of the growth of crystalline fibers at a cluster of workstations, the author developed a parallel molecular-dynamics (MD) algorithm. The structure of the MD algorithm is described briefly, together with its parallelization. Some specific features of the application is discussed and an illustration of the program performance is given. DOE

N95-22649# International Centre for Theoretical Physics, Trieste (Italy).
CONTINUOUS LOCAL SYMMETRY IN ISING-TYPE MODELS
S. RandjbarDaemi and J. Strathdee Jan. 1994 6 p
(DE94-629045; IC-94/27) Avail: CASI HC A02/MF A01 (US Sales Only)

A class of generalized Ising models is examined with a view to extracting a low energy sector comprising Dirac fermions coupled to Yang-Mills vectors. The main feature of this approach is a set of gap equations, covariant with respect to one of the 4-dimensional crystallographic space groups. DOE

N95-22653# Los Alamos National Lab., NM.
DISLOCATION DECOMPOSITION, DISSOCIATION, AND DEFORMATION IN MoSi2 AND (ALPHA)-Al2O3 SINGLE CRYSTALS
Stuart A. Maloy and Terence E. Mitchell 1994 11 p Presented at the Conference on Plastic Deformation of Ceramics, Snowbird, UT, 7-12 Aug. 1994
(Contract W-7405-eng-36)
(DE95-002715; LA-UR-94-3488; CONF-940865-5) Avail: CASI HC A03/MF A01

The mechanisms of deformation in single crystal MoSi2 along (001) at temperatures of 900 to 1450 C are compared and contrasted with the mechanisms of deformation of single crystal (alpha)-Al2O3 deformed by prismatic slip at temperatures of 1450-1700 C. Deformation occurs by dislocations with large Burgers vectors at lower temperatures. These

dislocations are dissociated into three collinear partials separated by antiphase boundaries or stacking faults. At higher temperatures, these dislocations with large Burgers vectors decompose into two perfect dislocations. This decomposition has the effect of forcing slip on another slip system in MoSi2 and increasing the work hardening rate in (alpha)-Al2O3. DOE

N95-22687# Oak Ridge National Lab., TN.
SUPERLATTICES IN THERMOELECTRIC APPLICATIONS
J. O. Sofo (Tennessee Univ., Knoxville, TN.) and G. D. Mahan (Tennessee Univ., Knoxville, TN.) Aug. 1994 8 p Presented at the 13th International Conference on Thermoelectrics, Kansas City, MO, 30 Aug. - 1 Sep. 1994
(Contract DE-AC05-84OR-21400)
(DE95-001356; CONF-940830-1) Avail: CASI HC A02/MF A01

The electrical conductivity, thermopower and the electronic contribution to the thermal conductivity of a superlattice, are calculated with the electric field and the thermal gradient applied parallel to the interfaces. Tunneling between quantum wells is included. The broadening of the lowest subband when the period of the superlattice is decreased produces a reduction of the thermoelectric figure of merit. However, we found that a moderate increase of the figure of merit may be expected for intermediate values of the period, due to the enhancement of the density of states produced by the superlattice structure. DOE

N95-22762# Argonne National Lab., IL.
PHOTOEMISSION STUDY OF QUANTUM CONFINEMENT BY A FINITE BARRIER: Cu/Co(WEDGE)/Cu(100)
D. Li, J. Pearson, J. E. Mattson, S. D. Bader, and P. D. Johnson (Brookhaven National Lab., Upton, NY.) Jul. 1994 16 p
(Contracts W-31-109-eng-38; DE-AC02-76CH-00016)
(DE95-002913; ANL/MSD/PP-83766) Avail: CASI HC A03/MF A01

The evolution of d-electron quantum-well (QW) states is observed with angle-resolved photoemission for ultrathin Cu epitaxially deposited on fcc Co(100). Quantum confinement is studied of the Cu d-QW state at 2.4 eV binding energy and the corresponding sp-state at 1.6 eV for 2ML of Cu separated from the Cu(100) substrate by an epitaxial wedge of Co (0-13ML) that serves as a finite barrier. The photoemission intensities indicate stronger confinement of the d-QW state than of the sp-state. Implications for the magnetic coupling are discussed. DOE

N95-22774# International Centre for Theoretical Physics, Trieste (Italy).
GENERAL CRYSTAL IN PREBIOTIC CONTEXT
I. Simon Sep. 1993 5 p
(DE94-628475; IC-93/322) Avail: CASI HC A01/MF A01 (US Sales Only)

General crystal is an extension of the crystal concept to any form of matter which exhibits neighbor structure determination. This extension makes many results of solid state physics applicable to heterogeneous matter. Among others it includes the description of phase transition from random to unique structure. The advantage of the general crystal approach is demonstrated on globular protein, on of the most important macromolecules of life, which are capable to adopt unique 3D structure spontaneously, regardless of the heterogeneous character of their chemical structure and conformation. It is suggested that the use of general crystal concept may help to find candidates among heterogeneous matters capable of spontaneous self-organization in the same way as crystallization results in unique structure of homogeneous matter, and to apply some of the results of solid state physics to describe the phase transition and other behavior of this matter. DOE

N95-22803*# National Aeronautics and Space Administration. Langley Research Center, Hampton, VA.
A RUGGEDNESS EVALUATION OF PROCEDURES FOR DAMAGE THRESHOLD TESTING OPTICAL MATERIALS
Matthew W. Hooker (Science and Technology Corp., Hampton, VA.), Milfred E. Thomas (Science and Technology Corp., Hampton, VA.), Stephanie A. Wise, and Nina D. Tappan Feb. 1995 9 p
(RTOP 323-17-04-01)
(NASA-TM-4639; L-17439; NAS 1.15:4639) Avail: CASI HC A02/MF A01

A ruggedness evaluation of approaches to damage threshold testing was performed to determine the influence of three procedural variables on damage threshold data. The differences between the number of test sites evaluated at an applied fluence level (1 site versus 10 sites), the number of laser pulses at each test site (1 pulse versus 200 pulses), and the beam diameter (0.35 mm versus 0.70 mm) were all found to significantly influence the damage threshold data over a 99-percent confidence interval. Author

N95-22839# International Centre for Theoretical Physics, Trieste (Italy).
VARIATIONAL CALCULATIONS FOR He-3 IMPURITIES ON He-4 DROPLETS
A. Belic, F. Dalfovo (Trento Univ., Povo, Italy.), S. Stringari (Trento Univ., Povo, Italy.), and S. Fantoni (International School for Advanced Studies, Trieste, Italy.) Jan. 1994 17 p
(DE94-628469; IC-94/1) Avail: CASI HC A03/MF A01 (US Sales Only)

Variational Monte Carlo method is used to calculate ground state properties of He-4 droplets, containing 70, 112, 168, 240, 330 and 728 particles. The resulting particle and kinetic energy densities are used as an input in the Feynman-Lekner theory for He-3 impurities. The kinetic energy density of He-4 atoms and the energy of the He-3 surface states are compared with the results of previous phenomenological calculations. DOE

N95-22845# International Centre for Theoretical Physics, Trieste (Italy).
BLOCK SPINS AND CHIRALITY IN HEISENBERG MODEL ON KAGOME AND TRIANGULAR LATTICES
V. Subrahmanyam Jan. 1994 12 p
(DE94-629044; IC-94/24) Avail: CASI HC A03/MF A01 (US Sales Only)

The spin-1/2 Heisenberg model (HM) is investigated using a block-spin renormalization approach on Kagome and triangular lattices. In both cases, after coarse graining the triangles on original lattice and truncation of the Hilbert space to the triangular ground state subspace, HM reduces to an effective model on a triangular lattice in terms of the triangular-block degrees of freedom viz. the spin and the chirality quantum numbers. The chirality part of the effective Hamiltonian captures the essential difference between the two lattices. It is seen that simple eigenstates can be constructed for the effective model whose energies serve as upper bounds on the exact ground state energy of HM, and chiral ordered variational states have high energies compared to the other variational states. DOE

N95-22846# International Centre for Theoretical Physics, Trieste (Italy).
CORRELATION EFFECTS IN HIGH-Tc SUPERCONDUCTORS AND HEAVY FERMION COMPOUNDS
A. L. Kuzemsky Oct. 1993 22 p
(DE94-629057; IC-93/336) Avail: CASI HC A03/MF A01 (US Sales Only)

This paper describes certain aspects of Highly Correlated Systems (HCS) such as high Tc superconductors (HTSC) and some new class of Heavy Fermion (HF) systems which have been studied recently. The problem is discussed on how the charge and spin degrees of freedom participate in the specific character of superconductivity in the copper oxides and competition of the magnetism and Kondo screening in heavy fermions. The electronic structure and possible superconducting mechanisms of HTSC compounds are discussed. The similarity and dissimilarity with HF compounds is pointed out. It is shown that the spins and carriers in the copper oxides are coupled in a very nontrivial way in order to introduce the discussion and the comparison of the Emery model, the t - J-model and the Kondo-Heisenberg model. It concerns attempts to derive from fundamental multi-band Hamiltonian the reduced effective Hamiltonians to extract and separate the relevant low-energy physics. A short review of the arguments which seem to support the spin-polaron pairing mechanism in HTSC are presented. Many other topics like the idea of mixed valence states in oxides, the role of charge transfer (CT) excitations, phase separation, self-consistent nonperturbative technique, etc. are also discussed. DOE

N95-22851 Stanford Univ., CA.
LIGAND K-EDGE X-RAY ADSORPTION SPECTROSCOPIC STUDIES OF THE ELECTRONIC STRUCTURE OF INORGANIC MODEL COMPLEXES AND METALLOPROTEIN ACTIVE SITES
S. E. Shadle Aug. 1994 288 p Limited Reproducibility: More than 20% of this document may be affected by poor print

(Contract DE-AC03-76SF-00515)
(DE95-003338; SU-SLAC-449) Avail: Issuing Activity (Department of Energy (DOE))

Ligand K-edge X-ray absorption spectroscopy (XAS) has been developed as a technique for the investigation of ligand-metal bonding and has been applied to the study of electronic structure in organic model complexes and metalloprotein active sites. Ligand K-edge XAS has been measured at the chloride K-edge for a series of complexes containing chloride ligands bound to open shell d(sup 9) copper ions. The intensity of the pre-edge feature in these spectra reflects the covalency in the half-occupied d(sub x)2(sub -y)2-derived molecular orbital (HOMO) of the complex. The energy of the pre-edge feature is related to both the charge on the ligand and the HOMO energy. An analysis of the intensity and energy of the pre-edge feature as well as the energy of the rising edge absorption provides quantitative information about the covalency of the ligand-metal interaction, the charge donated by the chloride, and the energy of the copper d-manifold. The results demonstrate that ligand K-edge XAS features can be used to obtain quantitative information about ligand-metal bonding. The results also identify the chemical basis for trends in the XAS data for the complexes: D(sub 4h)CuCl4(sup 2-), D(sub 2d)CuCl4(sup 2-), planar, trans-CuCl2(pdmp)(sub 2) (pdmp = N-phenyl-3,5-dimethylpyrazole), square pyramidal CuCl5(sup 3-), the planar dimer KCuCl3, the distorted tetrahedral dimer (Ph4P)CuCl3, and two dimers with mixed ligation, one containing a bridging chloride, and the other, terminally bound chloride. A geometric distortion from square planar to distorted tetrahedral results in a decrease in the chloride-copper HOMO covalency but an increase in the total charge donation by the chlorides. Thus, while the geometry can maximize the overlap for a highly covalent HOMO, this does not necessarily reflect the overall charge donation. The Cl-Cu(II) bonding interactions are dependent on the nature of the other coordinating ligands. DOE

N95-22854# Israel Association for Crystal Growth, Rehovot (Israel).
THE 1993 ANNUAL CONFERENCE OF THE ISRAELI ASSOCIATION FOR CRYSTAL GROWTH. PROGRAM AND ABSTRACTS
Nov. 1993 56 p Conference held in Rehovot, Israel, 16 Nov. 1993
(DE94-633510; INIS-mf-13903; CONF-9311228) Avail: CASI HC A04/MF A01 (US Sales Only)

Papers presented in oral and poster sessions of a one day conference, organized by the Israeli Association for Crystal Growth, are compiled in this document. Main topics covered in this document can be classified as: (i) Fundamental and numerical analysis of crystal growth. (ii) Techniques of crystal growth and structural analysis. (iii) Thin film growth and characterization. DOE

N95-22860# Lawrence Livermore National Lab., Livermore, CA.
PROGRESS TOWARDS THE SYNTHESIS OF POLYMERIC NITROGEN
H. E. Lorenzana, A. K. McMahan, C. S. Yoo, and T. W. Barbee, III Jun. 1994 7 p Presented at the Air Force High Energy Density Materials Contractors Conference, Crystal Bay, NV, 5-7 Jun. 1994
(Contract W-7405-eng-48)
(DE94-017547; UCRL-JC-116590; CONF-9406246-1) Avail: CASI HC A02/MF A01

Current conventional energetic compounds rely on strong covalent bonds within individual molecules for energy storage. A new class of energetic compounds has been recently proposed that entirely replaces weak van der Waals interactions with strong covalent bonds arranged in a continuous, uniform network, thus tremendously enhancing the energy per volume. In particular, recent theoretical calculations have suggested that a phosphorus-like or polymeric form of nitrogen may exist metastably at atmospheric pressure as a hard, insulating solid with an enhanced energy per unit volume. It is predicted that the polymeric phase of nitrogen should be stable at high pressure. And therefore the megabar diamond anvil cell might provide the ideal vehicle for carrying out proof-of-existence experiments. Currently, the authors are bringing to bear technologies for achieving multimegabar pressures and temperatures of several thousand K. These conditions are necessary to rearrange the bonds of strongly covalent systems into highly energetic configurations. There is no doubt that the transformations will show strong hysteresis making the initial synthesis difficult, but for these very same reasons, these new compounds potentially will be metastable at ambient conditions in their energetic state. They discuss their results and progress to date, indicating that they are well on their way to understanding the high pressure equation-of-state of sold N2. DOE

N95-22907*# Alabama Univ., Huntsville, AL. Dept. of Physics.
COMPUTATIONAL MODELING OF PROPERTIES Final Report, 12 Mar. 1993 - 11 Jul. 1994
Judy R. Franz 11 Jul. 1994 51 p
(Contract NAS8-38609)
(NAS-CR-196544; NAS 1.26:196544) Avail: CASI HC A04/MF A01

A simple model was developed to calculate the electronic transport parameters in disordered semiconductors in strong scattered regime. The calculation is based on a Green function solution to Kubo equation for the energy-dependent conductivity. This solution together with a rigorous calculation of the temperature-dependent chemical potential allows the determination of the dc conductivity and the thermopower. For wise-gap semiconductors with single defect bands, these transport properties are investigated as a function of defect concentration, defect energy, Fermi level, and temperature. Under certain conditions the calculated conductivity is quite similar to the measured conductivity in liquid II-VI semiconductors in that two distinct temperature regimes are found. Under different conditions the conductivity is found to decrease with temperature; this result agrees with measurements in amorphous Si. Finally the calculated thermopower can be positive or negative and may change sign with temperature or defect concentration. Author

N95-23020# International Centre for Theoretical Physics, Trieste (Italy).
PHOTOINDUCED BRAGG GRATING FORMATION IN OPTICAL FIBRES AS A CONSEQUENCE OF CONVECTIVE INSTABILITY
A. S. Furman Oct. 1993 5 p
(DE94-628479; IC-93/357) Avail: CASI HC A01/MF A01 (US Sales Only)

The photoinduced formation of Bragg gratings in optical fibers is explained as a consequence of convective instability. Close analogy is emphasized between this phenomenon and the photoinduced second harmonic generation in optical fibers. The observed grating formation is interpreted as amplification of very low frequency noise. Predictions concerning the transient processes are made which could be checked experimentally. DOE

N95-23021# International Centre for Theoretical Physics, Trieste (Italy).
SURFACE GROWTH OF TWO KINDS OF PARTICLES DEPOSITION MODELS
Wei Wang and H. A. Cerdeira Oct. 1993 21 p
(DE94-628480; IC-93/361) Avail: CASI HC A03/MF A01 (US Sales Only)

The surface kinetics with diffusion of two kinds of particles (A and C) deposition models, random-like and ballistic-like depositing on a (1 + 1)-dimensional substrate, is studied. The scaling behavior of the surface width for these two models is obtained for various deposition probability P of particle C (the probability of particle A being 1 - P). We found that both models have a scaling behavior: the surface width growth only depends on the time, W approximately t(exp alpha(P)) for the early stage and W approximately t(exp beta(P)) for the intermediate time, as well as W approximately L(exp z) for the later time with different exponents alpha(P), beta(P), and z for two models. In addition, there is a phase transition when the saturation surface widths are scaled to the deposition probability P for both models W(t = infinity) approximately P(exp gamma): before and after the transition the scaling exponent gamma is different. This transition is interpreted as that there are different morphologic structures when the depositing probability for one kind of particle, particle C, is larger than a critical value P(sub c). DOE

N95-23022# International Centre for Theoretical Physics, Trieste (Italy).
DYNAMICAL BEHAVIOUR OF THE COUPLED DIFFUSION MAP LATTICE
Wei Wang and H. A. Cerdeira Oct. 1993 30 p
(DE94-628481; IC-93/362) Avail: CASI HC A03/MF A01 (US Sales Only)

We report the dynamical study of a coupled diffusive map lattice with the coupling between the elements only through the bifurcation parameter of the mapping function. The diffusive process of the lattice from an initially random distribution state to a homogeneous one and the stable

range of the diffusive homogeneous attractor are discussed. For various coupling strengths we find that there are several types of spatio-temporal structures. In addition, the evolution of the lattice into chaos is studied and a largest Lyapunov exponent is used to characterize the dynamical behavior. DOE

N95-23047# International Centre for Theoretical Physics, Trieste (Italy).
EFFECTS OF LONG-RANGE COUPLING ON AGGREGATION
E. Canessa and Wei Wang Oct. 1993 6 p
(DE94-628483; IC-93/367) Avail: CASI HC A02/MF A01 (US Sales Only)

Numerical simulations of a 2D biharmonic equation (nabla)(sup 4)u = 0 show that a transition from dense to multibranched growth is a consequence of long-range coupling between displacements on the pattern formation of fractal aggregates. DOE

N95-23048# International Centre for Theoretical Physics, Trieste (Italy).
ON CORE LEVEL ELECTRON DIFFRACTION
L. Fonda Nov. 1993 37 p
(DE94-628484; IC-93/369) Avail: CASI HC A03/MF A01 (US Sales Only)

In this article the basic elements of the theory of core level electron diffraction are given in a comprehensive form. All relevant formulas are obtained rigorously. Some approximations are then considered such as those involving single scatterings and plane waves. The theory applies both to photo- and Auger-electron diffraction. DOE

N95-23059# International Centre for Theoretical Physics, Trieste (Italy).
ASYMPTOTICALLY EXACT SOLUTION OF A LOCAL COPPER-OXIDE MODEL
GuangMing Zhang and Lu Yu Mar. 1994 11 p
(DE94-628492; IC-94/63) Avail: CASI HC A03/MF A01 (US Sales Only)

We present an asymptotically exact solution of a local copper-oxide model abstracted from the multi-band models. The phase diagram is obtained through the renormalization-group analysis of the partition function. In the strong coupling regime, we find an exactly solved line, which crosses the quantum critical point of the mixed valence regime separating two different Fermi-liquid (FL) phases. At this critical point, a many-particle resonance is formed near the chemical potential, and a marginal-FL spectrum can be derived for the spin and charge susceptibilities. DOE

N95-23135# Sandia National Labs., Albuquerque, NM.
SURFACE STRUCTURAL DEPENDENCE OF CESIUM ADSORPTION ON THE (ALPHA)-AI2O3(0001) SURFACE
K. R. Zavadil and J. L. Ing (AEA Technology, Albuquerque, NM.) 1994 7 p Presented at the 12th Symposium on Space Nuclear Power and Propulsion, Albuquerque, NM, 8-12 Jan. 1995
(Contract DE-AC04-94AL-85000)
(DE95-002610; SAND-94-2506C; CONF-950110-13) Avail: CASI HC A02/MF A01

The structural dependence of Cs adsorption on the (alpha)-Al2O3 (0001) surface has been studied using a combination of surface analytical techniques. The unreconstructed or (1(times)1) surface shows a high initial Cs adsorption probability of 0.9 based on reflection mass spectrometry (RMS). This value decreases rapidly after a critical Cs coverage of 1.5 x 10(exp 14) atoms/sq cm is reached. Thermally-induced surface reconstruction to form an O deficient surface results in a decrease in the critical coverage, probability and capacity for Cs adsorption. Low energy electron diffraction (LEED) demonstrates that a predominantly (3(square root of) 3 x 3(square root of) 3)R30 deg surface yields an initial adsorption probability of 0.5 while a predominantly (square root of 31 x square root of 31)R(+/-s)9 deg yields a value of 0.3. Thermal desorption mass spectrometry (TDMS) shows that surface reconstruction suppresses the high binding energy states of Cs, consistent with the observed changes in adsorption probability. X-ray photoelectron spectroscopy (XPS) provides no direct evidence for formal oxidative/reductive chemistry taking place at the interface. We interpret the facile adsorption and strong binding of Cs on sapphire to result from Cs interacting with coordinatively unsaturated O. DOE

N95-23265# Los Alamos National Lab., NM.
ORIENTATION SELECTION AND MICROSTRUCTURAL EVOLUTION OF EPITAXIAL PLATINUM FILMS ON (001) MAGNESIUM OXIDE
P. C. McIntyre, C. J. Maggiore, and M. Natasi 1995 13 p Presented at the 1994 Fall Meeting of the Materials Research Society (MRS), Boston, MA, 28 Nov. - 2 Dec. 1994
(Contract W-7405-eng-36)
(DE95-003680; LA-UR-94-4052; CONF-941144-3) Avail: CASI HC A03/MF A01

Thin platinum films were deposited at several different deposition rates and with varying thickness on (001)-cut MgO single crystal substrates by electron beam evaporation. A mixture of two epitaxial Pt orientations were detected in the films by x-ray diffraction and planar ion channeling experiments: (001) zone axes(100) Pt // (001) zone axes(100) MgO (the 'cube-on-cube' orientation) and (111) zone axes(110) Pt // (001) zone axes(110) MgO. The effect of deposition rate on film orientation indicated the (111) Pt orientation was preferred under conditions of high driving force for nucleation. The volume fraction of the films occupied by the (111) orientation increased with nominal film thickness, at a constant substrate temperature and deposition rate. This result indicates crystallites having the (111) Pt orientation grew more quickly following nucleation than the (001). The mosaic spread of the Pt orientation decreased markedly as the nominal film thickness increased from approximately 1.5 nm (isolated islands) to 20 nm (continuous film). DOE

N95-23266# Los Alamos National Lab., NM.
CATION DISORDER DETERMINED BY MAS Al-27 NMR IN HIGH DOSE NEUTRON IRRADIATED SPINEL
E. A. Cooper, K. E. Sickafus, C. D. Hughes, W. L. Earl, G. W. Hollenberg (Pacific Northwest Lab., Richland, WA.), F. A. Garner (Pacific Northwest Lab., Richland, WA.), and R. C. Bradt (Alabama Univ., Tuscaloosa, AL.) 1995 7 p Presented at the 1994 Fall Meeting of the Materials Research Society (MRS), Boston, MA, 28 Nov. - 2 Dec. 1994
(Contract W-7405-eng-36)
(DE95-003681; LA-UR-94-4071; CONF-941144-4) Avail: CASI HC A02/MF A01

Spinel (MgAl2O4) single crystals which had been neutron irradiated to high doses (53-250 dpa) were examined using Al-27 magic angle spinning (MAS) nuclear magnetic resonance (NMR). The sensitivity of this procedure to a specific cation (Al) residing in different crystallographic environments allowed one to determine the distribution of the Al between the two cation sites in the spinel structure. The samples were irradiated at two different temperatures (400 and 750 C) and various doses. These results indicate that the Al was nearly fully disordered over the two lattice sites after irradiation. DOE

N95-23354# Brookhaven National Lab., Upton, NY.
SOME ASPECTS OF CRITICAL CURRENTS IN Ag SHEATHED Bi2Sr2Ca2Cu3O10 COMPOSITE TAPES: A SUMMARY
M. Suenaga, Qiang Li, Y. Fukumoto, K. Shibutani, Y. L. Wang, H. J. Wiesmann, P. Haldar (Intermagnetics General Corp., Latham, NY.), and L. Motowidlo (IGC Advanced Superconductors, Inc., Waterbury, CT.) 1995 8 p Presented at the Topical Conference on the Critical State in Superconductors, Honolulu, HI, 24-26 Oct. 1994
(Contract DE-AC02-76CH-00016)
(DE95-003952; BNL-60962; CONF-941014-1) Avail: CASI HC A02/MF A01

Detailed and high sensitivity (E greater than 10(exp -9)V/cm) measurements of J-E (I-V) characteristics were made for Bi2Sr2Ca2Cu3O10 /Ag composite tapes at 4.2, 27, 55-90, and 64-77 K in liquid cryogens and at H = 0-17 T. The results have helped to clarify the critical current limiting factors as well as reveal a new low voltage dissipation phenomena in these composites. A brief summary of the results are presented. DOE

N95-23365# Los Alamos National Lab., NM.
INTERNAL STRAIN MEASUREMENT USING PULSED NEUTRON DIFFRACTION AT LANSCE
J. A. Goldstone, M. A. M. Bourke, and N. Shi 1994 6 p Presented at the 1994 Fall Meeting of the Materials Research Society (MRS), Boston, MA, 28 Nov. - 2 Dec. 1994
(Contract W-7405-eng-36)

(DE95-003677; LA-UR-94-4043; CONF-941144-11) Avail: CASI HC A02/MF A01

The presence of residual stress in engineering components can effect their mechanical properties and structural integrity. Neutron diffraction is the only technique that can make nondestructive measurements in the interior of components. By recording the change in crystalline lattice spacings, elastic strains can be measured for individual lattice reflections. Using a pulsed neutron source, all lattice reflections are recorded in each measurement, which allows for easy examination of heterogeneous materials such as metal matrix composites. Measurements made at the Manuel Lujan Jr. Neutron Scattering Center (LANSCE) demonstrate the potential at pulsed sources for in-situ stress measurements at ambient and elevated temperatures. DOE

N95-23366# Los Alamos National Lab., NM.

EFFECT ON c-AXIS TRANSPORT PROPERTIES OF A CRITICAL STATE IN Bi2Sr2CaCu2O8

J. H. Cho, M. P. Maley, and L. N. Bulaevskii 1995 5 p Presented at the Applied Superconductivity Conference, Boston, MA, 16-21 Oct. 1994

(Contract W-7405-eng-36)
(DE95-003695; LA-UR-94-3850; CONF-941013-12) Avail: CASI HC A01/MF A01

At low temperatures, the c-axis transport properties of Bi2Sr2CaCu2O8 single crystals depend strongly on the magnetic field history for fields applied along the c-axis, indicating the effect of a critical state in the ab direction. In this study, the authors report zero field cooled (ZFC), field cooled warming (FCW), and field cooled cooling (FCC) c-axis transport properties. In addition, they also report magnetic relaxation measurements on the same samples to identify the c-axis dissipation mechanism. They observe a relaxation of the c-axis resistivity that follows the relaxation of the flux profile across the ab plane. By identifying the irreversible temperature vs. magnetic field for H // c, they construct a phase diagram of vortex states. Finally, they discuss the implication of the phase diagram and the features related to the transport properties of the Josephson-coupled system and the role of pancake vortices in highly two-dimensional superconductors. DOE

N95-23367# Los Alamos National Lab., NM.

TRANSPORT PROPERTIES OF Tl2Ba2CaCu2O8 MEANDER LINES

S. Fleshler, M. P. Maley, Quanxi Jia, Xin Di Wu, and A. Lacerda 1995 5 p Presented at the Applied Superconductivity Conference, Boston, MA, 16-21 Oct. 1994

(Contract W-7405-eng-36)
(DE95-003715; LA-UR-94-1390; CONF-941013-13) Avail: CASI HC A01/MF A01

The authors have measured the electrical transport properties of 10 cm long Tl2Ba2CaCu2O8 thin film meander lines in magnetic fields up to 18T. The large resistance of the meander line effectively increased the electric field, or equivalently, resistivity sensitivity by two orders of magnitude. In moderate magnetic fields the critical current density is found to depend only on the component of the magnetic field normal to the ab planes owing to the highly anisotropic nature of the system. The resistivity versus temperature was measured as a function of magnetic field up to 18T. The linear resistivity is found to vanish in a manner consistent with the occurrence of a second order phase transition. The critical exponent v(z-1) is virtually field independent with a value 5.3 +/- 1 consistent with previous measurements of a three dimensional vortex glass transition in YBa2Cu3O7 and Bi2Sr2CaCu2O8. The critical regime is 10-15K wide in agreement with values for Bi2Sr2CaCu2O8 at high magnetic field. DOE

N95-23563*# Alabama Univ., Huntsville, AL.

GROWTH OF SINGLE CRYSTALS OF ORGANIC SALTS WITH LARGE SECOND-ORDER OPTICAL NONLINEARITIES BY SOLUTION PROCESSES FOR DEVICES Final Report

Thomas M. Leslie 1995 15 p

(Contract NAS8-38609)
(NASA-CR-197963; NAS 1.26:197963) Avail: CASI HC A03/MF A01

Data obtained from the electric field induced second harmonic generation (EFISH) and Kurtz Powder Methods will be provided to MSFC for further refinement of their method. A theoretical model for predicting the second-order nonlinearities of organic salts is being worked on. Another task is the synthesis of a number of salts with various counterions. Several salts with promising SHG activities and new salts will be tested for the presence of two crystalline forms. The materials will be recrystallized from dry and wet solvents and compared for SHG efficiency. Salts that have a high SHG efficiency and no tendency to form hydrates will be documented. The synthesis of these materials are included in this report. A third task involves method to aid in the growth of large, high quality single crystals by solution processes. These crystals will be characterized for their applicability in the fabrication of devices that will be incorporated into optical computers in future programs. Single crystals of optimum quality may be obtained by crystal growth in low-gravity. The final task is the design of a temperature lowering single crystal growth apparatus for ground based work. At least one prototype will be built. Derived from text

N95-23579# Pacific Northwest Lab., Richland, WA.

SMALL ANGLE X RAY SCATTERING STUDIES OF AGGREGATION IN SUPERCRITICAL FLUID SOLUTIONS

J. L. Fulton and D. M. Pfund Oct. 1994 7 p Presented at the 3rd International Symposium on Supercritical Fluids, Strasbourg, France, 17-19 Oct. 1994

(Contract DE-AC06-76RL-01830)
(DE95-004576; PNL-SA-24552; CONF-9410114-4) Avail: CASI HC A02/MF A01

Small-angle x ray scattering (SAXS) can be used to derive structural information on molecular aggregates having sizes from 2 to 200 nm. Not only is the technique useful for probing fluid structure in pure and simple binary supercritical fluid systems, but the technique is also well suited to investigate a range of much more complex multi-molecular aggregates that form when surfactants are added to supercritical fluids. The authors describe the experimental apparatus that was constructed for these studies and the experimental approach used to collect the scattering data. They present scattering results for pure fluids and for fluids containing various types of microemulsion phases, including reverse micelle and normal micelle phases. These results demonstrate that SAXS is a powerful technique for probing various types of molecular aggregation in supercritical fluid solutions. DOE

N95-23585# Argonne National Lab., IL.

PHONON-INDUCED ANOMALOUS SPECIFIC HEAT OF A MODEL NANOCRYSTAL BY COMPUTER SIMULATION

J. Wang, D. Wolf, S. R. Phillpot, and H. Gleiter (Saarland Univ., Saarbruecken, Germany.) Oct. 1994 5 p Presented at the 2nd International Conference on Nanostructured Materials, Stuttgart, Germany, 3-7 Oct. 1994

(Contract W-31-109-eng-38)
(DE95-004653; ANL/MSD/CP-83452; CONF-941039-3) Avail: CASI HC A01/MF A01

The authors construct a simple model of a nanocrystalline material in which all the grains are the same size and shape, and in which all the grain boundaries are crystallographically identical. The authors show that the model nanocrystal has a low-temperature specific-heat anomaly similar to that seen in experiment, which arises from the presence of low-frequency phonons localized at the grain boundaries. DOE

N95-23586# Argonne National Lab., IL.

NMR STUDY OF NANOPHASE Al/Al-OXIDE POWDER AND CONSOLIDATED COMPOSITES

B. H. Suits, P. Apte, D. E. Wilken, and R. W. Siegel Oct. 1994 5 p Presented at the 2nd International Conference on Nanostructured Materials, Stuttgart, Germany, 3-7 Oct. 1994

(Contract W-31-109-eng-38)
(DE95-004655; ANL/MSD/CP-83568; CONF-941039-2) Avail: CASI HC A01/MF A01

Al-27 Nuclear Magnetic Resonance (NMR) measurements from aluminum powders and consolidated nanophase aluminum made from those powders are presented. The signals from the metal and surface oxidation are easily separated and are compared before and after consolidation. The results presented indicate that the oxide coating becomes the interface region within the nanophase composite material and that during consolidation the metal has undergone a deformation equivalent to that seen for bulk material under a compressive strain of between 4% and 8%. DOE

N95-23774# International Centre for Theoretical Physics, Trieste (Italy).
PHOTOIONIZATION OF O(6+) BELOW THE n=3 THRESHOLD OF THE REDUCED ION
N. A. B. Faye and A. Wague May 1994 11 p
(DE94-634436; LAMP-94/4) Avail: CASI HC A03/MF A01 (US Sales Only)

Near the n = 3 threshold of residual ion O(sup 7+), the resonant photoionization of the multicharged ion O(sup 6+) is considered by calculating the excitation energies, associated wave-functions, partial and total widths of the (sup 1)P(sup (-)) and (sup 3)P(sup (-)) autoionizing states. These calculations are made in the diagonalization approximation in the LS coupling scheme. The results are compared with the available theoretical results obtained by authors using other theoretical approaches. DOE

N95-23986# International Centre for Theoretical Physics, Trieste (Italy).
LATTICE RELAXATION STUDY ON SELF-TRAPPED EXCITON AND BIEXCITON IN NEUTRAL AND CHARGED FULLERENES
Wenzheng Wang, Zhaobin Su, Chuilin Wang, and Lu Yu May 1994 13 p
(DE94-635788; IC-94/92) Avail: CASI HC A03/MF A01 (US Sales Only)

The formation and dynamical properties of D(sub 5d)-symmetry self-trapped exciton (STE) derived from the electronic h(sub u) (yields) t(sub 1u) parity-forbidden transition of neutral buckyball are studied in the presence of Coulomb interactions using the Bogoliubov-de Gennes formalism. Within the lattice relaxation theory, the multi-mode vibronic structures in the luminescence and absorption spectra related to STE's are elucidated in good agreement with experiments. The STE's arising from the allowed t(sub 1u) (yields) t(sub 1g) transition of C(sup 1-)(sub 60) and C(sup 2-)(sub 60) as well as the possibility of forming a self-trapped biexciton (STBE) in C(sup 1-)(sub 60) are also considered. DOE

N95-24010# California Univ., Berkeley. Lawrence Berkeley Lab, CA.
ANNEALING OF NITROGEN-DOPED ZnSe AT HIGH PRESSURES: TOWARD SUPPRESSION OF NATIVE DEFECT FORMATION
A. L. Chen, W. Walukiewicz, E. E. Haller, H. Luo (Notre Dame Univ., IN.), G. Karczewski (Notre Dame Univ., IN.), and J. Furdyna (Notre Dame Univ., IN.) Jul. 1994 6 p Presented at the 21st International Symposium on Compound Semiconductors, San Diego, CA, 18-22 Sep. 1994
(Contract DE-AC03-76SF-00098)
(DE95-003420; LBL-35434; CONF-940981-4) Avail: CASI HC A02/MF A01

Pressure is shown to have a drastic effect on the annealing characteristics of p-type, nitrogen-doped ZnSe. Samples annealed in vacuum show decreased carrier concentrations and simultaneous formation of deep-donor-related luminescence, while samples annealed under pressure show suppression of this compensating donor. Results are interpreted as an increase in the formation energy of the compensating deep donor under pressure. In addition the samples annealed under pressure show emergence of a new, intense, green luminescence band centered at 2.44 eV. The magnitude of the shift of this Peak under applied stress suggests that it results from a recombination involving a deep acceptor. DOE

N95-24011# California Univ., Berkeley. Lawrence Berkeley Lab, CA.
INCREASING THE RETAINED DOSE BY PLASMA IMMERSION ION IMPLANTATION AND DEPOSITION
A. Anders, S. Anders, I. G. Brown, and Kin M. Yu 22 Jul. 1994 13 p Presented at the 2nd International Conference on Computer Simulation of Radiation Effects, Santa Barbara, CA, 24-29 Jul. 1994
(Contract DE-AC03-76SF-00098)
(DE95-003423; LBL-35679; CONF-940731-3) Avail: CASI HC A03/MF A01

The retained dose of ions can be increased by Plasma Immersion Ion Implantation and Deposition (PIIID). A substrate is immersed in a metal or carbon plasma and a negative repetitively pulsed bias voltage is applied. During the pulses, an electric sheath is formed around the substrate and ions are accelerated through the sheath and implanted into the substrate. Direct and recoil ion implantation and sputtering take place during the pulses whereas low-energy deposition occurs between the pulses. The condensable plasma can be produced using a cathodic arc plasma source combined with a magnetic macroparticle filter. PIIID can be applied to perform fast high-dose implantations or to deposit thin films with broad intermixing at the film-substrate interface. The bias voltage duty cycle can be tuned to sputter away the film deposited during pulse off-time (similar to the method of sacrificial layer). We have simulated the PIIID process using the Monte Carlo code T-DYN 4.0. This code allows a calculation of the dose-dependent depth profile for a process with deposition and implantation phases, taking sputtering into account. Predicted retained doses and experimentally obtained retained doses measured by Rutherford backscattering spectrometry are compared. DOE

N95-24013# California Univ., Berkeley. Lawrence Berkeley Lab, CA.
CARBON DOPING OF III-V COMPOUND SEMICONDUCTORS Ph.D. Thesis
A. J. Moll Sep. 1994 134 p
(Contract DE-AC03-76SF-00098)
(DE95-003431; LBL-36256) Avail: CASI HC A07/MF A02

Focus of the study is C acceptor doping of GaAs, since C diffusion coefficient is at least one order of magnitude lower than that of other common p-type dopants in GaAs. C ion implantation results in a concentration of free holes in the valence band is less than 10% of that of the implanted C atoms for doses greater than 10(exp 14)/sq cm. Rutherford backscattering, electrical measurements, Raman spectroscopy, and Fourier transform infrared spectroscopy were among the techniques used. Ga co-implantation increased the C activation in two steps: first, the additional radiation damage creates vacant As sites that the implanted C can occupy, and second, it maintains the stoichiometry of the implanted layer, reducing the number of compensating native defects. In InP, the behavior of C was different from that in GaAs. C acts as n-type dopant in the In site; however, its incorporation by implantation was difficult to control; experiments using P co-implants were inconsistent. The lattice position of inactive C in GaAs in implanted and epitaxial layers is discussed; evidence for formation of C precipitates in GaAs and InP was found. Correlation of the results with literature on C doping in III-V semiconductors led to a phenomenological description of C in III-V compounds (particularly GaAs): The behavior of C is controlled by the chemical nature of C and the intrinsic Fermi level stabilization energy of the material. DOE

N95-24073# Los Alamos National Lab., NM.
TEMPERATURE EFFECTS ON ION IRRADIATION DAMAGE IN MgAl2O4 SPINEL SINGLE CRYSTALS
Ning Yu, K. E. Sickafus, and M. Nastasi 1994 6 p Presented at the 1994 Fall Meeting of the Materials Research Society (MRS), Boston, MA, 28 Nov. - 2 Dec. 1994
(Contract W-7405-eng-36)
(DE95-003679; LA-UR-94-4051; CONF-941144-7) Avail: CASI HC A02/MF A01

MgAl2O4 monocrystals, group of zone (100) axes oriented, were irradiated at 100 and 670 K with 370-400 KeV Xe ions to doses of (1-2) x 10(exp 16) Xe/sq cm. Microstructures of irradiated samples were examined by cross-sectional TEM at RT. A uniform layer of amorphous phase was found on the surface of spinel irradiated at 100 K. At the end of the damage range underlying the amorphous layer, a disordered transition layer resided on the undamaged substrate. The transition layer retained single crystallinity having epitaxial relation with underlying substrate. However, group of zone (220) axes reflections in the transition layer diminished compared to undamaged spinel. No amorphization was found in spinel irradiated at 670 K to 2 x 10(exp 16) Xe/sq cm. Partial diminishing of intensity of group of zone (220) axes reflections was observed in the heavily damaged region. The missing or reduction of group of zone (220) axes reflections suggests that spinel experiences a structural transition from original cubic phase (a = 0.808 nm) to a new cubic phase (a = 0.404 nm). A phase sequence from the original spinel to a metastable spinel and then to an amorphous spinel has been found. Temperature dependence of metastable and amorphous phase formation showed that the accumulation efficiency of cation disorder decreases with increasing irradiation temperature due to the enhanced mechanism of interstitial-vacancy recombination. DOE

N95-24076# Los Alamos National Lab., NM.
PHONON CHARACTERISTICS OF HIGH (T SUB c) SUPERCONDUCTORS FROM NEUTRON DOPPLER BROADENING MEASUREMENTS

W. J. Trela, G. H. Kwei, J. E. Lynn, and K. Meggers (Kiel Univ., Germany.) 1994 9 p Presented at the 1994 Fall Meeting of the Materials Research Society (MRS), Boston, MA, 28 Nov. - 2 Dec. 1994
(Contract W-7405-eng-36)
(DE95-003703; LA-UR-94-3872; CONF-941144-14) Avail: CASI HC A02/MF A01

Statistical information on the phonon frequency spectrum of materials can be measured by neutron transmission techniques if they contain nuclei with low energy resonances, narrow enough to be Doppler-broadened, in their neutron cross sections. The authors have carried out some measurements using this technique for materials of the lanthanum barium cuprate class, La(2-x)Ba(x)CuO4. Two samples with slightly different concentrations of oxygen, one being superconductive, the other not, were examined. Pure lanthanum cuprate was also measured. Lanthanum, barium and copper all have relatively low energy narrow resonances. Thus it should be possible to detect differences in the phonons carried by different kinds of atom in the lattice. Neutron cross section measurements have been made with high energy resolution and statistical precision on the 59 m flight path of LANSCE, the pulsed spallation neutron source at Los Alamos National Laboratory. Measurements on all three materials were made over a range of temperatures from 15 to 300 K, with small steps through the critical temperature region near 27 K. No significant changes in the mean phonon energy of the lanthanum atoms were observed near the critical temperature of the super-conducting material. It appears however that the mean phonon energy of lanthanum in the superconductor is considerably higher than that in the non-superconductors. The samples used in this series of experiments were too thin in barium and copper to determine anything significant about their phonon spectra. DOE

N95-24079# Los Alamos National Lab., NM.
EXPERIMENTAL AND THEORETICAL STUDIES ON THE C15 INTERMETALLIC COMPOUNDS MV2 (M = Zr, Hf AND Ta): ELASTICITY AND PHASE STABILITY
F. Chu, T. E. Mitchell, S. P. Chen, M. Sob (Pennsylvania Univ., Philadelphia, PA.), R. Siegl (Pennsylvania Univ., Philadelphia, PA.), and D. P. Pope (Pennsylvania Univ., Philadelphia, PA.) 1994 7 p Presented at the 1994 Fall Meeting of the Materials Research Society (MRS), Boston, MA, 28 Nov. - 2 Dec. 1994
(Contract W-7405-eng-36)
(DE95-003723; LA-UR-94-3726; CONF-941144-16) Avail: CASI HC A02/MF A01

The phase stability of C15 HfV2 was studied by specific heat measurements. The elastic constants of C15 HfV2 were measured by the resonant ultrasound spectroscopy. Total energy and electronic structure of C15 intermetallic compounds MV2 (M = Zr, Hf and Ta) were calculated using the linear muffin tin orbital (LMTO) method. The band structures at X-point near the Fermi level were used to understand the anomalous shear moduli of the C15 HfV2 and ZrV2. It was found that the double degeneracy with a linear dispersion relation of electronic levels at the x-point near the Fermi surface is mainly responsible for the C15 anomalous elasticity at high temperatures. The densities of states at Fermi level and the geometry of the Fermi surface were used to explain the low temperature phase instability of C15 HfV2 and ZrV2 and the stability of C15 TaV2. The relationship between the anomalous elasticity and structural instability of C15 HfV2 and ZrV2 were also studied. DOE

N95-24143# Lehigh Univ., Bethlehem, PA.
HIGH RESOLUTION MICROSTRUCTURAL ANALYSIS OF ZIRCONIA EUTECTIC INTERFACES
M. R. Notis 1994 15 p
(Contract DE-FG02-84ER-45150)
(DE95-003143; DOE/ER-45150/T3) Avail: CASI HC A03/MF A01

This report is divided into: Cu-Ni-Sn ternary alloys (spinodal decomposition, ordering transformation), AlN extended defects (Al-N-O system), and Cu-Sn intermetallics research (solder joints). DOE

N95-24150# Argonne National Lab., IL.
EFFECTS OF Bi AND Bi2O3 ADDITIONS ON THE MICROSTRUCTURE AND SUPERCONDUCTING PROPERTIES OF POWDER-IN-TUBE BSCCO (2212) TAPES
J. Guo, J. A. Lewis, and K. C. Goretta Oct. 1994 5 p Presented at the Applied Superconductivity Conference, Boston, MA, 16-21 Oct. 1994
(Contract W-31-109-eng-38)
(DE95-004605; ANL/ET/CP-84563; CONF-941013-19) Avail: CASI HC A01/MF A01

The microstructural development and superconducting properties of Bi2Sr2CaCu2O(x) (Bi-2212) Ag-clad powder-in-tube tapes with 2 vol% bismuth (Bi) added from either Bi (s) or Bi2O3 powders were investigated. Such additives reduce the peritectic decomposition temperature of pure Bi-2212 by approximately 15-20 C. Scanning electron microscopy (SEM) and optical microscopy on polished top and cross-sections revealed that the volume fraction of Bi-free phases was lower in the Bi-added specimens relative to those based on pore Bi-2212. In addition, it appeared that the Bi-added samples had improved grain alignment, which was confirmed by x-ray diffraction analysis. Magnetic hysteresis (at 5 K between (+/-) 5.5 T) and transport measurements (at 4.2 K) were performed on each specimen. These results showed that Bi-additions yielded superior magnetization critical currents, which is attributed to improved grain alignment and reduced secondary phases. DOE

N95-24152# Argonne National Lab., IL.
MICROSTRUCTURE AND COMPOSITION OF A SNS JOSEPHSON JUNCTION USING CaRuO3 AS THE METALLIC BARRIER
S. Rozeveld, K. L. Merkle, and K. Char (Conductus, Inc., Sunnyvale, CA.) Oct. 1994 5 p Presented at the Applied Superconductivity Conference, Boston, MA, 16-21 Oct. 1994
(Contract W-31-109-eng-38)
(DE95-004611; ANL/MSD/CP-82573; CONF-941013-21) Avail: CASI HC A01/MF A01

Superconductor - normal - superconductor (SNS) edge junctions consisting of YBa2Cu3O(7-x)/CaRuO3/ YBa2Cu3O(7-x) were fabricated on (001) LaAlO3 substrates. These devices display an excess interface resistance which is not well understood but is related to the SN interface and interlayer structure. High-resolution and conventional transmission electron microscopy were employed to investigate the SN interface to determine the structure and possible interface defects. Energy-loss spectroscopy and energy dispersive x-ray analysis were performed on the CaRuO3 film and near interface regions to quantify the extent of interdiffusion between the CiRuO3 and YBCO films. Changes in either the interface structure or the normal layer chemistry are expected to greatly influence the junction properties. DOE

N95-24154# Argonne National Lab., IL.
PROCESSING OF SINGLE- AND MULTI-DOMAIN YBa2Cu3O(x) BULK MATERIALS FOR LEVITATION APPLICATIONS BY Nd(1+x)Ba(2-x)Cu3O(y) SEEDING
V. R. Todt, S. Sengupta, and D. J. Miller 1995 29 p Presented at the 7th Conference on Superconductivity and Applications, Buffalo, NY, 7-9 Sep. 1994
(Contract W-31-109-eng-38)
(DE95-004615; ANL/MSD/CP-84413; CONF-940926-4) Avail: CASI HC A03/MF A01

Melt processing of YBa2Cu3O(x) (Y123) is a well established technique to produce materials for levitation applications. We report our new results on the melt-processing of Y123. To achieve materials with high levitation forces we utilize a seeding technique using Nd(1+x)Ba(2-x)Cu3O(y) seeds (Nd123). Two different kinds of Nd123-seeds, one plate-shaped and the other cube-shaped, were developed and used for this study. The microstructures of the levitators depended strongly on the type of the seeding material used and on the seeding geometry. We were able to produce large single domains as well as materials containing five domains with three different c-axis orientations. Levitation forces up to 8.2 N for samples with a diameter of about 18 mm were found for the multi-domain samples, which is well within the area of the levitation forces measured for the single domain materials. DOE

N95-24156# Sandia National Labs., Albuquerque, NM.
EXTRACTION OF THE SURFACE RECOMBINATION VELOCITY OF PASSIVATED PHOSPHORUS-DOPED SILICON EMITTERS
A. Cuevas, G. Girault-Matlakowski, C. DuBois, and P. A. Basore 1995 4 p Presented at the 1st World Conference on Photovoltaic Energy Conversion, Waikoloa, HI, 5-9 Dec. 1994
(Contract DE-AC04-94AL-85000)

(DE95-004539; SAND-94-1563C; CONF-941203-10) Avail: CASI HC A01/MF A01

An analytical procedure to extract the surface recombination velocity of the SiO2/n type silicon interface, S(sub p), from PCD measurements of emitter recombination currents is described. The analysis shows that the extracted values of S(sub p) are significantly affected by the assumed material parameters for highly doped silicon, t(sub p), mu(sub p) and (Delta)E(sub g)(sup app). Updated values for these parameters are used to obtain the dependence of S(sub p) on the phosphorus concentration, N(sub D), using both previous and new experimental data. The new evidence supports the finding that S(sub p) increases strongly with N(sub D). DOE

N95-24168# Argonne National Lab., IL.

EPITAXIAL GROWTH OF bcc TRANSITION METAL FILMS AND SUPERLATTICES ONTO MgO (111), (011) AND (001) SUBSTRATES

J. E. Mattson, E. E. Fullerton, C. H. Sowers, and S. D. Bader Apr. 1994 24 p

(Contract W-31-109-eng-38)

(DE95-004629; ANL/MSD/PP-82718) Avail: CASI HC A03/MF A01

We demonstrate epitaxial growth of the bcc transition metals Nb, Mo, Fe, and Cr via sputtering onto single crystal MgO substrates. The epitaxial growth orientations are (011), (112) and (001) when grown onto MgO (111), (011) and (001), respectively. Further, we demonstrate that under appropriate growth conditions, superlattices of these materials (e.g., Fe/Cr, Fe/V and Mo/V) can be grown with the same epitaxial order as the films. DOE

N95-24169# Argonne National Lab., IL.

A PHENOMENOLOGICAL MODEL FOR THE EFFECT OF NANOCRYSTALLINE MICROSTRUCTURE ON IRRADIATION-INDUCED AMORPHIZATION IN U3Si

J. Rest Oct. 1994 7 p Presented at the 1994 Fall Meeting of the Materials Research Society (MRS), Boston, MA, 28 Nov. - 2 Dec. 1994

(Contracts W-31-109-eng-38; DE-AC05-84OR-21400)

(DE95-004631; ANL/ET/CP-83901; CONF-941144-20) Avail: CASI HC A02/MF A01

A rate theory model is formulated wherein amorphous clusters are formed by a damage event. These clusters are considered centers of expansion (CE's), or excess-free-volume zones. Simultaneously, centers of compression (CC's) are created in the material. The CC's are local regions of increased density that travel through the material as an elastic (e.g., acoustic) shock wave. The CE's can be annihilated upon contact with a sufficient number of CC's, to form either a crystallized region indistinguishable from the host material, or a region with a slight disorientation (recrystallized grain). Recrystallized grains grow by the accumulation of additional CC's. Full amorphization is calculated on the basis of achieving a fuel volume fraction consistent with the close packing of spherical entities. Amorphization of a recrystallized grain is hindered by the presence of a grain boundary. Preirradiation of U3Si above the critical temperature for amorphization results in the formation of nanometer-size grains. In addition, subsequent reirradiation of these samples in the same ion flux at temperatures below the critical temperature shows that the material has developed a resistance to radiation-induced amorphization (i.e., a higher dose is needed to amorphous preirradiated samples than those that have not been preirradiated). In the model, it is assumed that grain boundaries act as effective defect sinks, and that enhanced defect annihilation is responsible for retarding amorphization below the critical temperature. The calculations have been validated against data from ion-irradiation experiments with U3Si. For appropriate values of the activation energy of thermal crystallization, the model predicts the evolution of a two phase microstructure consisting of nanocrystalline grains and amorphous clusters. DOE

N95-24170# Argonne National Lab., IL.

A SIMPLE, CLOSED-FORM EXPRESSION FOR THE X RAY REFLECTIVITY FROM SUPERLATTICES WITH CUMULATIVE ROUGHNESS

D. M. Kelly, J. Santa-Maria, I. K. Schuller, and E. E. Fullerton May 1994 12 p

(Contract W-31-109-eng-38)

(DE95-004633; ANL/MSD/PP-83083) Avail: CASI HC A03/MF A01

The authors present a simple closed-form expression for the reflectivity from a multilayer which includes the effects of absorption, refraction, surface and substrate reflections but neglects dynamical effects. This expression reproduces the exact dynamical calculation except for the regions near the critical angle and for intense Bragg reflections. The expression is generalized to include cumulative interface roughness which follows a t(exp 1/2) power-law growth. DOE

N95-24171# Argonne National Lab., IL.

COOLING RATE EFFECTS ON THE MICROSTRUCTURE, CRITICAL CURRENT DENSITY, AND (T(SUB c)) TRANSITION OF ONE- AND TWO-POWDER BSCCO-2223 Ag SHEATHED TAPES

J. A. Parrell, D. C. Larbalestier, and S. E. Dorris Nov. 1994 5 p Presented at the Applied Superconductivity Conference, Boston, MA, 16-21 Oct. 1994

(Contract W-31-109-eng-38)

(DE95-004639; ANL/ET/CP-84861; CONF-941013-20) Avail: CASI HC A01/MF A01

An important variable controlling the critical current density (J(sub c)) of Ag-sheathed BSCCO-2223 tapes is the degree of phase purity of the reacted tapes. Most correlations between J(sub c) and microstructure show that it is highly desirable to reduce the amount of non-superconducting second phases to as low a level as practical. In recent studies of the influence of cooling rate after the final reaction, we find contradictions to this general rule. The J(sub c) (77 K, 0 T) of so-called 'one-powder' tapes can be raised by as much as 50% (from -8,000 A/sq cm to 12,000 A/sq cm) by slow cooling in 7.5% O2 at 0.05 C/min, even though large 2212 grains are usually seen in the slowly cooled microstructure. However, the higher J(sub c) of the slow-cooled state does correlate with a sharper T(sub c) transition. Experiments with 'two-powder' tapes have produced similar results. These apparently anomalous results emphasize the important role played by the connectivity of the polycrystalline core in determining J(sub c). DOE

N95-24173# Argonne National Lab., IL.

DEPENDENCE OF THE JOSEPHSON COUPLING OF UNCONVENTIONAL SUPERCONDUCTORS ON THE PROPERTIES OF THE TUNNELING BARRIER

M. Ledvij and R. A. Klemm 30 May 1994 14 p

(Contract W-31-109-eng-38)

(DE95-004649; ANL/MSD/PP-83268) Avail: CASI HC A03/MF A01

The Josephson coupling between a conventional and an unconventional superconductor is investigated as a function of the properties of the tunneling barrier. A simple model is adopted for the tunneling probability and it is shown that its variation dramatically affects the I(sub c)R(sub n) product of an s-d, as opposed to an s-s junction. Based on these conclusions, experiments are proposed to probe the symmetry of the order parameter in high temperature superconductors. DOE

N95-24188*# National Aeronautics and Space Administration. Lewis Research Center, Cleveland, OH.

SUBBAND QUANTUM SCATTERING TIMES FOR AlGaAs/GaAs OBTAINED USING DIGITAL FILTERING

R. A. Mena, S. E. Schacham, E. J. Haughland, S. A. Alterovitz, S. B. Bibyk (Ohio State Univ., Columbus, OH.), and S. A. Ringel (Ohio State Univ., Columbus, OH.) Mar. 1995 11 p

(RTOP 235-01-0B)

(NASA-TM-106873; E-9494; NAS 1.15:106873) Avail: CASI HC A03/MF A01

In this study we investigate both the transport and quantum scattering times as a function of the carrier concentration for a modulation doped Al(0.3)Ga(0.7)As/GaAs structure. Carriers in the well are generated as a result of the persistent photoconductivity effect. When more than one subband becomes populated, digital filtering is used to separate the components for each of the excited subbands. We find that the quantum scattering time for the ground subband increases initially as the carrier concentration is increased. However, once the second subband becomes populated, the ground subband scattering time begins to decrease. The quantum scattering time for the excited subband is also observed to decrease as the concentration is increased. From the ratio of the transport and quantum scattering times, it is seen that the transport in the well becomes more isotropic also as the concentration is increased. Author

N95-23285*# Montana State Univ., Bozeman, MT. Dept. of Electrical Engineering.
MEASUREMENTS OF STRIAE IN CR+ DOPED YAG LASER CRYSTALS Abstract Only
Fredrick M. Cady *In* Hampton Univ., 1994 NASA-HU American Society for Engineering Education (ASEE) Summer Faculty Fellowship Program Dec. 1994 p 65 (For primary document see N95-23276 07-99)
Avail: CASI HC A01/MF A02

77 THERMODYNAMICS AND STATISTICAL PHYSICS

Includes quantum mechanics; theoretical physics; and Bose and Fermi statistics.

For related information see also *25 Inorganic and Physical Chemistry* and *34 Fluid Mechanics and Heat Transfer.*

N95-22496# International Centre for Theoretical Physics, Trieste (Italy).
MAGNETIC FIELD EFFECTS ON STRONG-COUPLING POLARON IN QUANTUM DOTS
Ka-Di Zhu Nov. 1993 11 p
(DE94-629038; IC-93/393) Avail: CASI HC A03/MF A01 (US Sales Only)

Magnetic field effects on strong-coupling polaron in a parabolic quantum dot are investigated by the Landau-Pekar variation treatment. The polaron binding energy and the average number of virtual phonons around the electron as functions of magnetic field strength and the effective confinement length of the quantum dot are obtained in the Gaussian function approximation. It is shown that in the presence of magnetic fields, the polaron binding energy increases with enhancement of the magnetic field strength. The magnetic field effects on the average number of virtual phonons around the electron are very small for strong electron-LO-phonon coupling. DOE

N95-22545# International Centre for Theoretical Physics, Trieste (Italy).
THE CHIRALITY OPERATORS FOR HEISENBERG SPIN SYSTEMS
V. Subrahmanyam Jan. 1994 6 p
(DE94-629043; IC-94/23) Avail: CASI HC A02/MF A01 (US Sales Only)

The ground state of closed Heisenberg spin chains with an odd number of sites has a chiral degeneracy, in addition to a two-fold Kramers degeneracy. A non-zero chirality implies that the spins are not coplanar, and is a measure of handedness. The chirality operator, which can be treated as a spin-1/2 operator, is explicitly constructed in terms of the spin operators, and is given as commutator of permutation operators. DOE

N95-22566# Stanford Linear Accelerator Center, CA.
COMMENSURATE SCALE RELATIONS: PRECISE TESTS OF QUANTUM CHROMODYNAMICS WITHOUT SCALE OR SCHEME AMBIGUITY
Stanley J. Brodsky and Hung Jung Lu (Maryland Univ., College Park, MD.) Oct. 1994 8 p Presented at the Tennessee International Symposium on Radiative Corrections, Gatlinburg, TN, 27 Jun. - 1 Jul. 1994
(Contracts DE-AC03-76SF-00515; DE-FG02-93ER-40762)
(DE95-002785; SU-SLAC-PUB-6683; CONF-9406273-2) Avail: CASI HC A02/MF A01

We derive commensurate scale relations which relate perturbatively calculable QCD observables to each other, including the annihilation ratio R(sub e+e-), the heavy quark potential, (tau) decay, and radiative corrections to structure function sum rules. For each such observable one can define an effective charge, such as (alpha)(sub R)((radical)s)/(pi) (equivalent to) R (sub e+e-) ((radical)s)/(3(Sigma)e(sub q, sup 2)) -1. The commensurate scale relation connecting the effective charges for observables A and B has the form (alpha)(sub A)(Q(sub A)) = (alpha)(sub B)(Q(sub B))(1 + r(sub A/B(alpha B/pi)) +.....), where the coefficient r(sub A/B) is independent of the number of flavors (integral) contributing to coupling renormalization, as in BLM scale-fixing. The ratio of scales Q(sub A)/Q(sub B) is unique at leading order and guarantees that the observables A and B pass through new quark thresholds at the same physical scale. In higher orders a different renormalization scale Q(sup n*) is assigned for each order n in the perturbative series such that the coefficients of the series are identical to that of a invariant theory. The commensurate scale relations and scales satisfy the renormalization group transitivity rule which ensures that predictions in PQCD are independent of the choice of an intermediate renormalization scheme C. In particular, scale-fixed predictions can be made without reference to theoretically constructed singular renormalization schemes such as MS. QCD can thus be tested in a new and precise way by checking that the effective charges of observables track both in their relative normalization and in their commensurate scale dependence. The commensurate scale relations which relate the radiative corrections to the annihilation ratio R(sub e+e-) to the radiative corrections for the Bjorken and Gross-Llewellyn Smith sum rules are particularly elegant and interesting. DOE

N95-22620# International Centre for Theoretical Physics, Trieste (Italy).
BERRY PHASE BY DESCRIPTION OF THE QUANTUM SYSTEMS IN THE KUSTAANHEIMO-STIEFEL BUNDLE
I. E. Pris, E. A. Tolkachev, and Ya. M. Shnir Sep. 1993 5 p
(DE94-628410; IC-93/296) Avail: CASI HC A01/MF A01 (US Sales Only)

An analogy between the description of the quantum systems in the adiabatic approximation and by using the Hilbert line bundle associated to the Kustaanheimo-Stiefel fiber bundle is found if a constraint condition provides the factorizability of the wave functions. DOE

N95-22621# International Centre for Theoretical Physics, Trieste (Italy).
Q-ANALYTIC FUNCTIONS ON QUANTUM SPACES
A. ShafeiDehAbad and V. Milani Sep. 1993 13 p
(DE94-628412; IC-93/309) Avail: CASI HC A03/MF A01 (US Sales Only)

In this paper we give a different interpretation of the quantum plane introduced by Manin and characterize the Q-analytic functions on its 2-intervals. In the end we show that the *-product defined by Suzuki does not satisfy the associativity law and therefore is not really a *-product. But the A(sub 1)(q)-modules of Q-analytic functions defined in this paper are in fact non-commutative associative algebras with unity, which can be considered as deformations of the algebras of analytic functions on the 2-intervals of R(sup 2). DOE

N95-22635# International Centre for Theoretical Physics, Trieste (Italy).
ON THE (DE-) STABILIZATION OF QUANTUM MECHANICAL BINDING BY POTENTIAL BARRIERS
H. Hogreve Apr. 1994 16 p
(DE94-628433; IC-94/68) Avail: CASI HC A03/MF A01 (US Sales Only)

Stabilization and destabilization effects caused by adding or rising a potential barrier are studied for a simple one-dimensional quantum system. Calculating the motion of the corresponding S-matrix poles for varying barrier width and height, this reveals the scenario for the transition between bound, virtual and resonance states. Our results show that the presence of a barrier leads to nonanalyticity of the ground state with respect to the involved coupling constants. Furthermore, for increasing barrier width the size of the virtual regime shrinks drastically, so that it might be hardly detectable in many practical situations. DOE

N95-22655# Los Alamos National Lab., NM.
MORPHOLOGY OF LAPLACIAN GROWTH PROCESSES AND STATISTICS OF EQUIVALENT MANY-BODY SYSTEMS
Raphael Blumenfeld 1994 17 p Presented at the NEEDS 1994 Conference, Los Alamos, NM, 12-16 Sep. 1994
(Contract W-7405-eng-36)
(DE95-002734; LA-UR-94-3528; CONF-9409241-2) Avail: CASI HC A03/MF A01

The authors proposes a theory for the nonlinear evolution of two dimensional interfaces in Laplacian fields. The growing region is conformally mapped onto the unit disk, generating an equivalent many-body system whose dynamics and statistics are studied. The process is shown to be Hamiltonian, with the Hamiltonian being the imaginary part of the complex electrostatic potential. Surface effects are introduced through the Hamiltonian as an external field. An extension to a continuous density of particles is presented. The results are used to study the morphology of the interface using statistical mechanics for the many-body system. The distribution of

the curvature and the moments of the growth probability along the interface are calculated exactly from the distribution of the particles. In the dilute limit, the distribution of the curvature is shown to develop algebraic tails, which may, for the first time, explain the origin of fractality in diffusion controlled processes. DOE

N95-22698# Stanford Linear Accelerator Center, CA.
QCD TEST IN THREE-JET Z(SUP 0) DECAYS AT SLD AND DETECTOR DEVELOPMENT FOR H(SUP 0) YIELDS GAMMA GAMMA SEARCHES IN HIGH ENERGY HADRON COLLIDERS Ph.D. Thesis
Hyun Hwang Aug. 1994 157 p
(Contract DE-AC03-76SF-00515)
(DE95-003336; SU-SLAC-453) Avail: CASI HC A08/MF A02

Polarized Z(sup 0) decays into three jets have been detected and measured in the SLAC Large Detector (SLD) experiment operating at the SLAC Linear Collider (SLC). The hadrons from the jets were detected in the SLD liquid argon calorimeter, providing a sensitivity over 98% of the solid angle. The spin of the gluon was tested by studying the scaled jet energies (x(sub 1), x(sub 2), x(sub 3)), the Ellis-Karliner angle (cos theta(sub EK)) and the parameters of event plane orientation (alpha, alpha(sub N), beta). These measured variables are compared with quantum chromodynamics (QCD) and a scalar gluon model. Good agreement is found between data, and the vector QCD model for the distributions of (x(sub 1), x(sub 2), x(sub 3)) and (cos theta(sub EK)). Two detector prototypes for the GEM detector of the Superconducting Super Collider have been studied: a prototype silicon-tungsten preradiator and a liquid argon hadron calorimeter. The silicon-tungsten preradiator was designed for the GEM detector to distinguish between single photons from Higgs decay and background photon pairs from pi(sup 0) decay. This preradiator was tested in a beam at Brookhaven National Laboratory in July, 1992. A lead glass array placed behind the silicon was used to determine energy resolution effects. The results from the test on spatial distributions and energy resolution including correction for the energy deposited in the preradiator are presented, along with comparisons to EGS simulations. Data from a beam test of the liquid argon prototype was analyzed and compared to CALOR89 simulations. The studies concentrated on energy resolution optimization and electronic noise suppression. DOE

N95-22728# Washington Univ., Seattle, WA.
HOW TO MEASURE THE Q(BAR Q) POTENTIAL IN A LIGHT-FRONT CALCULATION
M. Burkardt 1994 7 p Presented at the Theory of Hardons and Light-front QCD Workshop, Polona Zgorzelisko, Poland, Aug. 1994
(Contract DE-FG06-90ER-40561)
(DE95-003200; DOE/ER-40561/160; CONF-9408188-1) Avail: CASI HC A02/MF A01

A scheme is developed which shows how one would, given a light-front Hamiltonian for QCD, extract the Q(bar Q) potential, i.e. the quantity which corresponds to the potential between two infinitely heavy quarks in a rest frame, from a light-front calculation. The resulting potential will in general depend on the direction along which the infinitely heavy sources are separated and thus provides a direct probe of violations of rotational invariance in a physical observable. Furthermore, easy comparison to data from c(bar c) and b(bar b) spectroscopy and to lattice data is possible. The scheme may thus be very helpful in constructing a light-front Hamiltonian through an iterative procedure. DOE

N95-22735# International Centre for Theoretical Physics, Trieste (Italy).
TWISTOR-LIKE TYPE 2 SUPERSTRING WITH THE HETEROTIC (2,0) AND (4,0) WORLDSHEET SUPERSYMMETRY
V. Chikalov and A. Pashnev Nov. 1993 5 p
(DE94-628510; IC-93/379) Avail: CASI HC A01/MF A01 (US Sales Only)

The twistor-like formulation of type 2 Green-Schwarz superstring with N = (2,0) and (4,0) heterotic worldsheet supersymmetry is constructed. Both of the Virasoro constraints are solved with the help of twistors in dimensions D = 4 and D = 6. As in the case of N = (1,0) worldsheet supersymmetry, considered earlier, any worldsheet gauge fields enter the actions. On the component level the resulting Lagrangians are classically equivalent to the Green-Schwarz one. DOE

N95-22738# International Centre for Theoretical Physics, Trieste (Italy).
FIRST QUANTIZED NONCRITICAL RELATIVISTIC POLYAKOV STRING
Z. Jaskolski and K. A. Meissner Jan. 1994 51 p
(DE94-628513; IC-94/11; HEP-TH-9401100) Avail: CASI HC A04/MF A01 (US Sales Only)

The first quantization of the relativistic Brink-DiVecchia Howe-Polyakov (BDHP) string in the range 1 less than d less than 25 is considered. It is shown that using the Polyakov sum over bordered surfaces in the Feynman path integral quantization scheme one gets a consistent quantum mechanics of relativistic 1-dim extended objects in the range 1 less than d less than 25. In particular, the BDHP string propagator is exactly calculated for arbitrary initial and final string configurations and the Hilbert space of physical states of noncritical BDHP string is explicitly constructed. The resulting theory is equivalent to the Fairlie-Chodos-Thorn massive string model. In contrast to the conventional conformal field theory approach to noncritical string and random surfaces in the Euclidean target space the path integral formulation of the Fairlie-Chodos-Thorn string obtained in this paper does not rely on the principle of conformal invariance. Some consequences of this feature for constructing a consistent relativistic string theory based on the 'splitting-joining' interaction are discussed. DOE

N95-22742# International Centre for Theoretical Physics, Trieste (Italy).
TOPOLOGICALLY STABLE Z - STRINGS IN THE SUPERSYMMETRIC STANDARD MODEL
G. Dvali (Pisa Univ., Italy.) and G. Senjanovic Mar. 1994 10 p
(DE94-628517; IC-94/56) Avail: CASI HC A02/MF A01 (US Sales Only)

We show that the minimal supergravity extension of the standard model automatically contains topologically stable electroweak strings if the hidden sector is invariant under the exact R-symmetry. These defects appear in the form of the semiglobal R-strings, which necessarily carry Z-flux inside their core. This result is independent from the particular structure of the hidden sector. Discussed strings differ fundamentally from the embedded Z-strings. If R-symmetry is explicitly broken (e.g. due to an anomaly), the decay of the semiglobal strings may have important implications for the baryogenesis. DOE

N95-22743# Joint Inst. for Nuclear Research, Dubna (USSR).
FINITE-TEMPERATURE SCALAR FIELD THEORY IN STATIC DE SITTER SPACE
D. V. Fursaev and G. Miele (Naples Univ., Italy.) 1993 22 p
(DE94-628522; JINR-E-2-93-46) Avail: CASI HC A03/MF A01 (US Sales Only)

The finite-temperature one-loop effective potential for a scalar field in the static de Sitter space-time is obtained. Within this framework, by using zeta-function regularization, one can get, in the conformally invariant case, the explicit expression for the stress tensor anomaly. Its value turns out to depend on the thermal state of the system. This conclusion is different from the one derived by other authors, who considered thermal properties of ultraviolet divergences in static spaces ignoring the effects of horizons. The behavior of the effective potential in the ground state and in de Sitter-invariant state is also studied, showing the role played by the curvature on the minima. DOE

N95-22744# International Centre for Theoretical Physics, Trieste (Italy).
CHIRAL SYMMETRY BREAKING IN QCD WITH LINEARLY RISING CONFINEMENT POTENTIAL
A. N. Ivanov, N. I. Troitskaya, M. Faber (Technische Univ., Vienna, Austria.), M. Schaler (Technische Univ., Vienna, Austria.), and M. Nagy (Slovak Academy of Sciences, Bratislava, Czechoslovakia.) Jan. 1994 14 p
(DE94-628559; IC-94/28) Avail: CASI HC A03/MF A01 (US Sales Only)

Chiral symmetry breaking is explored within QCD with linearly rising confinement potential at the Nambu-Jona-Lasinio (NJL) prescription. The dynamical quark mass is obtained from the gap-equation in terms of the string tension sigma, i.e. m=2 (square root of sigma)/pi = 0.33 GeV at sigma = 0.27 GeV(exp 2). The phenomenological constants of the NJL local four-quark interactions G(sub 1) and G(sub 2) are found equal and expressed in terms of the string tension and the confinement radius. It is shown that the spectra of low-lying quark-antiquark collective excitations coincide with those predicted by the NJL model. DOE

N95-22745# International Centre for Theoretical Physics, Trieste (Italy).
SPONTANEOUS BREAKING OF CHIRAL SYMMETRY AS A CONSEQUENCE OF CONFINEMENT
A. N. Ivanov, N. I. Troitskaya, M. Faber (Technische Univ., Vienna, Austria.), M. Schaler (Technische Univ., Vienna, Austria.), and M. Nagy (Slovak Academy of Sciences, Bratislava, Czechoslovakia.) Feb. 1994 8 p
(DE94-628560; IC-94/32) Avail: CASI HC A02/MF A01 (US Sales Only)

It is shown that at the leading order in large N-expansion a confinement potential, linearly rising at large distances, leads to a non-local four-quark interaction which realizes spontaneous breaking of chiral symmetry in the same way as the Nambu-Jona-Lasinio model does. The Nambu-Jona-Lasinio phenomenological constant G(sub 1), which is responsible for SBCS, is expressed in terms of the string tension and the confinement radius. The dynamical quark mass is found as a function on the string tension m = 2 (square root of sigma)/(pi) = 0.33 GeV at sigma = 0.27 GeV(exp 2). DOE

N95-22752# International Centre for Theoretical Physics, Trieste (Italy).
LECTURES ON 2D GAUGE THEORIES. TOPOLOGICAL ASPECTS AND PATH INTEGRAL TECHNIQUES
M. Blau and G. Thompson Oct. 1993 69 p
(DE94-628509; IC-93/356) Avail: CASI HC A04/MF A01 (US Sales Only)

In these lectures are discussed two classes of two-dimensional field theories which are not obviously topological, but which nevertheless exhibit an intriguing equivalence with certain topological theories. These classes are two-dimensional Yang-Mills theory and the so-called G/G gauged Wess-Zumino-Witten model. The aim is to exhibit and extract the topological information contained in these theories and to present a technique which allows us to calculate directly their partition functions and topological correlation functions on arbitrary closed surfaces. DOE

N95-22753# International Centre for Theoretical Physics, Trieste (Italy).
CHIRAL ANOMALIES IN NON-LEPTONIC DECAYS WITHIN CHIRAL PERTURBATION THEORY AT THE QUARK LEVEL
A. N. Ivanov, N. I. Troitskaya, and M. Nagy (Slovak Academy of Sciences, Bratislava, Czechoslovakia.) Jan. 1994 9 p
(DE94-628613; IC-94/30) Avail: CASI HC A02/MF A01 (US Sales Only)

By example of the K(sup +) yields pi(sup +)(pi)(sup 0) gamma decay there has been investigated at the quark level the contribution of chiral anomalies to non-leptonic weak decays of K-mesons. The theoretical prediction for the probability of the K(sup +) yields pi(sup +) pi(sup 0) gamma decay with the direct emission of a photon is B(K(sup +) yields pi(sup +) pi(sup 0) gamma(DE))(sub anom) is less than or equal to (1.1 +/- 0.2) x 10(exp -5). It is stressed that the mechanism of the Delta I = 1/2 transition in the K(sup +) yields pi(sup +) pi(sup 0) gamma decay differs from that governing the enhancement of the Delta I = 1/2 transitions in the K(sup 0) yields pi(sup +) pi(sup -) decay. DOE

N95-22759# International Centre for Theoretical Physics, Trieste (Italy).
OPTICAL ABSORPTION IN AN INDIRECT-GAP SEMICONDUCTOR QUANTUM WELL SYSTEMS
A. R. Hassan Aug. 1993 14 p
(DE94-628878; IC-93/261) Avail: CASI HC A03/MF A01 (US Sales Only)

We have derived the optical absorption coefficient due to phonon-assisted, excitonic transitions of a semiconductor layered quantum well (QW) and quantum well wire (QWW) systems having an indirect-band-gap. The spectral dependence of the absorption coefficients varies as ((h/2 pi) omega +/- (h/2 pi) Omega - E(sub G) + E(sup b)(sub ex))(sup (beta)), where (h/2(pi))(omega)((h/2 pi) Omega) is the photon (phonon) energy, E(sub G) is the effective indirect band gap and E(sup b)(sub ex) is the exciton binding energy, (beta) takes the values -1/2, 0 and 1/2 for 1D (one-dimensional), 2D and 3D structure systems. Our results for 1D and 2D converge to each other in the appropriate limits and also to 3D (bulk) limit as well. The analytical forms of the exciton-photon and exciton-phonon matrix elements involved in the excitonic transitions in each case are given. The dominant transition mechanism lead to a final indirect bound 1s exciton state assisted by optical phonons in both QW's. Numerical Application taking the parameters of Si(0.5)Ge(0.5) shows that, near the threshold the indirect exciton absorption coefficient in QWW, alpha(sup (1))(sub ex) is one and two orders of magnitude larger than that of QW, alpha(sup (2))(sub ex) and of bulk, alpha(sup (3))(sub ex), respectively. On the other hand, alpha(sup (2))(sub ex) is bigger than alpha(sup (3))(sub ex) by one order of magnitude. These enhancement of alpha(sup (1))(sub ex) and alpha(sup (2))(sub ex) is function of the dimension of the system and reflects the additional lateral confinement of the carriers in the QWW's. DOE

N95-22760# International Centre for Theoretical Physics, Trieste (Italy).
TWO-PHOTON ABSORPTION IN AN INDIRECT-GAP SEMICONDUCTOR QUANTUM WELL SYSTEMS 1. INTERBAND TRANSITIONS
A. R. Hassan Aug. 1993 13 p
(DE94-628879; IC-93/262) Avail: CASI HC A03/MF A01 (US Sales Only)

Phonon-assisted two-photon interband transitions in an indirect-band-gap semiconductor layered quantum well (QW) and quantum well wire (QWW) have been theoretically studied. The spectral dependence of the two-photon absorption (TPA) coefficients in one-dimensional (1D), alpha(sup (1)), 2D, alpha(sup (2)), and also 3D (bulk) alpha(sup (3)) systems have been found to vary according as (2(h/2pi) +/- (h/2pi)Omega - E(sub G))(sup beta) where (h/2pi)omega((h/2pi) Omega) is the photon (phonon) energy and E(sub G) is the effective indirect gap. beta takes the values 0,1,2 and 3 depending on the dimension of the system and the form of momentum matrix elements. The analytical expressions of the electron-phonon matrix elements in QW's systems are given. A numerical calculation in Si(0.5)Ge(0.5) for the TPA coefficients alpha(sup (1)), alpha(sup (2)) and alpha(sup (3)) shows that: alpha(sup (1)) (alpha(sup (2))) for polarization parallel to the confinement directions, is 4(2) orders bigger than alpha(sup (3)) for (allowed-allowed) transitions. Furthermore, (alpha)(sup (1)) is 2 orders of magnitude larger than (alpha)(sup (2)), for both photon polarizations w.r.t. the confinement directions in QW systems. This enhancement of (alpha)(sup (1)) over (alpha)(sup (2)) and (alpha)(sup (3)) is interpreted as due to the additional lateral quantum confinement of the carriers in QWW and also due to the intra subband momentum matrix elements. DOE

N95-22761# International Centre for Theoretical Physics, Trieste (Italy).
TWO-PHOTON ABSORPTION IN AN INDIRECT-GAP SEMICONDUCTOR QUANTUM WELL SYSTEMS 2. EXCITONIC TRANSITIONS
A. R. Hassan Aug. 1993 15 p
(DE94-628880; IC-93/263) Avail: CASI HC A03/MF A01 (US Sales Only)

A theory of phonon-assisted two-phonon exciton transitions in an indirect-band-gap semiconductor layered Quantum Wells (QW) and Quantum Well Wires (QWW) is developed. The expressions for the two-photon absorption coefficients in one-dimensional (1D), alpha(sup (1))(sub ex), 2D, alpha(sup (2))(sub ex) and 3D (bulk), alpha(sup (3))(sub ex) have been calculated. The spectra dependence of these expressions, at the vicinity of the band edge, are found to obey a law (2(h/2pi) omega +/- (h/2pi) Omega - E(sub G) + E(sup b)(sub ex))(sup beta) where (h/2(pi))omega ((h/2pi) Omega) is the photon (phonon) energy, E(sub G) is the effective indirect gap and E(sup b)(sub ex) is the exciton binding energy. The values of beta varies from -1/2 up to 3/2 depending on the dimension of the system and the type of the coupling matrix element involved in each transition process. Before the edge, the final exciton states are of s-symmetry or p-symmetry according to the photon polarizations with respect to the confinement directions in the QW's and to the selection rules allowed by the momentum matrix elements. A numerical estimation for the case Si(0.5)Ge(0.5) show that alpha(sup (1))(sub ex) for both photon polarizations (parallel and perpendicular to the confinement directions of the QW's) is enhanced over the values of alpha(sup (2))(sub ex) and alpha(sup (3))(sub ex) (allowed and forbidden transitions). Furthermore alpha(sup (2))(sub ex) is also enhanced over alpha(sup (3))(sub ex) values for bulk materials. This behaviour of alpha(sub ex)'s is interpreted as due to: (1) the additionalconfinement of the carriers which occur going from 3D (yields) 2D (yields) 1D systems; (2) the photon polarization configurations w.r.t. the confinement directions; and (3) the coupling matrixelements. DOE

N95-22775# International Centre for Theoretical Physics, Trieste (Italy).
THE ROLE OF TRIPLET CORRELATION FUNCTION IN DENSE FLUIDS
R. I. M. A. Rashid Sep. 1993 10 p

(DE94-628476; IC-93/325) Avail: CASI HC A02/MF A01 (US Sales Only)

In the theory of dense liquids, one usually introduces various correlation functions for describing properties of such systems. It has proved impossible to solve these correlation functions exactly and as such one often resorts to some meaningful approximations for their solutions. It is well known that unless proper precautions are taken, the approximate solutions will violate some useful sum rules and thermodynamic consistency conditions. Here the general rules for generating thermodynamically consistent approximate correlation functions are discussed. The role of triplet correlation is elucidated further by calculating a residual correction to the vacancy formation energy via three-particle correlation in rare gas solids. DOE

N95-22776# International Centre for Theoretical Physics, Trieste (Italy).
GAUGE DEPENDENCE AND NEW KIND OF TWO-DIMENSIONAL GRAVITY THEORY WITH TRIVIAL QUANTUM CORRECTIONS
A. T. Banin (Tomsk State Univ., USSR.) and I. L. Shapiro Dec. 1993 9 p
(DE94-628502; IC-93/217) Avail: CASI HC A02/MF A01 (US Sales Only)

We search for the new kinds of classical potentials in two-dimensional induced gravity, which provide the triviality of the one-loop quantum corrections. First of all the gauge dependence of the effective potential is studied. The unique effective potential, introduced by Vilkovisly in 1984 is found to manifest the gauge dependence due to some unusual properties of the theory under consideration. Then we take the gauge of harmonical type, which provides the one-loop finiteness off shell, and then the solution for the required classical potential is found. DOE

N95-22779# International Centre for Theoretical Physics, Trieste (Italy).
DEFORMED HEISENBERG ALGEBRA AND FRACTIONAL SPIN FIELD IN 2+1 DIMENSIONS
M. S. Plyushchay Sep. 1993 8 p
(DE94-628507; IC-93/328) Avail: CASI HC A02/MF A01 (US Sales Only)

With the help of the deformed Heisenberg algebra involving the Klein operator, we construct the minimal set of linear differential equations for the (2+1)-dimensional relativistic field with arbitrary fractional spin, whose value is defined by the deformation parameters. DOE

N95-22782# International Centre for Theoretical Physics, Trieste (Italy).
NON-ZERO TEMPERATURE TWO-MODE SQUEEZING FOR TIME-DEPENDENT TWO-LEVEL SYSTEMS
J. Aliaga, J. L. Gruver, A. N. Proto, and H. A. Cerdeira Jan. 1994 17 p
(DE94-628427; IC-94/5) Avail: CASI HC A03/MF A01 (US Sales Only)

A Maximum Entropy Principle density matrix method, valid for systems with temperature different from zero, is presented making it possible to find two-mode squeezed states in two-level systems with relevant operators and Hamiltonian connected with O(3,2). A method which allows one to relate the appearance of squeezing to the relevant operators, included in order to define the density matrix of the system is given. DOE

N95-22783# International Centre for Theoretical Physics, Trieste (Italy).
SUPERSYMMETRIC SINGLET MAJORONS AND COSMOLOGY
E. J. Chun, H. B. Kim (Seoul National Univ., Republic of Korea.), and A. Lukas (Technische Univ., Munich, Germany.) Feb. 1994 14 p
(DE94-628571; IC-94/40; SNUTP-94-15; TUM-TH-164/94) Avail: CASI HC A03/MF A01 (US Sales Only)

We examine cosmological constraints on the lepton number breaking scale in super-symmetric singlet majoron models. Special attention is drawn to the model dependence arising from the particular choice of a certain majoron extension and a cosmological scenario. We find that the bounds on the symmetry breaking scale can vary substantially. Large values of this scale can be allowed if the decoupling temperature of majoron and majorino exceeds the reheating temperature of inflation. In the opposite case an upper bound depending on the majoron model can be obtained which, however, is unlikely to be much larger than 10(exp 10) GeV. DOE

N95-22784# International Centre for Theoretical Physics, Trieste (Italy).
A SPACE-TIME LATTICE VERSION OF SCALAR ELECTRODYNAMICS
J. Kijowski and A. Thielmann (Polish Academy of Sciences, Warsaw, Poland.) Oct. 1993 30 p
(DE94-628577; IC-93/340) Avail: CASI HC A03/MF A01 (US Sales Only)

A Minkowski-lattice version of quantum scalar electrodynamics is constructed. Quantum field is consequently described in a gauge-independent way, i.e. the algebra of quantum observables of the theory is generated by gauge-invariant operators assigned to zero-, one-, and two-dimensional elements of the lattice. The operators satisfy canonical commutation relations. Field dynamics is formulated in terms of difference equations imposed on the field operators. The dynamics is obtained from a discrete version of the path-integral. DOE

N95-22812# International Centre for Theoretical Physics, Trieste (Italy).
THE OMEGA PI(SUP 0)-TRANSIENT FORM FACTOR WITHIN EFFECTIVE CHIRAL LAGRANGIAN APPROACH
A. N. Ivanov, N. I. Troitskaya, M. Nagy (Slovak Academy of Sciences, Bratislava, Czechoslovakia.), and M. P. Rekalo (Academy of Sciences of the Ukraine, Kharkov, Ukraine.) Jan. 1994 22 p
(DE94-628612; IC-94/29) Avail: CASI HC A03/MF A01 (US Sales Only)

The omega pi(sup 0)-transient form factor is explored within effective chiral Lagrangians, based on the extended Nambu-Jona-Lasinio model and incorporating a gauge-invariant vector dominance approach. It is shown that on the whole the experimental data can be described by the contribution of the virtual rho-meson with many channel parametrization of the imaginary part of the propagator. The processes omega yields pi(sup 0) mu(+) mu(-), e(+) e(-) yields pi(sup 0) omega and tau(-) yields nu(sub tau) pi(-) omega, connected with the omega pi(sup 0)-transient for factor, have been analyzed. The theoretical results are in reasonable agreement with experimental data. The explanation of the observed discrepancies between theoretical results and experimental data goes beyond the effective chiral Lagrangian approach. DOE

N95-23049# International Centre for Theoretical Physics, Trieste (Italy).
STRONG-COUPLING POLARON EFFECT IN QUANTUM DOTS
KaDi Zhu and ShiWei Gu (Tongji Univ., Shanghai, China.) Nov. 1993 10 p
(DE94-628485; IC-93/375) Avail: CASI HC A02/MF A01 (US Sales Only)

Strong-coupling polaron in a parabolic quantum dot is investigated by the Landau-Pekar variational treatment. The polaron binding energy and the average number of virtual phonons around the electron as a function of the effective confinement length of the quantum dot are obtained in Gaussian function approximation. It is shown that both the polaron binding energy and the average number of virtual phonons around the electron decrease by increasing the effective confinement length. The results indicate that the polaronic effects are more pronounced in quantum dots than those in two-dimensional and three-dimensional cases. DOE

N95-23154 Rutherford Appleton Lab., Chilton (England).
BOSE CONDENSATION, MACROSCOPIC QUANTUM PHENOMENA AND ATOMIC SPATIAL CORRELATIONS IN SUPERFLUID He-4
J. Mayers Jun. 1994 10 p
(PB95-139085; RAL-94-063) Avail: Issuing Activity (National Technical Information Service (NTIS))

It is shown that the assumption of a Bose-Einstein condensation of a macroscopic number of particles into a single momentum state necessarily implies that the many particle wavefunction describing the system contains a component with phase coherence over the sample volume. This component has all of the properties usually associated with the 'condensate wavefunction' which is postulated to account for coherent phase effects in superconductors and superfluid He-4. The derivation is completely general, independent of assumptions about the form of the particle interaction, isotropy or anisotropy, translational invariance or temperature. It is shown that the condensate part of the wave function makes no contribution to the static pair correlation function g(r bar), thus explaining the reduction in amplitude of the oscillations in g(r bar) which are observed in neutron scattering measurements on He-4, as the temperature is reduced below the lambda point. NTIS

N95-23335# Brookhaven National Lab., Upton, NY.
SPIN POLARIZED PHOTOEMISSION STUDIES OF MAGNETIC QUANTUM WELL STATES
P. D. Johnson 1994 17 p Presented at the 14th International Colloquium on Magnetic Films and Surfaces, Duesseldorf, Germany, 29 Aug. - 2 Sep. 1994
(Contract DE-AC02-76CH-00016)
(DE95-004218; BNL-60869; CONF-940829-1) Avail: CASI HC A03/MF A01

There is currently considerable technological interest in the properties of transition metal multilayers. In these multilayers, which include Fe/Cr(001) and Cu/Co(001), it is possible to achieve either ferromagnetic or antiferromagnetic coupling of the adjacent ferromagnetic layers depending on the thickness of the intervening layer. The related giant magnetoresistance properties and the large enhancement of the Kerr rotation in these systems make them particularly interesting. In this paper, quantum well states with discrete binding energies dependent on the thickness of the film are observed in copper films deposited on a Co(001) substrate. They are found to be spin polarized, preferentially with minority spin. These states pass up to and through the Fermi level with a frequency identical to the long period of oscillation in the associated magnetic multilayers. In the pre-asymptotic limit the dispersion of these states away from the center of the zone is described by enhanced effective masses. This has implications for theories of the oscillatory exchange coupling that invoke the bulk Fermi surface. DOE

N95-23352# Stanford Linear Accelerator Center, CA.
THE IMPACT OF QCD AND LIGHT-CONE QUANTUM MECHANICS ON NUCLEAR PHYSICS
S. J. Brodsky and F. Schlumpf (Maryland Univ., College Park, MD.) Dec. 1994 13 p Presented at the Electromagnetic Probes and the Structure of Hadrons and Nuclei, Erice, Italy, 15-23 Sep. 1994
(Contract DE-AC03-76SF-00515)
(DE95-004293; SU-SLAC-PUB-6729; CONF-9409259-1) Avail: CASI HC A03/MF A01

We discuss a number of novel applications of Quantum Chromodynamics to nuclear structure and dynamics, such as the reduced amplitude formalism for exclusive nuclear amplitudes. We particularly emphasize the importance of light-cone Hamiltonian and Fock State methods as a tool for describing the wavefunctions of composite relativistic many-body systems and their interactions. We also show that the use of covariant kinematics leads to nontrivial corrections to the standard formulae for the axial, magnetic, and quadrupole moments of nucleons and nuclei. DOE

N95-23454# International Centre for Theoretical Physics, Trieste (Italy).
SPONTANEOUS WAVE PACKET REDUCTION
G. C. Ghirardi Jun. 1994 23 p
(DE94-634280; IC-94/117) Avail: CASI HC A03/MF A01 (US Sales Only)

This article has taken into account the main conceptual difficulties met by standard quantum mechanics in dealing with physical processes involving macroscopic systems. An idea stressed has been how J. A. Wheeler's remarks and lucid analysis have been relevant in pinpointing and bringing to its extreme consequences the puzzling aspects of quantum phenomena. The recently proposed models of spontaneous dynamical reduction shown represent a consistent way to overcome the conceptual difficulties of the standard theory. Obviously, many nontrivial problems remain open, the first and more relevant one being that of generalizing the model theories considered to the relativistic case. This is the challenge of the dynamical reduction program. DOE

N95-23922# International Centre for Theoretical Physics, Trieste (Italy).
EFFECTIVE (MU)-TERM IN SUPERSTRING THEORY
I. Antoniadis (Ecole Polytechnique, Palaiseau, France.), E. Gava, K. S. Narain, and T. R. Taylor (Northeastern Univ., Boston, MA.) Apr. 1994 28 p
(DE94-634326; IC-94/72; NUB-3084; CPTH-A282-0194) Avail: CASI HC A03/MF A01 (US Sales Only)

In four-dimensional compactifications of the heterotic superstring theory the Kaehler potential has a form which generically induces a superpotential mass term for Higgs particles once supersymmetry is broken at low energies. This '(mu) term' is analyzed in a model-independent way at the three level and in the one loop approximation, and explicit expressions are obtained for orbifold compactifications. Additional contributions, which arise in the case of supersymmetry breaking induced by gaugino condensation are also discussed. DOE

N95-23964# Joint Inst. for Nuclear Research, Dubna (USSR).
DOES THE RELATIVITY PRINCIPLE VIOLATE?
V. S. Barashenkov and M. Z. Yurev 1994 30 p
(DE94-635420; JINR-E-2-94-21) Avail: CASI HC A03/MF A01 (US Sales Only)

Theoretical and experimental data about a possible existence in Nature of some preferred reference frame with a violation of the principle of relativity are considered. The Einstein's and Lorentz's points of view are compared. Some experiments are known which, in the opinion of their authors, indicate that the relativity principle violation. The proposals of new experiments in this region, particularly with electron spin precession, are discussed. DOE

N95-23967# Joint Inst. for Nuclear Research, Dubna (USSR).
THE POINT INTERACTIONS IN THE QUANTUM PROBLEM OF THREE PARTICLES WITH INTERNAL STRUCTURE
K. A. Makarov, V. V. Melezhik, and A. K. Motovilov 1994 24 p In RUSSIAN
(DE94-635423; JINR-R-5-94-51) Avail: CASI HC A03/MF A01 (US Sales Only)

The problem of three quantum particles with internal structure is considered where the pair interactions are described in terms of two-channel Hamiltonians. It is proved that if parameters of the model are such that the total three-body Hamiltonian is semi bounded, the Faddeev equations are of Fredholm type. The boundary value problems are formulated for the Faddeev differential equations which can be used for search of the scattering wave functions. DOE

N95-23968# Joint Inst. for Nuclear Research, Dubna (USSR).
TACHYONS - IT WAS THE END OF HISTORY?
V. S. Barashenkov 1994 18 p
(DE94-635439; JINR-R-2-94-18) Avail: CASI HC A03/MF A01 (US Sales Only)

Hypothesis about superluminal particle intensively discussed during the 70s and at the beginning of the 80s is almost forgotten now, though faster-than-light particles appear by string and other generalizations of modern theory. The present state of tachyon hypothesis is considered. Special consideration is given to effects and symmetries appearing by attempts of superluminal generalization of the Lorentz transformation. The possible ways to circumvent the difficulties are discussed. Tachyons cannot occur in macroscopic space-time regions, however one may hope to discover them in ultra small intervals where the concepts 'earlier' and 'later' acquire a relative meaning. DOE

N95-23969# Joint Inst. for Nuclear Research, Dubna (USSR).
WEYL CONNECTION AND NON-ABELIAN GAUGE FIELD
B. M. Barbashov and A. B. Pestov 1994 6 p
(DE94-635440; JINR-E-2-94-90) Avail: CASI HC A02/MF A01 (US Sales Only)

It is shown that the congruent transference introduced by Weyl in 1921 defines a non-Abelian gauge field. The simplest gauge-invariant equations are proposed for this field. Connection with the Riemann-Cartan geometry is discussed. DOE

N95-23970# Joint Inst. for Nuclear Research, Dubna (USSR).
GRAVITATIONAL FIELD OF THE ISOLATED MASS IN YORDAN-BRANS-DICKE THEORY
G. G. Arutyunyan and V. V. Papoyan 1994 11 p In RUSSIAN
(DE94-635441; JINR-R-2-94-84) Avail: CASI HC A03/MF A01 (US Sales Only)

The problem of determination of the gravitational field inside the static, spherically symmetric self-gravitating object is formulated. A number of exact solutions of the YBD equations are supplemented by the new solutions describing the object considered. This solution can be rewritten in the form of modified curvature, uniform and other type coordinates. In the special case, the obtained solution coincides with the well-known Schwarzschild solution. DOE

N95-22959*# Los Alamos National Lab., NM. Theoretical Div.
EXACT, E = 0, CLASSICAL AND QUANTUM SOLUTIONS FOR GENERAL POWER-LAW OSCILLATORS
Michael Martin Nieto and Jamil Daboul (Ben Gurion Univ. of the Negev, Beersheva, Israel.) *In* NASA. Goddard Space Flight Center, Second International Workshop on Harmonic Oscillators Jan. 1995 p 13-24 See also N95-16428 (For primary document see N95-22957 07-74)
Avail: CASI HC A03/MF A04

N95-22965*# Universidad Nacional Autonoma de Mexico, Mexico City (Mexico). Inst. de Fisica.
QUANTUM FIELD BETWEEN MOVING MIRRORS: A THREE DIMENSIONAL EXAMPLE
S. Hacyan, Roco Jauregui, and Carlos Villarreal *In* NASA. Goddard Space Flight Center, Second International Workshop on Harmonic Oscillators Jan. 1995 p 61-67 (For primary document see N95-22957 07-74)
Avail: CASI HC A02/MF A04

N95-22970*# Hungarian Academy of Sciences, Debrecen. Inst. of Nuclear Research.
A POSSIBLE GENERALIZATION OF THE HARMONIC OSCILLATOR POTENTIAL
Geza Levai *In* NASA. Goddard Space Flight Center, Second International Workshop on Harmonic Oscillators Jan. 1995 p 113-119 (For primary document see N95-22957 07-74)
(Grant OTKA-4303)
Avail: CASI HC A02/MF A04

N95-22973*# Tulane Univ., New Orleans, LA. Dept. of Physics.
GALACTIC OSCILLATOR SYMMETRY
George Rosensteel *In* NASA. Goddard Space Flight Center, Second International Workshop on Harmonic Oscillators Jan. 1995 p 137-143 (For primary document see N95-22957 07-74)
(Grant NSF PHY-92-12231)
Avail: CASI HC A02/MF A04

N95-22977*# Chile Univ., Santiago (Chile). Dept. de Fisica.
NON-NOETHERIAN SYMMETRIES FOR OSCILLATORS IN CLASSICAL MECHANICS AND IN FIELD THEORY
Sergio A. Hojman, Jamie DeLaJara, and Leda Pena *In* NASA. Goddard Space Flight Center, Second International Workshop on Harmonic Oscillators Jan. 1995 p 173-179 Sponsored by Fondo Facional de Ciencia y Tecnologia, Fundacion Andes, Comision Nacional de Investigacion Cientifica y Tecnologica-Fundacion Andes and Consejo Nacional de Ciencia y Tecnologia (For primary document see N95-22957 07-74)
Avail: CASI HC A02/MF A04

N95-22979*# Instituto Venezolano de Investigaciones Cientificas, Caracas (Venezuela). Centro de Fisica.
LOCALIZATION IN DEFORMED QUANTUM MECHANICS
Simon Codriansky *In* NASA. Goddard Space Flight Center, Second International Workshop on Harmonic Oscillators Jan. 1995 p 189-193 Sponsored by Vicerrectorado de Investigacion y Postgrado of Universidasd Pedagogica Experimental Libertador and CONICIT (For primary document see N95-22957 07-74)
Avail: CASI HC A01/MF A04

N95-22980*# Liverpool Univ. (England). Dept. of Electrical Engineering and Electronics.
NOISY BASES IN HILBERT SPACE: A NEW CLASS OF THERMAL COHERENT STATES AND THEIR PROPERTIES
A. Vourdas and R. F. Bishop (Manchester Coll. of Science and Technology, England.) *In* NASA. Goddard Space Flight Center, Second International Workshop on Harmonic Oscillators Jan. 1995 p 195-206 (For primary document see N95-22957 07-74)
Avail: CASI HC A03/MF A04

N95-22981*# Instituto Politecnico Nacional, Mexico City (Mexico). Dept de Fisica.
GEOMETRIC PHASES, EVOLUTION LOOPS AND GENERALIZED OSCILLATOR POTENTIALS
David J. Fernandez *In* NASA. Goddard Space Flight Center, Second International Workshop on Harmonic Oscillators Jan. 1995 p 207-213 Sponsored by CONACYT (For primary document see N95-22957 07-74)
Avail: CASI HC A02/MF A04

N95-22982*# Instituto Politecnico Nacional, Mexico City (Mexico). Dept. of Fisica.
COHERENT STATES FOR A GENERALIZATION OF THE HARMONIC OSCILLATOR
David J. Fernandez, Veronique Hussin (Montreal Univ., Quebec.), and Luis M. Nieto (Montreal Univ., Quebec.) *In* NASA. Goddard Space Flight Center, Second International Workshop on Harmonic Oscillators Jan. 1995 p 215-221 Sponsored by CONACYT, NSERC of Canada, FCAR du Gouverment du Quebec, and Ministerio de Educacion y Ciencia (For primary document see N95-22957 07-74)
Avail: CASI HC A02/MF A04

N95-22983*# Oklahoma Univ., Norman, OK.
FINITE-ELEMENT TIME EVOLUTION OPERATOR FOR THE ANHARMONIC OSCILLATOR
Kimball A. Milton *In* NASA. Goddard Space Flight Center, Second International Workshop on Harmonic Oscillators Jan. 1995 p 223-230 Sponsored by DOE (For primary document see N95-22957 07-74)
Avail: CASI HC A02/MF A04

N95-22991*# Universidad Nacional Autonoma de Mexico, Mexico City (Mexico). Inst. de Fisica.
THE RELATIVISTIC MANY BODY PROBLEM WITH AN OSCILLATOR INTERACTION
Marcos Moshinsky *In* NASA. Goddard Space Flight Center, Second International Workshop on Harmonic Oscillators Jan. 1995 p 283-292 (For primary document see N95-22957 07-74)
Avail: CASI HC A02/MF A04

N95-22992*# National Aeronautics and Space Administration. Goddard Space Flight Center, Greenbelt, MD.
COVARIANT HARMONIC OSCILLATORS AND COUPLED HARMONIC OSCILLATORS
Daesoo Han, Young S. Kim (Maryland Univ., College Park, MD.), and Marilyn E. Noz (New York Univ., New York, NY.) *In its* Second International Workshop on Harmonic Oscillators Jan. 1995 p 293-304 (For primary document see N95-22957 07-74)
Avail: CASI HC A03/MF A04

N95-22993*# Granada Univ. (Spain). Inst. de fisica Teorica y Computacional.
COHERENT STATES FOR THE RELATIVISTIC HARMONIC OSCILLATOR
Victor Aldaya and J. Guerrero *In* NASA. Goddard Space Flight Center, Second International Workshop on Harmonic Oscillators Jan. 1995 p 305-312 (For primary document see N95-22957 07-74)
Avail: CASI HC A02/MF A04

N95-22996*# Universidad Nacional Autonoma de Mexico, Cuernavaca (Mexico). Inst. de Fisica.
PSEUDOCLASSICAL DESCRIPTION OF THE DIRAC OSCILLATOR
Antonio DelSolMesa and R. P. MartinezyRomero *In* NASA. Goddard Space Flight Center, Second International Workshop on Harmonic Oscillators Jan. 1995 p 327-332 Sponsored by direccion General de Asuntos del Personal Academico and ESP (For primary document see N95-22957 07-74)
Avail: CASI HC A02/MF A04

N95-22998*# Surrey Univ., Guildford (England). Dept. of Physics.
THE DUFFIN-KEMMER-PETIAU OSCILLATOR
Youcef Nedjadi and Roger Barrett *In* NASA. Goddard Space Flight Center, Second International Workshop on Harmonic Oscillators Jan. 1995 p 341-348 (For primary document see N95-22957 07-74)
(Grant SERC GR/H53648)
Avail: CASI HC A02/MF A04

N95-22999*# Saint Petersburg State Univ., Saint Petersburg (Russia). Inst. of Physics.
HARMONIC OSCILLATORS AND RESONANCE SERIES GENERATED BY A PERIODIC UNSTABLE CLASSICAL ORBIT
A. K. Kazansky and Valentin N. Ostrovsky *In* NASA. Goddard Space Flight Center, Second International Workshop on Harmonic Oscillators (SEE N95-22957 07-74) Jan. 1995 Sponsored by Russian Foundation for Foundamental Researches (For primary document see N95-22957 07-74)
Avail: CASI HC A02/MF A04

N95-23003*# Montreal Univ. (Quebec).
OSCILLATOR-LIKE COHERENT STATES FOR THE JAYNES-CUMMINGS MODEL
Y. BerubeLauziere, V. Hussin, and Michael M. Nieto *In* NASA. Goddard Space Flight Center, Second International Workshop on Harmonic Oscillators Jan. 1995 p 381-386 Sponsored by NSERC, FCAR du Gouvernement du Quebec, and Ministerio de Educacion y Ciencia (For primary document see N95-22957 07-74)
Avail: CASI HC A02/MF A04

N95-23005*# Academy of Sciences (USSR), Vladivostok (USSR). Pacific Oceanological Inst.
COHERENT CONTROL IN SIMPLE QUANTUM SYSTEMS
Sergey V. Prants *In* NASA. Goddard Space Flight Center, Second International Workshop on Harmonic Oscillators Jan. 1995 p 395-402 Sponsored by International Science Foundation (For primary document see N95-22957 07-74)
Avail: CASI HC A02/MF A04

80 SOCIAL SCIENCES (GENERAL)

Includes educational matters.

N95-23286*# Pennsylvania State Univ., University Park, PA. Instructional Systems Program.
FORMATIVE AND SUMMATIVE EVALUATION EFFORTS FOR THE TEACHER ENHANCEMENT INSTITUTE CONDUCTED AT THE NASA LANGLEY RESEARCH CENTER, SUMMER 1994 Abstract Only
Randal D. Carlson *In* Hampton Univ., 1994 NASA-HU American Society for Engineering Education (ASEE) Summer Faculty Fellowship Program Dec. 1994 p 66-67 (For primary document see N95-23276 07-99)
Avail: CASI HC A01/MF A02

N95-23306*# Christopher Newport Coll., Newport News, VA.
DESIGN AND IMPLEMENTATION OF TWO TWO-WEEK TEACHER ENHANCEMENT INSTITUTES Abstract Only
Lynn Lambert *In* Hampton Univ., 1994 NASA-HU American Society for Engineering Education (ASEE) Summer Faculty Fellowship Program Dec. 1994 p 88 (For primary document see N95-23276 07-99)
Avail: CASI HC A01/MF A02

N95-23312*# Norfolk State Univ., VA. School of Education.
TEACHER ENHANCEMENT INSTITUTE Abstract Only
Tina Marshall-Bradley *In* Hampton Univ., 1994 NASA-HU American Society for Engineering Education (ASEE) Summer Faculty Fellowship Program Dec. 1994 p 94 (For primary document see N95-23276 07-99)
Avail: CASI HC A01/MF A02

N95-23316*# Norfolk State Univ., VA. School of Social Work.
LANGLEY RESEARCH CENTER STRATEGIC PLAN FOR EDUCATION Abstract Only
Sandra B. Proctor *In* Hampton Univ., 1994 NASA-HU American Society for Engineering Education (ASEE) Summer Faculty Fellowship Program Dec. 1994 p 98 (For primary document see N95-23276 07-99)
Avail: CASI HC A01/MF A02

N95-23320*# College of William and Mary, Williamsburg, VA. Dept. of Mathematics.
PREPARATION OF COURSE MATERIALS: ELEMENTARY MATHEMATICS OF POWERED FLIGHT Abstract Only
George T. Rublein *In* Hampton Univ., 1994 NASA-HU American Society for Engineering Education (ASEE) Summer Faculty Fellowship Program Dec. 1994 p 102 (For primary document see N95-23276 07-99)
Avail: CASI HC A01/MF A02

N95-23324*# Virginia Univ. Hospital, Charlottesville, VA.
TEACHER ENHANCEMENT INSTITUTE Abstract Only
Ron W. Simmons *In* Hampton Univ., 1994 NASA-HU American Society for Engineering Education (ASEE) Summer Faculty Fellowship Program Dec. 1994 p 106 (For primary document see N95-23276 07-99)
Avail: CASI HC A01/MF A02

81 ADMINISTRATION AND MANAGEMENT

Includes management planning and research.

N95-22891*# Science Applications, Inc., Huntsville, AL.
COST AND SCHEDULE ANALYTICAL TECHNIQUES DEVELOPMENT Final Report
30 Nov. 1994 21 p
(Contract NAS8-38784)
(NASA-CR-196548; NAS 1.26:196548) Avail: CASI HC A03/MF A01
This contract provided technical services and products to the Marshall Space Flight Center's Engineering Cost Office (PP03) and the Program Plans and Requirements Office (PP02) for the period of 3 Aug. 1991 - 30 Nov. 1994. Accomplishments summarized cover the REDSTAR data base, NASCOM hard copy data base, NASCOM automated data base, NASCOM cost model, complexity generators, program planning, schedules, NASA computer connectivity, other analytical techniques, and special project support. CASI

N95-23588# General Accounting Office, Washington, DC. National Security and International Affairs Div.
SECURITY CLEARANCES: CONSIDERATION OF SEXUAL ORIENTATION IN THE CLEARANCE PROCESS. REPORT TO CONGRESSIONAL REQUESTERS
24 Mar. 1995 61 p
(GAO/NSIAD-95-21; B-258273) Avail: CASI HC A04/MF A01; GAO, PO Box 6015, Gaithersburg, MD 20884-6015 HC
This General Accounting Office (GAO) report is in response to issues relating to how sexual orientation is treated in the security clearance process for federal civilian and contractor employees. Specific areas include: (1) whether clearances are currently being denied or revoked based on individuals' sexual orientation, (2) whether sexual orientation is being used as a criterion in granting or revoking security clearances, and (3) how concealment of sexual orientation affects the granting or revoking of security clearances. The review was performed at eight agencies that, except for the Central Intelligence Agency, accounted for over 95 percent of the security clearances granted to civilian and contractor employees during fiscal year 1993. Security clearances were not reviewed at the CIA, Defense Intelligence Agency, nor the National Security Agency. Also, the scope of this work did not include military personnel. Derived from text

N95-24043# Rochester Univ., NY. Dept. of Computer Science.
USING SIMULATION-BASED PROJECTION TO PLAN IN AN UNCERTAIN AND TEMPORALLY COMPLEX WORLD
Ed Yampratoom Sep. 1994 59 p
(Contract F30602-91-C-0010)
(TR-531) Avail: CASI HC A04/MF A01
Temporal projection is a crucial task in planning. In order to achieve its goals, the planner must be able to reason about the consequences of its actions. In the real world, the planner does not have complete information about the environment or even the consequences of its actions. The planner thus must be able to reason about the probabilistic nature of the world and the probabilistic effects of its action. Interactions between actions and events in the world are not only probabilistic; they also are temporally complex. Simultaneous events can interact in many different ways depending

on their temporal properties. An action's temporal relation to its preconditions and effects can also become quite complex. Existing projection systems are weak in their representations of temporally complex actions and events in a probabilistic world. Those that can handle probabilistic situations have a limited representation of temporal relations, while those that can handle complex temporal relations generally assume the world to be completely deterministic. Moreover, the speed of existing probabilistic projection systems are low. These systems are impractical to scale up to larger problems. In this thesis, we propose a practical projection system that can handle both the probabilistic nature of the world and the temporally complex nature of actions. The projection is based on simulation methods. Projection is done by simulating possible courses of events, one at a time. The simulation traces are then collected and processed by a projection module front-end, which provides the planner and the execution monitor with probabilistic estimates of propositions' values. The representation allowed by the system is rich in both the temporal and the probabilistic aspects. Author

N95-24054# General Accounting Office, Washington, DC. National Security and International Affairs Div.
NASA PROCUREMENT: CONTRACT AND MANAGEMENT IMPROVEMENTS AT THE JET PROPULSION LABORATORY. REPORT TO CONGRESSIONAL REQUESTERS
30 Dec. 1994 13 p
(GAO/NSIAD-95-40; B-259019) Avail: CASI HC A03/MF A01; GAO, PO Box 6015, Gaithersburg, MD 20884-6015

Selected contract provisions and internal controls at the Jet Propulsion Laboratory (JPL) are examined. JPL is NASA's only Federally Funded Research and Development Center (FFRDC) and is operated under contract by Caltech. JPL is NASA's field installation for solar system exploration and is a major operating division of Caltech. Together, these overlapping roles contribute to unique JPL management and oversight challenges. This report reviews the current contract between NASA and Caltech for the operation of the JPL. Derived from text

N95-24085# General Accounting Office, Washington, DC. Office of Special Investigations.
INSPECTOR GENERAL: ALLEGED MISCONDUCT BY NASA INSPECTOR GENERAL. REPORT TO CONGRESSIONAL REQUESTERS
10 Feb. 1995 9 p
(GAO/OSI-95-9; B-259046) Avail: CASI HC A02/MF A01; GAO, PO Box 6015, Gaithersburg, MD 20994-6015 HC

This GAO report addresses a March 25, 1994 request from John Glenn, Ranking Minority Member, Committee on Governmental Affairs, United States Senate, concerning the allegations of misconduct by the then-National Aeronautics and Space Administrations (NASA) Inspector General, William Colvin. This report discusses the investigative results concerning Mr. Colvin's activities, as follows: (1) prenotification of senior NASA employees who were targets of impending Office of the Inspector General (OIG) investigations; (2) unauthorized disclosure of grand jury-related information; and (3) premature closing of selected audits and investigations. CASI

N95-23282*# Old Dominion Coll., Norfolk, VA.
PROJECT: INTERNAL COMMUNICATIONS Abstract Only
Lydia Black *In* Hampton Univ., 1994 NASA-HU American Society for Engineering Education (ASEE) Summer Faculty Fellowship Program Dec. 1994 p 62 (For primary document see N95-23276 07-99)
Avail: CASI HC A01/MF A02

N95-23292*# Old Dominion Coll., Norfolk, VA. Dept. of Psychology.
TEAMS AND TEAMWORK AT NASA LANGLEY RESEARCH CENTER Abstract Only
Terry L. Dickinson *In* Hampton Univ., 1994 NASA-HU American Society for Engineering Education (ASEE) Summer Faculty Fellowship Program Dec. 1994 p 73 (For primary document see N95-23276 07-99)
Avail: CASI HC A01/MF A02

N95-23305*# Ohio Univ., Athens, OH. Dept. of Industrial and Systems Engineering.
STOCHASTIC DECISION ANALYSIS Abstract Only
Thomas A. Lacksonen *In* Hampton Univ., 1994 NASA-HU American Society for Engineering Education (ASEE) Summer Faculty Fellowship Program Dec. 1994 p 87 (For primary document see N95-23276 07-99)
Avail: CASI HC A01/MF A02

N95-23323*# Hampton Univ., VA. Dept. of Management.
UPWARD APPRAISAL AS A MEANS FOR IMPROVING SUPERVISORY PERFORMANCE AND PROMOTING PROCESS IMPROVEMENT, WITH LONG-TERM IMPLICATIONS FOR ORGANIZATIONAL CHANGE Abstract Only
Denise V. Siegfeldt *In its* 1994 NASA-HU American Society for Engineering Education (ASEE) Summer Faculty Fellowship Program Dec. 1994 p 105 (For primary document see N95-23276 07-99)
Avail: CASI HC A01/MF A02

N95-23331*# Paul D. Camp Community Coll., Suffolk, VA. Dept. of Computer Information Sytems.
THE SOFTWARE ANALYSIS PROJECT FOR THE OFFICE OF HUMAN RESOURCES Abstract Only
Robert L. Tureman, Jr. *In* Hampton Univ., 1994 NASA-HU American Society for Engineering Education (ASEE) Summer Faculty Fellowship Program Dec. 1994 p 113 (For primary document see N95-23276 07-99)
Avail: CASI HC A01/MF A02

N95-23677*# Siemens A.G., Vienna (Austria).
UTILIZING INHERITANCE IN REQUIREMENTS ENGINEERING
Hermann Kaindl *In* JPL, Third International Symposium on Artificial Intelligence, Robotics, and Automation for Space 1994 Oct. 1994 p 29-31 Sponsored by ESA and Innovation- und Technologiefonds (For primary document see N95-23672 07-63)
Avail: CASI HC A01/MF A03

N95-23747*# National Aeronautics and Space Administration. Marshall Space Flight Center, Huntsville, AL.
A FORMAT FOR THE INTERCHANGE OF SCHEDULING MODELS
John P. Jaap and Elizabeth K. Davis *In* JPL, Third International Symposium on Artificial Intelligence, Robotics, and Automation for Space 1994 Oct. 1994 p 369-372 (For primary document see N95-23672 07-63)
Avail: CASI HC A01/MF A03

82 DOCUMENTATION AND INFORMATION SCIENCE

Includes information management; information storage and retrieval technology; technical writing; graphic arts; and micrography.

For computer documentation see *61 Computer Programming and Software.*

N95-22494# Sprehe Information Management Associates, Inc., Washington, DC.
A STUDY OF POLICY ISSUES AFFECTING THE DEFENSE TECHNICAL INFORMATION CENTER Final Report, Mar. - Oct. 1994
J. Timothy Sprehe 26 Oct. 1994 82 p Revised Sponsored by DTIC
(AD-A286629; DTIC-1994-S-1-Rev) Avail: CASI HC A05/MF A01

This is a report of a research project for the purpose of exploring the federal information policy environment in which DTIC finds itself. The report surveys current federal information policy including 1994 legislative and policy initiatives affecting the Privacy Act, the Paperwork Reduction Act, OMB Circular A-130, the Government Information Locator Service, the information infrastructure and other areas. Special attention was devoted to the Freedom of Information Act, especially electronic FOIA, and to public versus non-public information. The report examines how recent events affecting intellectual property in electronic and network environments will affect DTIC. The report asks the question as to whether the federal government needs a policy document to cover the special situation of scientific and technical information; it concludes that the policy setting of STI is so different from other federal information activities and faces such urgent issues that a separate STI policy is needed. DTIC

N95-22515# Los Alamos National Lab., NM.
EXPERIENCE WITH CANDID: COMPARISON ALGORITHM FOR NAVIGATING DIGITAL IMAGE DATABASES
P. Kelly and M. Cannon 1994 13 p Presented at the 23rd AIPR Workshop on Image and Information Systems: Applications and Opportunities, Washington, DC, 12-14 Oct. 1994
(Contract W-7405-eng-36)
(DE95-000869; LA-UR-94-3086; CONF-9410211-1) Avail: CASI HC A03/MF A01

This paper presents results from the authors experience with CANDID (Comparison Algorithm for Navigating Digital Image Databases), which was designed to facilitate image retrieval by content using a query-by-example methodology. A global signature describing the texture, shape, or color content is first computed for every image stored in a database, and a normalized similarity measure between probability density functions of feature vectors is used to match signatures. This method can be used to retrieve images from a database that are similar to a user-provided example image. Results for three test applications are included. DOE

N95-22523# Vrije Univ., Amsterdam (Netherlands).
JACKSON SYSTEM DEVELOPMENT, ENTITY-RELATIONSHIP ANALYSIS AND DATA FLOW MODELS: A COMPARATIVE STUDY
R. J. Wieringa 11 Oct. 1993 26 p
(PB95-127338) Avail: CASI HC A03/MF A01

This paper compares Jackson System Development (JSD) with Entity-Relationship (ER) modelling and with data flow modelling. It is shown that the JSD method can be combined with ER modelling and that the result is a richer method than either of the two. The resulting method can serve as a basis for a practical object-oriented modelling method and has some resemblance to parts of well-known methods, like OMT. It is also argued that JSD and data flow modelling rest on opposite philosophies and cannot be combined in one modelling effort. This is illustrated by transforming a JSD model into a data flow model and listing the differences between the models. The results of this analysis are extrapolated to object-oriented models. NTIS

N95-22525 Vrije Univ., Amsterdam (Netherlands).
METHOD FOR BUILDING AND EVALUATING FORMAL SPECIFICATIONS OF OBJECT-ORIENTED CONCEPTUAL MODELS OF DATABASE SYSTEMS
R. J. Wieringa 15 Dec. 1993 138 p
(PB95-127353) Copyright Avail: Issuing Activity (National Technical Information Service (NTIS))

This report describes a Method for Conceptual Modeling (MCM) for building and evaluating formal specifications of object-oriented models of database system behavior. First, a general framework for information system development methods is given. In general, the following elements are needed: requirements determination, conceptual modeling, implementation, and project management methods. MCM is a conceptual modeling method, and must be supplemented with three other kinds of methods. These are: observation, induction, and evaluation methods. In this report, the author concentrates on induction and evaluation methods and merely makes a list of relevant observation methods. The result of following MCM is a conceptual model. NTIS

N95-22534# Technische Univ., Eindhoven (Netherlands).
BROWSING SEMANTICS IN THE TOWER MODEL
W. vanderAalst, P. DeBra, G. J. Houben, and Y. Kornatzky (Ben Gurion Univ. of the Negev, Beersheva, Israel.) 1994 32 p Prepared in cooperation with Ben-Gurion Univ.
(PB95-127221) Avail: CASI HC A03/MF A01

Browsing through a hyperdocument often leads to orientation problems. In order to detect potential problems in the use of a hyperdocument, the authors reduce different types of browsing actions to a unified and well know formalism: the Petri net. In the paper, the authors describe hyperdocuments using an object-oriented model. The model describes objects using a number of different description layers, which are not fixed by the model, and of which none are excluded from the model. In order to use Petri nets to describe browsing, the operations dealing with the hierarchical structure of objects (composites, towers and cities) are translated into operations that are equivalent to the simple follow-link. They combine the operations offered by the hypertext system (or presentation layer) with the link structure of the document, in order to characterize the browsing semantics of document and system as a unity. They do this by translating system features into (virtual) link structures. By using existing analysis tools for (different kinds of) Petri nets one can easily detect potential browsing problems like unreachable nodes and links, dead ends, unlimited numbers of simultaneously displayed nodes, infinite loops, etc. Such analysis is most valuable to hypertext authors, whose biggest problem is the creation of the most appropriate links. NTIS

N95-22871# Lawrence Livermore National Lab., Livermore, CA.
PHOTON AND ELECTRON INTERACTION DATABASES AND THEIR USE IN MEDICAL APPLICATIONS
Dermott E. Cullen May 1994 8 p Presented at the World Congress on Medical Physics and Biomedical Engineering Jointly With the International Conference on Medical Physics, Rio de Janeiro, Brazil, 22-26 Aug. 1994
(Contract W-7405-eng-48)
(DE94-015558; UCRL-JC-117419; CONF-940802-1) Avail: CASI HC A02/MF A01

This paper discusses the All Particle-Method photon and electron interaction, and atomic relaxation data bases, that were initially developed for use in medical applications. Currently these data bases are being used in both medical and industrial applications. The All Particle Method data bases are designed to allow modelling of individual collisions in as much detail as possible. Elastic scattering can be modelled as single, as opposed to multiple, scattering events. Ionization can be modelled at the atomic subshell level, to define which subshell was ionized, spectrum of the initially emitted electron, as well as the spectra of electron and photons emitted as the atom relaxes back to neutrality. These data bases are currently being used in applications involving rather small spatial regions, where detailed calculations of individual events are required. While initially designed for use in medical applications, these data bases are now being used in a variety of industrial applications, e.g., transport in microelectronics. DOE

N95-23024# Naval Postgraduate School, Monterey, CA.
EFFECTIVE MANAGEMENT OF CLASSIFIED DOCUMENTS USING THE LIBRARY DOCUMENT SYSTEM M.S. Thesis
Kenneth F. Elkern, Jr. Sep. 1994 90 p
(AD-A286021) Avail: CASI HC A05/MF A01

Previous automated classified document systems developed commercially or in-house to serve classified libraries with 50,000 documents or less, have been limited by excessive cost or insufficient functionality. The problem addressed by this research was to improve the automated systems available to classified libraries with 50,000 documents or less, by upgrading the Library Document System (LDS) to meet the tracking and document search needs of librarians. The approach taken was to first conduct a survey of 25 classified libraries to assess their document tracking procedures and requirements. Next, a thorough examination of the commercial and in-house automated classified document systems was performed to determine the state of solutions available. Finally, a strategy for modifying LDS was outlined to incorporate the tracking and document search features desired, using modern relational database constructs, structured programming techniques, and user-friendly interface design. As a result of this work, LDS was upgraded to fulfill the needs of classified librarians with 50,000 documents or less. In particular the schemata of the system were extended, a sophisticated search facility was implemented, and a mouse-oriented user-friendly interface was provided. DTIC

N95-23206*# Cortez 3 Services Corp., Brook Park, OH.
MICROGRAVITY EXPERIMENTS SAFETY AND INTEGRATION REQUIREMENTS DOCUMENT TREE
Jean M. Hogan Cleveland, OH NASA Mar. 1995 210 p
(Contract NAS3-26360; RTOP 323-61-05)
(NASA-CR-195447; E-9511; NAS 1.26:195447) Avail: CASI HC A10/MF A03

This report is a document tree of the safety and integration documents required to develop a space experiment. Pertinent document information for each of the top level (tier one) safety and integration documents, and their applicable and reference (tier two) documents has been identified. This information includes: document title, revision level, configuration management, electronic availability, listed applicable and reference documents, source for obtaining the document, and document owner. One of the main conclusions of this report is that no single document tree

exists for all safety and integration documents, regardless of the Shuttle carrier. This document also identifies the need for a single point of contact for customers wishing to access documents. The data in this report serves as a valuable information source for the NASA Lewis Research Center Project Documentation Center, as well as for all developers of space experiments. Author

N95-23209*# National Aeronautics and Space Administration. Goddard Space Flight Center, Greenbelt, MD.
NASAwide ELECTRONIC PUBLISHING SYSTEM: ELECTRONIC PRINTING AND DUPLICATING, STAGE-2 EVALUATION REPORT (GSFC)
Richard C. Tuey, Robert Lane, and Susan V. Hart Jan. 1995 57 p
(NASA-TM-104615; Rept-95B00026; NAS 1.15:104615) Avail: CASI HC A04/MF A01

The NASA Scientific and Technical Information Office was assigned the responsibility to continue with the expansion of the NASAwide networked electronic duplicating effort by including the Goddard Space Flight Center (GSFC) as an additional node to the existing configuration of networked electronic duplicating systems within NASA. The subject of this report is the evaluation of a networked electronic duplicating system which meets the duplicating requirements and expands electronic publishing capabilities without increasing current operating costs. This report continues the evaluation reported in 'NASA Electronic Publishing System - Electronic Printing and Duplicating Evaluation Report' (NASA TM-106242) and 'NASA Electronic Publishing System - Stage 1 Evaluation Report' (NASA TM-106510). This report differs from the previous reports through the inclusion of an external networked desktop editing, archival, and publishing functionality which did not exist with the previous networked electronic duplicating system. Additionally, a two-phase approach to the evaluation was undertaken; the first was a paper study justifying a 90-day, on-site evaluation, and the second phase was to validate, during the 90-day evaluation, the cost benefits and productivity increases that could be achieved in an operational mode. A benchmark of the functionality of the networked electronic publishing system and external networked desktop editing, archival, and publishing system was performed under a simulated daily production environment. This report can be used to guide others in determining the most cost effective duplicating/publishing alternative through the use of cost/benefit analysis and return on investment techniques. A treatise on the use of these techniques can be found by referring to 'NASA Electronic Publishing System -Cost/Benefit Methodology' (NASA TM-106662). Author

N95-23223*# NASA Scientific and Technical Information Facility, Baltimore-Washington International Airport, MD.
NASA THESAURUS, SUPPLEMENT Special Publication
Washington Feb. 1995 20 p
(NASA-SP-7096-Suppl-1; NAS 1.21:7096-Suppl-1) Avail: CASI HC A03/MF A01

The four part cumulative NASA Thesaurus Supplement to the 1994 edition of the NASA Thesaurus includes Part 1, Hierarchical Listing, Part 2, Access Vocabulary, Part 3, NASA Thesaurus Definitions, and Part 4, Changes. The semiannual supplement gives complete hierarchies for new terms. Uppercase-lowercase forms are provided in both Part 2 and Part 3. Author

N95-23225*# National Aeronautics and Space Administration. Marshall Space Flight Center, Huntsville, AL.
FY 1994 SCIENTIFIC AND TECHNICAL REPORTS, ARTICLES, PAPERS, AND PRESENTATIONS
Joyce E. Turner, Comp. Washington Oct. 1994 85 p
(NASA-TM-108480; NASA 1.15:108480) Avail: CASI HC A05/MF A01

This document presents formal NASA technical reports, papers published in technical journals, and presentations by Marshall Space Flight Center personnel in FY94. It also includes papers of MSFC contractors and author indexes. The information in this report may be of value to the scientific and engineering community in determining what information has been published and what is available. Author

N95-23340# Westinghouse Hanford Co., Richland, WA.
SEARCH HANFORD ACCESSIBLE REPORTS ELECTRONICALLY SYSTEM REQUIREMENTS SPECIFICATION
K. J. Willers 28 Feb. 1994 24 p
(Contract DE-AC06-87RL-10930)
(DE95-004367; WHC-SD-GN-CSRS-30008-Rev-1) Avail: CASI HC A03/MF A01

The Emergency, Safety, & Quality (ESQ) Services organization of Westinghouse Hanford Company (WHC) is experiencing changes related to new programs. The programs include Corrective Actions Management Systems, Self-Assessment, Trend Analysis, and Lessons Learned analysis. The programs are pushing up organizational costs while funding and manpower levels are projected to be dropping. A large cost involved in implementing the new programs is the cost for people to locate unstructured information required to make decisions or write documentation. But, most resources for retrieving information are found in structured database systems. This means that unstructured information that must be located has to be found by one of these methods: (1) searching manually through documents; (2) searching individual documents one at a time with word processing programs; (3) searching through text fields with query systems primarily designed for structured database information; or (4) develop a text search and retrieval system designed for unstructured information. One example of this is using Occurrence Reporting Processing System (ORPS) and Quality, Environmental, and Safety Tracking (QUEST) documents. DOE

N95-23341# Westinghouse Hanford Co., Richland, WA.
SEARCH HANFORD ACCESSIBLE REPORTS ELECTRONICALLY SYSTEM DESIGN DESCRIPTION, REVISION 1
T. L. Gilomen 1995 45 p
(Contract DE-AC06-87RL-10930)
(DE95-004369; WHC-SD-GN-CSDD-30006-Rev-1) Avail: CASI HC A03/MF A01

The Search Hanford Accessible Records Electronically (SHARE) system was produced by a combined team of personnel from Westinghouse Hanford Company (WHC) Corrective Action Data Systems (CADS) and Information Resource Management (IRM) Information and Scientific Systems (ISS) organizations. The ESQD Text Evaluation and exchange Tool (ETEXT) prototype was used as a basis for the requirements used to support this design/build effort. TOPIC was used to build the SHARE application. TOPIC is a text search and retrieval software product produced by the Verity Corporation. The TOPIC source code is not provided with the product, and the programs cannot be changed. TOPIC can be customized for special requirements. The software is fully documented. Help messages, menu and screen layouts, command edits and options, and internal system design are all described in the TOPIC documentation. This System Design Description (SDD) will not reiterate the TOPIC documentation and design. Instead, it will focus on the SHARE installation of TOPIC. This SDD is designed to assist the SHARE database/infobase administrator (DBA) in maintaining and supporting the application. It assumes that the assigned DBA is knowledgeable in using the TOPIC product, and is also knowledgeable in using a personal computer (PC), Disk Operating System (DOS) commands, and the document WHC-CM-3-10. SHARE is an Impact Level 4 system, and all activities related to SHARE must conform with the WHC-CM-3-10 procedures for an Impact Level 4 system. The Alternatives Analysis will be treated as a level 3-Q document, to allow for reference by potential future projects. DOE

N95-23364*# National Aeronautics and Space Administration, Washington, DC.
NASA UNIVERSITY PROGRAM MANAGEMENT INFORMATION SYSTEM, FY 1994
1994 642 p
(NASA-TM-110345; NAS 1.15:110345) Avail: CASI HC A99/MF A06

The University Program report, Fiscal Year 1994, provides current information and related statistics for 7841 grants/contracts/cooperative agreements active during the reporting period. NASA field centers and certain Headquarters program offices provide funds for those activities in universities which contribute to the mission needs of that particular NASA element. This annual report is one means of documenting the NASA-university relationship, frequently denoted, collectively, as NASA's University Program. Author

N95-23452# International Atomic Energy Agency, Vienna (Austria).
ONLINE NUCLEAR DATA SERVICE
C. L. Dunford and T. W. Burrows (Brookhaven National Lab., Upton, NY.)

Feb. 1994 82 p
(DE94-634268; IAEA-NDS-150(Rev-94/2)) Avail: CASI HC A05/MF A01 (US Sales Only)

The US National Nuclear Data Center and the IAEA Nuclear Data Section offer online computer access through international networks to their nuclear-physics and photo-atomic numeric databases, related bibliographic systems and other related information of interest to basic and applied research and technology. A detailed description of the access procedures, the technical requirements, and the available databases is given. DOE

N95-23453# International Atomic Energy Agency, Vienna (Austria).
INDEX OF NUCLEAR DATA LIBRARIES AVAILABLE FROM THE IAEA NUCLEAR DATA SECTION
H. D. Lemmel Jan. 1994 36 p
(DE94-634271; IAEA-NDS-7(Rev-94/1)) Avail: CASI HC A03/MF A01 (US Sales Only)

This document lists more than 100 nuclear data libraries together with references that give more detailed information about these libraries. The data libraries include neutron cross-sections, resonance parameters, fission-product yields, nuclear structure and decay data, gamma-rays from radionuclides, data of nuclear reactions induced by charged particles or heavy ions, photonuclear data, photoatomic interaction data, and many others, partly with related data processing computer codes. All data and documentation references are available upon request from the IAEA Nuclear Data Section, free of charge on magnetic tape, PC diskettes, or through the online Nuclear Data Information System (NDIS). DOE

N95-23490# Argonne National Lab., IL.
SQUEEZING OUT ALL THE PERFORMANCE: USING INGRES FOR A C(SUP 3)I REPORTING SYSTEM
J. J. Tatar 1994 13 p Presented at the 1994 Ingres World, Chicago, IL, 2-6 Oct. 1994
(Contract W-31-109-eng-38)
(DE95-004591; ANL/DIS/CP-84377; CONF-9410204-2) Avail: CASI HC A03/MF A01

Argonne National Laboratory was tasked with developing a data interface between the Joint Theater Level Simulation (JTLS), a military simulation model, and the Warrior Preparation Center C(sup 3)I reporting system, an Ingres-based application. The problem was to build an application that could take buffered input/output (I/O) from the simulation and trade it for direct I/O into an Ingres database. At the same time, the database could have up to 100 concurrent users through the C(sup 3)I reporting system, making retrievals and generating reports, so lock contention had to be minimized. One advantage was that events did not have to be reported immediately. Rather, delays in data updates were desired to emulate reporting delays that occur in the real world. Because of the massive amount of state information generated by time series simulations, a single interface could not maintain the database. Therefore, the problem was partitioned among several processes. One process separated the stream, and others maintained the database with state data from the simulation. A number of specific features in the application are reviewed that may be of interest to other developers faced with the problem of developing applications that have a large transaction throughput. DOE

N95-23574# Department of Energy, Washington, DC. Assistant Secretary for Human Resources and Administration.
INFORMATION TECHNOLOGY STANDARDS PROCESS GUIDE
Apr. 1994 33 p
(DE95-003967; DOE/HR-0083) Avail: CASI HC A03/MF A01

This document presents a logical and realistic approach to implementation of the Information Technology Standards Program throughout the Department and its management and operating contractors, as described in Department of Energy 1360.3C, Information Technology Standards, dated October 19, 1992. To take better advantage of commercial advances and investments in information technology resources, it is paramount that the Department of Energy move as rapidly as programmatically feasible to an open systems environment. The process revolves around the selection of interface standards in areas such as multi-system and multi-processor interconnects, operating and database management systems, graphics, and security. This new approach will result in reduced production, operation, and maintenance costs, and more effective system integration. The Information Technology Standards Process Guide provides a model that may be tailored to Department of Energy sites. It also assists sites in understanding the Information Technology Standards Program. It is not an architectural description to be used in implementing a corporate information systems environment. DOE

N95-24089# Westinghouse Hanford Co., Richland, WA.
SEARCH HANFORD ACCESSIBLE REPORTS ELECTRONICALLY SYSTEM CONFIGURATION MANAGEMENT PLAN
E. L. White 1995 22 p
(Contract DE-AC06-87RL-10930)
(DE95-004493; WHC-SD-GN-CSCM-30022) Avail: CASI HC A03/MF A01

This Software Configuration Management Plan (SCMP) provides the requirements for control of the Search Hanford Accessible Reports Electronically (SHARE) software and documentation. The SHARE system consists of the TOPIC Text Search and Retrieval software and the programs necessary to extract information from other sources to be placed in SHARE. DOE

N95-24108*# National Aeronautics and Space Administration. Goddard Space Flight Center, Greenbelt, MD.
FOURTH NASA GODDARD CONFERENCE ON MASS STORAGE SYSTEMS AND TECHNOLOGIES
Benjamin Kobler, ed. and P. C. Hariharan, ed. (Systems Engineering and Security, Inc., Greenbelt, MD.) Mar. 1994 387 p Conference held in College Park, MD, 28-30 Mar. 1995
(RTOP 505-00-00)
(NASA-CP-3295; Rept-95B00056; NAS 1.55:3295) Avail: CASI HC A17/MF A04

This report contains copies of all those technical papers received in time for publication just prior to the Fourth Goddard Conference on Mass Storage and Technologies, held March 28-30, 1995, at the University of Maryland, University College Conference Center, in College Park, Maryland. This series of conferences continues to serve as a unique medium for the exchange of information on topics relating to the ingestion and management of substantial amounts of data and the attendant problems involved. This year's discussion topics include new storage technology, stability of recorded media, performance studies, storage system solutions, the National Information infrastructure (Infobahn), the future for storage technology, and lessons learned from various projects. There also will be an update on the IEEE Mass Storage System Reference Model Version 5, on which the final vote was taken in July 1994. For individual titles, see N95-24109 through N95-24139.

N95-24109*# Massachusetts Inst. of Tech., Minneapolis, MN. Research Program on Communications Policy.
APPLICATIONS DRIVERS FOR DATA PARKING ON THE INFORMATION SUPERHIGHWAY
Clark E. Johnson, Jr. and Thomas Foeller (Configured Health Care, Inc., Balsam Lake, WI.) *In* NASA. Goddard Space Flight Center, Fourth NASA Goddard Conference on Mass Storage Systems and Technologies Mar. 1994 p 1-5 (For primary document see N95-24108 07-82)
Avail: CASI HC A01/MF A04

As the cost of data storage continues to decline (currently about one-millionth of its cost four decades ago) entirely new applications areas become economically feasible. Many of these new areas involved the extraordinarily high data rates and universal connectivity soon to be provided by the National Information Infrastructure (NII). The commonly held belief is that the main driver for the NII will be entertainment applications. We believe that entertainment applications as currently touted (multi-media, 500 video channels, video-on-demand, etc.) will play an important but far from dominant role in the development of the NII and its data storage components. The most pervasively effective drivers will be medical applications such as telemedicine and remote diagnosis, education and environmental monitoring. These applications have a significant funding base and offer a clearly perceived opportunity to improve the nation's standard of living. The NII's wideband connectivity both nationwide and worldwide requires a broad spectrum of data storage devices with a wide-range of performance capabilities. These storage centers will be dispersed throughout the system. Magnetic recording devices will fill the majority of these new data storage requirements for at least the rest of

this century. The storage needs of various application areas and their respective market sizes will be explored. The comparative performance of various magnetic technologies and competitive alternative storage systems will be discussed. Author

N95-24110*# Loral AeroSys, Landover, MD.
THE DESIGN OF A PETABYTE ARCHIVE AND DISTRIBUTION SYSTEM FOR THE NASA ECS PROJECT
Parris M. Caulk *In* NASA. Goddard Space Flight Center, Fourth NASA Goddard Conference on Mass Storage Systems and Technologies Mar. 1994 p 7-17 (For primary document see N95-24108 07-82)
Avail: CASI HC A03/MF A04

The NASA EOS Data and Information System (EOSDIS) Core System (ECS) will contain one of the largest data management systems ever built - the ECS Science and Data Processing System (SDPS). SDPS is designed to support long term Global Change Research by acquiring, producing, and storing earth science data, and by providing efficient means for accessing and manipulating that data. The first two releases of SDPS, Release A and Release B, will be operational in 1997 and 1998, respectively. Release B will be deployed at eight Distributed Active Archiving Centers (DAAC's). Individual DAAC's will archive different collections of earth science data, and will vary in archive capacity. The storage and management of these data collections is the responsibility of the SDPS Data Server subsystem. It is anticipated that by the year 2001, the Data Server subsystem at the Goddard DAAC must support a near-line data storage capacity of one petabyte. The development of SDPS is a system integration effort in which COTS products will be used in favor of custom components in very possible way. Some software and hardware capabilities required to meet ECS data volume and storage management requirements beyond 1999 are not yet supported by available COTS products. The ECS project will not undertake major custom development efforts to provide these capabilities. Instead, SDPS and its Data Server subsystem are designed to support initial implementations with current products, and provide an evolutionary framework that facilitates the introduction of advanced COTS products as they become available. This paper provides a high-level description of the Data Server subsystem design from a COTS integration standpoint, and discussed some of the major issues driving the design. The paper focuses on features of the design that will make the system scalable and adaptable to changing technologies. Author

N95-24111*# California Univ., Berkeley. Lawrence Berkeley Lab, CA.
A DISTRIBUTED PARALLEL STORAGE ARCHITECTURE AND ITS POTENTIAL APPLICATION WITHIN EOSDIS
William E. Johnston, Brian Tierney, Jay Feuquay (Hughes STX Corp., Sioux Falls, SD.), and Tony Butzer (Hughes STX Corp., Sioux Falls, SD.) *In* NASA. Goddard Space Flight Center, Fourth NASA Goddard Conference on Mass Storage Systems and Technologies Mar. 1994 p 19-33 Sponsored by ARPA (For primary document see N95-24108 07-82)
(Contract DE-AC03-76SF-00098)
Avail: CASI HC A03/MF A04

We describe the architecture, implementation, use of a scalable, high performance, distributed-parallel data storage system developed in the ARPA funded MAGIC gigabit testbed. A collection of wide area distributed disk servers operate in parallel to provide logical block level access to large data sets. Operated primarily as a network-based cache, the architecture supports cooperation among independently owned resources to provide fast, large-scale, on-demand storage to support data handling, simulation, and computation. Author

N95-24112*# Department of Defense, Fort Meade, MD.
ROBOTIC TAPE LIBRARY SYSTEM LEVEL TESTING AT NSA: PRESENT AND PLANNED
Michael F. Shields *In* NASA. Goddard Space Flight Center, Fourth NASA Goddard Conference on Mass Storage Systems and Technologies Mar. 1994 p 35-44 (For primary document see N95-24108 07-82)
Avail: CASI HC A02/MF A04

In the present of declining Defense budgets, increased pressure has been placed on the DOD to utilize Commercial Off the Shelf (COTS) solutions to incrementally solve a wide variety of our computer processing requirements. With the rapid growth in processing power, significant expansion of high performance networking, and the increased complexity of applications data sets, the requirement for high performance, large capacity, reliable and secure, and most of all affordable robotic tape storage libraries has greatly increased. Additionally, the migration to a heterogeneous, distributed computing environment has further complicated the problem. With today's open system compute servers approaching yesterday's supercomputer capabilities, the need for affordable, reliable secure Mass Storage Systems (MSS) has taken on an ever increasing importance to our processing center's ability to satisfy operational mission requirements. To that end, NSA has established an in-house capability to acquire, test, and evaluate COTS products. Its goal is to qualify a set of COTS MSS libraries, thereby achieving a modicum of standardization for robotic tape libraries which can satisfy our low, medium, and high performance file and volume serving requirements. In addition, NSA has established relations with other Government Agencies to complete this in-house effort and to maximize our research, testing, and evaluation work. While the preponderance of the effort is focused at the high end of the storage ladder, considerable effort will be extended this year and next at the server class or mid range storage systems. Author

N95-24113*# IBM Federal Systems Div., Houston, TX.
THE ARCHITECTURE OF THE HIGH PERFORMANCE STORAGE SYSTEM (HPSS)
Danny Teaff, Dick Watson (Lawrence Livermore National Lab., Livermore, CA.), and Bob Coyne *In* NASA. Goddard Space Flight Center, Fourth NASA Goddard Conference on Mass Storage Systems and Technologies Mar. 1994 p 45-73 Sponsored by DOE (For primary document see N95-24108 07-82)
Avail: CASI HC A03/MF A04

The rapid growth in the size of datasets has caused a serious imbalance in I/O and storage system performance and functionality relative to application requirements and the capabilities of other system components. The High Performance Storage System (HPSS) is a scalable, next-generation storage system that will meet the functionality and performance requirements or large-scale scientific and commercial computing environments. Our goal is to improve the performance and capacity of storage by two orders of magnitude or more over what is available in the general or mass marketplace today. We are also providing corresponding improvements in architecture and functionality. This paper describes the architecture and functionality of HPSS. Author

N95-24114*# Minnesota Univ., Minneapolis, MN. Graphics and Visualization Lab.
A 500 MEGABYTE/SECOND DISK ARRAY **c60**
Thomas M. Ruwart and Matthew T. OKeefe *In* NASA. Goddard Space Flight Center, Fourth NASA Goddard Conference on Mass Storage Systems and Technologies Mar. 1994 p 75-90 Sponsored by Army (For primary document see N95-24108 07-82)
(Contract USRA-C-5555-23)
Avail: CASI HC A03/MF A04

Applications at the Army High Performance Computing Research Center's (AHPCRC) Graphic and Visualization Laboratory (GVL) at the University of Minnesota require a tremendous amount of I/O bandwidth and this appetite for data is growing. Silicon Graphics workstations are used to perform the post-processing, visualization, and animation of multi-terabyte size datasets produced by scientific simulations performed of AHPCRC supercomputers. The M.A.X. (Maximum Achievable Xfer) was designed to find the maximum achievable I/O performance of the Silicon Graphics CHALLENGE/Onyx-class machines that run these applications. Running a fully configured Onyx machine with 12-150MHz R4400 processors, 512MB of 8-way interleaved memory, 31 fast/wide SCSI-2 channel each with a Ciprico disk array controller we were able to achieve a maximum sustained transfer rate of 509.8 megabytes per second. However, after analyzing the results it became clear that the true maximum transfer rate is somewhat beyond this figure and we will need to do further testing with more disk array controllers in order to find the true maximum. Author

N95-24115*# Data Storage Technologies, Inc., Ridgewood, NJ.
NEW ARCHITECTURAL PARADIGMS FOR MULTI-PETABYTE DISTRIBUTED STORAGE SYSTEMS
Richard R. Lee *In* NASA. Goddard Space Flight Center, Fourth NASA Goddard Conference on Mass Storage Systems and Technologies Mar. 1994 p 91-98 (For primary document see N95-24108 07-82)
Avail: CASI HC A02/MF A04

In the not too distant future, programs such as NASA's Earth Observing System, NSF/ARPA/NASA's Digital Libraries Initiative and Intelligence Community's (NSA, CIA, NRO, etc.) mass storage system upgrades will all require multi-petabyte (petabyte: 1015 bytes of bitfile data) (or larger) distributed storage solutions. None of these requirements, as currently defined, will meet their objectives utilizing either today's architectural paradigms or storage solutions. Radically new approaches will be required to not only store and manage veritable 'mountain ranges of data', but to make the cost of ownership affordable, much less practical in today's (and certainly the future's) austere budget environment! Within this paper we will explore new architectural paradigms and project systems performance benefits and dollars per petabyte of information stored. We will discuss essential 'top down' approaches to achieving an overall systems level performance capability sufficient to meet the challenges of these major programs. Author (revised)

N95-24116*# Mega Drive Systems, Inc., Beverly Hills, CA.
OPTIMIZING RAID PERFORMANCE WITH CACHE **c61**
Alex Bouzari *In* NASA. Goddard Space Flight Center, Fourth NASA Goddard Conference on Mass Storage Systems and Technologies Mar. 1994 p 99-103 (For primary document see N95-24108 07-82)
Avail: CASI HC A01/MF A04

We live in a world of increasingly complex applications and operating systems. Information is increasing at a mind-boggling rate. The consolidation of text, voice, and imaging represents an even greater challenge for our information systems. Which forced us to address three important questions: Where do we store all this information? How do we access it? And, how do we protect it against the threat of loss or damage? Introduced in the 1980s, RAID (Redundant Arrays of Independent Disks) represents a cost-effective solution to the needs of the information age. While fulfilling expectations for high storage, and reliability, RAID is sometimes subject to criticisms in the area of performance. However, there are design elements that can significantly enhance performance. They can be subdivided into two areas: (1) RAID levels or basic architecture. And, (2) enhancement schemes such as intelligent caching, support of tagged command queuing, and use of SCSI-2 Fast and Wide features. Derived from text

N95-24117*# National Library of Medicine, Bethesda, MD. National Center for Biomedical Communications.
DOCUMENT IMAGE ARCHIVE TRANSFER FROM DOS TO UNIX **c61**
Susan E. Hauser, Michael J. Gill, and George R. Thoma *In* NASA. Goddard Space Flight Center, Fourth NASA Goddard Conference on Mass Storage Systems and Technologies Mar. 1994 p 105-113 (For primary document see N95-24108 07-82)
Avail: CASI HC A02/MF A04

An R&D division of the National Library of Medicine has developed a prototype system for automated document image delivery as an adjunct to the labor-intensive manual interlibrary loan service of the library. The document image archive is implemented by a PC controlled bank of optical disk drives which use 12 inch WORM platters containing bitmapped images of over 200,000 pages of medical journals. Following three years of routine operation which resulted in serving patrons with articles both by mail and fax, an effort is underway to relocate the storage environment from the DOS-based system to a UNIX-based jukebox whose magneto-optical erasable 5 1/4 inch platters hold the images. This paper describes the deficiencies of the current storage system, the design issues of modifying several modules in the system, the alternatives proposed and the tradeoffs involved. Author

N95-24118*# Massachusetts Inst. of Tech., Westford, MA. Haystack Observatory.
HIGH DATA RATE RECORDER DEVELOPMENT AT MIT HAYSTACK OBSERVATORY **c35**
H. F. Hinteregger *In* NASA. Goddard Space Flight Center, Fourth NASA Goddard Conference on Mass Storage Systems and Technologies Mar. 1994 p 115-121 (For primary document see N95-24108 07-82)
Avail: CASI HC A02/MF A04

Current operational capabilities of tape recording for Very Long Baseline Interferometry (VLBI) at the Haystack Observatory allow 0.7 terabytes (12 hours at 128 Mb/s) of data to be stored in a 128 cu. inch volume. On-going efforts are aimed at full time 1 Gb/s operation with two 36-channel headstacks. Applications for linear digital tape recording, with suitable development of thin-film head arrays, suggest a volume density exceeding 1 TB/cu. inch to be achievable in the future. Author

N95-24119*# Primelink Technologies, Inc., Edmonton (Alberta).
PETABYTE MASS MEMORY SYSTEM USING THE NEWELL OPTICEL(TM) **c60**
Chester W. Newell *In* NASA. Goddard Space Flight Center, Fourth NASA Goddard Conference on Mass Storage Systems and Tecnologies Mar. 1994 p 123-136 (For primary document see N95-24108 07-82)
Avail: CASI HC A03/MF A04

A random access system is proposed for digital storage and retrieval of up to a Petabyte of user data. The system is comprised of stacked memory modules using laser heads writing to an optical medium, in a new shirt-pocket-sized optical storage device called the Opticel. The Opticel described is a completely sealed 'black box' in which an optical medium is accelerated and driven at very high rates to accommodate the desired transfer rates, yet in such a manner that wear is virtually eliminated. It essentially emulates a disk, but with storage area up to several orders of magnitude higher. Access time to the first bit can range from a few milliseconds to a fraction of a second, with time to the last bit within a fraction of a second to a few seconds. The actual times are dependent on the capacity of each Opticel, which ranges from 72 Gigabytes to 1.25 Terabytes. Data transfer rate is limited strictly by the head and electronics, and is 15 Megabits per second in the first version. Independent parallel write/read access to each Opticel is provided using dedicated drives and heads. A Petabyte based on the present Opticel and drive design would occupy 120 cubic feet on a footprint of 45 square feet; with further development, it could occupy as little as 9 cubic feet. Author

N95-24120*# CONVEX Computer Corp., Richardson, TX.
INTEGRATING UniTree WITH THE DATA MIGRATION API **c61**
David G. Schrodel *In* NASA. Goddard Space Flight Center, Fourth NASA Goddard Conference on Mass Storage Systems and Technologies Mar. 1994 p 137-155 (For primary document see N95-24108 07-82)
Avail: CASI HC A03/MF A04

The Data Migration Application Programming Interface (DMAPI) has the potential to allow developers of open systems Hierarchical Storage Management (HSM) products to virtualize native file systems without the requirement to make changes to the underlying operating system. This paper describes advantages of virtualizing native file systems in hierarchical storage management systems, the DMAPI at a high level, what the goals are for the interface, and the integration of the Convex UniTree+HSM with DMAPI along with some of the benefits derived in the resulting product. Author

N95-24121*# National Aeronautics and Space Administration. Goddard Space Flight Center, Greenbelt, MD.
CONSTRAINT BASED SCHEDULING FOR THE GODDARD SPACE FLIGHT CENTER DISTRIBUTED ACTIVE ARCHIVE CENTER'S DATA ARCHIVE AND DISTRIBUTION SYSTEM
Nick Short, Jr., Jean-Jacques Bedet (Hughes STX, Inc., Greenbelt, MD.), Lee Bodden (Hughes STX, Inc., Greenbelt, MD.), Mark Boddy (Honeywell Technology Center, Minneapolis, MN.), Jim White (Honeywell Technology Center, Minneapolis, MN.), and John Beane (Honeywell Technology Center, Minneapolis, MN.) *In its* Fourth NASA Goddard Conference on Mass Storage Systems and Technologies Mar. 1994 p 157-175 Sponsored by NASA, Washington (For primary document see N95-24108 07-82)
Avail: CASI HC A03/MF A04

The Goddard Space Flight Center (GSFC) Distributed Active Archive Center (DAAC) has been operational since October 1, 1993. Its mission is to support the Earth Observing System (EOS) by providing rapid access to EOS data and analysis products, and to test Earth Observing System Data and Information System (EOSDIS) design concepts. One of the challenges is to ensure quick and easy retrieval of any data archived within the DAAC's Data Archive and Distributed System (DADS). Over the 15-year life of EOS project, an estimated several Petabytes (10(exp 15)) of data will be permanently stored. Accessing that amount of information is a formidable task that will require innovative approaches. As a precursor of the full EOS system, the GSFC DAAC with a few Terabits of storage, has implemented a prototype of a constraint-based task and resource scheduler to improve the performance of the DADS. This Honeywell Task and Resource

Scheduler (HTRS), developed by Honeywell Technology Center in cooperation the Information Science and Technology Branch/935, the Code X Operations Technology Program, and the GSFC DAAC, makes better use of limited resources, prevents backlog of data, provides information about resources bottlenecks and performance characteristics. The prototype which is developed concurrently with the GSFC Version 0 (V0) DADS, models DADS activities such as ingestion and distribution with priority, precedence, resource requirements (disk and network bandwidth) and temporal constraints. HTRS supports schedule updates, insertions, and retrieval of task information via an Application Program Interface (API). The prototype has demonstrated with a few examples, the substantial advantages of using HTRS over scheduling algorithms such as a First In First Out (FIFO) queue. The kernel scheduling engine for HTRS, called Kronos, has been successfully applied to several other domains such as space shuttle mission scheduling, demand flow manufacturing, and avionics communications scheduling. Author

N95-24122*# Run Length Ltd., Burghfield (England).
A COMPARISON OF ROTARY- AND STATIONARY-HEAD TAPE RECORDERS **c35**
John R. Watkinson *In* NASA. Goddard Space Flight Center, Fourth NASA Goddard Conference on Mass Storage Systems and Technologies Mar. 1994 p 177-183 (For primary document see N95-24108 07-82)
Avail: CASI HC A02/MF A04

Digital recording may take advantage of many types of media, but usually a preferred type of drive or transport emerges for each. In magnetic tape recording, two approaches have emerged in which essentially the same medium is tracked in two radically different ways. This paper compares the characteristics of Rotary- and Stationary-Head transports in an attempt to establish which approach might be considered for a given application. The conclusion is that in many cases there is no obvious choice based on recording physics and that often the choice will be made on the experimental knowledge of the designer. Author

N95-24123*# Maximum Strategy, Inc., Milpitas, CA.
CLIENT/SERVER DATA SERVING FOR HIGH PERFORMANCE COMPUTING **c61**
Chris Wood *In* NASA. Goddard Space Flight Center, Fourth NASA Goddard Conference on Mass Storage Systems and Technologies Mar. 1994 p 185-201 (For primary document see N95-24108 07-82)
Avail: CASI HC A03/MF A04

This paper will attempt to examine the industry requirements for shared network data storage and sustained high speed (10's to 100's to thousands of megabytes per second) network data serving via the NFS and FTP protocol suite. It will discuss the current structural and architectural impediments to achieving these sorts of data rates cost effectively today on many general purpose servers and will describe and architecture and resulting product family that addresses these problems. The sustained performance levels that were achieved in the lab will be shown as well as a discussion of early customer experiences utilizing both the HIPPI-IP and ATM OC3-IP network interfaces. Author

N95-24124*# Sony Corp., Tagajyo (Japan).
A KINETIC STUDY OF HYDROLYSIS OF POLYESTER ELASTOMER IN MAGNETIC TAPE **c27**
K. Yamamoto and H. Watanabe *In* NASA. Goddard Space Flight Center, Fourth NASA Goddard Conference on Mass Storage Systems and Technologies 203-210 (SEE N95-24108 07-82) Mar. 1994 (For primary document see N95-24108 07-82)
Avail: CASI HC A02/MF A04

A useful method for kinetic study of the hydrolysis of polyester elastomer is established which uses the number-average molecular weight. The reasonableness of this method is confirmed and the effect of magnetic particles on hydrolysis is considered. Author

N95-24125*# Quantum Corp., Shrewbury, MA.
DIGITAL LINEAR TAPE (DLT) TECHNOLOGY AND PRODUCT FAMILY OVERVIEW **c60**
Demetrios Lignos *In* NASA. Goddard Space Flight Center, Fourth NASA Goddard Conference on Mass Storage Systems and Technologies Mar. 1994 p 211-231 (For primary document see N95-24108 07-82)
Avail: CASI HC A03/MF A04

The demand that began a couple of years ago for increased data storage capacity continues. Peripheral Strategies (a Santa Barbara, California, Storage Market Research Firm) projects the amount of data stored on the average enterprise network will grow by 50 percent to 100 percent per year. Furthermore, Peripheral Strategies says that a typical mid-range workstation system containing 30GB to 50GB of storage today will grow at the rate of 50 percent per year. Dan Friedlander, a Boulder, Colorado-based consultant specializing in PC-LAN backup, says, 'The average NetWare LAN is about 8GB, but there are many that have 30GB to 300GB.....' The substantial growth of storage requirements has created various tape technologies that seek to satisfy the needs of today's and, especially, the next generations's systems and applications. There are five leading tape technologies in the market today: QIC (Quarter Inch Cartridge), IBM 3480/90, 8mm, DAT (Digital Audio Tape) and DLT (Digital Linear Tape). Product performance specifications and user needs have combined to classify these technologies into low-end, mid-range, and high-end systems applications. Although the manufacturers may try to position their products differently, product specifications and market requirements have determined that QIC and DAT are primarily low-end systems products while 8mm and DLT are competing for mid-range systems applications and the high-end systems space, where IBM compatibility is not required. The 3480/90 products seem to be used primarily in the IBM market, for interchangeability purposes. There are advantages and disadvantages for each of the tape technologies in the market today. We believe that DLT technology offers a significant number of very important features and specifications that make it extremely attractive for most current as well as emerging new applications, such as Hierarchical Storage Management (HSM). This paper will demonstrate why we think that the DLT technology and family of DLT products will become the technology of choice for most new applications in the mid-range and high-end (non-IBM) markets. Author

N95-24126*# Exabyte Corp., Boulder, CO.
THE MAMMOTH PROJECT **c60**
Tim Gerchar *In* NASA. Goddard Space Flight Center, Fourth NASA Goddard Conference on Mass Storage Systems and Technologies Mar. 1994 p 233-236 (For primary document see N95-24108 07-82)
Avail: CASI HC A01/MF A04

On the surface MAMMOTH is a high performance 5.25-inch half-high 8mm helical scan tape drive that records a native 20 Gigabytes of data on Advanced Metal Evaporated media at a sustained throughput of 3 Megabyte per second over a high speed SCSI interface, that is scheduled for production in the second half of 1995. But it's much more than that. Inside its custom designed sheet metal enclosure lies one of the greatest technical achievements of its kind. Exabyte's strategic direction is to increase throughput and capacity while continuing to improve drive, data and media reliability to its products. MAMMOTH adheres to that direction and the description of its technical advances is described in this paper. MAMMOTH can be broken down into four main functional assemblies: high-performance integrated digital electronics, high-reliability tape transport mechanism, high-performance scanner, and advanced metal evaporated media. All this technology is packaged into a standard 5.25-inch half-high form factor that dissipates only 15 watts. Author

N95-24127*# International Business Machines Corp., Tucson, AZ.
INFLUENCE OF TECHNOLOGY ON MAGNETIC TAPE STORAGE DEVICE CHARACTERISTICS **c35**
John J. Gniewek and Stephen M. Vogel *In* NASA. Goddard Space Flight Center, Fourth NASA Goddard Conference on Mass Storage Systems and Technologies Mar. 1994 p 237-251 (For primary document see N95-24108 07-82)
Avail: CASI HC A03/MF A04

There are available today many data storage devices that serve the diverse application requirements of the consumer, professional entertainment, and computer data processing industries. Storage technologies include semiconductors, several varieties of optical disk, optical tape, magnetic disk, and many varieties of magnetic tape. In some cases, devices are developed with specific characteristics to meet specification requirements. In other cases, an existing storage device is modified and adapted to a different application. For magnetic tape storage devices, examples of the former case are 3480/3490 and QIC device types developed for the high end and low end segments of the data processing industry respectively, VHS, Beta, and 8 mm formats developed for consumer video applications,

and D-1, D-2, D-3 formats developed for professional video applications. Examples of modified and adapted devices include 4 mm, 8 mm, 12.7 mm and 19 mm computer data storage devices derived from consumer and professional audio and video applications. With the conversion of the consumer and professional entertainment industries from analog to digital storage and signal processing, there have been increasing references to the 'convergence' of the computer data processing and entertainment industry technologies. There has yet to be seen, however, any evidence of convergence of data storage device types. There are several reasons for this. The diversity of application requirements results in varying degrees of importance for each of the tape storage characteristics. Author

N95-24128*# Carnegie-Mellon Univ., Pittsburgh, PA. Engineering Research Center and Data Storage Systems.

APPROACHES TO 100 Gbit/SQ. IN. RECORDING DENSITY **c35**

Mark H. Kryder *In* NASA. Goddard Space Flight Center, Fourth NASA Goddard Conference on Mass Storage Systems and Technologies Mar. 1994 p 253-254 (For primary document see N95-24108 07-82)

Avail: CASI HC A01/MF A04

A recording density of 10 Gbit/sq. in. is being pursued by a number of companies and universities in the National Storage Industry Consortium. It is widely accepted that this goal will be achieved in the laboratory within a few years. In this paper approaches to achieving 100 Gbit/sq. in. storage densities are considered. A major obstacle to continued scaling of magnetic recording to higher densities is that as the bit size is reduced, the grain size in the magnetic media must be reduced in order that media noise does not become so large that the signal to noise ratio (SNR) degrades sufficiently to make detection impossible. At 100 Gbit/sq. in., the bit size is only 0.006 square micrometers, which, in order to achieve 30 dB SNR, requires a grain size of about 2.5 nm. Such small grains are subject to thermal instability, and the recorded information will degrade over time unless the magnetic anisotropy of the materials used is increased significantly, or the media thickness is made much larger than expected on the basis of scaling today's longitudinal media thickness. Author

N95-24129*# Carnegie-Mellon Univ., Pittsburgh, PA. Dept. of Chemical Engineering.

REPRODUCIBLE DIRECT EXPOSURE ENVIRONMENTAL TESTING OF METAL-BASED MAGNETIC MEDIA **c35**

Paul J. Sides *In* NASA. Goddard Space Flight Center, Fourth NASA Goddard Conference on Mass Storage Systems and Technologies Mar. 1994 p 255-264 (For primary document see N95-24108 07-82)

Avail: CASI HC A02/MF A04

A flow geometry and flow rate for mixed flowing gas testing is proposed. Use of an impinging jet of humid polluted air can provide a uniform and reproducible exposure of coupons of metal-based magnetic media. Numerical analysis of the fluid flow and mass transfer in such as system has shown that samples confined within a distance equal to the nozzle radius on the surface of impingement are uniformly accessible to pollutants in the impinging gas phase. The critical factor is the nozzle height above the surface of impingement. In particular, the uniformity of exposure is less than plus/minus 2% for a volumetric flow rate of 1600 cm(exp 3)/minute total flow with the following specifications: For a one inch nozzle, the height of the nozzle opening above the stage should be 0.177 inches; for a 2 inch nozzle - 0.390 inches. Not only is the distribution uniform, but one can calculate the maximum delivery rate of pollutants to the samples for comparison with the observed deterioration. Author

N95-24130*# National Inst. of Standards and Technology, Gaithersburg, MD.

OPTICAL STORAGE MEDIA DATA INTEGRITY STUDIES **c74**

Fernando L. Podio *In* NASA. Goddard Space Flight Center, Fourth NASA Goddard Conference on Mass Storage Systems and Technologies Mar. 1994 p 265-276 (For primary document see N95-24108 07-82)

Avail: CASI HC A03/MF A04

Optical disk-based information systems are being used in private industry and many Federal Government agencies for on-line and long-term storage of large quantities of data. The storage devices that are part of these systems are designed with powerful, but not unlimited, media error correction capacities. The integrity of data stored on optical disks does not only depend on the life expectancy specifications for the medium. Different factors, including handling and storage conditions, may result in an increase of medium errors in size and frequency. Monitoring the potential data degradation is crucial, especially for long term applications. Efforts are being made by the Association for Information and Image Management Technical Committee C21, Storage Devices and Applications, to specify methods for monitoring and reporting to the user medium errors detected by the storage device while writing, reading or verifying the data stored in that medium. The Computer Systems Laboratory (CSL) of the National Institute of Standard and Technology (NIST) has a leadership role in the development of these standard techniques. In addition, CSL is researching other data integrity issues, including the investigation of error-resilient compression algorithms. NIST has conducted care and handling experiments on optical disk media with the objective of identifying possible causes of degradation. NIST work in data integrity and related standards activities is described. Author

N95-24131*# California Univ., Berkeley. Lawrence Berkeley Lab, CA.

OPTIMIZING TERTIARY STORAGE ORGANIZATION AND ACCESS FOR SPATIO-TEMPORAL DATASETS

Ling Tony Chen, Doron Rotem, Arie Shoshani, Bob Drach (Lawrence Livermore National Lab., Livermore, CA.), Steve Louis (Lawrence Livermore National Lab., Livermore, CA.), and Meridith Keating (Lawrence Livermore National Lab., Livermore, CA.) *In* NASA. Goddard Space Flight Center, Fourth NASA Goddard Conference on Mass Storage Systems and Technologies Mar. 1994 p 277-302 (For primary document see N95-24108 07-82)

(Contracts W-7405-eng-48; DE-AC03-76SF-00098)

Avail: CASI HC A03/MF A04

We address in this paper data management techniques for efficiently retrieving requested subsets of large datasets stored on mass storage devices. This problem represents a major bottleneck that can negate the benefits of fast networks, because the time to access a subset from a large dataset stored on a mass storage system is much greater that the time to transmit that subset over a network. This paper focuses on very large spatial and temporal datasets generated by simulation programs in the area of climate modeling, but the techniques developed can be applied to other applications that deal with large multidimensional datasets. The main requirement we have addressed is the efficient access of subsets of information contained within much larger datasets, for the purpose of analysis and interactive visualization. We have developed data partitioning techniques that partition datasets into 'clusters' based on analysis of data access patterns and storage device characteristics. The goal is to minimize the number of clusters read from mass storage systems when subsets are requested. We emphasize in this paper proposed enhancements to current storage server protocols to permit control over physical placement of data on storage devices. We also discuss in some detail the aspects of the interface between the application programs and the mass storage system, as well as a workbench to help scientists to design the best reorganization of a dataset for anticipated access patterns. Author

N95-24132*# Federal Data Corp., Bethesda, MD.

BUILDING A COTS ARCHIVE FOR SATELLITE DATA

Ken Singer, Dave Terril, Jack Kelly (L.A. Systems, Alexandria, VA.), and Cathy Nichols (National Environmental Satellite Service, Suitland, MD.) *In* NASA. Goddard Space Flight Center, Fourth NASA Goddard Conference on Mass Storage Systems and Technologies Mar. 1994 p 303-309 (For primary document see N95-24108 07-82)

Avail: CASI HC A02/MF A04

The goal of the NOAA/NESDIS Active Archive was to provide a method of access to an online archive of satellite data. The archive had to manage and store the data, let users interrogate the archive, and allow users to retrieve data from the archive. Practical issues of the system design such as implementation time, cost and operational support were examined in addition to the technical issues. There was a fixed window of opportunity to create an operational system, along with budget and staffing constraints. Therefore, the technical solution had to be designed and implemented subject to constraint imposed by the practical issues. The NOAA/NESDIS Active Archive came online in July of 1994, meeting all of its original objectives. Author

N95-24133*# Alaska Univ., Fairbanks, AK. SAR Facility.

ASF ARCHIVE ISSUES: CURRENT STATUS, PAST HISTORY, AND QUESTIONS FOR THE FUTURE

Crystal A. Goula and Carl Wales *In* NASA. Goddard Space Flight Center, Fourth NASA Goddard Conference on Mass Storage Systems and Technologies Mar. 1994 p 311-322 (For primary document see N95-24108 07-82)
Avail: CASI HC A03/MF A04

The Alaska SAR Facility (ASF) collects, processes, archives, and distributes data from synthetic aperture radar (SAR) satellites in support of scientific research. ASF has been in operation since 1991 and presently has an archive of over 100 terabytes of data. ASF is performing an analysis of its magnetic tape storage system to ensure long-term preservation of this archive. Future satellite missions have the possibility of doubling to tripling the amounts of data that ASF acquires. ASF is examining the current data systems and the high volume storage, and exploring future concerns and solutions. Author

N95-24134*# National Aeronautics and Space Administration. Goddard Space Flight Center, Greenbelt, MD.
ARCHITECTURE AND EVOLUTION OF GODDARD SPACE FLIGHT CENTER DISTRIBUTED ACTIVE ARCHIVE CENTER
Jean-Jacques Bedet (Hughes STX, Inc., Greenbelt, MD.), Lee Bodden (Hughes STX, Inc., Greenbelt, MD.), Wayne Rosen (Hughes STX, Inc., Greenbelt, MD.), Mark Sherman (Hughes STX, Inc., Greenbelt, MD.), and Phil Pease *In its* Fourth NASA Goddard Conference on Mass Storage Systems and Technologies Mar. 1994 p 323-343 (For primary document see N95-24108 07-82)
Avail: CASI HC A03/MF A04

The Goddard Space Flight Center (GSFC) Distributed Active Archive Center (DAAC) has been developed to enhance Earth Science research by improved access to remote sensor earth science data. Building and operating an archive, even one of a moderate size (a few Terabytes), is a challenging task. One of the critical components of this system is Unitree, the Hierarchical File Storage Management System. Unitree, selected two years ago as the best available solution, requires constant system administrative support. It is not always suitable as an archive and distribution data center, and has moderate performance. The Data Archive and Distribution System (DADS) software developed to monitor, manage, and automate the ingestion, archive, and distribution functions turned out to be more challenging than anticipated. Having the software and tools is not sufficient to succeed. Human interaction within the system must be fully understood to improve efficiency to improve efficiency and ensure that the right tools are developed. One of the lessons learned is that the operability, reliability, and performance aspects should be thoroughly addressed in the initial design. However, the GSFC DAAC has demonstrated that it is capable of distributing over 40 GB per day. A backup system to archive a second copy of all data ingested is under development. This backup system will be used not only for disaster recovery but will also replace the main archive when it is unavailable during maintenance or hardware replacement. The GSFC DAAC has put a strong emphasis on quality at all level of its organization. A Quality team has also been formed to identify quality issues and to propose improvements. The DAAC has conducted numerous tests to benchmark the performance of the system. These tests proved to be extremely useful in identifying bottlenecks and deficiencies in operational procedures. Author

N95-24135*# National Aeronautics and Space Administration. Goddard Space Flight Center, Greenbelt, MD.
THE GROWTH OF THE UniTree MASS STORAGE SYSTEM AT THE NASA CENTER FOR COMPUTATIONAL SCIENCES: SOME LESSONS LEARNED
Adina Tarshish and Ellen Salmon *In its* Fourth NASA Goddard Conference on Mass Storage Systems and Technologies Mar. 1994 p 345-357 (For primary document see N95-24108 07-82)
Avail: CASI HC A03/MF A04

In October 1992, the NASA Center for Computational Sciences made its Convex-based UniTree system generally available to users. The ensuing months saw growth in every area. Within 26 months, data under UniTree control grew from nil to over 12 terabytes, nearly all of it stored on robotically mounted tape. HiPPI/UltraNet was added to enhance connectivity, and later HiPPI/TCP was added as well. Disks and robotic tape silos were added to those already under UniTree's control, and 18-track tapes were upgraded to 36-track. The primary data source for UniTree, the facility's Cray Y-MP/4-128, first doubled its processing power and then was replaced altogether by a C98/6-256 with nearly two-and-a-half times the Y-MP's combined peak gigaflops. The Convex/UniTree software was upgraded from version 1.5 to 1.7.5, and then to 1.7.6. Finally, the server itself, a Convex C3240, was upgraded to a C3830 with a second I/O bay, doubling the C3240's memory and capacity for I/O. This paper describes insights gained and reinforced with the burgeoning demands on the UniTree storage system and the significant increases in performance gained from the many upgrades. Author

N95-24136*# National Aeronautics and Space Administration. Goddard Space Flight Center, Greenbelt, MD.
NSSDC PROVIDES NETWORK ACCESS TO KEY DATA VIA NDADS
Jeanne Behnke and Joseph King *In its* Fourth NASA Goddard Conference on Mass Storage Systems and Technologies Mar. 1994 p 359-365 (For primary document see N95-24108 07-82)
Avail: CASI HC A02/MF A04

The National Space Science Data Center (NSSDC) is making a growing fraction of its most customer-desirable data electronically accessible via both the local and wide area networks. NSSDC is witnessing a great increase in its data dissemination owing to this network accessibility. To provide its customers the best data accessibility, the NSSDC makes data available from a nearline, mass storage system, the NSSDC Data Archive and Dissemination Service (NDADS). The NDADS, the initial version was made available in January 1992, is a customized system of hardware and software that provides users access to the nearline data via ANONYMOUS FTP, an e-mail interface (ARMS), and a C-based software library. In January 1992, the NDADS registered 416 requests for 1,957 files. By December of 1994, NDADS had been populated with 800 gigabytes of electronically accessible data and had registered 1458 requests for 20,887 files. In this report we describe the NDADS system, both hardware and software. Later in the report, we discuss some of the lessons that were learned as a result of operating NDADS, particularly in the area of ingest and dissemination. Author

N95-24137*# Florida Univ., Gainesville, FL. Dept. of CIS.
ANALYSIS OF THE REQUEST PATTERNS TO THE NSSDC ON-LINE ARCHIVE
Theodore Johnson *In* NASA. Goddard Space Flight Center, Fourth NASA Goddard Conference on Mass Storage Systems and Technologies Mar. 1994 p 367-381 (For primary document see N95-24108 07-82)
(Contract USRA-C-5555-19)
Avail: CASI HC A03/MF A04

NASA missions, both for earth science and for space science, collect huge amounts of data, and the rate at which data is being gathered is increasing. For example, the EOSDIS project is expected to collect petabytes per year. In addition, these archives are being made available to remote users over the Internet. The ability to manage the growth of the size and request activity of scientific archives depends on an understanding of the access patterns of scientific users. The National Space Science Data Center (NSSDC) of NASA Goddard Space Flight Center has run their on-line mass storage archive of space data, the National Data Archive and Distribution Service (NDADS), since November 1991. A large world-wide space research community makes use of NSSDC, requesting more than 20,000 files per month. Since the initiation of their service, they have maintained log files which record all accesses the archive. In this report, we present an analysis of the NDADS log files. We analyze the log files, and discuss several issues, including caching, reference patterns, clustering, and system loading. Author

N95-24138*# National Aeronautics and Space Administration. Goddard Space Flight Center, Greenbelt, MD.
EVALUATING THE EFFECT OF ONLINE DATA COMPRESSION ON THE DISK CACHE OF A MASS STORAGE SYSTEM
Odysseas I. Pentakalos (Maryland Univ. Baltimore County, Catonsville, MD.) and Yelena Yesha (Maryland Univ. Baltimore County, Catonsville, MD.) *In its* Fourth NASA Goddard Conference on Mass Storage Systems and Technologies Mar. 1994 p 383-391 (For primary document see N95-24108 07-82)
Avail: CASI HC A02/MF A04

A trace driven simulation of the disk cache of a mass storage system was used to evaluate the effect of an online compression algorithm on various performance measures. Traces from the system at NASA's Center

for Computational Sciences were used to run the simulation and disk cache hit ratios, number of files and bytes migrating to tertiary storage were measured. The measurements were performed for both an LRU and a size based migration algorithm. In addition to seeing the effect of online data compression on the disk cache performance measure, the simulation provided insight into the characteristics of the interactive references, suggesting that hint based prefetching algorithms are the only alternative for any future improvements to the disk cache hit ratio. Author

N95-24139*# Interferometrics, Inc., Vienna, VA.
A TERABYTE LINEAR TAPE RECORDER c35
John C. Webber *In* NASA. Goddard Space Flight Center, Fourth NASA Goddard Conference on Mass Storage Systems and Technologies Mar. 1994 p 393-397 (For primary document see N95-24108 07-82)
Avail: CASI HC A01/MF A04

A plan has been formulated and selected for a NASA Phase 2 SBIR award for using the VLBA tape recorder for recording general data. The VLBA tape recorder is a high-speed, high-density linear tape recorder developed for Very Long Baseline Interferometry (VLBI) which is presently capable of recording at rates up to 2 Gbit/sec and holding up to 1 Terabyte of data on one tape, using a special interface and not employing error correction. A general-purpose interface and error correction will be added so that the recorder can be used in other high-speed, high-capacity applications. Author

N95-24180# Japan Broadcasting Corp., Tokyo (Japan). Advanced Television Systems Research Div.
PROPOSAL OF A MODIFIED EBU METHOD FOR RELIABLE EVALUATION OF PICTURE QUALITY
Nagato Narita Dec. 1994 10 p
(ISSN 0027-657X)
(NHK-Labs-Note-431) Avail: CASI HC A02/MF A01

A new method suitable for subjective evaluation test using moving sequences, called the Modified EBU method, is proposed and the reliability of the scores obtained using this method is investigated. It is confirmed that this method has higher sensitivity to small impairments than conventional methods. Author

N95-23284*# Arkansas Univ., Pine Bluff, AR. Dept. of Mathematics and Computer Science.
AUTOMATION TECHNOLOGY USING GEOGRAPHIC INFORMATION SYSTEM (GIS) Abstract Only
Cynthia L. Brooks *In* Hampton Univ., 1994 NASA-HU American Society for Engineering Education (ASEE) Summer Faculty Fellowship Program Dec. 1994 p 64 (For primary document see N95-23276 07-99)
Avail: CASI HC A01/MF A02

N95-23678*# National Aeronautics and Space Administration. Ames Research Center, Moffett Field, CA.
USING DEDAL TO SHARE AND REUSE DISTRIBUTED ENGINEERING DESIGN INFORMATION
Vinod Baya (Stanford Univ., CA.), Catherine Baudin, Ade Mabogunje (Stanford Univ., CA.), Aseem Das, David M. Cannon (Stanford Univ., CA.), and Larry J. Leifer (Stanford Univ., CA.) *In* JPL, Third International Symposium on Artificial Intelligence, Robotics, and Automation for Space 1994 Oct. 1994 p 33-36 (For primary document see N95-23672 07-63)
Avail: CASI HC A01/MF A03

N95-23848*# Colorado Univ., Boulder, CO. Center for the Study of Earth from Space.
AUTOMATING SPECTRAL UNMIXING OF AVIRIS DATA USING CONVEX GEOMETRY CONCEPTS
Joseph W. Boardman *In* JPL, Summaries of the 4th Annual JPL Airborne Geoscience Workshop. Volume 1: AVIRIS Workshop 25 Oct. 1993 p 11-14 (For primary document see N95-23844 07-42)
(Contract NAS5-31711)
Avail: CASI HC A01/MF A03

N95-23849*# University of South Florida, Saint Petersburg, FL. Dept. of Marine Science.
AVIRIS CALIBRATION USING THE CLOUD-SHADOW METHOD
K. L. Carder, P. Reinersman, and R. F. Chen *In* JPL, Summaries of the 4th Annual JPL Airborne Geoscience Workshop. Volume 1: AVIRIS Workshop 25 Oct. 1993 p 15-18 (For primary document see N95-23844 07-42)
Avail: CASI HC A01/MF A03

N95-23854*# Jet Propulsion Lab., California Inst. of Tech., Pasadena, CA.
COMPARISON OF METHODS FOR CALIBRATING AVIRIS DATA TO GROUND REFLECTANCE
Roger N. Clark (Geological Survey, Denver, CO.), Gregg Swayze (Geological Survey, Denver, CO.), Kathy Heidebrecht (Colorado Univ., Boulder, CO.), Alexander F. H. Goetz (Colorado Univ., Boulder, CO.), and Robert O. Green *In its* Summaries of the 4th Annual JPL Airborne Geoscience Workshop. Volume 1: AVIRIS Workshop 25 Oct. 1993 p 35-36 (For primary document see N95-23844 07-42)
Avail: CASI HC A01/MF A03

N95-23855*# Geological Survey, Denver, CO.
THE US GEOLOGICAL SURVEY, DIGITAL SPECTRAL REFLECTANCE LIBRARY: VERSION 1: 0.2 TO 3.0 MICRONS Abstract Only
Roger N. Clark, Gregg A. Swayze, Trude V. V. King, Andrea J. Gallagher, and Wendy M. Calvin (Geological Survey, Flagstaff, AZ.) *In* JPL, Summaries of the 4th Annual JPL Airborne Geoscience Workshop. Volume 1: AVIRIS Workshop 25 Oct. 1993 p 3 (For primary document see N95-23844 07-42)
Avail: CASI HC A01/MF A03

N95-23858*# Naval Research Lab., Washington, DC. HYDICE Project Office.
DISCRIMINATION OF POORLY EXPOSED LITHOLOGIES IN AVIRIS DATA
William H. Farrand and Joseph C. Harsanyi *In* JPL, Summaries of the 4th Annual JPL Airborne Geoscience Workshop. Volume 1: AVIRIS Workshop 25 Oct. 1993 p 53-56 (For primary document see N95-23844 07-42)
Avail: CASI HC A01/MF A03

N95-23859*# Geological Survey, Flagstaff, AZ.
SPECTRAL DECOMPOSITION OF AVIRIS DATA
Lisa Gaddis, Laurence Soderblom, Hugh Kieffer, Kris Becker, Jim Torson, and Kevin Mullins *In* JPL, Summaries of the 4th Annual JPL Airborne Geoscience Workshop. Volume 1: AVIRIS Workshop 25 Oct. 1993 p 57-60 (For primary document see N95-23844 07-42)
Avail: CASI HC A01/MF A03

N95-23861*# Jet Propulsion Lab., California Inst. of Tech., Pasadena, CA.
USE OF DATA FROM THE AVIRIS ONBOARD CALIBRATOR
Robert O. Green *In its* Summaries of the 4th Annual JPL Airborne Geoscience Workshop. Volume 1: AVIRIS Workshop 25 Oct. 1993 p 65-68 (For primary document see N95-23844 07-42)
Avail: CASI HC A01/MF A03

N95-23868*# Purdue Univ., West Lafayette, IN. School of Electrical Engineering.
CLASSIFICATION OF HIGH DIMENSIONAL MULTISPECTRAL IMAGE DATA
Joseph P. Hoffbeck and David A. Landgrebe *In* JPL, Summaries of the 4th Annual JPL Airborne Geoscience Workshop. Volume 1: AVIRIS Workshop 25 Oct. 1993 p 93-96 (For primary document see N95-23844 07-42)
(Grant NAGw-925)
Avail: CASI HC A01/MF A03

N95-23869*# Aerospace Corp., Los Angeles, CA.
SIMULATION OF LANDSAT THEMATIC MAPPER IMAGERY USING AVIRIS HYPERSPECTRAL IMAGERY
Linda S. Kalman and Gerard R. Peltzer *In* JPL, Summaries of the 4th Annual JPL Airborne Geoscience Workshop. Volume 1: AVIRIS Workshop 25 Oct. 1993 p 97-100 Sponsored by Aerospace Sponsored Research

program (For primary document see N95-23844 07-42)
Avail: CASI HC A01/MF A03

N95-23872*# National Aeronautics and Space Administration. Ames Research Center, Moffett Field, CA.
AVIRIS AND TIMS DATA PROCESSING AND DISTRIBUTION AT THE LAND PROCESSES DISTRIBUTED ACTIVE ARCHIVE CENTER
G. R. Mah and J. Myers *In* JPL, Summaries of the 4th Annual JPL Airborne Geoscience Workshop. Volume 1: AVIRIS Workshop 25 Oct. 1993 p 109-112 (For primary document see N95-23844 07-42)
Avail: CASI HC A01/MF A03

N95-23875*# Jet Propulsion Lab., California Inst. of Tech., Pasadena, CA.
EXTRACTION OF AUXILIARY DATA FROM AVIRIS DISTRIBUTION TAPE FOR SPECTRAL, RADIOMETRIC, AND GEOMETRIC QUALITY ASSESSMENT
Peter Meyer, Robert O. Green, and Thomas G. Chrien *In its* Summaries of the 4th Annual JPL Airborne Geoscience Workshop. Volume 1: AVIRIS Workshop 25 Oct. 1993 p 121-125 (For primary document see N95-23844 07-42)
Avail: CASI HC A01/MF A03

N95-23876*# Jet Propulsion Lab., California Inst. of Tech., Pasadena, CA.
PREPROCESSING: GEOCODING OF AVIRIS DATA USING NAVIGATION, ENGINEERING, DEM, AND RADAR TRACKING SYSTEM DATA
Peter Meyer, Steven A. Larson, Earl G. Hansen, and Klaus I. Itten *In its* Summaries of the 4th Annual JPL Airborne Geoscience Workshop. Volume 1: AVIRIS Workshop 25 Oct. 1993 p 127-132 Sponsored by NASA, Ames Research Center and Litton Aero Products (For primary document see N95-23844 07-42)
(SNSF Proj. 82-20332.90)
Avail: CASI HC A02/MF A03

N95-23877*# Jet Propulsion Lab., California Inst. of Tech., Pasadena, CA.
THE DATA FACILITY OF THE AIRBORNE VISIBLE/INFRARED IMAGING SPECTROMETER (AVIRIS)
Pia J. Nielsen, Robert O. Green, Alex T. Murray, Bjorn T. Eng, H. Ian Novack, Manuel Solis, and Martin Olah *In its* Summaries of the 4th Annual JPL Airborne Geoscience Workshop. Volume 1: AVIRIS Workshop p133-136 (SEE N95-23844 07-42) 25 Oct. 1993 (For primary document see N95-23844 07-42)
Avail: CASI HC A01/MF A03

N95-23894*# Arizona State Univ., Tempe, AZ. Dept. of Geology.
LABORATORY SPECTRA OF FIELD SAMPLES AS A CHECK ON TWO ATMOSPHERIC CORRECTION METHODS
Pung Xu and Ronald Greeley *In* JPL, Summaries of the 4th Annual JPL Airborne Geoscience Workshop. Volume 1: AVIRIS Workshop 25 Oct. 1993 p 201-204 (For primary document see N95-23844 07-42)
Avail: CASI HC A01/MF A03

N95-23916*# National Aeronautics and Space Administration. Langley Research Center, Hampton, VA.
OVERVIEW OF THE LDEF MSIG DATABASING ACTIVITIES
Joan G. Funk *In its* LDEF: 69 Months in Space. Third Post-Retrieval Symposium, Part 2 Feb. 1995 p 859-865 (For primary document see N95-23896 07-99)
(Contract NAS1-19247)
Avail: CASI HC A02/MF A03

N95-23952*# Telespazio S.p.A., Rome (Italy).
MAC EUROPE 1991 CAMPAIGN: AIRSAR/AVIRIS DATA INTEGRATION FOR AGRICULTURAL TEST SITE CLASSIFICATION
S. Sangiovanni, M. F. Buongiorno, M. Ferrarini (La Sapienza Univ., Rome, Italy.), and A. Fiumara *In* JPL, Summaries of the 4th Annual JPL Airborne Geoscience Workshop. Volume 3: AIRSAR Workshop 25 Oct. 1993 p 53-56 (For primary document see N95-23938 07-42)
Avail: CASI HC A01/MF A01

N95-23955*# National Aeronautics and Space Administration. Goddard Space Flight Center, Greenbelt, MD.
POLARIMETRIC RADAR DATA DECOMPOSITION AND INTERPRETATION
Guoqing Sun (Science Systems and Applications, Inc., Lanham, MD.) and K. Jon Ranson *In* JPL, Summaries of the 4th Annual JPL Airborne Geoscience Workshop. Volume 3: AIRSAR Workshop 25 Oct. 1993 p 65-68 (For primary document see N95-23938 07-42)
Avail: CASI HC A01/MF A01

83 ECONOMICS AND COST ANALYSIS

Includes cost effectiveness studies.

N95-24062# General Accounting Office, Washington, DC. National Security and International Affairs Div.
DOD BUDGET: SELECTED CATEGORIES OF PLANNED FUNDING FOR FISCAL YEARS 1995-99. REPORT TO CONGRESSIONAL REQUESTERS
17 Feb. 1995 20 p
(GAO/NSIAD-95-92; B-260307) Avail: CASI HC A03/MF A01; GAO, PO Box 6015, Gaithersburg, MD 20884-6015 HC

This GAO (Government Accounting Office) investigative report identifies programs in the DOD's future funding plans for the fiscal years 1995-1999 for the thirteen broad categories selected by John Kasich (Chairman, Committee on the Budget, House of Representatives) and Charles E. Grassley (United States Senate). The categories are: (1) environmental; (2) defense conversion; (3) DOD dependents schools and Junior ROTC; (4) basic research; (5) counter-drug programs; (6) humanitarian and foreign assistance programs; (7) civilian separation pay and military temporary early retirement authority; (8) grants to universities and colleges; (9) operation of the 89th Military Airlift Wing at Andrews Air Force Base; (10) medical education and noncombat-related medical research; (11) support for foreign military sales; (12) antiterrorism activities; and (13) pay and allowances to incarcerated military personnel. Derived from text

84 LAW, POLITICAL SCIENCE AND SPACE POLICY

Includes NASA appropriation hearings; aviation law; space law and policy; international law; international cooperation; and patent policy.

No abstracts in this category.

85 URBAN TECHNOLOGY AND TRANSPORTATION

Includes applications of space technology to urban problems; technology transfer; technology assessment; and surface and mass transportation.

For related information see also *03 Air Transportation and Safety, 16 Space Transportation,* and *44 Energy Production and Conversion.*

N95-22526*# Research Triangle Inst., Research Triangle Park, NC. Center for Technology Applications.
NASA TECHNOLOGY APPLICATIONS TEAM: COMMERCIAL APPLICATIONS OF AEROSPACE TECHNOLOGY Annual Report, 1 Oct. 1993 - 31 Dec. 1994
31 Dec. 1994 162 p Original contains color illustrations
(Contract NASw-4367)
(NASA-CR-197589; NAS 1.26:197589; RTI/4321/Q4-94) Avail: CASI HC A08/MF A02; 1 functional color page

The Research Triangle Institute (RTI) is pleased to report the results of NASA contract NASW-4367, 'Operation of a Technology Applications

Team'. Through a period of significant change within NASA, the RTI Team has maintained its focus on helping NASA establish partnerships with U.S. industry for dual use development and technology commercialization. Our emphasis has been on outcomes, such as licenses, industry partnerships and commercialization of technologies that are important to NASA in its mission of contributing to the improved competitive position of U.S. industry. RTI's ongoing commitment to quality and customer responsiveness has driven our staff to continuously improve our technology transfer methodologies to meet NASA's requirements. For example, RTI has emphasized the following areas: (1) Methodology For Technology Assessment and Marketing: RTI has developed an implemented effective processes for assessing the commercial potential of NASA technologies. These processes resulted from an RTI study of best practices, hands-on experience, and extensive interaction with the NASA Field Centers to adapt to their specific needs; (2) Effective Marketing Strategies: RTI surveyed industry technology managers to determine effective marketing tools and strategies. The Technology Opportunity Announcement format and content were developed as a result of this industry input. For technologies with a dynamic visual impact, RTI has developed a stand-alone demonstration diskette that was successful in developing industry interest in licensing the technology; and (3) Responsiveness to NASA Requirements: RTI listened to our customer (NASA) and designed our processes to conform with the internal procedures and resources at each NASA Field Center and the direction provided by NASA's Agenda for Change. This report covers the activities of the Research Triangle Institute Technology Applications Team for the period 1 October 1993 through 31 December 1994. Author

N95-23091*# Research Triangle Inst., Research Triangle Park, NC.
NASA TECHNOLOGY APPLICATIONS TEAM: COMMERCIAL APPLICATIONS OF AEROSPACE TECHNOLOGY Annual Report, 1 Oct. 1993 - 31 Dec. 1994
31 Dec. 1994 162 p Original contains color illustrations
(Contract NASw-4367)
(NASA-CR-197870; NAS 1.26:197870) Avail: CASI HC A08/MF A02; 1 functional color page

The Research Triangle Institute (RTI) Team has maintained its focus on helping NASA establish partnerships with U.S. industry for dual use development and technology commercialization. Our emphasis has been on outcomes, such as licenses, industry partnerships and commercialization of technologies, that are important to NASA in its mission of contributing to the improved competitive position of U.S. industry. The RTI Team has been successful in the development of NASA/industry partnerships and commercialization of NASA technologies. RTI ongoing commitment to quality and customer responsiveness has driven our staff to continuously improve our technology transfer methodologies to meet NASA's requirements. For example, RTI has emphasized the following areas: (1) Methodology For Technology Assessment and Marketing: RTI has developed and implemented effective processes for assessing the commercial potential of NASA technologies. These processes resulted from an RTI study of best practices, hands-on experience, and extensive interaction with the NASA Field Centers to adapt to their specific needs. (2) Effective Marketing Strategies: RTI surveyed industry technology managers to determine effective marketing tools and strategies. The Technology Opportunity Announcement format and content were developed as a result of this industry input. For technologies with a dynamic visual impact, RTI has developed a stand-alone demonstration diskette that was successful in developing industry interest in licensing the technology. And (3) Responsiveness to NASA Requirements: RTI listened to our customer (NASA) and designed our processes to conform with the internal procedures and resources at each NASA Field Center and the direction provided by NASA's Agenda for Change. This report covers the activities of the Research Triangle Institute Technology Applications Team for the period 1 October 1993 through 31 December 1994. Author

N95-23168# Defense Advanced Research Projects Agency, Arlington, VA.
TECHNOLOGY REINVESTMENT PROJECT'S FOCUS AREA: AFFORDABLE POLYMER MATRIX COMPOSITES FOR AIRFRAME STRUCTURES
1994 202 p Workshops held in Seattle, WA, 16 Nov. 1994; and Oakland, CA, 18 Nov. 1994
(PB95-136032) Avail: CASI HC A10/MF A03

The mission of the Technology Reinvestment Project (TRP) is to stimulate the transition to a growing, integrated, national industrial capability that provides the most advanced, affordable military systems and the most competitive commercial products. Programs are structured to expand high quality employment opportunities in dual-use technologies that demonstrably enhance U.S. competitiveness and national security. The publication contains the transparencies from the TRP workshops held in Seattle, WA and Oakland, CA in November, 1994. It includes general sessions on TRP, Technology Development, Regional Technology Alliances, and Manufacturing Education and Training, as well as the break out session on Affordable Polymer Matrix Composites for Airframe Structures. Also included are registration forms for both workshops. NTIS

88 SPACE SCIENCES (GENERAL)

No abstracts in this category.

89 ASTRONOMY

Includes radio, gamma-ray, and infrared astronomy, and astrometry.

N95-22539*# Jet Propulsion Lab., California Inst. of Tech., Pasadena, CA.
IRAS SKY SURVEY ATLAS: EXPLANATORY SUPPLEMENT
S. L. Wheelock, T. N. Gautier, J. Chillemi, D. Kester, H. McCallon, C. Oken, J. White, D. Gregorich, F. Boulanger, and J. Good et al May 1994 158 p Sponsored in cooperation with Netherlands Agency for Aerospace Programs and Science and Engineering Research Council
(Contract NAS7-918)
(NASA-CR-197335; JPL-Publ-94-11; NAS 1.26:197335) Avail: CASI HC A08/MF A02

This Explanatory Supplement accompanies the IRAS Sky Survey Atlas (ISSA) and the ISSA Reject Set. The first ISSA release in 1991 covers completely the high ecliptic latitude sky, absolute value of beta is greater than 50 deg, with some coverage down to the absolute value of beta approx. equal to 40 deg. The second ISSA release in 1992 covers ecliptic latitudes of 50 deg greater than the absolute value of beta greater than 20 deg, with some coverage down to the absolute value of beta approx. equal to 13 deg. The remaining fields covering latitudes within 20 deg of the ecliptic plane are of reduced quality compared to the rest of the ISSA fields and therefore are released as a separate IPAC product, the ISSA Reject Set. The reduced quality is due to contamination by zodiacal emission residuals. Special care should be taken when using the ISSA Reject images. In addition to information on the ISSA images, some information is provided in this Explanatory Supplement on the IRAS Zodiacal History File (ZOHF), Version 3.0, which was described in the December 1988 release memo. The data described in this Supplement are available at the National Space Science Data Center (NSSDC) at the Goddard Space Flight Center. The interested reader is referred to the NSSDC for access to the IRAS Sky Survey Atlas (ISSA). Author

N95-23401*# Applied Research Corp., Landover, MD.
LONG TERM VARIABILITY OF B SUPERGIANT WINDS Final Report
Derck L. Massa 18 Jan. 1995 36 p
(NASA Order S-14634-F)
(NASA-CR-197925; NAS 1.26:197925; ARC-R-95-229) Avail: CASI HC A03/MF A01

The object of this observing proposal was to sample wind variability in B supergiants on a daily basis over a period of several days in order to determine the time scale with which density variability occurs in their winds. Three stars were selected for this project: 69 Cyg (B0 Ib), HD 164402 (B0 Ib), and HD 47240 (B1 Ib). Three grey scale representations of the Si IV lambda lambda 1400 doublet in each star are attached. In these figures, time (in days) increases upward, and the wavelength (in terms of velocity

relative to the rest wavelength of the violet component of the doublet) is the abscissa. The spectra are normalized by a minimum absorption (maximum flux) template, so that all changes appear as absorptions. As a result of these observations, we can now state with some certainty that typical B supergiants develop significant wind inhomogeneities with recurrence times of a few days, and that some of these events show signs of strong temporal coherence. Derived from text

N95-23402*# Lehigh Univ., Bethlehem, PA. Dept. of Mathematics.
MASS LOSS IN THE INTERACTING SEMI-DETACHED BINARY DELTA LIBRAE Final Report
George E. McCluskey, Jr., Carolina P. S. McCluskey, and Yoji Kondo 10 Feb. 1995 9 p Submitted for publication
(Grant NAG5-2100)
(NASA-CR-197924; NAS 1.26:197924) Avail: CASI HC A02/MF A01

The interacting Algol-type binary Delta Librae (AOV + G: V) has been observed with the International Ultraviolet Explorer (IUE) satellite. More than fifty high resolution spectra in the far-ultraviolet and mid-ultraviolet spectrum have been analyzed in order to model the mass flow in the Delta Librae system. The resonance lines of Si IV and C IV are present in absorption and vary in strength both secularly and with phase. The radial velocities of the Si IV and C IV absorption lines generally follow the orbital motion of the primary star but deviate by typically a few tens of kilometers per second in the direction of the observer. The presence of Si IV and C IV features indicates the existence of a region considerably hotter than the normal AOV photosphere and, since these lines are present at all phases, this region must be fairly extensive. These results are interpreted in terms of a 'pseudo-photosphere' around the equatorial region of the AOV star, created by matter being accreted from the G-type companion. The widths of the Si IV and C IV absorption features imply that some of the matter lost by the G-star leaves the system entirely. Author

N95-23468# Chalmers Univ. of Technology, Goeteborg (Sweden). Onsala Space Observatory.
MULTIBAND VLBI IMAGING OF THE JET IN 3C 345
F. T. Rantakyroe, L. B. Baath, and L. Matveenko 10 May 1994 18 p Prepared in cooperation with Akademiya Nauk SSSR
(PB95-139275) Avail: CASI HC A03/MF A01

The authors present two high dynamic range images of the quasar 3C 345 from observations at 0avelength 18 cm (1990.74) and a wavelength 49 cm (1990.72). The simultaneous observations at two wavelengths have made it possible to construct a spectral index map covering the core and the extended jet. At a distance of about 15 mas, the jet flares out and the emission beyond this is probably due to optically thick self-absorbed synchrotron radiation, while the radiation downstream is due to emission from an adiabatically expanding plasma. The authors conclude that the flaring out is either due to a standing shock caused by the jet passing into a region of different density, or due to large scale oscillations in a helical jet disrupting the collimated flow. NTIS

N95-23540*# Columbia Univ., New York, NY. Columbia Astrophysics Lab.
DEVELOPMENT OF MICROCHANNEL PLATE X-RAY OPTICS Final Technical Report, 1 Jul. 1992 - 31 Dec. 1994
Philip Kaaret 9 Feb. 1995 12 p
(Grant NAGw-2721)
(NASA-CR-197935; NAS 1.26:197935) Avail: CASI HC A03/MF A01

The goal of this research program was to develop a novel technique for focusing x-rays based on the optical system of a lobster's eye. A lobster eye employs many closely packed reflecting surfaces arranged within a spherical or cylindrical shell. These optics have two unique properties: they have unlimited fields of view and can be manufactured via replication of identical structures. Because the angular resolution is given by the ratio of the size of the individual optical elements to the focal length, optical elements with size on the order of one hundred microns are required to achieve good angular resolution with a compact telescope. We employed anisotropic etching of single crystal silicon wafers for the fabrication of micron-scale optical elements. This technique, commonly referred to as silicon micromachining, is based on silicon fabrication techniques developed by the microelectronics industry. We have succeeded in producing silicon lenses with a geometry suitable for a 1-d focusing x-ray optics. These lenses have an aspect ratio (40:1) suitable for x-ray reflection and have very good optical surface alignment. We have developed a number of process refinements which improved the quality of the lens geometry and the repeatability of the etch process. In addition to the silicon fabrication, an x-ray beam line was constructed at Columbia for testing the optics. Most recently, we have done several experiments to find the fundamental limits that the anisotropic etch process placed on the etched surface roughness. Derived from text

N95-23560*# Southwest Research Inst., San Antonio, TX. Instrumentation and Space Research Division.
[IUE OBSERVING PROGRAMS: NSOSS, VEOEB, AND PCOEB] Final Report
1995 18 p
(Grant NAG5-1913; SwRI Proj. 15-5301)
(NASA-CR-197424; NAS 1.26:197424) Avail: CASI HC A03/MF A01

The data reduction and analysis of IUE observations were completed. These results were presented from Venus SO2 (of the VEOEB program). The three IUE observing programs were NSOSS, VEOEB, and PCOEB. NSOSS consisted of comparative UV studies. The objectives of NSOSS included: making the first UV observations of 4179 Toutatis (a near-Earth asteroid), Himalia (a satellite of Jupiter), and Hyperion (the Saturnian satellite); obtaining the first radially-dependent information on the UV color of Saturn's rings; gathering uncontaminated UV spectra of Iapetus's bright and dark hemispheres; and obtaining a spectrum of Titania to initiate the comparative study of UV photometric properties in the Uranian system. VEOEB, as stated above, was a study of the SO2 of the Venus atmosphere and surface. Based on past Pioneer Venus and IUE observations, significant SO2 variations have been interpreted as indicating that the long term atmospheric SO2 abundance may be related to large, episodic infections from the surface or interior of Venus. If episodic events occur, then continuing observations of SO2 in the Venus atmosphere play a vital role in understanding Venus's current and past geologic evolution. PCOEB was a study of the Pluto-Charon system. The primary objective of PCOEB was to complete the coverage of the system's UV light curve in order to analyze the surface properties of Pluto-Charon. Publications, abstracts and articles, resulting from this grant are appended to this report. Derived from text

N95-23561*# Applied Research Corp., Landover, MD.
OBSERVATIONAL STUDIES OF THE CLEARING PHASE IN PROTO-PLANETARY DISK SYSTEMS Annual Report, 19 Mar. 1994 - Mar. 3 1995
Carol A. Grady 16 Mar. 1995 6 p
(Contract NASw-4756)
(NASA-CR-197900; NAS 1.26:197900; ARC-R95-234) Avail: CASI HC A02/MF A01

Progress in this study is summarized for its second year. An extensive program of high dispersion UV spectral studies using the IUE (International Ultraviolet Explorer) has resulted in acquisition of 40 Herbig Ae/Be star and related object spectra. We find that accreting, circumstellar gas is detected with velocities consistent with material in free-fall toward the stars in approximately 38% of the sample. With acquisition of optical measurements of the projected stellar rotational velocities, we find that the systems with accreting gas exhibit systematically higher projected rotational velocities than the systems showing signatures of outflowing material only. When combined with polarimetric and photometric data, the IUE spectra for these stars indicate that accretion in intermediate-mass pre-main sequence stars is confined to the plane of the circumstellar dust disk. This is in contrast to lower-mass PMS stars where accretion, persumably along magnetic field lines, is seen at polar latitudes. Our data alsc support significant clearing of the central regions of these circumstellar disks, as originally suggested. The model which most closely matches the observational data is accretion from a disk envelope, as developed by Calvet et al. (1994). Author (revised)

N95-23595*# Columbia Univ., New York, NY. Astrophysics Lab.
ROSAT OBSERVATION PROGRAM Annual Status Report, 1 Nov. 1993 - 31 Oct. 1994
Jules P. Halpern Mar. 1995 49 p
(Grant NAG5-1935)
(NASA-CR-197683; NAS 1.26:197683) Avail: CASI HC A03/MF A01

In this annual progress report (November 1, 1993 to October 31, 1994), the geminga pulsar was observed by the ROSAT PSPC for 37,000

s in September 1993, in order to make a more detailed study than was previously possible of the pulse profile and two-component spectrum, and to do phase-resolved spectroscopy. This exposure was 2.5 times longer than the original discovery observation. In addition, a shorter 4,000 s exposure was made in October 1992, simultaneously with a GRO observation of Geminga, in order to verify the absolute phasing of the X-ray and gamma-ray peaks. We verified that the spectrum can be described as the sum of two black bodies, whose temperatures are 6 x 10(exp 5) K and 3 - 4 x 10(exp 6) K, with the latter covering 3 x 10(exp -5) the area of the former. The pulse profiles indicate that the intensity of the two emitting regions peak is approximately 90 deg out of phase in rotation, but that the temperatures are otherwise independent of phase. An improved estimate of the distance can be made from the cooler (larger) blackbody component, yielding d = 440 +/- 120 pc. Another program of this report was to obtain PSPC spectra of an important class of Seyfert galaxies which have narrow lines and stron permitted Fe II emission. Sometines called I Zw 1 objects, or narrow-line Seyfert 1s, they are crucial to our understanding of Seyfert classification and models of Seyfert unification. We observed four new objects and, in addition, obtained data on 17 more from the ROSAT archive. A third program combined PSPC and HRI observations of selected Seyfert galaxies which have unusual and variable spectra. The purpose was to disentangle diffuse X-ray emission from the nuclear source, in order to properly interpret the soft X-ray spectral shapes in terms of partial covering and/or warm-absorber models. The targets of the program are NGC 3516, NGC 3227, and NGC 7314. So far, we have only performed a dtailed analysis on NGC 3516. The fourth program of this report is the NGC 1672, the second brightest Seyfert galaxy and one or the original 'composite' Seyfert/starburst galaxies which have evidence for both Seyfert activity and H II regions in their optical spectra. It is one of the lowest luminosity Seyfert 2 galaxies that can be studied in detail.

Derived from text

N95-23740*# Space Telescope Science Inst., Baltimore, MD.
PLANNING AND SCHEDULING THE HUBBLE SPACE TELESCOPE: PRACTICAL APPLICATION OF ADVANCED TECHNIQUES
Glenn E. Miller *In* JPL, Third International Symposium on Artificial Intelligence, Robotics, and Automation for Space 1994 Oct. 1994 p 339-343 (For primary document see N95-23672 07-63)
Avail: CASI HC A01/MF A03

N95-23741*# Computer Sciences Corp., Greenbelt, MD. Science Programs.
A CONSTRAINT-LOGIC BASED IMPLEMENTATION OF THE COARSE-GRAINED APPROACH TO DATA ACQUISITION SCHEDULING OF THE INTERNATIONAL ULTRAVIOLET EXPLORER ORBITING OBSERVATORY
Bruce McCollum and Mark Graves (Baylor Coll. of Medicine, Houston, TX.) *In* JPL, Third International Symposium on Artificial Intelligence, Robotics, and Automation for Space 1994 Oct. 1994 p 343-346 (For primary document see N95-23672 07-63)
Avail: CASI HC A01/MF A03

N95-23742*# National Aeronautics and Space Administration. Ames Research Center, Moffett Field, CA.
ROBUST TELESCOPE SCHEDULING
Keith Swanson, John Bresina (RECOM Technologies, Inc., Moffett Field, CA.), and Mark Drummond (RECOM Technologies, Inc., Moffett Field, CA.) *In* JPL, Third International Symposium on Artificial Intelligence, Robotics, and Automation for Space 1994 Oct. 1994 p 347-350 (For primary document see N95-23672 07-63)
Avail: CASI HC A01/MF A03

N95-23743*# RECOM Technologies, Inc., Moffett Field, CA.
THE ASSOCIATE PRINCIPAL ASTRONOMER TELESCOPE OPERATIONS MODEL
Mark Drummond, John Bresina, Keith Swanson, Will Edgington, and Greg Henry (Tennessee State Univ., Nashville, TN.) *In* JPL, Third International Symposium on Artificial Intelligence, Robotics, and Automation for Space 1994 Oct. 1994 p 351-354 (For primary document see N95-23672 07-63)
Avail: CASI HC A01/MF A03

N95-23757*# RECOM Technologies, Inc., Moffett Field, CA.
TELESCOPE LOADING: A PROBLEM REDUCTION APPROACH
John L. Bresina *In* JPL, Third International Symposium on Artificial Intelligence, Robotics, and Automation for Space 1994 Oct. 1994 p 415-418 (For primary document see N95-23672 07-63)
Avail: CASI HC A01/MF A03

90 ASTROPHYSICS

Includes cosmology; celestial mechanics; space plasmas; and interstellar and interplanetary gases and dust.

For related information see also *75 Plasma Physics*.

N95-22516# Los Alamos National Lab., NM.
ENERGETIC PARTICLE OBSERVATIONS AT GEOSYNCHRONOUS ORBIT
E. Geoffrey and D. Reeves 1994 7 p Presented at the Ribubetsu Workshop on Magnetic Storms, Rikubetsu, Japan, 6-8 Oct. 1994
(Contract W-7405-eng-36)
(DE95-000873; LA-UR-94-3067; CONF-9410214-1) Avail: CASI HC A02/MF A01

The region of space near geosynchronous altitudes is important for the processes which contribute to magnetic storms. During substorms magnetic energy is converted to particle kinetic energy resulting in the 'substorm injections' commonly observed at geosynchronous orbit. These injections are manifested in energies from a few tens of keV to hundreds of keV and, on occasion, to the MeV energy range. The injected particles are subject to gradient and curvature drifts and therefore contribute to the ring current. It is common to think of a magnetic storm as a superposition of substorms in which the injection rate into the ring current exceeds the loss rate due to scattering, diffusion, and precipitation. In this paper the authors review current understanding of substorm injections and examine geosynchronous energetic particle data for the signatures of magnetic storms and for clues to the storm-substorm connection. DOE

N95-22739# International Centre for Theoretical Physics, Trieste (Italy).
BLACK HOLE FORMATION AND SPACE-TIME FLUCTUATIONS IN TWO DIMENSIONAL DILATON GRAVITY AND COMPLEMENTARITY
S. R. Das (Tata Inst. of Fundamental Research, Bombay, India.) and S. Mukherji Jan. 1994 32 p
(DE94-628514; IC-94/16; TIFR/TH-94-01) Avail: CASI HC A03/MF A01 (US Sales Only)

We study black hole formation in a model of two dimensional dilaton gravity and 24 massless scalar fields with a boundary. We find the most general boundary condition consistent with perfect reflection of matter and the constraints. We show that in the semiclassical approximation and for the generic value of a parameter which characterizes the boundary conditions, the boundary starts receding to infinity at the speed of light whenever the total energy of the incoming matter flux exceeds a certain critical value. This is also the critical energy which marks the onset of black hole formation. We then compute the quantum fluctuations of the boundary and of the rescaled scalar curvature and show that as soon as the incoming energy exceeds this critical value, and asymptotic observer using normal time resolutions will always measure large quantum fluctuations of space-time near the horizon, even though the freely falling observer does not. This is an aspect of black hole complementarity relating directly to quantum gravity effects. DOE

N95-23013*# Pennsylvania State Univ., University Park, PA. Dept. of Astronomy and Astrophysics.
ORIGINS OF INTERSTELLAR AND SOLAR SYSTEM: CARBONACEOUS MATERIALS Final Technical Report, 1 Nov. 1990 - 31 Oct. 1994
Eric D. Feigelson 31 Oct. 1994 4 p
(Grant NAGw-2280)
(NASA-CR-197436; NAS 1.26:197436) Avail: CASI HC A01/MF A01

Carbon is a crucial atom in cosmochemistry. It is well-established that carbon is synthesized in stellar interiors after the main sequence, is ejected by red giants as small carbonaceous grains during their 'carbon star' phase, resides in the interstellar medium, and was later incorporated into the solar system. The mechanisms of carbon grain formation and later chemical processing are complex because, with only small thermodynamic differences,

carbon can take on a bewildering variety of forms: diamond; oxides; carbides; graphite; aliphatic hydrocarbons; polycyclic aromatic hydrocarbons (PAH's); fullerenes; amorphous carbon; and other compounds. These are evidence for many of the forms of carbon found in astronomical observations. We seek to understand the possible astrophysical sites and conditions of the origins of different forms of carbon by combining state-of-the-art capabilities of carbon chemistry with astrophysical modeling. The work is a collaboration between Prof. Frenklach, a leading carbon materials scientist with both laboratory and computer modeling expertise and Prof. Feigelson, an astrophysicist with interests in star formation. The largest effort under this grant was devoted to developing this concept into a comprehensive quantitative model. In addition to explaining the astronomical properties of red giants producing carbonaceous grains, our model also can incorporate recent meteoritic findings. Finally, our induced nucleation grain formation model provides a natural explanation for the widespread presence of PAH emission bands in the Galactic interstellar medium. A brief synopsis of other activities sponsored under this grant and a list of publications from this grant is included. Derived from text

N95-23205*# Lockheed Missiles and Space Co., Palo Alto, CA.
INVESTIGATION OF PHYSICAL PARAMETERS IN STELLAR FLARES OBSERVED BY GINGA Final Report, 7 Jul. 1993 - 19 Sep. 1994
Robert A. Stern 19 Sep. 1994 38 p
(Contract NAS8-39936)
(NASA-CR-196547; NAS 1.26:196547) Avail: CASI HC A03/MF A01

This program involves analysis and interpretation of results from GINGA Large Area Counter (LAC) observations from a group of large stellar X-ray flares. All LAC data are re-extracted using the standard Hayashida method of LAC background subtraction and analyzed using various models available with the XSPEC spectral fitting program.Temperature-emission measure histories are available for a total of 5 flares observed by GINGA. These will be used to compare physical parameters of these flares with solar and stellar flare models. Author

N95-23228# Chalmers Univ. of Technology, Goeteborg (Sweden). Onsala Space Observatory.
STRUCTURE AND EVOLUTION OF LONG-LIVED SPIRAL PATTERNS IN GALAXIES
K. J. Donner and M. Thomasson 15 Jun. 1994 14 p Prepared in cooperation with Helsinki Univ.
(PB95-139242) Avail: CASI HC A03/MF A01

The authors use N-body simulations to study the non-linear evolution of spontaneous and tidally induced spiral patterns in galaxies on time-scales of several rotation periods of the disc. The authors find that the patterns can sometimes survive with an almost constant amplitude for five revolutions or more, and tend to be regenerated after disappearing temporarily. The pattern velocity is such that the corotation radius is where the self-gravity as measured by the swing amplification of the m = 2 component is strongest, and the amplitude of the pattern is larger when swing amplification is stronger. The shape of the spirals is independent of the origin of the pattern, and corresponds to a critical wave number. The pattern survives longer if the self-gravity of the disc is strong. If self-gravity is weak, the dominant tidal effect is a kinematic spiral at the inter Lindblad resonance. NTIS

N95-23230 Chalmers Univ. of Technology, Goeteborg (Sweden). Onsala Space Observatory.
INTERSTELLAR MOLECULES IN THE LARGE MAGELLANIC CLOUD
L. E. B. Johansson, H. Olofsson, A. Hjalmarson, R. Gredel, and J. H. Black 14 Jun. 1994 18 p Prepared in cooperation with European Southern Observatory, La Silla, Chile, and Steward Observatory, Tucson, AZ
(PB95-139267) Avail: Issuing Activity (National Technical Information Service (NTIS))

The authors present the results of a mm-wave molecular line search in the Large Magellanic Cloud obtained with the SEST (Swedish ESO Submillimeter Telescope) in the area of the N 159 complex of HII regions. Isotopomers of CO, CS, SO, CN, HCN, HNC, HCO(+) and H2CO have been detected. Some of these molecules have been observed in two transitions allowing excitation temperature estimates. For (13)CO and (12)CO the authors find temperatures close to, or in excess of 10 K, while C(18)O, CS and HCO(+) show temperatures between 5 and 10 K. All observed isotopomer intensity ratios suggest small optical depths provided that Galactic isotopic abundance ratios apply. NTIS

N95-23570# Los Alamos National Lab., NM.
CDM AND OMEGA IN THE LOCAL NEIGHBORHOOD
A. M. Dunn (Cambridge Univ., Cambridge, England.) and R. Laflamme 1995 5 p Presented at the Meeting of the Division of Particles and Fields of the American Physical Society, Albuquerque, NM, 2-6 Aug. 1994
(Contract W-7405-eng-36)
(DE95-003683; LA-UR-94-3766; CONF-940816-57) Avail: CASI HC A01/MF A01

Peebles has suggested an interesting method to trace back in time positions of galaxies called the least action method. This method applied on the Local Group galaxies seems to indicate that we live in an Omega approx. 0.1 Universe. The authors have studied a cold dark matter (CDM) N-body simulation with Omega = 0.2 and H = 50km/s /Mpc and compare trajectories traced back from the Least Action Principle and the center of mass of the particle forming CDM halos. They have shown that the agreement between these sets of trajectories is at best qualitative. They have also shown that the line of sight peculiar velocities are underestimated. This discrepancy is due to orphans, CDM particles which do not end up in halos. By varying the density parameter Omega in the least action principle the authors show that using this method they would underestimate the density of the Universe by a factor of 4-5. DOE

N95-23607 Chalmers Univ. of Technology, Goeteborg (Sweden). Onsala Space Observatory.
SEARCH FOR MILLIMETERWAVE CO EMISSION IN DAMPED LYMAN-ALPHA SYSTEMS
T. Wiklind and F. Combes 18 Jul. 1994 6 p Prepared in cooperation with Observatoire de Paris Limited Reproducibility: More than 20% of this document may be affected by microfiche quality
(PB95-139259) Avail: Issuing Activity (National Technical Information Service (NTIS))

A sensitive search for millimeterwave CO emission in 8 damped Lyman-alpha systems, 3 heavy element absorption line systems and one emission line galaxy, at redshifts ranging from 0.5 to 2.8, have yielded upper limits to the amount of molecular gas. The limits still allow relatively high H2 masses, but our results show that damped Lyman-alpha systems are not similar to the hyperluminous infrared galaxies at high redshifts found in the Infrared Astronomical Satellite (IRAS) database. One tentative detection of CO emission at z(sub a)=2.47 remains, but is very uncertain. We are not able to confirm a claimed detection of CO emission at z(sub a)=2.14 towards Q0528-250. NTIS

N95-23656# Sandia National Labs., Albuquerque, NM.
IMPACT SHOCK AND PENETRATION FRAGMENTATION IN POROUS MEDIA
T. Trucano and D. Grady 1994 27 p Presented at the 1994 Hypervelocity Impact Symposium, Santa Fe, NM, 16-20 Oct. 1994
(Contract DE-AC04-94AL-85000)
(DE94-018900; SAND-93-3866C; CONF-9410131-6) Avail: CASI HC A03/MF A01

In this paper, we discuss experimental, analytical, and computational techniques for studying the high velocity interaction of solid bodies with low density media. We assume that the velocity of the interaction is such that compressible effects in the solid are important. We are particularly interested in the dynamic mechanisms of deformation, erosion, and breakup which dominate the solid response at these high velocities. This is a problem of considerable current interest. Applications include the atmospheric propagation of high velocity aerosols, such as those that might be created in certain kinds of nuclear reactor accidents and explosive weapon accidents. An even more novel application is to the study of the impact of astrophysical bodies, such as meteors, asteroids, and comet fragments into planetary atmospheres. There is significant concern over the threats posed by impacts of these kinds on the earth. We will discuss the application of our methodology to understanding these impacts. In particular, we suggest that the experimental technique we present is applicable to scaled laboratory simulations of some of the phenomena that are believed to be important in atmospheric impacts. DOE

N95-24066*# Virginia Univ., Charlottesville, VA. Dept. of Materials Science and Engineering.
CHARGING OF INTERPLANETARY GRAINS Progress Report, 1 Apr. 1994 - 31 Mar. 1995
R. A. Baragiola, R. E. Johnson, and John L. Newcomb Jan. 1995 70 p (Grants NAGw-3954; NSF DMR-91-21272)
(NASA-CR-198032; NAS 1.26:198032; UVA/528488/MSE95/101) Avail: CASI HC A04/MF A01

The objective of this program is to quantify, by laboratory experiments, the charging of ices and other insulators subject to irradiation with electrons, ions and ultraviolet photons and to model special conditions based on the data. The system and conditions to be studied are those relevant for charging of dust in magnetospheric plasmas. The measurements are supplemented by computer simulations of charging or grains under a variety of conditions. Our work for this period involved experiments on water ice, improved models of charging of ice grains for Saturn's E-ring, and the construction of apparatus for electron impact studies and measurements of electron energy distributions. Author

N95-23000*# Guanajuato Univ., Guanajuato (Mexico). Inst. de Fisica.
SHANNON-WEHRL ENTROPY FOR COSMOLOGICAL AND BLACK-HOLE SQUEEZING
Haret Rosu and Marco Reyes *In* NASA. Goddard Space Flight Center, Second International Workshop on Harmonic Oscillators Jan. 1995 p 359-362 Sponsored by CONACyT (For primary document see N95-22957 07-74)
Avail: CASI HC A01/MF A04

N95-23828*# National Aeronautics and Space Administration. Langley Research Center, Hampton, VA.
LDEF INTERPLANETARY DUST EXPERIMENT (IDE) RESULTS
John P. Oliver (Institute for Space Science and Technology, Inc., Gainesville, FL.), S. F. Singer (Institute for Space Science and Technology, Inc., Gainesville, FL.), J. L. Weinberg (Institute for Space Science and Technology, Inc., Gainesville, FL.), C. G. Simon (Institute for Space Science and Technology, Inc., Gainesville, FL.), W. J. Cooke (Institute for Space Science and Technology, Inc., Gainesville, FL.), P. C. Kassel, W. H. Kinard, J. D. Mulholland (POD Associates, Inc., Albuquerque, NM.), and J. J. Wortman (North Carolina State Univ., Raleigh, NC.) *In its* LDEF: 69 Months in Space. Third Post-Retrieval Symposium, Part 1 Feb. 1995 p 353-360 (For primary document see N95-23796 07-99)
(Grant NAG1-1218)
Avail: CASI HC A02/MF A04

N95-23829*# Institute for Space Science and Technology, Inc., Gainesville, FL.
THE ORBITAL CHARACTERISTICS OF DEBRIS PARTICLE RINGS AS DERIVED FROM IDE OBSERVATIONS OF MULTIPLE ORBIT INTERSECTIONS WITH LDEF
William J. Cooke, John P. Oliver, and Charles G. Simon *In* NASA. Langley Research Center, LDEF: 69 Months in Space. Third Post-Retrieval Symposium, Part 1 Feb. 1995 p 361-371 (For primary document see N95-23796 07-99)
(Grant NAG1-1218)
Avail: CASI HC A03/MF A04

N95-23830*# National Aeronautics and Space Administration. Lyndon B. Johnson Space Center, Houston, TX.
ORBITAL DEBRIS AND METEOROID POPULATION AS ESTIMATED FROM LDEF IMPACT DATA
Jingchang Zhang and Donald J. Kessler *In* NASA. Langley Research Center, LDEF: 69 Months in Space. Third Post-Retrieval Symposium, Part 1 Feb. 1995 p 373-384 (For primary document see N95-23796 07-99)
Avail: CASI HC A03/MF A04

N95-23832*# National Aeronautics and Space Administration. Lyndon B. Johnson Space Center, Houston, TX.
ANALYTICAL ELECTRON MICROSCOPY OF LDEF IMPACTOR RESIDUES
Ronald P. Bernhard (Lockheed Engineering and Sciences Co., Houston, TX.), Ruth A. Barrett (Lockheed Engineering and Sciences Co., Houston, TX.), and Michael E. Zolensky *In* NASA. Langley Research Center, LDEF: 69 Months in Space. Third Post-Retrieval Symposium, Part 1 Feb. 1995 p 401-413 (For primary document see N95-23796 07-99)
Avail: CASI HC A03/MF A04

N95-23833*# National Aeronautics and Space Administration. Lyndon B. Johnson Space Center, Houston, TX.
NATURAL AND ORBITAL DEBRIS PARTICLES ON LDEF'S TRAILING AND FORWARD-FACING SURFACES
Friedrich Hoerz, Thomas H. See (Lockheed Engineering and Sciences Co., Houston, TX.), Ronald P. Bernhard (Lockheed Engineering and Sciences Co., Houston, TX.), and Donald E. Brownlee (Washington Univ., Seattle, WA.) *In* NASA. Langley Research Center, LDEF: 69 Months in Space. Third Post-Retrieval Symposium, Part 1 Feb. 1995 p 415-429 (For primary document see N95-23796 07-99)
Avail: CASI HC A03/MF A04

N95-23834*# Departement d'Etudes et de Recherches en Technologie Spatiale, Toulouse (France).
DEBRIS AND METEOROID PROPORTIONS DEDUCED FROM IMPACT CRATER RESIDUE ANALYSIS
Lucinda Berthoud, Jean-Claude Mandeville, Christian Durin (Centre National d'Etudes Spatiales, Toulouse, France.), and Janet Borg (Centre National de la Recherche Scientifique, Orsay, France.) *In* NASA. Langley Research Center, LDEF: 69 Months in Space. Third Post-Retrieval Symposium, Part 1 Feb. 1995 p 431-444 Sponsored by European Commission (For primary document see N95-23796 07-99)
Avail: CASI HC A03/MF A04

91 LUNAR AND PLANETARY EXPLORATION

Includes planetology; and manned and unmanned flights.

For spacecraft design or space stations see *18 Spacecraft Design, Testing and Performance.*

N95-22828*# Iowa Univ., Iowa City, IA. Dept. of Physics and Astronomy.
LANGMUIR-LIKE WAVES AND RADIATION IN PLANETARY FORESHOCKS Annual Progress Report, 1 Jan. 1994 - 31 Jan. 1995
Iver H. Cairns, P. A. Robinson, R. R. Anderson, D. A. Gurnett, and W. S. Kurth 31 Jan. 1995 7 p
(Grant NAGw-2040)
(NASA-CR-197376; NAS 1.26:197376) Avail: CASI HC A02/MF A01

The basic objectives of this NASA Grant are to develop theoretical understandings (tested with spacecraft data) of the generation and characteristics of electron plasma waves, commonly known as Langmuir-like waves, and associated radiation near f(sub p) and 2f(sub p) in planetary foreshocks. (Here f(sub p) is plasma frequency.) Related waves and radiation in the source regions of interplanetary type III solar radio bursts provide a simpler observational and theoretical context for developing and testing such understandings. Accordingly, applications to type III bursts constitute a significant fraction of the research effort. The testing of the new Stochastic Growth Theory (SGT) for type III bursts, and its extension and testing for foreshock waves and radiation, constitutes a major longterm strategic goal of the research effort. Derived from text

N95-23689*# Tokyo Univ., Sagamihara (Japan).
PATH PLANNING FOR PLANETARY ROVER USING EXTENDED ELEVATION MAP
Ichiro Nakatani, Takashi Kubota, and Tetsuo Yoshimitsu *In* JPL, Third International Symposium on Artificial Intelligence, Robotics, and Automation for Space 1994 Oct. 1994 p 87-90 (For primary document see N95-23672 07-63)
Avail: CASI HC A01/MF A03

N95-23725*# Canadian Space Agency, Saint Hubert (Quebec).
ROBOTICS AND TELEPRESENCE FOR MOON MISSIONS
Christian Sallaberger *In* JPL, Third International Symposium on Artificial Intelligence, Robotics, and Automation for Space 1994 Oct. 1994 p 269-273 (For primary document see N95-23672 07-63)
Avail: CASI HC A01/MF A03

92 SOLAR PHYSICS

Includes solar activity, solar flares, solar radiation and sunspots. For related information see *93 Space Radiation.*

N95-22938# Los Alamos National Lab., NM.
SOLAR MASS LOSS, SOLAR LITHIUM, AND SOLAR OSCILLATIONS
A. N. Cox and J. A. Guzik 1994 5 p Presented at the 1994 GONG Conference, Los Angeles, CA, May 1994
(Contract W-7405-eng-36)
(DE94-018262; LA-UR-94-2741; CONF-9405222-1) Avail: CASI HC A01/MF A01

Swenson and Faulkner, and Boothroyd et al. investigated the possibility that early main-sequence mass loss via a stronger early solar wind could be responsible for the observed solar lithium and beryllium depletion. This depletion requires a total mass loss of approx. 0.1, nearly independent of the mass loss timescale. The authors have calculated the evolution and oscillation frequencies of solar models including helium and heavier element diffusion, and such early solar mass loss. For models with gradual early mass loss (during approx. 1 Gyr), the early mass loss phase decreases the total amount of helium and heavier elements diffused from the convection zone, and the extent of the diffusion-produced composition gradient just below the convection zone, deteriorating the agreement with observed frequencies for intermediate (ell) modes. The mass loss phase must be confined to approx. 0.2 Gyr or less to solve simultaneously the solar Li/Be problem and avoid discrepancies with solar oscillation frequencies. DOE

N95-23181*# Hughes STX, Inc., Lanham, MD.
PLASMA PROPERTIES AND MAGNETIC FIELD STRUCTURE OF THE SOLAR CORONA, BASED ON COORDINATED MAX 1991 OBSERVATIONS FROM SERTS, THE VLA, AND MAGNETOGRAPHS
Semiannual Report, 12 Jul. 1994 - 12 Jan. 1995
Jeffrey W. Brosius 12 Jan. 1995 12 p
(Contract NASw-4933)
(NASA-CR-197864; NAS 1.26:197864) Avail: CASI HC A03/MF A01

The purposes of this investigation are to determine the plasma properties and magnetic field structure of the solar corona using coordinated observations obtained with NASA/GSFC's Solar EUV rocket Telescope and Spectrograph (SERTS), the Very Large Array (VLA), and magnetographs. The observations were obtained under the auspices of NASA's Max '91 program. The methods of achieving the stated purposes of this investigation are: (1) to use SERTS spectra and spectroheliograms to determine coronal plasma properties such as temperature, density, and emission measure; (2) to use the coronal plasma properties to calculate the intensity of the thermal bremsstrahlung microwave emission from the coronal plasma (the minimum microwave intensity expected from the emitting plasma); (3) to establish which emission mechanism(s) contribute to the observed microwave emission by comparing the calculated thermal bremsstrahlung intensity with the observed microwave intensity; (4) to derive the coronal magnetic field for regions in which gyroemission contributes to the microwave emission by determining the appropriate harmonic of the local electron gyrofrequency; (5) to derive the coronal magnetic field for regions in which thermal bremsstrahlung emission alone is responsible for the observed microwave emission by calculating the magnetic field which yields the observed microwave polarization; (6) to derive three-dimensional models of the coronal plasma and magnetic field which are consistent with all of the EUV spectra and spectroheliograms, as well as with the intensity and polarization maps at all of the microwave observing frequencies; and (7) to compare the coronal magnetic field derived from the coordinated multiwaveband observations with extrapolations from photospheric magnetograms. Author

N95-23584# Argonne National Lab., IL.
LONG-BASELINE NEUTRINO OSCILLATION EXPERIMENTS
D. Crane and M. Goodman 1994 6 p Presented at the Snowmass 94: Particle and Astrophysics in the Next Millenium, Snowmass, CO, 29 Jun. - 14 Jul. 1994
(Contract W-31-109-eng-38)
(DE95-004636; ANL-HEP-CP-94-82; CONF-9406269-3) Avail: CASI HC A02/MF A01

There is no unambiguous definition for long baseline neutrino oscillation experiments. The term is generally used for accelerator neutrino oscillation experiments which are sensitive to Delta sq m less than 1.0 eV(sup 2), and for which the detector is not on the accelerator site. The Snowmass N2L working group met to discuss the issues facing such experiments. The Fermilab Program Advisory Committee adopted several recommendations concerning the Fermilab neutrino program at their Aspen meeting immediately prior to the Snowmass Workshop. This heightened the attention for the proposals to use Fermilab for a long-baseline neutrino experiment at the workshop. The plan for a neutrino oscillation program at Brookhaven was also thoroughly discussed. Opportunities at CERN were considered, particularly the use of detectors at the Gran Sasso laboratory. The idea to build a neutrino beam from KEK towards Superkamiokande was not discussed at the Snowmass meeting, but there has been considerable development of this idea since then. Brookhaven and KEK would use low energy neutrino beams, while FNAL and CERN would plan have medium energy beams. This report will summarize a few topics common to LBL proposals and attempt to give a snapshot of where things stand in this fast developing field. DOE

N95-23925# National Geophysical Data Center, Boulder, CO.
SOLAR-GEOPHYSICAL DATA NUMBER 602, OCTOBER 1994. PART 1: (PROMPT REPORTS). DATA FOR SEPTEMBER, AUGUST 1994, AND LATE DATA
Helen E. Coffey, ed. Oct. 1994 135 p
(ISSN 0038-0911)
(PB95-149357; SGD-602-Pt-1; LC-79-640375) Avail: CASI HC A07/MF A02

This document contains the following: Detailed Index for 1994; Data for September 1994 -- Solar-Terrestrial Environment, IUWDS Alert Periods (Advanced and Worldwide), Solar Activity Indices, Solar Flares, Solar Radio Emission, Stanford Mean Solar Magnetic Field, GOES-7 Daily Electron Fluence; Data for August 1994 -- Solar Active Regions, Sudden Ionospheric Disturbances, Solar Radio Spectral Observations, Solar Radioheliograph-164 MHz-Nancay, Cosmic Ray Measurements by Neutron Monitor, Geomagnetic Indices, Principal Magnetic Storms, Sudden Commencements/Solar Flare Effects; Late Data -- Geomagnetic Activity Indices March-April 1994, Cosmic Rays Graph Haleakala 17-20 May 1994. NTIS

N95-23926# National Geophysical Data Center, Boulder, CO.
SOLAR-GEOPHYSICAL DATA NUMBER 602, OCTOBER 1994. PART 2: (COMPREHENSIVE REPORTS). DATA FOR APRIL 1994, AND MISCELLANEOUS
Helen E. Coffey, ed. Oct. 1994 44 p
(ISSN 0038-0911)
(PB95-149365; SGD-602-Pt-2; LC-79-640375) Avail: CASI HC A03/MF A01

This document contains: Detailed Index for 1994; Data for April 1994 -- Solar Flares, Solar Radio Bursts at Fixed Frequencies, Solar X-Ray Radiation from GOES Satellite, Active Prominences and Filaments; Miscellaneous Data -- Solar X-Ray Radiation from SOLRAD Satellites -- SOLRAD Daily X-ray Background March 1968-February 1973. NTIS

N95-23808*# Naval Research Lab., Washington, DC.
RESULTS FROM THE HEAVY IONS IN SPACE (HIIS) EXPERIMENT ON THE IONIC CHARGE STATE OF SOLAR ENERGETIC PARTICLES
Allan J. Tylka, Paul R. Boberg, James H. Adams, Jr., Lorraine P. Beahm, and Thomas Kleis (George Mason Univ., Fairfax, VA.) *In* NASA. Langley Research Center, LDEF: 69 Months in Space. Third Post-Retrieval Symposium, Part 1 Feb. 1995 p 113-127 Sponsored by ONR (For primary document see N95-23796 07-99)
(NASA Order W-18409)
Avail: CASI HC A03/MF A04

N95-23865*# Jet Propulsion Lab., California Inst. of Tech., Pasadena, CA.
A PROPOSED UPDATE TO THE SOLAR IRRADIANCE SPECTRUM USED IN LOWTRAN AND MODTRAN
Robert O. Green and Bo-Cai Gao (National Aeronautics and Space Administration. Goddard Space Flight Center, Greenbelt, MD.) *In its* Summaries of the 4th Annual JPL Airborne Geoscience Workshop. Volume 1: AVIRIS Workshop 25 Oct. 1993 p 81-84 (For primary document see N95-23844 07-42)
Avail: CASI HC A01/MF A03

93 SPACE RADIATION

Includes cosmic radiation; and inner and outer earth's radiation belts.

For biological effects of radiation see *52 Aerospace Medicine.* For theory see *73 Nuclear and High-Energy Physics.*

N95-22910*# Stanford Univ., CA. Dept. of Physics.
GAMMA RAY EMISSION FROM RADIO PULSARS Final Technical Report, 1 Aug. 1992 - 30 Nov. 1994
Roger W. Romani 30 Nov. 1994 2 p
(Grant NAG5-2307)
(NASA-CR-197917; NAS 1.26:197917) Avail: CASI HC A01/MF A01

While the proposed research received partial funding under this grant, during the term of support substantial progress was made on the development of a new model for the emission of gamma-rays from isolated rotation-powered pulsars. In phase one of the work, we showed how a modified version of the 'outer gap' model of pulsar emission could reproduce the double peaked profiles seen in CGRO pulsar observations. This work also demonstrated the spectrum of gap radiation varies significantly with position in the magnetosphere, and produced approximate computations of the emission from outer magnetosphere gap zones, including primary curvature radiation, gamma - gamma pair production and synchrotron radiation and inverse Compton scattering by the resulting secondary particles. This work was followed in phase two by a more complete treatment of the geometry of the radiation zone, and improved connections with observations at other wavelengths. Author

N95-23216*# Hampden-Sydney Coll., VA. Dept. of Physics and Astronomy.
ANALYSIS OF DATA FROM THE ENERGETIC GAMMA-RAY EXPERIMENT OF THE GAMMA RAY OBSERVATORY Semiannual Status Report No. 7, 15 Aug. 1994 - 15 Feb. 1995
Donald A. Kniffen 15 Feb. 1995 12 p
(Grant NAG5-1742)
(NASA-CR-197347; NAS 1.26:197347) Avail: CASI HC A03/MF A01

The work under the Grant has involved continued participation with the Compton Gamma Ray Observatory Energetic Gamma-Ray Experiment Telescope (EGRET) Team in the analysis of data obtained during instrument operations and the preparation of scientific papers and proposals for future observations. The EGRET team continues to submit IAU Astronomical telegrams and present many papers at scientific meetings. The EGRET Team was also successful on many proposals for the Cycle 4 portion of the mission, including long high galactic latitude studies of the diffuse extragalactic radiation in both the Northern and Southern Galactic Sky. These studies will be used in an effort to establish whether this radiation is truly diffuse or the sum of radiation from unresolved discrete sources such as radio-loud quasars. Data analysis is complete for papers on behalf of the EGRET Team by the author on general sources in the anticenter region of the galaxy, with galactic latitudes from 125 to 220 deg. A paper on this subject is in preparation for publication in the Astrophysical Journal. Another is being prepared on EGRET observations of the COS-B source 2CG135. Work is in progress for a third on the contribution of unresolved pulsars to the galactic diffuse radiations; two other papers are in analysis phase. A number of papers have been published in the last reporting period, and several others are in press currently. A summary of the publications is described. Author

N95-23370# Fermi National Accelerator Lab., Batavia, IL.
PERFORMANCE OF A LARGE SCALE SCINTILLATING FIBER TRACKER USING VLPC READOUT
Sep. 1994 7 p Presented at the Meeting of the Division of Particles and Fields of the American Physical Society, Albuquerque, NM, 2-6 Aug. 1994
(Contract DE-AC02-76CH-03000)
(DE95-003746; FNAL/C-94/312; CONF-940816-64) Avail: CASI HC A02/MF A01

The authors report on results of a cosmic-ray test of a 3,072 channel scintillating fiber tracker using Visible Light Photon Counter (VLPC) readout. This system is a prototype for the D0 detector tracking upgrade, and represents a configuration that is similar to that planned for the final detector. A detailed description of the cosmic ray test, including trigger, fiber configuration, lightguides, VLPC cassettes and cryogenics, calibration system, and DAQ is given. Tracking results with a muon momentum cutoff of 2.5 GeV/c include R-(phi) and R-Z resolution studies, light yield/mip, and efficiency measurements. Preliminary analysis gives a most probable value of 19.2 photoelectrons/mip per fiber doublet, an R-(phi) resolution of 163 microns (before corrections for fiber position survey), and an efficiency of nearly 100% after accounting for known dead channels in the system. DOE

N95-23472*# Applied Research Corp., Landover, MD.
A STUDY OF EUV EMISSION FROM THE O4f STAR ZETA PUPPIS Final Report, 15 Feb. 1994 - 14 Feb. 1995
Wayne L. Waldron and John Vallerga (Eureka Scientific, Inc., Oakland, CA.) 9 Feb. 1995 9 p
(NASA Order S-14648-F)
(NASA-CR-197350; NAS 1.26:197350; ARC-R95-233) Avail: CASI HC A02/MF A01

Our 20 ks observation did not allow us to carry out our primary objective, i.e., to test the limitations of deeply embedded EUV and X-ray sources. However, it did provide a very useful constraint in our analysis of a newly acquired high S/N ROSAT PSPC X-ray spectrum of Zeta Pup. In addition, modifications to our stellar wind opacity code have been preformed to investigate the sensitivity of the EUV opacity energy range to different photospheric model flux inputs and different wind structures. These analyses provided the justification for a 140 ks follow up EUVE Cycle III observation of this star. We have recently been informed that our requested observation has been accepted as a Type 1 target for Cycle III. The remainder of this report focuses on the following: (1) a brief background on the status of X-ray emission from OB stars; (2) a discussion on the importance of EUV observations; (3) a discussion of our scientific objectives; and (4) a summary of our technical approach for our Cycle III observation (including the predicted EUV counts for various lines.) Author

N95-23546*# Maryland Univ., College Park, MD. East-West Space Science Center.
STATISTICAL PROPERTIES OF THE TIME HISTORIES OF COSMIC GAMMA-RAY BURSTS DETECTED BY THE BATSE EXPERIMENT OF THE COMPTON GAMMA-RAY OBSERVATORY Final Report, 10 Sep. 1993 - 31 Dec. 1994
Roald Sagdeev 1995 18 p
(Contract NCC8-25)
(NASA-CR-197425; NAS 1.26:197425) Avail: CASI HC A03/MF A01

The main scientific objectives of the project were: (1) Calculation of average time history for different subsets of BATSE gamma-ray bursts; (2) Comparison of averaged parameters and averaged time history for different Burst And Transient Source Experiments (BASTE) Gamma Ray Bursts (GRB's) sets; (3) Comparison of results obtained with BATSE data with those obtained with APEX experiment at PHOBOS mission; and (4) Use the results of (1)-(3) to compare current models of gamma-ray bursts sources. Author

N95-24191*# Ultramet Co., Pacoima, CA.
HIGH ENERGY COLLIMATING FINE GRIDS Final Technical Report, May 1993 - Mar. 1994
Victor M. Arrieta, Robert H. Tuffias, and Raffaele LaFeria Feb. 1995 12 p
(Contract NAS5-32530)
(NASA-CR-197688; NAS 1.26:197688; ULT/TR-94-6505) Avail: CASI HC A03/MF A01

The objective of this project was to demonstrate the fabrication of extremely tight tolerance collimating grids using a high-Z material, specifically tungsten. The approach taken was to fabricate grids by a replication method involving the coating of a silicon grid substrate with tungsten by chemical vapor deposition (CVD). A negative of the desired grid structure was fabricated in silicon using highly wafering techniques developed for the semiconductor industry and capable of producing the required tolerances. Using diamond wafering blades, a network of accurately spaced slots was machined into a single-crystal silicon surface. These slots were then filled with tungsten by CVD, via the hydrogen reduction of tungsten hexafluoride. Following tungsten deposition, the silicon negative was etched away to leave the tungsten collimating grid structure. The project was divided into five tasks: (1) identify materials of construction for the replica and final

collimating grid structures; (2) identify and implement a micromachining technique for manufacturing the negative collimator replicas (performed by NASA/JPL); (3) develop a CVD technique and processing parameters suitable for the complete tungsten densification of the collimator replicas; (4) develop a chemical etching technique for the removal of the collimator replicas after the tungsten deposition process; and (5) fabricate and deliver tungsten collimating grid specimens. Author

N95-23800*# Deutsche Forschungsanstalt fuer Luft- und Raumfahrt, Cologne (Germany). Inst. for Aerospace Medicine, Radiation and Biology.
DOSIMETRIC RESULTS ON EURECA
G. Reitz *In* NASA. Langley Research Center, LDEF: 69 Months in Space. Third Post-Retrieval Symposium, Part 1 Feb. 1995 p 37-42 (For primary document see N95-23796 07-99)
Avail: CASI HC A02/MF A04

N95-23801*# San Francisco Univ., CA. Physics Research Lab.
PRELIMINARY RESULTS OF RADIATION MEASUREMENTS ON EURECA
E. V. Benton and A. L. Frank *In* NASA. Langley Research Center, LDEF: 69 Months in Space. Third Post-Retrieval Symposium, Part 1 Feb. 1995 p 43-50 (For primary document see N95-23796 07-99)
(Grant NAG9-235)
Avail: CASI HC A02/MF A04

N95-23805*# National Aeronautics and Space Administration. Marshall Space Flight Center, Huntsville, AL.
LDEF CONTRIBUTIONS TO COSMIC RAY AND RADIATION ENVIRONMENTS RESEARCH Abstract Only
Thomas A. Parnell *In* NASA. Langley Research Center, LDEF: 69 Months in Space. Third Post-Retrieval Symposium, Part 1 Feb. 1995 p 89 (For primary document see N95-23796 07-99)
Avail: CASI HC A01/MF A04

N95-23806*# Kiel Univ. (Germany). Inst. fuer Reine und Angewandte Kernphysik.
TRAPPED IRON MEASURED ON LDEF
R. Beaujean, D. Jonathal, S. Barz, and W. Enge *In* NASA. Langley Research Center, LDEF: 69 Months in Space. Third Post-Retrieval Symposium, Part 1 Feb. 1995 p 91-99 Sponsored by BMFT (For primary document see N95-23796 07-99)
(Grant DARA-OS-9001)
Avail: CASI HC A02/MF A04

N95-23809*# Dublin Inst. for Advanced Studies (Ireland).
EARLY RESULTS FROM THE ULTRA HEAVY COSMIC RAY EXPERIMENT
D. OSullivan, A. Thompson, J. Bosch, R. Keegan, K.-P. Wenzel (European Space Agency. European Space Research and Technology Center, ESTEC, Noordwijk, Netherlands.), F. Jansen (European Space Agency. European Space Research and Technology Center, ESTEC, Noordwijk, Netherlands.), and C. Domingo (Autonoma de Barcelona Univ., Barcelona, Spain.) *In* NASA. Langley Research Center, LDEF: 69 Months in Space. Third Post-Retrieval Symposium, Part 1 Feb. 1995 p 129-133 (For primary document see N95-23796 07-99)
Avail: CASI HC A01/MF A04

99 GENERAL

N95-22920*# National Aeronautics and Space Administration. Ames Research Center, Moffett Field, CA.
DIRECTOR'S DISCRETIONARY FUND REPORT FOR FISCAL YEAR 1994 Report, Oct. 1993 - Sep. 1994
Feb. 1995 110 p
(RTOP 307-51-50)
(NASA-TM-108848; A-94135; NAS 1.15:108848) Avail: CASI HC A06/MF A02

This technical memorandum contains brief technical papers describing research and technology development programs sponsored by the Ames Research Center Director's Discretionary Fund during fiscal year 1991 (October 1993 through September 1994). An appendix provides administrative information for each of the sponsored research programs. Author

N95-23276*# Hampton Univ., VA. Dept. of Architecture.
1994 NASA-HU AMERICAN SOCIETY FOR ENGINEERING EDUCATION (ASEE) SUMMER FACULTY FELLOWSHIP PROGRAM Abstracts Only
John H. Spencer, comp. and Deborah B. Young, comp. (Old Dominion Coll., Norfolk, VA.) Dec. 1994 155 p Program held in Hampton, VA, 6 Jun. - 12 Aug. 1994
(Grant NGT-47-020-800)
(NASA-CR-194972; NAS 1.26:194972) Avail: CASI HC A08/MF A02

Since 1964, the National Aeronautics and Space Administration (NASA) has supported a program of summer faculty fellowships for engineering and science educators. In a series of collaborations between NASA research and development centers and nearby universities, engineering faculty members spend 10 weeks working with professional peers on research. The Summer Faculty Program Committee of the American Society for Engineering Education supervises the programs. Objectives: (1) To further the professional knowledge of qualified engineering and science faculty members; (2) To stimulate and exchange ideas between participants and NASA; (3) To enrich and refresh the research and teaching activities of participants' institutions; (4) To contribute to the research objectives of the NASA center. For individual titles, see N95-23277 through N95-23333.

N95-23277*# Iowa State Univ. of Science and Technology, Ames, IA. Dept. of Aerospace Engineering and Engineering Mechanics.
IDEALIZED TEXTILE COMPOSITES FOR EXPERIMENTAL/ANALYTICAL CORRELATION Abstract Only **c24**
Daniel O. Adams *In* Hampton Univ., 1994 NASA-HU American Society for Engineering Education (ASEE) Summer Faculty Fellowship Program Dec. 1994 p 57 (For primary document see N95-23276 07-99)
Avail: CASI HC A01/MF A02

Textile composites are fiber reinforced materials produced by weaving, braiding, knitting, or stitching. These materials offer possible reductions in manufacturing costs compared to conventional laminated composites. Thus, they are attractive candidate materials for aircraft structures. To date, numerous experimental studies have been performed to characterize the mechanical performance of specific textile architectures. Since many materials and architectures are of interest, there is a need for analytical models to predict the mechanical properties of a specific textile composite material. Models of varying sophistication have been proposed based on mechanics of materials, classical laminated plate theory, and the finite element method. These modeling approaches assume an idealized textile architecture and generally consider a single unit cell. Due to randomness of the textile architectures produced using conventional processing techniques, experimental data obtained has been of limited use for verifying the accuracy of these analytical approaches. This research is focused on fabricating woven textile composites with highly aligned and accurately placed fiber tows that closely represent the idealized architectures assumed in analytical models. These idealized textile composites have been fabricated with three types of layer nesting configurations: stacked, diagonal, and split-span. Compression testing results have identified strength variations as a function of nesting. Moire interferometry experiments are being used to determine localized deformations for detailed correlation with model predictions. Author

N95-23278*# South Dakota State Univ., Brookings, SD. Dept. of Electrical Engineering.
STUDY OF ATMOSPHERIC PARAMETERS MEASUREMENTS USING MM-WAVE RADAR IN SYNERGY WITH LITE-2 Abstract Only **c46**
Madeleine Y. Andrawis *In* Hampton Univ., 1994 NASA-HU American Society for Engineering Education (ASEE) Summer Faculty Fellowship Program Dec. 1994 p 58 (For primary document see N95-23276 07-99)
Avail: CASI HC A01/MF A02

The Lidar In-Space Technology Experiment, (LITE), has been developed, designed, and built by NASA Langley Research Center, to be flown on the space shuttle 'Discovery' on September 9, 1994. Lidar, which stands for light detecting and ranging, is a radar system that uses short pulses of laser light instead of radio waves in the case of the common radar. This

space-based lidar offers atmospheric measurements of stratospheric and tropospheric aerosols, the planetary boundary layer, cloud top heights, and atmospheric temperature and density in the 10-40 km altitude range. A study is being done on the use, advantages, and limitations of a millimeterwave radar to be utilized in synergy with the Lidar system, for the LITE-2 experiment to be flown on a future space shuttle mission. The lower atmospheric attenuation, compared to infrared and optical frequencies, permits the millimeter-wave signals to penetrate through the clouds and measure multi-layered clouds, cloud thickness, and cloud-base height. These measurements would provide a useful input to radiation computations used in the operational numerical weather prediction models, and for forecasting. High power levels, optimum modulation, data processing, and high antenna gain are used to increase the operating range, while space environment, radar tradeoffs, and power availability are considered. Preliminary, numerical calculations are made, using the specifications of an experimental system constructed at Georgia Tech. The noncoherent 94 GHz millimeter-wave radar system has a pulsed output with peak value of 1 kW. The backscatter cross section of the particles to be measured, that are present in the volume covered by the beam footprint, is also studied. Author

N95-23279*# Old Dominion Coll., Norfolk, VA. Dept. of Engineering Management.

A MANUFACTURING DATABASE OF ADVANCED MATERIALS USED IN SPACECRAFT STRUCTURES Abstract Only **c18**

Han P. Bao *In* Hampton Univ., 1994 NASA-HU American Society for Engineering Education (ASEE) Summer Faculty Fellowship Program Dec. 1994 p 59 (For primary document see N95-23276 07-99)

Avail: CASI HC A01/MF A02

Cost savings opportunities over the life cycle of a product are highest in the early exploratory phase when different design alternatives are evaluated not only for their performance characteristics but also their methods of fabrication which really control the ultimate manufacturing costs of the product. In the past, Design-To-Cost methodologies for spacecraft design concentrated on the sizing and weight issues more than anything else at the early so-called 'Vehicle Level' (Ref: DOD/NASA Advanced Composites Design Guide). Given the impact of manufacturing cost, the objective of this study is to identify the principal cost drivers for each materials technology and propose a quantitative approach to incorporating these cost drivers into the family of optimization tools used by the Vehicle Analysis Branch of NASA LaRC to assess various conceptual vehicle designs. The advanced materials being considered include aluminum-lithium alloys, thermoplastic graphite-polyether etherketone composites, graphite-bismaleimide composites, graphite- polyimide composites, and carbon-carbon composites. Two conventional materials are added to the study to serve as baseline materials against which the other materials are compared. These two conventional materials are aircraft aluminum alloys series 2000 and series 7000, and graphite-epoxy composites T-300/934. The following information is available in the database. For each material type, the mechanical, physical, thermal, and environmental properties are first listed. Next the principal manufacturing processes are described. Whenever possible, guidelines for optimum processing conditions for specific applications are provided. Finally, six categories of cost drivers are discussed. They include, design features affecting processing, tooling, materials, fabrication, joining/assembly, and quality assurance issues. It should be emphasized that this database is not an exhaustive database. Its primary use is to make the vehicle designer aware of some of the most important aspects of manufacturing associated with his/her choice of the structural materials. The other objective of this study is to propose a quantitative method to determine a Manufacturing Complexity Factor (MCF) for each material being contemplated. This MCF is derived on the basis of the six cost drivers mentioned above plus a Technology Readiness Factor which is very closely related to the Technology Readiness Level (TRL) as defined in the Access To Space final report. Short of any manufacturing information, our MCF is equivalent to the inverse of TRL. As more manufacturing information is available, our MCF is a better representation (than TRL) of the fabrication processes involved. The most likely application for MCF is in cost modeling for trade studies. On-going work is being pursued to expand the potential applications of MCF. Author

N95-23280*# Hampton Univ., VA.

INFINITE POSSIBILITIES: COMPUTATIONAL STRUCTURES TECHNOLOGY Abstract Only **c39**

Sherilee F. Beam *In its* 1994 NASA-HU American Society for Engineering Education (ASEE) Summer Faculty Fellowship Program Dec. 1994 p 60 (For primary document see N95-23276 07-99)

Avail: CASI HC A01/MF A02

Computational Fluid Dynamics (or CFD) methods are very familiar to the research community. Even the general public has had some exposure to CFD images, primarily through the news media. However, very little attention has been paid to CST--Computational Structures Technology. Yet, no important design can be completed without it. During the first half of this century, researchers only dreamed of designing and building structures on a computer. Today their dreams have become practical realities as computational methods are used in all phases of design, fabrication and testing of engineering systems. Increasingly complex structures can now be built in even shorter periods of time. Over the past four decades, computer technology has been developing, and early finite element methods have grown from small in-house programs to numerous commercial software programs. When coupled with advanced computing systems, they help engineers make dramatic leaps in designing and testing concepts. The goals of CST include: predicting how a structure will behave under actual operating conditions; designing and complementing other experiments conducted on a structure; investigating microstructural damage or chaotic, unpredictable behavior; helping material developers in improving material systems; and being a useful tool in design systems optimization and sensitivity techniques. Applying CST to a structure problem requires five steps: (1) observe the specific problem; (2) develop a computational model for numerical simulation; (3) develop and assemble software and hardware for running the codes; (4) post-process and interpret the results; and (5) use the model to analyze and design the actual structure. Researchers in both industry and academia continue to make significant contributions to advance this technology with improvements in software, collaborative computing environments and supercomputing systems. As these environments and systems evolve, computational structures technology will evolve. By using CST in the design and operation of future structures systems, engineers will have a better understanding of how a system responds and lasts, more cost-effective methods of designing and testing models, and improved productivity. For informational and educational purposes, a videotape is being produced using both static and dynamic images from research institutions, software and hardware companies, private individuals, and historical photographs and drawings. The extensive number of CST resources indicates its widespread use. Applications run the gamut from simpler university-simulated problems to those requiring solutions on supercomputers. In some cases, an image or an animation will be mapped onto the actual structure to show the relevance of the computer model to the structure. Transferring the digital files to videotape presents a number of problems related to maintaining the quality of the original image, while still producing a broadcast quality videotape. Since researchers normally do not create a computer image using traditional composition theories or video production requirements, often the image loses some of its original digital quality and impact when transferred to videotape. Although many CST images are currently available, those that are edited into the final project must meet two important criteria: they must complement the narration, and they must be broadcast quality when recorded on videotape. Author

N95-23281*# Carnegie-Mellon Univ., Pittsburgh, PA. Dept. of Mechanical Engineering.

SEPARATION OF CRACK EXTENSION MODES IN COMPOSITE DELAMINATION PROBLEMS Abstract Only **c39**

Jack L. Beuth *In* Hampton Univ., 1994 NASA-HU American Society for Engineering Education (ASEE) Summer Faculty Fellowship Program Dec. 1994 p 61 (For primary document see N95-23276 07-99)

Avail: CASI HC A01/MF A02

This work concerns fracture mechanics modeling of composite delamination problems. In order to predict delamination resistance, an applied stress intensity factor, K, or energy release rate, G, must be compared to a mode-dependent critical value of K or G from experiment. In the interfacial fracture analysis of most applications and some tests, the mode of crack extension is not uniquely defined. It is instead a function of distance from the crack tip due to the oscillating singularity existing at the tip. In this work, a consistent method is presented of extracting crack extension modes in such cases. In particular, use of the virtual crack closure technique (VCCT) to extract modes of crack extension is studied for cases of a

crack along the interface between two in-plane orthotropic materials. Modes of crack extension extracted from oscillatory analyses using VCCT are a function of the virtual crack extension length, delta. Most existing efforts to obtain delta-independent modes of crack extension involve changing the analysis in order to eliminate its oscillatory nature. One such method involves changing one or more properties of the layers to make the oscillatory exponent parameter, epsilon, equal zero. Standardized application of this method would require consistent criteria for identifying which properties can be altered without changing the physical aspects of the problem. Another method involves inserting a thin homogeneous layer (typically referred to as a resin interlayer) along the interface and placing the crack within it. The drawbacks of this method are that it requires increased modeling effort and introduces the thickness of the interlayer as an additional length parameter. The approach presented here does not attempt to alter the interfacial fracture analysis to eliminate its oscillatory behavior. Instead, the argument is made that the oscillatory behavior is non-physical and that if its effects were separated from VCCT quantities, then consistent, delta-independent modes of crack extension could be defined. Knowledge of the near-tip fields in a planar orthotropic material interfacial fracture analysis is used to determine the explicit delta dependence of VCCT parameters. Once this delta dependence is determined, energy release rates are defined with this delta dependence factored out. This modified VCCT method is applied to results from two finite element test cases. It is shown that, as predicted, delta-independent modes of crack extension result. The modified VCCT approach shows potential as a consistent method of extracting crack extension modes. It uses the same information from a finite element analysis (i.e., nodal forces and displacements) as the traditional VCCT method does. The A-independent modes extracted using the modified VCCT approach can also be used as guides to test the convergence of finite element solutions. Author

N95-23282*# Old Dominion Coll., Norfolk, VA.
PROJECT: INTERNAL COMMUNICATIONS Abstract Only **c81**
Lydia Black *In* Hampton Univ., 1994 NASA-HU American Society for Engineering Education (ASEE) Summer Faculty Fellowship Program Dec. 1994 p 62 (For primary document see N95-23276 07-99)
Avail: CASI HC A01/MF A02

The purpose of this study was to ascertain the perceived information needs of NASA Langley employees. One hundred and twelve face-to-face interviews were conducted with a representative sample of aero-space technologists, administrative professionals, technicians. and secretarial/clerical personnel. Results of employee perceptions are analyzed and summarized using affinity diagramming. Particular strategies to maximize use of existing internal communication networks are discussed. Author

N95-23283*# Mississippi State Univ., Mississippi State, MS. Dept. of Aerospace Engineering.
CROSSFLOW INSTABILITY CONTROL ON A SWEPT-WING: PRELIMINARY STUDIES Abstract Only **c02**
David H. Bridges *In* Hampton Univ., 1994 NASA-HU American Society for Engineering Education (ASEE) Summer Faculty Fellowship Program Dec. 1994 p 63 (For primary document see N95-23276 07-99)
Avail: CASI HC A01/MF A02

The pressure distribution on a swept wing causes the streamlines at the edge of the boundary layer to be curved. This pressure gradient normal to the external streamline creates a velocity component normal to the external streamline within the boundary layer which is referred to as the crossflow velocity. Because the crossflow velocity profile perpendicular to the wing surface has an inflection point, the profile is unstable. The stationary instability mode takes the form of crossflow vortices. Under these conditions, the boundary layer on the wing is extremely unstable and transition to turbulent flow takes place much closer to the leading edge of the wing than it would on an unswept wing. Higher skin friction drag is associated with turbulent flow, and so better aircraft performance could be obtained if the crossflow could be eliminated One method of controlling crossflow that is being investigated is boundary-layer suction. An extensive airfoil suction experiment in the 8 feet Transonic Pressure Tunnel (TPT) at NASA Langley Research Center will begin late in 1994. Because of the size, complexity, and expense associated with this test, a number of 'risk-reduction' tests are currently being conducted. The 20 x 28 in. Shear Flow Control Tunnel at NASA Langley is being used for some of these tests. Prior to the summer of 1994, a flat plate with a swept leading edge was installed in the 20 x 28 in. tunnel, with a displacement body mounted on the tunnel ceiling that created a pressure distribution on the plate similar to the pressure distribution on a swept wing. The flow over the plate was investigated during the summer of 1994 using a laser Doppler velocimeter (LDV) system. The LDV measurements indicated the possible presence of multiple disturbance modes, a rarely-seen phenomena since, in most tests, one disturbance mode dominates. The possible existence of multiple disturbance modes in the flat plate boundary layer, however, means that the flow in the 20 x 28 in. tunnel is of interest itself, and will be investigated more thoroughly in the future. With a view to these investigations, the boundary layer traverse mechanism in the 20 x 28 in. tunnel was modified to improve its performance, and strain gauges were mounted on the traverse in order to monitor its deflection during a test. Other preliminary work conducted in the 20 x 28 in. tunnel included the use of an infrared camera system. Previous work with this system showed that transition indeed could be detected, but the signal produced by the crossflow vortices was too weak to be detected. It was hoped that spraying the flat plate with naphthalene would augment the heat transfer associated with the crossflow vortices so that they would show up in a IR image; however, experiments showed that this would not work. Another set of tests was conducted in the 20 x 28 in. tunnel to determine the tripping requirements for a set of airfoil-shaped struts that will be used in the 8 feet TPT experiment. Since the Reynolds number associated with these struts is small, a laminar boundary layer would separate early, causing large fluctuations in the flow field. A turbulent boundary layer would remain attached further back, but tripping from laminar to turbulent flow at low Reynolds number is very difficult. However, trip strip configurations were found that should effectively trip the boundary layer at the required conditions. Currently underway is an investigation of the data acquisition requirements for the 8 feet TPT experiment, with the purpose of the finding the minimum amount of data needed to characterize sufficiently the swept-wing boundary layer. This study is being conducted using a numerically generated data set. Author

N95-23284*# Arkansas Univ., Pine Bluff, AR. Dept. of Mathematics and Computer Science.
AUTOMATION TECHNOLOGY USING GEOGRAPHIC INFORMATION SYSTEM (GIS) Abstract Only **c82**
Cynthia L. Brooks *In* Hampton Univ., 1994 NASA-HU American Society for Engineering Education (ASEE) Summer Faculty Fellowship Program Dec. 1994 p 64 (For primary document see N95-23276 07-99)
Avail: CASI HC A01/MF A02

Airport Surface Movement Area is but one of the actions taken to increase the capacity and safety of existing airport facilities. The System Integration Branch (SIB) has designed an integrated system consisting of an electronic moving display in the cockpit, and includes display of taxi routes which will warn controllers and pilots of the position of other traffic and warning information automatically. Although, this system has in test simulation proven to be accurate and helpful; the initial process of obtaining an airport layout of the taxi-routes and designing each of them is a very tedious and time-consuming process. Other methods of preparing the display maps are being researched. One such method is the use of the Geographical Information System (GIS). GIS is an integrated system of computer hardware and software linking topographical, demographic and other resource data that is being referenced. The software can support many areas of work with virtually unlimited information compatibility due to the system's open architecture. GIS will allow us to work faster with increased efficiency and accuracy while providing decision making capabilities. GIS is currently being used at the Langley Research Center with other applications and has been validated as an accurate system for that task. GIS usage for our task will involve digitizing aerial photographs of the topology for each taxi-runway and identifying each position according to its specific spatial coordinates. The information currently being used can be integrated with the GIS system, due to its ability to provide a wide variety of user interfaces. Much more research and data analysis will be needed before this technique will be used, however we are hopeful this will lead to better usage of man-power and technological capabilities for the future. Author

N95-23285*# Montana State Univ., Bozeman, MT. Dept. of Electrical Engineering.
MEASUREMENTS OF STRIAE IN CR+ DOPED YAG LASER CRYSTALS Abstract Only **c76**

Fredrick M. Cady *In* Hampton Univ., 1994 NASA-HU American Society for Engineering Education (ASEE) Summer Faculty Fellowship Program Dec. 1994 p 65 (For primary document see N95-23276 07-99)
Avail: CASI HC A01/MF A02

Striations in Czochralski (CZ) grown crystals have been observed in materials such as GaAs, silicon, photorefractive crystals used for data storage, potassium titanyl phosphate crystals and LiNbO3. Several techniques have been used for investigating these defects including electron microscopy, laser scanning tomography, selective photoetching, X-ray diffuse scattering, interference orthoscopy, laser interferometry and micro-Fourier transform infrared spectroscopy mapping. A 2mm thick sample of the material to be investigated is illuminated with light that is absorbed and non-absorbed by the ion concentration to be observed. The back surface of the sample is focused onto a solid-state image detector and images of the input beam and absorbed (and diffracted) beams are captured at two wavelengths. The variation of the coefficient of absorption asa function of distance on the sample can be derived from these measurements. A Big Sky Software Beamcode system is used to capture and display images. Software has been written to convert the Beamcode data files to a format that can be imported into a spreadsheet program such as Quatro Pro. The spreadsheet is then used to manipulate and display data. A model of the intensity map of the striae collected by the imaging system has been proposed and a data analysis procedure derived. From this, the variability of the attenuation coefficient alpha can be generated. Preliminary results show that alpha may vary by a factor of four or five over distances of 100 mu m. Potential errors and problems have been discovered and additional experiments and improvements to the experimental setup are in progress and we must now show that the measurement techniques and data analysis procedures provide 'real' information. Striae are clearly visible at all wavelengths including white light. Their basic spatial frequency does not change radically, at least when changing from blue to green to white light. Further experimental and theoretical work can be done to improve the data collection techniques and to verify the data analysis procedures. Author

N95-23286*# Pennsylvania State Univ., University Park, PA. Instructional Systems Program.
FORMATIVE AND SUMMATIVE EVALUATION EFFORTS FOR THE TEACHER ENHANCEMENT INSTITUTE CONDUCTED AT THE NASA LANGLEY RESEARCH CENTER, SUMMER 1994 Abstract Only **c80**
Randal D. Carlson *In* Hampton Univ., 1994 NASA-HU American Society for Engineering Education (ASEE) Summer Faculty Fellowship Program Dec. 1994 p 66-67 (For primary document see N95-23276 07-99)
Avail: CASI HC A01/MF A02

The Teacher Enhancement Institute (TEI) at NASA Langley Research Center was developed in response to Executive Order 12821 which mandates national laboratories to 'assist in the mathematics and science education of our Nation's students, teachers, parents, and the public by establishing programs at their agency to provide for training elementary and secondary school teachers to improve their knowledge of mathematics and science. Such programs, to the maximum extent possible, shall involve partnerships with universities, state and local elementary and secondary school authorities, corporations and community based organizations'. The faculty worked closely with one another and the invited speakers to insure that the sessions supported the objectives. Speakers were informed of the objectives and given guidance concerning form and function for the session. Faculty members monitored sessions to assist speakers and to provide a quality control function. Faculty provided feedback to speakers concerning general objective accomplishment. Participant comments were also provided when applicable. Post TEI surveys asked for specific comments about each TEI session. During the second of the two, two week institutes, daily critiques were provided to the participants for their reflection. This seemed to provide much improved feedback to speakers and faculty because the sessions were fresh in each participant's mind. Between sessions one and two, some changes were made to the program as a result of the formative evaluation process. Those changes, though, were minor in nature and comprised what may be called 'fine tuning' a well conceived and implemented program. After the objectives were written, an assessment instrument was developed to test the accomplishment of the objectives. This instrument was actually two surveys, one given before the TEI and one given after the TEI. In using such a series, it was expected that changes in the participants induced by attendance at TEI may be discovered. Because the institute was limited in time and depth of exposure, attitudinal changes (self-assessment of ability and confidence) were chosen to be surveyed. On the pre-survey, seven general categories of questions were asked. The post-survey repeated three of these categories, providing a pre and post evaluation of the same questions and added a fourth category which asked the participant to self-assess objective accomplishment. The assessment process for TEI was valuable when one looks at the final accomplishments of the TEI. A number of aspects stand out: (1) formative evaluation during project development allowed the goals and objectives to guide the development of the institute; (2) formative evaluation provided positive guidance to presenters in developing and implementing their session; (3) formative evaluation helped presenters to improve or focus their sessions; (4) summative evaluation provided managers a way to gauge the success of the institute; (5) summative evaluation provided a benchmark for future programs to be measured against. Author

N95-23287*# Illinois Univ., Chicago, IL.
HOLOGRAPHIC INTERFEROMETRIC TOMOGRAPHY FOR RECONSTRUCTING FLOW FIELDS Abstract Only **c35**
Soyoung S. Cha *In* Hampton Univ., 1994 NASA-HU American Society for Engineering Education (ASEE) Summer Faculty Fellowship Program Dec. 1994 p 68 (For primary document see N95-23276 07-99)
Avail: CASI HC A01/MF A02

Holographic interferometric tomography is a technique for instantaneously capturing and quantitatively reconstructing three-dimensional flow fields. It has a very useful application potential for high-speed aerodynamics. However, three major challenging tasks need to be accomplished before its practical applications. First, fluid flows are mostly unsteady or at least non repeatable. Consequently, a means for Instantaneously recording three-dimensional flow fields, that is, a simple holographic technique for simultaneously recording multi-directional projections, needs to be developed. Second, while holographic interferometry provides enormous data storage capabilities, expeditious data extraction from complicated interferograms is very important for timely near real-time applications. Third, unlike medical applications, flow tomography does not provide complete data sets but instead involves ill-posed reconstruction problems of incomplete projection and limited angular scanning. During this summer research period, new experimental techniques and corresponding hardware were developed and tested to address the above mentioned tasks. The first task was achieved by diffuser illumination. This concept allows instantaneous capture of many projections with a conventional setup for single-projection recording. For the second task, a phase-shifting technique was incorporated. This technique allows one to acquire multiple phase-stepped interferograms for a single projection and thus to extract phase information from intensity data almost at real-time. For the third task, the research that has been extensively conducted previously was utilized. In this research period, a complete experimental setup that provides the above three major capabilities was designed, built, and tested by integrating all the techniques. A simple laboratory experiment for simulating wind-tunnel testing was then conducted. A test flow was produced by employing a relatively simple device that generated a gravity-driven flow. The flow was then experimentally investigated to check the viability of the holographic interferometric tomographic technique before wind-tunnel application. Author

N95-23288*# Boston Univ., MA. Dept. of Aerospace and Mechanical Engineering.
FABRIC GEOMETRY DISTORTION DURING COMPOSITES PROCESSING Abstract Only **c24**
Julie Chen *In* Hampton Univ., 1994 NASA-HU American Society for Engineering Education (ASEE) Summer Faculty Fellowship Program Dec. 1994 p 69 (For primary document see N95-23276 07-99)
Avail: CASI HC A01/MF A02

Waviness and tow misalignment are often cited as possible causes of data scatter and lower compression stiffness and strength in textile composites. Strength differences of as much as 40 percent have been seen in composites that appear to have the same basic material and structural properties -- i.e., yarn orientation, yarn size, interlacing geometry. Fabric geometry distortion has been suggested as a possible reason for this discrepancy, but little quantitative data or substantial evidence exists. The focus of this research is to contribute to the present understanding of the causes and effects of geometric distortion in textile composites. The initial part of the study was an attempt to gather qualitative information on

a variety of textile structures. Existing and new samples confirmed that structures with a significant direction presence would be more susceptible to distortion due to the compaction process. Thus, uniweaves (fiber vol frac: 54-72 percent) biaxial braids (vf: 34-58 percent) demonstrated very little fabric geometry distortion. In stitched panels, only slight buckling of z-direction stitches was observed, primarily near the surface. In contrast, for structures with high compaction ratios -- e.g., large cylindrical yarns (2.5:1) orpowder towpreg (4:1) -- there were visible distortions where previously smooth and periodic undulations were transformed to abrupt changes in direction. A controlled study of the effect of forming pressure on distortion was conducted on type 162 glass plain weave fabrics. Panels (6 x 6 in) were produced via a resin infusion type setup, but with an EPON 815 epoxy resin. Pressures ranging from hand layup to 200 psi were used (vf: 34-54 percent). Photomicrographs indicated that at pressures up to 50 psi, large changes in thickness were due primarily to resin squeeze out. At higher pressures, when intimate contact was made between the layers, there was some tow flattening and in-plane shifting to optimize nesting. However, even at 200 psi the period and amplitude of the tow undulation remained constant, suggesting that for this relatively fine fabric, distortions from compaction were not a problem. Because of the interest in using larger tows (to reduce cost) and more complex structures, tests were also run on 2D triaxial glass braid (113 yd/lb at 0, 225 yd/lb at +/- 45). Forming pressures of 20, 50, 200, and 500 psi were used, and short block compression tests were run. The 500 psi specimen had a 10 percent decrease in modulus and an almost 50 percent decrease in strength (vs. 20 psi). Because the total fiber wgt/panel was kept constant, the thickness varied from 0.32 to 0.22 in (49-70 percent vf). Yet, the strength value is clearly below what would be expected, even with the decrease in thickness. Photomicrographs of these samples will be taken to determine if more fabric distortion exists in the 500 psi specimens. Finally, because the ultimate goal is to be able to predict and control distortion in a variety of textile structures, a model compaction test was developed to directly measure the deformation of the tows during compaction. Layers of dry glass fabric were placed in a mold with a clear plexiglass window. The yarn amplitude and period was then calculated using image analysis of the videotaped deformation. Preliminary tests demonstrated the feasibility of this technique for simple fabrics with large tows. Author

N95-23289*# Pennsylvania State Univ., University Park, PA. Dept. of Mechanical Engineering.

DIRECT NUMERICAL SIMULATIONS AND MODELING OF A SPATIALLY-EVOLVING TURBULENT WAKE Abstract Only **c34**

John M. Cimbala *In* Hampton Univ., 1994 NASA-HU American Society for Engineering Education (ASEE) Summer Faculty Fellowship Program Dec. 1994 p 70 (For primary document see N95-23276 07-99)

Avail: CASI HC A01/MF A02

Understanding of turbulent free shear flows (wakes, jets, and mixing layers) is important, not only for scientific interest, but also because of their appearance in numerous practical applications. Turbulent wakes, in particular, have recently received increased attention by researchers at NASA Langley. The turbulent wake generated by a two-dimensional airfoil has been selected as the test-case for detailed high-resolution particle image velocimetry (PIV) experiments. This same wake has also been chosen to enhance NASA's turbulence modeling efforts. Over the past year, the author has completed several wake computations, while visiting NASA through the 1993 and 1994 ASEE summer programs, and also while on sabbatical leave during the 1993-94 academic year. These calculations have included two-equation (K-omega and K-epsilon) models, algebraic stress models (ASM), full Reynolds stress closure models, and direct numerical simulations (DNS). Recently, there has been mutually beneficial collaboration of the experimental and computational efforts. In fact, these projects have been chosen for joint presentation at the NASA Turbulence Peer Review, scheduled for September 1994. DNS calculations are presently underway for a turbulent wake at Re(sub theta) = 1000 and at a Mach number of 0.20. (Theta is the momentum thickness, which remains constant in the wake of a two dimensional body.) These calculations utilize a compressible DNS code written by M. M. Rai of NASA Ames, and modified for the wake by J. Cimbala. The code employs fifth-order accurate upwind-biased finite differencing for the convective terms, fourth-order accurate central differencing for the viscous terms, and an iterative-implicit time-integration scheme. The computational domain for these calculations starts at x/theta = 10, and extends to x/theta = 610. Fully developed turbulent wake profiles, obtained from experimental data from several wake generators, are supplied at the computational inlet, along with appropriate noise. After some adjustment period, the flow downstream of the inlet develops into a fully three-dimensional turbulent wake. Of particular interest in the present study is the far wake spreading rate and the self-similar mean and turbulence profiles. At the time of this writing, grid resolution studies are underway, and a code is being written to calculate turbulence statistics from these wake calculations; the statistics will be compared to those from the ongoing PIV wake measurements, those of previous experiments, and those predicted by the various turbulence models. These calculations will lead to significant long-term benefits for the turbulence modeling effort. In particular, quantities such as the pressure-strain correlation and the dissipation rate tensor can be easily calculated from the DNS results, whereas these quantities are nearly impossible to measure experimentally. Improvements to existing turbulence models (and development of new models) require knowledge about flow quantities such as these. Present turbulence models do a very good job at prediction of the shape of the mean velocity and Reynolds stress profiles in a turbulent wake, but significantly underpredict the magnitude of the stresses and the spreading rate of the wake. Thus, the turbulent wake is an ideal flow for turbulence modeling research. By careful comparison and analysis of each term in the modeled Reynolds stress equations, the DNS data can show where deficiencies in the models exist; improvements to the models can then be attempted. Derived from text

N95-23290*# Rochester Univ., NY. Dept. of Imaging and Photographic Technology.

SCIENTIFIC AND TECHNICAL PHOTOGRAPHY AT NASA LANGLEY RESEARCH CENTER Abstract Only **c35**

Andrew Davidhazy *In* Hampton Univ., 1994 NASA-HU American Society for Engineering Education (ASEE) Summer Faculty Fellowship Program (SEE N95-23276 07-99) Dec. 1994 (For primary document see N95-23276 07-99)

Avail: CASI HC A01/MF A02

As part of my assignment connected with the Scientific and Technical Photography & Lab (STPL) at the NASA Langley Research Center I conducted a series of interviews and observed the day to day operations of the STPL with the ultimate objective of becoming exposed first hand to a scientific and technical photo/imaging department for which my school prepares its graduates. I was also asked to share my observations with the staff in order that these comments and observations might assist the STPL to better serve its customers. Meetings with several individuals responsible for various wind tunnels and with a group that provides photo-optical instrumentation services at the Center gave me an overview of the services provided by the Lab and possible areas for development. In summary form these are some of the observations that resulted from the interviews and daily contact with the STPL facility. (1) The STPL is perceived as a valuable and almost indispensable service group within the organization. This comment was invariably made by everyone. Everyone also seemed to support the idea that the STPL continue to provide its current level of service and quality. (2) The STPL generally is not perceived to be a highly technically oriented group but rather as a provider of high quality photographic illustration and documentation services. In spite of the importance and high marks assigned to the STPL there are several observations that merit consideration and evaluation for possible inclusion into the STPL's scope of expertise and future operating practices. (1) While the care and concern for artistic rendition of subjects is seen as laudable and sometimes valuable, the time that this often requires is seen as interfering with keeping the tunnels operating at maximum productivity. Tunnel managers would like to shorten down-time due to photography, have services available during evening hours and on short notice. It may be of interest to the STPL that tunnel managers are incorporating ever greater imaging capabilities in their facilities. To some extent this could mean a reduced demand for traditional photographic services. (2) The photographic archive is seen as a Center resource. Archiving of images, as well as data, is a matter of concern to the investigators. The early holdings of the Photographic Archives are quickly deteriorating. The relative inaccessibility of the material held in the archives is problematic. (3) In certain cases delivery or preparation of digital image files instead of, or along with, hardcopy is already being perceived by the STPL's customers

as desirable. The STPL should make this option available, and the fact that it has, or will have this capability widely known. (4) The STPL needs to continue to provide expert advice and technical imaging support in terms of application information to users of traditional photographic and new electronic imaging systems. Cooperative demo projects might be undertaken to maintain or improve the capabilities of the Lab. (5) STPL personnel do not yet have significant electronic imaging or electronic communication skills and improvements in this is an area could potentially have a positive impact on the Center. (6) High speed photographic or imaging services are often mentioned by the STPL as being of primary importance to their mission but the lab supports very few projects calling for high speed imaging services. Much high speed equipment is in poor state of repair. It is interesting to note that when the operation of lasers, digital imaging or quantitative techniques are requested these are directed to another NASA department. Could joint activities be initiated to solve problems? (7). The STPL could acquire more technical assignments if examples of the areas where they posses expertise would be circulated around the center. The fact that the STPL owns high speed video capability could be 'advertised' among its customer base if there truly was an interest in building up a customer base in this area. The STPL could participate in events like TOPS as an exhibitor, as well as a documenter, of the event.

Author

N95-23291*# Air Force Academy, CO. Dept. of Chemistry.

METHOD DEVELOPMENT FOR COMPENSATING TEMPERATURE EFFECTS IN PRESSURE SENSITIVE PAINT MEASUREMENTS Abstract Only **c27**

Carlo Greg N. Demandante *In* Hampton Univ., 1994 NASA-HU American Society for Engineering Education (ASEE) Summer Faculty Fellowship Program Dec. 1994 p 72 (For primary document see N95-23276 07-99)

Avail: CASI HC A01/MF A02

Pressure sensitive luminescent paints (PSP) have recently emerged as a viable technique for aerodynamic pressure measurements. The technique uses a surface coating which contains probe molecules that luminesce when excited by light of an appropriate wavelength. The photoluminescence of these materials is known to be quenched by the presence of molecular oxygen. Since oxygen is a fixed mole fraction of the air, the coating's luminescence intensity varies inversely with air pressure. Digital imaging of the luminescence varying across a coated surface produces a pressure distribution map over that surface. One difficulty encountered with this technique is the temperature effect on the luminescence intensity. Present PSP formulations have significant sensitivity to temperature. At the moment, the most practical way of correcting for temperature effects is to calibrate the paint in place at the operating temperatures by using a few well-placed pressure taps. This study is looking at development of temperature indicating coatings that can be applied and measured concurrently with PSP, and use the temperature measurement to compute the correct pressure. Two methods for this dual paint formulation are proposed. One method will use a coating that consists of temperature sensitive phosphors in a polymer matrix. This is similar in construction to PSP, except that the probe molecules used are selected primarily for their temperature sensitivity. Both organic phosphors (e.g., europium thenoyltrifluoroacetonate, bioprobes) and inorganic phosphors (e.g., Mg4(F)GeO6:Mn, La2O2S:Eu, Radelin Type phosphors, Sylvania Type phosphors) will be evaluated for their temperature sensing potential. The next method will involve a novel coating composing of five membered heterocyclic conducting polymers which are known to show temperature dependent luminescence (e.g., poly(3-alkylthiopene), poly(3-alkylselenophene), poly(3-alkylfuran)). Both methods will involve applying a bottom layer of temperature sensitive coating followed by a top coating of PSP. An oxygen-impermeable polymer can be used as the temperature sensitive coating matrix, or it can be layered in between the coatings to prevent oxygen quenching of the bottom coating's luminescence. The probe molecules of the coatings will be excited by a broad band of light, with the different emissions detected and measured at their distinct wavelengths. Developmental research of these coatings is still in progress; however, preliminary results look very promising.

Author

N95-23292*# Old Dominion Coll., Norfolk, VA. Dept. of Psychology.

TEAMS AND TEAMWORK AT NASA LANGLEY RESEARCH CENTER Abstract Only **c81**

Terry L. Dickinson *In* Hampton Univ., 1994 NASA-HU American Society for Engineering Education (ASEE) Summer Faculty Fellowship Program Dec. 1994 p 73 (For primary document see N95-23276 07-99)

Avail: CASI HC A01/MF A02

The recent reorganization and shift to managing total quality at the NASA Langley Research Center (LaRC) has placed an increasing emphasis on teams and teamwork in accomplishing day-to-day work activities and long-term projects. The purpose of this research was to review the nature of teams and teamwork at LaRC. Models of team performance and teamwork guided the gathering of information. Current and former team members served as participants; their collective experience reflected membership in over 200 teams at LaRC. The participants responded to a survey of open-ended questions which assessed various aspects of teams and teamwork. The participants also met in a workshop to clarify and elaborate on their responses. The work accomplished by the teams ranged from high-level managerial decision making (e.g., developing plans for LaRC reorganization) to creating scientific proposals (e.g., describing spaceflight projects to be designed, sold, and built). Teams typically had nine members who remained together for six months. Member turnover was around 20 percent; this turnover was attributed to heavy loads of other work assignments and little formal recognition and reward for team membership. Team members usually shared a common and valued goal, but there was not a clear standard (except delivery of a document) for knowing when the goal was achieved. However, members viewed their teams as successful. A major factor in team success was the setting of explicit a priori rules for communication. Task interdependencies between members were not complex (e.g., sharing of meeting notes and ideas about issues), except between members of scientific teams (i.e., reliance on the expertise of others). Thus, coordination of activities usually involved scheduling and attendance of team meetings. The team leader was designated by the team's sponsor. This leader usually shared power and responsibilities with other members, such that team members established their own operating procedures for decision making. Sponsors followed a hands-off policy during team operations, but they approved and reviewed team products. Most teams, particularly high-level decision-making teams, had little or no authority to carry out their decisions. Team members had few interpersonal conflicts. They monitored each other respectfully about meeting deadlines. Feedback and backup behaviors were seen as desirable aspects of teamwork, wanted by the members, and done appropriately.

Author

N95-23293*# Norfolk State Univ., VA. Dept. of Physics.

NONDESTRUCTIVE EVALUATION OF FATIGUE DAMAGE IN ALUMINUM 2024 BY X-RAY DIFFRACTION Abstract Only **c38**

Milton W. Ferguson *In* Hampton Univ., 1994 NASA-HU American Society for Engineering Education (ASEE) Summer Faculty Fellowship Program Dec. 1994 p 74 (For primary document see N95-23276 07-99)

Avail: CASI HC A01/MF A02

Aluminum alloys are widely used in the automobile and aerospace industries. This is due to their attractive low density-high modulus and low density-high strength characteristics. Unfortunately, cyclic stress-strain deformations alter the microstructure of aluminum alloys when they are placed into service. These structural changes can lead to fatigue damage and ultimately service failure. Since x-ray diffraction analysis is known to be a sensitive nondestructive indicator of structural changes due to deformations, this technique is being used to evaluate changes in the microstructure of cycled aluminum 2024 commercial alloys. Line shapes, widths, and positions in an x-ray diffraction pattern depend on microstructural properties such as grain size, grain orientation, residual stress, microstrain, etc. Changes in the microstructure due to fatigue will appear as changes in the diffraction pattern. One parameter used to characterize a reflection in a diffraction pattern is the full width at half maximum (FWHM). Preliminary x-ray diffraction results on cycled Al 2024 indicate that the (111) and (222) reflections of the matrix phase do not show any variations in the FWHM due to an increase in the fatigue cycles. However, the FWHM of the (200) and (400) reflections of the same phase unexpectedly showed a dramatic decrease. These results can be interpreted as due to the relaxation of some initial nonuniform residual stresses in the matrix phase lattice. Further work is in progress to evaluate the FWHM of the second phase of the cycled alloys.

Author

N95-23294*# Texas A&M Univ., College Station, TX. Dept. of Aerospace Engineering.

CONTROL OF FLOW SEPARATION IN AIRFOIL/WING DESIGN APPLICATIONS Abstract Only **c02**

Thomas A. Gally *In* Hampton Univ., 1994 NASA-HU American Society for Engineering Education (ASEE) Summer Faculty Fellowship Program Dec. 1994 p 75 (For primary document see N95-23276 07-99)
Avail: CASI HC A01/MF A02

Existing aerodynamic design methods have generally concentrated on the optimization of airfoil or wing shapes to produce a minimum drag while satisfying some basic constraints such as lift, pitching moment, or thickness. Since the minimization of drag almost always precludes the existence of separated flow, the evaluation and validation of these design methods for their robustness and accuracy when separated flow is present has not been aggressively pursued. However, two new applications for these design tools may be expected to include separated flow and the issues of aerodynamic design with this feature must be addressed. The first application of the aerodynamic design tools is the design of airfoils or wings to provide an optimal performance over a wide range of flight conditions (multipoint design). While the definition of 'optimal performance' in the multipoint setting is currently being hashed out, it is recognized that given a wide enough range of flight conditions, it will not be possible to ensure a minimum drag constraint at all conditions, and in fact some amount of separated flow (presumably small) may have to be allowed at the more demanding flight conditions. Thus a multipoint design method must be tolerant of the existence of separated flow and may include some controls upon its extent. The second application is in the design of wings with extended high speed buffet boundaries of their flight envelopes. Buffet occurs on a wing when regions of flow separation have grown to the extent that their time varying pressures induce possible destructive effects upon the wing structure or adversely effect either the aircraft controllability or the passenger comfort. A conservative approach to the expansion of the buffet flight boundary is to simply expand the flight envelope of nonseparated flow under the assumption that buffet will also thus be alleviated. However, having the ability to design a wing with separated flow and thus to control the location, extent, and severity of the separated flow regions may allow aircraft manufacturers to gain an advantage in the early design stages of an aircraft, when configuration changes are relatively inexpensive to make. Continuing the work begun last year, an airfoil design package has been modified to provide some control over the existence and extent of flow separation. This package consists of a 2-D Navier-Stokes flow solver which is coupled to the CDISC (constrained direct/iterative surface curvature) design method. The first modification is a prediction method for determining whether separation is likely based solely upon a given pressure distribution. If separation is predicted but is undesirable, the new routines will modify the pressure distribution to alleviate the problem. This new pressure distribution is then used in the design method to generate a new aerodynamic shape. Since separation may be acceptable in some cases, particularly if the separation does not extend to the trailing edge, another added logic estimates the extent of separation based upon a correlation with calculated separated flow cases. If the flow behind a shock induced separation is not predicted to reattach before the trailing edge, the logic weakens the shock strength and otherwise alters the pressure distribution in order to promote reattachment. This later addition is as yet unreliable due to secondary separation effects, but additional work is being pursued to improve the method. Author

N95-23295*# Moravian Coll., Bethlehem, PA. Dept. of Computer Science.

LOCATING BUILDINGS IN AERIAL PHOTOS Abstract Only **c43**

James S. Green *In* Hampton Univ., 1994 NASA-HU American Society for Engineering Education (ASEE) Summer Faculty Fellowship Program Dec. 1994 p 77 (For primary document see N95-23276 07-99)
Avail: CASI HC A01/MF A02

Algorithms and techniques for use in the identification and location of large buildings in digitized copies of aerial photographs are developed and tested. The building data would be used in the simulation of objects located in the vicinity of an airport that may be detected by aircraft radar. Two distinct approaches are considered. Most building footprints are rectangular in form. The first approach studied is to search for right-angled corners that characterize rectangular objects and then to connect these corners to complete the building. This problem is difficult because many nonbuilding objects, such as street corners, parking lots, and ballparks often have well defined corners which are often difficult to distinguish from rooftops. Furthermore, rooftops come in a number of shapes, sizes, shadings, and textures which also limit the discrimination task. The strategy used linear sequences of different samples to detect straight edge segments at multiple angles and to determine when these segments meet at approximately right-angles with respect to each other. This technique is effective in locating corners. The test image used has a fairly rectangular block pattern oriented about thirty degrees clockwise from a vertical alignment, and the overall measurement data reflect this. However, this technique does not discriminate between buildings and other objects at an operationally suitable rate. In addition, since multiple paths are tested for each image pixel, this is a time consuming task. The process can be speeded up by preprocessing the image to locate the more optimal sampling paths. The second approach is to rely on a human operator to identify and select the building objects and then to have the computer determine the outline and location of the selected structures. When presented with a copy of a digitized aerial photograph, the operator uses a mouse and cursor to select a target building. After a button on the mouse is pressed, with the cursor fully within the perimeter of the building, the program scans from the position of the cursor to a perimeter position where a shift in grayscale is detected. Once at the perimeter, the process traces along it, around the building, until it eventually returns to the perimeter starting point. Spatial resolution limits cause the perimeter trace to be somewhat course so that a line straightening algorithm is employed. One result is that the building corner positions become more distinctly defined. Author

N95-23296*# Tuskegee Inst., AL. Dept. of Aerospace Science Engineering.

DIRECT NUMERICAL SIMULATION OF SHEARED TURBULENT FLOW Abstract Only **c34**

Vascar G. Harris *In* Hampton Univ., 1994 NASA-HU American Society for Engineering Education (ASEE) Summer Faculty Fellowship Program Dec. 1994 p 78 (For primary document see N95-23276 07-99)
Avail: CASI HC A01/MF A02

The summer assignment to study sheared turbulent flow was divided into three phases which were: (1) literature survey, (2) computational familiarization, and (3) pilot computational studies. The governing equations of fluid dynamics or Navier-Stokes equations describe the velocity, pressure, and density as functions of position and time. In principle, when combined with conservation equations for mass, energy, and thermodynamic state of the fluid a determinate system could be obtained. In practice the Navier-Stokes equations have not been solved due to the nonlinear nature and complexity of these equations. Consequently, the importance of experiments in gaining insight for understanding the physics of the problem has been an ongoing process. Reasonable computer simulations of the problem have occured as the computational speed and storage of computers has evolved. The importance of the microstructure of the turbulence dictates the need for high resolution grids in extracting solutions which contain the physical mechanisms which are essential to a successful simulation. The recognized breakthrough occurred as a result of the pioneering work of Orzag and Patterson in which the Navier-Stokes equations were solved numerically utilizing a time saving toggling technique between physical and wave space, known as a spectral method. An equally analytically unsolvable problem, containing the same quasi-chaotic nature as turbulence, is known as the three body problem which was studied computationally as a first step this summer. This study was followed by computations of a two dimensional (2D) free shear layer. Author (revised)

N95-23297*# California Univ., Davis, CA. Dept. of Mechanical and Aeronautical Engineering.

ANALYSIS OF THE LONGITUDINAL HANDLING QUALITIES AND PILOT-INDUCED-OSCILLATION TENDENCIES OF THE HIGH-ANGLE-OF-ATTACK RESEARCH VEHICLE (HARV) Abstract Only **c08**

Ronald A. Hess *In* Hampton Univ., 1994 NASA-HU American Society for Engineering Education (ASEE) Summer Faculty Fellowship Program Dec. 1994 p 79 (For primary document see N95-23276 07-99)
Avail: CASI HC A01/MF A02

The NASA High-Angle-of Attack Research Vehicle (HARV), a modified F-18 aircraft, experienced handling qualities problems in recent flight tests

at NASA Dryden Research Center. Foremost in these problems was the tendency of the pilot-aircraft system to exhibit a potentially dangerous phenomenon known as a pilot-induced oscillation (PIO). When they occur, PIO's can severely restrict performance, sharply dimish mission capabilities, and can even result in aircraft loss. A pilot/vehicle analysis was undertaken with the goal of reducing these PIO tendencies and improving the overall vehicle handling qualities with as few changes as possible to the existing feedback/feedforward flight control laws. Utilizing a pair of analytical pilot models developed by the author, a pilot/vehicle analysis of the existing longitudinal flight control system was undertaken. The analysis included prediction of overall handling qualities levels and PIO susceptability. The analysis indicated that improvement in the flight control system was warranted and led to the formulation of a simple control stick command shaping filter. Analysis of the pilot/vehicle system with the shaping filter indicated significant improvements in handling qualities and PIO tendencies could be achieved. A non-real time simulation of the modified control system was undertaken with a realistic, nonlinear model of the current HARV. Special emphasis was placed upon those details of the command filter implementation which could effect safety of flight. The modified system is currently awaiting evaluation in the real-time, pilot-in-the-loop, Dual-Maneuvering-Simulator (DMS) facility at Langley. Author

N95-23298*# Rochester Univ., NY.

ELECTRONIC PHOTOGRAPHY AT NASA LANGLEY RESEARCH CENTER Abstract Only **c35**

Jack M. Holm *In* Hampton Univ., 1994 NASA-HU American Society for Engineering Education (ASEE) Summer Faculty Fellowship Program Dec. 1994 p 80 (For primary document see N95-23276 07-99)
Avail: CASI HC A01/MF A02

The field of photography began a metamorphosis several years ago which promises to fundamentally change how images are captured, transmitted, and output. At this time the metamorphosis is still in the early stages, but already new processes, hardware, and software are allowing many individuals and organizations to explore the entry of imaging into the information revolution. Exploration at this time is prerequisite to leading expertise in the future, and a number of branches at LaRC have ventured into electronic and digital imaging. Their progress until recently has been limited by two factors: the lack of an integrated approach and the lack of an electronic photographic capability. The purpose of the research conducted was to address these two items. In some respects, the lack of electronic photographs has prevented application of an integrated imaging approach. Since everything could not be electronic, the tendency was to work with hard copy. Over the summer, the Photographics Section has set up an Electronic Photography Laboratory. This laboratory now has the capability to scan film images, process the images, and output the images in a variety of forms. Future plans also include electronic capture capability. The current forms of image processing available include sharpening, noise reduction, dust removal, tone correction, color balancing, image editing, cropping, electronic separations, and halftoning. Output choices include customer specified electronic file formats which can be output on magnetic or optical disks or over the network, 4400 line photographic quality prints and transparencies to 8.5 by 11 inches, and 8000 line film negatives and transparencies to 4 by 5 inches. The problem of integrated imaging involves a number of branches at LaRC including Visual Imaging, Research Printing and Publishing, Data Visualization and Animation, Advanced Computing, and various research groups. These units must work together to develop common approaches to image processing and archiving. The ultimate goal is to be able to search for images using an on-line database and image catalog. These images could then be retrieved over the network as needed, along with information on the acquisition and processing prior to storage. For this goal to be realized, a number of standard processing protocols must be developed to allow the classification of images into categories. Standard series of processing algorithms can then be applied to each category (although many of these may be adaptive between images). Since the archived image files would be standardized, it should also be possible to develop standard output processing protocols for a number of output devices. If LaRC continues the research effort begun this summer, it may be one of the first organizations to develop an integrated approach to imaging. As such, it could serve as a model for other organizations in government and the private sector. Author

N95-23299*# Old Dominion Coll., Norfolk, VA. Dept. of Mechanical Engineering.

SYSTEM IDENTIFICATION OF THE LARGE-ANGLE MAGNETIC SUSPENSION TEST FIXTURE (LAMSTF) Abstract Only **c09**

Jen-Kuang Huang *In* Hampton Univ., 1994 NASA-HU American Society for Engineering Education (ASEE) Summer Faculty Fellowship Program Dec. 1994 p 81 (For primary document see N95-23276 07-99)
Avail: CASI HC A01/MF A02

The Large-Angle Magnetic Suspension Test Fixture (LAMSTF), a laboratory-scale research project to demonstrate the magnetic suspension of objects over wide ranges of attitudes, has been developed. This system represents a scaled model of a planned Large-Gap Magnetic Suspension System (LGMSS). The LAMSTF consists of a small cylindrical permanent magnet suspended element which is levitated above a planar array of five electromagnets mounted in a circular configuration. The cylinder is a rigid body and can be controlled to move in five independent degrees of freedom. Six position variables are sensed indirectly by using infrared light-emitting diodes and light-receiving phototransistors. The motion of the suspended cylinder is in general nonlinear and hence only the linear, time-invariant perturbed motion about an equilibrium state is considered. One of the main challenges in this project is the control of the suspended element over a wide range of orientations. An accurate dynamic model plays an essential role in controller design. The analytical model is first derived and open-loop characteristics discussed. The system is shown to be highly unstable and requires feedback control for system identification. Projection filters are first proposed to identify the state space model from closed-loop input/output test data in the time domain. This method is then extended to identify linear systems from the frequency test data. A canonical transformation matrix is also derived to transform the identified state space model into the physical coordinate. The LAMSTF system is stabilized by using a linear quadratic regulator (LQR) feedback controller for closed-loop identification. The rate information is obtained by calculating the back difference of the sensed position signals. Only the closed-loop random input/output data are recorded. Preliminary results from numerical simulations demonstrate that the identified system model is fairly accurate from either time domain or frequency-domain data. Experiments will be performed to validate the proposed closed-loop identification algorithms. Author

N95-23300*# Florida Univ., Gainesville, FL. Dept. of Aerospace Engineering, Mechanical and Engineering Science.

INTERLAMINAR SHEAR TEST METHOD DEVELOPMENT FOR LONG TERM DURABILITY TESTING OF COMPOSITES Abstract Only **c24**

Peter G. Ifju *In* Hampton Univ., 1994 NASA-HU American Society for Engineering Education (ASEE) Summer Faculty Fellowship Program Dec. 1994 p 82 (For primary document see N95-23276 07-99)
Avail: CASI HC A01/MF A02

The high speed civil transport is a commercial aircraft that is expected to carry 300 passengers at Mach 2.4 over a range of more than 6000 nautical miles. With the existing commercial structural material technology (i.e., aluminum) the performance characteristics of the high speed civil transport would not be realized. Therefore there has been a concerted effort in the development of light weight materials capable of withstanding elevated temperatures for long duration. Thermoplastic composite materials are such candidate materials and the understanding of how these materials perform over the long term under harsh environments is essential to safe and effective design. The matrix dominated properties of thermoplastic composites are most affected by both time and temperature. There is currently an effort to perform short term testing to predict long term behavior of in-plane mechanical properties E22 (transverse modulus of elasticity) and G12 (shear modulus). Out-of-plane properties such as E33, G13, and G23 are inherently more difficult to characterize. This is especially true for the out-of-plane shear modulus G23 and hence there is no existing acceptable standard test method. Since G23 is the most matrix dominated property, it is essential that a test method be developed. A shear test methodology is developed to do just that. The test method, called the double notched specimen, along with the previously developed shear gage was tested at room temperature. Mechanical testing confirmed the attributes of the methodology. A finite element parametric study was conducted for specimen optimization. Moire interferometry, a high sensitivity laser optical method, was used for full-field analysis of the specimen. From this work,

material parameters will be determined and thus enable the prediction of long term material behavior of laminates subjected to general loading states. Author (revised)

N95-23301*# Alabama Univ., Huntsville, AL. Dept. of Electrical and Computer Engineering.

TASK SCHEDULING IN DATAFLOW COMPUTER ARCHITECTURES Abstract Only **c60**

Constantine Katsinis *In* Hampton Univ., 1994 NASA-HU American Society for Engineering Education (ASEE) Summer Faculty Fellowship Program Dec. 1994 p 83 (For primary document see N95-23276 07-99)
Avail: CASI HC A01/MF A02

Dataflow computers provide a platform for the solution of a large class of computational problems, which includes digital signal processing and image processing. Many typical applications are represented by a set of tasks which can be repetitively executed in parallel as specified by an associated dataflow graph. Research in this area aims to model these architectures, develop scheduling procedures, and predict the transient and steady state performance. Researchers at NASA have created a model and developed associated software tools which are capable of analyzing a dataflow graph and predicting its runtime performance under various resource and timing constraints. These models and tools were extended and used in this work. Experiments using these tools revealed certain properties of such graphs that require further study. Specifically, the transient behavior at the beginning of the execution of a graph can have a significant effect on the steady state performance. Transformation and retiming of the application algorithm and its initial conditions can produce a different transient behavior and consequently different steady state performance. The effect of such transformations on the resource requirements or under resource constraints requires extensive study. Task scheduling to obtain maximum performance (based on user-defined criteria), or to satisfy a set of resource constraints, can also be significantly affected by a transformation of the application algorithm. Since task scheduling is performed by heuristic algorithms, further research is needed to determine if new scheduling heuristics can be developed that can exploit such transformations. This work has provided the initial development for further long-term research efforts. A simulation tool was completed to provide insight into the transient and steady state execution of a dataflow graph. A set of scheduling algorithms was completed which can operate in conjunction with the modeling and performance tools previously developed. Initial studies on the performance of these algorithms were done to examine the effects of application algorithm transformations as measured by such quantities as number of processors, time between outputs, time between input and output, communication time, and memory size. Author

N95-23302*# Thomas Nelson Community Coll., Hampton, VA. Dept. of Engineering and Technology.

RELIABILITY ANALYSIS IN THE OFFICE OF SAFETY, ENVIRONMENTAL, AND MISSION ASSURANCE (OSEMA) Abstract Only **c38**

Paul J. Kauffmann *In* Hampton Univ., 1994 NASA-HU American Society for Engineering Education (ASEE) Summer Faculty Fellowship Program Dec. 1994 p 84 (For primary document see N95-23276 07-99)
Avail: CASI HC A01/MF A02

The technical personnel in the SEMA office are working to provide the highest degree of value-added activities to their support of the NASA Langley Research Center mission. Management perceives that reliability analysis tools and an understanding of a comprehensive systems approach to reliability will be a foundation of this change process. Since the office is involved in a broad range of activities supporting space mission projects and operating activities (such as wind tunnels and facilities), it was not clear what reliability tools the office should be familiar with and how these tools could serve as a flexible knowledge base for organizational growth. Interviews and discussions with the office personnel (both technicians and engineers) revealed that job responsibilities ranged from incoming inspection to component or system analysis to safety and risk. It was apparent that a broad base in applied probability and reliability along with tools for practical application was required by the office. A series of ten class sessions with a duration of two hours each was organized and scheduled. Hand-out materials were developed and practical examples based on the type of work performed by the office personnel were included. Topics covered were: Reliability Systems - a broad system oriented approach to reliability; Probability Distributions - discrete and continuous distributions; Sampling and Confidence Intervals - random sampling and sampling plans; Data Analysis and Estimation - Model selection and parameter estimates; and Reliability Tools - block diagrams, fault trees, event trees, FMEA. In the future, this information will be used to review and assess existing equipment and processes from a reliability system perspective. An analysis of incoming materials sampling plans was also completed. This study looked at the issues associated with Mil Std 105 and changes for a zero defect acceptance sampling plan. Author

N95-23303*# Elizabeth City State Univ., NC. Dept. of Physical Sciences.

RAMAN-SHIFTING AN ArF EXCIMER LASER TO GENERATE NEW LINES FOR OBTAINING OPTICAL DIAGNOSTIC BASED INFORMATION IN FLOW FIELDS Abstract Only **c36**

Edmond B. Koker *In* Hampton Univ., 1994 NASA-HU American Society for Engineering Education (ASEE) Summer Faculty Fellowship Program Dec. 1994 p 85 (For primary document see N95-23276 07-99)
Avail: CASI HC A01/MF A02

The application of tunable excimer lasers in combustion and flow diagnostics is almost routine nowadays. The properties of this laser system that enable density and temperature measurements in supersonic and hypersonic flow fields to be conducted are its high power, high repetition rate, and high spectral brightness. The limitation imposed by this system on these measurements is the paucity of lines in the wavelength region, the vacuum-ultraviolet, where species of interest, such as OH, N2, O2, H2, H2O, CO, NO, etc., are susceptible to electronic excitation to high-lying states. To circumvent this problem one normally resorts to nonlinear optical techniques such as frequency conversion via stimulated Raman scattering (SRS), more commonly known as Raman shifting or Raman mixing, to extend these nonintrusive and nonperturbing techniques to the shorter wavelengths in the VUV region and, for that matter, to longer wavelengths in the infrared region, if the need arises. The theoretical basis of SRS and its application are well documented in the literature. In essence, the Raman shift is a consequence of the inelastic scattering of the incident radiation by the sample. Most of the scattered radiation from the molecules of the sample is unchanged in frequency. However, a small fraction of the incident radiation is changed in frequency. This shift is a result of the fact that some of the incident photons on colliding with the molecules of the sample give up some of their energy and emerge with a lower energy resulting in the lower-frequency Stokes radiation. Other incident photons may increase their energy by colliding with the vibrationally excited molecules of the medium and emerge as higher-frequency antistokes radiation. The generation of the latter is the main objective of this project. The process, however, depends on several factors, including the beam quality of the pump laser, the cross-section of the gaseous medium, the gas pressure, and the ambient temperature of the gas near the focal region. Furthermore, since the Raman shifting process is polarization sensitive, it is necessary to have all of the laser energy in a single polarization. These factors were taken into consideration in the execution of the project. The implementation of the Raman shift was accomplished by focusing the 193 nm output of an ArF excimer laser (Lamda-Physik LPX 150) into a 1-meter long high pressure recirculating Raman cell filled with H2 gas. The laser system was modified in order to improve the mode quality of the pump beam to enhance the Raman shifting. To accomplish this feat, a prism beam expander and grating on the oscillator discharge provided wavelength tuning over the excimer gain profile. Furthermore, a triple-pass configuration, as opposed to unstable resonator optics, was employed in the operation of the amplifier cavity so that when the oscillator output radiation, focused by a 51-cm focal length fused silica lens through a 50 micron pinhole (serving as a spatial filter) and recollimated with a 25-cm focal length lens, was fed into the amplifier, it was injection locked, thereby providing tunable radiation with relatively low divergence. The forward scattered radiation emanating from the impingement of the modified pump beam on the Raman cell was detected using an energy meter after the latter had been separated from it using a dispersing prism. Author (revised)

N95-23304*# Old Dominion Coll., Norfolk, VA. Dept. of Mechanical Engineering.

OPTIMIZED DESIGN OF A HYPERSONIC NOZZLE Abstract Only **c09**

Ramesh Krishnamurthy *In* Hampton Univ., 1994 NASA-HU American Society for Engineering Education (ASEE) Summer Faculty Fellowship

Program Dec. 1994 p 86 (For primary document see N95-23276 07-99)
Avail: CASI HC A01/MF A02

Conventional procedures for designing nozzles involve the design of an inviscid contour (using the method of characteristics) that is corrected with a displacement thickness calculated from boundary-layer theory. However, nozzles designed using this classical procedure have been shown to exhibit poor flow quality at Mach numbers characteristic of hypersonic applications. The nozzle to be designed will be a part of the NASA HYPULSE facility which is being used for hypervelocity flight research. Thus, the flow quality of the nozzle is a critical question that needs to be addressed. Design of nozzles for hypersonic applications requires a proper assessment of the effects of the thick boundary layer on the inviscid flowfield. Since the flow field is largely supersonic, the parabolized form of the Navier-Stokes (PNS) equations can be used. The requirement of a uniform flow at the exit plane of the nozzle can be used to define an objective function as part of an optimization procedure. The design procedure used in this study involves the coupling of a nonlinear (least-squares) optimization algorithm with an efficient, explicit PNS solver. The thick boundary layers growing on the walls of the nozzle limit the extent of the usable core region (region with uniform flow) for testing models (especially rectangular). In order to maximize the region of uniform flow, it was decided to have the exit plane of this nozzle to be (nearly) rectangular. Thus, an additional constraint on the nozzle shape resulted, namely the nozzle will have a shape transitioning from a circular one at the inlet to that of a rectangle at the exit. In order to provide for a smooth shape transition, the cross sectional contour of the nozzle is defined by a superellipse. The nozzle is taken to be a meter in length. The axial variations of the major and minor radii of the superellipse are governed by cubic splines. The design parameters are the coefficients of the splines associated with the local nozzle wall slopes. Extensive calculations have been made (with a three-dimensional Euler code) to understand the effects of various parameters such as location of the knot points of the spline function, different ways of characterizing the uniformity of the flow in the exit plane, as well as the effect of constraining the area of the nozzle to be invariant. Turbulent flow (measurements indicate that the flow at the nozzle inlet is turbulent) calculations are now being performed (with the inviscidly designed nozzle contours) to assess the flow quality.

Author (revised)

N95-23305*# Ohio Univ., Athens, OH. Dept. of Industrial and Systems Engineering.

STOCHASTIC DECISION ANALYSIS Abstract Only **c81**

Thomas A. Lacksonen *In* Hampton Univ., 1994 NASA-HU American Society for Engineering Education (ASEE) Summer Faculty Fellowship Program Dec. 1994 p 87 (For primary document see N95-23276 07-99)
Avail: CASI HC A01/MF A02

Small space flight project design at NASA Langley Research Center goes through a multi-phase process from preliminary analysis to flight operations. The process insures that each system achieves its technical objectives with demonstrated quality and within planned budgets and schedules. A key technical component of early phases is decision analysis, which is a structure procedure for determining the best of a number of feasible concepts based upon project objectives. Feasible system concepts are generated by the designers and analyzed for schedule, cost, risk, and technical measures. Each performance measure value is normalized between the best and worst values and a weighted average score of all measures is calculated for each concept. The concept(s) with the highest scores are retained, while others are eliminated from further analysis. This project automated and enhanced the decision analysis process. Automation of the decision analysis process was done by creating a user-friendly, menu-driven, spreadsheet macro based decision analysis software program. The program contains data entry dialog boxes, automated data and output report generation, and automated output chart generation. The enhancements to the decision analysis process permit stochastic data entry and analysis. Rather than enter single measure values, the designers enter the range and most likely value for each measure and concept. The data can be entered at the system or subsystem level. System level data can be calculated as either sum, maximum, or product functions of the subsystem data. For each concept, the probability distributions are approximated for each measure and the total score for each concept as either constant, triangular, normal, or log-normal distributions. Based on these distributions, formulas are derived for the probability that the concept meets any given constraint, the probability that the concept meets all constraints, and the probability that the concept is within a given amount of the best score. Formulas are also derived for the probability that one concept's total score is within a given amount of a second concept's total score. These probabilistic calculations provide more realistic data entry and output information for designers, enabling designers to better determine which concepts to eliminate and which concepts to retain at the decision points of each design phase.

Author

N95-23306*# Christopher Newport Coll., Newport News, VA.

DESIGN AND IMPLEMENTATION OF TWO TWO-WEEK TEACHER ENHANCEMENT INSTITUTES Abstract Only **c80**

Lynn Lambert *In* Hampton Univ., 1994 NASA-HU American Society for Engineering Education (ASEE) Summer Faculty Fellowship Program Dec. 1994 p 88 (For primary document see N95-23276 07-99)
Avail: CASI HC A01/MF A02

During this summer, I have been part of a four team effort that planned and executed two two-week Teacher Enhancement Institutes (TEI) for 40 K-8 teachers from this area. The TEI was designed to enhance teachers' background in aeronautics and technology so that they would be better equipped to encourage and to train students in the mathematics, science, and technology fields. The teachers were given a stipend and three graduate credits from Christopher Newport University for their participation in this program. The four ASEE fellows worked together to develop objectives and a schedule of activities for each two-week session based on the program outline given in the grants that were funding this effort. We divided the responsibilities in coordinating and implementing each part of the TEI based on the specific strengths and background of each ASEE fellow. My specific responsibilities were: (1) to develop the course syllabus and generally handle all matters involved with the graduate course; (2) coordinate the follow-up sessions; and (3) design and manage half of the technology sessions that we had scheduled (approximately 30% of the TEI was devoted to technology). Because the first two responsibilities were primarily administrative in nature, I will address only the last. The technology sessions were divided into computer-only and other technologies (e.g., television and digital technology including scanning, digital photography and CD-ROM). I had responsibility for the computer-only technology sessions. The emphasis of these sessions was on use of the Internet specifically to locate and use educational resources. To maximize learning, these sessions were hands-on with two teachers at each computer. Each teacher received instruction in, and actually used, the most popular tools available on the Internet: email (they were given temporary accounts at NASA LaRC), anonymous ftp and archie, gopher and veronica, mosaic, and telnet. Teachers participated in hands-on workshops to learn about these programs, but were also given time during the two-week session to explore on their own and to find resources on the Net that specifically met their needs. In order to ensure that Internet access continues after their return to the classroom, all teachers who did not have them also applied for Learning Link accounts (from WHRO, the local public television station) and Virginia Pen accounts (from the Department of Education of Virginia), both of which allow textbased access to Internet. In addition to getting exposure to and practice with Internet tools, teachers were also given a hands-on seminar (and also given practice time) on ClarisWorks, an integrated word processing, spreadsheet, database, and paint package. The technology sessions (and TEI as a whole) were enthusiastically received by both new and more experienced teachers as extremely helpful in improving their ability to use technology in developing lesson plans.

Author

N95-23307*# Old Dominion Coll., Norfolk, VA. Dept. of Electrical and Computer Engineering.

ACCELERATED PANEL METHODS USING THE FAST MULTIPOLE METHOD Abstract Only **c34**

James F. Leathrum, Jr. *In* Hampton Univ., 1994 NASA-HU American Society for Engineering Education (ASEE) Summer Faculty Fellowship Program Dec. 1994 p 89 (For primary document see N95-23276 07-99)
Avail: CASI HC A01/MF A02

Panel methods are commonly used in computational fluid dynamics for the solution of potential flow problems. The methods are a numerical

technique based on the surface distribution of singularity elements. The solution is the process of finding the strength of the singularity elements distributed over the body's surface. This process involves the solution of the matrix problem Pq = p' for a set of unknowns q. The Fast Multipole Method is used to directly compute q without using matrix solvers. The algorithm works in O(N) time for N points, a great improvement over standard matrix solvers. In panel methods, the surface of a body is divided into a series of quadrilateral panels. The methods involve the computation of the influence of all other panels on each individual panel. The influence is based on the surface distribution, though this can be approximated by the area for distant panels. An alternative approximation, though with arbitrary accuracy, is to develop a multipole expansion about the center of the panel to describe the effect of a given panel on distant points in space. The expansion is based on the moments of the panel, thus allow the use of various surface distributions without changing the basic algorithm, just the computation of the various moments. The expansions are then manipulated in a tree walk to develop Taylor series expansions about a point in space which describe the effect of all distant panels on any point within a volume of convergence. The effect of near panels then needs to be computed directly, but the effect of all distant panels can be computed by simply evaluating the resulting expansion. The Fast Multipole Method has been applied to panel methods for the solution of source and doublet distributions. A major feature of the algorithm is that the algorithm does not change to derive the potential and velocity for sources and doublets. The same expansions can be used for both sources and doublets. Since the velocity is related to the potential, and the doublet potential is related to the z-component of the source velocity, all values can be derived from the same expansion by taking a series of partial derivatives. This requires more expansion terms to be kept since terms are lost in the process of taking partial derivatives. Thus to maintain accuracy for the doublet computation, more terms are required than if just evaluating for sources. The resulting Fast Multipole code should then parallelize better than classical panel methods due to the locality of data dependencies found in the Fast Multipole Method. Theoretically the parallelized code should execute in O(log N) time with O(N) processors, though this is not practical. Ongoing work includes implementing the parallel accelerated panel method, including methods to improve the load balancing of the problem by taking advantage of the known geometry of panels, and to encorporate sensitivity analysis into the algorithm. Author

N95-23308*# Kansas Univ., Lawrence, KS. Dept. of Aerospace Engineering.

ON-LINE, ADAPTIVE STATE ESTIMATOR FOR ACTIVE NOISE CONTROL Abstract Only **c63**

Tae W. Lim *In* Hampton Univ., 1994 NASA-HU American Society for Engineering Education (ASEE) Summer Faculty Fellowship Program Dec. 1994 p 90 (For primary document see N95-23276 07-99)
Avail: CASI HC A01/MF A02

Dynamic characteristics of airframe structures are expected to vary as aircraft flight conditions change. Accurate knowledge of the changing dynamic characteristics is crucial to enhancing the performance of the active noise control system using feedback control. This research investigates the development of an adaptive, on-line state estimator using a neural network concept to conduct active noise control. In this research, an algorithm has been developed that can be used to estimate displacement and velocity responses at any locations on the structure from a limited number of acceleration measurements and input force information. The algorithm employs band-pass filters to extract from the measurement signal the frequency contents corresponding to a desired mode. The filtered signal is then used to train a neural network which consists of a linear neuron with three weights. The structure of the neural network is designed as simple as possible to increase the sampling frequency as much as possible. The weights obtained through neural network training are then used to construct the transfer function of a mode in z-domain and to identify modal properties of each mode. By using the identified transfer function and interpolating the mode shape obtained at sensor locations, the displacement and velocity responses are estimated with reasonable accuracy at any locations on the structure. The accuracy of the response estimates depends on the number of modes incorporated in the estimates and the number of sensors employed to conduct mode shape interpolation. Computer simulation demonstrates that the algorithm is capable of adapting to the varying dynamic characteristics of structural properties. Experimental implementation of the algorithm on a DSP (digital signal processing) board for a plate structure is underway. The algorithm is expected to reach the sampling frequency range of about 10 kHz to 20 kHz which needs to be maintained for a typical active noise control application. Author

N95-23309*# New Jersey Inst. of Tech., Newark, NJ. Dept. of Chemical Engineering, Chemistry and Environmental Science.

DESIGN OF A VARIABLE AREA DIFFUSER FOR A 15-INCH MACH 6 OPEN-JET TUNNEL Abstract Only **c09**

Norman W. Loney *In* Hampton Univ., 1994 NASA-HU American Society for Engineering Education (ASEE) Summer Faculty Fellowship Program Dec. 1994 p 91 (For primary document see N95-23276 07-99)
Avail: CASI HC A01/MF A02

The Langley 15-inch Mach 6 High Temperature Tunnel was recently converted from a Mach 10 Hypersonic Flow Apparatus. This conversion was effected to improve the capability of testing in Mach 6 air at relatively high reservoir temperatures not previously possible at Langley. Elevated temperatures allow the matching of the Mach numbers, Reynolds numbers, and ratio of wall-to-adiabatic-wall temperatures (TW/Taw) between this and the Langley 20-inch Mach 6 CF4 Tunnel. This ratio is also matched for Langley's 31-inch Mach 10 Tunnel and is an important parameter useful in the simulation of slender bodies such as National Aerospace Plane (NASP) configurations currently being studied. Having established the nozzle's operating characteristics, the decision was made to install another test section to provide model injection capability. This test section is an open-jet type, with an injection system capable of injecting a model from retracted position to nozzle centerline between 0.5 and 2 seconds. Preliminary calibrations with the new test section resulted in Tunnel blockage. This blockage phenomenon was eliminated when the conical center body in the diffuser was replaced. The issue then, is to provide a new and more efficient variable area diffuser configuration with the capability to withstand testing of larger models without sending the Tunnel into an unstart condition. Use of the 1-dimensional steady flow equation with due regard to friction and heat transfer was employed to estimate the required area ratios (exit area / throat area) in a variable area diffuser. Correlations between diffuser exit Mach number and area ratios, relative to the stagnation pressure ratios and diffuser inlet Mach number were derived. From these correlations, one can set upper and lower operating pressures and temperatures for a given diffuser throat area. In addition, they will provide appropriate input conditions for the full 3-dimensional computational fluid dynamics (CFD) code for further simulation studies. Author

N95-23310*# Memphis Univ., Memphis, TN. Dept. of Mechanical Engineering.

DEFLECTIONS OF ANISOTROPIC SANDWICH BEAMS WITH VARIABLE FACE SHEETS AND CORE THICKNESSES Abstract Only **c39**

Chu-Ho Lu *In* Hampton Univ., 1994 NASA-HU American Society for Engineering Education (ASEE) Summer Faculty Fellowship Program Dec. 1994 p 92 (For primary document see N95-23276 07-99)
Avail: CASI HC A01/MF A02

A sandwich construction consists of a low-density core material with high strength face sheets bounded to the top and bottom surfaces. The construction has been widely used in the aerospace and marine industries due to its outstanding characteristics such as noise absorption, weight minimization, heat insulation, and better bending stiffness. In sandwich structures used in high-performance aircraft, the face sheets are often made of fiber-reinforced composite materials and the core is made of honeycomb. The structures may also have variable thickness so as to satisfy aerodynamic requirements. In the stress analysis, the constant-thickness face sheets are usually considered as membrane and the core is assumed to be inextensible but deformable in the thickness direction. The static behavior of variable-thickness, isotropic and homogeneous sandwich beams was successfully studied by employing a constant-thickness theory but allowing stiffnesses to vary in accordance with local thickness variations. It has been recently found in a refined theory that the analyses based on the constant thickness theory locally can lead to significant errors in structural responses if the sandwich beam is thickness-tapered and the cores are deformable in transverse shear. The errors arise mainly from two factors: (1) the transverse shear components of the membrane forces in the face sheets alter the transverse shears carried by the core; and (2) the face-sheet membrane strains arise

from transverse shear deformation of the core. In practice the variable thickness may not only exist in core but also in face sheets. The thickness-variations may even be a type of step function. In this case the transverse shear stress in the face sheets and bending stress in the core should be taken into account in the refined theory mentioned. In the present study, energy principles are employed in deriving governing equations for general bending of anisotropic sandwich beams with variable thickness in both face sheets and cores. Solutions to these equations are based on a finite difference scheme. As an example in application, a simply supported thickness-tapered sandwich beam subject to a concentrated load at its center is considered. Let W' be the maximum deflection of the beam in which face sheets are considered as membrane, while W'' is that based on using the modified refined theory. It is found that W' is always larger than W'', however, the magnitude of (W'- W'') appears to be insensitive to the change of the taper of the beam. Author

N95-23311*# Arizona Univ., Tucson, AZ. Dept. of Aerospace and Mechanical Engineering.

RESIDUAL STRENGTH OF THIN PANELS WITH CRACKS Abstract Only **c39**

Erdogan Madenci *In* Hampton Univ., 1994 NASA-HU American Society for Engineering Education (ASEE) Summer Faculty Fellowship Program Dec. 1994 p 93 (For primary document see N95-23276 07-99)

Avail: CASI HC A01/MF A02

The previous design philosophies involving safe life, fail-safe and damage tolerance concepts become inadequate for assuring the safety of aging aircraft structures. For example, the failure mechanism for the Aloha Airline accident involved the coalescence of undetected small cracks at the rivet holes causing a section of the fuselage to peel open during flight. Therefore, the fuselage structure should be designed to have sufficient residual strength under worst case crack configurations and in-flight load conditions. Residual strength is interpreted as the maximum load carrying capacity prior to unstable crack growth. Internal pressure and bending moment constitute the two major components of the external loads on the fuselage section during flight. Although the stiffeners in the form of stringers, frames and tear straps sustain part of the external loads, the significant portion of the load is taken up by the skin. In the presence of a large crack in the skin, the crack lips bulge out with considerable yielding; thus, the geometric and material nonlinearities must be included in the analysis for predicting residual strength. Also, these nonlinearities do not permit the decoupling of in-plane and out-of-plane bending deformations. The failure criterion combining the concepts of absorbed specific energy and strain energy density addresses the aforementioned concerns. The critical absorbed specific energy (local toughness) for the material is determined from the global specimen response and deformation geometry based on the uniaxial tensile test data and detailed finite element modeling of the specimen response. The use of the local toughness and stress-strain response at the continuum level eliminates the size effect. With this critical parameter and stress-strain response, the finite element analysis of the component by using STAGS along with the application of this failure criterion provides the stable crack growth calculations for residual strength predictions. Author

N95-23312*# Norfolk State Univ., VA. School of Education.

TEACHER ENHANCEMENT INSTITUTE Abstract Only **c80**

Tina Marshall-Bradley *In* Hampton Univ., 1994 NASA-HU American Society for Engineering Education (ASEE) Summer Faculty Fellowship Program Dec. 1994 p 94 (For primary document see N95-23276 07-99)

Avail: CASI HC A01/MF A02

During the 1980's, a period of intense concern over educational quality in the United States, few indicators of U.S. student achievement garnered the interest of policy makers and pundits as successfully as the results of international testing in mathematics and science. This concern was so great that as a part of the Goals 2000 initiative, President George Bush indicated that 'By the year 2000, U.S. students should be first in the world in mathematics and science.' The Clinton Administration is placing a major emphasis, not only on rigorous academic standards and creating a new system for assessing students' progress, but also including professional development as a major focus. The argument being that teachers need more sustained, intensive training to prepare them to teach to higher standards. Executive order 12821 mandates that national laboratories 'assist in the mathematics and science education of our Nation's students, teachers, parents and the public by establishing programs at their agency to provide for training elementary and secondary school teachers to improve their knowledge of mathematics and science'. These and other issues led to the development of ideas for a project that addresses the need for excellence in mathematics, science and technology instruction. In response to these initiatives the NASA/LaRC Teacher Enhancement Institute was proposed. The TEI incorporated systemic reform perspectives, enhanced content knowledge for teachers, and teacher preparation. Emphasis was also placed on recruiting those educators who teach in impoverished urban school districts with at-risk student populations who have been traditionally under represented in science, mathematics, technology and engineering. Participants in the Teacher Enhancement Institute were 37 teachers from grades K-8, teaching in Region 2 in the state of Virginia, as well as 2 preservice teachers from Norfolk State University and one teacher from Dublin, Virginia, where a Science/Mathematics model school has been established. Teachers selected for this project represented school systems where income levels are extremely low, and students served tend not to receive innovative instruction in mathematics and science and their use of technology is limited. The Teacher Enhancement Institute contained several features, that when combined, allowed for a unique experience. Some of these features included local teachers, administrators and school board members as presenters, instruction and use of technology every day, tours of select features of the research facility, briefings by NASA/LaRC scientists, engineers and researchers as well as individuals from the Continuous Electron Beam Accelerator Facility (CEBAF). Another unique feature of this program is to have participants convene on three separate occasions throughout the academic year to discuss strategies for information dissemination and implementation results. Teachers' attitudes towards the use of technology, their ability to develop lessons using technology and their ability to develop lessons using information obtained through TEI were assessed using instruments developed by TEI summer faculty members. Data from these instruments were analyzed and reported in a final report submitted to the director of the Office of Education. Author

N95-23313*# Christopher Newport Coll., Newport News, VA. Dept. of Mathematics.

AEROACOUSTIC COMPUTATION OF GUST-BLADE INTERACTION Abstract Only **c71**

James E. Martin *In* Hampton Univ., 1994 NASA-HU American Society for Engineering Education (ASEE) Summer Faculty Fellowship Program Dec. 1994 p 95 (For primary document see N95-23276 07-99)

Avail: CASI HC A01/MF A02

To better understand and address the challenges faced in computing the acoustics of flow fields, test problems must be considered. In the present study, the sound radiated by the interaction of a flat plate with an oncoming gust containing a two component, mean velocity is computed. The gust has a uniform mean flow in x with Mach number M(infinity) equal to 0.5. The gust's mean velocity in y is of smaller amplitude and is given by: v = 0.1 sin(pi/8(x/M(sub infinity) - t)). This problem has been posed for an upcoming ICASE/LaRC workshop on benchmark problems in computational aeroacoustics. A plate with a length of 30 units in x is used. The plate is assumed to be infinitesimally thin and is centered at the origin. All variables are made dimensionless using the scales specified. Acoustic quantities are obtained by numerically integrating the linearized Euler equations. Integration is performed on the computational domain -100.0 less than or equal to x less than or equal to 100.0, -100.0 less than or equal to y less than or equal to 100.0, using unit length grid spacing in x and in y. An integration scheme is sought which will provide accurate solution to the small quantities of interest at a minimal computational expense. Results indicate that with the given discretization a scheme of minimal fourth order accuracy might be adequate to approximate the waves within the given flow. Thus, a variation of the MacCormack scheme with fourth order accuracy in space and second order accuracy in time was chosen. A scheme with sixth order accuracy in space has also been implemented and results compared with those of the fourth order accurate scheme. To ensure no mass flux, zero normal velocity is assigned at the plate. This condition will induce a discontinuity in the pressure across the plate location. Values for the perturbation pressure p' along the surface of the plate are obtained using a one-sided, third order Taylor expansion, such that p'(sub y) = O. In accordance with the Kutta condition, perturbation pressure at the trailing edge is assigned to zero. In the far field, radiation

boundary conditions have been implemented. The effectiveness of the far field conditions are validated by computing in a larger computational domain and comparing the results. Early in time, sound waves begin to radiate from the plate. A Doppler effect is observed. After the initial transients disappear, the strongest waves leave the trailing edge at an approximate 45 degree angle. The intensity pattern of pressure fluctuations shows five lobes (of increasing magnitude with increasing downstream direction) emerging from the plate. Undesirable short wave contaminants are observed in the computed pressure distribution along the plate surface. For a more accurate solution at small scales, a more refined discretization will be required. Author

N95-23314*# Old Dominion Coll., Norfolk, VA. Dept. of Aerospace Engineering.

INNER LOOP FLIGHT CONTROL FOR THE HIGH-SPEED CIVIL TRANSPORT Abstract Only **c08**

Brett A. Newman *In* Hampton Univ., 1994 NASA-HU American Society for Engineering Education (ASEE) Summer Faculty Fellowship Program Dec. 1994 p 96 (For primary document see N95-23276 07-99)

Avail: CASI HC A01/MF A02

High-speed aerospace vehicles which employ high strength, light weight, yet deformable materials may exhibit significant interaction between the rigid-body and vibrational dynamics. Preliminary High-Speed Civil Transport (HSCT) configurations are a prime example. Traditionally, separate control systems have been used to augment the rigid-body and vibrational dynamics. In the HSCT arena, the highly coupled motions may not allow this design freedom. The research activity addresses two specific issues associated with the design and development of an integrated flight control system (FCS) for HSCT configurations, which are discussed next. The HSCT is expected to have a short period instability at subsonic speeds. Flight vehicles with this characteristic (i.e., F-16, F-22, X-29, Space Shuttle) are stabilized with what is called a superaugmented pitch rate loop. One concern is 'Will this stability augmentation logic work for a HSCT?' Studies show that an idealized pitch rate design would be acceptable, but is not realistic. Investigations using a contaminated pitch rate design reveal serious hurdles to overcome in the FCS design. Mounting location for the pitch rate sensor is critical. Results indicate a forward location leads to destabilizing pick-up of aeroelastic modes, while aft locations lead to undesirable coupling of the dominate pitch mode with the first aeroelastic mode. Intermediate locations for the sensor may not be acceptable. The source of the problem is the presence of low frequency aeroelastic modes in HSCT configurations, which are not present in vehicles currently using the superaugmented logic. To say the least, a conventional superaugmented pitch rate loop strategy may have undesirable characteristics. An unconventional strategy, which attempts to eliminate the above deficiencies by blending several pitch rate signals, indicates an improvement in the FCS architecture feasibility, but is still lacking in some respects. The HSCT configuration does not have aerodynamic surfaces in the vicinity of the nose (i.e., no canard or vane). A second concern is 'Can the fuselage bending/torsion aeroelastic modes be effectively augmented without sufficient control input near the vehicle nose?' The superaugmented FCS results above may be suggesting the necessity of a secondary feedback loop to achieve an acceptable integrated FCS. Preliminary analysis of HSCT aeroelastic mode shapes indicate the use of existing wing leading edge devices as a second control input may be lacking in control authority for the rigid-body attitude and aeroelastic modes. An effort is underway to incorporate generic wing leading edge devices and canards into a generic HSCT model for the purpose of assessing additional control authority and it's use in candidate FCS designs. A generic HSCT mathematical model was necessary for the studies above. A HSCT category model is available in NASA-CR-172201. This model describes the linear, longitudinal dynamics about the following flight condition: ascent, W = 730,000 lbs, h = 6,500 ft, M = 0.6. The model incorporates the full rigid-body variable set, as well as eighteen aeroelastic modes. Elevator deflection serves as the control input. Modifications to the model include the incorporation of relaxed static stability (i.e., static margin from -7.3% to +10%) and additional control inputs. Author

N95-23315*# Pembroke State Univ., NC.

BENCHMARK PROBLEMS IN COMPUTATIONAL AEROACOUSTICS Abstract Only **c71**

Freda Porter-Locklear *In* Hampton Univ., 1994 NASA-HU American Society for Engineering Education (ASEE) Summer Faculty Fellowship Program Dec. 1994 p 97 (For primary document see N95-23276 07-99)

Avail: CASI HC A01/MF A02

A recent directive at NASA Langley is aimed at numerically predicting principal noise sources. During my summer stay, I worked with high-order ENO code, developed by Dr. Harold Atkins, for solving the unsteady compressible Navier-Stokes equations, as it applies to computational aeroacoustics (CAA). A CAA workshop, composed of six categories of benchmark problems, has been organized to test various numerical properties of code. My task was to determine the robustness of Atkins' code for these test problems. In one category, we tested the nonlinear wave propagation of the code for the one-dimensional Euler equations, with initial pressure, density, and velocity conditions. Using freestream boundary conditions, our results were plausible. In another category, we solved the linearized two-dimensional Euler equations to test the effectiveness of radiation boundary conditions. Here we utilized MAPLE to compute eigenvalues and eigenvectors of the Jacobian given variable and flux vectors. We experienced a minor problem with inflow and outflow boundary conditions. Next, we solved the quasi one dimensional unsteady flow equations with an incoming acoustic wave of amplitude 10(exp -6). The small amplitude sound wave was incident on a convergent-divergent nozzle. After finding a steady-state solution and then marching forward, our solution indicated that after 30 periods the acoustic wave had dissipated (a period is time required for sound wave to traverse one end of nozzle to other end). Author

N95-23316*# Norfolk State Univ., VA. School of Social Work.

LANGLEY RESEARCH CENTER STRATEGIC PLAN FOR EDUCATION Abstract Only **c80**

Sandra B. Proctor *In* Hampton Univ., 1994 NASA-HU American Society for Engineering Education (ASEE) Summer Faculty Fellowship Program Dec. 1994 p 98 (For primary document see N95-23276 07-99)

Avail: CASI HC A01/MF A02

Research assignment centered on the preparation of final draft of the NASA Langley Strategic Plan for Education. Primary research activity consisted of data collection, through interviews with LaRC Office of Education and NASA Headquarters staff, university administrators and faculty, and school administrators / teachers; and documentary analysis. Pre-college and university programs were critically reviewed to assure effectiveness, support of NASA and Langley's mission and goals; National Education Goals; and educational reform strategies. In addition to these mandates, pre-college programs were reviewed to address present and future LaRC activities for teacher enhancement and preparation. University programs were reviewed with emphasis on student support and recruitment; faculty development and enhancement; and LaRC's role in promoting the utilization of educational technologies and distance learning. The LaRC Strategic Plan for Education will enable the Office of Education to provide a focused and well planned continuum of education programs for students, teachers and faculty. It will serve to direct and focus present activities and programs while simultaneously offering the flexibility to address new and emerging directions based on changing national, state, and agency trends. Author

N95-23317*# Mississippi State Univ., Mississippi State, MS. Dept. of Aerospace Engineering.

THIN TAILORED COMPOSITE WING FOR CIVIL TILTROTOR Abstract Only **c05**

Masoud Rais-Rohani *In* Hampton Univ., 1994 NASA-HU American Society for Engineering Education (ASEE) Summer Faculty Fellowship Program Dec. 1994 p 99 (For primary document see N95-23276 07-99)

Avail: CASI HC A01/MF A02

The tiltrotor aircraft is a flight vehicle which combines the efficient low speed (i.e., take-off, landing, and hover) characteristics of a helicopter with the efficient cruise speed of a turboprop airplane. A well-known example of such vehicle is the Bell-Boeing V-22 Osprey. The high cruise speed and range constraints placed on the civil tiltrotor require a relatively thin wing to increase the drag-divergence Mach number which translates into lower compressibility drag. It is required to reduce the wing maximum thickness-to-chord ratio t/c from 23% (i.e., V-22 wing) to 18%. While a reduction in wing thickness results in improved aerodynamic efficiency, it has an adverse effect on the wing structure and it tends to reduce structural stiffness. If ignored, the reduction in wing stiffness leads to susceptibility

to aeroelastic and dynamic instabilities which may consequently cause a catastrophic failure. By taking advantage of the directional stiffness characteristics of composite materials the wing structure may be tailored to have the necessary stiffness, at a lower thickness, while keeping the weight low. The goal of this study is to design a wing structure for minimum weight subject to structural, dynamic and aeroelastic constraints. The structural constraints are in terms of strength and buckling allowables. The dynamic constraints are in terms of wing natural frequencies in vertical and horizontal bending and torsion. The aeroelastic constraints are in terms of frequency placement of the wing structure relative to those of the rotor system. The wing-rotor-pylon aeroelastic and dynamic interactions are limited in this design study by holding the cruise speed, rotor-pylon system, and wing geometric attributes fixed. To assure that the wing-rotor stability margins are maintained a more rigorous analysis based on a detailed model of the rotor system will need to ensue following the design study. The skin-stringer-rib type architecture is used for the wing-box structure. The design variables include upper and lower skin ply thicknesses and orientation angles, spar and rib web thicknesses and cap areas, and stringer cross-sectional areas. These design variables will allow the maximum tailoring of the structure to meet the design requirements most efficiently. Initial dynamic analysis has been conducted using MSC/NASTRAN to determine the baseline wing's frequencies and mode shapes. For the design study we intend to use the finite-element based code called WIDOWAC (Wing Design Optimization With Aeroeastic Constraints) that was developed at NASA Langley in early 1970's for airplane wing structural analysis and preliminary design. Currently, the focus is on modification and validation of this code which will be used for the civil tiltrotor design efforts. Author

N95-23318*# Saint Cloud State Coll., MN. Dept. of Electrical Engineering.

DIFFERENTIAL GPS AND SYSTEM INTEGRATION OF THE LOW VISIBILITY LANDING AND SURFACE OPERATIONS (LVLASO) DEMONSTRATION Abstract Only **c04**

James M. Rankin *In* Hampton Univ., 1994 NASA-HU American Society for Engineering Education (ASEE) Summer Faculty Fellowship Program Dec. 1994 p 100 (For primary document see N95-23276 07-99)

Avail: CASI HC A01/MF A02

The LVLASO Flight Demonstration of ASTA concepts (FDAC) integrates NASA-Langley's electronic moving map display and Transport Systems Research Vehicle (TSRV) (a modified Boeing 737 aircraft); ARINC's VHF data link, GPS ground station, and automated controller workstation; and Norden's surface radar/airport movement safety system. Aircraft location is shown on the electronic map display in the cockpit. An approved taxi route as well as other aircraft and surface traffic are also displayed. An Ashtech Z12 Global Positioning System (GPS) receiver on the TSRV estimates the aircraft's position. In Differential mode (DSPS), the Ashtech receiver accepts differential C/A code pseudorange corrections from a GPS ground station. The GPS ground station provides corrections up to ten satellites. The corrections are transmitted on a VHF data link at a 1 Hz. rate using the RTCM-104 format. DGPS position estimates will be within 5 meters of actual aircraft position. DGPS position estimates are blended with position, velocity, acceleration, and heading data from the TSRV Air Data/Inertial Reference System (ADIRS). The ADIRS data is accurate in the short-term, but drifts over time. The DGPS data is used to keep the ADIRS position accurate. Ownship position, velocity, heading, and turn rate are sent at a 20 Hz. rate to the electronic map display. Airport traffic is detected by the airport surface radar system. Aircraft and vehicles such as fuel trucks and baggage carts are detected. The traffic's location, velocity, and heading are sent to the TSRV. To prevent traffic symbology from jumping each second when a location update arrives, velocity and heading are used to predict a new traffic location for each display update. Possible runway incursions and collisions can be shown on the electronic map. Integrating the different systems used in the FDAC requires attention to the underlying coordinate systems. The airport diagram displayed on the electronic map is obtained from published navigational charts. The charts reference the North American Datum of 1927 (NAD27) or a local state-plane coordinate system. GPS uses the World Geodetic Standard of 1984 (WGS84). Both NAD27 and WGS84 model the Earth as an ellipsoid, however, they use a different origin and different size ellipsoids. Latitudes and longitudes given in these systems can be converted to a Cartesian system with the origin at the Earth's center. The surface radar detects traffic in a locally-level, rho-theta coordiante system. The electronic airport diagram is stored using a flat XY coordinate system. The map origin is at the tower and is referenced as True North up. All ownship and other traffic positions must be converted to the electronic map's frame of reference for display. Author

N95-23319*# Saint Louis Univ., Cahokia, IL. Dept. of Aerospace Engineering.

PRELIMINARY IDENTIFICATION OF BUFFET PROBLEMS IN HIGH SPEED CIVIL TRANSPORT Abstract Only **c08**

Krishnaswamy Ravindra *In* Hampton Univ., 1994 NASA-HU American Society for Engineering Education (ASEE) Summer Faculty Fellowship Program Dec. 1994 p 101 (For primary document see N95-23276 07-99)

Avail: CASI HC A01/MF A02

In the present study, some effort is made to identify whether empennage buffet is a relevant factor in the design and operation of the High Speed Civil Transport (HSCT). Based on some results of the only operational supersonic transport, Concorde and the innumerable studies that exist on the tail buffet of high performance airplanes, CFD analyses on the HSCT as well as low speed wind tunnel tests on models, it appears as though buffet will be a factor that needs attention in the proper design of empennage structure. Utilizing the existing empirical relation between the reduced frequency of the leading edge vortices and the geometric parameters, it is estimated that the characteristic frequencies of the vortices from the wing cranks are in the range of certain fundamental frequencies of the wing-fuselage-empennage structure. Buffet is believed to be critical during take-off, climb, descent and landing. Computational and experimental data available in open literature indicate coherent vortex flow structure in the empennage region at supersonic cruise speeds. This raises further concern on the fatigue life of the empennage structure. Three second generation supersonic transport designs taken from open literature are briefly compared with the 'empennage buffet' in mind. Future research efforts relating to buffet studies on the HSCT are summarized. A bibliography pertaining to the present research, including relevant studies on the first generation supersonic transport is presented. The effect of rounded wing leading edges on the present frequency estimates needs further study. The effect of engine exhaust on the flow field in the empennage region also needs further study. Author

N95-23320*# College of William and Mary, Williamsburg, VA. Dept. of Mathematics.

PREPARATION OF COURSE MATERIALS: ELEMENTARY MATHEMATICS OF POWERED FLIGHT Abstract Only **c80**

George T. Rublein *In* Hampton Univ., 1994 NASA-HU American Society for Engineering Education (ASEE) Summer Faculty Fellowship Program Dec. 1994 p 102 (For primary document see N95-23276 07-99)

Avail: CASI HC A01/MF A02

Non-science students at William and Mary will soon be required to take a mathematics course in order to earn a bachelor's degree. A standard menu of technique courses is the usual way in which universities provide for this requirement: Trigonometry, probability, geometry for teachers, and the like. In this work, we attempt to break away from these largely unsuccessful choices. Our intent is to prepare material that sets a variety of simple mathematical procedures in the context of a commonly experienced part of students' lives: riding in commercial airplanes. The work, begun last summer at Langley, is now close to completion and trial in upcoming fall term at William and Mary. As of this writing, the narrative is complete for 12 to 14 projected sections. We have prepared material on wind triangles, wind roses, navigation maps, drag induced loss of velocity for unpowered missiles (tennis balls), luggage and its effect on center of gravity, localized magnetic declination and VOR orientation, geometry of great circles, terminal velocity for falling bodies, pressure vessels: tires and balloons and blimps, global structure of declination lines, map projections (mercator, azimuthal equidistant, Lambert), ears and their reaction to altitude change. The next section will treat lift, drag and thrust. The last will treat control surfaces. The entire approach avoids any effort to investigate mathematical topics that arise in the solution of problems. And by the same token, we avoid any organized attempt to explain aeronautical engineering, even on an elementary level. We look only at enough mathematics to do a problem and we select only engineering topics that permit some kind of (elementary) mathematical analysis. In the end, we

will think of the material as successful if two things happen: Students must come away with some confidence that even lay people can quantify parts of their surroundings. Other potential instructors must be willing to gain enough familiarity with the physical content of the material so that it can be used at other universities. Author

N95-23321*# Virginia Polytechnic Inst. and State Univ., Blacksburg, VA. Dept. of Mechanical Engineering.

ASSOCIATED WITH AEROSPACE VEHICLES DEVELOPMENT OF METHODOLOGIES FOR THE ESTIMATION OF THERMAL PROPERTIES Abstract Only **c39**

Elaine P. Scott *In* Hampton Univ., 1994 NASA-HU American Society for Engineering Education (ASEE) Summer Faculty Fellowship Program Dec. 1994 p 103 (For primary document see N95-23276 07-99)
Avail: CASI HC A01/MF A02

Thermal stress analyses are an important aspect in the development of aerospace vehicles at NASA-LaRC. These analyses require knowledge of the temperature distributions within the vehicle structures which consequently necessitates the need for accurate thermal property data. The overall goal of this ongoing research effort is to develop methodologies for the estimation of the thermal property data needed to describe the temperature responses of these complex structures. The research strategy undertaken utilizes a building block approach. The idea here is to first focus on the development of property estimation methodologies for relatively simple conditions, such as isotropic materials at constant temperatures, and then systematically modify the technique for the analysis of more and more complex systems, such as anisotropic multi-component systems. The estimation methodology utilized is a statistically based method which incorporates experimental data and a mathematical model of the system. Several aspects of this overall research effort were investigated during the time of the ASEE summer program. One important aspect involved the calibration of the estimation procedure for the estimation of the thermal properties through the thickness of a standard material. Transient experiments were conducted using a Pyrex standard at various temperatures, and then the thermal properties (thermal conductivity and volumetric heat capacity) were estimated at each temperature. Confidence regions for the estimated values were also determined. These results were then compared to documented values. Another set of experimental tests were conducted on carbon composite samples at different temperatures. Again, the thermal properties were estimated for each temperature, and the results were compared with values obtained using another technique. In both sets of experiments, a 10-15 percent off-set between the estimated values and the previously determined values was found. Another effort was related to the development of the experimental techniques. Initial experiments required a resistance heater placed between two samples. The design was modified such that the heater was placed on the surface of only one sample, as would be necessary in the analysis of built up structures. Experiments using the modified technique were conducted on the composite sample used previously at different temperatures. The results were within 5 percent of those found using two samples. Finally, an initial heat transfer analysis, including conduction, convection and radiation components, was completed on a titanium sandwich structural sample. Experiments utilizing this sample are currently being designed and will be used to first estimate the material's effective thermal conductivity and later to determine the properties associated with each individual heat transfer component. Author

N95-23322*# Christopher Newport Coll., Newport News, VA. Dept. of Physics and Computer Science.

POTENTIAL AEROSPACE APPLICATIONS OF HIGH TEMPERATURE SUPERCONDUCTORS Abstract Only **c33**

Raouf Selim *In* Hampton Univ., 1994 NASA-HU American Society for Engineering Education (ASEE) Summer Faculty Fellowship Program Dec. 1994 p 104 (For primary document see N95-23276 07-99)
Avail: CASI HC A01/MF A02

The recent discovery of High Temperature Superconductors (HTS) with superconducting transition temperature, T(sub c), above the boiling point of liquid nitrogen has opened the door for using these materials in new and practical applications. These materials have zero resistance to electric current, have the capability of carrying large currents and as such have the potential to be used in high magnetic field applications. One of the space applications that can use superconductors is electromagnetic launch of payloads to low-earth-orbit. An electromagnetic gun-type launcher can be used in small payload systems that are launched at very high velocity, while sled-type magnetically levitated launcher can be used to launch larger payloads at smaller velocities. Both types of launchers are being studied by NASA and the aerospace industry. The use of superconductors will be essential in any of these types of launchers in order to produce the large magnetic fields required to obtain large thrust forces. Low Temperature Superconductor (LTS) technology is mature enough and can be easily integrated in such systems. As for the HTS, many leading companies are currently producing HTS coils and magnets that potentially can be mass-produced for these launchers. It seems that designing and building a small-scale electromagnetic launcher is the next logical step toward seriously considering this method for launching payloads into low-earth-orbit. A second potential application is the use of HTS to build sensitive portable devices for the use in Non Destructive Evaluation (NDE). Superconducting Quantum Interference Devices (SQUID's) are the most sensitive instruments for measuring changes in magnetic flux. By using HTS in SQUID's, one will be able to design a portable unit that uses liquid nitrogen or a cryocooler pump to explore the use of gradiometers or magnetometers to detect deep cracks or corrosion in structures. A third use is the replacement of Infra-Red (IR) sensor leads on Earth Orbit Systems (EOS) with HTS leads. IR detectors on these EOS missions are cooled to a 4.2K to improve their signal to noise ratio. They are connected to data acquisitions systems using manganin wires (low thermal conductors) to reduce the heat load on the cryogen. Replacing these wires with HTS leads will increase the lifetime of these missions by about 50 percent. This is a promising application that is ready for actual implementation on such systems. The analysis also show that an the number of IR detectors increase in larger EOS systems, substantial increase in the lifetime of each mission will be realized by using HTS leads instead of the manganin ones. Author

N95-23323*# Hampton Univ., VA. Dept. of Management.

UPWARD APPRAISAL AS A MEANS FOR IMPROVING SUPERVISORY PERFORMANCE AND PROMOTING PROCESS IMPROVEMENT, WITH LONG-TERM IMPLICATIONS FOR ORGANIZATIONAL CHANGE Abstract Only **c81**

Denise V. Siegfeldt *In its* 1994 NASA-HU American Society for Engineering Education (ASEE) Summer Faculty Fellowship Program Dec. 1994 p 105 (For primary document see N95-23276 07-99)
Avail: CASI HC A01/MF A02

This study represents the implementation phase of an organizational development project which was initiated last year in the Management Support Division (MSD) at Langley Research Center to diagnose organizational functioning. As a result of MSD survey data from last year's effort, a Quality Action Team was created to address the responses compiled from the MSD Organizational Assessment Questionnaire and Follow-Up Questionnaire. The team was officially named the MSD Employee Relations Improvement Team (MERIT). MERIT's goal was to analyze major concerns generated by the questionnaires and to present feasible solutions to management which would improve supervisory performance, promote process improvement; and ultimately, lead to a better organization. The team met weekly and was very disciplined in following guidelines needed to ensure a fully functioning team. Several TQM tools were used during the team process, including brainstorming and the cause and effect diagram. One of the products produced by MERIT was a 'report card', more formally known as an upward appraisal system, to evaluate supervisory performance in the division office, its three branches, and in teams. Major areas of emphasis on the 47 item report card were those identified by employees through the previously administered questionnaires as needing to be improved; specifically, training, recognition, teamwork, supervision and leadership, and communication. MERIT created an enlarged and modified version of the report card which enabled scores for each individual supervisor to be recorded on a separate form, along with summary results and employee comments. Report card results have been compiled and fed back to the Division Chief and Assistant Division Chief. These individuals will in turn, feed the results back to the remaining supervisors and the team leaders. Although results differ among supervisors, some similarities exist. Communication generally appears to be adequate, which represents an improvement over last year. In contrast, recognition and teamwork are the two major areas where improvement in supervisory performance seems to be most needed. The initial report card results will serve as a baseline

against which future performance ratings will be compared. Once supervisors have been presented with their data and given an opportunity to analyze and discus the results, they will be assisted in developing an action plan for improving their performance and work processes. They will be provided with ongoing support from management in following through with the action plan. Author

N95-23324*# Virginia Univ. Hospital, Charlottesville, VA.
TEACHER ENHANCEMENT INSTITUTE Abstract Only **c80**
Ron W. Simmons *In* Hampton Univ., 1994 NASA-HU American Society for Engineering Education (ASEE) Summer Faculty Fellowship Program Dec. 1994 p 106 (For primary document see N95-23276 07-99)
Avail: CASI HC A01/MF A02

In a team building, team teaching strategy with four faculty, can learning strategies such as educational technology and problem based learning be provided to forty local teachers of primary, elementary, and secondary students? The impetus for the effort is to provide information about science and engineering at NASA and motivate students to pursue careers in science and technology. Teachers, identified and selected through a rigorous application procedure, participated in a two week workshop for a graduate credit. Teachers were exposed to computer applications such as INTERNET, MOSAIC, Power Machintosh word processing, NASA scientists, and laboratory experiments. Teachers were evaluated on level and quality of their participation, design of teacher application materials and relevant lesson plans and presentations. The results show that teachers, regardless of preparation and background, can learn science and engineering applications and develop relevant materials to transfer information to their classroom. Follow-up during the academic year will show that teachers are successfully using materials. Author

N95-23325*# Tennessee Univ. Space Inst., Tullahoma, TN.
HANDLING QUALITIES OF THE HIGH SPEED CIVIL TRANSPORT Abstract Only **c08**
U. Peter Solies *In* Hampton Univ., 1994 NASA-HU American Society for Engineering Education (ASEE) Summer Faculty Fellowship Program Dec. 1994 p 107 (For primary document see N95-23276 07-99)
Avail: CASI HC A01/MF A02

The low speed handling qualities of a High Speed Civil Transport class aircraft have been investigated by using data of the former Advanced Supersonic Transport (AST) 105. The operation of such vehicles in the airport terminal area is characterized by 'backside' performance. Main objectives of this research effort were: (Q) determination of the nature and magnitude of the speed instability associated with the backside of the thrust required curve; (2) confirmation of the validity of existing MIL-SPEC handling qualities criteria; (3) safety of operation of the vehicle in the event of autothrottle failure; and (4) correlation of required engine responsiveness with level of speed instability. Preliminary findings comprise the following: (1) The critical velocity for speed instability was determined to be 196 knots, well above the projected approach speed of 155 knots. This puts the vehicle far on the backside of its thrust required curve. While the aircraft can be configured to have static and dynamic stability at this trim point, a significant speed instability emerges, if a pilot or autopilot attempts flight path control with elevator and/or canard control surfaces only. This requires a properly configured autothrottle and/or variable aerodynamic drag devices which can provide speed stability; (2) An AST 105 type vehicle meets MIL-SPEC criteria only in part. While the damping criteria for phugoid and short period motion are met easily, the AST 105 falls short of the required minimum short period frequency, meaning that the HSCT is too sluggish in pitch to meet the military criteria. Obviously the military specification do not consider a vehicle with such high pitch inertia. With regard to speed stability and flight path stability criteria, the vehicle meets levels 2 and 3 of the military requirements, indicating that it would be landed safety with manual controls in case of an autothrottle failure, even though the pilot workload would be high; and (3) This requires quick thrust response to throttle adjustment, however. If the engine responsiveness is slow, the aircraft handling qualities are further deteriorated. Progress has been made in correlating required engine responses dyanmics with the given level of speed instability of the vehicle. Author (revised)

N95-23326*# Montana State Univ., Bozeman, MT. Dept. of Chemistry.
COMPUTATIONAL MODELLING OF Er(3+): GARNET LASER MATERIALS Abstract Only **c36**
Lee H. Spangler *In* Hampton Univ., 1994 NASA-HU American Society for Engineering Education (ASEE) Summer Faculty Fellowship Program Dec. 1994 p 108 (For primary document see N95-23276 07-99)
Avail: CASI HC A01/MF A02

The Er(3+) ion has attracted a lot of interest for four reasons: (1) Its (4)I(sub 13/2) yields (4)I(sub 15/2) transition lases in the eyesafe region near 1.5 micron; (2) the (4)I(sub 13/2) transition lases near 2.8 micron, an important wavelength for surgical purposes; (3) it displays surprisingly efficient upconversion with lasing observed at 1.7, 1.2, 0.85, 0.56, 0.55, and 0.47 micron following 1.5 micron pumping; and (4) it has absorption bands at 0.96 and 0.81 micron and thus can be diode pumped. However, properties desirable for upconversion reduce the efficiency of 1.5 and 3 micron laser operation and vice versa. Since all of the processes are influenced by the host via the crystal field induced stark splittings in the Er levels, this project undertook modelling of the host influence on the Er lasinng behavior. While growth and measurement of all ten Er(3+) doped garnets is the surest way of identifying hosts which maximize upconversion (or conversly, 1.5 and 3 micron performance), it is also expensive - costing approximately $10,000/material or approximately $100,000 for the materials computationally investigated here. The calculations were performed using a quantum mechanical point charge model developed by Clyde Morrison at Harry Diamond Laboratories. The programs were used to fit the Er:YAG experimental energy levels so that the crystal field parameters, B(sub nm) could be extracted. From these radial factors, rho (sub n) were determined for Er(3+) in garnets. These, in combination with crystal field components, Anm, available from X-ray data, were used to predict energy levels for Er in the other nine garnet hosts. The levels in Er:YAG were fit with an rms error of 12.2/cm over a 22,000/cm range. Predicted levels for two other garnets for which literature values were available had rms errors of less than 17/cm , showing the calculations to be reliable. Based on resonances between pairs of calculated stark levels, the model predicts GSGG as the best host for 1.5 micron laser operation, GSGG or YSAG as the best host for a 2.8 micron operation, and LuGG as the best host for an upconversion material. Author

N95-23327*# Oklahoma Univ., Norman, OK. School of Aerospace and Mechanical Engineering.
A NEW LOOK AT THE SIMULTANEOUS ANALYSIS AND DESIGN OF STRUCTURES Abstract Only **c39**
Alfred G. Striz *In* Hampton Univ., 1994 NASA-HU American Society for Engineering Education (ASEE) Summer Faculty Fellowship Program Dec. 1994 p 109 (For primary document see N95-23276 07-99)
Avail: CASI HC A01/MF A02

The minimum weight optimization of structural systems, subject to strength and displacement constraints as well as size side constraints, was investigated by the Simultaneous ANalysis and Design (SAND) approach. As an optimizer, the code NPSOL was used which is based on a sequential quadratic programming (SQP) algorithm. The structures were modeled by the finite element method. The finite element related input to NPSOL was automatically generated from the input decks of such standard FEM/optimization codes as NASTRAN or ASTROS, with the stiffness matrices, at present, extracted from the FEM code ANALYZE. In order to avoid ill-conditioned matrices that can be encountered when the global stiffness equations are used as additional nonlinear equality constraints in the SAND approach (with the displacements as additional variables), the matrix displacement method was applied. In this approach, the element stiffness equations are used as constraints instead of the global stiffness equations, in conjunction with the nodal force equilibrium equations. This approach adds the element forces as variables to the system. Since, for complex structures and the associated large and very sparce matrices, the execution times of the optimization code became excessive due to the large number of required constraint gradient evaluations, the Kreisselmeier-Steinhauser function approach was used to decrease the computational effort by reducing the nonlinear equality constraint system to essentially a single combined constraint equation. As the linear equality and inequality constraints require much less computational effort to evaluate, they were kept in their previous form to limit the complexity of the KS function evaluation. To date, the standard three-bar, ten-bar, and 72-bar trusses have been tested. For the standard SAND approach, correct results were obtained for all three trusses although convergence became slower for the 72-bar truss. When the matrix displacement method was used,

correct results were still obtained, but the execution times became excessive due to the large number of constraint gradient evaluations required. Using the KS function, the computational effort dropped, but the optimization seemed to become less robust. The investigation of this phenomenon is continuing. As an alternate approach, the code MINOS for the optimization of sparse matrices can be applied to the problem in lieu of the Kreisselmeier-Steinhauser function. This investigation is underway. Author

N95-23328*# Hampton Univ., VA.

APPLICATION OF ELECTRON PARAMAGNETIC RESONANCE IMAGING TO THE CHARACTERIZATION OF THE ULTEM(R) EXPOSED TO 1 MeV ELECTRONS. CORRELATION OF RADICAL DENSITY DATA TO TIGER CODE CALCULATIONS Abstract Only **c72**

Naushadalli K. Suleman *In its* 1994 NASA-HU American Society for Engineering Education (ASEE) Summer Faculty Fellowship Program Dec. 1994 p 110 (For primary document see N95-23276 07-99)
Avail: CASI HC A01/MF A02

A major long-term goal of the Materials Division at the NASA Langley Research Center is the characterization of new high-performance materials that have potential applications in the aircraft industry, and in space. The materials used for space applications are often subjected to a harsh and potentially damaging radiation environment. The present study constitutes the application of a novel technique to obtain reliable data for ascertaining the molecular basis for the resilience and durability of materials that have been exposed to simulated space radiations. The radiations of greatest concern are energetic electrons and protons, as well as galactic cosmic rays. Presently, the effects of such radiation on matter are not understood in their entirety. It is clear however, that electron radiation causes ionization and homolytic bond rupture, resulting in the formation of paramagnetic spin centers in the polymer matrices of the structural materials. Since the detection and structure elucidation of paramagnetic species are most readily accomplished using Electron Paramagnetic Resonance (EPR) Spectroscopy, the NASA LaRC EPR system was brought back on-line during the 1991 ASEE term. The subsequent 1992 ASEE term was devoted to the adaptation of the EPR core system to meet the requirements for EPR Imaging (EPRI), which provides detailed information on the spatial distribution of paramagnetic species in bulk media. The present (1994) ASEE term was devoted to the calibration of this EPR Imaging system, as well as to the application of this technology to study the effects of electron irradiation on Ultem(exp R), a high performance polymer which is a candidate for applications in aerospace. The Ultem was exposed to a dose of 2.4 x 10(exp 9) Rads (1-MeV energy/electron) at the LaRC electron accelerator facility. Subsequently, the exposed specimens were stored in liquid nitrogen, until immediately prior to analyses by EPRI. The intensity and dimensions of the EPR Images that were generated for the irradiated specimens showed that the electrons penetrated the material to a depth of approximately 0.125 inch. These data show a very high degree of correlation to the energy deposition profile as predicted by the Tiger Code, a Monte Carlo code that provides guidelines for the transport of electrons in matter. Subsequent efforts will focus on delineating the transport properties of energetic protons in Ultem(R). Author

N95-23329*# Alabama Univ., Tuscaloosa, AL. Dept. of Physics and Astronomy.

THEORETICAL STUDIES OF SPECTROSCOPIC PROBLEMS OF IMPORTANCE FOR ATMOSPHERIC RADIATION MEASUREMENTS Abstract Only **c46**

Richard H. Tipping *In* Hampton Univ., 1994 NASA-HU American Society for Engineering Education (ASEE) Summer Faculty Fellowship Program Dec. 1994 p 111 (For primary document see N95-23276 07-99)
Avail: CASI HC A01/MF A02

Many of the instruments used to deduce the physical parameters of the Earth's atmosphere necessary for climate studies or for pollution monitoring (for instance, temperature versus pressure or number densities of trace molecules) rely on the existence of accurate spectroscopic data and an understanding of the physical processes responsible for the absorption or emission of radiation. During the summer, research was either continued or begun on three distinct problems: (1) an improved theoretical framework for the calculation of the far-wing absorption of allowed spectral lines; (2) a refinement of the calculation of the collision-induced fundamental spectrum of N2; and (3) an investigation of possible line-mixing effects in the fundamental spectrum of CH4. Progress in these three areas is summarized below. During the past few years, we have developed a theoretical framework for the calculation of the absorption of radiation by the far wings of spectral lines. Such absorption due to water vapor plays a crucial role in the greenhouse effect as well as limiting the retrieval of temperature profiles from satellite data. Several improvements in the theory have been made and the results are being prepared for publication. Last year we published results for the theoretical calculation of the absorption of radiation due to the dipoles induced during binary collisions of N2 molecules using independently measured molecular parameters; the results were in reasonable agreement with experimental data. However, recent measurements have revealed new fine structure that has been attributed to line-mixing effects. We do not think that this is correct, rather that the structure results from short-range anisotropic dipoles. We are in the process of including this refinement in our theoretical calculation in order to compare with the new experimental data. Subtle changes in the spectra of CH4 measured by researchers at Langley have also been attributed to line-mixing effects. By analyzing the same spectral lines we have attempted to verify or rule out possible line-mixing mechanisms. Due to the complexity and richness of the spectrum of this highly symmetric molecule, as well as the small magnitude of the effects, a detailed first-principle calculation of the mixing is a difficult problem. Before such a program is undertaken it is important to glean as much information as possible concerning the possible mechanisms by a systematic analysis of the existing data. Author

N95-23330*# Sage Junior Coll. of Albany, Albany, NY. Math/Science Div.

COMPUTER MODELING OF THE SENSITIVITY OF A LASER WATER VAPOR SENSOR TO VARIATIONS IN TEMPERATURE AND AIR SPEED Abstract Only **c36**

George F. Tucker *In* Hampton Univ., 1994 NASA-HU American Society for Engineering Education (ASEE) Summer Faculty Fellowship Program Dec. 1994 p 112 (For primary document see N95-23276 07-99)
Avail: CASI HC A01/MF A02

Currently, there is disagreement among existing methods of determining atmospheric water vapor concentration at dew-points below -40 C. A major source of error is wall effects which result from the necessity of bringing samples into the instruments. All of these instruments also have response times on the order of seconds. NASA Langley is developing a water vapor sensor which utilizes the absorption of the infrared radiation produced by a diode laser to estimate water vapor concentration. The laser beam is directed through an aircraft window to a retroreflector located on an engine. The reflected beam is detected by an infrared detector located near the laser. To maximize signal to noise, derivative signals are analyzed. By measuring the 2f/DC signal and correcting for ambient temperature, atmospheric pressure and air speed (which results in a Doppler shifting of the laser beam), the water vapor concentration can be retrieved. Since this is an in situ measurement there are no wall effects and measurements can be made at a rate of more than 20 per second. This allows small spatial variations of water vapor to be studied. In order to study the sensitivity of the instrument to variations in temperature and air speed, a computer program which generated the 2f, 3f, 4f, DC and 2f/DC signals of the instrument as a function of temperature, pressure and air speed was written. This model was used to determine the effect of errors in measurement of the temperature and air speed on the measured water vapor concentration. Future studies will quantify the effect of pressure measurement errors, which are expected to be very small. As a result of these studied, a retrieval algorithm has been formulated, and will be applied to data taken during the PEM-West atmospheric science field mission. Spectroscopic studies of the water vapor line used by the instrument will be used to refine this algorithm. To prepare for these studies, several lasers have been studied to determine their output frequency range and power. Author

N95-23331*# Paul D. Camp Community Coll., Suffolk, VA. Dept. of Computer Information Sytems.

THE SOFTWARE ANALYSIS PROJECT FOR THE OFFICE OF HUMAN RESOURCES Abstract Only **c81**

Robert L. Tureman, Jr. *In* Hampton Univ., 1994 NASA-HU American Society for Engineering Education (ASEE) Summer Faculty Fellowship Program Dec. 1994 p 113 (For primary document see N95-23276 07-99)
Avail: CASI HC A01/MF A02

There were two major sections of the project for the Office of Human Resources (OHR). The first section was to conduct a planning study to analyze software use with the goal of recommending software purchases and determining whether the need exists for a file server. The second section was analysis and distribution planning for retirement planning computer program entitled VISION provided by NASA Headquarters. The software planning study was developed to help OHR analyze the current administrative desktop computing environment and make decisions regarding software acquisition and implementation. There were three major areas addressed by the study: current environment new software requirements, and strategies regarding the implementation of a server in the Office. To gather data on current environment, employees were surveyed and an inventory of computers were produced. The surveys were compiled and analyzed by the ASEE fellow with interpretation help by OHR staff. New software requirements represented a compilation and analysis of the surveyed requests of OHR personnel. Finally, the information on the use of a server represents research done by the ASEE fellow and analysis of survey data to determine software requirements for a server. This included selection of a methodology to estimate the number of copies of each software program required given current use and estimated growth. The report presents the results of the computing survey, a description of the current computing environment, recommenations for changes in the computing environment, current software needs, management advantages of using a server, and management considerations in the implementation of a server. In addition, detailed specifications were presented for the hardware and software recommendations to offer a complete picture to OHR management. The retirement planning computer program available to NASA employees will aid in long-range retirement planning. The intended audience is the NASA civil service employee with several years until retirement. The employee enters current salary and savings information as well as goals concerning salary at retirement, assumptions on inflation, and the return on investments. The program produces a picture of the employee's retirement income from all sources based on the assumptions entered. A session showing features of the program was conducted for key personnel at the Center. After analysis, it was decided to offer the program through the Learning Center starting in August 1994. Author

N95-23332*# Old Dominion Coll., Norfolk, VA.

MULTIDISCIPLINARY DESIGN OPTIMIZATION USING GENETIC ALGORITHMS Abstract Only **c15**

Resit Unal *In* Hampton Univ., 1994 NASA-HU American Society for Engineering Education (ASEE) Summer Faculty Fellowship Program Dec. 1994 p 114 (For primary document see N95-23276 07-99)

Avail: CASI HC A01/MF A02

Multidisciplinary design optimization (MDO) is an important step in the conceptual design and evaluation of launch vehicles since it can have a significant impact on performance and life cycle cost. The objective is to search the system design space to determine values of design variables that optimize the performance characteristic subject to system constraints. Gradient-based optimization routines have been used extensively for aerospace design optimization. However, one limitation of gradient based optimizers is their need for gradient information. Therefore, design problems which include discrete variables can not be studied. Such problems are common in launch vehicle design. For example, the number of engines and material choices must be integer values or assume only a few discrete values. In this study, genetic algorithms are investigated as an approach to MDO problems involving discrete variables and discontinuous domains. Optimization by genetic algorithms (GA) uses a search procedure which is fundamentally different from those gradient based methods. Genetic algorithms seek to find good solutions in an efficient and timely manner rather than finding the best solution. GA are designed to mimic evolutionary selection. A population of candidate designs is evaluated at each iteration, and each individual's probability of reproduction (existence in the next generation) depends on its fitness value (related to the value of the objective function). Progress toward the optimum is achieved by the crossover and mutation operations. GA is attractive since it uses only objective function values in the search process, so gradient calculations are avoided. Hence, GA are able to deal with discrete variables. Studies report success in the use of GA for aircraft design optimization studies, trajectory analysis, space structure design and control systems design. In these studies reliable convergence was achieved, but the number of function evaluations was large compared with efficient gradient methods. Applicaiton of GA is underway for a cost optimization study for a launch-vehicle fuel-tank and structural design of a wing. The strengths and limitations of GA for launch vehicle design optimization is studied. Author

N95-23333*# California Univ., Davis, CA. Dept. of Mechanical and Aeronautical Engineering.

HIGH-LIFT FLOW-PHYSICS FLIGHT EXPERIMENTS ON A SUBSONIC CIVIL TRANSPORT AIRCRAFT (B737-100) Abstract Only **c02**

Cornelis P. vanDam *In* Hampton Univ., 1994 NASA-HU American Society for Engineering Education (ASEE) Summer Faculty Fellowship Program Dec. 1994 p 115 (For primary document see N95-23276 07-99)

Avail: CASI HC A01/MF A02

As part of the subsonic transport high-lift program, flight experiments are being conducted using NASA Langley's B737-100 to measure the flow characteristics of the multi-element high-lift system at full-scale high-Reynolds-number conditions. The instrumentation consists of hot-film anemometers to measure boundary-layer states, an infra-red camera to detect transition from laminar to turbulent flow, Preston tubes to measure wall shear stress, boundary-layer rakes to measure off-surface velocity profiles, and pressure orifices to measure surface pressure distributions. The initial phase of this research project was recently concluded with two flights on July 14. This phase consisted of a total of twenty flights over a period of about ten weeks. In the coming months the data obtained in this initial set of flight experiments will be analyzed and the results will be used to finalize the instrumentation layout for the next set of flight experiments scheduled for Winter and Spring of 1995. The main goal of these upcoming flights will be: (1) to measure more detailed surface pressure distributions across the wing for a range of flight conditions and flap settings; (2) to visualize the surface flows across the multi-element wing at high-lift conditions using fluorescent mini tufts; and (3) to measure in more detail the changes in boundary-layer state on the various flap elements as a result of changes in flight condition and flap deflection. These flight measured results are being correlated with experimental data measured in ground-based facilities as well as with computational data calculated with methods based on the Navier-Stokes equations or a reduced set of these equations. Also these results provide insight into the extent of laminar flow that exists on actual multi-element lifting surfaces at full-scale high-life conditions. Preliminary results indicate that depending on the deflection angle, the slat and flap elements have significant regions of laminar flow over a wide range of angles of attack. Boundary-layer transition mechanisms that were observed include attachment-line contamination on the slat and inflectional instability on the slat and fore flap. Also, the results agree fairly well with the predictions reported in a paper presented at last year's AIAA Fluid Dynamics Conference. The fact that extended regions of laminar flow are shown to exist on the various elements of the high-lift system raises the question what the effect is of loss of laminar flow as a result of insect contamiantion, rain or ice accumulation on high-life performance. Author

N95-23796*# National Aeronautics and Space Administration. Langley Research Center, Hampton, VA.

LDEF: 69 MONTHS IN SPACE. THIRD POST-RETRIEVAL SYMPOSIUM, PART 1

Arlene S. Levine, ed. Feb. 1995 530 p Symposium held in Williamsburg, VA, 8-12 Nov. 1993; sponsored by NASA, Washington and AIAA

(RTOP 233-03-02-03)

(NASA-CP-3275-Pt-1; L-17430A-Pt-1; NAS 1.55:3275-Pt-1) Avail: CASI HC A23/MF A04

This volume (Part 1 of 3) is a compilation of papers presented at the Third Long Duration Exposure Facility (LDEF) Post-Retrieval Symposium. The papers represent the data analysis of the 57 experiments flown on the LDEF. The experiments include materials, coatings, thermal systems, power and propulsion, science (cosmic ray, interstellar gas, heavy ions, micrometeoroid, etc.), electronics, optics, and life science. In addition, papers on preliminary data analysis of EURECA, EOIM-3, and other spacecraft are included. For individual titles, see N95-23797 through N95-23843.

N95-23797*# National Aeronautics and Space Administration. Marshall Space Flight Center, Huntsville, AL.

LDEF ENVIRONMENT MODELING UPDATES **c25**

Tim Gordon (Applied Science Technology, Inc., Littleton, CO.), Ray Rantanen

(ROR Enterprises, Athol, ID.), and Ann F. Whitaker *In* NASA. Langley Research Center, LDEF: 69 Months in Space. Third Post-Retrieval Symposium, Part 1 Feb. 1995 p 3-11 (For primary document see N95-23796 07-99)
Avail: CASI HC A02/MF A04

An updated gas dynamics model for gas interactions around the LDEF is presented that includes improved scattering algorithms. The primary improvement is more accurate predictions of surface fluxes in the wake region. The code used is the Integrated Spacecraft Environments Model (ISEM). Additionally, initial results of a detailed ISEM prediction model of the Solar Array Passive LDEF Experiment (SAMPLE), A0171, is presented. This model includes details of the A0171 geometry and outgassing characteristics of the many surfaces on the experiment. The detailed model includes the multiple scattering that exists between the ambient atmosphere, LDEF outgassing, and atomic oxygen erosion products. Predictions are made for gas densities, surface fluxes and deposition at three different time periods of the LDEF mission. Author

N95-23798*# National Aeronautics and Space Administration. Langley Research Center, Hampton, VA.
OUTGASSING PRODUCTS FROM ORBITER TPS MATERIALS c25
Gale A. Harvey, Tom J. Lash, and J. Richard Rawls *In its* LDEF: 69 Months in Space. Third Post-Retrieval Symposium, Part 1 Feb. 1995 p 13-20 (For primary document see N95-23796 07-99)
Avail: CASI HC A02/MF A04

The Space Transportation System (STS) orbiters are known to be significant sources of outgassing in low earth orbit (LEO). Infrared and mass spectra of residues and outgassing from orbiter thermal protection tile and an external blanket are presented. Several sources of methyl and phenyl methyl silicones are identified. About fifty pounds of silicones are estimated to be outgassed during an STS mission. Author

N95-23799*# European Space Agency. European Space Research and Technology Center, ESTEC, Noordwijk (Netherlands).
EURECA 11 MONTHS IN ORBIT: INITIAL POST FLIGHT INVESTIGATION RESULTS c18
Alan Dover, Roberto Aceti, and Gerhard Drolshagen *In* NASA. Langley Research Center, LDEF: 69 Months in Space. Third Post-Retrieval Symposium, Part 1 Feb. 1995 p 23-35 (For primary document see N95-23796 07-99)
Avail: CASI HC A03/MF A04

This paper gives a brief overview of the European free flying spacecraft 'EURECA' and the initial post flight investigations following its retrieval in June 1993. EURECA was in low earth orbit for 11 months commencing in August 1992, and is the first spacecraft to be retrieved and returned to Earth since the recovery of LDEF. The primary mission objective of EURECA was the investigation of materials and fluids in a very low micro-gravity environment. In addition other experiments were conducted in space science, technology and space environment disciplines. The European Space Agency (ESA) has taken the initiative in conducting a detailed post-flight investigation to ensure the full exploitation of this unique opportunity. Author

N95-23800*# Deutsche Forschungsanstalt fuer Luft- und Raumfahrt, Cologne (Germany). Inst. for Aerospace Medicine, Radiation and Biology.
DOSIMETRIC RESULTS ON EURECA c93
G. Reitz *In* NASA. Langley Research Center, LDEF: 69 Months in Space. Third Post-Retrieval Symposium, Part 1 Feb. 1995 p 37-42 (For primary document see N95-23796 07-99)
Avail: CASI HC A02/MF A04

Detector packages were exposed on the European Retrievable Carrier (EURECA) as part of the Biostack experiment inside the Exobiology and Radiation Assembly (ERA) and at several locations around EURECA. The packages consist of different plastic nuclear track detectors, nuclear emulsions and thermoluminescence dosimeters (TLD's). Evaluation of these detectors yields data on absorbed dose and particle and LET spectra. Preliminary results of absorbed dose measurements in the EURECA dosimeter packages are reported and compared to results of the LDEF experiments. The highest dose rate measured on EURECA is 63.3 plus or minus 0.4 mGy d(exp -1) behind a shielding thickness of 0.09 g cm(exp -2) in front of the detector package. Author

N95-23801*# San Francisco Univ., CA. Physics Research Lab.
PRELIMINARY RESULTS OF RADIATION MEASUREMENTS ON EURECA c93
E. V. Benton and A. L. Frank *In* NASA. Langley Research Center, LDEF: 69 Months in Space. Third Post-Retrieval Symposium, Part 1 Feb. 1995 p 43-50 (For primary document see N95-23796 07-99)
(Grant NAG9-235)
Avail: CASI HC A02/MF A04

The eleven-month duration of the EURECA mission allows long term radiation effects to be studied similarly to those of the Long Duration Exposure Facility (LDEF). Basic data can be generated for projections of crew doses and electronic and computer reliability on spacecraft missions. A radiation experiment has been designed for EURECA which uses passive integrating detectors to measure average radiation levels. The components include a Trackoscope, which employs fourteen plastic nuclear track detector (PNTD) stacks to measure the angular dependence of LET (greater than or equal to 6 keV/microns) radiation. Also included are TLD's for total absorbed doses, thermal/resonance neutron detectors (TRND's) for low energy neutron fluences and a thick PNTD stack for depth dependence measurements. LET spectra are derived from the PNTD measurements. Preliminary TLD results from seven levels within the detector array show that integrated doses inside the flight canister varied from 18.8 plus or minus 0.6 cGy to 38.9 plus or minus 1.2 cGy. The TLD's oriented toward the least shielded direction averaged 53 percent higher in dose than those oriented away from the least shielded direction (minimum shielding toward the least shielded direction varied from 1.13 to 7.9 g/cm(exp 2), Al equivalent). The maximum dose rate on EURECA (1.16 mGy/day) was 37 percent of the maximum measured on LDEF and dose rates at all depths were less than measured on LDEF. The shielding external to the flight canister covered a greater solid angle about the canister than in the LDEF experiments. Author

N95-23802*# National Aeronautics and Space Administration. Lewis Research Center, Cleveland, OH.
PERFORMANCE CHARACTERIZATION OF EURECA RETROREFLECTORS WITH FLUOROPOLYMER-FILLED SiO(x) PROTECTIVE COATINGS c27
Bruce A. Banks, Sharon K. Rutledge, and Michael Cales (Cleveland State Univ., OH.) *In* NASA. Langley Research Center, LDEF: 69 Months in Space. Third Post-Retrieval Symposium, Part 1 Feb. 1995 p 51-63 (For primary document see N95-23796 07-99)
Avail: CASI HC A03/MF A04

Aluminized corner-cube polymethylmethacrylate retroreflectors were coated with 92% SiO(x) - 8% fluoropolymer (by volume) and flown on the EURECA spacecraft. The fluoropolymer-filled SiO(x) protective coating was found to be durable to atomic oxygen when exposed in a ground-based plasma asher to an anticipated mission fluence of 2x10(exp 20) atoms/cm(exp 2). Unprotected retroreflector surfaces were found to develop highly diffuse reflectance characteristics, thus inhibiting their use for laser retroreflector purposes. A noncontacting retroreflector optical characterization system was constructed and used to measure the optical retroreflection characteristics of the following retroreflector materials: uncoated unexposed, coated unexposed, both uncoated and coated ground laboratory atomic oxygen exposed, and coated exposed to space atomic oxygen on the EURECA spacecraft. A comparison of the optical characterizations is presented. Author

N95-23803*# T and M Engineering, Glendora, CA.
EFFECT OF THE SPACE ENVIRONMENT ON MATERIALS FLOWN ON THE EURECA/TICCE-HVI EXPERIMENT c18
Carl R. Maag, Tim J. Stevenson (Mare Crisium, Old Carisbrooke, England.), William G. Tanner (Baylor Univ., Waco, TX.), and Janet Borg (Centre National de la Recherche Scientifique, Orsay, France.) *In* NASA. Langley Research Center, LDEF: 69 Months in Space. Third Post-Retrieval Symposium, Part 1 Feb. 1995 p 65-70 (For primary document see N95-23796 07-99)
Avail: CASI HC A02/MF A04

The primary benefit of accurately quantifying and characterizing the space environmental effects on materials is longer instrument and spacecraft life. Knowledge of the limits of materials allows the designer to optimize the spacecraft design so that the required life is achieved. Materials such as radiator coatings that have excellent durability result in the design of smaller radiators than a radiator coated with a lower durability coating.

This may reduce the weight of the spacecraft due to a more optimum design. Another benefit of characterizing materials is the quantification of outgassing properties. Spacecraft which have ultraviolet or visible sensor payloads are susceptible to contamination by outgassed volatile materials. Materials with known outgassing characteristics can be restricted in these spacecraft. Finally, good data on material characteristics improves the ability of analytical models to predict material performance. A flight experiment was conducted on the European Space Agency's European Retrievable Carrier (EuReCa) as part of the Timeband Capture Cell Experiment (TICCE). Our main objective was to gather additional data on the dust and debris environments, with the focus on understanding growth as a function of size (mass) for hypervelocity particles 1E-06 cm and larger. In addition to enumerating particle impacts, hypervelocity particles were to be captured and returned intact. Measurements were performed post-flight to determine the flux density, diameters, and subsequent effects on various optical, thermal control and structural materials. In addition to these principal measurements, the experiment also provided a structure and sample holders for the exposure of passive material samples to the space environment, e.g., the effects of thermal cycling, atomic oxygen, etc. Preliminary results are presented, including the techniques used for intact capture of particles. Author

N95-23804*# European Space Agency. European Space Research and Technology Center, ESTEC, Noordwijk (Netherlands).

MATERIAL INSPECTION OF EURECA FIRST FINDINGS AND RECOMMENDATIONS **c25**

Marc VanEesbeek, Michael Froggatt, and Georges Gourmelon *In* NASA. Langley Research Center, LDEF: 69 Months in Space. Third Post-Retrieval Symposium, Part 1 Feb. 1995 p 71-86 (For primary document see N95-23796 07-99)

Avail: CASI HC A03/MF A04

This paper gives the first results of the Post flight materials investigation on the European Retrievable Carrier (EURECA) after a stay of 11 months in LEO. The paper will concentrate on the first findings after the visual inspection performed at KSC and Astrotech and give some general design recommendations for potential future Carrier flights. Author

N95-23805*# National Aeronautics and Space Administration. Marshall Space Flight Center, Huntsville, AL.

LDEF CONTRIBUTIONS TO COSMIC RAY AND RADIATION ENVIRONMENTS RESEARCH Abstract Only **c93**

Thomas A. Parnell *In* NASA. Langley Research Center, LDEF: 69 Months in Space. Third Post-Retrieval Symposium, Part 1 Feb. 1995 p 89 (For primary document see N95-23796 07-99)

Avail: CASI HC A01/MF A04

LDEF-1 carried three experiments which are producing significant advances in our knowledge of ultra heavy and anomalous cosmic rays, solar flare particles, and heavy nuclei in the trapped belts. Nine other experiments made measurements on the radiation environments or performed dosmetric monitoring. Data from those experiments, and from measurements of induced radioactivity in LDEF components have significantly improved our knowledge of LEO radiation environment. Measurements at various locations shielding depths of radiation absorbed dose, linear energy transfer spectra, proton, neutron and heavy ion fluences, and induced radioactivity have been made, and many of these results have been compared to models. This has allowed the assessment of accuracy, and the potential for improvement, of the models. Serendipitous results from the radiation measurements include the discovery of atmospheric Be-7 plated on the front surface of LDEF, which has motivated a series of new investigations. A sample of measurements and modeling results will be presented, as well as the status of archiving the measurements and models. Author

N95-23806*# Kiel Univ. (Germany). Inst. fuer Reine und Angewandte Kernphysik.

TRAPPED IRON MEASURED ON LDEF **c93**

R. Beaujean, D. Jonathal, S. Barz, and W. Enge *In* NASA. Langley Research Center, LDEF: 69 Months in Space. Third Post-Retrieval Symposium, Part 1 Feb. 1995 p 91-99 Sponsored by BMFT (For primary document see N95-23796 07-99)

(Grant DARA-OS-9001)

Avail: CASI HC A02/MF A04

Heavy ions far below the cutoff energy were detected on the 28.5 deg inclination orbit of LDEF in a plastic track detector experiment. The Fe-group particles show a constant energy spectrum at 50 less than or equal to E less than or equal to 200 MeV/nuc. The steep energy spectrum of Fe-particles at 20 less than or equal to E less than or equal to 50 MeV/nuc and the arrival directions of these ions is consistent with a trapped component incident in the South Atlantic Anomaly at values of L=1.4-1.6. Author

N95-23807*# George Mason Univ., Fairfax, VA. CSI Inst.

CHARACTERISTICS OF LOW ENERGY IONS IN THE HEAVY IONS IN SPACE (HIIS) EXPERIMENT **c72**

Thomas Kleis, Allan J. Tylka (Naval Research Lab., Washington, DC.), Paul R. Boberg (Naval Research Lab., Washington, DC.), James H. Adams, Jr. (Naval Research Lab., Washington, DC.), and Lorraine P. Beahm (Naval Research Lab., Washington, DC.) *In* NASA. Langley Research Center, LDEF: 69 Months in Space. Third Post-Retrieval Symposium, Part 1 Feb. 1995 p 101-112 Sponsored by ONR (For primary document see N95-23796 07-99)

(NASA Order W-18409)

Avail: CASI HC A03/MF A04

We present preliminary data on heavy ions (Z greater than or equal to 10) detected in the topmost Lexan sheets of the track detector stacks of the Heavy Ions in space (HIIS) experiment (M0001) on LDEF. The energy interval covered by these observations varies with the element, with (for example) Ne observable at 18-100 MeV nuc and Fe at 45-200 MeV/nuc. All of the observed ions are at energies far below the geomagnetic cutoff for fully-ionized particles at the LDEF orbit. Above 50 MeV/nuc (where most of our observed particles are Fe), the ions arrive primarily from the direction of lowest geomagnetic cutoff. This suggests that these particles originate outside the magnetosphere from a source with a steeply-falling spectrum and may therefore be associated with solar energetic particle (SEP) events. Below 50 MeV/nuc, the distribution of arrival directions suggests that most of the observed heavy ions are trapped in the Earth's magnetic field. Preliminary analysis, however, shows that these trapped heavy ions have a very surprising composition: they include not only Ne and Ar, which are expected from the trapping of anomalous cosmic rays (ACR's), but also Mg and Si, which are not part of the anomalous component. Our preliminary analysis shows that trapped heavy ions at 12 less than or equal to Zeta less than or equal to 14 have a steeply-falling spectrum, similar to that reported by the Kiel experiment (exp 1,2,3) on LDEF (M0002) for trapped Ar and Fe at E less than 50 MeV/nuc. The trapped Mg, Si, and Fe may also be associated with SEP events, but the mechanism by which they have appeared to deep in the inner magnetosphere requires further theoretical investigation. Author

N95-23808*# Naval Research Lab., Washington, DC.

RESULTS FROM THE HEAVY IONS IN SPACE (HIIS) EXPERIMENT ON THE IONIC CHARGE STATE OF SOLAR ENERGETIC PARTICLES **c92**

Allan J. Tylka, Paul R. Boberg, James H. Adams, Jr., Lorraine P. Beahm, and Thomas Kleis (George Mason Univ., Fairfax, VA.) *In* NASA. Langley Research Center, LDEF: 69 Months in Space. Third Post-Retrieval Symposium, Part 1 Feb. 1995 p 113-127 Sponsored by ONR (For primary document see N95-23796 07-99)

(NASA Order W-18409)

Avail: CASI HC A03/MF A04

It has long been known that low-energy solar energetic particles (SEP's) are partially-ionized. For example, in large, so-called 'gradual' solar energetic particle events, at approximately 1 MeV/nucleon the measured mean ionic charge state, Q, of Fe ions is 14.1 +/- 0.2, corresponding to a plasma temperature of approximately 2 MK in the coronal or solar-wind source material. Recent studies, which have greatly clarified the origin of solar energetic particles and their relation to solar flares, suggest that ions in these SEP events are accelerated not at a flare site, but by shocks propagating through relatively low-density regions in the interplanetary medium. As a result, the partially-ionized states observed at low energies are expected to continue to higher energies. However, up to now there have been no high-energy measurements of ionic charge states to confirm this notion. We report here HIIS observations of Fe-group ions at 50-600 MeV/nucleon, at energies and fluences which cannot be explained by fully-ionized galactic cosmic rays, even in the presence of severe geomagnetic cutoff suppression. Above approximately 200 MeV/nucleon,

all features of our data -- fluence, energy spectrum, elemental composition, and arrival directions -- can be explained by the large SEP events of October 1989, provided that the mean ionic charge state at these high energies is comparable to the measured value at approximately 1 MeV/nucleon. By comparing the HIIS observations with measurements in interplanetary space in October 1989, we determine the mean ionic charge state of SEP Fe ions at approximately 200-600 MeV/nucleon to be Q = 13.4 plus or minus 1.0, in good agreement with the observed value at approximately 1 MeV/nucleon. The source of the ions below approximately 200 MeV/nucleon is not yet clear. Partially-ionized ions are less effectively deflected by the Earth's magnetic field than fully-ionized cosmic rays and therefore have greatly enhanced access to low-Earth orbit. Moreover, at the high energies observed in HIIS, these ions can penetrate typical amounts of shielding. We discuss the significance of the HIIS results for estimates of the radiation hazard posed by large SEP events to satellites in low-Earth orbit, including the proposed Space Station orbit. Finally, we comment on previous reports of low-energy below-cutoff Fe-group ions, which some authors have interpreted as evidence for partially-ionized galactic cosmic rays. The LDEF flux levels are much smaller than the corresponding fluxes in these previous reports, implying that the source of these ions has an unusual solar-cycle variation and/or strongly increases with decreasing altitude. Derived from text

N95-23809*# Dublin Inst. for Advanced Studies (Ireland).
EARLY RESULTS FROM THE ULTRA HEAVY COSMIC RAY EXPERIMENT **c93**

D. OSullivan, A. Thompson, J. Bosch, R. Keegan, K.-P. Wenzel (European Space Agency. European Space Research and Technology Center, ESTEC, Noordwijk, Netherlands.), F. Jansen (European Space Agency. European Space Research and Technology Center, ESTEC, Noordwijk, Netherlands.), and C. Domingo (Autonoma de Barcelona Univ., Barcelona, Spain.) *In* NASA. Langley Research Center, LDEF: 69 Months in Space. Third Post-Retrieval Symposium, Part 1 Feb. 1995 p 129-133 (For primary document see N95-23796 07-99)
Avail: CASI HC A01/MF A04

Data extraction and analysis of the LDEF Ultra Heavy Cosmic Ray Experiment is continuing. Almost twice the pre LDEF world sample has been investigated and some details of the charge spectrum in the region from Z approximately 70 up to and including the actinides are presented. The early results indicate r process enhancement over solar system source abundances. Author

N95-23810*# National Aeronautics and Space Administration. Marshall Space Flight Center, Huntsville, AL.
ABSORBED DOSE AND LET SPECTRA MEASUREMENTS ON LDEF **c72**

E. V. Benton (San Francisco Univ., CA.), I. Csige (San Francisco Univ., CA.), A. L. Frank (San Francisco Univ., CA.), E. R. Benton (San Francisco Univ., CA.), L. A. Frigo (San Francisco Univ., CA.), T. A. Parnell, J. Watts, and A. Harmon *In* NASA. Langley Research Center, LDEF: 69 Months in Space. Third Post-Retrieval Symposium, Part 1 Feb. 1995 p 135-148 (For primary document see N95-23796 07-99)
(Grant NAG5-282)
Avail: CASI HC A03/MF A04

Total absorbed doses measured with TLD's, linear energy transfer (LET) spectra measured with plastic track detectors, and low energy neutrons measured on LDEF have been compared with model calculations. The total absorbed doses measured in TLD's were higher than predicted in the calculations of Armstrong et al. and differ from the calculations of Atwell et al. LDEF LET spectra are dependent on detector orientation, shielding and experiment location. These factors need to be taken into account when modeling the LDEF LET spectra. LET spectra measured with plastic nuclear track detectors (PNTD's) also deviate significantly from calculations especially for high LET particles (LET(sub infinity) H2O greater than 100keV/micron). Modeling efforts to date do not include the contribution of proton induced secondaries. Analysis of polycarbonate PNTD's from the West-side of LDEF has revealed a very high fluence of tracks (greater than 1 x 10(exp 7) tracks/cm(exp 2) under 2 gm/cm(exp 2) shielding). Fluence drops off rapidly as shielding depth increases. Tracks only form in the region of the detector closest to the surface, not in the bulk of the detector. To date no adequate explanation for this observation has been found. We plan to measure range distribution of very high LET (LET (sub infinity) H2O greater than 500 keV/micron) secondary particles produced in silicon wafer by high energy primary cosmic ray particles. Refinements of experimental techniques and model calculations are being carried out in order to understand existing discrepancies between experimental measurements and calculations. Author

N95-23811*# Eril Research, Inc., San Rafael, CA.
FISSION FOIL MEASUREMENTS OF NEUTRON AND PROTON FLUENCES IN THE A0015 EXPERIMENT **c72**

A. L. Frank, E. V. Benton, T. W. Armstrong (Science Applications International Corp., Prospect, TN.), and B. L. Colborn (Science Applications International Corp., Prospect, TN.) *In* NASA. Langley Research Center, LDEF: 69 Months in Space. Third Post-Retrieval Symposium, Part 1 Feb. 1995 p 149-158 (For primary document see N95-23796 07-99)
(Contract NAS8-39610)
Avail: CASI HC A02/MF A04

Results are given from sets of fission foil detectors (FFD's) (Ta-181, Bi-209, Th-232, U-238) which were included in the A0015 experiment to measure combined proton/neutron fluences. Use has been made of recent FFD high energy proton calibrations for improved accuracy of response. Comparisons of track density measurements have been made with the predictions of environmental modeling based on simple 1-D (slab) geometry. At 1 g/cm(exp 2) (trailing edge) the calculations were approximately 25 percent lower than measurements; at 13 g/cm(exp 2) (Earthside) calculations were more than a factor of 2 lower. A future 3-D modeling of the experiment is needed for a more meaningful comparison. Approximate mission proton doses and neutron dose equivalents were found. At Earthside (13 g/cm(exp 2) the dose was 171 rad and dose equivalent was 82 rem. At the trailing edge (1 g/cm(exp 2) dose was 315 rad and dose equivalent was 33 rem. The proton doses are less than expected from TLD doses by 16 percent and 37 percent, respectively. These differences can be explained by uncertainties in the proton and neutron spectra and in the method used to separate proton and neutron contributions to the measurements. Author

N95-23812*# San Francisco Univ., CA. Physics Research Lab.
MEASUREMENT OF TRAPPED PROTON FLUENCES IN MAIN STACK OF P0006 EXPERIMENT **c72**

N. Nefedov, I. Csige, E. V. Benton, R. P. Henke, E. R. Benton, and L. A. Frigo *In* NASA. Langley Research Center, LDEF: 69 Months in Space. Third Post-Retrieval Symposium, Part 1 Feb. 1995 p 159-166 (For primary document see N95-23796 07-99)
(Grant NAG8-282)
Avail: CASI HC A02/MF A04

We have measured directional distribution and Eastward directed mission fluence of trapped protons at two different energies with plastic nuclear track detectors (CR-39 with DOP) in the main stack of the P0006 experiment on LDEF. Results show arriving directions of trapped protons have very high anisotropy with most protons arriving from the West direction. Selecting these particles we have determined the mission fluence of Eastward directed trapped protons. We found experimental fluences are slightly higher than results of the model calculations of Armstrong and Colborn. Author

N95-23813*# Eril Research, Inc., San Rafael, CA.
CONTRIBUTION OF PROTON-INDUCED SHORT RANGE SECONDARIES TO THE LET SPECTRA ON LDEF **c72**

E. R. Benton, I. Csige, E. V. Benton, and L. A. Frigo *In* NASA. Langley Research Center, LDEF: 69 Months in Space. Third Post-Retrieval Symposium, Part 1 Feb. 1995 p 167-177 (For primary document see N95-23796 07-99)
(Contract NAS8-38610)
Avail: CASI HC A03/MF A04

The contribution to the LET (linear energy transfer) spectrum from proton-induced short range secondaries was investigated by making measurements of total track density and LET spectra in CR-39 Plastic Nuclear Track Detectors (PNTD's) at varying shielding depths in the A0015 West-side stack. Proton-induced short range secondaries were found to make a significant contribution to the LET spectra, especially in the region above 100 keV/micron. At present, calculational models do not include this component. Total track density was measured at five shielding depths and was seen to increase as a function of shielding. LET spectra were measured under two shielding depths (2.6 and 9.2 g/cm(exp 2)) and stayed fairly constant as a function of shielding. Prerecovery estimates of LET

spectra dropped off rapidly in the 100-300 keV/micron region, while the measured LET spectra extended to higher LET's. Track density and LET spectra measurements of secondaries were made in a CR-39 PNTD stack exposed to 154 MeV accelerator protons. Similarities in LET spectra measured in the A0015 experiment and in the 154 MeV accelerator proton stack demonstrate that a useful first step in modeling the contribution to the LET spectra of secondaries induced by the spectrum of trapped protons would be to model a mono-energetic proton beam being transported through a one-dimensional geometry. Author

N95-23814*# San Francisco Univ., CA. Physics Research Lab.
CHARGE, ENERGY AND LET SPECTRA OF HIGH LET PRIMARY AND SECONDARY PARTICLES IN CR-39 PLASTIC NUCLEAR TRACK DETECTORS OF THE P0006 EXPERIMENT Abstract Only **c72**
I. Csige, L. A. Frigo, E. V. Benton, and K. Oda (Kobe Univ. of Mercantile Marine, Japan.) *In* NASA. Langley Research Center, LDEF: 69 Months in Space. Third Post-Retrieval Symposium, Part 1 Feb. 1995 p 179 Sponsored by NASA. Marshall Space Flight Center (For primary document see N95-23796 07-99)
Avail: CASI HC A01/MF A04

We have measured the charge, energy and linear energy transfer (LET) spectra of about 800 high LET (LET(sub infinity) H2O greater than 50 keV/micron) particles in CR-39 plastic nuclear track detectors in the P0006 experiment of LDEF. Primary particles with residual range at the reference surface greater than about 2 microns and secondary particles produced in the detector material with total range greater than about 4 microns were measured. We have used a multi-etch technique and an internal calibration to identify and measure the energy of the particles at the reference surface. The LET spectrum was obtained from the charge and energy distribution of the particles. Author

N95-23815*# Science Applications International Corp., Prospect, TN.
PREDICTIONS OF LET SPECTRA MEASURED ON LDEF **c72**
T. W. Armstrong, B. L. Colborn, and E. V. Benton (San Francisco Univ., CA.) *In* NASA. Langley Research Center, LDEF: 69 Months in Space. Third Post-Retrieval Symposium, Part 1 Feb. 1995 p 181-188 Sponsored by NASA. Marshall Space Flight Center (For primary document see N95-23796 07-99)
Avail: CASI HC A02/MF A04

The linear energy transfer (LET) spectra measured by plastic (CR-39) detectors in Exp. P0006 on LDEF are much higher at high LET than expected from methods commonly used to predict LET spectra produced by the space ionizing radiation environment. This discrepancy is being investigated by examining modeling approximations used in the predictions, and some interim results are presented. Author

N95-23816*# California Univ., Berkeley. Lawrence Berkeley Lab, CA.
DOING PHOTONS WITH MERLIN 2 AT OROVILLE **c72**
Alan R. Smith and Donna L. Hurley *In* NASA. Langley Research Center, LDEF: 69 Months in Space. Third Post-Retrieval Symposium, Part 1 Feb. 1995 p 189-197 (For primary document see N95-23796 07-99)
(Contract NASA Order H-06815-D; DE-ACO3-76SF-00098)
Avail: CASI HC A02/MF A04

A very large n-type high-purity Ge-semiconductor detector has recently been installed in the Lawrence Berkeley Laboratory's underground low-background facility at Oroville. The detector (named MERLIN II) is mounted in a low-activity cryostat and has a rated 'efficiency' of about 115 percent -- nearly 4 times higher than our original MERLIN detector, which was used extensively to measure the minute amounts of radioactivity in samples from the LDEF satellite. We discuss gamma-spectrometric analyses with MERLIN II on some of the same LDEF samples, providing direct evidence for improvement in performance achieved with the larger detector. Author

N95-23817*# National Aeronautics and Space Administration. Marshall Space Flight Center, Huntsville, AL.
STATUS OF LDEF ACTIVATION MEASUREMENTS AND ARCHIVE **c72**
B. Alan Harmon, Thomas A. Parnell, and Christopher E. Laird *In* NASA. Langley Research Center, LDEF: 69 Months in Space. Third Post-Retrieval Symposium, Part 1 Feb. 1995 p 199-201 (For primary document see N95-23796 07-99)
Avail: CASI HC A01/MF A04

We review the status of induced radioactivity measurements for the LDEF spacecraft which includes studies of the nuclide, target, directional and depth dependences of the activation. Analysis of the data has focused on extraction of the specific activities for many materials to develop a global picture of the low Earth orbital environment to which the LDEF was subjected. Preliminary comparisons of data in a previous review showed that it was possible to make meaningful intercomparisons between results obtained at different facilities. Generally these comparisons were good and gave results to within 10-20 percent, although some analysis remains. These results clearly provide constraints for recent calculations being performed of the radiation environment of the LDEF. We are not anticipating a period of production of final activation results. An archive is being prepared jointly between NASA/Marshall and Eastern Kentucky University which will include gamma ray spectra and other intermediate results. Author

N95-23818*# National Aeronautics and Space Administration. Marshall Space Flight Center, Huntsville, AL.
PREDICTIONS OF LDEF RADIOACTIVITY AND COMPARISON WITH MEASUREMENTS **c72**
T. W. Armstrong (Science Applications International Corp., Prospect, TN.), B. L. Colborn (Science Applications International Corp., Prospect, TN.), B. A. Harmon, and C. E. Laird (University of Eastern Kentucky, Richmond, KY.) *In* NASA. Langley Research Center, LDEF: 69 Months in Space. Third Post-Retrieval Symposium, Part 1 Feb. 1995 p 203-216 (For primary document see N95-23796 07-99)
Avail: CASI HC A03/MF A04

As part of the program to utilize LDEF data for evaluation and improvement of current ionizing radiation environmental models and related predictive methods for future LEO missions, calculations have been carried out to compare with the induced radioactivity measured in metal samples placed on LDEF. The predicted activation is about a factor of two lower than observed, which is attributed to deficiencies in the AP8 trapped proton model. It is shown that this finding based on activation sample data is consistent with comparisons made with other LDEF activation and dose data. Plans for confirming these results utilizing additional LDEF data sets, and plans for model modifications to improve the agreement with LDEF data, are discussed. Author

N95-23819*# National Aeronautics and Space Administration. Marshall Space Flight Center, Huntsville, AL.
STATUS OF LDEF RADIATION MODELING **c72**
John W. Watts, T. W. Armstrong (Science Applications International Corp., Prospect, TN.), and B. L. Colborn (Science Applications International Corp., Prospect, TN.) *In* NASA. Langley Research Center, LDEF: 69 Months in Space. Third Post-Retrieval Symposium, Part 1 Feb. 1995 p 217-226 (For primary document see N95-23796 07-99)
Avail: CASI HC A02/MF A04

The current status of model prediction and comparison with LDEF radiation dosimetry measurements is summarized with emphasis on major results obtained in evaluating the uncertainties of present radiation environment model. The consistency of results and conclusions obtained from model comparison with different sets of LDEF radiation data (dose, activation, fluence, LET spectra) is discussed. Examples where LDEF radiation data and modeling results can be utilized to provide improved radiation assessments for planned LEO missions (e.g., Space Station) are given. Author

N95-23820*# National Aeronautics and Space Administration. Marshall Space Flight Center, Huntsville, AL.
Be-10 IN TERRESTRIAL BAUXITE AND INDUSTRIAL ALUMINUM: AN LDEF FALLOUT **c26**
J. C. Gregory (Alabama Univ., Huntsville, AL.), A. Albrecht (Rutgers Univ., New Brunswick, NJ.), G. Herzog (Rutgers Univ., New Brunswick, NJ.), J. Klein (Pennsylvania Univ., Philadelphia, PA.), R. Middleton (Pennsylvania Univ., Philadelphia, PA.), B. A. Harmon, and T. A. Parnell *In* NASA. Langley Research Center, LDEF: 69 Months in Space. Third Post-Retrieval Symposium, Part 1 Feb. 1995 p 227-230 (For primary document see N95-23796 07-99)
Avail: CASI HC A01/MF A04

Work has continued on the search for Be-10 on metals other than aluminum flown on LDEF. Much time-consuming extractive chemistry has been performed at Rutgers University on turnings obtained from the ends

of two stainless steel trunnions from LDEF and the prepared samples will be run on the University of Pennsylvania accelerator mass spectrometer. We have continued to investigate our discovery of naturally-occurring Be-10 contamination in bauxite and industrial aluminums from different sources. Measurements of Be-10 in ores from three different sites, and from four different samples of commercial aluminum have been made. Our investigators indicate that the contamination in commercial aluminum metal originates in its principal ore, bauxite. The levels in some bauxite samples were much greater than the maximum possible for in situ production by cosmic ray secondaries. Absorption of atmospheric Be-10 by surface ores exposed to rainfall is a reasonable explanation. Author

N95-23821*# Morgan State Univ., Baltimore, MD.
GERMINATION, GROWTH RATES, AND ELECTRON MICROSCOPE ANALYSIS OF TOMATO SEEDS FLOWN ON THE LDEF **c51**
Ernest C. Hammond, Jr., Kevin Bridgers, and Cecelia Wright Brown *In* NASA. Langley Research Center, LDEF: 69 Months in Space. Third Post-Retrieval Symposium, Part 1 Feb. 1995 p 231-252 (For primary document see N95-23796 07-99)
Avail: CASI HC A03/MF A04

The tomato seeds were flown in orbit aboard the Long Duration Exposure Facility (LDEF) for nearly six years. During this time, the tomato seeds received an abundant exposure to cosmic radiation and solar wind. Upon the return of the LDEF to earth, the seeds were distributed throughout the United States and 30 foreign countries for analysis. The purpose of the experiment was to determine the long term effect of cosmic rays on living tissue. Our university analysis included germination and growth rates as well as Scanning Electron Microscopy and X-ray analysis of the control as well as Space-exposed tomato seeds. In analyzing the seeds under the Electron Microscope, usual observations were performed on the nutritional and epidermis layer of the seed. These layers appeared to be more porous in the Space-exposed seeds than on the Earth-based control seeds. This unusual characteristic may explain the increases in the space seeds growth pattern. (Several test results show that the Space-exposed seeds germinate sooner than the Earth-Based seeds. Also, the Space-exposed seeds grew at a faster rate). The porous nutritional region may allow the seeds to receive necessary nutrients and liquids more readily, thus enabling the plant to grow at a faster rate. Roots, leaves and stems were cut into small sections and mounted. After sputter coating the specimens with Argon/Gold Palladium Plasma, they were ready to be viewed under the Electron Microscope. Many micrographs were taken. The X-ray analysis displayed possible identifications of calcium, potassium, chlorine, copper, aluminum, silicon, phosphate, carbon, and sometimes sulfur and iron. The highest concentrations were shown in potassium and calcium. The Space-exposed specimens displayed a high concentration of copper and calcium in the two specimens. There was a significantly high concentration of copper in the Earth-based specimens, whereas there was no copper in the Space-exposed specimens. Author

N95-23822*# National Aeronautics and Space Administration. Langley Research Center, Hampton, VA.
STATUS OF LDEF CONTRIBUTIONS TO CURRENT KNOWLEDGE OF METEOROID AND MANMADE DEBRIS ENVIRONMENTS AND THEIR EFFECTS ON SPACECRAFT IN LEO Abstract Only **c18**
William H. Kinard *In its* LDEF: 69 Months in Space. Third Post-Retrieval Symposium, Part 1 Feb. 1995 p 255 (For primary document see N95-23796 07-99)
Avail: CASI HC A01/MF A04

The analyses, which are currently being performed by the LDEF Meteoroid and Debris Principal Investigators and the other LDEF Meteoroid and Debris Special Investigation Group Members of the data derived from the seven meteoroid and debris experiments that were flown on the LDEF and the post-retrieval scans of the impact sites found on other experiment and LDEF surfaces will, when they are completed, result in many very significant contributions to our knowledge of the meteoroid and debris status report on the analyses that have been performed to date and the preliminary contributions indicated by these analyses. This paper also discusses new questions that have been raised by the completed analyses regarding these environments and their effects on spacecraft. Author

N95-23823*# National Aeronautics and Space Administration. Lyndon B. Johnson Space Center, Houston, TX.
LDEF METEOROID AND DEBRIS SPECIAL INVESTIGATION GROUP INVESTIGATIONS AND ACTIVITIES AT THE JOHNSON SPACE CENTER **c18**
Thomas H. See (Lockheed Engineering and Sciences Co., Houston, TX.), Jack L. Warren (Lockheed Engineering and Sciences Co., Houston, TX.), Michael E. Zolensky, Clyde A. Sapp (Lockheed Engineering and Sciences Co., Houston, TX.), Ronald P. Bernhard (Lockheed Engineering and Sciences Co., Houston, TX.), and Claire B. Dardano (Lockheed Engineering and Sciences Co., Houston, TX.) *In* NASA. Langley Research Center, LDEF: 69 Months in Space. Third Post-Retrieval Symposium, Part 1 Feb. 1995 p 257-273 (For primary document see N95-23796 07-99)
Avail: CASI HC A03/MF A04

Since the return of the Long Duration Exposure Facility (LDEF) in January, 1990, members of the Meteoroid and Debris Special Investigation Group (M&D SIG) at the Johnson Space Center (JSC) in Houston, Texas have been examining LDEF hardware in an effort to expand the knowledge base regarding the low-Earth orbit (LEO) particulate environment. In addition to the various investigative activities, JSC is also the location of the general Meteoroid & Debris database. This publicly accessible database contains information obtained from the various M&D SIG investigations, as well as limited data obtained by individual LDEF Principal Investigators. LDEF exposed approximately 130 m(exp 2) of surface area to the LEO particulate environment, approximately 15.4 m(exp 2) of which was occupied by structural frame components (i.e., longerons and intercoastals) of the spacecraft. The data reported here was obtained as a result of detailed scans of LDEF intercoastals, 68 of which reside at JSC. The limited amount of data presently available on the A0178 thermal control blankets was reported last year and will not be reiterated here. The data presented here are limited to measurements of crater diameters and their frequency of occurrence (i.e., flux). Author

N95-23824*# Departement d'Etudes et de Recherches en Technologie Spatiale, Toulouse (France).
MICROMETEOROIDS AND DEBRIS ON LDEF COMPARISON WITH MIR DATA **c18**
Jean-Claude Mandeville and Lucinda Berthoud *In* NASA. Langley Research Center, LDEF: 69 Months in Space. Third Post-Retrieval Symposium, Part 1 Feb. 1995 p 275-285 Sponsored by European Commission (For primary document see N95-23796 07-99)
Avail: CASI HC A03/MF A04

Part of the LDEF tray allocated to French experiments (FRECOPA) has been devoted to the study of dust particles. The tray was located on the face of LDEF directly opposed to the velocity vector. Crater size distributions have made possible the evaluation of the incident microparticle flux in the near-Earth environment. Comparisons are made with measurements obtained on the other faces of LDEF (tray clamps), on the leading edge (MAP) and with results of a similar experiment flown on the MIR space station. The geometry of impact craters, depth in particular, provides useful information on the nature of impacting particles and the correlation of geometry with the chemical analysis of projectile remnants inside craters make possible a discrimination between meteoroids and orbital debris. Emphasis has been laid on the size distribution of small craters in order to assess a cut-off in the distribution of particles in LEO. Special attention has been paid to the phenomenon of secondary impacts. A comparison of flight data with current models of meteoroids and space debris shows a fair agreement for LDEF, except for the smaller particles: the possible contribution of orbital debris in GTO orbits to the LDEF trailing edge flux is discussed. For MIR, flight results show differences with current modeling: the possible enhancement of orbital debris could be due to the contaminating presence of a permanently manned space station. Author

N95-23825*# National Aeronautics and Space Administration. Langley Research Center, Hampton, VA.
SMALL CRATERS ON THE METEOROID AND SPACE DEBRIS IMPACT EXPERIMENT **c18**
Donald H. Humes *In its* LDEF: 69 Months in Space. Third Post-Retrieval Symposium, Part 1 Feb. 1995 p 287-322 (For primary document see N95-23796 07-99)
Avail: CASI HC A03/MF A04

Examination of 9.34 m(exp 2) of thick aluminum plates from the Long Duration Exposure Facility (LDEF) using a 25X microscope revealed 4341 craters that were 0.1 mm in diameter or larger. The largest was 3 mm in diameter. Most were roughly hemispherical with lips that were raised above the original plate surface. The crater diameter measured was the diameter at the top of the raised lips. There was a large variation in the number density of craters around the three-axis gravity-gradient stabilized spacecraft. A model of the near-Earth meteoroid environment is presented which uses a meteoroid size distribution based on the crater size distribution on the space end of the LDEF. An argument is made that nearly all the craters on the space end must have been caused by meteoroids and that very few could have been caused by man-made orbital debris. However, no chemical analysis of impactor residue that will distinguish between meteoroids and man-made debris is yet available. A small area (0.0447 m(exp 2)) of one of the plates on the space end was scanned with a 200X microscope revealing 155 craters between 10 micron and 100 micron in diameter and 3 craters smaller than 10 micron. This data was used to extend the size distribution of meteoroids down to approximately 1 micron. New penetration equations developed by Alan Watts were used to relate crater dimensions to meteoroid size. The equations suggest that meteoroids must have a density near 2.5 g/cm(exp 3) to produce craters of the shape found on the LDEF. The near-Earth meteoroid model suggests that about 80 to 85 percent of the 100 micron to 1 mm diameter craters on the twelve peripheral rows of the LDEF were caused by meteoroids, leaving 15 to 20 percent to be caused by man-made orbital debris. Author

N95-23826*# National Aeronautics and Space Administration. Langley Research Center, Hampton, VA.

LONG TERM MICROPARTICLE IMPACT FLUXES ON LDEF DETERMINED FROM OPTICAL SURVEY OF INTERPLANETARY DUST EXPERIMENT (IDE) SENSORS **c18**

C. G. Simon (Institute for Space Science and Technology, Inc., Gainesville, FL.), J. P. Oliver (Institute for Space Science and Technology, Inc., Gainesville, FL.), W. J. Cooke (Institute for Space Science and Technology, Inc., Gainesville, FL.), K. I. Downey (Institute for Space Science and Technology, Inc., Gainesville, FL.), and P. C. Kassel *In its* LDEF: 69 Months in Space. Third Post-Retrieval Symposium, Part 1 Feb. 1995 p 323-336 (For primary document see N95-23796 07-99)

(Grant NAG1-1218)

Avail: CASI HC A03/MF A04

Many of the IDE metal-oxide-silicon (MOS) capacitor-discharge impact sensors remained active during the entire Long Duration Exposure Facility (LDEF) mission. An optical survey of impact sites on the active surfaces of these sensors has been extended to include all sensors from the low-flux sides of LDEF (i.e. the west or trailing side, the earth end, and the space end) and 5-7 active sensors from each LDEF's high-flux sides (i.e. the east or leading side, the south side, and the north side). This survey was facilitated by the presence of a relatively large (greater than 50 micron diameter) optical signature associated with each impact site on the active sensor surfaces. Of the approximately 4700 impacts in the optical survey data set, 84% were from particles in the 0.5 to 3 micron size range. An estimate of the total number of hypervelocity impacts on LDEF from particles greater than 0.5 micron diameter yields a value of approximately 7 x 10(exp 6). Impact feature dimensions for several dozen large craters on MOS sensors and germanium witness plates are also presented. Impact fluxes calculated from the IDE survey data closely matched surveys of similar size impacts (greater than or equal to 3 micron diameter craters in Al, or marginal penetrations of a 2.4 micron thick Al foil) by other LDEF investigators. Since the first year IDE data were electronically recorded, the flux data could be divided into three long term time periods: the first year, the entire 5.8 year mission, and the intervening 4.8 years (by difference). The IDE data show that there was an order of magnitude decrease in the long term microparticle impact flux on the trailing side of LDEF, from 1.01 to 0.098 x 10(exp -4) m(exp 2)/s, from the first year in orbit compared to years 2-6. The long term flux on the leading edge showed an increase from 8.6 to 11.2 x 10(exp -4) m(exp -2)/s over this same time period. (Short term flux increases up to 10,000 times the background rate were recorded on the leading side during LDEF's first year in orbit.) The overall east/west ratio was 44, but during LDEF's first year in orbit the ratio was 8.5, and during years 2-6 the ratio was 114. Long term microparticle impact fluxes on the space end decreased from 1.12 to 0.55 x 10(exp -4) m(exp -2)/s from the first year in orbit compared to years 2-6. The earth end showed the opposite trend with an increase from 0.16 to 0.38 x 10(exp -4) m(exp -2)/s. Fluxes on rows 6 and 12 decreased from 6.1 to 3.4 and 6.7 to 3.7 x 10(exp -4) m(exp -2)/s, respectively, over the same time periods. This resulted in space/earth microparticle impact flux ratios of 7.1 during the first year and 1.5 during years 2-6, while the south/north, space/north and space/south ratios remained constant at 1.1, 0.16 and 0.17, respectively, during the entire mission. This information indicates the possible identification of long term changes in discrete microparticle orbital debris component contributions to the total impact flux experienced by LDEF. A dramatic decrease in the debris population capable of striking the trailing side was detected that could possibly be attributed to the hiatus of western launch activity experienced from 1986-1989. A significant increase in the debris population that preferentially struck the leading side was also observed and could possibly be attributed to a single breakup event that occurred in September of 1986. A substantial increase in the microparticle debris population that struck the earth end of LDEF, but not the space end, was also detected and could possibly be the result of a single breakup event at low altitude. These results point to the importance of including discrete orbital debris component contribution changes in flux models in order to achieve accurate predictions of the microparticle environment that a particular spacecraft will experience in earth orbit. The only reliable, verified empirical measurements of these changes are reported in this paper. Further time-resolved in-situ measurements of these debris populations are needed to accurately assess model predictions and mitigation practices. Author

N95-23827*# Kent Univ., Canterbury (England). Unit for Space Sciences.

PENETRATION RATES OVER 30 YEARS IN THE SPACE AGE **c18**

J. A. M. McDonnell and J. M. Baron *In* NASA. Langley Research Center, LDEF: 69 Months in Space. Third Post-Retrieval Symposium, Part 1 Feb. 1995 p 337-351 Sponsored by Science and Engineering Research Council (For primary document see N95-23796 07-99)

Avail: CASI HC A03/MF A04

Experimental data from spacecraft providing impact penetration rates and cratering for metallic targets is reviewed. Data includes NASA Explorers 16 and 23 and the Pegasus series, the second US-UK satellite Ariel 2, Space Shuttle STS-3 (MFE), recovered surfaces on Solar Max Satellite, The Long Duration Exposure Facility (LDEF) and EuReCa TiCCE. Factors concerning exposure to the environment are considered and, especially, material properties which affect the penetration resistance. Reference to a common material, Aluminum alloy 2024-T3, is effected and the data then compared to define firstly an average impact flux over the period. The data is examined, in the context of possible satellite and space debris growth rates, to determine the constancy of the flux. This also provides strong constraints on the current space debris component. It is found that the impact data are consistent with domination by natural meteoroid sources. Growth rates are not evident within the period 1980-1990 and Eureca TiCCE fluxes in 1993, for particles penetrating foils of around 10 microns thickness, supports the constancy of the flux. At larger dimensions the 1993 Eureca TiCCE fluxes show an 8-fold increase but this is considered not inconsistent with the selective exposure to meteoroid streams of a satellite stabilized in heliocentric co-ordinates for an 11 month period. Author

N95-23828*# National Aeronautics and Space Administration. Langley Research Center, Hampton, VA.

LDEF INTERPLANETARY DUST EXPERIMENT (IDE) RESULTS **c90**

John P. Oliver (Institute for Space Science and Technology, Inc., Gainesville, FL.), S. F. Singer (Institute for Space Science and Technology, Inc., Gainesville, FL.), J. L. Weinberg (Institute for Space Science and Technology, Inc., Gainesville, FL.), C. G. Simon (Institute for Space Science and Technology, Inc., Gainesville, FL.), W. J. Cooke (Institute for Space Science and Technology, Inc., Gainesville, FL.), P. C. Kassel, W. H. Kinard, J. D. Mulholland (POD Associates, Inc., Albuquerque, NM.), and J. J. Wortman (North Carolina State Univ., Raleigh, NC.) *In its* LDEF: 69 Months in Space. Third Post-Retrieval Symposium, Part 1 Feb. 1995 p 353-360 (For primary document see N95-23796 07-99)

(Grant NAG1-1218)

Avail: CASI HC A02/MF A04

The Interplanetary Dust Experiment (IDE) provided high time resolution

detection of microparticle impacts on the Long Duration Exposure Facility satellite. Particles, in the diameter range from 0.2 microns to several hundred microns, were detected impacting on six orthogonal surfaces of the gravity-gradient stabilized LDEF spacecraft. The total sensitive surface area was about one square meter, distributed between LDEF rows 3 (Wake or West), 6 (South), 9 (Ram or East), 12 (North), as well as the Space and Earth ends of LDEF. The time of each impact is known to an accuracy that corresponds to better than one degree in orbital longitude. Because LDEF was gravity-gradient stabilized and magnetically damped, the direction of the normal to each detector panel is precisely known for each impact. The 11 1/2 month tape-recorded data set represents the most extensive record gathered of the number, orbital location, and incidence direction for microparticle impacts in low Earth orbit. Perhaps the most striking result from IDE was the discovery that microparticle impacts, especially on the Ram, South, and North surfaces, were highly episodic. Most such impacts occurred in localized regions of the orbit for dozens or even hundreds of orbits in what we have termed Multiple Orbit Event Sequences (MOES). In addition, more than a dozen intense and short-lived 'spikes' were seen in which impact fluxes exceeded the background by several orders of magnitude. These events were distributed in a highly non-uniform fashion in time and terrestrial longitude and latitude. Author

N95-23829*# Institute for Space Science and Technology, Inc., Gainesville, FL.

THE ORBITAL CHARACTERISTICS OF DEBRIS PARTICLE RINGS AS DERIVED FROM IDE OBSERVATIONS OF MULTIPLE ORBIT INTERSECTIONS WITH LDEF **c90**

William J. Cooke, John P. Oliver, and Charles G. Simon *In* NASA. Langley Research Center, LDEF: 69 Months in Space. Third Post-Retrieval Symposium, Part 1 Feb. 1995 p 361-371 (For primary document see N95-23796 07-99)

(Grant NAG1-1218)

Avail: CASI HC A03/MF A04

During the first 346 days of the LDEF's almost 6 year stay in space, the metal oxide silicon detectors of the Interplanetary Dust Experiment (IDE) recorded over 15,000 impacts, most of which were separated in time by integer multiples of the LDEF orbital period (called multiple orbit event sequences, or MOES). Simple celestial mechanics provides ample reason to expect that a good deal of information about the orbits of the impacting debris particles can be extracted from these MOES, and so a procedure, based on the work of Greenberg, has been developed and applied to one of these events, the so-called 'May swarm'. This technique, the 'Method of Differential Precession,' allows for the determination of the geometrical elements of a particle orbit from the change in the position of the impact point with time. The application of this approach to the May swarm gave the following orbital elements for the orbit of the particles striking LDEF during this MOES: a = 6746.5 km; 0.0165 less than e less than 0.025; i = 66.55 deg; Omega(sub 0) = 179.0 deg plus or minus 0.2 deg; omega = 178.1 deg plus or minus 0.2 deg. Author

N95-23830*# National Aeronautics and Space Administration. Lyndon B. Johnson Space Center, Houston, TX.

ORBITAL DEBRIS AND METEOROID POPULATION AS ESTIMATED FROM LDEF IMPACT DATA **c90**

Jingchang Zhang and Donald J. Kessler *In* NASA. Langley Research Center, LDEF: 69 Months in Space. Third Post-Retrieval Symposium, Part 1 Feb. 1995 p 373-384 (For primary document see N95-23796 07-99)

Avail: CASI HC A03/MF A04

Examination of LDEF's various surfaces shows numerous craters and holes due to hypervelocity impacts of meteoroids and man-made orbital debris. In this paper, the crater numbers as reported by Humes have been analyzed in an effort to understand the orbital debris and natural meteoroid environment in LEO. To determine the fraction of man-made to natural impacts, the side to top ratio of impacts and results of the Chemistry of Micrometeoroids Experiment are used. For craters in the 100 micron to 500 micron size range, about 25 percent to 30 percent of the impacts on the forward-facing surfaces and about 10 percent of the impacts on the trailing surfaces were estimated due to man-made orbital debris. A technique has been developed to convert crater numbers to particle fluxes, taking the fact into account that the distributions of impact velocity and incidence angle vary over the different surfaces of LDEF, as well as the ratio of the surface area flux to the cross-sectional area flux. Applying this technique, Humes' data concerning craters with limiting lip diameters of 100 micron, 200 micron and 500 micron have been converted into orbital debris and meteoroid fluxes ranging from about 20 micron to 200 micron particle diameter. The results exhibit good agreement with orbital debris model and meteoroid model. The converted meteoroid flux is slightly larger than Grun's model (by 40 to 70 percent). The converted orbital debris flux is slightly lower than Kessler's model for particle diameter smaller than about 30 micron and slightly larger than the model for particle diameter larger than about 40 micron. Taking also into account the IDE data point at about 0.8 micron particle diameter, it suggests to change the slope log (flux) versus log (diameter) of orbital debris flux in the 1 micron to 100 micron particle diameter range from 2.5 to 1.9. Author

N95-23831*# National Aeronautics and Space Administration. Ames Research Center, Moffett Field, CA.

HYPERVELOCITY IMPACT SURVIVABILITY EXPERIMENTS FOR CARBONACEOUS IMPACTORS, PART 2 **c39**

T. E. Bunch, Julie M. Paque (Search for Extraterrestrial Intelligence Inst., Mountain View, CA.), Luann Becker (Scripps Institution of Oceanography, La Jolla, CA.), James F. Vedder, and Jozef Erlichman (TMA/Norcal, Richmond, CA.) *In* NASA. Langley Research Center, LDEF: 69 Months in Space. Third Post-Retrieval Symposium, Part 1 Feb. 1995 p 385-399 (For primary document see N95-23796 07-99)

Avail: CASI HC A03/MF A04

Hypervelocity impact experiments were performed to further test the survivability of carbonaceous impactors and to determine potential products that may have been synthesized during impact. Diamonds were launched by the Ames two-stage light gas gun into Al plate at velocities of 2.75 and 3.1 km sec(exp -1). FESEM imagery confirms that diamond fragments survived in both experiments. Earlier experiments found that diamonds were destroyed on impact above 4.3 km sec(exp -1). Thus, the upper stability limit for diamond on impact into Al, as determined from our experimental conditions, is between 3.1 and 4.3 km sec(exp -1). Particles of the carbonaceous chondrite Nogoya were also launched into Al at a velocity of 6.2 km sec (exp -1). Laser desorption (L (exp 2) MS) analyses of the impactor residues indicate that the lowest and highest mass polycyclic aromatic hydrocarbons (PAH's) were largely destroyed on impact; those of intermediate mass (202-220 amu) remained at the same level or increased in abundance. In addition, alkyl-substituted homologs of the most abundant pre-impacted PAH's were synthesized during impact. These results suggest that an unknown fraction of some organic compounds can survive low to moderate impact velocities and that synthesized products can be expected to form up to velocities of, at least, 6.5 km sec(exp -1). We also present examples of craters formed by a unique microparticle accelerator that could launch micron-sized particles of almost any coherent material at velocities up to approximately 15 km sec(exp -1). Many of the experiments have a direct bearing on the interpretation of LDEF craters. Author

N95-23832*# National Aeronautics and Space Administration. Lyndon B. Johnson Space Center, Houston, TX.

ANALYTICAL ELECTRON MICROSCOPY OF LDEF IMPACTOR RESIDUES **c90**

Ronald P. Bernhard (Lockheed Engineering and Sciences Co., Houston, TX.), Ruth A. Barrett (Lockheed Engineering and Sciences Co., Houston, TX.), and Michael E. Zolensky *In* NASA. Langley Research Center, LDEF: 69 Months in Space. Third Post-Retrieval Symposium, Part 1 Feb. 1995 p 401-413 (For primary document see N95-23796 07-99)

Avail: CASI HC A03/MF A04

The LDEF contained 57 individual experiment trays or tray portions specifically designed to characterize critical aspects of meteoroid and debris environment in low-Earth orbit (LEO). However, it was realized from the beginning that the most efficient use of the satellite would be to characterize impact features from the entire surface of the LDEF. With this in mind particular interest has focused on common materials facing in all 26 LDEF facing directions; among the most important of these materials has been the tray clamps. Therefore, in an effort to better understand the nature and flux of particulates in LEO, and their effects on spacecraft hardware, we are analyzing residues found in impact features on LDEF tray clamp surfaces. This paper summarizes all data from 79 clamps located on Bay A & B of the LDEF. We also describe current efforts to characterize impactor residues recovered from the impact craters, and we have found

that a low, but significant, fraction of these residues have survived in a largely unmelted state. These residues can be characterized sufficiently to permit resolution of the impactor origin. We have concentrated on the residue from chondritic interplanetary dust particles (micrometeoroids), as these represent the harshest test of our analytical capabilities. Author

N95-23833*# National Aeronautics and Space Administration. Lyndon B. Johnson Space Center, Houston, TX.

NATURAL AND ORBITAL DEBRIS PARTICLES ON LDEF'S TRAILING AND FORWARD-FACING SURFACES **c90**

Friedrich Hoerz, Thomas H. See (Lockheed Engineering and Sciences Co., Houston, TX.), Ronald P. Bernhard (Lockheed Engineering and Sciences Co., Houston, TX.), and Donald E. Brownlee (Washington Univ., Seattle, WA.) *In* NASA. Langley Research Center, LDEF: 69 Months in Space. Third Post-Retrieval Symposium, Part 1 Feb. 1995 p 415-429 (For primary document see N95-23796 07-99)

Avail: CASI HC A03/MF A04

Approximately 1000 impact craters on the Chemistry of Meteoroid Experiment (CME) have been analyzed by means of Scanning Electron Microscopy (SEM) and Energy Dispersive X-ray Analysis (EDXA) to determine the compositional make-up of projectile residues. This report completes our systematic survey of gold and aluminum surfaces exposed at the trailing-edge (A03) and forward-facing (A11) LDEF sites, respectively. The major categories for the projectile residues were (1) natural, with diverse subgroups such as chondritic, monomineralic silicates, and sulfides, and (2) man made, that were classified into aluminum (metallic or oxide) and miscellaneous materials (such as stainless steel, paint flakes, etc). On CME gold collectors on LDEF's trailing edge approximately 11 percent of all craters greater than 100 micron in diameter were due to man-made debris, the majority (8.6 percent) caused by pure aluminum, approximately 31.4 percent were due to cosmic dust, while the remaining 58 percent were indeterminate via the analytical techniques utilized in this study. The aluminum surfaces located at the A11 forward-facing site did not permit analysis of aluminum impactors, but approximately 9.4 percent of all craters were demonstratably caused by miscellaneous debris materials and approximately 39.2 percent were the result of natural particles, leaving approximately 50 percent which were indeterminate. Model considerations and calculations are presented that focus on the crater-production rates for features greater than 100 micron in diameter, and on assigning the intermediate crater population to man-made or natural particles. An enhancement factor of 6 in the crater-production rate of natural impactors for the 'forward-facing' versus the 'trailing-edge' CME collectors was found to best explain all observations (i.e., total crater number(s), as well as their computational characteristics). Enhancement factors of 10 and 4 are either too high or too low. It is also suggested that approximately 45 percent of all craters greater than 100 micron in diameter are caused by man-made impactors on the A11 surfaces. This makes the production rate for craters greater than 100 micron in diameter, resulting from orbital debris, a factor of 40 higher on the forward-facing sides as opposed to the trailing-edge direction. Author

N95-23834*# Departement d'Etudes et de Recherches en Technologie Spatiale, Toulouse (France).

DEBRIS AND METEOROID PROPORTIONS DEDUCED FROM IMPACT CRATER RESIDUE ANALYSIS **c90**

Lucinda Berthoud, Jean-Claude Mandeville, Christian Durin (Centre National d'Etudes Spatiales, Toulouse, France.), and Janet Borg (Centre National de la Recherche Scientifique, Orsay, France.) *In* NASA. Langley Research Center, LDEF: 69 Months in Space. Third Post-Retrieval Symposium, Part 1 Feb. 1995 p 431-444 Sponsored by European Commission (For primary document see N95-23796 07-99)

Avail: CASI HC A03/MF A04

This study is a further investigation of space-exposed samples recovered from the LDEF satellite and the Franco-Russian 'Aragatz' dust collection experiment on the Mir Space Station. Impact craters with diameters ranging from 1 to 900 micron were found on the retrieved samples. Elemental analysis of residues found in the impact craters was carried out using Energy Dispersive X-ray spectrometry (EDX). The analyses show evidence of micrometeoroid and orbital debris origins for the impacts. The proportions of these two components vary according to particle size and experimental position with respect to the leading edge of the spacecraft. On the LDEF leading edge 17 percent of the impacts were apparently caused by micrometeoroids and 11 percent by debris; on the LDEF trailing edge 23 percent of the impacts are apparently caused by micrometeoroids and 4 percent consist of debris particles - mostly larger than 3 micron in diameter - in elliptical orbits around the Earth. For Mir, the analyses indicate that micrometeoroids form 23 percent of impacts and debris 9 percent. However, we note that 60-70 percent of the craters are unidentifiable, so the definitive proportions of natural v. man-made particles are yet to be determined. Experiments carried out using a light gas gun to accelerate glass spheres and fragments demonstrate the influence of particle shape on crater morphology. The experiments also show that it is more difficult to analyze the residues produced by an irregular fragment than those produced by a spherical projectile. If the particle is travelling above a certain velocity, it vaporizes upon impact and no residues are left. Simulation experiments carried out with an electrostatic accelerator indicate that this limit is about 14 km/s for Fe particles impacting Al targets. This chemical analysis cut-off may bias interpretations of the relative populations of meteoroid and orbital debris. Oblique impacts and multiple foil detectors provide a higher likelihood of detection of residues as the velocities involved are lower. Author

N95-23835*# Kent Univ., Canterbury (England). Unit for Space Sciences.

MICRO-ABRASION PACKAGE CAPTURE CELL EXPERIMENT ON THE TRAILING EDGE OF LDEF: IMPACTOR CHEMISTRY AND WHIPPLE BUMPER SHIELD EFFICIENCIES **c18**

Howard J. Fitzgerald and Hajime Yano *In* NASA. Langley Research Center, LDEF: 69 Months in Space. Third Post-Retrieval Symposium, Part 1 Feb. 1995 p 445-457 Sponsored by European Social Fund, Overseas Research Studentship, Daiwa Anglo-Japanese Foundation, and the Anglo-American Educational Exchange Scholarship Fund (For primary document see N95-23796 07-99)

Avail: CASI HC A03/MF A04

Four of the eight available double layer microparticle capture cells, flown as the experiment A0023 on the trailing (West) face of LDEF, have been extensively studied. An investigation of the chemistry of impactors has been made using SEM/EDX techniques and the effectiveness of the capture cells as bumper shields has also been examined. Studies of these capture cells gave positive EDX results, with 53 percent of impact sites indicating the presence of some chemical residues, the predominant residue identified as being silicon in varying quantities. Author

N95-23836*# Institute for Space Science and Technology, Inc., Gainesville, FL.

SECONDARY ION MASS SPECTROMETRY (SIMS) ANALYSIS OF HYPERVELOCITY MICROPARTICLE IMPACT SITES ON LDEF SURFACES Abstract Only **c25**

C. G. Simon, A. J. Buonaquisti (North Carolina State Univ., Raleigh, NC.), D. A. Batchelor (North Carolina State Univ., Raleigh, NC.), J. L. Hunter (North Carolina State Univ., Raleigh, NC.), D. P. Griffis (North Carolina State Univ., Raleigh, NC.), V. Misra (North Carolina State Univ., Raleigh, NC.), D. R. Ricks (North Carolina State Univ., Raleigh, NC.), J. J. Wortman (North Carolina State Univ., Raleigh, NC.), D. E. Brownlee (Washington Univ., Seattle, WA.), and S. R. Best (Auburn Univ., AL.) et al *In* NASA. Langley Research Center, LDEF: 69 Months in Space. Third Post-Retrieval Symposium, Part 1 Feb. 1995 p 459-460 (For primary document see N95-23796 07-99)

(Grant NAG1-1218)

Avail: CASI HC A01/MF A04

Two dimensional elemental ion maps have been recorded for hundreds of microparticle impact sites and contamination features on LDEF surfaces. Since the majority of the analyzed surfaces were metal-oxide-silicon (MOS) impact detectors from the Interplanetary Dust Experiment, a series of 'standard' and 'blank' analyses of these surfaces are included. Hypervelocity impacts of forsterite olivine microparticles on activated flight sensors served as standards while stylus and pulsed laser simulated 'impacts' served as analytical blanks. Results showed that despite serious contamination issues, impactor residues can be identified in greater than 1/3 of the impact sites. While aluminum oxide particles could not be detected on aluminum surfaces, they were detected on germanium surfaces from row 12. Remnants of manmade debris impactors consisting of paint chips and bits of metal were identified on surfaces from LDEF Rows 3 (west or trailing side), 6 (south), 9 (ram or leading side), 12 (north) and the space end. Higher than expected ratios of manmade microparticle impacts to total microparticle

impacts were found on the space end and the trailing side. These results were consistent with time-tagged and time-segregated microparticle impact data from the IDE and other LDEF experiments. A myriad of contamination interferences were identified and their effects on impactor debris identification mitigated during the course of this study. These interferences include pre-, post and inflight deposited surface contaminants as well as indigenous heterogeneous material contaminants. Non-flight contaminations traced to human origins, including spittle and skin oils, contributed significant levels of alkali-rich carbonaceous interferences. A ubiquitous layer of in-flight deposited silicaceous contamination varied in thickness with location on LDEF, even on a micro scale. In-flight deposited (low velocity) contaminants include urine droplets and bits of metal film from eroded thermal blankets. Author

N95-23837*# Technische Hochschule, Darmstadt (Germany). Dept. of Material Science.

SIMS CHEMICAL AND ISOTOPIC ANALYSIS OF IMPACT FEATURES FROM LDEF EXPERIMENTS AO187-1 AND AO187-2 **c25**

Frank J. Stadermann, Sachiko Amari (Washington Univ., Saint Louis, MO.), John Foote (Washington Univ., Saint Louis, MO.), Pat Swan (Washington Univ., Saint Louis, MO.), Robert M. Walker (Washington Univ., Saint Louis, MO.), and Ernst Zinner (Washington Univ., Saint Louis, MO.) *In* NASA. Langley Research Center, LDEF: 69 Months in Space. Third Post-Retrieval Symposium, Part 1 Feb. 1995 p 461-473 (For primary document see N95-23796 07-99)

Avail: CASI HC A03/MF A04

Previous secondary ion mass spectrometry (SIMS) studies of extended impact features from LDEF capture cell experiment AO187-2 showed that it is possible to distinguish natural and man-made particle impacts based on the chemical composition of projectile residues. The same measurement technique has now been applied to specially prepared gold target impacts from experiment AO187-1 in order to identify the origins of projectiles that left deposits too thin to be analyzed by conventional energy-dispersive x-ray (EDX) spectroscopy. The results indicate that SIMS may be the method of choice for the analysis of impact deposits on a variety of sample surfaces. SIMS was also used to determine the isotopic compositions of impact residues from several natural projectiles. Within the precision of the measurements all analyzed residues show isotopically normal compositions. Author

N95-23838*# National Aeronautics and Space Administration. Ames Research Center, Moffett Field, CA.

IMAGE AND COMPOSITIONAL CHARACTERISTICS OF THE LDEF BIG GUY IMPACT CRATER **c39**

T. E. Bunch, Julie M. Paque (Search for Extraterrestrial Intelligence Inst., Mountain View, CA.), and Michael Zolensky (National Aeronautics and Space Administration. Lyndon B. Johnson Space Center, Houston, TX.) *In* NASA. Langley Research Center, LDEF: 69 Months in Space. Third Post-Retrieval Symposium, Part 1 Feb. 1995 p 475-481 (For primary document see N95-23796 07-99)

Avail: CASI HC A02/MF A04

A 5.2 mm crater in Al-metal represents the largest found on LDEF. We have examined this crater by field emission scanning electron microscopy (FESEM), energy dispersive spectroscopy (EDS) and time-of-flight/secondary ion mass spectroscopy (TOF-SIMS) in order to determine if there is any evidence of impactor residue. Droplet and dome-shaped columns, along with flow features, are evidence of melting. EDS from the crater cavity and rim show Mg, C, O and variable amounts of Si, in addition to Al. No evidence for a chondritic impactor was found, and it hypothesized that the crater may be the result of impact with space debris. Author

N95-23839*# Auburn Univ., AL. Space Power Inst.

THE EFFECT OF IMPACT ANGLE ON CRATERS FORMED BY HYPERVELOCITY PARTICLES **c39**

David C. Hill, M. Frank Rose, Steve R. Best, Michael S. Crumpler, Gary D. Crawford, Ralph H.-C. Zee, and Michael J. Bozack *In* NASA. Langley Research Center, LDEF: 69 Months in Space. Third Post-Retrieval Symposium, Part 1 Feb. 1995 p 483-498 (For primary document see N95-23796 07-99)

(Grant NAG1-1329)

Avail: CASI HC A03/MF A04

The Space Power Institute (SPI) at Auburn University has conducted experiments on the effects of impact angle on crater morphology and impactor residue retention for hypervelocity impacts. Copper target plates were set at angles of 30 deg, 45 deg, 60 deg, and 75 deg from the particle flight path. For the 30 deg and 45 deg impacts, in the velocity regime greater than 8 km s(exp -1) the resultant craters are almost identical to normal incidence impacts. The only difference found was in the apparent distribution of particle residue within the crater, and further research is needed to verify this. The 60 deg and 75 deg impacts showed marked differences in crater symmetry, crater lip shape, and particle residue distribution in the same velocity regime. Impactor residue shock fractionation effects have been quantified in first-order. It is concluded that a combination of analysis techniques can yield further information on impact velocity, direction, and angle of incidence. Author

N95-23840*# Kent Univ., Canterbury (England). Unit for Space Sciences.

EXPERIMENTAL INVESTIGATION OF THE RELATIONSHIP BETWEEN IMPACT CRATER MORPHOLOGY AND IMPACTING PARTICLE VELOCITY AND DIRECTION **c39**

N. G. Mackay, S. F. Green, D. J. Gardner, and J. A. M. McDonnell *In* NASA. Langley Research Center, LDEF: 69 Months in Space. Third Post-Retrieval Symposium, Part 1 Feb. 1995 p 499-508 (For primary document see N95-23796 07-99)

Avail: CASI HC A02/MF A04

Interpretation of the wealth of impact data available from the Long Duration Exposure Facility, in terms of the absolute and relative populations of space debris and natural micrometeoroids, requires three dimensional models of the distribution of impact directions, velocities and masses of such particles, as well as understanding of the impact processes. Although the stabilized orbit of LDEF provides limited directional information, it is possible to determine more accurate impact directions from detailed crater morphology. The applicability of this technique has already been demonstrated but the relationship between crater shape and impactor direction and velocity has not been derived in detail. We present the results of impact experiments and simulations: (1) impacts at micron dimensions using the Unit's 2MV Van de Graaff accelerator; (2) impacts at mm dimensions using a Light Gas Gun; and (3) computer simulations using AUTODYN-3D from which an empirical relationship between crater shape and impactor velocity, direction and particle properties we aim to derive. Such a relationship can be applied to any surface exposed to space debris or micrometeoroid particles for which a detailed pointing history is available. Author

N95-23841*# Technische Univ., Munich (Germany). Lehrstuhl fuer Raumfahrttechnik.

DETERMINING ORBITAL PARTICLE PARAMETERS OF IMPACTS INTO GERMANIUM USING MORPHOLOGY ANALYSIS AND CALIBRATION DATA FROM HYPERVELOCITY IMPACT EXPERIMENTS IN THE LABORATORY **c39**

Klaus G. Paul *In* NASA. Langley Research Center, LDEF: 69 Months in Space. Third Post-Retrieval Symposium, Part 1 Feb. 1995 p 509-520 (For primary document see N95-23796 07-99)

(Contract DARA-50-QV-9194-0)

Avail: CASI HC A03/MF A04

This paper describes the work that is done at the Lehrstuhl fur Raumfahrttechnik (lrt) at the Technische Universitat Munchen to examine particle impacts into germanium surfaces which were flown on board the LDEF satellite. Besides the description of the processing of the samples, a brief overview of the particle launchers at our institute is given together with descriptions of impact morphology of high- and hypervelocity particles into germanium. Since germanium is a brittle, almost glass-like material, the impact morphology may also be interesting for anyone dealing with materials such as optics and solar cells. The main focus of our investigations is to learn about the impacting particle's properties, for example mass, velocity and direction. This is done by examining the morphology, various geometry parameters, crater obliqueness and crater volume. Author

N95-23842*# National Aeronautics and Space Administration. Lyndon B. Johnson Space Center, Houston, TX.

CRATERING AND PENETRATION EXPERIMENTS IN TEFLON TARGETS AT VELOCITIES FROM 1 TO 7 km/s Abstract Only **c39**

Friedrich Hoerz, Ronald P. Bernhard (Lockheed Engineering and Sciences

Co., Houston, TX.), Mark J. Cintala, and Thomas H. See (Lockheed Engineering and Sciences Co., Houston, TX.) *In* NASA. Langley Research Center, LDEF: 69 Months in Space. Third Post-Retrieval Symposium, Part 1 Feb. 1995 p 521 (For primary document see N95-23796 07-99)
Avail: CASI HC A01/MF A04

Approximately 20 sq m of protective thermal blankets, largely composed of Teflon, were retrieved from the Long Duration Exposure Facility (LDEF) after the spacecraft had spent approximately 5.7 years in space. Examination of these blankets revealed that they contained thousands of hypervelocity impact features ranging from micron-sized craters to penetration holes several millimeters in diameter. We conducted impact experiments in an effort to reproduce such features and to -- hopefully -- understand the relationships between projectile size and the resulting crater or penetration-hole diameter over a wide range of impact velocity. Such relationships are needed to derive the size- and mass-frequency distribution and flux of natural and man-made particles in low-Earth orbit. Powder propellant and light-gas guns were used to launch soda-lime glass spheres of 3.175 mm (1/8 inch) nominal diameter (Dp) into pure Teflon FEP targets at velocities ranging from 1 to 7 km/s. Target thickness (T) was varied over more than three orders of magnitude from infinite halfspace targets (Dp/T less than 0.1) to very thin films (Dp/T greater than 100). Cratering and penetration of massive Teflon targets is dominated by brittle failure and the development of extensive spall zones at the target's front and, if penetrated, the target's rear side. Mass removal by spallation at the back side of Teflon targets may be so severe that the absolute penetration-hole diameter (Dh) can become larger than that of a standard crater (Dc) at relative target thicknesses of Dp/T = 0.6-0.9. The crater diameter is infinite halfspace Teflon targets increases -- at otherwise constant impact conditions -- with encounter velocity by a factor of V0.44. In contrast, the penetration-hole size is very thin foils (Dp/T greater than 50) is essentially unaffected by impact velocity. Penetrations at target thicknesses intermediate to these extremes will scale with variable exponents of V. Our experimental matrix is sufficiently systematic and complete, up to 7 km/s, to make reasonable recommendations for the velocity-scaling of Teflon craters and penetrations. We specifically suggest that cratering behavior and associated equations dominate all impacts in which the shock-pulse duration of the projectile (tp) is shorter than that of the target (tt). We also demonstrate that each penetration hole from space-retrieved surfaces may be assigned a unique projectile size, provided an impact velocity is known or assumed. This calibration seems superior to the traditional ballistic-limit approach.
Author (revised)

N95-23843*# POD Associates, Inc., Albuquerque, NM.
DIMENSIONAL SCALING FOR IMPACT CRATERING AND PERFORATION **c18**
Alan J. Watts and Dale Atkinson *In* NASA. Langley Research Center, LDEF: 69 Months in Space. Third Post-Retrieval Symposium, Part 1 Feb. 1995 p 523-535 (For primary document see N95-23796 07-99)
Avail: CASI HC A03/MF A04

POD Associates have revisited the issue of generic scaling laws able to adequately predict (within better than 20 percent) cratering in semi-infinite targets and perforations through finite thickness targets. The approach used was to apply physical logic for hydrodynamics in a consistent manner able to account for chunky-body impacts such that the only variables needed are those directly related to known material properties for both the impactor and target. The analyses were compared and verified versus CTH hydrodynamic code calculations and existing data. Comparisons with previous scaling laws were also performed to identify which (if any) were good for generic purposes. This paper is a short synopsis of the full report available through the NASA Langley Research Center, LDEF Science Office. Author

N95-23896*# National Aeronautics and Space Administration. Langley Research Center, Hampton, VA.
LDEF: 69 MONTHS IN SPACE. THIRD POST-RETRIEVAL SYMPOSIUM, PART 2
Arlene S. Levine, ed. Feb. 1995 339 p Symposium held in Williamsburg, VA, 8-12 Nov. 1993; sponsored by NASA, Washington and AIAA
(RTOP 233-03-02-03)
(NASA-CP-3275-Pt-2; L-17430B-Pt-2; NAS 1.55:3275-Pt-2) Avail: CASI HC A15/MF A03

This volume is a compilation of papers presented at the Third Long Duration Exposure Facility (LDEF) Post-Retrieval Symposium. The papers represent the data analysis of the 57 experiments flown on the LDEF. The experiments include materials, coatings, thermal systems, power and propulsion, science (cosmic ray, interstellar gas, heavy ions, micrometeoroid, etc.), electronics, optics, and life science. In addition, papers on preliminary data analysis of EURECA, EOIM-3, and other spacecraft are included. This second of three parts covers spacecraft construction materials. For individual titles, see N95-23897 through N95-23916.

N95-23897*# National Aeronautics and Space Administration. Langley Research Center, Hampton, VA.
SUMMARY AND REVIEW OF MATERIALS SPECIAL INVESTIGATION GROUP EVALUATIONS OF HARDWARE FROM THE LONG DURATION EXPOSURE FACILITY **c25**
Ann F. Whitaker (National Aeronautics and Space Administration. Marshall Space Flight Center, Huntsville, AL.), Joan Funk, H. Gary Pippin (Boeing Defense and Space Group, Seattle, WA.), and Harry Dursch (Boeing Defense and Space Group, Seattle, WA.) *In its* LDEF: 69 Months in Space. Third Post-Retrieval Symposium, Part 2 Feb. 1995 p 539-553 (For primary document see N95-23896 07-99)
(Contract NAS1-19247)
Avail: CASI HC A03/MF A03

Major materials findings obtained during LDEF post-flight investigations over the past three and one-half years are reported. The summary of findings to date includes results for thermal control coatings, thin polymeric films, composites, metals, adhesives, contamination, and environments definitions. Reaction rates of selected materials exposed to atomic oxygen are presented. Results useful for model verification and comparison with ground based facility data are specifically highlighted. Potential areas for future work are described. In conclusion, a rationale for a second long term flight experiment is presented. Author

N95-23898*# Boeing Defense and Space Group, Seattle, WA.
RECENT RESULTS FROM LONG DURATION EXPOSURE FACILITY MATERIALS TESTING **c25**
H. Gary Pippin and Harry W. Dursch *In* NASA. Langley Research Center, LDEF: 69 Months in Space. Third Post-Retrieval Symposium, Part 2 Feb. 1995 p 555-565 (For primary document see N95-23896 07-99)
(Contract NAS1-19247)
Avail: CASI HC A03/MF A03

The overall goals of the Long Duration Exposure Facility (LDEF) investigations, established by the Materials Special Investigation Group (MSIG) prior to LDEF retrieval, are to provide useful engineering data to people designing and building spacecraft, and secondarily, to obtain data of potential interest to materials researchers. The specific objectives are to support predictions of materials lifetimes under the various low earth orbit (LEO) environments to determine how long the material will physically survive; to estimate the engineering performance lifetimes of these same materials under specific LEO exposures; to identify materials and processes by which given materials degrade; and to provide insights into development of new, more inherently LEO environmentally resistant materials. To achieve the established objectives, two criteria were established to select which materials had the highest priorities for analyses. The first criteria was to examine materials which are still being used on new spacecraft. The second priority was to examine materials with multiple exposure locations on LDEF, because this provided the opportunity to develop predictions on how a material will behave as the exposure environment varies. The goals as defined led to the identification of silverized Teflon (Ag/FEP), chromic acid anodized aluminum, and certain thermal control paints used on LDEF as the material types of highest priority for examination. Ag/FEP was chosen because of an excellent a/e ratio (extremely low), and extensive flight history. Also influencing the decision was the fact that the Hubble Space Telescope uses Ag/FEP as its primary passive thermal control system (and was launched shortly after LDEF retrieval) and that a number of other spacecraft are using or considering this material for use. The various forms of Ag/FEP were used on virtually every side of the LDEF except the earth end. The potential uses of this material, and the location distribution and therefore, exposure conditions, have provided the rationale and opportunity for a comprehensive study of this material. Derived from text

N95-23899*# National Aeronautics and Space Administration. Langley Research Center, Hampton, VA.

LDEF POLYMERIC MATERIALS: A SUMMARY OF LANGLEY CHARACTERIZATION **c27**

Philip R. Young, Wayne S. Slemp, Karen S. Whitley, Carol R. Kalil (Analytical Services and Materials, Inc., Hampton, VA.), Emilie J. Siochi (Lockheed Engineering and Sciences Co., Hampton, VA.), James Y. Shen (Lockheed Engineering and Sciences Co., Hampton, VA.), and A. C. Chang (Lockheed Engineering and Sciences Co., Hampton, VA.) *In its* LDEF: 69 Months in Space. Third Post-Retrieval Symposium, Part 2 Feb. 1995 p 567-599 (For primary document see N95-23896 07-99)

Avail: CASI HC A03/MF A03

The NASA Long Duration Exposure Facility (LDEF) enabled the exposure of a wide variety of materials to the low earth orbit (LEO) environment. This paper provides a summary of research conducted at the Langley Research Center into the response of selected LDEF polymers to this environment. Materials examined include graphite fiber reinforced epoxy, polysulfone, and additional polyimide matrix composites, films of FEP Teflon, Kapton, several experimental high performance polyimides, and films of more traditional polymers such as poly(vinyl toluene) and polystyrene. Exposure duration was either 10 months or 5.8 years. Flight and control specimens were characterized by a number of analytical techniques including ultraviolet-visible and infrared spectroscopy, thermal analysis, scanning electron and scanning tunneling microscopy, x-ray photoelectron spectroscopy, and, in some instances, selected solution property measurements. Characterized effects were found to be primarily surface phenomena. These effects included atomic oxygen-induced erosion of unprotected surfaces and ultraviolet-induced discoloration and changes in selected molecular level parameters. No gross changes in molecular structure or glass transition temperature were noted. The intent of this characterization is to increase our fundamental knowledge of space environmental effects as an aid in developing new and improved polymers for space application. A secondary objective is to develop benchmarks to enhance our methodology for the ground-based simulation of environmental effects so that polymer performance in space can be more reliably predicted. Author

N95-23900*# National Aeronautics and Space Administration. Langley Research Center, Hampton, VA.

SURFACE CHARACTERIZATION OF LDEF CARBON FIBER/POLYMER MATRIX COMPOSITES **c24**

Holly L. Grammer (Virginia Polytechnic Inst. and State Univ., Blacksburg, VA.), James P. Wightman (Virginia Polytechnic Inst. and State Univ., Blacksburg, VA.), Philip R. Young, and Wayne S. Slemp *In its* LDEF: 69 Months in Space. Third Post-Retrieval Symposium, Part 2 Feb. 1995 p 601-612 (For primary document see N95-23896 07-99)

(Grant NAG1-1186)
Avail: CASI HC A03/MF A03

XPS (x-ray photoelectron spectroscopy) and SEM (scanning electron microscopy) analysis of both carbon fiber/epoxy matrix and carbon fiber/polysulfone matrix composites revealed significant changes in the surface composition as a result of exposure to low-earth orbit. The carbon 1s curve fit XPS analysis in conjunction with the SEM photomicrographs revealed significant erosion of the polymer matrix resins by atomic oxygen to expose the carbon fibers of the composite samples. This erosion effect on the composites was seen after 10 months in orbit and was even more obvious after 69 months. Author

N95-23901*# Toronto Univ., North York (Ontario). Inst. for Aerospace Studies.

SPACE ENVIRONMENTAL EFFECTS ON POLYMER MATRIX COMPOSITES AS A FUNCTION OF SAMPLE LOCATION ON LDEF **c27**

R. C. Tennyson, G. R. Cool, and D. G. Zimcik (Canadian Space Agency, Ottawa, Ontario.) *In* NASA. Langley Research Center, LDEF: 69 Months in Space. Third Post-Retrieval Symposium, Part 2 Feb. 1995 p 613-629 (For primary document see N95-23896 07-99)

Avail: CASI HC A03/MF A03

This paper presents results on the effect of circumferential location on the variation in solar absorptance (alpha(sub S)) and infrared emittance (epsilon) for five different polymer matrix composites (PMC), and variations in erosion depth due to atomic oxygen (AO) for fourteen different PMC materials. In addition, a chemical content design parameter (gamma) has been found that correlates well with the erosion yield obtained from space flight data and hyperthermal AO tests for hydrocarbon polymeric materials. This parameter defines the ratio of the total number of atoms in a repeat monomer unit to the difference between the total carbon content and the total number of intermolecular oxygen atoms in the same repeat unit. Author

N95-23902*# Texas A&M Univ., College Station, TX. Dept. of Aerospace Engineering.

NONLINEAR VISCOELASTIC CHARACTERIZATION OF POLYMER MATERIALS USING A DYNAMIC-MECHANICAL METHODOLOGY **c27**

Thomas W. Strganac, Debbie Flowers Payne, Bruce A. Biskup, and Alan Letton *In* NASA. Langley Research Center, LDEF: 69 Months in Space. Third Post-Retrieval Symposium, Part 2 Feb. 1995 p 631-644 (For primary document see N95-23896 07-99)

(Grant NAG5-673)
Avail: CASI HC A03/MF A03

Polymer materials retrieved from LDEF exhibit nonlinear constitutive behavior; thus the authors present a method to characterize nonlinear viscoelastic behavior using measurements from dynamic (oscillatory) mechanical tests. Frequency-derived measurements are transformed into time-domain properties providing the capability to predict long term material performance without a lengthy experimentation program. Results are presented for thin-film high-performance polymer materials used in the fabrication of high-altitude scientific balloons. Predictions based upon a linear test and analysis approach are shown to deteriorate for moderate to high stress levels expected for extended applications. Tests verify that nonlinear viscoelastic response is induced by large stresses. Hence, an approach is developed in which the stress-dependent behavior is examined in a manner analogous to modeling temperature-dependent behavior with time-temperature correspondence and superposition principles. The development leads to time-stress correspondence and superposition of measurements obtained through dynamic mechanical tests. Predictions of material behavior using measurements based upon linear and nonlinear approaches are compared with experimental results obtained from traditional creep tests. Excellent agreement is shown for the nonlinear model. Author

N95-23903*# Queensland Univ., Brisbane (Australia). Polymer Materials and Radiation Group.

THE EFFECT OF SIMULATED LOW EARTH ORBIT RADIATION ON POLYIMIDES (UV DEGRADATION STUDY) **c27**

John S. Forsythe, Graeme A. George, David J. T. Hill, James H. ODonnell, Peter J. Pomery, and Firas A. Rasoul *In* NASA. Langley Research Center, LDEF: 69 Months in Space. Third Post-Retrieval Symposium, Part 2 Feb. 1995 p 645-656 (For primary document see N95-23896 07-99)

Avail: CASI HC A03/MF A03

UV degradation of polyimide films in air and vacuum were studied using UV-visible, ESR, FTIR, and XPS spectroscopies. The UV-visible spectra of polyimide films showed a blue shift in the absorption compared to Kapton. This behavior was attributed to the presence of bulky groups and kinks along the polymer chains which disrupt the formation of a charge transfer complex. The UV-visible spectra showed also that UV irradiation of polyimides result extensively in surface degradation, leaving the bulk of the polymer intact. ESR spectra of polyimides irradiated in vacuum revealed the formation of stable carbon-centered radicals which give a singlet ESR spectrum, while polyimides irradiated in air produced an asymmetric signal shifted to a lower magnetic field, with a higher g value and line width. This signal was attributed to oxygen-cenetered radicals of peroxy and/or alkoxy type. The rate of radical formation in air was two fold higher than for vacuum irradiation, and reached a plateau after a short time. This suggests a continuous depletion of radicals on the surface via an ablative degradation process. FTIR, XPS, and weight loss studies supported this postulate. An XPS study of the surface indicated a substantial increase in the surface oxidation after irradiation in air. The sharp increase in the C-O binding energy peak relative to the C-C peak was believed to be associated with an aromatic ring opening reaction. Author

N95-23904*# Queensland Univ., Brisbane (Australia). Polymer Materials and Radiation Group.

THE SURFACE PROPERTIES OF FLUORINATED POLYIMIDES EXPOSED TO VUV AND ATOMIC OXYGEN **c27**

John S. Forsythe, Graeme A. George, David J. T. Hill, James H. ODonnell, Peter J. Pomery, and Firas A. Rasoul *In* NASA. Langley Research Center, LDEF: 69 Months in Space. Third Post-Retrieval Symposium, Part 2 Feb. 1995 p 657-665 (For primary document see N95-23896 07-99)
Avail: CASI HC A02/MF A03

The effect of atomic oxygen flux and VUV radiation alone and in combination on the surface of fluorinated polyimide films was studied using XPS spectroscopy. Exposure of fluorinated polyimides to VUV radiation alone caused no observable damage to the polymer surface, while an atomic oxygen flux resulted in substantial oxidation of the surface. On the other hand, exposure to VUV radiation and atomic oxygen in combination caused extensive oxidation of the polymer surface after only 2 minutes of exposure. The amount of oxidized carbon on the polymer surface indicated that there is aromatic ring opening oxidation. The changes in the O1s/C1s, N1s/C1s, and F1s/C1s ratios suggested that an ablative degradation process is highly favorable. A synergistic effect of VUV radiation in the presence of atomic oxygen is clearly evidenced from the XPS study. The atomic oxygen could be considered as the main factor in the degradation process of fluorinated polyimide films exposed to a low earth orbit environment.
Author

N95-23905*# Boeing Defense and Space Group, Seattle, WA.
COLLECTION AND REVIEW OF METALS DATA OBTAINED FROM LDEF EXPERIMENT SPECIMENS AND SUPPORT HARDWARE **c26**
Roger Bourassa and H. Gary Pippin *In* NASA. Langley Research Center, LDEF: 69 Months in Space. Third Post-Retrieval Symposium, Part 2 Feb. 1995 p 667-688 (For primary document see N95-23896 07-99)
(Contract NAS1-19247)
Avail: CASI HC A03/MF A03

LDEF greatly extended the range of data available for metals exposed to the low-Earth-orbital environment. The effects of low-Earth-orbital exposure on metals include meteoroid and debris impacts, solar ultraviolet radiation, thermal cycling, cosmic rays, solar particles, and surface oxidation and contamination. This paper is limited to changes in surface composition and texture caused by oxidation and contamination. Surface property changes afford a means to study the environments (oxidation and contamination) as well as in-space stability of metal surfaces. We compare thermal-optical properties for bare aluminum and anodized aluminum clamps flown on LDEF. We also show that the silicon observed on the LDEF tray clamps and tray clamp bolt heads is not necessarily evidence of silicon contamination of LDEF from the shuttle. The paper concludes with a listing of LDEF reports that have been published thus far that contain significant findings concerning metals.
Derived from text

N95-23906*# National Aeronautics and Space Administration. Marshall Space Flight Center, Huntsville, AL.
MEASUREMENTS OF THE OPTICAL PROPERTIES OF THIN FILMS OF SILVER AND SILVER OXIDE **c27**
Palmer N. Peters, Robert C. Sisk, Yolanda Brown, John C. Gregory (Alabama Univ., Huntsville, AL.), Pallob K. Nag (Alabama Univ., Huntsville, AL.), and Ligia Christl (Alabama Univ., Huntsville, AL.) *In* NASA. Langley Research Center, LDEF: 69 Months in Space. Third Post-Retrieval Symposium, Part 2 Feb. 1995 p 689-701 (For primary document see N95-23896 07-99)
Avail: CASI HC A03/MF A03

The optical properties of silver films and their oxides are measured to better characterize such films for use as sensors for atomic oxygen. Good agreement between properties of measured pure silver films and reported optical constants is observed. Similar comparisons for silver oxide have not been possible because of a lack of reported constants, but self-consistencies and discrepancies in our measured results are described.
Author

N95-23907*# National Aeronautics and Space Administration. Marshall Space Flight Center, Huntsville, AL.
CHANGES IN CHEMICAL AND OPTICAL PROPERTIES OF THIN FILM METAL MIRRORS ON LDEF **c27**
Palmer N. Peters, James M. Zwiener, John C. Gregory (Alabama Univ., Huntsville, AL.), Ganesh N. Raikar (Alabama Univ., Huntsville, AL.), Ligia C. Christl (Alabama Univ., Huntsville, AL.), and Donald R. Wilkes (AZ Technology, Huntsville, AL.) *In* NASA. Langley Research Center, LDEF: 69 Months in Space. Third Post-Retrieval Symposium, Part 2 Feb. 1995 p 703-725 (For primary document see N95-23896 07-99)
Avail: CASI HC A03/MF A03

Thin films of the metals Cu, Ni, Pt, Au, Sn, Mo, and W deposited on fused silica flats were exposed at ambient temperature on the leading and trailing faces of the LDEF. Reflectances of these films were measured from 250 to 2500 nm and compared with controls. The exposed films were subjected to the LDEF external environment including atomic oxygen, molecular contamination, and solar ultraviolet. Major changes in optical and infrared reflectance were seen for Cu, Mo, Ni, and W films on the leading face of LDEF and are attributed to partial conversion of metal to metal oxide. Smaller changes in optical properties are seen on all films and are probably caused by thin contaminant films deposited on top of the metal. The optical measurements are correlated with film thickness measurements, x-ray photoelectron spectroscopy, optical calculations, and, in the case of Cu, with x-ray diffraction measurements. In a few cases, comparisons with results from a similar UAH experiment on STS-8 have been drawn.
Author

N95-23908*# National Aeronautics and Space Administration. Marshall Space Flight Center, Huntsville, AL.
FURTHER INVESTIGATIONS OF EXPERIMENT A0034 ATOMIC OXYGEN STIMULATED OUTGASSING **c27**
Roger C. Linton, Miria M. Finckenor, and Rachel R. Kamenetzky *In* NASA. Langley Research Center, LDEF: 69 Months in Space. Third Post-Retrieval Symposium, Part 2 Feb. 1995 p 727-736 (For primary document see N95-23896 07-99)
(Contract NAS8-39924)
Avail: CASI HC A02/MF A03

Thermal control coatings within the recessed compartments of LDEF Experiment A0034 experienced the maximum leading edge fluence of atomic oxygen with considerably less solar UV radiation exposure than top-surface mounted materials of other LDEF experiments on either the leading or the trailing edge. This combination of exposure within A0034 resulted in generally lower levels of darkening attributable to solar UV radiation than for similar materials on other LDEF experiments exposed to greater cumulative solar UV radiation levels. Changes in solar absorptance and infrared thermal emittance of the exposed coatings are thus unique to this exposure. Analytical results for other applications have been found for environmentally induced changes in fluorescence, surface morphology, light scattering, and the effects of coating outgassing products on adjacent mirrors and windows of the A0034 experiment. Some atmospheric bleaching of the thermal control coatings, in addition to that presumably experience during reentry and recovery operations, has been found since initial post-flight observations and measurements.
Author

N95-23909*# National Aeronautics and Space Administration. Lewis Research Center, Cleveland, OH.
ATOMIC OXYGEN INTERACTIONS WITH PROTECTED ORGANIC MATERIALS ON THE LONG DURATION EXPOSURE FACILITY (LDEF) **c23**
Bruce A. Banks, Kim K. deGroh, Justine L. Bucholz (Ohio Aerospace Inst., Brook Park, OH.), and Michael R. Cales (Cleveland State Univ., OH.) *In* NASA. Langley Research Center, LDEF: 69 Months in Space. Third Post-Retrieval Symposium, Part 2 Feb. 1995 p 737-753 (For primary document see N95-23896 07-99)
Avail: CASI HC A03/MF A03

The Long Duration Exposure Facility (LDEF) has provided an excellent opportunity to understand the nature of directed atomic oxygen interactions with protected polymers and composites. Although there were relatively few samples of materials with protective coatings on their external surfaces on LDEF which were exposed to a high atomic oxygen fluence, analysis of such samples has enabled an examination of the shape of atomic oxygen undercut cavities at defect sites in the protective coatings. Samples of front-surface aluminized (Kapton) polyimide were inspected by scanning electron microscopy to identify and measure crack defects in the aluminum protective coatings. After chemical removal of the aluminum coating, measurements were also made of the width of the oxidized undercut cavities below the crack defects. The LDEF flight undercut cavity geometries were then compared with Monte Carlo computational model undercut cavity predictions. The comparison of the LDEF results and computational modeling indicates agreement in specific undercut cavity geometries for atomic oxygen

reaction probabilities dependent upon the 0.68 to 3.0 power of the energy. However, no single energy dependency was adequate to replicate flight results over a variety of aluminum crack widths. Author

N95-23910*# National Aeronautics and Space Administration. Marshall Space Flight Center, Huntsville, AL.

TREND ANALYSIS OF IN-SITU SPECTRAL REFLECTANCE DATA FROM THE THERMAL CONTROL SURFACES EXPERIMENT (TCSE) **c24**

Donald R. Wilkes (AZ Technology, Huntsville, AL.), P. S. LeMaster (AZ Technology, Huntsville, AL.), Richard J. Mell (AZ Technology, Huntsville, AL.), Edgar R. Miller (AZ Technology, Huntsville, AL.), and James M. Zwiener *In* NASA. Langley Research Center, LDEF: 69 Months in Space. Third Post-Retrieval Symposium, Part 2 Feb. 1995 p 755-769 (For primary document see N95-23896 07-99)

Avail: CASI HC A03/MF A03

The Thermal Control Surfaces Experiment (TCSE) on the LDEF was a comprehensive experiment that combined in-space measurements with extensive pre- and post-flight analyses of thermal control surfaces to determine the effects of exposure to the low earth orbit (LEO) space environment. The TCSE is the first space experiment to directly measure in-situ total hemispherical reflectance of thermal control surfaces in the same way they are routinely measured in the laboratory. In-space optical measurements performed by the TCSE provide the unique opportunity for trend analysis of the performance of materials in the space environment. Such trend analysis of flight data offers the potential to develop an empirical life time prediction model for several thermal control surfaces. For material research, trend analysis of the TCSE flight data, particularly the spectral data, can provide insight into the damage mechanisms of space exposure. Trend analysis for the TCSE samples has been limited to those materials that were not significantly eroded by the atomic oxygen (AO) environment. The performance of several materials on the LDEF mission was dominated by AO effects. Trend analysis was performed on both the detailed spectral reflectance measurements (in-space, pre-flight, and post-flight) and on the integrated solar absorptance. Results of this analysis for the five selected TCSE materials are presented along with the spectral flight data. Possible degradation and effects mechanisms will be discussed to better understand and predict the behavior of these materials in the LEO space environment. Author

N95-23911*# National Aeronautics and Space Administration. Marshall Space Flight Center, Huntsville, AL.

WHISKER/CONE GROWTH ON THE THERMAL CONTROL SURFACES EXPERIMENT NO. S0069 **c27**

James M. Zwiener, James E. Coston, Jr., Edgar R. Miller (AZ Technology, Huntsville, AL.), Richard J. Mell (AZ Technology, Huntsville, AL.), and Donald R. Wilkes (AZ Technology, Huntsville, AL.) *In* NASA. Langley Research Center, LDEF: 69 Months in Space. Third Post-Retrieval Symposium, Part 2 Feb. 1995 p 771-790 (For primary document see N95-23896 07-99)

Avail: CASI HC A03/MF A03

An unusual surface 'growth' was found during scanning electron microscope (SEM) investigations of the Thermal Control Surface Experiment (TCSE) S0069 front thermal cover. This 'growth' is similar to the cone type whisker growth phenomena as studied by G. K. Wehner beginning in the 1960's. Extensive analysis has identified the most probable composition of the whiskers to be a silicate type glass. Sources of the growth material are outgassing products from the experiment and orbital atomic oxygen, which occurs naturally at the orbital altitudes of the LDEF mission in the form of neutral atomic oxygen. The highly ordered symmetry and directionality of the whiskers are attributed to the long term (5.8 year) stable flight orientation of the LDEF. Author

N95-23912*# National Aeronautics and Space Administration. Marshall Space Flight Center, Huntsville, AL.

DURABILITY OF REFLECTOR MATERIALS IN THE SPACE ENVIRONMENT **c27**

Ann F. Whitaker, Miria M. Finckenor, David Edwards, Rachel R. Kamenetzky, and Roger C. Linton *In* NASA. Langley Research Center, LDEF: 69 Months in Space. Third Post-Retrieval Symposium, Part 2 Feb. 1995 p 791-802 (For primary document see N95-23896 07-99)

Avail: CASI HC A03/MF A03

Various reflector configurations were flown as part of the Long Duration Exposure Facility (LDEF) A0171 experiment. These reflectors consisted of nickel substrates with aluminum, enhanced aluminum (multiple layers of aluminum and silver), silver, and silver alloy coatings with glassy ceramic overcoatings. These samples have been evaluated for changes in reflectance due to 5.8 years in the space environment. The reflector materials have also been evaluated using angstrometer, Rutherford backscattering (RBS), and electron spectroscopy for chemical analysis (ESCA) techniques. Author

N95-23913*# National Aeronautics and Space Administration. Goddard Space Flight Center, Greenbelt, MD.

FOUR SPACE APPLICATION MATERIAL COATINGS ON THE LONG-DURATION EXPOSURE FACILITY (LDEF) **c27**

John J. Scialdone and Carroll Clatterbuck *In* NASA. Langley Research Center, LDEF: 69 Months in Space. Third Post-Retrieval Symposium, Part 2 Feb. 1995 p 803-823 (For primary document see N95-23896 07-99)

Avail: CASI HC A03/MF A03

Four material coatings of different thicknesses were flown on the LDEF to determine their ability to perform in the harsh space environment. The coatings, located in the ram direction of the spacecraft, were exposed for 10 months to the low-Earth orbit (LEO) environments experienced by the LDEF at an orbit of 260 nautical miles. They consisted of indium oxide (In2O3), silicon oxide (SiO(x)), clear RTV silicone, and silicone with silicate-treated zinc oxide (ZnO). These coatings were flown to assess their behavior when exposed to atomic oxygen and to confirm their good radiative properties, stability, electrical conductivity, and resistance to UV exposure. The flown samples were checked and compared with the reference unflown samples using high-magnification optical inspection, ESCA analysis, weight changes, and dimensional changes. These comparisons indicated the following. The 1000 A SiO(x) coating eroded uniformly, with minor changes in its radiative properties. The 100 A In2O3 coating eroded completely down to the Kapton backing, with resultant losses of reflectance. The RTV-615 showed erosion, with carbon (C) content losses, while the Si remained constant, with a doubling of the oxygen (O) concentration. The RTV-615 silicone with K2SiO3-treated ZnO changed from flat to glossy white in appearance. It lost C, was etched, and increased its O content. The upper layers showed no remaining Zn or K. Losses of reflectance occurred within certain wavelength bands. It was not possible to evaluate the experimental oxygen reaction rate using the calculated atomic oxygen fluence of 2.6 x 10(exp 20) atoms/cm(exp 2) for the exposure of these coatings during the flight. The bakeout of the coatings was not carried out prior to the flight. Hence, the coating weight and dimensional losses included losses by outgassing products. Author

N95-23914*# Boeing Defense and Space Group, Seattle, WA.

ORGANIC MATRIX COMPOSITE PROTECTIVE COATINGS FOR SPACE APPLICATIONS **c23**

Harry W. Dursch and Pete George *In* NASA. Langley Research Center, LDEF: 69 Months in Space. Third Post-Retrieval Symposium, Part 2 Feb. 1995 p 825-842 (For primary document see N95-23896 07-99)

(Contract NAS1-19427)

Avail: CASI HC A03/MF A03

Successful use of composites in low earth orbit (LEO) depends on their ability to survive long-term exposure to atomic oxygen (AO), ultraviolet radiation, charged particle radiation, thermal cycling, and micrometeoroid and space debris. The AO environment is especially severe for unprotected organic matrix composites surfaces in LEO. Ram facing unprotected graphite/epoxy flown on the 69-month Long Duration Exposure Facility (LDEF) mission lost up to one ply of thickness (5 mils) resulting in decreased mechanical properties. The expected AO fluence of the 30 year Space Station Alpha mission is approximately 20 times that seen on LDEF. This exposure would result in significant material loss of unprotected ram facing organic matrix composites. Several protective coatings for composites were flown on LDEF including anodized aluminum, vacuum deposited coatings, a variety of thermal control coatings, metalized Teflon, and leafing aluminum. Results from the testing and analysis of the coated and uncoated composite specimens flown on LDEF's leading and trailing edges provide the baseline for determining the effectiveness of protectively coated composites in LEO. In addition to LDEF results, results from shuttle flight experiments and ground based testing will be discussed. Author

N95-23915*# Altai State Univ., Barnaul (USSR).
STRUCTURE AND PROPERTIES OF POLYMERIC COMPOSITE MATERIALS DURING 1501 DAYS OUTER SPACE EXPOSURE AT SALYUT-7 ORBITAL STATION **c27**
Oleg V. Startsev and Eugene F. Nikishin (Salyut Design Office 18, Moscow, Russia.) *In* NASA. Langley Research Center, LDEF: 69 Months in Space. Third Post-Retrieval Symposium, Part 2 Feb. 1995 p 843-857 (For primary document see N95-23896 07-99)
Avail: CASI HC A03/MF A03

Specimens of polymeric composite materials for aviation and space applications such as glass fiber reinforced plastics (GFRP), carbon fiber reinforced plastics (CFRP), organic fiber reinforced plastics (OFRP), and hybrid plastics (HP) based on epoxy compounds were exposed to the space environment on the surface of Salyut-7 orbital station. The space exposure lasted 1501 days as a maximum. The data relating to the change in mechanical properties, mass losses, glass transition temperature, linear thermal expansion coefficient, and microstructure after various periods of exposure are given. It has been found that the change in properties is caused by the processes of binder postcuring and microerosion of the exposed surface of plastics. The phenomenon of strengthening of the surface layer of hybrid composites, due to which the nature of destruction changes at bending loads, has been revealed. Author

N95-23916*# National Aeronautics and Space Administration. Langley Research Center, Hampton, VA.
OVERVIEW OF THE LDEF MSIG DATABASING ACTIVITIES **c82**
Joan G. Funk *In its* LDEF: 69 Months in Space. Third Post-Retrieval Symposium, Part 2 Feb. 1995 p 859-865 (For primary document see N95-23896 07-99)
(Contract NAS1-19247)
Avail: CASI HC A02/MF A03

The Long Duration Exposure Facility (LDEF) and the accompanying experiments were composed of and contained a wide variety of materials, representing the largest collection of materials flown in low earth orbit (LEO) and retrieved for ground-based analysis to date. The results and implications of the mechanical, thermal, optical, and electrical data from these materials are the foundation on which future LEO spacecraft and missions will be built. The LDEF Materials Special Investigation Group (MSIG) has been charged with establishing and developing databases to document these materials and their performance to assure not only that the data are archived for future generations but also that the data are available to the spacecraft user community in an easily accessed, user-friendly form. This paper gives an overview of the current LDEF Materials Databases, their capabilities, and availability. An overview of the philosophy and format of a developing handbook on LEO effects on materials is also described. Author

N95-24080# General Accounting Office, Washington, DC. National Security and International Affairs Div.
BALLISTIC MISSILE DEFENSE: CURRENT STATUS OF STRATEGIC TARGET SYSTEM. REPORT TO CONGRESSIONAL REQUESTERS
Mar. 1995 18 p
(GAO/NSIAD-95-78; B-259821) Avail: CASI HC A03/MF A01; GAO, PO Box 6015, Gaithersburg, MD 20884-6015 HC

This GAO (Government Accounting Office) investigative report presents information on the Ballistic Missile Defense Organization's (BMDO) Strategic Target System (STARS). Specifically, the information contained in this report concerns: (1) the status of the STARS program, (2) the planned launches through fiscal year 2000, (3) the program costs, and (4) the status of major hardware acquisition and refurbishment. Derived from text

N95-24178# Department of Defense, Washington, DC. Defense Research and Engineering.
DEFENSE TECHNOLOGY PLAN
Sep. 1994 191 p
(AD-A285415) Avail: CASI HC A09/MF A02

This technology plan is a compilation of individual plans each covering one of the 19 technology areas comprising everything but basic research that collectively describe the total Department of Defense Science and Technology effort. The primary purpose of this plan is to document the objectives that we are trying to achieve and the science and technology efforts that are being pursued in order to reach these objectives. The plan also identifies the funding that has been allocated for these objectives and the timeframes in which these technologies will be available to be transitioned to new warfighting capabilities. The 19 technology area plans cover: aerospace propulsion and power; air and space vehicles; battlespace environments; biomedicine; chemical and biological defense; clothing, textiles, and food; command, control, and communications (C3); computing and software; conventional weapons; electronics; electronic warfare and directed energy weapons; environmental quality and civil engineering; human systems interface; manpower, personnel, and training; materials, processes, and structures; sensors; ships/watercraft and ground vehicles; manufacturing science and technology; and modeling and simulation. CASI

N95-24179# Department of Defense, Washington, DC. Defense Research and Engineering.
DEFENSE SCIENCE AND TECHNOLOGY STRATEGY
Sep. 1994 38 p
(AD-A285414) Avail: CASI HC A03/MF A01

The methods of the Department of Defense for managing science and technology in order to ensure the technological superiority of U.S. military forces is described. The following topics are addressed: the overall vision, the science and technology contribution to military capability needs, strategic investment priorities, the science and technology program, and guiding principles for science and technology management. These guiding principles include transitioning technology to address warfighting needs, reducing cost, strengthening the commercial-military industrial base, promoting basic research, and assuring quality. CASI

Typical Subject Index Listing

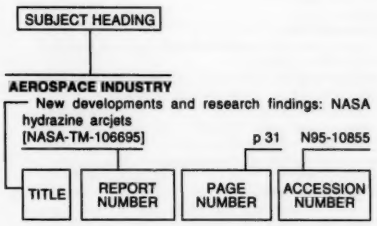

The subject heading is a key to the subject content of the document. Titles, report numbers, and accession numbers of pertinent documents are provided under each subject heading. When the title is insufficiently descriptive of the document content, a title extension is added, separated from the title by three hyphens. The report number helps to indicate the type of document cited (e.g., NASA report, NASA translation, NASA contractor report). The accession number is the number by which the document abstracts are arranged in this journal and by which the document is sold or requested. The page number helps you locate the citation in the abstract section. The titles, with title extensions if present, are arranged under each subject heading in ascending accession number order. The subject headings have been selected from the latest revision of the *NASA Thesaurus*.

A

ABEL FUNCTION
Weyl connection and non-Abelian gauge field
|DE94-635440| p 1851 N95-23969

ABIOGENESIS
Revitalization of the Gemenc-area, Baja, Hungary. 1: A study on hydrological possibilities to revitalise the ecosystem in the Keselyues-area. 2: Towards the restoration of the Gyueruesalj floodplain
|PB95-139283| p 1718 N95-23469

ABSORPTION CROSS SECTIONS
Comparison of exact solution with Eikonal approximation for elastic heavy ion scattering
|NASA-TP-3498| p 1817 N95-22929
Simulation of absorption edge densitometry
|DE95-004393| p 1635 N95-23360

ABSORPTION SPECTRA
Simulation of absorption edge densitometry
|DE95-004393| p 1635 N95-23360
Statistical properties of the time histories of cosmic gamma-ray bursts detected by the BATSE experiment of the Compton gamma-ray observatory
|NASA-CR-197425| p 1871 N95-23546
Mapping of the Ronda peridotite massif (Spain) from AVIRIS spectro-imaging survey: A first attempt p 1707 N95-23878
Spectral variations in a collection of AVIRIS imagery p 1707 N95-23879
Monitoring land use and degradation using satellite and airborne data p 1707 N95-23880
Optimal band selection for dimensionality reduction of hyperspectral imagery p 1709 N95-23887
Investigations on the 1.7 micron residual absorption feature in the vegetation reflection spectrum p 1710 N95-23891
Lattice relaxation study on self-trapped exciton and biexciton in neutral and charged fullerenes
|DE94-635788| p 1844 N95-23986

ABSORPTION SPECTROSCOPY
Solvation of isolated transition metal ions
|DE95-002978| p 1638 N95-22571
Ligand K-edge x-ray adsorption spectroscopic studies of the electronic structure of inorganic model complexes and metalloprotein active sites
|DE95-003338| p 1840 N95-22851

ABSORPTIVITY
Optical absorption in an indirect-gap semiconductor quantum well systems
|DE94-628878| p 1849 N95-22759
Two-photon absorption in an indirect-gap semiconductor quantum well systems 1. Interband transitions
|DE94-628879| p 1849 N95-22760
Two-photon absorption in an indirect-gap semiconductor quantum well systems 2. Excitonic transitions
|DE94-628880| p 1849 N95-22761
Transient radiation-induced absorption in materials for the DOI laser
|DE95-004549| p 1828 N95-24161

ABSTRACTS
Plinius intermediate report
|PB95-135216| p 1648 N95-23128

ABUNDANCE
Krypton isotope analysis using near-resonant stimulated Raman spectroscopy
|DE95-005061| p 1635 N95-23348
Temporal changes in endmember abundances, liquid water and water vapor over vegetation at Jasper Ridge p 1708 N95-23882

ACCELERATED LIFE TESTS
Advanced development of PV encapsulants
|DE95-000246| p 1728 N95-23062
Interlaminar shear test method development for long term durability testing of composites p 1631 N95-23300
Exfoliation corrosion and stress corrosion cracking behaviour of Al-Li alloys p 1641 N95-23498
Specific features of corrosion behavior of stainless maraging steels for aerospace application p 1642 N95-23501
Eddy current detection of pitting corrosion around fastener holes p 1643 N95-23507
Test method and test results for environmental assessment of aircraft materials p 1643 N95-23509

ACCELERATION (PHYSICS)
Quick look report of acceleration measurements on Mir Space Station during Mir-16
|NASA-TM-106835| p 1621 N95-22667
Summary of OARE flight calibration measurements
|NASA-TM-109159| p 1688 N95-23012
New pellet production and acceleration technologies for high speed pellet injection system HIPEL in Large Helical Device
|NISF-326| p 1835 N95-23566

ACCELEROMETERS
Quick look report of acceleration measurements on Mir Space Station during Mir-16
|NASA-TM-106835| p 1621 N95-22667
Summary of OARE flight calibration measurements
|NASA-TM-109159| p 1688 N95-23012
Material characterization system
|AD-D016536| p 1800 N95-23073
USML-1 microgravity glovebox experiment no. 1 Passive Accelerometer System
|NASA-CR-196575| p 1653 N95-23552

ACCEPTABILITY
Accepting the T3D
|DE95-000924| p 1762 N95-22679

ACCESS CONTROL
Modelling and analysis of a high speed data bus with predicate/transition nets
|PB95-140695| p 1764 N95-23538

ACCESS TIME
Improved small satellite access of the space network
|NASA-CR-197863| p 1657 N95-22944

ACCIDENT PREVENTION
Mishap risk control for advanced aerospace/composite materials p 1628 N95-23031

ACCOMMODATION COEFFICIENT
Calculation of satellite drag coefficients
|AD-A285118| p 1622 N95-23781

ACCOUNTING
DOD budget: Selected categories of planned funding for fiscal years 1995-99. Report to Congressional requesters
|GAO/NSIAD-95-92| p 1864 N95-24062

ACCRETION DISKS
Observational studies of the clearing phase in proto-planetary disk systems
|NASA-CR-197900| p 1866 N95-23561

ACCURACY
On the accuracy of CFD-based pressure drop predictions for right-angle ducts p 1682 N95-23634
CFD modeling of turbulent duct flows for coolant channel analysis p 1682 N95-23635

ACETATES
Transmethylation reactions during methanogenesis from acetate in Methanosarcina barkeri
|DE94-016222| p 1745 N95-22873
Advanced development of PV encapsulants
|DE95-000246| p 1728 N95-23062

ACETYLENE
Ethylene oxidation chemistry in a well-stirred reactor
|DE95-004823| p 1635 N95-23381

ACOUSTIC ATTENUATION
Theoretical estimates of high frequency acoustic attenuation and backscattering from suspended sand particles in the ocean and in an estuary
|DSTO-TR-0078| p 1743 N95-23667

ACOUSTIC FREQUENCIES
Capacitive acoustic wave detector and method of using same
|NASA-CASE-LAR-13890-1| p 1799 N95-22921
The sound insulations of studio doors. Part 2: Door seals
|BBC-RD-1994/15| p 1654 N95-24045

ACOUSTIC INSTABILITY
The sound insulations of studio doors. Part 1: Door blanks
|BBC-RD-1994/14| p 1654 N95-24093

ACOUSTIC MEASUREMENT
The sound insulations of studio doors. Part 1: Door blanks
|BBC-RD-1994/14| p 1654 N95-24093

ACOUSTIC PROPAGATION
Capacitive acoustic wave detector and method of using same
|NASA-CASE-LAR-13890-1| p 1799 N95-22921

ACOUSTIC SCATTERING
Theoretical estimates of high frequency acoustic attenuation and backscattering from suspended sand particles in the ocean and in an estuary
|DSTO-TR-0078| p 1743 N95-23667

ACOUSTICS
Dynamic response of a transducer mounted at one end of an acoustical cavity which is subjected to a specified pressure at the open end of the cavity
|DE95-004192| p 1799 N95-23379

ACOUSTO-OPTICS
Programmable hyperspectral image mapper with on-array processing
|NASA-CASE-NPO-17794-1-CU| p 1819 N95-22765
Field observations using an AOTF polarimetric imaging spectrometer p 1702 N95-23850

ACTINIDE SERIES
EXTRA.M: A computing code system for analysis of the Purex process with mixer settlers for reprocessing
|DE94-785273| p 1635 N95-23476

ACTIVATION (BIOLOGY)
Activation of the jun-D gene in human myeloid cells by 1-(beta)-D-arabinofuranosylcytosine
|DE94-016591| p 1746 N95-22912

ACTIVATION ANALYSIS
Investigation of mechanical properties and their relation to the internal structure of nanocrystalline metals and composites
|DE95-001151| p 1627 N95-22683

ACTIVATION ENERGY
Thermal activation of steady-state creep in polycrystalline copper
|DE94-627394| p 1839 N95-22607

ACTIVE CONTROL
Segregated rigid and structural control for a photolithography positioning system
|DE95-002603| p 1766 N95-23134
Active control of panel vibrations induced by a boundary layer flow
|NASA-CR-197867| p 1608 N95-23182
On-line, adaptive state estimator for active noise control p 1784 N95-23308
Supersonic laminar flow control research
|NASA-CR-197938| p 1609 N95-23669
Active vision in satellite scene analysis p 1778 N95-23738

ACTIVITY (BIOLOGY)
Neurodynamic oscillators p 1749 N95-22987

ACTIVITY CYCLES (BIOLOGY)
The 1993 Gordon Research Conference on Chronobiology
|NASA-CR-197990| p 1748 N95-24047

ACTS
Design and implementation of an experiment scheduling system for the ACTS satellite p 1620 N95-23756

ACTUATORS
High gain GaAs photoconductive semiconductor switches: Measurement of filament velocity and reduced trigger energy
|DE95-001884| p 1661 N95-22844
Environmental Systems Management Analysis and Reporting Network (E-SMART)
|AD-A279766| p 1732 N95-22856
Superconductivity devices: Commercial use of space
|NASA-CR-197885| p 1648 N95-22883
Design and application of electromechanical actuators for deep space missions
|NASA-CR-197957| p 1694 N95-22909
A microcontroller-based three degree-of-freedom manipulator testbed
|NASA-CR-197423| p 1696 N95-23409
Motor drive technologies for the power-by-wire (PBW) program: Options, trends and tradeoffs
|NASA-TM-106885| p 1616 N95-23671

ADA (PROGRAMMING LANGUAGE)
Comparing data synchronization in Ada 9X and Orca
|PB95-127999| p 1754 N95-22529

ADAPTIVE CONTROL
Investigation of Federal Standard 1045 high-frequency ALE radio performance in the Southern Trans-Auroral Zone
|PB94-204831| p 1655 N95-22636
Direct adaptive performance optimization of subsonic transports: A periodic perturbation technique
|NASA-TM-4676| p 1612 N95-22829
Adaptive control of linear systems based on approximate models
|PB95-139333| p 1767 N95-23199
Computational control of flexible aerospace systems
|NASA-CR-197902| p 1621 N95-23260

ADAPTIVE FILTERS
Maximum-likelihood spectral estimation and adaptive filtering techniques with application to airborne Doppler weather radar
|NASA-CR-197699| p 1658 N95-23670

ADDITIVES
Process for preparing an assembly of an article and a polyimide which resists dimensional change, delamination and debonding when exposed to changes in temperature
|NASA-CASE-LAR-14538-2| p 1649 N95-23254
Carbon doping of III-V compound semiconductors
|DE95-003431| p 1844 N95-24013

ADENOSINE TRIPHOSPHATE
Computational Fluid Dynamics (CFD) analyses in support of Space Shuttle Main Engine (SSME) heat exchanger (HX) vane cracking investigation p 1679 N95-23619

ADHESION TESTS
Corrosion protection measures for CFC/metal joints of fuel integral tank structures of advanced military aircraft p 1644 N95-23510

ADHESIVE BONDING
Permeability testing of composite material and adhesive bonds for the DC-XA composite feedline program
|NASA-TM-108483| p 1630 N95-23551

ADHESIVES
Evaluation of adhesive materials used on the Long Duration Exposure Facility
|NASA-CR-4646| p 1626 N95-22918
A kinetic study of hydrolysis of polyester elastomer in magnetic tape p 1652 N95-24124

ADIABATIC EQUATIONS
Berry phase by description of the quantum systems in the Kustaanheimo-Stiefel bundle
|DE94-628410| p 1847 N95-22620

ADSORPTION
Hydrogen vibrational density of states of adsorbed water on rare-earth modified zirconia
|DE95-001127| p 1632 N95-22681
Reflectivity studies on adsorbed block copolymers under shear
|DE95-003676| p 1649 N95-23568

ADVANCED SOLID ROCKET MOTOR (STS)
ASRM multi-port igniter flow field analysis p 1683 N95-23639
A fine-grid model for the ASRM aft segment with gimballed nozzle p 1685 N95-23648
Application of CFD analysis to design support and problem resolution for ASRM and RSRM p 1685 N95-23649

ADVANCED VERY HIGH RESOLUTION RADIOMETER
Improved AVHRR data navigation using automated land feature recognition to correct a satellite orbital model
|CSIRO-TR-34| p 1718 N95-24026
Determining coniferous forest cover and forest fragmentation with NOAA-9 advanced very high resolution radiometer data p 1720 N95-24103
Land surface temperature measurements from EOS MODIS data
|NASA-CR-197969| p 1721 N95-24190

ADVECTION
Unification of some advection schemes in two dimensions
|NASA-CR-195044| p 1790 N95-23465

AERIAL PHOTOGRAPHY
A multispectral scanner survey of the Tonopah Test Range, Nevada. Date of survey: August 1993
|DE95-003920| p 1717 N95-22503
Locating buildings in aerial photos p 1721 N95-23295

AERIAL RECONNAISSANCE
Annual tropical cyclone report, 1993
|AD-A285097| p 1742 N95-23255
Remote sensing of smoke, clouds, and fire using AVIRIS data p 1704 N95-23860
Application of MAC-Europe AVIRIS data to the analysis of various alteration stages in the Landdmannalauger Hydrothermal Area (South Iceland) p 1709 N95-23885

AEROACOUSTICS
Supersonic jet noise reductions predicted with increased jet spreading rate
|NASA-TM-106872| p 1800 N95-23178
Aeroacoustic computation of gust-blade interaction p 1800 N95-23313
Benchmark problems in computational aeroacoustics p 1800 N95-23315
Institute for Computational Mechanics in Propulsion (ICOMP)
|NASA-TM-106884| p 1677 N95-23464

AERODYNAMIC BALANCE
System for determining aerodynamic imbalance
|NASA-CASE-ARC-11913-1| p 1688 N95-23377

AERODYNAMIC CHARACTERISTICS
Thin tailored composite wing for civil tiltrotor p 1613 N95-23317
Aerodynamic flight control to increase payload capability of future launch vehicles
|NASA-CR-197704| p 1619 N95-24032

AERODYNAMIC COEFFICIENTS
Calculation of satellite drag coefficients
|AD-A285118| p 1622 N95-23781

AERODYNAMIC CONFIGURATIONS
Impeller flow field characterization with a laser two-focus velocimeter p 1675 N95-23440

AERODYNAMIC DRAG
Calculation of satellite drag coefficients
|AD-A285118| p 1622 N95-23781

AERODYNAMIC HEAT TRANSFER
Numerical computation of aerodynamics and heat transfer in a turbine cascade and a turn-around duct using advanced turbulence models p 1675 N95-23444

AERODYNAMIC INTERFERENCE
A wall interference assessment/correction system
|NASA-CR-197421| p 1667 N95-23183

AERODYNAMIC LOADS
System for determining aerodynamic imbalance
|NASA-CASE-ARC-11913-1| p 1688 N95-23377
Review of some results of the author's fatigue investigations with applications in engineering and material science
|TAE-698| p 1699 N95-23662

AERODYNAMIC NOISE
Supersonic jet noise reductions predicted with increased jet spreading rate
|NASA-TM-106872| p 1800 N95-23178

AERODYNAMICS
Mach 10 computational study of a three-dimensional scramjet inlet flow field
|NASA-TM-4602| p 1667 N95-23210
Aerodynamic design optimization with sensitivity analysis and computational fluid dynamics
|NASA-CR-197419| p 1608 N95-23218
A hybrid vehicle evaluation code and its application to vehicle design
|DE95-004205| p 1662 N95-23334
Aerodynamic surface distension system for high angle of attack forebody vortex control
|NASA-CASE-ARC-11979-1| p 1612 N95-23390
Aerodynamic design and analysis of a highly loaded turbine exhaust p 1673 N95-23435
Numerical computation of aerodynamics and heat transfer in a turbine cascade and a turn-around duct using advanced turbulence models p 1675 N95-23444
NTS-spill test facility wind tunnel exhaust plume characterization
|DE95-003630| p 1616 N95-24019

AEROELASTICITY
High-performance parallel analysis of coupled problems for aircraft propulsion
|NASA-CR-197440| p 1614 N95-23088
Flutter analysis of composite box beams
|NASA-CR-197931| p 1615 N95-23392
User's guide for ECAP2D: An Euler unsteady aerodynamic and aeroelastic analysis program for two dimensional oscillating cascades, version 1.0
|NASA-CR-189146| p 1699 N95-24189

AERONAUTICAL ENGINEERING
Research and Technology, 1994
|NASA-TM-106764| p 1607 N95-24025

AEROSOLS
Ocean observations with EOS/MODIS: Algorithm development and post launch studies
|NASA-CR-197402| p 1717 N95-22916
Modeling aerosol emissions from the combustion of composite materials p 1629 N95-23038
Ocean observations with EOS/MODIS: Algorithm development and post launch studies
|NASA-CR-197894| p 1718 N95-23473
Estimation of aerosol optical depth and additional atmospheric parameters for the calculation of apparent reflectance from radiance measured by the Airborne Visible/Infrared Imaging Spectrometer p 1704 N95-23863
Assessing the relative contribution of biogenic and fossil processes to visibility scattering aerosols found in remote areas: Near-term Organic Research Program
|DE95-003149| p 1735 N95-24146
Laboratory studies of the sensitivity of tropospheric ozone to the chemistry of sea salt aerosol
|DE95-003607| p 1735 N95-24147

AEROSPACE ENGINEERING
FY 1994 scientific and technical reports, articles, papers, and presentations
|NASA-TM-108480| p 1856 N95-23225
Third International Symposium on Artificial Intelligence, Robotics, and Automation for Space 1994
|NASA-CR-197340| p 1767 N95-23672
An expert system for diagnosing anomalies of spacecraft p 1770 N95-23684
Research and Technology, 1994
|NASA-TM-106764| p 1607 N95-24025

AEROSPACE ENVIRONMENTS
Low Earth orbit thermal control coatings exposure flight tests: A comparison of U.S. and Russian results
|NASA-CR-4647| p 1626 N95-22919
LDEF materials results for spacecraft applications: Executive summary
|NASA-CP-3261| p 1617 N95-23549
LDEF: 69 Months in Space. Third Post-Retrieval Symposium, part 1
|NASA-CP-3275-PT-1| p 1889 N95-23796
LDEF environment modeling updates p 1637 N95-23797
EURECA 11 months in orbit: Initial post flight investigation results p 1623 N95-23799
Effect of the space environment on materials flown on the EURECA/TICCE-HVI experiment p 1623 N95-23803

AEROSPACE INDUSTRY
Environmental, Safety, and Health Considerations: Composite Materials in the Aerospace Industry
|NASA-CP-3289| p 1628 N95-23025
Stochastic decision analysis p 1854 N95-23305
A format for the interchange of scheduling models p 1780 N95-23747
Vaccum Gas Tungsten Arc Welding, phase 1
|NASA-CR-197979| p 1696 N95-24064

AEROSPACE MEDICINE
Rearrangement of RAG-1 recombinase gene in radiation-sensitive wasted mice
|DE94-017083| p 1746 N95-22913
All systems go!
|NASA-TM-110542| p 1620 N95-23665

AEROSPACE PLANES
A summary of the slush hydrogen technology program for the National Aero-Space Plane
|NASA-TM-106863| p 1653 N95-24186
AEROSPACE SCIENCES
Director's discretionary fund report for fiscal year 1994
|NASA-TM-108848| p 1872 N95-22920
FY 1994 scientific and technical reports, articles, papers, and presentations
|NASA-TM-108480| p 1856 N95-23225
Design and implementation of two two-week Teacher Enhancement Institutes p 1853 N95-23306
Using high-performance networks to enable computational aerosciences applications
|NASA-CR-197951| p 1764 N95-24023
AEROSPACE SYSTEMS
Human-centered design of human-computer-human dialogs in aerospace systems
|NASA-CR-197379| p 1750 N95-22797
Computational control of flexible aerospace systems
|NASA-CR-197902| p 1621 N95-23260
Integrating O/S models during conceptual design, part 1
|NASA-CR-197903| p 1622 N95-23398
Integrating O/S models during conceptual design, part 2
|NASA-CR-197904| p 1622 N95-23399
AEROSPACE TECHNOLOGY TRANSFER
NASA Technology Applications Team: Commercial applications of aerospace technology
|NASA-CR-197589| p 1864 N95-22526
NASA Technology Applications Team: Commercial applications of aerospace technology
|NASA-CR-197870| p 1865 N95-23091
Design and implementation of two two-week Teacher Enhancement Institutes p 1853 N95-23306
Endeavor: Now and then
|NASA-TM-110539| p 1620 N95-23664
The next decade of space robotics p 1768 N95-23673
Commercialization of JPL Virtual Reality calibration and redundant manipulator control technologies p 1768 N95-23676
An intelligent ground operator support system p 1769 N95-23681
Distributed intelligence for ground/space systems p 1770 N95-23685
Overview of the LDEF MSIG databasing activities p 1864 N95-23916
AEROSPACE VEHICLES
Associated with aerospace vehicles development of methodologies for the estimation of thermal properties p 1700 N95-23321
Moving mass trim control for aerospace vehicles
|DE95-002602| p 1622 N95-23532
AEROTHERMOCHEMISTRY
Preconditioning for the Navier-Stokes equations with finite-rate chemistry p 1670 N95-23421
AFTERBODIES
Experimental results for a hypersonic nozzle/afterbody flow field
|NASA-TM-4638| p 1609 N95-23250
Validation of a Computational Fluid Dynamics (CFD) code for supersonic axisymmetric base flow p 1686 N95-23652
AGE FACTOR
Some performance effects of age and low blood alcohol levels on a computerized neuropsychological test
|DOT/FAA/AM-95/7| p 1749 N95-23788
Effects of age and low doses of alcohol on compensatory tracking during angular acceleration
|DOT/FAA/AM-95/3| p 1750 N95-23934
AGGREGATES
Effect of critical field on screened dielectric breakdown growth
|DE94-628482| p 1661 N95-23046
Effects of long-range coupling on aggregation
|DE94-628483| p 1842 N95-23047
Small angle x ray scattering studies of aggregation in supercritical fluid solutions
|DE95-004576| p 1843 N95-23579
AGING (MATERIALS)
Decomposition mechanisms in thermally-aged thin-film explosives
|DE95-000741| p 1652 N95-22838
Advanced development of PV encapsulants
|DE95-000246| p 1728 N95-23062
Long-term aging of type 308 stainless steel welds: Effects on properties and microstructure
|DE94-018961| p 1640 N95-23132
Effect of loading direction and long-term aging on fatigue-crack growth in Al-Li alloy 2090 p 1641 N95-23499
Problems of predicting material property retention during long term service p 1644 N95-23514
Oklahoma City air logistics center (USAF) aging aircraft corrosion program p 1607 N95-23519
AGING (METALLURGY)
Analysis of physiochemical processes during solder aging
|DE95-003811| p 1638 N95-22576
AGRICULTURE
The significance of hair mineral analysis as a means for assessing internal body burdens of environmental pollutants
|DE94-633512| p 1734 N95-23541
Monitoring land use and degradation using satellite and airborne data p 1707 N95-23880
MAX-91: Polarimetric SAR results on Montespertoli site p 1712 N95-23940
MAC Europe 1991 campaign: AIRSAR/AVIRIS data integration for agricultural test site classification p 1715 N95-23952
AIR
Krypton isotope analysis using near-resonant stimulated Raman spectroscopy
|DE95-005061| p 1635 N95-23348
Airborne rotary air separator study
|NASA-CR-189099| p 1614 N95-24053
Effects of jet strength on NOx formation in premixed impinging jet combustion with minimum heat losses
|NAL-TR-1237T| p 1637 N95-24181
AIR BREATHING ENGINES
Airborne rotary air separator study
|NASA-CR-189099| p 1614 N95-24053
AIR CONDITIONING
Load calculation and system evaluation for electric vehicle climate control
|DE95-004350| p 1695 N95-23358
AIR COOLING
Evaluation of thermal barrier and PS-200 self-lubricating coatings in an air-cooled rotary engine
|NASA-CR-195445| p 1614 N95-23222
AIR FILTERS
Applied research on air pollution using nuclear-related analytical techniques
|DE94-633513| p 1734 N95-23542
Extraction and detection of pesticide residues from air filter inserts using supercritical carbon dioxide
|DE95-004579| p 1735 N95-23580
Airborne rotary air separator study
|NASA-CR-189099| p 1614 N95-24053
AIR FLOW
CFD analysis of turbopump volutes p 1674 N95-23436
Phase 2: HGM air flow tests in support of HEX vane investigation p 1674 N95-23438
AIR INTAKES
Three-dimensional Navier-Stokes analysis and redesign of an imbedded bellmouth nozzle in a turbine cascade inlet section p 1671 N95-23423
AIR JETS
Reproducible direct exposure environmental testing of metal-based magnetic media p 1690 N95-24129
AIR LAND INTERACTIONS
HAPEX-Sahel: Basic description of methods and data sets
|PB95-127262| p 1701 N95-22639
AIR LAW
Oceanic operations: An authoritative guide to oceanic operations
|FAA-AFS-550| p 1610 N95-24065
AIR NAVIGATION
Cueing light configuration for aircraft navigation
|NASA-CASE-ARC-11982-1| p 1611 N95-23393
Oceanic operations: An authoritative guide to oceanic operations
|FAA-AFS-550| p 1610 N95-24065
AIR POLLUTION
Preliminary assessment of air toxic emissions in the natural gas industry, phase 1
|PB95-135547| p 1732 N95-22865
Oxidants and oxidation in the Earth's atmosphere
|NASA-CR-197945| p 1734 N95-23460
Review of research results for the photocatalytic oxidation of hazardous wastes in air
|DE95-004004| p 1734 N95-23480
Applied research on air pollution using nuclear-related analytical techniques
|DE94-633513| p 1734 N95-23542
Remote sensor test range update
|DE95-003629| p 1735 N95-24018
Reproducible direct exposure environmental testing of metal-based magnetic media p 1690 N95-24129
Assessing the relative contribution of biogenic and fossil processes to visibility scattering aerosols found in remote areas: Near-term Organic Research Program
|DE95-003149| p 1735 N95-24146
AIR PURIFICATION
Life support systems analysis and technical trades for a lunar outpost
|NASA-TM-109927| p 1751 N95-23194
AIR TRAFFIC CONTROL
The role of flight progress strips in en route air traffic control: A time-series analysis
|DOT/FAA/AM-95/4| p 1611 N95-23565
Functions of external cues in prospective memory
|DOT/FAA/AM-95/9| p 1750 N95-24088
AIR TRAFFIC CONTROLLERS (PERSONNEL)
The role of flight progress strips in en route air traffic control: A time-series analysis
|DOT/FAA/AM-95/4| p 1611 N95-23565
AIR TRANSPORTATION
Report of proceedings: Aviation Accident Investigation Symposium. Volume 2: Participant presentations
|PB94-917007| p 1610 N95-23598
Oceanic operations: An authoritative guide to oceanic operations
|FAA-AFS-550| p 1610 N95-24065
AIRBORNE EQUIPMENT
A multispectral scanner survey of the Tonopah Test Range, Nevada. Date of survey: August 1993
|DE95-003920| p 1717 N95-22503
Combining optical and microwave remote sensing data of forest vegetation: MAC Europe 1991
|PB95-127312| p 1717 N95-22538
Upgrade of the 92 GHz airborne multi-channel meteorological radiometer (AMMR)
|NASA-CR-197875| p 1742 N95-23208
Summaries of the 4th Annual JPL Airborne Geoscience Workshop. Volume 1: AVIRIS Workshop
|NASA-CR-197877-VOL-1| p 1701 N95-23844
Lithologic discrimination and alteration mapping from AVIRIS Data, Socorro, New Mexico p 1701 N95-23847
Automating spectral unmixing of AVIRIS data using convex geometry concepts p 1702 N95-23848
AVIRIS calibration using the cloud-shadow method p 1702 N95-23849
Instantaneous field of view and spatial sampling of the Airborne Visible/Infrared Imaging Spectrometer (AVIRIS) p 1702 N95-23851
Airborne Visible/Infrared Imaging Spectrometer (AVIRIS): Recent improvements to the sensor p 1690 N95-23852
Comparison of methods for calibrating AVIRIS data to ground reflectance p 1703 N95-23854
Discrimination of poorly exposed lithologies in AVIRIS data p 1703 N95-23858
Use of data from the AVIRIS onboard calibrator p 1704 N95-23861
Inflight calibration of AVIRIS in 1992 and 1993 p 1690 N95-23862
Estimation of aerosol optical depth and additional atmospheric parameters for the calculation of apparent reflectance from radiance measured by the Airborne Visible/Infrared Imaging Spectrometer p 1704 N95-23863
Use of the Airborne Visible/Infrared Imaging Spectrometer to calibrate the optical sensor on board the Japanese Earth Resources Satellite-1 p 1624 N95-23864
A role for AVIRIS in the Landsat and Advanced Land Remote Sensing Systems program p 1705 N95-23866
Classification of high dimensional multispectral image data p 1705 N95-23868
Simulation of landsat thematic mapper imagery using AVIRIS hyperspectral imagery p 1705 N95-23869
Summaries of the 4th Annual JPL Airborne Geoscience Workshop. Volume 3: AIRSAR Workshop
|NASA-CR-197354-VOL-3| p 1712 N95-23938
AIRBORNE RADAR
TOGA/COARE AMMR 1992 data processing
|NASA-CR-197289| p 1736 N95-22867
Summaries of the 4th Annual JPL Airborne Geoscience Workshop. Volume 3: AIRSAR Workshop
|NASA-CR-197354-VOL-3| p 1712 N95-23938
Interferometric synthetic aperture radar imagery of the Gulf Stream p 1712 N95-23939
MAX-91: Polarimetric SAR results on Montespertoli site p 1712 N95-23940
Glaciological studies in the central Andes using AIRSAR/TOPSAR p 1713 N95-23942
Comparison of inversion models using AIRSAR data for Death Valley, California p 1713 N95-23945
Geologic mapping using integrated AIRSAR, AVIRIS, and TIMS data p 1714 N95-23946
Unusual radar echoes from the Greenland ice sheet p 1714 N95-23951
An improved algorithm for retrieval of snow wetness using C-band AIRSAR p 1715 N95-23954
Relating P-band AIRSAR backscatter to forest stand parameters p 1716 N95-23959

AIRCRAFT ACCIDENT INVESTIGATION
Report of proceedings: Aviation Accident Investigation Symposium. Volume 2: Participant presentations
[PB94-917007] p 1610 N95-23598
Aircraft accident report. Runway overrun following rejected takeoff. Continental airlines flight 795, McDonnell Douglas MD-82, N18835, LaGuardia Airport, Flushing, NY, 2 March 1994
[PB95-910401] p 1610 N95-23609
Aviation Accident Investigation Symposium. Volume 1: Industry recommendations and Safety Board responses
[PB94-917005] p 1611 N95-24105
AIRCRAFT ACCIDENTS
Mishap risk control for advanced aerospace/composite materials p 1628 N95-23031
Aircraft accident report. Runway overrun following rejected takeoff. Continental airlines flight 795, McDonnell Douglas MD-82, N18835, LaGuardia Airport, Flushing, NY, 2 March 1994
[PB95-910401] p 1610 N95-23609
Aircraft fires, smoke toxicity, and survival: An overview
[DOT/FAA/AM-95/8] p 1610 N95-24024
A review of civil aviation fatal accidents in which lost/disoriented was a cause/factor: 1981-1990
[DOT/FAA/AM-95/1] p 1611 N95-24071
AIRCRAFT APPROACH SPACING
Guidance and control requirements for high-speed Rollout and Turnoff (ROTO)
[NASA-CR-195026] p 1614 N95-22674
AIRCRAFT COMPARTMENTS
Living in space
[NASA-TM-110536] p 1751 N95-23274
AIRCRAFT CONSTRUCTION MATERIALS
Mishap risk control for advanced aerospace/composite materials p 1628 N95-23031
Technology reinvestment project's focus area: Affordable polymer matrix composites for airframe structures
[PB95-136032] p 1865 N95-23168
Development and verification of a resin film infusion/resin transfer molding simulation model for fabrication of advanced textile composites
[NASA-CR-197439] p 1648 N95-23179
Test method and test results for environmental assessment of aircraft materials p 1643 N95-23509
US Navy operating experience with new aircraft construction materials p 1645 N95-23517
Review of some results of the author's fatigue investigations with applications in engineering and material science
[TAE-698] p 1699 N95-23662
AIRCRAFT CONTROL
Guidance and control requirements for high-speed Rollout and Turnoff (ROTO)
[NASA-CR-195026] p 1614 N95-22674
Nonlinear system guidance in the presence of transmission zero dynamics
[NASA-TM-4661] p 1654 N95-22804
Flight test of the X-29A at high angle of attack: Flight dynamics and controls
[NASA-TP-3537] p 1612 N95-22806
Design of high performance multivariable control systems for supermaneuverable aircraft at high angle of attack
[NASA-CR-197661] p 1615 N95-22908
Stable H(infinity) controller design for the longitudinal dynamics of an aircraft
[NASA-TM-106847] p 1615 N95-22954
Analysis of the longitudinal handling qualities and pilot-induced-oscillation tendencies of the High-Angle-of-Attack Research Vehicle (HARV) p 1616 N95-23297
Handling qualities of the High Speed Civil Transport p 1616 N95-23325
Feedback control laws for highly maneuverable aircraft
[NASA-CR-197944] p 1615 N95-23410
AIRCRAFT DESIGN
Euler Technology Assessment program for preliminary aircraft design employing SPLITFLOW code with Cartesian unstructured grid method
[NASA-CR-4649] p 1608 N95-22917
Euler technology assessment for preliminary aircraft design employing OVERFLOW code with multiblock structured-grid method
[NASA-CR-4651] p 1608 N95-23095
Control of flow separation in airfoil/wing design applications p 1609 N95-23294
Thin tailored composite wing for civil tiltrotor p 1613 N95-23317
AIRCRAFT ENGINES
High-performance parallel analysis of coupled problems for aircraft propulsion
[NASA-CR-197440] p 1614 N95-23088
Engines-only flight control system
[NASA-CASE-ARC-11944-1] p 1615 N95-23389
AIRCRAFT GUIDANCE
Guidance and control requirements for high-speed Rollout and Turnoff (ROTO)
[NASA-CR-195026] p 1614 N95-22674
Nonlinear system guidance in the presence of transmission zero dynamics
[NASA-TM-4661] p 1654 N95-22804
Knowledge-based guidance and control functions
[AGARD-AR-325] p 1751 N95-23601
AIRCRAFT ICING
Additional improvements to the NASA Lewis ice accretion code LEWICE
[NASA-TM-106849] p 1665 N95-22669
Collaborative research on aircraft icing and charging processes in ice
[AD-A285102] p 1609 N95-23201
Experimental technique and assessment for measuring the convective heat transfer coefficient from natural ice accretions
[NASA-TM-106864] p 1668 N95-23248
AIRCRAFT INDUSTRY
Report of proceedings: Aviation Accident Investigation Symposium. Volume 2: Participant presentations
[PB94-917007] p 1610 N95-23598
AIRCRAFT MAINTENANCE
POD assessment of NDI procedures using a round robin test
[AGARD-R-809] p 1697 N95-23602
Enhancement of F/A-18 operational flight measurements: Data report for phase 1
[DSTO-TR-0049] p 1613 N95-23666
AIRCRAFT MODELS
An investigation of helicopter dynamic coupling using an analytical model
[NASA-CR-197420] p 1612 N95-23217
Inner loop flight control for the High-Speed Civil Transport p 1616 N95-23314
AIRCRAFT NOISE
The use of cowl camber and taper to reduce rotor/stator interaction noise
[NASA-CR-195421] p 1799 N95-22675
AIRCRAFT PARTS
Review of some results of the author's fatigue investigations with applications in engineering and material science
[TAE-698] p 1699 N95-23662
AIRCRAFT PERFORMANCE
Guidance and control requirements for high-speed Rollout and Turnoff (ROTO)
[NASA-CR-195026] p 1614 N95-22674
Direct adaptive performance optimization of subsonic transports: A periodic perturbation technique
[NASA-TM-4676] p 1612 N95-22829
Design of high performance multivariable control systems for supermaneuverable aircraft at high angle of attack
[NASA-CR-197661] p 1615 N95-22908
AIRCRAFT PILOTS
Aviator's night vision imaging system preflight adjustment/assessment procedures
[AD-A285829] p 1750 N95-22513
AIRCRAFT POWER SUPPLIES
Motor drive technologies for the power-by-wire (PBW) program: Options, trends and tradeoffs
[NASA-TM-106885] p 1616 N95-23671
AIRCRAFT RELIABILITY
Oklahoma City air logistics center (USAF) aging aircraft corrosion program p 1607 N95-23519
AIRCRAFT SAFETY
Additional improvements to the NASA Lewis ice accretion code LEWICE
[NASA-TM-106849] p 1665 N95-22669
Handling qualities of the High Speed Civil Transport p 1616 N95-23325
Report of proceedings: Aviation Accident Investigation Symposium. Volume 2: Participant presentations
[PB94-917007] p 1610 N95-23598
Aircraft fires, smoke toxicity, and survival: An overview
[DOT/FAA/AM-95/8] p 1610 N95-24024
A multibody/finite element analysis approach for modeling of crash dynamic responses
[NIAR-94-3] p 1610 N95-24050
Aviation Accident Investigation Symposium. Volume 1: Industry recommendations and Safety Board responses
[PB94-917005] p 1611 N95-24105
AIRCRAFT STABILITY
System for determining aerodynamic imbalance
[NASA-CASE-ARC-11913-1] p 1688 N95-23377
Aerodynamic flight control to increase payload capability of future launch vehicles
[NASA-CR-197704] p 1619 N95-24032
AIRCRAFT STRUCTURES
Review of aeronautical fatigue investigation in the Netherlands during the period March 1991-March 1993
[PB95-139184] p 1612 N95-23161
Double pass retroreflection for corrosion detection in aircraft structures p 1642 N95-23503
Non-destructive detection of corrosion for life management p 1643 N95-23505
Health and usage monitoring systems: Corrosion surveillance p 1607 N95-23506
New nondestructive techniques for the detection and quantification of corrosion in aircraft structures p 1644 N95-23512
Organic coating technology for the protection of aircraft against corrosion p 1644 N95-23513
Corrosion detection and monitoring of aircraft structures: An overview p 1644 N95-23515
Experience of in-service corrosion on military aircraft p 1644 N95-23516
US Navy operating experience with new aircraft construction materials p 1645 N95-23517
Oklahoma City air logistics center (USAF) aging aircraft corrosion program p 1607 N95-23519
AIRFIELD SURFACE MOVEMENTS
Automation technology using Geographic Information System (GIS) p 1863 N95-23284
AIRFOIL PROFILES
Control of flow separation in airfoil/wing design applications p 1609 N95-23294
AIRFRAME MATERIALS
Technology reinvestment project's focus area: Affordable polymer matrix composites for airframe structures
[PB95-136032] p 1865 N95-23168
Corrosion detection and management of advanced airframe materials
[AGARD-CP-565] p 1641 N95-23496
The corrosion and protection of advanced aluminium - lithium airframe alloys p 1641 N95-23497
Non-destructive detection of corrosion for life management p 1643 N95-23505
New nondestructive techniques for the detection and quantification of corrosion in aircraft structures p 1644 N95-23512
AIRFRAMES
Oklahoma City air logistics center (USAF) aging aircraft corrosion program p 1607 N95-23519
AIRGLOW
Investigation of the role of gravity waves in the generation of equatorial bubbles
[NASA-CR-197962] p 1739 N95-23272
AIRLINE OPERATIONS
Aircraft accident report. Runway overrun following rejected takeoff. Continental airlines flight 795, McDonnell Douglas MD-82, N18835, LaGuardia Airport, Flushing, NY, 2 March 1994
[PB95-910401] p 1610 N95-23609
The airline quality report, 1994
[NIAR-94-11] p 1610 N95-24012
AIRPORTS
Evaluation of neutron techniques for illicit substance detection
[DE95-002988] p 1632 N95-22764
Automation technology using Geographic Information System (GIS) p 1863 N95-23284
AIRSPACE
Oceanic operations: An authoritative guide to oceanic operations
[FAA-AFS-550] p 1610 N95-24065
ALCOHOLS
Regulation of alcohol fermentation in Escherichia coli
[DE94-016227] p 1745 N95-22874
Some performance effects of age and low blood alcohol levels on a computerized neuropsychological test
[DOT/FAA/AM-95/7] p 1749 N95-23788
Effects of age and low doses of alcohol on compensatory tracking during angular acceleration
[DOT/FAA/AM-95/3] p 1750 N95-23934
ALERTNESS
Method of encouraging attention by correlating video game difficulty with attention level
[NASA-CASE-LAR-15022-1] p 1749 N95-22579
ALGAE
The red edge in arid region vegetation: 340-1060 nm spectra p 1708 N95-23881
ALGEBRA
Lectures on Fermat's last theorem
[DE94-628392] p 1795 N95-22617
Q-analytic functions on quantum spaces
[DE94-628412] p 1847 N95-22621
Graph isomorphism models for non interleaving process algebra
[PB95-110490] p 1786 N95-22714
A space-time lattice version of scalar electrodynamics
[DE94-628577] p 1850 N95-22784
Idempotents in Banach algebra
[DE94-628429] p 1787 N95-22794
Trisecant curve associated to a smooth curve in P(sub 3) of degree d greater than g+2
[DE94-628425] p 1787 N95-22809

Molecular vibrational states during a collision
p 1814 N95-22964
Covariant deformed oscillator algebras
p 1797 N95-22978
Algebraic semantics of basic message sequence charts
| PB95-138970 | p 1657 N95-23151
Taxonomy of finite automata construction algorithms
| PB95-139234 | p 1758 N95-23606
The exchange algebra for Liouville field on Riemann surfaces with h greater than 1 genus
| DE94-635446 | p 1792 N95-23971

ALGORITHMS

An adaptive projection method for the incompressible Navier-Stokes equations
| DE94-019049 | p 1665 N95-22491
Experience with CANDID: Comparison algorithm for navigating digital image databases
| DE95-000869 | p 1855 N95-22515
Treewidth and pathwidth of cocomparability graphs of bounded dimension
| PB95-127239 | p 1785 N95-22535
A worst-case example using linesearch methods for numerical optimization with inexact gradient evaluations
| DE95-002917 | p 1754 N95-22570
A Newton-type neural network learning algorithm
| DE94-628371 | p 1766 N95-22614
A certainty grid to object boundary algorithm
| PB94-203510 | p 1755 N95-22637
Software for the generalized eigenproblem on distributed memory architectures
| DE95-002999 | p 1755 N95-22690
Ocean observations with EOS/MODIS: Algorithm development and post launch studies
| NASA-CR-197402 | p 1717 N95-22916
Global electric field determination in the Earth's outer magnetosphere using energetic charged particles
| NASA-CR-197392 | p 1737 N95-22945
An algorithm for the basis of the finite Fourier transform p 1760 N95-22985
Kravchuk functions for the finite oscillator approximation p 1798 N95-23006
Algorithms for parallel and vector computations
| NASA-CR-197394 | p 1756 N95-23017
Ghost images and feasibility of reconstructions with the Richardson-Lucy algorithm
| DE95-002351 | p 1756 N95-23079
Hierarchical membership protocol for synchronous distributed systems
| PB95-138947 | p 1763 N95-23129
Taxonomy of finite automata minimization algorithms
| PB95-139226 | p 1756 N95-23131
Automatic verification of regular protocols in P/T nets
| PB95-138921 | p 1789 N95-23146
Performance of single-keyword and multiple-keyword pattern matching algorithms
| PB95-138954 | p 1756 N95-23150
Infrared algorithm development for ocean observations with EOS/MODIS
| NASA-CR-197851 | p 1743 N95-23212
Aerodynamic design optimization with sensitivity analysis and computational fluid dynamics
| NASA-CR-197419 | p 1608 N95-23218
Characterization of non-negative greedy matrices
| PB95-139366 | p 1757 N95-23232
Some recent results in the analysis of greedy algorithms for assignment problems
| PB95-140620 | p 1757 N95-23238
Two portable parallel tridiagonal solvers
| DE94-019044 | p 1763 N95-23243
Accelerated panel methods using the fast multipole method p 1687 N95-23307
On-line, adaptive state estimator for active noise control p 1784 N95-23308
A new look at the simultaneous analysis and design of structures p 1700 N95-23327
Verification and validation of decision support software: Expert Choice(trademark) and PCM(trademark)
| DE95-004469 | p 1757 N95-23346
Numerical simulation of steady and unsteady viscous flow in turbomachinery using pressure based algorithm p 1671 N95-23426
Liquid propellant rocket engine combustion simulation with a time-accurate CFD method p 1676 N95-23445
A controlled variation scheme for convection treatment in pressure-based algorithm p 1677 N95-23448
Ocean observations with EOS/MODIS: Algorithm development and post launch studies
| NASA-CR-197894 | p 1718 N95-23473
Technical report series on global modeling and data assimilation. Volume 4: Documentation of the Goddard Earth Observing System (GEOS) data assimilation system, version 1
| NASA-TM-104606-VOL-4 | p 1740 N95-23529
Modelling and analysis of a high speed data bus with predicate/transition nets
| PB95-140695 | p 1764 N95-23538
On adaptive weighted polynomial preconditioning for Hermitian positive definite matrices
| NASA-CR-197946 | p 1791 N95-23547
Taylor series expansion and modified extended Prony analysis for localization
| DE95-003671 | p 1758 N95-23567
Block LU factorization
| NASA-CR-197949 | p 1791 N95-23592
Quasi-kernel polynomials and convergence results for quasi-minimal residual iterations
| NASA-CR-197948 | p 1791 N95-23593
Microarchitecture support for dynamic scheduling of acyclic task graphs
| CSRD-1207 | p 1791 N95-23600
Taxonomy of finite automata construction algorithms
| PB95-139234 | p 1758 N95-23606
Submodular linear programs on forests
| PB95-139820 | p 1758 N95-23608
Recent advances in Lanczos-based iterative methods for nonsymmetric linear systems
| NASA-CR-197950 | p 1791 N95-23611
An implementation of the QMR method based on coupled two-term recurrences
| NASA-CR-197956 | p 1791 N95-23612
Spray combustion experiments and numerical predictions p 1637 N95-23643
Path planning for planetary rover using extended elevation map p 1771 N95-23689
Empirical results on scheduling and dynamic backtracking p 1618 N95-23761
Comparison of three methods for materials identification and mapping with imaging spectroscopy p 1702 N95-23853
Algorithms for categorizing multiprocessor communication under invalidate and update-based coherence protocols
| TR-533-REV | p 1759 N95-23928
An improved algorithm for retrieval of snow wetness using C-band AIRSAR p 1715 N95-23954
Reducibility classes of P-selective sets
| TR-524 | p 1792 N95-24002
Chemical recognition software
| DE95-003346 | p 1636 N95-24007
A modal test design strategy for model correlation
| DE95-003631 | p 1759 N95-24020
An efficient algorithm for concurrent priority queue heaps
| TR-560 | p 1759 N95-24033
Unsupervised classification learning from cross-modal environmental structure
| TR-536 | p 1784 N95-24040
Using simulation-based projection to plan in an uncertain and temporally complex world
| TR-531 | p 1853 N95-24043
Unifying data and control transformations for distributed shared-memory machines
| TR-542 | p 1765 N95-24061
Semi-membership algorithms: Some recent advances
| TR-526 | p 1760 N95-24092
Scheduler-conscious synchronization
| TR-550 | p 1765 N95-24183

ALKALI HALIDES

A model for the metal-nonmetal transition in metal-molten salt solutions
| DE94-628490 | p 1640 N95-23057

ALKALI METALS

Electrical resistivity of liquid alkali metals and non-local pseudopotential
| DE94-627417 | p 1639 N95-22608
A model for the metal-nonmetal transition in metal-molten salt solutions
| DE94-628490 | p 1640 N95-23057

ALLOCATIONS

Some recent results in the analysis of greedy algorithms for assignment problems
| PB95-140620 | p 1757 N95-23238

ALLOYS

Calculations of alloy phases with a direct Monte-Carlo method
| DE94-018963 | p 1640 N95-23121

ALPHA PARTICLES

Status of helium-production reaction studies with a spallation neutron source
| DE95-002816 | p 1806 N95-23137
Alpha spectral analysis via artificial neural networks
| DE95-004567 | p 1767 N95-23578
MHD-Vlasov simulation of the toroidal Alfven eigenmode
| NIFS-319 | p 1836 N95-23591
Pauli-blocking effects in neutron-alpha reactions
| DE94-016358 | p 1813 N95-24046

ALTERNATING CURRENT

An investigation of AC losses in two sub-size conductors for the ITER
| DE94-765449 | p 1831 N95-22849

ALTERNATING DIRECTION IMPLICIT METHODS

Two portable parallel tridiagonal solvers
| DE94-019044 | p 1763 N95-23243
Convergence acceleration of implicit schemes in the presence of high aspect ratio grid cells
p 1676 N95-23446

ALTERNATIVES

Consistency and Monte Carlo simulation of a data driven version of smooth goodness-of-fit tests
| PB95-141255 | p 1794 N95-23559

ALTIMETERS

Assimilation of altimeter data in a quasi-geostrophic model of the Gulf Stream system: A dynamical perspective
| NASA-CR-196313 | p 1744 N95-23766

ALTITUDE

Energetic particle observations at geosynchronous orbit
| DE95-000873 | p 1867 N95-22516

ALUMINUM

CO2 and waste policy: Monitoring results 1991/1992 and main problems
| PB95-133799 | p 1733 N95-23126
The corrosion protection of 2219-T87 aluminum by organic and inorganic zinc-rich primers
| NASA-TP-3543 | p 1641 N95-23186
Corrosion protection measures for CFC/metal joints of fuel integral tank structures of advanced military aircraft
p 1644 N95-23510
Recent results from Long Duration Exposure Facility materials testing p 1638 N95-23898
Durability of reflector materials in the space environment p 1651 N95-23912

ALUMINUM ALLOYS

Technology maturation project on optimization of sheet metal forming of aluminum for use in transportation systems
| DE95-003005 | p 1654 N95-22692
Three-dimensional CTOA and constraint effects during stable tearing in a thin-sheet material
| NASA-TM-109183 | p 1627 N95-22928
Nondestructive evaluation of fatigue damage in aluminum 2024 by x-ray diffraction p 1698 N95-23293
Test method and test results for environmental assessment of aircraft materials p 1643 N95-23509
Penetration rates over 30 years in the space age
p 1624 N95-23827

ALUMINUM COATINGS

Atomic oxygen interactions with protected organic materials on the Long Duration Exposure Facility (LDEF)
p 1627 N95-23909

ALUMINUM GALLIUM ARSENIDES

Resonant shallow donor magnetopolaron effect in a GaAs/AlGaAs quantum dot in high magnetic fields
| DE94-629039 | p 1798 N95-22497
Subband quantum scattering times for AlGaAs/GaAs obtained using digital filtering
| NASA-TM-106873 | p 1846 N95-24188

ALUMINUM ISOTOPES

NMR study of nanophase Al/Al-oxide powder and consolidated composites
| DE95-004655 | p 1843 N95-23586

ALUMINUM OXIDES

Infrared study of carbon deposits on bimetallic catalysts
| DE95-000902 | p 1631 N95-22517
Dislocation decomposition, dissociation, and deformation in MoSi2 and (alpha)-Al2O3 single crystals
| DE95-002715 | p 1839 N95-22653
Micro-sensor thin-film anemometer
| NASA-CASE-LAR-15112-1-CU | p 1666 N95-22906
Surface structural dependence of cesium adsorption on the (alpha)-Al2O3(0001) surface
| DE95-002610 | p 1842 N95-23135
Explosive bonding and its application in the Advanced Photon Source front-end and beamline components design
| DE95-004132 | p 1696 N95-23397
Temperature effects on ion irradiation damage in MgAl2O4 spinel single crystals
| DE95-003679 | p 1844 N95-24073
Modified molecular sieves: Stationary phase for the gas chromatographic separation of hydrogen isotopes
| DE94-627282 | p 1814 N95-24175

ALUMINUM-LITHIUM ALLOYS

The corrosion and protection of advanced aluminium - lithium airframe alloys p 1641 N95-23497
Exfoliation corrosion and stress corrosion cracking behaviour of Al-Li alloys p 1641 N95-23498
Effect of loading direction and long-term aging on fatigue-crack growth in Al-Li alloy 2090
p 1641 N95-23499

The use of electrochemical impedance spectroscopy to predict the corrosion of aluminum-lithium alloys in marine environments p 1637 N95-23504
AMINES
Transmethylation reactions during methanogenesis from acetate in Methanosarcina barkeri
| DE94-016222 | p 1745 N95-22873
AMINO ACIDS
Protein folding and protein metallocluster studies using synchrotron small angler x ray scattering
| DE95-003339 | p 1746 N95-22897
The origin of chirality in protein amino acids
| DE94-628491 | p 1747 N95-23058
AMORPHOUS MATERIALS
Polyazomethines containing trifluoromethylbenzene units
| NASA-CASE-LAR-14896-1 | p 1649 N95-23253
Temperature effects on ion irradiation damage in MgAl2O4 spinel single crystals
| DE95-003679 | p 1844 N95-24073
A phenomenological model for the effect of nanocrystalline microstructure on irradiation-induced amorphization in U3Si
| DE95-004631 | p 1846 N95-24169
AMORPHOUS SILICON
Southeast Regional Experiment Station
| DE95-000903 | p 1726 N95-22518
Large-area triple-junction a-Si alloy production scaleup
| DE95-000245 | p 1726 N95-22546
Research on defects and transport in amorphous-silicon-based semiconductors
| DE94-011888 | p 1660 N95-22586
Continuous roll-to-roll amorphous-silicon photovoltaic manufacturing technology
| DE95-000243 | p 1728 N95-23061
Amorphous silicon photovoltaic manufacturing technology, phase 2A
| DE95-000298 | p 1729 N95-23478
ANAEROBES
Resource recovery and epidemiology of anaerobic wastewater treatment process in a controlled ecological life support system
| NASA-CR-197930 | p 1751 N95-23474
ANALOG TO DIGITAL CONVERTERS
D(O) upgrade muon electronics design
| DE95-003744 | p 1817 N95-23369
Operation and tests of a DDC101 A/D
| DE95-003747 | p 1663 N95-23405
Video frame processor
| DE94-635414 | p 1753 N95-23962
A high speed digitizing photomultiplier tube base for the KTeV CsI calorimeter
| DE95-003739 | p 1664 N95-24081
ANALYTIC FUNCTIONS
Q-analytic functions on quantum spaces
| DE94-628412 | p 1847 N95-22621
ANDES MOUNTAINS (SOUTH AMERICA)
Glaciological studies in the central Andes using AIRSAR/TOPSAR p 1713 N95-23942
ANEMOMETERS
Micro-sensor thin-film anemometer
| NASA-CASE-LAR-15112-1-CU | p 1666 N95-22906
ANGIOSPERMS
Molecular relics from chemical evolution and the origin of life
| DE94-628493 | p 1747 N95-23060
ANGLE OF ATTACK
Wing pressure distributions from subsonic tests of a high-wing transport model --- in the Langley 14- by 22-Foot Subsonic Wind Tunnel
| NASA-TM-4583 | p 1607 N95-22802
Flight test of the X-29A at high angle of attack: Flight dynamics and controls
| NASA-TP-3537 | p 1612 N95-22806
An assessment of viscous effects in computational simulation of benign and burst vortex flows on generic fighter wind-tunnel models using TEAM code
| NASA-CR-4650 | p 1608 N95-23185
Aerodynamic surface distension system for high angle of attack forebody vortex control
| NASA-CASE-ARC-11979-1 | p 1612 N95-23390
ANGLES (GEOMETRY)
Prediction of incidence and surface roughness effects on turbine performance p 1671 N95-23424
ANGULAR ACCELERATION
Effects of age and low doses of alcohol on compensatory tracking during angular acceleration
| DOT/FAA/AM-95/3 | p 1750 N95-23934
ANGULAR MOMENTUM
Exact, E = 0, classical and quantum solutions for general power-law oscillators p 1820 N95-22959
Coherent state constructions of bases for some physically relevant group chains p 1814 N95-22966
The Duffin-Kemmer-Petiau oscillator p 1825 N95-22998
ANHYDRIDES
Process for preparing an assembly of an article and a polyimide which resists dimensional change, delamination and debonding when exposed to changes in temperature
| NASA-CASE-LAR-14538-2 | p 1649 N95-23254
ANIONS
Test procedure for anion exchange chromatography
| DE95-003767 | p 1809 N95-23407
ANISOTROPIC MEDIA
Phase space analysis in anisotropic optical systems p 1826 N95-23007
ANISOTROPY
An upper bound for the proton temperature anisotrophy
| DE95-002752 | p 1737 N95-22903
Dynamical properties of critical and paramagnetic spin fluctuations in anisotropic heisenberg magnets
| PB95-134623 | p 1798 N95-23127
Deflections of anisotropic sandwich beams with variable face sheets and core thicknesses p 1700 N95-23310
Generation of fast electrons in reversed field pinches by the equilibrium grad (vert bar)B(vert bar) force
| DE95-004467 | p 1809 N95-23363
ANNEALING
Superconducting Tl2Ba2CaCu2O8 thin films prepared by post-annealing in a flow-through multiple-zone furnace
| DE95-002745 | p 1838 N95-22520
X-ray diffraction characterization of defect behavior in nanocrystalline nickel during annealing
| DE95-002992 | p 1639 N95-22594
Rapid thermal processing of high-efficiency silicon solar cells with controlled in-situ annealing
| DE95-004729 | p 1730 N95-23489
Annealing of nitrogen-doped ZnSe at high pressures: Toward suppression of native defect formation
| DE95-003420 | p 1844 N95-24010
ANNIHILATION REACTIONS
Commensurate scale relations: Precise tests of quantum chromodynamics without scale or scheme ambiguity
| DE95-002785 | p 1847 N95-22566
Searches for the H-dibaryon at the AGS
| DE95-003091 | p 1802 N95-22727
Coherent states for a generalization of the harmonic oscillator p 1823 N95-22982
Coherent states for the relativistic harmonic oscillator p 1825 N95-22993
Oscillator-like coherent states for the Jaynes-Cummings Model p 1826 N95-23003
Search for top quark at CDF
| DE95-003748 | p 1809 N95-23406
ANNUAL VARIATIONS
A comparison of ionospheric F2-layer IRI model with experimental data for Ibadan Geog. Lat. 7.4 deg N
| DE94-627710 | p 1736 N95-22613
The atmosphere below
| NASA-TM-110538 | p 1740 N95-23663
Determination of semi-arid landscape endmembers and seasonal trends using convex geometry spectral unmixing techniques p 1711 N95-23895
ANODES
Corrosion control acceptance criteria for sacrificial anode type, cathodic protection systems (user guide)
| AD-A285275 | p 1662 N95-23117
ANODIZING
Effect of different ions on the anodic behaviour of alloy 800 chloride solutions at high temperature
| DE94-634944 | p 1645 N95-23983
ANOMALIES
An automated computer misuse detection system for UNICOS
| DE95-000929 | p 1762 N95-22680
Determinants of elliptic pseudo-differential operators
| PB95-109062 | p 1786 N95-22711
The U(3) x U(3) Nambu - Jona-Lasinio model with the gluon condensate and axial anomaly at finite temperature
| DE94-628588 | p 1804 N95-22787
STS-61 Space Shuttle mission report
| NASA-TM-110545 | p 1619 N95-23187
Phonon-induced anomalous specific heat of a model nanocrystal by computer simulation
| DE95-004653 | p 1843 N95-23585
An expert system for diagnosing anomalies of spacecraft p 1770 N95-23684
ANTENNA ARRAYS
Adaptive beamforming in a CDMA mobile satellite communications system p 1655 N95-22815
Synthesis of a large communications aperture using small antennas
| NASA-CR-197330 | p 1656 N95-22852
ANTENNA DESIGN
Passive intermodulation generation in wire mesh deployable reflector antennas p 1656 N95-22816
Observation model and parameter partials for the JPL VLBI parameter estimation software MODEST, 19 94
| NASA-CR-197328 | p 1756 N95-22853
Improved small satellite access of the space network
| NASA-CR-197863 | p 1657 N95-22944
ANTIBIOTICS
Effect of hyperbaric carbon dioxide on spores and vegetative cells of bacillus stearothermophilus
| AD-A280115 | p 1747 N95-23251
ANTIFERROELECTRICITY
Superconductivity devices: Commercial use of space
| NASA-CR-197885 | p 1648 N95-22883
ANTIFERROMAGNETISM
Spin polarized photoemission studies of magnetic quantum well states
| DE95-004218 | p 1851 N95-23335
ANTIMATTER
Traps for antimatter and antihydrogen production
| DE95-002814 | p 1805 N95-22927
A brief history in time of ion traps and their achievements in science
| DE95-002815 | p 1805 N95-22936
ANTIMONY COMPOUNDS
Test procedure for cation exchange chromatography
| DE95-003770 | p 1808 N95-23350
ANTIPROTONS
Traps for antimatter and antihydrogen production
| DE95-002814 | p 1805 N95-22927
ANTIREFLECTION COATINGS
Rapid thermal processing of high-efficiency silicon solar cells with controlled in-situ annealing
| DE95-004729 | p 1730 N95-23489
Silicon surface and bulk defect passivation by low temperature PECVD oxides and nitrides
| DE95-004531 | p 1731 N95-24090
Reflectance control for multicrystalline-silicon photovoltaic modules using textured-dielectric coatings
| DE95-004532 | p 1731 N95-24155
APERTURES
Synthesis of a large communications aperture using small antennas
| NASA-CR-197330 | p 1656 N95-22852
Stellar Interferometer Technology Experiment (SITE)
| NASA-CR-197856 | p 1827 N95-23089
APEXES
A preliminary measurement of the average B hadron lifetime
| DE95-003138 | p 1808 N95-23226
Trees are graceful if and only if trees with a perfect matching are strongly graceful
| PB95-139853 | p 1790 N95-23236
APPLICATION SPECIFIC INTEGRATED CIRCUITS
A high speed digitizing photomultiplier tube base for the KTeV CsI calorimeter
| DE95-003739 | p 1664 N95-24081
APPLICATIONS OF MATHEMATICS
Preparation of course materials: Elementary mathematics of powered flight p 1853 N95-23320
Ploxoma: Testbed for uncertain inference
| TR-537 | p 1794 N95-23927
APPLICATIONS PROGRAMS (COMPUTERS)
HiRel: Hybrid Automated Reliability Predictor (HARP) integrated reliability tool system, (version 7.0). Volume 1: HARP introduction and user's guide
| NASA-TP-3452-VOL-1 | p 1754 N95-22603
HiRel: Hybrid Automated Reliability Predictor (HARP) integrated reliability tool system, (version 7.0). Volume 2: HARP tutorial
| NASA-TP-3452-VOL-2 | p 1755 N95-22604
HiRel: Hybrid Automated Reliability Predictor (HARP) integrated reliability tool system, (version 7.0). Volume 4: HARP Output (HARPO) graphics display user's guide
| NASA-TP-3452-VOL-4 | p 1755 N95-22605
PRISMA GENIE data analysis manual
| PB95-130464 | p 1755 N95-22769
Development of an adaptive hp-version finite element method for computational optimal control
| NASA-CR-197898 | p 1766 N95-22831
Photon and electron interaction databases and their use in medical applications
| DE94-015558 | p 1855 N95-22871
The torsion space nucleic acids molecular mechanics program DUPLEX: Surveying conformation space by potential energy minimization
| DE94-017707 | p 1805 N95-22889
An improved system for exon recognition and gene modeling in human DNA sequences
| DE94-017863 | p 1746 N95-22890
COYOTE 2: A Finite Element Computer Program for nonlinear heat conduction problems
| DE95-002848 | p 1666 N95-22914
Conjugate gradient MATHEW
| DE95-003479 | p 1738 N95-23143
VLUGR2: A vectorizable adaptive grid solver for PDes in 2D
| PB95-136008 | p 1789 N95-23167

A hybrid vehicle evaluation code and its application to vehicle design
| DE95-004205 | p 1662 N95-23334
Measurement of correlated b quark cross sections at CDF
| DE95-004240 | p 1808 N95-23336
GPP: A General-Purpose Post Processor for wind turbine data analysis
| DE95-000223 | p 1729 N95-23383
Long range targeting for space based rendezvous
| NASA-CR-197890 | p 1757 N95-23388
EXTRA.M: A computing code system for analysis of the Purex process with mixer settlers for reprocessing
| DE94-785273 | p 1635 N95-23476
An interactive tool for discrete phase analysis in two-phase flows p 1683 N95-23641
Toward an automated signature recognition toolkit for mission operations p 1659 N95-23682
Learning time series for intelligent monitoring p 1770 N95-23686
Benefits of advanced software techniques for mission planning systems p 1618 N95-23752
Design and implementation of an experiment scheduling system for the ACTS satellite p 1620 N95-23756
ESTAR, PSTAR, ASTAR: A PC package for calculating stopping powers and ranges of electrons, protons and helium ions, version 2
| DE94-634435 | p 1811 N95-23773
GPP user's guide: A general-purpose postprocessor for wind turbine data analysis
| DE95-000293 | p 1730 N95-23776
An RL10A-3-3A rocket engine model using the rocket engine transient simulator (ROCETS) software
| NASA-CR-190786 | p 1625 N95-23790
A proposed update to the solar irradiance spectrum used in LOWTRAN and MODTRAN p 1705 N95-23865
SAR terrain classifier and mapper of biophysical attributes p 1715 N95-23957
TRACKER: A three-dimensional raytracing program for ionospheric radio propagation
| DE95-003510 | p 1658 N95-24015
Fracture mechanics life analytical methods verification testing
| NASA-CR-196555 | p 1697 N95-24106

APPROPRIATIONS
Director's discretionary fund report for fiscal year 1994
| NASA-TM-108848 | p 1872 N95-22920

APPROXIMATION
A certainty grid to object boundary algorithm
| PB94-203510 | p 1755 N95-22637
Kravchuk functions for the finite oscillator approximation p 1798 N95-23006
Adaptive control of linear systems based on approximate models
| PB95-139333 | p 1767 N95-23199
Aeroacoustic computation of gust-blade interaction p 1800 N95-23313

AQUEOUS SOLUTIONS
Hydrogen vibrational density of states of adsorbed water on rare-earth modified zirconia
| DE95-001127 | p 1632 N95-22681
On the formation of iron(3) oxides via oxidation of iron(2)
| DE94-018392 | p 1632 N95-22857
Aqueous alternatives for metal and composite cleaning p 1630 N95-23039
Effect of different ions on the anodic behaviour of alloy 800 chloride solutions at high temperature
| DE94-634944 | p 1645 N95-23983

ARAMID FIBER COMPOSITES
Method for forming a glove attachment
| NASA-CASE-MSC-21632-1 | p 1750 N95-22766

ARCHAEBACTERIA
Transmethylation reactions during methanogenesis from acetate in Methanosarcina barkeri
| DE94-016222 | p 1745 N95-22873

ARCHITECTURE (COMPUTERS)
Parallel digital modem using multirate digital filter banks
| NASA-CR-197331 | p 1761 N95-22478
Adaptive beamforming in a CDMA mobile satellite communications system p 1655 N95-22815
Task scheduling in dataflow computer architectures p 1753 N95-23301
MPI implementation of CFD program PHOENICS
| DE95-003896 | p 1668 N95-23372
Parallel computation of automatic differentiation applied to magnetic field calculations
| DE95-004689 | p 1763 N95-23486
Towards the Teraflop CFD
| NASA-CR-197947 | p 1764 N95-23594
Microarchitecture support for dynamic scheduling of acyclic task graphs
| CSRD-1207 | p 1791 N95-23600
Unstructured grids on SIMD torus machines
| NASA-CR-197954 | p 1758 N95-23610
An expert system for diagnosing anomalies of spacecraft p 1770 N95-23684
Distributed intelligence for ground/space systems p 1770 N95-23685
Performance results of cooperating expert systems in a distributed real-time monitoring system p 1761 N95-23688
Path planning for planetary rover using extended elevation map p 1771 N95-23689
Subsumption-based architecture for autonomous movement planning for planetary rovers p 1771 N95-23690
Control technique for planetary rover p 1771 N95-23692
Autonomous navigation system for the Marsokhod rover project p 1771 N95-23693
Algorithms for categorizing multiprocessor communication under invalidate and update-based coherence protocols
| TR-533-REV | p 1759 N95-23928
Scalability of atomic primitives on distributed shared memory multiprocessors
| TR-528 | p 1764 N95-23930
A distributed parallel storage architecture and its potential application within EOSDIS p 1858 N95-24111
The architecture of the High Performance Storage System (HPSS) p 1858 N95-24113
New architectural paradigms for multi-petabyte distributed storage systems p 1858 N95-24115

ARGON
Electron drift velocities of Ar-CO2-CF4 gas mixtures
| DE95-004353 | p 1809 N95-23359

ARID LANDS
The red edge in arid region vegetation: 340-1060 nm spectra p 1708 N95-23881
Determination of semi-arid landscape endmembers and seasonal trends using convex geometry spectral unmixing techniques p 1711 N95-23895

ARMOR
Projectile penetration into representative targets
| DE95-003089 | p 1698 N95-22726

AROMATIC COMPOUNDS
Tough, soluble, aromatic, thermoplastic copolyimides
| NASA-CASE-LAR-15205-1 | p 1648 N95-22882
Polyazomethines containing trifluoromethylbenzene units
| NASA-CASE-LAR-14896-1 | p 1649 N95-23253

ARTIFICIAL HEART VALVES
A constraint-logic based implementation of the coarse-grained approach to data acquisition scheduling of the International Ultraviolet Explorer orbiting observatory p 1779 N95-23741

ARTIFICIAL INTELLIGENCE
Towards method-independent knowledge acquisition
| AD-A285823 | p 1766 N95-22512
Roles and dynamic subclasses: A modal logic approach
| PB95-127320 | p 1754 N95-22522
Temporal model theory for default logic
| PB95-127346 | p 1766 N95-22524
A certainty grid to object boundary algorithm
| PB94-203510 | p 1755 N95-22637
An improved system for exon recognition and gene modeling in human DNA sequences
| DE94-017863 | p 1746 N95-22890
Knowledge-based guidance and control functions
| AGARD-AR-325 | p 1751 N95-23601
Third International Symposium on Artificial Intelligence, Robotics, and Automation for Space 1994
| NASA-CR-197340 | p 1767 N95-23672
The next decade of space robotics p 1768 N95-23673
Utilizing inheritance in requirements engineering p 1768 N95-23677
AMPHION: Specification-based programming for scientific subroutine libraries p 1761 N95-23680
An intelligent ground operator support system p 1769 N95-23681
Attention focusing and anomaly detection in systems monitoring p 1769 N95-23683
An expert system for diagnosing anomalies of spacecraft p 1770 N95-23684
Distributed intelligence for ground/space systems p 1770 N95-23685
Learning time series for intelligent monitoring p 1770 N95-23686
An operations and command systems for the extreme ultraviolet explorer p 1770 N95-23687
Performance results of cooperating expert systems in a distributed real-time monitoring system p 1761 N95-23688
Subsumption-based architecture for autonomous movement planning for planetary rovers p 1771 N95-23690
Very fast motion planning for highly dexterous-articulated robots p 1771 N95-23691
Lunar rover technology demonstrations with Dante and Ratler p 1697 N95-23694
POINTER: Portable Intelligent Trainer for External Robotics p 1752 N95-23714
A new generation of intelligent trainable tools for analyzing large scientific image databases p 1775 N95-23717
Intelligent monitoring system applied to super long distance telerobotic tasks p 1777 N95-23728
Planning and scheduling the Hubble Space Telescope: Practical application of advanced techniques p 1779 N95-23740
Automated synthesis of image processing procedures using AI planning techniques p 1779 N95-23745
Benefits of advanced software techniques for mission planning systems p 1618 N95-23752
A scheduling and diagnostic system for scientific satellite GEOTAIL using expert system p 1781 N95-23753
Artificial intelligence techniques for scheduling Space Shuttle missions p 1781 N95-23755
High performance techniques for space mission scheduling p 1618 N95-23758
Applications of dynamic scheduling technique to space related problems: Some case studies p 1618 N95-23759
Knowledge representation and reasoning for mixed-initiative planning
| TR-562 | p 1783 N95-24031
Robot skill learning through intelligent experimentation
| TR-567 | p 1784 N95-24038
OPUS: A new generation Knowledge Engineering Environment p 1760 N95-24176

ARTIFICIAL SATELLITES
Civilian satellite remote sensing: A strategic approach
| PB95-109633 | p 1717 N95-22713
On-orbit science in a small package: Managing the ALEXIS satellite and experiments
| DE94-014426 | p 1621 N95-22868
Design and development status of ETS-7, an RVD and space robot experiment satellite p 1623 N95-23700
Concept verification of three dimensional free motion simulator for space robot p 1618 N95-23702
Calculation of satellite drag coefficients
| AD-A285118 | p 1622 N95-23781

ASHES
Tritium transport, influx, and helium ash measurements on TFTR during DT operation
| DE95-003708 | p 1833 N95-23269

ASPECT RATIO
On the accuracy of CFD-based pressure drop predictions for right-angle ducts p 1682 N95-23634
CFD modeling of turbulent duct flows for coolant channel analysis p 1682 N95-23635

ASSAYING
Light emission-or-absorbance-based binding assays for polynucleic acids
| AD-D016557 | p 1632 N95-22710

ASSEMBLING
Coherent state constructions of bases for some physically relevant group chains p 1814 N95-22966

ASSESSMENTS
Criteria for evaluation of grid generation systems p 1669 N95-23416

ASSIMILATION
Technical report series on global modeling and data assimilation. Volume 4: Documentation of the Goddard Earth Observing System (GEOS) data assimilation system, version 1
| NASA-TM-104606-VOL-4 | p 1740 N95-23529
Assimilation of altimeter data in a quasi-geostrophic model of the Gulf Stream system: A dynamical perspective
| NASA-CR-196313 | p 1744 N95-23766

ASTHENOSPHERE
Axial focusing of energy from a hypervelocity impact on earth
| DE95-003347 | p 1740 N95-24008
Axial focusing of impact energy in the earth's interior: A possible link to flood basalts and hotspots
| DE95-003357 | p 1741 N95-24009

ASTRONAUT TRAINING
POINTER: Portable Intelligent Trainer for External Robotics p 1752 N95-23714
Formalizing procedures for operations automation, operator training and spacecraft autonomy p 1752 N95-23720

ASTRONOMICAL INTERFEROMETRY
Stellar Interferometer Technology Experiment (SITE)
| NASA-CR-197856 | p 1827 N95-23089

ASTRONOMICAL MODELS
Finite-temperature scalar field theory in static de Sitter space
| DE94-628522 | p 1848 N95-22743

Solar mass loss, solar lithium, and solar oscillations
|DE94-018262| p 1870 N95-22938
Galactic oscillator symmetry p 1822 N95-22973
Origins of interstellar and solar system: Carbonaceous materials
|NASA-CR-197436| p 1867 N95-23013
ROSAT observation program
|NASA-CR-197683| p 1866 N95-23595

ASTRONOMICAL OBSERVATORIES
Planning and scheduling the Hubble Space Telescope: Practical application of advanced techniques p 1779 N95-23740

ASTRONOMY
Origins of interstellar and solar system: Carbonaceous materials
|NASA-CR-197436| p 1867 N95-23013
Planning and scheduling the Hubble Space Telescope: Practical application of advanced techniques p 1779 N95-23740
Telescope loading: A problem reduction approach p 1781 N95-23757

ASTROPHYSICS
IRAS sky survey atlas: Explanatory supplement
|NASA-CR-197335| p 1865 N95-22539
Neutrino overview
|DE95-003201| p 1802 N95-22729
Ninth topical conference on atomic processes in plasmas
|DE95-002810| p 1833 N95-23246

ASYMMETRY
New preliminary results on the physics of charm hadroproduction subprocesses
|DE95-002530| p 1801 N95-22646
The first measurement of the left-right cross section asymmetry in Z(sup 0) boson production
|DE95-003335| p 1802 N95-22697
Measurement of the left-right asymmetry in Z boson production by electron-positron collisions
|DE95-003337| p 1802 N95-22699
Measurement of the left-right charge asymmetry in hadronic Z decays and A(sub e) determination
|DE95-003467| p 1806 N95-23140
Measuring the left-right cross section asymmetry in Z boson production by e(+)e(-) collisions at the SLC
|DE95-003468| p 1807 N95-23141

ASYMPTOTIC METHODS
Stress intensity factors and crack mouth openings for bridged cracks emanating from circular holes
|AR-008-408| p 1699 N95-22952
Influence of porosity and two-phase flow on diffusional/thermal instability of a deflagrating energetic material
|DE95-002592| p 1634 N95-23122
A uniform geometrical optics and an extended uniform geometrical theory of diffraction for evaluating high frequency EM fields near smooth caustics and composite shadow boundaries
|NASA-CR-197934| p 1657 N95-23391

ASYMPTOTIC SERIES
Asymptotically exact solution of the multi-channel resonant-level model
|DE94-629040| p 1801 N95-22498
Strong-coupling behaviour of two t-J chains with interchain single-electron hopping
|DE94-629041| p 1838 N95-22499
Asymptotically exact solution of a local copper-oxide model
|DE94-628492| p 1842 N95-23059

ATLANTIC OCEAN
Oceanic operations: An authoritative guide to oceanic operations
|FAA-AFS-550| p 1610 N95-24065

ATMOSPHERIC BOUNDARY LAYER
Dimethylsulfide oxidation over the tropical South Atlantic: OH and other oxidants
|NASA-CR-197417| p 1732 N95-22930
Observations of the magnetopause current layer: Cases with no boundary layer and tests of recent models
|NASA-CR-197391| p 1738 N95-23184
Physics of magnetospheric boundary layers
|NASA-CR-197920| p 1739 N95-23271
Bursting in the near-surface boundary layer: Comparisons between realistic models and observations
|DE95-003714| p 1741 N95-24078

ATMOSPHERIC CHEMISTRY
Measurement of HO2 and other trace gases in the stratosphere using a high resolution far-infrared spectrometer
|NASA-CR-197368| p 1735 N95-22482
The Atmospheric Lifetime Experiment and the Global Atmospheric Gas Experiment (ALE/GAGE)
|NASA-CR-197400| p 1731 N95-22673
Dimethylsulfide oxidation over the tropical South Atlantic: OH and other oxidants
|NASA-CR-197417| p 1732 N95-22930
The high latitude ionosphere-magnetosphere transition region: Simulation and data comparison
|NASA-CR-197404| p 1737 N95-22956
Compendium of NASA data base for the Global Tropospheric Experiment's Pacific Exploratory Mission West-A (PEM West-A)
|NASA-TM-109177| p 1733 N95-23009
RAS Division model evaluation database description
|DE95-003481| p 1733 N95-23124
Atmospheric peroxides
|DE95-004435| p 1733 N95-23362
Oxidants and oxidation in the Earth's atmosphere
|NASA-CR-197945| p 1734 N95-23460
Laboratory studies of the sensitivity of tropospheric ozone to the chemistry of sea salt aerosol
|DE95-003607| p 1735 N95-24147

ATMOSPHERIC CIRCULATION
Development of an advanced finite difference atmospheric general circulation model
|DE95-003187| p 1736 N95-22879
Format( )MEDIC( )Input
|DE95-003482| p 1737 N95-23063
Conjugate gradient MATHEW
|DE95-003479| p 1738 N95-23143
Bursting in the near-surface boundary layer: Comparisons between realistic models and observations
|DE95-003714| p 1741 N95-24078

ATMOSPHERIC COMPOSITION
The Atmospheric Lifetime Experiment and the Global Atmospheric Gas Experiment (ALE/GAGE)
|NASA-CR-197400| p 1731 N95-22673
Direct effects of atmospheric CO2 enrichment on plants and ecosystems: An updated bibliographic data base
|DE95-003060| p 1731 N95-22725
Compendium of NASA data base for the Global Tropospheric Experiment's Pacific Exploratory Mission West-A (PEM West-A)
|NASA-TM-109177| p 1733 N95-23009
IUE observing programs: NSOSS, VEOEB, and PCOEB
|NASA-CR-197424| p 1866 N95-23560

ATMOSPHERIC CORRECTION
Ocean observations with EOS/MODIS: Algorithm development and post launch studies
|NASA-CR-197402| p 1717 N95-22916
Ocean observations with EOS/MODIS: Algorithm development and post launch studies
|NASA-CR-197894| p 1718 N95-23473
AVIRIS calibration using the cloud-shadow method p 1702 N95-23849
Atmospheric correction of AVIRIS data of Monterey Bay contaminated by thin cirrus clouds p 1710 N95-23890
Laboratory spectra of field samples as a check on two atmospheric correction methods p 1711 N95-23894
Determination of semi-arid landscape endmembers and seasonal trends using convex geometry spectral unmixing techniques p 1711 N95-23895

ATMOSPHERIC EFFECTS
Ocean observations with EOS/MODIS: Algorithm development and post launch studies
|NASA-CR-197402| p 1717 N95-22916
Low Earth orbit thermal control coatings exposure flight tests: A comparison of U.S. and Russian results
|NASA-CR-4647| p 1626 N95-22919
Test method and test results for environmental assessment of aircraft materials p 1643 N95-23509
AVIRIS calibration using the cloud-shadow method p 1702 N95-23849
Estimation of crown closure from AVIRIS data using regression analysis p 1709 N95-23886

ATMOSPHERIC ELECTRICITY
A model for ball lightning
|DE95-003366| p 1742 N95-22701

ATMOSPHERIC GENERAL CIRCULATION MODELS
Development of an advanced finite difference atmospheric general circulation model
|DE95-003187| p 1736 N95-22879
Continued studies of polar cap thermospheric dynamics
|PL-TR-94-2076| p 1737 N95-22951
Technical report series on global modeling and data assimilation. Volume 4: Documentation of the Goddard Earth Observing System (GEOS) data assimilation system, version 1
|NASA-TM-104606-VOL-4| p 1740 N95-23529
Implementation of a soil-canopy scheme into the CSIRO GCM: Regional aspects of the model response
|CSIRO-TR-32| p 1721 N95-24192

ATMOSPHERIC IONIZATION
Magnetospheric space plasma investigations
|NASA-CR-197405| p 1831 N95-22955

ATMOSPHERIC MODELS
A comparison of ionospheric F2-layer IRI model with experimental data for Ibadan Geog. Lat. 7.4 deg N
|DE94-627710| p 1736 N95-22613
Observation model and parameter partials for the JPL VLBI parameter estimation software MODEST, 19 94
|NASA-CR-197328| p 1756 N95-22853
Magnetospheric space plasma investigations
|NASA-CR-197405| p 1831 N95-22955
The high latitude ionosphere-magnetosphere transition region: Simulation and data comparison
|NASA-CR-197404| p 1737 N95-22956
Semikinetic modeling and observations of high-latitude plasma outflow
|NASA-CR-197403| p 1831 N95-23008
Modeling of the coupled magnetospheric and neutral wind dynamos
|NASA-CR-197861| p 1738 N95-23090
RAS Division model evaluation database description
|DE95-003481| p 1733 N95-23124
Physics of magnetospheric boundary layers
|NASA-CR-197920| p 1739 N95-23271
Assimilation of altimeter data in a quasi-geostrophic model of the Gulf Stream system: A dynamical perspective
|NASA-CR-196313| p 1744 N95-23766
Comparison of methods for calibrating AVIRIS data to ground reflectance p 1703 N95-23854
Laboratory spectra of field samples as a check on two atmospheric correction methods p 1711 N95-23894

ATMOSPHERIC MOISTURE
Computer modeling of the sensitivity of a laser water vapor sensor to variations in temperature and air speed p 1692 N95-23330
Temporal changes in endmember abundances, liquid water and water vapor over vegetation at Jasper Ridge p 1708 N95-23882
Implementation of a soil-canopy scheme into the CSIRO GCM: Regional aspects of the model response
|CSIRO-TR-32| p 1721 N95-24192

ATMOSPHERIC PHYSICS
RAS Division model evaluation database description
|DE95-003481| p 1733 N95-23124
Physics of magnetospheric boundary layers
|NASA-CR-197920| p 1739 N95-23271

ATMOSPHERIC RADIATION
Design of a differential radiometer for atmospheric radiative flux measurements
|DE95-002701| p 1739 N95-23244
Theoretical studies of spectroscopic problems of importance for atmospheric radiation measurements p 1741 N95-23329
Implementation of a soil-canopy scheme into the CSIRO GCM: Regional aspects of the model response
|CSIRO-TR-32| p 1721 N95-24192

ATMOSPHERIC SCATTERING
Spectral decomposition of AVIRIS data p 1704 N95-23859
The red edge in arid region vegetation: 340-1060 nm spectra p 1708 N95-23881

ATMOSPHERIC TEMPERATURE
Land surface temperature measurements for EOS MODIS data
|NASA-CR-197443| p 1717 N95-23191

ATMOSPHERIC TURBULENCE
Bursting in the near-surface boundary layer: Comparisons between realistic models and observations
|DE95-003714| p 1741 N95-24078

ATOMIC CLUSTERS
Structure, melting, and reactivity of nickel clusters from numerical simulations
|DE95-002911| p 1638 N95-22531
Ionic core effects on the Mie resonance in lithium clusters
|DE94-014974| p 1805 N95-22870
An algebraic cluster model based on the harmonic oscillator basis p 1814 N95-22971
Calculations of alloy phases with a direct Monte-Carlo method
|DE94-018963| p 1640 N95-23121
Symmetry breaking in O4(+): An application of the Brueckner coupled-cluster method
|NASA-CR-197981| p 1810 N95-23459
Thermochemistry of transition metal clusters
|DE95-003144| p 1646 N95-24144

ATOMIC COLLISIONS
Studies of photon and electron interactions with atoms and ions
|DE95-003340| p 1802 N95-22700
Algebraic description of atom-molecule interactions p 1814 N95-22961
Molecular vibrational states during a collision p 1814 N95-22964
Studies of autoionizing states relevant to dielectronic recombination
|DE94-014162| p 1812 N95-23978

ATOMIC ENERGY LEVELS
The role of triplet correlation function in dense fluids
|DE94-628476| p 1849 N95-22775

ATOMIC EXCITATIONS
Optogalvanic monitoring of collisional transfer of laser excitation energy in a neon RF plasma
| DE95-003103 | p 1691 N95-22748
Slightly anharmonic systems in quantum optics
p 1826 N95-23004
Studies of autoionizing states relevant to dielectronic recombination
| DE94-014162 | p 1812 N95-23978
ATOMIC FORCE MICROSCOPY
Aspects of surface generation in orthogonal ultraprecision machining
| DE95-000922 | p 1654 N95-22678
ATOMIC PHYSICS
Geometrical interpretation for the outer SU(3) outer multiplicity label p 1814 N95-22968
Ninth topical conference on atomic processes in plasmas
| DE95-002810 | p 1833 N95-23246
Atomic physics at high brilliance synchrotron sources: Proceedings
| DE95-006077 | p 1813 N95-24174
ATOMIC STRUCTURE
Photoemission study of quantum confinement by a finite barrier: Cu/Co(wedge)/Cu(100)
| DE95-002913 | p 1840 N95-22762
Correlation effects in high-Tc superconductors and heavy fermion compounds
| DE94-629057 | p 1840 N95-22846
Ligand K-edge x-ray adsorption spectroscopic studies of the electronic structure of inorganic model complexes and metalloprotein active sites
| DE95-003338 | p 1840 N95-22851
Strongly interacting fermion systems
| DE95-003405 | p 1806 N95-23054
The electronic structure of heavy element complexes
| DE95-003407 | p 1806 N95-23082
Calculations of alloy phases with a direct Monte-Carlo method
| DE94-018963 | p 1640 N95-23121
Computational studies of metal-metal and metal-ligand interactions
| NASA-CR-197862 | p 1641 N95-23215
Experimental and theoretical studies on the C15 intermetallic compounds MV2 (M = Zr, Hf and Ta): Elasticity and phase stability
| DE95-003723 | p 1845 N95-24079
ATOMIC WEIGHTS
Precise determinations of the isotopic compositions and atomic weights of molybdenum, tellurium, tin and tungsten using ICP source magnetic sector multiple collector mass spectrometry
| DE95-003003 | p 1632 N95-22795
ATOMIZING
Development of an atomization methodology for spray combustion p 1637 N95-23646
ATOMS
Bose condensation, macroscopic quantum phenomena and atomic spatial correlations in superfluid He-4
| PB95-139085 | p 1850 N95-23154
Atoms as many-body systems
| DE95-004609 | p 1813 N95-24151
ATTACHMENT
Method for forming a glove attachment
| NASA-CASE-MSC-21632-1 | p 1750 N95-22766
ATTENTION
Method of encouraging attention by correlating video game difficulty with attention level
| NASA-CASE-LAR-15022-1 | p 1749 N95-22579
Attention focusing and anomaly detection in systems monitoring p 1769 N95-23683
ATTITUDE (INCLINATION)
Dynamic response tests of inertial and optical wind-tunnel model attitude measurement devices
| NASA-TM-109182 | p 1616 N95-23011
ATTITUDE CONTROL
Moving mass trim control for aerospace vehicles
| DE95-002602 | p 1622 N95-23532
ATTITUDE INDICATORS
Dynamic response tests of inertial and optical wind-tunnel model attitude measurement devices
| NASA-TM-109182 | p 1616 N95-23011
AUDIO SIGNALS
DRACULA: Dynamic range control for broadcasting and other applications
| BBC-RD-1994/13 | p 1658 N95-24044
AUDITORY PERCEPTION
A self-organizing neural network architecture for auditory and speech perception with applications to acoustic and other temporal prediction problems
| AD-A285640 | p 1800 N95-23782
AUDITORY SIGNALS
A self-organizing neural network architecture for auditory and speech perception with applications to acoustic and other temporal prediction problems
| AD-A285640 | p 1800 N95-23782
AUGER SPECTROSCOPY
On core level electron diffraction
| DE94-628484 | p 1842 N95-23048
AUGMENTATION
Design and implementation of two two-week Teacher Enhancement Institutes p 1853 N95-23306
Teacher Enhancement Institute p 1853 N95-23324
AUSTENITIC STAINLESS STEELS
Temperature effects on hydrogen-induced cracking in an iron-based superalloy
| DE95-003037 | p 1639 N95-22724
AUSTRALIA
AIRSAR deployment in Australia, September 1993: Management and objectives p 1714 N95-23948
AUTOCORRELATION
Optical image correlator using orthogonal data storage
| AD-A285795 | p 1819 N95-22508
AUTOIONIZATION
Photoionization of O(6+) below the n=3 threshold of the reduced ion
| DE94-634436 | p 1844 N95-23774
Studies of autoionizing states relevant to dielectronic recombination
| DE94-014162 | p 1812 N95-23978
AUTOMATA THEORY
Taxonomy of finite automata minimization algorithms
| PB95-139226 | p 1756 N95-23131
Automatic verification of regular protocols in P/T nets
| PB95-138921 | p 1789 N95-23146
Taxonomy of finite automata construction algorithms
| PB95-139234 | p 1758 N95-23606
Properties of probabilistic pushdown automata
| TR-554 | p 1760 N95-24056
AUTOMATED GUIDEWAY TRANSIT VEHICLES
Computation of magnetic forces on moving conductors by using ELEKTRA and other 3-D computer codes
| DE95-003308 | p 1798 N95-22895
AUTOMATED PILOT ADVISORY SYSTEM
Differential GPS and system integration of the Low Visibility Landing and Surface Operations (LVLASO) demonstration p 1611 N95-23318
AUTOMATIC CONTROL
Nonlinear system guidance in the presence of transmission zero dynamics
| NASA-TM-4661 | p 1654 N95-22804
Effective management of classified documents using the library document system
| AD-A286021 | p 1855 N95-23024
Material characterization system
| AD-D016536 | p 1800 N95-23073
Performance of the 0.3-meter transonic cryogenic tunnel with air, nitrogen, and sulfur hexafluoride media under closed loop automatic control
| NASA-CR-195052 | p 1668 N95-23257
Low-cost packaging of high-performance optoelectronic components
| DE95-003645 | p 1827 N95-23449
Knowledge-based guidance and control functions
| AGARD-AR-325 | p 1751 N95-23601
Distributed intelligence for ground/space systems
p 1770 N95-23685
Path planning for planetary rover using extended elevation map p 1771 N95-23689
Subsumption-based architecture for autonomous movement planning for planetary rovers
p 1771 N95-23690
Control technique for planetary rover
p 1771 N95-23692
Autonomous navigation system for the Marsokhod rover project p 1771 N95-23693
Design and development status of ETS-7, an RVD and space robot experiment satellite p 1623 N95-23700
The Charlotte (TM) intra-vehicular robot
p 1697 N95-23703
Robot arm system for automatic satellite capture and berthing p 1752 N95-23709
Robust control of multi-jointed arm with a decentralized autonomous control mechanism p 1659 N95-23710
Automatic satellite capture and berthing with robot arm (ASCABRA) p 1623 N95-23713
Automation and crew time saving in the space experiment p 1752 N95-23715
Space science experimentation automation and support p 1775 N95-23718
Robotics and telepresence for moon missions
p 1776 N95-23725
AUTOMATION
The role of flight progress strips in en route air traffic control: A time-series analysis
| DOT/FAA/AM-95/4 | p 1611 N95-23565
Knowledge-based guidance and control functions
| AGARD-AR-325 | p 1751 N95-23601
Network Event Recording Device: An automated system for network anomaly detection, and notification
| DE94-018274 | p 1658 N95-23772
Automated solar cell assembly teamed process research
| DE95-000299 | p 1730 N95-23777
Functions of external cues in prospective memory
| DOT/FAA/AM-95/9 | p 1750 N95-24088
AUTOMOBILE ENGINES
Advanced Turbine Technology Applications Project (ATTAP) 1993 annual report
| DE95-003198 | p 1693 N95-22880
AUTOMOBILES
Technology maturation project on optimization of sheet metal forming of aluminum for use in transportation systems
| DE95-003005 | p 1654 N95-22692
AUTONOMOUS NAVIGATION
Third International Symposium on Artificial Intelligence, Robotics, and Automation for Space 1994
| NASA-CR-197340 | p 1767 N95-23672
Subsumption-based architecture for autonomous movement planning for planetary rovers
p 1771 N95-23690
Very fast motion planning for highly dexterous-articulated robots p 1771 N95-23691
Control technique for planetary rover
p 1771 N95-23692
Autonomous navigation system for the Marsokhod rover project p 1771 N95-23693
Lunar rover technology demonstrations with Dante and Ratler p 1697 N95-23694
A perspective on space robotics in Japan
p 1697 N95-23695
Autonomous spacecraft executive and its application to rendezvous and docking p 1623 N95-23719
Terrain modelling and motion planning for an autonomous exploration rover p 1721 N95-23765
AUTONOMY
JPL space robotics: Present accomplishments and future thrusts p 1697 N95-23697
Robust control of multi-jointed arm with a decentralized autonomous control mechanism p 1659 N95-23710
Formalizing procedures for operations automation, operator training and spacecraft autonomy
p 1752 N95-23720
Interactive autonomy and robotic skills
p 1777 N95-23730
Active vision in satellite scene analysis
p 1778 N95-23738
CRI planning and scheduling for space
p 1617 N95-23751
A self-organizing neural network architecture for auditory and speech perception with applications to acoustic and other temporal prediction problems
| AD-A285640 | p 1800 N95-23782
AUXILIARY POWER SOURCES
Motor drive technologies for the power-by-wire (PBW) program: Options, trends and tradeoffs
| NASA-TM-106885 | p 1616 N95-23671
AXIAL FLOW
CFD modeling of turbulent duct flows for coolant channel analysis p 1682 N95-23635
AXIAL LOADS
The development of shell imperfection measurement techniques
| TAE-712 | p 1699 N95-23923
AXIOMS
Temporal operators viewed as predicate transformers
| PB95-138996 | p 1757 N95-23152
Bose condensation, macroscopic quantum phenomena and atomic spatial correlations in superfluid He-4
| PB95-139085 | p 1850 N95-23154
Marginalistic value for monotonic set games
| PB95-140646 | p 1794 N95-23239
Set games
| PB95-140786 | p 1794 N95-23539
AXISYMMETRIC BODIES
Status of axisymmetric CFD of an eleven inch diameter hybrid rocket motor p 1686 N95-23651
AXISYMMETRIC FLOW
BEM solution to simulate the curvature driven deformation of a profile that is pressed into a plate of hot glass
| PB95-138913 | p 1648 N95-23145
Supersonic jet noise reductions predicted with increased jet spreading rate
| NASA-TM-106872 | p 1800 N95-23178
A generic efficient adaptive grid scheme for rocket propulsion modeling p 1670 N95-23418
TIGER: A user-friendly interactive grid generation system for complicated turbomachinery and axis-symmetric configurations p 1670 N95-23419
Computational Fluid Dynamic (CFD) analysis of axisymmetric plume and base flow of film/dump cooled rocket nozzle p 1673 N95-23431
Validation of a Computational Fluid Dynamics (CFD) code for supersonic axisymmetric base flow
p 1686 N95-23652

B

B STARS
Long term variability of B supergiant winds
|NASA-CR-197925| p 1865 N95-23401
A study of EUV emission from the O4f star Zeta Puppis
|NASA-CR-197350| p 1871 N95-23472

BACILLUS
Biotransformation of an uncured composite material
p 1629 N95-23033

BACKGROUND NOISE
Motion-sensitive optical correlator using a VanderLugt correlator
|NASA-CASE-NPO-18769-1-CU| p 1827 N95-23045

BACKSCATTERING
Theoretical estimates of high frequency acoustic attenuation and backscattering from suspended sand particles in the ocean and in an estuary
|DSTO-TR-0078| p 1743 N95-23667
Interferometric synthetic aperture radar imagery of the Gulf Stream p 1712 N95-23939
AIRSAR views of aerolian terrain
p 1713 N95-23941
Estimation of biophysical properties of upland Sitka spruce (Picea sitchensis) plantations
p 1713 N95-23943
Polarimetric radar data decomposition and interpretation p 1715 N95-23955
Synergy between optical and microwave remote sensing to derive soil and vegetation parameters from MAC Europe 1991 Experiment p 1715 N95-23956
Relating P-band AIRSAR backscatter to forest stand parameters p 1716 N95-23959
Soil moisture retrieval in the Oberpfaffenhofen testsite using MAC Europe AIRSAR data p 1716 N95-23960
Microwave dielectric properties of boreal forest trees
p 1716 N95-23961

BACKWARD DIFFERENCING
BEm-BDF scheme for curvature driven moving stokes flows
|PB95-138905| p 1667 N95-23144
BEM solution to simulate the curvature driven deformation of a profile that is pressed into a plate of hot glass
|PB95-138913| p 1648 N95-23145
Numerical simulation of axisymmetric viscous sintering
|PB95-138889| p 1667 N95-23175

BACTERIA
Continuous production of cellulase in a fluidized-bed reactor by Pseudonomas fluorescens immobilized in hydrogel beads
|DE94-014105| p 1744 N95-22588

BALANCING
Normalized coprime factorizations and balancing for unstable nonlinear systems
|PB95-141222| p 1767 N95-23557

BALL BEARINGS
Finite-difference solutions of the alternate turbopump development high-pressure oxidizer turbopump pump-end ball-bearing cavity flows p 1678 N95-23617

BALL LIGHTNING
A model for ball lightning
|DE95-003366| p 1742 N95-22701

BALLISTIC MISSILES
Ballistic Missile Defense: Current status of strategic target system. Report to Congressional requesters
|GAO/NSIAD-95-78| p 1903 N95-24080

BALLISTIC VEHICLES
Moving mass trim control for aerospace vehicles
|DE95-002602| p 1622 N95-23532

BALLOON FLIGHT
Measurement of HO2 and other trace gases in the stratosphere using a high resolution far-infrared spectrometer
|NASA-CR-197368| p 1735 N95-22482

BALLOONING MODES
Experimental achievement of toroidal beta beyond that predicted by 'Troyon' scaling
|DE95-003880| p 1837 N95-24087

BANACH SPACE
Spectral application of the theorem for the essential quasi-Fredholm spectrum
|DE94-628430| p 1795 N95-22632
Iterative solutions of nonlinear equations with strongly accretive or strongly pseudocontractive maps
|DE94-628432| p 1786 N95-22634
Idempotents in Banach algebra
|DE94-628429| p 1787 N95-22794
Analytic sets and games in Banach spaces
|PB95-108080| p 1787 N95-22837
Iterative solutions of nonlinear equations in smooth Banach spaces
|DE94-634287| p 1790 N95-23455
Ishikawa iteration process for nonlinear Lipschitz strongly accretive mappings
|DE94-634284| p 1792 N95-23658

BAND RATIOING
Optimal band selection for dimensionality reduction of hyperspectral imagery p 1709 N95-23887

BAND STRUCTURE OF SOLIDS
Correlation effects in high-Tc superconductors and heavy fermion compounds
|DE94-629057| p 1840 N95-22846

BANDWIDTH
Limited bandwidth microwave filter
|AD-D016553| p 1660 N95-22708
Effects of modulation index on telecommunications
|AD-A286018| p 1657 N95-23023

BARIUM
Studies of autoionizing states relevant to dielectronic recombination
|DE94-014162| p 1812 N95-23978

BARIUM COMPOUNDS
Effect on c-axis transport properties of a critical state in Bi2Sr2CaCu2O8
|DE95-003695| p 1843 N95-23366
Transport properties of Tl2Ba2CaCu2O8 meander lines
|DE95-003715| p 1843 N95-23367

BARIUM OXIDES
Superconducting Tl2Ba2CaCu2O8 thin films prepared by post-annealing in a flow-through multiple-zone furnace
|DE95-002745| p 1838 N95-22520
Preparation of high quality YBa2Cu3O(7-delta) thick films on flexible Ni-based alloy substrates with textured buffer layers
|DE95-003686| p 1645 N95-23571
Phonon characteristics of high (T sub c) superconductors from neutron Doppler broadening measurements
|DE95-003703| p 1844 N95-24076

BARIUM TITANATES
A study of ceramic composite of ferroelectric BaTiO3 ceramic and superconductor YBa2Cu3O(6+delta) ceramic
|DE94-627563| p 1647 N95-22610
A special percolation problem in ceramic composites
|DE94-627641| p 1647 N95-22611

BARYON RESONANCE
Theoretical aspects of electroweak and other interactions in medium energy nuclear physics
|DE95-004341| p 1808 N95-23357

BARYONS
Searches for the H-dibaryon at the AGS
|DE95-003091| p 1802 N95-22727
Do narrow Sigma hypernuclear states exist?
|DE95-002930| p 1803 N95-22763
Baryon number fluctuations in a quark-hadron phase transition
|DE94-628585| p 1804 N95-22786
Charm-conserving strangeness-changing two body hadronic decays of charmed baryons
|DE94-628621| p 1811 N95-23770

BASALT
Axial focusing of impact energy in the earth's interior: A possible link to flood basalts and hotspots
|DE95-003357| p 1741 N95-24009

BASE FLOW
Axisymmetric computational fluid dynamics analysis of Saturn V/S1-C/F1 nozzle and plume
p 1672 N95-23430
Computational Fluid Dynamic (CFD) analysis of axisymmetric plume and base flow of film/dump cooled rocket nozzle p 1673 N95-23431
NLS base heating CFD analysis p 1673 N95-23432
Validation of a Computational Fluid Dynamics (CFD) code for supersonic axisymmetric base flow
p 1686 N95-23652
Code validation study for base flows
p 1686 N95-23653
Four-nozzle benchmark wind tunnel model USA code solutions for simulation of multiple rocket base flow recirculation at 145,000 feet altitude
p 1686 N95-23654
Numerical study of base pressure characteristic curve for a four-engine clustered nozzle configuration
p 1625 N95-23655

BASE HEATING
NLS base heating CFD analysis p 1673 N95-23432
Code validation study for base flows
p 1686 N95-23653
Four-nozzle benchmark wind tunnel model USA code solutions for simulation of multiple rocket base flow recirculation at 145,000 feet altitude
p 1686 N95-23654
Numerical study of base pressure characteristic curve for a four-engine clustered nozzle configuration
p 1625 N95-23655

BASE PRESSURE
CFD flowfield simulation of Delta Launch Vehicles in a power-on configuration p 1673 N95-23433
Numerical study of base pressure characteristic curve for a four-engine clustered nozzle configuration
p 1625 N95-23655

BAUXITE
Be-10 in terrestrial bauxite and industrial aluminum: An LDEF fallout p 1646 N95-23820

BAYES THEOREM
Learning time series for intelligent monitoring
p 1770 N95-23686
Optimal band selection for dimensionality reduction of hyperspectral imagery p 1709 N95-23887

BEACONS
Cueing light configuration for aircraft navigation
|NASA-CASE-ARC-11982-1| p 1611 N95-23393

BEAM CURRENTS
D3-D program overview
|DE95-003879| p 1837 N95-24086

BEAM INTERACTIONS
Multipole contribution from an off-axis orbit in an IR quadrupole and the consequences on the dynamic aperture
|DE95-002874| p 1816 N95-22567
Atomic physics at high brilliance synchrotron sources: Proceedings
|DE95-006077| p 1813 N95-24174

BEAMFORMING
Electron beam acceleration and compression for short wavelength FELs
|DE95-003371| p 1691 N95-22704
Adaptive beamforming in a CDMA mobile satellite communications system p 1655 N95-22815

BEAMS
Standardization of CDF and D(O) reported luminosities
|DE95-003388| p 1818 N95-24077

BEAMS (SUPPORTS)
A coupled layerwise analysis of the thermopiezoelectric response of smart composite beams beams
|NASA-TM-106889| p 1630 N95-23463

BENZENE
Pressure shifts and electron scattering in atomic and molecular gases
|DE95-003102| p 1803 N95-22747

BERGMAN OPERATOR
Noisy bases in Hilbert space: A new class of thermal coherent states and their properties
p 1823 N95-22980

BERYLLIUM
Solar mass loss, solar lithium, and solar oscillations
|DE94-018262| p 1870 N95-22938
Beryllium in the ITER blanket
|DE95-004620| p 1837 N95-24165

BERYLLIUM ISOTOPES
Be-10 in terrestrial bauxite and industrial aluminum: An LDEF fallout p 1646 N95-23820

BERYLLIUM OXIDES
Beryllium in the ITER blanket
|DE95-004620| p 1837 N95-24165

BETA FACTOR
Non-Taylor magnetohydrodynamic self-organization
|NIFS-314| p 1834 N95-23524
Theory of pressure-induced islands and self-healing in three-dimensional toroidal magnetohydrodynamic equilibria
|NIFS-321| p 1836 N95-23589

BETA PARTICLES
The q profile evolution and enhanced core confinement of high (beta)(sub p) plasmas in D3-D
|DE95-003878| p 1834 N95-23371
MHD-Vlasov simulation of the toroidal Alfven eigenmode
|NIFS-319| p 1836 N95-23591
Neutrinoless double beta decay and the solar neutrino problem
|DE94-628633| p 1812 N95-23785

BETHE-SALPETER EQUATION
Hadrons of arbitrary spin and heavy quark symmetry
|DE94-628597| p 1804 N95-22789
Scale-invariant Lipatov kernels from t-channel unitarity
|DE95-004625| p 1813 N95-24166

BIAS
High power Josephson effect sources
|AD-A285808| p 1838 N95-22511
VLPC characterization for the Dzero upgrade
|DE95-003742| p 1818 N95-24084

BIBLIOGRAPHIES
Direct effects of atmospheric CO2 enrichment on plants and ecosystems: An updated bibliographic data base
|DE95-003060| p 1731 N95-22725
FY 1994 scientific and technical reports, articles, papers, and presentations
|NASA-TM-108480| p 1856 N95-23225

Oak Ridge National Laboratory Energy Efficiency and Renewable Energy Program Bibliography: 1994 Edition
[DE95-002296] p 1730 N95-23605

BIHARMONIC EQUATIONS
Effects of long-range coupling on aggregation
[DE94-628483] p 1842 N95-23047

BIMETALS
Infrared study of carbon deposits on bimetallic catalysts
[DE95-000902] p 1631 N95-22517
Organometallic chemistry of bimetallic compounds
[DE95-004436] p 1634 N95-23345

BINARY FLUIDS
Small angle x ray scattering studies of aggregation in supercritical fluid solutions
[DE95-004576] p 1843 N95-23579

BINARY MIXTURES
Pressure shifts and electron scattering in atomic and molecular gases
[DE95-003102] p 1803 N95-22747

BINARY PHASE SHIFT KEYING
Effects of modulation index on telecommunications
[AD-A286018] p 1657 N95-23023

BINARY STARS
Long term variability of B supergiant winds
[NASA-CR-197925] p 1865 N95-23401

BIOASSAY
The development and applications of biomarkers
[DE94-014249] p 1744 N95-22589

BIOCHEMISTRY
The development and applications of biomarkers
[DE94-014249] p 1744 N95-22589
General crystal in prebiotic context
[DE94-628475] p 1840 N95-22774
Transmethylation reactions during methanogenesis from acetate in Methanosarcina barkeri
[DE94-016222] p 1745 N95-22873
Analysis of structural domains required for phytochrome function by in vitro mutagenesis
[DE94-016230] p 1745 N95-22884
Membrane phase separations, asymmetry and implications in the origin of life
[DE94-628486] p 1747 N95-23050
The origin of chirality in protein amino acids
[DE94-628491] p 1747 N95-23058
A comparative study of the effects of clofibrate, ciprofibrate, WY-14,643, and di-(2-ethylhexyl)-phthalate on liver protein expression in mice
[DE94-016587] p 1748 N95-23771
Use of spectral analogy to evaluate canopy reflectance sensitivity to leaf optical property p 1701 N95-23845
AVIRIS spectra correlated with the chlorophyll concentration of a forest canopy p 1705 N95-23871
The effect of signal noise on the remote sensing of Foliar biochemical concentration p 1708 N95-23884
Relationships between pigment composition variation and reflectance for plant species from a coastal savannah in California p 1709 N95-23889
Investigations on the 1.7 micron residual absorption feature in the vegetation reflection spectrum p 1710 N95-23891
The 1993 Gordon Research Conference on Chronobiology
[NASA-CR-197990] p 1748 N95-24047

BIOCONVERSION
Design and demonstration of an immobilized-cell fluidized-bed reactor for the efficient production of ethanol
[DE94-014023] p 1652 N95-22587

BIODEGRADATION
Biotransformation of an uncured composite material p 1629 N95-23033
Monitoring land use and degradation using satellite and airborne data p 1707 N95-23880

BIOLOGICAL EFFECTS
Activation of the jun-D gene in human myeloid cells by 1-(beta)-D-arabinofuranosylcytosine
[DE94-016591] p 1746 N95-22912
All systems go!
[NASA-TM-110542] p 1620 N95-23665
A comparative study of the effects of clofibrate, ciprofibrate, WY-14,643, and di-(2-ethylhexyl)-phthalate on liver protein expression in mice
[DE94-016587] p 1748 N95-23771
Biological interactions and human health effects of static magnetic fields
[DE95-003147] p 1749 N95-24145

BIOLOGICAL EVOLUTION
Membrane phase separations, asymmetry and implications in the origin of life
[DE94-628486] p 1747 N95-23050
Molecular relics from chemical evolution and the origin of life
[DE94-628493] p 1747 N95-23060

BIOLOGICAL MODELS (MATHEMATICS)
Design of a cervical spine gross motion simulator for standard size human and anthropomorphic dummy adult and child
[NIAR-94-16] p 1751 N95-24021

BIOMASS
Development of a multi-sensor in situ fiber optic fluorometer
[DE95-003105] p 1819 N95-22780
Renewable Energy Sources Brno 1993
[DE94-633975] p 1727 N95-22855
Development of the IGT RENUGAS(reg sign) process
[DE94-017652] p 1727 N95-22888
Estimating dry grass residues using landscape integration analysis p 1705 N95-23867
The red edge in arid region vegetation: 340-1060 nm spectra p 1708 N95-23881
Synergy between optical and microwave remote sensing to derive soil and vegetation parameters from MAC Europe 1991 Experiment p 1715 N95-23956
Relating P-band AIRSAR backscatter to forest stand parameters p 1716 N95-23959

BIOMASS ENERGY PRODUCTION
Design and demonstration of an immobilized-cell fluidized-bed reactor for the efficient production of ethanol
[DE94-014023] p 1652 N95-22587

BIOMETRICS
The development and applications of biomarkers
[DE94-014249] p 1744 N95-22589

BIOPHYSICS
Protein folding and protein metallocluster studies using synchrotron small angler x ray scattering
[DE95-003339] p 1746 N95-22897
Membrane phase separations, asymmetry and implications in the origin of life
[DE94-628486] p 1747 N95-23050
Estimation of biophysical properties of upland Sitka spruce (Picea sitchensis) plantations p 1713 N95-23943

BIOPROCESSING
Development of novel separation techniques for biological samples in capillary electrophoresis
[DE95-001672] p 1744 N95-22493
Continuous production of cellulase in a fluidized-bed reactor by Pseudonomas fluorescens immobilized in hydrogel beads
[DE94-014105] p 1744 N95-22588

BIOREACTORS
Design and demonstration of an immobilized-cell fluidized-bed reactor for the efficient production of ethanol
[DE94-014023] p 1652 N95-22587
Continuous production of cellulase in a fluidized-bed reactor by Pseudonomas fluorescens immobilized in hydrogel beads
[DE94-014105] p 1744 N95-22588
Biological determinants of photobioreactor design
[DE94-016032] p 1745 N95-22872

BIOSPHERE
Assessing the relative contribution of biogenic and fossil processes to visibility scattering aerosols found in remote areas: Near-term Organic Research Program
[DE95-003149] p 1735 N95-24146

BIOSYNTHESIS
A comparative study of the effects of clofibrate, ciprofibrate, WY-14,643, and di-(2-ethylhexyl)-phthalate on liver protein expression in mice
[DE94-016587] p 1748 N95-23771

BIOTECHNOLOGY
Biological determinants of photobioreactor design
[DE94-016032] p 1745 N95-22872

BIRDS
Old-growth and mature forests near spotted owl nests in western Oregon p 1719 N95-24098

BISMALEIMIDE
Biotransformation of an uncured composite material p 1629 N95-23033
The detection and analysis of galvanic damage in BMI/graphite fiber composites p 1631 N95-23502

BISMUTH OXIDES
Some aspects of critical currents in Ag sheathed Bi2Sr2Ca2Cu3O10 composite tapes: A summary
[DE95-003952] p 1842 N95-23354
Cooling rate effects on the microstructure, critical current density, and (T(sub c)) transition of one- and two-powder BSCCO-2223 Ag sheathed tapes
[DE95-004639] p 1846 N95-24171

BISPHENOLS
Biotransformation of an uncured composite material p 1629 N95-23033

BLACK BODY RADIATION
ROSAT observation program
[NASA-CR-197683] p 1866 N95-23595

BLACK HOLES (ASTRONOMY)
Black hole formation and space-time fluctuations in two dimensional dilaton gravity and complementarity
[DE94-628514] p 1867 N95-22739
Shannon-Wehrl entropy for cosmological and black-hole squeezing p 1826 N95-23000

BLADE TIPS
GGOT total pressure loss control concept evaluation p 1672 N95-23427
Navier-Stokes analysis of an oxidizer turbine blade with tip clearance with and without a mini-shroud p 1672 N95-23428
Supersonic flow and shock formation in turbine tip gaps p 1672 N95-23429

BLANKETS (FUSION REACTORS)
Beryllium in the ITER blanket
[DE95-004620] p 1837 N95-24165

BLOCK COPOLYMERS
Reflectivity studies on adsorbed block copolymers under shear
[DE95-003676] p 1649 N95-23568

BOATS
SWIFT BOAT 1994: Using a fast chase boat to investigate offshore weather features in conjunction with WSR-88D observations
[PB94-195146] p 1742 N95-22651

BODY CENTERED CUBIC LATTICES
Epitaxial growth of bcc transition metal films and superlattices onto MgO (111), (011) and (001) substrates
[DE95-004629] p 1846 N95-24168

BOEING 737 AIRCRAFT
Differential GPS and system integration of the Low Visibility Landing and Surface Operations (LVLASO) demonstration p 1611 N95-23318

BOLOMETERS
High Tc superconducting bolometric and nonbolometric infrared (IR) detectors
[NASA-CR-197868] p 1827 N95-23224

BONDED JOINTS
Support research for solid oxide fuel cells
[DE95-002910] p 1726 N95-22568
Explosive bonding and its application in the Advanced Photon Source front-end and beamline components design
[DE95-004132] p 1696 N95-23397

BONDING
Explosive bonding and its application in the Advanced Photon Source front-end and beamline components design
[DE95-004132] p 1696 N95-23397

BORON 10
Continuation of BNCT Research Program at NEMC and MIT
[DE94-016228] p 1748 N95-22875

BOSONS
Fermion-spin transformation to implement the charge-spin separation
[DE94-629035] p 1800 N95-22495
The first measurement of the left-right cross section asymmetry in Z(sup 0) boson production
[DE95-003335] p 1802 N95-22697
Measurement of the left-right asymmetry in Z boson production by electron-positron collisions
[DE95-003337] p 1802 N95-22699
Geometrical interpretation for the outer SU(3) outer multiplicity label p 1814 N95-22968
Boson mapping techniques applied to constant gauge fields in QCD p 1814 N95-22969
Shapes and stability of algebraic nuclear models p 1814 N95-22974
q-bosons and the q-analogue quantized field p 1814 N95-22984
The Duffin-Kemmer-Petiau oscillator p 1825 N95-22998
Heavy quark physics at SLD: Preliminary results
[DE95-003372] p 1806 N95-23138
Measuring the left-right cross section asymmetry in Z boson production by e(+)e(-) collisions at the SLC
[DE95-003468] p 1807 N95-23141
Properties of jets in Z events from 1.8 TeV (bar p)p collisions
[DE94-018982] p 1808 N95-23197
Search for Z' and W' at CDF
[DE94-018987] p 1808 N95-23203
Search for new gauge bosons at D(O)
[DE95-003745] p 1809 N95-23404
Measurement of W and Z boson production and extraction of the W width and branching ratios at CDF
[DE94-018989] p 1810 N95-23522
Electroweak physics from the Tevatron
[DE95-002213] p 1810 N95-23530
W mass measurements from D(circle slash) and CDF experiments at TeVatron
[DE95-003497] p 1813 N95-24000

A measurement of the mass of the W vector boson at CDF
|DE95-003498| p 1813 N95-24016
BOUNDARIES
Neural network for detection and correction of local boundary misalignments between images
|AD-D016539| p 1766 N95-22705
A uniform geometrical optics and an extended uniform geometrical theory of diffraction for evaluating high frequency EM fields near smooth caustics and composite shadow boundaries
|NASA-CR-197934| p 1657 N95-23391
BOUNDARY CONDITIONS
Treewidth and pathwidth of cocomparability graphs of bounded dimension
|PB95-127239| p 1785 N95-22535
Black hole formation and space-time fluctuations in two dimensional dilaton gravity and complementarity
|DE94-628514| p 1867 N95-22739
Sullivan model for wetting transition in closed system
|DE94-628472| p 1665 N95-22771
Quantum field between moving mirrors: A three dimensional example p 1821 N95-22965
Effect of critical field on screened dielectric breakdown growth
|DE94-628482| p 1661 N95-23046
Conjugate gradient MATHEW
|DE95-003479| p 1738 N95-23143
Observations of the magnetopause current layer: Cases with no boundary layer and tests of recent models
|NASA-CR-197391| p 1738 N95-23184
Three-dimensional viscous flow analysis inside a turbine volute p 1674 N95-23437
Advanced turbulence models for turbomachinery p 1675 N95-23443
Fourth order difference methods for hyperbolic IBVP's
|NASA-CR-197955| p 1791 N95-23548
Sensitivity of combustion-acoustic instabilities to boundary conditions for premixed gas turbine combustors
|NASA-TM-106890| p 1614 N95-23550
CFD parametric study of consortium impeller p 1680 N95-23626
BOUNDARY ELEMENT METHOD
BEm-BDF scheme for curvature driven moving stokes flows
|PB95-138905| p 1667 N95-23144
BEM solution to simulate the curvature driven deformation of a profile that is pressed into a plate of hot glass
|PB95-138913| p 1648 N95-23145
Numerical simulation of axisymmetric viscous sintering
|PB95-138889| p 1667 N95-23175
BOUNDARY LAYER COMBUSTION
Fundamental phenomena on fuel decomposition and boundary layer combustion processes with applications to hybrid rocket motors
|NASA-CR-197919| p 1625 N95-23261
BOUNDARY LAYER CONTROL
Supersonic laminar flow control research
|NASA-CR-197938| p 1609 N95-23669
BOUNDARY LAYER EQUATIONS
An approximate theoretical method for modeling the static thrust performance of non-axisymmetric two-dimensional convergent-divergent nozzles
|NASA-CR-195050| p 1608 N95-23193
BOUNDARY LAYER FLOW
Active control of panel vibrations induced by a boundary layer flow
|NASA-CR-197867| p 1608 N95-23182
BOUNDARY LAYER SEPARATION
Control of flow separation in airfoil/wing design applications p 1609 N95-23294
BOUNDARY LAYER STABILITY
Supersonic laminar flow control research
|NASA-CR-197938| p 1609 N95-23669
BOUNDARY LAYER TRANSITION
Crossflow instability control on a swept-wing: Preliminary studies p 1609 N95-23283
High-lift flow-physics flight experiments on a subsonic civil transport aircraft (B737-100) p 1609 N95-23333
Supersonic laminar flow control research
|NASA-CR-197938| p 1609 N95-23669
BOUNDARY LAYERS
Optimized design of a hypersonic nozzle p 1617 N95-23304
BOUNDARY VALUE PROBLEMS
Remarks on multiple solutions for asymptotically linear elliptic boundary value problems
|DE94-628416| p 1785 N95-22624
A prescribing geodesic curvature problem
|DE94-628503| p 1787 N95-22750
Quasistatic model for the motion of a viscous capillary liquid drop
|PB95-138848| p 1667 N95-23172
Stoermer-Cowell: Straight, summed and split. An overview
|PB95-139341| p 1789 N95-23200
The initial-value problem for viscous channel flows
|NASA-CR-195034| p 1667 N95-23207
Orders of predictor-corrector pairs for second-order ODE's
|PB95-140612| p 1790 N95-23237
Dynamic response of a transducer mounted at one end of an acoustical cavity which is subjected to a specified pressure at the open end of the cavity
|DE95-004192| p 1799 N95-23379
Fourth order difference methods for hyperbolic IBVP's
|NASA-CR-197955| p 1791 N95-23548
The point interactions in the quantum problem of three particles with internal structure
|DE94-635423| p 1851 N95-23967
BOW WAVES
Investigation of infra-red and nonequilibrium air radiation
|NASA-CR-197977| p 1741 N95-24041
BOX BEAMS
Flutter analysis of composite box beams
|NASA-CR-197931| p 1615 N95-23392
BRAGG ANGLE
Photoinduced Bragg grating formation in optical fibres as a consequence of convective instability
|DE94-628479| p 1841 N95-23020
BRAIN
Unsupervised classification learning from cross-modal environmental structure
|TR-536| p 1784 N95-24040
BRANCHING (MATHEMATICS)
Dynamics of L to H bifurcation
|DE94-019126| p 1832 N95-23163
Degenerate Hamiltonian Hopf bifurcations
|PB95-138871| p 1789 N95-23174
New determination of V(sub us) from K(sub e3)(+) decay
|DE94-628616| p 1811 N95-23769
BRAZING
Sensor-based control of rocket thrust chamber feature location for automated braze paste dispensing
|DE94-016559| p 1624 N95-22885
BREEDER REACTORS
Beryllium in the ITER blanket
|DE95-004620| p 1837 N95-24165
BREMSSTRAHLUNG
Hard e(+)e(-)-pair Bremsstrahlung as a lepton polarimeter
|DE94-635615| p 1812 N95-23984
BRIDGMAN METHOD
USML-1 Glovebox experiments
|NASA-CR-196574| p 1653 N95-24028
BRIGHTNESS
Preserving the high source brightness with x ray beam line optics
|DE95-003172| p 1820 N95-22877
BRITTLE MATERIALS
Determining orbital particle parameters of impacts into germanium using morphology analysis and calibration data from hypervelocity impact experiments in the laboratory p 1700 N95-23841
BRITTLENESS
Morphology of extinguished monolithic JA2 grains fired in a 30-mm Solid Propellant Electrothermal Chemical (SPETC) gun
|AD-A285792| p 1652 N95-22506
BROADCASTING
Addendum to the Proceedings of the Third International Mobile Satellite Conference (IMSC 1993)
|NASA-CR-197343| p 1655 N95-22813
Utilizing a TDRS satellite for direct broadcast satellite-radio propagation experiments and demonstrations p 1622 N95-22814
The possibilities for mobile and fixed services up to the 20/30 GHz frequency bands p 1656 N95-22817
DRACULA: Dynamic range control for broadcasting and other applications
|BBC-RD-1994/13| p 1658 N95-24044
The sound insulations of studio doors. Part 2: Door seals
|BBC-RD-1994/15| p 1654 N95-24045
The sound insulations of studio doors. Part 1: Door blanks
|BBC-RD-1994/14| p 1654 N95-24093
BROKEN SYMMETRY
A model of mesons based on chi SB in the light-front frame
|DE95-003203| p 1802 N95-22731
Chiral symmetry breaking in QCD with linearly rising confinement potential
|DE94-628559| p 1848 N95-22744
Spontaneous breaking of chiral symmetry as a consequence of confinement
|DE94-628560| p 1849 N95-22745
Supersymmetric singlet majorons and cosmology
|DE94-628571| p 1850 N95-22783
The origin of chirality in protein amino acids
|DE94-628491| p 1747 N95-23058
Higgs searches and WW scattering
|PB95-139143| p 1807 N95-23160
Symmetry breaking in O4(+): An application of the Brueckner coupled-cluster method
|NASA-CR-197981| p 1810 N95-23459
BSCCO SUPERCONDUCTORS
High-temperature ultrasonic characterization of Ag-clad superconductor tapes
|DE95-002909| p 1838 N95-22530
Design and production of efficient current leads for 1500-A, 50-Hz service in a 77-4 K temperature gradient
|DE95-004121| p 1662 N95-23355
Effects of Bi and Bi2O3 additions on the microstructure and superconducting properties of powder-in-tube BSCCO (2212) tapes
|DE95-004605| p 1845 N95-24150
BUBBLES
Investigation of the role of gravity waves in the generation of equatorial bubbles
|NASA-CR-197962| p 1739 N95-23272
A generalized Eulerian-Lagrangian analysis, with application to liquid flows with vapor bubbles p 1682 N95-23633
BUCKLING
The development of shell imperfection measurement techniques
|TAE-712| p 1699 N95-23923
BUFFETING
Preliminary identification of buffet problems in high speed civil transport p 1616 N95-23319
BUILDINGS
Mercury detection with thermal neutrons
|DE95-002061| p 1806 N95-23055
Locating buildings in aerial photos p 1721 N95-23295
BUMPERS
Micro-abrasion package capture cell experiment on the trailing edge of LDEF: Impactor chemistry and whipple bumper shield efficiencies p 1624 N95-23835
BUNDLES
Method for making fiber-optic bundle collimator assembly
|AD-D016491| p 1819 N95-22492
Grassman and hyperKaehler structures on some spaces of sections of holomorphic bundles
|PB95-109104| p 1795 N95-22712
Trisecant curve associated to a smooth curve in P(sub 3) of degree d greater than g+2
|DE94-628425| p 1787 N95-22809
A fiber-optic bundle and collimator assembly
|AD-D016500| p 1820 N95-22864
Collisionless magnetic reconnection associated with coalescence of flux bundles
|NIFS-315| p 1834 N95-23525
Universal Hodge bundle and Mumford isomorphisms on the abelian inductive limit of Teichmueller spaces
|DE94-634325| p 1796 N95-23660
BUOYANCY
Modeling NO(x) emissions in turbulent jet flames: Effects of buoyancy and radiation
|DE94-016621| p 1633 N95-22886
BURGER EQUATION
Fourth order difference methods for hyperbolic IBVP's
|NASA-CR-197955| p 1791 N95-23548
BURSTS
Bursting in the near-surface boundary layer: Comparisons between realistic models and observations
|DE95-003714| p 1741 N95-24078

C

C (PROGRAMMING LANGUAGE)
An expert system for diagnosing anomalies of spacecraft p 1770 N95-23684
CADMIUM
Corrosion prevention with environmentally compliant materials: A design challenge p 1644 N95-23511
CADMIUM ISOTOPES
Large-sized and highly radioactive H-3 and Cd-109 Langmuir-Blodgett films
|DE94-785270| p 1811 N95-23775
CADMIUM TELLURIDES
Study of photorefractive non-linearities in the 3-5 and 2-4 semi-insulator compounds: The effect of electron irradiation
|PB94-189057| p 1839 N95-22584
Polycrystalline CuInSe2 and CdTePV solar cells
|DE95-000244| p 1727 N95-22842

CALCIUM
MOCVD of gallium and calcium sulfides for improved phosphor processing
[DE95-000918] p 1631 N95-22677
CALCIUM COMPOUNDS
MHD seed recovery and regeneration, phase 2
[DE95-004308] p 1833 N95-23338
Effect on c-axis transport properties of a critical state in Bi2Sr2CaCu2O8
[DE95-003695] p 1843 N95-23366
Transport properties of Tl2Ba2CaCu2O8 meander lines
[DE95-003715] p 1843 N95-23367
CALCIUM ISOTOPES
Rate coefficients for the electron-impact excitation, ionization and recombination of He-like ions, S XV, Ca XIX and Fe XXV, and related processes
[ISAS-R-657] p 1811 N95-23604
CALCIUM OXIDES
Superconducting Tl2Ba2CaCu2O8 thin films prepared by post-annealing in a flow-through multiple-zone furnace
[DE95-002745] p 1838 N95-22520
Conversion of light hydrocarbon gases to metal carbides for production of liquid fuels and chemicals
[DE95-000362] p 1634 N95-23164
Some aspects of critical currents in Ag sheathed Bi2Sr2Ca2Cu3O10 composite tapes: A summary
[DE95-003952] p 1842 N95-23354
Microstructure and composition of a SNS Josephson junction using CaRuO3 as the metallic barrier
[DE95-004611] p 1845 N95-24152
Cooling rate effects on the microstructure, critical current density, and (T(sub c)) transition of one- and two-powder BSCCO-2223 Ag sheathed tapes
[DE95-004639] p 1846 N95-24171
CALCIUM SULFIDES
MOCVD of gallium and calcium sulfides for improved phosphor processing
[DE95-000918] p 1631 N95-22677
CALCULUS
Idempotents in Banach algebra
[DE94-628429] p 1787 N95-22794
Canonical typing and pi-conversion
[PB95-139218] p 1788 N95-23130
Temporal operators viewed as predicate transformers
[PB95-138996] p 1757 N95-23152
CALIBRATING
IRAS sky survey atlas: Explanatory supplement
[NASA-CR-197335] p 1865 N95-22539
SeaWiFS technical report series. Volume 25: Ocean optics protocols for SeaWiFS validation, revision 1
[NASA-TM-104566-VOL-25-REV-] p 1743 N95-22671
Investigation of depth-area relationships associated with nanoindentations
[DE95-001353] p 1639 N95-22686
TOGA/COARE AMMR 1992 data processing
[NASA-CR-197289] p 1736 N95-22867
Summary of OARE flight calibration measurements
[NASA-TM-109159] p 1688 N95-23012
Simultaneous inference in multivariate calibration
[DE95-003592] p 1794 N95-23066
Upgrade of the 92 GHz airborne multi-channel meteorological radiometer (AMMR)
[NASA-CR-197875] p 1742 N95-23208
Design of a variable area diffuser for a 15-inch Mach 6 open-jet tunnel p 1617 N95-23309
On the accuracy of CFD-based pressure drop predictions for right-angle ducts p 1682 N95-23634
Commercialization of JPL Virtual Reality calibration and redundant manipulator control technologies p 1768 N95-23676
AVIRIS calibration using the cloud-shadow method p 1702 N95-23849
Airborne Visible/Infrared Imaging Spectrometer (AVIRIS): Recent improvements to the sensor p 1690 N95-23852
Comparison of methods for calibrating AVIRIS data to ground reflectance p 1703 N95-23854
Use of data from the AVIRIS onboard calibrator p 1704 N95-23861
Inflight calibration of AVIRIS in 1992 and 1993 p 1690 N95-23862
Use of the Airborne Visible/Infrared Imaging Spectrometer to calibrate the optical sensor on board the Japanese Earth Resources Satellite-1 p 1624 N95-23864
A role for AVIRIS in the Landsat and Advanced Land Remote Sensing Systems program p 1705 N95-23866
The effects of AVIRIS atmospheric calibration methodology on identification and quantitative mapping of surface mineralogy, Drum Mountains, Utah p 1705 N95-23870
Extraction of auxiliary data from AVIRIS distribution tape for spectral, radiometric, and geometric quality assessment p 1706 N95-23875
The data facility of the Airborne Visible/Infrared Imaging Spectrometer (AVIRIS) p 1707 N95-23877
Using AVIRIS for in-flight calibration of the spectral shifts of SPOT-HRV and of AVHRR? p 1710 N95-23893
CALIFORNIA
Streamflow and selected precipitation data for Yucca Mountain Region, southern Nevada and eastern California, water years 1986-90
[DE95-001893] p 1742 N95-23385
CALORIMETERS
Calorimetric measurement of energy of ultrasonic cleaners
[DE95-003938] p 1800 N95-23375
Thermal effects on the STAR electromagnetic calorimeter
[DE95-004663] p 1688 N95-23492
The STAR EM calorimeter design and small prototype test results
[DE95-004592] p 1689 N95-23583
A high speed digitizing photomultiplier tube base for the KTeV CsI calorimeter
[DE95-003739] p 1664 N95-24081
CAMBER
The use of cowl camber and taper to reduce rotor/stator interaction noise
[NASA-CR-195421] p 1799 N95-22675
CAMERAS
Intelligent monitoring system applied to super long distance telerobotic tasks p 1777 N95-23728
Automatic commanding of the Mars Observer Camera p 1620 N95-23754
PRISM Spectrograph Optical Design
[NASA-CR-197965] p 1828 N95-24035
CANADIAN SPACE PROGRAM
Robotics research at Canadian Space Agency p 1772 N95-23699
CANARD CONFIGURATIONS
Inner loop flight control for the High-Speed Civil Transport p 1616 N95-23314
CANONICAL FORMS
Turbulent transport across invariant canonical flux surfaces
[DE95-000710] p 1832 N95-23072
Canonical typing and pi-conversion
[PB95-139218] p 1788 N95-23130
CANOPIES (VEGETATION)
Combining optical and microwave remote sensing data of forest vegetation: MAC Europe 1991
[PB95-127312] p 1717 N95-22538
Use of spectral analogy to evaluate canopy reflectance sensitivity to leaf optical property p 1701 N95-23845
Application of a two-stream radiative transfer model for leaf lignin and cellulose concentrations from spectral reflectance measurements, part 1 p 1703 N95-23856
AVIRIS spectra correlated with the chlorophyll concentration of a forest canopy p 1705 N95-23871
Measurements of canopy chemistry with 1992 AVIRIS data at Blackhawk Island and Harvard Forest p 1706 N95-23873
The effect of signal noise on the remote sensing of Foliar biochemical concentration p 1708 N95-23884
Investigations on the 1.7 micron residual absorption feature in the vegetation reflection spectrum p 1710 N95-23891
Thermal radiant exitance model performance: Soils and forests
[DE95-003619] p 1721 N95-24148
CANTILEVER BEAMS
Effects of delaminations on the damped dynamic characteristics of composite laminates: Mechanics and experiments
[NASA-TM-106862] p 1630 N95-23258
Method and apparatus for measuring the strain developed in a coated surface
[NASA-CASE-ARC-11938-1-C] p 1688 N95-23263
CAPACITANCE
Capacitive acoustic wave detector and method of using same
[NASA-CASE-LAR-13890-1] p 1799 N95-22921
CAPACITORS
Capacitive acoustic wave detector and method of using same
[NASA-CASE-LAR-13890-1] p 1799 N95-22921
CAPILLARY FLOW
Development of novel separation techniques for biological samples in capillary electrophoresis
[DE95-001672] p 1744 N95-22493
CAPILLARY TUBES
Development of novel separation techniques for biological samples in capillary electrophoresis
[DE95-001672] p 1744 N95-22493
CAPILLARY WAVES
Profiling and light scattering studies of Si surfaces
[DE95-002931] p 1828 N95-24005
CARBIDES
Conversion of light hydrocarbon gases to metal carbides for production of liquid fuels and chemicals
[DE95-000362] p 1634 N95-23164
CARBON
Infrared study of carbon deposits on bimetallic catalysts
[DE95-000902] p 1631 N95-22517
Neutron scattering analysis of rubber carbon black composite structure
[DE95-002735] p 1646 N95-22553
Regulation of photosynthetic carbon fixation on the ocean margins
[DE95-003185] p 1743 N95-22878
Origins of interstellar and solar system: Carbonaceous materials
[NASA-CR-197436] p 1867 N95-23013
Transmission electron microscope studies of extraterrestrial materials
[NASA-CR-188363] p 1633 N95-23092
High surface area, high permeability carbon monoliths
[DE95-004555] p 1650 N95-23577
Carbon doping of III-V compound semiconductors
[DE95-003431] p 1844 N95-24013
Assessing the relative contribution of biogenic and fossil processes to visibility scattering aerosols found in remote areas: Near-term Organic Research Program
[DE95-003149] p 1735 N95-24146
CARBON CYCLE
Regulation of photosynthetic carbon fixation on the ocean margins
[DE95-003185] p 1743 N95-22878
CARBON DIOXIDE
Emissions of greenhouse gases in the United States, 1987-1992
[DE95-003001] p 1731 N95-22691
Direct effects of atmospheric CO2 enrichment on plants and ecosystems: An updated bibliographic data base
[DE95-003060] p 1731 N95-22725
CO2 and waste policy: Monitoring results 1991/1992 and main problems
[PB95-133799] p 1733 N95-23126
Effect of hyperbaric carbon dioxide on spores and vegetative cells of bacillus stearothermophilus
[AD-A280115] p 1747 N95-23251
Electron drift velocities of Ar-CO2-CF4 gas mixtures
[DE95-004353] p 1809 N95-23359
Ethylene oxidation chemistry in a well-stirred reactor
[DE95-004823] p 1635 N95-23381
Extraction and detection of pesticide residues from air filter inserts using supercritical carbon dioxide
[DE95-004579] p 1735 N95-23580
The atmosphere below
[NASA-TM-110538] p 1740 N95-23663
CARBON DIOXIDE CONCENTRATION
Direct effects of atmospheric CO2 enrichment on plants and ecosystems: An updated bibliographic data base
[DE95-003060] p 1731 N95-22725
CARBON DIOXIDE LASERS
Edge fluctuation measurements by phase contrast imaging on DIII-D
[DE94-016681] p 1836 N95-23768
CARBON FIBER REINFORCED PLASTICS
Mishap risk control for advanced aerospace/composite materials p 1628 N95-23031
CARBON FIBERS
Corrosion protection measures for CFC/metal joints of fuel integral tank structures of advanced military aircraft p 1644 N95-23510
Surface characterization of LDEF carbon fiber/polymer matrix composites p 1631 N95-23900
CARBON MONOXIDE
Ethylene oxidation chemistry in a well-stirred reactor
[DE95-004823] p 1635 N95-23381
Carbon monoxide oxidation over three different states of copper: Development of a model metal oxide catalyst
[DE95-004682] p 1636 N95-23495
CARBON STEELS
In-situ detection of surface passivation or activation and of localized corrosion: Experiences and prospectives in aircraft p 1643 N95-23508
CARBONACEOUS CHONDRITES
Hypervelocity impact survivability experiments for carbonaceous impactors, part 2 p 1700 N95-23831
CARBONACEOUS MATERIALS
Origins of interstellar and solar system: Carbonaceous materials
[NASA-CR-197436] p 1867 N95-23013
CARBONATES
The US molten carbonate fuel-cell development and commercialization effort
[DE94-019096] p 1728 N95-23162

CARBOXYLATES
Regulation of photosynthetic carbon fixation on the ocean margins
[DE95-003185] p 1743 N95-22878
CARBOXYLIC ACIDS
Membrane phase separations, asymmetry and implications in the origin of life
[DE94-628486] p 1747 N95-23050
CARGO
Evaluation of neutron techniques for illicit substance detection
[DE95-002988] p 1632 N95-22764
CARIBBEAN REGION
Oceanic operations: An authoritative guide to oceanic operations
[FAA-AFS-550] p 1610 N95-24065
CARTESIAN COORDINATES
Boson mapping techniques applied to constant gauge fields in QCD p 1814 N95-22969
Unification of some advection schemes in two dimensions
[NASA-CR-195044] p 1790 N95-23465
CASCADE FLOW
Numerical computation of aerodynamics and heat transfer in a turbine cascade and a turn-around duct using advanced turbulence models p 1675 N95-23444
User's guide for ECAP2D: An Euler unsteady aerodynamic and aeroelastic analysis program for two dimensional oscillating cascades, version 1.0
[NASA-CR-189146] p 1699 N95-24189
CASCADE RANGE (CA-OR-WA)
Measuring forest landscape patterns in the Cascade Range of Oregon, USA p 1719 N95-24096
Old-growth and mature forests near spotted owl nests in western Oregon p 1719 N95-24098
Forest and wildlife habitat analysis using remote sensing and geographic information systems p 1720 N95-24100
Analysis of conifer forest regeneration using Landsat Thematic Mapper data p 1720 N95-24101
Determining coniferous forest cover and forest fragmentation with NOAA-9 advanced very high resolution radiometer data p 1720 N95-24103
CASES (CONTAINERS)
NASA low-speed axial compressor for fundamental research
[NASA-TM-4635] p 1616 N95-23192
CASTING
Method of producing a silicon carbide fiber reinforced strontium aluminosilicate glass-ceramic matrix composite
[NASA-CASE-LEW-15263-2] p 1627 N95-22563
CATABOLISM
Transmethylation reactions during methanogenesis from acetate in Methanosarcina barkeri
[DE94-016222] p 1745 N95-22873
CATALYSIS
Chemical recycling of scrap composites p 1629 N95-23034
Organometallic chemistry of bimetallic compounds
[DE95-004436] p 1634 N95-23345
CATALYSTS
Infrared study of carbon deposits on bimetallic catalysts
[DE95-000902] p 1631 N95-22517
Hydrogen vibrational density of states of adsorbed water on rare-earth modified zirconia
[DE95-001127] p 1632 N95-22681
Nanophase materials: Synthesis, properties, applications
[AD-A286013] p 1627 N95-22940
Charge distribution analysis of catalysts under simulated reaction conditions
[DE95-003526] p 1633 N95-23064
Ethanol synthesis and water gas shift over bifunctional sulfide catalysts
[DE94-017376] p 1634 N95-23202
Supported transition metal catalysts for para- to ortho-hydrogen conversion
[NASA-CR-197907] p 1634 N95-23252
Carbon monoxide oxidation over three different states of copper: Development of a model metal oxide catalyst
[DE95-004682] p 1636 N95-23495
AVIRIS spectra correlated with the chlorophyll concentration of a forest canopy p 1705 N95-23871
Processing of single- and multi-domain YBa2Cu3O(x) bulk materials for levitation applications by Nd(1+x)Ba(2-x)Cu3O(y) seeding
[DE95-004615] p 1845 N95-24154
CATALYTIC ACTIVITY
Particle size dependence in Fischer-Tropsch synthesis
[DE95-003124] p 1633 N95-22876
Ethanol synthesis and water gas shift over bifunctional sulfide catalysts
[DE94-017376] p 1634 N95-23202
Review of research results for the photocatalytic oxidation of hazardous wastes in air
[DE95-004004] p 1734 N95-23480
CATASTROPHE THEORY
Shapes and stability of algebraic nuclear models p 1814 N95-22974
CATHODIC COATINGS
Corrosion control acceptance criteria for sacrificial anode type, cathodic protection systems (user guide)
[AD-A285275] p 1662 N95-23117
CATIONS
Magnetic resonance and optical spectroscopic studies of carotenoids
[DE95-003729] p 1631 N95-22575
Cation disorder determined by MAS Al-27 NMR in high dose neutron irradiated spinel
[DE95-003681] p 1842 N95-23266
NO decomposition in non-reducing atmospheres
[DE95-004324] p 1634 N95-23339
Test procedure for cation exchange chromatography
[DE95-003770] p 1808 N95-23350
CAUCHY PROBLEM
Galactic oscillator symmetry p 1822 N95-22973
CAVITATION FLOW
Adaptation of the advanced spray combustion code to cavitating flow problems p 1681 N95-23629
Cavitation modeling in Euler and Navier-Stokes codes p 1681 N95-23630
An inducer CFD solution and effects associated with cavitation p 1681 N95-23631
Current status in cavitation modeling p 1681 N95-23632
A generalized Eulerian-Lagrangian analysis, with application to liquid flows with vapor bubbles p 1682 N95-23633
CAVITIES
Dynamic response of a transducer mounted at one end of an acoustical cavity which is subjected to a specified pressure at the open end of the cavity
[DE95-004192] p 1799 N95-23379
Finite-difference solutions of the alternate turbopump development high-pressure oxidizer turbopump pump-end ball-bearing cavity flows p 1678 N95-23617
Cavitation modeling in Euler and Navier-Stokes codes p 1681 N95-23630
CAVITY FLOW
A time-accurate finite volume method valid at all flow velocities p 1676 N95-23447
CELL MEMBRANES (BIOLOGY)
Plant metabolism and cell wall formation in space (microgravity) and on Earth
[NASA-CR-197618] p 1745 N95-22801
Membrane phase separations, asymmetry and implications in the origin of life
[DE94-628486] p 1747 N95-23050
Enhancement of biomembrane functions under phase-separated conditions: A self-organized criticality phenomenon?
[DE94-628489] p 1747 N95-23053
CELLS (BIOLOGY)
Structural studies of complex carbohydrates of plant cell walls
[DE95-003099] p 1748 N95-24075
CELLULOSE
Continuous production of cellulase in a fluidized-bed reactor by Pseudonomas fluorescens immobilized in hydrogel beads
[DE94-014105] p 1744 N95-22588
Application of a two-stream radiative transfer model for leaf lignin and cellulose concentrations from spectral reflectance measurements, part 1 p 1703 N95-23856
Application of a two-stream radiative transfer model for leaf lignin and cellulose concentrations from spectral reflectance measurements, part 2 p 1703 N95-23857
Relationships between pigment composition variation and reflectance for plant species from a coastal savannah in California p 1709 N95-23889
CELLULOSE NITRATE
Decomposition mechanisms in thermally-aged thin-film explosives
[DE95-000741] p 1652 N95-22838
CENTRAL NERVOUS SYSTEM
Rearrangement of RAG-1 recombinase gene in radiation-sensitive wasted mice
[DE94-017083] p 1746 N95-22913
CENTRAL PROCESSING UNITS
GPP user's guide: A general-purpose postprocessor for wind turbine data analysis
[DE95-000293] p 1730 N95-23776
Algorithms for categorizing multiprocessor communication under invalidate and update-based coherence protocols
[TR-533-REV] p 1759 N95-23928
Scalability of atomic primitives on distributed shared memory multiprocessors
[TR-528] p 1764 N95-23930
CENTRIFUGAL FORCE
Optimization of a centrifugal impeller design through CFD analysis p 1680 N95-23624
Use of blade lean in turbomachinery redesign p 1680 N95-23625
Incompressible Navier-Stokes calculations in pump flows p 1680 N95-23627
CENTRIFUGAL PUMPS
The influence of swirl brakes and a tip discharge orifice on the rotordynamic forces generated by discharge-to-suction leakage flows in shrouded centrifugal pumps p 1680 N95-23628
CERAMIC COATINGS
Performance of thin-ceramic-coated combustion chamber with gasoline and methanol as fuels in a two-stroke SI engine
[DE95-002903] p 1693 N95-22557
Durability of reflector materials in the space environment p 1651 N95-23912
CERAMIC MATRIX COMPOSITES
Method of producing a silicon carbide fiber reinforced strontium aluminosilicate glass-ceramic matrix composite
[NASA-CASE-LEW-15263-2] p 1627 N95-22563
A study of ceramic composite of ferroelectric BaTiO3 ceramic and superconductor YBa2Cu3O(6+delta) ceramic
[DE94-627563] p 1647 N95-22610
A special percolation problem in ceramic composites
[DE94-627641] p 1647 N95-22611
CERAMICS
A study of ceramic composite of ferroelectric BaTiO3 ceramic and superconductor YBa2Cu3O(6+delta) ceramic
[DE94-627563] p 1647 N95-22610
Transformation behavior in Al2O3-ZrO2 ceraamic composites
[DE95-001359] p 1647 N95-22688
Advanced Turbine Technology Applications Project (ATTAP) 1993 annual report
[DE95-003198] p 1693 N95-22880
Superconductivity devices: Commercial use of space
[NASA-CR-197885] p 1648 N95-22883
Plinius intermediate report
[PB95-135216] p 1648 N95-23128
Protective coating for ceramic materials
[NASA-CASE-ARC-11969-1-CU] p 1649 N95-23394
Advances in research for solid oxide fuel cells
[DE95-004590] p 1730 N95-23582
Development of sensors for ceramic components in advanced propulsion systems
[NASA-CR-195324] p 1689 N95-23795
A 4 MW fast wave current drive upgrade for D3-D
[DE95-003741] p 1837 N95-24083
Modeling of tritium recovery from lithium ceramics
[DE95-004626] p 1838 N95-24167
CESIUM
Surface structural dependence of cesium adsorption on the (alpha)-Al2O3(0001) surface
[DE95-002610] p 1842 N95-23135
CESIUM COMPOUNDS
Ethanol synthesis and water gas shift over bifunctional sulfide catalysts
[DE94-017376] p 1634 N95-23202
CESIUM IODIDES
A high speed digitizing photomultiplier tube base for the KTeV CsI calorimeter
[DE95-003739] p 1664 N95-24081
CHANGE DETECTION
A comparison of spectral mixture analysis an NDVI for ascertaining ecological variables p 1710 N95-23892
Glaciological studies in the central Andes using AIRSAR/TOPSAR p 1713 N95-23942
CHANNEL FLOW
The initial-value problem for viscous channel flows
[NASA-CR-195034] p 1667 N95-23207
CFD modeling of turbulent duct flows for coolant channel analysis p 1682 N95-23635
CHANNELS
MHD seed recovery and regeneration, phase 2
[DE95-004308] p 1833 N95-23338
CHANNELS (DATA TRANSMISSION)
Description of a MIL-STD-1553B data bus Ada driver for the LeRC EPS Testbed
[NASA-TM-106866] p 1762 N95-22668
Modelling and analysis of a high speed data bus with predicate/transition nets
[PB95-140695] p 1764 N95-23538
CHAOS
Lyapunov exponents from CHUA's circuit time series using artificial neural networks p 1784 N95-22988
Static parametric fluctuations give nonstatistical behaviour in uncoupled chaotic systems
[DE94-628478] p 1794 N95-23019
Dynamical behaviour of the coupled diffusion map lattice
[DE94-628481] p 1841 N95-23022

CHARACTERIZATION
Novel mass spectrometric instrument for gaseous and particulate characterization and monitoring
| DE95-001135 | p 1687 N95-22682
Investigation of arc length versus flange thickness while using an arc voltage controller
| DE95-003937 | p 1695 N95-23374
Flowfield characterization in a LOX/GH2 propellant rocket p 1684 N95-23642
VLPC characterization for the Dzero upgrade
| DE95-003742 | p 1818 N95-24084
CHARGE COUPLED DEVICES
A perspective on space robotics in Japan p 1697 N95-23695
CHARGE DISTRIBUTION
Charge distribution analysis of catalysts under simulated reaction conditions
| DE95-003526 | p 1633 N95-23064
Measurement of the left-right charge asymmetry in hadronic Z decays and A(sub e) determination
| DE95-003467 | p 1806 N95-23140
CHARGE TRANSFER
Collaborative research on aircraft icing and charging processes in ice
| AD-A285102 | p 1609 N95-23201
CHARGED PARTICLES
Relativistic particle with torsion and charged particle in a constant electromagnetic field: Identity of evolution
| DE94-628506 | p 1803 N95-22778
Inclusive rapidity correlations of (pi)(-) mesons in pp-interactions
| DE94-635654 | p 1812 N95-23974
CHARM (PARTICLE PHYSICS)
New preliminary results on the physics of charm hadroproduction subprocesses
| DE95-002530 | p 1801 N95-22646
The charm physics potential of a Tau-Charm Factory
| DE95-003369 | p 1802 N95-22703
J/psi, psi' yields mu(+)mu(-) and B yields J/psi, psi' cross sections
| DE94-018996 | p 1808 N95-23242
Recent results from Fermilab E-687, charm particle decays, lifetimes and photoproduction dynamics: A compilation results presented at DPF 1994
| DE95-004580 | p 1808 N95-23347
Charm-conserving strangeness-changing two body hadronic decays of charmed baryons
| DE94-628621 | p 1811 N95-23770
CHARON
IUE observing programs: NSOSS, VEOEB, and PCOEB
| NASA-CR-197424 | p 1866 N95-23560
CHARTS
Algebraic semantics of basic message sequence charts
| PB95-138970 | p 1657 N95-23151
CHEBYSHEV APPROXIMATION
Note on the computational complexity of j-radii of polytopes in (R sup n)
| PB95-139358 | p 1790 N95-23231
On adaptive weighted polynomial preconditioning for Hermitian positive definite matrices
| NASA-CR-197946 | p 1791 N95-23547
CHEMICAL ANALYSIS
Transmission electron microscope studies of extraterrestrial materials
| NASA-CR-188363 | p 1633 N95-23092
Ethanol synthesis and water gas shift over bifunctional sulfide catalysts
| DE94-017376 | p 1634 N95-23202
Simulation of absorption edge densitometry
| DE95-004393 | p 1635 N95-23360
Four space application material coatings on the Long-Duration Exposure Facility (LDEF) p 1651 N95-23913
CHEMICAL BONDS
Ligand K-edge x-ray adsorption spectroscopic studies of the electronic structure of inorganic model complexes and metalloprotein active sites
| DE95-003338 | p 1840 N95-22851
Computational studies of metal-metal and metal-ligand interactions
| NASA-CR-197862 | p 1641 N95-23215
Investigations on the 1.7 micron residual absorption feature in the vegetation reflection spectrum p 1710 N95-23891
CHEMICAL COMPOSITION
Glass science tutorial: Lecture 2, operating electric glass melters
| DE95-002965 | p 1647 N95-22648
EXTRA.M: A computing code system for analysis of the Purex process with mixer settlers for reprocessing
| DE94-785273 | p 1635 N95-23476
SIMS chemical and isotopic analysis of impact features from LDEF experiments AO187-1 and AO187-2 p 1637 N95-23837
Application of a two-stream radiative transfer model for leaf lignin and cellulose concentrations from spectral reflectance measurements, part 1 p 1703 N95-23856
Application of a two-stream radiative transfer model for leaf lignin and cellulose concentrations from spectral reflectance measurements, part 2 p 1703 N95-23857
Measurements of canopy chemistry with 1992 AVIRIS data at Blackhawk Island and Harvard Forest p 1706 N95-23873
Changes in chemical and optical properties of thin film metal mirrors on LDEF p 1651 N95-23907
CHEMICAL ENERGY
The effect of a non-zero shock width on wave propagation in multi-dimensions
| DE95-002748 | p 1666 N95-22902
AVIRIS spectra correlated with the chlorophyll concentration of a forest canopy p 1705 N95-23871
CHEMICAL ENGINEERING
Chemical recycling of scrap composites p 1629 N95-23034
Proceedings of the fuel cells 1994 contractors review meeting
| DE94-012285 | p 1730 N95-23977
CHEMICAL EQUILIBRIUM
Numerical study of the SSME nozzle flow fields during transient operations: A comparison of the animated results with test p 1673 N95-23434
CHEMICAL EVOLUTION
Origins of interstellar and solar system: Carbonaceous materials
| NASA-CR-197436 | p 1867 N95-23013
Molecular relics from chemical evolution and the origin of life
| DE94-628493 | p 1747 N95-23060
CHEMICAL EXPLOSIONS
Evaluation of neutron techniques for illicit substance detection
| DE95-002988 | p 1632 N95-22764
Decomposition mechanisms in thermally-aged thin-film explosives
| DE95-000741 | p 1652 N95-22838
CHEMICAL PROPERTIES
Glass science tutorial: Lecture 1, Chemistry and properties of oxide glasses
| DE95-002963 | p 1647 N95-22647
Aqueous alternatives for metal and composite cleaning p 1630 N95-23039
CHEMICAL REACTIONS
Energy Conversion and Storage Program
| DE95-003796 | p 1725 N95-22501
Particle size dependence in Fischer-Tropsch synthesis
| DE95-003124 | p 1633 N95-22876
Process for preparing an assembly of an article and a polyimide which resists dimensional change, delamination and debonding when exposed to changes in temperature
| NASA-CASE-LAR-14538-2 | p 1649 N95-23254
NO decomposition in non-reducing atmospheres
| DE95-004324 | p 1634 N95-23339
EXTRA.M: A computing code system for analysis of the Purex process with mixer settlers for reprocessing
| DE94-785273 | p 1635 N95-23476
Advanced multi-phase flow CFD model development for solid rocket motor flowfield analysis p 1683 N95-23638
The atmosphere below
| NASA-TM-110538 | p 1740 N95-23663
All systems go!
| NASA-TM-110542 | p 1620 N95-23665
Chemical Sciences Division
| DE95-002655 | p 1626 N95-24142
CHEMICAL REACTORS
Chemical vapor deposition in low pressure batch furnaces
| DE95-003035 | p 1632 N95-22722
CHEMISORPTION
Surface structural dependence of cesium adsorption on the (alpha)-Al2O3(0001) surface
| DE95-002610 | p 1842 N95-23135
CHIPS
Aspects of surface generation in orthogonal ultraprecision machining
| DE95-000922 | p 1654 N95-22678
CHIPS (ELECTRONICS)
A high speed digitizing photomultiplier tube base for the KTeV CsI calorimeter
| DE95-003739 | p 1664 N95-24081
CHIRAL DYNAMICS
The convergence radius of the chiral expansion in the Dyson-Schwinger approach
| DE94-012852 | p 1805 N95-22925
Theoretical aspects of electroweak and other interactions in medium energy nuclear physics
| DE95-004341 | p 1808 N95-23357
CHIRALITY
The chirality operators for Heisenberg spin systems
| DE94-629043 | p 1847 N95-22545
A model of mesons based on chi SB in the light-front frame
| DE95-003203 | p 1802 N95-22731
Chiral symmetry breaking in QCD with linearly rising confinement potential
| DE94-628559 | p 1848 N95-22744
Spontaneous breaking of chiral symmetry as a consequence of confinement
| DE94-628560 | p 1849 N95-22745
Block spins and chirality in Heisenberg model on Kagome and triangular lattices
| DE94-629044 | p 1840 N95-22845
The origin of chirality in protein amino acids
| DE94-628491 | p 1747 N95-23058
CHLORELLA
Biological determinants of photobioreactor design
| DE94-016032 | p 1745 N95-22872
CHLORIDES
Ligand K-edge x-ray adsorption spectroscopic studies of the electronic structure of inorganic model complexes and metalloprotein active sites
| DE95-003338 | p 1840 N95-22851
Effect of different ions on the anodic behaviour of alloy 800 chloride solutions at high temperature
| DE94-634944 | p 1645 N95-23983
CHLORINE
Laboratory studies of the sensitivity of tropospheric ozone to the chemistry of sea salt aerosol
| DE95-003607 | p 1735 N95-24147
CHLOROFLUOROCARBONS
The Atmospheric Lifetime Experiment and the Global Atmospheric Gas Experiment (ALE/GAGE)
| NASA-CR-197400 | p 1731 N95-22673
The atmosphere below
| NASA-TM-110538 | p 1740 N95-23663
CHLOROPHYLLS
SeaWiFS technical report series. Volume 25: Ocean optics protocols for SeaWiFS validation, revision 1
| NASA-TM-104566-VOL-25-REV- | p 1743 N95-22671
Development of a multi-sensor in situ fiber optic fluorometer
| DE95-003105 | p 1819 N95-22780
Photochemical energy conversion by membrane-bound photoredox systems
| DE95-004405 | p 1729 N95-23361
AVIRIS spectra correlated with the chlorophyll concentration of a forest canopy p 1705 N95-23871
The red edge in arid region vegetation: 340-1060 nm spectra p 1708 N95-23881
The effect of signal noise on the remote sensing of Foliar biochemical concentration p 1708 N95-23884
Relationships between pigment composition variation and reflectance for plant species from a coastal savannah in California p 1709 N95-23889
CHROMATES
Corrosion prevention with environmentally compliant materials: A design challenge p 1644 N95-23511
CHROMATOGRAPHY
Test procedure for cation exchange chromatography
| DE95-003770 | p 1808 N95-23350
Test procedure for anion exchange chromatography
| DE95-003767 | p 1809 N95-23407
CHROMIUM CARBIDES
The hydrogen embrittlement of alloy X-750
| DE95-003207 | p 1640 N95-22893
CHROMOPHORES
Comparison of the rate constants for energy transfer in the light-harvesting protein, C-phycocyanin, calculated from Foerster's theory and experimentally measured by time-resolved fluorescence spectroscopy
| DE94-014961 | p 1745 N95-22590
Analysis of structural domains required for phytochrome function by in vitro mutagenesis
| DE94-016230 | p 1745 N95-22884
CHROMOSOMES
Rearrangement of RAG-1 recombinase gene in radiation-sensitive wasted mice
| DE94-017083 | p 1746 N95-22913
CHRONOLOGY
Glaciological studies in the central Andes using AIRSAR/TOPSAR p 1713 N95-23942
CIRCADIAN RHYTHMS
Cellular interactions in the suprachiasmatic nucleus
| AD-A285639 | p 1749 N95-23780
The 1993 Gordon Research Conference on Chronobiology
| NASA-CR-197990 | p 1748 N95-24047
CIRCLES (GEOMETRY)
Light-traffic analysis for queues with spatially distributed arrivals
| PB95-140802 | p 1767 N95-23556

CIRCUIT BOARDS
Planar magnetic component development
[DE95-003311] p 1661 N95-22896
CIRCUITS
Current estimation for electromigration, hot carriers, and voltage drop
[AD-A285794] p 1659 N95-22507
Method and system for electron beam lithography
[AD-D016554] p 1660 N95-22709
Planar magnetic component development
[DE95-003311] p 1661 N95-22896
User's guide and physics manual for the ScatPlus circuit code
[DE95-003755] p 1663 N95-23479
High-performance GaAs/AlGaAs optical modulators: Their performance and packaging for microwave photonic integrated circuits
[DE95-004533] p 1828 N95-23575
CIRCULAR CYLINDERS
Flexural vibration of thin piezoelectric laminate circular cylinder of hexagonal symmetry
[DE94-628474] p 1698 N95-22773
Characterization of Type 304L stainless steel solid-state closure welds for radioactive waste containment
[DE94-016539] p 1645 N95-23980
Circular electrode geometry metal-semiconductor-metal photodetectors
[NASA-CASE-LAR-15172-1-CU] p 1663 N95-24048
CIRRUS CLOUDS
Atmospheric correction of AVIRIS data of Monterey Bay contaminated by thin cirrus clouds p 1710 N95-23890
CIVIL AVIATION
Inner loop flight control for the High-Speed Civil Transport p 1616 N95-23314
Handling qualities of the High Speed Civil Transport p 1616 N95-23325
The airline quality report, 1994
[NIAR-94-11] p 1610 N95-24012
Oceanic operations: An authoritative guide to oceanic operations
[FAA-AFS-550] p 1610 N95-24065
A review of civil aviation fatal accidents in which lost/disoriented was a cause/factor: 1981-1990
[DOT/FAA/AM-95/1] p 1611 N95-24071
CLASSICAL MECHANICS
Exact, E = 0, classical and quantum solutions for general power-law oscillators p 1820 N95-22959
Non-Noetherian symmetries for oscillators in classical mechanics and in field theory p 1823 N95-22977
Study of frustrated systems via dissipative maps
[PB95-139093] p 1799 N95-23155
CLASSIFICATIONS
Classification of SU(3) modular invariants revisited
[PB95-110771] p 1787 N95-22715
Classification of (2,2) compactifications by free fermions 2
[PB95-139119] p 1807 N95-23157
Classification of the LCVF AVIRIS test site with a Kohonen artificial neural network p 1706 N95-23874
MAC Europe 1991 campaign: AIRSAR/AVIRIS data integration for agricultural test site classification p 1715 N95-23952
SAR terrain classifier and mapper of biophysical attributes p 1715 N95-23957
Classification and soil moisture determination of agricultural fields p 1716 N95-23958
CLEAN FUELS
Diesel fuel component contributions to engine emissions and performance: Clean fuel study
[DE94-011868] p 1732 N95-22834
CLEANERS
Aqueous alternatives for metal and composite cleaning p 1630 N95-23039
Calorimetric measurement of energy of ultrasonic cleaners
[DE95-003938] p 1800 N95-23375
CLEANING
Innovative technology for contamination control in plasma processing
[DE95-000913] p 1829 N95-22519
Aqueous alternatives for metal and composite cleaning p 1630 N95-23039
Military bases: Environmental impact at closing installations. Report to Congressional requesters
[GAO/NSIAD-95-70] p 1735 N95-24057
CLEARANCES
Security clearances: Consideration of sexual orientation in the clearance process. Report to Congressional requesters
[GAO/NSIAD-95-21] p 1853 N95-23588
CLEBSCH-GORDAN COEFFICIENTS
The role of SU(2) 3n-j coefficients in SU(3)
[DE95-002726] p 1796 N95-22900
CLIMATE CHANGE
Direct effects of atmospheric CO2 enrichment on plants and ecosystems: An updated bibliographic data base
[DE95-003060] p 1731 N95-22725
Development of an advanced finite difference atmospheric general circulation model
[DE95-003187] p 1736 N95-22879
Format( )MEDIC( )Input
[DE95-003482] p 1737 N95-23063
RAS Division model evaluation database tools
[DE95-003480] p 1733 N95-23123
The atmosphere below
[NASA-TM-110538] p 1740 N95-23663
Glaciological studies in the central Andes using AIRSAR/TOPSAR p 1713 N95-23942
Laboratory studies of the sensitivity of tropospheric ozone to the chemistry of sea salt aerosol
[DE95-003607] p 1735 N95-24147
CLIMATE MODELS
RAS Division model evaluation database tools
[DE95-003480] p 1733 N95-23123
CLIMATOLOGY
A numerical study of interannual wind forcing effects on the California current system, 1980-1983
[AD-A286023] p 1743 N95-23074
Basic data sets description and preliminary results of EFEDA-Spain
[PB95-139291] p 1740 N95-23470
A comparison of spectral mixture analysis an NDVI for ascertaining ecological variables p 1710 N95-23892
CLOCKS
Precise clock synchronization protocol
[PB95-127247] p 1687 N95-22536
CLOSURE LAW
Study of the pressure field in rotating homogeneous turbulent flows
[PB94-189107] p 1665 N95-22585
Relating multifunctions and predicate transformers through closure operators
[PB95-135646] p 1757 N95-23467
CLOUD COVER
Atmospheric correction of AVIRIS data of Monterey Bay contaminated by thin cirrus clouds p 1710 N95-23890
CLOUDS (METEOROLOGY)
Dimethylsulfide oxidation over the tropical South Atlantic: OH and other oxidants
[NASA-CR-197417] p 1732 N95-22930
Remote sensing of smoke, clouds, and fire using AVIRIS data p 1704 N95-23860
CLUTTER
Maximum-likelihood spectral estimation and adaptive filtering techniques with application to airborne Doppler weather radar
[NASA-CR-197699] p 1658 N95-23670
CMOS
Current estimation for electromigration, hot carriers, and voltage drop
[AD-A285794] p 1659 N95-22507
Adaptive beamforming in a CDMA mobile satellite communications system p 1655 N95-22815
COALESCING
The hydrogen embrittlement of alloy X-750
[DE95-003207] p 1640 N95-22893
COASTAL PLAINS
Remote identification of a gravel laden Pleistocene river bed p 1712 N95-23921
COATING
Corrosivity sensor
[AD-D016549] p 1687 N95-22706
Organic coating technology for the protection of aircraft against corrosion p 1644 N95-23513
Corrosion in service experience with aircraft in France p 1645 N95-23518
COATINGS
Method and system for electron beam lithography
[AD-D016554] p 1660 N95-22709
EUV metrology of multilayer optics
[DE95-003036] p 1819 N95-22723
Method and apparatus for measuring the strain developed in a coated surface
[NASA-CASE-ARC-11938-1-C] p 1688 N95-23263
Method development for compensating temperature effects in pressure sensitive paint measurements p 1650 N95-23291
COBALT
Photoemission study of quantum confinement by a finite barrier: Cu/Co(wedge)/Cu(100)
[DE95-002913] p 1840 N95-22762
NO decomposition in non-reducing atmospheres
[DE95-004324] p 1634 N95-23339
COCKPITS
Differential GPS and system integration of the Low Visibility Landing and Surface Operations (LVLASO) demonstration p 1611 N95-23318
CODING
Method and system for pattern analysis using a coarse-coded neural network
[NASA-CASE-ARC-11961-1] p 1767 N95-23387
Reevaluation of the significance of sequence information for speech recognition
[TR-555] p 1658 N95-23794
COEFFICIENT OF FRICTION
On the accuracy of CFD-based pressure drop predictions for right-angle ducts p 1682 N95-23634
COEFFICIENTS
Characterization of non-negative greedy matrices
[PB95-139366] p 1757 N95-23232
Process for preparing an assembly of an article and a polyimide which resists dimensional change, delamination and debonding when exposed to changes in temperature
[NASA-CASE-LAR-14538-2] p 1649 N95-23254
Rate coefficients for the electron-impact excitation, ionization and recombination of He-like ions, S XV, Ca XIX and Fe XXV, and related processes
[ISAS-R-657] p 1811 N95-23604
COGNITION
Active vision in satellite scene analysis p 1778 N95-23738
Knowledge representation and reasoning for mixed-initiative planning
[TR-562] p 1783 N95-24031
COGNITIVE PSYCHOLOGY
Functions of external cues in prospective memory
[DOT/FAA/AM-95/9] p 1750 N95-24088
COHERENCE
Oscillator-like coherent states for the Jaynes-Cummings Model p 1826 N95-23003
COHERENT LIGHT
Nonclassical light in interferometric measurements p 1822 N95-22976
Undulators for short wavelength FEL amplifiers
[DE95-004690] p 1692 N95-23487
COHERENT RADIATION
q-bosons and the q-analogue quantized field p 1814 N95-22984
COKE
Infrared study of carbon deposits on bimetallic catalysts
[DE95-000902] p 1631 N95-22517
COLD FLOW TESTS
Non-intrusive measurements in a rocket engine combustor p 1625 N95-23439
COLD PLASMAS
Dynamics and variability of the plasmasphere observed from synchronous orbit
[DE95-002733] p 1829 N95-22665
COLLECTION
PUZZLES 4: Sperner collections and the keys puzzle
[PB95-139374] p 1790 N95-23233
COLLIMATION
High energy collimating fine grids
[NASA-CR-197688] p 1871 N95-24191
COLLIMATORS
Method for making fiber-optic bundle collimator assembly
[AD-D016491] p 1819 N95-22492
A fiber-optic bundle and collimator assembly
[AD-D016500] p 1820 N95-22864
High energy collimating fine grids
[NASA-CR-197688] p 1871 N95-24191
COLLISIONAL PLASMAS
The high latitude ionosphere-magnetosphere transition region: Simulation and data comparison
[NASA-CR-197404] p 1737 N95-22956
COLLISIONLESS PLASMAS
The high latitude ionosphere-magnetosphere transition region: Simulation and data comparison
[NASA-CR-197404] p 1737 N95-22956
Collisionless magnetic reconnection associated with coalescence of flux bundles
[NIFS-315] p 1834 N95-23525
Macro-EM particle simulation method and a study of collisionless magnetic reconnection
[NIFS-316] p 1834 N95-23526
COLLISIONS
Strong collision approach to calculation of depolarization function for neutron beam passing through ferromagnetic bulk domains
[DE94-628847] p 1803 N95-22758
COLOR
Supersymmetric oscillator in optics p 1826 N95-23002
Color orthophotography: To scan or not
[DE95-002749] p 1689 N95-24069
COMBINATORIAL ANALYSIS
Capacitated facility location: Valid inequalities and facets (revised)
[PB95-130225] p 1786 N95-22641

Combinatorial semantics
| TR-563 | p 1792 N95-23793
Ploxoma: Testbed for uncertain inference
| TR-537 | p 1794 N95-23927

COMBUSTIBLE FLOW
Adaptation of the advanced spray combustion code to cavitating flow problems p 1681 N95-23629

COMBUSTION
The influence of high-octane fuel blends on the performance of a two-stroke SI engine with knock-limited-compression ratio
| DE95-002902 | p 1692 N95-22556
Performance of thin-ceramic-coated combustion chamber with gasoline and methanol as fuels in a two-stroke SI engine
| DE95-002903 | p 1693 N95-22557
Modeling aerosol emissions from the combustion of composite materials p 1629 N95-23038
Influence of porosity and two-phase flow on diffusional/thermal instability of a deflagrating energetic material
| DE95-002592 | p 1634 N95-23122
Non-intrusive measurements in a rocket engine combustor p 1625 N95-23439
Liquid propellant rocket engine combustion simulation with a time-accurate CFD method p 1676 N95-23445
Oxygen enriched combustion system performance study. Phase 2: 100 percent oxygen enriched combustion in regenerative glass melters
| DE95-004212 | p 1635 N95-23481
Adaptation of the advanced spray combustion code to cavitating flow problems p 1681 N95-23629
Microgravity combustion science: 1995 program update
| NASA-TM-106858 | p 1626 N95-24004
Flow diagnostics, chemically reacting turbulent flow modeling and turbulent mixing: A summary of project studies in combustion
| NASA-CR-197348 | p 1687 N95-24022

COMBUSTION CHAMBERS
Performance of thin-ceramic-coated combustion chamber with gasoline and methanol as fuels in a two-stroke SI engine
| DE95-002903 | p 1693 N95-22557
Heat transfer in rocket engine combustion chambers and nozzles p 1668 N95-23413
Non-intrusive measurements in a rocket engine combustor p 1625 N95-23439
Sensitivity of combustion-acoustic instabilities to boundary conditions for premixed gas turbine combustors
| NASA-TM-106890 | p 1614 N95-23550
Spray combustion experiments and numerical predictions p 1637 N95-23643
CFD analysis of spray combustion and radiation in OMV thrust chamber p 1637 N95-23645
Modeling of non-spherical droplet dynamics p 1685 N95-23647
Flow diagnostics, chemically reacting turbulent flow modeling and turbulent mixing: A summary of project studies in combustion
| NASA-CR-197348 | p 1687 N95-24022
A computer model in general 3-D curvilinear coordinates for the prediction of the turbulent flow field in a jet induced ram combustor
| NAL-TR-1240T | p 1687 N95-24051
Effects of jet strength on NOx formation in premixed impinging jet combustion with minimum heat losses
| NAL-TR-1237T | p 1637 N95-24181

COMBUSTION CHEMISTRY
Ethylene oxidation chemistry in a well-stirred reactor
| DE95-004823 | p 1635 N95-23381
CFD analysis of spray combustion and radiation in OMV thrust chamber p 1637 N95-23645
Time-accurate unsteady flow simulations supporting the SRM T+68-second pressure spike anomaly investigation (STS-54B) p 1685 N95-23650

COMBUSTION EFFICIENCY
Sensitivity of combustion-acoustic instabilities to boundary conditions for premixed gas turbine combustors
| NASA-TM-106890 | p 1614 N95-23550

COMBUSTION PHYSICS
Fundamental phenomena on fuel decomposition and boundary layer combustion processes with applications to hybrid rocket motors
| NASA-CR-197919 | p 1625 N95-23261
Ethylene oxidation chemistry in a well-stirred reactor
| DE95-004823 | p 1635 N95-23381
Liquid propellant rocket engine combustion simulation with a time-accurate CFD method p 1676 N95-23445
Spray combustion experiments and numerical predictions p 1637 N95-23643
Progress in advanced spray combustion code integration p 1637 N95-23644
Development of an atomization methodology for spray combustion p 1637 N95-23646
Microgravity combustion science: 1995 program update
| NASA-TM-106858 | p 1626 N95-24004
Chemical Sciences Division
| DE95-002655 | p 1626 N95-24142

COMBUSTION PRODUCTS
Diesel fuel component contributions to engine emissions and performance: Clean fuel study
| DE94-011868 | p 1732 N95-22834
Analytical Boltzmann moments for electrons in N2-O2-H2O gas mixtures
| DE95-003474 | p 1732 N95-22898
Aircraft fires, smoke toxicity, and survival: An overview
| DOT/FAA/AM-95/8 | p 1610 N95-24024

COMBUSTION STABILITY
Sensitivity of combustion-acoustic instabilities to boundary conditions for premixed gas turbine combustors
| NASA-TM-106890 | p 1614 N95-23550
Flow diagnostics, chemically reacting turbulent flow modeling and turbulent mixing: A summary of project studies in combustion
| NASA-CR-197348 | p 1687 N95-24022

COMMAND GUIDANCE
An operations and command systems for the extreme ultraviolet explorer p 1770 N95-23687
Formalizing procedures for operations automation, operator training and spacecraft autonomy p 1752 N95-23720

COMMERCIAL AIRCRAFT
Preparation of course materials: Elementary mathematics of powered flight p 1853 N95-23320
Aircraft accident report. Runway overrun following rejected takeoff. Continental airlines flight 795, McDonnell Douglas MD-82, N18835, LaGuardia Airport, Flushing, NY, 2 March 1994
| PB95-910401 | p 1610 N95-23609

COMMUNICATING
Graph isomorphism models for non interleaving process algebra
| PB95-110490 | p 1786 N95-22714

COMMUNICATION
Project: Internal communications p 1854 N95-23282

COMMUNICATION NETWORKS
Non-blocking crossbar permutation engine with constant routing latency
| NASA-CASE-NPO-18864-1-CU | p 1762 N95-22564
Addendum to the Proceedings of the Third International Mobile Satellite Conference (IMSC 1993)
| NASA-CR-197343 | p 1655 N95-22813
Geolocation applications of the Gonets LEO messaging satellites p 1656 N95-22818
Low Earth Orbit satellite/terrestrial mobile service compatibility p 1656 N95-22819
Environmental Systems Management Analysis and Reporting Network (E-SMART)
| AD-A279766 | p 1732 N95-22856
Loop scheduling for heterogeneity
| TR-540 | p 1764 N95-23936

COMMUNICATION SATELLITES
Addendum to the Proceedings of the Third International Mobile Satellite Conference (IMSC 1993)
| NASA-CR-197343 | p 1655 N95-22813
Geolocation applications of the Gonets LEO messaging satellites p 1656 N95-22818
Low Earth Orbit satellite/terrestrial mobile service compatibility p 1656 N95-22819
Dynamical model and numerical simulations for Engineering Test Satellite-6
| NAL-TR-1239 | p 1622 N95-24049

COMMUNICATION THEORY
Second International Workshop on Harmonic Oscillators
| NASA-CP-3286 | p 1820 N95-22957

COMMUTATION
Finite-element time evolution operator for the anharmonic oscillator p 1823 N95-22983
Cumulant approach to dynamical correlation functions at finite temperatures
| DE94-628487 | p 1788 N95-23051

COMMUTATORS
The chirality operators for Heisenberg spin systems
| DE94-629043 | p 1847 N95-22545

COMPACTING
Investigation of mechanical properties and their relation to the internal structure of nanocrystalline metals and composites
| DE95-001151 | p 1627 N95-22683
Classification of (2,2) compactifications by free fermions 2
| PB95-139119 | p 1807 N95-23157

COMPENSATORY TRACKING
Effects of age and low doses of alcohol on compensatory tracking during angular acceleration
| DOT/FAA/AM-95/3 | p 1750 N95-23934

COMPETITION
The effect of a non-zero shock width on wave propagation in multi-dimensions
| DE95-002748 | p 1666 N95-22902

COMPILERS
Realizing parallel reduction operation in Sisal 1.2
| DE94-017524 | p 1763 N95-22858
Realizing parallel reduction operations in Sisal 1.2
| DE94-017525 | p 1763 N95-22859

COMPLEX NUMBERS
The satanic notations: Counting classes beyond #P and other definitional adventures
| TR-561 | p 1793 N95-24194

COMPLEX SYSTEMS
Long range potentials and multiple scattering theory in complex systems
| DE94-628881 | p 1804 N95-22791
Attention focusing and anomaly detection in systems monitoring p 1769 N95-23683
Optimizing raid performance with cache p 1761 N95-24116

COMPLEXITY
Effective category and measure in abstract complexity theory
| TR-529 | p 1792 N95-23929
Reducibility classes of P-selective sets
| TR-524 | p 1792 N95-24002
Witness-isomorphic reductions and the local search problem
| TR-522 | p 1793 N95-24003
Large sets in AC(exp 0): A Kolmogorov complexity related property and some applications
| TR-556 | p 1797 N95-24029
Teaching computational complexity: Resources to treasure
| TR-543 | p 1784 N95-24060

COMPONENT RELIABILITY
Integrating O/S models during conceptual design, part 3
| NASA-CR-197905 | p 1622 N95-23400

COMPOSITE MATERIALS
Environmental, Safety, and Health Considerations: Composite Materials in the Aerospace Industry
| NASA-CP-3289 | p 1628 N95-23025
Health, safety and environmental requirements for composite materials p 1628 N95-23028
Aerospace Industries Association (AIA) work practices report for composites p 1628 N95-23029
Biotransformation of an uncured composite material p 1629 N95-23033
Offgassing test methodology for composite materials p 1629 N95-23035
Outgassing considerations for composites in space applications p 1629 N95-23037
Modeling aerosol emissions from the combustion of composite materials p 1629 N95-23038
Aqueous alternatives for metal and composite cleaning p 1630 N95-23039
Review of aeronautical fatigue investigation in the Netherlands during the period March 1991-March 1993
| PB95-139184 | p 1612 N95-23161
Effects of delaminations on the damped dynamic characteristics of composite laminates: Mechanics and experiments
| NASA-TM-106862 | p 1630 N95-23258
A manufacturing database of advanced materials used in spacecraft structures p 1623 N95-23279
Separation of crack extension modes in composite delamination problems p 1700 N95-23281
Spin polarized photoemission studies of magnetic quantum well states
| DE95-004218 | p 1851 N95-23335
Permeability testing of composite material and adhesive bonds for the DC-XA composite feedline program
| NASA-TM-108483 | p 1630 N95-23551
The sound insulations of studio doors. Part 1: Door blanks
| BBC-RD-1994/14 | p 1654 N95-24093

COMPOSITE STRUCTURES
Neutron scattering analysis of rubber carbon black composite structure
| DE95-002735 | p 1646 N95-22553
Corrosivity sensor
| AD-D016549 | p 1687 N95-22706
Method for forming a glove attachment
| NASA-CASE-MSC-21632-1 | p 1750 N95-22766
Mishap risk control for advanced aerospace/composite materials p 1628 N95-23031
Development and verification of a resin film infusion/resin transfer molding simulation model for fabrication of advanced textile composites
| NASA-CR-197439 | p 1648 N95-23179

Structural Arrangement Trade Study. Volume 1: Reusable Hydrogen Composite Tank System (RHCTS) and Graphite Composite Primary Structures (GCPS). Executive summary
| NASA-CR-197685 | p 1621 N95-23188
Structural arrangement trade study. Volume 3: Reusable Hydrogen Composite Tank System (RHCTS) and Graphite Composite Primary Structures (GCPS). Addendum
| NASA-CR-197687 | p 1621 N95-23189
Thin tailored composite wing for civil tiltrotor p 1613 N95-23317
A coupled layerwise analysis of the thermopiezoelectric response of smart composite beams beams
| NASA-TM-106889 | p 1630 N95-23463
US Navy operating experience with new aircraft construction materials p 1645 N95-23517

COMPOSITION (PROPERTY)
Precise determinations of the isotopic compositions and atomic weights of molybdenum, tellurium, tin and tungsten using ICP source magnetic sector multiple collector mass spectrometry
| DE95-003003 | p 1632 N95-22795

COMPRESSIBILITY
Turbidity of a near critical ionic fluid
| DE94-014916 | p 1633 N95-22869
Incompressible Navier-Stokes calculations in pump flows p 1680 N95-23627

COMPRESSIBILITY EFFECTS
Evaluating the effect of online data compression on the disk cache of a mass storage system p 1862 N95-24138

COMPRESSIBLE BOUNDARY LAYER
Development of an algebraic stress/two-layer model for calculating thrust chamber flow fields p 1675 N95-23442

COMPRESSIBLE FLOW
An approximate theoretical method for modeling the static thrust performance of non-axisymmetric two-dimensional convergent-divergent nozzles
| NASA-CR-195050 | p 1608 N95-23193
Towards a generalized computational fluid dynamics technique for all Mach numbers p 1670 N95-23420
A controlled variation scheme for convection treatment in pressure-based algorithm p 1677 N95-23448
Unification of some advection schemes in two dimensions
| NASA-CR-195044 | p 1790 N95-23465
Navier-Stokes flow field analysis of compressible flow in a pressure relief valve p 1679 N95-23618

COMPRESSIBLE FLUIDS
Dynamic response of a transducer mounted at one end of an acoustical cavity which is subjected to a specified pressure at the open end of the cavity
| DE95-004192 | p 1799 N95-23379

COMPRESSING
Non-zero temperature two-mode squeezing for time-dependent two-level systems
| DE94-628427 | p 1850 N95-22782
Real lasers and other deformed objects p 1692 N95-23001

COMPRESSIVE STRENGTH
Fabric geometry distortion during composites processing p 1631 N95-23288

COMPRESSOR BLADES
NASA low-speed axial compressor for fundamental research
| NASA-TM-4635 | p 1616 N95-23192

COMPTON EFFECT
Neutron compton scattering
| PB95-139135 | p 1807 N95-23159

COMPUTATION
Electrical resistivity of liquid alkali metals and non-local pseudopotential
| DE94-627417 | p 1639 N95-22608
Realizing parallel reduction operation in Sisal 1.2
| DE94-017524 | p 1763 N95-22858
Realizing parallel reduction operations in Sisal 1.2
| DE94-017525 | p 1763 N95-22859
The fundamental group of complex hyperplanes arrangements
| DE94-628426 | p 1796 N95-22933
Accelerated panel methods using the fast multipole method p 1687 N95-23307
Institute for Computational Mechanics in Propulsion (ICOMP)
| NASA-TM-106884 | p 1677 N95-23464
Properties of probabilistic pushdown automata
| TR-554 | p 1760 N95-24056
Logspace reducibility and self-reducibility: Models and equivalences
| TR-544 | p 1760 N95-24059
Teaching computational complexity: Resources to treasure
| TR-543 | p 1784 N95-24060
The satanic notations: Counting classes beyond #P and other definitional adventures
| TR-561 | p 1793 N95-24194

COMPUTATIONAL ASTROPHYSICS
Origins of interstellar and solar system: Carbonaceous materials
| NASA-CR-197436 | p 1867 N95-23013

COMPUTATIONAL CHEMISTRY
Computational studies of metal-metal and metal-ligand interactions
| NASA-CR-197862 | p 1641 N95-23215
Diffusion behavior of lysozyme in aqueous ammonium sulfate solutions under varying solution conditions as determined by dynamic light scattering
| DE95-004821 | p 1635 N95-23380
A multi-region radial integration scheme
| NASA-CR-197982 | p 1809 N95-23408
Symmetry breaking in O4(+): An application of the Brueckner coupled-cluster method
| NASA-CR-197981 | p 1810 N95-23459

COMPUTATIONAL FLUID DYNAMICS
Particle kinetic simulation of high altitude hypervelocity flight
| NASA-CR-197383 | p 1664 N95-22481
An adaptive projection method for the incompressible Navier-Stokes equations
| DE94-019049 | p 1665 N95-22491
Nonlinear generalized functions and nonconservative shock simulations
| DE95-003307 | p 1795 N95-22734
Euler Technology Assessment program for preliminary aircraft design employing SPLITFLOW code with Cartesian unstructured grid method
| NASA-CR-4649 | p 1608 N95-22917
A perspective on unstructured grid flow solvers
| NASA-CR-195025 | p 1788 N95-22931
A CFD study of complex missile and store configurations in relative motion
| NASA-CR-197912 | p 1612 N95-22949
Mach 10 computational study of a three-dimensional scramjet inlet flow field
| NASA-TM-4602 | p 1666 N95-23015
Euler technology assessment for preliminary aircraft design employing OVERFLOW code with multiblock structured-grid method
| NASA-CR-4651 | p 1608 N95-23095
An assessment of viscous effects in computational simulation of benign and burst vortex flows on generic fighter wind-tunnel models using TEAM code
| NASA-CR-4650 | p 1608 N95-23185
The initial-value problem for viscous channel flows
| NASA-CR-195034 | p 1667 N95-23207
Mach 10 computational study of a three-dimensional scramjet inlet flow field
| NASA-TM-4602 | p 1667 N95-23210
Aerodynamic design optimization with sensitivity analysis and computational fluid dynamics
| NASA-CR-197419 | p 1608 N95-23218
Three-dimensional structure in a supersonic jet: Behavior near centerline
| NASA-TM-106869 | p 1668 N95-23220
Direct numerical simulations and modeling of a spatially-evolving turbulent wake p 1687 N95-23289
Direct numerical simulation of sheared turbulent flow p 1687 N95-23296
MPI implementation of CFD program PHOENICS
| DE95-003896 | p 1668 N95-23372
Eleventh Workshop for Computational Fluid Dynamic Applications in Rocket Propulsion
| NASA-CP-3221-PT-2 | p 1668 N95-23412
Criteria for evaluation of grid generation systems p 1669 N95-23416
TIGER: A user-friendly interactive grid generation system for complicated turbomachinery and axis-symmetric configurations p 1670 N95-23419
Towards a generalized computational fluid dynamics technique for all Mach numbers p 1670 N95-23420
Preconditioning for the Navier-Stokes equations with finite-rate chemistry p 1670 N95-23421
A numerical procedure for analysis of finite rate reacting flows p 1671 N95-23422
Three-dimensional Navier-Stokes analysis and redesign of an imbedded bellmouth nozzle in a turbine cascade inlet section p 1671 N95-23423
Numerical simulation of steady and unsteady viscous flow in turbomachinery using pressure based algorithm p 1671 N95-23426
GGOT total pressure loss control concept evaluation p 1672 N95-23427
Supersonic flow and shock formation in turbine tip gaps p 1672 N95-23429
Axisymmetric computational fluid dynamics analysis of Saturn V/S1-C/F1 nozzle and plume p 1672 N95-23430
Computational Fluid Dynamic (CFD) analysis of axisymmetric plume and base flow of film/dump cooled rocket nozzle p 1673 N95-23431
NLS base heating CFD analysis p 1673 N95-23432
CFD flowfield simulation of Delta Launch Vehicles in a power-on configuration p 1673 N95-23433
CFD analysis of turbopump volutes p 1674 N95-23436
Three-dimensional viscous flow analysis inside a turbine volute p 1674 N95-23437
Development of an algebraic stress/two-layer model for calculating thrust chamber flow fields p 1675 N95-23442
Advanced turbulence models for turbomachinery p 1675 N95-23443
Liquid propellant rocket engine combustion simulation with a time-accurate CFD method p 1676 N95-23445
Convergence acceleration of implicit schemes in the presence of high aspect ratio grid cells p 1676 N95-23446
A time-accurate finite volume method valid at all flow velocities p 1676 N95-23447
A controlled variation scheme for convection treatment in pressure-based algorithm p 1677 N95-23448
On the conservative interface treatment for multi-block viscous flow computations
| NASA-CR-195442 | p 1677 N95-23451
Institute for Computational Mechanics in Propulsion (ICOMP)
| NASA-TM-106884 | p 1677 N95-23464
A study of the vortex flow over 76/40-deg double-delta wing
| NASA-CR-195032 | p 1677 N95-23466
On the breakup of viscous liquid threads
| NASA-CR-195023 | p 1678 N95-23544
Combining comparison functions and finite element approximations in CFD
| NASA-TM-106851 | p 1792 N95-23614
Eleventh Workshop for Computational Fluid Dynamic Applications in Rocket Propulsion, part 1
| NASA-CP-3221-PT-1 | p 1678 N95-23615
Computational Fluid Dynamics (CFD) analyses in support of Space Shuttle Main Engine (SSME) heat exchanger (HX) vane cracking investigation p 1679 N95-23619
Unsteady flow simulations in support of the SSME HEX turning vane cracking investigation with the ATD HPOTP p 1679 N95-23621
Comparison between predicted and experimentally measured flow fields at the exit of the SSME HPFTP impeller p 1679 N95-23622
CFD parametric study of consortium impeller p 1680 N95-23626
An inducer CFD solution and effects associated with cavitation p 1681 N95-23631
On the accuracy of CFD-based pressure drop predictions for right-angle ducts p 1682 N95-23634
CFD modeling of turbulent duct flows for coolant channel analysis p 1682 N95-23635
Flow and heat transfer in 180-degree turn square ducts: Effects of turning configuration and system rotation p 1682 N95-23636
Methodology for CFD design analysis of National Launch System nozzle manifold p 1683 N95-23637
Advanced multi-phase flow CFD model development for solid rocket motor flowfield analysis p 1683 N95-23638
ASRM multi-port igniter flow field analysis p 1683 N95-23639
Ignition transient calculations in the Space Shuttle solid rocket motor p 1625 N95-23640
An interactive tool for discrete phase analysis in two-phase flows p 1683 N95-23641
Flowfield characterization in a LOX/GH2 propellant rocket p 1684 N95-23642
Spray combustion experiments and numerical predictions p 1637 N95-23643
CFD analysis of spray combustion and radiation in OMV thrust chamber p 1637 N95-23645
Development of an atomization methodology for spray combustion p 1637 N95-23646
A fine-grid model for the ASRM aft segment with gimballed nozzle p 1685 N95-23648
Application of CFD analysis to design support and problem resolution for ASRM and RSRM p 1685 N95-23649
Time-accurate unsteady flow simulations supporting the SRM T+68-second pressure spike anomaly investigation (STS-54B) p 1685 N95-23650
Status of axisymmetric CFD of an eleven inch diameter hybrid rocket motor p 1686 N95-23651
Validation of a Computational Fluid Dynamics (CFD) code for supersonic axisymmetric base flow p 1686 N95-23652
Code validation study for base flows p 1686 N95-23653

Four-nozzle benchmark wind tunnel model USA code solutions for simulation of multiple rocket base flow recirculation at 145,000 feet altitude
p 1686 N95-23654
Numerical study of base pressure characteristic curve for a four-engine clustered nozzle configuration
p 1625 N95-23655
Supersonic laminar flow control research
| NASA-CR-197938 | p 1609 N95-23669
Using high-performance networks to enable computational aerosciences applications
| NASA-CR-197951 | p 1764 N95-24023
A computer model in general 3-D curvilinear coordinates for the prediction of the turbulent flow field in a jet induced ram combustor
| NAL-TR-1240T | p 1687 N95-24051

COMPUTATIONAL GRIDS

An adaptive projection method for the incompressible Navier-Stokes equations
| DE94-019049 | p 1665 N95-22491
Partitioning methods for unstructured finite element meshes
| PB95-130555 | p 1785 N95-22544
A certainty grid to object boundary algorithm
| PB94-203510 | p 1755 N95-22637
Extensible PDE Solvers package users manual
| DE95-003333 | p 1786 N95-22696
Development of an adaptive hp-version finite element method for computational optimal control
| NASA-CR-197898 | p 1766 N95-22831
A perspective on unstructured grid flow solvers
| NASA-CR-195025 | p 1788 N95-22931
A CFD study of complex missile and store configurations in relative motion
| NASA-CR-197912 | p 1612 N95-22949
VLUGR2: A vectorizable adaptive grid solver for PDes in 2D
| PB95-136008 | p 1789 N95-23167
New robust multigrid method for 2D convection-diffusion problems
| PB95-138897 | p 1789 N95-23176
Mach 10 computational study of a three-dimensional scramjet inlet flow field
| NASA-TM-4602 | p 1667 N95-23210
IGES transformer and NURBS in grid generation
p 1669 N95-23415
Structured adaptive grid generation using algebraic methods p 1669 N95-23417
A generic efficient adaptive grid scheme for rocket propulsion modeling p 1670 N95-23418
TIGER: A user-friendly interactive grid generation system for complicated turbomachinery and axis-symmetric configurations p 1670 N95-23419
Towards a generalized computational fluid dynamics technique for all Mach numbers p 1670 N95-23420
CFD analysis of turbopump volutes
p 1674 N95-23436
Three-dimensional viscous flow analysis inside a turbine volute p 1674 N95-23437
Advanced turbulence models for turbomachinery
p 1675 N95-23443
Convergence acceleration of implicit schemes in the presence of high aspect ratio grid cells
p 1676 N95-23446
A controlled variation scheme for convection treatment in pressure-based algorithm p 1677 N95-23448
On the conservative interface treatment for multi-block viscous flow computations
| NASA-CR-195442 | p 1677 N95-23451
Unification of some advection schemes in two dimensions
| NASA-CR-195044 | p 1790 N95-23465
Unstructured grids on SIMD torus machines
| NASA-CR-197954 | p 1758 N95-23610
A fine-grid model for the ASRM aft segment with gimballed nozzle p 1685 N95-23648

COMPUTER AIDED DESIGN

HiRel: Hybrid Automated Reliability Predictor (HARP) integrated reliability tool system, (version 7.0). Volume 3: HARP Graphics Oriented (GO) input user's guide
| NASA-TP-3452-VOL-3 | p 1753 N95-22479
The viability of establishing collaborative, reconfigurable research environments for the Human Performance Research Laboratory at NASA Ames
| NASA-CR-197384 | p 1753 N95-22480
Layered Electrical Product Application Protocol (AP)
| DE95-001524 | p 1754 N95-22548
CDMS-CAD data set management system test plan
| DE95-003219 | p 1755 N95-22718
Weight minimization of structural components for launch in space shuttle
| NASA-TM-4586 | p 1698 N95-22805
CDMS: CAD data set system design description
| DE95-003218 | p 1756 N95-22894
Euler Technology Assessment program for preliminary aircraft design employing SPLITFLOW code with Cartesian unstructured grid method
| NASA-CR-4649 | p 1608 N95-22917
Euler technology assessment for preliminary aircraft design employing OVERFLOW code with multiblock structured-grid method
| NASA-CR-4651 | p 1608 N95-23095
Segregated rigid and structural control for a photolithography positioning system
| DE95-002603 | p 1766 N95-23134
Control of flow separation in airfoil/wing design applications p 1609 N95-23294
Thin tailored composite wing for civil tiltrotor
p 1613 N95-23317
Application Protocol, Initial Graphics Exchange Specification (IGES), Layered Electrical Product
| DE95-004266 | p 1757 N95-23337
IGES transformer and NURBS in grid generation
p 1669 N95-23415
CFD analysis of turbopump volutes
p 1674 N95-23436
Parallel computation of automatic differentiation applied to magnetic field calculations
| DE95-004689 | p 1763 N95-23486
Methodology for CFD design analysis of National Launch System nozzle manifold p 1683 N95-23637

COMPUTER AIDED MANUFACTURING

IGES transformer and NURBS in grid generation
p 1669 N95-23415
Amorphous silicon photovoltaic manufacturing technology, phase 2A
| DE95-000298 | p 1729 N95-23478

COMPUTER AIDED MAPPING

The effects of AVIRIS atmospheric calibration methodology on identification and quantitative mapping of surface mineralogy, Drum Mountains, Utah
p 1705 N95-23870
Classification of the LCVF AVIRIS test site with a Kohonen artificial neural network p 1706 N95-23874
Mapping and monitoring changes in vegetation communities of Jasper Ridge, CA, using spectral fractions derived from AVIRIS images p 1708 N95-23883

COMPUTER ANIMATION

Newton in space
| NASA-TM-110535 | p 1799 N95-23273
Endeavor: Now and then
| NASA-TM-110539 | p 1620 N95-23664

COMPUTER ASSISTED INSTRUCTION

Human-centered design of human-computer-human dialogs in aerospace systems
| NASA-CR-197379 | p 1750 N95-22797
Teacher Enhancement Institute p 1853 N95-23324
POINTER: Portable Intelligent Trainer for External Robotics p 1752 N95-23714

COMPUTER COMPONENTS

The MAMMOTH project p 1753 N95-24126

COMPUTER GRAPHICS

HiRel: Hybrid Automated Reliability Predictor (HARP) integrated reliability tool system, (version 7.0). Volume 3: HARP Graphics Oriented (GO) input user's guide
| NASA-TP-3452-VOL-3 | p 1753 N95-22479
IGES transformer and NURBS in grid generation
p 1669 N95-23415
Endeavor: Now and then
| NASA-TM-110539 | p 1620 N95-23664
Software agents for the dissemination of remote terrestrial sensing data p 1721 N95-23675
An expert system for diagnosing anomalies of spacecraft p 1770 N95-23684

COMPUTER INFORMATION SECURITY

Network Event Recording Device: An automated system for network anomaly detection, and notification
| DE94-018274 | p 1658 N95-23772
NSSDC provides network access to key data via NDADS p 1862 N95-24136

COMPUTER NETWORKS

Description of a MIL-STD-1553B data bus Ada driver for the LeRC EPS Testbed
| NASA-TM-106866 | p 1762 N95-22668
P2Info Resource Center: Linking the DOE Pollution Prevention community
| DE95-003133 | p 1732 N95-22781
Overview of Ph.D. theses and memoranda, 1993
| PB95-135190 | p 1756 N95-23071
Online Nuclear Data Service
| DE94-634268 | p 1856 N95-23452
Using Dedal to share and reuse distributed engineering design information p 1768 N95-23678
Performance results of cooperating expert systems in a distributed real-time monitoring system
p 1761 N95-23688
Network Event Recording Device: An automated system for network anomaly detection, and notification
| DE94-018274 | p 1658 N95-23772
Computer software design description for the Treated Effluent Disposal Facility (TEDF), Project L-045H, Operator Training Station (OTS)
| DE95-003065 | p 1759 N95-24006
Using high-performance networks to enable computational aerosciences applications
| NASA-CR-197951 | p 1764 N95-24023
A network-based distributed, media-rich computing and information environment
| DE95-003696 | p 1765 N95-24074
A distributed parallel storage architecture and its potential application within EOSDIS
p 1858 N95-24111
The architecture of the High Performance Storage System (HPSS) p 1858 N95-24113
Client/Server data serving for high performance computing p 1761 N95-24123
NSSDC provides network access to key data via NDADS p 1862 N95-24136

COMPUTER PROGRAM INTEGRITY

Network Event Recording Device: An automated system for network anomaly detection, and notification
| DE94-018274 | p 1658 N95-23772
Real-world shepherding: Combining vision, manipulation, and planning in real time
| TR-530 | p 1783 N95-24001

COMPUTER PROGRAMMING

Method for building and evaluating formal specifications of object-oriented conceptual models of database systems
| PB95-127353 | p 1855 N95-22525
Overview of Ph.D. theses and memoranda, 1993
| PB95-135190 | p 1756 N95-23071
Investigation of the role of gravity waves in the generation of equatorial bubbles
| NASA-CR-197962 | p 1739 N95-23272
Radioisotope thermoelectric generator transportation system subsystem 143 software development plan
| DE95-003774 | p 1662 N95-23351
A constraint-logic based implementation of the coarse-grained approach to data acquisition scheduling of the International Ultraviolet Explorer orbiting observatory p 1779 N95-23741
Automated synthesis of image processing procedures using AI planning techniques p 1779 N95-23745
OPUS: A new generation Knowledge Engineering Environment p 1760 N95-24176
Lazy release consistency for hardware-coherent multiprocessors
| TR-547 | p 1765 N95-24184

COMPUTER PROGRAMS

Analysis of physiochemical processes during solder aging
| DE95-003811 | p 1638 N95-22576
Additional improvements to the NASA Lewis ice accretion code LEWICE
| NASA-TM-106849 | p 1665 N95-22669
Measurements and modeling of impurity source distributions from the Tore Supra outboard pump limiter
| DE95-003097 | p 1831 N95-22800
Observation model and parameter partials for the JPL VLBI parameter estimation software MODEST, 19 94
| NASA-CR-197328 | p 1756 N95-22853
Computation of magnetic forces on moving conductors by using ELEKTRA and other 3-D computer codes
| DE95-003308 | p 1798 N95-22895
Format( )MEDIC( )Input
| DE95-003482 | p 1737 N95-23063
Properties of jets in Z events from 1.8 TeV (bar p)p collisions
| DE94-018982 | p 1808 N95-23197
Two portable parallel tridiagonal solvers
| DE94-019044 | p 1763 N95-23243
Computational control of flexible aerospace systems
| NASA-CR-197902 | p 1621 N95-23260
Infinite possibilities: Computational structures technology p 1700 N95-23280
Automation technology using Geographic Information System (GIS) p 1863 N95-23284
Measurements of striae in CR+ doped YAG laser crystals p 1847 N95-23285
Stochastic decision analysis p 1854 N95-23305
Residual strength of thin panels with cracks
p 1700 N95-23311
Benchmark problems in computational aeroacoustics
p 1800 N95-23315
Application of electron paramagnetic resonance imaging to the characterization of the Ultem(R) exposed to 1 MeV electrons. Correlation of radical density data to tiger code calculations p 1815 N95-23328
The software analysis project for the Office of Human Resources p 1854 N95-23331
Search Hanford accessible reports electronically system design description, revision 1
| DE95-004369 | p 1856 N95-23341

Verification and validation of decision support software: Expert Choice(trademark) and PCM(trademark)
| DE95-004469 | p 1757 N95-23346
Radioisotope thermoelectric generator transportation system subsystem 143 software development plan
| DE95-003774 | p 1662 N95-23351
MPI implementation of CFD program PHOENICS
| DE95-003896 | p 1668 N95-23372
GGOT total pressure loss control concept evaluation
p 1672 N95-23427
CFD analysis of turbopump volutes
p 1674 N95-23436
Advanced turbulence models for turbomachinery
p 1675 N95-23443
Liquid propellant rocket engine combustion simulation with a time-accurate CFD method p 1676 N95-23445
Index of nuclear data libraries available from the IAEA nuclear data section
| DE94-634271 | p 1857 N95-23453
Enhanced analysis and users manual for radial-inflow turbine conceptual design code RTD
| NASA-CR-195454 | p 1609 N95-23462
User's guide and physics manual for the ScatPlus circuit code
| DE95-003755 | p 1663 N95-23479
Parallel computation of automatic differentiation applied to magnetic field calculations
| DE95-004689 | p 1763 N95-23486
Squeezing out all the performance: Using Ingres for a C(sup 3)I reporting system
| DE95-004591 | p 1857 N95-23490
WHAMS3D Project: Parallel implementations of WHAMS3D on two shared-memory multiprocessors
| CSRD-1248 | p 1764 N95-23599
Knowledge-based guidance and control functions
| AGARD-AR-325 | p 1751 N95-23601
Recent advances in Lanczos-based iterative methods for nonsymmetric linear systems
| NASA-CR-197950 | p 1791 N95-23611
Spray combustion experiments and numerical predictions p 1637 N95-23643
Progress in advanced spray combustion code integration p 1637 N95-23644
Modeling of non-spherical droplet dynamics
p 1685 N95-23647
Attention focusing and anomaly detection in systems monitoring p 1769 N95-23683
Performance results of cooperating expert systems in a distributed real-time monitoring system
p 1761 N95-23688
Telerobotics test bed for space structure assembly
p 1618 N95-23734
Network Event Recording Device: An automated system for network anomaly detection, and notification
| DE94-018274 | p 1658 N95-23772
ESTAR, PSTAR, ASTAR: A PC package for calculating stopping powers and ranges of electrons, protons and helium ions, version 2
| DE94-634435 | p 1811 N95-23773
The US Geological Survey, digital spectral reflectance library: version 1: 0.2 to 3.0 microns
p 1703 N95-23855
Laboratory spectra of field samples as a check on two atmospheric correction methods p 1711 N95-23894
PCLOOK: An interactive code for spectral analysis
| DE94-635415 | p 1759 N95-23963
Real-world shepherding: Combining vision, manipulation, and planning in real time
| TR-530 | p 1783 N95-24001
Computer software design description for the Treated Effluent Disposal Facility (TEDF), Project L-045H, Operator Training Station (OTS)
| DE95-003065 | p 1759 N95-24006
Increasing the retained dose by plasma immersion ion implantation and deposition
| DE95-003423 | p 1844 N95-24011
Remote sensor test range update
| DE95-003629 | p 1735 N95-24018
Eliminating useless messages in write-update protocols on scalable multiprocessors
| TR-539 | p 1764 N95-24037
Using simulation-based projection to plan in an uncertain and temporally complex world
| TR-531 | p 1853 N95-24043
A computer model in general 3-D curvilinear coordinates for the prediction of the turbulent flow field in a jet induced ram combustor
| NAL-TR-1240T | p 1687 N95-24051
Transferring ecosystem simulation codes to supercomputers
| NASA-TM-4662 | p 1759 N95-24052
Search Hanford accessible reports electronically system configuration management plan
| DE95-004493 | p 1857 N95-24089
Modeling of tritium recovery from lithium ceramics
| DE95-004626 | p 1838 N95-24167
User's guide for ECAP2D: An Euler unsteady aerodynamic and aeroelastic analysis program for two dimensional oscillating cascades, version 1.0
| NASA-CR-189146 | p 1699 N95-24189

COMPUTER STORAGE DEVICES

Fourth NASA Goddard Conference on Mass Storage Systems and Technologies
| NASA-CP-3295 | p 1857 N95-24108
A distributed parallel storage architecture and its potential application within EOSDIS
p 1858 N95-24111
New architectural paradigms for multi-petabyte distributed storage systems p 1858 N95-24115
Approaches to 100 Gbit/sq. in. recording density
p 1690 N95-24128
Optimizing tertiary storage organization and access for spatio-temporal datasets p 1861 N95-24131

COMPUTER SYSTEMS DESIGN

Parallel digital modem using multirate digital filter banks
| NASA-CR-197331 | p 1761 N95-22478
HiRel: Hybrid Automated Reliability Predictor (HARP) integrated reliability tool system, (version 7.0). Volume 3: HARP Graphics Oriented (GO) input user's guide
| NASA-TP-3452-VOL-3 | p 1753 N95-22479
DIstributed VIRtual System (DIVIRS) project
| NASA-CR-197855 | p 1757 N95-23180
On-line, adaptive state estimator for active noise control p 1784 N95-23308
Integrating O/S models during conceptual design, part 3
| NASA-CR-197905 | p 1622 N95-23400
Software agents for the dissemination of remote terrestrial sensing data p 1721 N95-23675
Commercialization of JPL Virtual Reality calibration and redundant manipulator control technologies
p 1768 N95-23676
Utilizing inheritance in requirements engineering
p 1768 N95-23677
Operator procedure verification with a rapidly reconfigurable simulator p 1618 N95-23679
Toward an automated signature recognition toolkit for mission operations p 1659 N95-23682
An expert system for diagnosing anomalies of spacecraft p 1770 N95-23684
Distributed intelligence for ground/space systems
p 1770 N95-23685
Learning time series for intelligent monitoring
p 1770 N95-23686
Subsumption-based architecture for autonomous movement planning for planetary rovers
p 1771 N95-23690
Algorithms for categorizing multiprocessor communication under invalidate and update-based coherence protocols
| TR-533-REV | p 1759 N95-23928
Scalability of atomic primitives on distributed shared memory multiprocessors
| TR-528 | p 1764 N95-23930
The design of a petabyte archive and distribution system for the NASA ECS project p 1858 N95-24110
A distributed parallel storage architecture and its potential application within EOSDIS
p 1858 N95-24111
Robotic tape library system level testing at NSA: Present and planned p 1858 N95-24112
The architecture of the High Performance Storage System (HPSS) p 1858 N95-24113
A 500 megabyte/second disk array
p 1753 N95-24114
New architectural paradigms for multi-petabyte distributed storage systems p 1858 N95-24115
Optimizing raid performance with cache
p 1761 N95-24116
Document image archive transfer from DOS to UNIX
p 1761 N95-24117
Integrating UniTree with the data migration API
p 1761 N95-24120
Client/Server data serving for high performance computing p 1761 N95-24123

COMPUTER SYSTEMS PERFORMANCE

Integrating O/S models during conceptual design, part 3
| NASA-CR-197905 | p 1622 N95-23400
Institute for Computational Mechanics in Propulsion (ICOMP)
| NASA-TM-106884 | p 1677 N95-23464
Microarchitecture support for dynamic scheduling of acyclic task graphs
| CSRD-1207 | p 1791 N95-23600
Attention focusing and anomaly detection in systems monitoring p 1769 N95-23683
Performance results of cooperating expert systems in a distributed real-time monitoring system
p 1761 N95-23688
Eliminating useless messages in write-update protocols on scalable multiprocessors
| TR-539 | p 1764 N95-24037
The architecture of the High Performance Storage System (HPSS) p 1858 N95-24113
A 500 megabyte/second disk array
p 1753 N95-24114
Integrating UniTree with the data migration API
p 1761 N95-24120

COMPUTER SYSTEMS PROGRAMS

Description of a MIL-STD-1553B data bus Ada driver for the LeRC EPS Testbed
| NASA-TM-106866 | p 1762 N95-22668
Integrating UniTree with the data migration API
p 1761 N95-24120

COMPUTER SYSTEMS SIMULATION

Evaluation of a Multiple Instruction/Multiple Data (MIMD) parallel computer for CFD applications
| AD-A285796 | p 1762 N95-22509
Simulation and off-line programming systems comparison
| DE95-002267 | p 1766 N95-23078

COMPUTER TECHNIQUES

RAS Division model evaluation database tools
| DE95-003480 | p 1733 N95-23123
Infinite possibilities: Computational structures technology p 1700 N95-23280
Electronic photography at NASA Langley Research Center p 1690 N95-23298
Teacher Enhancement Institute p 1853 N95-23324
IGES transformer and NURBS in grid generation
p 1669 N95-23415
Criteria for evaluation of grid generation systems
p 1669 N95-23416
Computer software design description for the Treated Effluent Disposal Facility (TEDF), Project L-045H, Operator Training Station (OTS)
| DE95-003065 | p 1759 N95-24006
Optimizing raid performance with cache
p 1761 N95-24116

COMPUTER VISION

Progress report on a fully automatic Gas Tungsten Arc Welding (GTAW) system development
| DE95-004397 | p 1695 N95-23343
The next decade of space robotics
p 1768 N95-23673
Autonomous navigation system for the Marsokhod rover project p 1771 N95-23693
Lunar rover technology demonstrations with Dante and Ratler p 1697 N95-23694
A perspective on space robotics in Japan
p 1697 N95-23695
A fuzzy structural matching scheme for space robotics vision p 1778 N95-23737
Active vision in satellite scene analysis
p 1778 N95-23738
Real-time tracking using stereo and motion: Visual perception for space robotics p 1778 N95-23739
Terrain modelling and motion planning for an autonomous exploration rover p 1721 N95-23765
Vision-based planning and execution of precision grasps
| TR-546 | p 1784 N95-24185

COMPUTERIZED SIMULATION

Parallel digital modem using multirate digital filter banks
| NASA-CR-197331 | p 1761 N95-22478
The viability of establishing collaborative, reconfigurable research environments for the Human Performance Research Laboratory at NASA Ames
| NASA-CR-197384 | p 1753 N95-22480
Particle kinetic simulation of high altitude hypervelocity flight
| NASA-CR-197383 | p 1664 N95-22481
Effects of wind on rainfall simulation. Spatial distribution of water application, kinetic energy, and overland flow under single full-cone nozzle sprays
| PB95-127304 | p 1717 N95-22537
A parallel molecular dynamics simulation of crystal growth at a cluster of workstations
| DE94-628382 | p 1839 N95-22615
Computer simulation of the structure of ionic surfaces and interfaces
| DE95-002991 | p 1804 N95-22792
Hot proton anisotropies and cool proton temperatures in the outer magnetosphere
| DE95-002719 | p 1736 N95-22850
The 1993 Annual Conference of the Israeli Association for Crystal Growth. Program and abstracts
| DE94-633510 | p 1841 N95-22854
The torsion space nucleic acids molecular mechanics program DUPLEX: Surveying conformation space by potential energy minimization
| DE94-017707 | p 1805 N95-22889
Overview of Ph.D. theses and memoranda, 1993
| PB95-135190 | p 1756 N95-23071

Simulation and off-line programming systems comparison
[DE95-002267] p 1766 N95-23078
High-performance parallel analysis of coupled problems for aircraft propulsion
[NASA-CR-197440] p 1614 N95-23088
Development and verification of a resin film infusion/resin transfer molding simulation model for fabrication of advanced textile composites
[NASA-CR-197439] p 1648 N95-23179
A wall interference assessment/correction system
[NASA-CR-197421] p 1667 N95-23183
Life support systems analysis and technical trades for a lunar outpost
[NASA-TM-109927] p 1751 N95-23194
Three-dimensional structure in a supersonic jet: Behavior near centerline
[NASA-TM-106869] p 1668 N95-23220
Infinite possibilities: Computational structures technology p 1700 N95-23280
Direct numerical simulations and modeling of a spatially-evolving turbulent wake p 1687 N95-23289
Design of a variable area diffuser for a 15-inch Mach 6 open-jet tunnel p 1617 N95-23309
Computational modelling of Er(3+): Garnet laser materials p 1692 N95-23326
Computer modeling of the sensitivity of a laser water vapor sensor to variations in temperature and air speed p 1692 N95-23330
A hybrid vehicle evaluation code and its application to vehicle design
[DE95-004205] p 1662 N95-23334
Measurement of correlated b quark cross sections at CDF
[DE95-004240] p 1808 N95-23336
Simulation of absorption edge densitometry
[DE95-004393] p 1635 N95-23360
MPI implementation of CFD program PHOENICS
[DE95-003896] p 1668 N95-23372
Integrating O/S models during conceptual design, part 1
[NASA-CR-197903] p 1622 N95-23398
Numerical simulation of steady and unsteady viscous flow in turbomachinery using pressure based algorithm p 1671 N95-23426
Navier-Stokes analysis of an oxidizer turbine blade with tip clearance with and without a mini-shroud p 1672 N95-23428
CFD flowfield simulation of Delta Launch Vehicles in a power-on configuration p 1673 N95-23433
Numerical study of the SSME nozzle flow fields during transient operations: A comparison of the animated results with test p 1673 N95-23434
Three-dimensional viscous flow analysis inside a turbine volute p 1674 N95-23437
Liquid propellant rocket engine combustion simulation with a time-accurate CFD method p 1676 N95-23445
Institute for Computational Mechanics in Propulsion (ICOMP)
[NASA-TM-106884] p 1677 N95-23464
EXTRA.M: A computing code system for analysis of the Purex process with mixer settlers for reprocessing
[DE94-785273] p 1635 N95-23476
A wavenumber-partitioning scheme for two-dimensional statistical closures
[DE95-004514] p 1677 N95-23483
On inertial range scaling laws
[DE95-004515] p 1677 N95-23484
Parallel computation of automatic differentiation applied to magnetic field calculations
[DE95-004689] p 1763 N95-23486
Squeezing out all the performance: Using Ingres for a C(sup 3)I reporting system
[DE95-004591] p 1857 N95-23490
Macro-EM particle simulation method and a study of collisionless magnetic reconnection
[NIFS-316] p 1834 N95-23526
Complexity in plasma: A grand view of self-organization
[NIFS-318] p 1835 N95-23528
Current-profile flattening and hot core shift due to the nonlinear development of resistive kink mode
[NIFS-311] p 1835 N95-23564
Phonon-induced anomalous specific heat of a model nanocrystal by computer simulation
[DE95-004653] p 1843 N95-23585
Computer simulation of a magnetohydrodynamic dynamo 2
[NIFS-320] p 1836 N95-23590
MHD-Vlasov simulation of the toroidal Alfven eigenmode
[NIFS-319] p 1836 N95-23591
Development of qualification guidelines for personal computer-based aviation training devices
[DOT/FAA/AM-95/6] p 1758 N95-23603
Time-accurate unsteady flow simulations supporting the SRM T+68-second pressure spike anomaly investigation (STS-54B) p 1685 N95-23650
Four-nozzle benchmark wind tunnel model USA code solutions for simulation of multiple rocket base flow recirculation at 145,000 feet altitude p 1686 N95-23654
A toolbox and record for scientific models p 1775 N95-23716
Modeling actions and operations to support mission preparation p 1617 N95-23750
New determination of V(sub us) from K(sub e3)(+) decay
[DE94-628616] p 1811 N95-23769
An RL10A-3-3A rocket engine model using the rocket engine transient simulator (ROCETS) software
[NASA-CR-190786] p 1625 N95-23790
Experimental investigation of the relationship between impact crater morphology and impacting particle velocity and direction p 1700 N95-23840
Axial focusing of energy from a hypervelocity impact on earth
[DE95-003347] p 1740 N95-24008
Axial focusing of impact energy in the earth's interior: A possible link to flood basalts and hotspots
[DE95-003357] p 1741 N95-24009
Increasing the retained dose by plasma immersion ion implantation and deposition
[DE95-003423] p 1844 N95-24011
Gyrokinetic and global fluid simulations of tokamak microturbulence and transport
[DE95-003628] p 1837 N95-24017
Design of a cervical spine gross motion simulator for standard size human and anthropomorphic dummy adult and child
[NIAR-94-16] p 1751 N95-24021
Unsupervised classification learning from cross-modal environmental structure
[TR-536] p 1784 N95-24040
Using simulation-based projection to plan in an uncertain and temporally complex world
[TR-531] p 1853 N95-24043
Dynamical model and numerical simulations for Engineering Test Satellite-6
[NAL-TR-1239] p 1622 N95-24049
A computer model in general 3-D curvilinear coordinates for the prediction of the turbulent flow field in a jet induced ram combustor
[NAL-TR-1240T] p 1687 N95-24051
Transferring ecosystem simulation codes to supercomputers
[NASA-TM-4662] p 1759 N95-24052
Optimizing tertiary storage organization and access for spatio-temporal datasets p 1861 N95-24131

COMPUTERS

Evaluation of a Multiple Instruction/Multiple Data (MIMD) parallel computer for CFD applications
[AD-A285796] p 1762 N95-22509
Real-world shepherding: Combining vision, manipulation, and planning in real time
[TR-530] p 1783 N95-24001
Eliminating useless messages in write-update protocols on scalable multiprocessors
[TR-539] p 1764 N95-24037

CONCENTRATION (COMPOSITION)

Chemical recognition software
[DE95-003346] p 1636 N95-24007

CONCORDE AIRCRAFT

Preliminary identification of buffet problems in high speed civil transport p 1616 N95-23319

CONCURRENT PROCESSING

Automatic verification of regular protocols in P/T nets
[PB95-138921] p 1789 N95-23146
Performance results of cooperating expert systems in a distributed real-time monitoring system p 1761 N95-23688
An efficient algorithm for concurrent priority queue heaps
[TR-560] p 1759 N95-24033

CONDENSATES

The U(3) x U(3) Nambu - Jona-Lasinio model with the gluon condensate and axial anomaly at finite temperature
[DE94-628588] p 1804 N95-22787
Bose condensation, macroscopic quantum phenomena and atomic spatial correlations in superfluid He-4
[PB95-139085] p 1850 N95-23154

CONDENSED MATTER PHYSICS

Aspects of sigma models
[DE94-628511] p 1795 N95-22736
Magnetic multilayer physics
[DE95-003408] p 1798 N95-23083

CONDUCTIVE HEAT TRANSFER

COYOTE 2: A Finite Element Computer Program for nonlinear heat conduction problems
[DE95-002848] p 1666 N95-22914

CONDUCTORS

Computation of magnetic forces on moving conductors by using ELEKTRA and other 3-D computer codes
[DE95-003308] p 1798 N95-22895
Electrochemical studies of perovskite mixed conductors
[DE95-003704] p 1636 N95-23573

CONFERENCES

Proceedings of NATO Advanced Research Workshop on the Formation, Transport and Consequences of Particles in Plasmas
[AD-A285850] p 1829 N95-22514
The development and applications of biomarkers
[DE94-014249] p 1744 N95-22589
Addendum to the Proceedings of the Third International Mobile Satellite Conference (IMSC 1993)
[NASA-CR-197343] p 1655 N95-22813
The 1993 Annual Conference of the Israeli Association for Crystal Growth. Program and abstracts
[DE94-633510] p 1841 N95-22854
Renewable Energy Sources Brno 1993
[DE94-633975] p 1727 N95-22855
Open problems of computational molecular biology
[DE95-000895] p 1745 N95-22866
Second International Workshop on Harmonic Oscillators
[NASA-CP-3286] p 1820 N95-22957
Environmental, Safety, and Health Considerations: Composite Materials in the Aerospace Industry
[NASA-CP-3289] p 1628 N95-23025
7th International Symposium on Applications of Laser Techniques to Fluid Mechanics, volume 1
[AD-A285647] p 1691 N95-23118
Ninth topical conference on atomic processes in plasmas
[DE95-002810] p 1833 N95-23246
Hydrogen and fuel cells for energy storage
[DE95-723907] p 1729 N95-23382
Eleventh Workshop for Computational Fluid Dynamic Applications in Rocket Propulsion
[NASA-CP-3221-PT-2] p 1668 N95-23412
Oxidants and oxidation in the Earth's atmosphere
[NASA-CR-197945] p 1734 N95-23460
Corrosion detection and management of advanced airframe materials
[AGARD-CP-565] p 1641 N95-23496
LDEF materials results for spacecraft applications: Executive summary
[NASA-CP-3261] p 1617 N95-23549
Proceedings of the workshop on deductive databases and logic programming
[PB95-139382] p 1758 N95-23553
Scandinavian symposium on surface chemistry
[PB95-140687] p 1636 N95-23554
Report of proceedings: Aviation Accident Investigation Symposium. Volume 2: Participant presentations
[PB94-917007] p 1610 N95-23598
Eleventh Workshop for Computational Fluid Dynamic Applications in Rocket Propulsion, part 1
[NASA-CP-3221-PT-1] p 1678 N95-23615
Third International Symposium on Artificial Intelligence, Robotics, and Automation for Space 1994
[NASA-CR-197340] p 1767 N95-23672
LDEF: 69 Months in Space. Third Post-Retrieval Symposium, part 1
[NASA-CP-3275-PT-1] p 1889 N95-23796
Summaries of the 4th Annual JPL Airborne Geoscience Workshop. Volume 1: AVIRIS Workshop
[NASA-CR-197877-VOL-1] p 1701 N95-23844
LDEF: 69 Months in Space. Third Post-Retrieval Symposium, part 2
[NASA-CP-3275-PT-2] p 1899 N95-23896
Summaries of the 4th Annual JPL Airborne Geoscience Workshop. Volume 3: AIRSAR Workshop
[NASA-CR-197354-VOL-3] p 1712 N95-23938
Proceedings of the fuel cells 1994 contractors review meeting
[DE94-012285] p 1730 N95-23977
The 1993 Gordon Research Conference on Chronobiology
[NASA-CR-197990] p 1748 N95-24047
Aviation Accident Investigation Symposium. Volume 1: Industry recommendations and Safety Board responses
[PB94-917005] p 1611 N95-24105
Fourth NASA Goddard Conference on Mass Storage Systems and Technologies
[NASA-CP-3295] p 1857 N95-24108
Atomic physics at high brilliance synchrotron sources: Proceedings
[DE95-006077] p 1813 N95-24174

CONFIGURATION INTERACTION

Symmetry breaking in O4(+): An application of the Brueckner coupled-cluster method
[NASA-CR-197981] p 1810 N95-23459

CONFIGURATION MANAGEMENT
CDMS: CAD data set system design description
|DE95-003218| p 1756 N95-22894
Search Hanford accessible reports electronically system configuration management plan
|DE95-004493| p 1857 N95-24089
CONFIGURATIONS
Results from neutrino experiments
|DE94-628604| p 1804 N95-22790
CONFINEMENT
Spontaneous breaking of chiral symmetry as a consequence of confinement
|DE94-628560| p 1849 N95-22745
The q profile evolution and enhanced core confinement of high (beta)(sub p) plasmas in D3-D
|DE95-003878| p 1834 N95-23371
CONFORMAL MAPPING
On diagonalization in map (M,G)
|DE94-628515| p 1796 N95-22740
Schwarz-Christoffel methods for multiply-elongated regions
|DE94-019048| p 1790 N95-23536
CONGRESSIONAL REPORTS
NASA procurement: Contract and management improvements at the Jet Propulsion Laboratory. Report to Congressional requesters
|GAO/NSIAD-95-40| p 1854 N95-24054
DOD budget: Selected categories of planned funding for fiscal years 1995-99. Report to Congressional requesters
|GAO/NSIAD-95-92| p 1864 N95-24062
Inspector General: Alleged misconduct by NASA Inspector General. Report to Congressional requesters
|GAO/OSI-95-9| p 1854 N95-24085
Report to the Secretary of Defense. Unmanned aerial vehicles: No more Hunter systems should be bought until problems are fixed
|GAO/NSIAD-95-52| p 1613 N95-24091
CONGRUENCES
Coherent states for a generalization of the harmonic oscillator p 1823 N95-22982
CONIFERS
Estimation of crown closure from AVIRIS data using regression analysis p 1709 N95-23886
Estimation of biophysical properties of upland Sitka spruce (Picea sitchensis) plantations p 1713 N95-23943
Hierarchical analysis of spatial pattern and processes of Douglas-fir forests p 1719 N95-24099
Analysis of conifer forest regeneration using Landsat Thematic Mapper data p 1720 N95-24101
Determining successional stage of temperate coniferous forests with Landsat satellite data p 1720 N95-24102
Determining coniferous forest cover and forest fragmentation with NOAA-9 advanced very high resolution radiometer data p 1720 N95-24103
Dynamics and pattern of a managed coniferous forest landscape in Oregon p 1720 N95-24104
CONJUGATE GRADIENT METHOD
Algorithms for parallel and vector computations
|NASA-CR-197394| p 1756 N95-23017
Conjugate gradient MATHEW
|DE95-003479| p 1738 N95-23143
On adaptive weighted polynomial preconditioning for Hermitian positive definite matrices
|NASA-CR-197946| p 1791 N95-23547
CONJUGATES
On diagonalization in map (M,G)
|DE94-628515| p 1796 N95-22740
CONSERVATION EQUATIONS
A generalized Eulerian-Lagrangian analysis, with application to liquid flows with vapor bubbles p 1682 N95-23633
CONSERVATION LAWS
The effect of a non-zero shock width on wave propagation in multi-dimensions
|DE95-002748| p 1666 N95-22902
Exact, E = 0, classical and quantum solutions for general power-law oscillators p 1820 N95-22959
Non-Noetherian symmetries for oscillators in classical mechanics and in field theory p 1823 N95-22977
A time-accurate finite volume method valid at all flow velocities p 1676 N95-23447
CONSISTENCY
Verifying sequentially consistent memory using interface refinement
|PB95-139002| p 1752 N95-23153
Consistency and Monte Carlo simulation of a data driven version of smooth goodness-of-fit tests
|PB95-141255| p 1794 N95-23559
CONSOLIDATION
Investigation of mechanical properties and their relation to the internal structure of nanocrystalline metals and composites
|DE95-001151| p 1627 N95-22683
NMR study of nanophase Al/Al-oxide powder and consolidated composites
|DE95-004655| p 1843 N95-23586
Optimizing raid performance with cache p 1761 N95-24116
CONSTRAINTS
Solution and reasoning reuse in space planning and scheduling applications p 1618 N95-23760
Empirical results on scheduling and dynamic backtracking p 1618 N95-23761
CONSTRUCTION
Grassman and hyperKaehler structures on some spaces of sections of holomorphic bundles
|PB95-109104| p 1795 N95-22712
Parallal Arnoldi method for the construction of a Krylov subspace basis: An application in magnetohydrodynamics
|PB95-135786| p 1787 N95-22717
Hadrons of arbitrary spin and heavy quark symmetry
|DE94-628597| p 1804 N95-22789
Taxonomy of finite automata construction algorithms
|PB95-139234| p 1758 N95-23606
CONSTRUCTION MATERIALS
Fire hazard considerations for composites in vehicle design p 1628 N95-23032
CONTACT RESISTANCE
Advances in research for solid oxide fuel cells
|DE95-004590| p 1730 N95-23582
CONTACTORS
Functional testing of the space station plasma contactor
|NASA-TM-106841| p 1624 N95-23240
CONTAINERLESS MELTS
A new containerless image furnace with electro-static positioning device p 1690 N95-23674
CONTAINMENT
Characterization of Type 304L stainless steel solid-state closure welds for radioactive waste containment
|DE94-016539| p 1645 N95-23980
CONTAMINANTS
Novel mass spectrometric instrument for gaseous and particulate characterization and monitoring
|DE95-001135| p 1687 N95-22682
Analytical Boltzmann moments for electrons in N2-O2-H2O gas mixtures
|DE95-003474| p 1732 N95-22898
The significance of hair mineral analysis as a means for assessing internal body burdens of environmental pollutants
|DE94-633512| p 1734 N95-23541
Reproducible direct exposure environmental testing of metal-based magnetic media p 1690 N95-24129
CONTAMINATION
Innovative technology for contamination control in plasma processing
|DE95-000913| p 1829 N95-22519
Be-10 in terrestrial bauxite and industrial aluminum: An LDEF fallout p 1646 N95-23820
Secondary ion mass spectrometry (SIMS) analysis of hypervelocity microparticle impact sites on LDEF surfaces p 1637 N95-23836
Atmospheric correction of AVIRIS data of Monterey Bay contaminated by thin cirrus clouds p 1710 N95-23890
CONTINUOUS WAVE LASERS
Reduced dimer production in solar-simulator-pumped continuous wave iodine lasers based on model simulations and scaling and pumping studies
|NASA-TP-3486| p 1691 N95-23411
CONTINUUMS
Is omega* - (mu) absolutely countably compact?
|PB95-127981| p 1785 N95-22528
Harmonic oscillator representation in the theory of scattering and nuclear reactions p 1814 N95-22967
Discrimination of poorly exposed lithologies in AVIRIS data p 1703 N95-23858
CONTRACT MANAGEMENT
NASA procurement: Contract and management improvements at the Jet Propulsion Laboratory. Report to Congressional requesters
|GAO/NSIAD-95-40| p 1854 N95-24054
CONTRACTORS
Information technology standards process guide
|DE95-003967| p 1857 N95-23574
Proceedings of the fuel cells 1994 contractors review meeting
|DE94-012285| p 1730 N95-23977
NASA procurement: Contract and management improvements at the Jet Propulsion Laboratory. Report to Congressional requesters
|GAO/NSIAD-95-40| p 1854 N95-24054
CONTROL
Robotic all-terrain lunar exploration rover (RATLER) FY93 program status report
|DE95-003589| p 1694 N95-23065
CONTROL EQUIPMENT
Flow measuring structures
|PB95-127254| p 1665 N95-22638
Engines-only flight control system
|NASA-CASE-ARC-11944-1| p 1615 N95-23389
DRACULA: Dynamic range control for broadcasting and other applications
|BBC-RD-1994/13| p 1658 N95-24044
CONTROL SIMULATION
Computational control of flexible aerospace systems
|NASA-CR-197902| p 1621 N95-23260
CONTROL STABILITY
Stable H(infinity) controller design for the longitudinal dynamics of an aircraft
|NASA-TM-106847| p 1615 N95-22954
Using AVIRIS for in-flight calibration of the spectral shifts of SPOT-HRV and of AVHRR? p 1710 N95-23893
CONTROL SURFACES
Aerodynamic surface distension system for high angle of attack forebody vortex control
|NASA-CASE-ARC-11979-1| p 1612 N95-23390
CONTROL SYSTEMS DESIGN
Description of a MIL-STD-1553B data bus Ada driver for the LeRC EPS Testbed
|NASA-TM-106866| p 1762 N95-22668
Environmental Systems Management Analysis and Reporting Network (E-SMART)
|AD-A279766| p 1732 N95-22856
Design of high performance multivariable control systems for supermaneuverable aircraft at high angle of attack
|NASA-CR-197661| p 1615 N95-22908
Stable H(infinity) controller design for the longitudinal dynamics of an aircraft
|NASA-TM-106847| p 1615 N95-22954
System identification of the Large-Angle Magnetic Suspension Test Fixture (LAMSTF) p 1617 N95-23299
Engines-only flight control system
|NASA-CASE-ARC-11944-1| p 1615 N95-23389
Integrating O/S models during conceptual design, part 1
|NASA-CR-197903| p 1622 N95-23398
Integrating O/S models during conceptual design, part 2
|NASA-CR-197904| p 1622 N95-23399
Integrating O/S models during conceptual design, part 3
|NASA-CR-197905| p 1622 N95-23400
A microcontroller-based three degree-of-freedom manipulator testbed
|NASA-CR-197423| p 1696 N95-23409
Feedback control laws for highly maneuverable aircraft
|NASA-CR-197944| p 1615 N95-23410
Knowledge-based guidance and control functions
|AGARD-AR-325| p 1751 N95-23601
Development of Advanced Robotic Hand System for space application p 1752 N95-23704
Hardware interface unit for control of shuttle RMS vibrations p 1697 N95-23706
Robotic experiment with a force reflecting handcontroller onboard MIR space station p 1752 N95-23707
Development of Japanese experiment module remote manipulator system p 1752 N95-23708
Robot arm system for automatic satellite capture and berthing p 1752 N95-23709
Robust control of multi-jointed arm with a decentralized autonomous control mechanism p 1659 N95-23710
CONTROL THEORY
Stable H(infinity) controller design for the longitudinal dynamics of an aircraft
|NASA-TM-106847| p 1615 N95-22954
Integrating planning and reactive control p 1618 N95-23763
Unifying data and control transformations for distributed shared-memory machines
|TR-542| p 1765 N95-24061
CONTROLLABILITY
Flight test of the X-29A at high angle of attack: Flight dynamics and controls
|NASA-TP-3537| p 1612 N95-22806
Analysis of the longitudinal handling qualities and pilot-induced-oscillation tendencies of the High-Angle-of-Attack Research Vehicle (HARV) p 1616 N95-23297
CONTROLLED FUSION
Ion rings for magnetic fusion
|DE94-017606| p 1832 N95-23120
CONTROLLERS
Controlling under-actuated robot arms using a high speed dynamics process
|NASA-CASE-NPO-18498-1-CU| p 1692 N95-22543
Description of a MIL-STD-1553B data bus Ada driver for the LeRC EPS Testbed
|NASA-TM-106866| p 1762 N95-22668

Programmable hyperspectral image mapper with on-array processing
| NASA-CASE-NPO-17794-1-CU | p 1819 N95-22765
Design and application of electromechanical actuators for deep space missions
| NASA-CR-197957 | p 1694 N95-22909
Stable H(infinity) controller design for the longitudinal dynamics of an aircraft
| NASA-TM-106847 | p 1615 N95-22954
Investigation of arc length versus flange thickness while using an arc voltage controller
| DE95-003937 | p 1695 N95-23374
Robotic experiment with a force reflecting handcontroller onboard MIR space station p 1752 N95-23707
Robust control of multi-jointed arm with a decentralized autonomous control mechanism p 1659 N95-23710

CONVECTION
New robust multigrid method for 2D convection-diffusion problems
| PB95-138897 | p 1789 N95-23176
Radiation/convection coupling in rocket motors and plumes p 1669 N95-23414
Computer simulation of a magnetohydrodynamic dynamo 2
| NIFS-320 | p 1836 N95-23590

CONVECTION-DIFFUSION EQUATION
An adaptive projection method for the incompressible Navier-Stokes equations
| DE94-019049 | p 1665 N95-22491
New robust multigrid method for 2D convection-diffusion problems
| PB95-138897 | p 1789 N95-23176

CONVECTIVE FLOW
A controlled variation scheme for convection treatment in pressure-based algorithm p 1677 N95-23448
Modeling of non-spherical droplet dynamics p 1685 N95-23647
USML-1 Glovebox experiments
| NASA-CR-196574 | p 1653 N95-24028

CONVECTIVE HEAT TRANSFER
The high latitude ionosphere-magnetosphere transition region: Simulation and data comparison
| NASA-CR-197404 | p 1737 N95-22956
Experimental technique and assessment for measuring the convective heat transfer coefficient from natural ice accretions
| NASA-TM-106864 | p 1668 N95-23248

CONVERGENCE
Precise clock synchronization protocol
| PB95-127247 | p 1687 N95-22536
The convergence radius of the chiral expansion in the Dyson-Schwinger approach
| DE94-012852 | p 1805 N95-22925
Stability and efficiency of waveform relaxation methods
| PB95-138863 | p 1789 N95-23173
Convergence acceleration of implicit schemes in the presence of high aspect ratio grid cells p 1676 N95-23446
Quasi-kernel polynomials and convergence results for quasi-minimal residual iterations
| NASA-CR-197948 | p 1791 N95-23593
Ishikawa iteration process for nonlinear Lipschitz strongly accretive mappings
| DE94-634284 | p 1792 N95-23658
Martin-Lof tests can help too
| TR-541 | p 1797 N95-24063

CONVERGENT-DIVERGENT NOZZLES
An approximate theoretical method for modeling the static thrust performance of non-axisymmetric two-dimensional convergent-divergent nozzles
| NASA-CR-195050 | p 1608 N95-23193

CONVERSATION
Spoken dialogue understanding and local context
| TR-523 | p 1658 N95-23937
A computational theory of grounding in natural language conversation
| TR-545 | p 1760 N95-24058
The TRAINS project: A case study in building a conversational planning agent
| TR-532 | p 1659 N95-24193

CONVEXITY
Capacitated facility location: Valid inequalities and facets (revised)
| PB95-130225 | p 1786 N95-22641

CONVOLUTION INTEGRALS
AR-descriptions in translatable Frechet spaces
| PB95-138855 | p 1789 N95-23149

COOLANTS
Quick connect coupling
| NASA-CASE-ARC-11921-2 | p 1695 N95-23376
CFD modeling of turbulent duct flows for coolant channel analysis p 1682 N95-23635

COOLING
Gas cooled leads. Part 1: Theoretical Study. Part 2: Frost free lead optimized for a specific current. Part 3: Frost free lead optimized for a large current range
| DE95-002657 | p 1660 N95-22716
Traps for antimatter and antihydrogen production
| DE95-002814 | p 1805 N95-22927
Load calculation and system evaluation for electric vehicle climate control
| DE95-004350 | p 1695 N95-23358
Quick connect coupling
| NASA-CASE-ARC-11921-2 | p 1695 N95-23376
Thermal effects on the STAR electromagnetic calorimeter
| DE95-004663 | p 1688 N95-23492
Cooling rate effects on the microstructure, critical current density, and (T(sub c)) transition of one- and two-powder BSCCO-2223 Ag sheathed tapes
| DE95-004639 | p 1846 N95-24171

COOLING SYSTEMS
NASA advanced refrigerator/freezer technology development project overview
| NASA-TM-106309 | p 1747 N95-23177

COORDINATE TRANSFORMATIONS
Possibility of extending space-time coordinates
| DE94-628512 | p 1796 N95-22737

COORDINATES
Possibility of extending space-time coordinates
| DE94-628512 | p 1796 N95-22737
Gravitational field of the isolated mass in Yordan-Brans-Dicke theory
| DE94-635441 | p 1851 N95-23970

COPOLYMERS
Tough, soluble, aromatic, thermoplastic copolyimides
| NASA-CASE-LAR-15205-1 | p 1648 N95-22882
Polyazomethines containing trifluoromethylbenzene units
| NASA-CASE-LAR-14896-1 | p 1649 N95-23253
Reflectivity studies on adsorbed block copolymers under shear
| DE95-003676 | p 1649 N95-23568

COPPER
Thermal activation of steady-state creep in polycrystalline copper
| DE94-627394 | p 1839 N95-22607
Photoemission study of quantum confinement by a finite barrier: Cu/Co(wedge)/Cu(100)
| DE95-002913 | p 1840 N95-22762
Explosive bonding and its application in the Advanced Photon Source front-end and beamline components design
| DE95-004132 | p 1696 N95-23397
Carbon monoxide oxidation over three different states of copper: Development of a model metal oxide catalyst
| DE95-004682 | p 1636 N95-23495
Changes in chemical and optical properties of thin film metal mirrors on LDEF p 1651 N95-23907
Cu deposition using a permanent magnet electron cyclotron resonance microwave plasma source
| DE94-017768 | p 1650 N95-23981

COPPER ALLOYS
Explosive bonding and its application in the Advanced Photon Source front-end and beamline components design
| DE95-004132 | p 1696 N95-23397

COPPER COMPOUNDS
Ligand K-edge x-ray adsorption spectroscopic studies of the electronic structure of inorganic model complexes and metalloprotein active sites
| DE95-003338 | p 1840 N95-22851
Effect on c-axis transport properties of a critical state in Bi2Sr2CaCu2O8
| DE95-003695 | p 1843 N95-23366
Transport properties of Tl2Ba2CaCu2O8 meander lines
| DE95-003715 | p 1843 N95-23367

COPPER OXIDES
Superconducting Tl2Ba2CaCu2O8 thin films prepared by post-annealing in a flow-through multiple-zone furnace
| DE95-002745 | p 1838 N95-22520
Asymptotically exact solution of a local copper-oxide model
| DE94-628492 | p 1842 N95-23059
Some aspects of critical currents in Ag sheathed Bi2Sr2Ca2Cu3O10 composite tapes: A summary
| DE95-003952 | p 1842 N95-23354
Carbon monoxide oxidation over three different states of copper: Development of a model metal oxide catalyst
| DE95-004682 | p 1636 N95-23495
Preparation of high quality YBa2Cu3O(7-delta) thick films on flexible Ni-based alloy substrates with textured buffer layers
| DE95-003686 | p 1645 N95-23571
Phonon characteristics of high (T sub c) superconductors from neutron Doppler broadening measurements
| DE95-003703 | p 1844 N95-24076
Cooling rate effects on the microstructure, critical current density, and (T(sub c)) transition of one- and two-powder BSCCO-2223 Ag sheathed tapes
| DE95-004639 | p 1846 N95-24171

COPPER SELENIDES
Polycrystalline CuInSe2 and CdTePV solar cells
| DE95-000244 | p 1727 N95-22842

CORE SAMPLING
OU3 sediment dating and sedimentation rates
| DE95-001891 | p 1734 N95-23384

CORIOLIS EFFECT
Incompressible Navier-Stokes calculations in pump flows p 1680 N95-23627

COROTATION
Structure and evolution of long-lived spiral patterns in galaxies
| PB95-139242 | p 1868 N95-23228

CORRECTION
Baryon number fluctuations in a quark-hadron phase transition
| DE94-628585 | p 1804 N95-22786

CORRELATION
Fermion-spin transformation to implement the charge-spin separation
| DE94-629035 | p 1800 N95-22495
Strong-coupling behaviour of two t-J chains with interchain single-electron hopping
| DE94-629041 | p 1838 N95-22499
Lectures on 2D gauge theories. Topological aspects and path integral techniques
| DE94-628509 | p 1849 N95-22752
The role of triplet correlation function in dense fluids
| DE94-628476 | p 1849 N95-22775
Cumulant approach to dynamical correlation functions at finite temperatures
| DE94-628487 | p 1788 N95-23051
Bose condensation, macroscopic quantum phenomena and atomic spatial correlations in superfluid He-4
| PB95-139085 | p 1850 N95-23154
Estimation of crown closure from AVIRIS data using regression analysis p 1709 N95-23886
Inclusive rapidity correlations of (pi)(-) mesons in pp-interactions
| DE94-635654 | p 1812 N95-23974
Determining successional stage of temperate coniferous forests with Landsat satellite data p 1720 N95-24102

CORROSION
Corrosivity sensor
| AD-D016549 | p 1687 N95-22706
Corrosion control acceptance criteria for sacrificial anode type, cathodic protection systems (user guide)
| AD-A285275 | p 1662 N95-23117
Corrosion detection and management of advanced airframe materials
| AGARD-CP-565 | p 1641 N95-23496
The corrosion and protection of advanced aluminium - lithium airframe alloys p 1641 N95-23497
Corrosion of landing gear steels p 1642 N95-23500
Specific features of corrosion behavior of stainless maraging steels for aerospace application p 1642 N95-23501
Double pass retroreflection for corrosion detection in aircraft structures p 1642 N95-23503
The use of electrochemical impedance spectroscopy to predict the corrosion of aluminum-lithium alloys in marine environments p 1637 N95-23504
Non-destructive detection of corrosion for life management p 1643 N95-23505
Health and usage monitoring systems: Corrosion surveillance p 1607 N95-23506
Eddy current detection of pitting corrosion around fastener holes p 1643 N95-23507
In-situ detection of surface passivation or activation and of localized corrosion: Experiences and prospectives in aircraft p 1643 N95-23508
Test method and test results for environmental assessment of aircraft materials p 1643 N95-23509
New nondestructive techniques for the detection and quantification of corrosion in aircraft structures p 1644 N95-23512
Corrosion detection and monitoring of aircraft structures: An overview p 1644 N95-23515
Experience of in-service corrosion on military aircraft p 1644 N95-23516
US Navy operating experience with new aircraft construction materials p 1645 N95-23517
Corrosion in service experience with aircraft in France p 1645 N95-23518
Oklahoma City air logistics center (USAF) aging aircraft corrosion program p 1607 N95-23519

CORROSION PREVENTION
Pulsed Ion Beam Surface Treatment for preparing rapidly solidified corrosion resistant alloy surfaces
| DE94-012072 | p 1640 N95-22835
Corrosion control acceptance criteria for sacrificial anode type, cathodic protection systems (user guide)
| AD-A285275 | p 1662 N95-23117
The corrosion protection of 2219-T87 aluminum by organic and inorganic zinc-rich primers
| NASA-TP-3543 | p 1641 N95-23186
Corrosion detection and management of advanced airframe materials
| AGARD-CP-565 | p 1641 N95-23496
The corrosion and protection of advanced aluminium - lithium airframe alloys p 1641 N95-23497
Corrosion protection measures for CFC/metal joints of fuel integral tank structures of advanced military aircraft p 1644 N95-23510
Corrosion prevention with environmentally compliant materials: A design challenge p 1644 N95-23511
Organic coating technology for the protection of aircraft against corrosion p 1644 N95-23513
Corrosion detection and monitoring of aircraft structures: An overview p 1644 N95-23515
Experience of in-service corrosion on military aircraft p 1644 N95-23516
US Navy operating experience with new aircraft construction materials p 1645 N95-23517
Corrosion in service experience with aircraft in France p 1645 N95-23518
Robotic weld overlay coatings for erosion control
| DE95-002624 | p 1696 N95-24141
Solderability preservation through the use of organic inhibitors
| DE95-003633 | p 1664 N95-24149

CORROSION RESISTANCE
Pulsed Ion Beam Surface Treatment for preparing rapidly solidified corrosion resistant alloy surfaces
| DE94-012072 | p 1640 N95-22835
In-situ detection of surface passivation or activation and of localized corrosion: Experiences and prospectives in aircraft p 1643 N95-23508
Robotic weld overlay coatings for erosion control
| DE95-002624 | p 1696 N95-24141

CORROSION TESTS
The role of grain boundary chemistry and structure in the environmentally-assisted intergranular cracking of nickel-base alloys
| DE95-002941 | p 1638 N95-22532
Corrosion detection and management of advanced airframe materials
| AGARD-CP-565 | p 1641 N95-23496
Corrosion of landing gear steels p 1642 N95-23500
Specific features of corrosion behavior of stainless maraging steels for aerospace application p 1642 N95-23501
The use of electrochemical impedance spectroscopy to predict the corrosion of aluminum-lithium alloys in marine environments p 1637 N95-23504
Eddy current detection of pitting corrosion around fastener holes p 1643 N95-23507
Test method and test results for environmental assessment of aircraft materials p 1643 N95-23509
Corrosion protection measures for CFC/metal joints of fuel integral tank structures of advanced military aircraft p 1644 N95-23510
New nondestructive techniques for the detection and quantification of corrosion in aircraft structures p 1644 N95-23512
US Navy operating experience with new aircraft construction materials p 1645 N95-23517

COSMIC DUST
Modification and damping of Alfven waves in a magnetized dusty plasma
| NIFS-312 | p 1834 N95-23523

COSMIC RAYS
Performance of a large scale scintillating fiber tracker using VLPC readout
| DE95-003746 | p 1871 N95-23370
LDEF contributions to cosmic ray and radiation environments research p 1872 N95-23805
Early results from the ultra heavy cosmic ray experiment p 1872 N95-23809
Absorbed dose and LET spectra measurements on LDEF p 1815 N95-23810
Germination, growth rates, and electron microscope analysis of tomato seeds flown on the LDEF p 1748 N95-23821

COSMOCHEMISTRY
Origins of interstellar and solar system: Carbonaceous materials
| NASA-CR-197436 | p 1867 N95-23013

COSMOLOGY
Neutrino overview
| DE95-003201 | p 1802 N95-22729
Topologically stable Z - strings in the supersymmetric standard model
| DE94-628517 | p 1848 N95-22742
Finite-temperature scalar field theory in static de Sitter space
| DE94-628522 | p 1848 N95-22743
Supersymmetric singlet majorons and cosmology
| DE94-628571 | p 1850 N95-22783
Shannon-Wehrl entropy for cosmological and black-hole squeezing p 1826 N95-23000
High Energy Theory: Task B and Task L
| DE95-003453 | p 1817 N95-23148

COST ANALYSIS
Cost and schedule analytical techniques development
| NASA-CR-196548 | p 1853 N95-22891
NASAwide electronic publishing system: Electronic printing and duplicating, stage-2 evaluation report (GSFC)
| NASA-TM-104615 | p 1856 N95-23209
A manufacturing database of advanced materials used in spacecraft structures p 1623 N95-23279

COST EFFECTIVENESS
Evaluating photovoltaic applications: A guide for utilities
| DE95-003807 | p 1726 N95-22502
Southeast Regional Experiment Station
| DE95-000903 | p 1726 N95-22518

COST ESTIMATES
Synthesis of a large communications aperture using small antennas
| NASA-CR-197330 | p 1656 N95-22852

COST REDUCTION
Planar magnetic component development
| DE95-003311 | p 1661 N95-22896
Low-cost packaging of high-performance optoelectronic components
| DE95-003645 | p 1827 N95-23449
Advanced technologies for a compact RF linac FEL
| DE95-003674 | p 1692 N95-24072
Using simple page placement policies to reduce the cost of cache fills in coherent shared-memory systems
| TR-535 | p 1753 N95-24177

COSTS
Plinius intermediate report
| PB95-135216 | p 1648 N95-23128
Submodular linear programs on forests
| PB95-139820 | p 1758 N95-23608

COULOMB POTENTIAL
Computer simulation of the structure of ionic surfaces and interfaces
| DE95-002991 | p 1804 N95-22792
A possible generalization of the harmonic oscillator potential p 1822 N95-22970

COUNTERS
Investigation of physical parameters in stellar flares observed by GINGA
| NASA-CR-196547 | p 1868 N95-23205

COUNTING
Collecting operational event data for statistical analysis
| DE95-002020 | p 1793 N95-22550
Real lasers and other deformed objects p 1692 N95-23001
The satanic notations: Counting classes beyond #P and other definitional adventures
| TR-561 | p 1793 N95-24194

COUPLED MODES
Dynamical properties of critical and paramagnetic spin fluctuations in anisotropic heisenberg magnets
| PB95-134623 | p 1798 N95-23127
Synchronous dynamics of a coupled shaft/bearing/housing system with auxiliary support from a clearance bearing: Analysis and experiment
| NASA-CR-197858 | p 1695 N95-23214

COUPLING
Effects of long-range coupling on aggregation
| DE94-628483 | p 1842 N95-23047
Magnetic multilayer physics
| DE95-003408 | p 1798 N95-23083
TFTR Ion Cyclotron Range of Frequencies (ICRF) experimental data analysis collaboration
| DE95-003409 | p 1832 N95-23084
Quick connect coupling
| NASA-CASE-ARC-11921-2 | p 1695 N95-23376

COVARIANCE
Second derivative of the likelihood of an exact ARMA model
| PB95-135158 | p 1788 N95-23069
Asymptotic justification for a modified GLS procedure to estimate ARMA parameters
| PB95-135166 | p 1788 N95-23070
Taylor series expansion and modified extended Prony analysis for localization
| DE95-003671 | p 1758 N95-23567
Polarimetric radar data decomposition and interpretation p 1715 N95-23955

COVERINGS
On certain N-sheeted coverings of curves and symmetric numerical semigroups which cannot be realized as Weierstrass semigroups
| DE94-634328 | p 1797 N95-23661

COWLINGS
The use of cowl camber and taper to reduce rotor/stator interaction noise
| NASA-CR-195421 | p 1799 N95-22675

CRACK CLOSURE
Separation of crack extension modes in composite delamination problems p 1700 N95-23281

CRACK OPENING DISPLACEMENT
Separation of crack extension modes in composite delamination problems p 1700 N95-23281

CRACK PROPAGATION
Temperature effects on hydrogen-induced cracking in an iron-based superalloy
| DE95-003037 | p 1639 N95-22724
Notch-tip damage and translaminar fracture toughness measurements from carbon/epoxy laminates
| AD-A280101 | p 1627 N95-22833
Three-dimensional CTOA and constraint effects during stable tearing in a thin-sheet material
| NASA-TM-109183 | p 1627 N95-22928
Stress intensity factors and crack mouth openings for bridged cracks emanating from circular holes
| AR-008-408 | p 1699 N95-22952
Effects of delaminations on the damped dynamic characteristics of composite laminates: Mechanics and experiments
| NASA-TM-106862 | p 1630 N95-23258
Separation of crack extension modes in composite delamination problems p 1700 N95-23281
Residual strength of thin panels with cracks p 1700 N95-23311
Effect of loading direction and long-term aging on fatigue-crack growth in Al-Li alloy 2090 p 1641 N95-23499
Microstructural behavior of nonequilibrium systems
| DE95-004450 | p 1630 N95-23924
Fracture mechanics life analytical methods verification testing
| NASA-CR-196555 | p 1697 N95-24106

CRACK TIPS
Three-dimensional CTOA and constraint effects during stable tearing in a thin-sheet material
| NASA-TM-109183 | p 1627 N95-22928
Stress intensity factors and crack mouth openings for bridged cracks emanating from circular holes
| AR-008-408 | p 1699 N95-22952

CRACKING (FRACTURING)
Temperature effects on hydrogen-induced cracking in an iron-based superalloy
| DE95-003037 | p 1639 N95-22724
Separation of crack extension modes in composite delamination problems p 1700 N95-23281
Fracture mechanics life analytical methods verification testing
| NASA-CR-196555 | p 1697 N95-24106

CRACKS
Residual strength of thin panels with cracks p 1700 N95-23311

CRASH INJURIES
Design of a cervical spine gross motion simulator for standard size human and anthropomorphic dummy adult and child
| NIAR-94-16 | p 1751 N95-24021

CRASHES
Design of a cervical spine gross motion simulator for standard size human and anthropomorphic dummy adult and child
| NIAR-94-16 | p 1751 N95-24021
Aircraft fires, smoke toxicity, and survival: An overview
| DOT/FAA/AM-95/8 | p 1610 N95-24024
A multibody/finite element analysis approach for modeling of crash dynamic responses
| NIAR-94-3 | p 1610 N95-24050

CRASHWORTHINESS
A multibody/finite element analysis approach for modeling of crash dynamic responses
| NIAR-94-3 | p 1610 N95-24050

CRATERING
Penetration rates over 30 years in the space age p 1624 N95-23827
Dimensional scaling for impact cratering and perforation p 1624 N95-23843

CRATERS
Long term microparticle impact fluxes on LDEF determined from optical survey of Interplanetary Dust Experiment (IDE) sensors p 1623 N95-23826
Hypervelocity impact survivability experiments for carbonaceous impactors, part 2 p 1700 N95-23831
Image and compositional characteristics of the LDEF Big Guy impact crater p 1700 N95-23838

The effect of impact angle on craters formed by hypervelocity particles p 1700 N95-23839
Experimental investigation of the relationship between impact crater morphology and impacting particle velocity and direction p 1700 N95-23840
Determining orbital particle parameters of impacts into germanium using morphology analysis and calibration data from hypervelocity impact experiments in the laboratory p 1700 N95-23841

CRAY COMPUTERS
Accepting the T3D
|DE95-000924| p 1762 N95-22679
An automated computer misuse detection system for UNICOS
|DE95-000929| p 1762 N95-22680
WHAMS3D Project: Parallel implementations of WHAMS3D on two shared-memory multiprocessors
|CSRD-1248| p 1764 N95-23599
Transferring ecosystem simulation codes to supercomputers
|NASA-TM-4662| p 1759 N95-24052

CREEP ANALYSIS
Damage-mitigating control of a reusable rocket engine for high performance and extended life
|NASA-CR-4640| p 1654 N95-23195

CREEP PROPERTIES
The role of grain boundary chemistry and structure in the environmentally-assisted intergranular cracking of nickel-base alloys
|DE95-002941| p 1638 N95-22532
Evolution of oxidation and creep damage mechanisms in HIPed silicon nitride materials
|DE95-001360| p 1647 N95-22689
Microstructural behavior of nonequilibrium systems
|DE95-004450| p 1630 N95-23924

CREEP TESTS
The role of grain boundary chemistry and structure in the environmentally-assisted intergranular cracking of nickel-base alloys
|DE95-002941| p 1638 N95-22532
Thermal activation of steady-state creep in polycrystalline copper
|DE94-627394| p 1839 N95-22607
Study of radiation damages in AISI 316 and 347 steels
|DE94-627480| p 1639 N95-22609
Evolution of oxidation and creep damage mechanisms in HIPed silicon nitride materials
|DE95-001360| p 1647 N95-22689

CREW PROCEDURES (INFLIGHT)
Formalizing procedures for operations automation, operator training and spacecraft autonomy p 1752 N95-23720

CREW WORKSTATIONS
Living in space
|NASA-TM-110536| p 1751 N95-23274

CRITERIA
Security clearances: Consideration of sexual orientation in the clearance process. Report to Congressional requesters
|GAO/NSIAD-95-21| p 1853 N95-23588

CRITICAL EXPERIMENTS
Dry critical experiments and analyses performed in support of the Topaz-2 Safety Program
|DE95-002724| p 1817 N95-23245

CRITICAL PATH METHOD
A format for the interchange of scheduling models p 1780 N95-23747

CROSS CORRELATION
Optical image correlator using orthogonal data storage
|AD-A285795| p 1819 N95-22508
Using AVIRIS for in-flight calibration of the spectral shifts of SPOT-HRV and of AVHRR? p 1710 N95-23893

CROSS FLOW
Crossflow instability control on a swept-wing: Preliminary studies p 1609 N95-23283

CROSS POLARIZATION
AIRSAR views of aerolian terrain p 1713 N95-23941

CROSS SECTIONS
Measuring the left-right cross section asymmetry in Z boson production by e(+)e(-) collisions at the SLC
|DE95-003468| p 1807 N95-23141
Testing QCD with jet physics at CDF
|DE94-018980| p 1807 N95-23196
J/psi, psi' yields mu(+)mu(-) and B yields J/psi, psi' cross sections
|DE94-018996| p 1808 N95-23242
Measurement of correlated b quark cross sections at CDF
|DE95-004240| p 1808 N95-23336
Measurement of W and Z boson production and extraction of the W width and branching ratios at CDF
|DE94-018989| p 1810 N95-23522
Standardization of CDF and D(O) reported luminosities
|DE95-003388| p 1818 N95-24077

CROWDING
Schwarz-Christoffel methods for multiply-elongated regions
|DE94-019048| p 1790 N95-23536

CRYOGENIC COOLING
The DIII-D divertor cryopump system: Design and operational experience
|DE95-003007| p 1693 N95-22796
HTS current lead using a composite heat pipe
|DE95-003718| p 1662 N95-23368

CRYOGENIC EQUIPMENT
NASA advanced refrigerator/freezer technology development project overview
|NASA-TM-106309| p 1747 N95-23177

CRYOGENIC FLUIDS
Some aspects of critical currents in Ag sheathed Bi2Sr2Ca2Cu3O10 composite tapes: A summary
|DE95-003952| p 1842 N95-23354
Cavitation modeling in Euler and Navier-Stokes codes p 1681 N95-23630

CRYOPUMPING
The DIII-D divertor cryopump system: Design and operational experience
|DE95-003007| p 1693 N95-22796
Engineering design of a radiative divertor for DIII-D
|DE95-003008| p 1693 N95-22798
D3-D program overview
|DE95-003879| p 1837 N95-24086

CRYOSTATS
Doing photons with MERLIN 2 at Oroville p 1815 N95-23816

CRYSTAL DEFECTS
X-ray diffraction characterization of defect behavior in nanocrystalline nickel during annealing
|DE95-002992| p 1639 N95-22594
Measurements of striae in CR+ doped YAG laser crystals p 1847 N95-23285
Annealing of nitrogen-doped ZnSe at high pressures: Toward suppression of native defect formation
|DE95-003420| p 1844 N95-24010
High resolution microstructural analysis of zirconia eutectic interfaces
|DE95-003143| p 1845 N95-24143

CRYSTAL DISLOCATIONS
Dislocation decomposition, dissociation, and deformation in MoSi2 and (alpha)-Al2O3 single crystals
|DE95-002715| p 1839 N95-22653

CRYSTAL GROWTH
X-ray diffraction characterization of defect behavior in nanocrystalline nickel during annealing
|DE95-002992| p 1639 N95-22594
A parallel molecular dynamics simulation of crystal growth at a cluster of workstations
|DE94-628382| p 1839 N95-22615
World's first 15%-efficient multicrystalline silicon modules
|DE95-002604| p 1727 N95-22650
Polycrystalline CuInSe2 and CdTePV solar cells
|DE95-000244| p 1727 N95-22842
The 1993 Annual Conference of the Israeli Association for Crystal Growth. Program and abstracts
|DE94-633510| p 1841 N95-22854
Surface growth of two kinds of particles deposition models
|DE94-628480| p 1841 N95-23021
Measurements of striae in CR+ doped YAG laser crystals p 1847 N95-23285
Growth of single crystals of organic salts with large second-order optical nonlinearities by solution processes for devices
|NASA-CR-197963| p 1843 N95-23563
Whisker/Cone growth on the thermal control surfaces experiment no. S0069 p 1651 N95-23911
USML-1 Glovebox experiments
|NASA-CR-196574| p 1653 N95-24028
Epitaxial growth of bcc transition metal films and superlattices onto MgO (111), (011) and (001) substrates
|DE95-004629| p 1846 N95-24168

CRYSTAL LATTICES
Block spins and chirality in Heisenberg model on Kagome and triangular lattices
|DE94-629044| p 1840 N95-22845
Cation disorder determined by MAS Al-27 NMR in high dose neutron irradiated spinel
|DE95-003681| p 1842 N95-23266
Internal strain measurement using pulsed neutron diffraction at LANSCE
|DE95-003677| p 1842 N95-23365

CRYSTAL STRUCTURE
High pressure neutron powder diffraction at LANSCE
|DE95-002703| p 1839 N95-22565
General crystal in prebiotic context
|DE94-628475| p 1840 N95-22774
Computer simulation of the structure of ionic surfaces and interfaces
|DE95-002991| p 1804 N95-22792
The 1993 Annual Conference of the Israeli Association for Crystal Growth. Program and abstracts
|DE94-633510| p 1841 N95-22854
Asymptotically exact solution of a local copper-oxide model
|DE94-628492| p 1842 N95-23059
Internal strain measurement using pulsed neutron diffraction at LANSCE
|DE95-003677| p 1842 N95-23365
Deformation of C15 Laves phase alloys
|DE95-003636| p 1646 N95-24067

CRYSTALLINITY
MOCVD of gallium and calcium sulfides for improved phosphor processing
|DE95-000918| p 1631 N95-22677

CRYSTALLIZATION
Initial crystallization and growth in melt processing of large-domain YBa2Cu3O(x) for magnetic levitation
|DE95-002993| p 1839 N95-22572
General crystal in prebiotic context
|DE94-628475| p 1840 N95-22774
A phenomenological model for the effect of nanocrystalline microstructure on irradiation-induced amorphization in U3Si
|DE95-004631| p 1846 N95-24169

CRYSTALS
Optical image correlator using orthogonal data storage
|AD-A285795| p 1819 N95-22508
General crystal in prebiotic context
|DE94-628475| p 1840 N95-22774
Asymptotically exact solution of a local copper-oxide model
|DE94-628492| p 1842 N95-23059
Experimental and theoretical studies on the C15 intermetallic compounds MV2 (M = Zr, Hf and Ta): Elasticity and phase stability
|DE95-003723| p 1845 N95-24079

CURIE TEMPERATURE
Microstructural behavior of nonequilibrium systems
|DE95-004450| p 1630 N95-23924

CURING
Development and verification of a resin film infusion/resin transfer molding simulation model for fabrication of advanced textile composites
|NASA-CR-197439| p 1648 N95-23179

CURRENT ALGEBRA
(pi)- and a(sub 1)-meson physics in current algebra at the quark level
|DE94-628611| p 1804 N95-22811
Linearizing W-algebras
|DE94-634324| p 1790 N95-23457

CURRENT DENSITY
Some aspects of critical currents in Ag sheathed Bi2Sr2Ca2Cu3O10 composite tapes: A summary
|DE95-003952| p 1842 N95-23354
Effect on c-axis transport properties of a critical state in Bi2Sr2CaCu2O8
|DE95-003695| p 1843 N95-23366
Transport properties of Tl2Ba2CaCu2O8 meander lines
|DE95-003715| p 1843 N95-23367
A 4 MW fast wave current drive upgrade for D3-D
|DE95-003741| p 1837 N95-24083
Cooling rate effects on the microstructure, critical current density, and (T(sub c)) transition of one- and two-powder BSCCO-2223 Ag sheathed tapes
|DE95-004639| p 1846 N95-24171

CURVATURE
Energetic particle observations at geosynchronous orbit
|DE95-000873| p 1867 N95-22516
On the scalar curvature of minimal hypersurfaces
|DE94-628516| p 1796 N95-22741
A prescribing geodesic curvature problem
|DE94-628503| p 1787 N95-22750
Level set techniques applied to unsteady detonation propagation
|DE95-002741| p 1666 N95-22901
The effect of a non-zero shock width on wave propagation in multi-dimensions
|DE95-002748| p 1666 N95-22902
BEm-BDF scheme for curvature driven moving stokes flows
|PB95-138905| p 1667 N95-23144
BEM solution to simulate the curvature driven deformation of a profile that is pressed into a plate of hot glass
|PB95-138913| p 1648 N95-23145
Unsteady flow simulations in support of the SSME HEX turning vane cracking investigation with the ATD HPOTP p 1679 N95-23621

CURVE FITTING
Statistically generated weighted curve fit of residual functions for modal analysis of structures
|NASA-TM-108481| p 1699 N95-22950
CURVES
On certain N-sheeted coverings of curves and symmetric numerical semigroups which cannot be realized as Weierstrass semigroups
|DE94-634328| p 1797 N95-23661
CURVES (GEOMETRY)
Lectures on Fermat's last theorem
|DE94-628392| p 1795 N95-22617
Semi-symmetric manifolds satisfying certain curvature conditions
|DE94-628414| p 1788 N95-22922
CUTTING
Study on possible environmental effects of a WBM cutting discharge in the north sea, one year after termination of drilling
|PB95-133740| p 1733 N95-23125
CYCLIC LOADS
The spectral content of the torque loads on a turbine gear tooth
|DE95-002188| p 1694 N95-23056
CYCLONES
Annual tropical cyclone report, 1993
|AD-A285097| p 1742 N95-23255
CYCLOTRON FREQUENCY
Resonant shallow donor magnetopolaron effect in a GaAs/AlGaAs quantum dot in high magnetic fields
|DE94-629039| p 1798 N95-22497
TFTR Ion Cyclotron Range of Frequencies (ICRF) experimental data analysis collaboration
|DE95-003409| p 1832 N95-23084
A 4 MW fast wave current drive upgrade for D3-D
|DE95-003741| p 1837 N95-24083
CYCLOTRON RESONANCE
Cu deposition using a permanent magnet electron cyclotron resonance microwave plasma source
|DE94-017768| p 1650 N95-23981
CYCLOTRONS
Hot proton anisotropies and cool proton temperatures in the outer magnetosphere
|DE95-002719| p 1736 N95-22850
An upper bound for the proton temperature anisotrophy
|DE95-002752| p 1737 N95-22903
CYLINDRICAL BODIES
Method for making fiber-optic bundle collimator assembly
|AD-D016491| p 1819 N95-22492
Second order focusing property of 210 deg cylindrical energy analyzer
|NIFS-317| p 1834 N95-23527
CYLINDRICAL SHELLS
The development of shell imperfection measurement techniques
|TAE-712| p 1699 N95-23923
CZOCHRALSKI METHOD
Measurements of striae in CR+ doped YAG laser crystals p 1847 N95-23285

D

DAMAGE
Rationale for the Modular Air-system Vulnerability Estimation Network (MAVEN) methodology
|AD-A285797| p 1611 N95-22510
Damage-mitigating control of a reusable rocket engine for high performance and extended life
|NASA-CR-4640| p 1654 N95-23195
Residual strength of thin panels with cracks p 1700 N95-23311
The detection and analysis of galvanic damage in BMI/graphite fiber composites p 1631 N95-23502
Double pass retroreflection for corrosion detection in aircraft structures p 1642 N95-23503
POD assessment of NDI procedures using a round robin test
|AGARD-R-809| p 1697 N95-23602
DAMAGE ASSESSMENT
A ruggedness evaluation of procedures for damage threshold testing optical materials
|NASA-TM-4639| p 1840 N95-22803
Laser irradiation effects: A functional assessment
|AD-A285100| p 1691 N95-22937
The spectral content of the torque loads on a turbine gear tooth
|DE95-002188| p 1694 N95-23056
Nondestructive evaluation of fatigue damage in aluminum 2024 by x-ray diffraction p 1698 N95-23293
POD assessment of NDI procedures using a round robin test
|AGARD-R-809| p 1697 N95-23602
Aircraft accident report. Runway overrun following rejected takeoff. Continental airlines flight 795, McDonnell Douglas MD-82, N18835, LaGuardia Airport, Flushing, NY, 2 March 1994
|PB95-910401| p 1610 N95-23609
Atomic oxygen interactions with protected organic materials on the Long Duration Exposure Facility (LDEF) p 1627 N95-23909
Organic matrix composite protective coatings for space applications p 1627 N95-23914
DAMPING
Modification and damping of Alfven waves in a magnetized dusty plasma
|NIFS-312| p 1834 N95-23523
Three-D CFD analysis of hydrostatic bearings p 1678 N95-23616
DARK MATTER
CDM and Omega in the local neighborhood
|DE95-003683| p 1868 N95-23570
DATA ACQUISITION
Towards method-independent knowledge acquisition
|AD-A285823| p 1766 N95-22512
Collecting operational event data for statistical analysis
|DE95-002020| p 1793 N95-22550
GPS survey of the western Tien Shan
|NASA-CR-197901| p 1717 N95-22832
TOGA/COARE AMMR 1992 data processing
|NASA-CR-197289| p 1736 N95-22867
Summary of solar cell data from the Long Duration Exposure Facility (LDEF)
|NASA-CR-196539| p 1727 N95-22904
Material characterization system
|AD-D016536| p 1800 N95-23073
Investigation of physical parameters in stellar flares observed by GINGA
|NASA-CR-196547| p 1868 N95-23205
Langley Research Center Strategic Plan for Education p 1853 N95-23316
Progress report on a fully automatic Gas Tungsten Arc Welding (GTAW) system development
|DE95-004397| p 1695 N95-23343
Radioisotope thermoelectric generator transportation system subsystem 143 software development plan
|DE95-003774| p 1662 N95-23351
Validation data for land surface temperature determination from satellites
|CSIRO-TR-33| p 1718 N95-23597
Software agents for the dissemination of remote terrestrial sensing data p 1721 N95-23675
The development of shell imperfection measurement techniques
|TAE-712| p 1699 N95-23923
Video frame processor
|DE94-635414| p 1753 N95-23962
Improved AVHRR data navigation using automated land feature recognition to correct a satellite orbital model
|CSIRO-TR-34| p 1718 N95-24026
Energy efficiency of electric vehicles at the 1994 American Tour de Sol
|DE95-002905| p 1664 N95-24070
DATA BASE MANAGEMENT SYSTEMS
Jackson system development, entity-relationship analysis and data flow models: A comparative study
|PB95-127338| p 1855 N95-22523
Method for building and evaluating formal specifications of object-oriented conceptual models of database systems
|PB95-127353| p 1855 N95-22525
LCM 3.0: A language for describing conceptual models. Syntax definition
|PB95-128005| p 1755 N95-22652
CDMS-CAD data set management system test plan
|DE95-003219| p 1755 N95-22718
P2Info Resource Center: Linking the DOE Pollution Prevention community
|DE95-003133| p 1732 N95-22781
Overview of Ph.D. theses and memoranda, 1993
|PB95-135190| p 1756 N95-23071
Search Hanford accessible reports electronically system requirements specification
|DE95-004367| p 1856 N95-23340
Search Hanford accessible reports electronically system design description, revision 1
|DE95-004369| p 1856 N95-23341
Online Nuclear Data Service
|DE94-634268| p 1856 N95-23452
Index of nuclear data libraries available from the IAEA nuclear data section
|DE94-634271| p 1857 N95-23453
BROND-2.1. Russian evaluated neutron reaction data library
|DE94-634417| p 1810 N95-23458
Squeezing out all the performance: Using Ingres for a C(sup 3)I reporting system
|DE95-004591| p 1857 N95-23490
Information technology standards process guide
|DE95-003967| p 1857 N95-23574
The data facility of the Airborne Visible/Infrared Imaging Spectrometer (AVIRIS) p 1707 N95-23877
A network-based distributed, media-rich computing and information environment
|DE95-003696| p 1765 N95-24074
Search Hanford accessible reports electronically system configuration management plan
|DE95-004493| p 1857 N95-24089
Robotic tape library system level testing at NSA: Present and planned p 1858 N95-24112
The architecture of the High Performance Storage System (HPSS) p 1858 N95-24113
New architectural paradigms for multi-petabyte distributed storage systems p 1858 N95-24115
Constraint based scheduling for the Goddard Space Flight Center distributed Active Archive Center's data archive and distribution system p 1859 N95-24121
Building a COTS archive for satellite data p 1861 N95-24132
ASF archive issues: Current status, past history, and questions for the future p 1861 N95-24133
Architecture and evolution of Goddard Space Flight Center Distributed Active Archive Center p 1862 N95-24134
The growth of the UniTree mass storage system at the NASA Center for Computational Sciences: Some lessons learned p 1862 N95-24135
NSSDC provides network access to key data via NDADS p 1862 N95-24136
OPUS: A new generation Knowledge Engineering Environment p 1760 N95-24176
DATA BASES
Experience with CANDID: Comparison algorithm for navigating digital image databases
|DE95-000869| p 1855 N95-22515
Roles and dynamic subclasses: A modal logic approach
|PB95-127320| p 1754 N95-22522
Method for building and evaluating formal specifications of object-oriented conceptual models of database systems
|PB95-127353| p 1855 N95-22525
Review of uncertainty files and improved multigroup cross section files for FENDL
|DE94-628639| p 1830 N95-22757
P2Info Resource Center: Linking the DOE Pollution Prevention community
|DE95-003133| p 1732 N95-22781
Photon and electron interaction databases and their use in medical applications
|DE94-015558| p 1855 N95-22871
Cost and schedule analytical techniques development
|NASA-CR-196548| p 1853 N95-22891
Compendium of NASA data base for the Global Tropospheric Experiment's Pacific Exploratory Mission West-A (PEM West-A)
|NASA-TM-109177| p 1733 N95-23009
Effective management of classified documents using the library document system
|AD-A286021| p 1855 N95-23024
Format( )MEDIC( )Input
|DE95-003482| p 1737 N95-23063
RAS Division model evaluation database tools
|DE95-003480| p 1733 N95-23123
RAS Division model evaluation database description
|DE95-003481| p 1733 N95-23124
A manufacturing database of advanced materials used in spacecraft structures p 1623 N95-23279
Search Hanford accessible reports electronically system design description, revision 1
|DE95-004369| p 1856 N95-23341
Impeller flow field characterization with a laser two-focus velocimeter p 1675 N95-23440
Index of nuclear data libraries available from the IAEA nuclear data section
|DE94-634271| p 1857 N95-23453
BROND-2.1. Russian evaluated neutron reaction data library
|DE94-634417| p 1810 N95-23458
Squeezing out all the performance: Using Ingres for a C(sup 3)I reporting system
|DE95-004591| p 1857 N95-23490
Proceedings of the workshop on deductive databases and logic programming
|PB95-139382| p 1758 N95-23553
A new generation of intelligent trainable tools for analyzing large scientific image databases p 1775 N95-23717
DTS: Building custom, intelligent schedulers p 1779 N95-23744
Coordinating complex decision support activities across distributed applications p 1761 N95-23749
Status of LDEF activation measurements and archive p 1815 N95-23817

The data facility of the Airborne Visible/Infrared Imaging Spectrometer (AVIRIS) p 1707 N95-23877
Overview of the LDEF MSIG databasing activities p 1864 N95-23916
The design of a petabyte archive and distribution system for the NASA ECS project p 1858 N95-24110
Robotic tape library system level testing at NSA: Present and planned p 1858 N95-24112
Building a COTS archive for satellite data p 1861 N95-24132
Architecture and evolution of Goddard Space Flight Center Distributed Active Archive Center p 1862 N95-24134

DATA COMPRESSION
Evaluating the effect of online data compression on the disk cache of a mass storage system p 1862 N95-24138

DATA CORRELATION
A modal test design strategy for model correlation | DE95-003631 | p 1759 N95-24020

DATA FLOW ANALYSIS
Jackson system development, entity-relationship analysis and data flow models: A comparative study | PB95-127338 | p 1855 N95-22523
Algebra of lines and boxes | PB95-130456 | p 1787 N95-22768
Task scheduling in dataflow computer architectures p 1753 N95-23301

DATA INTEGRATION
MAC Europe 1991 campaign: AIRSAR/AVIRIS data integration for agricultural test site classification p 1715 N95-23952

DATA LINKS
Utilizing a TDRS satellite for direct broadcast satellite-radio propagation experiments and demonstrations p 1622 N95-22814
Differential GPS and system integration of the Low Visibility Landing and Surface Operations (LVLASO) demonstration p 1611 N95-23318

DATA MANAGEMENT
CDMS-CAD data set management system test plan | DE95-003219 | p 1755 N95-22718
CDMS: CAD data set system design description | DE95-003218 | p 1756 N95-22894
Using Dedal to share and reuse distributed engineering design information p 1768 N95-23678
The design of a petabyte archive and distribution system for the NASA ECS project p 1858 N95-24110
Robotic tape library system level testing at NSA: Present and planned p 1858 N95-24112
Optimizing tertiary storage organization and access for spatio-temporal datasets p 1861 N95-24131
The growth of the UniTree mass storage system at the NASA Center for Computational Sciences: Some lessons learned p 1862 N95-24135
Analysis of the request patterns to the NSSDC on-line archive p 1862 N95-24137

DATA PROCESSING
Measurement of HO2 and other trace gases in the stratosphere using a high resolution far-infrared spectrometer | NASA-CR-197368 | p 1735 N95-22482
Twelve month performance evaluation for the rotating shadowband radiometer | DE95-002847 | p 1726 N95-22554
PRISMA GENIE data analysis manual | PB95-130464 | p 1755 N95-22769
Environmental Systems Management Analysis and Reporting Network (E-SMART) | AD-A279766 | p 1732 N95-22856
TOGA/COARE AMMR 1992 data processing | NASA-CR-197289 | p 1736 N95-22867
Summary of solar cell data from the Long Duration Exposure Facility (LDEF) | NASA-CR-196539 | p 1727 N95-22904
The effect of sensor spacing on wind measurements at the Shuttle Landing Facility | NASA-TP-3529 | p 1742 N95-23010
TFTR Ion Cyclotron Range of Frequencies (ICRF) experimental data analysis collaboration | DE95-003409 | p 1832 N95-23084
Investigation of physical parameters in stellar flares observed by GINGA | NASA-CR-196547 | p 1868 N95-23205
Analysis of data from the energetic gamma-ray experiment of the Gamma Ray Observatory | NASA-CR-197347 | p 1871 N95-23216
Measurements of striae in CR+ doped YAG laser crystals p 1847 N95-23285
Stochastic decision analysis p 1854 N95-23305
Search Hanford accessible reports electronically system design description, revision 1 | DE95-004369 | p 1856 N95-23341
Vision-sensing image analysis for GTAW process control | DE95-003936 | p 1695 N95-23373
GPP: A General-Purpose Post Processor for wind turbine data analysis | DE95-000223 | p 1729 N95-23383
Index of nuclear data libraries available from the IAEA nuclear data section | DE94-634271 | p 1857 N95-23453
Search for supersymmetric (tilde W)(sub 1) and (tilde Z)(sub 2) states using the D0 detector | DE95-004581 | p 1811 N95-23581
Enhancement of F/A-18 operational flight measurements: Data report for phase 1 | DSTO-TR-0049 | p 1613 N95-23666
Utilizing inheritance in requirements engineering p 1768 N95-23677
A data analysis assistant p 1761 N95-23748
Calculation of satellite drag coefficients | AD-A285118 | p 1622 N95-23781
Status of LDEF activation measurements and archive p 1815 N95-23817
Lithologic discrimination and alteration mapping from AVIRIS Data, Socorro, New Mexico p 1701 N95-23847
Automating spectral unmixing of AVIRIS data using convex geometry concepts p 1702 N95-23848
Comparison of three methods for materials identification and mapping with imaging spectroscopy p 1702 N95-23853
Discrimination of poorly exposed lithologies in AVIRIS data p 1703 N95-23858
AVIRIS and TIMS data processing and distribution at the land processes distributed active archive center p 1706 N95-23872
Extraction of auxiliary data from AVIRIS distribution tape for spectral, radiometric, and geometric quality assessment p 1706 N95-23875
Preprocessing: Geocoding of AVIRIS data using navigation, engineering, DEM, and radar tracking system data p 1707 N95-23876
The data facility of the Airborne Visible/Infrared Imaging Spectrometer (AVIRIS) p 1707 N95-23877
Objective determination of image end-members in spectral mixture analysis of AVIRIS data p 1709 N95-23888
Investigations on the 1.7 micron residual absorption feature in the vegetation reflection spectrum p 1710 N95-23891
Laboratory spectra of field samples as a check on two atmospheric correction methods p 1711 N95-23894
Comparison of inversion models using AIRSAR data for Death Valley, California p 1713 N95-23945
Using simple page placement policies to reduce the cost of cache fills in coherent shared-memory systems | TR-535 | p 1753 N95-24177

DATA RECORDING
High data rate recorder development at MIT Haystack Observatory p 1690 N95-24118
A comparison of rotary- and stationary-head tape recorders p 1690 N95-24122
A terabyte linear tape recorder p 1690 N95-24139

DATA REDUCTION
Stochastic decision analysis p 1854 N95-23305
Optimal band selection for dimensionality reduction of hyperspectral imagery p 1709 N95-23887

DATA RETRIEVAL
Experience with CANDID: Comparison algorithm for navigating digital image databases | DE95-000869 | p 1855 N95-22515
Automated synthesis of image processing procedures using AI planning techniques p 1779 N95-23745
Document image archive transfer from DOS to UNIX p 1761 N95-24117

DATA SIMULATION
Task scheduling in dataflow computer architectures p 1753 N95-23301

DATA STORAGE
Optical image correlator using orthogonal data storage | AD-A285795 | p 1819 N95-22508
Holographic interferometric tomography for reconstructing flow fields p 1690 N95-23287
AVIRIS and TIMS data processing and distribution at the land processes distributed active archive center p 1706 N95-23872
The data facility of the Airborne Visible/Infrared Imaging Spectrometer (AVIRIS) p 1707 N95-23877
Applications drivers for data parking on the Information Superhighway p 1857 N95-24109
The design of a petabyte archive and distribution system for the NASA ECS project p 1858 N95-24110
Robotic tape library system level testing at NSA: Present and planned p 1858 N95-24112
The architecture of the High Performance Storage System (HPSS) p 1858 N95-24113
A 500 megabyte/second disk array p 1753 N95-24114
New architectural paradigms for multi-petabyte distributed storage systems p 1858 N95-24115
Optimizing raid performance with cache p 1761 N95-24116
Document image archive transfer from DOS to UNIX p 1761 N95-24117
High data rate recorder development at MIT Haystack Observatory p 1690 N95-24118
Petabyte mass memory system using the Newell Opticel(TM) p 1753 N95-24119
Integrating UniTree with the data migration API p 1761 N95-24120
Constraint based scheduling for the Goddard Space Flight Center distributed Active Archive Center's data archive and distribution system p 1859 N95-24121
Client/Server data serving for high performance computing p 1761 N95-24123
A kinetic study of hydrolysis of polyester elastomer in magnetic tape p 1652 N95-24124
Digital Linear Tape (DLT) technology and product family overview p 1753 N95-24125
The MAMMOTH project p 1753 N95-24126
Influence of technology on magnetic tape storage device characteristics p 1690 N95-24127
Approaches to 100 Gbit/sq. in. recording density p 1690 N95-24128
Optical storage media data integrity studies p 1829 N95-24130
Optimizing tertiary storage organization and access for spatio-temporal datasets p 1861 N95-24131
Building a COTS archive for satellite data p 1861 N95-24132
ASF archive issues: Current status, past history, and questions for the future p 1861 N95-24133
Architecture and evolution of Goddard Space Flight Center Distributed Active Archive Center p 1862 N95-24134
The growth of the UniTree mass storage system at the NASA Center for Computational Sciences: Some lessons learned p 1862 N95-24135
Evaluating the effect of online data compression on the disk cache of a mass storage system p 1862 N95-24138
Using simple page placement policies to reduce the cost of cache fills in coherent shared-memory systems | TR-535 | p 1753 N95-24177

DATA STRUCTURES
Path planning for planetary rover using extended elevation map p 1771 N95-23689
A constraint-logic based implementation of the coarse-grained approach to data acquisition scheduling of the International Ultraviolet Explorer orbiting observatory p 1779 N95-23741
Unifying data and control transformations for distributed shared-memory machines | TR-542 | p 1765 N95-24061
Scalable, extensible, and portable numerical libraries | DE95-004643 | p 1765 N95-24172

DATA SYSTEMS
Technical report series on global modeling and data assimilation. Volume 4: Documentation of the Goddard Earth Observing System (GEOS) data assimilation system, version 1 | NASA-TM-104606-VOL-4 | p 1740 N95-23529
Constraint based scheduling for the Goddard Space Flight Center distributed Active Archive Center's data archive and distribution system p 1859 N95-24121

DATA TRANSFER (COMPUTERS)
AVIRIS and TIMS data processing and distribution at the land processes distributed active archive center p 1706 N95-23872
The data facility of the Airborne Visible/Infrared Imaging Spectrometer (AVIRIS) p 1707 N95-23877
A 500 megabyte/second disk array p 1753 N95-24114
Document image archive transfer from DOS to UNIX p 1761 N95-24117
Petabyte mass memory system using the Newell Opticel(TM) p 1753 N95-24119
Integrating UniTree with the data migration API p 1761 N95-24120
Constraint based scheduling for the Goddard Space Flight Center distributed Active Archive Center's data archive and distribution system p 1859 N95-24121
Client/Server data serving for high performance computing p 1761 N95-24123
Optimizing tertiary storage organization and access for spatio-temporal datasets p 1861 N95-24131
NSSDC provides network access to key data via NDADS p 1862 N95-24136
Analysis of the request patterns to the NSSDC on-line archive p 1862 N95-24137

DATA TRANSMISSION
Addendum to the Proceedings of the Third International Mobile Satellite Conference (IMSC 1993) | NASA-CR-197343 | p 1655 N95-22813

A draft standard for message passing in a distributed memory environment
|DE94-019159| p 1657 N95-23075
Squeezing out all the performance: Using Ingres for a C(sup 3)I reporting system
|DE95-004591| p 1857 N95-23490
DEATH VALLEY (CA)
Comparison of inversion models using AIRSAR data for Death Valley, California p 1713 N95-23945
DEBONDING (MATERIALS)
Process for preparing an assembly of an article and a polyimide which resists dimensional change, delamination and debonding when exposed to changes in temperature
|NASA-CASE-LAR-14538-2| p 1649 N95-23254
DECAY
Neutrino masses and mixing
|DE94-628632| p 1812 N95-23784
DECAY RATES
Dynamical properties of critical and paramagnetic spin fluctuations in anisotropic heisenberg magnets
|PB95-134623| p 1798 N95-23127
DECISION MAKING
Teams and teamwork at NASA Langley Research Center p 1854 N95-23292
Langley Research Center Strategic Plan for Education p 1853 N95-23316
DECISION THEORY
Stochastic decision analysis p 1854 N95-23305
DTS: Building custom, intelligent schedulers p 1779 N95-23744
DECOMPOSITION
Dislocation decomposition, dissociation, and deformation in MoSi2 and (alpha)-Al2O3 single crystals
|DE95-002715| p 1839 N95-22653
NO decomposition in non-reducing atmospheres
|DE95-004324| p 1634 N95-23339
Application of a two-stream radiative transfer model for leaf lignin and cellulose concentrations from spectral reflectance measurements, part 1 p 1703 N95-23856
High resolution microstructural analysis of zirconia eutectic interfaces
|DE95-003143| p 1845 N95-24143
Effects of Bi and Bi2O3 additions on the microstructure and superconducting properties of powder-in-tube BSCCO (2212) tapes
|DE95-004605| p 1845 N95-24150
DECONTAMINATION
Mercury detection with thermal neutrons
|DE95-002061| p 1806 N95-23055
DECOUPLING
Dynamic disturbance decoupling of nonlinear systems and linearization
|PB95-141248| p 1767 N95-23558
DEEP SPACE
Effects of modulation index on telecommunications
|AD-A286018| p 1657 N95-23023
DEFECTS
Research on defects and transport in amorphous-silicon-based semiconductors
|DE94-011888| p 1660 N95-22586
New nondestructive techniques for the detection and quantification of corrosion in aircraft structures p 1644 N95-23512
Assessment of resin transfer molding process for the XM6 discharger, ERDEC SSP 93-64
|NIAR-94-2| p 1650 N95-23932
Particle transport in plasma reactors
|DE95-004541| p 1837 N95-24158
DEFENSE PROGRAM
Report to the Secretary of Defense. Unmanned aerial vehicles: No more Hunter systems should be bought until problems are fixed
|GAO/NSIAD-95-52| p 1613 N95-24091
Defense technology plan
|AD-A285415| p 1903 N95-24178
Defense science and technology strategy
|AD-A285414| p 1903 N95-24179
DEFINITION
LCM 3.0: A language for describing conceptual models. Syntax definition
|PB95-128005| p 1755 N95-22652
DEFLAGRATION
Influence of porosity and two-phase flow on diffusional/thermal instability of a deflagrating energetic material
|DE95-002592| p 1634 N95-23122
DEFLECTION
Method and apparatus for measuring the strain developed in a coated surface
|NASA-CASE-ARC-11938-1-C| p 1688 N95-23263
Deflections of anisotropic sandwich beams with variable face sheets and core thicknesses p 1700 N95-23310
DEFORMATION
Dislocation decomposition, dissociation, and deformation in MoSi2 and (alpha)-Al2O3 single crystals
|DE95-002715| p 1839 N95-22653
Covariant deformed oscillator algebras p 1797 N95-22978
Localization in deformed quantum mechanics p 1823 N95-22979
Real lasers and other deformed objects p 1692 N95-23001
BEm-BDF scheme for curvature driven moving stokes flows
|PB95-138905| p 1667 N95-23144
BEM solution to simulate the curvature driven deformation of a profile that is pressed into a plate of hot glass
|PB95-138913| p 1648 N95-23145
Electromagnetic production of pions on the nucleon
|DE95-004658| p 1811 N95-23587
Deformation of C15 Laves phase alloys
|DE95-003636| p 1646 N95-24067
DEGENERATION
Singlet quarks beyond the top at the tevatron
|PB95-139127| p 1807 N95-23158
Degenerate Hamiltonian Hopf bifurcations
|PB95-138871| p 1789 N95-23174
DEGRADATION
Evolution of oxidation and creep damage mechanisms in HIPed silicon nitride materials
|DE95-001360| p 1647 N95-22689
The hydrogen embrittlement of alloy X-750
|DE95-003207| p 1640 N95-22893
The detection and analysis of galvanic damage in BMI/graphite fiber composites p 1631 N95-23502
Non-destructive detection of corrosion for life management p 1643 N95-23505
In-situ detection of surface passivation or activation and of localized corrosion: Experiences and prospectives in aircraft p 1643 N95-23508
Oklahoma City air logistics center (USAF) aging aircraft corrosion program p 1607 N95-23519
Space environmental effects on polymer matrix composites as a function of sample location on LDEF p 1651 N95-23901
The effect of simulated low earth orbit radiation on polyimides (UV degradation study) p 1651 N95-23903
The surface properties of fluorinated polyimides exposed to VUV and atomic oxygen p 1651 N95-23904
Remote sensor test range update
|DE95-003629| p 1735 N95-24018
A kinetic study of hydrolysis of polyester elastomer in magnetic tape p 1652 N95-24124
DEGREES OF FREEDOM
Fermion-spin transformation to implement the charge-spin separation
|DE94-629035| p 1800 N95-22495
Algebraic approach to the vibrational excitations in methane p 1814 N95-22960
Pseudoclassical description of the Dirac Oscillator p 1825 N95-22996
Morphing hands and virtual tools (or What good is an extra degree of freedom?)
|TR-551| p 1783 N95-24036
DELAMINATING
Process for preparing an assembly of an article and a polyimide which resists dimensional change, delamination and debonding when exposed to changes in temperature
|NASA-CASE-LAR-14538-2| p 1649 N95-23254
Effects of delaminations on the damped dynamic characteristics of composite laminates: Mechanics and experiments
|NASA-TM-106862| p 1630 N95-23258
Separation of crack extension modes in composite delamination problems p 1700 N95-23281
Exfoliation corrosion and stress corrosion cracking behaviour of Al-Li alloys p 1641 N95-23498
Thermoelastic theory for the response of materials functionally graded in two directions with applications to the free-edge problem
|NASA-TM-106882| p 1699 N95-24055
DELAY
Automatic generation of efficient orderings of events for scheduling applications p 1618 N95-23764
DELTA FUNCTION
Bethe ansatz and quantum Davey-Stewartson 1 system with multicomponent in two dimensions
|DE94-628423| p 1786 N95-22631
DELTA LAUNCH VEHICLE
CFD flowfield simulation of Delta Launch Vehicles in a power-on configuration p 1673 N95-23433
DELTA WINGS
A study of the vortex flow over 76/40-deg double-delta wing
|NASA-CR-195032| p 1677 N95-23466
DENSE PLASMAS
Ninth topical conference on atomic processes in plasmas
|DE95-002810| p 1833 N95-23246
DENSITY MEASUREMENT
The TEXT neutral lithium beam edge density diagnostic
|DE95-003256| p 1830 N95-22719
Simulation of absorption edge densitometry
|DE95-004393| p 1635 N95-23360
Contribution of proton-induced short range secondaries to the LET spectra on LDEF p 1815 N95-23813
DEOXYRIBONUCLEIC ACID
Development of novel separation techniques for biological samples in capillary electrophoresis
|DE95-001672| p 1744 N95-22493
Open problems of computational molecular biology
|DE95-000895| p 1745 N95-22866
The torsion space nucleic acids molecular mechanics program DUPLEX: Surveying conformation space by potential energy minimization
|DE94-017707| p 1805 N95-22889
An improved system for exon recognition and gene modeling in human DNA sequences
|DE94-017863| p 1746 N95-22890
Activation of the jun-D gene in human myeloid cells by 1-(beta)-D-arabinofuranosylcytosine
|DE94-016591| p 1746 N95-22912
Rearrangement of RAG-1 recombinase gene in radiation-sensitive wasted mice
|DE94-017083| p 1746 N95-22913
A supersymmetric family of harmonic oscillators simulating H-bonds in DNA p 1748 N95-22963
Molecular relics from chemical evolution and the origin of life
|DE94-628493| p 1747 N95-23060
DEPLETION
Solar mass loss, solar lithium, and solar oscillations
|DE94-018262| p 1870 N95-22938
Krypton isotope analysis using near-resonant stimulated Raman spectroscopy
|DE95-005061| p 1635 N95-23348
DEPOLARIZATION
Strong collision approach to calculation of depolarization function for neutron beam passing through ferromagnetic bulk domains
|DE94-628847| p 1803 N95-22758
DEPOSITION
Infrared study of carbon deposits on bimetallic catalysts
|DE95-000902| p 1631 N95-22517
Surface growth of two kinds of particles deposition models
|DE94-628480| p 1841 N95-23021
Method of making a semiconductor device using a nanochannel glass matrix
|AD-D016383| p 1662 N95-23241
Cu deposition using a permanent magnet electron cyclotron resonance microwave plasma source
|DE94-017768| p 1650 N95-23981
Increasing the retained dose by plasma immersion ion implantation and deposition
|DE95-003423| p 1844 N95-24011
DEPOSITS
Infrared study of carbon deposits on bimetallic catalysts
|DE95-000902| p 1631 N95-22517
DEPTH
Aspects of surface generation in orthogonal ultraprecision machining
|DE95-000922| p 1654 N95-22678
Investigation of depth-area relationships associated with nanoindentations
|DE95-001353| p 1639 N95-22686
DERIVATION
Boson mapping techniques applied to constant gauge fields in QCD p 1814 N95-22969
Second derivative of the likelihood of an exact ARMA model
|PB95-135158| p 1788 N95-23069
Singular moduli and Arakelov intersection
|DE94-634286| p 1792 N95-23659
DERMATITIS
Skin exposure: Assessing the hazard in the workplace p 1628 N95-23030
DESIGN ANALYSIS
A high-power switch-mode DC power supply for dynamic loads
|DE94-016714| p 1659 N95-22504
Conceptual design of a 20-kA current lead using forced-flow cooling and Ag-alloy-sheathed Bi-2223 high-temperature superconductors
|DE95-002916| p 1660 N95-22569
Electromechanical Battery Program at the Lawrence Livermore National Laboratory
|DE95-003657| p 1727 N95-22574

Interdigital-H linac for unstable nuclei at INS
| DE94-765448 | p 1816 N95-22644
Using the shield for thermal energy storage in PULSAR
| DE95-002457 | p 1829 N95-22645
Advanced liquid oxygen (LO2) propellant conditioning concept testing
| NASA-TM-108477 | p 1652 N95-22672
Passive intermodulation generation in wire mesh deployable reflector antennas p 1656 N95-22816
Application requirements for wind turbine gearboxes
| DE94-011883 | p 1694 N95-22923
Euler technology assessment for preliminary aircraft design employing OVERFLOW code with multiblock structured-grid method
| NASA-CR-4651 | p 1608 N95-23095
The US molten carbonate fuel-cell development and commercialization effort
| DE94-019096 | p 1728 N95-23162
Aerodynamic design optimization with sensitivity analysis and computational fluid dynamics
| NASA-CR-197419 | p 1608 N95-23218
NASA 30 cm ion thruster development status
| NASA TM-106842 | p 1624 N95-23221
Functional testing of the space station plasma contactor
| NASA-TM-106841 | p 1624 N95-23240
Design of a differential radiometer for atmospheric radiative flux measurements
| DE95-002701 | p 1739 N95-23244
Design of a GaAs/Ge solar array for unmanned aerial vehicles
| NASA-TM-106870 | p 1728 N95-23259
Infinite possibilities: Computational structures technology p 1700 N95-23280
Inner loop flight control for the High-Speed Civil Transport p 1616 N95-23314
Multidisciplinary design optimization using genetic algorithms p 1619 N95-23332
Search Hanford accessible reports electronically system design description, revision 1
| DE95-004369 | p 1856 N95-23341
Design and production of efficient current leads for 1500-A, 50-Hz service in a 77-4 K temperature gradient
| DE95-004121 | p 1662 N95-23355
HTS current lead using a composite heat pipe
| DE95-003718 | p 1662 N95-23368
D(O) upgrade muon electronics design
| DE95-003744 | p 1817 N95-23369
Enhanced analysis and users manual for radial-inflow turbine conceptual design code RTD
| NASA-CR-195454 | p 1609 N95-23462
Mechanical design of the CDF SVX 2 silicon vertex detector
| DE94-018985 | p 1689 N95-23520
The next Large Helical Devices
| NIFS-323 | p 1835 N95-23535
Recent studies of the Large Helical Device
| NIFS-322 | p 1835 N95-23543
The STAR EM calorimeter design and small prototype test results
| DE95-004592 | p 1689 N95-23583
Methodology for CFD design analysis of National Launch System nozzle manifold p 1683 N95-23637
ASRM multi-port igniter flow field analysis p 1683 N95-23639
Application of CFD analysis to design support and problem resolution for ASRM and RSRM p 1685 N95-23649
Concept verification of three dimensional free motion simulator for space robot p 1618 N95-23702
A three-finger multisensory hand for dexterous space robotic tasks p 1752 N95-23705
Development of Japanese experiment module remote manipulator system p 1752 N95-23708
Automated solar cell assembly teamed process research
| DE95-000299 | p 1730 N95-23777
Micro heat spreader enhanced heat transfer in MCM's
| DE95-004520 | p 1663 N95-23779
PRISM Spectrograph Optical Design
| NASA-CR-197965 | p 1828 N95-24035
Design of a high-temperature superconductor current lead for electric utility SMES
| DE95-004604 | p 1664 N95-24163
Ultrafast, high precision gated integrator
| DE95-004616 | p 1664 N95-24164
Beryllium in the ITER blanket
| DE95-004620 | p 1837 N95-24165

DESIGN TO COST
A manufacturing database of advanced materials used in spacecraft structures p 1623 N95-23279

DESTABILIZATION
On the (DE-) stabilization of quantum mechanical binding by potential barriers
| DE94-628433 | p 1847 N95-22635

DETECTION
An automated computer misuse detection system for UNICOS
| DE95-000929 | p 1762 N95-22680
Light emission-or-absorbance-based binding assays for polynucleic acids
| AD-D016557 | p 1632 N95-22710
Evaluation of neutron techniques for illicit substance detection
| DE95-002988 | p 1632 N95-22764
Mercury detection with thermal neutrons
| DE95-002061 | p 1806 N95-23055
Health and usage monitoring systems: Corrosion surveillance p 1607 N95-23506
In-situ detection of surface passivation or activation and of localized corrosion: Experiences and prospectives in aircraft p 1643 N95-23508
New nondestructive techniques for the detection and quantification of corrosion in aircraft structures p 1644 N95-23512
Corrosion detection and monitoring of aircraft structures: An overview p 1644 N95-23515
Experience of in-service corrosion on military aircraft p 1644 N95-23516
The significance of hair mineral analysis as a means for assessing internal body burdens of environmental pollutants
| DE94-633512 | p 1734 N95-23541

DETERIORATION
Non-destructive detection of corrosion for life management p 1643 N95-23505
Reproducible direct exposure environmental testing of metal-based magnetic media p 1690 N95-24129

DETERMINANTS
Determinants of elliptic pseudo-differential operators
| PB95-109062 | p 1786 N95-22711
The U(3) x U(3) Nambu - Jona-Lasinio model with the gluon condensate and axial anomaly at finite temperature
| DE94-628588 | p 1804 N95-22787
Second derivative of the likelihood of an exact ARMA model
| PB95-135158 | p 1788 N95-23069

DETONATION
Level set techniques applied to unsteady detonation propagation
| DE95-002741 | p 1666 N95-22901

DETONATION WAVES
The effect of a non-zero shock width on wave propagation in multi-dimensions
| DE95-002748 | p 1666 N95-22902

DETONATORS
Computer modeling of detonators
| DE95-003031 | p 1652 N95-22721

DEUTERIUM
Structure, melting, and reactivity of nickel clusters from numerical simulations
| DE95-002911 | p 1638 N95-22531
The DIII-D divertor cryopump system: Design and operational experience
| DE95-003007 | p 1693 N95-22796
Engineering design of a radiative divertor for DIII-D
| DE95-003008 | p 1693 N95-22798
Exotic atoms
| DE95-003199 | p 1805 N95-22881

DIAGNOSIS
An intelligent ground operator support system p 1769 N95-23681
An expert system for diagnosing anomalies of spacecraft p 1770 N95-23684
Distributed intelligence for ground/space systems p 1770 N95-23685
Performance results of cooperating expert systems in a distributed real-time monitoring system p 1761 N95-23688
Ploxoma: Testbed for uncertain inference
| TR-537 | p 1794 N95-23927

DIAMINES
Polyazomethines containing trifluoromethylbenzene units
| NASA-CASE-LAR-14896-1 | p 1649 N95-23253
Process for preparing an assembly of an article and a polyimide which resists dimensional change, delamination and debonding when exposed to changes in temperature
| NASA-CASE-LAR-14538-2 | p 1649 N95-23254

DIAMONDS
Hypervelocity impact survivability experiments for carbonaceous impactors, part 2 p 1700 N95-23831

DIATOMIC MOLECULES
Fibonacci chain polynomials: Identities from self-similarity p 1814 N95-22962

DIELECTRIC PROPERTIES
Effect of critical field on screened dielectric breakdown growth
| DE94-628482 | p 1661 N95-23046
Microwave dielectric properties of boreal forest trees p 1716 N95-23961

DIELECTRICS
Turbidity of a near critical ionic fluid
| DE94-014916 | p 1633 N95-22869
Capacitive acoustic wave detector and method of using same
| NASA-CASE-LAR-13890-1 | p 1799 N95-22921
A new containerless image furnace with electro-static positioning device p 1690 N95-23674
Studies of autoionizing states relevant to dielectronic recombination
| DE94-014162 | p 1812 N95-23978
Reflectance control for multicrystalline-silicon photovoltaic modules using textured-dielectric coatings
| DE95-004532 | p 1731 N95-24155
Microporous polyimide films for reduced dielectric applications
| DE95-004543 | p 1650 N95-24159

DIESEL ENGINES
Diesel fuel component contributions to engine emissions and performance: Clean fuel study
| DE94-011868 | p 1732 N95-22834

DIESEL FUELS
Diesel fuel component contributions to engine emissions and performance: Clean fuel study
| DE94-011868 | p 1732 N95-22834

DIETHYL HYDROGEN PHOSPHITE (DEHP)
A comparative study of the effects of clofibrate, ciprofibrate, WY-14,643, and di-(2-ethylhexyl)-phthalate on liver protein expression in mice
| DE94-016587 | p 1748 N95-23771

DIFFERENCE EQUATIONS
Fourth order difference methods for hyperbolic IBVP's
| NASA-CR-197955 | p 1791 N95-23548

DIFFERENTIAL CALCULUS
On the theory of smooth structures 3
| DE94-628411 | p 1786 N95-22642

DIFFERENTIAL EQUATIONS
Diffusion terms in systems of reaction diffusion equations can lead to blow up
| DE94-628408 | p 1785 N95-22618
On oscillations of higher order neutral differential equations
| DE94-628421 | p 1786 N95-22629
Iterative solutions of nonlinear equations with strongly accretive or strongly pseudocontractive maps
| DE94-628432 | p 1786 N95-22634
Determinants of elliptic pseudo-differential operators
| PB95-109062 | p 1786 N95-22711
Deformed Heisenberg algebra and fractional spin field in 2+1 dimensions
| DE94-628507 | p 1850 N95-22779
Stoermer-Cowell: Straight, summed and split. An overview
| PB95-139341 | p 1789 N95-23200
A preliminary measurement of the average B hadron lifetime
| DE95-003138 | p 1808 N95-23226
Orders of predictor-corrector pairs for second-order ODE's
| PB95-140612 | p 1790 N95-23237
Aeroacoustic computation of gust-blade interaction p 1800 N95-23313
Iterative solutions of nonlinear equations in smooth Banach spaces
| DE94-634287 | p 1790 N95-23455

DIFFRACTION
Optical image correlator using orthogonal data storage
| AD-A285795 | p 1819 N95-22508
Long range potentials and multiple scattering theory in complex systems
| DE94-628881 | p 1804 N95-22791
A uniform geometrical optics and an extended uniform geometrical theory of diffraction for evaluating high frequency EM fields near smooth caustics and composite shadow boundaries
| NASA-CR-197934 | p 1657 N95-23391

DIFFRACTION PATTERNS
Nondestructive evaluation of fatigue damage in aluminum 2024 by x-ray diffraction p 1698 N95-23293

DIFFUSE RADIATION
Application of a two-stream radiative transfer model for leaf lignin and cellulose concentrations from spectral reflectance measurements, part 2 p 1703 N95-23857

DIFFUSION
Energetic particle observations at geosynchronous orbit
| DE95-000873 | p 1867 N95-22516
Modeling NO(x) emissions in turbulent jet flames: Effects of buoyancy and radiation
| DE94-016621 | p 1633 N95-22886
Dynamical behaviour of the coupled diffusion map lattice
| DE94-628481 | p 1841 N95-23022

Influence of porosity and two-phase flow on diffusional/thermal instability of a deflagrating energetic material
|DE95-002592| p 1634 N95-23122
New robust multigrid method for 2D convection-diffusion problems
|PB95-138897| p 1789 N95-23176

DIFFUSION COEFFICIENT
Analysis of physiochemical processes during solder aging
|DE95-003811| p 1638 N95-22576
Carbon doping of III-V compound semiconductors
|DE95-003431| p 1844 N95-24013

DIFFUSION FLAMES
Microgravity combustion science: 1995 program update
|NASA-TM-106858| p 1626 N95-24004

DIGITAL COMMAND SYSTEMS
DRACULA: Dynamic range control for broadcasting and other applications
|BBC-RD-1994/13| p 1658 N95-24044

DIGITAL DATA
Simulation of landsat thematic mapper imagery using AVIRIS hyperspectral imagery p 1705 N95-23869
Current and future use of TOPSAR digital topographic data for volcanological research p 1714 N95-23949
Comparison of 7.5-minute and 1-degree digital elevation models p 1719 N95-24095

DIGITAL ELECTRONICS
The MAMMOTH project p 1753 N95-24126

DIGITAL FILTERS
Parallel digital modem using multirate digital filter banks
|NASA-CR-197331| p 1761 N95-22478
VLSI for high-speed digital signal processing
|AD-A285643| p 1663 N95-23783
Subband quantum scattering times for AlGaAs/GaAs obtained using digital filtering
|NASA-TM-106873| p 1846 N95-24188

DIGITAL SIMULATION
Simulation of landsat thematic mapper imagery using AVIRIS hyperspectral imagery p 1705 N95-23869
Mapping and monitoring changes in vegetation communities of Jasper Ridge, CA, using spectral fractions derived from AVIRIS images p 1708 N95-23883
Using simple page placement policies to reduce the cost of cache fills in coherent shared-memory systems
|TR-535| p 1753 N95-24177

DIGITAL SYSTEMS
Parallel digital modem using multirate digital filter banks
|NASA-CR-197331| p 1761 N95-22478
Electronic photography at NASA Langley Research Center p 1690 N95-23298
DRACULA: Dynamic range control for broadcasting and other applications
|BBC-RD-1994/13| p 1658 N95-24044
Color orthophotography: To scan or not
|DE95-002749| p 1689 N95-24069
High data rate recorder development at MIT Haystack Observatory p 1690 N95-24118

DIGITAL TECHNIQUES
Adaptive beamforming in a CDMA mobile satellite communications system p 1655 N95-22815
Document image archive transfer from DOS to UNIX p 1761 N95-24117
Petabyte mass memory system using the Newell Opticel(TM) p 1753 N95-24119
The MAMMOTH project p 1753 N95-24126

DIMENSIONAL ANALYSIS
Assessment of resin transfer molding process for the XM6 discharger, ERDEC SSP 93-64
|NIAR-94-2| p 1650 N95-23932

DIMENSIONAL MEASUREMENT
Optimal band selection for dimensionality reduction of hyperspectral imagery p 1709 N95-23887

DIMENSIONLESS NUMBERS
A method of solving simple harmonic oscillator Schroedinger equation p 1797 N95-22989

DIMERS
Reduced dimer production in solar-simulator-pumped continuous wave iodine lasers based on model simulations and scaling and pumping studies
|NASA-TP-3486| p 1691 N95-23411

DIMETHYL COMPOUNDS
Dimethylsulfide oxidation over the tropical South Atlantic: OH and other oxidants
|NASA-CR-197417| p 1732 N95-22930

DIODES
Computational modelling of Er(3+): Garnet laser materials p 1692 N95-23326

DIPOLE MOMENTS
Harmonic oscillator representation in the theory of scattering and nuclear reactions p 1814 N95-22967
Computational studies of metal-metal and metal-ligand interactions
|NASA-CR-197862| p 1641 N95-23215

DIRAC EQUATION
Continuous local symmetry in Ising-type models
|DE94-629045| p 1839 N95-22649
Dirac canonical quantization and Faddeev-Jackiw symplectic quantization of higher order Lagrangians
|DE9?-628428| p 1796 N95-22788
Generalized phase transformations of spinor fields
|DE94-628505| p 1656 N95-22841
Pseudoclassical description of the Dirac Oscillator p 1825 N95-22996

DIRECTIONAL CONTROL
Flow measuring structures
|PB95-127254| p 1665 N95-22638
Feedback control laws for highly maneuverable aircraft
|NASA-CR-197944| p 1615 N95-23410

DIRICHLET PROBLEM
Quantum field between moving mirrors: A three dimensional example p 1821 N95-22965
Optimally scaled systems for second order scalar singularity perturbed problems
|PB95-138814| p 1789 N95-23169

DISCHARGERS
Assessment of resin transfer molding process for the XM6 discharger, ERDEC SSP 93-64
|NIAR-94-2| p 1650 N95-23932

DISCONTINUITY
Aeroacoustic computation of gust-blade interaction p 1800 N95-23313

DISCRETE FUNCTIONS
An interactive tool for discrete phase analysis in two-phase flows p 1683 N95-23641

DISEASES
Ploxoma: Testbed for uncertain inference
|TR-537| p 1794 N95-23927

DISK OPERATING SYSTEM (DOS)
Document image archive transfer from DOS to UNIX p 1761 N95-24117

DISLOCATIONS (MATERIALS)
Microstructural behavior of nonequilibrium systems
|DE95-004450| p 1630 N95-23924

DISORIENTATION
A review of civil aviation fatal accidents in which lost/disoriented was a cause/factor: 1981-1990
|DOT/FAA/AM-95/1| p 1611 N95-24071

DISPENSERS
Sensor-based control of rocket thrust chamber feature location for automated braze paste dispensing
|DE94-016559| p 1624 N95-22885

DISPLAY DEVICES
Virtual reality flight control display with six-degree-of-freedom controller and spherical orientation overlay
|NASA-CASE-NPO-18733-1-CU| p 1613 N95-22578
Automation technology using Geographic Information System (GIS) p 1863 N95-23284
Differential GPS and system integration of the Low Visibility Landing and Surface Operations (LVLASO) demonstration p 1611 N95-23318
Computational modelling of Er(3+): Garnet laser materials p 1692 N95-23326
An intelligent ground operator support system p 1769 N95-23681
Toward an automated signature recognition toolkit for mission operations p 1659 N95-23682
Full resolution hologram-like autostereoscopic display
|NASA-CR-197913| p 1689 N95-23789

DISRUPTING
Neural net prediction of tokamak plasma disruptions
|DE95-002616| p 1832 N95-23136

DISSIPATION
Study of frustrated systems via dissipative maps
|PB95-139093| p 1799 N95-23155

DISSOCIATION
Dislocation decomposition, dissociation, and deformation in MoSi2 and (alpha)-Al2O3 single crystals
|DE95-002715| p 1839 N95-22653
Thermochemistry of transition metal clusters
|DE95-003144| p 1646 N95-24144
Some thoughts of future experiments with the new generation of storage rings
|DE95-004602| p 1818 N95-24162

DISTILLATION
Airborne rotary air separator study
|NASA-CR-189099| p 1614 N95-24053

DISTORTION
Fabric geometry distortion during composites processing p 1631 N95-23288

DISTRIBUTED PARAMETER SYSTEMS
Utilizing inheritance in requirements engineering p 1768 N95-23677

DISTRIBUTED PROCESSING
Comparing data synchronization in Ada 9X and Orca
|PB95-127999| p 1754 N95-22529
Precise clock synchronization protocol
|PB95-127247| p 1687 N95-22536
Software for the generalized eigenproblem on distributed memory architectures
|DE95-002999| p 1755 N95-22690
A draft standard for message passing in a distributed memory environment
|DE94-019159| p 1657 N95-23075
Distributed VIRtual System (DIVIRS) project
|NASA-CR-197855| p 1757 N95-23180
Towards the Teraflop CFD
|NASA-CR-197947| p 1764 N95-23594
Using Dedal to share and reuse distributed engineering design information p 1768 N95-23678
Performance results of cooperating expert systems in a distributed real-time monitoring system p 1761 N95-23688
AVIRIS and TIMS data processing and distribution at the land processes distributed active archive center p 1706 N95-23872
The data facility of the Airborne Visible/Infrared Imaging Spectrometer (AVIRIS) p 1707 N95-23877
Scalability of atomic primitives on distributed shared memory multiprocessors
|TR-528| p 1764 N95-23930
Using high-performance networks to enable computational aerosciences applications
|NASA-CR-197951| p 1764 N95-24023
Unifying data and control transformations for distributed shared-memory machines
|TR-542| p 1765 N95-24061
A network-based distributed, media-rich computing and information environment
|DE95-003696| p 1765 N95-24074
Client/Server data serving for high performance computing p 1761 N95-24123

DISTRIBUTING
Description of a MIL-STD-1553B data bus Ada driver for the LeRC EPS Testbed
|NASA-TM-106866| p 1762 N95-22668

DISTRIBUTION FUNCTIONS
Nonparametric measure of spatial interaction in point patterns
|PB95-127965| p 1793 N95-22527
Wigner distribution function and entropy of the damped harmonic oscillator within the theory of the open quantum systems p 1798 N95-22990
(Phi)(sup 4) kinks: Statistical mechanics
|DE95-003693| p 1794 N95-23349
Gluon distribution as function of F(sub 2) and dF(sub 2)/dlnQ(exp 2) at small x
|DE94-635677| p 1812 N95-23975

DIVERTERS
The DIII-D divertor cryopump system: Design and operational experience
|DE95-003007| p 1693 N95-22796
Engineering design of a radiative divertor for DIII-D
|DE95-003008| p 1693 N95-22798
Divertor heat and particle control experiments on the DIII-D tokamak
|DE94-017518| p 1832 N95-23119
The next Large Helical Devices
|NIFS-323| p 1835 N95-23535
Recent studies of the Large Helical Device
|NIFS-322| p 1835 N95-23543

DIVERTORS (FUSION REACTORS)
D3-D program overview
|DE95-003879| p 1837 N95-24086

DOCUMENT STORAGE
Cost and schedule analytical techniques development
|NASA-CR-196548| p 1853 N95-22891

DOCUMENTS
NASAwide electronic publishing system: Electronic printing and duplicating, stage-2 evaluation report (GSFC)
|NASA-TM-104615| p 1856 N95-23209
Analysis of data from the energetic gamma-ray experiment of the Gamma Ray Observatory
|NASA-CR-197347| p 1871 N95-23216

DOMAINS
Coordinating complex decision support activities across distributed applications p 1761 N95-23749
Scheduling with genetic algorithms p 1761 N95-23762

DOORS
The sound insulations of studio doors. Part 2: Door seals
|BBC-RD-1994/15| p 1654 N95-24045
The sound insulations of studio doors. Part 1: Door blanks
|BBC-RD-1994/14| p 1654 N95-24093

DOPED CRYSTALS
MOCVD of gallium and calcium sulfides for improved phosphor processing
| DE95-000918 | p 1631 N95-22677
Hydrogen vibrational density of states of adsorbed water on rare-earth modified zirconia
| DE95-001127 | p 1632 N95-22681
Computational modelling of Er(3+): Garnet laser materials p 1692 N95-23326
Annealing of nitrogen-doped ZnSe at high pressures: Toward suppression of native defect formation
| DE95-003420 | p 1844 N95-24010
Carbon doping of III-V compound semiconductors
| DE95-003431 | p 1844 N95-24013
Silicon surface and bulk defect passivation by low temperature PECVD oxides and nitrides
| DE95-004531 | p 1731 N95-24090
Extraction of the surface recombination velocity of passivated phosphorus-doped silicon emitters
| DE95-004539 | p 1845 N95-24156

DOPPLER RADAR
SWIFT BOAT 1994: Using a fast chase boat to investigate offshore weather features in conjunction with WSR-88D observations
| PB94-195146 | p 1742 N95-22651
Maximum-likelihood spectral estimation and adaptive filtering techniques with application to airborne Doppler weather radar
| NASA-CR-197699 | p 1658 N95-23670

DOSIMETERS
Annual report of the Osaka Laboratory for Radiation Chemistry Japan Atomic Energy Research Institute, (No. 26)
| DE94-785277 | p 1626 N95-23477
Dosimetric results on EURECA p 1872 N95-23800

DOWNLINKING
Design and production of efficient current leads for 1500-A, 50-Hz service in a 77-4 K temperature gradient
| DE95-004121 | p 1662 N95-23355

DRAINAGE
Streamflow and selected precipitation data for Yucca Mountain Region, southern Nevada and eastern California, water years 1986-90
| DE95-001893 | p 1742 N95-23385

DRIFT RATE
Electron drift velocities of Ar-CO2-CF4 gas mixtures
| DE95-004353 | p 1809 N95-23359
Laser light induced drift for atoms of radioactive isotopes Na-22 and Na-24
| DE94-635759 | p 1812 N95-23976

DRILLING
Study on possible environmental effects of a WBM cutting discharge in the north sea, one year after termination of drilling
| PB95-133740 | p 1733 N95-23125

DROP SIZE
Development of an atomization methodology for spray combustion p 1637 N95-23646

DROPS (LIQUIDS)
Quasistatic model for the motion of a viscous capillary liquid drop
| PB95-138848 | p 1667 N95-23172
Modeling of non-spherical droplet dynamics p 1685 N95-23647
A new containerless image furnace with electro-static positioning device p 1690 N95-23674

DROSOPHILA
Genetic effects on heavy ions in drosophila
| NASA-CR-197916 | p 1746 N95-22911

DRUGS
Evaluation of neutron techniques for illicit substance detection
| DE95-002988 | p 1632 N95-22764

DRYING
Innovative technology for contamination control in plasma processing
| DE95-000913 | p 1829 N95-22519

DUCTED FLOW
Computational Fluid Dynamics (CFD) analyses in support of Space Shuttle Main Engine (SSME) heat exchanger (HX) vane cracking investigation p 1679 N95-23619
Unsteady flow simulations in support of the SSME HEX turning vane cracking investigation with the ATD HPOTP p 1679 N95-23621

DUCTED ROCKET ENGINES
Fundamental phenomena on fuel decomposition and boundary layer combustion processes with applications to hybrid rocket motors
| NASA-CR-197919 | p 1625 N95-23261

DUCTILITY
The hydrogen embrittlement of alloy X-750
| DE95-003207 | p 1640 N95-22893

DUCTS
The use of cowl camber and taper to reduce rotor/stator interaction noise
| NASA-CR-195421 | p 1799 N95-22675
Three-D flow analysis of the alternate SSME HPOT TAD p 1679 N95-23620
On the accuracy of CFD-based pressure drop predictions for right-angle ducts p 1682 N95-23634
CFD modeling of turbulent duct flows for coolant channel analysis p 1682 N95-23635
Flow and heat transfer in 180-degree turn square ducts: Effects of turning configuration and system rotation p 1682 N95-23636

DUMMIES
Design of a cervical spine gross motion simulator for standard size human and anthropomorphic dummy adult and child
| NIAR-94-16 | p 1751 N95-24021

DUMPING
Study on possible environmental effects of a WBM cutting discharge in the north sea, one year after termination of drilling
| PB95-133740 | p 1733 N95-23125

DUNES
Determination of semi-arid landscape endmembers and seasonal trends using convex geometry spectral unmixing techniques p 1711 N95-23895
Mineralogic variability of the Kelso Dunes, Mojave Desert, California derived from Thermal Infrared Multispectral Scanner (TIMS) data p 1711 N95-23920
AIRSAR views of aerolian terrain p 1713 N95-23941

DURABILITY
Glass science tutorial: Lecture 1, Chemistry and properties of oxide glasses
| DE95-002963 | p 1647 N95-22647
Atomic oxygen durability evaluation of protected polymers using thermal energy plasma systems
| NASA-TM-106855 | p 1626 N95-23270
Interlaminar shear test method development for long term durability testing of composites p 1631 N95-23300
Problems of predicting material property retention during long term service p 1644 N95-23514
Durability of reflector materials in the space environment p 1651 N95-23912

DUST
Proceedings of NATO Advanced Research Workshop on the Formation, Transport and Consequences of Particles in Plasmas
| AD-A285850 | p 1829 N95-22514

DYE LASERS
Non-intrusive measurements in a rocket engine combustor p 1625 N95-23439

DYNAMIC CONTROL
Computational control of flexible aerospace systems
| NASA-CR-197902 | p 1621 N95-23260

DYNAMIC LOADS
A high-power switch-mode DC power supply for dynamic loads
| DE94-016714 | p 1659 N95-22504
Unsteady flow simulations in support of the SSME HEX turning vane cracking investigation with the ATD HPOTP p 1679 N95-23621
Enhancement of F/A-18 operational flight measurements: Data report for phase 1
| DSTO-TR-0049 | p 1613 N95-23666

DYNAMIC MODELS
Roles and dynamic subclasses: A modal logic approach
| PB95-127320 | p 1754 N95-22522
Semikinetic modeling and observations of high-latitude plasma outflow
| NASA-CR-197403 | p 1831 N95-23008
Modeling of nonequilibrium space plasma flows
| NASA-CR-197432 | p 1833 N95-23211
Flutter analysis of composite box beams
| NASA-CR-197931 | p 1615 N95-23392

DYNAMIC PRESSURE
Unsteady flow simulations in support of the SSME HEX turning vane cracking investigation with the ATD HPOTP p 1679 N95-23621

DYNAMIC PROGRAMMING
An improved system for exon recognition and gene modeling in human DNA sequences
| DE94-017863 | p 1746 N95-22890

DYNAMIC RANGE
Operation and tests of a DDC101 A/D
| DE95-003747 | p 1663 N95-23405
Multiband VLBI imaging of the jet in 3C 345
| PB95-139275 | p 1866 N95-23468
DRACULA: Dynamic range control for broadcasting and other applications
| BBC-RD-1994/13 | p 1658 N95-24044
A high speed digitizing photomultiplier tube base for the KTeV CsI calorimeter
| DE95-003739 | p 1664 N95-24081

DYNAMIC RESPONSE
A high-power switch-mode DC power supply for dynamic loads
| DE94-016714 | p 1659 N95-22504
Dynamic response tests of inertial and optical wind-tunnel model attitude measurement devices
| NASA-TM-109182 | p 1616 N95-23011
Influence of backup bearings and support structure dynamics on the behavior of rotors with active supports
| NASA-CR-197438 | p 1694 N95-23190
Dynamic modelling and response characteristics of a magnetic bearing rotor system including auxiliary bearings
| NASA-CR-197859 | p 1694 N95-23213
Effects of delaminations on the damped dynamic characteristics of composite laminates: Mechanics and experiments
| NASA-TM-106862 | p 1630 N95-23258
Dynamic response of a transducer mounted at one end of an acoustical cavity which is subjected to a specified pressure at the open end of the cavity
| DE95-004192 | p 1799 N95-23379
Nonlinear thermoviscoelastic behaviour in complex materials
| PB95-140653 | p 1630 N95-23537
Current-profile flattening and hot core shift due to the nonlinear development of resistive kink mode
| NIFS-311 | p 1835 N95-23564
Time-accurate unsteady flow simulations supporting the SRM T+68-second pressure spike anomaly investigation (STS-54B) p 1685 N95-23650
A multibody/finite element analysis approach for modeling of crash dynamic responses
| NIAR-94-3 | p 1610 N95-24050

DYNAMIC STABILITY
Handling qualities of the High Speed Civil Transport p 1616 N95-23325

DYNAMIC STRUCTURAL ANALYSIS
Integrated aerodynamic/dynamic/structural optimization of helicopter rotor blades using multilevel decomposition
| NASA-TP-3465 | p 1612 N95-22953
Geometrical interpretation for the outer SU(3) outer multiplicity label p 1814 N95-22968
Structural arrangement trade study. Volume 3: Reusable Hydrogen Composite Tank System (RHCTS) and Graphite Composite Primary Structures (GCPS). Addendum
| NASA-CR-197687 | p 1621 N95-23189
Computational control of flexible aerospace systems
| NASA-CR-197902 | p 1621 N95-23260
Thin tailored composite wing for civil tiltrotor p 1613 N95-23317
A new look at the simultaneous analysis and design of structures p 1700 N95-23327
Flutter analysis of composite box beams
| NASA-CR-197931 | p 1615 N95-23392

DYNAMIC TESTS
Nonlinear viscoelastic characterization of polymer materials using a dynamic-mechanical methodology p 1651 N95-23902

DYNAMICAL SYSTEMS
Hausdorff dimension of Julia sets of complex Henon mappings
| DE94-628420 | p 1785 N95-22628
Symplectic computation of Lyapunov exponents
| DE95-002732 | p 1795 N95-22654
Nonlinear system guidance in the presence of transmission zero dynamics
| NASA-TM-4661 | p 1654 N95-22804
Lyapunov exponents from CHUA's circuit time series using artificial neural networks p 1784 N95-22988
Static parametric fluctuations give nonstatistical behaviour in uncoupled chaotic systems
| DE94-628478 | p 1794 N95-23019
Dynamical behaviour of the coupled diffusion map lattice
| DE94-628481 | p 1841 N95-23022
Adaptive control of linear systems based on approximate models
| PB95-139333 | p 1767 N95-23199

DYSON THEORY
The convergence radius of the chiral expansion in the Dyson-Schwinger approach
| DE94-012852 | p 1805 N95-22925

E

EARTH (PLANET)
Space Science for the 21st Century. Strategic Plan for 1995-2000
| NASA-TM-110546 | p 1617 N95-22947

Physics of magnetospheric boundary layers
| NASA-CR-197920 | p 1739 N95-23271
Investigation of the role of gravity waves in the generation of equatorial bubbles
| NASA-CR-197962 | p 1739 N95-23272
Real-world shepherding: Combining vision, manipulation, and planning in real time
| TR-530 | p 1783 N95-24001
Using simulation-based projection to plan in an uncertain and temporally complex world
| TR-531 | p 1853 N95-24043

EARTH ATMOSPHERE
Magnetospheric space plasma investigations
| NASA-CR-197405 | p 1831 N95-22955
Physics of magnetospheric boundary layers
| NASA-CR-197920 | p 1739 N95-23271
Study of atmospheric parameters measurements using MM-wave radar in synergy with LITE-2
p 1741 N95-23278
Theoretical studies of spectroscopic problems of importance for atmospheric radiation measurements
p 1741 N95-23329
Oxidants and oxidation in the Earth's atmosphere
| NASA-CR-197945 | p 1734 N95-23460
The atmosphere below
| NASA-TM-110538 | p 1740 N95-23663

EARTH CRUST
Tomographic analysis of the three-dimensional variation of the seismic velocity structure of the shallow crust underlying Southern New England
| AD-A279406 | p 1739 N95-23247
Mapping of the Ronda peridotite massif (Spain) from AVIRIS spectro-imaging survey: A first attempt
p 1707 N95-23878

EARTH GRAVITATION
Newton in space
| NASA-TM-110535 | p 1799 N95-23273
Living in space
| NASA-TM-110536 | p 1751 N95-23274

EARTH IONOSPHERE
Magnetospheric space plasma investigations
| NASA-CR-197405 | p 1831 N95-22955
The high latitude ionosphere-magnetosphere transition region: Simulation and data comparison
| NASA-CR-197404 | p 1737 N95-22956
Physics of magnetospheric boundary layers
| NASA-CR-197920 | p 1739 N95-23271
TRACKER: A three-dimensional raytracing program for ionospheric radio propagation
| DE95-003510 | p 1658 N95-24015

EARTH MAGNETOSPHERE
Hot proton anisotropies and cool proton temperatures in the outer magnetosphere
| DE95-002719 | p 1736 N95-22850
Global electric field determination in the Earth's outer magnetosphere using energetic charged particles
| NASA-CR-197392 | p 1737 N95-22945
Magnetospheric space plasma investigations
| NASA-CR-197405 | p 1831 N95-22955
The high latitude ionosphere-magnetosphere transition region: Simulation and data comparison
| NASA-CR-197404 | p 1737 N95-22956
Semikinetic modeling and observations of high-latitude plasma outflow
| NASA-CR-197403 | p 1831 N95-23008
Modeling of the coupled magnetospheric and neutral wind dynamos
| NASA-CR-197861 | p 1738 N95-23090
Characteristics of low energy ions in the Heavy Ions In Space (HIIS) experiment p 1815 N95-23807

EARTH MANTLE
Axial focusing of energy from a hypervelocity impact on earth
| DE95-003347 | p 1740 N95-24008
Axial focusing of impact energy in the earth's interior: A possible link to flood basalts and hotspots
| DE95-003357 | p 1741 N95-24009

EARTH OBSERVATIONS (FROM SPACE)
Civilian satellite remote sensing: A strategic approach
| PB95-109633 | p 1717 N95-22713
Ocean observations with EOS/MODIS: Algorithm development and post launch studies
| NASA-CR-197402 | p 1717 N95-22916
Active vision in satellite scene analysis
p 1778 N95-23738

EARTH OBSERVING SYSTEM (EOS)
Land surface temperature measurements for EOS MODIS data
| NASA-CR-197443 | p 1717 N95-23191
Infrared algorithm development for ocean observations with EOS/MODIS
| NASA-CR-197851 | p 1743 N95-23212
Ocean observations with EOS/MODIS: Algorithm development and post launch studies
| NASA-CR-197894 | p 1718 N95-23473
Technical report series on global modeling and data assimilation. Volume 4: Documentation of the Goddard Earth Observing System (GEOS) data assimilation system, version 1
| NASA-TM-104606-VOL-4 | p 1740 N95-23529
Land surface temperature measurements from EOS MODIS data
| NASA-CR-197969 | p 1721 N95-24190

EARTH ORBITAL ENVIRONMENTS
Evaluation of adhesive materials used on the Long Duration Exposure Facility
| NASA-CR-4646 | p 1626 N95-22918
Electromagnetic radiation in the plasma environment around the shuttle
| NASA-TM-106891 | p 1738 N95-23116
Atomic oxygen durability evaluation of protected polymers using thermal energy plasma systems
| NASA-TM-106855 | p 1626 N95-23270
Outgassing products from orbiter TPS materials
p 1637 N95-23798
Dosimetric results on EURECA p 1872 N95-23800
Preliminary results of radiation measurements on EURECA p 1872 N95-23801
LDEF contributions to cosmic ray and radiation environments research p 1872 N95-23805
Trapped iron measured on LDEF
p 1872 N95-23806
Results from the Heavy Ions In Space (HIIS) experiment on the ionic charge state of solar energetic particles
p 1870 N95-23808
Early results from the ultra heavy cosmic ray experiment p 1872 N95-23809
Fission foil measurements of neutron and proton fluences in the A0015 experiment p 1815 N95-23811
Measurement of trapped proton fluences in main stack of P0006 experiment p 1815 N95-23812
Predictions of LET spectra measured on LDEF
p 1815 N95-23815
Predictions of LDEF radioactivity and comparison with measurements p 1815 N95-23818
Status of LDEF radiation modeling
p 1815 N95-23819
Be-10 in terrestrial bauxite and industrial aluminum: An LDEF fallout p 1646 N95-23820
Status of LDEF contributions to current knowledge of meteoroid and manmade debris environments and their effects on spacecraft in LEO p 1623 N95-23822
LDEF meteoroid and debris special investigation group investigations and activities at the Johnson Space Center p 1623 N95-23823
Micrometeoroids and debris on LDEF comparison with MIR data p 1623 N95-23824
Small craters on the meteoroid and space debris impact experiment p 1623 N95-23825
LDEF Interplanetary Dust Experiment (IDE) results
p 1869 N95-23828
The orbital characteristics of debris particle rings as derived from IDE observations of multiple orbit intersections with LDEF p 1869 N95-23829
Analytical electron microscopy of LDEF impactor residues p 1869 N95-23832
Debris and meteoroid proportions deduced from impact crater residue analysis p 1869 N95-23834
SIMS chemical and isotopic analysis of impact features from LDEF experiments AO187-1 and AO187-2
p 1637 N95-23837
The effect of impact angle on craters formed by hypervelocity particles p 1700 N95-23839
Experimental investigation of the relationship between impact crater morphology and impacting particle velocity and direction p 1700 N95-23840
Determining orbital particle parameters of impacts into germanium using morphology analysis and calibration data from hypervelocity impact experiments in the laboratory
p 1700 N95-23841
Cratering and penetration experiments in Teflon targets at velocities from 1 to 7 km/s p 1700 N95-23842
LDEF: 69 Months in Space. Third Post-Retrieval Symposium, part 2
| NASA-CP-3275-PT-2 | p 1899 N95-23896
Summary and review of Materials Special Investigation Group evaluations of hardware from the Long Duration Exposure Facility p 1638 N95-23897
Recent results from Long Duration Exposure Facility materials testing p 1638 N95-23898
LDEF polymeric materials: A summary of Langley characterization p 1651 N95-23899
Surface characterization of LDEF carbon fiber/polymer matrix composites p 1631 N95-23900
Space environmental effects on polymer matrix composites as a function of sample location on LDEF
p 1651 N95-23901
The effect of simulated low earth orbit radiation on polyimides (UV degradation study) p 1651 N95-23903
The surface properties of fluorinated polyimides exposed to VUV and atomic oxygen p 1651 N95-23904
Collection and review of metals data obtained from LDEF experiment specimens and support hardware
p 1646 N95-23905
Changes in chemical and optical properties of thin film metal mirrors on LDEF p 1651 N95-23907
Further investigations of experiment A0034 atomic oxygen stimulated outgassing p 1651 N95-23908
Atomic oxygen interactions with protected organic materials on the Long Duration Exposure Facility (LDEF)
p 1627 N95-23909
Trend analysis of in-situ spectral reflectance data from the Thermal Control Surfaces Experiment (TCSE)
p 1631 N95-23910
Whisker/Cone growth on the thermal control surfaces experiment no. S0069 p 1651 N95-23911
Durability of reflector materials in the space environment p 1651 N95-23912
Four space application material coatings on the Long-Duration Exposure Facility (LDEF)
p 1651 N95-23913
Organic matrix composite protective coatings for space applications p 1627 N95-23914
Structure and properties of polymeric composite materials during 1501 days outer space exposure at Salyut-7 orbital station p 1652 N95-23915
Overview of the LDEF MSIG databasing activities
p 1864 N95-23916

EARTH ORBITAL RENDEZVOUS
Long range targeting for space based rendezvous
| NASA-CR-197890 | p 1757 N95-23388

EARTH ORBITS
Geolocation applications of the Gonets LEO messaging satellites p 1656 N95-22818
Low Earth Orbit satellite/terrestrial mobile service compatibility p 1656 N95-22819
Low Earth orbit thermal control coatings exposure flight tests: A comparison of U.S. and Russian results
| NASA-CR-4647 | p 1626 N95-22919
STS-61 Space Shuttle mission report
| NASA-TM-110545 | p 1619 N95-23187
USML-1 microgravity glovebox experiment no. 1 Passive Accelerometer System
| NASA-CR-196575 | p 1653 N95-23552

EARTH PLANETARY STRUCTURE
The effects of AVIRIS atmospheric calibration methodology on identification and quantitative mapping of surface mineralogy, Drum Mountains, Utah
p 1705 N95-23870

EARTH RESOURCES
Comparison of 7.5-minute and 1-degree digital elevation models p 1719 N95-24095

EARTH SCIENCES
The design of a petabyte archive and distribution system for the NASA ECS project p 1858 N95-24110

EARTH SURFACE
HAPEX-Sahel: Basic description of methods and data sets
| PB95-127262 | p 1701 N95-22639
Basic data sets description and preliminary results of EFEDA-Spain
| PB95-139291 | p 1740 N95-23470
Validation data for land surface temperature determination from satellites
| CSIRO-TR-33 | p 1718 N95-23597
The effects of AVIRIS atmospheric calibration methodology on identification and quantitative mapping of surface mineralogy, Drum Mountains, Utah
p 1705 N95-23870
Mapping and monitoring changes in vegetation communities of Jasper Ridge, CA, using spectral fractions derived from AVIRIS images p 1708 N95-23883
A comparison of spectral mixture analysis an NDVI for ascertaining ecological variables p 1710 N95-23892
Summaries of the 4th Annual JPL Airborne Geoscience Workshop. Volume 3: AIRSAR Workshop
| NASA-CR-197354-VOL-3 | p 1712 N95-23938
MAX-91: Polarimetric SAR results on Montespertoli site p 1712 N95-23940

EARTHQUAKE DAMAGE
Seismic hazards at Kilauea and Mauna Loa volcanoes, Hawaii
| DE94-012109 | p 1737 N95-22924

EARTHQUAKES
Intermediate-term earthquake prediction and seismic zoning in Northern Italy
| DE94-627689 | p 1736 N95-22612
Seismic hazards at Kilauea and Mauna Loa volcanoes, Hawaii
| DE94-012109 | p 1737 N95-22924
Seismic evidence of conjugate normal faulting: The 1994 Devil Canyon earthquake sequence near Challis, Idaho
| DE95-002052 | p 1740 N95-23386

ECLIPSING BINARY STARS
Mass loss in the interacting semi-detached binary delta librae
| NASA-CR-197924 | p 1866 N95-23402

ECOLOGY
Geographic information analysis: An ecological approach for the management of wildlife on the forest landscape
|NASA-CR-197941| p 1719 N95-24094
ECONOMIC ANALYSIS
The possibilities for mobile and fixed services up to the 20/30 GHz frequency bands p 1656 N95-22817
Geolocation applications of the Gonets LEO messaging satellites p 1656 N95-22818
ECONOMIC IMPACT
Military bases: Environmental impact at closing installations. Report to Congressional requesters
|GAO/NSIAD-95-70| p 1735 N95-24057
ECONOMICS
Net energy analysis: Powerful tool for selecting electric power options
|DE95-002516| p 1728 N95-23133
DOD budget: Selected categories of planned funding for fiscal years 1995-99. Report to Congressional requesters
|GAO/NSIAD-95-92| p 1864 N95-24062
ECOSYSTEMS
Direct effects of atmospheric CO2 enrichment on plants and ecosystems: An updated bibliographic data base
|DE95-003060| p 1731 N95-22725
An extension of Freedman's results on a model of predator-prey dynamics as modified by the action of a parasite
|DE94-628488| p 1796 N95-23052
Revitalization of the Gemenc-area, Baja, Hungary. 1: A study on hydrological possibilities to revitalise the ecosystem in the Keselyues-area. 2: Towards the restoration of the Gyueruesalj floodplain
|PB95-139283| p 1718 N95-23469
Measurements of canopy chemistry with 1992 AVIRIS data at Blackhawk Island and Harvard Forest p 1706 N95-23873
Mapping and monitoring changes in vegetation communities of Jasper Ridge, CA, using spectral fractions derived from AVIRIS images p 1708 N95-23883
Transferring ecosystem simulation codes to supercomputers
|NASA-TM-4662| p 1759 N95-24052
Old-growth and mature forests near spotted owl nests in western Oregon p 1719 N95-24098
Hierarchical analysis of spatial pattern and processes of Douglas-fir forests p 1719 N95-24099
Forest and wildlife habitat analysis using remote sensing and geographic information systems p 1720 N95-24100
EDDY CURRENTS
Computation of magnetic forces on moving conductors by using ELEKTRA and other 3-D computer codes
|DE95-003308| p 1798 N95-22895
TPX magnet system status
|DE95-002389| p 1661 N95-23080
Eddy current detection of pitting corrosion around fastener holes p 1643 N95-23507
EDGE DETECTION
A certainty grid to object boundary algorithm
|PB94-203510| p 1755 N95-22637
Ligand K-edge x-ray adsorption spectroscopic studies of the electronic structure of inorganic model complexes and metalloprotein active sites
|DE95-003338| p 1840 N95-22851
EDITING
RAS Division model evaluation database tools
|DE95-003480| p 1733 N95-23123
Graphical timeline editing p 1761 N95-23746
EDUCATION
Hey! What's Space Station Freedom?
|NASA-TM-110531| p 1620 N95-22542
Simultaneous inference in multivariate calibration
|DE95-003592| p 1794 N95-23066
Living in space
|NASA-TM-110536| p 1751 N95-23274
Toys in space, 2
|NASA-TM-110541| p 1620 N95-23275
1994 NASA-HU American Society for Engineering Education (ASEE) Summer Faculty Fellowship Program
|NASA-CR-194972| p 1872 N95-23276
Formative and summative evaluation efforts for the Teacher Enhancement Institute conducted at the NASA Langley Research Center, summer 1994 p 1853 N95-23286
Design and implementation of two two-week Teacher Enhancement Institutes p 1853 N95-23306
Teacher Enhancement Institute p 1853 N95-23312
Langley Research Center Strategic Plan for Education p 1853 N95-23316
Preparation of course materials: Elementary mathematics of powered flight p 1853 N95-23320
Upward appraisal as a means for improving supervisory performance and promoting process improvement, with long-term implications for organizational change p 1854 N95-23323
Teacher Enhancement Institute p 1853 N95-23324
EFFLUENTS
Remote detection of trace effluents using resonance Raman spectroscopy
|DE94-016858| p 1633 N95-22887
EIGENVALUES
Software for the generalized eigenproblem on distributed memory architectures
|DE95-002999| p 1755 N95-22690
Parallal Arnoldi method for the construction of a Krylov subspace basis: An application in magnetohydrodynamics
|PB95-135786| p 1787 N95-22717
On pseudosupersymmetric oscillators and reality of relativistic energies for vector mesons p 1815 N95-22994
Regular graphs with four eigenvalues
|PB95-135141| p 1788 N95-23068
Partition of real symmetric matrices according to the multiplicities of their eigenvalues
|PB95-139846| p 1790 N95-23235
Set games
|PB95-140786| p 1794 N95-23539
EIGENVECTORS
An algorithm for the basis of the finite Fourier transform p 1760 N95-22985
Coherent states for the relativistic harmonic oscillator p 1825 N95-22993
The initial-value problem for viscous channel flows
|NASA-CR-195034| p 1667 N95-23207
Set games
|PB95-140786| p 1794 N95-23539
Singular moduli and Arakelov intersection
|DE94-634286| p 1792 N95-23659
EIKONAL EQUATION
Comparison of exact solution with Eikonal approximation for elastic heavy ion scattering
|NASA-TP-3498| p 1817 N95-22929
EINSTEIN EQUATIONS
Possibility of extending space-time coordinates
|DE94-628512| p 1796 N95-22737
Does the relativity principle violate?
|DE94-635420| p 1851 N95-23964
ELASTIC BENDING
Deflections of anisotropic sandwich beams with variable face sheets and core thicknesses p 1700 N95-23310
Residual strength of thin panels with cracks p 1700 N95-23311
Thin tailored composite wing for civil tiltrotor p 1613 N95-23317
ELASTIC MEDIA
Propagation of waves at the loosely bonded interface of two porous elastic half-spaces
|DE94-628477| p 1800 N95-23018
ELASTIC PROPERTIES
Vibration-damping structural component
|AD-D016550| p 1693 N95-22707
Experimental and theoretical studies on the C15 intermetallic compounds MV2 (M = Zr, Hf and Ta): Elasticity and phase stability
|DE95-003723| p 1845 N95-24079
The effect of elastic stress on Ostwald Ripening Phenomena
|DE95-002599| p 1646 N95-24140
ELASTIC SCATTERING
Comparison of exact solution with Eikonal approximation for elastic heavy ion scattering
|NASA-TP-3498| p 1817 N95-22929
ELASTOMERS
A kinetic study of hydrolysis of polyester elastomer in magnetic tape p 1652 N95-24124
ELECTRIC BATTERIES
Energy Conversion and Storage Program
|DE95-003796| p 1725 N95-22501
Electromechanical Battery Program at the Lawrence Livermore National Laboratory
|DE95-003657| p 1727 N95-22574
Chemical Sciences Division
|DE95-002655| p 1626 N95-24142
ELECTRIC CONDUCTORS
Conceptual design of a 20-kA current lead using forced-flow cooling and Ag-alloy-sheathed Bi-2223 high-temperature superconductors
|DE95-002916| p 1660 N95-22569
ELECTRIC CONTACTS
Large-area triple-junction a-Si alloy production scaleup
|DE95-000245| p 1726 N95-22546
ELECTRIC CURRENT
Potential aerospace applications of high temperature superconductors p 1664 N95-23322
Design of a high-temperature superconductor current lead for electric utility SMES
|DE95-004604| p 1664 N95-24163
ELECTRIC EQUIPMENT
Layered Electrical Product Application Protocol (AP)
|DE95-001524| p 1754 N95-22548
Application Protocol, Initial Graphics Exchange Specification (IGES), Layered Electrical Product
|DE95-004266| p 1757 N95-23337
ELECTRIC FIELDS
Superlattices in thermoelectric applications
|DE95-001356| p 1840 N95-22687
Analytical and numerical studies of ion mobility near the tokamak plasma edge
|DE95-003019| p 1830 N95-22693
Calculated coupling efficiency between an elliptical-core optical fiber and a silicon oxynitride rib waveguide
|NASA-TM-106850| p 1820 N95-22915
Global electric field determination in the Earth's outer magnetosphere using energetic charged particles
|NASA-CR-197392| p 1737 N95-22945
Dynamics of L to H bifurcation
|DE94-019126| p 1832 N95-23163
Plasmo-magnetoelastic waves in a semiconducting heterostructure. 1: Plasmo-elastic longitudinal modes. 2: Sh-magnetoelastic modes
|PB95-138822| p 1833 N95-23170
Collisionless magnetic reconnection associated with coalescence of flux bundles
|NIFS-315| p 1834 N95-23525
Physical mechanism determining the radial electric field and its radial structure in a toroidal plasma
|NIFS-313| p 1835 N95-23534
Growth of single crystals of organic salts with large second-order optical nonlinearities by solution processes for devices
|NASA-CR-197963| p 1843 N95-23563
Studies of autoionizing states relevant to dielectronic recombination
|DE94-014162| p 1812 N95-23978
ELECTRIC FURNACES
Glass science tutorial: Lecture 2, operating electric glass melters
|DE95-002965| p 1647 N95-22648
ELECTRIC GENERATORS
Electromechanical Battery Program at the Lawrence Livermore National Laboratory
|DE95-003657| p 1727 N95-22574
ELECTRIC HYBRID VEHICLES
A hybrid vehicle evaluation code and its application to vehicle design
|DE95-004205| p 1662 N95-23334
ELECTRIC MOTOR VEHICLES
Electromechanical Battery Program at the Lawrence Livermore National Laboratory
|DE95-003657| p 1727 N95-22574
Load calculation and system evaluation for electric vehicle climate control
|DE95-004350| p 1695 N95-23358
Multi-fuel reformers for fuel cells used in transportation. Phase 1: Multi-fuel reformers
|DE95-004215| p 1729 N95-23482
Energy efficiency of electric vehicles at the 1994 American Tour de Sol
|DE95-002905| p 1664 N95-24070
ELECTRIC MOTORS
Motor drive technologies for the power-by-wire (PBW) program: Options, trends and tradeoffs
|NASA-TM-106885| p 1616 N95-23671
ELECTRIC POTENTIAL
Current estimation for electromigration, hot carriers, and voltage drop
|AD-A285794| p 1659 N95-22507
Energetic particle observations at geosynchronous orbit
|DE95-000873| p 1867 N95-22516
Functional testing of the space station plasma contactor
|NASA-TM-106841| p 1624 N95-23240
Fast potential change in sawteeth in JIPP T-IIU tokamak plasmas
|NIFS-327| p 1835 N95-23533
ELECTRIC POWER PLANTS
Net energy analysis: Powerful tool for selecting electric power options
|DE95-002516| p 1728 N95-23133
ELECTRIC POWER SUPPLIES
Net energy analysis: Powerful tool for selecting electric power options
|DE95-002516| p 1728 N95-23133
ELECTRIC PROPULSION
Ground-based and space-based laser beam power applications
|NASA-TM-106744| p 1691 N95-22670

ELECTRIC SWITCHES
Liquid nitrogen temperature operation of a switching power converter
| NASA-TM-106867 | p 1662 N95-23219
ELECTRICAL ENGINEERING
Proceedings of the fuel cells 1994 contractors review meeting
| DE94-012285 | p 1730 N95-23977
ELECTRICAL IMPEDANCE
Surface impedance studies on the electrodynamical response of organic superconductors
| DE95-002986 | p 1660 N95-22593
The detection and analysis of galvanic damage in BMI/graphite fiber composites p 1631 N95-23502
The use of electrochemical impedance spectroscopy to predict the corrosion of aluminum-lithium alloys in marine environments p 1637 N95-23504
ELECTRICAL INSULATION
HTS current lead using a composite heat pipe
| DE95-003718 | p 1662 N95-23368
ELECTRICAL MEASUREMENT
Energetic particle observations at geosynchronous orbit
| DE95-000873 | p 1867 N95-22516
Second order focusing property of 210 deg cylindrical energy analyzer
| NIFS-317 | p 1834 N95-23527
ELECTRICAL PROPERTIES
Progress report on conductive paints, September 1, 1994-November 30, 1994
| DE95-004297 | p 1649 N95-23356
ELECTRICAL RESISTIVITY
Electrical resistivity of liquid alkali metals and non-local pseudopotential
| DE94-627417 | p 1639 N95-22608
A special percolation problem in ceramic composites
| DE94-627641 | p 1647 N95-22611
Superlattices in thermoelectric applications
| DE95-001356 | p 1840 N95-22687
Corrosivity sensor
| AD-D016549 | p 1687 N95-22706
Gas cooled leads. Part 1: Theoretical Study. Part 2: Frost free lead optimized for a specific current. Part 3: Frost free lead optimized for a large current range
| DE95-002657 | p 1660 N95-22716
Computer modeling of detonators
| DE95-003031 | p 1652 N95-22721
A model for the metal-nonmetal transition in metal-molten salt solutions
| DE94-628490 | p 1640 N95-23057
Transport properties of Tl2Ba2CaCu2O8 meander lines
| DE95-003715 | p 1843 N95-23367
Computer simulation of a magnetohydrodynamic dynamo 2
| NIFS-320 | p 1836 N95-23590
ELECTRIFICATION
Collaborative research on aircraft icing and charging processes in ice
| AD-A285102 | p 1609 N95-23201
ELECTRO-OPTICAL PHOTOGRAPHY
Electronic photography at NASA Langley Research Center p 1690 N95-23298
ELECTROCHEMICAL CORROSION
The corrosion protection of 2219-T87 aluminum by organic and inorganic zinc-rich primers
| NASA-TP-3543 | p 1641 N95-23186
Corrosion protection measures for CFC/metal joints of fuel integral tank structures of advanced military aircraft p 1644 N95-23510
ELECTROCHEMISTRY
Energy Conversion and Storage Program
| DE95-003796 | p 1725 N95-22501
Ligand K-edge x-ray adsorption spectroscopic studies of the electronic structure of inorganic model complexes and metalloprotein active sites
| DE95-003338 | p 1840 N95-22851
The detection and analysis of galvanic damage in BMI/graphite fiber composites p 1631 N95-23502
Health and usage monitoring systems: Corrosion surveillance p 1607 N95-23506
In-situ detection of surface passivation or activation and of localized corrosion: Experiences and prospectives in aircraft p 1643 N95-23508
Test method and test results for environmental assessment of aircraft materials p 1643 N95-23509
ELECTRODES
Vision-sensing image analysis for GTAW process control
| DE95-003936 | p 1695 N95-23373
Investigation of arc length versus flange thickness while using an arc voltage controller
| DE95-003937 | p 1695 N95-23374
Electrochemical studies of perovskite mixed conductors
| DE95-003704 | p 1636 N95-23573
Circular electrode geometry metal-semiconductor-metal photodetectors
| NASA-CASE-LAR-15172-1-CU | p 1663 N95-24048
ELECTRODYNAMICS
Surface impedance studies on the electrodynamical response of organic superconductors
| DE95-002986 | p 1660 N95-22593
A space-time lattice version of scalar electrodynamics
| DE94-628577 | p 1850 N95-22784
ELECTROLUMINESCENCE
MOCVD of gallium and calcium sulfides for improved phosphor processing
| DE95-000918 | p 1631 N95-22677
ELECTROLYTES
Electrochemical studies of perovskite mixed conductors
| DE95-003704 | p 1636 N95-23573
ELECTROMAGNETIC ABSORPTION
Optical absorption in an indirect-gap semiconductor quantum well systems
| DE94-628878 | p 1849 N95-22759
ELECTROMAGNETIC COMPATIBILITY
Thermal effects on the STAR electromagnetic calorimeter
| DE95-004663 | p 1688 N95-23492
ELECTROMAGNETIC COUPLING
Electroweak coupling measurements from polarized Bhabha scattering at SLD
| DE95-003137 | p 1807 N95-23165
ELECTROMAGNETIC FIELDS
Relativistic particle with torsion and charged particle in a constant electromagnetic field: Identity of evolution
| DE94-628506 | p 1803 N95-22778
Generalized phase transformations of spinor fields
| DE94-628505 | p 1656 N95-22841
A uniform geometrical optics and an extended uniform geometrical theory of diffraction for evaluating high frequency EM fields near smooth caustics and composite shadow boundaries
| NASA-CR-197934 | p 1657 N95-23391
ELECTROMAGNETIC INTERACTIONS
Unification of electromagnetic, strong and weak interaction
| DE94-628570 | p 1655 N95-22746
ELECTROMAGNETIC INTERFERENCE
US Navy operating experience with new aircraft construction materials p 1645 N95-23517
ELECTROMAGNETIC NOISE
Electromagnetic radiation in the plasma environment around the shuttle
| NASA-TM-106891 | p 1738 N95-23116
ELECTROMAGNETIC RADIATION
Electromagnetic radiation in the plasma environment around the shuttle
| NASA-TM-106891 | p 1738 N95-23116
Atoms as many-body systems
| DE95-004609 | p 1813 N95-24151
ELECTROMAGNETIC SPECTRA
The effects of AVIRIS atmospheric calibration methodology on identification and quantitative mapping of surface mineralogy, Drum Mountains, Utah p 1705 N95-23870
ELECTROMAGNETS
Parallel computation of automatic differentiation applied to magnetic field calculations
| DE95-004689 | p 1763 N95-23486
Cu deposition using a permanent magnet electron cyclotron resonance microwave plasma source
| DE94-017768 | p 1650 N95-23981
ELECTROMECHANICAL DEVICES
Superconductivity devices: Commercial use of space
| NASA-CR-197885 | p 1648 N95-22883
Design and application of electromechanical actuators for deep space missions
| NASA-CR-197957 | p 1694 N95-22909
Operator procedure verification with a rapidly reconfigurable simulator p 1618 N95-23679
ELECTROMECHANICS
Electromechanical Battery Program at the Lawrence Livermore National Laboratory
| DE95-003657 | p 1727 N95-22574
Using Dedal to share and reuse distributed engineering design information p 1768 N95-23678
ELECTROMIGRATION
Current estimation for electromigration, hot carriers, and voltage drop
| AD-A285794 | p 1659 N95-22507
ELECTRON ACCELERATION
Electron beam acceleration and compression for short wavelength FELs
| DE95-003371 | p 1691 N95-22704
ELECTRON ACCELERATORS
Time-resolved EPR studies of the H atom: A stable heavy isotope of muonium
| DE95-004614 | p 1810 N95-23491
Design study of beam dynamics issues for 1 TeVnext linear collider based on the relativistic-klystron two-beam accelerator
| DE95-004673 | p 1817 N95-23493
ELECTRON BEAMS
Precision standard model tests with polarized e(+)e(-) beams
| DE95-003367 | p 1816 N95-22702
Electron beam acceleration and compression for short wavelength FELs
| DE95-003371 | p 1691 N95-22704
Method and system for electron beam lithography
| AD-D016554 | p 1660 N95-22709
Measurement of the left-right charge asymmetry in hadronic Z decays and A(sub e) determination
| DE95-003467 | p 1806 N95-23140
Electron drift velocities of Ar-CO2-CF4 gas mixtures
| DE95-004353 | p 1809 N95-23359
D(O) upgrade muon electronics design
| DE95-003744 | p 1817 N95-23369
Search for scalar and vector leptoquarks in electron-proton collisions at radical S = 300 GeV
| DE94-785267 | p 1810 N95-23475
Design study of longitudinal dynamics of the drive beam in 1 TeV relativistic klystron two-beam accelerator
| DE95-004683 | p 1817 N95-23485
Undulators for short wavelength FEL amplifiers
| DE95-004690 | p 1692 N95-23487
Design study of beam dynamics issues for 1 TeVnext linear collider based on the relativistic-klystron two-beam accelerator
| DE95-004673 | p 1817 N95-23493
High current induction linacs
| DE95-003442 | p 1818 N95-24014
ELECTRON BUNCHING
Electron beam acceleration and compression for short wavelength FELs
| DE95-003371 | p 1691 N95-22704
High current induction linacs
| DE95-003442 | p 1818 N95-24014
ELECTRON DENSITY (CONCENTRATION)
Runaway electrons in TEXT-U
| DE94-019218 | p 1831 N95-22862
The q profile evolution and enhanced core confinement of high (beta)(sub p) plasmas in D3-D
| DE95-003878 | p 1834 N95-23371
ELECTRON DENSITY PROFILES
The TEXT neutral lithium beam edge density diagnostic
| DE95-003256 | p 1830 N95-22719
ELECTRON DIFFRACTION
On core level electron diffraction
| DE94-628484 | p 1842 N95-23048
ELECTRON DISTRIBUTION
Generation of fast electrons in reversed field pinches by the equilibrium grad (vert bar)B(vert bar) force
| DE95-004467 | p 1809 N95-23363
ELECTRON EMISSION
Generation of fast electrons in reversed field pinches by the equilibrium grad (vert bar)B(vert bar) force
| DE95-004467 | p 1809 N95-23363
ELECTRON ENERGY
Charging of interplanetary grains
| NASA-CR-198032 | p 1869 N95-24066
Experimental and theoretical studies on the C15 intermetallic compounds MV2 (M = Zr, Hf and Ta): Elasticity and phase stability
| DE95-003723 | p 1845 N95-24079
ELECTRON GAS
The effect of magnetic field on the edge plasmons of two-dimensional electron gas systems
| DE94-018044 | p 1837 N95-23982
ELECTRON GUNS
A high-power switch-mode DC power supply for dynamic loads
| DE94-016714 | p 1659 N95-22504
ELECTRON IMPACT
Novel mass spectrometric instrument for gaseous and particulate characterization and monitoring
| DE95-001135 | p 1687 N95-22682
Rate coefficients for the electron-impact excitation, ionization and recombination of He-like ions, S XV, Ca XIX and Fe XXV, and related processes
| ISAS-R-657 | p 1811 N95-23604
Charging of interplanetary grains
| NASA-CR-198032 | p 1869 N95-24066
ELECTRON IRRADIATION
Study of photorefractive non-linearities in the 3-5 and 2-4 semi-insulator compounds: The effect of electron irradiation
| PB94-189057 | p 1839 N95-22584
Application of electron paramagnetic resonance imaging to the characterization of the Ultem(R) exposed to 1 MeV electrons. Correlation of radical density data to tiger code calculations p 1815 N95-23328

ELECTRON MICROSCOPES
Transmission electron microscope studies of extraterrestrial materials
| NASA-CR-188363 | p 1633 N95-23092
ELECTRON MICROSCOPY
Analytical electron microscopy of LDEF impactor residues p 1869 N95-23832
ELECTRON MOBILITY
Computational modeling of properties
| NAS-CR-196544 | p 1841 N95-22907
ELECTRON PARAMAGNETIC RESONANCE
Application of electron paramagnetic resonance imaging to the characterization of the Ultem(R) exposed to 1 MeV electrons. Correlation of radical density data to tiger code calculations p 1815 N95-23328
Time-resolved EPR studies of the H atom: A stable heavy isotope of muonium
| DE95-004614 | p 1810 N95-23491
ELECTRON PHONON INTERACTIONS
Magnetic field effects on strong-coupling polaron in quantum dots
| DE94-629038 | p 1847 N95-22496
Resonant shallow donor magnetopolaron effect in a GaAs/AlGaAs quantum dot in high magnetic fields
| DE94-629039 | p 1798 N95-22497
ELECTRON PLASMA
Langmuir-like waves and radiation in planetary foreshocks
| NASA-CR-197376 | p 1869 N95-22828
ELECTRON PRECIPITATION
Magnetospheric space plasma investigations
| NASA-CR-197405 | p 1831 N95-22955
The high latitude ionosphere-magnetosphere transition region: Simulation and data comparison
| NASA-CR-197404 | p 1737 N95-22956
Semikinetic modeling and observations of high-latitude plasma outflow
| NASA-CR-197403 | p 1831 N95-23008
ELECTRON SCATTERING
Studies of photon and electron interactions with atoms and ions
| DE95-003340 | p 1802 N95-22700
Pressure shifts and electron scattering in atomic and molecular gases
| DE95-003102 | p 1803 N95-22747
Neutron compton scattering
| PB95-139135 | p 1807 N95-23159
Electroweak coupling measurements from polarized Bhabha scattering at SLD
| DE95-003137 | p 1807 N95-23165
The energy broadening resulting from electron stripping process of a low energy Au(-) beam
| NIFS-325 | p 1836 N95-23569
ELECTRON SOURCES
Advanced technologies for a compact RF linac FEL
| DE95-003674 | p 1692 N95-24072
ELECTRON SPECTROSCOPY
On core level electron diffraction
| DE94-628484 | p 1842 N95-23048
ELECTRON STATES
Optogalvanic monitoring of collisional transfer of laser excitation energy in a neon RF plasma
| DE95-003103 | p 1691 N95-22748
Studies of autoionizing states relevant to dielectronic recombination
| DE94-014162 | p 1812 N95-23978
ELECTRON TRANSFER
Magnetic resonance and optical spectroscopic studies of carotenoids
| DE95-003729 | p 1631 N95-22575
ELECTRON TRANSITIONS
Optogalvanic monitoring of collisional transfer of laser excitation energy in a neon RF plasma
| DE95-003103 | p 1691 N95-22748
ELECTRON-ION RECOMBINATION
Studies of autoionizing states relevant to dielectronic recombination
| DE94-014162 | p 1812 N95-23978
ELECTRON-POSITRON PAIRS
Heavy quark physics at SLD: Preliminary results
| DE95-003372 | p 1806 N95-23138
Final result on the mass of the tau lepton from the BES collaboration
| DE95-003466 | p 1806 N95-23139
Measurement of the left-right charge asymmetry in hadronic Z decays and A(sub e) determination
| DE95-003467 | p 1806 N95-23140
Measuring the left-right cross section asymmetry in Z boson production by e(+)e(-) collisions at the SLC
| DE95-003468 | p 1807 N95-23141
Electroweak coupling measurements from polarized Bhabha scattering at SLD
| DE95-003137 | p 1807 N95-23165
Hard e(+)e(-)-pair Bremsstrahlung as a lepton polarimeter
| DE94-635615 | p 1812 N95-23984
ELECTRONIC EQUIPMENT
Layered Electrical Product Application Protocol (AP)
| DE95-001524 | p 1754 N95-22548
Differential GPS and system integration of the Low Visibility Landing and Surface Operations (LVLASO) demonstration p 1611 N95-23318
Application Protocol, Initial Graphics Exchange Specification (IGES), Layered Electrical Product
| DE95-004266 | p 1757 N95-23337
Solderability preservation through the use of organic inhibitors
| DE95-003633 | p 1664 N95-24149
ELECTRONIC FILTERS
Programmable hyperspectral image mapper with on-array processing
| NASA-CASE-NPO-17794-1-CU | p 1819 N95-22765
ELECTRONS
Fermion-spin transformation to implement the charge-spin separation
| DE94-629035 | p 1800 N95-22495
Magnetic field effects on strong-coupling polaron in quantum dots
| DE94-629038 | p 1847 N95-22496
The omega pi(sup 0)-transient form factor within effective chiral Lagrangian approach
| DE94-628612 | p 1850 N95-22812
Runaway electrons in TEXT-U
| DE94-019218 | p 1831 N95-22862
Ionic core effects on the Mie resonance in lithium clusters
| DE94-014974 | p 1805 N95-22870
Photon and electron interaction databases and their use in medical applications
| DE94-015558 | p 1855 N95-22871
Analytical Boltzmann moments for electrons in N2-O2-H2O gas mixtures
| DE95-003474 | p 1732 N95-22898
The electronic structure of heavy element complexes
| DE95-003407 | p 1806 N95-23082
Search for Z' and W' at CDF
| DE94-018987 | p 1808 N95-23203
Search for supersymmetric (tilde W)(sub 1) and (tilde Z)(sub 2) states using the D0 detector
| DE95-004581 | p 1811 N95-23581
ESTAR, PSTAR, ASTAR: A PC package for calculating stopping powers and ranges of electrons, protons and helium ions, version 2
| DE94-634435 | p 1811 N95-23773
Charging of interplanetary grains
| NASA-CR-198032 | p 1869 N95-24066
ELECTROPHORESIS
Development of novel separation techniques for biological samples in capillary electrophoresis
| DE95-001672 | p 1744 N95-22493
A comparative study of the effects of clofibrate, ciprofibrate, WY-14,643, and di-(2-ethylhexyl)-phthalate on liver protein expression in mice
| DE94-016587 | p 1748 N95-23771
ELECTROPHYSIOLOGY
Cellular interactions in the suprachiasmatic nucleus
| AD-A285639 | p 1749 N95-23780
ELECTROSTATIC PROBES
Advanced detector development, laboratory simulations, diagnostic development, and data analysis on wake physics
| PL-TR-94-2204 | p 1831 N95-22948
Electromagnetic radiation in the plasma environment around the shuttle
| NASA-TM-106891 | p 1738 N95-23116
ELECTROSTATICS
A new containerless image furnace with electro-static positioning device p 1690 N95-23674
ELECTROSTRICTION
Superconductivity devices: Commercial use of space
| NASA-CR-197885 | p 1648 N95-22883
ELECTROWEAK INTERACTIONS (FIELD THEORY)
Precision standard model tests with polarized e(+)e(-) beams
| DE95-003367 | p 1816 N95-22702
Topologically stable Z - strings in the supersymmetric standard model
| DE94-628517 | p 1848 N95-22742
Results from neutrino experiments
| DE94-628604 | p 1804 N95-22790
Higgs searches and WW scattering
| PB95-139143 | p 1807 N95-23160
Electroweak coupling measurements from polarized Bhabha scattering at SLD
| DE95-003137 | p 1807 N95-23165
Theoretical aspects of electroweak and other interactions in medium energy nuclear physics
| DE95-004341 | p 1808 N95-23357
Electroweak physics from the Tevatron
| DE95-002213 | p 1810 N95-23530
Neutrino mass
| DE94-628634 | p 1812 N95-23786
A measurement of the mass of the W vector boson at CDF
| DE95-003498 | p 1813 N95-24016
ELECTROWEAK MODEL
The first measurement of the left-right cross section asymmetry in Z(sup 0) boson production
| DE95-003335 | p 1802 N95-22697
Theoretical aspects of electroweak and other interactions in medium energy nuclear physics
| DE95-004341 | p 1808 N95-23357
ELEMENTARY PARTICLE INTERACTIONS
Dimuon production in proton-nucleus interactions
| DE95-002613 | p 1801 N95-22551
Studies of photon and electron interactions with atoms and ions
| DE95-003340 | p 1802 N95-22700
Outlook from the intersections
| DE95-003202 | p 1802 N95-22730
The omega pi(sup 0)-transient form factor within effective chiral Lagrangian approach
| DE94-628612 | p 1850 N95-22812
Search for second generation leptoquarks at CDF
| DE94-018983 | p 1805 N95-22939
Introduction to the physics of Higgs bosons
| DE95-003965 | p 1809 N95-23396
Search for scalar and vector leptoquarks in electron-proton collisions at radical S = 300 GeV
| DE94-785267 | p 1810 N95-23475
ELEMENTARY PARTICLES
Second International Workshop on Harmonic Oscillators
| NASA-CP-3286 | p 1820 N95-22957
Search for supersymmetric (tilde W)(sub 1) and (tilde Z)(sub 2) states using the D0 detector
| DE95-004581 | p 1811 N95-23581
ELEVATION
Current and future use of TOPSAR digital topographic data for volcanological research p 1714 N95-23949
Comparison of 7.5-minute and 1-degree digital elevation models p 1719 N95-24095
ELLIPSOIDS
Galactic oscillator symmetry p 1822 N95-22973
ELLIPTIC DIFFERENTIAL EQUATIONS
Extensible PDE Solvers package users manual
| DE95-003333 | p 1786 N95-22696
ELLIPTIC FUNCTIONS
Remarks on multiple solutions for asymptotically linear elliptic boundary value problems
| DE94-628416 | p 1785 N95-22624
Existence of solutions for some superlinear or sublinear elliptic systems on R(sup N)
| DE94-628417 | p 1785 N95-22625
ELONGATION
The hydrogen embrittlement of alloy X-750
| DE95-003207 | p 1640 N95-22893
EMBEDDING
Corrosivity sensor
| AD-D016549 | p 1687 N95-22706
EMBRITTLEMENT
Specific features of corrosion behavior of stainless maraging steels for aerospace application p 1642 N95-23501
EMBRYOLOGY
Open problems of computational molecular biology
| DE95-000895 | p 1745 N95-22866
EMERGENCIES
Search Hanford accessible reports electronically system requirements specification
| DE95-004367 | p 1856 N95-23340
EMISSION
Environmental, Safety, and Health Considerations: Composite Materials in the Aerospace Industry
| NASA-CP-3289 | p 1628 N95-23025
A hybrid vehicle evaluation code and its application to vehicle design
| DE95-004205 | p 1662 N95-23334
EMISSION SPECTRA
Gamma ray emission from radio pulsars
| NASA-CR-197917 | p 1871 N95-22910
ROSAT observation program
| NASA-CR-197683 | p 1866 N95-23595
A tool for manual endmember selection and spectral unmixing p 1701 N95-23846
Analysis of conifer forest regeneration using Landsat Thematic Mapper data p 1720 N95-24101
Determining coniferous forest cover and forest fragmentation with NOAA-9 advanced very high resolution radiometer data p 1720 N95-24103
EMISSIVITY
Estimation of spectral emissivity in the thermal infrared p 1711 N95-23918
The difference between laboratory and in-situ pixel-averaged emissivity: The effects on temperature-emissivity separation p 1711 N95-23919

Mineralogic variability of the Kelso Dunes, Mojave Desert, California derived from Thermal Infrared Multispectral Scanner (TIMS) data p 1711 N95-23920

EMITTANCE

Exotic atoms
| DE95-003199 | p 1805 N95-22881

Development of sensors for ceramic components in advanced propulsion systems
| NASA-CR-195324 | p 1689 N95-23795

EMITTERS

Extraction of the surface recombination velocity of passivated phosphorus-doped silicon emitters
| DE95-004539 | p 1845 N95-24156

EMPLOYEE RELATIONS

Upward appraisal as a means for improving supervisory performance and promoting process improvement, with long-term implications for organizational change p 1854 N95-23323

ENCAPSULATING

Advanced development of PV encapsulants
| DE95-000246 | p 1728 N95-23062

END EFFECTORS

Development of Advanced Robotic Hand System for space application p 1752 N95-23704

A three-finger multisensory hand for dexterous space robotic tasks p 1752 N95-23705

Robot arm system for automatic satellite capture and berthing p 1752 N95-23709

Visually guided grasping to study teleprogrammation within the BAROCO testbed p 1777 N95-23731

Morphing hands and virtual tools (or What good is an extra degree of freedom?)
| TR-551 | p 1783 N95-24036

Vision-based planning and execution of precision grasps
| TR-546 | p 1784 N95-24185

ENDEAVOUR (ORBITER)

Space Shuttle mission: STS-67
| NASA-TM-110509 | p 1620 N95-24027

ENERGETIC PARTICLES

Energetic particle observations at geosynchronous orbit
| DE95-000873 | p 1867 N95-22516

The q profile evolution and enhanced core confinement of high (beta)(sub p) plasmas in D3-D
| DE95-003878 | p 1834 N95-23371

Characteristics of low energy ions in the Heavy Ions In Space (HIIS) experiment p 1815 N95-23807

Results from the Heavy Ions In Space (HIIS) experiment on the ionic charge state of solar energetic particles p 1870 N95-23808

ENERGY ABSORPTION

Computer modeling of detonators
| DE95-003031 | p 1652 N95-22721

ENERGY BUDGETS

Thermal radiant exitance model performance: Soils and forests
| DE95-003619 | p 1721 N95-24148

ENERGY CONSERVATION

The Louisiana State University waste-to-energy incinerator
| DE95-004417 | p 1728 N95-23344

ENERGY CONSUMPTION

Geolocation applications of the Gonets LEO messaging satellites p 1656 N95-22818

Oxygen enriched combustion system performance study. Phase 2: 100 percent oxygen enriched combustion in regenerative glass melters
| DE95-004212 | p 1635 N95-23481

ENERGY CONVERSION

Energy Conversion and Storage Program
| DE95-003796 | p 1725 N95-22501

Photochemical energy conversion by membrane-bound photoredox systems
| DE95-004405 | p 1729 N95-23361

ENERGY CONVERSION EFFICIENCY

Prediction of incidence and surface roughness effects on turbine performance p 1671 N95-23424

Rapid thermal processing of high-efficiency silicon solar cells with controlled in-situ annealing
| DE95-004729 | p 1730 N95-23489

Energy efficiency of electric vehicles at the 1994 American Tour de Sol
| DE95-002905 | p 1664 N95-24070

ENERGY DISSIPATION

An investigation of AC losses in two sub-size conductors for the ITER
| DE94-785449 | p 1831 N95-22849

The q profile evolution and enhanced core confinement of high (beta)(sub p) plasmas in D3-D
| DE95-003878 | p 1834 N95-23371

The energy broadening resulting from electron stripping process of a low energy Au(-) beam
| NIFS-325 | p 1836 N95-23569

Toward an automated signature recognition toolkit for mission operations p 1659 N95-23682

ENERGY DISTRIBUTION

Charging of interplanetary grains
| NASA-CR-198032 | p 1869 N95-24066

ENERGY LEVELS

On the (DE-) stabilization of quantum mechanical binding by potential barriers
| DE94-628433 | p 1847 N95-22635

More about the q-deformed H-atom wave functions: Normal and abnormal series
| DE94-628434 | p 1801 N95-22643

Geometric phases, evolution loops and generalized oscillator potentials p 1823 N95-22981

Studies of autoionizing states relevant to dielectronic recombination
| DE94-014162 | p 1812 N95-23978

Quantum fluctuations of D(sub 5d) polarons on C(sub 60) molecules
| DE94-635787 | p 1812 N95-23985

ENERGY POLICY

Multi-fuel reformers for fuel cells used in transportation. Phase 1: Multi-fuel reformers
| DE95-004215 | p 1729 N95-23482

ENERGY REQUIREMENTS

The possibilities for mobile and fixed services up to the 20/30 GHz frequency bands p 1656 N95-22817

ENERGY SOURCES

Hydrogen and fuel cells for energy storage
| DE95-723907 | p 1729 N95-23382

ENERGY SPECTRA

Algebraic approach to the vibrational excitations in methane p 1814 N95-22960

Status of helium-production reaction studies with a spallation neutron source
| DE95-002816 | p 1806 N95-23137

A wavenumber-partitioning scheme for two-dimensional statistical closures
| DE95-004514 | p 1677 N95-23483

On inertial range scaling laws
| DE95-004515 | p 1677 N95-23484

The energy broadening resulting from electron stripping process of a low energy Au(-) beam
| NIFS-325 | p 1836 N95-23569

Alpha spectral analysis via artificial neural networks
| DE95-004567 | p 1767 N95-23578

Trapped iron measured on LDEF p 1872 N95-23806

Characteristics of low energy ions in the Heavy Ions In Space (HIIS) experiment p 1815 N95-23807

Early results from the ultra heavy cosmic ray experiment p 1872 N95-23809

Absorbed dose and LET spectra measurements on LDEF p 1815 N95-23810

Fission foil measurements of neutron and proton fluences in the A0015 experiment p 1815 N95-23811

Contribution of proton-induced short range secondaries to the LET spectra on LDEF p 1815 N95-23813

Charge, energy and LET spectra of high LET primary and secondary particles in CR-39 plastic nuclear track detectors of the P0006 experiment p 1815 N95-23814

Predictions of LET spectra measured on LDEF p 1815 N95-23815

ENERGY STORAGE

Energy Conversion and Storage Program
| DE95-003796 | p 1725 N95-22501

Electromechanical Battery Program at the Lawrence Livermore National Laboratory
| DE95-003657 | p 1727 N95-22574

Using the shield for thermal energy storage in PULSAR
| DE95-002457 | p 1829 N95-22645

Multi-fuel reformers for fuel cells used in transportation: Assessment of hydrogen storage technologies
| DE94-017655 | p 1727 N95-22861

Photochemical energy conversion by membrane-bound photoredox systems
| DE95-004405 | p 1729 N95-23361

Hydrogen and fuel cells for energy storage
| DE95-723907 | p 1729 N95-23382

Solar photochemistry: Twenty years of progress, what's been accomplished, and where does it lead?
| DE95-004007 | p 1730 N95-23778

Processing of single- and multi-domain YBa2Cu3O(x) bulk materials for levitation applications by Nd(1+x)Ba(2-x)Cu3O(y) seeding
| DE95-004615 | p 1845 N95-24154

ENERGY TECHNOLOGY

Southeast Regional Experiment Station
| DE95-000903 | p 1726 N95-22518

Renewable Energy Sources Brno 1993
| DE94-633975 | p 1727 N95-22855

Development of the IGT RENUGAS(reg sign) process
| DE94-017652 | p 1727 N95-22888

Hydrogen and fuel cells for energy storage
| DE95-723907 | p 1729 N95-23382

Information technology standards process guide
| DE95-003967 | p 1857 N95-23574

Oak Ridge National Laboratory Energy Efficiency and Renewable Energy Program Bibliography: 1994 Edition
| DE95-002296 | p 1730 N95-23605

Proceedings of the fuel cells 1994 contractors review meeting
| DE94-012285 | p 1730 N95-23977

ENERGY TRANSFER

Comparison of the rate constants for energy transfer in the light-harvesting protein, C-phycocyanin, calculated from Foerster's theory and experimentally measured by time-resolved fluorescence spectroscopy
| DE94-014961 | p 1745 N95-22590

Optogalvanic monitoring of collisional transfer of laser excitation energy in a neon RF plasma
| DE95-003103 | p 1691 N95-22748

Quantum field between moving mirrors: A three dimensional example p 1821 N95-22965

Energy transfer dynamics in isolated and in colliding highly vibrationally excited molecules
| AD-A285771 | p 1806 N95-23077

Overview of the solar dynamic ground test demonstration program at the NASA Lewis Research Center
| NASA-TM-106876 | p 1625 N95-23450

The energy broadening resulting from electron stripping process of a low energy Au(-) beam
| NIFS-325 | p 1836 N95-23569

Charge, energy and LET spectra of high LET primary and secondary particles in CR-39 plastic nuclear track detectors of the P0006 experiment p 1815 N95-23814

Progress in ion beam power coupling and ion-driven hohlraums on PBFA 2
| DE95-004544 | p 1818 N95-24160

ENGINE ANALYZERS

Gearbox vibration diagnostic analyzer
| NASA-CR-189141 | p 1696 N95-23792

ENGINE DESIGN

Aerodynamic design and analysis of a highly loaded turbine exhaust p 1673 N95-23435

Phase 2: HGM air flow tests in support of HEX vane investigation p 1674 N95-23438

ENGINE MONITORING INSTRUMENTS

Gearbox vibration diagnostic analyzer
| NASA-CR-189141 | p 1696 N95-23792

ENGINE NOISE

The use of cowl camber and taper to reduce rotor/stator interaction noise
| NASA-CR-195421 | p 1799 N95-22675

Supersonic jet noise reductions predicted with increased jet spreading rate
| NASA-TM-106872 | p 1800 N95-23178

ENGINE PARTS

Influence of backup bearings and support structure dynamics on the behavior of rotors with active supports
| NASA-CR-197438 | p 1694 N95-23190

Damage-mitigating control of a reusable rocket engine for high performance and extended life
| NASA-CR-4640 | p 1654 N95-23195

Evaluation of thermal barrier and PS-200 self-lubricating coatings in an air-cooled rotary engine
| NASA-CR-195445 | p 1614 N95-23222

ENGINE TESTS

Numerical study of the SSME nozzle flow fields during transient operations: A comparison of the animated results with test p 1673 N95-23434

Phase 2: HGM air flow tests in support of HEX vane investigation p 1674 N95-23438

Non-intrusive measurements in a rocket engine combustor p 1625 N95-23439

Impeller flow field characterization with a laser two-focus velocimeter p 1675 N95-23440

ENGINEERING

1994 NASA-HU American Society for Engineering Education (ASEE) Summer Faculty Fellowship Program
| NASA-CR-194972 | p 1872 N95-23276

ENGINEERING DRAWINGS

CDMS-CAD data set management system test plan
| DE95-003219 | p 1755 N95-22718

ENGINEERING MANAGEMENT

Reliability analysis in the Office of Safety, Environmental, and Mission Assurance (OSEMA) p 1698 N95-23302

ENTROPY

Entropy of Z(sup d) subshifts of finite type
| PB95-108072 | p 1787 N95-22836

The effect of a non-zero shock width on wave propagation in multi-dimensions
| DE95-002748 | p 1666 N95-22902

Wigner distribution function and entropy of the damped harmonic oscillator within the theory of the open quantum systems p 1798 N95-22990

Shannon-Wehrl entropy for cosmological and black-hole squeezing p 1826 N95-23000

Entropy jump across an inviscid shock wave
| NASA-CR-195046 | p 1678 N95-23596

ENUMERATION
Civilian satellite remote sensing: A strategic approach
|PB95-109633| p 1717 N95-22713
ENVIRONMENT EFFECTS
Direct effects of atmospheric CO2 enrichment on plants and ecosystems: An updated bibliographic data base
|DE95-003060| p 1731 N95-22725
Summary of solar cell data from the Long Duration Exposure Facility (LDEF)
|NASA-CR-196539| p 1727 N95-22904
Application requirements for wind turbine gearboxes
|DE94-011883| p 1694 N95-22923
Modeling aerosol emissions from the combustion of composite materials p 1629 N95-23038
Aqueous alternatives for metal and composite cleaning p 1630 N95-23039
Study on possible environmental effects of a WBM cutting discharge in the north sea, one year after termination of drilling
|PB95-133740| p 1733 N95-23125
LDEF materials results for spacecraft applications: Executive summary
|NASA-CP-3261| p 1617 N95-23549
Effect of the space environment on materials flown on the EURECA/TICCE-HVI experiment p 1623 N95-23803
ENVIRONMENT MANAGEMENT
Environmental Systems Management Analysis and Reporting Network (E-SMART)
|AD-A279766| p 1732 N95-22856
Outline for a global environmental strategic planning exercise (GESPE-project)
|PB95-133773| p 1733 N95-23067
CO2 and waste policy: Monitoring results 1991/1992 and main problems
|PB95-133799| p 1733 N95-23126
Comparison of 7.5-minute and 1-degree digital elevation models p 1719 N95-24095
Old-growth and mature forests near spotted owl nests in western Oregon p 1719 N95-24098
Forest and wildlife habitat analysis using remote sensing and geographic information systems p 1720 N95-24100
ENVIRONMENT MODELS
LDEF environment modeling updates p 1637 N95-23797
Predictions of LDEF radioactivity and comparison with measurements p 1815 N95-23818
Status of LDEF radiation modeling p 1815 N95-23819
Transferring ecosystem simulation codes to supercomputers
|NASA-TM-4662| p 1759 N95-24052
ENVIRONMENT POLLUTION
The significance of hair mineral analysis as a means for assessing internal body burdens of environmental pollutants
|DE94-633512| p 1734 N95-23541
Military bases: Environmental impact at closing installations. Report to Congressional requesters
|GAO/NSIAD-95-70| p 1735 N95-24057
ENVIRONMENT PROTECTION
Diesel fuel component contributions to engine emissions and performance: Clean fuel study
|DE94-011868| p 1732 N95-22834
Corrosion in service experience with aircraft in France p 1645 N95-23518
ENVIRONMENT SIMULATION
Effects of wind on rainfall simulation. Spatial distribution of water application, kinetic energy, and overland flow under single full-cone nozzle sprays
|PB95-127304| p 1717 N95-22537
Debris and meteoroid proportions deduced from impact crater residue analysis p 1869 N95-23834
Experimental investigation of the relationship between impact crater morphology and impacting particle velocity and direction p 1700 N95-23840
ENVIRONMENT SIMULATORS
Operator procedure verification with a rapidly reconfigurable simulator p 1618 N95-23679
ENVIRONMENTAL CONTROL
Health, safety and environmental requirements for composite materials p 1628 N95-23028
ENVIRONMENTAL MONITORING
HAPEX-Sahel: Basic description of methods and data sets
|PB95-127262| p 1701 N95-22639
Environmental Systems Management Analysis and Reporting Network (E-SMART)
|AD-A279766| p 1732 N95-22856
Environmental, Safety, and Health Considerations: Composite Materials in the Aerospace Industry
|NASA-CP-3289| p 1628 N95-23025
Aerospace Industries Association (AIA) work practices report for composites p 1628 N95-23029
Remote sensing of smoke, clouds, and fire using AVIRIS data p 1704 N95-23860
Estimating dry grass residues using landscape integration analysis p 1705 N95-23867
Monitoring land use and degradation using satellite and airborne data p 1707 N95-23880
Temporal changes in endmember abundances, liquid water and water vapor over vegetation at Jasper Ridge p 1708 N95-23882
Mapping and monitoring changes in vegetation communities of Jasper Ridge, CA, using spectral fractions derived from AVIRIS images p 1708 N95-23883
Estimation of crown closure from AVIRIS data using regression analysis p 1709 N95-23886
A comparison of spectral mixture analysis an NDVI for ascertaining ecological variables p 1710 N95-23892
Comparison of 7.5-minute and 1-degree digital elevation models p 1719 N95-24095
ENVIRONMENTAL TESTS
HAPEX-Sahel: Basic description of methods and data sets
|PB95-127262| p 1701 N95-22639
Atomic oxygen durability evaluation of protected polymers using thermal energy plasma systems
|NASA-TM-106855| p 1626 N95-23270
Problems of predicting material property retention during long term service p 1644 N95-23514
LDEF: 69 Months in Space. Third Post-Retrieval Symposium, part 2
|NASA-CP-3275-PT-2| p 1899 N95-23896
Recent results from Long Duration Exposure Facility materials testing p 1638 N95-23898
LDEF polymeric materials: A summary of Langley characterization p 1651 N95-23899
Surface characterization of LDEF carbon fiber/polymer matrix composites p 1631 N95-23900
Space environmental effects on polymer matrix composites as a function of sample location on LDEF p 1651 N95-23901
Further investigations of experiment A0034 atomic oxygen stimulated outgassing p 1651 N95-23908
Trend analysis of in-situ spectral reflectance data from the Thermal Control Surfaces Experiment (TCSE) p 1631 N95-23910
Whisker/Cone growth on the thermal control surfaces experiment no. S0069 p 1651 N95-23911
Structure and properties of polymeric composite materials during 1501 days outer space exposure at Salyut-7 orbital station p 1652 N95-23915
ENZYME ACTIVITY
Transmethylation reactions during methanogenesis from acetate in Methanosarcina barkeri
|DE94-016222| p 1745 N95-22873
Regulation of photosynthetic carbon fixation on the ocean margins
|DE95-003185| p 1743 N95-22878
ENZYMES
Regulation of alcohol fermentation in Escherichia coli
|DE94-016227| p 1745 N95-22874
EOS DATA AND INFORMATION SYSTEM
The design of a petabyte archive and distribution system for the NASA ECS project p 1858 N95-24110
A distributed parallel storage architecture and its potential application within EOSDIS p 1858 N95-24111
Constraint based scheduling for the Goddard Space Flight Center distributed Active Archive Center's data archive and distribution system p 1859 N95-24121
EPIDEMIOLOGY
Resource recovery and epidemiology of anaerobic wastewater treatment process in a controlled ecological life support system
|NASA-CR-197930| p 1751 N95-23474
EPITAXY
Advanced growth and surface analysis system for in situ studies of interface formation
|DE95-002850| p 1838 N95-22555
Photoemission study of quantum confinement by a finite barrier: Cu/Co(wedge)/Cu(100)
|DE95-002913| p 1840 N95-22762
Orientation selection and microstructural evolution of epitaxial platinum films on (001) magnesium oxide
|DE95-003680| p 1842 N95-23265
Carbon doping of III-V compound semiconductors
|DE95-003431| p 1844 N95-24013
EPOXY MATRIX COMPOSITES
Notch-tip damage and translaminar fracture toughness measurements from carbon/epoxy laminates
|AD-A280101| p 1627 N95-22833
Surface characterization of LDEF carbon fiber/polymer matrix composites p 1631 N95-23900
EPOXY RESINS
Chemical recycling of scrap composites p 1629 N95-23034
Permeability testing of composite material and adhesive bonds for the DC-XA composite feedline program
|NASA-TM-108483| p 1630 N95-23551
EQUATIONS OF MOTION
Morphology of Laplacian growth processes and statistics of equivalent many-body systems
|DE95-002734| p 1847 N95-22655
Harmonic oscillator representation in the theory of scattering and nuclear reactions p 1814 N95-22967
Spinning particles in the Euclidean Taub-NUT space
|DE94-634320| p 1810 N95-23456
Moving mass trim control for aerospace vehicles
|DE95-002602| p 1622 N95-23532
Incompressible Navier-Stokes calculations in pump flows p 1680 N95-23627
A generalized Eulerian-Lagrangian analysis, with application to liquid flows with vapor bubbles p 1682 N95-23633
EQUATIONS OF STATE
Coherent state constructions of bases for some physically relevant group chains p 1814 N95-22966
On-line, adaptive state estimator for active noise control p 1784 N95-23308
EQUATORIAL REGIONS
Investigation of the role of gravity waves in the generation of equatorial bubbles
|NASA-CR-197962| p 1739 N95-23272
EQUIPMENT SPECIFICATIONS
NASA advanced refrigerator/freezer technology development project overview
|NASA-TM-106309| p 1747 N95-23177
EQUIVALENCE
Taxonomy of finite automata minimization algorithms
|PB95-139226| p 1756 N95-23131
Logspace reducibility and self-reducibility: Models and equivalences
|TR-544| p 1760 N95-24059
ERBIUM
Computational modelling of Er(3+): Garnet laser materials p 1692 N95-23326
EROSION
Low Earth orbit thermal control coatings exposure flight tests: A comparison of U.S. and Russian results
|NASA-CR-4647| p 1626 N95-22919
Atomic oxygen durability evaluation of protected polymers using thermal energy plasma systems
|NASA-TM-106855| p 1626 N95-23270
Robotic weld overlay coatings for erosion control
|DE95-002624| p 1696 N95-24141
ERROR ANALYSIS
IRAS sky survey atlas: Explanatory supplement
|NASA-CR-197335| p 1865 N95-22539
Dynamic response of a transducer mounted at one end of an acoustical cavity which is subjected to a specified pressure at the open end of the cavity
|DE95-004192| p 1799 N95-23379
Technical report series on global modeling and data assimilation. Volume 4: Documentation of the Goddard Earth Observing System (GEOS) data assimilation system, version 1
|NASA-TM-104606-VOL-4| p 1740 N95-23529
Block LU factorization
|NASA-CR-197949| p 1791 N95-23592
On the accuracy of CFD-based pressure drop predictions for right-angle ducts p 1682 N95-23634
A proposed update to the solar irradiance spectrum used in LOWTRAN and MODTRAN p 1705 N95-23865
Improved AVHRR data navigation using automated land feature recognition to correct a satellite orbital model
|CSIRO-TR-34| p 1718 N95-24026
ERROR CORRECTING CODES
Mappings between codewords of two distinct (N,K) Reed-Solomon codes over GF(2(sup J))
|NASA-CASE-NPO-18771-1-CU| p 1754 N95-22577
Ocean observations with EOS/MODIS: Algorithm development and post launch studies
|NASA-CR-197402| p 1717 N95-22916
Optical storage media data integrity studies p 1829 N95-24130
ERRORS
Bottom-quark production from muon-jet and dimuon events in p(bar p)-interactions at the square root of s = 1.8 TeV
|DE95-001286| p 1801 N95-22685
The effect of a non-zero shock width on wave propagation in multi-dimensions
|DE95-002748| p 1666 N95-22902
Simultaneous inference in multivariate calibration
|DE95-003592| p 1794 N95-23066
Second derivative of the likelihood of an exact ARMA model
|PB95-135158| p 1788 N95-23069
Heavy quark physics at SLD: Preliminary results
|DE95-003372| p 1806 N95-23138
Robust telescope scheduling p 1779 N95-23742

Comparison of methods for calibrating AVIRIS data to ground reflectance p 1703 N95-23854

ESCHERICHIA

Regulation of alcohol fermentation in Escherichia coli
|DE94-016227| p 1745 N95-22874

ESTERS

Activation of the jun-D gene in human myeloid cells by 1-(beta)-D-arabinofuranosylcytosine
|DE94-016591| p 1746 N95-22912

ESTIMATES

Accuracy of radar rainfall estimates compared to raingauge measurements and a hydrological application
|PB95-127296| p 1741 N95-22640

Emissions of greenhouse gases in the United States, 1987-1992
|DE95-003001| p 1731 N95-22691

Asymptotic justification for a modified GLS procedure to estimate ARMA parameters
|PB95-135166| p 1788 N95-23070

Using AVIRIS for in-flight calibration of the spectral shifts of SPOT-HRV and of AVHRR? p 1710 N95-23893

ESTIMATING

Rationale for the Modular Air-system Vulnerability Estimation Network (MAVEN) methodology
|AD-A285797| p 1611 N95-22510

Simultaneous inference in multivariate calibration
|DE95-003592| p 1794 N95-23066

Integrating O/S models during conceptual design, part 3
|NASA-CR-197905| p 1622 N95-23400

Estimating dry grass residues using landscape integration analysis p 1705 N95-23867

Estimation of crown closure from AVIRIS data using regression analysis p 1709 N95-23886

Estimation of spectral emissivity in the thermal infrared p 1711 N95-23918

ESTUARIES

Theoretical estimates of high frequency acoustic attenuation and backscattering from suspended sand particles in the ocean and in an estuary
|DSTO-TR-0078| p 1743 N95-23667

ETCHING

Development of microchannel plate x-ray optics
|NASA-CR-197935| p 1866 N95-23540

Microstructural behavior of nonequilibrium systems
|DE95-004450| p 1630 N95-23924

ETHANE

Ethylene oxidation chemistry in a well-stirred reactor
|DE95-004823| p 1635 N95-23381

ETHYL ALCOHOL

Design and demonstration of an immobilized-cell fluidized-bed reactor for the efficient production of ethanol
|DE94-014023| p 1652 N95-22587

Ethanol synthesis and water gas shift over bifunctional sulfide catalysts
|DE94-017376| p 1634 N95-23202

ETHYLENE

Ethylene oxidation chemistry in a well-stirred reactor
|DE95-004823| p 1635 N95-23381

EUCLIDEAN GEOMETRY

Note on the computational complexity of j-radii of polytopes in (R sup n)
|PB95-139358| p 1790 N95-23231

Spinning particles in the Euclidean Taub-NUT space
|DE94-634320| p 1810 N95-23456

EULER EQUATIONS OF MOTION

Euler Technology Assessment program for preliminary aircraft design employing SPLITFLOW code with Cartesian unstructured grid method
|NASA-CR-4649| p 1608 N95-22917

A perspective on unstructured grid flow solvers
|NASA-CR-195025| p 1788 N95-22931

Harmonic oscillator in quantum rotational spectra: Molecules and nuclei p 1814 N95-22972

Euler technology assessment for preliminary aircraft design employing OVERFLOW code with multiblock structured-grid method
|NASA-CR-4651| p 1608 N95-23095

An assessment of viscous effects in computational simulation of benign and burst vortex flows on generic fighter wind-tunnel models using TEAM code
|NASA-CR-4650| p 1608 N95-23185

Benchmark problems in computational aeroacoustics p 1800 N95-23315

Convergence acceleration of implicit schemes in the presence of high aspect ratio grid cells p 1676 N95-23446

Entropy jump across an inviscid shock wave
|NASA-CR-195046| p 1678 N95-23596

Cavitation modeling in Euler and Navier-Stokes codes p 1681 N95-23630

Modeling of non-spherical droplet dynamics p 1685 N95-23647

User's guide for ECAP2D: An Euler unsteady aerodynamic and aeroelastic analysis program for two dimensional oscillating cascades, version 1.0
|NASA-CR-189146| p 1699 N95-24189

EULER-LAGRANGE EQUATION

Conjugate gradient MATHEW
|DE95-003479| p 1738 N95-23143

Structured adaptive grid generation using algebraic methods p 1669 N95-23417

EURECA (ESA)

LDEF: 69 Months in Space. Third Post-Retrieval Symposium, part 1
|NASA-CP-3275-PT-1| p 1889 N95-23796

EURECA 11 months in orbit: Initial post flight investigation results p 1623 N95-23799

Dosimetric results on EURECA p 1872 N95-23800

Preliminary results of radiation measurements on EURECA p 1872 N95-23801

Performance characterization of EURECA retroreflectors with fluoropolymer-filled SiO(x) protective coatings p 1651 N95-23802

Effect of the space environment on materials flown on the EURECA/TICCE-HVI experiment p 1623 N95-23803

Material inspection of EURECA first findings and recommendations p 1637 N95-23804

EUROPEAN SPACE AGENCY

Third International Symposium on Artificial Intelligence, Robotics, and Automation for Space 1994
|NASA-CR-197340| p 1767 N95-23672

EUROPEAN SPACE PROGRAMS

Robotics and telepresence for moon missions p 1776 N95-23725

EUTECTICS

High resolution microstructural analysis of zirconia eutectic interfaces
|DE95-003143| p 1845 N95-24143

EVALUATION

Accuracy of radar rainfall estimates compared to raingauge measurements and a hydrological application
|PB95-127296| p 1741 N95-22640

EVENTS

Neutrino oscillation experiments with atmospheric neutrinos
|DE95-002994| p 1801 N95-22573

EXCIMER LASERS

Magnetic resonance and optical spectroscopic studies of carotenoids
|DE95-003729| p 1631 N95-22575

Raman-shifting an ArF excimer laser to generate new lines for obtaining optical diagnostic based information in flow fields p 1692 N95-23303

Annual report of the Osaka Laboratory for Radiation Chemistry Japan Atomic Energy Research Institute, (No. 26)
|DE94-785277| p 1626 N95-23477

10x reduction imaging at 13.4 nm
|DE94-016612| p 1828 N95-23767

EXCITATION

Do narrow Sigma hypernuclear states exist?
|DE95-002930| p 1803 N95-22763

Hadrons of arbitrary spin and heavy quark symmetry
|DE94-628597| p 1804 N95-22789

Dynamic response of a transducer mounted at one end of an acoustical cavity which is subjected to a specified pressure at the open end of the cavity
|DE95-004192| p 1799 N95-23379

MHD-Vlasov simulation of the toroidal Alfven eigenmode
|NIFS-319| p 1836 N95-23591

Rate coefficients for the electron-impact excitation, ionization and recombination of He-like ions, S XV, Ca XIX and Fe XXV, and related processes
|ISAS-R-657| p 1811 N95-23604

Photoionization of O(6+) below the n=3 threshold of the reduced ion
|DE94-634436| p 1844 N95-23774

EXCITONS

Optical absorption in an indirect-gap semiconductor quantum well systems
|DE94-628878| p 1849 N95-22759

Two-photon absorption in an indirect-gap semiconductor quantum well systems 2. Excitonic transitions
|DE94-628880| p 1849 N95-22761

Lattice relaxation study on self-trapped exciton and biexciton in neutral and charged fullerenes
|DE94-635788| p 1844 N95-23986

EXHAUST DIFFUSERS

Design of a variable area diffuser for a 15-inch Mach 6 open-jet tunnel p 1617 N95-23309

EXHAUST EMISSION

Diesel fuel component contributions to engine emissions and performance: Clean fuel study
|DE94-011868| p 1732 N95-22834

Preliminary assessment of air toxic emissions in the natural gas industry, phase 1
|PB95-135547| p 1732 N95-22865

EXHAUST GASES

Diesel fuel component contributions to engine emissions and performance: Clean fuel study
|DE94-011868| p 1732 N95-22834

Radiation/convection coupling in rocket motors and plumes p 1669 N95-23414

Numerical study of the SSME nozzle flow fields during transient operations: A comparison of the animated results with test p 1673 N95-23434

NTS-spill test facility wind tunnel exhaust plume characterization
|DE95-003630| p 1616 N95-24019

D3-D program overview
|DE95-003879| p 1837 N95-24086

EXHAUST NOZZLES

Numerical study of the SSME nozzle flow fields during transient operations: A comparison of the animated results with test p 1673 N95-23434

EXHAUST SYSTEMS

Aerodynamic design and analysis of a highly loaded turbine exhaust p 1673 N95-23435

EXHAUST VELOCITY

Aerodynamic design and analysis of a highly loaded turbine exhaust p 1673 N95-23435

EXHAUSTING

Study of frustrated systems via dissipative maps
|PB95-139093| p 1799 N95-23155

EXPANDABLE STRUCTURES

Self-generating oscillating pressure exercise device
|NASA-CASE-ARC-12000-1| p 1751 N95-23264

EXPECTATION

Singlet quarks beyond the top at the tevatron
|PB95-139127| p 1807 N95-23158

Light-traffic analysis for queues with spatially distributed arrivals
|PB95-140802| p 1767 N95-23556

EXPERIMENT DESIGN

Design and application of electromechanical actuators for deep space missions
|NASA-CR-197957| p 1694 N95-22909

Dynamic modelling and response characteristics of a magnetic bearing rotor system including auxiliary bearings
|NASA-CR-197859| p 1694 N95-23213

Design and implementation of two two-week Teacher Enhancement Institutes p 1853 N95-23306

USML-1 microgravity glovebox experiment no. 1 Passive Accelerometer System
|NASA-CR-196575| p 1653 N95-23552

Design and development status of ETS-7, an RVD and space robot experiment satellite p 1623 N95-23700

Robotic experiment with a force reflecting handcontroller onboard MIR space station p 1752 N95-23707

Automation and crew time saving in the space experiment p 1752 N95-23715

Space science experimentation automation and support p 1775 N95-23718

Robotic servicing system for space material experiment p 1697 N95-23722

EXPERIMENTATION

Robot skill learning through intelligent experimentation
|TR-567| p 1784 N95-24038

EXPERT SYSTEMS

Plinius intermediate report
|PB95-135216| p 1648 N95-23128

Verification and validation of decision support software: Expert Choice(trademark) and PCM(trademark)
|DE95-004469| p 1757 N95-23346

An expert system for diagnosing anomalies of spacecraft p 1770 N95-23684

Performance results of cooperating expert systems in a distributed real-time monitoring system p 1761 N95-23688

Autonomous spacecraft executive and its application to rendezvous and docking p 1623 N95-23719

The Starpicker expert system: A problem in expertise capture p 1623 N95-23721

A scheduling and diagnostic system for scientific satellite GEOTAIL using expert system p 1781 N95-23753

Knowledge representation and reasoning for mixed-initiative planning
|TR-562| p 1783 N95-24031

OPUS: A new generation Knowledge Engineering Environment p 1760 N95-24176

EXPLODING WIRES

Computer modeling of detonators
|DE95-003031| p 1652 N95-22721

EXPLORER SATELLITES

A constraint-logic based implementation of the coarse-grained approach to data acquisition scheduling of the International Ultraviolet Explorer orbiting observatory p 1779 N95-23741

EXPLOSIONS
Simulation of cookoff results in a small scale test
| DSTO-TR-0090 | p 1653 N95-23668
EXPLOSIVE WELDING
Explosive bonding and its application in the Advanced Photon Source front-end and beamline components design
| DE95-004132 | p 1696 N95-23397
EXPLOSIVES
Simulation of cookoff results in a small scale test
| DSTO-TR-0090 | p 1653 N95-23668
EXPONENTIAL FUNCTIONS
Symplectic computation of Lyapunov exponents
| DE95-002732 | p 1795 N95-22654
On the size of sets with weak membership properties
| TR-557 | p 1793 N95-24034
EXPONENTS
Lyapunov exponents from CHUA's circuit time series using artificial neural networks p 1784 N95-22988
EXPOSURE
Low Earth orbit thermal control coatings exposure flight tests: A comparison of U.S. and Russian results
| NASA-CR-4647 | p 1626 N95-22919
Skin exposure: Assessing the hazard in the workplace p 1628 N95-23030
The corrosion and protection of advanced aluminium - lithium airframe alloys p 1641 N95-23497
Effect of loading direction and long-term aging on fatigue-crack growth in Al-Li alloy 2090 p 1641 N95-23499
The detection and analysis of galvanic damage in BMI/graphite fiber composites p 1631 N95-23502
Corrosion protection measures for CFC/metal joints of fuel integral tank structures of advanced military aircraft p 1644 N95-23510
Performance characterization of EURECA retroreflectors with fluoropolymer-filled SiO(x) protective coatings p 1651 N95-23802
Reproducible direct exposure environmental testing of metal-based magnetic media p 1690 N95-24129
EXTERNAL STORE SEPARATION
A CFD study of complex missile and store configurations in relative motion
| NASA-CR-197912 | p 1612 N95-22949
EXTRACTION
On-line, adaptive state estimator for active noise control p 1784 N95-23308
Nonlinear thermoviscoelastic behaviour in complex materials
| PB95-140653 | p 1630 N95-23537
Extraction and detection of pesticide residues from air filter inserts using supercritical carbon dioxide
| DE95-004579 | p 1735 N95-23580
Extraction of auxiliary data from AVIRIS distribution tape for spectral, radiometric, and geometric quality assessment p 1706 N95-23875
Extraction of the surface recombination velocity of passivated phosphorus-doped silicon emitters
| DE95-004539 | p 1845 N95-24156
EXTRATERRESTRIAL MATTER
CDM and Omega in the local neighborhood
| DE95-003683 | p 1868 N95-23570
EXTRATERRESTRIAL RADIATION
Preliminary results of radiation measurements on EURECA p 1872 N95-23801
Predictions of LET spectra measured on LDEF p 1815 N95-23815
Status of LDEF activation measurements and archive p 1815 N95-23817
EXTRAVEHICULAR ACTIVITY
STS-61 Space Shuttle mission report
| NASA-TM-110545 | p 1619 N95-23187
Real-time tracking using stereo and motion: Visual perception for space robotics p 1778 N95-23739
EXTREME ULTRAVIOLET EXPLORER SATELLITE
An operations and command systems for the extreme ultraviolet explorer p 1770 N95-23687
EXTREME ULTRAVIOLET RADIATION
EUV metrology of multilayer optics
| DE95-003036 | p 1819 N95-22723
A study of EUV emission from the O4f star Zeta Puppis
| NASA-CR-197350 | p 1871 N95-23472
10x reduction imaging at 13.4 nm
| DE94-016612 | p 1828 N95-23767
EXTREMELY HIGH FREQUENCIES
The possibilities for mobile and fixed services up to the 20/30 GHz frequency bands p 1656 N95-22817

F

F REGION
Continued studies of polar cap thermospheric dynamics
| PL-TR-94-2076 | p 1737 N95-22951
Semikinetic modeling and observations of high-latitude plasma outflow
| NASA-CR-197403 | p 1831 N95-23008
Investigation of the role of gravity waves in the generation of equatorial bubbles
| NASA-CR-197962 | p 1739 N95-23272
F 2 REGION
A comparison of ionospheric F2-layer IRI model with experimental data for Ibadan Geog. Lat. 7.4 deg N
| DE94-627710 | p 1736 N95-22613
F-18 AIRCRAFT
Analysis of the longitudinal handling qualities and pilot-induced-oscillation tendencies of the High-Angle-of-Attack Research Vehicle (HARV) p 1616 N95-23297
Enhancement of F/A-18 operational flight measurements: Data report for phase 1
| DSTO-TR-0049 | p 1613 N95-23666
FABRICATION
Large-area triple-junction a-Si alloy production scaleup
| DE95-000245 | p 1726 N95-22546
Advanced Turbine Technology Applications Project (ATTAP) 1993 annual report
| DE95-003198 | p 1693 N95-22880
Idealized textile composites for experimental/analytical correlation p 1631 N95-23277
Infinite possibilities: Computational structures technology p 1700 N95-23280
Amorphous silicon photovoltaic manufacturing technology, phase 2A
| DE95-000298 | p 1729 N95-23478
Rapid thermal processing of high-efficiency silicon solar cells with controlled in-situ annealing
| DE95-004729 | p 1730 N95-23489
FABRICS
Fabric geometry distortion during composites processing p 1631 N95-23288
FABRY-PEROT INTERFEROMETERS
Continued studies of polar cap thermospheric dynamics
| PL-TR-94-2076 | p 1737 N95-22951
FACE CENTERED CUBIC LATTICES
A special percolation problem in ceramic composites
| DE94-627641 | p 1647 N95-22611
Photoemission study of quantum confinement by a finite barrier: Cu/Co(wedge)/Cu(100)
| DE95-002913 | p 1840 N95-22762
FACTORIZATION
A generic efficient adaptive grid scheme for rocket propulsion modeling p 1670 N95-23418
Normalized coprime factorizations and balancing for unstable nonlinear systems
| PB95-141222 | p 1767 N95-23557
Block LU factorization
| NASA-CR-197949 | p 1791 N95-23592
Singular moduli and Arakelov intersection
| DE94-634286 | p 1792 N95-23659
FADDEEV EQUATIONS
Dirac canonical quantization and Faddeev-Jackiw symplectic quantization of higher order Lagrangians
| DE94-628428 | p 1796 N95-22788
FAIL-SAFE SYSTEMS
Residual strength of thin panels with cracks p 1700 N95-23311
FAILURE
Robotic weld overlay coatings for erosion control
| DE95-002624 | p 1696 N95-24141
FAILURE ANALYSIS
Application requirements for wind turbine gearboxes
| DE94-011883 | p 1694 N95-22923
Handling qualities of the High Speed Civil Transport p 1616 N95-23325
Integrating O/S models during conceptual design, part 3
| NASA-CR-197905 | p 1622 N95-23400
FAILURE MODES
Precise clock synchronization protocol
| PB95-127247 | p 1687 N95-22536
The hydrogen embrittlement of alloy X-750
| DE95-003207 | p 1640 N95-22893
Residual strength of thin panels with cracks p 1700 N95-23311
FALLOUT
OU3 sediment dating and sedimentation rates
| DE95-001891 | p 1734 N95-23384
FAR ULTRAVIOLET RADIATION
Raman-shifting an ArF excimer laser to generate new lines for obtaining optical diagnostic based information in flow fields p 1692 N95-23303
Some thoughts of future experiments with the new generation of storage rings
| DE95-004602 | p 1818 N95-24162
FARM CROPS
Synergy between optical and microwave remote sensing to derive soil and vegetation parameters from MAC Europe 1991 Experiment p 1715 N95-23956
Classification and soil moisture determination of agricultural fields p 1716 N95-23958
FAST NEUTRONS
Evaluation of neutron techniques for illicit substance detection
| DE95-002988 | p 1632 N95-22764
Status of helium-production reaction studies with a spallation neutron source
| DE95-002816 | p 1806 N95-23137
FASTENERS
Eddy current detection of pitting corrosion around fastener holes p 1643 N95-23507
FATIGUE (MATERIALS)
Review of aeronautical fatigue investigation in the Netherlands during the period March 1991-March 1993
| PB95-139184 | p 1612 N95-23161
Review of some results of the author's fatigue investigations with applications in engineering and material science
| TAE-698 | p 1699 N95-23662
FATIGUE LIFE
Review of some results of the author's fatigue investigations with applications in engineering and material science
| TAE-698 | p 1699 N95-23662
Fracture mechanics life analytical methods verification testing
| NASA-CR-196555 | p 1697 N95-24106
FAULT DETECTION
STS-61 Space Shuttle mission report
| NASA-TM-110545 | p 1619 N95-23187
An intelligent ground operator support system p 1769 N95-23681
Attention focusing and anomaly detection in systems monitoring p 1769 N95-23683
An expert system for diagnosing anomalies of spacecraft p 1770 N95-23684
Distributed intelligence for ground/space systems p 1770 N95-23685
FAULT TOLERANCE
HiRel: Hybrid Automated Reliability Predictor (HARP) integrated reliability tool system, (version 7.0). Volume 3: HARP Graphics Oriented (GO) input user's guide
| NASA-TP-3452-VOL-3 | p 1753 N95-22479
HiRel: Hybrid Automated Reliability Predictor (HARP) integrated reliability tool system, (version 7.0). Volume 1: HARP introduction and user's guide
| NASA-TP-3452-VOL-1 | p 1754 N95-22603
HiRel: Hybrid Automated Reliability Predictor (HARP) integrated reliability tool system, (version 7.0). Volume 2: HARP tutorial
| NASA-TP-3452-VOL-2 | p 1755 N95-22604
Predicted performance of an integrated modular engine system
| NASA-CR-190787 | p 1625 N95-23791
FAULT TREES
Rationale for the Modular Air-system Vulnerability Estimation Network (MAVEN) methodology
| AD-A285797 | p 1611 N95-22510
FEASIBILITY
FAME: A forest assessment and monitoring environment scenario
| PB95-139309 | p 1718 N95-23471
FEASIBILITY ANALYSIS
The possibilities for mobile and fixed services up to the 20/30 GHz frequency bands p 1656 N95-22817
Geolocation applications of the Gonets LEO messaging satellites p 1656 N95-22818
Damage-mitigating control of a reusable rocket engine for high performance and extended life
| NASA-CR-4640 | p 1654 N95-23195
Inner loop flight control for the High-Speed Civil Transport p 1616 N95-23314
An intelligent ground operator support system p 1769 N95-23681
Distributed intelligence for ground/space systems p 1770 N95-23685
Autonomous navigation system for the Marsokhod rover project p 1771 N95-23693
Measurements of canopy chemistry with 1992 AVIRIS data at Blackhawk Island and Harvard Forest p 1706 N95-23873
FEDERAL BUDGETS
Director's discretionary fund report for fiscal year 1994
| NASA-TM-108848 | p 1872 N95-22920
Defense technology plan
| AD-A285415 | p 1903 N95-24178
FEED SYSTEMS
Advanced liquid oxygen (LO2) propellant conditioning concept testing
| NASA-TM-108477 | p 1652 N95-22672
FEEDBACK CONTROL
Performance of the 0.3-meter transonic cryogenic tunnel with air, nitrogen, and sulfur hexafluoride media under closed loop automatic control
| NASA-CR-195052 | p 1668 N95-23257

System identification of the Large-Angle Magnetic Suspension Test Fixture (LAMSTF)
p 1617 N95-23299
On-line, adaptive state estimator for active noise control p 1784 N95-23308
Progress report on a fully automatic Gas Tungsten Arc Welding (GTAW) system development
|DE95-004397| p 1695 N95-23343
Feedback control laws for highly maneuverable aircraft
|NASA-CR-197944| p 1615 N95-23410
Lunar rover technology demonstrations with Dante and Ratler p 1697 N95-23694
Mark Tracking: Position/orientation measurements using 4-circle mark and its tracking experiments
p 1778 N95-23736

FERMENTATION
Design and demonstration of an immobilized-cell fluidized-bed reactor for the efficient production of ethanol
|DE94-014023| p 1652 N95-22587
Regulation of alcohol fermentation in Escherichia coli
|DE94-016227| p 1745 N95-22874

FERMI LIQUIDS
Asymptotically exact solution of the multi-channel resonant-level model
|DE94-629040| p 1801 N95-22498

FERMI SURFACES
KKR-CPA calculations of density of states and soft X ray emission from disordered Li-Mg alloys
|DE94-628882| p 1640 N95-22934
Spin polarized photoemission studies of magnetic quantum well states
|DE95-004218| p 1851 N95-23335

FERMIONS
Fermion-spin transformation to implement the charge-spin separation
|DE94-629035| p 1800 N95-22495
Strong-coupling behaviour of two t-J chains with interchain single-electron hopping
|DE94-629041| p 1838 N95-22499
Continuous local symmetry in Ising-type models
|DE94-629045| p 1839 N95-22649
Correlation effects in high-Tc superconductors and heavy fermion compounds
|DE94-629057| p 1840 N95-22846
Strongly interacting fermion systems
|DE95-003405| p 1806 N95-23054
Classification of (2,2) compactifications by free fermions 2
|PB95-139119| p 1807 N95-23157

FERROELECTRICITY
A study of ceramic composite of ferroelectric BaTiO3 ceramic and superconductor YBa2Cu3O(6 + delta) ceramic
|DE94-627563| p 1647 N95-22610

FERROMAGNETIC MATERIALS
Strong collision approach to calculation of depolarization function for neutron beam passing through ferromagnetic bulk domains
|DE94-628847| p 1803 N95-22758
Dynamical properties of critical and paramagnetic spin fluctuations in anisotropic heisenberg magnets
|PB95-134623| p 1798 N95-23127

FERROMAGNETISM
Spin polarized photoemission studies of magnetic quantum well states
|DE95-004218| p 1851 N95-23335

FEYNMAN DIAGRAMS
The omega pi(sup 0)-transient form factor within effective chiral Lagrangian approach
|DE94-628612| p 1850 N95-22812

FIBER COMPOSITES
Method of producing a silicon carbide fiber reinforced strontium aluminosilicate glass-ceramic matrix composite
|NASA-CASE-LEW-15263-2| p 1627 N95-22563
Deflections of anisotropic sandwich beams with variable face sheets and core thicknesses p 1700 N95-23310
The detection and analysis of galvanic damage in BMI/graphite fiber composites p 1631 N95-23502
Corrosion protection measures for CFC/metal joints of fuel integral tank structures of advanced military aircraft
p 1644 N95-23510
Surface characterization of LDEF carbon fiber/polymer matrix composites p 1631 N95-23900
Assessment of resin transfer molding process for the XM6 discharger, ERDEC SSP 93-64
|NIAR-94-2| p 1650 N95-23932
Thermoelastic theory for the response of materials functionally graded in two directions with applications to the free-edge problem
|NASA-TM-106882| p 1699 N95-24055

FIBER OPTICS
Method for making fiber-optic bundle collimator assembly
|AD-D016491| p 1819 N95-22492
Development of a multi-sensor in situ fiber optic fluorometer
|DE95-003105| p 1819 N95-22780
Optical fiber strain sensor with improved linearity range
|NASA-CASE-LAR-14857-1-SB| p 1819 N95-22807
The possibilities for mobile and fixed services up to the 20/30 GHz frequency bands p 1656 N95-22817
A fiber-optic bundle and collimator assembly
|AD-D016500| p 1820 N95-22864
Photoinduced Bragg grating formation in optical fibres as a consequence of convective instability
|DE94-628479| p 1841 N95-23020
Low-cost packaging of high-performance optoelectronic components
|DE95-003645| p 1827 N95-23449
The STAR EM calorimeter design and small prototype test results
|DE95-004592| p 1689 N95-23583

FIBER PULLOUT
USML-1 Glovebox experiments
|NASA-CR-196574| p 1653 N95-24028

FIBERS (MATHEMATICS)
Berry phase by description of the quantum systems in the Kustaanheimo-Stiefel bundle
|DE94-628410| p 1847 N95-22620

FIBONACCI NUMBERS
Fibonacci chain polynomials: Identities from self-similarity p 1814 N95-22962

FIELD OF VIEW
SeaWiFS technical report series. Volume 25: Ocean optics protocols for SeaWiFS validation, revision 1
|NASA-TM-104566-VOL-25-REV-| p 1743 N95-22671
Instantaneous field of view and spatial sampling of the Airborne Visible/Infrared Imaging Spectrometer (AVIRIS)
p 1702 N95-23851

FIELD THEORY (PHYSICS)
Fermion-spin transformation to implement the charge-spin separation
|DE94-629035| p 1800 N95-22495
Problems in particle theory
|DE95-003106| p 1803 N95-22749
Nahm's product and W-algebra
|DE94-628504| p 1787 N95-22777
Non-Noetherian symmetries for oscillators in classical mechanics and in field theory p 1823 N95-22977
(Phi)(sup 4) kinks: Statistical mechanics
|DE95-003693| p 1794 N95-23349
Effective (mu)-term in superstring theory
|DE94-634326| p 1851 N95-23922
The exchange algebra for Liouville field on Riemann surfaces with h greater than 1 genus
|DE94-635446| p 1792 N95-23971

FIGHTER AIRCRAFT
An assessment of viscous effects in computational simulation of benign and burst vortex flows on generic fighter wind-tunnel models using TEAM code
|NASA-CR-4650| p 1608 N95-23185

FILAMENTS
High gain GaAs photoconductive semiconductor switches: Measurement of filament velocity and reduced trigger energy
|DE95-001884| p 1661 N95-22844

FILLERS
Chemical recycling of scrap composites
p 1629 N95-23034

FILM COOLING
Computational Fluid Dynamic (CFD) analysis of axisymmetric plume and base flow of film/dump cooled rocket nozzle p 1673 N95-23431
Methodology for CFD design analysis of National Launch System nozzle manifold p 1683 N95-23637

FILMS
Microporous polyimide films for reduced dielectric applications
|DE95-004543| p 1650 N95-24159

FINANCIAL MANAGEMENT
DOD budget: Selected categories of planned funding for fiscal years 1995-99. Report to Congressional requesters
|GAO/NSIAD-95-92| p 1864 N95-24062

FINITE DIFFERENCE THEORY
Evaluation of a Multiple Instruction/Multiple Data (MIMD) parallel computer for CFD applications
|AD-A285796| p 1762 N95-22509
Development of an advanced finite difference atmospheric general circulation model
|DE95-003187| p 1736 N95-22879
Harmonic oscillator representation in the theory of scattering and nuclear reactions p 1814 N95-22967
Conjugate gradient MATHEW
|DE95-003479| p 1738 N95-23143
VLUGR2: A vectorizable adaptive grid solver for PDes in 2D
|PB95-136008| p 1789 N95-23167
Finite-difference solutions of the alternate turbopump development high-pressure oxidizer turbopump pump-end ball-bearing cavity flows p 1678 N95-23617
Incompressible Navier-Stokes calculations in pump flows p 1680 N95-23627
Simulation of cookoff results in a small scale test
|DSTO-TR-0090| p 1653 N95-23668

FINITE ELEMENT METHOD
Partitioning methods for unstructured finite element meshes
|PB95-130555| p 1785 N95-22544
Development of an adaptive hp-version finite element method for computational optimal control
|NASA-CR-197898| p 1766 N95-22831
Computation of magnetic forces on moving conductors by using ELEKTRA and other 3-D computer codes
|DE95-003308| p 1798 N95-22895
COYOTE 2: A Finite Element Computer Program for nonlinear heat conduction problems
|DE95-002848| p 1666 N95-22914
Three-dimensional CTOA and constraint effects during stable tearing in a thin-sheet material
|NASA-TM-109183| p 1627 N95-22928
Finite-element time evolution operator for the anharmonic oscillator p 1823 N95-22983
Structural arrangement trade study. Volume 3: Reusable Hydrogen Composite Tank System (RHCTS) and Graphite Composite Primary Structures (GCPS). Addendum
|NASA-CR-197687| p 1621 N95-23189
Idealized textile composites for experimental/analytical correlation p 1631 N95-23277
Infinite possibilities: Computational structures technology p 1700 N95-23280
Residual strength of thin panels with cracks
p 1700 N95-23311
A new look at the simultaneous analysis and design of structures p 1700 N95-23327
Combining comparison functions and finite element approximations in CFD
|NASA-TM-106851| p 1792 N95-23614
A modal test design strategy for model correlation
|DE95-003631| p 1759 N95-24020
A multibody/finite element analysis approach for modeling of crash dynamic responses
|NIAR-94-3| p 1610 N95-24050

FINITE VOLUME METHOD
A time-accurate finite volume method valid at all flow velocities p 1676 N95-23447

FINNED BODIES
ASRM multi-port igniter flow field analysis
p 1683 N95-23639

FIRE FIGHTING
Fire hazard considerations for composites in vehicle design p 1628 N95-23032

FIRE PREVENTION
Fire hazard considerations for composites in vehicle design p 1628 N95-23032

FIRES
Rationale for the Modular Air-system Vulnerability Estimation Network (MAVEN) methodology
|AD-A285797| p 1611 N95-22510
Fire hazard considerations for composites in vehicle design p 1628 N95-23032
Remote sensing of smoke, clouds, and fire using AVIRIS data p 1704 N95-23860
Aircraft fires, smoke toxicity, and survival: An overview
|DOT/FAA/AM-95/8| p 1610 N95-24024

FISCHER-TROPSCH PROCESS
Particle size dependence in Fischer-Tropsch synthesis
|DE95-003124| p 1633 N95-22876

FISSION
Fission foil measurements of neutron and proton fluences in the A0015 experiment p 1815 N95-23811

FIXED POINTS (MATHEMATICS)
Relating multifunctions and predicate transformers through closure operators
|PB95-135646| p 1757 N95-23467

FIXED WINGS
Aviator's night vision imaging system preflight adjustment/assessment procedures
|AD-A285829| p 1750 N95-22513

FLAME PROPAGATION
Microgravity combustion science: 1995 program update
|NASA-TM-106858| p 1626 N95-24004

FLAMES
Modeling NO(x) emissions in turbulent jet flames: Effects of buoyancy and radiation
|DE94-016621| p 1633 N95-22886

FLAMMABILITY
The influence of high-octane fuel blends on the performance of a two-stroke SI engine with knock-limited-compression ratio
|DE95-002902| p 1692 N95-22556

FLANGES
Investigation of arc length versus flange thickness while using an arc voltage controller
| DE95-003937 | p 1695 N95-23374
FLAT PANEL DISPLAYS
MOCVD of gallium and calcium sulfides for improved phosphor processing
| DE95-000918 | p 1631 N95-22677
FLAT PLATES
Crossflow instability control on a swept-wing: Preliminary studies p 1609 N95-23283
Aeroacoustic computation of gust-blade interaction p 1800 N95-23313
FLAVOR (PARTICLE PHYSICS)
Dimuon production in proton-nucleus interactions
| DE95-002613 | p 1801 N95-22551
Mechanical design of the CDF SVX 2 silicon vertex detector
| DE94-018985 | p 1689 N95-23520
FLEXIBLE BODIES
Statistically generated weighted curve fit of residual functions for modal analysis of structures
| NASA-TM-108481 | p 1699 N95-22950
Segregated rigid and structural control for a photolithography positioning system
| DE95-002603 | p 1766 N95-23134
Manipulating flexible parts using a teleoperated system with time delay: An experiment p 1777 N95-23729
FLEXIBLE SPACECRAFT
Computational control of flexible aerospace systems
| NASA-CR-197902 | p 1621 N95-23260
FLEXIBLE WINGS
Flutter analysis of composite box beams
| NASA-CR-197931 | p 1615 N95-23392
FLEXING
Flexural vibration of thin piezoelectric laminate circular cylinder of hexagonal symmetry
| DE94-628474 | p 1698 N95-22773
FLIGHT CHARACTERISTICS
Flight test of the X-29A at high angle of attack: Flight dynamics and controls
| NASA-TP-3537 | p 1612 N95-22806
Analysis of the longitudinal handling qualities and pilot-induced-oscillation tendencies of the High-Angle-of-Attack Research Vehicle (HARV) p 1616 N95-23297
Preparation of course materials: Elementary mathematics of powered flight p 1853 N95-23320
Handling qualities of the High Speed Civil Transport p 1616 N95-23325
FLIGHT CONDITIONS
Direct adaptive performance optimization of subsonic transports: A periodic perturbation technique
| NASA-TM-4676 | p 1612 N95-22829
Control of flow separation in airfoil/wing design applications p 1609 N95-23294
FLIGHT CONTROL
Virtual reality flight control display with six-degree-of-freedom controller and spherical orientation overlay
| NASA-CASE-NPO-18733-1-CU | p 1613 N95-22578
Flight test of the X-29A at high angle of attack: Flight dynamics and controls
| NASA-TP-3537 | p 1612 N95-22806
Analysis of the longitudinal handling qualities and pilot-induced-oscillation tendencies of the High-Angle-of-Attack Research Vehicle (HARV) p 1616 N95-23297
Inner loop flight control for the High-Speed Civil Transport p 1616 N95-23314
Differential GPS and system integration of the Low Visibility Landing and Surface Operations (LVLASO) demonstration p 1611 N95-23318
Engines-only flight control system
| NASA-CASE-ARC-11944-1 | p 1615 N95-23389
Aerodynamic surface distension system for high angle of attack forebody vortex control
| NASA-CASE-ARC-11979-1 | p 1612 N95-23390
Feedback control laws for highly maneuverable aircraft
| NASA-CR-197944 | p 1615 N95-23410
Aerodynamic flight control to increase payload capability of future launch vehicles
| NASA-CR-197704 | p 1619 N95-24032
FLIGHT CREWS
Aviator's night vision imaging system preflight adjustment/assessment procedures
| AD-A285829 | p 1750 N95-22513
Aircraft accident report. Runway overrun following rejected takeoff. Continental airlines flight 795, McDonnell Douglas MD-82, N18835, LaGuardia Airport, Flushing, NY, 2 March 1994
| PB95-910401 | p 1610 N95-23609
FLIGHT INSTRUMENTS
Summary of OARE flight calibration measurements
| NASA-TM-109159 | p 1688 N95-23012
TRISTAR 1: Evaluation methods for testing head-up display (HUD) flight symbology
| NASA-TM-4665 | p 1613 N95-24030
FLIGHT OPERATIONS
Guidance and control requirements for high-speed Rollout and Turnoff (ROTO)
| NASA-CR-195026 | p 1614 N95-22674
Oceanic operations: An authoritative guide to oceanic operations
| FAA-AFS-550 | p 1610 N95-24065
FLIGHT PATHS
Nonlinear system guidance in the presence of transmission zero dynamics
| NASA-TM-4661 | p 1654 N95-22804
Engines-only flight control system
| NASA-CASE-ARC-11944-1 | p 1615 N95-23389
FLIGHT RECORDERS
The role of flight progress strips in en route air traffic control: A time-series analysis
| DOT/FAA/AM-95/4 | p 1611 N95-23565
FLIGHT SAFETY
Additional improvements to the NASA Lewis ice accretion code LEWICE
| NASA-TM-106849 | p 1665 N95-22669
Oklahoma City air logistics center (USAF) aging aircraft corrosion program p 1607 N95-23519
A multibody/finite element analysis approach for modeling of crash dynamic responses
| NIAR-94-3 | p 1610 N95-24050
FLIGHT SIMULATION
Virtual reality flight control display with six-degree-of-freedom controller and spherical orientation overlay
| NASA-CASE-NPO-18733-1-CU | p 1613 N95-22578
Direct adaptive performance optimization of subsonic transports: A periodic perturbation technique
| NASA-TM-4676 | p 1612 N95-22829
Review of aeronautical fatigue investigation in the Netherlands during the period March 1991-March 1993
| PB95-139184 | p 1612 N95-23161
Development of qualification guidelines for personal computer-based aviation training devices
| DOT/FAA/AM-95/6 | p 1758 N95-23603
FLIGHT STRESS (BIOLOGY)
All systems go!
| NASA-TM-110542 | p 1620 N95-23665
FLIGHT TESTS
Flight test of the X-29A at high angle of attack: Flight dynamics and controls
| NASA-TP-3537 | p 1612 N95-22806
Low Earth orbit thermal control coatings exposure flight tests: A comparison of U.S. and Russian results
| NASA-CR-4647 | p 1626 N95-22919
High-lift flow-physics flight experiments on a subsonic civil transport aircraft (B737-100) p 1609 N95-23333
TRISTAR 1: Evaluation methods for testing head-up display (HUD) flight symbology
| NASA-TM-4665 | p 1613 N95-24030
FLIGHT TRAINING
Development of qualification guidelines for personal computer-based aviation training devices
| DOT/FAA/AM-95/6 | p 1758 N95-23603
FLOAT ZONES
USML-1 Glovebox experiments
| NASA-CR-196574 | p 1653 N95-24028
FLOCCULATING
Scandinavian symposium on surface chemistry
| PB95-140687 | p 1636 N95-23554
FLOOD PLAINS
Revitalization of the Gemenc-area, Baja, Hungary. 1: A study on hydrological possibilities to revitalise the ecosystem in the Keselyues-area. 2: Towards the restoration of the Gyueruesalj floodplain
| PB95-139283 | p 1718 N95-23469
FLOODS
Axial focusing of impact energy in the earth's interior: A possible link to flood basalts and hotspots
| DE95-003357 | p 1741 N95-24009
FLOW CHARACTERISTICS
Impeller flow field characterization with a laser two-focus velocimeter p 1675 N95-23440
FLOW DISTRIBUTION
Flow visualization studies of VTOL aircraft models during Hover in ground effect
| NASA-TM-108860 | p 1607 N95-22666
A CFD study of complex missile and store configurations in relative motion
| NASA-CR-197912 | p 1612 N95-22949
Mach 10 computational study of a three-dimensional scramjet inlet flow field
| NASA-TM-4602 | p 1666 N95-23015
Three-dimensional structure in a supersonic jet: Behavior near centerline
| NASA-TM-106869 | p 1668 N95-23220
Experimental results for a hypersonic nozzle/afterbody flow field
| NASA-TM-4638 | p 1609 N95-23250
Holographic interferometric tomography for reconstructing flow fields p 1690 N95-23287
Aeroacoustic computation of gust-blade interaction p 1800 N95-23313
Structured adaptive grid generation using algebraic methods p 1669 N95-23417
A generic efficient adaptive grid scheme for rocket propulsion modeling p 1670 N95-23418
Three-dimensional unsteady flow calculations in an advanced gas generator turbine p 1671 N95-23425
Axisymmetric computational fluid dynamics analysis of Saturn V/S1-C/F1 nozzle and plume p 1672 N95-23430
NLS base heating CFD analysis p 1673 N95-23432
CFD flowfield simulation of Delta Launch Vehicles in a power-on configuration p 1673 N95-23433
A study of the vortex flow over 76/40-deg double-delta wing
| NASA-CR-195032 | p 1677 N95-23466
Navier-Stokes flow field analysis of compressible flow in a pressure relief valve p 1679 N95-23618
Comparison between predicted and experimentally measured flow fields at the exit of the SSME HPFTP impeller p 1679 N95-23622
Three-dimensional flow analysis inside consortium impeller at design and off-design conditions p 1679 N95-23623
Use of blade lean in turbomachinery redesign p 1680 N95-23625
CFD parametric study of consortium impeller p 1680 N95-23626
A generalized Eulerian-Lagrangian analysis, with application to liquid flows with vapor bubbles p 1682 N95-23633
CFD modeling of turbulent duct flows for coolant channel analysis p 1682 N95-23635
Flow and heat transfer in 180-degree turn square ducts: Effects of turning configuration and system rotation p 1682 N95-23636
Methodology for CFD design analysis of National Launch System nozzle manifold p 1683 N95-23637
Advanced multi-phase flow CFD model development for solid rocket motor flowfield analysis p 1683 N95-23638
ASRM multi-port igniter flow field analysis p 1683 N95-23639
Ignition transient calculations in the Space Shuttle solid rocket motor p 1625 N95-23640
An interactive tool for discrete phase analysis in two-phase flows p 1683 N95-23641
Flowfield characterization in a LOX/GH2 propellant rocket p 1684 N95-23642
Spray combustion experiments and numerical predictions p 1637 N95-23643
CFD analysis of spray combustion and radiation in OMV thrust chamber p 1637 N95-23645
Development of an atomization methodology for spray combustion p 1637 N95-23646
Application of CFD analysis to design support and problem resolution for ASRM and RSRM p 1685 N95-23649
Status of axisymmetric CFD of an eleven inch diameter hybrid rocket motor p 1686 N95-23651
Validation of a Computational Fluid Dynamics (CFD) code for supersonic axisymmetric base flow p 1686 N95-23652
Code validation study for base flows p 1686 N95-23653
Four-nozzle benchmark wind tunnel model USA code solutions for simulation of multiple rocket base flow recirculation at 145,000 feet altitude p 1686 N95-23654
Numerical study of base pressure characteristic curve for a four-engine clustered nozzle configuration p 1625 N95-23655
A computer model in general 3-D curvilinear coordinates for the prediction of the turbulent flow field in a jet induced ram combustor
| NAL-TR-1240T | p 1687 N95-24051
FLOW EQUATIONS
Modeling of nonequilibrium space plasma flows
| NASA-CR-197432 | p 1833 N95-23211
Benchmark problems in computational aeroacoustics p 1800 N95-23315
On the breakup of viscous liquid threads
| NASA-CR-195023 | p 1678 N95-23544
Progress in advanced spray combustion code integration p 1637 N95-23644
FLOW GEOMETRY
The influence of swirl brakes and a tip discharge orifice on the rotordynamic forces generated by discharge-to-suction leakage flows in shrouded centrifugal pumps p 1680 N95-23628

FLOW MEASUREMENT
Flow measuring structures
| PB95-127254 | p 1665 N95-22638
7th International Symposium on Applications of Laser Techniques to Fluid Mechanics, volume 1
| AD-A285647 | p 1691 N95-23118
Raman-shifting an ArF excimer laser to generate new lines for obtaining optical diagnostic based information in flow fields p 1692 N95-23303
Impeller flow field characterization with a laser two-focus velocimeter p 1675 N95-23440

FLOW STABILITY
Influence of porosity and two-phase flow on diffusional/thermal instability of a deflagrating energetic material
| DE95-002592 | p 1634 N95-23122
A time-accurate finite volume method valid at all flow velocities p 1676 N95-23447
On the breakup of viscous liquid threads
| NASA-CR-195023 | p 1678 N95-23544

FLOW VELOCITY
Superconducting Tl2Ba2CaCu2O8 thin films prepared by post-annealing in a flow-through multiple-zone furnace
| DE95-002745 | p 1838 N95-22520
Accelerated panel methods using the fast multipole method p 1687 N95-23307
Aeroacoustic computation of gust-blade interaction p 1800 N95-23313
Three-dimensional viscous flow analysis inside a turbine volute p 1674 N95-23437
Phase 2: HGM air flow tests in support of HEX vane investigation p 1674 N95-23438
Impeller flow field characterization with a laser two-focus velocimeter p 1675 N95-23440
A time-accurate finite volume method valid at all flow velocities p 1676 N95-23447

FLOW VISUALIZATION
Flow visualization studies of VTOL aircraft models during Hover in ground effect
| NASA-TM-108860 | p 1607 N95-22666
Experimental study of vortex breakdown in a swirling water jet
| PB95-130407 | p 1665 N95-22767
Experimental results for a hypersonic nozzle/afterbody flow field
| NASA-TM-4638 | p 1609 N95-23250
Flow diagnostics, chemically reacting turbulent flow modeling and turbulent mixing: A summary of project studies in combustion
| NASA-CR-197348 | p 1687 N95-24022

FLUENCE
Results from the Heavy Ions In Space (HIIS) experiment on the ionic charge state of solar energetic particles p 1870 N95-23808
Absorbed dose and LET spectra measurements on LDEF p 1815 N95-23810
Fission foil measurements of neutron and proton fluences in the A0015 experiment p 1815 N95-23811
Measurement of trapped proton fluences in main stack of P0006 experiment p 1815 N95-23812

FLUID DYNAMICS
Experimental study of vortex breakdown in a swirling water jet
| PB95-130407 | p 1665 N95-22767
High-lift flow-physics flight experiments on a subsonic civil transport aircraft (B737-100) p 1609 N95-23333
Application of CFD analysis to design support and problem resolution for ASRM and RSRM p 1685 N95-23649

FLUID FLOW
Effects of wind on rainfall simulation. Spatial distribution of water application, kinetic energy, and overland flow under single full-cone nozzle sprays
| PB95-127304 | p 1717 N95-22537
The effect of a non-zero shock width on wave propagation in multi-dimensions
| DE95-002748 | p 1666 N95-22902
7th International Symposium on Applications of Laser Techniques to Fluid Mechanics, volume 1
| AD-A285647 | p 1691 N95-23118
Holographic interferometric tomography for reconstructing flow fields p 1690 N95-23287
Numerical study of the SSME nozzle flow fields during transient operations: A comparison of the animated results with test p 1673 N95-23434
Phase 2: HGM air flow tests in support of HEX vane investigation p 1674 N95-23438
A time-accurate finite volume method valid at all flow velocities p 1676 N95-23447
Gyrokinetic and global fluid simulations of tokamak microturbulence and transport
| DE95-003628 | p 1837 N95-24017

FLUID JETS
On the breakup of viscous liquid threads
| NASA-CR-195023 | p 1678 N95-23544

FLUID MECHANICS
7th International Symposium on Applications of Laser Techniques to Fluid Mechanics, volume 1
| AD-A285647 | p 1691 N95-23118
A wavenumber-partitioning scheme for two-dimensional statistical closures
| DE95-004514 | p 1677 N95-23483
On inertial range scaling laws
| DE95-004515 | p 1677 N95-23484

FLUIDIZED BED PROCESSORS
Design and demonstration of an immobilized-cell fluidized-bed reactor for the efficient production of ethanol
| DE94-014023 | p 1652 N95-22587
Continuous production of cellulase in a fluidized-bed reactor by Pseudonomas fluorescens immobilized in hydrogel beads
| DE94-014105 | p 1744 N95-22588
Development of the IGT RENUGAS(reg sign) process
| DE94-017652 | p 1727 N95-22888
Robotic weld overlay coatings for erosion control
| DE95-002624 | p 1696 N95-24141

FLUORESCENCE
Comparison of the rate constants for energy transfer in the light-harvesting protein, C-phycocyanin, calculated from Foerster's theory and experimentally measured by time-resolved fluorescence spectroscopy
| DE94-014961 | p 1745 N95-22590
Development of a multi-sensor in situ fiber optic fluorometer
| DE95-003105 | p 1819 N95-22780

FLUORIDES
Electron drift velocities of Ar-CO2-CF4 gas mixtures
| DE95-004353 | p 1809 N95-23359

FLUOROCARBONS
Reduced dimer production in solar-simulator-pumped continuous wave iodine lasers based on model simulations and scaling and pumping studies
| NASA-TP-3486 | p 1691 N95-23411

FLUOROPOLYMERS
Polyazomethines containing trifluoromethylbenzene units
| NASA-CASE-LAR-14896-1 | p 1649 N95-23253
The surface properties of fluorinated polyimides exposed to VUV and atomic oxygen p 1651 N95-23904

FLUTTER
Flutter analysis of composite box beams
| NASA-CR-197931 | p 1615 N95-23392

FLUTTER ANALYSIS
Flutter analysis of composite box beams
| NASA-CR-197931 | p 1615 N95-23392

FLUX DENSITY
Energy flux and hydrogeology of thermal anomalies in the Gulf of Mexico Basin - South Texas example
| DE95-003341 | p 1743 N95-22695
Design of a differential radiometer for atmospheric radiative flux measurements
| DE95-002701 | p 1739 N95-23244

FLYBY MISSIONS
Using AVIRIS for in-flight calibration of the spectral shifts of SPOT-HRV and of AVHRR? p 1710 N95-23893

FLYWHEELS
Electromechanical Battery Program at the Lawrence Livermore National Laboratory
| DE95-003657 | p 1727 N95-22574

FOAMS
Scandinavian symposium on surface chemistry
| PB95-140687 | p 1636 N95-23554

FOCAL PLANE DEVICES
Programmable hyperspectral image mapper with on-array processing
| NASA-CASE-NPO-17794-1-CU | p 1819 N95-22765

FOCUSING
Attention focusing and anomaly detection in systems monitoring p 1769 N95-23683

FOIL BEARINGS
Influence of backup bearings and support structure dynamics on the behavior of rotors with active supports
| NASA-CR-197438 | p 1694 N95-23190

FOKKER-PLANCK EQUATION
Wigner distribution function and entropy of the damped harmonic oscillator within the theory of the open quantum systems p 1798 N95-22990

FOLDING
Protein folding and protein metallocluster studies using synchrotron small angler x ray scattering
| DE95-003339 | p 1746 N95-22897

FOLIAGE
Application of a two-stream radiative transfer model for leaf lignin and cellulose concentrations from spectral reflectance measurements, part 1 p 1703 N95-23856
The effect of signal noise on the remote sensing of Foliar biochemical concentration p 1708 N95-23884

FOREBODIES
Aerodynamic surface distension system for high angle of attack forebody vortex control
| NASA-CASE-ARC-11979-1 | p 1612 N95-23390

FORECASTING
Intermediate-term earthquake prediction and seismic zoning in Northern Italy
| DE94-627689 | p 1736 N95-22612

FOREST MANAGEMENT
FAME: A forest assessment and monitoring environment scenario
| PB95-139309 | p 1718 N95-23471
Forest investigations by polarimetric AIRSAR data in the Harz mountains p 1713 N95-23944
Polarimetric radar data decomposition and interpretation p 1715 N95-23955
Geographic information analysis: An ecological approach for the management of wildlife on the forest landscape
| NASA-CR-197941 | p 1719 N95-24094
Measuring forest landscape patterns in the Cascade Range of Oregon, USA p 1719 N95-24096
A preliminary comparison of Landsat Thematic Mapper and SPOT-1 HRV multispectral data for estimating coniferous forest volume p 1719 N95-24097
Old-growth and mature forests near spotted owl nests in western Oregon p 1719 N95-24098
Hierarchical analysis of spatial pattern and processes of Douglas-fir forests p 1719 N95-24099
Forest and wildlife habitat analysis using remote sensing and geographic information systems p 1720 N95-24100
Analysis of conifer forest regeneration using Landsat Thematic Mapper data p 1720 N95-24101
Determining successional stage of temperate coniferous forests with Landsat satellite data p 1720 N95-24102
Determining coniferous forest cover and forest fragmentation with NOAA-9 advanced very high resolution radiometer data p 1720 N95-24103
Dynamics and pattern of a managed coniferous forest landscape in Oregon p 1720 N95-24104

FORESTS
Combining optical and microwave remote sensing data of forest vegetation: MAC Europe 1991
| PB95-127312 | p 1717 N95-22538
FAME: A forest assessment and monitoring environment scenario
| PB95-139309 | p 1718 N95-23471
Submodular linear programs on forests
| PB95-139820 | p 1758 N95-23608
AVIRIS spectra correlated with the chlorophyll concentration of a forest canopy p 1705 N95-23871
Measurements of canopy chemistry with 1992 AVIRIS data at Blackhawk Island and Harvard Forest p 1706 N95-23873
Estimation of crown closure from AVIRIS data using regression analysis p 1709 N95-23886
Forest investigations by polarimetric AIRSAR data in the Harz mountains p 1713 N95-23944
Relating P-band AIRSAR backscatter to forest stand parameters p 1716 N95-23959
Microwave dielectric properties of boreal forest trees p 1716 N95-23961
Geographic information analysis: An ecological approach for the management of wildlife on the forest landscape
| NASA-CR-197941 | p 1719 N95-24094
Measuring forest landscape patterns in the Cascade Range of Oregon, USA p 1719 N95-24096
Old-growth and mature forests near spotted owl nests in western Oregon p 1719 N95-24098
Hierarchical analysis of spatial pattern and processes of Douglas-fir forests p 1719 N95-24099
Forest and wildlife habitat analysis using remote sensing and geographic information systems p 1720 N95-24100
Analysis of conifer forest regeneration using Landsat Thematic Mapper data p 1720 N95-24101
Determining successional stage of temperate coniferous forests with Landsat satellite data p 1720 N95-24102
Determining coniferous forest cover and forest fragmentation with NOAA-9 advanced very high resolution radiometer data p 1720 N95-24103
Dynamics and pattern of a managed coniferous forest landscape in Oregon p 1720 N95-24104
Thermal radiant exitance model performance: Soils and forests
| DE95-003619 | p 1721 N95-24148

FORM FACTORS
On the D yields K-bar(sup *)e(sup +)(nu)(sub e) form factors
| DE94-628614 | p 1803 N95-22754
To the problem of D-meson leptonic and semileptonic decays
| DE94-628615 | p 1803 N95-22755

The omega pi(sup 0)-transient form factor within effective chiral Lagrangian approach
| DE94-628612 | p 1850 N95-22812
Flavour dependence of form factors in heavy meson decays
| PB95-139101 | p 1807 N95-23156

FORMALDEHYDE
Ethylene oxidation chemistry in a well-stirred reactor
| DE95-004823 | p 1635 N95-23381

FORMALISM
Roles and dynamic subclasses: A modal logic approach
| PB95-127320 | p 1754 N95-22522
Temporal model theory for default logic
| PB95-127346 | p 1766 N95-22524
Browsing semantics in the tower model
| PB95-127221 | p 1855 N95-22534
DUALITY: A simple formalism for the analysis of UNITY
| PB95-135703 | p 1763 N95-23166
Ploxoma: Testbed for uncertain inference
| TR-537 | p 1794 N95-23927

FORMAT
Utilizing inheritance in requirements engineering p 1768 N95-23677

FORMING TECHNIQUES
Technology maturation project on optimization of sheet metal forming of aluminum for use in transportation systems
| DE95-003005 | p 1654 N95-22692

FOSSIL FUELS
Assessing the relative contribution of biogenic and fossil processes to visibility scattering aerosols found in remote areas: Near-term Organic Research Program
| DE95-003149 | p 1735 N95-24146

FOSSILS
Molecular relics from chemical evolution and the origin of life
| DE94-628493 | p 1747 N95-23060

FOURIER TRANSFORMATION
Optical image correlator using orthogonal data storage
| AD-A285795 | p 1819 N95-22508
A Ramanujan-type measure for the Askey-Wilson polynomials p 1797 N95-22975
An algorithm for the basis of the finite Fourier transform p 1760 N95-22985
A note on the angular Fourier transformation p 1797 N95-22986

FRACTALS
A fractal model for intergranular fractures in nanocrystals
| DE94-627393 | p 1839 N95-22606
Hausdorff dimension of Julia sets of complex Henon mappings
| DE94-628420 | p 1785 N95-22628
Effect of critical field on screened dielectric breakdown growth
| DE94-628482 | p 1661 N95-23046
Effects of long-range coupling on aggregation
| DE94-628483 | p 1842 N95-23047

FRACTIONS
Mapping and monitoring changes in vegetation communities of Jasper Ridge, CA, using spectral fractions derived from AVIRIS images p 1708 N95-23883
Objective determination of image end-members in spectral mixture analysis of AVIRIS data p 1709 N95-23888

FRACTURE MECHANICS
A fractal model for intergranular fractures in nanocrystals
| DE94-627393 | p 1839 N95-22606
Notch-tip damage and translaminar fracture toughness measurements from carbon/epoxy laminates
| AD-A280101 | p 1627 N95-22833
Three-dimensional CTOA and constraint effects during stable tearing in a thin-sheet material
| NASA-TM-109183 | p 1627 N95-22928
Separation of crack extension modes in composite delamination problems p 1700 N95-23281
Fracture mechanics life analytical methods verification testing
| NASA-CR-196555 | p 1697 N95-24106

FRACTURE STRENGTH
A fractal model for intergranular fractures in nanocrystals
| DE94-627393 | p 1839 N95-22606
An investigation into the effects of hydrogen on the fracture and deformation of Alloy X-750
| DE95-003206 | p 1639 N95-22732
Notch-tip damage and translaminar fracture toughness measurements from carbon/epoxy laminates
| AD-A280101 | p 1627 N95-22833
The hydrogen embrittlement of alloy X-750
| DE95-003207 | p 1640 N95-22893

FRACTURES (MATERIALS)
A fractal model for intergranular fractures in nanocrystals
| DE94-627393 | p 1839 N95-22606

FRACTURING
Morphology of extinguished monolithic JA2 grains fired in a 30-mm Solid Propellant Electrothermal Chemical (SPETC) gun
| AD-A285792 | p 1652 N95-22506
The hydrogen embrittlement of alloy X-750
| DE95-003207 | p 1640 N95-22893

FRAGMENTATION
Impact shock and penetration fragmentation in porous media
| DE94-018900 | p 1868 N95-23656
Measuring forest landscape patterns in the Cascade Range of Oregon, USA p 1719 N95-24096
Determining coniferous forest cover and forest fragmentation with NOAA-9 advanced very high resolution radiometer data p 1720 N95-24103

FRAGMENTS
Rationale for the Modular Air-system Vulnerability Estimation Network (MAVEN) methodology
| AD-A285797 | p 1611 N95-22510

FRAMES (DATA PROCESSING)
Utilizing inheritance in requirements engineering p 1768 N95-23677

FREE BOUNDARIES
Flexural vibration of thin piezoelectric laminate circular cylinder of hexagonal symmetry
| DE94-628474 | p 1698 N95-22773

FREE ELECTRON LASERS
Electron beam acceleration and compression for short wavelength FELs
| DE95-003371 | p 1691 N95-22704
Undulators for short wavelength FEL amplifiers
| DE95-004690 | p 1692 N95-23487
The project of high free electron laser using race-track microtron-recuperator
| DE94-634034 | p 1692 N95-23657
Advanced technologies for a compact RF linac FEL
| DE95-003674 | p 1692 N95-24072

FREE FLOW
Direct numerical simulations and modeling of a spatially-evolving turbulent wake p 1687 N95-23289
Benchmark problems in computational aeroacoustics p 1800 N95-23315

FREE VIBRATION
Flexural vibration of thin piezoelectric laminate circular cylinder of hexagonal symmetry
| DE94-628474 | p 1698 N95-22773

FREQUENCIES
Time-periodic solutions of some forced nonlinear wave equations: Analysis, approximations and applications
| PB95-135083 | p 1788 N95-22932

FREQUENCY MODULATION
Wavelet time-frequency analysis of phase-shift-key modulated signals
| AD-A285791 | p 1655 N95-22505

FREQUENCY STABILITY
Sensitivity of combustion-acoustic instabilities to boundary conditions for premixed gas turbine combustors
| NASA-TM-106890 | p 1614 N95-23550

FROST
Gas cooled leads. Part 1: Theoretical Study. Part 2: Frost free lead optimized for a specific current. Part 3: Frost free lead optimized for a large current range
| DE95-002657 | p 1660 N95-22716

FRUSTRATION
Study of frustrated systems via dissipative maps
| PB95-139093 | p 1799 N95-23155

FUEL CELL POWER PLANTS
The US molten carbonate fuel-cell development and commercialization effort
| DE94-019096 | p 1728 N95-23162

FUEL CELLS
Energy Conversion and Storage Program
| DE95-003796 | p 1725 N95-22501
Support research for solid oxide fuel cells
| DE95-002910 | p 1726 N95-22568
Multi-fuel reformers for fuel cells used in transportation: Assessment of hydrogen storage technologies
| DE94-017655 | p 1727 N95-22861
The US molten carbonate fuel-cell development and commercialization effort
| DE94-019096 | p 1728 N95-23162
Hydrogen and fuel cells for energy storage
| DE95-723907 | p 1729 N95-23382
Multi-fuel reformers for fuel cells used in transportation. Phase 1: Multi-fuel reformers
| DE95-004215 | p 1729 N95-23482
Electrochemical studies of perovskite mixed conductors
| DE95-003704 | p 1636 N95-23573
Advances in research for solid oxide fuel cells
| DE95-004590 | p 1730 N95-23582
Proceedings of the fuel cells 1994 contractors review meeting
| DE94-012285 | p 1730 N95-23977

FUEL COMBUSTION
Fundamental phenomena on fuel decomposition and boundary layer combustion processes with applications to hybrid rocket motors
| NASA-CR-197919 | p 1625 N95-23261

FUEL CONSUMPTION
A hybrid vehicle evaluation code and its application to vehicle design
| DE95-004205 | p 1662 N95-23334

FUEL INJECTION
New pellet production and acceleration technologies for high speed pellet injection system HIPEL in Large Helical Device
| NISF-326 | p 1835 N95-23566

FUEL PRODUCTION
Development of the IGT RENUGAS(reg sign) process
| DE94-017652 | p 1727 N95-22888

FUEL PUMPS
Detailed measurements in the SSME high pressure fuel turbine with smooth rotor blades p 1675 N95-23441
Comparison between predicted and experimentally measured flow fields at the exit of the SSME HPFTP impeller p 1679 N95-23622

FUEL SPRAYS
Spray combustion experiments and numerical predictions p 1637 N95-23643
Progress in advanced spray combustion code integration p 1637 N95-23644
CFD analysis of spray combustion and radiation in OMV thrust chamber p 1637 N95-23645
Development of an atomization methodology for spray combustion p 1637 N95-23646

FUEL SYSTEMS
Multi-fuel reformers for fuel cells used in transportation: Assessment of hydrogen storage technologies
| DE94-017655 | p 1727 N95-22861

FUEL TANKS
Multi-fuel reformers for fuel cells used in transportation: Assessment of hydrogen storage technologies
| DE94-017655 | p 1727 N95-22861

FUEL TESTS
Diesel fuel component contributions to engine emissions and performance: Clean fuel study
| DE94-011868 | p 1732 N95-22834
A summary of the slush hydrogen technology program for the National Aero-Space Plane
| NASA-TM-106863 | p 1653 N95-24186

FULLERENES
Lattice relaxation study on self-trapped exciton and biexciton in neutral and charged fullerenes
| DE94-635788 | p 1844 N95-23986

FUNCTION SPACE
Is omega* - (mu) absolutely countably compact?
| PB95-127981 | p 1785 N95-22528
Algebraic description of the elliptic cohomology of classifying spaces
| PB95-110797 | p 1788 N95-23076

FUNCTIONAL ANALYSIS
Translation invariant Frechet subspaces of distributions
| PB95-138830 | p 1789 N95-23171

FUNCTIONAL DESIGN SPECIFICATIONS
Parallel digital modem using multirate digital filter banks
| NASA-CR-197331 | p 1761 N95-22478
Utilizing inheritance in requirements engineering p 1768 N95-23677
Development of Advanced Robotic Hand System for space application p 1752 N95-23704
Digital Linear Tape (DLT) technology and product family overview p 1753 N95-24125

FUSELAGES
Residual strength of thin panels with cracks p 1700 N95-23311

FUSION REACTORS
Numerical Tokamak Project code comparison
| DE95-003475 | p 1831 N95-22899
TFTR Ion Cyclotron Range of Frequencies (ICRF) experimental data analysis collaboration
| DE95-003409 | p 1832 N95-23084
Tritium transport, influx, and helium ash measurements on TFTR during DT operation
| DE95-003708 | p 1833 N95-23269
New pellet production and acceleration technologies for high speed pellet injection system HIPEL in Large Helical Device
| NISF-326 | p 1835 N95-23566
Experimental achievement of toroidal beta beyond that predicted by 'Troyon' scaling
| DE95-003880 | p 1837 N95-24087

FUZZY SYSTEMS
Fuzziness and randomness in an optimization framework
|DE94-628383| p 1755 N95-22616
A fuzzy structural matching scheme for space robotics vision p 1778 N95-23737

G

GALACTIC EVOLUTION
Space Science for the 21st Century. Strategic Plan for 1995-2000
|NASA-TM-110546| p 1617 N95-22947
Structure and evolution of long-lived spiral patterns in galaxies
|PB95-139242| p 1868 N95-23228
GALACTIC ROTATION
Structure and evolution of long-lived spiral patterns in galaxies
|PB95-139242| p 1868 N95-23228
GALACTIC STRUCTURE
Structure and evolution of long-lived spiral patterns in galaxies
|PB95-139242| p 1868 N95-23228
GALAXIES
CDM and Omega in the local neighborhood
|DE95-003683| p 1868 N95-23570
Search for millimeterwave CO emission in damped Lyman-alpha systems
|PB95-139259| p 1868 N95-23607
GALLIUM
MOCVD of gallium and calcium sulfides for improved phosphor processing
|DE95-000918| p 1631 N95-22677
GALLIUM ARSENIDES
Resonant shallow donor magnetopolaron effect in a GaAs/AlGaAs quantum dot in high magnetic fields
|DE94-629039| p 1798 N95-22497
High gain GaAs Photoconductive Semiconductor Switches for impulse sources
|DE95-001885| p 1659 N95-22549
Study of photorefractive non-linearities in the 3-5 and 2-4 semi-insulator compounds: The effect of electron irradiation
|PB94-189057| p 1839 N95-22584
High gain GaAs photoconductive semiconductor switches: Measurement of filament velocity and reduced trigger energy
|DE95-001884| p 1661 N95-22844
Design of a GaAs/Ge solar array for unmanned aerial vehicles
|NASA-TM-106870| p 1728 N95-23259
Carbon doping of III-V compound semiconductors
|DE95-003431| p 1844 N95-24013
Subband quantum scattering times for AlGaAs/GaAs obtained using digital filtering
|NASA-TM-106873| p 1846 N95-24188
GALLIUM SELENIDES
Polycrystalline CuInSe2 and CdTePV solar cells
|DE95-000244| p 1727 N95-22842
GAME THEORY
PUZZLES 4: Sperner collections and the keys puzzle
|PB95-139374| p 1790 N95-23233
Marginalistic value for monotonic set games
|PB95-140646| p 1794 N95-23239
Set games
|PB95-140786| p 1794 N95-23539
Note on the tau-value and tau-related solution concepts
|PB95-140752| p 1795 N95-23555
GAMETOCYTES
Genetic effects on heavy ions in drosophila
|NASA-CR-197916| p 1746 N95-22911
GAMMA RAY ASTRONOMY
Gamma ray emission from radio pulsars
|NASA-CR-197917| p 1871 N95-22910
Statistical properties of the time histories of cosmic gamma-ray bursts detected by the BATSE experiment of the Compton gamma-ray observatory
|NASA-CR-197425| p 1871 N95-23546
GAMMA RAY BURSTS
Statistical properties of the time histories of cosmic gamma-ray bursts detected by the BATSE experiment of the Compton gamma-ray observatory
|NASA-CR-197425| p 1871 N95-23546
GAMMA RAY OBSERVATORY
Analysis of data from the energetic gamma-ray experiment of the Gamma Ray Observatory
|NASA-CR-197347| p 1871 N95-23216
GAMMA RAY TELESCOPES
Analysis of data from the energetic gamma-ray experiment of the Gamma Ray Observatory
|NASA-CR-197347| p 1871 N95-23216
GAMMA RAYS
Gamma ray emission from radio pulsars
|NASA-CR-197917| p 1871 N95-22910
Analysis of data from the energetic gamma-ray experiment of the Gamma Ray Observatory
|NASA-CR-197347| p 1871 N95-23216
ROSAT observation program
|NASA-CR-197683| p 1866 N95-23595
GARNETS
Computational modelling of Er(3+): Garnet laser materials p 1692 N95-23326
GAS ANALYSIS
Measurement of HO2 and other trace gases in the stratosphere using a high resolution far-infrared spectrometer
|NASA-CR-197368| p 1735 N95-22482
GAS BEARINGS
Concept verification of three dimensional free motion simulator for space robot p 1618 N95-23702
GAS CHROMATOGRAPHY
Modified molecular sieves: Stationary phase for the gas chromatographic separation of hydrogen isotopes
|DE94-627282| p 1814 N95-24175
GAS COOLING
Conceptual design of a 20-kA current lead using forced-flow cooling and Ag-alloy-sheathed Bi-2223 high-temperature superconductors
|DE95-002916| p 1660 N95-22569
GAS DETECTORS
Measurements of the optical properties of thin films of silver and silver oxide p 1651 N95-23906
GAS DYNAMICS
High-performance parallel analysis of coupled problems for aircraft propulsion
|NASA-CR-197440| p 1614 N95-23088
LDEF environment modeling updates p 1637 N95-23797
Investigation of infra-red and nonequilibrium air radiation
|NASA-CR-197977| p 1741 N95-24041
GAS FLOW
High-performance parallel analysis of coupled problems for aircraft propulsion
|NASA-CR-197440| p 1614 N95-23088
Entropy jump across an inviscid shock wave
|NASA-CR-195046| p 1678 N95-23596
Advanced multi-phase flow CFD model development for solid rocket motor flowfield analysis p 1683 N95-23638
Time-accurate unsteady flow simulations supporting the SRM T+68-second pressure spike anomaly investigation (STS-54B) p 1685 N95-23650
Monte Carlo simulation of rarefied nitrogen gases contained between parallel plates using the statistical inelastic cross-section model
|NAL-TR-1229T| p 1687 N95-24082
GAS GENERATORS
Three-dimensional unsteady flow calculations in an advanced gas generator turbine p 1671 N95-23425
GAS MIXTURES
Pressure shifts and electron scattering in atomic and molecular gases
|DE95-003102| p 1803 N95-22747
Analytical Boltzmann moments for electrons in N2-O2-H2O gas mixtures
|DE95-003474| p 1732 N95-22898
Electron drift velocities of Ar-CO2-CF4 gas mixtures
|DE95-004353| p 1809 N95-23359
GAS RECOVERY
Preliminary assessment of air toxic emissions in the natural gas industry, phase 1
|PB95-135547| p 1732 N95-22865
GAS STREAMS
Experimental results for a hypersonic nozzle/afterbody flow field
|NASA-TM-4638| p 1609 N95-23250
GAS TEMPERATURE
Non-intrusive measurements in a rocket engine combustor p 1625 N95-23439
Instantaneous 2D velocity and temperature measurements in high speed flows based on spectrally resolved molecular Rayleigh scattering
|NASA-TM-106883| p 1688 N95-23461
GAS TUNGSTEN ARC WELDING
Progress report on a fully automatic Gas Tungsten Arc Welding (GTAW) system development
|DE95-004397| p 1695 N95-23343
Vision-sensing image analysis for GTAW process control
|DE95-003936| p 1695 N95-23373
Investigation of arc length versus flange thickness while using an arc voltage controller
|DE95-003937| p 1695 N95-23374
Vaccum Gas Tungsten Arc Welding, phase 1
|NASA-CR-197979| p 1696 N95-24064
GAS TURBINE ENGINES
Evolution of oxidation and creep damage mechanisms in HIPed silicon nitride materials
|DE95-001360| p 1647 N95-22689
Advanced Turbine Technology Applications Project (ATTAP) 1993 annual report
|DE95-003198| p 1693 N95-22880
GAS TURBINES
Advanced Turbine Technology Applications Project (ATTAP) 1993 annual report
|DE95-003198| p 1693 N95-22880
Sensitivity of combustion-acoustic instabilities to boundary conditions for premixed gas turbine combustors
|NASA-TM-106890| p 1614 N95-23550
GASEOUS ROCKET PROPELLANTS
Flowfield characterization in a LOX/GH2 propellant rocket p 1684 N95-23642
GASES
Review of research results for the photocatalytic oxidation of hazardous wastes in air
|DE95-004004| p 1734 N95-23480
Microgravity combustion science: 1995 program update
|NASA-TM-106858| p 1626 N95-24004
GASIFICATION
Development of the IGT RENUGAS(reg sign) process
|DE94-017652| p 1727 N95-22888
GASOLINE
The influence of high-octane fuel blends on the performance of a two-stroke SI engine with knock-limited-compression ratio
|DE95-002902| p 1692 N95-22556
Performance of thin-ceramic-coated combustion chamber with gasoline and methanol as fuels in a two-stroke SI engine
|DE95-002903| p 1693 N95-22557
GATES
Flow measuring structures
|PB95-127254| p 1665 N95-22638
GATES (CIRCUITS)
Ultrafast, high precision gated integrator
|DE95-004616| p 1664 N95-24164
GAUGE INVARIANCE
First quantized noncritical relativistic Polyakov string
|DE94-628513| p 1848 N95-22738
Topologically stable Z - strings in the supersymmetric standard model
|DE94-628517| p 1848 N95-22742
One loop renormalization of Chern-Simons field theory in operator regularization
|DE94-628508| p 1796 N95-22751
Lectures on 2D gauge theories. Topological aspects and path integral techniques
|DE94-628509| p 1849 N95-22752
Gauge dependence and new kind of two-dimensional gravity theory with trivial quantum corrections
|DE94-628502| p 1850 N95-22776
The omega pi(sup 0)-transient form factor within effective chiral Lagrangian approach
|DE94-628612| p 1850 N95-22812
Scale-invariant Lipatov kernels from t-channel unitarity
|DE95-004625| p 1813 N95-24166
GAUGE THEORY
On diagonalization in map (M,G)
|DE94-628515| p 1796 N95-22740
Lectures on 2D gauge theories. Topological aspects and path integral techniques
|DE94-628509| p 1849 N95-22752
High Energy Theory: Task B and Task L
|DE95-003453| p 1817 N95-23148
Search for new gauge bosons at D(O)
|DE95-003745| p 1809 N95-23404
GEAR TEETH
The spectral content of the torque loads on a turbine gear tooth
|DE95-002188| p 1694 N95-23056
GEARS
Pressurized fluid torque driver control and method
|NASA-CASE-MSC-22385-1| p 1694 N95-22892
Application requirements for wind turbine gearboxes
|DE94-011883| p 1694 N95-22923
Gearbox vibration diagnostic analyzer
|NASA-CR-189141| p 1696 N95-23792
GENE EXPRESSION
Regulation of alcohol fermentation in Escherichia coli
|DE94-016227| p 1745 N95-22874
Rearrangement of RAG-1 recombinase gene in radiation-sensitive wasted mice
|DE94-017083| p 1746 N95-22913
GENERAL OVERVIEWS
Neutrino overview
|DE95-003201| p 1802 N95-22729
Outlook from the intersections
|DE95-003202| p 1802 N95-22730

Summary and review of Materials Special Investigation Group evaluations of hardware from the Long Duration Exposure Facility p 1638 N95-23897
Collection and review of metals data obtained from LDEF experiment specimens and support hardware p 1646 N95-23905
Overview of the LDEF MSIG databasing activities p 1864 N95-23916
Aircraft fires, smoke toxicity, and survival: An overview | DOT/FAA/AM-95/8 | p 1610 N95-24024

GENES
Regulation of alcohol fermentation in Escherichia coli | DE94-016227 | p 1745 N95-22874
Activation of the jun-D gene in human myeloid cells by 1-(beta)-D-arabinofuranosylcytosine | DE94-016591 | p 1746 N95-22912
Rearrangement of RAG-1 recombinase gene in radiation-sensitive wasted mice | DE94-017083 | p 1746 N95-22913

GENETIC ALGORITHMS
Multidisciplinary design optimization using genetic algorithms p 1619 N95-23332
Scheduling with genetic algorithms p 1761 N95-23762

GENETIC CODE
Activation of the jun-D gene in human myeloid cells by 1-(beta)-D-arabinofuranosylcytosine | DE94-016591 | p 1746 N95-22912
Rearrangement of RAG-1 recombinase gene in radiation-sensitive wasted mice | DE94-017083 | p 1746 N95-22913

GENETICS
Genetic effects on heavy ions in drosophila | NASA-CR-197916 | p 1746 N95-22911
Activation of the jun-D gene in human myeloid cells by 1-(beta)-D-arabinofuranosylcytosine | DE94-016591 | p 1746 N95-22912
Rearrangement of RAG-1 recombinase gene in radiation-sensitive wasted mice | DE94-017083 | p 1746 N95-22913
Performance of single-keyword and multiple-keyword pattern matching algorithms | PB95-138954 | p 1756 N95-23150

GEOCHEMISTRY
Measurements of canopy chemistry with 1992 AVIRIS data at Blackhawk Island and Harvard Forest p 1706 N95-23873
Application of MAC-Europe AVIRIS data to the analysis of various alteration stages in the Landdmannalauger Hydrothermal Area (South Iceland) p 1709 N95-23885

GEOCHRONOLOGY
OU3 sediment dating and sedimentation rates | DE95-001891 | p 1734 N95-23384

GEODESIC LINES
A prescribing geodesic curvature problem | DE94-628503 | p 1787 N95-22750

GEOGRAPHIC INFORMATION SYSTEMS
Automation technology using Geographic Information System (GIS) p 1863 N95-23284
Geographic information analysis: An ecological approach for the management of wildlife on the forest landscape | NASA-CR-197941 | p 1719 N95-24094
Measuring forest landscape patterns in the Cascade Range of Oregon, USA p 1719 N95-24096
Forest and wildlife habitat analysis using remote sensing and geographic information systems p 1720 N95-24100

GEOLOGICAL FAULTS
Seismic evidence of conjugate normal faulting: The 1994 Devil Canyon earthquake sequence near Challis, Idaho | DE95-002052 | p 1740 N95-23386

GEOLOGICAL SURVEYS
GPS survey of the western Tien Shan | NASA-CR-197901 | p 1717 N95-22832
Geophysical investigations in the 100 Areas: Fiscal year 1991 through December 1993 | DE95-001573 | p 1736 N95-22843
The US Geological Survey, digital spectral reflectance library: version 1: 0.2 to 3.0 microns p 1703 N95-23855
Classification of the LCVF AVIRIS test site with a Kohonen artificial neural network p 1706 N95-23874
Mapping of the Ronda peridotite massif (Spain) from AVIRIS spectro-imaging survey: A first attempt p 1707 N95-23878
Comparison of inversion models using AIRSAR data for Death Valley, California p 1713 N95-23945
Geologic mapping using integrated AIRSAR, AVIRIS, and TIMS data p 1714 N95-23946

GEOLOGY
Summaries of the 4th Annual JPL Airborne Geoscience Workshop. Volume 1: AVIRIS Workshop | NASA-CR-197877-VOL-1 | p 1701 N95-23844
Classification of the LCVF AVIRIS test site with a Kohonen artificial neural network p 1706 N95-23874
Mapping of the Ronda peridotite massif (Spain) from AVIRIS spectro-imaging survey: A first attempt p 1707 N95-23878

GEOMAGNETIC TAIL
Physics of magnetospheric boundary layers | NASA-CR-197920 | p 1739 N95-23271
An explanation for tailward flows with positive B(sub z) in the distant tail neutral sheet during quite times | ATR-95(7270)-1 | p 1740 N95-23933

GEOMAGNETISM
Dynamics and variability of the plasmasphere observed from synchronous orbit | DE95-002733 | p 1829 N95-22665
Physics of magnetospheric boundary layers | NASA-CR-197920 | p 1739 N95-23271
Characteristics of low energy ions in the Heavy Ions In Space (HIIS) experiment p 1815 N95-23807
Results from the Heavy Ions In Space (HIIS) experiment on the ionic charge state of solar energetic particles p 1870 N95-23808
An explanation for tailward flows with positive B(sub z) in the distant tail neutral sheet during quite times | ATR-95(7270)-1 | p 1740 N95-23933

GEOMETRIC ACCURACY
Spectral variations in a collection of AVIRIS imagery p 1707 N95-23879

GEOMETRIC RECTIFICATION (IMAGERY)
Extraction of auxiliary data from AVIRIS distribution tape for spectral, radiometric, and geometric quality assessment p 1706 N95-23875
Preprocessing: Geocoding of AVIRIS data using navigation, engineering, DEM, and radar tracking system data p 1707 N95-23876
Spectral variations in a collection of AVIRIS imagery p 1707 N95-23879

GEOMETRICAL OPTICS
A uniform geometrical optics and an extended uniform geometrical theory of diffraction for evaluating high frequency EM fields near smooth caustics and composite shadow boundaries | NASA-CR-197934 | p 1657 N95-23391

GEOMETRICAL THEORY OF DIFFRACTION
A uniform geometrical optics and an extended uniform geometrical theory of diffraction for evaluating high frequency EM fields near smooth caustics and composite shadow boundaries | NASA-CR-197934 | p 1657 N95-23391

GEOMORPHOLOGY
The effects of AVIRIS atmospheric calibration methodology on identification and quantitative mapping of surface mineralogy, Drum Mountains, Utah p 1705 N95-23870

GEOPHYSICS
Geophysical investigations in the 100 Areas: Fiscal year 1991 through December 1993 | DE95-001573 | p 1736 N95-22843
Summaries of the 4th Annual JPL Airborne Geoscience Workshop. Volume 1: AVIRIS Workshop | NASA-CR-197877-VOL-1 | p 1701 N95-23844
Summaries of the 4th Annual JPL Airborne Geoscience Workshop. Volume 3: AIRSAR Workshop | NASA-CR-197354-VOL-3 | p 1712 N95-23938

GEOSYNCHRONOUS ORBITS
Energetic particle observations at geosynchronous orbit | DE95-000873 | p 1867 N95-22516
Dynamics and variability of the plasmasphere observed from synchronous orbit | DE95-002733 | p 1829 N95-22665
Geolocation applications of the Gonets LEO messaging satellites p 1656 N95-22818

GEOTHERMAL TECHNOLOGY
Renewable Energy Sources Brno 1993 | DE94-633975 | p 1727 N95-22855

GERMANIDES
Research on defects and transport in amorphous-silicon-based semiconductors | DE94-011888 | p 1660 N95-22586

GERMANIUM
Advanced growth and surface analysis system for in situ studies of interface formation | DE95-002850 | p 1838 N95-22555
Metallization and incomplete melting of a semiconductor surface at high temperature | DE94-627342 | p 1660 N95-22591
Determining orbital particle parameters of impacts into germanium using morphology analysis and calibration data from hypervelocity impact experiments in the laboratory p 1700 N95-23841

GERMANIUM ALLOYS
Advanced growth and surface analysis system for in situ studies of interface formation | DE95-002850 | p 1838 N95-22555
Design of a GaAs/Ge solar array for unmanned aerial vehicles | NASA-TM-106870 | p 1728 N95-23259

GERMINATION
Effect of hyperbaric carbon dioxide on spores and vegetative cells of bacillus stearothermophilus | AD-A280115 | p 1747 N95-23251
Germination, growth rates, and electron microscope analysis of tomato seeds flown on the LDEF p 1748 N95-23821

GHOSTS
Ghost images and feasibility of reconstructions with the Richardson-Lucy algorithm | DE95-002351 | p 1756 N95-23079

GINGA SATELLITE
Investigation of physical parameters in stellar flares observed by GINGA | NASA-CR-196547 | p 1868 N95-23205

GLACIAL DRIFT
Glaciological studies in the central Andes using AIRSAR/TOPSAR p 1713 N95-23942

GLASS
Method of producing a silicon carbide fiber reinforced strontium aluminosilicate glass-ceramic matrix composite | NASA-CASE-LEW-15263-2 | p 1627 N95-22563
Glass science tutorial: Lecture 1, Chemistry and properties of oxide glasses | DE95-002963 | p 1647 N95-22647
Glass science tutorial: Lecture 2, operating electric glass melters | DE95-002965 | p 1647 N95-22648
BEM solution to simulate the curvature driven deformation of a profile that is pressed into a plate of hot glass | PB95-138913 | p 1648 N95-23145
Method of making a semiconductor device using a nanochannel glass matrix | AD-D016383 | p 1662 N95-23241
Oxygen enriched combustion system performance study. Phase 2: 100 percent oxygen enriched combustion in regenerative glass melters | DE95-004212 | p 1635 N95-23481

GLASS TRANSITION TEMPERATURE
Structure and properties of polymeric composite materials during 1501 days outer space exposure at Salyut-7 orbital station p 1652 N95-23915

GLASSWARE
Characterization of Type 304L stainless steel solid-state closure welds for radioactive waste containment | DE94-016539 | p 1645 N95-23980

GLOBAL AIR POLLUTION
Emissions of greenhouse gases in the United States, 1987-1992 | DE95-003001 | p 1731 N95-22691

GLOBAL POSITIONING SYSTEM
GPS survey of the western Tien Shan | NASA-CR-197901 | p 1717 N95-22832
Differential GPS and system integration of the Low Visibility Landing and Surface Operations (LVLASO) demonstration p 1611 N95-23318

GLOBAL WARMING
The atmosphere below | NASA-TM-110538 | p 1740 N95-23663

GLOVES
Method for forming a glove attachment | NASA-CASE-MSC-21632-1 | p 1750 N95-22766

GLUONS
New preliminary results on the physics of charm hadroproduction subprocesses | DE95-002530 | p 1801 N95-22646
The U(3) x U(3) Nambu - Jona-Lasinio model with the gluon condensate and axial anomaly at finite temperature | DE94-628588 | p 1804 N95-22787
Boson mapping techniques applied to constant gauge fields in QCD p 1814 N95-22969
Gluon distribution as function of F(sub 2) and dF(sub 2)/dlnQ(exp 2) at small x | DE94-635677 | p 1812 N95-23975

GOGGLES
Aviator's night vision imaging system preflight adjustment/assessment procedures | AD-A285829 | p 1750 N95-22513

GOLD
The energy broadening resulting from electron stripping process of a low energy Au(-) beam | NIFS-325 | p 1836 N95-23569
Changes in chemical and optical properties of thin film metal mirrors on LDEF p 1651 N95-23907

GOODNESS OF FIT
Consistency and Monte Carlo simulation of a data driven version of smooth goodness-of-fit tests | PB95-141255 | p 1794 N95-23559

GOVERNMENT PROCUREMENT
NASA procurement: Contract and management improvements at the Jet Propulsion Laboratory. Report to Congressional requesters
|GAO/NSIAD-95-40| p 1854 N95-24054
GOVERNMENT/INDUSTRY RELATIONS
NASA Technology Applications Team: Commercial applications of aerospace technology
|NASA-CR-197870| p 1865 N95-23091
Langley Research Center Strategic Plan for Education p 1853 N95-23316
Proceedings of the fuel cells 1994 contractors review meeting
|DE94-012285| p 1730 N95-23977
Defense science and technology strategy
|AD-A285414| p 1903 N95-24179
GOVERNMENTS
DOD budget: Selected categories of planned funding for fiscal years 1995-99. Report to Congressional requesters
|GAO/NSIAD-95-92| p 1864 N95-24062
GRADIENTS
Energetic particle observations at geosynchronous orbit
|DE95-000873| p 1867 N95-22516
Neural network for detection and correction of local boundary misalignments between images
|AD-D016539| p 1766 N95-22705
GRAIN BOUNDARIES
The role of grain boundary chemistry and structure in the environmentally-assisted intergranular cracking of nickel-base alloys
|DE95-002941| p 1638 N95-22532
X-ray diffraction characterization of defect behavior in nanocrystalline nickel during annealing
|DE95-002992| p 1639 N95-22594
A fractal model for intergranular fractures in nanocrystals
|DE94-627393| p 1839 N95-22606
The hydrogen embrittlement of alloy X-750
|DE95-003207| p 1640 N95-22893
Mass transport through polycrystalline microstructures
|DE95-004552| p 1811 N95-23576
Phonon-induced anomalous specific heat of a model nanocrystal by computer simulation
|DE95-004653| p 1843 N95-23585
GRAIN SIZE
X-ray diffraction characterization of defect behavior in nanocrystalline nickel during annealing
|DE95-002992| p 1639 N95-22594
A fractal model for intergranular fractures in nanocrystals
|DE94-627393| p 1839 N95-22606
Investigation of mechanical properties and their relation to the internal structure of nanocrystalline metals and composites
|DE95-001151| p 1627 N95-22683
Mass transport through polycrystalline microstructures
|DE95-004552| p 1811 N95-23576
GRAND UNIFIED THEORY
Unification of electromagnetic, strong and weak interaction
|DE94-628570| p 1655 N95-22746
High Energy Theory: Task B and Task L
|DE95-003453| p 1817 N95-23148
GRAPH THEORY
Treewidth and pathwidth of cocomparability graphs of bounded dimension
|PB95-127239| p 1785 N95-22535
Graph isomorphism models for non interleaving process algebra
|PB95-110490| p 1786 N95-22714
Entropy of Z(sup d) subshifts of finite type
|PB95-108072| p 1787 N95-22836
Regular graphs with four eigenvalues
|PB95-135141| p 1788 N95-23068
PUZZLES 4: Sperner collections and the keys puzzle
|PB95-139374| p 1790 N95-23233
GRAPHICAL USER INTERFACE
HiRel: Hybrid Automated Reliability Predictor (HARP) integrated reliability tool system, (version 7.0). Volume 3: HARP Graphics Oriented (GO) input user's guide
|NASA-TP-3452-VOL-3| p 1753 N95-22479
TIGER: A user-friendly interactive grid generation system for complicated turbomachinery and axis-symmetric configurations p 1670 N95-23419
An interactive tool for discrete phase analysis in two-phase flows p 1683 N95-23641
PCLOOK: An interactive code for spectral analysis
|DE94-635415| p 1759 N95-23963
GRAPHITE
Structural Arrangement Trade Study. Volume 1: Reusable Hydrogen Composite Tank System (RHCTS) and Graphite Composite Primary Structures (GCPS). Executive summary
|NASA-CR-197685| p 1621 N95-23188
Structural arrangement trade study. Volume 3: Reusable Hydrogen Composite Tank System (RHCTS) and Graphite Composite Primary Structures (GCPS). Addendum
|NASA-CR-197687| p 1621 N95-23189
The detection and analysis of galvanic damage in BMI/graphite fiber composites p 1631 N95-23502
GRAPHITE-EPOXY COMPOSITES
LDEF polymeric materials: A summary of Langley characterization p 1651 N95-23899
Organic matrix composite protective coatings for space applications p 1627 N95-23914
GRAPHS (CHARTS)
Treewidth and pathwidth of cocomparability graphs of bounded dimension
|PB95-127239| p 1785 N95-22535
DTS: Building custom, intelligent schedulers p 1779 N95-23744
GRASSES
Estimating dry grass residues using landscape integration analysis p 1705 N95-23867
GRASSLANDS
Estimating dry grass residues using landscape integration analysis p 1705 N95-23867
A comparison of spectral mixture analysis an NDVI for ascertaining ecological variables p 1710 N95-23892
Determination of semi-arid landscape endmembers and seasonal trends using convex geometry spectral unmixing techniques p 1711 N95-23895
Transferring ecosystem simulation codes to supercomputers
|NASA-TM-4662| p 1759 N95-24052
GRATINGS (SPECTRA)
Photoinduced Bragg grating formation in optical fibres as a consequence of convective instability
|DE94-628479| p 1841 N95-23020
PRISM Spectrograph Optical Design
|NASA-CR-197965| p 1828 N95-24035
GRAVELS
Remote identification of a gravel laden Pleistocene river bed p 1712 N95-23921
GRAVITATION
Black hole formation and space-time fluctuations in two dimensional dilaton gravity and complementarity
|DE94-628514| p 1867 N95-22739
Gauge dependence and new kind of two-dimensional gravity theory with trivial quantum corrections
|DE94-628502| p 1850 N95-22776
Traps for antimatter and antihydrogen production
|DE95-002814| p 1805 N95-22927
GRAVITATIONAL EFFECTS
Plant metabolism and cell wall formation in space (microgravity) and on Earth
|NASA-CR-197618| p 1745 N95-22801
Microgravity sciences application visiting scientist program
|NASA-CR-197854| p 1653 N95-23204
Microgravity experiments safety and integration requirements document tree
|NASA-CR-195447| p 1855 N95-23206
Investigation of the role of gravity waves in the generation of equatorial bubbles
|NASA-CR-197962| p 1739 N95-23272
Newton in space
|NASA-TM-110535| p 1799 N95-23273
Living in space
|NASA-TM-110536| p 1751 N95-23274
Toys in space, 2
|NASA-TM-110541| p 1620 N95-23275
USML-1 Glovebox experiments
|NASA-CR-196574| p 1653 N95-24028
Airborne rotary air separator study
|NASA-CR-189099| p 1614 N95-24053
GRAVITATIONAL FIELDS
Non-Noetherian symmetries for oscillators in classical mechanics and in field theory p 1823 N95-22977
Gravitational field of the isolated mass in Yordan-Brans-Dicke theory
|DE94-635441| p 1851 N95-23970
GRAVITATIONAL PHYSIOLOGY
All systems go!
|NASA-TM-110542| p 1620 N95-23665
GRAVITATIONAL WAVES
Nonclassical light in interferometric measurements p 1822 N95-22976
GRAVITY WAVES
Investigation of the role of gravity waves in the generation of equatorial bubbles
|NASA-CR-197962| p 1739 N95-23272
GREEN'S FUNCTIONS
Correlation effects in high-Tc superconductors and heavy fermion compounds
|DE94-629057| p 1840 N95-22846
Computational modeling of properties
|NAS-CR-196544| p 1841 N95-22907
Singular moduli and Arakelov intersection
|DE94-634286| p 1792 N95-23659
GREENHOUSE EFFECT
Emissions of greenhouse gases in the United States, 1987-1992
|DE95-003001| p 1731 N95-22691
Outline for a global environmental strategic planning exercise (GESPE-project)
|PB95-133773| p 1733 N95-23067
GRID GENERATION (MATHEMATICS)
An adaptive projection method for the incompressible Navier-Stokes equations
|DE94-019049| p 1665 N95-22491
Euler Technology Assessment program for preliminary aircraft design employing SPLITFLOW code with Cartesian unstructured grid method
|NASA-CR-4649| p 1608 N95-22917
A perspective on unstructured grid flow solvers
|NASA-CR-195025| p 1788 N95-22931
A CFD study of complex missile and store configurations in relative motion
|NASA-CR-197912| p 1612 N95-22949
High-performance parallel analysis of coupled problems for aircraft propulsion
|NASA-CR-197440| p 1614 N95-23088
Euler technology assessment for preliminary aircraft design employing OVERFLOW code with multiblock structured-grid method
|NASA-CR-4651| p 1608 N95-23095
Eleventh Workshop for Computational Fluid Dynamic Applications in Rocket Propulsion
|NASA-CP-3221-PT-2| p 1668 N95-23412
IGES transformer and NURBS in grid generation p 1669 N95-23415
Criteria for evaluation of grid generation systems p 1669 N95-23416
Structured adaptive grid generation using algebraic methods p 1669 N95-23417
A generic efficient adaptive grid scheme for rocket propulsion modeling p 1670 N95-23418
TIGER: A user-friendly interactive grid generation system for complicated turbomachinery and axis-symmetric configurations p 1670 N95-23419
CFD analysis of turbopump volutes p 1674 N95-23436
Unification of some advection schemes in two dimensions
|NASA-CR-195044| p 1790 N95-23465
Eleventh Workshop for Computational Fluid Dynamic Applications in Rocket Propulsion, part 1
|NASA-CP-3221-PT-1| p 1678 N95-23615
A fine-grid model for the ASRM aft segment with gimballed nozzle p 1685 N95-23648
High energy collimating fine grids
|NASA-CR-197688| p 1871 N95-24191
GROUND BASED CONTROL
Low Earth Orbit satellite/terrestrial mobile service compatibility p 1656 N95-22819
Improved small satellite access of the space network
|NASA-CR-197863| p 1657 N95-22944
Distributed intelligence for ground/space systems p 1770 N95-23685
The Charlotte (TM) intra-vehicular robot p 1697 N95-23703
Truss structure tele-manipulation experiment using ETS-7 p 1623 N95-23726
Preprocessing: Geocoding of AVIRIS data using navigation, engineering, DEM, and radar tracking system data p 1707 N95-23876
Using AVIRIS for in-flight calibration of the spectral shifts of SPOT-HRV and of AVHRR? p 1710 N95-23893
GROUND EFFECT (AERODYNAMICS)
Flow visualization studies of VTOL aircraft models during Hover in ground effect
|NASA-TM-108860| p 1607 N95-22666
GROUND OPERATIONAL SUPPORT SYSTEM
An intelligent ground operator support system p 1769 N95-23681
Modeling actions and operations to support mission preparation p 1617 N95-23750
GROUND STATE
Variational calculations for He-3 impurities on He-4 droplets
|DE94-628469| p 1840 N95-22839
Study of frustrated systems via dissipative maps
|PB95-139093| p 1799 N95-23155
Neutron compton scattering
|PB95-139135| p 1807 N95-23159
GROUND SUPPORT SYSTEMS
Robotic system for the servicing of the orbiter thermal protection system p 1697 N95-23724
GROUND TESTS
Overview of the solar dynamic ground test demonstration program at the NASA Lewis Research Center
|NASA-TM-106876| p 1625 N95-23450
Automatic commanding of the Mars Observer Camera p 1620 N95-23754

GROUND TRUTH
Validation data for land surface temperature determination from satellites
| CSIRO-TR-33 | p 1718 N95-23597
GROUND-AIR-GROUND COMMUNICATION
Low Earth Orbit satellite/terrestrial mobile service compatibility p 1656 N95-22819
GROUP DYNAMICS
Teams and teamwork at NASA Langley Research Center p 1854 N95-23292
GROUP THEORY
Finite-temperature scalar field theory in static de Sitter space
| DE94-628522 | p 1848 N95-22743
Jacobson radicals in matrix near rings
| DE94-628424 | p 1796 N95-22808
The fundamental group of complex hyperplanes arrangements
| DE94-628426 | p 1796 N95-22933
Second International Workshop on Harmonic Oscillators
| NASA-CP-3286 | p 1820 N95-22957
Coherent control in simple quantum systems p 1826 N95-23005
Algebraic description of the elliptic cohomology of classifying spaces
| PB95-110797 | p 1788 N95-23076
AR-descriptions in translatable Frechet spaces
| PB95-138855 | p 1789 N95-23149
On certain N-sheeted coverings of curves and symmetric numerical semigroups which cannot be realized as Weierstrass semigroups
| DE94-634328 | p 1797 N95-23661
GROUP VELOCITY
Tomographic analysis of the three-dimensional variation of the seismic velocity structure of the shallow crust underlying Southern New England
| AD-A279406 | p 1739 N95-23247
GROWTH
Investigation of the role of gravity waves in the generation of equatorial bubbles
| NASA-CR-197962 | p 1739 N95-23272
GUIDANCE (MOTION)
Moving mass trim control for aerospace vehicles
| DE95-002602 | p 1622 N95-23532
GUIDANCE SENSORS
The Starpicker expert system: A problem in expertise capture p 1623 N95-23721
GUIDE VANES
Computational Fluid Dynamics (CFD) analyses in support of Space Shuttle Main Engine (SSME) heat exchanger (HX) vane cracking investigation p 1679 N95-23619
GULF OF MEXICO
Energy flux and hydrogeology of thermal anomalies in the Gulf of Mexico Basin - South Texas example
| DE95-003341 | p 1743 N95-22695
Oceanic operations: An authoritative guide to oceanic operations
| FAA-AFS-550 | p 1610 N95-24065
GULF STREAM
Assimilation of altimeter data in a quasi-geostrophic model of the Gulf Stream system: A dynamical perspective
| NASA-CR-196313 | p 1744 N95-23766
Interferometric synthetic aperture radar imagery of the Gulf Stream p 1712 N95-23939
GUST LOADS
Review of aeronautical fatigue investigation in the Netherlands during the period March 1991-March 1993
| PB95-139184 | p 1612 N95-23161
GUSTS
Aeroacoustic computation of gust-blade interaction p 1800 N95-23313

H

H II REGIONS
Interstellar molecules in the large magellanic cloud
| PB95-139267 | p 1868 N95-23230
H-INFINITY CONTROL
Stable H(infinity) controller design for the longitudinal dynamics of an aircraft
| NASA-TM-106847 | p 1615 N95-22954
Feedback control laws for highly maneuverable aircraft
| NASA-CR-197944 | p 1615 N95-23410
HABITATS
Old-growth and mature forests near spotted owl nests in western Oregon p 1719 N95-24098
Forest and wildlife habitat analysis using remote sensing and geographic information systems p 1720 N95-24100
Dynamics and pattern of a managed coniferous forest landscape in Oregon p 1720 N95-24104
HADRONS
New preliminary results on the physics of charm hadroproduction subprocesses
| DE95-002530 | p 1801 N95-22646
QCD test in three-jet Z(sup 0) decays at SLD and detector development for H(sup 0) yields gamma gamma searches in high energy hadron colliders
| DE95-003336 | p 1848 N95-22698
Baryon number fluctuations in a quark-hadron phase transition
| DE94-628585 | p 1804 N95-22786
Hadrons of arbitrary spin and heavy quark symmetry
| DE94-628597 | p 1804 N95-22789
Measurement of the left-right charge asymmetry in hadronic Z decays and A(sub e) determination
| DE95-003467 | p 1806 N95-23140
A preliminary measurement of the average B hadron lifetime
| DE95-003138 | p 1808 N95-23226
J/psi, psi' yields mu(+)mu(-) and B yields J/psi, psi' cross sections
| DE94-018996 | p 1808 N95-23242
A report on the Indiana University Workshop on future U.S. hadron facilities
| DE95-003951 | p 1817 N95-23353
Introduction to the physics of Higgs bosons
| DE95-003965 | p 1809 N95-23396
Study of b(anti b) production in e(+)e(-) annihilation at radical s = 29 GeV with the aid of neural networks
| DE95-004691 | p 1810 N95-23488
Search for supersymmetric (tilde W)(sub 1) and (tilde Z)(sub 2) states using the D0 detector
| DE95-004581 | p 1811 N95-23581
Charm-conserving strangeness-changing two body hadronic decays of charmed baryons
| DE94-628621 | p 1811 N95-23770
HAFNIUM ALLOYS
Deformation of C15 Laves phase alloys
| DE95-003636 | p 1646 N95-24067
Experimental and theoretical studies on the C15 intermetallic compounds MV2 (M = Zr, Hf and Ta): Elasticity and phase stability
| DE95-003723 | p 1845 N95-24079
HAIR
The significance of hair mineral analysis as a means for assessing internal body burdens of environmental pollutants
| DE94-633512 | p 1734 N95-23541
HALF PLANES
Singular moduli and Arakelov intersection
| DE94-634286 | p 1792 N95-23659
HALF SPACES
Propagation of waves at the loosely bonded interface of two porous elastic half-spaces
| DE94-628477 | p 1800 N95-23018
HALOCARBONS
Emissions of greenhouse gases in the United States, 1987-1992
| DE95-003001 | p 1731 N95-22691
HAMILTONIAN FUNCTIONS
Asymptotically exact solution of the multi-channel resonant-level model
| DE94-629040 | p 1801 N95-22498
Strong-coupling behaviour of two t-J chains with interchain single-electron hopping
| DE94-629041 | p 1838 N95-22499
Existence of solutions for some superlinear or sublinear elliptic systems on R(sup N)
| DE94-628417 | p 1785 N95-22625
Bethe ansatz and quantum Davey-Stewartson 1 system with multicomponent in two dimensions
| DE94-628423 | p 1786 N95-22631
On the (DE-) stabilization of quantum mechanical binding by potential barriers
| DE94-628433 | p 1847 N95-22635
Symplectic computation of Lyapunov exponents
| DE95-002732 | p 1795 N95-22654
Morphology of Laplacian growth processes and statistics of equivalent many-body systems
| DE95-002734 | p 1847 N95-22655
How to measure the Q(bar Q) potential in a light-front calculation
| DE95-003200 | p 1848 N95-22728
Neutrinos with Zee-mass matrix in vacuum and matter
| DE94-628635 | p 1803 N95-22756
Non-zero temperature two-mode squeezing for time-dependent two-level systems
| DE94-628427 | p 1850 N95-22782
Block spins and chirality in Heisenberg model on Kagome and triangular lattices
| DE94-629044 | p 1840 N95-22845
Correlation effects in high-Tc superconductors and heavy fermion compounds
| DE94-629057 | p 1840 N95-22846
Algebraic theory of molecules p 1814 N95-22958
Algebraic approach to the vibrational excitations in methane p 1814 N95-22960
Algebraic description of atom-molecule interactions p 1814 N95-22961
A supersymmetric family of harmonic oscillators simulating H-bonds in DNA p 1748 N95-22983
Molecular vibrational states during a collision p 1814 N95-22964
Harmonic oscillator representation in the theory of scattering and nuclear reactions p 1814 N95-22967
Boson mapping techniques applied to constant gauge fields in QCD p 1814 N95-22969
An algebraic cluster model based on the harmonic oscillator basis p 1814 N95-22971
Harmonic oscillator in quantum rotational spectra: Molecules and nuclei p 1814 N95-22972
Galactic oscillator symmetry p 1822 N95-22973
Shapes and stability of algebraic nuclear models p 1814 N95-22974
Localization in deformed quantum mechanics p 1823 N95-22979
Geometric phases, evolution loops and generalized oscillator potentials p 1823 N95-22981
Coherent states for a generalization of the harmonic oscillator p 1823 N95-22982
Finite-element time evolution operator for the anharmonic oscillator p 1823 N95-22983
Oscillator-like coherent states for the Jaynes-Cummings Model p 1826 N95-23003
Slightly anharmonic systems in quantum optics p 1826 N95-23004
Coherent control in simple quantum systems p 1826 N95-23005
Phase space analysis in anisotropic optical systems p 1826 N95-23007
Asymptotically exact solution of a local copper-oxide model
| DE94-628492 | p 1842 N95-23059
Degenerate Hamiltonian Hopf bifurcations
| PB95-138871 | p 1789 N95-23174
The impact of QCD and light-cone quantum mechanics on nuclear physics
| DE95-004293 | p 1851 N95-23352
Charm-conserving strangeness-changing two body hadronic decays of charmed baryons
| DE94-628621 | p 1811 N95-23770
Scattering problem for quantum system with time-dependent periodic Hamiltonian
| DE94-635421 | p 1797 N95-23965
The kinetics of quantum system with time-dependent periodic Hamiltonian
| DE94-635422 | p 1797 N95-23966
The point interactions in the quantum problem of three particles with internal structure
| DE94-635423 | p 1851 N95-23967
A theory for the morphology of Laplacian growth from statistics of equivalent many-body Hamiltonian systems
| DE94-014473 | p 1799 N95-23979
TRACKER: A three-dimensional raytracing program for ionospheric radio propagation
| DE95-003510 | p 1658 N95-24015
HANDBOOKS
Microgravity experiments safety and integration requirements document tree
| NASA-CR-195447 | p 1855 N95-23206
HANDEDNESS
Hard e(+)e(-)-pair Bremsstrahlung as a lepton polarimeter
| DE94-635615 | p 1812 N95-23984
HARDNESS
Investigation of depth-area relationships associated with nanoindentations
| DE95-001353 | p 1639 N95-22686
HARDWARE
Mir hardware heritage
| NASA-RP-1357 | p 1621 N95-23249
Hardware interface unit for control of shuttle RMS vibrations p 1697 N95-23706
Lazy release consistency for hardware-coherent multiprocessors
| TR-547 | p 1765 N95-24184
HARDWARE DESCRIPTION LANGUAGES
Specification and verification of gate-level VHDL models of synchronous and asynchronous circuits
| NASA-CR-191608 | p 1762 N95-22830
HARMONIC GENERATIONS
Growth of single crystals of organic salts with large second-order optical nonlinearities by solution processes for devices
| NASA-CR-197963 | p 1843 N95-23563
HARMONIC OSCILLATION
A Ramanujan-type measure for the Askey-Wilson polynomials p 1797 N95-22975

HARMONIC OSCILLATORS
Second International Workshop on Harmonic Oscillators
| NASA-CP-3286 | p 1820 N95-22957
Algebraic approach to the vibrational excitations in methane p 1814 N95-22960
A supersymmetric family of harmonic oscillators simulating H-bonds in DNA p 1748 N95-22963
Molecular vibrational states during a collision p 1814 N95-22964
Harmonic oscillator representation in the theory of scattering and nuclear reactions p 1814 N95-22967
A possible generalization of the harmonic oscillator potential p 1822 N95-22970
An algebraic cluster model based on the harmonic oscillator basis p 1814 N95-22971
Harmonic oscillator in quantum rotational spectra: Molecules and nuclei p 1814 N95-22972
Galactic oscillator symmetry p 1822 N95-22973
Noisy bases in Hilbert space: A new class of thermal coherent states and their properties p 1823 N95-22980
Geometric phases, evolution loops and generalized oscillator potentials p 1823 N95-22981
Coherent states for a generalization of the harmonic oscillator p 1823 N95-22982
Finite-element time evolution operator for the anharmonic oscillator p 1823 N95-22983
q-bosons and the q-analogue quantized field p 1814 N95-22984
A method of solving simple harmonic oscillator Schroedinger equation p 1797 N95-22989
Wigner distribution function and entropy of the damped harmonic oscillator within the theory of the open quantum systems p 1798 N95-22990
Covariant harmonic oscillators and coupled harmonic oscillators p 1825 N95-22992
Coherent states for the relativistic harmonic oscillator p 1825 N95-22993
The Duffin-Kemmer-Petiau oscillator p 1825 N95-22998
Harmonic oscillators and resonance series generated by a periodic unstable classical orbit p 1825 N95-22999
Oscillator-like coherent states for the Jaynes-Cummings Model p 1826 N95-23003
Kravchuk functions for the finite oscillator approximation p 1798 N95-23006

HARTREE APPROXIMATION
The impact of QCD and light-cone quantum mechanics on nuclear physics
| DE95-004293 | p 1851 N95-23352

HAZARDS
Mishap risk control for advanced aerospace/composite materials p 1628 N95-23031
Fire hazard considerations for composites in vehicle design p 1628 N95-23032
Corrosion prevention with environmentally compliant materials: A design challenge p 1644 N95-23511

HEAD (ANATOMY)
Design of a cervical spine gross motion simulator for standard size human and anthropomorphic dummy adult and child
| NIAR-94-16 | p 1751 N95-24021

HEAD-UP DISPLAYS
TRISTAR 1: Evaluation methods for testing head-up display (HUD) flight symbology
| NASA-TM-4665 | p 1613 N95-24030

HEALTH
Environmental, Safety, and Health Considerations: Composite Materials in the Aerospace Industry
| NASA-CP-3289 | p 1628 N95-23025
Health, safety and environmental requirements for composite materials p 1628 N95-23028
Skin exposure: Assessing the hazard in the workplace p 1628 N95-23030
The significance of hair mineral analysis as a means for assessing internal body burdens of environmental pollutants
| DE94-633512 | p 1734 N95-23541
Biological interactions and human health effects of static magnetic fields
| DE95-003147 | p 1749 N95-24145

HEAT EXCHANGERS
Phase 2: HGM air flow tests in support of HEX vane investigation p 1674 N95-23438
Unsteady flow simulations in support of the SSME HEX turning vane cracking investigation with the ATD HPOTP p 1679 N95-23621

HEAT FLUX
Engineering design of a radiative divertor for DIII-D
| DE95-003008 | p 1693 N95-22798
Measurements and modeling of impurity source distributions from the Tore Supra outboard pump limiter
| DE95-003097 | p 1831 N95-22800
Divertor heat and particle control experiments on the DIII-D tokamak
| DE94-017518 | p 1832 N95-23119
Flow and heat transfer in 180-degree turn square ducts: Effects of turning configuration and system rotation p 1682 N95-23636
Development of sensors for ceramic components in advanced propulsion systems
| NASA-CR-195324 | p 1689 N95-23795

HEAT OF COMBUSTION
Level set techniques applied to unsteady detonation propagation
| DE95-002741 | p 1666 N95-22901

HEAT PIPES
Summary of solar cell data from the Long Duration Exposure Facility (LDEF)
| NASA-CR-196539 | p 1727 N95-22904
HTS current lead using a composite heat pipe
| DE95-003718 | p 1662 N95-23368
Micro heat spreader enhanced heat transfer in MCM's
| DE95-004520 | p 1663 N95-23779

HEAT RESISTANT ALLOYS
Temperature effects on hydrogen-induced cracking in an iron-based superalloy
| DE95-003037 | p 1639 N95-22724
An investigation into the effects of hydrogen on the fracture and deformation of Alloy X-750
| DE95-003206 | p 1639 N95-22732

HEAT SHIELDING
Protective coating for ceramic materials
| NASA-CASE-ARC-11969-1-CU | p 1649 N95-23394

HEAT TRANSFER
Gas cooled leads. Part 1: Theoretical Study. Part 2: Frost free lead optimized for a specific current. Part 3: Frost free lead optimized for a large current range
| DE95-002657 | p 1660 N95-22716
Level set techniques applied to unsteady detonation propagation
| DE95-002741 | p 1666 N95-22901
Development and verification of a resin film infusion/resin transfer molding simulation model for fabrication of advanced textile composites
| NASA-CR-197439 | p 1648 N95-23179
Eleventh Workshop for Computational Fluid Dynamic Applications in Rocket Propulsion
| NASA-CP-3221-PT-2 | p 1668 N95-23412
Heat transfer in rocket engine combustion chambers and nozzles p 1668 N95-23413
Thermal modeling of the lithium/polymer battery
| DE95-004680 | p 1663 N95-23494
Eleventh Workshop for Computational Fluid Dynamic Applications in Rocket Propulsion, part 1
| NASA-CP-3221-PT-1 | p 1678 N95-23615
Computational Fluid Dynamics (CFD) analyses in support of Space Shuttle Main Engine (SSME) heat exchanger (HX) vane cracking investigation p 1679 N95-23619
CFD modeling of turbulent duct flows for coolant channel analysis p 1682 N95-23635
Flow and heat transfer in 180-degree turn square ducts: Effects of turning configuration and system rotation p 1682 N95-23636
Micro heat spreader enhanced heat transfer in MCM's
| DE95-004520 | p 1663 N95-23779
Effects of jet strength on NOx formation in premixed impinging jet combustion with minimum heat losses
| NAL-TR-1237T | p 1637 N95-24181

HEAT TRANSMISSION
Modeling of nonequilibrium space plasma flows
| NASA-CR-197432 | p 1833 N95-23211

HEAT TREATMENT
High-temperature ultrasonic characterization of Ag-clad superconductor tapes
| DE95-002909 | p 1838 N95-22530

HEATING
Load calculation and system evaluation for electric vehicle climate control
| DE95-004350 | p 1695 N95-23358

HEAVY ELEMENTS
The electronic structure of heavy element complexes
| DE95-003407 | p 1806 N95-23082
Search for millimeterwave CO emission in damped Lyman-alpha systems
| PB95-139259 | p 1868 N95-23607

HEAVY IONS
Interdigital-H linac for unstable nuclei at INS
| DE94-765448 | p 1816 N95-22644
(pi)N correlations at AGS
| DE95-002933 | p 1801 N95-22656
A heavy ion linac complex for unstable nuclei
| DE94-765443 | p 1816 N95-22848
Genetic effects on heavy ions in drosophila
| NASA-CR-197916 | p 1746 N95-22911
Comparison of exact solution with Eikonal approximation for elastic heavy ion scattering
| NASA-TP-3498 | p 1817 N95-22929
The energy broadening resulting from electron stripping process of a low energy Au(-) beam
| NIFS-325 | p 1836 N95-23569
Trapped iron measured on LDEF p 1872 N95-23806
Characteristics of low energy ions in the Heavy Ions In Space (HIIS) experiment p 1815 N95-23807
Results from the Heavy Ions In Space (HIIS) experiment on the ionic charge state of solar energetic particles p 1870 N95-23808

HEAVY LIFT LAUNCH VEHICLES
Advanced liquid oxygen (LO2) propellant conditioning concept testing
| NASA-TM-108477 | p 1652 N95-22672

HEAVY NUCLEI
Geometrical interpretation for the outer SU(3) outer multiplicity label p 1814 N95-22968
LDEF contributions to cosmic ray and radiation environments research p 1872 N95-23805
Early results from the ultra heavy cosmic ray experiment p 1872 N95-23809

HEISENBERG THEORY
Deformed Heisenberg algebra and fractional spin field in 2+1 dimensions
| DE94-628507 | p 1850 N95-22779
Block spins and chirality in Heisenberg model on Kagome and triangular lattices
| DE94-629044 | p 1840 N95-22845

HELICAL WINDINGS
The next Large Helical Devices
| NIFS-323 | p 1835 N95-23535
Recent studies of the Large Helical Device
| NIFS-322 | p 1835 N95-23543

HELICOPTER CONTROL
An investigation of helicopter dynamic coupling using an analytical model
| NASA-CR-197420 | p 1612 N95-23217

HELICOPTER PROPELLER DRIVE
Gearbox vibration diagnostic analyzer
| NASA-CR-189141 | p 1696 N95-23792

HELICOPTERS
An investigation of helicopter dynamic coupling using an analytical model
| NASA-CR-197420 | p 1612 N95-23217
Thin tailored composite wing for civil tiltrotor p 1613 N95-23317

HELIOSTATS
Advanced reflector materials for solar concentrators
| DE95-000248 | p 1726 N95-22547

HELIOTRONS
Physical mechanism determining the radial electric field and its radial structure in a toroidal plasma
| NIFS-313 | p 1835 N95-23534
The next Large Helical Devices
| NIFS-323 | p 1835 N95-23535
Recent studies of the Large Helical Device
| NIFS-322 | p 1835 N95-23543

HELIUM
Tritium transport, influx, and helium ash measurements on TFTR during DT operation
| DE95-003708 | p 1833 N95-23269
Theoretical calculations of pressure broadening coefficients for H2O perturbed by hydrogen or helium gas
| NASA-CR-197345 | p 1636 N95-23545
Effect of dynamically charged helium on mechanical properties of vanadium-base alloys
| DE95-004613 | p 1646 N95-24153

HELIUM IONS
ESTAR, PSTAR, ASTAR: A PC package for calculating stopping powers and ranges of electrons, protons and helium ions, version 2
| DE94-634435 | p 1811 N95-23773

HELIUM ISOTOPES
Variational calculations for He-3 impurities on He-4 droplets
| DE94-628469 | p 1840 N95-22839
Status of helium-production reaction studies with a spallation neutron source
| DE95-002816 | p 1806 N95-23137

HELIUM PLASMA
Divertor heat and particle control experiments on the DIII-D tokamak
| DE94-017518 | p 1832 N95-23119

HERBICIDES
Extraction and detection of pesticide residues from air filter inserts using supercritical carbon dioxide
| DE95-004579 | p 1735 N95-23580

HERMITIAN POLYNOMIAL
Coherent states for the relativistic harmonic oscillator p 1825 N95-22993
On adaptive weighted polynomial preconditioning for Hermitian positive definite matrices
| NASA-CR-197946 | p 1791 N95-23547

An implementation of the QMR method based on coupled two-term recurrences
|NASA-CR-197956| p 1791 N95-23612

HETEROGENEITY
Coordinating complex decision support activities across distributed applications p 1761 N95-23749
Loop scheduling for heterogeneity
|TR-540| p 1764 N95-23936

HETEROJUNCTIONS
Optical absorption in an indirect-gap semiconductor quantum well systems
|DE94-628878| p 1849 N95-22759
Photoemission study of quantum confinement by a finite barrier: Cu/Co(wedge)/Cu(100)
|DE95-002913| p 1840 N95-22762

HEURISTIC METHODS
Unstructured grids on SIMD torus machines
|NASA-CR-197954| p 1758 N95-23610
An efficient algorithm for concurrent priority queue heaps
|TR-560| p 1759 N95-24033

HIERARCHIES
Browsing semantics in the tower model
|PB95-127221| p 1855 N95-22534
Solutions for the vector k-constrained KP hierarchy
|DE94-628431| p 1786 N95-22633
Hierarchical membership protocol for synchronous distributed systems
|PB95-138947| p 1763 N95-23129
NASA Thesaurus, Supplement
|NASA-SP-7096-SUPPL-1| p 1856 N95-23223

HIGGS BOSONS
Neutrinos with Zee-mass matrix in vacuum and matter
|DE94-628635| p 1803 N95-22756
Introduction to the physics of Higgs bosons
|DE95-003965| p 1809 N95-23396
A measurement of the mass of the W vector boson at CDF
|DE95-003498| p 1813 N95-24016

HIGH ALTITUDE
Particle kinetic simulation of high altitude hypervelocity flight
|NASA-CR-197383| p 1664 N95-22481
Four-nozzle benchmark wind tunnel model USA code solutions for simulation of multiple rocket base flow recirculation at 145,000 feet altitude p 1686 N95-23654
Numerical study of base pressure characteristic curve for a four-engine clustered nozzle configuration p 1625 N95-23655

HIGH ALTITUDE TESTS
NLS base heating CFD analysis p 1673 N95-23432

HIGH ASPECT RATIO
Convergence acceleration of implicit schemes in the presence of high aspect ratio grid cells p 1676 N95-23446

HIGH CURRENT
Gas cooled leads. Part 1: Theoretical Study. Part 2: Frost free lead optimized for a specific current. Part 3: Frost free lead optimized for a large current range
|DE95-002657| p 1660 N95-22716
The q profile evolution and enhanced core confinement of high (beta)(sub p) plasmas in D3-D
|DE95-003878| p 1834 N95-23371
Preparation of high quality YBa2Cu3O(7-delta) thick films on flexible Ni-based alloy substrates with textured buffer layers
|DE95-003686| p 1645 N95-23571
High current induction linacs
|DE95-003442| p 1818 N95-24014

HIGH ENERGY INTERACTIONS
A brief history in time of ion traps and their achievements in science
|DE95-002815| p 1805 N95-22936
High Energy Theory: Task B and Task L
|DE95-003453| p 1817 N95-23148
A report on the Indiana University Workshop on future U.S. hadron facilities
|DE95-003951| p 1817 N95-23353

HIGH FREQUENCIES
Investigation of Federal Standard 1045 high-frequency ALE radio performance in the Southern Trans-Auroral Zone
|PB94-204831| p 1655 N95-22636

HIGH GAIN
High gain GaAs Photoconductive Semiconductor Switches for impulse sources
|DE95-001885| p 1659 N95-22549
High gain GaAs photoconductive semiconductor switches: Measurement of filament velocity and reduced trigger energy
|DE95-001884| p 1661 N95-22844

HIGH POWER LASERS
Production of high contrast ultrashort laser pulses for short scale length plasma experiments
|DE95-003640| p 1690 N95-22595

HIGH PRESSURE
High pressure neutron powder diffraction at LANSCE
|DE95-002703| p 1839 N95-22565
Progress towards the synthesis of polymeric nitrogen
|DE94-017547| p 1841 N95-22860
Finite-difference solutions of the alternate turbopump development high-pressure oxidizer turbopump pump-end ball-bearing cavity flows p 1678 N95-23617
Navier-Stokes flow field analysis of compressible flow in a pressure relief valve p 1679 N95-23618
Three-D flow analysis of the alternate SSME HPOT TAD p 1679 N95-23620
Comparison between predicted and experimentally measured flow fields at the exit of the SSME HPFTP impeller p 1679 N95-23622

HIGH PRESSURE OXYGEN
Computational Fluid Dynamics (CFD) analyses in support of Space Shuttle Main Engine (SSME) heat exchanger (HX) vane cracking investigation p 1679 N95-23619

HIGH RESOLUTION
X-ray transmission microscope development
|NASA-CR-197884| p 1826 N95-23016
MAX-91: Polarimetric SAR results on Montespertoli site p 1712 N95-23940

HIGH SPEED
High-velocity penetrators
|DE95-001886| p 1698 N95-22500
Controlling under-actuated robot arms using a high speed dynamics process
|NASA-CASE-NPO-18498-1-CU| p 1692 N95-22543
Micro-sensor thin-film anemometer
|NASA-CASE-LAR-15112-1-CU| p 1666 N95-22906
Inner loop flight control for the High-Speed Civil Transport p 1616 N95-23314
Modelling and analysis of a high speed data bus with predicate/transition nets
|PB95-140695| p 1764 N95-23538
A high speed digitizing photomultiplier tube base for the KTeV CsI calorimeter
|DE95-003739| p 1664 N95-24081

HIGH SPEED CAMERAS
Amplified MOS Imager
|NHK-LABS-NOTE-432| p 1690 N95-24107

HIGH STRENGTH
Deflections of anisotropic sandwich beams with variable face sheets and core thicknesses p 1700 N95-23310

HIGH STRENGTH ALLOYS
Exfoliation corrosion and stress corrosion cracking behaviour of Al-Li alloys p 1641 N95-23498

HIGH STRENGTH STEELS
Test method and test results for environmental assessment of aircraft materials p 1643 N95-23509

HIGH TEMPERATURE
Metallization and incomplete melting of a semiconductor surface at high temperature
|DE94-627342| p 1660 N95-22591
MOCVD of gallium and calcium sulfides for improved phosphor processing
|DE95-000918| p 1631 N95-22677
Evolution of oxidation and creep damage mechanisms in HIPed silicon nitride materials
|DE95-001360| p 1647 N95-22689
Progress towards the synthesis of polymeric nitrogen
|DE94-017547| p 1841 N95-22860
Design of a variable area diffuser for a 15-inch Mach 6 open-jet tunnel p 1617 N95-23309
Electrochemical studies of perovskite mixed conductors
|DE95-003704| p 1636 N95-23573
Advances in research for solid oxide fuel cells
|DE95-004590| p 1730 N95-23582
Effect of different ions on the anodic behaviour of alloy 800 chloride solutions at high temperature
|DE94-634944| p 1645 N95-23983

HIGH TEMPERATURE GASES
Phase 2: HGM air flow tests in support of HEX vane investigation p 1674 N95-23438
Advanced multi-phase flow CFD model development for solid rocket motor flowfield analysis p 1683 N95-23638

HIGH TEMPERATURE PLASMAS
Semikinetic modeling and observations of high-latitude plasma outflow
|NASA-CR-197403| p 1831 N95-23008

HIGH TEMPERATURE SUPERCONDUCTORS
Asymptotically exact solution of the multi-channel resonant-level model
|DE94-629040| p 1801 N95-22498
Superconducting Tl2Ba2CaCu2O8 thin films prepared by post-annealing in a flow-through multiple-zone furnace
|DE95-002745| p 1838 N95-22520
High pressure neutron powder diffraction at LANSCE
|DE95-002703| p 1839 N95-22565
Conceptual design of a 20-kA current lead using forced-flow cooling and Ag-alloy-sheathed Bi-2223 high-temperature superconductors
|DE95-002916| p 1660 N95-22569
Analyses, algorithms, and computations for models of high-temperature superconductivity
|DE95-003290| p 1661 N95-22733
Correlation effects in high-Tc superconductors and heavy fermion compounds
|DE94-629057| p 1840 N95-22846
High Tc superconducting bolometric and nonbolometric infrared (IR) detectors
|NASA-CR-197868| p 1827 N95-23224
Potential aerospace applications of high temperature superconductors p 1664 N95-23322
Some aspects of critical currents in Ag sheathed Bi2Sr2Ca2Cu3O10 composite tapes: A summary
|DE95-003952| p 1842 N95-23354
HTS current lead using a composite heat pipe
|DE95-003718| p 1662 N95-23368
Electrochemical studies of perovskite mixed conductors
|DE95-003704| p 1636 N95-23573
Phonon characteristics of high (T sub c) superconductors from neutron Doppler broadening measurements
|DE95-003703| p 1844 N95-24076
Design of a high-temperature superconductor current lead for electric utility SMES
|DE95-004604| p 1664 N95-24163
Dependence of the Josephson coupling of unconventional superconductors on the properties of the tunneling barrier
|DE95-004649| p 1846 N95-24173

HIGH VOLTAGES
Method and system for electron beam lithography
|AD-D016554| p 1660 N95-22709

HIGHLY MANEUVERABLE AIRCRAFT
Feedback control laws for highly maneuverable aircraft
|NASA-CR-197944| p 1615 N95-23410

HILBERT SPACE
Spectral application of the theorem for the essential quasi-Fredholm spectrum
|DE94-628430| p 1795 N95-22632
First quantized noncritical relativistic Polyakov string
|DE94-628513| p 1848 N95-22738
Noisy bases in Hilbert space: A new class of thermal coherent states and their properties p 1823 N95-22980

HISTORIES
IRAS sky survey atlas: Explanatory supplement
|NASA-CR-197335| p 1865 N95-22539
Mir hardware heritage
|NASA-RP-1357| p 1621 N95-23249
Endeavor: Now and then
|NASA-TM-110539| p 1620 N95-23664

HOHLRAUMS
Laser-plasma instability in hohlraums
|DE95-000914| p 1829 N95-22676
Progress in ion beam power coupling and ion-driven hohlraums on PBFA 2
|DE95-004544| p 1818 N95-24160

HOLES (MECHANICS)
Stress intensity factors and crack mouth openings for bridged cracks emanating from circular holes
|AR-008-408| p 1699 N95-22952
Eddy current detection of pitting corrosion around fastener holes p 1643 N95-23507
POD assessment of NDI procedures using a round robin test
|AGARD-R-809| p 1697 N95-23602

HOLLOW CATHODES
Functional testing of the space station plasma contactor
|NASA-TM-106841| p 1624 N95-23240

HOLOGRAPHIC INTERFEROMETRY
Holographic interferometric tomography for reconstructing flow fields p 1690 N95-23287

HOLOGRAPHY
Optical image correlator using orthogonal data storage
|AD-A285795| p 1819 N95-22508
Full resolution hologram-like autostereoscopic display
|NASA-CR-197913| p 1689 N95-23789

HOMEOSTASIS
Interrelations between nervous system and immune system in stress situations
|PB95-135521| p 1748 N95-22770

HOMOLOGY
Lectures on homology with internal symmetries
|DE94-628409| p 1785 N95-22619
Geometry of Moishezon and 1-convex spaces 2: Projectivity of Moishezon spaces and its non-compact version
|DE94-628415| p 1795 N95-22623
The Euler series of restricted Chow varieties
|DE94-628418| p 1785 N95-22626

Algebraic description of the elliptic cohomology of classifying spaces
|PB95-110797| p 1788 N95-23076

HOMOMORPHISMS
Lectures on homology with internal symmetries
|DE94-628409| p 1785 N95-22619

HONEYCOMB STRUCTURES
Deflections of anisotropic sandwich beams with variable face sheets and core thicknesses p 1700 N95-23310

HOT ELECTRONS
Semikinetic modeling and observations of high-latitude plasma outflow
|NASA-CR-197403| p 1831 N95-23008

HOT ISOSTATIC PRESSING
Evolution of oxidation and creep damage mechanisms in HIPed silicon nitride materials
|DE95-001360| p 1647 N95-22689

HOT PRESSING
BEM solution to simulate the curvature driven deformation of a profile that is pressed into a plate of hot glass
|PB95-138913| p 1648 N95-23145

HOUSINGS
Synchronous dynamics of a coupled shaft/bearing/housing system with auxiliary support from a clearance bearing: Analysis and experiment
|NASA-CR-197858| p 1695 N95-23214

HOVERING
Flow visualization studies of VTOL aircraft models during Hover in ground effect
|NASA-TM-108860| p 1607 N95-22666

HUBBLE SPACE TELESCOPE
Ghost images and feasibility of reconstructions with the Richardson-Lucy algorithm
|DE95-002351| p 1756 N95-23079
STS-61 Space Shuttle mission report
|NASA-TM-110545| p 1619 N95-23187
STS-61 mission director's post-mission report
|NASA-TM-104803| p 1617 N95-23262
Planning and scheduling the Hubble Space Telescope: Practical application of advanced techniques p 1779 N95-23740

HUBS
NASA low-speed axial compressor for fundamental research
|NASA-TM-4635| p 1616 N95-23192

HULLS (STRUCTURES)
Capacitated facility location: Valid inequalities and facets (revised)
|PB95-130225| p 1786 N95-22641

HUMAN BEHAVIOR
Method of encouraging attention by correlating video game difficulty with attention level
|NASA-CASE-LAR-15022-1| p 1749 N95-22579

HUMAN BODY
All systems go!
|NASA-TM-110542| p 1620 N95-23665
Design of a cervical spine gross motion simulator for standard size human and anthropomorphic dummy adult and child
|NIAR-94-16| p 1751 N95-24021

HUMAN FACTORS ENGINEERING
The viability of establishing collaborative, reconfigurable research environments for the Human Performance Research Laboratory at NASA Ames
|NASA-CR-197384| p 1753 N95-22480
Human-centered design of human-computer-human dialogs in aerospace systems
|NASA-CR-197379| p 1750 N95-22797
TRISTAR 1: Evaluation methods for testing head-up display (HUD) flight symbology
|NASA-TM-4665| p 1613 N95-24030
A computational theory of grounding in natural language conversation
|TR-545| p 1760 N95-24058

HUMAN PERFORMANCE
The viability of establishing collaborative, reconfigurable research environments for the Human Performance Research Laboratory at NASA Ames
|NASA-CR-197384| p 1753 N95-22480
Method of encouraging attention by correlating video game difficulty with attention level
|NASA-CASE-LAR-15022-1| p 1749 N95-22579
Some performance effects of age and low blood alcohol levels on a computerized neuropsychological test
|DOT/FAA/AM-95/7| p 1749 N95-23788
Effects of age and low doses of alcohol on compensatory tracking during angular acceleration
|DOT/FAA/AM-95/3| p 1750 N95-23934

HUMAN RELATIONS
Teams and teamwork at NASA Langley Research Center p 1854 N95-23292

HUMAN RESOURCES
The software analysis project for the Office of Human Resources p 1854 N95-23331

HUMAN-COMPUTER INTERFACE
Human-centered design of human-computer-human dialogs in aerospace systems
|NASA-CR-197379| p 1750 N95-22797
Simulation and off-line programming systems comparison
|DE95-002267| p 1766 N95-23078
Knowledge-based guidance and control functions
|AGARD-AR-325| p 1751 N95-23601
Software agents for the dissemination of remote terrestrial sensing data p 1721 N95-23675
Commercialization of JPL Virtual Reality calibration and redundant manipulator control technologies p 1768 N95-23676
Knowledge representation and reasoning for mixed-initiative planning
|TR-562| p 1783 N95-24031
Architecture and evolution of Goddard Space Flight Center Distributed Active Archive Center p 1862 N95-24134

HUMIDITY
Corrosion of landing gear steels p 1642 N95-23500
Assessing the relative contribution of biogenic and fossil processes to visibility scattering aerosols found in remote areas: Near-term Organic Research Program
|DE95-003149| p 1735 N95-24146

HUNGARY
Revitalization of the Gemenc-area, Baja, Hungary. 1: A study on hydrological possibilities to revitalise the ecosystem in the Keselyues-area. 2: Towards the restoration of the Gyueruesalj floodplain
|PB95-139283| p 1718 N95-23469

HYBRID PROPULSION
Fundamental phenomena on fuel decomposition and boundary layer combustion processes with applications to hybrid rocket motors
|NASA-CR-197919| p 1625 N95-23261

HYDRAULIC JETS
Experimental study of vortex breakdown in a swirling water jet
|PB95-130407| p 1665 N95-22767

HYDROCARBON COMBUSTION
Ethylene oxidation chemistry in a well-stirred reactor
|DE95-004823| p 1635 N95-23381

HYDROCARBON FUEL PRODUCTION
Design and demonstration of an immobilized-cell fluidized-bed reactor for the efficient production of ethanol
|DE94-014023| p 1652 N95-22587
Preliminary assessment of air toxic emissions in the natural gas industry, phase 1
|PB95-135547| p 1732 N95-22865

HYDROCARBON FUELS
Multi-fuel reformers for fuel cells used in transportation: Assessment of hydrogen storage technologies
|DE94-017655| p 1727 N95-22861

HYDROCARBONS
Magnetic resonance and optical spectroscopic studies of carotenoids
|DE95-003729| p 1631 N95-22575
Particle size dependence in Fischer-Tropsch synthesis
|DE95-003124| p 1633 N95-22876
Conversion of light hydrocarbon gases to metal carbides for production of liquid fuels and chemicals
|DE95-000362| p 1634 N95-23164

HYDROCYANIC ACID
Interstellar molecules in the large magellanic cloud
|PB95-139267| p 1868 N95-23230

HYDRODYNAMICS
Laser-plasma instability in hohlraums
|DE95-000914| p 1829 N95-22676
Dimensional scaling for impact cratering and perforation p 1624 N95-23843

HYDROELECTRICITY
Renewable Energy Sources Brno 1993
|DE94-633975| p 1727 N95-22855

HYDROGEN
More about the q-deformed H-atom wave functions: Normal and abnormal series
|DE94-628434| p 1801 N95-22643
Hydrogen vibrational density of states of adsorbed water on rare-earth modified zirconia
|DE95-001127| p 1632 N95-22681
Investigation of mechanical properties and their relation to the internal structure of nanocrystalline metals and composites
|DE95-001151| p 1627 N95-22683
Ethylene oxidation chemistry in a well-stirred reactor
|DE95-004823| p 1635 N95-23381
Hydrogen and fuel cells for energy storage
|DE95-723907| p 1729 N95-23382
Multi-fuel reformers for fuel cells used in transportation. Phase 1: Multi-fuel reformers
|DE95-004215| p 1729 N95-23482
Time-resolved EPR studies of the H atom: A stable heavy isotope of muonium
|DE95-004614| p 1810 N95-23491
Theoretical calculations of pressure broadening coefficients for H2O perturbed by hydrogen or helium gas
|NASA-CR-197345| p 1636 N95-23545
Search for millimeterwave CO emission in damped Lyman-alpha systems
|PB95-139259| p 1868 N95-23607

HYDROGEN ATOMS
Exotic atoms
|DE95-003199| p 1805 N95-22881

HYDROGEN BONDS
A supersymmetric family of harmonic oscillators simulating H-bonds in DNA p 1748 N95-22963

HYDROGEN EMBRITTLEMENT
Temperature effects on hydrogen-induced cracking in an iron-based superalloy
|DE95-003037| p 1639 N95-22724
An investigation into the effects of hydrogen on the fracture and deformation of Alloy X-750
|DE95-003206| p 1639 N95-22732
The hydrogen embrittlement of alloy X-750
|DE95-003207| p 1640 N95-22893

HYDROGEN ENGINES
A hybrid vehicle evaluation code and its application to vehicle design
|DE95-004205| p 1662 N95-23334

HYDROGEN FUELS
Multi-fuel reformers for fuel cells used in transportation: Assessment of hydrogen storage technologies
|DE94-017655| p 1727 N95-22861
Structural Arrangement Trade Study. Volume 1: Reusable Hydrogen Composite Tank System (RHCTS) and Graphite Composite Primary Structures (GCPS). Executive summary
|NASA-CR-197685| p 1621 N95-23188
Structural arrangement trade study. Volume 3: Reusable Hydrogen Composite Tank System (RHCTS) and Graphite Composite Primary Structures (GCPS). Addendum
|NASA-CR-197687| p 1621 N95-23189
Flowfield characterization in a LOX/GH2 propellant rocket p 1684 N95-23642
A summary of the slush hydrogen technology program for the National Aero-Space Plane
|NASA-TM-106863| p 1653 N95-24186

HYDROGEN ISOTOPES
Large-sized and highly radioactive H-3 and Cd-109 Langmuir-Blodgett films
|DE94-785270| p 1811 N95-23775
Modified molecular sieves: Stationary phase for the gas chromatographic separation of hydrogen isotopes
|DE94-627282| p 1814 N95-24175

HYDROGEN OXYGEN ENGINES
Predicted performance of an integrated modular engine system
|NASA-CR-190787| p 1625 N95-23791

HYDROGEN PEROXIDE
Atmospheric peroxides
|DE95-004435| p 1733 N95-23362

HYDROGEN PRODUCTION
Supported transition metal catalysts for para- to ortho-hydrogen conversion
|NASA-CR-197907| p 1634 N95-23252
Multi-fuel reformers for fuel cells used in transportation. Phase 1: Multi-fuel reformers
|DE95-004215| p 1729 N95-23482

HYDROGEOLOGY
Energy flux and hydrogeology of thermal anomalies in the Gulf of Mexico Basin - South Texas example
|DE95-003341| p 1743 N95-22695

HYDROGRAPHY
Assimilation of altimeter data in a quasi-geostrophic model of the Gulf Stream system: A dynamical perspective
|NASA-CR-196313| p 1744 N95-23766

HYDROLOGY
Effects of wind on rainfall simulation. Spatial distribution of water application, kinetic energy, and overland flow under single full-cone nozzle sprays
|PB95-127304| p 1717 N95-22537
HAPEX-Sahel: Basic description of methods and data sets
|PB95-127262| p 1701 N95-22639
Accuracy of radar rainfall estimates compared to raingauge measurements and a hydrological application
|PB95-127296| p 1741 N95-22640
Streamflow and selected precipitation data for Yucca Mountain Region, southern Nevada and eastern California, water years 1986-90
|DE95-001893| p 1742 N95-23385

HYDROLYSIS
Continuous production of cellulase in a fluidized-bed reactor by Pseudonomas fluorescens immobilized in hydrogel beads
[DE94-014105] p 1744 N95-22588
On the formation of iron(3) oxides via oxidation of iron(2)
[DE94-018392] p 1632 N95-22857
A kinetic study of hydrolysis of polyester elastomer in magnetic tape p 1652 N95-24124
HYDROMETEOROLOGY
Accuracy of radar rainfall estimates compared to raingauge measurements and a hydrological application
[PB95-127296] p 1741 N95-22640
HYDROSTATICS
Three-D CFD analysis of hydrostatic bearings
p 1678 N95-23616
HYDROTHERMAL SYSTEMS
Application of MAC-Europe AVIRIS data to the analysis of various alteration stages in the Landdmannalauger Hydrothermal Area (South Iceland)
p 1709 N95-23885
HYDROXYL RADICALS
Dimethylsulfide oxidation over the tropical South Atlantic: OH and other oxidants
[NASA-CR-197417] p 1732 N95-22930
HYPERBARIC CHAMBERS
Effect of hyperbaric carbon dioxide on spores and vegetative cells of bacillus stearothermophilus
[AD-A280115] p 1747 N95-23251
HYPERBOLIC DIFFERENTIAL EQUATIONS
Nonlinear generalized functions and nonconservative shock simulations
[DE95-003307] p 1795 N95-22734
Fourth order difference methods for hyperbolic IBVP's
[NASA-CR-197955] p 1791 N95-23548
HYPERION
IUE observing programs: NSOSS, VEOEB, and PCOEB
[NASA-CR-197424] p 1866 N95-23560
HYPERNUCLEI
Do narrow Sigma hypernuclear states exist?
[DE95-002930] p 1803 N95-22763
HYPERPLANES
The fundamental group of complex hyperplanes arrangements
[DE94-628426] p 1796 N95-22933
HYPERSONIC FLIGHT
Particle kinetic simulation of high altitude hypervelocity flight
[NASA-CR-197383] p 1664 N95-22481
HYPERSONIC FLOW
Experimental results for a hypersonic nozzle/afterbody flow field
[NASA-TM-4638] p 1609 N95-23250
Design of a variable area diffuser for a 15-inch Mach 6 open-jet tunnel p 1617 N95-23309
HYPERSONIC NOZZLES
Optimized design of a hypersonic nozzle
p 1617 N95-23304
HYPERSONIC SPEED
Mach 10 computational study of a three-dimensional scramjet inlet flow field
[NASA-TM-4602] p 1666 N95-23015
Mach 10 computational study of a three-dimensional scramjet inlet flow field
[NASA-TM-4602] p 1667 N95-23210
Design of a variable area diffuser for a 15-inch Mach 6 open-jet tunnel p 1617 N95-23309
HYPERSONIC VEHICLES
Particle kinetic simulation of high altitude hypervelocity flight
[NASA-CR-197383] p 1664 N95-22481
HYPERSONIC WIND TUNNELS
Optimized design of a hypersonic nozzle
p 1617 N95-23304
HYPERSPACES
Browsing semantics in the tower model
[PB95-127221] p 1855 N95-22534
On the scalar curvature of minimal hypersurfaces
[DE94-628516] p 1796 N95-22741
HYPERVELOCITY IMPACT
Impact shock and penetration fragmentation in porous media
[DE94-018900] p 1868 N95-23656
Effect of the space environment on materials flown on the EURECA/TICCE-HVI experiment
p 1623 N95-23803
Long term microparticle impact fluxes on LDEF determined from optical survey of Interplanetary Dust Experiment (IDE) sensors p 1623 N95-23826
Hypervelocity impact survivability experiments for carbonaceous impactors, part 2 p 1700 N95-23831
Micro-abrasion package capture cell experiment on the trailing edge of LDEF: Impactor chemistry and whipple bumper shield efficiencies p 1624 N95-23835
Secondary ion mass spectrometry (SIMS) analysis of hypervelocity microparticle impact sites on LDEF surfaces p 1637 N95-23836
The effect of impact angle on craters formed by hypervelocity particles p 1700 N95-23839
Determining orbital particle parameters of impacts into germanium using morphology analysis and calibration data from hypervelocity impact experiments in the laboratory
p 1700 N95-23841
Cratering and penetration experiments in Teflon targets at velocities from 1 to 7 km/s p 1700 N95-23842
Axial focusing of energy from a hypervelocity impact on earth
[DE95-003347] p 1740 N95-24008
Axial focusing of impact energy in the earth's interior: A possible link to flood basalts and hotspots
[DE95-003357] p 1741 N95-24009
HYPOTHALAMUS
Cellular interactions in the suprachiasmatic nucleus
[AD-A285639] p 1749 N95-23780
HYPOTHESES
Is omega* - (mu) absolutely countably compact?
[PB95-127981] p 1785 N95-22528
HYSTERESIS
Effects of Bi and Bi2O3 additions on the microstructure and superconducting properties of powder-in-tube BSCCO (2212) tapes
[DE95-004605] p 1845 N95-24150

I

ICE
Collaborative research on aircraft icing and charging processes in ice
[AD-A285102] p 1609 N95-23201
Experimental technique and assessment for measuring the convective heat transfer coefficient from natural ice accretions
[NASA-TM-106864] p 1668 N95-23248
Charging of interplanetary grains
[NASA-CR-198032] p 1869 N95-24066
ICE FORMATION
Experimental technique and assessment for measuring the convective heat transfer coefficient from natural ice accretions
[NASA-TM-106864] p 1668 N95-23248
IDAHO
Seismic evidence of conjugate normal faulting: The 1994 Devil Canyon earthquake sequence near Challis, Idaho
[DE95-002052] p 1740 N95-23386
IDENTIFYING
Toward an automated signature recognition toolkit for mission operations p 1659 N95-23682
Automatic generation of efficient orderings of events for scheduling applications p 1618 N95-23764
IDENTITIES
Fibonacci chain polynomials: Identities from self-similarity p 1814 N95-22962
IGNITERS
Laser-plasma instability in hohlraums
[DE95-000914] p 1829 N95-22676
The railplug: Development of a new ignitor for internal combustion engines
[DE95-004375] p 1695 N95-23342
IGNITION SYSTEMS
Diesel fuel component contributions to engine emissions and performance: Clean fuel study
[DE94-011868] p 1732 N95-22834
The railplug: Development of a new ignitor for internal combustion engines
[DE95-004375] p 1695 N95-23342
Ignition transient calculations in the Space Shuttle solid rocket motor p 1625 N95-23640
ILL-POSED PROBLEMS (MATHEMATICS)
Diffusion terms in systems of reaction diffusion equations can lead to blow up
[DE94-628408] p 1785 N95-22618
IMAGE ANALYSIS
A multispectral scanner survey of the Tonopah Test Range, Nevada. Date of survey: August 1993
[DE95-003920] p 1717 N95-22503
Combining optical and microwave remote sensing data of forest vegetation: MAC Europe 1991
[PB95-127312] p 1717 N95-22538
Scientific and technical photography at NASA Langley Research Center p 1690 N95-23290
Vision-sensing image analysis for GTAW process control
[DE95-003936] p 1695 N95-23373
A new generation of intelligent trainable tools for analyzing large scientific image databases
p 1775 N95-23717
Investigations on the 1.7 micron residual absorption feature in the vegetation reflection spectrum
p 1710 N95-23891
Remote identification of a gravel laden Pleistocene river bed p 1712 N95-23921
Summaries of the 4th Annual JPL Airborne Geoscience Workshop. Volume 3: AIRSAR Workshop
[NASA-CR-197354-VOL-3] p 1712 N95-23938
AIRSAR views of aerolian terrain
p 1713 N95-23941
Statistics of multi-look AIRSAR imagery: A comparison of theory with measurements p 1714 N95-23947
Preliminary analysis of the sensitivity of AIRSAR images to soil moisture variations p 1714 N95-23950
Relating P-band AIRSAR backscatter to forest stand parameters p 1716 N95-23959
Soil moisture retrieval in the Oberpfaffenhofen testsite using MAC Europe AIRSAR data p 1716 N95-23960
Dynamics and pattern of a managed coniferous forest landscape in Oregon p 1720 N95-24104
IMAGE CLASSIFICATION
Classification of high dimensional multispectral image data p 1705 N95-23868
MAC Europe 1991 campaign: AIRSAR/AVIRIS data integration for agricultural test site classification
p 1715 N95-23952
Polarimetric radar data decomposition and interpretation p 1715 N95-23955
SAR terrain classifier and mapper of biophysical attributes p 1715 N95-23957
IMAGE CORRELATORS
Optical image correlator using orthogonal data storage
[AD-A285795] p 1819 N95-22508
IMAGE ENHANCEMENT
A multispectral scanner survey of the Tonopah Test Range, Nevada. Date of survey: August 1993
[DE95-003920] p 1717 N95-22503
IMAGE FURNACES
A new containerless image furnace with electro-static positioning device p 1690 N95-23674
Robotic servicing system for space material experiment p 1697 N95-23722
IMAGE INTENSIFIERS
Video frame processor
[DE94-635414] p 1753 N95-23962
IMAGE PROCESSING
A certainty grid to object boundary algorithm
[PB94-203510] p 1755 N95-22637
Ghost images and feasibility of reconstructions with the Richardson-Lucy algorithm
[DE95-002351] p 1756 N95-23079
Locating buildings in aerial photos
p 1721 N95-23295
Electronic photography at NASA Langley Research Center p 1690 N95-23298
Vision-sensing image analysis for GTAW process control
[DE95-003936] p 1695 N95-23373
Manipulating flexible parts using a teleoperated system with time delay: An experiment p 1777 N95-23729
Mark Tracking: Position/orientation measurements using 4-circle mark and its tracking experiments
p 1778 N95-23736
A fuzzy structural matching scheme for space robotics vision p 1778 N95-23737
Active vision in satellite scene analysis
p 1778 N95-23738
Automated synthesis of image processing procedures using AI planning techniques p 1779 N95-23745
10x reduction imaging at 13.4 nm
[DE94-016612] p 1828 N95-23767
Edge fluctuation measurements by phase contrast imaging on DIII-D
[DE94-016681] p 1836 N95-23768
Spectral decomposition of AVIRIS data
p 1704 N95-23859
AVIRIS and TIMS data processing and distribution at the land processes distributed active archive center
p 1706 N95-23872
Classification of the LCVF AVIRIS test site with a Kohonen artificial neural network p 1706 N95-23874
Extraction of auxiliary data from AVIRIS distribution tape for spectral, radiometric, and geometric quality assessment p 1706 N95-23875
Preprocessing: Geocoding of AVIRIS data using navigation, engineering, DEM, and radar tracking system data p 1707 N95-23876
Mapping and monitoring changes in vegetation communities of Jasper Ridge, CA, using spectral fractions derived from AVIRIS images p 1708 N95-23883
Optimal band selection for dimensionality reduction of hyperspectral imagery p 1709 N95-23887

Atmospheric correction of AVIRIS data of Monterey Bay contaminated by thin cirrus clouds p 1710 N95-23890
Statistics of multi-look AIRSAR imagery: A comparison of theory with measurements p 1714 N95-23947
Polarimetric radar data decomposition and interpretation p 1715 N95-23955
Video frame processor
|DE94-635414| p 1753 N95-23962

IMAGE RESOLUTION
Full resolution hologram-like autostereoscopic display
|NASA-CR-197913| p 1689 N95-23789
Preprocessing: Geocoding of AVIRIS data using navigation, engineering, DEM, and radar tracking system data p 1707 N95-23876

IMAGE TRANSDUCERS
Amplified MOS Imager
|NHK-LABS-NOTE-432| p 1690 N95-24107

IMAGES
Optical image correlator using orthogonal data storage
|AD-A285795| p 1819 N95-22508
Color orthophotography: To scan or not
|DE95-002749| p 1689 N95-24069
Document image archive transfer from DOS to UNIX p 1761 N95-24117
Proposal of a Modified EBU method for reliable evaluation of picture quality
|NHK-LABS-NOTE-431| p 1863 N95-24180

IMAGING RADAR
Summaries of the 4th Annual JPL Airborne Geoscience Workshop. Volume 3: AIRSAR Workshop
|NASA-CR-197354-VOL-3| p 1712 N95-23938

IMAGING SPECTROMETERS
Ocean observations with EOS/MODIS: Algorithm development and post launch studies
|NASA-CR-197402| p 1717 N95-22916
Land surface temperature measurements for EOS MODIS data
|NASA-CR-197443| p 1717 N95-23191
Infrared algorithm development for ocean observations with EOS/MODIS
|NASA-CR-197851| p 1743 N95-23212
Ocean observations with EOS/MODIS: Algorithm development and post launch studies
|NASA-CR-197894| p 1718 N95-23473
Summaries of the 4th Annual JPL Airborne Geoscience Workshop. Volume 1: AVIRIS Workshop
|NASA-CR-197877-VOL-1| p 1701 N95-23844
A tool for manual endmember selection and spectral unmixing p 1701 N95-23846
Automating spectral unmixing of AVIRIS data using convex geometry concepts p 1702 N95-23848
AVIRIS calibration using the cloud-shadow method p 1702 N95-23849
Field observations using an AOTF polarimetric imaging spectrometer p 1702 N95-23850
Instantaneous field of view and spatial sampling of the Airborne Visible/Infrared Imaging Spectrometer (AVIRIS) p 1702 N95-23851
Airborne Visible/Infrared Imaging Spectrometer (AVIRIS): Recent improvements to the sensor p 1690 N95-23852
Comparison of three methods for materials identification and mapping with imaging spectroscopy p 1702 N95-23853
Comparison of methods for calibrating AVIRIS data to ground reflectance p 1703 N95-23854
Discrimination of poorly exposed lithologies in AVIRIS data p 1703 N95-23858
Spectral decomposition of AVIRIS data p 1704 N95-23859
Remote sensing of smoke, clouds, and fire using AVIRIS data p 1704 N95-23860
Use of data from the AVIRIS onboard calibrator p 1704 N95-23861
Inflight calibration of AVIRIS in 1992 and 1993 p 1690 N95-23862
Estimation of aerosol optical depth and additional atmospheric parameters for the calculation of apparent reflectance from radiance measured by the Airborne Visible/Infrared Imaging Spectrometer p 1704 N95-23863
Use of the Airborne Visible/Infrared Imaging Spectrometer to calibrate the optical sensor on board the Japanese Earth Resources Satellite-1 p 1624 N95-23864
A role for AVIRIS in the Landsat and Advanced Land Remote Sensing Systems program p 1705 N95-23866
Estimating dry grass residues using landscape integration analysis p 1705 N95-23867
Classification of high dimensional multispectral image data p 1705 N95-23868
Geologic mapping using integrated AIRSAR, AVIRIS, and TIMS data p 1714 N95-23946
Land surface temperature measurements from EOS MODIS data
|NASA-CR-197969| p 1721 N95-24190

IMAGING TECHNIQUES
Aviator's night vision imaging system preflight adjustment/assessment procedures
|AD-A285829| p 1750 N95-22513
Programmable hyperspectral image mapper with on-array processing
|NASA-CASE-NPO-17794-1-CU| p 1819 N95-22765
Continuation of BNCT Research Program at NEMC and MIT
|DE94-016228| p 1748 N95-22875
Ghost images and feasibility of reconstructions with the Richardson-Lucy algorithm
|DE95-002351| p 1756 N95-23079
TIMED Imaging Photometer Experiment (TIPE)
|NASA-CR-197431| p 1688 N95-23087
Measurements of striae in CR+ doped YAG laser crystals p 1847 N95-23285
Scientific and technical photography at NASA Langley Research Center p 1690 N95-23290
Method development for compensating temperature effects in pressure sensitive paint measurements p 1650 N95-23291
Application of electron paramagnetic resonance imaging to the characterization of the Ultem(R) exposed to 1 MeV electrons. Correlation of radical density data to tiger code calculations p 1815 N95-23328
Vision-sensing image analysis for GTAW process control
|DE95-003936| p 1695 N95-23373
Multiband VLBI imaging of the jet in 3C 345
|PB95-139275| p 1866 N95-23468
Automatic commanding of the Mars Observer Camera p 1620 N95-23754
10x reduction imaging at 13.4 nm
|DE94-016612| p 1828 N95-23767
Edge fluctuation measurements by phase contrast imaging on DIII-D
|DE94-016681| p 1836 N95-23768
Full resolution hologram-like autostereoscopic display
|NASA-CR-197913| p 1689 N95-23789
Hypervelocity impact survivability experiments for carbonaceous impactors, part 2 p 1700 N95-23831
Field observations using an AOTF polarimetric imaging spectrometer p 1702 N95-23850
Comparison of three methods for materials identification and mapping with imaging spectroscopy p 1702 N95-23853
Simulation of landsat thematic mapper imagery using AVIRIS hyperspectral imagery p 1705 N95-23869
Classification of the LCVF AVIRIS test site with a Kohonen artificial neural network p 1706 N95-23874
Estimation of crown closure from AVIRIS data using regression analysis p 1709 N95-23886
Optimal band selection for dimensionality reduction of hyperspectral imagery p 1709 N95-23887
Objective determination of image end-members in spectral mixture analysis of AVIRIS data p 1709 N95-23888
Relationships between pigment composition variation and reflectance for plant species from a coastal savannah in California p 1709 N95-23889
Investigations on the 1.7 micron residual absorption feature in the vegetation reflection spectrum p 1710 N95-23891
Laboratory spectra of field samples as a check on two atmospheric correction methods p 1711 N95-23894
Determination of semi-arid landscape endmembers and seasonal trends using convex geometry spectral unmixing techniques p 1711 N95-23895
Interferometric synthetic aperture radar imagery of the Gulf Stream p 1712 N95-23939
AIRSAR deployment in Australia, September 1993: Management and objectives p 1714 N95-23948
Comparison of 7.5-minute and 1-degree digital elevation models p 1719 N95-24095
Amplified MOS Imager
|NHK-LABS-NOTE-432| p 1690 N95-24107

IMMUNE SYSTEMS
Interrelations between nervous system and immune system in stress situations
|PB95-135521| p 1748 N95-22770

IMPACT DAMAGE
Impact shock and penetration fragmentation in porous media
|DE94-018900| p 1868 N95-23656
Status of LDEF contributions to current knowledge of meteoroid and manmade debris environments and their effects on spacecraft in LEO p 1623 N95-23822
Long term microparticle impact fluxes on LDEF determined from optical survey of Interplanetary Dust Experiment (IDE) sensors p 1623 N95-23826
Penetration rates over 30 years in the space age p 1624 N95-23827
LDEF Interplanetary Dust Experiment (IDE) results p 1869 N95-23828
Orbital debris and meteoroid population as estimated from LDEF impact data p 1869 N95-23830
Hypervelocity impact survivability experiments for carbonaceous impactors, part 2 p 1700 N95-23831
Analytical electron microscopy of LDEF impactor residues p 1869 N95-23832

IMPACT TESTS
High-velocity penetrators
|DE95-001886| p 1698 N95-22500
Analytical electron microscopy of LDEF impactor residues p 1869 N95-23832
Debris and meteoroid proportions deduced from impact crater residue analysis p 1869 N95-23834
Experimental investigation of the relationship between impact crater morphology and impacting particle velocity and direction p 1700 N95-23840
Cratering and penetration experiments in Teflon targets at velocities from 1 to 7 km/s p 1700 N95-23842
Axial focusing of energy from a hypervelocity impact on earth
|DE95-003347| p 1740 N95-24008

IMPACTORS
Hypervelocity impact survivability experiments for carbonaceous impactors, part 2 p 1700 N95-23831
Dimensional scaling for impact cratering and perforation p 1624 N95-23843

IMPEDANCE MEASUREMENT
The use of electrochemical impedance spectroscopy to predict the corrosion of aluminum-lithium alloys in marine environments p 1637 N95-23504

IMPELLERS
Comparison between predicted and experimentally measured flow fields at the exit of the SSME HPFTP impeller p 1679 N95-23622
Three-dimensional flow analysis inside consortium impeller at design and off-design conditions p 1679 N95-23623
Optimization of a centrifugal impeller design through CFD analysis p 1680 N95-23624
The influence of swirl brakes and a tip discharge orifice on the rotordynamic forces generated by discharge-to-suction leakage flows in shrouded centrifugal pumps p 1680 N95-23628
An inducer CFD solution and effects associated with cavitation p 1681 N95-23631

IMPINGEMENT
Effects of jet strength on NOx formation in premixed impinging jet combustion with minimum heat losses
|NAL-TR-1237T| p 1637 N95-24181

IMPULSE GENERATORS
High gain GaAs Photoconductive Semiconductor Switches for impulse sources
|DE95-001885| p 1659 N95-22549

IMPURITIES
Engineering design of a radiative divertor for DIII-D
|DE95-003008| p 1693 N95-22798
Measurements and modeling of impurity source distributions from the Tore Supra outboard pump limiter
|DE95-003097| p 1831 N95-22800
Variational calculations for He-3 impurities on He-4 droplets
|DE94-628469| p 1840 N95-22839
D3-D program overview
|DE95-003879| p 1837 N95-24086

IN SITU MEASUREMENT
The difference between laboratory and in-situ pixel-averaged emissivity: The effects on temperature-emissivity separation p 1711 N95-23919

IN-FLIGHT MONITORING
Summary of OARE flight calibration measurements
|NASA-TM-109159| p 1688 N95-23012
Enhancement of F/A-18 operational flight measurements: Data report for phase 1
|DSTO-TR-0049| p 1613 N95-23666
An intelligent ground operator support system p 1769 N95-23681
Attention focusing and anomaly detection in systems monitoring p 1769 N95-23683
An expert system for diagnosing anomalies of spacecraft p 1770 N95-23684
Distributed intelligence for ground/space systems p 1770 N95-23685
Learning time series for intelligent monitoring p 1770 N95-23686
An operations and command systems for the extreme ultraviolet explorer p 1770 N95-23687
Performance results of cooperating expert systems in a distributed real-time monitoring system p 1761 N95-23688
Use of data from the AVIRIS onboard calibrator p 1704 N95-23861
Inflight calibration of AVIRIS in 1992 and 1993 p 1690 N95-23862

INCENDIARY AMMUNITION
Rationale for the Modular Air-system Vulnerability Estimation Network (MAVEN) methodology
| AD-A285797 | p 1611 N95-22510
INCIDENCE
Prediction of incidence and surface roughness effects on turbine performance p 1671 N95-23424
INCIDENT RADIATION
Resonant infrared detector with substantially unit quantum efficiency
| NASA-CASE-ARC-11940-1-SB | p 1827 N95-23378
INCINERATORS
The Louisiana State University waste-to-energy incinerator
| DE95-004417 | p 1728 N95-23344
INCOMPRESSIBLE FLOW
An adaptive projection method for the incompressible Navier-Stokes equations
| DE94-019049 | p 1665 N95-22491
BEm-BDF scheme for curvature driven moving stokes flows
| PB95-138905 | p 1667 N95-23144
Quasistatic model for the motion of a viscous capillary liquid drop
| PB95-138848 | p 1667 N95-23172
Numerical simulation of axisymmetric viscous sintering
| PB95-138889 | p 1667 N95-23175
The initial-value problem for viscous channel flows
| NASA-CR-195034 | p 1667 N95-23207
A controlled variation scheme for convection treatment in pressure-based algorithm p 1677 N95-23448
On the conservative interface treatment for multi-block viscous flow computations
| NASA-CR-195442 | p 1677 N95-23451
Incompressible Navier-Stokes calculations in pump flows p 1680 N95-23627
INDENTATION
Investigation of depth-area relationships associated with nanoindentations
| DE95-001353 | p 1639 N95-22686
INDEXES (DOCUMENTATION)
NASA Thesaurus, Supplement
| NASA-SP-7096-SUPPL-1 | p 1856 N95-23223
Index of nuclear data libraries available from the IAEA nuclear data section
| DE94-634271 | p 1857 N95-23453
Using Dedal to share and reuse distributed engineering design information p 1768 N95-23678
INDIUM COMPOUNDS
Polycrystalline CuInSe2 and CdTePV solar cells
| DE95-000244 | p 1727 N95-22842
Four space application material coatings on the Long-Duration Exposure Facility (LDEF) p 1651 N95-23913
INDIUM PHOSPHIDES
Study of photorefractive non-linearities in the 3-5 and 2-4 semi-insulator compounds: The effect of electron irradiation
| PB94-189057 | p 1839 N95-22584
Carbon doping of III-V compound semiconductors
| DE95-003431 | p 1844 N95-24013
INDUCTION MOTORS
Motor drive technologies for the power-by-wire (PBW) program: Options, trends and tradeoffs
| NASA-TM-106885 | p 1616 N95-23671
INDUSTRIAL PLANTS
Preliminary assessment of air toxic emissions in the natural gas industry, phase 1
| PB95-135547 | p 1732 N95-22865
Aerospace Industries Association (AIA) work practices report for composites p 1628 N95-23029
INDUSTRIAL SAFETY
Environmental, Safety, and Health Considerations: Composite Materials in the Aerospace Industry
| NASA-CP-3289 | p 1628 N95-23025
Health, safety and environmental requirements for composite materials p 1628 N95-23026
Offgassing test methodology for composite materials p 1629 N95-23035
INDUSTRIAL WASTES
Biotransformation of an uncured composite material p 1629 N95-23033
Chemical recycling of scrap composites p 1629 N95-23034
INDUSTRIES
Solar photochemistry: Twenty years of progress, what's been accomplished, and where does it lead?
| DE95-004007 | p 1730 N95-23778
INELASTIC SCATTERING
Experimental results on polarized structure functions in deep inelastic lepton-nucleon scattering
| DE95-002782 | p 1801 N95-22521
Gluon distribution as function of F(sub 2) and dF(sub 2)/dlnQ(exp 2) at small x
| DE94-635677 | p 1812 N95-23975
INEQUALITIES
Capacitated facility location: Valid inequalities and facets (revised)
| PB95-130225 | p 1786 N95-22641
INERTIAL CONFINEMENT FUSION
High current induction linacs
| DE95-003442 | p 1818 N95-24014
Progress in ion beam power coupling and ion-driven hohlraums on PBFA 2
| DE95-004544 | p 1818 N95-24160
INERTIAL PLATFORMS
Dynamic response tests of inertial and optical wind-tunnel model attitude measurement devices
| NASA-TM-109182 | p 1616 N95-23011
INERTIAL REFERENCE SYSTEMS
Terrain modelling and motion planning for an autonomous exploration rover p 1721 N95-23765
INFECTIOUS DISEASES
Interrelations between nervous system and immune system in stress situations
| PB95-135521 | p 1748 N95-22770
An extension of Freedman's results on a model of predator-prey dynamics as modified by the action of a parasite
| DE94-628488 | p 1796 N95-23052
INFERENCE
Simultaneous inference in multivariate calibration
| DE95-003592 | p 1794 N95-23066
Combinatorial semantics
| TR-563 | p 1792 N95-23793
INFILTRATION
Effects of wind on rainfall simulation. Spatial distribution of water application, kinetic energy, and overland flow under single full-cone nozzle sprays
| PB95-127304 | p 1717 N95-22537
Development and verification of a resin film infusion/resin transfer molding simulation model for fabrication of advanced textile composites
| NASA-CR-197439 | p 1648 N95-23179
INFORMATION DISSEMINATION
NASAwide electronic publishing system: Electronic printing and duplicating, stage-2 evaluation report (GSFC)
| NASA-TM-104615 | p 1856 N95-23209
A network-based distributed, media-rich computing and information environment
| DE95-003696 | p 1765 N95-24074
The design of a petabyte archive and distribution system for the NASA ECS project p 1858 N95-24110
NSSDC provides network access to key data via NDADS p 1862 N95-24136
Analysis of the request patterns to the NSSDC on-line archive p 1862 N95-24137
INFORMATION FLOW
A study of policy issues affecting the Defense Technical Information Center
| AD-A286629 | p 1854 N95-22494
Jackson system development, entity-relationship analysis and data flow models: A comparative study
| PB95-127338 | p 1855 N95-22523
INFORMATION MANAGEMENT
Online Nuclear Data Service
| DE94-634268 | p 1856 N95-23452
The data facility of the Airborne Visible/Infrared Imaging Spectrometer (AVIRIS) p 1707 N95-23877
A network-based distributed, media-rich computing and information environment
| DE95-003696 | p 1765 N95-24074
Applications drivers for data parking on the Information Superhighway p 1857 N95-24109
INFORMATION PROCESSING (BIOLOGY)
Functions of external cues in prospective memory
| DOT/FAA/AM-95/9 | p 1750 N95-24088
INFORMATION RETRIEVAL
A multispectral scanner survey of the Tonopah Test Range, Nevada. Date of survey: August 1993
| DE95-003920 | p 1717 N95-22503
NASA Thesaurus, Supplement
| NASA-SP-7096-SUPPL-1 | p 1856 N95-23223
Search Hanford accessible reports electronically system requirements specification
| DE95-004367 | p 1856 N95-23340
Index of nuclear data libraries available from the IAEA nuclear data section
| DE94-634271 | p 1857 N95-23453
A network-based distributed, media-rich computing and information environment
| DE95-003696 | p 1765 N95-24074
INFORMATION SYSTEMS
Layered Electrical Product Application Protocol (AP)
| DE95-001524 | p 1754 N95-22548
Review of uncertainty files and improved multigroup cross section files for FENDL
| DE94-628639 | p 1830 N95-22757
Cost and schedule analytical techniques development
| NASA-CR-196548 | p 1853 N95-22891
Distributed VIRtual System (DIVIRS) project
| NASA-CR-197855 | p 1757 N95-23180
Automation technology using Geographic Information System (GIS) p 1863 N95-23284
Application Protocol, Initial Graphics Exchange Specification (IGES), Layered Electrical Product
| DE95-004266 | p 1757 N95-23337
Search Hanford accessible reports electronically system requirements specification
| DE95-004367 | p 1856 N95-23340
Search Hanford accessible reports electronically system design description, revision 1
| DE95-004369 | p 1856 N95-23341
Index of nuclear data libraries available from the IAEA nuclear data section
| DE94-634271 | p 1857 N95-23453
BROND-2.1. Russian evaluated neutron reaction data library
| DE94-634417 | p 1810 N95-23458
Information technology standards process guide
| DE95-003967 | p 1857 N95-23574
AMPHION: Specification-based programming for scientific subroutine libraries p 1761 N95-23680
Search Hanford accessible reports electronically system configuration management plan
| DE95-004493 | p 1857 N95-24089
Optimizing raid performance with cache p 1761 N95-24116
INFORMATION TRANSFER
A study of policy issues affecting the Defense Technical Information Center
| AD-A286629 | p 1854 N95-22494
A network-based distributed, media-rich computing and information environment
| DE95-003696 | p 1765 N95-24074
A 500 megabyte/second disk array p 1753 N95-24114
Document image archive transfer from DOS to UNIX p 1761 N95-24117
INFRARED ASTRONOMY
IRAS sky survey atlas: Explanatory supplement
| NASA-CR-197335 | p 1865 N95-22539
Near infrared and optical spectroscopy of FSC10214+4724
| NASA-CR-197966 | p 1828 N95-24068
INFRARED ASTRONOMY SATELLITE
IRAS sky survey atlas: Explanatory supplement
| NASA-CR-197335 | p 1865 N95-22539
INFRARED DETECTORS
High Tc superconducting bolometric and nonbolometric infrared (IR) detectors
| NASA-CR-197868 | p 1827 N95-23224
Resonant infrared detector with substantially unit quantum efficiency
| NASA-CASE-ARC-11940-1-SB | p 1827 N95-23378
INFRARED IMAGERY
IRAS sky survey atlas: Explanatory supplement
| NASA-CR-197335 | p 1865 N95-22539
Infrared algorithm development for ocean observations with EOS/MODIS
| NASA-CR-197851 | p 1743 N95-23212
AVIRIS and TIMS data processing and distribution at the land processes distributed active archive center p 1706 N95-23872
Monitoring land use and degradation using satellite and airborne data p 1707 N95-23880
The red edge in arid region vegetation: 340-1060 nm spectra p 1708 N95-23881
Temporal changes in endmember abundances, liquid water and water vapor over vegetation at Jasper Ridge p 1708 N95-23882
Mapping and monitoring changes in vegetation communities of Jasper Ridge, CA, using spectral fractions derived from AVIRIS images p 1708 N95-23883
The effect of signal noise on the remote sensing of Foliar biochemical concentration p 1708 N95-23884
Application of MAC-Europe AVIRIS data to the analysis of various alteration stages in the Landdmannalauger Hydrothermal Area (South Iceland) p 1709 N95-23885
Estimation of crown closure from AVIRIS data using regression analysis p 1709 N95-23886
Objective determination of image end-members in spectral mixture analysis of AVIRIS data p 1709 N95-23888
Atmospheric correction of AVIRIS data of Monterey Bay contaminated by thin cirrus clouds p 1710 N95-23890
A comparison of spectral mixture analysis an NDVI for ascertaining ecological variables p 1710 N95-23892
Laboratory spectra of field samples as a check on two atmospheric correction methods p 1711 N95-23894
INFRARED RADIATION
Infrared study of carbon deposits on bimetallic catalysts
| DE95-000902 | p 1631 N95-22517

Relationships between pigment composition variation and reflectance for plant species from a coastal savannah in California p 1709 N95-23889
Estimation of spectral emissivity in the thermal infrared p 1711 N95-23918
The difference between laboratory and in-situ pixel-averaged emissivity: The effects on temperature-emissivity separation p 1711 N95-23919
Investigation of infra-red and nonequilibrium air radiation
| NASA-CR-197977 | p 1741 N95-24041

INFRARED SCANNERS
Summaries of the 4th Annual JPL Airborne Geoscience Workshop. Volume 2: TIMS Workshop
| NASA-CR-197876-VOL-2 | p 1711 N95-23917
Mineralogic variability of the Kelso Dunes, Mojave Desert, California derived from Thermal Infrared Multispectral Scanner (TIMS) data p 1711 N95-23920
Geologic mapping using integrated AIRSAR, AVIRIS, and TIMS data p 1714 N95-23946

INFRARED SIGNATURES
Investigation of infra-red and nonequilibrium air radiation
| NASA-CR-197977 | p 1741 N95-24041

INFRARED SOURCES (ASTRONOMY)
Near infrared and optical spectroscopy of FSC10214+4724
| NASA-CR-197966 | p 1828 N95-24068

INFRARED SPECTRA
Outgassing products from orbiter TPS materials p 1637 N95-23798
A proposed update to the solar irradiance spectrum used in LOWTRAN and MODTRAN p 1705 N95-23865
AVIRIS spectra correlated with the chlorophyll concentration of a forest canopy p 1705 N95-23871
AVIRIS and TIMS data processing and distribution at the land processes distributed active archive center p 1706 N95-23872
Classification of the LCVF AVIRIS test site with a Kohonen artificial neural network p 1706 N95-23874
Extraction of auxiliary data from AVIRIS distribution tape for spectral, radiometric, and geometric quality assessment p 1706 N95-23875
Mapping of the Ronda peridotite massif (Spain) from AVIRIS spectro-imaging survey: A first attempt p 1707 N95-23878
Spectral variations in a collection of AVIRIS imagery p 1707 N95-23879
The red edge in arid region vegetation: 340-1060 nm spectra p 1708 N95-23881
Temporal changes in endmember abundances, liquid water and water vapor over vegetation at Jasper Ridge p 1708 N95-23882
Mapping and monitoring changes in vegetation communities of Jasper Ridge, CA, using spectral fractions derived from AVIRIS images p 1708 N95-23883
The effect of signal noise on the remote sensing of Foliar biochemical concentration p 1708 N95-23884
Application of MAC-Europe AVIRIS data to the analysis of various alteration stages in the Landdmannalauger Hydrothermal Area (South Iceland) p 1709 N95-23885
Estimation of crown closure from AVIRIS data using regression analysis p 1709 N95-23886
Objective determination of image end-members in spectral mixture analysis of AVIRIS data p 1709 N95-23888
Atmospheric correction of AVIRIS data of Monterey Bay contaminated by thin cirrus clouds p 1710 N95-23890
Investigations on the 1.7 micron residual absorption feature in the vegetation reflection spectrum p 1710 N95-23891
A comparison of spectral mixture analysis an NDVI for ascertaining ecological variables p 1710 N95-23892
Using AVIRIS for in-flight calibration of the spectral shifts of SPOT-HRV and of AVHRR? p 1710 N95-23893
Laboratory spectra of field samples as a check on two atmospheric correction methods p 1711 N95-23894
Determination of semi-arid landscape endmembers and seasonal trends using convex geometry spectral unmixing techniques p 1711 N95-23895
MAC Europe 1991 campaign: AIRSAR/AVIRIS data integration for agricultural test site classification p 1715 N95-23952

INFRARED SPECTROMETERS
Summaries of the 4th Annual JPL Airborne Geoscience Workshop. Volume 1: AVIRIS Workshop
| NASA-CR-197877-VOL-1 | p 1701 N95-23844
Lithologic discrimination and alteration mapping from AVIRIS Data, Socorro, New Mexico p 1701 N95-23847
Automating spectral unmixing of AVIRIS data using convex geometry concepts p 1702 N95-23848
AVIRIS calibration using the cloud-shadow method p 1702 N95-23849
Instantaneous field of view and spatial sampling of the Airborne Visible/Infrared Imaging Spectrometer (AVIRIS) p 1702 N95-23851
Airborne Visible/Infrared Imaging Spectrometer (AVIRIS): Recent improvements to the sensor p 1690 N95-23852
Comparison of three methods for materials identification and mapping with imaging spectroscopy p 1702 N95-23853
Comparison of methods for calibrating AVIRIS data to ground reflectance p 1703 N95-23854
Discrimination of poorly exposed lithologies in AVIRIS data p 1703 N95-23858
Spectral decomposition of AVIRIS data p 1704 N95-23859
Remote sensing of smoke, clouds, and fire using AVIRIS data p 1704 N95-23860
Use of data from the AVIRIS onboard calibrator p 1704 N95-23861
Inflight calibration of AVIRIS in 1992 and 1993 p 1690 N95-23862
Estimation of aerosol optical depth and additional atmospheric parameters for the calculation of apparent reflectance from radiance measured by the Airborne Visible/Infrared Imaging Spectrometer p 1704 N95-23863
Use of the Airborne Visible/Infrared Imaging Spectrometer to calibrate the optical sensor on board the Japanese Earth Resources Satellite-1 p 1624 N95-23864
A role for AVIRIS in the Landsat and Advanced Land Remote Sensing Systems program p 1705 N95-23866
Classification of high dimensional multispectral image data p 1705 N95-23868
Summaries of the 4th Annual JPL Airborne Geoscience Workshop. Volume 2: TIMS Workshop
| NASA-CR-197876-VOL-2 | p 1711 N95-23917
Geologic mapping using integrated AIRSAR, AVIRIS, and TIMS data p 1714 N95-23946

INFRARED SPECTROSCOPY
Measurement of HO2 and other trace gases in the stratosphere using a high resolution far-infrared spectrometer
| NASA-CR-197368 | p 1735 N95-22482
The effect of signal noise on the remote sensing of Foliar biochemical concentration p 1708 N95-23884
Near infrared and optical spectroscopy of FSC10214+4724
| NASA-CR-197966 | p 1828 N95-24068

INHIBITORS
Solderability preservation through the use of organic inhibitors
| DE95-003633 | p 1664 N95-24149

INITIATION
Investigation of the role of gravity waves in the generation of equatorial bubbles
| NASA-CR-197962 | p 1739 N95-23272

INJECTION
Finite-difference solutions of the alternate turbopump development high-pressure oxidizer turbopump pump-end ball-bearing cavity flows p 1678 N95-23617

INJECTORS
Heat transfer in rocket engine combustion chambers and nozzles p 1668 N95-23413
Mechanical design of the CDF SVX 2 silicon vertex detector
| DE94-018985 | p 1689 N95-23520
New pellet production and acceleration technologies for high speed pellet injection system HIPEL in Large Helical Device
| NISF-326 | p 1835 N95-23566

INLET FLOW
Flow visualization studies of VTOL aircraft models during Hover in ground effect
| NASA-TM-108860 | p 1607 N95-22666
Mach 10 computational study of a three-dimensional scramjet inlet flow field
| NASA-TM-4602 | p 1666 N95-23015
Mach 10 computational study of a three-dimensional scramjet inlet flow field
| NASA-TM-4602 | p 1667 N95-23210
Three-dimensional Navier-Stokes analysis and redesign of an imbedded bellmouth nozzle in a turbine cascade inlet section p 1671 N95-23423
Supersonic flow and shock formation in turbine tip gaps p 1672 N95-23429
Three-dimensional viscous flow analysis inside a turbine volute p 1674 N95-23437
Detailed measurements in the SSME high pressure fuel turbine with smooth rotor blades p 1675 N95-23441
CFD parametric study of consortium impeller p 1680 N95-23626

INNER RADIATION BELT
Characteristics of low energy ions in the Heavy Ions In Space (HIIS) experiment p 1815 N95-23807

INOCULATION
MHD seed recovery and regeneration, phase 2
| DE95-004308 | p 1833 N95-23338

INORGANIC COMPOUNDS
Ligand K-edge x-ray adsorption spectroscopic studies of the electronic structure of inorganic model complexes and metalloprotein active sites
| DE95-003338 | p 1840 N95-22851

INPUT/OUTPUT ROUTINES
Distributed VIRtual System (DIVIRS) project
| NASA-CR-197855 | p 1757 N95-23180
Integrating O/S models during conceptual design, part 2
| NASA-CR-197904 | p 1622 N95-23399
A 500 megabyte/second disk array p 1753 N95-24114

INSERTS
Extraction and detection of pesticide residues from air filter inserts using supercritical carbon dioxide
| DE95-004579 | p 1735 N95-23580

INSPECTION
Double pass retroreflection for corrosion detection in aircraft structures p 1642 N95-23503
The use of electrochemical impedance spectroscopy to predict the corrosion of aluminum-lithium alloys in marine environments p 1637 N95-23504
Non-destructive detection of corrosion for life management p 1643 N95-23505
Health and usage monitoring systems: Corrosion surveillance p 1607 N95-23506
Eddy current detection of pitting corrosion around fastener holes p 1643 N95-23507
Corrosion detection and monitoring of aircraft structures: An overview p 1644 N95-23515
Experience of in-service corrosion on military aircraft p 1644 N95-23516
POD assessment of NDI procedures using a round robin test
| AGARD-R-809 | p 1697 N95-23602
Robotic system for the servicing of the orbiter thermal protection system p 1697 N95-23724
10x reduction imaging at 13.4 nm
| DE94-016612 | p 1828 N95-23767

INSTRUCTORS
Formative and summative evaluation efforts for the Teacher Enhancement Institute conducted at the NASA Langley Research Center, summer 1994 p 1853 N95-23286
Teacher Enhancement Institute p 1853 N95-23312
Teacher Enhancement Institute p 1853 N95-23324

INTEGERS
Capacitated facility location: Valid inequalities and facets (revised)
| PB95-130225 | p 1786 N95-22641

INTEGRAL EQUATIONS
Lectures on 2D gauge theories. Topological aspects and path integral techniques
| DE94-628509 | p 1849 N95-22752
Nonlinear thermoviscoelastic behaviour in complex materials
| PB95-140653 | p 1630 N95-23537

INTEGRATED CIRCUITS
Current estimation for electromigration, hot carriers, and voltage drop
| AD-A285794 | p 1659 N95-22507
Limited bandwidth microwave filter
| AD-D016553 | p 1660 N95-22708
Segregated rigid and structural control for a photolithography positioning system
| DE95-002603 | p 1766 N95-23134
High-performance GaAs/AlGaAs optical modulators: Their performance and packaging for microwave photonic integrated circuits
| DE95-004533 | p 1828 N95-23575
Micro heat spreader enhanced heat transfer in MCM's
| DE95-004520 | p 1663 N95-23779
Cu deposition using a permanent magnet electron cyclotron resonance microwave plasma source
| DE94-017768 | p 1650 N95-23981

INTEGRATED LIBRARY SYSTEMS
Online Nuclear Data Service
| DE94-634268 | p 1856 N95-23452
Index of nuclear data libraries available from the IAEA nuclear data section
| DE94-634271 | p 1857 N95-23453
BROND-2.1. Russian evaluated neutron reaction data library
| DE94-634417 | p 1810 N95-23458
An expert system for diagnosing anomalies of spacecraft p 1770 N95-23684
AVIRIS and TIMS data processing and distribution at the land processes distributed active archive center p 1706 N95-23872
The data facility of the Airborne Visible/Infrared Imaging Spectrometer (AVIRIS) p 1707 N95-23877

A network-based distributed, media-rich computing and information environment
[DE95-003696] p 1765 N95-24074
OPUS: A new generation Knowledge Engineering Environment p 1760 N95-24176

INTEGRATORS
Ultrafast, high precision gated integrator
[DE95-004616] p 1664 N95-24164

INTELLIGENCE
The viability of establishing collaborative, reconfigurable research environments for the Human Performance Research Laboratory at NASA Ames
[NASA-CR-197384] p 1753 N95-22480

INTELSAT SATELLITES
Endeavor: Now and then
[NASA-TM-110539] p 1620 N95-23664

INTERACTIVE CONTROL
Commercialization of JPL Virtual Reality calibration and redundant manipulator control technologies
p 1768 N95-23676

INTERATOMIC FORCES
Structural properties of silicon clusters: An empirical potential study
[DE94-628902] p 1805 N95-22935
Calculations of alloy phases with a direct Monte-Carlo method
[DE94-018963] p 1640 N95-23121

INTERFACES
Advanced growth and surface analysis system for in situ studies of interface formation
[DE95-002850] p 1838 N95-22555
Magnetic multilayer physics
[DE95-003408] p 1798 N95-23083

INTERFACIAL TENSION
Morphology of Laplacian growth processes and statistics of equivalent many-body systems
[DE95-002734] p 1847 N95-22655
Quasistatic model for the motion of a viscous capillary liquid drop
[PB95-138848] p 1667 N95-23172
Numerical simulation of axisymmetric viscous sintering
[PB95-138889] p 1667 N95-23175

INTERFEROMETERS
Stellar Interferometer Technology Experiment (SITE)
[NASA-CR-197856] p 1827 N95-23089

INTERFEROMETRY
Interferometric synthetic aperture radar imagery of the Gulf Stream p 1712 N95-23939

INTERGRANULAR CORROSION
The role of grain boundary chemistry and structure in the environmentally-assisted intergranular cracking of nickel-base alloys
[DE95-002941] p 1638 N95-22532

INTERLAMINAR STRESS
Notch-tip damage and translaminar fracture toughness measurements from carbon/epoxy laminates
[AD-A280101] p 1627 N95-22833

INTERLAYERS
Magnetic multilayer physics
[DE95-003408] p 1798 N95-23083

INTERMETALLICS
Analysis of physiochemical processes during solder aging
[DE95-003811] p 1638 N95-22576
Nanophase materials: Synthesis, properties, applications
[AD-A286013] p 1627 N95-22940
Deformation of C15 Laves phase alloys
[DE95-003636] p 1646 N95-24067
Experimental and theoretical studies on the C15 intermetallic compounds MV2 (M = Zr, Hf and Ta): Elasticity and phase stability
[DE95-003723] p 1845 N95-24079
High resolution microstructural analysis of zirconia eutectic interfaces
[DE95-003143] p 1845 N95-24143

INTERMODULATION
Passive intermodulation generation in wire mesh deployable reflector antennas p 1656 N95-22816

INTERNAL COMBUSTION ENGINES
The influence of high-octane fuel blends on the performance of a two-stroke SI engine with knock-limited-compression ratio
[DE95-002902] p 1692 N95-22556
Performance of thin-ceramic-coated combustion chamber with gasoline and methanol as fuels in a two-stroke SI engine
[DE95-002903] p 1693 N95-22557
A hybrid vehicle evaluation code and its application to vehicle design
[DE95-004205] p 1662 N95-23334
The railplug: Development of a new ignitor for internal combustion engines
[DE95-004375] p 1695 N95-23342
Multi-fuel reformers for fuel cells used in transportation. Phase 1: Multi-fuel reformers
[DE95-004215] p 1729 N95-23482

INTERNAL FLOW
Mach 10 computational study of a three-dimensional scramjet inlet flow field
[NASA-TM-4602] p 1666 N95-23015
NASA low-speed axial compressor for fundamental research
[NASA-TM-4635] p 1616 N95-23192
CFD analysis of turbopump volutes
p 1674 N95-23436
Three-dimensional viscous flow analysis inside a turbine volute p 1674 N95-23437
Impeller flow field characterization with a laser two-focus velocimeter p 1675 N95-23440
A fine-grid model for the ASRM aft segment with gimballed nozzle p 1685 N95-23648
Application of CFD analysis to design support and problem resolution for ASRM and RSRM
p 1685 N95-23649
Time-accurate unsteady flow simulations supporting the SRM T+68-second pressure spike anomaly investigation (STS-54B) p 1685 N95-23650
Status of axisymmetric CFD of an eleven inch diameter hybrid rocket motor p 1686 N95-23651

INTERNAL PRESSURE
Residual strength of thin panels with cracks
p 1700 N95-23311

INTERNATIONAL COOPERATION
Basic data sets description and preliminary results of EFEDA-Spain
[PB95-139291] p 1740 N95-23470

INTERNATIONAL SPACE STATION
Hey! What's Space Station Freedom?
[NASA-TM-110531] p 1620 N95-22542
Functional testing of the space station plasma contactor
[NASA-TM-106841] p 1624 N95-23240
Automation and crew time saving in the space experiment p 1752 N95-23715
Graphical timeline editing p 1761 N95-23746
A format for the interchange of scheduling models
p 1780 N95-23747

INTERNETS
Applications drivers for data parking on the Information Superhighway p 1857 N95-24109
Analysis of the request patterns to the NSSDC on-line archive p 1862 N95-24137

INTERPLANETARY DUST
Transmission electron microscope studies of extraterrestrial materials
[NASA-CR-188363] p 1633 N95-23092
Micrometeoroids and debris on LDEF comparison with MIR data p 1623 N95-23824
Long term microparticle impact fluxes on LDEF determined from optical survey of Interplanetary Dust Experiment (IDE) sensors p 1623 N95-23826
LDEF Interplanetary Dust Experiment (IDE) results
p 1869 N95-23828
The orbital characteristics of debris particle rings as derived from IDE observations of multiple orbit intersections with LDEF p 1869 N95-23829

INTERPLANETARY MAGNETIC FIELDS
An explanation for tailward flows with positive B(sub z) in the distant tail neutral sheet during quite times
[ATR-95(7270)-1] p 1740 N95-23933

INTERPLANETARY MEDIUM
Results from the Heavy Ions in Space (HIIS) experiment on the ionic charge state of solar energetic particles
p 1870 N95-23808

INTERPOLATION
Stress intensity factors and crack mouth openings for bridged cracks emanating from circular holes
[AR-008-408] p 1699 N95-22952
On-line, adaptive state estimator for active noise control p 1784 N95-23308

INTERPROCESSOR COMMUNICATION
Description of a MIL-STD-1553B data bus Ada driver for the LeRC EPS Testbed
[NASA-TM-106866] p 1762 N95-22668
Using Dedal to share and reuse distributed engineering design information p 1768 N95-23678
Performance results of cooperating expert systems in a distributed real-time monitoring system
p 1761 N95-23688
Algorithms for categorizing multiprocessor communication under invalidate and update-based coherence protocols
[TR-533-REV] p 1759 N95-23928
Client/Server data serving for high performance computing p 1761 N95-24123

INTERSTELLAR GAS
Search for millimeterwave CO emission in damped Lyman-alpha systems
[PB95-139259] p 1868 N95-23607

INTERSTELLAR MATTER
Interstellar molecules in the large magellanic cloud
[PB95-139267] p 1868 N95-23230

INTRAVEHICULAR ACTIVITY
The Charlotte (TM) intra-vehicular robot
p 1697 N95-23703

INTRUSION
An automated computer misuse detection system for UNICOS
[DE95-000929] p 1762 N95-22680

INVARIANCE
Anti-invariant submanifolds of trans-Sasakian manifolds
[DE94-628413] p 1829 N95-22622
Classification of SU(3) modular invariants revisited
[PB95-110771] p 1787 N95-22715
Linearizing W-algebras
[DE94-634324] p 1790 N95-23457

INVARIANT IMBEDDINGS
Existence of solutions for some superlinear or sublinear elliptic systems on R(sup N)
[DE94-628417] p 1785 N95-22625
The Euler series of restricted Chow varieties
[DE94-628418] p 1785 N95-22626
On the theory of smooth structures 3
[DE94-628411] p 1786 N95-22642
Trisecant curve associated to a smooth curve in P(sub 3) of degree d greater than g+2
[DE94-628425] p 1787 N95-22809

INVENTIONS
Limited bandwidth microwave filter
[AD-D016553] p 1660 N95-22708
Motion-sensitive optical correlator using a VanderLugt correlator
[NASA-CASE-NPO-18769-1-CU] p 1827 N95-23045

INVERSIONS
Determinants of elliptic pseudo-differential operators
[PB95-109062] p 1786 N95-22711
Tomographic analysis of the three-dimensional variation of the seismic velocity structure of the shallow crust underlying Southern New England
[AD-A279406] p 1739 N95-23247
Comparison of inversion models using AIRSAR data for Death Valley, California p 1713 N95-23945

INVESTIGATION
Military bases: Environmental impact at closing installations. Report to Congressional requesters
[GAO/NSIAD-95-70] p 1735 N95-24057
DOD budget: Selected categories of planned funding for fiscal years 1995-99. Report to Congressional requesters
[GAO/NSIAD-95-92] p 1864 N95-24062
Ballistic Missile Defense: Current status of strategic target system. Report to Congressional requesters
[GAO/NSIAD-95-78] p 1903 N95-24080
Inspector General: Alleged misconduct by NASA Inspector General. Report to Congressional requesters
[GAO/OSI-95-9] p 1854 N95-24085

INVISCID FLOW
Numerical simulation of steady and unsteady viscous flow in turbomachinery using pressure based algorithm
p 1671 N95-23426
Entropy jump across an inviscid shock wave
[NASA-CR-195046] p 1678 N95-23596

IODIDES
Pressure shifts and electron scattering in atomic and molecular gases
[DE95-003102] p 1803 N95-22747

IODINE LASERS
Reduced dimer production in solar-simulator-pumped continuous wave iodine lasers based on model simulations and scaling and pumping studies
[NASA-TP-3486] p 1691 N95-23411

ION ACOUSTIC WAVES
Theory of HF induced turbulence in the ionosphere: Status and challenges
[DE95-002705] p 1739 N95-23256

ION BEAMS
Pulsed Ion Beam Surface Treatment for preparing rapidly solidified corrosion resistant alloy surfaces
[DE94-012072] p 1640 N95-22835
Genetic effects on heavy ions in drosophila
[NASA-CR-197916] p 1746 N95-22911
Ion rings for magnetic fusion
[DE94-017606] p 1832 N95-23120
The energy broadening resulting from electron stripping process of a low energy Au(-) beam
[NIFS-325] p 1836 N95-23569
High current induction linacs
[DE95-003442] p 1818 N95-24014
Thermochemistry of transition metal clusters
[DE95-003144] p 1646 N95-24144
Progress in ion beam power coupling and ion-driven hohlraums on PBFA 2
[DE95-004544] p 1818 N95-24160

ION CHARGE
Results from the Heavy Ions In Space (HIIS) experiment on the ionic charge state of solar energetic particles
p 1870 N95-23808

ION CURRENTS
Advanced detector development, laboratory simulations, diagnostic development, and data analysis on wake physics
|PL-TR-94-2204| p 1831 N95-22948

ION CYCLOTRON RADIATION
TFTR Ion Cyclotron Range of Frequencies (ICRF) experimental data analysis collaboration
|DE95-003409| p 1832 N95-23084
Cu deposition using a permanent magnet electron cyclotron resonance microwave plasma source
|DE94-017768| p 1650 N95-23981
A 4 MW fast wave current drive upgrade for D3-D
|DE95-003741| p 1837 N95-24083

ION ENGINES
NASA 30 cm ion thruster development status
|NASA TM-106842| p 1624 N95-23221

ION EXCHANGE RESINS
Test procedure for anion exchange chromatography
|DE95-003767| p 1809 N95-23407

ION EXCHANGING
NO decomposition in non-reducing atmospheres
|DE95-004324| p 1634 N95-23339
Test procedure for cation exchange chromatography
|DE95-003770| p 1808 N95-23350

ION IMPLANTATION
Increasing the retained dose by plasma immersion ion implantation and deposition
|DE95-003423| p 1844 N95-24011
Carbon doping of III-V compound semiconductors
|DE95-003431| p 1844 N95-24013

ION IRRADIATION
Genetic effects on heavy ions in drosophila
|NASA-CR-197916| p 1746 N95-22911
Temperature effects on ion irradiation damage in MgAl2O4 spinel single crystals
|DE95-003679| p 1844 N95-24073
A phenomenological model for the effect of nanocrystalline microstructure on irradiation-induced amorphization in U3Si
|DE95-004631| p 1846 N95-24169

ION PROPULSION
NASA 30 cm ion thruster development status
|NASA TM-106842| p 1624 N95-23221

ION RECOMBINATION
Rate coefficients for the electron-impact excitation, ionization and recombination of He-like ions, S XV, Ca XIX and Fe XXV, and related processes
|ISAS-R-657| p 1811 N95-23604

ION SCATTERING
Comparison of exact solution with Eikonal approximation for elastic heavy ion scattering
|NASA-TP-3498| p 1817 N95-22929

ION SOURCES
Progress in ion beam power coupling and ion-driven hohlraums on PBFA 2
|DE95-004544| p 1818 N95-24160

ION STORAGE
A brief history in time of ion traps and their achievements in science
|DE95-002815| p 1805 N95-22936

ION STRIPPING
The energy broadening resulting from electron stripping process of a low energy Au(-) beam
|NIFS-325| p 1836 N95-23569

ION TEMPERATURE
Numerical Tokamak Project code comparison
|DE95-003475| p 1831 N95-22899

IONIC COLLISIONS
Dimuon production in proton-nucleus interactions
|DE95-002613| p 1801 N95-22551
(pi)N correlations at AGS
|DE95-002933| p 1801 N95-22656
Studies of photon and electron interactions with atoms and ions
|DE95-003340| p 1802 N95-22700
The problem of phase transition and the heavy ion collisions at very high energies
|DE94-628584| p 1816 N95-22785

IONIC CRYSTALS
Computer simulation of the structure of ionic surfaces and interfaces
|DE95-002991| p 1804 N95-22792

IONIC DIFFUSION
Diffusion behavior of lysozyme in aqueous ammonium sulfate solutions under varying solution conditions as determined by dynamic light scattering
|DE95-004821| p 1635 N95-23380

IONIC MOBILITY
Analytical and numerical studies of ion mobility near the tokamak plasma edge
|DE95-003019| p 1830 N95-22693

IONIZATION
Novel mass spectrometric instrument for gaseous and particulate characterization and monitoring
|DE95-001135| p 1687 N95-22682
Rate coefficients for the electron-impact excitation, ionization and recombination of He-like ions, S XV, Ca XIX and Fe XXV, and related processes
|ISAS-R-657| p 1811 N95-23604
Near infrared and optical spectroscopy of FSC10214+4724
|NASA-CR-197966| p 1828 N95-24068
Atoms as many-body systems
|DE95-004609| p 1813 N95-24151

IONIZING RADIATION
LDEF: 69 Months in Space. Third Post-Retrieval Symposium, part 1
|NASA-CP-3275-PT-1| p 1889 N95-23796
Dosimetric results on EURECA p 1872 N95-23800
Contribution of proton-induced short range secondaries to the LET spectra on LDEF p 1815 N95-23813
Charge, energy and LET spectra of high LET primary and secondary particles in CR-39 plastic nuclear track detectors of the P0006 experiment
p 1815 N95-23814
Predictions of LET spectra measured on LDEF
p 1815 N95-23815
Predictions of LDEF radioactivity and comparison with measurements p 1815 N95-23818
Status of LDEF radiation modeling
p 1815 N95-23819

IONOSPHERES
Observation model and parameter partials for the JPL VLBI parameter estimation software MODEST, 19 94
|NASA-CR-197328| p 1756 N95-22853
Theory of HF induced turbulence in the ionosphere: Status and challenges
|DE95-002705| p 1739 N95-23256

IONOSPHERIC HEATING
Magnetospheric space plasma investigations
|NASA-CR-197405| p 1831 N95-22955
The high latitude ionosphere-magnetosphere transition region: Simulation and data comparison
|NASA-CR-197404| p 1737 N95-22956

IONOSPHERIC SOUNDING
Investigation of Federal Standard 1045 high-frequency ALE radio performance in the Southern Trans-Auroral Zone
|PB94-204831| p 1655 N95-22636

IONS
Turbidity of a near critical ionic fluid
|DE94-014916| p 1633 N95-22869
Ionic core effects on the Mie resonance in lithium clusters
|DE94-014974| p 1805 N95-22870
Effect of different ions on the anodic behaviour of alloy 800 chloride solutions at high temperature
|DE94-634944| p 1645 N95-23983
Increasing the retained dose by plasma immersion ion implantation and deposition
|DE95-003423| p 1844 N95-24011
Charging of interplanetary grains
|NASA-CR-198032| p 1869 N95-24066
Temperature effects on ion irradiation damage in MgAl2O4 spinel single crystals
|DE95-003679| p 1844 N95-24073

IRON
Trapped iron measured on LDEF
p 1872 N95-23806

IRON ALLOYS
Nanophase materials: Synthesis, properties, applications
|AD-A286013| p 1627 N95-22940

IRON ISOTOPES
Rate coefficients for the electron-impact excitation, ionization and recombination of He-like ions, S XV, Ca XIX and Fe XXV, and related processes
|ISAS-R-657| p 1811 N95-23604

IRON OXIDES
On the formation of iron(3) oxides via oxidation of iron(2)
|DE94-018392| p 1632 N95-22857
Particle size dependence in Fischer-Tropsch synthesis
|DE95-003124| p 1633 N95-22876
Nanophase materials: Synthesis, properties, applications
|AD-A286013| p 1627 N95-22940
Charge distribution analysis of catalysts under simulated reaction conditions
|DE95-003526| p 1633 N95-23064

IRRADIANCE
Twelve month performance evaluation for the rotating shadowband radiometer
|DE95-002847| p 1726 N95-22554
A proposed update to the solar irradiance spectrum used in LOWTRAN and MODTRAN p 1705 N95-23865

IRRADIATION
Laser irradiation effects: A functional assessment
|AD-A285100| p 1691 N95-22937
The effect of simulated low earth orbit radiation on polyimides (UV degradation study) p 1651 N95-23903
Charging of interplanetary grains
|NASA-CR-198032| p 1869 N95-24066
Effect of dynamically charged helium on mechanical properties of vanadium-base alloys
|DE95-004613| p 1646 N95-24153
Transient radiation-induced absorption in materials for the DOI laser
|DE95-004549| p 1828 N95-24161

ISING MODEL
Continuous local symmetry in Ising-type models
|DE94-629045| p 1839 N95-22649
Turbidity of a near critical ionic fluid
|DE94-014916| p 1633 N95-22869

ISOMORPHISM
Grassman and hyperKaehler structures on some spaces of sections of holomorphic bundles
|PB95-109104| p 1795 N95-22712
Graph isomorphism models for non interleaving process algebra
|PB95-110490| p 1786 N95-22714

ISOTHERMAL FLOW
A computer model in general 3-D curvilinear coordinates for the prediction of the turbulent flow field in a jet induced ram combustor
|NAL-TR-1240T| p 1687 N95-24051

ISOTHERMAL PROCESSES
Decomposition mechanisms in thermally-aged thin-film explosives
|DE95-000741| p 1652 N95-22838

ISOTOPE RATIOS
Recent developments in inductively coupled plasma source magnetic sector multiple collector mass spectrometry
|DE95-003002| p 1830 N95-22793
Precise determinations of the isotopic compositions and atomic weights of molybdenum, tellurium, tin and tungsten using ICP source magnetic sector multiple collector mass spectrometry
|DE95-003003| p 1632 N95-22795

ISOTOPE SEPARATION
Modified molecular sieves: Stationary phase for the gas chromatographic separation of hydrogen isotopes
|DE94-627282| p 1814 N95-24175

ISOTOPES
Recent developments in inductively coupled plasma source magnetic sector multiple collector mass spectrometry
|DE95-003002| p 1830 N95-22793

ISOTOPIC LABELING
Precise determinations of the isotopic compositions and atomic weights of molybdenum, tellurium, tin and tungsten using ICP source magnetic sector multiple collector mass spectrometry
|DE95-003003| p 1632 N95-22795
SIMS chemical and isotopic analysis of impact features from LDEF experiments AO187-1 and AO187-2
p 1637 N95-23837

ISOTOPIC SPIN
Search for top quark at CDF
|DE95-003748| p 1809 N95-23406

ITALY
Intermediate-term earthquake prediction and seismic zoning in Northern Italy
|DE94-627689| p 1736 N95-22612

ITERATION
Iterative solutions of nonlinear equations in smooth Banach spaces
|DE94-634287| p 1790 N95-23455
Quasi-kernel polynomials and convergence results for quasi-minimal residual iterations
|NASA-CR-197948| p 1791 N95-23593
Ishikawa iteration process for nonlinear Lipschitz strongly accretive mappings
|DE94-634284| p 1792 N95-23658

ITERATIVE SOLUTION
A worst-case example using linesearch methods for numerical optimization with inexact gradient evaluations
|DE95-002917| p 1754 N95-22570
Iterative solutions of nonlinear equations with strongly accretive or strongly pseudocontractive maps
|DE94-628432| p 1786 N95-22634
Stability and efficiency of waveform relaxation methods
|PB95-138863| p 1789 N95-23173
Iterative solutions of nonlinear equations in smooth Banach spaces
|DE94-634287| p 1790 N95-23455
Recent advances in Lanczos-based iterative methods for nonsymmetric linear systems
|NASA-CR-197950| p 1791 N95-23611

An implementation of the QMR method based on coupled two-term recurrences
|NASA-CR-197956| p 1791 N95-23612

IUE
IUE observing programs: NSOSS, VEOEB, and PCOEB
|NASA-CR-197424| p 1866 N95-23560
Observational studies of the clearing phase in proto-planetary disk systems
|NASA-CR-197900| p 1866 N95-23561
A constraint-logic based implementation of the coarse-grained approach to data acquisition scheduling of the International Ultraviolet Explorer orbiting observatory p 1779 N95-23741

J

JAHN-TELLER EFFECT
Quantum fluctuations of D(sub 5d) polarons on C(sub 60) molecules
|DE94-635787| p 1812 N95-23985

JAPANESE SPACE PROGRAM
Third International Symposium on Artificial Intelligence, Robotics, and Automation for Space 1994
|NASA-CR-197340| p 1767 N95-23672
A perspective on space robotics in Japan p 1697 N95-23695
Space robotic experiment in JEM flight demonstration p 1697 N95-23701
Development of Japanese experiment module remote manipulator system p 1752 N95-23708
Automatic satellite capture and berthing with robot arm (ASCABRA) p 1623 N95-23713

JAPANESE SPACECRAFT
Use of the Airborne Visible/Infrared Imaging Spectrometer to calibrate the optical sensor on board the Japanese Earth Resources Satellite-1 p 1624 N95-23864
Dynamical model and numerical simulations for Engineering Test Satellite-6
|NAL-TR-1239| p 1622 N95-24049

JET AIRCRAFT NOISE
Supersonic jet noise reductions predicted with increased jet spreading rate
|NASA-TM-106872| p 1800 N95-23178

JET ENGINES
High-performance parallel analysis of coupled problems for aircraft propulsion
|NASA-CR-197440| p 1614 N95-23088

JET FLOW
Experimental study of vortex breakdown in a swirling water jet
|PB95-130407| p 1665 N95-22767
Modeling NO(x) emissions in turbulent jet flames: Effects of buoyancy and radiation
|DE94-016621| p 1633 N95-22886
Testing QCD with jet physics at CDF
|DE94-018980| p 1807 N95-23196
Measurement of correlated b quark cross sections at CDF
|DE95-004240| p 1808 N95-23336
On the breakup of viscous liquid threads
|NASA-CR-195023| p 1678 N95-23544

JET MIXING FLOW
Supersonic jet noise reductions predicted with increased jet spreading rate
|NASA-TM-106872| p 1800 N95-23178

JET PROPULSION
NASA procurement: Contract and management improvements at the Jet Propulsion Laboratory. Report to Congressional requesters
|GAO/NSIAD-95-40| p 1854 N95-24054

JETS
Testing QCD with jet physics at CDF
|DE94-018980| p 1807 N95-23196
Properties of jets in Z events from 1.8 TeV (bar p)p collisions
|DE94-018982| p 1808 N95-23197

JOINTS (JUNCTIONS)
Controlling under-actuated robot arms using a high speed dynamics process
|NASA-CASE-NPO-18498-1-CU| p 1692 N95-22543

JOSEPHSON JUNCTIONS
High power Josephson effect sources
|AD-A285808| p 1838 N95-22511
Microstructure and composition of a SNS Josephson junction using CaRuO3 as the metallic barrier
|DE95-004611| p 1845 N95-24152
Dependence of the Josephson coupling of unconventional superconductors on the properties of the tunneling barrier
|DE95-004649| p 1846 N95-24173

JUPITER SATELLITES
IUE observing programs: NSOSS, VEOEB, and PCOEB
|NASA-CR-197424| p 1866 N95-23560

K

K-EPSILON TURBULENCE MODEL
GGOT total pressure loss control concept evaluation p 1672 N95-23427
Advanced turbulence models for turbomachinery p 1675 N95-23443
Numerical computation of aerodynamics and heat transfer in a turbine cascade and a turn-around duct using advanced turbulence models p 1675 N95-23444

KALMAN FILTERS
Tutorial on filtering, restoration, and state estimation
|TR-534| p 1793 N95-24042

KAONS
Limit on the muon neutrino mass from K(exp 0)muon 3 decay spectra
|DE95-000816| p 1801 N95-22583
Chiral anomalies in non-leptonic decays within chiral perturbation theory at the quark level
|DE94-628613| p 1849 N95-22753
Do narrow Sigma hypernuclear states exist?
|DE95-002930| p 1803 N95-22763
New determination of V(sub us) from K(sub e3)(+) decay
|DE94-628616| p 1811 N95-23769

KAPTON (TRADEMARK)
LDEF polymeric materials: A summary of Langley characterization p 1651 N95-23899
Atomic oxygen interactions with protected organic materials on the Long Duration Exposure Facility (LDEF) p 1627 N95-23909

KERNEL FUNCTIONS
Quasi-kernel polynomials and convergence results for quasi-minimal residual iterations
|NASA-CR-197948| p 1791 N95-23593
Scale-invariant Lipatov kernels from t-channel unitarity
|DE95-004625| p 1813 N95-24166

KERR EFFECTS
Spin polarized photoemission studies of magnetic quantum well states
|DE95-004218| p 1851 N95-23335

KINEMATICS
Effects of delaminations on the damped dynamic characteristics of composite laminates: Mechanics and experiments
|NASA-TM-106862| p 1630 N95-23258

KINETIC ENERGY
Energetic particle observations at geosynchronous orbit
|DE95-000873| p 1867 N95-22516
Effects of wind on rainfall simulation. Spatial distribution of water application, kinetic energy, and overland flow under single full-cone nozzle sprays
|PB95-127304| p 1717 N95-22537
Variational calculations for He-3 impurities on He-4 droplets
|DE94-628469| p 1840 N95-22839
Galactic oscillator symmetry p 1822 N95-22973

KINETIC EQUATIONS
MHD-Vlasov simulation of the toroidal Alfven eigenmode
|NIFS-319| p 1836 N95-23591
The kinetics of quantum system with time-dependent periodic Hamiltonian
|DE94-635422| p 1797 N95-23966

KINETIC THEORY
Theory of HF induced turbulence in the ionosphere: Status and challenges
|DE95-002705| p 1739 N95-23256

KINETICS
Magnetospheric space plasma investigations
|NASA-CR-197405| p 1831 N95-22955
The kinetics of quantum system with time-dependent periodic Hamiltonian
|DE94-635422| p 1797 N95-23966

KLEIN-GORDON EQUATION
Deformed Heisenberg algebra and fractional spin field in 2+1 dimensions
|DE94-628507| p 1850 N95-22779
Notes on oscillator-like interactions of various spin relativistic particles p 1815 N95-22997

KLYSTRONS
Design study of longitudinal dynamics of the drive beam in 1 TeV relativistic klystron two-beam accelerator
|DE95-004683| p 1817 N95-23485
Design study of beam dynamics issues for 1 TeVnext linear collider based on the relativistic-klystron two-beam accelerator
|DE95-004673| p 1817 N95-23493

KNOWLEDGE BASED SYSTEMS
Towards method-independent knowledge acquisition
|AD-A285823| p 1766 N95-22512
Knowledge-based guidance and control functions
|AGARD-AR-325| p 1751 N95-23601
A toolbox and record for scientific models p 1775 N95-23716
Space science experimentation automation and support p 1775 N95-23718
Intelligent monitoring system applied to super long distance telerobotic tasks p 1777 N95-23728

KNOWLEDGE BASES (ARTIFICIAL INTELLIGENCE)
AMPHION: Specification-based programming for scientific subroutine libraries p 1761 N95-23680
An expert system for diagnosing anomalies of spacecraft p 1770 N95-23684
Performance results of cooperating expert systems in a distributed real-time monitoring system p 1761 N95-23688
Classification of the LCVF AVIRIS test site with a Kohonen artificial neural network p 1706 N95-23874

KNOWLEDGE REPRESENTATION
Knowledge representation and reasoning for mixed-initiative planning
|TR-562| p 1783 N95-24031
OPUS: A new generation Knowledge Engineering Environment p 1760 N95-24176
The TRAINS project: A case study in building a conversational planning agent
|TR-532| p 1659 N95-24193

KOLMOGOROV THEORY
On inertial range scaling laws
|DE95-004515| p 1677 N95-23484
Large sets in AC(exp 0): A Kolmogorov complexity related property and some applications
|TR-556| p 1797 N95-24029
Martin-Lof tests can help too
|TR-541| p 1797 N95-24063

KRYPTON
Krypton isotope analysis using near-resonant stimulated Raman spectroscopy
|DE95-005061| p 1635 N95-23348

KRYPTON ISOTOPES
Krypton isotope analysis using near-resonant stimulated Raman spectroscopy
|DE95-005061| p 1635 N95-23348

KUTTA-JOUKOWSKI CONDITION
Aeroacoustic computation of gust-blade interaction p 1800 N95-23313

L

LABORATORIES
Southeast Regional Experiment Station
|DE95-000903| p 1726 N95-22518

LABORATORY EQUIPMENT
Atomic oxygen durability evaluation of protected polymers using thermal energy plasma systems
|NASA-TM-106855| p 1626 N95-23270

LAGRANGE COORDINATES
Quasistatic model for the motion of a viscous capillary liquid drop
|PB95-138848| p 1667 N95-23172

LAGRANGIAN FUNCTION
Twistor-like type 2 superstring with the heterotic (2,0) and (4,0) worldsheet supersymmetry
|DE94-628510| p 1848 N95-22735
Aspects of sigma models
|DE94-628511| p 1795 N95-22736
Dirac canonical quantization and Faddeev-Jackiw symplectic quantization of higher order Lagrangians
|DE94-628428| p 1796 N95-22788
The decays of D(sup *)-mesons
|DE94-628610| p 1804 N95-22810
The omega pi(sup 0)-transient form factor within effective chiral Lagrangian approach
|DE94-628612| p 1850 N95-22812
Once more about the omega approaches 3(pi) contact term
|DE94-633202| p 1804 N95-22847
Modeling NO(x) emissions in turbulent jet flames: Effects of buoyancy and radiation
|DE94-016621| p 1633 N95-22886
Non-Noetherian symmetries for oscillators in classical mechanics and in field theory p 1823 N95-22977
Pseudoclassical description of the Dirac Oscillator p 1825 N95-22996
A generalized Eulerian-Lagrangian analysis, with application to liquid flows with vapor bubbles p 1682 N95-23633
Modeling of non-spherical droplet dynamics p 1685 N95-23647

LAMINAR BOUNDARY LAYER
Bursting in the near-surface boundary layer: Comparisons between realistic models and observations
[DE95-003714] p 1741 N95-24078
LAMINAR FLOW
The initial-value problem for viscous channel flows
[NASA-CR-195034] p 1667 N95-23207
High-lift flow-physics flight experiments on a subsonic civil transport aircraft (B737-100) p 1609 N95-23333
CFD modeling of turbulent duct flows for coolant channel analysis p 1682 N95-23635
Supersonic laminar flow control research
[NASA-CR-197938] p 1609 N95-23669
Bursting in the near-surface boundary layer: Comparisons between realistic models and observations
[DE95-003714] p 1741 N95-24078
LAMINATES
Vibration-damping structural component
[AD-D016550] p 1693 N95-22707
Notch-tip damage and translaminar fracture toughness measurements from carbon/epoxy laminates
[AD-A280101] p 1627 N95-22833
Advanced development of PV encapsulants
[DE95-000246] p 1728 N95-23062
Effects of delaminations on the damped dynamic characteristics of composite laminates: Mechanics and experiments
[NASA-TM-106862] p 1630 N95-23258
Interlaminar shear test method development for long term durability testing of composites
p 1631 N95-23300
New nondestructive techniques for the detection and quantification of corrosion in aircraft structures
p 1644 N95-23512
Thermoelastic theory for the response of materials functionally graded in two directions with applications to the free-edge problem
[NASA-TM-106882] p 1699 N95-24055
LAND ICE
Glaciological studies in the central Andes using AIRSAR/TOPSAR p 1713 N95-23942
Unusual radar echoes from the Greenland ice sheet
p 1714 N95-23951
LAND SURFACE TEMPERATURE
Land surface temperature measurements for EOS MODIS data
[NASA-CR-197443] p 1717 N95-23191
Validation data for land surface temperature determination from satellites
[CSIRO-TR-33] p 1718 N95-23597
Land surface temperature measurements from EOS MODIS data
[NASA-CR-197969] p 1721 N95-24190
LAND USE
Monitoring land use and degradation using satellite and airborne data p 1707 N95-23880
Estimation of crown closure from AVIRIS data using regression analysis p 1709 N95-23886
LANDAU DAMPING
MHD-Vlasov simulation of the toroidal Alfven eigenmode
[NIFS-319] p 1836 N95-23591
LANDAU-GINZBURG EQUATIONS
Analyses, algorithms, and computations for models of high-temperature superconductivity
[DE95-003290] p 1661 N95-22733
LANDING AIDS
Guidance and control requirements for high-speed Rollout and Turnoff (ROTO)
[NASA-CR-195026] p 1614 N95-22674
LANDING GEAR
Corrosion of landing gear steels p 1642 N95-23500
LANDING SITES
The effect of sensor spacing on wind measurements at the Shuttle Landing Facility
[NASA-TP-3529] p 1742 N95-23010
LANDSAT SATELLITES
A role for AVIRIS in the Landsat and Advanced Land Remote Sensing Systems program
p 1705 N95-23866
A preliminary comparison of Landsat Thematic Mapper and SPOT-1 HRV multispectral data for estimating coniferous forest volume p 1719 N95-24097
Determining successional stage of temperate coniferous forests with Landsat satellite data p 1720 N95-24102
LANGMUIR TURBULENCE
Langmuir-like waves and radiation in planetary foreshocks
[NASA-CR-197376] p 1869 N95-22828
Theory of HF induced turbulence in the ionosphere: Status and challenges
[DE95-002705] p 1739 N95-23256
LANGMUIR-BLODGETT FILMS
Large-sized and highly radioactive H-3 and Cd-109 Langmuir-Blodgett films
[DE94-785270] p 1811 N95-23775
LANGUAGE PROGRAMMING
Realizing parallel reduction operation in Sisal 1.2
[DE94-017524] p 1763 N95-22858
Realizing parallel reduction operations in Sisal 1.2
[DE94-017525] p 1763 N95-22859
LANGUAGES
Automatic verification of regular protocols in P/T nets
[PB95-138921] p 1789 N95-23146
Proceedings of the workshop on deductive databases and logic programming
[PB95-139382] p 1758 N95-23553
Combinatorial semantics
[TR-563] p 1792 N95-23793
LANTHANUM OXIDES
Phonon characteristics of high (T sub c) superconductors from neutron Doppler broadening measurements
[DE95-003703] p 1844 N95-24076
LAPLACE TRANSFORMATION
Morphology of Laplacian growth processes and statistics of equivalent many-body systems
[DE95-002734] p 1847 N95-22655
Fourth order difference methods for hyperbolic IBVP's
[NASA-CR-197955] p 1791 N95-23548
A theory for the morphology of Laplacian growth from statistics of equivalent many-body Hamiltonian systems
[DE94-014473] p 1799 N95-23979
LARGE SCALE INTEGRATION
Integrating O/S models during conceptual design, part 1
[NASA-CR-197903] p 1622 N95-23398
Integrating O/S models during conceptual design, part 2
[NASA-CR-197904] p 1622 N95-23399
LASER APPLICATIONS
Production of high contrast ultrashort laser pulses for short scale length plasma experiments
[DE95-003640] p 1690 N95-22595
Ground-based and space-based laser beam power applications
[NASA-TM-106744] p 1691 N95-22670
7th International Symposium on Applications of Laser Techniques to Fluid Mechanics, volume 1
[AD-A285647] p 1691 N95-23118
Transient radiation-induced absorption in materials for the DOI laser
[DE95-004549] p 1828 N95-24161
LASER BEAMS
Ground-based and space-based laser beam power applications
[NASA-TM-106744] p 1691 N95-22670
Laser irradiation effects: A functional assessment
[AD-A285100] p 1691 N95-22937
10x reduction imaging at 13.4 nm
[DE94-016612] p 1828 N95-23767
Laser light induced drift for atoms of radioactive isotopes Na-22 and Na-24
[DE94-635759] p 1812 N95-23976
LASER DAMAGE
A ruggedness evaluation of procedures for damage threshold testing optical materials
[NASA-TM-4639] p 1840 N95-22803
LASER DEPOSITION
Large-area triple-junction a-Si alloy production scaleup
[DE95-000245] p 1726 N95-22546
LASER DOPPLER VELOCIMETERS
Impeller flow field characterization with a laser two-focus velocimeter p 1675 N95-23440
Flow diagnostics, chemically reacting turbulent flow modeling and turbulent mixing: A summary of project studies in combustion
[NASA-CR-197348] p 1687 N95-24022
LASER MATERIALS
Computational modelling of Er(3+): Garnet laser materials p 1692 N95-23326
Reduced dimer production in solar-simulator-pumped continuous wave iodine lasers based on model simulations and scaling and pumping studies
[NASA-TP-3486] p 1691 N95-23411
LASER OUTPUTS
Proceedings of NATO Advanced Research Workshop on the Formation, Transport and Consequences of Particles in Plasmas
[AD-A285850] p 1829 N95-22514
Ground-based and space-based laser beam power applications
[NASA-TM-106744] p 1691 N95-22670
Laser irradiation effects: A functional assessment
[AD-A285100] p 1691 N95-22937
Annual report of the Osaka Laboratory for Radiation Chemistry Japan Atomic Energy Research Institute, (No. 26)
[DE94-785277] p 1626 N95-23477
LASER PLASMAS
10x reduction imaging at 13.4 nm
[DE94-016612] p 1828 N95-23767
LASER RANGE FINDERS
Small image laser range finder for planetary rover
p 1692 N95-23712
LASER SPECTROMETERS
AIRSAR deployment in Australia, September 1993: Management and objectives p 1714 N95-23948
LASER SPECTROSCOPY
Raman-shifting an ArF excimer laser to generate new lines for obtaining optical diagnostic based information in flow fields p 1692 N95-23303
LASER TARGET INTERACTIONS
Optogalvanic monitoring of collisional transfer of laser excitation energy in a neon RF plasma
[DE95-003103] p 1691 N95-22748
LASER TARGETS
Progress in ion beam power coupling and ion-driven hohlraums on PBFA 2
[DE95-004544] p 1818 N95-24160
LASERS
Laser-plasma instability in hohlraums
[DE95-000914] p 1829 N95-22676
Real lasers and other deformed objects
p 1692 N95-23001
7th International Symposium on Applications of Laser Techniques to Fluid Mechanics, volume 1
[AD-A285647] p 1691 N95-23118
Computational modelling of Er(3+): Garnet laser materials p 1692 N95-23326
Krypton isotope analysis using near-resonant stimulated Raman spectroscopy
[DE95-005061] p 1635 N95-23348
LASING
Reduced dimer production in solar-simulator-pumped continuous wave iodine lasers based on model simulations and scaling and pumping studies
[NASA-TP-3486] p 1691 N95-23411
LATERAL CONTROL
Aerodynamic surface distension system for high angle of attack forebody vortex control
[NASA-CASE-ARC-11979-1] p 1612 N95-23390
Feedback control laws for highly maneuverable aircraft
[NASA-CR-197944] p 1615 N95-23410
LATTICE PARAMETERS
Transformation behavior in Al2O3-ZrO2 ceraamic composites
[DE95-001359] p 1647 N95-22688
Block spins and chirality in Heisenberg model on Kagome and triangular lattices
[DE94-629044] p 1840 N95-22845
Lattice relaxation study on self-trapped exciton and biexciton in neutral and charged fullerenes
[DE94-635788] p 1844 N95-23986
LATTICE VIBRATIONS
A report on the Indiana University Workshop on future U.S. hadron facilities
[DE95-003951] p 1817 N95-23353
LATTICES (MATHEMATICS)
Static parametric fluctuations give nonstatistical behaviour in uncoupled chaotic systems
[DE94-628478] p 1794 N95-23019
Dynamical behaviour of the coupled diffusion map lattice
[DE94-628481] p 1841 N95-23022
LAUNCH VEHICLES
Multidisciplinary design optimization using genetic algorithms p 1619 N95-23332
NLS base heating CFD analysis p 1673 N95-23432
Aerodynamic flight control to increase payload capability of future launch vehicles
[NASA-CR-197704] p 1619 N95-24032
Airborne rotary air separator study
[NASA-CR-189099] p 1614 N95-24053
Ballistic Missile Defense: Current status of strategic target system. Report to Congressional requesters
[GAO/NSIAD-95-78] p 1903 N95-24080
LAUNCHING
On-orbit science in a small package: Managing the ALEXIS satellite and experiments
[DE94-014426] p 1621 N95-22868
LEADERSHIP
Upward appraisal as a means for improving supervisory performance and promoting process improvement, with long-term implications for organizational change
p 1854 N95-23323
LEADING EDGE FLAPS
Wing pressure distributions from subsonic tests of a high-wing transport model --- in the Langley 14- by 22-Foot Subsonic Wind Tunnel
[NASA-TM-4583] p 1607 N95-22802
LEADING EDGE SLATS
Lift enhancing tabs for airfoils
[NASA-CASE-ARC-11990-1] p 1613 N95-23395
LEAKAGE
Optimization of a centrifugal impeller design through CFD analysis p 1680 N95-23624

The influence of swirl brakes and a tip discharge orifice on the rotordynamic forces generated by discharge-to-suction leakage flows in shrouded centrifugal pumps p 1680 N95-23628

LEARNING

Design and implementation of two two-week Teacher Enhancement Institutes p 1853 N95-23306

Teacher Enhancement Institute p 1853 N95-23312

Unsupervised classification learning from cross-modal environmental structure
|TR-536| p 1784 N95-24040

LEARNING THEORY

Unsupervised classification learning from cross-modal environmental structure
|TR-536| p 1784 N95-24040

LEAST SQUARES METHOD

Objective determination of image end-members in spectral mixture analysis of AVIRIS data p 1709 N95-23888

LEAVES

Use of spectral analogy to evaluate canopy reflectance sensitivity to leaf optical property p 1701 N95-23845

Application of a two-stream radiative transfer model for leaf lignin and cellulose concentrations from spectral reflectance measurements, part 1 p 1703 N95-23856

Application of a two-stream radiative transfer model for leaf lignin and cellulose concentrations from spectral reflectance measurements, part 2 p 1703 N95-23857

Relationships between pigment composition variation and reflectance for plant species from a coastal savannah in California p 1709 N95-23889

LECTURES

Glass science tutorial: Lecture 1, Chemistry and properties of oxide glasses
|DE95-002963| p 1647 N95-22647

Glass science tutorial: Lecture 2, operating electric glass melters
|DE95-002965| p 1647 N95-22648

Higgs searches and WW scattering
|PB95-139143| p 1807 N95-23160

LENSES

Development of microchannel plate x-ray optics
|NASA-CR-197935| p 1866 N95-23540

LENTICULAR BODIES

Evolution of oxidation and creep damage mechanisms in HIPed silicon nitride materials
|DE95-001360| p 1647 N95-22689

LEPTONS

Experimental results on polarized structure functions in deep inelastic lepton-nucleon scattering
|DE95-002782| p 1801 N95-22521

Supersymmetric singlet majorons and cosmology
|DE94-628571| p 1850 N95-22783

Results from neutrino experiments
|DE94-628604| p 1804 N95-22790

Search for second generation leptoquarks at CDF
|DE94-018983| p 1805 N95-22939

Final result on the mass of the tau lepton from the BES collaboration
|DE95-003466| p 1806 N95-23139

High Energy Theory: Task B and Task L
|DE95-003453| p 1817 N95-23148

Search for Z' and W' at CDF
|DE94-018987| p 1808 N95-23203

Recent results from Fermilab E-687, charm particle decays, lifetimes and photoproduction dynamics: A compilation results presented at DPF 1994
|DE95-004580| p 1808 N95-23347

New determination of V(sub us) from K(sub e3)(+) decay
|DE94-628616| p 1811 N95-23769

Neutrino masses and mixing
|DE94-628632| p 1812 N95-23784

Neutrino mass
|DE94-628634| p 1812 N95-23786

Hard e(+)e(-)-pair Bremsstrahlung as a lepton polarimeter
|DE94-635615| p 1812 N95-23984

W mass measurements from D(circle slash) and CDF experiments at TeVatron
|DE95-003497| p 1813 N95-24000

LEUKEMIAS

Activation of the jun-D gene in human myeloid cells by 1-(beta)-D-arabinofuranosylcytosine
|DE94-016591| p 1746 N95-22912

LEVITATION

Initial crystallization and growth in melt processing of large-domain YBa2Cu3O(x) for magnetic levitation
|DE95-002993| p 1839 N95-22572

Processing of single- and multi-domain YBa2Cu3O(x) bulk materials for levitation applications by Nd(1+x)Ba(2-x)Cu3O(y) seeding
|DE95-004615| p 1845 N95-24154

LIAPUNOV FUNCTIONS

Symplectic computation of Lyapunov exponents
|DE95-002732| p 1795 N95-22654

Lyapunov exponents from CHUA's circuit time series using artificial neural networks p 1784 N95-22988

LIBRARIES

Review of uncertainty files and improved multigroup cross section files for FENDL
|DE94-628639| p 1830 N95-22757

Effective management of classified documents using the library document system
|AD-A286021| p 1855 N95-23024

AMPHION: Specification-based programming for scientific subroutine libraries p 1761 N95-23680

LIE GROUPS

On the theory of smooth structures 3
|DE94-628411| p 1786 N95-22642

Grassman and hyperKaehler structures on some spaces of sections of holomorphic bundles
|PB95-109104| p 1795 N95-22712

On diagonalization in map (M,G)
|DE94-628515| p 1796 N95-22740

Second International Workshop on Harmonic Oscillators
|NASA-CP-3286| p 1820 N95-22957

Algebraic theory of molecules p 1814 N95-22958

Algebraic approach to the vibrational excitations in methane p 1814 N95-22960

Linearizing W-algebras
|DE94-634324| p 1790 N95-23457

LIFE (DURABILITY)

NASA 30 cm ion thruster development status
|NASA TM-106842| p 1624 N95-23221

Recent results from Fermilab E-687, charm particle decays, lifetimes and photoproduction dynamics: A compilation results presented at DPF 1994
|DE95-004580| p 1808 N95-23347

Test method and test results for environmental assessment of aircraft materials p 1643 N95-23509

LIFE CYCLE COSTS

Multidisciplinary design optimization using genetic algorithms p 1619 N95-23332

Integrating O/S models during conceptual design, part 3
|NASA-CR-197905| p 1622 N95-23400

LIFE SUPPORT SYSTEMS

Life support systems analysis and technical trades for a lunar outpost
|NASA-TM-109927| p 1751 N95-23194

LIFT

High-lift flow-physics flight experiments on a subsonic civil transport aircraft (B737-100) p 1609 N95-23333

Lift enhancing tabs for airfoils
|NASA-CASE-ARC-11990-1| p 1613 N95-23395

LIGANDS

Ligand K-edge x-ray adsorption spectroscopic studies of the electronic structure of inorganic model complexes and metalloprotein active sites
|DE95-003338| p 1840 N95-22851

Computational studies of metal-metal and metal-ligand interactions
|NASA-CR-197862| p 1641 N95-23215

LIGHT (VISIBLE RADIATION)

VLPC characterization for the Dzero upgrade
|DE95-003742| p 1818 N95-24084

LIGHT BEAMS

Proceedings of NATO Advanced Research Workshop on the Formation, Transport and Consequences of Particles in Plasmas
|AD-A285850| p 1829 N95-22514

Supersymmetric oscillator in optics p 1826 N95-23002

LIGHT CURVE

IUE observing programs: NSOSS, VEOEB, and PCOEB
|NASA-CR-197424| p 1866 N95-23560

LIGHT GAS GUNS

Hypervelocity impact survivability experiments for carbonaceous impactors, part 2 p 1700 N95-23831

Cratering and penetration experiments in Teflon targets at velocities from 1 to 7 km/s p 1700 N95-23842

LIGHT SCATTERING

Diffusion behavior of lysozyme in aqueous ammonium sulfate solutions under varying solution conditions as determined by dynamic light scattering
|DE95-004821| p 1635 N95-23380

Measurement and analysis of scatter from silicon wafers
|DE95-002411| p 1827 N95-23531

Profiling and light scattering studies of Si surfaces
|DE95-002931| p 1828 N95-24005

LIGHT SOURCES

Preserving the high source brightness with x ray beam line optics
|DE95-003172| p 1820 N95-22877

Undulators for short wavelength FEL amplifiers
|DE95-004690| p 1692 N95-23487

Chemical Sciences Division
|DE95-002655| p 1626 N95-24142

LIGHT TRANSMISSION

Method for making fiber-optic bundle collimator assembly
|AD-D016491| p 1819 N95-22492

Optical absorption in an indirect-gap semiconductor quantum well systems
|DE94-628878| p 1849 N95-22759

A fiber-optic bundle and collimator assembly
|AD-D016500| p 1820 N95-22864

LIGHT-CONE EXPANSION

A model of mesons based on chi SB in the light-front frame
|DE95-003203| p 1802 N95-22731

The impact of QCD and light-cone quantum mechanics on nuclear physics
|DE95-004293| p 1851 N95-23352

LIGNIN

Application of a two-stream radiative transfer model for leaf lignin and cellulose concentrations from spectral reflectance measurements, part 1 p 1703 N95-23856

Application of a two-stream radiative transfer model for leaf lignin and cellulose concentrations from spectral reflectance measurements, part 2 p 1703 N95-23857

AVIRIS spectra correlated with the chlorophyll concentration of a forest canopy p 1705 N95-23871

Measurements of canopy chemistry with 1992 AVIRIS data at Blackhawk Island and Harvard Forest p 1706 N95-23873

Relationships between pigment composition variation and reflectance for plant species from a coastal savannah in California p 1709 N95-23889

LIMITERS (FUSION REACTORS)

Runaway electrons in TEXT-U
|DE94-019218| p 1831 N95-22862

LINE SPECTRA

Theoretical studies of spectroscopic problems of importance for atmospheric radiation measurements p 1741 N95-23329

ROSAT observation program
|NASA-CR-197683| p 1866 N95-23595

Search for millimeterwave CO emission in damped Lyman-alpha systems
|PB95-139259| p 1868 N95-23607

LINEAR ACCELERATORS

Interdigital-H linac for unstable nuclei at INS
|DE94-765448| p 1816 N95-22644

A heavy ion linac complex for unstable nuclei
|DE94-765443| p 1816 N95-22848

Design study of longitudinal dynamics of the drive beam in 1 TeV relativistic klystron two-beam accelerator
|DE95-004683| p 1817 N95-23485

Parallel computation of automatic differentiation applied to magnetic field calculations
|DE95-004689| p 1763 N95-23486

Undulators for short wavelength FEL amplifiers
|DE95-004690| p 1692 N95-23487

High current induction linacs
|DE95-003442| p 1818 N95-24014

Advanced technologies for a compact RF linac FEL
|DE95-003674| p 1692 N95-24072

LINEAR ARRAYS

High power Josephson effect sources
|AD-A285808| p 1838 N95-22511

LINEAR ENERGY TRANSFER (LET)

Dosimetric results on EURECA p 1872 N95-23800

Absorbed dose and LET spectra measurements on LDEF p 1815 N95-23810

Contribution of proton-induced short range secondaries to the LET spectra on LDEF p 1815 N95-23813

Charge, energy and LET spectra of high LET primary and secondary particles in CR-39 plastic nuclear track detectors of the P0006 experiment p 1815 N95-23814

Predictions of LET spectra measured on LDEF p 1815 N95-23815

LINEAR EQUATIONS

Deformed Heisenberg algebra and fractional spin field in 2+1 dimensions
|DE94-628507| p 1850 N95-22779

An implementation of the QMR method based on coupled two-term recurrences
|NASA-CR-197956| p 1791 N95-23612

Objective determination of image end-members in spectral mixture analysis of AVIRIS data p 1709 N95-23888

LINEAR OPERATORS

AR-descriptions in translatable Frechet spaces
|PB95-138855| p 1789 N95-23149

LINEAR PROGRAMMING

Fuzziness and randomness in an optimization framework
|DE94-628383| p 1755 N95-22616

Characterization of non-negative greedy matrices
|PB95-139366| p 1757 N95-23232

Some recent results in the analysis of greedy algorithms for assignment problems
|PB95-140620| p 1757 N95-23238
Submodular linear programs on forests
|PB95-139820| p 1758 N95-23608
LINEAR QUADRATIC GAUSSIAN CONTROL
Normalized coprime factorizations and balancing for unstable nonlinear systems
|PB95-141222| p 1767 N95-23557
LINEAR QUADRATIC REGULATOR
System identification of the Large-Angle Magnetic Suspension Test Fixture (LAMSTF)
p 1617 N95-23299
LINEAR SYSTEMS
Adaptive control of linear systems based on approximate models
|PB95-139333| p 1767 N95-23199
On adaptive weighted polynomial preconditioning for Hermitian positive definite matrices
|NASA-CR-197946| p 1791 N95-23547
Normalized coprime factorizations and balancing for unstable nonlinear systems
|PB95-141222| p 1767 N95-23557
Quasi-kernel polynomials and convergence results for quasi-minimal residual iterations
|NASA-CR-197948| p 1791 N95-23593
Recent advances in Lanczos-based iterative methods for nonsymmetric linear systems
|NASA-CR-197950| p 1791 N95-23611
An implementation of the QMR method based on coupled two-term recurrences
|NASA-CR-197956| p 1791 N95-23612
LINEAR VIBRATION
Active control of panel vibrations induced by a boundary layer flow
|NASA-CR-197867| p 1608 N95-23182
LINEARITY
A certainty grid to object boundary algorithm
|PB94-203510| p 1755 N95-22637
LINEARIZATION
Design of high performance multivariable control systems for supermaneuverable aircraft at high angle of attack
|NASA-CR-197661| p 1615 N95-22908
Linearizing W-algebras
|DE94-634324| p 1790 N95-23457
Dynamic disturbance decoupling of nonlinear systems and linearization
|PB95-141248| p 1767 N95-23558
LINGUISTICS
Spoken dialogue understanding and local context
|TR-523| p 1658 N95-23937
LIOUVILLE EQUATIONS
The exchange algebra for Liouville field on Riemann surfaces with h greater than 1 genus
|DE94-635446| p 1792 N95-23971
LIPIDS
Membrane phase separations, asymmetry and implications in the origin of life
|DE94-628486| p 1747 N95-23050
LIQUID FLOW
A generalized Eulerian-Lagrangian analysis, with application to liquid flows with vapor bubbles
p 1682 N95-23633
LIQUID FUELS
Particle size dependence in Fischer-Tropsch synthesis
|DE95-003124| p 1633 N95-22876
Conversion of light hydrocarbon gases to metal carbides for production of liquid fuels and chemicals
|DE95-000362| p 1634 N95-23164
LIQUID METALS
Electrical resistivity of liquid alkali metals and non-local pseudopotential
|DE94-627417| p 1639 N95-22608
Non local pseudopotentials, transport properties of liquid noble metals
|DE94-627416| p 1640 N95-22840
LIQUID NITROGEN
Liquid nitrogen temperature operation of a switching power converter
|NASA-TM-106867| p 1662 N95-23219
Performance of the 0.3-meter transonic cryogenic tunnel with air, nitrogen, and sulfur hexafluoride media under closed loop automatic control
|NASA-CR-195052| p 1668 N95-23257
Modified molecular sieves: Stationary phase for the gas chromatographic separation of hydrogen isotopes
|DE94-627282| p 1814 N95-24175
LIQUID OXYGEN
Advanced liquid oxygen (LO2) propellant conditioning concept testing
|NASA-TM-108477| p 1652 N95-22672
Flowfield characterization in a LOX/GH2 propellant rocket p 1684 N95-23642
LIQUID PHASES
High-temperature ultrasonic characterization of Ag-clad superconductor tapes
|DE95-002909| p 1838 N95-22530
Quick connect coupling
|NASA-CASE-ARC-11921-2| p 1695 N95-23376
A generalized Eulerian-Lagrangian analysis, with application to liquid flows with vapor bubbles
p 1682 N95-23633
Development of an atomization methodology for spray combustion p 1637 N95-23646
LIQUID PROPELLANT ROCKET ENGINES
Damage-mitigating control of a reusable rocket engine for high performance and extended life
|NASA-CR-4640| p 1654 N95-23195
Eleventh Workshop for Computational Fluid Dynamic Applications in Rocket Propulsion
|NASA-CP-3221-PT-2| p 1668 N95-23412
Heat transfer in rocket engine combustion chambers and nozzles p 1668 N95-23413
Liquid propellant rocket engine combustion simulation with a time-accurate CFD method p 1676 N95-23445
A generalized Eulerian-Lagrangian analysis, with application to liquid flows with vapor bubbles
p 1682 N95-23633
CFD modeling of turbulent duct flows for coolant channel analysis p 1682 N95-23635
LIQUID ROCKET PROPELLANTS
Flowfield characterization in a LOX/GH2 propellant rocket p 1684 N95-23642
LIQUID-GAS MIXTURES
Development of an atomization methodology for spray combustion p 1637 N95-23646
Modeling of non-spherical droplet dynamics
p 1685 N95-23647
LIQUID-VAPOR INTERFACES
Sullivan model for wetting transition in closed system
|DE94-628472| p 1665 N95-22771
LIQUIDS
Sullivan model for wetting transition in closed system
|DE94-628472| p 1665 N95-22771
The role of triplet correlation function in dense fluids
|DE94-628476| p 1849 N95-22775
LITHIUM
The TEXT neutral lithium beam edge density diagnostic
|DE95-003256| p 1830 N95-22719
Ionic core effects on the Mie resonance in lithium clusters
|DE94-014974| p 1805 N95-22870
Solar mass loss, solar lithium, and solar oscillations
|DE94-018262| p 1870 N95-22938
Thermal modeling of the lithium/polymer battery
|DE95-004680| p 1663 N95-23494
LITHIUM COMPOUNDS
Transient radiation-induced absorption in materials for the DOI laser
|DE95-004549| p 1828 N95-24161
LITHIUM ISOTOPES
Harmonic oscillator representation in the theory of scattering and nuclear reactions p 1814 N95-22967
LITHIUM OXIDES
Modeling of tritium recovery from lithium ceramics
|DE95-004626| p 1838 N95-24167
LITHOGRAPHY
Method and system for electron beam lithography
|AD-D016554| p 1660 N95-22709
LITHOLOGY
Lithologic discrimination and alteration mapping from AVIRIS Data, Socorro, New Mexico
p 1701 N95-23847
Discrimination of poorly exposed lithologies in AVIRIS data p 1703 N95-23858
LIVER
A comparative study of the effects of clofibrate, ciprofibrate, WY-14,643, and di-(2-ethylhexyl)-phthalate on liver protein expression in mice
|DE94-016587| p 1748 N95-23771
LOAD DISTRIBUTION (FORCES)
Application requirements for wind turbine gearboxes
|DE94-011883| p 1694 N95-22923
LOAD TESTS
Exfoliation corrosion and stress corrosion cracking behaviour of Al-Li alloys p 1641 N95-23498
LOADS (FORCES)
Investigation of depth-area relationships associated with nanoindentations
|DE95-001353| p 1639 N95-22686
Current status in cavitation modeling
p 1681 N95-23632
LOCAL AREA NETWORKS
Digital Linear Tape (DLT) technology and product family overview p 1753 N95-24125
LOCI
Rearrangement of RAG-1 recombinase gene in radiation-sensitive wasted mice
|DE94-017083| p 1746 N95-22913
LOGIC PROGRAMMING
Roles and dynamic subclasses: A modal logic approach
|PB95-127320| p 1754 N95-22522
Temporal model theory for default logic
|PB95-127346| p 1766 N95-22524
Proceedings of the workshop on deductive databases and logic programming
|PB95-139382| p 1758 N95-23553
LOGISTICS
Addendum to the Proceedings of the Third International Mobile Satellite Conference (IMSC 1993)
|NASA-CR-197343| p 1655 N95-22813
LONG DURATION EXPOSURE FACILITY
Summary of solar cell data from the Long Duration Exposure Facility (LDEF)
|NASA-CR-196539| p 1727 N95-22904
Evaluation of adhesive materials used on the Long Duration Exposure Facility
|NASA-CR-4646| p 1626 N95-22918
LDEF materials results for spacecraft applications: Executive summary
|NASA-CP-3261| p 1617 N95-23549
LDEF: 69 Months in Space. Third Post-Retrieval Symposium, part 1
|NASA-CP-3275-PT-1| p 1889 N95-23796
LDEF environment modeling updates
p 1637 N95-23797
LDEF contributions to cosmic ray and radiation environments research p 1872 N95-23805
Trapped iron measured on LDEF
p 1872 N95-23806
Status of LDEF activation measurements and archive
p 1815 N95-23817
Predictions of LDEF radioactivity and comparison with measurements p 1815 N95-23818
Status of LDEF radiation modeling
p 1815 N95-23819
Status of LDEF contributions to current knowledge of meteoroid and manmade debris environments and their effects on spacecraft in LEO p 1623 N95-23822
LDEF meteoroid and debris special investigation group investigations and activities at the Johnson Space Center p 1623 N95-23823
Micrometeoroids and debris on LDEF comparison with MIR data p 1623 N95-23824
Small craters on the meteoroid and space debris impact experiment p 1623 N95-23825
Long term microparticle impact fluxes on LDEF determined from optical survey of Interplanetary Dust Experiment (IDE) sensors p 1623 N95-23826
LDEF Interplanetary Dust Experiment (IDE) results
p 1869 N95-23828
The orbital characteristics of debris particle rings as derived from IDE observations of multiple orbit intersections with LDEF p 1869 N95-23829
Orbital debris and meteoroid population as estimated from LDEF impact data p 1869 N95-23830
Analytical electron microscopy of LDEF impactor residues p 1869 N95-23832
Natural and orbital debris particles on LDEF's trailing and forward-facing surfaces p 1869 N95-23833
Debris and meteoroid proportions deduced from impact crater residue analysis p 1869 N95-23834
Micro-abrasion package capture cell experiment on the trailing edge of LDEF: Impactor chemistry and whipple bumper shield efficiencies p 1624 N95-23835
Secondary ion mass spectrometry (SIMS) analysis of hypervelocity microparticle impact sites on LDEF surfaces p 1637 N95-23836
SIMS chemical and isotopic analysis of impact features from LDEF experiments AO187-1 and AO187-2
p 1637 N95-23837
Image and compositional characteristics of the LDEF Big Guy impact crater p 1700 N95-23838
Determining orbital particle parameters of impacts into germanium using morphology analysis and calibration data from hypervelocity impact experiments in the laboratory
p 1700 N95-23841
Cratering and penetration experiments in Teflon targets at velocities from 1 to 7 km/s p 1700 N95-23842
LDEF: 69 Months in Space. Third Post-Retrieval Symposium, part 2
|NASA-CP-3275-PT-2| p 1899 N95-23896
Summary and review of Materials Special Investigation Group evaluations of hardware from the Long Duration Exposure Facility p 1638 N95-23897
Recent results from Long Duration Exposure Facility materials testing p 1638 N95-23898
LDEF polymeric materials: A summary of Langley characterization p 1651 N95-23899

Surface characterization of LDEF carbon fiber/polymer matrix composites p 1631 N95-23900
Space environmental effects on polymer matrix composites as a function of sample location on LDEF p 1651 N95-23901
Collection and review of metals data obtained from LDEF experiment specimens and support hardware p 1646 N95-23905
Changes in chemical and optical properties of thin film metal mirrors on LDEF p 1651 N95-23907
Further investigations of experiment A0034 atomic oxygen stimulated outgassing p 1651 N95-23908
Atomic oxygen interactions with protected organic materials on the Long Duration Exposure Facility (LDEF) p 1627 N95-23909
Trend analysis of in-situ spectral reflectance data from the Thermal Control Surfaces Experiment (TCSE) p 1631 N95-23910
Whisker/Cone growth on the thermal control surfaces experiment no. S0069 p 1651 N95-23911
Durability of reflector materials in the space environment p 1651 N95-23912
Four space application material coatings on the Long-Duration Exposure Facility (LDEF) p 1651 N95-23913
Organic matrix composite protective coatings for space applications p 1627 N95-23914
Overview of the LDEF MSIG databasing activities p 1864 N95-23916

LONG DURATION SPACE FLIGHT
Material inspection of EURECA first findings and recommendations p 1637 N95-23804

LONG TERM EFFECTS
Long-term aging of type 308 stainless steel welds: Effects on properties and microstructure
|DE94-018961| p 1640 N95-23132
Effect of loading direction and long-term aging on fatigue-crack growth in Al-Li alloy 2090 p 1641 N95-23499
Preliminary results of radiation measurements on EURECA p 1872 N95-23801
Germination, growth rates, and electron microscope analysis of tomato seeds flown on the LDEF p 1748 N95-23821

LONGITUDINAL CONTROL
Analysis of the longitudinal handling qualities and pilot-induced-oscillation tendencies of the High-Angle-of-Attack Research Vehicle (HARV) p 1616 N95-23297
Aerodynamic surface distension system for high angle of attack forebody vortex control
|NASA-CASE-ARC-11979-1| p 1612 N95-23390

LONGITUDINAL WAVES
Plasmo-magnetoelastic waves in a semiconducting heterostructure. 1: Plasmo-elastic longitudinal modes. 2: Sh-magnetoelastic modes
|PB95-138822| p 1833 N95-23170

LOOPS
Loop scheduling for heterogeneity
|TR-540| p 1764 N95-23936
Unifying data and control transformations for distributed shared-memory machines
|TR-542| p 1765 N95-24061

LORENTZ TRANSFORMATIONS
A note on the angular Fourier transformation p 1797 N95-22986
Does the relativity principle violate?
|DE94-635420| p 1851 N95-23964
Tachyons - it was the end of history?
|DE94-635439| p 1851 N95-23968

LOSSES
GGOT total pressure loss control concept evaluation p 1672 N95-23427
Navier-Stokes analysis of an oxidizer turbine blade with tip clearance with and without a mini-shroud p 1672 N95-23428
Use of blade lean in turbomachinery redesign p 1680 N95-23625
On the accuracy of CFD-based pressure drop predictions for right-angle ducts p 1682 N95-23634

LOW ALTITUDE
Geolocation applications of the Gonets LEO messaging satellites p 1656 N95-22818
Low Earth Orbit satellite/terrestrial mobile service compatibility p 1656 N95-22819

LOW COST
The associate principal astronomer telescope operations model p 1779 N95-23743

LOW CURRENTS
The q profile evolution and enhanced core confinement of high (beta)(sub p) plasmas in D3-D
|DE95-003878| p 1834 N95-23371

LOW DENSITY MATERIALS
Deflections of anisotropic sandwich beams with variable face sheets and core thicknesses p 1700 N95-23310
Impact shock and penetration fragmentation in porous media
|DE94-018900| p 1868 N95-23656

LOW EARTH ORBITS
Status of LDEF radiation modeling p 1815 N95-23819
Micrometeoroids and debris on LDEF comparison with MIR data p 1623 N95-23824
LDEF Interplanetary Dust Experiment (IDE) results p 1869 N95-23828
The orbital characteristics of debris particle rings as derived from IDE observations of multiple orbit intersections with LDEF p 1869 N95-23829

LOW GRAVITY MANUFACTURING
A new containerless image furnace with electro-static positioning device p 1690 N95-23674

LOW PRESSURE
Proceedings of NATO Advanced Research Workshop on the Formation, Transport and Consequences of Particles in Plasmas
|AD-A285850| p 1829 N95-22514

LOW SPEED
NASA low-speed axial compressor for fundamental research
|NASA-TM-4635| p 1616 N95-23192
Handling qualities of the High Speed Civil Transport p 1616 N95-23325
Towards a generalized computational fluid dynamics technique for all Mach numbers p 1670 N95-23420

LOW VISIBILITY
Differential GPS and system integration of the Low Visibility Landing and Surface Operations (LVLASO) demonstration p 1611 N95-23318

LOWER CALIFORNIA (MEXICO)
Revitalization of the Gemenc-area, Baja, Hungary. 1: A study on hydrological possibilities to revitalise the ecosystem in the Keselyues-area. 2: Towards the restoration of the Gyueruesalj floodplain
|PB95-139283| p 1718 N95-23469

LOWER IONOSPHERE
Semikinetic modeling and observations of high-latitude plasma outflow
|NASA-CR-197403| p 1831 N95-23008

LUMBAR REGION
A multibody/finite element analysis approach for modeling of crash dynamic responses
|NIAR-94-3| p 1610 N95-24050

LUMINAIRES
A new containerless image furnace with electro-static positioning device p 1690 N95-23674

LUMINOSITY
A model for ball lightning
|DE95-003366| p 1742 N95-22701
Preserving the high source brightness with x ray beam line optics
|DE95-003172| p 1820 N95-22877
Properties of jets in Z events from 1.8 TeV (bar p)p collisions
|DE94-018982| p 1808 N95-23197
Search for Z' and W' at CDF
|DE94-018987| p 1808 N95-23203
Standardization of CDF and D(O) reported luminosities
|DE95-003388| p 1818 N95-24077

LUMINOUS INTENSITY
Optical fiber strain sensor with improved linearity range
|NASA-CASE-LAR-14857-1-SB| p 1819 N95-22807

LUNAR BASES
Life support systems analysis and technical trades for a lunar outpost
|NASA-TM-109927| p 1751 N95-23194

LUNAR CRATERS
Classification of the LCVF AVIRIS test site with a Kohonen artificial neural network p 1706 N95-23874

LUNAR EXPLORATION
Robotic all-terrain lunar exploration rover (RATLER) FY93 program status report
|DE95-003589| p 1694 N95-23065
Robotics and telepresence for moon missions p 1776 N95-23725

LUNAR ROVING VEHICLES
Robotics and telepresence for moon missions p 1776 N95-23725

LUNAR SOIL
Transmission electron microscope studies of extraterrestrial materials
|NASA-CR-188363| p 1633 N95-23092

LUNAR SURFACE
Lunar rover technology demonstrations with Dante and Ratler p 1697 N95-23694

LYMAN ALPHA RADIATION
Search for millimeterwave CO emission in damped Lyman-alpha systems
|PB95-139259| p 1868 N95-23607

LYSOZYME
Diffusion behavior of lysozyme in aqueous ammonium sulfate solutions under varying solution conditions as determined by dynamic light scattering
|DE95-004821| p 1635 N95-23380

M

MACH NUMBER
Wing pressure distributions from subsonic tests of a high-wing transport model --- in the Langley 14- by 22-Foot Subsonic Wind Tunnel
|NASA-TM-4583| p 1607 N95-22802
Advanced detector development, laboratory simulations, diagnostic development, and data analysis on wake physics
|PL-TR-94-2204| p 1831 N95-22948
Performance of the 0.3-meter transonic cryogenic tunnel with air, nitrogen, and sulfur hexafluoride media under closed loop automatic control
|NASA-CR-195052| p 1668 N95-23257
Design of a variable area diffuser for a 15-inch Mach 6 open-jet tunnel p 1617 N95-23309
Towards a generalized computational fluid dynamics technique for all Mach numbers p 1670 N95-23420
Preconditioning for the Navier-Stokes equations with finite-rate chemistry p 1670 N95-23421
A numerical procedure for analysis of finite rate reacting flows p 1671 N95-23422

MACHINE LEARNING
Towards method-independent knowledge acquisition
|AD-A285823| p 1766 N95-22512
A Newton-type neural network learning algorithm
|DE94-628371| p 1766 N95-22614
Learning time series for intelligent monitoring p 1770 N95-23686
Subsumption-based architecture for autonomous movement planning for planetary rovers p 1771 N95-23690
A new generation of intelligent trainable tools for analyzing large scientific image databases p 1775 N95-23717
Applications of dynamic scheduling technique to space related problems: Some case studies p 1618 N95-23759
Robot skill learning through intelligent experimentation
|TR-567| p 1784 N95-24038

MACHINING
Aspects of surface generation in orthogonal ultraprecision machining
|DE95-000922| p 1654 N95-22678

MACROMOLECULES
Protein folding and protein metallocluster studies using synchrotron small angler x ray scattering
|DE95-003339| p 1746 N95-22897
A supersymmetric family of harmonic oscillators simulating H-bonds in DNA p 1748 N95-22963

MAGELLANIC CLOUDS
Interstellar molecules in the large magellanic cloud
|PB95-139267| p 1868 N95-23230

MAGNESIUM
Studies of autoionizing states relevant to dielectronic recombination
|DE94-014162| p 1812 N95-23978

MAGNESIUM OXIDES
Conversion of light hydrocarbon gases to metal carbides for production of liquid fuels and chemicals
|DE95-000362| p 1634 N95-23164
Orientation selection and microstructural evolution of epitaxial platinum films on (001) magnesium oxide
|DE95-003680| p 1842 N95-23265
Temperature effects on ion irradiation damage in MgAl2O4 spinel single crystals
|DE95-003679| p 1844 N95-24073
Epitaxial growth of bcc transition metal films and superlattices onto MgO (111), (011) and (001) substrates
|DE95-004629| p 1846 N95-24168

MAGNETIC ANOMALIES
Trapped iron measured on LDEF p 1872 N95-23806

MAGNETIC BEARINGS
Influence of backup bearings and support structure dynamics on the behavior of rotors with active supports
|NASA-CR-197438| p 1694 N95-23190
Dynamic modelling and response characteristics of a magnetic bearing rotor system including auxiliary bearings
|NASA-CR-197859| p 1694 N95-23213
Synchronous dynamics of a coupled shaft/bearing/housing system with auxiliary support from a clearance bearing: Analysis and experiment
|NASA-CR-197858| p 1695 N95-23214

MAGNETIC COMPRESSION
Runaway electrons in TEXT-U
[DE94-019218] p 1831 N95-22862
MAGNETIC COOLING
Effect on c-axis transport properties of a critical state in Bi2Sr2CaCu2O8
[DE95-003695] p 1843 N95-23366
MAGNETIC CORES
A brief history in time of ion traps and their achievements in science
[DE95-002815] p 1805 N95-22936
MAGNETIC DISKS
Optimizing raid performance with cache p 1761 N95-24116
Document image archive transfer from DOS to UNIX p 1761 N95-24117
MAGNETIC DOMAINS
Microstructural behavior of nonequilibrium systems
[DE95-004450] p 1630 N95-23924
MAGNETIC EFFECTS
Resonant shallow donor magnetopolaron effect in a GaAs/AlGaAs quantum dot in high magnetic fields
[DE94-629039] p 1798 N95-22497
The effect of magnetic field on the edge plasmons of two-dimensional electron gas systems
[DE94-018044] p 1837 N95-23982
Biological interactions and human health effects of static magnetic fields
[DE95-003147] p 1749 N95-24145
MAGNETIC ENERGY STORAGE
Design of a high-temperature superconductor current lead for electric utility SMES
[DE95-004604] p 1664 N95-24163
MAGNETIC FIELD CONFIGURATIONS
Turbulent transport across invariant canonical flux surfaces
[DE95-000710] p 1832 N95-23072
TPX magnet system status
[DE95-002389] p 1661 N95-23080
Plasma properties and magnetic field structure of the solar corona, based on coordinated Max 1991 observations from SERTS, the VLA, and magnetographs
[NASA-CR-197864] p 1870 N95-23181
Recent studies of the Large Helical Device
[NIFS-322] p 1835 N95-23543
An explanation for tailward flows with positive B(sub z) in the distant tail neutral sheet during quite times
[ATR-95(7270)-1] p 1740 N95-23933
MAGNETIC FIELD RECONNECTION
Non-Taylor magnetohydrodynamic self-organization
[NIFS-314] p 1834 N95-23524
Collisionless magnetic reconnection associated with coalescence of flux bundles
[NIFS-315] p 1834 N95-23525
Macro-EM particle simulation method and a study of collisionless magnetic reconnection
[NIFS-316] p 1834 N95-23526
MAGNETIC FIELDS
Magnetic field effects on strong-coupling polaron in quantum dots
[DE94-629038] p 1847 N95-22496
High magnetic fields in the USA
[DE95-002716] p 1798 N95-22552
A brief history in time of ion traps and their achievements in science
[DE95-002815] p 1805 N95-22936
On pseudosupersymmetric oscillators and reality of relativistic energies for vector mesons p 1815 N95-22994
On parasupersymmetric oscillators and relativistic vector mesons in constant magnetic fields p 1815 N95-22995
Plasmo-magnetoelastic waves in a semiconducting heterostructure. 1: Plasmo-elastic longitudinal modes. 2: Sh-magnetoelastic modes
[PB95-138822] p 1833 N95-23170
Potential aerospace applications of high temperature superconductors p 1664 N95-23322
Generation of fast electrons in reversed field pinches by the equilibrium grad (vert bar)B(vert bar) force
[DE95-004467] p 1809 N95-23363
Effect on c-axis transport properties of a critical state in Bi2Sr2CaCu2O8
[DE95-003695] p 1843 N95-23366
Transport properties of Tl2Ba2CaCu2O8 meander lines
[DE95-003715] p 1843 N95-23367
Parallel computation of automatic differentiation applied to magnetic field calculations
[DE95-004689] p 1763 N95-23486
Modification and damping of Alfven waves in a magnetized dusty plasma
[NIFS-312] p 1834 N95-23523
Non-Taylor magnetohydrodynamic self-organization
[NIFS-314] p 1834 N95-23524
Collisionless magnetic reconnection associated with coalescence of flux bundles
[NIFS-315] p 1834 N95-23525
The next Large Helical Devices
[NIFS-323] p 1835 N95-23535
Current-profile flattening and hot core shift due to the nonlinear development of resistive kink mode
[NIFS-311] p 1835 N95-23564
Quasisymmetry equations for conventional stellarators
[NIFS-324] p 1836 N95-23572
Effect of satellite helical harmonics on the stellarator configuration
[NIFS-328] p 1609 N95-23787
The effect of magnetic field on the edge plasmons of two-dimensional electron gas systems
[DE94-018044] p 1837 N95-23982
Biological interactions and human health effects of static magnetic fields
[DE95-003147] p 1749 N95-24145
MAGNETIC FLUX
Turbulent transport across invariant canonical flux surfaces
[DE95-000710] p 1832 N95-23072
Collisionless magnetic reconnection associated with coalescence of flux bundles
[NIFS-315] p 1834 N95-23525
MAGNETIC ISLANDS
Theory of pressure-induced islands and self-healing in three-dimensional toroidal magnetohydrodynamic equilibria
[NIFS-321] p 1836 N95-23589
MAGNETIC PROPERTIES
Correlation effects in high-Tc superconductors and heavy fermion compounds
[DE94-629057] p 1840 N95-22846
Magnetic multilayer physics
[DE95-003408] p 1798 N95-23083
MAGNETIC RECORDING
A comparison of rotary- and stationary-head tape recorders p 1690 N95-24122
Approaches to 100 Gbit/sq. in. recording density p 1690 N95-24128
A terabyte linear tape recorder p 1690 N95-24139
MAGNETIC RESONANCE
Magnetic resonance and optical spectroscopic studies of carotenoids
[DE95-003729] p 1631 N95-22575
MAGNETIC SIGNATURES
Plasma properties and magnetic field structure of the solar corona, based on coordinated Max 1991 observations from SERTS, the VLA, and magnetographs
[NASA-CR-197864] p 1870 N95-23181
MAGNETIC STORAGE
Fourth NASA Goddard Conference on Mass Storage Systems and Technologies
[NASA-CP-3295] p 1857 N95-24108
Applications drivers for data parking on the Information Superhighway p 1857 N95-24109
Influence of technology on magnetic tape storage device characteristics p 1690 N95-24127
Reproducible direct exposure environmental testing of metal-based magnetic media p 1690 N95-24129
MAGNETIC STORMS
Energetic particle observations at geosynchronous orbit
[DE95-000873] p 1867 N95-22516
MAGNETIC SUSPENSION
Computation of magnetic forces on moving conductors by using ELEKTRA and other 3-D computer codes
[DE95-003308] p 1798 N95-22895
System identification of the Large-Angle Magnetic Suspension Test Fixture (LAMSTF) p 1617 N95-23299
MAGNETIC TAPES
Index of nuclear data libraries available from the IAEA nuclear data section
[DE94-634271] p 1857 N95-23453
A comparison of rotary- and stationary-head tape recorders p 1690 N95-24122
A kinetic study of hydrolysis of polyester elastomer in magnetic tape p 1652 N95-24124
Digital Linear Tape (DLT) technology and product family overview p 1753 N95-24125
The MAMMOTH project p 1753 N95-24126
Influence of technology on magnetic tape storage device characteristics p 1690 N95-24127
ASF archive issues: Current status, past history, and questions for the future p 1861 N95-24133
The growth of the UniTree mass storage system at the NASA Center for Computational Sciences: Some lessons learned p 1862 N95-24135
MAGNETIZATION
Effects of Bi and Bi2O3 additions on the microstructure and superconducting properties of powder-in-tube BSCCO (2212) tapes
[DE95-004605] p 1845 N95-24150
MAGNETOACOUSTIC WAVES
Plasmo-magnetoelastic waves in a semiconducting heterostructure. 1: Plasmo-elastic longitudinal modes. 2: Sh-magnetoelastic modes
[PB95-138822] p 1833 N95-23170
MAGNETOHYDRODYNAMIC FLOW
Modeling of nonequilibrium space plasma flows
[NASA-CR-197432] p 1833 N95-23211
Non-Taylor magnetohydrodynamic self-organization
[NIFS-314] p 1834 N95-23524
An explanation for tailward flows with positive B(sub z) in the distant tail neutral sheet during quite times
[ATR-95(7270)-1] p 1740 N95-23933
MAGNETOHYDRODYNAMIC GENERATORS
Particle transport in plasma reactors
[DE95-004541] p 1837 N95-24158
MAGNETOHYDRODYNAMIC STABILITY
Comparisons of nonlinear toroidal turbulence simulations with experiment
[DE95-003020] p 1830 N95-22694
An upper bound for the proton temperature anisotrophy
[DE95-002752] p 1737 N95-22903
Global electric field determination in the Earth's outer magnetosphere using energetic charged particles
[NASA-CR-197392] p 1737 N95-22945
High beta and second stability region transport and stability analysis
[DE95-003411] p 1832 N95-23147
Current-profile flattening and hot core shift due to the nonlinear development of resistive kink mode
[NIFS-311] p 1835 N95-23564
Theory of pressure-induced islands and self-healing in three-dimensional toroidal magnetohydrodynamic equilibria
[NIFS-321] p 1836 N95-23589
Effect of satellite helical harmonics on the stellarator configuration
[NIFS-328] p 1609 N95-23787
MAGNETOHYDRODYNAMIC WAVES
Modification and damping of Alfven waves in a magnetized dusty plasma
[NIFS-312] p 1834 N95-23523
MHD-Vlasov simulation of the toroidal Alfven eigenmode
[NIFS-319] p 1836 N95-23591
MAGNETOHYDRODYNAMICS
Analytical and numerical studies of ion mobility near the tokamak plasma edge
[DE95-003019] p 1830 N95-22693
Parallal Arnoldi method for the construction of a Krylov subspace basis: An application in magnetohydrodynamics
[PB95-135786] p 1787 N95-22717
High beta and second stability region transport and stability analysis
[DE95-003411] p 1832 N95-23147
Physics of magnetospheric boundary layers
[NASA-CR-197920] p 1739 N95-23271
MHD seed recovery and regeneration, phase 2
[DE95-004308] p 1833 N95-23338
Fast potential change in sawteeth in JIPP T-IIU tokamak plasmas
[NIFS-327] p 1835 N95-23533
Current-profile flattening and hot core shift due to the nonlinear development of resistive kink mode
[NIFS-311] p 1835 N95-23564
Theory of pressure-induced islands and self-healing in three-dimensional toroidal magnetohydrodynamic equilibria
[NIFS-321] p 1836 N95-23589
Computer simulation of a magnetohydrodynamic dynamo 2
[NIFS-320] p 1836 N95-23590
MHD-Vlasov simulation of the toroidal Alfven eigenmode
[NIFS-319] p 1836 N95-23591
MAGNETOMECHANICS (PHYSICS)
Biological interactions and human health effects of static magnetic fields
[DE95-003147] p 1749 N95-24145
MAGNETOPAUSE
Observations of the magnetopause current layer: Cases with no boundary layer and tests of recent models
[NASA-CR-197391] p 1738 N95-23184
MAGNETOSHEATH
An upper bound for the proton temperature anisotrophy
[DE95-002752] p 1737 N95-22903
Observations of the magnetopause current layer: Cases with no boundary layer and tests of recent models
[NASA-CR-197391] p 1738 N95-23184
Physics of magnetospheric boundary layers
[NASA-CR-197920] p 1739 N95-23271

MAGNETOSPHERE-IONOSPHERE COUPLING
Magnetospheric space plasma investigations
[NASA-CR-197405] p 1831 N95-22955
The high latitude ionosphere-magnetosphere transition region: Simulation and data comparison
[NASA-CR-197404] p 1737 N95-22956
Semikinetic modeling and observations of high-latitude plasma outflow
[NASA-CR-197403] p 1831 N95-23008
Modeling of the coupled magnetospheric and neutral wind dynamos
[NASA-CR-197861] p 1738 N95-23090
MAGNETOSPHERIC INSTABILITY
Hot proton anisotropies and cool proton temperatures in the outer magnetosphere
[DE95-002719] p 1736 N95-22850
Global electric field determination in the Earth's outer magnetosphere using energetic charged particles
[NASA-CR-197392] p 1737 N95-22945
MAGNETS
Dynamical properties of critical and paramagnetic spin fluctuations in anisotropic heisenberg magnets
[PB95-134623] p 1798 N95-23127
MAGNIFICATION
X-ray transmission microscope development
[NASA-CR-197884] p 1826 N95-23016
MAINTAINABILITY
Integrating O/S models during conceptual design, part 2
[NASA-CR-197904] p 1622 N95-23399
Integrating O/S models during conceptual design, part 3
[NASA-CR-197905] p 1622 N95-23400
MAINTENANCE
Application requirements for wind turbine gearboxes
[DE94-011883] p 1694 N95-22923
MAN ENVIRONMENT INTERACTIONS
Emissions of greenhouse gases in the United States, 1987-1992
[DE95-003001] p 1731 N95-22691
MAN MACHINE SYSTEMS
Human-centered design of human-computer-human dialogs in aerospace systems
[NASA-CR-197379] p 1750 N95-22797
Design of teleoperation system with a force-reflecting real-time simulator p 1778 N95-23733
Telepresence control of a dual-arm dexterous robot p 1752 N95-23735
Knowledge representation and reasoning for mixed-initiative planning
[TR-562] p 1783 N95-24031
MANAGEMENT
Inspector General: Alleged misconduct by NASA Inspector General. Report to Congressional requesters
[GAO/OSI-95-9] p 1854 N95-24085
MANAGEMENT INFORMATION SYSTEMS
NASA university program management information system, FY 1994
[NASA-TM-110345] p 1856 N95-23364
AVIRIS and TIMS data processing and distribution at the land processes distributed active archive center p 1706 N95-23872
The data facility of the Airborne Visible/Infrared Imaging Spectrometer (AVIRIS) p 1707 N95-23877
The design of a petabyte archive and distribution system for the NASA ECS project p 1858 N95-24110
The architecture of the High Performance Storage System (HPSS) p 1858 N95-24113
Client/Server data serving for high performance computing p 1761 N95-24123
MANAGEMENT METHODS
Method for building and evaluating formal specifications of object-oriented conceptual models of database systems
[PB95-127353] p 1855 N95-22525
Stochastic decision analysis p 1854 N95-23305
Upward appraisal as a means for improving supervisory performance and promoting process improvement, with long-term implications for organizational change p 1854 N95-23323
Optimizing tertiary storage organization and access for spatio-temporal datasets p 1861 N95-24131
MANAGEMENT PLANNING
Outline for a global environmental strategic planning exercise (GESPE-project)
[PB95-133773] p 1733 N95-23067
STS-61 mission director's post-mission report
[NASA-TM-104803] p 1617 N95-23262
Upward appraisal as a means for improving supervisory performance and promoting process improvement, with long-term implications for organizational change p 1854 N95-23323
The software analysis project for the Office of Human Resources p 1854 N95-23331
CRI planning and scheduling for space p 1617 N95-23751
Artificial intelligence techniques for scheduling Space Shuttle missions p 1781 N95-23755
Search Hanford accessible reports electronically system configuration management plan
[DE95-004493] p 1857 N95-24089
Defense technology plan
[AD-A285415] p 1903 N95-24178
MANAGEMENT SYSTEMS
The viability of establishing collaborative, reconfigurable research environments for the Human Performance Research Laboratory at NASA Ames
[NASA-CR-197384] p 1753 N95-22480
Investigation of Federal Standard 1045 high-frequency ALE radio performance in the Southern Trans-Auroral Zone
[PB94-204831] p 1655 N95-22636
CDMS: CAD data set system design description
[DE95-003218] p 1756 N95-22894
MANIFOLDS
Trisecant curve associated to a smooth curve in P(sub 3) of degree d greater than g+2
[DE94-628425] p 1787 N95-22809
Aerodynamic design and analysis of a highly loaded turbine exhaust p 1673 N95-23435
Phase 2: HGM air flow tests in support of HEX vane investigation p 1674 N95-23438
Methodology for CFD design analysis of National Launch System nozzle manifold p 1683 N95-23637
MANIFOLDS (MATHEMATICS)
Lectures on homology with internal symmetries
[DE94-628409] p 1785 N95-22619
Geometry of Moishezon and 1-convex spaces 2: Projectivity of Moishezon spaces and its non-compact version
[DE94-628415] p 1795 N95-22623
Vector bundles as direct images of line bundles
[DE94-628422] p 1795 N95-22630
Grassman and hyperKaehler structures on some spaces of sections of holomorphic bundles
[PB95-109104] p 1795 N95-22712
Possibility of extending space-time coordinates
[DE94-628512] p 1796 N95-22737
On diagonalization in map (M,G)
[DE94-628515] p 1796 N95-22740
MANIPULATORS
Controlling under-actuated robot arms using a high speed dynamics process
[NASA-CASE-NPO-18498-1-CU] p 1692 N95-22543
A microcontroller-based three degree-of-freedom manipulator testbed
[NASA-CR-197423] p 1696 N95-23409
ASI's space automation and robotics programs: The second step p 1697 N95-23696
Hardware interface unit for control of shuttle RMS vibrations p 1697 N95-23706
Development of Japanese experiment module remote manipulator system p 1752 N95-23708
Robust control of multi-jointed arm with a decentralized autonomous control mechanism p 1659 N95-23710
Development of the dynamic motion simulator of 3D micro-gravity with a combined passive/active suspension system p 1618 N95-23711
Dexterous Orbital Servicing System (DOSS) p 1752 N95-23723
Visually guided grasping to study teleprogrammation within the BAROCO testbed p 1777 N95-23731
Telepresence control of a dual-arm dexterous robot p 1752 N95-23735
Morphing hands and virtual tools (or What good is an extra degree of freedom?)
[TR-551] p 1783 N95-24036
Vision-based planning and execution of precision grasps
[TR-546] p 1784 N95-24185
MANPOWER
Integrating O/S models during conceptual design, part 3
[NASA-CR-197905] p 1622 N95-23400
MANUALS
Rationale for the Modular Air-system Vulnerability Estimation Network (MAVEN) methodology
[AD-A285797] p 1611 N95-22510
Tutorial on filtering, restoration, and state estimation
[TR-534] p 1793 N95-24042
MANUFACTURING
Chemical vapor deposition in low pressure batch furnaces
[DE95-003035] p 1632 N95-22722
Aerospace Industries Association (AIA) work practices report for composites p 1628 N95-23029
Continuous roll-to-roll amorphous-silicon photovoltaic manufacturing technology
[DE95-000243] p 1728 N95-23061
A manufacturing database of advanced materials used in spacecraft structures p 1623 N95-23279
Fabric geometry distortion during composites processing p 1631 N95-23288
Application Protocol, Initial Graphics Exchange Specification (IGES), Layered Electrical Product
[DE95-004266] p 1757 N95-23337
Scheduling with genetic algorithms p 1761 N95-23762
Particle transport in plasma reactors
[DE95-004541] p 1837 N95-24158
MANY BODY PROBLEM
Bethe ansatz and quantum Davey-Stewartson 1 system with multicomponent in two dimensions
[DE94-628423] p 1786 N95-22631
Morphology of Laplacian growth processes and statistics of equivalent many-body systems
[DE95-002734] p 1847 N95-22655
The relativistic many body problem with an oscillator interaction p 1824 N95-22991
Structure and evolution of long-lived spiral patterns in galaxies
[PB95-139242] p 1868 N95-23228
CDM and Omega in the local neighborhood
[DE95-003683] p 1868 N95-23570
A theory for the morphology of Laplacian growth from statistics of equivalent many-body Hamiltonian systems
[DE94-014473] p 1799 N95-23979
Atoms as many-body systems
[DE95-004609] p 1813 N95-24151
MAPPING
Vector bundles as direct images of line bundles
[DE94-628422] p 1795 N95-22630
Iterative solutions of nonlinear equations with strongly accretive or strongly pseudocontractive maps
[DE94-628432] p 1786 N95-22634
Programmable hyperspectral image mapper with on-array processing
[NASA-CASE-NPO-17794-1-CU] p 1819 N95-22765
Boson mapping techniques applied to constant gauge fields in QCD p 1814 N95-22969
Ishikawa iteration process for nonlinear Lipschitz strongly accretive mappings
[DE94-634284] p 1792 N95-23658
Comparison of three methods for materials identification and mapping with imaging spectroscopy p 1702 N95-23853
Comparison of 7.5-minute and 1-degree digital elevation models p 1719 N95-24095
MAPS
Automation technology using Geographic Information System (GIS) p 1863 N95-23284
MARAGING STEELS
Specific features of corrosion behavior of stainless maraging steels for aerospace application p 1642 N95-23501
MARANGONI CONVECTION
USML-1 Glovebox experiments
[NASA-CR-196574] p 1653 N95-24028
MARINE ENVIRONMENTS
SWIFT BOAT 1994: Using a fast chase boat to investigate offshore weather features in conjunction with WSR-88D observations
[PB94-195146] p 1742 N95-22651
The use of electrochemical impedance spectroscopy to predict the corrosion of aluminum-lithium alloys in marine environments p 1637 N95-23504
MARINE METEOROLOGY
Dimethylsulfide oxidation over the tropical South Atlantic: OH and other oxidants
[NASA-CR-197417] p 1732 N95-22930
MARKET RESEARCH
The airline quality report, 1994
[NIAR-94-11] p 1610 N95-24012
MARKETING
NASA Technology Applications Team: Commercial applications of aerospace technology
[NASA-CR-197589] p 1864 N95-22526
MARKING
Light emission-or-absorbance-based binding assays for polynucleic acids
[AD-D016557] p 1632 N95-22710
MARKOV CHAINS
Open problems of computational molecular biology
[DE95-000895] p 1745 N95-22866
Discrete-time Markovian stochastic Petri nets
[NASA-CR-195039] p 1758 N95-23613
MARKOV PROCESSES
Nonparametric measure of spatial interaction in point patterns
[PB95-127965] p 1793 N95-22527
Strong collision approach to calculation of depolarization function for neutron beam passing through ferromagnetic bulk domains
[DE94-628847] p 1803 N95-22758
MARS EXPLORATION
Autonomous navigation system for the Marsokhod rover project p 1771 N95-23693

MARS OBSERVER
Automatic commanding of the Mars Observer Camera
p 1620 N95-23754
MASS
Alert-derivative bimodal space power and propulsion systems
| DE95-002754 | p 1624 N95-22905
MASS DISTRIBUTION
The Atmospheric Lifetime Experiment and the Global Atmospheric Gas Experiment (ALE/GAGE)
| NASA-CR-197400 | p 1731 N95-22673
Neutrinos with Zee-mass matrix in vacuum and matter
| DE94-628635 | p 1803 N95-22756
MASS FLOW
Mass loss in the interacting semi-detached binary delta librae
| NASA-CR-197924 | p 1866 N95-23402
MASS SPECTRA
Do narrow Sigma hypernuclear states exist?
| DE95-002930 | p 1803 N95-22763
Search for Z' and W' at CDF
| DE94-018987 | p 1808 N95-23203
J/psi, psi' yields mu(+)mu(-) and B yields J/psi, psi' cross sections
| DE94-018996 | p 1808 N95-23242
Outgassing products from orbiter TPS materials
p 1637 N95-23798
A measurement of the mass of the W vector boson at CDF
| DE95-003498 | p 1813 N95-24016
MASS SPECTROMETERS
Novel mass spectrometric instrument for gaseous and particulate characterization and monitoring
| DE95-001135 | p 1687 N95-22682
MASS SPECTROSCOPY
Novel mass spectrometric instrument for gaseous and particulate characterization and monitoring
| DE95-001135 | p 1687 N95-22682
Recent developments in inductively coupled plasma source magnetic sector multiple collector mass spectrometry
| DE95-003002 | p 1830 N95-22793
Precise determinations of the isotopic compositions and atomic weights of molybdenum, tellurium, tin and tungsten using ICP source magnetic sector multiple collector mass spectrometry
| DE95-003003 | p 1632 N95-22795
MASS TRANSFER
Mass transport through polycrystalline microstructures
| DE95-004552 | p 1811 N95-23576
MASSIFS
Mapping of the Ronda peridotite massif (Spain) from AVIRIS spectro-imaging survey: A first attempt
p 1707 N95-23878
MASSIVELY PARALLEL PROCESSORS
Evaluation of a Multiple Instruction/Multiple Data (MIMD) parallel computer for CFD applications
| AD-A285796 | p 1762 N95-22509
MATCHING
A fuzzy structural matching scheme for space robotics vision p 1778 N95-23737
MATERIALS RECOVERY
Chemical recycling of scrap composites
p 1629 N95-23034
MHD seed recovery and regeneration, phase 2
| DE95-004308 | p 1833 N95-23338
MATERIALS SCIENCE
Deflections of anisotropic sandwich beams with variable face sheets and core thicknesses p 1700 N95-23310
MATERIALS TESTS
A ruggedness evaluation of procedures for damage threshold testing optical materials
| NASA-TM-4639 | p 1840 N95-22803
Offgassing test methodology for composite materials
p 1629 N95-23035
Calorimetric measurement of energy of ultrasonic cleaners
| DE95-003938 | p 1800 N95-23375
Explosive bonding and its application in the Advanced Photon Source front-end and beamline components design
| DE95-004132 | p 1696 N95-23397
LDEF materials results for spacecraft applications: Executive summary
| NASA-CP-3261 | p 1617 N95-23549
The sound insulations of studio doors. Part 1: Door blanks
| BBC-RD-1994/14 | p 1654 N95-24093
MATHEMATICAL LOGIC
Temporal model theory for default logic
| PB95-127346 | p 1766 N95-22524
Temporal operators viewed as predicate transformers
| PB95-138996 | p 1757 N95-23152
Combinatorial semantics
| TR-563 | p 1792 N95-23793
Martin-Lof tests can help too
| TR-541 | p 1797 N95-24063
MATHEMATICAL MODELS
Particle kinetic simulation of high altitude hypervelocity flight
| NASA-CR-197383 | p 1664 N95-22481
Roles and dynamic subclasses: A modal logic approach
| PB95-127320 | p 1754 N95-22522
Jackson system development, entity-relationship analysis and data flow models: A comparative study
| PB95-127338 | p 1855 N95-22523
Temporal model theory for default logic
| PB95-127346 | p 1766 N95-22524
Method for building and evaluating formal specifications of object-oriented conceptual models of database systems
| PB95-127353 | p 1855 N95-22525
Nonparametric measure of spatial interaction in point patterns
| PB95-127965 | p 1793 N95-22527
Browsing semantics in the tower model
| PB95-127221 | p 1855 N95-22534
Effects of wind on rainfall simulation. Spatial distribution of water application, kinetic energy, and overland flow under single full-cone nozzle sprays
| PB95-127304 | p 1717 N95-22537
The chirality operators for Heisenberg spin systems
| DE94-629043 | p 1847 N95-22545
Analysis of physiochemical processes during solder aging
| DE95-003811 | p 1638 N95-22576
HiRel: Hybrid Automated Reliability Predictor (HARP) integrated reliability tool system, (version 7.0). Volume 1: HARP introduction and user's guide
| NASA-TP-3452-VOL-1 | p 1754 N95-22603
HiRel: Hybrid Automated Reliability Predictor (HARP) integrated reliability tool system, (version 7.0). Volume 2: HARP tutorial
| NASA-TP-3452-VOL-2 | p 1755 N95-22604
Glass science tutorial: Lecture 1, Chemistry and properties of oxide glasses
| DE95-002963 | p 1647 N95-22647
LCM 3.0: A language for describing conceptual models. Syntax definition
| PB95-128005 | p 1755 N95-22652
A model for ball lightning
| DE95-003366 | p 1742 N95-22701
Computer modeling of detonators
| DE95-003031 | p 1652 N95-22721
Chemical vapor deposition in low pressure batch furnaces
| DE95-003035 | p 1632 N95-22722
A model of mesons based on chi SB in the light-front frame
| DE95-003203 | p 1802 N95-22731
Analyses, algorithms, and computations for models of high-temperature superconductivity
| DE95-003290 | p 1661 N95-22733
Measurements and modeling of impurity source distributions from the Tore Supra outboard pump limiter
| DE95-003097 | p 1831 N95-22800
Specification and verification of gate-level VHDL models of synchronous and asynchronous circuits
| NASA-CR-191608 | p 1762 N95-22830
Observation model and parameter partials for the JPL VLBI parameter estimation software MODEST, 19 94
| NASA-CR-197328 | p 1756 N95-22853
Photon and electron interaction databases and their use in medical applications
| DE94-015558 | p 1855 N95-22871
Modeling NO(x) emissions in turbulent jet flames: Effects of buoyancy and radiation
| DE94-016621 | p 1633 N95-22886
Computational modeling of properties
| NAS-CR-196544 | p 1841 N95-22907
Statistically generated weighted curve fit of residual functions for modal analysis of structures
| NASA-TM-108481 | p 1699 N95-22950
Magnetospheric space plasma investigations
| NASA-CR-197405 | p 1831 N95-22955
Second International Workshop on Harmonic Oscillators
| NASA-CP-3286 | p 1820 N95-22957
Algebraic approach to the vibrational excitations in methane p 1814 N95-22960
Algebraic description of atom-molecule interactions
p 1814 N95-22961
Fibonacci chain polynomials: Identities from self-similarity p 1814 N95-22962
A supersymmetric family of harmonic oscillators simulating H-bonds in DNA p 1748 N95-22963
Molecular vibrational states during a collision
p 1814 N95-22964
Quantum field between moving mirrors: A three dimensional example p 1821 N95-22965
Harmonic oscillator representation in the theory of scattering and nuclear reactions p 1814 N95-22967
Geometrical interpretation for the outer SU(3) outer multiplicity label p 1814 N95-22968
Boson mapping techniques applied to constant gauge fields in QCD p 1814 N95-22969
An algebraic cluster model based on the harmonic oscillator basis p 1814 N95-22971
Oscillator-like coherent states for the Jaynes-Cummings Model p 1826 N95-23003
Slightly anharmonic systems in quantum optics
p 1826 N95-23004
Origins of interstellar and solar system: Carbonaceous materials
| NASA-CR-197436 | p 1867 N95-23013
Surface growth of two kinds of particles deposition models
| DE94-628480 | p 1841 N95-23021
Modeling aerosol emissions from the combustion of composite materials p 1629 N95-23038
An extension of Freedman's results on a model of predator-prey dynamics as modified by the action of a parasite
| DE94-628488 | p 1796 N95-23052
A numerical study of interannual wind forcing effects on the California current system, 1980-1983
| AD-A286023 | p 1743 N95-23074
The probabilistic structure of sprays: Implications for measurements by in site particle counters
| DE95-002483 | p 1666 N95-23081
The electronic structure of heavy element complexes
| DE95-003407 | p 1806 N95-23082
Modeling of the coupled magnetospheric and neutral wind dynamos
| NASA-CR-197861 | p 1738 N95-23090
Segregated rigid and structural control for a photolithography positioning system
| DE95-002603 | p 1766 N95-23134
Supersonic jet noise reductions predicted with increased jet spreading rate
| NASA-TM-106872 | p 1800 N95-23178
Development and verification of a resin film infusion/resin transfer molding simulation model for fabrication of advanced textile composites
| NASA-CR-197439 | p 1648 N95-23179
An approximate theoretical method for modeling the static thrust performance of non-axisymmetric two-dimensional convergent-divergent nozzles
| NASA-CR-195050 | p 1608 N95-23193
Damage-mitigating control of a reusable rocket engine for high performance and extended life
| NASA-CR-4640 | p 1654 N95-23195
An investigation of helicopter dynamic coupling using an analytical model
| NASA-CR-197420 | p 1612 N95-23217
Idealized textile composites for experimental/analytical correlation p 1631 N95-23277
Infinite possibilities: Computational structures technology p 1700 N95-23280
Deflections of anisotropic sandwich beams with variable face sheets and core thicknesses p 1700 N95-23310
Aeroacoustic computation of gust-blade interaction
p 1800 N95-23313
Inner loop flight control for the High-Speed Civil Transport p 1616 N95-23314
Preparation of course materials: Elementary mathematics of powered flight p 1853 N95-23320
Associated with aerospace vehicles development of methodologies for the estimation of thermal properties
p 1700 N95-23321
Computational modelling of Er(3+): Garnet laser materials p 1692 N95-23326
A hybrid vehicle evaluation code and its application to vehicle design
| DE95-004205 | p 1662 N95-23334
Dynamic response of a transducer mounted at one end of an acoustical cavity which is subjected to a specified pressure at the open end of the cavity
| DE95-004192 | p 1799 N95-23379
Diffusion behavior of lysozyme in aqueous ammonium sulfate solutions under varying solution conditions as determined by dynamic light scattering
| DE95-004821 | p 1635 N95-23380
Ethylene oxidation chemistry in a well-stirred reactor
| DE95-004823 | p 1635 N95-23381
Integrating O/S models during conceptual design, part 1
| NASA-CR-197903 | p 1622 N95-23398
Integrating O/S models during conceptual design, part 2
| NASA-CR-197904 | p 1622 N95-23399
Integrating O/S models during conceptual design, part 3
| NASA-CR-197905 | p 1622 N95-23400

Reduced dimer production in solar-simulator-pumped continuous wave iodine lasers based on model simulations and scaling and pumping studies
| NASA-TP-3486 | p 1691 N95-23411
Heat transfer in rocket engine combustion chambers and nozzles p 1668 N95-23413
A generic efficient adaptive grid scheme for rocket propulsion modeling p 1670 N95-23418
Numerical study of the SSME nozzle flow fields during transient operations: A comparison of the animated results with test p 1673 N95-23434
Aerodynamic design and analysis of a highly loaded turbine exhaust p 1673 N95-23435
Three-dimensional viscous flow analysis inside a turbine volute p 1674 N95-23437
Phase 2: HGM air flow tests in support of HEX vane investigation p 1674 N95-23438
Detailed measurements in the SSME high pressure fuel turbine with smooth rotor blades p 1675 N95-23441
Liquid propellant rocket engine combustion simulation with a time-accurate CFD method p 1676 N95-23445
Spontaneous wave packet reduction
| DE94-634280 | p 1851 N95-23454
Spinning particles in the Euclidean Taub-NUT space
| DE94-634320 | p 1810 N95-23456
A wavenumber-partitioning scheme for two-dimensional statistical closures
| DE95-004514 | p 1677 N95-23483
Study of b(anti b) production in e(+)e(-) annihilation at radical s = 29 GeV with the aid of neural networks
| DE95-004691 | p 1810 N95-23488
Thermal modeling of the lithium/polymer battery
| DE95-004680 | p 1663 N95-23494
Moving mass trim control for aerospace vehicles
| DE95-002602 | p 1622 N95-23532
Electromagnetic production of pions on the nucleon
| DE95-004658 | p 1811 N95-23587
CFD analysis of spray combustion and radiation in OMV thrust chamber p 1637 N95-23645
Modeling of non-spherical droplet dynamics p 1685 N95-23647
Theoretical estimates of high frequency acoustic attenuation and backscattering from suspended sand particles in the ocean and in an estuary
| DSTO-TR-0078 | p 1743 N95-23667
Simulation of cookoff results in a small scale test
| DSTO-TR-0090 | p 1653 N95-23668
Operator procedure verification with a rapidly reconfigurable simulator p 1618 N95-23679
Learning time series for intelligent monitoring p 1770 N95-23686
Path planning for planetary rover using extended elevation map p 1771 N95-23689
Autonomous navigation system for the Marsokhod rover project p 1771 N95-23693
A toolbox and record for scientific models p 1775 N95-23716
Assimilation of altimeter data in a quasi-geostrophic model of the Gulf Stream system: A dynamical perspective
| NASA-CR-196313 | p 1744 N95-23766
Application of a two-stream radiative transfer model for leaf lignin and cellulose concentrations from spectral reflectance measurements, part 1 p 1703 N95-23856
Application of a two-stream radiative transfer model for leaf lignin and cellulose concentrations from spectral reflectance measurements, part 2 p 1703 N95-23857
Objective determination of image end-members in spectral mixture analysis of AVIRIS data p 1709 N95-23888
Statistics of multi-look AIRSAR imagery: A comparison of theory with measurements p 1714 N95-23947
A modal test design strategy for model correlation
| DE95-003631 | p 1759 N95-24020
Improved AVHRR data navigation using automated land feature recognition to correct a satellite orbital model
| CSIRO-TR-34 | p 1718 N95-24026
Unsupervised classification learning from cross-modal environmental structure
| TR-536 | p 1784 N95-24040
Pauli-blocking effects in neutron-alpha reactions
| DE94-016358 | p 1813 N95-24046
A multibody/finite element analysis approach for modeling of crash dynamic responses
| NIAR-94-3 | p 1610 N95-24050
Transferring ecosystem simulation codes to supercomputers
| NASA-TM-4662 | p 1759 N95-24052
Thermal radiant exitance model performance: Soils and forests
| DE95-003619 | p 1721 N95-24148
Modeling of tritium recovery from lithium ceramics
| DE95-004626 | p 1838 N95-24167
A phenomenological model for the effect of nanocrystalline microstructure on irradiation-induced amorphization in U3Si
| DE95-004631 | p 1846 N95-24169

MATHEMATICAL PROGRAMMING
Capacitated facility location: Valid inequalities and facets (revised)
| PB95-130225 | p 1786 N95-22641

MATHEMATICS
Teacher Enhancement Institute p 1853 N95-23312
Schwarz-Christoffel methods for multiply-elongated regions
| DE94-019048 | p 1790 N95-23536

MATRICES (MATHEMATICS)
Is omega* - (mu) absolutely countably compact?
| PB95-127981 | p 1785 N95-22528
Parallal Arnoldi method for the construction of a Krylov subspace basis: An application in magnetohydrodynamics
| PB95-135786 | p 1787 N95-22717
Jacobson radicals in matrix near rings
| DE94-628424 | p 1796 N95-22808
Finite-element time evolution operator for the anharmonic oscillator p 1823 N95-22983
Second derivative of the likelihood of an exact ARMA model
| PB95-135158 | p 1788 N95-23069
Asymptotic justification for a modified GLS procedure to estimate ARMA parameters
| PB95-135166 | p 1788 N95-23070
Characterization of non-negative greedy matrices
| PB95-139366 | p 1757 N95-23232
Partition of real symmetric matrices according to the multiplicities of their eigenvalues
| PB95-139846 | p 1790 N95-23235
Taylor series expansion and modified extended Prony analysis for localization
| DE95-003671 | p 1758 N95-23567
Block LU factorization
| NASA-CR-197949 | p 1791 N95-23592
Tutorial on filtering, restoration, and state estimation
| TR-534 | p 1793 N95-24042

MATRIX MATERIALS
Method of making a semiconductor device using a nanochannel glass matrix
| AD-D016383 | p 1662 N95-23241
US Navy operating experience with new aircraft construction materials p 1645 N95-23517

MATRIX METHODS
A new look at the simultaneous analysis and design of structures p 1700 N95-23327

MATTER (PHYSICS)
Neutrinos with Zee-mass matrix in vacuum and matter
| DE94-628635 | p 1803 N95-22756

MAXIMUM ENTROPY METHOD
Non-zero temperature two-mode squeezing for time-dependent two-level systems
| DE94-628427 | p 1850 N95-22782

MAXIMUM LIKELIHOOD ESTIMATES
Ghost images and feasibility of reconstructions with the Richardson-Lucy algorithm
| DE95-002351 | p 1756 N95-23079
A preliminary measurement of the average B hadron lifetime
| DE95-003138 | p 1808 N95-23226
Maximum-likelihood spectral estimation and adaptive filtering techniques with application to airborne Doppler weather radar
| NASA-CR-197699 | p 1658 N95-23670

MAXWELL EQUATION
Generalized phase transformations of spinor fields
| DE94-628505 | p 1656 N95-22841

MEASURE AND INTEGRATION
A generalized Eulerian-Lagrangian analysis, with application to liquid flows with vapor bubbles p 1682 N95-23633
Weyl connection and non-Abelian gauge field
| DE94-635440 | p 1851 N95-23969

MEASURING INSTRUMENTS
Radioisotope thermoelectric generator transportation system subsystem 143 software development plan
| DE95-003774 | p 1662 N95-23351

MECHANICAL DEVICES
Toys in space, 2
| NASA-TM-110541 | p 1620 N95-23275

MECHANICAL PROPERTIES
High-velocity penetrators
| DE95-001886 | p 1698 N95-22500
Glass science tutorial: Lecture 1, Chemistry and properties of oxide glasses
| DE95-002963 | p 1647 N95-22647
Glass science tutorial: Lecture 2, operating electric glass melters
| DE95-002965 | p 1647 N95-22648
Investigation of mechanical properties and their relation to the internal structure of nanocrystalline metals and composites
| DE95-001151 | p 1627 N95-22683
Investigation of depth-area relationships associated with nanoindentations
| DE95-001353 | p 1639 N95-22686
Plinius intermediate report
| PB95-135216 | p 1648 N95-23128
Idealized textile composites for experimental/analytical correlation p 1631 N95-23277
Explosive bonding and its application in the Advanced Photon Source front-end and beamline components design
| DE95-004132 | p 1696 N95-23397
Structure and properties of polymeric composite materials during 1501 days outer space exposure at Salyut-7 orbital station p 1652 N95-23915

MEDICAL EQUIPMENT
Continuation of BNCT Research Program at NEMC and MIT
| DE94-016228 | p 1748 N95-22875
Biological interactions and human health effects of static magnetic fields
| DE95-003147 | p 1749 N95-24145

MEDICAL SCIENCE
The development and applications of biomarkers
| DE94-014249 | p 1744 N95-22589

MELTING
Metallization and incomplete melting of a semiconductor surface at high temperature
| DE94-627342 | p 1660 N95-22591
Glass science tutorial: Lecture 2, operating electric glass melters
| DE95-002965 | p 1647 N95-22648
Oxygen enriched combustion system performance study. Phase 2: 100 percent oxygen enriched combustion in regenerative glass melters
| DE95-004212 | p 1635 N95-23481
Microstructural behavior of nonequilibrium systems
| DE95-004450 | p 1630 N95-23924
Processing of single- and multi-domain YBa2Cu3O(x) bulk materials for levitation applications by Nd(1+x)Ba(2-x)Cu3O(y) seeding
| DE95-004615 | p 1845 N95-24154

MELTS (CRYSTAL GROWTH)
Initial crystallization and growth in melt processing of large-domain YBa2Cu3O(x) for magnetic levitation
| DE95-002993 | p 1839 N95-22572
The 1993 Annual Conference of the Israeli Association for Crystal Growth. Program and abstracts
| DE94-633510 | p 1841 N95-22854

MEMORY
Functions of external cues in prospective memory
| DOT/FAA/AM-95/9 | p 1750 N95-24088

MEMORY (COMPUTERS)
A draft standard for message passing in a distributed memory environment
| DE94-019159 | p 1657 N95-23075
Verifying sequentially consistent memory using interface refinement
| PB95-139002 | p 1752 N95-23153
GPP user's guide: A general-purpose postprocessor for wind turbine data analysis
| DE95-000293 | p 1730 N95-23776
Scalability of atomic primitives on distributed shared memory multiprocessors
| TR-528 | p 1764 N95-23930
Unifying data and control transformations for distributed shared-memory machines
| TR-542 | p 1765 N95-24061
Petabyte mass memory system using the Newell Opticel(TM) p 1753 N95-24119
Using simple page placement policies to reduce the cost of cache fills in coherent shared-memory systems
| TR-535 | p 1753 N95-24177
Lazy release consistency for hardware-coherent multiprocessors
| TR-547 | p 1765 N95-24184

MENTAL PERFORMANCE
Some performance effects of age and low blood alcohol levels on a computerized neuropsychological test
| DOT/FAA/AM-95/7 | p 1749 N95-23788

MERCURY (METAL)
Mercury detection with thermal neutrons
| DE95-002061 | p 1806 N95-23055

MESON-MESON INTERACTIONS
(pi)- and a(sub 1)-meson physics in current algebra at the quark level
| DE94-628611 | p 1804 N95-22811

MESONS
New preliminary results on the physics of charm hadroproduction subprocesses
| DE95-002530 | p 1801 N95-22646

QCD improved exclusive rare B-decays at the heavy b-quark limit
|DE94-628609| p 1802 N95-22720
A model of mesons based on chi SB in the light-front frame
|DE95-003203| p 1802 N95-22731
On the D yields K-bar(sup *)e(sup +)(nu)(sub e) form factors
|DE94-628614| p 1803 N95-22754
To the problem of D-meson leptonic and semileptonic decays
|DE94-628615| p 1803 N95-22755
The U(3) x U(3) Nambu - Jona-Lasinio model with the gluon condensate and axial anomaly at finite temperature
|DE94-628588| p 1804 N95-22787
The decays of D(sup *)-mesons
|DE94-628610| p 1804 N95-22810
(pi)- and a(sub 1)-meson physics in current algebra at the quark level
|DE94-628611| p 1804 N95-22811
The omega pi(sup 0)-transient form factor within effective chiral Lagrangian approach
|DE94-628612| p 1850 N95-22812
Heavy quark physics at SLD: Preliminary results
|DE95-003372| p 1806 N95-23138
Flavour dependence of form factors in heavy meson decays
|PB95-139101| p 1807 N95-23156
J/psi, psi' yields mu(+)mu(-) and B yields J/psi, psi' cross sections
|DE94-018996| p 1808 N95-23242
Recent results from Fermilab E-687, charm particle decays, lifetimes and photoproduction dynamics: A compilation results presented at DPF 1994
|DE95-004580| p 1808 N95-23347
Inclusive rapidity correlations of (pi)(-) mesons in pp-interactions
|DE94-635654| p 1812 N95-23974

MESSAGE PROCESSING
Learning time series for intelligent monitoring p 1770 N95-23686

MESSAGES
Hierarchical membership protocol for synchronous distributed systems
|PB95-138947| p 1763 N95-23129
Algebraic semantics of basic message sequence charts
|PB95-138970| p 1657 N95-23151
Eliminating useless messages in write-update protocols on scalable multiprocessors
|TR-539| p 1764 N95-24037

METABOLISM
Plant metabolism and cell wall formation in space (microgravity) and on Earth
|NASA-CR-197618| p 1745 N95-22801

METAL BONDING
Support research for solid oxide fuel cells
|DE95-002910| p 1726 N95-22568

METAL CLUSTERS
Structure, melting, and reactivity of nickel clusters from numerical simulations
|DE95-002911| p 1638 N95-22531
Ionic core effects on the Mie resonance in lithium clusters
|DE94-014974| p 1805 N95-22870
Thermochemistry of transition metal clusters
|DE95-003144| p 1646 N95-24144

METAL COATINGS
The corrosion protection of 2219-T87 aluminum by organic and inorganic zinc-rich primers
|NASA-TP-3543| p 1641 N95-23186
Durability of reflector materials in the space environment p 1651 N95-23912
Cu deposition using a permanent magnet electron cyclotron resonance microwave plasma source
|DE94-017768| p 1650 N95-23981

METAL FATIGUE
Nondestructive evaluation of fatigue damage in aluminum 2024 by x-ray diffraction p 1698 N95-23293
Effect of loading direction and long-term aging on fatigue-crack growth in Al-Li alloy 2090 p 1641 N95-23499

METAL FILMS
Vacuum vapor deposition
|NASA-CASE-MFS-28652-1| p 1647 N95-22558
Orientation selection and microstructural evolution of epitaxial platinum films on (001) magnesium oxide
|DE95-003680| p 1842 N95-23265
Spin polarized photoemission studies of magnetic quantum well states
|DE95-004218| p 1851 N95-23335
Measurements of the optical properties of thin films of silver and silver oxide p 1651 N95-23906
Changes in chemical and optical properties of thin film metal mirrors on LDEF p 1651 N95-23907
Epitaxial growth of bcc transition metal films and superlattices onto MgO (111), (011) and (001) substrates
|DE95-004629| p 1846 N95-24168

METAL FOILS
Protective coating for ceramic materials
|NASA-CASE-ARC-11969-1-CU| p 1649 N95-23394
Micro-abrasion package capture cell experiment on the trailing edge of LDEF: Impactor chemistry and whipple bumper shield efficiencies p 1624 N95-23835

METAL FUELS
Microgravity combustion science: 1995 program update
|NASA-TM-106858| p 1626 N95-24004

METAL IONS
Solvation of isolated transition metal ions
|DE95-002978| p 1638 N95-22571

METAL OXIDES
Electrochemical studies of perovskite mixed conductors
|DE95-003704| p 1636 N95-23573
Four space application material coatings on the Long-Duration Exposure Facility (LDEF) p 1651 N95-23913

METAL PLATES
The effect of impact angle on craters formed by hypervelocity particles p 1700 N95-23839
Characterization of Type 304L stainless steel solid-state closure welds for radioactive waste containment
|DE94-016539| p 1645 N95-23980

METAL SHEETS
Technology maturation project on optimization of sheet metal forming of aluminum for use in transportation systems
|DE95-003005| p 1654 N95-22692

METAL SURFACES
Advanced growth and surface analysis system for in situ studies of interface formation
|DE95-002850| p 1838 N95-22555
Pulsed Ion Beam Surface Treatment for preparing rapidly solidified corrosion resistant alloy surfaces
|DE94-012072| p 1640 N95-22835
Nanophase materials: Synthesis, properties, applications
|AD-A286013| p 1627 N95-22940
Charge distribution analysis of catalysts under simulated reaction conditions
|DE95-003526| p 1633 N95-23064
Experimental technique and assessment for measuring the convective heat transfer coefficient from natural ice accretions
|NASA-TM-106864| p 1668 N95-23248
Natural and orbital debris particles on LDEF's trailing and forward-facing surfaces p 1869 N95-23833
Secondary ion mass spectrometry (SIMS) analysis of hypervelocity microparticle impact sites on LDEF surfaces p 1637 N95-23836
Collection and review of metals data obtained from LDEF experiment specimens and support hardware p 1646 N95-23905
Solderability preservation through the use of organic inhibitors
|DE95-003633| p 1664 N95-24149

METAL WORKING
Technology maturation project on optimization of sheet metal forming of aluminum for use in transportation systems
|DE95-003005| p 1654 N95-22692
Characterization of Type 304L stainless steel solid-state closure welds for radioactive waste containment
|DE94-016539| p 1645 N95-23980

METAL-WATER REACTIONS
The use of electrochemical impedance spectroscopy to predict the corrosion of aluminum-lithium alloys in marine environments p 1637 N95-23504

METALLIC GLASSES
Microstructural behavior of nonequilibrium systems
|DE95-004450| p 1630 N95-23924

METALLIZING
Vacuum vapor deposition
|NASA-CASE-MFS-28652-1| p 1647 N95-22558

METALLOGRAPHY
X-ray transmission microscope development
|NASA-CR-197884| p 1826 N95-23016
Nondestructive evaluation of fatigue damage in aluminum 2024 by x-ray diffraction p 1698 N95-23293

METALORGANIC CHEMICAL VAPOR DEPOSITION
MOCVD of gallium and calcium sulfides for improved phosphor processing
|DE95-000918| p 1631 N95-22677

METALS
Novel mass spectrometric instrument for gaseous and particulate characterization and monitoring
|DE95-001135| p 1687 N95-22682
Investigation of mechanical properties and their relation to the internal structure of nanocrystalline metals and composites
|DE95-001151| p 1627 N95-22683
Recent developments in inductively coupled plasma source magnetic sector multiple collector mass spectrometry
|DE95-003002| p 1830 N95-22793
Aqueous alternatives for metal and composite cleaning p 1630 N95-23039
Strongly interacting fermion systems
|DE95-003405| p 1806 N95-23054
Computational studies of metal-metal and metal-ligand interactions
|NASA-CR-197862| p 1641 N95-23215
Collection and review of metals data obtained from LDEF experiment specimens and support hardware p 1646 N95-23905
Reproducible direct exposure environmental testing of metal-based magnetic media p 1690 N95-24129

METAMORPHISM (GEOLOGY)
Lithologic discrimination and alteration mapping from AVIRIS Data, Socorro, New Mexico p 1701 N95-23847

METASTABLE STATE
Study of frustrated systems via dissipative maps
|PB95-139093| p 1799 N95-23155
Temperature effects on ion irradiation damage in MgAl2O4 spinel single crystals
|DE95-003679| p 1844 N95-24073

METEORITE COLLISIONS
Small craters on the meteoroid and space debris impact experiment p 1623 N95-23825
Penetration rates over 30 years in the space age p 1624 N95-23827
Debris and meteoroid proportions deduced from impact crater residue analysis p 1869 N95-23834

METEORITE CRATERS
Micrometeoroids and debris on LDEF comparison with MIR data p 1623 N95-23824
Small craters on the meteoroid and space debris impact experiment p 1623 N95-23825

METEORITIC DAMAGE
Status of LDEF contributions to current knowledge of meteoroid and manmade debris environments and their effects on spacecraft in LEO p 1623 N95-23822
LDEF meteoroid and debris special investigation group investigations and activities at the Johnson Space Center p 1623 N95-23823
Micrometeoroids and debris on LDEF comparison with MIR data p 1623 N95-23824
Natural and orbital debris particles on LDEF's trailing and forward-facing surfaces p 1869 N95-23833

METEOROID CONCENTRATION
Small craters on the meteoroid and space debris impact experiment p 1623 N95-23825
Orbital debris and meteoroid population as estimated from LDEF impact data p 1869 N95-23830

METEOROIDS
Status of LDEF contributions to current knowledge of meteoroid and manmade debris environments and their effects on spacecraft in LEO p 1623 N95-23822
LDEF meteoroid and debris special investigation group investigations and activities at the Johnson Space Center p 1623 N95-23823
Orbital debris and meteoroid population as estimated from LDEF impact data p 1869 N95-23830
Natural and orbital debris particles on LDEF's trailing and forward-facing surfaces p 1869 N95-23833

METEOROLOGICAL PARAMETERS
Compendium of NASA data base for the Global Tropospheric Experiment's Pacific Exploratory Mission West-A (PEM West-A)
|NASA-TM-109177| p 1733 N95-23009
Study of atmospheric parameters measurements using MM-wave radar in synergy with LITE-2 p 1741 N95-23278
Estimation of aerosol optical depth and additional atmospheric parameters for the calculation of apparent reflectance from radiance measured by the Airborne Visible/Infrared Imaging Spectrometer p 1704 N95-23863

METEOROLOGICAL RADAR
Accuracy of radar rainfall estimates compared to raingauge measurements and a hydrological application
|PB95-127296| p 1741 N95-22640
SWIFT BOAT 1994: Using a fast chase boat to investigate offshore weather features in conjunction with WSR-88D observations
|PB94-195146| p 1742 N95-22651
Maximum-likelihood spectral estimation and adaptive filtering techniques with application to airborne Doppler weather radar
|NASA-CR-197699| p 1658 N95-23670

METEOROLOGICAL SATELLITES
Calculation of satellite drag coefficients
| AD-A285118 | p 1622 N95-23781
METEOROLOGY
Development of an advanced finite difference atmospheric general circulation model
| DE95-003187 | p 1736 N95-22879
RAS Division model evaluation database description
| DE95-003481 | p 1733 N95-23124
Extraction of auxiliary data from AVIRIS distribution tape for spectral, radiometric, and geometric quality assessment p 1706 N95-23875
METHANATION
Transmethylation reactions during methanogenesis from acetate in Methanosarcina barkeri
| DE94-016222 | p 1745 N95-22873
METHANE
Emissions of greenhouse gases in the United States, 1987-1992
| DE95-003001 | p 1731 N95-22691
Transmethylation reactions during methanogenesis from acetate in Methanosarcina barkeri
| DE94-016222 | p 1745 N95-22873
Algebraic approach to the vibrational excitations in methane p 1814 N95-22960
Ethylene oxidation chemistry in a well-stirred reactor
| DE95-004823 | p 1635 N95-23381
Effects of jet strength on NOx formation in premixed impinging jet combustion with minimum heat losses
| NAL-TR-1237T | p 1637 N95-24181
METHODOLOGY
Addendum to the Proceedings of the Third International Mobile Satellite Conference (IMSC 1993)
| NASA-CR-197343 | p 1655 N95-22813
METHYL ALCOHOL
The influence of high-octane fuel blends on the performance of a two-stroke SI engine with knock-limited-compression ratio
| DE95-002902 | p 1692 N95-22556
Performance of thin-ceramic-coated combustion chamber with gasoline and methanol as fuels in a two-stroke SI engine
| DE95-002903 | p 1693 N95-22557
Transmethylation reactions during methanogenesis from acetate in Methanosarcina barkeri
| DE94-016222 | p 1745 N95-22873
METHYL COMPOUNDS
Pressure shifts and electron scattering in atomic and molecular gases
| DE95-003102 | p 1803 N95-22747
Transmethylation reactions during methanogenesis from acetate in Methanosarcina barkeri
| DE94-016222 | p 1745 N95-22873
Atmospheric peroxides
| DE95-004435 | p 1733 N95-23362
METRIC SPACE
Q-analytic functions on quantum spaces
| DE94-628412 | p 1847 N95-22621
Geometry of Moishezon and 1-convex spaces 2: Projectivity of Moishezon spaces and its non-compact version
| DE94-628415 | p 1795 N95-22623
A new method of constructing scalar-flat Kaehler surfaces
| DE94-628419 | p 1785 N95-22627
Hausdorff dimension of Julia sets of complex Henon mappings
| DE94-628420 | p 1785 N95-22628
A prescribing geodesic curvature problem
| DE94-628503 | p 1787 N95-22750
Spinning particles in the Euclidean Taub-NUT space
| DE94-634320 | p 1810 N95-23456
Relating multifunctions and predicate transformers through closure operators
| PB95-135646 | p 1757 N95-23467
METROLOGY
EUV metrology of multilayer optics
| DE95-003036 | p 1819 N95-22723
MICE
Rearrangement of RAG-1 recombinase gene in radiation-sensitive wasted mice
| DE94-017083 | p 1746 N95-22913
A comparative study of the effects of clofibrate, ciprofibrate, WY-14,643, and di-(2-ethylhexyl)-phthalate on liver protein expression in mice
| DE94-016587 | p 1748 N95-23771
MICHELSON INTERFEROMETERS
Nonclassical light in interferometric measurements p 1822 N95-22976
MICROANALYSIS
Analytical electron microscopy of LDEF impactor residues p 1869 N95-23832
Natural and orbital debris particles on LDEF's trailing and forward-facing surfaces p 1869 N95-23833
Micro-abrasion package capture cell experiment on the trailing edge of LDEF: Impactor chemistry and whipple bumper shield efficiencies p 1624 N95-23835
SIMS chemical and isotopic analysis of impact features from LDEF experiments AO187-1 and AO187-2 p 1637 N95-23837
Image and compositional characteristics of the LDEF Big Guy impact crater p 1700 N95-23838
High resolution microstructural analysis of zirconia eutectic interfaces
| DE95-003143 | p 1845 N95-24143
MICROCHANNEL PLATES
Development of microchannel plate x-ray optics
| NASA-CR-197935 | p 1866 N95-23540
MICROCRYSTALS
A fractal model for intergranular fractures in nanocrystals
| DE94-627393 | p 1839 N95-22606
MICROGRAVITY
Quick look report of acceleration measurements on Mir Space Station during Mir-16
| NASA-TM-106835 | p 1621 N95-22667
Plant metabolism and cell wall formation in space (microgravity) and on Earth
| NASA-CR-197618 | p 1745 N95-22801
Microgravity sciences application visiting scientist program
| NASA-CR-197854 | p 1653 N95-23204
Microgravity experiments safety and integration requirements document tree
| NASA-CR-195447 | p 1855 N95-23206
Newton in space
| NASA-TM-110535 | p 1799 N95-23273
Living in space
| NASA-TM-110536 | p 1751 N95-23274
Toys in space, 2
| NASA-TM-110541 | p 1620 N95-23275
USML-1 microgravity glovebox experiment no. 1 Passive Accelerometer System
| NASA-CR-196575 | p 1653 N95-23552
All systems go!
| NASA-TM-110542 | p 1620 N95-23665
A new containerless image furnace with electro-static positioning device p 1690 N95-23674
Development of the dynamic motion simulator of 3D micro-gravity with a combined passive/active suspension system p 1618 N95-23711
Microgravity combustion science: 1995 program update
| NASA-TM-106858 | p 1626 N95-24004
USML-1 Glovebox experiments
| NASA-CR-196574 | p 1653 N95-24028
MICROMACHINING
Development of microchannel plate x-ray optics
| NASA-CR-197935 | p 1866 N95-23540
MICROMECHANICS
Thermoelastic theory for the response of materials functionally graded in two directions with applications to the free-edge problem
| NASA-TM-106882 | p 1699 N95-24055
MICROMETEOROIDS
Micrometeoroids and debris on LDEF comparison with MIR data p 1623 N95-23824
Orbital debris and meteoroid population as estimated from LDEF impact data p 1869 N95-23830
Analytical electron microscopy of LDEF impactor residues p 1869 N95-23832
Experimental investigation of the relationship between impact crater morphology and impacting particle velocity and direction p 1700 N95-23840
MICROPARTICLES
Long term microparticle impact fluxes on LDEF determined from optical survey of Interplanetary Dust Experiment (IDE) sensors p 1623 N95-23826
LDEF Interplanetary Dust Experiment (IDE) results p 1869 N95-23828
Hypervelocity impact survivability experiments for carbonaceous impactors, part 2 p 1700 N95-23831
Micro-abrasion package capture cell experiment on the trailing edge of LDEF: Impactor chemistry and whipple bumper shield efficiencies p 1624 N95-23835
Secondary ion mass spectrometry (SIMS) analysis of hypervelocity microparticle impact sites on LDEF surfaces p 1637 N95-23836
MICROPOROSITY
High surface area, high permeability carbon monoliths
| DE95-004555 | p 1650 N95-23577
Microporous polyimide films for reduced dielectric applications
| DE95-004543 | p 1650 N95-24159
MICROSCOPES
X-ray transmission microscope development
| NASA-CR-197884 | p 1826 N95-23016
MICROSCOPY
X-ray transmission microscope development
| NASA-CR-197884 | p 1826 N95-23016
MICROSTRUCTURE
The role of grain boundary chemistry and structure in the environmentally-assisted intergranular cracking of nickel-base alloys
| DE95-002941 | p 1638 N95-22532
Initial crystallization and growth in melt processing of large-domain YBa2Cu3O(x) for magnetic levitation
| DE95-002993 | p 1839 N95-22572
An investigation into the effects of hydrogen on the fracture and deformation of Alloy X-750
| DE95-003206 | p 1639 N95-22732
Long-term aging of type 308 stainless steel welds: Effects on properties and microstructure
| DE94-018961 | p 1640 N95-23132
Surface structural dependence of cesium adsorption on the (alpha)-Al2O3(0001) surface
| DE95-002610 | p 1842 N95-23135
Orientation selection and microstructural evolution of epitaxial platinum films on (001) magnesium oxide
| DE95-003680 | p 1842 N95-23265
Nondestructive evaluation of fatigue damage in aluminum 2024 by x-ray diffraction p 1698 N95-23293
Internal strain measurement using pulsed neutron diffraction at LANSCE
| DE95-003677 | p 1842 N95-23365
Mass transport through polycrystalline microstructures
| DE95-004552 | p 1811 N95-23576
Structure and properties of polymeric composite materials during 1501 days outer space exposure at Salyut-7 orbital station p 1652 N95-23915
Microstructural behavior of nonequilibrium systems
| DE95-004450 | p 1630 N95-23924
Thermoelastic theory for the response of materials functionally graded in two directions with applications to the free-edge problem
| NASA-TM-106882 | p 1699 N95-24055
The effect of elastic stress on Ostwald Ripening Phenomena
| DE95-002599 | p 1646 N95-24140
High resolution microstructural analysis of zirconia eutectic interfaces
| DE95-003143 | p 1845 N95-24143
Effects of Bi and Bi2O3 additions on the microstructure and superconducting properties of powder-in-tube BSCCO (2212) tapes
| DE95-004605 | p 1845 N95-24150
Microstructure and composition of a SNS Josephson junction using CaRuO3 as the metallic barrier
| DE95-004611 | p 1845 N95-24152
Processing of single- and multi-domain YBa2Cu3O(x) bulk materials for levitation applications by Nd(1 + x)Ba(2-x)Cu3O(y) seeding
| DE95-004615 | p 1845 N95-24154
A phenomenological model for the effect of nanocrystalline microstructure on irradiation-induced amorphization in U3Si
| DE95-004631 | p 1846 N95-24169
Cooling rate effects on the microstructure, critical current density, and (T(sub c)) transition of one- and two-powder BSCCO-2223 Ag sheathed tapes
| DE95-004639 | p 1846 N95-24171
MICROTRONS
The project of high free electron laser using race-track microtron-recuperator
| DE94-634034 | p 1692 N95-23657
MICROWAVE CIRCUITS
Limited bandwidth microwave filter
| AD-D016553 | p 1660 N95-22708
High-performance GaAs/AlGaAs optical modulators: Their performance and packaging for microwave photonic integrated circuits
| DE95-004533 | p 1828 N95-23575
MICROWAVE EMISSION
A new containerless image furnace with electro-static positioning device p 1690 N95-23674
MICROWAVE EQUIPMENT
A 4 MW fast wave current drive upgrade for D3-D
| DE95-003741 | p 1837 N95-24083
MICROWAVE FILTERS
Limited bandwidth microwave filter
| AD-D016553 | p 1660 N95-22708
MICROWAVE IMAGERY
Combining optical and microwave remote sensing data of forest vegetation: MAC Europe 1991
| PB95-127312 | p 1717 N95-22538
Synergy between optical and microwave remote sensing to derive soil and vegetation parameters from MAC Europe 1991 Experiment p 1715 N95-23956
Soil moisture retrieval in the Oberpfaffenhofen testsite using MAC Europe AIRSAR data p 1716 N95-23960
Microwave dielectric properties of boreal forest trees p 1716 N95-23961
MICROWAVE RADIOMETERS
TOGA/COARE AMMR 1992 data processing
| NASA-CR-197289 | p 1736 N95-22867

Upgrade of the 92 GHz airborne multi-channel meteorological radiometer (AMMR)
| NASA-CR-197875 | p 1742 N95-23208

MICROWAVES
Studies of autoionizing states relevant to dielectronic recombination
| DE94-014162 | p 1812 N95-23978
Cu deposition using a permanent magnet electron cyclotron resonance microwave plasma source
| DE94-017768 | p 1650 N95-23981

MILITARY OPERATIONS
Military bases: Environmental impact at closing installations. Report to Congressional requesters
| GAO/NSIAD-95-70 | p 1735 N95-24057
DOD budget: Selected categories of planned funding for fiscal years 1995-99. Report to Congressional requesters
| GAO/NSIAD-95-92 | p 1864 N95-24062
Ballistic Missile Defense: Current status of strategic target system. Report to Congressional requesters
| GAO/NSIAD-95-78 | p 1903 N95-24080

MILITARY TECHNOLOGY
Alert-derivative bimodal space power and propulsion systems
| DE95-002754 | p 1624 N95-22905
Defense technology plan
| AD-A285415 | p 1903 N95-24178
Defense science and technology strategy
| AD-A285414 | p 1903 N95-24179

MILITARY VEHICLES
Fire hazard considerations for composites in vehicle design p 1628 N95-23032

MILLIMETER WAVES
Interstellar molecules in the large magellanic cloud
| PB95-139267 | p 1868 N95-23230
Study of atmospheric parameters measurements using MM-wave radar in synergy with LITE-2 p 1741 N95-23278
Search for millimeterwave CO emission in damped Lyman-alpha systems
| PB95-139259 | p 1868 N95-23607

MIMD (COMPUTERS)
Evaluation of a Multiple Instruction/Multiple Data (MIMD) parallel computer for CFD applications
| AD-A285796 | p 1762 N95-22509
Towards the Teraflop CFD
| NASA-CR-197947 | p 1764 N95-23594

MINERAL EXPLORATION
Lithologic discrimination and alteration mapping from AVIRIS Data, Socorro, New Mexico p 1701 N95-23847

MINERALOGY
The effects of AVIRIS atmospheric calibration methodology on identification and quantitative mapping of surface mineralogy, Drum Mountains, Utah p 1705 N95-23870
Mapping of the Ronda peridotite massif (Spain) from AVIRIS spectro-imaging survey: A first attempt p 1707 N95-23878
Application of MAC-Europe AVIRIS data to the analysis of various alteration stages in the Landdmannalauger Hydrothermal Area (South Iceland) p 1709 N95-23885
Mineralogic variability of the Kelso Dunes, Mojave Desert, California derived from Thermal Infrared Multispectral Scanner (TIMS) data p 1711 N95-23920

MINERALS
The significance of hair mineral analysis as a means for assessing internal body burdens of environmental pollutants
| DE94-633512 | p 1734 N95-23541
Scandinavian symposium on surface chemistry
| PB95-140687 | p 1636 N95-23554
Comparison of three methods for materials identification and mapping with imaging spectroscopy p 1702 N95-23853
The effects of AVIRIS atmospheric calibration methodology on identification and quantitative mapping of surface mineralogy, Drum Mountains, Utah p 1705 N95-23870
The red edge in arid region vegetation: 340-1060 nm spectra p 1708 N95-23881

MINIMUM DRAG
Control of flow separation in airfoil/wing design applications p 1609 N95-23294

MIR SPACE STATION
Quick look report of acceleration measurements on Mir Space Station during Mir-16
| NASA-TM-106835 | p 1621 N95-22667
Mir hardware heritage
| NASA-RP-1357 | p 1621 N95-23249
Micrometeoroids and debris on LDEF comparison with MIR data p 1623 N95-23824

MIRRORS
Quantum field between moving mirrors: A three dimensional example p 1821 N95-22965
Changes in chemical and optical properties of thin film metal mirrors on LDEF p 1651 N95-23907
PRISM Spectrograph Optical Design
| NASA-CR-197965 | p 1828 N95-24035

MISALIGNMENT
Neural network for detection and correction of local boundary misalignments between images
| AD-D016539 | p 1766 N95-22705

MISSILE CONTROL
Moving mass trim control for aerospace vehicles
| DE95-002602 | p 1622 N95-23532

MISSILE DEFENSE
Ballistic Missile Defense: Current status of strategic target system. Report to Congressional requesters
| GAO/NSIAD-95-78 | p 1903 N95-24080

MISSILE TRAJECTORIES
A CFD study of complex missile and store configurations in relative motion
| NASA-CR-197912 | p 1612 N95-22949

MISSION PLANNING
Space Science for the 21st Century. Strategic Plan for 1995-2000
| NASA-TM-110546 | p 1617 N95-22947
STS-61 mission director's post-mission report
| NASA-TM-104803 | p 1617 N95-23262
Integrating O/S models during conceptual design, part 2
| NASA-CR-197904 | p 1622 N95-23399
Operator procedure verification with a rapidly reconfigurable simulator p 1618 N95-23679
An operations and command systems for the extreme ultraviolet explorer p 1770 N95-23687
Autonomous spacecraft executive and its application to rendezvous and docking p 1623 N95-23719
Robotics and telepresence for moon missions p 1776 N95-23725
Modeling actions and operations to support mission preparation p 1617 N95-23750
CRI planning and scheduling for space p 1617 N95-23751
Benefits of advanced software techniques for mission planning systems p 1618 N95-23752
Artificial intelligence techniques for scheduling Space Shuttle missions p 1781 N95-23755
Design and implementation of an experiment scheduling system for the ACTS satellite p 1620 N95-23756
High performance techniques for space mission scheduling p 1618 N95-23758
Applications of dynamic scheduling technique to space related problems: Some case studies p 1618 N95-23759
Solution and reasoning reuse in space planning and scheduling applications p 1618 N95-23760
Integrating planning and reactive control p 1618 N95-23763
Ballistic Missile Defense: Current status of strategic target system. Report to Congressional requesters
| GAO/NSIAD-95-78 | p 1903 N95-24080

MIXING
Biological determinants of photobioreactor design
| DE94-016032 | p 1745 N95-22872

MIXING RATIOS
Objective determination of image end-members in spectral mixture analysis of AVIRIS data p 1709 N95-23888

MIXTURES
The influence of high-octane fuel blends on the performance of a two-stroke SI engine with knock-limited-compression ratio
| DE95-002902 | p 1692 N95-22556
Chemical recognition software
| DE95-003346 | p 1636 N95-24007

MOBILE COMMUNICATION SYSTEMS
Addendum to the Proceedings of the Third International Mobile Satellite Conference (IMSC 1993)
| NASA-CR-197343 | p 1655 N95-22813
Adaptive beamforming in a CDMA mobile satellite communications system p 1655 N95-22815
Passive intermodulation generation in wire mesh deployable reflector antennas p 1656 N95-22816
The possibilities for mobile and fixed services up to the 20/30 GHz frequency bands p 1656 N95-22817
Low Earth Orbit satellite/terrestrial mobile service compatibility p 1656 N95-22819

MOBILITY
Revitalization of the Gemenc-area, Baja, Hungary. 1: A study on hydrological possibilities to revitalise the ecosystem in the Keselyues-area. 2: Towards the restoration of the Gyueruesalj floodplain
| PB95-139283 | p 1718 N95-23469

MODAL RESPONSE
A modal test design strategy for model correlation
| DE95-003631 | p 1759 N95-24020

MODELS
Simultaneous inference in multivariate calibration
| DE95-003592 | p 1794 N95-23066
High beta and second stability region transport and stability analysis
| DE95-003411 | p 1832 N95-23147
Carbon monoxide oxidation over three different states of copper: Development of a model metal oxide catalyst
| DE95-004682 | p 1636 N95-23495

MODEMS
Parallel digital modem using multirate digital filter banks
| NASA-CR-197331 | p 1761 N95-22478

MODULARITY
Predicted performance of an integrated modular engine system
| NASA-CR-190787 | p 1625 N95-23791

MODULATION
Effects of modulation index on telecommunications
| AD-A286018 | p 1657 N95-23023

MODULATORS
High-performance GaAs/AlGaAs optical modulators: Their performance and packaging for microwave photonic integrated circuits
| DE95-004533 | p 1828 N95-23575

MODULES
Hey! What's Space Station Freedom?
| NASA-TM-110531 | p 1620 N95-22542
World's first 15%-efficient multicrystalline silicon modules
| DE95-002604 | p 1727 N95-22650
Amorphous silicon photovoltaic manufacturing technology, phase 2A
| DE95-000298 | p 1729 N95-23478
Proceedings of the workshop on deductive databases and logic programming
| PB95-139382 | p 1758 N95-23553

MODULUS OF ELASTICITY
Interlaminar shear test method development for long term durability testing of composites p 1631 N95-23300

MOISTURE
Outgassing considerations for composites in space applications p 1629 N95-23037

MOISTURE CONTENT
An improved algorithm for retrieval of snow wetness using C-band AIRSAR p 1715 N95-23954
Determining successional stage of temperate coniferous forests with Landsat satellite data p 1720 N95-24102

MOJAVE DESERT (CA)
Monitoring land use and degradation using satellite and airborne data p 1707 N95-23880

MOLECULAR BIOLOGY
Open problems of computational molecular biology
| DE95-000895 | p 1745 N95-22866
Regulation of alcohol fermentation in Escherichia coli
| DE94-016227 | p 1745 N95-22874
Activation of the jun-D gene in human myeloid cells by 1-(beta)-D-arabinofuranosylcytosine
| DE94-016591 | p 1746 N95-22912
Rearrangement of RAG-1 recombinase gene in radiation-sensitive wasted mice
| DE94-017083 | p 1746 N95-22913

MOLECULAR CHAINS
Fibonacci chain polynomials: Identities from self-similarity p 1814 N95-22962
Coherent state constructions of bases for some physically relevant group chains p 1814 N95-22966

MOLECULAR COLLISIONS
Structure, melting, and reactivity of nickel clusters from numerical simulations
| DE95-002911 | p 1638 N95-22531
Algebraic description of atom-molecule interactions p 1814 N95-22961
Molecular vibrational states during a collision p 1814 N95-22964
Energy transfer dynamics in isolated and in colliding highly vibrationally excited molecules
| AD-A285771 | p 1806 N95-23077

MOLECULAR DYNAMICS
Structure, melting, and reactivity of nickel clusters from numerical simulations
| DE95-002911 | p 1638 N95-22531
Metallization and incomplete melting of a semiconductor surface at high temperature
| DE94-627342 | p 1660 N95-22591
A parallel molecular dynamics simulation of crystal growth at a cluster of workstations
| DE94-628382 | p 1839 N95-22615
A multi-region radial integration scheme
| NASA-CR-197982 | p 1809 N95-23408

MOLECULAR ENERGY LEVELS
Geometrical interpretation for the outer SU(3) outer multiplicity label p 1814 N95-22968

MOLECULAR EXCITATION
Algebraic approach to the vibrational excitations in methane p 1814 N95-22960

Energy transfer dynamics in isolated and in colliding highly vibrationally excited molecules
| AD-A285771 | p 1806 N95-23077

MOLECULAR GASES
Pressure shifts and electron scattering in atomic and molecular gases
| DE95-003102 | p 1803 N95-22747
Search for millimeterwave CO emission in damped Lyman-alpha systems
| PB95-139259 | p 1868 N95-23607

MOLECULAR ORBITALS
Ligand K-edge x-ray adsorption spectroscopic studies of the electronic structure of inorganic model complexes and metalloprotein active sites
| DE95-003338 | p 1840 N95-22851
Exact, E = 0, classical and quantum solutions for general power-law oscillators p 1820 N95-22959

MOLECULAR OSCILLATIONS
Enhanced oscillation of neutrinos of different masses in matter
| DE94-635648 | p 1812 N95-23973

MOLECULAR OSCILLATORS
Algebraic description of atom-molecule interactions p 1814 N95-22961

MOLECULAR RELAXATION
Energy transfer dynamics in isolated and in colliding highly vibrationally excited molecules
| AD-A285771 | p 1806 N95-23077

MOLECULAR STRUCTURE
Structure, melting, and reactivity of nickel clusters from numerical simulations
| DE95-002911 | p 1638 N95-22531
Asymptotically exact solution of a local copper-oxide model
| DE94-628492 | p 1842 N95-23059
Organometallic chemistry of bimetallic compounds
| DE95-004436 | p 1634 N95-23345

MOLECULAR TRAJECTORIES
Exact, E = 0, classical and quantum solutions for general power-law oscillators p 1820 N95-22959

MOLECULES
The torsion space nucleic acids molecular mechanics program DUPLEX: Surveying conformation space by potential energy minimization
| DE94-017707 | p 1805 N95-22889
Algebraic theory of molecules p 1814 N95-22958
Harmonic oscillator in quantum rotational spectra: Molecules and nuclei p 1814 N95-22972
Quantum fluctuations of D(sub 5d) polarons on C(sub 60) molecules
| DE94-635787 | p 1812 N95-23985
Monte Carlo simulation of rarefied nitrogen gases contained between parallel plates using the statistical inelastic cross-section model
| NAL-TR-1229T | p 1687 N95-24082

MOLTEN SALTS
A model for the metal-nonmetal transition in metal-molten salt solutions
| DE94-628490 | p 1640 N95-23057

MOLYBDENUM
Precise determinations of the isotopic compositions and atomic weights of molybdenum, tellurium, tin and tungsten using ICP source magnetic sector multiple collector mass spectrometry
| DE95-003003 | p 1632 N95-22795
Changes in chemical and optical properties of thin film metal mirrors on LDEF p 1651 N95-23907

MOLYBDENUM ALLOYS
Thermal outgassing studies on machinable tungsten and TZM molybdenum alloy
| DE95-002984 | p 1638 N95-22592

MOLYBDENUM COMPOUNDS
Dislocation decomposition, dissociation, and deformation in MoSi2 and (alpha)-Al2O3 single crystals
| DE95-002715 | p 1839 N95-22653

MOLYBDENUM DISULFIDES
Ethanol synthesis and water gas shift over bifunctional sulfide catalysts
| DE94-017376 | p 1634 N95-23202

MOMENTS OF INERTIA
Harmonic oscillator in quantum rotational spectra: Molecules and nuclei p 1814 N95-22972

MOMENTUM
Bose condensation, macroscopic quantum phenomena and atomic spatial correlations in superfluid He-4
| PB95-139085 | p 1850 N95-23154
Neutron compton scattering
| PB95-139135 | p 1807 N95-23159
Measurement of correlated b quark cross sections at CDF
| DE95-004240 | p 1808 N95-23336

MOMENTUM TRANSFER
Collisionless magnetic reconnection associated with coalescence of flux bundles
| NIFS-315 | p 1834 N95-23525

MONATOMIC GASES
Pressure shifts and electron scattering in atomic and molecular gases
| DE95-003102 | p 1803 N95-22747

MONKEYS
Laser irradiation effects: A functional assessment
| AD-A285100 | p 1691 N95-22937

MONOMERS
Polyazomethines containing trifluoromethylbenzene units
| NASA-CASE-LAR-14896-1 | p 1649 N95-23253

MONTE CARLO METHOD
Particle kinetic simulation of high altitude hypervelocity flight
| NASA-CR-197383 | p 1664 N95-22481
Variational calculations for He-3 impurities on He-4 droplets
| DE94-628469 | p 1840 N95-22839
Photon and electron interaction databases and their use in medical applications
| DE94-015558 | p 1855 N95-22871
Calculations of alloy phases with a direct Monte-Carlo method
| DE94-018963 | p 1640 N95-23121
Consistency and Monte Carlo simulation of a data driven version of smooth goodness-of-fit tests
| PB95-141255 | p 1794 N95-23559
Increasing the retained dose by plasma immersion ion implantation and deposition
| DE95-003423 | p 1844 N95-24011
Monte Carlo simulation of rarefied nitrogen gases contained between parallel plates using the statistical inelastic cross-section model
| NAL-TR-1229T | p 1687 N95-24082

MONTMORILLONITE
Application of MAC-Europe AVIRIS data to the analysis of various alteration stages in the Landdmannalauger Hydrothermal Area (South Iceland) p 1709 N95-23885

MORPHOLOGICAL INDEXES
Learning time series for intelligent monitoring p 1770 N95-23686

MORPHOLOGY
Morphology of extinguished monolithic JA2 grains fired in a 30-mm Solid Propellant Electrothermal Chemical (SPETC) gun
| AD-A285792 | p 1652 N95-22506
Glass science tutorial: Lecture 1, Chemistry and properties of oxide glasses
| DE95-002963 | p 1647 N95-22647
Determination of semi-arid landscape endmembers and seasonal trends using convex geometry spectral unmixing techniques p 1711 N95-23895
A theory for the morphology of Laplacian growth from statistics of equivalent many-body Hamiltonian systems
| DE94-014473 | p 1799 N95-23979
Structural studies of complex carbohydrates of plant cell walls
| DE95-003099 | p 1748 N95-24075

MORSE POTENTIAL
Algebraic theory of molecules p 1814 N95-22958
A supersymmetric family of harmonic oscillators simulating H-bonds in DNA p 1748 N95-22963

MOTION SIMULATION
Concept verification of three dimensional free motion simulator for space robot p 1618 N95-23702

MOTION SIMULATORS
Concept verification of three dimensional free motion simulator for space robot p 1618 N95-23702
Development of the dynamic motion simulator of 3D micro-gravity with a combined passive/active suspension system p 1618 N95-23711
Design of a cervical spine gross motion simulator for standard size human and anthropomorphic dummy adult and child
| NIAR-94-16 | p 1751 N95-24021

MOUNTAINS
GPS survey of the western Tien Shan
| NASA-CR-197901 | p 1717 N95-22832
Comparison of 7.5-minute and 1-degree digital elevation models p 1719 N95-24095

MSM (SEMICONDUCTORS)
Circular electrode geometry metal-semiconductor-metal photodetectors
| NASA-CASE-LAR-15172-1-CU | p 1663 N95-24048

MULTICHANNEL COMMUNICATION
Passive intermodulation generation in wire mesh deployable reflector antennas p 1656 N95-22816

MULTIDISCIPLINARY DESIGN OPTIMIZATION
Multidisciplinary design optimization using genetic algorithms p 1619 N95-23332

MULTIGRID METHODS
New robust multigrid method for 2D convection-diffusion problems
| PB95-138897 | p 1789 N95-23176

MULTILAYER INSULATION
The sound insulations of studio doors. Part 2: Door seals
| BBC-RD-1994/15 | p 1654 N95-24045
The sound insulations of studio doors. Part 1: Door blanks
| BBC-RD-1994/14 | p 1654 N95-24093

MULTIPATH TRANSMISSION
Adaptive beamforming in a CDMA mobile satellite communications system p 1655 N95-22815

MULTIPHASE FLOW
Advanced multi-phase flow CFD model development for solid rocket motor flowfield analysis p 1683 N95-23638

MULTIPLEXING
Optical image correlator using orthogonal data storage
| AD-A285795 | p 1819 N95-22508

MULTIPOLES
Multipole contribution from an off-axis orbit in an IR quadrupole and the consequences on the dynamic aperture
| DE95-002874 | p 1816 N95-22567
Accelerated panel methods using the fast multipole method p 1687 N95-23307
The effect of magnetic field on the edge plasmons of two-dimensional electron gas systems
| DE94-018044 | p 1837 N95-23982

MULTIPROCESSING (COMPUTERS)
Verifying sequentially consistent memory using interface refinement
| PB95-139002 | p 1752 N95-23153
Distributed VIRtual System (DIVIRS) project
| NASA-CR-197855 | p 1757 N95-23180
Block LU factorization
| NASA-CR-197949 | p 1791 N95-23592
WHAMS3D Project: Parallel implementations of WHAMS3D on two shared-memory multiprocessors
| CSRD-1248 | p 1764 N95-23599
Very fast motion planning for highly dexterous-articulated robots p 1771 N95-23691
Algorithms for categorizing multiprocessor communication under invalidate and update-based coherence protocols
| TR-533-REV | p 1759 N95-23928
Scalability of atomic primitives on distributed shared memory multiprocessors
| TR-528 | p 1764 N95-23930
Eliminating useless messages in write-update protocols on scalable multiprocessors
| TR-539 | p 1764 N95-24037
Using simple page placement policies to reduce the cost of cache fills in coherent shared-memory systems
| TR-535 | p 1753 N95-24177
Scheduler-conscious synchronization
| TR-550 | p 1765 N95-24183
Lazy release consistency for hardware-coherent multiprocessors
| TR-547 | p 1765 N95-24184

MULTIPROGRAMMING
Scheduler-conscious synchronization
| TR-550 | p 1765 N95-24183

MULTISENSOR APPLICATIONS
Development of a multi-sensor in situ fiber optic fluorometer
| DE95-003105 | p 1819 N95-22780
A three-finger multisensory hand for dexterous space robotic tasks p 1752 N95-23705
MAC Europe 1991 campaign: AIRSAR/AVIRIS data integration for agricultural test site classification p 1715 N95-23952

MULTISPECTRAL BAND SCANNERS
A multispectral scanner survey of the Tonopah Test Range, Nevada. Date of survey: August 1993
| DE95-003920 | p 1717 N95-22503
Optimal band selection for dimensionality reduction of hyperspectral imagery p 1709 N95-23887
Summaries of the 4th Annual JPL Airborne Geoscience Workshop. Volume 2: TIMS Workshop
| NASA-CR-197876-VOL-2 | p 1711 N95-23917
Estimation of spectral emissivity in the thermal infrared p 1711 N95-23918
Mineralogic variability of the Kelso Dunes, Mojave Desert, California derived from Thermal Infrared Multispectral Scanner (TIMS) data p 1711 N95-23920
Geologic mapping using integrated AIRSAR, AVIRIS, and TIMS data p 1714 N95-23946

MULTIVARIABLE CONTROL
Design of high performance multivariable control systems for supermaneuverable aircraft at high angle of attack
| NASA-CR-197661 | p 1615 N95-22908

MULTIVARIATE STATISTICAL ANALYSIS
Chemical recognition software
| DE95-003346 | p 1636 N95-24007

MUONIUM
Time-resolved EPR studies of the H atom: A stable heavy isotope of muonium
| DE95-004614 | p 1810 N95-23491
MUONS
Dimuon production in proton-nucleus interactions
| DE95-002613 | p 1801 N95-22551
Limit on the muon neutrino mass from K(exp 0)muon 3 decay spectra
| DE95-000816 | p 1801 N95-22583
Bottom-quark production from muon-jet and dimuon events in p(bar p)-interactions at the square root of s = 1.8 TeV
| DE95-001286 | p 1801 N95-22685
Exotic atoms
| DE95-003199 | p 1805 N95-22881
J/psi, psi' yields mu(+)mu(-) and B yields J/psi, psi' cross sections
| DE94-018996 | p 1808 N95-23242
Measurement of correlated b quark cross sections at CDF
| DE95-004240 | p 1808 N95-23336
D(O) upgrade muon electronics design
| DE95-003744 | p 1817 N95-23369
Measurement of W and Z boson production and extraction of the W width and branching ratios at CDF
| DE94-018989 | p 1810 N95-23522
Search for supersymmetric (tilde W)(sub 1) and (tilde Z)(sub 2) states using the D0 detector
| DE95-004581 | p 1811 N95-23581
MUTATIONS
Analysis of structural domains required for phytochrome function by in vitro mutagenesis
| DE94-016230 | p 1745 N95-22884

N

N-TYPE SEMICONDUCTORS
Doing photons with MERLIN 2 at Oroville
p 1815 N95-23816
NASA PROGRAMS
1994 NASA-HU American Society for Engineering Education (ASEE) Summer Faculty Fellowship Program
| NASA-CR-194972 | p 1872 N95-23276
Teams and teamwork at NASA Langley Research Center p 1854 N95-23292
Electronic photography at NASA Langley Research Center p 1690 N95-23298
NASA university program management information system, FY 1994
| NASA-TM-110345 | p 1856 N95-23364
Research and Technology, 1994
| NASA-TM-106764 | p 1607 N95-24025
NASA SPACE PROGRAMS
Third International Symposium on Artificial Intelligence, Robotics, and Automation for Space 1994
| NASA-CR-197340 | p 1767 N95-23672
NASTRAN
Thin tailored composite wing for civil tiltrotor
p 1613 N95-23317
A new look at the simultaneous analysis and design of structures p 1700 N95-23327
NATIONAL AEROSPACE PLANE PROGRAM
A summary of the slush hydrogen technology program for the National Aero-Space Plane
| NASA-TM-106863 | p 1653 N95-24186
NATURAL GAS
Preliminary assessment of air toxic emissions in the natural gas industry, phase 1
| PB95-135547 | p 1732 N95-22865
NATURAL GAS EXPLORATION
Preliminary assessment of air toxic emissions in the natural gas industry, phase 1
| PB95-135547 | p 1732 N95-22865
NATURAL LANGUAGE (COMPUTERS)
A computational theory of grounding in natural language conversation
| TR-545 | p 1760 N95-24058
The TRAINS project: A case study in building a conversational planning agent
| TR-532 | p 1659 N95-24193
NAVIER-STOKES EQUATION
An adaptive projection method for the incompressible Navier-Stokes equations
| DE94-019049 | p 1665 N95-22491
A perspective on unstructured grid flow solvers
| NASA-CR-195025 | p 1788 N95-22931
An assessment of viscous effects in computational simulation of benign and burst vortex flows on generic fighter wind-tunnel models using TEAM code
| NASA-CR-4650 | p 1608 N95-23185
Mach 10 computational study of a three-dimensional scramjet inlet flow field
| NASA-TM-4602 | p 1667 N95-23210
Direct numerical simulation of sheared turbulent flow
p 1687 N95-23296
Benchmark problems in computational aeroacoustics
p 1800 N95-23315
A generic efficient adaptive grid scheme for rocket propulsion modeling p 1670 N95-23418
Preconditioning for the Navier-Stokes equations with finite-rate chemistry p 1670 N95-23421
Navier-Stokes analysis of an oxidizer turbine blade with tip clearance with and without a mini-shroud
p 1672 N95-23428
Advanced turbulence models for turbomachinery
p 1675 N95-23443
Numerical computation of aerodynamics and heat transfer in a turbine cascade and a turn-around duct using advanced turbulence models p 1675 N95-23444
Convergence acceleration of implicit schemes in the presence of high aspect ratio grid cells
p 1676 N95-23446
A time-accurate finite volume method valid at all flow velocities p 1676 N95-23447
On the conservative interface treatment for multi-block viscous flow computations
| NASA-CR-195442 | p 1677 N95-23451
Navier-Stokes flow field analysis of compressible flow in a pressure relief valve p 1679 N95-23618
Incompressible Navier-Stokes calculations in pump flows p 1680 N95-23627
Cavitation modeling in Euler and Navier-Stokes codes
p 1681 N95-23630
On the accuracy of CFD-based pressure drop predictions for right-angle ducts p 1682 N95-23634
NAVIGATION
Experience with CANDID: Comparison algorithm for navigating digital image databases
| DE95-000869 | p 1855 N95-22515
Small image laser range finder for planetary rover
p 1692 N95-23712
NAVIGATION AIDS
Cueing light configuration for aircraft navigation
| NASA-CASE-ARC-11982-1 | p 1611 N95-23393
TRISTAR 1: Evaluation methods for testing head-up display (HUD) flight symbology
| NASA-TM-4665 | p 1613 N95-24030
NEAR FIELDS
Taylor series expansion and modified extended Prony analysis for localization
| DE95-003671 | p 1758 N95-23567
NEAR INFRARED RADIATION
Study of photorefractive non-linearities in the 3-5 and 2-4 semi-insulator compounds: The effect of electron irradiation
| PB94-189057 | p 1839 N95-22584
AVIRIS and TIMS data processing and distribution at the land processes distributed active archive center
p 1706 N95-23872
Near infrared and optical spectroscopy of FSC10214+4724
| NASA-CR-197966 | p 1828 N95-24068
NEARSHORE WATER
SWIFT BOAT 1994: Using a fast chase boat to investigate offshore weather features in conjunction with WSR-88D observations
| PB94-195146 | p 1742 N95-22651
NECK (ANATOMY)
Design of a cervical spine gross motion simulator for standard size human and anthropomorphic dummy adult and child
| NIAR-94-16 | p 1751 N95-24021
NEODYMIUM LASERS
Transient radiation-induced absorption in materials for the DOI laser
| DE95-004549 | p 1828 N95-24161
NERVOUS SYSTEM
Interrelations between nervous system and immune system in stress situations
| PB95-135521 | p 1748 N95-22770
NETHERLANDS
Review of aeronautical fatigue investigation in the Netherlands during the period March 1991-March 1993
| PB95-139184 | p 1612 N95-23161
NETS
Modelling and analysis of a high speed data bus with predicate/transition nets
| PB95-140695 | p 1764 N95-23538
NETWORK ANALYSIS
Lyapunov exponents from CHUA's circuit time series using artificial neural networks p 1784 N95-22988
Loop scheduling for heterogeneity
| TR-540 | p 1764 N95-23936
NEURAL NETS
A Newton-type neural network learning algorithm
| DE94-628371 | p 1766 N95-22614
Neural network for detection and correction of local boundary misalignments between images
| AD-D016539 | p 1766 N95-22705
An improved system for exon recognition and gene modeling in human DNA sequences
| DE94-017863 | p 1746 N95-22890
Neurodynamic oscillators p 1749 N95-22987
Lyapunov exponents from CHUA's circuit time series using artificial neural networks p 1784 N95-22988
Neural net prediction of tokamak plasma disruptions
| DE95-002616 | p 1832 N95-23136
On-line, adaptive state estimator for active noise control p 1784 N95-23308
Method and system for pattern analysis using a coarse-coded neural network
| NASA-CASE-ARC-11961-1 | p 1767 N95-23387
Study of b(anti b) production in e(+)e(-) annihilation at radical s = 29 GeV with the aid of neural networks
| DE95-004691 | p 1810 N95-23488
Alpha spectral analysis via artificial neural networks
| DE95-004567 | p 1767 N95-23578
Interactive autonomy and robotic skills
p 1777 N95-23730
A self-organizing neural network architecture for auditory and speech perception with applications to acoustic and other temporal prediction problems
| AD-A285640 | p 1800 N95-23782
Classification of the LCVF AVIRIS test site with a Kohonen artificial neural network p 1706 N95-23874
Mapping and monitoring changes in vegetation communities of Jasper Ridge, CA, using spectral fractions derived from AVIRIS images p 1708 N95-23883
NEURONS
Neurodynamic oscillators p 1749 N95-22987
NEUROPSYCHIATRY
Some performance effects of age and low blood alcohol levels on a computerized neuropsychological test
| DOT/FAA/AM-95/7 | p 1749 N95-23788
NEUTRAL ATMOSPHERES
Modeling of the coupled magnetospheric and neutral wind dynamos
| NASA-CR-197861 | p 1738 N95-23090
NEUTRAL BEAMS
The TEXT neutral lithium beam edge density diagnostic
| DE95-003256 | p 1830 N95-22719
NEUTRAL SHEETS
An explanation for tailward flows with positive B(sub z) in the distant tail neutral sheet during quite times
| ATR-95(7270)-1 | p 1740 N95-23933
NEUTRINO BEAMS
Neutrino oscillation experiments with atmospheric neutrinos
| DE95-002994 | p 1801 N95-22573
Long-baseline neutrino oscillation experiments
| DE95-004636 | p 1870 N95-23584
NEUTRINOS
Neutrino oscillation experiments with atmospheric neutrinos
| DE95-002994 | p 1801 N95-22573
Limit on the muon neutrino mass from K(exp 0)muon 3 decay spectra
| DE95-000816 | p 1801 N95-22583
Neutrino overview
| DE95-003201 | p 1802 N95-22729
On the D yields K-bar(sup *)e(sup +)(nu)(sub e) form factors
| DE94-628614 | p 1803 N95-22754
Neutrinos with Zee-mass matrix in vacuum and matter
| DE94-628635 | p 1803 N95-22756
Results from neutrino experiments
| DE94-628604 | p 1804 N95-22790
Structural properties of silicon clusters: An empirical potential study
| DE94-628902 | p 1805 N95-22935
Long-baseline neutrino oscillation experiments
| DE95-004636 | p 1870 N95-23584
Neutrino masses and mixing
| DE94-628632 | p 1812 N95-23784
Neutrino mass
| DE94-628634 | p 1812 N95-23786
Enhanced oscillation of neutrinos of different masses in matter
| DE94-635648 | p 1812 N95-23973
NEUTRON BEAMS
Strong collision approach to calculation of depolarization function for neutron beam passing through ferromagnetic bulk domains
| DE94-628847 | p 1803 N95-22758
Continuation of BNCT Research Program at NEMC and MIT
| DE94-016228 | p 1748 N95-22875
NEUTRON DIFFRACTION
High pressure neutron powder diffraction at LANSCE
| DE95-002703 | p 1839 N95-22565
Transformation behavior in Al2O3-ZrO2 ceramic composites
| DE95-001359 | p 1647 N95-22688

PRISMA GENIE data analysis manual
| PB95-130464 | p 1755 N95-22769
Internal strain measurement using pulsed neutron diffraction at LANSCE
| DE95-003677 | p 1842 N95-23365

NEUTRON IRRADIATION
Study of radiation damages in AISI 316 and 347 steels
| DE94-627480 | p 1639 N95-22609
Cation disorder determined by MAS Al-27 NMR in high dose neutron irradiated spinel
| DE95-003681 | p 1842 N95-23266

NEUTRON SCATTERING
Neutron scattering analysis of rubber carbon black composite structure
| DE95-002735 | p 1646 N95-22553
Neutron compton scattering
| PB95-139135 | p 1807 N95-23159

NEUTRON SOURCES
Status of helium-production reaction studies with a spallation neutron source
| DE95-002816 | p 1806 N95-23137
Neutron compton scattering
| PB95-139135 | p 1807 N95-23159

NEUTRONS
Experimental results on polarized structure functions in deep inelastic lepton-nucleon scattering
| DE95-002782 | p 1801 N95-22521
Geometrical interpretation for the outer SU(3) outer multiplicity label p 1814 N95-22968
Reflectivity studies on adsorbed block copolymers under shear
| DE95-003676 | p 1649 N95-23568
Pauli-blocking effects in neutron-alpha reactions
| DE94-016358 | p 1813 N95-24046
Phonon characteristics of high (T sub c) superconductors from neutron Doppler broadening measurements
| DE95-003703 | p 1844 N95-24076

NEVADA
Streamflow and selected precipitation data for Yucca Mountain Region, southern Nevada and eastern California, water years 1986-90
| DE95-001893 | p 1742 N95-23385

NEWTON
Newton in space
| NASA-TM-110535 | p 1799 N95-23273

NEWTON METHODS
A Newton-type neural network learning algorithm
| DE94-628371 | p 1766 N95-22614

NEWTONIAN FLUIDS
BEm-BDF scheme for curvature driven moving stokes flows
| PB95-138905 | p 1667 N95-23144
On the breakup of viscous liquid threads
| NASA-CR-195023 | p 1678 N95-23544

NICKEL
Structure, melting, and reactivity of nickel clusters from numerical simulations
| DE95-002911 | p 1638 N95-22531
X-ray diffraction characterization of defect behavior in nanocrystalline nickel during annealing
| DE95-002992 | p 1639 N95-22594
Changes in chemical and optical properties of thin film metal mirrors on LDEF p 1651 N95-23907
Durability of reflector materials in the space environment p 1651 N95-23912

NICKEL ALLOYS
The role of grain boundary chemistry and structure in the environmentally-assisted intergranular cracking of nickel-base alloys
| DE95-002941 | p 1638 N95-22532
An investigation into the effects of hydrogen on the fracture and deformation of Alloy X-750
| DE95-003206 | p 1639 N95-22732

NIGHT VISION
Aviator's night vision imaging system preflight adjustment/assessment procedures
| AD-A285829 | p 1750 N95-22513

NIOBATES
Transient radiation-induced absorption in materials for the DOI laser
| DE95-004549 | p 1828 N95-24161

NIOBIUM ALLOYS
Deformation of C15 Laves phase alloys
| DE95-003636 | p 1646 N95-24067

NITRATES
Test procedure for anion exchange chromatography
| DE95-003767 | p 1809 N95-23407

NITRIC OXIDE
NO decomposition in non-reducing atmospheres
| DE95-004324 | p 1634 N95-23339
Carbon monoxide oxidation over three different states of copper: Development of a model metal oxide catalyst
| DE95-004682 | p 1636 N95-23495

NITROGEN
Progress towards the synthesis of polymeric nitrogen
| DE94-017547 | p 1841 N95-22860
Analytical Boltzmann moments for electrons in N2-O2-H2O gas mixtures
| DE95-003474 | p 1732 N95-22898
High surface area, high permeability carbon monoliths
| DE95-004555 | p 1650 N95-23577
Application of a two-stream radiative transfer model for leaf lignin and cellulose concentrations from spectral reflectance measurements, part 1 p 1703 N95-23856
AVIRIS spectra correlated with the chlorophyll concentration of a forest canopy p 1705 N95-23871
Measurements of canopy chemistry with 1992 AVIRIS data at Blackhawk Island and Harvard Forest p 1706 N95-23873
Relationships between pigment composition variation and reflectance for plant species from a coastal savannah in California p 1709 N95-23889
Monte Carlo simulation of rarefied nitrogen gases contained between parallel plates using the statistical inelastic cross-section model
| NAL-TR-1229T | p 1687 N95-24082

NITROGEN COMPOUNDS
The atmosphere below
| NASA-TM-110538 | p 1740 N95-23663

NITROGEN OXIDES
Modeling NO(x) emissions in turbulent jet flames: Effects of buoyancy and radiation
| DE94-016621 | p 1633 N95-22886
Effects of jet strength on NOx formation in premixed impinging jet combustion with minimum heat losses
| NAL-TR-1237T | p 1637 N95-24181

NITROUS OXIDES
Emissions of greenhouse gases in the United States, 1987-1992
| DE95-003001 | p 1731 N95-22691

NOBLE METALS
Non local pseudopotentials, transport properties of liquid noble metals
| DE94-627416 | p 1640 N95-22840

NOISE MEASUREMENT
High Tc superconducting bolometric and nonbolometric infrared (IR) detectors
| NASA-CR-197868 | p 1827 N95-23224

NOISE PREDICTION (AIRCRAFT)
Supersonic jet noise reductions predicted with increased jet spreading rate
| NASA-TM-106872 | p 1800 N95-23178

NOISE REDUCTION
The use of cowl camber and taper to reduce rotor/stator interaction noise
| NASA-CR-195421 | p 1799 N95-22675
Supersonic jet noise reductions predicted with increased jet spreading rate
| NASA-TM-106872 | p 1800 N95-23178
On-line, adaptive state estimator for active noise control p 1784 N95-23308

NOMENCLATURES
Glass science tutorial: Lecture 2, operating electric glass melters
| DE95-002965 | p 1647 N95-22648

NONDESTRUCTIVE TESTS
High-temperature ultrasonic characterization of Ag-clad superconductor tapes
| DE95-002909 | p 1838 N95-22530
Nondestructive evaluation of fatigue damage in aluminum 2024 by x-ray diffraction p 1698 N95-23293
Internal strain measurement using pulsed neutron diffraction at LANSCE
| DE95-003677 | p 1842 N95-23365
Double pass retroreflection for corrosion detection in aircraft structures p 1642 N95-23503
Non-destructive detection of corrosion for life management p 1643 N95-23505
New nondestructive techniques for the detection and quantification of corrosion in aircraft structures p 1644 N95-23512
POD assessment of NDI procedures using a round robin test
| AGARD-R-809 | p 1697 N95-23602

NONEQUILIBRIUM FLOW
Preconditioning for the Navier-Stokes equations with finite-rate chemistry p 1670 N95-23421

NONEQUILIBRIUM PLASMAS
Modeling of nonequilibrium space plasma flows
| NASA-CR-197432 | p 1833 N95-23211

NONEQUILIBRIUM RADIATION
Investigation of infra-red and nonequilibrium air radiation
| NASA-CR-197977 | p 1741 N95-24041

NONINTRUSIVE MEASUREMENT
Non-intrusive measurements in a rocket engine combustor p 1625 N95-23439
Impeller flow field characterization with a laser two-focus velocimeter p 1675 N95-23440

NONLINEAR EQUATIONS
Iterative solutions of nonlinear equations with strongly accretive or strongly pseudocontractive maps
| DE94-628432 | p 1786 N95-22634
Nonlinear generalized functions and nonconservative shock simulations
| DE95-003307 | p 1795 N95-22734
Development of an adaptive hp-version finite element method for computational optimal control
| NASA-CR-197898 | p 1766 N95-22831
Time-periodic solutions of some forced nonlinear wave equations: Analysis, approximations and applications
| PB95-135083 | p 1788 N95-22932
Algorithms for parallel and vector computations
| NASA-CR-197394 | p 1756 N95-23017
Iterative solutions of nonlinear equations in smooth Banach spaces
| DE94-634287 | p 1790 N95-23455
Linearizing W-algebras
| DE94-634324 | p 1790 N95-23457
Moving mass trim control for aerospace vehicles
| DE95-002602 | p 1622 N95-23532
Nonlinear thermoviscoelastic behaviour in complex materials
| PB95-140653 | p 1630 N95-23537

NONLINEAR EVOLUTION EQUATIONS
Morphology of Laplacian growth processes and statistics of equivalent many-body systems
| DE95-002734 | p 1847 N95-22655

NONLINEAR FEEDBACK
Design of high performance multivariable control systems for supermaneuverable aircraft at high angle of attack
| NASA-CR-197661 | p 1615 N95-22908

NONLINEAR OPTICS
Study of photorefractive non-linearities in the 3-5 and 2-4 semi-insulator compounds: The effect of electron irradiation
| PB94-189057 | p 1839 N95-22584
Two-photon absorption in an indirect-gap semiconductor quantum well systems 1. Interband transitions
| DE94-628879 | p 1849 N95-22760

NONLINEAR SYSTEMS
Nonlinear system guidance in the presence of transmission zero dynamics
| NASA-TM-4661 | p 1654 N95-22804
Disorder-induced breakdown of soliton and polaron particles
| DE95-003694 | p 1808 N95-23267
Complexity in plasma: A grand view of self-organization
| NIFS-318 | p 1835 N95-23528
On the breakup of viscous liquid threads
| NASA-CR-195023 | p 1678 N95-23544
Normalized coprime factorizations and balancing for unstable nonlinear systems
| PB95-141222 | p 1767 N95-23557
Dynamic disturbance decoupling of nonlinear systems and linearization
| PB95-141248 | p 1767 N95-23558

NONLINEARITY
COYOTE 2: A Finite Element Computer Program for nonlinear heat conduction problems
| DE95-002848 | p 1666 N95-22914
Structure and evolution of long-lived spiral patterns in galaxies
| PB95-139242 | p 1868 N95-23228
Nonlinear thermoviscoelastic behaviour in complex materials
| PB95-140653 | p 1630 N95-23537
Normalized coprime factorizations and balancing for unstable nonlinear systems
| PB95-141222 | p 1767 N95-23557
Dynamic disturbance decoupling of nonlinear systems and linearization
| PB95-141248 | p 1767 N95-23558
Ishikawa iteration process for nonlinear Lipschitz strongly accretive mappings
| DE94-634284 | p 1792 N95-23658
Nonlinear viscoelastic characterization of polymer materials using a dynamic-mechanical methodology p 1651 N95-23902

NORMAL DENSITY FUNCTIONS
Wigner distribution function and entropy of the damped harmonic oscillator within the theory of the open quantum systems p 1798 N95-22990
Stochastic decision analysis p 1854 N95-23305

NORMALITY
Second derivative of the likelihood of an exact ARMA model
| PB95-135158 | p 1788 N95-23069

NORTH ATLANTIC TREATY ORGANIZATION (NATO)
Proceedings of NATO Advanced Research Workshop on the Formation, Transport and Consequences of Particles in Plasmas
| AD-A285850 | p 1829 N95-22514

NORTH SEA
Study on possible environmental effects of a WBM cutting discharge in the north sea, one year after termination of drilling
|PB95-133740| p 1733 N95-23125

NOTCH SENSITIVITY
Notch-tip damage and translaminar fracture toughness measurements from carbon/epoxy laminates
|AD-A280101| p 1627 N95-22833

NOTCH TESTS
Notch-tip damage and translaminar fracture toughness measurements from carbon/epoxy laminates
|AD-A280101| p 1627 N95-22833
Interlaminar shear test method development for long term durability testing of composites
p 1631 N95-23300

NOZZLE DESIGN
An approximate theoretical method for modeling the static thrust performance of non-axisymmetric two-dimensional convergent-divergent nozzles
|NASA-CR-195050| p 1608 N95-23193
Optimized design of a hypersonic nozzle
p 1617 N95-23304
Design of a variable area diffuser for a 15-inch Mach 6 open-jet tunnel p 1617 N95-23309
Three-dimensional Navier-Stokes analysis and redesign of an imbedded bellmouth nozzle in a turbine cascade inlet section p 1671 N95-23423
Methodology for CFD design analysis of National Launch System nozzle manifold p 1683 N95-23637

NOZZLE EFFICIENCY
An approximate theoretical method for modeling the static thrust performance of non-axisymmetric two-dimensional convergent-divergent nozzles
|NASA-CR-195050| p 1608 N95-23193

NOZZLE FLOW
Experimental study of vortex breakdown in a swirling water jet
|PB95-130407| p 1665 N95-22767
An approximate theoretical method for modeling the static thrust performance of non-axisymmetric two-dimensional convergent-divergent nozzles
|NASA-CR-195050| p 1608 N95-23193
Experimental results for a hypersonic nozzle/afterbody flow field
|NASA-TM-4638| p 1609 N95-23250
Axisymmetric computational fluid dynamics analysis of Saturn V/S1-C/F1 nozzle and plume
p 1672 N95-23430
Computational Fluid Dynamic (CFD) analysis of axisymmetric plume and base flow of film/dump cooled rocket nozzle p 1673 N95-23431
Numerical study of the SSME nozzle flow fields during transient operations: A comparison of the animated results with test p 1673 N95-23434
Development of an algebraic stress/two-layer model for calculating thrust chamber flow fields
p 1675 N95-23442
Application of CFD analysis to design support and problem resolution for ASRM and RSRM
p 1685 N95-23649

NOZZLE GEOMETRY
Axisymmetric computational fluid dynamics analysis of Saturn V/S1-C/F1 nozzle and plume
p 1672 N95-23430

NOZZLE WALLS
Supersonic laminar flow control research
|NASA-CR-197938| p 1609 N95-23669

NUCLEAR BINDING ENERGY
Strong-coupling polaron effect in quantum dots
|DE94-628485| p 1850 N95-23049
Surface structural dependence of cesium adsorption on the (alpha)-Al2O3(0001) surface
|DE95-002610| p 1842 N95-23135
Thermochemistry of transition metal clusters
|DE95-003144| p 1646 N95-24144

NUCLEAR DEFORMATION
Geometrical interpretation for the outer SU(3) outer multiplicity label p 1814 N95-22968

NUCLEAR ELECTRIC POWER GENERATION
Review of uncertainty files and improved multigroup cross section files for FENDL
|DE94-628639| p 1830 N95-22757

NUCLEAR EMULSIONS
Dosimetric results on EURECA p 1872 N95-23800

NUCLEAR FUELS
EXTRA.M: A computing code system for analysis of the Purex process with mixer settlers for reprocessing
|DE94-785273| p 1635 N95-23476
New pellet production and acceleration technologies for high speed pellet injection system HIPEL in Large Helical Device
|NISF-326| p 1835 N95-23566

NUCLEAR FUSION
Ion rings for magnetic fusion
|DE94-017606| p 1832 N95-23120

NUCLEAR INTERACTIONS
(pi)N correlations at AGS
|DE95-002933| p 1801 N95-22656
Comparison of exact solution with Eikonal approximation for elastic heavy ion scattering
|NASA-TP-3498| p 1817 N95-22929
An algebraic cluster model based on the harmonic oscillator basis p 1814 N95-22971

NUCLEAR MAGNETIC RESONANCE
Cation disorder determined by MAS Al-27 NMR in high dose neutron irradiated spinel
|DE95-003681| p 1842 N95-23266
NMR study of nanophase Al/Al-oxide powder and consolidated composites
|DE95-004655| p 1843 N95-23586

NUCLEAR MEDICINE
Continuation of BNCT Research Program at NEMC and MIT
|DE94-016228| p 1748 N95-22875

NUCLEAR MODELS
Geometrical interpretation for the outer SU(3) outer multiplicity label p 1814 N95-22968
Shapes and stability of algebraic nuclear models
p 1814 N95-22974

NUCLEAR PARTICLES
Second International Workshop on Harmonic Oscillators
|NASA-CP-3286| p 1820 N95-22957
Measurement of trapped proton fluences in main stack of P0006 experiment p 1815 N95-23812
Contribution of proton-induced short range secondaries to the LET spectra on LDEF p 1815 N95-23813
Charge, energy and LET spectra of high LET primary and secondary particles in CR-39 plastic nuclear track detectors of the P0006 experiment
p 1815 N95-23814

NUCLEAR PHYSICS
Neutrino overview
|DE95-003201| p 1802 N95-22729
Outlook from the intersections
|DE95-003202| p 1802 N95-22730
Exotic atoms
|DE95-003199| p 1805 N95-22881
Galactic oscillator symmetry p 1822 N95-22973
Heavy quark physics at SLD: Preliminary results
|DE95-003372| p 1806 N95-23138
The impact of QCD and light-cone quantum mechanics on nuclear physics
|DE95-004293| p 1851 N95-23352
Online Nuclear Data Service
|DE94-634268| p 1856 N95-23452
Index of nuclear data libraries available from the IAEA nuclear data section
|DE94-634271| p 1857 N95-23453
BROND-2.1. Russian evaluated neutron reaction data library
|DE94-634417| p 1810 N95-23458

NUCLEAR REACTIONS
Harmonic oscillator representation in the theory of scattering and nuclear reactions p 1814 N95-22967
BROND-2.1. Russian evaluated neutron reaction data library
|DE94-634417| p 1810 N95-23458
Pauli-blocking effects in neutron-alpha reactions
|DE94-016358| p 1813 N95-24046

NUCLEAR REACTORS
Closing the circle on the splitting of the atom: The environmental legacy of nuclear weapons production in the United States and what the Department of Energy is doing about it p 1818 N95-23562

NUCLEAR RESEARCH
Review of uncertainty files and improved multigroup cross section files for FENDL
|DE94-628639| p 1830 N95-22757

NUCLEAR SCATTERING
Harmonic oscillator representation in the theory of scattering and nuclear reactions p 1814 N95-22967

NUCLEAR STRUCTURE
The impact of QCD and light-cone quantum mechanics on nuclear physics
|DE95-004293| p 1851 N95-23352

NUCLEAR WARHEADS
Closing the circle on the splitting of the atom: The environmental legacy of nuclear weapons production in the United States and what the Department of Energy is doing about it p 1818 N95-23562

NUCLEAR WEAPONS
Closing the circle on the splitting of the atom: The environmental legacy of nuclear weapons production in the United States and what the Department of Energy is doing about it p 1818 N95-23562

NUCLEATION
Origins of interstellar and solar system: Carbonaceous materials
|NASA-CR-197436| p 1867 N95-23013

NUCLEI (NUCLEAR PHYSICS)
A heavy ion linac complex for unstable nuclei
|DE94-765443| p 1816 N95-22848
An algebraic cluster model based on the harmonic oscillator basis p 1814 N95-22971
Harmonic oscillator in quantum rotational spectra: Molecules and nuclei p 1814 N95-22972

NUCLEIC ACIDS
General crystal in prebiotic context
|DE94-628475| p 1840 N95-22774

NUCLEON-NUCLEON INTERACTIONS
Pauli-blocking effects in neutron-alpha reactions
|DE94-016358| p 1813 N95-24046

NUCLEONS
Dimuon production in proton-nucleus interactions
|DE95-002613| p 1801 N95-22551
Theoretical aspects of electroweak and other interactions in medium energy nuclear physics
|DE95-004341| p 1808 N95-23357
Electromagnetic production of pions on the nucleon
|DE95-004658| p 1811 N95-23587
Pauli-blocking effects in neutron-alpha reactions
|DE94-016358| p 1813 N95-24046

NUMBER THEORY
Lectures on Fermat's last theorem
|DE94-628392| p 1795 N95-22617

NUMERICAL ANALYSIS
A worst-case example using linesearch methods for numerical optimization with inexact gradient evaluations
|DE95-002917| p 1754 N95-22570
Gas cooled leads. Part 1: Theoretical Study. Part 2: Frost free lead optimized for a specific current. Part 3: Frost free lead optimized for a large current range
|DE95-002657| p 1660 N95-22716
Net energy analysis: Powerful tool for selecting electric power options
|DE95-002516| p 1728 N95-23133
Stoermer-Cowell: Straight, summed and split. An overview
|PB95-139341| p 1789 N95-23200
Orders of predictor-corrector pairs for second-order ODE's
|PB95-140612| p 1790 N95-23237
Institute for Computational Mechanics in Propulsion (ICOMP)
|NASA-TM-106884| p 1677 N95-23464
Note on the tau-value and tau-related solution concepts
|PB95-140752| p 1795 N95-23555
Spray combustion experiments and numerical predictions p 1637 N95-23643

NUMERICAL CONTROL
Material characterization system
|AD-D016536| p 1800 N95-23073
Progress report on a fully automatic Gas Tungsten Arc Welding (GTAW) system development
|DE95-004397| p 1695 N95-23343
A microcontroller-based three degree-of-freedom manipulator testbed
|NASA-CR-197423| p 1696 N95-23409

NUMERICAL INTEGRATION
Stability and efficiency of waveform relaxation methods
|PB95-138863| p 1789 N95-23173
Numerical simulation of axisymmetric viscous sintering
|PB95-138889| p 1667 N95-23175
Stoermer-Cowell: Straight, summed and split. An overview
|PB95-139341| p 1789 N95-23200
A multi-region radial integration scheme
|NASA-CR-197982| p 1809 N95-23408

NUMERICAL STABILITY
Stability and efficiency of waveform relaxation methods
|PB95-138863| p 1789 N95-23173

O

O STARS
A study of EUV emission from the O4f star Zeta Puppis
|NASA-CR-197350| p 1871 N95-23472

OBJECT-ORIENTED PROGRAMMING
Roles and dynamic subclasses: A modal logic approach
|PB95-127320| p 1754 N95-22522
Method for building and evaluating formal specifications of object-oriented conceptual models of database systems
|PB95-127353| p 1855 N95-22525
Comparing data synchronization in Ada 9X and Orca
|PB95-127999| p 1754 N95-22529
A certainty grid to object boundary algorithm
|PB94-203510| p 1755 N95-22637

LCM 3.0: A language for describing conceptual models. Syntax definition
| PB95-128005 | p 1755 N95-22652
Utilizing inheritance in requirements engineering
p 1768 N95-23677
AMPHION: Specification-based programming for scientific subroutine libraries p 1761 N95-23680
Learning time series for intelligent monitoring
p 1770 N95-23686

OBLIQUE SHOCK WAVES
Supersonic flow and shock formation in turbine tip gaps p 1672 N95-23429

OCCURRENCES
Seismic hazards at Kilauea and Mauna Loa volcanoes, Hawaii
| DE94-012109 | p 1737 N95-22924

OCEAN COLOR SCANNER
SeaWiFS technical report series. Volume 25: Ocean optics protocols for SeaWiFS validation, revision 1
| NASA-TM-104566-VOL-25-REV- | p 1743 N95-22671

OCEAN CURRENTS
A numerical study of interannual wind forcing effects on the California current system, 1980-1983
| AD-A286023 | p 1743 N95-23074

OCEAN DATA ACQUISITIONS SYSTEMS
TOGA/COARE AMMR 1992 data processing
| NASA-CR-197289 | p 1736 N95-22867

OCEAN MODELS
Observation model and parameter partials for the JPL VLBI parameter estimation software MODEST, 19 94
| NASA-CR-197328 | p 1756 N95-22853
A numerical study of interannual wind forcing effects on the California current system, 1980-1983
| AD-A286023 | p 1743 N95-23074
Assimilation of altimeter data in a quasi-geostrophic model of the Gulf Stream system: A dynamical perspective
| NASA-CR-196313 | p 1744 N95-23766

OCEAN SURFACE
Assimilation of altimeter data in a quasi-geostrophic model of the Gulf Stream system: A dynamical perspective
| NASA-CR-196313 | p 1744 N95-23766
Measurement of ocean wave spectra using polarimetric AIRSAR data p 1715 N95-23953

OCEANOGRAPHY
SWIFT BOAT 1994: Using a fast chase boat to investigate offshore weather features in conjunction with WSR-88D observations
| PB94-195146 | p 1742 N95-22651
SeaWiFS technical report series. Volume 25: Ocean optics protocols for SeaWiFS validation, revision 1
| NASA-TM-104566-VOL-25-REV- | p 1743 N95-22671
Development of a multi-sensor in situ fiber optic fluorometer
| DE95-003105 | p 1819 N95-22780

OCEANS
Ocean observations with EOS/MODIS: Algorithm development and post launch studies
| NASA-CR-197894 | p 1718 N95-23473
Theoretical estimates of high frequency acoustic attenuation and backscattering from suspended sand particles in the ocean and in an estuary
| DSTO-TR-0078 | p 1743 N95-23667
AVIRIS calibration using the cloud-shadow method
p 1702 N95-23849

OFFGASSING
Offgassing test methodology for composite materials
p 1629 N95-23035

OHMIC DISSIPATION
The DIII-D divertor cryopump system: Design and operational experience
| DE95-003007 | p 1693 N95-22796

OIL EXPLORATION
Energy flux and hydrogeology of thermal anomalies in the Gulf of Mexico Basin - South Texas example
| DE95-003341 | p 1743 N95-22695

OILS
The influence of high-octane fuel blends on the performance of a two-stroke SI engine with knock-limited-compression ratio
| DE95-002902 | p 1692 N95-22556

OMEGA-MESONS
Once more about the omega approaches 3(pi) contact term
| DE94-633202 | p 1804 N95-22847

ON-LINE PROGRAMMING
Evaluating the effect of online data compression on the disk cache of a mass storage system
p 1862 N95-24138

ON-LINE SYSTEMS
An automated computer misuse detection system for UNICOS
| DE95-000929 | p 1762 N95-22680
Environmental Systems Management Analysis and Reporting Network (E-SMART)
| AD-A279766 | p 1732 N95-22856
On-line, adaptive state estimator for active noise control p 1784 N95-23308
Online Nuclear Data Service
| DE94-634268 | p 1856 N95-23452
Index of nuclear data libraries available from the IAEA nuclear data section
| DE94-634271 | p 1857 N95-23453
BROND-2.1. Russian evaluated neutron reaction data library
| DE94-634417 | p 1810 N95-23458
Building a COTS archive for satellite data
p 1861 N95-24132
Analysis of the request patterns to the NSSDC on-line archive p 1862 N95-24137
Evaluating the effect of online data compression on the disk cache of a mass storage system
p 1862 N95-24138

ONE DIMENSIONAL FLOW
Benchmark problems in computational aeroacoustics
p 1800 N95-23315
On the breakup of viscous liquid threads
| NASA-CR-195023 | p 1678 N95-23544

OPEN CHANNEL FLOW
Flow measuring structures
| PB95-127254 | p 1665 N95-22638

OPERATING COSTS
The associate principal astronomer telescope operations model p 1779 N95-23743
DOD budget: Selected categories of planned funding for fiscal years 1995-99. Report to Congressional requesters
| GAO/NSIAD-95-92 | p 1864 N95-24062

OPERATING SYSTEMS (COMPUTERS)
Integrating O/S models during conceptual design, part 1
| NASA-CR-197903 | p 1622 N95-23398
Integrating O/S models during conceptual design, part 2
| NASA-CR-197904 | p 1622 N95-23399

OPERATING TEMPERATURE
Advances in research for solid oxide fuel cells
| DE95-004590 | p 1730 N95-23582
VLPC characterization for the Dzero upgrade
| DE95-003742 | p 1818 N95-24084

OPERATIONS RESEARCH
STS-61 mission director's post-mission report
| NASA-TM-104803 | p 1617 N95-23262

OPERATORS (MATHEMATICS)
Spectral application of the theorem for the essential quasi-Fredholm spectrum
| DE94-628430 | p 1795 N95-22632
Iterative solutions of nonlinear equations with strongly accretive or strongly pseudocontractive maps
| DE94-628432 | p 1786 N95-22634
Determinants of elliptic pseudo-differential operators
| PB95-109062 | p 1786 N95-22711
A supersymmetric family of harmonic oscillators simulating H-bonds in DNA p 1748 N95-22963
A note on the angular Fourier transformation
p 1797 N95-22986
Oscillator-like coherent states for the Jaynes-Cummings Model p 1826 N95-23003
Slightly anharmonic systems in quantum optics
p 1826 N95-23004
Canonical typing and pi-conversion
| PB95-139218 | p 1788 N95-23130
Taxonomy of finite automata construction algorithms
| PB95-139234 | p 1758 N95-23606
Ishikawa iteration process for nonlinear Lipschitz strongly accretive mappings
| DE94-634284 | p 1792 N95-23658
Operator procedure verification with a rapidly reconfigurable simulator p 1618 N95-23679

OPERATORS (PERSONNEL)
Formalizing procedures for operations automation, operator training and spacecraft autonomy
p 1752 N95-23720

OPTICAL COMMUNICATION
Non-blocking crossbar permutation engine with constant routing latency
| NASA-CASE-NPO-18864-1-CU | p 1762 N95-22564

OPTICAL CONTROL
Stellar Interferometer Technology Experiment (SITE)
| NASA-CR-197856 | p 1827 N95-23089

OPTICAL CORRELATORS
Motion-sensitive optical correlator using a VanderLugt correlator
| NASA-CASE-NPO-18769-1-CU | p 1827 N95-23045

OPTICAL COUPLING
Calculated coupling efficiency between an elliptical-core optical fiber and a silicon oxynitride rib waveguide
| NASA-TM-106850 | p 1820 N95-22915

OPTICAL DISKS
Document image archive transfer from DOS to UNIX
p 1761 N95-24117
Optical storage media data integrity studies
p 1829 N95-24130

OPTICAL EQUIPMENT
The STAR EM calorimeter design and small prototype test results
| DE95-004592 | p 1689 N95-23583

OPTICAL FIBERS
Method for making fiber-optic bundle collimator assembly
| AD-D016491 | p 1819 N95-22492
Measurements and modeling of impurity source distributions from the Tore Supra outboard pump limiter
| DE95-003097 | p 1831 N95-22800
Optical fiber strain sensor with improved linearity range
| NASA-CASE-LAR-14857-1-SB | p 1819 N95-22807
A fiber-optic bundle and collimator assembly
| AD-D016500 | p 1820 N95-22864
Calculated coupling efficiency between an elliptical-core optical fiber and a silicon oxynitride rib waveguide
| NASA-TM-106850 | p 1820 N95-22915
Photoinduced Bragg grating formation in optical fibres as a consequence of convective instability
| DE94-628479 | p 1841 N95-23020

OPTICAL FILTERS
Transient radiation-induced absorption in materials for the DOI laser
| DE95-004549 | p 1828 N95-24161

OPTICAL MATERIALS
Advanced reflector materials for solar concentrators
| DE95-000248 | p 1726 N95-22547
A ruggedness evaluation of procedures for damage threshold testing optical materials
| NASA-TM-4639 | p 1840 N95-22803

OPTICAL MEASUREMENT
HAPEX-Sahel: Basic description of methods and data sets
| PB95-127262 | p 1701 N95-22639
EUV metrology of multilayer optics
| DE95-003036 | p 1819 N95-22723
Dynamic response tests of inertial and optical wind-tunnel model attitude measurement devices
| NASA-TM-109182 | p 1616 N95-23011
High Tc superconducting bolometric and nonbolometric infrared (IR) detectors
| NASA-CR-197868 | p 1827 N95-23224

OPTICAL MEASURING INSTRUMENTS
Development of a multi-sensor in situ fiber optic fluorometer
| DE95-003105 | p 1819 N95-22780
Electrochemical studies of perovskite mixed conductors
| DE95-003704 | p 1636 N95-23573

OPTICAL MEMORY (DATA STORAGE)
Fourth NASA Goddard Conference on Mass Storage Systems and Technologies
| NASA-CP-3295 | p 1857 N95-24108
Petabyte mass memory system using the Newell Opticel(TM) p 1753 N95-24119
Optical storage media data integrity studies
p 1829 N95-24130

OPTICAL PROPERTIES
SeaWiFS technical report series. Volume 25: Ocean optics protocols for SeaWiFS validation, revision 1
| NASA-TM-104566-VOL-25-REV- | p 1743 N95-22671
Two-photon absorption in an indirect-gap semiconductor quantum well systems 1. Interband transitions
| DE94-628879 | p 1849 N95-22760
Strongly interacting fermion systems
| DE95-003405 | p 1806 N95-23054
Use of spectral analogy to evaluate canopy reflectance sensitivity to leaf optical property p 1701 N95-23845
Measurements of the optical properties of thin films of silver and silver oxide p 1651 N95-23906

OPTICAL PUMPING
Photoinduced Bragg grating formation in optical fibres as a consequence of convective instability
| DE94-628479 | p 1841 N95-23020

OPTICAL RADAR
Combining optical and microwave remote sensing data of forest vegetation: MAC Europe 1991
| PB95-127312 | p 1717 N95-22538
Study of atmospheric parameters measurements using MM-wave radar in synergy with LITE-2
p 1741 N95-23278

OPTICAL THICKNESS
Estimation of aerosol optical depth and additional atmospheric parameters for the calculation of apparent reflectance from radiance measured by the Airborne Visible/Infrared Imaging Spectrometer
p 1704 N95-23863

OPTICAL WAVEGUIDES
Calculated coupling efficiency between an elliptical-core optical fiber and a silicon oxynitride rib waveguide
| NASA-TM-106850 | p 1820 N95-22915
OPTIMAL CONTROL
Development of an adaptive hp-version finite element method for computational optimal control
| NASA-CR-197898 | p 1766 N95-22831
Active control of panel vibrations induced by a boundary layer flow
| NASA-CR-197867 | p 1608 N95-23182
OPTIMIZATION
IRAS sky survey atlas: Explanatory supplement
| NASA-CR-197335 | p 1865 N95-22539
A worst-case example using linesearch methods for numerical optimization with inexact gradient evaluations
| DE95-002917 | p 1754 N95-22570
Direct adaptive performance optimization of subsonic transports: A periodic perturbation technique
| NASA-TM-4676 | p 1612 N95-22829
Realizing parallel reduction operation in Sisal 1.2
| DE94-017524 | p 1763 N95-22858
Realizing parallel reduction operations in Sisal 1.2
| DE94-017525 | p 1763 N95-22859
Integrated aerodynamic/dynamic/structural optimization of helicopter rotor blades using multilevel decomposition
| NASA-TP-3465 | p 1612 N95-22953
Geometrical interpretation for the outer SU(3) outer multiplicity label p 1814 N95-22968
Taxonomy of finite automata minimization algorithms
| PB95-139226 | p 1756 N95-23131
Aerodynamic design optimization with sensitivity analysis and computational fluid dynamics
| NASA-CR-197419 | p 1608 N95-23218
The data facility of the Airborne Visible/Infrared Imaging Spectrometer (AVIRIS) p 1707 N95-23877
Optimal band selection for dimensionality reduction of hyperspectral imagery p 1709 N95-23887
Logspace reducibility and self-reducibility: Models and equivalences
| TR-544 | p 1760 N95-24059
A 4 MW fast wave current drive upgrade for D3-D
| DE95-003741 | p 1837 N95-24083
OPTOELECTRONIC DEVICES
Low-cost packaging of high-performance optoelectronic components
| DE95-003645 | p 1827 N95-23449
OPTOGALVANIC SPECTROSCOPY
Optogalvanic monitoring of collisional transfer of laser excitation energy in a neon RF plasma
| DE95-003103 | p 1691 N95-22748
ORBITAL ASSEMBLY
Hey! What's Space Station Freedom?
| NASA-TM-110531 | p 1620 N95-22542
Truss structure tele-manipulation experiment using ETS-7 p 1623 N95-23726
Antenna-assembling mechanism test on ETS-7 p 1623 N95-23727
ORBITAL ELEMENTS
The orbital characteristics of debris particle rings as derived from IDE observations of multiple orbit intersections with LDEF p 1869 N95-23829
ORBITAL MANEUVERING VEHICLES
CFD analysis of spray combustion and radiation in OMV thrust chamber p 1637 N95-23645
ORBITAL RENDEZVOUS
Autonomous spacecraft executive and its application to rendezvous and docking p 1623 N95-23719
ORBITAL SERVICING
The next decade of space robotics p 1768 N95-23673
Commercialization of JPL Virtual Reality calibration and redundant manipulator control technologies p 1768 N95-23676
ASI's space automation and robotics programs: The second step p 1697 N95-23696
JPL space robotics: Present accomplishments and future thrusts p 1697 N95-23697
A US-Japan collaborative robotics research program p 1772 N95-23698
Dexterous Orbital Servicing System (DOSS) p 1752 N95-23723
ORBITS
Harmonic oscillators and resonance series generated by a periodic unstable classical orbit p 1825 N95-22999
ORDER-DISORDER TRANSFORMATIONS
Fermion-spin transformation to implement the charge-spin separation
| DE94-629035 | p 1800 N95-22495
Protein folding and protein metallocluster studies using synchrotron small angler x ray scattering
| DE95-003339 | p 1746 N95-22897
Computational modeling of properties
| NAS-CR-196544 | p 1841 N95-22907
KKR-CPA calculations of density of states and soft X ray emission from disordered Li-Mg alloys
| DE94-628882 | p 1640 N95-22934
High resolution microstructural analysis of zirconia eutectic interfaces
| DE95-003143 | p 1845 N95-24143
OREGON
Dynamics and pattern of a managed coniferous forest landscape in Oregon p 1720 N95-24104
ORGANIC COMPOUNDS
Development of novel separation techniques for biological samples in capillary electrophoresis
| DE95-001672 | p 1744 N95-22493
Turbidity of a near critical ionic fluid
| DE94-014916 | p 1633 N95-22869
Assessing the relative contribution of biogenic and fossil processes to visibility scattering aerosols found in remote areas: Near-term Organic Research Program
| DE95-003149 | p 1735 N95-24146
ORGANIC MATERIALS
Organic coating technology for the protection of aircraft against corrosion p 1644 N95-23513
Atomic oxygen interactions with protected organic materials on the Long Duration Exposure Facility (LDEF) p 1627 N95-23909
Organic matrix composite protective coatings for space applications p 1627 N95-23914
ORGANIC PEROXIDES
Atmospheric peroxides
| DE95-004435 | p 1733 N95-23362
ORGANIC SUPERCONDUCTORS
Surface impedance studies on the electrodynamical response of organic superconductors
| DE95-002986 | p 1660 N95-22593
ORGANIC WASTES (FUEL CONVERSION)
Review of research results for the photocatalytic oxidation of hazardous wastes in air
| DE95-004004 | p 1734 N95-23480
ORGANIZATIONS
Optimization of a centrifugal impeller design through CFD analysis p 1680 N95-23624
CFD parametric study of consortium impeller p 1680 N95-23626
ORGANOMETALLIC COMPOUNDS
The electronic structure of heavy element complexes
| DE95-003407 | p 1806 N95-23082
Organometallic chemistry of bimetallic compounds
| DE95-004436 | p 1634 N95-23345
ORIFICES
The influence of swirl brakes and a tip discharge orifice on the rotordynamic forces generated by discharge-to-suction leakage flows in shrouded centrifugal pumps p 1680 N95-23628
ORTHO HYDROGEN
Supported transition metal catalysts for para- to ortho-hydrogen conversion
| NASA-CR-197907 | p 1634 N95-23252
ORTHO PARA CONVERSION
Supported transition metal catalysts for para- to ortho-hydrogen conversion
| NASA-CR-197907 | p 1634 N95-23252
ORTHOGONAL FUNCTIONS
A Ramanujan-type measure for the Askey-Wilson polynomials p 1797 N95-22975
Kravchuk functions for the finite oscillator approximation p 1798 N95-23006
ORTHOGONALITY
Parallal Arnoldi method for the construction of a Krylov subspace basis: An application in magnetohydrodynamics
| PB95-135786 | p 1787 N95-22717
Tutorial on filtering, restoration, and state estimation
| TR-534 | p 1793 N95-24042
ORTHOPHOTOGRAPHY
Color orthophotography: To scan or not
| DE95-002749 | p 1689 N95-24069
Old-growth and mature forests near spotted owl nests in western Oregon p 1719 N95-24098
OSCILLATIONS
Neutrino oscillation experiments with atmospheric neutrinos
| DE95-002994 | p 1801 N95-22573
On oscillations of higher order neutral differential equations
| DE94-628421 | p 1786 N95-22629
Self-generating oscillating pressure exercise device
| NASA-CASE-ARC-12000-1 | p 1751 N95-23264
Fast potential change in sawteeth in JIPP T-IIU tokamak plasmas
| NIFS-327 | p 1835 N95-23533
Long-baseline neutrino oscillation experiments
| DE95-004636 | p 1870 N95-23584
OSCILLATORS
Capacitive acoustic wave detector and method of using same
| NASA-CASE-LAR-13890-1 | p 1799 N95-22921
Exact, E = 0, classical and quantum solutions for general power-law oscillators p 1820 N95-22959
Non-Noetherian symmetries for oscillators in classical mechanics and in field theory p 1823 N95-22977
Covariant deformed oscillator algebras p 1797 N95-22978
Neurodynamic oscillators p 1749 N95-22987
Lyapunov exponents from CHUA's circuit time series using artificial neural networks p 1784 N95-22988
The relativistic many body problem with an oscillator interaction p 1824 N95-22991
Covariant harmonic oscillators and coupled harmonic oscillators p 1825 N95-22992
On pseudosupersymmetric oscillators and reality of relativistic energies for vector mesons p 1815 N95-22994
On parasupersymmetric oscillators and relativistic vector mesons in constant magnetic fields p 1815 N95-22995
Pseudoclassical description of the Dirac Oscillator p 1825 N95-22996
Notes on oscillator-like interactions of various spin relativistic particles p 1815 N95-22997
The Duffin-Kemmer-Petiau oscillator p 1825 N95-22998
Supersymmetric oscillator in optics p 1826 N95-23002
OSTWALD RIPENING
The effect of elastic stress on Ostwald Ripening Phenomena
| DE95-002599 | p 1646 N95-24140
OUTGASSING
Thermal outgassing studies on machinable tungsten and TZM molybdenum alloy
| DE95-002984 | p 1638 N95-22592
Society of the plastic industry process emission initiatives p 1629 N95-23036
Outgassing considerations for composites in space applications p 1629 N95-23037
LDEF environment modeling updates p 1637 N95-23797
Outgassing products from orbiter TPS materials p 1637 N95-23798
Effect of the space environment on materials flown on the EURECA/TICCE-HVI experiment p 1623 N95-23803
Further investigations of experiment A0034 atomic oxygen stimulated outgassing p 1651 N95-23908
OUTLET FLOW
Three-dimensional viscous flow analysis inside a turbine volute p 1674 N95-23437
OXIDATION
Evolution of oxidation and creep damage mechanisms in HIPed silicon nitride materials
| DE95-001360 | p 1647 N95-22689
On the formation of iron(3) oxides via oxidation of iron(2)
| DE94-018392 | p 1632 N95-22857
Analytical Boltzmann moments for electrons in N2-O2-H2O gas mixtures
| DE95-003474 | p 1732 N95-22898
Dimethylsulfide oxidation over the tropical South Atlantic: OH and other oxidants
| NASA-CR-197417 | p 1732 N95-22930
Ethylene oxidation chemistry in a well-stirred reactor
| DE95-004823 | p 1635 N95-23381
Oxidants and oxidation in the Earth's atmosphere
| NASA-CR-197945 | p 1734 N95-23460
Multi-fuel reformers for fuel cells used in transportation. Phase 1: Multi-fuel reformers
| DE95-004215 | p 1729 N95-23482
Carbon monoxide oxidation over three different states of copper: Development of a model metal oxide catalyst
| DE95-004682 | p 1636 N95-23495
NMR study of nanophase Al/Al-oxide powder and consolidated composites
| DE95-004655 | p 1843 N95-23586
The surface properties of fluorinated polyimides exposed to VUV and atomic oxygen p 1651 N95-23904
Collection and review of metals data obtained from LDEF experiment specimens and support hardware p 1646 N95-23905
Solderability preservation through the use of organic inhibitors
| DE95-003633 | p 1664 N95-24149
OXIDE FILMS
Vapor deposition of thin-film Y-doped ZrO2 for electrochemical device applications
| DE95-003705 | p 1649 N95-23268
OXIDES
Support research for solid oxide fuel cells
| DE95-002910 | p 1726 N95-22568
Glass science tutorial: Lecture 1, Chemistry and properties of oxide glasses
| DE95-002963 | p 1647 N95-22647

Reflectivity studies on adsorbed block copolymers under shear
[DE95-003676] p 1649 N95-23568

Advances in research for solid oxide fuel cells
[DE95-004590] p 1730 N95-23582

OXIDIZERS

Navier-Stokes analysis of an oxidizer turbine blade with tip clearance with and without a mini-shroud
p 1672 N95-23428

Finite-difference solutions of the alternate turbopump development high-pressure oxidizer turbopump pump-end ball-bearing cavity flows p 1678 N95-23617

Three-D flow analysis of the alternate SSME HPOT TAD p 1679 N95-23620

OXYGEN

Evolution of oxidation and creep damage mechanisms in HIPed silicon nitride materials
[DE95-001360] p 1647 N95-22689

Analytical Boltzmann moments for electrons in N2-O2-H2O gas mixtures
[DE95-003474] p 1732 N95-22898

Oxygen enriched combustion system performance study. Phase 2: 100 percent oxygen enriched combustion in regenerative glass melters
[DE95-004212] p 1635 N95-23481

Navier-Stokes flow field analysis of compressible flow in a pressure relief valve p 1679 N95-23618

OXYGEN ATOMS

Atomic oxygen durability evaluation of protected polymers using thermal energy plasma systems
[NASA-TM-106855] p 1626 N95-23270

Performance characterization of EURECA retroreflectors with fluoropolymer-filled SiO(x) protective coatings p 1651 N95-23802

Summary and review of Materials Special Investigation Group evaluations of hardware from the Long Duration Exposure Facility p 1638 N95-23897

The surface properties of fluorinated polyimides exposed to VUV and atomic oxygen p 1651 N95-23904

Measurements of the optical properties of thin films of silver and silver oxide p 1651 N95-23906

Further investigations of experiment A0034 atomic oxygen stimulated outgassing p 1651 N95-23908

Atomic oxygen interactions with protected organic materials on the Long Duration Exposure Facility (LDEF) p 1627 N95-23909

Atomic oxygen textured polymers
[NASA-TM-106769] p 1650 N95-24187

OXYGEN IONS

Symmetry breaking in O4(+): An application of the Brueckner coupled-cluster method
[NASA-CR-197981] p 1810 N95-23459

Photoionization of O(6+) below the n=3 threshold of the reduced ion
[DE94-634436] p 1844 N95-23774

OXYGEN PLASMA

Atomic oxygen durability evaluation of protected polymers using thermal energy plasma systems
[NASA-TM-106855] p 1626 N95-23270

Atomic oxygen textured polymers
[NASA-TM-106769] p 1650 N95-24187

OXYGEN SUPPLY EQUIPMENT

Oxygen enriched combustion system performance study. Phase 2: 100 percent oxygen enriched combustion in regenerative glass melters
[DE95-004212] p 1635 N95-23481

OZONE

Compendium of NASA data base for the Global Tropospheric Experiment's Pacific Exploratory Mission West-A (PEM West-A)
[NASA-TM-109177] p 1733 N95-23009

Oxidants and oxidation in the Earth's atmosphere
[NASA-CR-197945] p 1734 N95-23460

The atmosphere below
[NASA-TM-110538] p 1740 N95-23663

Laboratory studies of the sensitivity of tropospheric ozone to the chemistry of sea salt aerosol
[DE95-003607] p 1735 N95-24147

OZONE DEPLETION

The Atmospheric Lifetime Experiment and the Global Atmospheric Gas Experiment (ALE/GAGE)
[NASA-CR-197400] p 1731 N95-22673

The atmosphere below
[NASA-TM-110538] p 1740 N95-23663

OZONOSPHERE

The Atmospheric Lifetime Experiment and the Global Atmospheric Gas Experiment (ALE/GAGE)
[NASA-CR-197400] p 1731 N95-22673

The atmosphere below
[NASA-TM-110538] p 1740 N95-23663

P

P-I-N JUNCTIONS

Research on defects and transport in amorphous-silicon-based semiconductors
[DE94-011888] p 1660 N95-22586

P-TYPE SEMICONDUCTORS

Annealing of nitrogen-doped ZnSe at high pressures: Toward suppression of native defect formation
[DE95-003420] p 1844 N95-24010

PACIFIC OCEAN

Oceanic operations: An authoritative guide to oceanic operations
[FAA-AFS-550] p 1610 N95-24065

PACKAGING

Radioisotope thermoelectric generator licensed hardware package and certification tests
[DE95-003039] p 1661 N95-22799

Low-cost packaging of high-performance optoelectronic components
[DE95-003645] p 1827 N95-23449

High-performance GaAs/AlGaAs optical modulators: Their performance and packaging for microwave photonic integrated circuits
[DE95-004533] p 1828 N95-23575

Micro heat spreader enhanced heat transfer in MCM's
[DE95-004520] p 1663 N95-23779

PACKET SWITCHING

Non-blocking crossbar permutation engine with constant routing latency
[NASA-CASE-NPO-18864-1-CU] p 1762 N95-22564

PACKET TRANSMISSION

Non-blocking crossbar permutation engine with constant routing latency
[NASA-CASE-NPO-18864-1-CU] p 1762 N95-22564

Geolocation applications of the Gonets LEO messaging satellites p 1656 N95-22818

PACKETS (COMMUNICATION)

Non-blocking crossbar permutation engine with constant routing latency
[NASA-CASE-NPO-18864-1-CU] p 1762 N95-22564

PAINTS

Low Earth orbit thermal control coatings exposure flight tests: A comparison of U.S. and Russian results
[NASA-CR-4647] p 1626 N95-22919

Method development for compensating temperature effects in pressure sensitive paint measurements p 1650 N95-23291

Progress report on conductive paints, September 1, 1994-November 30, 1994
[DE95-004297] p 1649 N95-23356

PAIR PRODUCTION

Dimuon production in proton-nucleus interactions
[DE95-002613] p 1801 N95-22551

QCD test in three-jet Z(sup 0) decays at SLD and detector development for H(sup 0) yields gamma gamma searches in high energy hadron colliders
[DE95-003336] p 1848 N95-22698

Search for second generation leptoquarks at CDF
[DE94-018983] p 1805 N95-22939

Final result on the mass of the tau lepton from the BES collaboration
[DE95-003466] p 1806 N95-23139

Search for top quark at CDF
[DE95-003748] p 1809 N95-23406

Search for scalar and vector leptoquarks in electron-proton collisions at radical S = 300 GeV
[DE94-785267] p 1810 N95-23475

Search for supersymmetric (tilde W)(sub 1) and (tilde Z)(sub 2) states using the D0 detector
[DE95-004581] p 1811 N95-23581

PANEL METHOD (FLUID DYNAMICS)

Accelerated panel methods using the fast multipole method p 1687 N95-23307

PANELS

Active control of panel vibrations induced by a boundary layer flow
[NASA-CR-197867] p 1608 N95-23182

Residual strength of thin panels with cracks p 1700 N95-23311

PARA HYDROGEN

Supported transition metal catalysts for para- to ortho-hydrogen conversion
[NASA-CR-197907] p 1634 N95-23252

PARALLEL COMPUTERS

Evaluation of a Multiple Instruction/Multiple Data (MIMD) parallel computer for CFD applications
[AD-A285796] p 1762 N95-22509

Block LU factorization
[NASA-CR-197949] p 1791 N95-23592

Scalable, extensible, and portable numerical libraries
[DE95-004643] p 1765 N95-24172

PARALLEL FLOW

Experimental technique and assessment for measuring the convective heat transfer coefficient from natural ice accretions
[NASA-TM-106864] p 1668 N95-23248

PARALLEL PLATES

Capacitive acoustic wave detector and method of using same
[NASA-CASE-LAR-13890-1] p 1799 N95-22921

Quantum field between moving mirrors: A three dimensional example p 1821 N95-22965

Monte Carlo simulation of rarefied nitrogen gases contained between parallel plates using the statistical inelastic cross-section model
[NAL-TR-1229T] p 1687 N95-24082

PARALLEL PROCESSING (COMPUTERS)

Partitioning methods for unstructured finite element meshes
[PB95-130555] p 1785 N95-22544

A parallel molecular dynamics simulation of crystal growth at a cluster of workstations
[DE94-628382] p 1839 N95-22615

Accepting the T3D
[DE95-000924] p 1762 N95-22679

Software for the generalized eigenproblem on distributed memory architectures
[DE95-002999] p 1755 N95-22690

Realizing parallel reduction operation in Sisal 1.2
[DE94-017524] p 1763 N95-22858

Realizing parallel reduction operations in Sisal 1.2
[DE94-017525] p 1763 N95-22859

Algorithms for parallel and vector computations
[NASA-CR-197394] p 1756 N95-23017

Overview of Ph.D. theses and memoranda, 1993
[PB95-135190] p 1756 N95-23071

A draft standard for message passing in a distributed memory environment
[DE94-019159] p 1657 N95-23075

High-performance parallel analysis of coupled problems for aircraft propulsion
[NASA-CR-197440] p 1614 N95-23088

Distributed VIRtual System (DIVIRS) project
[NASA-CR-197855] p 1757 N95-23180

Two portable parallel tridiagonal solvers
[DE94-019044] p 1763 N95-23243

Task scheduling in dataflow computer architectures p 1753 N95-23301

MPI implementation of CFD program PHOENICS
[DE95-003896] p 1668 N95-23372

Parallel computation of automatic differentiation applied to magnetic field calculations
[DE95-004689] p 1763 N95-23486

Towards the Teraflop CFD
[NASA-CR-197947] p 1764 N95-23594

WHAMS3D Project: Parallel implementations of WHAMS3D on two shared-memory multiprocessors
[CSRD-1248] p 1764 N95-23599

Microarchitecture support for dynamic scheduling of acyclic task graphs
[CSRD-1207] p 1791 N95-23600

Unstructured grids on SIMD torus machines
[NASA-CR-197954] p 1758 N95-23610

Very fast motion planning for highly dexterous-articulated robots p 1771 N95-23691

Algorithms for categorizing multiprocessor communication under invalidate and update-based coherence protocols
[TR-533-REV] p 1759 N95-23928

Loop scheduling for heterogeneity
[TR-540] p 1764 N95-23936

Unifying data and control transformations for distributed shared-memory machines
[TR-542] p 1765 N95-24061

A distributed parallel storage architecture and its potential application within EOSDIS p 1858 N95-24111

Client/Server data serving for high performance computing p 1761 N95-24123

Scalable, extensible, and portable numerical libraries
[DE95-004643] p 1765 N95-24172

PARALLEL PROGRAMMING

Comparing data synchronization in Ada 9X and Orca
[PB95-127999] p 1754 N95-22529

Realizing parallel reduction operation in Sisal 1.2
[DE94-017524] p 1763 N95-22858

Realizing parallel reduction operations in Sisal 1.2
[DE94-017525] p 1763 N95-22859

DUALITY: A simple formalism for the analysis of UNITY
[PB95-135703] p 1763 N95-23166

Loop scheduling for heterogeneity
[TR-540] p 1764 N95-23936

Unifying data and control transformations for distributed shared-memory machines
[TR-542] p 1765 N95-24061

Scalable, extensible, and portable numerical libraries
|DE95-004643| p 1765 N95-24172
PARTIAL DIFFERENTIAL EQUATIONS
Existence of solutions for some superlinear or sublinear elliptic systems on R(sup N)
|DE94-628417| p 1785 N95-22625
Nonlinear generalized functions and nonconservative shock simulations
|DE95-003307| p 1795 N95-22734
Level set techniques applied to unsteady detonation propagation
|DE95-002741| p 1666 N95-22901
Time-periodic solutions of some forced nonlinear wave equations: Analysis, approximations and applications
|PB95-135083| p 1788 N95-22932
VLUGR2: A vectorizable adaptive grid solver for PDes in 2D
|PB95-136008| p 1789 N95-23167
Stability and efficiency of waveform relaxation methods
|PB95-138863| p 1789 N95-23173
Fourth order difference methods for hyperbolic IBVP's
|NASA-CR-197955| p 1791 N95-23548
PARTICLE ACCELERATION
Interdigital-H linac for unstable nuclei at INS
|DE94-765448| p 1816 N95-22644
Introduction to the physics of Higgs bosons
|DE95-003965| p 1809 N95-23396
PARTICLE ACCELERATORS
A report on the Indiana University Workshop on future U.S. hadron facilities
|DE95-003951| p 1817 N95-23353
D(O) upgrade muon electronics design
|DE95-003744| p 1817 N95-23369
PARTICLE BEAMS
Interdigital-H linac for unstable nuclei at INS
|DE94-765448| p 1816 N95-22644
PARTICLE COLLISIONS
Search for second generation leptoquarks at CDF
|DE94-018983| p 1805 N95-22939
Final result on the mass of the tau lepton from the BES collaboration
|DE95-003466| p 1806 N95-23139
Measurement of the left-right charge asymmetry in hadronic Z decays and A(sub e) determination
|DE95-003467| p 1806 N95-23140
Measuring the left-right cross section asymmetry in Z boson production by e(+)e(-) collisions at the SLC
|DE95-003468| p 1807 N95-23141
Testing QCD with jet physics at CDF
|DE94-018980| p 1807 N95-23196
Properties of jets in Z events from 1.8 TeV (bar p)p collisions
|DE94-018982| p 1808 N95-23197
Search for Z' and W' at CDF
|DE94-018987| p 1808 N95-23203
J/psi, psi' yields mu(+)mu(-) and B yields J/psi, psi' cross sections
|DE94-018996| p 1808 N95-23242
D(O) upgrade muon electronics design
|DE95-003744| p 1817 N95-23369
Introduction to the physics of Higgs bosons
|DE95-003965| p 1809 N95-23396
Search for scalar and vector leptoquarks in electron-proton collisions at radical S = 300 GeV
|DE94-785267| p 1810 N95-23475
Measurement of W and Z boson production and extraction of the W width and branching ratios at CDF
|DE94-018989| p 1810 N95-23522
Inclusive rapidity correlations of (pi)(-) mesons in pp-interactions
|DE94-635654| p 1812 N95-23974
PARTICLE DECAY
Limit on the muon neutrino mass from K(exp 0)muon 3 decay spectra
|DE95-000816| p 1801 N95-22583
The first measurement of the left-right cross section asymmetry in Z(sup 0) boson production
|DE95-003335| p 1802 N95-22697
The charm physics potential of a Tau-Charm Factory
|DE95-003369| p 1802 N95-22703
QCD improved exclusive rare B-decays at the heavy b-quark limit
|DE94-628609| p 1802 N95-22720
Chiral anomalies in non-leptonic decays within chiral perturbation theory at the quark level
|DE94-628613| p 1849 N95-22753
On the D yields K-bar(sup *)e(sup +)(nu)(sub e) form factors
|DE94-628614| p 1803 N95-22754
To the problem of D-meson leptonic and semileptonic decays
|DE94-628615| p 1803 N95-22755
The decays of D(sup *)-mesons
|DE94-628610| p 1804 N95-22810
(pi)- and a(sub 1)-meson physics in current algebra at the quark level
|DE94-628611| p 1804 N95-22811
The omega pi(sup 0)-transient form factor within effective chiral Lagrangian approach
|DE94-628612| p 1850 N95-22812
Once more about the omega approaches 3(pi) contact term
|DE94-633202| p 1804 N95-22847
Heavy quark physics at SLD: Preliminary results
|DE95-003372| p 1806 N95-23138
Measurement of the left-right charge asymmetry in hadronic Z decays and A(sub e) determination
|DE95-003467| p 1806 N95-23140
High Energy Theory: Task B and Task L
|DE95-003453| p 1817 N95-23148
Flavour dependence of form factors in heavy meson decays
|PB95-139101| p 1807 N95-23156
Search for Z' and W' at CDF
|DE94-018987| p 1808 N95-23203
J/psi, psi' yields mu(+)mu(-) and B yields J/psi, psi' cross sections
|DE94-018996| p 1808 N95-23242
Measurement of correlated b quark cross sections at CDF
|DE95-004240| p 1808 N95-23336
Recent results from Fermilab E-687, charm particle decays, lifetimes and photoproduction dynamics: A compilation results presented at DPF 1994
|DE95-004580| p 1808 N95-23347
Search for new gauge bosons at D(O)
|DE95-003745| p 1809 N95-23404
New determination of V(sub us) from K(sub e3)(+) decay
|DE94-628616| p 1811 N95-23769
Charm-conserving strangeness-changing two body hadronic decays of charmed baryons
|DE94-628621| p 1811 N95-23770
Neutrinoless double beta decay and the solar neutrino problem
|DE94-628633| p 1812 N95-23785
W mass measurements from D(circle slash) and CDF experiments at TeVatron
|DE95-003497| p 1813 N95-24000
PARTICLE DIFFUSION
Surface growth of two kinds of particles deposition models
|DE94-628480| p 1841 N95-23021
PARTICLE ENERGY
Energetic particle observations at geosynchronous orbit
|DE95-000873| p 1867 N95-22516
Variational calculations for He-3 impurities on He-4 droplets
|DE94-628469| p 1840 N95-22839
Second order focusing property of 210 deg cylindrical energy analyzer
|NIFS-317| p 1834 N95-23527
Alpha spectral analysis via artificial neural networks
|DE95-004567| p 1767 N95-23578
PARTICLE IMAGE VELOCIMETRY
Direct numerical simulations and modeling of a spatially-evolving turbulent wake p 1687 N95-23289
PARTICLE INTERACTIONS
Chiral symmetry breaking in QCD with linearly rising confinement potential
|DE94-628559| p 1848 N95-22744
Spontaneous breaking of chiral symmetry as a consequence of confinement
|DE94-628560| p 1849 N95-22745
Inclusive rapidity correlations of (pi)(-) mesons in pp-interactions
|DE94-635654| p 1812 N95-23974
Lattice relaxation study on self-trapped exciton and biexciton in neutral and charged fullerenes
|DE94-635788| p 1844 N95-23986
PARTICLE MASS
Limit on the muon neutrino mass from K(exp 0)muon 3 decay spectra
|DE95-000816| p 1801 N95-22583
Final result on the mass of the tau lepton from the BES collaboration
|DE95-003466| p 1806 N95-23139
Introduction to the physics of Higgs bosons
|DE95-003965| p 1809 N95-23396
Search for new gauge bosons at D(O)
|DE95-003745| p 1809 N95-23404
Electroweak physics from the Tevatron
|DE95-002213| p 1810 N95-23530
Neutrino masses and mixing
|DE94-628632| p 1812 N95-23784
Neutrinoless double beta decay and the solar neutrino problem
|DE94-628633| p 1812 N95-23785
Neutrino mass
|DE94-628634| p 1812 N95-23786
Enhanced oscillation of neutrinos of different masses in matter
|DE94-635648| p 1812 N95-23973
W mass measurements from D(circle slash) and CDF experiments at TeVatron
|DE95-003497| p 1813 N95-24000
A measurement of the mass of the W vector boson at CDF
|DE95-003498| p 1813 N95-24016
PARTICLE MOTION
Photon and electron interaction databases and their use in medical applications
|DE94-015558| p 1855 N95-22871
Design study of longitudinal dynamics of the drive beam in 1 TeV relativistic klystron two-beam accelerator
|DE95-004683| p 1817 N95-23485
A generalized Eulerian-Lagrangian analysis, with application to liquid flows with vapor bubbles p 1682 N95-23633
PARTICLE PRECIPITATION
Diffusion behavior of lysozyme in aqueous ammonium sulfate solutions under varying solution conditions as determined by dynamic light scattering
|DE95-004821| p 1635 N95-23380
PARTICLE PRODUCTION
New preliminary results on the physics of charm hadroproduction subprocesses
|DE95-002530| p 1801 N95-22646
(pi)N correlations at AGS
|DE95-002933| p 1801 N95-22656
Perturbative QCD tests from the LEP, HERA, and TEVATRON colliders
|DE95-001285| p 1816 N95-22684
Bottom-quark production from muon-jet and dimuon events in p(bar p)-interactions at the square root of s = 1.8 TeV
|DE95-001286| p 1801 N95-22685
The first measurement of the left-right cross section asymmetry in Z(sup 0) boson production
|DE95-003335| p 1802 N95-22697
Measurement of the left-right asymmetry in Z boson production by electron-positron collisions
|DE95-003337| p 1802 N95-22699
Searches for the H-dibaryon at the AGS
|DE95-003091| p 1802 N95-22727
Status of helium-production reaction studies with a spallation neutron source
|DE95-002816| p 1806 N95-23137
Measuring the left-right cross section asymmetry in Z boson production by e(+)e(-) collisions at the SLC
|DE95-003468| p 1807 N95-23141
Electroweak coupling measurements from polarized Bhabha scattering at SLD
|DE95-003137| p 1807 N95-23165
Properties of jets in Z events from 1.8 TeV (bar p)p collisions
|DE94-018982| p 1808 N95-23197
Measurement of correlated b quark cross sections at CDF
|DE95-004240| p 1808 N95-23336
Introduction to the physics of Higgs bosons
|DE95-003965| p 1809 N95-23396
Study of b(anti b) production in e(+)e(-) annihilation at radical s = 29 GeV with the aid of neural networks
|DE95-004691| p 1810 N95-23488
Measurement of W and Z boson production and extraction of the W width and branching ratios at CDF
|DE94-018989| p 1810 N95-23522
Independent production and Poisson distribution
|DE94-635632| p 1794 N95-23972
PARTICLE SPIN
Fermion-spin transformation to implement the charge-spin separation
|DE94-629035| p 1800 N95-22495
Experimental results on polarized structure functions in deep inelastic lepton-nucleon scattering
|DE95-002782| p 1801 N95-22521
Spin physics in the next decade
|DE95-003727| p 1809 N95-23403
Spinning particles in the Euclidean Taub-NUT space
|DE94-634320| p 1810 N95-23456
PARTICLE THEORY
The charm physics potential of a Tau-Charm Factory
|DE95-003369| p 1802 N95-22703
How to measure the Q(bar Q) potential in a light-front calculation
|DE95-003200| p 1848 N95-22728
Neutrino overview
|DE95-003201| p 1802 N95-22729
Outlook from the intersections
|DE95-003202| p 1802 N95-22730
Aspects of sigma models
|DE94-628511| p 1795 N95-22736

Problems in particle theory
| DE95-003106 | p 1803 N95-22749
Disorder-induced breakdown of soliton and polaron particles
| DE95-003694 | p 1808 N95-23267

PARTICLE TRACKS
Performance of a large scale scintillating fiber tracker using VLPC readout
| DE95-003746 | p 1871 N95-23370
Thermal effects on the STAR electromagnetic calorimeter
| DE95-004663 | p 1688 N95-23492
Absorbed dose and LET spectra measurements on LDEF p 1815 N95-23810
Measurement of trapped proton fluences in main stack of P0006 experiment p 1815 N95-23812
Charge, energy and LET spectra of high LET primary and secondary particles in CR-39 plastic nuclear track detectors of the P0006 experiment p 1815 N95-23814
VLPC characterization for the Dzero upgrade
| DE95-003742 | p 1818 N95-24084

PARTICLE TRAJECTORIES
Spinning particles in the Euclidean Taub-NUT space
| DE94-634320 | p 1810 N95-23456
A generalized Eulerian-Lagrangian analysis, with application to liquid flows with vapor bubbles p 1682 N95-23633
LDEF Interplanetary Dust Experiment (IDE) results p 1869 N95-23828
The orbital characteristics of debris particle rings as derived from IDE observations of multiple orbit intersections with LDEF p 1869 N95-23829
The effect of impact angle on craters formed by hypervelocity particles p 1700 N95-23839

PARTICLES
Particle size dependence in Fischer-Tropsch synthesis
| DE95-003124 | p 1633 N95-22876
Divertor heat and particle control experiments on the DIII-D tokamak
| DE94-017518 | p 1832 N95-23119

PARTICULATES
Novel mass spectrometric instrument for gaseous and particulate characterization and monitoring
| DE95-001135 | p 1687 N95-22682
Applied research on air pollution using nuclear-related analytical techniques
| DE94-633513 | p 1734 N95-23542
Advanced multi-phase flow CFD model development for solid rocket motor flowfield analysis p 1683 N95-23638
An interactive tool for discrete phase analysis in two-phase flows p 1683 N95-23641

PARTITIONS (MATHEMATICS)
Partitioning methods for unstructured finite element meshes
| PB95-130555 | p 1785 N95-22544
Classification of SU(3) modular invariants revisited
| PB95-110771 | p 1787 N95-22715

PARTONS
Dimuon production in proton-nucleus interactions
| DE95-002613 | p 1801 N95-22551

PASSENGERS
A multibody/finite element analysis approach for modeling of crash dynamic responses
| NIAR-94-3 | p 1610 N95-24050

PASSIVITY
In-situ detection of surface passivation or activation and of localized corrosion: Experiences and prospectives in aircraft p 1643 N95-23508
Silicon surface and bulk defect passivation by low temperature PECVD oxides and nitrides
| DE95-004531 | p 1731 N95-24090

PASTES
Sensor-based control of rocket thrust chamber feature location for automated braze paste dispensing
| DE94-016559 | p 1624 N95-22885

PATHOLOGICAL EFFECTS
All systems go!
| NASA-TM-110542 | p 1620 N95-23665

PATTERN RECOGNITION
An improved system for exon recognition and gene modeling in human DNA sequences
| DE94-017863 | p 1746 N95-22890
Locating buildings in aerial photos p 1721 N95-23295
Method and system for pattern analysis using a coarse-coded neural network
| NASA-CASE-ARC-11961-1 | p 1767 N95-23387
Toward an automated signature recognition toolkit for mission operations p 1659 N95-23682
Unsupervised classification learning from cross-modal environmental structure
| TR-536 | p 1784 N95-24040
Hierarchical analysis of spatial pattern and processes of Douglas-fir forests p 1719 N95-24099
Dynamics and pattern of a managed coniferous forest landscape in Oregon p 1720 N95-24104

PAYLOAD RETRIEVAL (STS)
Endeavor: Now and then
| NASA-TM-110539 | p 1620 N95-23664

PAYLOADS
Adaptive beamforming in a CDMA mobile satellite communications system p 1655 N95-22815
Toys in space, 2
| NASA-TM-110541 | p 1620 N95-23275
An operations and command systems for the extreme ultraviolet explorer p 1770 N95-23687
Aerodynamic flight control to increase payload capability of future launch vehicles
| NASA-CR-197704 | p 1619 N95-24032

PELLETS
New pellet production and acceleration technologies for high speed pellet injection system HIPEL in Large Helical Device
| NISF-326 | p 1835 N95-23566

PENETRATION
High-velocity penetrators
| DE95-001886 | p 1698 N95-22500
Rationale for the Modular Air-system Vulnerability Estimation Network (MAVEN) methodology
| AD-A285797 | p 1611 N95-22510
Projectile penetration into representative targets
| DE95-003089 | p 1698 N95-22726
Impact shock and penetration fragmentation in porous media
| DE94-018900 | p 1868 N95-23656
Small craters on the meteoroid and space debris impact experiment p 1623 N95-23825
Penetration rates over 30 years in the space age p 1624 N95-23827
Cratering and penetration experiments in Teflon targets at velocities from 1 to 7 km/s p 1700 N95-23842

PERCEPTION
Project: Internal communications p 1854 N95-23282

PERFORMANCE PREDICTION
HiRel: Hybrid Automated Reliability Predictor (HARP) integrated reliability tool system, (version 7.0). Volume 1: HARP introduction and user's guide
| NASA-TP-3452-VOL-1 | p 1754 N95-22603
Neural net prediction of tokamak plasma disruptions
| DE95-002616 | p 1832 N95-23136
An approximate theoretical method for modeling the static thrust performance of non-axisymmetric two-dimensional convergent-divergent nozzles
| NASA-CR-195050 | p 1608 N95-23193
Damage-mitigating control of a reusable rocket engine for high performance and extended life
| NASA-CR-4640 | p 1654 N95-23195
An RL10A-3-3A rocket engine model using the rocket engine transient simulator (ROCETS) software
| NASA-CR-190786 | p 1625 N95-23790
Predicted performance of an integrated modular engine system
| NASA-CR-190787 | p 1625 N95-23791
Design of a high-temperature superconductor current lead for electric utility SMES
| DE95-004604 | p 1664 N95-24163

PERFORMANCE TESTS
Design and demonstration of an immobilized-cell fluidized-bed reactor for the efficient production of ethanol
| DE94-014023 | p 1652 N95-22587
Accepting the T3D
| DE95-000924 | p 1762 N95-22679
Conversion of light hydrocarbon gases to metal carbides for production of liquid fuels and chemicals
| DE95-000362 | p 1634 N95-23164
NASA 30 cm ion thruster development status
| NASA TM-106842 | p 1624 N95-23221
Functional testing of the space station plasma contactor
| NASA-TM-106841 | p 1624 N95-23240
Performance of the 0.3-meter transonic cryogenic tunnel with air, nitrogen, and sulfur hexafluoride media under closed loop automatic control
| NASA-CR-195052 | p 1668 N95-23257
Verification and validation of decision support software: Expert Choice(trademark) and PCM(trademark)
| DE95-004469 | p 1757 N95-23346
Calorimetric measurement of energy of ultrasonic cleaners
| DE95-003938 | p 1800 N95-23375
Operation and tests of a DDC101 A/D
| DE95-003747 | p 1663 N95-23405
Remote sensor test range update
| DE95-003629 | p 1735 N95-24018
A high speed digitizing photomultiplier tube base for the KTeV CsI calorimeter
| DE95-003739 | p 1664 N95-24081
VLPC characterization for the Dzero upgrade
| DE95-003742 | p 1818 N95-24084
Experimental achievement of toroidal beta beyond that predicted by 'Troyon' scaling
| DE95-003880 | p 1837 N95-24087
Silicon surface and bulk defect passivation by low temperature PECVD oxides and nitrides
| DE95-004531 | p 1731 N95-24090
Report to the Secretary of Defense. Unmanned aerial vehicles: No more Hunter systems should be bought until problems are fixed
| GAO/NSIAD-95-52 | p 1613 N95-24091
Robotic tape library system level testing at NSA: Present and planned p 1858 N95-24112
Digital Linear Tape (DLT) technology and product family overview p 1753 N95-24125

PERIDOTITE
Mapping of the Ronda peridotite massif (Spain) from AVIRIS spectro-imaging survey: A first attempt p 1707 N95-23878

PERIODIC VARIATIONS
Static parametric fluctuations give nonstatistical behaviour in uncoupled chaotic systems
| DE94-628478 | p 1794 N95-23019
Telescope loading: A problem reduction approach p 1781 N95-23757

PERMANENT MAGNETS
Multipole contribution from an off-axis orbit in an IR quadrupole and the consequences on the dynamic aperture
| DE95-002874 | p 1816 N95-22567
Cu deposition using a permanent magnet electron cyclotron resonance microwave plasma source
| DE94-017768 | p 1650 N95-23981

PERMEABILITY
Permeability testing of composite material and adhesive bonds for the DC-XA composite feedline program
| NASA-TM-108483 | p 1630 N95-23551
High surface area, high permeability carbon monoliths
| DE95-004555 | p 1650 N95-23577

PERMUTATIONS
The chirality operators for Heisenberg spin systems
| DE94-629043 | p 1847 N95-22545
Non-blocking crossbar permutation engine with constant routing latency
| NASA-CASE-NPO-18864-1-CU | p 1762 N95-22564
Classification of SU(3) modular invariants revisited
| PB95-110771 | p 1787 N95-22715

PEROVSKITES
Electrochemical studies of perovskite mixed conductors
| DE95-003704 | p 1636 N95-23573

PEROXIDES
Measurement of HO2 and other trace gases in the stratosphere using a high resolution far-infrared spectrometer
| NASA-CR-197368 | p 1735 N95-22482

PERSONAL COMPUTERS
Novel mass spectrometric instrument for gaseous and particulate characterization and monitoring
| DE95-001135 | p 1687 N95-22682
Development of qualification guidelines for personal computer-based aviation training devices
| DOT/FAA/AM-95/6 | p 1758 N95-23603

PERSONNEL
Project: Internal communications p 1854 N95-23282
The software analysis project for the Office of Human Resources p 1854 N95-23331
Security clearances: Consideration of sexual orientation in the clearance process. Report to Congressional requesters
| GAO/NSIAD-95-21 | p 1853 N95-23588
Inspector General: Alleged misconduct by NASA Inspector General. Report to Congressional requesters
| GAO/OSI-95-9 | p 1854 N95-24085

PERSONNEL MANAGEMENT
Upward appraisal as a means for improving supervisory performance and promoting process improvement, with long-term implications for organizational change p 1854 N95-23323
The software analysis project for the Office of Human Resources p 1854 N95-23331

PERTURBATION
Direct adaptive performance optimization of subsonic transports: A periodic perturbation technique
| NASA-TM-4676 | p 1612 N95-22829
Partition of real symmetric matrices according to the multiplicities of their eigenvalues
| PB95-139846 | p 1790 N95-23235

PERTURBATION THEORY
Chiral anomalies in non-leptonic decays within chiral perturbation theory at the quark level
| DE94-628613 | p 1849 N95-22753

On the D yields K-bar(sup *)e(sup +)(nu)(sub e) form factors
[DE94-628614] p 1803 N95-22754
To the problem of D-meson leptonic and semileptonic decays
[DE94-628615] p 1803 N95-22755
(pi)- and a(sub 1)-meson physics in current algebra at the quark level
[DE94-628611] p 1804 N95-22811
Optimally scaled systems for second order scalar singularity perturbed problems
[PB95-138814] p 1789 N95-23169

PESTICIDES
Extraction and detection of pesticide residues from air filter inserts using supercritical carbon dioxide
[DE95-004579] p 1735 N95-23580

PETN
Simulation of cookoff results in a small scale test
[DSTO-TR-0090] p 1653 N95-23668

PETRI NETS
Browsing semantics in the tower model
[PB95-127221] p 1855 N95-22534
Automatic verification of regular protocols in P/T nets
[PB95-138921] p 1789 N95-23146
Discrete-time Markovian stochastic Petri nets
[NASA-CR-195039] p 1758 N95-23613

PHASE COHERENCE
Bose condensation, macroscopic quantum phenomena and atomic spatial correlations in superfluid He-4
[PB95-139085] p 1850 N95-23154

PHASE CONTRAST
Edge fluctuation measurements by phase contrast imaging on DIII-D
[DE94-016681] p 1836 N95-23768

PHASE DIAGRAMS
Asymptotically exact solution of a local copper-oxide model
[DE94-628492] p 1842 N95-23059

PHASE MODULATION
Wavelet time-frequency analysis of phase-shift-key modulated signals
[AD-A285791] p 1655 N95-22505

PHASE SEPARATION (MATERIALS)
Turbidity of a near critical ionic fluid
[DE94-014916] p 1633 N95-22869
Enhancement of biomembrane functions under phase-separated conditions: A self-organized criticality phenomenon?
[DE94-628489] p 1747 N95-23053
Microporous polyimide films for reduced dielectric applications
[DE95-004543] p 1650 N95-24159

PHASE SHIFT
Using AVIRIS for in-flight calibration of the spectral shifts of SPOT-HRV and of AVHRR? p 1710 N95-23893

PHASE SHIFT KEYING
Wavelet time-frequency analysis of phase-shift-key modulated signals
[AD-A285791] p 1655 N95-22505
Effects of modulation index on telecommunications
[AD-A286018] p 1657 N95-23023

PHASE STABILITY (MATERIALS)
Experimental and theoretical studies on the C15 intermetallic compounds MV2 (M = Zr, Hf and Ta): Elasticity and phase stability
[DE95-003723] p 1845 N95-24079

PHASE TRANSFORMATIONS
Sullivan model for wetting transition in closed system
[DE94-628472] p 1665 N95-22771
Generalized phase transformations of spinor fields
[DE94-628505] p 1656 N95-22841
Progress towards the synthesis of polymeric nitrogen
[DE94-017547] p 1841 N95-22860
Enhancement of biomembrane functions under phase-separated conditions: A self-organized criticality phenomenon?
[DE94-628489] p 1747 N95-23053
A model for the metal-nonmetal transition in metal-molten salt solutions
[DE94-628490] p 1640 N95-23057
The origin of chirality in protein amino acids
[DE94-628491] p 1747 N95-23058
Calculations of alloy phases with a direct Monte-Carlo method
[DE94-018963] p 1640 N95-23121
Dynamics of L to H bifurcation
[DE94-019126] p 1832 N95-23163
Experimental and theoretical studies on the C15 intermetallic compounds MV2 (M = Zr, Hf and Ta): Elasticity and phase stability
[DE95-003723] p 1845 N95-24079
Microporous polyimide films for reduced dielectric applications
[DE95-004543] p 1650 N95-24159

PHASED ARRAYS
Adaptive beamforming in a CDMA mobile satellite communications system p 1655 N95-22815

PHENOMENOLOGY
Higgs searches and WW scattering
[PB95-139143] p 1807 N95-23160

PHONEMES
Reevaluation of the significance of sequence information for speech recognition
[TR-555] p 1658 N95-23794

PHONETICS
Phonetic set hashing: A novel scheme for transforming phone sequences to words
[TR-538] p 1658 N95-24039

PHONONS
Magnetic field effects on strong-coupling polaron in quantum dots
[DE94-629038] p 1847 N95-22496
Optical absorption in an indirect-gap semiconductor quantum well systems
[DE94-628878] p 1849 N95-22759
Two-photon absorption in an indirect-gap semiconductor quantum well systems 1. Interband transitions
[DE94-628879] p 1849 N95-22760
Two-photon absorption in an indirect-gap semiconductor quantum well systems 2. Excitonic transitions
[DE94-628880] p 1849 N95-22761
Strong-coupling polaron effect in quantum dots
[DE94-628485] p 1850 N95-23049
Phonon characteristics of high (T sub c) superconductors from neutron Doppler broadening measurements
[DE95-003703] p 1844 N95-24076

PHOSPHATES
Light emission-or-absorbance-based binding assays for polynucleic acids
[AD-D016557] p 1632 N95-22710

PHOSPHORS
MOCVD of gallium and calcium sulfides for improved phosphor processing
[DE95-000918] p 1631 N95-22677

PHOTOABSORPTION
Pressure shifts and electron scattering in atomic and molecular gases
[DE95-003102] p 1803 N95-22747
Atoms as many-body systems
[DE95-004609] p 1813 N95-24151
Atomic physics at high brilliance synchrotron sources: Proceedings
[DE95-006077] p 1813 N95-24174

PHOTOCHEMICAL OXIDANTS
Oxidants and oxidation in the Earth's atmosphere
[NASA-CR-197945] p 1734 N95-23460

PHOTOCHEMICAL REACTIONS
Photochemical energy conversion by membrane-bound photoredox systems
[DE95-004405] p 1729 N95-23361
Atmospheric peroxides
[DE95-004435] p 1733 N95-23362
Oxidants and oxidation in the Earth's atmosphere
[NASA-CR-197945] p 1734 N95-23460
Annual report of the Osaka Laboratory for Radiation Chemistry Japan Atomic Energy Research Institute, (No. 26)
[DE94-785277] p 1626 N95-23477
Review of research results for the photocatalytic oxidation of hazardous wastes in air
[DE95-004004] p 1734 N95-23480
Solar photochemistry: Twenty years of progress, what's been accomplished, and where does it lead?
[DE95-004007] p 1730 N95-23778
AVIRIS spectra correlated with the chlorophyll concentration of a forest canopy p 1705 N95-23871

PHOTOCONDUCTIVITY
High gain GaAs Photoconductive Semiconductor Switches for impulse sources
[DE95-001885] p 1659 N95-22549
High gain GaAs photoconductive semiconductor switches: Measurement of filament velocity and reduced trigger energy
[DE95-001884] p 1661 N95-22844

PHOTODIODES
VLPC characterization for the Dzero upgrade
[DE95-003742] p 1818 N95-24084

PHOTODISSOCIATION
Thermochemistry of transition metal clusters
[DE95-003144] p 1646 N95-24144

PHOTOELECTRIC EMISSION
Advanced growth and surface analysis system for in situ studies of interface formation
[DE95-002850] p 1838 N95-22555
Photoemission study of quantum confinement by a finite barrier: Cu/Co(wedge)/Cu(100)
[DE95-002913] p 1840 N95-22762
On core level electron diffraction
[DE94-628484] p 1842 N95-23048
A preliminary measurement of the average B hadron lifetime
[DE95-003138] p 1808 N95-23226
Spin polarized photoemission studies of magnetic quantum well states
[DE95-004218] p 1851 N95-23335

PHOTOELECTRONS
Long range potentials and multiple scattering theory in complex systems
[DE94-628881] p 1804 N95-22791

PHOTOEXCITATION
Photochemical energy conversion by membrane-bound photoredox systems
[DE95-004405] p 1729 N95-23361

PHOTOGRAMMETRY
Comparison of 7.5-minute and 1-degree digital elevation models p 1719 N95-24095

PHOTOGRAPHS
Scientific and technical photography at NASA Langley Research Center p 1690 N95-23290

PHOTOGRAPHY
Scientific and technical photography at NASA Langley Research Center p 1690 N95-23290

PHOTOINTERPRETATION
Locating buildings in aerial photos p 1721 N95-23295

PHOTOIONIZATION
Studies of photon and electron interactions with atoms and ions
[DE95-003340] p 1802 N95-22700
Pressure shifts and electron scattering in atomic and molecular gases
[DE95-003102] p 1803 N95-22747
Photoionization of O(6+) below the n=3 threshold of the reduced ion
[DE94-634436] p 1844 N95-23774
Some thoughts of future experiments with the new generation of storage rings
[DE95-004602] p 1818 N95-24162
Atomic physics at high brilliance synchrotron sources: Proceedings
[DE95-006077] p 1813 N95-24174

PHOTOLITHOGRAPHY
Segregated rigid and structural control for a photolithography positioning system
[DE95-002603] p 1766 N95-23134

PHOTOLUMINESCENCE
Method development for compensating temperature effects in pressure sensitive paint measurements p 1650 N95-23291

PHOTOLYSIS
Magnetic resonance and optical spectroscopic studies of carotenoids
[DE95-003729] p 1631 N95-22575

PHOTOMETERS
TIMED Imaging Photometer Experiment (TIPE)
[NASA-CR-197431] p 1688 N95-23087
Circular electrode geometry metal-semiconductor-metal photodetectors
[NASA-CASE-LAR-15172-1-CU] p 1663 N95-24048

PHOTOMULTIPLIER TUBES
A high speed digitizing photomultiplier tube base for the KTeV CsI calorimeter
[DE95-003739] p 1664 N95-24081

PHOTON BEAMS
Preserving the high source brightness with x ray beam line optics
[DE95-003172] p 1820 N95-22877

PHOTON-ELECTRON INTERACTION
Photon and electron interaction databases and their use in medical applications
[DE94-015558] p 1855 N95-22871

PHOTONS
Perturbative QCD tests from the LEP, HERA, and TEVATRON colliders
[DE95-001285] p 1816 N95-22684
Chiral anomalies in non-leptonic decays within chiral perturbation theory at the quark level
[DE94-628613] p 1849 N95-22753
Two-photon absorption in an indirect-gap semiconductor quantum well systems 1. Interband transitions
[DE94-628879] p 1849 N95-22760
Two-photon absorption in an indirect-gap semiconductor quantum well systems 2. Excitonic transitions
[DE94-628880] p 1849 N95-22761
The omega pi(sup 0)-transient form factor within effective chiral Lagrangian approach
[DE94-628612] p 1850 N95-22812
Photon and electron interaction databases and their use in medical applications
[DE94-015558] p 1855 N95-22871
Protein folding and protein metallocluster studies using synchrotron small angler x ray scattering
[DE95-003339] p 1746 N95-22897
Real lasers and other deformed objects p 1692 N95-23001

Doing photons with MERLIN 2 at Oroville
p 1815 N95-23816
Charging of interplanetary grains
|NASA-CR-198032| p 1869 N95-24066
VLPC characterization for the Dzero upgrade
|DE95-003742| p 1818 N95-24084

PHOTOOXIDATION
Review of research results for the photocatalytic oxidation of hazardous wastes in air
|DE95-004004| p 1734 N95-23480

PHOTOPRODUCTION
QCD test in three-jet Z(sup 0) decays at SLD and detector development for H(sup 0) yields gamma gamma searches in high energy hadron colliders
|DE95-003336| p 1848 N95-22698
Recent results from Fermilab E-687, charm particle decays, lifetimes and photoproduction dynamics: A compilation results presented at DPF 1994
|DE95-004580| p 1808 N95-23347

PHOTORECEPTORS
AVIRIS spectra correlated with the chlorophyll concentration of a forest canopy p 1705 N95-23871

PHOTOSYNTHESIS
Magnetic resonance and optical spectroscopic studies of carotenoids
|DE95-003729| p 1631 N95-22575
Comparison of the rate constants for energy transfer in the light-harvesting protein, C-phycocyanin, calculated from Foerster's theory and experimentally measured by time-resolved fluorescence spectroscopy
|DE94-014961| p 1745 N95-22590
Biological determinants of photobioreactor design
|DE94-016032| p 1745 N95-22872
Regulation of photosynthetic carbon fixation on the ocean margins
|DE95-003185| p 1743 N95-22878
Photochemical energy conversion by membrane-bound photoredox systems
|DE95-004405| p 1729 N95-23361
Relationships between pigment composition variation and reflectance for plant species from a coastal savannah in California p 1709 N95-23889

PHOTOVOLTAIC CELLS
Evaluating photovoltaic applications: A guide for utilities
|DE95-003807| p 1726 N95-22502
World's first 15%-efficient multicrystalline silicon modules
|DE95-002604| p 1727 N95-22650
Amorphous silicon photovoltaic manufacturing technology, phase 2A
|DE95-000298| p 1729 N95-23478
Crystalline-silicon photovoltaics: Necessary and sufficient
|DE95-004540| p 1731 N95-24157

PHOTOVOLTAIC CONVERSION
Evaluating photovoltaic applications: A guide for utilities
|DE95-003807| p 1726 N95-22502
Southeast Regional Experiment Station
|DE95-000903| p 1726 N95-22518
Advanced development of PV encapsulants
|DE95-000246| p 1728 N95-23062
Amorphous silicon photovoltaic manufacturing technology, phase 2A
|DE95-000298| p 1729 N95-23478
Automated solar cell assembly teamed process research
|DE95-000299| p 1730 N95-23777
Crystalline-silicon photovoltaics: Necessary and sufficient
|DE95-004540| p 1731 N95-24157

PHOTOVOLTAIC EFFECT
Continuous roll-to-roll amorphous-silicon photovoltaic manufacturing technology
|DE95-000243| p 1728 N95-23061

PHYSICAL CHEMISTRY
Diffusion behavior of lysozyme in aqueous ammonium sulfate solutions under varying solution conditions as determined by dynamic light scattering
|DE95-004821| p 1635 N95-23380

PHYSICAL EXERCISE
Self-generating oscillating pressure exercise device
|NASA-CASE-ARC-12000-1| p 1751 N95-23264

PHYSICAL PROPERTIES
Glass science tutorial: Lecture 2, operating electric glass melters
|DE95-002965| p 1647 N95-22648
Aqueous alternatives for metal and composite cleaning p 1630 N95-23039
Material characterization system
|AD-D016536| p 1800 N95-23073

PHYSIOCHEMISTRY
Analysis of physiochemical processes during solder aging
|DE95-003811| p 1638 N95-22576

PHYSIOLOGICAL EFFECTS
Cellular interactions in the suprachiasmatic nucleus
|AD-A285639| p 1749 N95-23780
The 1993 Gordon Research Conference on Chronobiology
|NASA-CR-197990| p 1748 N95-24047

PHYSIOLOGICAL RESPONSES
All systems go!
|NASA-TM-110542| p 1620 N95-23665

PHYTOPLANKTON
Development of a multi-sensor in situ fiber optic fluorometer
|DE95-003105| p 1819 N95-22780
Regulation of photosynthetic carbon fixation on the ocean margins
|DE95-003185| p 1743 N95-22878

PICRATES
Turbidity of a near critical ionic fluid
|DE94-014916| p 1633 N95-22869

PIEZOELECTRIC CERAMICS
Superconductivity devices: Commercial use of space
|NASA-CR-197885| p 1648 N95-22883

PIEZOELECTRICITY
Flexural vibration of thin piezoelectric laminate circular cylinder of hexagonal symmetry
|DE94-628474| p 1698 N95-22773
Superconductivity devices: Commercial use of space
|NASA-CR-197885| p 1648 N95-22883
A coupled layerwise analysis of the thermopiezoelectric response of smart composite beams beams
|NASA-TM-106889| p 1630 N95-23463

PIGMENTS
Magnetic resonance and optical spectroscopic studies of carotenoids
|DE95-003729| p 1631 N95-22575

PILOT INDUCED OSCILLATION
Analysis of the longitudinal handling qualities and pilot-induced-oscillation tendencies of the High-Angle-of-Attack Research Vehicle (HARV)
p 1616 N95-23297

PILOT PERFORMANCE
TRISTAR 1: Evaluation methods for testing head-up display (HUD) flight symbology
|NASA-TM-4665| p 1613 N95-24030
A review of civil aviation fatal accidents in which lost/disoriented was a cause/factor: 1981-1990
|DOT/FAA/AM-95/1| p 1611 N95-24071

PILOT TRAINING
Human-centered design of human-computer-human dialogs in aerospace systems
|NASA-CR-197379| p 1750 N95-22797

PILOTLESS AIRCRAFT
Design of a GaAs/Ge solar array for unmanned aerial vehicles
|NASA-TM-106870| p 1728 N95-23259
Report to the Secretary of Defense. Unmanned aerial vehicles: No more Hunter systems should be bought until problems are fixed
|GAO/NSIAD-95-52| p 1613 N95-24091

PIONS
Electromagnetic production of pions on the nucleon
|DE95-004658| p 1811 N95-23587

PIPELINES
Preliminary assessment of air toxic emissions in the natural gas industry, phase 1
|PB95-135547| p 1732 N95-22865

PISTON ENGINES
The influence of high-octane fuel blends on the performance of a two-stroke SI engine with knock-limited-compression ratio
|DE95-002902| p 1692 N95-22556

PITCH (INCLINATION)
Pitch sensor system
|AD-D016488| p 1799 N95-22863

PITTING
Eddy current detection of pitting corrosion around fastener holes p 1643 N95-23507

PIXELS
Neural network for detection and correction of local boundary misalignments between images
|AD-D016539| p 1766 N95-22705
AVIRIS calibration using the cloud-shadow method
p 1702 N95-23849
Discrimination of poorly exposed lithologies in AVIRIS data p 1703 N95-23858
The difference between laboratory and in-situ pixel-averaged emissivity: The effects on temperature-emissivity separation p 1711 N95-23919

PLANE WAVES
A uniform geometrical optics and an extended uniform geometrical theory of diffraction for evaluating high frequency EM fields near smooth caustics and composite shadow boundaries
|NASA-CR-197934| p 1657 N95-23391

PLANETARY MAPPING
The effects of AVIRIS atmospheric calibration methodology on identification and quantitative mapping of surface mineralogy, Drum Mountains, Utah
p 1705 N95-23870

PLANETARY SURFACES
Path planning for planetary rover using extended elevation map p 1771 N95-23689
Subsumption-based architecture for autonomous movement planning for planetary rovers
p 1771 N95-23690
Control technique for planetary rover
p 1771 N95-23692
Lunar rover technology demonstrations with Dante and Ratler p 1697 N95-23694
Small image laser range finder for planetary rover
p 1692 N95-23712

PLANETS
Space Science for the 21st Century. Strategic Plan for 1995-2000
|NASA-TM-110546| p 1617 N95-22947

PLANFORMS
A study of the vortex flow over 76/40-deg double-delta wing
|NASA-CR-195032| p 1677 N95-23466

PLANNING
Outline for a global environmental strategic planning exercise (GESPE-project)
|PB95-133773| p 1733 N95-23067
Planning and scheduling the Hubble Space Telescope: Practical application of advanced techniques
p 1779 N95-23740
Knowledge representation and reasoning for mixed-initiative planning
|TR-562| p 1783 N95-24031
Using simulation-based projection to plan in an uncertain and temporally complex world
|TR-531| p 1853 N95-24043
The TRAINS project: A case study in building a conversational planning agent
|TR-532| p 1659 N95-24193

PLANT DESIGN
Using the shield for thermal energy storage in PULSAR
|DE95-002457| p 1829 N95-22645

PLANTS (BOTANY)
Direct effects of atmospheric CO2 enrichment on plants and ecosystems: An updated bibliographic data base
|DE95-003060| p 1731 N95-22725
Plant metabolism and cell wall formation in space (microgravity) and on Earth
|NASA-CR-197618| p 1745 N95-22801
Structural studies of complex carbohydrates of plant cell walls
|DE95-003099| p 1748 N95-24075

PLASMA ACCELERATION
The high latitude ionosphere-magnetosphere transition region: Simulation and data comparison
|NASA-CR-197404| p 1737 N95-22956

PLASMA CONTROL
Analytical and numerical studies of ion mobility near the tokamak plasma edge
|DE95-003019| p 1830 N95-22693
Comparisons of nonlinear toroidal turbulence simulations with experiment
|DE95-003020| p 1830 N95-22694
Divertor heat and particle control experiments on the DIII-D tokamak
|DE94-017518| p 1832 N95-23119
Ion rings for magnetic fusion
|DE94-017606| p 1832 N95-23120
Dynamics of L to H bifurcation
|DE94-019126| p 1832 N95-23163
The q profile evolution and enhanced core confinement of high (beta)(sub p) plasmas in D3-D
|DE95-003878| p 1834 N95-23371
Quasisymmetry equations for conventional stellarators
|NIFS-324| p 1836 N95-23572
Effect of satellite helical harmonics on the stellarator configuration
|NIFS-328| p 1609 N95-23787
D3-D program overview
|DE95-003879| p 1837 N95-24086

PLASMA CURRENTS
TFTR Ion Cyclotron Range of Frequencies (ICRF) experimental data analysis collaboration
|DE95-003409| p 1832 N95-23084
Observations of the magnetopause current layer: Cases with no boundary layer and tests of recent models
|NASA-CR-197391| p 1738 N95-23184
Experimental achievement of toroidal beta beyond that predicted by 'Troyon' scaling
|DE95-003880| p 1837 N95-24087

PLASMA DENSITY
Dynamics and variability of the plasmasphere observed from synchronous orbit
| DE95-002733 | p 1829 N95-22665
The TEXT neutral lithium beam edge density diagnostic
| DE95-003256 | p 1830 N95-22719
Advanced detector development, laboratory simulations, diagnostic development, and data analysis on wake physics
| PL-TR-94-2204 | p 1831 N95-22948
Electromagnetic radiation in the plasma environment around the shuttle
| NASA-TM-106891 | p 1738 N95-23116
PLASMA DIAGNOSTICS
The TEXT neutral lithium beam edge density diagnostic
| DE95-003256 | p 1830 N95-22719
Measurements and modeling of impurity source distributions from the Tore Supra outboard pump limiter
| DE95-003097 | p 1831 N95-22800
Advanced detector development, laboratory simulations, diagnostic development, and data analysis on wake physics
| PL-TR-94-2204 | p 1831 N95-22948
Ninth topical conference on atomic processes in plasmas
| DE95-002810 | p 1833 N95-23246
Tritium transport, influx, and helium ash measurements on TFTR during DT operation
| DE95-003708 | p 1833 N95-23269
Edge fluctuation measurements by phase contrast imaging on DIII-D
| DE94-016681 | p 1836 N95-23768
PLASMA DYNAMICS
Collisionless magnetic reconnection associated with coalescence of flux bundles
| NIFS-315 | p 1834 N95-23525
Macro-EM particle simulation method and a study of collisionless magnetic reconnection
| NIFS-316 | p 1834 N95-23526
Complexity in plasma: A grand view of self-organization
| NIFS-318 | p 1835 N95-23528
Investigation of infra-red and nonequilibrium air radiation
| NASA-CR-197977 | p 1741 N95-24041
D3-D program overview
| DE95-003879 | p 1837 N95-24086
PLASMA FREQUENCIES
Langmuir-like waves and radiation in planetary foreshocks
| NASA-CR-197376 | p 1869 N95-22828
PLASMA GENERATORS
Functional testing of the space station plasma contactor
| NASA-TM-106841 | p 1624 N95-23240
Atomic oxygen durability evaluation of protected polymers using thermal energy plasma systems
| NASA-TM-106855 | p 1626 N95-23270
PLASMA HEATING
Magnetospheric space plasma investigations
| NASA-CR-197405 | p 1831 N95-22955
The high latitude ionosphere-magnetosphere transition region: Simulation and data comparison
| NASA-CR-197404 | p 1737 N95-22956
Semikinetic modeling and observations of high-latitude plasma outflow
| NASA-CR-197403 | p 1831 N95-23008
TFTR Ion Cyclotron Range of Frequencies (ICRF) experimental data analysis collaboration
| DE95-003409 | p 1832 N95-23084
Experimental achievement of toroidal beta beyond that predicted by 'Troyon' scaling
| DE95-003880 | p 1837 N95-24087
PLASMA INTERACTIONS
Electromagnetic radiation in the plasma environment around the shuttle
| NASA-TM-106891 | p 1738 N95-23116
Observations of the magnetopause current layer: Cases with no boundary layer and tests of recent models
| NASA-CR-197391 | p 1738 N95-23184
Performance characterization of EURECA retroreflectors with fluoropolymer-filled SiO(x) protective coatings p 1651 N95-23802
PLASMA JETS
The DIII-D divertor cryopump system: Design and operational experience
| DE95-003007 | p 1693 N95-22796
Neural net prediction of tokamak plasma disruptions
| DE95-002616 | p 1832 N95-23136
PLASMA PHYSICS
Plasma properties and magnetic field structure of the solar corona, based on coordinated Max 1991 observations from SERTS, the VLA, and magnetographs
| NASA-CR-197864 | p 1870 N95-23181
Ninth topical conference on atomic processes in plasmas
| DE95-002810 | p 1833 N95-23246
Modification and damping of Alfven waves in a magnetized dusty plasma
| NIFS-312 | p 1834 N95-23523
Macro-EM particle simulation method and a study of collisionless magnetic reconnection
| NIFS-316 | p 1834 N95-23526
Physical mechanism determining the radial electric field and its radial structure in a toroidal plasma
| NIFS-313 | p 1835 N95-23534
The next Large Helical Devices
| NIFS-323 | p 1835 N95-23535
Recent studies of the Large Helical Device
| NIFS-322 | p 1835 N95-23543
Effect of satellite helical harmonics on the stellarator configuration
| NIFS-328 | p 1609 N95-23787
PLASMA PINCH
Generation of fast electrons in reversed field pinches by the equilibrium grad (vert bar)B(vert bar) force
| DE95-004467 | p 1809 N95-23363
PLASMA PRESSURE
The q profile evolution and enhanced core confinement of high (beta)(sub p) plasmas in D3-D
| DE95-003878 | p 1834 N95-23371
Non-Taylor magnetohydrodynamic self-organization
| NIFS-314 | p 1834 N95-23524
Experimental achievement of toroidal beta beyond that predicted by 'Troyon' scaling
| DE95-003880 | p 1837 N95-24087
PLASMA RESONANCE
Hot proton anisotropies and cool proton temperatures in the outer magnetosphere
| DE95-002719 | p 1736 N95-22850
PLASMA SHEATHS
Physics of magnetospheric boundary layers
| NASA-CR-197920 | p 1739 N95-23271
PLASMA TEMPERATURE
Advanced detector development, laboratory simulations, diagnostic development, and data analysis on wake physics
| PL-TR-94-2204 | p 1831 N95-22948
PLASMA TURBULENCE
Comparisons of nonlinear toroidal turbulence simulations with experiment
| DE95-003020 | p 1830 N95-22694
Turbulent transport across invariant canonical flux surfaces
| DE95-000710 | p 1832 N95-23072
Dynamics of L to H bifurcation
| DE94-019126 | p 1832 N95-23163
Gyrokinetic and global fluid simulations of tokamak microturbulence and transport
| DE95-003628 | p 1837 N95-24017
PLASMA WAVES
Langmuir-like waves and radiation in planetary foreshocks
| NASA-CR-197376 | p 1869 N95-22828
PLASMA-ELECTROMAGNETIC INTERACTION
Modification and damping of Alfven waves in a magnetized dusty plasma
| NIFS-312 | p 1834 N95-23523
PLASMA-PARTICLE INTERACTIONS
The q profile evolution and enhanced core confinement of high (beta)(sub p) plasmas in D3-D
| DE95-003878 | p 1834 N95-23371
PLASMAPAUSE
Global electric field determination in the Earth's outer magnetosphere using energetic charged particles
| NASA-CR-197392 | p 1737 N95-22945
PLASMAS (PHYSICS)
Morphology of extinguished monolithic JA2 grains fired in a 30-mm Solid Propellant Electrothermal Chemical (SPETC) gun
| AD-A285792 | p 1652 N95-22506
Proceedings of NATO Advanced Research Workshop on the Formation, Transport and Consequences of Particles in Plasmas
| AD-A285850 | p 1829 N95-22514
Innovative technology for contamination control in plasma processing
| DE95-000913 | p 1829 N95-22519
Laser-plasma instability in hohlraums
| DE95-000914 | p 1829 N95-22676
A model for ball lightning
| DE95-003366 | p 1742 N95-22701
The problem of phase transition and the heavy ion collisions at very high energies
| DE94-628584 | p 1816 N95-22785
Baryon number fluctuations in a quark-hadron phase transition
| DE94-628585 | p 1804 N95-22786
Analytical Boltzmann moments for electrons in N2-O2-H2O gas mixtures
| DE95-003474 | p 1732 N95-22898
Ion rings for magnetic fusion
| DE94-017606 | p 1832 N95-23120
Neural net prediction of tokamak plasma disruptions
| DE95-002616 | p 1832 N95-23136
High beta and second stability region transport and stability analysis
| DE95-003411 | p 1832 N95-23147
The railplug: Development of a new ignitor for internal combustion engines
| DE95-004375 | p 1695 N95-23342
Multiband VLBI imaging of the jet in 3C 345
| PB95-139275 | p 1866 N95-23468
New pellet production and acceleration technologies for high speed pellet injection system HIPEL in Large Helical Device
| NISF-326 | p 1835 N95-23566
MHD-Vlasov simulation of the toroidal Alfven eigenmode
| NIFS-319 | p 1836 N95-23591
A new containerless image furnace with electro-static positioning device p 1690 N95-23674
10x reduction imaging at 13.4 nm
| DE94-016612 | p 1828 N95-23767
Cu deposition using a permanent magnet electron cyclotron resonance microwave plasma source
| DE94-017768 | p 1650 N95-23981
Increasing the retained dose by plasma immersion ion implantation and deposition
| DE95-003423 | p 1844 N95-24011
Investigation of infra-red and nonequilibrium air radiation
| NASA-CR-197977 | p 1741 N95-24041
D3-D program overview
| DE95-003879 | p 1837 N95-24086
PLASMASPHERE
Dynamics and variability of the plasmasphere observed from synchronous orbit
| DE95-002733 | p 1829 N95-22665
PLASMONS
The effect of magnetic field on the edge plasmons of two-dimensional electron gas systems
| DE94-018044 | p 1837 N95-23982
PLASTIC DEFORMATION
Aspects of surface generation in orthogonal ultraprecision machining
| DE95-000922 | p 1654 N95-22678
PLATE THEORY
Idealized textile composites for experimental/analytical correlation p 1631 N95-23277
PLATEAUS
The hydrogen embrittlement of alloy X-750
| DE95-003207 | p 1640 N95-22893
PLATENS
Segregated rigid and structural control for a photolithography positioning system
| DE95-002603 | p 1766 N95-23134
PLATINUM
Orientation selection and microstructural evolution of epitaxial platinum films on (001) magnesium oxide
| DE95-003680 | p 1842 N95-23265
Changes in chemical and optical properties of thin film metal mirrors on LDEF p 1651 N95-23907
PLOTTING
Old-growth and mature forests near spotted owl nests in western Oregon p 1719 N95-24098
PLUMES
Axisymmetric computational fluid dynamics analysis of Saturn V/S1-C/F1 nozzle and plume p 1672 N95-23430
Computational Fluid Dynamic (CFD) analysis of axisymmetric plume and base flow of film/dump cooled rocket nozzle p 1673 N95-23431
CFD flowfield simulation of Delta Launch Vehicles in a power-on configuration p 1673 N95-23433
Numerical study of the SSME nozzle flow fields during transient operations: A comparison of the animated results with test p 1673 N95-23434
NTS-spill test facility wind tunnel exhaust plume characterization
| DE95-003630 | p 1616 N95-24019
PLUTO (PLANET)
IUE observing programs: NSOSS, VEOEB, and PCOEB
| NASA-CR-197424 | p 1866 N95-23560
PLUTONIUM
Test procedure for anion exchange chromatography
| DE95-003767 | p 1809 N95-23407
Alpha spectral analysis via artificial neural networks
| DE95-004567 | p 1767 N95-23578
PNEUMATIC EQUIPMENT
Pressurized fluid torque driver control and method
| NASA-CASE-MSC-22385-1 | p 1694 N95-22892

POINT IMPACT
Axial focusing of energy from a hypervelocity impact on earth
|DE95-003347| p 1740 N95-24008
POINT SOURCES
Nonparametric measure of spatial interaction in point patterns
|PB95-127965| p 1793 N95-22527
POINTING CONTROL SYSTEMS
Stellar Interferometer Technology Experiment (SITE)
|NASA-CR-197856| p 1827 N95-23089
POINTS (MATHEMATICS)
The point interactions in the quantum problem of three particles with internal structure
|DE94-635423| p 1851 N95-23967
POISSON DENSITY FUNCTIONS
Light-traffic analysis for queues with spatially distributed arrivals
|PB95-140802| p 1767 N95-23556
Independent production and Poisson distribution
|DE94-635632| p 1794 N95-23972
POLAR CAPS
Continued studies of polar cap thermospheric dynamics
|PL-TR-94-2076| p 1737 N95-22951
Semikinetic modeling and observations of high-latitude plasma outflow
|NASA-CR-197403| p 1831 N95-23008
POLAR REGIONS
Continued studies of polar cap thermospheric dynamics
|PL-TR-94-2076| p 1737 N95-22951
The high latitude ionosphere-magnetosphere transition region: Simulation and data comparison
|NASA-CR-197404| p 1737 N95-22956
Semikinetic modeling and observations of high-latitude plasma outflow
|NASA-CR-197403| p 1831 N95-23008
Oceanic operations: An authoritative guide to oceanic operations
|FAA-AFS-550| p 1610 N95-24065
POLARIMETERS
SAR terrain classifier and mapper of biophysical attributes p 1715 N95-23957
Hard e(+)e(-)-pair Bremsstrahlung as a lepton polarimeter
|DE94-635615| p 1812 N95-23984
POLARIMETRY
Field observations using an AOTF polarimetric imaging spectrometer p 1702 N95-23850
MAX-91: Polarimetric SAR results on Montespertoli site p 1712 N95-23940
Estimation of biophysical properties of upland Sitka spruce (Picea sitchensis) plantations p 1713 N95-23943
Forest investigations by polarimetric AIRSAR data in the Harz mountains p 1713 N95-23944
Comparison of inversion models using AIRSAR data for Death Valley, California p 1713 N95-23945
Statistics of multi-look AIRSAR imagery: A comparison of theory with measurements p 1714 N95-23947
Unusual radar echoes from the Greenland ice sheet p 1714 N95-23951
Measurement of ocean wave spectra using polarimetric AIRSAR data p 1715 N95-23953
An improved algorithm for retrieval of snow wetness using C-band AIRSAR p 1715 N95-23954
Polarimetric radar data decomposition and interpretation p 1715 N95-23955
Classification and soil moisture determination of agricultural fields p 1716 N95-23958
Soil moisture retrieval in the Oberpfaffenhofen testsite using MAC Europe AIRSAR data p 1716 N95-23960
POLARIZATION
Field observations using an AOTF polarimetric imaging spectrometer p 1702 N95-23850
POLARIZATION (CHARGE SEPARATION)
Measurement of the left-right charge asymmetry in hadronic Z decays and A(sub e) determination
|DE95-003467| p 1806 N95-23140
POLARIZATION (SPIN ALIGNMENT)
Spin polarized photoemission studies of magnetic quantum well states
|DE95-004218| p 1851 N95-23335
POLARIZED LIGHT
Diffusion behavior of lysozyme in aqueous ammonium sulfate solutions under varying solution conditions as determined by dynamic light scattering
|DE95-004821| p 1635 N95-23380
POLARONS
Magnetic field effects on strong-coupling polaron in quantum dots
|DE94-629038| p 1847 N95-22496
Resonant shallow donor magnetopolaron effect in a GaAs/AlGaAs quantum dot in high magnetic fields
|DE94-629039| p 1798 N95-22497
Strong-coupling polaron effect in quantum dots
|DE94-628485| p 1850 N95-23049
Disorder-induced breakdown of soliton and polaron particles
|DE95-003694| p 1808 N95-23267
Quantum fluctuations of D(sub 5d) polarons on C(sub 60) molecules
|DE94-635787| p 1812 N95-23985
POLICIES
A study of policy issues affecting the Defense Technical Information Center
|AD-A286629| p 1854 N95-22494
Mishap risk control for advanced aerospace/composite materials p 1628 N95-23031
CO2 and waste policy: Monitoring results 1991/1992 and main problems
|PB95-133799| p 1733 N95-23126
Inspector General: Alleged misconduct by NASA Inspector General. Report to Congressional requesters
|GAO/OSI-95-9| p 1854 N95-24085
Using simple page placement policies to reduce the cost of cache fills in coherent shared-memory systems
|TR-535| p 1753 N95-24177
POLLUTION CONTROL
P2Info Resource Center: Linking the DOE Pollution Prevention community
|DE95-003133| p 1732 N95-22781
Society of the plastic industry process emission initiatives p 1629 N95-23036
POLLUTION MONITORING
Modeling aerosol emissions from the combustion of composite materials p 1629 N95-23038
Review of research results for the photocatalytic oxidation of hazardous wastes in air
|DE95-004004| p 1734 N95-23480
Applied research on air pollution using nuclear-related analytical techniques
|DE94-633513| p 1734 N95-23542
Remote sensor test range update
|DE95-003629| p 1735 N95-24018
POLOIDAL FLUX
TPX magnet system status
|DE95-002389| p 1661 N95-23080
POLYATOMIC MOLECULES
Non-intrusive measurements in a rocket engine combustor p 1625 N95-23439
POLYCARBONATES
Absorbed dose and LET spectra measurements on LDEF p 1815 N95-23810
POLYCRYSTALS
Thermal activation of steady-state creep in polycrystalline copper
|DE94-627394| p 1839 N95-22607
World's first 15%-efficient multicrystalline silicon modules
|DE95-002604| p 1727 N95-22650
Polycrystalline CuInSe2 and CdTePV solar cells
|DE95-000244| p 1727 N95-22842
Mass transport through polycrystalline microstructures
|DE95-004552| p 1811 N95-23576
POLYESTERS
A kinetic study of hydrolysis of polyester elastomer in magnetic tape p 1652 N95-24124
POLYGONS
Schwarz-Christoffel methods for multiply-elongated regions
|DE94-019048| p 1790 N95-23536
POLYHEDRONS
Capacitated facility location: Valid inequalities and facets (revised)
|PB95-130225| p 1786 N95-22641
POLYIMIDES
Process for preparing an assembly of an article and a polyimide which resists dimensional change, delamination and debonding when exposed to changes in temperature
|NASA-CASE-LAR-14538-2| p 1649 N95-23254
LDEF polymeric materials: A summary of Langley characterization p 1651 N95-23899
The effect of simulated low earth orbit radiation on polyimides (UV degradation study) p 1651 N95-23903
The surface properties of fluorinated polyimides exposed to VUV and atomic oxygen p 1651 N95-23904
Microporous polyimide films for reduced dielectric applications
|DE95-004543| p 1650 N95-24159
POLYISOPRENES
Neutron scattering analysis of rubber carbon black composite structure
|DE95-002735| p 1646 N95-22553
POLYMER CHEMISTRY
Progress towards the synthesis of polymeric nitrogen
|DE94-017547| p 1841 N95-22860
Process for preparing an assembly of an article and a polyimide which resists dimensional change, delamination and debonding when exposed to changes in temperature
|NASA-CASE-LAR-14538-2| p 1649 N95-23254
Atomic oxygen textured polymers
|NASA-TM-106769| p 1650 N95-24187
POLYMER MATRIX COMPOSITES
Mishap risk control for advanced aerospace/composite materials p 1628 N95-23031
Society of the plastic industry process emission initiatives p 1629 N95-23036
Technology reinvestment project's focus area. Affordable polymer matrix composites for airframe structures
|PB95-136032| p 1865 N95-23168
Application of electron paramagnetic resonance imaging to the characterization of the Ultem(R) exposed to 1 MeV electrons. Correlation of radical density data to tiger code calculations p 1815 N95-23328
The detection and analysis of galvanic damage in BMI/graphite fiber composites p 1631 N95-23502
LDEF polymeric materials: A summary of Langley characterization p 1651 N95-23899
Surface characterization of LDEF carbon fiber/polymer matrix composites p 1631 N95-23900
Space environmental effects on polymer matrix composites as a function of sample location on LDEF p 1651 N95-23901
Structure and properties of polymeric composite materials during 1501 days outer space exposure at Salyut-7 orbital station p 1652 N95-23915
POLYMERIC FILMS
LDEF polymeric materials: A summary of Langley characterization p 1651 N95-23899
Nonlinear viscoelastic characterization of polymer materials using a dynamic-mechanical methodology p 1651 N95-23902
The effect of simulated low earth orbit radiation on polyimides (UV degradation study) p 1651 N95-23903
The surface properties of fluorinated polyimides exposed to VUV and atomic oxygen p 1651 N95-23904
POLYMERIZATION
Annual report of the Osaka Laboratory for Radiation Chemistry Japan Atomic Energy Research Institute. (No. 26)
|DE94-785277| p 1626 N95-23477
POLYMERS
Polyazomethines containing trifluoromethylbenzene units
|NASA-CASE-LAR-14896-1| p 1649 N95-23253
Atomic oxygen durability evaluation of protected polymers using thermal energy plasma systems
|NASA-TM-106855| p 1626 N95-23270
Atomic oxygen textured polymers
|NASA-TM-106769| p 1650 N95-24187
POLYNOMIALS
Treewidth and pathwidth of cocomparability graphs of bounded dimension
|PB95-127239| p 1785 N95-22535
Fibonacci chain polynomials: Identities from self-similarity p 1814 N95-22962
A Ramanujan-type measure for the Askey-Wilson polynomials p 1797 N95-22975
Taylor series expansion and modified extended Prony analysis for localization
|DE95-003671| p 1758 N95-23567
Quasi-kernel polynomials and convergence results for quasi-minimal residual iterations
|NASA-CR-197948| p 1791 N95-23593
Optimal advice
|TR-527| p 1792 N95-23931
Witness-isomorphic reductions and the local search problem
|TR-522| p 1793 N95-24003
Large sets in AC(exp 0): A Kolmogorov complexity related property and some applications
|TR-556| p 1797 N95-24029
On the size of sets with weak membership properties
|TR-557| p 1793 N95-24034
Properties of probabilistic pushdown automata
|TR-554| p 1760 N95-24056
Polynomial-time membership comparable sets
|TR-552| p 1793 N95-24182
The satanic notations: Counting classes beyond #P and other definitional adventures
|TR-561| p 1793 N95-24194
POLYSACCHARIDES
Structural studies of complex carbohydrates of plant cell walls
|DE95-003099| p 1748 N95-24075
POLYSTYRENE
LDEF polymeric materials: A summary of Langley characterization p 1651 N95-23899

POLYTOPES
Note on the computational complexity of j-radii of polytopes in (R sup n)
[PB95-139358] p 1790 N95-23231
POPULATIONS
Orbital debris and meteoroid population as estimated from LDEF impact data p 1869 N95-23830
POROSITY
Thermal outgassing studies on machinable tungsten and TZM molybdenum alloy
[DE95-002984] p 1638 N95-22592
Investigation of mechanical properties and their relation to the internal structure of nanocrystalline metals and composites
[DE95-001151] p 1627 N95-22683
Influence of porosity and two-phase flow on diffusional/thermal instability of a deflagrating energetic material
[DE95-002592] p 1634 N95-23122
High surface area, high permeability carbon monoliths
[DE95-004555] p 1650 N95-23577
POROUS MATERIALS
Propagation of waves at the loosely bonded interface of two porous elastic half-spaces
[DE94-628477] p 1800 N95-23018
Impact shock and penetration fragmentation in porous media
[DE94-018900] p 1868 N95-23656
POSITION (LOCATION)
Capacitated facility location: Valid inequalities and facets (revised)
[PB95-130225] p 1786 N95-22641
Sensor-based control of rocket thrust chamber feature location for automated braze paste dispensing
[DE94-016559] p 1624 N95-22885
Localization in deformed quantum mechanics p 1823 N95-22979
Taylor series expansion and modified extended Prony analysis for localization
[DE95-003671] p 1758 N95-23567
Space environmental effects on polymer matrix composites as a function of sample location on LDEF p 1651 N95-23901
POSITION INDICATORS
TRISTAR 1: Evaluation methods for testing head-up display (HUD) flight symbology
[NASA-TM-4665] p 1613 N95-24030
POSITIONING
Segregated rigid and structural control for a photolithography positioning system
[DE95-002603] p 1766 N95-23134
POSITIONING DEVICES (MACHINERY)
A new containerless image furnace with electro-static positioning device p 1690 N95-23674
POSITRON ANNIHILATION
Study of radiation damages in AISI 316 and 347 steels
[DE94-627480] p 1639 N95-22609
Measurement of the left-right asymmetry in Z boson production by electron-positron collisions
[DE95-003337] p 1802 N95-22699
Precision standard model tests with polarized e(+)e(-) beams
[DE95-003367] p 1816 N95-22702
Heavy quark physics at SLD: Preliminary results
[DE95-003372] p 1806 N95-23138
Introduction to the physics of Higgs bosons
[DE95-003965] p 1809 N95-23396
Study of b(anti b) production in e(+)e(-) annihilation at radical s = 29 GeV with the aid of neural networks
[DE95-004691] p 1810 N95-23488
POSITRONS
Traps for antimatter and antihydrogen production
[DE95-002814] p 1805 N95-22927
POSTFLIGHT ANALYSIS
Low Earth orbit thermal control coatings exposure flight tests: A comparison of U.S. and Russian results
[NASA-CR-4647] p 1626 N95-22919
STS-61 mission director's post-mission report
[NASA-TM-104803] p 1617 N95-23262
Integrating O/S models during conceptual design, part 1
[NASA-CR-197903] p 1622 N95-23398
Integrating O/S models during conceptual design, part 3
[NASA-CR-197905] p 1622 N95-23400
EURECA 11 months in orbit: Initial post flight investigation results p 1623 N95-23799
POSTMISSION ANALYSIS (SPACECRAFT)
Evaluation of adhesive materials used on the Long Duration Exposure Facility
[NASA-CR-4646] p 1626 N95-22918
Integrating O/S models during conceptual design, part 3
[NASA-CR-197905] p 1622 N95-23400
EURECA 11 months in orbit: Initial post flight investigation results p 1623 N95-23799
Material inspection of EURECA first findings and recommendations p 1637 N95-23804
POTASSIUM
MHD seed recovery and regeneration, phase 2
[DE95-004308] p 1833 N95-23338
POTENTIAL ENERGY
On the (DE-) stabilization of quantum mechanical binding by potential barriers
[DE94-628433] p 1847 N95-22635
How to measure the Q(bar Q) potential in a light-front calculation
[DE95-003200] p 1848 N95-22728
Structural properties of silicon clusters: An empirical potential study
[DE94-628902] p 1805 N95-22935
POTENTIAL FIELDS
Finite-temperature scalar field theory in static de Sitter space
[DE94-628522] p 1848 N95-22743
POTENTIAL FLOW
Conjugate gradient MATHEW
[DE95-003479] p 1738 N95-23143
Accelerated panel methods using the fast multipole method p 1687 N95-23307
Combining comparison functions and finite element approximations in CFD
[NASA-TM-106851] p 1792 N95-23614
POTENTIAL GRADIENTS
A worst-case example using linesearch methods for numerical optimization with inexact gradient evaluations
[DE95-002917] p 1754 N95-22570
POWDER (PARTICLES)
High pressure neutron powder diffraction at LANSCE
[DE95-002703] p 1839 N95-22565
Transformation behavior in Al2O3-ZrO2 ceraamic composites
[DE95-001359] p 1647 N95-22688
Charge distribution analysis of catalysts under simulated reaction conditions
[DE95-003526] p 1633 N95-23064
NMR study of nanophase Al/Al-oxide powder and consolidated composites
[DE95-004655] p 1843 N95-23586
POWDER METALLURGY
Cooling rate effects on the microstructure, critical current density, and (T(sub c)) transition of one- and two-powder BSCCO-2223 Ag sheathed tapes
[DE95-004639] p 1846 N95-24171
POWDERED ALUMINUM
NMR study of nanophase Al/Al-oxide powder and consolidated composites
[DE95-004655] p 1843 N95-23586
POWER CONVERTERS
Liquid nitrogen temperature operation of a switching power converter
[NASA-TM-106867] p 1662 N95-23219
POWER EFFICIENCY
Calorimetric measurement of energy of ultrasonic cleaners
[DE95-003938] p 1800 N95-23375
Energy efficiency of electric vehicles at the 1994 American Tour de Sol
[DE95-002905] p 1664 N95-24070
POWER FACTOR CONTROLLERS
DRACULA: Dynamic range control for broadcasting and other applications
[BBC-RD-1994/13] p 1658 N95-24044
POWER GAIN
A high-power switch-mode DC power supply for dynamic loads
[DE94-016714] p 1659 N95-22504
POWER LIMITERS
Design and production of efficient current leads for 1500-A, 50-Hz service in a 77-4 K temperature gradient
[DE95-004121] p 1662 N95-23355
POWER LINES
Current estimation for electromigration, hot carriers, and voltage drop
[AD-A285794] p 1659 N95-22507
Universal Hodge bundle and Mumford isomorphisms on the abelian inductive limit of Teichmueller spaces
[DE94-634325] p 1796 N95-23660
POWER SERIES
The convergence radius of the chiral expansion in the Dyson-Schwinger approach
[DE94-012852] p 1805 N95-22925
POWER SUPPLY CIRCUITS
A high-power switch-mode DC power supply for dynamic loads
[DE94-016714] p 1659 N95-22504
PRE-MAIN SEQUENCE STARS
Observational studies of the clearing phase in proto-planetary disk systems
[NASA-CR-197900] p 1866 N95-23561
PRECESSION
Exact, E = 0, classical and quantum solutions for general power-law oscillators p 1820 N95-22959
PRECIPITATION (CHEMISTRY)
Polyazomethines containing trifluoromethylbenzene units
[NASA-CASE-LAR-14896-1] p 1649 N95-23253
Diffusion behavior of lysozyme in aqueous ammonium sulfate solutions under varying solution conditions as determined by dynamic light scattering
[DE95-004821] p 1635 N95-23380
PRECIPITATION (METEOROLOGY)
HAPEX-Sahel: Basic description of methods and data sets
[PB95-127262] p 1701 N95-22639
Streamflow and selected precipitation data for Yucca Mountain Region, southern Nevada and eastern California, water years 1986-90
[DE95-001893] p 1742 N95-23385
PRECISION
Traps for antimatter and antihydrogen production
[DE95-002814] p 1805 N95-22927
PRECONDITIONING
Preconditioning for the Navier-Stokes equations with finite-rate chemistry p 1670 N95-23421
On adaptive weighted polynomial preconditioning for Hermitian positive definite matrices
[NASA-CR-197946] p 1791 N95-23547
PREDATORS
An extension of Freedman's results on a model of predator-prey dynamics as modified by the action of a parasite
[DE94-628488] p 1796 N95-23052
PREDICATE CALCULUS
Relating multifunctions and predicate transformers through closure operators
[PB95-135646] p 1757 N95-23467
PREDICTION ANALYSIS TECHNIQUES
HiRel: Hybrid Automated Reliability Predictor (HARP) integrated reliability tool system, (version 7.0). Volume 1: HARP introduction and user's guide
[NASA-TP-3452-VOL-1] p 1754 N95-22603
HiRel: Hybrid Automated Reliability Predictor (HARP) integrated reliability tool system, (version 7.0). Volume 2: HARP tutorial
[NASA-TP-3452-VOL-2] p 1755 N95-22604
HiRel: Hybrid Automated Reliability Predictor (HARP) integrated reliability tool system, (version 7.0). Volume 4: HARP Output (HARPO) graphics display user's guide
[NASA-TP-3452-VOL-4] p 1755 N95-22605
Additional improvements to the NASA Lewis ice accretion code LEWICE
[NASA-TM-106849] p 1665 N95-22669
Net energy analysis: Powerful tool for selecting electric power options
[DE95-002516] p 1728 N95-23133
Neural net prediction of tokamak plasma disruptions
[DE95-002616] p 1832 N95-23136
Development and verification of a resin film infusion/resin transfer molding simulation model for fabrication of advanced textile composites
[NASA-CR-197439] p 1648 N95-23179
On the accuracy of CFD-based pressure drop predictions for right-angle ducts p 1682 N95-23634
Predictions of LDEF radioactivity and comparison with measurements p 1815 N95-23818
Dimensional scaling for impact cratering and perforation p 1624 N95-23843
Tutorial on filtering, restoration, and state estimation
[TR-534] p 1793 N95-24042
PREDICTIONS
Intermediate-term earthquake prediction and seismic zoning in Northern Italy
[DE94-627689] p 1736 N95-22612
The use of cowl camber and taper to reduce rotor/stator interaction noise
[NASA-CR-195421] p 1799 N95-22675
PREDICTOR-CORRECTOR METHODS
Orders of predictor-corrector pairs for second-order ODE's
[PB95-140612] p 1790 N95-23237
Numerical study of the SSME nozzle flow fields during transient operations: A comparison of the animated results with test p 1673 N95-23434
PREFLIGHT ANALYSIS
Integrating O/S models during conceptual design, part 1
[NASA-CR-197903] p 1622 N95-23398
Integrating O/S models during conceptual design, part 3
[NASA-CR-197905] p 1622 N95-23400
PRELAUNCH TESTS
Integrating O/S models during conceptual design, part 1
[NASA-CR-197903] p 1622 N95-23398

Integrating O/S models during conceptual design, part 3
[NASA-CR-197905] p 1622 N95-23400

PREMIXED FLAMES
Sensitivity of combustion-acoustic instabilities to boundary conditions for premixed gas turbine combustors
[NASA-TM-106890] p 1614 N95-23550
Microgravity combustion science: 1995 program update
[NASA-TM-106858] p 1626 N95-24004

PREMIXING
Effects of jet strength on NOx formation in premixed impinging jet combustion with minimum heat losses
[NAL-TR-1237T] p 1637 N95-24181

PREPREGS
Biotransformation of an uncured composite material p 1629 N95-23033

PREPROCESSING
Preprocessing: Geocoding of AVIRIS data using navigation, engineering, DEM, and radar tracking system data p 1707 N95-23876

PRESIDENTIAL REPORTS
Hey! What's Space Station Freedom?
[NASA-TM-110531] p 1620 N95-22542

PRESSURE BROADENING
Theoretical calculations of pressure broadening coefficients for H2O perturbed by hydrogen or helium gas
[NASA-CR-197345] p 1636 N95-23545

PRESSURE DISTRIBUTION
Study of the pressure field in rotating homogeneous turbulent flows
[PB94-189107] p 1665 N95-22585
Wing pressure distributions from subsonic tests of a high-wing transport model --- in the Langley 14- by 22-Foot Subsonic Wind Tunnel
[NASA-TM-4583] p 1607 N95-22802
Three-dimensional unsteady flow calculations in an advanced gas generator turbine p 1671 N95-23425
Modeling of non-spherical droplet dynamics p 1685 N95-23647
Numerical study of base pressure characteristic curve for a four-engine clustered nozzle configuration p 1625 N95-23655

PRESSURE EFFECTS
Method development for compensating temperature effects in pressure sensitive paint measurements p 1650 N95-23291
A controlled variation scheme for convection treatment in pressure-based algorithm p 1677 N95-23448
Theory of pressure-induced islands and self-healing in three-dimensional toroidal magnetohydrodynamic equilibria
[NIFS-321] p 1836 N95-23589
Annealing of nitrogen-doped ZnSe at high pressures: Toward suppression of native defect formation
[DE95-003420] p 1844 N95-24010

PRESSURE GRADIENTS
Application of CFD analysis to design support and problem resolution for ASRM and RSRM p 1685 N95-23649

PRESSURE OSCILLATIONS
Active control of panel vibrations induced by a boundary layer flow
[NASA-CR-197867] p 1608 N95-23182
Time-accurate unsteady flow simulations supporting the SRM T+68-second pressure spike anomaly investigation (STS-54B) p 1685 N95-23650

PRESSURE PULSES
System for determining aerodynamic imbalance
[NASA-CASE-ARC-11913-1] p 1688 N95-23377

PRESSURE REDUCTION
Morphology of extinguished monolithic JA2 grains fired in a 30-mm Solid Propellant Electrothermal Chemical (SPETC) gun
[AD-A285792] p 1652 N95-22506

PRESSURE SENSORS
Dynamic response of a transducer mounted at one end of an acoustical cavity which is subjected to a specified pressure at the open end of the cavity
[DE95-004192] p 1799 N95-23379
Impeller flow field characterization with a laser two-focus velocimeter p 1675 N95-23440

PRESTRESSING
Finite-difference solutions of the alternate turbopump development high-pressure oxidizer turbopump pump-end ball-bearing cavity flows p 1678 N95-23617

PREVENTION
Adaptation of the advanced spray combustion code to cavitating flow problems p 1681 N95-23629

PRIMERS (COATINGS)
Organic coating technology for the protection of aircraft against corrosion p 1644 N95-23513

PRIMITIVE EQUATIONS
A numerical study of interannual wind forcing effects on the California current system, 1980-1983
[AD-A286023] p 1743 N95-23074

PRINTED CIRCUITS
Planar magnetic component development
[DE95-003311] p 1661 N95-22896

PRINTING
NASAwide electronic publishing system: Electronic printing and duplicating, stage-2 evaluation report (GSFC)
[NASA-TM-104615] p 1856 N95-23209

PRISMS
PRISM Spectrograph Optical Design
[NASA-CR-197965] p 1828 N95-24035

PRIVACY
Security clearances: Consideration of sexual orientation in the clearance process. Report to Congressional requesters
[GAO/NSIAD-95-21] p 1853 N95-23588

PROBABILITY DENSITY FUNCTIONS
Statistics of multi-look AIRSAR imagery: A comparison of theory with measurements p 1714 N95-23947

PROBABILITY THEORY
Stochastic decision analysis p 1854 N95-23305
Combinatorial semantics
[TR-563] p 1792 N95-23793
Properties of probabilistic pushdown automata
[TR-554] p 1760 N95-24056
Martin-Lof tests can help too
[TR-541] p 1797 N95-24063

PROBLEM SOLVING
Towards method-independent knowledge acquisition
[AD-A285823] p 1766 N95-22512
BEM solution to simulate the curvature driven deformation of a profile that is pressed into a plate of hot glass
[PB95-138913] p 1648 N95-23145
The initial-value problem for viscous channel flows
[NASA-CR-195034] p 1667 N95-23207
Two portable parallel tridiagonal solvers
[DE94-019044] p 1763 N95-23243
Spontaneous wave packet reduction
[DE94-634280] p 1851 N95-23454
Linearizing W-algebras
[DE94-634324] p 1790 N95-23457
Quasisymmetry equations for conventional stellarators
[NIFS-324] p 1836 N95-23572
Recent advances in Lanczos-based iterative methods for nonsymmetric linear systems
[NASA-CR-197950] p 1791 N95-23611
High performance techniques for space mission scheduling p 1618 N95-23758
Solution and reasoning reuse in space planning and scheduling applications p 1618 N95-23760
Empirical results on scheduling and dynamic backtracking p 1618 N95-23761
Integrating planning and reactive control p 1618 N95-23763
Automatic generation of efficient orderings of events for scheduling applications p 1618 N95-23764

PROCEDURES
Scientific and technical photography at NASA Langley Research Center p 1690 N95-23290
Integrating O/S models during conceptual design, part 2
[NASA-CR-197904] p 1622 N95-23399

PROCESS CONTROL (INDUSTRY)
Society of the plastic industry process emission initiatives p 1629 N95-23036
Vision-sensing image analysis for GTAW process control
[DE95-003936] p 1695 N95-23373
Investigation of arc length versus flange thickness while using an arc voltage controller
[DE95-003937] p 1695 N95-23374
Assessment of resin transfer molding process for the XM6 discharger, ERDEC SSP 93-64
[NIAR-94-2] p 1650 N95-23932

PRODUCT DEVELOPMENT
Product stewardship in the composites industry p 1628 N95-23027
The US molten carbonate fuel-cell development and commercialization effort
[DE94-019096] p 1728 N95-23162
Problems of predicting material property retention during long term service p 1644 N95-23514

PRODUCTION COSTS
A manufacturing database of advanced materials used in spacecraft structures p 1623 N95-23279
Information technology standards process guide
[DE95-003967] p 1857 N95-23574

PRODUCTION PLANNING
Scheduling with genetic algorithms p 1761 N95-23762
Automatic generation of efficient orderings of events for scheduling applications p 1618 N95-23764

PRODUCTIVITY
The associate principal astronomer telescope operations model p 1779 N95-23743

PROGRAM VERIFICATION (COMPUTERS)
Specification and verification of gate-level VHDL models of synchronous and asynchronous circuits
[NASA-CR-191608] p 1762 N95-22830
Temporal operators viewed as predicate transformers
[PB95-138996] p 1757 N95-23152
Operator procedure verification with a rapidly reconfigurable simulator p 1618 N95-23679
Attention focusing and anomaly detection in systems monitoring p 1769 N95-23683
Fracture mechanics life analytical methods verification testing
[NASA-CR-196555] p 1697 N95-24106

PROGRAMMING ENVIRONMENTS
OPUS: A new generation Knowledge Engineering Environment p 1760 N95-24176

PROGRAMMING LANGUAGES
LCM 3.0: A language for describing conceptual models. Syntax definition
[PB95-128005] p 1755 N95-22652
Algebra of lines and boxes
[PB95-130456] p 1787 N95-22768
DUALITY: A simple formalism for the analysis of UNITY
[PB95-135703] p 1763 N95-23166
Using Dedal to share and reuse distributed engineering design information p 1768 N95-23678
On helping by parity-like languages
[TR-553] p 1759 N95-23935

PROGRESS
Military bases: Environmental impact at closing installations. Report to Congressional requesters
[GAO/NSIAD-95-70] p 1735 N95-24057

PROJECT MANAGEMENT
Computer software design description for the Treated Effluent Disposal Facility (TEDF), Project L-045H, Operator Training Station (OTS)
[DE95-003065] p 1759 N95-24006
Search Hanford accessible reports electronically system configuration management plan
[DE95-004493] p 1857 N95-24089

PROJECT PLANNING
Structural Arrangement Trade Study. Volume 1: Reusable Hydrogen Composite Tank System (RHCTS) and Graphite Composite Primary Structures (GCPS). Executive summary
[NASA-CR-197685] p 1621 N95-23188

PROJECTILE CRATERING
Natural and orbital debris particles on LDEF's trailing and forward-facing surfaces p 1869 N95-23833
Debris and meteoroid proportions deduced from impact crater residue analysis p 1869 N95-23834
Image and compositional characteristics of the LDEF Big Guy impact crater p 1700 N95-23838
The effect of impact angle on craters formed by hypervelocity particles p 1700 N95-23839
Experimental investigation of the relationship between impact crater morphology and impacting particle velocity and direction p 1700 N95-23840
Determining orbital particle parameters of impacts into germanium using morphology analysis and calibration data from hypervelocity impact experiments in the laboratory p 1700 N95-23841
Cratering and penetration experiments in Teflon targets at velocities from 1 to 7 km/s p 1700 N95-23842

PROJECTILES
High-velocity penetrators
[DE95-001886] p 1698 N95-22500
Projectile penetration into representative targets
[DE95-003089] p 1698 N95-22726
SIMS chemical and isotopic analysis of impact features from LDEF experiments AO187-1 and AO187-2 p 1637 N95-23837

PROJECTIVE GEOMETRY
The Euler series of restricted Chow varieties
[DE94-628418] p 1785 N95-22626

PROPAGATION MODES
D3-D program overview
[DE95-003879] p 1837 N95-24086

PROPAGATION VELOCITY
Quench propagation study for full-length RHIC dipole magnets
[DE94-014089] p 1816 N95-22926

PROPELLANT CHEMISTRY
Advanced liquid oxygen (LO2) propellant conditioning concept testing
[NASA-TM-108477] p 1652 N95-22672

PROPELLANT COMBUSTION
A numerical procedure for analysis of finite rate reacting flows p 1671 N95-23422

PROPELLANT GRAINS
Ignition transient calculations in the Space Shuttle solid rocket motor p 1625 N95-23640
PROPELLANTS
Morphology of extinguished monolithic JA2 grains fired in a 30-mm Solid Propellant Electrothermal Chemical (SPETC) gun
| AD-A285792 | p 1652 N95-22506
PROPELLER BLADES
System for determining aerodynamic imbalance
| NASA-CASE-ARC-11913-1 | p 1688 N95-23377
PROPULSION
Eleventh Workshop for Computational Fluid Dynamic Applications in Rocket Propulsion
| NASA-CP-3221-PT-2 | p 1668 N95-23412
A generic efficient adaptive grid scheme for rocket propulsion modeling p 1670 N95-23418
Institute for Computational Mechanics in Propulsion (ICOMP)
| NASA-TM-106884 | p 1677 N95-23464
Eleventh Workshop for Computational Fluid Dynamic Applications in Rocket Propulsion, part 1
| NASA-CP-3221-PT-1 | p 1678 N95-23615
Airborne rotary air separator study
| NASA-CR-189099 | p 1614 N95-24053
PROPULSION SYSTEM CONFIGURATIONS
Alert-derivative bimodal space power and propulsion systems
| DE95-002754 | p 1624 N95-22905
Predicted performance of an integrated modular engine system
| NASA-CR-190787 | p 1625 N95-23791
Development of sensors for ceramic components in advanced propulsion systems
| NASA-CR-195324 | p 1689 N95-23795
PROPULSION SYSTEM PERFORMANCE
Alert-derivative bimodal space power and propulsion systems
| DE95-002754 | p 1624 N95-22905
Damage-mitigating control of a reusable rocket engine for high performance and extended life
| NASA-CR-4640 | p 1654 N95-23195
Radiation/convection coupling in rocket motors and plumes p 1669 N95-23414
An RL10A-3-3A rocket engine model using the rocket engine transient simulator (ROCETS) software
| NASA-CR-190786 | p 1625 N95-23790
Predicted performance of an integrated modular engine system
| NASA-CR-190787 | p 1625 N95-23791
Development of sensors for ceramic components in advanced propulsion systems
| NASA-CR-195324 | p 1689 N95-23795
PROTACTINIUM
The electronic structure of heavy element complexes
| DE95-003407 | p 1806 N95-23082
PROTECTIVE CLOTHING
Skin exposure: Assessing the hazard in the workplace p 1628 N95-23030
PROTECTIVE COATINGS
Advanced reflector materials for solar concentrators
| DE95-000248 | p 1726 N95-22547
The corrosion protection of 2219-T87 aluminum by organic and inorganic zinc-rich primers
| NASA-TP-3543 | p 1641 N95-23186
Evaluation of thermal barrier and PS-200 self-lubricating coatings in an air-cooled rotary engine
| NASA-CR-195445 | p 1614 N95-23222
Protective coating for ceramic materials
| NASA-CASE-ARC-11969-1-CU | p 1649 N95-23394
Corrosion protection measures for CFC/metal joints of fuel integral tank structures of advanced military aircraft p 1644 N95-23510
Performance characterization of EURECA retroreflectors with fluoropolymer-filled SiO(x) protective coatings p 1651 N95-23802
Effect of the space environment on materials flown on the EURECA/TICCE-HVI experiment p 1623 N95-23803
Atomic oxygen interactions with protected organic materials on the Long Duration Exposure Facility (LDEF) p 1627 N95-23909
Organic matrix composite protective coatings for space applications p 1627 N95-23914
Robotic weld overlay coatings for erosion control
| DE95-002624 | p 1696 N95-24141
PROTEIN SYNTHESIS
Open problems of computational molecular biology
| DE95-000895 | p 1745 N95-22866
Analysis of structural domains required for phytochrome function by in vitro mutagenesis
| DE94-016230 | p 1745 N95-22884
PROTEINS
Comparison of the rate constants for energy transfer in the light-harvesting protein, C-phycocyanin, calculated from Foerster's theory and experimentally measured by time-resolved fluorescence spectroscopy
| DE94-014961 | p 1745 N95-22590
General crystal in prebiotic context
| DE94-628475 | p 1840 N95-22774
Regulation of alcohol fermentation in Escherichia coli
| DE94-016227 | p 1745 N95-22874
Analysis of structural domains required for phytochrome function by in vitro mutagenesis
| DE94-016230 | p 1745 N95-22884
An improved system for exon recognition and gene modeling in human DNA sequences
| DE94-017863 | p 1746 N95-22890
Protein folding and protein metallocluster studies using synchrotron small angler x ray scattering
| DE95-003339 | p 1746 N95-22897
Activation of the jun-D gene in human myeloid cells by 1-(beta)-D-arabinofuranosylcytosine
| DE94-016591 | p 1746 N95-22912
Rearrangement of RAG-1 recombinase gene in radiation-sensitive wasted mice
| DE94-017083 | p 1746 N95-22913
The origin of chirality in protein amino acids
| DE94-628491 | p 1747 N95-23058
Diffusion behavior of lysozyme in aqueous ammonium sulfate solutions under varying solution conditions as determined by dynamic light scattering
| DE95-004821 | p 1635 N95-23380
A comparative study of the effects of clofibrate, ciprofibrate, WY-14,643, and di-(2-ethylhexyl)-phthalate on liver protein expression in mice
| DE94-016587 | p 1748 N95-23771
Relationships between pigment composition variation and reflectance for plant species from a coastal savannah in California p 1709 N95-23889
PROTOCOL (COMPUTERS)
Precise clock synchronization protocol
| PB95-127247 | p 1687 N95-22536
Layered Electrical Product Application Protocol (AP)
| DE95-001524 | p 1754 N95-22548
Specification and verification of gate-level VHDL models of synchronous and asynchronous circuits
| NASA-CR-191608 | p 1762 N95-22830
Hierarchical membership protocol for synchronous distributed systems
| PB95-138947 | p 1763 N95-23129
Automatic verification of regular protocols in P/T nets
| PB95-138921 | p 1789 N95-23146
Verifying sequentially consistent memory using interface refinement
| PB95-139002 | p 1752 N95-23153
Application Protocol, Initial Graphics Exchange Specification (IGES), Layered Electrical Product
| DE95-004266 | p 1757 N95-23337
Modelling and analysis of a high speed data bus with predicate/transition nets
| PB95-140695 | p 1764 N95-23538
Using Dedal to share and reuse distributed engineering design information p 1768 N95-23678
Algorithms for categorizing multiprocessor communication under invalidate and update-based coherence protocols
| TR-533-REV | p 1759 N95-23928
Eliminating useless messages in write-update protocols on scalable multiprocessors
| TR-539 | p 1764 N95-24037
A computational theory of grounding in natural language conversation
| TR-545 | p 1760 N95-24058
Using simple page placement policies to reduce the cost of cache fills in coherent shared-memory systems
| TR-535 | p 1753 N95-24177
Lazy release consistency for hardware-coherent multiprocessors
| TR-547 | p 1765 N95-24184
PROTON BEAMS
Search for scalar and vector leptoquarks in electron-proton collisions at radical S = 300 GeV
| DE94-785267 | p 1810 N95-23475
High current induction linacs
| DE95-003442 | p 1818 N95-24014
PROTON RESONANCE
Phonon characteristics of high (T sub c) superconductors from neutron Doppler broadening measurements
| DE95-003703 | p 1844 N95-24076
PROTON-PROTON REACTIONS
Searches for the H-dibaryon at the AGS
| DE95-003091 | p 1802 N95-22727
Search for second generation leptoquarks at CDF
| DE94-018983 | p 1805 N95-22939
Testing QCD with jet physics at CDF
| DE94-018980 | p 1807 N95-23196
Search for top quark at CDF
| DE95-003748 | p 1809 N95-23406
PROTONS
Dimuon production in proton-nucleus interactions
| DE95-002613 | p 1801 N95-22551
Hot proton anisotropies and cool proton temperatures in the outer magnetosphere
| DE95-002719 | p 1736 N95-22850
Exotic atoms
| DE95-003199 | p 1805 N95-22881
An upper bound for the proton temperature anisotrophy
| DE95-002752 | p 1737 N95-22903
Geometrical interpretation for the outer SU(3) outer multiplicity label p 1814 N95-22968
ESTAR, PSTAR, ASTAR: A PC package for calculating stopping powers and ranges of electrons, protons and helium ions, version 2
| DE94-634435 | p 1811 N95-23773
Measurement of trapped proton fluences in main stack of P0006 experiment p 1815 N95-23812
Contribution of proton-induced short range secondaries to the LET spectra on LDEF p 1815 N95-23813
PROTOTYPES
The STAR EM calorimeter design and small prototype test results
| DE95-004592 | p 1689 N95-23583
Toward an automated signature recognition toolkit for mission operations p 1659 N95-23682
PROVING
Stoermer-Cowell: Straight, summed and split. An overview
| PB95-139341 | p 1789 N95-23200
Fourth order difference methods for hyperbolic IBVP's
| NASA-CR-197955 | p 1791 N95-23548
PSEUDOMONAS
Biotransformation of an uncured composite material p 1629 N95-23033
PSEUDOPOTENTIALS
Electrical resistivity of liquid alkali metals and non-local pseudopotential
| DE94-627417 | p 1639 N95-22608
Non local pseudopotentials, transport properties of liquid noble metals
| DE94-627416 | p 1640 N95-22840
PUBLIC HEALTH
How health risk from radiation is assessed
| DE95-003477 | p 1749 N95-23142
Closing the circle on the splitting of the atom: The environmental legacy of nuclear weapons production in the United States and what the Department of Energy is doing about it p 1818 N95-23562
PULSARS
Using the shield for thermal energy storage in PULSAR
| DE95-002457 | p 1829 N95-22645
Gamma ray emission from radio pulsars
| NASA-CR-197917 | p 1871 N95-22910
ROSAT observation program
| NASA-CR-197683 | p 1866 N95-23595
PULSE COMMUNICATION
Proposal of a Modified EBU method for reliable evaluation of picture quality
| NHK-LABS-NOTE-431 | p 1863 N95-24180
PULSED LASERS
Coherent control in simple quantum systems p 1826 N95-23005
PULSED RADIATION
Production of high contrast ultrashort laser pulses for short scale length plasma experiments
| DE95-003640 | p 1690 N95-22595
Pulsed Ion Beam Surface Treatment for preparing rapidly solidified corrosion resistant alloy surfaces
| DE94-012072 | p 1640 N95-22835
ROSAT observation program
| NASA-CR-197683 | p 1866 N95-23595
PUMP IMPELLERS
Impeller flow field characterization with a laser two-focus velocimeter p 1675 N95-23440
Comparison between predicted and experimentally measured flow fields at the exit of the SSME HPFTP impeller p 1679 N95-23622
Use of blade lean in turbomachinery redesign p 1680 N95-23625
CFD parametric study of consortium impeller p 1680 N95-23626
Incompressible Navier-Stokes calculations in pump flows p 1680 N95-23627
PUMPS
Current status in cavitation modeling p 1681 N95-23632
PYROLYSIS
Novel mass spectrometric instrument for gaseous and particulate characterization and monitoring
| DE95-001135 | p 1687 N95-22682

High surface area, high permeability carbon monoliths
[DE95-004555] p 1650 N95-23577
PYROXENES
Mapping of the Ronda peridotite massif (Spain) from AVIRIS spectro-imaging survey: A first attempt
p 1707 N95-23878

Q

Q FACTORS
Alpha spectral analysis via artificial neural networks
[DE95-004567] p 1767 N95-23578
QUADRATIC PROGRAMMING
A new look at the simultaneous analysis and design of structures p 1700 N95-23327
QUADRUPOLES
Multipole contribution from an off-axis orbit in an IR quadrupole and the consequences on the dynamic aperture
[DE95-002874] p 1816 N95-22567
Interdigital-H linac for unstable nuclei at INS
[DE94-765448] p 1816 N95-22644
A heavy ion linac complex for unstable nuclei
[DE94-765443] p 1816 N95-22848
Phase space analysis in anisotropic optical systems
p 1826 N95-23007
QUALITY
The airline quality report, 1994
[NIAR-94-11] p 1610 N95-24012
Approaches to 100 Gbit/sq. in. recording density
p 1690 N95-24128
QUALITY CONTROL
Product stewardship in the composites industry
p 1628 N95-23027
Technical report series on global modeling and data assimilation. Volume 4: Documentation of the Goddard Earth Observing System (GEOS) data assimilation system, version 1
[NASA-TM-104606-VOL-4] p 1740 N95-23529
Extraction of auxiliary data from AVIRIS distribution tape for spectral, radiometric, and geometric quality assessment p 1706 N95-23875
Assessment of resin transfer molding process for the XM6 discharger, ERDEC SSP 93-64
[NIAR-94-2] p 1650 N95-23932
Optical storage media data integrity studies
p 1829 N95-24130
QUANTITATIVE ANALYSIS
Evaluation of neutron techniques for illicit substance detection
[DE95-002988] p 1632 N95-22764
Nonlinear thermoviscoelastic behaviour in complex materials
[PB95-140653] p 1630 N95-23537
The effects of AVIRIS atmospheric calibration methodology on identification and quantitative mapping of surface mineralogy, Drum Mountains, Utah
p 1705 N95-23870
Extraction of auxiliary data from AVIRIS distribution tape for spectral, radiometric, and geometric quality assessment p 1706 N95-23875
Laboratory spectra of field samples as a check on two atmospheric correction methods p 1711 N95-23894
Chemical recognition software
[DE95-003346] p 1636 N95-24007
QUANTUM CHROMODYNAMICS
Commensurate scale relations: Precise tests of quantum chromodynamics without scale or scheme ambiguity
[DE95-002785] p 1847 N95-22566
New preliminary results on the physics of charm hadroproduction subprocesses
[DE95-002530] p 1801 N95-22646
Perturbative QCD tests from the LEP, HERA, and TEVATRON colliders
[DE95-001285] p 1816 N95-22684
Bottom-quark production from muon-jet and dimuon events in p(bar p)-interactions at the square root of s = 1.8 TeV
[DE95-001286] p 1801 N95-22685
QCD test in three-jet Z(sup 0) decays at SLD and detector development for H(sup 0) yields gamma gamma searches in high energy hadron colliders
[DE95-003336] p 1848 N95-22698
QCD improved exclusive rare B-decays at the heavy b-quark limit
[DE94-628609] p 1802 N95-22720
How to measure the Q(bar Q) potential in a light-front calculation
[DE95-003200] p 1848 N95-22728
Chiral symmetry breaking in QCD with linearly rising confinement potential
[DE94-628559] p 1848 N95-22744
Spontaneous breaking of chiral symmetry as a consequence of confinement
[DE94-628560] p 1849 N95-22745
The problem of phase transition and the heavy ion collisions at very high energies
[DE94-628584] p 1816 N95-22785
Baryon number fluctuations in a quark-hadron phase transition
[DE94-628585] p 1804 N95-22786
Search for second generation leptoquarks at CDF
[DE94-018983] p 1805 N95-22939
Boson mapping techniques applied to constant gauge fields in QCD p 1814 N95-22969
Singlet quarks beyond the top at the tevatron
[PB95-139127] p 1807 N95-23158
Testing QCD with jet physics at CDF
[DE94-018980] p 1807 N95-23196
Properties of jets in Z events from 1.8 TeV (bar p)p collisions
[DE94-018982] p 1808 N95-23197
Measurement of correlated b quark cross sections at CDF
[DE95-004240] p 1808 N95-23336
The impact of QCD and light-cone quantum mechanics on nuclear physics
[DE95-004293] p 1851 N95-23352
Theoretical aspects of electroweak and other interactions in medium energy nuclear physics
[DE95-004341] p 1808 N95-23357
Spin physics in the next decade
[DE95-003727] p 1809 N95-23403
Study of b(anti b) production in e(+)e(-) annihilation at radical s = 29 GeV with the aid of neural networks
[DE95-004691] p 1810 N95-23488
QUANTUM EFFICIENCY
Resonant infrared detector with substantially unit quantum efficiency
[NASA-CASE-ARC-11940-1-SB] p 1827 N95-23378
QUANTUM ELECTRODYNAMICS
A space-time lattice version of scalar electrodynamics
[DE94-628577] p 1850 N95-22784
The omega pi(sup 0)-transient form factor within effective chiral Lagrangian approach
[DE94-628612] p 1850 N95-22812
QUANTUM MECHANICS
Resonant shallow donor magnetopolaron effect in a GaAs/AlGaAs quantum dot in high magnetic fields
[DE94-629039] p 1798 N95-22497
Berry phase by description of the quantum systems in the Kustaanheimo-Stiefel bundle
[DE94-628410] p 1847 N95-22620
On the (DE-) stabilization of quantum mechanical binding by potential barriers
[DE94-628433] p 1847 N95-22635
First quantized noncritical relativistic Polyakov string
[DE94-628513] p 1848 N95-22738
The torsion space nucleic acids molecular mechanics program DUPLEX: Surveying conformation space by potential energy minimization
[DE94-017707] p 1805 N95-22889
Algebraic theory of molecules p 1814 N95-22958
Exact, E = 0, classical and quantum solutions for general power-law oscillators p 1820 N95-22959
A supersymmetric family of harmonic oscillators simulating H-bonds in DNA p 1748 N95-22963
Molecular vibrational states during a collision
p 1814 N95-22964
A possible generalization of the harmonic oscillator potential p 1822 N95-22970
Harmonic oscillator in quantum rotational spectra: Molecules and nuclei p 1814 N95-22972
Covariant deformed oscillator algebras
p 1797 N95-22978
Localization in deformed quantum mechanics
p 1823 N95-22979
Wigner distribution function and entropy of the damped harmonic oscillator within the theory of the open quantum systems p 1798 N95-22990
Covariant harmonic oscillators and coupled harmonic oscillators p 1825 N95-22992
On pseudosupersymmetric oscillators and reality of relativistic energies for vector mesons
p 1815 N95-22994
Supersymmetric oscillator in optics
p 1826 N95-23002
Coherent control in simple quantum systems
p 1826 N95-23005
The impact of QCD and light-cone quantum mechanics on nuclear physics
[DE95-004293] p 1851 N95-23352
Spontaneous wave packet reduction
[DE94-634280] p 1851 N95-23454
QUANTUM NUMBERS
Coherent state constructions of bases for some physically relevant group chains p 1814 N95-22966
QUANTUM OPTICS
Second International Workshop on Harmonic Oscillators
[NASA-CP-3286] p 1820 N95-22957
Slightly anharmonic systems in quantum optics
p 1826 N95-23004
Phase space analysis in anisotropic optical systems
p 1826 N95-23007
QUANTUM STATISTICS
q-bosons and the q-analogue quantized field
p 1814 N95-22984
QUANTUM THEORY
Unification of electromagnetic, strong and weak interaction
[DE94-628570] p 1655 N95-22746
One loop renormalization of Chern-Simons field theory in operator regularization
[DE94-628508] p 1796 N95-22751
Lectures on 2D gauge theories. Topological aspects and path integral techniques
[DE94-628509] p 1849 N95-22752
Gauge dependence and new kind of two-dimensional gravity theory with trivial quantum corrections
[DE94-628502] p 1850 N95-22776
A space-time lattice version of scalar electrodynamics
[DE94-628577] p 1850 N95-22784
(pi)- and a(sub 1)-meson physics in current algebra at the quark level
[DE94-628611] p 1804 N95-22811
Quantum field between moving mirrors: A three dimensional example p 1821 N95-22965
Scattering problem for quantum system with time-dependent periodic Hamiltonian
[DE94-635421] p 1797 N95-23965
The kinetics of quantum system with time-dependent periodic Hamiltonian
[DE94-635422] p 1797 N95-23966
The point interactions in the quantum problem of three particles with internal structure
[DE94-635423] p 1851 N95-23967
Quantum fluctuations of D(sub 5d) polarons on C(sub 60) molecules
[DE94-635787] p 1812 N95-23985
Subband quantum scattering times for AlGaAs/GaAs obtained using digital filtering
[NASA-TM-106873] p 1846 N95-24188
QUANTUM WELLS
Optical absorption in an indirect-gap semiconductor quantum well systems
[DE94-628878] p 1849 N95-22759
Two-photon absorption in an indirect-gap semiconductor quantum well systems 1. Interband transitions
[DE94-628879] p 1849 N95-22760
Two-photon absorption in an indirect-gap semiconductor quantum well systems 2. Excitonic transitions
[DE94-628880] p 1849 N95-22761
Photoemission study of quantum confinement by a finite barrier: Cu/Co(wedge)/Cu(100)
[DE95-002913] p 1840 N95-22762
Spin polarized photoemission studies of magnetic quantum well states
[DE95-004218] p 1851 N95-23335
QUARK MODELS
Experimental results on polarized structure functions in deep inelastic lepton-nucleon scattering
[DE95-002782] p 1801 N95-22521
QCD improved exclusive rare B-decays at the heavy b-quark limit
[DE94-628609] p 1802 N95-22720
(pi)- and a(sub 1)-meson physics in current algebra at the quark level
[DE94-628611] p 1804 N95-22811
The convergence radius of the chiral expansion in the Dyson-Schwinger approach
[DE94-012852] p 1805 N95-22925
QUARKS
Dimuon production in proton-nucleus interactions
[DE95-002613] p 1801 N95-22551
Commensurate scale relations: Precise tests of quantum chromodynamics without scale or scheme ambiguity
[DE95-002785] p 1847 N95-22566
New preliminary results on the physics of charm hadroproduction subprocesses
[DE95-002530] p 1801 N95-22646
Bottom-quark production from muon-jet and dimuon events in p(bar p)-interactions at the square root of s = 1.8 TeV
[DE95-001286] p 1801 N95-22685
QCD improved exclusive rare B-decays at the heavy b-quark limit
[DE94-628609] p 1802 N95-22720
How to measure the Q(bar Q) potential in a light-front calculation
[DE95-003200] p 1848 N95-22728
Chiral symmetry breaking in QCD with linearly rising confinement potential
[DE94-628559] p 1848 N95-22744
Spontaneous breaking of chiral symmetry as a consequence of confinement
[DE94-628560] p 1849 N95-22745

Chiral anomalies in non-leptonic decays within chiral perturbation theory at the quark level
[DE94-628613] p 1849 N95-22753
On the D yields K-bar(sup *)e(sup +)(nu)(sub e) form factors
[DE94-628614] p 1803 N95-22754
To the problem of D-meson leptonic and semileptonic decays
[DE94-628615] p 1803 N95-22755
The problem of phase transition and the heavy ion collisions at very high energies
[DE94-628584] p 1816 N95-22785
The U(3) x U(3) Nambu - Jona-Lasinio model with the gluon condensate and axial anomaly at finite temperature
[DE94-628588] p 1804 N95-22787
Hadrons of arbitrary spin and heavy quark symmetry
[DE94-628597] p 1804 N95-22789
The decays of D(sup *)-mesons
[DE94-628610] p 1804 N95-22810
The convergence radius of the chiral expansion in the Dyson-Schwinger approach
[DE94-012852] p 1805 N95-22925
Search for second generation leptoquarks at CDF
[DE94-018983] p 1805 N95-22939
Heavy quark physics at SLD: Preliminary results
[DE95-003372] p 1806 N95-23138
Flavour dependence of form factors in heavy meson decays
[PB95-139101] p 1807 N95-23156
Singlet quarks beyond the top at the tevatron
[PB95-139127] p 1807 N95-23158
Measurement of correlated b quark cross sections at CDF
[DE95-004240] p 1808 N95-23336
Search for top quark at CDF
[DE95-003748] p 1809 N95-23406
Search for scalar and vector leptoquarks in electron-proton collisions at radical S = 300 GeV
[DE94-785267] p 1810 N95-23475
Electroweak physics from the Tevatron
[DE95-002213] p 1810 N95-23530
A measurement of the mass of the W vector boson at CDF
[DE95-003498] p 1813 N95-24016

QUARTZ
Reflectivity studies on adsorbed block copolymers under shear
[DE95-003676] p 1649 N95-23568

QUASARS
Multiband VLBI imaging of the jet in 3C 345
[PB95-139275] p 1866 N95-23468

QUATERNIONS
Notes on oscillator-like interactions of various spin relativistic particles p 1815 N95-22997

QUENCHING (COOLING)
Quench propagation study for full-length RHIC dipole magnets
[DE94-014089] p 1816 N95-22926

QUERY LANGUAGES
Overview of Ph.D. theses and memoranda, 1993
[PB95-135190] p 1756 N95-23071
Modelling and analysis of a high speed data bus with predicate/transition nets
[PB95-140695] p 1764 N95-23538

R

RACAH COEFFICIENT
The role of SU(2) 3n-j coefficients in SU(3)
[DE95-002726] p 1796 N95-22900

RACETRACKS (PARTICLE ACCELERATORS)
The project of high free electron laser using race-track microtron-recuperator
[DE94-634034] p 1692 N95-23657

RADAR DATA
Combining optical and microwave remote sensing data of forest vegetation: MAC Europe 1991
[PB95-127312] p 1717 N95-22538
Monitoring land use and degradation using satellite and airborne data p 1707 N95-23880
Summaries of the 4th Annual JPL Airborne Geoscience Workshop. Volume 3: AIRSAR Workshop
[NASA-CR-197354-VOL-3] p 1712 N95-23938
AIRSAR views of aerolian terrain p 1713 N95-23941
Forest investigations by polarimetric AIRSAR data in the Harz mountains p 1713 N95-23944
Comparison of inversion models using AIRSAR data for Death Valley, California p 1713 N95-23945
Geologic mapping using integrated AIRSAR, AVIRIS, and TIMS data p 1714 N95-23946
Statistics of multi-look AIRSAR imagery: A comparison of theory with measurements p 1714 N95-23947
Current and future use of TOPSAR digital topographic data for volcanological research p 1714 N95-23949
MAC Europe 1991 campaign: AIRSAR/AVIRIS data integration for agricultural test site classification p 1715 N95-23952
Measurement of ocean wave spectra using polarimetric AIRSAR data p 1715 N95-23953
An improved algorithm for retrieval of snow wetness using C-band AIRSAR p 1715 N95-23954
Polarimetric radar data decomposition and interpretation p 1715 N95-23955
Classification and soil moisture determination of agricultural fields p 1716 N95-23958
Relating P-band AIRSAR backscatter to forest stand parameters p 1716 N95-23959
Soil moisture retrieval in the Oberpfaffenhofen testsite using MAC Europe AIRSAR data p 1716 N95-23960
Microwave dielectric properties of boreal forest trees p 1716 N95-23961
ASF archive issues: Current status, past history, and questions for the future p 1861 N95-24133

RADAR ECHOES
Unusual radar echoes from the Greenland ice sheet p 1714 N95-23951

RADAR EQUIPMENT
A perspective on space robotics in Japan p 1697 N95-23695

RADAR IMAGERY
Remote identification of a gravel laden Pleistocene river bed p 1712 N95-23921
Summaries of the 4th Annual JPL Airborne Geoscience Workshop. Volume 3: AIRSAR Workshop
[NASA-CR-197354-VOL-3] p 1712 N95-23938
Interferometric synthetic aperture radar imagery of the Gulf Stream p 1712 N95-23939
AIRSAR views of aerolian terrain p 1713 N95-23941
Glaciological studies in the central Andes using AIRSAR/TOPSAR p 1713 N95-23942
Estimation of biophysical properties of upland Sitka spruce (Picea sitchensis) plantations p 1713 N95-23943
Forest investigations by polarimetric AIRSAR data in the Harz mountains p 1713 N95-23944
Statistics of multi-look AIRSAR imagery: A comparison of theory with measurements p 1714 N95-23947
AIRSAR deployment in Australia, September 1993: Management and objectives p 1714 N95-23948
Preliminary analysis of the sensitivity of AIRSAR images to soil moisture variations p 1714 N95-23950
MAC Europe 1991 campaign: AIRSAR/AVIRIS data integration for agricultural test site classification p 1715 N95-23952
Measurement of ocean wave spectra using polarimetric AIRSAR data p 1715 N95-23953
Polarimetric radar data decomposition and interpretation p 1715 N95-23955
Synergy between optical and microwave remote sensing to derive soil and vegetation parameters from MAC Europe 1991 Experiment p 1715 N95-23956
SAR terrain classifier and mapper of biophysical attributes p 1715 N95-23957
Relating P-band AIRSAR backscatter to forest stand parameters p 1716 N95-23959
Soil moisture retrieval in the Oberpfaffenhofen testsite using MAC Europe AIRSAR data p 1716 N95-23960

RADAR MAPS
Differential GPS and system integration of the Low Visibility Landing and Surface Operations (LVLASO) demonstration p 1611 N95-23318
MAX-91: Polarimetric SAR results on Montespertoli site p 1712 N95-23940
Geologic mapping using integrated AIRSAR, AVIRIS, and TIMS data p 1714 N95-23946
Unusual radar echoes from the Greenland ice sheet p 1714 N95-23951

RADAR MEASUREMENT
Study of atmospheric parameters measurements using MM-wave radar in synergy with LITE-2 p 1741 N95-23278

RADAR SCATTERING
A uniform geometrical optics and an extended uniform geometrical theory of diffraction for evaluating high frequency EM fields near smooth caustics and composite shadow boundaries
[NASA-CR-197934] p 1657 N95-23391
Interferometric synthetic aperture radar imagery of the Gulf Stream p 1712 N95-23939
Estimation of biophysical properties of upland Sitka spruce (Picea sitchensis) plantations p 1713 N95-23943
Preliminary analysis of the sensitivity of AIRSAR images to soil moisture variations p 1714 N95-23950
Unusual radar echoes from the Greenland ice sheet p 1714 N95-23951
Polarimetric radar data decomposition and interpretation p 1715 N95-23955
Synergy between optical and microwave remote sensing to derive soil and vegetation parameters from MAC Europe 1991 Experiment p 1715 N95-23956
SAR terrain classifier and mapper of biophysical attributes p 1715 N95-23957
Classification and soil moisture determination of agricultural fields p 1716 N95-23958
Relating P-band AIRSAR backscatter to forest stand parameters p 1716 N95-23959
Soil moisture retrieval in the Oberpfaffenhofen testsite using MAC Europe AIRSAR data p 1716 N95-23960
Microwave dielectric properties of boreal forest trees p 1716 N95-23961

RADAR SIGNATURES
AIRSAR views of aerolian terrain p 1713 N95-23941
Measurement of ocean wave spectra using polarimetric AIRSAR data p 1715 N95-23953

RADAR TRACKING
SWIFT BOAT 1994: Using a fast chase boat to investigate offshore weather features in conjunction with WSR-88D observations
[PB94-195146] p 1742 N95-22651
Motion-sensitive optical correlator using a VanderLugt correlator
[NASA-CASE-NPO-18769-1-CU] p 1827 N95-23045

RADIAL FLOW
Enhanced analysis and users manual for radial-inflow turbine conceptual design code RTD
[NASA-CR-195454] p 1609 N95-23462
Physical mechanism determining the radial electric field and its radial structure in a toroidal plasma
[NIFS-313] p 1835 N95-23534
Current-profile flattening and hot core shift due to the nonlinear development of resistive kink mode
[NIFS-311] p 1835 N95-23564

RADIAL VELOCITY
Unsteady flow simulations in support of the SSME HEX turning vane cracking investigation with the ATD HPOTP p 1679 N95-23621

RADIANCE
A tool for manual endmember selection and spectral unmixing p 1701 N95-23846
AVIRIS calibration using the cloud-shadow method p 1702 N95-23849
Instantaneous field of view and spatial sampling of the Airborne Visible/Infrared Imaging Spectrometer (AVIRIS) p 1702 N95-23851
Comparison of methods for calibrating AVIRIS data to ground reflectance p 1703 N95-23854
Estimation of aerosol optical depth and additional atmospheric parameters for the calculation of apparent reflectance from radiance measured by the Airborne Visible/Infrared Imaging Spectrometer p 1704 N95-23863
A proposed update to the solar irradiance spectrum used in LOWTRAN and MODTRAN p 1705 N95-23865

RADIANT FLUX DENSITY
Radiation/convection coupling in rocket motors and plumes p 1669 N95-23414

RADIATION
How health risk from radiation is assessed
[DE95-003477] p 1749 N95-23142

RADIATION ABSORPTION
Theoretical studies of spectroscopic problems of importance for atmospheric radiation measurements p 1741 N95-23329
Computer modeling of the sensitivity of a laser water vapor sensor to variations in temperature and air speed p 1692 N95-23330

RADIATION CHEMISTRY
Test procedure for cation exchange chromatography
[DE95-003770] p 1808 N95-23350
Annual report of the Osaka Laboratory for Radiation Chemistry Japan Atomic Energy Research Institute, (No. 26)
[DE94-785277] p 1626 N95-23477

RADIATION COUNTERS
QCD test in three-jet Z(sup 0) decays at SLD and detector development for H(sup 0) yields gamma gamma searches in high energy hadron colliders
[DE95-003336] p 1848 N95-22698
The probabilistic structure of sprays: Implications for measurements by in site particle counters
[DE95-002483] p 1666 N95-23081
VLPC characterization for the Dzero upgrade
[DE95-003742] p 1818 N95-24084

RADIATION DAMAGE
Study of radiation damages in AISI 316 and 347 steels
[DE94-627480] p 1639 N95-22609
Rearrangement of RAG-1 recombinase gene in radiation-sensitive wasted mice
[DE94-017083] p 1746 N95-22913

Cation disorder determined by MAS Al-27 NMR in high dose neutron irradiated spinel
| DE95-003681 | p 1842 N95-23266
Application of electron paramagnetic resonance imaging to the characterization of the Ultem(R) exposed to 1 MeV electrons. Correlation of radical density data to tiger code calculations p 1815 N95-23328
The effect of simulated low earth orbit radiation on polyimides (UV degradation study) p 1651 N95-23903
The surface properties of fluorinated polyimides exposed to VUV and atomic oxygen p 1651 N95-23904
Temperature effects on ion irradiation damage in MgAl2O4 spinel single crystals
| DE95-003679 | p 1844 N95-24073

RADIATION DETECTORS
SVX(prime), the new CDF silicon vertex detector
| DE94-018986 | p 1689 N95-23521
Doing photons with MERLIN 2 at Oroville p 1815 N95-23816
TRACKER: A three-dimensional raytracing program for ionospheric radio propagation
| DE95-003510 | p 1658 N95-24015

RADIATION DISTRIBUTION
Gamma ray emission from radio pulsars
| NASA-CR-197917 | p 1871 N95-22910
q-bosons and the q-analogue quantized field p 1814 N95-22984

RADIATION DOSAGE
How health risk from radiation is assessed
| DE95-003477 | p 1749 N95-23142
Preliminary results of radiation measurements on EURECA p 1872 N95-23801
Absorbed dose and LET spectra measurements on LDEF p 1815 N95-23810
Fission foil measurements of neutron and proton fluences in the A0015 experiment p 1815 N95-23811
Germination, growth rates, and electron microscope analysis of tomato seeds flown on the LDEF p 1748 N95-23821

RADIATION EFFECTS
Study of photorefractive non-linearities in the 3-5 and 2-4 semi-insulator compounds: The effect of electron irradiation
| PB94-189057 | p 1839 N95-22584
Modeling NO(x) emissions in turbulent jet flames: Effects of buoyancy and radiation
| DE94-016621 | p 1633 N95-22886
Summary of solar cell data from the Long Duration Exposure Facility (LDEF)
| NASA-CR-196539 | p 1727 N95-22904
Genetic effects on heavy ions in drosophila
| NASA-CR-197916 | p 1746 N95-22911
COYOTE 2: A Finite Element Computer Program for noonlinear heat conduction problems
| DE95-002848 | p 1666 N95-22914
How health risk from radiation is assessed
| DE95-003477 | p 1749 N95-23142
Annual report of the Osaka Laboratory for Radiation Chemistry Japan Atomic Energy Research Institute, (No. 26)
| DE94-785277 | p 1626 N95-23477
Preliminary results of radiation measurements on EURECA p 1872 N95-23801
Contribution of proton-induced short range secondaries to the LET spectra on LDEF p 1815 N95-23813
Germination, growth rates, and electron microscope analysis of tomato seeds flown on the LDEF p 1748 N95-23821
Temperature effects on ion irradiation damage in MgAl2O4 spinel single crystals
| DE95-003679 | p 1844 N95-24073
Effect of dynamically charged helium on mechanical properties of vanadium-base alloys
| DE95-004613 | p 1646 N95-24153
A phenomenological model for the effect of nanocrystalline microstructure on irradiation-induced amorphization in U3Si
| DE95-004631 | p 1846 N95-24169

RADIATION HARDENING
SVX(prime), the new CDF silicon vertex detector
| DE94-018986 | p 1689 N95-23521

RADIATION HAZARDS
Genetic effects on heavy ions in drosophila
| NASA-CR-197916 | p 1746 N95-22911

RADIATION MEASUREMENT
Preliminary results of radiation measurements on EURECA p 1872 N95-23801
LDEF contributions to cosmic ray and radiation environments research p 1872 N95-23805
Fission foil measurements of neutron and proton fluences in the A0015 experiment p 1815 N95-23811
Predictions of LDEF radioactivity and comparison with measurements p 1815 N95-23818
Status of LDEF radiation modeling p 1815 N95-23819

RADIATION SHIELDING
Thermal outgassing studies on machinable tungsten and TZM molybdenum alloy
| DE95-002984 | p 1638 N95-22592
Using the shield for thermal energy storage in PULSAR
| DE95-002457 | p 1829 N95-22645
Closing the circle on the splitting of the atom: The environmental legacy of nuclear weapons production in the United States and what the Department of Energy is doing about it p 1818 N95-23562
Preliminary results of radiation measurements on EURECA p 1872 N95-23801
Contribution of proton-induced short range secondaries to the LET spectra on LDEF p 1815 N95-23813

RADIATION SOURCES
Large-sized and highly radioactive H-3 and Cd-109 Langmuir-Blodgett films
| DE94-785270 | p 1811 N95-23775
Some thoughts of future experiments with the new generation of storage rings
| DE95-004602 | p 1818 N95-24162
Atomic physics at high brilliance synchrotron sources: Proceedings
| DE95-006077 | p 1813 N95-24174

RADIATION SPECTRA
Alpha spectral analysis via artificial neural networks
| DE95-004567 | p 1767 N95-23578

RADIATIVE TRANSFER
Radiation/convection coupling in rocket motors and plumes p 1669 N95-23414
Application of a two-stream radiative transfer model for leaf lignin and cellulose concentrations from spectral reflectance measurements, part 1 p 1703 N95-23856
Application of a two-stream radiative transfer model for leaf lignin and cellulose concentrations from spectral reflectance measurements, part 2 p 1703 N95-23857
A proposed update to the solar irradiance spectrum used in LOWTRAN and MODTRAN p 1705 N95-23865
Atmospheric correction of AVIRIS data of Monterey Bay contaminated by thin cirrus clouds p 1710 N95-23890
Thermal radiant exitance model performance: Soils and forests
| DE95-003619 | p 1721 N95-24148
Land surface temperature measurements from EOS MODIS data
| NASA-CR-197969 | p 1721 N95-24190

RADICALS
Magnetic resonance and optical spectroscopic studies of carotenoids
| DE95-003729 | p 1631 N95-22575
Jacobson radicals in matrix near rings
| DE94-628424 | p 1796 N95-22808

RADII
Note on the computational complexity of j-radii of polytopes in (R sup n)
| PB95-139358 | p 1790 N95-23231

RADIO ASTRONOMY
Gamma ray emission from radio pulsars
| NASA-CR-197917 | p 1871 N95-22910

RADIO COMMUNICATION
Investigation of Federal Standard 1045 high-frequency ALE radio performance in the Southern Trans-Auroral Zone
| PB94-204831 | p 1655 N95-22636
Utilizing a TDRS satellite for direct broadcast satellite-radio propagation experiments and demonstrations p 1622 N95-22814

RADIO FREQUENCIES
Investigation of Federal Standard 1045 high-frequency ALE radio performance in the Southern Trans-Auroral Zone
| PB94-204831 | p 1655 N95-22636
A heavy ion linac complex for unstable nuclei
| DE94-765443 | p 1816 N95-22848
Advanced technologies for a compact RF linac FEL
| DE95-003674 | p 1692 N95-24072

RADIO RECEIVERS
Investigation of Federal Standard 1045 high-frequency ALE radio performance in the Southern Trans-Auroral Zone
| PB94-204831 | p 1655 N95-22636

RADIO TRANSMISSION
TRACKER: A three-dimensional raytracing program for ionospheric radio propagation
| DE95-003510 | p 1658 N95-24015

RADIO TRANSMITTERS
Investigation of Federal Standard 1045 high-frequency ALE radio performance in the Southern Trans-Auroral Zone
| PB94-204831 | p 1655 N95-22636

RADIO WAVES
Utilizing a TDRS satellite for direct broadcast satellite-radio propagation experiments and demonstrations p 1622 N95-22814
TRACKER: A three-dimensional raytracing program for ionospheric radio propagation
| DE95-003510 | p 1658 N95-24015

RADIOACTIVE AGE DETERMINATION
OU3 sediment dating and sedimentation rates
| DE95-001891 | p 1734 N95-23384

RADIOACTIVE CONTAMINANTS
OU3 sediment dating and sedimentation rates
| DE95-001891 | p 1734 N95-23384

RADIOACTIVE DECAY
The decays of D(sup *)-mesons
| DE94-628610 | p 1804 N95-22810
Neutrinoless double beta decay and the solar neutrino problem
| DE94-628633 | p 1812 N95-23785

RADIOACTIVE ISOTOPES
Laser light induced drift for atoms of radioactive isotopes Na-22 and Na-24
| DE94-635759 | p 1812 N95-23976

RADIOACTIVE MATERIALS
Radioisotope thermoelectric generator licensed hardware package and certification tests
| DE95-003039 | p 1661 N95-22799

RADIOACTIVE WASTES
Closing the circle on the splitting of the atom: The environmental legacy of nuclear weapons production in the United States and what the Department of Energy is doing about it p 1818 N95-23562
Characterization of Type 304L stainless steel solid-state closure welds for radioactive waste containment
| DE94-016539 | p 1645 N95-23980

RADIOACTIVITY
Large-sized and highly radioactive H-3 and Cd-109 Langmuir-Blodgett films
| DE94-785270 | p 1811 N95-23775
Status of LDEF activation measurements and archive p 1815 N95-23817
Predictions of LDEF radioactivity and comparison with measurements p 1815 N95-23818

RADIOISOTOPE BATTERIES
Radioisotope thermoelectric generator transportation system subsystem 143 software development plan
| DE95-003774 | p 1662 N95-23351

RADIOLYSIS
Magnetic resonance and optical spectroscopic studies of carotenoids
| DE95-003729 | p 1631 N95-22575
Test procedure for cation exchange chromatography
| DE95-003770 | p 1808 N95-23350
Time-resolved EPR studies of the H atom: A stable heavy isotope of muonium
| DE95-004614 | p 1810 N95-23491

RADIOMETERS
Twelve month performance evaluation for the rotating shadowband radiometer
| DE95-002847 | p 1726 N95-22554
SeaWiFS technical report series. Volume 25: Ocean optics protocols for SeaWiFS validation, revision 1
| NASA-TM-104566-VOL-25-REV- | p 1743 N95-22671
Design of a differential radiometer for atmospheric radiative flux measurements
| DE95-002701 | p 1739 N95-23244
Doing photons with MERLIN 2 at Oroville p 1815 N95-23816
Airborne Visible/Infrared Imaging Spectrometer (AVIRIS): Recent improvements to the sensor p 1690 N95-23852

RADIOMETRIC CORRECTION
Use of data from the AVIRIS onboard calibrator p 1704 N95-23861
Use of the Airborne Visible/Infrared Imaging Spectrometer to calibrate the optical sensor on board the Japanese Earth Resources Satellite-1 p 1624 N95-23864
A role for AVIRIS in the Landsat and Advanced Land Remote Sensing Systems program p 1705 N95-23866
Classification of high dimensional multispectral image data p 1705 N95-23868
Extraction of auxiliary data from AVIRIS distribution tape for spectral, radiometric, and geometric quality assessment p 1706 N95-23875

RADIOMETRIC RESOLUTION
Design of a differential radiometer for atmospheric radiative flux measurements
| DE95-002701 | p 1739 N95-23244

RAILGUN ACCELERATORS
The railplug: Development of a new ignitor for internal combustion engines
| DE95-004375 | p 1695 N95-23342

RAIN
Accuracy of radar rainfall estimates compared to raingauge measurements and a hydrological application
| PB95-127296 | p 1741 N95-22640

RAIN GAGES
Accuracy of radar rainfall estimates compared to raingauge measurements and a hydrological application
|PB95-127296| p 1741 N95-22640
RAIN IMPACT DAMAGE
Effects of wind on rainfall simulation. Spatial distribution of water application, kinetic energy, and overland flow under single full-cone nozzle sprays
|PB95-127304| p 1717 N95-22537
RAINDROPS
Effects of wind on rainfall simulation. Spatial distribution of water application, kinetic energy, and overland flow under single full-cone nozzle sprays
|PB95-127304| p 1717 N95-22537
RAMAN SPECTRA
Progress towards the synthesis of polymeric nitrogen
|DE94-017547| p 1841 N95-22860
RAMAN SPECTROSCOPY
Remote detection of trace effluents using resonance Raman spectroscopy
|DE94-016858| p 1633 N95-22887
Raman-shifting an ArF excimer laser to generate new lines for obtaining optical diagnostic based information in flow fields p 1692 N95-23303
Krypton isotope analysis using near-resonant stimulated Raman spectroscopy
|DE95-005061| p 1635 N95-23348
RANDOM ACCESS
Petabyte mass memory system using the Newell Opticel(TM) p 1753 N95-24119
RANDOM NOISE
The effect of signal noise on the remote sensing of Foliar biochemical concentration p 1708 N95-23884
RANDOM PROCESSES
Martin-Lof tests can help too
|TR-541| p 1797 N95-24063
RANDOM VARIABLES
Fuzziness and randomness in an optimization framework
|DE94-628383| p 1755 N95-22616
RANDOM WALK
Strong collision approach to calculation of depolarization function for neutron beam passing through ferromagnetic bulk domains
|DE94-628847| p 1803 N95-22758
RANGE (EXTREMES)
ESTAR, PSTAR, ASTAR: A PC package for calculating stopping powers and ranges of electrons, protons and helium ions, version 2
|DE94-634435| p 1811 N95-23773
RARE EARTH ELEMENTS
Hydrogen vibrational density of states of adsorbed water on rare-earth modified zirconia
|DE95-001127| p 1632 N95-22681
RARE GAS-HALIDE LASERS
Raman-shifting an ArF excimer laser to generate new lines for obtaining optical diagnostic based information in flow fields p 1692 N95-23303
RAREFIED GAS DYNAMICS
Particle kinetic simulation of high altitude hypervelocity flight
|NASA-CR-197383| p 1664 N95-22481
Monte Carlo simulation of rarefied nitrogen gases contained between parallel plates using the statistical inelastic cross-section model
|NAL-TR-1229T| p 1687 N95-24082
RAREFIED GASES
Monte Carlo simulation of rarefied nitrogen gases contained between parallel plates using the statistical inelastic cross-section model
|NAL-TR-1229T| p 1687 N95-24082
RATES (PER TIME)
Improved small satellite access of the space network
|NASA-CR-197863| p 1657 N95-22944
High data rate recorder development at MIT Haystack Observatory p 1690 N95-24118
Analysis of the request patterns to the NSSDC on-line archive p 1882 N95-24137
RATINGS
Criteria for evaluation of grid generation systems p 1669 N95-23416
The airline quality report, 1994
|NIAR-94-11| p 1610 N95-24012
RAYLEIGH SCATTERING
Instantaneous 2D velocity and temperature measurements in high speed flows based on spectrally resolved molecular Rayleigh scattering
|NASA-TM-106883| p 1688 N95-23461
RDX
Simulation of cookoff results in a small scale test
|DSTO-TR-0090| p 1653 N95-23668
REACTING FLOW
Towards a generalized computational fluid dynamics technique for all Mach numbers p 1670 N95-23420
Preconditioning for the Navier-Stokes equations with finite-rate chemistry p 1670 N95-23421
A numerical procedure for analysis of finite rate reacting flows p 1671 N95-23422
A controlled variation scheme for convection treatment in pressure-based algorithm p 1677 N95-23448
Flow diagnostics, chemically reacting turbulent flow modeling and turbulent mixing: A summary of project studies in combustion
|NASA-CR-197348| p 1687 N95-24022
REACTION KINETICS
Energy Conversion and Storage Program
|DE95-003796| p 1725 N95-22501
Comparison of the rate constants for energy transfer in the light-harvesting protein, C-phycocyanin, calculated from Foerster's theory and experimentally measured by time-resolved fluorescence spectroscopy
|DE94-014961| p 1745 N95-22590
Glass science tutorial: Lecture 2, operating electric glass melters
|DE95-002965| p 1647 N95-22648
On the formation of iron(3) oxides via oxidation of iron(2)
|DE94-018392| p 1632 N95-22857
Ethylene oxidation chemistry in a well-stirred reactor
|DE95-004823| p 1635 N95-23381
Reduced dime production in solar-simulator-pumped continuous wave iodine lasers based on model simulations and scaling and pumping studies
|NASA-TP-3486| p 1691 N95-23411
A numerical procedure for analysis of finite rate reacting flows p 1671 N95-23422
CFD flowfield simulation of Delta Launch Vehicles in a power-on configuration p 1673 N95-23433
Sensitivity of combustion-acoustic instabilities to boundary conditions for premixed gas turbine combustors
|NASA-TM-106890| p 1614 N95-23550
REACTION-DIFFUSION EQUATIONS
Diffusion terms in systems of reaction diffusion equations can lead to blow up
|DE94-628408| p 1785 N95-22618
Dynamical behaviour of the coupled diffusion map lattice
|DE94-628481| p 1841 N95-23022
REACTIVITY
Structure, melting, and reactivity of nickel clusters from numerical simulations
|DE95-002911| p 1638 N95-22531
REACTOR CORES
Dry critical experiments and analyses performed in support of the Topaz-2 Safety Program
|DE95-002724| p 1817 N95-23245
The q profile evolution and enhanced core confinement of high (beta)(sub p) plasmas in D3-D
|DE95-003878| p 1834 N95-23371
REACTOR DESIGN
Conversion of light hydrocarbon gases to metal carbides for production of liquid fuels and chemicals
|DE95-000362| p 1634 N95-23164
Dry critical experiments and analyses performed in support of the Topaz-2 Safety Program
|DE95-002724| p 1817 N95-23245
REACTOR MATERIALS
Effect of dynamically charged helium on mechanical properties of vanadium-base alloys
|DE95-004613| p 1646 N95-24153
REACTOR SAFETY
Dry critical experiments and analyses performed in support of the Topaz-2 Safety Program
|DE95-002724| p 1817 N95-23245
Closing the circle on the splitting of the atom: The environmental legacy of nuclear weapons production in the United States and what the Department of Energy is doing about it p 1818 N95-23562
READING
Verifying sequentially consistent memory using interface refinement
|PB95-139002| p 1752 N95-23153
REAL NUMBERS
Set games
|PB95-140786| p 1794 N95-23539
REAL TIME OPERATION
Investigation of Federal Standard 1045 high-frequency ALE radio performance in the Southern Trans-Auroral Zone
|PB94-204831| p 1655 N95-22636
An automated computer misuse detection system for UNICOS
|DE95-000929| p 1762 N95-22680
Novel mass spectrometric instrument for gaseous and particulate characterization and monitoring
|DE95-001135| p 1687 N95-22682
Toward an automated signature recognition toolkit for mission operations p 1659 N95-23682
Performance results of cooperating expert systems in a distributed real-time monitoring system p 1761 N95-23688
Subsumption-based architecture for autonomous movement planning for planetary rovers p 1771 N95-23690
Design of teleoperation system with a force-reflecting real-time simulator p 1778 N95-23733
Real-time tracking using stereo and motion: Visual perception for space robotics p 1778 N95-23739
A self-organizing neural network architecture for auditory and speech perception with applications to acoustic and other temporal prediction problems
|AD-A285640| p 1800 N95-23782
Field observations using an AOTF polarimetric imaging spectrometer p 1702 N95-23850
Real-world shepherding: Combining vision, manipulation, and planning in real time
|TR-530| p 1783 N95-24001
Chemical recognition software
|DE95-003346| p 1636 N95-24007
The TRAINS project: A case study in building a conversational planning agent
|TR-532| p 1659 N95-24193
RECEIVERS
Parallel digital modem using multirate digital filter banks
|NASA-CR-197331| p 1761 N95-22478
RECOMBINATION REACTIONS
Time-resolved EPR studies of the H atom: A stable heavy isotope of muonium
|DE95-004614| p 1810 N95-23491
RECOMMENDATIONS
A roadmap for regulatory survival in the 1990s p 1628 N95-23026
Aviation Accident Investigation Symposium. Volume 1: Industry recommendations and Safety Board responses
|PB94-917005| p 1611 N95-24105
RECONSTRUCTION
Holographic interferometric tomography for reconstructing flow fields p 1690 N95-23287
RECORDING HEADS
High data rate recorder development at MIT Haystack Observatory p 1690 N95-24118
A comparison of rotary- and stationary-head tape recorders p 1690 N95-24122
RECORDING INSTRUMENTS
High data rate recorder development at MIT Haystack Observatory p 1690 N95-24118
RECRYSTALLIZATION
Growth of single crystals of organic salts with large second-order optical nonlinearities by solution processes for devices
|NASA-CR-197963| p 1843 N95-23563
RECURSIVE FUNCTIONS
Tutorial on filtering, restoration, and state estimation
|TR-534| p 1793 N95-24042
RECYCLING
Chemical recycling of scrap composites p 1629 N95-23034
The Louisiana State University waste-to-energy incinerator
|DE95-004417| p 1728 N95-23344
RED SHIFT
Ionic core effects on the Mie resonance in lithium clusters
|DE94-014974| p 1805 N95-22870
Search for millimeterwave CO emission in damped Lyman-alpha systems
|PB95-139259| p 1868 N95-23607
REDUNDANCY
Morphing hands and virtual tools (or What good is an extra degree of freedom?)
|TR-551| p 1783 N95-24036
REDUNDANCY ENCODING
Commercialization of JPL Virtual Reality calibration and redundant manipulator control technologies p 1768 N95-23676
REED-SOLOMON CODES
Mappings between codewords of two distinct (N,K) Reed-Solomon codes over GF(2(sup J))
|NASA-CASE-NPO-18771-1-CU| p 1754 N95-22577
REENTRY VEHICLES
Moving mass trim control for aerospace vehicles
|DE95-002602| p 1622 N95-23532
REFINING
Transformation behavior in Al2O3-ZrO2 ceraamic composites
|DE95-001359| p 1647 N95-22688
REFLECTANCE
Advanced reflector materials for solar concentrators
|DE95-000248| p 1726 N95-22547
Laser-plasma instability in hohlraums
|DE95-000914| p 1829 N95-22676
A uniform geometrical optics and an extended uniform geometrical theory of diffraction for evaluating high frequency EM fields near smooth caustics and composite shadow boundaries
|NASA-CR-197934| p 1657 N95-23391

Reflectivity studies on adsorbed block copolymers under shear
| DE95-003676 | p 1649 N95-23568
Use of spectral analogy to evaluate canopy reflectance sensitivity to leaf optical property p 1701 N95-23845
Comparison of methods for calibrating AVIRIS data to ground reflectance p 1703 N95-23854
The US Geological Survey, digital spectral reflectance library: version 1: 0.2 to 3.0 microns p 1703 N95-23855
Spectral decomposition of AVIRIS data p 1704 N95-23859
The effects of AVIRIS atmospheric calibration methodology on identification and quantitative mapping of surface mineralogy, Drum Mountains, Utah p 1705 N95-23870
AVIRIS spectra correlated with the chlorophyll concentration of a forest canopy p 1705 N95-23871
Changes in chemical and optical properties of thin film metal mirrors on LDEF p 1651 N95-23907
Unusual radar echoes from the Greenland ice sheet p 1714 N95-23951
A simple, closed-form expression for the x ray reflectivity from superlattices with cumulative roughness
| DE95-004633 | p 1846 N95-24170

REFLECTOR ANTENNAS
Passive intermodulation generation in wire mesh deployable reflector antennas p 1656 N95-22816

REFLECTORS
Passive intermodulation generation in wire mesh deployable reflector antennas p 1656 N95-22816
Durability of reflector materials in the space environment p 1651 N95-23912

REFRACTIVITY
Study of photorefractive non-linearities in the 3-5 and 2-4 semi-insulator compounds: The effect of electron irradiation
| PB94-189057 | p 1839 N95-22584
Reflectance control for multicrystalline-silicon photovoltaic modules using textured-dielectric coatings
| DE95-004532 | p 1731 N95-24155

REFRIGERATORS
NASA advanced refrigerator/freezer technology development project overview
| NASA-TM-106309 | p 1747 N95-23177

REFUELING
New pellet production and acceleration technologies for high speed pellet injection system HIPEL in Large Helical Device
| NISF-326 | p 1835 N95-23566

REGRESSION ANALYSIS
Estimation of crown closure from AVIRIS data using regression analysis p 1709 N95-23886
Determining coniferous forest cover and forest fragmentation with NOAA-9 advanced very high resolution radiometer data p 1720 N95-24103

REGRESSION COEFFICIENTS
Asymptotic justification for a modified GLS procedure to estimate ARMA parameters
| PB95-135166 | p 1788 N95-23070

REGULATIONS
A roadmap for regulatory survival in the 1990s p 1628 N95-23026

REGULATORY MECHANISMS (BIOLOGY)
Activation of the jun-D gene in human myeloid cells by 1-(beta)-D-arabinofuranosylcytosine
| DE94-016591 | p 1746 N95-22912

REINFORCED PLASTICS
Society of the plastic industry process emission initiatives p 1629 N95-23036

REINFORCING FIBERS
Method of producing a silicon carbide fiber reinforced strontium aluminosilicate glass-ceramic matrix composite
| NASA-CASE-LEW-15263-2 | p 1627 N95-22563
Chemical recycling of scrap composites p 1629 N95-23034

RELATIONSHIPS
Jackson system development, entity-relationship analysis and data flow models: A comparative study
| PB95-127338 | p 1855 N95-22523

RELATIVE BIOLOGICAL EFFECTIVENESS (RBE)
Genetic effects on heavy ions in drosophila
| NASA-CR-197916 | p 1746 N95-22911

RELATIVISTIC PARTICLES
(pi)N correlations at AGS
| DE95-002933 | p 1801 N95-22656
Relativistic particle with torsion and charged particle in a constant electromagnetic field: Identity of evolution
| DE94-628506 | p 1803 N95-22778
The relativistic many body problem with an oscillator interaction p 1824 N95-22991
Notes on oscillator-like interactions of various spin relativistic particles p 1815 N95-22997
Design study of longitudinal dynamics of the drive beam in 1 TeV relativistic klystron two-beam accelerator
| DE95-004683 | p 1817 N95-23485
Design study of beam dynamics issues for 1 TeVnext linear collider based on the relativistic-klystron two-beam accelerator
| DE95-004673 | p 1817 N95-23493

RELATIVISTIC THEORY
First quantized noncritical relativistic Polyakov string
| DE94-628513 | p 1848 N95-22738
Does the relativity principle violate?
| DE94-635420 | p 1851 N95-23964

RELATIVITY
Does the relativity principle violate?
| DE94-635420 | p 1851 N95-23964

RELAXATION METHOD (MATHEMATICS)
Stability and efficiency of waveform relaxation methods
| PB95-138863 | p 1789 N95-23173

RELIABILITY
The MAMMOTH project p 1753 N95-24126
Architecture and evolution of Goddard Space Flight Center Distributed Active Archive Center p 1862 N95-24134
Design of a high-temperature superconductor current lead for electric utility SMES
| DE95-004604 | p 1664 N95-24163

RELIABILITY ANALYSIS
HiRel: Hybrid Automated Reliability Predictor (HARP) integrated reliability tool system, (version 7.0). Volume 3: HARP Graphics Oriented (GO) input user's guide
| NASA-TP-3452-VOL-3 | p 1753 N95-22479
Current estimation for electromigration, hot carriers, and voltage drop
| AD-A285794 | p 1659 N95-22507
HiRel: Hybrid Automated Reliability Predictor (HARP) integrated reliability tool system, (version 7.0). Volume 1: HARP introduction and user's guide
| NASA-TP-3452-VOL-1 | p 1754 N95-22603
HiRel: Hybrid Automated Reliability Predictor (HARP) integrated reliability tool system, (version 7.0). Volume 2: HARP tutorial
| NASA-TP-3452-VOL-2 | p 1755 N95-22604
HiRel: Hybrid Automated Reliability Predictor (HARP) integrated reliability tool system, (version 7.0). Volume 4: HARP Output (HARPO) graphics display user's guide
| NASA-TP-3452-VOL-4 | p 1755 N95-22605
Reliability analysis in the Office of Safety, Environmental, and Mission Assurance (OSEMA) p 1698 N95-23302
Integrating O/S models during conceptual design, part 2
| NASA-CR-197904 | p 1622 N95-23399

RELIABILITY ENGINEERING
HiRel: Hybrid Automated Reliability Predictor (HARP) integrated reliability tool system, (version 7.0). Volume 3: HARP Graphics Oriented (GO) input user's guide
| NASA-TP-3452-VOL-3 | p 1753 N95-22479
HiRel: Hybrid Automated Reliability Predictor (HARP) integrated reliability tool system, (version 7.0). Volume 4: HARP Output (HARPO) graphics display user's guide
| NASA-TP-3452-VOL-4 | p 1755 N95-22605
Reliability analysis in the Office of Safety, Environmental, and Mission Assurance (OSEMA) p 1698 N95-23302

RELIEF MAPS
Path planning for planetary rover using extended elevation map p 1771 N95-23689

RELIEF VALVES
Navier-Stokes flow field analysis of compressible flow in a pressure relief valve p 1679 N95-23618

REMOTE CONTROL
The next decade of space robotics p 1768 N95-23673
JPL space robotics: Present accomplishments and future thrusts p 1697 N95-23697
A US-Japan collaborative robotics research program p 1772 N95-23698
Space science experimentation automation and support p 1775 N95-23718
Robotic servicing system for space material experiment p 1697 N95-23722
Robotics and telepresence for moon missions p 1776 N95-23725
Intelligent monitoring system applied to super long distance telerobotic tasks p 1777 N95-23726
Manipulating flexible parts using a teleoperated system with time delay: An experiment p 1777 N95-23729
Visually guided grasping to study teleprogrammation within the BAROCO testbed p 1777 N95-23731
Design of teleoperation system with a force-reflecting real-time simulator p 1778 N95-23733
Telerobotics test bed for space structure assembly p 1618 N95-23734

REMOTE HANDLING
Design of teleoperation system with a force-reflecting real-time simulator p 1778 N95-23733

REMOTE MANIPULATOR SYSTEM
Commercialization of JPL Virtual Reality calibration and redundant manipulator control technologies p 1768 N95-23676
A perspective on space robotics in Japan p 1697 N95-23695
Space robotic experiment in JEM flight demonstration p 1697 N95-23701
Hardware interface unit for control of shuttle RMS vibrations p 1697 N95-23706
Development of Japanese experiment module remote manipulator system p 1752 N95-23708
Design of teleoperation system with a force-reflecting real-time simulator p 1778 N95-23733

REMOTE SENSING
Measurement of HO2 and other trace gases in the stratosphere using a high resolution far-infrared spectrometer
| NASA-CR-197368 | p 1735 N95-22482
A multispectral scanner survey of the Tonopah Test Range, Nevada. Date of survey: August 1993
| DE95-003920 | p 1717 N95-22503
Combining optical and microwave remote sensing data of forest vegetation: MAC Europe 1991
| PB95-127312 | p 1717 N95-22538
HAPEX-Sahel: Basic description of methods and data sets
| PB95-127262 | p 1701 N95-22639
Civilian satellite remote sensing: A strategic approach
| PB95-109633 | p 1717 N95-22713
Programmable hyperspectral image mapper with on-array processing
| NASA-CASE-NPO-17794-1-CU | p 1819 N95-22765
Remote detection of trace effluents using resonance Raman spectroscopy
| DE94-016858 | p 1633 N95-22887
TIMED Imaging Photometer Experiment (TIPE)
| NASA-CR-197431 | p 1688 N95-23087
Upgrade of the 92 GHz airborne multi-channel meteorological radiometer (AMMR)
| NASA-CR-197875 | p 1742 N95-23208
Study of atmospheric parameters measurements using MM-wave radar in synergy with LITE-2 p 1741 N95-23278
FAME: A forest assessment and monitoring environment scenario
| PB95-139309 | p 1718 N95-23471
Ocean observations with EOS/MODIS: Algorithm development and post launch studies
| NASA-CR-197894 | p 1718 N95-23473
Software agents for the dissemination of remote terrestrial sensing data p 1721 N95-23675
Attention focusing and anomaly detection in systems monitoring p 1769 N95-23683
A data analysis assistant p 1761 N95-23748
Summaries of the 4th Annual JPL Airborne Geoscience Workshop. Volume 1: AVIRIS Workshop
| NASA-CR-197877-VOL-1 | p 1701 N95-23844
Use of spectral analogy to evaluate canopy reflectance sensitivity to leaf optical property p 1701 N95-23845
A tool for manual endmember selection and spectral unmixing p 1701 N95-23846
Lithologic discrimination and alteration mapping from AVIRIS Data, Socorro, New Mexico p 1701 N95-23847
Automating spectral unmixing of AVIRIS data using convex geometry concepts p 1702 N95-23848
AVIRIS calibration using the cloud-shadow method p 1702 N95-23849
Field observations using an AOTF polarimetric imaging spectrometer p 1702 N95-23850
Instantaneous field of view and spatial sampling of the Airborne Visible/Infrared Imaging Spectrometer (AVIRIS) p 1702 N95-23851
Discrimination of poorly exposed lithologies in AVIRIS data p 1703 N95-23858
AVIRIS and TIMS data processing and distribution at the land processes distributed active archive center p 1706 N95-23872
Classification of the LCVF AVIRIS test site with a Kohonen artificial neural network p 1706 N95-23874
Extraction of auxiliary data from AVIRIS distribution tape for spectral, radiometric, and geometric quality assessment p 1706 N95-23875
Preprocessing: Geocoding of AVIRIS data using navigation, engineering, DEM, and radar tracking system data p 1707 N95-23876
Mapping of the Ronda peridotite massif (Spain) from AVIRIS spectro-imaging survey: A first attempt p 1707 N95-23878
Spectral variations in a collection of AVIRIS imagery p 1707 N95-23879
The red edge in arid region vegetation: 340-1060 nm spectra p 1708 N95-23881
Temporal changes in endmember abundances, liquid water and water vapor over vegetation at Jasper Ridge p 1708 N95-23882
The effect of signal noise on the remote sensing of Foliar biochemical concentration p 1708 N95-23884

Application of MAC-Europe AVIRIS data to the analysis of various alteration stages in the Landdmannalauger Hydrothermal Area (South Iceland) p 1709 N95-23885
Estimation of crown closure from AVIRIS data using regression analysis p 1709 N95-23886
Relationships between pigment composition variation and reflectance for plant species from a coastal savannah in California p 1709 N95-23889
Investigations on the 1.7 micron residual absorption feature in the vegetation reflection spectrum p 1710 N95-23891
A comparison of spectral mixture analysis an NDVI for ascertaining ecological variables p 1710 N95-23892
Using AVIRIS for in-flight calibration of the spectral shifts of SPOT-HRV and of AVHRR? p 1710 N95-23893
Determination of semi-arid landscape endmembers and seasonal trends using convex geometry spectral unmixing techniques p 1711 N95-23895
Summaries of the 4th Annual JPL Airborne Geoscience Workshop. Volume 2: TIMS Workshop
|NASA-CR-197876-VOL-2| p 1711 N95-23917
Mineralogic variability of the Kelso Dunes, Mojave Desert, California derived from Thermal Infrared Multispectral Scanner (TIMS) data p 1711 N95-23920
Remote identification of a gravel laden Pleistocene river bed p 1712 N95-23921
Interferometric synthetic aperture radar imagery of the Gulf Stream p 1712 N95-23939
AIRSAR views of aerolian terrain p 1713 N95-23941
Forest investigations by polarimetric AIRSAR data in the Harz mountains p 1713 N95-23944
Geologic mapping using integrated AIRSAR, AVIRIS, and TIMS data p 1714 N95-23946
AIRSAR deployment in Australia, September 1993: Management and objectives p 1714 N95-23948
Synergy between optical and microwave remote sensing to derive soil and vegetation parameters from MAC Europe 1991 Experiment p 1715 N95-23956
Soil moisture retrieval in the Oberpfaffenhofen testsite using MAC Europe AIRSAR data p 1716 N95-23960
Chemical recognition software
|DE95-003346| p 1636 N95-24007
Geographic information analysis: An ecological approach for the management of wildlife on the forest landscape
|NASA-CR-197941| p 1719 N95-24094
Comparison of 7.5-minute and 1-degree digital elevation models p 1719 N95-24095
Measuring forest landscape patterns in the Cascade Range of Oregon, USA p 1719 N95-24096
A preliminary comparison of Landsat Thematic Mapper and SPOT-1 HRV multispectral data for estimating coniferous forest volume p 1719 N95-24097
Old-growth and mature forests near spotted owl nests in western Oregon p 1719 N95-24098
Forest and wildlife habitat analysis using remote sensing and geographic information systems p 1720 N95-24100
Determining coniferous forest cover and forest fragmentation with NOAA-9 advanced very high resolution radiometer data p 1720 N95-24103
Land surface temperature measurements from EOS MODIS data
|NASA-CR-197969| p 1721 N95-24190

REMOTE SENSORS
SeaWiFS technical report series. Volume 25: Ocean optics protocols for SeaWiFS validation, revision 1
|NASA-TM-104566-VOL-25-REV-| p 1743 N95-22671
Remote detection of trace effluents using resonance Raman spectroscopy
|DE94-016858| p 1633 N95-22887
Long range targeting for space based rendezvous
|NASA-CR-197890| p 1757 N95-23388
Airborne Visible/Infrared Imaging Spectrometer (AVIRIS): Recent improvements to the sensor p 1690 N95-23852
Remote sensor test range update
|DE95-003629| p 1735 N95-24018

RENORMALIZATION GROUP METHODS
Asymptotically exact solution of the multi-channel resonant-level model
|DE94-629040| p 1801 N95-22498
One loop renormalization of Chern-Simons field theory in operator regularization
|DE94-628508| p 1796 N95-22751

REPLACING
Corrosion prevention with environmentally compliant materials: A design challenge p 1644 N95-23511

REPORTS
FY 1994 scientific and technical reports, articles, papers, and presentations
|NASA-TM-108480| p 1856 N95-23225
Military bases: Environmental impact at closing installations. Report to Congressional requesters
|GAO/NSIAD-95-70| p 1735 N95-24057
DOD budget: Selected categories of planned funding for fiscal years 1995-99. Report to Congressional requesters
|GAO/NSIAD-95-92| p 1864 N95-24062
Ballistic Missile Defense: Current status of strategic target system. Report to Congressional requesters
|GAO/NSIAD-95-78| p 1903 N95-24080

REPRODUCTION (COPYING)
NASAwide electronic publishing system: Electronic printing and duplicating, stage-2 evaluation report (GSFC)
|NASA-TM-104615| p 1856 N95-23209

RESEARCH
Microgravity sciences application visiting scientist program
|NASA-CR-197854| p 1653 N95-23204
1994 NASA-HU American Society for Engineering Education (ASEE) Summer Faculty Fellowship Program
|NASA-CR-194972| p 1872 N95-23276
Research and Technology, 1994
|NASA-TM-106764| p 1607 N95-24025

RESEARCH AIRCRAFT
Analysis of the longitudinal handling qualities and pilot-induced-oscillation tendencies of the High-Angle-of-Attack Research Vehicle (HARV) p 1616 N95-23297

RESEARCH AND DEVELOPMENT
The viability of establishing collaborative, reconfigurable research environments for the Human Performance Research Laboratory at NASA Ames
|NASA-CR-197384| p 1753 N95-22480
Design and implementation of two two-week Teacher Enhancement Institutes p 1853 N95-23306
Teacher Enhancement Institute p 1853 N95-23324
Institute for Computational Mechanics in Propulsion (ICOMP)
|NASA-TM-106884| p 1677 N95-23464
Advances in research for solid oxide fuel cells
|DE95-004590| p 1730 N95-23582
Oak Ridge National Laboratory Energy Efficiency and Renewable Energy Program Bibliography: 1994 Edition
|DE95-002296| p 1730 N95-23605
A perspective on space robotics in Japan p 1697 N95-23695
A US-Japan collaborative robotics research program p 1772 N95-23698
Robotics research at Canadian Space Agency p 1772 N95-23699
Proceedings of the fuel cells 1994 contractors review meeting
|DE94-012285| p 1730 N95-23977
Chemical Sciences Division
|DE95-002655| p 1626 N95-24142
Defense technology plan
|AD-A285415| p 1903 N95-24178
Defense science and technology strategy
|AD-A285414| p 1903 N95-24179

RESEARCH MANAGEMENT
Defense technology plan
|AD-A285415| p 1903 N95-24178
Defense science and technology strategy
|AD-A285414| p 1903 N95-24179
The TRAINS project: A case study in building a conversational planning agent
|TR-532| p 1659 N95-24193

RESEARCH PROJECTS
High magnetic fields in the USA
|DE95-002716| p 1798 N95-22552
Director's discretionary fund report for fiscal year 1994
|NASA-TM-108848| p 1872 N95-22920
Stochastic decision analysis p 1854 N95-23305
Teacher Enhancement Institute p 1853 N95-23312
Langley Research Center Strategic Plan for Education p 1853 N95-23316
NASA university program management information system, FY 1994
|NASA-TM-110345| p 1856 N95-23364

RESEARCH VEHICLES
Differential GPS and system integration of the Low Visibility Landing and Surface Operations (LVLASO) demonstration p 1611 N95-23318

RESERVOIRS
OU3 sediment dating and sedimentation rates
|DE95-001891| p 1734 N95-23384

RESIDUAL STRENGTH
Residual strength of thin panels with cracks p 1700 N95-23311

RESIDUAL STRESS
Statistically generated weighted curve fit of residual functions for modal analysis of structures
|NASA-TM-108481| p 1699 N95-22950

RESIDUES
Extraction and detection of pesticide residues from air filter inserts using supercritical carbon dioxide
|DE95-004579| p 1735 N95-23580
Analytical electron microscopy of LDEF impactor residues p 1869 N95-23832
Natural and orbital debris particles on LDEF's trailing and forward-facing surfaces p 1869 N95-23833
Debris and meteoroid proportions deduced from impact crater residue analysis p 1869 N95-23834
Micro-abrasion package capture cell experiment on the trailing edge of LDEF: Impactor chemistry and whipple bumper shield efficiencies p 1624 N95-23835
Secondary ion mass spectrometry (SIMS) analysis of hypervelocity microparticle impact sites on LDEF surfaces p 1637 N95-23836
SIMS chemical and isotopic analysis of impact features from LDEF experiments AO187-1 and AO187-2 p 1637 N95-23837
Image and compositional characteristics of the LDEF Big Guy impact crater p 1700 N95-23838
The effect of impact angle on craters formed by hypervelocity particles p 1700 N95-23839

RESIN MATRIX COMPOSITES
Chemical recycling of scrap composites p 1629 N95-23034
Nonlinear thermoviscoelastic behaviour in complex materials
|PB95-140653| p 1630 N95-23537
Surface characterization of LDEF carbon fiber/polymer matrix composites p 1631 N95-23900

RESIN TRANSFER MOLDING
Development and verification of a resin film infusion/resin transfer molding simulation model for fabrication of advanced textile composites
|NASA-CR-197439| p 1648 N95-23179
Assessment of resin transfer molding process for the XM6 discharger, ERDEC SSP 93-64
|NIAR-94-2| p 1650 N95-23932

RESINS
Biotransformation of an uncured composite material p 1629 N95-23033

RESISTANCE HEATING
The DIII-D divertor cryopump system: Design and operational experience
|DE95-003007| p 1693 N95-22796
Current-profile flattening and hot core shift due to the nonlinear development of resistive kink mode
|NIFS-311| p 1835 N95-23564
Characterization of Type 304L stainless steel solid-state closure welds for radioactive waste containment
|DE94-016539| p 1645 N95-23980

RESONANCE
Ionic core effects on the Mie resonance in lithium clusters
|DE94-014974| p 1805 N95-22870
Time-periodic solutions of some forced nonlinear wave equations: Analysis, approximations and applications
|PB95-135083| p 1788 N95-22932
Harmonic oscillators and resonance series generated by a periodic unstable classical orbit p 1825 N95-22999
Structure and evolution of long-lived spiral patterns in galaxies
|PB95-139242| p 1868 N95-23228
Computational modelling of Er(3+): Garnet laser materials p 1692 N95-23326
Electromagnetic production of pions on the nucleon
|DE95-004658| p 1811 N95-23587
Navier-Stokes flow field analysis of compressible flow in a pressure relief valve p 1679 N95-23618

RESONANCE SCATTERING
Remote detection of trace effluents using resonance Raman spectroscopy
|DE94-016858| p 1633 N95-22887

RESONANT FREQUENCIES
Resonant shallow donor magnetopolaron effect in a GaAs/AlGaAs quantum dot in high magnetic fields
|DE94-629039| p 1798 N95-22497
Interdigital-H linac for unstable nuclei at INS
|DE94-765448| p 1816 N95-22644
Phonon characteristics of high (T sub c) superconductors from neutron Doppler broadening measurements
|DE95-003703| p 1844 N95-24076

RESOURCE ALLOCATION
Applications of dynamic scheduling technique to space related problems: Some case studies p 1618 N95-23759

RESOURCES MANAGEMENT
Net energy analysis: Powerful tool for selecting electric power options
|DE95-002516| p 1728 N95-23133

RESPONSE TIME (COMPUTERS)
Optimizing tertiary storage organization and access for spatio-temporal datasets p 1861 N95-24131

RESTORATION
Ghost images and feasibility of reconstructions with the Richardson-Lucy algorithm
| DE95-002351 | p 1756 N95-23079
Revitalization of the Gemenc-area, Baja, Hungary. 1: A study on hydrological possibilities to revitalise the ecosystem in the Keselyues-area. 2: Towards the restoration of the Gyueruesalj floodplain
| PB95-139283 | p 1718 N95-23469
Tutorial on filtering, restoration, and state estimation
| TR-534 | p 1793 N95-24042
RETENTION (PSYCHOLOGY)
Functions of external cues in prospective memory
| DOT/FAA/AM-95/9 | p 1750 N95-24088
RETROREFLECTION
Double pass retroreflection for corrosion detection in aircraft structures p 1642 N95-23503
Performance characterization of EURECA retroreflectors with fluoropolymer-filled SiO(x) protective coatings p 1651 N95-23802
RETROREFLECTORS
Performance characterization of EURECA retroreflectors with fluoropolymer-filled SiO(x) protective coatings p 1651 N95-23802
REUSABLE HEAT SHIELDING
Robotic system for the servicing of the orbiter thermal protection system p 1697 N95-23724
REUSABLE ROCKET ENGINES
Damage-mitigating control of a reusable rocket engine for high performance and extended life
| NASA-CR-4640 | p 1654 N95-23195
REVERSE FIELD PINCH
Generation of fast electrons in reversed field pinches by the equilibrium grad (vert bar)B(vert bar) force
| DE95-004467 | p 1809 N95-23363
REYNOLDS NUMBER
Wing pressure distributions from subsonic tests of a high-wing transport model --- in the Langley 14- by 22-Foot Subsonic Wind Tunnel
| NASA-TM-4583 | p 1607 N95-22802
Design of a variable area diffuser for a 15-inch Mach 6 open-jet tunnel p 1617 N95-23309
On the accuracy of CFD-based pressure drop predictions for right-angle ducts p 1682 N95-23634
REYNOLDS STRESS
Development of an algebraic stress/two-layer model for calculating thrust chamber flow fields p 1675 N95-23442
RHYTHM (BIOLOGY)
The 1993 Gordon Research Conference on Chronobiology
| NASA-CR-197990 | p 1748 N95-24047
RIBONUCLEIC ACIDS
Open problems of computational molecular biology
| DE95-000895 | p 1745 N95-22866
The torsion space nucleic acids molecular mechanics program DUPLEX: Surveying conformation space by potential energy minimization
| DE94-017707 | p 1805 N95-22889
Rearrangement of RAG-1 recombinase gene in radiation-sensitive wasted mice
| DE94-017083 | p 1746 N95-22913
Molecular relics from chemical evolution and the origin of life
| DE94-628493 | p 1747 N95-23060
Cellular interactions in the suprachiasmatic nucleus
| AD-A285639 | p 1749 N95-23780
RIBS (SUPPORTS)
The influence of swirl brakes and a tip discharge orifice on the rotordynamic forces generated by discharge-to-suction leakage flows in shrouded centrifugal pumps p 1680 N95-23628
RIEMANN MANIFOLD
Anti-invariant submanifolds of trans-Sasakian manifolds
| DE94-628413 | p 1829 N95-22622
A new method of constructing scalar-flat Kaehler surfaces
| DE94-628419 | p 1785 N95-22627
Hausdorff dimension of Julia sets of complex Henon mappings
| DE94-628420 | p 1785 N95-22628
On the scalar curvature of minimal hypersurfaces
| DE94-628516 | p 1796 N95-22741
Semi-symmetric manifolds satisfying certain curvature conditions
| DE94-628414 | p 1788 N95-22922
Universal Hodge bundle and Mumford isomorphisms on the abelian inductive limit of Teichmueller spaces
| DE94-634325 | p 1796 N95-23660
On certain N-sheeted coverings of curves and symmetric numerical semigroups which cannot be realized as Weierstrass semigroups
| DE94-634328 | p 1797 N95-23661
The exchange algebra for Liouville field on Riemann surfaces with h greater than 1 genus
| DE94-635446 | p 1792 N95-23971
RIGID STRUCTURES
High-velocity penetrators
| DE95-001886 | p 1698 N95-22500
Segregated rigid and structural control for a photolithography positioning system
| DE95-002603 | p 1766 N95-23134
RINGS (MATHEMATICS)
Algebraic description of the elliptic cohomology of classifying spaces
| PB95-110797 | p 1788 N95-23076
RISK
How health risk from radiation is assessed
| DE95-003477 | p 1749 N95-23142
RIVER BASINS
Remote identification of a gravel laden Pleistocene river bed p 1712 N95-23921
RL-10-A-3 ENGINE
An RL10A-3-3A rocket engine model using the rocket engine transient simulator (ROCETS) software
| NASA-CR-190786 | p 1625 N95-23790
ROBOT ARMS
Controlling under-actuated robot arms using a high speed dynamics process
| NASA-CASE-NPO-18498-1-CU | p 1692 N95-22543
A microcontroller-based three degree-of-freedom manipulator testbed
| NASA-CR-197423 | p 1696 N95-23409
Commercialization of JPL Virtual Reality calibration and redundant manipulator control technologies p 1768 N95-23676
Very fast motion planning for highly dexterous-articulated robots p 1771 N95-23691
ASI's space automation and robotics programs: The second step p 1697 N95-23696
Space robotic experiment in JEM flight demonstration p 1697 N95-23701
Development of Advanced Robotic Hand System for space application p 1752 N95-23704
A three-finger multisensory hand for dexterous space robotic tasks p 1752 N95-23705
Robot arm system for automatic satellite capture and berthing p 1752 N95-23709
Robust control of multi-jointed arm with a decentralized autonomous control mechanism p 1659 N95-23710
Automatic satellite capture and berthing with robot arm (ASCABRA) p 1623 N95-23713
Dexterous Orbital Servicing System (DOSS) p 1752 N95-23723
Truss structure tele-manipulation experiment using ETS-7 p 1623 N95-23726
Antenna-assembling mechanism test on ETS-7 p 1623 N95-23727
Mark Tracking: Position/orientation measurements using 4-circle mark and its tracking experiments p 1778 N95-23736
Real-world shepherding: Combining vision, manipulation, and planning in real time
| TR-530 | p 1783 N95-24001
Morphing hands and virtual tools (or What good is an extra degree of freedom?)
| TR-551 | p 1783 N95-24036
ROBOT CONTROL
A certainty grid to object boundary algorithm
| PB94-203510 | p 1755 N95-22637
A microcontroller-based three degree-of-freedom manipulator testbed
| NASA-CR-197423 | p 1696 N95-23409
Commercialization of JPL Virtual Reality calibration and redundant manipulator control technologies p 1768 N95-23676
Very fast motion planning for highly dexterous-articulated robots p 1771 N95-23691
Control technique for planetary rover p 1771 N95-23692
Autonomous navigation system for the Marsokhod rover project p 1771 N95-23693
Lunar rover technology demonstrations with Dante and Ratler p 1697 N95-23694
ASI's space automation and robotics programs: The second step p 1697 N95-23696
A US-Japan collaborative robotics research program p 1772 N95-23698
Design and development status of ETS-7, an RVD and space robot experiment satellite p 1623 N95-23700
The Charlotte (TM) intra-vehicular robot p 1697 N95-23703
A three-finger multisensory hand for dexterous space robotic tasks p 1752 N95-23705
Hardware interface unit for control of shuttle RMS vibrations p 1697 N95-23706
Development of Japanese experiment module remote manipulator system p 1752 N95-23708
Interactive autonomy and robotic skills p 1777 N95-23730
Telerobotics test bed for space structure assembly p 1618 N95-23734
Telepresence control of a dual-arm dexterous robot p 1752 N95-23735
Terrain modelling and motion planning for an autonomous exploration rover p 1721 N95-23765
Morphing hands and virtual tools (or What good is an extra degree of freedom?)
| TR-551 | p 1783 N95-24036
Robot skill learning through intelligent experimentation
| TR-567 | p 1784 N95-24038
ROBOT DYNAMICS
Path planning for planetary rover using extended elevation map p 1771 N95-23689
Subsumption-based architecture for autonomous movement planning for planetary rovers p 1771 N95-23690
Very fast motion planning for highly dexterous-articulated robots p 1771 N95-23691
Control technique for planetary rover p 1771 N95-23692
Lunar rover technology demonstrations with Dante and Ratler p 1697 N95-23694
A US-Japan collaborative robotics research program p 1772 N95-23698
Robotic experiment with a force reflecting handcontroller onboard MIR space station p 1752 N95-23707
ROBOT SENSORS
A microcontroller-based three degree-of-freedom manipulator testbed
| NASA-CR-197423 | p 1696 N95-23409
Control technique for planetary rover p 1771 N95-23692
Lunar rover technology demonstrations with Dante and Ratler p 1697 N95-23694
Terrain modelling and motion planning for an autonomous exploration rover p 1721 N95-23765
ROBOTICS
Controlling under-actuated robot arms using a high speed dynamics process
| NASA-CASE-NPO-18498-1-CU | p 1692 N95-22543
Sensor-based control of rocket thrust chamber feature location for automated braze paste dispensing
| DE94-016559 | p 1624 N95-22885
Robotic all-terrain lunar exploration rover (RATLER) FY93 program status report
| DE95-003589 | p 1694 N95-23065
Simulation and off-line programming systems comparison
| DE95-002267 | p 1766 N95-23078
A microcontroller-based three degree-of-freedom manipulator testbed
| NASA-CR-197423 | p 1696 N95-23409
Third International Symposium on Artificial Intelligence, Robotics, and Automation for Space 1994
| NASA-CR-197340 | p 1767 N95-23672
Path planning for planetary rover using extended elevation map p 1771 N95-23689
Subsumption-based architecture for autonomous movement planning for planetary rovers p 1771 N95-23690
Very fast motion planning for highly dexterous-articulated robots p 1771 N95-23691
Control technique for planetary rover p 1771 N95-23692
Autonomous navigation system for the Marsokhod rover project p 1771 N95-23693
Lunar rover technology demonstrations with Dante and Ratler p 1697 N95-23694
A perspective on space robotics in Japan p 1697 N95-23695
ASI's space automation and robotics programs: The second step p 1697 N95-23696
Robotics research at Canadian Space Agency p 1772 N95-23699
Design and development status of ETS-7, an RVD and space robot experiment satellite p 1623 N95-23700
Space robotic experiment in JEM flight demonstration p 1697 N95-23701
A three-finger multisensory hand for dexterous space robotic tasks p 1752 N95-23705
Hardware interface unit for control of shuttle RMS vibrations p 1697 N95-23706
Robotic experiment with a force reflecting handcontroller onboard MIR space station p 1752 N95-23707
Development of Japanese experiment module remote manipulator system p 1752 N95-23708
Robust control of multi-jointed arm with a decentralized autonomous control mechanism p 1659 N95-23710
Automation and crew time saving in the space experiment p 1752 N95-23715
Robotic servicing system for space material experiment p 1697 N95-23722

Robotic system for the servicing of the orbiter thermal protection system p 1697 N95-23724
Robotics and telepresence for moon missions p 1776 N95-23725
Interactive autonomy and robotic skills p 1777 N95-23730
Planetary stations and Abyssal Benthic Laboratories: An overview of parallel approaches for long-term investigation in extreme environments p 1752 N95-23732
Design of teleoperation system with a force-reflecting real-time simulator p 1778 N95-23733
Telerobotics test bed for space structure assembly p 1618 N95-23734
A fuzzy structural matching scheme for space robotics vision p 1778 N95-23737
Real-time tracking using stereo and motion: Visual perception for space robotics p 1778 N95-23739
Terrain modelling and motion planning for an autonomous exploration rover p 1721 N95-23765
Robot skill learning through intelligent experimentation |TR-567| p 1784 N95-24038
The growth of the UniTree mass storage system at the NASA Center for Computational Sciences: Some lessons learned p 1862 N95-24135

ROBOTS
Controlling under-actuated robot arms using a high speed dynamics process
|NASA-CASE-NPO-18498-1-CU| p 1692 N95-22543
Simulation and off-line programming systems comparison
|DE95-002267| p 1766 N95-23078
The next decade of space robotics p 1768 N95-23673
Very fast motion planning for highly dexterous-articulated robots p 1771 N95-23691
Lunar rover technology demonstrations with Dante and Ratler p 1697 N95-23694
JPL space robotics: Present accomplishments and future thrusts p 1697 N95-23697
Concept verification of three dimensional free motion simulator for space robot p 1618 N95-23702
The Charlotte (TM) intra-vehicular robot p 1697 N95-23703
Robotic servicing system for space material experiment p 1697 N95-23722
Robotic system for the servicing of the orbiter thermal protection system p 1697 N95-23724
Visually guided grasping to study teleprogrammation within the BAROCO testbed p 1777 N95-23731
Telepresence control of a dual-arm dexterous robot p 1752 N95-23735
Mark Tracking: Position/orientation measurements using 4-circle mark and its tracking experiments p 1778 N95-23736
A fuzzy structural matching scheme for space robotics vision p 1778 N95-23737
Terrain modelling and motion planning for an autonomous exploration rover p 1721 N95-23765

ROBUSTNESS (MATHEMATICS)
Design of high performance multivariable control systems for supermaneuverable aircraft at high angle of attack
|NASA-CR-197661| p 1615 N95-22908
Benchmark problems in computational aeroacoustics p 1800 N95-23315
Progress in advanced spray combustion code integration p 1637 N95-23644
Robust control of multi-jointed arm with a decentralized autonomous control mechanism p 1659 N95-23710

ROCKET ENGINE DESIGN
Status of axisymmetric CFD of an eleven inch diameter hybrid rocket motor p 1686 N95-23651
Predicted performance of an integrated modular engine system
|NASA-CR-190787| p 1625 N95-23791

ROCKET ENGINES
STS-59 Space Shuttle mission report
|NASA-TM-110527| p 1619 N95-23093
STS-62 Space Shuttle mission report
|NASA-TM-110450| p 1619 N95-23094
Radiation/convection coupling in rocket motors and plumes p 1669 N95-23414
Non-intrusive measurements in a rocket engine combustor p 1625 N95-23439
Impeller flow field characterization with a laser two-focus velocimeter p 1675 N95-23440
Three-D CFD analysis of hydrostatic bearings p 1678 N95-23616
CFD parametric study of consortium impeller p 1680 N95-23626
On the accuracy of CFD-based pressure drop predictions for right-angle ducts p 1682 N95-23634

ROCKET EXHAUST
Radiation/convection coupling in rocket motors and plumes p 1669 N95-23414

ROCKET NOZZLES
Heat transfer in rocket engine combustion chambers and nozzles p 1668 N95-23413
Computational Fluid Dynamic (CFD) analysis of axisymmetric plume and base flow of film/dump cooled rocket nozzle p 1673 N95-23431
Four-nozzle benchmark wind tunnel model USA code solutions for simulation of multiple rocket base flow recirculation at 145,000 feet altitude p 1686 N95-23654
Numerical study of base pressure characteristic curve for a four-engine clustered nozzle configuration p 1625 N95-23655

ROCKET THRUST
Sensor-based control of rocket thrust chamber feature location for automated braze paste dispensing
|DE94-016559| p 1624 N95-22885
Development of an algebraic stress/two-layer model for calculating thrust chamber flow fields p 1675 N95-23442

ROCKS
Lithologic discrimination and alteration mapping from AVIRIS Data, Socorro, New Mexico p 1701 N95-23847

ROLL
Pitch sensor system
|AD-D016488| p 1799 N95-22863
Feedback control laws for highly maneuverable aircraft
|NASA-CR-197944| p 1615 N95-23410

RONCHI TEST
EUV metrology of multilayer optics
|DE95-003036| p 1819 N95-22723

ROOM TEMPERATURE
Liquid nitrogen temperature operation of a switching power converter
|NASA-TM-106867| p 1662 N95-23219

ROSAT MISSION
ROSAT observation program
|NASA-CR-197683| p 1866 N95-23595

ROTARY ENGINES
Evaluation of thermal barrier and PS-200 self-lubricating coatings in an air-cooled rotary engine
|NASA-CR-195445| p 1614 N95-23222

ROTARY WING AIRCRAFT
System for determining aerodynamic imbalance
|NASA-CASE-ARC-11913-1| p 1688 N95-23377

ROTARY WINGS
Integrated aerodynamic/dynamic/structural optimization of helicopter rotor blades using multilevel decomposition
|NASA-TP-3465| p 1612 N95-22953
System for determining aerodynamic imbalance
|NASA-CASE-ARC-11913-1| p 1688 N95-23377

ROTATING FLUIDS
Study of the pressure field in rotating homogeneous turbulent flows
|PB94-189107| p 1665 N95-22585

ROTATING GENERATORS
Computer simulation of a magnetohydrodynamic dynamo 2
|NIFS-320| p 1836 N95-23590

ROTATION
Harmonic oscillator in quantum rotational spectra: Molecules and nuclei p 1814 N95-22972
Flavour dependence of form factors in heavy meson decays
|PB95-139101| p 1807 N95-23156
Structure and evolution of long-lived spiral patterns in galaxies
|PB95-139242| p 1868 N95-23228
Computer simulation of a magnetohydrodynamic dynamo 2
|NIFS-320| p 1836 N95-23590
Flow and heat transfer in 180-degree turn square ducts: Effects of turning configuration and system rotation p 1682 N95-23636
D3-D program overview
|DE95-003879| p 1837 N95-24086

ROTATIONAL STATES
Energy transfer dynamics in isolated and in colliding highly vibrationally excited molecules
|AD-A265771| p 1806 N95-23077

ROTOR BLADES (TURBOMACHINERY)
Navier-Stokes analysis of an oxidizer turbine blade with tip clearance with and without a mini-shroud p 1672 N95-23428
Enhanced analysis and users manual for radial-inflow turbine conceptual design code RTD
|NASA-CR-195454| p 1609 N95-23462
Optimization of a centrifugal impeller design through CFD analysis p 1680 N95-23624
CFD parametric study of consortium impeller p 1680 N95-23626

ROTOR BODY INTERACTIONS
An investigation of helicopter dynamic coupling using an analytical model
|NASA-CR-197420| p 1612 N95-23217

ROTOR DYNAMICS
Coherent state constructions of bases for some physically relevant group chains p 1814 N95-22966
Influence of backup bearings and support structure dynamics on the behavior of rotors with active supports
|NASA-CR-197438| p 1694 N95-23190
Dynamic modelling and response characteristics of a magnetic bearing rotor system including auxiliary bearings
|NASA-CR-197859| p 1694 N95-23213
Synchronous dynamics of a coupled shaft/bearing/housing system with auxiliary support from a clearance bearing: Analysis and experiment
|NASA-CR-197858| p 1695 N95-23214
Evaluation of thermal barrier and PS-200 self-lubricating coatings in an air-cooled rotary engine
|NASA-CR-195445| p 1614 N95-23222
The influence of swirl brakes and a tip discharge orifice on the rotordynamic forces generated by discharge-to-suction leakage flows in shrouded centrifugal pumps p 1680 N95-23628

ROTORS
Influence of backup bearings and support structure dynamics on the behavior of rotors with active supports
|NASA-CR-197438| p 1694 N95-23190
Thin tailored composite wing for civil tiltrotor p 1613 N95-23317

ROUTES
High surface area, high permeability carbon monoliths
|DE95-004555| p 1650 N95-23577

ROVER PROJECT
Autonomous navigation system for the Marsokhod rover project p 1771 N95-23693

ROVING VEHICLES
Robotic all-terrain lunar exploration rover (RATLER) FY93 program status report
|DE95-003589| p 1694 N95-23065
Path planning for planetary rover using extended elevation map p 1771 N95-23689
Subsumption-based architecture for autonomous movement planning for planetary rovers p 1771 N95-23690
Control technique for planetary rover p 1771 N95-23692
A perspective on space robotics in Japan p 1697 N95-23695
Small image laser range finder for planetary rover p 1692 N95-23712
Terrain modelling and motion planning for an autonomous exploration rover p 1721 N95-23765

RUBBER
Neutron scattering analysis of rubber carbon black composite structure
|DE95-002735| p 1646 N95-22553

RUNGE-KUTTA METHOD
Numerical computation of aerodynamics and heat transfer in a turbine cascade and a turn-around duct using advanced turbulence models p 1675 N95-23444

RUNWAY CONDITIONS
Guidance and control requirements for high-speed Rollout and Turnoff (ROTO)
|NASA-CR-195026| p 1614 N95-22674

RUNWAYS
Aircraft accident report. Runway overrun following rejected takeoff. Continental airlines flight 795, McDonnell Douglas MD-82, N18835, LaGuardia Airport, Flushing, NY, 2 March 1994
|PB95-910401| p 1610 N95-23609

RUSSIAN FEDERATION
BROND-2.1. Russian evaluated neutron reaction data library
|DE94-634417| p 1810 N95-23458

RUTHENIUM
Supported transition metal catalysts for para- to ortho-hydrogen conversion
|NASA-CR-197907| p 1634 N95-23252
Microstructure and composition of a SNS Josephson junction using CaRuO3 as the metallic barrier
|DE95-004611| p 1845 N95-24152

S

S MATRIX THEORY
Harmonic oscillator representation in the theory of scattering and nuclear reactions p 1814 N95-22967
Scattering problem for quantum system with time-dependent periodic Hamiltonian
|DE94-635421| p 1797 N95-23965

S WAVES
More about the q-deformed H-atom wave functions: Normal and abnormal series
| DE94-628434 | p 1801 N95-22643
(pi)- and a(sub 1)-meson physics in current algebra at the quark level
| DE94-628611 | p 1804 N95-22811
Tomographic analysis of the three-dimensional variation of the seismic velocity structure of the shallow crust underlying Southern New England
| AD-A279406 | p 1739 N95-23247

SADDLE POINTS
A prescribing geodesic curvature problem
| DE94-628503 | p 1787 N95-22750

SAFETY
Radioisotope thermoelectric generator licensed hardware package and certification tests
| DE95-003039 | p 1661 N95-22799
Skin exposure: Assessing the hazard in the workplace p 1628 N95-23030
Mishap risk control for advanced aerospace/composite materials p 1628 N95-23031
Fire hazard considerations for composites in vehicle design p 1628 N95-23032
Microgravity experiments safety and integration requirements document tree
| NASA-CR-195447 | p 1855 N95-23206
Search Hanford accessible reports electronically system requirements specification
| DE95-004367 | p 1856 N95-23340

SAFETY FACTORS
Corrosion detection and monitoring of aircraft structures: An overview p 1644 N95-23515
Closing the circle on the splitting of the atom: The environmental legacy of nuclear weapons production in the United States and what the Department of Energy is doing about it p 1818 N95-23562

SAFETY MANAGEMENT
A review of civil aviation fatal accidents in which lost/disoriented was a cause/factor: 1981-1990
| DOT/FAA/AM-95/1 | p 1611 N95-24071
Aviation Accident Investigation Symposium. Volume 1: Industry recommendations and Safety Board responses
| PB94-917005 | p 1611 N95-24105

SALMONELLA
Regulation of alcohol fermentation in Escherichia coli
| DE94-016227 | p 1745 N95-22874

SALT BATHS
Corrosion of landing gear steels p 1642 N95-23500

SALT SPRAY TESTS
Corrosion of landing gear steels p 1642 N95-23500

SALTS
Diffusion behavior of lysozyme in aqueous ammonium sulfate solutions under varying solution conditions as determined by dynamic light scattering
| DE95-004821 | p 1635 N95-23380
Laboratory studies of the sensitivity of tropospheric ozone to the chemistry of sea salt aerosol
| DE95-003607 | p 1735 N95-24147

SALYUT SPACE STATION
Structure and properties of polymeric composite materials during 1501 days outer space exposure at Salyut-7 orbital station p 1652 N95-23915

SAMPLING
Novel mass spectrometric instrument for gaseous and particulate characterization and monitoring
| DE95-001135 | p 1687 N95-22682
Instantaneous field of view and spatial sampling of the Airborne Visible/Infrared Imaging Spectrometer (AVIRIS) p 1702 N95-23851

SANDS
Theoretical estimates of high frequency acoustic attenuation and backscattering from suspended sand particles in the ocean and in an estuary
| DSTO-TR-0078 | p 1743 N95-23667

SANDWICH STRUCTURES
Deflections of anisotropic sandwich beams with variable face sheets and core thicknesses p 1700 N95-23310

SAPPHIRE
Surface structural dependence of cesium adsorption on the (alpha)-Al2O3(0001) surface
| DE95-002610 | p 1842 N95-23135

SATELLITE ATTITUDE CONTROL
The Starpicker expert system: A problem in expertise capture p 1623 N95-23721
Improved AVHRR data navigation using automated land feature recognition to correct a satellite orbital model
| CSIRO-TR-34 | p 1718 N95-24026

SATELLITE COMMUNICATION
Adaptive beamforming in a CDMA mobile satellite communications system p 1655 N95-22815
The possibilities for mobile and fixed services up to the 20/30 GHz frequency bands p 1656 N95-22817
Improved small satellite access of the space network
| NASA-CR-197863 | p 1657 N95-22944

SATELLITE CONTROL
Robot arm system for automatic satellite capture and berthing p 1752 N95-23709
A scheduling and diagnostic system for scientific satellite GEOTAIL using expert system p 1781 N95-23753

SATELLITE DRAG
Calculation of satellite drag coefficients
| AD-A285118 | p 1622 N95-23781

SATELLITE IMAGERY
SeaWiFS technical report series. Volume 25: Ocean optics protocols for SeaWiFS validation, revision 1
| NASA-TM-104566-VOL-25-REV- | p 1743 N95-22671
Infrared algorithm development for ocean observations with EOS/MODIS
| NASA-CR-197851 | p 1743 N95-23212
FAME: A forest assessment and monitoring environment scenario
| PB95-139309 | p 1718 N95-23471
AVIRIS calibration using the cloud-shadow method p 1702 N95-23849
Simulation of landsat thematic mapper imagery using AVIRIS hyperspectral imagery p 1705 N95-23869
Measurements of canopy chemistry with 1992 AVIRIS data at Blackhawk Island and Harvard Forest p 1706 N95-23873
Preprocessing: Geocoding of AVIRIS data using navigation, engineering, DEM, and radar tracking system data p 1707 N95-23876
The data facility of the Airborne Visible/Infrared Imaging Spectrometer (AVIRIS) p 1707 N95-23877
Spectral variations in a collection of AVIRIS imagery p 1707 N95-23879
Monitoring land use and degradation using satellite and airborne data p 1707 N95-23880
The red edge in arid region vegetation: 340-1060 nm spectra p 1708 N95-23881
Temporal changes in endmember abundances, liquid water and water vapor over vegetation at Jasper Ridge p 1708 N95-23882
Mapping and monitoring changes in vegetation communities of Jasper Ridge, CA, using spectral fractions derived from AVIRIS images p 1708 N95-23883
The effect of signal noise on the remote sensing of Foliar biochemical concentration p 1708 N95-23884
Application of MAC-Europe AVIRIS data to the analysis of various alteration stages in the Landdmannalauger Hydrothermal Area (South Iceland) p 1709 N95-23885
Estimation of crown closure from AVIRIS data using regression analysis p 1709 N95-23886
Atmospheric correction of AVIRIS data of Monterey Bay contaminated by thin cirrus clouds p 1710 N95-23890
Investigations on the 1.7 micron residual absorption feature in the vegetation reflection spectrum p 1710 N95-23891
A comparison of spectral mixture analysis an NDVI for ascertaining ecological variables p 1710 N95-23892
Using AVIRIS for in-flight calibration of the spectral shifts of SPOT-HRV and of AVHRR? p 1710 N95-23893
Laboratory spectra of field samples as a check on two atmospheric correction methods p 1711 N95-23894
Determination of semi-arid landscape endmembers and seasonal trends using convex geometry spectral unmixing techniques p 1711 N95-23895
Forest and wildlife habitat analysis using remote sensing and geographic information systems p 1720 N95-24100
Analysis of conifer forest regeneration using Landsat Thematic Mapper data p 1720 N95-24101
Determining successional stage of temperate coniferous forests with Landsat satellite data p 1720 N95-24102
Determining coniferous forest cover and forest fragmentation with NOAA-9 advanced very high resolution radiometer data p 1720 N95-24103
Dynamics and pattern of a managed coniferous forest landscape in Oregon p 1720 N95-24104

SATELLITE INSTRUMENTS
On-orbit science in a small package: Managing the ALEXIS satellite and experiments
| DE94-014426 | p 1621 N95-22868
TIMED Imaging Photometer Experiment (TIPE)
| NASA-CR-197431 | p 1688 N95-23087

SATELLITE NAVIGATION SYSTEMS
Improved AVHRR data navigation using automated land feature recognition to correct a satellite orbital model
| CSIRO-TR-34 | p 1718 N95-24026

SATELLITE NETWORKS
Improved small satellite access of the space network
| NASA-CR-197863 | p 1657 N95-22944

SATELLITE OBSERVATION
Civilian satellite remote sensing: A strategic approach
| PB95-109633 | p 1717 N95-22713
GPS survey of the western Tien Shan
| NASA-CR-197901 | p 1717 N95-22832
Global electric field determination in the Earth's outer magnetosphere using energetic charged particles
| NASA-CR-197392 | p 1737 N95-22945
TIMED Imaging Photometer Experiment (TIPE)
| NASA-CR-197431 | p 1688 N95-23087
Infrared algorithm development for ocean observations with EOS/MODIS
| NASA-CR-197851 | p 1743 N95-23212
Investigation of the role of gravity waves in the generation of equatorial bubbles
| NASA-CR-197962 | p 1739 N95-23272
Ocean observations with EOS/MODIS: Algorithm development and post launch studies
| NASA-CR-197894 | p 1718 N95-23473
Validation data for land surface temperature determination from satellites
| CSIRO-TR-33 | p 1718 N95-23597
Use of the Airborne Visible/Infrared Imaging Spectrometer to calibrate the optical sensor on board the Japanese Earth Resources Satellite-1 p 1624 N95-23864
Measurements of canopy chemistry with 1992 AVIRIS data at Blackhawk Island and Harvard Forest p 1706 N95-23873
Atmospheric correction of AVIRIS data of Monterey Bay contaminated by thin cirrus clouds p 1710 N95-23890
Determination of semi-arid landscape endmembers and seasonal trends using convex geometry spectral unmixing techniques p 1711 N95-23895
Architecture and evolution of Goddard Space Flight Center Distributed Active Archive Center p 1862 N95-24134

SATELLITE ORBITS
Improved AVHRR data navigation using automated land feature recognition to correct a satellite orbital model
| CSIRO-TR-34 | p 1718 N95-24026

SATELLITE ORIENTATION
The Starpicker expert system: A problem in expertise capture p 1623 N95-23721

SATELLITE TRANSMISSION
Utilizing a TDRS satellite for direct broadcast satellite-radio propagation experiments and demonstrations p 1622 N95-22814

SATELLITE-BORNE INSTRUMENTS
Validation data for land surface temperature determination from satellites
| CSIRO-TR-33 | p 1718 N95-23597
An intelligent ground operator support system p 1769 N95-23681

SATELLITES
Active vision in satellite scene analysis p 1778 N95-23738

SATURN RINGS
Charging of interplanetary grains
| NASA-CR-198032 | p 1869 N95-24066

SATURN 5 LAUNCH VEHICLES
Axisymmetric computational fluid dynamics analysis of Saturn V/S1-C/F1 nozzle and plume p 1672 N95-23430

SAWTOOTH WAVEFORMS
Fast potential change in sawteeth in JIPP T-IIU tokamak plasmas
| NIFS-327 | p 1835 N95-23533

SCALARS
On the scalar curvature of minimal hypersurfaces
| DE94-628516 | p 1796 N95-22741
Finite-temperature scalar field theory in static de Sitter space
| DE94-628522 | p 1848 N95-22743
A space-time lattice version of scalar electrodynamics
| DE94-628577 | p 1850 N95-22784
Level set techniques applied to unsteady detonation propagation
| DE95-002741 | p 1666 N95-22901
The relativistic many body problem with an oscillator interaction p 1824 N95-22991
The Duffin-Kemmer-Petiau oscillator p 1825 N95-22998
Optimally scaled systems for second order scalar singularity perturbed problems
| PB95-138814 | p 1789 N95-23169
Two portable parallel tridiagonal solvers
| DE94-019044 | p 1763 N95-23243
Search for scalar and vector leptoquarks in electron-proton collisions at radical S = 300 GeV
| DE94-785267 | p 1810 N95-23475

SCALE MODELS
The viability of establishing collaborative, reconfigurable research environments for the Human Performance Research Laboratory at NASA Ames
| NASA-CR-197384 | p 1753 N95-22480

SCALING LAWS
On inertial range scaling laws
| DE95-004515 | p 1677 N95-23484
Dimensional scaling for impact cratering and perforation p 1624 N95-23843

Experimental achievement of toroidal beta beyond that predicted by 'Troyon' scaling
| DE95-003880 | p 1837 N95-24087

SCANNERS
Color orthophotography: To scan or not
| DE95-002749 | p 1689 N95-24069

SCANNING
Color orthophotography: To scan or not
| DE95-002749 | p 1689 N95-24069

SCANNING ELECTRON MICROSCOPY
Morphology of extinguished monolithic JA2 grains fired in a 30-mm Solid Propellant Electrothermal Chemical (SPETC) gun
| AD-A285792 | p 1652 N95-22506
Germination, growth rates, and electron microscope analysis of tomato seeds flown on the LDEF
p 1748 N95-23821
Image and compositional characteristics of the LDEF Big Guy impact crater p 1700 N95-23838

SCATTERING
Investigation of mechanical properties and their relation to the internal structure of nanocrystalline metals and composites
| DE95-001151 | p 1627 N95-22683
Long range potentials and multiple scattering theory in complex systems
| DE94-628881 | p 1804 N95-22791
Protein folding and protein metallocluster studies using synchrotron small angler x ray scattering
| DE95-003339 | p 1746 N95-22897
An upper bound for the proton temperature anisotrophy
| DE95-002752 | p 1737 N95-22903
Higgs searches and WW scattering
| PB95-139143 | p 1807 N95-23160
LDEF environment modeling updates
p 1637 N95-23797
Scattering problem for quantum system with time-dependent periodic Hamiltonian
| DE94-635421 | p 1797 N95-23965
Pauli-blocking effects in neutron-alpha reactions
| DE94-016358 | p 1813 N95-24046

SCATTERING FUNCTIONS
The point interactions in the quantum problem of three particles with internal structure
| DE94-635423 | p 1851 N95-23967
Subband quantum scattering times for AlGaAs/GaAs obtained using digital filtering
| NASA-TM-106873 | p 1846 N95-24188

SCENE ANALYSIS
Active vision in satellite scene analysis
p 1778 N95-23738
A self-organizing neural network architecture for auditory and speech perception with applications to acoustic and other temporal prediction problems
| AD-A285640 | p 1800 N95-23782

SCHEDULES
Cost and schedule analytical techniques development
| NASA-CR-196548 | p 1853 N95-22891
DTS: Building custom, intelligent schedulers
p 1779 N95-23744
A scheduling and diagnostic system for scientific satellite GEOTAIL using expert system p 1781 N95-23753
Automatic generation of efficient orderings of events for scheduling applications p 1618 N95-23764

SCHEDULING
Task scheduling in dataflow computer architectures
p 1753 N95-23301
Microarchitecture support for dynamic scheduling of acyclic task graphs
| CSRD-1207 | p 1791 N95-23600
An intelligent ground operator support system
p 1769 N95-23681
Distributed intelligence for ground/space systems
p 1770 N95-23685
Planning and scheduling the Hubble Space Telescope: Practical application of advanced techniques
p 1779 N95-23740
A constraint-logic based implementation of the coarse-grained approach to data acquisition scheduling of the International Ultraviolet Explorer orbiting observatory p 1779 N95-23741
Robust telescope scheduling p 1779 N95-23742
DTS: Building custom, intelligent schedulers
p 1779 N95-23744
Graphical timeline editing p 1761 N95-23746
A format for the interchange of scheduling models
p 1780 N95-23747
Coordinating complex decision support activities across distributed applications p 1761 N95-23749
CRI planning and scheduling for space
p 1617 N95-23751
A scheduling and diagnostic system for scientific satellite GEOTAIL using expert system p 1781 N95-23753
Design and implementation of an experiment scheduling system for the ACTS satellite p 1620 N95-23756
High performance techniques for space mission scheduling p 1618 N95-23758
Applications of dynamic scheduling technique to space related problems: Some case studies
p 1618 N95-23759
Solution and reasoning reuse in space planning and scheduling applications p 1618 N95-23760
Empirical results on scheduling and dynamic backtracking p 1618 N95-23761
Scheduling with genetic algorithms
p 1761 N95-23762
Automatic generation of efficient orderings of events for scheduling applications p 1618 N95-23764
Loop scheduling for heterogeneity
| TR-540 | p 1764 N95-23936
Constraint based scheduling for the Goddard Space Flight Center distributed Active Archive Center's data archive and distribution system p 1859 N95-24121
Scheduler-conscious synchronization
| TR-550 | p 1765 N95-24183

SCHROEDINGER EQUATION
Solutions for the vector k-constrained KP hierarchy
| DE94-628431 | p 1786 N95-22633
More about the q-deformed H-atom wave functions: Normal and abnormal series
| DE94-628434 | p 1801 N95-22643
Dirac canonical quantization and Faddeev-Jackiw symplectic quantization of higher order Lagrangians
| DE94-628428 | p 1796 N95-22788
Algebraic theory of molecules p 1814 N95-22958
Harmonic oscillator representation in the theory of scattering and nuclear reactions p 1814 N95-22967
A possible generalization of the harmonic oscillator potential p 1822 N95-22970
A method of solving simple harmonic oscillator Schroedinger equation p 1797 N95-22989
The relativistic many body problem with an oscillator interaction p 1824 N95-22991
Disorder-induced breakdown of soliton and polaron particles
| DE95-003694 | p 1808 N95-23267
Spontaneous wave packet reduction
| DE94-634280 | p 1851 N95-23454

SCHWARZ-CHRISTOFFEL TRANSFORMATION
Schwarz-Christoffel methods for multiply-elongated regions
| DE94-019048 | p 1790 N95-23536

SCIENCE
Teacher Enhancement Institute p 1853 N95-23312

SCIENTIFIC SATELLITES
On-orbit science in a small package: Managing the ALEXIS satellite and experiments
| DE94-014426 | p 1621 N95-22868
A constraint-logic based implementation of the coarse-grained approach to data acquisition scheduling of the International Ultraviolet Explorer orbiting observatory p 1779 N95-23741
A scheduling and diagnostic system for scientific satellite GEOTAIL using expert system p 1781 N95-23753

SCINTILLATING FIBERS
Performance of a large scale scintillating fiber tracker using VLPC readout
| DE95-003746 | p 1871 N95-23370

SCINTILLATION COUNTERS
Performance of a large scale scintillating fiber tracker using VLPC readout
| DE95-003746 | p 1871 N95-23370
Thermal effects on the STAR electromagnetic calorimeter
| DE95-004663 | p 1688 N95-23492

SCRAP
Chemical recycling of scrap composites
p 1629 N95-23034

SEA ICE
Unusual radar echoes from the Greenland ice sheet
p 1714 N95-23951

SEA SURFACE TEMPERATURE
Infrared algorithm development for ocean observations with EOS/MODIS
| NASA-CR-197851 | p 1743 N95-23212

SEALERS
Method for forming a glove attachment
| NASA-CASE-MSC-21632-1 | p 1750 N95-22766

SEALING
The sound insulations of studio doors. Part 2: Door seals
| BBC-RD-1994/15 | p 1654 N95-24045

SECONDARY FLOW
Three-dimensional unsteady flow calculations in an advanced gas generator turbine p 1671 N95-23425

SECONDARY ION MASS SPECTROMETRY
Secondary ion mass spectrometry (SIMS) analysis of hypervelocity microparticle impact sites on LDEF surfaces p 1637 N95-23836
SIMS chemical and isotopic analysis of impact features from LDEF experiments AO187-1 and AO187-2
p 1637 N95-23837

SECURITY
Information technology standards process guide
| DE95-003967 | p 1857 N95-23574
Security clearances: Consideration of sexual orientation in the clearance process. Report to Congressional requesters
| GAO/NSIAD-95-21 | p 1853 N95-23588

SEDIMENTARY ROCKS
Energy flux and hydrogeology of thermal anomalies in the Gulf of Mexico Basin - South Texas example
| DE95-003341 | p 1743 N95-22695

SEDIMENTS
OU3 sediment dating and sedimentation rates
| DE95-001891 | p 1734 N95-23384
Remote identification of a gravel laden Pleistocene river bed p 1712 N95-23921

SEEDS
Germination, growth rates, and electron microscope analysis of tomato seeds flown on the LDEF
p 1748 N95-23821

SEISMIC ENERGY
Axial focusing of energy from a hypervelocity impact on earth
| DE95-003347 | p 1740 N95-24008

SEISMIC WAVES
Intermediate-term earthquake prediction and seismic zoning in Northern Italy
| DE94-627689 | p 1736 N95-22612
Axial focusing of impact energy in the earth's interior: A possible link to flood basalts and hotspots
| DE95-003357 | p 1741 N95-24009

SEISMOLOGY
Intermediate-term earthquake prediction and seismic zoning in Northern Italy
| DE94-627689 | p 1736 N95-22612
Seismic hazards at Kilauea and Mauna Loa volcanoes, Hawaii
| DE94-012109 | p 1737 N95-22924
Seismic evidence of conjugate normal faulting: The 1994 Devil Canyon earthquake sequence near Challis, Idaho
| DE95-002052 | p 1740 N95-23386
Axial focusing of impact energy in the earth's interior: A possible link to flood basalts and hotspots
| DE95-003357 | p 1741 N95-24009

SELECTION
Gas cooled leads. Part 1: Theoretical Study. Part 2: Frost free lead optimized for a specific current. Part 3: Frost free lead optimized for a large current range
| DE95-002657 | p 1660 N95-22716
Supersymmetric singlet majorons and cosmology
| DE94-628571 | p 1850 N95-22783
Real lasers and other deformed objects
p 1692 N95-23001

SELECTIVE DISSEMINATION OF INFORMATION
Software agents for the dissemination of remote terrestrial sensing data p 1721 N95-23675

SELF CONSISTENT FIELDS
Computational studies of metal-metal and metal-ligand interactions
| NASA-CR-197862 | p 1641 N95-23215
Symmetry breaking in O4(+): An application of the Brueckner coupled-cluster method
| NASA-CR-197981 | p 1810 N95-23459

SELF ORGANIZING SYSTEMS
Complexity in plasma: A grand view of self-organization
| NIFS-318 | p 1835 N95-23528

SELF PROPAGATION
Level set techniques applied to unsteady detonation propagation
| DE95-002741 | p 1666 N95-22901

SEMANTICS
Browsing semantics in the tower model
| PB95-127221 | p 1855 N95-22534
Algebra of lines and boxes
| PB95-130456 | p 1787 N95-22768
Algebraic semantics of basic message sequence charts
| PB95-138970 | p 1657 N95-23151
DUALITY: A simple formalism for the analysis of UNITY
| PB95-135703 | p 1763 N95-23166
Relating multifunctions and predicate transformers through closure operators
| PB95-135646 | p 1757 N95-23467
Modelling and analysis of a high speed data bus with predicate/transition nets
| PB95-140695 | p 1764 N95-23538
Combinatorial semantics
| TR-563 | p 1792 N95-23793

SEMICONDUCTOR DEVICES
Plasmo-magnetoelastic waves in a semiconducting heterostructure. 1: Plasmo-elastic longitudinal modes. 2: Sh-magnetoelastic modes
| PB95-138822 | p 1833 N95-23170
Method of making a semiconductor device using a nanochannel glass matrix
| AD-D016383 | p 1662 N95-23241
Measurement and analysis of scatter from silicon wafers
| DE95-002411 | p 1827 N95-23531
Extraction of the surface recombination velocity of passivated phosphorus-doped silicon emitters
| DE95-004539 | p 1845 N95-24156
Particle transport in plasma reactors
| DE95-004541 | p 1837 N95-24158
SEMICONDUCTORS (MATERIALS)
Magnetic field effects on strong-coupling polaron in quantum dots
| DE94-629038 | p 1847 N95-22496
Resonant shallow donor magnetopolaron effect in a GaAs/AlGaAs quantum dot in high magnetic fields
| DE94-629039 | p 1798 N95-22497
Large-area triple-junction a-Si alloy production scaleup
| DE95-000245 | p 1726 N95-22546
High gain GaAs Photoconductive Semiconductor Switches for impulse sources
| DE95-001885 | p 1659 N95-22549
Metallization and incomplete melting of a semiconductor surface at high temperature
| DE94-627342 | p 1660 N95-22591
A special percolation problem in ceramic composites
| DE94-627641 | p 1647 N95-22611
Method and system for electron beam lithography
| AD-D016554 | p 1660 N95-22709
Chemical vapor deposition in low pressure batch furnaces
| DE95-003035 | p 1632 N95-22722
Optical absorption in an indirect-gap semiconductor quantum well systems
| DE94-628878 | p 1849 N95-22759
Two-photon absorption in an indirect-gap semiconductor quantum well systems 1. Interband transitions
| DE94-628879 | p 1849 N95-22760
Two-photon absorption in an indirect-gap semiconductor quantum well systems 2. Excitonic transitions
| DE94-628880 | p 1849 N95-22761
Photoemission study of quantum confinement by a finite barrier: Cu/Co(wedge)/Cu(100)
| DE95-002913 | p 1840 N95-22762
High gain GaAs photoconductive semiconductor switches: Measurement of filament velocity and reduced trigger energy
| DE95-001884 | p 1661 N95-22844
Computational modeling of properties
| NAS-CR-196544 | p 1841 N95-22907
Nanophase materials: Synthesis, properties, applications
| AD-A286013 | p 1627 N95-22940
Strong-coupling polaron effect in quantum dots
| DE94-628485 | p 1850 N95-23049
Thermal effects on the STAR electromagnetic calorimeter
| DE95-004663 | p 1688 N95-23492
Mechanical design of the CDF SVX 2 silicon vertex detector
| DE94-018985 | p 1689 N95-23520
SVX(prime), the new CDF silicon vertex detector
| DE94-018986 | p 1689 N95-23521
Profiling and light scattering studies of Si surfaces
| DE95-002931 | p 1828 N95-24005
Carbon doping of III-V compound semiconductors
| DE95-003431 | p 1844 N95-24013
SENSITIVITY
Computer modeling of the sensitivity of a laser water vapor sensor to variations in temperature and air speed p 1692 N95-23330
Long-baseline neutrino oscillation experiments
| DE95-004636 | p 1870 N95-23584
Search for millimeterwave CO emission in damped Lyman-alpha systems
| PB95-139259 | p 1868 N95-23607
Preliminary analysis of the sensitivity of AIRSAR images to soil moisture variations p 1714 N95-23950
SEQUENCING
An improved system for exon recognition and gene modeling in human DNA sequences
| DE94-017863 | p 1746 N95-22890
Protein folding and protein metallocluster studies using synchrotron small angler x ray scattering
| DE95-003339 | p 1746 N95-22897
Performance of single-keyword and multiple-keyword pattern matching algorithms
| PB95-138954 | p 1756 N95-23150
Ishikawa iteration process for nonlinear Lipschitz strongly accretive mappings
| DE94-634284 | p 1792 N95-23658
Reevaluation of the significance of sequence information for speech recognition
| TR-555 | p 1658 N95-23794
Phonetic set hashing: A novel scheme for transforming phone sequences to words
| TR-538 | p 1658 N95-24039
Proposal of a Modified EBU method for reliable evaluation of picture quality
| NHK-LABS-NOTE-431 | p 1863 N95-24180
SEQUENTIAL ANALYSIS
Analytic sets and games in Banach spaces
| PB95-108080 | p 1787 N95-22837
SEQUENTIAL COMPUTERS
Microarchitecture support for dynamic scheduling of acyclic task graphs
| CSRD-1207 | p 1791 N95-23600
SEQUENTIAL CONTROL
Integrating O/S models during conceptual design, part 2
| NASA-CR-197904 | p 1622 N95-23399
An operations and command systems for the extreme ultraviolet explorer p 1770 N95-23687
SERIES EXPANSION
Coherent state constructions of bases for some physically relevant group chains p 1814 N95-22966
Taylor series expansion and modified extended Prony analysis for localization
| DE95-003671 | p 1758 N95-23567
SERUMS
Activation of the jun-D gene in human myeloid cells by 1-(beta)-D-arabinofuranosylcytosine
| DE94-016591 | p 1746 N95-22912
SERVICE LIFE
Product stewardship in the composites industry p 1628 N95-23027
Damage-mitigating control of a reusable rocket engine for high performance and extended life
| NASA-CR-4640 | p 1654 N95-23195
Oklahoma City air logistics center (USAF) aging aircraft corrosion program p 1607 N95-23519
SERVOCONTROL
Vision-based planning and execution of precision grasps
| TR-546 | p 1784 N95-24185
SERVOMECHANISMS
Controlling under-actuated robot arms using a high speed dynamics process
| NASA-CASE-NPO-18498-1-CU | p 1692 N95-22543
SET THEORY
Is omega* - (mu) absolutely countably compact?
| PB95-127981 | p 1785 N95-22528
Countable space with a closed subspace without continuous extender
| PB95-127973 | p 1785 N95-22533
Entropy of Z(sup d) subshifts of finite type
| PB95-108072 | p 1787 N95-22836
Analytic sets and games in Banach spaces
| PB95-108080 | p 1787 N95-22837
Reevaluation of the significance of sequence information for speech recognition
| TR-555 | p 1658 N95-23794
Effective category and measure in abstract complexity theory
| TR-529 | p 1792 N95-23929
Optimal advice
| TR-527 | p 1792 N95-23931
Reducibility classes of P-selective sets
| TR-524 | p 1792 N95-24002
Witness-isomorphic reductions and the local search problem
| TR-522 | p 1793 N95-24003
Large sets in AC(exp 0): A Kolmogorov complexity related property and some applications
| TR-556 | p 1797 N95-24029
On the size of sets with weak membership properties
| TR-557 | p 1793 N95-24034
Logspace reducibility and self-reducibility: Models and equivalences
| TR-544 | p 1760 N95-24059
Semi-membership algorithms: Some recent advances
| TR-526 | p 1760 N95-24092
Polynomial-time membership comparable sets
| TR-552 | p 1793 N95-24182
The satanic notations: Counting classes beyond #P and other definitional adventures
| TR-561 | p 1793 N95-24194
SEWAGE TREATMENT
Resource recovery and epidemiology of anaerobic wastewater treatment process in a controlled ecological life support system
| NASA-CR-197930 | p 1751 N95-23474
SEYFERT GALAXIES
ROSAT observation program
| NASA-CR-197683 | p 1866 N95-23595
Near infrared and optical spectroscopy of FSC10214+4724
| NASA-CR-197966 | p 1828 N95-24068
SH WAVES
Plasmo-magnetoelastic waves in a semiconducting heterostructure. 1: Plasmo-elastic longitudinal modes. 2: Sh-magnetoelastic modes
| PB95-138822 | p 1833 N95-23170
SHAFTS (MACHINE ELEMENTS)
Synchronous dynamics of a coupled shaft/bearing/housing system with auxiliary support from a clearance bearing: Analysis and experiment
| NASA-CR-197858 | p 1695 N95-23214
SHAPES
Shapes and stability of algebraic nuclear models p 1814 N95-22974
Phonon-induced anomalous specific heat of a model nanocrystal by computer simulation
| DE95-004653 | p 1843 N95-23585
SHEAR FLOW
Three-dimensional structure in a supersonic jet: Behavior near centerline
| NASA-TM-106869 | p 1668 N95-23220
Direct numerical simulations and modeling of a spatially-evolving turbulent wake p 1687 N95-23289
Direct numerical simulation of sheared turbulent flow p 1687 N95-23296
SHEAR LAYERS
Computational Fluid Dynamic (CFD) analysis of axisymmetric plume and base flow of film/dump cooled rocket nozzle p 1673 N95-23431
SHEAR STRENGTH
Interlaminar shear test method development for long term durability testing of composites p 1631 N95-23300
SHEAR STRESS
High-lift flow-physics flight experiments on a subsonic civil transport aircraft (B737-100) p 1609 N95-23333
SHELL STABILITY
The development of shell imperfection measurement techniques
| TAE-712 | p 1699 N95-23923
SHIPS
Endeavor: Now and then
| NASA-TM-110539 | p 1620 N95-23664
SHOCK LAYERS
Entropy jump across an inviscid shock wave
| NASA-CR-195046 | p 1678 N95-23596
SHOCK LOADS
Impact shock and penetration fragmentation in porous media
| DE94-018900 | p 1868 N95-23656
SHOCK WAVE INTERACTION
Mach 10 computational study of a three-dimensional scramjet inlet flow field
| NASA-TM-4602 | p 1667 N95-23210
A generic efficient adaptive grid scheme for rocket propulsion modeling p 1670 N95-23418
Supersonic flow and shock formation in turbine tip gaps p 1672 N95-23429
SHOCK WAVE PROPAGATION
The effect of a non-zero shock width on wave propagation in multi-dimensions
| DE95-002748 | p 1666 N95-22902
Entropy jump across an inviscid shock wave
| NASA-CR-195046 | p 1678 N95-23596
SHOCK WAVES
Nonlinear generalized functions and nonconservative shock simulations
| DE95-003307 | p 1795 N95-22734
Langmuir-like waves and radiation in planetary foreshocks
| NASA-CR-197376 | p 1869 N95-22828
Entropy jump across an inviscid shock wave
| NASA-CR-195046 | p 1678 N95-23596
Axial focusing of impact energy in the earth's interior: A possible link to flood basalts and hotspots
| DE95-003357 | p 1741 N95-24009
Investigation of infra-red and nonequilibrium air radiation
| NASA-CR-197977 | p 1741 N95-24041
SHROUDED TURBINES
Navier-Stokes analysis of an oxidizer turbine blade with tip clearance with and without a mini-shroud p 1672 N95-23428
SHROUDS
Optimization of a centrifugal impeller design through CFD analysis p 1680 N95-23624
Use of blade lean in turbomachinery redesign p 1680 N95-23625
SHUTTLE IMAGING RADAR
AIRSAR deployment in Australia, September 1993: Management and objectives p 1714 N95-23948

Preliminary analysis of the sensitivity of AIRSAR images to soil moisture variations p 1714 N95-23950

SIDESLIP

Wing pressure distributions from subsonic tests of a high-wing transport model --- in the Langley 14- by 22-Foot Subsonic Wind Tunnel
| NASA-TM-4583 | p 1607 N95-22802

SIGNAL ANALYSIS

Simulation of landsat thematic mapper imagery using AVIRIS hyperspectral imagery p 1705 N95-23869

SIGNAL DETECTION

Parallel digital modem using multirate digital filter banks
| NASA-CR-197331 | p 1761 N95-22478

Capacitive acoustic wave detector and method of using same
| NASA-CASE-LAR-13890-1 | p 1799 N95-22921

SIGNAL PROCESSING

Parallel digital modem using multirate digital filter banks
| NASA-CR-197331 | p 1761 N95-22478

Maximum-likelihood spectral estimation and adaptive filtering techniques with application to airborne Doppler weather radar
| NASA-CR-197699 | p 1658 N95-23670

Active vision in satellite scene analysis p 1778 N95-23738

VLSI for high-speed digital signal processing
| AD-A285643 | p 1663 N95-23783

SIGNAL TO NOISE RATIOS

The effect of signal noise on the remote sensing of Foliar biochemical concentration p 1708 N95-23884

SIGNAL TRANSMISSION

A self-organizing neural network architecture for auditory and speech perception with applications to acoustic and other temporal prediction problems
| AD-A285640 | p 1800 N95-23782

SIGNATURE ANALYSIS

Toward an automated signature recognition toolkit for mission operations p 1659 N95-23682

Remote sensor test range update
| DE95-003629 | p 1735 N95-24018

SIGNATURES

Experience with CANDID: Comparison algorithm for navigating digital image databases
| DE95-000869 | p 1855 N95-22515

SILICATES

Supported transition metal catalysts for para- to ortho-hydrogen conversion
| NASA-CR-197907 | p 1634 N95-23252

SILICIDES

Dislocation decomposition, dissociation, and deformation in MoSi2 and (alpha)-Al2O3 single crystals
| DE95-002715 | p 1839 N95-22653

SILICON

Twelve month performance evaluation for the rotating shadowband radiometer
| DE95-002847 | p 1726 N95-22554

Advanced growth and surface analysis system for in situ studies of interface formation
| DE95-002850 | p 1838 N95-22555

World's first 15%-efficient multicrystalline silicon modules
| DE95-002604 | p 1727 N95-22650

Structural properties of silicon clusters: An empirical potential study
| DE94-628902 | p 1805 N95-22935

Mechanical design of the CDF SVX 2 silicon vertex detector
| DE94-018985 | p 1689 N95-23520

SVX(prime), the new CDF silicon vertex detector
| DE94-018986 | p 1689 N95-23521

Measurement and analysis of scatter from silicon wafers
| DE95-002411 | p 1827 N95-23531

Development of microchannel plate x-ray optics
| NASA-CR-197935 | p 1866 N95-23540

Cu deposition using a permanent magnet electron cyclotron resonance microwave plasma source
| DE94-017768 | p 1650 N95-23981

Profiling and light scattering studies of Si surfaces
| DE95-002931 | p 1828 N95-24005

Silicon surface and bulk defect passivation by low temperature PECVD oxides and nitrides
| DE95-004531 | p 1731 N95-24090

Extraction of the surface recombination velocity of passivated phosphorus-doped silicon emitters
| DE95-004539 | p 1845 N95-24156

Crystalline-silicon photovoltaics: Necessary and sufficient
| DE95-004540 | p 1731 N95-24157

SILICON ALLOYS

Continuous roll-to-roll amorphous-silicon photovoltaic manufacturing technology
| DE95-000243 | p 1728 N95-23061

SILICON CARBIDES

Method of producing a silicon carbide fiber reinforced strontium aluminosilicate glass-ceramic matrix composite
| NASA-CASE-LEW-15263-2 | p 1627 N95-22563

Research on defects and transport in amorphous-silicon-based semiconductors
| DE94-011888 | p 1660 N95-22586

SILICON DIOXIDE

Protective coating for ceramic materials
| NASA-CASE-ARC-11969-1-CU | p 1649 N95-23394

SILICON FILMS

Chemical vapor deposition in low pressure batch furnaces
| DE95-003035 | p 1632 N95-22722

SILICON NITRIDES

Evolution of oxidation and creep damage mechanisms in HIPed silicon nitride materials
| DE95-001360 | p 1647 N95-22689

Silicon surface and bulk defect passivation by low temperature PECVD oxides and nitrides
| DE95-004531 | p 1731 N95-24090

SILICON OXIDES

Four space application material coatings on the Long-Duration Exposure Facility (LDEF) p 1651 N95-23913

Silicon surface and bulk defect passivation by low temperature PECVD oxides and nitrides
| DE95-004531 | p 1731 N95-24090

SILICONE RUBBER

Method for forming a glove attachment
| NASA-CASE-MSC-21632-1 | p 1750 N95-22766

SILICONES

Four space application material coatings on the Long-Duration Exposure Facility (LDEF) p 1651 N95-23913

SILVER

Some aspects of critical currents in Ag sheathed Bi2Sr2Ca2Cu3O10 composite tapes: A summary
| DE95-003952 | p 1842 N95-23354

Measurements of the optical properties of thin films of silver and silver oxide p 1651 N95-23906

Durability of reflector materials in the space environment p 1651 N95-23912

SILVER ALLOYS

Durability of reflector materials in the space environment p 1651 N95-23912

SILVER OXIDES

Measurements of the optical properties of thin films of silver and silver oxide p 1651 N95-23906

SIMD (COMPUTERS)

Towards the Teraflop CFD
| NASA-CR-197947 | p 1764 N95-23594

Unstructured grids on SIMD torus machines
| NASA-CR-197954 | p 1758 N95-23610

SIMULATION

Structure and evolution of long-lived spiral patterns in galaxies
| PB95-139242 | p 1868 N95-23228

Holographic interferometric tomography for reconstructing flow fields p 1690 N95-23287

Structured adaptive grid generation using algebraic methods p 1669 N95-23417

Consistency and Monte Carlo simulation of a data driven version of smooth goodness-of-fit tests
| PB95-141255 | p 1794 N95-23559

Unsteady flow simulations in support of the SSME HEX turning vane cracking investigation with the ATD HPOTP p 1679 N95-23621

Simulation of cookoff results in a small scale test
| DSTO-TR-0090 | p 1653 N95-23668

SIMULATORS

Combining optical and microwave remote sensing data of forest vegetation: MAC Europe 1991
| PB95-127312 | p 1717 N95-22538

Design of teleoperation system with a force-reflecting real-time simulator p 1778 N95-23733

SIMULTANEOUS EQUATIONS

Nonlinear thermoviscoelastic behaviour in complex materials
| PB95-140653 | p 1630 N95-23537

SINGLE CRYSTALS

Dislocation decomposition, dissociation, and deformation in MoSi2 and (alpha)-Al2O3 single crystals
| DE95-002715 | p 1839 N95-22653

Motion-sensitive optical correlator using a VanderLugt correlator
| NASA-CASE-NPO-18769-1-CU | p 1827 N95-23045

Cation disorder determined by MAS Al-27 NMR in high dose neutron irradiated spinel
| DE95-003681 | p 1842 N95-23266

Effect on c-axis transport properties of a critical state in Bi2Sr2CaCu2O8
| DE95-003695 | p 1843 N95-23366

Growth of single crystals of organic salts with large second-order optical nonlinearities by solution processes for devices
| NASA-CR-197963 | p 1843 N95-23563

Electrochemical studies of perovskite mixed conductors
| DE95-003704 | p 1636 N95-23573

Temperature effects on ion irradiation damage in MgAl2O4 spinel single crystals
| DE95-003679 | p 1844 N95-24073

SINGLE STAGE TO ORBIT VEHICLES

Structural Arrangement Trade Study. Volume 1: Reusable Hydrogen Composite Tank System (RHCTS) and Graphite Composite Primary Structures (GCPS). Executive summary
| NASA-CR-197685 | p 1621 N95-23188

Structural arrangement trade study. Volume 3: Reusable Hydrogen Composite Tank System (RHCTS) and Graphite Composite Primary Structures (GCPS). Addendum
| NASA-CR-197687 | p 1621 N95-23189

SINGULARITY (MATHEMATICS)

A wall interference assessment/correction system
| NASA-CR-197421 | p 1667 N95-23183

SINTERING

Numerical simulation of axisymmetric viscous sintering
| PB95-138889 | p 1667 N95-23175

SISO (CONTROL SYSTEMS)

Adaptive control of linear systems based on approximate models
| PB95-139333 | p 1767 N95-23199

SITTING POSITION

A multibody/finite element analysis approach for modeling of crash dynamic responses
| NIAR-94-3 | p 1610 N95-24050

SIZE (DIMENSIONS)

Petabyte mass memory system using the Newell Optical(TM) p 1753 N95-24119

SIZE DISTRIBUTION

Mass transport through polycrystalline microstructures
| DE95-004552 | p 1811 N95-23576

High surface area, high permeability carbon monoliths
| DE95-004555 | p 1650 N95-23577

SKIN (ANATOMY)

Skin exposure: Assessing the hazard in the workplace p 1628 N95-23030

SKY SURVEYS (ASTRONOMY)

IRAS sky survey atlas: Explanatory supplement
| NASA-CR-197335 | p 1865 N95-22539

ROSAT observation program
| NASA-CR-197683 | p 1866 N95-23595

Telescope loading: A problem reduction approach p 1781 N95-23757

SLABS

Numerical Tokamak Project code comparison
| DE95-003475 | p 1831 N95-22899

SLAGS

Application of CFD analysis to design support and problem resolution for ASRM and RSRM p 1685 N95-23649

SLITS

Thermal outgassing studies on machinable tungsten and TZM molybdenum alloy
| DE95-002984 | p 1638 N95-22592

SLOTS

Ignition transient calculations in the Space Shuttle solid rocket motor p 1625 N95-23640

SLUSH

A summary of the slush hydrogen technology program for the National Aero-Space Plane
| NASA-TM-106863 | p 1653 N95-24186

SLUSH HYDROGEN

A summary of the slush hydrogen technology program for the National Aero-Space Plane
| NASA-TM-106863 | p 1653 N95-24186

SMART STRUCTURES

A coupled layerwise analysis of the thermopiezoelectric response of smart composite beams beams
| NASA-TM-106889 | p 1630 N95-23463

SMOKE

Modeling aerosol emissions from the combustion of composite materials p 1629 N95-23038

Remote sensing of smoke, clouds, and fire using AVIRIS data p 1704 N95-23860

Aircraft fires, smoke toxicity, and survival: An overview
| DOT/FAA/AM-95/8 | p 1610 N95-24024

SMOOTHING

Iterative solutions of nonlinear equations in smooth Banach spaces
| DE94-634287 | p 1790 N95-23455

Tutorial on filtering, restoration, and state estimation
| TR-534 | p 1793 N95-24042

SNOW

Unusual radar echoes from the Greenland ice sheet p 1714 N95-23951

An improved algorithm for retrieval of snow wetness using C-band AIRSAR p 1715 N95-23954

SNOW COVER
Glaciological studies in the central Andes using AIRSAR/TOPSAR p 1713 N95-23942
Unusual radar echoes from the Greenland ice sheet p 1714 N95-23951
An improved algorithm for retrieval of snow wetness using C-band AIRSAR p 1715 N95-23954
SODIUM
Ethanol synthesis and water gas shift over bifunctional sulfide catalysts
|DE94-017376| p 1634 N95-23202
SODIUM 22
Laser light induced drift for atoms of radioactive isotopes Na-22 and Na-24
|DE94-635759| p 1812 N95-23976
SODIUM 24
Laser light induced drift for atoms of radioactive isotopes Na-22 and Na-24
|DE94-635759| p 1812 N95-23976
SOFTWARE ENGINEERING
Jackson system development, entity-relationship analysis and data flow models: A comparative study
|PB95-127338| p 1855 N95-22523
Software for the generalized eigenproblem on distributed memory architectures
|DE95-002999| p 1755 N95-22690
Investigation of the role of gravity waves in the generation of equatorial bubbles
|NASA-CR-197962| p 1739 N95-23272
Radioisotope thermoelectric generator transportation system subsystem 143 software development plan
|DE95-003774| p 1662 N95-23351
Three-dimensional viscous flow analysis inside a turbine volute p 1674 N95-23437
Software agents for the dissemination of remote terrestrial sensing data p 1721 N95-23675
Utilizing inheritance in requirements engineering p 1768 N95-23677
Using Dedal to share and reuse distributed engineering design information p 1768 N95-23678
AMPHION: Specification-based programming for scientific subroutine libraries p 1761 N95-23680
An operations and command systems for the extreme ultraviolet explorer p 1770 N95-23687
A toolbox and record for scientific models p 1775 N95-23716
Computer software design description for the Treated Effluent Disposal Facility (TEDF), Project L-045H, Operator Training Station (OTS)
|DE95-003065| p 1759 N95-24006
OPUS: A new generation Knowledge Engineering Environment p 1760 N95-24176
SOFTWARE REUSE
Software agents for the dissemination of remote terrestrial sensing data p 1721 N95-23675
Using Dedal to share and reuse distributed engineering design information p 1768 N95-23678
AMPHION: Specification-based programming for scientific subroutine libraries p 1761 N95-23680
Constraint based scheduling for the Goddard Space Flight Center distributed Active Archive Center's data archive and distribution system p 1859 N95-24121
SOFTWARE TOOLS
HiRel: Hybrid Automated Reliability Predictor (HARP) integrated reliability tool system, (version 7.0). Volume 3: HARP Graphics Oriented (GO) input user's guide
|NASA-TP-3452-VOL-3| p 1753 N95-22479
Browsing semantics in the tower model
|PB95-127221| p 1855 N95-22534
Partitioning methods for unstructured finite element meshes
|PB95-130555| p 1785 N95-22544
Extensible PDE Solvers package users manual
|DE95-003333| p 1786 N95-22696
Performance of single-keyword and multiple-keyword pattern matching algorithms
|PB95-138954| p 1756 N95-23150
Long range targeting for space based rendezvous
|NASA-CR-197890| p 1757 N95-23388
Criteria for evaluation of grid generation systems p 1669 N95-23416
Toward an automated signature recognition toolkit for mission operations p 1659 N95-23682
An expert system for diagnosing anomalies of spacecraft p 1770 N95-23684
A toolbox and record for scientific models p 1775 N95-23716
DTS: Building custom, intelligent schedulers p 1779 N95-23744
A data analysis assistant p 1761 N95-23748
Modeling actions and operations to support mission preparation p 1617 N95-23750
CRI planning and scheduling for space p 1617 N95-23751
Artificial intelligence techniques for scheduling Space Shuttle missions p 1781 N95-23755
GPP user's guide: A general-purpose postprocessor for wind turbine data analysis
|DE95-000293| p 1730 N95-23776
The US Geological Survey, digital spectral reflectance library: version 1: 0.2 to 3.0 microns p 1703 N95-23855
Extraction of auxiliary data from AVIRIS distribution tape for spectral, radiometric, and geometric quality assessment p 1706 N95-23875
SOIL EROSION
Effects of wind on rainfall simulation. Spatial distribution of water application, kinetic energy, and overland flow under single full-cone nozzle sprays
|PB95-127304| p 1717 N95-22537
SOIL MAPPING
Geophysical investigations in the 100 Areas: Fiscal year 1991 through December 1993
|DE95-001573| p 1736 N95-22843
Classification of high dimensional multispectral image data p 1705 N95-23868
Mapping of the Ronda peridotite massif (Spain) from AVIRIS spectro-imaging survey: A first attempt p 1707 N95-23878
Synergy between optical and microwave remote sensing to derive soil and vegetation parameters from MAC Europe 1991 Experiment p 1715 N95-23956
SOIL MOISTURE
HAPEX-Sahel: Basic description of methods and data sets
|PB95-127262| p 1701 N95-22639
Preliminary analysis of the sensitivity of AIRSAR images to soil moisture variations p 1714 N95-23950
Synergy between optical and microwave remote sensing to derive soil and vegetation parameters from MAC Europe 1991 Experiment p 1715 N95-23956
Classification and soil moisture determination of agricultural fields p 1716 N95-23958
Soil moisture retrieval in the Oberpfaffenhofen testsite using MAC Europe AIRSAR data p 1716 N95-23960
Implementation of a soil-canopy scheme into the CSIRO GCM: Regional aspects of the model response
|CSIRO-TR-32| p 1721 N95-24192
SOIL SAMPLING
Application of MAC-Europe AVIRIS data to the analysis of various alteration stages in the Landdmannalauger Hydrothermal Area (South Iceland) p 1709 N95-23885
SOIL SCIENCE
HAPEX-Sahel: Basic description of methods and data sets
|PB95-127262| p 1701 N95-22639
SOILS
Basic data sets description and preliminary results of EFEDA-Spain
|PB95-139291| p 1740 N95-23470
Temporal changes in endmember abundances, liquid water and water vapor over vegetation at Jasper Ridge p 1708 N95-23882
Thermal radiant exitance model performance: Soils and forests
|DE95-003619| p 1721 N95-24148
SOLAR ACTIVITY
Space Science for the 21st Century. Strategic Plan for 1995-2000
|NASA-TM-110546| p 1617 N95-22947
Solar-geophysical data number 602, October 1994. Part 1: (Prompt reports). Data for September, August 1994, and late data
|PB95-149357| p 1870 N95-23925
Solar-geophysical data number 602, October 1994. Part 2: (Comprehensive reports). Data for April 1994, and miscellaneous
|PB95-149365| p 1870 N95-23926
SOLAR ARRAYS
Summary of solar cell data from the Long Duration Exposure Facility (LDEF)
|NASA-CR-196539| p 1727 N95-22904
Design of a GaAs/Ge solar array for unmanned aerial vehicles
|NASA-TM-106870| p 1728 N95-23259
SOLAR CELLS
Research on defects and transport in amorphous-silicon-based semiconductors
|DE94-011888| p 1660 N95-22586
Polycrystalline CuInSe2 and CdTePV solar cells
|DE95-000244| p 1727 N95-22842
Summary of solar cell data from the Long Duration Exposure Facility (LDEF)
|NASA-CR-196539| p 1727 N95-22904
Continuous roll-to-roll amorphous-silicon photovoltaic manufacturing technology
|DE95-000243| p 1728 N95-23061
Design of a GaAs/Ge solar array for unmanned aerial vehicles
|NASA-TM-106870| p 1728 N95-23259
Hydrogen and fuel cells for energy storage
|DE95-723907| p 1729 N95-23382
Rapid thermal processing of high-efficiency silicon solar cells with controlled in-situ annealing
|DE95-004729| p 1730 N95-23489
Telerobotics test bed for space structure assembly p 1618 N95-23734
Automated solar cell assembly teamed process research
|DE95-000299| p 1730 N95-23777
Silicon surface and bulk defect passivation by low temperature PECVD oxides and nitrides
|DE95-004531| p 1731 N95-24090
Reflectance control for multicrystalline-silicon photovoltaic modules using textured-dielectric coatings
|DE95-004532| p 1731 N95-24155
SOLAR COLLECTORS
Advanced reflector materials for solar concentrators
|DE95-000248| p 1726 N95-22547
Twelve month performance evaluation for the rotating shadowband radiometer
|DE95-002847| p 1726 N95-22554
SOLAR CORONA
Plasma properties and magnetic field structure of the solar corona, based on coordinated Max 1991 observations from SERTS, the VLA, and magnetographs
|NASA-CR-197864| p 1870 N95-23181
SOLAR CORPUSCULAR RADIATION
Characteristics of low energy ions in the Heavy Ions In Space (HIIS) experiment p 1815 N95-23807
Results from the Heavy Ions In Space (HIIS) experiment on the ionic charge state of solar energetic particles p 1870 N95-23808
SOLAR DYNAMIC POWER SYSTEMS
Overview of the solar dynamic ground test demonstration program at the NASA Lewis Research Center
|NASA-TM-106876| p 1625 N95-23450
SOLAR ENERGY
Southeast Regional Experiment Station
|DE95-000903| p 1726 N95-22518
Hydrogen and fuel cells for energy storage
|DE95-723907| p 1729 N95-23382
Solar photochemistry: Twenty years of progress, what's been accomplished, and where does it lead?
|DE95-004007| p 1730 N95-23778
SOLAR ENERGY CONVERSION
Renewable Energy Sources Brno 1993
|DE94-633975| p 1727 N95-22855
SOLAR FLARES
Investigation of physical parameters in stellar flares observed by GINGA
|NASA-CR-196547| p 1868 N95-23205
LDEF contributions to cosmic ray and radiation environments research p 1872 N95-23805
Solar-geophysical data number 602, October 1994. Part 1: (Prompt reports). Data for September, August 1994, and late data
|PB95-149357| p 1870 N95-23925
Solar-geophysical data number 602, October 1994. Part 2: (Comprehensive reports). Data for April 1994, and miscellaneous
|PB95-149365| p 1870 N95-23926
SOLAR FLUX
Comparison of methods for calibrating AVIRIS data to ground reflectance p 1703 N95-23854
SOLAR MAGNETIC FIELD
Plasma properties and magnetic field structure of the solar corona, based on coordinated Max 1991 observations from SERTS, the VLA, and magnetographs
|NASA-CR-197864| p 1870 N95-23181
Solar-geophysical data number 602, October 1994. Part 1: (Prompt reports). Data for September, August 1994, and late data
|PB95-149357| p 1870 N95-23925
SOLAR NEUTRINOS
Neutrino masses and mixing
|DE94-628632| p 1812 N95-23784
Neutrinoless double beta decay and the solar neutrino problem
|DE94-628633| p 1812 N95-23785
SOLAR OSCILLATIONS
Solar mass loss, solar lithium, and solar oscillations
|DE94-018262| p 1870 N95-22938
SOLAR PROMINENCES
Solar-geophysical data number 602, October 1994. Part 2: (Comprehensive reports). Data for April 1994, and miscellaneous
|PB95-149365| p 1870 N95-23926
SOLAR RADIATION
Plasma properties and magnetic field structure of the solar corona, based on coordinated Max 1991 observations from SERTS, the VLA, and magnetographs
|NASA-CR-197864| p 1870 N95-23181
A proposed update to the solar irradiance spectrum used in LOWTRAN and MODTRAN p 1705 N95-23865

SOLAR RADIO BURSTS
Solar-geophysical data number 602, October 1994. Part 2: (Comprehensive reports). Data for April 1994, and miscellaneous
|PB95-149365| p 1870 N95-23926
SOLAR RADIO EMISSION
Solar-geophysical data number 602, October 1994. Part 1: (Prompt reports). Data for September, August 1994, and late data
|PB95-149357| p 1870 N95-23925
SOLAR REFLECTORS
Advanced reflector materials for solar concentrators
|DE95-000248| p 1726 N95-22547
SOLAR SYSTEM
Space Science for the 21st Century. Strategic Plan for 1995-2000
|NASA-TM-110546| p 1617 N95-22947
Origins of interstellar and solar system: Carbonaceous materials
|NASA-CR-197436| p 1867 N95-23013
SOLAR SYSTEM EVOLUTION
Origins of interstellar and solar system: Carbonaceous materials
|NASA-CR-197436| p 1867 N95-23013
SOLAR WIND
Solar mass loss, solar lithium, and solar oscillations
|DE94-018262| p 1870 N95-22938
Physics of magnetospheric boundary layers
|NASA-CR-197920| p 1739 N95-23271
Germination, growth rates, and electron microscope analysis of tomato seeds flown on the LDEF p 1748 N95-23821
SOLAR X-RAYS
Solar-geophysical data number 602, October 1994. Part 2: (Comprehensive reports). Data for April 1994, and miscellaneous
|PB95-149365| p 1870 N95-23926
SOLDERING
Solderability preservation through the use of organic inhibitors
|DE95-003633| p 1664 N95-24149
SOLDERS
Analysis of physiochemical processes during solder aging
|DE95-003811| p 1638 N95-22576
SOLID CRYOGENS
Exotic atoms
|DE95-003199| p 1805 N95-22881
SOLID ELECTROLYTES
Vapor deposition of thin-film Y-doped ZrO2 for electrochemical device applications
|DE95-003705| p 1649 N95-23268
SOLID LUBRICANTS
Evaluation of thermal barrier and PS-200 self-lubricating coatings in an air-cooled rotary engine
|NASA-CR-195445| p 1614 N95-23222
SOLID MECHANICS
Institute for Computational Mechanics in Propulsion (ICOMP)
|NASA-TM-106884| p 1677 N95-23464
SOLID PHASES
Quick connect coupling
|NASA-CASE-ARC-11921-2| p 1695 N95-23376
Deformation of C15 Laves phase alloys
|DE95-003636| p 1646 N95-24067
SOLID PROPELLANT ROCKET ENGINES
Eleventh Workshop for Computational Fluid Dynamic Applications in Rocket Propulsion
|NASA-CP-3221-PT-2| p 1668 N95-23412
Advanced multi-phase flow CFD model development for solid rocket motor flowfield analysis p 1683 N95-23638
Ignition transient calculations in the Space Shuttle solid rocket motor p 1625 N95-23640
SOLID PROPELLANTS
Morphology of extinguished monolithic JA2 grains fired in a 30-mm Solid Propellant Electrothermal Chemical (SPETC) gun
|AD-A285792| p 1652 N95-22506
SOLID STATE
Characterization of Type 304L stainless steel solid-state closure welds for radioactive waste containment
|DE94-016539| p 1645 N95-23980
SOLID STATE DEVICES
Measurements of striae in CR+ doped YAG laser crystals p 1847 N95-23285
SOLID STATE LASERS
Non-intrusive measurements in a rocket engine combustor p 1625 N95-23439
SOLID SURFACES
Profiling and light scattering studies of Si surfaces
|DE95-002931| p 1828 N95-24005
SOLID WASTES
Biotransformation of an uncured composite material p 1629 N95-23033
The Louisiana State University waste-to-energy incinerator
|DE95-004417| p 1728 N95-23344
SOLID-SOLID INTERFACES
Propagation of waves at the loosely bonded interface of two porous elastic half-spaces
|DE94-628477| p 1800 N95-23018
SOLIDS
Influence of porosity and two-phase flow on diffusional/thermal instability of a deflagrating energetic material
|DE95-002592| p 1634 N95-23122
SOLITARY WAVES
Solutions for the vector k-constrained KP hierarchy
|DE94-628431| p 1786 N95-22633
Disorder-induced breakdown of soliton and polaron particles
|DE95-003694| p 1808 N95-23267
(Phi)(sup 4) kinks: Statistical mechanics
|DE95-003693| p 1794 N95-23349
Theoretical aspects of electroweak and other interactions in medium energy nuclear physics
|DE95-004341| p 1808 N95-23357
SOLUBILITY
Tough, soluble, aromatic, thermoplastic copolyimides
|NASA-CASE-LAR-15205-1| p 1648 N95-22882
SOLUTES
EXTRA.M: A computing code system for analysis of the Purex process with mixer settlers for reprocessing
|DE94-785273| p 1635 N95-23476
SOLVATION
Solvation of isolated transition metal ions
|DE95-002978| p 1638 N95-22571
SOLVENT EXTRACTION
EXTRA.M: A computing code system for analysis of the Purex process with mixer settlers for reprocessing
|DE94-785273| p 1635 N95-23476
SOLVENTS
Tough, soluble, aromatic, thermoplastic copolyimides
|NASA-CASE-LAR-15205-1| p 1648 N95-22882
Polyazomethines containing trifluoromethylbenzene units
|NASA-CASE-LAR-14896-1| p 1649 N95-23253
SOUND DETECTING AND RANGING
Pitch sensor system
|AD-D016488| p 1799 N95-22863
SOUND FIXING AND RANGING
DRACULA: Dynamic range control for broadcasting and other applications
|BBC-RD-1994/13| p 1658 N95-24044
SOUND TRANSMISSION
The sound insulations of studio doors. Part 2: Door seals
|BBC-RD-1994/15| p 1654 N95-24045
SOUND WAVES
Capacitive acoustic wave detector and method of using same
|NASA-CASE-LAR-13890-1| p 1799 N95-22921
Benchmark problems in computational aeroacoustics p 1800 N95-23315
A self-organizing neural network architecture for auditory and speech perception with applications to acoustic and other temporal prediction problems
|AD-A285640| p 1800 N95-23782
The sound insulations of studio doors. Part 2: Door seals
|BBC-RD-1994/15| p 1654 N95-24045
SPACE BASES
Planetary stations and Abyssal Benthic Laboratories: An overview of parallel approaches for long-term investigation in extreme environments p 1752 N95-23732
SPACE CHARGE
Design study of longitudinal dynamics of the drive beam in 1 TeV relativistic klystron two-beam accelerator
|DE95-004683| p 1817 N95-23485
SPACE COMMERCIALIZATION
Superconductivity devices: Commercial use of space
|NASA-CR-197885| p 1648 N95-22883
SPACE COMMUNICATION
Effects of modulation index on telecommunications
|AD-A286018| p 1657 N95-23023
SPACE DEBRIS
Effect of the space environment on materials flown on the EURECA/TICCE-HVI experiment p 1623 N95-23803
Status of LDEF contributions to current knowledge of meteoroid and manmade debris environments and their effects on spacecraft in LEO p 1623 N95-23822
LDEF meteoroid and debris special investigation group investigations and activities at the Johnson Space Center p 1623 N95-23823
Micrometeoroids and debris on LDEF comparison with MIR data p 1623 N95-23824
Small craters on the meteoroid and space debris impact experiment p 1623 N95-23825
Penetration rates over 30 years in the space age p 1624 N95-23827
LDEF Interplanetary Dust Experiment (IDE) results p 1869 N95-23828
The orbital characteristics of debris particle rings as derived from IDE observations of multiple orbit intersections with LDEF p 1869 N95-23829
Orbital debris and meteoroid population as estimated from LDEF impact data p 1869 N95-23830
Analytical electron microscopy of LDEF impactor residues p 1869 N95-23832
Natural and orbital debris particles on LDEF's trailing and forward-facing surfaces p 1869 N95-23833
Debris and meteoroid proportions deduced from impact crater residue analysis p 1869 N95-23834
SIMS chemical and isotopic analysis of impact features from LDEF experiments AO187-1 and AO187-2 p 1637 N95-23837
Image and compositional characteristics of the LDEF Big Guy impact crater p 1700 N95-23838
The effect of impact angle on craters formed by hypervelocity particles p 1700 N95-23839
Experimental investigation of the relationship between impact crater morphology and impacting particle velocity and direction p 1700 N95-23840
SPACE ENVIRONMENT SIMULATION
Overview of the solar dynamic ground test demonstration program at the NASA Lewis Research Center
|NASA-TM-106876| p 1625 N95-23450
SPACE ERECTABLE STRUCTURES
Hey! What's Space Station Freedom?
|NASA-TM-110531| p 1620 N95-22542
SPACE EXPLORATION
Space Science for the 21st Century. Strategic Plan for 1995-2000
|NASA-TM-110546| p 1617 N95-22947
The next decade of space robotics p 1768 N95-23673
Very fast motion planning for highly dexterous-articulated robots p 1771 N95-23691
JPL space robotics: Present accomplishments and future thrusts p 1697 N95-23697
Robotics research at Canadian Space Agency p 1772 N95-23699
Active vision in satellite scene analysis p 1778 N95-23738
SPACE LABORATORIES
Hey! What's Space Station Freedom?
|NASA-TM-110531| p 1620 N95-22542
Interactive autonomy and robotic skills p 1777 N95-23730
SPACE MAINTENANCE
STS-61 Space Shuttle mission report
|NASA-TM-110545| p 1619 N95-23187
SPACE MISSIONS
STS-59 Space Shuttle mission report
|NASA-TM-110527| p 1619 N95-23093
STS-62 Space Shuttle mission report
|NASA-TM-110450| p 1619 N95-23094
STS-61 Space Shuttle mission report
|NASA-TM-110545| p 1619 N95-23187
Reliability analysis in the Office of Safety, Environmental, and Mission Assurance (OSEMA) p 1698 N95-23302
Robotics and telepresence for moon missions p 1776 N95-23725
High performance techniques for space mission scheduling p 1618 N95-23758
SPACE PLASMAS
Langmuir-like waves and radiation in planetary foreshocks
|NASA-CR-197376| p 1869 N95-22828
Magnetospheric space plasma investigations
|NASA-CR-197405| p 1831 N95-22955
The high latitude ionosphere-magnetosphere transition region: Simulation and data comparison
|NASA-CR-197404| p 1737 N95-22956
Semikinetic modeling and observations of high-latitude plasma outflow
|NASA-CR-197403| p 1831 N95-23008
Electromagnetic radiation in the plasma environment around the shuttle
|NASA-TM-106891| p 1738 N95-23116
Modeling of nonequilibrium space plasma flows
|NASA-CR-197432| p 1833 N95-23211
Modification and damping of Alfven waves in a magnetized dusty plasma
|NIFS-312| p 1834 N95-23523
Charging of interplanetary grains
|NASA-CR-198032| p 1869 N95-24066
SPACE PLATFORMS
Hey! What's Space Station Freedom?
|NASA-TM-110531| p 1620 N95-22542
Attention focusing and anomaly detection in systems monitoring p 1769 N95-23683

SPACE PROGRAMS
Effects of modulation index on telecommunications
| AD-A286018 | p 1657 N95-23023
SPACE SHUTTLE BOOSTERS
Ignition transient calculations in the Space Shuttle solid rocket motor p 1625 N95-23640
SPACE SHUTTLE MAIN ENGINE
STS-59 Space Shuttle mission report
| NASA-TM-110527 | p 1619 N95-23093
STS-62 Space Shuttle mission report
| NASA-TM-110450 | p 1619 N95-23094
Prediction of incidence and surface roughness effects on turbine performance p 1671 N95-23424
Numerical study of the SSME nozzle flow fields during transient operations: A comparison of the animated results with test p 1673 N95-23434
Phase 2: HGM air flow tests in support of HEX vane investigation p 1674 N95-23438
Detailed measurements in the SSME high pressure fuel turbine with smooth rotor blades p 1675 N95-23441
Development of an algebraic stress/two-layer model for calculating thrust chamber flow fields p 1675 N95-23442
Computational Fluid Dynamics (CFD) analyses in support of Space Shuttle Main Engine (SSME) heat exchanger (HX) vane cracking investigation p 1679 N95-23619
Three-D flow analysis of the alternate SSME HPOT TAD p 1679 N95-23620
Unsteady flow simulations in support of the SSME HEX turning vane cracking investigation with the ATD HPOTP p 1679 N95-23621
Comparison between predicted and experimentally measured flow fields at the exit of the SSME HPFTP impeller p 1679 N95-23622
SPACE SHUTTLE MISSIONS
Summary of OARE flight calibration measurements
| NASA-TM-109159 | p 1688 N95-23012
STS-61 mission director's post-mission report
| NASA-TM-104803 | p 1617 N95-23262
Newton in space
| NASA-TM-110535 | p 1799 N95-23273
Living in space
| NASA-TM-110536 | p 1751 N95-23274
Toys in space, 2
| NASA-TM-110541 | p 1620 N95-23275
All systems go!
| NASA-TM-110542 | p 1620 N95-23665
Artificial intelligence techniques for scheduling Space Shuttle missions p 1781 N95-23755
Space Shuttle mission: STS-67
| NASA-TM-110509 | p 1620 N95-24027
SPACE SHUTTLE ORBITERS
Summary of OARE flight calibration measurements
| NASA-TM-109159 | p 1688 N95-23012
Robotic system for the servicing of the orbiter thermal protection system p 1697 N95-23724
SPACE SHUTTLE PAYLOADS
STS-59 Space Shuttle mission report
| NASA-TM-110527 | p 1619 N95-23093
STS-62 Space Shuttle mission report
| NASA-TM-110450 | p 1619 N95-23094
Dexterous Orbital Servicing System (DOSS) p 1752 N95-23723
Space Shuttle mission: STS-67
| NASA-TM-110509 | p 1620 N95-24027
SPACE SHUTTLES
STS-59 Space Shuttle mission report
| NASA-TM-110527 | p 1619 N95-23093
STS-62 Space Shuttle mission report
| NASA-TM-110450 | p 1619 N95-23094
Electromagnetic radiation in the plasma environment around the shuttle
| NASA-TM-106891 | p 1738 N95-23116
STS-61 Space Shuttle mission report
| NASA-TM-110545 | p 1619 N95-23187
Toys in space, 2
| NASA-TM-110541 | p 1620 N95-23275
Toward an automated signature recognition toolkit for mission operations p 1659 N95-23682
Modeling actions and operations to support mission preparation p 1617 N95-23750
SPACE STATION FREEDOM
Hey! What's Space Station Freedom?
| NASA-TM-110531 | p 1620 N95-22542
Weight minimization of structural components for launch in space shuttle
| NASA-TM-4586 | p 1698 N95-22805
SPACE STATION PAYLOADS
Hey! What's Space Station Freedom?
| NASA-TM-110531 | p 1620 N95-22542
Automation and crew time saving in the space experiment p 1752 N95-23715
SPACE STATION POWER SUPPLIES
Description of a MIL-STD-1553B data bus Ada driver for the LeRC EPS Testbed
| NASA-TM-106866 | p 1762 N95-22668
Overview of the solar dynamic ground test demonstration program at the NASA Lewis Research Center
| NASA-TM-106876 | p 1625 N95-23450
SPACE STATION STRUCTURES
Weight minimization of structural components for launch in space shuttle
| NASA-TM-4586 | p 1698 N95-22805
Mir hardware heritage
| NASA-RP-1357 | p 1621 N95-23249
SPACE SUITS
Method for forming a glove attachment
| NASA-CASE-MSC-21632-1 | p 1750 N95-22766
SPACE SURVEILLANCE
Annual tropical cyclone report, 1993
| AD-A285097 | p 1742 N95-23255
SPACE TRANSPORTATION SYSTEM
Long range targeting for space based rendezvous
| NASA-CR-197890 | p 1757 N95-23388
Applications of dynamic scheduling technique to space related problems: Some case studies p 1618 N95-23759
Outgassing products from orbiter TPS materials p 1637 N95-23798
SPACE TRANSPORTATION SYSTEM FLIGHTS
STS-59 Space Shuttle mission report
| NASA-TM-110527 | p 1619 N95-23093
STS-62 Space Shuttle mission report
| NASA-TM-110450 | p 1619 N95-23094
STS-61 Space Shuttle mission report
| NASA-TM-110545 | p 1619 N95-23187
STS-61 mission director's post-mission report
| NASA-TM-104803 | p 1617 N95-23262
Newton in space
| NASA-TM-110535 | p 1799 N95-23273
Toys in space, 2
| NASA-TM-110541 | p 1620 N95-23275
Modeling actions and operations to support mission preparation p 1617 N95-23750
Space Shuttle mission: STS-67
| NASA-TM-110509 | p 1620 N95-24027
SPACE-TIME FUNCTIONS
Possibility of extending space-time coordinates
| DE94-628512 | p 1796 N95-22737
Black hole formation and space-time fluctuations in two dimensional dilaton gravity and complementarity
| DE94-628514 | p 1867 N95-22739
Finite-temperature scalar field theory in static de Sitter space
| DE94-628522 | p 1848 N95-22743
Spinning particles in the Euclidean Taub-NUT space
| DE94-634320 | p 1810 N95-23456
SPACEBORNE ASTRONOMY
Stellar Interferometer Technology Experiment (SITE)
| NASA-CR-197856 | p 1827 N95-23089
Statistical properties of the time histories of cosmic gamma-ray bursts detected by the BATSE experiment of the Compton gamma-ray observatory
| NASA-CR-197425 | p 1871 N95-23546
A constraint-logic based implementation of the coarse-grained approach to data acquisition scheduling of the International Ultraviolet Explorer orbiting observatory p 1779 N95-23741
SPACEBORNE EXPERIMENTS
Quick look report of acceleration measurements on Mir Space Station during Mir-16
| NASA-TM-106835 | p 1621 N95-22667
Summary of solar cell data from the Long Duration Exposure Facility (LDEF)
| NASA-CR-196539 | p 1727 N95-22904
Evaluation of adhesive materials used on the Long Duration Exposure Facility
| NASA-CR-4646 | p 1626 N95-22918
STS-61 Space Shuttle mission report
| NASA-TM-110545 | p 1619 N95-23187
Microgravity sciences application visiting scientist program
| NASA-CR-197854 | p 1653 N95-23204
Microgravity experiments safety and integration requirements document tree
| NASA-CR-195447 | p 1855 N95-23206
Newton in space
| NASA-TM-110535 | p 1799 N95-23273
Living in space
| NASA-TM-110536 | p 1751 N95-23274
Toys in space, 2
| NASA-TM-110541 | p 1620 N95-23275
LDEF materials results for spacecraft applications: Executive summary
| NASA-CP-3261 | p 1617 N95-23549
Endeavor: Now and then
| NASA-TM-110539 | p 1620 N95-23664
All systems go!
| NASA-TM-110542 | p 1620 N95-23665
Space robotic experiment in JEM flight demonstration p 1697 N95-23701
Automatic satellite capture and berthing with robot arm (ASCABRA) p 1623 N95-23713
Automation and crew time saving in the space experiment p 1752 N95-23715
Space science experimentation automation and support p 1775 N95-23718
Robotic servicing system for space material experiment p 1697 N95-23722
Truss structure tele-manipulation experiment using ETS-7 p 1623 N95-23726
Antenna-assembling mechanism test on ETS-7 p 1623 N95-23727
LDEF: 69 Months in Space. Third Post-Retrieval Symposium, part 1
| NASA-CP-3275-PT-1 | p 1889 N95-23796
LDEF environment modeling updates p 1637 N95-23797
EURECA 11 months in orbit: Initial post flight investigation results p 1623 N95-23799
Dosimetric results on EURECA p 1872 N95-23800
LDEF contributions to cosmic ray and radiation environments research p 1872 N95-23805
Characteristics of low energy ions in the Heavy Ions In Space (HIIS) experiment p 1815 N95-23807
Results from the Heavy Ions In Space (HIIS) experiment on the ionic charge state of solar energetic particles p 1870 N95-23808
Early results from the ultra heavy cosmic ray experiment p 1872 N95-23809
Absorbed dose and LET spectra measurements on LDEF p 1815 N95-23810
Fission foil measurements of neutron and proton fluences in the A0015 experiment p 1815 N95-23811
Measurement of trapped proton fluences in main stack of P0006 experiment p 1815 N95-23812
Charge, energy and LET spectra of high LET primary and secondary particles in CR-39 plastic nuclear track detectors of the P0006 experiment p 1815 N95-23814
Predictions of LET spectra measured on LDEF p 1815 N95-23815
Germination, growth rates, and electron microscope analysis of tomato seeds flown on the LDEF p 1748 N95-23821
Determining orbital particle parameters of impacts into germanium using morphology analysis and calibration data from hypervelocity impact experiments in the laboratory p 1700 N95-23841
LDEF: 69 Months in Space. Third Post-Retrieval Symposium, part 2
| NASA-CP-3275-PT-2 | p 1899 N95-23896
Further investigations of experiment A0034 atomic oxygen stimulated outgassing p 1651 N95-23908
Whisker/Cone growth on the thermal control surfaces experiment no. S0069 p 1651 N95-23911
Overview of the LDEF MSIG databasing activities p 1864 N95-23916
Space Shuttle mission: STS-67
| NASA-TM-110509 | p 1620 N95-24027
USML-1 Glovebox experiments
| NASA-CR-196574 | p 1653 N95-24026
SPACECRAFT ANTENNAS
Antenna-assembling mechanism test on ETS-7 p 1623 N95-23727
SPACECRAFT COMPONENTS
Be-10 in terrestrial bauxite and industrial aluminum: An LDEF fallout p 1646 N95-23820
Small craters on the meteoroid and space debris impact experiment p 1623 N95-23825
SPACECRAFT CONFIGURATIONS
Mir hardware heritage
| NASA-RP-1357 | p 1621 N95-23249
SPACECRAFT CONSTRUCTION MATERIALS
Evaluation of adhesive materials used on the Long Duration Exposure Facility
| NASA-CR-4646 | p 1626 N95-22918
Outgassing considerations for composites in space applications p 1629 N95-23037
Atomic oxygen durability evaluation of protected polymers using thermal energy plasma systems
| NASA-TM-106855 | p 1626 N95-23270
LDEF materials results for spacecraft applications: Executive summary
| NASA-CP-3261 | p 1617 N95-23549
Outgassing products from orbiter TPS materials p 1637 N95-23798
Effect of the space environment on materials flown on the EURECA/TICCE-HVI experiment p 1623 N95-23803
LDEF: 69 Months in Space. Third Post-Retrieval Symposium, part 2
| NASA-CP-3275-PT-2 | p 1899 N95-23896

Summary and review of Materials Special Investigation Group evaluations of hardware from the Long Duration Exposure Facility p 1638 N95-23897
Recent results from Long Duration Exposure Facility materials testing p 1638 N95-23898
LDEF polymeric materials: A summary of Langley characterization p 1651 N95-23899
Surface characterization of LDEF carbon fiber/polymer matrix composites p 1631 N95-23900
Space environmental effects on polymer matrix composites as a function of sample location on LDEF p 1651 N95-23901
Collection and review of metals data obtained from LDEF experiment specimens and support hardware p 1646 N95-23905
Changes in chemical and optical properties of thin film metal mirrors on LDEF p 1651 N95-23907
Further investigations of experiment A0034 atomic oxygen stimulated outgassing p 1651 N95-23908
Trend analysis of in-situ spectral reflectance data from the Thermal Control Surfaces Experiment (TCSE) p 1631 N95-23910
Durability of reflector materials in the space environment p 1651 N95-23912
Four space application material coatings on the Long-Duration Exposure Facility (LDEF) p 1651 N95-23913
Organic matrix composite protective coatings for space applications p 1627 N95-23914
Overview of the LDEF MSIG databasing activities p 1864 N95-23916
Vaccum Gas Tungsten Arc Welding, phase 1 | NASA-CR-197979 | p 1696 N95-24064

SPACECRAFT CONTAMINATION
Outgassing considerations for composites in space applications p 1629 N95-23037
Summary and review of Materials Special Investigation Group evaluations of hardware from the Long Duration Exposure Facility p 1638 N95-23897
Collection and review of metals data obtained from LDEF experiment specimens and support hardware p 1646 N95-23905

SPACECRAFT CONTROL
Operator procedure verification with a rapidly reconfigurable simulator p 1618 N95-23679
Distributed intelligence for ground/space systems p 1770 N95-23685
Formalizing procedures for operations automation, operator training and spacecraft autonomy p 1752 N95-23720

SPACECRAFT DESIGN
Weight minimization of structural components for launch in space shuttle | NASA-TM-4586 | p 1698 N95-22805
A manufacturing database of advanced materials used in spacecraft structures p 1623 N95-23279
LDEF materials results for spacecraft applications: Executive summary | NASA-CP-3261 | p 1617 N95-23549
An operations and command systems for the extreme ultraviolet explorer p 1770 N95-23687
Design and development status of ETS-7, an RVD and space robot experiment satellite p 1623 N95-23700
Space robotic experiment in JEM flight demonstration p 1697 N95-23701
Effect of the space environment on materials flown on the EURECA/TICCE-HVI experiment p 1623 N95-23803

SPACECRAFT DOCKING
Automatic satellite capture and berthing with robot arm (ASCABRA) p 1623 N95-23713
Autonomous spacecraft executive and its application to rendezvous and docking p 1623 N95-23719

SPACECRAFT ELECTRONIC EQUIPMENT
Design and application of electromechanical actuators for deep space missions | NASA-CR-197957 | p 1694 N95-22909

SPACECRAFT ENVIRONMENTS
Quick look report of acceleration measurements on Mir Space Station during Mir-16 | NASA-TM-106835 | p 1621 N95-22667
Summary of OARE flight calibration measurements | NASA-TM-109159 | p 1688 N95-23012

SPACECRAFT GUIDANCE
Autonomous spacecraft executive and its application to rendezvous and docking p 1623 N95-23719

SPACECRAFT INSTRUMENTS
Design and development status of ETS-7, an RVD and space robot experiment satellite p 1623 N95-23700
Automatic commanding of the Mars Observer Camera p 1620 N95-23754
Use of the Airborne Visible/Infrared Imaging Spectrometer to calibrate the optical sensor on board the Japanese Earth Resources Satellite-1 p 1624 N95-23864

SPACECRAFT MAINTENANCE
STS-61 Space Shuttle mission report | NASA-TM-110545 | p 1619 N95-23187
Integrating O/S models during conceptual design, part 1 | NASA-CR-197903 | p 1622 N95-23398
Integrating O/S models during conceptual design, part 3 | NASA-CR-197905 | p 1622 N95-23400
Robotic system for the servicing of the orbiter thermal protection system p 1697 N95-23724

SPACECRAFT MODELS
An operations and command systems for the extreme ultraviolet explorer p 1770 N95-23687
Dynamical model and numerical simulations for Engineering Test Satellite-6 | NAL-TR-1239 | p 1622 N95-24049

SPACECRAFT MODULES
Living in space | NASA-TM-110536 | p 1751 N95-23274

SPACECRAFT POWER SUPPLIES
Ground-based and space-based laser beam power applications | NASA-TM-106744 | p 1691 N95-22670
Alert-derivative bimodal space power and propulsion systems | DE95-002754 | p 1624 N95-22905

SPACECRAFT PROPULSION
An RL10A-3-3A rocket engine model using the rocket engine transient simulator (ROCETS) software | NASA-CR-190786 | p 1625 N95-23790
Predicted performance of an integrated modular engine system | NASA-CR-190787 | p 1625 N95-23791

SPACECRAFT RECOVERY
Robot arm system for automatic satellite capture and berthing p 1752 N95-23709
Automatic satellite capture and berthing with robot arm (ASCABRA) p 1623 N95-23713

SPACECRAFT SHIELDING
Robotic system for the servicing of the orbiter thermal protection system p 1697 N95-23724
LDEF meteoroid and debris special investigation group investigations and activities at the Johnson Space Center p 1623 N95-23823
Micro-abrasion package capture cell experiment on the trailing edge of LDEF: Impactor chemistry and whipple bumper shield efficiencies p 1624 N95-23835

SPACECRAFT STRUCTURES
Structural Arrangement Trade Study. Volume 1: Reusable Hydrogen Composite Tank System (RHCTS) and Graphite Composite Primary Structures (GCPS). Executive summary | NASA-CR-197685 | p 1621 N95-23188
Structural arrangement trade study. Volume 3: Reusable Hydrogen Composite Tank System (RHCTS) and Graphite Composite Primary Structures (GCPS). Addendum | NASA-CR-197687 | p 1621 N95-23189
A manufacturing database of advanced materials used in spacecraft structures p 1623 N95-23279
Telerobotics test bed for space structure assembly p 1618 N95-23734
LDEF meteoroid and debris special investigation group investigations and activities at the Johnson Space Center p 1623 N95-23823
Penetration rates over 30 years in the space age p 1624 N95-23827
LDEF Interplanetary Dust Experiment (IDE) results p 1869 N95-23828
SIMS chemical and isotopic analysis of impact features from LDEF experiments AO187-1 and AO187-2 p 1637 N95-23837
Image and compositional characteristics of the LDEF Big Guy impact crater p 1700 N95-23838

SPACECREWS
The Charlotte (TM) intra-vehicular robot p 1697 N95-23703
Telepresence control of a dual-arm dexterous robot p 1752 N95-23735
Space Shuttle mission: STS-67 | NASA-TM-110509 | p 1620 N95-24027

SPACELAB
Graphical timeline editing p 1761 N95-23746

SPALLATION
Status of helium-production reaction studies with a spallation neutron source | DE95-002816 | p 1806 N95-23137
Neutron compton scattering | PB95-139135 | p 1807 N95-23159
Phonon characteristics of high (T sub c) superconductors from neutron Doppler broadening measurements | DE95-003703 | p 1844 N95-24076

SPATIAL DISTRIBUTION
Nonparametric measure of spatial interaction in point patterns | PB95-127965 | p 1793 N95-22527
Measurements and modeling of impurity source distributions from the Tore Supra outboard pump limiter | DE95-003097 | p 1831 N95-22800
Measuring forest landscape patterns in the Cascade Range of Oregon, USA p 1719 N95-24096
Hierarchical analysis of spatial pattern and processes of Douglas-fir forests p 1719 N95-24099

SPATIAL RESOLUTION
Instantaneous field of view and spatial sampling of the Airborne Visible/Infrared Imaging Spectrometer (AVIRIS) p 1702 N95-23851

SPECIFIC HEAT
Associated with aerospace vehicles development of methodologies for the estimation of thermal properties p 1700 N95-23321
Phonon-induced anomalous specific heat of a model nanocrystal by computer simulation | DE95-004653 | p 1843 N95-23585
Experimental and theoretical studies on the C15 intermetallic compounds MV2 (M = Zr, Hf and Ta): Elasticity and phase stability | DE95-003723 | p 1845 N95-24079

SPECIFICATIONS
Method for building and evaluating formal specifications of object-oriented conceptual models of database systems | PB95-127353 | p 1855 N95-22525
LCM 3.0: A language for describing conceptual models. Syntax definition | PB95-128005 | p 1755 N95-22652
Handling qualities of the High Speed Civil Transport p 1616 N95-23325
Influence of technology on magnetic tape storage device characteristics p 1690 N95-24127

SPECTRA
Multiband VLBI imaging of the jet in 3C 345 | PB95-139275 | p 1866 N95-23468

SPECTRAL BANDS
Programmable hyperspectral image mapper with on-array processing | NASA-CASE-NPO-17794-1-CU | p 1819 N95-22765
A tool for manual endmember selection and spectral unmixing p 1701 N95-23846
Optimal band selection for dimensionality reduction of hyperspectral imagery p 1709 N95-23887
Estimation of spectral emissivity in the thermal infrared p 1711 N95-23918
A preliminary comparison of Landsat Thematic Mapper and SPOT-1 HRV multispectral data for estimating coniferous forest volume p 1719 N95-24097

SPECTRAL EMISSION
Summaries of the 4th Annual JPL Airborne Geoscience Workshop. Volume 2: TIMS Workshop | NASA-CR-197876-VOL-2 | p 1711 N95-23917
Estimation of spectral emissivity in the thermal infrared p 1711 N95-23918
The difference between laboratory and in-situ pixel-averaged emissivity: The effects on temperature-emissivity separation p 1711 N95-23919
Mineralogic variability of the Kelso Dunes, Mojave Desert, California derived from Thermal Infrared Multispectral Scanner (TIMS) data p 1711 N95-23920

SPECTRAL LINE WIDTH
Theoretical calculations of pressure broadening coefficients for H2O perturbed by hydrogen or helium gas | NASA-CR-197345 | p 1636 N95-23545

SPECTRAL METHODS
Spectral application of the theorem for the essential quasi-Fredholm spectrum | DE94-628430 | p 1795 N95-22632
The spectral content of the torque loads on a turbine gear tooth | DE95-002188 | p 1694 N95-23056
The detection and analysis of galvanic damage in BMI/graphite fiber composites p 1631 N95-23502
The use of electrochemical impedance spectroscopy to predict the corrosion of aluminum-lithium alloys in marine environments p 1637 N95-23504
Investigation of infra-red and nonequilibrium air radiation | NASA-CR-197977 | p 1741 N95-24041

SPECTRAL REFLECTANCE
Use of spectral analogy to evaluate canopy reflectance sensitivity to leaf optical property p 1701 N95-23845
The US Geological Survey, digital spectral reflectance library: version 1: 0.2 to 3.0 microns p 1703 N95-23855
Application of a two-stream radiative transfer model for leaf lignin and cellulose concentrations from spectral reflectance measurements, part 1 p 1703 N95-23856
Application of a two-stream radiative transfer model for leaf lignin and cellulose concentrations from spectral reflectance measurements, part 2 p 1703 N95-23857

Estimation of aerosol optical depth and additional atmospheric parameters for the calculation of apparent reflectance from radiance measured by the Airborne Visible/Infrared Imaging Spectrometer
p 1704 N95-23863
Measurements of canopy chemistry with 1992 AVIRIS data at Blackhawk Island and Harvard Forest
p 1706 N95-23873
Temporal changes in endmember abundances, liquid water and water vapor over vegetation at Jasper Ridge
p 1708 N95-23882
The effect of signal noise on the remote sensing of Foliar biochemical concentration p 1708 N95-23884
Estimation of crown closure from AVIRIS data using regression analysis p 1709 N95-23886
Objective determination of image end-members in spectral mixture analysis of AVIRIS data
p 1709 N95-23888
Relationships between pigment composition variation and reflectance for plant species from a coastal savannah in California p 1709 N95-23889
Atmospheric correction of AVIRIS data of Monterey Bay contaminated by thin cirrus clouds p 1710 N95-23890
Investigations on the 1.7 micron residual absorption feature in the vegetation reflection spectrum
p 1710 N95-23891
A comparison of spectral mixture analysis an NDVI for ascertaining ecological variables p 1710 N95-23892
Using AVIRIS for in-flight calibration of the spectral shifts of SPOT-HRV and of AVHRR? p 1710 N95-23893
Laboratory spectra of field samples as a check on two atmospheric correction methods p 1711 N95-23894
Determination of semi-arid landscape endmembers and seasonal trends using convex geometry spectral unmixing techniques p 1711 N95-23895
Trend analysis of in-situ spectral reflectance data from the Thermal Control Surfaces Experiment (TCSE)
p 1631 N95-23910
Reflectance control for multicrystalline-silicon photovoltaic modules using textured-dielectric coatings
|DE95-004532| p 1731 N95-24155

SPECTRAL RESOLUTION
The US Geological Survey, digital spectral reflectance library: version 1: 0.2 to 3.0 microns
p 1703 N95-23855
Measurements of canopy chemistry with 1992 AVIRIS data at Blackhawk Island and Harvard Forest
p 1706 N95-23873
Spectral variations in a collection of AVIRIS imagery
p 1707 N95-23879
The red edge in arid region vegetation: 340-1060 nm spectra p 1708 N95-23881

SPECTRAL SENSITIVITY
Using AVIRIS for in-flight calibration of the spectral shifts of SPOT-HRV and of AVHRR? p 1710 N95-23893

SPECTRAL SIGNATURES
A tool for manual endmember selection and spectral unmixing p 1701 N95-23846
Investigations on the 1.7 micron residual absorption feature in the vegetation reflection spectrum
p 1710 N95-23891
Determining coniferous forest cover and forest fragmentation with NOAA-9 advanced very high resolution radiometer data p 1720 N95-24103

SPECTROGRAPHS
PRISM Spectrograph Optical Design
|NASA-CR-197965| p 1828 N95-24035

SPECTROSCOPIC ANALYSIS
Recent developments in inductively coupled plasma source magnetic sector multiple collector mass spectrometry
|DE95-003002| p 1830 N95-22793
Decomposition mechanisms in thermally-aged thin-film explosives
|DE95-000741| p 1652 N95-22838
The corrosion protection of 2219-T87 aluminum by organic and inorganic zinc-rich primers
|NASA-TP-3543| p 1641 N95-23186
Theoretical studies of spectroscopic problems of importance for atmospheric radiation measurements
p 1741 N95-23329
Secondary ion mass spectrometry (SIMS) analysis of hypervelocity microparticle impact sites on LDEF surfaces p 1637 N95-23836
Experimental and theoretical studies on the C15 intermetallic compounds MV2 (M = Zr, Hf and Ta): Elasticity and phase stability
|DE95-003723| p 1845 N95-24079

SPECTROSCOPY
The TEXT neutral lithium beam edge density diagnostic
|DE95-003256| p 1830 N95-22719
The use of electrochemical impedance spectroscopy to predict the corrosion of aluminum-lithium alloys in marine environments p 1637 N95-23504

SPECTRUM ANALYSIS
Measurement of HO2 and other trace gases in the stratosphere using a high resolution far-infrared spectrometer
|NASA-CR-197368| p 1735 N95-22482
Alpha spectral analysis via artificial neural networks
|DE95-004567| p 1767 N95-23578
A tool for manual endmember selection and spectral unmixing p 1701 N95-23846
Automating spectral unmixing of AVIRIS data using convex geometry concepts p 1702 N95-23848
The US Geological Survey, digital spectral reflectance library: version 1: 0.2 to 3.0 microns
p 1703 N95-23855
Discrimination of poorly exposed lithologies in AVIRIS data p 1703 N95-23858
Estimating dry grass residues using landscape integration analysis p 1705 N95-23867
Mapping and monitoring changes in vegetation communities of Jasper Ridge, CA, using spectral fractions derived from AVIRIS images p 1708 N95-23883
The effect of signal noise on the remote sensing of Foliar biochemical concentration p 1708 N95-23884
Application of MAC-Europe AVIRIS data to the analysis of various alteration stages in the Landdmannalauger Hydrothermal Area (South Iceland)
p 1709 N95-23885
Objective determination of image end-members in spectral mixture analysis of AVIRIS data
p 1709 N95-23888
A comparison of spectral mixture analysis an NDVI for ascertaining ecological variables p 1710 N95-23892
PCLOOK: An interactive code for spectral analysis
|DE94-635415| p 1759 N95-23963
Phonon characteristics of high (T sub c) superconductors from neutron Doppler broadening measurements
|DE95-003703| p 1844 N95-24076
Determining successional stage of temperate coniferous forests with Landsat satellite data p 1720 N95-24102

SPEECH
Spoken dialogue understanding and local context
|TR-523| p 1658 N95-23937

SPEECH DEFECTS
Spoken dialogue understanding and local context
|TR-523| p 1658 N95-23937

SPEECH RECOGNITION
Reevaluation of the significance of sequence information for speech recognition
|TR-555| p 1658 N95-23794
Spoken dialogue understanding and local context
|TR-523| p 1658 N95-23937
Phonetic set hashing: A novel scheme for transforming phone sequences to words
|TR-538| p 1658 N95-24039

SPHERICAL COORDINATES
A computer model in general 3-D curvilinear coordinates for the prediction of the turbulent flow field in a jet induced ram combustor
|NAL-TR-1240T| p 1687 N95-24051

SPHERICAL SHELLS
Computer simulation of a magnetohydrodynamic dynamo 2
|NIFS-320| p 1836 N95-23590

SPIN
The chirality operators for Heisenberg spin systems
|DE94-629043| p 1847 N95-22545

SPIN DECOUPLING
Strong-coupling behaviour of two t-J chains with interchain single-electron hopping
|DE94-629041| p 1838 N95-22499

SPIN DYNAMICS
Strong-coupling behaviour of two t-J chains with interchain single-electron hopping
|DE94-629041| p 1838 N95-22499
Experimental results on polarized structure functions in deep inelastic lepton-nucleon scattering
|DE95-002782| p 1801 N95-22521
Deformed Heisenberg algebra and fractional spin field in 2+1 dimensions
|DE94-628507| p 1850 N95-22779
Block spins and chirality in Heisenberg model on Kagome and triangular lattices
|DE94-629044| p 1840 N95-22845

SPIN-LATTICE RELAXATION
Lattice relaxation study on self-trapped exciton and biexciton in neutral and charged fullerenes
|DE94-635788| p 1844 N95-23986

SPIN-SPIN COUPLING
Boson mapping techniques applied to constant gauge fields in QCD p 1814 N95-22969

SPINE
Design of a cervical spine gross motion simulator for standard size human and anthropomorphic dummy adult and child
|NIAR-94-16| p 1751 N95-24021
A multibody/finite element analysis approach for modeling of crash dynamic responses
|NIAR-94-3| p 1610 N95-24050

SPINEL
Cation disorder determined by MAS Al-27 NMR in high dose neutron irradiated spinel
|DE95-003681| p 1842 N95-23266
Mapping of the Ronda peridotite massif (Spain) from AVIRIS spectro-imaging survey: A first attempt
p 1707 N95-23878
Temperature effects on ion irradiation damage in MgAl2O4 spinel single crystals
|DE95-003679| p 1844 N95-24073

SPINOR GROUPS
Generalized phase transformations of spinor fields
|DE94-628505| p 1656 N95-22841

SPIRAL GALAXIES
Structure and evolution of long-lived spiral patterns in galaxies
|PB95-139242| p 1868 N95-23228

SPORES
Effect of hyperbaric carbon dioxide on spores and vegetative cells of bacillus stearothermophilus
|AD-A280115| p 1747 N95-23251

SPOT (FRENCH SATELLITE)
A preliminary comparison of Landsat Thematic Mapper and SPOT-1 HRV multispectral data for estimating coniferous forest volume p 1719 N95-24097

SPRAY CHARACTERISTICS
Spray combustion experiments and numerical predictions p 1637 N95-23643

SPRAYERS
The probabilistic structure of sprays: Implications for measurements by in site particle counters
|DE95-002483| p 1666 N95-23081
Adaptation of the advanced spray combustion code to cavitating flow problems p 1681 N95-23629

SPUTTERING
Large-area triple-junction a-Si alloy production scaleup
|DE95-000245| p 1726 N95-22546
MOCVD of gallium and calcium sulfides for improved phosphor processing
|DE95-000918| p 1631 N95-22677

SQUEEZED STATES (QUANTUM THEORY)
Nonclassical light in interferometric measurements
p 1822 N95-22976
Noisy bases in Hilbert space: A new class of thermal coherent states and their properties
p 1823 N95-22980

STABILITY
Shapes and stability of algebraic nuclear models
p 1814 N95-22974
Thin tailored composite wing for civil tiltrotor
p 1613 N95-23317
Dynamic disturbance decoupling of nonlinear systems and linearization
|PB95-141248| p 1767 N95-23558

STABILITY TESTS
High beta and second stability region transport and stability analysis
|DE95-003411| p 1832 N95-23147

STABILIZATION
On the (DE-) stabilization of quantum mechanical binding by potential barriers
|DE94-628433| p 1847 N95-22635

STABILIZED PLATFORMS
Preprocessing: Geocoding of AVIRIS data using navigation, engineering, DEM, and radar tracking system data p 1707 N95-23876

STAGNATION PRESSURE
GGOT total pressure loss control concept evaluation
p 1672 N95-23427

STAINLESS STEELS
Study of radiation damages in AISI 316 and 347 steels
|DE94-627480| p 1639 N95-22609
Pulsed Ion Beam Surface Treatment for preparing rapidly solidified corrosion resistant alloy surfaces
|DE94-012072| p 1640 N95-22835
Long-term aging of type 308 stainless steel welds: Effects on properties and microstructure
|DE94-018961| p 1640 N95-23132
Explosive bonding and its application in the Advanced Photon Source front-end and beamline components design
|DE95-004132| p 1696 N95-23397
Specific features of corrosion behavior of stainless maraging steels for aerospace application
p 1642 N95-23501
Be-10 in terrestrial bauxite and industrial aluminum: An LDEF fallout p 1646 N95-23820
Characterization of Type 304L stainless steel solid-state closure welds for radioactive waste containment
|DE94-016539| p 1645 N95-23980

STANDARD MODEL (PARTICLE PHYSICS)
Precision standard model tests with polarized e(+)e(-) beams
| DE95-003367 | p 1816 N95-22702
The charm physics potential of a Tau-Charm Factory
| DE95-003369 | p 1802 N95-22703
Introduction to the physics of Higgs bosons
| DE95-003965 | p 1809 N95-23396
A measurement of the mass of the W vector boson at CDF
| DE95-003498 | p 1813 N95-24016
STANDARDIZATION
Algebraic semantics of basic message sequence charts
| PB95-138970 | p 1657 N95-23151
STANDARDS
A draft standard for message passing in a distributed memory environment
| DE94-019159 | p 1657 N95-23075
STAR FORMATION
Origins of interstellar and solar system: Carbonaceous materials
| NASA-CR-197436 | p 1867 N95-23013
STAR TRACKERS
The Starpicker expert system: A problem in expertise capture p 1623 N95-23721
STATE ESTIMATION
Tutorial on filtering, restoration, and state estimation
| TR-534 | p 1793 N95-24042
STATIC PRESSURE
Numerical simulation of steady and unsteady viscous flow in turbomachinery using pressure based algorithm p 1671 N95-23426
GGOT total pressure loss control concept evaluation p 1672 N95-23427
STATIC STABILITY
Handling qualities of the High Speed Civil Transport p 1616 N95-23325
STATIC TESTS
Corrosion protection measures for CFC/metal joints of fuel integral tank structures of advanced military aircraft p 1644 N95-23510
STATIC THRUST
An approximate theoretical method for modeling the static thrust performance of non-axisymmetric two-dimensional convergent-divergent nozzles
| NASA-CR-195050 | p 1608 N95-23193
STATISTICAL ANALYSIS
Nonparametric measure of spatial interaction in point patterns
| PB95-127965 | p 1793 N95-22527
Collecting operational event data for statistical analysis
| DE95-002020 | p 1793 N95-22550
An improved system for exon recognition and gene modeling in human DNA sequences
| DE94-017863 | p 1746 N95-22890
Static parametric fluctuations give nonstatistical behaviour in uncoupled chaotic systems
| DE94-628478 | p 1794 N95-23019
The probabilistic structure of sprays: Implications for measurements by in site particle counters
| DE95-002483 | p 1666 N95-23081
On-line, adaptive state estimator for active noise control p 1784 N95-23308
A wavenumber-partitioning scheme for two-dimensional statistical closures
| DE95-004514 | p 1677 N95-23483
Technical report series on global modeling and data assimilation. Volume 4: Documentation of the Goddard Earth Observing System (GEOS) data assimilation system, version 1
| NASA-TM-104606-VOL-4 | p 1740 N95-23529
POD assessment of NDI procedures using a round robin test
| AGARD-R-809 | p 1697 N95-23602
A tool for manual endmember selection and spectral unmixing p 1701 N95-23846
Spectral variations in a collection of AVIRIS imagery p 1707 N95-23879
Optimal band selection for dimensionality reduction of hyperspectral imagery p 1709 N95-23887
Laboratory spectra of field samples as a check on two atmospheric correction methods p 1711 N95-23894
A theory for the morphology of Laplacian growth from statistics of equivalent many-body Hamiltonian systems
| DE94-014473 | p 1799 N95-23979
STATISTICAL DISTRIBUTIONS
Statistical properties of the time histories of cosmic gamma-ray bursts detected by the BATSE experiment of the Compton gamma-ray observatory
| NASA-CR-197425 | p 1871 N95-23546
STATISTICAL MECHANICS
Study of frustrated systems via dissipative maps
| PB95-139093 | p 1799 N95-23155
(Phi)(sup 4) kinks: Statistical mechanics
| DE95-003693 | p 1794 N95-23349
A theory for the morphology of Laplacian growth from statistics of equivalent many-body Hamiltonian systems
| DE94-014473 | p 1799 N95-23979
STATISTICAL TESTS
Consistency and Monte Carlo simulation of a data driven version of smooth goodness-of-fit tests
| PB95-141255 | p 1794 N95-23559
STATORS
Enhanced analysis and users manual for radial-inflow turbine conceptual design code RTD
| NASA-CR-195454 | p 1609 N95-23462
STDN (NETWORK)
Improved AVHRR data navigation using automated land feature recognition to correct a satellite orbital model
| CSIRO-TR-34 | p 1718 N95-24026
STEADY FLOW
A perspective on unstructured grid flow solvers
| NASA-CR-195025 | p 1788 N95-22931
Numerical simulation of steady and unsteady viscous flow in turbomachinery using pressure based algorithm p 1671 N95-23426
Aerodynamic design and analysis of a highly loaded turbine exhaust p 1673 N95-23435
STEADY STATE
Status of axisymmetric CFD of an eleven inch diameter hybrid rocket motor p 1686 N95-23651
Experimental achievement of toroidal beta beyond that predicted by 'Troyon' scaling
| DE95-003880 | p 1837 N95-24087
STEADY STATE CREEP
Thermal activation of steady-state creep in polycrystalline copper
| DE94-627394 | p 1839 N95-22607
STEAROTHERMOPHILUS
Effect of hyperbaric carbon dioxide on spores and vegetative cells of bacillus stearothermophilus
| AD-A280115 | p 1747 N95-23251
STEEL STRUCTURES
Corrosion control acceptance criteria for sacrificial anode type, cathodic protection systems (user guide)
| AD-A285275 | p 1662 N95-23117
STEELS
Corrosion of landing gear steels p 1642 N95-23500
STELLAR EVOLUTION
Origins of interstellar and solar system: Carbonaceous materials
| NASA-CR-197436 | p 1867 N95-23013
STELLAR FLARES
Investigation of physical parameters in stellar flares observed by GINGA
| NASA-CR-196547 | p 1868 N95-23205
STELLAR MASS
Solar mass loss, solar lithium, and solar oscillations
| DE94-018262 | p 1870 N95-22938
STELLAR MASS ACCRETION
Observational studies of the clearing phase in proto-planetary disk systems
| NASA-CR-197900 | p 1866 N95-23561
STELLAR MODELS
Gamma ray emission from radio pulsars
| NASA-CR-197917 | p 1871 N95-22910
STELLAR PHYSICS
Origins of interstellar and solar system: Carbonaceous materials
| NASA-CR-197436 | p 1867 N95-23013
Investigation of physical parameters in stellar flares observed by GINGA
| NASA-CR-196547 | p 1868 N95-23205
STELLAR RADIATION
Gamma ray emission from radio pulsars
| NASA-CR-197917 | p 1871 N95-22910
STELLAR SPECTRA
Long term variability of B supergiant winds
| NASA-CR-197925 | p 1865 N95-23401
Mass loss in the interacting semi-detached binary delta librae
| NASA-CR-197924 | p 1866 N95-23402
A study of EUV emission from the O4f star Zeta Puppis
| NASA-CR-197350 | p 1871 N95-23472
STELLAR WINDS
Long term variability of B supergiant winds
| NASA-CR-197925 | p 1865 N95-23401
A study of EUV emission from the O4f star Zeta Puppis
| NASA-CR-197350 | p 1871 N95-23472
STELLARATORS
Conceptual design of a 20-kA current lead using forced-flow cooling and Ag-alloy-sheathed Bi-2223 high-temperature superconductors
| DE95-002916 | p 1660 N95-22569
Physical mechanism determining the radial electric field and its radial structure in a toroidal plasma
| NIFS-313 | p 1835 N95-23534
Quasisymmetry equations for conventional stellarators
| NIFS-324 | p 1836 N95-23572
Theory of pressure-induced islands and self-healing in three-dimensional toroidal magnetohydrodynamic equilibria
| NIFS-321 | p 1836 N95-23589
Effect of satellite helical harmonics on the stellarator configuration
| NIFS-328 | p 1609 N95-23787
STEREOSCOPIC VISION
Autonomous navigation system for the Marsokhod rover project p 1771 N95-23693
A fuzzy structural matching scheme for space robotics vision p 1778 N95-23737
Full resolution hologram-like autostereoscopic display
| NASA-CR-197913 | p 1689 N95-23789
STEREOSCOPY
Full resolution hologram-like autostereoscopic display
| NASA-CR-197913 | p 1689 N95-23789
STIFFNESS
Vibration-damping structural component
| AD-D016550 | p 1693 N95-22707
Integrated aerodynamic/dynamic/structural optimization of helicopter rotor blades using multilevel decomposition
| NASA-TP-3465 | p 1612 N95-22953
Fabric geometry distortion during composites processing p 1631 N95-23288
Deflections of anisotropic sandwich beams with variable face sheets and core thicknesses p 1700 N95-23310
Three-D CFD analysis of hydrostatic bearings p 1678 N95-23616
STOCHASTIC PROCESSES
The propagation of travelling waves for stochastic generalized KPP equations
| DE94-628473 | p 1787 N95-22772
Langmuir-like waves and radiation in planetary foreshocks
| NASA-CR-197376 | p 1869 N95-22828
Stochastic decision analysis p 1854 N95-23305
Spontaneous wave packet reduction
| DE94-634280 | p 1851 N95-23454
Light-traffic analysis for queues with spatially distributed arrivals
| PB95-140802 | p 1767 N95-23556
STOICHIOMETRY
Particle size dependence in Fischer-Tropsch synthesis
| DE95-003124 | p 1633 N95-22876
NO decomposition in non-reducing atmospheres
| DE95-004324 | p 1634 N95-23339
Carbon doping of III-V compound semiconductors
| DE95-003431 | p 1844 N95-24013
STOKES FLOW
BEm-BDF scheme for curvature driven moving stokes flows
| PB95-138905 | p 1667 N95-23144
Numerical simulation of axisymmetric viscous sintering
| PB95-138889 | p 1667 N95-23175
On the breakup of viscous liquid threads
| NASA-CR-195023 | p 1678 N95-23544
STOPPING POWER
ESTAR, PSTAR, ASTAR: A PC package for calculating stopping powers and ranges of electrons, protons and helium ions, version 2
| DE94-634435 | p 1811 N95-23773
STORAGE RINGS (PARTICLE ACCELERATORS)
Thermal outgassing studies on machinable tungsten and TZM molybdenum alloy
| DE95-002984 | p 1638 N95-22592
Ion rings for magnetic fusion
| DE94-017606 | p 1832 N95-23120
Spin physics in the next decade
| DE95-003727 | p 1809 N95-23403
STORAGE STABILITY
Test procedure for anion exchange chromatography
| DE95-003767 | p 1809 N95-23407
Fourth NASA Goddard Conference on Mass Storage Systems and Technologies
| NASA-CP-3295 | p 1857 N95-24108
A kinetic study of hydrolysis of polyester elastomer in magnetic tape p 1652 N95-24124
STORAGE TANKS
Multi-fuel reformers for fuel cells used in transportation: Assessment of hydrogen storage technologies
| DE94-017655 | p 1727 N95-22861
STRAIN GAGES
Optical fiber strain sensor with improved linearity range
| NASA-CASE-LAR-14857-1-SB | p 1819 N95-22807
STRAIN MEASUREMENT
Method and apparatus for measuring the strain developed in a coated surface
| NASA-CASE-ARC-11938-1-C | p 1688 N95-23263
Internal strain measurement using pulsed neutron diffraction at LANSCE
| DE95-003677 | p 1842 N95-23365

Development of sensors for ceramic components in advanced propulsion systems
| NASA-CR-195324 | p 1689 N95-23795

STRAIN RATE
Exfoliation corrosion and stress corrosion cracking behaviour of Al-Li alloys p 1641 N95-23498

STRANDS
Light emission-or-absorbance-based binding assays for polynucleic acids
| AD-D016557 | p 1632 N95-22710

STRATEGY
Defense science and technology strategy
| AD-A285414 | p 1903 N95-24179

STRATIFICATION
Partition of real symmetric matrices according to the multiplicities of their eigenvalues
| PB95-139846 | p 1790 N95-23235

STRATOSPHERE
Measurement of HO2 and other trace gases in the stratosphere using a high resolution far-infrared spectrometer
| NASA-CR-197368 | p 1735 N95-22482
Oxidants and oxidation in the Earth's atmosphere
| NASA-CR-197945 | p 1734 N95-23460

STREAMS
CO2 and waste policy: Monitoring results 1991/1992 and main problems
| PB95-133799 | p 1733 N95-23126
Streamflow and selected precipitation data for Yucca Mountain Region, southern Nevada and eastern California, water years 1986-90
| DE95-001893 | p 1742 N95-23385

STRESS (PHYSIOLOGY)
Interrelations between nervous system and immune system in stress situations
| PB95-135521 | p 1748 N95-22770

STRESS ANALYSIS
Deflections of anisotropic sandwich beams with variable face sheets and core thicknesses p 1700 N95-23310
Associated with aerospace vehicles development of methodologies for the estimation of thermal properties p 1700 N95-23321

STRESS CORROSION CRACKING
The role of grain boundary chemistry and structure in the environmentally-assisted intergranular cracking of nickel-base alloys
| DE95-002941 | p 1638 N95-22532
The corrosion and protection of advanced aluminium - lithium airframe alloys p 1641 N95-23497
Exfoliation corrosion and stress corrosion cracking behaviour of Al-Li alloys p 1641 N95-23498
Corrosion of landing gear steels p 1642 N95-23500
Specific features of corrosion behavior of stainless maraging steels for aerospace application p 1642 N95-23501

STRESS INTENSITY FACTORS
Stress intensity factors and crack mouth openings for bridged cracks emanating from circular holes
| AR-008-408 | p 1699 N95-22952

STRESS MEASUREMENT
Internal strain measurement using pulsed neutron diffraction at LANSCE
| DE95-003677 | p 1842 N95-23365

STRESS TENSORS
Finite-temperature scalar field theory in static de Sitter space
| DE94-628522 | p 1848 N95-22743

STRESSES
The effect of elastic stress on Ostwald Ripening Phenomena
| DE95-002599 | p 1646 N95-24140

STRIATION
Measurements of striae in CR+ doped YAG laser crystals p 1847 N95-23285

STRING THEORY
Twistor-like type 2 superstring with the heterotic (2,0) and (4,0) worldsheet supersymmetry
| DE94-628510 | p 1848 N95-22735
First quantized noncritical relativistic Polyakov string
| DE94-628513 | p 1848 N95-22738
Topologically stable Z - strings in the supersymmetric standard model
| DE94-628517 | p 1848 N95-22742
Chiral symmetry breaking in QCD with linearly rising confinement potential
| DE94-628559 | p 1848 N95-22744
Spontaneous breaking of chiral symmetry as a consequence of confinement
| DE94-628560 | p 1849 N95-22745
Effective (mu)-term in superstring theory
| DE94-634326 | p 1851 N95-23922

STRINGS
Performance of single-keyword and multiple-keyword pattern matching algorithms
| PB95-138954 | p 1756 N95-23150

STRONG INTERACTIONS (FIELD THEORY)
Unification of electromagnetic, strong and weak interaction
| DE94-628570 | p 1655 N95-22746
The problem of phase transition and the heavy ion collisions at very high energies
| DE94-628584 | p 1816 N95-22785

STRONTIUM COMPOUNDS
Effect on c-axis transport properties of a critical state in Bi2Sr2CaCu2O8
| DE95-003695 | p 1843 N95-23366

STRONTIUM OXIDES
Some aspects of critical currents in Ag sheathed Bi2Sr2Ca2Cu3O10 composite tapes: A summary
| DE95-003952 | p 1842 N95-23354
Cooling rate effects on the microstructure, critical current density, and (T(sub c)) transition of one- and two-powder BSCCO-2223 Ag sheathed tapes
| DE95-004639 | p 1846 N95-24171

STRUCTURAL ANALYSIS
Statistically generated weighted curve fit of residual functions for modal analysis of structures
| NASA-TM-108481 | p 1699 N95-22950
Computational control of flexible aerospace systems
| NASA-CR-197902 | p 1621 N95-23260
Vision-sensing image analysis for GTAW process control
| DE95-003936 | p 1695 N95-23373

STRUCTURAL BASINS
Energy flux and hydrogeology of thermal anomalies in the Gulf of Mexico Basin - South Texas example
| DE95-003341 | p 1743 N95-22695

STRUCTURAL DESIGN
Hey! What's Space Station Freedom?
| NASA-TM-110531 | p 1620 N95-22542
Weight minimization of structural components for launch in space shuttle
| NASA-TM-4586 | p 1698 N95-22805
Integrated aerodynamic/dynamic/structural optimization of helicopter rotor blades using multilevel decomposition
| NASA-TP-3465 | p 1612 N95-22953
A new look at the simultaneous analysis and design of structures p 1700 N95-23327

STRUCTURAL ENGINEERING
Infinite possibilities: Computational structures technology p 1700 N95-23280

STRUCTURAL STRAIN
Method and apparatus for measuring the strain developed in a coated surface
| NASA-CASE-ARC-11938-1-C | p 1688 N95-23263

STRUCTURAL VIBRATION
Active control of panel vibrations induced by a boundary layer flow
| NASA-CR-197867 | p 1608 N95-23182
Gearbox vibration diagnostic analyzer
| NASA-CR-189141 | p 1696 N95-23792

STRUCTURAL WEIGHT
Weight minimization of structural components for launch in space shuttle
| NASA-TM-4586 | p 1698 N95-22805

STRUCTURED PROGRAMMING
Effective management of classified documents using the library document system
| AD-A286021 | p 1855 N95-23024

STRUCTURES
Flow measuring structures
| PB95-127254 | p 1665 N95-22638

SUBMERGING
Grassman and hyperKaehler structures on some spaces of sections of holomorphic bundles
| PB95-109104 | p 1795 N95-22712

SUBMILLIMETER WAVES
High power Josephson effect sources
| AD-A285808 | p 1838 N95-22511
Interstellar molecules in the large magellanic cloud
| PB95-139267 | p 1868 N95-23230

SUBROUTINES
AMPHION: Specification-based programming for scientific subroutine libraries p 1761 N95-23680

SUBSONIC FLOW
Wing pressure distributions from subsonic tests of a high-wing transport model --- in the Langley 14- by 22-Foot Subsonic Wind Tunnel
| NASA-TM-4583 | p 1607 N95-22802
Towards a generalized computational fluid dynamics technique for all Mach numbers p 1670 N95-23420

SUBSONIC SPEED
Inner loop flight control for the High-Speed Civil Transport p 1616 N95-23314
High-lift flow-physics flight experiments on a subsonic civil transport aircraft (B737-100) p 1609 N95-23333

SUBSTITUTES
Fibonacci chain polynomials: Identities from self-similarity p 1814 N95-22962

SUBSTRATES
Vibration-damping structural component
| AD-D016550 | p 1693 N95-22707
Method and system for electron beam lithography
| AD-D016554 | p 1660 N95-22709
Surface growth of two kinds of particles deposition models
| DE94-628480 | p 1841 N95-23021
Surface structural dependence of cesium adsorption on the (alpha)-Al2O3(0001) surface
| DE95-002610 | p 1842 N95-23135
Preparation of high quality YBa2Cu3O(7-delta) thick films on flexible Ni-based alloy substrates with textured buffer layers
| DE95-003686 | p 1645 N95-23571
Silicon surface and bulk defect passivation by low temperature PECVD oxides and nitrides
| DE95-004531 | p 1731 N95-24090

SULFATES
MHD seed recovery and regeneration, phase 2
| DE95-004308 | p 1833 N95-23338

SULFIDATION
Charge distribution analysis of catalysts under simulated reaction conditions
| DE95-003526 | p 1633 N95-23064

SULFUR
Compendium of NASA data base for the Global Tropospheric Experiment's Pacific Exploratory Mission West-A (PEM West-A)
| NASA-TM-109177 | p 1733 N95-23009

SULFUR HEXAFLUORIDE
Performance of the 0.3-meter transonic cryogenic tunnel with air, nitrogen, and sulfur hexafluoride media under closed loop automatic control
| NASA-CR-195052 | p 1668 N95-23257

SULFUR ISOTOPES
Rate coefficients for the electron-impact excitation, ionization and recombination of He-like ions, S XV, Ca XIX and Fe XXV, and related processes
| ISAS-R-657 | p 1811 N95-23604

SUM RULES
Fermion-spin transformation to implement the charge-spin separation
| DE94-629035 | p 1800 N95-22495

SUMS
Second derivative of the likelihood of an exact ARMA model
| PB95-135158 | p 1788 N95-23069

SUN
Space Science for the 21st Century. Strategic Plan for 1995-2000
| NASA-TM-110546 | p 1617 N95-22947

SUPERCOMPUTERS
Evaluation of a Multiple Instruction/Multiple Data (MIMD) parallel computer for CFD applications
| AD-A285796 | p 1762 N95-22509
Towards the Teraflop CFD
| NASA-CR-197947 | p 1764 N95-23594
Unstructured grids on SIMD torus machines
| NASA-CR-197954 | p 1758 N95-23610
Transferring ecosystem simulation codes to supercomputers
| NASA-TM-4662 | p 1759 N95-24052

SUPERCONDUCTING DEVICES
Superconductivity devices: Commercial use of space
| NASA-CR-197885 | p 1648 N95-22883
Undulators for short wavelength FEL amplifiers
| DE95-004690 | p 1692 N95-23487

SUPERCONDUCTING FILMS
Superconducting Tl2Ba2CaCu2O8 thin films prepared by post-annealing in a flow-through multiple-zone furnace
| DE95-002745 | p 1838 N95-22520
Analyses, algorithms, and computations for models of high-temperature superconductivity
| DE95-003290 | p 1661 N95-22733
High Tc superconducting bolometric and nonbolometric infrared (IR) detectors
| NASA-CR-197868 | p 1827 N95-23224
Preparation of high quality YBa2Cu3O(7-delta) thick films on flexible Ni-based alloy substrates with textured buffer layers
| DE95-003686 | p 1645 N95-23571
Microstructure and composition of a SNS Josephson junction using CaRuO3 as the metallic barrier
| DE95-004611 | p 1845 N95-24152

SUPERCONDUCTING MAGNETS
Multipole contribution from an off-axis orbit in an IR quadrupole and the consequences on the dynamic aperture
| DE95-002874 | p 1816 N95-22567
An investigation of AC losses in two sub-size conductors for the ITER
| DE94-765449 | p 1831 N95-22849

Quench propagation study for full-length RHIC dipole magnets
| DE94-014089 | p 1816 N95-22926
TPX magnet system status
| DE95-002389 | p 1661 N95-23080
Undulators for short wavelength FEL amplifiers
| DE95-004690 | p 1692 N95-23487
Recent studies of the Large Helical Device
| NIFS-322 | p 1835 N95-23543
Design of a high-temperature superconductor current lead for electric utility SMES
| DE95-004604 | p 1664 N95-24163

SUPERCONDUCTIVITY
Multipole contribution from an off-axis orbit in an IR quadrupole and the consequences on the dynamic aperture
| DE95-002874 | p 1816 N95-22567
Surface impedance studies on the electrodynamical response of organic superconductors
| DE95-002986 | p 1660 N95-22593
A study of ceramic composite of ferroelectric BaTiO3 ceramic and superconductor YBa2Cu3O(6+delta) ceramic
| DE94-627563 | p 1647 N95-22610
Analyses, algorithms, and computations for models of high-temperature superconductivity
| DE95-003290 | p 1661 N95-22733
Correlation effects in high-Tc superconductors and heavy fermion compounds
| DE94-629057 | p 1840 N95-22846
The next Large Helical Devices
| NIFS-323 | p 1835 N95-23535
Electrochemical studies of perovskite mixed conductors
| DE95-003704 | p 1636 N95-23573
Effects of Bi and Bi2O3 additions on the microstructure and superconducting properties of powder-in-tube BSCCO (2212) tapes
| DE95-004605 | p 1845 N95-24150

SUPERCONDUCTORS (MATERIALS)
Fermion-spin transformation to implement the charge-spin separation
| DE94-629035 | p 1800 N95-22495
High power Josephson effect sources
| AD-A285808 | p 1838 N95-22511
Correlation effects in high-Tc superconductors and heavy fermion compounds
| DE94-629057 | p 1840 N95-22846
An investigation of AC losses in two sub-size conductors for the ITER
| DE94-765449 | p 1831 N95-22849
Strongly interacting fermion systems
| DE95-003405 | p 1806 N95-23054
Bose condensation, macroscopic quantum phenomena and atomic spatial correlations in superfluid He-4
| PB95-139085 | p 1850 N95-23154

SUPERCRITICAL FLUIDS
Small angle x ray scattering studies of aggregation in supercritical fluid solutions
| DE95-004576 | p 1843 N95-23579

SUPERFLUIDITY
Bose condensation, macroscopic quantum phenomena and atomic spatial correlations in superfluid He-4
| PB95-139085 | p 1850 N95-23154

SUPERGRAVITY
Topologically stable Z - strings in the supersymmetric standard model
| DE94-628517 | p 1848 N95-22742

SUPERHIGH FREQUENCIES
Utilizing a TDRS satellite for direct broadcast satellite-radio propagation experiments and demonstrations p 1622 N95-22814

SUPERLATTICES
Superlattices in thermoelectric applications
| DE95-001356 | p 1840 N95-22687
Epitaxial growth of bcc transition metal films and superlattices onto MgO (111), (011) and (001) substrates
| DE95-004629 | p 1846 N95-24168
A simple, closed-form expression for the x ray reflectivity from superlattices with cumulative roughness
| DE95-004633 | p 1846 N95-24170

SUPERPLASTIC FORMING
Technology maturation project on optimization of sheet metal forming of aluminum for use in transportation systems
| DE95-003005 | p 1654 N95-22692

SUPERSONIC COMBUSTION RAMJET ENGINES
Mach 10 computational study of a three-dimensional scramjet inlet flow field
| NASA-TM-4602 | p 1666 N95-23015
Mach 10 computational study of a three-dimensional scramjet inlet flow field
| NASA-TM-4602 | p 1667 N95-23210

SUPERSONIC FLOW
Supersonic flow and shock formation in turbine tip gaps p 1672 N95-23429
Instantaneous 2D velocity and temperature measurements in high speed flows based on spectrally resolved molecular Rayleigh scattering
| NASA-TM-106883 | p 1688 N95-23461
Validation of a Computational Fluid Dynamics (CFD) code for supersonic axisymmetric base flow p 1686 N95-23652
Supersonic laminar flow control research
| NASA-CR-197938 | p 1609 N95-23669

SUPERSONIC INLETS
Mach 10 computational study of a three-dimensional scramjet inlet flow field
| NASA-TM-4602 | p 1667 N95-23210
Supersonic flow and shock formation in turbine tip gaps p 1672 N95-23429

SUPERSONIC JET FLOW
Supersonic jet noise reductions predicted with increased jet spreading rate
| NASA-TM-106872 | p 1800 N95-23178
Three-dimensional structure in a supersonic jet: Behavior near centerline
| NASA-TM-106869 | p 1668 N95-23220

SUPERSONIC TRANSPORTS
Inner loop flight control for the High-Speed Civil Transport p 1616 N95-23314
Preliminary identification of buffet problems in high speed civil transport p 1616 N95-23319
Handling qualities of the High Speed Civil Transport p 1616 N95-23325

SUPERSONIC WIND TUNNELS
Supersonic laminar flow control research
| NASA-CR-197938 | p 1609 N95-23669

SUPERSYMMETRY
Twistor-like type 2 superstring with the heterotic (2,0) and (4,0) worldsheet supersymmetry
| DE94-628510 | p 1848 N95-22735
Aspects of sigma models
| DE94-628511 | p 1795 N95-22736
Topologically stable Z - strings in the supersymmetric standard model
| DE94-628517 | p 1848 N95-22742
Supersymmetric singlet majorons and cosmology
| DE94-628571 | p 1850 N95-22783
Supersymmetric oscillator in optics p 1826 N95-23002
Classification of (2,2) compactifications by free fermions 2
| PB95-139119 | p 1807 N95-23157
Higgs searches and WW scattering
| PB95-139143 | p 1807 N95-23160
Search for supersymmetric (tilde W)(sub 1) and (tilde Z)(sub 2) states using the D0 detector
| DE95-004581 | p 1811 N95-23581
Effective (mu)-term in superstring theory
| DE94-634326 | p 1851 N95-23922

SUPPLEMENTS
NASA Thesaurus, Supplement
| NASA-SP-7096-SUPPL-1 | p 1856 N95-23223

SUPPORT SYSTEMS
Integrating O/S models during conceptual design, part 1
| NASA-CR-197903 | p 1622 N95-23398
Integrating O/S models during conceptual design, part 2
| NASA-CR-197904 | p 1622 N95-23399
Constraint based scheduling for the Goddard Space Flight Center distributed Active Archive Center's data archive and distribution system p 1859 N95-24121

SURFACE CRACKS
Atomic oxygen interactions with protected organic materials on the Long Duration Exposure Facility (LDEF) p 1627 N95-23909

SURFACE DEFECTS
The effect of simulated low earth orbit radiation on polyimides (UV degradation study) p 1651 N95-23903
The surface properties of fluorinated polyimides exposed to VUV and atomic oxygen p 1651 N95-23904
Atomic oxygen interactions with protected organic materials on the Long Duration Exposure Facility (LDEF) p 1627 N95-23909
The development of shell imperfection measurement techniques
| TAE-712 | p 1699 N95-23923
Silicon surface and bulk defect passivation by low temperature PECVD oxides and nitrides
| DE95-004531 | p 1731 N95-24090

SURFACE DIFFUSION
Analysis of physiochemical processes during solder aging
| DE95-003811 | p 1638 N95-22576

SURFACE DISTORTION
Double pass retroreflection for corrosion detection in aircraft structures p 1642 N95-23503

SURFACE ENERGY
Thermal radiant exitance model performance: Soils and forests
| DE95-003619 | p 1721 N95-24148
Implementation of a soil-canopy scheme into the CSIRO GCM: Regional aspects of the model response
| CSIRO-TR-32 | p 1721 N95-24192

SURFACE LAYERS
Metallization and incomplete melting of a semiconductor surface at high temperature
| DE94-627342 | p 1660 N95-22591

SURFACE NAVIGATION
Lunar rover technology demonstrations with Dante and Ratler p 1697 N95-23694
Terrain modelling and motion planning for an autonomous exploration rover p 1721 N95-23765

SURFACE PROPERTIES
Surface impedance studies on the electrodynamical response of organic superconductors
| DE95-002986 | p 1660 N95-22593
Glass science tutorial: Lecture 1, Chemistry and properties of oxide glasses
| DE95-002963 | p 1647 N95-22647
Guidance and control requirements for high-speed Rollout and Turnoff (ROTO)
| NASA-CR-195026 | p 1614 N95-22674
Computer simulation of the structure of ionic surfaces and interfaces
| DE95-002991 | p 1804 N95-22792
Surface structural dependence of cesium adsorption on the (alpha)-Al2O3(0001) surface
| DE95-002610 | p 1842 N95-23135
Carbon monoxide oxidation over three different states of copper: Development of a model metal oxide catalyst
| DE95-004682 | p 1636 N95-23495
Spectral decomposition of AVIRIS data p 1704 N95-23859

SURFACE REACTIONS
Advanced growth and surface analysis system for in situ studies of interface formation
| DE95-002850 | p 1838 N95-22555
Surface structural dependence of cesium adsorption on the (alpha)-Al2O3(0001) surface
| DE95-002610 | p 1842 N95-23135
In-situ detection of surface passivation or activation and of localized corrosion: Experiences and prospectives in aircraft p 1643 N95-23508
Scandinavian symposium on surface chemistry
| PB95-140687 | p 1636 N95-23554
The surface properties of fluorinated polyimides exposed to VUV and atomic oxygen p 1651 N95-23904
Collection and review of metals data obtained from LDEF experiment specimens and support hardware p 1646 N95-23905

SURFACE ROUGHNESS
Surface growth of two kinds of particles deposition models
| DE94-628480 | p 1841 N95-23021
Measurement and analysis of scatter from silicon wafers
| DE95-002411 | p 1827 N95-23531
Profiling and light scattering studies of Si surfaces
| DE95-002931 | p 1828 N95-24005
A simple, closed-form expression for the x ray reflectivity from superlattices with cumulative roughness
| DE95-004633 | p 1846 N95-24170

SURFACE ROUGHNESS EFFECTS
Prediction of incidence and surface roughness effects on turbine performance p 1671 N95-23424

SURFACE TEMPERATURE
Particle kinetic simulation of high altitude hypervelocity flight
| NASA-CR-197383 | p 1664 N95-22481
Land surface temperature measurements for EOS MODIS data
| NASA-CR-197443 | p 1717 N95-23191
Validation data for land surface temperature determination from satellites
| CSIRO-TR-33 | p 1718 N95-23597
Thermal radiant exitance model performance: Soils and forests
| DE95-003619 | p 1721 N95-24148

SURFACE TREATMENT
Pulsed Ion Beam Surface Treatment for preparing rapidly solidified corrosion resistant alloy surfaces
| DE94-012072 | p 1640 N95-22835
Experience of in-service corrosion on military aircraft p 1644 N95-23516

SURFACE VEHICLES
Fire hazard considerations for composites in vehicle design p 1628 N95-23032

SURFACE WATER
Streamflow and selected precipitation data for Yucca Mountain Region, southern Nevada and eastern California, water years 1986-90
| DE95-001893 | p 1742 N95-23385

SURFACE WAVES
Propagation of waves at the loosely bonded interface of two porous elastic half-spaces
|DE94-628477| p 1800 N95-23018
Tomographic analysis of the three-dimensional variation of the seismic velocity structure of the shallow crust underlying Southern New England
|AD-A279406| p 1739 N95-23247
SURFACTANTS
Small angle x ray scattering studies of aggregation in supercritical fluid solutions
|DE95-004576| p 1843 N95-23579
SURVEYS
A multispectral scanner survey of the Tonopah Test Range, Nevada. Date of survey: August 1993
|DE95-003920| p 1717 N95-22503
Study on possible environmental effects of a WBM cutting discharge in the north sea, one year after termination of drilling
|PB95-133740| p 1733 N95-23125
Some recent results in the analysis of greedy algorithms for assignment problems
|PB95-140620| p 1757 N95-23238
Teams and teamwork at NASA Langley Research Center p 1854 N95-23292
SURVIVAL
Aircraft fires, smoke toxicity, and survival: An overview
|DOT/FAA/AM-95/8| p 1610 N95-24024
SUSPENDING (HANGING)
Development of the dynamic motion simulator of 3D micro-gravity with a combined passive/active suspension system p 1618 N95-23711
SWEPT FORWARD WINGS
Flight test of the X-29A at high angle of attack: Flight dynamics and controls
|NASA-TP-3537| p 1612 N95-22806
SWEPT WINGS
Crossflow instability control on a swept-wing: Preliminary studies p 1609 N95-23283
SWIRLING
Experimental study of vortex breakdown in a swirling water jet
|PB95-130407| p 1665 N95-22767
Aerodynamic design and analysis of a highly loaded turbine exhaust p 1673 N95-23435
SWITCHES
High gain GaAs Photoconductive Semiconductor Switches for impulse sources
|DE95-001885| p 1659 N95-22549
High gain GaAs photoconductive semiconductor switches: Measurement of filament velocity and reduced trigger energy
|DE95-001884| p 1661 N95-22844
SWITCHING CIRCUITS
A high-power switch-mode DC power supply for dynamic loads
|DE94-016714| p 1659 N95-22504
Non-blocking crossbar permutation engine with constant routing latency
|NASA-CASE-NPO-18864-1-CU| p 1762 N95-22564
SYMBOLS
Determinants of elliptic pseudo-differential operators
|PB95-109062| p 1786 N95-22711
TRISTAR 1: Evaluation methods for testing head-up display (HUD) flight symbology
|NASA-TM-4665| p 1613 N95-24030
SYMMETRY
Lectures on homology with internal symmetries
|DE94-628409| p 1785 N95-22619
Continuous local symmetry in Ising-type models
|DE94-629045| p 1839 N95-22649
Hadrons of arbitrary spin and heavy quark symmetry
|DE94-628597| p 1804 N95-22789
An algebraic cluster model based on the harmonic oscillator basis p 1814 N95-22971
Galactic oscillator symmetry p 1822 N95-22973
Covariant harmonic oscillators and coupled harmonic oscillators p 1825 N95-22992
Quasisymmetry equations for conventional stellarators
|NIFS-324| p 1836 N95-23572
Electromagnetic production of pions on the nucleon
|DE95-004658| p 1811 N95-23587
SYNCHRONISM
Comparing data synchronization in Ada 9X and Orca
|PB95-127999| p 1754 N95-22529
Precise clock synchronization protocol
|PB95-127247| p 1687 N95-22536
Scalability of atomic primitives on distributed shared memory multiprocessors
|TR-528| p 1764 N95-23930
Scheduler-conscious synchronization
|TR-550| p 1765 N95-24183
SYNCHRONOUS PLATFORMS
Geolocation applications of the Gonets LEO messaging satellites p 1656 N95-22818
SYNCHROTRON RADIATION
Advanced growth and surface analysis system for in situ studies of interface formation
|DE95-002850| p 1838 N95-22555
A report on the Indiana University Workshop on future U.S. hadron facilities
|DE95-003951| p 1817 N95-23353
Multiband VLBI imaging of the jet in 3C 345
|PB95-139275| p 1866 N95-23468
Some thoughts of future experiments with the new generation of storage rings
|DE95-004602| p 1818 N95-24162
Atomic physics at high brilliance synchrotron sources: Proceedings
|DE95-006077| p 1813 N95-24174
SYNCHROTRONS
Preserving the high source brightness with x ray beam line optics
|DE95-003172| p 1820 N95-22877
Protein folding and protein metallocluster studies using synchrotron small angler x ray scattering
|DE95-003339| p 1746 N95-22897
SYNOPTIC MEASUREMENT
An intelligent ground operator support system p 1769 N95-23681
SYNTAX
LCM 3.0: A language for describing conceptual models. Syntax definition
|PB95-128005| p 1755 N95-22652
Graph isomorphism models for non interleaving process algebra
|PB95-110490| p 1786 N95-22714
Algebra of lines and boxes
|PB95-130456| p 1787 N95-22768
SYNTHESIS (CHEMISTRY)
Progress towards the synthesis of polymeric nitrogen
|DE94-017547| p 1841 N95-22860
Particle size dependence in Fischer-Tropsch synthesis
|DE95-003124| p 1633 N95-22876
Development of the IGT RENUGAS(reg sign) process
|DE94-017652| p 1727 N95-22888
Nanophase materials: Synthesis, properties, applications
|AD-A286013| p 1627 N95-22940
Ethanol synthesis and water gas shift over bifunctional sulfide catalysts
|DE94-017376| p 1634 N95-23202
Supported transition metal catalysts for para- to ortho-hydrogen conversion
|NASA-CR-197907| p 1634 N95-23252
Process for preparing an assembly of an article and a polyimide which resists dimensional change, delamination and debonding when exposed to changes in temperature
|NASA-CASE-LAR-14538-2| p 1649 N95-23254
Organometallic chemistry of bimetallic compounds
|DE95-004436| p 1634 N95-23345
SYNTHETIC APERTURE RADAR
Combining optical and microwave remote sensing data of forest vegetation: MAC Europe 1991
|PB95-127312| p 1717 N95-22538
Summaries of the 4th Annual JPL Airborne Geoscience Workshop. Volume 3: AIRSAR Workshop
|NASA-CR-197354-VOL-3| p 1712 N95-23938
Interferometric synthetic aperture radar imagery of the Gulf Stream p 1712 N95-23939
MAX-91: Polarimetric SAR results on Montespertoli site p 1712 N95-23940
AIRSAR views of aerolian terrain p 1713 N95-23941
Estimation of biophysical properties of upland Sitka spruce (Picea sitchensis) plantations p 1713 N95-23943
Forest investigations by polarimetric AIRSAR data in the Harz mountains p 1713 N95-23944
Comparison of inversion models using AIRSAR data for Death Valley, California p 1713 N95-23945
Geologic mapping using integrated AIRSAR, AVIRIS, and TIMS data p 1714 N95-23946
Statistics of multi-look AIRSAR imagery: A comparison of theory with measurements p 1714 N95-23947
AIRSAR deployment in Australia, September 1993: Management and objectives p 1714 N95-23948
Current and future use of TOPSAR digital topographic data for volcanological research p 1714 N95-23949
Preliminary analysis of the sensitivity of AIRSAR images to soil moisture variations p 1714 N95-23950
Unusual radar echoes from the Greenland ice sheet p 1714 N95-23951
Measurement of ocean wave spectra using polarimetric AIRSAR data p 1715 N95-23953
An improved algorithm for retrieval of snow wetness using C-band AIRSAR p 1715 N95-23954
SAR terrain classifier and mapper of biophysical attributes p 1715 N95-23957
Classification and soil moisture determination of agricultural fields p 1716 N95-23958
Relating P-band AIRSAR backscatter to forest stand parameters p 1716 N95-23959
Soil moisture retrieval in the Oberpfaffenhofen testsite using MAC Europe AIRSAR data p 1716 N95-23960
ASF archive issues: Current status, past history, and questions for the future p 1861 N95-24133
SYNTHETIC FUELS
Energy Conversion and Storage Program
|DE95-003796| p 1725 N95-22501
SYSTEM IDENTIFICATION
System identification of the Large-Angle Magnetic Suspension Test Fixture (LAMSTF) p 1617 N95-23299
SYSTEMS ANALYSIS
Southeast Regional Experiment Station
|DE95-000903| p 1726 N95-22518
Synthesis of a large communications aperture using small antennas
|NASA-CR-197330| p 1656 N95-22852
Life support systems analysis and technical trades for a lunar outpost
|NASA-TM-109927| p 1751 N95-23194
Integrating O/S models during conceptual design, part 1
|NASA-CR-197903| p 1622 N95-23398
The effects of AVIRIS atmospheric calibration methodology on identification and quantitative mapping of surface mineralogy, Drum Mountains, Utah p 1705 N95-23870
SYSTEMS ENGINEERING
Layered Electrical Product Application Protocol (AP)
|DE95-001524| p 1754 N95-22548
CDMS: CAD data set system design description
|DE95-003218| p 1756 N95-22894
Overview of Ph.D. theses and memoranda, 1993
|PB95-135190| p 1756 N95-23071
Inner loop flight control for the High-Speed Civil Transport p 1616 N95-23314
Multidisciplinary design optimization using genetic algorithms p 1619 N95-23332
Progress report on a fully automatic Gas Tungsten Arc Welding (GTAW) system development
|DE95-004397| p 1695 N95-23343
Radioisotope thermoelectric generator transportation system subsystem 143 software development plan
|DE95-003774| p 1662 N95-23351
Integrating O/S models during conceptual design, part 1
|NASA-CR-197903| p 1622 N95-23398
Aerodynamic design and analysis of a highly loaded turbine exhaust p 1673 N95-23435
An operations and command systems for the extreme ultraviolet explorer p 1770 N95-23687
Full resolution hologram-like autostereoscopic display
|NASA-CR-197913| p 1689 N95-23789
Search Hanford accessible reports electronically system configuration management plan
|DE95-004493| p 1857 N95-24089
OPUS: A new generation Knowledge Engineering Environment p 1760 N95-24176
SYSTEMS INTEGRATION
Automation technology using Geographic Information System (GIS) p 1863 N95-23284
Differential GPS and system integration of the Low Visibility Landing and Surface Operations (LVLASO) demonstration p 1611 N95-23318
Network Event Recording Device: An automated system for network anomaly detection, and notification
|DE94-018274| p 1658 N95-23772
Automated solar cell assembly teamed process research
|DE95-000299| p 1730 N95-23777
The design of a petabyte archive and distribution system for the NASA ECS project p 1858 N95-24110
SYSTEMS MANAGEMENT
Environmental Systems Management Analysis and Reporting Network (E-SMART)
|AD-A279766| p 1732 N95-22856
Distributed VIRtual System (DIVIRS) project
|NASA-CR-197855| p 1757 N95-23180
SYSTEMS STABILITY
D3-D program overview
|DE95-003879| p 1837 N95-24086
Experimental achievement of toroidal beta beyond that predicted by 'Troyon' scaling
|DE95-003880| p 1837 N95-24087

T

TABS (CONTROL SURFACES)
Lift enhancing tabs for airfoils
|NASA-CASE-ARC-11990-1| p 1613 N95-23395

TACHYONS
Tachyons - it was the end of history?
|DE94-635439| p 1851 N95-23968
TACTILE SENSORS (ROBOTICS)
Very fast motion planning for highly dexterous-articulated robots p 1771 N95-23691
A perspective on space robotics in Japan p 1697 N95-23695
Vision-based planning and execution of precision grasps
|TR-546| p 1784 N95-24185
TAIL ASSEMBLIES
Preliminary identification of buffet problems in high speed civil transport p 1616 N95-23319
TAKEOFF
Aircraft accident report. Runway overrun following rejected takeoff. Continental airlines flight 795, McDonnell Douglas MD-82, N18835, LaGuardia Airport, Flushing, NY, 2 March 1994
|PB95-910401| p 1610 N95-23609
TANGENTS
Grassman and hyperKaehler structures on some spaces of sections of holomorphic bundles
|PB95-109104| p 1795 N95-22712
TANTALUM ALLOYS
Experimental and theoretical studies on the C15 intermetallic compounds MV2 (M = Zr, Hf and Ta): Elasticity and phase stability
|DE95-003723| p 1845 N95-24079
TAPE RECORDERS
High data rate recorder development at MIT Haystack Observatory p 1690 N95-24118
A comparison of rotary- and stationary-head tape recorders p 1690 N95-24122
A terabyte linear tape recorder p 1690 N95-24139
TAPERING
The use of cowl camber and taper to reduce rotor/stator interaction noise
|NASA-CR-195421| p 1799 N95-22675
TARGET ACQUISITION
Discrimination of poorly exposed lithologies in AVIRIS data p 1703 N95-23858
TARGETS
Light emission-or-absorbance-based binding assays for polynucleic acids
|AD-D016557| p 1632 N95-22710
Projectile penetration into representative targets
|DE95-003089| p 1698 N95-22726
CO2 and waste policy: Monitoring results 1991/1992 and main problems
|PB95-133799| p 1733 N95-23126
TASK PLANNING (ROBOTICS)
Software agents for the dissemination of remote terrestrial sensing data p 1721 N95-23675
TASKS
Integrating planning and reactive control p 1618 N95-23763
Using simulation-based projection to plan in an uncertain and temporally complex world
|TR-531| p 1853 N95-24043
TATB
Simulation of cookoff results in a small scale test
|DSTO-TR-0090| p 1653 N95-23668
TAXONOMY
Taxonomy of finite automata minimization algorithms
|PB95-139226| p 1756 N95-23131
Taxonomy of finite automata construction algorithms
|PB95-139234| p 1758 N95-23606
TAYLOR SERIES
Accelerated panel methods using the fast multipole method p 1687 N95-23307
Non-Taylor magnetohydrodynamic self-organization
|NIFS-314| p 1834 N95-23524
Taylor series expansion and modified extended Prony analysis for localization
|DE95-003671| p 1758 N95-23567
TDR SATELLITES
Improved small satellite access of the space network
|NASA-CR-197863| p 1657 N95-22944
TEACHING MACHINES
POINTER: Portable Intelligent Trainer for External Robotics p 1752 N95-23714
TEAMS
Teams and teamwork at NASA Langley Research Center p 1854 N95-23292
TEARING
Three-dimensional CTOA and constraint effects during stable tearing in a thin-sheet material
|NASA-TM-109183| p 1627 N95-22928
TECHNETIUM
EXTRA.M: A computing code system for analysis of the Purex process with mixer settlers for reprocessing
|DE94-785273| p 1635 N95-23476
TECHNOLOGY ASSESSMENT
Evaluating photovoltaic applications: A guide for utilities
|DE95-003807| p 1726 N95-22502
NASA Technology Applications Team: Commercial applications of aerospace technology
|NASA-CR-197589| p 1864 N95-22526
Euler Technology Assessment program for preliminary aircraft design employing SPLITFLOW code with Cartesian unstructured grid method
|NASA-CR-4649| p 1608 N95-22917
NASA Technology Applications Team: Commercial applications of aerospace technology
|NASA-CR-197870| p 1865 N95-23091
Euler technology assessment for preliminary aircraft design employing OVERFLOW code with multiblock structured-grid method
|NASA-CR-4651| p 1608 N95-23095
NASA advanced refrigerator/freezer technology development project overview
|NASA-TM-106309| p 1747 N95-23177
Spin physics in the next decade
|DE95-003727| p 1809 N95-23403
Motor drive technologies for the power-by-wire (PBW) program: Options, trends and tradeoffs
|NASA-TM-106885| p 1616 N95-23671
Robotics and telepresence for moon missions p 1776 N95-23725
Advanced technologies for a compact RF linac FEL
|DE95-003674| p 1692 N95-24072
Report to the Secretary of Defense. Unmanned aerial vehicles: No more Hunter systems should be bought until problems are fixed
|GAO/NSIAD-95-52| p 1613 N95-24091
Crystalline-silicon photovoltaics: Necessary and sufficient
|DE95-004540| p 1731 N95-24157
TECHNOLOGY TRANSFER
Southeast Regional Experiment Station
|DE95-000903| p 1726 N95-22518
Accuracy of radar rainfall estimates compared to raingauge measurements and a hydrological application
|PB95-127296| p 1741 N95-22640
Technology reinvestment project's focus area: Affordable polymer matrix composites for airframe structures
|PB95-136032| p 1865 N95-23168
Teacher Enhancement Institute p 1853 N95-23312
Planetary stations and Abyssal Benthic Laboratories: An overview of parallel approaches for long-term investigation in extreme environments p 1752 N95-23732
Research and Technology, 1994
|NASA-TM-106764| p 1607 N95-24025
Defense science and technology strategy
|AD-A285414| p 1903 N95-24179
TECHNOLOGY UTILIZATION
Innovative technology for contamination control in plasma processing
|DE95-000913| p 1829 N95-22519
NASA Technology Applications Team: Commercial applications of aerospace technology
|NASA-CR-197589| p 1864 N95-22526
Technology maturation project on optimization of sheet metal forming of aluminum for use in transportation systems
|DE95-003005| p 1654 N95-22692
Addendum to the Proceedings of the Third International Mobile Satellite Conference (IMSC 1993)
|NASA-CR-197343| p 1655 N95-22813
NASA Technology Applications Team: Commercial applications of aerospace technology
|NASA-CR-197870| p 1865 N95-23091
Corrosion control acceptance criteria for sacrificial anode type, cathodic protection systems (user guide)
|AD-A285275| p 1662 N95-23117
The US molten carbonate fuel-cell development and commercialization effort
|DE94-019096| p 1728 N95-23162
Technology reinvestment project's focus area: Affordable polymer matrix composites for airframe structures
|PB95-136032| p 1865 N95-23168
Teacher Enhancement Institute p 1853 N95-23312
Potential aerospace applications of high temperature superconductors p 1664 N95-23322
Teacher Enhancement Institute p 1853 N95-23324
Hydrogen and fuel cells for energy storage
|DE95-723907| p 1729 N95-23382
Endeavor: Now and then
|NASA-TM-110539| p 1620 N95-23664
Third International Symposium on Artificial Intelligence, Robotics, and Automation for Space 1994
|NASA-CR-197340| p 1767 N95-23672
The next decade of space robotics p 1768 N95-23673
Proceedings of the fuel cells 1994 contractors review meeting
|DE94-012285| p 1730 N95-23977
OPUS: A new generation Knowledge Engineering Environment p 1760 N95-24176
Defense science and technology strategy
|AD-A285414| p 1903 N95-24179
TECTONICS
Seismic hazards at Kilauea and Mauna Loa volcanoes, Hawaii
|DE94-012109| p 1737 N95-22924
TEFLON (TRADEMARK)
Cratering and penetration experiments in Teflon targets at velocities from 1 to 7 km/s p 1700 N95-23842
Recent results from Long Duration Exposure Facility materials testing p 1638 N95-23898
LDEF polymeric materials: A summary of Langley characterization p 1651 N95-23899
TELECOMMUNICATION
Synthesis of a large communications aperture using small antennas
|NASA-CR-197330| p 1656 N95-22852
Effects of modulation index on telecommunications
|AD-A286018| p 1657 N95-23023
Algebraic semantics of basic message sequence charts
|PB95-138970| p 1657 N95-23151
TELEMETRY
Improved small satellite access of the space network
|NASA-CR-197863| p 1657 N95-22944
Toward an automated signature recognition toolkit for mission operations p 1659 N95-23682
TELEOPERATORS
An intelligent ground operator support system p 1769 N95-23681
Subsumption-based architecture for autonomous movement planning for planetary rovers p 1771 N95-23690
Very fast motion planning for highly dexterous-articulated robots p 1771 N95-23691
Lunar rover technology demonstrations with Dante and Ratler p 1697 N95-23694
A perspective on space robotics in Japan p 1697 N95-23695
ASI's space automation and robotics programs: The second step p 1697 N95-23696
JPL space robotics: Present accomplishments and future thrusts p 1697 N95-23697
Robotic experiment with a force reflecting handcontroller onboard MIR space station p 1752 N95-23707
Design of teleoperation system with a force-reflecting real-time simulator p 1778 N95-23733
Telepresence control of a dual-arm dexterous robot p 1752 N95-23735
Terrain modelling and motion planning for an autonomous exploration rover p 1721 N95-23765
TELEROBOTICS
The next decade of space robotics p 1768 N95-23673
Commercialization of JPL Virtual Reality calibration and redundant manipulator control technologies p 1768 N95-23676
JPL space robotics: Present accomplishments and future thrusts p 1697 N95-23697
A US-Japan collaborative robotics research program p 1772 N95-23698
The Charlotte (TM) intra-vehicular robot p 1697 N95-23703
Development of Advanced Robotic Hand System for space application p 1752 N95-23704
POINTER: Portable Intelligent Trainer for External Robotics p 1752 N95-23714
Space science experimentation automation and support p 1775 N95-23718
Dexterous Orbital Servicing System (DOSS) p 1752 N95-23723
Truss structure tele-manipulation experiment using ETS-7 p 1623 N95-23726
Antenna-assembling mechanism test on ETS-7 p 1623 N95-23727
Intelligent monitoring system applied to super long distance telerobotic tasks p 1777 N95-23728
Manipulating flexible parts using a teleoperated system with time delay: An experiment p 1777 N95-23729
Visually guided grasping to study teleprogrammation within the BAROCO testbed p 1777 N95-23731
Telerobotics test bed for space structure assembly p 1618 N95-23734
Telepresence control of a dual-arm dexterous robot p 1752 N95-23735
Morphing hands and virtual tools (or What good is an extra degree of freedom?)
|TR-551| p 1783 N95-24036
TELESCOPES
Interstellar molecules in the large magellanic cloud
|PB95-139267| p 1868 N95-23230

Robust telescope scheduling p 1779 N95-23742
The associate principal astronomer telescope operations model p 1779 N95-23743
Telescope loading: A problem reduction approach p 1781 N95-23757
Near infrared and optical spectroscopy of FSC10214+4724
| NASA-CR-197966 | p 1828 N95-24068

TELEVISION CAMERAS
Amplified MOS Imager
| NHK-LABS-NOTE-432 | p 1690 N95-24107

TELLURIUM
Precise determinations of the isotopic compositions and atomic weights of molybdenum, tellurium, tin and tungsten using ICP source magnetic sector multiple collector mass spectrometry
| DE95-003003 | p 1632 N95-22795

TEMPERATURE CONTROL
Protective coating for ceramic materials
| NASA-CASE-ARC-11969-1-CU | p 1649 N95-23394

TEMPERATURE DEPENDENCE
Surface impedance studies on the electrodynamical response of organic superconductors
| DE95-002986 | p 1660 N95-22593
Enhancement of biomembrane functions under phase-separated conditions: A self-organized criticality phenomenon?
| DE94-628489 | p 1747 N95-23053
Non-intrusive measurements in a rocket engine combustor p 1625 N95-23439
Simulation of cookoff results in a small scale test
| DSTO-TR-0090 | p 1653 N95-23668
The effect of elastic stress on Ostwald Ripening Phenomena
| DE95-002599 | p 1646 N95-24140

TEMPERATURE DISTRIBUTION
Associated with aerospace vehicles development of methodologies for the estimation of thermal properties p 1700 N95-23321
Computer modeling of the sensitivity of a laser water vapor sensor to variations in temperature and air speed p 1692 N95-23330

TEMPERATURE EFFECTS
Temperature effects on hydrogen-induced cracking in an iron-based superalloy
| DE95-003037 | p 1639 N95-22724
Long-term aging of type 308 stainless steel welds: Effects on properties and microstructure
| DE94-018961 | p 1640 N95-23132
Liquid nitrogen temperature operation of a switching power converter
| NASA-TM-106867 | p 1662 N95-23219
Process for preparing an assembly of an article and a polyimide which resists dimensional change, delamination and debonding when exposed to changes in temperature
| NASA-CASE-LAR-14538-2 | p 1649 N95-23254
Method development for compensating temperature effects in pressure sensitive paint measurements p 1650 N95-23291
NLS base heating CFD analysis p 1673 N95-23432
A coupled layerwise analysis of the thermopiezoelectric response of smart composite beams beams
| NASA-TM-106889 | p 1630 N95-23463
Rapid thermal processing of high-efficiency silicon solar cells with controlled in-situ annealing
| DE95-004729 | p 1730 N95-23489
Thermal effects on the STAR electromagnetic calorimeter
| DE95-004663 | p 1688 N95-23492
Thermal modeling of the lithium/polymer battery
| DE95-004680 | p 1663 N95-23494
Thermoelastic theory for the response of materials functionally graded in two directions with applications to the free-edge problem
| NASA-TM-106882 | p 1699 N95-24055
Temperature effects on ion irradiation damage in MgAl2O4 spinel single crystals
| DE95-003679 | p 1844 N95-24073
Effects of Bi and Bi2O3 additions on the microstructure and superconducting properties of powder-in-tube BSCCO (2212) tapes
| DE95-004605 | p 1845 N95-24150
Design of a high-temperature superconductor current lead for electric utility SMES
| DE95-004604 | p 1664 N95-24163

TEMPERATURE GRADIENTS
Superlattices in thermoelectric applications
| DE95-001356 | p 1840 N95-22687
Numerical Tokamak Project code comparison
| DE95-003475 | p 1831 N95-22899
Design and production of efficient current leads for 1500-A, 50-Hz service in a 77-4 K temperature gradient
| DE95-004121 | p 1662 N95-23355

TEMPERATURE MEASUREMENT
Land surface temperature measurements for EOS MODIS data
| NASA-CR-197443 | p 1717 N95-23191
Instantaneous 2D velocity and temperature measurements in high speed flows based on spectrally resolved molecular Rayleigh scattering
| NASA-TM-106883 | p 1688 N95-23461
Validation data for land surface temperature determination from satellites
| CSIRO-TR-33 | p 1718 N95-23597
Development of sensors for ceramic components in advanced propulsion systems
| NASA-CR-195324 | p 1689 N95-23795
Land surface temperature measurements from EOS MODIS data
| NASA-CR-197969 | p 1721 N95-24190

TEMPERATURE PROFILES
Land surface temperature measurements for EOS MODIS data
| NASA-CR-197443 | p 1717 N95-23191

TEMPERATURE SENSORS
Computer modeling of the sensitivity of a laser water vapor sensor to variations in temperature and air speed p 1692 N95-23330

TEMPORAL DISTRIBUTION
Light-traffic analysis for queues with spatially distributed arrivals
| PB95-140802 | p 1767 N95-23556
Reevaluation of the significance of sequence information for speech recognition
| TR-555 | p 1658 N95-23794

TEMPORAL LOGIC
Temporal model theory for default logic
| PB95-127346 | p 1766 N95-22524
Temporal operators viewed as predicate transformers
| PB95-138996 | p 1757 N95-23152

TEMPORAL RESOLUTION
Temporal changes in endmember abundances, liquid water and water vapor over vegetation at Jasper Ridge p 1708 N95-23882

TENSILE CREEP
Thermal activation of steady-state creep in polycrystalline copper
| DE94-627394 | p 1839 N95-22607
Evolution of oxidation and creep damage mechanisms in HIPed silicon nitride materials
| DE95-001360 | p 1647 N95-22689

TENSILE DEFORMATION
An investigation into the effects of hydrogen on the fracture and deformation of Alloy X-750
| DE95-003206 | p 1639 N95-22732

TENSILE PROPERTIES
Long-term aging of type 308 stainless steel welds: Effects on properties and microstructure
| DE94-018961 | p 1640 N95-23132

TENSILE STRENGTH
Review of some results of the author's fatigue investigations with applications in engineering and material science
| TAE-698 | p 1699 N95-23662

TENSILE TESTS
Study of radiation damages in AISI 316 and 347 steels
| DE94-627480 | p 1639 N95-22609
An investigation into the effects of hydrogen on the fracture and deformation of Alloy X-750
| DE95-003206 | p 1639 N95-22732

TENSORS
Grassman and hyperKaehler structures on some spaces of sections of holomorphic bundles
| PB95-109104 | p 1795 N95-22712

TERMINAL BALLISTICS
Projectile penetration into representative targets
| DE95-003089 | p 1698 N95-22726

TERMINOLOGY
Glass science tutorial: Lecture 1, Chemistry and properties of oxide glasses
| DE95-002963 | p 1647 N95-22647
NASA Thesaurus, Supplement
| NASA-SP-7096-SUPPL-1 | p 1856 N95-23223

TERNARY ALLOYS
The effect of elastic stress on Ostwald Ripening Phenomena
| DE95-002599 | p 1646 N95-24140
High resolution microstructural analysis of zirconia eutectic interfaces
| DE95-003143 | p 1845 N95-24143

TERRAIN
Robotic all-terrain lunar exploration rover (RATLER) FY93 program status report
| DE95-003589 | p 1694 N95-23065
SAR terrain classifier and mapper of biophysical attributes p 1715 N95-23957
Measuring forest landscape patterns in the Cascade Range of Oregon, USA p 1719 N95-24096

TERRAIN ANALYSIS
Path planning for planetary rover using extended elevation map p 1771 N95-23689
Control technique for planetary rover p 1771 N95-23692
Autonomous navigation system for the Marsokhod rover project p 1771 N95-23693
Terrain modelling and motion planning for an autonomous exploration rover p 1721 N95-23765
Comparison of inversion models using AIRSAR data for Death Valley, California p 1713 N95-23945

TERRAIN FOLLOWING
Path planning for planetary rover using extended elevation map p 1771 N95-23689
Control technique for planetary rover p 1771 N95-23692
Lunar rover technology demonstrations with Dante and Ratler p 1697 N95-23694
Terrain modelling and motion planning for an autonomous exploration rover p 1721 N95-23765

TERRESTRIAL PLANETS
Software agents for the dissemination of remote terrestrial sensing data p 1721 N95-23675

TEST CHAMBERS
Design of a variable area diffuser for a 15-inch Mach 6 open-jet tunnel p 1617 N95-23309

TEST FACILITIES
NASA low-speed axial compressor for fundamental research
| NASA-TM-4635 | p 1616 N95-23192
System identification of the Large-Angle Magnetic Suspension Test Fixture (LAMSTF) p 1617 N95-23299
Detailed measurements in the SSME high pressure fuel turbine with smooth rotor blades p 1675 N95-23441
The influence of swirl brakes and a tip discharge orifice on the rotordynamic forces generated by discharge-to-suction leakage flows in shrouded centrifugal pumps p 1680 N95-23628
NASA procurement: Contract and management improvements at the Jet Propulsion Laboratory. Report to Congressional requesters
| GAO/NSIAD-95-40 | p 1854 N95-24054

TEST FIRING
Non-intrusive measurements in a rocket engine combustor p 1625 N95-23439

TEST STANDS
Non-intrusive measurements in a rocket engine combustor p 1625 N95-23439
Development of the dynamic motion simulator of 3D micro-gravity with a combined passive/active suspension system p 1618 N95-23711
Telerobotics test bed for space structure assembly p 1618 N95-23734
Using simple page placement policies to reduce the cost of cache fills in coherent shared-memory systems
| TR-535 | p 1753 N95-24177

TEXAS
Energy flux and hydrogeology of thermal anomalies in the Gulf of Mexico Basin - South Texas example
| DE95-003341 | p 1743 N95-22695

TEXTBOOKS
Teaching computational complexity: Resources to treasure
| TR-543 | p 1784 N95-24060

TEXTILES
Development and verification of a resin film infusion/resin transfer molding simulation model for fabrication of advanced textile composites
| NASA-CR-197439 | p 1648 N95-23179
Fabric geometry distortion during composites processing p 1631 N95-23288

TEXTS
Plinius intermediate report
| PB95-135216 | p 1648 N95-23128
Performance of single-keyword and multiple-keyword pattern matching algorithms
| PB95-138954 | p 1756 N95-23150

TEXTURES
Experience with CANDID: Comparison algorithm for navigating digital image databases
| DE95-000869 | p 1855 N95-22515
Mapping of the Ronda peridotite massif (Spain) from AVIRIS spectro-imaging survey: A first attempt p 1707 N95-23878

THALLIUM
Superconducting Tl2Ba2CaCu2O8 thin films prepared by post-annealing in a flow-through multiple-zone furnace
| DE95-002745 | p 1838 N95-22520

THALLIUM COMPOUNDS
Transport properties of Tl2Ba2CaCu2O8 meander lines
| DE95-003715 | p 1843 N95-23367

THEMATIC MAPPERS (LANDSAT)
Simulation of landsat thematic mapper imagery using AVIRIS hyperspectral imagery p 1705 N95-23869
A preliminary comparison of Landsat Thematic Mapper and SPOT-1 HRV multispectral data for estimating coniferous forest volume p 1719 N95-24097
THEMATIC MAPPING
Lithologic discrimination and alteration mapping from AVIRIS Data, Socorro, New Mexico p 1701 N95-23847
Simulation of landsat thematic mapper imagery using AVIRIS hyperspectral imagery p 1705 N95-23869
AVIRIS and TIMS data processing and distribution at the land processes distributed active archive center p 1706 N95-23872
Mapping and monitoring changes in vegetation communities of Jasper Ridge, CA, using spectral fractions derived from AVIRIS images p 1708 N95-23883
Application of MAC-Europe AVIRIS data to the analysis of various alteration stages in the Landdmannalauger Hydrothermal Area (South Iceland) p 1709 N95-23885
Measuring forest landscape patterns in the Cascade Range of Oregon, USA p 1719 N95-24096
A preliminary comparison of Landsat Thematic Mapper and SPOT-1 HRV multispectral data for estimating coniferous forest volume p 1719 N95-24097
Forest and wildlife habitat analysis using remote sensing and geographic information systems p 1720 N95-24100
Analysis of conifer forest regeneration using Landsat Thematic Mapper data p 1720 N95-24101
Determining successional stage of temperate coniferous forests with Landsat satellite data p 1720 N95-24102
Determining coniferous forest cover and forest fragmentation with NOAA-9 advanced very high resolution radiometer data p 1720 N95-24103
THEODORSEN TRANSFORMATION
Flutter analysis of composite box beams
|NASA-CR-197931| p 1615 N95-23392
THEOREM PROVING
Semi-symmetric manifolds satisfying certain curvature conditions
|DE94-628414| p 1788 N95-22922
Optimal advice
|TR-527| p 1792 N95-23931
A theory for the morphology of Laplacian growth from statistics of equivalent many-body Hamiltonian systems
|DE94-014473| p 1799 N95-23979
Reducibility classes of P-selective sets
|TR-524| p 1792 N95-24002
Large sets in AC(exp 0): A Kolmogorov complexity related property and some applications
|TR-556| p 1797 N95-24029
On the size of sets with weak membership properties
|TR-557| p 1793 N95-24034
Semi-membership algorithms: Some recent advances
|TR-526| p 1760 N95-24092
Polynomial-time membership comparable sets
|TR-552| p 1793 N95-24182
THEOREMS
Countable space with a closed subspace without continuous extender
|PB95-127973| p 1785 N95-22533
Lectures on Fermat's last theorem
|DE94-628392| p 1795 N95-22617
Effective category and measure in abstract complexity theory
|TR-529| p 1792 N95-23929
Optimal advice
|TR-527| p 1792 N95-23931
On helping by parity-like languages
|TR-553| p 1759 N95-23935
Reducibility classes of P-selective sets
|TR-524| p 1792 N95-24002
Witness-isomorphic reductions and the local search problem
|TR-522| p 1793 N95-24003
Semi-membership algorithms: Some recent advances
|TR-526| p 1760 N95-24092
THEORETICAL PHYSICS
The charm physics potential of a Tau-Charm Factory
|DE95-003369| p 1802 N95-22703
Nahm's product and W-algebra
|DE94-628504| p 1787 N95-22777
THEORIES
Ploxoma: Testbed for uncertain inference
|TR-537| p 1794 N95-23927
THERAPY
Continuation of BNCT Research Program at NEMC and MIT
|DE94-016228| p 1748 N95-22875
THERMAL ANALYSIS
Initial crystallization and growth in melt processing of large-domain YBa2Cu3O(x) for magnetic levitation
|DE95-002993| p 1839 N95-22572
Using the shield for thermal energy storage in PULSAR
|DE95-002457| p 1829 N95-22645
Design of a high-temperature superconductor current lead for electric utility SMES
|DE95-004604| p 1664 N95-24163
THERMAL BATTERIES
Thermal modeling of the lithium/polymer battery
|DE95-004680| p 1663 N95-23494
THERMAL CONDUCTIVITY
Superlattices in thermoelectric applications
|DE95-001356| p 1840 N95-22687
Associated with aerospace vehicles development of methodologies for the estimation of thermal properties p 1700 N95-23321
Design and production of efficient current leads for 1500-A, 50-Hz service in a 77-4 K temperature gradient
|DE95-004121| p 1662 N95-23355
Progress report on conductive paints, September 1, 1994-November 30, 1994
|DE95-004297| p 1649 N95-23356
Thermal modeling of the lithium/polymer battery
|DE95-004680| p 1663 N95-23494
Micro heat spreader enhanced heat transfer in MCM's
|DE95-004520| p 1663 N95-23779
THERMAL CONTROL COATINGS
Low Earth orbit thermal control coatings exposure flight tests: A comparison of U.S. and Russian results
|NASA-CR-4647| p 1626 N95-22919
Evaluation of thermal barrier and PS-200 self-lubricating coatings in an air-cooled rotary engine
|NASA-CR-195445| p 1614 N95-23222
Recent results from Long Duration Exposure Facility materials testing p 1638 N95-23898
Further investigations of experiment A0034 atomic oxygen stimulated outgassing p 1651 N95-23908
Trend analysis of in-situ spectral reflectance data from the Thermal Control Surfaces Experiment (TCSE) p 1631 N95-23910
Whisker/Cone growth on the thermal control surfaces experiment no. S0069 p 1651 N95-23911
THERMAL CYCLING TESTS
Permeability testing of composite material and adhesive bonds for the DC-XA composite feedline program
|NASA-TM-108483| p 1630 N95-23551
THERMAL DECOMPOSITION
Decomposition mechanisms in thermally-aged thin-film explosives
|DE95-000741| p 1652 N95-22838
THERMAL DEGRADATION
Test procedure for cation exchange chromatography
|DE95-003770| p 1808 N95-23350
THERMAL DIFFUSION
Silicon surface and bulk defect passivation by low temperature PECVD oxides and nitrides
|DE95-004531| p 1731 N95-24090
THERMAL DIFFUSIVITY
Tritium transport, influx, and helium ash measurements on TFTR during DT operation
|DE95-003708| p 1833 N95-23269
THERMAL EMISSION
Plasma properties and magnetic field structure of the solar corona, based on coordinated Max 1991 observations from SERTS, the VLA, and magnetographs
|NASA-CR-197864| p 1870 N95-23181
AVIRIS and TIMS data processing and distribution at the land processes distributed active archive center p 1706 N95-23872
Summaries of the 4th Annual JPL Airborne Geoscience Workshop. Volume 2: TIMS Workshop
|NASA-CR-197876-VOL-2| p 1711 N95-23917
Estimation of spectral emissivity in the thermal infrared p 1711 N95-23918
The difference between laboratory and in-situ pixel-averaged emissivity: The effects on temperature-emissivity separation p 1711 N95-23919
Mineralogic variability of the Kelso Dunes, Mojave Desert, California derived from Thermal Infrared Multispectral Scanner (TIMS) data p 1711 N95-23920
THERMAL ENERGY
Using the shield for thermal energy storage in PULSAR
|DE95-002457| p 1829 N95-22645
Atomic oxygen textured polymers
|NASA-TM-106769| p 1650 N95-24187
THERMAL EXPANSION
Transformation behavior in Al2O3-ZrO2 ceraamic composites
|DE95-001359| p 1647 N95-22688
Process for preparing an assembly of an article and a polyimide which resists dimensional change, delamination and debonding when exposed to changes in temperature
|NASA-CASE-LAR-14538-2| p 1649 N95-23254
Structure and properties of polymeric composite materials during 1501 days outer space exposure at Salyut-7 orbital station p 1652 N95-23915
THERMAL INSTABILITY
Influence of porosity and two-phase flow on diffusional/thermal instability of a deflagrating energetic material
|DE95-002592| p 1634 N95-23122
THERMAL INSULATION
Performance of thin-ceramic-coated combustion chamber with gasoline and methanol as fuels in a two-stroke SI engine
|DE95-002903| p 1693 N95-22557
THERMAL MAPPING
Combining optical and microwave remote sensing data of forest vegetation: MAC Europe 1991
|PB95-127312| p 1717 N95-22538
THERMAL NEUTRONS
Mercury detection with thermal neutrons
|DE95-002061| p 1806 N95-23055
THERMAL PLASMAS
Conversion of light hydrocarbon gases to metal carbides for production of liquid fuels and chemicals
|DE95-000362| p 1634 N95-23164
Atomic oxygen durability evaluation of protected polymers using thermal energy plasma systems
|NASA-TM-106855| p 1626 N95-23270
THERMAL PROTECTION
Robotic system for the servicing of the orbiter thermal protection system p 1697 N95-23724
Outgassing products from orbiter TPS materials p 1637 N95-23798
THERMAL RADIATION
Land surface temperature measurements for EOS MODIS data
|NASA-CR-197443| p 1717 N95-23191
Design of a differential radiometer for atmospheric radiative flux measurements
|DE95-002701| p 1739 N95-23244
The difference between laboratory and in-situ pixel-averaged emissivity: The effects on temperature-emissivity separation p 1711 N95-23919
THERMAL REACTORS
Conversion of light hydrocarbon gases to metal carbides for production of liquid fuels and chemicals
|DE95-000362| p 1634 N95-23164
THERMAL STABILITY
Hydrogen vibrational density of states of adsorbed water on rare-earth modified zirconia
|DE95-001127| p 1632 N95-22681
THERMAL STRESSES
Thermal activation of steady-state creep in polycrystalline copper
|DE94-627394| p 1839 N95-22607
Associated with aerospace vehicles development of methodologies for the estimation of thermal properties p 1700 N95-23321
Automated solar cell assembly teamed process research
|DE95-000299| p 1730 N95-23777
THERMIONIC CONVERTERS
Surface structural dependence of cesium adsorption on the (alpha)-Al2O3(0001) surface
|DE95-002610| p 1842 N95-23135
THERMOCHEMISTRY
Energy Conversion and Storage Program
|DE95-003796| p 1725 N95-22501
Thermochemistry of transition metal clusters
|DE95-003144| p 1646 N95-24144
THERMODYNAMIC EQUILIBRIUM
(Phi)(sup 4) kinks: Statistical mechanics
|DE95-003693| p 1794 N95-23349
Current status in cavitation modeling p 1681 N95-23632
THERMODYNAMIC PROPERTIES
Finite-temperature scalar field theory in static de Sitter space
|DE94-628522| p 1848 N95-22743
Heat transfer in rocket engine combustion chambers and nozzles p 1668 N95-23413
Thermochemistry of transition metal clusters
|DE95-003144| p 1646 N95-24144
Microporous polyimide films for reduced dielectric applications
|DE95-004543| p 1650 N95-24159
THERMODYNAMICS
Energy Conversion and Storage Program
|DE95-003796| p 1725 N95-22501
Glass science tutorial: Lecture 2, operating electric glass melters
|DE95-002965| p 1647 N95-22648
The role of triplet correlation function in dense fluids
|DE94-628476| p 1849 N95-22775
Cumulant approach to dynamical correlation functions at finite temperatures
|DE94-628487| p 1788 N95-23051

Multi-fuel reformers for fuel cells used in transportation. Phase 1: Multi-fuel reformers
| DE95-004215 | p 1729 N95-23482

THERMOELASTICITY
Thermoelastic theory for the response of materials functionally graded in two directions with applications to the free-edge problem
| NASA-TM-106882 | p 1699 N95-24055

THERMOELECTRIC GENERATORS
Radioisotope thermoelectric generator licensed hardware package and certification tests
| DE95-003039 | p 1661 N95-22799
Radioisotope thermoelectric generator transportation system subsystem 143 software development plan
| DE95-003774 | p 1662 N95-23351

THERMOELECTRIC POWER GENERATION
Computational modeling of properties
| NAS-CR-196544 | p 1841 N95-22907

THERMOELECTRICITY
Superlattices in thermoelectric applications
| DE95-001356 | p 1840 N95-22687
Computational modeling of properties
| NAS-CR-196544 | p 1841 N95-22907

THERMOLUMINESCENCE
Dosimetric results on EURECA p 1872 N95-23800

THERMOPLASTIC RESINS
Chemical recycling of scrap composites p 1629 N95-23034

THERMOPLASTICITY
Tough, soluble, aromatic, thermoplastic copolyimides
| NASA-CASE-LAR-15205-1 | p 1648 N95-22882
Society of the plastic industry process emission initiatives p 1629 N95-23036

THERMOSPHERE
Continued studies of polar cap thermospheric dynamics
| PL-TR-94-2076 | p 1737 N95-22951
Calculation of satellite drag coefficients
| AD-A285118 | p 1622 N95-23781

THESAURI
NASA Thesaurus, Supplement
| NASA-SP-7096-SUPPL-1 | p 1856 N95-23223

THESES
Overview of Ph.D. theses and memoranda, 1993
| PB95-135190 | p 1756 N95-23071

THICK FILMS
Preparation of high quality YBa2Cu3O(7-delta) thick films on flexible Ni-based alloy substrates with textured buffer layers
| DE95-003686 | p 1645 N95-23571

THICKNESS
Investigation of arc length versus flange thickness while using an arc voltage controller
| DE95-003937 | p 1695 N95-23374

THIN FILMS
Southeast Regional Experiment Station
| DE95-000903 | p 1726 N95-22518
Superconducting Tl2Ba2CaCu2O8 thin films prepared by post-annealing in a flow-through multiple-zone furnace
| DE95-002745 | p 1838 N95-22520
Vacuum vapor deposition
| NASA-CASE-MFS-28652-1 | p 1647 N95-22558
MOCVD of gallium and calcium sulfides for improved phosphor processing
| DE95-000918 | p 1631 N95-22677
Decomposition mechanisms in thermally-aged thin-film explosives
| DE95-000741 | p 1652 N95-22838
Polycrystalline CuInSe2 and CdTePV solar cells
| DE95-000244 | p 1727 N95-22842
The 1993 Annual Conference of the Israeli Association for Crystal Growth. Program and abstracts
| DE94-633510 | p 1841 N95-22854
Micro-sensor thin-film anemometer
| NASA-CASE-LAR-15112-1-CU | p 1666 N95-22906
Orientation selection and microstructural evolution of epitaxial platinum films on (001) magnesium oxide
| DE95-003680 | p 1842 N95-23265
Vapor deposition of thin-film Y-doped ZrO2 for electrochemical device applications
| DE95-003705 | p 1649 N95-23268
Electrochemical studies of perovskite mixed conductors
| DE95-003704 | p 1636 N95-23573
Advances in research for solid oxide fuel cells
| DE95-004590 | p 1730 N95-23582
Nonlinear viscoelastic characterization of polymer materials using a dynamic-mechanical methodology p 1651 N95-23902
Measurements of the optical properties of thin films of silver and silver oxide p 1651 N95-23906
Changes in chemical and optical properties of thin film metal mirrors on LDEF p 1651 N95-23907

THIN WINGS
Thin tailored composite wing for civil tiltrotor p 1613 N95-23317

THREE BODY PROBLEM
The point interactions in the quantum problem of three particles with internal structure
| DE94-635423 | p 1851 N95-23967

THREE DIMENSIONAL FLOW
Mach 10 computational study of a three-dimensional scramjet inlet flow field
| NASA-TM-4602 | p 1666 N95-23015
Mach 10 computational study of a three-dimensional scramjet inlet flow field
| NASA-TM-4602 | p 1667 N95-23210
Holographic interferometric tomography for reconstructing flow fields p 1690 N95-23287
Three-dimensional unsteady flow calculations in an advanced gas generator turbine p 1671 N95-23425
Three-dimensional viscous flow analysis inside a turbine volute p 1674 N95-23437
Phase 2: HGM air flow tests in support of HEX vane investigation p 1674 N95-23438
On inertial range scaling laws
| DE95-004515 | p 1677 N95-23484
Three-dimensional flow analysis inside consortium impeller at design and off-design conditions p 1679 N95-23623
A fine-grid model for the ASRM aft segment with gimballed nozzle p 1685 N95-23648

THREE DIMENSIONAL MODELS
Three-dimensional CTOA and constraint effects during stable tearing in a thin-sheet material
| NASA-TM-109183 | p 1627 N95-22928
Algebraic description of atom-molecule interactions p 1814 N95-22961
Quantum field between moving mirrors: A three dimensional example p 1821 N95-22965
Three-dimensional structure in a supersonic jet: Behavior near centerline
| NASA-TM-106869 | p 1668 N95-23220
Physics of magnetospheric boundary layers
| NASA-CR-197920 | p 1739 N95-23271
Three-dimensional viscous flow analysis inside a turbine volute p 1674 N95-23437
Autonomous navigation system for the Marsokhod rover project p 1771 N95-23693
Development of the dynamic motion simulator of 3D micro-gravity with a combined passive/active suspension system p 1618 N95-23711
A computer model in general 3-D curvilinear coordinates for the prediction of the turbulent flow field in a jet induced ram combustor
| NAL-TR-1240T | p 1687 N95-24051

THREE DIMENSIONAL MOTION
Concept verification of three dimensional free motion simulator for space robot p 1618 N95-23702

THROATS
Design of a variable area diffuser for a 15-inch Mach 6 open-jet tunnel p 1617 N95-23309

THRUST CHAMBERS
Sensor-based control of rocket thrust chamber feature location for automated braze paste dispensing
| DE94-016559 | p 1624 N95-22885
Radiation/convection coupling in rocket motors and plumes p 1669 N95-23414
Development of an algebraic stress/two-layer model for calculating thrust chamber flow fields p 1675 N95-23442
CFD analysis of spray combustion and radiation in OMV thrust chamber p 1637 N95-23645

THUNDERSTORMS
Collaborative research on aircraft icing and charging processes in ice
| AD-A285102 | p 1609 N95-23201

TIMBER INVENTORY
A preliminary comparison of Landsat Thematic Mapper and SPOT-1 HRV multispectral data for estimating coniferous forest volume p 1719 N95-24097
Analysis of conifer forest regeneration using Landsat Thematic Mapper data p 1720 N95-24101

TIMBER VIGOR
Determining successional stage of temperate coniferous forests with Landsat satellite data p 1720 N95-24102

TIME DEPENDENCE
Non-zero temperature two-mode squeezing for time-dependent two-level systems
| DE94-628427 | p 1850 N95-22782
Algebraic description of atom-molecule interactions p 1814 N95-22961
Quantum field between moving mirrors: A three dimensional example p 1821 N95-22965
Harmonic oscillators and resonance series generated by a periodic unstable classical orbit p 1825 N95-22999
Temporal operators viewed as predicate transformers
| PB95-138996 | p 1757 N95-23152
Scattering problem for quantum system with time-dependent periodic Hamiltonian
| DE94-635421 | p 1797 N95-23965

TIME FUNCTIONS
Wavelet time-frequency analysis of phase-shift-key modulated signals
| AD-A285791 | p 1655 N95-22505

TIME LAG
Intelligent monitoring system applied to super long distance telerobotic tasks p 1777 N95-23728
Manipulating flexible parts using a teleoperated system with time delay: An experiment p 1777 N95-23729
Design of teleoperation system with a force-reflecting real-time simulator p 1778 N95-23733

TIME SERIES ANALYSIS
Nonlinear thermoviscoelastic behaviour in complex materials
| PB95-140653 | p 1630 N95-23537
The role of flight progress strips in en route air traffic control: A time-series analysis
| DOT/FAA/AM-95/4 | p 1611 N95-23565
Learning time series for intelligent monitoring p 1770 N95-23686
Monitoring land use and degradation using satellite and airborne data p 1707 N95-23880

TIN
Precise determinations of the isotopic compositions and atomic weights of molybdenum, tellurium, tin and tungsten using ICP source magnetic sector multiple collector mass spectrometry
| DE95-003003 | p 1632 N95-22795
Changes in chemical and optical properties of thin film metal mirrors on LDEF p 1651 N95-23907

TISSUES (BIOLOGY)
Enhancement of biomembrane functions under phase-separated conditions: A self-organized criticality phenomenon?
| DE94-628489 | p 1747 N95-23053

TITANIA
IUE observing programs: NSOSS, VEOEB, and PCOEB
| NASA-CR-197424 | p 1866 N95-23560

TITANIUM OXIDES
Nanophase materials: Synthesis, properties, applications
| AD-A286013 | p 1627 N95-22940

TOBACCO
Analysis of structural domains required for phytochrome function by in vitro mutagenesis
| DE94-016230 | p 1745 N95-22884

TOKAMAK DEVICES
Using the shield for thermal energy storage in PULSAR
| DE95-002457 | p 1829 N95-22645
Analytical and numerical studies of ion mobility near the tokamak plasma edge
| DE95-003019 | p 1830 N95-22693
Comparisons of nonlinear toroidal turbulence simulations with experiment
| DE95-003020 | p 1830 N95-22694
The DIII-D divertor cryopump system: Design and operational experience
| DE95-003007 | p 1693 N95-22796
Engineering design of a radiative divertor for DIII-D
| DE95-003008 | p 1693 N95-22798
Measurements and modeling of impurity source distributions from the Tore Supra outboard pump limiter
| DE95-003097 | p 1831 N95-22800
An investigation of AC losses in two sub-size conductors for the ITER
| DE94-765449 | p 1831 N95-22849
Runaway electrons in TEXT-U
| DE94-019218 | p 1831 N95-22862
Numerical Tokamak Project code comparison
| DE95-003475 | p 1831 N95-22899
TPX magnet system status
| DE95-002389 | p 1661 N95-23080
TFTR Ion Cyclotron Range of Frequencies (ICRF) experimental data analysis collaboration
| DE95-003409 | p 1832 N95-23084
Divertor heat and particle control experiments on the DIII-D tokamak
| DE94-017518 | p 1832 N95-23119
Neural net prediction of tokamak plasma disruptions
| DE95-002616 | p 1832 N95-23136
Tritium transport, influx, and helium ash measurements on TFTR during DT operation
| DE95-003708 | p 1833 N95-23269
Fast potential change in sawteeth in JIPP T-IIU tokamak plasmas
| NIFS-327 | p 1835 N95-23533
Physical mechanism determining the radial electric field and its radial structure in a toroidal plasma
| NIFS-313 | p 1835 N95-23534

Current-profile flattening and hot core shift due to the nonlinear development of resistive kink mode
[NIFS-311] p 1835 N95-23564
Edge fluctuation measurements by phase contrast imaging on DIII-D
[DE94-016681] p 1836 N95-23768
Gyrokinetic and global fluid simulations of tokamak microturbulence and transport
[DE95-003628] p 1837 N95-24017
A 4 MW fast wave current drive upgrade for D3-D
[DE95-003741] p 1837 N95-24083
D3-D program overview
[DE95-003879] p 1837 N95-24086
Experimental achievement of toroidal beta beyond that predicted by 'Troyon' scaling
[DE95-003880] p 1837 N95-24087
Beryllium in the ITER blanket
[DE95-004620] p 1837 N95-24165

TOMATOES
Germination, growth rates, and electron microscope analysis of tomato seeds flown on the LDEF p 1748 N95-23821

TOMOGRAPHY
Evaluation of neutron techniques for illicit substance detection
[DE95-002988] p 1632 N95-22764
Tomographic analysis of the three-dimensional variation of the seismic velocity structure of the shallow crust underlying Southern New England
[AD-A279406] p 1739 N95-23247

TOOLS
Pressurized fluid torque driver control and method
[NASA-CASE-MSC-22385-1] p 1694 N95-22892

TOPOGRAPHY
AVIRIS and TIMS data processing and distribution at the land processes distributed active archive center p 1706 N95-23872
Preprocessing: Geocoding of AVIRIS data using navigation, engineering, DEM, and radar tracking system data p 1707 N95-23876
A comparison of spectral mixture analysis an NDVI for ascertaining ecological variables p 1710 N95-23892
Determination of semi-arid landscape endmembers and seasonal trends using convex geometry spectral unmixing techniques p 1711 N95-23895
Glaciological studies in the central Andes using AIRSAR/TOPSAR p 1713 N95-23942
Estimation of biophysical properties of upland Sitka spruce (Picea sitchensis) plantations p 1713 N95-23943
Current and future use of TOPSAR digital topographic data for volcanological research p 1714 N95-23949
Profiling and light scattering studies of Si surfaces
[DE95-002931] p 1828 N95-24005

TOPOLOGY
Countable space with a closed subspace without continuous extender
[PB95-127973] p 1785 N95-22533
Lectures on homology with internal symmetries
[DE94-628409] p 1785 N95-22619
On diagonalization in map (M,G)
[DE94-628515] p 1796 N95-22740
On the scalar curvature of minimal hypersurfaces
[DE94-628516] p 1796 N95-22741
Lectures on 2D gauge theories. Topological aspects and path integral techniques
[DE94-628509] p 1849 N95-22752
AR-descriptions in translatable Frechet spaces
[PB95-138855] p 1789 N95-23149
Translation invariant Frechet subspaces of distributions
[PB95-138830] p 1789 N95-23171
CFD analysis of turbopump volutes p 1674 N95-23436
Universal Hodge bundle and Mumford isomorphisms on the abelian inductive limit of Teichmueller spaces
[DE94-634325] p 1796 N95-23660

TORCHES
Vacuum vapor deposition
[NASA-CASE-MFS-28652-1] p 1647 N95-22558

TOROIDAL PLASMAS
Analytical and numerical studies of ion mobility near the tokamak plasma edge
[DE95-003019] p 1830 N95-22693
TPX magnet system status
[DE95-002389] p 1661 N95-23080
TFTR Ion Cyclotron Range of Frequencies (ICRF) experimental data analysis collaboration
[DE95-003409] p 1832 N95-23084
Non-Taylor magnetohydrodynamic self-organization
[NIFS-314] p 1834 N95-23524
Fast potential change in sawteeth in JIPP T-IIU tokamak plasmas
[NIFS-327] p 1835 N95-23533
Physical mechanism determining the radial electric field and its radial structure in a toroidal plasma
[NIFS-313] p 1835 N95-23534
The next Large Helical Devices
[NIFS-323] p 1835 N95-23535
Current-profile flattening and hot core shift due to the nonlinear development of resistive kink mode
[NIFS-311] p 1835 N95-23564
Theory of pressure-induced islands and self-healing in three-dimensional toroidal magnetohydrodynamic equilibria
[NIFS-321] p 1836 N95-23589
Effect of satellite helical harmonics on the stellarator configuration
[NIFS-328] p 1609 N95-23787
Gyrokinetic and global fluid simulations of tokamak microturbulence and transport
[DE95-003628] p 1837 N95-24017

TORQUE
The spectral content of the torque loads on a turbine gear tooth
[DE95-002188] p 1694 N95-23056

TORQUERS
Pressurized fluid torque driver control and method
[NASA-CASE-MSC-22385-1] p 1694 N95-22892

TORSION
Relativistic particle with torsion and charged particle in a constant electromagnetic field: Identity of evolution
[DE94-628506] p 1803 N95-22778

TORUSES
The Euler series of restricted Chow varieties
[DE94-628418] p 1785 N95-22626
Unstructured grids on SIMD torus machines
[NASA-CR-197954] p 1758 N95-23610

TOTAL QUALITY MANAGEMENT
Upward appraisal as a means for improving supervisory performance and promoting process improvement, with long-term implications for organizational change p 1854 N95-23323

TOXIC HAZARDS
Skin exposure: Assessing the hazard in the workplace p 1628 N95-23030
Chemical recycling of scrap composites p 1629 N95-23034
Offgassing test methodology for composite materials p 1629 N95-23035

TOXICITY
Preliminary assessment of air toxic emissions in the natural gas industry, phase 1
[PB95-135547] p 1732 N95-22865
Modeling aerosol emissions from the combustion of composite materials p 1629 N95-23038
Aqueous alternatives for metal and composite cleaning p 1630 N95-23039
The significance of hair mineral analysis as a means for assessing internal body burdens of environmental pollutants
[DE94-633512] p 1734 N95-23541
Applied research on air pollution using nuclear-related analytical techniques
[DE94-633513] p 1734 N95-23542
Aircraft fires, smoke toxicity, and survival: An overview
[DOT/FAA/AM-95/8] p 1610 N95-24024

TOXICITY AND SAFETY HAZARD
A roadmap for regulatory survival in the 1990s p 1628 N95-23026

TRACE ELEMENTS
Measurement of HO2 and other trace gases in the stratosphere using a high resolution far-infrared spectrometer
[NASA-CR-197368] p 1735 N95-22482
Applied research on air pollution using nuclear-related analytical techniques
[DE94-633513] p 1734 N95-23542

TRACKING (POSITION)
Twelve month performance evaluation for the rotating shadowband radiometer
[DE95-002847] p 1726 N95-22554
Mark Tracking: Position/orientation measurements using 4-circle mark and its tracking experiments p 1778 N95-23736
Automatic commanding of the Mars Observer Camera p 1620 N95-23754

TRAILING EDGE FLAPS
Wing pressure distributions from subsonic tests of a high-wing transport model --- in the Langley 14- by 22-Foot Subsonic Wind Tunnel
[NASA-TM-4583] p 1607 N95-22802

TRAILING EDGES
Aeroacoustic computation of gust-blade interaction p 1800 N95-23313
Lift enhancing tabs for airfoils
[NASA-CASE-ARC-11990-1] p 1613 N95-23395

TRAINING DEVICES
Virtual reality flight control display with six-degree-of-freedom controller and spherical orientation overlay
[NASA-CASE-NPO-18733-1-CU] p 1613 N95-22578
Development of qualification guidelines for personal computer-based aviation training devices
[DOT/FAA/AM-95/6] p 1758 N95-23603

TRAINING EVALUATION
Formative and summative evaluation efforts for the Teacher Enhancement Institute conducted at the NASA Langley Research Center, summer 1994 p 1853 N95-23286

TRAJECTORY CONTROL
Nonlinear system guidance in the presence of transmission zero dynamics
[NASA-TM-4661] p 1654 N95-22804
Terrain modelling and motion planning for an autonomous exploration rover p 1721 N95-23765

TRAJECTORY PLANNING
Path planning for planetary rover using extended elevation map p 1771 N95-23689
Subsumption-based architecture for autonomous movement planning for planetary rovers p 1771 N95-23690
Very fast motion planning for highly dexterous-articulated robots p 1771 N95-23691
Control technique for planetary rover p 1771 N95-23692
Autonomous navigation system for the Marsokhod rover project p 1771 N95-23693
Lunar rover technology demonstrations with Dante and Ratler p 1697 N95-23694
A perspective on space robotics in Japan p 1697 N95-23695
Terrain modelling and motion planning for an autonomous exploration rover p 1721 N95-23765

TRANSDUCERS
Capacitive acoustic wave detector and method of using same
[NASA-CASE-LAR-13890-1] p 1799 N95-22921
Investigation of arc length versus flange thickness while using an arc voltage controller
[DE95-003937] p 1695 N95-23374
Dynamic response of a transducer mounted at one end of an acoustical cavity which is subjected to a specified pressure at the open end of the cavity
[DE95-004192] p 1799 N95-23379

TRANSFER FUNCTIONS
On-line, adaptive state estimator for active noise control p 1784 N95-23308

TRANSFORMERS
Temporal operators viewed as predicate transformers
[PB95-138996] p 1757 N95-23152
IGES transformer and NURBS in grid generation p 1669 N95-23415

TRANSIENT RESPONSE
Numerical study of the SSME nozzle flow fields during transient operations: A comparison of the animated results with test p 1673 N95-23434
User's guide and physics manual for the ScatPlus circuit code
[DE95-003755] p 1663 N95-23479

TRANSITION FLOW
Crossflow instability control on a swept-wing: Preliminary studies p 1609 N95-23283
Bursting in the near-surface boundary layer: Comparisons between realistic models and observations
[DE95-003714] p 1741 N95-24078

TRANSITION METALS
Solvation of isolated transition metal ions
[DE95-002978] p 1638 N95-22571
Magnetic multilayer physics
[DE95-003408] p 1798 N95-23083
Supported transition metal catalysts for para- to ortho-hydrogen conversion
[NASA-CR-197907] p 1634 N95-23252
Spin polarized photoemission studies of magnetic quantum well states
[DE95-004218] p 1851 N95-23335
Thermochemistry of transition metal clusters
[DE95-003144] p 1646 N95-24144
Epitaxial growth of bcc transition metal films and superlattices onto MgO (111), (011) and (001) substrates
[DE95-004629] p 1846 N95-24168

TRANSITION TEMPERATURE
Superconducting Tl2Ba2CaCu2O8 thin films prepared by post-annealing in a flow-through multiple-zone furnace
[DE95-002745] p 1838 N95-22520
Potential aerospace applications of high temperature superconductors p 1664 N95-23322
Electrochemical studies of perovskite mixed conductors
[DE95-003704] p 1636 N95-23573

Phonon characteristics of high (T sub c) superconductors from neutron Doppler broadening measurements
| DE95-003703 | p 1844 N95-24076
Cooling rate effects on the microstructure, critical current density, and (T(sub c)) transition of one- and two-powder BSCCO-2223 Ag sheathed tapes
| DE95-004639 | p 1846 N95-24171

TRANSLATING
Proceedings of the workshop on deductive databases and logic programming
| PB95-139382 | p 1758 N95-23553

TRANSMISSION ELECTRON MICROSCOPY
Transmission electron microscope studies of extraterrestrial materials
| NASA-CR-188363 | p 1633 N95-23092

TRANSMISSION RATE (COMMUNICATIONS)
Using high-performance networks to enable computational aerosciences applications
| NASA-CR-197951 | p 1764 N95-24023

TRANSMITTERS
A 4 MW fast wave current drive upgrade for D3-D
| DE95-003741 | p 1837 N95-24083

TRANSONIC WIND TUNNELS
Performance of the 0.3-meter transonic cryogenic tunnel with air, nitrogen, and sulfur hexafluoride media under closed loop automatic control
| NASA-CR-195052 | p 1668 N95-23257
Three-dimensional Navier-Stokes analysis and redesign of an imbedded bellmouth nozzle in a turbine cascade inlet section p 1671 N95-23423

TRANSPARENCE
Coordinating complex decision support activities across distributed applications p 1761 N95-23749

TRANSPONDERS
Improved small satellite access of the space network
| NASA-CR-197863 | p 1657 N95-22944

TRANSPORT AIRCRAFT
Wing pressure distributions from subsonic tests of a high-wing transport model --- in the Langley 14- by 22-Foot Subsonic Wind Tunnel
| NASA-TM-4583 | p 1607 N95-22802
Handling qualities of the High Speed Civil Transport p 1616 N95-23325
High-lift flow-physics flight experiments on a subsonic civil transport aircraft (B737-100) p 1609 N95-23333

TRANSPORT PROPERTIES
Research on defects and transport in amorphous-silicon-based semiconductors
| DE94-011888 | p 1660 N95-22586
Non local pseudopotentials, transport properties of liquid noble metals
| DE94-627416 | p 1640 N95-22840
Computational modeling of properties
| NAS-CR-196544 | p 1841 N95-22907
Turbulent transport across invariant canonical flux surfaces
| DE95-000710 | p 1832 N95-23072
Modeling of nonequilibrium space plasma flows
| NASA-CR-197432 | p 1833 N95-23211
Effect on c-axis transport properties of a critical state in Bi2Sr2CaCu2O8
| DE95-003695 | p 1843 N95-23366
Transport properties of Tl2Ba2CaCu2O8 meander lines
| DE95-003715 | p 1843 N95-23367
Mass transport through polycrystalline microstructures
| DE95-004552 | p 1811 N95-23576
High current induction linacs
| DE95-003442 | p 1818 N95-24014
Gyrokinetic and global fluid simulations of tokamak microturbulence and transport
| DE95-003628 | p 1837 N95-24017
Particle transport in plasma reactors
| DE95-004541 | p 1837 N95-24158

TRANSPORT THEORY
Comparisons of nonlinear toroidal turbulence simulations with experiment
| DE95-003020 | p 1830 N95-22694
Turbulent transport across invariant canonical flux surfaces
| DE95-000710 | p 1832 N95-23072

TRANSPORTATION
Radioisotope thermoelectric generator licensed hardware package and certification tests
| DE95-003039 | p 1661 N95-22799
Submodular linear programs on forests
| PB95-139820 | p 1758 N95-23608

TRANSPORTATION ENERGY
Multi-fuel reformers for fuel cells used in transportation: Assessment of hydrogen storage technologies
| DE94-017655 | p 1727 N95-22861

TRAPPED PARTICLES
Magnetospheric space plasma investigations
| NASA-CR-197405 | p 1831 N95-22955
Measurement of trapped proton fluences in main stack of P0006 experiment p 1815 N95-23812

TRAPPING
Traps for antimatter and antihydrogen production
| DE95-002814 | p 1805 N95-22927

TRAPS
Traps for antimatter and antihydrogen production
| DE95-002814 | p 1805 N95-22927
A brief history in time of ion traps and their achievements in science
| DE95-002815 | p 1805 N95-22936

TRAVELING WAVES
The propagation of travelling waves for stochastic generalized KPP equations
| DE94-628473 | p 1787 N95-22772

TREES (MATHEMATICS)
Trees are graceful if and only if trees with a perfect matching are strongly graceful
| PB95-139853 | p 1790 N95-23236
Effective (mu)-term in superstring theory
| DE94-634326 | p 1851 N95-23922

TREND ANALYSIS
Search Hanford accessible reports electronically system requirements specification
| DE95-004367 | p 1856 N95-23340
Trend analysis of in-situ spectral reflectance data from the Thermal Control Surfaces Experiment (TCSE) p 1631 N95-23910

TRITIUM
Exotic atoms
| DE95-003199 | p 1805 N95-22881
Tritium transport, influx, and helium ash measurements on TFTR during DT operation
| DE95-003708 | p 1833 N95-23269
Modeling of tritium recovery from lithium ceramics
| DE95-004626 | p 1838 N95-24167

TROPICAL METEOROLOGY
TOGA/COARE AMMR 1992 data processing
| NASA-CR-197289 | p 1736 N95-22867
Upgrade of the 92 GHz airborne multi-channel meteorological radiometer (AMMR)
| NASA-CR-197875 | p 1742 N95-23208
Annual tropical cyclone report, 1993
| AD-A285097 | p 1742 N95-23255

TROPICAL STORMS
Annual tropical cyclone report, 1993
| AD-A285097 | p 1742 N95-23255

TROPOSPHERE
Observation model and parameter partials for the JPL VLBI parameter estimation software MODEST, 19 94
| NASA-CR-197328 | p 1756 N95-22853
Compendium of NASA data base for the Global Tropospheric Experiment's Pacific Exploratory Mission West-A (PEM West-A)
| NASA-TM-109177 | p 1733 N95-23009
Oxidants and oxidation in the Earth's atmosphere
| NASA-CR-197945 | p 1734 N95-23460
Laboratory studies of the sensitivity of tropospheric ozone to the chemistry of sea salt aerosol
| DE95-003607 | p 1735 N95-24147

TRUSSES
Truss structure tele-manipulation experiment using ETS-7 p 1623 N95-23726
A fuzzy structural matching scheme for space robotics vision p 1778 N95-23737

TUNABLE LASERS
Raman-shifting an ArF excimer laser to generate new lines for obtaining optical diagnostic based information in flow fields p 1692 N95-23303

TUNERS
A 4 MW fast wave current drive upgrade for D3-D
| DE95-003741 | p 1837 N95-24083

TUNGSTEN
Thermal outgassing studies on machinable tungsten and TZM molybdenum alloy
| DE95-002984 | p 1638 N95-22592
Precise determinations of the isotopic compositions and atomic weights of molybdenum, tellurium, tin and tungsten using ICP source magnetic sector multiple collector mass spectrometry
| DE95-003003 | p 1632 N95-22795
Changes in chemical and optical properties of thin film metal mirrors on LDEF p 1651 N95-23907
High energy collimating fine grids
| NASA-CR-197688 | p 1871 N95-24191

TUNNEL JUNCTIONS
Dependence of the Josephson coupling of unconventional superconductors on the properties of the tunneling barrier
| DE95-004649 | p 1846 N95-24173

TURBIDITY
Turbidity of a near critical ionic fluid
| DE94-014916 | p 1633 N95-22869

TURBINE BLADES
Navier-Stokes analysis of an oxidizer turbine blade with tip clearance with and without a mini-shroud p 1672 N95-23428
Supersonic flow and shock formation in turbine tip gaps p 1672 N95-23429

TURBINE EXHAUST NOZZLES
Numerical study of base pressure characteristic curve for a four-engine clustered nozzle configuration p 1625 N95-23655

TURBINE PUMPS
Prediction of incidence and surface roughness effects on turbine performance p 1671 N95-23424
CFD analysis of turbopump volutes p 1674 N95-23436
Phase 2: HGM air flow tests in support of HEX vane investigation p 1674 N95-23438
Detailed measurements in the SSME high pressure fuel turbine with smooth rotor blades p 1675 N95-23441
Three-D CFD analysis of hydrostatic bearings p 1678 N95-23616
Finite-difference solutions of the alternate turbopump development high-pressure oxidizer turbopump pump-end ball-bearing cavity flows p 1678 N95-23617
Incompressible Navier-Stokes calculations in pump flows p 1680 N95-23627
The influence of swirl brakes and a tip discharge orifice on the rotordynamic forces generated by discharge-to-suction leakage flows in shrouded centrifugal pumps p 1680 N95-23628
Adaptation of the advanced spray combustion code to cavitating flow problems p 1681 N95-23629
An inducer CFD solution and effects associated with cavitation p 1681 N95-23631

TURBINES
Prediction of incidence and surface roughness effects on turbine performance p 1671 N95-23424
Three-dimensional unsteady flow calculations in an advanced gas generator turbine p 1671 N95-23425
GGOT total pressure loss control concept evaluation p 1672 N95-23427
Aerodynamic design and analysis of a highly loaded turbine exhaust p 1673 N95-23435
CFD analysis of turbopump volutes p 1674 N95-23436
Three-dimensional viscous flow analysis inside a turbine volute p 1674 N95-23437
Detailed measurements in the SSME high pressure fuel turbine with smooth rotor blades p 1675 N95-23441
Numerical computation of aerodynamics and heat transfer in a turbine cascade and a turn-around duct using advanced turbulence models p 1675 N95-23444
Enhanced analysis and users manual for radial-inflow turbine conceptual design code RTD
| NASA-CR-195454 | p 1609 N95-23462
Three-D flow analysis of the alternate SSME HPOT TAD p 1679 N95-23620
Unsteady flow simulations in support of the SSME HEX turning vane cracking investigation with the ATD HPOTP p 1679 N95-23621
Use of blade lean in turbomachinery redesign p 1680 N95-23625

TURBOCOMPRESSORS
NASA low-speed axial compressor for fundamental research
| NASA-TM-4635 | p 1616 N95-23192

TURBOMACHINERY
Eleventh Workshop for Computational Fluid Dynamic Applications in Rocket Propulsion
| NASA-CP-3221-PT-2 | p 1668 N95-23412
Numerical simulation of steady and unsteady viscous flow in turbomachinery using pressure based algorithm p 1671 N95-23426
Advanced turbulence models for turbomachinery p 1675 N95-23443
Use of blade lean in turbomachinery redesign p 1680 N95-23625
CFD parametric study of consortium impeller p 1680 N95-23626
Current status in cavitation modeling p 1681 N95-23632

TURBULENCE
Study of the pressure field in rotating homogeneous turbulent flows
| PB94-189107 | p 1665 N95-22585
Micro-sensor thin-film anemometer
| NASA-CASE-LAR-15112-1-CU | p 1666 N95-22906
On inertial range scaling laws
| DE95-004515 | p 1677 N95-23484

TURBULENCE EFFECTS
Turbulent transport across invariant canonical flux surfaces
| DE95-000710 | p 1832 N95-23072
Development of an algebraic stress/two-layer model for calculating thrust chamber flow fields p 1675 N95-23442

TURBULENCE MODELS
Theory of HF induced turbulence in the ionosphere: Status and challenges
| DE95-002705 | p 1739 N95-23256

Direct numerical simulations and modeling of a spatially-evolving turbulent wake p 1687 N95-23289
Development of an algebraic stress/two-layer model for calculating thrust chamber flow fields p 1675 N95-23442
Numerical computation of aerodynamics and heat transfer in a turbine cascade and a turn-around duct using advanced turbulence models p 1675 N95-23444
Liquid propellant rocket engine combustion simulation with a time-accurate CFD method p 1676 N95-23445
Advanced multi-phase flow CFD model development for solid rocket motor flowfield analysis p 1683 N95-23638
Flow diagnostics, chemically reacting turbulent flow modeling and turbulent mixing: A summary of project studies in combustion
|NASA-CR-197348| p 1687 N95-24022
Bursting in the near-surface boundary layer: Comparisons between realistic models and observations
|DE95-003714| p 1741 N95-24078

TURBULENT BOUNDARY LAYER
Detailed measurements in the SSME high pressure fuel turbine with smooth rotor blades p 1675 N95-23441
Bursting in the near-surface boundary layer: Comparisons between realistic models and observations
|DE95-003714| p 1741 N95-24078

TURBULENT COMBUSTION
Modeling NO(x) emissions in turbulent jet flames: Effects of buoyancy and radiation
|DE94-016621| p 1633 N95-22886
Effects of jet strength on NOx formation in premixed impinging jet combustion with minimum heat losses
|NAL-TR-1237T| p 1637 N95-24181

TURBULENT FLOW
Study of the pressure field in rotating homogeneous turbulent flows
|PB94-189107| p 1665 N95-22585
Experimental study of vortex breakdown in a swirling water jet
|PB95-130407| p 1665 N95-22767
Crossflow instability control on a swept-wing: Preliminary studies p 1609 N95-23283
Direct numerical simulations and modeling of a spatially-evolving turbulent wake p 1687 N95-23289
Direct numerical simulation of sheared turbulent flow p 1687 N95-23296
High-lift flow-physics flight experiments on a subsonic civil transport aircraft (B737-100) p 1609 N95-23333
Numerical simulation of steady and unsteady viscous flow in turbomachinery using pressure based algorithm p 1671 N95-23426
Advanced turbulence models for turbomachinery p 1675 N95-23443
Numerical computation of aerodynamics and heat transfer in a turbine cascade and a turn-around duct using advanced turbulence models p 1675 N95-23444
Convergence acceleration of implicit schemes in the presence of high aspect ratio grid cells p 1676 N95-23446
A controlled variation scheme for convection treatment in pressure-based algorithm p 1677 N95-23448
A wavenumber-partitioning scheme for two-dimensional statistical closures
|DE95-004514| p 1677 N95-23483
CFD parametric study of consortium impeller p 1680 N95-23626
On the accuracy of CFD-based pressure drop predictions for right-angle ducts p 1682 N95-23634
CFD modeling of turbulent duct flows for coolant channel analysis p 1682 N95-23635
Advanced multi-phase flow CFD model development for solid rocket motor flowfield analysis p 1683 N95-23638
Flow diagnostics, chemically reacting turbulent flow modeling and turbulent mixing: A summary of project studies in combustion
|NASA-CR-197348| p 1687 N95-24022
A computer model in general 3-D curvilinear coordinates for the prediction of the turbulent flow field in a jet induced ram combustor
|NAL-TR-1240T| p 1687 N95-24051
Bursting in the near-surface boundary layer: Comparisons between realistic models and observations
|DE95-003714| p 1741 N95-24078

TURBULENT MIXING
Flow diagnostics, chemically reacting turbulent flow modeling and turbulent mixing: A summary of project studies in combustion
|NASA-CR-197348| p 1687 N95-24022

TURBULENT WAKES
Direct numerical simulations and modeling of a spatially-evolving turbulent wake p 1687 N95-23289

TURING MACHINES
On helping by parity-like languages
|TR-553| p 1759 N95-23935
Logspace reducibility and self-reducibility: Models and equivalences
|TR-544| p 1760 N95-24059

TVD SCHEMES
Liquid propellant rocket engine combustion simulation with a time-accurate CFD method p 1676 N95-23445

TWO DIMENSIONAL FLOW
BEM solution to simulate the curvature driven deformation of a profile that is pressed into a plate of hot glass
|PB95-138913| p 1648 N95-23145
New robust multigrid method for 2D convection-diffusion problems
|PB95-138897| p 1789 N95-23176
On inertial range scaling laws
|DE95-004515| p 1677 N95-23484
User's guide for ECAP2D: An Euler unsteady aerodynamic and aeroelastic analysis program for two dimensional oscillating cascades, version 1.0
|NASA-CR-189146| p 1699 N95-24189

TWO DIMENSIONAL JETS
Instantaneous 2D velocity and temperature measurements in high speed flows based on spectrally resolved molecular Rayleigh scattering
|NASA-TM-106883| p 1688 N95-23461

TWO DIMENSIONAL MODELS
VLUGR2: A vectorizable adaptive grid solver for PDes in 2D
|PB95-136008| p 1789 N95-23167
Unification of some advection schemes in two dimensions
|NASA-CR-195044| p 1790 N95-23465
ROSAT observation program
|NASA-CR-197683| p 1866 N95-23595
The effect of magnetic field on the edge plasmons of two-dimensional electron gas systems
|DE94-018044| p 1837 N95-23982
Gyrokinetic and global fluid simulations of tokamak microturbulence and transport
|DE95-003628| p 1837 N95-24017

TWO PHASE FLOW
Influence of porosity and two-phase flow on diffusional/thermal instability of a deflagrating energetic material
|DE95-002592| p 1634 N95-23122
Current status in cavitation modeling p 1681 N95-23632
An interactive tool for discrete phase analysis in two-phase flows p 1683 N95-23641
Progress in advanced spray combustion code integration p 1637 N95-23644
Development of an atomization methodology for spray combustion p 1637 N95-23646

TYPE 3 BURSTS
Langmuir-like waves and radiation in planetary foreshocks
|NASA-CR-197376| p 1869 N95-22828

U

U.S.S.R.
GPS survey of the western Tien Shan
|NASA-CR-197901| p 1717 N95-22832

ULTRAHIGH FREQUENCIES
Utilizing a TDRS satellite for direct broadcast satellite-radio propagation experiments and demonstrations p 1622 N95-22814
The possibilities for mobile and fixed services up to the 20/30 GHz frequency bands p 1656 N95-22817

ULTRAHIGH VACUUM
Thermal outgassing studies on machinable tungsten and TZM molybdenum alloy
|DE95-002984| p 1638 N95-22592

ULTRASHORT PULSED LASERS
Production of high contrast ultrashort laser pulses for short scale length plasma experiments
|DE95-003640| p 1690 N95-22595

ULTRASONIC CLEANING
Calorimetric measurement of energy of ultrasonic cleaners
|DE95-003938| p 1800 N95-23375

ULTRASONIC RADIATION
Calorimetric measurement of energy of ultrasonic cleaners
|DE95-003938| p 1800 N95-23375

ULTRASONIC TESTS
High-temperature ultrasonic characterization of Ag-clad superconductor tapes
|DE95-002909| p 1838 N95-22530

ULTRAVIOLET ASTRONOMY
IUE observing programs: NSOSS, VEOEB, and PCOEB
|NASA-CR-197424| p 1866 N95-23560
Observational studies of the clearing phase in proto-planetary disk systems
|NASA-CR-197900| p 1866 N95-23561

ULTRAVIOLET RADIATION
The effect of simulated low earth orbit radiation on polyimides (UV degradation study) p 1651 N95-23903

ULTRAVIOLET SPECTRA
IUE observing programs: NSOSS, VEOEB, and PCOEB
|NASA-CR-197424| p 1866 N95-23560
Observational studies of the clearing phase in proto-planetary disk systems
|NASA-CR-197900| p 1866 N95-23561

ULTRAVIOLET SPECTROSCOPY
On the formation of iron(3) oxides via oxidation of iron(2)
|DE94-018392| p 1632 N95-22857
Advanced development of PV encapsulants
|DE95-000246| p 1728 N95-23062
Raman-shifting an ArF excimer laser to generate new lines for obtaining optical diagnostic based information in flow fields p 1692 N95-23303
Mass loss in the interacting semi-detached binary delta librae
|NASA-CR-197924| p 1866 N95-23402

UNDERWATER ACOUSTICS
Theoretical estimates of high frequency acoustic attenuation and backscattering from suspended sand particles in the ocean and in an estuary
|DSTO-TR-0078| p 1743 N95-23667

UNDERWATER ENGINEERING
Planetary stations and Abyssal Benthic Laboratories: An overview of parallel approaches for long-term investigation in extreme environments p 1752 N95-23732

UNDERWATER OPTICS
SeaWiFS technical report series. Volume 25: Ocean optics protocols for SeaWiFS validation, revision 1
|NASA-TM-104566-VOL-25-REV-| p 1743 N95-22671

UNDERWATER RESEARCH LABORATORIES
Planetary stations and Abyssal Benthic Laboratories: An overview of parallel approaches for long-term investigation in extreme environments p 1752 N95-23732

UNIFORM FLOW
Aeroacoustic computation of gust-blade interaction p 1800 N95-23313

UNIQUENESS
Time-periodic solutions of some forced nonlinear wave equations: Analysis, approximations and applications
|PB95-135083| p 1788 N95-22932
Regular graphs with four eigenvalues
|PB95-135141| p 1788 N95-23068

UNITED STATES
Closing the circle on the splitting of the atom: The environmental legacy of nuclear weapons production in the United States and what the Department of Energy is doing about it p 1818 N95-23562

UNIVERSAL TIME
Observation model and parameter partials for the JPL VLBI parameter estimation software MODEST, 19 94
|NASA-CR-197328| p 1756 N95-22853

UNIVERSE
Baryon number fluctuations in a quark-hadron phase transition
|DE94-628585| p 1804 N95-22786
Space Science for the 21st Century. Strategic Plan for 1995-2000
|NASA-TM-110546| p 1617 N95-22947
CDM and Omega in the local neighborhood
|DE95-003683| p 1868 N95-23570

UNIVERSITIES
1994 NASA-HU American Society for Engineering Education (ASEE) Summer Faculty Fellowship Program
|NASA-CR-194972| p 1872 N95-23276
NASA university program management information system, FY 1994
|NASA-TM-110345| p 1856 N95-23364

UNIVERSITY PROGRAM
Langley Research Center Strategic Plan for Education p 1853 N95-23316
Teacher Enhancement Institute p 1853 N95-23324
NASA university program management information system, FY 1994
|NASA-TM-110345| p 1856 N95-23364
Integrating O/S models during conceptual design, part 2
|NASA-CR-197904| p 1622 N95-23399

UNIX (OPERATING SYSTEM)
Document image archive transfer from DOS to UNIX p 1761 N95-24117

UNSTEADY AERODYNAMICS
Flutter analysis of composite box beams
|NASA-CR-197931| p 1615 N95-23392
User's guide for ECAP2D: An Euler unsteady aerodynamic and aeroelastic analysis program for two dimensional oscillating cascades, version 1.0
|NASA-CR-189146| p 1699 N95-24189

UNSTEADY FLOW
A perspective on unstructured grid flow solvers
| NASA-CR-195025 | p 1788 N95-22931
A CFD study of complex missile and store configurations in relative motion
| NASA-CR-197912 | p 1612 N95-22949
Holographic interferometric tomography for reconstructing flow fields p 1690 N95-23287
Benchmark problems in computational aeroacoustics p 1800 N95-23315
Three-dimensional unsteady flow calculations in an advanced gas generator turbine p 1671 N95-23425
Numerical simulation of steady and unsteady viscous flow in turbomachinery using pressure based algorithm p 1671 N95-23426
Numerical study of the SSME nozzle flow fields during transient operations: A comparison of the animated results with test p 1673 N95-23434
Aerodynamic design and analysis of a highly loaded turbine exhaust p 1673 N95-23435
Liquid propellant rocket engine combustion simulation with a time-accurate CFD method p 1676 N95-23445
A time-accurate finite volume method valid at all flow velocities p 1676 N95-23447
Unsteady flow simulations in support of the SSME HEX turning vane cracking investigation with the ATD HPOTP p 1679 N95-23621
Time-accurate unsteady flow simulations supporting the SRM T+68-second pressure spike anomaly investigation (STS-54B) p 1685 N95-23650

UPPER ATMOSPHERE
Particle kinetic simulation of high altitude hypervelocity flight
| NASA-CR-197383 | p 1664 N95-22481

UPPER ATMOSPHERE RESEARCH SATELLITE (UARS)
Measurement of HO2 and other trace gases in the stratosphere using a high resolution far-infrared spectrometer
| NASA-CR-197368 | p 1735 N95-22482

URANIUM
Closing the circle on the splitting of the atom: The environmental legacy of nuclear weapons production in the United States and what the Department of Energy is doing about it p 1818 N95-23562

URANIUM OXIDES
A phenomenological model for the effect of nanocrystalline microstructure on irradiation-induced amorphization in U3Si
| DE95-004631 | p 1846 N95-24169

USER MANUALS (COMPUTER PROGRAMS)
HiRel: Hybrid Automated Reliability Predictor (HARP) integrated reliability tool system, (version 7.0). Volume 1: HARP introduction and user's guide
| NASA-TP-3452-VOL-1 | p 1754 N95-22603
HiRel: Hybrid Automated Reliability Predictor (HARP) integrated reliability tool system, (version 7.0). Volume 2: HARP tutorial
| NASA-TP-3452-VOL-2 | p 1755 N95-22604
HiRel: Hybrid Automated Reliability Predictor (HARP) integrated reliability tool system, (version 7.0). Volume 4: HARP Output (HARPO) graphics display user's guide
| NASA-TP-3452-VOL-4 | p 1755 N95-22605
Extensible PDE Solvers package users manual
| DE95-003333 | p 1786 N95-22696
PRISMA GENIE data analysis manual
| PB95-130464 | p 1755 N95-22769
Long range targeting for space based rendezvous
| NASA-CR-197890 | p 1757 N95-23388
Enhanced analysis and users manual for radial-inflow turbine conceptual design code RTD
| NASA-CR-195454 | p 1609 N95-23462
User's guide and physics manual for the ScatPlus circuit code
| DE95-003755 | p 1663 N95-23479
GPP user's guide: A general-purpose postprocessor for wind turbine data analysis
| DE95-000293 | p 1730 N95-23776
User's guide for ECAP2D: An Euler unsteady aerodynamic and aeroelastic analysis program for two dimensional oscillating cascades, version 1.0
| NASA-CR-189146 | p 1699 N95-24189

USER REQUIREMENTS
Addendum to the Proceedings of the Third International Mobile Satellite Conference (IMSC 1993)
| NASA-CR-197343 | p 1655 N95-22813
The possibilities for mobile and fixed services up to the 20/30 GHz frequency bands p 1656 N95-22817
The next decade of space robotics p 1768 N95-23673
Software agents for the dissemination of remote terrestrial sensing data p 1721 N95-23675
Utilizing inheritance in requirements engineering p 1768 N95-23677
AMPHION: Specification-based programming for scientific subroutine libraries p 1761 N95-23680
Building a COTS archive for satellite data p 1861 N95-24132

UTILITIES
Evaluating photovoltaic applications: A guide for utilities
| DE95-003807 | p 1726 N95-22502

V

V-22 AIRCRAFT
Thin tailored composite wing for civil tiltrotor p 1613 N95-23317

VACUUM
Neutrinos with Zee-mass matrix in vacuum and matter
| DE94-628635 | p 1803 N95-22756

VACUUM DEPOSITION
Vacuum vapor deposition
| NASA-CASE-MFS-28652-1 | p 1647 N95-22558

VACUUM EFFECTS
Vaccum Gas Tungsten Arc Welding, phase 1
| NASA-CR-197979 | p 1696 N95-24064

VALUE
Marginalistic value for monotonic set games
| PB95-140646 | p 1794 N95-23239

VALVES
Navier-Stokes flow field analysis of compressible flow in a pressure relief valve p 1679 N95-23618

VANADIUM ALLOYS
Deformation of C15 Laves phase alloys
| DE95-003636 | p 1646 N95-24067
Experimental and theoretical studies on the C15 intermetallic compounds MV2 (M = Zr, Hf and Ta): Elasticity and phase stability
| DE95-003723 | p 1845 N95-24079
Effect of dynamically charged helium on mechanical properties of vanadium-base alloys
| DE95-004613 | p 1646 N95-24153

VANES
Phase 2: HGM air flow tests in support of HEX vane investigation p 1674 N95-23438
Unsteady flow simulations in support of the SSME HEX turning vane cracking investigation with the ATD HPOTP p 1679 N95-23621

VAPOR DEPOSITION
Large-area triple-junction a-Si alloy production scaleup
| DE95-000245 | p 1726 N95-22546
MOCVD of gallium and calcium sulfides for improved phosphor processing
| DE95-000918 | p 1631 N95-22677
Chemical vapor deposition in low pressure batch furnaces
| DE95-003035 | p 1632 N95-22722
Vapor deposition of thin-film Y-doped ZrO2 for electrochemical device applications
| DE95-003705 | p 1649 N95-23268
Silicon surface and bulk defect passivation by low temperature PECVD oxides and nitrides
| DE95-004531 | p 1731 N95-24090
High energy collimating fine grids
| NASA-CR-197688 | p 1871 N95-24191

VAPOR PHASES
A generalized Eulerian-Lagrangian analysis, with application to liquid flows with vapor bubbles p 1682 N95-23633

VAPORS
Analytical Boltzmann moments for electrons in N2-O2-H2O gas mixtures
| DE95-003474 | p 1732 N95-22898
A generalized Eulerian-Lagrangian analysis, with application to liquid flows with vapor bubbles p 1682 N95-23633
NTS-spill test facility wind tunnel exhaust plume characterization
| DE95-003630 | p 1616 N95-24019

VARIABILITY
Spectral variations in a collection of AVIRIS imagery p 1707 N95-23879

VARIANCE (STATISTICS)
Objective determination of image end-members in spectral mixture analysis of AVIRIS data p 1709 N95-23888

VECTOR ANALYSIS
Algorithms for parallel and vector computations
| NASA-CR-197394 | p 1756 N95-23017

VECTOR MESONS
Once more about the omega approaches 3(pi) contact term
| DE94-633202 | p 1804 N95-22847
On pseudosupersymmetric oscillators and reality of relativistic energies for vector mesons p 1815 N95-22994
On parasupersymmetric oscillators and relativistic vector mesons in constant magnetic fields p 1815 N95-22995

VECTOR PROCESSING (COMPUTERS)
VLUGR2: A vectorizable adaptive grid solver for PDes in 2D
| PB95-136008 | p 1789 N95-23167

VECTOR QUANTIZATION
Reevaluation of the significance of sequence information for speech recognition
| TR-555 | p 1658 N95-23794

VECTOR SPACES
Countable space with a closed subspace without continuous extender
| PB95-127973 | p 1785 N95-22533
Vector bundles as direct images of line bundles
| DE94-628422 | p 1795 N95-22630
Phase space analysis in anisotropic optical systems p 1826 N95-23007
Degenerate Hamiltonian Hopf bifurcations
| PB95-138871 | p 1789 N95-23174

VECTORS (MATHEMATICS)
Two portable parallel tridiagonal solvers
| DE94-019044 | p 1763 N95-23243
An implementation of the QMR method based on coupled two-term recurrences
| NASA-CR-197956 | p 1791 N95-23612

VEGETATION
Basic data sets description and preliminary results of EFEDA-Spain
| PB95-139291 | p 1740 N95-23470
Estimating dry grass residues using landscape integration analysis p 1705 N95-23867
The red edge in arid region vegetation: 340-1060 nm spectra p 1708 N95-23881
Temporal changes in endmember abundances, liquid water and water vapor over vegetation at Jasper Ridge p 1708 N95-23882
Mapping and monitoring changes in vegetation communities of Jasper Ridge, CA, using spectral fractions derived from AVIRIS images p 1708 N95-23883

VEGETATION GROWTH
Plant metabolism and cell wall formation in space (microgravity) and on Earth
| NASA-CR-197618 | p 1745 N95-22801

VEGETATIVE INDEX
Investigations on the 1.7 micron residual absorption feature in the vegetation reflection spectrum p 1710 N95-23891
A comparison of spectral mixture analysis an NDVI for ascertaining ecological variables p 1710 N95-23892

VELOCITY DISTRIBUTION
Unsteady flow simulations in support of the SSME HEX turning vane cracking investigation with the ATD HPOTP p 1679 N95-23621

VELOCITY MEASUREMENT
Experimental study of vortex breakdown in a swirling water jet
| PB95-130407 | p 1665 N95-22767
High gain GaAs photoconductive semiconductor switches: Measurement of filament velocity and reduced trigger energy
| DE95-001884 | p 1661 N95-22844
7th International Symposium on Applications of Laser Techniques to Fluid Mechanics, volume 1
| AD-A285647 | p 1691 N95-23118
Impeller flow field characterization with a laser two-focus velocimeter p 1675 N95-23440
Detailed measurements in the SSME high pressure fuel turbine with smooth rotor blades p 1675 N95-23441
Instantaneous 2D velocity and temperature measurements in high speed flows based on spectrally resolved molecular Rayleigh scattering
| NASA-TM-106883 | p 1688 N95-23461

VENTILATION
Load calculation and system evaluation for electric vehicle climate control
| DE95-004350 | p 1695 N95-23358

VENUS (PLANET)
IUE observing programs: NSOSS, VEOEB, and PCOEB
| NASA-CR-197424 | p 1866 N95-23560

VENUS ATMOSPHERE
IUE observing programs: NSOSS, VEOEB, and PCOEB
| NASA-CR-197424 | p 1866 N95-23560

VERTICAL DISTRIBUTION
Tomographic analysis of the three-dimensional variation of the seismic velocity structure of the shallow crust underlying Southern New England
| AD-A279406 | p 1739 N95-23247
Edge fluctuation measurements by phase contrast imaging on DIII-D
| DE94-016681 | p 1836 N95-23768

VERTICAL LANDING
Flow visualization studies of VTOL aircraft models during Hover in ground effect
| NASA-TM-108860 | p 1607 N95-22666

VERTICAL TAKEOFF
Flow visualization studies of VTOL aircraft models during Hover in ground effect
[NASA-TM-108860] p 1607 N95-22666
VERTICAL TAKEOFF AIRCRAFT
Flow visualization studies of VTOL aircraft models during Hover in ground effect
[NASA-TM-108860] p 1607 N95-22666
VERY LARGE SCALE INTEGRATION
Current estimation for electromigration, hot carriers, and voltage drop
[AD-A285794] p 1659 N95-22507
VLSI for high-speed digital signal processing
[AD-A285643] p 1663 N95-23783
VERY LONG BASE INTERFEROMETRY
Observation model and parameter partials for the JPL VLBI parameter estimation software MODEST, 19 94
[NASA-CR-197328] p 1756 N95-22853
Multiband VLBI imaging of the jet in 3C 345
[PB95-139275] p 1866 N95-23468
High data rate recorder development at MIT Haystack Observatory p 1690 N95-24118
A terabyte linear tape recorder p 1690 N95-24139
VERY LOW FREQUENCIES
The effect of magnetic field on the edge plasmons of two-dimensional electron gas systems
[DE94-018044] p 1837 N95-23982
VHSIC (CIRCUITS)
Specification and verification of gate-level VHDL models of synchronous and asynchronous circuits
[NASA-CR-191608] p 1762 N95-22830
VIABILITY
The viability of establishing collaborative, reconfigurable research environments for the Human Performance Research Laboratory at NASA Ames
[NASA-CR-197384] p 1753 N95-22480
VIBRATION
Vibration-damping structural component
[AD-D016550] p 1693 N95-22707
Finite-difference solutions of the alternate turbopump development high-pressure oxidizer turbopump pump-end ball-bearing cavity flows p 1678 N95-23617
VIBRATION DAMPING
Vibration-damping structural component
[AD-D016550] p 1693 N95-22707
Active control of panel vibrations induced by a boundary layer flow
[NASA-CR-197867] p 1608 N95-23182
VIBRATION ISOLATORS
Hardware interface unit for control of shuttle RMS vibrations p 1697 N95-23706
VIBRATION MODE
Statistically generated weighted curve fit of residual functions for modal analysis of structures
[NASA-TM-108481] p 1699 N95-22950
Synchronous dynamics of a coupled shaft/bearing/housing system with auxiliary support from a clearance bearing: Analysis and experiment
[NASA-CR-197858] p 1695 N95-23214
VIBRATIONAL SPECTRA
Algebraic approach to the vibrational excitations in methane p 1814 N95-22960
Algebraic description of atom-molecule interactions p 1814 N95-22961
VIBRATIONAL STATES
Hydrogen vibrational density of states of adsorbed water on rare-earth modified zirconia
[DE95-001127] p 1632 N95-22681
Molecular vibrational states during a collision p 1814 N95-22964
Energy transfer dynamics in isolated and in colliding highly vibrationally excited molecules
[AD-A285771] p 1806 N95-23077
VIDEO COMMUNICATION
Automated synthesis of image processing procedures using AI planning techniques p 1779 N95-23745
VIDEO DATA
Video frame processor
[DE94-635414] p 1753 N95-23962
VIDEO EQUIPMENT
Method of encouraging attention by correlating video game difficulty with attention level
[NASA-CASE-LAR-15022-1] p 1749 N95-22579
Video frame processor
[DE94-635414] p 1753 N95-23962
VIDEO SIGNALS
Video frame processor
[DE94-635414] p 1753 N95-23962
VINYL POLYMERS
LDEF polymeric materials: A summary of Langley characterization p 1651 N95-23899
VIRTUAL MEMORY SYSTEMS
Distributed VIRtual System (DIVIRS) project
[NASA-CR-197855] p 1757 N95-23180
VIRTUAL REALITY
Virtual reality flight control display with six-degree-of-freedom controller and spherical orientation overlay
[NASA-CASE-NPO-18733-1-CU] p 1613 N95-22578
Commercialization of JPL Virtual Reality calibration and redundant manipulator control technologies p 1768 N95-23676
VISCOELASTIC DAMPING
Vibration-damping structural component
[AD-D016550] p 1693 N95-22707
VISCOELASTICITY
Nonlinear viscoelastic characterization of polymer materials using a dynamic-mechanical methodology p 1651 N95-23902
VISCOSITY
Development and verification of a resin film infusion/resin transfer molding simulation model for fabrication of advanced textile composites
[NASA-CR-197439] p 1648 N95-23179
VISCOUS FLOW
Quasistatic model for the motion of a viscous capillary liquid drop
[PB95-138848] p 1667 N95-23172
An assessment of viscous effects in computational simulation of benign and burst vortex flows on generic fighter wind-tunnel models using TEAM code
[NASA-CR-4650] p 1608 N95-23185
The initial-value problem for viscous channel flows
[NASA-CR-195034] p 1667 N95-23207
Preconditioning for the Navier-Stokes equations with finite-rate chemistry p 1670 N95-23421
Numerical simulation of steady and unsteady viscous flow in turbomachinery using pressure based algorithm p 1671 N95-23426
Three-dimensional viscous flow analysis inside a turbine volute p 1674 N95-23437
On the conservative interface treatment for multi-block viscous flow computations
[NASA-CR-195442] p 1677 N95-23451
VISCOUS FLUIDS
BEm-BDF scheme for curvature driven moving stokes flows
[PB95-138905] p 1667 N95-23144
VISIBILITY
Atmospheric correction of AVIRIS data of Monterey Bay contaminated by thin cirrus clouds p 1710 N95-23890
Assessing the relative contribution of biogenic and fossil processes to visibility scattering aerosols found in remote areas: Near-term Organic Research Program
[DE95-003149] p 1735 N95-24146
VISIBLE SPECTRUM
A proposed update to the solar irradiance spectrum used in LOWTRAN and MODTRAN p 1705 N95-23865
Relationships between pigment composition variation and reflectance for plant species from a coastal savannah in California p 1709 N95-23889
VISUAL ACUITY
Laser irradiation effects: A functional assessment
[AD-A285100] p 1691 N95-22937
VISUAL CONTROL
Visually guided grasping to study teleprogrammation within the BAROCO testbed p 1777 N95-23731
Mark Tracking: Position/orientation measurements using 4-circle mark and its tracking experiments p 1778 N95-23736
Vision-based planning and execution of precision grasps
[TR-546] p 1784 N95-24185
VISUAL DISCRIMINATION
Laser irradiation effects: A functional assessment
[AD-A285100] p 1691 N95-22937
VISUAL OBSERVATION
Material inspection of EURECA first findings and recommendations p 1637 N95-23804
Long term microparticle impact fluxes on LDEF determined from optical survey of Interplanetary Dust Experiment (IDE) sensors p 1623 N95-23826
Near infrared and optical spectroscopy of FSC10214+4724
[NASA-CR-197966] p 1828 N95-24068
VISUAL PERCEPTION
Laser irradiation effects: A functional assessment
[AD-A285100] p 1691 N95-22937
Real-time tracking using stereo and motion: Visual perception for space robotics p 1778 N95-23739
VISUAL SIGNALS
Cueing light configuration for aircraft navigation
[NASA-CASE-ARC-11982-1] p 1611 N95-23393
VISUAL STIMULI
Functions of external cues in prospective memory
[DOT/FAA/AM-95/9] p 1750 N95-24088
VITRIFICATION
Glass science tutorial: Lecture 1, Chemistry and properties of oxide glasses
[DE95-002963] p 1647 N95-22647
VLASOV EQUATIONS
Hot proton anisotropies and cool proton temperatures in the outer magnetosphere
[DE95-002719] p 1736 N95-22850
VOICE COMMUNICATION
Addendum to the Proceedings of the Third International Mobile Satellite Conference (IMSC 1993)
[NASA-CR-197343] p 1655 N95-22813
VOLCANOES
Classification of the LCVF AVIRIS test site with a Kohonen artificial neural network p 1706 N95-23874
Application of MAC-Europe AVIRIS data to the analysis of various alteration stages in the Landdmannalauger Hydrothermal Area (South Iceland) p 1709 N95-23885
Current and future use of TOPSAR digital topographic data for volcanological research p 1714 N95-23949
VOLCANOLOGY
Application of MAC-Europe AVIRIS data to the analysis of various alteration stages in the Landdmannalauger Hydrothermal Area (South Iceland) p 1709 N95-23885
Current and future use of TOPSAR digital topographic data for volcanological research p 1714 N95-23949
VOLTAGE CONVERTERS (DC TO DC)
A high-power switch-mode DC power supply for dynamic loads
[DE94-016714] p 1659 N95-22504
Liquid nitrogen temperature operation of a switching power converter
[NASA-TM-106867] p 1662 N95-23219
VOLTAGE REGULATORS
Investigation of arc length versus flange thickness while using an arc voltage controller
[DE95-003937] p 1695 N95-23374
VORTEX BREAKDOWN
Experimental study of vortex breakdown in a swirling water jet
[PB95-130407] p 1665 N95-22767
VORTICES
Study of the pressure field in rotating homogeneous turbulent flows
[PB94-189107] p 1665 N95-22585
Euler technology assessment for preliminary aircraft design employing OVERFLOW code with multiblock structured-grid method
[NASA-CR-4651] p 1608 N95-23095
An assessment of viscous effects in computational simulation of benign and burst vortex flows on generic fighter wind-tunnel models using TEAM code
[NASA-CR-4650] p 1608 N95-23185
The initial-value problem for viscous channel flows
[NASA-CR-195034] p 1667 N95-23207
Crossflow instability control on a swept-wing: Preliminary studies p 1609 N95-23283
Preliminary identification of buffet problems in high speed civil transport p 1616 N95-23319
Aerodynamic surface distension system for high angle of attack forebody vortex control
[NASA-CASE-ARC-11979-1] p 1612 N95-23390
Three-dimensional Navier-Stokes analysis and redesign of an imbedded bellmouth nozzle in a turbine cascade inlet section p 1671 N95-23423
A study of the vortex flow over 76/40-deg double-delta wing
[NASA-CR-195032] p 1677 N95-23466
VORTICITY
A wavenumber-partitioning scheme for two-dimensional statistical closures
[DE95-004514] p 1677 N95-23483
VULNERABILITY
Rationale for the Modular Air-system Vulnerability Estimation Network (MAVEN) methodology
[AD-A285797] p 1611 N95-22510
An automated computer misuse detection system for UNICOS
[DE95-000929] p 1762 N95-22680

W

WAFERS
Innovative technology for contamination control in plasma processing
[DE95-000913] p 1829 N95-22519
Chemical vapor deposition in low pressure batch furnaces
[DE95-003035] p 1632 N95-22722
Superconductivity devices: Commercial use of space
[NASA-CR-197885] p 1648 N95-22883
Measurement and analysis of scatter from silicon wafers
[DE95-002411] p 1827 N95-23531

WAKES
Advanced detector development, laboratory simulations, diagnostic development, and data analysis on wake physics
| PL-TR-94-2204 | p 1831 N95-22948
WALL FLOW
A wall interference assessment/correction system
| NASA-CR-197421 | p 1667 N95-23183
Development of an algebraic stress/two-layer model for calculating thrust chamber flow fields
p 1675 N95-23442
WALL PRESSURE
A wall interference assessment/correction system
| NASA-CR-197421 | p 1667 N95-23183
WALLS
Structural studies of complex carbohydrates of plant cell walls
| DE95-003099 | p 1748 N95-24075
WASTE DISPOSAL
Environmental, Safety, and Health Considerations: Composite Materials in the Aerospace Industry
| NASA-CP-3289 | p 1628 N95-23025
A roadmap for regulatory survival in the 1990s
p 1628 N95-23026
Chemical recycling of scrap composites
p 1629 N95-23034
Simulation and off-line programming systems comparison
| DE95-002267 | p 1766 N95-23078
The Louisiana State University waste-to-energy incinerator
| DE95-004417 | p 1728 N95-23344
Closing the circle on the splitting of the atom: The environmental legacy of nuclear weapons production in the United States and what the Department of Energy is doing about it p 1818 N95-23562
Characterization of Type 304L stainless steel solid-state closure welds for radioactive waste containment
| DE94-016539 | p 1645 N95-23980
WASTE TREATMENT
Biotransformation of an uncured composite material
p 1629 N95-23033
Life support systems analysis and technical trades for a lunar outpost
| NASA-TM-109927 | p 1751 N95-23194
Review of research results for the photocatalytic oxidation of hazardous wastes in air
| DE95-004004 | p 1734 N95-23480
WASTE UTILIZATION
Chemical recycling of scrap composites
p 1629 N95-23034
The Louisiana State University waste-to-energy incinerator
| DE95-004417 | p 1728 N95-23344
WASTE WATER
Resource recovery and epidemiology of anaerobic wastewater treatment process in a controlled ecological life support system
| NASA-CR-197930 | p 1751 N95-23474
WATER
Hydrogen vibrational density of states of adsorbed water on rare-earth modified zirconia
| DE95-001127 | p 1632 N95-22681
Study on possible environmental effects of a WBM cutting discharge in the north sea, one year after termination of drilling
| PB95-133740 | p 1733 N95-23125
Revitalization of the Gemenc-area, Baja, Hungary. 1: A study on hydrological possibilities to revitalise the ecosystem in the Keselyues-area. 2: Towards the restoration of the Gyueruesalj floodplain
| PB95-139283 | p 1718 N95-23469
Theoretical calculations of pressure broadening coefficients for H2O perturbed by hydrogen or helium gas
| NASA-CR-197345 | p 1636 N95-23545
A new containerless image furnace with electro-static positioning device p 1690 N95-23674
Monitoring land use and degradation using satellite and airborne data p 1707 N95-23880
Temporal changes in endmember abundances, liquid water and water vapor over vegetation at Jasper Ridge
p 1708 N95-23882
Airborne rotary air separator study
| NASA-CR-189099 | p 1614 N95-24053
WATER BALANCE
HAPEX-Sahel: Basic description of methods and data sets
| PB95-127262 | p 1701 N95-22639
Implementation of a soil-canopy scheme into the CSIRO GCM: Regional aspects of the model response
| CSIRO-TR-32 | p 1721 N95-24192
WATER COLOR
SeaWiFS technical report series. Volume 25: Ocean optics protocols for SeaWiFS validation, revision 1
| NASA-TM-104566-VOL-25-REV- | p 1743 N95-22671
WATER FLOW
Flow measuring structures
| PB95-127254 | p 1665 N95-22638
WATER MANAGEMENT
Flow measuring structures
| PB95-127254 | p 1665 N95-22638
WATER QUALITY
Effects of wind on rainfall simulation. Spatial distribution of water application, kinetic energy, and overland flow under single full-cone nozzle sprays
| PB95-127304 | p 1717 N95-22537
WATER TREATMENT
Life support systems analysis and technical trades for a lunar outpost
| NASA-TM-109927 | p 1751 N95-23194
Resource recovery and epidemiology of anaerobic wastewater treatment process in a controlled ecological life support system
| NASA-CR-197930 | p 1751 N95-23474
WATER VAPOR
Computer modeling of the sensitivity of a laser water vapor sensor to variations in temperature and air speed
p 1692 N95-23330
Temporal changes in endmember abundances, liquid water and water vapor over vegetation at Jasper Ridge
p 1708 N95-23882
Investigations on the 1.7 micron residual absorption feature in the vegetation reflection spectrum
p 1710 N95-23891
WATER WAVES
Measurement of ocean wave spectra using polarimetric AIRSAR data p 1715 N95-23953
WATERPROOFING
Robotic system for the servicing of the orbiter thermal protection system p 1697 N95-23724
WATERSHEDS
Synergy between optical and microwave remote sensing to derive soil and vegetation parameters from MAC Europe 1991 Experiment p 1715 N95-23956
WATERWAYS
Flow measuring structures
| PB95-127254 | p 1665 N95-22638
WAVE DEGRADATION
Using AVIRIS for in-flight calibration of the spectral shifts of SPOT-HRV and of AVHRR? p 1710 N95-23893
WAVE DISPERSION
Tomographic analysis of the three-dimensional variation of the seismic velocity structure of the shallow crust underlying Southern New England
| AD-A279406 | p 1739 N95-23247
WAVE EQUATIONS
Time-periodic solutions of some forced nonlinear wave equations: Analysis, approximations and applications
| PB95-135083 | p 1788 N95-22932
Pseudoclassical description of the Dirac Oscillator
p 1825 N95-22996
WAVE FRONTS
Observation model and parameter partials for the JPL VLBI parameter estimation software MODEST, 19 94
| NASA-CR-197328 | p 1756 N95-22853
WAVE FUNCTIONS
Berry phase by description of the quantum systems in the Kustaanheimo-Stiefel bundle
| DE94-628410 | p 1847 N95-22620
More about the q-deformed H-atom wave functions: Normal and abnormal series
| DE94-628434 | p 1801 N95-22643
Hadrons of arbitrary spin and heavy quark symmetry
| DE94-628597 | p 1804 N95-22789
An algebraic cluster model based on the harmonic oscillator basis p 1814 N95-22971
A Ramanujan-type measure for the Askey-Wilson polynomials p 1797 N95-22975
Coherent states for the relativistic harmonic oscillator
p 1825 N95-22993
Slightly anharmonic systems in quantum optics
p 1826 N95-23004
Bose condensation, macroscopic quantum phenomena and atomic spatial correlations in superfluid He-4
| PB95-139085 | p 1850 N95-23154
Spontaneous wave packet reduction
| DE94-634280 | p 1851 N95-23454
The point interactions in the quantum problem of three particles with internal structure
| DE94-635423 | p 1851 N95-23967
WAVE PACKETS
Spontaneous wave packet reduction
| DE94-634280 | p 1851 N95-23454
WAVE PROPAGATION
The propagation of travelling waves for stochastic generalized KPP equations
| DE94-628473 | p 1787 N95-22772
Utilizing a TDRS satellite for direct broadcast satellite-radio propagation experiments and demonstrations p 1622 N95-22814
Propagation of waves at the loosely bonded interface of two porous elastic half-spaces
| DE94-628477 | p 1800 N95-23018
Tomographic analysis of the three-dimensional variation of the seismic velocity structure of the shallow crust underlying Southern New England
| AD-A279406 | p 1739 N95-23247
Benchmark problems in computational aeroacoustics
p 1800 N95-23315
A generic efficient adaptive grid scheme for rocket propulsion modeling p 1670 N95-23418
WAVE SCATTERING
A uniform geometrical optics and an extended uniform geometrical theory of diffraction for evaluating high frequency EM fields near smooth caustics and composite shadow boundaries
| NASA-CR-197934 | p 1657 N95-23391
WAVEFORMS
Stability and efficiency of waveform relaxation methods
| PB95-138863 | p 1789 N95-23173
WAVEGUIDES
Supersymmetric oscillator in optics
p 1826 N95-23002
WAVELENGTHS
Using AVIRIS for in-flight calibration of the spectral shifts of SPOT-HRV and of AVHRR? p 1710 N95-23893
WAVELET ANALYSIS
Wavelet time-frequency analysis of phase-shift-key modulated signals
| AD-A285791 | p 1655 N95-22505
Hierarchical analysis of spatial pattern and processes of Douglas-fir forests p 1719 N95-24099
WEAK INTERACTIONS (FIELD THEORY)
Unification of electromagnetic, strong and weak interaction
| DE94-628570 | p 1655 N95-22746
WEAR TESTS
Evaluation of thermal barrier and PS-200 self-lubricating coatings in an air-cooled rotary engine
| NASA-CR-195445 | p 1614 N95-23222
WEATHER FORECASTING
SWIFT BOAT 1994: Using a fast chase boat to investigate offshore weather features in conjunction with WSR-88D observations
| PB94-195146 | p 1742 N95-22651
Annual tropical cyclone report, 1993
| AD-A285097 | p 1742 N95-23255
WEATHERING
Exfoliation corrosion and stress corrosion cracking behaviour of Al-Li alloys p 1641 N95-23498
WEIGHT (MASS)
Load calculation and system evaluation for electric vehicle climate control
| DE95-004350 | p 1695 N95-23358
WEIGHT REDUCTION
Weight minimization of structural components for launch in space shuttle
| NASA-TM-4586 | p 1698 N95-22805
Effect of the space environment on materials flown on the EURECA/TICCE-HVI experiment
p 1623 N95-23803
WEIGHTING FUNCTIONS
Statistically generated weighted curve fit of residual functions for modal analysis of structures
| NASA-TM-108481 | p 1699 N95-22950
On-line, adaptive state estimator for active noise control p 1784 N95-23308
On adaptive weighted polynomial preconditioning for Hermitian positive definite matrices
| NASA-CR-197946 | p 1791 N95-23547
WEIGHTLESSNESS
Self-generating oscillating pressure exercise device
| NASA-CASE-ARC-12000-1 | p 1751 N95-23264
Newton in space
| NASA-TM-110535 | p 1799 N95-23273
Toys in space, 2
| NASA-TM-110541 | p 1620 N95-23275
Microgravity combustion science: 1995 program update
| NASA-TM-106858 | p 1626 N95-24004
WELDABILITY
Vaccum Gas Tungsten Arc Welding, phase 1
| NASA-CR-197979 | p 1696 N95-24064
WELDED JOINTS
Vision-sensing image analysis for GTAW process control
| DE95-003936 | p 1695 N95-23373
Investigation of arc length versus flange thickness while using an arc voltage controller
| DE95-003937 | p 1695 N95-23374
Explosive bonding and its application in the Advanced Photon Source front-end and beamline components design
| DE95-004132 | p 1696 N95-23397

Characterization of Type 304L stainless steel solid-state closure welds for radioactive waste containment
| DE94-016539 | p 1645 N95-23980

WELDED STRUCTURES
Long-term aging of type 308 stainless steel welds: Effects on properties and microstructure
| DE94-018961 | p 1640 N95-23132

WELDING
Vaccum Gas Tungsten Arc Welding, phase 1
| NASA-CR-197979 | p 1696 N95-24064

WETTING
Sullivan model for wetting transition in closed system
| DE94-628472 | p 1665 N95-22771

WHISKERS (CRYSTALS)
Whisker/Cone growth on the thermal control surfaces experiment no. S0069 p 1651 N95-23911

WHITE NOISE
The propagation of travelling waves for stochastic generalized KPP equations
| DE94-628473 | p 1787 N95-22772

WIDE ANGLE LENSES
Automatic commanding of the Mars Observer Camera p 1620 N95-23754

WIENER FILTERING
Tutorial on filtering, restoration, and state estimation
| TR-534 | p 1793 N95-24042

WIGGLER MAGNETS
Undulators for short wavelength FEL amplifiers
| DE95-004690 | p 1692 N95-23487

WIGNER COEFFICIENT
Coherent state constructions of bases for some physically relevant group chains p 1814 N95-22966

WILDLIFE
Geographic information analysis: An ecological approach for the management of wildlife on the forest landscape
| NASA-CR-197941 | p 1719 N95-24094
Old-growth and mature forests near spotted owl nests in western Oregon p 1719 N95-24098
Forest and wildlife habitat analysis using remote sensing and geographic information systems p 1720 N95-24100

WIND (METEOROLOGY)
HAPEX-Sahel: Basic description of methods and data sets
| PB95-127262 | p 1701 N95-22639
Conjugate gradient MATHEW
| DE95-003479 | p 1738 N95-23143

WIND DIRECTION
Applied research on air pollution using nuclear-related analytical techniques
| DE94-633513 | p 1734 N95-23542

WIND EFFECTS
Effects of wind on rainfall simulation. Spatial distribution of water application, kinetic energy, and overland flow under single full-cone nozzle sprays
| PB95-127304 | p 1717 N95-22537
A numerical study of interannual wind forcing effects on the California current system, 1980-1983
| AD-A286023 | p 1743 N95-23074
AIRSAR views of aerolian terrain p 1713 N95-23941

WIND EROSION
Monitoring land use and degradation using satellite and airborne data p 1707 N95-23880

WIND MEASUREMENT
Continued studies of polar cap thermospheric dynamics
| PL-TR-94-2076 | p 1737 N95-22951
The effect of sensor spacing on wind measurements at the Shuttle Landing Facility
| NASA-TP-3529 | p 1742 N95-23010

WIND PRESSURE
The spectral content of the torque loads on a turbine gear tooth
| DE95-002188 | p 1694 N95-23056

WIND SHEAR
Maximum-likelihood spectral estimation and adaptive filtering techniques with application to airborne Doppler weather radar
| NASA-CR-197699 | p 1658 N95-23670

WIND TUNNEL MODELS
Dynamic response tests of inertial and optical wind-tunnel model attitude measurement devices
| NASA-TM-109182 | p 1616 N95-23011
Four-nozzle benchmark wind tunnel model USA code solutions for simulation of multiple rocket base flow recirculation at 145,000 feet altitude p 1686 N95-23654

WIND TUNNEL NOZZLES
Optimized design of a hypersonic nozzle p 1617 N95-23304
Three-dimensional Navier-Stokes analysis and redesign of an imbedded bellmouth nozzle in a turbine cascade inlet section p 1671 N95-23423
Supersonic laminar flow control research
| NASA-CR-197938 | p 1609 N95-23669

WIND TUNNEL TESTS
Wing pressure distributions from subsonic tests of a high-wing transport model --- in the Langley 14- by 22-Foot Subsonic Wind Tunnel
| NASA-TM-4583 | p 1607 N95-22802
Dynamic response tests of inertial and optical wind-tunnel model attitude measurement devices
| NASA-TM-109182 | p 1616 N95-23011
Experimental technique and assessment for measuring the convective heat transfer coefficient from natural ice accretions
| NASA-TM-106864 | p 1668 N95-23248
Experimental results for a hypersonic nozzle/afterbody flow field
| NASA-TM-4638 | p 1609 N95-23250
Performance of the 0.3-meter transonic cryogenic tunnel with air, nitrogen, and sulfur hexafluoride media under closed loop automatic control
| NASA-CR-195052 | p 1668 N95-23257
Crossflow instability control on a swept-wing: Preliminary studies p 1609 N95-23283
Preliminary identification of buffet problems in high speed civil transport p 1616 N95-23319
Instantaneous 2D velocity and temperature measurements in high speed flows based on spectrally resolved molecular Rayleigh scattering
| NASA-TM-106883 | p 1688 N95-23461
A study of the vortex flow over 76/40-deg double-delta wing
| NASA-CR-195032 | p 1677 N95-23466
Four-nozzle benchmark wind tunnel model USA code solutions for simulation of multiple rocket base flow recirculation at 145,000 feet altitude p 1686 N95-23654

WIND TUNNEL WALLS
A wall interference assessment/correction system
| NASA-CR-197421 | p 1667 N95-23183

WIND TUNNELS
NTS-spill test facility wind tunnel exhaust plume characterization
| DE95-003630 | p 1616 N95-24019

WIND TURBINES
Application requirements for wind turbine gearboxes
| DE94-011883 | p 1694 N95-22923
The spectral content of the torque loads on a turbine gear tooth
| DE95-002188 | p 1694 N95-23056
GPP: A General-Purpose Post Processor for wind turbine data analysis
| DE95-000223 | p 1729 N95-23383
GPP user's guide: A general-purpose postprocessor for wind turbine data analysis
| DE95-000293 | p 1730 N95-23776

WIND VARIATIONS
Long term variability of B supergiant winds
| NASA-CR-197925 | p 1865 N95-23401

WIND VELOCITY
The effect of sensor spacing on wind measurements at the Shuttle Landing Facility
| NASA-TP-3529 | p 1742 N95-23010
Format( )MEDIC( )Input
| DE95-003482 | p 1737 N95-23063
A numerical study of interannual wind forcing effects on the California current system, 1980-1983
| AD-A286023 | p 1743 N95-23074
NTS-spill test facility wind tunnel exhaust plume characterization
| DE95-003630 | p 1616 N95-24019

WINDING
Planar magnetic component development
| DE95-003311 | p 1661 N95-22896

WINDPOWER UTILIZATION
Renewable Energy Sources Brno 1993
| DE94-633975 | p 1727 N95-22855
Hydrogen and fuel cells for energy storage
| DE95-723907 | p 1729 N95-23382

WINDS ALOFT
Modeling of the coupled magnetospheric and neutral wind dynamos
| NASA-CR-197861 | p 1738 N95-23090

WINGS
Wing pressure distributions from subsonic tests of a high-wing transport model --- in the Langley 14- by 22-Foot Subsonic Wind Tunnel
| NASA-TM-4583 | p 1607 N95-22802
Control of flow separation in airfoil/wing design applications p 1609 N95-23294
High-lift flow-physics flight experiments on a subsonic civil transport aircraft (B737-100) p 1609 N95-23333
Lift enhancing tabs for airfoils
| NASA-CASE-ARC-11990-1 | p 1613 N95-23395

WIRE
Two-photon absorption in an indirect-gap semiconductor quantum well systems 1. Interband transitions
| DE94-628879 | p 1849 N95-22760
Two-photon absorption in an indirect-gap semiconductor quantum well systems 2. Excitonic transitions
| DE94-628880 | p 1849 N95-22761

WIRE CLOTH
Passive intermodulation generation in wire mesh deployable reflector antennas p 1656 N95-22816

WORD PROCESSING
Phonetic set hashing: A novel scheme for transforming phone sequences to words
| TR-538 | p 1658 N95-24039

WORDS (LANGUAGE)
Phonetic set hashing: A novel scheme for transforming phone sequences to words
| TR-538 | p 1658 N95-24039

WORKING FLUIDS
Current status in cavitation modeling p 1681 N95-23632

WORKSTATIONS
HiRel: Hybrid Automated Reliability Predictor (HARP) integrated reliability tool system, (version 7.0). Volume 3: HARP Graphics Oriented (GO) input user's guide
| NASA-TP-3452-VOL-3 | p 1753 N95-22479
HiRel: Hybrid Automated Reliability Predictor (HARP) integrated reliability tool system, (version 7.0). Volume 2: HARP tutorial
| NASA-TP-3452-VOL-2 | p 1755 N95-22604
HiRel: Hybrid Automated Reliability Predictor (HARP) integrated reliability tool system, (version 7.0). Volume 4: HARP Output (HARPO) graphics display user's guide
| NASA-TP-3452-VOL-4 | p 1755 N95-22605
Performance of single-keyword and multiple-keyword pattern matching algorithms
| PB95-138954 | p 1756 N95-23150
JPL space robotics: Present accomplishments and future thrusts p 1697 N95-23697

WOVEN COMPOSITES
Idealized textile composites for experimental/analytical correlation p 1631 N95-23277

X

X RAY ABSORPTION
Solvation of isolated transition metal ions
| DE95-002978 | p 1638 N95-22571
Ligand K-edge x-ray adsorption spectroscopic studies of the electronic structure of inorganic model complexes and metalloprotein active sites
| DE95-003338 | p 1840 N95-22851

X RAY ANALYSIS
X-ray transmission microscope development
| NASA-CR-197884 | p 1826 N95-23016
Germination, growth rates, and electron microscope analysis of tomato seeds flown on the LDEF p 1748 N95-23821
Debris and meteoroid proportions deduced from impact crater residue analysis p 1869 N95-23834
Micro-abrasion package capture cell experiment on the trailing edge of LDEF: Impactor chemistry and whipple bumper shield efficiencies p 1624 N95-23835
Microstructure and composition of a SNS Josephson junction using CaRuO3 as the metallic barrier
| DE95-004611 | p 1845 N95-24152

X RAY DETECTORS
Runaway electrons in TEXT-U
| DE94-019218 | p 1831 N95-22862

X RAY DIFFRACTION
Nondestructive evaluation of fatigue damage in aluminum 2024 by x-ray diffraction p 1698 N95-23293

X RAY IMAGERY
On-orbit science in a small package: Managing the ALEXIS satellite and experiments
| DE94-014426 | p 1621 N95-22868

X RAY INSPECTION
POD assessment of NDI procedures using a round robin test
| AGARD-R-809 | p 1697 N95-23602

X RAY LASERS
Ninth topical conference on atomic processes in plasmas
| DE95-002810 | p 1833 N95-23246

X RAY OPTICS
Preserving the high source brightness with x ray beam line optics
| DE95-003172 | p 1820 N95-22877
Development of microchannel plate x-ray optics
| NASA-CR-197935 | p 1866 N95-23540

X RAY SCATTERING
Protein folding and protein metallocluster studies using synchrotron small angler x ray scattering
| DE95-003339 | p 1746 N95-22897

Small angle x ray scattering studies of aggregation in supercritical fluid solutions
[DE95-004576] p 1843 N95-23579

X RAY SOURCES
Protein folding and protein metallocluster studies using synchrotron small angler x ray scattering
[DE95-003339] p 1746 N95-22897
X-ray transmission microscope development
[NASA-CR-197884] p 1826 N95-23016
A study of EUV emission from the O4f star Zeta Puppis
[NASA-CR-197350] p 1871 N95-23472

X RAY SPECTRA
KKR-CPA calculations of density of states and soft X ray emission from disordered Li-Mg alloys
[DE94-628882] p 1640 N95-22934

X RAY SPECTROSCOPY
Long range potentials and multiple scattering theory in complex systems
[DE94-628881] p 1804 N95-22791
Transmission electron microscope studies of extraterrestrial materials
[NASA-CR-188363] p 1633 N95-23092
Atomic physics at high brilliance synchrotron sources: Proceedings
[DE95-006077] p 1813 N95-24174

X RAY TELESCOPES
On-orbit science in a small package: Managing the ALEXIS satellite and experiments
[DE94-014426] p 1621 N95-22868

X RAYS
Preserving the high source brightness with x ray beam line optics
[DE95-003172] p 1820 N95-22877
KKR-CPA calculations of density of states and soft X ray emission from disordered Li-Mg alloys
[DE94-628882] p 1640 N95-22934
ROSAT observation program
[NASA-CR-197683] p 1866 N95-23595
A simple, closed-form expression for the x ray reflectivity from superlattices with cumulative roughness
[DE95-004633] p 1846 N95-24170

X-29 AIRCRAFT
Flight test of the X-29A at high angle of attack: Flight dynamics and controls
[NASA-TP-3537] p 1612 N95-22806

XENON
NASA 30 cm ion thruster development status
[NASA TM-106842] p 1624 N95-23221
Temperature effects on ion irradiation damage in MgAl2O4 spinel single crystals
[DE95-003679] p 1844 N95-24073

Y

YAG LASERS
Measurements of striae in CR+ doped YAG laser crystals p 1847 N95-23285

YANG-MILLS THEORY
Continuous local symmetry in Ising-type models
[DE94-629045] p 1839 N95-22649
Lectures on 2D gauge theories. Topological aspects and path integral techniques
[DE94-628509] p 1849 N95-22752

YAW
Pitch sensor system
[AD-D016488] p 1799 N95-22863
Feedback control laws for highly maneuverable aircraft
[NASA-CR-197944] p 1615 N95-23410

YBCO SUPERCONDUCTORS
Initial crystallization and growth in melt processing of large-domain YBa2Cu3O(x) for magnetic levitation
[DE95-002993] p 1839 N95-22572
A study of ceramic composite of ferroelectric BaTiO3 ceramic and superconductor YBa2Cu3O(6+delta) ceramic
[DE94-627563] p 1647 N95-22610
Microstructure and composition of a SNS Josephson junction using CaRuO3 as the metallic barrier
[DE95-004611] p 1845 N95-24152
Processing of single- and multi-domain YBa2Cu3O(x) bulk materials for levitation applications by Nd(1+x)Ba(2-x)Cu3O(y) seeding
[DE95-004615] p 1845 N95-24154

YIELD POINT
A ruggedness evaluation of procedures for damage threshold testing optical materials
[NASA-TM-4639] p 1840 N95-22803

YTTRIA-STABILIZED ZIRCONIA
Vapor deposition of thin-film Y-doped ZrO2 for electrochemical device applications
[DE95-003705] p 1649 N95-23268

YTTRIUM
Evolution of oxidation and creep damage mechanisms in HIPed silicon nitride materials
[DE95-001360] p 1647 N95-22689

YTTRIUM OXIDES
Preparation of high quality YBa2Cu3O(7-delta) thick films on flexible Ni-based alloy substrates with textured buffer layers
[DE95-003686] p 1645 N95-23571

Z

ZEOLITES
NO decomposition in non-reducing atmospheres
[DE95-004324] p 1634 N95-23339

ZINC
The corrosion protection of 2219-T87 aluminum by organic and inorganic zinc-rich primers
[NASA-TP-3543] p 1641 N95-23186

ZINC SELENIDES
Annealing of nitrogen-doped ZnSe at high pressures: Toward suppression of native defect formation
[DE95-003420] p 1844 N95-24010

ZIRCONIUM ALLOYS
Experimental and theoretical studies on the C15 intermetallic compounds MV2 (M = Zr, Hf and Ta): Elasticity and phase stability
[DE95-003723] p 1845 N95-24079

ZIRCONIUM OXIDES
Performance of thin-ceramic-coated combustion chamber with gasoline and methanol as fuels in a two-stroke SI engine
[DE95-002903] p 1693 N95-22557
Hydrogen vibrational density of states of adsorbed water on rare-earth modified zirconia
[DE95-001127] p 1632 N95-22681
Transformation behavior in Al2O3-ZrO2 ceraamic composites
[DE95-001359] p 1647 N95-22688
High resolution microstructural analysis of zirconia eutectic interfaces
[DE95-003143] p 1845 N95-24143

PERSONAL AUTHOR INDEX

Typical Personal Author Index Listing

ACKERMAN, PHILLIP L. ..... p 147 N95-10536

PERSONAL AUTHOR | PAGE NUMBER | ACCESSION NUMBER

Listings in this index are arranged alphabetically by personal author. The page number helps you locate the citation in the abstract section. The accession number denotes the number by which the citation is identified.

A

AARDAL, K. ..... p 1786 N95-22641
AARTS, H. F. M. ..... p 1794 N95-23239
p 1794 N95-23539
AARUP, MADS ..... p 1770 N95-23685
p 1617 N95-23751
ABBASI, S. J. ..... p 1796 N95-22808
ABE, TOSHIO ..... p 1690 N95-23674
p 1697 N95-23722
ABEELE, G. D. V. D. ..... p 1740 N95-23470
ABEL, S. A. ..... p 1807 N95-23157
ABER, JOHN D. ..... p 1706 N95-23873
ABOUDI, JACOB ..... p 1699 N95-24055
ABRAMOVICH, HAIM ..... p 1699 N95-23923
ACETI, ROBERTO ..... p 1623 N95-23799
ACEVES, S. M. ..... p 1662 N95-23334
p 1695 N95-23358
ACHARYA, A. ..... p 1614 N95-24053
ACKER, JAMES G. ..... p 1743 N95-22671
ACOSTA, A. J. ..... p 1680 N95-23628
ADACHI, TADASHI ..... p 1771 N95-23692
p 1692 N95-23712
ADAIR, R. T. ..... p 1655 N95-22636
ADAMS, C. D. ..... p 1631 N95-22677
ADAMS, DANIEL O. ..... p 1631 N95-23277
ADAMS, JAMES H., JR. ..... p 1815 N95-23807
p 1870 N95-23808
ADAMS, JOHN B. ..... p 1708 N95-23882
p 1708 N95-23883
ADAMS, R. G. ..... p 1818 N95-24160
ADELMAN, HOWARD M. ..... p 1612 N95-22953
ADENIYI, J. O. ..... p 1736 N95-22613
ADIMULA, I. A. ..... p 1736 N95-22613
ADJEPONG, S. K. ..... p 1839 N95-22607
ADKINS, D. R. ..... p 1663 N95-23779
ADLER, RICHARD M. ..... p 1761 N95-23749
ADLER, STEPHEN L. ..... p 1803 N95-22749
AGARWAL, R. K. ..... p 1673 N95-23433
AGARWALA, V. S. ..... p 1644 N95-23515
AGARWALA, VINOID S. ..... p 1687 N95-22706
AGASHE, ALOK ..... p 1753 N95-23962
AGRO, S. ..... p 1728 N95-23062
AHERN, F. ..... p 1716 N95-23961
AINSWORTH, T. L. ..... p 1712 N95-23939
AKDENIZ, Z. ..... p 1640 N95-23057
AKITA, KENZO ..... p 1752 N95-23704
p 1752 N95-23705
ALAM, M. ANIS ..... p 1639 N95-22608
ALBRECHT, A. ..... p 1646 N95-23820
ALDAYA, VICTOR ..... p 1825 N95-22993
ALDRICH, DONALD C. ..... p 1628 N95-23027
ALEKSEEVSKY, D. V. ..... p 1795 N95-22712
ALEXANDER, D. J. ..... p 1640 N95-23132
ALEXANDER, J. IWAN D. ..... p 1653 N95-23552
ALEXANDER, K. B. ..... p 1647 N95-22688
ALIAGA, J. ..... p 1850 N95-22782
ALLEN, JAMES F. ..... p 1659 N95-24193
ALLEN, S. L. ..... p 1832 N95-23119
ALLRED, RONALD E. ..... p 1629 N95-23034
ALLSHOUSE, G. O. ..... p 1818 N95-24160
ALMGREN, A. S. ..... p 1665 N95-22491
ALSTEIN, D. ..... p 1763 N95-23129
ALTEROVITZ, S. A. ..... p 1846 N95-24188
ALVAREZ, M. G. ..... p 1645 N95-23983
AMAI, W. A. ..... p 1694 N95-23065
AMARI, SACHIKO ..... p 1637 N95-23837
AMES, GREGORY H. ..... p 1819 N95-22492
p 1820 N95-22864
AMO, H. ..... p 1835 N95-23528
AMUSIA, M. YA. ..... p 1813 N95-24151
ANDERS, A. ..... p 1844 N95-24011
ANDERS, S. ..... p 1844 N95-24011
ANDERSON, P. G. ..... p 1668 N95-23413
ANDERSON, P. M. ..... p 1693 N95-22798
ANDERSON, R. R. ..... p 1869 N95-22828
ANDERSON, ROBERT L. ..... p 1623 N95-23719
ANDOH, FUMIHIKO ..... p 1690 N95-24107
ANDRAWIS, MADELEINE Y. ..... p 1741 N95-23278
ANDREAE, MEINRAT O. ..... p 1732 N95-22930
ANDREOLI, G. ..... p 1710 N95-23891
ANERELLA, M. ..... p 1816 N95-22926
ANGELO, J. E. ..... p 1639 N95-22724
ANIK, M. ..... p 1641 N95-23499
ANISALAM, M. ANIS ..... p 1640 N95-22840
ANNAJIRAO, K. ..... p 1814 N95-24175
ANSARI, N. A. ..... p 1822 N95-22976
ANTONIADIS, H. ..... p 1660 N95-22586
ANTONIADIS, I. ..... p 1851 N95-23922
ANTONIO, JOSEPH C. ..... p 1750 N95-22513
ANTONOV, A. N. ..... p 1813 N95-24046
AOKI, SHIGERU ..... p 1623 N95-23726
APPEL, JEFFREY A. ..... p 1801 N95-22646
APPLIN, ZACHARY T. ..... p 1607 N95-22802
APTE, P. ..... p 1843 N95-23586
ARAI, S. ..... p 1816 N95-22644
p 1816 N95-22848
ARENDT, P. ..... p 1645 N95-23571
ARENDT, P. N. ..... p 1838 N95-22520
ARENT, K. ..... p 1767 N95-23199
ARGO, P. E. ..... p 1658 N95-24015
ARMENTROUT, P. B. ..... p 1646 N95-24144
ARMSTRONG, T. W. ..... p 1815 N95-23811
p 1815 N95-23815
p 1815 N95-23818
p 1815 N95-23819
ARMSTRONG, THOMAS D. ..... p 1691 N95-22748
ARMUS, L. ..... p 1828 N95-24068
ARNOLD, A. J. ..... p 1650 N95-23932
ARNOLD, STEVEN M. ..... p 1699 N95-24055
ARRIETA, VICTOR M. ..... p 1871 N95-24191
ARROYO, RUBEN ..... p 1749 N95-22987
ARSENOVIC, PETAR ..... p 1629 N95-23037
ARUTYUNYAN, G. G. ..... p 1851 N95-23970
ASAF, U. ..... p 1803 N95-22747
ASAKURA, M. ..... p 1777 N95-23729
ASCOLI, EDWARD P. ..... p 1669 N95-23416
p 1673 N95-23432
p 1674 N95-23436
p 1686 N95-23653
ASHJAEE, JAVAD M. ..... p 1656 N95-22818
ASLAM, T. ..... p 1666 N95-22901
ASPER, V. L. ..... p 1819 N95-22780
ATAKISHIYEV, NATIG M. ..... p 1797 N95-22975
p 1798 N95-23006
ATKINSON, DALE ..... p 1624 N95-23843
ATKINSON, DAVID J. ..... p 1775 N95-23717
ATKINSON, WILLIAM H. ..... p 1689 N95-23795
ATWOOD, C. L. ..... p 1793 N95-22550
AUBERT, J. H. ..... p 1650 N95-24159
p 1818 N95-24160
AUSTIN, ROSWELL W. ..... p 1743 N95-22671
AVERETTE, H. S. ..... p 1661 N95-22799
AVRIGEANU, M. ..... p 1813 N95-24046
AVRIGEANU, V. ..... p 1813 N95-24046
AVVA, RAM K. ..... p 1681 N95-23632
AYENSU, A. ..... p 1839 N95-22607

B

BAATH, L. B. ..... p 1866 N95-23468
BACHE, GEORGE ..... p 1679 N95-23622
BACON, L. D. ..... p 1818 N95-24160
BADDELEY, A. J. ..... p 1793 N95-22527
BADER, S. D. ..... p 1840 N95-22762
p 1846 N95-24168
BADGETT, W. F. ..... p 1810 N95-23522
BAETEN, J. C. M. ..... p 1786 N95-22714
BAILEY, J. E. ..... p 1818 N95-24160
BAIN, RICHARD L. ..... p 1727 N95-22888
BAIRI, B. R. ..... p 1753 N95-23962
BAITY, F. W. ..... p 1837 N95-24083
BAKER, D. R. ..... p 1832 N95-23119
BAKER, S. M. ..... p 1649 N95-23568
BAL, H. E. ..... p 1754 N95-22529
BALACHANDRAN, U. ..... p 1839 N95-22572
p 1662 N95-23355
BALAKRISHNA, S. ..... p 1668 N95-23257
BALAS, GARY J. ..... p 1615 N95-23410
BALCAR, E. ..... p 1798 N95-23127
BALDIN, B. ..... p 1817 N95-23369
BALEANU, D. ..... p 1810 N95-23456
BALICK, L. K. ..... p 1721 N95-24148
BALLARD, DANA H. ..... p 1658 N95-23794
p 1658 N95-24039
BAMBA, H. ..... p 1777 N95-23729
BANIN, A. T. ..... p 1850 N95-22776
BANKS, BRUCE A. ..... p 1626 N95-23270
p 1651 N95-23802
p 1627 N95-23909
p 1650 N95-24187
BANSAL, NAROTTAM P. ..... p 1627 N95-22563
BANTLY, J. ..... p 1818 N95-24077
BAO, HAN P. ..... p 1623 N95-23279
BAO, YAHUA ..... p 1647 N95-22610
p 1647 N95-22611
BARAGIOLA, R. A. ..... p 1869 N95-24066
BARANKO, G. J. ..... p 1806 N95-23140
BARASHENKOV, V. S. ..... p 1851 N95-23964
p 1851 N95-23968
BARBASHOV, B. M. ..... p 1851 N95-23969
BARBEE, T. W., III ..... p 1841 N95-22860
BARES, JOHN ..... p 1697 N95-23694
BARET, FREDERIC ..... p 1701 N95-23845
BARGER, V. ..... p 1807 N95-23158
BARLETTA, W. ..... p 1818 N95-24014
BARNES, LESLIE A. ..... p 1641 N95-23215
p 1809 N95-23408
p 1810 N95-23459
BARON, J. M. ..... p 1624 N95-23827
BARON, S. ..... p 1728 N95-23133
BARONTI, S. ..... p 1712 N95-23940
BARRETT, DAVID J. ..... p 1693 N95-22707
BARRETT, ROGER ..... p 1825 N95-22998
BARRETT, RUTH A. ..... p 1869 N95-23832
BARSON, STEVEN L. ..... p 1669 N95-23416
BARTELS, D. M. ..... p 1810 N95-23491
BARTLETT, D. L. ..... p 1641 N95-23497
BARZ, S. ..... p 1872 N95-23806
BASORE, P. A. ..... p 1845 N95-24156
p 1731 N95-24157
BASSON, A. ..... p 1671 N95-23426
BASTASZ, B. ..... p 1832 N95-23119
BATCHELOR, D. A. ..... p 1637 N95-23836
BATEMAN, F. B. ..... p 1806 N95-23137
BATESON, C. ANN ..... p 1701 N95-23846
p 1710 N95-23892
BATHE, C. G. ..... p 1829 N95-22645
BATY, R. S. ..... p 1795 N95-22734
BAUD, TIM ..... p 1770 N95-23685
BAUDIN, CATHERINE ..... p 1768 N95-23678
BAUER, D. J. ..... p 1742 N95-23385
BAUER, JEFFREY E. ..... p 1612 N95-22806
BAUMEISTER, JOSEPH F. ..... p 1792 N95-23614
BAUMEISTER, KENNETH J. ..... p 1792 N95-23614
BAVUSO, SALVATORE J. ..... p 1753 N95-22479
p 1754 N95-22603
p 1755 N95-22604
p 1755 N95-22605
BAXI, C. B. ..... p 1693 N95-22796
p 1693 N95-22798

BAYA, VINOD p 1768 N95-23678
BAYSAL, OKTAY p 1612 N95-22949
p 1608 N95-23218
BDZIL, J. B. p 1666 N95-22901
BEAHM, LORRAINE P. p 1815 N95-23807
p 1870 N95-23808
BEALE, CHRIS p 1768 N95-23676
BEAM, SHERILEE F. p 1700 N95-23280
BEANE, JOHN p 1859 N95-24121
BEAUJEAN, R. p 1872 N95-23806
BECHER, P. F. p 1647 N95-22688
BECKER, KRIS p 1704 N95-23859
BECKER, LUANN p 1700 N95-23831
BECKERS, JULES p 1815 N95-22994
p 1815 N95-22995
BECKMAN, BRIAN C. p 1613 N95-22578
BECKMANN, CARL J. p 1791 N95-23600
BEDET, JEAN-JACQUES p 1859 N95-24121
p 1862 N95-24134
BEER, M. A. p 1830 N95-22694
p 1831 N95-22899
BEHEIM, GLENN p 1820 N95-22915
BEHNKE, JEANNE p 1862 N95-24136
BELIC, A. p 1840 N95-22839
BELITSKIJ, A. V. p 1812 N95-23984
BELL, J. B. p 1665 N95-22491
BELL, Z. W. p 1806 N95-23055
BELLINGER, N. C. p 1642 N95-23503
BEN-DAVID, R. J. p 1802 N95-22697
BENALLEGUE, M. p 1715 N95-23956
BENDER, D. A. p 1727 N95-22574
BENEDETTI, G. A. p 1799 N95-23379
BENJAMIN, THEODORE G. p 1678 N95-23617
p 1679 N95-23619
BENNETT, J. p 1613 N95-23666
BENNETT, RICHARD p 1697 N95-23724
BENNING, TRACY L. p 1710 N95-23892
BENO, M. A. p 1639 N95-22594
BENOLIEL, S. p 1721 N95-23765
BENSON, J. L. p 1689 N95-24069
BENSON, J. Z. p 1799 N95-23379
BENTON, E. R. p 1815 N95-23810
p 1815 N95-23812
BENTON, E. V. p 1815 N95-23813
p 1872 N95-23801
p 1815 N95-23810
p 1815 N95-23811
p 1815 N95-23812
p 1815 N95-23813
p 1815 N95-23814
p 1815 N95-23815
BENTS, DAVID J. p 1728 N95-23259
BERATAN, K. K. p 1701 N95-23847
BERDOZ, A. p 1802 N95-22727
BERGER, M. J. p 1811 N95-23773
BERGSTRA, J. A. p 1786 N95-22714
BERKA, REGINALD B. p 1752 N95-23723
BERKANI, M. p 1795 N95-22632
p 1787 N95-22794
BERKE, LASZLO p 1698 N95-22805
BERKLEY, WILLIAM E. p 1750 N95-22513
BERKOWITZ, J. p 1818 N95-24162
BERMAN, L. E. p 1820 N95-22877
BERNHARD, RONALD P. p 1623 N95-23823
p 1869 N95-23832
p 1869 N95-23833
p 1700 N95-23842
BERNT, M. L. p 1827 N95-23531
BERRY, G. p 1813 N95-24174
BERRY, L. A. p 1650 N95-23981
BERTHOUD, LUCINDA p 1623 N95-23824
p 1869 N95-23834
BERTSCH, G. F. p 1805 N95-22870
BERUBELAUZIERE, Y. p 1826 N95-23003
BESHTOEV, KH. M. p 1812 N95-23973
BEST, S. R. p 1637 N95-23836
BEST, STEVE R. p 1700 N95-23839
BETTENHAUSEN, M. p 1832 N95-23084
BEUTH, JACK L. p 1700 N95-23281
BHAGAT, P. K. p 1644 N95-23515
BHASKER, T. p 1692 N95-22556
BHATTACHARJEE, A. p 1836 N95-23589
BIANCHINI, R. p 1759 N95-23928
BIANCHINI, RICARDO p 1764 N95-24037
p 1753 N95-24177
p 1765 N95-24184
BIBYK, S. B. p 1846 N95-24188
BIDWELL, COLIN S. p 1665 N95-22669
BIEDENHARN, L. C. p 1796 N95-22900
BIGELOW, C. A. p 1627 N95-22928
BIJLSMA, A. p 1757 N95-23152
BILLONE, M. C. p 1837 N95-24165
p 1838 N95-24167
BINDER, MICHAEL p 1625 N95-23790
p 1625 N95-23791
BISHOP, A. R. p 1808 N95-23267
BISHOP, R. F. p 1823 N95-22980
BISHOP, WILLIAM L. p 1663 N95-24048
BISKUP, BRUCE A. p 1651 N95-23902
BISWAS, I. p 1796 N95-23660
BJORKHOLM, J. p 1819 N95-22723
BJORSTAD, PETTER E. p 1758 N95-23610
BLACK, J. H. p 1868 N95-23230
BLACK, LYDIA p 1854 N95-23262
BLAIR, R. B. p 1734 N95-23384
BLAKE, D. M. p 1730 N95-23778
BLANCH, H. W. p 1635 N95-23380
BLANCHARD, J. P. p 1829 N95-22645
BLANCHARD, ROBERT C. p 1688 N95-23012
BLANCHARD, ROBERT E. p 1758 N95-23603
BLAU, HANNAH p 1794 N95-23927
BLAU, M. p 1796 N95-22740
p 1849 N95-22752
BLESSING, S. K. p 1811 N95-23581
BLOCH, JEFFREY J. p 1621 N95-22868
BLODGETT, TROY A. p 1713 N95-23942
BLOM, CASPAR JACOBUS p 1788 N95-22932
BLOM, J. G. p 1789 N95-23167
BLOM, R. p 1701 N95-23847
BLOM, RONALD G. p 1707 N95-23880
BLOOM, STEPHEN p 1740 N95-23529
BLOOMQUIST, D. D. p 1818 N95-24160
BLUMBERG, DAN G. p 1713 N95-23941
BLUMENFELD, R. p 1799 N95-23979
BLUMENFELD, RAPHAEL p 1847 N95-22655
BLUMENTHAL, R. F. p 1672 N95-23427
BOARDMAN, JOE p 1702 N95-23853
BOARDMAN, JOSEPH W. p 1702 N95-23848
p 1711 N95-23895
BOBERG, PAUL R. p 1815 N95-23807
p 1870 N95-23808
BODDEN, LEE p 1859 N95-24121
p 1862 N95-24134
BODDY, MARK p 1859 N95-24121
BODDY, MARK S. p 1618 N95-23761
BOEUF, JEAN-PIERRE p 1829 N95-22514
BOGART, EDWARD H. p 1749 N95-22579
BOITEN, W. p 1665 N95-22638
BOMBAY, J. N. p 1659 N95-22504
BONGIOVANNI, ROBERTA p 1632 N95-22857
BONSANGUE, M. p 1757 N95-23467
BOODEY, J. B. p 1642 N95-23500
BOOKOUT, P. S. p 1699 N95-22950
BOOTEN, J. G. L. p 1787 N95-22717
BORG, JANET p 1623 N95-23803
p 1869 N95-23834
BORGARELLO, ENRICO p 1632 N95-22857
BOSCH, J. p 1872 N95-23809
BOSLOUGH, M. B. p 1740 N95-24008
p 1741 N95-24009
BOULANGER, F. p 1865 N95-22539
BOURASSA, ROGER p 1646 N95-23905
BOURKE, M. A. M. p 1842 N95-23365
BOUZARI, ALEX p 1761 N95-24116
BOWEN, BRENT D. p 1610 N95-24012
BOWERS-IRONS, GAIL p 1629 N95-23033
BOWERS, A. K. p 1739 N95-23247
BOWMAN, J. C. p 1677 N95-23483
p 1677 N95-23484
BOYD, IAIN p 1664 N95-22481
BOYD, MARK A. p 1754 N95-22603
BOYES, J. p 1818 N95-24160
BOYLE, R. J. p 1671 N95-23424
BOZACK, MICHAEL J. p 1700 N95-23839
BOZEK, JOHN M. p 1691 N95-22670
BRADSHAW, G. A. p 1719 N95-24096
p 1719 N95-24099
p 1720 N95-24104
BRADT, R. C. p 1842 N95-23266
BRANKOVIC, ANDREJA p 1682 N95-23634
BRANNON, P. J. p 1828 N95-24161
BRASHER, D. p 1696 N95-23397
BRAUN, REINHOLD p 1641 N95-23498
BRENNEN, C. E. p 1680 N95-23628
BRESINA, JOHN p 1779 N95-23742
p 1779 N95-23743
BRESINA, JOHN L. p 1781 N95-23757
BREWSTER, S. B., JR. p 1717 N95-22503
BRIDGERS, KEVIN p 1748 N95-23821
BRIDGES, DAVID H. p 1609 N95-23283
BRIMER, C. p 1829 N95-22645
BRINKER, DAVID J. p 1728 N95-23259
BRINKMAN, G. E. p 1650 N95-23932
BROADWELL, JAMES E. p 1633 N95-22886
BRODSKY, S. J. p 1851 N95-23352
BRODSKY, STANLEY J. p 1847 N95-22566
BROERSMA, H. J. p 1790 N95-23236
BROOKS, CHRISTOPHER J. p 1634 N95-23252
BROOKS, CYNTHIA L. p 1863 N95-23284
BROOKS, N. H. p 1832 N95-23119
BROSHA, E. L. p 1649 N95-23268
p 1636 N95-23573
BROSIUS, JEFFREY W. p 1870 N95-23181
BROWN, CECELIA WRIGHT p 1748 N95-23821
BROWN, CHRISTOPHER M. p 1793 N95-24042
BROWN, D. R. p 1649 N95-23268
BROWN, G. G. p 1745 N95-22872
BROWN, I. G. p 1844 N95-24011
BROWN, J. p 1716 N95-23961
BROWN, OTIS B. p 1743 N95-23212
BROWN, RAY p 1751 N95-23274
BROWN, ROBERT p 1768 N95-23676
BROWN, ROBERT MICHAEL, JR. p 1696 N95-23409
BROWN, YOLANDA p 1651 N95-23906
BROWNE, G. T. p 1645 N95-23517
BROWNLEE, D. E. p 1637 N95-23836
BROWNLEE, DONALD E. p 1869 N95-23833
BROYDE, SUSE p 1805 N95-22889
BROZOWSKI, L. A. p 1675 N95-23440
BRUCE, DAVID A. p 1643 N95-23505
BRUDER, S. p 1660 N95-22593
BRUEGE, UWE p 1769 N95-23681
BRYANT, ROBERT G. p 1648 N95-22882
p 1649 N95-23253
BUBELEV, V. G. p 1817 N95-23245
BUCH, A. p 1699 N95-23662
BUCHENAUER, D. p 1832 N95-23119
BUCHHEIT, R. G. p 1640 N95-22835
BUCHOLZ, JUSTINE L. p 1627 N95-23909
BUEHRLE, R. D. p 1616 N95-23011
BUELOW, B. E. O. p 1676 N95-23446
BUHL, M. L., JR. p 1729 N95-23383
p 1730 N95-23776
BUITRAGO, C. p 1664 N95-24070
BUKIET, B. G. p 1666 N95-22902
BUKSA, J. J. p 1624 N95-22905
BULAEVSKII, L. N. p 1843 N95-23366
BULMER, R. H. p 1661 N95-23080
BULZAN, DANIEL L. p 1637 N95-23643
BUNCH, T. E. p 1700 N95-23831
p 1700 N95-23838
BUONAQUISTI, A. J. p 1637 N95-23836
BUONGIORNO, M. F. p 1715 N95-23952
BURCHAM, FRANK W. p 1615 N95-23389
BURKARDT, M. p 1848 N95-22728
p 1802 N95-22731
BURKEN, JOHN J. p 1612 N95-22806
BURNER, A. W. p 1616 N95-23011
BURNETTE, D. W. p 1679 N95-23621
p 1685 N95-23650
BURROWS, T. W. p 1856 N95-23452
BURSTEN, B. E. p 1806 N95-23082
BURWINKLE, D. P. p 1694 N95-23056
BUTZER, TONY p 1858 N95-24111
BYERS, J. A. p 1831 N95-22899
p 1837 N95-24017

C

CADY, FREDRICK M. p 1847 N95-23285
CAHEN, G. L., JR. p 1631 N95-23502
CAI, D. p 1808 N95-23267
CAI, Y. p 1816 N95-22567
CAIRELLI, J. E. p 1747 N95-23177
CAIRNS, E. J. p 1725 N95-22501
CAIRNS, IVER H. p 1869 N95-22828
p 1739 N95-23271
CALDWELL, D. J. p 1629 N95-23038
CALES, MICHAEL p 1651 N95-23802
CALES, MICHAEL R. p 1627 N95-23909
p 1650 N95-24187
CALLEN, J. D. p 1832 N95-23072
CALLIS, R. W. p 1837 N95-24083
CALUDE, CRISTIAN p 1792 N95-23929
CALVIN, WENDY M. p 1703 N95-23855
CAMACHO, H. S. p 1698 N95-22773
CAMPBELL, D. L. p 1741 N95-24009
CAMPBELL, G. L. p 1693 N95-22796
CAMPBELL, I. H. p 1645 N95-23571
CAMPBELL, LAURENCE J. p 1798 N95-22552
CAMPBELL, LISA M. p 1732 N95-22865
CAMPBELL, M. J. p 1635 N95-23481
CAMPBELL, PERRY D. p 1697 N95-23703
CAMPBELL, R. B. p 1832 N95-23119
CANESSA, E. p 1842 N95-23047
CANNELLA, M. E. p 1712 N95-23939
CANNON, B. D. p 1635 N95-23348
CANNON, DAVID M. p 1768 N95-23678
CANNON, M. p 1855 N95-22515
CANRIGHT, G. S. p 1799 N95-23155
CANTRELL, GIDGET p 1650 N95-24187
CAPLINGER, MICHAEL p 1620 N95-23754
CAPOTONDI, ANTONIETTA p 1744 N95-23766
CARANDE, R. E. p 1712 N95-23939
CARDER, K. L. p 1702 N95-23849
CARLSON, K. D. p 1660 N95-22593
CARLSON, RANDAL D. p 1853 N95-23286

CARNE, T. G. ..... p 1759 N95-24020
CARPENTER, C. P., II ..... p 1730 N95-23977
CARRADO, KATHLEEN A. ..... p 1638 N95-22571
CARRERAS, B. A. ..... p 1832 N95-23163
CARTER, DALE ..... p 1607 N95-22666
CARTER, R. L., JR. ..... p 1759 N95-24006
CARTER, RICHARD G. ..... p 1754 N95-22570
CARTY, RONALD H. ..... p 1727 N95-22888
CARY, W. P. ..... p 1837 N95-24083
CASE, R. P. ..... p 1694 N95-23065
CASEY, C. P. ..... p 1634 N95-23345
CASPER, T. A. ..... p 1834 N95-23371
CASPI, S. ..... p 1816 N95-22567
CASSINGHAM, RANDY ..... p 1655 N95-22813
CASTANOS, OCTAVIO ..... p 1814 N95-22974
CAUGHEY, T. K. ..... p 1680 N95-23628
CAULK, PARRIS M. ..... p 1858 N95-24110
CERDEIRA, H. A. ..... p 1850 N95-22782
p 1794 N95-23019
p 1841 N95-23021
p 1841 N95-23022
CERRINA, F. ..... p 1819 N95-22723
CEULENEER, G. ..... p 1707 N95-23878
CHA, SOYOUNG S. ..... p 1690 N95-23287
CHA, Y. S. ..... p 1664 N95-24163
CHABRILLAT, S. ..... p 1707 N95-23878
CHADWICK, M. B. ..... p 1806 N95-23137
p 1813 N95-24046
CHAEL, E. P. ..... p 1740 N95-24008
p 1741 N95-24009
CHALLOU, DANIEL J. ..... p 1771 N95-23691
CHAN, CHUNG ..... p 1831 N95-22948
CHAN, D. C. ..... p 1680 N95-23624
CHAN, DANIEL C. ..... p 1674 N95-23436
p 1682 N95-23635
CHAN, STEPHEN C. ..... p 1669 N95-23417
CHAN, TONY ..... p 1672 N95-23428
CHANCE, KELLY V. ..... p 1735 N95-22482
CHANDLER, G. A. ..... p 1818 N95-24160
CHANG-LIU, CHIN-MEI ..... p 1746 N95-22913
CHANG, A. C. ..... p 1651 N95-23899
CHANG, BRITTON ..... p 1732 N95-22898
CHANG, HUAN-TSUNG ..... p 1744 N95-22493
CHANG, K. C. ..... p 1787 N95-22750
CHANG, LEON ..... p 1680 N95-23627
CHAPIN, C. E. ..... p 1701 N95-23847
CHAPLIN, M. R. ..... p 1661 N95-23080
CHAR, K. ..... p 1845 N95-24152
CHATFIELD, ROBERT B. ..... p 1732 N95-22930
CHATURVEDI, ARVIND K. ..... p 1610 N95-24024
CHEHBOUNI, A. ..... p 1708 N95-23881
CHELAFLORES, J. ..... p 1747 N95-23053
p 1747 N95-23058
p 1747 N95-23060
CHEN, A. L. ..... p 1844 N95-24010
CHEN, ANG ..... p 1647 N95-22610
p 1647 N95-22611
CHEN, C. P. ..... p 1671 N95-23422
p 1675 N95-23442
p 1637 N95-23646
CHEN, CARL L. ..... p 1633 N95-22887
CHEN, H. ..... p 1764 N95-23599
CHEN, JULIE ..... p 1631 N95-23288
CHEN, KUO-HUEY ..... p 1637 N95-23643
CHEN, LING TONY ..... p 1861 N95-24131
CHEN, P.-S. ..... p 1614 N95-23088
CHEN, R. F. ..... p 1702 N95-23849
CHEN, S. P. ..... p 1845 N95-24079
CHEN, W. C. ..... p 1680 N95-23624
CHEN, W. F. ..... p 1796 N95-22751
CHEN, W. Y. C. ..... p 1796 N95-22900
CHEN, X. M. ..... p 1837 N95-23982
CHEN, Y. S. ..... p 1671 N95-23422
p 1676 N95-23445
p 1680 N95-23626
p 1683 N95-23638
p 1637 N95-23646
CHEN, Z. ..... p 1730 N95-23489
p 1731 N95-24090
CHEN, Z. J. ..... p 1671 N95-23422
CHENG, E. T. ..... p 1829 N95-22645
CHENG, G. C. ..... p 1668 N95-23413
CHENG, GARY C. ..... p 1680 N95-23626
CHENG, LI-JEN ..... p 1702 N95-23850
CHENG, QUING-MING ..... p 1796 N95-22741
CHENG, YI ..... p 1786 N95-22631
p 1786 N95-22633
CHESLACK, BRIAN ..... p 1629 N95-23033
CHEUNG, BENNY K. ..... p 1688 N95-23377
CHIAVERINI, MARTIN J. ..... p 1625 N95-23261
CHIDUME, C. E. ..... p 1786 N95-22634
p 1790 N95-23455
p 1792 N95-23658
CHIEN, STEVE ..... p 1779 N95-23745
CHIKALOV, V. ..... p 1848 N95-22735
CHILLEMI, J. ..... p 1865 N95-22539
CHIN, E. ..... p 1693 N95-22798
CHING, CHANG KUNG ..... p 1785 N95-22624
CHIPMAN, RUSSELL A. ..... p 1828 N95-24035
CHLADEK, JOHN T. ..... p 1752 N95-23723
CHO, J. H. ..... p 1843 N95-23366
CHOI, JUNHO ..... p 1657 N95-23023
CHOI, SEUNG J. ..... p 1837 N95-24158
CHOMAZ, J. M. ..... p 1665 N95-22767
CHOU, LYNN C. ..... p 1685 N95-23647
CHOVIT, CHRIS ..... p 1690 N95-23862
CHOVIT, CHRISTOPHER ..... p 1690 N95-23852
CHOW, ALAN S. ..... p 1670 N95-23418
CHOW, PAO-LIU ..... p 1608 N95-23182
CHOY, B. K. ..... p 1742 N95-22651
CHRIEN, THOMAS G. ..... p 1702 N95-23851
p 1690 N95-23852
p 1706 N95-23875
CHRIEN, TOM ..... p 1690 N95-23862
CHRISTENSEN, BRIAN ..... p 1768 N95-23676
CHRISTENSEN, J. C. ..... p 1830 N95-22793
CHRISTENSEN, NORMAN L., JR. ..... p 1716 N95-23959
CHRISTENSEN, PHILIP R. ..... p 1711 N95-23920
CHRISTL, LIGIA ..... p 1651 N95-23906
CHRISTL, LIGIA C. ..... p 1651 N95-23907
CHRISTOPH, G. G. ..... p 1762 N95-22680
CHU, F. ..... p 1646 N95-24067
p 1845 N95-24079
CHU, HUAI-PU ..... p 1628 N95-23025
p 1629 N95-23037
CHUBB, S. R. ..... p 1712 N95-23939
CHUMAKOV, SERGEY M. ..... p 1826 N95-23002
p 1826 N95-23004
p 1826 N95-23007
CHUN, E. J. ..... p 1850 N95-22783
CHUNG, B. W. ..... p 1649 N95-23268
p 1636 N95-23573
CHUNG, H. M. ..... p 1646 N95-24153
CHURCH, E. L. ..... p 1827 N95-23531
p 1828 N95-24005
CHURCHILL, GARY B. ..... p 1688 N95-23377
CHURCHILL, MARK ..... p 1746 N95-22913
CHURCHWARD, REX A. ..... p 1649 N95-23394
CHYU, MING-KING ..... p 1682 N95-23636
CIARDO, GIANFRANCO ..... p 1758 N95-23613
CIARPALLINI, PAOLA ..... p 1735 N95-22482
CIERNIAK, MICHAL ..... p 1765 N95-24061
CIERNIAK, MICHAL J. ..... p 1764 N95-23936
CIHANGIR, S. ..... p 1689 N95-23521
CIMBALA, JOHN M. ..... p 1687 N95-23289
CINTALA, MARK J. ..... p 1700 N95-23842
CISKOWSKI, DOUG ..... p 1621 N95-22868
CLAESSEN, M. ..... p 1763 N95-23129
CLARK, DAVID P. ..... p 1745 N95-22874
CLARK, R. ..... p 1654 N95-24045
p 1654 N95-24093
CLARK, ROGER N. ..... p 1702 N95-23853
p 1703 N95-23854
p 1703 N95-23855
CLARKE, ROBERT ..... p 1612 N95-22806
CLATTERBUCK, CARROLL ..... p 1651 N95-23913
CLAYTON, B. R. ..... p 1630 N95-23537
CLEGHORN, T. ..... p 1659 N95-23682
CLEMONS, T. G. ..... p 1697 N95-24106
CLIPSON, COLIN ..... p 1753 N95-22480
CLOSE, F. E. ..... p 1807 N95-23156
COBBAERT, J. ..... p 1740 N95-23470
COBBLE, J. A. ..... p 1829 N95-22676
COCHRAN, JOHN E., JR. ..... p 1619 N95-24032
CODA, S. ..... p 1836 N95-23768
CODRIANSKY, SIMON ..... p 1823 N95-22979
COFFEY, H. T. ..... p 1798 N95-22895
COFFEY, HELEN E. ..... p 1870 N95-23925
p 1870 N95-23926
COGGIOLA, M. J. ..... p 1687 N95-22682
COHEN, B. I. ..... p 1831 N95-22899
p 1837 N95-24017
COHEN, J. G. ..... p 1828 N95-24068
COHEN, MICHAEL ..... p 1800 N95-23782
COHEN, R. H. ..... p 1837 N95-24017
COLBORN, B. L. ..... p 1815 N95-23811
p 1815 N95-23815
p 1815 N95-23818
p 1815 N95-23819
COLELLA, P. ..... p 1665 N95-22491
COLEY, WILLIAM R. ..... p 1739 N95-23272
COLLINS, M. ..... p 1635 N95-23360
COLLINS, WILLIAM E. ..... p 1749 N95-23788
p 1750 N95-23934
p 1611 N95-24071
COLOZZA, ANTHONY J. ..... p 1728 N95-23259
COMBES, F. ..... p 1868 N95-23607
COMFORT, RICHARD H. ..... p 1831 N95-22955
COMFORT, W. J., III ..... p 1695 N95-23358
CONEL, JAMES E. ..... p 1703 N95-23856
p 1703 N95-23857
p 1690 N95-23862
p 1704 N95-23863
p 1624 N95-23864
CONLEY, JOSEPH L. ..... p 1615 N95-23389
CONSTANTINIDES, E. D. ..... p 1657 N95-23391
COOK, JOSEPH S., JR. ..... p 1694 N95-22892
COOKE, W. J. ..... p 1623 N95-23826
p 1869 N95-23828
COOKE, WILLIAM J. ..... p 1869 N95-23829
COOL, G. R. ..... p 1651 N95-23901
COOPER, E. A. ..... p 1842 N95-23266
COOPER, ERIC ..... p 1697 N95-23724
COOPER, T. D. ..... p 1808 N95-23350
p 1809 N95-23407
CORIANO, C. ..... p 1813 N95-24166
CORNELISON, J. ..... p 1679 N95-23619
COSGROVE, JOHN M. ..... p 1744 N95-22588
COSTA, GIOVANI ..... p 1736 N95-22612
COSTEN, ROBERT C. ..... p 1691 N95-23411
COSTON, JAMES E., JR. ..... p 1651 N95-23911
COUILLAUD, STEPHANE ..... p 1607 N95-22666
COULTER, J. Y. ..... p 1645 N95-23571
COULTER, R. C. ..... p 1741 N95-24078
COWAN, CREGG ..... p 1697 N95-23724
COWAN, P. ..... p 1813 N95-24174
COX, A. N. ..... p 1870 N95-22938
COX, BRIAN ..... p 1752 N95-23735
COX, G. B., JR. ..... p 1674 N95-23438
COYNE, BOB ..... p 1858 N95-24113
CRABTREE, G. W. ..... p 1839 N95-22572
CRAMER, K. E. ..... p 1644 N95-23512
CRANE, D. ..... p 1870 N95-23584
CRAWFORD, D. A. ..... p 1740 N95-24008
p 1741 N95-24009
CRAWFORD, GARY D. ..... p 1700 N95-23839
CRAWLEY, EDWARD F. ..... p 1827 N95-23089
CRIM, F. F. ..... p 1806 N95-23077
CRIMINALE, W. O. ..... p 1667 N95-23207
CRIPPEN, ROBERT E. ..... p 1707 N95-23880
CROTINGER, J. A. ..... p 1837 N95-24017
CROW, JACK E. ..... p 1798 N95-22552
CRUMPLER, MICHAEL S. ..... p 1700 N95-23839
CRUZ, VINCENT B. ..... p 1666 N95-22906
CSEH, J. ..... p 1814 N95-22971
CSIGE, I. ..... p 1815 N95-23810
p 1815 N95-23812
p 1815 N95-23813
p 1815 N95-23814
CUCINOTTA, FRANCIS A. ..... p 1817 N95-22929
CUEVAS, A. ..... p 1845 N95-24156
CULBERT, C. ..... p 1659 N95-23682
CULLEN, DERMOTT E. ..... p 1855 N95-22871
CUMMINS, KEVIN ..... p 1628 N95-23030
CURE, JENNIFER D. ..... p 1731 N95-22725
CURRAN, PAUL J. ..... p 1705 N95-23871
p 1708 N95-23884
CURTISS, BRIAN ..... p 1701 N95-23846
p 1710 N95-23892
CUSHMAN, ROBERT M. ..... p 1731 N95-22725
CUTHBERTSON, J. W. ..... p 1832 N95-23119
CUTTS, JAMES A. ..... p 1819 N95-22765
CWIK, T. W. ..... p 1656 N95-22852
CYR, M. A. ..... p 1689 N95-23795

D

DAAN, R. ..... p 1733 N95-23125
DABOUL, JAMIL ..... p 1820 N95-22959
DAHL, MILO D. ..... p 1800 N95-23178
DAI, XI ..... p 1647 N95-22610
p 1647 N95-22611
DAI, XIAOWEN ..... p 1654 N95-23195
DAKHOUL, YOUSSEF ..... p 1678 N95-23617
DALFOVO, F. ..... p 1840 N95-22839
DANEY, D. E. ..... p 1662 N95-23368
DANFORD, M. D. ..... p 1641 N95-23186
DANIELS, T. ..... p 1808 N95-23242
DANTZER, R. ..... p 1748 N95-22770
DARDANO, CLAIRE B. ..... p 1623 N95-23823
DARIAN, ARMEN ..... p 1674 N95-23436
DARLING, DOUGLAS ..... p 1614 N95-23550
DARVILL, A. G. ..... p 1748 N95-24075
DAS, ASEEM ..... p 1768 N95-23678
DAS, S. R. ..... p 1867 N95-22739
DASGUPTA, B. ..... p 1834 N95-23523
DASILVA, ARLINDO ..... p 1740 N95-23529
DAUGHERTY, M. A. ..... p 1662 N95-23368
DAUMEYER, G. J. ..... p 1695 N95-23374
DAUMEYER, G. J., III ..... p 1695 N95-23343
DAVID, S. A. ..... p 1640 N95-23132
DAVIDHAZY, ANDREW ..... p 1690 N95-23290
DAVIS, CURTISS O. ..... p 1710 N95-23890
DAVIS, ELIZABETH K. ..... p 1780 N95-23747
DAVIS, FRANK W. ..... p 1716 N95-23959
DAVISON, B. H. ..... p 1652 N95-22587
DAWICKE, D. S. ..... p 1627 N95-22928
DAWN, FREDERIC S. ..... p 1750 N95-22766

DAWSON, S. p 1809 N95-23396
DEATON, JERRY W. p 1648 N95-23179
DEBERGH, NATHALIE p 1815 N95-22994
p 1815 N95-22995
DEBRA, P. p 1855 N95-22534
DEBRECZENY, MARTIN PAUL p 1745 N95-22590
DECROIX, MICHELE E. p 1669 N95-23416
p 1675 N95-23443
DEEMER, M. p 1634 N95-23202
DEES, H. C. p 1744 N95-22588
DEESE, J. E. p 1673 N95-23433
DEGROH, KIM K. p 1626 N95-23270
p 1627 N95-23909
DEJONG, FREDERIK J. p 1672 N95-23428
p 1682 N95-23633
p 1683 N95-23641
DEJONG, H. p 1648 N95-23128
DEJONGE, J. B. p 1612 N95-23161
DEJONGE, W. p 1754 N95-22522
DELAJARA, JAMIE p 1823 N95-22977
DELAPP, D. p 1658 N95-24015
DELAPP, J. G. p 1762 N95-22679
DELAYE, P. p 1839 N95-22584
DELILLO, N. p 1701 N95-23847
DELIMA, J. L. M. P. p 1717 N95-22537
DELOMBARD, RICHARD p 1621 N95-22667
DELONG, K. p 1690 N95-22595
DELPECH, M. p 1752 N95-23707
p 1777 N95-23731
DELSOLMESA, ANTONIO p 1825 N95-22996
p 1815 N95-22997
DEMANDANTE, CARLO GREG N. p 1650 N95-23291
DEMMEL, JAMES W. p 1791 N95-23592
DENG, ZHENG-TAO p 1685 N95-23647
DENINGER, W. J. p 1663 N95-23479
DENNY-BROWN, DEREK p 1760 N95-24092
DENTON, S. M. p 1763 N95-22858
p 1763 N95-22859
DERIJCKE, M. M. A. p 1789 N95-23149
DESA, VIRGINIA RUTH p 1784 N95-24040
DESAINTVINCENT, A. p 1618 N95-23752
DESAINTVINCENT, ARNAUD p 1752 N95-23720
DESHPANDE, MANISH p 1681 N95-23630
DESTAEBLER, H. p 1816 N95-22567
DEVOTO, JORGE A. p 1788 N95-23076
DEVRIES, H. J. M. p 1733 N95-23067
DEVY, M. p 1777 N95-23731
DEWITT, KENNETH J. p 1668 N95-23248
DEWSON, T. p 1630 N95-23537
DEXTER, H. BENSON p 1648 N95-23179
DHERE, N. G. p 1727 N95-22842
DIAMOND, P. H. p 1832 N95-23163
DIAZ, A. F. p 1634 N95-23164
DICKINSON, TERRY L. p 1854 N95-23292
DIFIORE, L. p 1822 N95-22976
DIFTLER, MYRON p 1752 N95-23735
DIJKSTRA, R. M. p 1763 N95-23166
DILIDDO, A. p 1785 N95-22618
DILL, RICHARD A. p 1685 N95-23649
DILLEY, A. C. p 1718 N95-24026
DIMITS, A. M. p 1831 N95-22899
p 1837 N95-24017
DING, E. J. p 1665 N95-22771
DINGLER, ROBERT p 1621 N95-22868
DIPIPPO, S. p 1752 N95-23732
DIPIPPO, SIMONETTA p 1697 N95-23696
DIWAN, M. p 1801 N95-22583
DIXON, K. D. p 1664 N95-24163
DOBISZ, ELIZABETH A. p 1660 N95-22709
DOBRANICH, D. p 1663 N95-23779
DOBSON, M. CRAIG p 1715 N95-23957
DOHNER, J. p 1766 N95-23134
DOHRMANN, C. R. p 1759 N95-24020
DOI, M. p 1816 N95-22644
p 1816 N95-22848
DOMINGO, C. p 1872 N95-23809
DOMINGUEZ, R. R. p 1830 N95-22694
DONALD, M. p 1816 N95-22567
DONG, J. Q. p 1830 N95-22694
DONGARRA, J. J. p 1657 N95-23075
DONNER, K. J. p 1868 N95-23228
DOOLING, D. p 1617 N95-23549
DORAN, DENISE p 1683 N95-23638
p 1683 N95-23639
DORLAND, W. p 1830 N95-22694
p 1831 N95-22899
DORRIS, S. p 1839 N95-22572
DORRIS, S. E. p 1846 N95-24171
DORUK, M. p 1641 N95-23499
DOSHI, P. p 1730 N95-23489
DOSHI, R. p 1730 N95-23582
DOSSANTOS, GONCALO RODRIGUES p 1639 N95-22609
DOUGHERTY, N. S. p 1679 N95-23621
p 1685 N95-23650
p 1686 N95-23654
DOVER, ALAN p 1623 N95-23799
DOWLING, KEVIN p 1697 N95-23724
DOWNEY, K. I. p 1623 N95-23826
DOYLE, RICHARD J. p 1769 N95-23683
DOZIER, JEFF p 1715 N95-23954
DRAAYER, JERRY P. p 1814 N95-22968
DRACH, BOB p 1861 N95-24131
DRENNAN, ARTHUR P. p 1750 N95-22766
DRESSEL, M. p 1660 N95-22593
DROBOTIJ, ERIN p 1650 N95-24187
DROLSHAGEN, GERHARD p 1623 N95-23799
DROOGERS, P. p 1701 N95-22639
p 1740 N95-23470
DRUMMOND, MARK p 1779 N95-23742
p 1779 N95-23743
DUAN, LIAN p 1705 N95-23867
DUBEY, RAJENDRA R. p 1817 N95-22929
DUBOIS, D. F. p 1739 N95-23256
DUBOLS, C. p 1845 N95-24156
DUC, DUONG ANH p 1655 N95-22746
DUGAN, JOANNE BECHTA p 1754 N95-22603
p 1755 N95-22604
DUKHAN, NIHAD p 1668 N95-23248
DUMAS, CATHERINE p 1673 N95-23434
p 1683 N95-23639
DUNFORD, C. L. p 1856 N95-23452
DUNG, NGUYEN VIET p 1796 N95-22933
DUNN, A. M. p 1868 N95-23570
DUOBA, M. p 1664 N95-24070
DURAN, G. p 1729 N95-23478
DURAND, RICK p 1770 N95-23684
DURIN, CHRISTIAN p 1869 N95-23834
DURSCH, H. W. p 1626 N95-22918
DURSCH, HARRY p 1638 N95-23897
DURSCH, HARRY W. p 1638 N95-23898
p 1627 N95-23914
DVALI, G. p 1848 N95-22742
DVOEGLAZOV, VALERI V. p 1815 N95-22997
DWYER, JOHN L. p 1705 N95-23870
DYE, R. C. p 1631 N95-22677

E

EARL, W. L. p 1842 N95-23266
EASTLAND, A. H. p 1680 N95-23624
EASTMAN, J. A. p 1639 N95-22594
EASTMAN, TIMOTHY E. p 1737 N95-22945
p 1738 N95-23184
EASTWOOD, MICHAEL L. p 1690 N95-23852
EBELING, CHARLES E. p 1622 N95-23398
p 1622 N95-23399
p 1622 N95-23400
EDGINGTON, WILL p 1779 N95-23743
EDWARDS, C. F. p 1666 N95-23081
EDWARDS, DAVID p 1651 N95-23912
EDWARDS, E. L. p 1732 N95-22781
EDWARDS, MARK B. p 1611 N95-23565
p 1750 N95-24088
EFREMOV, A. V. p 1812 N95-23984
EFTHIMION, P. C. p 1833 N95-23269
EGALON, CLAUDIO OLIVEIRA p 1819 N95-22807
EICHENLAUB, JESSE B. p 1689 N95-23789
EINSTEIN, J. RALPH p 1746 N95-22890
EISCHENS, R. P. p 1631 N95-22517
EISENHART, D. W. p 1674 N95-23438
EISMANN, PAUL p 1768 N95-23676
EJIRI, A. p 1835 N95-23533
EKSUZIAN, D. J. p 1613 N95-24030
EL-GUEBALY, L. A. p 1829 N95-22645
ELBULUK, MALIK E. p 1616 N95-23671
ELIA, R. D. p 1802 N95-22699
ELIEZER, DAVID p 1746 N95-22897
ELIZONDO, J. p 1785 N95-22626
ELKERN, KENNETH F., JR. p 1855 N95-23024
ELLMAN, THOMAS p 1775 N95-23716
ELSUM, C. C. p 1718 N95-24026
ELTGROTH, P. G. p 1763 N95-23243
ELWORTHY, K. D. p 1787 N95-22772
ENDRES, S. p 1709 N95-23885
ENG, ANTHONY T. p 1644 N95-23513
ENG, BJORN T. p 1690 N95-23852
p 1707 N95-23877
ENGE, W. p 1872 N95-23806
ENGELFRIET, J. p 1766 N95-22524
ENGELMORE, ROBERT p 1618 N95-23679
ENGMAN, EDWIN T. p 1714 N95-23950
ERCOLINE, W. R. p 1613 N95-24030
ERG, G. I. p 1692 N95-23657
ERICKSON, K. L. p 1638 N95-22576
p 1652 N95-22838
ERLICHMAN, JOZEF p 1700 N95-23831
ERMOLAEV, I. M. p 1812 N95-23976
ERRICHELLO, ROBERT p 1694 N95-22923
ERWIN, J. p 1732 N95-22834
ESPANA, MARTIN D. p 1612 N95-22829
ESPANOZA, B. F. p 1631 N95-22677
ESPINOSA, ISMAEL p 1749 N95-22987
ESPINOSA, ISMAEL E. p 1784 N95-22988
ETRO, JAMES F. p 1742 N95-23255
EVANS, R. H. p 1613 N95-24030
EVANS, T. E. p 1832 N95-23119
EVERETT, LOUIS J. p 1757 N95-23388
EYMAN, DARRELL P. p 1634 N95-23252
EZE, M. O. p 1747 N95-23050
p 1747 N95-23053

F

FABER, M. p 1848 N95-22744
p 1849 N95-22745
FAIGLE, U. p 1790 N95-23231
p 1757 N95-23232
p 1757 N95-23238
p 1758 N95-23608
FALTENS, A. p 1818 N95-24014
FANTONI, S. p 1840 N95-22839
FARHANGI, S. p 1625 N95-23439
FARHAT, C. p 1614 N95-23088
FARHOOMAND, JAM p 1827 N95-23378
FARMER, R. C. p 1668 N95-23413
p 1669 N95-23414
FARR, THOMAS G. p 1707 N95-23880
FARRAND, WILLIAM H. p 1703 N95-23858
p 1706 N95-23874
FARRER, R. G. p 1658 N95-24015
FAUGERAS, O. p 1721 N95-23765
FAULKNER, J. S. p 1640 N95-23121
FAVENESI, J. A. p 1697 N95-24106
FAYE, N. A. B. p 1844 N95-23774
FAYYAD, USAMA M. p 1775 N95-23717
FEENSTRA, R. B. p 1755 N95-22652
FEHR, GARY p 1618 N95-23679
FEIGELSON, ERIC D. p 1867 N95-23013
FEILER, CHARLES E. p 1677 N95-23464
FELDER, JAMES L. p 1625 N95-23791
FELICIANI, F. p 1656 N95-22817
FELIPPA, C. A. p 1614 N95-23088
FENG, JINZHANG p 1681 N95-23630
FENG, S. p 1800 N95-22495
FENG, SHIPING p 1838 N95-22499
FENNEL, THERON R. p 1761 N95-23762
FENSTERMACHER, M. E. p 1832 N95-23119
p 1834 N95-23371
FEO, J. T. p 1763 N95-22858
p 1763 N95-22859
FERBER, M. K. p 1639 N95-22686
p 1647 N95-22689
FERGUSON, DALE C. p 1738 N95-23116
FERGUSON, GEORGE p 1659 N95-24193
FERGUSON, GEORGE M. p 1783 N95-24031
FERGUSON, MILTON W. p 1698 N95-23293
FERGUSON, T. V. p 1675 N95-23440
FERNANDEZ-BACA, J. A. p 1647 N95-22688
FERNANDEZ, DAVID J. p 1823 N95-22981
p 1823 N95-22982
FERNANDEZ, J. C. p 1829 N95-22676
FERO, M. J. p 1816 N95-22702
p 1807 N95-23141
FERRALL, J. F. p 1751 N95-23194
FERRARINI, M. p 1715 N95-23952
FERRY, KATHY R. p 1732 N95-22865
FEUQUAY, JAY p 1858 N95-24111
FIDDAMAN, T. p 1733 N95-23067
FIEDLER, GEORGE M. p 1750 N95-22513
FIKES, RICHARD p 1618 N95-23679
p 1760 N95-24176
FIKSEL, G. p 1809 N95-23363
FILHO, ELSO DRIGO p 1748 N95-22963
FILMAN, ROBERT p 1760 N95-24176
FILUK, A. B. p 1818 N95-24160
FINCKENOR, MIRIA M. p 1651 N95-23908
p 1651 N95-23912
FINK, C. L. p 1632 N95-22764
FINLAYSON-PITTS, B. J. p 1735 N95-24147
FINLEY, DENNIS B. p 1608 N95-22917
FINLEY, T. D. p 1616 N95-23011
FIORELLA, MARIA p 1720 N95-24100
p 1720 N95-24101
p 1720 N95-24102
FIORINI, PAOLO p 1768 N95-23676
FIRESTONE, ELAINE R. p 1743 N95-22671
FISCHER, BERND p 1791 N95-23547
FISCHER, SOPHIE p 1793 N95-24003
FISHER, DOUG p 1770 N95-23686
FITZGERALD, HOWARD J. p 1624 N95-23835
FIUMARA, A. p 1715 N95-23952
FLESHLER, S. p 1843 N95-23367
FLOWERS, GEORGE T. p 1694 N95-23190
p 1694 N95-23213
p 1695 N95-23214

FOELLER, THOMAS ..... p 1857 N95-24109
FOLEY, E. W. ..... p 1712 N95-23939
FOLTYN, S. R. ..... p 1645 N95-23571
FONDA, L. ..... p 1804 N95-22791
p 1842 N95-23048
FOOTE, JOHN ..... p 1637 N95-23837
FOREST, C. B. ..... p 1834 N95-23371
FOREST, E. ..... p 1816 N95-22567
FORNEFELD, U. M. ..... p 1635 N95-23380
FORNEK, T. ..... p 1688 N95-23492
FOROUHAR, KAMRAN ..... p 1697 N95-23706
FORSTER, RICHARD R. ..... p 1713 N95-23942
FORSYTH, DONALD W. ..... p 1709 N95-23888
FORSYTHE, JOHN S. ..... p 1651 N95-23903
p 1651 N95-23904
FOSTER, K. ..... p 1737 N95-23063
FOSTER, K. T. ..... p 1733 N95-23123
p 1733 N95-23124
FOSTER, WINFRED A., JR. ..... p 1625 N95-23640
FOUST, M. J. ..... p 1684 N95-23642
FOWLER, R. F. ..... p 1785 N95-22544
FRAINIER, RICHARD J. ..... p 1775 N95-23718
FRANK, A. L. ..... p 1872 N95-23801
p 1815 N95-23810
p 1815 N95-23811
FRANK, ALEJANDRO ..... p 1814 N95-22960
p 1814 N95-22961
FRANKENA, J. F. ..... p 1789 N95-23200
p 1790 N95-23237
FRANKLIN, G. ..... p 1802 N95-22727
FRANZ, JUDY R. ..... p 1841 N95-22907
FREDMONSKI, A. J. ..... p 1679 N95-23619
FREE, APRIL M. ..... p 1694 N95-23213
FREEMAN, M. R. ..... p 1831 N95-22862
FREUND, F. ..... p 1633 N95-23064
FREUND, ROLAND W. ..... p 1791 N95-23547
p 1791 N95-23593
p 1791 N95-23611
p 1791 N95-23612
FRICKE, ROBERT W., JR. ..... p 1619 N95-23093
p 1619 N95-23094
p 1619 N95-23187
FRIEDLAND, SHMUEL ..... p 1787 N95-22836
FRIEDMAN, ROBERT ..... p 1626 N95-24004
FRIGO, L. A. ..... p 1815 N95-23810
p 1815 N95-23812
p 1815 N95-23813
p 1815 N95-23814
FRITTS, D. C. ..... p 1688 N95-23087
FRITZ, R. ..... p 1709 N95-23886
FROGGATT, MICHAEL ..... p 1637 N95-23804
FRUSTIE, M. J. ..... p 1645 N95-23518
FRYBERGER, D. ..... p 1742 N95-22701
FUCHS, JOACHIM ..... p 1770 N95-23685
FUENTES, ALBERTO M. ..... p 1784 N95-22988
FUENTES, OLAC ..... p 1783 N95-24036
p 1784 N95-24185
FUJISAWA, A. ..... p 1834 N95-23527
FUJITA, JUNJI ..... p 1836 N95-23569
FUJITA, YOSHIHIRO ..... p 1690 N95-24107
FUKUMOTO, Y. ..... p 1842 N95-23354
FUKUYAMA, ATSUSHI ..... p 1835 N95-23534
FULLER, DANA ..... p 1611 N95-23565
FULLERTON, CHARLES G. ..... p 1615 N95-23389
FULLERTON, E. E. ..... p 1846 N95-24168
p 1846 N95-24170
FULTON, J. L. ..... p 1843 N95-23579
FUNAKI, Y. ..... p 1794 N95-23239
p 1794 N95-23539
FUNAYA, KOUICHI ..... p 1752 N95-23715
FUNK, JOAN ..... p 1638 N95-23897
FUNK, JOAN G. ..... p 1864 N95-23916
FURDYNA, J. ..... p 1844 N95-24010
FURMAN, A. S. ..... p 1841 N95-23020
FURMAN, EUGENE ..... p 1648 N95-22883
FURNBERG, CARLTON M. ..... p 1652 N95-22721
FURSAEV, D. V. ..... p 1848 N95-22743
FURUYA, MASATOSHI ..... p 1623 N95-23719

G

GADDIS, LISA ..... p 1704 N95-23859
GAISSER, TOM ..... p 1801 N95-22573
GALICA, J. ..... p 1728 N95-23062
GALLAGHER, ANDREA J. ..... p 1703 N95-23855
GALLAGHER, T. F. ..... p 1812 N95-23978
GALLY, THOMAS A. ..... p 1609 N95-23294
GAMACHE, ROBERT R. ..... p 1636 N95-23545
GANAPATHI, G. B. ..... p 1751 N95-23194
GANESAN, S. ..... p 1830 N95-22757
GANETIS, G. ..... p 1816 N95-22926
GANGRSKIJ, YU. P. ..... p 1812 N95-23976
GANNON, TERRY ..... p 1787 N95-22715
GAO, BO-CAI ..... p 1704 N95-23860
p 1705 N95-23865
GAO, H. ..... p 1764 N95-23599
GAPOSCHKIN, EDWARD M. ..... p 1622 N95-23781
GARBEIL, HAROLD ..... p 1714 N95-23949
GARBER, M. ..... p 1816 N95-22926
GARCIA, MANUEL ..... p 1732 N95-22898
GARCIA, ROBERTO ..... p 1678 N95-23617
p 1679 N95-23619
p 1679 N95-23623
p 1680 N95-23624
p 1680 N95-23626
GARDINER, JOHN G. ..... p 1656 N95-22819
GARDNER, D. J. ..... p 1700 N95-23840
GARG, SANJAY ..... p 1615 N95-22954
GARNER, F. A. ..... p 1842 N95-23266
GARRARD, WILLIAM L. ..... p 1615 N95-23410
GARRATT, J. R. ..... p 1721 N95-24192
GARRETT, J. ..... p 1681 N95-23631
GARRIC, V. ..... p 1777 N95-23731
GARTLING, D. K. ..... p 1666 N95-22914
GARY, J. B. ..... p 1738 N95-23090
GARY, S. P. ..... p 1737 N95-22903
GARY, S. PETER ..... p 1736 N95-22850
GARZON, F. H. ..... p 1649 N95-23268
p 1636 N95-23573
GASIEWSKI, A. J. ..... p 1742 N95-23208
GASPARONI, F. ..... p 1752 N95-23732
GASQUET, A. ..... p 1618 N95-23752
GAUTHIER, P. ..... p 1645 N95-23518
GAUTIER, T. N. ..... p 1865 N95-22539
GAVA, E. ..... p 1851 N95-23922
GAVRILOV, N. G. ..... p 1692 N95-23657
GEBAUER, LINDA ..... p 1626 N95-23270
GEE, J. M. ..... p 1731 N95-24155
p 1731 N95-24157
GEIST, ROBERT M. ..... p 1754 N95-22603
GELLER, A. S. ..... p 1837 N95-24158
GEMMELL, D. ..... p 1813 N95-24174
GEMMELL, M. ANNE ..... p 1748 N95-23771
GENDY, ATEF S. ..... p 1698 N95-22805
GENTRY, GARL L., JR. ..... p 1607 N95-22802
GEOFFREY, E. ..... p 1867 N95-22516
GEORGE, GRAEME A. ..... p 1651 N95-23903
p 1651 N95-23904
GEORGE, PETE ..... p 1627 N95-23914
GERBER, SCOTT S. ..... p 1662 N95-23219
GERCHAR, TIM ..... p 1753 N95-24126
GERDES, D. ..... p 1808 N95-23336
GERSPACHER, MICHEL ..... p 1646 N95-22553
GERTH, R. ..... p 1752 N95-23153
GESKE, U. ..... p 1758 N95-23553
GHIRARDI, G. C. ..... p 1851 N95-23454
GHORASHI, BAHMAN ..... p 1687 N95-24022
GHOSH, A. K. ..... p 1816 N95-22926
GIEL, P. W. ..... p 1671 N95-23423
GIELDA, T. P. ..... p 1673 N95-23433
GIL, YOLANDA ..... p 1766 N95-22512
GILCHRIST, N. H. C. ..... p 1658 N95-24044
GILL, MICHAEL J. ..... p 1761 N95-24117
GILLESPIE, G. ..... p 1689 N95-23521
GILLICH, CHRISTOPHER J. ..... p 1652 N95-22506
GILOMEN, T. L. ..... p 1856 N95-23341
GILYARD, GLENN ..... p 1612 N95-22829
GILYARD, GLENN B ..... p 1615 N95-23389
GINI, MARIA ..... p 1771 N95-23691
GIOMETTI, CAROL S. ..... p 1748 N95-23771
GIRIDHARAN, M. G. ..... p 1637 N95-23645
GIROULT-MATLAKOWSKI, G. ..... p 1845 N95-24156
GLASS, MICHAEL J. ..... p 1629 N95-23033
GLASSMAN, ARTHUR J. ..... p 1609 N95-23462
GLEITER, H. ..... p 1843 N95-23585
GLICKSMAN, MARTIN ..... p 1653 N95-23204
GLUSHKOV, E. S. ..... p 1817 N95-23245
GNIEWEK, JOHN J. ..... p 1690 N95-24127
GODFREY, A. G. ..... p 1670 N95-23420
GODFREY, ANDREW G. ..... p 1670 N95-23421
GOEBEL, F. ..... p 1790 N95-23233
GOERLACH, THOMAS ..... p 1769 N95-23681
GOETZ, ALEXANDER F. H. ..... p 1703 N95-23854
p 1711 N95-23895
GOFFENEY, N. ..... p 1817 N95-23493
GOHIL, P. ..... p 1834 N95-23371
GOKOGLU, SULEYMAN A. ..... p 1626 N95-24004
GOLDMAN, ROBERT P. ..... p 1618 N95-23761
GOLDMANN, L. H. ..... p 1661 N95-22799
GOLDSTEIN, R. M. ..... p 1712 N95-23939
GOLDSTONE, J. A. ..... p 1842 N95-23365
GOLDTHORPE, STEVE H. ..... p 1614 N95-22674
GOLDWIRE, H. ..... p 1616 N95-24019
GOLOKHVASTOV, A. I. ..... p 1794 N95-23972
p 1812 N95-23974
GOLUB, GENE H. ..... p 1791 N95-23611
GOMBOSI, TAMAS ..... p 1833 N95-23211
GONAZALEZ, J. JESUS ..... p 1749 N95-22987
GONG, X. G. ..... p 1805 N95-22935
GONZALEZ, H. ..... p 1689 N95-23521
GONZALEZ, HORTENSIA ..... p 1749 N95-22987
GONZALEZ, J. JESUS ..... p 1784 N95-22988
GOOD, J. ..... p 1865 N95-22539
GOODMAN, M. ..... p 1870 N95-23584
GOODMAN, MAURY ..... p 1801 N95-22573
GOPALAKRISHNAN, K. V. ..... p 1692 N95-22556
p 1693 N95-22557
GORBATKIN, S. M. ..... p 1650 N95-23981
GORDEEV, YU. P. ..... p 1644 N95-23514
GORDON, HOWARD R. ..... p 1717 N95-22916
p 1718 N95-23473
GORDON, R. ..... p 1731 N95-24155
GORDON, REX B. ..... p 1628 N95-23032
GORDON, TIM ..... p 1637 N95-23797
GORETTA, K. C. ..... p 1845 N95-24150
GORNEY, DAVID ..... p 1770 N95-23684
GORNIKER, E. I. ..... p 1692 N95-23657
GOTTZMANN, C. F. ..... p 1614 N95-24053
GOULA, CRYSTAL A. ..... p 1861 N95-24133
GOULD, R. W. ..... p 1642 N95-23503
GOURMELON, GEORGES ..... p 1637 N95-23804
GOWERS, W. T. ..... p 1787 N95-22837
GOYAL, ANUJA ..... p 1827 N95-23224
GRADY, CAROL A. ..... p 1866 N95-23561
GRADY, D. ..... p 1868 N95-23656
GRAEV, M. M. ..... p 1795 N95-22712
GRAHAM, TODD ..... p 1697 N95-23724
GRAMMER, HOLLY L. ..... p 1631 N95-23900
GRANDJEAN, P. ..... p 1721 N95-23765
GRATSON, D. A. ..... p 1734 N95-23480
GRAVES, MARK ..... p 1779 N95-23741
GRAY, E. L. ..... p 1755 N95-22718
p 1756 N95-22894
GRAY, J. A. ..... p 1641 N95-23497
GRCAR, J. F. ..... p 1632 N95-22722
GREDEL, R. ..... p 1868 N95-23230
GREELEY, RONALD ..... p 1711 N95-23894
p 1713 N95-23941
GREEN, D. ..... p 1817 N95-23369
GREEN, JAMES S. ..... p 1721 N95-23295
GREEN, ROBERT M. ..... p 1713 N95-23943
GREEN, ROBERT O. ..... p 1701 N95-23844
p 1702 N95-23851
p 1690 N95-23852
p 1703 N95-23854
p 1704 N95-23860
p 1704 N95-23861
p 1690 N95-23862
p 1704 N95-23863
p 1624 N95-23864
p 1705 N95-23865
p 1705 N95-23866
p 1706 N95-23875
p 1707 N95-23877
p 1708 N95-23882
GREEN, S. F. ..... p 1700 N95-23840
GREENE, A. ..... p 1816 N95-22926
GREENLY, J. B. ..... p 1640 N95-22835
GREENMAN, MATTHEW ..... p 1615 N95-23392
GREENOUGH, C. ..... p 1785 N95-22544
GREENWALD, D. A. ..... p 1674 N95-23437
p 1679 N95-23623
GREGORICH, D. ..... p 1865 N95-22539
GREGORY, G. L. ..... p 1733 N95-23009
GREGORY, J. C. ..... p 1646 N95-23820
GREGORY, JOHN C. ..... p 1651 N95-23906
p 1651 N95-23907
GRIBBLE, R. F. ..... p 1663 N95-23479
GRIFFIN, L. ..... p 1674 N95-23437
GRIFFIS, D. P. ..... p 1637 N95-23836
GROLEAU, NICOLAS ..... p 1775 N95-23718
GRONBECH-JENSEN, N. ..... p 1808 N95-23267
GROOT, J. S. ..... p 1716 N95-23958
GROPP, W. ..... p 1765 N95-24172
GROSS, K. ..... p 1637 N95-23645
GROSSBERG, STEPHEN ..... p 1800 N95-23782
GROSSMAN, YAFFA ..... p 1709 N95-23889
GROVE, CINDY I. ..... p 1703 N95-23856
p 1703 N95-23857
GRUENER, G. ..... p 1660 N95-22593
GRUVER, J. L. ..... p 1850 N95-22782
GRYK, THOMAS J. ..... p 1819 N95-22492
GU, Q. ..... p 1660 N95-22586
GU, SHIWEI ..... p 1850 N95-23049
GUARINO, V. ..... p 1688 N95-23492
GUERRERO, J. ..... p 1825 N95-22993
GUEVENC, Z. B. ..... p 1638 N95-22531
GUILHEM, D. ..... p 1831 N95-22800
GUMASTE, U. ..... p 1614 N95-23088
GUNZBURGER, M. D. ..... p 1661 N95-22733
GUO, J. ..... p 1845 N95-24150
GUPTA, R. ..... p 1816 N95-22926
GURNETT, D. A. ..... p 1869 N95-22828
GUSTAFSSON, BERTIL ..... p 1791 N95-23548
GUY, WALTER W. ..... p 1750 N95-22766
GUZIK, J. A. ..... p 1870 N95-22938
GYLYS, V. T. ..... p 1625 N95-23439

H

HA, HUY VUI ..... p 1796 N95-22933
HAAG, THOMAS W. ..... p 1624 N95-23221
HAAS, BRIAN L. ..... p 1664 N95-22481
HABERBUSCH, MARK S. ..... p 1653 N95-24186
HABIB, S. ..... p 1794 N95-23349
HABIB, SALMAN ..... p 1795 N95-22654
HACYAN, S. ..... p 1821 N95-22965
HADID, ALI H. ..... p 1675 N95-23443
HADJIPANAYIS, GEORGE C. ..... p 1627 N95-22940
HADZIIOANNOU, G. ..... p 1649 N95-23568
HAERTLING, GENE ..... p 1648 N95-22883
HAGEN, M. ..... p 1755 N95-22769
HAGENIERS, O. L. ..... p 1642 N95-23503
HAGER, BRADFORD H. ..... p 1717 N95-22832
HAGGERTY, H. ..... p 1809 N95-23359
p 1817 N95-23369
HAH, C. ..... p 1674 N95-23437
p 1679 N95-23623
HAIGHT, R. C. ..... p 1806 N95-23137
HAINES, ROBERT T. ..... p 1743 N95-23074
HAIRE, SCOT L. ..... p 1683 N95-23637
HAJJ, IBRAHIM N. ..... p 1659 N95-22507
HAKVOORT, H. A. M. ..... p 1741 N95-22640
HALDAR, P. ..... p 1842 N95-23354
HALL, C. M. ..... p 1830 N95-22793
HALLER, E. E. ..... p 1844 N95-24010
HALLIDAY, A. N. ..... p 1830 N95-22793
p 1632 N95-22795
HALLIOP, E. ..... p 1637 N95-23504
HALPERN, JULES P. ..... p 1866 N95-23595
HAMADA, Y. ..... p 1834 N95-23527
p 1835 N95-23533
HAMADA, YASUJI ..... p 1836 N95-23569
HAMBURGER, MICHAEL W. ..... p 1717 N95-22832
HAMILTON, D. ..... p 1737 N95-22945
HAMILTON, MIKE ..... p 1702 N95-23850
HAMLEY, JOHN A. ..... p 1624 N95-23240
HAMM, CLAUS D. ..... p 1644 N95-23510
HAMMEN, D. ..... p 1659 N95-23682
HAMMETT, G. W. ..... p 1830 N95-22694
HAMMOND, ERNEST C., JR. ..... p 1748 N95-23821
HAN, DAESOO ..... p 1820 N95-22957
p 1825 N95-22992
HAN, YENJO ..... p 1760 N95-24092
HANGE, CRAIG ..... p 1607 N95-22666
HANSEN, EARL G. ..... p 1707 N95-23876
HANSEN, JOSEPH M. ..... p 1697 N95-23706
HANSEN, S. ..... p 1817 N95-23369
HANSSON, OTHAR ..... p 1779 N95-23744
HARDING, W. B. ..... p 1800 N95-23375
HARDY, G. L. ..... p 1644 N95-23515
HARDY, TERRY L. ..... p 1653 N95-24186
HARGIS, P. J., JR. ..... p 1636 N95-24007
HARIHARAN, P. C. ..... p 1857 N95-24108
HARMON, A. ..... p 1815 N95-23810
HARMON, B. A. ..... p 1815 N95-23818
p 1646 N95-23820
HARMON, B. ALAN ..... p 1815 N95-23817
HARRIS, BRENDA W. ..... p 1608 N95-23185
HARRIS, HOWARD C., JR. ..... p 1749 N95-23788
p 1750 N95-23934
HARRIS, VASCAR G. ..... p 1687 N95-23296
HARSANYI, JOSEPH C. ..... p 1703 N95-23858
HART, QUINN J. ..... p 1705 N95-23867
p 1709 N95-23889
HART, SUSAN V. ..... p 1856 N95-23209
HARTING, GEORGE C. ..... p 1625 N95-23261
HARTMANN, BRUCE ..... p 1800 N95-23073
HARTMANN, RALF ..... p 1770 N95-23685
HARVEY, GALE A. ..... p 1637 N95-23798
HASAN, M. Z. ..... p 1829 N95-22645
HASANSHAHID, M. ..... p 1829 N95-22622
HASHEM, S. ..... p 1767 N95-23578
HASHIMOTO, M. ..... p 1781 N95-23753
HASHIMOTO, Y. ..... p 1816 N95-22848
HASKEW, TIM A. ..... p 1694 N95-22909
HASKO, GROGORY H. ..... p 1648 N95-23179
HASSAN, A. R. ..... p 1849 N95-22759
p 1849 N95-22760
p 1849 N95-22761
HATTORI, T. ..... p 1816 N95-22644
p 1816 N95-22848
HAUGER, S. A. ..... p 1808 N95-23197
HAUGHLAND, E. J. ..... p 1846 N95-24188
HAUSER, SUSAN E. ..... p 1761 N95-24117
HAWORTH, L. A. ..... p 1613 N95-24030
HAXTON, W. C. ..... p 1802 N95-22729
p 1802 N95-22730
HAYARD, M. ..... p 1721 N95-23765
HAYASHI, MASATO ..... p 1752 N95-23709
HAYASHI, SHIGERU ..... p 1637 N95-24181
HAYASHI, T. ..... p 1834 N95-23524
p 1835 N95-23528
p 1835 N95-23528
HAYATI, S. A. ..... p 1836 N95-23589
p 1836 N95-23590
HAZELTINE, R. D. ..... p 1697 N95-23697
HAZER, KATHLEEN A. ..... p 1830 N95-22693
HAZUMI, MASASHI ..... p 1628 N95-23028
HE, YI ZHEN ..... p 1810 N95-23475
HEADLEY, DEAN E. ..... p 1805 N95-22935
HECHT, JAMES H. ..... p 1610 N95-24012
HECHT, KARL T. ..... p 1688 N95-23087
HEELIS, R. A. ..... p 1814 N95-22966
HEEMAN, PETER ..... p 1738 N95-23090
HEEMAN, PETER A. ..... p 1659 N95-24193
HEGEDUS, CHARLES R. ..... p 1658 N95-23937
HEGNA, C. C. ..... p 1644 N95-23513
HEIBA, ADEL H. ..... p 1836 N95-23589
p 1673 N95-23432
p 1686 N95-23653
HEIDA, J. H. ..... p 1643 N95-23507
HEIDBRINK, W. W. ..... p 1834 N95-23371
HEIDEBRECHT, KATHY ..... p 1703 N95-23854
HEINBOCKEL, JOHN H. ..... p 1691 N95-23411
HELGESON, W. D. ..... p 1659 N95-22549
p 1661 N95-22844
HELLER, REINHARD ..... p 1660 N95-22569
HELM, R. ..... p 1816 N95-22567
HELMLINGER, MARK ..... p 1690 N95-23862
HEMASPAANDRA, LANE A. ..... p 1792 N95-23931
p 1792 N95-24002
p 1793 N95-24003
p 1760 N95-24059
p 1784 N95-24060
p 1760 N95-24092
p 1793 N95-24194
HEMMING, BROOKE L. ..... p 1732 N95-22930
HEMPEL, R. ..... p 1657 N95-23075
HENESTROZA, E. ..... p 1817 N95-23493
p 1818 N95-24014
HENKE, ANDREA L. ..... p 1781 N95-23755
HENKE, R. P. ..... p 1815 N95-23812
HENKEL, JOCHEN ..... p 1716 N95-23960
HENRY, GREG ..... p 1779 N95-23743
HERBERT, DEXTER ..... p 1799 N95-23273
p 1620 N95-23275
HERITAGE, J. ..... p 1690 N95-22595
HERMAN, R. G. ..... p 1634 N95-23202
p 1634 N95-23339
HERNANDEZ, J. V. ..... p 1832 N95-23136
HERSHEY, K. T. ..... p 1719 N95-24098
HERZOG, G. ..... p 1646 N95-23820
HESS, PETER OTTO ..... p 1814 N95-22969
HESS, RONALD A. ..... p 1616 N95-23297
HESS, W. R. ..... p 1831 N95-22800
HEWETT, J. L. ..... p 1802 N95-22703
HEY, A. J. G. ..... p 1657 N95-23075
HIBBS, ROBERT I., JR. ..... p 1678 N95-23616
HIDEUMA, SHIGERU ..... p 1835 N95-23534
HIEL, CLEMENT C. ..... p 1688 N95-23263
HIETALA, V. M. ..... p 1828 N95-23575
HIGHAM, NICHOLAS J. ..... p 1791 N95-23592
HILDEMANN, LYNN M. ..... p 1732 N95-22930
HILL, D. D. ..... p 1662 N95-23368
HILL, DAVID C. ..... p 1727 N95-22904
p 1700 N95-23839
HILL, DAVID J. T. ..... p 1651 N95-23903
p 1651 N95-23904
HILL, S. D. ..... p 1613 N95-23666
HINEDI, SAMI ..... p 1761 N95-22478
HINGERTY, BRIAN E. ..... p 1805 N95-22889
HINKINS, R. L. ..... p 1763 N95-23486
HINTEREGGER, H. F. ..... p 1690 N95-24118
HIRAI, S. ..... p 1618 N95-23734
HIRAI, SHIGEOKI ..... p 1772 N95-23698
p 1777 N95-23728
HIRATA, MITSUNORI ..... p 1778 N95-23733
HIROSE, SHIGEO ..... p 1618 N95-23711
HIRSCHOWITZ, A. ..... p 1795 N95-22630
HIXON, R. ..... p 1668 N95-23220
HJALMARSON, A. ..... p 1868 N95-23230
HJELM, REX P., JR. ..... p 1646 N95-22553
HO, Y. ..... p 1671 N95-23426
HOCK, VINCENT F. ..... p 1662 N95-23117
HODGES, DEWEY H. ..... p 1766 N95-22831
p 1615 N95-23392
HODGSON, P. E. ..... p 1813 N95-24046
HOEDE, C. ..... p 1790 N95-23236
p 1794 N95-23239
p 1794 N95-23539
HOENE, ALBRECHT ..... p 1792 N95-24002
HOERZ, FRIEDRICH ..... p 1869 N95-23833
p 1700 N95-23842
HOFFBECK, JOSEPH P. ..... p 1705 N95-23868
HOFFMAN, D. J. ..... p 1837 N95-24083
HOFMANN, J. ..... p 1835 N95-23534
HOGAN, J. T. ..... p 1831 N95-22800
HOGAN, JEAN M. ..... p 1855 N95-23206
HOGAN, R. E. ..... p 1666 N95-22914
HOGREVE, H. ..... p 1847 N95-22635
HOJMAN, SERGIO A. ..... p 1823 N95-22977
HOLLAND, SCOTT D. ..... p 1666 N95-23015
p 1667 N95-23210
HOLLANSWORTH, JAMES E. ..... p 1622 N95-22814
HOLLENBERG, G. W. ..... p 1842 N95-23266
HOLLENBERG, J. B. ..... p 1832 N95-23072
HOLLERBACH, M. A. ..... p 1693 N95-22798
HOLLEY, W. ..... p 1728 N95-23062
HOLLIDAY, M. A. ..... p 1766 N95-23078
HOLM, E. A. ..... p 1811 N95-23576
HOLM, JACK M. ..... p 1690 N95-23298
HOLT, C. M. ..... p 1787 N95-22768
HOLT, J. B. ..... p 1679 N95-23621
p 1685 N95-23650
HOLZSCHEITER, M. H. ..... p 1805 N95-22927
p 1805 N95-22936
HOMMA, KHOZO ..... p 1778 N95-23737
HONDA, MASAHISA ..... p 1692 N95-23712
HOOKER, MATTHEW W. ..... p 1840 N95-22803
HOOKER, STANFORD B. ..... p 1743 N95-22671
HOPKINS, D. A. ..... p 1630 N95-23258
HOPKINS, DALE A. ..... p 1698 N95-22805
HOPKINS, P. L. ..... p 1638 N95-22576
HOPPEL, K. W. ..... p 1714 N95-23947
HOPSON, PURNELL, JR. ..... p 1666 N95-22906
HORAN, STEPHEN ..... p 1657 N95-22944
HORIUCHI, R. ..... p 1835 N95-23528
p 1836 N95-23590
p 1836 N95-23591
HORIUCHI, RITOKU ..... p 1834 N95-23524
HORNIK, K. E. ..... p 1660 N95-22716
HORST, JOHN ALBERT ..... p 1755 N95-22637
HORTON, W. ..... p 1830 N95-22694
p 1832 N95-23136
HORVATH, E. A. ..... p 1640 N95-23121
HORWITZ, JAMES L. ..... p 1831 N95-22955
p 1737 N95-22956
p 1831 N95-23008
HOSGOOD, B. ..... p 1710 N95-23891
HOSKING, F. M. ..... p 1664 N95-24149
HOUBEN, G. J. ..... p 1855 N95-22534
HOUCK, T. ..... p 1817 N95-23493
HOUF, W. G. ..... p 1632 N95-22722
HOUTS, M. G. ..... p 1624 N95-22905
HOWALD, A. M. ..... p 1830 N95-22719
HOWARD, DOUGLAS A. ..... p 1711 N95-23920
HOWARD, J. B. ..... p 1634 N95-23164
HOWARD, M. E. ..... p 1717 N95-22503
HOWELL, L. H. ..... p 1665 N95-22491
p 1790 N95-23536
HRADECNY, C. ..... p 1812 N95-23976
HSING, W. W. ..... p 1829 N95-22676
HSU, WAYNE W. ..... p 1669 N95-23416
p 1674 N95-23436
HSU, YANN-FU ..... p 1673 N95-23432
HSUE, SIN-TAO ..... p 1635 N95-23360
HUANG, HUI-MIN ..... p 1755 N95-22637
HUANG, J. ..... p 1675 N95-23442
HUANG, JEN-KUANG ..... p 1617 N95-23299
HUBBARD, C. R. ..... p 1647 N95-22688
HUBER, ERIC ..... p 1778 N95-23739
HUBER, F. W. ..... p 1673 N95-23435
HUBERMAN, ELIEZER ..... p 1746 N95-22912
HUDSON, G. MARTIN ..... p 1623 N95-23721
HUDSON, SUSAN T. ..... p 1675 N95-23441
HUEHN, T. ..... p 1801 N95-22685
HUERRE, P. ..... p 1665 N95-22767
HUGHES, C. D. ..... p 1842 N95-23266
HUGHES, CLIFFORD D. ..... p 1656 N95-22817
HUGHES, M. H. ..... p 1832 N95-23147
HUGHES, T. C. ..... p 1613 N95-24030
HUI, FRANK C. L. ..... p 1609 N95-23250
HUI, RAYMOND ..... p 1772 N95-23699
HUIBERTS, H. J. C. ..... p 1767 N95-23558
HULL, J. R. ..... p 1664 N95-24163
HULL, JOHN R. ..... p 1660 N95-22569
HUMES, DONALD H. ..... p 1623 N95-23825
HUMM, P. ..... p 1632 N95-22764
HUND, T. D. ..... p 1727 N95-22650
p 1731 N95-24155
HUNT, GALEN C. ..... p 1759 N95-24033
HUNT, JASON D. ..... p 1650 N95-24187
HUNT, L. R. ..... p 1654 N95-22804
HUNT, MADELYN D. ..... p 1751 N95-23474
HUNTER, CRAIG A. ..... p 1608 N95-23193
HUNTER, J. L. ..... p 1637 N95-23836
HURLEY, DONNA L. ..... p 1815 N95-23816
HUSSAIN, F. ..... p 1803 N95-22754
p 1804 N95-22789
HUSSIN, V. ..... p 1826 N95-23003
HUSSIN, VERONIQUE ..... p 1823 N95-22982
HUTCHINS, JAMIE ..... p 1689 N95-23789
HUTT, J. ..... p 1676 N95-23445
HWANG, CHUNG HEE ..... p 1659 N95-24193
HWANG, HYUN ..... p 1848 N95-22698

HYATT, A. W. ..... p 1693 N95-22798
p 1834 N95-23371

I

IACHELLO, FRANCO ..... p 1814 N95-22958
IANNO, N. J. ..... p 1649 N95-23356
IDA, KATSUMI ..... p 1835 N95-23534
IDEI, HIROSHI ..... p 1835 N95-23534
IFJU, PETER G. ..... p 1631 N95-23300
IGUCHI, H. ..... p 1834 N95-23527
IGUCHI, HARUKAZU ..... p 1835 N95-23534
IIJIMA, TAKAHIKO ..... p 1692 N95-23712
p 1623 N95-23713
IIYOSHI, ATSUO ..... p 1835 N95-23535
p 1835 N95-23543
IMANISHI, A. ..... p 1816 N95-22848
INABA, NORIYASU ..... p 1623 N95-23713
INAGAKI, T. ..... p 1623 N95-23700
ING, J. L. ..... p 1842 N95-23135
INGRAFFEA, A. R. ..... p 1697 N95-24106
IOLLO, ANGELO ..... p 1678 N95-23596
IRVING, A. D. ..... p 1630 N95-23537
IRWIN, J. ..... p 1816 N95-22567
ISAACSON, DENNIS L. ..... p 1719 N95-24095
p 1719 N95-24097
ISACKS, BRYAN L. ..... p 1713 N95-23942
ISAR, AURELIAN ..... p 1798 N95-22990
ISLER, R. C. ..... p 1831 N95-22800
ISONO, TAKAAKI ..... p 1831 N95-22849
ITIKAWA, Y. ..... p 1811 N95-23604
ITOH, K. ..... p 1835 N95-23533
ITOH, SANAE-I. ..... p 1835 N95-23534
ITOKO, T. ..... p 1618 N95-23734
ITON, L. E. ..... p 1632 N95-22681
ITTEN, KLAUS I. ..... p 1707 N95-23876
IVANOV, A. N. ..... p 1848 N95-22744
p 1849 N95-22745
p 1849 N95-22753
p 1803 N95-22754
p 1803 N95-22755
p 1804 N95-22811
p 1850 N95-22812
IVANOV, V. V. ..... p 1766 N95-22614
IWASAKI, YUMI ..... p 1618 N95-23679
IWATA, TSUTOMU ..... p 1697 N95-23695
IWATA, YOSHITAKA ..... p 1778 N95-23737
IYER, R. M. ..... p 1814 N95-24175
IZU, M. ..... p 1728 N95-23061

J

JAAP, JOHN P. ..... p 1761 N95-23746
p 1780 N95-23747
JAARSMA, M. N. ..... p 1701 N95-22639
JACKSON, K. A. ..... p 1762 N95-22680
JACKSON, S. M. ..... p 1740 N95-23386
JACKSON, T. L. ..... p 1667 N95-23207
JACOBS, C. S. ..... p 1756 N95-22853
JACOBSON, A. ..... p 1701 N95-23847
JACOBY, W. A. ..... p 1734 N95-23480
JACQUEMOUD, S. ..... p 1710 N95-23891
JACQUEMOUD, STEPHANE ..... p 1701 N95-23845
JAIN, A. ..... p 1816 N95-22926
JAIN, ABHINANDAN ..... p 1692 N95-22543
JAMES, R. A. ..... p 1834 N95-23371
JAMNEJAD, V. ..... p 1656 N95-22852
JANSEN, F. ..... p 1872 N95-23809
JANSEN, J. K. M. ..... p 1789 N95-23173
JANSEN, R. W. ..... p 1712 N95-23939
JANSSEN, R. ..... p 1733 N95-23067
JASKOLSKI, Z. ..... p 1848 N95-22738
JAUREGUI, ROCIO ..... p 1814 N95-22964
JAUREGUI, ROCO ..... p 1821 N95-22965
JELLINEK, J. ..... p 1638 N95-22531
JENKINS, L. N. ..... p 1677 N95-23466
JENKINS, RHONALD M. ..... p 1625 N95-23640
JENSEN, R. J. ..... p 1625 N95-23439
JERNIGAN, G. G. ..... p 1636 N95-23495
JEZEK, K. C. ..... p 1714 N95-23951
JIA, QUANXI ..... p 1843 N95-23367
JIA, W. X. ..... p 1645 N95-23571
JIANG, ZHIGEN ..... p 1760 N95-24059
JIAQUAN, LIU ..... p 1785 N95-22624
JIRKA, I. ..... p 1634 N95-23339
JOHANSSON, L. E. B. ..... p 1868 N95-23230
JOHNSON, CLARK E., JR. ..... p 1857 N95-24109
JOHNSON, DAVID G. ..... p 1735 N95-22482
JOHNSON, DAVID H. ..... p 1719 N95-24098
JOHNSON, FRANCIS S. ..... p 1739 N95-23272
JOHNSON, KEN I. ..... p 1654 N95-22692
JOHNSON, L. C. ..... p 1833 N95-23269
JOHNSON, MARJORY J. ..... p 1764 N95-24023
JOHNSON, P. D. ..... p 1840 N95-22762
p 1851 N95-23335
JOHNSON, R. E. ..... p 1869 N95-24066
JOHNSON, RAYMOND W. ..... p 1721 N95-23675
JOHNSON, S. L. ..... p 1686 N95-23654
JOHNSON, THEODORE ..... p 1862 N95-24137
JOHNSON, W. C. ..... p 1646 N95-24140
JOHNSON, WALTER J. ..... p 1611 N95-23393
JOHNSTON, P. H. ..... p 1644 N95-23512
JOHNSTON, WILLIAM E. ..... p 1858 N95-24111
JONATHAL, D. ..... p 1872 N95-23806
JONES, C. E. ..... p 1830 N95-22793
JONES, DAVID A. ..... p 1653 N95-23668
JONES, MARK T. ..... p 1755 N95-22690
JONG, R. A. ..... p 1834 N95-23371
JONKER, P. ..... p 1790 N95-23235
JOOSTEN, J. M. ..... p 1733 N95-23126
JORALMON, DEFOREST Q. ..... p 1750 N95-22513
JORGENSEN, GARY ..... p 1726 N95-22547
JOSHI, V. M. ..... p 1753 N95-23962
JUCKS, KENNETH W. ..... p 1735 N95-22482
JUNG, CHANG KEE ..... p 1813 N95-24000
JUNGE, R. ..... p 1693 N95-22798
JUSTUS, BRIAN L. ..... p 1662 N95-23241

K

KAARET, PHILIP ..... p 1866 N95-23540
KAFKA, A. L. ..... p 1739 N95-23247
KAGEYAMA, A. ..... p 1834 N95-23524
p 1835 N95-23528
KAGEYAMA, AKIRA ..... p 1836 N95-23590
KAHN, S. ..... p 1816 N95-22926
KAINDL, HERMANN ..... p 1768 N95-23677
KAISER, MARY K. ..... p 1611 N95-23393
KALACHEV, L. V. ..... p 1789 N95-23169
KALE, P. G. ..... p 1746 N95-22911
KALIL, CAROL R. ..... p 1651 N95-23899
KALINOVSKIJ, YU. L. ..... p 1804 N95-22787
KALLENBERG, W. C. M. ..... p 1794 N95-23559
KALMAN, LINDA S. ..... p 1705 N95-23869
KAMALIKHAMSEH, F. ..... p 1786 N95-22642
KAMAREDDINE, F. ..... p 1788 N95-23130
KAMATH, GAUTHAM ..... p 1659 N95-22507
KAMENETZKY, RACHEL R. ..... p 1651 N95-23908
p 1651 N95-23912
KANDA, SHINJI ..... p 1778 N95-23736
KANE, T. G., III ..... p 1742 N95-23385
KANEKO, ATSUKO ..... p 1690 N95-23674
KANGAS, L. J. ..... p 1767 N95-23578
KANIA, LEE ..... p 1683 N95-23639
KANKAM, M. DAVID ..... p 1616 N95-23671
KARCZEWSKI, G. ..... p 1844 N95-24010
KARLEN, JAMES ..... p 1768 N95-23676
KARPALA, F. ..... p 1642 N95-23503
KASISCHKE, ERIC S. ..... p 1716 N95-23959
KASSEL, P. C. ..... p 1623 N95-23826
p 1869 N95-23828
KATAYAMA, T. ..... p 1816 N95-22644
p 1816 N95-22848
KATO, S. ..... p 1811 N95-23775
KATO, T. ..... p 1811 N95-23604
KATO, TSUNEAKI ..... p 1659 N95-24193
KATRAGADDA, LALITESH ..... p 1697 N95-23694
KATSINIS, CONSTANTINE ..... p 1753 N95-23301
KATSURAGAWA, T. ..... p 1618 N95-23734
KAUFFMANN, PAUL J. ..... p 1698 N95-23302
KAUFMAN, YORMAN J. ..... p 1704 N95-23860
KAUKLER, WILLIAM F. ..... p 1826 N95-23016
KAWAHATA, K. ..... p 1835 N95-23533
KAWAKAMI, H. ..... p 1811 N95-23775
KAWAMURA, TAKEYA ..... p 1752 N95-23715
KAWASUMI, Y. ..... p 1835 N95-23533
KAZANSKY, A. K. ..... p 1825 N95-22999
KEATING, MERIDITH ..... p 1861 N95-24131
KEEGAN, R. ..... p 1872 N95-23809
KEENER, EARL R. ..... p 1609 N95-23250
KEIL, M. ..... p 1713 N95-23944
KELLER, JEFFREY D. ..... p 1612 N95-23217
KELLER, LINDSAY P. ..... p 1633 N95-23092
KELLER, P. E. ..... p 1767 N95-23578
KELLEY, N. D. ..... p 1729 N95-23383
KELLNER, A. ..... p 1777 N95-23730
KELLY, D. M. ..... p 1846 N95-24170
KELLY, E. ..... p 1816 N95-22926
KELLY, JACK ..... p 1861 N95-24132
KELLY, P. ..... p 1855 N95-22515
KENNISON, MEG ..... p 1621 N95-22868
KEOUGH, B. K. ..... p 1626 N95-22918
KERN, S. B. ..... p 1677 N95-23466
KERN, W. ..... p 1790 N95-23231
p 1757 N95-23232
p 1758 N95-23608
KERNIK, ALAN C. ..... p 1614 N95-22674
KERR, R. ..... p 1616 N95-24019
KERR, S. A. ..... p 1622 N95-23532
KESSLER, DONALD J. ..... p 1869 N95-23830
KESSLER, G. K. ..... p 1613 N95-24030
KESTER, D. ..... p 1865 N95-22539
KEUP, R. M. ..... p 1813 N95-24016
KHALELL, MOHAMMAD A. ..... p 1654 N95-22692
KHALIL, M. ASLAM K. ..... p 1731 N95-22673
KHANDELWAL, GOVIND S. ..... p 1817 N95-22929
KHANNA, M. P. ..... p 1804 N95-22810
p 1811 N95-23770
KHARBANDA, SURENDER ..... p 1746 N95-22912
KHOMUTOV, A. M. ..... p 1644 N95-23514
KIBE, K. ..... p 1623 N95-23700
KIBE, SEISHIROH ..... p 1623 N95-23726
KIDA, TAKASHI ..... p 1623 N95-23726
p 1622 N95-24049
KIDWELL, DAVID A. ..... p 1632 N95-22710
KIEFFER, HUGH ..... p 1704 N95-23859
KIEREIN-YOUNG, KATHRYN S. ..... p 1713 N95-23945
KIJOWSKI, J. ..... p 1850 N95-22784
KILGORE, S. H. ..... p 1838 N95-22530
KILGORE, W. ALLEN ..... p 1668 N95-23257
KILLEEN, T. L. ..... p 1737 N95-22951
p 1688 N95-23087
KIM, C. P. ..... p 1701 N95-22639
p 1740 N95-23470
KIM, H. B. ..... p 1850 N95-22783
KIM, JONGSU ..... p 1785 N95-22627
KIM, S.-W. ..... p 1676 N95-23447
KIM, WON S. ..... p 1768 N95-23676
KIM, YOUNG S. ..... p 1825 N95-22992
KIMURA, SHINICHI ..... p 1659 N95-23710
p 1623 N95-23727
KINARD, TIM A. ..... p 1608 N95-23185
KINARD, W. H. ..... p 1869 N95-23828
KINARD, WILLIAM H. ..... p 1623 N95-23822
KING, C. N. ..... p 1631 N95-22677
KING, D. A. ..... p 1662 N95-23351
KING, D. L. ..... p 1727 N95-22650
KING, JOSEPH ..... p 1862 N95-24136
KING, TRUDE V. V. ..... p 1703 N95-23855
KIRANE, M. ..... p 1785 N95-22618
KIRIS, CETIN ..... p 1680 N95-23627
KIRKLAND, T. P. ..... p 1647 N95-22689
KISPERT, L. D. ..... p 1631 N95-22575
KITAMI, M. ..... p 1618 N95-23734
KLARER, P. R. ..... p 1694 N95-23065
KLEIN, ANDREW G. ..... p 1713 N95-23942
KLEIN, FRED W. ..... p 1737 N95-22924
KLEIN, J. ..... p 1646 N95-23820
KLEIN, O. ..... p 1660 N95-22593
KLEIS, THOMAS ..... p 1815 N95-23807
p 1870 N95-23808
KLEMM, R. A. ..... p 1846 N95-24173
KLEPPER, C. C. ..... p 1831 N95-22800
KLIER, K ..... p 1634 N95-23202
KLIER, K. ..... p 1634 N95-23339
KLIMOV, ANDREY B. ..... p 1826 N95-23004
KLOKS, T. ..... p 1785 N95-22535
KNAPP, G. S. ..... p 1639 N95-22594
KNIFFEN, DONALD A. ..... p 1871 N95-23216
KOBAYASHI, A. ..... p 1633 N95-22876
KOBAYASHI, H. ..... p 1635 N95-23481
KOBLER, BENJAMIN ..... p 1857 N95-24108
KOERNER, J. G. ..... p 1804 N95-22789
KOK, J. N. ..... p 1757 N95-23467
KOKER, EDMOND B. ..... p 1692 N95-23303
KOMADA, SATORU ..... p 1752 N95-23704
p 1752 N95-23705
KOMORIYA, K. ..... p 1777 N95-23729
KOMOROWSKI, J. P. ..... p 1642 N95-23503
KOMPANIETZ, G. B. ..... p 1817 N95-23245
KOMURA, FUMINOBU ..... p 1623 N95-23719
KONDO, YOJI ..... p 1866 N95-23402
KONTOTHANASSIS, L. I. ..... p 1759 N95-23928
KONTOTHANASSIS, LEONIDAS ..... p 1753 N95-24177
KONTOTHANASSIS, LEONIDAS I. ..... p 1765 N95-24183
p 1765 N95-24184
KONTSEVICH, MAXIM ..... p 1786 N95-22711
KOONS, HARRY C. ..... p 1770 N95-23684
KOPPEN, SANDRA HOWELL ..... p 1753 N95-22479
KORNATZKY, Y. ..... p 1855 N95-22534
KORNILOV, E. ..... p 1803 N95-22758
KORSMEYER, DAVID J. ..... p 1770 N95-23687
KORTSCHOT, M. T. ..... p 1627 N95-22833
KOSMO, JOSEPH ..... p 1750 N95-22766
KOTIKOV, A. V. ..... p 1812 N95-23975
KOTOKU, T. ..... p 1777 N95-23729
KOTSCHENREUTHER, M. ..... p 1830 N95-22694
KOURA, KATSUHISA ..... p 1687 N95-24082
KOURTIDES, DEMETRIUS A. ..... p 1649 N95-23394
KOUZES, R. T. ..... p 1767 N95-23578
KOVACS, E. ..... p 1807 N95-23196
KOWALCZYK, E. A. ..... p 1721 N95-24192
KOZOL, J. ..... p 1642 N95-23500
KRATSCH, D. ..... p 1785 N95-22535
KRAVITZ, S. H. ..... p 1828 N95-23575

KRIPLANI, HARISH p 1659 N95-22507
KRISHNAKUMAR, S. p 1642 N95-23503
KRISHNAMURTHY, RAMESH p 1617 N95-23304
KRISHNAN, A. p 1637 N95-23645
KRIVONOS, S. O. p 1790 N95-23457
KROESE, D. P. p 1767 N95-23556
KROTKOV, ERIC p 1697 N95-23694
KROTZ, P. D. p 1696 N95-24064
KRUGER, ALBERT A. p 1647 N95-22647
p 1647 N95-22648
KRUGER, CHARLES H. p 1741 N95-24041
KRUMMEL, P. B. p 1721 N95-24192
KRUMPELT, M. p 1726 N95-22568
p 1730 N95-23582
KRUSE, FRED p 1702 N95-23853
KRUSE, FRED A. p 1705 N95-23870
p 1714 N95-23946
KRUTOV, A. M. p 1817 N95-23245
KRYDER, MARK H. p 1690 N95-24128
KRYSKOWSKI, DAVID p 1711 N95-23918
KRZYCKI, JOSEPH A. p 1745 N95-22873
KUBIAK, G. D. p 1828 N95-23767
KUBINSKI, CHERYL A. p 1679 N95-23620
KUBO, TOMOAKI p 1752 N95-23709
KUBOTA, TAKASHI p 1771 N95-23689
p 1771 N95-23692
KUDLAC, MAUREEN T. p 1653 N95-24186
KUEHNER, D. E. p 1635 N95-23380
KUEPER, T. W. p 1726 N95-22568
p 1730 N95-23582
KUFE, DONALD p 1746 N95-22912
KUHLMANN, K. J. p 1629 N95-23038
KUHLMANN, S. p 1816 N95-22684
KUIPER, HILBERT p 1752 N95-23714
KUMAR, SANJIV p 1687 N95-24051
KUMAR, VIPIN p 1771 N95-23691
KUNKEE, D. B. p 1736 N95-22867
p 1742 N95-23208
KUNSELMAN, R. p 1805 N95-22881
KUO, KENNETH K. p 1625 N95-23261
KUPIEC, JOHN p 1705 N95-23871
KUPPERMAN, D. S. p 1838 N95-22530
KURAEV, E. A. p 1804 N95-22847
KUROSAKI, Y. p 1618 N95-23734
KURTH, W. S. p 1869 N95-22828
KURYLA, J. p 1681 N95-23631
KUSHNER, M. J. p 1837 N95-24158
KUSSMAUL, MICHAEL T. p 1624 N95-23221
KUWAO, FUMIHIRO p 1752 N95-23708
KUZAY, T. M. p 1638 N95-22592
p 1696 N95-23397
KUZEMSKY, A. L. p 1840 N95-22846
KWAK, DOCHAN p 1680 N95-23627
KWAN, ROBERT p 1655 N95-22813
KWEI, G. H. p 1844 N95-24076
KYBURG, HENRY E., JR. p 1792 N95-23793
p 1794 N95-23927

L

LACERDA, A. p 1843 N95-23367
LACKNER, K. S. p 1666 N95-22902
LACKSONEN, THOMAS A. p 1854 N95-23305
LADELFE, P. C. p 1739 N95-23244
LAFERLA, RAFFAELE p 1871 N95-24191
LAFLAMME, R. p 1868 N95-23570
LAFONT, C. J. p 1645 N95-23983
LAGASSE, R. R. p 1650 N95-23577
LAGNADO, RONALD R. p 1673 N95-23432
p 1686 N95-23653
LAI, G. p 1764 N95-23599
LAI, JONATHAN Y. p 1658 N95-23670
LAIRD, C. E. p 1815 N95-23818
LAIRD, CHRISTOPHER E. p 1815 N95-23817
LAIRD, P p 1659 N95-23682
LAKEOU, SAMUEL p 1827 N95-23224
LAKSHMINARAYANA, B. p 1671 N95-23426
p 1675 N95-23444
LALWANI, NARENDRA D. p 1748 N95-23771
LAM, ALEX W. p 1655 N95-22505
LAM, N. p 1832 N95-23084
LAMBERT, D. J. p 1810 N95-23488
LAMBERT, LYNN p 1853 N95-23306
LAMBOLEY, M. p 1771 N95-23693
LAMICH, DAVID p 1740 N95-23529
LAMOREAUX, CYNTHIA M. p 1626 N95-23270
LANAGAN, M. T. p 1838 N95-22530
p 1662 N95-23355
LANCASTER, NICHOLAS p 1711 N95-23920
LANDGREBE, DAVID A. p 1705 N95-23868
LANE, ROBERT p 1856 N95-23209
LANG, D. D. p 1661 N95-23080
LANG, WOLFDIETER p 1814 N95-22962
LANGE, A. C. p 1659 N95-22504
LANSKY, AMY L. p 1761 N95-23748
LAO, L. L. p 1834 N95-23371
LARA, RITALUZ p 1749 N95-22987
LARBALESTIER, D. C. p 1846 N95-24171
LARSEN, R. p 1664 N95-24070
LARSON, STEVEN A. p 1707 N95-23876
LASH, TOM J. p 1637 N95-23798
LASKIN, ROBERT p 1827 N95-23089
LASSEIGNE, D. G. p 1667 N95-23207
LAU, FRANCIS S. p 1727 N95-22888
LAUGHON, G. J. p 1693 N95-22796
LAULAINEN, N. p 1735 N95-24146
LAURIENTE, MICHAEL p 1770 N95-23684
LAVENDER, CURT A. p 1654 N95-22692
LAVERY, DAVE p 1768 N95-23673
LAWEN, JAMES, JR. p 1695 N95-23214
LAYTIMI, F. p 1787 N95-22809
LEATHRUM, JAMES F., JR. p 1687 N95-23307
LEBEDEV, V. p 1832 N95-23163
LEBLANC, N. p 1664 N95-24070
LEBLANC, THOMAS J. p 1764 N95-24037
LECOUAT, FRANCOIS p 1752 N95-23720
LEDVIJ, M. p 1846 N95-24173
LEDWINA, T. p 1794 N95-23559
LEE, DER-CHUEN p 1830 N95-22793
p 1632 N95-22795
LEE, E. p 1818 N95-24014
LEE, E. U. p 1642 N95-23500
LEE, GILBERT F. p 1800 N95-23073
LEE, H.-J. p 1630 N95-23463
LEE, J. K. p 1660 N95-22586
LEE, J. S. p 1714 N95-23947
LEE, JA H. p 1691 N95-23411
LEE, R. L. p 1738 N95-23143
LEE, R. N. p 1735 N95-23580
LEE, RICHARD R. p 1858 N95-24115
LEE, T. S. H. p 1811 N95-23587
LEFFLER, J. S. p 1732 N95-22856
LEIFER, LARRY J. p 1768 N95-23678
LEMASTER, P. S. p 1631 N95-23910
LEMMEL, H. D. p 1857 N95-23453
LEMUS, RENATO p 1814 N95-22960
p 1814 N95-22961
LENARD, D. R. p 1637 N95-23504
LEOINNE, M. p 1614 N95-23088
LESLIE, THOMAS M. p 1843 N95-23563
LETTON, ALAN p 1651 N95-23902
LEVAI, GEZA p 1822 N95-22970
p 1814 N95-22971
LEVINE, ARLENE S. p 1889 N95-23796
p 1899 N95-23896
LEWIS, J. A. p 1845 N95-24150
LEWIS, NORMAN G. p 1745 N95-22801
LEWIS, P. S. p 1758 N95-23567
LI, D. p 1840 N95-22762
LI, GUANG p 1648 N95-22883
LI, H. p 1817 N95-23485
p 1817 N95-23493
LI, J. C. M. p 1630 N95-23924
LI, KU-YEN p 1751 N95-23474
LI, LARRY p 1752 N95-23735
LI, PING-CHUNG p 1659 N95-22507
LI, QIANG p 1842 N95-23354
LI, WEI p 1764 N95-23936
p 1765 N95-24061
LI, Y. p 1638 N95-22592
p 1696 N95-23397
LIANG, H. p 1731 N95-24155
LIANG, PAK-YAN p 1681 N95-23629
p 1637 N95-23644
LIANG, YI MING p 1832 N95-23163
LIAO, LI p 1801 N95-22643
LIAW, GOANG-SHIN p 1685 N95-23647
LIAW, PAUL p 1676 N95-23445
p 1683 N95-23638
LIAW, Y. K. p 1696 N95-24064
LIBERTIN, CLAUDIA R. p 1746 N95-22913
LIEB, ROBERT J. p 1652 N95-22506
LIGHT, MARC p 1659 N95-24193
LIGNOS, DEMETRIOS p 1753 N95-24125
LIM, TAE W. p 1784 N95-23308
LIN, SHYI-JANG p 1678 N95-23616
LIN, Z. p 1832 N95-23136
LINDH, ROLAND p 1810 N95-23459
LINDSAY, THOMAS S. p 1697 N95-23706
LINTON, ROGER C. p 1651 N95-23908
p 1651 N95-23912
LITTLE, CINDY p 1621 N95-22868
LIU, C. p 1638 N95-22592
LIU, DONGSHENG p 1802 N95-22720
LIU, J. p 1677 N95-23451
LIU, J. Q. p 1787 N95-22750
LIU, TSUEN-HSI p 1827 N95-23045
LIU, YULIANG p 1812 N95-23985
LLACER, J. p 1756 N95-23079
LLEWELLYN, EDWARD J. p 1688 N95-23087
LO, C. F. p 1667 N95-23183
p 1609 N95-23669
LOELLBACH, J. p 1674 N95-23437
p 1679 N95-23623
LOERCHER, G. p 1709 N95-23885
LOGAN, R. T. p 1656 N95-22852
LOHE, M. A. p 1796 N95-22900
LOHRENZ, S. E. p 1819 N95-22780
LOMAX, CURTIS p 1695 N95-23376
LONEY, NORMAN W. p 1617 N95-23309
LONG, D. D. p 1695 N95-23373
LOOMIS, B. A. p 1646 N95-24153
LOONG, C. K. p 1632 N95-22681
LOOS, ALFRED C. p 1648 N95-23179
LOOYEN, W. J. p 1718 N95-23471
LOPEZ-MORENO, ENRIQUE p 1814 N95-22974
LOPEZ, J. C. p 1814 N95-22969
LORENZANA, H. E. p 1841 N95-22860
LOUBRIEL, G. M. p 1659 N95-22549
p 1661 N95-22844
LOUCK, J. D. p 1796 N95-22900
LOUIS, STEVE p 1861 N95-24131
LOVESEY, S. W. p 1798 N95-23127
p 1807 N95-23159
LOWE, DAVID M. p 1649 N95-23394
LOWE, ROBERT P. p 1688 N95-23087
LOWRY, M. p 1827 N95-23449
LOWRY, MICHAEL p 1761 N95-23680
LOYNSTEV, V. A. p 1817 N95-23245
LU, CHU-HO p 1700 N95-23310
LU, HUNG JUNG p 1847 N95-22566
LU, SHIN-YEE p 1827 N95-23449
LU, Y. C. p 1625 N95-23261
LUCA, JACKIE p 1628 N95-23029
LUCCA, D. A. p 1654 N95-22678
LUCIANI, S. p 1712 N95-23940
LUHANDJULA, M. K. p 1755 N95-22616
LUIT, E. J. p 1687 N95-22536
LUKAS, A. p 1850 N95-22783
LUKENS, JAMES p 1838 N95-22511
LUKINS, R. p 1626 N95-22919
LUND, P. p 1729 N95-23382
LUNDGREN, RONALD G. p 1698 N95-22500
LUNG, C. W. p 1839 N95-22606
LUO, H. p 1844 N95-24010
LUO, J. p 1675 N95-23444
LUPI, ALEX p 1680 N95-23625
LURIE, YURI, A. p 1814 N95-22967
LUTZ, ANDREW E. p 1633 N95-22886
LYNCH, EDWARD D. p 1673 N95-23432
LYNN, J. E. p 1844 N95-24076
LYON, PORTER p 1657 N95-23023
LYONS, L. R. p 1740 N95-23933

M

MA, DEREN p 1610 N95-24050
MAAG, CARL R. p 1623 N95-23803
MABOGUNJE, ADE p 1768 N95-23678
MACARIE, IOAN I. p 1760 N95-24056
MACCHIAVELLI, A. O. p 1759 N95-23963
MACHA, M. p 1659 N95-23682
MACHIDA, K. p 1618 N95-23734
MACHIDA, KAZUO p 1752 N95-23704
p 1752 N95-23705
p 1777 N95-23728
MACKAMUL, K. p 1729 N95-23478
MACKAY, N. G. p 1700 N95-23840
MACKIN, MICHAEL A. p 1762 N95-22668
MACRAE, JOHN DOUGLAS p 1648 N95-23179
MADENCI, ERDOGAN p 1700 N95-23311
MAEDIGER, B. p 1777 N95-23730
MAESHIMA, K. p 1808 N95-23203
MAESTAS, L. M. p 1640 N95-22835
MAGAHIZ, R. p 1802 N95-22727
MAGGIORE, C. J. p 1842 N95-23265
MAH, G. R. p 1706 N95-23872
MAHAJAN, D. p 1633 N95-22876
MAHAN, G. D. p 1840 N95-22687
MAHDAVI, M. A p 1832 N95-23119
MAHDAVI, M. A. p 1693 N95-22796
p 1693 N95-22798
MAHONEY, COLIN p 1702 N95-23850
MAINGI, R. p 1693 N95-22796
MAKAROV, K. A. p 1851 N95-23967
MAKROUM, H. p 1665 N95-22585
MALAPATI, SRINIVAS REDDY p 1751 N95-24021
MALEY, M. P. p 1843 N95-23366
p 1843 N95-23367
p 1645 N95-23571
MALIN, JANE T. p 1617 N95-23750
MALINOWSKI, M. E. p 1828 N95-23767
MALOY, STUART A. p 1839 N95-22653
MALTE, P. p 1635 N95-23381
MANDEVILLE, JEAN-CLAUDE p 1623 N95-23824
p 1869 N95-23834
MANGANARIS, STEFANOS p 1770 N95-23686

MANGO, S. A. p 1714 N95-23947
MANKBADI, REDA R. p 1668 N95-23220
MANKO, MARGARITA A. p 1822 N95-22976
MANKO, VLADIMIR I. p 1822 N95-22976
MANLY, STEVEN L. p 1808 N95-23226
MANNING, CAROL A. p 1611 N95-23565
p 1750 N95-24088
MANOKHIN, V. N. p 1810 N95-23458
MANOUCHEHRI, DAVOUD p 1697 N95-23706
p 1697 N95-23724
MANTAY, WAYNE R. p 1612 N95-22953
MARCHETTI, MICHAEL p 1753 N95-24177
MAREELS, I. M. Y. p 1767 N95-23199
MARENGONI, HILCEA F. p 1784 N95-24185
MARGASON, RICHARD J. p 1607 N95-22666
MARGOLIS, S. B. p 1634 N95-23122
MARHEFKA, R. J. p 1657 N95-23391
MARINOV, N. p 1635 N95-23381
MARK, WILLIAM S. p 1721 N95-23675
MARKELOFF, R. p 1809 N95-23359
MARKOV, B. N. p 1812 N95-23976
MARRIAN, CHRISTIE R. p 1660 N95-22709
MARS, N. J. I. p 1648 N95-23128
MARSHALL-BRADLEY, TINA p 1853 N95-23312
MARTENS, W. G. p 1733 N95-23126
MARTIN, J. D. p 1757 N95-23346
MARTIN, J. M. M. p 1687 N95-22536
MARTIN, JAMES E. p 1800 N95-23313
MARTIN, M. M. p 1632 N95-22764
MARTIN, MARY E. p 1706 N95-23873
MARTIN, NATHANIEL G. p 1659 N95-24193
MARTINEZ, C. M. p 1742 N95-23385
MARTINEZ, R. p 1799 N95-22675
MARTINEZYROMERO, R. P. p 1825 N95-22996
MARUSZEWSKI, B. p 1833 N95-23170
MARUYAMA, TSUGITO p 1778 N95-23733
p 1778 N95-23736
MASIULANIEC, K. CYRIL p 1668 N95-23248
MASLAKOWSKI, JOHN E. p 1624 N95-22885
MASSA, DERCK L. p 1865 N95-23401
MASUDA, H. p 1816 N95-22848
MATIENZO, JOSE p 1685 N95-23650
MATSUEDA, TATSUO p 1752 N95-23708
MATSUHIRA, N. p 1777 N95-23729
MATSUMOTO, KOHTARO p 1752 N95-23715
p 1623 N95-23726
MATSUNAGA, TSUNEO p 1711 N95-23919
MATTHEIJ, R. M. M. p 1667 N95-23144
p 1789 N95-23169
p 1789 N95-23173
MATTHEWS, K. p 1828 N95-24068
MATTHEWS, R. D. p 1695 N95-23342
MATTSON, J. E. p 1840 N95-22762
p 1846 N95-24168
MATVEENKO, L. p 1866 N95-23468
MATZ, C. W. p 1644 N95-23511
MATZAKIS, Y. p 1752 N95-23707
MAUNG, KHIN MAUNG p 1817 N95-22929
MAURY, JUAN CARLOS F. p 1797 N95-22989
MAUW, S. p 1657 N95-23151
MAXWELL, J. R. p 1711 N95-23918
MAYER, ANDREW p 1779 N95-23744
MAYERS, J. p 1850 N95-23154
MAYFIELD, M. J. p 1728 N95-23162
p 1730 N95-23977
MCADDO, JAMES A. p 1663 N95-24048
MCBEE, LARRY S. p 1614 N95-22674
MCBRIDE, PHILIP p 1760 N95-24176
MCCALLON, H. p 1865 N95-22539
MCCHESNEY, J. M. p 1830 N95-22719
MCCLUSKEY, CAROLINA P. S. p 1866 N95-23402
MCCLUSKEY, GEORGE E., JR. p 1866 N95-23402
MCCOLLISTER, S. B. p 1628 N95-23026
MCCOLLUM, BRUCE p 1779 N95-23741
MCCOMAS, DAVID J. p 1829 N95-22665
p 1736 N95-22850
MCCONNAUGHEY, PAUL K. p 1678 N95-23617
MCCOOL, S. C. p 1832 N95-23136
MCCRADY, R. p 1802 N95-22727
MCDADE, IAN C. p 1688 N95-23087
MCDERMOTT, JOSEPH p 1629 N95-23036
MCDONNELL, J. A. M. p 1624 N95-23827
p 1700 N95-23840
MCGINLEY, CATHERINE B. p 1666 N95-22906
MCGLYNN, S. P. p 1803 N95-22747
MCINTYRE, D. C. p 1640 N95-22835
MCINTYRE, P. C. p 1842 N95-23265
MCLEOD, MALCOLM E. p 1662 N95-23117
MCMAHAN, A. K. p 1841 N95-22860
MCMURRAY, ROBERT E., JR. p 1827 N95-23378
MCNAMARA, W. F. p 1650 N95-24159
MCNELIS, NANCY B. p 1653 N95-24186
MEADOR, WILLARD E., JR. p 1691 N95-23411
MEGGERS, K. p 1844 N95-24076
MEHLHORN, T. A. p 1818 N95-24160
MEIJER, P. M. p 1787 N95-22717
MEISEL, DAN p 1632 N95-22857
MEISSNER, K. A. p 1848 N95-22738
MEISSNER, T. p 1805 N95-22925
MELACK, JOHN M. p 1716 N95-23959
MELEZHIK, V. V. p 1851 N95-23967
MELL, RICHARD J. p 1631 N95-23910
p 1651 N95-23911
MENA, R. A. p 1846 N95-24188
MENDE, STEPHEN B. p 1688 N95-23087
MENDREK, M. J. p 1641 N95-23186
MENEON, M. M. p 1693 N95-22796
MENIKOFF, R. p 1666 N95-22902
MERCERET, FRANCIS J. p 1742 N95-23010
MERENYI, ERZSEBET p 1706 N95-23874
MERKLE, C. L. p 1676 N95-23446
MERKLE, CHARLES L. p 1681 N95-23630
MERKLE, K. L. p 1845 N95-24152
MERRILL, F. p 1802 N95-22727
MERRIMAN, EDMUND A. p 1628 N95-23027
MERRITT, B. T. p 1727 N95-22574
MESLOW, E. CHARLES p 1719 N95-24098
METCALF, D. p 1729 N95-23478
MEYER, C. p 1802 N95-22727
MEYER, G. p 1654 N95-22804
MEYER, PATRICK E. p 1761 N95-23746
MEYER, PETER p 1706 N95-23875
p 1707 N95-23876
MEYYAPPAN, MEYYA p 1682 N95-23633
MICHAEL, MAGED M. p 1764 N95-23930
p 1759 N95-24033
MICKLICH, B. J. p 1632 N95-22764
MIDDLETON, R. p 1646 N95-23820
MIELE, G. p 1848 N95-22743
MIKAMI, TATSUO p 1752 N95-23704
MIKHOV, S. G. p 1656 N95-22841
MILANI, V. p 1847 N95-22621
MILLER, BRADFORD W. p 1659 N95-24193
MILLER, D. J. p 1845 N95-24154
MILLER, DAVID p 1827 N95-23089
MILLER, EDGAR R. p 1631 N95-23910
p 1651 N95-23911
MILLER, GLENN E. p 1779 N95-23740
MILLER, P. J. p 1763 N95-22858
p 1763 N95-22859
MILLER, R. B. p 1656 N95-22852
MILNE, A. K. p 1714 N95-23948
MILTON, KIMBALL A. p 1823 N95-22983
MINER, GILDA A. p 1691 N95-23411
MINER, W. H., JR. p 1830 N95-22694
MINHTIEN, TRAN p 1788 N95-23051
MINNIX, TIMOTHY p 1657 N95-22944
MISRA, V. p 1637 N95-23836
MITCHELL, CHRISTINE M. p 1750 N95-22797
MITCHELL, R. T. p 1663 N95-23779
MITCHELL, T. E. p 1845 N95-24079
MITCHELL, T. H. p 1736 N95-22843
MITCHELL, TERENCE E. p 1839 N95-22653
MITTAL, NITIN p 1753 N95-22479
p 1754 N95-22603
p 1755 N95-22604
MIURA, YUKITOSHI p 1835 N95-23534
MIYATA, MAKOTO p 1752 N95-23709
MIYAZAKI, KEN p 1659 N95-23710
MO, J. D. p 1670 N95-23418
MOBLEY, CURTIS D. p 1710 N95-23890
MODESTINO, A. J. p 1634 N95-23164
MOEBES, T. p 1659 N95-23682
MOLDWIN, MARK B. p 1829 N95-22665
p 1736 N95-22850
MOLL, A. J. p 1844 N95-24013
MOLLER, PAUL S. p 1614 N95-23222
MOLNAR, PETER H. p 1717 N95-22832
MONACOS, STEVE P. p 1762 N95-22564
MONIER-GARBET, P. p 1831 N95-22800
MONINCX, J. F. p 1701 N95-22639
MONTESDEOCA, X. A. p 1673 N95-23435
MOODY, N. R. p 1639 N95-22724
MOORE, JOAN G. p 1680 N95-23625
MOORE, JOHN p 1672 N95-23429
p 1680 N95-23625
MOORES, J. G. p 1637 N95-23504
MORAN, MATTHEW E. p 1653 N95-24186
MORE, K. L. p 1647 N95-22689
MORETTI, S. p 1712 N95-23940
MORIKAWA, HAJIME p 1623 N95-23727
MORRIS, J. p 1726 N95-22546
MORRIS, M. J. p 1819 N95-22780
MORRIS, PAUL p 1760 N95-24176
MORRIS, PHILIP J. p 1800 N95-23178
MORRIS, ROBERT A. p 1618 N95-23764
MORSE, PETER A. p 1742 N95-23255
MORTENSEN, HELEN p 1779 N95-23745
MOSER, M. D. p 1684 N95-23642
MOSHER, J. C. p 1758 N95-23567
MOSHINSKY, MARCOS p 1824 N95-22991
MOSS, J. M. p 1809 N95-23403
MOTOHASI, SHOICHI p 1752 N95-23708
MOTOVILOV, A. K. p 1851 N95-23967
MOTOWIDLO, L. p 1842 N95-23354
MOUGINIS-MARK, PETER J. p 1714 N95-23949
MOULTEN, D. S. p 1732 N95-22834
MOURTOS, NIKOS J. p 1607 N95-22666
MSEZANE, A. Z. p 1802 N95-22700
MUELLER, JAMES L. p 1743 N95-22671
MUENCHAUSEN, R. E. p 1838 N95-22520
MUILENBURG, DENNIS A. p 1608 N95-23095
MUKAI, T. p 1781 N95-23753
MUKHERJI, S. p 1867 N95-22739
MUKHOPADHYAY, N. C. p 1808 N95-23357
MULARZ, EDWARD J. p 1637 N95-23643
MULCAHY, T. p 1798 N95-22895
MULDER, M. p 1733 N95-23125
MULHOLLAND, J. D. p 1869 N95-23828
MULLER, JANE p 1694 N95-22923
MULLINS, KEVIN p 1704 N95-23859
MUNCH, KLAUS HEJE p 1770 N95-23685
MUNOZ-GARCIA, SAMUEL G. p 1655 N95-22815
MURAL, R. J. p 1746 N95-22890
MURASE, YUICHI p 1752 N95-23705
MURATORE, J. p 1816 N95-22926
MURPHY, W. P. p 1627 N95-22683
MURRAY, ALEX T. p 1707 N95-23877
MURRAY, BRUCE C. p 1708 N95-23881
MUSCETTOLA, NICOLA p 1770 N95-23687
MUSTARD, JOHN F. p 1709 N95-23888
MYERS, IRA T. p 1662 N95-23219
MYERS, J. p 1706 N95-23872
MYERS, KAREN L. p 1618 N95-23763
MYSHINSKIJ, G. V. p 1812 N95-23976

N

NACHTIGAL, NOEEL M. p 1791 N95-23612
NACHTIGAL, NOEL M. p 1791 N95-23611
NADO, ROBERT p 1760 N95-24176
NAG, PALLOB K. p 1651 N95-23906
NAG, S. p 1796 N95-23660
NAGALINGAM, B. p 1692 N95-22556
p 1693 N95-22557
NAGARAJ, D. S. p 1787 N95-22809
NAGASHIMA, FUMIO p 1778 N95-23733
NAGATOMO, MASANORI p 1697 N95-23701
NAGEL, ROBERT L. p 1661 N95-22896
NAGY, M. p 1848 N95-22744
p 1849 N95-22745
p 1849 N95-22753
p 1803 N95-22755
p 1850 N95-22812
NAILLON, MARTINE p 1778 N95-23736
NAJMABADI, F. p 1829 N95-22645
NAKA, MASAO p 1778 N95-23737
NAKAJIMA, N. p 1836 N95-23589
NAKAMURA, KAZUO p 1623 N95-23727
NAKAMURA, KAZUYUKI p 1697 N95-23701
NAKASUKA, SHINICHI p 1771 N95-23690
p 1618 N95-23759
NAKATANI, I p 1781 N95-23753
NAKATANI, ICHIRO p 1771 N95-23689
p 1771 N95-23692
p 1697 N95-23695
NAKAYA, TERUOMI p 1618 N95-23702
NAKAYAMA, YUICHIRO p 1835 N95-23564
NAMKUNG, M. p 1644 N95-23512
NARAIN, K. S. p 1851 N95-23922
NARASIMHAN, M. S. p 1795 N95-22630
NARAYANAN, T. p 1633 N95-22869
NARIHARA, K. p 1835 N95-23533
NARITA, NAGATO p 1863 N95-24180
NASTASI, M. p 1844 N95-24073
NATASI, M. p 1842 N95-23265
NAUMANN, ROBERT J. p 1653 N95-24028
NAUMOV, S. F. p 1626 N95-22919
NEDERPELT, R. P. p 1788 N95-23130
NEDJADI, YOUCEF p 1825 N95-22998
NEFEDOV, N. p 1815 N95-23812
NELSON, CHARLES A. p 1814 N95-22984
NELSON, R. J. p 1831 N95-22849
NELSON, RANDAL C. p 1783 N95-24036
p 1784 N95-24185
NELSON, W. E. p 1636 N95-24007
NEMANICH, R. J. p 1838 N95-22555
NESMAN, T. p 1679 N95-23621
NESTHUS, THOMAS E. p 1749 N95-23788
NETTLES, A. T. p 1630 N95-23551
NEUGEBAUER, G. p 1828 N95-24068
NEUMAN, CLIFFORD B. p 1757 N95-23180
NEUMAN, M. C. p 1762 N95-22680
NEWCOMB, JOHN L. p 1869 N95-24066
NEWELL, CHESTER W. p 1753 N95-24119
NEWMAN, BRETT A. p 1616 N95-23314
NEWMAN, D. p 1832 N95-23163

NEWMAN, J. C., JR. p 1627 N95-22928
NEWMAN, R. L. p 1613 N95-24030
NEWMAN, RONALD L. p 1617 N95-23262
NG, W. p 1819 N95-22723
NGUYEN, D. C. p 1692 N95-24072
NGUYEN, H. p 1663 N95-23405
NGUYEN, Q. H. p 1757 N95-23346
NICHOLS, CATHY p 1861 N95-24132
NICHOLS, S. P. p 1695 N95-23342
NICHOLSON, JOHN Y. p 1688 N95-23012
NICIEJEWSKI, R. J. p 1737 N95-22951
NIELSEN, PIA J. p 1707 N95-23877
NIELSEN, R. W. p 1638 N95-22592
NIEMANN, R. C. p 1664 N95-24163
NIESER, DONALD E. p 1607 N95-23519
NIETO, LUIS M. p 1823 N95-22982
NIETO, MICHAEL M. p 1826 N95-23003
NIETO, MICHAEL MARTIN p 1820 N95-22959
NIJMEIJER, H. p 1767 N95-23558
NIJMEIJER, M. J. P. p 1839 N95-22615
NIKI, K. p 1816 N95-22644
p 1816 N95-22848
NIKISHIN, EUGENE F. p 1652 N95-23915
NIMLOS, M. R. p 1734 N95-23480
NINOMIYA, TETSUJIRO p 1618 N95-23759
NISHIDA, M. p 1623 N95-23700
NISHIDA, SHINICHIRO p 1752 N95-23709
NISHIGORI, N. p 1781 N95-23753
NISHIHARA, H. KEITH p 1778 N95-23739
NISHIZAWA, A. p 1835 N95-23533
NJOKU, ENI p 1708 N95-23881
NOBLE, MICHAEL p 1662 N95-23117
NODULMAN, L. p 1810 N95-23530
NORMAND, M. p 1715 N95-23956
NORMANDY, JANET p 1744 N95-22589
NOTIS, M. R. p 1845 N95-24143
NOVACK, H. IAN p 1707 N95-23877
NOVAK, JIM L. p 1624 N95-22885
NOWLAN, M. p 1730 N95-23777
NOWOBILSKI, J. J. p 1614 N95-24053
NOZ, MARILYN E. p 1825 N95-22992
NUNEZ, J. p 1756 N95-23079

O

OBARA, T. p 1781 N95-23753
OCONNELL, L. J. p 1757 N95-23337
ODA, K. p 1815 N95-23814
ODA, M. p 1623 N95-23700
ODONNELL, JAMES H. p 1651 N95-23903
p 1651 N95-23904
OEZBAY, HITAY p 1615 N95-22954
OGAWA, TADASHI p 1618 N95-23711
OGIHARA, MITSUNORI p 1759 N95-23935
p 1792 N95-24002
p 1760 N95-24056
p 1793 N95-24182
OGIMOTO, K. p 1618 N95-23734
OH, K. M. M. p 1733 N95-23126
OHKAMI, YOSHIAKI p 1697 N95-23695
OHLENDORF, GERHARD p 1769 N95-23681
OHTSU, KIICHI p 1831 N95-22849
OKABAYASHI, KEIJYU p 1778 N95-23736
OKAMOTO, OSAMU p 1618 N95-23702
OKAMOTO, SINYA p 1771 N95-23692
OKAMURA, RYO p 1752 N95-23708
OKE, J. B. p 1828 N95-24068
OKEEFE, MATTHEW T. p 1753 N95-24114
OKEN, C. p 1865 N95-22539
OLAH, MARTIN p 1707 N95-23877
OLIVER, J. P. p 1623 N95-23826
OLIVER, JOHN P. p 1869 N95-23828
p 1869 N95-23829
OLOFSSON, H. p 1868 N95-23230
OLSON, ERIC C. p 1770 N95-23687
OLSON, JOHN M. p 1628 N95-23031
OLSON, R. D. p 1628 N95-23026
OLSSON, PELLE p 1791 N95-23548
OMALLEY, M. W. p 1659 N95-22549
p 1661 N95-22844
ONEILL, R. C. p 1837 N95-24083
ONISCHAK, MICHAEL p 1727 N95-22888
OROZOVA-STANISHKOVA, IVANKA p 1736 N95-22612
ORTEGA, JAMES M. p 1756 N95-23017
OSBORNE, WILLIAM P. p 1657 N95-22944
OSILIKE, M. O. p 1792 N95-23658
OSTRO, S. J. p 1714 N95-23951
OSTROVSKY, VALENTIN N. p 1825 N95-22999
OSULLIVAN, D. p 1872 N95-23809
OSWALD, R. p 1726 N95-22546
OUAHAB, A. p 1795 N95-22632
OYEDIRAN, AYO p 1614 N95-23550
OZAWA, MASAKUNI p 1632 N95-22681

P

PAINE, D. P. p 1719 N95-24097
PAL, S. p 1684 N95-23642
PALOSCIA, S. p 1712 N95-23940
PALS, C. R. p 1663 N95-23494
PALSSON, BERNHARD O. p 1745 N95-22872
PANZA, GIULIANO F. p 1736 N95-22612
PAPAGEORGIOU, DEMETRIOS T. p 1678 N95-23544
PAPOYAN, V. V. p 1851 N95-23970
PAQUE, JULIE M. p 1700 N95-23831
p 1700 N95-23838
PARDIPURAM, RAJAN p 1714 N95-23950
PARHI, N. p 1786 N95-22629
PARIS, CECILE p 1766 N95-22512
PARK, S. p 1805 N95-22939
PARKER, G. p 1766 N95-23134
PARKER, ROBERT P. p 1653 N95-23668
PARKER, S. E. p 1831 N95-22899
PARKIN, DON E. p 1798 N95-22552
PARNELL, T. A. p 1815 N95-23810
p 1646 N95-23820
PARNELL, THOMAS A. p 1872 N95-23805
p 1815 N95-23817
PARRELL, J. A. p 1846 N95-24171
PARROD, Y. p 1618 N95-23752
PARSONS, E. L., JR. p 1728 N95-23162
PARTHASARATHY, SRINIVASAN p 1759 N95-24033
PARTRIDGE, MICHAEL E. p 1661 N95-22896
PASHNEV, A. p 1848 N95-22735
PATNAIK, SURYA N. p 1698 N95-22805
PATRA, B. K. p 1804 N95-22786
PATTERSON, MICHAEL J. p 1624 N95-23221
p 1624 N95-23240
PATTERSON, RICHARD L. p 1662 N95-23219
PAUL, J. H. p 1743 N95-22878
PAUL, KLAUS G. p 1700 N95-23841
PAULSON, ANNE p 1760 N95-24176
PAVISH, D. L. p 1673 N95-23433
PAVLICHENKOV, IGOR M. p 1814 N95-22972
PAYNE, DEBBIE FLOWERS p 1651 N95-23902
PEACH, D. F. p 1655 N95-22636
PEACHEY, N. M. p 1631 N95-22677
PEARLSTEIN, FRED p 1687 N95-22706
PEARSON, J. p 1840 N95-22762
PEASE, PHIL p 1862 N95-24134
PECHAN, M. J. p 1798 N95-23083
PECKERAR, MARTIN C. p 1660 N95-22709
PEETERS, JOHN p 1744 N95-22589
PELIZZETTI, EXIO p 1632 N95-22857
PELOWITZ, D. B. p 1817 N95-23245
PELTZER, GERARD R. p 1705 N95-23869
PENA, LEDA p 1823 N95-22977
PENDERS, M. T. M. p 1789 N95-23173
PENG, J. C. p 1801 N95-22551
PENTAKALOS, ODYSSEAS I. p 1862 N95-24138
PEREZ, G. p 1794 N95-23019
PERLMAN, MARVIN p 1754 N95-22577
PERRA, M. W. p 1639 N95-22724
PERRINE, L. p 1659 N95-23682
PERRY, G. L. E. p 1652 N95-22672
PERVAIZ, MEHTAB M. p 1681 N95-23631
PESTOV, A. B. p 1851 N95-23969
PETCOV, S. T. p 1812 N95-23785
PETERS, PALMER N. p 1651 N95-23906
p 1651 N95-23907
PETERS, W. A. p 1634 N95-23164
PETERSON, J. S. p 1661 N95-22733
PETERSON, JAMES R. p 1709 N95-23887
PETTY, C. C. p 1837 N95-24083
PFAENDTNER, JAMES p 1740 N95-23529
PFUND, D. M. p 1843 N95-23579
PHELPS, R. D. p 1837 N95-24083
PHI, DUONG VAN p 1655 N95-22746
PHILLIPS, M. W. p 1832 N95-23147
PHILLIPS, R. J. N. p 1807 N95-23158
p 1807 N95-23160
PHILLIPS, R. L. p 1765 N95-24074
PHILLPOT, S. R. p 1843 N95-23585
PHILPOT, ANDREW p 1761 N95-23680
PICKTHALL, COLIN R. p 1699 N95-22952
PIERCE, LELAND p 1715 N95-23957
PIETERS, CARLE M. p 1709 N95-23888
PINDERA, MAREK-JERZY p 1699 N95-24055
PINET, P. C. p 1707 N95-23878
PINSKER, R. I. p 1837 N95-24083
PIPPIN, H. G. p 1626 N95-22918
PIPPIN, H. GARY p 1638 N95-23897
p 1638 N95-23898
p 1646 N95-23905
PITTS, KEVIN T. p 1807 N95-23165
PITZER, K. S. p 1633 N95-22869
PLASSMANN, PAUL E. p 1755 N95-22690
PLASSMEIER, FRANK p 1769 N95-23681
PLETTA, J. B. p 1694 N95-23065
PLUMB, G. D. p 1654 N95-24045
p 1654 N95-24093
PLUNKETT, R. p 1818 N95-24077
PLUYM, T. C. p 1838 N95-22520
PLYUSHCHAY, M. S. p 1803 N95-22778
p 1850 N95-22779
POCHA, M. p 1827 N95-23449
POCHET, Y. p 1786 N95-22641
PODIO, FERNANDO L. p 1829 N95-24130
POESIO, MASSIMO p 1659 N95-24193
POKINES, BRETT p 1618 N95-23702
POL, R. p 1785 N95-22533
POLDERMAN, J. W. p 1767 N95-23199
POLL, D. p 1713 N95-23944
POLLACK, JAMES B. p 1636 N95-23545
POLYAKOV, D. N. p 1817 N95-23245
POLYCHRONOPOULOS, CONSTANTINE D. p 1791 N95-23600
POMERY, PETER J. p 1651 N95-23903
p 1651 N95-23904
POMJAKUSHIN, V. p 1803 N95-22758
PONOMAREV-STEPNOI, N. N. p 1817 N95-23245
PONTECORVO, M. p 1785 N95-22627
POOLA, RAMESH B. p 1692 N95-22556
p 1693 N95-22557
POORMAN, RICHARD M. p 1647 N95-22558
POPE, ALAN T. p 1749 N95-22579
POPE, D. P. p 1646 N95-24067
p 1845 N95-24079
POPE, S. C. p 1762 N95-22679
POPERNACK, T. G., JR. p 1616 N95-23011
PORKOLAB, M. p 1836 N95-23768
PORTER-LOCKLEAR, FREDA p 1800 N95-23315
PORTREE, DAVID S. F. p 1621 N95-23249
POST, R. F. p 1727 N95-22574
POSTON, WENDY L. p 1766 N95-22705
POURBAIX, A. p 1643 N95-23508
p 1643 N95-23509
PRANTS, SERGEY V. p 1826 N95-23005
PRASAD, R. p 1640 N95-22934
PRATA, A. J. p 1718 N95-23597
PRAUSNITZ, J. M. p 1635 N95-23380
PRENDIN, W. p 1752 N95-23732
PRENGER, F. C. p 1662 N95-23368
PRESSBURGER, THOMAS p 1761 N95-23680
PRESTON, ORV W. p 1614 N95-22674
PREVOT, L. p 1715 N95-23956
PRICE, CHARLES R. p 1752 N95-23723
PRICE, D. F. p 1690 N95-22595
PRICE, JOHN C. p 1707 N95-23879
PRIDE, J. p 1634 N95-23164
PRIDMORE-BROWN, D. C. p 1740 N95-23933
PRIEBE, CAREY E. p 1766 N95-22705
PRIEDHORSKY, WILLIAM C. p 1621 N95-22868
PRIS, I. E. p 1847 N95-22620
PRITCHARD, JOCELYN I. p 1612 N95-22953
PROCTOR, SANDRA B. p 1853 N95-23316
PROKERT, G. p 1667 N95-23172
PROTO, A. N. p 1850 N95-22782
PROY, C. p 1771 N95-23693
p 1777 N95-23731
PRUSS, S. p 1818 N95-24077
PRYOR, ROBERT p 1629 N95-23033
PRZEKWAS, A. J. p 1637 N95-23645
PUREHVDORZH, B. p 1766 N95-22614
PURVIS, J. W. p 1694 N95-23065
PUSHPA, K. K. p 1814 N95-24175
PUSTOVITOV, V. D. p 1836 N95-23572
p 1609 N95-23787
PUZYNIN, I. V. p 1766 N95-22614
PYSSYSALO, T. p 1764 N95-23538

Q

QUAINOO, G. K. p 1839 N95-22607
QUAN, A. G. p 1761 N95-23688
QUESNE, CHRISTIANE p 1797 N95-22978
QUINN, B. p 1802 N95-22727
QUINN, J. J. p 1837 N95-23982
QUITMEYER, JOANN p 1630 N95-23039
QUIZA, JORGE p 1749 N95-22987
QUONG, S. p 1664 N95-24070

R

RADER, D. J. p 1837 N95-24158
RADHAKRISHNAN, KRISHNAN p 1614 N95-23550
RAHM-CRITES, L. p 1749 N95-23142
RAHMAN, M. S. p 1788 N95-22922
RAIKAR, GANESH N. p 1651 N95-23907
RAINWATER, B. A. p 1622 N95-23532
RAIS-ROHANI, MASOUD p 1613 N95-23317
RAJ, PRADEEP p 1608 N95-23185

RAJESWARI, M. p 1827 N95-23224
RAJPUT, S. S. p 1640 N95-22934
RAKULJIC, GEORGE A. p 1819 N95-22508
RAMBAGS, P. M. P. p 1789 N95-23146
RAMSEY, MICHAEL S. p 1711 N95-23920
RANDALL, D. A. p 1736 N95-22879
RANDJBARDAEMI, S. p 1839 N95-22649
p 1795 N95-22736
RANGWALLA, AKIL A. p 1671 N95-23425
RANKEN, W. A. p 1624 N95-22905
RANKIN, JAMES M. p 1611 N95-23318
RANSON, K. JON p 1715 N95-23955
RANTAKYROE, F. T. p 1866 N95-23468
RANTANEN, RAY p 1637 N95-23797
RAPHAELI, DAN p 1761 N95-22478
RASHID, M. S. p 1796 N95-22788
RASHID, R. I. M. A. p 1849 N95-22775
RASMUSSEN, R. A. p 1731 N95-22673
RASOUL, FIRAS A. p 1651 N95-23903
p 1851 N95-23904
RASTEL, L. p 1771 N95-23693
RAUBENHEIMER, T. O. p 1691 N95-22704
RAUPENSTRAUCH, J. p 1713 N95-23944
RAUSCHER, CHRISTEN p 1660 N95-22708
RAVINDRA, KRISHNASWAMY p 1616 N95-23319
RAWLIN, VINCENT K. p 1624 N95-23221
RAWLINGS, J. p 1616 N95-24019
RAWLS, J. RICHARD p 1637 N95-23798
RAY-CHAUDHURI, A. K. p 1819 N95-22723
RAY, ASOK p 1654 N95-23195
RAY, BISWAJIT p 1662 N95-23219
RAY, TERRILL W. p 1707 N95-23880
p 1708 N95-23881
REALMUTO, VINCENT J. p 1711 N95-23917
RECAMIER, JOSE A. p 1814 N95-22964
REDDY, JANARDAN K. p 1748 N95-23771
REDDY, T. S. R. p 1699 N95-24189
REDFIELD, R. C. p 1757 N95-23388
REDLER, K. p 1693 N95-22798
REDMOND, J. p 1766 N95-23134
REESE, G. p 1766 N95-23134
REEVES, D. p 1867 N95-22516
REEVES, GEOFF D. p 1829 N95-22665
REHAK, M. L. p 1660 N95-22716
REID, C. ANN p 1778 N95-23739
REID, MAX B. p 1767 N95-23387
REILINGER, ROBERT E. p 1717 N95-22832
REINEKE, M. p 1726 N95-22502
REINERSMAN, P. p 1702 N95-23849
REIS, E. E. p 1693 N95-22798
REITZ, G. p 1872 N95-23800
REKALO, M. P. p 1850 N95-22812
REMSEN, D. B. p 1837 N95-24083
RENIERS, M. A. p 1657 N95-23151
RENLUND, A. M. p 1652 N95-22838
RESCH, GEORGE M. p 1656 N95-22852
RESKE, EDWARD J. p 1685 N95-23648
REST, J. p 1846 N95-24169
REUSKEN, A. A. p 1789 N95-23176
REVELLE, D. O. p 1741 N95-24078
REY, C. M. p 1664 N95-24163
REYES, GEORGE p 1702 N95-23850
REYES, MARCO p 1826 N95-23000
RHEA, W. JOSEPH p 1710 N95-23890
RHEE, KEE W. p 1660 N95-22709
RHOADES, R. L. p 1650 N95-23981
RHORER, R. L. p 1654 N95-22678
RICH, D. O. p 1762 N95-22679
RICHARD, F. p 1721 N95-23765
RICKS, D. R. p 1637 N95-23836
RIDDELL, W. T. p 1697 N95-24106
RIESTER, L. p 1639 N95-22686
RIGLEY, JACK p 1655 N95-22813
RIGNOT, E. J. p 1714 N95-23951
RIKKEN, PATRICK J. p 1752 N95-23714
RINGEL, S. A. p 1846 N95-24188
RINGER, MARK J. p 1620 N95-23756
RIPPLE, WILLIAM J. p 1719 N95-24094
p 1719 N95-24095
p 1719 N95-24096
p 1719 N95-24097
p 1719 N95-24098
p 1720 N95-24101
p 1720 N95-24102
p 1720 N95-24103
p 1720 N95-24104
RIVERA, ANA LEONOR p 1826 N95-23007
ROACH, LISA K. p 1611 N95-22510
ROBBINS, DAVID O. p 1691 N95-22937
ROBERG, JEFFREY M. p 1726 N95-22554
ROBERGE, P. R. p 1637 N95-23504
ROBERTS, DAR A. p 1704 N95-23863
p 1708 N95-23882
p 1708 N95-23883
ROBIN, D. p 1816 N95-22567
ROBINETT, R. D. p 1622 N95-23532
ROBINS, W. H. p 1735 N95-23580
ROBINSON, P. A. p 1869 N95-22828
ROBINSON, S. L. p 1639 N95-22724
ROBSON, J. p 1616 N95-24019
RODRIGUEZ, C. W. p 1739 N95-23244
RODRIGUEZ, G. p 1697 N95-23697
RODRIGUEZ, GUILLERMO p 1692 N95-22543
RODRIGUEZ, R. R. p 1698 N95-22773
ROE, P. L. p 1790 N95-23465
ROESSLEROVA, R. p 1740 N95-23470
ROGER, R. P. p 1669 N95-23417
ROGERS, GEORGE W. p 1766 N95-22705
ROGERS, MELISSA J. B. p 1621 N95-22667
p 1653 N95-23552
ROGOWSKI, ROBERT S. p 1819 N95-22807
ROGSTAD, DAVE H. p 1656 N95-22852
ROHATGI, A. p 1730 N95-23489
p 1731 N95-24090
ROHATGI, N. K. p 1751 N95-23194
ROJAS, L. p 1675 N95-23440
ROMANI, ROGER W. p 1871 N95-22910
ROMANO, R. p 1822 N95-22976
ROOP, J. A. p 1629 N95-23038
ROPP, M. p 1730 N95-23489
ROSE, M. FRANK p 1727 N95-22904
p 1700 N95-23839
ROSEN, WAYNE p 1862 N95-24134
ROSENBERGER, FRANZ E. p 1826 N95-23016
ROSENSTEEL, GEORGE p 1822 N95-22973
ROSENTHAL, ANDREW L. p 1726 N95-22554
ROSKEY, CHESTER T. p 1747 N95-23251
ROSMALEN, T. p 1718 N95-23469
ROSS, HOWARD D. p 1626 N95-24004
ROSS, JAMES C. p 1613 N95-23395
ROSS, MARTIN N. p 1688 N95-23087
ROSU, HARET p 1826 N95-23000
ROTEM, DORON p 1861 N95-24131
ROTHMANN, ELIZABETH p 1753 N95-22479
p 1754 N95-22603
p 1755 N95-22604
ROTT, HELMUT p 1715 N95-23954
ROTWAIN, IRA p 1736 N95-22612
ROUSSEL-DUPRE, DIANE p 1621 N95-22868
ROWEY, R. J. p 1673 N95-23435
ROWLAND, SCOTT K. p 1714 N95-23949
ROZEVELD, S. p 1845 N95-24152
RUBLEIN, GEORGE T. p 1853 N95-23320
RUBY, D. p 1730 N95-23489
p 1731 N95-24090
RUF, J. p 1674 N95-23437
RUF, JOSEPH p 1686 N95-23651
RUF, JOSEPH H. p 1672 N95-23430
RUGGIERO, JOSE R. p 1748 N95-22963
RUPNIK, K. p 1803 N95-22747
RUSSINOFF, DAVID M. p 1762 N95-22830
RUTLEDGE, SHARON K. p 1626 N95-23270
p 1651 N95-23802
p 1650 N95-24187
RUWART, THOMAS M. p 1753 N95-24114
RYAN, D. P. p 1617 N95-23750
RYAN, H. M. p 1684 N95-23642
RYAN, SEAN p 1621 N95-22868
RYAN, T. W., III p 1732 N95-22834
RYDING, D. p 1638 N95-22592
p 1696 N95-23397
RYNE, ROBERT D. p 1795 N95-22654

S

SABOL, DONALD E. p 1708 N95-23882
SABOL, DONALD E., JR. p 1708 N95-23883
SADR, RAMIN p 1761 N95-22478
SAGALOVSKY, L. p 1632 N95-22764
SAGDEEV, ROALD p 1871 N95-23546
SAGER, G. T. p 1829 N95-22645
SAITOU, HIROAKI p 1771 N95-23692
SAKIMOTO, K. p 1811 N95-23604
SALADINO, A. J. p 1669 N95-23414
SALAS, MANUEL D. p 1678 N95-23596
SALAS, RICHARD M. p 1629 N95-23034
SALAWITCH, ROSS J. p 1735 N95-22482
SALIMULLAH, M. p 1834 N95-23523
SALKOLA, M. I. p 1808 N95-23267
SALLABERGER, CHRISTIAN p 1776 N95-23725
SALMON, ELLEN p 1862 N95-24135
SAMUELS, J. A. p 1631 N95-22677
SANDERS, DONALD C. p 1610 N95-24024
SANDERSON, ERIC W. p 1709 N95-23889
SANGIOVANNI, S. p 1715 N95-23952
SANTA-MARIA, J. p 1846 N95-24170
SANTER, RICHARD p 1710 N95-23893
SANTHANAM, BALU p 1797 N95-22986
SANTHANAM, THALANAYAR S. p 1760 N95-22985
p 1797 N95-22986
SANTIAGO, R. D. p 1814 N95-22961
SANTORO, A. M. p 1831 N95-22899
SANTORO, R. J. p 1684 N95-23642
SANUKI, HEIJI p 1835 N95-23534
SAPIR, J. p 1817 N95-23245
SAPP, CLYDE A. p 1623 N95-23823
SARABANDI, KAMAL p 1715 N95-23957
SARAVANOS, D. A. p 1630 N95-23258
p 1630 N95-23463
SARTURE, CHARLES M. p 1690 N95-23852
SARUKKAI, RAMESH R. p 1658 N95-23794
p 1658 N95-24039
SARVARANTA, L. p 1636 N95-23554
SARVER-VERHEY, TIMOTHY R. p 1624 N95-23240
SASAKI, TOMOYUKI p 1831 N95-22849
SASAKI, TOSHIRO p 1623 N95-23719
SASAO, M. p 1834 N95-23527
SASAO, MAMIKO p 1836 N95-23569
SATO, HITOSHI p 1623 N95-23726
SATO, K. p 1835 N95-23533
SATO, T. p 1834 N95-23523
p 1836 N95-23589
p 1836 N95-23591
SATO, TETSUYA p 1834 N95-23524
p 1835 N95-23528
p 1835 N95-23564
p 1836 N95-23590
SATO, YUICHI p 1778 N95-23733
SAUL, R. p 1659 N95-23682
SAUNDERS, C. P. p 1609 N95-23201
SAUNDERS, R. S. p 1650 N95-24159
SAWAFTA, R. p 1803 N95-22763
SAYAD, R. S. p 1628 N95-23026
SAYANO, KOICHI p 1819 N95-22508
SAYERS, D. E. p 1838 N95-22555
SCHACHAM, S. E. p 1846 N95-24188
SCHAFFER, M. J. p 1693 N95-22796
SCHAFFER, T. p 1616 N95-24019
SCHALER, M. p 1848 N95-22744
p 1849 N95-22745
SCHAUBEL, K. M. p 1693 N95-22796
SCHAUS, C. F. p 1631 N95-22677
SCHEER, DALE A. p 1629 N95-23035
SCHEER, GEORGE p 1705 N95-23867
SCHEICH, C. M. A. p 1807 N95-23157
SCHEIMAN, DAVID A. p 1728 N95-23259
SCHENKER, PAUL S. p 1772 N95-23698
SCHERPEN, J. M. A. p 1767 N95-23557
SCHIAVON, G. p 1712 N95-23940
SCHIEX, THOMAS p 1618 N95-23760
SCHIFF, E. A. p 1660 N95-22586
SCHILDERS, W. H. A. p 1789 N95-23173
SCHLUETER, R. p 1692 N95-23487
SCHLUMPF, F. p 1851 N95-23352
SCHMIDT, V. p 1767 N95-23556
SCHMITT, DAN J. p 1624 N95-22885
SCHNEIDER-MUNTAU, HANS J. p 1798 N95-22552
SCHNEIDER, JEFF G. p 1784 N95-24038
SCHOLEN, DOUGLAS E. p 1712 N95-23921
SCHORR, HERBERT p 1757 N95-23180
SCHRAML, STEPHEN J. p 1762 N95-22509
SCHRECKENGHOST, D. L. p 1617 N95-23750
SCHREIBER, ROBERT p 1764 N95-23594
p 1758 N95-23610
SCHREIBER, ROBERT S. p 1791 N95-23592
SCHRODEL, DAVID G. p 1761 N95-24120
SCHROEDER, DAVID J. p 1749 N95-23788
p 1750 N95-23934
SCHROEDER, J. L. p 1650 N95-23577
SCHUBERT, LENHART K. p 1659 N95-24193
SCHUBERT, W. K. p 1727 N95-22650
SCHULBACH, C. H. p 1759 N95-24052
SCHULER, D. L. p 1715 N95-23953
SCHULLER, I. K. p 1846 N95-24170
SCHUMACHER, R. p 1802 N95-22727
SCHWARTZ, WILLIAM J. p 1748 N95-24047
SCHWUTTKE, U. M. p 1761 N95-23688
SCIALDONE, JOHN J. p 1651 N95-23913
SCOTT, A. D., JR. p 1733 N95-23009
SCOTT, C. D. p 1652 N95-22587
p 1744 N95-22588
SCOTT, ELAINE P. p 1700 N95-23321
SCOTT, MICHAEL L. p 1764 N95-23930
p 1759 N95-24033
p 1753 N95-24177
p 1765 N95-24183
p 1765 N95-24184
SCOTT, T. C. p 1652 N95-22587
p 1744 N95-22588
SEABLOM, MICHAEL p 1740 N95-23529
SEASHOLTZ, RICHARD G. p 1688 N95-23461
SEDLACEK, ARTHUR J. p 1633 N95-22887
SEE, THOMAS H. p 1623 N95-23823
p 1869 N95-23833
p 1700 N95-23842
SEIPEL, D. p 1758 N95-23553
SEKI, T. p 1835 N95-23533

SELIM, RAOUF ..... p 1664 N95-23322
SELLONI, A. ..... p 1660 N95-22591
SELWYN, G. S. ..... p 1829 N95-22519
SENGUPTA, S. ..... p 1839 N95-22572
p 1845 N95-24154
SENJANOVIC, G. ..... p 1848 N95-22742
p 1812 N95-23786
SENYITKO, RICHARD G. ..... p 1616 N95-23192
SEO, Y. W. ..... p 1654 N95-22678
SERAJI, HOMAYOUN ..... p 1768 N95-23676
SERGEEV, V. K. ..... p 1626 N95-22919
SESHAN, P. K. ..... p 1751 N95-23194
SESSLER, A. ..... p 1817 N95-23493
SESSLER, A. M. ..... p 1817 N95-23485
SEUNG, S. P. ..... p 1637 N95-23646
SHADLE, S. E. ..... p 1840 N95-22851
SHAFEIDEHABAD, A. ..... p 1847 N95-22621
p 1786 N95-22642
SHAH, IIJAZ ..... p 1639 N95-22608
SHAH, IJAZ ..... p 1640 N95-22840
SHAH, MANESH ..... p 1746 N95-22890
SHALTENS, RICHARD K. ..... p 1625 N95-23450
SHANG, H. M. ..... p 1671 N95-23422
p 1675 N95-23442
p 1676 N95-23445
p 1683 N95-23638
SHAO, MICHAEL ..... p 1827 N95-23089
SHAO, Y. ..... p 1809 N95-23359
SHAPIRO, I. L. ..... p 1850 N95-22776
SHAPIRO, JEFF C. ..... p 1775 N95-23718
SHARAPOV, V. V. ..... p 1642 N95-23501
SHAREEF, GUNSELI SAGUN ..... p 1732 N95-22865
SHARER, J. E. ..... p 1832 N95-23084
SHARFUDDIN, A. ..... p 1829 N95-22622
SHARP, J. M., JR. ..... p 1743 N95-22695
SHARPE, LONNIE, JR. ..... p 1621 N95-23260
SHELDON, R. ..... p 1737 N95-22945
SHELTON, R. ..... p 1659 N95-23682
SHELTON, SUSAN ..... p 1752 N95-23735
SHEN, D. S. ..... p 1663 N95-23779
SHEN, JAMES Y. ..... p 1651 N95-23899
SHEN, JI YAO ..... p 1621 N95-23260
SHEN, JIANMIN ..... p 1792 N95-23971
SHENG, ZHENGMAO ..... p 1792 N95-23971
SHEPLAK, MARK ..... p 1666 N95-22906
SHERIFF, RAY E. ..... p 1656 N95-22819
SHERMAN, MARK ..... p 1862 N95-24134
SHESTAKOV, A. I. ..... p 1837 N95-24017
SHI, D. ..... p 1839 N95-22572
SHI, JIANCHENG ..... p 1715 N95-23954
SHI, N. ..... p 1842 N95-23365
SHIBATA, S. ..... p 1811 N95-23775
SHIBUTANI, K. ..... p 1842 N95-23354
SHIELDS, MICHAEL F. ..... p 1858 N95-24112
SHIH, MING H. ..... p 1670 N95-23419
SHIH, MING-HSIN ..... p 1679 N95-23618
SHIH, S. H. ..... p 1668 N95-23220
SHIMADA, MASANOBU ..... p 1624 N95-23864
SHIMER, D. W. ..... p 1659 N95-22504
SHIMOJI, HARUHIKO ..... p 1697 N95-23722
SHINES, J. E. ..... p 1717 N95-22503
SHIRASAKA, SEIKOH ..... p 1771 N95-23690
SHIROKOV, A. M. ..... p 1814 N95-22967
SHNIR, YA. M. ..... p 1847 N95-22620
SHORT, NICK, JR. ..... p 1859 N95-24121
SHOSHANI, ARIE ..... p 1861 N95-24131
SHU, D. ..... p 1696 N95-23397
SHUJIE, LI ..... p 1785 N95-22624
p 1785 N95-22625
SHUTT, R. P. ..... p 1660 N95-22716
SHYY, W. ..... p 1677 N95-23451
SHYY, WEI ..... p 1677 N95-23448
SIAGADZE, Z. K. ..... p 1804 N95-22847
SICKAFUS, K. E. ..... p 1842 N95-23266
p 1844 N95-24073
SIDES, PAUL J. ..... p 1690 N95-24129
SIDILKOVER, D. ..... p 1790 N95-23465
SIEBER, A. ..... p 1710 N95-23891
SIEGEL, R. W. ..... p 1843 N95-23586
SIEGFELDT, DENISE V. ..... p 1854 N95-23323
SIEGL, R. ..... p 1845 N95-24079
SIEGL, RICHARD W. ..... p 1627 N95-22940
SIENKIEWICZ, META ..... p 1740 N95-23529
SIGISMONDI, S. ..... p 1712 N95-23940
SIKES, ANTHONY ..... p 1747 N95-23251
SIMEON, T. ..... p 1721 N95-23765
SIMMONDS, D. D. ..... p 1762 N95-22680
SIMMONDS, JOHN J. ..... p 1705 N95-23866
SIMMONS, D. G. ..... p 1658 N95-23772
SIMMONS, REID ..... p 1697 N95-23694
SIMMONS, RON W. ..... p 1853 N95-23324
SIMMS, D. A. ..... p 1729 N95-23383
SIMON, C. G. ..... p 1623 N95-23826
p 1869 N95-23828
p 1637 N95-23836
SIMON, CHARLES G. ..... p 1869 N95-23829
SIMON, HORST D. ..... p 1764 N95-23594
SIMON, I. ..... p 1840 N95-22774
SIMONNET, G. ..... p 1748 N95-22770
SIMOUDIS, EVANGELOS ..... p 1721 N95-23675
SIMUNOVIC, S. ..... p 1668 N95-23372
SINDIR, MUNIR M. ..... p 1675 N95-23443
SINGER, JOSEF ..... p 1699 N95-23923
SINGER, KEN ..... p 1861 N95-24132
SINGER, ROBERT B. ..... p 1706 N95-23874
SINGER, S. F. ..... p 1869 N95-23828
SINGH, C. P. ..... p 1804 N95-22786
SINGHAL, ASHOK K. ..... p 1681 N95-23632
SINGRU, R. M. ..... p 1640 N95-22934
SIOCHI, EMILIE J. ..... p 1651 N95-23899
SIRBAUGH, J. R. ..... p 1671 N95-23423
SISK, ROBERT C. ..... p 1651 N95-23906
SITARAMAYYA, M. ..... p 1795 N95-22623
SIVO, JOSEPH M. ..... p 1680 N95-23628
SKARHA, J. E. ..... p 1689 N95-23520
SKILES, J. W. ..... p 1759 N95-24052
SKINNER, C. H. ..... p 1833 N95-23269
SKOBLIN, A. A. ..... p 1797 N95-23965
p 1797 N95-23966
SLACK, D. C. ..... p 1670 N95-23420
SLAUGHTER, D. ..... p 1735 N95-24018
SLEMP, WAYNE S. ..... p 1651 N95-23899
p 1631 N95-23900
SLOVAK, J. ..... p 1812 N95-23976
SMART, J. D. ..... p 1607 N95-23506
SMIRNOV, A. YU. ..... p 1803 N95-22756
p 1804 N95-22790
p 1812 N95-23784
p 1812 N95-23785
SMIRNOV, YURI F. ..... p 1814 N95-22967
SMITH, ALAN R. ..... p 1815 N95-23816
SMITH, B. ..... p 1786 N95-22696
p 1765 N95-24172
SMITH, C. J. E. ..... p 1641 N95-23497
SMITH, D. ..... p 1616 N95-24019
SMITH, D. C. ..... p 1631 N95-22677
SMITH, D. L. ..... p 1646 N95-24153
SMITH, DAVID ..... p 1623 N95-23721
SMITH, G. S. ..... p 1649 N95-23568
SMITH, GEOFFREY M. ..... p 1705 N95-23871
p 1708 N95-23884
SMITH, J. A. ..... p 1721 N95-24148
SMITH, J. P. ..... p 1693 N95-22796
p 1693 N95-22798
SMITH, J. R. ..... p 1662 N95-23334
SMITH, MARK T. ..... p 1654 N95-22692
SMITH, MILTON O. ..... p 1708 N95-23883
SMITH, P. C. ..... p 1655 N95-22636
SMITH, SHELDON M. ..... p 1688 N95-23263
SMITH, STEPHEN F. ..... p 1618 N95-23758
SMOTHERMAN, MARK D. ..... p 1754 N95-22603
SMYTH, PADHRAIC ..... p 1775 N95-23717
SOB, M. ..... p 1845 N95-24079
SODERBLOM, LAURENCE ..... p 1704 N95-23859
SODERSTROM, E. ..... p 1806 N95-23139
SOET, M. ..... p 1701 N95-22639
SOFO, J. O. ..... p 1840 N95-22687
SOIFER, B. T. ..... p 1828 N95-24068
SOLIES, U. PETER ..... p 1616 N95-23325
SOLIMENO, S. ..... p 1822 N95-22976
SOLIS, MANUEL ..... p 1707 N95-23877
SOLKA, JEFFREY L. ..... p 1766 N95-22705
SOLOMON, ALLAN I. ..... p 1692 N95-23001
SOLOVYOV, YU. ..... p 1785 N95-22619
SOMMER, S. ..... p 1709 N95-23885
SONG, XING-CHANG ..... p 1801 N95-22643
SONI, B. K. ..... p 1673 N95-23433
SONI, BHARAT K. ..... p 1669 N95-23415
p 1669 N95-23417
p 1670 N95-23419
p 1679 N95-23618
SONOBE, MASAYOSHI ..... p 1752 N95-23715
SORENSEN, N. R. ..... p 1664 N95-24149
SORIN, A. S. ..... p 1790 N95-23457
SOUKUP, R. J. ..... p 1649 N95-23356
SOULAS, GEORGE C. ..... p 1624 N95-23240
SOVERS, O. J. ..... p 1756 N95-22853
SOWERS, C. H. ..... p 1846 N95-24168
SPADAFORA, STEPHEN J. ..... p 1644 N95-23513
SPAID, FRANK W. ..... p 1609 N95-23250
SPANGLER, LEE H. ..... p 1692 N95-23326
SPECTOR, S. ..... p 1819 N95-22723
SPEEL, P. H. ..... p 1648 N95-23128
SPENCER, JOHN H. ..... p 1872 N95-23276
SPIES, THOMAS A. ..... p 1719 N95-24096
p 1720 N95-24104
SPILLER, J. ..... p 1656 N95-22817
SPINA, ERIC F. ..... p 1666 N95-22906
SPINKA, H. ..... p 1688 N95-23492
SPINRAD, J. ..... p 1785 N95-22535
SPIRIDONOV, V. B. ..... p 1642 N95-23501
SPIRKOVSKA, LILJANA ..... p 1767 N95-23387
SPREHE, J. TIMOTHY ..... p 1854 N95-22494
SPROLES, DARRELL W. ..... p 1755 N95-22605
SPRUIT, P. ..... p 1754 N95-22522
ST.CLAIR, ANNE K. ..... p 1649 N95-23254
STADERMANN, FRANK J. ..... p 1637 N95-23837
STAENZ, K. ..... p 1709 N95-23886
STALLARD, B. W. ..... p 1834 N95-23371
STALLINGS, C. A. ..... p 1762 N95-22680
STALPERS, L. ..... p 1718 N95-23469
STAMBAUGH, R. D. ..... p 1693 N95-22796
p 1837 N95-24086
STAMOULIS, GEORGE ..... p 1659 N95-22507
STARR, GREGORY P. ..... p 1624 N95-22885
STARTSEV, OLEG V. ..... p 1652 N95-23915
STEARNS, STEPHEN D. ..... p 1709 N95-23887
STEELE, L. L. ..... p 1674 N95-23438
STEKL, I. ..... p 1812 N95-23976
STENIUS, P. ..... p 1636 N95-23554
STEPHENS, RALPH M. ..... p 1666 N95-22906
STERN, P. ..... p 1614 N95-23088
STERN, ROBERT A. ..... p 1868 N95-23205
STEVEN, MICHAEL D. ..... p 1701 N95-23845
STEVENSON, TIM J. ..... p 1623 N95-23803
STEWART, D. S. ..... p 1666 N95-22901
STEWART, JAMES F. ..... p 1615 N95-23389
STICKEL, MARK ..... p 1761 N95-23680
STIDHAM, CURTIS R. ..... p 1626 N95-23270
STILL, G. ..... p 1790 N95-23235
STINNETT, R. W. ..... p 1640 N95-22835
STOAKLEY, DIANE M. ..... p 1649 N95-23254
STOBIE, JAMES ..... p 1740 N95-23529
STOCKS, G. M. ..... p 1640 N95-23121
STOITSOV, M. V. ..... p 1813 N95-24046
STONE, GEORGE W. ..... p 1698 N95-22726
STOTTLER, RICHARD H. ..... p 1781 N95-23755
STOVER, J. C. ..... p 1827 N95-23531
p 1828 N95-24005
STRAIN, BOYD R. ..... p 1731 N95-22725
STRAND, O. T. ..... p 1827 N95-23449
STRANGE, R. R. ..... p 1689 N95-23795
STRATHDEE, J. ..... p 1839 N95-22649
p 1795 N95-22736
STRENG, M. ..... p 1790 N95-23231
STRGANAC, THOMAS W. ..... p 1651 N95-23902
STRICKER, J. N. M. ..... p 1741 N95-22640
STRIFFLER, FOSTER ..... p 1799 N95-22863
STRINGARI, S. ..... p 1840 N95-22839
STRIZ, ALFRED G. ..... p 1700 N95-23327
STUART, L. ..... p 1801 N95-22521
STULEN, R. H. ..... p 1819 N95-22723
SU, R. ..... p 1654 N95-22804
SU, Z. B. ..... p 1800 N95-22495
SU, ZAOBIN ..... p 1812 N95-23985
SU, ZHAOBIN ..... p 1801 N95-22498
p 1844 N95-23986
SUAREZ, MAX J. ..... p 1740 N95-23529
SUBRAHMANYAM, V. ..... p 1847 N95-22545
p 1840 N95-22845
SUDAN, RAVI N. ..... p 1832 N95-23120
SUDO, S. ..... p 1835 N95-23566
SUENAGA, M. ..... p 1842 N95-23354
SUGAWARA, MASAYUKI ..... p 1690 N95-24107
SUGIYAMA, G. ..... p 1738 N95-23143
SUITS, B. H. ..... p 1843 N95-23586
SUKATON, R. ..... p 1802 N95-22727
SULEMAN, NAUSHADALLI K. ..... p 1815 N95-23328
SULLIVAN, A. ..... p 1690 N95-22595
SULLIVAN, D. ..... p 1796 N95-23660
SULLIVAN, M. ..... p 1816 N95-22567
SULLIVAN, MATTHEW R. ..... p 1686 N95-23651
SULLIVAN, NEIL S. ..... p 1798 N95-22552
SUN, GUOQING ..... p 1715 N95-23955
SUND, R. ..... p 1832 N95-23084
SURY, B. ..... p 1795 N95-22617
SUSSKIND, L. ..... p 1802 N95-22731
SUTER, J. D. ..... p 1652 N95-22672
SUTHERLAND, C. D. ..... p 1658 N95-24015
SUTHERLAND, H. J. ..... p 1694 N95-23056
SUZUKI, TSUYOSHI ..... p 1752 N95-23715
SUZUKI, YOSHIAKI ..... p 1659 N95-23710
p 1623 N95-23727
SWAIM, PATRICK L. ..... p 1697 N95-23703
SWAN, PAT ..... p 1637 N95-23837
SWANSON, KEITH ..... p 1779 N95-23742
p 1779 N95-23743
SWAYZE, GREGG ..... p 1702 N95-23853
p 1703 N95-23854
SWAYZE, GREGG A. ..... p 1703 N95-23855
SWENSON, GARY R. ..... p 1688 N95-23087
SWILER, T. P. ..... p 1811 N95-23576
SYDORA, R. D. ..... p 1831 N95-22899
SYMONS, D. M. ..... p 1639 N95-22732
SYMONS, DOUGLAS M. ..... p 1640 N95-22893
SYPHERS, M. J. ..... p 1817 N95-23353
SZE, D.-K. ..... p 1829 N95-22645

T

TABIBI, BAGHER M. ..... p 1691 N95-23411
TABITA, F. R. ..... p 1743 N95-22878
TACHIMORI, SHOICHI ..... p 1635 N95-23476
TACONET, O. ..... p 1715 N95-23956
TAJIRI, FUMIO ..... p 1831 N95-22849
TAJUDDIN, M. ..... p 1800 N95-23018
TAKACS, P. Z. ..... p 1827 N95-23531
p 1828 N95-24005
TAKAHASHI, TETSUO ..... p 1623 N95-23727
TAKAHASHI, YOSHIKAZU ..... p 1831 N95-22849
TAKALLU, M. A. ..... p 1607 N95-22802
TAKAMARU, H. ..... p 1834 N95-23524
p 1835 N95-23528
p 1836 N95-23590
TAKAMUNE, K. ..... p 1777 N95-23729
TAKEKA, Y. ..... p 1816 N95-22848
TAKEUCHI, NOBORU ..... p 1660 N95-22591
TALBOT, JOHN M. ..... p 1831 N95-22948
TAN, Z. ..... p 1819 N95-22723
TANAKA, MASAKI ..... p 1697 N95-23701
TANAKA, MOTOHIKO ..... p 1834 N95-23526
TANIE, K. ..... p 1777 N95-23729
TANIIKE, AKIRA ..... p 1836 N95-23569
TANKA, MOTOHIKO ..... p 1834 N95-23525
TANNER, WILLIAM G. ..... p 1623 N95-23803
TAO, ZHIJIAN ..... p 1803 N95-22756
TAPLEY, I. J. ..... p 1714 N95-23948
TAPPAN, NINA D. ..... p 1840 N95-22803
TARDY, H. L. ..... p 1731 N95-24155
TARES, T. ..... p 1713 N95-23944
TARSHISH, ADINA ..... p 1862 N95-24135
TARTAGLIA, M. ..... p 1818 N95-24077
TATAR, J. J. ..... p 1857 N95-23490
TAYLOR, D. J. ..... p 1837 N95-24083
TAYLOR, JOHN ..... p 1748 N95-23771
TAYLOR, S. R. ..... p 1631 N95-23502
TAYLOR, T. R. ..... p 1851 N95-23922
TAYLOR, T. S. ..... p 1837 N95-24087
TCHENG, P. ..... p 1616 N95-23011
TEAFF, DANNY ..... p 1858 N95-24113
TEAGLE, D. ..... p 1830 N95-22793
TENFORDE, T. S. ..... p 1749 N95-24145
TENG, WILLIAM L. ..... p 1714 N95-23950
TENNANT, D. ..... p 1819 N95-22723
TENNYSON, R. C. ..... p 1651 N95-23901
TERIELE, H. J. J. ..... p 1787 N95-22717
TERRIL, DAVE ..... p 1861 N95-24132
TERSTAL, W. G. ..... p 1648 N95-23128
TESTER, J. W. ..... p 1634 N95-23164
TETHAL, T. ..... p 1812 N95-23976
THAKUR, SIDDHARTH ..... p 1677 N95-23448
THART, W. G. J. ..... p 1643 N95-23507
THAYER, J. P. ..... p 1738 N95-23090
THIELMANN, A. ..... p 1850 N95-22784
THOMA, GEORGE R. ..... p 1761 N95-24117
THOMA, L. ..... p 1728 N95-23062
THOMAS, E. V. ..... p 1794 N95-23066
THOMAS, HANS ..... p 1778 N95-23739
THOMAS, MILFRED E. ..... p 1840 N95-22803
THOMASSON, M. ..... p 1868 N95-23228
THOMPSON, A. ..... p 1872 N95-23809
THOMPSON, ANTHONY W. ..... p 1640 N95-22893
THOMPSON, CLARK J. ..... p 1697 N95-23703
THOMPSON, G. ..... p 1796 N95-22740
p 1849 N95-22752
p 1804 N95-22789
THOMPSON, J. L. ..... p 1762 N95-22680
THOMPSON, L. J. ..... p 1639 N95-22594
THOMSEN, MICHELLE F. ..... p 1829 N95-22665
p 1736 N95-22850
THOREN, STEPHEN J. ..... p 1683 N95-23641
THURAISINGHAM, R. A. ..... p 1743 N95-23667
TICHENOR, D. A. ..... p 1828 N95-23767
TIERNEY, BRIAN ..... p 1858 N95-24111
TIGELAAR, H. ..... p 1788 N95-23070
TIPPING, RICHARD H. ..... p 1741 N95-23329
TISONE, G. C. ..... p 1636 N95-24007
TIWARI, P. ..... p 1645 N95-23571
TOBIN, S. J. ..... p 1831 N95-22800
TODD, D. T. ..... p 1696 N95-24064
TODO, Y. ..... p 1834 N95-23524
p 1835 N95-23528
p 1836 N95-23590
p 1836 N95-23591
TODT, V. R. ..... p 1839 N95-22572
p 1845 N95-24154
TOI, K. ..... p 1835 N95-23533
TOKUDA, N. ..... p 1816 N95-22848
TOLKACHEV, E. A. ..... p 1847 N95-22620
TOLLAKSEN, SANDRA L. ..... p 1748 N95-23771
TOLLIN, G. ..... p 1729 N95-23361
TOMASI, D. ..... p 1759 N95-23963
TOMIZAWA, M. ..... p 1816 N95-22644
TOMPKINS, STEFANIE ..... p 1709 N95-23888
TOMSIK, THOMAS M. ..... p 1653 N95-24186
TONUCCI, RONALD J. ..... p 1662 N95-23241
TOOMEY, CHRISTOPHER N. ..... p 1721 N95-23675
TOPRAKCIOGLU, C. ..... p 1649 N95-23568
TORENVLIET, L. ..... p 1760 N95-24092
TORENVLIET, LEEN ..... p 1792 N95-23931
TORENVLIET, LEON ..... p 1793 N95-24003
TORFS, P. J. J. ..... p 1717 N95-22537
TORIU, HIDETOSHI ..... p 1752 N95-23709
TORRES, F. ..... p 1797 N95-23661
TORSON, JIM ..... p 1704 N95-23859
TOSATTI, E. ..... p 1660 N95-22591
TOSI, M. P. ..... p 1640 N95-23057
TOWE, ELIAS ..... p 1663 N95-24048
TOWNSEND, J. ..... p 1645 N95-23571
TRAHAN, M. W. ..... p 1636 N95-24007
TRAN, DUAN K. ..... p 1629 N95-23033
TRAN, KEN ..... p 1674 N95-23436
TRAUB, WESLEY A. ..... p 1735 N95-22482
TRAUM, DAVID ROOD ..... p 1760 N95-24058
TREBINO, R. ..... p 1690 N95-22595
TREIBER, DAVID A. ..... p 1608 N95-23095
TREITEL, RICHARD ..... p 1760 N95-24176
TRELA, W. J. ..... p 1844 N95-24076
TRENT, VICTOR S. ..... p 1694 N95-23213
TREUR, J. ..... p 1766 N95-22524
TREXLER, E. ..... p 1735 N95-24146
TREXLER, M. ..... p 1742 N95-22651
TRIBBLE, A. C. ..... p 1626 N95-22919
TRIPP, J. S. ..... p 1616 N95-23011
TRIVEDI, KISHOR S. ..... p 1754 N95-22603
p 1755 N95-22604
TROITSKAYA, N. I. ..... p 1848 N95-22744
p 1849 N95-22745
p 1849 N95-22753
p 1803 N95-22754
p 1803 N95-22755
p 1804 N95-22811
p 1850 N95-22812
TROLTENIER, D. ..... p 1814 N95-22968
TROMPERT, R. A. ..... p 1789 N95-23167
TROTT, W. M. ..... p 1652 N95-22838
TROYER, G. L. ..... p 1767 N95-23578
TRUCANO, T. ..... p 1868 N95-23656
TRUCANO, T. G. ..... p 1740 N95-24008
p 1741 N95-24009
TRUCHON, M. ..... p 1709 N95-23886
TSAI, TSUNG-MING ..... p 1755 N95-22637
TSCHIRCH, RICHARD P. ..... p 1750 N95-22766
TSUDA, SHINICHI ..... p 1697 N95-23701
TSUGAWA, ROY K. ..... p 1623 N95-23719
TSUKISHIMA, CHIHIRO ..... p 1690 N95-23674
TSUNG, F.-L. ..... p 1679 N95-23623
TUCK, M. R. ..... p 1663 N95-23779
TUCKER, GEORGE F. ..... p 1692 N95-23330
TUCKER, KEVIN ..... p 1677 N95-23448
TUCKER, P. K. ..... p 1673 N95-23431
TUCKER, P. KEVIN ..... p 1686 N95-23652
TUENGE, R. T. ..... p 1631 N95-22677
TUEY, RICHARD C. ..... p 1856 N95-23209
TUFFIAS, ROBERT H. ..... p 1871 N95-24191
TUMA, MARGARET L. ..... p 1820 N95-22915
TURCHI, C. ..... p 1734 N95-23480
TUREMAN, ROBERT L., JR. ..... p 1854 N95-23331
TURNBULL, DAVID N. ..... p 1688 N95-23087
TURNER, GREGORY M. ..... p 1656 N95-22816
TURNER, JOYCE E. ..... p 1856 N95-23225
TURNER, S. G. ..... p 1652 N95-22672
TUSON, G. B. ..... p 1635 N95-23481
TWILT, F. ..... p 1790 N95-23235
TYLKA, ALLAN J. ..... p 1815 N95-23807
p 1870 N95-23808

U

UBERBACHER, E. C. ..... p 1746 N95-22890
UCHIYAMA, TAKASHI ..... p 1752 N95-23705
p 1778 N95-23736
UDDIN, S. ..... p 1804 N95-22786
UENO, HIROSHI ..... p 1623 N95-23726
UIJLENHOET, R. ..... p 1741 N95-22640
ULABY, FAWWAZ T. ..... p 1715 N95-23957
UNAL, RESIT ..... p 1619 N95-23332
UNDERBRINK, A. J., JR. ..... p 1761 N95-23762
UNDERWOOD, D. ..... p 1688 N95-23492
UNDERWOOD, D. G. ..... p 1689 N95-23583
UNDERWOOD, IAN ..... p 1761 N95-23680
UNDERWOOD, J. H. ..... p 1627 N95-22833
UNGEWITTER, RONALD J. ..... p 1682 N95-23635
p 1686 N95-23653
USTIN, SUSAN L. ..... p 1705 N95-23867
p 1709 N95-23889

V

VACCARI, FRANCO ..... p 1736 N95-22612
VAIDYANATHAN, P. P. ..... p 1761 N95-24278
VALANJU, P. M. ..... p 1830 N95-22693
p 1830 N95-22694
VALAVANI, LENA ..... p 1615 N95-22908
VALENZUELA, G. R. ..... p 1712 N95-23939
VALLERGA, JOHN ..... p 1871 N95-23472
VAMPOLA, AL ..... p 1770 N95-23684
VANALSTINE, JAMES ..... p 1653 N95-23204
VANDAM, CORNELIS P. ..... p 1609 N95-23333
VANDAM, E. R. ..... p 1788 N95-23068
VANDENBOSCH, JEANNETTE ..... p 1703 N95-23856
p 1703 N95-23857
p 1690 N95-23862
p 1624 N95-23864
p 1710 N95-23890
VANDENBRINK, R. ..... p 1795 N95-23555
VANDENBROEK, A. C. ..... p 1716 N95-23958
VANDENPOL, ANTHONY N. ..... p 1749 N95-23780
VANDERAALST, W. ..... p 1855 N95-22534
VANDERBILT, VERN C. ..... p 1701 N95-23845
VANDERBURG, G. ..... p 1718 N95-23471
VANDERLEEUW, J. ..... p 1788 N95-23069
p 1788 N95-23070
VANDERMEER, J. C. ..... p 1789 N95-23174
VANDERSCHAFT, A. J. ..... p 1767 N95-23557
VANDERSTOK, P. ..... p 1763 N95-23129
VANDERVET, P. E. ..... p 1648 N95-23128
VANDERVORST, H. A. ..... p 1787 N95-22717
VANDEVEN, A. A. F. ..... p 1833 N95-23170
VANDEVORST, G. A. L. ..... p 1667 N95-23144
p 1648 N95-23145
p 1667 N95-23175
VANEESBEEK, MARC ..... p 1637 N95-23804
VANEIJNDHOVEN, S. J. L. ..... p 1789 N95-23171
VANFOSSEN, G. JAMES, JR. ..... p 1668 N95-23248
VANLIESHOUT, M. N. M. ..... p 1793 N95-22527
VANMAREN, G. ..... p 1717 N95-22538
VANMILL, J. ..... p 1785 N95-22528
p 1785 N95-22533
VANNHUNG, TRAN ..... p 1796 N95-23052
VANNUCCI, A. ..... p 1832 N95-23136
VANZYL, J. J. ..... p 1714 N95-23951
VANZYL, JAKOB ..... p 1712 N95-23938
VAREKAMP, C. ..... p 1717 N95-22538
VASTANO, JOHN A. ..... p 1732 N95-22930
VAUGHAN, J. E. ..... p 1785 N95-22528
VAUGHAN, K. H. ..... p 1730 N95-23605
VAWTER, G. A. ..... p 1828 N95-23575
VAYNER, BORIS V. ..... p 1738 N95-23116
VEDDER, JAMES F. ..... p 1700 N95-23831
VEENSTRA, JACK E. ..... p 1764 N95-24037
VELEV, G. V. ..... p 1811 N95-23769
VELLA, E. ..... p 1806 N95-23138
VENEMA, J. C. ..... p 1718 N95-23471
VENKATAKRISHNAN, V. ..... p 1788 N95-22931
VENKATESWARAN, S. ..... p 1676 N95-23446
VERDEBOUT, J. ..... p 1710 N95-23891
VEREGGE, J. R. ..... p 1761 N95-23688
VERFAILLIE, GERARD ..... p 1618 N95-23760
VERHAAGEN, N. G. ..... p 1677 N95-23466
VERJOVSKY, A. ..... p 1785 N95-22628
VERMILLION, DONALD ..... p 1766 N95-22705
VERWER, J. G. ..... p 1789 N95-23167
VIANCO, P. T. ..... p 1638 N95-22576
VICKREY, J. F. ..... p 1738 N95-23090
VIDAL-MADJAR, D. ..... p 1715 N95-23956
VIDAL, A. ..... p 1715 N95-23956
VIDEBAEK, FLEMMING ..... p 1801 N95-22656
VIERSTRA, RICHARD D. ..... p 1745 N95-22884
VILLARREAL, CARLOS ..... p 1821 N95-22965
VINIAR, I. ..... p 1835 N95-23566
VISHIK, SIMEON ..... p 1786 N95-22711
VITEK, J. M. ..... p 1640 N95-23132
VLASOV, VLADIMIR N. ..... p 1656 N95-22818
VOGEL, STEPHEN M. ..... p 1690 N95-24127
VOLKOV, M. K. ..... p 1804 N95-22787
p 1804 N95-22810
VOLLMER, HERIBERT ..... p 1793 N95-24194
VONDREELE, ROBERT B. ..... p 1839 N95-22565
VONEHRENFRIED, DUTCH ..... p 1620 N95-22542
VONKAENEL, PETER ..... p 1783 N95-24001
VORTAC, O. U. ..... p 1611 N95-23565
p 1750 N95-24088
VOSS, H. J. ..... p 1644 N95-23516
VOURDAS, A. ..... p 1823 N95-22980
VU, BRUCE T. ..... p 1678 N95-23617
p 1679 N95-23618

W

WACKER, J. F. ..... p 1635 N95-23348

WADA, MOTOI	p 1836	N95-23569
WAGES, S.	p 1649	N95-23568
WAGNER, J. S.	p 1636	N95-24007
WAGUE, A.	p 1844	N95-23774
WAHEED, A.	p 1816	N95-22785
WAKABAYASHI, SACHIKO	p 1623	N95-23726
WAKABAYASHI, YASUFUMI	p 1697	N95-23695
	p 1692	N95-23712
	p 1623	N95-23713
WAKITA, YUJIN	p 1777	N95-23728
WALDER, A. J.	p 1830	N95-22793
WALDINGER, RICHARD	p 1761	N95-23680
WALDMAN, J.	p 1642	N95-23500
WALDRON, WAYNE L.	p 1871	N95-23472
WALES, CARL	p 1861	N95-24133
WALKER, DAVID W.	p 1657	N95-23075
WALKER, H.	p 1738	N95-23143
WALKER, ROBERT M.	p 1637	N95-23837
WALSH, D. W.	p 1641	N95-23186
WALSH, JOANNE L.	p 1612	N95-22953
WALTERS, R. A.	p 1819	N95-22780
WALTERS, R. W.	p 1670	N95-23420
WALTZ, R. E.	p 1830	N95-22694
	p 1831	N95-22899
WALUKIEWICZ, W.	p 1844	N95-24010
WAMBACH, A.	p 1807	N95-23156
WAMPLER, WESLEY A.	p 1646	N95-22553
WAN, ZHENGMING	p 1717	N95-23191
	p 1721	N95-24190
WANDER, JOHN	p 1694	N95-22909
WANG, CHUILIN	p 1812	N95-23985
	p 1844	N95-23986
WANG, H. H.	p 1660	N95-22593
WANG, J.	p 1843	N95-23585
WANG, JAMES R.	p 1714	N95-23950
WANG, LIANG-GUO	p 1663	N95-24048
WANG, PEI	p 1787	N95-22777
WANG, Q.	p 1660	N95-22586
WANG, S.	p 1719	N95-24097
WANG, T. S.	p 1671	N95-23422
WANG, TEN SEE	p 1686	N95-23651
WANG, TEN-SEE	p 1673	N95-23434
	p 1678	N95-23617
	p 1679	N95-23618
	p 1682	N95-23636
	p 1625	N95-23655
WANG, WEI	p 1841	N95-23021
	p 1841	N95-23022
	p 1661	N95-23046
	p 1842	N95-23047
	p 1634	N95-23252
WANG, WENZHENG	p 1812	N95-23985
	p 1844	N95-23986
WANG, X.	p 1664	N95-24164
WANG, X. L.	p 1647	N95-22688
WANG, Y. L.	p 1842	N95-23354
WANG, YANG	p 1640	N95-23121
WANG, YONG	p 1716	N95-23959
WANG, YONGCHENG	p 1796	N95-22737
WANG, Z.	p 1838	N95-22555
	p 1798	N95-22895
WANG, ZHONGHUA	p 1792	N95-23971
WARDWELL, DOUG	p 1607	N95-22666
WARNER, MICHAEL S.	p 1766	N95-22831
WARNER, RICHARD	p 1621	N95-22868
WARREN, JACK L.	p 1623	N95-23823
WARSI, S. A.	p 1673	N95-23431
WAS, G. S.	p 1638	N95-22532
WASHBURN, A. E.	p 1677	N95-23466
WASSERBAUER, CHARLES A.	p 1616	N95-23192
WASSERMAN, STEPHEN R.	p 1638	N95-22571
WATANABE, H.	p 1652	N95-24124
WATANABE, K.	p 1834	N95-23523
	p 1836	N95-23590
WATANABE, KUNIHIKO	p 1836	N95-23591
WATANABE, T. H.	p 1835	N95-23564
	p 1835	N95-23528
	p 1836	N95-23590
	p 1836	N95-23591
WATANABE, T.-H.	p 1834	N95-23524
WATANANE, K.	p 1835	N95-23528
WATANEBE, K.	p 1834	N95-23524
WATENPAUGH, DONALD E.	p 1751	N95-23264
WATKINSON, JOHN R.	p 1690	N95-24122
WATSON, B. W.	p 1756	N95-23131
	p 1756	N95-23150
	p 1758	N95-23606
WATSON, DICK	p 1858	N95-24113
WATSON, G. I.	p 1799	N95-23155
WATT, A. S.	p 1734	N95-23480
WATTS, ALAN J.	p 1624	N95-23843
WATTS, E.	p 1626	N95-22919
WATTS, J.	p 1815	N95-23810
WATTS, JOHN W.	p 1815	N95-23819
WAWRZYNEK, P. A.	p 1697	N95-24106
WEAVER, HAROLD F.	p 1616	N95-23192
WEAVER, PAUL	p 1746	N95-22913
WEBB, O. F.	p 1652	N95-22587
WEBBER, JOHN C.	p 1690	N95-24139
WEBBON, BRUCE	p 1695	N95-23376
WEBER, P. G.	p 1739	N95-23244
WEEKS, J. L.	p 1696	N95-24064
WEEKS, JACK L.	p 1647	N95-22558
WEERTMAN, J. R.	p 1627	N95-22683
WEETMAN, D. C.	p 1607	N95-23506
WEINBERG, J. L.	p 1869	N95-23828
WEINSTEIN-LLOYD, J.	p 1733	N95-23362
WEINSTEIN, L. F.	p 1613	N95-24030
WEISBIN, C. R.	p 1697	N95-23697
WEISBIN, CHARLES	p 1768	N95-23673
WELDON, W. F.	p 1695	N95-23342
WELP, U.	p 1839	N95-22572
WELSH, CLEMENT J.	p 1629	N95-23033
WENDELIN, TIM	p 1726	N95-22547
WENG, LIN	p 1792	N95-23659
WENZEL, K.-P.	p 1872	N95-23809
WERESZCZAK, A. A.	p 1647	N95-22689
WESSMAN, CAROL A.	p 1710	N95-23892
WEST, S. L.	p 1645	N95-23980
WEST, W. P.	p 1830	N95-22719
WESTENSKOW, G.	p 1817	N95-23493
WEVER, TOBIAS	p 1716	N95-23960
WHALEN, MARGARET V.	p 1653	N95-24186
WHEELOCK, S. L.	p 1865	N95-22539
WHITAKER, A. F.	p 1617	N95-23549
WHITAKER, ANN F.	p 1637	N95-23797
	p 1638	N95-23897
	p 1651	N95-23912
WHITE, A. R.	p 1813	N95-24166
WHITE, E. L.	p 1857	N95-24089
WHITE, J.	p 1865	N95-22539
WHITE, JIM	p 1859	N95-24121
WHITE, R.	p 1728	N95-23062
WHITE, W. E.	p 1690	N95-22595
WHITEHEAD, C. A.	p 1635	N95-23348
WHITESIDES, R. HAROLD	p 1685	N95-23649
WHITLEY, KAREN S.	p 1651	N95-23899
WHITMORE, J.	p 1664	N95-24081
WHITTAKER, RED	p 1697	N95-23694
WIERINGA, R. J.	p 1754	N95-22522
	p 1855	N95-22523
	p 1855	N95-22525
	p 1755	N95-22652
WIESMANN, H. J.	p 1842	N95-23354
WIGHTMAN, JAMES P.	p 1631	N95-23900
WIKLIND, T.	p 1868	N95-23607
WILCZEK, FRANK	p 1803	N95-22749
WILKEN, D. E.	p 1843	N95-23586
WILKES, DONALD R.	p 1651	N95-23907
	p 1631	N95-23910
	p 1651	N95-23911
WILKINS, DAVID E.	p 1618	N95-23763
WILKINS, R.	p 1658	N95-23772
WILLART-SOUFFLET, VERONIQUE	p 1710	N95-23893
WILLERS, K. J.	p 1856	N95-23340
WILLIAMS, D. J.	p 1709	N95-23886
WILLIAMS, F. A.	p 1634	N95-23122
WILLIAMS, GEORGE P. W., JR.	p 1761	N95-23762
WILLIAMS, J. M.	p 1660	N95-22593
WILLIAMS, KEVIN W.	p 1758	N95-23603
WILLIAMS, M. C.	p 1728	N95-23162
WILLIAMS, MICHAEL D.	p 1691	N95-23411
WILLIAMS, MORGAN	p 1686	N95-23653
WILLIAMS, R. W.	p 1668	N95-23412
WILLIAMS, ROBERT W.	p 1678	N95-23615
	p 1680	N95-23626
WILLIAMS, T. J.	p 1837	N95-24017
WILLIAMS, TOM	p 1726	N95-22547
WILLIS, J. O.	p 1645	N95-23571
WILSON, ALAN N., JR.	p 1663	N95-23783
WILSON, BRUCE E.	p 1709	N95-23887
WILSON, GORDON R.	p 1737	N95-22956
WINFREE, W. P.	p 1644	N95-23512
WINSKE, DAN	p 1736	N95-22850
WINTER, R.	p 1713	N95-23944
WISE, STEPHANIE A.	p 1840	N95-22803
WISNIEWSKI, ROBERT W.	p 1783	N95-24001
	p 1765	N95-24183
WOLF, D.	p 1804	N95-22792
	p 1843	N95-23585
WOLF, KURT BERNARDO	p 1820	N95-22957
	p 1826	N95-23002
	p 1798	N95-23006
	p 1826	N95-23007
WOLFRUM, E. J.	p 1734	N95-23480
WOLOSCHAK, GAYLE E.	p 1746	N95-22913
WOLOSHUN, K. A.	p 1662	N95-23368
WOLSEY, L. A.	p 1786	N95-22641
WONG, C. P. C.	p 1829	N95-22645
WONG, GARY	p 1770	N95-23687
WONG, H. V.	p 1831	N95-22899
WOOD, CHRIS	p 1761	N95-24123
WOODYATT, B. A.	p 1613	N95-23666
WORTMAN, J. J.	p 1869	N95-23828
	p 1637	N95-23836
WRIGHT, B. W.	p 1735	N95-23580
WRIGHT, S. A.	p 1811	N95-23576
WRIGHT, WILLIAM B.	p 1665	N95-22669
WU, H.	p 1785	N95-22628
WU, M. M.	p 1665	N95-22767
WU, X. D.	p 1645	N95-23571
WU, XIN DI	p 1843	N95-23367

X

XIA, X.	p 1837	N95-23982
XIAO, H.	p 1830	N95-22693
XIE, LIN	p 1637	N95-24181
XIONG, L. Y.	p 1839	N95-22606
XU, G.	p 1716	N95-23961
XU, PUNG	p 1711	N95-23894
XU, W. Q.	p 1837	N95-24017
XU, YING	p 1746	N95-22890
XUE, JIM CHANGQIN	p 1735	N95-22482

Y

YABANA, K.	p 1805	N95-22870
YACONI, G. A.	p 1838	N95-22530
YAMADA, HIROSHI	p 1835	N95-23534
YAMAGATA, F.	p 1623	N95-23700
YAMAGUCHI, ISAO	p 1623	N95-23726
	p 1622	N95-24049
YAMAMOTO, HIROMICHI	p 1778	N95-23737
YAMAMOTO, K.	p 1652	N95-24124
YAMAWAKI, TOSHIHIKO	p 1690	N95-23674
	p 1697	N95-23722
YAMAZAKI, JUNICHI	p 1690	N95-24107
YAMAZAKI, KOZO	p 1835	N95-23535
	p 1835	N95-23543
YAMPRATOOM, ED	p 1853	N95-24043
YAN, MU-LIN	p 1786	N95-22631
YANG, JIANN-CHERNG	p 1669	N95-23417
YANHENG, YING	p 1785	N95-22625
YANO, HAJIME	p 1624	N95-23835
YAO, JIN	p 1666	N95-22901
YAPUNCICH, M. L.	p 1663	N95-23479
YASUMOTO, F.	p 1618	N95-23734
YESHA, YELENA	p 1862	N95-24138
YI, WEN	p 1830	N95-22793
YONKE, MARTIN	p 1760	N95-24176
YOO, C. S.	p 1841	N95-22860
YORGENSEN, R.	p 1728	N95-23062
YOSHIDA, KAZUYA	p 1618	N95-23711
YOSHIDA, TETSUJI	p 1623	N95-23726
YOSHIMITSU, TETSUO	p 1771	N95-23689
YOSHIZAWA, M.	p 1816	N95-22644
YOST, WILLIAM T.	p 1799	N95-22921
YOUNG, C. P., JR.	p 1616	N95-23011
YOUNG, DEBORAH B.	p 1872	N95-23276
YOUNG, KATHERINE C.	p 1612	N95-22953
YOUNG, M. F.	p 1811	N95-23576
YOUNG, PHILIP R.	p 1651	N95-23899
	p 1631	N95-23900
YOUNGDAHL, C. A.	p 1662	N95-23355
YU, KIN M.	p 1844	N95-24011
YU, L.	p 1800	N95-22495
YU, LU	p 1801	N95-22498
	p 1838	N95-22499
	p 1842	N95-23059
	p 1812	N95-23985
	p 1844	N95-23986
YU, NING	p 1844	N95-24073
YU, S.	p 1817	N95-23493
YU, S. S.	p 1817	N95-23485
YU, TZU-YI	p 1669	N95-23415
YUHAS, ROBERTA H.	p 1711	N95-23895
YULE, T. J.	p 1632	N95-22764
YURDABAK, D.	p 1640	N95-23057
YUREV, M. Z.	p 1851	N95-23964

Z

ZACCARIA, F.	p 1822	N95-22976
ZACHARIA, T.	p 1668	N95-23372
ZAFAR, S.	p 1660	N95-22586
ZAITSEV, S. A.	p 1814	N95-22967
ZAKI, MOHAMMED JAVEED	p 1764	N95-23936
ZAMENHOF, ROBERT G.	p 1748	N95-22875
ZAVADIL, K. R.	p 1842	N95-23135
ZEE, RALPH H.-C.	p 1700	N95-23839
ZELL, PETER T.	p 1612	N95-23390
ZEMANIAN, T. S.	p 1735	N95-23580
ZEMLYANOJ, S. G.	p 1812	N95-23976
ZEPPENFELDT, F. O.	p 1718	N95-23471

ZEPS, V.	p 1802	N95-22727
ZHANG, GUANGMING	p 1801	N95-22498
	p 1838	N95-22499
	p 1842	N95-23059
ZHANG, JINGCHANG	p 1869	N95-23830
ZHANG, YOU JIN	p 1786	N95-22633
ZHAO, BAO-HENG	p 1786	N95-22631
ZHAO, H. Z.	p 1787	N95-22772
ZHENG, Q. Q.	p 1805	N95-22935
ZHI, YU	p 1647	N95-22610
	p 1647	N95-22611
ZHOLENTS, A.	p 1816	N95-22567
ZHONG, W.	p 1839	N95-22572
ZHOU, X. Z.	p 1839	N95-22606
ZHU, KA-DI	p 1847	N95-22496
	p 1798	N95-22497
ZHU, KADI	p 1850	N95-23049
ZHU, SHAO-PING	p 1834	N95-23524
ZHU, Z. Y.	p 1796	N95-22751
ZIMAND, MARIUS	p 1792	N95-23929
	p 1797	N95-24029
	p 1793	N95-24034
	p 1797	N95-24063
ZIMCIK, D. G.	p 1651	N95-23901
ZINNER, ERNST	p 1637	N95-23837
ZOLENSKY, MICHAEL	p 1700	N95-23838
ZOLENSKY, MICHAEL E.	p 1623	N95-23823
	p 1869	N95-23832
ZSUFFA, I.	p 1718	N95-23469
ZUCKERMAN, E.	p 1633	N95-22876
ZUTAVERN, F. J.	p 1659	N95-22549
	p 1661	N95-22844
ZUZAAN, P.	p 1812	N95-23976
ZWIENER, JAMES M.	p 1651	N95-23907
	p 1631	N95-23910
	p 1651	N95-23911

Typical Corporate Source Index Listing

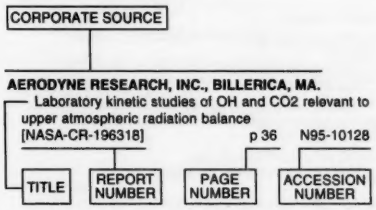

Listings in this index are arranged alphabetically by corporate source. The title of the document provides the user with a brief description of the subject matter. The report number helps to indicate the type of document cited (e.g., NASA report, translation, NASA contractor report). The accession number denotes the number by which the citation is identified. The page number helps you locate the citation in the abstract section. The titles are arranged under each corporate source in ascending accession number order.

A

ACADEMIA R. P. R., BUCHAREST (ROMANIA).
Wigner distribution function and entropy of the damped harmonic oscillator within the theory of the open quantum systems p 1798 N95-22990

ACADEMY OF SCIENCES (USSR), NOVOSIBIRSK (USSR).
Once more about the omega approaches 3(pi) contact term
|DE94-633202| p 1804 N95-22847
The project of high free electron laser using race-track microtron-recuperator
|DE94-634034| p 1692 N95-23657

ACADEMY OF SCIENCES (USSR), VLADIVOSTOK (USSR).
Coherent control in simple quantum systems p 1826 N95-23005

ACCUWAVE CORP., SANTA MONICA, CA.
Optical image correlator using orthogonal data storage
|AD-A285795| p 1819 N95-22508

ADHERENT TECHNOLOGIES, INC., ALBUQUERQUE, NM.
Chemical recycling of scrap composites p 1629 N95-23034

ADVANCED SCIENTIFIC COMPUTING CORP., EL DORADO HILLS, CA.
Comparison between predicted and experimentally measured flow fields at the exit of the SSME HPFTP impeller p 1679 N95-23622

ADVISORY GROUP FOR AERONAUTICAL RESEARCH AND DEVELOPMENT, OXFORD (ENGLAND).
POD assessment of NDI procedures using a round robin test
|AGARD-R-809| p 1697 N95-23602

ADVISORY GROUP FOR AEROSPACE RESEARCH AND DEVELOPMENT, NEUILLY-SUR-SEINE (FRANCE).
Corrosion detection and management of advanced airframe materials
|AGARD-CP-565| p 1641 N95-23496
Knowledge-based guidance and control functions
|AGARD-AR-325| p 1751 N95-23601

AERO THERMO TECHNOLOGY, INC., HUNTSVILLE, AL.
Preconditioning for the Navier-Stokes equations with finite-rate chemistry p 1670 N95-23421

AEROJET-GENERAL CORP., SACRAMENTO, CA.
GGOT total pressure loss control concept evaluation p 1672 N95-23427

AEROSOFT, INC., BLACKSBURG, VA.
Towards a generalized computational fluid dynamics technique for all Mach numbers p 1670 N95-23420

AEROSPACE CORP., EL SEGUNDO, CA.
An explanation for tailward flows with positive B(sub z) in the distant tail neutral sheet during quite times
|ATR-95(7270)-1| p 1740 N95-23933

AEROSPACE CORP., LOS ANGELES, CA.
Simulation of landsat thematic mapper imagery using AVIRIS hyperspectral imagery p 1705 N95-23869

AEROSPATIALE, TOULOUSE (FRANCE).
Corrosion in service experience with aircraft in France p 1645 N95-23518

AGRICULTURAL RESEARCH SERVICE, BELTSVILLE, MD.
Spectral variations in a collection of AVIRIS imagery p 1707 N95-23879

AIR FORCE ACADEMY, CO.
Method development for compensating temperature effects in pressure sensitive paint measurements p 1650 N95-23291

AIR FORCE INST. OF TECH., WRIGHT-PATTERSON AFB, OH.
Modeling aerosol emissions from the combustion of composite materials p 1629 N95-23038

AIR FORCE SYSTEMS COMMAND, MCCLELLAN AFB, CA.
Mishap risk control for advanced aerospace/composite materials p 1628 N95-23031

AIR PRODUCTS AND CHEMICALS, INC., ALLENTOWN, PA.
Organic coating technology for the protection of aircraft against corrosion p 1644 N95-23513

ALABAMA A & M UNIV., NORMAL, AL.
Genetic effects on heavy ions in drosophila
|NASA-CR-197916| p 1746 N95-22911

ALABAMA UNIV., HUNTSVILLE, AL.
Computational modeling of properties
|NAS-CR-196544| p 1841 N95-22907
Magnetospheric space plasma investigations
|NASA-CR-197405| p 1831 N95-22955
The high latitude ionosphere-magnetosphere transition region: Simulation and data comparison
|NASA-CR-197404| p 1737 N95-22956
Semikinetic modeling and observations of high-latitude plasma outflow
|NASA-CR-197403| p 1831 N95-23008
X-ray transmission microscope development
|NASA-CR-197884| p 1826 N95-23016
Task scheduling in dataflow computer architectures p 1753 N95-23301
Development of an algebraic stress/two-layer model for calculating thrust chamber flow fields p 1675 N95-23442
USML-1 microgravity glovebox experiment no. 1 Passive Accelerometer System
|NASA-CR-196575| p 1653 N95-23552
Growth of single crystals of organic salts with large second-order optical nonlinearities by solution processes for devices
|NASA-CR-197963| p 1843 N95-23563
Development of an atomization methodology for spray combustion p 1637 N95-23646
USML-1 Glovebox experiments
|NASA-CR-196574| p 1653 N95-24028
PRISM Spectrograph Optical Design
|NASA-CR-197965| p 1828 N95-24035

ALABAMA UNIV., TUSCALOOSA, AL.
Design and application of electromechanical actuators for deep space missions
|NASA-CR-197957| p 1694 N95-22909
Theoretical studies of spectroscopic problems of importance for atmospheric radiation measurements p 1741 N95-23329

ALABAMA UNIV., UNIVERSITY, AL.
Magnetic resonance and optical spectroscopic studies of carotenoids
|DE95-003729| p 1631 N95-22575

ALASKA UNIV., FAIRBANKS, AK.
ASF archive issues: Current status, past history, and questions for the future p 1861 N95-24133

ALCATEL ESPACE, TOULOUSE (FRANCE).
Terrain modelling and motion planning for an autonomous exploration rover p 1721 N95-23765

ALLIED-SIGNAL AEROSPACE CO., KANSAS CITY, MO.
Progress report on a fully automatic Gas Tungsten Arc Welding (GTAW) system development
|DE95-004397| p 1695 N95-23343
Vision-sensing image analysis for GTAW process control
|DE95-003936| p 1695 N95-23373
Investigation of arc length versus flange thickness while using an arc voltage controller
|DE95-003937| p 1695 N95-23374
Calorimetric measurement of energy of ultrasonic cleaners
|DE95-003938| p 1800 N95-23375

ALTAI STATE UNIV., BARNAUL (USSR).
Structure and properties of polymeric composite materials during 1501 days outer space exposure at Salyut-7 orbital station p 1652 N95-23915

AMERICAN CHEMICAL SOCIETY, WASHINGTON, DC.
Oxidants and oxidation in the Earth's atmosphere
|NASA-CR-197945| p 1734 N95-23460

APPLIED RESEARCH CORP., LANDOVER, MD.
Long term variability of B supergiant winds
|NASA-CR-197925| p 1865 N95-23401
A study of EUV emission from the O4f star Zeta Puppis
|NASA-CR-197350| p 1871 N95-23472
Observational studies of the clearing phase in proto-planetary disk systems
|NASA-CR-197900| p 1866 N95-23561

ARGONNE NATIONAL LAB., IL.
High-temperature ultrasonic characterization of Ag-clad superconductor tapes
|DE95-002909| p 1838 N95-22530
Structure, melting, and reactivity of nickel clusters from numerical simulations
|DE95-002911| p 1638 N95-22531
The influence of high-octane fuel blends on the performance of a two-stroke SI engine with knock-limited-compression ratio
|DE95-002902| p 1692 N95-22556
Performance of thin-ceramic-coated combustion chamber with gasoline and methanol as fuels in a two-stroke SI engine
|DE95-002903| p 1693 N95-22557
Support research for solid oxide fuel cells
|DE95-002910| p 1726 N95-22568
Conceptual design of a 20-kA current lead using forced-flow cooling and Ag-alloy-sheathed Bi-2223 high-temperature superconductors
|DE95-002916| p 1660 N95-22569
A worst-case example using linesearch methods for numerical optimization with inexact gradient evaluations
|DE95-002917| p 1754 N95-22570
Solvation of isolated transition metal ions
|DE95-002978| p 1638 N95-22571
Initial crystallization and growth in melt processing of large-domain YBa2Cu3O(x) for magnetic levitation
|DE95-002993| p 1839 N95-22572
Neutrino oscillation experiments with atmospheric neutrinos
|DE95-002994| p 1801 N95-22573
Thermal outgassing studies on machinable tungsten and TZM molybdenum alloy
|DE95-002984| p 1638 N95-22592
Surface impedance studies on the electrodynamical response of organic superconductors
|DE95-002986| p 1660 N95-22593
X-ray diffraction characterization of defect behavior in nanocrystalline nickel during annealing
|DE95-002992| p 1639 N95-22594

Hydrogen vibrational density of states of adsorbed water on rare-earth modified zirconia
| DE95-001127 | p 1632 N95-22681
Software for the generalized eigenproblem on distributed memory architectures
| DE95-002999 | p 1755 N95-22690
Extensible PDE Solvers package users manual
| DE95-003333 | p 1786 N95-22696
Photoemission study of quantum confinement by a finite barrier: Cu/Co(wedge)/Cu(100)
| DE95-002913 | p 1840 N95-22762
Evaluation of neutron techniques for illicit substance detection
| DE95-002988 | p 1632 N95-22764
Computer simulation of the structure of ionic surfaces and interfaces
| DE95-002991 | p 1804 N95-22792
On the formation of iron(3) oxides via oxidation of iron(2)
| DE94-018392 | p 1632 N95-22857
Computation of magnetic forces on moving conductors by using ELEKTRA and other 3-D computer codes
| DE95-003308 | p 1798 N95-22895
Activation of the jun-D gene in human myeloid cells by 1-(beta)-D-arabinofuranosylcytosine
| DE94-016591 | p 1746 N95-22912
Rearrangement of RAG-1 recombinase gene in radiation-sensitive wasted mice
| DE94-017083 | p 1746 N95-22913
Design and production of efficient current leads for 1500-A, 50-Hz service in a 77-4 K temperature gradient
| DE95-004121 | p 1662 N95-23355
Explosive bonding and its application in the Advanced Photon Source front-end and beamline components design
| DE95-004132 | p 1696 N95-23397
Squeezing out all the performance: Using Ingres for a C(sup 3)I reporting system
| DE95-004591 | p 1857 N95-23490
Time-resolved EPR studies of the H atom: A stable heavy isotope of muonium
| DE95-004614 | p 1810 N95-23491
Thermal effects on the STAR electromagnetic calorimeter
| DE95-004663 | p 1688 N95-23492
Advances in research for solid oxide fuel cells
| DE95-004590 | p 1730 N95-23582
The STAR EM calorimeter design and small prototype test results
| DE95-004592 | p 1689 N95-23583
Long-baseline neutrino oscillation experiments
| DE95-004636 | p 1870 N95-23584
Phonon-induced anomalous specific heat of a model nanocrystal by computer simulation
| DE95-004653 | p 1843 N95-23585
NMR study of nanophase Al/Al-oxide powder and consolidated composites
| DE95-004655 | p 1843 N95-23586
Electromagnetic production of pions on the nucleon
| DE95-004658 | p 1811 N95-23587
A comparative study of the effects of clofibrate, ciprofibrate, WY-14,643, and di-(2-ethylhexyl)-phthalate on liver protein expression in mice
| DE94-016587 | p 1748 N95-23771
Energy efficiency of electric vehicles at the 1994 American Tour de Sol
| DE95-002905 | p 1664 N95-24070
Effects of Bi and Bi2O3 additions on the microstructure and superconducting properties of powder-in-tube BSCCO (2212) tapes
| DE95-004605 | p 1845 N95-24150
Atoms as many-body systems
| DE95-004609 | p 1813 N95-24151
Microstructure and composition of a SNS Josephson junction using CaRuO3 as the metallic barrier
| DE95-004611 | p 1845 N95-24152
Effect of dynamically charged helium on mechanical properties of vanadium-base alloys
| DE95-004613 | p 1646 N95-24153
Processing of single- and multi-domain YBa2Cu3O(x) bulk materials for levitation applications by Nd(1+x)Ba(2-x)Cu3O(y) seeding
| DE95-004615 | p 1845 N95-24154
Some thoughts of future experiments with the new generation of storage rings
| DE95-004602 | p 1818 N95-24162
Design of a high-temperature superconductor current lead for electric utility SMES
| DE95-004604 | p 1664 N95-24163
Ultrafast, high precision gated integrator
| DE95-004616 | p 1664 N95-24164
Beryllium in the ITER blanket
| DE95-004620 | p 1837 N95-24165
Scale-invariant Lipatov kernels from t-channel unitarity
| DE95-004625 | p 1813 N95-24166
Modeling of tritium recovery from lithium ceramics
| DE95-004626 | p 1838 N95-24167
Epitaxial growth of bcc transition metal films and superlattices onto MgO (111), (011) and (001) substrates
| DE95-004629 | p 1846 N95-24168
A phenomenological model for the effect of nanocrystalline microstructure on irradiation-induced amorphization in U3Si
| DE95-004631 | p 1846 N95-24169
A simple, closed-form expression for the x ray reflectivity from superlattices with cumulative roughness
| DE95-004633 | p 1846 N95-24170
Cooling rate effects on the microstructure, critical current density, and (T(sub c)) transition of one- and two-powder BSCCO-2223 Ag sheathed tapes
| DE95-004639 | p 1846 N95-24171
Scalable, extensible, and portable numerical libraries
| DE95-004643 | p 1765 N95-24172
Dependence of the Josephson coupling of unconventional superconductors on the properties of the tunneling barrier
| DE95-004649 | p 1846 N95-24173
Atomic physics at high brilliance synchrotron sources: Proceedings
| DE95-006077 | p 1813 N95-24174

ARIZONA STATE UNIV., TEMPE, AZ.
Laboratory spectra of field samples as a check on two atmospheric correction methods p 1711 N95-23894
Mineralogic variability of the Kelso Dunes, Mojave Desert, California derived from Thermal Infrared Multispectral Scanner (TIMS) data p 1711 N95-23920
AIRSAR views of aerolian terrain p 1713 N95-23941

ARIZONA UNIV., TUCSON, AZ.
Residual strength of thin panels with cracks p 1700 N95-23311
Photochemical energy conversion by membrane-bound photoredox systems
| DE95-004405 | p 1729 N95-23361
Classification of the LCVF AVIRIS test site with a Kohonen artificial neural network p 1706 N95-23874

ARKANSAS UNIV., PINE BLUFF, AR.
Automation technology using Geographic Information System (GIS) p 1863 N95-23284

ARMY ARMAMENT RESEARCH, DEVELOPMENT AND ENGINEERING CENTER, WATERVLIET, NY.
Notch-tip damage and translaminar fracture toughness measurements from carbon/epoxy laminates
| AD-A280101 | p 1627 N95-22833

ARMY CONSTRUCTION ENGINEERING RESEARCH LAB., CHAMPAIGN, IL.
Corrosion control acceptance criteria for sacrificial anode type, cathodic protection systems (user guide)
| AD-A285275 | p 1662 N95-23117

ARMY NATICK LABS., MA.
Effect of hyperbaric carbon dioxide on spores and vegetative cells of bacillus stearothermophilus
| AD-A280115 | p 1747 N95-23251

ARMY RESEARCH LAB., ABERDEEN PROVING GROUND, MD.
Morphology of extinguished monolithic JA2 grains fired in a 30-mm Solid Propellant Electrothermal Chemical (SPETC) gun
| AD-A285792 | p 1652 N95-22506

ARMY RESEARCH LAB., WATERTOWN, MA.
Evaluation of a Multiple Instruction/Multiple Data (MIMD) parallel computer for CFD applications
| AD-A285796 | p 1762 N95-22509
Rationale for the Modular Air-system Vulnerability Estimation Network (MAVEN) methodology
| AD-A285797 | p 1611 N95-22510

AUBURN UNIV., AL.
Summary of solar cell data from the Long Duration Exposure Facility (LDEF)
| NASA-CR-196539 | p 1727 N95-22904
Influence of backup bearings and support structure dynamics on the behavior of rotors with active supports
| NASA-CR-197438 | p 1694 N95-23190
Dynamic modelling and response characteristics of a magnetic bearing rotor system including auxiliary bearings
| NASA-CR-197859 | p 1694 N95-23213
Synchronous dynamics of a coupled shaft/bearing/housing system with auxiliary support from a clearance bearing: Analysis and experiment
| NASA-CR-197858 | p 1695 N95-23214
Ignition transient calculations in the Space Shuttle solid rocket motor p 1625 N95-23640
The effect of impact angle on craters formed by hypervelocity particles p 1700 N95-23839
Aerodynamic flight control to increase payload capability of future launch vehicles
| NASA-CR-197704 | p 1619 N95-24032

AVRO INTERNATIONAL AEROSPACE, WOODFORD (ENGLAND).
Health and usage monitoring systems: Corrosion surveillance p 1607 N95-23506

B

BELGIAN CENTER FOR CORROSION STUDY, BRUSSELS (BELGIUM).
In-situ detection of surface passivation or activation and of localized corrosion: Experiences and prospectives in aircraft p 1643 N95-23508
Test method and test results for environmental assessment of aircraft materials p 1643 N95-23509

BETTIS ATOMIC POWER LAB., WEST MIFFLIN, PA.
The hydrogen embrittlement of alloy X-750
| DE95-003207 | p 1640 N95-22893

BHABHA ATOMIC RESEARCH CENTRE, BOMBAY (INDIA).
Video frame processor
| DE94-635414 | p 1753 N95-23962
Modified molecular sieves: Stationary phase for the gas chromatographic separation of hydrogen isotopes
| DE94-627282 | p 1814 N95-24175

BOEING CO., HUNTSVILLE, AL.
Scheduling with genetic algorithms p 1761 N95-23762

BOEING DEFENSE AND SPACE GROUP, SEATTLE, WA.
Evaluation of adhesive materials used on the Long Duration Exposure Facility
| NASA-CR-4646 | p 1626 N95-22918
Euler technology assessment for preliminary aircraft design employing OVERFLOW code with multiblock structured-grid method
| NASA-CR-4651 | p 1608 N95-23095
Recent results from Long Duration Exposure Facility materials testing p 1638 N95-23898
Collection and review of metals data obtained from LDEF experiment specimens and support hardware p 1646 N95-23905
Organic matrix composite protective coatings for space applications p 1627 N95-23914

BOSTON UNIV., MA.
Fabric geometry distortion during composites processing p 1631 N95-23288
A self-organizing neural network architecture for auditory and speech perception with applications to acoustic and other temporal prediction problems
| AD-A285640 | p 1800 N95-23782

BRADFORD UNIV. (ENGLAND).
Low Earth Orbit satellite/terrestrial mobile service compatibility p 1656 N95-22819

BRITISH BROADCASTING CORP., TADWORTH (ENGLAND).
DRACULA: Dynamic range control for broadcasting and other applications
| BBC-RD-1994/13 | p 1658 N95-24044
The sound insulations of studio doors. Part 2: Door seals
| BBC-RD-1994/15 | p 1654 N95-24045
The sound insulations of studio doors. Part 1: Door blanks
| BBC-RD-1994/14 | p 1654 N95-24093

BROOKHAVEN NATIONAL LAB., UPTON, NY.
Limit on the muon neutrino mass from K(exp 0)muon 3 decay spectra
| DE95-000816 | p 1801 N95-22583
Symplectic computation of Lyapunov exponents
| DE95-002732 | p 1795 N95-22654
(pi)N correlations at AGS
| DE95-002933 | p 1801 N95-22656
Gas cooled leads. Part 1: Theoretical Study. Part 2: Frost free lead optimized for a specific current. Part 3: Frost free lead optimized for a large current range
| DE95-002657 | p 1660 N95-22716
Searches for the H-dibaryon at the AGS
| DE95-003091 | p 1802 N95-22727
Do narrow Sigma hypernuclear states exist?
| DE95-002930 | p 1803 N95-22763
Particle size dependence in Fischer-Tropsch synthesis
| DE95-003124 | p 1633 N95-22876
Preserving the high source brightness with x ray beam line optics
| DE95-003172 | p 1820 N95-22877
Remote detection of trace effluents using resonance Raman spectroscopy
| DE94-016858 | p 1633 N95-22887
Quench propagation study for full-length RHIC dipole magnets
| DE94-014089 | p 1816 N95-22926
Net energy analysis: Powerful tool for selecting electric power options
| DE95-002516 | p 1728 N95-23133

Spin polarized photoemission studies of magnetic quantum well states
|DE95-004218| p 1851 N95-23335
A report on the Indiana University Workshop on future U.S. hadron facilities
|DE95-003951| p 1817 N95-23353
Some aspects of critical currents in Ag sheathed Bi2Sr2Ca2Cu3O10 composite tapes: A summary
|DE95-003952| p 1842 N95-23354
Introduction to the physics of Higgs bosons
|DE95-003965| p 1809 N95-23396
Measurement and analysis of scatter from silicon wafers
|DE95-002411| p 1827 N95-23531
Profiling and light scattering studies of Si surfaces
|DE95-002931| p 1828 N95-24005

BROWN UNIV., PROVIDENCE, RI.
Objective determination of image end-members in spectral mixture analysis of AVIRIS data
p 1709 N95-23888
A comparison of spectral mixture analysis an NDVI for ascertaining ecological variables p 1710 N95-23892

BRUSSELS UNIV. (BELGIUM).
Covariant deformed oscillator algebras
p 1797 N95-22978

C

CALIFORNIA INST. OF TECH., PASADENA, CA.
The influence of swirl brakes and a tip discharge orifice on the rotordynamic forces generated by discharge-to-suction leakage flows in shrouded centrifugal pumps p 1680 N95-23628
Near infrared and optical spectroscopy of FSC10214+4724
|NASA-CR-197966| p 1828 N95-24068

CALIFORNIA STATE UNIV., FULLERTON, CA.
Laboratory studies of the sensitivity of tropospheric ozone to the chemistry of sea salt aerosol
|DE95-003607| p 1735 N95-24147

CALIFORNIA UNIV., BERKELEY. LAWRENCE BERKELEY LAB, CA.
Energy Conversion and Storage Program
|DE95-003796| p 1725 N95-22501
Comparison of the rate constants for energy transfer in the light-harvesting protein, C-phycocyanin, calculated from Foerster's theory and experimentally measured by time-resolved fluorescence spectroscopy
|DE94-014961| p 1745 N95-22590
Turbidity of a near critical ionic fluid
|DE94-014916| p 1633 N95-22869
Ghost images and feasibility of reconstructions with the Richardson-Lucy algorithm
|DE95-002351| p 1756 N95-23079
Diffusion behavior of lysozyme in aqueous ammonium sulfate solutions under varying solution conditions as determined by dynamic light scattering
|DE95-004821| p 1635 N95-23380
Design study of longitudinal dynamics of the drive beam in 1 TeV relativistic klystron two-beam accelerator
|DE95-004683| p 1817 N95-23485
Parallel computation of automatic differentiation applied to magnetic field calculations
|DE95-004689| p 1763 N95-23486
Undulators for short wavelength FEL amplifiers
|DE95-004690| p 1692 N95-23487
Study of b(anti b) production in e(+)e(-) annihilation at radical s = 29 GeV with the aid of neural networks
|DE95-004691| p 1810 N95-23488
Design study of beam dynamics issues for 1 TeVnext linear collider based on the relativistic-klystron two-beam accelerator
|DE95-004673| p 1817 N95-23493
Thermal modeling of the lithium/polymer battery
|DE95-004680| p 1663 N95-23494
Carbon monoxide oxidation over three different states of copper: Development of a model metal oxide catalyst
|DE95-004682| p 1636 N95-23495
Doing photons with MERLIN 2 at Oroville
p 1815 N95-23816
Annealing of nitrogen-doped ZnSe at high pressures: Toward suppression of native defect formation
|DE95-003420| p 1844 N95-24010
Increasing the retained dose by plasma immersion ion implantation and deposition
|DE95-003423| p 1844 N95-24011
Carbon doping of III-V compound semiconductors
|DE95-003431| p 1844 N95-24013
High current induction linacs
|DE95-003442| p 1818 N95-24014
A distributed parallel storage architecture and its potential application within EOSDIS
p 1858 N95-24111
Optimizing tertiary storage organization and access for spatio-temporal datasets p 1861 N95-24131
Chemical Sciences Division
|DE95-002655| p 1626 N95-24142

CALIFORNIA UNIV., DAVIS, CA.
Analysis of the longitudinal handling qualities and pilot-induced-oscillation tendencies of the High-Angle-of-Attack Research Vehicle (HARV)
p 1616 N95-23297
High-lift flow-physics flight experiments on a subsonic civil transport aircraft (B737-100) p 1609 N95-23333
Estimating dry grass residues using landscape integration analysis p 1705 N95-23867
Relationships between pigment composition variation and reflectance for plant species from a coastal savannah in California p 1709 N95-23889

CALIFORNIA UNIV., LOS ANGELES, CA.
VLSI for high-speed digital signal processing
|AD-A285643| p 1663 N95-23783

CALIFORNIA UNIV., SANTA BARBARA, CA.
Land surface temperature measurements for EOS MODIS data
|NASA-CR-197443| p 1717 N95-23191
An improved algorithm for retrieval of snow wetness using C-band AIRSAR p 1715 N95-23954
Relating P-band AIRSAR backscatter to forest stand parameters p 1716 N95-23959
Land surface temperature measurements from EOS MODIS data
|NASA-CR-197969| p 1721 N95-24190

CAMBRIDGE ACOUSTICAL ASSOCIATES, INC., CAMBRIDGE, MA.
The use of cowl camber and taper to reduce rotor/stator interaction noise
|NASA-CR-195421| p 1799 N95-22675

CANADA CENTRE FOR REMOTE SENSING, OTTAWA (ONTARIO).
Estimation of crown closure from AVIRIS data using regression analysis p 1709 N95-23886
Microwave dielectric properties of boreal forest trees
p 1716 N95-23961

CANADIAN SPACE AGENCY, SAINT HUBERT (QUEBEC).
Robotics research at Canadian Space Agency
p 1772 N95-23699
Robotics and telepresence for moon missions
p 1776 N95-23725

CARNEGIE-MELLON UNIV., PITTSBURGH, PA.
Separation of crack extension modes in composite delamination problems p 1700 N95-23281
Lunar rover technology demonstrations with Dante and Ratler p 1697 N95-23694
High performance techniques for space mission scheduling p 1618 N95-23758
Approaches to 100 Gbit/sq. in. recording density
p 1690 N95-24128
Reproducible direct exposure environmental testing of metal-based magnetic media p 1690 N95-24129
The effect of elastic stress on Ostwald Ripening Phenomena
|DE95-002599| p 1646 N95-24140

CENTER FOR MATHEMATICS AND COMPUTER SCIENCE, AMSTERDAM (NETHERLANDS).
Parallel Arnoldi method for the construction of a Krylov subspace basis: An application in magnetohydrodynamics
|PB95-135786| p 1787 N95-22717
VLUGR2: A vectorizable adaptive grid solver for PDes in 2D
|PB95-136008| p 1789 N95-23167

CENTRE DE RECHERCHES EN PHYSIQUE DE L'ENVIRONNEMENT TERRESTRE ET PLANETAIRE, ORLEANS (FRANCE).
Synergy between optical and microwave remote sensing to derive soil and vegetation parameters from MAC Europe 1991 Experiment p 1715 N95-23956

CENTRE NATIONAL D'ETUDES SPATIALES, TOULOUSE (FRANCE).
Autonomous navigation system for the Marsokhod rover project p 1771 N95-23693
Robotic experiment with a force reflecting handcontroller onboard MIR space station p 1752 N95-23707

CENTRE NATIONAL DE LA RECHERCHE SCIENTIFIQUE, TOULOUSE (FRANCE).
Visually guided grasping to study teleprogrammation within the BAROCO testbed p 1777 N95-23731
Mapping of the Ronda peridotite massif (Spain) from AVIRIS spectro-imaging survey: A first attempt
p 1707 N95-23878

CFD RESEARCH CORP., HUNTSVILLE, AL.
Current status in cavitation modeling
p 1681 N95-23632

CHALMERS UNIV. OF TECHNOLOGY, GOETEBORG (SWEDEN).
Structure and evolution of long-lived spiral patterns in galaxies
|PB95-139242| p 1868 N95-23228
Interstellar molecules in the large magellanic cloud
|PB95-139267| p 1868 N95-23230
Multiband VLBI imaging of the jet in 3C 345
|PB95-139275| p 1866 N95-23468
Search for millimeterwave CO emission in damped Lyman-alpha systems
|PB95-139259| p 1868 N95-23607

CHILE UNIV., SANTIAGO (CHILE).
Non-Noetherian symmetries for oscillators in classical mechanics and in field theory p 1823 N95-22977

CHRISTOPHER NEWPORT COLL., NEWPORT NEWS, VA.
Design and implementation of two two-week Teacher Enhancement Institutes p 1853 N95-23306
Aeroacoustic computation of gust-blade interaction
p 1800 N95-23313
Potential aerospace applications of high temperature superconductors p 1664 N95-23322

CIUDAD UNIV., MEXICO CITY (MEXICO).
Notes on oscillator-like interactions of various spin relativistic particles p 1815 N95-22997

CIVIL AEROMEDICAL INST., OKLAHOMA CITY, OK.
The role of flight progress strips in en route air traffic control: A time-series analysis
|DOT/FAA/AM-95/4| p 1611 N95-23565
Development of qualification guidelines for personal computer-based aviation training devices
|DOT/FAA/AM-95/6| p 1758 N95-23603
Some performance effects of age and low blood alcohol levels on a computerized neuropsychological test
|DOT/FAA/AM-95/7| p 1749 N95-23788
Effects of age and low doses of alcohol on compensatory tracking during angular acceleration
|DOT/FAA/AM-95/3| p 1750 N95-23934
Aircraft fires, smoke toxicity, and survival: An overview
|DOT/FAA/AM-95/8| p 1610 N95-24024
A review of civil aviation fatal accidents in which lost/disoriented was a cause/factor: 1981-1990
|DOT/FAA/AM-95/1| p 1611 N95-24071
Functions of external cues in prospective memory
|DOT/FAA/AM-95/9| p 1750 N95-24088

CLARK-ATLANTA UNIV., GA.
Studies of photon and electron interactions with atoms and ions
|DE95-003340| p 1802 N95-22700

CLEMSON UNIV., SC.
Superconductivity devices: Commercial use of space
|NASA-CR-197885| p 1648 N95-22883
Maximum-likelihood spectral estimation and adaptive filtering techniques with application to airborne Doppler weather radar
|NASA-CR-197699| p 1658 N95-23670

CLEVELAND STATE UNIV., OH.
Flow diagnostics, chemically reacting turbulent flow modeling and turbulent mixing: A summary of project studies in combustion
|NASA-CR-197348| p 1687 N95-24022

COLLEGE OF WILLIAM AND MARY, WILLIAMSBURG, VA.
Preparation of course materials: Elementary mathematics of powered flight p 1853 N95-23320

COLORADO STATE UNIV., FORT COLLINS, CO.
Development of an advanced finite difference atmospheric general circulation model
|DE95-003187| p 1736 N95-22879

COLORADO UNIV., BOULDER, CO.
High-performance parallel analysis of coupled problems for aircraft propulsion
|NASA-CR-197440| p 1614 N95-23088
A tool for manual endmember selection and spectral unmixing p 1701 N95-23846
Automating spectral unmixing of AVIRIS data using convex geometry concepts p 1702 N95-23848
The effects of AVIRIS atmospheric calibration methodology on identification and quantitative mapping of surface mineralogy, Drum Mountains, Utah
p 1705 N95-23870
Determination of semi-arid landscape endmembers and seasonal trends using convex geometry spectral unmixing techniques p 1711 N95-23895
Comparison of inversion models using AIRSAR data for Death Valley, California p 1713 N95-23945
Geologic mapping using integrated AIRSAR, AVIRIS, and TIMS data p 1714 N95-23946

COLUMBIA UNIV., NEW YORK, NY.
Development of microchannel plate x-ray optics
|NASA-CR-197935| p 1866 N95-23540
ROSAT observation program
|NASA-CR-197683| p 1866 N95-23595

COMISION NACIONAL DE ENERGIA ATOMICA, BUENOS AIRES (ARGENTINA).
PCLOOK: An interactive code for spectral analysis
|DE94-635415| p 1759 N95-23963
Effect of different ions on the anodic behaviour of alloy 800 chloride solutions at high temperature
|DE94-634944| p 1645 N95-23983

COMMISSION OF THE EUROPEAN COMMUNITIES, ISPRA (ITALY).
Investigations on the 1.7 micron residual absorption feature in the vegetation reflection spectrum p 1710 N95-23891
COMMONWEALTH SCIENTIFIC AND INDUSTRIAL RESEARCH ORGANIZATION, MORDIALOC (AUSTRALIA).
Validation data for land surface temperature determination from satellites
|CSIRO-TR-33| p 1718 N95-23597
Improved AVHRR data navigation using automated land feature recognition to correct a satellite orbital model
|CSIRO-TR-34| p 1718 N95-24026
Implementation of a soil-canopy scheme into the CSIRO GCM: Regional aspects of the model response
|CSIRO-TR-32| p 1721 N95-24192
COMMUNICATIONS RESEARCH CENTRE, OTTAWA (ONTARIO).
Addendum to the Proceedings of the Third International Mobile Satellite Conference (IMSC 1993)
|NASA-CR-197343| p 1655 N95-22813
COMMUNICATIONS RESEARCH LAB., KOGANEI (JAPAN).
Robust control of multi-jointed arm with a decentralized autonomous control mechanism p 1659 N95-23710
Antenna-assembling mechanism test on ETS-7 p 1623 N95-23727
COMPOSITES SERVICES CORP.
Society of the plastic industry process emission initiatives p 1629 N95-23036
COMPUTATIONAL LOGIC, INC., AUSTIN, TX.
Specification and verification of gate-level VHDL models of synchronous and asynchronous circuits
|NASA-CR-191608| p 1762 N95-22830
COMPUTER SCIENCES CORP., GREENBELT, MD.
A constraint-logic based implementation of the coarse-grained approach to data acquisition scheduling of the International Ultraviolet Explorer orbiting observatory p 1779 N95-23741
CONSIGLIO NAZIONALE DELLE RICERCHE, ROME (ITALY).
MAX-91: Polarimetric SAR results on Montespertoli site p 1712 N95-23940
CONVEX COMPUTER CORP., RICHARDSON, TX.
Integrating UniTree with the data migration API p 1761 N95-24120
CORNELL UNIV., ITHACA, NY.
Ion rings for magnetic fusion
|DE94-017606| p 1832 N95-23120
Glaciological studies in the central Andes using AIRSAR/TOPSAR p 1713 N95-23942
Fracture mechanics life analytical methods verification testing
|NASA-CR-196555| p 1697 N95-24106
CORTEZ 3 SERVICES CORP., BROOK PARK, OH.
Microgravity experiments safety and integration requirements document tree
|NASA-CR-195447| p 1855 N95-23206
COSTA RICA NATIONAL UNIV., HEREDIA (COSTA RICA).
A method of solving simple harmonic oscillator Schroedinger equation p 1797 N95-22989
CRI SPACE, (DENMARK).
Distributed intelligence for ground/space systems p 1770 N95-23685
CRI planning and scheduling for space p 1617 N95-23751
CZECHOSLOVAK SOLAR ENERGY SOCIETY, PRAGUE.
Renewable Energy Sources Brno 1993
|DE94-633975| p 1727 N95-22855

D

DASSAULT AVIATION, SAINT-CLOUD (FRANCE).
Active vision in satellite scene analysis p 1778 N95-23738
DATA STORAGE TECHNOLOGIES, INC., RIDGEWOOD, NJ.
New architectural paradigms for multi-petabyte distributed storage systems p 1858 N95-24115
DAYTON UNIV., OH.
Integrating O/S models during conceptual design, part 1
|NASA-CR-197903| p 1622 N95-23398
Integrating O/S models during conceptual design, part 2
|NASA-CR-197904| p 1622 N95-23399
Integrating O/S models during conceptual design, part 3
|NASA-CR-197905| p 1622 N95-23400
DAYTON UNIV. RESEARCH INST., OH.
Aviator's night vision imaging system preflight adjustment/assessment procedures
|AD-A285829| p 1750 N95-22513
DEFENCE RESEARCH AGENCY, FARNBOROUGH, HAMPSHIRE (ENGLAND).
The corrosion and protection of advanced aluminium - lithium airframe alloys p 1641 N95-23497
Non-destructive detection of corrosion for life management p 1643 N95-23505
DEFENCE RESEARCH ESTABLISHMENT PACIFIC, VICTORIA (BRITISH COLUMBIA).
The use of electrochemical impedance spectroscopy to predict the corrosion of aluminum-lithium alloys in marine environments p 1637 N95-23504
DEFENCE SCIENCE AND TECHNOLOGY ORGANIZATION, MELBOURNE (AUSTRALIA).
Stress intensity factors and crack mouth openings for bridged cracks emanating from circular holes
|AR-008-408| p 1699 N95-22952
Enhancement of F/A-18 operational flight measurements: Data report for phase 1
|DSTO-TR-0049| p 1613 N95-23666
Theoretical estimates of high frequency acoustic attenuation and backscattering from suspended sand particles in the ocean and in an estuary
|DSTO-TR-0078| p 1743 N95-23667
Simulation of cookoff results in a small scale test
|DSTO-TR-0090| p 1653 N95-23668
DEFENSE ADVANCED RESEARCH PROJECTS AGENCY, ARLINGTON, VA.
Technology reinvestment project's focus area: Affordable polymer matrix composites for airframe structures
|PB95-136032| p 1865 N95-23168
DELAWARE UNIV., NEWARK, DE.
Nanophase materials: Synthesis, properties, applications
|AD-A286013| p 1627 N95-22940
DEPARTEMENT D'ETUDES ET DE RECHERCHES EN TECHNOLOGIE SPATIALE, TOULOUSE (FRANCE).
Micrometeoroids and debris on LDEF comparison with MIR data p 1623 N95-23824
Debris and meteoroid proportions deduced from impact crater residue analysis p 1869 N95-23834
DEPARTMENT OF DEFENSE, FORT MEADE, MD.
Robotic tape library system level testing at NSA: Present and planned p 1858 N95-24112
DEPARTMENT OF DEFENSE, WASHINGTON, DC.
Defense technology plan
|AD-A285415| p 1903 N95-24178
Defense science and technology strategy
|AD-A285414| p 1903 N95-24179
DEPARTMENT OF ENERGY, LAS VEGAS, NV.
Streamflow and selected precipitation data for Yucca Mountain Region, southern Nevada and eastern California, water years 1986-90
|DE95-001893| p 1742 N95-23385
DEPARTMENT OF ENERGY, WASHINGTON, DC.
The development and applications of biomarkers
|DE94-014249| p 1744 N95-22589
The Louisiana State University waste-to-energy incinerator
|DE95-004417| p 1728 N95-23344
Closing the circle on the splitting of the atom: The environmental legacy of nuclear weapons production in the United States and what the Department of Energy is doing about it p 1818 N95-23562
Information technology standards process guide
|DE95-003967| p 1857 N95-23574
Proceedings of the fuel cells 1994 contractors review meeting
|DE94-012285| p 1730 N95-23977
DEPARTMENT OF THE AIR FORCE, TINKER AFB, OK.
Oklahoma City air logistics center (USAF) aging aircraft corrosion program p 1607 N95-23519
DEPARTMENT OF THE NAVY, WASHINGTON, DC.
Method for making fiber-optic bundle collimator assembly
|AD-D016491| p 1819 N95-22492
Neural network for detection and correction of local boundary misalignments between images
|AD-D016539| p 1766 N95-22705
Corrosivity sensor
|AD-D016549| p 1687 N95-22706
Vibration-damping structural component
|AD-D016550| p 1693 N95-22707
Limited bandwidth microwave filter
|AD-D016553| p 1660 N95-22708
Method and system for electron beam lithography
|AD-D016554| p 1660 N95-22709
Light emission-or-absorbance-based binding assays for polynucleic acids
|AD-D016557| p 1632 N95-22710
Pitch sensor system
|AD-D016488| p 1799 N95-22863
Material characterization system
|AD-D016536| p 1800 N95-23073
Method of making a semiconductor device using a nanochannel glass matrix
|AD-D016383| p 1662 N95-23241
DEUTSCHE AEROSPACE A.G., BREMEN (GERMANY).
Interactive autonomy and robotic skills p 1777 N95-23730
DEUTSCHE AEROSPACE A.G., MUNICH (GERMANY).
Corrosion protection measures for CFC/metal joints of fuel integral tank structures of advanced military aircraft p 1644 N95-23510
Experience of in-service corrosion on military aircraft p 1644 N95-23516
DEUTSCHE AIRBUS G.M.B.H., BREMEN (GERMANY).
Corrosion prevention with environmentally compliant materials: A design challenge p 1644 N95-23511
DEUTSCHE FORSCHUNGS- UND VERSUCHSANSTALT FUER LUFT- UND RAUMFAHRT, COLOGNE (GERMANY).
Exfoliation corrosion and stress corrosion cracking behaviour of Al-Li alloys p 1641 N95-23498
DEUTSCHE FORSCHUNGSANSTALT FUER LUFT- UND RAUMFAHRT, COLOGNE (GERMANY).
Dosimetric results on EURECA p 1872 N95-23800
DEUTSCHE FORSCHUNGSANSTALT FUER LUFT- UND RAUMFAHRT, OBERPFAFFENHOFEN (GERMANY).
Forest investigations by polarimetric AIRSAR data in the Harz mountains p 1713 N95-23944
DIMENSION TECHNOLOGIES, INC., ROCHESTER, NY.
Full resolution hologram-like autostereoscopic display
|NASA-CR-197913| p 1689 N95-23789
DIRECTION DES RECHERCHES, ETUDES ET TECHNIQUES, PARIS (FRANCE).
Study of photorefractive non-linearities in the 3-5 and 2-4 semi-insulator compounds: The effect of electron irradiation
|PB94-189057| p 1839 N95-22584
Study of the pressure field in rotating homogeneous turbulent flows
|PB94-189107| p 1665 N95-22585
Experimental study of vortex breakdown in a swirling water jet
|PB95-130407| p 1665 N95-22767
Interrelations between nervous system and immune system in stress situations
|PB95-135521| p 1748 N95-22770
DISTRICT OF COLUMBIA UNIV., WASHINGTON, DC.
High Tc superconducting bolometric and nonbolometric infrared (IR) detectors
|NASA-CR-197868| p 1827 N95-23224
DOW CHEMICAL CO., MIDLAND, MI.
A roadmap for regulatory survival in the 1990s p 1628 N95-23026
DU PONT DE NEMOURS (E. I.) AND CO., WILMINGTON, DE.
Product stewardship in the composites industry p 1628 N95-23027
DUBLIN INST. FOR ADVANCED STUDIES (IRELAND).
Early results from the ultra heavy cosmic ray experiment p 1872 N95-23809

E

ECOLE POLYTECHNIQUE, PALAISEAU (FRANCE).
Experimental study of vortex breakdown in a swirling water jet
|PB95-130407| p 1665 N95-22767
EG AND G ENERGY MEASUREMENTS, INC., IDAHO FALLS, ID.
Seismic evidence of conjugate normal faulting: The 1994 Devil Canyon earthquake sequence near Challis, Idaho
|DE95-002052| p 1740 N95-23386
EG AND G ENERGY MEASUREMENTS, INC., LAS VEGAS, NV.
Thermal radiant exitance model performance: Soils and forests
|DE95-003619| p 1721 N95-24148
EG AND G ROCKY FLATS, INC., GOLDEN, CO.
OU3 sediment dating and sedimentation rates
|DE95-001891| p 1734 N95-23384
ELECTROMAGNETIC SYSTEMS LABS., INC., SUNNYVALE, CA.
Optimal band selection for dimensionality reduction of hyperspectral imagery p 1709 N95-23887
ELECTROTECHNICAL LAB., TSUKUBA (JAPAN).
Intelligent monitoring system applied to super long distance telerobotic tasks p 1777 N95-23728
ELIZABETH CITY STATE UNIV., NC.
Raman-shifting an ArF excimer laser to generate new lines for obtaining optical diagnostic based information in flow fields p 1692 N95-23303
ELORET CORP., PALO ALTO, CA.
Particle kinetic simulation of high altitude hypervelocity flight
|NASA-CR-197383| p 1664 N95-22481

Computational studies of metal-metal and metal-ligand interactions
| NASA-CR-197862 | p 1641 N95-23215
A multi-region radial integration scheme
| NASA-CR-197982 | p 1809 N95-23408
Symmetry breaking in O4(+): An application of the Brueckner coupled-cluster method
| NASA-CR-197981 | p 1810 N95-23459

ENERGY INFORMATION ADMINISTRATION, WASHINGTON, DC.
Emissions of greenhouse gases in the United States, 1987-1992
| DE95-003001 | p 1731 N95-22691

ENGINEERING RESEARCH AND CONSULTING, INC., HUNTSVILLE, AL.
Application of CFD analysis to design support and problem resolution for ASRM and RSRM
p 1685 N95-23649

ENTWICKLUNGSRING NORD, BREMEN (GERMANY).
An intelligent ground operator support system
p 1769 N95-23681

ENVIRONMENTAL RESEARCH INST. OF MICHIGAN, ANN ARBOR, MI.
Estimation of spectral emissivity in the thermal infrared p 1711 N95-23918

ERIL RESEARCH, INC., SAN RAFAEL, CA.
Fission foil measurements of neutron and proton fluences in the A0015 experiment p 1815 N95-23811
Contribution of proton-induced short range secondaries to the LET spectra on LDEF p 1815 N95-23813

EUROPEAN SPACE AGENCY. EUROPEAN SPACE RESEARCH AND TECHNOLOGY CENTER, ESTEC, NOORDWIJK (NETHERLANDS).
Adaptive beamforming in a CDMA mobile satellite communications system p 1655 N95-22815
The possibilities for mobile and fixed services up to the 20/30 GHz frequency bands p 1656 N95-22817
EURECA 11 months in orbit: Initial post flight investigation results p 1623 N95-23799
Material inspection of EURECA first findings and recommendations p 1637 N95-23804

EXABYTE CORP., BOULDER, CO.
The MAMMOTH project p 1753 N95-24126

EXTRA RESEARCH, INC., SALT LAKE CITY, UT.
Biotransformation of an uncured composite material
p 1629 N95-23033

F

FEDERAL AVIATION ADMINISTRATION, WASHINGTON, DC.
Oceanic operations: An authoritative guide to oceanic operations
| FAA-AFS-550 | p 1610 N95-24065

FEDERAL DATA CORP., BETHESDA, MD.
Building a COTS archive for satellite data
p 1861 N95-24132

FERMI NATIONAL ACCELERATOR LAB., BATAVIA, IL.
New preliminary results on the physics of charm hadroproduction subprocesses
| DE95-002530 | p 1801 N95-22646
Perturbative QCD tests from the LEP, HERA, and TEVATRON colliders
| DE95-001285 | p 1816 N95-22684
Bottom-quark production from muon-jet and dimuon events in p(bar p)-interactions at the square root of s = 1.8 TeV
| DE95-001286 | p 1801 N95-22685
Search for second generation leptoquarks at CDF
| DE94-018983 | p 1805 N95-22939
Testing QCD with jet physics at CDF
| DE94-018980 | p 1807 N95-23196
Properties of jets in Z events from 1.8 TeV (bar p)p collisions
| DE94-018982 | p 1808 N95-23197
Search for Z' and W' at CDF
| DE94-018987 | p 1808 N95-23203
J/psi, psi' yields mu(+)mu(-) and B yields J/psi, psi' cross sections
| DE94-018996 | p 1808 N95-23242
Measurement of correlated b quark cross sections at CDF
| DE95-004240 | p 1808 N95-23336
Recent results from Fermilab E-687, charm particle decays, lifetimes and photoproduction dynamics: A compilation results presented at DPF 1994
| DE95-004580 | p 1808 N95-23347
Electron drift velocities of Ar-CO2-CF4 gas mixtures
| DE95-004353 | p 1809 N95-23359
D(O) upgrade muon electronics design
| DE95-003744 | p 1817 N95-23369
Performance of a large scale scintillating fiber tracker using VLPC readout
| DE95-003746 | p 1871 N95-23370
Search for new gauge bosons at D(O)
| DE95-003745 | p 1809 N95-23404
Operation and tests of a DDC101 A/D
| DE95-003747 | p 1663 N95-23405
Search for top quark at CDF
| DE95-003748 | p 1809 N95-23406
Test procedure for anion exchange chromatography
| DE95-003767 | p 1809 N95-23407
Mechanical design of the CDF SVX 2 silicon vertex detector
| DE94-018985 | p 1689 N95-23520
SVX(prime), the new CDF silicon vertex detector
| DE94-018986 | p 1689 N95-23521
Measurement of W and Z boson production and extraction of the W width and branching ratios at CDF
| DE94-018989 | p 1810 N95-23522
Electroweak physics from the Tevatron
| DE95-002213 | p 1810 N95-23530
Search for supersymmetric (tilde W)(sub 1) and (tilde Z)(sub 2) states using the D0 detector
| DE95-004581 | p 1811 N95-23581
W mass measurements from D(circle slash) and CDF experiments at TeVatron
| DE95-003497 | p 1813 N95-24000
A measurement of the mass of the W vector boson at CDF
| DE95-003498 | p 1813 N95-24016
Standardization of CDF and D(O) reported luminosities
| DE95-003388 | p 1818 N95-24077
A high speed digitizing photomultiplier tube base for the KTeV CsI calorimeter
| DE95-003739 | p 1664 N95-24081
VLPC characterization for the Dzero upgrade
| DE95-003742 | p 1818 N95-24084

FLORIDA INST. OF TECH., MELBOURNE, FL.
Automatic generation of efficient orderings of events for scheduling applications p 1618 N95-23764

FLORIDA SOLAR ENERGY CENTER, CAPE CANAVERAL, FL.
Southeast Regional Experiment Station
| DE95-000903 | p 1726 N95-22518

FLORIDA UNIV., GAINESVILLE, FL.
Interlaminar shear test method development for long term durability testing of composites
p 1631 N95-23300
On the conservative interface treatment for multi-block viscous flow computations
| NASA-CR-195442 | p 1677 N95-23451
Analysis of the request patterns to the NSSDC on-line archive p 1862 N95-24137

FOREST SERVICE, ATLANTA, GA.
Remote identification of a gravel laden Pleistocene river bed p 1712 N95-23921

FRACTURE ANALYSIS CONSULTANTS, ITHACA, NY.
Fracture mechanics life analytical methods verification testing
| NASA-CR-196555 | p 1697 N95-24106

FUJITSU LTD., KAWASAKI (JAPAN).
A three-finger multisensory hand for dexterous space robotic tasks p 1752 N95-23705
Design of teleoperation system with a force-reflecting real-time simulator p 1778 N95-23733
Mark Tracking: Position/orientation measurements using 4-circle mark and its tracking experiments
p 1778 N95-23736

G

GAS RESEARCH INST., CHICAGO, IL.
Preliminary assessment of air toxic emissions in the natural gas industry, phase 1
| PB95-135547 | p 1732 N95-22865

GENERAL ACCOUNTING OFFICE, WASHINGTON, DC.
Security clearances: Consideration of sexual orientation in the clearance process. Report to Congressional requesters
| GAO/NSIAD-95-21 | p 1853 N95-23588
NASA procurement: Contract and management improvements at the Jet Propulsion Laboratory. Report to Congressional requesters
| GAO/NSIAD-95-40 | p 1854 N95-24054
Military bases: Environmental impact at closing installations. Report to Congressional requesters
| GAO/NSIAD-95-70 | p 1735 N95-24057
DOD budget: Selected categories of planned funding for fiscal years 1995-99. Report to Congressional requesters
| GAO/NSIAD-95-92 | p 1864 N95-24062
Ballistic Missile Defense: Current status of strategic target system. Report to Congressional requesters
| GAO/NSIAD-95-78 | p 1903 N95-24080
Inspector General: Alleged misconduct by NASA Inspector General. Report to Congressional requesters
| GAO/OSI-95-9 | p 1854 N95-24085
Report to the Secretary of Defense. Unmanned aerial vehicles: No more Hunter systems should be bought until problems are fixed
| GAO/NSIAD-95-52 | p 1613 N95-24091

GENERAL ATOMICS CO., SAN DIEGO, CA.
The TEXT neutral lithium beam edge density diagnostic
| DE95-003256 | p 1830 N95-22719
The DIII-D divertor cryopump system: Design and operational experience
| DE95-003007 | p 1693 N95-22796
Engineering design of a radiative divertor for DIII-D
| DE95-003008 | p 1693 N95-22798
Environmental Systems Management Analysis and Reporting Network (E-SMART)
| AD-A279766 | p 1732 N95-22856
Divertor heat and particle control experiments on the DIII-D tokamak
| DE94-017518 | p 1832 N95-23119
The q profile evolution and enhanced core confinement of high (beta)(sub p) plasmas in D3-D
| DE95-003878 | p 1834 N95-23371
Edge fluctuation measurements by phase contrast imaging on DIII-D
| DE94-016681 | p 1836 N95-23768
A 4 MW fast wave current drive upgrade for D3-D
| DE95-003741 | p 1837 N95-24083
D3-D program overview
| DE95-003879 | p 1837 N95-24086
Experimental achievement of toroidal beta beyond that predicted by 'Troyon' scaling
| DE95-003880 | p 1837 N95-24087

GENERAL ATOMICS TECHNOLOGIES CORP., SAN DIEGO, CA.
Using the shield for thermal energy storage in PULSAR
| DE95-002457 | p 1829 N95-22645

GEOLOGICAL SURVEY, DENVER, CO.
Comparison of three methods for materials identification and mapping with imaging spectroscopy
p 1702 N95-23853
The US Geological Survey, digital spectral reflectance library: version 1: 0.2 to 3.0 microns
p 1703 N95-23855

GEOLOGICAL SURVEY, FLAGSTAFF, AZ.
Spectral decomposition of AVIRIS data
p 1704 N95-23859

GEOLOGICAL SURVEY, MENLO PARK, CA.
Seismic hazards at Kilauea and Mauna Loa volcanoes, Hawaii
| DE94-012109 | p 1737 N95-22924

GEOLOGICAL SURVEY OF JAPAN, KAWASAKI (JAPAN).
The difference between laboratory and in-situ pixel-averaged emissivity: The effects on temperature-emissivity separation p 1711 N95-23919

GEORGE MASON UNIV., FAIRFAX, VA.
Characteristics of low energy ions in the Heavy Ions In Space (HIIS) experiment p 1815 N95-23807

GEORGIA INST. OF TECH., ATLANTA, GA.
Human-centered design of human-computer-human dialogs in aerospace systems
| NASA-CR-197379 | p 1750 N95-22797
Development of an adaptive hp-version finite element method for computational optimal control
| NASA-CR-197898 | p 1766 N95-22831
TOGA/COARE AMMR 1992 data processing
| NASA-CR-197289 | p 1736 N95-22867
A note on the angular Fourier transformation
p 1797 N95-22986
Upgrade of the 92 GHz airborne multi-channel meteorological radiometer (AMMR)
| NASA-CR-197875 | p 1742 N95-23208

GEORGIA TECH RESEARCH INST., ATLANTA, GA.
Flutter analysis of composite box beams
| NASA-CR-197931 | p 1615 N95-23392

GEORGIA UNIV., ATHENS, GA.
Structural studies of complex carbohydrates of plant cell walls
| DE95-003099 | p 1748 N95-24075

GESELLSCHAFT FUER MATHEMATIK UND DATENVERARBEITUNG, SAINT AUGUSTIN (GERMANY).
Proceedings of the workshop on deductive databases and logic programming
| PB95-139382 | p 1758 N95-23553

GORDON (REX B.).
Fire hazard considerations for composites in vehicle design p 1628 N95-23032

GRACE (W. R.) AND CO., LEXINGTON, MA.
Aqueous alternatives for metal and composite cleaning p 1630 N95-23039

GRANADA UNIV. (SPAIN).
Coherent states for the relativistic harmonic oscillator
p 1825 N95-22993

GRONINGEN RIJKSUNIV. (NETHERLANDS).
DUALITY: A simple formalism for the analysis of UNITY
[PB95-135703] p 1763 N95-23166
GRUMMAN AEROSPACE CORP., PRINCETON, NJ.
High beta and second stability region transport and stability analysis
[DE95-003411] p 1832 N95-23147
GUANAJUATO UNIV., GUANAJUATO (MEXICO).
Shannon-Wehrl entropy for cosmological and black-hole squeezing p 1826 N95-23000

H

HAMPDEN-SYDNEY COLL., VA.
Analysis of data from the energetic gamma-ray experiment of the Gamma Ray Observatory
[NASA-CR-197347] p 1871 N95-23216
HAMPTON UNIV., VA.
1994 NASA-HU American Society for Engineering Education (ASEE) Summer Faculty Fellowship Program
[NASA-CR-194972] p 1872 N95-23276
Infinite possibilities: Computational structures technology p 1700 N95-23280
Upward appraisal as a means for improving supervisory performance and promoting process improvement, with long-term implications for organizational change p 1854 N95-23323
Application of electron paramagnetic resonance imaging to the characterization of the Ultem(R) exposed to 1 MeV electrons. Correlation of radical density data to tiger code calculations p 1815 N95-23328
HARRIS CORP., MELBOURNE, FL.
Passive intermodulation generation in wire mesh deployable reflector antennas p 1656 N95-22816
HAWAII UNIV., HONOLULU, HI.
Current and future use of TOPSAR digital topographic data for volcanological research p 1714 N95-23949
HELSINKI UNIV. OF TECHNOLOGY, ESPOO (FINLAND).
Modelling and analysis of a high speed data bus with predicate/transition nets
[PB95-140695] p 1764 N95-23538
Scandinavian symposium on surface chemistry
[PB95-140687] p 1636 N95-23554
HELSINKI UNIV. OF TECHNOLOGY, OTANIEMI (FINLAND).
Hydrogen and fuel cells for energy storage
[DE95-723907] p 1729 N95-23382
HERCULES, INC., WILMINGTON, DE.
Structural Arrangement Trade Study. Volume 1: Reusable Hydrogen Composite Tank System (RHCTS) and Graphite Composite Primary Structures (GCPS). Executive summary
[NASA-CR-197685] p 1621 N95-23188
Structural arrangement trade study. Volume 3: Reusable Hydrogen Composite Tank System (RHCTS) and Graphite Composite Primary Structures (GCPS). Addendum
[NASA-CR-197687] p 1621 N95-23189
HEURISTICRATS RESEARCH, INC., BERKELEY, CA.
DTS: Building custom, intelligent schedulers p 1779 N95-23744
HITACHI LTD., KAWASAKI (JAPAN).
Autonomous spacecraft executive and its application to rendezvous and docking p 1623 N95-23719
HONEYWELL TECHNOLOGY CENTER, MINNEAPOLIS, MN.
Empirical results on scheduling and dynamic backtracking p 1618 N95-23761
HUGHES INFORMATION TECHNOLOGY CORP., AURORA, IL.
The Starpicker expert system: A problem in expertise capture p 1623 N95-23721
HUGHES STX, INC., LANHAM, MD.
Plasma properties and magnetic field structure of the solar corona, based on coordinated Max 1991 observations from SERTS, the VLA, and magnetographs
[NASA-CR-197864] p 1870 N95-23181
HUNGARIAN ACADEMY OF SCIENCES, DEBRECEN.
A possible generalization of the harmonic oscillator potential p 1822 N95-22970
An algebraic cluster model based on the harmonic oscillator basis p 1814 N95-22971

I

IBM FEDERAL SYSTEMS DIV., HOUSTON, TX.
The architecture of the High Performance Storage System (HPSS) p 1858 N95-24113
IDAHO NATIONAL ENGINEERING LAB., IDAHO FALLS, ID.
A multispectral scanner survey of the Tonopah Test Range, Nevada. Date of survey: August 1993
[DE95-003920] p 1717 N95-22503
Collecting operational event data for statistical analysis
[DE95-002020] p 1793 N95-22550
ILLINOIS UNIV., CHICAGO, IL.
Holographic interferometric tomography for reconstructing flow fields p 1690 N95-23287
ILLINOIS UNIV., URBANA, IL.
Current estimation for electromigration, hot carriers, and voltage drop
[AD-A285794] p 1659 N95-22507
ILLINOIS UNIV., URBANA-CHAMPAIGN, IL.
WHAMS3D Project: Parallel implementations of WHAMS3D on two shared-memory multiprocessors
[CSRD-1248] p 1764 N95-23599
Microarchitecture support for dynamic scheduling of acyclic task graphs
[CSRD-1207] p 1791 N95-23600
INSTITUT DES HAUTES ETUDES SCIENTIFIQUES, BURES-SUR-YVETTE (FRANCE).
Determinants of elliptic pseudo-differential operators
[PB95-109062] p 1786 N95-22711
Grassman and hyperKaehler structures on some spaces of sections of holomorphic bundles
[PB95-109104] p 1795 N95-22712
Classification of SU(3) modular invariants revisited
[PB95-110771] p 1787 N95-22715
Entropy of Z(sup d) subshifts of finite type
[PB95-108072] p 1787 N95-22836
Analytic sets and games in Banach spaces
[PB95-108080] p 1787 N95-22837
Algebraic description of the elliptic cohomology of classifying spaces
[PB95-110797] p 1788 N95-23076
INSTITUT NATIONAL DE LA SANTE ET DE LA RESEARCH MEDICALE, BORDEAUX (FRANCE).
Interrelations between nervous system and immune system in stress situations
[PB95-135521] p 1748 N95-22770
INSTITUTE FOR ADVANCED STUDY, PRINCETON, NJ.
Problems in particle theory
[DE95-003106] p 1803 N95-22749
INSTITUTE FOR AEROSPACE RESEARCH, OTTAWA (ONTARIO).
Double pass retroreflection for corrosion detection in aircraft structures p 1642 N95-23503
INSTITUTE FOR COMPUTER APPLICATIONS IN SCIENCE AND ENGINEERING, HAMPTON, VA.
A perspective on unstructured grid flow solvers
[NASA-CR-195025] p 1788 N95-22931
The initial-value problem for viscous channel flows
[NASA-CR-195034] p 1667 N95-23207
Unification of some advection schemes in two dimensions
[NASA-CR-195044] p 1790 N95-23465
A study of the vortex flow over 76/40-deg double-delta wing
[NASA-CR-195032] p 1677 N95-23466
On the breakup of viscous liquid threads
[NASA-CR-195023] p 1678 N95-23544
Entropy jump across an inviscid shock wave
[NASA-CR-195046] p 1678 N95-23596
Discrete-time Markovian stochastic Petri nets
[NASA-CR-195039] p 1758 N95-23613
INSTITUTE FOR SPACE SCIENCE AND TECHNOLOGY, INC., GAINESVILLE, FL.
The orbital characteristics of debris particle rings as derived from IDE observations of multiple orbit intersections with LDEF p 1869 N95-23829
Secondary ion mass spectrometry (SIMS) analysis of hypervelocity microparticle impact sites on LDEF surfaces p 1637 N95-23836
INSTITUTE FOR TELECOMMUNICATION SCIENCES, BOULDER, CO.
Investigation of Federal Standard 1045 high-frequency ALE radio performance in the Southern Trans-Auroral Zone
[PB94-204831] p 1655 N95-22636
INSTITUTE OF GAS TECHNOLOGY, CHICAGO, IL.
Development of the IGT RENUGAS(reg sign) process
[DE94-017652] p 1727 N95-22888
INSTITUTO DE ENGENHARIA NUCLEAR, RIO DE JANEIRO (BRAZIL).
Study of radiation damages in AISI 316 and 347 steels
[DE94-627480] p 1639 N95-22609
INSTITUTO POLITECNICO NACIONAL, MEXICO CITY (MEXICO).
Geometric phases, evolution loops and generalized oscillator potentials p 1823 N95-22981
Coherent states for a generalization of the harmonic oscillator p 1823 N95-22982
INSTITUTO VENEZOLANO DE INVESTIGACIONES CIENTIFICAS, CARACAS (VENEZUELA).
Localization in deformed quantum mechanics p 1823 N95-22979
INTELLICORP, MOUNTAIN VIEW, CA.
OPUS: A new generation Knowledge Engineering Environment p 1760 N95-24176
INTERFEROMETRICS, INC., VIENNA, VA.
A terabyte linear tape recorder p 1690 N95-24139
INTERNATIONAL ATOMIC ENERGY AGENCY, VIENNA (AUSTRIA).
Review of uncertainty files and improved multigroup cross section files for FENDL
[DE94-628639] p 1830 N95-22757
Online Nuclear Data Service
[DE94-634268] p 1856 N95-23452
Index of nuclear data libraries available from the IAEA nuclear data section
[DE94-634271] p 1857 N95-23453
BROND-2.1. Russian evaluated neutron reaction data library
[DE94-634417] p 1810 N95-23458
The significance of hair mineral analysis as a means for assessing internal body burdens of environmental pollutants
[DE94-633512] p 1734 N95-23541
Applied research on air pollution using nuclear-related analytical techniques
[DE94-633513] p 1734 N95-23542
ESTAR, PSTAR, ASTAR: A PC package for calculating stopping powers and ranges of electrons, protons and helium ions, version 2
[DE94-634435] p 1811 N95-23773
INTERNATIONAL BUSINESS MACHINES CORP., TUCSON, AZ.
Influence of technology on magnetic tape storage device characteristics p 1690 N95-24127
INTERNATIONAL CENTRE FOR THEORETICAL PHYSICS, TRIESTE (ITALY).
Fermion-spin transformation to implement the charge-spin separation
[DE94-629035] p 1800 N95-22495
Magnetic field effects on strong-coupling polaron in quantum dots
[DE94-629038] p 1847 N95-22496
Resonant shallow donor magnetopolaron effect in a GaAs/AlGaAs quantum dot in high magnetic fields
[DE94-629039] p 1798 N95-22497
Asymptotically exact solution of the multi-channel resonant-level model
[DE94-629040] p 1801 N95-22498
Strong-coupling behaviour of two t-J chains with interchain single-electron hopping
[DE94-629041] p 1838 N95-22499
The chirality operators for Heisenberg spin systems
[DE94-629043] p 1847 N95-22545
Metallization and incomplete melting of a semiconductor surface at high temperature
[DE94-627342] p 1660 N95-22591
A fractal model for intergranular fractures in nanocrystals
[DE94-627393] p 1839 N95-22606
Thermal activation of steady-state creep in polycrystalline copper
[DE94-627394] p 1839 N95-22607
Electrical resistivity of liquid alkali metals and non-local pseudopotential
[DE94-627417] p 1639 N95-22608
A study of ceramic composite of ferroelectric BaTiO3 ceramic and superconductor YBa2Cu3O(6+delta) ceramic
[DE94-627563] p 1647 N95-22610
A special percolation problem in ceramic composites
[DE94-627641] p 1647 N95-22611
Intermediate-term earthquake prediction and seismic zoning in Northern Italy
[DE94-627689] p 1736 N95-22612
A comparison of ionospheric F2-layer IRI model with experimental data for Ibadan Geog. Lat. 7.4 deg N
[DE94-627710] p 1736 N95-22613
A parallel molecular dynamics simulation of crystal growth at a cluster of workstations
[DE94-628382] p 1839 N95-22615
Fuzziness and randomness in an optimization framework
[DE94-628383] p 1755 N95-22616
Lectures on Fermat's last theorem
[DE94-628392] p 1795 N95-22617
Diffusion terms in systems of reaction diffusion equations can lead to blow up
[DE94-628408] p 1785 N95-22618
Lectures on homology with internal symmetries
[DE94-628409] p 1785 N95-22619
Berry phase by description of the quantum systems in the Kustaanheimo-Stiefel bundle
[DE94-628410] p 1847 N95-22620
Q-analytic functions on quantum spaces
[DE94-628412] p 1847 N95-22621

Anti-invariant submanifolds of trans-Sasakian manifolds
|DE94-628413| p 1829 N95-22622
Geometry of Moishezon and 1-convex spaces 2: Projectivity of Moishezon spaces and its non-compact version
|DE94-628415| p 1795 N95-22623
Remarks on multiple solutions for asymptotically linear elliptic boundary value problems
|DE94-628416| p 1785 N95-22624
Existence of solutions for some superlinear or sublinear elliptic systems on R(sup N)
|DE94-628417| p 1785 N95-22625
The Euler series of restricted Chow varieties
|DE94-628418| p 1785 N95-22626
A new method of constructing scalar-flat Kaehler surfaces
|DE94-628419| p 1785 N95-22627
Hausdorff dimension of Julia sets of complex Henon mappings
|DE94-628420| p 1785 N95-22628
On oscillations of higher order neutral differential equations
|DE94-628421| p 1786 N95-22629
Vector bundles as direct images of line bundles
|DE94-628422| p 1795 N95-22630
Bethe ansatz and quantum Davey-Stewartson 1 system with multicomponent in two dimensions
|DE94-628423| p 1786 N95-22631
Spectral application of the theorem for the essential quasi-Fredholm spectrum
|DE94-628430| p 1795 N95-22632
Solutions for the vector k-constrained KP hierarchy
|DE94-628431| p 1786 N95-22633
Iterative solutions of nonlinear equations with strongly accretive or strongly pseudocontractive maps
|DE94-628432| p 1786 N95-22634
On the (DE-) stabilization of quantum mechanical binding by potential barriers
|DE94-628433| p 1847 N95-22635
On the theory of smooth structures 3
|DE94-628411| p 1786 N95-22642
More about the q-deformed H-atom wave functions: Normal and abnormal series
|DE94-628434| p 1801 N95-22643
Continuous local symmetry in Ising-type models
|DE94-629045| p 1839 N95-22649
QCD improved exclusive rare B-decays at the heavy b-quark limit
|DE94-628609| p 1802 N95-22720
Twistor-like type 2 superstring with the heterotic (2,0) and (4,0) worldsheet supersymmetry
|DE94-628510| p 1848 N95-22735
Aspects of sigma models
|DE94-628511| p 1795 N95-22736
Possibility of extending space-time coordinates
|DE94-628512| p 1796 N95-22737
First quantized noncritical relativistic Polyakov string
|DE94-628513| p 1848 N95-22738
Black hole formation and space-time fluctuations in two dimensional dilaton gravity and complementarity
|DE94-628514| p 1867 N95-22739
On diagonalization in map (M,G)
|DE94-628515| p 1796 N95-22740
On the scalar curvature of minimal hypersurfaces
|DE94-628516| p 1796 N95-22741
Topologically stable Z - strings in the supersymmetric standard model
|DE94-628517| p 1848 N95-22742
Chiral symmetry breaking in QCD with linearly rising confinement potential
|DE94-628559| p 1848 N95-22744
Spontaneous breaking of chiral symmetry as a consequence of confinement
|DE94-628560| p 1849 N95-22745
Unification of electromagnetic, strong and weak interaction
|DE94-628570| p 1655 N95-22746
A prescribing geodesic curvature problem
|DE94-628503| p 1787 N95-22750
One loop renormalization of Chern-Simons field theory in operator regularization
|DE94-628508| p 1796 N95-22751
Lectures on 2D gauge theories. Topological aspects and path integral techniques
|DE94-628509| p 1849 N95-22752
Chiral anomalies in non-leptonic decays within chiral perturbation theory at the quark level
|DE94-628613| p 1849 N95-22753
On the D yields K-bar(sup *)e(sup +)(nu)(sub e) form factors
|DE94-628614| p 1803 N95-22754
To the problem of D-meson leptonic and semileptonic decays
|DE94-628615| p 1803 N95-22755
Neutrinos with Zee-mass matrix in vacuum and matter
|DE94-628635| p 1803 N95-22756
Strong collision approach to calculation of depolarization function for neutron beam passing through ferromagnetic bulk domains
|DE94-628847| p 1803 N95-22758
Optical absorption in an indirect-gap semiconductor quantum well systems
|DE94-628878| p 1849 N95-22759
Two-photon absorption in an indirect-gap semiconductor quantum well systems 1. Interband transitions
|DE94-628879| p 1849 N95-22760
Two-photon absorption in an indirect-gap semiconductor quantum well systems 2. Excitonic transitions
|DE94-628880| p 1849 N95-22761
Sullivan model for wetting transition in closed system
|DE94-628472| p 1665 N95-22771
The propagation of travelling waves for stochastic generalized KPP equations
|DE94-628473| p 1787 N95-22772
Flexural vibration of thin piezoelectric laminate circular cylinder of hexagonal symmetry
|DE94-628474| p 1698 N95-22773
General crystal in prebiotic context
|DE94-628475| p 1840 N95-22774
The role of triplet correlation function in dense fluids
|DE94-628476| p 1849 N95-22775
Gauge dependence and new kind of two-dimensional gravity theory with trivial quantum corrections
|DE94-628502| p 1850 N95-22776
Nahm's product and W-algebra
|DE94-628504| p 1787 N95-22777
Relativistic particle with torsion and charged particle in a constant electromagnetic field: Identity of evolution
|DE94-628506| p 1803 N95-22778
Deformed Heisenberg algebra and fractional spin field in 2+1 dimensions
|DE94-628507| p 1850 N95-22779
Non-zero temperature two-mode squeezing for time-dependent two-level systems
|DE94-628427| p 1850 N95-22782
Supersymmetric singlet majorons and cosmology
|DE94-628571| p 1850 N95-22783
A space-time lattice version of scalar electrodynamics
|DE94-628577| p 1850 N95-22784
The problem of phase transition and the heavy ion collisions at very high energies
|DE94-628584| p 1816 N95-22785
Baryon number fluctuations in a quark-hadron phase transition
|DE94-628585| p 1804 N95-22786
Dirac canonical quantization and Faddeev-Jackiw symplectic quantization of higher order Lagrangians
|DE94-628428| p 1796 N95-22788
Hadrons of arbitrary spin and heavy quark symmetry
|DE94-628597| p 1804 N95-22789
Results from neutrino experiments
|DE94-628604| p 1804 N95-22790
Long range potentials and multiple scattering theory in complex systems
|DE94-628881| p 1804 N95-22791
Idempotents in Banach algebra
|DE94-628429| p 1787 N95-22794
Jacobson radicals in matrix near rings
|DE94-628424| p 1796 N95-22808
Trisecant curve associated to a smooth curve in P(sub 3) of degree d greater than g+2
|DE94-628425| p 1787 N95-22809
The decays of D(sup *)-mesons
|DE94-628610| p 1804 N95-22810
(pi)- and a(sub 1)-meson physics in current algebra at the quark level
|DE94-628611| p 1804 N95-22811
The omega pi(sup 0)-transient form factor within effective chiral Lagrangian approach
|DE94-628612| p 1850 N95-22812
Variational calculations for He-3 impurities on He-4 droplets
|DE94-628469| p 1840 N95-22839
Non local pseudopotentials, transport properties of liquid noble metals
|DE94-627416| p 1640 N95-22840
Generalized phase transformations of spinor fields
|DE94-628505| p 1656 N95-22841
Block spins and chirality in Heisenberg model on Kagome and triangular lattices
|DE94-629044| p 1840 N95-22845
Correlation effects in high-Tc superconductors and heavy fermion compounds
|DE94-629057| p 1840 N95-22846
Semi-symmetric manifolds satisfying certain curvature conditions
|DE94-628414| p 1788 N95-22922
The fundamental group of complex hyperplanes arrangements
|DE94-628426| p 1796 N95-22933
KKR-CPA calculations of density of states and soft X ray emission from disordered Li-Mg alloys
|DE94-628882| p 1640 N95-22934
Structural properties of silicon clusters: An empirical potential study
|DE94-628902| p 1805 N95-22935
Propagation of waves at the loosely bonded interface of two porous elastic half-spaces
|DE94-628477| p 1800 N95-23018
Static parametric fluctuations give nonstatistical behaviour in uncoupled chaotic systems
|DE94-628478| p 1794 N95-23019
Photoinduced Bragg grating formation in optical fibres as a consequence of convective instability
|DE94-628479| p 1841 N95-23020
Surface growth of two kinds of particles deposition models
|DE94-628480| p 1841 N95-23021
Dynamical behaviour of the coupled diffusion map lattice
|DE94-628481| p 1841 N95-23022
Effect of critical field on screened dielectric breakdown growth
|DE94-628482| p 1661 N95-23046
Effects of long-range coupling on aggregation
|DE94-628483| p 1842 N95-23047
On core level electron diffraction
|DE94-628484| p 1842 N95-23048
Strong-coupling polaron effect in quantum dots
|DE94-628485| p 1850 N95-23049
Membrane phase separations, asymmetry and implications in the origin of life
|DE94-628486| p 1747 N95-23050
Cumulant approach to dynamical correlation functions at finite temperatures
|DE94-628487| p 1788 N95-23051
An extension of Freedman's results on a model of predator-prey dynamics as modified by the action of a parasite
|DE94-628488| p 1796 N95-23052
Enhancement of biomembrane functions under phase-separated conditions: A self-organized criticality phenomenon?
|DE94-628489| p 1747 N95-23053
A model for the metal-nonmetal transition in metal-molten salt solutions
|DE94-628490| p 1640 N95-23057
The origin of chirality in protein amino acids
|DE94-628491| p 1747 N95-23058
Asymptotically exact solution of a local copper-oxide model
|DE94-628492| p 1842 N95-23059
Molecular relics from chemical evolution and the origin of life
|DE94-628493| p 1747 N95-23060
Spontaneous wave packet reduction
|DE94-634280| p 1851 N95-23454
Iterative solutions of nonlinear equations in smooth Banach spaces
|DE94-634287| p 1790 N95-23455
Spinning particles in the Euclidean Taub-NUT space
|DE94-634320| p 1810 N95-23456
Linearizing W-algebras
|DE94-634324| p 1790 N95-23457
Ishikawa iteration process for nonlinear Lipschitz strongly accretive mappings
|DE94-634284| p 1792 N95-23658
Singular moduli and Arakelov intersection
|DE94-634286| p 1792 N95-23659
Universal Hodge bundle and Mumford isomorphisms on the abelian inductive limit of Teichmueller spaces
|DE94-634325| p 1796 N95-23660
On certain N-sheeted coverings of curves and symmetric numerical semigroups which cannot be realized as Weierstrass semigroups
|DE94-634328| p 1797 N95-23661
Charm-conserving strangeness-changing two body hadronic decays of charmed baryons
|DE94-628621| p 1811 N95-23770
Photoionization of O(6+) below the n=3 threshold of the reduced ion
|DE94-634436| p 1844 N95-23774
Neutrino masses and mixing
|DE94-628632| p 1812 N95-23784
Neutrinoless double beta decay and the solar neutrino problem
|DE94-628633| p 1812 N95-23785
Neutrino mass
|DE94-628634| p 1812 N95-23786
Effective (mu)-term in superstring theory
|DE94-634326| p 1851 N95-23922
The exchange algebra for Liouville field on Riemann surfaces with h greater than 1 genus
|DE94-635446| p 1792 N95-23971

Quantum fluctuations of D(sub 5d) polarons on C(sub 60) molecules
[DE94-635787] p 1812 N95-23985
Lattice relaxation study on self-trapped exciton and biexciton in neutral and charged fullerenes
[DE94-635788] p 1844 N95-23986

IOWA STATE UNIV. OF SCIENCE AND TECHNOLOGY, AMES, IA.
Development of novel separation techniques for biological samples in capillary electrophoresis
[DE95-001672] p 1744 N95-22493
Idealized textile composites for experimental/analytical correlation p 1631 N95-23277

IOWA UNIV., IOWA CITY, IA.
Langmuir-like waves and radiation in planetary foreshocks
[NASA-CR-197376] p 1869 N95-22828
Supported transition metal catalysts for para- to ortho-hydrogen conversion
[NASA-CR-197907] p 1634 N95-23252
Physics of magnetospheric boundary layers
[NASA-CR-197920] p 1739 N95-23271

ISRAEL ASSOCIATION FOR CRYSTAL GROWTH, REHOVOT (ISRAEL).
The 1993 Annual Conference of the Israeli Association for Crystal Growth. Program and abstracts
[DE94-633510] p 1841 N95-22854

ITALIAN SPACE AGENCY, ROME.
ASI's space automation and robotics programs: The second step p 1697 N95-23696
Planetary stations and Abyssal Benthic Laboratories: An overview of parallel approaches for long-term investigation in extreme environments p 1752 N95-23732

J

JAPAN ATOMIC ENERGY RESEARCH INST., TOKYO (JAPAN).
An investigation of AC losses in two sub-size conductors for the ITER
[DE94-765449] p 1831 N95-22849
EXTRA.M: A computing code system for analysis of the Purex process with mixer settlers for reprocessing
[DE94-785273] p 1635 N95-23476
Annual report of the Osaka Laboratory for Radiation Chemistry Japan Atomic Energy Research Institute, (No. 26)
[DE94-785277] p 1626 N95-23477

JAPAN BROADCASTING CORP., TOKYO (JAPAN).
Amplified MOS Imager
[NHK-LABS-NOTE-432] p 1690 N95-24107
Proposal of a Modified EBU method for reliable evaluation of picture quality
[NHK-LABS-NOTE-431] p 1863 N95-24180

JET PROPULSION LAB., CALIFORNIA INST. OF TECH., PASADENA, CA.
Parallel digital modem using multirate digital filter banks
[NASA-CR-197331] p 1761 N95-22478
IRAS sky survey atlas: Explanatory supplement
[NASA-CR-197335] p 1865 N95-22539
Controlling under-actuated robot arms using a high speed dynamics process
[NASA-CASE-NPO-18498-1-CU] p 1692 N95-22543
Non-blocking crossbar permutation engine with constant routing latency
[NASA-CASE-NPO-18864-1-CU] p 1762 N95-22564
Mappings between codewords of two distinct (N,K) Reed-Solomon codes over GF(2(sup J))
[NASA-CASE-NPO-18771-1-CU] p 1754 N95-22577
Virtual reality flight control display with six-degree-of-freedom controller and spherical orientation overlay
[NASA-CASE-NPO-18733-1-CU] p 1613 N95-22578
Programmable hyperspectral image mapper with on-array processing
[NASA-CASE-NPO-17794-1-CU] p 1819 N95-22765
Addendum to the Proceedings of the Third International Mobile Satellite Conference (IMSC 1993)
[NASA-CR-197343] p 1655 N95-22813
Synthesis of a large communications aperture using small antennas
[NASA-CR-197330] p 1656 N95-22852
Observation model and parameter partials for the JPL VLBI parameter estimation software MODEST, 19 94
[NASA-CR-197328] p 1756 N95-22853
Motion-sensitive optical correlator using a VanderLugt correlator
[NASA-CASE-NPO-18769-1-CU] p 1827 N95-23045
Life support systems analysis and technical trades for a lunar outpost
[NASA-TM-109927] p 1751 N95-23194
Third International Symposium on Artificial Intelligence, Robotics, and Automation for Space 1994
[NASA-CR-197340] p 1767 N95-23672
Commercialization of JPL Virtual Reality calibration and redundant manipulator control technologies p 1768 N95-23676
Attention focusing and anomaly detection in systems monitoring p 1769 N95-23683
Performance results of cooperating expert systems in a distributed real-time monitoring system p 1761 N95-23688
JPL space robotics: Present accomplishments and future thrusts p 1697 N95-23697
A US-Japan collaborative robotics research program p 1772 N95-23698
A new generation of intelligent trainable tools for analyzing large scientific image databases p 1775 N95-23717
Automated synthesis of image processing procedures using AI planning techniques p 1779 N95-23745
Summaries of the 4th Annual JPL Airborne Geoscience Workshop. Volume 1: AVIRIS Workshop
[NASA-CR-197877-VOL-1] p 1701 N95-23844
Lithologic discrimination and alteration mapping from AVIRIS Data, Socorro, New Mexico p 1701 N95-23847
Field observations using an AOTF polarimetric imaging spectrometer p 1702 N95-23850
Instantaneous field of view and spatial sampling of the Airborne Visible/Infrared Imaging Spectrometer (AVIRIS) p 1702 N95-23851
Airborne Visible/Infrared Imaging Spectrometer (AVIRIS): Recent improvements to the sensor p 1690 N95-23852
Comparison of methods for calibrating AVIRIS data to ground reflectance p 1703 N95-23854
Application of a two-stream radiative transfer model for leaf lignin and cellulose concentrations from spectral reflectance measurements, part 1 p 1703 N95-23856
Application of a two-stream radiative transfer model for leaf lignin and cellulose concentrations from spectral reflectance measurements, part 2 p 1703 N95-23857
Remote sensing of smoke, clouds, and fire using AVIRIS data p 1704 N95-23860
Use of data from the AVIRIS onboard calibrator p 1704 N95-23861
Inflight calibration of AVIRIS in 1992 and 1993 p 1690 N95-23862
Estimation of aerosol optical depth and additional atmospheric parameters for the calculation of apparent reflectance from radiance measured by the Airborne Visible/Infrared Imaging Spectrometer p 1704 N95-23863
Use of the Airborne Visible/Infrared Imaging Spectrometer to calibrate the optical sensor on board the Japanese Earth Resources Satellite-1 p 1624 N95-23864
A proposed update to the solar irradiance spectrum used in LOWTRAN and MODTRAN p 1705 N95-23865
A role for AVIRIS in the Landsat and Advanced Land Remote Sensing Systems program p 1705 N95-23866
Extraction of auxiliary data from AVIRIS distribution tape for spectral, radiometric, and geometric quality assessment p 1706 N95-23875
Preprocessing: Geocoding of AVIRIS data using navigation, engineering, DEM, and radar tracking system data p 1707 N95-23876
The data facility of the Airborne Visible/Infrared Imaging Spectrometer (AVIRIS) p 1707 N95-23877
Monitoring land use and degradation using satellite and airborne data p 1707 N95-23880
The red edge in arid region vegetation: 340-1060 nm spectra p 1708 N95-23881
Temporal changes in endmember abundances, liquid water and water vapor over vegetation at Jasper Ridge p 1708 N95-23882
Atmospheric correction of AVIRIS data of Monterey Bay contaminated by thin cirrus clouds p 1710 N95-23890
Summaries of the 4th Annual JPL Airborne Geoscience Workshop. Volume 2: TIMS Workshop
[NASA-CR-197876-VOL-2] p 1711 N95-23917
Summaries of the 4th Annual JPL Airborne Geoscience Workshop. Volume 3: AIRSAR Workshop
[NASA-CR-197354-VOL-3] p 1712 N95-23938
Interferometric synthetic aperture radar imagery of the Gulf Stream p 1712 N95-23939
Unusual radar echoes from the Greenland ice sheet p 1714 N95-23951

JOINT INST. FOR ADVANCEMENT OF FLIGHT SCIENCES, HAMPTON, VA.
An approximate theoretical method for modeling the static thrust performance of non-axisymmetric two-dimensional convergent-divergent nozzles
[NASA-CR-195050] p 1608 N95-23193

JOINT INST. FOR NUCLEAR RESEARCH, DUBNA (USSR).
A Newton-type neural network learning algorithm
[DE94-628371] p 1766 N95-22614
Finite-temperature scalar field theory in static de Sitter space
[DE94-628522] p 1848 N95-22743
The U(3) x U(3) Nambu - Jona-Lasinio model with the gluon condensate and axial anomaly at finite temperature
[DE94-628588] p 1804 N95-22787
New determination of V(sub us) from K(sub e3)(+) decay
[DE94-628616] p 1811 N95-23769
Does the relativity principle violate?
[DE94-635420] p 1851 N95-23964
Scattering problem for quantum system with time-dependent periodic Hamiltonian
[DE94-635421] p 1797 N95-23965
The kinetics of quantum system with time-dependent periodic Hamiltonian
[DE94-635422] p 1797 N95-23966
The point interactions in the quantum problem of three particles with internal structure
[DE94-635423] p 1851 N95-23967
Tachyons - it was the end of history?
[DE94-635439] p 1851 N95-23968
Weyl connection and non-Abelian gauge field
[DE94-635440] p 1851 N95-23969
Gravitational field of the isolated mass in Yordan-Brans-Dicke theory
[DE94-635441] p 1851 N95-23970
Independent production and Poisson distribution
[DE94-635632] p 1794 N95-23972
Enhanced oscillation of neutrinos of different masses in matter
[DE94-635648] p 1812 N95-23973
Inclusive rapidity correlations of (pi)(-) mesons in pp-interactions
[DE94-635654] p 1812 N95-23974
Gluon distribution as function of F(sub 2) and dF(sub 2)/dlnQ(exp 2) at small x
[DE94-635677] p 1812 N95-23975
Laser light induced drift for atoms of radioactive isotopes Na-22 and Na-24
[DE94-635759] p 1812 N95-23976
Hard e(+)e(-)-pair Bremsstrahlung as a lepton polarimeter
[DE94-635615] p 1812 N95-23984

K

KANSAS UNIV., LAWRENCE, KS.
On-line, adaptive state estimator for active noise control p 1784 N95-23308

KARLSRUHE UNIV. (GERMANY).
Fibonacci chain polynomials: Identities from self-similarity p 1814 N95-22962

KAWASAKI HEAVY INDUSTRIES LTD., KAKAMIGAHARA (JAPAN).
Telerobotics test bed for space structure assembly p 1618 N95-23734

KEELE UNIV. (ENGLAND).
PRISMA GENIE data analysis manual
[PB95-130464] p 1755 N95-22769

KENT UNIV., CANTERBURY (ENGLAND).
Penetration rates over 30 years in the space age p 1624 N95-23827
Micro-abrasion package capture cell experiment on the trailing edge of LDEF: Impactor chemistry and whipple bumper shield efficiencies p 1624 N95-23835
Experimental investigation of the relationship between impact crater morpholcgy and impacting particle velocity and direction p 1700 N95-23840

KIEL UNIV. (GERMANY).
Trapped iron measured on LDEF p 1872 N95-23806

KOMPOZIT CORP., KALININGRAD (RUSSIA).
Specific features of corrosion behavior of stainless maraging steels for aerospace application p 1642 N95-23501
Problems of predicting material property retention during long term service p 1644 N95-23514

KURCHATOV (I. V.) INST. OF ATOMIC ENERGY, MOSCOW (USSR).
Harmonic oscillator in quantum rotational spectra: Molecules and nuclei p 1814 N95-22972

L

LAMAR UNIV., BEAUMONT, TX.
Resource recovery and epidemiology of anaerobic wastewater treatment process in a controlled ecological life support system
[NASA-CR-197930] p 1751 N95-23474

LAWRENCE LIVERMORE NATIONAL LAB., LIVERMORE, CA.
An adaptive projection method for the incompressible Navier-Stokes equations
|DE94-019049| p 1665 N95-22491
A high-power switch-mode DC power supply for dynamic loads
|DE94-016714| p 1659 N95-22504
Electromechanical Battery Program at the Lawrence Livermore National Laboratory
|DE95-003657| p 1727 N95-22574
Production of high contrast ultrashort laser pulses for short scale length plasma experiments
|DE95-003640| p 1690 N95-22595
Realizing parallel reduction operation in Sisal 1.2
|DE94-017524| p 1763 N95-22858
Realizing parallel reduction operations in Sisal 1.2
|DE94-017525| p 1763 N95-22859
Progress towards the synthesis of polymeric nitrogen
|DE94-017547| p 1841 N95-22860
Photon and electron interaction databases and their use in medical applications
|DE94-015558| p 1855 N95-22871
Analytical Boltzmann moments for electrons in N2-O2-H2O gas mixtures
|DE95-003474| p 1732 N95-22898
Numerical Tokamak Project code comparison
|DE95-003475| p 1831 N95-22899
Format( )MEDIC( )Input
|DE95-003482| p 1737 N95-23063
Simulation and off-line programming systems comparison
|DE95-002267| p 1766 N95-23078
TPX magnet system status
|DE95-002389| p 1661 N95-23080
RAS Division model evaluation database tools
|DE95-003480| p 1733 N95-23123
RAS Division model evaluation database description
|DE95-003481| p 1733 N95-23124
How health risk from radiation is assessed
|DE95-003477| p 1749 N95-23142
Conjugate gradient MATHEW
|DE95-003479| p 1738 N95-23143
Two portable parallel tridiagonal solvers
|DE94-019044| p 1763 N95-23243
A hybrid vehicle evaluation code and its application to vehicle design
|DE95-004205| p 1662 N95-23334
Load calculation and system evaluation for electric vehicle climate control
|DE95-004350| p 1695 N95-23358
Ethylene oxidation chemistry in a well-stirred reactor
|DE95-004823| p 1635 N95-23381
Low-cost packaging of high-performance optoelectronic components
|DE95-003645| p 1827 N95-23449
Schwarz-Christoffel methods for multiply-elongated regions
|DE94-019048| p 1790 N95-23536
Gyrokinetic and global fluid simulations of tokamak microturbulence and transport
|DE95-003628| p 1837 N95-24017
Remote sensor test range update
|DE95-003629| p 1735 N95-24018
Pauli-blocking effects in neutron-alpha reactions
|DE94-016358| p 1813 N95-24046

LEHIGH UNIV., BETHLEHEM, PA.
Infrared study of carbon deposits on bimetallic catalysts
|DE95-000902| p 1631 N95-22517
Ethanol synthesis and water gas shift over bifunctional sulfide catalysts
|DE94-017376| p 1634 N95-23202
NO decomposition in non-reducing atmospheres
|DE95-004324| p 1634 N95-23339
Mass loss in the interacting semi-detached binary delta librae
|NASA-CR-197924| p 1866 N95-23402
Robotic weld overlay coatings for erosion control
|DE95-002624| p 1696 N95-24141
High resolution microstructural analysis of zirconia eutectic interfaces
|DE95-003143| p 1845 N95-24143

LIEGE UNIV. (BELGIUM).
On pseudosupersymmetric oscillators and reality of relativistic energies for vector mesons
p 1815 N95-22994
On parasupersymmetric oscillators and relativistic vector mesons in constant magnetic fields
p 1815 N95-22995

LITTLE (ARTHUR D.), INC., CAMBRIDGE, MA.
Multi-fuel reformers for fuel cells used in transportation: Assessment of hydrogen storage technologies
|DE94-017655| p 1727 N95-22861
Multi-fuel reformers for fuel cells used in transportation. Phase 1: Multi-fuel reformers
|DE95-004215| p 1729 N95-23482

LITTORAL UNIV., WIMEREUX (FRANCE).
Using AVIRIS for in-flight calibration of the spectral shifts of SPOT-HRV and of AVHRR? p 1710 N95-23893

LIVERPOOL UNIV. (ENGLAND).
Noisy bases in Hilbert space: A new class of thermal coherent states and their properties
p 1823 N95-22980

LOCKHEED AERONAUTICAL SYSTEMS CO., MARIETTA, GA.
An assessment of viscous effects in computational simulation of benign and burst vortex flows on generic fighter wind-tunnel models using TEAM code
|NASA-CR-4650| p 1608 N95-23185

LOCKHEED ENGINEERING AND SCIENCES CO., HOUSTON, TX.
STS-59 Space Shuttle mission report
|NASA-TM-110527| p 1619 N95-23093
STS-62 Space Shuttle mission report
|NASA-TM-110450| p 1619 N95-23094
STS-61 Space Shuttle mission report
|NASA-TM-110545| p 1619 N95-23187

LOCKHEED-FORT WORTH CO., FORT WORTH, TX.
Euler Technology Assessment program for preliminary aircraft design employing SPLITFLOW code with Cartesian unstructured grid method
|NASA-CR-4649| p 1608 N95-22917

LOCKHEED MISSILES AND SPACE CO., PALO ALTO, CA.
TIMED Imaging Photometer Experiment (TIPE)
|NASA-CR-197431| p 1688 N95-23087
Investigation of physical parameters in stellar flares observed by GINGA
|NASA-CR-196547| p 1868 N95-23205
Software agents for the dissemination of remote terrestrial sensing data p 1721 N95-23675

LORAL AEROSYS, LANDOVER, MD.
The design of a petabyte archive and distribution system for the NASA ECS project p 1858 N95-24110

LOS ALAMOS NATIONAL LAB., NM.
Experience with CANDID: Comparison algorithm for navigating digital image databases
|DE95-000869| p 1855 N95-22515
Energetic particle observations at geosynchronous orbit
|DE95-000873| p 1867 N95-22516
Innovative technology for contamination control in plasma processing
|DE95-000913| p 1829 N95-22519
Superconducting Tl2Ba2CaCu2O8 thin films prepared by post-annealing in a flow-through multiple-zone furnace
|DE95-002745| p 1838 N95-22520
Dimuon production in proton-nucleus interactions
|DE95-002613| p 1801 N95-22551
High magnetic fields in the USA
|DE95-002716| p 1798 N95-22552
Neutron scattering analysis of rubber carbon black composite structure
|DE95-002735| p 1646 N95-22553
High pressure neutron powder diffraction at LANSCE
|DE95-002703| p 1839 N95-22565
Dislocation decomposition, dissociation, and deformation in MoSi2 and (alpha)-Al2O3 single crystals
|DE95-002715| p 1839 N95-22653
Morphology of Laplacian growth processes and statistics of equivalent many-body systems
|DE95-002734| p 1847 N95-22655
Dynamics and variability of the plasmasphere observed from synchronous orbit
|DE95-002733| p 1829 N95-22665
Laser-plasma instability in hohlraums
|DE95-000914| p 1829 N95-22676
MOCVD of gallium and calcium sulfides for improved phosphor processing
|DE95-000918| p 1631 N95-22677
Aspects of surface generation in orthogonal ultraprecision machining
|DE95-000922| p 1654 N95-22678
Accepting the T3D
|DE95-000924| p 1762 N95-22679
An automated computer misuse detection system for UNICOS
|DE95-000929| p 1762 N95-22680
Hot proton anisotropies and cool proton temperatures in the outer magnetosphere
|DE95-002719| p 1736 N95-22850
On-orbit science in a small package: Managing the ALEXIS satellite and experiments
|DE94-014426| p 1621 N95-22868
The role of SU(2) 3n-j coefficients in SU(3)
|DE95-002726| p 1796 N95-22900
Level set techniques applied to unsteady detonation propagation
|DE95-002741| p 1666 N95-22901
The effect of a non-zero shock width on wave propagation in multi-dimensions
|DE95-002748| p 1666 N95-22902
An upper bound for the proton temperature anisotrophy
|DE95-002752| p 1737 N95-22903
Alert-derivative bimodal space power and propulsion systems
|DE95-002754| p 1624 N95-22905
Traps for antimatter and antihydrogen production
|DE95-002814| p 1805 N95-22927
A brief history in time of ion traps and their achievements in science
|DE95-002815| p 1805 N95-22936
Solar mass loss, solar lithium, and solar oscillations
|DE94-018262| p 1870 N95-22938
Exact, E = 0, classical and quantum solutions for general power-law oscillators p 1820 N95-22959
Status of helium-production reaction studies with a spallation neutron source
|DE95-002816| p 1806 N95-23137
Design of a differential radiometer for atmospheric radiative flux measurements
|DE95-002701| p 1739 N95-23244
Dry critical experiments and analyses performed in support of the Topaz-2 Safety Program
|DE95-002724| p 1817 N95-23245
Theory of HF induced turbulence in the ionosphere: Status and challenges
|DE95-002705| p 1739 N95-23256
Orientation selection and microstructural evolution of epitaxial platinum films on (001) magnesium oxide
|DE95-003680| p 1842 N95-23265
Cation disorder determined by MAS Al-27 NMR in high dose neutron irradiated spinel
|DE95-003681| p 1842 N95-23266
Disorder-induced breakdown of soliton and polaron particles
|DE95-003694| p 1808 N95-23267
Vapor deposition of thin-film Y-doped ZrO2 for electrochemical device applications
|DE95-003705| p 1649 N95-23268
Tritium transport, influx, and helium ash measurements on TFTR during DT operation
|DE95-003708| p 1833 N95-23269
(Phi)(sup 4) kinks: Statistical mechanics
|DE95-003693| p 1794 N95-23349
Simulation of absorption edge densitometry
|DE95-004393| p 1635 N95-23360
Internal strain measurement using pulsed neutron diffraction at LANSCE
|DE95-003677| p 1842 N95-23365
Effect on c-axis transport properties of a critical state in Bi2Sr2CaCu2O8
|DE95-003695| p 1843 N95-23366
Transport properties of Tl2Ba2CaCu2O8 meander lines
|DE95-003715| p 1843 N95-23367
HTS current lead using a composite heat pipe
|DE95-003718| p 1662 N95-23368
Spin physics in the next decade
|DE95-003727| p 1809 N95-23403
User's guide and physics manual for the ScatPlus circuit code
|DE95-003755| p 1663 N95-23479
Taylor series expansion and modified extended Prony analysis for localization
|DE95-003671| p 1758 N95-23567
Reflectivity studies on adsorbed block copolymers under shear
|DE95-003676| p 1649 N95-23568
CDM and Omega in the local neighborhood
|DE95-003683| p 1868 N95-23570
Preparation of high quality YBa2Cu3O(7-delta) thick films on flexible Ni-based alloy substrates with textured buffer layers
|DE95-003686| p 1645 N95-23571
Electrochemical studies of perovskite mixed conductors
|DE95-003704| p 1636 N95-23573
Network Event Recording Device: An automated system for network anomaly detection, and notification
|DE94-018274| p 1658 N95-23772
A theory for the morphology of Laplacian growth from statistics of equivalent many-body Hamiltonian systems
|DE94-014473| p 1799 N95-23979
TRACKER: A three-dimensional raytracing program for ionospheric radio propagation
|DE95-003510| p 1658 N95-24015
NTS-spill test facility wind tunnel exhaust plume characterization
|DE95-003630| p 1616 N95-24019

Deformation of C15 Laves phase alloys
[DE95-003636] p 1646 N95-24067
Color orthophotography: To scan or not
[DE95-002749] p 1689 N95-24069
Advanced technologies for a compact RF linac FEL
[DE95-003674] p 1692 N95-24072
Temperature effects on ion irradiation damage in MgAl2O4 spinel single crystals
[DE95-003679] p 1844 N95-24073
A network-based distributed, media-rich computing and information environment
[DE95-003696] p 1765 N95-24074
Phonon characteristics of high (T sub c) superconductors from neutron Doppler broadening measurements
[DE95-003703] p 1844 N95-24076
Bursting in the near-surface boundary layer: Comparisons between realistic models and observations
[DE95-003714] p 1741 N95-24078
Experimental and theoretical studies on the C15 intermetallic compounds MV2 (M = Zr, Hf and Ta): Elasticity and phase stability
[DE95-003723] p 1845 N95-24079

LOUISIANA STATE UNIV., BATON ROUGE, LA.
Pressure shifts and electron scattering in atomic and molecular gases
[DE95-003102] p 1803 N95-22747
Optogalvanic monitoring of collisional transfer of laser excitation energy in a neon RF plasma
[DE95-003103] p 1691 N95-22748
Geometrical interpretation for the outer SU(3) outer multiplicity label p 1814 N95-22968

LUDWIG-MAXIMILIANS-UNIV., MUNICH (GERMANY).
Application of MAC-Europe AVIRIS data to the analysis of various alteration stages in the Landdmannalauger Hydrothermal Area (South Iceland)
p 1709 N95-23885

M

MALIN SPACE SCIENCE SYSTEMS, SAN DIEGO, CA.
Automatic commanding of the Mars Observer Camera
p 1620 N95-23754

MANCHESTER UNIV. (ENGLAND).
Collaborative research on aircraft icing and charging processes in ice
[AD-A285102] p 1609 N95-23201

MARYLAND UNIV., COLLEGE PARK, MD.
Statistical properties of the time histories of cosmic gamma-ray bursts detected by the BATSE experiment of the Compton gamma-ray observatory
[NASA-CR-197425] p 1871 N95-23546

MARYLAND UNIV. BALTIMORE COUNTY, CATONSVILLE, MD.
Global electric field determination in the Earth's outer magnetosphere using energetic charged particles
[NASA-CR-197392] p 1737 N95-22945
Observations of the magnetopause current layer: Cases with no boundary layer and tests of recent models
[NASA-CR-197391] p 1738 N95-23184

MASSACHUSETTS INST. OF TECH., CAMBRIDGE, MA.
GPS survey of the western Tien Shan
[NASA-CR-197901] p 1717 N95-22832
Design of high performance multivariable control systems for supermaneuverable aircraft at high angle of attack
[NASA-CR-197661] p 1615 N95-22908
Stellar Interferometer Technology Experiment (SITE)
[NASA-CR-197856] p 1827 N95-23089
Conversion of light hydrocarbon gases to metal carbides for production of liquid fuels and chemicals
[DE95-000362] p 1634 N95-23164
Edge fluctuation measurements by phase contrast imaging on DIII-D
[DE94-016681] p 1836 N95-23768

MASSACHUSETTS INST. OF TECH., LEXINGTON, MA.
Calculation of satellite drag coefficients
[AD-A285118] p 1622 N95-23781

MASSACHUSETTS INST. OF TECH., MINNEAPOLIS, MN.
Applications drivers for data parking on the Information Superhighway p 1857 N95-24109

MASSACHUSETTS INST. OF TECH., WESTFORD, MA.
High data rate recorder development at MIT Haystack Observatory p 1690 N95-24118

MASSACHUSETTS UNIV., LOWELL, MA.
Theoretical calculations of pressure broadening coefficients for H2O perturbed by hydrogen or helium gas
[NASA-CR-197345] p 1636 N95-23545

MATRA MARCONI SPACE, TOULOUSE (FRANCE).
Formalizing procedures for operations automation, operator training and spacecraft autonomy
p 1752 N95-23720
Benefits of advanced software techniques for mission planning systems p 1618 N95-23752

MAXIMUM STRATEGY, INC., MILPITAS, CA.
Client/Server data serving for high performance computing p 1761 N95-24123

MCAT INST., MOFFETT FIELD, CA.
Three-dimensional unsteady flow calculations in an advanced gas generator turbine p 1671 N95-23425

MCDONNELL-DOUGLAS AEROSPACE, HOUSTON, TX.
The Charlotte (TM) intra-vehicular robot
p 1697 N95-23703

MCDONNELL-DOUGLAS AEROSPACE, HUNTINGTON BEACH, CA.
CFD flowfield simulation of Delta Launch Vehicles in a power-on configuration p 1673 N95-23433

MCDONNELL-DOUGLAS AEROSPACE, LONG BEACH, CA.
Guidance and control requirements for high-speed Rollout and Turnoff (ROTO)
[NASA-CR-195026] p 1614 N95-22674

MCDONNELL-DOUGLAS AEROSPACE, SAINT LOUIS, MO.
Offgassing test methodology for composite materials
p 1629 N95-23035

MEGA DRIVE SYSTEMS, INC., BEVERLY HILLS, CA.
Optimizing raid performance with cache
p 1761 N95-24116

MEMPHIS UNIV., MEMPHIS, TN.
Deflections of anisotropic sandwich beams with variable face sheets and core thicknesses p 1700 N95-23310

MIAMI UNIV., CORAL GABLES, FL.
Ocean observations with EOS/MODIS: Algorithm development and post launch studies
[NASA-CR-197402] p 1717 N95-22916
Ocean observations with EOS/MODIS: Algorithm development and post launch studies
[NASA-CR-197894] p 1718 N95-23473

MIAMI UNIV., FL.
Magnetic multilayer physics
[DE95-003408] p 1798 N95-23083
Infrared algorithm development for ocean observations with EOS/MODIS
[NASA-CR-197851] p 1743 N95-23212

MICHIGAN UNIV., ANN ARBOR, MI.
The viability of establishing collaborative, reconfigurable research environments for the Human Performance Research Laboratory at NASA Ames
[NASA-CR-197384] p 1753 N95-22480
The role of grain boundary chemistry and structure in the environmentally-assisted intergranular cracking of nickel-base alloys
[DE95-002941] p 1638 N95-22532
Recent developments in inductively coupled plasma source magnetic sector multiple collector mass spectrometry
[DE95-003002] p 1830 N95-22793
Precise determinations of the isotopic compositions and atomic weights of molybdenum, tellurium, tin and tungsten using ICP source magnetic sector multiple collector mass spectrometry
[DE95-003003] p 1632 N95-22795
Biological determinants of photobioreactor design
[DE94-016032] p 1745 N95-22872
Continued studies of polar cap thermospheric dynamics
[PL-TR-94-2076] p 1737 N95-22951
Coherent state constructions of bases for some physically relevant group chains p 1814 N95-22966
Modeling of nonequilibrium space plasma flows
[NASA-CR-197432] p 1833 N95-23211
SAR terrain classifier and mapper of biophysical attributes p 1715 N95-23957

MIDDLE EAST TECHNICAL UNIV., ANKARA (TURKEY).
Effect of loading direction and long-term aging on fatigue-crack growth in Al-Li alloy 2090
p 1641 N95-23499

MINISTRY OF INTERNATIONAL TRADE AND INDUSTRY, TSUKUBA (JAPAN).
Development of Advanced Robotic Hand System for space application p 1752 N95-23704
Manipulating flexible parts using a teleoperated system with time delay: An experiment p 1777 N95-23729

MINNESOTA UNIV., MINNEAPOLIS, MN.
Feedback control laws for highly maneuverable aircraft
[NASA-CR-197944] p 1615 N95-23410
Very fast motion planning for highly dexterous-articulated robots p 1771 N95-23691
A 500 megabyte/second disk array
p 1753 N95-24114

MISSISSIPPI STATE UNIV., MISSISSIPPI STATE, MS.
Crossflow instability control on a swept-wing: Preliminary studies p 1609 N95-23283
Thin tailored composite wing for civil tiltrotor
p 1613 N95-23317
IGES transformer and NURBS in grid generation
p 1669 N95-23415
Structured adaptive grid generation using algebraic methods p 1669 N95-23417
TIGER: A user-friendly interactive grid generation system for complicated turbomachinery and axis-symmetric configurations p 1670 N95-23419

MOLLER INTERNATIONAL, INC., DAVIS, CA.
Evaluation of thermal barrier and PS-200 self-lubricating coatings in an air-cooled rotary engine
[NASA-CR-195445] p 1614 N95-23222

MONTANA STATE UNIV., BOZEMAN, MT.
Measurements of striae in CR+ doped YAG laser crystals p 1847 N95-23285
Computational modelling of Er(3+): Garnet laser materials p 1692 N95-23326

MONTREAL UNIV. (QUEBEC).
Oscillator-like coherent states for the Jaynes-Cummings Model p 1826 N95-23003

MORAVIAN COLL., BETHLEHEM, PA.
Locating buildings in aerial photos
p 1721 N95-23295

MORGAN STATE UNIV., BALTIMORE, MD.
Germination, growth rates, and electron microscope analysis of tomato seeds flown on the LDEF
p 1748 N95-23821

MORGANTOWN TECHNOLOGY CENTER, WV.
The US molten carbonate fuel-cell development and commercialization effort
[DE94-019096] p 1728 N95-23162

MVA, INC., NORCROSS, GA.
Transmission electron microscope studies of extraterrestrial materials
[NASA-CR-188363] p 1633 N95-23092

N

NAPLES UNIV. (ITALY).
Nonclassical light in interferometric measurements
p 1822 N95-22976

NASA SCIENTIFIC AND TECHNICAL INFORMATION FACILITY, BALTIMORE-WASHINGTON INTERNATIONAL AIRPORT, MD.
NASA Thesaurus, Supplement
[NASA-SP-7096-SUPPL-1] p 1856 N95-23223

NATIONAL AERONAUTICS AND SPACE ADMINISTRATION, WASHINGTON, DC.
Hey! What's Space Station Freedom?
[NASA-TM-110531] p 1620 N95-22542
Space Science for the 21st Century. Strategic Plan for 1995-2000
[NASA-TM-110546] p 1617 N95-22947
NASA university program management information system, FY 1994
[NASA-TM-110345] p 1856 N95-23364
The next decade of space robotics
p 1768 N95-23673
Space Shuttle mission: STS-67
[NASA-TM-110509] p 1620 N95-24027

NATIONAL AERONAUTICS AND SPACE ADMINISTRATION. AMES RESEARCH CENTER, MOFFETT FIELD, CA.
Flow visualization studies of VTOL aircraft models during Hover in ground effect
[NASA-TM-108860] p 1607 N95-22666
Nonlinear system guidance in the presence of transmission zero dynamics
[NASA-TM-4661] p 1654 N95-22804
Director's discretionary fund report for fiscal year 1994
[NASA-TM-108848] p 1872 N95-22920
Experimental results for a hypersonic nozzle/afterbody flow field
[NASA-TM-4638] p 1609 N95-23250
Method and apparatus for measuring the strain developed in a coated surface
[NASA-CASE-ARC-11938-1-C] p 1688 N95-23263
Self-generating oscillating pressure exercise device
[NASA-CASE-ARC-12000-1] p 1751 N95-23264
Quick connect coupling
[NASA-CASE-ARC-11921-2] p 1695 N95-23376
System for determining aerodynamic imbalance
[NASA-CASE-ARC-11913-1] p 1688 N95-23377
Resonant infrared detector with substantially unit quantum efficiency
[NASA-CASE-ARC-11940-1-SB] p 1827 N95-23378
Method and system for pattern analysis using a coarse-coded neural network
[NASA-CASE-ARC-11961-1] p 1767 N95-23387
Engines-only flight control system
[NASA-CASE-ARC-11944-1] p 1615 N95-23389
Aerodynamic surface distension system for high angle of attack forebody vortex control
[NASA-CASE-ARC-11979-1] p 1612 N95-23390
Cueing light configuration for aircraft navigation
[NASA-CASE-ARC-11982-1] p 1611 N95-23393
Protective coating for ceramic materials
[NASA-CASE-ARC-11969-1-CU] p 1649 N95-23394

Lift enhancing tabs for airfoils
[NASA-CASE-ARC-11990-1] p 1613 N95-23395
Incompressible Navier-Stokes calculations in pump flows p 1680 N95-23627
Using Dedal to share and reuse distributed engineering design information p 1768 N95-23678
An operations and command systems for the extreme ultraviolet explorer p 1770 N95-23687
Space science experimentation automation and support p 1775 N95-23718
Robust telescope scheduling p 1779 N95-23742
Hypervelocity impact survivability experiments for carbonaceous impactors, part 2 p 1700 N95-23831
Image and compositional characteristics of the LDEF Big Guy impact crater p 1700 N95-23838
Use of spectral analogy to evaluate canopy reflectance sensitivity to leaf optical property p 1701 N95-23845
AVIRIS and TIMS data processing and distribution at the land processes distributed active archive center p 1706 N95-23872
TRISTAR 1: Evaluation methods for testing head-up display (HUD) flight symbology
[NASA-TM-4665] p 1613 N95-24030
Transferring ecosystem simulation codes to supercomputers
[NASA-TM-4662] p 1759 N95-24052

NATIONAL AERONAUTICS AND SPACE ADMINISTRATION. FLIGHT RESEARCH CENTER, EDWARDS, CA.

Flight test of the X-29A at high angle of attack: Flight dynamics and controls
[NASA-TP-3537] p 1612 N95-22806
Direct adaptive performance optimization of subsonic transports: A periodic perturbation technique
[NASA-TM-4676] p 1612 N95-22829

NATIONAL AERONAUTICS AND SPACE ADMINISTRATION. GODDARD SPACE FLIGHT CENTER, GREENBELT, MD.

SeaWiFS technical report series. Volume 25: Ocean optics protocols for SeaWiFS validation, revision 1
[NASA-TM-104566-VOL-25-REV-] p 1743 N95-22671
Second International Workshop on Harmonic Oscillators
[NASA-CP-3286] p 1820 N95-22957
Covariant harmonic oscillators and coupled harmonic oscillators p 1825 N95-22992
Environmental, Safety, and Health Considerations: Composite Materials in the Aerospace Industry
[NASA-CP-3289] p 1628 N95-23025
Outgassing considerations for composites in space applications p 1629 N95-23037
NASAwide electronic publishing system: Electronic printing and duplicating, stage-2 evaluation report (GSFC)
[NASA-TM-104615] p 1856 N95-23209
Technical report series on global modeling and data assimilation. Volume 4: Documentation of the Goddard Earth Observing System (GEOS) data assimilation system, version 1
[NASA-TM-104606-VOL-4] p 1740 N95-23529
An expert system for diagnosing anomalies of spacecraft p 1770 N95-23684
Four space application material coatings on the Long-Duration Exposure Facility (LDEF) p 1651 N95-23913
Preliminary analysis of the sensitivity of AIRSAR images to soil moisture variations p 1714 N95-23950
Polarimetric radar data decomposition and interpretation p 1715 N95-23955
Fourth NASA Goddard Conference on Mass Storage Systems and Technologies
[NASA-CP-3295] p 1857 N95-24108
Constraint based scheduling for the Goddard Space Flight Center distributed Active Archive Center's data archive and distribution system p 1859 N95-24121
Architecture and evolution of Goddard Space Flight Center Distributed Active Archive Center p 1862 N95-24134
The growth of the UniTree mass storage system at the NASA Center for Computational Sciences: Some lessons learned p 1862 N95-24135
NSSDC provides network access to key data via NDADS p 1862 N95-24136
Evaluating the effect of online data compression on the disk cache of a mass storage system p 1862 N95-24138

NATIONAL AERONAUTICS AND SPACE ADMINISTRATION. JOHN F. KENNEDY SPACE CENTER, COCOA BEACH, FL.

The effect of sensor spacing on wind measurements at the Shuttle Landing Facility
[NASA-TP-3529] p 1742 N95-23010
Robotic system for the servicing of the orbiter thermal protection system p 1697 N95-23724

NATIONAL AERONAUTICS AND SPACE ADMINISTRATION. LYNDON B. JOHNSON SPACE CENTER, HOUSTON, TX.

Method for forming a glove attachment
[NASA-CASE-MSC-21632-1] p 1750 N95-22766
Pressurized fluid torque driver control and method
[NASA-CASE-MSC-22385-1] p 1694 N95-22892
Mir hardware heritage
[NASA-RP-1357] p 1621 N95-23249
STS-61 mission director's post-mission report
[NASA-TM-104803] p 1617 N95-23262
Newton in space
[NASA-TM-110535] p 1799 N95-23273
Living in space
[NASA-TM-110536] p 1751 N95-23274
Toys in space, 2
[NASA-TM-110541] p 1620 N95-23275
The atmosphere below
[NASA-TM-110538] p 1740 N95-23663
Endeavor: Now and then
[NASA-TM-110539] p 1620 N95-23664
All systems go!
[NASA-TM-110542] p 1620 N95-23665
Toward an automated signature recognition toolkit for mission operations p 1659 N95-23682
Dexterous Orbital Servicing System (DOSS) p 1752 N95-23723
Telepresence control of a dual-arm dexterous robot p 1752 N95-23735
Modeling actions and operations to support mission preparation p 1617 N95-23750
LDEF meteoroid and debris special investigation group investigations and activities at the Johnson Space Center p 1623 N95-23823
Orbital debris and meteoroid population as estimated from LDEF impact data p 1869 N95-23830
Analytical electron microscopy of LDEF impactor residues p 1869 N95-23832
Natural and orbital debris particles on LDEF's trailing and forward-facing surfaces p 1869 N95-23833
Cratering and penetration experiments in Teflon targets at velocities from 1 to 7 km/s p 1700 N95-23842

NATIONAL AERONAUTICS AND SPACE ADMINISTRATION. LANGLEY RESEARCH CENTER, HAMPTON, VA.

HiRel: Hybrid Automated Reliability Predictor (HARP) integrated reliability tool system, (version 7.0). Volume 3: HARP Graphics Oriented (GO) input user's guide
[NASA-TP-3452-VOL-3] p 1753 N95-22479
Method of encouraging attention by correlating video game difficulty with attention level
[NASA-CASE-LAR-15022-1] p 1749 N95-22579
HiRel: Hybrid Automated Reliability Predictor (HARP) integrated reliability tool system, (version 7.0). Volume 1: HARP introduction and user's guide
[NASA-TP-3452-VOL-1] p 1754 N95-22603
HiRel: Hybrid Automated Reliability Predictor (HARP) integrated reliability tool system, (version 7.0). Volume 2: HARP tutorial
[NASA-TP-3452-VOL-2] p 1755 N95-22604
HiRel: Hybrid Automated Reliability Predictor (HARP) integrated reliability tool system, (version 7.0). Volume 4: HARP Output (HARPO) graphics display user's guide
[NASA-TP-3452-VOL-4] p 1755 N95-22605
Wing pressure distributions from subsonic tests of a high-wing transport model
[NASA-TM-4583] p 1607 N95-22802
A ruggedness evaluation of procedures for damage threshold testing optical materials
[NASA-TM-4639] p 1840 N95-22803
Optical fiber strain sensor with improved linearity range
[NASA-CASE-LAR-14857-1-SB] p 1819 N95-22807
Tough, soluble, aromatic, thermoplastic copolyimides
[NASA-CASE-LAR-15205-1] p 1648 N95-22882
Micro-sensor thin-film anemometer
[NASA-CASE-LAR-15112-1-CU] p 1666 N95-22906
Capacitive acoustic wave detector and method of using same
[NASA-CASE-LAR-13890-1] p 1799 N95-22921
Three-dimensional CTOA and constraint effects during stable tearing in a thin-sheet material
[NASA-TM-109183] p 1627 N95-22928
Comparison of exact solution with Eikonal approximation for elastic heavy ion scattering
[NASA-TP-3498] p 1817 N95-22929
Integrated aerodynamic/dynamic/structural optimization of helicopter rotor blades using multilevel decomposition
[NASA-TP-3465] p 1612 N95-22953
Compendium of NASA data base for the Global Tropospheric Experiment's Pacific Exploratory Mission West-A (PEM West-A)
[NASA-TM-109177] p 1733 N95-23009
Dynamic response tests of inertial and optical wind-tunnel model attitude measurement devices
[NASA-TM-109182] p 1616 N95-23011
Summary of OARE flight calibration measurements
[NASA-TM-109159] p 1688 N95-23012
Mach 10 computational study of a three-dimensional scramjet inlet flow field
[NASA-TM-4602] p 1666 N95-23015
Mach 10 computational study of a three-dimensional scramjet inlet flow field
[NASA-TM-4602] p 1667 N95-23210
Polyazomethines containing trifluoromethylbenzene units
[NASA-CASE-LAR-14896-1] p 1649 N95-23253
Process for preparing an assembly of an article and a polyimide which resists dimensional change, delamination and debonding when exposed to changes in temperature
[NASA-CASE-LAR-14538-2] p 1649 N95-23254
Reduced dimer production in solar-simulator-pumped continuous wave iodine lasers based on model simulations and scaling and pumping studies
[NASA-TP-3486] p 1691 N95-23411
New nondestructive techniques for the detection and quantification of corrosion in aircraft structures p 1644 N95-23512
LDEF: 69 Months in Space. Third Post-Retrieval Symposium, part 1
[NASA-CP-3275-PT-1] p 1889 N95-23796
Outgassing products from orbiter TPS materials p 1637 N95-23798
Status of LDEF contributions to current knowledge of meteoroid and manmade debris environments and their effects on spacecraft in LEO p 1623 N95-23822
Small craters on the meteoroid and space debris impact experiment p 1623 N95-23825
Long term microparticle impact fluxes on LDEF determined from optical survey of Interplanetary Dust Experiment (IDE) sensors p 1623 N95-23826
LDEF Interplanetary Dust Experiment (IDE) results p 1869 N95-23828
LDEF: 69 Months in Space. Third Post-Retrieval Symposium, part 2
[NASA-CP-3275-PT-2] p 1899 N95-23896
Summary and review of Materials Special Investigation Group evaluations of hardware from the Long Duration Exposure Facility p 1638 N95-23897
LDEF polymeric materials: A summary of Langley characterization p 1651 N95-23899
Surface characterization of LDEF carbon fiber/polymer matrix composites p 1631 N95-23900
Overview of the LDEF MSIG databasing activities p 1864 N95-23916
Circular electrode geometry metal-semiconductor-metal photodetectors
[NASA-CASE-LAR-15172-1-CU] p 1663 N95-24048

NATIONAL AERONAUTICS AND SPACE ADMINISTRATION. LEWIS RESEARCH CENTER, CLEVELAND, OH.

Method of producing a silicon carbide fiber reinforced strontium aluminosilicate glass-ceramic matrix composite
[NASA-CASE-LEW-15263-2] p 1627 N95-22563
Quick look report of acceleration measurements on Mir Space Station during Mir-16
[NASA-TM-106835] p 1621 N95-22667
Description of a MIL-STD-1553B data bus Ada driver for the LeRC EPS Testbed
[NASA-TM-106866] p 1762 N95-22668
Additional improvements to the NASA Lewis ice accretion code LEWICE
[NASA-TM-106849] p 1665 N95-22669
Ground-based and space-based laser beam power applications
[NASA-TM-106744] p 1691 N95-22670
Weight minimization of structural components for launch in space shuttle
[NASA-TM-4586] p 1698 N95-22805
Utilizing a TDRS satellite for direct broadcast satellite-radio propagation experiments and demonstrations p 1622 N95-22814
Advanced Turbine Technology Applications Project (ATTAP) 1993 annual report
[DE95-003198] p 1693 N95-22880
Calculated coupling efficiency between an elliptical-core optical fiber and a silicon oxynitride rib waveguide
[NASA-TM-106850] p 1820 N95-22915
Stable H(infinity) controller design for the longitudinal dynamics of an aircraft
[NASA-TM-106847] p 1615 N95-22954
Electromagnetic radiation in the plasma environment around the shuttle
[NASA-TM-106891] p 1738 N95-23116
NASA advanced refrigerator/freezer technology development project overview
[NASA-TM-106309] p 1747 N95-23177

Supersonic jet noise reductions predicted with increased jet spreading rate
| NASA-TM-106872 | p 1800 N95-23178
NASA low-speed axial compressor for fundamental research
| NASA-TM-4635 | p 1616 N95-23192
Liquid nitrogen temperature operation of a switching power converter
| NASA-TM-106867 | p 1662 N95-23219
Three-dimensional structure in a supersonic jet: Behavior near centerline
| NASA-TM-106869 | p 1668 N95-23220
NASA 30 cm ion thruster development status
| NASA TM-106842 | p 1624 N95-23221
Functional testing of the space station plasma contactor
| NASA-TM-106841 | p 1624 N95-23240
Experimental technique and assessment for measuring the convective heat transfer coefficient from natural ice accretions
| NASA-TM-106864 | p 1668 N95-23248
Effects of delaminations on the damped dynamic characteristics of composite laminates: Mechanics and experiments
| NASA-TM-106862 | p 1630 N95-23258
Design of a GaAs/Ge solar array for unmanned aerial vehicles
| NASA-TM-106870 | p 1728 N95-23259
Atomic oxygen durability evaluation of protected polymers using thermal energy plasma systems
| NASA-TM-106855 | p 1626 N95-23270
Prediction of incidence and surface roughness effects on turbine performance p 1671 N95-23424
Three-dimensional viscous flow analysis inside a turbine volute p 1674 N95-23437
A time-accurate finite volume method valid at all flow velocities p 1676 N95-23447
Overview of the solar dynamic ground test demonstration program at the NASA Lewis Research Center
| NASA-TM-106876 | p 1625 N95-23450
Instantaneous 2D velocity and temperature measurements in high speed flows based on spectrally resolved molecular Rayleigh scattering
| NASA-TM-106883 | p 1688 N95-23461
A coupled layerwise analysis of the thermopiezoelectric response of smart composite beams beams
| NASA-TM-106889 | p 1630 N95-23463
Institute for Computational Mechanics in Propulsion (ICOMP)
| NASA-TM-106884 | p 1677 N95-23464
Sensitivity of combustion-acoustic instabilities to boundary conditions for premixed gas turbine combustors
| NASA-TM-106890 | p 1614 N95-23550
Combining comparison functions and finite element approximations in CFD
| NASA-TM-106851 | p 1792 N95-23614
Three-dimensional flow analysis inside consortium impeller at design and off-design conditions p 1679 N95-23623
Spray combustion experiments and numerical predictions p 1637 N95-23643
Motor drive technologies for the power-by-wire (PBW) program: Options, trends and tradeoffs
| NASA-TM-106885 | p 1616 N95-23671
Performance characterization of EURECA retroreflectors with fluoropolymer-filled SiO(x) protective coatings p 1651 N95-23802
Atomic oxygen interactions with protected organic materials on the Long Duration Exposure Facility (LDEF) p 1627 N95-23909
Microgravity combustion science: 1995 program update
| NASA-TM-106858 | p 1626 N95-24004
Research and Technology, 1994
| NASA-TM-106764 | p 1607 N95-24025
Thermoelastic theory for the response of materials functionally graded in two directions with applications to the free-edge problem
| NASA-TM-106882 | p 1699 N95-24055
A summary of the slush hydrogen technology program for the National Aero-Space Plane
| NASA-TM-106863 | p 1653 N95-24186
Atomic oxygen textured polymers
| NASA-TM-106769 | p 1650 N95-24187
Subband quantum scattering times for AlGaAs/GaAs obtained using digital filtering
| NASA-TM-106873 | p 1846 N95-24188

NATIONAL AERONAUTICS AND SPACE ADMINISTRATION. MARSHALL SPACE FLIGHT CENTER, HUNTSVILLE, AL.

Vacuum vapor deposition
| NASA-CASE-MFS-28652-1 | p 1647 N95-22558
Advanced liquid oxygen (LO2) propellant conditioning concept testing
| NASA-TM-108477 | p 1652 N95-22672
Statistically generated weighted curve fit of residual functions for modal analysis of structures
| NASA-TM-108481 | p 1699 N95-22950
The corrosion protection of 2219-T87 aluminum by organic and inorganic zinc-rich primers
| NASA-TP-3543 | p 1641 N95-23186
FY 1994 scientific and technical reports, articles, papers, and presentations
| NASA-TM-108480 | p 1856 N95-23225
Eleventh Workshop for Computational Fluid Dynamic Applications in Rocket Propulsion
| NASA-CP-3221-PT-2 | p 1668 N95-23412
A generic efficient adaptive grid scheme for rocket propulsion modeling p 1670 N95-23418
A numerical procedure for analysis of finite rate reacting flows p 1671 N95-23422
Axisymmetric computational fluid dynamics analysis of Saturn V/S1-C/F1 nozzle and plume p 1672 N95-23430
Computational Fluid Dynamic (CFD) analysis of axisymmetric plume and base flow of film/dump cooled rocket nozzle p 1673 N95-23431
Numerical study of the SSME nozzle flow fields during transient operations: A comparison of the animated results with test p 1673 N95-23434
Detailed measurements in the SSME high pressure fuel turbine with smooth rotor blades p 1675 N95-23441
Liquid propellant rocket engine combustion simulation with a time-accurate CFD method p 1676 N95-23445
A controlled variation scheme for convection treatment in pressure-based algorithm p 1677 N95-23448
LDEF materials results for spacecraft applications: Executive summary
| NASA-CP-3261 | p 1617 N95-23549
Permeability testing of composite material and adhesive bonds for the DC-XA composite feedline program
| NASA-TM-108483 | p 1630 N95-23551
Eleventh Workshop for Computational Fluid Dynamic Applications in Rocket Propulsion, part 1
| NASA-CP-3221-PT-1 | p 1678 N95-23615
Finite-difference solutions of the alternate turbopump development high-pressure oxidizer turbopump pump-end ball-bearing cavity flows p 1678 N95-23617
Navier-Stokes flow field analysis of compressible flow in a pressure relief valve p 1679 N95-23618
Computational Fluid Dynamics (CFD) analyses in support of Space Shuttle Main Engine (SSME) heat exchanger (HX) vane cracking investigation p 1679 N95-23619
Unsteady flow simulations in support of the SSME HEX turning vane cracking investigation with the ATD HPOTP p 1679 N95-23621
Optimization of a centrifugal impeller design through CFD analysis p 1680 N95-23624
CFD parametric study of consortium impeller p 1680 N95-23626
Flow and heat transfer in 180-degree turn square ducts: Effects of turning configuration and system rotation p 1682 N95-23636
Advanced multi-phase flow CFD model development for solid rocket motor flowfield analysis p 1683 N95-23638
ASRM multi-port igniter flow field analysis p 1683 N95-23639
CFD analysis of spray combustion and radiation in OMV thrust chamber p 1637 N95-23645
Modeling of non-spherical droplet dynamics p 1685 N95-23647
A fine-grid model for the ASRM aft segment with gimballed nozzle p 1685 N95-23648
Time-accurate unsteady flow simulations supporting the SRM T+68-second pressure spike anomaly investigation (STS-54B) p 1685 N95-23650
Status of axisymmetric CFD of an eleven inch diameter hybrid rocket motor p 1686 N95-23651
Validation of a Computational Fluid Dynamics (CFD) code for supersonic axisymmetric base flow p 1686 N95-23652
Numerical study of base pressure characteristic curve for a four-engine clustered nozzle configuration p 1625 N95-23655
Graphical timeline editing p 1761 N95-23746
A format for the interchange of scheduling models p 1780 N95-23747
LDEF environment modeling updates p 1637 N95-23797
LDEF contributions to cosmic ray and radiation environments research p 1872 N95-23805
Absorbed dose and LET spectra measurements on LDEF p 1815 N95-23810
Status of LDEF activation measurements and archive p 1815 N95-23817
Predictions of LDEF radioactivity and comparison with measurements p 1815 N95-23818
Status of LDEF radiation modeling p 1815 N95-23819
Be-10 in terrestrial bauxite and industrial aluminum: An LDEF fallout p 1646 N95-23820
Measurements of the optical properties of thin films of silver and silver oxide p 1651 N95-23906
Changes in chemical and optical properties of thin film metal mirrors on LDEF p 1651 N95-23907
Further investigations of experiment A0034 atomic oxygen stimulated outgassing p 1651 N95-23908
Trend analysis of in-situ spectral reflectance data from the Thermal Control Surfaces Experiment (TCSE) p 1631 N95-23910
Whisker/Cone growth on the thermal control surfaces experiment no. S0069 p 1651 N95-23911
Durability of reflector materials in the space environment p 1651 N95-23912

NATIONAL AERONAUTICS AND SPACE ADMINISTRATION. PASADENA OFFICE, CA.

Controlling under-actuated robot arms using a high speed dynamics process
| NASA-CASE-NPO-18498-1-CU | p 1692 N95-22543
Non-blocking crossbar permutation engine with constant routing latency
| NASA-CASE-NPO-18864-1-CU | p 1762 N95-22564
Mappings between codewords of two distinct (N,K) Reed-Solomon codes over GF(2(sup J))
| NASA-CASE-NPO-18771-1-CU | p 1754 N95-22577
Virtual reality flight control display with six-degree-of-freedom controller and spherical orientation overlay
| NASA-CASE-NPO-18733-1-CU | p 1613 N95-22578
Programmable hyperspectral image mapper with on-array processing
| NASA-CASE-NPO-17794-1-CU | p 1819 N95-22765
Motion-sensitive optical correlator using a VanderLugt correlator
| NASA-CASE-NPO-18769-1-CU | p 1827 N95-23045

NATIONAL AEROSPACE LAB., AMSTERDAM (NETHERLANDS).

Review of aeronautical fatigue investigation in the Netherlands during the period March 1991-March 1993
| PB95-139184 | p 1612 N95-23161
FAME: A forest assessment and monitoring environment scenario
| PB95-139309 | p 1718 N95-23471
Eddy current detection of pitting corrosion around fastener holes p 1643 N95-23507

NATIONAL AEROSPACE LAB., TOKYO (JAPAN).

Concept verification of three dimensional free motion simulator for space robot p 1618 N95-23702
Truss structure tele-manipulation experiment using ETS-7 p 1623 N95-23726
A fuzzy structural matching scheme for space robotics vision p 1778 N95-23737
Dynamical model and numerical simulations for Engineering Test Satellite-6
| NAL-TR-1239 | p 1622 N95-24049
A computer model in general 3-D curvilinear coordinates for the prediction of the turbulent flow field in a jet induced ram combustor
| NAL-TR-1240T | p 1687 N95-24051
Monte Carlo simulation of rarefied nitrogen gases contained between parallel plates using the statistical inelastic cross-section model
| NAL-TR-1229T | p 1687 N95-24082
Effects of jet strength on NOx formation in premixed impinging jet combustion with minimum heat losses
| NAL-TR-1237T | p 1637 N95-24181

NATIONAL GEOPHYSICAL DATA CENTER, BOULDER, CO.

Solar-geophysical data number 602, October 1994. Part 1: (Prompt reports). Data for September, August 1994, and late data
| PB95-149357 | p 1870 N95-23925
Solar-geophysical data number 602, October 1994. Part 2: (Comprehensive reports). Data for April 1994, and miscellaneous
| PB95-149365 | p 1870 N95-23926

NATIONAL INST. FOR FUSION SCIENCE, NAGOYA (JAPAN).

Modification and damping of Alfven waves in a magnetized dusty plasma
| NIFS-312 | p 1834 N95-23523
Non-Taylor magnetohydrodynamic self-organization
| NIFS-314 | p 1834 N95-23524
Collisionless magnetic reconnection associated with coalescence of flux bundles
| NIFS-315 | p 1834 N95-23525
Macro-EM particle simulation method and a study of collisionless magnetic reconnection
| NIFS-316 | p 1834 N95-23526
Second order focusing property of 210 deg cylindrical energy analyzer
| NIFS-317 | p 1834 N95-23527
Complexity in plasma: A grand view of self-organization
| NIFS-318 | p 1835 N95-23528

Fast potential change in sawteeth in JIPP T-IIU tokamak plasmas
[NIFS-327] p 1835 N95-23533
Physical mechanism determining the radial electric field and its radial structure in a toroidal plasma
[NIFS-313] p 1835 N95-23534
The next Large Helical Devices
[NIFS-323] p 1835 N95-23535
Recent studies of the Large Helical Device
[NIFS-322] p 1835 N95-23543
Current-profile flattening and hot core shift due to the nonlinear development of resistive kink mode
[NIFS-311] p 1835 N95-23564
New pellet production and acceleration technologies for high speed pellet injection system HIPEL in Large Helical Device
[NISF-326] p 1835 N95-23566
The energy broadening resulting from electron stripping process of a low energy Au(-) beam
[NIFS-325] p 1836 N95-23569
Quasisymmetry equations for conventional stellarators
[NIFS-324] p 1836 N95-23572
Theory of pressure-induced islands and self-healing in three-dimensional toroidal magnetohydrodynamic equilibria
[NIFS-321] p 1836 N95-23589
Computer simulation of a magnetohydrodynamic dynamo 2
[NIFS-320] p 1836 N95-23590
MHD-Vlasov simulation of the toroidal Alfven eigenmode
[NIFS-319] p 1836 N95-23591
Effect of satellite helical harmonics on the stellarator configuration
[NIFS-328] p 1609 N95-23787

NATIONAL INST. OF STANDARDS AND TECHNOLOGY, GAITHERSBURG, MD.
A certainty grid to object boundary algorithm
[PB94-203510] p 1755 N95-22637
Optical storage media data integrity studies p 1829 N95-24130

NATIONAL LIBRARY OF MEDICINE, BETHESDA, MD.
Document image archive transfer from DOS to UNIX p 1761 N95-24117

NATIONAL RENEWABLE ENERGY LAB., GOLDEN, CO.
Large-area triple-junction a-Si alloy production scaleup
[DE95-000245] p 1726 N95-22546
Advanced reflector materials for solar concentrators
[DE95-000248] p 1726 N95-22547
Research on defects and transport in amorphous-silicon-based semiconductors
[DE94-011888] p 1660 N95-22586
Diesel fuel component contributions to engine emissions and performance: Clean fuel study
[DE94-011868] p 1732 N95-22834
Polycrystalline CuInSe2 and CdTePV solar cells
[DE95-000244] p 1727 N95-22842
Application requirements for wind turbine gearboxes
[DE94-011883] p 1694 N95-22923
Continuous roll-to-roll amorphous-silicon photovoltaic manufacturing technology
[DE95-000243] p 1728 N95-23061
Advanced development of PV encapsulants
[DE95-000246] p 1728 N95-23062
GPP: A General-Purpose Post Processor for wind turbine data analysis
[DE95-000223] p 1729 N95-23383
Amorphous silicon photovoltaic manufacturing technology, phase 2A
[DE95-000298] p 1729 N95-23478
Review of research results for the photocatalytic oxidation of hazardous wastes in air
[DE95-004004] p 1734 N95-23480
GPP user's guide: A general-purpose postprocessor for wind turbine data analysis
[DE95-000293] p 1730 N95-23776
Automated solar cell assembly teamed process research
[DE95-000299] p 1730 N95-23777
Solar photochemistry: Twenty years of progress, what's been accomplished, and where does it lead?
[DE95-004007] p 1730 N95-23778

NATIONAL SCIENCE FOUNDATION, WASHINGTON, DC.
Investigation of Federal Standard 1045 high-frequency ALE radio performance in the Southern Trans-Auroral Zone
[PB94-204831] p 1655 N95-22636

NATIONAL SPACE DEVELOPMENT AGENCY, TOKYO (JAPAN).
Design and development status of ETS-7, an RVD and space robot experiment satellite p 1623 N95-23700

NATIONAL SPACE DEVELOPMENT AGENCY, TSUKUBA (JAPAN).
A new containerless image furnace with electro-static positioning device p 1690 N95-23674
Space robotic experiment in JEM flight demonstration p 1697 N95-23701
Development of Japanese experiment module remote manipulator system p 1752 N95-23708
Small image laser range finder for planetary rover p 1692 N95-23712
Automatic satellite capture and berthing with robot arm (ASCABRA) p 1623 N95-23713
Automation and crew time saving in the space experiment p 1752 N95-23715
Robotic servicing system for space material experiment p 1697 N95-23722

NATIONAL TRANSPORTATION SAFETY BOARD, WASHINGTON, DC.
Report of proceedings: Aviation Accident Investigation Symposium. Volume 2: Participant presentations
[PB94-917007] p 1610 N95-23598
Aircraft accident report. Runway overrun following rejected takeoff. Continental airlines flight 795, McDonnell Douglas MD-82, N18835, LaGuardia Airport, Flushing, NY, 2 March 1994
[PB95-910401] p 1610 N95-23609
Aviation Accident Investigation Symposium. Volume 1: Industry recommendations and Safety Board responses
[PB94-917005] p 1611 N95-24105

NATIONAL WEATHER SERVICE, FORT WORTH, TX.
SWIFT BOAT 1994: Using a fast chase boat to investigate offshore weather features in conjunction with WSR-88D observations
[PB94-195146] p 1742 N95-22651

NAUCHNO-PROIZVODSTVENNOE OBEDINENIE PRECISION INSTRUMENTS, MOSCOW (RUSSIA).
Geolocation applications of the Gonets LEO messaging satellites p 1656 N95-22818

NAVAL AIR STATION, NORFOLK, VA.
US Navy operating experience with new aircraft construction materials p 1645 N95-23517

NAVAL AIR WARFARE CENTER, WARMINSTER, PA.
Corrosion of landing gear steels p 1642 N95-23500
Corrosion detection and monitoring of aircraft structures: An overview p 1644 N95-23515

NAVAL OCEANOGRAPHY COMMAND CENTER/JOINT TYPHOON WARNING CENTER, FPO SAN FRANCISCO, CA.
Annual tropical cyclone report, 1993
[AD-A285097] p 1742 N95-23255

NAVAL POSTGRADUATE SCHOOL, MONTEREY, CA.
Wavelet time-frequency analysis of phase-shift-key modulated signals
[AD-A285791] p 1655 N95-22505
Effective management of classified documents using the library document system
[AD-A286021] p 1855 N95-23024
A numerical study of interannual wind forcing effects on the California current system, 1980-1983
[AD-A286023] p 1743 N95-23074

NAVAL RESEARCH LAB., WASHINGTON, DC.
Effects of modulation index on telecommunications
[AD-A286018] p 1657 N95-23023
Results from the Heavy Ions In Space (HIIS) experiment on the ionic charge state of solar energetic particles p 1870 N95-23808
Discrimination of poorly exposed lithologies in AVIRIS data p 1703 N95-23858
Statistics of multi-look AIRSAR imagery: A comparison of theory with measurements p 1714 N95-23947
Measurement of ocean wave spectra using polarimetric AIRSAR data p 1715 N95-23953

NEBRASKA UNIV., LINCOLN, NE.
Progress report on conductive paints, September 1, 1994-November 30, 1994
[DE95-004297] p 1649 N95-23356

NEDERLANDS INST. VOOR ONDERZOEK DER ZEE, TEXEL (NETHERLANDS).
Study on possible environmental effects of a WBM cutting discharge in the north sea, one year after termination of drilling
[PB95-133740] p 1733 N95-23125

NEW ENGLAND MEDICAL CENTER HOSPITALS, BOSTON, MA.
Continuation of BNCT Research Program at NEMC and MIT
[DE94-016228] p 1748 N95-22875

NEW HAMPSHIRE UNIV., DURHAM, NH.
Measurements of canopy chemistry with 1992 AVIRIS data at Blackhawk Island and Harvard Forest p 1706 N95-23873

NEW JERSEY INST. OF TECH., NEWARK, NJ.
Design of a variable area diffuser for a 15-inch Mach 6 open-jet tunnel p 1617 N95-23309

NEW MEXICO STATE UNIV., LAS CRUCES, NM.
Improved small satellite access of the space network
[NASA-CR-197863] p 1657 N95-22944

NEW SOUTH WALES UNIV., KENSINGTON (AUSTRALIA).
AIRSAR deployment in Australia, September 1993: Management and objectives p 1714 N95-23948

NEWCASTLE-UPON-TYNE UNIV., NEWCASTLE (ENGLAND).
Algebra of lines and boxes
[PB95-130456] p 1787 N95-22768

NICHOLS RESEARCH CORP., HUNTSVILLE, AL.
Fracture mechanics life analytical methods verification testing
[NASA-CR-196555] p 1697 N95-24106

NIIGATA UNIV. (JAPAN).
Ionic core effects on the Mie resonance in lithium clusters
[DE94-014974] p 1805 N95-22870

NORFOLK STATE UNIV., VA.
Nondestructive evaluation of fatigue damage in aluminum 2024 by x-ray diffraction p 1698 N95-23293
Teacher Enhancement Institute p 1853 N95-23312
Langley Research Center Strategic Plan for Education p 1853 N95-23316

NORTH AMERICAN AVIATION, INC., TULSA, OK.
Structural Arrangement Trade Study. Volume 1: Reusable Hydrogen Composite Tank System (RHCTS) and Graphite Composite Primary Structures (GCPS). Executive summary
[NASA-CR-197685] p 1621 N95-23188
Structural arrangement trade study. Volume 3: Reusable Hydrogen Composite Tank System (RHCTS) and Graphite Composite Primary Structures (GCPS). Addendum
[NASA-CR-197687] p 1621 N95-23189

NORTH CAROLINA AGRICULTURAL AND TECHNICAL STATE UNIV., GREENSBORO, NC.
A microcontroller-based three degree-of-freedom manipulator testbed
[NASA-CR-197423] p 1696 N95-23409

NORTH CAROLINA STATE UNIV., RALEIGH, NC.
Advanced growth and surface analysis system for in situ studies of interface formation
[DE95-002850] p 1838 N95-22555

NORTH CAROLINA UNIV., GREENSBORO, NC.
Computational control of flexible aerospace systems
[NASA-CR-197902] p 1621 N95-23260

NORTHEASTERN UNIV., BOSTON, MA.
Advanced detector development, laboratory simulations, diagnostic development, and data analysis on wake physics
[PL-TR-94-2204] p 1831 N95-22948

NORTHROP GRUMMAN CORP., LOS ANGELES, CA.
Health, safety and environmental requirements for composite materials p 1628 N95-23028
Aerospace Industries Association (AIA) work practices report for composites p 1628 N95-23029
Structural Arrangement Trade Study. Volume 1: Reusable Hydrogen Composite Tank System (RHCTS) and Graphite Composite Primary Structures (GCPS). Executive summary
[NASA-CR-197685] p 1621 N95-23188
Structural arrangement trade study. Volume 3: Reusable Hydrogen Composite Tank System (RHCTS) and Graphite Composite Primary Structures (GCPS). Addendum
[NASA-CR-197687] p 1621 N95-23189

NORTHWESTERN UNIV., EVANSTON, IL.
Investigation of mechanical properties and their relation to the internal structure of nanocrystalline metals and composites
[DE95-001151] p 1627 N95-22683

NYMA, INC., CLEVELAND, OH.
Design and implementation of an experiment scheduling system for the ACTS satellite p 1620 N95-23756

O

OAK RIDGE NATIONAL LAB., TN.
Design and demonstration of an immobilized-cell fluidized-bed reactor for the efficient production of ethanol
[DE94-014023] p 1652 N95-22587
Continuous production of cellulase in a fluidized-bed reactor by Pseudonomas fluorescens immobilized in hydrogel beads
[DE94-014105] p 1744 N95-22588
Investigation of depth-area relationships associated with nanoindentations
[DE95-001353] p 1639 N95-22686
Superlattices in thermoelectric applications
[DE95-001356] p 1840 N95-22687
Transformation behavior in Al2O3-ZrO2 ceraamic composites
[DE95-001359] p 1647 N95-22688
Evolution of oxidation and creep damage mechanisms in HIPed silicon nitride materials
[DE95-001360] p 1647 N95-22689

Direct effects of atmospheric CO2 enrichment on plants and ecosystems: An updated bibliographic data base
|DE95-003060| p 1731 N95-22725
Measurements and modeling of impurity source distributions from the Tore Supra outboard pump limiter
|DE95-003097| p 1831 N95-22800
The torsion space nucleic acids molecular mechanics program DUPLEX: Surveying conformation space by potential energy minimization
|DE94-017707| p 1805 N95-22889
An improved system for exon recognition and gene modeling in human DNA sequences
|DE94-017863| p 1746 N95-22890
A draft standard for message passing in a distributed memory environment
|DE94-019159| p 1657 N95-23075
Calculations of alloy phases with a direct Monte-Carlo method
|DE94-018963| p 1640 N95-23121
Long-term aging of type 308 stainless steel welds: Effects on properties and microstructure
|DE94-018961| p 1640 N95-23132
Dynamics of L to H bifurcation
|DE94-019126| p 1832 N95-23163
MPI implementation of CFD program PHOENICS
|DE95-003896| p 1668 N95-23372
Oak Ridge National Laboratory Energy Efficiency and Renewable Energy Program Bibliography: 1994 Edition
|DE95-002296| p 1730 N95-23605
Cu deposition using a permanent magnet electron cyclotron resonance microwave plasma source
|DE94-017768| p 1650 N95-23981
The effect of magnetic field on the edge plasmons of two-dimensional electron gas systems
|DE94-018044| p 1837 N95-23982

OAK RIDGE Y-12 PLANT, TN.
Mercury detection with thermal neutrons
|DE95-002061| p 1806 N95-23055

OCCUPATIONAL SAFETY AND HEALTH ADMINISTRATION, SALT LAKE CITY, UT.
Skin exposure: Assessing the hazard in the workplace p 1628 N95-23030

OFFICE NATIONAL D'ETUDES ET DE RECHERCHES AEROSPATIALES, TOULOUSE (FRANCE).
Solution and reasoning reuse in space planning and scheduling applications p 1618 N95-23760

OFFICE OF NAVAL RESEARCH, ARLINGTON, VA.
A fiber-optic bundle and collimator assembly
|AD-D016500| p 1820 N95-22864

OFFICE OF TECHNOLOGY ASSESSMENT, WASHINGTON, DC.
Civilian satellite remote sensing: A strategic approach
|PB95-109633| p 1717 N95-22713

OHIO STATE UNIV., COLUMBUS, OH.
Transmethylation reactions during methanogenesis from acetate in Methanosarcina barkeri
|DE94-016222| p 1745 N95-22873
Regulation of photosynthetic carbon fixation on the ocean margins
|DE95-003185| p 1743 N95-22878
Strongly interacting fermion systems
|DE95-003405| p 1806 N95-23054
The electronic structure of heavy element complexes
|DE95-003407| p 1806 N95-23082
High Energy Theory: Task B and Task L
|DE95-003453| p 1817 N95-23148
A uniform geometrical optics and an extended uniform geometrical theory of diffraction for evaluating high frequency EM fields near smooth caustics and composite shadow boundaries
|NASA-CR-197934| p 1657 N95-23391

OHIO UNIV., ATHENS, OH.
Stochastic decision analysis p 1854 N95-23305

OHIO WESLEYAN UNIV., DELAWARE, DE.
Laser irradiation effects: A functional assessment
|AD-A285100| p 1691 N95-22937

OKLAHOMA UNIV., NORMAN, OK.
Finite-element time evolution operator for the anharmonic oscillator p 1823 N95-22983
A new look at the simultaneous analysis and design of structures p 1700 N95-23327

OLD DOMINION COLL., NORFOLK, VA.
A manufacturing database of advanced materials used in spacecraft structures p 1623 N95-23279
Project: Internal communications p 1854 N95-23282
Teams and teamwork at NASA Langley Research Center p 1854 N95-23292
System identification of the Large-Angle Magnetic Suspension Test Fixture (LAMSTF) p 1617 N95-23299
Optimized design of a hypersonic nozzle p 1617 N95-23304
Accelerated panel methods using the fast multipole method p 1687 N95-23307
Inner loop flight control for the High-Speed Civil Transport p 1616 N95-23314
Multidisciplinary design optimization using genetic algorithms p 1619 N95-23332

OLD DOMINION UNIV., NORFOLK, VA.
A CFD study of complex missile and store configurations in relative motion
|NASA-CR-197912| p 1612 N95-22949
Aerodynamic design optimization with sensitivity analysis and computational fluid dynamics
|NASA-CR-197419| p 1608 N95-23218

OPEN UNIV., MILTON KEYNES (ENGLAND).
Real lasers and other deformed objects p 1692 N95-23001

OREGON GRADUATE INST. OF SCIENCE AND TECHNOLOGY, PORTLAND, OR.
The Atmospheric Lifetime Experiment and the Global Atmospheric Gas Experiment (ALE/GAGE)
|NASA-CR-197400| p 1731 N95-22673

OREGON STATE UNIV., CORVALLIS, OR.
Geographic information analysis: An ecological approach for the management of wildlife on the forest landscape
|NASA-CR-197941| p 1719 N95-24094
Comparison of 7.5-minute and 1-degree digital elevation models p 1719 N95-24095
Measuring forest landscape patterns in the Cascade Range of Oregon, USA p 1719 N95-24096
A preliminary comparison of Landsat Thematic Mapper and SPOT-1 HRV multispectral data for estimating coniferous forest volume p 1719 N95-24097
Old-growth and mature forests near spotted owl nests in western Oregon p 1719 N95-24098
Hierarchical analysis of spatial pattern and processes of Douglas-fir forests p 1719 N95-24099
Forest and wildlife habitat analysis using remote sensing and geographic information systems p 1720 N95-24100
Analysis of conifer forest regeneration using Landsat Thematic Mapper data p 1720 N95-24101
Determining successional stage of temperate coniferous forests with Landsat satellite data p 1720 N95-24102
Determining coniferous forest cover and forest fragmentation with NOAA-9 advanced very high resolution radiometer data p 1720 N95-24103

ORGANISATIE VOOR TOEGEPAST NATUURWETENSCHAPPELIJK ONDERZOEK, THE HAGUE (NETHERLANDS).
POINTER: Portable Intelligent Trainer for External Robotics p 1752 N95-23714
Classification and soil moisture determination of agricultural fields p 1716 N95-23958

P

PACIFIC NORTHWEST ENVIRONMENTAL RESEARCH LAB., CORVALLIS, OR.
Dynamics and pattern of a managed coniferous forest landscape in Oregon p 1720 N95-24104

PACIFIC NORTHWEST LAB., RICHLAND, WA.
Technology maturation project on optimization of sheet metal forming of aluminum for use in transportation systems
|DE95-003005| p 1654 N95-22692
P2Info Resource Center: Linking the DOE Pollution Prevention community
|DE95-003133| p 1732 N95-22781
Krypton isotope analysis using near-resonant stimulated Raman spectroscopy
|DE95-005061| p 1635 N95-23348
Alpha spectral analysis via artificial neural networks
|DE95-004567| p 1767 N95-23578
Small angle x ray scattering studies of aggregation in supercritical fluid solutions
|DE95-004576| p 1843 N95-23579
Extraction and detection of pesticide residues from air filter inserts using supercritical carbon dioxide
|DE95-004579| p 1735 N95-23580
Biological interactions and human health effects of static magnetic fields
|DE95-003147| p 1749 N95-24145
Assessing the relative contribution of biogenic and fossil processes to visibility scattering aerosols found in remote areas: Near-term Organic Research Program
|DE95-003149| p 1735 N95-24146

PARIS II UNIV., ORSAY (FRANCE).
Study of photorefractive non-linearities in the 3-5 and 2-4 semi-insulator compounds: The effect of electron irradiation
|PB94-189057| p 1839 N95-22584

PARIS VI UNIV. (FRANCE).
Study of the pressure field in rotating homogeneous turbulent flows
|PB94-189107| p 1665 N95-22585

PAUL D. CAMP COMMUNITY COLL., SUFFOLK, VA.
The software analysis project for the Office of Human Resources p 1854 N95-23331

PEMBROKE STATE UNIV., NC.
Benchmark problems in computational aeroacoustics p 1800 N95-23315

PENNSYLVANIA STATE UNIV., STATE COLLEGE, PA.
Cavitation modeling in Euler and Navier-Stokes codes p 1681 N95-23630

PENNSYLVANIA STATE UNIV., UNIVERSITY PARK, PA.
Origins of interstellar and solar system: Carbonaceous materials
|NASA-CR-197436| p 1867 N95-23013
Damage-mitigating control of a reusable rocket engine for high performance and extended life
|NASA-CR-4640| p 1654 N95-23195
Fundamental phenomena on fuel decomposition and boundary layer combustion processes with applications to hybrid rocket motors
|NASA-CR-197919| p 1625 N95-23261
Formative and summative evaluation efforts for the Teacher Enhancement Institute conducted at the NASA Langley Research Center, summer 1994 p 1853 N95-23286
Direct numerical simulations and modeling of a spatially-evolving turbulent wake p 1687 N95-23289
Numerical simulation of steady and unsteady viscous flow in turbomachinery using pressure based algorithm p 1671 N95-23426
Numerical computation of aerodynamics and heat transfer in a turbine cascade and a turn-around duct using advanced turbulence models p 1675 N95-23444
Convergence acceleration of implicit schemes in the presence of high aspect ratio grid cells p 1676 N95-23446
Flowfield characterization in a LOX/GH2 propellant rocket p 1684 N95-23642

POD ASSOCIATES, INC., ALBUQUERQUE, NM.
Dimensional scaling for impact cratering and perforation p 1624 N95-23843

PRATT AND WHITNEY AIRCRAFT, WEST PALM BEACH, FL.
Aerodynamic design and analysis of a highly loaded turbine exhaust p 1673 N95-23435
Phase 2: HGM air flow tests in support of HEX vane investigation p 1674 N95-23438
Three-D flow analysis of the alternate SSME HPOT TAD p 1679 N95-23620
An inducer CFD solution and effects associated with cavitation p 1681 N95-23631
On the accuracy of CFD-based pressure drop predictions for right-angle ducts p 1682 N95-23634
Methodology for CFD design analysis of National Launch System nozzle manifold p 1683 N95-23637

PRAXAIR, INC., TONAWANDA, NY.
Oxygen enriched combustion system performance study. Phase 2: 100 percent oxygen enriched combustion in regenerative glass melters
|DE95-004212| p 1635 N95-23481

PRIMELINK TECHNOLOGIES, INC., EDMONTON (ALBERTA).
Petabyte mass memory system using the Newell Opticel(TM) p 1753 N95-24119

PRINCETON UNIV., NJ.
An investigation of helicopter dynamic coupling using an analytical model
|NASA-CR-197420| p 1612 N95-23217

PURDUE UNIV., WEST LAFAYETTE, IN.
Classification of high dimensional multispectral image data p 1705 N95-23868

Q

QUANTUM CORP., SHREWBURY, MA.
Digital Linear Tape (DLT) technology and product family overview p 1753 N95-24125

QUEENSLAND UNIV., BRISBANE (AUSTRALIA).
The effect of simulated low earth orbit radiation on polyimides (UV degradation study) p 1651 N95-23903
The surface properties of fluorinated polyimides exposed to VUV and atomic oxygen p 1651 N95-23904

R

RADIAN CORP., RESEARCH TRIANGLE PARK, NC.
Preliminary assessment of air toxic emissions in the natural gas industry, phase 1
|PB95-135547| p 1732 N95-22865

RECOM TECHNOLOGIES, INC., MOFFETT FIELD, CA.
AMPHION: Specification-based programming for scientific subroutine libraries p 1761 N95-23680
The associate principal astronomer telescope operations model p 1779 N95-23743
A data analysis assistant p 1761 N95-23748

Telescope loading: A problem reduction approach
p 1781 N95-23757

RENSSELAER POLYTECHNIC INST., TROY, NY.
Theoretical aspects of electroweak and other interactions in medium energy nuclear physics
| DE95-004341 | p 1808 N95-23357

RESEARCH INST. FOR ADVANCED COMPUTER SCIENCE, MOFFETT FIELD, CA.
On adaptive weighted polynomial preconditioning for Hermitian positive definite matrices
| NASA-CR-197946 | p 1791 N95-23547
Fourth order difference methods for hyperbolic IBVP's
| NASA-CR-197955 | p 1791 N95-23548
Block LU factorization
| NASA-CR-197949 | p 1791 N95-23592
Quasi-kernel polynomials and convergence results for quasi-minimal residual iterations
| NASA-CR-197948 | p 1791 N95-23593
Towards the Teraflop CFD
| NASA-CR-197947 | p 1764 N95-23594
Unstructured grids on SIMD torus machines
| NASA-CR-197954 | p 1758 N95-23610
Recent advances in Lanczos-based iterative methods for nonsymmetric linear systems
| NASA-CR-197950 | p 1791 N95-23611
An implementation of the QMR method based on coupled two-term recurrences
| NASA-CR-197956 | p 1791 N95-23612
Using high-performance networks to enable computational aerosciences applications
| NASA-CR-197951 | p 1764 N95-24023

RESEARCH TRIANGLE INST., RESEARCH TRIANGLE PARK, NC.
NASA Technology Applications Team: Commercial applications of aerospace technology
| NASA-CR-197589 | p 1864 N95-22526
NASA Technology Applications Team: Commercial applications of aerospace technology
| NASA-CR-197870 | p 1865 N95-23091

RHODE ISLAND UNIV., KINGSTON, RI.
The 1993 Gordon Research Conference on Chronobiology
| NASA-CR-197990 | p 1748 N95-24047

RIJKSINSTITUUT VOOR DE VOLKSGEZONDHEID, BILTHOVEN (NETHERLANDS).
Outline for a global environmental strategic planning exercise (GESPE-project)
| PB95-133773 | p 1733 N95-23067
CO2 and waste policy: Monitoring results 1991/1992 and main problems
| PB95-133799 | p 1733 N95-23126

ROCHESTER UNIV., NY.
Scientific and technical photography at NASA Langley Research Center p 1690 N95-23290
Electronic photography at NASA Langley Research Center p 1690 N95-23298
Combinatorial semantics
| TR-563 | p 1792 N95-23793
Reevaluation of the significance of sequence information for speech recognition
| TR-555 | p 1658 N95-23794
Microstructural behavior of nonequilibrium systems
| DE95-004450 | p 1630 N95-23924
Ploxoma: Testbed for uncertain inference
| TR-537 | p 1794 N95-23927
Algorithms for categorizing multiprocessor communication under invalidate and update-based coherence protocols
| TR-533-REV | p 1759 N95-23928
Effective category and measure in abstract complexity theory
| TR-529 | p 1792 N95-23929
Scalability of atomic primitives on distributed shared memory multiprocessors
| TR-528 | p 1764 N95-23930
Optimal advice
| TR-527 | p 1792 N95-23931
On helping by parity-like languages
| TR-553 | p 1759 N95-23935
Loop scheduling for heterogeneity
| TR-540 | p 1764 N95-23936
Spoken dialogue understanding and local context
| TR-523 | p 1658 N95-23937
Real-world shepherding: Combining vision, manipulation, and planning in real time
| TR-530 | p 1783 N95-24001
Reducibility classes of P-selective sets
| TR-524 | p 1792 N95-24002
Witness-isomorphic reductions and the local search problem
| TR-522 | p 1793 N95-24003
Large sets in AC(exp 0): A Kolmogorov complexity related property and some applications
| TR-556 | p 1797 N95-24029
Knowledge representation and reasoning for mixed-initiative planning
| TR-562 | p 1783 N95-24031
An efficient algorithm for concurrent priority queue heaps
| TR-560 | p 1759 N95-24033
On the size of sets with weak membership properties
| TR-557 | p 1793 N95-24034
Morphing hands and virtual tools (or What good is an extra degree of freedom?)
| TR-551 | p 1783 N95-24036
Eliminating useless messages in write-update protocols on scalable multiprocessors
| TR-539 | p 1764 N95-24037
Robot skill learning through intelligent experimentation
| TR-567 | p 1784 N95-24038
Phonetic set hashing: A novel scheme for transforming phone sequences to words
| TR-538 | p 1658 N95-24039
Unsupervised classification learning from cross-modal environmental structure
| TR-536 | p 1784 N95-24040
Tutorial on filtering, restoration, and state estimation
| TR-534 | p 1793 N95-24042
Using simulation-based projection to plan in an uncertain and temporally complex world
| TR-531 | p 1853 N95-24043
Properties of probabilistic pushdown automata
| TR-554 | p 1760 N95-24056
A computational theory of grounding in natural language conversation
| TR-545 | p 1760 N95-24058
Logspace reducibility and self-reducibility: Models and equivalences
| TR-544 | p 1760 N95-24059
Teaching computational complexity: Resources to treasure
| TR-543 | p 1784 N95-24060
Unifying data and control transformations for distributed shared-memory machines
| TR-542 | p 1765 N95-24061
Martin-Lof tests can help too
| TR-541 | p 1797 N95-24063
Semi-membership algorithms: Some recent advances
| TR-526 | p 1760 N95-24092
Using simple page placement policies to reduce the cost of cache fills in coherent shared-memory systems
| TR-535 | p 1753 N95-24177
Polynomial-time membership comparable sets
| TR-552 | p 1793 N95-24182
Scheduler-conscious synchronization
| TR-550 | p 1765 N95-24183
Lazy release consistency for hardware-coherent multiprocessors
| TR-547 | p 1765 N95-24184
Vision-based planning and execution of precision grasps
| TR-546 | p 1784 N95-24185
The TRAINS project: A case study in building a conversational planning agent
| TR-532 | p 1659 N95-24193
The satanic notations: Counting classes beyond #P and other definitional adventures
| TR-561 | p 1793 N95-24194

ROCKWELL INTERNATIONAL CORP., CANOGA PARK, CA.
Criteria for evaluation of grid generation systems
p 1669 N95-23416
NLS base heating CFD analysis p 1673 N95-23432
CFD analysis of turbopump volutes
p 1674 N95-23436
Non-intrusive measurements in a rocket engine combustor p 1625 N95-23439
Impeller flow field characterization with a laser two-focus velocimeter p 1675 N95-23440
Advanced turbulence models for turbomachinery
p 1675 N95-23443
Three-D CFD analysis of hydrostatic bearings
p 1678 N95-23616
Adaptation of the advanced spray combustion code to cavitating flow problems p 1681 N95-23629
CFD modeling of turbulent duct flows for coolant channel analysis p 1682 N95-23635
Progress in advanced spray combustion code integration p 1637 N95-23644
Code validation study for base flows
p 1686 N95-23653
Vaccum Gas Tungsten Arc Welding, phase 1
| NASA-CR-197979 | p 1696 N95-24064

ROCKWELL INTERNATIONAL CORP., DOWNEY, CA.
Low Earth orbit thermal control coatings exposure flight tests: A comparison of U.S. and Russian results
| NASA-CR-4647 | p 1626 N95-22919
Structural Arrangement Trade Study. Volume 1: Reusable Hydrogen Composite Tank System (RHCTS) and Graphite Composite Primary Structures (GCPS). Executive summary
| NASA-CR-197685 | p 1621 N95-23188
Structural arrangement trade study. Volume 3: Reusable Hydrogen Composite Tank System (RHCTS) and Graphite Composite Primary Structures (GCPS). Addendum
| NASA-CR-197687 | p 1621 N95-23189
Hardware interface unit for control of shuttle RMS vibrations p 1697 N95-23706

ROCKWELL INTERNATIONAL CORP., HUNTSVILLE, AL.
Four-nozzle benchmark wind tunnel model USA code solutions for simulation of multiple rocket base flow recirculation at 145,000 feet altitude
p 1686 N95-23654

RUN LENGTH LTD., BURGHFIELD (ENGLAND).
A comparison of rotary- and stationary-head tape recorders p 1690 N95-24122

RUTGERS - THE STATE UNIV., PISCATAWAY, NJ.
A toolbox and record for scientific models
p 1775 N95-23716

RUTHERFORD APPLETON LAB., CHILTON (ENGLAND).
Bose condensation, macroscopic quantum phenomena and atomic spatial correlations in superfluid He-4
| PB95-139085 | p 1850 N95-23154
Study of frustrated systems via dissipative maps
| PB95-139093 | p 1799 N95-23155
Flavour dependence of form factors in heavy meson decays
| PB95-139101 | p 1807 N95-23156
Classification of (2,2) compactifications by free fermions 2
| PB95-139119 | p 1807 N95-23157
Singlet quarks beyond the top at the tevatron
| PB95-139127 | p 1807 N95-23158
Neutron compton scattering
| PB95-139135 | p 1807 N95-23159
Higgs searches and WW scattering
| PB95-139143 | p 1807 N95-23160
Nonlinear thermoviscoelastic behaviour in complex materials
| PB95-140653 | p 1630 N95-23537

RUTHERFORD APPLETON LAB., OXFORD (ENGLAND).
Partitioning methods for unstructured finite element meshes
| PB95-130555 | p 1785 N95-22544
PRISMA GENIE data analysis manual
| PB95-130464 | p 1755 N95-22769
Dynamical properties of critical and paramagnetic spin fluctuations in anisotropic heisenberg magnets
| PB95-134623 | p 1798 N95-23127

S

SAGE JUNIOR COLL. OF ALBANY, ALBANY, NY.
Computer modeling of the sensitivity of a laser water vapor sensor to variations in temperature and air speed
p 1692 N95-23330

SAINT CLOUD STATE COLL., MN.
Differential GPS and system integration of the Low Visibility Landing and Surface Operations (LVLASO) demonstration p 1611 N95-23318

SAINT LOUIS UNIV., CAHOKIA, IL.
An algorithm for the basis of the finite Fourier transform p 1760 N95-22985
Preliminary identification of buffet problems in high speed civil transport p 1616 N95-23319

SAINT PETERSBURG STATE UNIV., SAINT PETERSBURG (RUSSIA).
Harmonic oscillators and resonance series generated by a periodic unstable classical orbit
p 1825 N95-22999

SAN FRANCISCO UNIV., CA.
Preliminary results of radiation measurements on EURECA p 1872 N95-23801
Measurement of trapped proton fluences in main stack of P0006 experiment p 1815 N95-23812
Charge, energy and LET spectra of high LET primary and secondary particles in CR-39 plastic nuclear track detectors of the P0006 experiment
p 1815 N95-23814

SANDIA LABS., ALBUQUERQUE, NM.
COYOTE 2: A Finite Element Computer Program for nonlinear heat conduction problems
| DE95-002848 | p 1666 N95-22914

SANDIA NATIONAL LABS., ALBUQUERQUE, NM.
High-velocity penetrators
| DE95-001886 | p 1698 N95-22500
Evaluating photovoltaic applications: A guide for utilities
| DE95-003807 | p 1726 N95-22502
Layered Electrical Product Application Protocol (AP)
| DE95-001524 | p 1754 N95-22548

High gain GaAs Photoconductive Semiconductor Switches for impulse sources
|DE95-001885| p 1659 N95-22549
Twelve month performance evaluation for the rotating shadowband radiometer
|DE95-002847| p 1726 N95-22554
Analysis of physiochemical processes during solder aging
|DE95-003811| p 1638 N95-22576
World's first 15%-efficient multicrystalline silicon modules
|DE95-002604| p 1727 N95-22650
Projectile penetration into representative targets
|DE95-003089| p 1698 N95-22726
Nonlinear generalized functions and nonconservative shock simulations
|DE95-003307| p 1795 N95-22734
Pulsed Ion Beam Surface Treatment for preparing rapidly solidified corrosion resistant alloy surfaces
|DE94-012072| p 1640 N95-22835
Decomposition mechanisms in thermally-aged thin-film explosives
|DE95-000741| p 1652 N95-22838
High gain GaAs photoconductive semiconductor switches: Measurement of filament velocity and reduced trigger energy
|DE95-001884| p 1661 N95-22844
Sensor-based control of rocket thrust chamber feature location for automated braze paste dispensing
|DE94-016559| p 1624 N95-22885
Modeling NO(x) emissions in turbulent jet flames: Effects of buoyancy and radiation
|DE94-016621| p 1633 N95-22886
Planar magnetic component development
|DE95-003311| p 1661 N95-22896
The spectral content of the torque loads on a turbine gear tooth
|DE95-002188| p 1694 N95-23056
Robotic all-terrain lunar exploration rover (RATLER) FY93 program status report
|DE95-003589| p 1694 N95-23065
Simultaneous inference in multivariate calibration
|DE95-003592| p 1794 N95-23066
The probabilistic structure of sprays: Implications for measurements by in site particle counters
|DE95-002483| p 1666 N95-23081
Influence of porosity and two-phase flow on diffusional/thermal instability of a deflagrating energetic material
|DE95-002592| p 1634 N95-23122
Segregated rigid and structural control for a photolithography positioning system
|DE95-002603| p 1766 N95-23134
Surface structural dependence of cesium adsorption on the (alpha)-Al2O3(0001) surface
|DE95-002610| p 1842 N95-23135
Application Protocol, Initial Graphics Exchange Specification (IGES), Layered Electrical Product
|DE95-004266| p 1757 N95-23337
Rapid thermal processing of high-efficiency silicon solar cells with controlled in-situ annealing
|DE95-004729| p 1730 N95-23489
Moving mass trim control for aerospace vehicles
|DE95-002602| p 1622 N95-23532
High-performance GaAs/AlGaAs optical modulators: Their performance and packaging for microwave photonic integrated circuits
|DE95-004533| p 1828 N95-23575
Mass transport through polycrystalline microstructures
|DE95-004552| p 1811 N95-23576
High surface area, high permeability carbon monoliths
|DE95-004555| p 1650 N95-23577
Impact shock and penetration fragmentation in porous media
|DE94-018900| p 1868 N95-23656
10x reduction imaging at 13.4 nm
|DE94-016612| p 1828 N95-23767
Micro heat spreader enhanced heat transfer in MCM's
|DE95-004520| p 1663 N95-23779
Chemical recognition software
|DE95-003346| p 1636 N95-24007
Axial focusing of energy from a hypervelocity impact on earth
|DE95-003347| p 1740 N95-24008
Axial focusing of impact energy in the earth's interior: A possible link to flood basalts and hotspots
|DE95-003357| p 1741 N95-24009
A modal test design strategy for model correlation
|DE95-003631| p 1759 N95-24020
Silicon surface and bulk defect passivation by low temperature PECVD oxides and nitrides
|DE95-004531| p 1731 N95-24090
Solderability preservation through the use of organic inhibitors
|DE95-003633| p 1664 N95-24149
Reflectance control for multicrystalline-silicon photovoltaic modules using textured-dielectric coatings
|DE95-004532| p 1731 N95-24155
Extraction of the surface recombination velocity of passivated phosphorus-doped silicon emitters
|DE95-004539| p 1845 N95-24156
Crystalline-silicon photovoltaics: Necessary and sufficient
|DE95-004540| p 1731 N95-24157
Particle transport in plasma reactors
|DE95-004541| p 1837 N95-24158
Microporous polyimide films for reduced dielectric applications
|DE95-004543| p 1650 N95-24159
Progress in ion beam power coupling and ion-driven hohlraums on PBFA 2
|DE95-004544| p 1818 N95-24160
Transient radiation-induced absorption in materials for the DOI laser
|DE95-004549| p 1828 N95-24161

SANDIA NATIONAL LABS., LIVERMORE, CA.
Computer modeling of detonators
|DE95-003031| p 1652 N95-22721
Chemical vapor deposition in low pressure batch furnaces
|DE95-003035| p 1632 N95-22722
EUV metrology of multilayer optics
|DE95-003036| p 1819 N95-22723
Temperature effects on hydrogen-induced cracking in an iron-based superalloy
|DE95-003037| p 1639 N95-22724
Dynamic response of a transducer mounted at one end of an acoustical cavity which is subjected to a specified pressure at the open end of the cavity
|DE95-004192| p 1799 N95-23379

SCIENCE APPLICATIONS, INC., HUNTSVILLE, AL.
Cost and schedule analytical techniques development
|NASA-CR-196548| p 1853 N95-22891

SCIENCE APPLICATIONS INTERNATIONAL CORP., PROSPECT, TN.
Predictions of LET spectra measured on LDEF
p 1815 N95-23815

SCIENTIFIC RESEARCH ASSOCIATES, INC., GLASTONBURY, CT.
Navier-Stokes analysis of an oxidizer turbine blade with tip clearance with and without a mini-shroud
p 1672 N95-23428
A generalized Eulerian-Lagrangian analysis, with application to liquid flows with vapor bubbles
p 1682 N95-23633
An interactive tool for discrete phase analysis in two-phase flows p 1683 N95-23641

SECA, INC., HUNTSVILLE, AL.
Heat transfer in rocket engine combustion chambers and nozzles p 1668 N95-23413
Radiation/convection coupling in rocket motors and plumes p 1669 N95-23414

SIEMENS A.G., VIENNA (AUSTRIA).
Utilizing inheritance in requirements engineering
p 1768 N95-23677
Operator procedure verification with a rapidly reconfigurable simulator p 1618 N95-23679

SMITHSONIAN INSTITUTION, CAMBRIDGE, MA.
Measurement of HO2 and other trace gases in the stratosphere using a high resolution far-infrared spectrometer
|NASA-CR-197368| p 1735 N95-22482

SONY CORP., TAGAJYO (JAPAN).
A kinetic study of hydrolysis of polyester elastomer in magnetic tape p 1652 N95-24124

SOUTH DAKOTA STATE UNIV., BROOKINGS, SD.
Study of atmospheric parameters measurements using MM-wave radar in synergy with LITE-2
p 1741 N95-23278

SOUTHWEST RESEARCH INST., SAN ANTONIO, TX.
Diesel fuel component contributions to engine emissions and performance: Clean fuel study
|DE94-011868| p 1732 N95-22834
IUE observing programs: NSOSS, VEOEB, and PCOEB
|NASA-CR-197424| p 1866 N95-23560

SPACE TELESCOPE SCIENCE INST., BALTIMORE, MD.
Planning and scheduling the Hubble Space Telescope: Practical application of advanced techniques
p 1779 N95-23740

SPREHE INFORMATION MANAGEMENT ASSOCIATES, INC., WASHINGTON, DC.
A study of policy issues affecting the Defense Technical Information Center
|AD-A286629| p 1854 N95-22494

SRI INTERNATIONAL CORP., MENLO PARK, CA.
Novel mass spectrometric instrument for gaseous and particulate characterization and monitoring
|DE95-001135| p 1687 N95-22682
Modeling of the coupled magnetospheric and neutral wind dynamos
|NASA-CR-197861| p 1738 N95-23090
Integrating planning and reactive control
p 1618 N95-23763

STANFORD LINEAR ACCELERATOR CENTER, CA.
Experimental results on polarized structure functions in deep inelastic lepton-nucleon scattering
|DE95-002782| p 1801 N95-22521
Commensurate scale relations: Precise tests of quantum chromodynamics without scale or scheme ambiguity
|DE95-002785| p 1847 N95-22566
Multipole contribution from an off-axis orbit in an IR quadrupole and the consequences on the dynamic aperture
|DE95-002874| p 1816 N95-22567
The first measurement of the left-right cross section asymmetry in Z(sup 0) boson production
|DE95-003335| p 1802 N95-22697
QCD test in three-jet Z(sup 0) decays at SLD and detector development for H(sup 0) yields gamma gamma searches in high energy hadron colliders
|DE95-003336| p 1848 N95-22698
Measurement of the left-right asymmetry in Z boson production by electron-positron collisions
|DE95-003337| p 1802 N95-22699
A model for ball lightning
|DE95-003366| p 1742 N95-22701
Precision standard model tests with polarized e(+)e(-) beams
|DE95-003367| p 1816 N95-22702
The charm physics potential of a Tau-Charm Factory
|DE95-003369| p 1802 N95-22703
Electron beam acceleration and compression for short wavelength FELs
|DE95-003371| p 1691 N95-22704
Protein folding and protein metallocluster studies using synchrotron small angler x ray scattering
|DE95-003339| p 1746 N95-22897
Heavy quark physics at SLD: Preliminary results
|DE95-003372| p 1806 N95-23138
Final result on the mass of the tau lepton from the BES collaboration
|DE95-003466| p 1806 N95-23139
Measurement of the left-right charge asymmetry in hadronic Z decays and A(sub e) determination
|DE95-003467| p 1806 N95-23140
Measuring the left-right cross section asymmetry in Z boson production by e(+)e(-) collisions at the SLC
|DE95-003468| p 1807 N95-23141
Electroweak coupling measurements from polarized Bhabha scattering at SLD
|DE95-003137| p 1807 N95-23165
A preliminary measurement of the average B hadron lifetime
|DE95-003138| p 1808 N95-23226
The impact of QCD and light-cone quantum mechanics on nuclear physics
|DE95-004293| p 1851 N95-23352

STANFORD UNIV., CA.
Ligand K-edge x-ray adsorption spectroscopic studies of the electronic structure of inorganic model complexes and metalloprotein active sites
|DE95-003338| p 1840 N95-22851
Gamma ray emission from radio pulsars
|NASA-CR-197917| p 1871 N95-22910
Dimethylsulfide oxidation over the tropical South Atlantic: OH and other oxidants
|NASA-CR-197417| p 1732 N95-22930
Cellular interactions in the suprachiasmatic nucleus
|AD-A285639| p 1749 N95-23780
Investigation of infra-red and nonequilibrium air radiation
|NASA-CR-197977| p 1741 N95-24041

STATE AGRICULTURAL UNIV., WAGENINGEN (NETHERLANDS).
Revitalization of the Gemenc-area, Baja, Hungary. 1: A study on hydrological possibilities to revitalise the ecosystem in the Keselyues-area. 2: Towards the restoration of the Gyueruesalj floodplain
|PB95-139283| p 1718 N95-23469
Basic data sets description and preliminary results of EFEDA-Spain
|PB95-139291| p 1740 N95-23470

STATE UNIV. OF NEW YORK, BINGHAMTON, NY.
q-bosons and the q-analogue quantized field
p 1814 N95-22984

STATE UNIV. OF NEW YORK, BUFFALO, NY.
High power Josephson effect sources
|AD-A285808| p 1838 N95-22511

STATE UNIV. OF NEW YORK, OLD WESTBURY, NY.
Atmospheric peroxides
|DE95-004435| p 1733 N95-23362

STOTTLER HENKE ASSOCIATES, INC., BELMONT, CA.
Artificial intelligence techniques for scheduling Space Shuttle missions p 1781 N95-23755

SURFACE/INTERFACE, INC., MOUNTAIN VIEW, CA.
Charge distribution analysis of catalysts under simulated reaction conditions
|DE95-003526| p 1633 N95-23064
SURREY UNIV., GUILDFORD (ENGLAND).
The Duffin-Kemmer-Petiau oscillator
p 1825 N95-22998
SVERDRUP TECHNOLOGY, INC., BROOK PARK, OH.
Three-dimensional Navier-Stokes analysis and redesign of an imbedded bellmouth nozzle in a turbine cascade inlet section p 1671 N95-23423
An RL10A-3-3A rocket engine model using the rocket engine transient simulator (ROCETS) software
|NASA-CR-190786| p 1625 N95-23790
Predicted performance of an integrated modular engine system
|NASA-CR-190787| p 1625 N95-23791
SYMBIOTICS, INC., CAMBRIDGE, MA.
Coordinating complex decision support activities across distributed applications p 1761 N95-23749

T

T AND M ENGINEERING, GLENDORA, CA.
Effect of the space environment on materials flown on the EURECA/TICCE-HVI experiment
p 1623 N95-23803
TECHNICAL UNIV. OF BRNO (CZECHOSLOVAKIA).
Renewable Energy Sources Brno 1993
|DE94-633975| p 1727 N95-22855
TECHNICAL UNIV. OF LISBON (PORTUGAL).
7th International Symposium on Applications of Laser Techniques to Fluid Mechanics, volume 1
|AD-A285647| p 1691 N95-23118
TECHNION - ISRAEL INST. OF TECH., HAIFA (ISRAEL).
Review of some results of the author's fatigue investigations with applications in engineering and material science
|TAE-698| p 1699 N95-23662
The development of shell imperfection measurement techniques
|TAE-712| p 1699 N95-23923
TECHNISCHE HOCHSCHULE, DARMSTADT (GERMANY).
SIMS chemical and isotopic analysis of impact features from LDEF experiments AO187-1 and AO187-2
p 1637 N95-23837
TECHNISCHE HOGESCHOOL, EINDHOVEN (NETHERLANDS).
Graph isomorphism models for non interleaving process algebra
|PB95-110490| p 1786 N95-22714
TECHNISCHE UNIV., DELFT (NETHERLANDS).
Time-periodic solutions of some forced nonlinear wave equations: Analysis, approximations and applications
|PB95-135083| p 1788 N95-22932
TECHNISCHE UNIV., EINDHOVEN (NETHERLANDS).
Browsing semantics in the tower model
|PB95-127221| p 1855 N95-22534
Treewidth and pathwidth of cocomparability graphs of bounded dimension
|PB95-127239| p 1785 N95-22535
Precise clock synchronization protocol
|PB95-127247| p 1687 N95-22536
Hierarchical membership protocol for synchronous distributed systems
|PB95-138947| p 1763 N95-23129
Canonical typing and pi-conversion
|PB95-139218| p 1788 N95-23130
Taxonomy of finite automata minimization algorithms
|PB95-139226| p 1756 N95-23131
BEm-BDF scheme for curvature driven moving stokes flows
|PB95-138905| p 1667 N95-23144
BEM solution to simulate the curvature driven deformation of a profile that is pressed into a plate of hot glass
|PB95-138913| p 1648 N95-23145
Automatic verification of regular protocols in P/T nets
|PB95-138921| p 1789 N95-23146
AR-descriptions in translatable Frechet spaces
|PB95-138855| p 1789 N95-23149
Performance of single-keyword and multiple-keyword pattern matching algorithms
|PB95-138954| p 1756 N95-23150
Algebraic semantics of basic message sequence charts
|PB95-138970| p 1657 N95-23151
Temporal operators viewed as predicate transformers
|PB95-138996| p 1757 N95-23152
Verifying sequentially consistent memory using interface refinement
|PB95-139002| p 1752 N95-23153
Optimally scaled systems for second order scalar singularity perturbed problems
|PB95-138814| p 1789 N95-23169
Plasmo-magnetoelastic waves in a semiconducting heterostructure. 1: Plasmo-elastic longitudinal modes. 2: Sh-magnetoelastic modes
|PB95-138822| p 1833 N95-23170
Translation invariant Frechet subspaces of distributions
|PB95-138830| p 1789 N95-23171
Quasistatic model for the motion of a viscous capillary liquid drop
|PB95-138848| p 1667 N95-23172
Stability and efficiency of waveform relaxation methods
|PB95-138863| p 1789 N95-23173
Degenerate Hamiltonian Hopf bifurcations
|PB95-138871| p 1789 N95-23174
Numerical simulation of axisymmetric viscous sintering
|PB95-138889| p 1667 N95-23175
New robust multigrid method for 2D convection-diffusion problems
|PB95-138897| p 1789 N95-23176
Taxonomy of finite automata construction algorithms
|PB95-139234| p 1758 N95-23606
TECHNISCHE UNIV., MUNICH (GERMANY).
Determining orbital particle parameters of impacts into germanium using morphology analysis and calibration data from hypervelocity impact experiments in the laboratory
p 1700 N95-23841
Soil moisture retrieval in the Oberpfaffenhofen testsite using MAC Europe AIRSAR data p 1716 N95-23960
TECHNISCHE UNIV., TWENTE (NETHERLANDS).
Overview of Ph.D. theses and memoranda, 1993
|PB95-135190| p 1756 N95-23071
Plinius intermediate report
|PB95-135216| p 1648 N95-23128
Adaptive control of linear systems based on approximate models
|PB95-139333| p 1767 N95-23199
Stoermer-Cowell: Straight, summed and split. An overview
|PB95-139341| p 1789 N95-23200
Note on the computational complexity of j-radii of polytopes in (R sup n)
|PB95-139358| p 1790 N95-23231
Characterization of non-negative greedy matrices
|PB95-139366| p 1757 N95-23232
PUZZLES 4: Sperner collections and the keys puzzle
|PB95-139374| p 1790 N95-23233
Partition of real symmetric matrices according to the multiplicities of their eigenvalues
|PB95-139846| p 1790 N95-23235
Trees are graceful if and only if trees with a perfect matching are strongly graceful
|PB95-139853| p 1790 N95-23236
Orders of predictor-corrector pairs for second-order ODE's
|PB95-140612| p 1790 N95-23237
Some recent results in the analysis of greedy algorithms for assignment problems
|PB95-140620| p 1757 N95-23238
Marginalistic value for monotonic set games
|PB95-140646| p 1794 N95-23239
Set games
|PB95-140786| p 1794 N95-23539
Light-traffic analysis for queues with spatially distributed arrivals
|PB95-140802| p 1767 N95-23556
Normalized coprime factorizations and balancing for unstable nonlinear systems
|PB95-141222| p 1767 N95-23557
Dynamic disturbance decoupling of nonlinear systems and linearization
|PB95-141248| p 1767 N95-23558
Consistency and Monte Carlo simulation of a data driven version of smooth goodness-of-fit tests
|PB95-141255| p 1794 N95-23559
Submodular linear programs on forests
|PB95-139820| p 1758 N95-23608
TECHNOLOGY INTEGRATION AND DEVELOPMENT GROUP, INC., BEDFORD, MA.
Gearbox vibration diagnostic analyzer
|NASA-CR-189141| p 1696 N95-23792
TELEOS RESEARCH, PALO ALTO, CA.
Real-time tracking using stereo and motion: Visual perception for space robotics p 1778 N95-23739
TELESPAZIO S.P.A., ROME (ITALY).
MAC Europe 1991 campaign: AIRSAR/AVIRIS data integration for agricultural test site classification
p 1715 N95-23952
TELLURIDE SUMMER RESEARCH CENTER, TELLURIDE, CO.
Open problems of computational molecular biology
|DE95-000895| p 1745 N95-22866
TENNESSEE UNIV., TULLAHOMA, TN.
A wall interference assessment/correction system
|NASA-CR-197421| p 1667 N95-23183
Supersonic laminar flow control research
|NASA-CR-197938| p 1609 N95-23669
TENNESSEE UNIV. SPACE INST., TULLAHOMA, TN.
Handling qualities of the High Speed Civil Transport
p 1616 N95-23325
TEXAS A&M UNIV., COLLEGE STATION, TX.
Control of flow separation in airfoil/wing design applications p 1609 N95-23294
Long range targeting for space based rendezvous
|NASA-CR-197890| p 1757 N95-23388
Nonlinear viscoelastic characterization of polymer materials using a dynamic-mechanical methodology
p 1651 N95-23902
TEXAS UNIV., AUSTIN, TX.
Analytical and numerical studies of ion mobility near the tokamak plasma edge
|DE95-003019| p 1830 N95-22693
Comparisons of nonlinear toroidal turbulence simulations with experiment
|DE95-003020| p 1830 N95-22694
Energy flux and hydrogeology of thermal anomalies in the Gulf of Mexico Basin - South Texas example
|DE95-003341| p 1743 N95-22695
Runaway electrons in TEXT-U
|DE94-019218| p 1831 N95-22862
Neural net prediction of tokamak plasma disruptions
|DE95-002616| p 1832 N95-23136
Ninth topical conference on atomic processes in plasmas
|DE95-002810| p 1833 N95-23246
The railplug: Development of a new ignitor for internal combustion engines
|DE95-004375| p 1695 N95-23342
A wavenumber-partitioning scheme for two-dimensional statistical closures
|DE95-004514| p 1677 N95-23483
On inertial range scaling laws
|DE95-004515| p 1677 N95-23484
TEXAS UNIV. AT DALLAS, RICHARDSON, TX.
Investigation of the role of gravity waves in the generation of equatorial bubbles
|NASA-CR-197962| p 1739 N95-23272
THOMAS NELSON COMMUNITY COLL., HAMPTON, VA.
Reliability analysis in the Office of Safety, Environmental, and Mission Assurance (OSEMA) p 1698 N95-23302
TILBURG UNIV. (NETHERLANDS).
Capacitated facility location: Valid inequalities and facets (revised)
|PB95-130225| p 1786 N95-22641
Regular graphs with four eigenvalues
|PB95-135141| p 1788 N95-23068
Second derivative of the likelihood of an exact ARMA model
|PB95-135158| p 1788 N95-23069
Asymptotic justification for a modified GLS procedure to estimate ARMA parameters
|PB95-135166| p 1788 N95-23070
Note on the tau-value and tau-related solution concepts
|PB95-140752| p 1795 N95-23555
TOKYO INST. OF TECH. (JAPAN).
A perspective on space robotics in Japan
p 1697 N95-23695
Development of the dynamic motion simulator of 3D micro-gravity with a combined passive/active suspension system p 1618 N95-23711
TOKYO UNIV. (JAPAN).
Search for scalar and vector leptoquarks in electron-proton collisions at radical S = 300 GeV
|DE94-785267| p 1810 N95-23475
Subsumption-based architecture for autonomous movement planning for planetary rovers
p 1771 N95-23690
Applications of dynamic scheduling technique to space related problems: Some case studies
p 1618 N95-23759
Large-sized and highly radioactive H-3 and Cd-109 Langmuir-Blodgett films
|DE94-785270| p 1811 N95-23775
TOKYO UNIV., SAGAMIHARA (JAPAN).
Rate coefficients for the electron-impact excitation, ionization and recombination of He-like ions, S XV, Ca XIX and Fe XXV, and related processes
|ISAS-R-657| p 1811 N95-23604
Path planning for planetary rover using extended elevation map p 1771 N95-23689
Control technique for planetary rover
p 1771 N95-23692
A scheduling and diagnostic system for scientific satellite GEOTAIL using expert system p 1781 N95-23753
TOKYO UNIV., TANASHI (JAPAN).
Interdigital-H linac for unstable nuclei at INS
|DE94-765448| p 1816 N95-22644

A heavy ion linac complex for unstable nuclei
| DE94-765443 | p 1816 N95-22848

TOLEDO UNIV., OH.
Enhanced analysis and users manual for radial-inflow turbine conceptual design code RTD
| NASA-CR-195454 | p 1609 N95-23462
User's guide for ECAP2D: An Euler unsteady aerodynamic and aeroelastic analysis program for two dimensional oscillating cascades, version 1.0
| NASA-CR-189146 | p 1699 N95-24189

TORONTO UNIV., NORTH YORK (ONTARIO).
Space environmental effects on polymer matrix composites as a function of sample location on LDEF
p 1651 N95-23901

TOSHIBA CORP., KAWASAKI (JAPAN).
Robot arm system for automatic satellite capture and berthing p 1752 N95-23709

TOULOUSE UNIV. (FRANCE).
Proceedings of NATO Advanced Research Workshop on the Formation, Transport and Consequences of Particles in Plasmas
| AD-A285850 | p 1829 N95-22514

TRW SYSTEMS GROUP, REDONDO BEACH, CA.
MHD seed recovery and regeneration, phase 2
| DE95-004308 | p 1833 N95-23338

TULANE UNIV., NEW ORLEANS, LA.
Galactic oscillator symmetry p 1822 N95-22973

TUSKEGEE INST., AL.
Direct numerical simulation of sheared turbulent flow
p 1687 N95-23296

U

ULTRAMET CO., PACOIMA, CA.
High energy collimating fine grids
| NASA-CR-197688 | p 1871 N95-24191

UNION CARBIDE INDUSTRIAL GASES, INC., TONAWANDA, NY.
Airborne rotary air separator study
| NASA-CR-189099 | p 1614 N95-24053

UNITED TECHNOLOGIES CORP., EAST HARTFORD, CT.
Development of sensors for ceramic components in advanced propulsion systems
| NASA-CR-195324 | p 1689 N95-23795

UNIVERSIDAD AUTONOMA DEL ESTADO DE MORELOS, CUERNAVACA (MEXICO).
Molecular vibrational states during a collision
p 1814 N95-22964

UNIVERSIDAD DE GUADALAJARA, GUADALAJARA, JALISCO (MEXICO).
Slightly anharmonic systems in quantum optics
p 1826 N95-23004

UNIVERSIDAD NACIONAL AUTONOMA DE MEXICO, CUERNAVACA (MEXICO).
Shapes and stability of algebraic nuclear models
p 1814 N95-22974
A Ramanujan-type measure for the Askey-Wilson polynomials p 1797 N95-22975
Neurodynamic oscillators p 1749 N95-22987
Lyapunov exponents from CHUA's circuit time series using artificial neural networks p 1784 N95-22988
Pseudoclassical description of the Dirac Oscillator
p 1825 N95-22996
Supersymmetric oscillator in optics
p 1826 N95-23002
Kravchuk functions for the finite oscillator approximation p 1798 N95-23006
Phase space analysis in anisotropic optical systems
p 1826 N95-23007

UNIVERSIDAD NACIONAL AUTONOMA DE MEXICO, MEXICO CITY (MEXICO).
Algebraic approach to the vibrational excitations in methane p 1814 N95-22960
Algebraic description of atom-molecule interactions
p 1814 N95-22961
Quantum field between moving mirrors: A three dimensional example p 1821 N95-22965
Harmonic oscillator representation in the theory of scattering and nuclear reactions p 1814 N95-22967
Boson mapping techniques applied to constant gauge fields in QCD p 1814 N95-22969
The relativistic many body problem with an oscillator interaction p 1824 N95-22991

UNIVERSIDADE ESTADUAL DE PAULISTA, SAO PAULO (BRAZIL).
A supersymmetric family of harmonic oscillators simulating H-bonds in DNA p 1748 N95-22963

UNIVERSITIES SPACE RESEARCH ASSOCIATION, HUNTSVILLE, AL.
Microgravity sciences application visiting scientist program
| NASA-CR-197854 | p 1653 N95-23204

UNIVERSITY COLL. OF SWANSEA (WALES).
AVIRIS spectra correlated with the chlorophyll concentration of a forest canopy p 1705 N95-23871
The effect of signal noise on the remote sensing of Foliar biochemical concentration p 1708 N95-23884
Estimation of biophysical properties of upland Sitka spruce (Picea sitchensis) plantations
p 1713 N95-23943

UNIVERSITY OF SOUTH FLORIDA, SAINT PETERSBURG, FL.
AVIRIS calibration using the cloud-shadow method
p 1702 N95-23849

UNIVERSITY OF SOUTHERN CALIFORNIA, MARINA DEL REY, CA.
Towards method-independent knowledge acquisition
| AD-A285823 | p 1766 N95-22512
DIstributed VIRtual System (DIVIRS) project
| NASA-CR-197855 | p 1757 N95-23180

UNIVERSITY OF SOUTHERN ILLINOIS, CARBONDALE, IL.
Regulation of alcohol fermentation in Escherichia coli
| DE94-016227 | p 1745 N95-22874

UNIVERSITY OF SOUTHERN MISSISSIPPI, BAY SAINT LOUIS, MS.
Development of a multi-sensor in situ fiber optic fluorometer
| DE95-003105 | p 1819 N95-22780

UTAH UNIV., SALT LAKE CITY, UT.
Thermochemistry of transition metal clusters
| DE95-003144 | p 1646 N95-24144

V

VANDERBILT UNIV., NASHVILLE, TN.
Learning time series for intelligent monitoring
p 1770 N95-23686

VIGYAN RESEARCH ASSOCIATES, INC., HAMPTON, VA.
Performance of the 0.3-meter transonic cryogenic tunnel with air, nitrogen, and sulfur hexafluoride media under closed loop automatic control
| NASA-CR-195052 | p 1668 N95-23257

VIRGINIA POLYTECHNIC INST., BLACKSBURG, VA.
Development and verification of a resin film infusion/resin transfer molding simulation model for fabrication of advanced textile composites
| NASA-CR-197439 | p 1648 N95-23179

VIRGINIA POLYTECHNIC INST. AND STATE UNIV., BLACKSBURG, VA.
Analyses, algorithms, and computations for models of high-temperature superconductivity
| DE95-003290 | p 1661 N95-22733
Associated with aerospace vehicles development of methodologies for the estimation of thermal properties
p 1700 N95-23321
Supersonic flow and shock formation in turbine tip gaps p 1672 N95-23429
Use of blade lean in turbomachinery redesign
p 1680 N95-23625

VIRGINIA UNIV., CHARLOTTESVILLE, VA.
The detection and analysis of galvanic damage in BMI/graphite fiber composites p 1631 N95-23502
Studies of autoionizing states relevant to dielectronic recombination
| DE94-014162 | p 1812 N95-23978
Charging of interplanetary grains
| NASA-CR-198032 | p 1869 N95-24066

VIRGINIA UNIV. HOSPITAL, CHARLOTTESVILLE, VA.
Algorithms for parallel and vector computations
| NASA-CR-197394 | p 1756 N95-23017
Teacher Enhancement Institute p 1853 N95-23324

VRIJE UNIV., AMSTERDAM (NETHERLANDS).
Roles and dynamic subclasses: A modal logic approach
| PB95-127320 | p 1754 N95-22522
Jackson system development, entity-relationship analysis and data flow models: A comparative study
| PB95-127338 | p 1855 N95-22523
Temporal model theory for default logic
| PB95-127346 | p 1766 N95-22524
Method for building and evaluating formal specifications of object-oriented conceptual models of database systems
| PB95-127353 | p 1855 N95-22525
Nonparametric measure of spatial interaction in point patterns
| PB95-127965 | p 1793 N95-22527
Is omega* - (mu) absolutely countably compact?
| PB95-127981 | p 1785 N95-22528
Comparing data synchronization in Ada 9X and Orca
| PB95-127999 | p 1754 N95-22529
Countable space with a closed subspace without continuous extender
| PB95-127973 | p 1785 N95-22533
LCM 3.0: A language for describing conceptual models. Syntax definition
| PB95-128005 | p 1755 N95-22652
Relating multifunctions and predicate transformers through closure operators
| PB95-135646 | p 1757 N95-23467

W

WAGENINGEN AGRICULTURAL UNIV. (NETHERLANDS).
Effects of wind on rainfall simulation. Spatial distribution of water application, kinetic energy, and overland flow under single full-cone nozzle sprays
| PB95-127304 | p 1717 N95-22537
Combining optical and microwave remote sensing data of forest vegetation: MAC Europe 1991
| PB95-127312 | p 1717 N95-22538
Flow measuring structures
| PB95-127254 | p 1665 N95-22638
HAPEX-Sahel: Basic description of methods and data sets
| PB95-127262 | p 1701 N95-22639
Accuracy of radar rainfall estimates compared to raingauge measurements and a hydrological application
| PB95-127296 | p 1741 N95-22640

WASHINGTON STATE UNIV., PULLMAN, WA.
Plant metabolism and cell wall formation in space (microgravity) and on Earth
| NASA-CR-197618 | p 1745 N95-22801

WASHINGTON UNIV., SEATTLE, WA.
How to measure the Q(bar Q) potential in a light-front calculation
| DE95-003200 | p 1848 N95-22728
Neutrino overview
| DE95-003201 | p 1802 N95-22729
Outlook from the intersections
| DE95-003202 | p 1802 N95-22730
A model of mesons based on chi SB in the light-front frame
| DE95-003203 | p 1802 N95-22731
The convergence radius of the chiral expansion in the Dyson-Schwinger approach
| DE94-012852 | p 1805 N95-22925
Mapping and monitoring changes in vegetation communities of Jasper Ridge, CA, using spectral fractions derived from AVIRIS images p 1708 N95-23883

WAYNE STATE UNIV., DETROIT, MI.
Active control of panel vibrations induced by a boundary layer flow
| NASA-CR-197867 | p 1608 N95-23182

WESTINGHOUSE HANFORD CO., RICHLAND, WA.
Glass science tutorial: Lecture 1, Chemistry and properties of oxide glasses
| DE95-002963 | p 1647 N95-22647
Glass science tutorial: Lecture 2, operating electric glass melters
| DE95-002965 | p 1647 N95-22648
CDMS-CAD data set management system test plan
| DE95-003219 | p 1755 N95-22718
An investigation into the effects of hydrogen on the fracture and deformation of Alloy X-750
| DE95-003206 | p 1639 N95-22732
Radioisotope thermoelectric generator licensed hardware package and certification tests
| DE95-003039 | p 1661 N95-22799
Geophysical investigations in the 100 Areas: Fiscal year 1991 through December 1993
| DE95-001573 | p 1736 N95-22843
CDMS: CAD data set system design description
| DE95-003218 | p 1756 N95-22894
Search Hanford accessible reports electronically system requirements specification
| DE95-004367 | p 1856 N95-23340
Search Hanford accessible reports electronically system design description, revision 1
| DE95-004369 | p 1856 N95-23341
Test procedure for cation exchange chromatography
| DE95-003770 | p 1808 N95-23350
Radioisotope thermoelectric generator transportation system subsystem 143 software development plan
| DE95-003774 | p 1662 N95-23351
Computer software design description for the Treated Effluent Disposal Facility (TEDF), Project L-045H, Operator Training Station (OTS)
| DE95-003065 | p 1759 N95-24006
Search Hanford accessible reports electronically system configuration management plan
| DE95-004493 | p 1857 N95-24089

WESTINGHOUSE SAVANNAH RIVER CO., AIKEN, SC.
Characterization of Type 304L stainless steel solid-state closure welds for radioactive waste containment
| DE94-016539 | p 1645 N95-23980

WESTON OBSERVATORY, MA.
Tomographic analysis of the three-dimensional variation of the seismic velocity structure of the shallow crust underlying Southern New England
| AD-A279406 | p 1739 N95-23247
WICHITA STATE UNIV., WICHITA, KS.
Assessment of resin transfer molding process for the XM6 discharger, ERDEC SSP 93-64
| NIAR-94-2 | p 1650 N95-23932
The airline quality report, 1994
| NIAR-94-11 | p 1610 N95-24012
Design of a cervical spine gross motion simulator for standard size human and anthropomorphic dummy adult and child
| NIAR-94-16 | p 1751 N95-24021
A multibody/finite element analysis approach for modeling of crash dynamic responses
| NIAR-94-3 | p 1610 N95-24050
WISCONSIN UNIV., MADISON, WI.
Analysis of structural domains required for phytochrome function by in vitro mutagenesis
| DE94-016230 | p 1745 N95-22884
Turbulent transport across invariant canonical flux surfaces
| DE95-000710 | p 1832 N95-23072
Energy transfer dynamics in isolated and in colliding highly vibrationally excited molecules
| AD-A285771 | p 1806 N95-23077
TFTR Ion Cyclotron Range of Frequencies (ICRF) experimental data analysis collaboration
| DE95-003409 | p 1832 N95-23084
Organometallic chemistry of bimetallic compounds
| DE95-004436 | p 1634 N95-23345
Verification and validation of decision support software: Expert Choice(trademark) and PCM(trademark)
| DE95-004469 | p 1757 N95-23346
Generation of fast electrons in reversed field pinches by the equilibrium grad (vert bar)B(vert bar) force
| DE95-004467 | p 1809 N95-23363
WOODS HOLE OCEANOGRAPHIC INST., MA.
Assimilation of altimeter data in a quasi-geostrophic model of the Gulf Stream system: A dynamical perspective
| NASA-CR-196313 | p 1744 N95-23766
WYOMING UNIV., LARAMIE, WY.
Exotic atoms
| DE95-003199 | p 1805 N95-22881

Y

YALE UNIV., NEW HAVEN, CT.
Algebraic theory of molecules p 1814 N95-22958

Typical Contract Number Index Listing

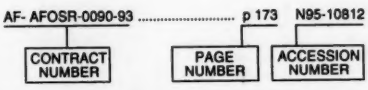

Listings in this index are arranged alphanumerically by contract number. Under each contract number the accession numbers denoting documents that have been produced as a result of research done under that contract are arranged in ascending order. The page number helps to locate the citation in the abstract section. The accession number denotes the number by which the citation is identified.

AF PROJ. 2310 ..... p 1737 N95-22951
AF PROJ. 2822 ..... p 1831 N95-22948
AF-AFOSR-0288-91 ..... p 1784 N95-24038
AF-AFOSR-0376-91 ..... p 1609 N95-23201
ARPA ORDER 8607 ..... p 1618 N95-23679
ARPA ORDER 8930 ..... p 1759 N95-23928
p 1764 N95-23930
p 1759 N95-24033
p 1764 N95-24037
p 1753 N95-24177
p 1765 N95-24183
p 1765 N95-24184
CEC-EV5V-CT92-0182 ..... p 1741 N95-22640
CONACYT-400340-5-3401E ..... p 1814 N95-22960
p 1814 N95-22961
DA PROJ. 1L1-6241-A-47-AB ..... p 1612 N95-22953
DA PROJ. 1L1-62618-AH-80 ..... p 1611 N95-22510
DAAB10-87-C-0053 ..... p 1761 N95-23749
DAAH04-96-G-0800 ..... p 1771 N95-23691
DAAL03-89-C-0038 ..... p 1754 N95-22570
p 1771 N95-23691
DAAL03-91-C-0047 ..... p 1791 N95-23592
DABT63-91-C-0025 ..... p 1766 N95-22512
DAJA45-83-C-0011 ..... p 1643 N95-23509
DAJA45-83-C-0041 ..... p 1643 N95-23509
DAMD17-92-C-2096 ..... p 1691 N95-22937
DARA-OS-9001 ..... p 1872 N95-23806
DARA-50-QV-9194-0 ..... p 1700 N95-23841
DE-ACO3-76SF-00098 ..... p 1815 N95-23816
DE-AC02-76CH-00016 ..... p 1801 N95-22583
p 1801 N95-22656
p 1660 N95-22716
p 1802 N95-22727
p 1840 N95-22762
p 1803 N95-22763
p 1633 N95-22876
p 1820 N95-22877
p 1633 N95-22887
p 1816 N95-22926
p 1728 N95-23133
p 1851 N95-23335
p 1817 N95-23353
p 1842 N95-23354
p 1809 N95-23396
p 1827 N95-23531
p 1828 N95-24005
DE-AC02-76CH-03000 ..... p 1801 N95-22646
p 1816 N95-22684
p 1801 N95-22685
p 1805 N95-22939
p 1807 N95-23196
p 1808 N95-23197
p 1808 N95-23203
p 1808 N95-23242
p 1808 N95-23336
p 1808 N95-23347
p 1809 N95-23359
p 1817 N95-23369
p 1871 N95-23370
p 1809 N95-23404
p 1663 N95-23405
p 1809 N95-23406
p 1689 N95-23520
p 1689 N95-23521
p 1810 N95-23522
p 1810 N95-23530
p 1811 N95-23581
p 1813 N95-24000
p 1813 N95-24016
p 1818 N95-24077
p 1664 N95-24081
p 1818 N95-24084
DE-AC02-76CH-03073 ..... p 1830 N95-22694
p 1661 N95-23080
DE-AC02-76ER-03069 ..... p 1806 N95-23139
p 1807 N95-23165
p 1808 N95-23226
DE-AC02-80CS-83004 ..... p 1727 N95-22888
DE-AC02-92CE-50343 ..... p 1727 N95-22861
p 1729 N95-23482
DE-AC03-76SF-00098 ..... p 1725 N95-22501
p 1816 N95-22567
p 1745 N95-22590
p 1633 N95-22869
p 1756 N95-23079
p 1808 N95-23226
p 1635 N95-23380
p 1817 N95-23485
p 1763 N95-23486
p 1692 N95-23487
p 1810 N95-23488
p 1817 N95-23493
p 1663 N95-23494
p 1636 N95-23495
p 1844 N95-24010
p 1844 N95-24011
p 1844 N95-24013
p 1818 N95-24014
p 1858 N95-24111
p 1861 N95-24131
p 1626 N95-24142
DE-AC03-76SF-00515 ..... p 1801 N95-22521
p 1847 N95-22566
p 1816 N95-22567
p 1802 N95-22697
p 1848 N95-22698
p 1802 N95-22699
p 1742 N95-22701
p 1816 N95-22702
p 1802 N95-22703
p 1691 N95-22704
p 1840 N95-22851
p 1746 N95-22897
p 1806 N95-23138
p 1806 N95-23139
p 1806 N95-23140
p 1807 N95-23141
p 1851 N95-23352
DE-AC03-89ER-51114 ..... p 1693 N95-22796
p 1693 N95-22798
p 1832 N95-23119
p 1834 N95-23371
p 1836 N95-23768
p 1837 N95-24083
p 1837 N95-24086
p 1837 N95-24087
DE-AC03-89ER-52153 ..... p 1829 N95-22645
DE-AC04-76DP-00613 ..... p 1695 N95-23343
p 1695 N95-23373
p 1695 N95-23374
p 1800 N95-23375
DE-AC04-76DP-00789 ..... p 1666 N95-23081
p 1832 N95-23119
DE-AC04-76ER-00881 ..... p 1807 N95-23158
DE-AC04-94AL-85000 ..... p 1698 N95-22500
p 1726 N95-22502
p 1754 N95-22548
p 1659 N95-22549
p 1726 N95-22554
p 1638 N95-22576
p 1727 N95-22650
p 1652 N95-22721
p 1632 N95-22722
p 1819 N95-22723
p 1639 N95-22724
p 1698 N95-22726
p 1795 N95-22734
p 1640 N95-22835
p 1652 N95-22838
p 1661 N95-22844
p 1624 N95-22885
p 1633 N95-22886
p 1661 N95-22896
p 1666 N95-22914
p 1694 N95-23056
p 1694 N95-23065
p 1794 N95-23066
p 1634 N95-23122
p 1766 N95-23134
p 1842 N95-23135
p 1757 N95-23337
p 1799 N95-23379
p 1730 N95-23489
p 1622 N95-23532
p 1828 N95-23575
p 1811 N95-23576
p 1650 N95-23577
p 1868 N95-23656
p 1828 N95-23767
p 1663 N95-23779
p 1636 N95-24007
p 1740 N95-24008
p 1741 N95-24009
p 1759 N95-24020
p 1837 N95-24086
p 1731 N95-24090
p 1664 N95-24149
p 1731 N95-24155
p 1845 N95-24156
p 1731 N95-24157
p 1837 N95-24158
p 1650 N95-24159
p 1818 N95-24160
p 1828 N95-24161
DE-AC05-84OR-21400 ..... p 1652 N95-22587
p 1744 N95-22588
p 1639 N95-22686
p 1840 N95-22687
p 1647 N95-22688
p 1647 N95-22689
p 1731 N95-22725
p 1693 N95-22796
p 1831 N95-22800
p 1805 N95-22889
p 1746 N95-22890
p 1657 N95-23075
p 1832 N95-23119
p 1640 N95-23121
p 1640 N95-23132
p 1799 N95-23155
p 1832 N95-23163
p 1668 N95-23372
p 1730 N95-23605
p 1650 N95-23981
p 1837 N95-23982
p 1837 N95-24083
p 1837 N95-24086
p 1837 N95-24087
p 1846 N95-24169
DE-AC05-84OS-21400 ..... p 1806 N95-23055
DE-AC06-76RL-01830 ..... p 1654 N95-22692
p 1732 N95-22781
p 1635 N95-23348
p 1767 N95-23578
p 1843 N95-23579
p 1735 N95-23580
p 1749 N95-24145
p 1735 N95-24146
DE-AC06-87RL-10930 ..... p 1647 N95-22647
p 1647 N95-22648
p 1755 N95-22718
p 1661 N95-22799
p 1736 N95-22843
p 1756 N95-22894
p 1856 N95-23340
p 1856 N95-23341
p 1757 N95-23346

DE-AC07-76ID-01570 p 1808 N95-23350
p 1662 N95-23351
p 1809 N95-23407
p 1759 N95-24006
p 1857 N95-24089
p 1793 N95-22550
p 1740 N95-23386
DE-AC08-93NV-11265 p 1717 N95-22503
p 1721 N95-24148
DE-AC09-89SR-18035 p 1645 N95-23980
DE-AC11-93PN-38195 p 1639 N95-22732
p 1640 N95-22893
DE-AC21-92MC-29116 p 1687 N95-22682
DE-AC22-87PC-79672 p 1833 N95-23338
DE-AC22-92PC-92106 p 1633 N95-23064
DE-AC22-92PC-92111 p 1634 N95-23164
DE-AC34-90DP-62349 p 1734 N95-23384
DE-AC35-89ER-40486 p 1806 N95-23139
DE-AC36-83CH-10093 p 1726 N95-22546
p 1726 N95-22547
p 1660 N95-22586
p 1732 N95-22834
p 1727 N95-22842
p 1694 N95-22923
p 1723 N95-23061
p 1728 N95-23062
p 1729 N95-23383
p 1729 N95-23478
p 1734 N95-23480
p 1730 N95-23776
p 1730 N95-23777
p 1730 N95-23778
DE-AI05-93OR-22089 p 1737 N95-22924
DE-AI08-92NV-10874 p 1742 N95-23385
DE-AS03-76ER-70285 p 1816 N95-22567
DE-FC02-91CH-10407 p 1727 N95-22888
DE-FC04-82AL-20729 p 1726 N95-22518
DE-FC07-88ID-12833 p 1635 N95-23481
DE-FG01-92CE-15974 p 1649 N95-23356
DE-FG02-76SF-00098 p 1807 N95-23165
DE-FG02-84ER-45150 p 1845 N95-24143
DE-FG02-84ER-45166 p 1646 N95-24140
DE-FG02-85ER-13406 p 1634 N95-23345
DE-FG02-85ER-25001 p 1791 N95-23600
DE-FG02-85ER-45184 p 1638 N95-22532
DE-FG02-85ER-45201 p 1630 N95-23924
DE-FG02-85ER-53198 p 1809 N95-23363
DE-FG02-86ER-13529 p 1806 N95-23082
DE-FG02-86ER-13612 p 1631 N95-22517
DE-FG02-86ER-13631 p 1729 N95-23361
DE-FG02-86ER-40224 p 1807 N95-23165
DE-FG02-86ER-45229 p 1627 N95-22683
DE-FG02-86ER-45281 p 1798 N95-23083
DE-FG02-86ER-53218 p 1832 N95-23072
p 1836 N95-23589
DE-FG02-86ER-53222 p 1836 N95-23589
DE-FG02-87ER-40333 p 1805 N95-22881
DE-FG02-87ER-60600 p 1748 N95-22875
DE-FG02-88ER-13941 p 1745 N95-22874
DE-FG02-88ER-13968 p 1745 N95-22884
DE-FG02-88ER-40448 p 1808 N95-23357
DE-FG02-88ER-45347 p 1806 N95-23054
DE-FG02-89ER-51124 p 1832 N95-23147
DE-FG02-90ER-40542 p 1803 N95-22749
DE-FG02-90ER-45427 p 1839 N95-22572
DE-FG02-90ER-60931 p 1805 N95-22889
DE-FG02-91ER-14193 p 1646 N95-24144
DE-FG02-91ER-20042 p 1745 N95-22873
DE-FG02-91ER-40608 p 1814 N95-22958
DE-FG02-91ER-40617 p 1807 N95-23165
DE-FG02-91ER-40661 p 1807 N95-23165
DE-FG02-91ER-40672 p 1807 N95-23165
p 1808 N95-23226
DE-FG02-91ER-40676 p 1806 N95-23139
p 1807 N95-23165
p 1808 N95-23226
DE-FG02-91ER-40677 p 1808 N95-23226
DE-FG02-91ER-40690 p 1817 N95-23148
DE-FG02-91ER-54109 p 1836 N95-23768
DE-FG02-91ER-61206 p 1733 N95-23362
DE-FG02-91ER-61218 p 1736 N95-22879
DE-FG02-92ER-25139 p 1790 N95-23465
DE-FG02-92ER-40715 p 1807 N95-23165
p 1808 N95-23226
DE-FG02-92ER-61443 p 1819 N95-22780
DE-FG02-93ER-40762 p 1847 N95-22566
DE-FG02-93ER-54196 p 1832 N95-23084
DE-FG02-93ER-54221 p 1832 N95-23120
DE-FG02-93ER-61700 p 1743 N95-22878
DE-FG02-94ER-14412 p 1830 N95-22793
p 1632 N95-22795
DE-FG03-86ER-53225 p 1837 N95-24086
DE-FG03-88ER-53275 p 1832 N95-23163
DE-FG03-89ER-51121 p 1832 N95-23119
DE-FG03-91ER-40618 p 1807 N95-23165
p 1808 N95-23226
DE-FG03-91ER-40679 p 1806 N95-23139
DE-FG03-92ER-25140 p 1665 N95-22491
DE-FG03-92ER-40689 p 1808 N95-23226
DE-FG03-92ER-40701 p 1806 N95-23139
p 1807 N95-23165
p 1808 N95-23226
DE-FG03-92ER-54150 p 1830 N95-22719
DE-FG03-93ER-40788 p 1808 N95-23226
DE-FG03-93ER-54200 p 1833 N95-23246
DE-FG03-93ER-61638 p 1745 N95-22866
DE-FG03-93ER-61728 p 1735 N95-24147
DE-FG03-94ER-54241 p 1831 N95-22862
DE-FG05-80ET-53088 p 1830 N95-22693
p 1830 N95-22694
p 1832 N95-23136
p 1677 N95-23483
p 1677 N95-23484
DE-FG05-84ER-13266 p 1802 N95-22700
DE-FG05-85ER-13394 p 1812 N95-23978
DE-FG05-86ER-13465 p 1631 N95-22575
DE-FG05-87ER-60503 p 1803 N95-22747
p 1691 N95-22748
DE-FG05-89ER-45392 p 1640 N95-23121
DE-FG05-91ER-12115 p 1695 N95-23342
DE-FG05-92ER-14278 p 1743 N95-22695
DE-FG05-92ER-40736 p 1806 N95-23139
DE-FG05-93ER-25175 p 1661 N95-22733
DE-FG05-93ER-79236 p 1838 N95-22555
DE-FG06-90ER-40561 p 1848 N95-22728
p 1802 N95-22729
p 1802 N95-22730
p 1802 N95-22731
p 1805 N95-22870
p 1805 N95-22925
DE-FG09-85ER-13426 p 1748 N95-24075
DE-FG22-91PC-91301 p 1634 N95-23202
DE-FG22-92PC-92542 p 1696 N95-24141
DE-FG22-93PC-93212 p 1745 N95-22872
DE-FG22-93PC-93222 p 1634 N95-23339
DGAPA PROJ-IN100593-UNAM p 1784 N95-22988
DTFA02-91-C-91089 p 1750 N95-24088
F08635-91-C-0224 p 1732 N95-22856
F08635-93-C-0109 p 1629 N95-23034
F19628-89-K-0047 p 1737 N95-22951
F19628-90-C-0002 p 1622 N95-23781
F19628-90-K-0033 p 1838 N95-22511
F19628-90-K-0035 p 1739 N95-23247
F19628-91-K-0019 p 1831 N95-22948
F19628-94-C-0057 p 1764 N95-23936
p 1765 N95-24061
F30602-85-C-0065 p 1760 N95-24176
F30602-90-C-0086 p 1618 N95-23763
F30602-90-C-0119 p 1618 N95-23758
F30602-91-C-0010 p 1783 N95-24031
p 1853 N95-24043
F30602-92-C-0059 p 1659 N95-24193
F30602-93-C-0021 p 1659 N95-22507
F33615-90-C-0005 p 1819 N95-22508
F49620-92-J-0040 p 1750 N95-22513
F49620-92-J-0225 p 1806 N95-23077
F49620-93-1-0283 p 1800 N95-23782
F49620-94-1-0242 p 1749 N95-23780
GRI-5091-254-2293 p 1678 N95-23544
GS-14-08-0001-A-0746 p 1732 N95-22865
JPL-958208 p 1705 N95-23870
JPL-958456 p 1744 N95-23766
p 1713 N95-23945
p 1714 N95-23946
JPL-959060 p 1620 N95-23754
JSPS-ENG-207 p 1759 N95-23935
p 1792 N95-24002
p 1797 N95-24029
p 1793 N95-24034
p 1760 N95-24059
p 1784 N95-24060
p 1797 N95-24063
JSPS-ENGR-207 p 1793 N95-24182
p 1792 N95-23931
p 1793 N95-24003
p 1760 N95-24092
p 1793 N95-24194
MDA972-92-J-1012 p 1783 N95-24001
p 1783 N95-24036
p 1784 N95-24038
p 1765 N95-24183
p 1784 N95-24185
MIT PROJ. OSP-8129 p 1717 N95-22832
NAGW-1143 p 1714 N95-23946
NAGW-1162 p 1714 N95-23949
NAGW-1348 p 1731 N95-22673
NAGW-1356 p 1684 N95-23642
NAGW-1460 p 1719 N95-24094
NAGW-1483 p 1739 N95-23271
NAGW-1554 p 1831 N95-23008
NAGW-1601 p 1714 N95-23946
NAGW-1848 p 1738 N95-23184
NAGW-2040 p 1869 N95-22828
NAGW-2070 p 1711 N95-23895
NAGW-2162 p 1833 N95-23211
NAGW-2280 p 1867 N95-23013
NAGW-2468 p 1714 N95-23949
NAGW-2721 p 1866 N95-23540
NAGW-3470 p 1737 N95-22956
NAGW-3508 p 1738 N95-23090
NAGW-3645 p 1748 N95-24047
NAGW-3672 p 1745 N95-22801
NAGW-3954 p 1869 N95-24066
NAGW-4002 p 1739 N95-23272
NAGW-4209 p 1734 N95-23460
NAGW-925 p 1705 N95-23868
NAG1-1088 p 1615 N95-22908
NAG1-1112 p 1756 N95-23017
NAG1-1150 p 1612 N95-22949
NAG1-1175 p 1608 N95-23182
NAG1-1186 p 1631 N95-23900
NAG1-1188 p 1608 N95-23218
NAG1-1218 p 1623 N95-23826
p 1869 N95-23828
p 1869 N95-23829
p 1637 N95-23836
NAG1-1283 p 1696 N95-23409
NAG1-1301 p 1648 N95-22883
NAG1-1327 p 1622 N95-23398
p 1622 N95-23399
p 1622 N95-23400
NAG1-1329 p 1700 N95-23839
NAG1-1380 p 1615 N95-23410
NAG1-1400 p 1666 N95-22906
NAG1-1434 p 1663 N95-24048
NAG1-1435 p 1766 N95-22831
NAG1-1436 p 1621 N95-23260
NAG1-343 p 1648 N95-23179
NAG1-928 p 1658 N95-23670
NAG2-561 p 1612 N95-23217
NAG2-581 p 1618 N95-23679
NAG2-635 p 1753 N95-22480
NAG2-733 p 1667 N95-23183
NAG2-834 p 1770 N95-23686
NAG2-881 p 1609 N95-23669
NAG2-910 p 1741 N95-24041
NAG3-1010 p 1687 N95-24022
NAG3-1137 p 1699 N95-24189
NAG3-1165 p 1609 N95-23462
NAG3-1240 p 1654 N95-23195
NAG3-1273 p 1614 N95-23088
NAG3-1350 p 1698 N95-22805
NAG3-1377 p 1699 N95-24055
NAG3-1507 p 1694 N95-23190
p 1694 N95-23213
p 1695 N95-23214
NAG3-72 p 1668 N95-23248
NAG3-893 p 1634 N95-23252
NAG5-1490 p 1736 N95-22867
p 1742 N95-23208
NAG5-1491 p 1657 N95-22944
NAG5-1500 p 1833 N95-23211
NAG5-1558 p 1737 N95-22945
NAG5-1742 p 1871 N95-23216
NAG5-1913 p 1866 N95-23560
NAG5-1935 p 1866 N95-23595
NAG5-1941 p 1717 N95-22832
NAG5-1947 p 1717 N95-22832
NAG5-2100 p 1866 N95-23402
NAG5-2307 p 1871 N95-22910
NAG5-2348 p 1827 N95-23224
NAG5-282 p 1815 N95-23810
NAG5-673 p 1651 N95-23902
NAG8-239 p 1831 N95-22955
NAG8-240 p 1694 N95-22909
NAG8-282 p 1815 N95-23812
NAG9-235 p 1872 N95-23801
NAG9-246 p 1746 N95-22911
NAG9-566 p 1757 N95-23388
NAG9-696 p 1751 N95-23474
NASA ORDER H-06815-D p 1815 N95-23816
NASA ORDER S-14634-F p 1865 N95-23401
NASA ORDER S-14648-F p 1871 N95-23472
NASA ORDER W-18409 p 1815 N95-23807
p 1870 N95-23808
NASW-4367 p 1864 N95-22526
p 1865 N95-23091
NASW-4756 p 1866 N95-23561
NASW-4886 p 1827 N95-23089
NASW-4933 p 1870 N95-23181
NAS1-18224 p 1626 N95-22918
NAS1-18762 p 1608 N95-23095
NAS1-18878 p 1762 N95-22830
NAS1-19000 p 1608 N95-22917
p 1608 N95-23185
NAS1-19243 p 1626 N95-22919
p 1697 N95-23706
NAS1-19247 p 1626 N95-22918

NAS1-19427 ..... p 1638 N95-23897
NAS1-19480 ..... p 1638 N95-23898
p 1646 N95-23905
p 1864 N95-23916
p 1627 N95-23914
p 1788 N95-22931
p 1667 N95-23207
p 1790 N95-23465
p 1677 N95-23466
p 1678 N95-23544
p 1678 N95-23596
p 1758 N95-23613
NAS1-19672 ..... p 1668 N95-23257
NAS1-19703 ..... p 1614 N95-22674
NAS10-11606 ..... p 1761 N95-23749
NAS10-11882 ..... p 1761 N95-23749
NAS2-13642 ..... p 1689 N95-23789
NAS2-13721 ..... p 1791 N95-23548
p 1758 N95-23610
NAS3-25141 ..... p 1689 N95-23795
NAS3-25266 ..... p 1616 N95-23192
p 1626 N95-23270
p 1625 N95-23790
p 1625 N95-23791
NAS3-25560 ..... p 1614 N95-24053
NAS3-26134 ..... p 1696 N95-23792
NAS3-26309 ..... p 1614 N95-23222
NAS3-26360 ..... p 1855 N95-23206
NAS3-27186 ..... p 1665 N95-22669
p 1662 N95-23219
p 1624 N95-23221
p 1728 N95-23259
p 1614 N95-23550
NAS3-27229 ..... p 1799 N95-22675
NAS5-30376 ..... p 1820 N95-22957
NAS5-30552 ..... p 1711 N95-23895
NAS5-31361 ..... p 1743 N95-23212
NAS5-31363 ..... p 1717 N95-22916
p 1718 N95-23473
NAS5-31370 ..... p 1717 N95-23191
p 1721 N95-24190
NAS5-31711 ..... p 1702 N95-23848
NAS5-31920 ..... p 1761 N95-23749
NAS5-32332 ..... p 1740 N95-23529
NAS5-32530 ..... p 1871 N95-24191
NAS5-32573 ..... p 1688 N95-23087
NAS7-918 ..... p 1761 N95-22478
p 1865 N95-22539
p 1692 N95-22543
p 1762 N95-22564
p 1754 N95-22577
p 1613 N95-22578
p 1819 N95-22765
p 1655 N95-22813
p 1656 N95-22852
p 1756 N95-22853
p 1827 N95-23045
p 1767 N95-23672
p 1701 N95-23844
p 1711 N95-23917
p 1712 N95-23938
NAS8-36801 ..... p 1674 N95-23438
NAS8-38103 ..... p 1697 N95-24106
NAS8-38609 ..... p 1841 N95-22907
p 1843 N95-23563
p 1828 N95-24035
NAS8-38610 ..... p 1815 N95-23813
NAS8-38773 ..... p 1653 N95-23552
p 1653 N95-24028
NAS8-38784 ..... p 1853 N95-22891
NAS8-38785 ..... p 1653 N95-23204
NAS8-38862 ..... p 1684 N95-23642
NAS8-38864 ..... p 1675 N95-23440
NAS8-38865 ..... p 1672 N95-23428
NAS8-38959 ..... p 1682 N95-23633
NAS8-39131 ..... p 1727 N95-22904
p 1619 N95-24032
NAS8-39398 ..... p 1683 N95-23638
NAS8-39610 ..... p 1815 N95-23811
NAS8-39924 ..... p 1651 N95-23908
NAS8-39932 ..... p 1696 N95-24064
NAS8-39936 ..... p 1868 N95-23205
NAS8-39945 ..... p 1625 N95-23261
NAS8-399905 ..... p 1761 N95-23749
NAS8-40185 ..... p 1826 N95-23016
NAS9-18992 ..... p 1633 N95-23092
NCC1-14 ..... p 1608 N95-23193
NCC1-193 ..... p 1621 N95-23188
p 1621 N95-23189
NCC1-24 ..... p 1608 N95-23193
NCC2-387 ..... p 1791 N95-23547
p 1791 N95-23592
p 1791 N95-23593
p 1764 N95-23594
p 1791 N95-23611
p 1791 N95-23612
NCC2-5023 ..... p 1764 N95-24023
NCC2-5029 ..... p 1732 N95-22930
NCC2-531 ..... p 1636 N95-23545
NCC2-537 ..... p 1618 N95-23758
NCC2-539 ..... p 1618 N95-23679
NCC2-582 ..... p 1757 N95-23180
NCC2-741 ..... p 1664 N95-22481
p 1641 N95-23215
p 1809 N95-23408
p 1810 N95-23459
NCC2-802 ..... p 1775 N95-23716
NCC2-824 ..... p 1750 N95-22797
NCC3-370 ..... p 1668 N95-23220
p 1677 N95-23451
p 1677 N95-23464
NCC8-25 ..... p 1871 N95-23546
NCC8-39 ..... p 1621 N95-23188
p 1621 N95-23189
NERC-GT4/91/TLS/62 ..... p 1713 N95-23943
NGT-47-020-800 ..... p 1872 N95-23276
NGT-50728 ..... p 1713 N95-23945
NGT-50981 ..... p 1615 N95-23392
NGT-70312 ..... p 1695 N95-23214
NSF ASC-90-05933 ..... p 1791 N95-23592
NSF ATM-91-20072 ..... p 1740 N95-23933
NSF CCR-88-21078 ..... p 1791 N95-23611
NSF CCR-89-57310 ..... p 1791 N95-23600
NSF CCR-89-57604 ..... p 1792 N95-23929
p 1792 N95-23931
p 1792 N95-24002
p 1793 N95-24003
p 1797 N95-24029
p 1793 N95-24034
p 1760 N95-24059
p 1797 N95-24063
p 1760 N95-24092
p 1793 N95-24194
NSF CCR-90-02292 ..... p 1792 N95-24002
NSF CCR-93-02057 ..... p 1793 N95-24194
NSF CCR-93-19445 ..... p 1764 N95-23930
p 1759 N95-24033
p 1765 N95-24183
NSF CCR-93-22513 ..... p 1797 N95-24029
p 1793 N95-24034
p 1760 N95-24059
p 1784 N95-24060
p 1797 N95-24063
p 1793 N95-24194
NSF CCR-94-09120 ..... p 1765 N95-24061
NSF CDA-88-22724 ..... p 1759 N95-23928
p 1764 N95-23930
p 1783 N95-24001
p 1759 N95-24033
p 1764 N95-24037
p 1753 N95-24177
p 1765 N95-24183
p 1765 N95-24184
NSF CDA-90-22509 ..... p 1771 N95-23691
NSF DMR-91-21272 ..... p 1869 N95-24066
NSF EAR-91-15159 ..... p 1717 N95-22832
NSF EAR-91-17889 ..... p 1717 N95-22832
NSF INT-91-16781 ..... p 1792 N95-23931
p 1759 N95-23935
p 1792 N95-24002
p 1793 N95-24003
p 1797 N95-24029
p 1793 N95-24034
p 1760 N95-24059
p 1784 N95-24060
p 1797 N95-24063
p 1760 N95-24092
p 1793 N95-24182
p 1793 N95-24194
NSF IRI-89-03582 ..... p 1783 N95-24001
p 1658 N95-24039
p 1784 N95-24040
NSF IRI-89-03592 ..... p 1658 N95-23794
NSF IRI-90-02659 ..... p 1792 N95-23793
NSF IRI-90-03841 ..... p 1783 N95-24031
p 1760 N95-24058
NSF IRI-90-13160 ..... p 1658 N95-23937
p 1659 N95-24193
NSF IRI-92-16941 ..... p 1771 N95-23691
NSF IRI-93-06454 ..... p 1784 N95-24038
NSF PHY-92-12231 ..... p 1822 N95-22973
NSG-1498 ..... p 1657 N95-23391
NSG-5175 ..... p 1735 N95-22482
N00014-90-J-1811 ..... p 1760 N95-24058
N00014-91-J-1721 ..... p 1742 N95-23255
N00014-91-J-1852 ..... p 1663 N95-23783
N00014-92-J-1512 ..... p 1658 N95-23937
p 1783 N95-24031
p 1760 N95-24058
N00014-92-J-1801 ..... p 1659 N95-24193
p 1759 N95-23928
p 1764 N95-23930
N00014-93-1-0221 ..... p 1759 N95-24033
p 1764 N95-24037
p 1753 N95-24177
p 1765 N95-24183
p 1765 N95-24184
p 1783 N95-24001
p 1783 N95-24036
p 1784 N95-24038
p 1784 N95-24185
N00014-93-1-0667 ..... p 1627 N95-22940
N68171-94-M-6048 ..... p 1691 N95-23118
OTKA-3008 ..... p 1814 N95-22971
OTKA-4303 ..... p 1822 N95-22970
PHS-1-R24-RR-06853-02 ..... p 1658 N95-23794
p 1658 N95-24039
p 1784 N95-24040
PROJ UNAM-DGAPA IN1042-93 .. p 1798 N95-23006
RTOP 199-45-16-11 ..... p 1817 N95-22929
RTOP 232-01-04-04 ..... p 1691 N95-23411
RTOP 232-02-03 ..... p 1624 N95-23221
RTOP 233-01-0E ..... p 1738 N95-23116
RTOP 233-01-03-05 ..... p 1759 N95-24052
RTOP 233-01-05 ..... p 1691 N95-22670
RTOP 233-02-0A ..... p 1728 N95-23259
RTOP 233-02-0C ..... p 1662 N95-23219
RTOP 233-02-03 ..... p 1616 N95-23671
RTOP 233-03-0A ..... p 1747 N95-23177
RTOP 233-03-0B ..... p 1625 N95-23450
RTOP 233-03-02-02 ..... p 1626 N95-22919
RTOP 233-03-02-03 ..... p 1889 N95-23796
p 1899 N95-23896
RTOP 233-03-02-04 ..... p 1626 N95-22918
RTOP 233-03-04-00-00 ..... p 1767 N95-23672
RTOP 235-01-0B ..... p 1846 N95-24188
RTOP 242-80-01-01 ..... p 1688 N95-23012
RTOP 243-30-0A ..... p 1650 N95-24187
RTOP 307-51-50 ..... p 1872 N95-22920
RTOP 313-00-00 ..... p 1628 N95-23025
RTOP 314-40-31-30-26D ..... p 1756 N95-22853
RTOP 315-91-40-20 ..... p 1761 N95-22478
RTOP 315-91-60-10-07 ..... p 1656 N95-22852
RTOP 323-17-04-01 ..... p 1840 N95-22803
RTOP 323-61-05 ..... p 1855 N95-23206
RTOP 324-02-00 ..... p 1614 N95-23222
RTOP 464-54-03-70 ..... p 1733 N95-23009
RTOP 465-01-00 ..... p 1701 N95-23844
RTOP 465-66-00-01 ..... p 1711 N95-23917
RTOP 474-46-10 ..... p 1698 N95-22805
RTOP 478-29-10 ..... p 1762 N95-22668
RTOP 478-43-10 ..... p 1624 N95-23240
RTOP 505-00-00 ..... p 1857 N95-24108
RTOP 505-50-5K ..... p 1668 N95-23220
RTOP 505-59-10-13 ..... p 1607 N95-22802
RTOP 505-59-50-02 ..... p 1668 N95-23257
RTOP 505-59-54-01 ..... p 1616 N95-23011
RTOP 505-62-50 ..... p 1820 N95-22915
p 1615 N95-22954
p 1654 N95-23195
p 1688 N95-23461
p 1689 N95-23795
RTOP 505-62-52 ..... p 1800 N95-23178
p 1616 N95-23192
p 1792 N95-23614
RTOP 505-63-12 ..... p 1699 N95-24055
RTOP 505-63-36-06 ..... p 1612 N95-22953
RTOP 505-63-36 ..... p 1696 N95-23792
RTOP 505-63-5B ..... p 1630 N95-23258
p 1630 N95-23463
RTOP 505-64-30 ..... p 1612 N95-22806
RTOP 505-64-36 ..... p 1613 N95-24030
RTOP 505-64-52 ..... p 1654 N95-22804
RTOP 505-66-21-02 ..... p 1753 N95-22479
p 1754 N95-22603
p 1755 N95-22604
p 1755 N95-22605
RTOP 505-68-10 ..... p 1665 N95-22669
p 1668 N95-23248
RTOP 505-68-30-03 ..... p 1608 N95-22917
p 1608 N95-23095
p 1608 N95-23185
RTOP 505-68-32 ..... p 1607 N95-22666
RTOP 505-69-10 ..... p 1612 N95-22829
RTOP 505-69-50 ..... p 1609 N95-23462
RTOP 505-70-62 ..... p 1609 N95-23250
RTOP 505-90-5K ..... p 1677 N95-23451
p 1677 N95-23464
RTOP 505-90-52-01 ..... p 1788 N95-22931
p 1667 N95-23207
p 1790 N95-23465
p 1677 N95-23466
p 1678 N95-23544
p 1678 N95-23596
p 1758 N95-23613
RTOP 506-40-41-02 ..... p 1666 N95-23015
p 1667 N95-23210
RTOP 506-41-4A ..... p 1626 N95-23270

RTOP 506-43-61-02 ..... p 1626 N95-22918
RTOP 506-64-10-13 ..... p 1762 N95-22830
RTOP 535-03-10 ..... p 1799 N95-22675
RTOP 537-02-21 ..... p 1614 N95-23550
RTOP 537-07-20 ..... p 1608 N95-23193
RTOP 538-02-10-01 ..... p 1627 N95-22928
RTOP 538-04-13-01 ..... p 1614 N95-22674
RTOP 538-06-13 ..... p 1699 N95-24189
RTOP 584-04-11 ..... p 1625 N95-23791
RTOP 593-12-00 ..... p 1625 N95-23790
RTOP 666-31-00 ..... p 1712 N95-23938
RTOP 669-00-00 ..... p 1655 N95-22813
RTOP 763-22-21 ..... p 1653 N95-24186
RTOP 962-22-00 ..... p 1626 N95-24004
RTOP 963-60-0D ..... p 1621 N95-22667
SERC GR/H53648 ..... p 1825 N95-22998
SNSF PROJ. 82-20332.90 ..... p 1707 N95-23876
SWRI PROJ. 15-5301 ..... p 1866 N95-23560
USRA-C-5555-19 ..... p 1862 N95-24137
USRA-C-5555-23 ..... p 1753 N95-24114
W-31-109-ENG-38 ..... p 1838 N95-22530
p 1638 N95-22531
p 1692 N95-22556
p 1693 N95-22557
p 1726 N95-22568
p 1660 N95-22569
p 1754 N95-22570
p 1638 N95-22571
p 1839 N95-22572
p 1801 N95-22573
p 1638 N95-22592
p 1660 N95-22593
p 1639 N95-22594
p 1632 N95-22681
p 1755 N95-22690
p 1786 N95-22696
p 1840 N95-22762
p 1632 N95-22764
p 1804 N95-22792
p 1632 N95-22857
p 1727 N95-22861
p 1798 N95-22895
p 1746 N95-22912
p 1746 N95-22913
p 1662 N95-23355
p 1696 N95-23397
p 1857 N95-23490
p 1810 N95-23491
p 1688 N95-23492
p 1810 N95-23530
p 1730 N95-23582
p 1689 N95-23583
p 1870 N95-23584
p 1843 N95-23585
p 1843 N95-23586
p 1811 N95-23587
p 1748 N95-23771
p 1664 N95-24070
p 1845 N95-24150
p 1813 N95-24151
p 1845 N95-24152
p 1646 N95-24153
p 1845 N95-24154
p 1818 N95-24162
p 1664 N95-24163
p 1664 N95-24164
p 1837 N95-24165
p 1813 N95-24166
p 1838 N95-24167
p 1846 N95-24168
p 1846 N95-24169
p 1846 N95-24170
p 1846 N95-24171
p 1765 N95-24172
p 1846 N95-24173
p 1813 N95-24174
W-7405-ENG-36 ..... p 1855 N95-22515
p 1867 N95-22516
p 1829 N95-22519
p 1838 N95-22520
p 1801 N95-22551
p 1798 N95-22552
p 1646 N95-22553
p 1839 N95-22565
p 1839 N95-22653
p 1795 N95-22654
p 1847 N95-22655
p 1829 N95-22665
p 1829 N95-22676
p 1631 N95-22677
p 1654 N95-22678
p 1762 N95-22679
p 1762 N95-22680
p 1736 N95-22850
p 1621 N95-22868
p 1796 N95-22900
p 1666 N95-22901
p 1666 N95-22902
p 1737 N95-22903
p 1624 N95-22905
p 1805 N95-22927
p 1805 N95-22936
p 1870 N95-22938
p 1806 N95-23137
p 1739 N95-23244
p 1817 N95-23245
p 1739 N95-23256
p 1842 N95-23265
p 1842 N95-23266
p 1808 N95-23267
p 1649 N95-23268
p 1833 N95-23269
p 1794 N95-23349
p 1635 N95-23360
p 1842 N95-23365
p 1843 N95-23366
p 1843 N95-23367
p 1662 N95-23368
p 1809 N95-23403
p 1663 N95-23479
p 1758 N95-23567
p 1649 N95-23568
p 1868 N95-23570
p 1645 N95-23571
p 1636 N95-23573
p 1658 N95-23772
p 1799 N95-23979
p 1658 N95-24015
p 1646 N95-24067
p 1689 N95-24069
p 1692 N95-24072
p 1844 N95-24073
p 1765 N95-24074
p 1844 N95-24076
p 1741 N95-24078
p 1845 N95-24079
W-7405-ENG-48 ..... p 1665 N95-22491
p 1659 N95-22504
p 1727 N95-22574
p 1690 N95-22595
p 1693 N95-22798
p 1763 N95-22858
p 1763 N95-22859
p 1841 N95-22860
p 1855 N95-22871
p 1732 N95-22898
p 1831 N95-22899
p 1737 N95-23063
p 1766 N95-23078
p 1661 N95-23080
p 1832 N95-23119
p 1733 N95-23123
p 1733 N95-23124
p 1749 N95-23142
p 1738 N95-23143
p 1763 N95-23243
p 1662 N95-23334
p 1695 N95-23358
p 1834 N95-23371
p 1635 N95-23381
p 1827 N95-23449
p 1790 N95-23536
p 1837 N95-24017
p 1735 N95-24018
p 1616 N95-24019
p 1813 N95-24046
p 1837 N95-24083
p 1837 N95-24086
p 1837 N95-24087
p 1861 N95-24131
W-7405-ENG-82 ..... p 1744 N95-22493
WHAMS3D PROJ. ..... p 1764 N95-23599

Typical Report Number Index Listing

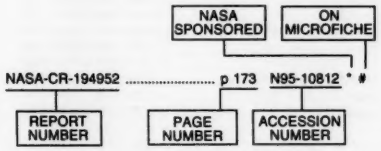

Listings in this index are arranged alphanumerically by report number. The accession number denotes the number by which the citation is identified. The page number helps to locate the citation in the abstract section. An asterisk (*) indicates that the item is a NASA report. A pound sign (#) indicates that the item is available on microfiche.

A-94119 ..... p 1609 N95-23250 * #
A-94135 ..... p 1872 N95-22920 * #
A-94141 ..... p 1613 N95-24030 * #
A-94142 ..... p 1759 N95-24052 * #
A-95014 ..... p 1654 N95-22804 * #
A-95025 ..... p 1607 N95-22666 * #

AD-A279406 ..... p 1739 N95-23247
AD-A279436 ..... p 1744 N95-23766 *
AD-A279766 ..... p 1732 N95-22856 #
AD-A280101 ..... p 1627 N95-22833
AD-A280115 ..... p 1747 N95-23251
AD-A285097 ..... p 1742 N95-23255 #
AD-A285100 ..... p 1691 N95-22937 #
AD-A285102 ..... p 1609 N95-23201 #
AD-A285118 ..... p 1622 N95-23781 #
AD-A285275 ..... p 1662 N95-23117 #
AD-A285414 ..... p 1903 N95-24179 #
AD-A285415 ..... p 1903 N95-24178 #
AD-A285639 ..... p 1749 N95-23780 #
AD-A285640 ..... p 1800 N95-23782 #
AD-A285643 ..... p 1663 N95-23783 #
AD-A285647 ..... p 1691 N95-23118 #
AD-A285771 ..... p 1806 N95-23077 #
AD-A285791 ..... p 1655 N95-22505 #
AD-A285792 ..... p 1652 N95-22506 #
AD-A285794 ..... p 1659 N95-22507
AD-A285795 ..... p 1819 N95-22508 #
AD-A285796 ..... p 1762 N95-22509 #
AD-A285797 ..... p 1611 N95-22510 #
AD-A285808 ..... p 1838 N95-22511
AD-A285823 ..... p 1766 N95-22512 #
AD-A285829 ..... p 1750 N95-22513 #
AD-A285850 ..... p 1829 N95-22514
AD-A286013 ..... p 1627 N95-22940 #
AD-A286018 ..... p 1657 N95-23023 #
AD-A286021 ..... p 1855 N95-23024 #
AD-A286023 ..... p 1743 N95-23074 #
AD-A286629 ..... p 1854 N95-22494 #

AD-D016383 ..... p 1662 N95-23241
AD-D016488 ..... p 1799 N95-22863
AD-D016491 ..... p 1819 N95-22492
AD-D016500 ..... p 1820 N95-22864
AD-D016536 ..... p 1800 N95-23073
AD-D016539 ..... p 1766 N95-22705
AD-D016549 ..... p 1687 N95-22706
AD-D016550 ..... p 1693 N95-22707
AD-D016553 ..... p 1660 N95-22708
AD-D016554 ..... p 1660 N95-22709
AD-D016557 ..... p 1632 N95-22710

AD-E201924 ..... p 1739 N95-23247

AFOSR-94-0641TR ..... p 1749 N95-23780 #
AFOSR-94-0647TR ..... p 1800 N95-23782 #
AFOSR-94-0669TR ..... p 1806 N95-23077 #

AGARD-AR-325 ..... p 1751 N95-23601 #

AGARD-CP-565 ..... p 1641 N95-23496 #

AGARD-R-809 ..... p 1697 N95-23602 #

AIAA PAPER 94-2849 ..... p 1624 N95-23221 * #
AIAA PAPER 94-3308 ..... p 1624 N95-23240 * #
AIAA PAPER 95-0300 ..... p 1688 N95-23461 * #
AIAA PAPER 95-0537 ..... p 1668 N95-23248 * #
AIAA PAPER 95-0560 ..... p 1677 N95-23466 * #
AIAA PAPER 95-0681 ..... p 1668 N95-23220 * #
AIAA PAPER 95-0752 ..... p 1665 N95-22669 * #
AIAA PAPER 95-1101 ..... p 1630 N95-23463 * #
AIAA PAPER 95-6056 ..... p 1653 N95-24186 * #

AL-CF-TR-1994-0159 ..... p 1613 N95-24030 * #

AL/EQ-TR-1993-0027 ..... p 1732 N95-22856 #

AL/HR-TR-1994-0111 ..... p 1750 N95-22513 #

ANL-HEP-CP-94-51 ..... p 1810 N95-23530 #
ANL-HEP-CP-94-72 ..... p 1801 N95-22573 #
ANL-HEP-CP-94-78 ..... p 1689 N95-23583 #
ANL-HEP-CP-94-82 ..... p 1870 N95-23584 #

ANL-HEP-PR-94-79 ..... p 1813 N95-24166 #

ANL-HEP-TR-94-42 ..... p 1688 N95-23492 #

ANL-94/40 ..... p 1786 N95-22696 #

ANL/APS/TM-14 ..... p 1813 N95-24174 #

ANL/ASD/CP-83682 ..... p 1664 N95-24164 #

ANL/BIM/PP-71687 ..... p 1748 N95-23771 #
ANL/BIM/PP-76678 ..... p 1746 N95-22912 #

ANL/CHM/CP-84071 ..... p 1818 N95-24162 #
ANL/CHM/CP-84263 ..... p 1638 N95-22531 #
ANL/CHM/CP-84364 ..... p 1660 N95-22593 #
ANL/CHM/CP-84392 ..... p 1810 N95-23491 #

ANL/CHM/PP-79404 ..... p 1632 N95-22857 #
ANL/CHM/PP-79757 ..... p 1638 N95-22571 #

ANL/CMB/PP-82201 ..... p 1746 N95-22913 #

ANL/CMT/CP-83639 ..... p 1730 N95-23582 #
ANL/CMT/CP-83648 ..... p 1726 N95-22568 #

ANL/DIS/CP-84377 ..... p 1857 N95-23490 #

ANL/EP/SUMM-84774 ..... p 1838 N95-24167 #

ANL/EP/VU-84785 ..... p 1837 N95-24165 #

ANL/ES/CP-83720 ..... p 1693 N95-22557 #
ANL/ES/CP-84138 ..... p 1664 N95-24070 #
ANL/ES/CP-84174 ..... p 1692 N95-22556 #

ANL/ESD/TM-72 ..... p 1798 N95-22895 #

ANL/ET/CP-82008 ..... p 1646 N95-24153 #
ANL/ET/CP-82120 ..... p 1664 N95-24163 #
ANL/ET/CP-82300 ..... p 1660 N95-22569 #
ANL/ET/CP-82313 ..... p 1838 N95-22530 #
ANL/ET/CP-83629 ..... p 1662 N95-23355 #
ANL/ET/CP-83901 ..... p 1846 N95-24169 #
ANL/ET/CP-84520 ..... p 1839 N95-22572 #
ANL/ET/CP-84563 ..... p 1845 N95-24150 #
ANL/ET/CP-84861 ..... p 1846 N95-24171 #

ANL/IPNS/CP-83105 ..... p 1632 N95-22681 #

ANL/MCS/CP-84113 ..... p 1755 N95-22690 #
ANL/MCS/CP-85098 ..... p 1765 N95-24172 #
ANL/MCS/PP-75185 ..... p 1754 N95-22570 #

ANL/MSD/CP-82573 ..... p 1845 N95-24152 #
ANL/MSD/CP-82603 ..... p 1639 N95-22594 #
ANL/MSD/CP-83452 ..... p 1843 N95-23585 #
ANL/MSD/CP-83568 ..... p 1843 N95-23586 #
ANL/MSD/CP-84182 ..... p 1804 N95-22792 #
ANL/MSD/CP-84413 ..... p 1845 N95-24154 #

ANL/MSD/PP-82718 ..... p 1846 N95-24168 #
ANL/MSD/PP-83083 ..... p 1846 N95-24170 #
ANL/MSD/PP-83268 ..... p 1846 N95-24173 #
ANL/MSD/PP-83766 ..... p 1840 N95-22762 #

ANL/PHY/CP-84545 ..... p 1813 N95-24151 #
ANL/PHY/CP-84618 ..... p 1811 N95-23587 #

ANL/TD/CP-83462 ..... p 1632 N95-22764 #

ANL/XFD/CP-82916 ..... p 1638 N95-22592 #
ANL/XFD/CP-82946 ..... p 1696 N95-23397 #

AR-008-408 ..... p 1699 N95-22952
AR-008-910 ..... p 1613 N95-23666
AR-008-946 ..... p 1743 N95-23667
AR-008-959 ..... p 1653 N95-23668

ARC-R-95-229 ..... p 1865 N95-23401 * #

ARC-R95-233 ..... p 1871 N95-23472 * #
ARC-R95-234 ..... p 1866 N95-23561 * #

ARCCB-TR-94010 ..... p 1627 N95-22833

ARL-TR-518 ..... p 1612 N95-22953 * #
ARL-TR-581 ..... p 1611 N95-22510 #
ARL-TR-589 ..... p 1762 N95-22509 #
ARL-TR-606 ..... p 1652 N95-22506 #

ATR-95(7270)-1 ..... p 1740 N95-23933 #

B-256333 ..... p 1735 N95-24057 #
B-258273 ..... p 1853 N95-23588 #
B-259019 ..... p 1854 N95-24054 #
B-259046 ..... p 1854 N95-24085 #
B-259256 ..... p 1613 N95-24091 #
B-259821 ..... p 1903 N95-24080 #
B-260307 ..... p 1864 N95-24062 #

BARC-1993/E/018 ..... p 1814 N95-24175 #
BARC-1993/E/031 ..... p 1753 N95-23962 #

BBC-RD-1994/13 ..... p 1658 N95-24044
BBC-RD-1994/14 ..... p 1654 N95-24093
BBC-RD-1994/15 ..... p 1654 N95-24045

BER-620-163 ..... p 1694 N95-22909 * #

BNL-49323 ..... p 1816 N95-22926 #
BNL-49542 ..... p 1633 N95-22887 #
BNL-52424-REV-9/94-PT-1-3 ..... p 1660 N95-22716 #
BNL-60058 ..... p 1728 N95-23133 #
BNL-60794 ..... p 1633 N95-22876 #
BNL-60835 ..... p 1803 N95-22763 #
BNL-60843 ..... p 1801 N95-22583 #
BNL-60859 ..... p 1820 N95-22877 #
BNL-60869 ..... p 1851 N95-23335 #
BNL-60899 ..... p 1827 N95-23531 #
BNL-60904 ..... p 1828 N95-24005 #
BNL-60958 ..... p 1801 N95-22656 #
BNL-60962 ..... p 1842 N95-23354 #
BNL-60963 ..... p 1817 N95-23353 #
BNL-61012 ..... p 1809 N95-23396 #
BNL-61018 ..... p 1802 N95-22727 #

BUDKERINP-93-52 ..... p 1804 N95-22847 #
BUDKERINP-93-75 ..... p 1692 N95-23657 #

CCMS-95-01 ..... p 1648 N95-23179 * #

CERL-FEAP-UG-FM-94/10 ..... p 1662 N95-23117 #

COLO-HEP-342 ..... p 1806 N95-23140 #

CONF-9111175-2 ..... p 1838 N95-24167 #
CONF-9111209-1-VUGRAPHS ..... p 1837 N95-24165 #
CONF-9206173-12 ..... p 1640 N95-23132 #
CONF-921101-144 ..... p 1640 N95-23121 #
CONF-9211198-4 ..... p 1657 N95-23075 #
CONF-9303296 ..... p 1734 N95-23542 #
CONF-9303301-1 ..... p 1727 N95-22888 #
CONF-9303322 ..... p 1729 N95-23382 #
CONF-9306364-1 ..... p 1805 N95-22889 #
CONF-9307199-EXTD-ABSTS ..... p 1745 N95-22866 #
CONF-9308231 ..... p 1727 N95-22855 #
CONF-9309119-SUMM-1 ..... p 1833 N95-23246 #
CONF-930926-37 ..... p 1816 N95-22926 #
CONF-9309407 ..... p 1759 N95-23963 #
CONF-9310181 ..... p 1645 N95-23983 #
CONF-9310220-7 ..... p 1765 N95-24172 #
CONF-9311147-11 ..... p 1832 N95-23163 #
CONF-9311173-2 ..... p 1633 N95-22887 #
CONF-9311217 ..... p 1830 N95-22757 #
CONF-9311228 ..... p 1841 N95-22854 #
CONF-931260-2 ..... p 1755 N95-22690 #
CONF-940285-1 ..... p 1741 N95-24009 #
CONF-9403180-1 ..... p 1742 N95-22701 #
CONF-9403185-1 ..... p 1741 N95-24078 #
CONF-940397-3 ..... p 1633 N95-22886 #
CONF-9404162-14 ..... p 1616 N95-24019 #
CONF-9404162-15 ..... p 1735 N95-24018 #
CONF-9404178-ABSTS ..... p 1744 N95-22589 #
CONF-9404198-4 ..... p 1818 N95-24162 #
CONF-9404198 ..... p 1813 N95-24174 #
CONF-940440-5 ..... p 1650 N95-23981 #
CONF-940507-36 ..... p 1813 N95-24046 #
CONF-9404514-15 ..... p 1802 N95-22727 #
CONF-940514-17 ..... p 1802 N95-22730 #
CONF-9405168-6 ..... p 1689 N95-23521 #
CONF-9405222-1 ..... p 1870 N95-22938 #
CONF-9405247-2 ..... p 1813 N95-24151 #
CONF-940526-5 ..... p 1652 N95-22587 #
CONF-940526-6 ..... p 1744 N95-22588 #
CONF-9405267-1 ..... p 1809 N95-23396 #
CONF-940552-19 ..... p 1836 N95-23768 #
CONF-940552-34 ..... p 1830 N95-22719 #
CONF-940556-ABSTS ..... p 1830 N95-22793 #
CONF-940556-4 ..... p 1632 N95-22795 #
CONF-940580-14 ..... p 1832 N95-23119 #
CONF-940580-21 ..... p 1831 N95-22800 #
CONF-940618-96 ..... p 1816 N95-22567 #
CONF-9406246-1 ..... p 1841 N95-22860 #
CONF-9406269-1 ..... p 1801 N95-22583 #
CONF-9406269-2 ..... p 1801 N95-22573 #
CONF-9406269-3 ..... p 1870 N95-23584 #
CONF-9406273-1 ..... p 1810 N95-23530 #
CONF-9406273-2 ..... p 1847 N95-22566 #
CONF-9406273-3 ..... p 1801 N95-22521 #
CONF-9406276-1 ..... p 1766 N95-23078 #
CONF-9406279-1 ..... p 1666 N95-22902 #
CONF-9406294-1 ..... p 1810 N95-23491 #
CONF-940633-6 ..... p 1633 N95-22869 #
CONF-940657-7 ..... p 1646 N95-24153 #
CONF-940664-33 ..... p 1829 N95-22645 #
CONF-940681-5 ..... p 1817 N95-23493 #
CONF-940693-2 ..... p 1816 N95-22684 #
CONF-940693-4 ..... p 1816 N95-22702 #
CONF-9407103-32 ..... p 1818 N95-24014 #
CONF-9407108-2 ..... p 1638 N95-22531 #
CONF-9407117-5 ..... p 1660 N95-22593 #
CONF-940714-39 ..... p 1820 N95-22877 #
CONF-940714-45 ..... p 1696 N95-23397 #
CONF-9407141-1 ..... p 1666 N95-23081 #
CONF-9407142-1 ..... p 1801 N95-22646 #
CONF-9407142-2 ..... p 1808 N95-23226 #
CONF-9407142-3 ..... p 1807 N95-23141 #
CONF-9407146-1 ..... p 1666 N95-22901 #
CONF-9407151-1 ..... p 1802 N95-22729 #
CONF-9407197 ..... p 1665 N95-22491 #
CONF-940719-7 ..... p 1790 N95-23536 #
CONF-940719-8 ..... p 1813 N95-24000 #
CONF-940722-34 ..... p 1621 N95-22868 #
CONF-940723-2 ..... p 1756 N95-23079 #
CONF-940723-30 ..... p 1827 N95-23531 #
CONF-940723-31 ..... p 1827 N95-23449 #
CONF-940723-34 ..... p 1803 N95-22763 #
CONF-940725-4 ..... p 1844 N95-24011 #
CONF-940731-3 ..... p 1645 N95-23980
CONF-940793-2 ..... p 1855 N95-22871 #
CONF-940802-1 ..... p 1632 N95-22722 #
CONF-940809-7 ..... p 1806 N95-23139 #
CONF-9408100-1 ..... p 1806 N95-23138 #
CONF-9408100-2 ..... p 1746 N95-22890 #
CONF-9408117-3 ..... p 1728 N95-23162 #
CONF-940812-22 ..... p 1727 N95-22574 #
CONF-940812-24 ..... p 1690 N95-22595 #
CONF-9408121-3 ..... p 1652 N95-22838 #
CONF-9408123-3 ..... p 1652 N95-22721 #
CONF-9408126-5 ..... p 1691 N95-22704 #
CONF-9408146-13 ..... p 1692 N95-23487 #
CONF-9408146-14 ..... p 1763 N95-22858 #
CONF-9408147-1-REV-1 ..... p 1763 N95-22859 #
CONF-9408147-1 ..... p 1808 N95-23347 #
CONF-940816-PT-1 ..... p 1807 N95-23196 #
CONF-940816-10 ..... p 1689 N95-23520 #
CONF-940816-11 ..... p 1810 N95-23522 #
CONF-940816-12 ..... p 1808 N95-23242 #
CONF-940816-13 ..... p 1805 N95-22939 #
CONF-940816-19 ..... p 1806 N95-23139 #
CONF-940816-1 ..... p 1801 N95-22685 #
CONF-940816-36 ..... p 1806 N95-23140 #
CONF-940816-52 ..... p 1868 N95-23570 #
CONF-940816-57 ..... p 1813 N95-24016 #
CONF-940816-58 ..... p 1818 N95-24084 #
CONF-940816-62 ..... p 1809 N95-23404 #
CONF-940816-63 ..... p 1871 N95-23370 #
CONF-940816-64 ..... p 1808 N95-23336 #
CONF-940816-67 ..... p 1811 N95-23581 #
CONF-940816-68 ..... p 1808 N95-23203 #
CONF-940816-7 ..... p 1808 N95-23197 #
CONF-940816-9 ..... p 1837 N95-24087 #
CONF-9408176-4 ..... p 1739 N95-23256 #
CONF-9408181-1 ..... p 1829 N95-22665 #
CONF-9408182-2 ..... p 1736 N95-22850 #
CONF-9408182-3 ..... p 1805 N95-22936 #
CONF-9408184-1 ..... p 1805 N95-22927 #
CONF-9408184-2 ..... p 1801 N95-22551 #
CONF-9408185-1 ..... p 1848 N95-22728 #
CONF-9408188-1 ..... p 1802 N95-22703 #
CONF-9408190-1 ..... p 1692 N95-24072 #
CONF-9408196-1 ..... p 1851 N95-23335 #
CONF-940829-1 ..... p 1840 N95-22687 #
CONF-940830-1 ..... p 1693 N95-22796 #
CONF-940843-10 ..... p 1693 N95-22798 #
CONF-940843-11 ..... p 1837 N95-24083 #
CONF-940843-12 ..... p 1661 N95-23080 #
CONF-940843-9 ..... p 1837 N95-23982 #
CONF-940847-4 ..... p 1654 N95-22678 #
CONF-940854-2 ..... p 1811 N95-23587 #
CONF-940858-1 ..... p 1639 N95-22686 #
CONF-940865-3 ..... p 1647 N95-22689 #
CONF-940865-4 ..... p 1839 N95-22653 #
CONF-940865-5 ..... p 1763 N95-23243 #
CONF-940875-1 ..... p 1726 N95-22568 #
CONF-940883-7 ..... p 1730 N95-23582 #
CONF-940883-8 ..... p 1730 N95-23977 #
CONF-940883 ..... p 1807 N95-23165 #
CONF-9409103-5 ..... p 1809 N95-23403 #
CONF-9409103-8 ..... p 1809 N95-23406 #
CONF-9409134-1 ..... p 1624 N95-22885 #
CONF-9409163-2 ..... p 1633 N95-22876 #
CONF-9409168-9 ..... p 1828 N95-23767 #
CONF-9409177-2 ..... p 1819 N95-22723 #
CONF-9409177-5 ..... p 1808 N95-23267 #
CONF-9409182-2 ..... p 1829 N95-22676 #
CONF-9409226-2 ..... p 1847 N95-22655 #
CONF-9409241-2 ..... p 1795 N95-22654 #
CONF-9409241-3 ..... p 1794 N95-23349 #
CONF-9409241-4 ..... p 1801 N95-22656 #
CONF-9409242-1 ..... p 1798 N95-22552 #
CONF-9409243-1 ..... p 1796 N95-22900 #
CONF-9409246-1 ..... p 1804 N95-22792 #
CONF-9409248-1 ..... p 1749 N95-24145 #
CONF-9409253-1 ..... p 1735 N95-24146 #
CONF-9409255-1 ..... p 1813 N95-24166 #
CONF-9409257-2 ..... p 1851 N95-23352 #
CONF-9409259-1 ..... p 1845 N95-24154 #
CONF-940926-4 ..... p 1721 N95-24148 #
CONF-9409265-1 ..... p 1664 N95-24081 #
CONF-9409268-1 ..... p 1689 N95-23583 #
CONF-9409268-3 ..... p 1837 N95-24017 #
CONF-940933-17 ..... p 1833 N95-23269 #
CONF-940933-18 ..... p 1837 N95-24086 #
CONF-940933-19 ..... p 1639 N95-22724 #
CONF-940945-3 ..... p 1726 N95-22547 #
CONF-940970-6 ..... p 1844 N95-24010 #
CONF-940981-4 ..... p 1834 N95-23371 #
CONF-940994-3 ..... p 1638 N95-22592 #
CONF-941001-7 ..... p 1843 N95-23579 #
CONF-9410114-4 ..... p 1735 N95-23580 #
CONF-9410114-5 ..... p 1839 N95-22565 #
CONF-9410115-1 ..... p 1660 N95-22569 #
CONF-941013-10 ..... p 1843 N95-23366 #
CONF-941013-12 ..... p 1843 N95-23367 #
CONF-941013-13 ..... p 1662 N95-23368 #
CONF-941013-14 ..... p 1664 N95-24163 #
CONF-941013-18 ..... p 1845 N95-24150 #
CONF-941013-19 ..... p 1645 N95-23571 #
CONF-941013-1 ..... p 1846 N95-24171 #
CONF-941013-20 ..... p 1845 N95-24152 #
CONF-941013-21 ..... p 1838 N95-22520 #
CONF-941013-3 ..... p 1838 N95-22530 #
CONF-941013-6 ..... p 1839 N95-22572 #
CONF-941013-9 ..... p 1740 N95-24008 #
CONF-9410131-11 ..... p 1868 N95-23656 #
CONF-9410131-6 ..... p 1837 N95-24158 #
CONF-9410132-4 ..... p 1659 N95-22549 #
CONF-9410134-3 ..... p 1842 N95-23354 #
CONF-9410141-5 ..... p 1732 N95-22781 #
CONF-9410154-4 ..... p 1661 N95-22844 #
CONF-9410156-3 ..... p 1758 N95-23567 #
CONF-941016-1 ..... p 1631 N95-22677 #
CONF-9410165-5 ..... p 1632 N95-22681 #
CONF-9410165-7 ..... p 1647 N95-22688 #
CONF-9410168-1 ..... p 1659 N95-22504 #
CONF-9410173-2 ..... p 1693 N95-22557 #
CONF-9410173-3 ..... p 1692 N95-22556 #
CONF-9410204-2 ..... p 1857 N95-23490 #
CONF-9410210-1 ..... p 1829 N95-22519 #
CONF-9410211-1 ..... p 1855 N95-22515 #
CONF-9410212-1 ..... p 1762 N95-22679 #
CONF-9410212-2 ..... p 1762 N95-22680 #
CONF-9410214-1 ..... p 1867 N95-22516 #
CONF-9410219-23 ..... p 1664 N95-24164 #
CONF-9410239-1 ..... p 1646 N95-22553 #
CONF-9410241-1 ..... p 1664 N95-24070 #
CONF-9410243-1 ..... p 1737 N95-22903 #
CONF-941039-1 ..... p 1639 N95-22594 #
CONF-941039-2 ..... p 1843 N95-23586 #
CONF-941039-3 ..... p 1843 N95-23585 #
CONF-941061-11 ..... p 1809 N95-23359 #
CONF-941061-13 ..... p 1767 N95-23578 #
CONF-941061-9 ..... p 1817 N95-23369 #
CONF-941063-1 ..... p 1640 N95-22835 #
CONF-941101-2 ..... p 1817 N95-23485 #
CONF-9411120-2 ..... p 1817 N95-23353 #
CONF-9411142-1 ..... p 1698 N95-22500 #
CONF-9411142-4 ..... p 1622 N95-23532 #
CONF-9411144-2 ..... p 1739 N95-23244 #
CONF-9411144-3 ..... p 1636 N95-24007 #
CONF-9411145-1 ..... p 1806 N95-23137 #
CONF-9411152-2 ..... p 1818 N95-24160 #
CONF-941117-2 ..... p 1728 N95-23133 #
CONF-9411118-9 ..... p 1765 N95-24074 #
CONF-941129-9 ..... p 1632 N95-22764 #
CONF-9411142-27 ..... p 1650 N95-24159 #
CONF-941144-11 ..... p 1842 N95-23365 #
CONF-941144-12 ..... p 1649 N95-23568 #
CONF-941144-13 ..... p 1649 N95-23268 #
CONF-941144-14 ..... p 1844 N95-24076 #
CONF-941144-15 ..... p 1636 N95-23573 #
CONF-941144-16 ..... p 1845 N95-24079 #
CONF-941144-20 ..... p 1846 N95-24169 #
CONF-941144-22 ..... p 1811 N95-23576 #
CONF-941144-23 ..... p 1650 N95-23577 #
CONF-941144-2 ..... p 1646 N95-24067 #
CONF-941144-3 ..... p 1842 N95-23265 #
CONF-941144-4 ..... p 1842 N95-23266 #
CONF-941144-7 ..... p 1844 N95-24073 #
CONF-941176-1 ..... p 1662 N95-23355 #
CONF-941203-10 ..... p 1845 N95-24156 #
CONF-941203-12 ..... p 1730 N95-23489 #
CONF-941203-1 ..... p 1731 N95-24155 #
CONF-941203-7 ..... p 1727 N95-22650 #
CONF-941203-8 ..... p 1731 N95-24090 #
CONF-941203-9 ..... p 1731 N95-24157 #
CONF-941220-1 ..... p 1766 N95-23134 #
CONF-941243-1 ..... p 1765 N95-24074 #
CONF-941247-1 ..... p 1828 N95-23575 #
CONF-950110-11 ..... p 1817 N95-23245 #
CONF-950110-13 ..... p 1842 N95-23135 #
CONF-950110-14 ..... p 1661 N95-22799 #
CONF-950110-9 ..... p 1624 N95-22905 #
CONF-950116-2 ..... p 1729 N95-23383 #
CONF-950116-3 ..... p 1694 N95-23056 #
CONF-950154-1 ..... p 1663 N95-23779 #
CONF-950221-1 ..... p 1799 N95-23979 #
CONF-950233-1 ..... p 1658 N95-23772 #
CONF-950240-4 ..... p 1759 N95-24020 #
CONF-950246-1 ..... p 1828 N95-24005 #
CONF-950256-1 ..... p 1662 N95-23334 #
CONF-950256-2 ..... p 1695 N95-23358 #
CONF-950344-4 ..... p 1664 N95-24149 #
CONF-950364-1 ..... p 1689 N95-24069 #

CPTH-A282-0194 ..... p 1851 N95-23922 #

CS-R9404 ..... p 1763 N95-23166 #

CSIRO-TR-32 ..... p 1721 N95-24192
CSIRO-TR-33 ..... p 1718 N95-23597
CSIRO-TR-34 ..... p 1718 N95-24026

CSRD-1207 ..... p 1791 N95-23600 #
CSRD-1248 ..... p 1764 N95-23599 #

CU-CAS-95-03 ..... p 1614 N95-23088 * #

CWI-NM-R9403 ..... p 1789 N95-23167
CWI-NM-R9406 ..... p 1787 N95-22717

DE94-011868 ..... p 1732 N95-22834 #

DE94-011883 ..... p 1694 N95-22923 #
DE94-011888 ..... p 1660 N95-22586 #
DE94-012072 ..... p 1640 N95-22835 #
DE94-012109 ..... p 1737 N95-22924 #
DE94-012285 ..... p 1730 N95-23977 #
DE94-012852 ..... p 1805 N95-22925 #
DE94-014023 ..... p 1652 N95-22587 #
DE94-014089 ..... p 1816 N95-22926 #
DE94-014105 ..... p 1744 N95-22588 #
DE94-014162 ..... p 1812 N95-23978 #
DE94-014249 ..... p 1744 N95-22589 #
DE94-014426 ..... p 1621 N95-22868 #
DE94-014473 ..... p 1799 N95-23979 #
DE94-014916 ..... p 1633 N95-22869 #
DE94-014961 ..... p 1745 N95-22590 #
DE94-014974 ..... p 1805 N95-22870 #
DE94-015558 ..... p 1855 N95-22871 #
DE94-016032 ..... p 1745 N95-22872 #
DE94-016222 ..... p 1745 N95-22873 #
DE94-016227 ..... p 1745 N95-22874 #
DE94-016228 ..... p 1748 N95-22875 #
DE94-016230 ..... p 1745 N95-22884 #
DE94-016358 ..... p 1813 N95-24046 #
DE94-016539 ..... p 1645 N95-23980
DE94-016559 ..... p 1624 N95-22885 #
DE94-016587 ..... p 1748 N95-23771 #
DE94-016591 ..... p 1746 N95-22912 #
DE94-016612 ..... p 1828 N95-23767 #
DE94-016621 ..... p 1633 N95-22886 #
DE94-016681 ..... p 1836 N95-23768 #
DE94-016714 ..... p 1659 N95-22504 #
DE94-016858 ..... p 1633 N95-22887 #
DE94-017083 ..... p 1746 N95-22913 #
DE94-017376 ..... p 1634 N95-23202 #
DE94-017518 ..... p 1832 N95-23119 #
DE94-017524 ..... p 1763 N95-22858 #
DE94-017525 ..... p 1763 N95-22859 #
DE94-017547 ..... p 1841 N95-22860 #
DE94-017606 ..... p 1832 N95-23120 #
DE94-017652 ..... p 1727 N95-22888 #
DE94-017655 ..... p 1727 N95-22861 #
DE94-017707 ..... p 1805 N95-22889 #
DE94-017768 ..... p 1650 N95-23981 #
DE94-017863 ..... p 1746 N95-22890 #
DE94-018044 ..... p 1837 N95-23982 #
DE94-018262 ..... p 1870 N95-22938 #
DE94-018274 ..... p 1658 N95-23772 #
DE94-018392 ..... p 1632 N95-22857 #
DE94-018900 ..... p 1868 N95-23656 #
DE94-018961 ..... p 1640 N95-23132 #
DE94-018963 ..... p 1640 N95-23121 #
DE94-018980 ..... p 1807 N95-23196 #
DE94-018982 ..... p 1808 N95-23197 #
DE94-018983 ..... p 1805 N95-22939 #
DE94-018985 ..... p 1689 N95-23520 #
DE94-018986 ..... p 1689 N95-23521 #
DE94-018987 ..... p 1808 N95-23203 #
DE94-018989 ..... p 1810 N95-23522 #
DE94-018996 ..... p 1808 N95-23242 #
DE94-019044 ..... p 1763 N95-23243 #
DE94-019048 ..... p 1790 N95-23536 #
DE94-019049 ..... p 1665 N95-22491 #
DE94-019096 ..... p 1728 N95-23162 #
DE94-019126 ..... p 1832 N95-23163 #
DE94-019159 ..... p 1657 N95-23075 #
DE94-019218 ..... p 1831 N95-22862 #
DE94-627282 ..... p 1814 N95-24175 #
DE94-627342 ..... p 1660 N95-22591 #
DE94-627393 ..... p 1839 N95-22606 #
DE94-627394 ..... p 1839 N95-22607 #
DE94-627416 ..... p 1640 N95-22840
DE94-627417 ..... p 1639 N95-22608 #
DE94-627480 ..... p 1639 N95-22609 #
DE94-627563 ..... p 1647 N95-22610 #
DE94-627641 ..... p 1647 N95-22611 #
DE94-627689 ..... p 1736 N95-22612 #
DE94-627710 ..... p 1736 N95-22613 #
DE94-628371 ..... p 1766 N95-22614 #
DE94-628382 ..... p 1839 N95-22615 #
DE94-628383 ..... p 1755 N95-22616 #
DE94-628392 ..... p 1795 N95-22617 #
DE94-628408 ..... p 1785 N95-22618 #
DE94-628409 ..... p 1785 N95-22619 #
DE94-628410 ..... p 1847 N95-22620 #
DE94-628411 ..... p 1786 N95-22642 #
DE94-628412 ..... p 1847 N95-22621 #
DE94-628413 ..... p 1829 N95-22622 #
DE94-628414 ..... p 1788 N95-22922
DE94-628415 ..... p 1795 N95-22623 #
DE94-628416 ..... p 1785 N95-22624 #
DE94-628417 ..... p 1785 N95-22625 #
DE94-628418 ..... p 1785 N95-22626 #
DE94-628419 ..... p 1785 N95-22627 #
DE94-628420 ..... p 1785 N95-22628 #
DE94-628421 ..... p 1786 N95-22629 #
DE94-628422 ..... p 1795 N95-22630 #
DE94-628423 ..... p 1786 N95-22631 #
DE94-628424 ..... p 1796 N95-22808 #
DE94-628425 ..... p 1787 N95-22809 #
DE94-628426 ..... p 1796 N95-22933 #
DE94-628427 ..... p 1850 N95-22782 #
DE94-628428 ..... p 1796 N95-22788 #
DE94-628429 ..... p 1787 N95-22794 #
DE94-628430 ..... p 1795 N95-22632 #
DE94-628431 ..... p 1786 N95-22633 #
DE94-628432 ..... p 1786 N95-22634 #
DE94-628433 ..... p 1847 N95-22635 #
DE94-628434 ..... p 1801 N95-22643 #
DE94-628469 ..... p 1840 N95-22839 #
DE94-628472 ..... p 1665 N95-22771 #
DE94-628473 ..... p 1787 N95-22772 #
DE94-628474 ..... p 1698 N95-22773 #
DE94-628475 ..... p 1840 N95-22774 #
DE94-628476 ..... p 1849 N95-22775 #
DE94-628477 ..... p 1800 N95-23018 #
DE94-628478 ..... p 1794 N95-23019 #
DE94-628479 ..... p 1841 N95-23020 #
DE94-628480 ..... p 1841 N95-23021 #
DE94-628481 ..... p 1841 N95-23022 #
DE94-628482 ..... p 1661 N95-23046 #
DE94-628483 ..... p 1842 N95-23047 #
DE94-628484 ..... p 1842 N95-23048 #
DE94-628485 ..... p 1850 N95-23049 #
DE94-628486 ..... p 1747 N95-23050 #
DE94-628487 ..... p 1788 N95-23051 #
DE94-628488 ..... p 1796 N95-23052 #
DE94-628489 ..... p 1747 N95-23053 #
DE94-628490 ..... p 1640 N95-23057 #
DE94-628491 ..... p 1747 N95-23058 #
DE94-628492 ..... p 1842 N95-23059 #
DE94-628493 ..... p 1747 N95-23060 #
DE94-628502 ..... p 1850 N95-22776 #
DE94-628503 ..... p 1787 N95-22750 #
DE94-628504 ..... p 1787 N95-22777 #
DE94-628505 ..... p 1656 N95-22841
DE94-628506 ..... p 1803 N95-22778 #
DE94-628507 ..... p 1850 N95-22779 #
DE94-628508 ..... p 1796 N95-22751 #
DE94-628509 ..... p 1849 N95-22752 #
DE94-628510 ..... p 1848 N95-22735 #
DE94-628511 ..... p 1795 N95-22736 #
DE94-628512 ..... p 1796 N95-22737 #
DE94-628513 ..... p 1848 N95-22738 #
DE94-628514 ..... p 1867 N95-22739 #
DE94-628515 ..... p 1796 N95-22740 #
DE94-628516 ..... p 1796 N95-22741 #
DE94-628517 ..... p 1848 N95-22742 #
DE94-628522 ..... p 1848 N95-22743 #
DE94-628559 ..... p 1848 N95-22744 #
DE94-628560 ..... p 1849 N95-22745 #
DE94-628570 ..... p 1655 N95-22746 #
DE94-628571 ..... p 1850 N95-22783 #
DE94-628577 ..... p 1850 N95-22784 #
DE94-628584 ..... p 1816 N95-22785 #
DE94-628585 ..... p 1804 N95-22786 #
DE94-628588 ..... p 1804 N95-22787 #
DE94-628597 ..... p 1804 N95-22789 #
DE94-628604 ..... p 1804 N95-22790 #
DE94-628609 ..... p 1802 N95-22720 #
DE94-628610 ..... p 1804 N95-22810 #
DE94-628611 ..... p 1804 N95-22811 #
DE94-628612 ..... p 1850 N95-22812 #
DE94-628613 ..... p 1849 N95-22753 #
DE94-628614 ..... p 1803 N95-22754 #
DE94-628615 ..... p 1803 N95-22755 #
DE94-628616 ..... p 1811 N95-23769 #
DE94-628621 ..... p 1811 N95-23770 #
DE94-628632 ..... p 1812 N95-23784 #
DE94-628633 ..... p 1812 N95-23785 #
DE94-628634 ..... p 1812 N95-23786 #
DE94-628635 ..... p 1803 N95-22756 #
DE94-628639 ..... p 1830 N95-22757 #
DE94-628847 ..... p 1803 N95-22758 #
DE94-628878 ..... p 1849 N95-22759 #
DE94-628879 ..... p 1849 N95-22760 #
DE94-628880 ..... p 1849 N95-22761 #
DE94-628881 ..... p 1804 N95-22791 #
DE94-628882 ..... p 1640 N95-22934 #
DE94-628902 ..... p 1805 N95-22935 #
DE94-629035 ..... p 1800 N95-22495 #
DE94-629038 ..... p 1847 N95-22496 #
DE94-629039 ..... p 1798 N95-22497 #
DE94-629040 ..... p 1801 N95-22498 #
DE94-629041 ..... p 1838 N95-22499 #
DE94-629043 ..... p 1847 N95-22545 #
DE94-629044 ..... p 1840 N95-22845 #
DE94-629045 ..... p 1839 N95-22649 #
DE94-629057 ..... p 1840 N95-22846 #
DE94-633202 ..... p 1804 N95-22847 #
DE94-633510 ..... p 1841 N95-22854 #
DE94-633512 ..... p 1734 N95-23541 #
DE94-633513 ..... p 1734 N95-23542 #
DE94-633975 ..... p 1727 N95-22855 #
DE94-634034 ..... p 1692 N95-23657 #
DE94-634268 ..... p 1856 N95-23452 #
DE94-634271 ..... p 1857 N95-23453 #
DE94-634280 ..... p 1851 N95-23454 #
DE94-634284 ..... p 1792 N95-23658 #
DE94-634286 ..... p 1792 N95-23659 #
DE94-634287 ..... p 1790 N95-23455 #
DE94-634320 ..... p 1810 N95-23456 #
DE94-634324 ..... p 1790 N95-23457 #
DE94-634325 ..... p 1796 N95-23660 #
DE94-634326 ..... p 1851 N95-23922 #
DE94-634328 ..... p 1797 N95-23661 #
DE94-634417 ..... p 1810 N95-23458 #
DE94-634435 ..... p 1811 N95-23773 #
DE94-634436 ..... p 1844 N95-23774 #
DE94-634944 ..... p 1645 N95-23983 #
DE94-635414 ..... p 1753 N95-23962 #
DE94-635415 ..... p 1759 N95-23963 #
DE94-635420 ..... p 1851 N95-23964 #
DE94-635421 ..... p 1797 N95-23965 #
DE94-635422 ..... p 1797 N95-23966 #
DE94-635423 ..... p 1851 N95-23967 #
DE94-635439 ..... p 1851 N95-23968 #
DE94-635440 ..... p 1851 N95-23969 #
DE94-635441 ..... p 1851 N95-23970 #
DE94-635446 ..... p 1792 N95-23971 #
DE94-635615 ..... p 1812 N95-23984 #
DE94-635632 ..... p 1794 N95-23972 #
DE94-635648 ..... p 1812 N95-23973 #
DE94-635654 ..... p 1812 N95-23974 #
DE94-635677 ..... p 1812 N95-23975 #
DE94-635759 ..... p 1812 N95-23976 #
DE94-635787 ..... p 1812 N95-23985 #
DE94-635788 ..... p 1844 N95-23986 #
DE94-765443 ..... p 1816 N95-22848 #
DE94-765448 ..... p 1816 N95-22644 #
DE94-765449 ..... p 1831 N95-22849 #
DE94-785267 ..... p 1810 N95-23475 #
DE94-785270 ..... p 1811 N95-23775 #
DE94-785273 ..... p 1635 N95-23476 #
DE94-785277 ..... p 1626 N95-23477 #
DE95-000223 ..... p 1729 N95-23383 #
DE95-000243 ..... p 1728 N95-23061 #
DE95-000244 ..... p 1727 N95-22842 #
DE95-000245 ..... p 1726 N95-22546 #
DE95-000246 ..... p 1728 N95-23062 #
DE95-000248 ..... p 1726 N95-22547 #
DE95-000293 ..... p 1730 N95-23776 #
DE95-000298 ..... p 1729 N95-23478 #
DE95-000299 ..... p 1730 N95-23777 #
DE95-000362 ..... p 1634 N95-23164 #
DE95-000710 ..... p 1832 N95-23072 #
DE95-000741 ..... p 1652 N95-22838 #
DE95-000816 ..... p 1801 N95-22583 #
DE95-000869 ..... p 1855 N95-22515 #
DE95-000873 ..... p 1867 N95-22516 #
DE95-000895 ..... p 1745 N95-22866 #
DE95-000902 ..... p 1631 N95-22517 #
DE95-000903 ..... p 1726 N95-22518 #
DE95-000913 ..... p 1829 N95-22519 #
DE95-000914 ..... p 1829 N95-22676 #
DE95-000918 ..... p 1631 N95-22677 #
DE95-000922 ..... p 1654 N95-22678 #
DE95-000924 ..... p 1762 N95-22679 #
DE95-000929 ..... p 1762 N95-22680 #
DE95-001127 ..... p 1632 N95-22681 #
DE95-001135 ..... p 1687 N95-22682 #
DE95-001151 ..... p 1627 N95-22683 #
DE95-001285 ..... p 1816 N95-22684 #
DE95-001286 ..... p 1801 N95-22685 #
DE95-001353 ..... p 1639 N95-22686 #
DE95-001356 ..... p 1840 N95-22687 #
DE95-001359 ..... p 1647 N95-22688 #
DE95-001360 ..... p 1647 N95-22689 #
DE95-001524 ..... p 1754 N95-22548 #
DE95-001573 ..... p 1736 N95-22843 #
DE95-001672 ..... p 1744 N95-22493 #
DE95-001884 ..... p 1661 N95-22844 #
DE95-001885 ..... p 1659 N95-22549 #
DE95-001886 ..... p 1698 N95-22500 #
DE95-001891 ..... p 1734 N95-23384 #
DE95-001893 ..... p 1742 N95-23385 #
DE95-002020 ..... p 1793 N95-22550 #
DE95-002052 ..... p 1740 N95-23386 #
DE95-002061 ..... p 1806 N95-23055 #
DE95-002188 ..... p 1694 N95-23056 #
DE95-002213 ..... p 1810 N95-23530 #
DE95-002267 ..... p 1766 N95-23078 #
DE95-002296 ..... p 1730 N95-23605 #
DE95-002351 ..... p 1756 N95-23079 #
DE95-002389 ..... p 1661 N95-23080 #
DE95-002411 ..... p 1827 N95-23531 #
DE95-002457 ..... p 1829 N95-22645 #
DE95-002483 ..... p 1666 N95-23081 #
DE95-002516 ..... p 1728 N95-23133 #

DE95-002530 ..... p 1801 N95-22646 #
DE95-002592 ..... p 1634 N95-23122 #
DE95-002599 ..... p 1646 N95-24140 #
DE95-002602 ..... p 1622 N95-23532 #
DE95-002603 ..... p 1766 N95-23134 #
DE95-002604 ..... p 1727 N95-22650 #
DE95-002610 ..... p 1842 N95-23135 #
DE95-002613 ..... p 1801 N95-22551 #
DE95-002616 ..... p 1832 N95-23136 #
DE95-002624 ..... p 1696 N95-24141 #
DE95-002655 ..... p 1626 N95-24142 #
DE95-002657 ..... p 1660 N95-22716 #
DE95-002701 ..... p 1739 N95-23244 #
DE95-002703 ..... p 1839 N95-22565 #
DE95-002705 ..... p 1739 N95-23256 #
DE95-002715 ..... p 1839 N95-22653 #
DE95-002716 ..... p 1798 N95-22552 #
DE95-002719 ..... p 1736 N95-22850 #
DE95-002724 ..... p 1817 N95-23245 #
DE95-002726 ..... p 1796 N95-22900 #
DE95-002732 ..... p 1795 N95-22654 #
DE95-002733 ..... p 1829 N95-22665 #
DE95-002734 ..... p 1847 N95-22655 #
DE95-002735 ..... p 1646 N95-22553 #
DE95-002741 ..... p 1666 N95-22901 #
DE95-002745 ..... p 1838 N95-22520 #
DE95-002748 ..... p 1666 N95-22902 #
DE95-002749 ..... p 1689 N95-24069 #
DE95-002752 ..... p 1737 N95-22903 #
DE95-002754 ..... p 1624 N95-22905 #
DE95-002782 ..... p 1801 N95-22521 #
DE95-002785 ..... p 1847 N95-22566 #
DE95-002810 ..... p 1833 N95-23246 #
DE95-002814 ..... p 1805 N95-22927 #
DE95-002815 ..... p 1805 N95-22936 #
DE95-002816 ..... p 1806 N95-23137 #
DE95-002847 ..... p 1726 N95-22554 #
DE95-002848 ..... p 1666 N95-22914 #
DE95-002850 ..... p 1838 N95-22555 #
DE95-002874 ..... p 1816 N95-22567 #
DE95-002902 ..... p 1692 N95-22556 #
DE95-002903 ..... p 1693 N95-22557 #
DE95-002905 ..... p 1664 N95-24070 #
DE95-002909 ..... p 1838 N95-22530 #
DE95-002910 ..... p 1726 N95-22568 #
DE95-002911 ..... p 1638 N95-22531 #
DE95-002913 ..... p 1840 N95-22762 #
DE95-002916 ..... p 1660 N95-22569 #
DE95-002917 ..... p 1754 N95-22570 #
DE95-002930 ..... p 1803 N95-22763 #
DE95-002931 ..... p 1828 N95-24005 #
DE95-002933 ..... p 1801 N95-22656 #
DE95-002941 ..... p 1638 N95-22532 #
DE95-002963 ..... p 1647 N95-22647 #
DE95-002965 ..... p 1647 N95-22648 #
DE95-002978 ..... p 1638 N95-22571 #
DE95-002984 ..... p 1638 N95-22592 #
DE95-002986 ..... p 1660 N95-22593 #
DE95-002988 ..... p 1632 N95-22764 #
DE95-002991 ..... p 1804 N95-22792 #
DE95-002992 ..... p 1639 N95-22594 #
DE95-002993 ..... p 1839 N95-22572 #
DE95-002994 ..... p 1801 N95-22573 #
DE95-002999 ..... p 1755 N95-22690 #
DE95-003001 ..... p 1731 N95-22691 #
DE95-003002 ..... p 1830 N95-22793 #
DE95-003003 ..... p 1632 N95-22795 #
DE95-003005 ..... p 1654 N95-22692 #
DE95-003007 ..... p 1693 N95-22796 #
DE95-003008 ..... p 1693 N95-22798 #
DE95-003019 ..... p 1830 N95-22693 #
DE95-003020 ..... p 1830 N95-22694 #
DE95-003031 ..... p 1652 N95-22721 #
DE95-003035 ..... p 1632 N95-22722 #
DE95-003036 ..... p 1819 N95-22723 #
DE95-003037 ..... p 1639 N95-22724 #
DE95-003039 ..... p 1661 N95-22799 #
DE95-003060 ..... p 1731 N95-22725 #
DE95-003065 ..... p 1759 N95-24006
DE95-003089 ..... p 1698 N95-22726 #
DE95-003091 ..... p 1802 N95-22727 #
DE95-003097 ..... p 1831 N95-22800 #
DE95-003099 ..... p 1748 N95-24075 #
DE95-003102 ..... p 1803 N95-22747 #
DE95-003103 ..... p 1691 N95-22748 #
DE95-003105 ..... p 1819 N95-22780 #
DE95-003106 ..... p 1803 N95-22749 #
DE95-003124 ..... p 1633 N95-22876 #
DE95-003133 ..... p 1732 N95-22781 #
DE95-003137 ..... p 1807 N95-23165 #
DE95-003138 ..... p 1808 N95-23226 #
DE95-003143 ..... p 1845 N95-24143 #
DE95-003144 ..... p 1646 N95-24144 #
DE95-003147 ..... p 1749 N95-24145 #
DE95-003149 ..... p 1735 N95-24146 #
DE95-003172 ..... p 1820 N95-22877 #
DE95-003185 ..... p 1743 N95-22878 #
DE95-003187 ..... p 1736 N95-22879 #
DE95-003198 ..... p 1693 N95-22880 #
DE95-003199 ..... p 1805 N95-22881 #
DE95-003200 ..... p 1848 N95-22728 #
DE95-003201 ..... p 1802 N95-22729 #
DE95-003202 ..... p 1802 N95-22730 #
DE95-003203 ..... p 1802 N95-22731 #
DE95-003206 ..... p 1639 N95-22732 #
DE95-003207 ..... p 1640 N95-22893 #
DE95-003218 ..... p 1756 N95-22894 #
DE95-003219 ..... p 1755 N95-22718 #
DE95-003256 ..... p 1830 N95-22719 #
DE95-003290 ..... p 1661 N95-22733 #
DE95-003307 ..... p 1795 N95-22734 #
DE95-003308 ..... p 1798 N95-22895 #
DE95-003311 ..... p 1661 N95-22896 #
DE95-003333 ..... p 1786 N95-22696 #
DE95-003335 ..... p 1802 N95-22697 #
DE95-003336 ..... p 1848 N95-22698 #
DE95-003337 ..... p 1802 N95-22699 #
DE95-003338 ..... p 1840 N95-22851
DE95-003339 ..... p 1746 N95-22897 #
DE95-003340 ..... p 1802 N95-22700 #
DE95-003341 ..... p 1743 N95-22695 #
DE95-003346 ..... p 1636 N95-24007 #
DE95-003347 ..... p 1740 N95-24008 #
DE95-003357 ..... p 1741 N95-24009 #
DE95-003366 ..... p 1742 N95-22701 #
DE95-003367 ..... p 1816 N95-22702 #
DE95-003369 ..... p 1802 N95-22703 #
DE95-003371 ..... p 1691 N95-22704 #
DE95-003372 ..... p 1806 N95-23138 #
DE95-003388 ..... p 1818 N95-24077 #
DE95-003405 ..... p 1806 N95-23054 #
DE95-003407 ..... p 1806 N95-23082 #
DE95-003408 ..... p 1798 N95-23083 #
DE95-003409 ..... p 1832 N95-23084 #
DE95-003411 ..... p 1832 N95-23147 #
DE95-003420 ..... p 1844 N95-24010 #
DE95-003423 ..... p 1844 N95-24011 #
DE95-003431 ..... p 1844 N95-24013 #
DE95-003442 ..... p 1818 N95-24014 #
DE95-003453 ..... p 1817 N95-23148 #
DE95-003466 ..... p 1806 N95-23139 #
DE95-003467 ..... p 1806 N95-23140 #
DE95-003468 ..... p 1807 N95-23141 #
DE95-003474 ..... p 1732 N95-22898 #
DE95-003475 ..... p 1831 N95-22899 #
DE95-003477 ..... p 1749 N95-23142 #
DE95-003479 ..... p 1738 N95-23143 #
DE95-003480 ..... p 1733 N95-23123 #
DE95-003481 ..... p 1733 N95-23124 #
DE95-003482 ..... p 1737 N95-23063 #
DE95-003497 ..... p 1813 N95-24000 #
DE95-003498 ..... p 1813 N95-24016 #
DE95-003510 ..... p 1658 N95-24015 #
DE95-003526 ..... p 1633 N95-23064 #
DE95-003589 ..... p 1694 N95-23065 #
DE95-003592 ..... p 1794 N95-23066 #
DE95-003607 ..... p 1735 N95-24147 #
DE95-003619 ..... p 1721 N95-24148 #
DE95-003628 ..... p 1837 N95-24017 #
DE95-003629 ..... p 1735 N95-24018 #
DE95-003630 ..... p 1616 N95-24019 #
DE95-003631 ..... p 1759 N95-24020 #
DE95-003633 ..... p 1664 N95-24149 #
DE95-003636 ..... p 1646 N95-24067 #
DE95-003640 ..... p 1690 N95-22595 #
DE95-003645 ..... p 1827 N95-23449 #
DE95-003657 ..... p 1727 N95-22574 #
DE95-003671 ..... p 1758 N95-23567 #
DE95-003674 ..... p 1692 N95-24072 #
DE95-003676 ..... p 1649 N95-23568 #
DE95-003677 ..... p 1842 N95-23365 #
DE95-003679 ..... p 1844 N95-24073 #
DE95-003680 ..... p 1842 N95-23265 #
DE95-003681 ..... p 1842 N95-23266 #
DE95-003683 ..... p 1868 N95-23570 #
DE95-003686 ..... p 1645 N95-23571 #
DE95-003693 ..... p 1794 N95-23349 #
DE95-003694 ..... p 1808 N95-23267 #
DE95-003695 ..... p 1843 N95-23366 #
DE95-003696 ..... p 1765 N95-24074 #
DE95-003703 ..... p 1844 N95-24076 #
DE95-003704 ..... p 1636 N95-23573 #
DE95-003705 ..... p 1649 N95-23268 #
DE95-003708 ..... p 1833 N95-23269 #
DE95-003714 ..... p 1741 N95-24078 #
DE95-003715 ..... p 1843 N95-23367 #
DE95-003718 ..... p 1662 N95-23368 #
DE95-003723 ..... p 1845 N95-24079 #
DE95-003727 ..... p 1809 N95-23403 #
DE95-003729 ..... p 1631 N95-22575 #
DE95-003739 ..... p 1664 N95-24081 #
DE95-003741 ..... p 1837 N95-24083 #
DE95-003742 ..... p 1818 N95-24084 #
DE95-003744 ..... p 1817 N95-23369 #
DE95-003745 ..... p 1809 N95-23404 #
DE95-003746 ..... p 1871 N95-23370 #
DE95-003747 ..... p 1663 N95-23405 #
DE95-003748 ..... p 1809 N95-23406 #
DE95-003755 ..... p 1663 N95-23479 #
DE95-003767 ..... p 1809 N95-23407 #
DE95-003770 ..... p 1808 N95-23350 #
DE95-003774 ..... p 1662 N95-23351 #
DE95-003796 ..... p 1725 N95-22501 #
DE95-003807 ..... p 1726 N95-22502 #
DE95-003811 ..... p 1638 N95-22576 #
DE95-003878 ..... p 1834 N95-23371 #
DE95-003879 ..... p 1837 N95-24086 #
DE95-003880 ..... p 1837 N95-24087 #
DE95-003896 ..... p 1668 N95-23372 #
DE95-003920 ..... p 1717 N95-22503 #
DE95-003936 ..... p 1695 N95-23373 #
DE95-003937 ..... p 1695 N95-23374 #
DE95-003938 ..... p 1800 N95-23375 #
DE95-003951 ..... p 1817 N95-23353 #
DE95-003952 ..... p 1842 N95-23354 #
DE95-003965 ..... p 1809 N95-23396 #
DE95-003967 ..... p 1857 N95-23574 #
DE95-004004 ..... p 1734 N95-23480 #
DE95-004007 ..... p 1730 N95-23778 #
DE95-004121 ..... p 1662 N95-23355 #
DE95-004132 ..... p 1696 N95-23397 #
DE95-004192 ..... p 1799 N95-23379 #
DE95-004205 ..... p 1662 N95-23334 #
DE95-004212 ..... p 1635 N95-23481 #
DE95-004215 ..... p 1729 N95-23482 #
DE95-004218 ..... p 1851 N95-23335 #
DE95-004240 ..... p 1808 N95-23336 #
DE95-004266 ..... p 1757 N95-23337 #
DE95-004293 ..... p 1851 N95-23352 #
DE95-004297 ..... p 1649 N95-23356 #
DE95-004308 ..... p 1833 N95-23338
DE95-004324 ..... p 1634 N95-23339 #
DE95-004341 ..... p 1808 N95-23357 #
DE95-004350 ..... p 1695 N95-23358 #
DE95-004353 ..... p 1809 N95-23359 #
DE95-004367 ..... p 1856 N95-23340 #
DE95-004369 ..... p 1856 N95-23341 #
DE95-004375 ..... p 1695 N95-23342 #
DE95-004393 ..... p 1635 N95-23360 #
DE95-004397 ..... p 1695 N95-23343 #
DE95-004405 ..... p 1729 N95-23361 #
DE95-004417 ..... p 1728 N95-23344 #
DE95-004435 ..... p 1733 N95-23362 #
DE95-004436 ..... p 1634 N95-23345 #
DE95-004450 ..... p 1630 N95-23924 #
DE95-004467 ..... p 1809 N95-23363 #
DE95-004469 ..... p 1757 N95-23346 #
DE95-004493 ..... p 1857 N95-24089 #
DE95-004514 ..... p 1677 N95-23483 #
DE95-004515 ..... p 1677 N95-23484 #
DE95-004520 ..... p 1663 N95-23779 #
DE95-004531 ..... p 1731 N95-24090 #
DE95-004532 ..... p 1731 N95-24155 #
DE95-004533 ..... p 1828 N95-23575 #
DE95-004539 ..... p 1845 N95-24156 #
DE95-004540 ..... p 1731 N95-24157 #
DE95-004541 ..... p 1837 N95-24158 #
DE95-004543 ..... p 1650 N95-24159 #
DE95-004544 ..... p 1818 N95-24160 #
DE95-004549 ..... p 1828 N95-24161 #
DE95-004552 ..... p 1811 N95-23576 #
DE95-004555 ..... p 1650 N95-23577 #
DE95-004567 ..... p 1767 N95-23578 #
DE95-004576 ..... p 1843 N95-23579 #
DE95-004579 ..... p 1735 N95-23580 #
DE95-004580 ..... p 1808 N95-23347 #
DE95-004581 ..... p 1811 N95-23581 #
DE95-004590 ..... p 1730 N95-23582 #
DE95-004591 ..... p 1857 N95-23490 #
DE95-004592 ..... p 1689 N95-23583 #
DE95-004602 ..... p 1818 N95-24162 #
DE95-004604 ..... p 1664 N95-24163 #
DE95-004605 ..... p 1845 N95-24150 #
DE95-004609 ..... p 1813 N95-24151 #
DE95-004611 ..... p 1845 N95-24152 #
DE95-004613 ..... p 1646 N95-24153 #
DE95-004614 ..... p 1810 N95-23491 #
DE95-004615 ..... p 1845 N95-24154 #
DE95-004616 ..... p 1664 N95-24164 #
DE95-004620 ..... p 1837 N95-24165 #
DE95-004625 ..... p 1813 N95-24166 #
DE95-004626 ..... p 1838 N95-24167 #
DE95-004629 ..... p 1846 N95-24168 #
DE95-004631 ..... p 1846 N95-24169 #
DE95-004633 ..... p 1846 N95-24170 #
DE95-004636 ..... p 1870 N95-23584 #
DE95-004639 ..... p 1846 N95-24171 #
DE95-004643 ..... p 1765 N95-24172 #

DE95-004649 ..... p 1846 N95-24173 #
DE95-004653 ..... p 1843 N95-23585 #
DE95-004655 ..... p 1843 N95-23586 #
DE95-004658 ..... p 1811 N95-23587 #
DE95-004663 ..... p 1688 N95-23492 #
DE95-004673 ..... p 1817 N95-23493 #
DE95-004680 ..... p 1663 N95-23494 #
DE95-004682 ..... p 1636 N95-23495 #
DE95-004683 ..... p 1817 N95-23485 #
DE95-004689 ..... p 1763 N95-23486 #
DE95-004690 ..... p 1692 N95-23487 #
DE95-004691 ..... p 1810 N95-23488 #
DE95-004729 ..... p 1730 N95-23489 #
DE95-004821 ..... p 1635 N95-23380 #
DE95-004823 ..... p 1635 N95-23381 #
DE95-005061 ..... p 1635 N95-23348 #
DE95-006077 ..... p 1813 N95-24174 #
DE95-723907 ..... p 1729 N95-23382 #

DOE/AL-20729/T2 ..... p 1726 N95-22518 #

DOE/CE-15974/T9 ..... p 1649 N95-23356 #
DOE/CE-50343/1 ..... p 1727 N95-22861 #
DOE/CE-50343/2 ..... p 1729 N95-23482 #

DOE/EA-0952 ..... p 1728 N95-23344 #

DOE/EH-0377T ..... p 1744 N95-22589 #

DOE/EIA-0573(11-94) ..... p 1731 N95-22691 #

DOE/ER-12115/T1 ..... p 1695 N95-23342 #
DOE/ER-13266/T5 ..... p 1802 N95-22700 #
DOE/ER-13394/T3 ..... p 1812 N95-23978 #
DOE/ER-13406/9 ..... p 1634 N95-23345 #
DOE/ER-13426/T3 ..... p 1748 N95-24075 #
DOE/ER-13465/9 ..... p 1631 N95-22575 #
DOE/ER-13529/T3 ..... p 1806 N95-23082 #
DOE/ER-13612/T1 ..... p 1631 N95-22517 #
DOE/ER-13631/T2 ..... p 1729 N95-23361 #
DOE/ER-13941/5 ..... p 1745 N95-22874 #
DOE/ER-13968/3 ..... p 1745 N95-22884 #
DOE/ER-14193/T1 ..... p 1646 N95-24144 #
DOE/ER-14278/4 ..... p 1743 N95-22695 #
DOE/ER-20042/2 ..... p 1745 N95-22873 #
DOE/ER-25175/1 ..... p 1661 N95-22733 #
DOE/ER-40333/147 ..... p 1805 N95-22881 #
DOE/ER-40448/T1 ..... p 1808 N95-23357 #
DOE/ER-40542/89 ..... p 1803 N95-22749 #
DOE/ER-40561/140 ..... p 1805 N95-22925 #
DOE/ER-40561/144 ..... p 1805 N95-22870 #
DOE/ER-40561/160 ..... p 1848 N95-22728 #
DOE/ER-40561/161 ..... p 1802 N95-22729 #
DOE/ER-40561/162 ..... p 1802 N95-22730 #
DOE/ER-40561/163 ..... p 1802 N95-22731 #
DOE/ER-40690/T1 ..... p 1817 N95-23148 #
DOE/ER-45150/T3 ..... p 1845 N95-24143 #
DOE/ER-45166/6 ..... p 1646 N95-24140 #
DOE/ER-45184/10 ..... p 1638 N95-22532 #
DOE/ER-45201/T2 ..... p 1630 N95-23924 #
DOE/ER-45229/34 ..... p 1627 N95-22683 #
DOE/ER-45281/T1 ..... p 1798 N95-23083 #
DOE/ER-45347/T3 ..... p 1806 N95-23054 #
DOE/ER-51124/19 ..... p 1832 N95-23147 #
DOE/ER-53198/251 ..... p 1809 N95-23363 #
DOE/ER-54196/2 ..... p 1832 N95-23084 #
DOE/ER-54221/1 ..... p 1832 N95-23120 #
DOE/ER-54241/133 ..... p 1831 N95-22862 #
DOE/ER-60503/365 ..... p 1803 N95-22747 #
DOE/ER-60503/367 ..... p 1691 N95-22748 #
DOE/ER-60600/4 ..... p 1748 N95-22875 #
DOE/ER-61206/3 ..... p 1733 N95-23362 #
DOE/ER-61218/4 ..... p 1736 N95-22879 #
DOE/ER-61443/3 ..... p 1819 N95-22780 #
DOE/ER-61700/1 ..... p 1743 N95-22878 #
DOE/ER-61728/T1 ..... p 1735 N95-24147 #
DOE/ER-79236/1 ..... p 1838 N95-22555 #

DOE/ET-53088/670 ..... p 1677 N95-23483 #
DOE/ET-53088/676 ..... p 1832 N95-23136 #
DOE/ET-53088/677 ..... p 1830 N95-22694 #
DOE/ET-53088/681 ..... p 1830 N95-22693 #
DOE/ET-53088/685 ..... p 1677 N95-23484 #

DOE/HR-0083 ..... p 1857 N95-23574 #

DOE/ID-12833/1 ..... p 1635 N95-23481 #

DOE/MC-29116/3913 ..... p 1687 N95-22682 #

DOE/METC-C/94/7134 ..... p 1728 N95-23162 #

DOE/METC-94-1010 ..... p 1730 N95-23977 #

DOE/NASA-0335/6 ..... p 1693 N95-22880 #

DOE/OR-22089/3D ..... p 1737 N95-22924 #

DOE/PC-79672/T9 ..... p 1833 N95-23338
DOE/PC-91301/11 ..... p 1634 N95-23202 #
DOE/PC-92106/T6 ..... p 1633 N95-23064 #
DOE/PC-92111/T6 ..... p 1634 N95-23164 #
DOE/PC-92542/T7 ..... p 1696 N95-24141 #
DOE/PC-93212/T3 ..... p 1745 N95-22872 #
DOE/PC-93222/4 ..... p 1634 N95-23339 #

DOT/FAA/AM-95/1 ..... p 1611 N95-24071 #
DOT/FAA/AM-95/3 ..... p 1750 N95-23934 #
DOT/FAA/AM-95/4 ..... p 1611 N95-23565 #
DOT/FAA/AM-95/6 ..... p 1758 N95-23603 #
DOT/FAA/AM-95/7 ..... p 1749 N95-23788 #
DOT/FAA/AM-95/8 ..... p 1610 N95-24024 #
DOT/FAA/AM-95/9 ..... p 1750 N95-24088 #

DSTO-RR-0005 ..... p 1699 N95-22952

DSTO-TR-0049 ..... p 1613 N95-23666
DSTO-TR-0078 ..... p 1743 N95-23667
DSTO-TR-0090 ..... p 1653 N95-23668

DTI/FR-95/2014 ..... p 1689 N95-23789 * #

DTIC-1994-S-1-REV ..... p 1854 N95-22494 #

E-24-X30 ..... p 1750 N95-22797 * #
E-8713 ..... p 1698 N95-22805 * #
E-8773 ..... p 1689 N95-23795 * #
E-9016 ..... p 1616 N95-23192 * #
E-9156 ..... p 1691 N95-22670 * #
E-9204 ..... p 1747 N95-23177 * #
E-9207 ..... p 1607 N95-24025 * #
E-9217 ..... p 1650 N95-24187 * #
E-9336 ..... p 1654 N95-23195 * #
E-9364 ..... p 1799 N95-22675 * #
E-9396 ..... p 1621 N95-22667 * #
E-9405 ..... p 1624 N95-23240 * #
E-9421 ..... p 1615 N95-22954 * #
E-9425 ..... p 1665 N95-22669 * #
E-9438 ..... p 1820 N95-22915 * #
E-9440 ..... p 1792 N95-23614 * #
E-9456 ..... p 1626 N95-24004 * #
E-9467 ..... p 1630 N95-23258 * #
E-9469 ..... p 1653 N95-24186 * #
E-9476 ..... p 1668 N95-23248 * #
E-9478 ..... p 1762 N95-22668 * #
E-9481 ..... p 1688 N95-23461 * #
E-9482 ..... p 1662 N95-23219 * #
E-9485 ..... p 1677 N95-23451 * #
E-9487 ..... p 1668 N95-23220 * #
E-9489 ..... p 1728 N95-23259 * #
E-9491 ..... p 1800 N95-23178 * #
E-9493 ..... p 1614 N95-23222 * #
E-9494 ..... p 1846 N95-24188 * #
E-9501 ..... p 1625 N95-23450 * #
E-9511 ..... p 1855 N95-23206 * #
E-9518 ..... p 1699 N95-24055 * #
E-9520 ..... p 1677 N95-23464 * #
E-9521 ..... p 1616 N95-23671 * #
E-9528 ..... p 1630 N95-23463 * #
E-9530 ..... p 1614 N95-23550 * #
E-9533 ..... p 1738 N95-23116 * #
E-9538 ..... p 1609 N95-23462 * #
E-9552 ..... p 1699 N95-24189 * #
E-9583 ..... p 1614 N95-24053 * #
E-9585 ..... p 1625 N95-23790 * #
E-9586 ..... p 1625 N95-23791 * #
E-9589 ..... p 1696 N95-23792 * #

EGG-EES-11478 ..... p 1740 N95-23386 #

EGG-RAAM-11086 ..... p 1793 N95-22550 #

EGG-11265-1075 ..... p 1721 N95-24148 #
EGG-11265-1092 ..... p 1717 N95-22503 #

EOARD-TR-94-07 ..... p 1609 N95-23201 #

ESC-TR-93-293 ..... p 1622 N95-23781 #

FAA-AC-91-70 ..... p 1610 N95-24065 #

FAA-AFS-550 ..... p 1610 N95-24065 #

FE-MIT-92111-7 ..... p 1634 N95-23164 #

FEW-644 ..... p 1786 N95-22641 #
FEW-652 ..... p 1795 N95-23555 #
FEW-659 ..... p 1788 N95-23068 #
FEW-661 ..... p 1788 N95-23069 #
FEW-662 ..... p 1788 N95-23070 #

FNAL-TM-1906 ..... p 1818 N95-24077 #

FNAL-TM-1913 ..... p 1663 N95-23405 #

FNAL/C-93/334-E ..... p 1813 N95-24000 #
FNAL/C-94/205-E ..... p 1689 N95-23521 #
FNAL/C-94/212-E ..... p 1808 N95-23242 #
FNAL/C-94/215-E ..... p 1807 N95-23196 #
FNAL/C-94/227-E ..... p 1808 N95-23203 #
FNAL/C-94/228-E ..... p 1805 N95-22939 #
FNAL/C-94/235-E ..... p 1808 N95-23197 #
FNAL/C-94/242-E ..... p 1689 N95-23520 #
FNAL/C-94/258-E ..... p 1810 N95-23522 #
FNAL/C-94/282-E ..... p 1813 N95-24016 #
FNAL/C-94/289-E ..... p 1809 N95-23404 #
FNAL/C-94/293-E ..... p 1811 N95-23581 #
FNAL/C-94/310-E ..... p 1816 N95-22684 #
FNAL/C-94/312 ..... p 1871 N95-23370 #
FNAL/C-94/317-E ..... p 1810 N95-23530 #
FNAL/C-94/318-E ..... p 1818 N95-24084 #
FNAL/C-94/319E ..... p 1801 N95-22685 #
FNAL/C-94/328-E ..... p 1808 N95-23336 #
FNAL/C-94/347-E ..... p 1801 N95-22646 #
FNAL/C-94/365-E ..... p 1808 N95-23347 #
FNAL/C-94/370 ..... p 1817 N95-23369 #
FNAL/C-94/372 ..... p 1664 N95-24081 #
FNAL/C-94/374-E ..... p 1809 N95-23406 #
FNAL/C-94/399 ..... p 1809 N95-23359 #

GA-A-21671 ..... p 1829 N95-22645 #
GA-A-21695 ..... p 1836 N95-23768 #
GA-A-21706 ..... p 1832 N95-23119 #
GA-A-21711 ..... p 1830 N95-22719 #
GA-A-21787 ..... p 1693 N95-22796 #
GA-A-21788 ..... p 1693 N95-22798 #
GA-A-21789 ..... p 1837 N95-24083 #
GA-A-21799 ..... p 1834 N95-23371 #
GA-A-21821 ..... p 1837 N95-24087 #
GA-A-21840 ..... p 1837 N95-24086 #

GA-C21601 ..... p 1732 N95-22856 #

GAO/NSIAD-95-21 ..... p 1853 N95-23588 #
GAO/NSIAD-95-40 ..... p 1854 N95-24054 #
GAO/NSIAD-95-52 ..... p 1613 N95-24091 #
GAO/NSIAD-95-70 ..... p 1735 N95-24057 #
GAO/NSIAD-95-78 ..... p 1903 N95-24080 #
GAO/NSIAD-95-92 ..... p 1864 N95-24062 #

GAO/OSI-95-9 ..... p 1854 N95-24085 #

GLOBO-2 ..... p 1733 N95-23067 #

GMD-231 ..... p 1758 N95-23553

GRI-94/0268 ..... p 1732 N95-22865 #

H-1984 ..... p 1612 N95-22806 * #
H-2040 ..... p 1612 N95-22829 * #

HEP-PH-9310368 ..... p 1812 N95-23784 #
HEP-PH-9311204 ..... p 1812 N95-23785 #
HEP-PH-9311359 ..... p 1804 N95-22790 #

HEP-TH-9401100 ..... p 1848 N95-22738 #
HEP-TH-9406005 ..... p 1790 N95-23457 #

HIFAN-666 ..... p 1818 N95-24014 #

IAEA-CN-60/A3/5-P-11 ..... p 1834 N95-23371 #

IAEA-NDS-144 ..... p 1811 N95-23773 #
IAEA-NDS-150(REV-94/2) ..... p 1856 N95-23452 #
IAEA-NDS-7(REV-94/1) ..... p 1857 N95-23453 #
IAEA-NDS-90(REV-7) ..... p 1810 N95-23458 #

IC-93/128 ..... p 1785 N95-22618 #
IC-93/217 ..... p 1850 N95-22776 #
IC-93/261 ..... p 1849 N95-22759 #
IC-93/262 ..... p 1849 N95-22760 #
IC-93/263 ..... p 1849 N95-22761 #
IC-93/271 ..... p 1816 N95-22785 #
IC-93/285 ..... p 1787 N95-22750 #
IC-93/293 ..... p 1640 N95-22840
IC-93/294 ..... p 1639 N95-22608 #
IC-93/295 ..... p 1785 N95-22619 #
IC-93/296 ..... p 1847 N95-22620 #
IC-93/297 ..... p 1787 N95-22777 #
IC-93/308 ..... p 1786 N95-22642 #
IC-93/309 ..... p 1847 N95-22621 #
IC-93/310 ..... p 1829 N95-22622 #
IC-93/311 ..... p 1655 N95-22746 #
IC-93/314 ..... p 1804 N95-22789 #
IC-93/317 ..... p 1665 N95-22771 #
IC-93/318 ..... p 1787 N95-22772 #
IC-93/319 ..... p 1788 N95-22922
IC-93/320 ..... p 1656 N95-22841
IC-93/321 ..... p 1698 N95-22773 #

IC-93/322 ..... p 1840 N95-22774 #
IC-93/323 ..... p 1802 N95-22720 #
IC-93/324 ..... p 1839 N95-22606 #
IC-93/325 ..... p 1849 N95-22775 #
IC-93/326 ..... p 1795 N95-22617 #
IC-93/327 ..... p 1803 N95-22778 #
IC-93/328 ..... p 1850 N95-22779 #
IC-93/331 ..... p 1805 N95-22935 #
IC-93/333 ..... p 1795 N95-22623 #
IC-93/335 ..... p 1800 N95-23018 #
IC-93/336 ..... p 1840 N95-22846 #
IC-93/337 ..... p 1794 N95-23019 #
IC-93/340 ..... p 1850 N95-22784 #
IC-93/344 ..... p 1785 N95-22624 #
IC-93/347 ..... p 1839 N95-22607 #
IC-93/349 ..... p 1785 N95-22625 #
IC-93/350 ..... p 1811 N95-23770 #
IC-93/351 ..... p 1785 N95-22626 #
IC-93/353 ..... p 1796 N95-22751 #
IC-93/354 ..... p 1800 N95-22495 #
IC-93/355 ..... p 1804 N95-22810 #
IC-93/356 ..... p 1849 N95-22752 #
IC-93/357 ..... p 1841 N95-23020 #
IC-93/358 ..... p 1785 N95-22627 #
IC-93/359 ..... p 1812 N95-23784 #
IC-93/360 ..... p 1812 N95-23785 #
IC-93/361 ..... p 1841 N95-23021 #
IC-93/362 ..... p 1841 N95-23022 #
IC-93/363 ..... p 1661 N95-23046 #
IC-93/365 ..... p 1660 N95-22591 #
IC-93/367 ..... p 1842 N95-23047 #
IC-93/368 ..... p 1736 N95-22613 #
IC-93/369 ..... p 1842 N95-23048 #
IC-93/375 ..... p 1850 N95-23049 #
IC-93/379 ..... p 1848 N95-22735 #
IC-93/380 ..... p 1785 N95-22628 #
IC-93/381 ..... p 1747 N95-23050 #
IC-93/384 ..... p 1803 N95-22758 #
IC-93/385 ..... p 1647 N95-22610 #
IC-93/386 ..... p 1647 N95-22611 #
IC-93/388 ..... p 1804 N95-22790 #
IC-93/389 ..... p 1788 N95-23051 #
IC-93/391 ..... p 1796 N95-23052 #
IC-93/392 ..... p 1786 N95-22629 #
IC-93/393 ..... p 1847 N95-22496 #
IC-93/394 ..... p 1798 N95-22497 #
IC-93/398 ..... p 1747 N95-23053 #
IC-93/399 ..... p 1795 N95-22736 #
IC-93/402 ..... p 1796 N95-22737 #
IC-93/414 ..... p 1736 N95-22612 #
IC-93/423 ..... p 1804 N95-22791 #
IC-93/426 ..... p 1795 N95-22630 #
IC-94/10 ..... p 1804 N95-22811 #
IC-94/112 ..... p 1790 N95-23457 #
IC-94/115 ..... p 1796 N95-23660 #
IC-94/117 ..... p 1851 N95-23454 #
IC-94/11 ..... p 1848 N95-22738 #
IC-94/126 ..... p 1812 N95-23985 #
IC-94/15 ..... p 1804 N95-22786 #
IC-94/16 ..... p 1867 N95-22739 #
IC-94/19 ..... p 1801 N95-22498 #
IC-94/1 ..... p 1840 N95-22839 #
IC-94/20 ..... p 1838 N95-22499 #
IC-94/23 ..... p 1847 N95-22545 #
IC-94/24 ..... p 1840 N95-22845 #
IC-94/25 ..... p 1640 N95-22934 #
IC-94/27 ..... p 1839 N95-22649 #
IC-94/28 ..... p 1848 N95-22744 #
IC-94/29 ..... p 1850 N95-22812 #
IC-94/30 ..... p 1849 N95-22753 #
IC-94/31 ..... p 1803 N95-22754 #
IC-94/32 ..... p 1849 N95-22745 #
IC-94/33 ..... p 1812 N95-23786 #
IC-94/35 ..... p 1786 N95-22631 #
IC-94/36 ..... p 1839 N95-22615 #
IC-94/37 ..... p 1796 N95-22740 #
IC-94/39 ..... p 1796 N95-22808 #
IC-94/40 ..... p 1850 N95-22783 #
IC-94/42 ..... p 1803 N95-22756 #
IC-94/44 ..... p 1787 N95-22809 #
IC-94/45 ..... p 1755 N95-22616 #
IC-94/47 ..... p 1796 N95-22933 #
IC-94/50 ..... p 1640 N95-23057 #
IC-94/51 ..... p 1796 N95-22788 #
IC-94/52 ..... p 1796 N95-22741 #
IC-94/56 ..... p 1848 N95-22742 #
IC-94/57 ..... p 1787 N95-22794 #
IC-94/58 ..... p 1795 N95-22632 #
IC-94/59 ..... p 1747 N95-23058 #
IC-94/5 ..... p 1850 N95-22782 #
IC-94/61 ..... p 1786 N95-22633 #
IC-94/63 ..... p 1842 N95-23059 #
IC-94/66 ..... p 1786 N95-22634 #
IC-94/68 ..... p 1847 N95-22635 #
IC-94/72 ..... p 1851 N95-23922 #
IC-94/75 ..... p 1747 N95-23060 #

IC-94/80 ..... p 1797 N95-23661 #
IC-94/83 ..... p 1810 N95-23456 #
IC-94/86 ..... p 1792 N95-23971 #
IC-94/8 ..... p 1801 N95-22643 #
IC-94/91 ..... p 1792 N95-23658 #
IC-94/92 ..... p 1844 N95-23986 #
IC-94/94 ..... p 1792 N95-23659 #
IC-94/96 ..... p 1790 N95-23455 #
IC-94/9 ..... p 1803 N95-22755 #

ICASE-95-10 ..... p 1790 N95-23465 * #
ICASE-95-12 ..... p 1678 N95-23596 * #
ICASE-95-1 ..... p 1678 N95-23544 * #
ICASE-95-3 ..... p 1788 N95-22931 * #
ICASE-95-5 ..... p 1677 N95-23466 * #
ICASE-95-6 ..... p 1667 N95-23207 * #
ICASE-95-9 ..... p 1758 N95-23613 * #

ICOMP-95-01 ..... p 1677 N95-23464 * #
ICOMP-95-4 ..... p 1677 N95-23451 * #
ICOMP-95-5 ..... p 1668 N95-23220 * #

IFSR-670 ..... p 1677 N95-23483 #
IFSR-677 ..... p 1830 N95-22694 #
IFSR-681 ..... p 1830 N95-22693 #
IFSR-685 ..... p 1677 N95-23484 #

IHES/M/94/30 ..... p 1786 N95-22711 #
IHES/M/94/31 ..... p 1795 N95-22712 #
IHES/M/94/37 ..... p 1787 N95-22836 #
IHES/M/94/40 ..... p 1788 N95-23076 #
IHES/M/94/42 ..... p 1787 N95-22837

IHES/P/94/32 ..... p 1787 N95-22715 #

INDC(NDS)-297 ..... p 1830 N95-22757 #

INIS-AR-066 ..... p 1645 N95-23983 #
INIS-AR-073 ..... p 1759 N95-23963 #

INIS-BR-3343 ..... p 1639 N95-22609 #

INIS-MF-13868 ..... p 1727 N95-22855 #
INIS-MF-13903 ..... p 1841 N95-22854 #

INS-J-177 ..... p 1810 N95-23475 #

INS-1024 ..... p 1811 N95-23775 #
INS-978 ..... p 1816 N95-22848 #
INS-981 ..... p 1816 N95-22644 #

INT-PATENT-CLASS-A63B-21/008 p 1751 N95-23264 *

INT-PATENT-CLASS-B29C-39/12 p 1750 N95-22766 *
INT-PATENT-CLASS-B29C-67/14 p 1750 N95-22766 *
INT-PATENT-CLASS-B32B-18/00 p 1649 N95-23394 *
INT-PATENT-CLASS-B64C-11/00 p 1688 N95-23377 *
INT-PATENT-CLASS-B64C-19/00 p 1615 N95-23389 *
INT-PATENT-CLASS-B64C-5/00 . p 1612 N95-23390 *
INT-PATENT-CLASS-B64C-9/16 . p 1613 N95-23395 *

INT-PATENT-CLASS-C08G-10/02 p 1649 N95-23253 *
INT-PATENT-CLASS-C09J-5/00 .. p 1649 N95-23254 *
INT-PATENT-CLASS-C23C-14/00 p 1647 N95-22558 *

INT-PATENT-CLASS-F28D-17/00 p 1695 N95-23376 *

INT-PATENT-CLASS-G01N-3/20 . p 1688 N95-23263 *
INT-PATENT-CLASS-G02B-6/16 . p 1819 N95-22807 *
INT-PATENT-CLASS-G06F-11/10 p 1754 N95-22577 *
INT-PATENT-CLASS-G06F-15/00 p 1692 N95-22543 * #
INT-PATENT-CLASS-G06F-15/336 p 1827 N95-23045 *
INT-PATENT-CLASS-G06F-15/44 p 1749 N95-22579 *
INT-PATENT-CLASS-G06K-9/46 . p 1767 N95-23387 *
INT-PATENT-CLASS-G06K-9/64 . p 1827 N95-23045 *
INT-PATENT-CLASS-G08B-21/00 p 1611 N95-23393 *

INT-PATENT-CLASS-H01L-27/14 p 1827 N95-23378 *
INT-PATENT-CLASS-H01L-31/00 p 1827 N95-23378 *
INT-PATENT-CLASS-H03M-13/00 p 1754 N95-22577 *
INT-PATENT-CLASS-H04N-9/04 . p 1819 N95-22765 *

IS-T-1710 ..... p 1744 N95-22493 #

ISAS-R-657 ..... p 1811 N95-23604 #

ISBN-0-16-045310-0 ..... p 1717 N95-22713 #
ISBN-0-643-05257-7 ..... p 1721 N95-24192
ISBN-0-643-05600-9 ..... p 1718 N95-23597
ISBN-0-643-05601-7 ..... p 1718 N95-24026
ISBN-92-836-1009-1 ..... p 1751 N95-23601 #
ISBN-92-836-1010-5 ..... p 1697 N95-23602 #
ISBN-92-836-1011-3 ..... p 1641 N95-23496 #
ISBN-951-22-2028-8 ..... p 1764 N95-23538 #
ISBN-951-22-2166-7 ..... p 1636 N95-23554

ISI/RR-94-377 ..... p 1766 N95-22512 #

IYAF-93-52 ..... p 1804 N95-22847 #
IYAF-93-75 ..... p 1692 N95-23657 #

JAERI-M-93-219 ..... p 1831 N95-22849 #
JAERI-M-94-017 ..... p 1626 N95-23477 #

JAERI-1331 ..... p 1635 N95-23476 #

JINR-D-11-93-317 ..... p 1766 N95-22614 #

JINR-E-1-93-305 ..... p 1811 N95-23769 #
JINR-E-2-93-38 ..... p 1804 N95-22787 #
JINR-E-2-93-46 ..... p 1848 N95-22743 #
JINR-E-2-94-21 ..... p 1851 N95-23964 #
JINR-E-2-94-27 ..... p 1812 N95-23974 #
JINR-E-2-94-43 ..... p 1794 N95-23972 #
JINR-E-2-94-46 ..... p 1812 N95-23973 #
JINR-E-2-94-71 ..... p 1812 N95-23984 #
JINR-E-2-94-90 ..... p 1851 N95-23969 #
JINR-E-2-94-92 ..... p 1812 N95-23975 #

JINR-R-15-94-47 ..... p 1812 N95-23976 #
JINR-R-2-94-18 ..... p 1851 N95-23968 #
JINR-R-2-94-84 ..... p 1851 N95-23970 #
JINR-R-4-94-63 ..... p 1797 N95-23965 #
JINR-R-4-94-65 ..... p 1797 N95-23966 #
JINR-R-5-94-51 ..... p 1851 N95-23967 #

JPL-PUBL-83-39-REV-5 ..... p 1756 N95-22853 * #
JPL-PUBL-93-009-ADD ..... p 1655 N95-22813 * #
JPL-PUBL-93-26-VOL-1 ..... p 1701 N95-23844 * #
JPL-PUBL-93-26-VOL-2 ..... p 1711 N95-23917 * #
JPL-PUBL-93-26-VOL-3 ..... p 1712 N95-23938 * #
JPL-PUBL-94-11 ..... p 1865 N95-22539 * #
JPL-PUBL-94-15 ..... p 1656 N95-22852 * #
JPL-PUBL-94-20 ..... p 1761 N95-22478 * #
JPL-PUBL-94-23 ..... p 1767 N95-23672 * #

KCP-613-4805 ..... p 1800 N95-23375 #
KCP-613-4808 ..... p 1695 N95-23374 #
KCP-613-4884 ..... p 1695 N95-23343 #
KCP-613-5302 ..... p 1695 N95-23373 #

L-16553A-VOL-1 ..... p 1754 N95-22603 * #
L-16553B-VOL-2 ..... p 1755 N95-22604 * #
L-16553C-VOL-3 ..... p 1753 N95-22479 * #
L-16553D-VOL-4 ..... p 1755 N95-22605 * #
L-17233 ..... p 1612 N95-22953 * #
L-17348 ..... p 1666 N95-23015 * #
L-17348 ..... p 1667 N95-23210 * #
L-17380 ..... p 1607 N95-22802 * #
L-17391 ..... p 1691 N95-23411 * #
L-17428 ..... p 1817 N95-22929 * #
L-17430A-PT-1 ..... p 1889 N95-23796 * #
L-17430B-PT-2 ..... p 1899 N95-23896 * #
L-17439 ..... p 1840 N95-22803 * #
L-9452 ..... p 1626 N95-23270 * #

LA-UR-94-1390 ..... p 1843 N95-23367 #
LA-UR-94-1947 ..... p 1663 N95-23479 #
LA-UR-94-2077 ..... p 1799 N95-23979 #
LA-UR-94-2180 ..... p 1621 N95-22868 #
LA-UR-94-2741 ..... p 1870 N95-22938 #
LA-UR-94-2790 ..... p 1658 N95-23772 #
LA-UR-94-2956 ..... p 1741 N95-24078 #
LA-UR-94-3067 ..... p 1867 N95-22516 #
LA-UR-94-3086 ..... p 1855 N95-22515 #
LA-UR-94-3166 ..... p 1654 N95-22678 #
LA-UR-94-3179 ..... p 1631 N95-22677 #
LA-UR-94-3182 ..... p 1829 N95-22676 #
LA-UR-94-3185 ..... p 1829 N95-22519 #
LA-UR-94-3326 ..... p 1817 N95-23245 #
LA-UR-94-3374 ..... p 1762 N95-22679 #
LA-UR-94-3385 ..... p 1762 N95-22680 #
LA-UR-94-3406 ..... p 1739 N95-23244 #
LA-UR-94-3422 ..... p 1839 N95-22565 #
LA-UR-94-3445 ..... p 1739 N95-23256 #
LA-UR-94-3486 ..... p 1798 N95-22552 #
LA-UR-94-3488 ..... p 1839 N95-22653 #
LA-UR-94-3493 ..... p 1736 N95-22850 #
LA-UR-94-3510 ..... p 1829 N95-22665 #
LA-UR-94-3523 ..... p 1646 N95-22553 #
LA-UR-94-3528 ..... p 1847 N95-22655 #
LA-UR-94-3546 ..... p 1666 N95-22901 #
LA-UR-94-3568 ..... p 1838 N95-22520 #
LA-UR-94-3585 ..... p 1666 N95-22902 #
LA-UR-94-3622 ..... p 1796 N95-22900 #
LA-UR-94-3641 ..... p 1795 N95-22654 #
LA-UR-94-3650 ..... p 1801 N95-22551 #
LA-UR-94-3653 ..... p 1689 N95-24069 #
LA-UR-94-3658 ..... p 1737 N95-22903 #
LA-UR-94-3660 ..... p 1624 N95-22905 #
LA-UR-94-3664 ..... p 1833 N95-23269 #
LA-UR-94-3676 ..... p 1805 N95-22936 #

LA-UR-94-3677 ..... p 1805 N95-22927 #
LA-UR-94-3678 ..... p 1806 N95-23137 #
LA-UR-94-3706 ..... p 1658 N95-24015 #
LA-UR-94-3725 ..... p 1662 N95-23368 #
LA-UR-94-3726 ..... p 1845 N95-24079 #
LA-UR-94-3728 ..... p 1809 N95-23403 #
LA-UR-94-3766 ..... p 1868 N95-23570 #
LA-UR-94-3789 ..... p 1645 N95-23571 #
LA-UR-94-3816 ..... p 1794 N95-23349 #
LA-UR-94-3835 ..... p 1765 N95-24074 #
LA-UR-94-3850 ..... p 1843 N95-23366 #
LA-UR-94-3852 ..... p 1808 N95-23267 #
LA-UR-94-3872 ..... p 1844 N95-24076 #
LA-UR-94-3930 ..... p 1636 N95-23573 #
LA-UR-94-3935 ..... p 1649 N95-23268 #
LA-UR-94-3978 ..... p 1758 N95-23567 #
LA-UR-94-3985 ..... p 1692 N95-24072 #
LA-UR-94-3999 ..... p 1649 N95-23568 #
LA-UR-94-4043 ..... p 1842 N95-23365 #
LA-UR-94-4051 ..... p 1844 N95-24073 #
LA-UR-94-4052 ..... p 1842 N95-23265 #
LA-UR-94-4071 ..... p 1842 N95-23266 #
LA-UR-94-4084 ..... p 1646 N95-24067 #

LA-12874-MS ..... p 1635 N95-23360 #

LAMP-94/4 ..... p 1844 N95-23774 #

LBL-35242 ..... p 1725 N95-22501 #
LBL-35434 ..... p 1844 N95-24010 #
LBL-35519 ..... p 1633 N95-22869 #
LBL-35672 ..... p 1745 N95-22590 #
LBL-35679 ..... p 1844 N95-24011 #
LBL-35769 ..... p 1626 N95-24142 #
LBL-35841 ..... p 1756 N95-23079 #
LBL-35911 ..... p 1816 N95-22567 #
LBL-35960 ..... p 1818 N95-24014 #
LBL-36024 ..... p 1763 N95-23486 #
LBL-36055 ..... p 1692 N95-23487 #
LBL-36180 ..... p 1817 N95-23485 #
LBL-36233 ..... p 1817 N95-23493 #
LBL-36256 ..... p 1844 N95-24013 #
LBL-36293 ..... p 1663 N95-23494 #
LBL-36353 ..... p 1810 N95-23488 #
LBL-36383 ..... p 1636 N95-23495 #
LBL-36510 ..... p 1635 N95-23380 #

LC-79-640375 ..... p 1870 N95-23925 #
LC-79-640375 ..... p 1870 N95-23926 #

M-726-PT-1 ..... p 1678 N95-23615 * #
M-726-PT-2 ..... p 1668 N95-23412 * #
M-745 ..... p 1617 N95-23549 * #
M-771 ..... p 1641 N95-23186 * #

MEMO-INF-94-01 ..... p 1756 N95-23071 #
MEMO-INF-94-35 ..... p 1648 N95-23128

MEMO-1155 ..... p 1767 N95-23557 #
MEMO-1157 ..... p 1767 N95-23558
MEMO-1158 ..... p 1794 N95-23559 #
MEMO-1159 ..... p 1790 N95-23237 #
MEMO-1160 ..... p 1757 N95-23238 #
MEMO-1162 ..... p 1794 N95-23239 #
MEMO-1163 ..... p 1758 N95-23608
MEMO-1166 ..... p 1790 N95-23235 #
MEMO-1167 ..... p 1790 N95-23236 #

MIT-TR-998 ..... p 1622 N95-23781 #

MZ-TH-93-23 ..... p 1804 N95-22789 #

NAHRES-18 ..... p 1734 N95-23541 #
NAHRES-19 ..... p 1734 N95-23542 #

NAL-TR-1229T ..... p 1687 N95-24082 #
NAL-TR-1237T ..... p 1637 N95-24181 #
NAL-TR-1239 ..... p 1622 N95-24049 #
NAL-TR-1240T ..... p 1687 N95-24051 #

NAS 1.15:104566-VOL-25-REV-1 p 1743 N95-22671 * #
NAS 1.15:104606-VOL-4 ..... p 1740 N95-23529 * #
NAS 1.15:104615 ..... p 1856 N95-23209 * #
NAS 1.15:104803 ..... p 1617 N95-23262 * #
NAS 1.15:106309 ..... p 1747 N95-23177 * #
NAS 1.15:106744 ..... p 1691 N95-22670 * #
NAS 1.15:106764 ..... p 1607 N95-24025 * #
NAS 1.15:106769 ..... p 1650 N95-24187 * #
NAS 1.15:106835 ..... p 1621 N95-22667 * #
NAS 1.15:106841 ..... p 1624 N95-23240 * #
NAS 1.15:106842 ..... p 1624 N95-23221 * #
NAS 1.15:106847 ..... p 1615 N95-22954 * #
NAS 1.15:106849 ..... p 1665 N95-22669 * #
NAS 1.15:106850 ..... p 1820 N95-22915 * #
NAS 1.15:106851 ..... p 1792 N95-23614 * #
NAS 1.15:106855 ..... p 1626 N95-23270 * #
NAS 1.15:106858 ..... p 1626 N95-24004 * #
NAS 1.15:106862 ..... p 1630 N95-23258 * #
NAS 1.15:106863 ..... p 1653 N95-24186 * #
NAS 1.15:106864 ..... p 1668 N95-23248 * #
NAS 1.15:106866 ..... p 1762 N95-22668 * #
NAS 1.15:106867 ..... p 1662 N95-23219 * #
NAS 1.15:106869 ..... p 1668 N95-23220 * #
NAS 1.15:106870 ..... p 1728 N95-23259 * #
NAS 1.15:106872 ..... p 1800 N95-23178 * #
NAS 1.15:106873 ..... p 1846 N95-24188 * #
NAS 1.15:106876 ..... p 1625 N95-23450 * #
NAS 1.15:106882 ..... p 1699 N95-24055 * #
NAS 1.15:106883 ..... p 1688 N95-23461 * #
NAS 1.15:106884 ..... p 1677 N95-23464 * #
NAS 1.15:106885 ..... p 1616 N95-23671 * #
NAS 1.15:106889 ..... p 1630 N95-23463 * #
NAS 1.15:106890 ..... p 1614 N95-23550 * #
NAS 1.15:106891 ..... p 1738 N95-23116 * #
NAS 1.15:108477 ..... p 1652 N95-22672 * #
NAS 1.15:108481 ..... p 1699 N95-22950 * #
NAS 1.15:108483 ..... p 1630 N95-23551 * #
NAS 1.15:108848 ..... p 1872 N95-22920 * #
NAS 1.15:108860 ..... p 1607 N95-22666 * #
NAS 1.15:109159 ..... p 1688 N95-23012 * #
NAS 1.15:109177 ..... p 1733 N95-23009 * #
NAS 1.15:109182 ..... p 1616 N95-23011 * #
NAS 1.15:109183 ..... p 1627 N95-22928 * #
NAS 1.15:109927 ..... p 1751 N95-23194 * #
NAS 1.15:110345 ..... p 1856 N95-23364 * #
NAS 1.15:110450 ..... p 1619 N95-23094 * #
NAS 1.15:110509 ..... p 1620 N95-24027 *
NAS 1.15:110527 ..... p 1619 N95-23093 * #
NAS 1.15:110545 ..... p 1619 N95-23187 * #
NAS 1.15:110546 ..... p 1617 N95-22947 * #
NAS 1.15:4583 ..... p 1607 N95-22802 * #
NAS 1.15:4586 ..... p 1698 N95-22805 * #
NAS 1.15:4602 ..... p 1666 N95-23015 * #
NAS 1.15:4602 ..... p 1667 N95-23210 * #
NAS 1.15:4635 ..... p 1616 N95-23192 * #
NAS 1.15:4638 ..... p 1609 N95-23250 * #
NAS 1.15:4639 ..... p 1840 N95-22803 * #
NAS 1.15:4661 ..... p 1654 N95-22804 * #
NAS 1.15:4662 ..... p 1759 N95-24052 * #
NAS 1.15:4665 ..... p 1613 N95-24030 * #
NAS 1.15:4676 ..... p 1612 N95-22829 * #
NAS 1.17:MSC-22385-1 ..... p 1694 N95-22892 * #
NAS 1.21:7096-SUPPL-1 ..... p 1856 N95-23223 *
NAS 1.26:188363 ..... p 1633 N95-23092 * #
NAS 1.26:189099 ..... p 1614 N95-24053 * #
NAS 1.26:189141 ..... p 1696 N95-23792 * #
NAS 1.26:189146 ..... p 1699 N95-24189 * #
NAS 1.26:190786 ..... p 1625 N95-23790 * #
NAS 1.26:190787 ..... p 1625 N95-23791 * #
NAS 1.26:191608 ..... p 1762 N95-22830 * #
NAS 1.26:194972 ..... p 1872 N95-23276 * #
NAS 1.26:195023 ..... p 1678 N95-23544 * #
NAS 1.26:195025 ..... p 1788 N95-22931 * #
NAS 1.26:195026 ..... p 1614 N95-22674 * #
NAS 1.26:195032 ..... p 1677 N95-23466 * #
NAS 1.26:195034 ..... p 1667 N95-23207 * #
NAS 1.26:195039 ..... p 1758 N95-23613 * #
NAS 1.26:195044 ..... p 1790 N95-23465 * #
NAS 1.26:195046 ..... p 1678 N95-23596 * #
NAS 1.26:195050 ..... p 1608 N95-23193 * #
NAS 1.26:195052 ..... p 1668 N95-23257 * #
NAS 1.26:195324 ..... p 1689 N95-23795 * #
NAS 1.26:195421 ..... p 1799 N95-22675 * #
NAS 1.26:195442 ..... p 1677 N95-23451 * #
NAS 1.26:195445 ..... p 1614 N95-23222 * #
NAS 1.26:195447 ..... p 1855 N95-23206 * #
NAS 1.26:195454 ..... p 1609 N95-23462 * #
NAS 1.26:196313 ..... p 1744 N95-23766 *
NAS 1.26:196539 ..... p 1727 N95-22904 * #
NAS 1.26:196544 ..... p 1841 N95-22907 * #
NAS 1.26:196547 ..... p 1868 N95-23205 * #
NAS 1.26:196548 ..... p 1853 N95-22891 * #
NAS 1.26:196555 ..... p 1697 N95-24106 * #
NAS 1.26:196574 ..... p 1653 N95-24028 * #
NAS 1.26:196575 ..... p 1653 N95-23552 * #
NAS 1.26:197289 ..... p 1736 N95-22867 * #
NAS 1.26:197328 ..... p 1756 N95-22853 * #
NAS 1.26:197330 ..... p 1656 N95-22852 * #
NAS 1.26:197331 ..... p 1761 N95-22478 * #
NAS 1.26:197335 ..... p 1865 N95-22539 * #
NAS 1.26:197340 ..... p 1767 N95-23672 * #
NAS 1.26:197343 ..... p 1655 N95-22813 * #
NAS 1.26:197345 ..... p 1636 N95-23545 * #
NAS 1.26:197347 ..... p 1871 N95-23216 * #
NAS 1.26:197348 ..... p 1687 N95-24022 * #
NAS 1.26:197350 ..... p 1871 N95-23472 * #
NAS 1.26:197354-VOL-3 ..... p 1712 N95-23936 * #
NAS 1.26:197368 ..... p 1735 N95-22482 * #
NAS 1.26:197376 ..... p 1869 N95-22828 * #
NAS 1.26:197379 ..... p 1750 N95-22797 * #
NAS 1.26:197383 ..... p 1664 N95-22481 * #
NAS 1.26:197384 ..... p 1753 N95-22480 * #
NAS 1.26:197391 ..... p 1738 N95-23184 * #
NAS 1.26:197392 ..... p 1737 N95-22945 * #
NAS 1.26:197394 ..... p 1756 N95-23017 * #
NAS 1.26:197400 ..... p 1731 N95-22673 * #
NAS 1.26:197402 ..... p 1717 N95-22916 * #
NAS 1.26:197403 ..... p 1831 N95-23008 * #
NAS 1.26:197404 ..... p 1737 N95-22956 * #
NAS 1.26:197405 ..... p 1831 N95-22955 * #
NAS 1.26:197417 ..... p 1732 N95-22930 * #
NAS 1.26:197419 ..... p 1608 N95-23218 * #
NAS 1.26:197420 ..... p 1612 N95-23217 * #
NAS 1.26:197421 ..... p 1667 N95-23183 * #
NAS 1.26:197423 ..... p 1696 N95-23409 * #
NAS 1.26:197424 ..... p 1866 N95-23560 * #
NAS 1.26:197425 ..... p 1871 N95-23546 * #
NAS 1.26:197431 ..... p 1688 N95-23087 * #
NAS 1.26:197432 ..... p 1833 N95-23211 * #
NAS 1.26:197436 ..... p 1867 N95-23013 * #
NAS 1.26:197438 ..... p 1694 N95-23190 * #
NAS 1.26:197439 ..... p 1648 N95-23179 * #
NAS 1.26:197440 ..... p 1614 N95-23088 * #
NAS 1.26:197443 ..... p 1717 N95-23191 * #
NAS 1.26:197589 ..... p 1864 N95-22526 * #
NAS 1.26:197618 ..... p 1745 N95-22801 * #
NAS 1.26:197661 ..... p 1615 N95-22908 * #
NAS 1.26:197683 ..... p 1866 N95-23595 * #
NAS 1.26:197685 ..... p 1621 N95-23188 * #
NAS 1.26:197687 ..... p 1621 N95-23189 * #
NAS 1.26:197688 ..... p 1871 N95-24191 * #
NAS 1.26:197699 ..... p 1658 N95-23670 * #
NAS 1.26:197704 ..... p 1619 N95-24032 * #
NAS 1.26:197851 ..... p 1743 N95-23212 * #
NAS 1.26:197854 ..... p 1653 N95-23204 * #
NAS 1.26:197855 ..... p 1757 N95-23180 * #
NAS 1.26:197856 ..... p 1827 N95-23089 * #
NAS 1.26:197858 ..... p 1695 N95-23214 * #
NAS 1.26:197859 ..... p 1694 N95-23213 * #
NAS 1.26:197861 ..... p 1738 N95-23090 * #
NAS 1.26:197862 ..... p 1641 N95-23215 * #
NAS 1.26:197863 ..... p 1657 N95-22944 * #
NAS 1.26:197864 ..... p 1870 N95-23181 * #
NAS 1.26:197867 ..... p 1608 N95-23182 * #
NAS 1.26:197868 ..... p 1827 N95-23224 * #
NAS 1.26:197870 ..... p 1865 N95-23091 * #
NAS 1.26:197875 ..... p 1742 N95-23208 * #
NAS 1.26:197876-VOL-2 ..... p 1711 N95-23917 * #
NAS 1.26:197877-VOL-1 ..... p 1701 N95-23844 * #
NAS 1.26:197884 ..... p 1826 N95-23016 * #
NAS 1.26:197885 ..... p 1648 N95-22883 * #
NAS 1.26:197890 ..... p 1757 N95-23388 * #
NAS 1.26:197894 ..... p 1718 N95-23473 * #
NAS 1.26:197898 ..... p 1766 N95-22831 * #
NAS 1.26:197900 ..... p 1866 N95-23561 * #
NAS 1.26:197901 ..... p 1717 N95-22832 * #
NAS 1.26:197902 ..... p 1621 N95-23260 * #
NAS 1.26:197903 ..... p 1622 N95-23398 * #
NAS 1.26:197904 ..... p 1622 N95-23399 * #
NAS 1.26:197905 ..... p 1622 N95-23400 * #
NAS 1.26:197907 ..... p 1634 N95-23252 * #
NAS 1.26:197912 ..... p 1612 N95-22949 * #
NAS 1.26:197913 ..... p 1689 N95-23789 * #
NAS 1.26:197916 ..... p 1746 N95-22911 * #
NAS 1.26:197917 ..... p 1871 N95-22910 * #
NAS 1.26:197919 ..... p 1625 N95-23261 * #
NAS 1.26:197920 ..... p 1739 N95-23271 * #
NAS 1.26:197924 ..... p 1866 N95-23402 * #
NAS 1.26:197925 ..... p 1865 N95-23401 * #
NAS 1.26:197930 ..... p 1751 N95-23474 * #
NAS 1.26:197931 ..... p 1615 N95-23392 * #
NAS 1.26:197934 ..... p 1657 N95-23391 * #
NAS 1.26:197935 ..... p 1866 N95-23540 * #
NAS 1.26:197938 ..... p 1609 N95-23669 * #
NAS 1.26:197941 ..... p 1719 N95-24094 * #
NAS 1.26:197944 ..... p 1615 N95-23410 * #
NAS 1.26:197945 ..... p 1734 N95-23460 * #
NAS 1.26:197946 ..... p 1791 N95-23547 * #
NAS 1.26:197947 ..... p 1764 N95-23594 * #
NAS 1.26:197948 ..... p 1791 N95-23593 * #
NAS 1.26:197949 ..... p 1791 N95-23592 * #
NAS 1.26:197950 ..... p 1791 N95-23611 * #
NAS 1.26:197951 ..... p 1764 N95-24023 * #
NAS 1.26:197954 ..... p 1758 N95-23610 * #
NAS 1.26:197955 ..... p 1791 N95-23548 * #
NAS 1.26:197956 ..... p 1791 N95-23612 * #
NAS 1.26:197957 ..... p 1694 N95-22909 * #
NAS 1.26:197962 ..... p 1739 N95-23272 * #
NAS 1.26:197963 ..... p 1843 N95-23563 * #
NAS 1.26:197965 ..... p 1828 N95-24035 * #
NAS 1.26:197966 ..... p 1828 N95-24068 * #
NAS 1.26:197969 ..... p 1721 N95-24190 * #
NAS 1.26:197977 ..... p 1741 N95-24041 * #
NAS 1.26:197979 ..... p 1696 N95-24064 * #
NAS 1.26:197981 ..... p 1810 N95-23459 * #
NAS 1.26:197982 ..... p 1809 N95-23408 * #
NAS 1.26:197990 ..... p 1748 N95-24047 * #
NAS 1.26:198032 ..... p 1869 N95-24066 * #

NAS 1.26:4640 ..... p 1654 N95-23195 * #
NAS 1.26:4646 ..... p 1626 N95-22918 * #
NAS 1.26:4647 ..... p 1626 N95-22919 * #
NAS 1.26:4649 ..... p 1608 N95-22917 * #
NAS 1.26:4650 ..... p 1608 N95-23185 * #
NAS 1.26:4651 ..... p 1608 N95-23095 * #
NAS 1.55:3221-PT-1 ..... p 1678 N95-23615 * #
NAS 1.55:3221-PT-2 ..... p 1668 N95-23412 * #
NAS 1.55:3261 ..... p 1617 N95-23549 * #
NAS 1.55:3275-PT-1 ..... p 1889 N95-23796 * #
NAS 1.55:3275-PT-2 ..... p 1899 N95-23896 * #
NAS 1.55:3286 ..... p 1820 N95-22957 * #
NAS 1.55:3289 ..... p 1628 N95-23025 * #
NAS 1.55:3295 ..... p 1857 N95-24108 * #
NAS 1.60:3452-VOL-1 ..... p 1754 N95-22603 * #
NAS 1.60:3452-VOL-2 ..... p 1755 N95-22604 * #
NAS 1.60:3452-VOL-3 ..... p 1753 N95-22479 * #
NAS 1.60:3452-VOL-4 ..... p 1755 N95-22605 * #
NAS 1.60:3465 ..... p 1612 N95-22953 * #
NAS 1.60:3486 ..... p 1691 N95-23411 * #
NAS 1.60:3498 ..... p 1817 N95-22929 * #
NAS 1.60:3529 ..... p 1742 N95-23010 * #
NAS 1.60:3537 ..... p 1612 N95-22806 * #
NAS 1.60:3543 ..... p 1641 N95-23186 * #
NAS 1.61:1357 ..... p 1621 N95-23249 * #
NAS 1.71:LAR-13890-1 ..... p 1799 N95-22921 * #
NAS 1.71:LAR-15112-1-CU ..... p 1666 N95-22906 * #
NAS 1.71:LAR-15172-1-CU ..... p 1663 N95-24048 * #
NAS 1.71:LAR-15205-1 ..... p 1648 N95-22882 * #

NAS-CR-196544 ..... p 1841 N95-22907 * #

NASA TM-106842 ..... p 1624 N95-23221 * #

NASA 1.15:108480 ..... p 1856 N95-23225 * #

NASA-CASE-ARC-11913-1 ..... p 1688 N95-23377 *
NASA-CASE-ARC-11921-2 ..... p 1695 N95-23376 *
NASA-CASE-ARC-11938-1-C ..... p 1688 N95-23263 *
NASA-CASE-ARC-11940-1-SB ..... p 1827 N95-23378 *
NASA-CASE-ARC-11944-1 ..... p 1615 N95-23389 *
NASA-CASE-ARC-11961-1 ..... p 1767 N95-23387 *
NASA-CASE-ARC-11969-1-CU ..... p 1649 N95-23394 *
NASA-CASE-ARC-11979-1 ..... p 1612 N95-23390 *
NASA-CASE-ARC-11982-1 ..... p 1611 N95-23393 *
NASA-CASE-ARC-11990-1 ..... p 1613 N95-23395 *
NASA-CASE-ARC-12000-1 ..... p 1751 N95-23264 *

NASA-CASE-LAR-13890-1 ..... p 1799 N95-22921 * #
NASA-CASE-LAR-14538-2 ..... p 1649 N95-23254 *
NASA-CASE-LAR-14857-1-SB ..... p 1819 N95-22807 *
NASA-CASE-LAR-14896-1 ..... p 1649 N95-23253 *
NASA-CASE-LAR-15022-1 ..... p 1749 N95-22579 *
NASA-CASE-LAR-15112-1-CU ..... p 1666 N95-22906 * #
NASA-CASE-LAR-15172-1-CU ..... p 1663 N95-24048 * #
NASA-CASE-LAR-15205-1 ..... p 1648 N95-22882 * #

NASA-CASE-LEW-15263-2 ..... p 1627 N95-22563 *

NASA-CASE-MFS-28652-1 ..... p 1647 N95-22558 *

NASA-CASE-MSC-21632-1 ..... p 1750 N95-22766 *
NASA-CASE-MSC-22385-1 ..... p 1694 N95-22892 * #

NASA-CASE-NPO-17794-1-CU ..... p 1819 N95-22765 *
NASA-CASE-NPO-18498-1-CU ..... p 1692 N95-22543 * #
NASA-CASE-NPO-18733-1-CU ..... p 1613 N95-22578 *
NASA-CASE-NPO-18769-1-CU ..... p 1827 N95-23045 *
NASA-CASE-NPO-18771-1-CU ..... p 1754 N95-22577 *
NASA-CASE-NPO-18864-1-CU ..... p 1762 N95-22564 *

NASA-CP-3221-PT-1 ..... p 1678 N95-23615 * #
NASA-CP-3221-PT-2 ..... p 1668 N95-23412 * #
NASA-CP-3261 ..... p 1617 N95-23549 * #
NASA-CP-3275-PT-1 ..... p 1889 N95-23796 * #
NASA-CP-3275-PT-2 ..... p 1899 N95-23896 * #
NASA-CP-3286 ..... p 1820 N95-22957 * #
NASA-CP-3289 ..... p 1628 N95-23025 * #
NASA-CP-3295 ..... p 1857 N95-24108 * #

NASA-CR-188363 ..... p 1633 N95-23092 * #
NASA-CR-189099 ..... p 1614 N95-24053 * #
NASA-CR-189141 ..... p 1696 N95-23792 * #
NASA-CR-189146 ..... p 1699 N95-24189 * #
NASA-CR-190786 ..... p 1625 N95-23790 * #
NASA-CR-190787 ..... p 1625 N95-23791 * #
NASA-CR-191608 ..... p 1762 N95-22830 * #
NASA-CR-194972 ..... p 1872 N95-23276 * #
NASA-CR-195023 ..... p 1678 N95-23544 * #
NASA-CR-195025 ..... p 1788 N95-22931 * #
NASA-CR-195026 ..... p 1614 N95-22674 * #
NASA-CR-195032 ..... p 1677 N95-23466 * #
NASA-CR-195034 ..... p 1667 N95-23207 * #
NASA-CR-195039 ..... p 1758 N95-23613 * #
NASA-CR-195044 ..... p 1790 N95-23465 * #
NASA-CR-195046 ..... p 1678 N95-23596 * #
NASA-CR-195050 ..... p 1608 N95-23193 * #
NASA-CR-195052 ..... p 1668 N95-23257 * #
NASA-CR-195324 ..... p 1689 N95-23795 * #
NASA-CR-195421 ..... p 1799 N95-22675 * #
NASA-CR-195442 ..... p 1677 N95-23451 * #
NASA-CR-195445 ..... p 1614 N95-23222 * #
NASA-CR-195447 ..... p 1855 N95-23206 * #
NASA-CR-195454 ..... p 1609 N95-23462 * #
NASA-CR-196313 ..... p 1744 N95-23766 *
NASA-CR-196539 ..... p 1727 N95-22904 * #
NASA-CR-196547 ..... p 1868 N95-23205 * #
NASA-CR-196548 ..... p 1853 N95-22891 * #
NASA-CR-196555 ..... p 1697 N95-24106 * #
NASA-CR-196574 ..... p 1653 N95-24028 * #
NASA-CR-196575 ..... p 1653 N95-23552 * #
NASA-CR-197289 ..... p 1736 N95-22867 * #
NASA-CR-197328 ..... p 1756 N95-22853 * #
NASA-CR-197330 ..... p 1656 N95-22852 * #
NASA-CR-197331 ..... p 1761 N95-22478 * #
NASA-CR-197335 ..... p 1865 N95-22539 * #
NASA-CR-197340 ..... p 1767 N95-23672 * #
NASA-CR-197343 ..... p 1655 N95-22813 * #
NASA-CR-197345 ..... p 1636 N95-23545 * #
NASA-CR-197347 ..... p 1871 N95-23216 * #
NASA-CR-197348 ..... p 1687 N95-24022 * #
NASA-CR-197350 ..... p 1871 N95-23472 * #
NASA-CR-197354-VOL-3 ..... p 1712 N95-23938 * #
NASA-CR-197368 ..... p 1735 N95-22482 * #
NASA-CR-197376 ..... p 1869 N95-22828 * #
NASA-CR-197379 ..... p 1750 N95-22797 * #
NASA-CR-197383 ..... p 1664 N95-22481 * #
NASA-CR-197384 ..... p 1753 N95-22480 * #
NASA-CR-197391 ..... p 1738 N95-23184 * #
NASA-CR-197392 ..... p 1737 N95-22945 * #
NASA-CR-197394 ..... p 1756 N95-23017 * #
NASA-CR-197400 ..... p 1731 N95-22673 * #
NASA-CR-197402 ..... p 1717 N95-22916 * #
NASA-CR-197403 ..... p 1831 N95-23008 * #
NASA-CR-197404 ..... p 1737 N95-22956 * #
NASA-CR-197405 ..... p 1831 N95-22955 * #
NASA-CR-197417 ..... p 1732 N95-22930 * #
NASA-CR-197419 ..... p 1608 N95-23218 * #
NASA-CR-197420 ..... p 1612 N95-23217 * #
NASA-CR-197421 ..... p 1667 N95-23183 * #
NASA-CR-197423 ..... p 1696 N95-23409 * #
NASA-CR-197424 ..... p 1866 N95-23560 * #
NASA-CR-197425 ..... p 1871 N95-23546 * #
NASA-CR-197431 ..... p 1688 N95-23087 * #
NASA-CR-197432 ..... p 1833 N95-23211 * #
NASA-CR-197436 ..... p 1867 N95-23013 * #
NASA-CR-197438 ..... p 1694 N95-23190 * #
NASA-CR-197439 ..... p 1648 N95-23179 * #
NASA-CR-197440 ..... p 1614 N95-23088 * #
NASA-CR-197443 ..... p 1717 N95-23191 * #
NASA-CR-197589 ..... p 1864 N95-22526 * #
NASA-CR-197618 ..... p 1745 N95-22801 * #
NASA-CR-197661 ..... p 1615 N95-22908 * #
NASA-CR-197683 ..... p 1866 N95-23595 * #
NASA-CR-197685 ..... p 1621 N95-23188 * #
NASA-CR-197687 ..... p 1621 N95-23189 * #
NASA-CR-197688 ..... p 1871 N95-24191 * #
NASA-CR-197699 ..... p 1658 N95-23670 * #
NASA-CR-197704 ..... p 1619 N95-24032 * #
NASA-CR-197851 ..... p 1743 N95-23212 * #
NASA-CR-197854 ..... p 1653 N95-23204 * #
NASA-CR-197855 ..... p 1757 N95-23180 * #
NASA-CR-197856 ..... p 1827 N95-23089 * #
NASA-CR-197858 ..... p 1695 N95-23214 * #
NASA-CR-197859 ..... p 1694 N95-23213 * #
NASA-CR-197861 ..... p 1738 N95-23090 * #
NASA-CR-197862 ..... p 1641 N95-23215 * #
NASA-CR-197863 ..... p 1657 N95-22944 * #
NASA-CR-197864 ..... p 1870 N95-23181 * #
NASA-CR-197867 ..... p 1608 N95-23182 * #
NASA-CR-197868 ..... p 1827 N95-23224 * #
NASA-CR-197870 ..... p 1865 N95-23091 * #
NASA-CR-197875 ..... p 1742 N95-23208 * #
NASA-CR-197876-VOL-2 ..... p 1711 N95-23917 * #
NASA-CR-197877-VOL-1 ..... p 1701 N95-23844 * #
NASA-CR-197884 ..... p 1826 N95-23016 * #
NASA-CR-197885 ..... p 1648 N95-22883 * #
NASA-CR-197890 ..... p 1757 N95-23388 * #
NASA-CR-197894 ..... p 1718 N95-23473 * #
NASA-CR-197898 ..... p 1766 N95-22831 * #
NASA-CR-197900 ..... p 1866 N95-23561 * #
NASA-CR-197901 ..... p 1717 N95-22832 * #
NASA-CR-197902 ..... p 1621 N95-23260 * #
NASA-CR-197903 ..... p 1622 N95-23398 * #
NASA-CR-197904 ..... p 1622 N95-23399 * #
NASA-CR-197905 ..... p 1622 N95-23400 * #
NASA-CR-197907 ..... p 1634 N95-23252 * #
NASA-CR-197912 ..... p 1612 N95-22949 * #
NASA-CR-197913 ..... p 1689 N95-23789 * #
NASA-CR-197916 ..... p 1746 N95-22911 * #
NASA-CR-197917 ..... p 1871 N95-22910 * #
NASA-CR-197919 ..... p 1625 N95-23261 * #
NASA-CR-197920 ..... p 1739 N95-23271 * #
NASA-CR-197924 ..... p 1866 N95-23402 * #
NASA-CR-197925 ..... p 1865 N95-23401 * #
NASA-CR-197930 ..... p 1751 N95-23474 * #
NASA-CR-197931 ..... p 1615 N95-23392 * #
NASA-CR-197934 ..... p 1657 N95-23391 * #
NASA-CR-197935 ..... p 1866 N95-23540 * #
NASA-CR-197938 ..... p 1609 N95-23669 * #
NASA-CR-197941 ..... p 1719 N95-24094 * #
NASA-CR-197944 ..... p 1615 N95-23410 * #
NASA-CR-197945 ..... p 1734 N95-23460 * #
NASA-CR-197946 ..... p 1791 N95-23547 * #
NASA-CR-197947 ..... p 1764 N95-23594 * #
NASA-CR-197948 ..... p 1791 N95-23593 * #
NASA-CR-197949 ..... p 1791 N95-23592 * #
NASA-CR-197950 ..... p 1791 N95-23611 * #
NASA-CR-197951 ..... p 1764 N95-24023 * #
NASA-CR-197954 ..... p 1758 N95-23610 * #
NASA-CR-197955 ..... p 1791 N95-23548 * #
NASA-CR-197956 ..... p 1791 N95-23612 * #
NASA-CR-197957 ..... p 1694 N95-22909 * #
NASA-CR-197962 ..... p 1739 N95-23272 * #
NASA-CR-197963 ..... p 1843 N95-23563 * #
NASA-CR-197965 ..... p 1828 N95-24035 * #
NASA-CR-197966 ..... p 1828 N95-24068 * #
NASA-CR-197969 ..... p 1721 N95-24190 * #
NASA-CR-197977 ..... p 1741 N95-24041 * #
NASA-CR-197979 ..... p 1696 N95-24064 * #
NASA-CR-197981 ..... p 1810 N95-23459 * #
NASA-CR-197982 ..... p 1809 N95-23408 * #
NASA-CR-197990 ..... p 1748 N95-24047 * #
NASA-CR-198032 ..... p 1869 N95-24066 * #
NASA-CR-4640 ..... p 1654 N95-23195 * #
NASA-CR-4646 ..... p 1626 N95-22918 * #
NASA-CR-4647 ..... p 1626 N95-22919 * #
NASA-CR-4649 ..... p 1608 N95-22917 * #
NASA-CR-4650 ..... p 1608 N95-23185 * #
NASA-CR-4651 ..... p 1608 N95-23095 * #

NASA-NEWS-RELEASE-95-18 ..... p 1620 N95-24027 *

NASA-RP-1357 ..... p 1621 N95-23249 * #

NASA-SP-7096-SUPPL-1 ..... p 1856 N95-23223 *

NASA-TM-104566-VOL-25-REV-1 p 1743 N95-22671 * #
NASA-TM-104606-VOL-4 ..... p 1740 N95-23529 * #
NASA-TM-104615 ..... p 1856 N95-23209 * #
NASA-TM-104803 ..... p 1617 N95-23262 * #
NASA-TM-106309 ..... p 1747 N95-23177 * #
NASA-TM-106744 ..... p 1691 N95-22670 * #
NASA-TM-106764 ..... p 1607 N95-24025 * #
NASA-TM-106769 ..... p 1650 N95-24187 * #
NASA-TM-106835 ..... p 1621 N95-22667 * #
NASA-TM-106841 ..... p 1624 N95-23240 * #
NASA-TM-106847 ..... p 1615 N95-22954 * #
NASA-TM-106849 ..... p 1665 N95-22669 * #
NASA-TM-106850 ..... p 1820 N95-22915 * #
NASA-TM-106851 ..... p 1792 N95-23614 * #
NASA-TM-106855 ..... p 1626 N95-23270 * #
NASA-TM-106858 ..... p 1626 N95-24004 * #
NASA-TM-106862 ..... p 1630 N95-23258 * #
NASA-TM-106863 ..... p 1653 N95-24186 * #
NASA-TM-106864 ..... p 1668 N95-23248 * #
NASA-TM-106866 ..... p 1762 N95-22668 * #
NASA-TM-106867 ..... p 1662 N95-23219 * #
NASA-TM-106869 ..... p 1668 N95-23220 * #
NASA-TM-106870 ..... p 1728 N95-23259 * #
NASA-TM-106872 ..... p 1800 N95-23178 * #
NASA-TM-106873 ..... p 1846 N95-24188 * #
NASA-TM-106876 ..... p 1625 N95-23450 * #
NASA-TM-106882 ..... p 1699 N95-24055 * #
NASA-TM-106883 ..... p 1688 N95-23461 * #
NASA-TM-106884 ..... p 1677 N95-23464 * #
NASA-TM-106885 ..... p 1616 N95-23671 * #
NASA-TM-106889 ..... p 1630 N95-23463 * #
NASA-TM-106890 ..... p 1614 N95-23550 * #
NASA-TM-106891 ..... p 1738 N95-23116 * #
NASA-TM-108477 ..... p 1652 N95-22672 * #
NASA-TM-108480 ..... p 1856 N95-23225 * #
NASA-TM-108481 ..... p 1699 N95-22950 * #
NASA-TM-108483 ..... p 1630 N95-23551 * #
NASA-TM-108848 ..... p 1872 N95-22920 * #
NASA-TM-108860 ..... p 1607 N95-22666 * #
NASA-TM-109159 ..... p 1688 N95-23012 * #
NASA-TM-109177 ..... p 1733 N95-23009 * #
NASA-TM-109182 ..... p 1616 N95-23011 * #
NASA-TM-109183 ..... p 1627 N95-22928 * #
NASA-TM-109927 ..... p 1751 N95-23194 * #
NASA-TM-110345 ..... p 1856 N95-23364 * #
NASA-TM-110450 ..... p 1619 N95-23094 * #
NASA-TM-110509 ..... p 1620 N95-24027 *
NASA-TM-110527 ..... p 1619 N95-23093 * #
NASA-TM-110531 ..... p 1620 N95-22542 *
NASA-TM-110535 ..... p 1799 N95-23273 *
NASA-TM-110536 ..... p 1751 N95-23274 *

NASA-TM-110538 ..... p 1740 N95-23663 *
NASA-TM-110539 ..... p 1620 N95-23664 *
NASA-TM-110541 ..... p 1620 N95-23275 *
NASA-TM-110542 ..... p 1620 N95-23665 *
NASA-TM-110545 ..... p 1619 N95-23187 * #
NASA-TM-110546 ..... p 1617 N95-22947 * #
NASA-TM-4583 ..... p 1607 N95-22802 * #
NASA-TM-4586 ..... p 1698 N95-22805 * #
NASA-TM-4602 ..... p 1666 N95-23015 * #
NASA-TM-4602 ..... p 1667 N95-23210 * #
NASA-TM-4635 ..... p 1616 N95-23192 * #
NASA-TM-4638 ..... p 1609 N95-23250 * #
NASA-TM-4639 ..... p 1840 N95-22803 * #
NASA-TM-4661 ..... p 1654 N95-22804 * #
NASA-TM-4662 ..... p 1759 N95-24052 * #
NASA-TM-4665 ..... p 1613 N95-24030 * #
NASA-TM-4676 ..... p 1612 N95-22829 * #

NASA-TP-3452-VOL-1 ..... p 1754 N95-22603 * #
NASA-TP-3452-VOL-2 ..... p 1755 N95-22604 * #
NASA-TP-3452-VOL-3 ..... p 1753 N95-22479 * #
NASA-TP-3452-VOL-4 ..... p 1755 N95-22605 * #
NASA-TP-3465 ..... p 1612 N95-22953 * #
NASA-TP-3486 ..... p 1691 N95-23411 * #
NASA-TP-3498 ..... p 1817 N95-22929 * #
NASA-TP-3529 ..... p 1742 N95-23010 * #
NASA-TP-3537 ..... p 1612 N95-22806 * #
NASA-TP-3543 ..... p 1641 N95-23186 * #

NATICK/TR-94/019 ..... p 1747 N95-23251

NAWCADPAX-95-10-RTR ..... p 1613 N95-24030 * #

NEI-FI-248 ..... p 1729 N95-23382 #

NHK-LABS-NOTE-431 ..... p 1863 N95-24180 #
NHK-LABS-NOTE-432 ..... p 1690 N95-24107 #

NIAR-94-11 ..... p 1610 N95-24012 #
NIAR-94-16 ..... p 1751 N95-24021 #
NIAR-94-2 ..... p 1650 N95-23932 #
NIAR-94-3 ..... p 1610 N95-24050 #

NIFS-311 ..... p 1835 N95-23564 #
NIFS-312 ..... p 1834 N95-23523 #
NIFS-313 ..... p 1835 N95-23534 #
NIFS-314 ..... p 1834 N95-23524 #
NIFS-315 ..... p 1834 N95-23525 #
NIFS-316 ..... p 1834 N95-23526 #
NIFS-317 ..... p 1834 N95-23527 #
NIFS-318 ..... p 1835 N95-23528 #
NIFS-319 ..... p 1836 N95-23591 #
NIFS-320 ..... p 1836 N95-23590 #
NIFS-321 ..... p 1836 N95-23589 #
NIFS-322 ..... p 1835 N95-23543 #
NIFS-323 ..... p 1835 N95-23535 #
NIFS-324 ..... p 1836 N95-23572 #
NIFS-325 ..... p 1836 N95-23569 #
NIFS-327 ..... p 1835 N95-23533 #
NIFS-328 ..... p 1609 N95-23787 #

NIOZ-1993-16 ..... p 1733 N95-23125

NISF-326 ..... p 1835 N95-23566 #

NISTIR-5447 ..... p 1755 N95-22637

NLR-TP-93047-U ..... p 1718 N95-23471
NLR-TP-93109-U ..... p 1612 N95-23161 #

NOAA-TM-NWS-SR-159 ..... p 1742 N95-22651

NONP-NASA-VT-95-42907 ..... p 1620 N95-22542 *
NONP-NASA-VT-95-43938 ..... p 1799 N95-23273 *
NONP-NASA-VT-95-43939 ..... p 1751 N95-23274 *
NONP-NASA-VT-95-43941 ..... p 1740 N95-23663 *
NONP-NASA-VT-95-43942 ..... p 1620 N95-23664 *
NONP-NASA-VT-95-43944 ..... p 1620 N95-23275 *
NONP-NASA-VT-95-43945 ..... p 1620 N95-23665 *

NPSEC-94-013 ..... p 1655 N95-22505 #

NREL/TP-411-7188 ..... p 1728 N95-23061 #
NREL/TP-411-7350 ..... p 1726 N95-22546 #
NREL/TP-411-7352 ..... p 1728 N95-23062 #
NREL/TP-411-7472 ..... p 1729 N95-23478 #
NREL/TP-411-7473 ..... p 1730 N95-23777 #
NREL/TP-425-6355 ..... p 1732 N95-22834 #
NREL/TP-433-6943 ..... p 1734 N95-23480 #
NREL/TP-433-7209 ..... p 1730 N95-23778 #
NREL/TP-442-7076 ..... p 1694 N95-22923 #
NREL/TP-442-7111 ..... p 1730 N95-23776 #
NREL/TP-442-7112 ..... p 1729 N95-23383 #
NREL/TP-451-7164 ..... p 1660 N95-22586 #
NREL/TP-451-7189 ..... p 1727 N95-22842 #
NREL/TP-471-7018 ..... p 1726 N95-22547 #

NRL/FR/8140-94-9739 ..... p 1657 N95-23023 #

NSTS-08288 ..... p 1619 N95-23187 * #
NSTS-08290 ..... p 1619 N95-23094 * #
NSTS-08291 ..... p 1619 N95-23093 * #

NTIA-94-304 ..... p 1655 N95-22636

NTSB/AAR-95/01 ..... p 1610 N95-23609 #

NTSB/RP-94/01-VOL-1 ..... p 1611 N95-24105 #
NTSB/RP-94/02-VOL-2 ..... p 1610 N95-23598 #

NUB-3084 ..... p 1851 N95-23922 #

ORNL/CDIAC-70 ..... p 1731 N95-22725 #

ORNL/CON-394 ..... p 1730 N95-23605 #

ORNL/M-3986 ..... p 1668 N95-23372 #

ORNL/TM-12795 ..... p 1831 N95-22800 #

OTA-ISS-607 ..... p 1717 N95-22713 #

PB94-189057 ..... p 1839 N95-22584
PB94-189107 ..... p 1665 N95-22585
PB94-195146 ..... p 1742 N95-22651
PB94-203510 ..... p 1755 N95-22637
PB94-204831 ..... p 1655 N95-22636
PB94-917005 ..... p 1611 N95-24105 #
PB94-917007 ..... p 1610 N95-23598 #
PB95-108072 ..... p 1787 N95-22836 #
PB95-108080 ..... p 1787 N95-22837
PB95-109062 ..... p 1786 N95-22711 #
PB95-109104 ..... p 1795 N95-22712 #
PB95-109633 ..... p 1717 N95-22713 #
PB95-110490 ..... p 1786 N95-22714 #
PB95-110771 ..... p 1787 N95-22715 #
PB95-110797 ..... p 1788 N95-23076 #
PB95-127221 ..... p 1855 N95-22534 #
PB95-127239 ..... p 1785 N95-22535 #
PB95-127247 ..... p 1687 N95-22536 #
PB95-127254 ..... p 1665 N95-22638 #
PB95-127262 ..... p 1701 N95-22639 #
PB95-127296 ..... p 1741 N95-22640 #
PB95-127304 ..... p 1717 N95-22537 #
PB95-127312 ..... p 1717 N95-22538 #
PB95-127320 ..... p 1754 N95-22522 #
PB95-127338 ..... p 1855 N95-22523 #
PB95-127346 ..... p 1766 N95-22524 #
PB95-127353 ..... p 1855 N95-22525
PB95-127965 ..... p 1793 N95-22527 #
PB95-127973 ..... p 1785 N95-22533 #
PB95-127981 ..... p 1785 N95-22528 #
PB95-127999 ..... p 1754 N95-22529 #
PB95-128005 ..... p 1755 N95-22652 #
PB95-130225 ..... p 1786 N95-22641 #
PB95-130407 ..... p 1665 N95-22767
PB95-130456 ..... p 1787 N95-22768
PB95-130464 ..... p 1755 N95-22769
PB95-130555 ..... p 1785 N95-22544 #
PB95-133740 ..... p 1733 N95-23125
PB95-133773 ..... p 1733 N95-23067 #
PB95-133799 ..... p 1733 N95-23126
PB95-134623 ..... p 1798 N95-23127
PB95-135083 ..... p 1788 N95-22932 #
PB95-135141 ..... p 1788 N95-23068 #
PB95-135158 ..... p 1788 N95-23069 #
PB95-135166 ..... p 1788 N95-23070 #
PB95-135190 ..... p 1756 N95-23071 #
PB95-135216 ..... p 1648 N95-23128
PB95-135521 ..... p 1748 N95-22770
PB95-135547 ..... p 1732 N95-22865 #
PB95-135646 ..... p 1757 N95-23467 #
PB95-135703 ..... p 1763 N95-23166 #
PB95-135786 ..... p 1787 N95-22717
PB95-136008 ..... p 1789 N95-23167
PB95-136032 ..... p 1865 N95-23168 #
PB95-138814 ..... p 1789 N95-23169
PB95-138822 ..... p 1833 N95-23170 #
PB95-138830 ..... p 1789 N95-23171 #
PB95-138848 ..... p 1667 N95-23172 #
PB95-138855 ..... p 1789 N95-23149 #
PB95-138863 ..... p 1789 N95-23173
PB95-138871 ..... p 1789 N95-23174 #
PB95-138889 ..... p 1667 N95-23175 #
PB95-138897 ..... p 1789 N95-23176 #
PB95-138905 ..... p 1667 N95-23144 #
PB95-138913 ..... p 1648 N95-23145
PB95-138921 ..... p 1789 N95-23146 #
PB95-138947 ..... p 1763 N95-23129 #
PB95-138954 ..... p 1756 N95-23150 #
PB95-138970 ..... p 1657 N95-23151
PB95-138996 ..... p 1757 N95-23152 #
PB95-139002 ..... p 1752 N95-23153 #
PB95-139085 ..... p 1850 N95-23154
PB95-139093 ..... p 1799 N95-23155
PB95-139101 ..... p 1807 N95-23156
PB95-139119 ..... p 1807 N95-23157
PB95-139127 ..... p 1807 N95-23158
PB95-139135 ..... p 1807 N95-23159
PB95-139143 ..... p 1807 N95-23160
PB95-139184 ..... p 1612 N95-23161 #
PB95-139218 ..... p 1788 N95-23130 #
PB95-139226 ..... p 1756 N95-23131 #
PB95-139234 ..... p 1758 N95-23606
PB95-139242 ..... p 1868 N95-23228 #
PB95-139259 ..... p 1868 N95-23607
PB95-139267 ..... p 1868 N95-23230
PB95-139275 ..... p 1866 N95-23468 #
PB95-139283 ..... p 1718 N95-23469 #
PB95-139291 ..... p 1740 N95-23470 #
PB95-139309 ..... p 1718 N95-23471
PB95-139333 ..... p 1767 N95-23199 #
PB95-139341 ..... p 1789 N95-23200
PB95-139358 ..... p 1790 N95-23231 #
PB95-139366 ..... p 1757 N95-23232 #
PB95-139374 ..... p 1790 N95-23233 #
PB95-139382 ..... p 1758 N95-23553
PB95-139820 ..... p 1758 N95-23608
PB95-139846 ..... p 1790 N95-23235 #
PB95-139853 ..... p 1790 N95-23236 #
PB95-140612 ..... p 1790 N95-23237 #
PB95-140620 ..... p 1757 N95-23238 #
PB95-140646 ..... p 1794 N95-23239 #
PB95-140653 ..... p 1630 N95-23537
PB95-140687 ..... p 1636 N95-23554
PB95-140695 ..... p 1764 N95-23538 #
PB95-140752 ..... p 1795 N95-23555 #
PB95-140786 ..... p 1794 N95-23539 #
PB95-140802 ..... p 1767 N95-23556
PB95-141222 ..... p 1767 N95-23557 #
PB95-141248 ..... p 1767 N95-23558
PB95-141255 ..... p 1794 N95-23559 #
PB95-149357 ..... p 1870 N95-23925 #
PB95-149365 ..... p 1870 N95-23926 #
PB95-910401 ..... p 1610 N95-23609 #

PL-TR-93-2201 ..... p 1739 N95-23247
PL-TR-94-2076 ..... p 1737 N95-22951 #
PL-TR-94-2204 ..... p 1831 N95-22948 #

PNL-SA-24038 ..... p 1735 N95-24146 #
PNL-SA-24176 ..... p 1767 N95-23578 #
PNL-SA-24394 ..... p 1735 N95-23580 #
PNL-SA-24515 ..... p 1732 N95-22781 #
PNL-SA-24552 ..... p 1843 N95-23579 #
PNL-SA-24931 ..... p 1749 N95-24145 #

PNL-10165 ..... p 1654 N95-22692 #
PNL-10203 ..... p 1635 N95-23348 #

PWA-6113-73 ..... p 1689 N95-23795 * #

R/D-7414-AN-02-VOL-1 ..... p 1691 N95-23118 #

RAL-94-037 ..... p 1799 N95-23155
RAL-94-041 ..... p 1807 N95-23156
RAL-94-043 ..... p 1807 N95-23157
RAL-94-045 ..... p 1807 N95-23158
RAL-94-048 ..... p 1807 N95-23160
RAL-94-051 ..... p 1807 N95-23159
RAL-94-063 ..... p 1850 N95-23154
RAL-94-073 ..... p 1630 N95-23537
RAL-94-086 ..... p 1755 N95-22769
RAL-94-092 ..... p 1785 N95-22544 #
RAL-94-098 ..... p 1798 N95-23127

RANA-93-13 ..... p 1833 N95-23170 #
RANA-93-14 ..... p 1789 N95-23169
RANA-93-15 ..... p 1789 N95-23171 #
RANA-93-16 ..... p 1667 N95-23172 #
RANA-93-17 ..... p 1789 N95-23173
RANA-93-18 ..... p 1789 N95-23174 #
RANA-93-19 ..... p 1789 N95-23149 #
RANA-94-03 ..... p 1648 N95-23145
RANA-94-04 ..... p 1789 N95-23176 #
RANA-94-05 ..... p 1667 N95-23144 #
RANA-94-06 ..... p 1667 N95-23175 #

RC-275-114 ..... p 1732 N95-22865 #

REPT-725311-3 ..... p 1657 N95-23391 * #
REPT-95B00017 ..... p 1820 N95-22957 * #
REPT-95B00026 ..... p 1856 N95-23209 * #
REPT-95B00035 ..... p 1628 N95-23025 * #
REPT-95B00040-VOL-4 ..... p 1740 N95-23529 * #
REPT-95B00043-VOL-25-REV-1 .. p 1743 N95-22671 * #
REPT-95B00056 ..... p 1857 N95-24108 * #

RFP-4882 ..... p 1734 N95-23384 #

RI/RD95-146 ..... p 1696 N95-24064 * #

RIACS-TR-92-01 ..... p 1764 N95-24023 * #
RIACS-TR-92-02 ..... p 1791 N95-23611 * #
RIACS-TR-92-03 ..... p 1791 N95-23592 * #
RIACS-TR-92-07 ..... p 1791 N95-23593 * #
RIACS-TR-92-09 ..... p 1791 N95-23547 * #
RIACS-TR-92-12 ..... p 1764 N95-23594 * #
RIACS-TR-92-15 ..... p 1791 N95-23612 * #
RIACS-TR-94-04 ..... p 1791 N95-23548 * #
RIACS-TR-94-05 ..... p 1758 N95-23610 * #

RIVM-776201007 ..... p 1733 N95-23126

RL-TR-94-124 ..... p 1659 N95-22507
RL-TR-94-154 ..... p 1819 N95-22508 #
RL-TR-94-171 ..... p 1838 N95-22511

RTI/4321/Q4-94 ..... p 1864 N95-22526 * #

S-780 ..... p 1617 N95-23262 * #
S-789 ..... p 1621 N95-23249 * #

SAND-93-0120 ..... p 1726 N95-22502 #
SAND-93-2557C ..... p 1741 N95-24009 #
SAND-93-3866C ..... p 1868 N95-23656 #
SAND-93-8685C ..... p 1632 N95-22722 #
SAND-94-0468C ..... p 1652 N95-22838 #
SAND-94-0691 ..... p 1638 N95-22576 #
SAND-94-0882C ..... p 1659 N95-22549 #
SAND-94-0883C ..... p 1661 N95-22844 #
SAND-94-1179 ..... p 1666 N95-22914 #
SAND-94-1248 ..... p 1726 N95-22554 #
SAND-94-1328C ..... p 1640 N95-22835 #
SAND-94-1392C ..... p 1818 N95-24160 #
SAND-94-1490 ..... p 1698 N95-22726 #
SAND-94-1546C ..... p 1731 N95-24090 #
SAND-94-1562C ..... p 1731 N95-24157 #
SAND-94-1563C ..... p 1845 N95-24156 #
SAND-94-1570C ..... p 1731 N95-24155 #
SAND-94-1646C ..... p 1624 N95-22885 #
SAND-94-1692C ..... p 1650 N95-23577 #
SAND-94-1706 ..... p 1694 N95-23065 #
SAND-94-1816C ..... p 1740 N95-24008 #
SAND-94-2246 ..... p 1661 N95-22896 #
SAND-94-2258 ..... p 1795 N95-22734 #
SAND-94-2333C ..... p 1694 N95-23056 #
SAND-94-2375C ..... p 1754 N95-22548 #
SAND-94-2375 ..... p 1757 N95-23337 #
SAND-94-2506C ..... p 1842 N95-23135 #
SAND-94-2531C ..... p 1828 N95-23575 #
SAND-94-2642 ..... p 1794 N95-23066 #
SAND-94-2702C ..... p 1759 N95-24020 #
SAND-94-2724C ..... p 1698 N95-22500 #
SAND-94-2731 ..... p 1828 N95-24161 #
SAND-94-2746C ..... p 1622 N95-23532 #
SAND-94-2749C ..... p 1664 N95-24149 #
SAND-94-2777C ..... p 1727 N95-22650 #
SAND-94-2817C ..... p 1636 N95-24007 #
SAND-94-2827C ..... p 1766 N95-23134 #
SAND-94-2831C ..... p 1650 N95-24159 #
SAND-94-2922C ..... p 1663 N95-23779 #
SAND-94-2944C ..... p 1837 N95-24158 #
SAND-94-3047C ..... p 1811 N95-23576 #
SAND-94-3077C ..... p 1730 N95-23489 #
SAND-94-8409 ..... p 1634 N95-23122 #
SAND-94-8586C ..... p 1633 N95-22886 #
SAND-94-8602C ..... p 1828 N95-23767 #
SAND-94-8643C ..... p 1666 N95-23081 #
SAND-94-8725C ..... p 1652 N95-22721 #
SAND-95-8200 ..... p 1799 N95-23379 #
SAND-95-8422C ..... p 1819 N95-22723 #
SAND-95-8435C ..... p 1639 N95-22724 #

SGD-602-PT-1 ..... p 1870 N95-23925 #
SGD-602-PT-2 ..... p 1870 N95-23926 #

SISSA-113/93/EP ..... p 1812 N95-23785 #

SLAC-PUB-6638 ..... p 1801 N95-22521 #

SNUTP-94-15 ..... p 1850 N95-22783 #

SR-3 ..... p 1739 N95-23247

SRI PROJ. ESU-4604 ..... p 1738 N95-23090 * #

SSD95D0069-VOL-1 ..... p 1621 N95-23188 * #
SSD95D0069-VOL-3 ..... p 1621 N95-23189 * #

SU-SLAC-PUB-6473 ..... p 1742 N95-22701 #
SU-SLAC-PUB-6533 ..... p 1816 N95-22567 #
SU-SLAC-PUB-6542 ..... p 1806 N95-23139 #
SU-SLAC-PUB-6636 ..... p 1806 N95-23140 #
SU-SLAC-PUB-6668 ..... p 1808 N95-23226 #
SU-SLAC-PUB-6678 ..... p 1816 N95-22702 #
SU-SLAC-PUB-6679 ..... p 1807 N95-23141 #
SU-SLAC-PUB-6683 ..... p 1847 N95-22566 #
SU-SLAC-PUB-6695 ..... p 1802 N95-22703 #
SU-SLAC-PUB-6699 ..... p 1807 N95-23165 #
SU-SLAC-PUB-6709 ..... p 1691 N95-22704 #
SU-SLAC-PUB-6711 ..... p 1806 N95-23138 #
SU-SLAC-PUB-6729 ..... p 1851 N95-23352 #

SU-SLAC-422 ..... p 1802 N95-22697 #
SU-SLAC-429 ..... p 1802 N95-22699 #
SU-SLAC-448 ..... p 1746 N95-22897 #
SU-SLAC-449 ..... p 1840 N95-22851
SU-SLAC-453 ..... p 1848 N95-22698 #

TAE-698 ..... p 1699 N95-23662 #
TAE-712 ..... p 1699 N95-23923 #

TIFR/TH-94-01 ..... p 1867 N95-22739 #

TII-R9201-001-RD ..... p 1696 N95-23792 * #

TN-94-3 ..... p 1659 N95-24193 #

TR-112894-3570P ..... p 1658 N95-23670 * #
TR-522 ..... p 1793 N95-24003 #
TR-523 ..... p 1658 N95-23937 #
TR-524 ..... p 1792 N95-24002 #
TR-526 ..... p 1760 N95-24092 #
TR-527 ..... p 1792 N95-23931 #
TR-528 ..... p 1764 N95-23930 #
TR-529 ..... p 1792 N95-23929 #
TR-530 ..... p 1783 N95-24001 #
TR-531 ..... p 1853 N95-24043 #
TR-532 ..... p 1659 N95-24193 #
TR-533-REV ..... p 1759 N95-23928 #
TR-534 ..... p 1793 N95-24042 #
TR-535 ..... p 1753 N95-24177 #
TR-536 ..... p 1784 N95-24040 #
TR-537 ..... p 1794 N95-23927 #
TR-538 ..... p 1658 N95-24039 #
TR-539 ..... p 1764 N95-24037 #
TR-540 ..... p 1764 N95-23936 #
TR-541 ..... p 1797 N95-24063 #
TR-542 ..... p 1765 N95-24061 #
TR-543 ..... p 1784 N95-24060 #
TR-544 ..... p 1760 N95-24059 #
TR-545 ..... p 1760 N95-24058 #
TR-546 ..... p 1784 N95-24185 #
TR-547 ..... p 1765 N95-24184 #
TR-550 ..... p 1765 N95-24183 #
TR-551 ..... p 1783 N95-24036 #
TR-552 ..... p 1793 N95-24182 #
TR-553 ..... p 1759 N95-23935 #
TR-554 ..... p 1760 N95-24056 #
TR-555 ..... p 1658 N95-23794 #
TR-556 ..... p 1797 N95-24029 #
TR-557 ..... p 1793 N95-24034 #
TR-560 ..... p 1759 N95-24033 #
TR-561 ..... p 1793 N95-24194 #
TR-562 ..... p 1783 N95-24031 #
TR-563 ..... p 1792 N95-23793 #
TR-567 ..... p 1784 N95-24038 #
TR-94-A-019 ..... p 1613 N95-24030 * #

TRS-483 ..... p 1787 N95-22768

TUM-TH-164/94 ..... p 1850 N95-22783 #

UCRL-ID-117124 ..... p 1732 N95-22898 #
UCRL-ID-117670 ..... p 1831 N95-22899 #
UCRL-ID-118487 ..... p 1749 N95-23142 #
UCRL-ID-118564 ..... p 1635 N95-23381 #
UCRL-ID-118629 ..... p 1738 N95-23143 #
UCRL-ID-118630 ..... p 1733 N95-23123 #
UCRL-ID-118631 ..... p 1733 N95-23124 #
UCRL-ID-118632 ..... p 1737 N95-23063 #

UCRL-JC-112328 ..... p 1665 N95-22491 #
UCRL-JC-115595 ..... p 1659 N95-22504 #
UCRL-JC-116015-REV-1 ..... p 1763 N95-22858 #
UCRL-JC-116015 ..... p 1763 N95-22859 #
UCRL-JC-116590 ..... p 1841 N95-22860 #
UCRL-JC-116614 ..... p 1790 N95-23536 #
UCRL-JC-116834 ..... p 1695 N95-23358 #
UCRL-JC-116947 ..... p 1661 N95-23080 #
UCRL-JC-117113 ..... p 1837 N95-24017 #
UCRL-JC-117308 ..... p 1766 N95-23078 #
UCRL-JC-117419 ..... p 1855 N95-22871 #
UCRL-JC-117463 ..... p 1813 N95-24046 #
UCRL-JC-117506 ..... p 1727 N95-22574 #
UCRL-JC-117858 ..... p 1690 N95-22595 #
UCRL-JC-117859 ..... p 1827 N95-23449 #
UCRL-JC-117918 ..... p 1662 N95-23334 #
UCRL-JC-118017 ..... p 1763 N95-23243 #
UCRL-JC-118476 ..... p 1616 N95-24019 #
UCRL-JC-118477 ..... p 1735 N95-24018 #

ULT/TR-94-6505 ..... p 1871 N95-24191 * #

US-PATENT-APPL-SN-004009 ..... p 1632 N95-22710
US-PATENT-APPL-SN-014581 ..... p 1613 N95-23395 *
US-PATENT-APPL-SN-014584 ..... p 1612 N95-23390 *
US-PATENT-APPL-SN-025210 ..... p 1660 N95-22708
US-PATENT-APPL-SN-029808 ..... p 1749 N95-22579 *
US-PATENT-APPL-SN-046331 ..... p 1827 N95-23045 *
US-PATENT-APPL-SN-053752 ..... p 1662 N95-23241
US-PATENT-APPL-SN-056503 ..... p 1613 N95-22578 *
US-PATENT-APPL-SN-061401 ..... p 1751 N95-23264 *
US-PATENT-APPL-SN-087237 ..... p 1687 N95-22706
US-PATENT-APPL-SN-105251 ..... p 1649 N95-23253 *
US-PATENT-APPL-SN-106865 ..... p 1695 N95-23376 *
US-PATENT-APPL-SN-111318 ..... p 1762 N95-22564 *
US-PATENT-APPL-SN-128007 ..... p 1627 N95-22563 *
US-PATENT-APPL-SN-141430 ..... p 1649 N95-23254 *
US-PATENT-APPL-SN-179598 ..... p 1663 N95-24048 * #
US-PATENT-APPL-SN-191309 ..... p 1647 N95-22558 *
US-PATENT-APPL-SN-217511 ..... p 1799 N95-22863
US-PATENT-APPL-SN-287028 ..... p 1819 N95-22492
US-PATENT-APPL-SN-287029 ..... p 1820 N95-22864
US-PATENT-APPL-SN-288114 ..... p 1694 N95-22892 * #
US-PATENT-APPL-SN-317491 ..... p 1799 N95-22921 * #
US-PATENT-APPL-SN-359752 ..... p 1648 N95-22882 * #
US-PATENT-APPL-SN-361601 ..... p 1666 N95-22906 * #
US-PATENT-APPL-SN-652821 ..... p 1800 N95-23073
US-PATENT-APPL-SN-703649 ..... p 1695 N95-23376 *
US-PATENT-APPL-SN-736880 ..... p 1649 N95-23254 *
US-PATENT-APPL-SN-779672 ..... p 1688 N95-23263 *
US-PATENT-APPL-SN-800902 ..... p 1693 N95-22707
US-PATENT-APPL-SN-827177 ..... p 1827 N95-23378 *
US-PATENT-APPL-SN-865535 ..... p 1649 N95-23394 *
US-PATENT-APPL-SN-866779 ..... p 1692 N95-22543 * #
US-PATENT-APPL-SN-882230 ..... p 1660 N95-22709
US-PATENT-APPL-SN-889347 ..... p 1615 N95-23389 *
US-PATENT-APPL-SN-892054 ..... p 1627 N95-22563 *
US-PATENT-APPL-SN-904550 ..... p 1819 N95-22765 *
US-PATENT-APPL-SN-908141 ..... p 1767 N95-23387 *
US-PATENT-APPL-SN-920700 ..... p 1766 N95-22705
US-PATENT-APPL-SN-926117 ..... p 1688 N95-23377 *
US-PATENT-APPL-SN-929556 ..... p 1750 N95-22766 *
US-PATENT-APPL-SN-935939 ..... p 1611 N95-23393 *
US-PATENT-APPL-SN-942500 ..... p 1754 N95-22577 *
US-PATENT-APPL-SN-994593 ..... p 1819 N95-22807 *

US-PATENT-CLASS-118-723VE .. p 1647 N95-22558 *
US-PATENT-CLASS-137-614.04 .. p 1695 N95-23376 *
US-PATENT-CLASS-156-330.9 .... p 1649 N95-23254 *
US-PATENT-CLASS-156-60 ..... p 1649 N95-23254 *
US-PATENT-CLASS-165-104.17 .. p 1695 N95-23376 *
US-PATENT-CLASS-165-10 ..... p 1695 N95-23376 *
US-PATENT-CLASS-204-192.38 .. p 1647 N95-22558 *
US-PATENT-CLASS-204-298.41 .. p 1647 N95-22558 *
US-PATENT-CLASS-205-118 ..... p 1687 N95-22706
US-PATENT-CLASS-244-182 ..... p 1615 N95-23389 *
US-PATENT-CLASS-244-199 ..... p 1612 N95-23390 *
US-PATENT-CLASS-244-215 ..... p 1613 N95-23395 *
US-PATENT-CLASS-244-216 ..... p 1613 N95-23395 *
US-PATENT-CLASS-244-51 ..... p 1615 N95-23389 *
US-PATENT-CLASS-244-7R ..... p 1615 N95-23389 *
US-PATENT-CLASS-244-75R ..... p 1615 N95-23389 *
US-PATENT-CLASS-244-75R ..... p 1612 N95-23390 *
US-PATENT-CLASS-250-227.16 .. p 1819 N95-22807 *
US-PATENT-CLASS-250-370.14 .. p 1827 N95-23378 *
US-PATENT-CLASS-250-492.2 .... p 1660 N95-22709
US-PATENT-CLASS-250-561 ..... p 1827 N95-23045 *
US-PATENT-CLASS-257-436 ..... p 1827 N95-23378 *
US-PATENT-CLASS-257-437 ..... p 1827 N95-23378 *
US-PATENT-CLASS-264-130 ..... p 1750 N95-22766 *
US-PATENT-CLASS-264-135 ..... p 1750 N95-22766 *
US-PATENT-CLASS-264-137 ..... p 1750 N95-22766 *
US-PATENT-CLASS-264-166 ..... p 1627 N95-22563 *
US-PATENT-CLASS-264-257 ..... p 1750 N95-22766 *
US-PATENT-CLASS-264-332 ..... p 1627 N95-22563 *
US-PATENT-CLASS-264-60 ..... p 1627 N95-22563 *
US-PATENT-CLASS-264-63 ..... p 1627 N95-22563 *
US-PATENT-CLASS-333-166 ..... p 1660 N95-22708
US-PATENT-CLASS-340-825.8 .... p 1762 N95-22564 *
US-PATENT-CLASS-340-827 ..... p 1762 N95-22564 *
US-PATENT-CLASS-340-946 ..... p 1611 N95-23393 *
US-PATENT-CLASS-340-953 ..... p 1611 N95-23393 *
US-PATENT-CLASS-340-961 ..... p 1611 N95-23393 *
US-PATENT-CLASS-340-981 ..... p 1611 N95-23393 *
US-PATENT-CLASS-345-8 ..... p 1613 N95-22578 *
US-PATENT-CLASS-348-207 ..... p 1819 N95-22765 *
US-PATENT-CLASS-348-269 ..... p 1819 N95-22765 *
US-PATENT-CLASS-359-561 ..... p 1827 N95-23045 *
US-PATENT-CLASS-362-62 ..... p 1611 N95-23393 *
US-PATENT-CLASS-364-410 ..... p 1749 N95-22579 *
US-PATENT-CLASS-364-578 ..... p 1613 N95-22578 *
US-PATENT-CLASS-370-16 ..... p 1762 N95-22564 *
US-PATENT-CLASS-370-58.3 ..... p 1762 N95-22564 *
US-PATENT-CLASS-370-60 ..... p 1762 N95-22564 *
US-PATENT-CLASS-370-94.1 ..... p 1762 N95-22564 *
US-PATENT-CLASS-371-37.1 ..... p 1754 N95-22577 *

US-PATENT-CLASS-379-221 ..... p 1762 N95-22564 *
US-PATENT-CLASS-382-15 ..... p 1767 N95-23387 *
US-PATENT-CLASS-382-27 ..... p 1767 N95-23387 *
US-PATENT-CLASS-382-415 ..... p 1766 N95-22705
US-PATENT-CLASS-382-42 ..... p 1827 N95-23045 *
US-PATENT-CLASS-385-123 ..... p 1819 N95-22807 *
US-PATENT-CLASS-385-13 ..... p 1819 N95-22807 *
US-PATENT-CLASS-385-28 ..... p 1819 N95-22807 *
US-PATENT-CLASS-395-152 ..... p 1613 N95-22578 *
US-PATENT-CLASS-395-95 ..... p 1692 N95-22543 * #
US-PATENT-CLASS-395-97 ..... p 1692 N95-22543 * #
US-PATENT-CLASS-395-98 ..... p 1692 N95-22543 * #
US-PATENT-CLASS-416-34 ..... p 1688 N95-23377 *
US-PATENT-CLASS-416-61 ..... p 1688 N95-23377 *
US-PATENT-CLASS-427-207.1 .... p 1649 N95-23254 *
US-PATENT-CLASS-427-430.1 .... p 1649 N95-23254 *
US-PATENT-CLASS-427-580 ..... p 1647 N95-22558 *
US-PATENT-CLASS-427-96 ..... p 1649 N95-23254 *
US-PATENT-CLASS-428-262 ..... p 1649 N95-23394 *
US-PATENT-CLASS-428-268 ..... p 1649 N95-23394 *
US-PATENT-CLASS-428-289 ..... p 1649 N95-23394 *
US-PATENT-CLASS-428-325 ..... p 1649 N95-23394 *
US-PATENT-CLASS-428-331 ..... p 1649 N95-23394 *
US-PATENT-CLASS-428-469 ..... p 1649 N95-23394 *
US-PATENT-CLASS-434-307R .... p 1613 N95-22578 *
US-PATENT-CLASS-434-372 ..... p 1613 N95-22578 *
US-PATENT-CLASS-434-38 ..... p 1613 N95-22578 *
US-PATENT-CLASS-434-43 ..... p 1613 N95-22578 *
US-PATENT-CLASS-435-6 ..... p 1632 N95-22710
US-PATENT-CLASS-437-90 ..... p 1662 N95-23241
US-PATENT-CLASS-482-111 ..... p 1751 N95-23264 *
US-PATENT-CLASS-501-8 ..... p 1627 N95-22563 *
US-PATENT-CLASS-501-95 ..... p 1627 N95-22563 *
US-PATENT-CLASS-528-230 ..... p 1649 N95-23253 *
US-PATENT-CLASS-528-232 ..... p 1649 N95-23253 *
US-PATENT-CLASS-528-243 ..... p 1649 N95-23253 *
US-PATENT-CLASS-528-244 ..... p 1649 N95-23253 *
US-PATENT-CLASS-528-266 ..... p 1649 N95-23253 *
US-PATENT-CLASS-601-23 ..... p 1751 N95-23264 *
US-PATENT-CLASS-62-250.3 ..... p 1695 N95-23376 *
US-PATENT-CLASS-62-299 ..... p 1695 N95-23376 *
US-PATENT-CLASS-73-150A ..... p 1688 N95-23263 *
US-PATENT-CLASS-73-178H ..... p 1611 N95-23393 *
US-PATENT-CLASS-73-574 ..... p 1800 N95-23073
US-PATENT-CLASS-73-827 ..... p 1688 N95-23263 *
US-PATENT-CLASS-73-851 ..... p 1688 N95-23263 *

US-PATENT-5,199,305 ..... p 1688 N95-23263 *
US-PATENT-5,291,055 ..... p 1827 N95-23378 *
US-PATENT-5,294,080 ..... p 1613 N95-23395 *
US-PATENT-5,296,288 ..... p 1649 N95-23394 *
US-PATENT-5,306,661 ..... p 1662 N95-23241
US-PATENT-5,315,296 ..... p 1611 N95-23393 *
US-PATENT-5,326,050 ..... p 1612 N95-23390 *
US-PATENT-5,330,131 ..... p 1615 N95-23389 *
US-PATENT-5,332,659 ..... p 1632 N95-22710
US-PATENT-5,333,210 ..... p 1767 N95-23387 *
US-PATENT-5,336,892 ..... p 1660 N95-22709
US-PATENT-5,338,432 ..... p 1687 N95-22706
US-PATENT-5,338,599 ..... p 1693 N95-22707
US-PATENT-5,339,057 ..... p 1660 N95-22708
US-PATENT-5,345,825 ..... p 1800 N95-23073
US-PATENT-5,351,311 ..... p 1766 N95-22705
US-PATENT-5,352,090 ..... p 1688 N95-23377 *
US-PATENT-5,356,361 ..... p 1751 N95-23264 *
US-PATENT-5,376,209 ..... p 1649 N95-23254 *
US-PATENT-5,376,807 ..... p 1827 N95-23045 *
US-PATENT-5,377,100 ..... p 1749 N95-22579 *
US-PATENT-5,377,182 ..... p 1762 N95-22564 *
US-PATENT-5,377,207 ..... p 1754 N95-22577 *
US-PATENT-5,377,310 ..... p 1692 N95-22543 * #
US-PATENT-5,378,795 ..... p 1649 N95-23253 *
US-PATENT-5,379,065 ..... p 1819 N95-22765 *
US-PATENT-5,380,415 ..... p 1647 N95-22558 *
US-PATENT-5,381,493 ..... p 1819 N95-22807 *
US-PATENT-5,384,083 ..... p 1750 N95-22766 *
US-PATENT-5,388,990 ..... p 1613 N95-22578 *
US-PATENT-5,389,321 ..... p 1627 N95-22563 *
US-PATENT-5,392,844 ..... p 1695 N95-23376 *

USGS-OFR-94-216 ..... p 1737 N95-22924 #
USGS-OFR-94-312 ..... p 1742 N95-23385 #

UVA/528340/CS95/108 ..... p 1756 N95-23017 * #
UVA/528488/MSE95/101 ..... p 1869 N95-24066 * #

UW-CPTC-94-7 ..... p 1832 N95-23072 #

VPI-E-94-09 ..... p 1648 N95-23179 * #

WAPD-T-3003 ..... p 1639 N95-22732 #
WAPD-T-3053 ..... p 1640 N95-22893 #

WHC-MR-0479 ..... p 1647 N95-22647 #
WHC-MR-0480 ..... p 1647 N95-22648 #

WHC-SA-2614 ..... p 1661 N95-22799 #

WHC-SD-CP-TP-079 ..... p 1809 N95-23407 #
WHC-SD-CP-TP-080 ..... p 1808 N95-23350 #

WHC-SD-EN-TI-247 ..... p 1736 N95-22843 #

WHC-SD-GN-CSCM-30022 ..... p 1857 N95-24089 #

WHC-SD-GN-CSDD-30006-REV-1 p 1856 N95-23341 #

WHC-SD-GN-CSRS-30008-REV-1 p 1856 N95-23340 #

WHC-SD-GN-CSWD-30076 ..... p 1755 N95-22718 #

WHC-SD-GN-ER-30033 ..... p 1757 N95-23346 #

WHC-SD-GN-SDD-30007-REV-1 . p 1756 N95-22894 #

WHC-SD-L045H-CSDD-001 ..... p 1759 N95-24006

WHC-SD-RTG-SDP-001 ..... p 1662 N95-23351 #

WHOI-93-29 ..... p 1744 N95-23766 *

WSRC-MS-94-0149 ..... p 1645 N95-23980

Y/DW-1340 ..... p 1806 N95-23055 #

APPENDIX

NASA SCIENTIFIC AND TECHNICAL INFORMATION OFFICE PRODUCTS AND SERVICES

The NASA Scientific and Technical Information (STI) Office provides for the collection and announcement of aerospace-related reports and literature obtained worldwide through agreements and exchanges. The result of the collection is the comprehensive NASA STI Database that covers aeronautics, space, and supporting disciplines.

The STI Database, documents generated or obtained by NASA, and products and services derived from or supporting the database are made available to the NASA research community and to the public. Descriptions and sources of these items are presented in the following pages.

Scientific and Technical Aerospace Reports (STAR) is an abstract journal, listing citations with abstracts for aerospace-related reports obtained from worldwide sources. *STAR* is issued on the first of each month, and announces current documents that have been entered into the NASA STI Database during the previous month. The reports are of the following types:

- NASA, NASA contractor, and NASA grantee reports;
- Reports issued by other U.S. Government agencies, domestic and foreign institutions, universities, and private firms;
- Translations in report form;
- NASA-owned patents and patent applications
- Other U.S. Government agency and foreign patents and patent applications
- Domestic and foreign dissertations and theses.

Journal, book, and conference literature, journal translations, and certain foreign dissertations having the same subject scope as *STAR* are announced in a companion journal, *NASA Open Volumes on Aerospace (NOVA). NOVA* is issued on the 15th of each month and is available from the NASA Center for AeroSpace Information, at the address below.

ELIGIBILITY AND REGISTRATION FOR NASA STI PRODUCTS AND SERVICES

Organizations of the type listed below that have registered with NASA can receive products and services.

- NASA offices and installations, contractors, subcontractors, grantees, and consultants;
- Other U.S. Government agencies and their contractors;
- Libraries in the United States that have arrangements with NASA to maintain collections of NASA documents for public reference;
- Other organizations in the United States having a need for NASA documents in work related to aeronautics and space research;
- Organizations abroad that have established reciprocal documents exchange arrangements with NASA.

The central service points—central points of document acquisition and control within qualified organizations—or individuals are eligible to register for NASA STI products and services. Domestic organizations or individuals may be eligible to receive various classes of NASA publications and services and should address their requests for registration or further information to:

ATTN: Registration Services
NASA Center for AeroSpace Information
800 Elkridge Landing Road
Linthicum Heights, MD 21090-2934
301-621-0390

Organizations abroad should direct requests to:

National Aeronautics and Space Administration
Scientific and Technical Information Office (JT)
International STI Office
Washington, DC 20546-0001
USA
703-271-5640

SUBJECT SCOPE

The subject scope of *STAR* and *NOVA* includes all aspects of aeronautics and space research and development, supporting basic and applied research, and applications. Aerospace aspects of Earth resources, energy development, conservation, oceanography, environmental protection, urban transportation, and other topics of high national priority are also covered.

HOW TO USE *STAR* SUBJECT CATEGORIES

Abstracts in *STAR* are categorized by 10 major subject divisions that are divided further into 76 specific subject categories. The subject divisions and categories are listed in the Table of Contents together with a note for each that defines its scope and provides any cross-references. For example:

> **16 SPACE TRANSPORTATION**
>
> Includes passenger and cargo space transportation, e.g., shuttle operations; and space rescue techniques. For related information see also *03 Air Transportation and Safety* and *18 Spacecraft Design, Testing and Performance.* For space suits see *54 Man/System Technology and Life Support.*

CROSS-REFERENCES

Individual *STAR* abstracts are not ordinarily cross-referenced, except for certain conference reports or book translations that have had separate abstracts written for their component papers or chapters. Citations and abstracts of the components follow immediately after those of the parent document. When the subject content of a component differs sufficiently from the general content of the parent, a cross-reference citation also is printed at the end of the category to which it normally would have been assigned if it were independent.

DOCUMENTS ON MICROFICHE

Documents available on microfiche are designated by a pound sign (#) following the accession number.

LIMITED REPRODUCIBILITY

A note of limited reproducibility appears in the citation, if there are factors affecting the reproducibility of more than 20% of the document. These factors include faint or broken type, color photographs, black and white photographs, foldouts, dot matrix print, or some other factor that limits the reproducibility of the document. This notation also appears on the microfiche header.

NASA PATENTS AND PATENT APPLICATIONS

Patents and patent applications owned by NASA are announced in *STAR* under appropriate subject categories and are referenced in the *STAR* indexes. In the Report Number Index, patents are indexed by the NASA Case Number, and the U.S. Patent Class. Patent applications are indexed by the NASA Case Number and the U.S. Patent Application Serial Number.

Printed copies of patents (which are not microfiched) are available for purchase from the U.S. Patent and Trademark Office.

When ordering patents, the U.S. Patent Number should be used, and payment must be remitted in advance, by money order or check payable to the Commissioner of Patents and Trademarks. Prepaid purchase coupons for ordering are also available from the U.S. Patent and Trademark Office.

NASA patent application specifications are sold in both paper copy and microfiche by the NASA Center for AeroSpace Information (CASI). The N accession number should be used in ordering either paper copy or microfiche from CASI.

The patents and patent applications announced in *STAR* are owned by NASA and are available for royalty-free licensing. Requests for licensing terms and further information should be addressed to:

National Aeronautics and Space Administration
Associate General Counsel for Intellectual Property
Code GP
Washington, DC 20546-0001

SOURCES FOR DOCUMENTS

One or more sources from which a document announced in *STAR* is available to the public is ordinarily given on the last line of the citation. The most commonly indicated sources and their acronyms or abbreviations are listed below, and their addresses are listed on page A-6. If the publication is available from a source other than those listed, the publisher and his address will be displayed on the availability line or in combination with the corporate source line.

Avail: CASI. Sold by the NASA Center for AeroSpace Information. Prices for hard copy (HC) and microfiche (MF) are indicated by a price code following the letters HC or MF in the *STAR* citation. Current values for the price codes are given in the tables on page A-7.

NOTE ON ORDERING DOCUMENTS: When ordering publications from NASA CASI, use the N accession number or other report number. It is also advisable to cite the title and other bibliographic identification.

Avail: SOD (or GPO). Sold by the Superintendent of Documents, U.S. Government Printing Office, in hard copy.

Avail: BLL (formerly NLL): British Library Lending Division, Boston Spa, Wetherby, Yorkshire, England. Photocopies available from this organization at the price shown. (If none is given, inquiry should be addressed to the BLL.)

Avail: DOE Depository Libraries. Organizations in U.S. cities and abroad that maintain collections of Department of Energy reports, usually in microfiche form, are listed in *Energy Research Abstracts*. Services available from the DOE and its depositories are described in a booklet, *DOE Technical Information Center - Its Functions and Services* (TID-4660), which may be obtained without charge from the DOE Technical Information Center.

Avail: ESDU. Pricing information on specific data, computer programs, and details on Engineering Sciences Data Unit (ESDU) topic categories can be obtained from ESDU International Ltd. Requesters in North America should use the Virginia address while all other requesters should use the London address, both of which are on page A-6.

Avail: Fachinformationszentrum Karlsruhe. Gesellschaft für wissenschaftlich-technische Information mbH 76344 Eggenstein-Leopoldshafen, Germany.

Avail: HMSO. Publications of Her Majesty's Stationery Office are sold in the U.S. by Pendragon House, Inc. (PHI), Redwood City, CA. The U.S. price (including a service and mailing charge) is given, or a conversion table may be obtained from PHI.

Avail: Issuing Activity, or Corporate Author, or no indication of availability. Inquiries as to the availability of these documents should be addressed to the organization shown in the citation as the corporate author of the document.

Avail: NASA Public Document Rooms. Documents so indicated may be examined at or purchased from the National Aeronautics and Space Administration (JBD-4), Public Documents Room (Room 1H23), Washington, DC 20546-0001, or public document rooms located at NASA installations, and the NASA Pasadena Office at the Jet Propulsion Laboratory.

Avail: NTIS. Sold by the National Technical Information Service. Initially distributed microfiche under the NTIS SRIM (Selected Research in Microfiche) are available. For information concerning this service, consult the NTIS Subscription Section, Springfield, VA 22161.

Avail: Univ. Microfilms. Documents so indicated are dissertations selected from *Dissertation Abstracts* and are sold by University Microfilms as xerographic copy (HC) and microfilm. All requests should cite the author and the Order Number as they appear in the citation.

Avail: US Patent and Trademark Office. Sold by Commissioner of Patents and Trademarks, U.S. Patent and Trademark Office, at the standard price of $1.50 each, postage free. (See discussion of NASA patents and patent applications on page A-3.)

Avail: (US Sales Only). These foreign documents are available to users within the United States from the National Technical Information Service (NTIS). They are available to users outside the United States through the International Nuclear Information Service (INIS) representative in their country, or by applying directly to the issuing organization.

Avail: USGS. Originals of many reports from the U.S. Geological Survey, which may contain color illustrations, or otherwise may not have the quality of illustrations preserved in the microfiche or facsimile reproduction, may be examined by the public at the libraries of the USGS field offices whose addresses are listed on page A-6. The libraries may be queried concerning the availability of specific documents and the possible utilization of local copying services, such as color reproduction.

FEDERAL DEPOSITORY LIBRARY PROGRAM

In order to provide the general public with greater access to U.S. Government publications, Congress established the Federal Depository Library Program under the Government Printing Office (GPO), with 53 regional depositories responsible for permanent retention of material, inter-library loan, and reference services. At least one copy of nearly every NASA and NASA-sponsored publication, either in printed or microfiche format, is received and retained by the 53 regional depositories. A list of the regional GPO libraries, arranged alphabetically by state, appears on page A-8. These libraries are *not* sales outlets. A local library can contact a regional depository to help locate specific reports, or direct contact may be made by an individual.

PUBLIC COLLECTION OF NASA DOCUMENTS

An extensive collection of NASA and NASA-sponsored publications is maintained by the British Library Lending Division, Boston Spa, Wetherby, Yorkshire, England for public access. The British Library Lending Division also has available many of the non-NASA publications cited in *STAR*. European requesters may purchase facsimile copy or microfiche of NASA and NASA-sponsored documents, those identified by both the symbols # and * from ESA — Information Retrieval Service European Space Agency, 8-10 rue Mario-Nikis, 75738 CEDEX 15, France.

SUBMITTING DOCUMENTS

All users of this abstract service are urged to forward reports to be considered for announcement in *STAR*. This will aid NASA in its efforts to provide the fullest possible coverage of all scientific and technical publications that might support aeronautics and space research and development. If you have prepared relevant reports (other than those you will transmit to NASA, DOD, or DOE through the

usual contract- or grant-reporting channels), please send them for consideration to the NASA Center for AeroSpace Information, 800 Elkridge Landing Road, Linthicum Heights, MD 21090-2934.

Reprints of journal articles, book chapters, and conference papers are also welcome. These will be considered for announcement in *STAR's* companion journal, *NOVA*.

You may specify a particular source to be included in a report announcement if you wish; otherwise the report will be placed on a public sale at the NASA Center for AeroSpace Information. Copyrighted publications will be announced but not distributed or sold.

PURCHASE OF *STAR*

STAR is publicly available on annual subscription from the NASA Center for AeroSpace Information (CASI). 1995 *STAR* subscription prices are $100.00/domestic and $125.00/foreign. Single copy prices: $33.00/domestic, $41.00/foreign.

An annual, cumulative *STAR Index* is also available at $70.00/domestic and foreign.

STAR is available to registered users on annual subscription from the NASA Center for AeroSpace Information, ATTN: Registration Services, 800 Elkridge Landing Road, Linthicum Heights, MD 21090-2934.

ADDRESSES OF ORGANIZATIONS

British Library Lending Division
Boston Spa, Wetherby, Yorkshire
England

Commissioner of Patents and Trademarks
U.S. Patent and Trademark Office
Washington, DC 20231

Department of Energy
Technical Information Center
P.O. Box 62
Oak Ridge, TN 37830

European Space Agency-
Information Retrieval Service ESRIN
Via Galileo Galilei
00044 Frascati (Rome) Italy

Engineering Sciences Data Unit International
P.O. Box 1633
Manassas, VA 22110

Engineering Sciences Data Unit
International, Ltd.
251-259 Regent Street
London, W1R 7AD, England

Fachinformationszentrum Karlsruhe
Gesellschaft für wissenschaftlich-technische
Information mbH
76344 Eggenstein-Leopoldshafen, Germany

Her Majesty's Stationery Office
P.O. Box 569, S.E. 1
London, England

NASA Center for AeroSpace Information
800 Elkridge Landing Road
Linthicum Heights, MD 21090-2934

National Aeronautics and Space Administration
Scientific and Technical Information Office
(JT)
Washington, DC 20546-0001

National Technical Information Service
5285 Port Royal Road
Springfield, VA 22161

Pendragon House, Inc.
899 Broadway Avenue
Redwood City, CA 94063

Superintendent of Documents
U.S. Government Printing Office
Washington, DC 20402

University Microfilms
A Xerox Company
300 North Zeeb Road
Ann Arbor, MI 48106

University Microfilms, Ltd.
Tylers Green
London, England

U.S. Geological Survey Library National Center
MS 950
12201 Sunrise Valley Drive
Reston, VA 22092

U.S. Geological Survey Library
2255 North Gemini Drive
Flagstaff, AZ 86001

U.S. Geological Survey
345 Middlefield Road
Menlo Park, CA 94025

U.S. Geological Survey Library
Box 25046
Denver Federal Center, MS914
Denver, CO 80225

NASA CASI PRICE CODE TABLE

(Effective January 1, 1995)

CASI PRICE CODE	NORTH AMERICAN PRICE	FOREIGN PRICE
A01	$ 6.00	$ 12.00
A02	9.00	18.00
A03	17.50	35.00
A04-A05	19.50	39.00
A06-A09	27.00	54.00
A10-A13	36.50	73.00
A14-A17	44.50	89.00
A18-A21	52.00	104.00
A22-A25	61.00	122.00
A99	Call For Price	Call For Price

IMPORTANT NOTICE

For users not registered at the NASA CASI, prepayment is required. Additionally, a shipping and handling fee of $1.00 per document for delivery within the United States and $9.00 per document for delivery outside the United States is charged.

For users registered at the NASA CASI, document orders may be invoiced at the end of the month, charged against a deposit account, or paid by check or credit card. NASA CASI accepts American Express, Diners' Club, MasterCard, and VISA credit cards. There are no shipping and handling charges. To register at the NASA CASI, please request a registration form through the NASA Access Help Desk at the address or numbers below.

NASA Center for AeroSpace Information
800 Elkridge Landing Road
Linthicum Heights, MD 21090-2934
Telephone: (301) 621-0390
E-mail: help@sti.nasa.gov
Fax: (301) 621-0134

FEDERAL REGIONAL DEPOSITORY LIBRARIES

ALABAMA

AUBURN UNIV. AT MONTGOMERY LIBRARY
Documents Dept.
7300 University Dr.
Montgomery, AL 36117-3596
(205) 244-3650 Fax: (205) 244-0678

UNIV. OF ALABAMA
Amelia Gayle Gorgas Library
Govt. Documents
P.O. Box 870266
Tuscaloosa, AL 35487-0266
(205) 348-6046 Fax: (205) 348-0760

ARIZONA

DEPT. OF LIBRARY, ARCHIVES, AND PUBLIC RECORDS
Research Division
Third Floor, State Capitol
1700 West Washington
Phoenix, AZ 85007
(602) 542-3701 Fax: (602) 542-4400

ARKANSAS

ARKANSAS STATE LIBRARY
State Library Service Section
Documents Service Section
One Capitol Mall
Little Rock, AR 72201-1014
(501) 682-2053 Fax: (501) 682-1529

CALIFORNIA

CALIFORNIA STATE LIBRARY
Govt. Publications Section
P.O. Box 942837 - 914 Capitol Mall
Sacramento, CA 94337-0091
(916) 654-0069 Fax: (916) 654-0241

COLORADO

UNIV. OF COLORADO - BOULDER
Libraries - Govt. Publications
Campus Box 184
Boulder, CO 80309-0184
(303) 492-8834 Fax: (303) 492-1881

DENVER PUBLIC LIBRARY
Govt. Publications Dept. BSG
1357 Broadway
Denver, CO 80203-2165
(303) 640-8846 Fax: (303) 640-8817

CONNECTICUT

CONNECTICUT STATE LIBRARY
231 Capitol Avenue
Hartford, CT 06106
(203) 566-4971 Fax: (203) 566-3322

FLORIDA

UNIV. OF FLORIDA LIBRARIES
Documents Dept.
240 Library West
Gainesville, FL 32611-2048
(904) 392-0366 Fax: (904) 392-7251

GEORGIA

UNIV. OF GEORGIA LIBRARIES
Govt. Documents Dept.
Jackson Street
Athens, GA 30602-1645
(706) 542-8949 Fax: (706) 542-4144

HAWAII

UNIV. OF HAWAII
Hamilton Library
Govt. Documents Collection
2550 The Mall
Honolulu, HI 96822
(808) 948-8230 Fax: (808) 956-5968

IDAHO

UNIV. OF IDAHO LIBRARY
Documents Section
Rayburn Street
Moscow, ID 83844-2353
(208) 885-6344 Fax: (208) 885-6817

ILLINOIS

ILLINOIS STATE LIBRARY
Federal Documents Dept.
300 South Second Street
Springfield, IL 62701-1796
(217) 782-7596 Fax: (217) 782-6437

INDIANA

INDIANA STATE LIBRARY
Serials/Documents Section
140 North Senate Avenue
Indianapolis, IN 46204-2296
(317) 232-3679 Fax: (317) 232-3728

IOWA

UNIV. OF IOWA LIBRARIES
Govt. Publications
Washington & Madison Streets
Iowa City, IA 52242-1166
(319) 335-5926 Fax: (319) 335-5900

KANSAS

UNIV. OF KANSAS
Govt. Documents & Maps Library
6001 Malott Hall
Lawrence, KS 66045-2800
(913) 864-4660 Fax: (913) 864-3855

KENTUCKY

UNIV. OF KENTUCKY
King Library South
Govt. Publications/Maps Dept.
Patterson Drive
Lexington, KY 40506-0039
(606) 257-3139 Fax: (606) 257-3139

LOUISIANA

LOUISIANA STATE UNIV.
Middleton Library
Govt. Documents Dept.
Baton Rouge, LA 70803-3312
(504) 388-2570 Fax: (504) 388-6992

LOUISIANA TECHNICAL UNIV.
Prescott Memorial Library
Govt. Documents Dept.
Ruston, LA 71272-0046
(318) 257-4962 Fax: (318) 257-2447

MAINE

UNIV. OF MAINE
Raymond H. Fogler Library
Govt. Documents Dept.
Orono, ME 04469-5729
(207) 581-1673 Fax: (207) 581-1653

MARYLAND

UNIV. OF MARYLAND - COLLEGE PARK
McKeldin Library
Govt. Documents/Maps Unit
College Park, MD 20742
(301) 405-9165 Fax: (301) 314-9416

MASSACHUSETTS

BOSTON PUBLIC LIBRARY
Govt. Documents
666 Boylston Street
Boston, MA 02117-0286
(617) 536-5400, ext. 226
Fax: (617) 536-7758

MICHIGAN

DETROIT PUBLIC LIBRARY
5201 Woodward Avenue
Detroit, MI 48202-4093
(313) 833-1025 Fax: (313) 833-0156

LIBRARY OF MICHIGAN
Govt. Documents Unit
P.O. Box 30007
717 West Allegan Street
Lansing, MI 48909
(517) 373-1300 Fax: (517) 373-3381

MINNESOTA

UNIV. OF MINNESOTA
Govt. Publications
409 Wilson Library
309 19th Avenue South
Minneapolis, MN 55455
(612) 624-5073 Fax: (612) 626-9353

MISSISSIPPI

UNIV. OF MISSISSIPPI
J.D. Williams Library
106 Old Gym Bldg.
University, MS 38677
(601) 232-5857 Fax: (601) 232-7465

MISSOURI

UNIV. OF MISSOURI - COLUMBIA
106B Ellis Library
Govt. Documents Sect.
Columbia, MO 65201-5149
(314) 882-6733 Fax: (314) 882-8044

MONTANA

UNIV. OF MONTANA
Mansfield Library
Documents Division
Missoula, MT 59812-1195
(406) 243-6700 Fax: (406) 243-2060

NEBRASKA

UNIV. OF NEBRASKA - LINCOLN
D.L. Love Memorial Library
Lincoln, NE 68588-0410
(402) 472-2562 Fax: (402) 472-5131

NEVADA

THE UNIV. OF NEVADA LIBRARIES
Business and Govt. Information Center
Reno, NV 89557-0044
(702) 784-6579 Fax: (702) 784-1751

NEW JERSEY

NEWARK PUBLIC LIBRARY
Science Div. - Public Access
P.O. Box 630
Five Washington Street
Newark, NJ 07101-7812
(201) 733-7782 Fax: (201) 733-5648

NEW MEXICO

UNIV. OF NEW MEXICO
General Library
Govt. Information Dept.
Albuquerque, NM 87131-1466
(505) 277-5441 Fax: (505) 277-6019

NEW MEXICO STATE LIBRARY
325 Don Gaspar Avenue
Santa Fe, NM 87503
(505) 827-3824 Fax: (505) 827-3888

NEW YORK

NEW YORK STATE LIBRARY
Cultural Education Center
Documents/Gift & Exchange Section
Empire State Plaza
Albany, NY 12230-0001
(518) 474-5355 Fax: (518) 474-5786

NORTH CAROLINA

UNIV. OF NORTH CAROLINA - CHAPEL HILL
Walter Royal Davis Library
CB 3912, Reference Dept.
Chapel Hill, NC 27514-8890
(919) 962-1151 Fax: (919) 962-4451

NORTH DAKOTA

NORTH DAKOTA STATE UNIV. LIB.
Documents
P.O. Box 5599
Fargo, ND 58105-5599
(701) 237-8886 Fax: (701) 237-7138

UNIV. OF NORTH DAKOTA
Chester Fritz Library
University Station
P.O. Box 9000 - Centennial and University Avenue
Grand Forks, ND 58202-9000
(701) 777-4632 Fax: (701) 777-3319

OHIO

STATE LIBRARY OF OHIO
Documents Dept.
65 South Front Street
Columbus, OH 43215-4163
(614) 644-7051 Fax: (614) 752-9178

OKLAHOMA

OKLAHOMA DEPT. OF LIBRARIES
U.S. Govt. Information Division
200 Northeast 18th Street
Oklahoma City, OK 73105-3298
(405) 521-2502, ext. 253
Fax: (405) 525-7804

OKLAHOMA STATE UNIV.
Edmon Low Library
Stillwater, OK 74078-0375
(405) 744-6546 Fax: (405) 744-5183

OREGON

PORTLAND STATE UNIV.
Branford P. Millar Library
934 Southwest Harrison
Portland, OR 97207-1151
(503) 725-4123 Fax: (503) 725-4524

PENNSYLVANIA

STATE LIBRARY OF PENN.
Govt. Publications Section
116 Walnut & Commonwealth Ave.
Harrisburg, PA 17105-1601
(717) 787-3752 Fax: (717) 783-2070

SOUTH CAROLINA

CLEMSON UNIV.
Robert Muldrow Cooper Library
Public Documents Unit
P.O. Box 343001
Clemson, SC 29634-3001
(803) 656-5174 Fax: (803) 656-3025

UNIV. OF SOUTH CAROLINA
Thomas Cooper Library
Green and Sumter Streets
Columbia, SC 29208
(803) 777-4841 Fax: (803) 777-9503

TENNESSEE

UNIV. OF MEMPHIS LIBRARIES
Govt. Publications Dept.
Memphis, TN 38152-0001
(901) 678-2206 Fax: (901) 678-2511

TEXAS

TEXAS STATE LIBRARY
United States Documents
P.O. Box 12927 - 1201 Brazos
Austin, TX 78701-0001
(512) 463-5455 Fax: (512) 463-5436

TEXAS TECH. UNIV. LIBRARIES
Documents Dept.
Lubbock, TX 79409-0002
(806) 742-2282 Fax: (806) 742-1920

UTAH

UTAH STATE UNIV.
Merrill Library Documents Dept.
Logan, UT 84322-3000
(801) 797-2678 Fax: (801) 797-2677

VIRGINIA

UNIV. OF VIRGINIA
Alderman Library
Govt. Documents
University Ave. & McCormick Rd.
Charlottesville, VA 22903-2498
(804) 824-3133 Fax: (804) 924-4337

WASHINGTON

WASHINGTON STATE LIBRARY
Govt. Publications
P.O. Box 42478
16th and Water Streets
Olympia, WA 98504-2478
(206) 753-4027 Fax: (206) 586-7575

WEST VIRGINIA

WEST VIRGINIA UNIV. LIBRARY
Govt. Documents Section
P.O. Box 6069 - 1549 University Ave.
Morgantown, WV 26506-6069
(304) 293-3051 Fax: (304) 293-6638

WISCONSIN

ST. HIST. SOC. OF WISCONSIN LIBRARY
Govt. Publication Section
816 State Street
Madison, WI 53706
(608) 264-6525 Fax: (608) 264-6520

MILWAUKEE PUBLIC LIBRARY
Documents Division
814 West Wisconsin Avenue
Milwaukee, WI 53233
(414) 286-3073 Fax: (414) 286-8074

*U.S. GOVERNMENT PRINTING OFFICE: 1995-387-253/20009

The New NASA Video Catalog is Here

Free!

To order your free copy call
the NASA Access Help Desk at
(301) 621-0390 or
fax to (301) 621-0134 or
e-mail to helpdesk@sti.nasa.gov

EXPLORE THE UNIVERSE

This publication was prepared by the NASA Center for AeroSpace Information,
800 Elkridge Landing Road, Linthicum Heights, MD 21090-2934, (301) 621-0390.

National Aeronautics and
Space Administration
Code JT
Washington, DC 20546-0001